50 years of the International Society of Biomechanics

Japanese Society of Biomechanics since1972

FUKUOKA

XXIX Congress of International/Japanese Society of Biomechanics

ISB/JSB2023

PROGRAM & ABSTRACT BOOK

プログラムとアブストラクトの本

ISB・JSB FUKUOKA 2023

Fukuoka University

Fukuoka International Congress Center

30th July – 3rd August, 2023

Fukuoka, Japan

Sponsors

Diamond Sponsor

VICON

Sapphire Sponsors

OptiTrack

QUALISYS
Motion Capture Systems

Crystal Sponsors

XSENSOR

4 Assist
株式会社フォーアシスト

BERTEC

NORAXON
SAKAImed
The exclusive distributor of Noraxon in Japan since1998

DELSYS
Inter Reha

cometa

Movella
Bringing meaning to movement

Exhibition Sponsors

Tekscan

Tec Gihan

KISTLER
measure. analyze. innovate.

ゼロシーセブン株式会社

novel.de
&
Creact

SiMi

BTS Bioengineering

Sportip

SPICE
NOBBYTECH

h/p/cosmos

AMTI
FORCE AND MOTION

PRECIX

The Motion Monitor
THE TOTAL SOLUTION IN MOTION CAPTURE

Minor Sponsor

National Biomechanics Day April 5, 2023

THEIA
Markerless

ISB Gold Sponsors

VICON

WORLD ATHLETICS

BERTEC

DELSYS
Inter Reha

QUALISYS
Motion Capture Systems

ELSEVIER

AMTI
FORCE AND MOTION

Proud to be Sapphire Sponsors of ISB 2023 Fukuoka

Win Win Win

For your chance to win yourself an Apple Watch pop by our booth and test out our 2 fully interactive baseball demonstrations

More information about Vicon and our guide to Fukuoka visit www.vicon/com.ISB2023

Join Us and our Distributor IRC on Wednesday 2nd August for drinks and nibbles - scan the code to get your ticket

www.vicon.com

NEXUS

OptiTrack x Acuity inc.

CLOSING THE LOOP FOR BIOMECHANISTS

RUN TO BOOTH C

Test Optitrack's new solver and real-time analysis with Acuity

Learn more at **OptiTrack.com** or **Acuity-inc.co.jp**

QUALISYS

www.qualisys.com

We turn motion into science.

Qualisys is proud to support the biomechanics community by being a Sapphire sponsor of ISB 2023. For more than 30 years, we have been supplying motion capture systems for researchers, coaches, and clinicians. Visit *Qualisys Booth B* as our staff members below host various hands-on demonstrations.

MONDAY 30 JULY

Digital Integrations - Bertec Force Plates

Learn how to digitally integrate Bertec force plates with QTM. We will demonstrate the workflow live using our Functional Assessment module to display force integration within our web reporting platform.

TUESDAY 31 JULY

Scripting in QTM

In this interactive demonstration, we will show you how to leverage the flexibility of Python or Lua scripts in QTM to add functionality, automate pipelines, create custom tools, and more!

WEDNESDAY 1 AUGUST

OpenSim

Learn how to simplify your simulation workflow with QTM and OpenSim. We will present a streamlined workflow to prepare data recorded with QTM and to load it into OpenSim software.

Nils Betzler

Product Manager of Life Sciences

Chiranjibi Nayak

Area Sales Manager - India

Stephanie Knustrom

Marketing & Communication Manager

Table of Contents

Welcome

from the Congress Chair

Dear Scholars,

Please accept my sincere welcome to the XXIX Conference of the International Society of Biomechanics (ISB) and the XXIX Conference of the Japanese Society of Biomechanics (JSB).

After a long, difficult time, we finally have a chance to exchange our latest findings, ideas and recent advances with friends and colleagues in person. This is exactly what I had hoped I could do as the ISB/JSB2023 conference host. I am so happy with this. My first time at an ISB conference was in Tokyo in 1997. The leader of our laboratory at the University of Tokyo, Professor Miyashita organized the conference as the congress chair. At that time, I had just started my academic career as a research associate at Nagoya University. I was overcome by the scale and the level of science at the ISB conference. I never imagined that I would have a chance to one day organize the ISB conference myself! If I had a chance to go back to that time, I would tell myself “Keep staying in academics because you will organize this conference in the future”. But who can believe it? Anyway, throughout my career, the ISB always shown me the path I have walked.

Also, it is my great pleasure to organize the JSB conference as a joint conference with the ISB conference. Since 1957, JSB continues to enhance academic research on human movement and promotes academic interactions among scientists in order to promote research in biomechanics as a leading scientific society in Japan. Throughout ISB’s history, JSB scholars have actively promoted the ISB’s mission. It is worth noting, JSB scholars successfully organized ISB conferences twice in history and the organizers achieved an excellent reputation from participants for their heart-warming and well-organized conference management. This is the third time for JSB, and I aim to ensure that you will come to have the exact same feeling during the current conference.

Fukuoka University kindly gave me the chance to host a conference in this charming city. Fukuoka is best known for its unique food, culture, beautiful beaches and islands. I am sure you will enjoy your stay. I can’t wait for the start on Sunday 31st July with The Wartenweiler Memorial Lecture. See you all very soon.

Welcome to ISB/JSB2023.

Hiro Nunome, PhD

Professor, Fukuoka University

Congress Chair

Welcome

from the ISB President

Dear Delegates,

On behalf of the International Society of Biomechanics Executive Council and the Congress organizers, I welcome you to Fukuoka, Japan, for the XXIX Congress of the International Society of Biomechanics (ISB2023) to be held in conjunction with the XXIX Congress of the Japanese Society of Biomechanics (JSB2023). Many thanks to the Congress Chair Prof. Hiroyuki Nunome, Fukuoka University, and Congress co-Chair, Dr. Hiroaki Hobara, Tokyo University of Science. Thanks also to the JSB president Prof. Shinji Sakurai, Chukyo University. The Organizing and the Scientific committees have worked very hard for securing this memorable event.

In the past few years, biomechanics has continued to grow despite international crisis and the pandemic. Rather, biomechanics always contributes to bring together professionals from a variety of scientific and technical disciplines including anatomy, physiology, engineering, computer science, orthopaedics, sport science, rehabilitation medicine, kinesiology and others also from industry. They work together to understand the development of diseases on mechanical bases, and to devise products, programmes, devices for a better quality of life and better functional and sport performances. To achieve this, state-of-the-art technology is exploited, and novel tools are developed; we now look forward to take advantage also of AI for more comprehensive models and thorough knowledge of the complex biological systems of the human body.

In 2021, the XXVIII Congress of ISB was held in Stockholm, and, although over 1000 delegates participated digitally we only had about ten people attend in person, because of the terrible international situations. This year we expect two thousand participants, as in most of the Congresses before 2021. It is so important that the necessary contact between these scientists can have a physical space able to welcome, involve and introduce people of all ages and backgrounds. Japan is a perfect location, due to its long and superb history and the passion and competence of its people, presenting a clear example of a tight-knit community. Please take the chance to become acquainted with the Japanese biomechanists, and also to meet the people and to taste their fascinating cities and culture. By gathering in person again, we finally can better exchange ideas and projects, to get to know each other, to hear research stories with sympathy, and thus perhaps to strengthen friendships amongst people in the world.

The ISB wants to promote biomechanics internationally and to contribute to this spirit of collaboration. In addition to the biennial international Congresses, the Society has a number of initiatives in this respect, including publications, student awards and mentoring, honours, social media, educational series, specialised Technical Groups, local national communities, special supports for members in economically developing countries, recommendation papers etc. Please search and ask about these, the Council members and other seniors will be pleased to tell you. The Congress is also the time for the General Assembly, where these activities are reported and discussed all together.

To make this Congress even more memorable, we celebrate 50 years of the ISB with a number of special guests and surprise events!

Alberto Leardini, DPhil

Istituto Ortopedico Rizzoli, Bologna - Italy

President, International Society of Biomechanics

Welcome

from the JSB President

Dear Delegates,

As the president of the Japanese Society of Biomechanics (JSB), I am honored to welcome you to our joint conference with the International Society of Biomechanics (ISB). This marks the third time that the ISB conference is being held in Japan, following the 8th conference in Nagoya in 1981 and the 16th conference in Tokyo in 1997.

The JSB was founded in 1957, and this year's conference marks our 29th meeting, coinciding with the 29th biannual conference of the ISB, which was established in 1973. We are thrilled to be hosting this esteemed event in Fukuoka.

2020 saw the World Health Organization declare a global emergency due to the COVID-19 pandemic. After more than three years of uncertainty, we are finally able to gather in person for this conference. While online events have their advantages, there is nothing that can replace the value of face-to-face discussions and information exchange that takes place at such gatherings.

I am confident that this conference will provide a stimulating forum for the exchange of ideas and the presentation of cutting-edge research in biomechanics. I encourage all attendees to take full advantage of this opportunity to engage with fellow researchers, share knowledge, deepen friendship, and forge new collaborations.

In closing, I thank each of you for attending and contributing to what is sure to be an outstanding showcase and celebration of the field of biomechanics. On behalf of the JSB executive board, we wish all attendees an enjoyable and intellectually stimulating meeting.

Shinji Sakurai, PhD

Professor, Chukyo University

President, Japanese Society of Biomechanics

Organizing Committee

Hiroyuki Nunome	Congress Chair, Fukuoka University
Hiroaki Hobara	Congress Co-Chair, Tokyo University of Science
Shinji Sakurai	JSB president, Chukyo University
Senshi Fukashiro	Advisory Board, Japan Women's College of Physical Education
Tadao Isaka	Advisory Board, Ritsumeikan University
Chiho Fukusaki	Secretary General, Chukyo University
Nahoko Sato	Secretary General, Nagoya Gakuin University
Satoru Hashizume	JSB Secretary, Ritsumeikan University
Hiroshi Suito	Mie University
Hironari Shinkai	Tokyo Gakugei University
Koichiro Inoue	Yamagata University
Norio Tsujimoto	Fukui University of Technology
Shinya Sano	Gifu City Women's College
Hiroki Ozaki	Japan Institute of Sports Science
Ryo Iwasaki	Fukuoka University
Yuji Tamura	Fukuoka University

Scientific Committee

Todd Pataky	Chair of Scientific Committee, Kyoto University
Yuki Inaba	Vice-Chair of Scientific Committee, Japan Institute of Sports Science
Ismail Shariman	Secretary General, Universiti Teknologi MARA
Raihana Sharir	Secretary General, Universiti Teknologi MARA

Hiroshi AKIMA
Yumna ALBERTUS
Kirsten ALBRACHT
Jacqueline ALDERSON
Michael Skipper ANDERSON
Charlotte APPS
Toni ARNDT
Takeshi ASAI
Alexandra ATACK
Simon AUGUSTUS
Michael BAGGALEY
Kevin BALL
Bruno BEDO
Erica BELL
Claudio BELVEDERE
Daniel BENOIT
Jillian BEVERRIDGE
Daniel BOARI
Maarten BOBBERT
Bart BOLSTERLEE
Xavier BONNET
Salvatore FEDERICO
Véronique FEIPEL
Kayla FEWSTER
Daniel FONG
Masahiro FUJIMOTO
Mako FUKANO
Reginaldo FUKUCHI
Atsuki FUKUTANI
Johannes FUNKEN
Phob GANOKROJ
Ying GAO
Deanna GATES
Andresa GERMANO
Claudia GIACOMOZZI
Richie GILL
James GOH
Tomohiro GONJO
Shane GORE
Annamaria GUIOTTO
Elena GUTIERREZ-FAREWIK
Mike HAHN
Shigetada KUDO
Young-Hoo KWON
Mark LAKE
Peter LAMB
Scott LANDRY
Annemarie LAUDANSKI
Alberto LEARDINI
Bill LEDOUX
Ki-Kwang LEE
Hae Dong LEE
Zong-Ming LI
Glen LICHTWARK
Yi-Xing LIU
Tung-Wu LU
Filip Gertz LYSDAL
Christian MAIWALD
Matthew MAJOR
Alberto Encarnación MARTINEZ
Konstantinos MICHALAKIS
Karen MICKLE
Isabel SACCO
Natsuki SADO
Lenny Suryani SAFRI
Kanae SANO
Shinya SANO
Karen SARRO
Nahoko SATO
Takahiko SATO
Zimi SAWACHA
Veerle SEGERS
Wolfgang SEIBERL
Oliver SEYNNES
Hironari SHINKAI
Masahiro SHINYA
Hiroto SHIOTANI
Anne SILVERMAN
Peter SINCLAIR
Annemie SMEETS
Neal SMITH
Gisela SOLE
Fabiola SPOLAOR

Fransiska BOSSUYT
Bjoern BRAUNSTEIN
Samuel CALLAGHAN
Paolo CARAVAGGI
Felipe P CARPES
Dan CATELLI
Dario CAZZOLA
Francesco CENNI
John CHALLIS
Hsiang-Ho CHEN
Weng-Pin CHEN
Nachippan CHOCKALINGAM
Li-Shan CHOU
Elizabeth CLARKE
Michele CONCONI
Andrew CRESSWELL
Joseph CRISCO
Neil CRONIN
Kris D'AOUT
Kat DANIELS
Sina DAVID
Brian DAVIS
Heiliane DE BRITO FONTANA
Mark DE ZEE
Vijay DHAMODHARAN
Taylor DICK
Fernando DIEFENTHAELER
Catherine DISSELHORST-KLUG
Sharon DIXON
Phil DIXON
Janessa DRAKE
Marcos DUARTE
Janet DUFEK
Kim DUFFY
Yoshihiro EHARA
Ryoichi EMA
Yasushi ENOMOTO
Hayri ERTAN
Amir ESRAFILIAN
Timothy EXELL
Dominic FARRIS

Joseph HAMILL
Seong-Won HAN
Keiichiro HATA
Aoife HEALY
Ewald HENNIG
Walter HERZOG
Tetsuya HIRONO
Genki HISANO
Joakim HOLMBERG
Han HOUDIJK
Ching-Chi HSU
Daisuke ICHIMURA
Masahiro IKENAGA
Akiko IMURA
Takuma INAI
Bernardo INNOCENTI
Koichiro INOUE
Kazuhiro ISHIMURA
Hashbullah ISMAIL
Parunchaya JAMKRAJANG
Ina JANSSEN
Ilse JONKERS
Matt JORDAN
Venus JOUMAA
Taija JUUTINEN
Kumiyo KAI
Emika KATO
Kenton KAUFMAN
Angela KEDGLEY
Luke KELLY
Tom KERNOZEK
Uwe KERSTING
Bryce KILLEN
Mark KING
Enda KING
Duane KNUDSON
Yoshiyuki KOBAYASHI
Shunichi KOBAYASHI
Taiki KOMATSU
Pui Wah KONG
Michihiko KOSEKI
Sentaro KOSHIDA
Stuart MCERLAIN-NAYLOR
Shoma KUDO

Takumi MIEDA
Peter MILBURN
Kathryn MILLS
Sophie De MITS
Luis MOCHIZUKI
Luca MODENESE
Eng Kuan MOO
Marion MUNDT
Akinori NAGANO
Motomu NAKASHIMA
Niels Jensby NEDERGAARD
Mohad Anizu Mohd NOR
Shinya OGAYA
Baaba OTOO
Sakiko OYAMA
Olga PANAGIOTOPOULOU
Sukyung PARK
Jaebum PARK
Cecilia PERSSON
Annamària PETER
Nicola PETRONE
Andrew PHILLIPS
Jarmo PIIRAINEN
Helene PILLET
Claudio PIZZOLATO
Andrew POHL
Wolfgang POTTHAST
Geoffrey POWER
Ezio PREATONI
Jose Ignacio Priego QUESADA
Mike RAINBOW
Brent RAITERI
Timo RANTALAINEN
Guillaume RAO
Chris RICHTER
Mark ROBINSON
Mary RODGERS
Karen ROEMER
Stephanie ROSS
Michelle SABICK

Leonidas SPYROU
Julie STEELE
Darren STEFANYSHYN
Lauri STENROTH
Thorsten STERZING
Eneida SUDA
Hiroshi SUITO
Wannes SWINNEN
Keizo TAKAHASHI
Katsuki TAKAHASHI
Takahiro TANAKA
Petri TANSKA
Hiroshige TATEUCHI
Alexander TSOUKNIDAS
Norio TSUJIMOTO
Brian UMBERGER
Jun UMEHARA
Ton VAN DEN BOGERT
Giuseppe VANNOZZI
Jos VANRENTERGHEM
Benedicte VANWANSEELE
Marco VAZ
Jasper VERHEUL
Mikko VIRMAVIRTA
Logan WADE
Taku WAKAHARA
Brian WALLACE
Ruoli WANG
Bill WANNOP
Kohei WATANABE
Frederick WERNER
Lindsey WESTOVER
Steffen WILLWACHER
Janie WILSON
Momoko YAMAGATA
Bing-Shiang YANG
Ichiro YOSHIMURA
Jackie ZEHR
Ron ZERNICKE

General Information

CITY OF FUKUOKA

Fukuoka is an extremely compact and well-organized city where places to live and work, as well as places of entertainment and leisure, are both temporally and geographically in close proximity. In fact, a short walk from the city center will bring you face-to-face with the expansive Hakata Harbour. Beautiful landscapes replete with water and greenery dot Fukuoka, which is that rare tourist city that offers the urban and the natural together. On your visit, be sure to enjoy Fukuoka's diverse natural environment and well-organized city area to the fullest.

CONGRESS VENUE

Fukuoka International Congress Center
2-1 Sekijo-machi, Hakata-ku, Fukuoka, 812-0032, Japan
TEL: +81-92-262-4111
Access from Fukuoka airport:
15 minutes by taxi / 30 minutes by subway & bus
www.marinemesse.or.jp/eng/congress/access/

GENERAL INFORMATION/REGISTRATION DESK

General information and registration desks are located at the entrance hall on the 1st floor. Participants are requested to complete the online registration in advance. QR code must be downloaded from the registration "My page" after completing the registration to receive the name badge and the certificate of attendance at the registration desk on-site.
Desks will be open during the following times:

Sunday, July 30th	09:30 – 18:00
Monday, July 31st	07:30 – 17:00
Tuesday, August 1st	07:30 – 17:00
Wednesday, August 2nd	07:30 – 17:00
Thursday, August 3rd	07:30 – 14:00

EXHIBITION

The exhibition will be held in the multi-purpose hall on the 2nd floor. It will be open at the following times:

Monday, July 31st	08:00 – 17:00
Tuesday, August 1st	08:00 – 17:00
Wednesday, August 2nd	08:00 – 17:00
Thursday, August 3rd	08:00 – 13:30

TRAVEL DESK

The travel desk will be located at the entrance hall on the 1st floor.

INTERNET

Wireless internet (Wi-Fi) will be available free of charge.

SSID: FCC_Free_WiFi *No password required

INSTRUCTIONS FOR CHAIRS

Chairs are requested to take their seats at the front-right row of each session room at least 15 minutes before the session starts. Chairs are asked to stay within the time allotted for the session and each presentation. During the Q&A, please ask the participants questions and/or comments to stand in line by the microphone in advance.

CORPORATE SUPPORT DISCLOSURE FOR ALL SPEAKERS

All presenters, regardless of format, must disclose within their presentations whether corporate support was provided for their research, including conference-related travel expenses. Example disclosure statements:

- "No corporate support was received for this research."
- "Company ABC funded subject recruitment and data collection. Other than funding no Company ABC employee was directly involved in this research in any way that could have influenced or biased the reported results."

INSTRUCTIONS FOR ORAL PRESENTATIONS

Session	Presentation	Discussion
Keynote	45 minutes	5 minutes
Symposium/Workshop/Others	Assigned individually	
Oral	8 minutes	3 minutes

- You must use congress PCs (Windows). Use of your own PC is not permitted.
- Screen ratio of 16:9 is recommended.
- Preferred file format: PPTX, PowerPoint 2010 or higher. If you create your PowerPoint file on a Mac please check your presentation on a Windows PC beforehand.
- Other file formats: PDF format is also possible.
- Presenter view is not allowed. Please bring your printed notes with you if necessary.
- Please bring your media (USB flash memory drive or CD-R).
- When writing onto a CD-R, use only the hybrid format (ISO 9660), as using special functions such as "Packet Write" may cause problems with data display.
- To avoid the possible spread of computer viruses, always scan your presentation files beforehand with updated anti-virus software.
- After saving your presentation file on the appropriate medium, do a test run on another PC to make sure it works properly.

- Please ensure you arrive at your presentation room and be seated at the next speaker seat at least 15 minutes prior to the start of the session.
- Any copies of your presentation data that the secretariat has received will be deleted after the congress.

SPEAKER READY ROOM

Speaker Ready Room is located on the 2nd floor. Each oral session speaker must report to the Speaker Ready Room to load their presentation on the laptop computer that will be used in their session room at least 1 hour prior to the start of the session. The Speaker Ready Room will be open during the following hours:

Sunday, July 30th	15:00 – 18:00
Monday, July 31st	07:30 – 17:00
Tuesday, August 1st	07:30 – 17:00
Wednesday, August 2nd	07:30 – 17:00
Thursday, August 3rd	07:30 – 15:00

INSTRUCTIONS FOR POSTER DISPLAY

All posters will be displayed during the general poster sessions. There will be no oral presentations, flash talks, or formal rotating audience panels for posters. Instead poster sessions will run in a free format. Each presenter is encouraged to engage with all attendees who are interested in your work.

Monday, July 31st	Install	07:30-
	Session	17:20-18:50
	Dismantle	18:50-19:10
Tuesday, August 1st	Install	07:30-
	Session	18:15-19:55
	Dismantle	19:55-20:15
Wednesday, August 2nd	Install	07:30-
	Session	18:10-19:40
	Dismantle	19:40-20:00

*If your poster is not removed by the relevant deadline, your poster will be removed and disposed of by the secretariat.
Poster size: H 180 cm (71 in) × W 90 cm (35 in).
Poster number: a 20 cm × 20 cm (8 in × 8 in) poster number will be provided at the congress venue on your allotted poster panel. Please place this number on the upper left corner of your poster (see figure below).

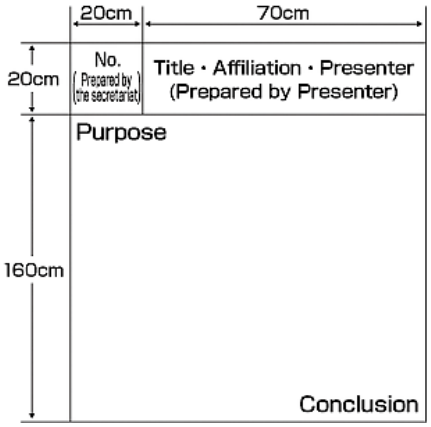

CATERING

Coffee will be offered at the posters/exhibition room on the 2nd floor and lobby on the 5th floor. Lunch will be offered on the 3rd and 4th Floors. For break times please refer to the day-at-a-glance pages of the program.

DRESS CODE

The dress code is smart casual.

DUPLICATION / RECORDING

No photography, videotaping or recording is allowed in oral or poster sessions except by the official society photographer or society-approved audio-visual vendor. This includes cameras, cell phones and all other devices.

SOCIAL PROGRAMS

Welcome Reception
18:00- , Sunday, July 30th
2F, Palace Room, Fukuoka Sunpalace
*Adjacent to the congress venue
1F, Restaurant. Fukuoka International Congress Center

GALA Dinner
19:00- , Thursday, August 3rd
Kawabata Shopping Arcade
kawabatadori.com/en/
*25 min. walk from the congress venue

ISB Student-Mentor Lunch *Registration only
12:40-13:30 , Monday, July 31st (Room 8)

JSB Night
19:00- , Monday, July 31st (Morris Hippo)

Student-NightOut (sponsored by Vicon Motion Systems) *Registration only
20:00- , Tuesday, August 1st

Venue Maps

Fukuoka International Congress Center

4th Floor

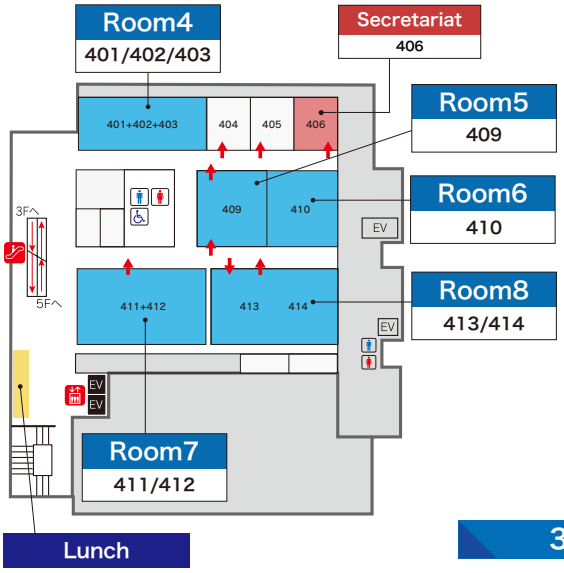

5th Floor

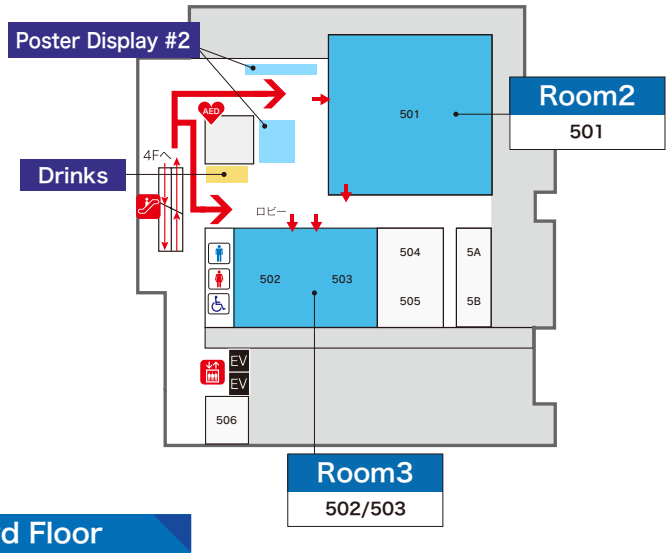

3rd Floor

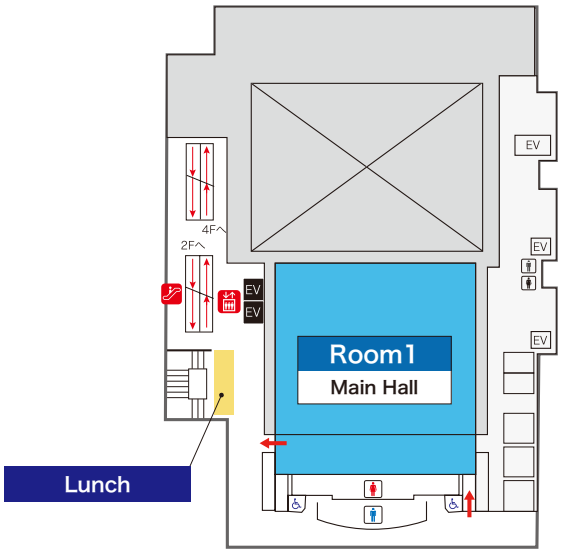

1st Floor

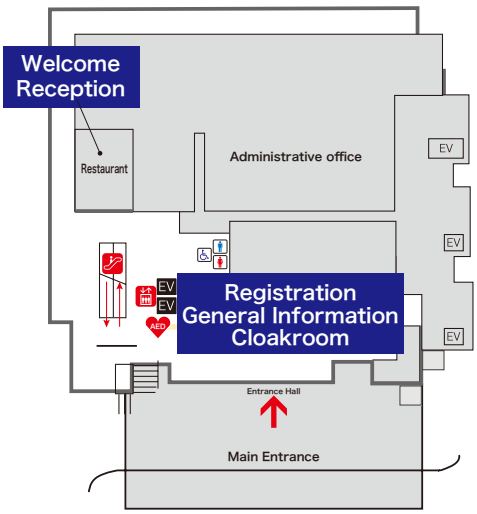

2nd Floor

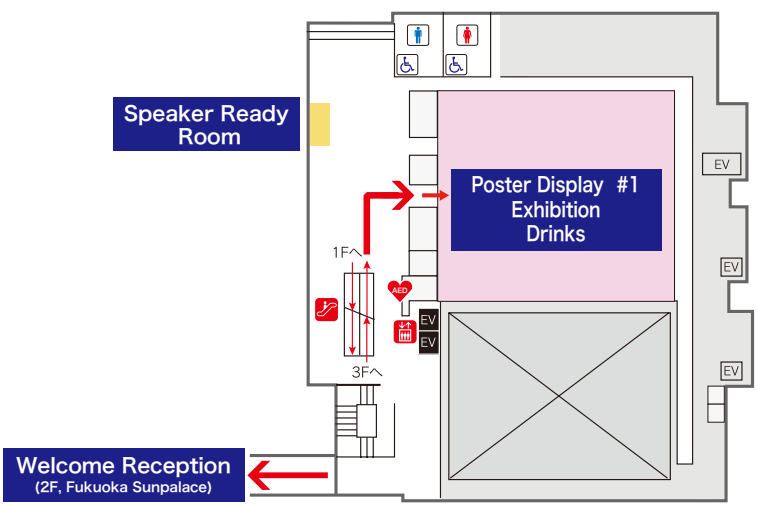

Invited Speakers

Wartenweiler Memorial Lecture

16:45-17:45, Sunday, July 30th

Pioneering Women of ISB: Tales from the Archives and Beyond

Julie Steele

Emeritus Professor, University of Wollongong, Australia

Julie Steele is an Emeritus Professor at the University of Wollongong, retiring in 2020 after 38 years at the University. With over 200 journal publications, Julie's research is focused on developing innovative strategies to decrease injury potential and optimize the quality of life of individuals of all ages. She has investigated lower limb injuries caused by high-impact landings; developed innovative wearable technologies for health applications; examined the effects of obesity, aging and occupational loading on lower limb structure and function; and investigated breast health biomechanics so women can exercise in comfort. A member of the World Council of Biomechanics and a Fellow of ISB, Julie served on the Executive Council of ISB for 14 years and as ISB President from 2009-2011. In 2019 Julie was awarded a Member of the Order of Australia (AM) for significant service to science in the field of biomechanics, higher education, and professional associations.

ISB President's Lecture

13:30-14:20, Thursday, August 3rd

Alberto Leardini

IRCCS Istituto Ortopedico Rizzoli – Bologna, Italy

He has been working at Istituto Ortopedico Rizzoli - Bologna (Italy) since 1990, where he is now Director of the Movement Analysis Laboratory, and Research Coordinator of the Line of Research "Innovative and prosthetic surgery".

He received the Doctor of Philosophy (DPhil) in Orthopaedic Engineering at the University of Oxford. His initial research focused on methodological issues and clinical applications of human motion analysis. His interests evolved to three-dimensional videofluoroscopy, radiostereometry, and ccomputer-assistedsurgery. He also made fundamental progress in the mechanical modelling and prosthesis design of the ankle joint, and his original total ankle replacement is implanted with successful clinical and functional outcomes. He is now exploiting medical imaging, including modern weight-bearing CT, and additive manufacturing for the custom-design of orthotics and implants in Orthopaedics. He is author of 241 papers in peer-review journals (H-index 47 and more than 13200 citations - SCOPUS August 2022) and of 4 international patents.

He has served in many national and international scientific communities: he has been President of the Società Italiana di Analisi del Movimento in Clinica (SIAMOC), of the Technical Group 3-D Analysis of Human Movement (3DAHM) and of the Italian Digital Biomanufacturing Network (IDBN), and in the Research Committee of the European Foot and Ankle Society (EFAS). He has been in the Steering Group of the International Foot & Ankle Biomechanics community (i-FAB) since the foundation, and more recently in the Scientific Board of the International Weight Bearing CT Society (IWBCTS). He is now the President of the International Society of Biomechanics (ISB).

Muybridge Award Lecture

15:10-16:10, Tuesday, August 1st

Born to Move: Embracing our Evolutionary Legacy

Irene S. Davis

The University of South Florida, USA

Dr. Irene Davis is a Professor in the School of Physical Therapy and Rehabilitation Science in the Morsani College of Medicine at the University of South Florida. Prior to this, she was the founding Director of the Spaulding National Running Center, Department of Physical Medicine and Rehabilitation, Harvard Medical School. Dr. Davis received her Bachelor of Science in Exercise Science from the University of Massachusetts, and in Physical Therapy from the University of Florida. She earned her Master's degree in Biomechanics from the University of Virginia, and her PhD in Biomechanics from Pennsylvania State University. She is a Professor Emeritus in Physical Therapy at the University of Delaware where she served on the faculty for over 20 years. Her research is focused on the relationship between lower extremity structure, mechanics and injury. Her research also extends to the development of interventions to alter faulty mechanics through gait retraining. She has been studying the use of wearable sensors in both the evaluation and treatment of injured runners. Her interests also include the effect of minimal footwear on mechanics and injury. Dr. Davis has received funding from the Department of Defense, and National Institutes of Health to support her research. She has given over 350 lectures both nationally and internationally and authored 160 publications on the topic of lower extremity mechanics during walking and running gait. She has been named one of the 50 Most Influential People in Running. She is a Fellow and Past President of the American Society of Biomechanics, and the 2019 ASB Borelli award winner. She is also a Fellow, past Vice President and current President-Elect of the American College of Sports Medicine. Finally, she is a Catherine Worthingham Fellow of the American Physical Therapy Association.

Keynote Lecture 1

09:40-10:30, Monday, July 31st

Animals as Machines: Robotic Approaches to Understanding Comparative Locomotor Mechanics

Bill Sellers

The University of Manchester, United Kingdom

Bill Sellers is a Professor of Natural Science at the University of Manchester where he researches the use of robotic simulation techniques for understanding animal biomechanics. His first degree was in zoology from the University of Cambridge, and he did his PhD on primate locomotion at the University of Liverpool. He uses machine learning to generate control systems that allow anatomically realistic digital twins to produce spontaneous gait patterns that match those recorded experimentally. He has used this approach to answer a range of questions about animal locomotion in both living and fossil animals including human and non-human primates, birds, turtles, spiders, dinosaurs, and plesiosaurs. He has also done a range of experimental and field studies on animal locomotion and vertebrate palaeontology.

Keynote Lecture 2

09:40-10:30, Tuesday, August 1st

Complementary Roles of Biomechanics and Machine Learning in Human Motion Monitoring

Sukyung (Sue) Park

Korea Advanced Institute of Science & Technology (KAIST), South Korea

Sukyung (Sue) Park is a professor in the department of Mechanical Engineering at KAIST, Korea. Her research interests are to understand human movement through the descriptive dynamics model that demonstrates movement mechanics and control, with an ultimate aim to develop wearable healthcare devices. Among a wide range of human movements, she is interested in walking, running, postural control, and sports activities including golf. Her recent studies focus on resolving the challenges of wearable devices for biomechanical variable prediction by integrating biomechanical knowledge with machine learning technology. She earned her BS. and MS. in Mechanical Engineering at KAIST and Ph.D. in Mechanical Engineering from the University of Michigan and was a post-doctoral fellow at the Massachusetts Eye and Ear Infirmary, Harvard Medical School. Recently she served as the Advisor to the President for Science and Technology at the Office of the President.

Keynote Lecture 3

09:40-10:30, Wednesday, August 2nd

Brain-Computer Interface Design: Thinking out of the box

Natalie Mrachacz-Kersting

The University of Freiburg, Germany

Prof. Dr. Natalie Mrachacz-Kersting member of IEEE received her Ph.D. degree in biomedical engineering from Aalborg University, in 2005, and currently holds a position as full Professor in Neuroscience at the Albert-Ludwigs University of Freiburg. She has previously held positions at Aalborg University, Denmark, FH Dortmund and at the University of Auckland, New Zealand. Natalie does research in Medical Technology, Biomedical Engineering and Neuroscience. She has authored over 80 articles in peer-reviewed journals, over 150 conference articles/abstracts, and ten book chapters. She is working on several projects specifically within the area of Brain-Computer-Interfaces (BCIs) involving patient populations such as those suffering from stroke or ALS. Dr. Mrachacz-Kersting received several awards including the international BCI award in 2017. She is on the board of the international society for Brain-Computer Interfaces (BCI Society) and has been voted on the Administrative Committee (AdCom) of the IEEE EMBS where she will commence her term from 1. January, 2023.

Keynote Lecture 4

13:30-14:20, Wednesday, August 2nd

The Mechanics of Running Fast and Jumping High: from small Differences in Ground Force to Big Differences in Performance

Peter Weyand

Southern Methodist University, USA

Dr. Peter Weyand is the Glenn Simmons Endowed Professor of Applied Physiology and Biomechanics and the Director of the Locomotor Performance Laboratory at Southern Methodist University. Prior to joining SMU, Dr. Weyand directed research efforts at Harvard University's Concord Field Station, a large animal facility specializing in terrestrial locomotion, and the Locomotion Laboratory of Rice University. Dr. Weyand's expertise on the mechanical basis of performance has led to him serving as a lead investigator on a number of high-profile projects at the intersection of biomechanics and sport policy. These include the mechanics of basketball flopping and the effects of artificial limbs on running and jumping performance. Dr. Weyand's past research subjects have included antelope, emus, rodents, and professional athletes with and without limb amputations.

Keynote Lecture 5

09:40-10:30, Thursday, August 3rd

Designing Treatment Strategies for Large Skeletal Defects by Combining in Silico, in Vitro and in Vivo Models

Liesbet Geris

The University of Liège and KU Leuven, Belgium

Liesbet Geris is professor in Biomechanics and Computational Tissue Engineering at the University of Liège and KU Leuven (Belgium). Her research focuses on the development of multi-scale and multi-physics in silico and in vitro models. Together with her team and their clinical and industrial collaborators, she uses these models to investigate the etiology of skeletal pathologies, design cell-based treatments, and optimize their manufacturing processes. She has received 2 prestigious ERC grants to finance her research and a number of young investigator and research awards. She is a member of the TERMIS-EU strategic alliance committee. She is the executive director of the VPH Institute, advocating the use of in silico modeling in healthcare through liaising with the clinical community, European Commission and Parliament, regulatory agencies, and patients. Besides her research work, she is often invited to give public lectures on the challenges of interdisciplinarity in research, women in academia, and digital healthcare.

Tutorials

Workshop 1

10:00-12:00, Sunday, July 30th

Machine Learning Applications in Movement Biomechanics

Marion Mundt (University of Western Australia, Australia)

This tutorial will provide an overview of different applications of machine learning to support movement biomechanics analysis. You will learn to use an off-the-shelf pose estimation model to determine anatomically-related landmarks in 2D videos and to code a simple artificial neural network to classify normal and abnormal gait from inertial sensor data. The pros and cons of machine learning in biomechanics will be discussed and opportunities and challenges explained using the two examples provided. All analyses will be undertaken using samples Python files.

Workshop 2

10:00-12:00, Sunday, July 30th

Power to the Foot! Understanding and Applying Distal Power Calculations in Biomechanics

Kota Takahashi (University of Utah, USA)
Eric C. Honert (BOA Technology Inc., USA)

'Distal power' calculation (also called unified deformable segment analysis in the literature) has a myriad of potential applications in biomechanics: (1) to understand energetic functions of the foot and ankle in various tasks (e.g., walking, running, and other sports-specific tasks), species or populations (e.g., individuals with and without pathologies) and (2) to quantify energy storage and return from assistive devices, such as prostheses, orthoses, and footwear. In this tutorial, we encourage participants from various specialties within ISB (e.g., sports or clinical biomechanics, orthopedics, comparative biomechanics, and orthotics & prosthetics) to learn and apply distal power calculations in their research areas. Sample data files from human walking will be provided during the tutorial, but attendees are highly encouraged to bring their unique data for an interactive discussion of the results and interpretations.

Workshop 3

13:00-15:00, Sunday, July 30th

Statistical Parametric Mapping - for MATLAB Users and SPM Novices

Todd Pataky (Kyoto University, Japan)
Mark Robinson (Liverpool John Moores University, UK)
Jos Vanrenterghem (KU Leuven, Belgium)

This tutorial will get you started with spm1d for MATLAB for the analysis of 1D data including forces, kinematics and EMG. We will begin with spm1d's implementations of 0D tests to help you become accustomed to the spm1d interface and its outputs. We'll then walk-through 1D t-tests, regression and ANOVA, highlighting important points regarding statistical outputs and their interpretations. We will also provide a conceptual overview of SPM theory by demonstrating the commonalities between 0D and 1D analysis. We will finish with slides regarding more advanced tests and future spm1d developments. Digital documentation and worksheets will be distributed to attendees; both MATLAB and Python files will be distributed but the workshop demonstrations will conducted in MATLAB only. MATLAB and basic statistics experience is expected but SPM experience is not. WARNING: there will be substantial overlap with our Online Workshop materials (https://spm1d.org/Workshops.html).

Workshop 4

13:00-15:00, Sunday, July 30th

An Introduction to Time-frequency Low-pass Filter Methods in Biomechanics

Neal Smith (University of Chichester, UK)
Simon Augustus (Kingston University, UK)

In a variety of human movements, ranging from walking to running, landing to kicking, we will attempt to apply some kind of mathematical filter to our kinematic (and kinetic) data, reducing the inherent noise within the signal that propagates errors in further calculations. However, the extent to which these body collisions alter the frequency content of the signal has remained relatively unknown. Once this information is identified, it is plausible to optimise the use of contemporary low-pass filter techniques that vary the magnitude of noise reduction over different phases of a task (i.e., transitions from aerial to ground contact). This workshop will explore the theory of the frequency content of these types of collision, along with practical demonstrations, and involvement of the audience with pre-prepared data sets. Participants will require a working version of MATLAB to participate in the workshop.

Exhibitor Location Map (2F)

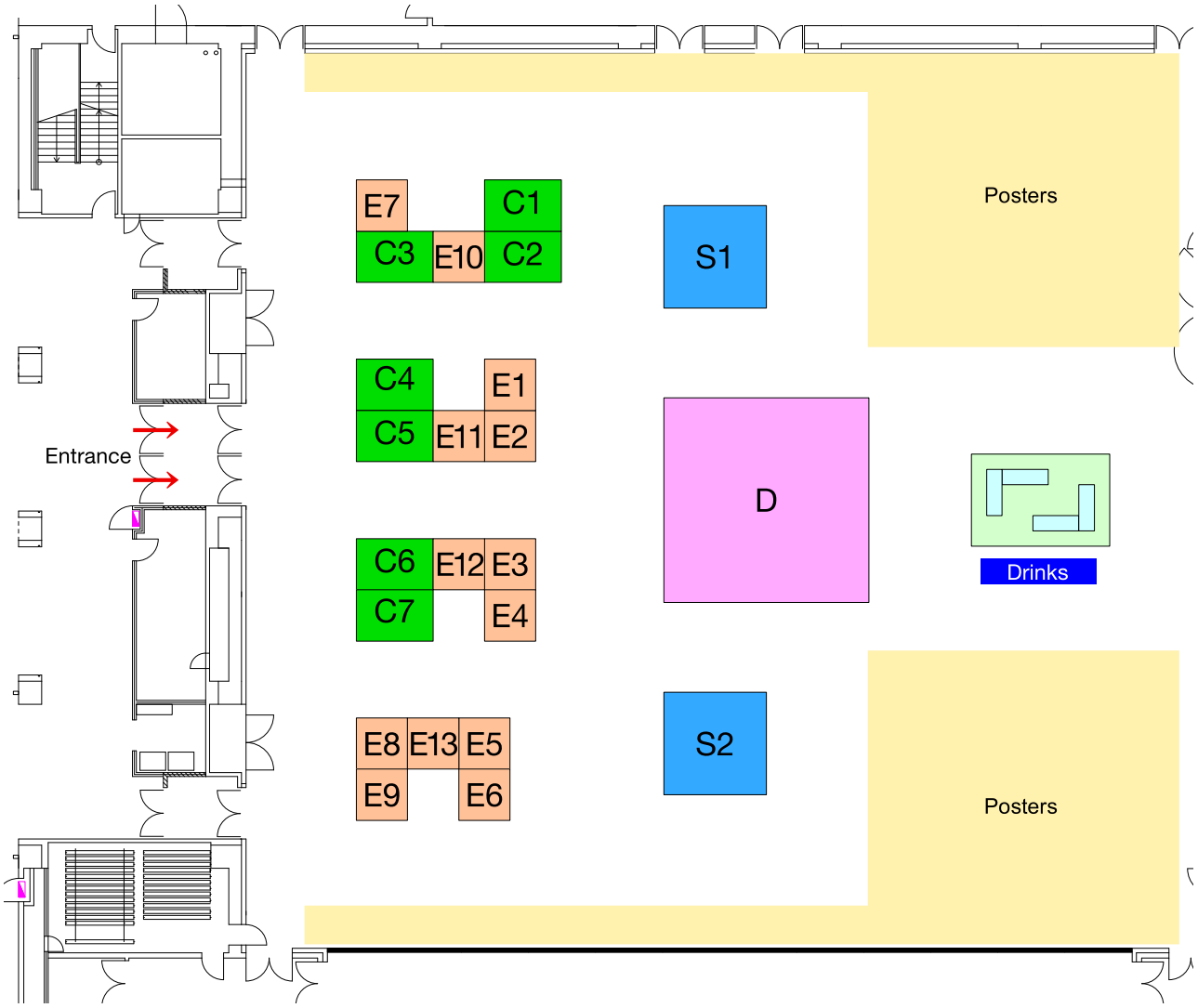

Booth Number	Company Name
C1	Archivetips(Cometa)
C2	BERTEC
C3	Sakai Medical Co.,Ltd.
C4	Movella
C5	XSENSOR Technology Corporation
C6	4Assist, Inc.
C7	Delsys/Inter Reha
D	Vicon Motion Systems Ltd
E1	Tec Gihan Co.,Ltd
E2	Tekscan INC
E3	Kistler Japan G.K.
E4	Zero C Seven Inc.

Booth Number	Company Name
E5	Simi Reality Motion Systems GmbH
E6	**Novel/Creact**
E7	Sportip, Inc.
E8	BTS Bioengineering
E9	Spice/Nobby Tech. Ltd.
E10	h/p/cosmos sports & medical gmbh
E11	AMTI
E12	PreciX
E13	The MotionMonitor (Innovative Sports Training, Inc)
S1	Qualisys
S2	OPTITRACK

Exhibitors

AMTI

Booth Number: E11
Web: www.AMTI.biz

Because Quality Matters... since over 45 years!

AMTI understands that the best research and testing in Orthopedics begins with the best equipment. For this reason, AMTI builds the most accurate Biomechanics Force Platforms, Instrumented Treadmills and state-of the art 6DOF Joint Simulators for your Biomechanical Research. We care about data quality for significant scientific conclusions, shouldn't you?

Archivetips(Cometa)

Booth Number: C1
Web: www.cometasystems.com

Cometa Systems is an Italian company producing and selling wireless EMG and inertial systems. Our systems have the smallest form factor on the market, and exclusive features such as fixed delay and configurable analog output, impedance check and waterproof coating for swimming applications. Our Mini Wave and Pico systems have been used worldwide by the most famous institutions for many years and a number of different applications. WaveX is our latest EMG development, with integrated IMU, wifi memory download, and IP68 certification for underwater use.

BERTEC

Booth Number: C2
Web: www.bertec.com

Thirty-five years of measurement excellence.

Bertec's products have represented a legacy of excellence in biomechanics for over thirty years. We provide solutions founded in accuracy and precision. Our engineering is trusted worldwide to enable a deeper understanding of human movement.
Bertec is a provider of the highest standard instrumented force plates, treadmills, stairs and other devices for the international research community.

BTS Bioengineering

Booth Number: E8
Web: www.btsbioengineering.com

BTS Bioengineering connects the world of healthcare and sport with cutting-edge motion capture technologies.
The ultimate goal of BTS Bioengeneering technologies is to help people overcome their restricted mobility and enhance their performance so that they can face life and competition to the best of their ability. We develop technologies as we are very familiar with the needs of the people for whom they are intended.
For patients and sports people, of course, but primarily for doctors, rehabilitators, physiotherapists, and athletic trainers, who need to find the same simplicity and fluidity in their use as someone who moves confidently.

Delsys/Inter Reha

Booth Number: C7
Web: www.delsys.com

Delsys is the worldwide leader in the design, manufacture, and marketing of a portfolio of high-performance electromyography (EMG) instruments. These include a range of wireless physiological and biomechanical sensors that are used in all types of human movement research and education. These products play a fundamental role in helping researchers, clinicians, and educators understand and solve complex questions surrounding human movement. Our EMG sensors contain a patented electrode design with several different form factors to choose from. Delsys develops its own software to support standalone use as well as a vast number of popular integrations.

4Assist, Inc.

Booth Number: C6
Web: www.4assist.co.jp

We deal with biomechanics such as Motion capture, Forceplate and other sports training science products.

h/p/cosmos sports & medical gmbh

Booth Number: E10
Web: www.hpcosmos.com

h/p/cosmos has been developing and building treadmills since 1988 in Germany for various fields including fitness, competitive sports, sports medicine, orthopaedic and neurological rehabilitation, sport science, biomechanics, uniformed services, performance diagnostics, cardiopulmonary diagnostics and rehabilitation. Over the time, the Traunstein based company has developed into the German specialists in manufacturing treadmill ergometers and systems and set up standards for innovation, technology, safety and support. Many developments and pioneering work from h/p/cosmos have significally influenced product design, functionality and methodologies.

Kistler Japan G.K.

Booth Number: E3
Web: www.kistler.com

As a global leader in dynamic measurement technology for measuring pressure, force, torque and acceleration, we support our customers in industry and science to improve their products and make their manufacturing processes more efficient. The piezoelectric sensor is at the heart of every measurement system from Kistler. To offer you sensors, measurement systems and services that are exactly tailored to your needs, we fully focus upon the complex current and future challenges in the areas of automobile development, industrial automation and in fields related to extreme environments and of course biomechanics and life sciences.

The MotionMonitor (Innovative Sports Training, Inc)

Booth Number: E13
Web: https://innsport.com/

The MotionMonitor makes a real-time biomechanics software for data collection, visualization and analysis. The MotionMonitor provides turn-key motion capture systems with all hardware and software included. Applications include finger, hand and upper extremity movement, gait, balance, sports-specific analysis including baseball, golf, basketball and more. The MotionMonitor team is excited about our recent integration of markerless motion capture, providing a research-grade hardware and software system that is optimized for flexibility and speed.

Movella

Booth Number: C4
Web: www.movella.com

Movella™ is a full-stack hardware, software, and data analytics company created by the consolidation of mCube, Xsens, and Kinduct. Movella is a global innovator of advanced technologies and products that sense, capture and analyze all aspects of movement. Movella serves the entertainment, sports, health, and industrial markets by capturing and transforming movement data into meaningful and actionable insights. Working with the leading global brands such as Electronic Arts, NBC Universal, Toyota, Siemens, and over 500 sports teams, we are creating extraordinary outcomes that move humanity forward.

Novel/Creact

Booth Number: E6
Web: www.novel.de

novel is the global leader in accurate and reliable load distribution measurement systems, with more than 40 years of experience. Our company has developed systems, that are able to measure contact forces between many surfaces,
Our world-wide customers include medical device manufacturers as well as world-class scientists and physicians. All novel systems operate with high quality, calibrated sensors and provide reliable and reproducible long term measurements.
Outstanding scientific software for the analysis of medical and industrial data allows our customers to be always one step ahead.

OptiTrack

Booth Number: S2
Web: www.optitrack.com

OptiTrack delivers the highest performing 3D motion capture hardware and software for both indoors and outdoors activities. With industry-leading 3D precision and accuracy, simpler workflows, on-site manufacturing enabling the best pricing, free and open developer access, and native integration of Force plates or EMG, OptiTrack is the favorite of key leaders in the movement science community. The OptiTrack product line includes motion capture software and world class high-speed tracking cameras ranging offering active markers, passive markers and markerless solutions.

PreciX Pte Ltd

Booth Number: E12

Web: https://precix.io/

PreciX is a Singapore based MedTech company, founded with a mission to revolutionize the approach to joint health and mobility assessment. Our flagship product, GATOR, is a non-invasive multi-sensor wearable platform that leverages automated pipelines and AI-powered data processing to enable the measurement of soft-tissue-corrected knee biomechanics with exceptional precision, eliminating the need for invasive bone pins or continuous X-rays. GATOR is designed for easy setup, without the requirement of body markers or cameras. By prioritizing simplicity, speed, and accessibility in joint assessment and data analysis, PreciX strives to advance and translate biomechanics research for improved patient care and outcomes.

Qualisys

Booth Number: S1

Web: www.qualisys.com

Qualisys is a leading provider of motion capture technology and has a long history of supplying research, animation, engineering and sports facilities with high-end camera systems and expertise in capturing and analyzing movements.

Qualisys offers a wide range of products and services and has offices in Gothenburg, Chicago and Shanghai. Our customers are found in the biomechanical research, sports biomechanics and medical sectors. Our systems are also used for engineering and specialized industrial purposes, along with entertainment applications such as virtual reality and animation.

Qualisys is certified according to ISO 9001:2015, our clinical products are compliant with Medical Device Directive 93/42/EEC and have FDA clearance (K171547), which demonstrates our commitment to provide highest possible quality products and services to our customers. The certifications reflect our ongoing investment in technology, process and people.

Sakai Medical Co.,Ltd.

Booth Number: C3

Web: www.noraxon.com

For over 30 years, Noraxon USA has been an industry leader in human movement metrics and biomechanics research solutions. Innovation is our number one goal and we are constantly hard at work to continue bringing valuable tools to the market for capturing biomechanics. Our system allows you to create a smarter workflow with reliable data by integration of electromyography, force, pressure, motion and high speed video. Whether you are in the lab, on the field, or in the clinic, we provide you with hardware and software solutions that are practical and flexible for all of your measurement applications.

Simi Reality Motion Systems GmbH

Booth Number: E5

Web: www.simi.com

Simi - Pioneers of Motion Capture and Analysis technology

Experts at the intersection of biomechanics and technology. Simi's not only been through the whole journey of motion capture since 1992; we've shaped it. Offering 30+ years of expertise in the field, we are one of the pioneers for markerless motion capture technology.

Simi delivers high-end 3D mocap technology using leading computer vision and machine learning algorithms to detect and quantify human movements in any condition.

We are establishing AI-powered technologies in all kinds of sports. Our solutions offer full 3D analytics, processing and visualization.
Go Markerless, go Simi: Choose experience.
www.simishape.com

Spice/Nobby Tech. Ltd.

Booth Number: E9
Web: mocap.jp

スパイスは30年以上の実績を持ったモーションキャプチャの老舗で、OptiTrackをはじめ多くの製品の日本総代理店です。
ノビテックは、モーションキャプチャやハイスピードカメラを取り扱う、画像計測を専門としたプロ集団です。
本学会では2社で共同出展をしております。

Sportip

Booth Number: E7
Web: www.sportip.jp

Sportip develops markerless 3D motion analysis technology using AI-based human pose estimation and 3D reconstruction. Sportip provides a wide range of products and services, mainly in the fitness, sports, and medical fields, using motion analysis as a solution that enables easy and quick analyzes.

Tec Gihan Co.,Ltd.

Booth Number: E1
Web: tecgihan.co.jp/en/

TEC Gihan is a leading manufacturer of measuring instruments, specializing in multi-axis small sensors, special load cells, and data loggers. We collaborate with cutting-edge companies, research institutes, and universities, supporting their research and development efforts. Our comprehensive range of products includes high-quality measuring instruments, measurement and control software, testing equipment, and inspection tools. With a focus on innovation and reliability, we deliver custom solutions tailored to our customers' unique needs. Through our consistent services and dedication to technological advancement, we strive to be the preferred partner in the field of measurement and instrumentation.

Tekscan INC

Booth Number: E2
Web: www.tekscan.com

Tekscan, Inc. is a leading manufacturer of tactile pressure and force measurement systems, which are used by researchers and clinicians around the world to aid in the diagnosis and treatment of pathomechanical disorders, and to ensure effective offloading of peak plantar pressure areas at increased risk for ulceration. Our in-shoe (F-Scan™) and modular platform and mat (Strideway™ and MobileMat™) systems accurately measure plantar pressure distribution, timing and Center of Force (CoF) trajectory during the stance phases of gait, giving you new information to help design better treatments. Enhance your ability to evaluate, substantiate and document your diagnosis with Tekscan pressure mapping systems. Learn more at www.tekscan.com/medical.

Vicon Motion Systems Ltd

Booth Number: D
Web: www.vicon.com

Vicon delivers highly accurate 3D movement analysis systems for use in dynamic injury assessment and evaluating therapy progress. Over 150 sports training department's world-wide use Vicon technology. Its flagship camera line, the Vicon Valkyrie, offers the highest resolution, frame rates and accuracy available, allowing detailed motion capture in almost any environment. Vero is Vicon's next generation camera, combining size, power, and price performance into one amazing solution.

Vicon was established in Oxford, UK, in 1984 and is now a subsidiary of the Oxford Metrics Group Plc. Some of Vicon's global clients include: University of Calgary's Running Injury Clinic; University of Brussels; Northumbria University; Imperial College, London; Loughborough University; University of Western Australia; Katholieke Universiteit Leuven; and University of New Brunswick. For more information please visit www.vicon.com

Zero C Seven Inc

Booth Number: E4
Web: www.0c7.co.jp

ゼロシーセブン株式会社センシング・ソリューション事業部は、Movella社XSENSモーションキャプチャ、Xsensor社足圧インソール、SIMI社マーカーレスモーションキャプチャなどを扱っています。

The Sensing Solutions Division of Zero C Seven Inc.. handles Movella XSENS motion capture, Xsensor foot pressure insoles, and SIMI marker-less motion capture.

XSENSOR Technology Corporation

Booth Number: C5
Web: www.xsensor.com

Reveal accurate gait and motion data, visualize in high-quality and get access to advanced, easy-to-use AI-powered analysis tools with Intelligent Dynamic Sensing.

Powered by leading-edge technology XSENSOR's Foot and Gait research-grade assistive tools provide access to key insights of the lower extremities, enabling you to augment Movement Research, optimize Athletic Performance, and aid Clinical Assessment.

Scientific Program

Day 1 Sunday, July 30th

Program-at-a-glance

	Room 1 3F Main Hall	Room 2 5F 501	Room 3 5F 502+503	Room 4 4F 401+402+403	Room 5 4F 409	Room 6 4F 410	Room 7 4F 411+412	Room 8 4F 413+414
8:00								
9:00								
10:00		10:00-12:00 **Workshop 1** **Machine Learning Applications in Movement Biomechanics** Marion Mundt						10:00-12:00 **Workshop 2** **Power to the Foot! Understanding and Applying Distal Power Calculations in Biomechanics** Kota Takahashi Eric C. Honert
11:00								
12:00								
13:00		13:00-15:00 **Workshop 3** **Statistical Parametric Mapping - for MATLAB Users and SPM Novices** Todd Pataky Mark Robinson Jos Vanrenterghem						13:00-15:00 **Workshop 4** **An Introduction to Time-frequency Low-pass Filter Methods in Biomechanics** Neal Smith Simon Augustus
14:00								
15:00								
16:00								
17:00	16:30-16:45 **Opening Ceremony** 16:45-17:45 **Wartenweiler Memorial Lecture**	**"Pioneering Women of ISB: Tales from the Archives and Beyond"** Julie Steele Chair: Karen Mickle						
18:00	18:00-20:00 **Welcome Reception (2F Fukuoka Sunpalace / 1F Restaurant, Fukuoka International Congress Center)**							
19:00								
20:00								
21:00								

Scientific Program

Day 2 Monday, July 31st

Program-at-a-glance

	Room 1 3F Main Hall	Room 2 5F 501	Room 3 5F 502+503	Room 4 4F 401+402+403	Room 5 4F 409	Room 6 4F 410	Room 7 4F 411+412	Room 8 4F 413+414
8:00	8:00-9:30 **Symposium 01** **Standardizing Foot & Ankle Bone References**	8:00-9:24 **Oral 01** **Locomotion: General 1**	8:00-9:12 **Oral 02** **Musculoskeletal modeling 1**	8:00-9:12 **Oral 03** **Cellular and molecular**	8:00-9:12 **Oral 04** **Orthopaedics: Bone & cartilage**	8:00-9:24 **Oral 05** **Medical devices**	8:00-9:24 **Oral 06** **Muscle tissue and architecture 1**	8:00-9:12 **Oral 07** **Injuries and rehabilitation 1**
9:00								
10:00	9:40-10:30 **Keynote Lecture 1**	**"Animals as Machines: Robotic Approaches to Understanding Comparative Locomotor Mechanics"** Bill Sellers Chair: Todd Pataky						
11:00	10:30-11:00 **Coffee Break (2F Poster & Exhibition Hall, 5F Lobby)**							
12:00	11:00-12:30 **Symposium 02** **ISB Motor Control Technical Group**	11:00-12:36 **Oral 08** **Sport biomechanics 1**	11:00-12:12 **Oral 09** **Musculoskeletal modeling 2**	11:00-12:12 **Oral 10** **Locomotion: Clinical gait 1**	11:00-12:36 **Oral 11** **Balance and posture 1**	11:00-11:48 **Oral 12** **Clinical biomechanics 1**	11:00-12:24 **Oral 13** **Artificial intelligence and machine learning 1**	11:00-12:12 **Oral 14** **Others 1**
13:00	12:40-13:30 **Lunch Break (3F/4F)**							
14:00	13:30-15:00 **The 50th ISB Anniversary Session #1**							
15:00	15:00-15:40 **Coffee Break & Sweets Serve (2F/5F)**							
16:00	15:40-17:10 **The 50th ISB Anniversary Session #2**							
17:00								
18:00	17:20-18:50 **Poster 01-08 (2nd Floor, Poster Display #1)** **Poster 09-10 (5th Floor, Poster Display #2)** **Dismantle:** 18:50-19:10							
19:00		19:00-20:30 **Advancing Women in Biomechanics**						
20:00								
21:00								

Scientific Program

Day 3 Tuesday, August 1st

Program-at-a-glance

	Room 1 3F Main Hall	Room 2 5F 501	Room 3 5F 502+503	Room 4 4F 401+402+403	Room 5 4F 409	Room 6 4F 410	Room 7 4F 411+412	Room 8 4F 413+414
8:00	8:00-9:30 **Symposium 03** **Artificial Intelligence in Biomechanics**	8:00-9:00 **Oral 15** **DWIA Nominee (Oral)**	8:00-9:24 **Oral 16** **Musculoskeletal modeling 3**	8:00-9:00 **Oral 17** **Methodologies and data analysis 1**	8:00-8:48 **Oral 18** **Impact biomechanics 1**	8:00-9:30 **CNB Symposium Slot 1**	8:00-9:12 **Oral 19** **Injuries and rehabilitation 2**	8:00-9:24 **Oral 20** **Running: Biomechanics 1**
9:00								
10:00	9:40-10:30 **Keynote Lecture 2**	**"Complementary Roles of Biomechanics and Machine Learning in Human Motion Monitoring"** Sukyung (Sue) Park Chair: Maarten Bobbert						
	10:30-11:00 **Coffee Break (2F Poster & Exhibition Hall, 5F Lobby)**							
11:00	11:00-12:30 **Symposium 04** **Biomechanics of Ball Kicking**	11:00-12:12 **Oral 21** **Musculoskeletal modeling 4**	11:00-12:12 **Oral 22** **Wireless sensors and wearable devices 1**	11:00-12:36 **Oral 23** **Spine and trunk 1**		11:00-12:30 **CNB Symposium Slot 2**	11:00-12:24 **Oral 24** **Clinical biomechanics 2**	11:00-12:36 **Oral 25** **Locomotion: General 2**
12:00								
13:00	12:40-13:30 **Lunch Break (3F/4F)**							
14:00	13:30-15:00 **Symposium 05** **Knee Injury**	13:30-14:42 **Oral 26** **JSB Awards Nominee (Oral)**	13:30-14:54 **Oral 27** **Sport biomechanics 2**	13:30-14:18 **Oral 28** **Orthopaedics: Tendon & ligament**	13:30-14:30 **Oral 29** **Running: Footwear 1**	13:30-15:00 **CNB Symposium Slot 3**	13:30-14:30 **Oral 30** **Prosthetics and orthotics 1**	13:30-14:42 **Oral 31** **Rehabilitation technology: Biorobotics and exoskeletons 1**
15:00								
16:00	15:10-16:10 **Muybridge Award Lecture**	**"Born to Move: Embracing our Evolutionary Legacy"** Irene s. Davis Chair: Toni Arndt						
	16:10-16:40 **Coffee Break (2F Poster & Exhibition Hall, 5F Lobby)**							
17:00	16:40-18:10 **Symposium 06** **Bio-Mec (Materials)**	16:40-18:04 **Oral 32** **Sport biomechanics 3**	16:40-18:04 **Oral 33** **Locomotion: Clinical gait 2**	16:40-17:40 **Oral 34** **Simulation techniques and applications 1**	16:40-18:04 **Oral 35** **Others 2**	16:40-18:04 **Oral 36** **Artificial intelligence and machine learning 2**	16:40-17:40 **Oral 37** **Running: Footwear 2**	16:40-18:04 **Oral 38** **Muscle tissue and architecture 2**
18:00								
19:00	18:20-19:50 **Poster 11-16 (2nd floor, Poster Display #1)** **Poster 17-21 (5th Floor, Poster Display #2)** **Dismantle:** 19:55-20:15							
20:00	20:00- **Student-Night out (sponsored by Vicon Motion Systems)**							
21:00								

Scientific Program

Day 4 Wednesday, August 2nd

Program-at-a-glance

	Room 1 3F Main Hall	Room 2 5F 501	Room 3 5F 502+503	Room 4 4F 401+402+403	Room 5 4F 409	Room 6 4F 410	Room 7 4F 411+412	Room 8 4F 413+414
8:00	8:00-9:30 **Symposium 07** **Musculoskeletal Modeling and Simulation applied**	8:00-9:24 **Oral 39** **Sport biomechanics 4**	8:00-9:00 **Oral 40** **Motor control 1**	8:00-9:00 **Oral 41** **Others 3**	8:00-9:12 **Oral 42** **Rehabilitation technology: Biorobotics and exoskeletons 2**	8:00-9:30 **Hand & Wrist Symposium Slot 1**	8:00-9:12 **Oral 43** **Muscle tissue and architecture 3**	8:00-9:00 **Oral 44** **Lower extremities 1**
9:00								
10:00	9:40-10:30 **Keynote Lecture 3**	**"Brain-Computer Interface Design: Thinking out of the box"** Natalie Mrachacz-Kersting Chiar: Gregory Sawicki						
11:00	10:30-11:00 **Coffee Break (2F Poster & Exhibition Hall, 5F Lobby)**							
12:00	11:00-12:30 **Symposium 08** **Performance Enhancement Footwear in Running**	11:00-12:24 **Oral 45** **Locomotion: Clinical gait 3**	11:00-11:48 **Oral 46** **Methodologies and data analysis 2**		11:00-12:00 **Oral 47** **Prosthetics and orthotics 3**	11:00-12:30 **Hand & Wrist Symposium Slot 2**	11:00-12:24 **Oral 48** **Biomedical engineering**	11:00-12:00 **Oral 49** **Impact biomechanics 2**
13:00	12:40-13:30 **Lunch Break (3F/4F)**							
14:00	13:30-14:20 **Keynote Lecture 4**	**"The Mechanics of Running Fast and Jumping High: from small Differences in Ground Force to Big Differences in Performance"** Peter Weyand Chiar: Wolfgang Potthast						
15:00	14:30-16:00 **Symposium 09** **Wearable Intertial Sensors**	14:30-15:42 **Oral 50** **Sport biomechanics 5**	14:30-15:42 **Oral 51** **Balance and posture 2**	14:30-15:30 **Oral 52** **Running: Biomechanics 2**	14:30-15:18 **Oral 53** **Simulation techniques and applications 2**	14:30-16:00 **Hand & Wrist Symposium Slot 3**	14:30-15:54 **Oral 54** **Artificial intelligence and machine learning 3**	14:30-15:30 **Oral 55** **Prosthetics and orthotics 2**
16:00	16:00-16:30 **Coffee Break (2F Poster & Exhibition Hall, 5F Lobby)**							
17:00	16:30-18:00 **Symposium 10** **Ankle Injury Biomechanics**	16:30-17:42 **Oral 56** **Sport biomechanics 6**	16:30-17:54 **Oral 57** **Locomotion: General 3**	16:30-18:06 **Oral 58** **Wireless sensors and wearable devices 2**		16:30-17:20 **Hand & Wrist Symposium Slot 4**	16:30-17:42 **Oral 59** **Clinical biomechanics 3**	16:30-18:06 **Oral 60** **Musculoskeletal modeling 5**
18:00								
19:00	18:10-19:40 **Poster 22-31 (2nd floor, Poster Display #1)** **Poster 32-33 (5th Floor, Poster Display #2)** **Dismantle:** 19:40-20:00							
20:00								
21:00								

Scientific Program

Day 5 Thursday, August 3rd

Program-at-a-glance

	Room 1 3F Main Hall	Room 2 5F 501	Room 3 5F 502+503	Room 4 4F 401+402+403	Room 5 4F 409	Room 6 4F 410	Room 7 4F 411+412	Room 8 4F 413+414
8:00	8:00-9:30 **Symposium 11** **ISEK: Lab and Clinic EMG Updates**	8:00-9:24 **Oral 61** **Balance and posture 3**	8:00-9:00 **Oral 62** **Rehabilitation technology: Biorobotics and exoskeletons 3**	8:00-9:12 **Oral 63** **Ergonomics**	8:00-9:12 **Oral 64** **Others 4**	8:00-9:12 **Oral 65** **Spine and trunk 2**	8:00-8:48 **Oral 66** **Orthopaedics: Surgeon guided biomechanics**	8:00-9:24 **Oral 67** **Upper extremity**
9:00								
10:00	9:40-10:30 **Keynote Lecture 5**	**"Designing Treatment Strategies for Large Skeletal Defects by Combining in Silico, in Vitro and in Vivo Models"** Liesbet Geris Chair: Eng Kuan Moo						
11:00	10:30-11:00 **Coffee Break (2F Poster & Exhibition Hall, 5F Lobby)**							
		11:00-12:12 **Oral 68** **Sport biomechanics 7**	11:00-12:24 **Oral 69** **Motor control 2**	11:00-12:24 **Oral 70** **Lower extremities 2**	11:00-12:12 **Oral 71** **Rehabilitation and neurorehabilitation**	11:00-11:48 **Oral 72** **Running: Biomechanics 3**	11:00-12:24 **Oral 73** **Musculoskeletal modeling 6**	11:00-12:12 **Oral 74** **Artificial intelligence and machine learning 4**
12:00								
13:00	12:40-13:30 **Lunch Break (3F/4F)**							
14:00	13:30-14:20 **ISB President's Lecture**	Alberto Leardini Chair: Shinji Sakurai						
15:00	14:20-16:20 **AGM** **Awards Presentations**							
16:00								
17:00	16:20-17:00 **Closing Ceremony**							
18:00								
19:00	19:00-21:00 **GALA Dinner (Kawabata Shopping Arcade)**							
20:00								
21:00								

Poster Map

Monday, July 31st

Venue	Session		Presentation Number
2nd floor, Poster Display #1	Poster 01	Sport biomechanics 1	P01-01 → P01-37
	Poster 02	Biomedical engineering	P02-02 → P02-13
	Poster 03	Injuries and rehabilitation	P03-01 → P03-08
	Poster 04	Orthopaedics: Bone & cartilage	P04-01 → P04-07
	Poster 05	Prosthetics and orthotics	P05-01 → P05-17
	Poster 06	Artificial intelligence and machine learning	P06-01 → P06-11
	Poster 07	Ergonomics	P07-02 → P07-05
	Poster 08	Imaging	P08-01 → P08-07
5th Floor, Poster Display #2	Poster 09	Balance and posture	P09-01 → P09-23
	Poster 10	Clinical biomechanics	P10-01 → P10-19

2nd floor, Poster Display #1

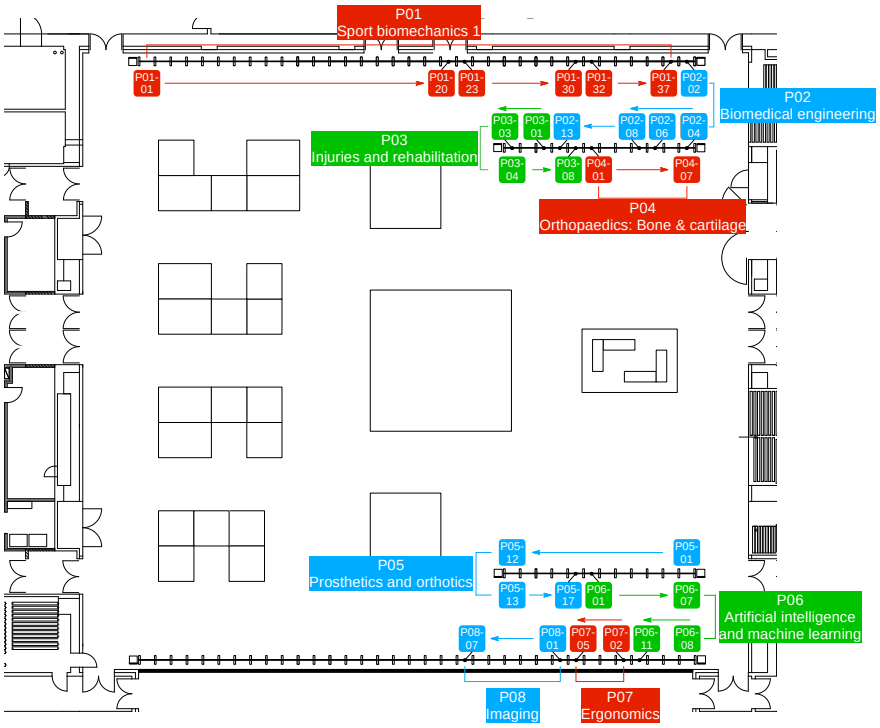

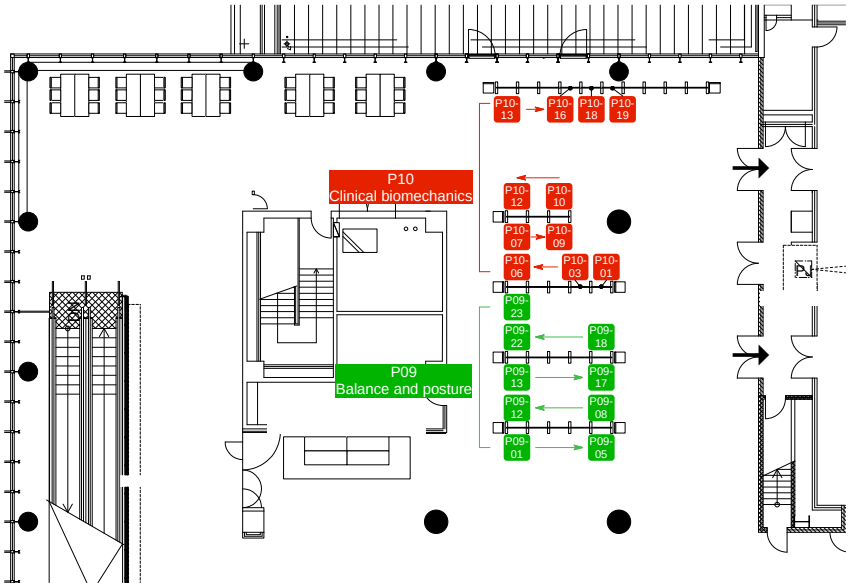

5th Floor, Poster Display #2

Tuesday, August 1st

Venue	Session		Presentation Number
2nd Floor, Poster Display #1	Poster 11	Sport biomechanics 2	P11-01 → P11-41
	Poster 12	Musculoskeletal modeling	P12-02 → P12-23
	Poster 13	Locomotion: Clinical gait	P13-01 → P13-19
	Poster 14	Lower extremities	P14-01 → P14-16
	Poster 15	Medical devices	P15-01 → P15-06
	Poster 16	Methodologies and data analysis	P16-01 → P16-07
5th Floor, Poster Display #2	Poster 17	David Winter Young Investigator Awards Nominee (Poster)	P17-01 → P17-05
	Poster 18	JSB Award Nominee (Poster)	P18-01 → P18-08
	Poster 19	Motor control	P19-01 → P19-12
	Poster 20	Muscle tissue and architecture	P20-01 → P20-09
	Poster 21	Others 1	P21-01 → P21-04

2nd floor, Poster Display #1

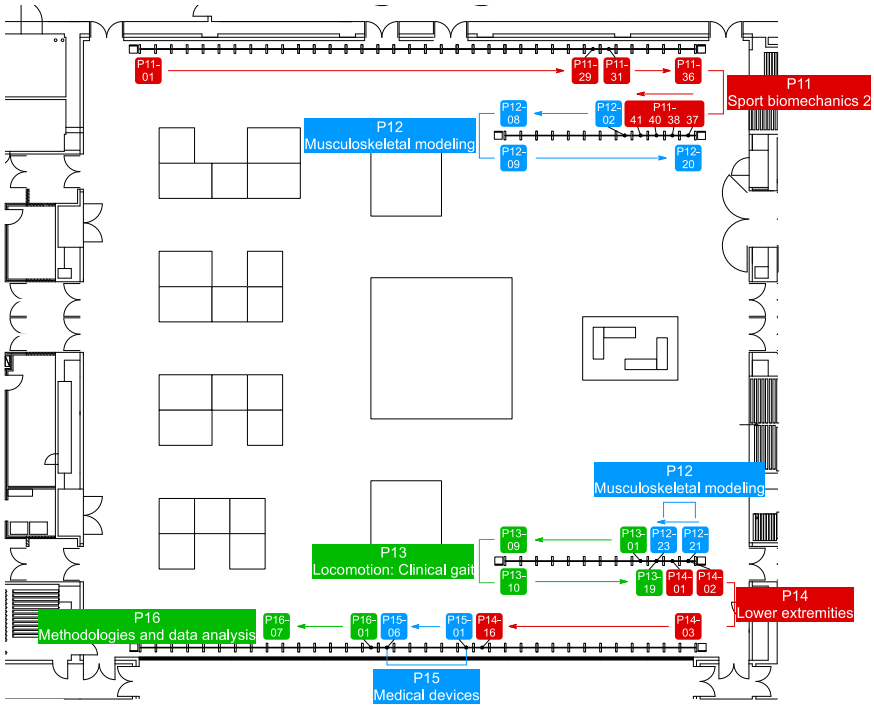

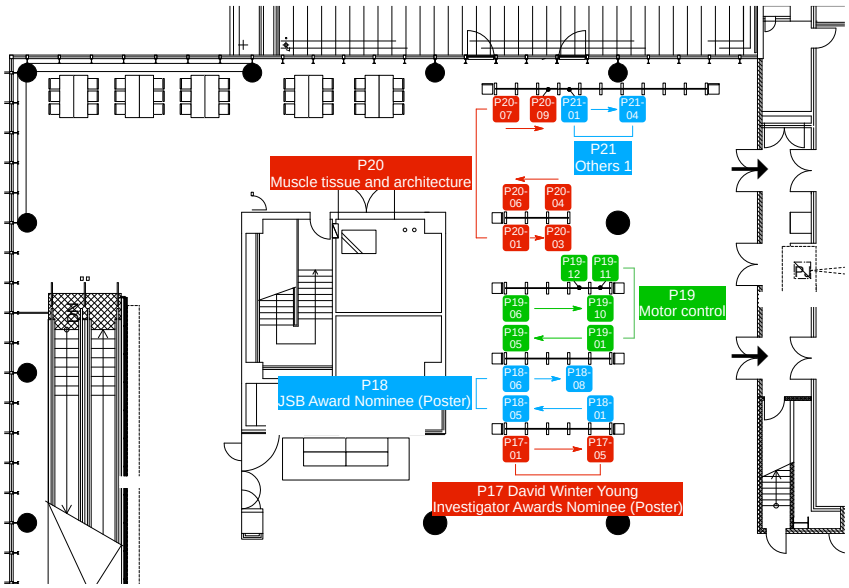

5th Floor, Poster Display #2

Wednesday, August 2nd

Venue	Session		Presentation Number
2nd Floor, Poster Display #1	Poster 22	Sport biomechanics 3	P22-01 → P22-36
	Poster 23	Sports and exercise for persons with impairment	P23-01 → P23-05
	Poster 24	Orthopaedics: Tendon & ligament	P24-01 → P24-04
	Poster 25	Rehabilitation and neurorehabilitation	P25-01 → P25-11
	Poster 26	Rehabilitation technology: Biorobotics and exoskeletons	P26-01 → P26-05
	Poster 27	Simulation techniques and applications	P27-01 → P27-08
	Poster 28	Spine and trunk	P28-01 → P28-05
	Poster 29	Upper extremity	P29-01 → P29-05
	Poster 30	Wireless sensors and wearable devices	P30-01 → P30-14
	Poster 31	Others 2	P31-01 → P31-13
5th Floor, Poster Display #2	Poster 32	Locomotion: General	P32-01 → P32-18
	Poster 33	Running: Biomechanics	P33-01 → P33-13

2nd floor, Poster Display #1

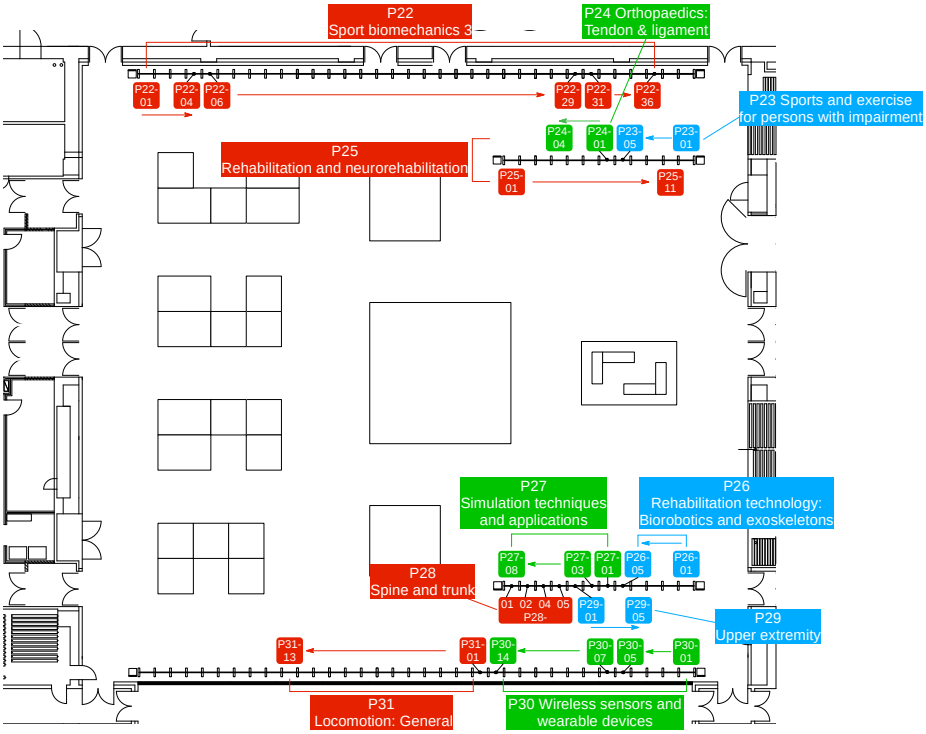

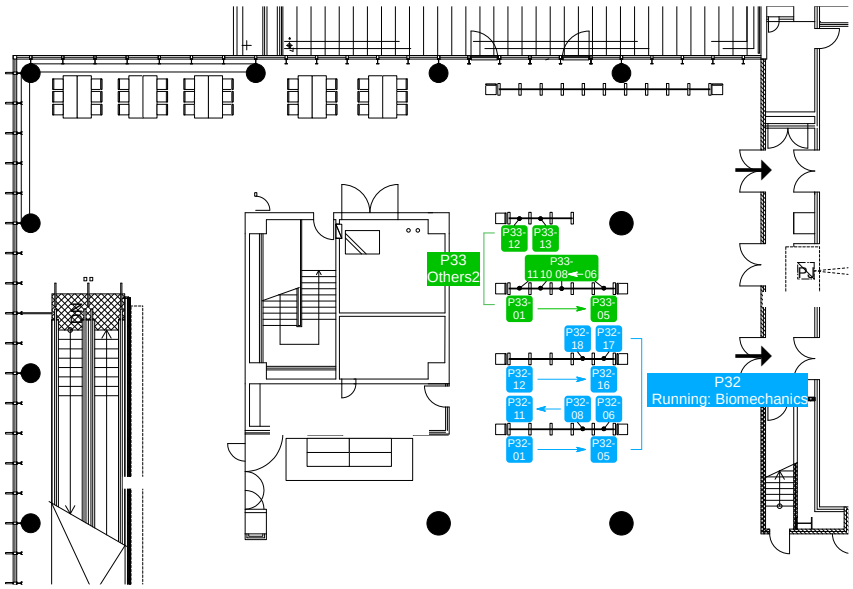

5th Floor, Poster Display #2

Detailed Program

Sunday, July 30th

1000-1200	**Workshop 1**	**Room 2**
WS1	Machine Learning Applications in Movement Biomechanics	Marion Mundt
1000-1200	**Workshop 2**	**Room 8**
WS2	Power to the Foot! Understanding and Applying Distal Power Calculations in Biomechanics	Kota Takahashi, Eric C. Honert
1300-1500	**Workshop 3**	**Room 2**
WS3	Statistical Parametric Mapping - for MATLAB Users and SPM Novices	Todd Pataky, Mark Robinson, Jos Vanrenterghem
1300-1500	**Workshop 4**	**Room 8**
WS4	An Introduction to Time-frequency Low-pass Filter Methods in Biomechanics	Neal Smith, Simon Augustus
1645-1745	**Wartenweiler Memorial Lecture** Chair: **Karen Mickle**	**Room 1**
WL	Pioneering Women of ISB: Tales from the Archives and Beyond	Julie Steele

Monday, July 31st

0800-0930	**Symposium 01 Standardizing Terminology, 3D Spatial Orientation, and Relative Positioning of the Foot and Ankle Bones** Chairs: **Amy Lenz, Lauren Welte**	**Room 1**
SY01-1	Standardizing terminology, 3D spatial orientation, and relative positioning of the foot and ankle bones: An expert consensus task force	Amy Lenz
SY01-2	Foot and ankle automatic anatomical coordinate system definition	Andrew Peterson
SY01-3	In vivo tarsal bone kinematics and the influence of articular talus morphology	Anja-Verena Behling
SY01-4	Weight-bearing CT in support of age-related 3D foot measurements	Claudio Belvedere
0800-0924	**Oral 01 Locomotion: General 1** Chairs: **Hannah Rice, Keitaro Seki**	**Room 2**
O01-1	The impact of body composition on stand-to-sit biomechanics and muscle activity of nurses - a quantitative-explorative study	Anna Brinkmann
O01-2	The effect of changing bicycle saddle position on submaximal cycling behaviour	Cristian Riveros-Matthey
O01-3	Effects of age-related muscle degeneration on dynamic stability during walking: A computer simulation study	Shoma Kudo
O01-4	Anatomical knee model for forward dynamics gait simulation	Beomsoo Shin
O01-5	The effect of changing gait parameters on tensor fascia latae, gluteus maximus, and the iliotibial band	Laura Hutchinson
O01-6	Walking symmetry is speed and index dependent	Gaspare Pavei
O01-7	Body center of mass to minimal moment axis distance is determinant of age-related evolution in stepping	Bruno Watier
0800-0912	**Oral 02 Musculoskeletal modeling 1** Chairs: **Masaki Ishikawa, Tetsuya Hirono**	**Room 3**
O02-1	Effectiveness of co-contraction in mitigating the effect of age-related increase in passive muscle stiffness	Tiina Murtola
O02-2	A composite reflexive and synergistic controller for predictive simulations of cycling	Giacomo Severini
O02-3	Investigating the effects of patellofemoral geometry incongruence on joint function using computational modelling	Annagh Macie
O02-4	A gradient-based method for automated muscle path calibration	Ziyu Chen
O02-5	Stabilization of the foot-ankle complex in response to perturbations	Michael Asmussen
O02-6	The influence of muscle injuries on the shoulder joint mechanics: A musculoskeletal modelling study and experimental validation	Melody Charlotte Labrune
0800-0912	**Oral 03 Cellular and molecular** Chair: **Walter Herzog**	**Room 4**
O03-1	High-fat diet induced vascular smooth muscle cell stiffening in apoe-/- mice	Zhongkui Hong
O03-2	Identification of collective mechanical traits of an injured muscle model	Tae Yoon Kwon
O03-3	Effects of solute molecular shapes on osmosis across fibrous membranes: An application to fluid transport in an endothelial glycocalyx layer	Panadda Dechadilok
O03-4	Contribution of titin to passive and active forces in single myofibrils	Seong-won Han

O03-5	The distinctive mechanical and structural signatures of residual force enhancement in myofibers	Anthony Hessel
O03-6	How collagen IX alters the micromechanical properties of collagen II arrays?	Fatemeh Jalali
0800-0912	**Oral 04 Orthopaedics: Bone & cartilage** Chairs: **Salvatore Federico, Genki Hisano**	**Room 5**
O04-1	An integrated finite element approach to simulate internal bone strain in response to joint loading	Timo van Leeuwen
O04-2	Effusion-synovitis mediates the association between quadriceps weakness and worsening knee pain	Ze Gong
O04-3	Ultrasonographic assessment of acute femoral cartilage response after running and cutting	Miyuki Hori
O04-4	3D MR analysis reveals sex-specific cam location differences in femoroacetabular impingmenent patients	Jessica Bugeja
O04-5	Timing and accuracy of 3D printed pelvic fracture plates	Dale Robinson
O04-6	Trochlear orientation of total knee designs is opposite to that of the natural femur	Nikhil Gattu
0800-0924	**Oral 05 Medical devices** Chairs: **Bing-Shiang Yang, Masataka Yamamoto**	**Room 6**
O05-1	Accelerometer based assessment of upper extremity movement in patients with obstetric plexus palsy	Catherine Disselhorst-Klug
O05-2	Differences in trochlear sulcus geometry of total knee designs	Shuyang Han
O05-3	Design and evaluation of a novel patient-specific, unloading knee brace	Michael Skipper Andersen
O05-4	Experimental validation of a knee implant damage prediction framework	Michael J. Dreyer
O05-5	Evaluation of plantar pressure redistribution in novel footwear for people with diabetes	Sarah Hemler
O05-6	Quantifying muscle tone of upper limb for stroke patients via an impedance-based arm circumference motor evaluation system (i-ACMES)	Chieh-Hsiang Hsu
O05-7	Novel arthrometer provides quantitative and objective measures of uniplanar and multiplanar knee laxity	Carl Imhauser
0800-0924	**Oral 06 Muscle tissue and architecture 1** Chairs: **Toni Arndt, Hiroto Shiotani**	**Room 7**
O06-1	Human lower leg muscles grow asynchronously	Brian V. Y. Chow
O06-2	Residual force depression during submaximal voluntary contractions is not simply related to the preceding positive muscle work	Brent James Raiteri
O06-3	Post-activation potentiation does not contribute to *in vivo* residual force enhancement	Daniel Hahn
O06-4	Understanding aging-related skeletal muscle weakness using shear wave elastography	Filiz Ates
O06-5	Shear modulus differs between regions of the tibialis anterior muscle during contraction	Patricio Pincheira
O06-6	Changes in biceps femoris long head fascicle length during sprinting	Mianfang Ruan
O06-7	How does the medial gastrocnemius and achilles tendon interplay contribute to the muscle-tendon unit during gait in cerebral palsy?	Francesco Cenni
0800-0912	**Oral 07 Injuries and rehabilitation 1** Chairs: **Yuki Sugimoto, Ayako Higashihara**	**Room 8**
O07-1	Passive muscle stiffness does not change after eccentric-only resistance training at long muscle lengths with a long duration	Raki Kawama
O07-2	Constant force muscle stretching induces greater acute deformations and changes in passive mechanical properties compared to constant length stretching	Guido Mirko Geusebroek
O07-3	Hamstring activation deficits during jumping and landing in athletes with hamstring strain injuries using time-frequency analysis method	Amornthep Jankaew
O07-4	The relationship between center of pressure position and knee extensor moment during double-leg squatting	Tomoya Ishida
O07-5	Inter-session reliability of markerless lower limb kinematics and kinetics in return-to-sport tasks often evaluated after serious knee injury	Jiaming Xu
O07-6	Effect of increasing walking cadence on impact loading in adults with knee osteoarthritis	Khara James
0940-1030	**Keynote Lecture 1** Chair: **Todd Pataky**	**Room 1**
KL1	Animals as Machines: Robotic Approaches to Understanding Comparative Locomotor Mechanics	Bill Sellers
1100-1230	**Symposium 02 ISB Motor Control Technical Group** Chairs: **Jim Richards, Walter Herzog**	**Room 1**
SY02-1	Development of a musculoskeletal model that estimates muscle tension from electromyography, joint torque, impedance, and equilibrium position	Yasuharu Koike
SY02-2	Interaction analysis between sEMG signals and cerebral dynamics in brain regions during isometric contraction of elbow joint	Le Li
SY02-3	Does a foot-eye coordination variable add value to the prediction of mild cognitive impairment?	Daniel Koska
SY02-4	Reflex modulation during gait with mechanical perturbations	Dana Lorenz

SY02-5	Embedding the control of balance into the muscle coordination for walking is associated with better walking function	Jessica Allen
SY02-6	Modelling patient-specific neural control in children with cerebral palsy	Miriam Febrer Nafria
SY02-7	Pre-programmed hamstring activation during sidecutting is associated with reflexive response during a single-legged pertubation test	Jesper Bencke
1100-1236	**Oral 08 Sport biomechanics 1** Chairs: **Kat Daniels, Takahiko Sato**	**Room 2**
O08-1	Relationship between countermovement jump and fastball velocity in adolescent baseball pitchers	Hui-Wen Hsiao
O08-2	Comparison between backward and forward propulsion in wheelchair badminton	Ilona Alberca
O08-3	Estimating distribution of mass between castor- and rear wheels using inertial sensors during manual wheelchair propulsion	Marit van Dijk
O08-4	Aerodynamics of dimple structure on soccer ball using 3D printer	Sungchan Hong
O08-5	The largest segmental components of energy directly contributing to height do not explain the variance of its total in the high jump	Natsuki Sado
O08-6	Hamstring muscle kinematics and activation during the acceleration phase in sprinting of soccer players	Van Thiet Le
O08-7	Sex-specific anthropometric and kinematic performance determinants in national elite javelin athletes	Chinedu Godwin Uzomba
O08-8	Classifying punch types and ranges in boxers: A machine learning approach with IMU sensor data	Saravanan Manoharan
1100-1212	**Oral 09 Musculoskeletal modeling 2** Chairs: **Luke Kelly, Satoru Hashizume**	**Room 3**
O09-1	A systematic review and evaluation of open-source transtibial amputee musculoskeletal models for use on female populations	Misha Hasan
O09-2	Complete 3D kinematics parameters of the temporo-mandibular joints using in vivo data fusion	Gaël Bescond
O09-3	Muscle contributions to the barbell back squat in trained females	William Goodman
O09-4	Predicting knee joint loading during different activities of daily living: A validation framework based on the CAMS-knee dataset	Enrico De Pieri
O09-5	Effect of the loading direction on the predicted local mechanical properties of the tibia in the ovariecto-mised mouse model	Saira Mary Farage-O'Reilly
O09-6	Automated tool for musculoskeletal finite element modeling of knee	Amir Esrafilian
1100-1212	**Oral 10 Locomotion: Clinical gait 1** Chairs: **Heng-ju Lee, Hiroaki Noro**	**Room 4**
O10-1	A CNN-based approach to classification of Parkinson's disease patients with and without freezing of gait during 360° turning task	Hwayoung Park
O10-2	Rotary spinal dynamics in gait - Reference data and functional descriptions based on surface topograpy	Ulrich Betz
O10-3	Gait and dynamic postural stability during obstacle crossing in the individuals with early-stage Parkinson's disease	Nok-Yeung Law
O10-4	Gait strategies identified by machine learning in older adults after spinal fixation	Naoto Mano
O10-5	Are adaptations in fall predictors following a 12-week mixed power training related to gait parameters in community-dwelling older men?	Aubertin-Leheudre Mylène
O10-6	Gait propulsion in patients with unilateral cerebral palsy when walking with and without an ankle foot orthosis	Jacqueline Romkes
1100-1236	**Oral 11 Balance and posture 1** Chairs: **Genevieve Williams, Sentarou Koshida**	**Room 5**
O11-1	Virtual reality skateboard balance training for improving balance stability in the elderly	Yi-Ching Tsai
O11-2	EMG normalization approaches show differing results in older adults during a stepping task	Marcel Bahia Lanza
O11-3	Adaptation in reactive balance control over repeated standing slips in ballet dancers	Caroline Simpkins
O11-4	Cortical involvement for postural control	Thomas Legrand
O11-5	The effect of applying external cutaneous tension on lower-limb movement and balance	Ning Tung
O11-6	Plantar tactile sensation, joint range of motion, and pain are unique fall risk factors for people with knee osteoarthritis	Peixin Shen
O11-7	Synthetic simulation of stepping maneuver using reinforcement learning	Yoshimori Kiriyama
O11-8	Human electrical brain and muscle activity during underwater standing balance	Seongmi Song
1100-1148	**Oral 12 Clinical biomechanics 1** Chairs: **Nahoko Sato, Hajime Ohtsu**	**Room 6**
O12-1	Muscle power and strength deficiencies in fallers with lower limb loss	Isabel Lin

O12-2	Initial changes in knee loading from a personalized gait modification are associated with changes in MRI metrics of cartilage health after 1 year	Kirsten Seagers
O12-3	Characterizing mechanical adaptation of muscles affected by myasthenia gravis using shear wave elastography	Manuela Zimmer
O12-4	Effects of small and normalized Q-Factor changes on knee biomechanics in stationary cycling	Songning Zhang
1100-1224	**Oral 13 Artificial intelligence and machine learning 1** Chairs: **Neil Cronin, Yoichi Iino**	**Room 7**
O13-1	Gait time series prediction using random forest model: A sensitivity analysis on IMU sensor location, window size, and number of features	Shima Mohammadi Moghadam
O13-2	Can computer vision be as good as multi-camera infra-red systems for motion analysis?	John Komar
O13-3	Comparison of the validity of ground reaction forces from two different sets of body landmarks during sidestepping via artificial neural networks	Yulin Zhou
O13-4	The estimation of ground reaction forces during stair walking	Marion Mundt
O13-5	Estimating knee arthroplasty patients' EQ-5D-5L VAS using IMUs and machine learning	Ted Yeung
O13-6	Using deep learning to personalize stroke rehabilitation	Sina David
O13-7	A machine learning approach to characterising rugby head impacts for laboratory recreation	Danyon Stitt
1100-1212	**Oral 14 Others 1** Chairs: **Mitsuo Otsuka, Kikwang Lee**	**Room 8**
O14-1	Brain tissue mechanics in postmortem interval estimation	Natalia Kabaliuk
O14-2	Degrading quality of proteoglycans in osteoarthritic cartilage	Eng Kuan Moo
O14-3	Skeletal muscle anisotropic mechanical properties quantification in vivo: Combining magnetic resonance elastography and diffusion tensor imaging	Zhongzheng Wang
O14-4	Brain stress measurements during biofidelic head surrogate impacts	Giuseppe Zullo
O14-5	A novel predict-update deep learning model for joint angle predictions from inertial measurement units	Vaibhav Shah
O14-6	A method to estimate the kinetics of a collective load carrying in ants	Jordan Drapin
1330-1500	**The 50th ISB Anniversary Session 1** **ISB 50 Years of International Biomechanics: History** Chair: **Veronique Feipel**	**Room 1**
AS1-1	Historical perspective of the founding of ISB	Joe Hamill Benno Nigg
AS1-2	History of the JSB-ISB relationship	Mitsumasa Miyashita
AS1-3	Muscle mechanics	Walter Herzog
AS1-4	Sports biomechanics and modeling	Jill McNitt Gray
AS1-5	Human motion and Gait analysis	Brian Davis
AS1-6	Neuromechanics	Daniel Hahn Catherine Disselhorst-Klug
1540-1710	**The 50th ISB Anniversary Session 2** **ISB 50 Years of International Biomechanics: Future** Chair: **Katherine Boyer**	**Room 1**
AS2-1	Muscles Alive-how far have we come since then?	Yasuo Kawakami
AS2-2	New perspectives in tendon biomechanics	Taija Finni
AS2-3	The future of Gait analysis and Human motion analysis	John Challis
AS2-4	Neuromusculoskeletal biomechanical modeling and Neuromechanics	Luca Modenese
AS2-5	Biomechanics in the wild by digital human and artificial intelligence	Mitsunori Tada
AS2-6	Internet of things and remote monitoring, field monitoring	Kamiar Aminian
AS2-7	Data, privacy and the future	Jacqueline Alderson

1720-1850	**Poster 01 Sport biomechanics 1**	2nd Floor, Poster Display #1
P01-01	Differences in joint kinematics between snatch and clean lifts in weightlifting	Ganbat Tumen-Ulzii
P01-02	Comparison of ballistic training and complex training on explosive performance in upper limbs	Hsiang-Hsian Wang
P01-03	Using landing error scoring system with automated joint angle tracking as a screening tool to predicating lower extremity sports injuries for athletes: A prospective study	Hsiao-Yun Chang
P01-04	Profile of hip rotational range of motion for the healthy collegiate baseball players	Chun-Wen Chiu
P01-05	Biomechanical patterns associated with knee injury in female futsal players diagnostic with the change of direction and acceleration test (CODAT): A cross-sectional analytical study	Ferrandez-Laliena Loreto
P01-06	Reducing variability may not increase the success rate of motor task: Toward a proper interpretation of function	Arata Kimura
P01-07	Effect of a physiotherapy program on the reversal of risk factors for patellar tendinopathy in amateur female soccer players. Clinical trial	Lucia Vicente Pina
P01-08	The scapulohumeral rhythm of javelin throwers	Tang-Yun Lo
P01-09	Relationships between the lower extremity biomechanics and forward propulsion in the preparatory motion for an effective judo throw	Takanori Ishii
P01-10	The effect of decreasing COR of baseball on batting stats and batting performance: In a case of professional baseball league	Shu-Wei Chen
P01-11	Evaluation of the muscle work in gym exercises with a “water ball” compared with a medicine ball	Alexis Herbaut
P01-12	Narrow stance width during the bar twist exercise decreases the trunk twist torque	Kazutaka Takahashi
P01-13	Acute: Chronic workload ratio and accumulated neuromuscular fatigue in college male rugby sevens athletes: A pilot study	Qianhui Sun
P01-14	Estimation of time consistency in taekwondo group poomsae with inertial measurement unit	He Minyan
P01-15	Influence of turf fibres on mechanical traction of artificial turf surfaces	Michael Esposito
P01-16	Club head parameter of effecting amateur golfer’s smash factor in real golf course situations	Tsung Yu Huang
P01-17	Biomechanical factors affecting long jump distance in Japanese male university athletes	Yamato Takayama
P01-18	Relationship between the position of hip joint and range of motion of lower limb joint during cycling	Hayato Seki
P01-19	Investigation of archery experience on shoulder girdle motion and acromiohumeral distance at full draw	Takeru Abekura
P01-20	Differences of maximum inclination and center of mass accelerations between professional and amateur ballet dancers during pirouette in classical ballet	Yurina Tsubaki
P01-23	Evaluation of trunk muscle activities during the arabesque	Kanae Ouchi
P01-24	The investigation of the mobility in the first tarsometatarsal joint in forced turnout of ballet dancers	Honoka Ishihara
P01-25	Regulate velocity on combined training improving the college basketball players jumping performance	Chenfu Huang
P01-26	Anteroposterior hand position at set posture affects the subsequent block start performance	Takuma Hayashi
P01-27	Validity of approach-run speed in pole vaulting using laser displacement meter or body-only model	Atsuto Noro
P01-28	Does the lower limb muscularity relate to long-sprint performance in 400-m sprinters?	Keishi Kuroki
P01-29	Age-related differences in electromyographic latencies of the lower limb muscles in standing sprint initiation throughout childhood and adolescence	Mizuki Kitamura
P01-30	Correlation between cue tip speed and kinematics of 9-ball break shot	Pui Wah Kong
P01-32	Potential injury mechanisms in ulnar collateral ligament injuries; magnitude and variability of elbow load in repetitive baseball pitching	Bart van Trigt
P01-33	Sex-specific effects of fatigue on muscle activation during a single-leg lateral jump landing task	Davine Yang
P01-34	Effect of taping on muscle activity during squatting exercise	Mao Zeniya
P01-35	Effects of the incline board on discus throwing motion	Shota Kikuchi
P01-36	Relation between throwing arm angle and trajectory of the pitched ball in baseball	Hirotaka Nakashima
P01-37	Biomechanical analysis of the golf swing in one-length and conventional irons	Yu Kashiwagi
1720-1850	**Poster 02 Biomedical engineering**	**2nd Floor, Poster Display #1**
P02-02	Quantitative estimation of the forearm performance fatigability in a screwing model	Yen-Wei Chiu
P02-04	Effect of insertion speed on the insertion torque value and initial stability quotient of dental implant	Jui-Ting Hsu
P02-05	Development of an advanced prototype simulator for dental education	Mi-El Kim
P02-06	Computational model verifying effects of ultrasound settings on temperature changes in nitinol implants	Shaye Tiell
P02-08	Gait event detection using the single IMU on the unilateral electromechanical KAFO	Sumin Yang
P02-09	Kinematical differences between water surface and underwater conditions in flutter kick swimming	Hiroshi Ichikawa
P02-10	Relationship between sEMG amplitude and muscle fiber conduction velocity each short-term waveform with muscle fatigue	Aya Shirai

P02-11	Development of a statistical shape model of the knee for predicting bone/cartilage morphology and articular contact trajectories during activities	Kuan Hsien Wu
P02-12	A biomechanical study of novel braided PET artificial ligament for ACL reconstruction	Shenglin Li
P02-13	Pre-impact fall detection during electric scooter riding	Seung Hee Lee
1720-1850	**Poster 03 Injuries and rehabilitation**	**2nd Floor, Poster Display #1**
P03-01	Head impacts during judo practice in college judokas: A preliminary study	Sentaro Koshida
P03-02	Injury-related gait variables during running and loaded walking in U.S. army trainees differ by sex, but not physical activity level	Caleb Johnson
P03-03	Establishing scientifically meaningful effect sizes for knee abduction moment curve reductions in side-stepping using 1D power analysis	Mark Robinson
P03-04	Longitudinal recovery of laterality in the upper extremity activity after distal radius fractures	Terufumi Iitsuka
P03-05	Relationship between plantar foot pressure and high-risk and early knee osteoarthritis	Teng Phillis
P03-06	Simulated tunnel vision and lower limb kinematics during gap cross-over	Tadashi Uno
P03-07	Comparison of the effects of vibration therapy with stretching exercise in school teachers with myofascial pain syndrome of the trapezius	Chia-Lin Chen
P03-08	Influence of pelvic and lower limb joint kinematics on hamstring muscle-tendon strain during the late swing phase of maximal speed sprinting	Terumitsu Miyazaki
1720-1850	**Poster 04 Orthopaedics: Bone & cartilage**	**2nd Floor, Poster Display #1**
P04-01	Kinematic comparison of lower extremity before and after total hip replacement for hip dysplasia: A case report	Tserenchimed Purevsuren
P04-02	Stair ambulation reveals greater medial meniscus extrusion in healthy young volunteers	Takato Hashizume
P04-03	Numerical simulation of bone metabolism over time with aging	Teppei Mano
P04-04	Morphological characteristics of the femoral cartilage in trained and untrained individuals	Junhyeong Lim
P04-05	The fatigue life of cortical bone does not increase with test interruptions	W. Brent Edwards
P04-06	Depth dependent tensile properties of articular cartilage	Francesca De Vecchi
P04-07	Effects of high tibial osteotomy on three-dimensional knee kinematics in patients with knee osteoarthritis during isolated knee flexion measured using bi-plane fluoroscopy	Kao-Shang Shih
1720-1850	**Poster 05 Prosthetics and orthotics**	**2nd Floor, Poster Display #1**
P05-01	Adapting the prosthesis evaluation questionnaire to assess sex differences in the prosthetic needs and priorities of lower limb amputees	Tess Carswell
P05-02	Kinematics of downhill skiing with lower limb prosthesis on two skis	Filip Hrusa
P05-03	Non-linear finite element approach for a priori modal analysis of prosthetic foot	Balaramakrishnan T M
P05-04	Unilateral above-knee amputees gait analysis with a statistical parametric mapping	Jin-Joo Yang
P05-05	Effect of silanized ZrO2 addition on the physical properties of 3D printing resin	Jinkyung Park
P05-06	Functional effectiveness of custom ACL bracing: A finite element analysis	Alexandria Mallinos
P05-07	Dynamic finite element analysis for the metamaterial prosthetic liner optimization	Vasja Plesec
P05-08	An affordable soft robotics prosthetic hand with rigid structures	Vani Virdyawan
P05-09	Accuracy of inertial measurement units (IMUS) to measure ankle range of motion: Application in transtibi-al prosthesis user	Manunchaya Samala
P05-10	Biomechanical analysis based on the skull model to derive the optimal screw configuration of the 3D printing patient-specific reconstruction plate used for maxillofacial bone defects	Dong-Young Je
P05-11	Development of a finite element model for simulations of cold flow and neck-liner impingement in hip prosthesis	Lu Shen
P05-12	Reliability analysis of two stability measurement methods depending on dental implant length and bone density	Jungwon Lee
P05-13	Influence of prosthetic ankle-angle and walking speed on pylon moments in the two axis adaptable ankle	Kieran Nichols
P05-14	Patient-specific optimisation of cushioning stiffness in diabetic footwear	Nachiappan Chockalingam
P05-15	A simple method to overcome weakness in FDM 3D printed parts for stronger prosthetic sockets	Mukul Talaty
P05-16	Energetics of a novel passive dynamic custom AFO in gait: Analysis in a sample of foot-drop patients	Luca Zamagni
P05-17	Footwear comfort and the effect of customised foot orthotic insoles and BMI	Lloyd Reed
1720-1850	**Poster 06 Artificial intelligence and machine learning**	**2nd Floor, Poster Display #1**
P06-01	Remote technologies for testing physical function	Neil Cronin
P06-02	Development of a neural network for prediction of ovine hip joint centers	Aaron Henry
P06-03	The influence of protective equipment on performance in ice hockey	Rebecca Lennartz

P06-04	Modeling healthy and impaired gait dynamics using recurrent neural networks	Taniel Winner
P06-05	High efficiency barbell recognition model by considering convolutional neural network	Jin-Yi Lin
P06-06	Prediction of GRF and joint moments from different combinations of kinematic data.	Juan Cordero-Sanchez
P06-07	Evaluation of deep neural networks-based frame interpolation of X-ray fluoroscopic images of dynamic knee motions	Yu-Chien Chen
P06-08	Joint angle calculation and prediction via openpose estimation and machine learning model for riding pose adjustment in cycling	Yun-Ju Lee
P06-09	Estimating hand reaction forces from arm segment accelerations during handcycle propulsion using machine learning	Griffin Sipes
P06-10	Validity and reliability of deep learning methods to analyse knee osteoarthritis using magnetic resonance imaging: A systematic review	Surabhi Thatte
P06-11	Classification of EMG signals during contra-lateral arm movement	Azmin Rambely
1720-1850	**Poster 07 Ergonomics**	**2nd Floor, Poster Display #1**
P07-02	Estimating L5/S1 flexion-extension moment with an artificial neural network method in manual lifting tasks: A preliminary validation study	Chien-Chi Chang
P07-03	The effect of slanted computer mouse in a quick click task: A pilot study	Kuang-Wei Lin
P07-04	Muscle fatigue comparison between slanted and non-slanted gaming mice	Winny Chang
P07-05	Musculoskeletal analysis of upper limb motion during repetitive tasks	Akisue Kuramoto
1720-1850	**Poster 08 Imaging**	**2nd Floor, Poster Display #1**
P08-01	Effect of superficial tissue and intermuscular connections on the shear modulus distribution within the rectus femoris muscle	Taiki Kodesho
P08-02	Short-term impact of basketball workout on knee medial meniscus	Hsin-Min Wang
P08-03	The effect of different file types and DXA protocols on an image processing fracture risk prediction tool	Ali Ammar
P08-04	MRI-based spine models for patient specific surgical planning	David Williams
P08-05	The association of normalized cross-correlation with biplanar videoradiography tracking error	Kaito Lee
P08-06	Towards dynamic CT imaging in revalidation tracking of jaw movements: An experimental phantom study	Benyameen Keelson
P08-07	Effects of physical activity level and motor function on hippocampal volume in the older adults	Kota Anjiki
1720-1850	**Poster 09 Balance and posture**	**5th Floor, Poster Display #2**
P09-01	Task-oriented whole body reaching improves postural performance in hemiparesis patients after stroke	Jen-Suh Chern
P09-02	The effects of internal perturbations on balance for the fallers and non-fallers with Parkinson's disease: A preliminary study	Yu-Chuan Tsai
P09-03	Plantar pressure distribution response to various gait speeds and its relationship with gait balance in overweight adults	Hyun Kyung Kim
P09-04	Reducing fall risk using 12-weeks of online dance classes for women aged 65 and above	Emma Chen
P09-05	Development of the two-dimensional mechanical model of human stability	Martyna Sopa
P09-08	Leg muscle activities during single leg stance	Jooyeon Ko
P09-09	Alteration of inter-joint interaction during standing due to spinal cord injury	Kimiya Fujio
P09-10	Research on the balance ability of freestyle skiing aerial skills athletes based on specific frequency band EEG	Youcai Guo
P09-11	A static model predicts roof-to-ladder transition friction requirements	Sarah Griffin
P09-12	Evidence for modifying extension ladder design to reduce slipping risk	Violet Williams
P09-13	Decompose centre of pressure component affecting centre of mass acceleration in quiet standing	Taku Miyazawa
P09-14	The effectiveness of artificial intelligence sport training mirror combine with chinese martial arts for lower extremities balance	Cheng-Wei Chen
P09-15	Gait stability restrictions did not elicit compensation from remaining strategies	Aaron Best
P09-16	Effects of bilateral subthalamic deep brain stimulation on balance control during sit-to-stand in patients with advanced Parkinson's disease	Ya Hung Wang
P09-17	Effect of small perturbation balance training using wearable device on muscle activity related to reactive postural control	Taku Washida
P09-18	The effect of suspensory strategy on postural control under lateral perturbations: A study on COM height and balance performance	Linjing Jiang
P09-19	Age-induced modifications in postural sway and force steadiness during plantar and dorsiflexion	Ioannis Amiridis
P09-20	Effects of eye dominance on whole-body balance control during level walking in the elderly	Ju Yang Tiong
P09-21	Effects of scoliosis on upper body balance control in middle-age adults during obstacle crossing	Wen-Horng Lo

P09-22	Neuromuscular responses during standing with sensory restrictions are not related to field test performance in children with cerebral palsy	Anastasia Papavasileiou
P09-23	A bi-planar inverted pendulum model for evaluating the dynamic stability in patients with duchenne muscular dystrophy during level walking	Shu-Jiun Lin
1720-1850	**Poster 10 Clinical biomechanics**	**5th Floor, Poster Display #2**
P10-01	Muscle-tendon biomechanics and daily steps in patients recovering from achilles tendon rupture	Taija Finni
P10-03	Effect of isometric quadriceps exercise on stiffness and hemoglobin concentration of the infrapatellar fat pad in knee osteoarthritis	Syoya Nakanishi
P10-04	Effect of creep after twenty minutes of full lumbar flexion on subsequent lifting	Mitsuhiro Ota
P10-05	Computer simulation on obturator prosthesis for velopharyngeal defect	Ho Beom Kwon
P10-06	Biomechanical effects of an aramany class VI obturator prosthesis: A 3D finite element analysis	Aein Mon
P10-07	Biomechanical analysis of the effects of post & core in short clinical crown	Jaebok Lee
P10-08	Stress analysis in the mandible of complete denture prosthesis wearers - A biomechanics perspective	Mary Delia Bondoc
P10-09	Diagnosis of anterior cruciate ligament deficiency using a composite index calculated from the knee flexion and muscle force	Haoran Li
P10-10	Degree of association between knee health with pelvis mobility and plantar pressure	Arnab Sarmah
P10-11	Knee joint moments calculated using markerless motion capture can distinguish osteoarthritis severity during walking gait	Jereme Outerleys
P10-12	In vivo kinematics of total ankle prosthesis with different talar implant shapes	Rea Ikeda
P10-13	Asymmetry on forearm rotation movement in patients with Parkinson's disease and swedd	Ji-Won Kim
P10-14	IMU-instrumented timed-up and go test identified task-specific mobility declines in older adults	Yu-Pin Liang
P10-15	A statistical analysis of the shape and density distribution of the talus	Jordan Stolle
P10-16	Kinematic and kinetic analysis of upper limb elevation exercises in baduanjin	Geonhui Kang
P10-18	Biomechanical effect of floor sit-to-stand movement on the optimal surgical site in ACLR surgery: A computational analysis	Jaewoong Han
P10-19	Optimal hinge positions on tibial wedge in biplane open-wedge high tibial osteotomy as varus deformity angle	Tae Soo Bae

Tuesday, August 1st

0800-0930	**Symposium 03 Artificial Intelligence in Biomechanics: Current and future applications** — Chairs: **Neil Cronin, Jacqueline Alderson**	**Room 1**
SY03-1	Team sports analytics using machine learning	Keisuke Fujii
SY03-2	Estimation of kinetic parameters from video data using supervised machine learning techniques	Marion Mundt
SY03-3	Applications of AI in clinical settings	Eni Halilaj
0800-0900	**Oral 15 David Winter Young Investigator Awards Nominee (Oral)** — Chair: **Elizabeth Clarke**	**Room 2**
O15-1	Influences of alteration in running foot strike angles on internal loading of the tibia	Sanghyuk Han
O15-2	Muscle shape changes and gearing are mediated by internal muscle properties in the human gastrocnemii	Nicole Yvette Kelp
O15-3	Foot and ankle kinetics are coupled during propulsion for walking and running	Quinn Yetman
O15-4	Inertial measurement unit calibration methods for the wrist joint: Which one should I use?	Alessandro Bonfiglio
O15-5	Windlass mechanism engagement influences calcaneocuboid joint kinematics within a robotic-driven tibial movement envelope: A preliminary study	Anthony Le
0800-0924	**Oral 16 Musculoskeletal modeling 3** — Chairs: **Daniel Hahn, Taku Wakahara**	**Room 3**
O16-1	Validation of EMG-driven model-based estimations of joint, muscle, and tendon stiffness	Christopher Pablo Cop
O16-2	Alterations of muscle activation to reduce knee loading for people with limb loss: A musculoskeletal simulation study	Jiayu Hu
O16-3	Creating subject-specific musculoskeletal models via morphometric transformation	Julia van Beesel
O16-4	Video fluoroscopy and advanced musculoskeletal modelling unveil new insights into the mechanics of total knee arthroplasty during the golf swing	Seyyed Hamed Hosseini Nasab
O16-5	Wearable motion capture-driven musculoskeletal framework for multiscale orthopedic biomechanics	Liming Shu
O16-6	Automated generation of personalized foot-ground contact models	Spencer Williams
O16-7	Towards rehabilitation of upper limb disorders via neuro-musculoskeletal modelling	Harnoor Saini
0800-0900	**Oral 17 Methodologies and data analysis 1** — Chair: **Ismail Shariman**	**Room 4**
O17-1	Validation of smartphone-based analysis of human kinematics during 45° changes of direction	Cameron Stephen
O17-2	Estimating how sensorimotor impairments influence walking speed in persons with spinal cord injury with machine learning techniques	Tat Nhat Minh Truong
O17-3	Validity of artificial intelligence-based motion analysis system ~ AI analysis vs. Human analysis	Takumi Ino
O17-4	Deep learning successfully classifies acoustic emission data from knee joints	Ivan Vatolik
O17-5	Evaluation of the estimated length of the plantar aponeurosis using a multi-segment foot model	Yuka Matsumoto
0800-0848	**Oral 18 Impact biomechanics 1** — Chair: **Hironari Shinkai**	**Room 5**
O18-1	Helmet performance and body effects in head impacts in E-scooter falls	Wei Wei
O18-2	Influence of midsole compression on acceleration magnitude in running	Robin Trama
O18-3	Effect of slip anticipation on muscle activation pattern during walking down a slippery slope	Dain Shim
O18-4	Simulation of the impact process of water cannon on cranio cerebral injuries	Yinze Lei
	Comparative Neuromuscular Biomechanics (CNB) Group Symposium: Muscles, Models, Machines — Chairs: **Jonas Rubenson, Greg Sawicki**	**Room 6**
0800-0930	**Slot 1**	
	Topic 1; *In vivo* paradigms	
CNB1-1	**Keynote**: Get real: New experiments, models and parameters for understanding in vivo muscle function.	Kiisa Nishikawa
CNB1-2	3D whole muscle shape changes - exploring a novel approach	Jeroen Aeles
CNB1-3	Direct in vivo assessments of plantar flexor function to guide patient care	Josh Baxter
	Topic 2; modelling paradigms	
CNB1-4	**Keynote**: Task-level feedback control of gait is an emergent property of effort minimization in the presence of noise	Friedl De Groote
1100-1230	**Slot 2**	
CNB2-1	Biophysical muscle models for simulating muscle and muscle spindle response to stretch	Surabhi N. Simha

CNB2-2	Muscle force estimation using convolutional neural networs and hill-type models	Anne Koelewijn
	Topic 3; Engineering/Machine paradigms	
CNB2-3	**Keynote**: Frogs as models for robotics, limb control and muscular ageing	Christopher Richards
CNB2-4	Measuring the motion of human muscle: Devices, disruptions, and deformations	Taylor Dick
CNB2-5	Viewing the elephant trunk as an engineer turned biologist	Andrew Schulz
1330-1500	**Slot 3 Poster viewing and moderated poster flash presentations**	
CNB3-1	Investigating intrinsic muscle mechanics of force production	Caitlin Bemis
CNB3-2	Energetics, mechanics, and muscle: Locomotor adaptations to chronic limb loading during development	Kavya Katugam-Dechene
CNB3-3	Does the *in-vivo* or *in-vitro* environment impact the tendon force-strain relationship?	Fransiska M. Bossuyt
CNB3-4	Blood python *(python brongersmai)* strike kinematics and forces are robust to variations in substrate geometry	Derek J. Jurestovsky
CNB3-5	Creating musculoskeletal models of humans and animals with opensim creator	Ajay Seth
CNB3-6	Residual force enhancement: Active versus passive contribution	Wejdaan Faridi
CNB3-7	Kinetics of a collective load carrying in ants	Jordan Drapin
CNB3-8	Characterizing residula and passive force enhancement in cardiac myofibrils	Seong-won Han
CNB3-9	The intrinsic and neurally-mediated contributions to the balance-correcting torque response differ between the ankle and hip	Kristen L. Jakubowski
0800-0912	**Oral 19 Injuries and rehabilitation 2** **Room 7** Chairs: **Masatoshi Nakamura, Jun Umehara**	
O19-1	Subject-specific FE analysis to investigate how different rehabilitation exercises influence tendon strains in achilles tendinopathy patients	Alessia Funaro
O19-2	Effects of brace wearing and rehabilitation on foot muscle thickness and cross-sectional area after ankle inversion trauma	Rosemary Dubbeldam
O19-3	Identifying movement strategies to offset the performance-injury risk conflict in side-step cutting via optimal control simulations	Aaron Fox
O19-4	Electrical stimulation induced isometric muscle contraction can improve mechanical properties and reduce tendon adhesion followed adipose-derived stromal vascular fraction gel treatment in the rat achilles tendinopathy	Ho-Yi Tuan-Mu
O19-5	Wearable ultrasound sensor for lateral epicondyle tendinopathy surveillance	Yeseop Park
O19-6	Does female handball players with low hip external rotation strength display higher knee abduction moments during side-cutting than players with high strength?	Niels Nedergaard
0800-0924	**Oral 20 Running: Biomechanics 1** **Room 8** Chairs: **Mike Hahn, Kazuhiro Ishimura**	
O20-1	Reduced tibial loading during a 10km run in competitive and recreational runners	Hannah Rice
O20-2	Effects of soft tissue artifacts on the calculated kinematics of the knee during gait	Wenjin Wang
O20-3	Adaptive biofeedback gait retraining on slopes: A proof-of-concept study	Zoe Y.S. Chan
O20-4	Trained novice runners increase step frequency and decrease force application	Janet Zhang-Lea
O20-5	Inter-individual differences in step length and step frequency change across running speeds	Masanori Sakaguchi
O20-6	Variation in tibia-fibular geometry is associated with strain-related changes during running	Meghan Keast
O20-7	Increasing step frequency reduces cumulated patellofemoral joint stress more at low running speed	Michiel Hagen
0940-1030	**Keynote Lecture 2** **Room 1** Chair: **Maarten Bobbert**	
KL2	Complementary Roles of Biomechanics and Machine Learning in Human Motion Monitoring	Sukyung (Sue) Park
1100-1230	**Symposium 04 Contemporary Issues In Ball Kicking Biomechanics Research Across The Football Codes** **Room 1** Chairs: **Alexandra Atack, Hiroyuki Nunome**	
SY04-1	Energy flow in soccer kicking	Neal Smith
SY04-2	Looking beyond the kicking leg: Whole-body strategies for ball kicking performance	Simon Augustus
SY04-3	Sex differences in ball kicking biomechanics (strength, technique and training effects)	Alexandra Atack
SY04-4	Myths and facts on football kicking: Filling the gaps between the player's perspective, coach's observation and scientific evidence	Hiroyuki Nunome
1100-1212	**Oral 21 Musculoskeletal modeling 4** **Room 2** Chairs: **Yasuo Kawakami, Emika Kato**	
O21-1	An advanced modelling framework for assessing knee articular mechanics and soft tissue loading after total knee arthroplasty	Ning Guo

O21-2	Dynamic simulation of running using a full-body model with trunk muscles	Harry George Driscoll
O21-3	Unravelling adaptation strategies in sit-to-walk using predictive neuromuscular simulations: Pain	Eline van der Kruk
O21-4	Towards a musculoskeletal shoulder model depicting glenohumeral translations considering bony, ligamentous and muscular stability constraints	Johanna Menze
O21-5	A dynamic foot model for predictive simulations of gait	Lars D'Hondt
O21-6	Insights into the different state-of-the-art optimisation approaches for solving the shoulder muscle redundancy problem	Maxence Lavaill
1100-1212	**Oral 22 Wireless sensors and wearable devices 1** Chairs: **Yuji Ohgi, Shoji Konda**	**Room 3**
O22-1	Three-dimensional training load of female university volleyball players during practice games	Chuan Fang Hou
O22-2	Sensor number-dependent accuracy of ground reaction forces and center of pressure in simplified pressure sensor insoles	Philip X. Fuchs
O22-3	IMU metrics assessed during 2km of indoor track vs. Sidewalk running	Hannah Dimmick
O22-4	A hybrid machine learning model predicts ankle and knee moments in multiple tasks from a single IMU	Ting Long
O22-5	The relationship between "hitting the wall" phenomenon and gait changes during a full marathon	Nao Hirakawa
O22-6	Probability of cardiac-locomotor coupling during daily activities	Aurora Rosato
1100-1236	**Oral 23 Spine and trunk 1** Chairs: **Pui Wah (veni) Kong, Tadahiko Kato**	**Room 4**
O23-1	New perspective from old data: A contemporary, quantitative analysis of the first reported cervical facet dislocation produced in the laboratory	Ryan Quarrington
O23-2	Differences in trunk rotation between people with and without low back pain during various movements	Batbayar Khuyagbaatar
O23-3	Effect of the draw-in maneuver on lumbar spine and hip motion during sit-to-stand for prevention of low back pain and urinary incontinence	Jin Ishibashi
O23-4	Effects of age and gender on back muscle activations during various spinal movements	Chih-Hsiu Cheng
O23-5	Biomechanical influence of the cage lordosis in an anterior lumbar interbody fusion at L4-L5 - A simulation study	Robin Remus
O23-6	Deep paraspinal muscle volume asymmetry in adolescent idiopathic scoliosis	Phoebe Duncombe
O23-7	Reliability of ultrasonography to assess spinal compression during heavy load carriage	Walters Sherrilyn
O23-8	Targeted multifidus muscle activation reduces fibrosis of multifidus muscle following intervertebral disc injury	Paul Hodges
1100-1224	**Oral 24 Clinical biomechanics 2** Chairs: **Mary Rodgers, Shigeyuki Kato**	**Room 7**
O24-1	Changes in muscular coordination patterns of the elderly population	Elisa Romero Avila
O24-2	Natural knee biomechanics can be restored by customized high-tibial osteotomy: PRE/POST-op functional and morphological evaluations	Claudio Belvedere
O24-3	Effects of unexpected slip and trip-induced perturbations on dynamic stability and support moment	Shabnam Shokouhi
O24-4	An experimental setup for assessment of traction force and associated fetal brain deformation in vacuum-assisted delivery	Estelle Pitti
O24-5	The BASMI limits patient specific examination compared to motion capture of a four-segment spine	Logan Wade
O24-6	The importance of reporting performance-based outcomes following intramedullary nailing of tibial shaft fractures	Simon Thwaites
O24-7	Femoroacetabular impingement patients show altered kinematics during lateral hop and drop jump	Katrin Däetwyler
1100-1236	**Oral 25 Locomotion: General 2** Chairs: **Masahiro Shinya, Kazutaka Takahashi**	**Room 8**
O25-1	Poincaré Analysis detects pathological loading rate variability in post-ACLR individuals	Noah Davidson
O25-2	Test-retest reliability of markerless three-dimensional gait kinematics and kinetics, in healthy older adults	Andreia Filipa Carvalho
O25-3	Differences in frontal joint kinetics between markerless and marker-based motion capture systems during treadmill running	Hui Tang
O25-4	Simple walking model to explain hip torque compensation for reduced propulsive force	Hajime Ohtsu
O25-5	Relationship between bicycle control and gaze behavior during a narrow-path ride	Takashi Kojima
O25-6	Effect of air resistance on braking and propulsive impulses during treadmill running	Jared Steele
O25-7	Influence of neglecting free moment and transverse ground reaction forces in the detection of the instability of gait	Helene Pillet
O25-8	Comparison of two hypomimia indicators in Parkinson's disease	Elena Pegolo

1330-1500	**Symposium 05 Healthy knees after knee injury – challenging the biomechanist's perspectives** Chairs: **Jos Vanrenterghem, Niels Nedergaard**		**Room 1**
SY5-1	To avoid re-injury after reconstruction of the Anterior Cruciate Ligament (ACL), one should screen patients on movement patterns that excessive load the knee ligaments	Jesper Bencke	
SY5-2	Risk of (re-)rupturing the ACL during a side cutting manoeuvre can be assessed by screening standardized hops and jumps	Kevin Ford	
SY5-3	The development of post-traumatic osteoarthritis is primarily caused by pathological load distributions on the tibiofemoral cartilage	David Saxby	
SY5-4	Pathological knee loading observed during gait/running will propagate itself in most if not all other activities a patient/athlete engages in	David Lloyd	
1330-1442	**Oral 26 JSB Awards Nominee (Oral)** Chair: **Yuki Inaba**		**Room 2**
O26-1	Unique mass distribution in the lower limbs of distance runners and its effect on moment of inertia	Takeshi Edagawa	
O26-2	Mechanical interaction between achilles tendon and plantar fascia during isometric ankle plantar flexion	Hiroto Shiotani	
O26-3	Markerless sagittal plane kinematic analysis of sprint running: Comparison between a deep learning analysis and manual digitization	Hiroaki Noro	
O26-4	Extreme elongation of triceps surae muscle-tendon unit was attributable to the elongation of the muscle rather than that of the tendon in rat	Satoru Hashizume	
O26-5	Switch point of impact height of adjusting segments to reach ball heights during a two-handed backhand stroke at various impact heights	Sichao Zhang	
O26-6	Reliability of ultrasound-based muscle cross-sectional area in lower-limb: A comparative analysis between ultrasound and MRI	Yoko Kunimasa	
1330-1454	**Oral 27 Sport biomechanics 2** Chairs: **Daisuke Takeshita, Hiroshi Suito**		**Room 3**
O27-1	The relationship between reaction time and landing mechanics associated with anterior cruciate ligament injury during single-leg landing	Yan-Long Chen	
O27-2	The impulse of the lateral ground reaction force makes runners' lateral velocity change and their variability during the approach phase into the curved path in sprint running	Tatsuro Ishidzuka	
O27-3	Performance strategy in the high jump varies between individuals: Mechanical work exertion vs. Energy conversion	Toshihide Fujimori	
O27-4	Why are force-velocity profiles determined in dynamometer experiments different from those determined in jumping experiments?	Maarten Bobbert	
O27-5	Are lower extremity joint kinetics influenced by shoe collar height in collegiate female volleyball players?	Tanner Thorsen	
O27-6	Pectroralis major and deltoid muscularity in shot putters: Reversal of whether cross-sectional area or volume is related to performance	Shogo Hashimoto	
O27-7	Front knee control in cricket fast bowling	Rene Ferdinands	
1330-1418	**Oral 28 Orthopaedics: Tendon & ligament** Chair: **Mei-ying Kuo**		**Room 4**
O28-1	Biomechanical and histological properties of different human tendons	Samantha Hefferan	
O28-2	Factors associated with good recovery from achilles tendon rupture at 1-year post rupture	Ra'ad Khair	
O28-3	In-vivo patellar tendon strain measured using ultrasound differs by sex and region of the tendon	Naoaki Ito	
O28-4	Near-infrared spectroscopic assessment of patellar tendon mechanics	Adam Kositsky	
1330-1430	**Oral 29 Running: Footwear 1** Chair: **Uwe Kersting**		**Room 5**
O29-1	Effect of minimalist school shoes on intrinsic foot muscle size	Roy Cheung	
O29-2	Investigation of optimal perceived comfort in sports shoes with plantar pressure distribution	Wei Ting Tu	
O29-3	Rate of knee flexion at the instant of landing during running can influence initial knee joint stiffness estimates due to running shoe cushioning	Zhenyuan Zhang	
O29-4	Effects of the Nike Vaporfly 4% features on muscle activity	Ashna Subramanium	
O29-5	The effects of habitual foot strike pattern and footwear on running pattern and economy	Hyunji Kim	
1330-1430	**Oral 30 Prosthetics and orthotics 1** Chair: **Paolo Caravaggi**		**Room 7**
O30-1	Using gaze-tracking to assess cognitive load in lower limb prosthetic users	Sabina Manz	
O30-2	Upper extremity kinematics are affected by socket suspended prostheses during reaching motions	Julia Dunn	
O30-3	Straight-line walking on cross-slope in unilateral transfemoral prosthesis users	Genki Hisano	

O30-4	Unilateral transfemoral amputees might be at risk of lateral compartment degeneration of the knee joint	Diana Toderita
O30-5	A non inferiority approach to investigate the influence of stem fixation and stem type on revision rates in elective THA procedures depending on patient age	Michael Morlock
1330-1442	**Oral 31 Rehabilitation technology: Biorobotics and exoskeletons 1** Chair: **Hiroshi Takemura**	**Room 8**
O31-1	Center of mass kinematics robustly predict reactive joint torques at the ankle, knee, and hip during perturbed standing	Kristen Jakubowski
O31-2	Personal standing mobility Qolo enables people with lower limb impairments to voluntarily stand up	Yukiyo Shimizu
O31-3	Effect of an assistive robotic system's compliance on subject's muscular activation and comfort	Maximilian Siebert
O31-4	Finding assistance strategies based on musculoskeletal simulation and machine learning	Xianyu Zhang
O31-5	Neuromusculoskeletal model-informed bayesian neural networks-based control of a knee exoskeleton	Longbin Zhang
O31-6	Evaluation of a passive upper-limb exoskeleton during a simulated dynamic work task over a large shoulder workspace	Leon Lauret
1510-1610	**Muybridge Award Lecture** Chair: **Toni Arndt**	**Room 1**
MAL	Born to Move: Embracing our Evolutionary Legacy	Irene S. Davis
1640-1810	**Symposium 06 Beyond the Surface: Uncovering the Role of Materials in Biomechanics, Sports, and Rehabilitation** Chairs: **Solehuddin Shuib, Abd Halim Abdullah**	**Room 1**
SY06-1	Development of knee implant using additive manufacturing technology: Lattice design, material and manufacturing	Solehuddin Shuib
SY06-2	Simulating material properties of in-vivo shoe-surface interaction using a robotic platform - opportunities and limitations	Uwe Gustav Kersting
SY06-3	3D printing material in developing assistive adaptive devices for rehabilitation medicine	Abd Halim Abdullah
SY06-4	New materials that modify horizontal forces for injury prevention	Thor Buch Grønlykke
SY06-5	Additive metal: Process, microstructure and properties	Izhar Aziz
1640-1804	**Oral 32 Sport biomechanics 3** Chairs: **Simon Augustus, Koichiro Inoue**	**Room 2**
O32-1	Leg joint kinetic determinants of sprint acceleration running	Ryu Nagahara
O32-2	Biomechanical analysis of an elite paralympic amputee sprinter in steady state running on treadmill and track	Samira Giuliana Breban
O32-3	The influence of lateral wedged insoles on the performance of a shuffle movement	Reyna Crawford
O32-4	Effect of cleat and rider positioning on leg joint function	Colin Firminger
O32-5	Impulse generation and initial velocities in basketball two-foot running jumps	Jun Ming Liu
O32-6	Centre of pressure and roll over shape from wearable sensors during overground running of an elite paralympic amputee sprinter	Sara Barbacane
O32-7	Acceleration transmission during cricket fast bowling	Matthew Lamb
1640-1804	**Oral 33 Locomotion: Clinical gait 2** Chairs: **Brian Davis, Shoma Kudo**	**Room 3**
O33-1	Are sagittal plane leg alignment and the active peak force generated during running associated with medial tibial stress syndrome development?	Joshua Mattock
O33-2	A consumer-grade wearable technology is valid for the assessment of walking gait "in the wild"	Josh Carter
O33-3	Reduced number of motor modules recruited during stair descent in patients with knee osteoarthritis	Lasse Hansen
O33-4	Achievement of bipedal locomotion in a two-dimensional neuromusculoskeletal model of unilateral transfemoral amputation	Daisuke Ichimura
O33-5	The effect of exercises derived from clinical gait analysis on low back pain - A randomized control trial	Christina Kaltenbach
O33-6	Altering foot orientation changes knee loading in people with and without knee osteoarthritis during three daily activities	Yi Wan
O33-7	Impact of age on muscle activation patterns with a prolonged walk	Katherine Boyer
1640-1740	**Oral 34 Simulation techniques and applications 1** Chair: **Shinsuke Yoshioka**	**Room 4**
O34-1	Predicted ground reaction force is plausible to use in inverse dynamics based musculoskeletal simulation during gait	Ryo Ueno
O34-2	Prediction of ground reaction force and moment by inertial measurement units using a 3D forward dynamics model	Naoto Haraguchi

O34-3	Participant-informed models of the tibia-fibula complex: Influence of geometry and density prediction errors on bone strain	Olivia Bruce
O34-4	Sensorimotor noise might explain effort in amputee gait: A simulation study	Wouter Muijres
O34-5	A cadaveric shoulder motion study using open-loop control for simulating in-vivo muscle loading	David Timothy Axford
1640-1804	**Oral 35 Others 2** Chairs: **Hiroki Ozaki, Shinya Sano**	**Room 5**
O35-1	Treadmill versus overground gait characteristics in autistic individuals	Kevin Valenzuela
O35-2	In situ validation of power quantification for dynamic wheelchair sports	Mathieu Deves
O35-3	The immediate effect of a hop-stabilization program on ground reaction force during cutting movements in individuals with chronic ankle instability	Teerapat Laddawong
O35-4	Neuromuscular adaptations to aerial landing performance following a shark bite injury: A case-control study	James Forsyth
O35-5	fMRI reveals fidgeting motor skills in ADHD improves prefrontal cortex activation during executive functioning	Xirui Zhao
O35-6	Breaking ground without breaking the bank - validation of a novel low-cost 3-axis force plate	Yumna Albertus
O35-7	Texture analysis of ultrasound images to evaluate multifidus muscle composition: A comparison between healthy subjects and patients with low back pain	Jong Hun Kim
1640-1804	**Oral 36 Artificial intelligence and machine learning 2** Chairs: **Sina David, Keizo Takahashi**	**Room 6**
O36-1	Improving cycling force sensor accuracy using multilayer perceptrons	Jonas Ebbecke
O36-2	Estimation of ground reaction forces and center of pressure during stair walking using convolutional neural network based model	Ye Ma
O36-3	Comparing the advantages and disadvantages of physics-based and neural network-based modeling for predicting cycling power	Patrick Mayerhofer
O36-4	AI based automated error detection for medical skills training using markerless biomechanics	Travis Eliason
O36-5	Myosuite: Combining neuromusculoskeletal modelling with reinforcement learning to mimic motor control	Guillaume Durandau
O36-6	Estimation of whole-body posture during walking in unilateral transfemoral amputees using sparse inertial measurement units and deep learning	Yuji Kumano
O36-7	Fast bowling performance analysis using inertial sensors and machine learning	Shruti Bhandurge
1640-1740	**Oral 37 Running: Footwear 2** Chair: **Mark John Lake**	**Room 7**
O37-1	A novel method to measuring the slip of foot inside the shoes: Evaluation of socks friction using pressure sensors	Dongwook Seo
O37-2	Influence of the type of running shoes in the lower limb muscular activity	Goncalo Marta
O37-3	Influence of shoe cushioniong on proximal running kinematics and kinetics	Kathy Reyes
O37-4	A pilot study: Effects of an 8-week training intervention in carbon-plated running shoes	Justin Matties
O37-5	Midsole stack height, running economy and step parameters	Montgomery Bertschy
1640-1804	**Oral 38 Muscle tissue and architecture 2** Chairs: **Kohei Watanabe, Katsuki Takahashi**	**Room 8**
O38-1	The effect of initial condition at the onset of stimulation on the ratio of muscle stiffness to force during isometric contraction	Siwoo Jeong
O38-2	Preload affects muscle fascicle mechanics during maximal voluntary MTU lengthening actions	Paolo Tecchio
O38-3	Multiscale hamstring muscle adaptations following a nine week eccentric training program	Max Andrews
O38-4	Typically developing children and children with cerebral palsy have similar leg muscle moment arms	Bart Bolsterlee
O38-5	Muscle- and sex-specific leg muscle volumes in children with cerebral palsy	Jonathan Yu
O38-6	A new model for the molecular mechanism of muscle contraction	Walter Herzog
O38-7	Is the aponeurosis protected from great length changes when active muscle forces change dramatically?	Fransiska Bossuyt

1820-1950	**Poster 11 Sport biomechanics 2**	2nd Floor, Poster Display #1
P11-01	Ground reaction forces during the full driver shot of Japanese male professional golfers	Tomoya Hirano
P11-02	Is there a linear relationship between swimming velocity and vertical body position in front crawl for each stroke phase?	Sohei Washino
P11-03	Evaluation of muscle activations of upper arm in collegiate athlete during 200-m front crawl: A pilot study	Jia-Hao Chang
P11-04	The effects of two-step golf swing drills on swing rhythm and clubhead speed in competitive juniors	Kanji Mori
P11-05	Conserved biomechanical strategies for standing and walking balance in the upright and inverted posture	Charlotte Le Mouel
P11-06	Shoulder, scapulothoracic, and glenohumeral joint movements during badminton overhead swing motion in standing versus wheelchair sitting positions	Yuki Tamura
P11-07	Mass-spring characteristics explain the temporal step parameters but are not specific to individuals across phases in accelerated sprinting	Arata Tatsumi
P11-08	Accuracy of the centre of mass estimation based on pictures among iqfoil windsurfing athletes	Martyna Bialecka
P11-09	Assessing the likelihood of ACL injury in volleyball players at UITM by utilizing the landing error scoring system	Raihana Sharir
P11-10	Measurement of horizontal ground reaction force moment in the golf swing	Sung Eun Kim
P11-11	Longitudinal associations among land-jump biomechanics and imaging of the patellar tendon in male basketball players during the preseason	Andrew Kraszewskia
P11-12	Biomechanical know-how of learning bicycle kick and jumping side volley in soccer	Gongbing Shan
P11-13	A nine-week ACL injury prevention program for female handball players: Effect on knee joint loading, cutting technique and performance	Patrick Mai
P11-14	Reference values of jump tests stratified by sex using an insole-embedded IMU	Meihui Li
P11-15	Associations of rotational range and strength of shoulder with regard to elbow valgus stress during pitching in youth baseball players	Yu-Chun Lin
P11-16	Impact of cold exposure and warm-up on muscle temperature and countermovement jump variables	Itaru Chiba
P11-17	Towards a contact model of the rugby union scrum	Zak Joseph Mascarenas Sheehy
P11-18	Effect of different speed in eccentric phase in squat protocols on hip flexors and extensors activation	Anna Pisz
P11-19	Sagittal plane lower extremity biomechanical response to soccer cleat stud length during a cutting task	Emily Karolidis
P11-20	Biomechanical analysis of the take-off phase in Japanese male pole vaulters	Tomoki Yamamoto
P11-21	A new approach to evaluate the ACL risk of re-injury after reconstruction	Sahar Ostadrahimi
P11-22	Effect of resin on ball velocity of the step-shooting in female handball players	Aoi Fujimoto
P11-23	Head striking patterns of Japanese kendo between elite traditional kendoka and elite tournament players	Ting-Cheng Chou
P11-24	Effect of different knee angles on hamstring muscle activity during nordic hamstring exercise with a sloped platform	Taspol Keerasomboon
P11-25	Angulation of handle force application from the cable direction in achieving a turn in the hammer throw	Eri Nonaka
P11-26	A biomechanical analysis on the straight jump of gymnastics trampoline	Yuji Ohgi
P11-27	The effects of footwear on the plantar pressure under the metatarsal heads during rope skipping	Kaicheng Wu
P11-28	Reduced medial-lateral displacement of the body's center of mass during walking in starting soccer players in high school football league	Anne Dixie Lim
P11-29	Throwing performance and kinematic analysis of overhead throwing in male elite and varsity cup cricketers	Jordan Leondiris
P11-31	Case study: Can tensiomyography predict sports performance?	Kyoungkyu Jeon
P11-32	Comparison of differences in muscle activity according to the types of conventional deadlifts	Seungho An
P11-33	Kinetic determinants of acceleration performance in sideward sprint start from standing position	Takahiko Sato
P11-34	Angular momentum analysis of four styles of baseball pitching	Tomohisa Miyanishi
P11-35	An interaction between landing height and ground condition in ground reaction force during two-leg landing	Jeongeun Moon
P11-36	Differences in lower extremity muscle activation patterns during anticipated or unanticipated single-leg drop jump tasks	Jae Wook Lee
P11-37	Neuromuscular fatigue of vastus lateralis during fatiguing squat exercises in trained and untrained people: Time-frequency analysis	Jihong Park
P11-38	Track GRFs from an elite transfemoral paralympic sprinter using a wearable clamp dynamometer	Mattia Scapinello
P11-40	Comparison between rotational shot put technique and discus throw	Tadahiko Kato
P11-41	The effect of single-leg rotational landing on knee kinematics	Parunchaya Jamkrajang

1820-1950	**Poster 12 Musculoskeletal modeling**	2nd Floor, Poster Display #1
P12-02	Bone-remodelling in the foot: Application to exercise during the covid-19 lockdown	Julie Kim
P12-03	Validation of markerless motion capture for the assessment of joint reaction forces under varying body-borne loads	Isabel Coll
P12-04	The effect of subscapularis repair following posterosuperior rotator cuff tear severities on superior joint shear force during abduction in reverse shoulder arthroplasty	Donghwan Lee
P12-05	Morphological musculoskeletal database of upper extremity using homologous modeling	Shoji Konda
P12-06	Effects of chronic ankle instability on ankle joint angles and ligament strains during unanticipated cutting tasks	Hoon Kim
P12-07	Comparison of synergy extrapolation and static optimization for estimating multiple unmeasured muscle activations during walking	Di Ao
P12-08	Pelvis stabilizing muscles activity and forces in hip flexion resistance training anybody modeling	Dobrochna Fryc
P12-09	The effect of multiple measurement angles on the prediction of joint torque-angle parameters	Amy Parkinson
P12-10	3D modeling of lever arm and moment-generating capacity of sternocleidomastoid and scalenus muscles in respiratory movement	David Biteau
P12-11	A modelling approach to determine femoroacetabular impingement in badminton-specific motions	Dominic Bachmann
P12-12	Analysis of force characteristics and muscular activity of temporomandibular joint in three masticatory motions: Multibody dynamics simulation	Sung-Ho Lee
P12-13	Impact of acromioclavicular and coracoclavicular ligament implementation on the shoulder musculoskeletal simulation	Takayuki Aimi
P12-14	Differences of muscle behaviors by muscle activation minimization and metabolic energy minimization in musculoskeletal dynamics simulation	Young-Jun Koo
P12-15	Optimal control simulations using wearable sensors and personalized musculoskeletal models - a novel approach to modelling gait	Grace McConnochie
P12-16	Creation of a head-ground contact model for equestian fall impacts	James Cowburn
P12-17	The prosthetic metatarsophalangeal joint stiffness during walking on various environments: A simulation study	Pankwon Kim
P12-18	Validity evaluation of muscle force and muscle activity estimated using two-dimensional vertical GRF	Zeming Jin
P12-19	Hindfoot articular joint loading during walking: A combined in vivo and in silico study	Barbara Postolka
P12-20	Control strategy of the locomotor system for obstacle-crossing in adolescents with severe idiopathic thoracic scoliosis: Trade-offs between mechanical energy expenditure and foot clearance	Cheng-Hao Yu
P12-21	Muscle fatigue: Experiment and simulation	Zeinab Saghaei Nooshabadi
P12-22	Lower limb mechanical load in ballet jumps with turnout and neutral positions (work in progress)	Filipa Joao
P12-23	Consequences of limiting electromyography and ground reaction forces on modelled anterior cruciate ligament forces	Azadeh Nasseri
1820-1950	**Poster 13 Locomotion: Clinical gait**	**2nd Floor, Poster Display #1**
P13-01	Activity of superficial trunk muscles in patients with stroke during gait: A case series	Christopher Cruz
P13-02	Classification of people with parkinson's disease based on images converted from time-series data during 360° turning task	Hyejin Choi
P13-03	Stretch strain sensor for abduction of the talonavicular joint	Shintarou Kudo
P13-04	Time series for the whole-body synergy of the hip angle during gait in patients with hip osteoarthritis	Takuya Ibara
P13-05	Biomechanical analysis of contralateral cane use	Hyeoun Soo Shin
P13-06	Relationship between leg muscle co-contraction and jerk during gait	Toshinori Miyashita
P13-07	Towards precision assessment of gait impairments in stroke survivors	Jun Liang Lau
P13-08	Oxygen consumption and center of foot pressure trajectory changes with a 3D-printed insole based on the 3D-scanned individual soleprint	Mizuki Kondo
P13-09	Comparisons of energy expenditures among children diagnosed with idiopathic toe walking and typical children using inertial sensors	Dylan Normandin
P13-10	Relationship between gait kinematics and fall risk in patients with parkinson's disease	Ryo Yamasaki
P13-11	Trunk movement during nordic walking evaluated using a gyroscope in patients with hip osteoarthritis	Chiho Fukusaki
P13-12	Effects of the monocular vision in endpoints control during obstructed gait	Yi-Ling Lu
P13-13	Aligning local segment frames based on different optimisation criteria to standardise kinematic signals	Adrian Sauer
P13-14	Centre of pressure displacement and velocity during gait in subjects with low back pain	Clara Leyh
P13-15	A comparison of two multi-segment spine models to assess movement during gait in adolescent idiopathic scoliosis	Robert Alan Needham
P13-16	Multi-segment spine movement in adolescence idiopathic scoliosis and effect of walking speed	Aoife Healy

P13-17	Instrumented assessment of falls risk in subjects with mild parkinson's disease	Sai Wei Yang
P13-18	Machine learning classification of gait in leprosy patients with foot drop	Adriane Muniz
P13-19	Multiscale entropy can be used to distinguish between fallers and non-fallers	Arezoo Amirpourabasi
1820-1950	**Poster 14 Lower extremities**	**2nd Floor, Poster Display #1**
P14-01	Measurements of tibial rotational range of motion and healthy adult characteristics	Shingo Kawakami
P14-02	Does the lower extremity muscular function symmetry exist in athletes with ACLR?	Ning Chu
P14-03	Analyses of lower limb asymmetry in division I women basketball players: A pilot study	Pin-Chun Tseng
P14-04	Gender differences in kinematics and muscle activity during the preparation phase of the single-leg landing task in badminton	Zhe Hu
P14-05	Predicting post-surgery muscle activations following internal hemipelvectomy surgery	Geng Li
P14-06	Effect of shoe sole thickness on the external ankle joint inversion moment during drop landings on a tilted surface	Nahoko Sato
P14-07	Aging effects on hip power during slope walking	Zihan Yang
P14-08	Acute effects of proprioceptive neuromuscular facilitation stretching on lower limb muscle activation in older and younger adults	Fiona Higgs
P14-09	Sagittal range of motion changes in cycling with asymmetric crank arms	Sean A Brown
P14-10	Effect of calf electrical stimulation training on sprint and jump performance	Sheng-Wei Jia
P14-11	Middle-aged adults altered the joint strategy but not muscle-tendon interaction during gait	Iseul Jo
P14-12	Comparison of differences in lower extremity EMG according to foot angle during self-weight squat in adult women with genu valgum	Chanki Kim
P14-13	Eccentric preload increases work during shortening by counteracting residual force depression	Wolfgang Seiberl
P14-14	The impact of spring tension on muscles activation in the lower limbs during footwork movements in pilates	Yongseok Park
P14-15	Comparative analysis on lower extremities kinematic of adult women during stair ascend according to heel height	Sangha Park
P14-16	Kinematic analysis of metatarsophalangeal joint during level and slope walking	Sang Woo Jung
1820-1950	**Poster 15 Medical devices**	**2nd Floor, Poster Display #1**
P15-01	Biomechamical evaluation of a hybrid suture anchor with expandable barbed in osteoporotic swine bone block	Yu-San Chen
P15-02	Biomechanical evaluation of a 3D printed adjustable assembly thin bone plates for transverse patella fracture	Chiao-Min Chang
P15-03	Pullout evaluation of a novel pedicle screw with a proximal pedicle sleeve augmentation	Ting-Shuo Hsu
P15-04	Lateral trunk muscles thickness change during seated virtual reality-guided exercise	Masashi Kitano
P15-05	Optimisation of the electrode configuration of a semg sensor system to be used in rehabilitation settings	Elmar Junker
P15-06	Developing and verification of the innovative blood flow restriction training device	Lan-Yuen Guo
1820-1950	**Poster 16 Methodologies and data analysis**	**2nd Floor, Poster Display #1**
P16-01	The validity of inverse dynamics calculations for lower limbs during gait using a markerless motion system	Tianchen Huang
P16-02	Reliability of opencap with smartphone videos to measure hip and knee angle during two-step test	Ibuki Ono
P16-03	Accuracy evaluation of lower limb joint angles with markerless motion capture during spin turn	Takuya Kikuchi
P16-04	Investigating the relationship between local and global gait stability	Ann-Kathrin Harsch
P16-05	Uncovering cluster structures within EMG signatures of gestures	Jonas Grosse Sundrup
P16-06	Prediction of the hip joint center position using statistical geometric transformation: Validation in canine models	Cheng-Chung Lin
P16-07	Automated gap-filling algorithm for kinetic data of finger movement: Pianist hand motion cleaning using spatio-temporal imputation	Taegyun Kwon
1820-1950	**Poster 17 David Winter Young Investigator Awards Nominee (Poster)**	**5th Floor, Poster Display #2**
P17-01	Steadiness of isometric plantarflexion is reduced when changing posture from supine to prone position	Moeka Samoto
P17-02	Energetics, mechanics, and muscle: Locomotor adaptations to chronic limb loading during development	Kavya Katugam-Dechene
P17-03	Effects of differences in friction conditions of fingertips on upper limb movement during fastball pitching in baseball	Souta Suzuki
P17-04	Biomechanics of handcycling high intensity interval training	Kellie Halloran
P17-05	Characteristic of thigh muscle hypertrophy induced by electrical muscle stimulation training	Kosuke Kano

1820-1950	**Poster 18 JSB Award Nominee (Poster)**	**5th Floor, Poster Display #2**
P18-01	Advent of carbon thick shoe changes morphological advantages for long-distance running ability	Ayaka Nobue
P18-02	Different effects of a single ingestion of quercetin on motor unit recruitment in upper and lower limbs	Taichi Nishikawa
P18-03	Differences in visco-elastic properites of muscle and tendon between 100m and 400m sprinters	Toshiaki Oda
P18-04	Effect of restricted thoracic expansion during shoulder external rotation on scapulothoracic and gleno-humeral joint motion	Mitsuhiro Yoshimi
P18-05	Motor unit firing properties of tibialis anterior during peripheral nerve stretching	Tetsuya Hirono
P18-06	The difference in the precision of the soccer shot between dominant and non-dominant feet	Yusuke Shimotashiro
P18-07	Kinematic contribution to javelin velocity at different run-up velocities in male javelin throwers	Mizuki Makino
P18-08	The intrinsic foot muscles contribute to controlling postural sway during single-leg stance	Momoka Nakamura
1820-1950	**Poster 19 Motor control**	**5th Floor, Poster Display #2**
P19-01	Muscle synergy analysis of two single-leg yoga postures: Comparison between practitioners and non-practitioners	Luciano Menegaldo
P19-02	Break dance motion analysis through motor synergy	Keli Shen
P19-03	Long-lasting VR-induced postural control impairment after mtbi	Gustavo Sandri Heidner
P19-04	Awareness of visual offset does not improve shoulder joint position sense in virtual reality environment	Motoki Sakurai
P19-05	Effects of dual-task challenges on the multi-objective optimal control strategies during obstructed gait	Yi-Chun Kuan
P19-06	Gender differences in postural control during single-leg squat	Sakiko Nishimura
P19-07	Force encoding in secondary muscle spindle endings	Jacob Stephens
P19-08	Sex differences in laterality of motor unit firing behaviour of first dorsal interosseous muscle in young adults	Yuichi Nishikawa
P19-09	Kinematic analysis of controlling foot-ball acceleration at ball impact during soccer juggling	Kazuki Aoi
P19-10	Sensorimotor learning of whole-body goal-directed movements with upper and lower extremities	Nagisa Inubashiri
P19-11	Control of standing posture depends on adaptation of goal-directed lower extremity movements	Mai Moriyama
P19-12	Effects of batting practice with pitch location feedback and peripheral vision on hitting variability in baseball	Masahiro Kokubu
1820-1950	**Poster 20 Muscle tissue and architecture**	**5th Floor, Poster Display #2**
P20-01	Direct measurements of tendon length changes during stretch-shortening cycles in rat	Atsuki Fukutani
P20-02	Acute effects of dynamic versus static stretching in muscle architecture in adolescents	ZhiYu Tao
P20-03	Torque loss during simultaneous activation of agonistic muscles	Michael Baggaley
P20-04	Is force-generating capacity of the plantarflexor muscles affected by the surrounded skin mechanical property and orientation of gravity?	Yasuhide Yoshitake
P20-05	Musculotendinous architecture and strength of supraspinatus after tear and arthroscopy repair in patients with full-thickness tendon tear	Yen-Ling Chou
P20-06	Mechanical properties of the achilles tendon in middle-aged men and its relation to jump performance	Hae Dong Lee
P20-07	In vivo 3-dimensional ultrasonography of human biceps femoris reveals a twisted proximal aponeurosis	Carmela Julia Mantecon Tagarro
P20-08	Relationship between baseline flexibility and changes after chronic stretching intervention program	Masatoshi Nakamura
P20-09	Force-generating capacity of plantarflexion force is lowered by gravity during standing positions	Kiichi Saji
1820-1950	**Poster 21 Others 1**	**5th Floor, Poster Display #2**
P21-01	A biomechanical 3D analysis of a lab recorded lateral ankle sprain during a handball specific fake-and-cut maneuver	Timo Bagehorn
P21-02	A novel approach for characterizing the individual plantar intrinsic foot muscles: Cluster analysis based on physiological cross-sectional area and muscle fiber length	Yuki Kusagawa
P21-03	Predicting cervical spine dynamics using gaussian processes	Andrea Braschi
P21-04	The influence of bariatric surgery on postural stability - a pilot study	Veronika Szabóvá

Wednesday, August 2nd

0800-0930	**Symposium 07 Musculoskeletal modeling and simulation for injury prevention: State-of-the-art and future needs** Chair: **: Nicos Haralabidis**	**Room 1**
SY07-1	Simulation of lower extremity sports injuries: can we translate theory into practice?	Ton van den Bogert
SY07-2	Including variability into simulations 101: How to handle uncertainty in movement simulations	Anne Koelewijn
SY07-3	Towards the adoption of musculoskeletal modelling in the contact sport industry: Is it dream or reality?	Dario Cazzola
SY07-4	Designing a model of the shoulder joint for sports applications and injury analyses	Jennifer Maier
SY07-5	Musculoskeletal simulation to discover risk factors of hamstring strain injury during sprinting	Reed Gurchiek
SY07-6	OpenCap: 3D musculoskeletal simulation from smartphone video – Applications for injury prevention	Antoine Falisse
0800-0924	**Oral 39 Sport biomechanics 4** Chairs: **Neal Smith, Hironari Shinkai**	**Room 2**
O39-1	Relathionship between knee valgus angle and lateral trunk bending angle during volleyball spike jump	Miki Kawai
O39-2	Framework to solve the optimum armstroke in crawl swimming considering subject-specific shoulder joint torque characteristics	Motomu Nakashima
O39-3	Barbell squats for crossfit athletes: Effect of footwear type and load magnitude on lower limb joint torques	Eduardo Campos Martins
O39-4	Simulation of running prosthetic feet ground reaction forces using a multi-axial robotic walking simulator	Giacomo Fabris
O39-5	Knee biomechanical differences during unilateral landing between symmetrical and asymmetrical groups classified by hop tests	Karine Stoelben
O39-6	Risk factor identification of adductor strain in professional soccer	Rebecca Davis
O39-7	Individualized immediate feedback on sidestep cutting technique reduces knee abduction moments in female handball players	Kevin Bill
0800-0900	**Oral 40 Motor control 1** Chairs: **Motoki Kouzaki, Daichi Yamashita**	**Room 3**
O40-1	Corticokinematic coherence: A proprioceptive biomarker for motor performance	Scott Mongold
O40-2	Evaluating the musculoskeletal impact of local muscle vibration	Andrew Lowry
O40-3	Compensatory covariation of ball launch variables in tennis strokes	Yusuke Sudo
O40-4	Investigation of sensor-embedded key to quantify dynamic pinch force during key turning in young vs older healthy adults	Li Jing Soh
O40-5	Calibrated muscle-synergies method for missing muscle excitations prediction during walking	Marco Romanato
0800-0900	**Oral 41 Others 3** Chairs: **Ismail Shariman, Ryo Iwasaki**	**Room 4**
O41-1	Impact of a high-fat high-sucrose diet on joint and muscle integrity in juvenile sprague dawley rats	Mauricio Delgado
O41-2	Substantial reductions in adult physical activity follow an exercise-restricted growth period in guinea fowl	Derek Jurestovsky
O41-3	Continuum mechanical approach to rigid body mechanics in biomechanics	Salvatore Federico
O41-4	The effects of 10 weeks movement training for a junior student with motor impairment on functional mobility	Sheng-Yang Tso
O41-5	Does a 100-day mentoring program change girls' attitudes & self-identification in science, engineering & biomechanics?	Karen Mickle
0800-0912	**Oral 42 Rehabilitation technology: Biorobotics and exoskeletons 2** Chair: **Chien-chi Chang**	**Room 5**
O42-1	The mechanical energetics of walking on incline surfaces with passive ankle exoskeleton assistance	James Williamson
O42-2	Predicting individualized joint kinetics over continuous variations of walking and running	Emma Reznick
O42-3	Gait adaptation on repeat exposure to a robotic hip exoskeleton	Mark Price
O42-4	An improved design of an upper limb exoskeleton for overhead tasks	Georgios Aronis
O42-5	Walking with exoskeletons: Establishing biomechanical metrics for quantifying assisted-gait familiarization	Giorgos Marinou
O42-6	Metabolic power response to added mass on the lower extremities during running	Raziel Riemer

Hand and Wrist Biomechanics International (HWBI) Symposium		Room 6
0800-0930	**Slot 1** Chairs: **Toshiyasu Nakamura, Veronique Feipel**	
	Welcome	Trey Crisco, Angela Kedgley
HWS1-1	Recovery of thumb joint movement for patients with severe carpal tunnel syndrome	Hiroshi Kurumadani
HWS1-2	Median nerve deformation increases during repeated efforts of a pulp-pinch grip task	Denise Balogh
HWS1-3	Stability of the midcarpal joint post scaphoidectomy in different wrist types	Ronit Wollstein
HWS1-4	Effect of age and sex on the subluxation of the thumb carpometacarpal (CMC) joint	Li-Chieh Kuo
HWS1-5	Using an RGB-depth camera for marker-less estimation of contact between hand and handrim during an in-lab wheelchair tennis propulsion	Enrico Ferlinghetti
HWS1-6	Investigating the long-term impacts of hand tractor operation on the upper limb of farm operators	Josefa Angelie Revilla
1100-1230	**Slot 2** Chairs: **Ronit Wollstein, Angela Kedgley**	
HWS2-1	Keynote: Unsolved clinical mysteries in the hand and wrist	Nina Suh
HWS2-2	The difference in the efficiency of reactive grip force adaptation during static and dynamic tasks between children and adults	Hsiu-Yun Hsu
HWS2-3	Do muscle activity patterns vary according to the severity of carpometacarpal osteoarthritis disease?	Tamara Ordonez Diaz
HWS2-4	Fatigue of hand muscles following pinch grip quantified by surface electromyogram	Kiatbodin Wanglertpanich
HWS2-5	Method for assessing the fine motor skills synergies based on computer vision	Andrey Pomerantsev
HWS2-6	Coordinated muscle activity during chopstick manipulation	Kazuya Kurauchi
1430-1600	**Slot 3** Chairs: **Nina Suh, Darshan Shah**	
HWS3-1	Keynote: Non-surgical carpal arch space augmentation for median nerve decompression	Zong-Ming Li
HWS3-2	Challenges in developing a healthy finite element wrist model: Ligaments	James Yang
HWS3-3	Multi-object and multi-feature models of thumb anatomy for population-based morphological assessment	Cait Farrell
HWS3-4	Evaluation and comparison of in-vitro joint kinematics using motion-based coordinate frames vs. anatomical landmarks	Mohammad Haddara
HWS3-5	Familiarity effect on handwriting performance in school-aged children	Hao-Ling Chen
HWS3-6	Wi-fi based continuous detection of hand movements for motor assessment in Parkinson's disease	Chi-Lun Lin
1630-1720	**Slot 4** Chair: **Zong-Ming Li**	
HWS4	Keynote: Biomechanics of the distal radioulnar joint (DRUJ)	Toshiyasu Nakamura
	Awards	Angela Kedgley, Zong-Ming Li
	Closing	Zong-Ming Li
0800-0912	**Oral 43 Muscle tissue and architecture 3** Chair: **Bart Bolsterlee**	**Room 7**
O43-1	Timing of shortening influences force depression	Joumaa Venus
O43-2	The effects of gait retraining on the behaviours and mechanical properties of medial gastrocnemius-tendon unit during running	Liqin Deng
O43-3	Muscle volumes and moment arms of human rotator cuff muscles in vivo	Yilan Zhang
O43-4	Correlations between achilles tendon moment arm and plantarflexor muscle architecture	Logan Faux-Dugan
O43-5	Regional hamstring hypertrophic adaptation following a nine-week eccentric nordic hamstring training program	Anoosha Pai S
O43-6	Ultrasound based muscle quality and the confounding effect of subcutaneous fat layer in individuals with obesity	Heiliane de Brito Fontana
0800-0900	**Oral 44 Lower extremities 1** Chair: **Aaron Fox**	**Room 8**
O44-1	Orthotropic bone remodelling around uncemented acetabular component	Sanjay Gupta
O44-2	3D personalized foot models using surface-based statistical shape modelling	Liangliang Xiang
O44-3	Changes in hallux movement in people with chronic ankle instability during walking at different speeds	Tunpisith Jeamsupakorn
O44-4	Passive properties of the achilles tendon in athletes	Maria Sukanen
O44-5	Determining torque-angle relationships of human toe flexors	Samuel Wisdish

0940-1030	**Keynote Lecture 3** Chair: **Gregory Sawicki**	**Room 1**
KL3	Brain-Computer Interface Design: Thinking out of the box	Natalie Mrachacz-Kersting
1100-1230	**Symposium 08 Performance Enhancement Footwear in Running** Chairs: **Kim Hébert-Losier, Irene Davis**	**Room 1**
SY08-1	The effects of advanced footwear technology on running performance and lower extremity loading: Current knowledge and future directions	Steffen Willwacher
SY08-2	Footwear energy storage and return: How footwear mechanically cooperates and/or competes with the runner	Emily Matijevich
SY08-3	Effect of increased longitudinal bending stiffness on running economy and biomechanics when running uphill and on unstable terrain: Implications for trail running footwear	Marlène Giandolini
SY08-4	Can we predict who is responding to advanced footwear technology from biomechanics?	Wouter Hoogkamer
1100-1224	**Oral 45 Locomotion: Clinical gait 3** Chairs: **Aoife Healy, Norio Tsujimoto**	**Room 2**
O45-1	Individual rocker shoe parameters that are most effective in reducing plantar peak pressure	Thomas Johnson
O45-2	A segment frame optimisation method to standardise kinematic signals	Ariana Ortigas Vasquez
O45-3	Is peak anterior foot position related to anterior foot position at initial contact during gait training with visual feedback?	Erik Hummer
O45-4	Gait kinematics for severe knee OA and post-Tka from markerless motion capture	Elise Laende
O45-5	Gait characteristics of older adults with sagittal malalignment progression after spinal fixation	Shun Ito
O45-6	Analysis of gait coordination changes after training using HAL in patients with gait impairment due to central nervous system disorders	Hideki Kadone
O45-7	Effects of posterior spinal fusion surgery on gait biomechanics in patients with adolescent idiopathic scoliosis	Manish Gupta
1100-1148	**Oral 46 Methodologies and data analysis 2** Chair: **Kazuhiro Ishimura**	**Room 3**
O46-1	Three-dimensional vector analysis of ground reaction force moment arms: Conceptual considerations and experimental verification	Shinichi Kawamoto
O46-2	Automated generation of patient-specific intervertebral disc FEM models based on CT images	Kati Nispel
O46-3	Backpack carrying: A comparison between marker-based and markerless systems	Jose Heredia-Jimenez
O46-4	Adaptive p-splines for challenging filtering problems in biomechanics	Andrew Pohl
1100-1200	**Oral 47 Prosthetics and orthotics 3** Chair: **Hiroaki Hobara**	**Room 5**
O47-1	Shape optimization of dental implant thread geometry	Andi Isra Mahyuddin
O47-2	Thermal assessment of an ankle-foot orthosis for varied climatic conditions	Ganesh Bapat
O47-3	Gait analysis and energetics of a novel passive dynamic custom foot and ankle orthosis in a population of foot-drop patients	Paolo Caravaggi
O47-4	Simulating prosthesis conditions in cycling: A comparative study	Heloisa Seratiuk Flores
O47-5	3D printed customized insoles: A FEM and gait analysis combined approach	Zimi Sawacha
1100-1224	**Oral 48 Biomedical engineering** Chairs: **Taylor Dick, Haruki Toda**	**Room 7**
O48-1	Biomechanical investigation of a novel plate for posterior tibial plateau fracture with posterior cruciate ligament avulsion fracture	Peter Andreas Timotius
O48-2	Predicting the mechanical properties of atherosclerotic coronary arteries	Ricardo Caballero
O48-3	Mechanical characterization of passive myocardial response at different animal ages in porcine hearts	Nicolas Laita
O48-4	Evaluation of biomechanical effieciency of dual mobility total hip arthroplasty: Multibody dynamic analysis	Jeong Ah Pak
O48-5	Improving prosthetic feet with polymer materials: A study of mechanical properties	Agus Setyo Nugroho
O48-6	Pilot study of cartilage creep and recovery determined with noninvasive magnetic resonance imaging and classical mechanical testing	Bo Eitel Seiferheld
O48-7	Finger palpation on an artery as gaussian space filter	Debadutta Subudhi
1100-1200	**Oral 49 Impact biomechanics 2** Chair: **Hiroki Ozaki**	**Room 8**
O49-1	Deformable headform design choices: An evaluation of brain simulant stiffness influence on intracranial displacements and strain	Sheng Xu
O49-2	The influence of the tertiary bronchi on strain-induced pulmonary injury	MacKenzie Brannen

O49-3	Identification of joint motions affected knee valgus after multi-directional single-legged drop landing by principal component analysis	Takayuki Koike
O49-4	Vinyl sports floor cushioning thickness affects shoe-surface traction in futsal but not mechanically evaluated ankle inversion moment	Filip Gertz Lysdal
O49-5	In vivo investigation of microstructural brain changes following football heading	Hugh McCloskey
1330-1420	**Keynote Lecture 4** Chair: **Wolfgang Potthast**	**Room 1**
KL4	The Mechanics of Running Fast and Jumping High: from small Differences in Ground Force to Big Differences in Performance	Peter Weyand
1430-1600	**Symposium 09 Human Motion Analysis With Wearable Inertial Sensors: Standardizations and Advances** Chairs: **Reed Gurchiek, Kamiar Aminian**	**Room 1**
SY09-1	Deep kinematics: Uncovering human biomechanics with IMUs and deep learning – preliminary result	Yong Kuk Kim
SY09-2	Inertial measurement unit calibration methods for the wrist joint: Which one should I use?	Alessandro Bonfiglio
SY09-3	Three-dimensional scapular tracking using inertial measurement units: A regression-modelling approach	Zhou Fang
SY09-4	Do different methods for mimu-based posturography lead to the same results?	Annamaria Guiotto
SY09-5	Opensim-based estimation of lower body kinematics using magneto-inertial recordings – recovery from ankle fractures and achilles tendon ruptures as a pilot case	Timo Rantalainen
SY09-6	Body segment orientation tracking with IMU: An adaptive robust ekf for dynamic long-duration activities	Hossein Rouhani
SY09-7	Bout duration during out-of-lab walking affects gait kinematics	Mayumi Wagatsuma
SY09-8	ISB recommendations on the assessment and reporting of joint kinematics in human motion analysis applications using IMUs	Reed Gurchiek Kamiar Aminian
1430-1542	**Oral 50 Sport biomechanics 5** Chair: **Ryu Nagahara**	**Room 2**
O50-1	Influence of sport surface properties on utilized traction and lower extremity biomechanics of american football players	John Wannop
O50-2	Exploring the acute neuromuscular effect of accentuated eccentric loading during unconstrained vertical jump with different loading locations on the body	Eric Yung-Sheng Su
O50-3	Dynamic sagittal plane joint loading biomechanics in individuals with ACL reconstruction with and without a history of ankle sprains compared to healthy controls	Yuki Sugimoto
O50-4	Use of a novel mobile application to assess calf muscle function in sport	Hebert-Losier Kim
O50-5	Influence of immediate dry needling therapy for hamstring muscle fatigue on standing balance control	Shih-Wun Hong
O50-6	Contribution to the racket head velocity in the tennis forehand drive between intermediate and high-performance players	Pedro Bruno
1430-1542	**Oral 51 Balance and posture 2** Chairs: **Masahiro Fujimoto, Arata Kimura**	**Room 3**
O51-1	Vsimulators to explore human static and dynamic balance control	Genevieve Williams
O51-2	A model predictive control scheme for human balance recovery in response to a continuous time-varying platform motion	Naser Taleshi
O51-3	Influence of spring-loaded ankle exoskeletons on gastrocnemius fascicle behaviour during balance tasks	Jemima Po
O51-4	A single session treadmill perturbation-based balance training for fall prevention: Efficacy and mechanisms	Deepak Ravi
O51-5	Emulating human postural control adjustment with perturbation using quadratic objective function	Seongwoong Hong
O51-6	Motor performance after treatment of pilocytic astrocytoma in childhood	Fredrik Oehberg
1430-1530	**Oral 52 Running: Biomechanics 2** Chair: **Wouter Hoogkamer**	**Room 4**
O52-1	Accuracy of a 2d camera for obtaining 3D data in running	Iain Hunter
O52-2	Improving estimation accuracy of energy expenditure during running from a single IMU by estimating mechanical power via estimating ground reaction force	Bumjoon Kim
O52-3	Groucho running reveals disparate results between ground reaction force and tibial bone strain: A finite element analysis	Arash Khassetarash
O52-4	Effect of running speed and inclination on biomechanical risk factors for medial tibial stress syndrome	Leon Robertz
O52-5	Influence of walking and running speeds on tibia impact stress	Qichang Mei

1430-1518	**Oral 53 Simulation techniques and applications 2** Chair: **Todd Pataky**	**Room 5**
O53-1	How does the inclusion of glenohumeral joint stability affect the estimates of individual muscle forces during shoulder movements?	Italo Belli
O53-2	The effect of touchdown configuration on top sprinting speed: A simulation study	Nicos Haralabidis
O53-3	Design and simulation of flow field for sinusoidal scaffold using computational fluid dynamics	Theresia Baumgartner
O53-4	Development of a workflow to morph volumetric meshes consistently across a population of pediatric femurs	Yidan Xu
1430-1554	**Oral 54 Artificial intelligence and machine learning 3** Chairs: **Marion Mundt, Daisuke Ichimura**	**Room 7**
O54-1	Physics-based features improve the generalizability of a neural network predicting ground reaction forces	Janelle Kaneda
O54-2	Gait abnormality detection by inertial measurement unit and machine learning	Ferryanto Ferryanto
O54-3	Using IMU to predict the effect of prosthetic alligment on knee moments	Gilmar Fernandes dos Santos
O54-4	The approach chosen for data dimensionality reduction affects the results of running technique clustering	Adrian Rivadulla
O54-5	Conditional generative deep learning in biomechanics: Generating synthetic motion capture datasets by controlling subject anthropometrics	Metin Bicer
O54-6	Gait-based person re-identification across force platform datasets from different countries	Kayne Duncanson
O54-7	Deep learning-based vertical ground reaction force estimation during walking with inertial measurement units of the left wrist and both heels	Yuta Takanobu
1430-1530	**Oral 55 Prosthetics and orthotics 2** Chair: **Steffen Willwacher**	**Room 8**
O55-1	Investigating the effects of transfemoral amputee anatomy on stress and strain distribution in osseointegrated implants using a 3D FE model	Tiereny McGuire
O55-2	Relationship between time since amputation and gait asymmetry in unilateral transfemoral amputees	Takeshi Hara
O55-3	Metabolic cost and musculoskeletal metabolic quantification of walking with an above knee prosthesis simulator	Xavier Bonnet
O55-4	Influence of hip flexion contracture on gait parameters of transfemoral amputees: A preliminary study	Kevin Arribart
O55-5	Bilateral asymmetry of ground reaction forces during running in unilateral transfemoral amputees	Mai Watanabe
1630-1800	**Symposium 10 Ankle injury biomechanics – a 2023 update on injury mechanism, risk factors, and long-term consequences** Chairs: **Filip Gertz Lysdal, Masafumi Terada**	**Room 1**
SY10-1	Debunking the myth - the noncontact lateral ankle sprain is not just the result of a bad landing: A systematic video analysis of 445 injuries	Filip Gertz Lysdal
SY10-2	Fatigue increases risk of lateral ankle sprain injuries i badminton - a biomechanical analysis	Alexis Herbaut
SY10-3	Why friction matters: Zooming in on the shoe-surface interaction of the ankle sprain injury	Filip Gertz Lysdal
SY10-4	Breathing out ankle instability: Addressing impairments in diaphragm function associated with chronic ankle instability	Masafumi Terada
1630-1742	**Oral 56 Sport biomechanics 6** Chair: **Mark Robinson**	**Room 2**
O56-1	The effect of a 6-week intrinsic foot muscle training intervention on static and dynamic balance in team sports players	Matthew Stoner
O56-2	Lumbar and pelvis movement comparison between cross-court and long-line topspin forehand stroke: Based on musculoskeletal model	Yuqi He
O56-3	Influence of release positions on optimal release conditions in basketball	Yuki Inaba
O56-4	The influence of pocket characteristics on lacrosse shot performance	Dean Hay
O56-5	Simulated knee mechanics during a maximal forward braking and backward acceleration in elite athletes	Rodrigo Bonacho Mateus
O56-6	Neuromuscular effect of warm-up on regulation of motor unit properties during isometric torque production tasks	Jiseop Lee
1630-1754	**Oral 57 Locomotion: General 3** Chairs: **Veerle Segers, Keiichiro Hata**	**Room 3**
O57-1	Effects of speed on ground reaction forces during skipping gait	Genki Tokuda
O57-2	Neuromuscular responses to unexpected slips during human walking	India Lindemann
O57-3	The differences in the characteristics of the body part angular momentum in the frontal plane during walking between young and older adults	Kodai Kawase

O57-4	Pendular energy exchange at very slow walking speeds reveal positive work shift from double support to single stance	Timothy Byles-Ho
O57-5	The effect of knee extensor fatigue on metabolic cost in running	Key Nahan
O57-6	The achilles subtendons exhibit distinct loading patterns during walking	Lauren Welte
O57-7	Patellofemoral kinetics walking in maximal, minimal and traditional shoes	JJ Hannigan
1630-1806	**Oral 58 Wireless sensors and wearable devices 2** Chairs: **Kota Takahashi, Takeo Matsubayashi**	**Room 4**
O58-1	How well do machine learning models trained on treadmill walking perform on overground data?	Sailee Sansgiri
O58-2	Timed-up-and-go test segmentation algorithm based on a wearable sensor technology: A technical validation in people with multiple sclerosis	Fabien Masse
O58-3	Detecting the progression of gait impairments in Parkinson's disease using Wi-Fi	Tzu-Yang Weng
O58-4	Capacitive sensing for natural environment rehabilitation monitoring	Owen Pearl
O58-5	Estimating energy expenditure using wearable sensors during indoor and outdoor locomotion	Mohammad Mohammad
O58-6	Validation of the lower limb joint kinematics in the sagittal and frontal planes calculated by a self-developed dual kinect azure sensors system	Hsuan-Lun Lu
O58-7	Changes in foot pressure during downhill walking after using a biofeedback which reduces acceleration	Alexandra Giraldo-Pedroza
O58-8	Automated gait event detection using wearables/ IMU for data acquisition and deep learning for placement classification	Yong Kuk Kim
1630-1742	**Oral 59 Clinical biomechanics 3** Chairs: **Yumna Albertus, Takuya Ibara**	**Room 7**
O59-1	Evaluation of hip joint kinetics in rehabilitation exercises for children with cerebral palsy	Jasper Kwasny
O59-2	Longitudinal changes in kinematics of the lumbopelvic hip complex and their association with the onset of cam deformity: A two-year follow-up of high-risk adolescent elite football players	Dalia Al Otti
O59-3	Validity and reliability of bodiometer mobile app for postural analysis	Nesa Keshavarz Moghadam
O59-4	A machine learning approach to differentiate stable from unstable total knees for data mining	Erica M. Ramirez
O59-5	Engagement of the cruciates and medial meniscus is related to anterior-posterior knee laxity but not cruciate ligament volume	Erin Berube
O59-6	Investigating the influence of different foot positions during the golf swing on the skin-marker-based kinematics after total knee arthroplasty	Nils Horn
1630-1806	**Oral 60 Musculoskeletal modeling 5** Chairs: **Barbara Postolka, Yoko Kunimasa**	**Room 8**
O60-1	Inclusion of distal fibular translations in multi-segmented foot modeling for lateral ankle ligament strains	Renee Alexander
O60-2	Identifying the slack postures of human skeletal muscle across three-dimensional joint	Jun Umehara
O60-3	Easy-to-use matlab software for personalizing opensim neuromusculoskeletal models	Claire V. Hammond
O60-4	Combined statistical shape model can predict lower limb bone shape variation in a paediatric population	Julie Choisne
O60-5	Muscle force estimation based on angle-EMG-force relationship and electromechanical delay	Takuya Mitani
O60-6	Relative energy cost of the gait phases across walking speeds	Israel Luis
O60-7	Towards automatic generation of subject-specific knee joint kinematic models from medical imaging	Beichen Shi
O60-8	Advanced signal processing techniques integrated into a textile-embedded EMG garment for ankle torque estimation in post-stroke individuals	Donatella Simonetti

1810-1940	**Poster 22 Sport biomechanics 3**	2nd Floor, Poster Display #1
P22-01	Relationship of jump performance and ground reaction force variables between young adults and different maturity adolescent soccer players	Takahiro Namiki
P22-02	Quantifying the contralateral repeated bout effect of the triceps surae	Nicole S. Jones
P22-03	Influence from wetsuit on the assessment of biomechanical parameters through imu measurements	Alexander Weiss
P22-04	Effect of motor synergies on posture and performance stability: A comparison of self- and external-triggered shooting in simulated archery	Junkyung Song
P22-05	Muscle activity timing and amplitude in the early acceleration phase of curve sprinting	Benjamin Millot
P22-06	Developing a simulation model considering frictional force during turning in dance	Akiko Imura
P22-07	Comparison of the difference between countermovement and squat jump in trained and untrained adults	Ching-Feng Cheng
P22-08	Get on up; Relating objective hip-hop dance biomechanics to subjective scoring	Joshua Vicente
P22-09	Changes in 5-10m elapse time in kick start of a swimming race at different back plate positionings	Masayuki Umemoto
P22-10	The influence of projectile mass on throw distance	John H Challis
P22-11	Changes in kinematic patterns in response to ball velocity in tennis forehand drive	Yoon-Seok Choi
P22-12	Characteristics of the steps in each section in a tailwind sprint	Koichi Nakayama
P22-13	Effects of strength training targeting medial quadriceps/hamstrings on knee joint biomechanics during single-leg landing	Jiyoung Jeong
P22-14	Effects of wearing a mask on heart rate variability during kendo practice	Minato Kawaguchi
P22-15	Quantification of external work using mechanical crank power with a bicycle ergometer underestimates the net external work exerted by a human	Yuta Yamaguchi
P22-16	Assessment of strain components for kinesiology taping techniques with digital image correlation	Chia-Han Hu
P22-17	Contact force during maximal snatches	Michael Webb
P22-18	How do grip-enhancing agents affect friction between a fingertip and a baseball?	Takeshi Yamaguchi
P22-19	A pilot study on the plantar pressures in females during sprinting on natural grass, 3G and cork surfaces	Jo Reeves
P22-20	Relationship between bilateral asymmetry in lower limb joint biomechanics and jumping height during single-leg countermovement jump	Shota Yamamoto
P22-21	A biomechanical study of uchimata in judo - comparison of different skill levels-	Kazuto Hamaguchi
P22-22	Effects of nordic hamstring exercise on hamstring stiffness, strength, and flexibility	Konstantinos Kaliarntas
P22-23	Effect of the upper limb joints on the control of ball speed in throwing distance control of throw-in	Rintaro Miyake
P22-24	Relationship between ball velocity and kinematics of pelvis and upper torso in female collegiate baseball players	Takuya Sekiguchi
P22-25	Characteristics of leg movements that induce red cards in race walking	Naoki Takahashi
P22-27	A comparison of rotation sequences for shoulder 3D kinematics in the volleyball attack	Kiara Barrett
P22-28	Associations between unilateral drop landing mechanics and diaphragmatic contractility in individuals with recurrent lateral ankle sprains	Shunya Nonoyama
P22-29	Grading of jumping height by quick movement	Yoshiho Muraoka
P22-31	Acceleration comparison between peak height velocities in male youth soccer players	Kavon Bonakdar
P22-32	Electromyographic activity during different phases in the bench press exercise	Dusan Blazek
P22-33	Waltz swing characteristics of the competitive ballroom dance world champion couple	Yasuyuki Yoshida
P22-34	Validity of spring-like behaviour performance during hopping using a smart watch	Atsuki Kageyama
P22-35	Cross-sectional area of hand intrinsic muscles and upper limb length associated with throwing record of female discus throwers	Yukiho Arano
P22-36	Relationship between propulsive force and hip joint motion during eggbeater kick in artistic swimming	Hiroki Hyodo
1810-1940	**Poster 23 Sports and exercise for persons with impairment**	**2nd Floor, Poster Display #1**
P23-01	Development of an adjustable sledge for paralympic cross-country skiing with a particular focus on neurological and physiological improvement of the sitting position	Leonie Hirsch
P23-02	Effects of trunk extension on body and wheelchair centers of gravity during wheelchair propulsion movements	Koichi Kawabata
P23-03	Effect of short-term combined intervention program on erector spinae contractile properties in patients with non-specific chronic low back pain	Hyungwoo Lee
P23-04	Biomechanics of wheelchair propulsion in athletes of wheelchair racing	Mikito Hikosaka
P23-05	Influence of seat pan angle and lower leg stabilizer on lower limb muscles activation during simulated sit-ski	Masashi Naoe

1810-1940	**Poster 24 Orthopaedics: Tendon & ligament**	2nd Floor, Poster Display #1
P24-01	Size dependent transport dynamics in the rat achilles tendon	Jarod Forer
P24-02	Sensitivity analysis of four graft parameters on knee kinematics following pediatric anterior cruciate ligament reconstruction: A linked neuromusculoskeletal-finite element modelling approach	Ayda Karimi Dastgerdi
P24-03	Effects of different carpal tunnel release surgeries on migration patterns of flexor tendons	Hsiao-Feng Chieh
P24-04	Compressive force inhibits excessive volar displacement of the fds tendon in patients after carpal tunnel release surgery	Chien-Ju Lin
1810-1940	**Poster 25 Rehabilitation and neurorehabilitation**	**2nd Floor, Poster Display #1**
P25-01	Assistance of the paretic knee in the sit-to-stand motion of acute stroke survivors prevents their trunk overuse	Hiroki Hanawa
P25-02	Clinical efficacy of 3 different types of digital mirror therapy on motor and daily functions in stroke survivors: A preliminary study	Yu-Wei Hsieh
P25-03	The effect of draw-in maneuver on knee joint function and thoracic kyphosis angle in patients with osteoarthritis of the knee	Yasuha Murakami
P25-04	Validity and reliability of mobile applications in physical therapy: A systematic review	Ibiza Gonzaga
P25-05	Change in ankle dorsiflexion motion during cycling generated by ankle assist ergometer	Keisuke Hirata
P25-06	Virtual reality balance training improves balance in patients with lumbar spinal stenosis: A pilot study	Po Jung Chen
P25-07	Effect of increasing weight-bearing during the seat-off task with sit-to-stand training augmented feedback and epidural electrical stimulation in people with incomplete spinal cord injury: A preliminary study	Tzu-Ming Chang
P25-08	Acute effects of dynamic stretching on muscle contractile properties of ankle plantar- and dorsi- flexors	Shuya Fukuoka
P25-09	Characteristics of trunk muscle activity in children with cerebral palsy during horseback riding -multiresolution analysis of semg-	Kenichi Kaneko
P25-10	Statistical shape modelling and reconstruction of subject-specific foot soles for two-point discrimination neuromuscular sensory tests	Yun-Chen Hsu
P25-11	A scoping review on effects of exercise training on hand dexterity in patients with parkinson	Ying-Ming Liu
1810-1940	**Poster 26 Rehabilitation technology: Biorobotics and exoskeletons**	**2nd Floor, Poster Display #1**
P26-01	Towards crutch-less exoskeleton-assisted geriatric sit-to-stand motions -- an experimental and optimization-based study	Jan Lau
P26-02	A usability evaluation of the powered-wheelchair for severely disabled in Korea	Eung-Pyo Hong
P26-03	Development of autonomous driving sensor system for wheelchair application	Yongcheol Kim
P26-04	Performance and usability evaluation of an intelligent wheelchair	Ki-Tae Nam
P26-05	A new coupling mechanics model for lower limb exoskeletons to account for initial surface forces	Christian Mele
1810-1940	**Poster 27 Simulation techniques and applications**	**2nd Floor, Poster Display #1**
P27-01	Biomechanical evaluation of difference between customized angled abutments and commercial angled abutment for dental implant in maxillary incisor region	Heng Li Huang
P27-03	Generalised ligament model for finite element modelling of the knee	Luca Kiener
P27-04	Is computer vision-based motion capture applicable for musculoskeletal simulation?	Ryotaro Numata
P27-05	Critical regions in the mandible during mastication and blunt impact	Samrat Sagar
P27-06	Appropriate metrics to evaluate spring assistance to lower limbs for improving human gait	Rajbeer Singh Anand
P27-07	Influence of bone inhomogeneity on strain calculation of CT-based vertebral finite element models	Cheng Yen
P27-08	The study of tip-over stability analysis for sitting position transition wheelchair	Dae-Jin Jang
1810-1940	**Poster 28 Spine and trunk**	**2nd Floor, Poster Display #1**
P28-01	Analysis of posture, spinal curvatures and gait in lumbar arthrodesis patients	Guillaume Claus
P28-02	Dependence of static compressive condition on breast support performance of sports bras during running	Yasuho Takii
P28-04	Comparison of scoliosis angles with and without menarche	Eunbi Park
P28-05	Effects of varying in load weight on spine kinematics in deadlift	Kazuma Shoji
1810-1940	**Poster 29 Upper extremity**	**2nd Floor, Poster Display #1**
P29-01	Less pain, but only small changes in shoulder kinematics following topical anesthetic in patients with ongoing shoulder pain	Norman D'hondt
P29-02	Motor unit behavior of the lower trapezius and serratus anterior in individuals with scapular dyskinesis	Masahiro Kuniki
P29-03	Characteristics of medial elbow pain in professional and amateur baseball players: Focusing on valgus instability and ulnar neuropathy	Issei Noda
P29-04	Effect of multiplane arm elevations on glenohumeral kinematics and contact patterns	Chia-Ling Fan

P29-05	Pilot follow up of a patient with post-stroke hemiparesis using the ssulf scale in comparison with other clinical assessment	Paris Joaquin Velasco Acosta
1810-1940	**Poster 30 Wireless sensors and wearable devices**	**2nd Floor, Poster Display #1**
P30-01	Using outdoor cycling power output and heart rate to estimate maximal oxygen consumption	Tzyy Yuang Shiang
P30-02	Integrated gaze tracking and motion analysis during walking	Zhaoyuan Wan
P30-03	Changes in spatiotemporal parameters during long distance running	Yuta Suzuki
P30-04	Changes in acceleration load during an agility test on artificial turf	Claudiane Fukuchi
P30-05	Development of an instructional support system for skiing using gnns data	Hiroshi Hoshino
P30-06	Reliability of the loadsol insole for measuring kinetics during stationary cycling	Walter Menke
P30-07	In-socket pressure sensor system for lower limb prosthetic	Min Jo
P30-08	Wearable intra-foot temperature gradients during free-living conditions	Emily Matijevich
P30-09	Is a wirelessly-charged implant safe?	Maedeh Amirpour
P30-10	Development and validation of a method to detect initial contact during graded running using a sacral mounted inertial measurement unit	Aida Chebbi
P30-11	Two hands gesture control for a robotic hand	Senol Piskin
P30-12	Whole-body kinematics prediction while walking and running using a virtual accelerometer on various positions	Gunwoo Park
P30-13	Real-time musical feedback from pressure-sensing insoles for ankle fracture rehabilitation: A case report	Markus Wimmer
P30-14	A hybrid LSTM-ANN model for predicting balance variables and spatiotemporal parameters during gait using a single waist-worn IMU	Tung-Wu Lu
1810-1940	**Poster 31 Others 2**	**2nd Floor, Poster Display #1**
P31-01	Prophylactic cerclage fixation for prevention of periprosthetic femoral fractures: The significance of cable location	Kartik Reddy
P31-02	Passive collar stiffness of a custom-designed high-collar shoe	Alireza Nasirzadeh
P31-03	Mouse horizontal aiming performance between two gaming mice of different slanted design	Yu-Lin Chen
P31-04	Compare of the clinical efficacy of volar plating with the pronator quadratus preservation versus the pronator quadratus repair or transection for distal radius fractures in different age groups	Kazuya Umeyama
P31-05	The optimal tunnel entry point in cranial cruciate ligament reconstruction for dogs: A simulation analysis for femoral tunnel placement	Ching-Ho Wu
P31-06	Changes in lower leg kinematic frequency content during pre-ground contact and weight acceptance phases of acl injury risk screening tasks	Simon Augustus
P31-07	The effect of racket mass on effective striking mass in tennis	Yoshiyuki Kawano
P31-08	Wheelchair operating capabilities of elderly caregivers	Misono Sakai
P31-09	Eight-week of concurrent and traditional training enhances specific adaptions of individuals with sub-healthy sedentary adults	Chia-Lun Lee
P31-10	Kinematic characteristics of the swing movement in comtemporary dance	Mayumi Kuno-Mizumura
P31-11	Effect of measurement approach on jawbone density for the dental implant evaluation	Shiuan-Hui Wang
P31-12	A digital, diverse, assemblable intelligent movement evaluation and training system for individuals with disabilities	Hsin-Yi Kathy Cheng
P31-13	Multivariate kinematic analysis of piano performance : A case study of a professional pianist	Park Dawon
1810-1940	**Poster 32 Locomotion: General**	**5th Floor, Poster Display #2**
P32-01	Progressive energization evaluation and benefits of group exercise session for seniors - Post-event movement observation and analysis method	YingTing Hsueh
P32-02	Age-related differences in knee and ankle dynamic joint stiffness during walking	Haruki Toda
P32-03	Gait modification after verbal instruction of “knee extension” or “hip extension” at early stance phase to knee flexed gait	Shinya Ogaya
P32-04	Association of muscle function with gait ability based on various speeds in older women over 75 years	Bohyun Kim
P32-05	Gender differences in trunk and lower extremity kinematics during hurdle step and squat lifting	Ganbat Danaa
P32-06	Effect of lower limb joints pain on toe area of foot pressure during walking in the elderly	Kazuya Imaizumi
P32-08	Effect of light touch on inappropriate mediolateral foot placement	Yudai Toyoda
P32-09	Classification of young adult motor fluctuation phenotypes in gait	Christopher Bailey
P32-10	Very short bout durations decrease the efficiency of walking up stairs	Francesco Luciano
P32-11	Open dataset for bipedal locomotion on an instrumented treadmill	Dominik Krumm

P32-12	Has the knowledge of barefoot gait in healthy adults changed with technological advancements? - A systematic review	Alycia Fong Yan
P32-13	Muscle activation patterns in decoupled stride frequency and duty factor	German Pequera
P32-14	Standing balance in response to physical and visual perturbations	Calaina Brooke
P32-15	The effect of different walking speed on gait stability between young and elderly population anlaysed by a zero moment point method	Sang Kuy Han
P32-16	Effect of midsole hardness on the center of pressure during walking	Yohei Yamazaki
P32-17	A.R.G! Augmented reality and gait: Cues elicit gait adaptations in AR	Wendy Pham
P32-18	Effects of artificial knee joint constraint on shared neural drive of ankle plantar flexors during gait	Carlos Cruz Montecinos
1810-1940	**Poster 33 Running: Biomechanics**	**5th Floor, Poster Display #2**
P33-01	Detrended fluctuation analysis of running stride time at and near the maximal lactate steady state	Cody van Rassel
P33-02	Frontal forefoot strike patterns and its associations with 100-m sprint performance in male sprinters	Haruto Arai
P33-03	Can an accelerometer replace lower extremity joint moment upon running?	Young-Seong Lee
P33-04	Foot medial longitudinal arch deformation and plantar load distribution pattern during running	Akira Kiuchi
P33-05	Biceps femoris shortens actively during the late swing phase of high-speed running	Junhee Yoon
P33-06	Prospective identification of musculoskeletal injury risk in elite college distance runners using ground reaction forces	Harper Stewart
P33-07	Graded running does not impact joint work asymmetry in healthy runners	Rachel Robinson
P33-08	Speed dependent changes to ankle joint mechanics during incline running	Hidetaka Hayashi
P33-10	The effects of foot torsional stiffness on foot kinematics and impact force during running	Tomohito Nakatsugawa
P33-11	The influence of fast running speed on joint coupling angle between ankle and knee joints in unilateral patellofemoral pain	Chich-Haung Richard Yang
P33-12	Step-to-step changes in lower limb muscle activity during the acceleration stage of sprinting	Keiichiro Hata
P33-13	Kinematics of maximal velocity running: Factors to further enhance step length and frequency	Takeo Matsubayashi

Thursday, August 3rd

0800-0930	**Symposium 11 Latest updates for recording, analysis, and interpretation of electromyographic (EMG) data: in the lab and the clinic** **Room 1** Chairs: **Kohei Watanabe, Kylie Tucker**	
SY11-1	ISEK Introduction	Kylie Tucker
SY11-2	An introduction to the consensus for experimental design in electromyography (CEDE) project	Paul Hodges
SY11-3	Using EMG to estimate muscle force	Taylor Dick
SY11-4	An overview of surface EMG in clinical assessment and neurorehabilitation	Elisa Romero Avila
SY11-5	High-density EMG in biomechanics	Kohei Watanabe
SY11-6	High-density EMG in clinical assessments	Yuichi Nishikawa
0800-0924	**Oral 61 Balance and posture 3** **Room 2** Chairs: **Julie Choisne, Momoko Yamagata**	
O61-1	Digital solution: A 3-dimensional kinematic rating algorithm for single-limb stance test	Yu Yuan Lee
O61-2	Novel analysis of centre of pressure in textured shoes: A pilot study	Chockalingam Nachiappan
O61-3	Dynamic optimization of human gait to solve kinematic-kinetic mismatch	Zuming Xiao
O61-4	Markerless motion capture is sensitive to postural balance parameters in a clinical stroke population	Mihic Anastasija
O61-5	Age-related changes in ankle proprioception and their relationship to postural control	Chrysostomos Sahinis
O61-6	Proprioceptive interference via tendon vibration during standing in children with cerebral palsy	Dimitrios Patikas
O61-7	Relative importance of the visual system for balance control is reflected in the continuous margins of stability while walking	Saskia Neumann
0800-0900	**Oral 62 Rehabilitation technology: Biorobotics and exoskeletons 3** **Room 3** Chair: **Amir Esrafilian**	
O62-1	Joint kinematic and kinetic responses to added mass on the lower extremities during running	Itay Coifman
O62-2	Effects of gait variability and encouraged exploration on adaptation to ankle exoskeletons	Gillian Phillips
O62-3	Design of a 2-dof soft ankle exoskeleton for people with dropfoot and excessive inversion	Xiaochen Zhang
O62-4	Green exoskeleton based on biomechanical energy harvester	Yakir Knafo
O62-5	Biologically inspired trajectories for active assistance of standing up and sitting down by robotic rollators	Marko Ackermann
0800-0912	**Oral 63 Ergonomics** **Room 4** Chairs: **Felipe Carpes, Toshiaki Oda**	
O63-1	Effects of finger flexion force on median nerve compression	Shengwei Li
O63-2	Energy transfer during a collective stretcher transport	Nour Sghaier
O63-3	Biomechanical changes associated with heavy load carriage using differing rucksack designs	Matthew Ellison
O63-4	Subjective and objective evaluation of sitting-induced sustained low-intensity muscle fatigue	Lyu Hui
O63-5	Influence of walking speed and load on spinal curvature and pelvic orientation during pushing tasks	Daniel Köerner
O63-6	Correlation between psychosocial factors and physical load of workers in the electronic components industry	Jansen Estrázulas
0800-0912	**Oral 64 Others 4** **Room 5** Chairs: **Kosuke Nakazato, Yuji Tamura**	
O64-1	The changes in balance, lower extremity strength and power of college tennis players after agility training	Mu Tzu Su
O64-2	Performance differences among U-15 and U-18 soccer players: A study of speed, change of direction, and explosive power	Muhammad Iftiqar Ahmad Termizi
O64-3	Influence of Penn State University on the international society of biomechanics	Brian Davis
O64-4	Kinematic analysis of chinese handwriting in adults with mild cognitive impairment	Tsai-Yu Shih
O64-5	Novel spring cleat testing with custom-built shoe test device yields null result	Gregory Chingas
O64-6	Tracking golf swing trajectory using a single imu by applying biomechanics and machine learning	Myeongsub Kim
0800-0912	**Oral 65 Spine and trunk 2** **Room 6** Chairs: **Ryan Quarrington, Chih-Hsiu Cheng**	
O65-1	Semi-automatic definition of subject-specific muscle parameters for musculoskeletal models of adult spinal deformity patients	Birgitt Peeters
O65-2	The role of spinal muscles for lumbar loads during static loading tasks in large patient cohorts: A musculoskeletal modeling study	Tanja Lerchl
O65-3	Quantifying spinal parameters for scoliosis using a low-cost 3-dimensional motion capture system	Pitchaya Rayothee
O65-4	Passive neck stiffness and range of motion in 80 adults up to 80 years of age	Mingyue Liu

O65-5	Validity and reliability of neck range of motion and repositioning error measured by a virtual reality system	Veronique Feipel
O65-6	Neuromuscular adaptations in ankle dorsiflexor in persons with spinal cord injury	Asta Kizyte
0800-0848	**Oral 66 Orthopaedics: Surgeon guided biomechanics** Chair: **Yukiyo Shimizu**	**Room 7**
O66-1	Patient-specific modeling of mandibular musculoskeletal system and its applications in trismus estimation	Jianqiao Guo
O66-2	A musculoskeletal modelling framework for evaluating instability after reverse total shoulder arthroplasty	Yichen Huang
O66-3	A pipeline to morph the finite element model of lumbar spine and generate personalised spinal implant	Yihang Yu
O66-4	Effect of pelvic tilt on femoral head coverage after periacetabular osteotomy	Ryan Blackwell
0800-0924	**Oral 67 Upper extremity** Chairs: **Angela Kedgley, Hiroshi Ichikawa**	**Room 8**
O67-1	Differentiating activity of forearm finger flexors and extensors for SEMG biofeedback training	Christian Sure
O67-2	Lower limb amputees have similar upper limb function 8y post injury as uninjured group: The advance cohort study	Fraje Watson
O67-3	Validation of a marker cluster-based approach to estimate scapula motion	Jennifer Maier
O67-4	Investigating the torque-velocity relationship within the human shoulder during high-demand	Kayla Lee
O67-5	Post-operative kinematics of coracobrachialis and short head of biceps after reverse total shoulder arthroplasty	Roopam Dey
O67-6	Investigating shoulder muscle coactivation ratio changes following and overhead fatigue task	Matthew Russell
O67-7	Disentangling allometry and sex-based differences in scapula shape	Erin Lee
0940-1030	**Keynote Lecture 5** Chair: **Eng Kuan Moo**	**Room 1**
KL5	Designing Treatment Strategies for Large Skeletal Defects by Combining in Silico, in Vitro and in Vivo Models	Liesbet Geris
1100-1212	**Oral 68 Sport biomechanics 7** Chair: **Filip Gertz Lysdal**	**Room 2**
O68-1	A study of suitable takeoff motion of a ski jumper using principal component analysis and computational fluid dynamics	Shin Ikeda
O68-2	Flexible multibody modeling of the skier musculoskeletal system and its applications in alpine skiing	Gao Nan
O68-3	Sex differences in netball players' foot shape: Implications for shoe design	Maddison Kirk
O68-4	Optimal attitude reorientation of free-floating humans by rectilinear joint actuation	Yuki Kubo
O68-5	Impact of menstrual cycle on anaerobic power among youth cricketers	Vijay Dhamodharan
O68-6	Gravel bike ground reaction forces	Josef Viellehner
1100-1224	**Oral 69 Motor control 2** Chairs: **Kiisa Nishikawa, Soichi Ando**	**Room 3**
O69-1	Performing both resisted and non-resisted trunk extension in prone are recommended to elicit maximum voluntary contraction of the spinal extensors in adolescents with idiopathic scoliosis and controls	Phoebe Ng
O69-2	Greater asymmetrical spinal muscle activity during submaximal trunk extension in adolescents with idiopathic scoliosis than those without	Kylie Tucker
O69-3	Lower extremity muscle activity in case of slipping during 90-degree change of direction tasks with and without an ankle brace	Uwe G. Kersting
O69-4	Supraspinal integration of proprioception is crucial for locomotor robustness	Alessandro Santuz
O69-5	Gait kinematics and surface emg alterations associated to different mosaicism type in children with fragile X syndrome	Fabiola Spolaor
O69-6	Ankle power in gait is more relevant to the maximum instance firing rate of soleus than gastrocnemius	Hayase Funakoshi
O69-7	Regional neuromuscular control of the human hamstring muscles	Patrick Smart
1100-1224	**Oral 70 Lower extremities 2** Chair: **Raihana Sharir**	**Room 4**
O70-1	New approach for calculating a functional subtalar joint axis	Anja Seeger
O70-2	Acute effects of high-definition transcranial direct current stimulation on ankle force sense and cortical activation	Chuyi Zhang
O70-3	How do bones of the sub-talar joint complex cope with size?	Paige Treherne
O70-4	The mechanism of leg stiffness adjustment during hopping with different hop frequencies	Kazuki Kuriyama
O70-5	Effects of compression garments on lower limb biomechanics during running under fatigue	Jichao Wang

O70-6	Effects of HD-tDCS on the changes of eeg-semg coherence after running-induced fatigue	Jianglong Zhan
O70-7	Tibial-tuberosity trochlear-groove distance in healthy subjects and patients with patellofemoral pain syndrome: a weight-bearing 4DCT study	Luca Buzzatti
1100-1212	**Oral 71 Rehabilitation and neurorehabilitation** Chairs: **Andrew Cresswell, Shun Kunugi**	**Room 5**
O71-1	Concurrent validity and reliability of a mobile iOS application used to assess calf raise test kinematics	Roxanne Fernandez
O71-2	Effects of task difficulties on first-grade children's handwriting performance in copy activities	Yu-An Tsai
O71-3	Investigation of the activation in upper limb muscles while using augmented reality mirror therapy	Tsai-Yu Chen
O71-4	Effectiveness of the low-dose camp-based bilateral intensive training on motor function in children with unilateral cerebral palsy	Zhi-Chi Weng
O71-5	Motor planning in children with unilateral cerebral palsy	Cherng-I Chou
O71-6	Predicting factors of handwriting legibility in children at preschooland first grade	Pin-Chen Hung
1100-1148	**Oral 72 Running: Biomechanics 3** Chair: **Natsuki Sado**	**Room 6**
O72-1	The static method of computing leg stiffness in running measures a smaller value than the dynamic method	Seungjoo Noh
O72-2	Sidestep cutting manoeuvres during running exhibit spring-mass behaviour	Kat Daniels
O72-3	How connecting the legs with a spring improves human running economy	Jon Stingel
O72-4	Changes in leg stiffness as a result of differences in leg bmd in various age groups during running	Jinsung Jung
1100-1224	**Oral 73 Musculoskeletal modeling 6** Chairs: **Seyyed Hamed Hosseini Nasab, Atsuki Fukutani**	**Room 7**
O73-1	Influence of synergy control assumptions on predicted walking function following pelvic sarcoma surgery	Marleny Vega
O73-2	Predicting knee adduction moment during walking by lower limb alignment using forward dynamics simulation	JongHyeon Park
O73-3	The foot's midtarsal joint alters the metabolic cost of walking	Daniel Davis
O73-4	4D shape and growth modelling in cerebral palsy paediatrics	Salim Bin Ghouth
O73-5	Estimation of musculoskeletal parameter values using hindlimb rat models	Gil Serrancoli
O73-6	Musculoskeletal simulations integrating a smooth knee pressure contact model	Mohanad Harba
O73-7	Quadriceps adaptation in response to split-belt asymmetric walking in long-term post-aclr patients	Yannis Halkiadakis
1100-1212	**Oral 74 Artificial intelligence and machine learning 4** Chairs: **Jos Vanrenterghem, Yuta Suzuki**	**Room 8**
O74-1	Achilles tendon force during walking can be predicted using two smartphone cameras	Zhengliang Xia
O74-2	Explaining deep learning models for age-related gait classification based on time-series acceleration	Xiaoping Zheng
O74-3	Transfer learning with simulated and recorded data improves predictions of upper extremity biomechanics	Kalyn Kearney
O74-4	Validity and reliability of 3D markerless motion capture using low-cost cameras	Victor Cossich
O74-5	Automatic multi-structure pediatric knee bone segmentation using optimal multi-level otsu thresholding technique	K Nandhini
O74-6	A method of detecting human movement intentions in real environments	Yi-Xing Liu
1330-1420	**President's Lecture** Chair: **Shinji Sakurai**	**Room 1**
PL		Alberto Leardini

Summary

The understanding of foot and ankle biomechanics is flourishing as new technology provides more detailed information about in vivo foot morphology and motion. The recent availability of cone beam CT in orthopaedics now enables 3D weight bearing measurements for the foot and ankle. Additionally, biplane fluoroscopy now provides the ability to measure dynamic bone motion. While there is increased research and clinical activity using these technologies, there are no commonly accepted 3D definition of foot bones axes and orientations or defined methodologies to calculate angulations and relationships between the bones. Despite this, a host of commercial software are being produced without any specific reference guidelines. This limits comparison of studies across different research centers. There is a growing interest in the orthopaedic and biomechanics communities to develop standardized terminologies, 3D orientation and measurements that can be reliably applied and generalized, ensuring consistency across international clinicians whatever the platform used.

A task force was established with representatives from three international societies (International Society of Biomechanics, Orthopaedic Research Society, and International Weightbearing CT Society). It consisted of orthopaedic surgeons, radiologists, and engineers with significant clinical and research expertise in foot and ankle. The task force aimed to establish accepted guidelines for these standards based on relevant measures of importance, a review of the literature, and when appropriate, develop new methodologies. It also aimed to evaluate current methodologies across multiple foot pathologies.

To achieve universal and disseminated acceptance for foot and ankle terminologies, 3D bone spatial orientation and tarsal inter-bone relationships, the standards defined by a group of experts on the foot and ankle and biomechanics environment must be understandable, interpretable, and most importantly reproducible. Reference definitions can be highly variable based on the shape of each individual tarsal bone, which can vary based on foot morphotype, age, deformity or pathology. Principal Componant Analysis is advantageous because it does not require user definitions however, may not represent the biomechanical joint axes. Identification of anatomic landmarks and/or fitting geometric primitives allow for better representation of bone morphology variations however it is vital that methods established be automation-compatible because one of the main objectives of clinicians is to improve accessibility through time-efficiency, in analyzing 3D datasets.

This symposium will present a summary of this group’s ongoing and future work to evaluate existing and new proposed references.

STANDARDIZING TERMINOLOGY, 3D SPATIAL ORIENTATION, AND RELATIVE POSITIONING OF THE FOOT AND ANKLE BONES: AN EXPERT CONSENSUS TASK FORCE

[1]Amy Lenz, [2,3]Karen Kruger, [3]Kevin Dibbern, [4]Cesar de Cesar Netto, [5]William Ledoux, [5]Eric Thorhauer, [6]Arne Burssens, [1]Andrew Peterson, [7]Michele Conconi, [8]Sorin Siegler, [9]Michael Rainbow, [10]Lauren Welte, [11]François Lintz, [7]Alberto Leardini

[1]University of Utah, [2]Shriners Children's Chicago, [3]Marquette University, [4]University of Iowa, [5]VA Puget Sound, [6]Ghent University Hospital, [7]Istituto Ortopedico Rizzoli, [8]Drexel University, [9]Queen's University, [10]University of Wisconsin-Madison, [11]Clinique de l'Union

INTRODUCTION

The understanding of foot and ankle biomechanics is becoming richer as new technology provides more detailed information about in vivo foot morphology and motion. The recent availability of cone beam CT in orthopaedics now enables 3D weight bearing measurements for the foot and ankle. Additionally, biplane fluoroscopy now provides the ability to measure dynamic bone motion. While there is increased research and clinical activity using these technologies, there are no commonly accepted 3D definition of tarsal bones axes and orientations or defined methodologies for calculation angulations and relationship between the bones [1]. Despite this, a host of commercial software are being produced without any specific guidelines. There is a growing interest in the orthopaedic and biomechanics communities to develop standardized terminologies, 3D orientation and measurements that can be reliably applied and generalized, ensuring consistency across international clinicians whatever the platform used. The goals of this group are to provide recommendations on terminologies, 3D orientation, and inter-bone measurements backed by evidence-based information that is clinically relevant. We also aim to provide a toolkit what will provide the agreed upon methodologies to to the foot and ankle community.

METHODS

A task force was established with representatives from three international societies. It consisted of orthopaedic surgeons and engineers with significant clinical and research expertise in foot and ankle. The task force aimed to establish important criteria for these standards, to determine relevant measures of importance, to review the literature, and when appropriate, develop new methodologies [2-4].

RESULTS AND DISCUSSION

Relevant criteria established included: desired reliable automatic refence frame generation, low processing times, relevant joint motion, and ability to accommodate various pathologies. A literature review showed methodologies in use include identification of specific anatomical landmarks, fitting of geometric primitives to surface anatomy, and principal component analysis (PCA). Many published methods in the literature lacked automated methodology.

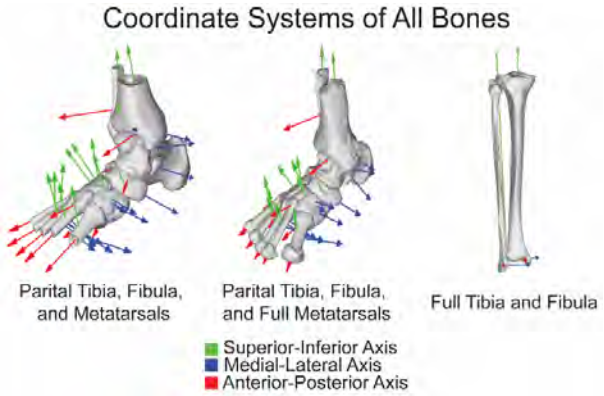

Figure 1 The anatomical coordinate system applied to all fourteen bones individually, with green signifying the superior-inferior axis, blue signifying the medial-lateral axis, and red signifying the anterior-posterior axis for full and partial bones

CONCLUSIONS

To achieve universal and disseminated acceptance for foot and ankle terminologies, 3D bone spatial orientation and tarsal inter-bone relationships, the standards defined by a group of experts on the foot and ankle and biomechanics environment must be understandable, interpretable, and most importantly reproducible. Reference definitions can be highly variable based on the shape of each individual tarsal bone, which can vary based on foot morphotype, age, deformity or pathology. PCA is advantageous because it does not require user definitions however, may not represent the biomechanical joint axes. Identification of anatomic landmarks and/or fitting geometric primitives allow for better representation of bone morphology variations however it is vital that methods established be automation-compatible because one of the main objectives of clinicians is to improve accessability in analyzing 3D datasets. Ongoing and future work within the task force will aim to evaluate existing and new proposed references in the light of available clinical data including various foot pathologies to establish a scientifically grounded consensus.

REFERENCES

[1] Lenz. J Biomech 120: 110344, 2021.
[2] Conconi. J Foot Ankle Res 14, 66 (2021).
[3] Thorhauer. J Biomech Eng. 2023 145(4):044502.
[4] Peterson. ORS 2023. #0694.

ACKNOWLEDGEMENTS

Funding was provided by the National Institutes of Health (1K01AR080221-01A1) and Shriners Children's (#79146)

FOOT AND ANKLE AUTOMATIC ANATOMICAL COORDINATE SYSTEM DEFINITION

Andrew C. Peterson[1], Karen M. Kruger[2,3], and Amy L. Lenz[1]
[1] Department of Orthopaedics, University of Utah, Salt Lake City, UT, USA.
[2] Department of Biomedical Engineering, Marquette University, Milwaukee, WI, USA.
[3]Motion Analysis Center, Shriners Children's, Chicago, IL, USA.
Email: andrew.c.peterson@utah.edu

INTRODUCTION

Anatomical coordinate systems (ACS) are necessary for analyzing bone position and orientation during static and dynamic movements. Unfortunately, there is no agreed-upon automatic definition for individual foot and ankle bones [1]. Many primary foot and ankle coordinate systems currently used require manual inputs of bony landmarks, are not practical in clinical settings, depend on other bones, and do not analyze pathologies [2]. This study aimed to develop an automatic ACS definition for the fourteen foot and ankle bones individually and analyze the ACS across different segmentation processes and throughout multiple populations demonstrating different deformities.

METHODS

A toolbox was developed to calculate these ACSs automatically in MATLAB (R2022b, MathWorks, Natick, MA, USA). This study used twenty-four models: eight asymptomatic, eight with PCFD, and eight with a cavovarus deformity. These twenty-four models were segmented automatically with DISIOR (Bonelogic Ortho Foot and Ankle 2.1, Helsinki, Finland) and manually cleaned up using Mimics (v22.0, Materialise, Leuven, Belgium), referred to as the DISIOR and Mimics models henceforth. The only required input for the toolbox was the bone model. The toolbox aligns the input and assigns it a coordinate system, as seen in Figure 1. To determine the consistency of this toolbox, each population was analyzed separately. A mean axis was determined for all three axes for each population, and the angle difference between an individual's coordinate system axes and the mean axes was calculated. A similar process of determining angle differences between the DISIOR and Mimics models was performed.

RESULTS AND DISCUSSION

The angle differences between the individual coordinate system axis and the mean axis for all fourteen bones combined are reported in Table 1. The maximum angle difference from the mean is from one of the medial-lateral cavovarus cuboid axes with a difference of 8.79°. The minimum angle difference from the mean is from one of the anterior-posterior PCFD fourth metatarsal axes with a difference of 0.01°. Additionally, the angle differences between the DISIOR and Mimics models are reported in Table 1. The maximum angle difference is from the medial-lateral second metatarsal axes with a difference of 6.02°. The minimum angle difference is from the anterior-posterior second metatarsal axes with a difference of 0.22°.

	DISIOR vs. MIMICS	Mean vs. Individual
Healthy	1.69° ± 0.97°	2.19° ± 0.63°
PCFD	2.21° ± 1.37°	2.33° ± 0.96°
Cavovarus	1.69° ± 0.88°	2.41° ± 0.79°

Table 1: Angle difference between the DISIOR and Mimics models and angle differences between individual axes compared to the mean axes.

CONCLUSIONS

This study aimed to develop a toolbox to automatically calculate an ACS for fourteen bones in the foot and ankle. This definition requires no user input, which eliminates errors in repeatability. Additionally, this toolbox is not drastically affected by pathological morphologies or segmentation processes, as seen by the minimal angle variation in Table 1. Primary future work of this methodology includes creating a statistical shape model to determine mean bones for the initial alignment step and expanding the analysis using kinematic data to evaluate crosstalk.

REFERENCES

[1] Lenz A et al. *J Biomech* **120**: 110344, 2021.
[2] Wu G et al. *J Biomech* **35(4)**: 543-548, 2002.

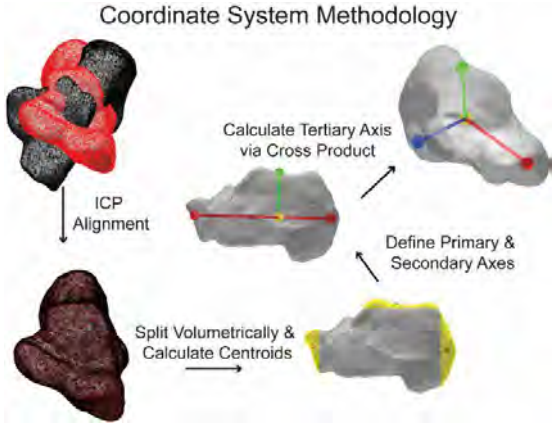

Figure 1 Simplified toolbox steps to calculate a coordinate system

IN VIVO TARSAL BONE KINEMATICS AND THE INFLUENCE OF ARTICULAR TALUS MORPHOLOGY

Anja-Verena Behling[1,2], Luke Kelly[1], LaurenWelte[3], and Michael Rainbow[2]
[1] School of Human Movement and Nutrition Sciences, University of Queensland, Brisbane, Australia.
[2] Mechanical and Materials Engineering, Queen's University, Kingston, Canada.
[3] Mechanical Engineering, University of Wisconsin-Madison, Wisconsin United States.
a.behling@uq.net.au

INTRODUCTION

Previous *in vivo* single -plane videoradiography (BVR) work reported that the calcaneus, navicular, and cuboid's (tarsal bones) motion relative to the talus occurs about the same axis of rotation [1]. Efforts have been made to quantify this axis using morphological features [2,3]. However, given the complexity of the articular geometry, muscle insertions, and ligament geometry of the tarsal bones, we questioned whether the axis based on talus articular morphology is sufficient to capture tarsal bone rotation. Here, we took advantage of the large range of motion during single leg hopping to compute the helical axis of motion (HAM) from BVR measurements. We hypothesized that the tarsal bones would rotate relative to the talus about the morphology-based axis. Secondarily, we compared the range of motion among the joints in the tarsal bone complex.

METHODS

Computed tomography scans (0.356mm x 0.356mm x 0.625mm) were obtained from nine asymptomatic feet (5 females, mean ± std height 171 ± 11cm, body mass 71 ± 15kg). We used BVR (125 Hz) to capture the motion of the talus, calcaneus, cuboid, and navicular during single leg hopping (156 bpm). All bones were tracked with Autoscoper (Brown University) using an established approach [4]. We computed the HAM for the calcaneus, navicular, and cuboid relative to the talus from landing to foot flat and from foot flat to push-off. All HAMs were resolved in the morphology-based coordinate system, whose z-axis is defined by the line joining the centroid of two spheres fit to the calcaneus and navicular facets on the talus, designed to capture the subtalar axis (Figure 1) [2,3]. We expected most tarsal bone rotation to occur about this axis. Differences for all metrics between landing and push-off were tested via paired t-tests. Differences in orientation between the morphological axis and z-direction of each bone's HAM were investigated via boxplots (not shown here). To compare each joint's range of motion, paired t-tests were performed. Non-parametric tests and Bonferroni corrections were applied when required.

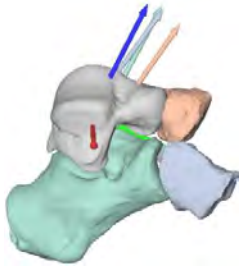

Figure 1 Color-coded HAM matching the bones, and the morphology-based coordinate system; blue indicates the morphological axis (representative participant).

RESULTS AND DISCUSSION

There were no differences between the tested variables regarding landing and push-off ($p \geq 0.04$). Most motion occurred about the morphological axis (Table 1), confirming that navicular, cuboid, and calcaneus motion is primarily driven by the articular morphology of the talus. This may imply that changes in the shape of the talonavicular or subtalar facets disturbs the normal uni-axial function of the tarsal complex. The cuboid rotated 89% and the calcaneus rotated 66% ($p \leq 0.008$) relative to the talus compared to talonavicular motion. This indicates the great mobility of the talonavicular and talocuboid joint in comparison to the more restricted subtalar joint. These findings strengthen previous results [1,5] of the foot being highly mobile during ground contact, exhibiting joint rotations about a single axis without "midtarsal locking".

CONCLUSIONS

Our data shows that most motion of the tarsal bones occurs about a morphological axis based on articular geometry of the talus, suggesting a strong influence of joint facet shapes on tarsal kinematics.

REFERENCES

[1] Wang et al. *Gait & Posture*. **49**: 54-60, 2016.
[2] Modenese and Renault. *J Biomech*. **116**.1186, 2021.
[3] Conconi et al. *J of Foot Ankle Res*. **14**.:66. 2021.
[4] Miranda et al. *J Biomech Eng*. **133**: 12: 121002, 2011.
[5] Okita et al. *J Orthop Res*. **32**: 1. 110-115, 2014.

Table 1: HAM kinematics (°) resolved in morphological subtalar coordinate system for push-off (n = 9; mean ± std).

	X-Axis	Y-Axis	Z-Axis (morphological subtalar axis)
Navicular	-2.5 ± 3.6	-0.0 ± 2.8	14.4 ± 4.1
Cuboid	-3.1 ± 1.6	-1.0 ± 2.5	13.1 ± 3.7
Calcaneus	-2.1 ± 0.6	-0.5 ± 1.5	9.5 ± 2.1

WEIGHT-BEARING CT IN SUPPORT OF AGE-RELATED 3D FOOT MEASUREMENTS

Leardini A.[1], Sacchetti G.[1], Bazzocchi A.[2], Gazzotti S.[2], Ortolani M.[1], Berti L.[1], Belvedere C.[1]
[1] Movement Analysis Laboratory, IRCCS Istituto Ortopedico Rizzoli, Bologna, Italy
[2] Department of Diagnostic and Interventional Radiology, IRCCS Istituto Ortopedico Rizzoli, Bologna, Italy
Email: belvedere@ior.it

INTRODUCTION

The foot complex in the elderly and its age-related degenerative processes need careful attention to prevent and treat major disorders and disabilities [1]. Current computed tomography (CT) allows three -dimensional (3D) analysis with varying levels of accuracy depending on the machine and settings used, but generally in the absence of physiological load on lower limb, including the foot. Patients are in fact supine within the CT bore, which greatly limits realistic reconstruction of joint relationships and deformities of normally loaded structures. Weight-bearing CT (WBCT) devices based on cone-beam technology have recently been developed for clinical evaluations of human limbs. These allow patient scans in standing posture and thus also foot scans finally in loading conditions [2]. These also allow very accurate 3D morphological reconstructions with minimal alterations [3] via reduced exposure doses. WBCT in foot assessments, especially in the elderly, can thus provide access to important measurements, like plantar tissue thickness, bone inclinations and identification of vascular calcifications, all of which are subject to age-related alterations. The aim of this study is to perform these measurements in three different populations and detect any correlations with age.

METHODS

Twenty-one flatfeet, seventeen diabetic feet, and four normal feet underwent WBCT (OnSight 3D Extremity System, Carestream, Rochester, NY-USA) scans on single-leg up-right posture. DICOM slicing of 0.26 mm and high-resolution image size of 884x884x960 voxels were set. 3D models of the distal tibia and all foot bones were reconstructed through semi-automatic segmentation with a state-of-the-art software (Mimics Innovation Suite - MIS, Materialise, Leuven, Belgium) based on initial HU masks. The same segmentation software was also used to reconstruct possible vascular calcifications in 3D and to quantify their volumes with an ad hoc software function. Principal Component Analysis was used to define anatomical reference systems on all 3D bone models using recent proposals [4], from which absolute and relative orientations and bone-to-ground heights (Hg) were calculated.

RESULTS AND DISCUSSION

In the flatfoot population, medial longitudinal arch collapse, talus supination, and 1st metatarsophalangeal joint and calcaneal valgism were revealed by calculated bone orientations; the 2nd metatarsal head was found correlated with age (R^2=0.23; p=0.04). In the diabetic population (Figure 1), the plantar tissue was found to thin with age, with significant ($p<0.05$) correlations for the 4th (R^2=0.26) and 5th metatarsal (R^2=0.28) heads. The diabetic subject most affected by vascular calcifications (volume 3920 mm^3) was the oldest and the one with the longest disease course.

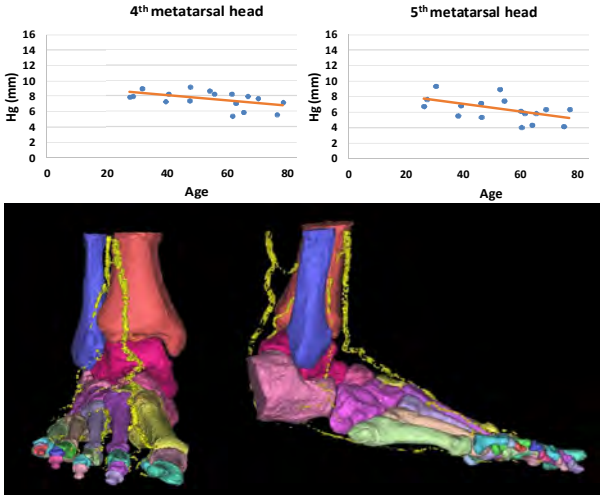

Figure 1 From the diabetic foot population: correlations between 4th and 5th metatarsal and age (top). Frontal and lateral views of 3D bones, with vascular calcifications in yellow (bottom).

CONCLUSIONS

These preliminary findings demonstrate the potential of WBCT for 3D foot measurements. Very accurate instrumental analysis can now be performed to monitor the progression of skeletal changes and vascular disorders over time, thus predicting, and possibly preventing, major problems, like instability, ulceration, cartilage degeneration, bone deformities and pain.

ACKNOWLEDGEMENTS

RETE AGING IRCCS – The Aging Network of Research and Care Institutes in Italy.

REFERENCES

[1] Belvedere C et al. *J Foot Ankle Res*. **13**:64-75,2020
[2] Leardini A et al. *Semin Musc Rad*, **23**:643-56,2019.
[3] Durastanti G et al. *QIMS*. **9**:1368-82,2019
[4] Carrara C et al. *Foot Ankle Surg*, **27**:168–74, 2021.

Summary

The goal of the ISB Technical Group in Motor Control is to provide a forum to highlight and foster the increased interest in scientific work that bridges the fields of Motor Control and Biomechanics. The Motor Control Technical Group was established as a Seed Group affiliated with the International Society of Biomechanics (ISB) at the XXIV Congress of ISB in Natal (Brazil), in 2013. It was recognized as a Working Group of ISB at the XXV Congress of ISB in Glasgow in 2015; and as a Technical Group of ISB at the 2019 ISB/ASB Congress in Calgary, Canada.

This 90 minute symposium includes a 30 min keynote talk and 6 oral presentations selected from submitted abstracts to ISB/JSB 2023. This will cover advancements in the understanding of human movement through an integrated approach that includes both the study of the organization of the nervous system and the biomechanical properties of the musculoskeletal system. This symposium will highlight novel scientific work that bridges elements of motor control and biomechanics to facilitate and encourage an integrated approach to the study of human movement. This symposium will include talks on the development of musculoskeletal models of muscle function, the interaction between muscle activity and cerebral dynamics in the brain, coordination and modelling of impairment, and the modulation of mechanical and reflexive responses to perturbations.

Executive Board Members: Professor Jim Richards, University of Central Lancashire, UK; Professor Walter Herzog, University of Calgary, Canada; Associate Professor Matt S. Stock, University of Central Florida, USA.
Advisors: Dr Paola Contessa, Padua University Hospital, Italy; Professor Patria Hume, Auckland University of Technology, New Zealand; Professor Jean-Benoit Morin, Université Jean Monnet in Saint-Etienne, France; Dr Archit Navandar, Aspire Academy, Qatar.

Scheduling
11:00 – 11:05 Introduction to Motor Control Technical Group: Professor Walter Herzog
11:05 – 11:25 Keynote
11:25 – 11:30 Discussion
6 oral presentations 8 mins each including question time.

Interaction analysis between sEMG signals and cerebral dynamics in brain regions during isometric contraction of elbow joint

Le Li [1,*], Xiaohan Wang[1], Ze Gong[1], Di Ao[1], and Huijing Hu[1]
[1] Institute of Medical Research, Northwestern Polytechnical University, Xi'an, China.
*Email: lile5@nwpu.edu.cn

INTRODUCTION

The motor function of the human body requires constant interaction between the brain and muscles. Functional near-infrared spectroscopy (fNIRS) can quantitatively analyse changes in HbO_2 and HbR concentrations in brain [1]. Surface electromyography (sEMG) is a complex bioelectrical signal that is directly related to body motor control [2].In this study, correlation analysis was conducted around cerebral cortex blood oxygen signals and the fuzzy approximate entropy (fApEn) of sEMG signals. We investigated the interaction between brain region activation and peripheral muscle contractions during elbow isometric motor tasks in healthy adults under different conditions.

METHODS

Twenty-one healthy subjects (12 males, 9 females) were recruited in this study. Subjects completed elbow isometric contractions with visual feedback adjustment. Subjects were required to complete both 20% maximum voluntary contraction (MVC) and 80% MVC conditions in each trial. Each trial consisted of a three-minute relaxation phase, a 15-second task phase and a 30-second rest phase. In this study, a total of 30 channels were used to cover the left and right prefrontal cortex (LPFC, RPFC), left and right motor cortex (LMC, RMC), and left and right occipital lobe (LOL, ROL). Then, circular silver-silver chloride (Ag-AgCl) electrodes were attached to the abdominals of the subjects' biceps (BIC) and triceps (TRI) muscles. The sEMG signal was recorded by a dual channel custom EMG amplifier and sampled by a data converter at a resolution of 1000Hz.

We analysed activation intensity of each brain region and sEMG signal eigenvalues under different motor tasks. Pearson correlation analysis was used to test the correlation between the activation intensity of each brain region and the fApEn of EMG signals under different task conditions.

RESULTS AND DISCUSSION

The results of fNIRS study showed that the activation of all brain regions was significantly enhanced under the condition of higher force during motor tasks, especially the contralateral motor cortex. Meanwhile, the fApEn of BIC and TRI were compared under different conditions, and the fApEn under the condition of more force were higher than those under the condition of less force ($P < 0.001$). As the strength level increases, more muscles are required to maintain the strength output, resulting in a significant increase in the complexity of sEMG signals and muscle coordination. The results showed a significant positive correlation between fApEn and HbO_2 in the contralateral motor cortex ($r = 0.594$, $p < 0.01$) (Fig.1). It showed that fApEn of BIC were significantly positively correlated with changes in HbO_2 in the contralateral motor cortex, suggesting correlation between the central nervous system and peripheral muscle contraction when performing motor tasks.

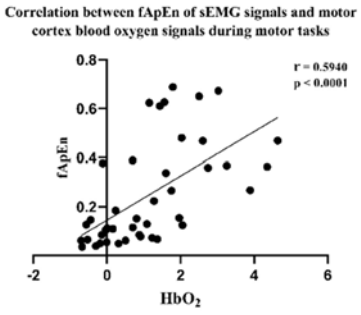

Figure 1 Correlation between fApEn of sEMG signals and motor cortex blood oxygen signals during motor tasks in healthy adults under different conditions.

CONCLUSIONS

In this study, we examined the correlation between sEMG signals and the intensity of activation in brain regions during motor tasks. We found that in motor tasks, the higher the force intensity, the more muscle motor units are involved in the motor task, and the higher the complexity of sEMG signals. At the same time, as the complexity of the motor task increased, the degree of activation of the corresponding brain regions increased. This finding provides evidence for further clinical rehabilitation of patients with impaired motor function.

ACKNOWLEDGEMENTS

This work was supported by the Education and Teaching Reform Funds for the Central Universities (22GZ230101) and NSFC (No.32071316, 32211530049)

REFERENCES

[1] Nippert AR et al. Mechanisms Mediating Functional Hyperemia in the Brain. *Neuroscientist* **24**: 73-83, 2018.
[2] Donaldson S et al. SEMG evaluations: an overview. *Appl Psychophysiol Biofeedback* **28**: 121-7, 2003.

Does a foot-eye coordination variable add value to the prediction of mild cognitive impairment?

Daniel Koska[1], Ann-Kathrin Harsch[1], Andresa Germano[1], Daniel Schmidt[1] and Christian Maiwald [1]
[1] Chemnitz University of Technology, Institute of Human Movement Science, Chemnitz, Germany
Email: daniel.koska@hsw.tu-chemnitz.de

INTRODUCTION

Early diagnosis of declining cognitive abilities in old age is important, since modifying risk factors may delay the onset of dementia [1]. Abnormal cognitive decline is currently diagnosed using either cognitive tests or objective but complex and expensive screening methods, such as brain imaging or blood-based biomarkers. Therefore, identifying reliable, sensitive, and objective low-cost markers is of great interest. We therefore investigated a simple foot-eye coordination test and its benefit for predicting mild cognitive impairment (MCI), a possible pre-stage of dementia.

METHODS

222 participants ≥ 80 years performed a cognitive test (MoCA, Montreal Cognitive Assessment) based on which they were stratified into two groups using the recommended MoCA-cutoff of MCI < 26: Cognitive healthy individuals (**CHI**: n=162, 82.3 (2.2) years, male/female: 75/87, MoCA score: 27.2 (1.6)) and **MCI** (n=59, 82.3 (2.2) years, male/female: 38/21, MoCA: 22.4 (1.4)). In addition, they performed a foot-eye coordination task, in which they rotated a foot pedal to follow a 0.15 Hz sinusoidal target curve presented on a screen. The difference between the target and the actual movement curve was quantified using Sample Entropy (SampEn) with parameters m=2 and r=0.3 [2]. Low SampEn values indicate that the signal is regular and predictable, while high values indicate greater complexity or randomness.
To quantify the added value of SampEn, two binary logistic regression models ('A', 'B') were fit: **'A'** models the probability of MCI using predictor variables age and sex. **'B'** is equal to model 'A' plus SampEn. Age and SampEn were modelled using restricted cubic splines. The added value of SampEn was quantified using the Fraction of New Information (FNI) [4]: FNI=1 - (LR_A/LR_B), where LR is a likelihood ratio chi-square test. The internal validity of the model was evaluated using overfitting-corrected estimates of the mean squared difference between the predicted probability and the actual outcome (MSE) and Nagelkerke's pseudo-R^2.

RESULTS AND DISCUSSION

The results indicate that SampEn adds diagnostic value (Figure 1). FNI from SampEn was 0.57, which represents a substantial gain in information regarding MCI status.

Table 1: Results for both statistical models.

	LR X^2	pseudo-R^2	MSE
Model 'A'	9.85	0.02	0.2
Model 'B'	22.9	0.07	0.19

The performance of the model, however, was poor, as evidenced by the high MSE and low pseudo-R^2 values (Table 1). This was caused largely by the simplicity of the baseline model, which predicts the complex outcome variable using only two basic variables. Therefore, more powerful predictor variables should be collected in future studies, e.g., genetic, lifestyle, or clinical variables. In addition, uncertainty is introduced by the MoCA scores. [5] estimate the random variation of MoCA scores across repeated tests to ±4 points, resulting in a substantial risk of assigning individuals to the wrong group. We generally recommend moving away from dichotomization toward modeling cognitive scores as ordered categorical responses to use the full information in the data.

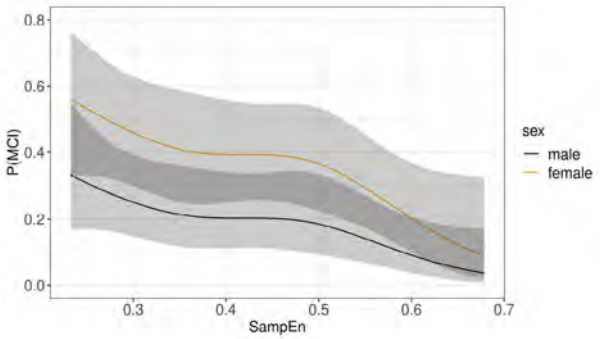

Figure 1 Predicted probability of MCI as a function of SampEn and sex for an 82 year old individual.

CONCLUSIONS

SampEn provides additional value for the prediction of cognitive status, but the performance of the prediction model must be improved to be able to assess the actual benefit of the new parameter.

REFERENCES

[1] Mangialasche F et al. *Alzheimers Res Ther* **86**: 34-9, 2012.
[2] Richman J and Moorman R *Am J Physiol Heart Circ Physiol* **278**: H2039-H2049, 2000.
[4] Harrell F, fharrell.com/post/addvalue/, 2020.
[5] Feeney J et al. *J Alzheimer's Dis* **53**: 1107-1114, 2016.

REFLEX MODULATION DURING GAIT WITH MECHANICAL PERTURBATIONS

Dana L. Lorenz[1], Antonie J. van den Bogert[2]
[1] Department of Chemical and Biomedical Engineering, Cleveland State University, Cleveland, USA.
[2] Department of Mechanical Engineering, Cleveland State University, Cleveland, USA.
Email: D.L.Lorenz@vikes.csuohio.edu

INTRODUCTION

Reflexes play an important role in the control and stability of human walking. H-reflex studies, which involve a controlled electrical stimulation of the muscle spindle afferents, have shown that reflexes are modulated through the gait cycle [1]. Direct mechanical perturbation with an exoskeleton showed quadriceps stretch reflex modulation between stance and swing phase [2], but is technically challenging and not clinically applicable. Treadmill-induced mechanical perturbations allow for reflexes to be observed in a more natural situation [3]. Potential clinical applications are the diagnosis of abnormal reflexes and the development of bio-inspired control systems for exoskeletons and prostheses. The aim of this study is to examine the normal reflex responses in eight lower extremity muscles, and how these are modulated through the stance phase of gait.

METHODS

Ten participants each walked for 30 minutes (six 5-minute trials) on an instrumented treadmill at a speed of 1.2 m/s. Each gait cycle had a 17% probability of being perturbed. The perturbations consisted of an increase of belt speed (by 0.75 m/s for 50 ms), delivered with equal probability at 10%, 20%, 30%, 40%, 50%, 60%, 70%, or 80% of the stance phase. Data were recorded using motion capture with 25 markers and electromyography (EMG) from the tibialis anterior (TA), soleus (SOL), lateral gastrocnemius (LG), rectus femoris (RF), vastus lateralis (VL), vastus medialis (VM), biceps femoris (BF), and gluteus maximus (GM). EMG signals were bandpass filtered, rectified, and separately ensemble-averaged for the unperturbed gait cycles and the perturbed gait cycles from each type of perturbation. Reflex responses were determined by subtracting the EMG envelope of the unperturbed gait from the EMG envelope for each perturbation type. A single-factor ANOVA with repeated measures was performed to test for the effect of perturbation time on the peak magnitude of the reflex response.

RESULTS AND DISCUSSION

For each of the 8 types of perturbation, 20-30 gait cycles were recorded, which was sufficient to obtain clear ensemble averages. The remaining gait cycles (more than 1000) were not perturbed. For most muscles, the ensemble-averaged EMG envelopes of the perturbed gait cycles showed a noticeable difference compared to the unperturbed gait cycles. SOL, LG, VL, and VM (Figure 1) responded immediately following a joint angle change induced by the perturbation, suggesting a stretch reflex mechanism. Other muscles had a more delayed response, suggesting an indirect response to an altered gait cycle.

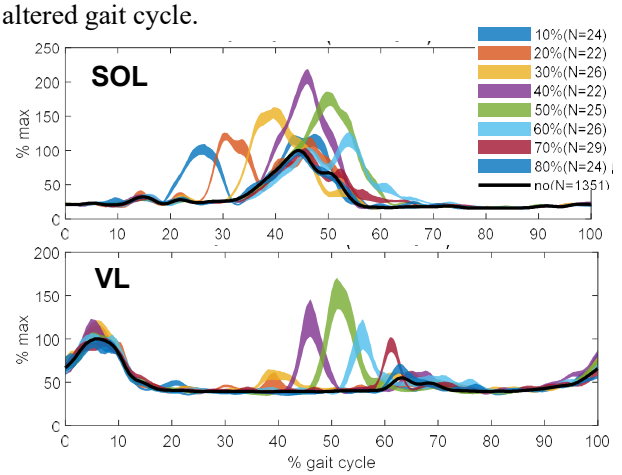

Figure 1 Normalized EMG of the Soleus (top) and Vastus Lateralis (bottom) in one participant during normal walking (black) and during perturbations starting at 10% to 80% of the stance phase.

Statistically significant effects of perturbation time were found in TA, LG, SOL, RF, VM, and BF. The results appear to show that the calf muscles have large responses during most perturbation types, indicating that ankle stabilization is important throughout the stance phase. The quadriceps and hamstring muscles, important in knee and hip stabilization, have stronger reflex responses later in the stance phase.

CONCLUSIONS

We conclude that mechanically induced reflexes are modulated during the stance phase. We suggest that control systems for prostheses and exoskeletons should be designed with similar modulation, i.e., time-varying feedback gains. Further work will be directed at determining control laws that explain the observed EMG responses.

ACKNOWLEDGEMENTS

The work was partially supported by a Faculty Research Development grant from Cleveland State University.

REFERENCES

[1] Zehr EP, *Prog Neurobiol* 58: 185-205, 1999.
[2] Mrachacz-Kersting N, *et al.*, *Exp Brain Res* 159: 108-122, 2004.
[3] Sloot LH, *et al.*, *PLOS One* 10(12): e0144815, 2015.

EMBEDDING THE CONTROL OF BALANCE INTO THE MUSCLE COORDINATION FOR WALKING IS ASSOCIATED WITH BETTER WALKING FUNCTION.

Jessica L. Allen
Department of Mechanical and Aerospace Engineering, University of Florida, Gainesville, FL, USA.
Email: jessal@ufl.edu

INTRODUCTION

Maintaining balance is critical for successful walking and converging evidence suggests that the neuromuscular control of walking and balance may share common structure. For example, several studies using motor module (a.k.a. muscle synergy) analysis have demonstrated that young adults recruit balance-specific motor modules during walking [1,2]. Whether recruiting balance-specific modules during walking is important for walking function is unknown but may have important implications for gait rehabilitation. This study tested the hypothesis that recruiting fewer balance-specific motor modules during walking would be associated with worse walking function.

METHODS

Electromyography was recorded from trunk and leg muscles while walking at preferred speed and during a standing reactive balance task in 9 chronic stroke survivors (57±12.7 years old, 46.3±23.1 months post-stroke), 8 neurotypical older adults (62±6.6 years old), and 20 young adults (21.9±2.8 years old). Muscle coordination was quantified using motor modules identified with nonnegative matrix factorization [2]. Motor module number in each behaviour was chosen such that at least 90% of the variability in muscle activity was accounted for. The number of balance-specific motor modules recruited during walking was identified using Pearson's correlations [1,2]. The relationship between module number and three metrics of walking performance were analysed: preferred walking speed (all groups, where higher values are better), range of frontal-plane whole-body angular momentum during walking (WBAM; stroke and older adults only, where lower values are better [3]) and distance walked on a narrow balance beam (young adults only, where higher values are better).

RESULTS AND DISCUSSION

In support of the study hypothesis, recruiting balance-specific motor modules during walking was associated with walking function (Fig. 1). In the stroke and older adult cohorts, the number of balance-specific modules recruited during walking was significantly associated with walking speed (Fig. 1A; r = 0.59, p<0.01) and frontal plane WBAM (r = -0.58, p=0.02). Or in other words, those individuals who walked at slower speeds and with larger range of frontal-plane WBAM recruited fewer balance-specific modules during walking. Moreover, neither walking speed or WBAM were related to the number of modules identified in walking alone (r = -0.01, r = -0.04), providing support that embedding the control of balance into the muscle coordination for walking is important.

In the young adult cohort, the number of balance-specific modules recruited during walking was significantly associated with distance walked on the balance beam (Fig. 1B; r = 0.45, p=0.02). Or in other words, those young adults who could walk farther on the beam recruited more balance-specific modules during walking. Moreover, such a relationship only emerged when balance was specifically challenged in the beam-walking task (r=0.09, p=0.35 for walking speed), providing support that this may reflect a neuromuscular strategy for the control of walking balance.

CONCLUSIONS

This study identified a positive relationship between walking function and recruiting balance-specific motor modules during walking. That such a relationship was found in both neurologically impaired and intact individuals suggests that this may reflect a general neuromuscular strategy contributing to the maintenance of balance while walking. As such, it may be an effective target for gait rehabilitation.

ACKNOWLEDGEMENTS

Supported by NSF/DARE 2245620

REFERENCES

[1] Chvatal and Ting. *Front Comput* **7**:48, 2013.
[2] Allen et al., *Gait Posture* **82**:242-7, 2022.
[3] Vistamehr et al., *J Biomech* **49**:396-400, 2016.

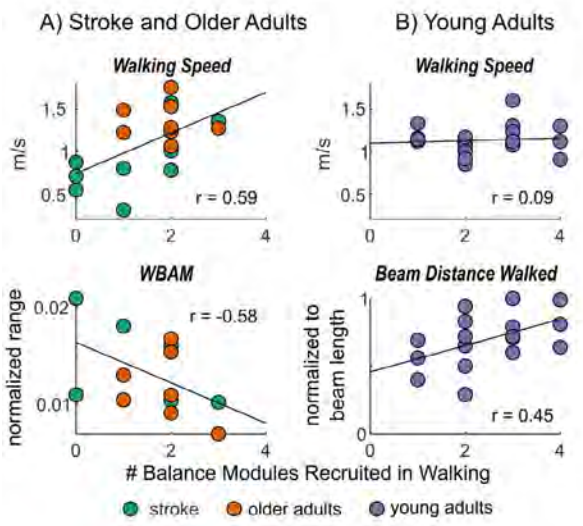

Figure 1: Relationship between walking function and the number of balance-specific modules recruiting during walking in A) stroke survivors and older adults and B) young adults.

MODELLING PATIENT-SPECIFIC NEURAL CONTROL IN CHILDREN WITH CEREBRAL PALSY

Míriam Febrer-Nafría[1], Zachary Roth[2], Bram Van Den Bosch[2], Lars D'Hondt[2], Kaat Desloovere[3], Anja Van Campenhout[4,5] and Friedl De Groote[2]

[1] Department of Mechanical Engineering, Universitat Politècnica de Catalunya, Barcelona, Spain. [2] Department of Movement Sciences, KU Leuven, Leuven, Belgium. [3] Department of Rehabilitation Sciences, KU Leuven, Leuven, Belgium. [4] Department of Orthopaedic Surgery, UZ Leuven, Leuven, Belgium. [5] Department of Development and Regeneration, KU Leuven, Leuven, Belgium.
Email: miriam.febrer@upc.edu

INTRODUCTION

Physics-based computer simulations that can predict the effect of treatments (e.g., bony and soft tissue correction, ankle-foot-orthoses) on gait in children with cerebral palsy (CP) have the potential to improve the clinical decision-making. For that, an important challenge is to accurately model patient-specific non-selective muscle control. Muscle synergies, which are groups of muscles activated in a fixed ratio (described by synergy weights) by a single input signal, can be used to describe the ability to selectively control muscles. Children with CP present fewer synergies [1], which are more variable [2], than typically developing individuals. Recently, it has been shown that reducing the number of synergies in musculoskeletal simulations had a minor effect on gait kinematics [3]. Therefore, we expect that capturing the effects of impaired muscle control on individual gait patterns will require imposing not only a customised number of synergies but also personalised synergy weights.

METHODS

We predicted gait [3] based on a musculoskeletal model scaled to the anthropometry of a healthy adult. We imposed a speed of 1.33m/s. We imposed the number of synergies to simulate healthy and impaired control. A healthy control strategy was simulated using five synergies per leg, whereas an impaired control strategy was represented with asymmetric and/or fewer synergies. We also explored the influence of imposing patient-specific synergy weights (co-activation patterns) obtained from data of two children with diplegic CP with low selectivity at the left ankle on a clinical scale. Patient-specific synergy weights were consistent across different activities within patients but varied between patients. The first child (CP1) had increased knee flexion at initial contact, while the second child (CP2) walked slowly with reduced motion in the knee and ankle during stance (Fig. 1b).

RESULTS AND DISCUSSION

We found that synergy-based control could produce a healthy walking pattern (Fig. 1a). Moreover, the predicted kinematics and muscle activation patterns remained almost unchanged when a reduced number of synergies (e.g. four or three) were imposed, even if the number of synergies was asymmetric (e.g. five right, three left). Finally, imposing patient-specific weights resulted in different knee kinematics for the two sets of weights. When imposing synergy weights as well as gait speed from CP2, the simulated knee pattern resembled experimental data (Fig. 1b). This suggests that impaired selective control contributed to this gait deficit. We did not expect our simulations to capture all the deficits in the gait pattern because we did not model musculoskeletal impairments whereas these were present in both children. Simulated muscle activations patterns were different when imposing CP1 and CP2 weights and resembled measured EMG.

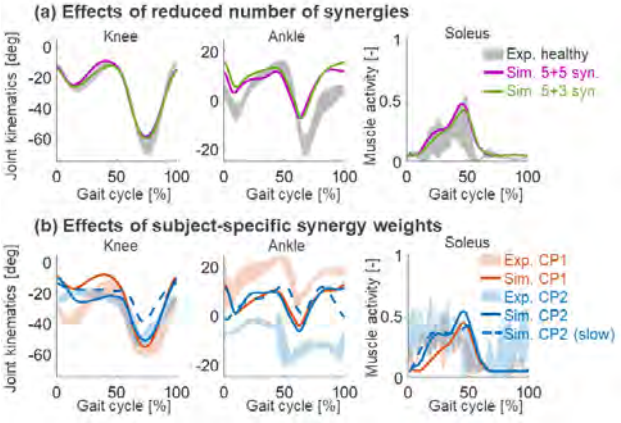

Fig. 1: Experimental (Exp.) and simulated (Sim.) kinematics and muscle activity (most impaired side of children with CP).

CONCLUSIONS

Muscle co-activation patterns derived from synergies might capture non-selective muscle control in children with CP and offer a way to include for motor control deficits in our current simulation workflow [3]. Accounting for motor control deficits might be crucial to achieve accurate gait predictions.

ACKNOWLEDGEMENTS

Margarita Salas (MFN), KU Leuven Internal Funds (C24M/19/064), FWO G0B422N, FWO 1SF1822 (BVDB).

REFERENCES

[1] Steele et al. *Dev Med Child Neurol* **57(12)**, 2015.

[2] Pitto et al. *PLoS ONE* **15(2):** e0228851, 2020.

[3] Falisse et al. *Front. Hum. Neurosci.* **14:**40, 20

PRE-PROGRAMMED HAMSTRING ACTIVATION DURING SIDECUTTING IS ASSOCIATED WITH REFLEXIVE RESPONSE DURING A SINGLE-LEGGED PERTUBATION TEST

Jesper Bencke[1], Mette K. Zebis[2], Jesper Lundbye-Jensen[3], Anke Karabanov[3], Merete Speedtsberg[1], Niels J. Nedergaard [1]

[1] Human Movement Analysis Laboratory, Copenhagen University Hospital, Hvidovre, Denmark.
[2] Department of Physiotherapy, University College Copenhagen, Copenhagen, Denmark
[3]NEXS, University of Copenhagen, Copenhagen, Denmark
Email: jesper.bencke@regionh.dk

INTRODUCTION

Increased knee joint stiffness is required to reduce injury risk in demanding sports situations like sidecutting or landing. Improving knee joint stiffness may be obtained through both preparatory and reflexive responses that are mediated by proprioceptive feed-forward and feedback mechanisms, respectively [1]. Previous studies have shown that an optimal pre-programmed activation of the medial hamstring (i.e. semitendinosus (ST)) during sidecutting is important to reduce risk of knee injuries [2]. To further explore the relation between proprioceptive reflexive and pre-programmed activation in injury risk situations, the aim of this pilot study was to investigate, if the ST muscle activity response obtained during a new knee joint pertubation test could explain the level of ST activity during sports movements with various demands of knee joint stability.

METHODS

Fourteen elite-level female handball players were recruited (age:18-30). All performed a knee perturbation test (KPT) standing with the dominant foot on a sliding surface keeping the shank near vertical and a knee flexion of 30 degrees and the other foot supported on a 40 cm box (see figure 1). Subjects would hold this position and look straight ahead, and the test leader would quickly pull the sliding surface 5-9 cm anteriorly for 5 trials and thereafter 5 trials of a lateral pull perturbation. The test was performed in a biomechanical lab. The velocity and distance of the anterior movement was measured using 3D recordings of a reflective marker on the ankle, and muscle activity of the ST was recorded simultaneously using EMG (Cometa, IT). Also, the subjects performed a dynamic horizontal single-legged landing on the dominant leg (SLL) with some demand of knee joint stiffness and a handball specific sidecutting movement (SC) requiring high knee joint stiffness. EMG data was high-pass filtered with a cut-off of 20 Hz and a RMS filtered with window of 30 ms and 29 ms overlap. Subsequently, EMG data was normalised to the maximal EMG activity obtained during maximal isometric contractions. The peak ST activity recorded during the first 150 ms after the perturbation was calculated for the KPT (figure 1), and the mean activity during the last 50 ms prior to landing during SC and SLL was collected [1]. Linear regression analysis was used to test to what extent ST activity during KPT (independent parameter) could explain sports specific ST pre-landing activity (dependent parameter). The test protocol was approved by the local ethics committee.

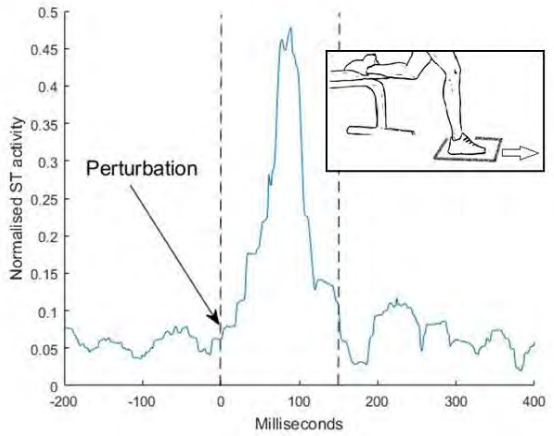

Figure 1 Representative trial of filtered, normalised ST activity for the anterior KPT. Vertical dashed lines indicate the 150 ms period after perturbation where peak ST activity was recorded.

RESULTS AND DISCUSSION

The KPT was feasible and simple. Mean peak perturbation velocity (SD) was 1.6 (0.2) and 1.2 (0.1) m/s, and the distance of the foot movement was 76 (9) mm and 66 (10) mm, for anterior and lateral pull, respectively.

Peak ST activity during the anterior (R^2=0.76, F=31.1, p<0.001) and lateral KPT (R^2=0.62, F=14.9, p=0.004) showed a high association with ST pre-activity during SC. Whereas the anterior (R^2=0.33, F=5.9, p=0.031) and lateral KPT (R^2=0.08, F=0.9, p=0.36) was poorly associated with ST pre-activity during SLL.

CONCLUSIONS

The results showed that medial hamstring reflexive response during a standing test is highly associated with pre-programmed activity during an ACL injury-risk movement (SC), but not to a low-risk movement (SLL).

REFERENCES

[1] Schultz SJ et al. J Athl Train 36:37-43. 2001.

[2] Zebis M et al. Knee Surg Sports Traumatol Arthrosc 21: 550–555, 2022.

Summary

In recent years, artificial intelligence (AI) has penetrated every domain of our lives, and forms an important component of any modern technology. For example, mobile phones are no longer just telephones, but are advanced computers capable of real-time analysis of movement data, image interpretation and much more. These developments are timely for biomechanists, who have long sought ways to analyse human movement in conditions outside of a laboratory, and over longer timespans than a few minutes or hours. This symposium will feature presentations from leading scientists in the field of biomechanics-related AI. They will introduce novel applications of AI techniques to solve biomechanical problems in various sub-domains. These applications will include markerless motion analysis methods, estimation of ground reaction forces from video data, and sport-related applications. We aim to give audience members an up-to-date picture of the AI landscape, and inspire new ideas and possible applications in the broader field of biomechanics. We will also address some of the challenges of using algorithms that, despite being trained on large volumes of data, do not always make perfect decisions.

Speakers and topics:

- SY03-1: Team Sports Analytics using machine learning.
  Keisuke Fujii, Associate Professor, Nagoya University
- SY03-2: Estimation of kinetic parameters from video data using supervised machine learning techniques
  Marion Mundt, Research Associate, University of Western Australia
- SY03-3: Applications of AI in clinical settings.
  Eni Halilaj, Assistant Professor, Carnegie Mellon University

Summary

This symposium will consist of a series of presentations from invited speakers with expertise in the biomechanics of ball kicking across football codes. We aim to address a number of contemporary issues across the field, highlighting both the current knowledge and pertinent questions that should be considered in future research.

SY04-1

- Neal Smith - Energy flow in soccer kicking
  The action of kicking in the football codes has been well described over the years. With angles and angular velocity values in good agreement amongst studies, it is important to understand the energetics of the motion and how these very fast foot velocities are obtained. We will look across the football codes and attempt to unpack energy flow in the kicking leg towards ball contact, and the transfer to the ball. Skill development will also be observed as key degrees of freedom are involved at higher skill levels.

SY04-2

- Simon Augustus – Looking beyond the kicking leg: whole-body strategies for ball kicking performance
  Descriptions of kick leg function during ball kicking are extensive, but less is known about how the support leg, pelvis and upper body contribute to kicking performance. Understanding whole-body strategies used to perform fast and accurate kicks can help players and coaches develop and train effective kicking actions. This presentation will provide an overview of research conducted over the last decade that has attempted clarify such strategies. Attention will be paid to a) common 'observable features' of ball kicking that have been identified as the foundation of successful performance b) different inter-individual strategies and classification of different 'types' of kicker.

SY04-3

- Alexandra Atack – Sex differences in ball kicking biomechanics (strength, technique and training effects)
  For a number of years research has sought to understand differences in ball kicking performance and technique between male and female players. Early research found female soccer players demonstrated different kicking leg mechanics and ultimately reduced ball velocities compared with males. Some researchers aligned this to differences in their physical performance capacities, others suggested it may be an effect of their training experiences. This presentation will take a holistic overview of these factors (strength, technique and training experience) through a comparison of elite female and male rugby place kickers.

SY04-4

- Hiroyuki Nunome – Myths and facts on football kicking: Filling the gaps between the player's perspective, coach's observation and scientific evidence
  There are many myths about how to perform football kicking better. A series of our studies demonstrated a more representative nature of the leg swing kinematics and ball impact dynamics, which concurrently proposed substantial gaps between what players try to do and phenomena actually happening during kicking. These natures should be carefully interpreted from practical and scientific perspectives. In some cases, coaching cues, which are not consistent with scientific evidence likely provide some benefit for players. In the current talk, we would like to emphasize the discussion about whether scientific evidence is relevant to improve the performance of football kicking.

Summary

In this symposium the aim is to critically revisit common biomechanical perspectives on how to maintain healthy knees after knee injury. Experts in the field of knee joint biomechanics will therefore challenge the audience by offering convincing arguments explicitly favouring or opposing statements such as:

- To avoid re-injury after reconstruction of the Anterior Cruciate Ligament (ACL), one should screen patients on movement patterns that excessive load the knee ligaments.
- Risk of (re-)rupturing the ACL during a side cutting manoeuvre can be assessed by screening standardized hops and jumps.
- The development of post-traumatic osteoarthritis is primarily caused by pathological load distributions on the tibiofemoral cartilage.
- Pathological knee loading observed during gait/running will propagate itself in most if not all other activities a patient/athlete engages in.

The experts will avoid technical language and build their arguments towards a non-expert audience, as such inviting everyone in the audience to actively participate in the debate, even if one is not working in the field of knee joint biomechanics.

Speakers:

- SY05-1: Jesper Bencke
- SY05-2: Kevin Ford
- SY05-3: David Saxby
- SY05-4: David Lloyd

Summary

The symposium - ***"Beyond the Surface: Uncovering the Role of Materials in Biomechanics, Sports, and Rehabilitation"*** brought together experts from various fields to discuss the latest advancements and applications in understanding human movement, optimizing sports performance, injury prevention and enhancing rehabilitation strategies. The symposium covered a wide range of topics and highlighted key research findings, technological advancements, and practical implications in these interconnected disciplines. Here is the list of material presented:

SY06-1: Solehuddin Shuib (Universiti Teknologi MARA, Malaysia)
Development of knee implant using additive manufacturing technology: lattice design, material and manufacturing

SY06-2: Uwe Gustav Kersting (German Sport University Cologne)
Simulating material properties of in-vivo shoe-surface interaction using a robotic platform - opportunities and limitations

SY06-3: Abd Halim Abdullah (Universiti Teknologi MARA, Malaysia)
3D printing material in developing assistive adaptive devices for rehabilitation medicine

SY06-4: Thor Buch Grønlykke (Spraino ApS)
New materials that modify horizontal forces for injury prevention

SY06-5: Izhar Aziz (3D Gens)
Additive metal: Process, microstructure and properties

Overall, the symposium provided an in-depth exploration of the interdisciplinary nature of biomechanics, sport biomechanics, and rehabilitation. It showcased the importance of biomechanical analysis in optimizing sports performance, designing effective rehabilitation protocols, and advancing our understanding of human movement. The event fostered collaboration and knowledge sharing among experts, paving the way for further advancements in these fields.

Summary

The theme of this symposium will be the application of modeling and simulation approaches to study sports injuries, and it will feature six invited talks followed by a discussion. The primary goals of the symposium are to: a) cover existing state-of-the-art modeling and simulation methods in the context of sports injury research and b) highlight necessary avenues for improvements in existing methods to enable real world impact.

SY07-1 ***Ton van den Bogert*** *(Parker-Hannifin Endowed Chair in Human Motion and Control in the Department of Mechanical Engineering, Cleveland State University, USA):*

Simulation has enormous potential for research on sports injuries. Tissue loads can be predicted and experiments conducted without risk to human subjects. Numerous scenarios can be rapidly evaluated to determine injury risk and the effects of risk factors or protective interventions. Now that software tools and methods are widely available, the focus needs to shift towards asking good research questions and designing good studies to answer those questions. Using previous work on ankle sprains and ACL injuries, we will discuss current obstacles on the path towards validated and trusted models that can be successfully translated into injury prevention practice. Translational research must consider the trade-off between sports performance and injury risk.

SY07-2 ***Anne Koelewijn*** *(Biomechanical Motion Analysis and Creation, Department Artificial Intelligence in Biomedical Engineering, FAU Erlangen-Nürmberg, Germany):*

In biomechanical investigations relying on predictive simulations it is common to solve a single optimal movement trajectory. However, in reality, when an individual performs a movement several times there is variability, which most predictive simulation frameworks do not capture. To capture this variability it is possible to perform the predictive simulations in a stochastic environment. In this talk I will briefly outline how predictive simulations in a stochastic environment can be performed and how this approach could benefit research in sporting settings.

SY07-3 ***Dario Cazzola*** *(Department for Health, University of Bath, UK):*

Musculoskeletal modeling has shown great potential when applied to sport and injury prevention scenarios. For this reason, such modeling approaches have started to have some traction in the sport technology industry, which needs fast and reliable models to monitor athletes' load during training and matches, and inform training or injury prevention strategies. In this talk, I will explore and discuss how musculoskeletal modeling can be used in contact sports for the estimation of contact and joint forces from video footages, and its integration with pose estimation algorithms and Gaussian processes.

SY07-4 ***Jennifer Maier*** *(Department of Mechanical Engineering, Stanford University, USA):*

The shoulder joint is the most complex joint in the human body. It is therefore challenging to find a model representation of this joint that can represent the high flexibility of the shoulder joint while allowing only for physically feasible types of motion. A particular challenge is the analysis of overhead athletes, as they perform highly dynamic movements that go far beyond the range of motion required in daily life. The high loads associated with the high range of motion makes them more susceptible for injuries like rotator cuff tears or labrum tears. Previous work has presented models on both ends of the spectrum: Models that are

constrained and physically feasible while not allowing for highly flexible and dynamic motion, and models that are highly flexible and individualizable but in need of accurate data for feasible solutions that is challenging to collect. We will talk about the challenges and considerations for designing a model of the shoulder joint that lies somewhere between the two extremes and is physically limited yet flexible and customizable to enable high ranges of motion for sports applications and injury analysis. Special focus will lie on the role of the scapula in shoulder motion.

SY07-5 ***Reed Gurchiek*** *(Department of Bioengineering, Stanford University, USA):*

Hamstring strain injuries are one of the most prevalent time-loss injuries in athletes, and re-injury is common. Research on injury mechanisms and kinetic and kinematic risk factors is often limited by drawbacks of prospective designs. In this talk, I will present preliminary results demonstrating the utility of simulation and optimization to overcome these limitations. Specifically, musculoskeletal simulations of maximal velocity sprinting revealed features of hip-knee coordination that could be used for injury risk assessment. These findings provide new insight regarding injury mechanisms and approaches for incorporating simulation and optimization for evaluating injury risk.

SY07-6 ***Antoine Falisse*** *(Department of Bioengineering, Stanford University, USA):*

There has been a lot of interest in developing methods to perform analyses of human motion based on non-invasive techniques in recent times. The development of such techniques permits large scale studies to be conducted more easily and with more participants, and they could also enable participants to be more monitored more regularly to track injury progression/rehabilitation. In this talk, I will first present OpenCap, an open source software system to measure human movement kinematics and kinetics from smartphone videos. I will then describe how this tool can be useful for diverse applications, including injury prevention and rehabilitation. I will then conclude by outlining the next steps for having this system deployed in sport settings.

Summary

The emergence of advanced footwear technology has altered the running landscape in the last decade and has divided the running community. Performance enhancement footwear in running – also known as “super shoes” – typically contain a stiff plate, lightweight, high-energy returning foam, and have a curved geometry that together enhance performance and reduce metabolic cost. The scientific community has been seeking to better understand the underlying mechanisms and conditions that lead to meaningful performance enhancements in runners, while considering the potential risks linked with rapid adoption of technologically advanced shoes.

This symposium will provide an overview of studies that have investigated the effects of advanced footwear technology on running economy, performance, and biomechanics. It will dive into misconceptions about the role of footwear energy storage and return (mechanical work) on running performance. The symposium will explore opportunities for evaluating how footwear energy storage and return cooperate and/or compete with the runner. A framework for evaluating foot and footwear mechanical power profiles during running will be presented to support biomechanics researchers and footwear developers. Furthermore, considerations with regards to the widespread adoption of advanced footwear technology in running will be discussed. Notably, the use of advanced footwear technology is now filtering to trail running, despite the limited amount of research examining the effects of such footwear on the economy and biomechanics of runners in trail-like conditions. The symposium will also speculate on how the use of advanced footwear technologies potentially affects lower extremity loading with implications for injury risk, whether it is possible to predict from biomechanics who is benefiting from wearing these shoes, and “where to from here”.

This symposium involves four invited presentations moderated by two running experts. The presentations will be followed by a panel discussion and questions from the audience.

- Kim Hébert-Losier and Irene Davis (moderators): Introduction
- SY08-1 Steffen Willwacher: The effects of advanced footwear technology on running performance and lower extremity loading: Current knowledge and future directions
- SY08-2 Emily Matijevich: Footwear energy storage and return: How footwear mechanically cooperates and/or competes with the runner
- SY08-3 Marlène Giandolini: Effect of increased longitudinal bending stiffness on running economy and biomechanics when running uphill and on unstable terrain: Implications for trail running footwear
- SY08-4 Wouter Hoogkamer: Can we predict who is responding to advanced footwear technology from biomechanics?

Summary

Motion analysis based on the use of inertial measurement units (IMUs) has expanded rapidly in recent years. In both academia and industry, IMUs have enabled development of software applications for joint kinematics estimation targeting the medical, health and wellness sectors. Proprietary algorithms and software or the lack of technological transparency of some applications can preclude assessing accuracy, validity, and reliability of the estimated parameters and comparing products and results of research studies. The rapid and growing development of IMUs and related methods has not yet resulted in consistent standards or recommendations of use. Proper use of IMUs relies on knowledge of sensor calibration procedures, sensor-to-segment alignment, data fusion algorithms, biomechanical models, reporting kinematic variables, and validation procedures. Hence, there is an urgent need to define standards and reporting guidelines for IMU-based kinematic analysis.

The two symposium chairs along with an international team of five other experts in inertial motion capture are developing these recommendations and standards. A written proposal has been reviewed and approved by the ISB committee. We believe this symposium is the ideal medium through which to present our ideas to and gather feedback from the ISB community.

Our intent is to advance the field and maximize transparency, reproducibility, generalizability, and validity of joint kinematics estimated using IMUs. Accordingly, this symposium will feature seven additional talks with IMU applications that span upper and lower limb kinematic analysis, remote gait assessment, and deep learning approaches. These will highlight novel techniques in our field and will facilitate a rich discussion amongst symposium attendees regarding our proposed recommendations.

Deep Kinematics: Uncovering Human Biomechanics with IMUs and Deep Learning – Preliminary Result

Yong Kuk Kim[1], Manuel Kaufmann[2], Alex Häfliger[1], William R Taylor[1], Navrag B Singh[1,3]
[1] *Laboratory for Movement Biomechanics, Institute for Biomechanics, ETH Zürich, Switzerland*
[2] *Advanced Interactive Technologies, Institute for Intelligent Interactive System, ETH Zürich, Switzerland*
[3] *Singapore-ETH Centre, Future Health Technologies, CREATE campus, #06-01 CREATE Tower, Singapore 138602*
Email: yong.kim@hest.ethz.ch

INTRODUCTION

Gait analysis is a crucial tool for clinicians evaluating gait impairments stemming from neurological and musculoskeletal disorders. Healthcare professionals can gain invaluable insights into a patient's well-being by analysing parameters such as stride length, variability, and swing time. Though regarded as the gold standard, traditional marker-based 3D optical motion tracking systems are hindered by time-consuming setups and restrictions to clinical facilities. Interestingly, the Hawthorne effect highlights the need for gait analysis in natural settings, as patients' performance often differs between home and clinical environments. Inertial Measurement Units (IMUs) offer a compelling alternative as wearable devices, supplying essential data regardless of location. These compact devices facilitate more practical and accessible gait analysis, promoting enhanced clinical assessments and patient care in various settings. Deep learning (DL) and IMU technology are widely used in computer graphics and vision[1]. However, clinical gait analysis requires higher accuracy than typically reported in these fields.

This study explores the potential of DL to address the limitations of traditional gait analysis methods and evaluate the accuracy and applicability of 3D human pose reconstruction using IMUs.

METHODS

3-D kinematic and IMU data were collected from 69 healthy participants (41 young: 20±2.26 years, 17 elderly: 68±5.91 years) during a 29-minute treadmill walk, a total of 1624 minutes at a sampling frequency of 200Hz. We assigned 70% of the data to the training set, 15% to the validation set, and 15% to the test. The kinematic trajectory of joint centres from motion capture data was used as ground truth. Pelvis was used as the root to serve as the origin, and height was normalised to the length of the femur. Two models were developed: the first (feed-forward) comprises three linear layers with a hidden size of 1024 and ReLU activation. The second model was built upon unidirectional Recurrent Neural Networks (RNN) with two LSTMs[2], each having a hidden size of 1024. Both models feature a final layer with an output dimension of 24 outputs: eight joint centres, each consisting of three axes.

RESULTS AND DISCUSSION

Table 1: Predicted joint centres' kinematic trajectory evaluated in Euclidean distance; The numbers presented with averages and standard deviation (SD) in centimetres, JC = Joint Centres.

	Feed Forward (FF)		RNN	
	Left	Right	Left	Right
Hip	1.47 ± 0.6	1.4 ± 0.58	1.15 ± 0.33	1.09 ± 0.29
Knee	4.52 ± 2.97	4.02 ± 2.72	3.41 ± 1.45	3.44 ± 1.45
Ankle	6.42 ± 4.32	5.36 ± 3.43	4.22 ± 2.2	3.84 ± 1.82
Toe	6.93 ± 4.27	6.21 ± 3.69	4.17 ± 2.33	4.08 ± 2.95

Both models predict joint centres with an average of 5cm error. A general pattern of increase in error distally, away from the root (pelvis), was observed. Additionally, both models do not show a significant difference between left and right predicted joint centres, although, for the ankle, the difference is more prominent. RNN displays a much lower error in Ankle and Toe than FF. Our results were based on a primitive DL model and approach, thus losing participant-specific information. Therefore, it is future work to apply body-model fitting with more advanced models to improve the accuracy in both kinematic and containing participant-specific information. Furthermore, it is of practical relevance to derive the required gait parameters mentioned in the introduction.

CONCLUSION

Both models have shown a similar pattern and promising 3D human reconstruction feasibility, where RNN outperforms the FF model. Further investigation with more advanced models and approaches is required to meet the accuracy level for clinical gait analysis.

REFERENCES

1. Huang Y et al. ACM Trans Graph. 2018;37: 1–15.
2. Hochreiter et al. 1997;9: 1735–1780

Inertial Measurement Unit calibration methods for the wrist joint: Which one should I use?

Alessandro Bonfiglio[123], Elisabetta Farella [3], David Tacconi[1], Raoul M. Bongers[4]
[1]Euleria Health, Rovereto, Italy; [2]University of Trento, Trento, Italy; [3] Fondazione Bruno Kessler, Trento, Italy.
[4] University of Groningen, University Medical Center Groningen, Groningen, Netherlands
email: abonfiglio@euleria.it

INTRODUCTION

Inertial Measurement Units (IMU) require complex calibration algorithms to convert orientation data expressed in their local reference frame into a clinically meaningful reference system. The algorithms require the wearer to perform a series of movements or poses. Several calibration methods have been developed to find the perfect trade-off between ease of use, accuracy and speed. Still, little work has been done to compare different calibration methods with each other and against a gold standard reference system [1,2]. Therefore, this paper contributes to covering this gap by assessing the accuracy and precision of a number of calibration techniques (static and dynamic) and comparing them against a gold-standard camera system.

METHODS

Seven healthy subjects with no signs of upper limb injury were recruited for this study. Five IMU sensors (Xsens DOT, Movella, The Netherlands) and five active 3-marker clusters (Optotrak Certus®, NDI, Canada), used as a gold standard reference system, were attached to the participants on the thorax, scapula, upper arm, forearm and wrist. The bony landmarks for the optical reference system presented in [3] were digitized after subjects were instrumented. Four IMU models were developed by employing different calibration techniques: 1) N-pose calibration (NP): the subject stands in neutral pose for three seconds; 2) Functional calibration (FC): the subject performs single plane movements for each joint to estimate individual rotation axes; 3) Manual alignment (MA): each sensor reference frame is manually aligned with the underlying bone frame; 4) One-Axis alignment (OA): one axis of the sensor is aligned with the long axis of the segment. The data acquisition protocol consisted of 1) Sensor calibration: a static N-pose and a series of controlled single-plane dynamic movements for shoulder, elbow and wrist; 2) Tasks: subjects were required to execute single-plane tasks for each upper limb joint and a series of multi-joint tasks that resemble common activities of daily living. A graph of an unconstrained wrist flexion/extension task at full range of motion is presented for one subject in the following paragraph.

RESULTS AND DISCUSSION

The four IMU models accurately estimated the wrist flexion/extension angle during a wrist flexion/extension task (Figure 1A). The maximum root mean squared error (RMSE) for the flexion/extension angle is 12.84±5.20° for NP, whereas the lowest RMSE is 8.76±4.16° for MA (Table 1). However, when performing the same task, the four models perform differently in estimating the radial/ulnar deviation angle (Figure 1B). In the same scenario, the highest RMSE is 34.76±9.53° for NP, whereas the lowest RMSE is 20.75±10.61° for FC.

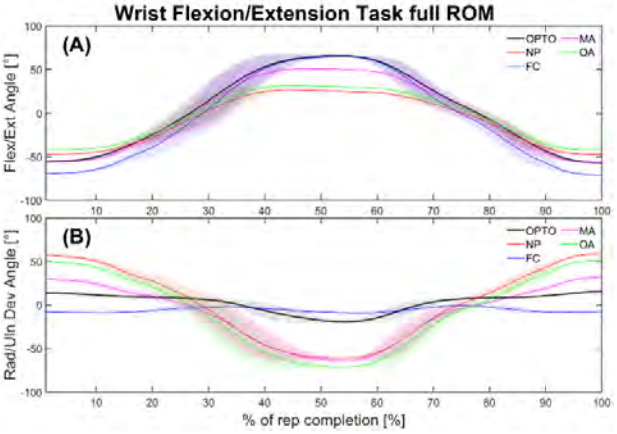

Figure 1: Plot of a wrist flexion/extension task starting from wrist fully flexed (0%) to fully extended (50%) and ending with full flexion (100%). Graph (A) displays the flexion/extension axis and graph (B) displays the radial/ulnar deviation axis.

CONCLUSIONS

All the four models presented perform rather similar in estimating the wrist flexion/extension angle, but their performance differs on the secondary rotation axis. Therefore, we advise a functional calibration approach for the best estimation of the overall wrist joint motion. However, for the highest accuracy possible on the flexion/extension axis, then we recommend the manual alignment (MA) method.

ACKNOWLEDGEMENTS

This project has received funding from the European Union's Horizon 2020 research and innovation programme under the Marie Skłodowska-Curie grant agreement No 956003.

REFERENCES

[1] Filippeschi et al. *Sensors*, **17**(6), 2017
[2] Bouvier et al. *Sensors*, **15**(8), 2015
[3] Wu et al. *J of Biomechanics*, **38**(5), 2006

Table 1: RMSE, correlation and offset (mean±standard deviation) of each IMU model calculated with respect to the optical reference system for both flexion/extension angle (FE) and radial/ulnar deviation angle (RUD) measured during a full ROM wrist flexion/extension movement.

Model	RMSE[°](FE)	RMSE[°](RUD)	R [-] (FE)	R [-] (RUD)	Offset[°](FE)	Offset[°] (RUD)
NP	12.842±5.200	34.762±9.526	0.997±0.004	0.188±0.823	7.396±5.574	10.958±11.460
FC	12.603±2.763	20.751±10.613	0.997±0.006	0.285±0.566	-6.121±8.188	-2.762±14.667
MA	8.760±4.158	26.131±10.245	0.997±0.002	0.782±0.446	1.409±6.105	15.48±10.229
OA	11.591±5.604	34.400±12.633	0.996±0.003	0.225±0.835	-1.226±7.764	8.846±15.820

THREE-DIMENSIONAL SCAPULAR MOTION TRACKING USING INERTIAL MEASUREMENT UNITS: A REGRESSION-MODELLING APPROACH

Zhou Fang[1], Damith Senanayake[1], Peter Lee[1], David Ackland[1]
[1] Department of Biomedical Engineering, The University of Melbourne, Melbourne, Australia.
Email: zhouf1@student.unimelb.edu.au

INTRODUCTION

Skin-marker-based scapular motion measurement can be challenging due to skin-motion artefact. Previous studies have validated the accuracy of optoelectronic-based methods [1] and shown that scapular motion can be predicted using a thorax-humeral regression model with RMS errors of less than 10º [2]. However, optoelectronic systems can be expensive, require considerable technical expertise and are generally confined to the laboratory environment. In recent years, wireless and lightweight inertial measurement units (IMUs) have become increasingly used to address these limitations and provide motion measurement capacity in the home setting. The aim of this study was to develop a scapulo-humeral regression model based on healthy subjects, calculate the three-diamensional scapular motion during daily activities using IMUs, and validate the results against an optoelectronic system.

METHODS

Thirty healthy subjects (age: 28±4 years) were recruited for testing. A set of 11 retro-reflective markers were placed on anatomical landmarks of the right upper limb of each subject. Three bony landmarks of the scapula, the TS (Trigonum Scapulae), AA (Angulus Acromialis) and AI (Angulus Inferior), were digitized at 21 humeral positions using an adjustable scapula locator and a 10-camera video motion analysis system. In addition, two IMUs were placed on the chest and the upper arm of the subjects. The orientations of the IMUs relative to body segments was computed using the ISB recommended coordinate systems [3] via two-stage static poses [4] and a T-pose. Subjects performed a range of activities of daily living including flexion-extension, abduction-adduction, head touching and reaching, synchronised to a metronome. The video motion data was processed using inverse kinematics with subject-specific musculoskeletal models. Then, an averaged regression model derived from 29 subjects was developed to predict scapular protraction, external rotation and tilt in the thorax reference frame given plane of humeral elevation and humeral elevation angle as input. This 'reference-standard' scapular motion was then compared to IMU-based scapular motion measurement, which was calculated by inputting each subject's humeral plane and elevation angles measured by the IMUs into the regression model.

RESULTS AND DISCUSSION

At the humerothracic joint, the RMSE in prediction of plane of elevation and elevation angle during reaching using IMU was 7.60º and 4.19º, respectively (Figure 1). For the scapular angles, the RMSE in prediction of protraction, external rotation and posterior tilt was 1.79º, 1.34º and 1.65º, respectively (Table 1). The reported IMU-based kinematics accuracy at the scapulothoracic joint (< 2º) is considered equivalent to that of direct scapula registration [2].

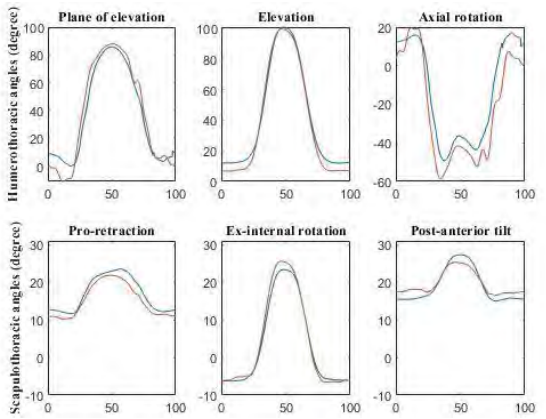

Figure 1 Three-dimensional humerothoracic and scapulothoracic angles during reaching. Horizontal axes: scaled task timeline (%); Blue curves: optoelectronic kinematics; red curves, IMU kinematics.

CONCLUSIONS

This study presents a new method to measure the three-dimensional scapular motion in healthy adults using IMUs and linear regression modelling. Scapula motion can be predicted with accuracy in three rotational degrees-of-freedom with errors less than 2º, which is within the range of optoelectronic motion tracking accuracy. Future studies will focus on evaluation of pathological kinematics, and upper limb muscle force predictions using predicted kinematics.

REFERENCES

[1] Brochard et al. *J Biomech* **44:** 751-754, 2011
[2] de Groot et al. *Clinical Biomech* **16**: 735-743, 2001
[3] Wu et al. *J Biomech* **38:** 981-992, 2005
[4] Palermo et al. *Measurement* **52:** 145-155, 2014

Table 1: 3D RMS error and correlation coefficient (R) of the IMU scapulothoracic angles for a reaching task.

	Pro-retraction	Ex-internal rotation	Post-anterior tilt
RMSE (R)	1.79º (0.987)	1.34º (0.997)	1.65º (0.991)

DO DIFFERENT METHODS FOR MIMU-BASED POSTUROGRAPHY LEAD TO THE SAME RESULTS?

Annamaria Guiotto[1] Elena Pegolo[1] and Zimi Sawacha[1,2]
[1] Department of Information Engineering, University of Padua, Padua, Italy.
[2] Department of Medicine, University of Padua, Padua, Italy.

Email: annamaria.guiotto@unipd.it

INTRODUCTION

Posturography is considered the objective measurement of standing posture control. The main parameters for assessing balance generally are obtained from the center of pressure (COP) (i.e. in time or frequency domain), registered through force/balance plates [1-2] (COP approach, A-COP). In recent years, the extraction of such parameters has been performed through [3]:
- Inertial Measurement Units (IMU) by extracting metrics directly from the acceleration measured through a sensor applied close to the COM [4] (acceleration approach, A-ACC);
- Magneto-IMU (MIMU) by reconstructing the position of the center of gravity (COG - projection of COM on the base of support, COG approach, A-COG) [5-6];
- the center of mass (COM) by registering the trajectory of a marker applied on the 5th lumbar vertebra (L5) with video-based methods [2] (A-L5). The aim of this study was to compare the posturographic parameters calculated with the above mentioned approaches: **1.** A-L5 [2], **2.** A-ACC [4], **3.** A-COG [5], **4.** A-COP [1-2].

METHODS

Thirteen healthy subjects (4M-9M, mean age 27.5±4.3 years, mean BMI 22.5±1.8 kg/m^2, 41.4±1.8 shoe size) stood for 60 seconds in upright position with eyes open and closed (arms along the body, feet 30° appart through a cardboard triangle, looking at a target at eye level, 5 meters away). Data were simultaneously acquired through a MIMU sensor (Muse, 221e srl, Italy, 100 Hz) applied on the L5/COM, fixed through an elastic band (A-ACC and A-COG), through a force plate (Bertec corp, FP6040, 200 Hz) as reference gold standard (A-COP) [2-3] and a stereophotogrammetric system (SMART-D, Bts srl, 200 Hz) (for A-L5). After a calibration refinement, MIMU data were processed as in [4] for A-ACC and by applying a Kalman extended filter for A-COG [5-6]; hence the posturographic parameters were extracted [4]. A-COP and A-L5 parameters were calculated as in [2-3]. Root mean square distance (RMSD) was calculated from the measures obtained in A-L5 and A-COG. Pearson's correlation analysis was performed among all the different posturographic measures.

RESULTS

A RMSD of 22.1±2.1 mm and 26.1±10.7 mm (mean±sd among all the subjects' data) was detected in the medial-lateral and anterior-posterior direction respectively, between A-L5 and A-COG. Results of the Pearson's correlations coefficients showed excellent to good correlation on the ellipse area and sway area between A-COP/A-L5/A-COG, very good correlation on the sway path between A-L5/A-COG, moderate correlation on the ellipse area between A-COP/A-L5/A-ACC (Table 1).

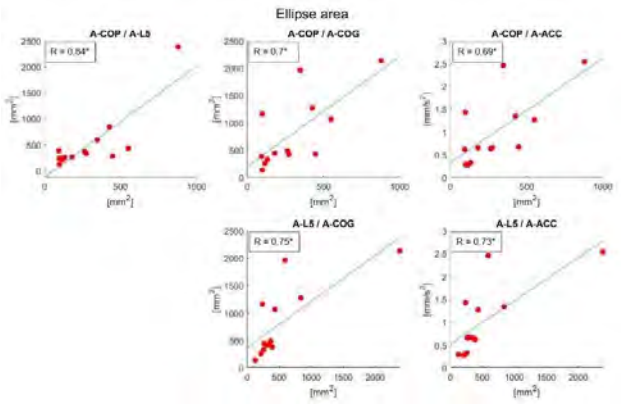

Figure 1. Scatterplot with regression line and Person's correlation coefficient (R). * Statistically significant correlation.

CONCLUSIONS

Results of the correlation between MIMU and the parameters computed through the standard methodology (i.e. A-COP) look promising toward an application in everyday living environments. Further studies are needed to assess their reliability in pathological conditions.

REFERENCES

[1] Chiari, L. et al. *Clin Biomech* **17**, 666–677, 2002.
[2] Romanato M. et al. *Clin Biomech* (in press).
[3] Ghislieri M. et al. *Sensors* **19**: 4075, 2019.
[4] Mancini M. et al., *J Neuroeng Rehab*, 9(1), 59, 2012.
[5] Palmerini, L.et al. *IEEE trans.inf.tech.* **15**,481, 2011.
[6] Caruso, M. et al. *Sensors* **21**, 2543, 202

Table 1: Results of the Pearson's correlation in some parameters as example. Bold numbers indicate a statistically significant correlation.

	A-COP / A-L5	A-COP / A-COG	A-L5 / A-COG	A-COP / A-ACC	A-L5 / A-ACC
Ellipse area	**0.84**	**0.71**	**0.75**	**0.69**	**0.73**
Sway area	**0.90**	**0.83**	**0.95**	0.33	0.46
Sway path	0.35	0.48	**0.83**	-0.45	0.06
AP median frequency	0.13	-0.03	0.19	-0.05	0.00

OPENSIM-BASED ESTIMATION OF LOWER BODY KINEMATICS USING MAGNETO-INERTIAL RECORDINGS – RECOVERY FROM ANKLE FRACTURES AND ACHILLES TENDON RUPTURES AS A PILOT CASE

Olli-Pekka Mattila[1], Paavo Vartiainen[1,2], Toni Mujunen[1], Harri Piitulainen[1], Neil Cronin[1], Taina Rantanen[1] and Timo Rantalainen[1]

[1] Faculty of Sport and Health Science, University of Jyväskylä, Jyväskylä, Finland. [2] Department of Technical Physics, Faculty of Science, Forestry and Technology, University of Eastern Finland, Kuopio, Finland.
Email:timo.rantalainen@jyu.fi

INTRODUCTION

Gait kinematics assessments provide relevant information for evaluating the recovery of lower limb injuries. Optical 3D motion capture is most often used for the purpose but the method is resource-intensive and only applicable in a laboratory setting. Wearable magneto-inertial measurement units (MIMU) could provide a more flexible and cost-effective alternative for gait kinematics evaluation compared to motion capture, however, more work is still required to establish the standard operating procedures that result in valid and reliable kinematics estimates [1]. Therefore, the purpose of the study was to develop a MIMU-based lower body gait kinematics assessment pipeline based on the cutting-edge best practices proposed in the literature (e.g., Opensim/OpenSense) [2]. The pipeline was piloted with apparently healthy adults and in monitoring a series of cases recovering from a lower limb trauma.

METHODS

Six adults with a lower limb trauma (three Achilles tendon ruptures [ATR], three ankle fractures [AF]) and 28 apparently healthy adults (controls) volunteered as participants. The participants were asked to walk 10 times back-and-forth a 20 m long straight path at their preferred/allowed by pain pace. MIMUs (NGIMU, x-io Technologies, UK) recording at 200 Hz were mounted on the feet, legs, thighs, and the waist using elastic Velcro bands. Madgwick's gradient descent algorithm [3] was used to estimate sensor orientations and OpenSim software to provide 3D joint kinematics [2]. Steps were segmented based on distance between virtual OpenSim heel markers. Fukuchi's open optical motion capture-based dataset (N = 42 healthy adults) [4] was used as a reference dataset for the controls.

RESULTS AND DISCUSSION

Some offset and a scaling biases were observed between the controls and the reference data (Figure 1). The step cycle segmentation appeared reasonable as the expected healthy gait flexion patterns were produced for the lower body joints (Figure 1). The AF and ATR cases differed clearly from the controls at 8 weeks post trauma and the kinematics recovered towards that of controls from 8 weeks to 6 months post trauma, although the recovery was heterogeneous. The detected improvements in the joint angles during the recovery were 4–12-fold larger than the minimal detectable change measurable with the MIMU-based method.

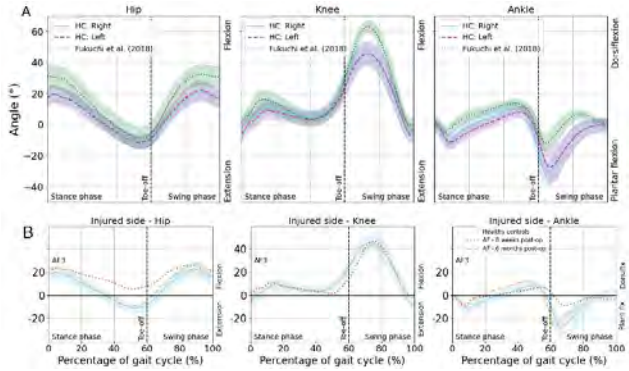

Figure 1 A) Hip (left), knee (mid) and ankle (right) flexion angle of the controls (red) compared to the reference dataset [4] (blue). Systematic offset and scaling biases are evident, however, the expected healthy gait pattern is reproduced. B) An ankle fracture case at 8 weeks (blue controls, red 8 weeks past trauma, yellow 6 months past trauma). Recovery towards the controls' kinematics is evident from 8 weeks to 6 months.

CONCLUSIONS

The simplicity of use and low cost coupled with the present findings warrant further investigation of MIMU-derived gait kinematics for use in applied settings, such as in the clinics, or in the ecologically valid free-living conditions.

ACKNOWLEDGEMENTS

Funding from the Academy of Finland (grant #321336, #326988 #349470), and PROFI funding; The Finnish Cultural Foundation/Edith Sorrin Foundation

REFERENCES

[1] Weygers I et al. *Sensors* **20**: 673, 2020.
[2] Al Borno M et al. *J Neuroeng Rehabil* **19**: 22, 2022.
[3] Madgwick SO et al. *IEEE Int Conf Rehabil Robot* 5975346, 2011.
[4] Fukuchi CA et al. *PeerJ* **6**: e4640, 2018.

BODY SEGMENT ORIENTATION TRACKING WITH IMU: AN ADAPTIVE ROBUST EKF FOR DYNAMIC LONG-DURATION ACTIVITIES

Milad Nazarahari[1] and Hossein Rouhani[1]
[1] Department of Mechanical Engineering, University of Alberta, Edmonton, Alberta, Canada.
Email: hrouhani@ualberta.ca

INTRODUCTION

Wearable inertial measurement units (IMUs) are ideal for human motion analysis, especially for out-of-lab applications. Yet, due to measurement errors of the gyroscope, accelerometer, and magnetometer embedded in an IMU, a sensor fusion algorithm (SFA) is required to estimate the body segment orientation accurately. Despite its importance, the literature lacked a systematic SFA design methodology and benchmarking of SFAs performance. Thus, we developed a full-state robust extended Kalman filter (REKF) and a method for optimal adaptation of its gains (e.g., covariance matrices). Then, we compared the performance of our REKF against three highly-cited SFAs from the literature. Finally, we benchmarked 30+ SFAs against a reference camera motion-capture system. We shared codes and sample data on our lab's website (ncbl.ualberta.ca/codes).

METHODS

We structured a novel full-state EKF by including the orientation quaternion, gyroscope bias, non-gravitational acceleration, and magnetic disturbance in the state vector (hence called a full-state EKF) [1]. 2nd-order strap-down integration of the corrected angular velocity and the 1st-order Markov process of the non-gravitational acceleration and magnetic disturbance were used to construct the state-transition matrix. The measurement-update equation was derived using a single-iteration gradient descent algorithm. Next, we improved the developed EKF to a REKF using H_∞ filter structure (i.e., manipulating the a posteriori error covariance matrix equation) to achieve robust estimations under various motions. To ensure that the REKF performance is not affected by improper gains, we developed a framework (which can be applied to every SFA) for optimal adaptive gain tuning. We used a hard switch with two levels for each gain and optimized the gains and switching thresholds by minimizing the error between the estimated and true orientations [2]. We compared the performance of our adaptive REKF using IMU raw data against three highly-cited SFAs (with optimal gain tuning), including, Madgwick2011, Mahony2008, and SFA from MATLAB Sensor Fusion and Tracking Toolbox; see [1] for further details. Then, after removing the gyroscope bias, we benchmarked 30+ SAF from the literature [3]. Experiments included continuous walking at a normal and fast pace (~10 min) with an IMU attached to the foot.

RESULTS AND DISCUSSION

Table 1 shows the mean (standard deviation) of the root-mean-square error between the estimated and true orientations. Our proposed REFK obtained significantly ($p<0.05$) lower estimation errors for roll, pitch, and yaw angles. Then, using the same data, we showed that removing the gyroscope's static bias before orientation estimation can significantly improve SFAs' accuracy, even for SFAs with a mechanism for online gyroscope bias removal, such as our REKF [4]. We compared the accuracy of estimated orientations by our REFK and 30+ SFAs against a motion-capture system [4]. The median errors between estimated and true orientations for the nine best SFAs (including our REFK) were less than 5 degrees, mainly due to the short duration of tests (~10 min); see [4] for reference to methods and detailed results.

Table 1: Mean (standard deviation) of root-mean-square error of orientation tracking using IMU raw data obtained by various SFAs.

	REKF	Madgwick2011	Mahony2008	MATLAB
Roll	7.3(2.9)	23.2(5.1)	23.8(4.7)	37.9(19.1)
Pitch	6.1(2.0)	22.3(6.1)	21.1(5.7)	16.1(7.8)
Yaw	7.8(3.3)	28.0(7.4)	27.7(7.8)	48.6(23.8)

CONCLUSIONS

This work presents a systematic approach to designing an adaptive REKF and its benchmarking against the literature. We showed that for IMU raw data, our REFK is superior to the literature. We also showed that for ~10 min tests, gyroscope static bias removal effectively reduced the estimation error of SFAs in general. In the future, longer tests (i.e., 30 min to 1 hour) must be performed to reveal the benefits of our full-state REKF with online gyroscope bias estimation and removal.

ACKNOWLEDGEMENTS

Vanier Canada Graduate Scholarship, Alberta Innovates Graduate Student Scholarship, and Izaak Walton Killam Memorial Scholarship financially supported this work.

REFERENCES

[1] Nazarahari M & Rouhani H. *IEEE TNSRE* **29**: 1280-1289, 2021.
[2] Nazarahari & Rouhani H. *IEEE TIM* **70**: 1-13, 2020.
[3] Nazarahari M & Rouhani H. *Information Fusion* **76**: 8–23, 2021.
[4] Nazarahari M. *Ph.D. Thesis, Uni. Of Alberta*, 2021.

BOUT DURATION DURING OUT-OF-LAB WALKING AFFECTS GAIT KINEMATICS

Mayumi Wagatsuma[1], Julien A. Mihy[1], Stephen M. Cain[2] and Jocelyn F. Hafer[1]
[1] Kinesiology & Applied Physiology, University of Delaware, Newark, DE, USA.
[2] Chemical and Biomedical Engineering, West Virginia University, Morgantown, WV, USA.
Email: mayumiw@udel.edu

INTRODUCTION

Gait kinematics differ between in-lab and out-of-lab settings [1,2]. Out-of-lab collections may provide a more complete insight into daily function as opposed to acute in-lab setting designs. Data collected out-of-lab have varying bout characteristics (i.e. time, speed, or step count) and there are no standardized procedures for segmenting or selecting out-of-lab walking data. We do not know how the duration of walking bouts included in analyses affects gait analysis results. Therefore, the purpose of this study was to compare the effects of walking bout duration on gait kinematics among healthy young adults, and older adults with and without knee osteoarthritis (OA).

METHODS

Ten healthy younger (28.1±3.5yrs) and older (60.8±3.3yrs) adults, and seven older adults with knee OA (64.1±3.6yrs) participated in this study. Four IMUs [Opal v2, APDM] were placed on the pelvis, and right (healthy) or more affected (knee OA) limb's thigh, shank, and foot. Participants walked a set, ~10 min route in a campus building. A zero-velocity update algorithm was used to calculate spatiotemporal variables from foot-mounted IMU data [3]. Medial-lateral axes for the pelvis, thigh, shank, and foot were defined using a functional sensor-to-segment alignment [4]. Level strides without turns were selected and walking velocity, stride length, and knee, hip, and ankle angular excursion (ROM) were calculated per stride and averaged for each subject. Variables were compared between long (>60 secs) and short (≤60 secs) bouts among young and older healthy adults, and older adults with knee OA using a 2x3 ANOVA (α=0.05).

RESULTS AND DISCUSSION

Short bouts were 32.1±19.1 sec and long bouts were 188.8±137.6 sec, on average. Walking speed (p<0.001), stride length (p<0.001), knee (p=0.017) and ankle ROM (p=0.012) were greater for the long compared to short bouts (Fig 1). Group x condition interactions were observed for walking speed (p=0.027) and stride length (p=0.036). Healthy older adults had significantly greater walking speed (p<0.001) and stride length (p<0.001) in long compared to short bouts. Older adults with knee OA showed significantly greater walking speed (p=0.001) and stride length (p=0.004) with longer bout duration. Our finding of greater walking speed and stride length with longer bout duration agrees with the suggestion of a previous study [2], but interestingly only for older adults.

CONCLUSIONS

Kinematics differed when out-of-lab gait data were divided into strides that occurred as part of short (≤60 s) or long (>60 s) bouts. Previous studies suggested that most walking bouts in daily life have more variety of bout duration (e.g. <10 secs, <30 secs, < 5 mins, >10 mins, etc.) [2,5,6]. A previous real-world study suggested the use of longer walking duration (10mins) to explain spatiotemporal gait characteristics [6]. We had minimal variability in bout duration length, therefore the out-of-lab setting in this study may not characterize real-world bout duration effectively. Bout duration selection criterion is important and should be carefully considered based on the research question for out-of-lab gait.

REFERENCES

[1] Carcreff et al., Sci Rep 2020, 10(1), 2091
[2] Del Din et al., J Neuroeng Rehabil 2016, 13(1):46
[3] Rebula et al., Gait Posture 2013, 38, 974-980
[4] Mihy et al., medRxiv 2022.11.29.22282894
[5] Baroudi et al., Gait Posture 2022, 98, 69-77
[6]Orendurff et al., J Rehabil Res Dev 2008, 45 (7)

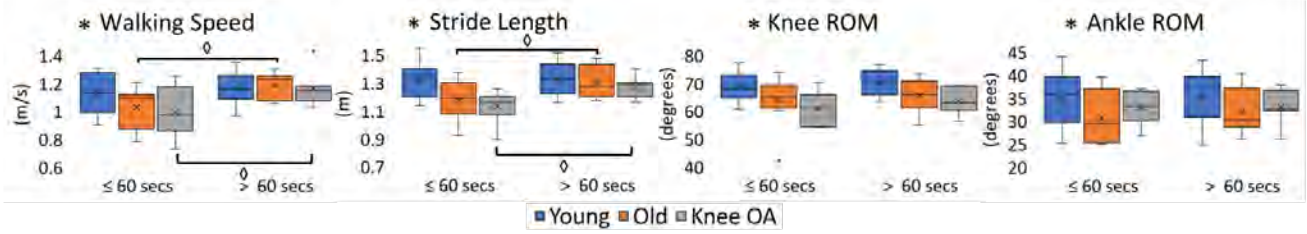

Figure 1: Comparison of gait kinematics between short (≤ 60) and long (>60) bout among healthy young and older adults and older adults with knee OA
* Significant difference between short and long bout durations ◊ Significant post-hoc

ISB RECOMMENDATIONS ON THE ASSESSMENT AND REPORTING OF JOINT KINEMATICS IN HUMAN MOTION ANALYSIS APPLICATIONS USING IMUS

Reed Gurchiek[1], Annegret Mündermann[2], Andrea Cereatti[3], Scott Delp[1], Silvia Fantozzi[4], Fay Horak[5] and Kamiar Aminian[6]
[1] Department of Bioengineering, Stanford University, Stanford, CA, USA.
[2] Department of Orthopaedics and Traumatology, University Hospital Basel, Basel, Switzerland.
[3] Department of Electronics and Telecommunications, Polytechnic University of Turin, Turin, Italy.
[4] Department of Electrical, Electronic, and Information Engineering, University of Bologna, Bologna, Italy.
[5] Department of Neurology, Oregon Health & Science University (OHSU), Portland, OR, USA.
[6] Laboratory of Movement Analysis and Measurement, Ecole Polytechnique Fédérale de Lausanne (EPFL), Lausanne, Switzerland.
Email: gurchiek@stanford.edu

INTRODUCTION

Motion analysis based on the use of inertial measurement units (IMUs) has expanded rapidly in recent years. In both academia and industry, IMUs have enabled development of software applications for joint kinematics estimation targeting the medical, health and wellness sectors. Proprietary algorithms and software or lacking technological transparency of some applications can preclude assessing accuracy, validity, and reliability of the estimated parameters and comparing products and results of research studies. The rapid and growing development of IMUs and related methods has not yet resulted in consistent standards or recommendations of use. Proper use of IMUs relies on knowledge of sensor calibration procedures, data fusion algorithms, biomechanical models, reporting kinematic variables, and validation procedures. Hence, there is an urgent need to define standards and reporting guidelines for IMU-based kinematic analysis. The aim of this project is to develop these standards and recommendations incorporating feedback from the ISB community.

RECOMMENDATIONS

Following the procedure to propose an "ISB Recommendations" paper [1], our written proposal has been reviewed and approved by the ISB committee. Our recommendations address basic principles and serve generally as reporting guidelines. We maintain consistency with established standards in human motion analysis where appropriate and have organized our recommendations under five topics described here.

Measurement device. Estimation performance depends on the hardware specifications of the device and the mechanism of bodily attachment. These specifications comprise parameters of the measurement model and are often calibrated (e.g., sensor bias and sensitivity). Our recommendations encourage reporting hardware specifications (sampling rate, range, noise levels, etc.), calibration procedures, sensor attachment modalities and synchronization for multi-sensor configurations.

Kinematic model. As for any kinematic analysis, the adoption of joint kinematic models facilitates interpretation of the results and provides the basis for implementing the subsequent stages of the analysis. Our recommendations concern describing the kinematic model, its parameterization, and joint and segment coordinate systems.

Sensor to segment calibration. This is to determine the orientation and position of sensor axes relative to joint/anatomical coordinate systems. It enables a biomechanical and clinical interpretation of sensor measurements. Our recommendations will support continued advancement in this field and encourage reporting the calibration procedures, algorithms, and justification based on the kinematic model.

Signal processing. Many algorithms exist for estimating kinematic variables with IMU data (e.g., Kalman filtering/smoothing, global optimization methods) with customization for specific tasks and/or joints. We encourage a clear description of the algorithm that is fully reproducible and (where applicable) the process for adjusting tuning parameters of the algorithm.

Assessment of validity and reliability. This concerns the correct use of the reference system for comparison and the related statistical characterization of estimation errors assessed by a range of different metrics and analyses. We encourage a description and justification of the statistical analysis, a clinically meaningful interpretation of errors, and description of the reference system used for comparison.

DISCUSSION & CONCLUSION

Our intent is to advance the field and maximize transparency, reproducibility, generalizability, and validity of joint kinematics estimated using IMUs. Although several other societies have shown interest in the use of IMUs, biomechanically grounded ISB recommendations would be most effective in establishing good practice for both biomechanics and human health research.

REFERENCES

[1] isbweb.org/activities/to-propose-an-isb-recommendation-paper

Summary

Join us for an enlightening symposium dedicated to the Biomechanics of Ankle Injuries. This event, open to medical practitioners, researchers, sports professionals, healthcare industry stakeholders, and footwear manufacturers, brings together the latest in biomechanics and its role in better understanding, treating, and preventing ankle injuries.

One of the highlights of this event will be an in-depth exploration of lateral ankle sprains, a common yet misunderstood injury. Our invited speakers will debunk pervasive myths, presenting detailed video analyses that demonstrate how these injuries are not merely the result of bad landings. This topic will provoke a vital discussion about preconceptions and open up new perspectives on the causes of these injuries.

The symposium will delve into the relationship between physical fatigue and increased risk of ankle sprains, using badminton as a case study. It will illuminate the biomechanical shifts occurring under fatigue conditions, providing crucial insights for athletes and trainers.

We'll also bring the spotlight onto the shoe-surface interactions, emphasizing their importance in ankle sprain injuries. Attendees will gain an understanding of how friction can be a game-changer, transforming their view on injury prevention and footwear choice.

The prevention of sports injuries in youth athletes, particularly lateral ankle sprains, is a pressing issue. Additionally, we will explore the critical role of diaphragm function and how it influences chronic ankle instability. This intriguing talk will delve into the physiological connections between our respiratory system and ankle stability, offering insights that could significantly inform rehabilitation strategies and injury prevention.

The symposium will wrap up with an engaging networking and co-creation session, providing a platform for speakers and attendees alike to exchange ideas, foster collaborations, and spark innovative research projects in the fascinating realm of ankle injury biomechanics.

This symposium promises a dynamic learning environment, networking opportunities, and the chance to reunite with members of the International Ankle Consortium. We look forward to welcoming you to the ankle injury symposium.

Kind regards,
Filip Gertz Lysdal, Alexis Herbaut, and Masafumi Terada

Latest updates for recording, analysis, and interpretation of electromyographic (EMG) data: in the lab and the clinic

International Society of Electrophysiology and Kinesiology

Tucker K[a], Hodges P[a], Elisa Romero Avila[b], Dick T[a], Nishikawa Y[c], Watanabe K[d]

[a] University of Queensland, Australia, [b] RWTH Aachen University, Germany, [c] Kanazawa University, Japan, [d] Chukyo University, Japan

Email: isek@podiumconferences.com

ISEK

The International Society of Electrophysiology and Kinesiology (ISEK) is a multidisciplinary organization composed of members from all over the world in health-related fields and basic science with a common desire to study human movement and the neuromuscular system.

The purpose of the Society is to promote research and teaching in the disciplines of Electrophysiology and Kinesiology in normal, experimental, and pathological conditions of the sensory and motor systems, with emphasis on the interactive use of the two disciplines.

With this purpose in mind, the ISEK-ISB joint symposium aims to bring together experts from around the world to discuss the use of electromyography.

This symposium will include:

(i) A short introductory presentation about ISEK by their current vice president A/Prof Kylie Tucker
(ii) An introduction to the Consensus for Experimental Design in Electromyography (CEDE) project by Professor Paul Hodges
(iii) A presentation by Dr. Taylor Dick about gaining consensus through this process with regard to using EMG to estimate muscle force
(iv) An overview of Surface EMG in Clinical Assessment and Neurorehabilitation by M.Sc. Elisa Romero Avila.
(v) A series of talks from those submitted to ISB including the use of high-density EMG in biomechanics, by Professor Kohei Watanabe[7] and clinical assessments by Dr. Yuichi Nishikawa[8].
(vi) A moderated panel discussion (chaired by A/Prof Tucker) where the attendees can ask questions about the use of EMG
(vii) And, will finish up with an invitation to attend the ISEK congress, to be held in Japan in 2024 by Professor Kohei Watanabe.

What is EMG?

Electromyography (EMG) is a tool used to record the electrical activity produced by skeletal muscles. It typically involves placing surface electrodes on the skin above a test muscle, or needle electrodes within the muscle, with the aim to detect the electrical signals generated by muscle fibers during their contraction.

EMG may be used in a variety of clinical and research settings to evaluate muscle function and assist with the diagnosis of neuromuscular disorders. EMG is most typically used by researchers to detect the timing and pattern of muscle activation during different tasks.

What is the CEDE project?

The CEDE project is an international initiative aimed at promoting standardization and best practices in the use of electromyography (EMG) for research and clinical purposes. The project involves a collaborative effort by experts in the field of EMG.

Through the CEDE project, consensus on the essential components of experimental design and methodology for EMG research has been reached. This includes defining the key parameters to be measured, selecting appropriate recording equipment and techniques, and establishing standardized protocols for data analysis and interpretation.

To date, the CEDE project, led by Professor Paul Hodges and coordinated by Dr. Manuela Besomi, has included a series of workshops, online surveys, and expert consensus meetings to establish best practices and recommendations for EMG research. Most recently, the team has called for researchers working with EMG and interested in translating the latest research into practice, to take part in a collaborative project with CEDE team members to develop knowledge translation strategies for CEDE.

CEDE project has resulted in six publications[1-6] in the Journal of Electromyography and Kinesiology (JEK) since 2019, including a consensus statement on electrode selection[1], normalisation[2], terminology[4], the use of HDsEMG[5], and identifying single motor unit beahviour[6].

REFERENCES

[1]Besomi M *et al*, 2019, *JEK;* [2]Besomi M *et al*, 2020, *JEK;* [3]Hodges PW, 2020, *JEK;* [4]Mcmanus L *et al*, 2021, *JEK;* [5]Gallina A *et al*, 2022, *JEK;* [6]Martinez-Valdes E *et al*, 2023, *JEK;* [7]Watanabe et al. *2021 ESSR;* [8]Nishikawa et al. *Clin Neurophysiol 2022.*

ACKNOWLEDGMENTS

The CEDE project is supported by:

Summary

The Comparative Neuromuscular Biomechanics Working Group of the ISB is excited to present CNB-ISB II in Fukuoka! The CNB-ISB meeting will feature synergistic research in comparative (non-human) and human biomechanics. The meeting will center on three themes: 1) direct in vivo and ex vivo experimental approaches; 2) computational modelling; 3) robotic/engineering approaches to understanding muscle function in movement. In particular, we will focus on areas where coordination between fields offers potential for innovation.

The meeting consists of three thematic keynote presentations and accompanying oral presentations, as well as a moderated 'flash' poster presentation session (see program schedule). Dedicated time is set aside to allow for Q&A and discussion.

The CNB aims to increase the visibility of comparative biomechanics and neuromechanics at the ISB. Our goal is to accelerate cross-pollination between comparative and human biomechanics fields. We believe that an exchange between comparative and human research fields will accelerate discovery, both of biomechanical principles as well as novel health and engineering applications.

[The CNB-ISB II Fukuoka meeting is sponsored by the ISB and the Journal of Experimental Biology; The Company of Biologists]

Get real: New experiments, models and parameters for understanding in vivo muscle function

Kiisa Nishikawa[1], Siwoo Jeong[2], Caitlin Bemis[1], Monica Daley[3] and Simon Sponberg[4]
[1] Department of Biological Sciences, Northern Arizona University, Flagstaff, USA.
[2] Department of Physical Therapy, Jeonju University, Jeonju, Korea.
[3]Department of Ecology and Evolutionary Biology, University of California, Irvine, USA
[4]School of Physics and Department of Biological Sciences, Georgia Institute of Technology, Atlanta, GA, USA
Email: Kiisa.Nishikawa@nau.edu

INTRODUCTION

Several recent studies have combined in vivo measurements of muscle fascicle length, force and activation with different Hill-type muscle models [1,2,3]. While the results vary among studies, the relatively low accuracy of in vivo force predictions suggests that key features of muscle function are not captured by existing models. Here, we use ex vivo data from cockroaches [4] and mice [5], and in vivo data from guinea fowl [6] to explore new experiments and models that suggest alternative approaches for predicting muscle force during in vivo movements.

NEW EXPERIMENTAL APPROACHES

To provide insights into in vivo muscle function, experiments should include perturbations that emulate in vivo conditions. We performed three experiments. First, we used ex vivo data from cockroach leg muscles (Fig. 1) that were stretched at the same length and phase of activation in work loops over a range of frequencies [4]. These experiments challenge Hill models because length, velocity and activation are constant, so Hill model-predicted force must also be constant. Yet, the observed force depends on frequency (Fig. 1, right).

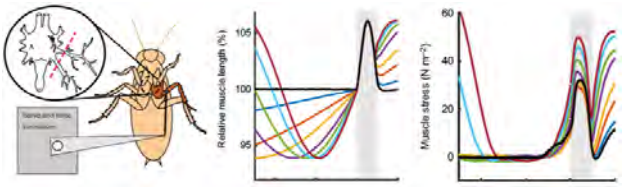

Figure 1 Cockroach stretch perturbation experiments from [4]. **Left**: In situ preparation. **Center**: Length vs. time. **Right**: Force vs. time.

Next, we investigated how the muscle force response depends on stiffness, activation, and length perturbations [5]. Submaximal isometric contraction was established for mouse soleus muscles, followed by active shortened at three velocities. Muscle stiffness increased with activation but decreased as shortening velocity increased. The results suggest that length history determines muscle stiffness, and that history-dependent stiffness influences the contributions of both activation and length perturbations to muscle force.

Thirdly, we used length and activation inputs from guinea fowl running on a treadmill with obstacle perturbations [6] as input parameters in ex vivo work loop experiments using mouse extensor digitorum longus (EDL) as an avatar.

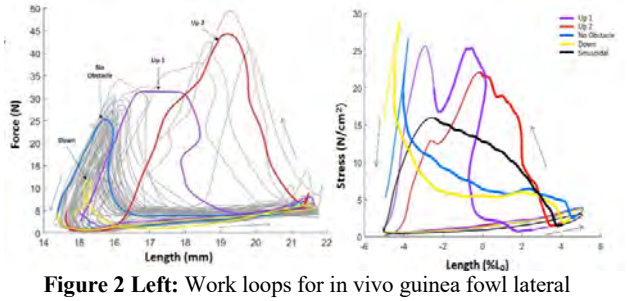

Figure 2 Left: Work loops for in vivo guinea fowl lateral gastrocnemius muscles during treadmill running over obstacles. **Right**: Mouse EDL muscles with the strain and constant activation.

ALTERNATIVE MUSCLE MODELS

We modelled data from in vivo guinea fowl and ex vivo experiments using 1st, 2nd, and 3rd order Hill-type models [3], phenomenological models that included muscle equilibrium length as a parameter [4,5], and a titin-inspired muscle model. We compared R^2 and RMSE among the different models, quantified overfitting using a training/testing protocol, and evaluated the biological relevance of the models by determining the effects of removing selected parameters.

CONCLUSIONS

R^2 increased as the order of Hill-type models increased, but overfitting also increased and biological relevance decreased with the order of the model. Phenomenological and titin-inspired models predicted muscle force with higher R^2 and lower RMSE than all Hill-type models, suggesting that muscle equilibrium length is a useful parameter for predicting history-dependence of muscle force. Calcium-dependent titin-actin binding and interactions between cross-bridges and titin have been suggested as factors that may regulate the equilibrium length of muscle sarcomeres.

ACKNOWLEDGEMENTS

Funded by NSF IOS-2016049 and NSF DBI-2021832.

REFERENCES

[1] Lee et al. 2011. *J Biomech* 46:2288-2295.
[2] Dick et al. 2017. *J. Exp. Biol.* **220**, 1643–1653.
[3] Wakeling et al. 2021. *J. Biomech.* **117**, 110242.
[4] Libby et al. 2020. *J. Exp. Biol.* **223**, 509646.
[5] Jeong & Nishikawa. 2023. *J. Exp. Biol.* In press.
[6] Daley & Biewener. 2011. *Phil. Trans. R. Soc. B* **366**, 1580–1591.

3D WHOLE MUSCLE SHAPE CHANGES – EXPLORING A NOVEL APPROACH

Jeroen Aeles[1,2], Peter Aerts [1,3], and Sam Van Wassenbergh[1]
[1] Department of Biology, University of Antwerp, Antwerp, Belgium.
[2] Department of Movement and Sport Sciences, Vrije Universiteit Brussel, Brussels, Belgium.
[3] Department of Movement and Sports Sciences, University of Ghent, Ghent, Belgium.
Email: Jeroen.aeles@vub.be

INTRODUCTION

When animals, including humans, move, their muscles contract, and by doing so change shape. While such shape changes are obvious and are inevitable for a muscle when generating force, we know little about its functional role in force production. Little is currently known about 3D whole muscle shape changes, which are evidently complex and non-linear in nature. The ability to ultimately measure shape changes during contraction would drastically improve our understanding of *in vivo* muscle biomechanics. Here we explore a novel approach for experimentally measuring 3D whole muscle shape changes using X-ray imaging. We present preliminary data on a validation experiment.

METHODS

Fresh cadaveric lower limbs of the domestic chicken (*Gallus gallus domesticus*) were used for this experiment. After surgically opening the skin over the posterior side of the lower leg, and removing most of the connective tissue surrounding the muscle, 35 opaque beads (⌀ = 0.35mm) were fixated all around the lateral gastrocnemius with a cyanoacrylate. The distal gastrocnemius tendon was severed distally as well as at the muscle-tendon junctions of the other gastrocnemius muscles. Two beads were implanted into the tendon, and three into the distal tibia (reference). Barium sulphate powder was applied to the entire muscle. High-speed stereo (3D) X-ray videos (750Hz) were recorded while the muscle was stretched cyclically by applying a force on the tendon. Ultrafast computed tomography (<2s) scans were reconstructed from images acquired while rotating the lower leg 360 degrees approximately along its longitudinal axis, with the muscle at resting length. 39 out of the 40 markers (beads) were successfully tracked during two shortening-lengthening cycles using XMALab [1]. The 3D Euclidean distance between each of the 35 muscle markers and the most distal reference marker was calculated for the entire cycle, and compared between the start and end of the cycle. CT slices were segmented in Matlab with Sashimi V1.1 [2].

RESULTS AND DISCUSSION

The distal tendon marker was used as a reference for the stretch-shortening cycles. This marker was displaced along the muscle-tendon line of action over 8.30 and 8.34 mm in cycle 1 and 2 respectively. One of the 34tracked muscle markers only had a displacement of 2.14 and 2.18 mm over cycle 1 and 2 respectively, which was considered too small given the amplitude of the displacement of the reference marker. On closer inspection, it appeared the marker got detached from the muscle and was therefore removed from further analyses. Of the remaining 33 muscle markers, the displacement ranged from 6.15 to 8.86 mm and from 6.11 to 9.05 mm for cycle 1 and 2 respectively.
Very small differences in the distance between the muscle markers and the distal reference marker were found when comparing the distance at the start and end of each cycle (mean: 0.07 ± 0.12 mm and 0.05 ± 0.05 mm for cycle 1 and 2 respectively), indicating no shifts in bead placement along the muscle surface.

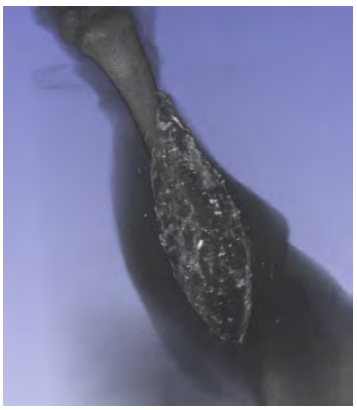

Figure 1 CT reconstruction of the gastrocnemius muscle.

CONCLUSIONS

These preliminary results suggest that the proposed approach can be used to track 3D whole muscle shape changes dynamically, at least during muscle stretching. Currently, we are working on comparing the 3D whole muscle shape between the CT reconstructed scans and reconstructed muscle shapes based on the marker data, as well as creating statistical shape models of these data. Ultimately, we aim to validate this technique for muscle shortening and *in situ* muscle contraction induced by electrical stimulation.

ACKNOWLEDGEMENTS

This research was funded by the European Commission through a Marie-Skłodowska Curie Actions Individual Fellowship to J Aeles. We thank Dr J Sanctorum of DynXLab for assistance in the CT reconstructions.

REFERENCES

[1] Knörlein BJ et al. *J Exp Biol* **219**: 3701-3711, 2016.
[2] Bolsterlee B. https://github.com/bartbols/SASHIMI

DIRECT IN VIVO ASSESSMENTS OF PLANTAR FLEXOR FUNCTION TO GUIDE PATIENT CARE

My My Tang and Josh R. Baxter
Department of Orthopeadic Surgery, University of Pennsylvania, Philadelphia, Pennsylvania, USA
Email: josh.baxter@pennmedicine.upenn.edu

INTRODUCTION

Achilles tendon ruptures are devastating injuries that cause long-term functional deficits in two-thirds of patients. Treatment for these injuries in the United States focuses on surgical care within the first 7 days of injury and rehabilitative care during the first 10 weeks of injury. Our thorough investigation of the literature and clinical collaborations suggest that new research models are needed to mechanistically establish optimal treatment strategies. This current study aimed to build confidence in a rat model to test the effects of surgical repair and rehabilitation loading. In this symposium presentation, we will describe our small animal dynamometer, how we use it, and why we think it will strengthen our clinical studies and impact patient care. We tested 2 hypotheses: 1) plantar flexor deficits are caused by an acute Achilles tendon rupture and 2) that repairing the rupture will mitigate some of the functional deficits compared to non-surgical treatment.

METHODS

We designed, fabricated, and validated a small animal dynamometer (see [1] for complete description and validation data). We surgically induced Achilles tendon ruptures in 20 adult male Sprague Dawley rats and repaired the rupture in half of these animals. Then, all animals completed 2-weeks of joint immobilization in plantarflexion followed by 2-weeks of unrestricted cage activity. We quantified isometric plantar flexor torque across the range of ankle motion by maximally stimulating the sciatic nerve. We approximated plantar flexor work as the summed area under the torque-angle curve because patient functional deficits are typically quantified by heel raise height ability. Estimating potential plantar flexor work is a good surrogate measure of this clinical test.

RESULTS AND DISCUSSION

Plantar flexor deficits following non-surgically repaired Achilles tendon ruptures in rats (n=10) closely match our dynamometer measurements we collected in a cohort of patients that were also treated non-surgically [1]. These findings are important because they establish this animal model as a clinically relevant model beyond it's typical use to study isolated Achilles tendon healing biomechanics. Because we have confidence in this animal model, we can now test the isolated effects of different clinical parameters and treatment strategies on functional outcomes. In this first set of experiments, we tested the isolated effects of surgically repaired the ruptured tendon followed by 2-weeks of unloaded immobilization. We found that animals who were surgically repaired suffered plantar flexor functional deficits compared to the control limb, but these functional deficits were lessened compared to animals that were treated non-surgically ($p = 0.037$, **Figure 1**).

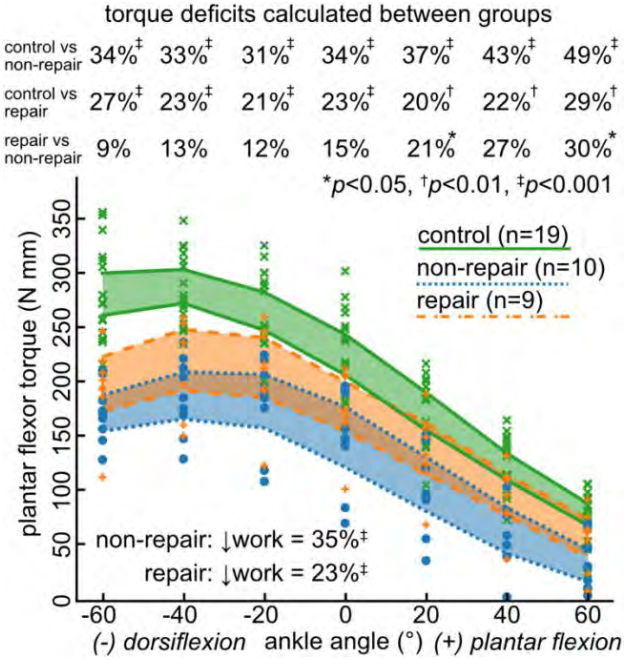

Figure 1. Plantar flexor function across the ankle range of motion decreased following Achilles tendon injury. These functional deficits were lessened in animals that were surgically repaired suggesting that stabilizing the tendon immediately following injury improves muscle-tendon healing.

CONCLUSIONS

Achilles tendon ruptures are typically viewed as an isolated tendon injury. But clinical observations [2] and our small animal experiments suggest that changes to muscle structure explain functional deficits. Our findings support surgical treatment to minimize functional deficits following Achilles tendon ruptures. This model system provides a unique opportunity to understand the basic mechanisms that govern muscle-tendon structure and function across multiple species. Our ongoing work is defining the link between tendon injury, rehabilitation loading, and muscle remodeling.

ACKNOWLEDGEMENTS

Funding support NIH/NIAMS K01AR075877, R21AR081497, and P30AR069619. Liala Sofi, and Ahmad Hammo assisted in animal care and experiments.

REFERENCES

[1] Tang MM+ *J Biomech* **145**: 111393, 2022.
[2] Hullfish TJ+ *J Appl. Physio* **127**:4 1005-1011, 2019

TASK-LEVEL FEEDBACK CONTROL OF GAIT IS AN EMERGENT PROPERTY OF EFFORT MINIMIZATION IN THE PRESENCE OF NOISE

Friedl De Groote[1], Tom Van Wouwe[2] and Lena Ting[3]

[1] Department of Movement Sciences, KU Leuven, Leuven, Belgium.
[2] Department of Bioengineering, Stanford University, Stanford, California USA.
[3] W.H. Coulter Department of Biomedical Engineering, Emory University and Georgia Institute of Technology, Atlanta, Georgia, USA.
Email: friedl.degroote@kuleuven.

INTRODUCTION

Deterministic simulations of human and animal locomotion based on effort minimization capture many features of experimentally observed gait mechanics and energetics. However, such simulations do not capture how locomotion is stabilized against sensorimotor noise or external perturbations. The ankle torque response to perturbations of walking balance can be explained by delayed feedback from center of mass (CoM) kinematics [1]. Here, we tested whether this apparent center of mass control strategy emerges from minimal effort simulations of walking in the presence of noise.

METHODS

We performed stochastic optimal control simulations based on a torque-driven skeletal model with five segments (trunk, upper legs, and lower legs) and five degrees of freedom (stance ankle angle, knee angles, and hip angles) [2]. Torques were controlled by feedforward and full state (joint angles and angular velocities) time-varying linear feedback and were corrupted by Gaussian noise. The reference state trajectory for the feedback controller was the state trajectory that would result from applying the feedforward torques in the absence of noise. We solved for control parameters, i.e. feedforward torque trajectories and time-varying feedback gains, that minimized a cost function while imposing mean stride time, mean stride length, and left-right symmetry (of the state distribution) using our recently developed framework for stochastic optimal control [3]. We considered two cost functions. (1) Minimizing expected effort resulted in a minimal effort controller. Effort was modelled as the sum of squared total (feedforward and feedback) torques. (2) Minimizing a weighted sum of feedforward effort and deviations from the reference state trajectory resulted in a trajectory controller. We then generated forward simulations of unperturbed and perturbed walking using the two optimal control laws. Perturbations consisted of support surface accelerations and decelerations of different magnitudes, similar to an experimental protocol we previously applied [1]. We evaluated whether CoM kinematics feedback could explain stance ankle feedback torques in the simulated dataset.

RESULTS AND DISCUSSION

The stochastic optimal control laws stabilized walking across a range of perturbations even though only motor noise was accounted for during the optimization. The feedback ankle torque could be explained by CoM feedback for the minimal effort controller (R^2 = 0.99) but not for the trajectory controller (R^2 = 0.18) (Figure 1).

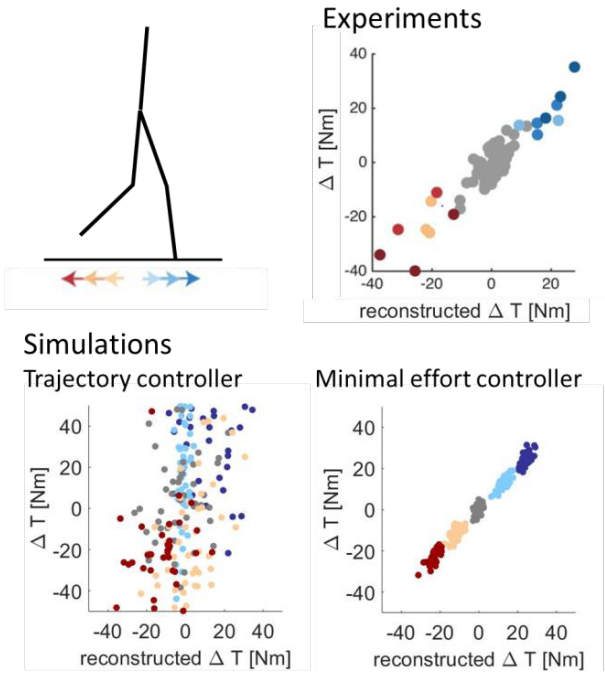

Figure 1 Experimental/simulated feedback torques versus best reconstruction by a linear sum of CoM position and velocity.

CONCLUSIONS

Task-level feedback control for stability is an emergent property of effort minimization in the presence of noise.

ACKNOWLEDGEMENTS

Supported by FWO G088420N.

REFERENCES

[1] Afschrift et al. *PLoS Comput Biol* **17**: 6, 2021.
[2] Kelly. *SIAM REVIEW* **59**: 4, 2017.
[3] Van Wouwe et al. *PLoS Comput Biol* **18**: 61, 2022.

Biophysical muscle models for simulating muscle and muscle spindle response to stretch

Surabhi N. Simha[1], Kenneth S. Campbell[2], Timothy C. Cope[1] and Lena H. Ting[1]
[1] Department of Biomedical Engineering, Emory University and Georgia Institute of Technology, Atlanta, USA
[2] Division of Cardiovascular Medicine, University of Kentucky, Lexington, USA
Email: ssimha@emory.edu

INTRODUCTION

The fastest two mechanisms that the body uses to recover from a physical perturbation are muscle response to stretch and stretch reflex. Muscle short-range stiffness—rapid, large, and brief increase in force due to cross-bridge dynamics in response to a stretch—is important in both these stabilization mechanisms. However, Hill-type muscle models, based on steady-state forces, do not exhibit short-range stiffness. De Groote et al. phenomenologically added short-range stiffness to a Hill-type model to better predict the initial joint torque and kinematics in a biomechanical model of perturbed balance [1]. Short-range stiffness is also critical in muscle spindle response to stretch, as muscle spindles contain *intrafusal* muscle fibres innervated by sensory neurons, that together drive the stretch reflex. Blum et al. found that these sensory neurons' output can be predicted as a linear sum of force and rate of change of force—yank—from the intrafusal fibres [2]. Despite the significance of muscle short-range stiffness to perturbation responses, we lack widespread use of muscle models capable of predicting short-range stiffness in musculoskeletal modeling.

Biophysical muscle models predict short-range stiffness as emerging from cross-bridge dynamics, making them generalizable across fibre types and behaviors. Short-range stiffness arises when the number of bound cross-bridges is high, e.g., in isometric muscle. It rapidly decreases when sarcomeres are stretched beyond a few nanometres and cross-bridges detach. Here, we compared muscle force response to stretch using biophysical and Hill-type models. We then varied the contractile properties of a biophysical model to evaluate their effect on sensory signals from a muscle spindle.

METHODS AND RESULTS

We used a ramp-and-hold protocol to evaluate muscle response to stretch. Using MATMyoSim, we parameterized a biophysical model to match force from an isolated rat soleus muscle fibre when it was stretched at constant velocity (ramp) and then held stationary (hold) (Fig. 1A). To compare the biophysical and Hill-type models' response to stretch, we generated force-length and force-velocity curves from the biophysical model. We found that, in the biophysical model, force rose sharply at ramp onset, continued a slower rise through ramp, and dropped slowly at hold (Fig. 1A, green). In contrast, force in the Hill-type model rose sharply at ramp onset, plateued through ramp, and dropped quickly at hold (Fig. 1A, purple). Unlike the Hill-type model, the biophysical model also predicted empirically-observed changes in short-range stiffness with muscle activation and prior movement [3].

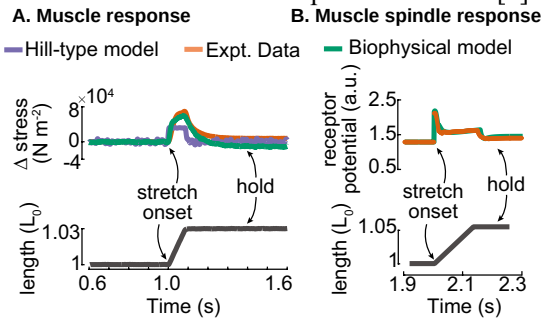

Figure 1: Top rows show experimental data and modelling results of muscle force (left) and muscle spindle sensory output (right) in response to muscle stretch as shown in the bottom rows.

We used a similar ramp-and-hold protocol to evaluate muscle spindle response to stretch. We tuned two biophysical models and used them to predict a phenomenological receptor current, modeled as a weighted sum of the force and yank of a dynamic bag1 fibre, and the force of a static bag2/chain fibre [2]. We tuned the biophysical model parameters to match experimentally measured Ia afferent output from the soleus muscle of an anaesthetized rat in response to a ramp-and-hold stretch (Fig. 1B). Intrafusal fibres express a broad range of myosin types; in our model, varying actin and myosin properties changed the predicted Ia sensory output. The model also predicted empirically-observed dependencies of muscle spindle sensory output on muscle inter-stretch interval, pre-stretch amplitude, sinusoidal stretches, and alpha and gamma drive [2]; such dependencies in behaviorally-relevant conditions would not arise using Hill models.

CONCLUSION

Biophysical muscle models are generalizable across fibre types and behaviors. They may help generate testable predictions about the role of muscles and muscle spindles in sensorimotor control.

ACKNOWLEDGEMENTS

Supported by NIH R01 HD090642.

REFERENCES

[1] De Groote et al. *J Biomech* **52**: 71-7, 2017
[2] Blum et al. *Elife* **9,** 2020
[3] Horslen et al. *bioRxiv*, 2022

Muscle Force Estimation using Convolutional Neural Networks and Hill-Type Models

Anne D. Koelewijn[1], Maria Eleni Athanasiadou[1], and Monica A. Daley[2]
[1] Department Artificial Intelligence in Biomedical Engineering, FAU Erlangen-Nürnberg, Erlangen, Germany
[2] Department of Ecology and Evolutionary Biology, University of California, Irvine, California, USA.
Email: anne.koelewijn@fau.de

INTRODUCTION

Musculoskeletal simulations are gaining popularity for movement predictions and reconstructions (e.g. [1]). These models are usually actuated using Hill-type muscle models. Hill-type models are fitted to static experimental muscle data [2], and could therefore be viewed as early machine learning models. Since different datasets have been used for this fitting process, many variations of the Hill-type model exist [3], while validations and comparisons are limited. Furthermore, static data, and thus Hill-type models, do not represent certain dynamic aspects of muscle mechanics (e.g. [4]). Therefore, we would like to (1) compare the quality of force estimations of different Hill-type model variations, and (2) investigate if we can outperform Hill-type models using a modern machine learning model.

METHODS

We used a dataset of muscle fibre length and velocity (sonomicrometry), activation (electromyography), and tendon force (tendon buckle) of five guinea fowls who ran with different speeds on level surfaces, and surfaces with a sudden height increase or obstacle [5]. Here, we mainly use data of the lateral gastrocnemius of one bird, running at 1.8 m/s and 3.8 m/s on the level surface.

For (1), we implemented 6 different Hill-type models from literature [1, 6-10]. For model [9], we adapted the slack length of the parallel elastic element to 1.2 l_{opt} to obtain realistic forces. We estimated muscle force for each of these models for the trial at 3.8 m/s and compared those forces to the experimental forces.

For (2), we trained a convolutional neural network (CNN) to estimate muscle force from activation, muscle length and velocity using the 1.8 m/s trial. We optimized hyperparameters with a Bayesian approach and an 80/20 data split. We tested the CNN using the trial at 3.8 m/s.

RESULTS AND DISCUSSION

We found comparable mean absolute errors and correlations between three Hill-type models [1,6,7], a higher error and lower correlation for models [8,9], and the worst performance for model [10]. The CNN model matched the experimental data better (Figure 1), leading to the smallest error and highest correlation (Table 1).

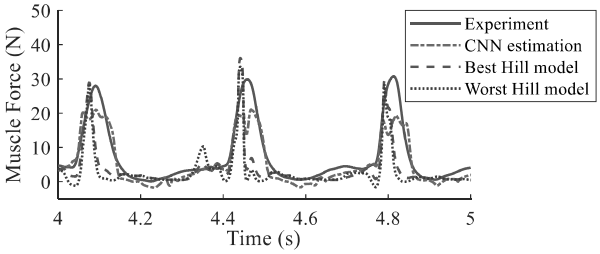

Figure 1 Experimental and estimated muscle force with the Hill-type model with lowest and highest error, as well as the CNN

In this abstract, we have tested the CNN on data of the same muscle and bird. However, for movement simulations, training cannot be performed for each species and their muscles. When we tested on data of another muscle (digital flexor) in another bird, we found that the CNN still outperformed the Hill-type models, but the errors and correlations were more similar.

CONCLUSIONS

We have shown that muscle force estimation lead to small differences between different variations of Hill-type models. The resulting effect on simulation outcomes should be further investigated. We also found that a CNN outperforms Hill-type models. Therefore, more accurate muscle models could potentially be developed using modern machine learning and representative datasets of muscle force generation.

ACKNOWLEDGEMENTS

We acknowledge Jessica Korten's contribution to the Hill-type model comparison.

REFERENCES

[1] Koelewijn AD & Van den Bogert AJ. *Gait & Posture* **49**: 219-225, 2016.
[2] Hill AV. *Proc Roy Soc B* **126**: 136-195, 1938
[3] Miller, Handbook of Human Motion 373-394, 2018.
[4] Abbot BC & Aubert XM. *J Physiol* **117**: 77, 1952.
[5] Daley MA & Biewener AA. *J Exp Biol* **206**: 2941-2958, 2003.
[6] Wakeling J et al. *Ann Biomed Eng* **40**: 1708-1720, 2012.
[7] Esposito ER & Miller RH. *PloS One* **13**: e0191310, 2018.
[8] De Groote F et al. *Ann Biomed Eng* **44**: 2922-2936, 2016.
[9] Geyer & Herr, *IEEE TNSRE* **18**: 263-273, 2010.
[10] Thelen DG. *J Biomech Eng* **125**: 70-77, 2013.

Table 1: Correlation and mean absolute error in muscle force for Hill-type models and the CNN

	Model [1]	Model [6]	Model [7]	Model [8]	Model [9]	Model [10]	CNN
Correlation	0.65	0.65	0.65	0.59	0.60	0.52	0.88
Mean absolute error (N)	3.75	3.75	3.89	3.82	3.92	4.46	2.44

FROGS AS MODELS FOR ROBOTICS, LIMB CONTROL AND MUSCULAR AGEING

Christopher T. Richards[1]
[1] Comparative Biomedical Sciences, The Royal Veterinary College, London, UK.
Email: ctrichards@rvc.ac.uk

INTRODUCTION

Frogs are known for their stunning diversity in ecology and locomotor behaviour, despite conserved musculoskeletal features across thousands of species. Even frogs of a single species have impressively versatile limbs; they can perform multiple locomotor tasks with little evidence of functional tradeoffs. Frogs are thus an ideal model for studying how vertebrate limbs achieve mechanical multifunctionality. In this talk, I will discuss the integration of experimental, computational and robotic techniques to a) better understand the neuromuscular and biomechanical basis for limb multifunctionality (i.e. swimming versus jumping versus walking) and b) develop hybrid experimental-computational tools to ultimately explore how limb anatomy, musculoskeletal architecture and motor control interact to govern limb motion. The talk will be in four parts. 1) I will present recent work on the mechanics and kinematics of frog jumping versus running. 2) I will overview prior work from my group towards developing "musculo-robotics" [1, 2] approaches involving closed-loop interactions between *in vitro* muscle tissue and a simple swimming robotic model. 3) I will introduce work using a frog jumping simulation interfaced with either a robotic arm or *in vitro* muscle tissue. 4) I will discuss current work investigating how ageing properties of muscle affects the neuro-mechanics of human reaching. From these above approaches we are working to gather evidence for how limb internal morphology (e.g. moment arms, limb inertia) as well as external morphology (e.g. foot shape) interact with locomotor substrate to influence limb dynamics. Furthermore, we are working to better understand how the above anatomically dependent interactions influence the motor control strategy of coordinated tasks such as jumping and reaching. In terms of real-world applications, our we are currently applying our suite of methodology to investigate the ageing process to better understand how age-related neuromuscular degradation leads to loss of limb function.

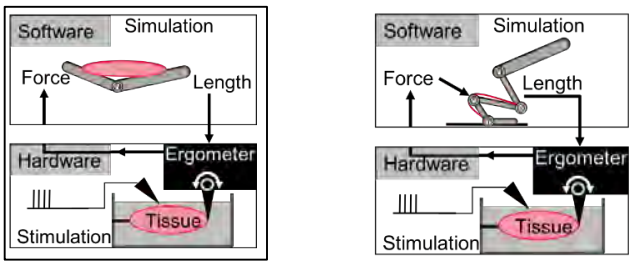

Figure 1 Closed-loop *in vitro* muscle techniques [1].

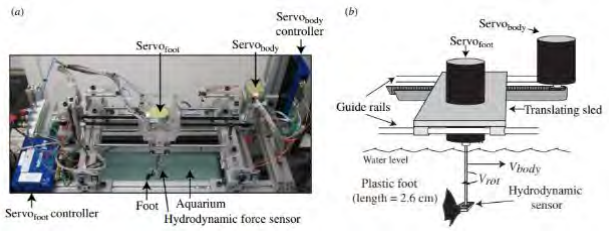

Figure 2 Closed-loop *Musculo-robotic* techniques [2].

ACKNOWLEDGEMENTS

This work was funded by The Rowland Institute at Harvard, a European Research Council Starting Grant and a Wellcome Trust Investigator award.

REFERENCES

[1] Richards, C. T., & Eberhard, E. A. (2020). *Journal of Experimental Biology*, 223(10), jeb210054.

[2] Richards, C. T., & Clemente, C. J. (2012). *Bioinspiration & biomimetics*, 7(1), 016010.

MEASURING THE MOTION OF HUMAN MUSCLE: DEVICES, DISRUPTIONS, AND DEFORMATIONS

Taylor J.M. Dick, Nicole Y. Kelp, India Lindemann, James L. Williamson
School of Biomedical Sciences, University of Queensland, Brisbane, Australia
Email: t.dick@uq.edu.au

INTRODUCTION

Skeletal muscle is the actuator that powers human and animal locomotion. Muscles function to change length and produce force to enable movement, posture, and balance. Given the intimate links between contractile length, velocity, and force—measurements of muscle length provide insights into the energetics, mechanics, and control of movement. As technology has advanced, measures of muscle length have expanded from two-point measures of length into broader dimensional analysis of muscle motion in both time and space.

The first direct measures of *in vivo* muscle fibre length [1] demonstrated that muscle fibres can shorten while the whole muscle-tendon unit lengthens. A series of studies in animals have since demonstrated that muscle motion and joint motion are uncoupled—owing to fibre rotations and stretching of elastic elements. Just a few years after the first sonomicrometry experiments in animals, B-mode ultrasound emerged as a technique to non-invasively look 'under the skin' and measure muscle-tendon architecture in humans, both at rest and during contractions [2]. The first studies to combine ultrasound with motion analysis demonstrated, perhaps unsurprisingly, that the ankle plantar flexor fascicles behaved near isometrically despite substantial length changes in the muscle-tendon unit during walking in humans [3]. Studies have since illuminated that changes in length of elastic tissues or the rotation of muscle fibres can alter the timing and rate of muscle length changes—with implications for locomotor function. The goal of this presentation is to showcase novel ways our research team is using B-mode ultrasound to look under the skin and measure *in vivo* muscle motion.

METHODS

We have experimentally measured *in vivo* muscle behavior during static and dynamic tasks using B-mode ultrasound. B-mode ultrasound images are analyzed using manual and semi-automated approaches to quantify muscle or tendon length changes, pennation angles, and muscle thickness. In some cases, measurements of muscle dynamics are combined with information about muscle activation, muscle stiffness, or muscle volume from electromyography, shear wave elastography, or magnetic resonance imaging, respectively. Using these tools, we have: (1) explored the influence of spring-loaded ankle exoskeletons on muscle behaviour during steady and perturbed hopping; (2) compared the synchronous fascicle strain patterns in agonist and antagonist ankle muscles during unexpected perturbations to walking; and (3) investigated the influence of internal muscle properties on shape changes and gearing in synergist muscles.

RESULTS AND DISCUSSION

Results from our exoskeleton-perturbation study have shown that assistance at the ankle leads to a reduction in soleus muscle activation, increases in fascicle length change and decreases in muscle forces during perturbed hopping. These changes have competing effects on the mechanics and energetics of lower limb muscles, likely limiting the capacity for series elastic tissues to absorb energy during a perturbation.

During unexpected 'slip' perturbations in walking, we found that the tibialis anterior and medial gastrocnemius fascicle length changes shift from their out of phase behaviour during normal walking to an in phase pattern whereby fascicles in both muscles undergo rapid shortening. These results suggest that effective perturbation recovery may be enabled via a muscle-based latch mechanism which is mediated by co-activation of agonist-antagonist muscles.

Results from our shape chage and gearing study shows that during high force contractions, stiffer muscles bulge less, muscles with higher amounts of intramuscular fat undergo less fibre rotation, and muscles with greater force-generating capacity operate at higher gearing. Interestingly, at submaximal contraction levels, differences in internal muscle properties had a minimal influence on shape changes and gearing.

CONCLUSIONS

Using ultrasound-based measures of muscle in motion, we have shown that measures of muscle fibre length change, architecture, and shape, when coupled with an understanding of muscle physiology, can offer critical insights into the energetics, mechanics, and motor control of movement during a variety of locomotor tasks.

REFERENCES

[1] Griffiths (1991). J Physiol, 436(1), 219-236.
[2] Kuno and Fukunaga (1995). Eur J App Physiol, 70, 45-48.
[3] Fukunaga et al. (2001). Proc Roy Soc B, 268 (1464), 229-233.

VIEWING THE ELEPHANT TRUNK AS AN ENGINEER TURNED BIOLOGIST

Andrew Schulz[1,2,*], Krishma Singal[3], Mike Dimitriyev[3], Margaret Zhang[2], David Hu[2,4], Sabetta Matsumoto[3]
Haptic Intelligence Department[1] Max Planck Institute for Intelligent Systems, Stuttgart, Germany
Departments of Mechanical Engineering[2], Physics[3], and Biological Science[4], Georgia Tech, Atlanta, GA
Email: aschulz@is.mpg.de

INTRODUCTION

The elephant trunk is an immensely complex appendage with deeply folded skin on the dorsal portion for protection and intermediate wrinkles for gripping slippery objects [1]. The skin covers the inner portion of the trunk, comprised of several thousand muscle fibers that, through actuation, can erect vibrissae or whiskers for added sensing [2]. With no bones or joints, this hydrostat is an infinite degree of freedom system, as any two constraints will have a third in between them [3]. Here, we discuss utilizing different engineering-based techniques, including innovative types of microscopy, work loops, and knitted mimics, to generate a more holistic understanding of the limitations and capabilities of the elephant trunk.

METHODS

The methods described will be that of two different sets of experiments, including both with living African elephants *(Loxodonta africana)* at Zoo Atlanta, as well as diseased African and Asian elephant trunk specimens taken at Humboldt University in Berlin, Imperial College London, and Icahn School of Medicine at Mount Sinai. Additionally, we utilized uni-axial strain testing of elephant trunk skin to determine the mechanical properties of the different load-bearing layers of the skin. Finally, to understand collagen alignment and interaction, pieces of skin were stained and imaged using Second Harmonic Generation Microscopy, Micro-CT, and classical hematoxylin and eosin staining. All experiments and dissections performed were under approved research by Georgia Tech's IACUC and Zoo Atlanta's ethics team.

RESULTS

The elephant trunk has asymmetries in function from the micro to the macro levels. Macro size asymmetries were observed from the muscular to the skin levels. During elongation trials with living elephants, we see the dorsal portion of the trunk elongates 20% more than the ventral portion of the skin. This is due to the asymmetries of skin function at each of these sites. When performing uni-axial tests of the elephant skin, we see a divergence of strain stiffening versus strain softening behavior, with the dorsal skin exhibiting strain softening due to the wrinkled geometry, whereas the ventral skin is strain stiffening. To understand these asymmetries in skin function, we utilized Second Harmonic Generation (SHG) microscopy to view collagen alignment and interaction in the skin. We find that the elephant skin's collagen is entangled across all sections. The uni-axial asymmetries are explained by the pre-tension the collagen in the skin experiences. The dorsal portion of collagen is relaxed with room to stretch and elongate, whereas the ventral collagen is stiff. We conclude that the dorsal folds are built for protection and stretching, whereas the ventral skin is built for wrapping, gripping, and protection. By collaborating with the Matsumoto lab at Georgia Tech, we have worked to understand utilizing knitting's asymmetries to re-create the morphologies and compositional asymmetries in the skin. This has enabled us to generate connections between the collagen orientation of the skin and specific knitting stitches. Additionally, in working with Zoo Atlanta, we have worked to understand the elephant trunk using an in-vivo work loop technique Figure (1).

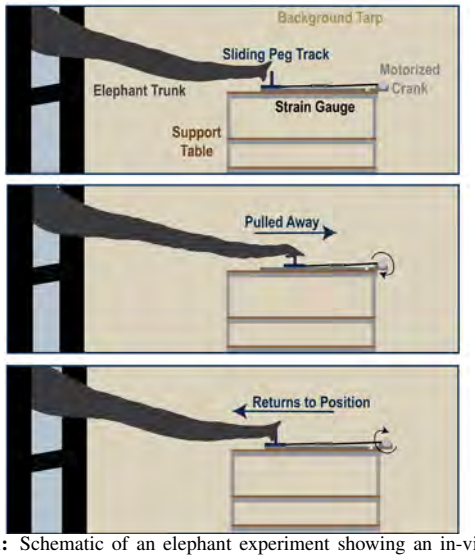

Figure 1: Schematic of an elephant experiment showing an in-vivo work loop technique of hydrostats.

These techniques utilize basic engineering principles, and the model hydrostatic of the elephant trunk has generated new types of bio-inspiration for soft robotics, bio-materials, and conservation technologies.

CONCLUSIONS

Overall the ability of engineers and biologists to share knowledge and techniques allows more scientifically encompassing comparative biomechanics studies to occur. Using uni-axial strain tests, complex materials mimic, advanced microscopy, and work-loop techniques can all be applied to various biological organisms to help advance biomechanics, bio-inspired robotics, and even wildlife conservation. By utilizing these engineering-based techniques and collaborating with biologists, we can discover connections between a macro function and micron-sized discovery, such as non-homogenality of elephant skin explained by collagen entanglement in the skin.

ACKNOWLEDGEMENTS

Thank you to those who assisted in making this work possible, including early influencers of G. Sawicki, C. Higgins, J. Reidenberg, and Y. Chang. Thank you to the Haptic Intelligence Department and Max Planck Institute for Intelligent Systems for travel support.

REFERENCES

[1] Schulz AK et al. *PNAS* **119**: 31, 2022.
[2] Schulz AK et al. *Bioinsp. & Biom.* **113**: 110845, 2023.
[3] Kier B. et al. *Zoo. Jour. of Lin.* **130**: 1985.

INVESTIGATING INTRINSIC MUSCLE MECHANICS OF FORCE PRODUCTION

Caitlin Bemis[1], Nicolai Konow[2], Monica Daley[3], and Kiisa Nishikawa[1]
[1] Department of Biological Sciences, Northern Arizona University, Flagstaff, USA
[2]Department of Biological Sciences, University of Massachusetts at Lowell, Lowell, USA
[3] Department of Ecology and Evolutionary Biology, University of California, Irvine, USA
Email: cmb992@nau.edu

INTRODUCTION

Movement through environments requires responses to varied forces facilitated by rapid processing of multi-modal sensory information and coordinated actuation of limbs and joints [1,2,3]. Responses can be mediated by intrinsic mechanical properties of the musculoskeletal system as well as by neural control to produce force and regulate work output [1]. Muscles have been viewed as motors producing force depending on their activation, strain, and velocity under isometric and isotonic conditions [2]. *In vivo* strain trajectories arise dynamicallly from interactions among neural activation, musculoskeletal kinematics and loads applied by the environment resulting in force production that is not accurately represented in traditional views of muscle [3]. Titin function in active muscle suggests alternatively that muscle develops force through combined effects of activation and viscoelastic resistance to applied loads [2]. Here we present a novel work loop technique that replicates *in vivo* muscle force using a mouse muscle "avatar" during controlled *ex vivo* experiments.

METHODS

In vivo fascicle strain trajectories were chosen from individual rat medial gastrocnemius (MG) (strides =3) [4], and guinea fowl lateral gastrocnemius (LG) (strides = 2) and digital flexor-IV (DF-IV) (strides = 2) [1] muscles during locomotion at various speeds on a level treadmill. Measured *in vivo* strain trajectories and activation patterns from rat and guinea fowl were used as length and stimulation inputs in *ex vivo* work loops on mouse extensor digitorum longus (EDL) (n = 24). Mouse EDL muscles were surgically removed without their tendons prior to experiments. Amplitudes of *ex vivo* strain trajectories were scaled to match *in vivo* passive force rise. Constant (1-ms square wave) submaximal stimulation (45V, 110Hz) was used during *ex vivo* work loops. Stimulation protocols were optimized to account for differences in activation and deactivation kinetics among muscles. For each strain trajectory and stimulation protocol, force was measured and work per cycle was calculated. Relative work per cycle (mJ/g) of *in vivo* and *ex vivo* muscles was compared by dividing work per cycle (mJ) by muscle mass (g).

RESULTS AND DISCUSSION

Our *ex vivo* "avatar" work loop experiments accurately replicated force production and work output in several conditions across rat and guinea fowl muscles at varying speeds based on measured strain trajectories, with an optimized stimulation protocol based on measured EMG *in vivo*. *Ex vivo* experiments using *in vivo* rat strain trajectories and an optimized stimulation protocol at various speeds resulted in high R^2 (R^2 = 0.74 – 0.97) (Figure 1) for force production.

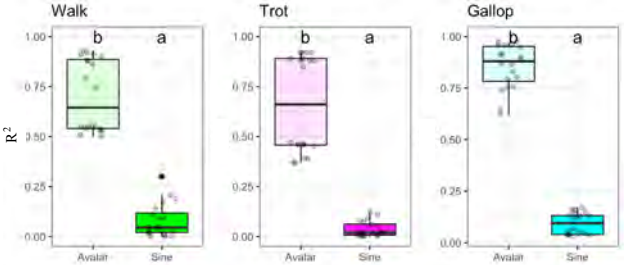

Figure 1: R^2 values of walking (green), trotting (magenta), and galloping (blue) using *in vivo* strain trajectories using both simulation protocols in "avatar" work loop experiments compared to sinusoidal length trajectories at the same frequency.

Additionally, *in vivo* rat relative work per cycle was accurately predicted by *ex vivo* work loops under most strain trajectories and stimulation protocols.

CONCLUSIONS

Results of "avatar" experiments demonstrate that viscoelastic responses to deformation from applied loads can be represented by strain and velocity transients in fasicles. These transients have large effects on muscle force production and regulation of work ouput. Our "avatar" experiments improve prediction of force in general, and particularly as frequency increases. This result suggests that muscles depend more heavily on intrinsic mechanical properties, such as titin, at higher frequencies, because tendons and sensory feedback are not present in "avatar" experiments.

ACKNOWLEDGEMENTS

Funded by NSF IOS-2016049 and NSF DBI-2021832.

REFERENCES

[1] Daley & Biewener. 2011. *Phil. Trans. R. Soc. B* **366**, 1580–1591. [2] Nishikawa. 2020. *Physiology.* **35,** 209–217. [3] Sponberg et al. 2011 *Phil. Trans. R. Soc. B* **366,** 1606-1620 [4] Wakeling et al. 2021. *J. Biomech.* **117**, 110-242.

ENERGETICS, MECHANICS, AND MUSCLE: LOCOMOTOR ADAPTATIONS TO CHRONIC LIMB LOADING DURING DEVELOPMENT

Kavya Katugam-Dechene[1], Talayah A. Johnson[1,2], Ian Dechene[1], Suzanne M. Cox[1,3], Stephen J. Piazza[1], and Jonas Rubenson[1]

[1]Biomechanics Laboratory, Dept. of Kinesiology, The Pennsylvania State University, University Park, PA, USA.
[2]McKay Orthopaedic Research Laboratory, Dept. of Bioengineering, University of Pennsylvania, Philadelphia, PA, USA.
[3]Dept. of Biology, Duke University, Durham, NC, USA.
Email: kavya@psu.edu

INTRODUCTION

Humans and other animals adapt to expend the least amount of metabolic energy to complete a movement task, both over acute [1-3] and evolutionary timeframes [1,4]. Whether adaptations in locomotor economy occur in response to altered life history, especially during development (e.g. environmental fluctuations, or training in humans) remains less clear. Further, the mechanical underpinning to adaptations in locomotor economy that may occure during development have not been well explored.

We have previously demonstrated that chronic limb loading during development substantially alters locomotor economy; it was found that chronically limb-loaded animals (LL) cary additional limb mass remarkably more economically than control animal (CON) [5]. Here we test the hypothesis that a reduction in mechanical limb work contributes to the observed lower metabolic cost of carrying externally applied limb mass after chronic limb loading. Specifically, we hypothesize that (1) LL animals locomote with added limb mass using less mechanical power than CON animals, and (2) the increase in mechanical power between unweighted and weighted conditions will be smaller for LL animals than CON animals.

METHODS

To study the effect of load stimulus during development on locomotor mechanics, we applied an average load of 3.5% body mass unilaterally to the lower right limb of a group of guinea fowl, continuously from 1-16 weeks of age (limb-loaded group, LL; n = 10). CON birds were raised in the same conditions but with no external limb loading (n = 10). At 16 weeks old, half of the birds (N = 5 per group) were video recorded (100 Hz) walking on a treadmill in both unilaterally loaded and non-loaded conditions. An inverse dynamic formulation was used to analyse swing-phase kinetics. We compared mechanical data to previously collected metabolic data on the same animals in the same conditions [5].

RESULTS AND DISCUSSION

At 16-weeks old, LL animals used 24% less metabolic energy than CON animals to walk with 3.5% BM loading [5]. Our hypothesis that LL had lower mechanical power than CON was, however, refuted. Surprisingly, our data is suggestive of LL animals having even greater mechanical power than CON animals, although this difference was not statistically significant at an alpha of 0.05 ($p = 0.12$, ES = 1.18; figure 1).

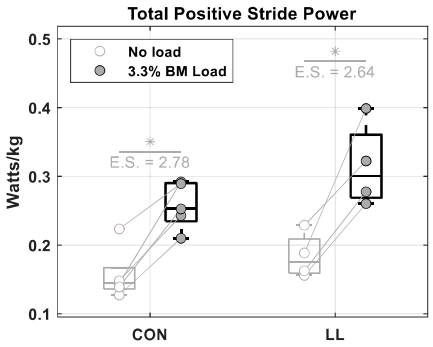

Figure 1 Total positive stride power (watts/kg) for both CON and LL animals. *significant difference due to loading ($p < 0.05$).

CONCLUSIONS

LL animals required no less limb power to carry additional mass compared to CON, despite the observed large reduction in metabolic energy consumption [5]. Increases in limb power in LL animals were isolated to the right (chronically loaded) limb, specifically driven by a larger increase in power at the ankle from unloaded to loaded walking. We propose that muscle-level adaptations may explain the improved locomotor economy in LL animals compared to CON animals. Further work is being conducted to investigate whether adaptations to muscular architecture explain how animals were able to achieve improvements in locomotor economy after growth-period loading. Preliminary findings indicate adaptations not only in muscle mass, but also in sarcomere properties after limb loading.

ACKNOWLEDGEMENTS

Supported by NIH Grants R21AR071588 and R01AR080711.

REFERENCES

[1] Alexander *Prin Animal Loc*, 2003.
[2] Barnes & Kilding *Sports Med* **45**: 37-56, 2015.
[3] McCann & Higginson *Sports Med* **7**: 158-162, 2008.
[4] Dawson & Taylor *Nature* **246**: 313-314, 1973.
[5] Johnson *PSU KINES Master's Thesis,* 2021.

DOES THE *IN-VIVO* OR *IN-VITRO* ENVIRONMENT IMPACT THE TENDON FORCE-STRAIN RELATIONSHIP?

Fransiska M. Bossuyt[1*], Tim Leonard[1], Andrew Sawatsky[1], W. Michael Scott[2], and Walter Herzog[1]
[1]Human performance Lab, Faculty of Kinesiology, University of Calgary, CA
[2]Faculty of Veterinary Medicine, University of Calgary, CA
email: *fransiska.bossuyt@ucalgary.ca

Introduction

By quantifying tendon properties, such as hysteresis and stiffness, we can improve our understanding of the functional capacity of the musculoskeletal system [1]. However, there is a great disparity in previously quantified tendon properties. For example, tendon hysteresis values obtained *in-vitro* are typically smaller and have less variation than the corresponding hysteresis obtained *in-vivo* [2]. It is unclear if these inconsistencies in tendon properties obtained *in-vivo* and *in-vitro* are caused by differences in methodology or if the mechanical properties of tendons are indeed different in *in-vivo* and *in-vitro* environments. The aim of this study was to determine the hysteresis of a sheep hindlimb tendon *in-vivo* and to compare the *in-vivo* results with those obtained from *in-vitro* experiments that replicated the *in-vivo* conditions. Based on data in the literature, it was hypothesized that the hysteresis obtained *in-vivo* is greater than the corresponding hysteresis obtained *in-vitro*.

Methods

Six sheep were trained to walk on a motor-driven treadmill after which the medial gastrocnemius tendon was surgically instrumented with a custom-made "E"-shaped buckle-type force transducer [3] and Sonomicrometry crystals [4] (Figure 1). All signals were transmitted by telemetry to a custom-built amplifier and synchronized with the use of an electronic synchronization pulse. Following post-surgical recovery, *in-vivo* muscle forces (1040Hz) and tendon lengths (520Hz) were collected while the sheep walked on a motor-driven treadmill (Figure 1). Results from one sheep and three steps walking at a speed of 1.96 m/s where good signals were obtained are presented. Force and sonomicrometry data were low pass filtered (10 and 50Hz, respectively) using a 4th order recursive Butterworth filter. The muscle tendon unit, including part of the calcaneus, was harvested for the *in-vitro* experiments which took place 24h post-mortem and included calibration of the tendon force transducer. The tendon was clamped in a mechanical testing machine with a 10kN load cell and preloaded with 14.9N (Instron). A 20-min rest period was followed by 101 conditioning cycles to 1% strain at 0.5 Hz, and 51 test cycles using strain rates and peak forces that had been measured during the *in-vivo* walking conditions. The tendon was kept hydrated using a 0.9% saline solution that was generously applied every 2-min. Tendon strain was calculated as (length-length$_{ref}$)/length$_{ref}$)*100. *In-vivo* tendon strains were measured for a segment of the tendon length (length$_{ref}$ = shortest segment length observed *in-vivo*), while *in-vitro* tendon strains were measured for the entire tendon length (length$_{ref}$ = tendon length at zero strain). Hysteresis was defined as the difference in area between the force vs strain loading and unloading curves relative to the area under the force vs strain loading curve. This study was approved by the University of Calgary Veterinary Sciences Animal Care committee.

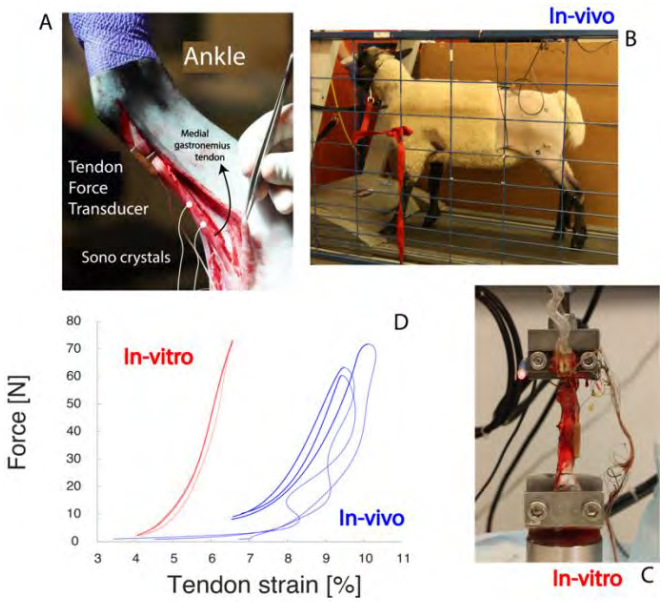

Figure 1: (A) surgically instrumented medial gastrocnemius tendon, (C) tendon clamped in Instron, (D) Force vs strain curve for 3 step cycles of a sheep walking on treadmill at 1.96 m/s (B)(blue line) and replication of the *in-vivo* strain rate and peak force *in-vitro* (red dashed line)(thick lines represent the loading and thin lines the unloading phases).

Results and Discussion

In agreement with published research, we found that the hysteresis for the sheep MG obtained for *in-vivo* conditions (Mean±SD; 57±8%) were greater than those obtained *in-vitro* for comparable loading conditions (14±1%). While our *in-vitro* results agree in magnitude with previous *in-vitro* studies, our *in-vivo* hysteresis values exceed previous estimates from *in-vivo* human studies [2]. Average tendon hysteresis values in humans typically do not exceed 40%, but they often vary greatly between step cycles (e.g., 2-45% [5]). These results suggest that muscular contractions and the *in-vivo* environment may impact the force-strain relationship of tendons.

Significance

The difference between *in-vivo* and *in-vitro* tendon properties for comparable loading conditions warrants caution when relating *in-vitro* tendon properties to *in-vivo* tendon function. Further research examining the detailed reasons for these differences is needed.

Acknowledgments

Early postdoc mobility funding from the Swiss National Science Foundation to FMB (187793). The Killam Foundation, the Canada Research Chair programme (CIHR), and NSERC (RGPIN-2020-03920).

References

[1] Voigt et al. (1995) J Biomech. 28(3): 281-291. [2] Finni et. al. (2012). J Appl Physiol. 114: 515-517. [3] Kaya et al, 2006. J Biomech. 39(15): 2752-66. [4] Caputi et al. (1991). J Biomech. 25: 1067-1074. [5] Farris et al. (2011) J Biomech. 44: 822-826.

BLOOD PYTHON (*PYTHON BRONGERSMAI*) STRIKE KINEMATICS AND FORCES ARE ROBUST TO VARIATIONS IN SUBSTRATE GEOMETRY

[1,2]Jurestovsky, DJ, [2]Joy, SP, [2]Astley, HC

[1] Dept. of Kinesiology, The Pennsylvania State University, University Park, PA, USA.
[2]Dept. of Biology, The University of Akron, Akron, OH, USA.

Email: derek.jurestovsky@psu.edu

INTRODUCTION

Fast impulsive behaviors are some of the most challening for animals to perform given the high forces that are necessary to produce these movements [1,2]. Movements that predominantly occur in the horizontal plane present an additional challenge on flat substrates due to slip occurring if the ratio between the horizontal and vertical components exceeds the coefficient of friction [3,4]. Additionally the surface's coefficient of friction and geometry can influence the angle that slip occurs. Striking snakes propel a large fraction of their anterior body forward with high accelerations [5]. Snakes are found in a wide range of substrates with highly variable surface friction and geometries which can be difficult to strike from. We hypothesize that snakes will strike faster and with more force on a surface with vertically-oriented walls than on an open platform.

METHODS

We obtained four wild-caught blood pythons (*P. brongersmai*) from a commercial provider. This species is suitable for strike studies due to being easily obtainable, non-venomous, and readily strikes defensively. We constructed a rigid strike platform out of a 30.5x30.5x0.7 cm carbon fiber sandwich panel of DragonPlate with a coefficient of friction of 0.3±0.09. Two setups were made, an open setup and a walled setup where we attached two walls on one corner of the strike platform. The strike platform was attached to a 6-axis force sensor (Nano 43). We recorded the strikes at 500 images s^{-1} in dorsal view using an overhead SC1 Edgertronic high-speed camera. Trials were performed in sets of three to five per 24 h and individuals were allowed a minimum of 5 minutes of rest between trials to prevent fatigue. A total of 47 trials were recorded (24 open setup, 23 walled setup). We measured 13 variables: maximum (max.) fore-aft force, max. lateral force, max. vertical force, max. total force, max. head velocity, max. head acceleration, fore-aft impulse, strike distance, max. tail velocity, max. tail acceleration, max. tail displacement, max. fore-aft to vertical force ratio, and percent of the strike above the slip threshold. Last we ran a mixed model ANOVA for each variable with setup, individual, and setup*individual.

RESULTS AND DISCUSSION

Contrary to our hypothesis, snakes displayed high strike performance in both setups (Fig. 1). Our results displayed high individual variability within and between individuals and setups. As a result, the open and walled setups were statistically indistinguishable in most variables measured. Only max. lateral force, max. tail distance, max. fore-aft to vertical force ratio, and percent of the strike above the slip threshold were significantly affected by setup. Our results match what would be expected if the tail and posterior body were being used as an inertial appendage based on the ratio of fore-aft to vertical forces which exceeds the coefficient of friction for a small portion of the strike (~6%) in the open setup which increased dramatically in the walled setup (~39%). This suggests the snakes tail movement is keeping this ratio at or just below the coefficient of friction in the open setup.

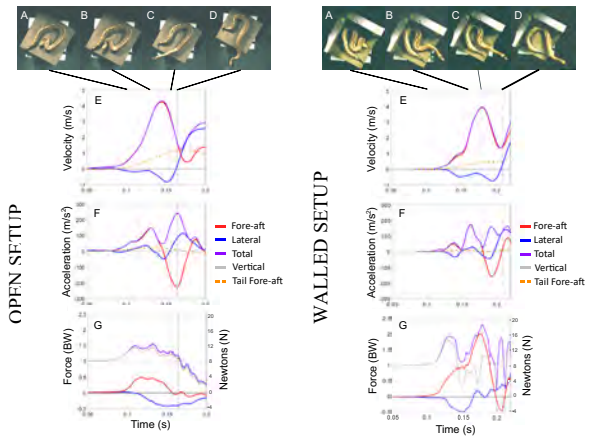

Figure 1. Snake strikes showing the snake during the strike (A-D), velocity (E), acceleration (F), and Force (G).

CONCLUSIONS

We found almost no statistical difference between the majority of variables analyzed for the blood python strikes between an open and walled setup. These results might be explained by the movement of the tail during the strike acting as an inertial appendage. A large variety of snakes encounter open habitats and this mechanism would allow them to exploit a wider range of microhabitats to successfully capture prey.

ACKNOWLEDGMENTS

Supported by NSF Grant#2045581.

REFERENCES

[1] Astley HC et al. *JEB* **217**: 4372-8, 2014.
[2] Patek SN et al. *Nature* **428**: 819-20, 2004.
[3] Hildebrand M *BioSci* **39**: 766, 1989.
[4] Wilson AM et al. *Nature* **498**: 185-9, 2013.
[5] Young BA *JEZ:Eco.Gen.Phys.* **313**: 114-21, 2010.

Creating musculoskeletal models of humans and animals with OpenSim Creator

Adam Kewley[1], Julia van Beesel[1,2], and Ajay Seth[1]
[1] Biomechanical Engineering, TU Delft, Delft, Netherlands.
[2] Dept. of Human Origins, Max Plank Institute for Evolutionary Anthropology, Leipzig, Germany.
Email: a.seth@tudelft.nl

INTRODUCTION

Musculoskeletal modeling is an important tool for investigating the biomechanics of human and animal movement. To study patient- or species-specific mechanics, researchers rely on anatomical information from cadavers or biomedical imaging (CT, MRI and Cryo scans). Therefore, there is a growing need to develop specimen-specific musculoskeletal models to predict patient outcomes and to understand how species evolved at a comparative level. While models with specimen-specific musculoskeletal geometries may yield more accurate results [1], the creation of specimen-specific models remains a huge challenge.

METHODS

We developed OpenSim Creator [2] to provide graphical tools to rapidly create, edit and analyze OpenSim [3,4] musculoskeletal models by interfacing directly with the OpenSim API. Model building tools include importing high-resolution meshes (e.g. from CT scans), landmark identification for joint axis and muscle path definition, and adding associated joints and muscles. Whilst editing, live plotting enables model builders to visualize how muscle paths, lengths and moment-arms change with respect to changing landmark selection. Furthermore, OpenSim Creator provides a workflow based on morphometric transformations [5] to morph existing musculoskeletal models to specimen-specific anatomy. We used OpenSim Creator to build and compare specimen-specific shoulder models. Beginning with a generic shoulder model [6] we fit subject-specific CT and MRI scans (superimposed in Fig.1) using its morphometric-transformation tool. We defined the line of action for each muscle from MRI-based muscle volumes and adjusted them to align with the moment arm curves from the generic model. Similarly, OpenSim Creator was used to enhance an existing gorilla model [7] with scapulothoracic joint kinematics as described in the human shoulder model (Fig 2), so that shoulder kinematics could be directly compared.

RESULTS AND DISCUSSION

OpenSimCreator's mesh importer tool enabled real-time placement and orientation of subject-specific bodies and joints based on boney landmarks, which automatically produced an OpenSim model. OpenSim Creator's live plotting provided real-time visual feedback on the effect of attachment points and wrapping surfaces on each muscle's moment arm (Fig. 1 right panel). (Fig. 2). We can now analyze species-specific differences through comparison of the biomechanical capacity of both models (Fig 2).

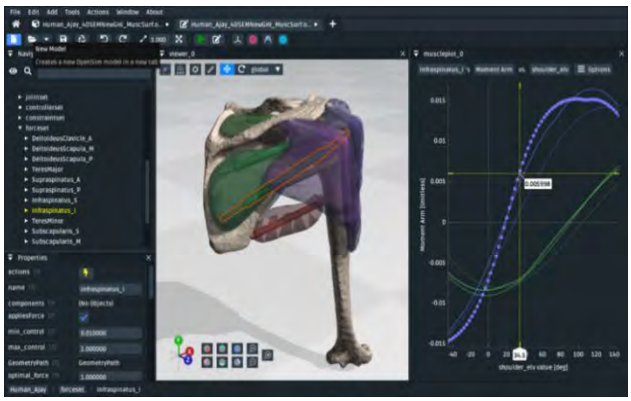

Figure 1: OpenSim Creator tools for creating a subject-specific shoulder model. The navigator (left) presents the composition of the model, model viewers (middle) provide the 3D visualization, and model output plotters like the muscle plotter (right) are updated whenever the model is modified.

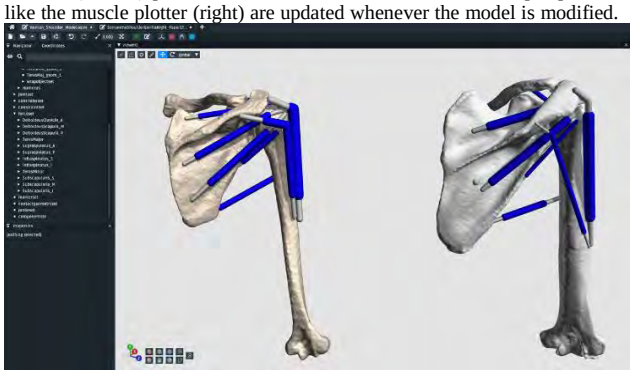

Figure 2: A specimen-specific human model (left) is used to update a gorilla model (right) in OpenSim Creator.

CONCLUSIONS

We developed a graphical model building tool, OpenSim Creator, that includes graphical editing and a morphometric transformation workflow to create new specimen-specific musculoskeletal models. We believe OpenSim Creator, as free and easy to use opensource software [2], will enable more studies with larger numbers and variety of specimen-specific models.

ACKNOWLEDGEMENTS

This project was made possible by grants: 2020-218896 and 2022-252796 from the Chan Zuckerberg Initiative DAF, an advised fund of Silicon Valley Community Foundation, and the Dutch Research Council, NWO XS: OCENW.XS21.4.161.

REFERENCES

[1] Gerus P et al. *J Biomech* 46(16): 2778-86, 2013.
[2] Kewley A. OpenSim Creator 0.3.2 *Zenodo*, 2023.
[3] Delp SL et. al. *IEEE Trans Biomed. Eng*. 54(11), 2007
[4] Seth A et al. *PLoS Comp.Biol.* 14(7), 2018.
[5] Mitteroecker P, Gunz P. *Evolutionary Biology*, 2009
[6] Seth A et al. *Front Neurorobot* 13: 90, 2019.
[7] van Beesel J et al. *J Anat.* 237(1), 2021.

RESIDUAL FORCE ENHANCEMENT: ACTIVE VERSUS PASSIVE CONTRIBUTION

Wejdaan Faridi, Venus Joumaa, Shuyue Liu and Walter Herzog
Faculty of Kinesiology, University of Calgary, Calgary, Canada
Email: Wejdaan.Faridi@ucalgary.ca

INTRODUCTION

Residual force enhancement (rFE) is the increase in isometric force observed following active stretch compared to purely isometric contractions at the same final muscle length and level of activation [1]. rFE is thought to be caused by an active component, associated with actin-myosin cross-bridges, and a passive component, associated with titin [1]. The relative contribution of the active and passive components to rFE is currently unclear.

In the muscle rigor state (devoid of ATP), all possible cross-bridges are attached to actin [2] in a uniform post-power stroke conformation, and therefore, the contribution of cross-bridges to force in the rigor state is thought to be the same following active stretch and purely isometric contractions. Any remaining difference in rFE in the rigor state would be attributable to the passive component.

Our purpose was to investigate the contribution of the active and passive components to rFE by exposing single muscle fibres in the force-enhanced and isometric reference states to rigor conditions. We hypothesized that the rFE in rigor would decrease but would not be abolished.

METHODS

Single fibers (n=8) from rabbit psoas muscle were harvested, skinned, and prepared for mechanical testing as previously described [e.g., Liu et al., 2022]. Fibres were then activated at an average sarcomere length of 2.4 um, stretched to a sarcomere length of 3.0 um, and then exposed to a rigor solution for 90s. For reference trials fibers were activated at an average sarcomere length of 3.0 and then exposed to the rigor conditions for 90s (Figure 1). rFE was compared between the two trials before and after incubation in the rigor solution.

RESULTS AND DISCUSSION

Contrary to our hypothesis, rFE increased from 8.5±4.5% to 17.1±4.0% (0.042±0.020 to 0.073±0.023 mN) following submersion in the rigor solution.

Assuming that the active component contribution is similar for the isometric reference and the force-enhanced conditions in the rigor solution, a possible explanation for the increase in rFE may come from an increase in titin stiffness when the number of cross-bridges increases in rigor solution [3].

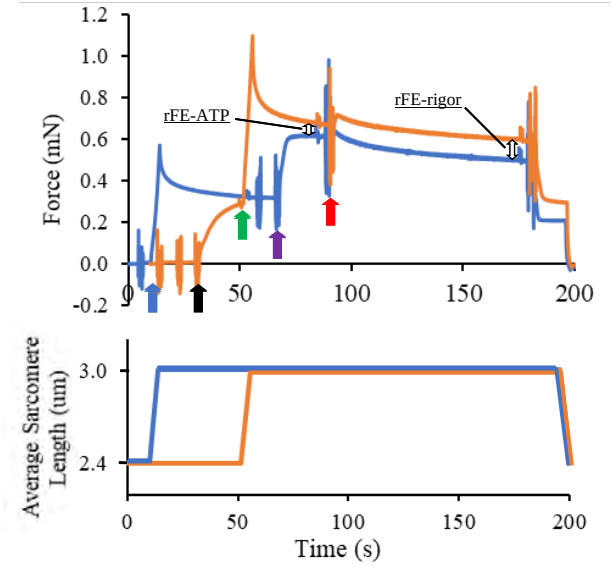

Figure 1 Force and average sarcomere length as a function of time for an active stretch (orange) and a purely isometric (blue) reference contraction performed with a single fibre from the rabbit psoas muscle. For the active stretch condition, the fibre was activated at a sarcomere length of 2.4 um (black arrow), and then actively stretched to a sarcomere length of 3.0 um (green arrow). For the purely isometric contraction, the fibre was passively stretched to a sarcomere length of 3.0 um (blue arrow), and then activated (purple arrow). At steady-state for both conditions, the fibre was transferred into a rigor solution (red arrow). rFE was measured in the activating (rFE-ATP) and the rigor (rFE-rigor) solutions (double headed black arrows).

CONCLUSIONS

The results of this study suggest that the passive component primarily contributes to the development of rFE. However, this conclusion relies on the assumption that the active component was effectively controlled with the induction of a rigor state. Further research is required to better understand the behaviour of cross-bridges in a rigor state.

REFERENCES

[1] Herzog et al. *Front Physiol* **6**: 2015.

[2] Yamada et al. *Biophys J* **85**: 1741-1753, 2003.

[3] Leonard et al. *Am J Physiol Cell Physiol* **299**: 14-20, 2010

Kinetics of a collective load carrying in ants

J. Drapin[1], V. Fourcassié[1] and P. Moretto[1]
[1] Centre de Recherches sur la Cognition Animale (CRCA)- Centre de Biologie Intégrative (CBI), Toulouse, France.
Email: pierre.moretto@univ-tlse3.fr

INTRODUCTION

Cooperative performances of social insects are transforming robotics perspectives because of their remarkable organisation to solve complex tasks. A cooperative transport occurs when a group of individuals works together to move an otherwise unmanageable object. Yet, the phenomenon of collective transport among worker ants is still poorly understood, although its existence has been reported in at least 40 genera of different subfamilies of Formicidae [1]. Advances in technology allow to acquire precise kinematics of the whole-body segments as well as detailed morphometric data [2]. A 2D kinematic analysis of a collective transport observed in *Paratrechina longicornis* has been performed. It enables us to attempt a first estimation of the forces and momentums applied by ants to move and turn a carried item.

METHODS

A camera and 3 infrared strobe spots all synchronized and sampled at 300Hz recorded the kinematic of a group of 4 ants that collectively carry a load (Fig.1a). The Vicon Motus (v10) software enabled calibration with a Lego® brick and to define a 2D external frame. The corners of the carried object, as well as the mandible distal (m_d) and head proximal extremities (neck) of each ant, were tracked to build a poly-articulated model including the 4 ant's heads and the load they transport. The forces ($\vec{F}_i=m_i.\vec{a}_i$) and momentum ($\overrightarrow{Mz}_i=Obj.\vec{m}_d\wedge\vec{F}_i$) applied by ants were determined from their body masses (m_i), as well as the accelerations ($\vec{a}_i$) of the head and object center of mass (Obj). The Fundamental Principle of Dynamic (PFD) enabled us to verify the accuracy of the estimates by comparing the sum of ant forces then momentum to the linear and angular accelerations of the object having its own mass and inertia momentum.

RESULTS AND DISCUSSION

It occurred that ants first moved the object to the left during 2.5" then rotated it clockwise. Our results are in good agreement with the observations and would enable us to precise the coordination and synergies across ants. During the first "translation" phase to the left, the ant's forces were negative in X and similar for all ants (Fig.1b). The negative momentums of ants 1 and 4 induced counter-clockwise rotation compensated by ant 2 (yellow, Mz > 0) while ant 3 was neutral (red, Mz ~ 0). The Mz of ant 2 (yellow, Fig.1d) decreases after 2.5" to become negative after 3.5" inducing the clockwise rotation of the object while all ants were acting in the same way.

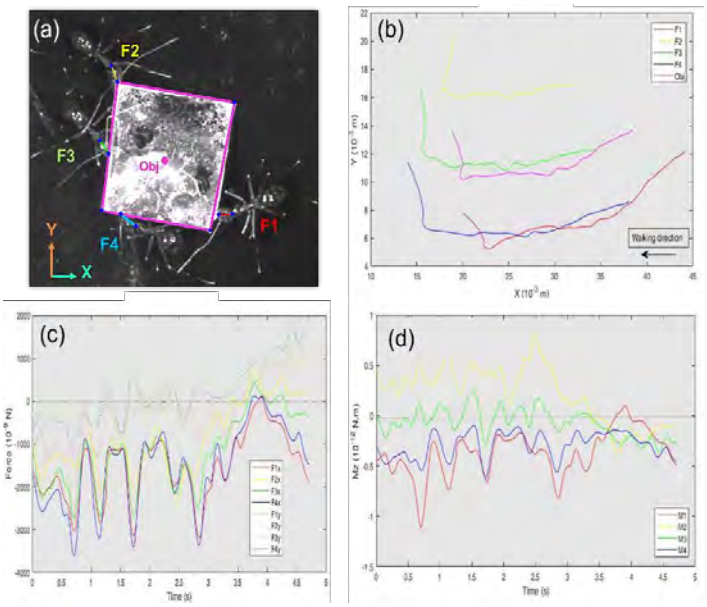

Figure 1 (a) Locations of the tracked points (i.e., mandibles and ant's necks, 4 corners of the load). Ants were moving towards the nest located on the left, which explains the negative values of the X coordinates. **(b)** Ant's and load center of mass trajectories. Time course of the forces **(c)** and momentum **(d)** respectively on the X, Y and Z axis.

CONCLUSIONS

The purpose of this study was to test a method to estimate the forces applied by four ants on a load they collectively carry to measure the 6 components of the torso applied by each ant. Our estimates in respect to the PFD appear accurate and the method seems to enable us to discern the action forces applied by ants on the object they collectively carry. It is confirmed by the moment of forces they apply, which is in agreement with the object rotation around its center of mass. Further investigations will enable us to precise the method to consider both 3D translations and rotations and finally address the synergies and the efficiency of the ant team.

ACKNOWLEDGEMENTS

This work has been supported by the CNRS AO MITI Biomim and the GDR Biomim 2088. JD work was supported by the Collectivité Territoriale de Martinique.

REFERENCES

[1] Hölldobler B et al. *Springer-Verlag* **72**: 2, 1990.
[2] Arroyave-Tobon S et al. *Front.Bioeng.Biotechnol.* 10: 767-914, 2022.

Characterizing residual and passive force enhancements in cardiac myofibrils

Seong-won Han[1,2], Kevin Boldt[2,3,4], Venus Joumaa[2], Walter Herzog[2]
[1] Institute of Physiology II, University of Münster, Münster, North Rhine-Westphalia, Germany
[2] Faculty of Kinesiology, University of Calgary, Calgary, Alberta, Canada
[3] Kinesiology Program, Trent University, Peterborough, Ontario, Canada
[4] Department of Human Health and Nutritional Science, University of Guelph, Guelph, Ontario, Canada
Email: seongwon.han@uni-muenster.de

Introduction

Residual force enhancement (RFE) is defined as the increase in the steady-state, isometric force of a muscle following an active stretch compared to the corresponding (same length, same activation) force of a purely isometric contraction. RFE has been consistently observed in skeletal muscle. However, there are conflicting observations regarding the occurrence of RFE in cardiac muscle [e.g., 1, 2]. The presence of RFE in cardiac muscle may not necessarily improve cardiac function but may provide insight into the possible mechanism of RFE. It has been suggested that the molecular spring, titin, plays a major role in RFE in skeletal muscle. Cardiac muscle has shorter titin isoforms than skeletal muscle, and thus might show different RFE properties compared to skeletal muscle. The purpose of this study was to re-examine RFE in cardiac myofibrils, thereby resolving the controversy that exists in the literature, and gain novel insights into cardiac RFE based on the eventual findings.

Methods

The experimental setup is demonstrated as previously [3]. Briefly, single myofibrils were prepared from the left ventricle of rabbits, and mounted on a custom-built setup on an inverted microscope. RFE was measured following active stretching of rabbit cardiac myofibrils across three different sarcomere length (SL) ranges, 1.8, 2.0, and 2.2 µm, while the stretching amplitude was kept the same, at 0.2 µm (n = 8 for each). We then repeated the same measurement at the final SL of 2.2 µm when actively stretching 0.4 µm (n = 8), to see the effect of stretching magnitude to RFE in cardiac myofibrils.

Results and Discussion

All 32 myofibrils that were tested in this study exhibited RFE. Following stretches of 0.2 µm/sarcomere, the total stresses after active stretching were significantly greater than the reference stresses, ranging from 13% - 19% (Fig 1A). There was no statistical difference in the magnitude of RFE among the three different sarcomere length rages (p = .20; Fig 1A). When the stretching magnitude was different (i.e., 0.2 µm or 0.4 µm) while the final SL was the same (2.2 µm/sarcomere), greater magnitude of RFE was observed with increasing stretching magnitude (p = .038; Fig 1B).

RFE is thought to be caused by a stiffening of titin upon muscle activation, by either calcium binding to titin and/or titin binding to actin [e.g., 4]. Since cardiac muscle clearly produced RFE in our study, we suggest that cardiac titin can lead to RFE, by interacting with actin filament. The specific mechanism by which titin indeed regulate active force needs further investigation.

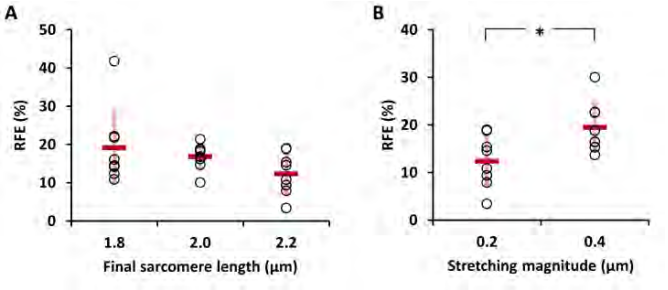

Figure 1. (A) RFE (%) at each final sarcomere length (SL) when the myofibrils were actively stretched by 0.2 µm. (B) RFE (%) at the same final SL (2.2 µm) when the stretching magnitude was different. The opened circle represents each data point measured from a single myofibril, and the red horizontal and vertical bars represent the average and one standard deviation, respectively.

A few studies observed the opposite findings to ours that they found no RFE in cardiac myofibrils/fibre bundles after active stretching. We believe that it is because of the different methodologies used in each study, such as the different speed of stretching of myofibrils, or different timing of active stretching during their experimental protocols.

Conclusions

We conclude from the results of our study that cardiac myofibrils have RFE properties similar to those found in skeletal muscle. Therefore, whatever the mechanisms are for these properties, they are likely contained in both cardiac and skeletal myofibrils, suggesting (but by no means proving) that RFE are caused by the same mechanism(s) in all striated muscles.

Acknowledgments

This work was supported by the Canadian Institutes of Health Research (10013332); The Canada Research Chair Program (RT730101); The Killam Foundation (10001203); The Nigg Chair for Mobility and Longevity; Dean's Doctoral Studentship in Kinesiology, University of Calgary; The Eyes High International Doctoral Studentship, University of Calgary; and The CONNECT! NSERC CREATE Program.

References

[1] Cornachinone A. S. et al. (2016). *Am J Physiol Cell Physiol*, **310**: C19-C26.
[2] Boldt K. et al., (2020). *J Biomech*, **109**: 109953.
[3] Han S. et al. (2023). *Biophys J*, e-published.
[4] Herzog W. et al. (2006). J Physiol, 574(Pt 3): 635-42

THE INTRINSIC AND NEURALLY-MEDIATED CONTRIBUTIONS TO THE BALANCE-CORRECTING TORQUE RESPONSE DIFFER BETWEEN THE ANKLE AND HIP

Kristen L. Jakubowski[1*], Giovanni Martino[1], Owen N. Beck, Gregory S. Sawicki[2], Lena H. Ting[1]
[1] Wallace H. Coulter Department of Biomedical Engineering, Emory University & Georgia Institute of Technology, Atlanta, USA [2] George W. Woodruff School of Mechanical Engineering, Georgia Institute of Technology, Atlanta, USA *Email: kjakubo@emory.edu

INTRODUCTION

To maintain balance in response to a perturbation (e.g., not fall), one needs to produce a corrective torque rapidly. The torque arises from the musculoskeletal system's intrinsic mechanical properties—including muscle short-range stiffness—at the time of the perturbation and from delayed muscle activation from neurally-mediated sensory feedback pathways, with the delay varying depending on the feedback pathway (e.g., short-latency, long-latency, or volitional responses) [1]. While these mechanisms are well-established, to our knowledge, no one has independently quantified the intrinsic and neural contributions to the balance-correcting torque response across different joints. Thus, this study aimed to quantify the intrinsic and neural contributions to the torque response at the ankle and hip.

METHODS

We assessed reactive leg joint torques to backward support surface perturbations in 7 healthy young adults (25 ± 4 years). Participants maintained standing balance during randomized ramp and hold perturbations at 12 cm or 75%, 85%, and 95% of their step threshold, each tested four times. Whole-body kinetics and kinematics were used to estimate ankle, knee, and hip torques using the OpenSim Inverse Dynamics (ID) tool [2].

To differentiate the intrinsic and neural contributions, we implemented a modified version of the previously developed sensorimotor response model (SRM) [3]. Similar to previous work, center of mass (COM) kinematics were used as the input into the SRM [3]. Parallel loops were added to the SRM to predict 1) non-negative signals, as prior versions only estimated positive signals, like electromyography (EMG; and 2) the response to both CoM acceleration and deceleration since torque is the net effect of muscle activation (Fig 1). Our modified SRM model can differentiate the intrinsic and neural contributions by evaluating the time delays (λ) of the parallel loops since the intrinsic components will have a nearly zero-delay. In contrast, the neurally-mediated components will have delays specific to the feedback pathway.

RESULTS

At all perturbation magnitudes, we found that the intrinsic and neural contributions to the reactive torque response differed between the hip and ankle. Namely, we observed an intrinsic component at the hip (blue) but not at the ankle (red; Fig 1). At the hip, two loops occurred at nearly "zero-delay", with one occurring in sync with the positive peak in COM acceleration (solid blue line) and the other with the negative peak in COM acceleration (dashed blue line). However, we did not observe a "zero-delay" loop at the ankle.

At the hip and ankle, two delayed loops were required to accurately model the response, separated into a "short" and "long delay" component. Since the delays associated with the short and long-delayed loops are different, they likely arise from different sensory feedback pathways (e.g., long-latency vs. volitional).

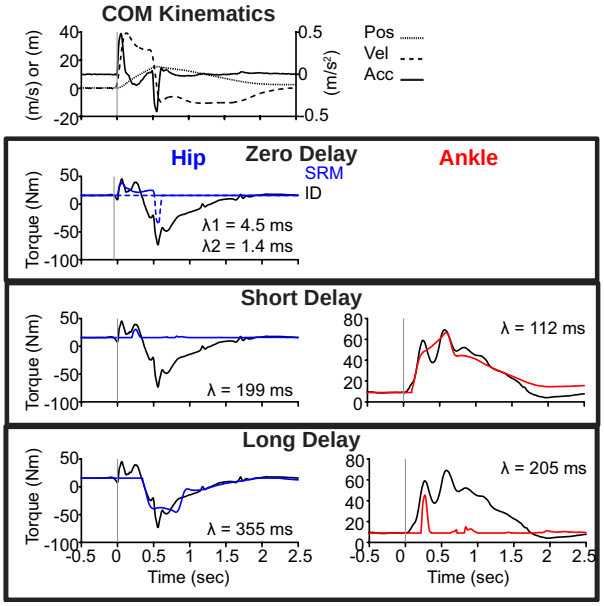

Figure 1 Exemplary data from a perturbation at 95% of step threshold. For the hip (blue) and ankle (red), a multi-loop SRM model was implemented to reconstruct the inverse dynamics (ID) derived joint torques. Center of mass (COM) acceleration (solid), velocity (dashed), and position (dotted) were used as the input into the SRM. The SRM loops were separated based on their delays (λ). The grey line represents the start of the perturbation.

DISCUSSION & CONCLUSION

The lack of an intrinsic (zero-delay) component at the ankle may occur because the compliance of the Achilles tendon is attenuating the short-range stiffness response. However, there is an intrinsic contribution to the hip response since the tendons are stiffer. This results in both intrinsic and neurally-mediated components contributing to the response at the hip, while the neurally-mediated components primarily dictate the response at the ankle.

ACKNOWLEDGEMENTS

Supported by NSF: #EEC-2127509 to ASEE and NIH R01 HD046922

REFERENCES

(1) Horak & Macpherson. *Handbook of phys* **1**: 1996
(2) Delp et al. *IEEE T Bio-med Eng* **54**: 11, 2007
(3) Welch & Ting. *J Neurophys* **101**: 6, 2009

Summary

The hand and wrist present some of the most challenging structures in the study of biomechanics, as well as in the evaluation of many biomechanical principles. Historically, biomechanics research of the hand and wrist has been underdeveloped when compared with that into other areas of the musculoskeletal system. While numerous biomechanical studies have been initiated by surgeons and engineers, cooperative efforts among scientists, anatomists, engineers, and clinicians in surgery and therapy are required to progress research avenues and further improvement of treatment modalities and functional outcomes. The symposium for hand and wrist biomechanics was first held in Brussels, Belgium 30 years ago in 1992. In 2012, Hand and Wrist Biomechanics International (HWBI) was founded with the aim to provide opportunities for global scientific exchange of knowledge in this field and to promote collaborative, interdisciplinary work to better understand and treat these complex joint systems. As a Technical Group of the ISB we are hosting a one-day Symposium within the 2023 ISB Congress. The four sessions consist of keynote and short talks, representing research from across the globe, and continuing our tradition of reporting on the latest research. The day will also provide opportunities to discuss tools and techniques, review challenges, and celebrate successes in this intriguing area of biomechanics.

Recovery of thumb joint movement for patients with severe carpal tunnel syndrome

Hiroshi Kurumadani[1], Akira Kodama[2], Teruyasu Tanaka[2] and Toru Sunagawa[1]
[1] Graduate School of Biomedical & Health Sciences, Hiroshima University, Hiroshima, Japan.
[2] Department of Orthopedic Surgery, Hiroshima University, Hiroshima, Japan.
Email: hkuruma@hiroshima-u.ac.jp

INTRODUCTION

Carpal tunnel syndrome (CTS) is a common entrapment neuropathy of the upper extremity that causes the symptoms, such as numbness, pain, and paralysis of thenar muscles. In severe CTS cases, the thenar muscle paralysis results in a loss of the thumb joint movement, which affects the activities of daily life. Previous reports have indicated that the surgical treatment, such as carpal tunnel release, reduces the symptoms of CTS[1]. Although surgical treatment, such as carpal tunnel release, reduces numbness or pain in severe CTS cases[2], it is unclear whether the thumb joint movement is improved by the surgical treatment. The purpose of this study was to examine the recovery of thumb joint movement in patients with severe CTS.

METHODS

16 hands of 12 patients with severe CTS (Padua classification: severe 8 hands, extreme 8 hands) and 16 hands of 8 healthy adults participated in this study. Data of the severe CTS patients were collected before, 6 months after, and 12 months after surgical treatment by carpal tunnel release. For thumb joint movement, the thumb joint angles were obtained during the thumb circumduction movement as a task. Ten spherical reflective markers were attached to the thumb tip, proximal phalanx, metacarpal, and dorsal surface of the middle metacarpal. A three-dimensional motion capture system recorded the displacements of the markers during the task. From the marker displacements, the joint angle of flexion/extension, abduction/adduction, and pronation/supination in the thumb carpometacarpal (CM) joint, and that of flexion/extension in the thumb metacarpophalangeal (MP) and interphalangeal (IP) joint were calculated using Euler angles. The joint angle ranges of each joint during the task were calculated. From the markers on the thumb tip, the trajectory area and perimeter of the thumb tip during the task were calculated, and the roundness was also calculated from the area and perimeter. The results were compared between healthy adults and patients with severe CTS by ANOVA.

RESULTS AND DISCUSSION

The joint angle range of the abduction/adduction of thumb CM joint in severe CTS did not differ from that in healthy adults at 12 months postoperatively. The joint angle range of flexion/extension of the MP joint in severe CTS was significantly improved at 12 months postoperatively compared with preoperatively and 6 months postoperatively; however, it was lower than that in healthy adults (Figure 1). The joint angle range of the thumb CM joint flexion/extension, pronation/supination, and IP joint flexion/extension was significantly lower in severe CTS than in healthy adults both preoperatively and postoperatively. The thumb MP joint movement may be improved due to recovery of tendon gliding disorder. The trajectory area of the thumb tip was significantly greater at 12 months postoperatively than at preoperatively and 6 months postoperatively (Figure 1). The roundness was significantly improved at 12 months postoperatively than at preoperatively. There were no significant differences in the perimeter. The recovery of the trajectory area may reflect the improvement in the MP joint movement.

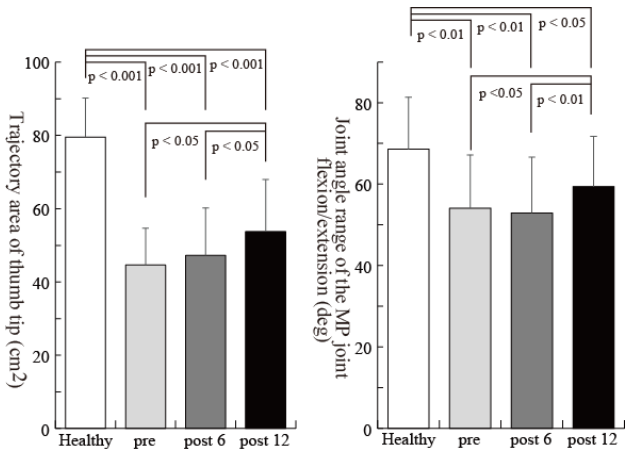

Figure 1 Results of trajectory area (left) and flexion/extension angle range of the MP joint (right).

CONCLUSIONS

Patients with severe carpal tunnel syndrome may have improved thumb joint movement due to recovery of thumb MP joint movement rather than thumb CM joint movement.

REFERENCES

[1] Kodama A et al. *J Hand Surg Eur* **46**: 743-748, 2021.
[2] Uemura T et al. *J Hand Surg Eur* **35**: 632-636, 2010

MEDIAN NERVE DEFORMATION INCREASES DURING REPEATED EFFORTS OF A PULP-PINCH GRIP TASK

Denise Balogh[1] and Aaron M. Kociolek [1]

[1] Department of Physical and Health Education, Nipissing University, North Bay, Canada.
Email: dbalogh798@my.nipissingu.ca

INTRODUCTION

Carpal tunnel syndrome (CTS) is a common peripheral neuropathy in workers exposed to occupational risk factors, including repetitive and forceful gripping **[1]**. The development of CTS is therefore quite multi-faceted, with several injury mechanisms contributing to the compression of the median nerve within the carpal tunnel **[2]**. Increased carpal tunnel pressure is a well-established injury mechanism, which increases with grip force magnitude during a pulp-pinch grip **[3].** This increase and redistribution of pressure in the carpal tunnel may further result in displacement and deformation of the median nerve.

Several studies have used ultrasound to investigate the effects of occupational risk factors on carpal tunnel dynamics **[4,5].** Turcotte & Kociolek **[4]** investigated the effects of non-neutral wrist postures and grip force magnitude on both median nerve deformation and displacement **[4].** However, there remains a need to assess the effects of repetitive gripping tasks including varying rates of force development.

METHODS

Twelve healthy participants performed a repeated grip task using a digital dynamometer (MIE Medical) while their carpal tunnel was scanned with ultrasound (L15, Clarius). The grip task involved pulp-pinching 3 consecutive times from 0% to 40% of maximal voluntary force (MVF), which was also performed at 3 different rates of force development (RFD): acquiring the 40% MVF target over 1sec; 2sec; and 5sec. A custom program (LabView, National Instruments) provided visual feedback of the force matching profiles and collected grip forces at 1000Hz.

Static images were extracted from ultrasound Cineloops at intervals of 10% MVF (from 0% to 40% MVF) along the ramp up phases of the grip tasks as well as .5sec before the start of each ramp and .5sec after 40% MVF was reached. From the images, deformation measures of median nerve circularity, width, and height as well as displacement were calculated (ImageJ, National Institutes of Health). A 3-way repeated measures ANOVA tested the effects of grip force magnitude, ramp (pinch) number, and RFD on all outcome measures of the median nerve (α=0.05).

RESULTS AND DISCUSSION

Median nerve width significantly decreased as a function of grip force magnitude ($F_{1,11}$=10.85, p=.007) and ramp number ($F_{1,11}$=8.35, p=.015; Figure 1). There was also a main effect of ramp number on median nerve height, with increased height in ramp three vs. ramp one ($F_{1,11}$=7.98, p=.017). These results indicate that the nerve continued to deform with increasing force and repeated pinch grips.

Median nerve displacement also increased with grip force magnitude from 0% to 40 % MVF ($F_{1,11}$=8.62, p=.014). However, displacement of the median nerve was greatest during the first ramp ($F_{1,11}$=13.89, p=.003), with very little displacement in the second and third ramps. These results indicate an initial re-arrangement of structures within the carpal tunnel upon initiation of a repeated grip task. There were no significant differences between the three RFD.

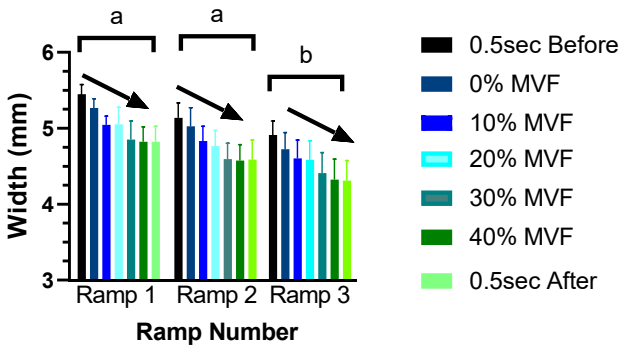

Figure 1. Mean (± SEM) median nerve width as a function of grip force and ramp number. Letters (a,b) indicate significant differences between ramps 1 to 3. Downward arrows indicate a significant decreasing linear trend of width with increasing force magnitude.

CONCLUSIONS

Median nerve displacement and deformation increased with grip force magnitude and repetition (i.e., pinch ramp number). We believe increased localized pressures during the grip task may lead to median nerve deformation as well as entrapment within the carpal tunnel during a repeated grip task.

ACKNOWLEDGEMENTS

Natural Science and Engineering Research Council of Canada Discovery Grant #2017-0409.

REFERENCES

[1]Harris-Adamson et al. *Occup Env Med* **72**:33-41, 2014
[2]Schrier & Amadio. *J Electro Kine* **38**:232-239, 2018
[3]Keir et al. *J Orthop Res* **16**:112-115, 1998
[4]Turcotte & Kociolek. *PeerJ* **9**:e11038, 2021
[5]Cowley et al.*Med Eng Phys* **38**(10):1055-1062,2017

STABILITY OF THE MIDCARPAL JOINT POST SCAPHOIDECTOMY IN DIFFERENT WRIST TYPES

Nicholas Parody, MSc; Catherine Petchprapa MD; Steven Glickel MD; Ronit Wollstein, MD
Orthopedic Surgery, NYU Langone Health

INTRODUCTION

Partial scaphoid excision has been employed to treat arthritis of the scaphoid-trapezium-trapezoid and radioscaphoid joints [1-4]. Because some patients developed midcarpal instability, utilization of this technique has been limited [2, 5, 6]. Recent studies have identified two distinct structural patterns of the midcarpal joint. Type 1 wrists have a lunate-capitate facet, and type 2 wrists have a lunate-hamate-capitate facet [7]. The structure of the midcarpal joint affects the transfer of forces through the wrist [8, 9]. We hypothesize that midcarpal joint structure will affect force transference through wrists with distal and proximal pole excision. Understanding these mechanical patterns may help in identifying those wrists that are prone to develop significant midcarpal joint instability following partial scaphoid excision, allowing a more personalized approach to scaphoid nonunion and wrist arthritis.

METHODS

Sixteen wrist CT scans were anonymized and converted to .stl files to be used with Fusion360 (Autodesk, v.2.0.14109). Ten were categorized as type 1, with the remaining six being type 2. Five wrists were selected at random from each group to be used in the simulation. Each bone was made into a separate body and given the mechanical properties of cortical bone. The scaphoid was split into proximal and distal halves by cutting the bone at a 40° angle from its base with the ulna. A 100N load was applied to the dorsal crests of the trapezoid and capitate. The displacement of the trapezoid, trapezium, scaphoid, capitate, and hamate were recorded in the x, y, and z directions after the load was applied. These displacement values were then averaged across each bone. The two-sample t-test was used to compare the displacement values between both wrist types and wrists that have and have not undergone a scaphoidectomy.

RESULTS AND DISCUSSION

The transfer of force through the trapezoid/STT joint and hamate was significantly different after proximal scaphoidectomy. There were no statistically significant differences in the displacements of the evaluated bones in type 1 and 2 wrists ($p = 0.05$) that underwent scaphoidectomies when compared to each other. It is likely we were underpowered to detect significant differences in a distal partial scaphoidectomy.

CONCLUSIONS

1) Partial excision of the scaphoid was found to affect the transfer of forces through the STT and midcarpal joints in type 1 wrists.
2) Further study is needed to better understand the transfer of forces in these two procedures and observe any potential trends.

REFERENCES

[1] Garcia-Elias M, Lluch A. *Hand Clin*. **17**: 687-95, 2001.
[2] Corbin C, Warwick D. *J Hand Surg Eur.* **34**: 537-8, 2009.
[3] Malerich MM, et al. *J Hand Surg Am*. **39**: 1668-76, 2014.
[4] Malerich MM, et al. *J Hand Surg Am*. **24**: 1196-205, 1999.
[5] Viegas SF. *J Hand Surg Am*. **19**: 127-33, 1994.
[6] McCombe D, et al. *J Hand Surg Am*. **26**: 877-82, 2001.
[7] Viegas SF, *Arthroscopy.* **6**: 5-10, 1990.
[8] Pendola M, et al. *J Wrist Surg.* **10**: 523-7, 2021.
[9] Wollstein R, et al. *J Wrist Surg.* **8**: 477-81, 2019.

Effect of age and sex on the subluxation of the thumb carpometacarpal (CMC) joint

Yu-Chen, Lin[1], Chi-Han, Chen[2], Chieh-Hsiang, Hsu[3],Cheng-Shih, Lai[4], Chien-Kuo, Wang[4], Tai-Hua, Yang[2] and Li-Chieh, Kuo [2,3,5]

[1] Department of Occupational Therapy, Da-Yeh University, Changhua, Taiwan.
[2] Department of Biomedical Engineering, National Cheng Kung University, Tainan, Taiwan.
[3] Department of Occupational Therapy, National Cheng Kung University, Tainan, Taiwan.
[4] Department of Radiology, National Cheng Kung University Hospital, College of Medicine, National Cheng Kung University, Tainan, Taiwan.
[5] Medical Device Innovation Center, National Cheng Kung University, Tainan, Taiwan.
Email: jkkuo@mail.ncku.edu.tw

INTRODUCTION

The Eaton-Littler stress-view radiography has been widely used to measure joint laxity and subluxation of the thumb carpometacarpal (CMC) joint for assisting in the diagnosis and severity classification of osteoarthritis. However, recent studies have shown its disadvantages, such as inconsistent or poor intra-observer or inter-observer reliability and a lack of compelling correlation with patients' clinical characteristics[1]. Furthermore, the scientific evidence regarding our understanding of the relationships among the extent of CMC joint subluxation, joint contact pattern, amount of applied stress, and assessing postures when performing a thumb CMC stress-view radiograph is still scant. Besides, sex and age may affect joint mobility. Therefore, this study aimed to assess the effect of age and sex on the subluxation of the thumb CMC joint via a novel stress-view measuring system, in which the amount of stress applied to the joint and the subsequent joint subluxation would be recorded and analysed, respectively.

METHODS

Twenty-eight healthy participants were recruited in this study. They were divided into three groups, the young group (20-39 years old; 5 males & 5 females), the middle-aged group (40-59 years old; 3 males & 5 females) and the elderly group (over 60 years old; 5 males & 5 females). The custom stress-view evaluation system(SvES)[2] collected the stress applied to the CMC joint and the subsequent joint subluxation. The SvES includes a hand-supported frame and a force transducer. Three-hand postures were set to induce subluxation of the first metacarpal bone respective to the trapezium by conducting a stressed force on the thumb. They were determined as follows: (1) MP_S: the participants positioned their thumbs, with the nails parallel to each other, and pressed against the transducer using their metacarpophalangeal joints at the lateral side of both thumbs with the frame(Fig.1); and (2) KP_S: the participants held the force transducer between their thumb pad and the proximal interphalangeal joint of the index finger in the key pinch posture with hand on the frame; and (3) KP: the similar posture as KP_S without the frame and the palm side was touching the table. A fluoroscopic system obtained real-time moving images of the hand, with the main focus on the CMC joint. The image recording frequency was set at 10 Hz. The fluoroscopic images and the force data were collected synchronously.

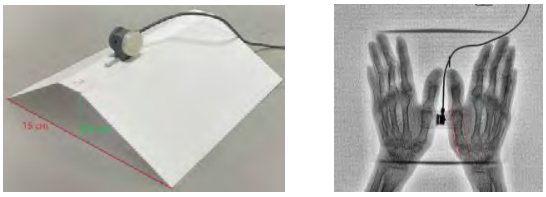

Figure 1 The main body of the custom stress-view evaluation system(left). The radiographic image used to determine the CMC joint radial subluxation ratio, where A indicates the amounts of the first metacarpal subluxation from the trapezium, and B represents the total width of the base of the first metacarpal bone (right)

RESULTS AND DISCUSSION

Table 1 shows the subluxation ratio occurring at the pressed force reaches maximal. Preliminary results suggested that the subluxation ratio of MP_S in the elder group was lower than in the other two age groups. This result might be caused by the soft tissue characteristics related to ageing. The effect of gender shows no particular trend, which may be due to the limited cases.

Table 1: The subluxation ratio of different age groups and gender.

	Male						Female					
	MP_S		KP_S		KP		MP_S		KP_S		KP	
Group	M	SD	M	SD	M	SD	M	SD	M	SD	M	SD
young	55.4	16.9	41.1	15.4	38.9	8.5	46.6	19.6	31.5	12.1	33	8.3
middle-aged	47.9	4.5	28.8	11.4	29.7	16.5	42.2	7.6	17.4	10.9	30.1	7.3
elderly	33.5	17.2	22.2	19.6	30.2	11.7	38.6	14.1	26	17.5	36.4	10.4

CONCLUSIONS

The study's result suggested that age affects the status of joint subluxation, and the effect of age should be considered in future clinical analysis. For future work, we will continue collecting data from subjects for more evidence.

ACKNOWLEDGEMENTS

This study was financially supported by the National Science and Technology Council of Taiwan under Grants MOST 109－2628－E－006－002－MY3.

REFERENCES

[1] Ladd, A.L. *Clin Orthop Relat Res* **472**(4): p. 1097-100. 2014.
[2] Kuo LC et al. *J Med Bio Eng* **38**: p.724-734,2018.

USING AN RGB-DEPTH CAMERA FOR MARKER-LESS ESTIMATION OF CONTACT BETWEEN HAND AND HANDRIM DURING IN-LAB WHEELCHAIR TENNIS PROPULSION

Enrico Ferlinghetti[1], Matteo Lancini[2], Riemer Vegter[3]
(1) DIMI, (2) DSMC, Università degli Studi di Brescia, Brescia, Italy.
(3) Center for Human Movement Sciences, University Medical Center Groningen, Groningen, The Netherlands.
Email: enrico.ferlinghetti@unibs.it

INTRODUCTION

The present work investigates marker-less measurements using vision systems for contact detection between hand and hand-rim in wheelchair propulsion. Measurement wheels or instrumented ergometers are good ways to measure kinetics, but lack the position of the hand in space.

METHODS

17 able-bodied participants with no prior experience in wheelchair propulsion pushed the wheelchair on the ergometer in six tests divided in two blocks: Byr (holding a tennis racket) and Bnr (free hands). Each block was tested in three different conditions: C1 (4 km/h for 90 s), C2 (5.4 km/h for 90 s), C3 (max speed for 10 s). The used measurement systems were an ergometer collecting torque and speed on both sides at a frequency of 100 Hz and a camera collecting both RGB and depth images at a frequency of 60 Hz, placed on the right side of the participant. For each RGB frame collected by the camera, the hand was identified by means of Mediapipe (MP) [1], able to detect 21 landmarks, as shown in (Figure 1). Using the maximum and the minimum value of the coordinates of each landmark, a region of interest (ROI) was located around the hand. The depth data of this ROI, obtained from the corresponding depth frame, were used to identify the hand point-cloud. The position of the hand had to be expressed with respect to the wheel. To do so, the centre and the circle of the hand-rim were recognized on the RGB image. Using the values of the corresponding pixels in the depth image, the best fitting plane in the hand-rim was then computed with a RANSAC method. Five features are extracted: radial and normal distance of the hand with respect to the wheel, their derivates and the ratio between the ROI height and width. These features were used to train different classifiers with two classes: Contact and No-Contact, whose ground-truth was obtained by the analysis of the torque applied, recorded by the ergometer [2]. The most accurate (MLP with 10,100 and 10 neurons, accuracy = 83%) was validated with a 5-fold validation on the 5 days of test. Finally, after a post-processing phase, the detection error in time was used to estimate the uncertainty.

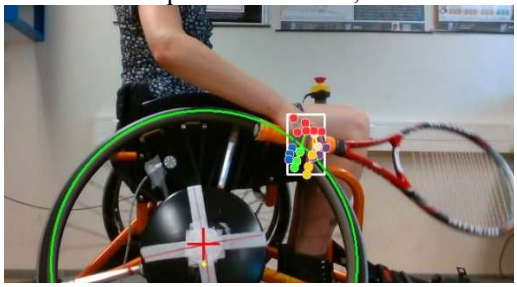

Figure 1: Hand recognized by Mediapipe during the propulsion of a wheelchair while holding a tennis racket

RESULTS AND DISCUSSION

The distributions of errors in contact detection for all the blocks and conditions was the following: -0.01 ± 0.12 s for start and 0.00 ± 0.12 s for end of contact, RMSE = 0.12 s for both). A distinction between the different test situations is presented in (Table 1). Since every frame in which the hand is not recognized by MP implies a gap for the contact detection algorithm, a relation between the performances of the two was expected. A lower RMSE for the tests executed with the racket (Byr) suggests that the contact detection algorithm performs better when the hand is holding the racket, even though the percentage of frames in which the hand is not recognized by MP is similar for the case with and without racket (≃9%). On the contrary, the percentage of frames not recognized by MP is proportional to the speed of the wheel, (and consequently the speed of the hand) but this does not affect the performances of the algorithm: the RMSE is similar for C1C2 and C3.

CONCLUSIONS

The present work shows the feasibility of the development of an algorithm able to detect the start and the end of the contact between hand and hand-rim using the relative position between the two obtained by means of marker-less vision systems. Further analysis should be carried out on the relation between the performances of the hand recognition algorithm (MP or an equivalent), and the contact detection algorithm.

REFERENCES

[1] F. Zhang et al., Jun. 2020, http://arxiv.org/abs/2006.10214

[2] R.J.K. Vegter et al., Mar. 2015, 10.1186/s12984-015-0017-5

Table 1: mean ± std dev [RMSE] of error in contact detection for Byr = with racket, Bnr = no racket, C1C2 = submaximal speed, C3 = sprint

	C1C2 (submax) Byr	C3 (sprint) Byr	C1C2 (submax) Bnr	C3 (sprint) Bnr
Start (s)	0.00 ± 0.12 [0.11]	-0.020 ± 0.075 [0.07]	-0.02 ± 0.14 [0.14]	-0.05 ± 0.13 [0.14]
End (s)	-0.02 ± 0.11 [0.11]	0.047 ± 0.070 [0.08]	0.01 ± 0.13 [0.13]	0.03 ± 0.14 [0.14]

Investigating the Long-Term Impacts of Hand Tractor Operation on the Upper Limb of Farm Operators

Josefa Angelie D. Revilla[1], Clarissa M. Pesigan[1], Stephanie Caridad DR. Landicho[1], and John Kenneth P. Punongbayan[1]
[1] Department of Industrial Engineering, College of Engineering and Agro-Industrial Technology, University of the Philippines Los Baños, Laguna, Philippines.
Email: jdrevilla@up.edu.ph

INTRODUCTION

In the Philippines, agriculture is one of the major sectors that provide livelihood to the people. Farming various crops is the most common activity. This uses different agricultural machinery such as the hand tractor or the two-wheel tractor. This is an equipment, driven or controlled by an operator, that helps in cultivating the farm land. A hand tractor is powered by either a diesel or gasoline engine. It is pushed forward by an operator on a puddy field. During operation, a downward push or vertical lift of the handle is sometimes necessary for easy maneuverability. The engine creates vibration of around 21 m/s^2 [1] that is proven to be transmitted to the handle. There have been little reports on how this level of vibration affects the operators in the long run. Hence, this investigation aims to identify how such vibration level influences the hand functionality of farm operators who have used a hand tractor for a long time.

METHODS

The study investigated 15 farm operators with a mean age and working experience of 36.7 ± 11.6 years old and 20.1 ± 12.2 years. Basic measurement such as height, weight, hand anthropometry, and handedness were recorded. Afterwards, grip strength (GS), pinch strength (PS), finger sensitivity, finger dexterity, and subjective discomfort along the upper limb were measured. Grip and pinch strength were measured using a Vernier hand dynamometer and Lab Quest 2 data logger. Finger sensitivity was assessed using the two-point discriminator test (TPDT) while finger dexterity was evaluated using the 9-hole peg board test (NHPT). The perceived discomfort along the upper limbs was rated using the Wong-Baker FACES scale. All tests were done for both the dominant and non-dominant hand side. The results were compared with related studies which determined a reference GS and PS value, NHPT performance, and TPDT result of healthy individuals with the same age range as the participants.

RESULTS AND DISCUSSION

Hand Strength

The mean GS of the experienced farm operators is 21.98 ± 5.79 kgf for the dominant and 19.46 ± 5.33 kgf for the non-dominant hand. Meanwhile, the mean PS is 12.13 ± 2.45 kgf and 10.89 ± 2.13 kgf for the dominant and non-dominant hand. Related studies determined that the GS of healthy men of the same age range is around 46-53 kgf and 42-50 kgf for the dominant and non-dominant side [2, 3, 4]. In addition, PS of healthy males is about 9-10 kgf and 9 kgf for the dominant and non-dominant side [4].

Finger Dexterity

Using the NHPT, the result led to 17.37 ± 1.38 seconds and 19.11 ± 1.99 seconds for the dominant and non-dominant hand. A similar study found that the NHPT of healthy males is 17-18 seconds and 18-20 seconds for the dominant and non-dominant hand [5].

Finger Sensitivity

Table 1 presents the TPDT results for the dominant and non-dominant hand. From related research, the normal minimal distance for the fingertips is 2-6 mm [6, 7].

Table 1. Median TPDT value (in mm)

Hand side	Thumb	Index	Middle	Ring	Small
Dominant	3	3	3	3	3
Non-dominant	3	2	2	2	3

Synthesis

Although the testing method may be different across the studies, the resulting GS of exposed farm operators is evidently lower than those of healthy men while PS and NHPT did not present a clear difference. Additionally, the TPDT values fell within the normal range. Subjectively, the upper limb discomfort perceived by the farm operators ranged from none to mild discomfort.

CONCLUSIONS

In conclusion, the long-term impact of constant exposure to hand tractor vibration is most evident on the reduction of grip strength. This signifies a strong tendency to develop upper limb MSD.

ACKNOWLEDGEMENTS

This study acknowledges the ECWRG Funding Program of the Office of the Vice President for Academic Affairs of the University of the Philippines.

REFERENCES

[1] Revilla JAD et al. *Philipp Agric Sci* **92**: 166-73, 2015.
[2] Amaral CA et al. *PLoS One* **14**: e0211452, 2019.
[3] Wang YC et al. *J Orthop Sports Phys Ther* **48**: 685-93, 2018.
[4] Mohammadian M et al. *Iran J Public Health* **43**: 1113-22, 2014.
[5] Mathiowetz V et al. *OTJR* **5**: 24-38, 1985.
[6] Thube S et al. *Int J Health Sci Res* **10**: 60-3, 2020.
[7] Jagad K et al. *J Emerg Technol Innov Res* **5**: 603-10, 2018.

Keynote speakers

Nina Suh, MD

Department of Orthopaedics, Emory University School of Medicine, Atlanta, GA, United States of America

Dr Suh received her medical degree and residency training at the Schulich School of Medicine & Dentistry at Western University. She then completed two years of fellowship training, subspecializing in wrist and hand reconstruction and trauma. Her first fellowship was completed at the Hospital for Special Surgery, New York, New York and her second at the Mayo Clinic in Rochester, Minnesota. She returned to Western in 2014 to join the Department of Surgery and in 2021 she relocated to Emory. Dr Suh's clinical interests encompass disorders of the wrist and hand, while her research interests include both biomechanical and clinical outcomes.

Unsolved Clinical Mysteries in the Hand and Wrist

The hand and wrist are composed of numerous bony and soft tissue elements, contributing to it being one of the most complex anatomical regions in the body. Musculoskeletal injuries of the hand and wrist also comprise the most common areas of injury with significant functional morbidity to the patient. Despite the gains in identifying and characterizing clinical conditions, there remains an incomplete understanding of the pathomechanics of injuries and the biomechanical impact of treatment options. The role of biomechanical investigation is increasingly being utilized to provide foundational work for the clinician given the anatomical complexity and is being leveraged to delineate the interplay of the various hand and wrist structures. This talk will discuss the current unsolved clinical mysteries in the hand and wrist that would benefit from further biomechanical investigation.

THE DIFFERENCE IN THE EFFICIENCY OF REACTIVE GRIP FORCE ADAPTATION DURING STATIC AND DYNAMIC TASKS BETWEEN CHILDREN AND ADULTS

Jie-Ning Yu[1], Chieh-Hsiang Hsu[1], Yu-Ching, Lin[2], Yu-Chen Lin[3], Kang-Chin Yang[4], Li-Chieh Kuo[1,2], Hsiu-Yun Hsu[1,2]

[1] Department of Occupational therapy, National Cheng Kung University, Tainan, Taiwan.
[2] Department of Physical Medicine and Rehabilitation, National Cheng Kung University Hospital, Tainan, Taiwan.
[3]Department of Occupational therapy, Da-Yeh University, Changhua, Taiwan
[4]Medical device innovation center, National Cheng Kung University, Tainan, Taiwan
Email: hyhsu@mail.ncku.edu.tw

INTRODUCTION

Daily activities are full of unexpected perturbations. Manipulating the objects with fingertips in an unpredicted context requires well-reactive grip force adaptation, which immediately adjusts the grip force based on adequate sensory feedback. Analysis of reactive grip force adaptation has been considered an indicator of hand sensorimotor control ability in response to environmental perturbation [1]. The use of the adaptation strategy is less efficient in younger children. With age, this strategy will become mature. The difference in the efficiency of force adaptation between children and adults was studied purely in one context[2]. However, perturbations in daily living may emerge during static or dynamic tasks. It has never been investigated separately. Thus, this study aimed (1) to understand if there is any difference in adaption strategies used in static and dynamic movements and (2) to investigate the efficiency of force adaptation between children and adults in static and dynamic tasks.

METHODS

This study recruited five adults (age = 23.8±1.9 years) and five children (age= 4.3±0.5 years). A novel pinch apparatus was used for measuring reactive grip force adaptation in static and dynamic tasks.

The novel pinch apparatus is made of a 3D-printed cuboid (size = 25×25×65 mm^3 weight = 90g) which contains a force sensor to record grip force. It is connected to a fixed-base platform that contains a 35g block with a string and is controlled by a button that releases the block to cause a perturbation.

In the static task, subjects grip and lift the pinch apparatus to 15cm and hold for 15s. In the 5^{th} second, the examiner presses the button unexpectedly to release the block. The other task is the dynamic task in which subjects lift the apparatus to 25cm and hold it for 10s. At 15cm, the perturbation is released. There are three trials in each task.

The efficiency of force adaptation was represented by (1) reaction time: the time delay between the impact and peak grip force; and (2) grip force rate: the ratio of peak grip force and the maximum grip force.

RESULTS AND DISCUSSION

In Table 1, comparing the reaction time and grip force rate between static and dynamic tasks, there was no significant difference found for children. However, for adults, no significant difference in reaction time but in grip force rate was found between static and dynamic tasks. Besides, children showed a significant delay in the reaction time and higher values of grip force rate in the dynamic task compared with adults.

CONCLUSIONS

We found that the grip force rate in the static task is larger than in the dynamic one for adults. The reason may be the amplitude of the grip force exerted is relatively small in the static task. Thus, the perturbation seemed to have a higher magnitude of impact on maintaining grip stability in the static task.

Moreover, children perform longer latency of reaction time and a higher percentage of grip force rate. It is consistent with the previous study in which age effects are evident in the delay to max grip force and a larger percentage of maximal grip force[2]. Therefore, the efficiency of utilizing forces is less efficient in children. However, the number of subjects in this study is still insufficient and limited to a specific age group. Therefore, it still needs further investigation to identify the difference better.

REFERENCES

[1] Bleyenheuft Y et al. *Journal of motor behavior* **42**(3): 169-177, 2010.
[2] Chiu, H.Y. et al. *Journal of Orthopaedic Research* **27**(8): 1116-1121, 2009.

Table 1: Descriptive statistics and the difference between group and within the group

	Children (n=5)			Adults (n=5)			Difference between adults and children	
	Static	Dynamic	*p*	Static	Dynamic	*p*	Static *p*	Dynamic *p*
Reaction time(sec)	0.13 ± 0.03	0.13 ± 0.03	0.686	0.1 ± 0.01	0.09 ± 0.01	0.068	0.31	0.016*
Grip force rate	0.5 ± 0.09	0.5 ± 0.06	0.465	0.67 ± 0.11	0.17 ± 0.04	0.043*	0.31	0.016*

*$p<0.05$

DO MUSCLE ACTIVITY PATTERNS VARY ACCORDING TO THE SEVERITY OF CARPOMETACARPAL OSTEOARTHRITIS DISEASE?

Tamara Ordonez Diaz[1], Kalyn Kearney[1], Thomas W. Wright[2] and Jennifer A. Nichols [1,2]
[1] J. Crayton Pruitt Family Department of Biomedical Engineering, University of Florida, Gainesville, USA
[2] Department of Orthopaedic Surgery & Sports Medicine, University of Florida, Gainesville, USA.
Email: tordonezdiaz@ufl.edu

INTRODUCTION

The thumb is essential for manipulating objects and performing tasks such as pinching and grasping. Its strength and dexterity stem from the interaction of 9 thumb muscles, particularly at the carpometacarpal (CMC) joint with 3 degrees of freedom. Unfortunately, when CMC osteoarthritis (OA) occurs, it can cause debilitating pain, diminished strength, and limited range of motion. [1]. Despite the importance of the thumb muscles, limited research has been conducted on healthy or pathologic cohorts [2-4] due to the challenges posed by the size and location of these muscles and the constraints of surface electromyography. Currently, there is a gap in our understanding of muscle activity in patients with CMC OA, including how these muscles may (or may not) compensate for pain and its impact on hand biomechanics. The purpose of this study was to investigate differences in muscle activity across the clinical spectrum of CMC OA.

METHODS

Women with clinically diagnosed CMC OA [n = 16; age 65.6 ± 11 years] and healthy, pain-free thumbs [n = 15, age 62.1 ± 12 years] were recruited for this IRB-approved study. Participants completed self-reported questionnaires on pain and function, including the Australian/Canadian Osteoarthritis Hand Index (AUSCAN). Disease severity was classified from radiographs using the Eaton-Littler scale. Muscle activity was recorded during range of motion (ROM) tasks: flexion/extension, ad/abduction, opposition, and circumduction. Each task was performed three times. Muscle activity was recorded from 4 extrinsic and 4 intrinsic muscles using fine-wire electromyography (fEMG) sampled at 3,000 Hz. Data were filtered, rectified, amplitude normalized, and time normalized to percent task completion. Analyses evaluated differences in muscle activity across participants.

RESULTS AND DISCUSSION

No clear differences in muscle activation existed between the two recruited cohorts. However, imaging and self-reported pain data demonstrated an overlap between the recruited cohorts (Fig. 1A), suggesting little correlation between pain and disease severity. To determine if there were any muscle activation patterns that separated participants into meaningful subgroups, various clustering methods were employed, including dynamic time warping (DTW), functional principal component analysis (fPCA), and non-negative matrix factorization (NMF). Results were examined to decide if self-reported pain, disease severity, or other measured characteristics could describe the identified clusters.

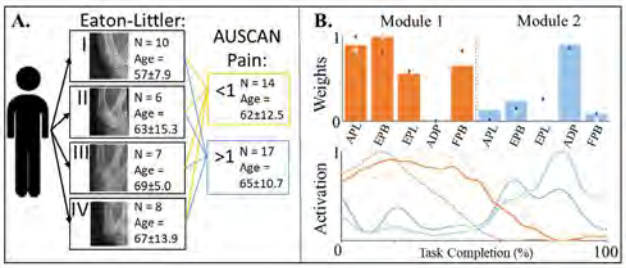

Figure 1A. Patient groups based on disease (Eaton-Littler classification) or pain severity (AUSCAN). **B.** Average muscle synergy using two modules (blue and orange) with examples of individuals with early- (light) versus end-stage (dark) disease.

When presented with 8 muscle activation patterns for each participant, both fPCA and DTW failed to identify meaningful subgroups. This outcome and the variability in muscle activation patterns across and within participants highlight the complexity and redundancy of thumb muscle actions. Clusters could be identified when examining each muscle individually, but valuable information about muscle coordination and co-activation was lost. Importantly, NMF analysis of muscle synergies, revealed that participants with diverse pain and disease severity levels could be grouped together. NMF results also showed agonist and antagonist muscles were activating simultaneously (Fig. 1B), emphasizing the significance of accurately measuring co-activation. To further understand the biomechanical changes in CMC OA, adding more features to clustering analysis, such as kinematic data and co-activation indices, is of immediate interest.

CONCLUSIONS

Our results elucidate the complex presentation of CMC OA and indicate a need for feature extraction techniques capable of analyzing multimodal datasets. Through these efforts, a more comprehensive understanding of CMC OA may be achieved.

ACKNOWLEDGEMENTS

Funding from the National Institutes of Health NRSA Parent F31-Diversity and R01 AR078817.

REFERENCES

[1]Kloppenburg et al. *Osteoarthr Cartil* **23**:772-86, 2015. [2]Kerkhof et al. *J Electromyogr Kinesiol* **30**:131-136. [3]Birdwell et al. *J Neurophysiol* **110**: 1385-1392. [4]Johanson et al. *J Hand Surg Am* **26**:698-70

Fatigue of Hand Muscles Following Pinch Grip Quantified by Surface Electromyogram

Kiatbodin Wanglertpanich[1], Yerkarn Bekenov[1,2] and Angela E. Kedgley [1,*]
[1,*] Department of Bioengineering, Imperial College London, London, United Kingdom.
[2] Leicester Medical School, College of Life Sciences, University of Leicester, Leicester, United Kingdom.
Email: kiatbodin.wanglertpanich19@imperial.ac.uk

INTRODUCTION

Pinch grip is a basic hand motion that allows string instrumentalists to perform music. However, muscle fatigue degrades their performance and can lead to overuse syndrome (OS)[1]. Muscle fatigue can be detected by increases in surface electromyographic (EMG) signals, since muscles are prone to electrically activate to compensate for decreases in muscle capacity[2]. We aimed to define muscle fatigue by changes in EMG signal and maximum endurance time (MET), used in a computational model to define decreases in muscle capacity. We hypothesised that (1) the EMG signals of muscles, induced by the requirements of the fingers' motions, would increase during maximum pinch force (MPF) tasks due to muscle fatigue; (2) the relative increase in EMG signals would increase with required pinch force; (3) fatigue, expressed as MPF following a trial divided by initial MPF, would increase with required pinch force.

METHODS

Twenty-two participants performed five static pinch trials to exhaustion, with the required force defined as a percentage of the individual's initial MPF. EMG sensors were attached on the left arm to monitor the flexor digitorum profungus (FDP), flexor digitorum superficialis (FDS), flexor pollicis longus (FPL), extensor digitorum communis (EDC), extensor indicis (EI), extensor pollicis longus (EPL), abductor pollicis longus (APL), abductor pollicis brevis (ABP) and first dorsal interosseous (DI) muscles. A second MPF task was performed immediately following the endurance task. At least 5-minutes of rest after each task ensured recovery from any fatigue.

RESULTS AND DISCUSSION

The EMG signals for all muscles increased from the baseline amplitude recorded during the first MPF task, when MPF was less than 50% (Figure 1). These increases agreed with increases in the post-task MPF ($p<0.01$, Table 1). In contrast, MET exponentially decreased in order of the level of the task (Table 1). Both EMG signals and MET demonstrated the level of muscle fatigue. However, eight of nine muscles did not indicate differences in EMG signals from 50 to 70% MPF; the exception being APL ($p<0.05$). Since APL is not a prime mover in flexing or extending the thumb, participants might have different techniques to stabilise their joints. The EMG signal was not sufficient to indicate the level of muscle fatigue from 50 to 70% MPF task while the MET showed differences for all levels of pinch ($p < 0.001$).

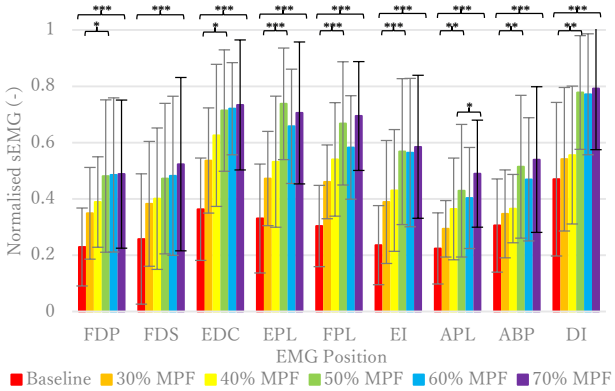

Figure 1 Normalised EMG signals during maximum voluntary contraction after static endurance tasks of varying %MPF

CONCLUSIONS

Muscle fatigue was related to decreasing post-task MPFs, which agreed with both rise of EMG signals and drop of MET for 30 to 50% MPF tasks. EMG was not sufficient to differentiate levels of fatigue from 50 to 70% MPF tasks, whereas the METs were able to show this. Combining these two factors will, therefore, be able to predict the decrease in MPF. These factors may be included to a computational model to calculate decreases in muscle capacity and applied to activities of instrumentalists.

REFERENCES

[1] Fry H J. *J R Soc Med:* ***81****:* 572-5, 1988.
[2] Masuda K et al. *J Electromyogr Kinesiol* **9**: 39-46, 1999.

Table 1: Normalised post-task maximum pinch force (MPF) and maximum endurance time (MET) following static endurance tasks of varying %MPF

Sub-maximum task [%MPF]	30	40	50	60	70
Normalised MPF [%]	61 (10)	69 (9)	76 (11)	80 (11)	84 (10)
MET [s]	192.7 (95.8)	90.2 (44.1)	53.6 (30.1)	32.3 (13.2)	22.4 (7.3)

METHOD FOR ASSESSING THE FINE MOTOR SKILLS SYNERGIES BASED ON COMPUTER VISION

Andrey Pomerantsev
Independent researcher
Email: a.pomerantsev.1981@gmail.com

INTRODUCTION

The coordinated work of the fingers is an indicator of human health and the key to professional skill. The aim of the work was to create a method for quantitative control of fine motor synergies based on computer vision. The study of fine motor skills is actual theme at different ages and for different purposes. At preschool age, fine motor skills allow to estimate the degree of child readiness for school. Cognitive abilities, memory, speech, logic, mathematical abilities, concentration, imaginative thinking evolves concurrently with fine motor skills. Fine motor skills determine the level of skill in many professions. Musicians (conductors, pianists, accordionists), doctors (dentists, surgeons), cyber sportsmen, IT specialists, jewelers and representatives of many other professions have well-developed and specific fine motor skills.

METHODS

The proposed method is based on the MediaPipe open source framework, exactly the Mediapipe Hands neural network. Computer vision allows to determine the palm by analysis of the video stream. First, neural network detects the palm area in the frame, and then localizes 21 nodal points to determine the gesture (Figure 1). Due neural network and the author's method of assessing fine motor skills [1], computer application FingerFit 4.0 was developed. During changing gestures, certain synergy is used [2]. The possible combination of straightened and bent fingers of one hand is 2^5 =32. The number of gestures changes combinations is $2^5x2^5=2^{10}$=32x32=1024. From this number, it is necessary to exclude 32 repetitive gestures and 160 gestures when only one finger is involved in the work. Thus, the final number of synergies is 832. The app fixes the synergy only if all fingers participate in the gesture construction at once. The time to rebuild the gesture is 1 second. If a person does not have time, the app asks to return to the original gesture. The complexity of synergy is estimated by the total time that a person spends on changing a gesture.

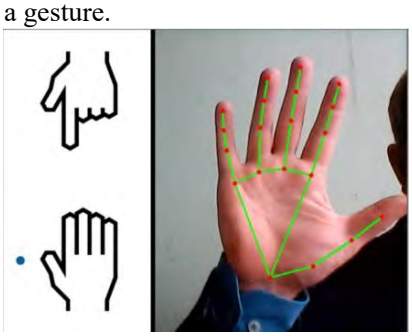

Figure 1 Computer application interface.

RESULTS AND DISCUSSION

A 7-year-old girl with no health abnormalities or delays participated in the method approbation. We evaluated 145 synergies by a sequence of 32 random gestures. The most complex synergies are presented in Table 1.

CONCLUSIONS

A fine motor skills assessment method was developed with using the MediaPipe framework. The method is based on the definition and quantity control of synergies. The presented approach will be advisable to use for the control of professional skills, assessment of the child's readiness for school, as well as the diagnosis of neurological diseases. The accumulated test results in the future will allow to establish the boundaries of the norm and draw objective conclusions about fine motor skills level.

REFERENCES

[1] Patent 2717365 C1 RU.
[2] Latash, M. L. *Exp. Brain Res.* **239(10)**: 2951-2967, 202.

Table 1: The most complex synergies.

Synergy	Time implimintation, sec
+px+med-a+min	75
+p-i+med+ax	21
-p+ix-a+min	20

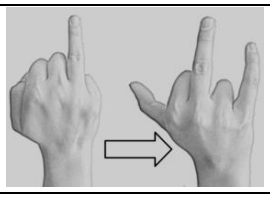

Note. Finger designations are given in accordance with their Latin names: p –pollex , I – index, med – medius, a – annularis, min – minimus; «+» – extension, «–»–flexion.

Coordinated muscle activity during chopstick manipulation

Kazuya Kurauchi, Hiroshi Kurumadani, Shota Date and Toru Sunagawa
Graduate School of Biomedical and Health Sciences, Hiroshima University, Hiroshima, Japan.
Email: kazu.hiro.bmk@gmail.com

INTRODUCTION

Chopsticks manipulation is one of the skillful finger movements. In rehabilitation, reacquisition of chopstick manipulation for disabled hands includes exercises such as manipulating chopsticks and picking up objects. Many intrinsic and extrinsic hand muscles are involved in chopstick manipulation. Previous reports of hand-muscle coordination have indicated that the intrinsic and extrinsic hand muscles have intermuscular coordination between these muscles[1]. Highly skilled finger movements require intrinsic hand muscle activities, such as the lumbrical muscle, and intermuscular coordination between intrinsic hand muscles[2]. Hand muscle activities may thus have several intermuscular coordination during chopsticks manipulation. This study aimed to examine the intermuscular coordination between the intrinsic and extrinsic hand muscles during chopstick manipulation.

METHODS

Twenty healthy right-handed adults performed six object-grasping tasks by using chopsticks. The grasping tasks consisted of three object widths (1, 2, and 3 cm) and two weights (10 and 40g). Each task was conducted in 10 trials. The surface electromyography measured 12 muscle activities during the task with a sampling frequency of 1000 Hz. The tested muscles were eight intrinsic (first, second, and third lumbrical muscles, first, second, and third dorsal interosseous muscles, flexor and abductor pollicis brevis) and four extrinsic (flexor digitorum superficialis, extensor digitorum, flexor carpi ulnaris, and extensor carpi radialis muscle) hand muscles.

Furthermore, the movements of the chopstick tips were measured with a three-dimensional motion capture system to identify the opening and closing movements of the chopsticks. The obtained electromyographic signals were filtered and smoothed and then extracted from the initial chopstick opening to the end of the closing movement. The muscle activity waveforms during the chopstick opening/closing movement were extracted for five trials for each task. Next, muscle synergy analysis using non-negative matrix factorization was performed on all muscle activity waveforms for all tasks, and the muscle weighting components and time-varying patterns with a variance accounted for above 90% were extracted. Muscle-weighting components greater than 0.4 were defined as those with high contributions to the extracted synergy.

RESULTS AND DISCUSSION

Five muscle synergies were extracted from the opening to closing chopstick movements (Figure 1). The five synergies were divided into three main categories. The first was intrinsic intermuscular coordination, such as between the lumbrical muscles and between the thenar and the interosseous muscles. The second was extrinsic intermuscular coordination between the extensor digitorum and extensor carpi radialis. The third was intermuscular coordination between intrinsic and extrinsic muscles, such as between the interosseous muscle and the flexor digitorum profundus. This coordination may be due to the same or close location of the nerve roots innervating the respective muscles.

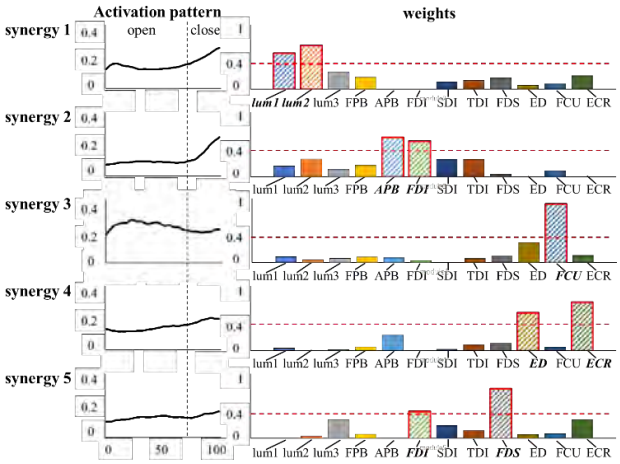

Figure 1 Results of non-negative matrix factorization. Basic pattern (left) and contributions of muscles (right). lum1: first lumbrical muscle, lum2: second lumbrical muscle, lum3: third lumbrical muscle, FDI: first dorsal interosseous muscle, SDI: second dorsal interosseous muscle, TDI: third dorsal interosseous muscle, FPB: flexor pollicis brevis muscle, APB: abductor pollicis brevis muscle, FDS: flexor digitorum superficialis muscle, ED: extensor digitorum muscle, FCU: flexor carpi ulnaris, ECR: extensor carpi radialis

CONCLUSIONS

We found three intermuscular coordination during chopstick manipulation: coordination between intrinsic hand muscles, extrinsic hand muscles, and intrinsic and extrinsic muscles. The results of this study may lead to the establishment of an efficient method for improving chopstick manipulation.

REFERENCES

[1] Santello M et al. *Frontiers in Computational Neuroscience* **7**: 23, 2013.

[2] Maier MA et al. *Experimental Brain Research* **103**: 108-122, 1995.

Keynote speakers

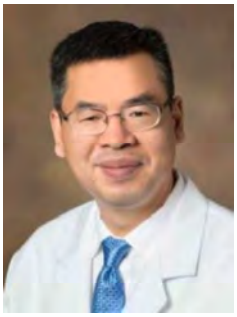

Zong-Ming Li, PhD

Orthopaedic Surgery, University of Arizona, Tuscan, AZ, United States of America

Zong-Ming Li is the William and Sylvia Rubin Chair of Orthopedic Research, and Professor of Orthopedic Surgery, Biomedical Engineering, and BIO5 Institute at the University of Arizona. Dr. Li is the Vice Chair for Research in Department of Orthopedic Surgery and Associate Director of University of Arizona Arthritis Center. Dr. Li is a Fellow of the American Institute for Medical and Biological Engineering (AIMBE), Fellow of American Society of Biomechanics (ASB), Fellow of the Institute of Electrical and Electronics Engineers (IEEE), Fellow of Asia-Pacific Artificial Intelligence Association (AAIA), and Fellow of American Society of Mechanical Engineers (ASME). Dr. Li is the recipient of ASME Savio L-Y. Woo Translational Biomechanics Medal. Dr. Li is interested in musculoskeletal system in general with a research focus on biomechanics and motor control of the hand.

Non-Surgical Carpal Arch Space Augmentation for Median Nerve Decompression

The carpal tunnel is a tightly bounded space, making the median nerve prone to compression and eventually leading to carpal tunnel syndrome. Carpal tunnel release surgery transects the transverse carpal ligament to expand the tunnel arch space, decompress the median nerve, and relieve the associated symptoms. However, the surgical procedure unavoidably disrupts essential anatomical, biomechanical and physiological functions of the wrist, potentially causing reduced grip strength, pillar pain, carpal bone instability, scar tissue formation, and perineural fibrosis. It is desirable to decompress the median nerve without surgically transecting the transverse carpal ligament. This talk is to review several approaches we have developed for nonsurgical carpal arch space augmentation (CASA), namely, radio ulnar wrist compression, muscle-ligament interaction, palmar pulling, and collagenolysis of the transverse carpal ligament. Briefly summarized is the research work on the CASA topic about theoretical considerations, in vitro and in situ experiment, computational modeling, and human subject studies with asymptomatic and carpal tunnel syndrome hands.

CHALLENGES IN DEVELOPING A HEALTHY FINITE ELEMENT WRIST MODEL: LIGAMENTS

Andrés Mena[1], Ronit Wollstein[2], and James Yang[1*]
[1]Texas Tech University, Lubbock, Texas 79409, USA
[2]New York University, New York, USA
*Email: james.yang@ttu.edu

INTRODUCTION

The wrist is a complex human joint that participates in most functional daily activities and is thus prone to pathology and injuries. Understanding how the wrist operates under normal conditions is crucial to study novel treatments and prevention, but wrist biomechanics remains vastly unexplored. Experimental methods have been used extensively to study the wrist [1]. However, the expensive equipment and natural limitations of *in vivo* and *in vitro* testing pose a challenge for the study of the wrist. Numerical methods like the finite element method (FEM) have been used to study other human joints [2] and are now being considered as a viable option to analyze important mechanical variables of the complex wrist joint. Since there is no accepted universal methodology to create finite element models, authors have opted for different modeling techniques, making comparison and validation extremely difficult. A fundamental part of most models is ligaments, but the number included in each work and their material properties vary depending on the authors [3]–[4]. Therefore, a study is performed to investigate the effects of different ligament configurations on the wrist's stress distribution and load transfer.

METHODS

Several finite element models were developed using computed tomography (CT) scans from a healthy right wrist (68-year-old male). The CT images were imported into 3D Slicer [5], manually segmented, and smoothed to create surface meshes of each bone. The bones considered were the distal radius, ulna, eight carpal bones, and a section of the metacarpals. The surface meshes were then imported into IA-FEMesh [6] to create volumetric meshes of each bone using 8-node brick elements. The volumetric meshes were imported into LS-DYNA (Livermore Software Technology Corporation, Livermore, CA, USA) to assemble the model. Cortical bone was modeled by extruding specific bone surfaces with shell elements with constant thickness. Linear elastic isotropic material properties were assigned to cortical (E=18 000 MPa, ν= 0.2) and cancellous (E=100 MPa, ν= 0.25) bone [5]. Soft tissues like cartilage and ligaments were manually incorporated into the model after consulting the original CT scans and other sources [7]. Cartilage was modeled using 8-node brick elements by extruding specific regions of the bone surface. Ligaments were implemented in the model using multiple linear springs. An original healthy model containing sixty ligaments [4] is considered as a control model. Then several modifications based on different experimental and computational studies [8] were evaluated. The following regions are evaluated: metacarpal, carpometacarpal, ulnar wrist, and radial wrist. Loads accrued from in vivo studies were applied to the metacarpal heads/carpometacarpal joints. As boundary conditions, the bottom ends of the radius and ulna were fixed. Further constraints were applied to the metacarpals and carpals to prevent displacement in the final model [4]. Contact was considered in the models using a frictionless or frictional surface-to-surface [9] scheme.

RESULTS AND DISCUSSION

The variables that will be retrieved from the simulation are stress distribution, contact pressure, and load transfer. These variables will be obtained for the whole model, important wrist regions (radial and ulnar side), and individual carpal bones.

CONCLUSIONS

The effects of completely removing ligament groups will be investigated to understand their contribution to computational stability and wrist biomechanics.

REFERENCES

[1] Kaufmann *et al. J Hand Surg Am* **31**: 1142–1148. 2006.

[2] Liu *et al. Front Bioeng Biotechnol* **10**: 2022.

[3] Bajuri *et al. Med Biol Eng Comput* **51**: 175–186. 2013.

[4] Gislason *et al. Med Eng Phys* **32**: 523–531. 2010.

[5] Fedorov *et al. Magn Reson Imaging* **30**: 1323–41. 2012.

[6] Grosland *et al. Comput Methods Programs Biomed* **94**: 96–107. 2009.

[7] Hirt *et al. Thieme Medical Publishers.* 2016.

[8] Wei *et al. Ann Biomed Eng* **48**: 1181–1195. 2019.

[9] Chamoret *et al. Computer Assisted Surgery* **21**: 22–29. 2016.

MULTI-OBJECT AND MULTI-FEATURE MODELS OF THUMB ANATOMY FOR POPULATION-BASED MORPHOLOGICAL ASSESSMENT

C. Farrell[1], B. Borotikar[2], E. Vereecke[3] T.Mutsvangwa[1]
[1]Human Biology, University of Cape Town, Cape Town, South Africa
[2]Symbiosis Centre for Medical Image Analysis, Symbiosis International University, Pune, India
[3]Development and Regeneration, KU Leuven, Kortrijk, Belgium
Email: cait.natalie.farrell@gmail.com

INTRODUCTION

Trapeziometacarpal (TMC) joint osteoarthritis (OA) is characterised by the degeneration of bone and cartilage in the basal thumb joint [1]. However, potential biomechanical factors that contribute to the onset and progression of OA are difficult to measure *in vivo*. We have developed image-based data driven methods to compare TMC joint morphology between OA-affected and healthy subjects. Dynamic multi feature-class Gaussian process models (DMFC-GPMs) [2] are used to model variation in the shape, pose, and intensity feature classes of the first metacarpal (MC1) and trapezium and anatomical features indicative of the onset and development of OA in the joint are determined.

METHODS

Three feature classes (shape, pose, and intensity) were extracted from the CT scan data of 38 participants (12 with TMC OA). Each participant was imaged in a series of standardized positions which allowed for the subject-specific pose variation as a feature class. This feature class cannot be represented in a single-object model. The bones were segmented semi-automatically to reconstruct 3D bone surface meshes and tetrahedral volume meshes. Dense correspondence within surface meshes and volumetric-shape-intensity meshes was established and latent space computation was used to build the individual DMFC-GPMs. Three DMFC-GPMs were built representative of the healthy, TMC OA, and the combined datasets.

The differences in the mean morphologies of the TMC OA and healthy groups were evaluated through the comparison of five anatomical features. A custom-written MATLAB code was used to determine the shortest distance between the articular surface of the trapezium and MC1 for each model. An anatomical 3D CAD software package was used determine the planes of best fit to manually measure both the volar beak angle and trapezial inclination of the mean shape of the MC1 and trapezium, respectively. The surface area of the articular facets was measured manually by delineating the edge of the facet. A custom-written sphere-fitting python code was used to calculate the average local curvature along the volar-dorsal and radio-ulnar axes of each bone. Preliminary models of the healthy and TMC OA datasets were built comprising of 3 participants each in a series of standardized positions.

RESULTS AND DISCUSSION

Four additional samples taken from each model were used to analyse the differences between datasets using a two sample, two-tailed T-test assuming equal variance (Table 1). TMC joint space was decreased whilst the surface area of the articular facets was increased for both the MC1 and trapezium bones of TMC OA. The trapezial inclination of TMC OA patients showed a more obtuse angle, indicating possible growth of osteophytes along the contour of the trapezial articular facet in late-stage OA. Analysis of the curvature of the articular facets indicates an increased radius of curvature along the radial-ulnar axis and the dorsal-volar axis of an OA-affected trapezium and MC1, respectively.

CONCLUSIONS

The DMFC GPM of TMC could be effectively used to assess five quantifiable anatomical features which are associated with TMC OA using standard CT scans.

ACKNOWLEDGEMENTS

This research uses retrospective data collected by researchers at KU Leuven (ethical approval S65627). We acknowledge South African DST/NRF SARChI (grant no. 98788) for funding this research.

REFERENCES

[1] Martel-Pelletier, J, et al. *Nat Rev Dis Primers* 2:16072, 2016
[2] Fouefack, JR, et al. *Med Image Anal* 85:102730, 2023

Table 1: Assessment of anatomical measures in a control and OA-affected dataset (Note: a negative sign indicates a concave curvature).

Anatomical Measure		Control Group	OA-Affected Group	p-value of two sample, two tailed T-test
Surface area of articular facets (mm^2)	MC1	112	186	1.06 E-4
	Trapezium	132	165	4.16 E-3
Curvature of articular facets (mm^{-1})	MC1 dorsal-volar	-0.112	-0.088	3.53 E-5
	MC1 radial-ulnar	0.111	0.086	1.41 E-2
	Trapezium dorsal-volar	0.099	0.087	1.22 E-4
	Trapezium radial-ulnar	-0.077	-0.054	2.34 E-3
Minimum distance between articular facets (mm)		0.8326	0.0590	1.36 E-5
Angle of trapezial inclination (°)		63.6	68.3	0.86
Angle of volar beak protrusion (°)		4.70	13.9	2.62 E-6

EVALUATION AND COMPARISON OF IN-VITRO JOINT KINEMATICS USING MOTION-BASED COORDINATE FRAMES VS. ANATOMICAL LANDMARKS

Mohammad M. Haddara PhD[1,2], David T. Axford MESc.[1,3], Louis M. Ferreira PhD, PEng[1,3]
[1]Roth|McFarlane Hand and Upper Limb Centre, St Joseph's Health Care, London ON, Canada
[2]School of Biomedical Engineering, Western University, London ON, Canada
[3]Department of Mechanical and Materials Engineering, Western University, London ON, Canada
Email: mhaddara@uwo.ca

INTRODUCTION

Anatomical frames for upper limb segments have previously been proposed by the International Society of Biomechanics (ISB) [1]. However, a limitation of creating anatomy-based frames is the need to denude to locate and digitize unique features on bones; introducing both intra- and inter-user variabilities that hamper reproducibility across research groups. Therefore, the purpose of this study was to quantify and validate the use of a new Motion-based Coordinate System (MCS) functional frame definition for finger joints using helical axes (HA) in an *in-vitro* setting. This model was directly compared to the standardized ISB anatomical frames.

METHODS

Eleven digits from 4 fresh-frozen upper extremities were utilized. Active finger flexion was controlled using a previously reported finger motion simulation protocol with flexor tendons moving in displacement control at a rate of 0.6 in/sec against a constant 10 N extensor antagonist load and vice versa for finger extension [2]. Joint kinematics was tracked using an electromagnetic transmitter system where rigid fixation of the trackers in bone was achieved by an interference tolerance fit. Discrete motion pathways of each segment were dictated in each bone segment to obtain the associated mean helical axis orientations required for coordinate system building. Two sets of frames were constructed: the landmark definition corresponded to implementation of ISB' anatomical frames whereas functional frames included a functional joint axis. Both constructed frames were further validated with goniometer measurements. Finger joint flexion/extension were measured and mean differences and deviations between methodologies were computed for all digits. A three-way repeated measures ANOVA (factors: Joint (MCP, PIP, DIP); Axes (X, Y, Z); Frame Definition (MCS, ISB)) was conducted to evaluate differences in each cardan angle. Furthermore, a paired t-test and a linear regression for correlation were also computed for a further validation of the local frame definition in the Z-axis (i.e. flexion/extension).

RESULTS AND DISCUSSION

The mean joint angle about the X-axis (add-abd), Y-axis (int-ext rot), and Z-axis (flex-ext) were computed (Figure 1). Non-significant differences were reported for both MCS and ISB compared to goniometer readings at 95% CI. Unlike ISB, all joints under MCS and goniometer readings were strongly and significantly correlated. Average joint angle deviations of about 2.7° were measured for both MCS and ISB across all three axes. Largest deviations were observed at the PIP and DIP joints along the int-ext rot and abd-add axes, with flexion-extension axes achieving the lowest deviations in all joints. In addition, A three-way ANOVA resulted in an insignificant mean difference of 0.151° between MCS and ISB (p=0.923). Repeatability of MCS and ISB along the flexion-extension axis following 5 motion cycles were measured to be 0.64° and 0.86°, respectively.

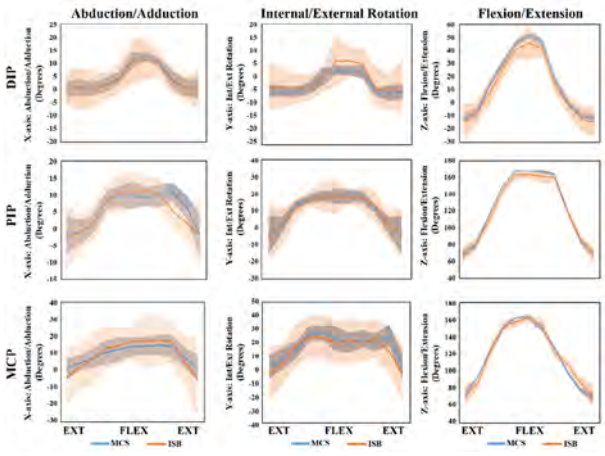

Figure 1 Mean angles measured by MCS and ISB local frames for each joint (DIP, PIP, MCP) along its respective X-, Y-, and Z-axes throughout one full active motion cycle are illustrated above. MCS are denoted by blue lines where ISB are denoted by orange lines.

CONCLUSIONS

Our findings support the use of the MCS methodology presented in this study in measuring accurate and reproducible finger joint kinematics, compared to ISB recommendations. To our knowledge, this is the first study that evaluates the accuracy of helical axes during active in-vitro finger motion without the use of virtually constructed motion pathways of bone segments in computed tomography (CT) scans.

REFERENCES

[1] Wu G et al. *J Biomech* **5**: 38, 2005.
[2] Haddara MM et al. *HAND* **5**:17, 2020.

FAMILIARITY EFFECT ON HANDWRITING PERFORMANCE IN SCHOOL-AGED CHILDREN

Wen-Feng Huang[1], Pin-Chen Hung[1], Tien-Ni Wang[1], Hao-Ling Chen[1]
[1] School of Occupational Therapy, National Taiwan University, Taipei, Taiwan, R.O.C
Email: hlchen@ntu.edu.tw

INTRODUCTION

Handwriting is very important for school-aged children. Children in Taiwan have to keep learning to write different characters in their early school years. Considering the busy schedules of school-aged children, efficiently producing handwritten scripts is essential for them. Children who are unfamiliar with the newly learned characters are considered to write inefficiently. However, relevant research was insufficient. Therefore, this study aimed to investigate the familiarity effect of characters on handwriting performance from the kinematic and kinetic perspectives for school-aged children in Taiwan.

METHODS

A convenience sample of 30 lower-grade children was recruited. They were asked to perform copy tasks at their own pace while copying characters as legibly as possible. To investigate the familiarity effect on handwriting kinematics and kinetics, two copy tasks, namely the *familiar task* and the *unfamiliar task,* were administered using a newly-developed tablet-based evaluation of Chinese handwriting (TECH) [1]. The TECH was shipped in a pressure-sensitive tablet with a wireless pen. The *familiar task* consisted of 20 high-frequency Chinese characters taught in the first-grade curriculum in Taiwan. The *unfamiliar task* consisted of 20 Hanguls (i.e., Korean characters) that have similar visual-spatial features to Chinese characters (e.g., square arrangement, multiple compounds, sharp turns, complex stroke directions, etc.). The assembly of the copy tasks considered the visual-spatial features of the construction of a copying character to ensure the equity of task difficulties. Additionally, the average stroke number of a copying character was identical in the two tasks. The TECH recorded the *On-surface* and *In-air movements* (Figure 1) of the pen-tip to obtain the temporal, spatial, and force measures [2]. The familiarity effects were examined using paired samples T-test. The significance level was .05.

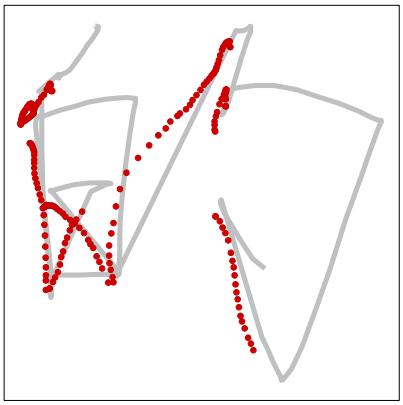

Figure 1 Illustration of the pen-tip movement. The gray-solid and the red-dotted lines respectively represent the trajectories of *On-surface* and *In-air movements.*

RESULTS AND DISCUSSION

The stroke velocity was comparable in the two tasks, suggesting that familiarity with characters might not significantly affect the time efficiency. When copying Hanguls (i.e., the *unfamiliar task*), children represented more peaks of stroke velocity, higher ratio of elapsed time in the air, higher ratio of excursion length in the air, and longer inter-stroke time. The tremble strokes and redundant *In-air movement* indicated that fluency and automaticity of handwriting were compromised. Additionally, stronger pen-tip force and more varied pen-tip force also indicated less efficient motor control during copying unfamiliar characters.

CONCLUSIONS

The familiarity with characters was important for children as it could influence the motor control of handwriting, including fluency, automaticity, and force regulation. To help children enhance familiarity to characters, handwriting instruction that involved direct practice of copying characters might be suggested.

REFERENCES

[1] Huang WF et al. *J Taiwan Occup Ther* **38**:36, 2020.
[2] Chang SH et al. *Sci Rep* **12**:15675, 2022.

Table 1: Difference in handwriting performance between the *familiar* and the *unfamiliar* tasks.

		Familiar task	*Unfamiliar task*	*t-value*	Effect size (*d*)
On-surface movement	Stroke velocity (mm/ms)	23.02 ± 6.89	23.23 ± 6.88	0.299	0.05
	Number of peaks of stroke velocity	3.10 ± 1.13	3.63 ± 1.21	4.50*	0.84
	Pen-tip force[+] (%)	0.55 ± 0.12	0.60 ± 0.13	6.62*	1.23
	Coefficient of force variation	0.48 ± 0.05	0.45 ± 0.06	7.10*	1.32
In-air movement	Ratio of *In-air* time to *On-paper* time (%)	68.11 ± 18.67	80.28 ± 21.33	6.06*	1.13
	Ratio of *In-air* length to *On-paper* length (%)	62.46 ± 10.50	70.83 ± 10.41	8.22*	1.53
	Averaged inter-stroke time per character (ms)	0.31 ± 0.11	0.47 ± 0.16	8.89*	1.65

[+] the pen-tip force was obtained with the tablet's built-in functionality, of which the pressure sensitivity was 1024-levels.
* $p < .005$.

Wi-Fi-Based Continuous Detection of Hand Movements for Motor Assessment in Parkinson's Disease

Chun-Hsiang Chang, Chi-Lun Lin
Department of Mechanical Engineering, National Cheng Kung University, Tainan, Taiwan.
Email: n16114704@gs.ncku.edu.tw
linc@ncku.edu.tw

INTRODUCTION

Parkinson's disease (PD) can significantly impair a patient's daily life. Assessing hand movement is an important part of the motor examination to understand the severity of PD. Accurate assessment can be challenging due to motor fluctuation or symptom variation throughout the day, resulting in incomplete characterization of the disease's actual condition during clinical examination. Therefore, a continuous sensing method to quantify the hand motor symptoms is needed. Channel state information (CSI) refers to the combined impact of the propagation of Wi-Fi signals from the transmitter to the receiver. The Wi-Fi-based sensing is passive , contactless, and privacy preserving. Studies have shown the capability of Wi-Fi CSI to capture human subtle motion, such as respiration [1]. Therefore, this paper proposes a method to continously detect subtle changes in the hand motor symptoms of PD, particularly tremor and bradykinesia and extract quantitative information for assessing the disease progression.

METHODS

A single Tx-Rx pair of Wi-Fi devices was used to collect CSI data during hand movements performed, and the environmental settings followed our previous study [2]. We first divided complex-valued CSI sequences gathered by two antennas to obtain the CSI ratio [1], which could eliminate the random phase offset that may occur. Second, The Butterworth filter was applied to remove low and high-frequency noise. After that, the principal component analysis was conducted to find the best presentation of signal response to the target motion. Finally, the Savitzky-Golay filter was used to smooth the data.

A processed sequence of complex-valued CSI ratio was analyzed in two steps. First, the data sequence was converted into magnitudes and the peaks were identified as the number of movements for determining the duration and frequency. Secondly, the data points of the sequence should visualize the movement as an arc in the complex plane, theoretically. By fitting the data points to a circle, the proportion of the arc (L_{arc}) to the circle's circumference C can be calculated by Eq. 1, where a and b are half of LoS length and the perpendicular distance from LoS to action point; λ is wavelength of carrier frequency (5.765 GHz), providing an estimate of the displacment of the movement (Δb).

$$\frac{L_{arc}}{C} * \lambda = 2 * (\sqrt{a^2 + (b + \Delta b)^2} - \sqrt{a^2 + b^2}) \quad (1)$$

RESULTS AND DISCUSSION

In the analysis of finger tapping, the amplitude graph (Figure 1) of a tapping action displays two distinct peaks that correspond to the opening and closing actions of the index finger and thumb. The frequency of approximately 1.12 Hz can be quantified by computing the number of peaks presented in the graph with average action duration 0.16 second.

Figure 2 illustrates the complex plane representation of an opening action in a finger-tapping test, which controlled the maximum opening to 5 cm. Another two finger-tapping tests were conducted with the maximum opening between two fingers set as 4 and 7 cm. In the former case, the complex plane representation showed a semicircular arc. In the latter case, the data points on the complex plane formed an approximately 0.8 full circle. The results suggested that the movements of fingers during tapping could be distinguished and measured in the tested range of opening action, i.e., 4 – 7 cm.

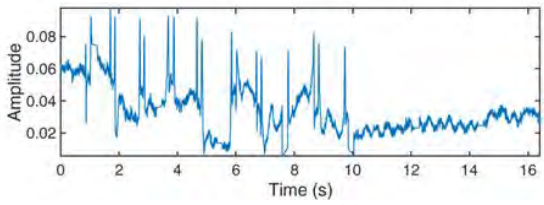

Figure 1 Amplitude plot of finger tapping

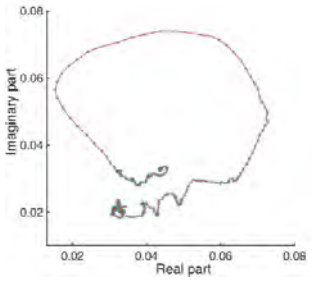

Figure 2 Finger tapping in complex plane

CONCLUSIONS

The proposed method successfully detected and quantified the frequencies and displacement of finger tapping. With continuous detection, the patient's daily condition can be tracked to understand the disease progression and drug efficacy, which help the doctor prescribe more accurately.

REFERENCES

[1] Y. Zeng, D. Wu, J. Xiong *et al.*, "FarSense: Pushing the Range Limit of WiFi-based Respiration Sensing with CSI Ratio of Two Antennas," Proc. 3(3), 121 (2019).

[2] H.-H. Chen, C.-L. Lin, and C.-H. Chang, "WiFi-Based Detection of Human Subtle Motion for Health Applications," Bioengineering, 10(2), 228 (2023).

Keynote speakers

Toshiyasu Nakamura, MD, PhD

Department of Orthopaedic Surgery, School of Medicine, International University of Health and Welfare, Tokyo, Japan

Dr Nakamura graduated from Keio University School of Medicine in 1988, and from the Graduate School of Medicine specializing in Orthopaedic Surgery in 1994. His PhD addressed the functional anatomy of the triangular fibrocartilage complex. He completed research fellowships at the Mayo Clinic, Rochester, Minnesota and the Hand Center of Western New York, Buffalo, New York. In 2000 Dr Nakamura joined the academic staff of Keio University, where he taught until 2014, when he moved to the International University of Health and Welfare.

Biomechanics of the Distal Radioulnar joint (DRUJ)

The human wrist is a complex joint allowing six freedom motion including flexion-extension, radial-ulnar deviation and forearm pronosupination. The wrist consists of radiocarpal, midcarpal and distal radioulnar joints. The carpometacarpal (CMC) joints are also included into the wrist, and especially the thumb CMC joint allows multidirectional motion to achieve opposition. In this presentation, the author presents biomechanics of the distal radioulnar joint (DRUJ).

Functional anatomy

The DRUJ consists of the triangular fibrocartilage complex (TFCC), sigmoid notch of the radius, ulnar head and joint capsule. The TFCC is the 3-D structure and characteristics of the radioulnar ligament (RUL) indicated nearly vertical insertion to the fovea of the ulna. Some fibers of the RUL also attach to the base of the ulnar styloid. The vertical insertion of the RUL fibers allows easy twisting during pronosupination and provides adequate stability of the DRUJ during motion.

Static analysis of stability

The TFC has been considered the primary stabilizer of the DRUJ. Several studies revealed that attaching fibers of the RUL to the fovea is the most important part among the TFCC. As the TFCC is a 3-D structure, care should be taken that its 3-D structure is maintained during biomechanical studies. The author presents that sectioning the TFCC can affect static stability of the DRUJ. Also, importance of the fovea attachment of the TFCC and lesser function of the ulnar styloid process are presented.

Dynamic analysis using wrist simulator

Stability contributions of the fovea attachment and styloid attachment of the RUL for DRUJ was examined using static MTC machine analysis and dynamic wrist simulator, indicating fovea attachment of the RUL was much important compared to the styloid attachment, which was consistent with the clinical findings that ulnar styloid is not necessary to fix in distal radius fracture when the foveal attachment of the RUL remained intact.

How to repair and reconstruct the RUL or TFCC to the ulna

Functional anatomy and biomechanical studies in this presentation suggest that the avulsed RUL should be introduced to the central lesion of the fovea, with stitches (arthroscopic or open repair) or tendon(s) (reconstruction). Once the RUL is reattached or reconstructed to the fovea, patient indicates full of forearm rotation with adequate stability of the DRUJ.

THE IMPACT OF BODY COMPOSITION ON STAND-TO-SIT BIOMECHANICS AND MUSCLE ACTIVITY OF NURSES – A QUANTITATIVE-EXPLORATIVE STUDY

Anna Brinkmann[1], Sandra Lau[2], Ole Meyer[1], Rebecca Diekmann and Andreas Hein[1]
[1] Assistive Systems and Medical Device Technology, Carl von Ossietzky University of Oldenburg, Germany.
[2] Geriatric Medicine, Carl von Ossietzky University of Oldenburg, Germany.
Email: anna.brinkmann1@uni-oldenburg.de

INTRODUCTION

Manual patient handling is one of the most significant challenges leading to musculoskeletal burden among nurses, who are already at high risk for physical impairments like muscle weakness, overweight, or obesity. Technical innovations can enhance traditional working techniques, e.g., a robotic system providing physical relief by collaboratively assisting nurses [1]. Worksite-tailored exercise training is another option to prevent physical burden in care [2, 3]. Traditional stand-to-sit (STS) tasks are promising exercises as they are easy to understand, reduce the risk of injury, and provide sufficient intensity for bodyweight resistance training. In addition, they can be easily integrated into daily routines, being elementary components of many activities of daily living and various actions in the day-to-day caregiving processes. However, research and evidence on STS tasks' biomechanical and muscular characteristics are limited – especially for nurses. Therefore, this explorative study aimed to quantify nurses' STS movement strategies in a laboratory setting to provide initial insights on identifying physical deterioration by data.

METHODS

We analyzed 292 STS transitions of eleven nurses (two male). The total number of STS transitions was counted, and ground reaction forces and non-invasive surface electromyography were collected. The displacement of the center of mass (COM), its velocity and acceleration, and the displacement of the center of foot pressure (COP) was calculated to quantify balance control. Muscle activation of the knee extensor, knee flexor, and lumbar erector muscles was quantified by root mean square. Individual data set elaboration led to group classification according to BMI characteristics (WHO: BMI ≥ 25 kg/m^2 is considered overweight).

RESULTS AND DISCUSSION

Compared to the normal-weight subjects, a BMI ≥ 25 kg/m^2 resulted in lower STS repetitions in 60 s (Tab. 1), a slower pace, and a longer cycle duration: Mean STS cycle duration took 0.59 s longer in the last 15 s of the STS movement compared to the normal-weight group. In the first 15 s of the movement, the mean difference between both groups was 0.32 s. COM displacement was extended in the anterior-posterior direction (Fig. 1a), and the COP range was ten times higher in the medial-lateral direction (Fig. 1b).
Movement strategies were adapted for balance control, increasing the muscle activity of the biarticular knee extensor, knee flexor, and lumbar erector. These findings imply that adapted trunk flexion due to overweight or obesity increases knee extensor activity as a compensatory mechanism for balance control.

Table 1. Descriptive data of the study participants (mean ± SD).

	BMI < 25 kg/m^2 (n = 8)	BMI ≥ 25 kg/m^2 (n = 3)
Age [years]	32 ± 11	36 ± 12
BMI [kg/m^2]	22.10 ± 1.24	30.93 ± 4.39
60 s STS repetitions [n]	28 ± 3	24 ± 6

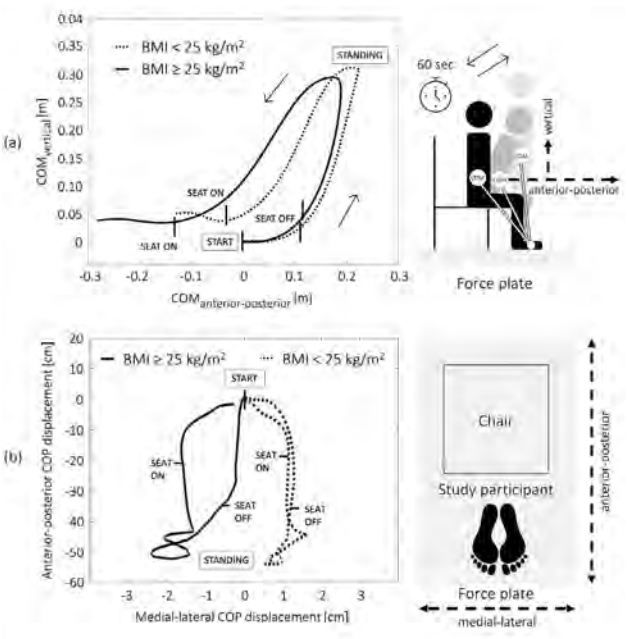

Figure 1. (a) COM trajectory in the anterior-posterior and vertical direction and (b) COP trajectory in the medial-lateral and anterior-posterior direction during the STS cycle.

CONCLUSIONS

In our data set, the functional performance of nurses in STS transitions is decreased with physical deteriorations (BMI ≥ 25 kg/m^2), resulting in lower STS repetitions in 60 s, a slower pace, and longer cycle duration. In this context, movement strategies were adapted for balance control, altering the velocity and acceleration, knee extensor, knee flexor, and lumbar erector muscle activity. These findings provide initial insights into STS performance strategies of nurses and can be used to conceive future worksite-tailored exercises.

REFERENCES

[1] Brinkmann A et al. Sci Rep 12, 8644, 2022.
[2] Zare A et al. BMJ Open 9, 2019.
[3] Christensen JR et al. JOEM 57(12): 146-7, 2015.

THE EFFECT OF CHANGING BICYCLE SADDLE POSITION ON SUBMAXIMAL CYCLING BEHAVIOUR.

Cristian Riveros-Matthey[1], Glen A. Lichtwark[1], Mark J. Connick [1] and Timothy J. Carroll [1]
[1] School of Human Movement and Nutrition Sciences, The University of Queensland, Brisbane, Australia.
Email: c.riverosmatthey@uq.net.au.

INTRODUCTION

According to optimal control theory, we organise our movements to maximise motor performance according to specific objectives (like economy and precision). Meeting these behavioural objectives can also be thought of as minimising the costs of movement. In walking, for example, people select a stride length and rate that are aligned with the minimum energy consumption [1]. However, in tasks such as cycling, other criteria may drive the selection of a preferred cadence. The amount of muscle activation has been proposed as a cost that regulates movement in cycling. Computer simulations and experimental cycling suggest that people tend to minimise the amount of muscle activation in each pedal stroke, rather than minimising the total energy expenditure. However, it is not clear whether a cost function based on EMG activations can explain cycling behaviour when the mechanical conditions of cycling change. This question is important because if a cost function explains behaviour under novel conditions, there is greater evidence that the function helps to determine behaviour rather than merely correlating with it. Here we tested whether changes in cycling behaviour driven by altering saddle height are consistent with various cost functions for optimising movement.

METHODS

Twelve level 3-4 cyclists took part in three days of assessments (normal, low, and high saddle conditions). They exerted 3min cycling bouts at submaximal power output (2.5 $W \cdot kg^{-1}$) under 7 cadences (from 50 to 110rpm plus the self-selected cadence (SSC)). Breath-by-breath gas analysis, 3D motion capture, surface electromyography (EMG) and force-instrumented pedals were included. The net metabolic power was calculated based on VO2 and CO2 uptake. The sum of normalised muscle activations squared (CF1) and the sum of the volume-weighted muscle activations (CF2) were calculated from EMG [2]. The EMG-based cost functions and metabolic power data were fitted with a second-order polynomial nonlinear regression. This study was approved by the local ethics committee (2022/HE001934) and participants provided written informed consent.

RESULTS AND DISCUSSION

Preliminary results show that saddle changes affect metabolic power (Fig. 1) and EMG-based cost functions across cadences. Changes in SSC were also observed (normal saddle: 94 rpm, low saddle: 102 rpm, high saddle: 83 rpm), with the CF1 tending to be minimised under all saddle height conditions (Fig. 2).

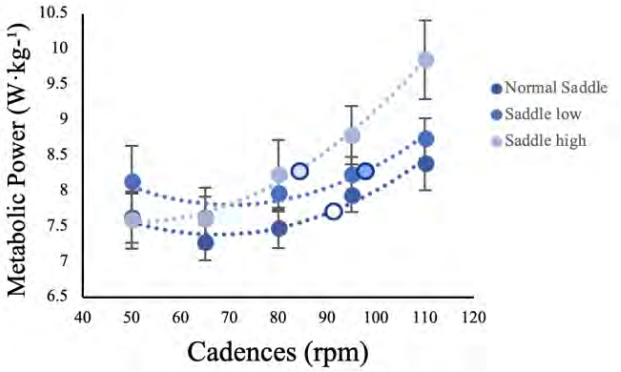

Figure 1: Metabolic power across cadences at 2.5 $W \cdot kg^{-1}$(n=9). Circles with borders represent the SSC in each mechanical condition.

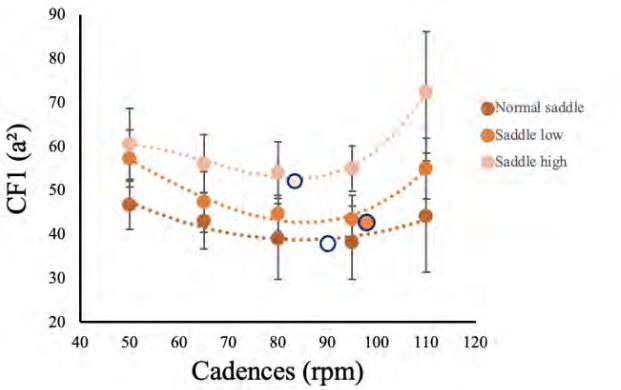

Figure 2: Mean "fatigue-like" CF1 per task cycle across cadences at 2.5 $W \cdot kg^{-1}$(n=6). Circles with borders represent the SSC in each mechanical condition.

CONCLUSIONS

Preliminary findings indicate that saddle height variations provide a sufficient change in mechanical conditions to substantially affect SSC, metabolic power, and EMG-based cost functions. Critically, the "fatigue-like" CF1 was minimized in all saddle conditions, whereas the "effort-like" CF2 was reduced only in normal and low saddle conditions. These preliminary data suggest the CNS prioritises avoidance of high muscle activation irrespective of the volume of muscle tissue that is activated.

REFERENCES

[1] Alexander McN. R. *Physiol Rev* **4**:1199–227, 1989
[2] Ackermann M. *J Biomech* **43**:1055–1060, 2010

EFFECTS OF AGE-RELATED MUSCLE DEGENERATION ON DYNAMIC STABILITY DURING WALKING: A MUSCULOSKELETAL COMPUTER SIMULATION STUDY

Shoma Kudo[1], Akinori Nagano[2], and Masahiro Fujimoto[1]
[1] National Institute of Advanced Industrial Science and Technology, Chiba, Japan.
[2] College of Sport and Health Science, Ritsumeikan University, Shiga, Japan.
Email: shoma-kudou@aist.go.jp

INTRODUCTION

Age-related deficits in muscle function have been considered to negatively affect dynamic stability during walking and increase the risk of falls [1]. Older adults exhibit reduced muscle strength, slower rate of muscle force development, and prolonged twitch contractions compared to younger adults [2]. However, it remains unclear how and to what extent these deficits of muscle property affect dynamic stability. The purpose of this study was to quantify the effect of age-related deficits in muscle function on dynamic stability during walking. A musculoskeletal computer simulation was utilized to alter specific muscular parameters.

METHODS

Walking movement was simulated by using two-dimensional musculoskeletal models, which consists of seven rigid bodies (trunk, thighs, shanks, and feet) and 18 Hill-type muscles (m. iliopsoas, mm. glutei, hamstrings, m. rectus femoris, mm. vasti, m. biceps femoris short head, m. gastrocnemius, m. soleus, and m. tibialis anterior in each leg). Maximum isometric muscle force (F_{iso}), maximum muscle contraction velocity (V_{max}), and deactivation time (T_{deact}) in the model's muscle properties were adjusted to assess the effect of age-related deficits in muscle function on the dynamic stability during walking.

Five models which differed in their muscle properties were created: young adult (YA) and older adult (OA) models, and the models with reduced F_{iso}, reduced V_{max}, and prolonged T_{deact} (ΔF, ΔV, and ΔT models, respectively). The muscle parameters for the YA model were adapted from the previous study [3]. The OA model was defined as the model with 30% reduced F_{iso}, 20% reduced V_{max}, and 20% extended T_{deact} from the YA model [2]. Each of these adjustments for F_{iso}, V_{max}, and T_{deact}, was independently applied for ΔF, ΔV, and ΔT models, respectively.

Numerical optimization was executed to find the muscle activation patterns that yielded successful three steps of walking with minimum energy expenditure. Optimizations were executed with a modified version of the algorithm of [4], implemented in MATLAB (MathWorks Inc., Natick, MA).

The margin of stability (MoS) [5] in the anteroposterior direction at toe-off instant was calculated as a measure of dynamic stability during walking. The MoS value was compared between the models.

RESULTS AND DISCUSSION

The MoS was 0.059 m and 0.020 m for the YA and the OA model, respectively. This indicates that the OA model performed walking with less dynamic stability than the YA model. The MoS was 0.001 m, 0.043 m, and 0.014 m, for the ΔF, ΔV, and ΔT model, respectively. These results indicate that the walking was less stable when the muscle force was adjusted than when the muscle contraction velocity or deactivation time was adjusted. These findings suggest that the degeneration in isometric muscle force would have the most adverse effect on the dynamic stability during walking.

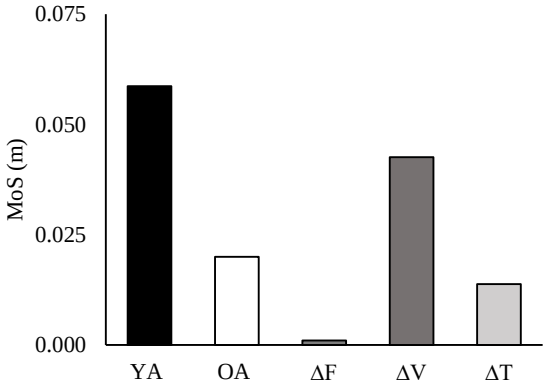

Figure 1 Margin of stability during walking for each model condition.

CONCLUSIONS

Age-related degeneration of muscle properties impaired the dynamic stability during walking. It appeared that the isometric muscle force had a larger effect on dynamic stability than muscle contraction velocity and deactivation time. These findings would be useful for developing an intervention program to effectively reduce the fall risk in older adults.

ACKNOWLEDGEMENTS

This work was supported by JSPS KAKENHI Grant Number JP21J01097.

REFERENCES

[1] Campbell et al., *Age Ageing*, 19: 136-141, 1990.
[2] Thelen, *J Biomech Eng*, 125: 70-77, 2003.
[3] Delp, *Dissertation, Stanford University*, 1990.
[4] Bremermann, *Math. Biosci*, 9: 1-15, 1970
[5] Hof et al., *J Biomech*, 38: 1-8, 2005.

Anatomical knee model for forward dynamics gait simulation

Beomsoo Shin[1], Seungbum Koo[1]
[1] Department of Mechanical engineering, Korea Advanced Institute of Science and Technology, Daejeon, Republic of Korea.
Email: skoo@kaist.ac.kr

INTRODUCTION

Ligaments provide passive constraint and stability to the knee. Roles of individual ligaments are controversial [1]. Abnormal kinematics and instability have been reported from patients with ligament ruptrue durting walking [2]. Clinical meausrements could show deviations by different ligament states such as reconstruction [3]. However, the kinematics of uninjured and injured knee conditions are difficult to obtain for the same subject. A dynamics model of the knee with ligaments and muscles would help understand the roles of individual ligaments. A forward dynamics simulation with muscle exctiation controller for walking could predict the kinematics of injured conditions. The objective of this study is to quantify the change of knee joint kinematics according to knee ligament injuries during level walking.

METHODS

A dynamics musculoskeletal model with 25 degrees of freedom (DOF) and 92 lower limb muscles were created [4]. The knee joint was made as a six-DOF joint and constrained with thirty-one ligaments. Ligament force was determined according to its strain. Ligament strain, stiffness, and attachment location were obtained from cadaveric anatomy data in a previous study [5]. The knee model was validated by comparing its kinematic response to external forces and torques [5]. A gait controller that determines temporal muscle excitations was made of a deep neural network and was trained by reinforcement learning to track a measured walking motion of a healthy participant. In the knee, only the flexion-extension angle was provided and the other five-DOF knee kinematics were not constrained during the training. The knee joint kinematics in the simulation of walking of a normal knee were compared with those in a previous study using bi-planar fluoroscopic system [6]. One of the anterior cruciate ligament (ACL), posterior cruciate ligament (PCL), lateral collateral ligament (LCL), and medial collateral ligament (MCL) was removed for each individual ligament injury simulation. The injured knee kinematics were compared with those of the intact knee simulation.

RESULTS AND DISCUSSION

Ligament strain and attachment locations were adjusted less than 9.52% and 8 mm, respectively, with respect to a reference model [5]. Walking motion was generated with a trained neural network, whose root mean square error of knee flexion was 5.6 deg during a gait cycle. Each injury simulation gave produced altered knee kinematics (Figure 1). ACL deficient model (ACLD) showed larger anterior translation during the stance phase. PCL deficient model (PCLD) showed larger posterior translation during the terminal swing phase. LCL deficient (LCLD) model showed varus rotation during the stance phase. MCL deficient (MCLD) model showed valgus rotation during the initial swing phase.

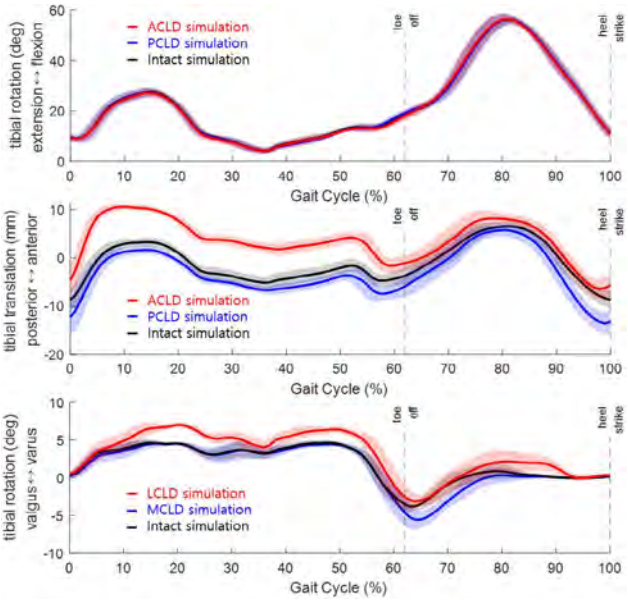

Figure 1 Knee flexion (Top), tibial translation (Mid) and tibial rotation (Bot) among ligament injury simulations during gait cycle

CONCLUSIONS

Six-DOF knee kinematics of normal knee could be reproduced in our forward dynamics simulation [6]. Temporal changes of the knee kinematics could be observed by individual ligament injuries. Cruciate ligaments provided translational stability and collateral ligaments provided rotational stability during gait cycle. It shows a role of ligaments in pure gait dynamics. Human response and adaptation to injury would make the prediction of kinematics changes complicated [2].

ACKNOWLEDGEMENTS

This research was supported by the NRF (MSIT Project No. 2022M3C1A3080598) and by IITP (MSIT Project No. 2022-0-00025) funded by the Korea government.

REFERENCES

[1] Rudolph et al. *Univ Delaware*, 1998. [2] Katz et al. *Am J Sports Med* **14**: 88-91, 1986. [3] Shabani al. *Int Orthop* **39**: 1187-93, 2015. [4] Rajagopal et al. IEEE TBME **63**: 2068-79, 2016. [5] Harris et al. *J Biomech* **138**: 081004, 2016. [6] Kozanek et al. *J Biomech* **42**: 1877-84, 2009.

THE EFFECT OF CHANGING GAIT PARAMETERS ON TENSOR FASCIA LATAE, GLUTEUS MAXIMUS, AND THE ILIOTIBIAL BAND

LA Hutchinson[1], LA Kelly[1], and GA Lichtwark[1]

[1] School of Human Movement and Nutrition Sciences, The University of Queensland, St. Lucia, QLD, Australia.
Email: laura.hutchinson@uq.edu.au

INTRODUCTION

The iliotibial band (ITB) is commonly injured in runners due to overuse, yet little is understood about the conditions that cause this syndrome. Typically, peak strain responses of the ITB to changes in gait kinematics have been modelled via musculoskeletal (MSK) models that only consider the ITB as a passive ligamentous structure originating on the iliac crest. However, these simplified models have ignored the potentially large strains transmitted through the ITB by its two in-series muscles; tensor fascia latae (TFL) and gluteus maximus (GMax) [1]. Here, we use an EMG-driven MSK model to assess the mechanical behaviour of the ITB during walking and running with perturbations chosen from literature aimed at increasing the strain in the ITB (i.e., changes in inclination and stance width). We hypothesized that narrower stance width and moving downhill would increase the strain in the ITB (both the ligamentous component and tendonous components).

METHODS

Fifteen healthy participants (4f, 11m, age:30±7 years, Height: 178±8 cm, Weight: 76±12 kg) provided informed, written consent to participate in this study. We recorded fine-wire electromyography (superior region of GMax-GMS), and three-dimensional kinematic and kinetic measures, which were used to drive an OpenSim musculoskeletal model during walking and running for each gait condition (wide stance, narrow stance, uphill, and downhill). We converted a lower body model by Eng *et al.* [1] from SIMM to OpenSim (SimTK, USA) and combined the ITB muscle tendon units (MTUs) of both TFL and GMS) with the Rajagopal *et al.* [2] model. We computed ITB ligamentous strain, and for each MTU we computed the force and length in response to the EMG stimulation during each walking and running condition. We performed separate repeated measures two-way ANOVAs (α=0.05) to test the effect of stance width and inclination on peak EMG and peak muscle force in the TFL and GMS as well peak strain in the ITB ligament structure. Pairwise differences were determined using a Bonferroni-Holm post-hoc comparison (α=0.05).

RESULTS AND DISCUSSION

A summary of the key statistical findings are shown in Figure 1. We found that uphill walking and running increased the demand on all three ITB trajectories (ligamentous, TFL and GMS MTUs) through increasing muscle activity, MTU force, and ITB ligament strain consistently. Additionally, we found limited effects of changing stance width on the MTU behaviour but found that increasing stance width resulted in lower ITB ligament strain.

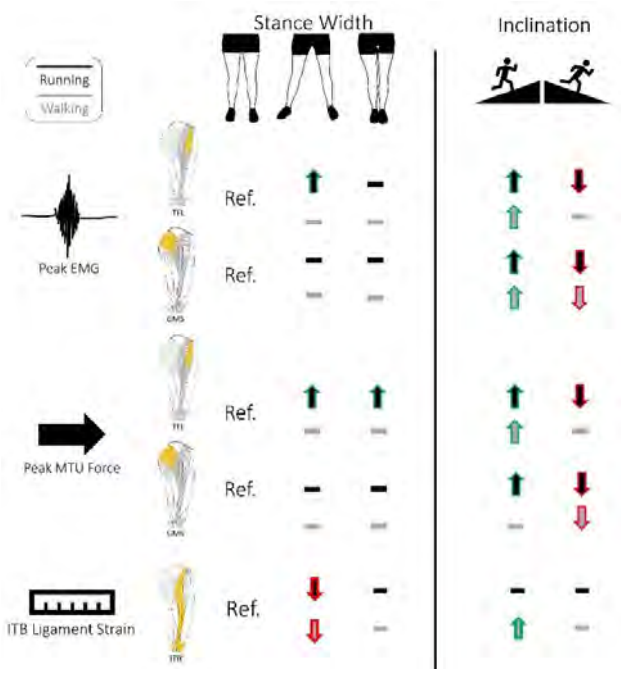

Figure 1 General summary of EMG, ITB MTU forces, and ITB ligament strain findings compared to normal level ground conditions for both walking (grey) and running (black).

CONCLUSIONS

Using our novel experimental and modelling approach, we found that surface inclination had a substantial influence on TFL and GMax activations and force in the ITB portion of these MTUs. During uphill walking and running, peak muscle activation was increased by an average of 51%, and during downhill running was decreased by an average of 33%. In contrast, little evidence of changes in passive ITB ligamentous strain were found due to changes in inclination angle. This work shows new insights into the contrasting mechanical behaviour of the passive (ligamentous) and active (MTU) components of the ITB, and these vary with gait modifications associated with ITB syndrome.

REFERENCES

[1] Eng et al. *J Biomech* **48**: 3341-3348, 2015.

[2] Rajagopal et al. *IEEE Trans. Biomed.* **63**:2068-79, 2016.

WALKING SYMMETRY IS SPEED AND INDEX DEPENDENT

Gaspare Pavei[1], Andrea Cereatti[2], Elena Bergamini[3]
[1]Department of Pathophysiology and Transplantation, University of Milan, Milan, Italy.
[2] Department of Electronics and Telecommunications, Polytechnic University of Turin, Turin, Italy.
[3] Department of Movement, Human, and Health Science, University of Rome "Foro Italico", Rome, Italy.
Email: gaspare.pavei@unimi.it

INTRODUCTION

Gait symmetry is one of the most informative aspects of gait quality. Quantifying gait symmetry contributes to the identification of deficits in typical and pathological locomotion. Many metrics have been proposed based on different data sources and approaches [1]. However, no consensus exists on their appropriate biomechanical interpretation and whether gait speed has an effect on symmetry indices computation.
The aim of this study is to compare two different gait symmetry indexes adopted in the literature, based on different data sources and approaches (from the whole-body centre of mass (BCoM) trajectory [2], and the accelerations measured by an inertial sensor located on the pelvis [3]) during walking at different speeds.

METHODS

Ten healthy participants (4 women, 1.71±0.08 m height, 68.2±10.2 kg body mass, 34.5±8.5 years old; mean±SD) walked for 60 s on a treadmill at seven different speeds (from 0.28 to 1.95 m/s with steps of 0.28 m/s) in a randomised order. Each participant was then asked to simulate an asymmetric walk at 0.83 m/s (ASYM). The position of 18 markers located on the main joint centres was recorded (200 Hz) with a Vicon system and the 3D BCoM trajectory was computed as a weighted mean [4]. For each stride, the BCoM trajectory was closed in a 3D loop and described by a 10-harmonic Fourier series, whose coefficients were used to calculate the Symmetry Index (SI) for each anatomical axis (antero-posterior (AP), medio-lateral (ML), and cranio-caudal (CC)) [2]. Simultaneously, lower trunk 3D linear accelerations were collected (200 Hz) by an inertial measurement unit (IMU) (APDM Opal) located at the L1-L2 level. To guarantee a repeatable system of reference among participants, the IMU was verticalized, and the resulting axes were considered to approximate anatomical axes. Gait symmetry was obtained for each stride by computing the improved Harmonic Ratio (iHR) [3]. SI and iHR ranges from 0%, total asymmetry, to 100%, perfect symmetry. The influence of speed and index on symmetry was assessed with a two-way repeated measure ANOVA after checking for data normality.

RESULTS AND DISCUSSION

Perfect symmetry (100%) was never achieved. In both indexes, symmetry increased significantly ($p<0.001$) with walking speed in AP and CC axes, whereas in ML axis, symmetry slightly decreased (SI) or increased (iHR) (Figure 1). Symmetry values were substantially different between indexes ($p<0.001$), with iHR showing higher values in AP and CC, and lower in ML. ASYM deviation from typical walking was highlighted by both indexes in AP and CC axes only ($p<0.05$). The difference in symmetry values between indexes can be ascribed to the different data sources (position vs. acceleration, and BCoM vs. pelvis) and analysis (harmonic content in SI vs. harmonic power in iHR).

CONCLUSIONS

Although a similar trend is shown by both indexes in the AP and CC axes at increasing speed, iHR systematically described a more symmetrical gait. This suggests caution when comparing values obtained by different metrics. Moreover, since symmetry indices are influenced by walking speed, particularly at low speeds, any comparison (e.g. among age-groups or diseases) should be performed only by matching the speed.

REFERENCES

[1] Viteckova S et al. *Biomed Signal Process Control* **42**: 89-100, 2018.
[2] Minetti AE et al. *J Biomech* **44**: 1471-7, 2011.
[3] Pasciuto I et al. *J Biomech* **53**: 184-9, 2017.
[4] Pavei G et al. *Front Physiol* **8**: 129, 2017.

Figure 1 Symmetry (%) as a function of the index (SI from BCoM trajectory; iHR from the IMU accelerations) and walking speed.

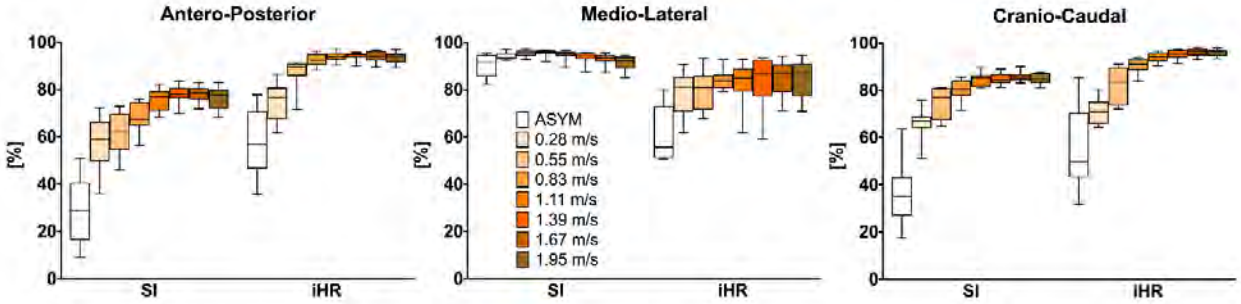

BODY CENTER OF MASS TO MINIMAL MOMENT AXIS DISTANCE IS DETERMINANT OF AGE-RELATED EVOLUTION IN STEPPING

Bruno Watier[1,2], Jérémie Begue[3], Teddy Caderby[3], Helene Pillet[4]
[1] LAAS-CNRS, CNRS, UPS, Université de Toulouse, France.
[2] CNRS-AIST JRL (Joint Robotics Laboratory), IRL, Tsukuba, Japan.
[3.] IRISSE – EA4075, UFR SHE, Université de la Réunion, France.
[4] Arts et Métiers, Institut de Biomécanique Humaine Georges Charpak, Paris, France.
Email: bruno.watier@univ-tlse3.fr

INTRODUCTION

Understanding mechanical phenomena underlying the initiation of gait is essential to better prevent risk of falling. Thus, mechanical variables such as kinematics of the center of mass or whole-body angular momentum evolutions have been demonstrated to be related to anticipatory adaptations of the body while stepping [1,2]. A degradation of these adaptations could therefore reveal an increased risk of falling and has been observed in motor-impaired population [2]. However, in spite of encouraging results, the transfer towards real-time applications for prevention or monitoring is hindered by the complexity of the proposed indicators in both their interpretability and their quantification process. In this abstract, we proposed to test the feasibility of using a mechanical-based index: the distance of the Body Center of Mass (BCoM) to the Minimal Moment Axis (MMA) of the external contact wrench, referred hereafter as $d_{BCoM-MMA}$ [3]. This index should overcome the above-mentioned difficulties while keeping a discriminating nature when comparing young and elderly stepping.

METHODS

15 healthy young (mean age: 25 years old; range: 19-29) and 15 healthy old (mean age: 69 years old; range: 63-77) adults volunteered. They were asked to initiate gait 10 times at a self-selected preferred (Pref) and at a fastest speed (Fast). Each participant performed this stepping and $d_{BCoM-MMA}$ was then obtained at each instant of time using: $d_{BCoM-MMA} = \frac{\|\boldsymbol{F} \times \boldsymbol{M_{BCoM}}\|}{\|\boldsymbol{F}\|^2}$ where $\boldsymbol{F} \times \boldsymbol{M_{BCoM}}$ is the cross product between the external forces and the external moment computed at the BCoM, $\boldsymbol{M_{BCoM}}$ being equal to the variation of the angular momentum ($\boldsymbol{K}$) at the BCOM obtained as described in [5]. Two parameters were then extracted for each trial and each participant: the norm of $d_{BCoM-MMA}$ (d_{norm}) and the value of the Antero-Posterior algebraic distance d_{AP}. Under the hypothesis of normal distribution, t tests were performed to compare the values of the range across groups and across conditions.

RESULTS AND DISCUSSION

Whereas average velocities were close for both groups for the Pref condition, the ranges of the norm and the antero-posterior component of $d_{BCoM-MMA}$ were significantly higher ($p<0.05$) for the group of old adults compared to the group of young adults. On the contrary, for the Fast condition, even if their average velocity was greater, the values of both parameters remained significantly lower for young compared to the old people (Table 1).

This study is the first to quantify the ranges of parameters extracted from $d_{BCoM-MMA}$ during stepping. The values of the ranges are consistent with the ones retrieved during gait of healthy adults. The magnitude of the increase with speed and age is also consistent with the tendency of the distance to be higher for motor-impaired people or in destabilizing situations [5]. Finally, the evolution of the proposed parameters with age is in direct relation with the larger angular momenta exhibited in this population [3]. It therefore confirms that this indicator could be used to monitor gait dynamics in real-time.

CONCLUSIONS

In this abstract we compared stepping instability using the distance between the BCOM and the MMA on old and young population at spontaneous and fast speed. Our results demonstrate that the distance tends to increase for older population at both cadences. This tendency is consistent with the higher instability of older adults during stepping and the distance could be used to quantify it.

REFERENCES

[1] Begue et al, Exp Gerontol 127:110714, 2019.
[2] Bouisset and Do, Neurosci Lett, 22: 345-362, 2008.
[3] Bailly et al. 7th IEEE int. conf. Biorob, 350-356, 2018.

Table 1: Mean (standard deviations) of the velocities (m/s) and ranges of d_{norm} and d_{AP} in mm for both groups (young and old) and both speed conditions (preferred and fast)

Parameters mean (std)	Pref		Fast	
	Young	Old	Young	Old
Velocity (m/s)	0.7	0.75	1.2	1.0
d_{norm} (mm)	42 (10)	52 (8)	75 (17)	79 (30)
d_{AP} (mm)	73 (15)	90 (18)	126 (22)	145 (50)

EFFECTIVENESS OF CO-CONTRACTION IN MITIGATING THE EFFECT OF AGE-RELATED INCREASE IN PASSIVE MUSCLE STIFFNESS

Tiina Murtola and Christopher Richards
Department of Comparative Biomedical Sciences, Royal Veterinary College, London, UK.
Email: tmurtola@rvc.ac.uk

INTRODUCTION

Ageing causes changes in the musculoskeletal system and its control. These changes include increasing the passive stiffness muscles [1], which has been observed to cause deterioration of reaching performance in simulations when studied independent of other ageing changes [2]. Older individuals have also been observed to utilise increased co-contraction of antagonistic muscles [e.g. 3]. In the present work, we use computational simulations to investigate the extent to which this co-contraction strategy has the potential to mitigate the effects of increased muscle stiffness.

METHODS

A three joint, six muscle model of the human upper limb is used in conjunction with a predictive PD controller which computes muscle excitations for horizontal reaching movements [2]. In order to introduce planned co-contraction into the model with minimal changes to the controller, each of the muscles (i=1,…,6) is set to produce force f_i according to

$$f_i = f_{a,i}a_i + f_{p,i} + f_{c,i},$$

where $f_{a,i}$ is the active force-velocity-length relationship, a_i is the active state, $f_{p,i}$ is the length dependent passive force, and $f_{c,i}$ is the co-contraction force for muscle i. Three cases of $f_{p,i}$ are considered: (i) no passive stiffness, (ii) slight passive stiffness representing young adults (YA) and (iii) severe passive stiffness representing older adults (OA). Co-contraction forces are kept constant throughout simulations, and three levels are compared: (i) no co-contraction, (ii) co-contraction at 5% of the isometric strength of the weaker muscle in an antagonistic pair, and (iii) co-contraction at 10% of the weaker muscle strength. Control parameters are optimised for each case separately, and accuracy of reaching towards four different targets is studied.

RESULTS

The deteriorating effects of increasing muscle stiffness can be seen both in average accuracy of the final endpoint position (Table 1) as well as for each individual reach (Figure 1). This deterioration is particularly large for contra-lateral reaching (target 2), where the final position error for the OA model is 700-fold compared to the YA model. Increasing co-contraction force had variable effects: it reduced accuracy in the model with no passive stiffness, caused target-dependent improvement or deterioration in the YA model, and resulted in a minor loss of accuracy for targets in the OA model except for target 2, where both 5% and 10% co-contraction levels improved accuracy significantly.

Table 1: Average reaching accuracy (mm) for the three passive stiffness and three co-contraction conditions considered.

f_c	No f_p	YA	OA
None	0.0087	0.0493	6.8133
5 %	0.0404	0.0602	2.1209
10 %	0.0588	0.0635	3.1615

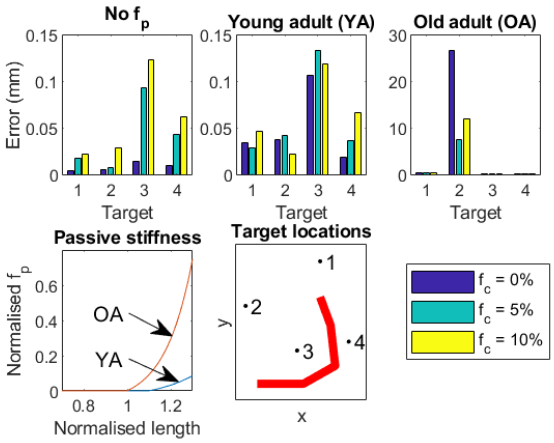

Figure 1 Accuracy of reaching towards four targets under three passive stiffness conditions and co-contraction force levels.

CONCLUSIONS

Our simulations indicate that age-related muscle stiffening causes deterioration in reaching accuracy, but this effect can be partially reversed in some movements by co-contraction of antagonistic muscles. However, in other cases, co-contraction may lead to reduced accuracy, suggesting that increased co-contraction observed in older adults serves a more complex purpose than simply compensating for muscle stiffness.

ACKNOWLEDGEMENTS

This work was funded by a Wellcome Trust Investigator Award 215618/Z/19/Z.

REFERENCES

[1] Lim JY et al. *Eur J Appl Physiol* **119**: 2339-48, 2019.
[2] Murtola T, Richards C. *R Soc Open Sci*, **10**: 221453 (in press) 2023.
[3] Klein CS et al. *J Appl Physiol* **91**: 1341-9, 2001.

A COMPOSITE REFLEXIVE AND SYNERGISTIC CONTROLLER FOR PREDICTIVE SIMULATIONS OF CYCLING

Giacomo Severini[1], Donal Holland[2], Cristiano De Marchis[3]
[1] School of Electrical and Electronic Engineering, University College Dublin, Dublin, Ireland.
[2] School of Mechanical and Materials Engineering, University College Dublin, Dublin, Ireland.
[3] Department of Engineering, University of Messina, Messina, Italy.
Email: giacomo.severini@ucd.ie

INTRODUCTION

Predictive neuromechanical simulations are useful for estimating the biomechanics of the human body in the absence of experimental data. These simulations are usually set up as optimal control problems aiming at finding the simulation parameters that optimize the movement of a neuromechanical model of the human body by minimizing a task-dependent cost function. A common approach is that of using the optimal control problem for estimating the parameters of a neural controller that can, or not, be biologically inspired. In this work we propose a novel biologically-inspired neural controller for predictive simulation of cycling. The controller we developed pairs descending, rythmic activity, with reflexes to obtain a physiological cycling motion.

METHODS

The biomechanical model used in this work was adapted from a standard gait biomechanical model developed in Opensim. The neural controller used in the simulations is a composite controller constituted by a feedforward synergistic controller and a reflexive feedback controller. The feedforward controller consists of 10 synergies (5 per side). The synergies are shaped as synergy modules, where the contribution of a muscle to the module is reflected by a weight value, activated by a time-varying activation signal. The contribution of the muscles to the modules of the synergies was restricted by those observed experimentally in [1]. Specifically, each module was constituted by 2-4 muscles of unknown weight, selected as the muscles considered more active in an experimental synergy, while the weights for all the other muscles was set to zero. The activation signals of the synergies were modelled as sine waves with zeroed negative phase. All the 10 synergies shared the same frequency for the cosine, while each synergy has its own phase. The optimization procedure estimates the weights of the muscles in each synergy, the common frequency of the 10 synergies activation signals and the amplitude and phases of the activation of the single synergies. To minimize the parameters to be optimized, the amplitude and phases were estimated only for the synergies on the left side. The amplitudes for the right side were the same as the left, and the phases were delayed by π. The reflexive controller was modelled as a controller that inhibits the activation of a muscle if its antagonistic muscle is active. The optimization was carried out using the CMA-ES algorithm [2] by estimating the synergy parameters minimizing a cost function which penalizes ankle dorsi-flexion angles outside the [-30;20] degrees range and minimizes the energy expenditure, the interaction forces between the pedal and the foot and the difference between the actual and target speed (75 rpm). The simulations were set to last 8 seconds. The muscular activations obtained in these simulations were compared with those obtained during a baseline cycling task performed at 75 rpm in a previous work [1]. The simulations were performed using the Hyfydy simulation engine and the SCONE software [3]. We performed 15 simulations with random initial parameters. The parameters of the simulation better minimizing the cost function were then used as initial parameters for 10 post-hoc simulations, that have been analyzed using custom Matlab code.

RESULTS AND DISCUSSION

The optimization procedure resulted in simulations which synthesized kinematic data consistent with a physiological normal cycling pattern (not shown) and muscular activations that are similar to the experimental ones (Figure 1).

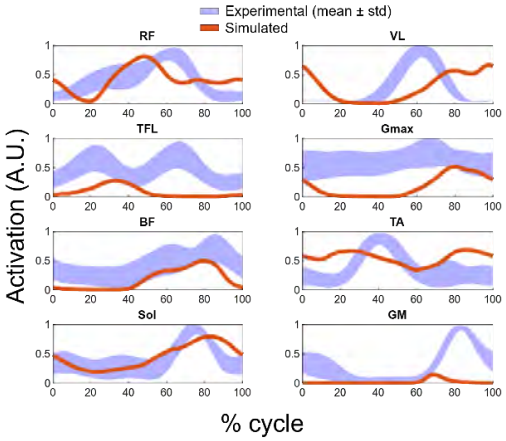

Figure 1 Comparison between experimental (blue) and simulated (red) muscular activations.

CONCLUSIONS

Here we show that a simple synergistic/reflexive controller, paired with a general cost function, can replicate cycling kinematics and, to a degree, the physiological muscular activations. Further work will test improved cost functions, and the ability of the controller to generalize to different cycling scenarios.

REFERENCES

[1] Zych M et al. *J Neurophys* **121**: 163-176, 2019.
[2] Hansen N et al. *Parallel Prob Solv* 202-291, 2004
[3] Geijtenbeek T. *J Open Source Soft* **4**:1421, 2019

INVESTIGATING THE EFFECTS OF PATELLOFEMORAL GEOMETRY INCONGRUENCE ON JOINT FUNCTION USING COMPUTATIONAL MODELLING

Annagh Macie[1], Allison Clouthier[1]
[1] School of Human Kinetics, University of Ottawa, Ottawa, Canada.
Email: amaci014@uottawa.ca

INTRODUCTION

Bone and cartilage geometry varies widely among people and these morphological differences have implications for risk of injury and pathology. In the knee, geometrical features have been associated with patellofemoral (PF) pain and instability, and knee osteoarthritis. Furthermore, changes to bone geometry that occurs in knee surgeries like trochleoplasty (sulcus deepening) have been noted to increase PF contact pressure and shear stress [1]. Investigations into how incongruent PF geometry affects joint function can provide insight into why certain variance in bone geometries may put a person at risk for injury or pathology. This research seeks to use computational modelling to demonstrate the effects of PF geometry incongruency in regards to changes in PF kinematics and cartilage contact pressure during gait.

METHODS

A statistical shape model was generated from magnetic resonance images of the right knee of 14 asymptomatic participants [2]. Meshes of the femur, tibia and patella bone and cartilage were created [2]. Principal component (PC) analysis was then applied to the whole joint [2]. For PC2 (trochlear groove (TG) depth), new knee geometries for the femur and patella were created by adding ± 3 standard deviations of the PC2 score multiplied by the loading vector for PC2 to the mean mesh. This resulted with 3 geometries of TG depth (shallow, mean and deep) as well as a congruent patella for each TG. Combinations of one femur and one patella were then created to produce models with congruent and incongruent geometries (i.e., deep TG with deep patella and deep TG with shallow patella), for a total of nine knee models. These models where then integrated into a previously validated musculoskeletal model and the same overground walking trial was simulated using each model. The cartilage contact pressure and knee kinematics were simulated for the walking trial using the Concurrent Optimization of Muscle Activations and Kinematics (COMAK) routine [3]. The resulting knee kinematics and contact mechanics from the different models were compared throughout the gait cycle to assess the influence of PF incongruence on functional knee mechanics.

RESULTS AND DISCUSSION

The findings from this research indicated that a lack of bone geometry congruency results in changes in joint kinematics and cartilage contact pressure during gait. With the models using the deep patella there was an increase in lateral patellar translation and patellar tilt as bone congruency decreased. Furthermore, contact pressure also increased and presented more laterally as bone congruency decreased (Fig. 1). With the models using the shallow patella, lateral patellar translation and patellar tilt was greater using the congruent shallow TG and decreased with less congruent femur models, with the least amount of patellar translation and tilt being present with the deep TG. Similarly, for contact pressure the shallow patella also showed that the highest and most lateral pressure occurred with the congruent femur and this reduced and presented more medially as incongruence increased. These results indicated that instances where the shallow TG was used resulted in the most lateral translation and largest amount of contact pressure regardless of congruency.

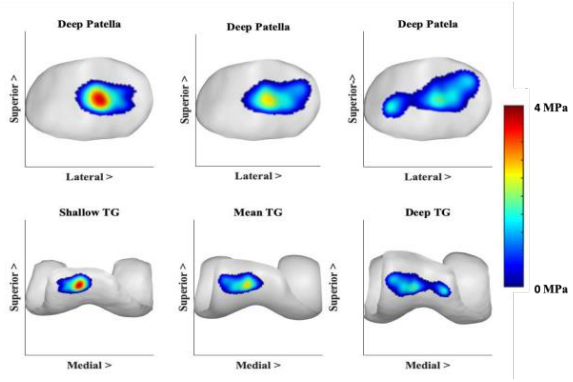

Figure 1 Instant of maximum contact pressure for models using a shallow, mean and deep TG and a deep patella during gait.

CONCLUSIONS

This research explores the effects of bone geometry and congruence on PF function. Changes in PF geometry congruency did result in altered PF joint kinematics and cartilage contact pressure in all of the models. However, in the scope of decreasing lateral patellar translation and patellar tilt as well as decreasing and medializing cartilage contact pressure, the absence of a shallow TG was the key component for this outcome. Understanding the effect of congruence on function could provide insight into treatment effectiveness or the likelihood of an individual experiencing a knee injury or degenerative knee disorder.

REFERENCES

[1] Kaiser, D. et al. *J Exp Ortop* **9:** 76, 2022.
[2] Clouthier, A, et al. *Med Eng Phys*, **66:** 47-55, 2019.
[3] Smith, C. et al. *J Knee Surg,* **29:** 99-106, 2016.

A Gradient-Based Method for Automated Muscle Path Calibration

Ziyu Chen[1,2], Tingli Hu[2,3], Sami Haddadin[2,3] and David W. Franklin[1,2]
[1] Neuromuscular Diagnostics, Technical University of Munich, Munich, Germany.
[2] Munich Institute of Robotics and Machine Intelligence (MIRMI), Technical University of Munich, Munich, Germany.
[3] Chair of Robotics and Systems Intelligence (RSI), Technical University of Munich, Munich, Germany.
Email: ziyu.chen@tum.de

INTRODUCTION

In musculoskeletal modeling, the path of a muscle is represented as a series of straight and curved lines, defined by origin, via, and insertion points as well as obstacles around which the lines wrap [1]. A correct configuration of muscle path is crucial for simulation accuracy as it determines muscle moment arm, on which a muscle's kinetic capacity is dependent. However, muscle path modeling can be laborious, where a large number of path-related parameters must be tuned; often manually. In this work, we propose a method that automatically calibrates muscle path, with high speed and accuracy.

METHODS

We formulate the process of parameter tuning as a least-squares problem with the following cost function:

$$\delta(\boldsymbol{p}) = \sum_{n=1}^{N} \|\boldsymbol{r}_{\text{data}}(\boldsymbol{q}_n) - \boldsymbol{r}_{\text{model}}(\boldsymbol{q}_n, \boldsymbol{p})\|_2^{\,2} \rightarrow \min$$

where $\boldsymbol{p}$ denotes muscle path parameters, including locations of origin, via, and insertion points, as well as the size, location, and orientation of the wrapping obstacle(s), and $\boldsymbol{r}(\boldsymbol{q})$ is the moment arm at joint position $\boldsymbol{q}$. Note that $\boldsymbol{r}$ and $\boldsymbol{q}$ are vectors with the dimension of DoF number, whereas N is the size of the dataset.

To reduce computational load, we first take a geometric approach to compute $\boldsymbol{r}_{\text{model}}(\boldsymbol{q})$ from the muscle path defined by $\boldsymbol{p}$, and then specify the gradient of $\delta(\boldsymbol{p})$ in its analytical form. To this end, we revise the muscle path algorithm in [1] into a continuous form, such that the derivative $\partial \boldsymbol{r}_{\text{model}}(\boldsymbol{q}, \boldsymbol{p})/\partial \boldsymbol{p}$ exists for all $\boldsymbol{p}$.

For result quantification, we use a 12-DoF human shoulder-arm model [2] as a reference to examine algorithm performance in replicating the geometry of all 42 muscle paths. Measurements of $\boldsymbol{q}$ in [3] are put into the reference model to generate artificial $\boldsymbol{r}_{\text{data}}(\boldsymbol{q})$ for calibration and validation.

RESULTS AND DISCUSSION

On a 2.9-GHz Intel Core i9 (64 GB RAM), the path calibration of all 42 muscles took 37.2 min; with parallel computing, the total time decreased to 5.5 min. For most muscles, the calibration took less than 1 min. Muscles with multiple via points and wrapping obstacles are configured with more than 18 parameters, requiring more iterations, but were still calibrated within 5 min.

The calibrated muscle path geometry shared much resemblance to the reference model (Figure 1, top). In validation, most muscles contain less than 1 mm of absolute error in moment arm about any actuating DOF (Figure 1, bottom); the mean is 0.37 mm.

With the analytical form of the gradient specified, our muscle path calibration method achieves speed and accuracy beyond manual capability. A major challenge in muscle path modeling is that a muscle may span multiple joint DoFs and have multiple moment arms, each determined by all actuating DoFs. Importantly, our method is not limited to fit moment arm–angle curves or surfaces but is designed to fit hypercubes. The path calibration we demonstrate is based on a vector of moment arms about 12 DoFs, which dependents on a vector of 12 generalized coordinates ($\boldsymbol{r}(\boldsymbol{q})$: $\mathrm{R}^{12} \mapsto \mathrm{R}^{12}$). This is an impossible task for manual tuning.

Though the performance is demonstrated in silico, the method is conveniently compatible with experimental data, since the only mandatory input is the relationship between moment arms and joint angles. We also derived the gradient for a path coordinate–based cost function, which enables calibration with medical imaging data (e.g., MRI) and expands the possibility of application.

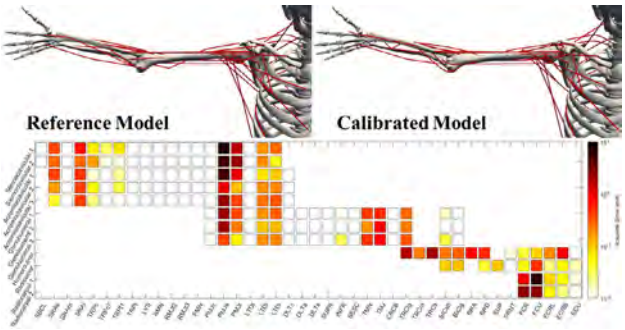

Figure 1 Top: Reference and calibrated muscle path geometry. Bottom: Absolute error of moment arm about each actuating DoF.

CONCLUSIONS

An automated method of muscle path calibration is developed with the gradient analytically specified, and its performance is demonstrated by fast and accurate replication of muscle path geometry.

ACKNOWLEDGEMENTS

This work was supported by the Lighthouse Initiative Geriatronics by StMWi Bayern (Project X, grant no. 5140951) and the German Federal Ministry of Education and Research funding (Project AI.D, grant no. 16ME0539K).

REFERENCES

[1] Garner B & Pandy M *Comput. Methods Biomech. Biomed. Engin.* **3**: 1-30, 2000.
[2] Hu T et al. *Comput. Methods Biomech. Biomed. Engin.* **23**: 785–803, 2020.
[3] Hu T et al. *IEEE BioRob 2018*: 1011–1018, 2018.

Stabilization of the foot-ankle complex in response to perturbations

Michael J. Asmussen[1,2], Phuong Tran[3], and Simon M. Danner [3]
[1] Department of Biology, Mount Royal University [2] Faculty of Kinesiology, University of Calgary, Calgary, Canada. [3] Neurobiology and Anatomy, College of Medicine, Drexel University, Philadelphia, USA.
Email: masmussen@mtroyal.ca

INTRODUCTION

A large array of small and large muscles can control the foot and ankle to aid in locomotion across complex terrain. These muscles can control the foot by either co-activating muscles prior to a perturbation or rely on feedback to stabilize the foot and ankle. *In vivo* experiments to understand these mechanisms are limited by multiple factors such as having humans experience unsafe, unexpected perturbations that could lead to injury [1]. *In silico* experiments allow researchers to overcome these limitations imposed by *in vivo* studies. The purpose of this study is to determine how humans can compensate for peturbations to the foot-ankle complex using computer simulation and a neuromusculoskeletal model.

METHODS

Musculoskeletal model: We used a modified version of a musculoskeletal model [2] with 12 muscles that crossed a 3 degree of freedom (DoF) ankle with a 3 DoF bushing force representing a lumped ligament contributing force at the end range of motion.

Neural model: We added a simulated neural network consisting of motoneurons and basic reflex circuitry. Each muscle was controlled by a population of motoneurons; Ia spindle feedback calculated from the musculoskeletal model was connected to the neural network model to simulate Ia homonymous excitation (stretch reflex) and reciprocal inhibition to all antagonist muscles. Renshaw cells (exhibiting recurrent inhibition of the agonist muscles) and phasic presynaptic inhibition of Ia afferents were modelled. Motoneuron pools were activated by descending drives.

Task: We applied simulated torque perturbations to the ankle of the neuromechanical model that varied in amplitude and were consistent with locomotion literature. We used optimization (with a multi-objective version of covariance adaptation evolution strategy) to find connection weights (feedback, central, and drives) that minimize metabolic cost, angular accelerations, and ligament force in response to random perturbations into dorsiflexion (similar to stance phase of locomotion).

RESULTS AND DISCUSSION

Without the neural reflex model, the muscle activations in response to a novel perturbation resulted large angular deviations. With the additional of a neural feedback model, the perturbation was compensated resulting in an angular acceleration profile that was relatively smooth, creating increased stabilization of the foot. Figure 1 shows an example of the simulation with a 50 Nm perturbation to the foot with neural feedback.

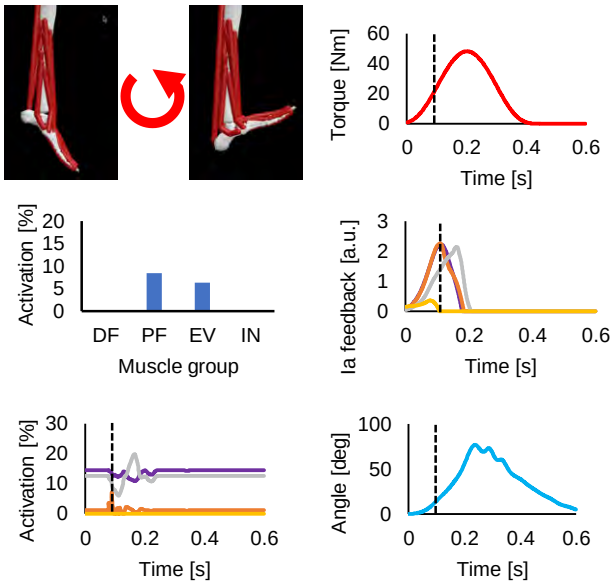

Figure 1: Top left panel shows the ankle model initial position and perturbation. Top right panel shows the torque perturbation time course. Middle left panel shows pre-activation of dorsiflexors (DF), plantarflexors (PF), evertors (EV), invertors (IN) prior to the perturbation. Middle right panel shows the Ia feedback from tibialis posterior (yellow), gastrocnemius medialis (orange), peroneus brevis (grey), and soleus (purple). Bottom left panel shows the activations from these same muscles. Bottom right panel shows the joint angle change from the perturbation.

Our preliminary findings showed that the combination of pre-activation of multiple muscles crossing the ankle followed by a coordinated activation of select muscles to produce force can oppose a rapid, applied perturbation to the foot similar to what is experienced during locomotion. During bipedal locomotion across varied terrain, humans can alter their foot posture and muscle activations to prepare for unexpected perturbations from the environment. Although there are other plausible mechanisms, these results provide a basis for understanding how humans can adapt to quick, unexpected perturbations to the foot and ankle via feedback similar to what occurs in locomotion.

CONCLUSIONS

Feedback is important for controlling perturbations to the foot and ankle and a combination of muscle pre-activation and the low-level neural circuitry are likely essential for controlling the foot during locomotion.

ACKNOWLEDGEMENTS

NSERC and Canada Research Chair to MJA, and the National Institutes of Health (NIH) grant nos. R01NS115900 and R01NS112304 to SMD.

REFERENCES

[1] Lee et al. (2018), *IEEE T. Neu. Sys. Reh. Eng. 44-52*
[2] Rajagopal et al., (2016), *IEEE Bio Med, 2068-79*

THE INFLUENCE OF MUSCLE INJURIES ON THE SHOULDER JOINT MECHANICS: A MUSCULOSKELETAL MODELLING STUDY AND EXPERIMENTAL VALIDATION

Mélody C. Labrune[1], Seyyed Hamed Hosseini Nasab[2], David T. Axford[1,3], Robert Potra[1], Joseph Cadman[1], Danè Dabirrahmani[1], William R. Taylor[2], Louis M. Ferreira[1,3], Sumit Raniga[1], Richard Appleyard[1]

[1] Faculty of Medicine, Health and Human Sciences, Macquarie University, Sydney, Australia.
[2] ETH, Institute for Biomechanics, Zürich, Switzerland.
[3] Dept of Mechanical and Materials Engineering, Western University, London, Canada.
Email: melody.labrune@hdr.mq.edu.au

INTRODUCTION

Non-invasive modelling tools, such as *in-silico* and *in-vitro* studies, have been developed to predict shoulder biomechanics and to better understand the impacts of clinical challenges on it. Previous studies have developed musculoskeletal shoulder models however, the experimental validations were generally insufficient. The goal of this study was to investigate the impact of soft tissue injuries on shoulder joint mechanics using a musculoskeletal model validated against *in-vitro* data from an advanced cadaveric shoulder simulator.

METHODS

A subject-specific musculoskeletal model was developed using OpenSim [1]. The model (Fig. 1), expanded on previous published models [2], comprises a six degree of freedom (DoF) shoulder joint actuated by eight Millard 2012 Equilibrium type muscles {Anterior, Lateral and Posterior Deltoids (AD, LD, PD respectively), Subscapularis Superior (SBS) and Inferior (SBI), Supraspinatus (SSP), Infraspinatus (ISP), Teres Minor (TM)}. Concurrent Optimization of Muscles Activation and Kinematics (COMAK) algorithm [3] was used to predict muscle and joint contact forces for two ranges of motion (RoM) {Abduction (ABD) and Forward Flexion (FF)} under three conditions {healthy, supraspinatus tear, Type C tear (SSP, ISP, SBS tears) [4]}. Tears were simulated by setting up maximum isometric force to zero. The kinematics from our in-house eight muscle-actuated, six DoF advanced cadaveric shoulder simulator were input into the model for validation. Pearson correlation coefficients were calculated to compare the muscle forces from the model against the shoulder simulator forces during the different RoMs and thereby assess the validity of the *in-silico* study.

RESULTS AND DISCUSSION

For ABD and FF, forces in the dominant muscle groups estimated by the musculoskeletal model and those measured by the cadaveric shoulder simulator showed strong correlations (Pearson's r >0.5, Fig.1). However, for some non-dominant muscle groups (all conditions: PD; Type C: TM and SBI), Pearson's r <0.5 demonstrated weak correlation between the shoulder model and the experimental muscle forces. This may be explained by their low force magnitudes and the small changes in their activation patterns.

Our results indicated increases of AD and LD forces with the severity of the conditions tested (ABD results in Fig. 1, an average increase of 30% for the AD and 47% for the LD).

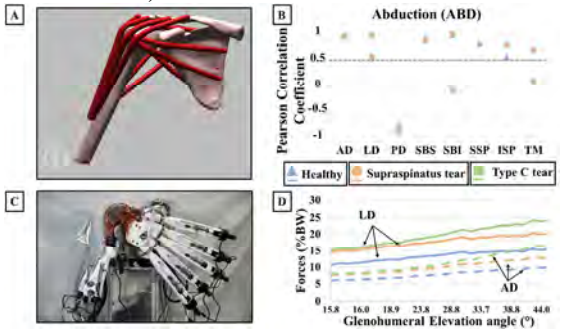

Figure 1 (A) OpenSim musculoskeletal model; (B) Correlation between muscle forces estimated by the model and the corresponding *in-vitro* data during ABD {Grey dashed line – Pearson's r = 0.5}; (C) Cadaveric shoulder simulator; (D) AD and LD muscle forces for ABD.

CONCLUSIONS

The results obtained from the shoulder model and those from the cadaveric simulator showed a good agreement for the dominant muscle groups. We found that the AD and LD forces increase when the rotator cuff muscles' function is compromised. This increase in muscle load may generate higher stress on the bones leading to potential fracture. Our *in-silico* approach provides a non-invasive tool for further investigations on shoulder pathologies and effectiveness of different surgical techniques.

ACKNOWLEDGEMENTS

We thank Sara Sadat Farshidfar for her technical support. This work was supported by Macquarie University scholarship.

REFERENCES

[1]Delp SL, et al. IEEE Trans Biomed Eng. 2007; 54(11): 1940-50.
[2]Saul KR, et al. Comput Methods Biomech Biomed Engin. 2015;18(13):1445-58.
[3]Smith, C. R., et al. J Biomech, 82, 124-133
[4]Collin P, et al. J Shoulder Elbow Surg (2014)23,1195-1202

HIGH-FAT DIET INDUCED VASCULAR SMOOTH MUSCLE CELL STIFFENING IN APOE$^{-/-}$ MICE

Nisha Khatiwada[1,2], Alex P. Rickel[1], Zhongkui Hong[1,2]*

[1]Department of Biomedical Engineering, University of South Dakota, Sioux Falls, SD, USA

[2]Department of Mechanical Engineering, Texas Tech University, Lubbock, TX, USA

Email: zhongkui.hong@ttu.edu

INTRODUCTION

Cardiovascular disease (CVD) causes about 30% of global death (estimated 17.9 million) and about 80% of CVD is atherosclerosis-related diseases [1]. Vascular smooth muscle cells (VSMCs) are the major cellular components of arterial wall and perform the major function for arterial contraction and extracellular matrix (ECM) production. During atherosclerosis, VSMCs undergo phenotypic switching to a synthetic phenotype capable of proliferation and migration. The surrounding environment of VSMCs in vivo undergoes alterations in ECM stiffness and composition in addition to an increase in cholesterol content. Our work is focused on the analyzing difference in the mechanics of VSMCs isolated from western diet fed apolipoprotein-E knockout (ApoE$^{-/-}$) and wild type (WT) mice during atherosclerosis.

METHODS

VSMCs were enzymatically isolated from the descending thoracic aorta of male ApoE$^{-/-}$ and male WT mice [2]. VSMCs were cultured on elastically tunable substrates. Atomic force microscope (AFM) was employed to study N-cadherin (N-Cad) mediated cell-cell adhesion, integrin mediated cell-ECM adhesion forces, and stiffness of VSMCs. AFM was also used to examine live VSMC submembranous cytoskeleton organization. Two-way ANOVA was used to test statistical significance for all experiments.

RESULTS AND DISCUSSION

No significant difference in cell stiffenss was observed between normal diet-fed ApoE$^{-/-}$ and WT VSMCs. After three-month high fat diet, ApoE$^{-/-}$ VSMCs were found to have a significantly higher stiffness compared to WT VSMCs (Figure 1) [2]. Increased stiffness of ApoE$^{-/-}$ VSMCs correlated with a greater degree of stress fiber alignment as evidenced by AFM-generated force maps and stress fiber topography images. ApoE$^{-/-}$ VSMCs had a significantly lower adhesion force to N-Cad compared to WT on the 28 and 103 kPa substrates.

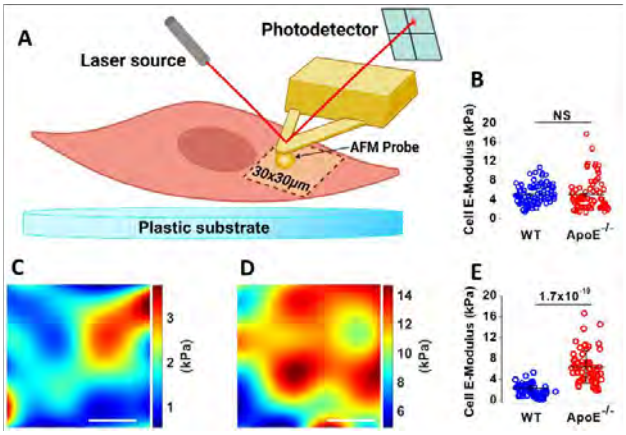

Figure 1 Live WT and ApoE$^{-/-}$ VSMC stiffness maps. **(A)** 30 × 30 μm cell surface areas were automatically scanned and indented at 6×6 positions with a glass bead. **(B)** Average stiffness for normal diet-fed ApoE$^{-/-}$ and WT VSMCs. **(C, D)** Stiffness force maps for WT and ApoE$^{-/-}$ VSMCs, respectively. **(E)** Average stiffness for Western diet-fed WT and ApoE$^{-/-}$ VSMCs. All data are presented as means ± SE (n > 60 cells across six different mice). Scale bar in lower right corner represents 10 μm. A was created with BioRender. com.

CONCLUSIONS

The results demonstrated a significant difference in cell mechanics, cytoskeletal organization, and migratory behavior of VSMCs isolated from WT and ApoE$^{-/-}$ mice. This supports our hypothesis that atherosclerosis alters the mechanical properties of VSMCs and provide insight into underlying mechanisms that may lead to future novel therapeutic approaches.

ACKNOWLEDGEMENTS

This work was supported, in part, by the National Science Foundation Grant 2127031 (USA) and the National Institutes of Health Grant R15HL147214 (USA).

REFERENCES

[1] Roth GA, et al. Global burden of cardiovascular diseases and risk factors, 1990-2019: update from the GBD 2019 study. J Am Coll Cardiol **76**: 2982–3021, 2020 [Erratum in J Am Coll Cardiol **77**: 1958–1959, 2021

[2] Rickel AP, et al. Am J Physiology-Cell Physiology **323**: C1393–C1401, 2022.

Identification of collective mechanical traits of an injured muscle model

Tae Yoon Kwon[1], Hyuntae Jeong[1], Youngbin Cho[1] and Jennifer H. Shin[1]
[1] Department of Mechanical Engineering, Korea Advanced Institute of Science and Technology, Daejeon, Korea.
Email: j_shin@kaist.ac.kr

INTRODUCTION

Collective cell migration is essential in diverse biological processes, including wound healing, development, cancer metastasis, and tissue regeneration. Skeletal muscle tissues contain myoblasts and satellite cells, which are undifferentiated forms of muscle cells that help self-regeneration after muscle injury. Collective motions in skeletal muscle regeneration are composed of cellular heterogeneity due to the presence of undifferentiated cells. This migration of skeletal muscle cells is important for regeneration because it serves as targeted migration toward injured regions as well as an aligning motion for improved differentiation. However, little is known about the dynamic collective behavior of skeletal muscle regeneration.

In this study, we constructed in vitro injured muscle model which can mimic a skeletal muscle injury and regeneration environment with conditioned media. In addition, we identified the collective mechanical traits of the muscle cell clusters with the muscle model.

METHODS

C2C12 cells were obtained from American Type Culture Collection (CRL-1772) and cultured under a normal culture condition. Normal muscle (NM) and damaged muscle (DM) conditioned media were manually obtained by fully differentiated and scratch-damaged-differentiated C2C12 skeletal muscle cultured with base media (BM), respectively. Polyacrylamide gel (PA gel, 11kPa) and collagen type I were used to construct in vitro cell traction measurement platform. We cultured C2C12 cells on circular patterned (Diameter: 700μm) collagen, which was created by utilizing a PDMS stencil to allow selective attachment of the cells only inside the circular pattern. The stencil was then removed to induce the migration of cells toward free space. The displacements of the fluorescent beads contained in the PA gel were used to calculate traction and intercellular stress.

RESULTS AND DISCUSSION

We examined the migration behavior of the cell clusters under three different media conditions (DM, NM, and BM) for 24 hours. Distinct patterns were observed in the spreading area, velocity, and directionality under each condition. Furthermore, the traction and stress of migrating cells also showed uniquely different trends and were closely related to the migrating behavior. We identified that the heterogeneous population of skeletal muscle cell clusters exhibited distinct behaviors in the injured muscle-mimicking condition compared to the normal muscle-mimicking condition.

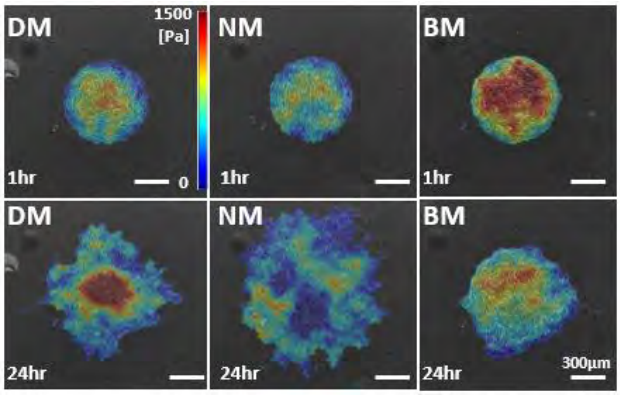

Figure 1 Temporal evolution of intercellular stress map.

CONCLUSIONS

In this study, we constructed in vitro injured muscle model which can mimic the skeletal muscle regeneration environment and measure cell traction to analyze the collective migration of muscle cells. As a result, we identified distinct patterns of migratory behavior and the mechanical traits of the cell clusters under different media conditions. Based on these findings, we suggest that biochemical cues from normal and injured skeletal muscles can induce these unique migratory patterns and mechanical properties by selectively activating specific cells at migrating clusters.

ACKNOWLEDGEMENTS

This work was supported by National Research Foundation of Korea (NRF) grants funded by the Korean Government (NRF-2020M3A9E4039658).

REFERENCES

[1] Tambe, D. T. et al. *Nature Materials* **10**: 469-475, 2011.

[2] Goetsch, K. P. et al. *J Muscle Res Cell Motil* **34**: 333-347, 2013.

EFFECTS OF SOLUTE MOLECULAR SHAPES ON OSMOSIS ACROSS FIBROUS MEMBRANES: AN APPLICATION TO FLUID TRANSPORT IN AN ENDOTHELIAL GLYCOCALYX LAYER

Panadda Dechadilok[1] and Kittipitch Yooprasertchuti[2]
[1]Department of Physics, Faculty of Science, Chulalongkorn University, Bangkok,Thailand
[2]Department of Physics, Faculty of Science, National University of Singapore, Singapore
E-mail: panadda.d@chula.ac.th

INTRODUCTION

Endothelial glycocalyx layer (EGL) is a fiber matrix of proteoglycans and glycoproteins observed at vascular endothelial cell surfaces. Interaction between EGL and plasma globular proteins is believed to help preventing transcapillary fluid extravasation. Low level of serum albumins, for instance, is believed to cause hypovolemia and facilitate pulmonary edema [1]. The present work focuses on studying the effect of EGL-globular protein interaction on the abilities of globular proteins as osmotic agents due to their molecular shapes through a theoretical investigation.

METHODS

Volume flux (J_v) of the osmotic flow across a fibrous membrane can be written as

$$J_v = L_P\left(\Delta P_\infty - \sigma_0 \Delta\Pi_\infty\right) \qquad (1)$$

where ΔP_∞ is the hydrodynamic pressure difference across the layer and $\Delta\Pi_\infty$ is the osmotic pressure difference related to the external solute concentration difference (ΔC_∞) as $kT\Delta C_\infty$. L_P is the hydraulic permeability, and σ_0 is the osmotic reflection coefficient. Based on analysis of electron microscopic images showing that, near the endothelial cell surfaces of frog mesenteric capillaries, EGL structure was a quasi-periodic fibrous meshwork [2], EGL simplified geometry was that of a hexagonal array of rigid cylinders [3, 4]. In the present study, globular proteins are modelled as spheroids**.** Lubrication approximation can be employed and, using Green's second identity, σ_0 can be computed as [4,5]

$$\sigma_0 = 1 - \left\langle u_z \left\{ \exp\left(-E/kT\right) \right\} \right\rangle \Big/ \left\langle u_z \right\rangle \qquad (2)$$

where u_z is the axial velocity of Stokes flow in a hexagonal array of cylinders. E is the solute-fiber potential energy of interaction. To examine effects of solute molecular shape alone, E was assumed to be due to a solute-fiber steric interaction. The curved and angle brackets denote an average over all solute orientations and a cross-sectional average, respectively. u_z was obtained as a finite element solution and σ_0 was computed using Eq. (2).

RESULTS AND DISCUSSION

In Figure 1, σ_0 is presented as a function of the solute Stokes-Einstein radius (a_{SE}) scaled with the distance between two closest fibers (d). An increase in solute shape asymmetry (an increase in deviation of b/a from unity) causes an increase in σ_0. At a_{SE} = 3.6 nm (a_{SE} of serum albumins) and d = 6 nm (d of EGL [2, 4]), σ_0 of an uncharged sphere = 0.66. If the solute shape resembles that of an albumin (approximated as an oblate spheroid with b/a = 0.5), σ_0 = 0.81 [6], close to σ_0 of albumins obtained experimentally (σ_0 = 0.816 ± 0.027 for frog mesenteric capillaries and σ_0 > 0.9 for mammalians [7,8]) even without including charge effects.

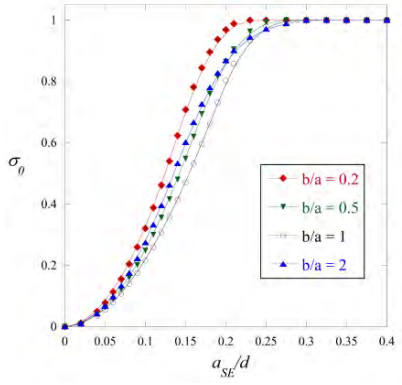

Figure 1 Osmotic reflection coefficient (σ_0) as a function of Stokes-Einstein radius scaled with a distance between fibers (a_{SE}/d). a is the spheroid equatorial radius, and b is the distance from center to pole along the symmetry axis of the spheroid [6].

CONCLUSIONS

Globular protein molecular shapes affect the osmotic fluid flux across a fibrous membrane and are likely to contribute to prevention of transcapillary fluid leakage. Figure 1 also shows a decline in σ_0 as a_{SE}/d decreases, indicating fiber volume fraction reduction caused by EGL damage (that is one of earliest signs of sepsis) can lead to transvascular fluid extravasation and edema.

ACKNOWLEGEMENTS

Supports from the Institute for the Promotion of Teaching Science and Technology, Thailand, and Faculty of Science, Chulalongkorn University, are gratefully acknowledged.

REFERENCES

[1] Arques S. *Eur. J. Inter. Med.* **52**: 8-12, 2018.
[2] Squire J M et al. *J Struct Biol* **136**: 239-225, 2001.
[3] Weinbaum S et al. *PNAS* **100**: 7988-7995, 2003.
[4] Sugihara-seki M et al. *J Fluid Mech* **664**: 174-192, 2010.
[5] Anderson J L. *J Theor Biol* **90**: 405-426, 1981.
[6]Yooprasertchuti K et al. *Chem. Eng. Sci.* **217**: 115521, 2020.
[7] Michel M M. J *Physiol. London* **404**: 1- 29, 1988.
[8] Michel M M et al. *Physiol. Rev.* **79**: 703-761, 1999.

Contribution of Titin to Passive and Active Forces in Single Myofibrils

Seong-won Han[1], Johanna K. Freundt[1], Wolfgang A. Linke[1]
[1] Institute of Physiology II, University of Münster, Germany.
Email: seongwon.han@uni-muenster.de

INTRODUCTION

Titin is a molecular spring and ruler that connects the Z-disk and the M-band in the sarcomere. Titin has been considered as the third component after actin and myosin, contributing to force generation of a sarcomere. Many attempts have been made to quantify the contribution of titin to passive and active forces, by removing titin through chemical degradation [1] or genetic impairment [2]. However, these approaches have limitations, because (i) other proteins are also affected by the chemical degradation, and (ii) most of the genetically modified animals exhibit secondary disease phenotypes, which complicate the interpretion of the results. Recently, the titin cleavage (TC) mouse model was established, where a cleavage site is cloned into I-band titin close to the A-band, and adding the tobacco etch virus protease to muscles allows for rapid and specific titin cleavage [3]. Using the TC model, we confirmed that titin contributes to passive and active force generation and also maintains sarcomeric structure organized [4]. However, even when all titin was cleaved, passive force did not drop to zero, but decreased by 50-55%, while titin was thought to contribute >90% of passive force previously [5]. One reason for this discrepancy could be the presence of stiff extracellular matrix proteins in the skinned muscle fibre bundles that were used [4]. Thus, we aimed at re-examining the contribution of titin to passive and active forces in single myofibrils, where the primary passive structure is clearly titin.

METHODS

Single myofibrils (n=3) from the psoas muscle of the TC mouse were attached to cantilevers (76 nN/µm) and set at an average sarcomere length (SL) of 2.4 µm. Then, the myofibril was slowly stretched to 3.0 µm, held for 30 s to measure passive force, and returned to the slack SL. The measurement was then repeated on the same myofibril, after titin was cleaved. Active force was quantified during activation with Ca^{2+} at an average SL of 2.4 µm. All force data were converted into stress considering the cross-sectional area of the myofibrils.

RESULTS AND DISCUSSION

After titin was cleaved, passive and active stresses were reduced by 59.2% and 47.8% on average, respectively (Fig 1A, B). Substantial changes in myofibrillar structure were observed during activation after TC (Fig 1C, D). Before the myofibril was activated, the Z-disks (red arrows) and the A-bands (blue arrows) were clearly defined (Fig 1C), but as the activation proceeded, the myofibril structures became indistinguishable (Fig 1D).

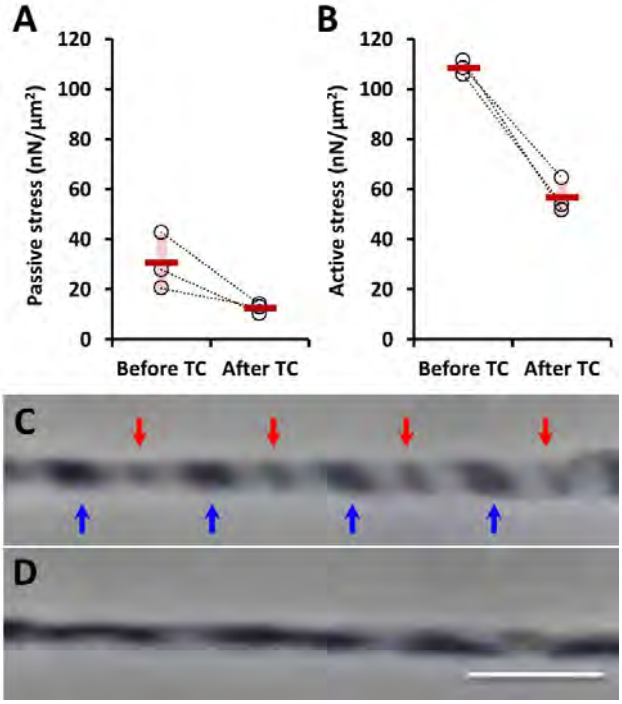

Figure 1 Summary of the results. Passive (A) and active (B) stresses are shown: each circle represents a result from a myofibril, and the horizontal bar and vertical bar represent the mean with 1SD, respectively. Structural changes in the myofibril before (C) and after (D) activation are shown when titin was removed. The red arrows point to the Z-disks, the blue arrows to the A-bands. The scale bar is 5 µm.

CONCLUSIONS

Our results confirm that cleaving titin reduces passive and active stress [4], but the decrease in stress reached no more than 67% in single myofibril preparation. Thus, further studies are required to determine the source of the remnant passive stress in myofibrils. Also, activating myofibrils is deleterious to the sarcomeric structures when titin was removed, resulting in substantial decrease in active stress.

ACKNOWLEDGEMENTS

This work was supported by the German Research Foundation (SFB1002-A08; Wolfgang A. Linke).

REFERENCES

[1] Higuchi H. *J Biochem.* **111**: 291-295, 1992.
[2] Radke MH et al. *Circulation*. **139**: 1813-1827, 2019.
[3] Rivas-Pardo JA et al. *Nat Commun.* **11**:2060, 2020.
[4] Li Y et al. *eLife.* **9**:e64107, 2020.
[5] Irving T et al. *Biophys J.* **100**:1499-1508, 2011.

THE DISTINCTIVE MECHANICAL AND STRUCTURAL SIGNATURES OF RESIDUAL FORCE ENHANCEMENT IN MYOFIBERS

Anthony L. Hessel[1], Michel Kuehn[1], Bradley M. Palmer[2], Devin Nissen[3], Dhruv Mishra[4], Venus Joumaa[5], Johanna Freundt[1], Weikang Ma[3], Kiisa C. Nishikawa[4], Thomas Irving[3], Wolfgang A. Linke[1]
[1] Institute of Physiology II, University of Muenster, Muenster, Germany.
[2]Department of Molecular Physiology and Biophysics, University of Vermont, Burlington, USA.
[3]BioCAT, Department of Biology, Illinois Institute of Technology, Chicago, USA.
[4] Department of Biological Sciences, University of Northern Arizona, Flagstaff, USA.
[5]Human Performance Laboratory, Faculty of Kinesiology, University of Calgary, Calgary, Canada
Email: anthony.hessel@uni-muenster.de

INTRODUCTION

In skeletal muscle, titin proteins connect sarcomeric myofilaments together and are thought to be critical for contraction, especially during residual force enhancement (RFE) when force is elevated after an active stretch compared to a purely isometric contraction at the stretched final length [1]. We investigated titin's function during contraction using small-angle X-ray diffraction to track structural changes before and after 50% I-band titin cleavage using the titin cleavage transgenic mouse (TC) and the RFE-deficient, muscular dystrophy with myositis (*mdm*) mouse mutant [2-3].

METHODS

We used fast-twitch and permeabilized skeletal muscle fibers from TC (heterozygotes) and *mdm* (wild type and homozygous) mice. TC muscles have a splice site engineered into I-band titin [3] that allows for specific and rapid cutting of titins, and so decreases titin-based force and stiffness in the sarcomere. *Mdm* muscles have a small mutation in the titin gene that manifest as a small deletion in the I-band region that reduces RFE. Using these mutations, we ran typical mechanical experiments while also evaluating sarcomeric structures using small-angle X-ray diffraction. We captured mechanical and structural details of fibers during pure isometric contractions at short (Iso_{Short}) and long (Iso_{Long}) sarcomere lengths, as well as after an eccentric contraction from the shorter to longer sarcomere lengths (Iso_{RFE}). Full-factorial ANOVA with individual random effects were used on best Box-Cox transformed variables to test for differences in structure and function between titin treatments (TC) or genotypes (*mdm*).

RESULTS AND DISCUSSION

50% titin cleavage reduced RFE from 30.69 ± 3.35% to 17.44 ± 2.24% of reference force (Iso_{Long}; $P < 0.01$). We report that Iso_{RFE} is structurally distinct from pure isometric contractions, with increased thick filament strain and decreased lattice spacing compared to Iso_{Long} ($P < 0.01$). Furthermore, these distinctive RFE structural features were not detected in *mdm* fibers, but were present in wild-type fibers ($P < 0.01$). The results suggest that decreased lattice spacing and increased thick filament length, improving force production and transmission enough to account for ~40-70% of RFE. The remaining ~30-60% of RFE could be accounted for by an activation-dependent ~2-3-fold increase in titin-based stiffness before eccentric stretch (Fig. 1).

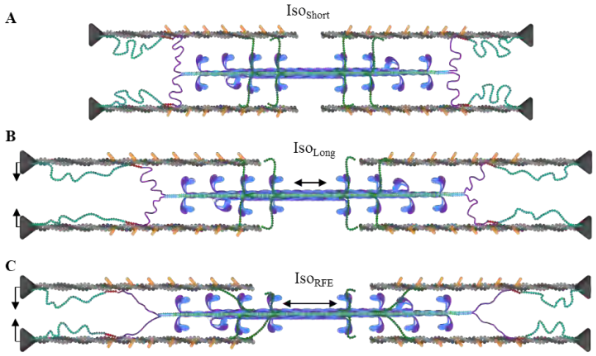

Figure 1 Possible mechanism of RFE. Configuration of sarcomeric proteins during (A) Iso_{Short}, (B) Iso_{Long}, and (C) Iso_{RFE} that may account for the distinctive mechanical and structural signatures.

CONCLUSIONS

These data demonstrate that titin is a critical regulator of sarcomeric tension, and as such, an essential contributor to RFE. The presence of RFE aligns with a distinctive structural state that is altered by titin cleavage and the *mdm* mutation. The analysis provides evidence that RFE is caused by increasing titin-based forces after eccentric stretch that also leads to decreased lattice spacing and elongated thick filaments. Finally, our data provide evidence for an activation-dependent increase in titin-based stiffness, but the mechanism remains unclear (possible mechanism shown in Fig. 1).

ACKNOWLEDGEMENTS

We thank BioCAT and Institute of Physiology II lab members for their contributions to our project. Funding was provided by the German Research Foundation (454867250 to ALH, SFB1002A08 to WAL), National Institutes of Health (P41 GM103622, P30 GM138395 to TI), National Science Foundation (IOS-2016049 to KN), and IZKF Münster (Li1/029/20 to WAL).

REFERENCES

[1] Hessel et al. *Front Physiol*. **8** 70, 2017
[2] Mishra et al. J. Exp. Biol. **15**: jeb243732, 2022
[3] Rivas-Pardo et al. Nat Commun. **11**: 2060, 2020

HOW COLLAGEN IX ALTERS THE MICROMECHANICAL PROPERTIES OF COLLAGEN II ARRAYS?

Fatemeh Jalali[1], Mohammad Ali Nazari[1]
[1] Department of Biomechanics, University of Tehran / School of Mechanical Engineering, College of Engineering, Tehran, Iran.
Email: f.jalali156@gmail.com

INTRODUCTION

Osteoarthritis (OA) is one of the most common skeletal diseases that can overshadow people's daily activities. This disorder is associated with the wear of the upper surface of the articular cartilage. Knowing the mechanical properties of the cartilage components by considering their structure can help to understand cartilage damage and regeneration. Thin collagen fibrils in the cartilage surface are heteromeric molecular structures composed of collagens type II, IX, and XI. Collagen type IX is fibril-associated collagen with interrupted triple helices (FACIT), which has remarkable properties. Type IX collagen is present not only in healthy fetal and mature cartilage but in OA-damaged cartilage at the edge of fibrillations. In this study mechanical properties of type II collagens with and without type IX collagen, have been investigated.

METHODS

Unlike fibrillar collagens, collagen IX is composed of three collagenous domains (COL1, COL2, and COL3) and four non-collagenous domains (NC1 to NC4). The NC1, NC2, COL1, and COL2 are vital in the mechanical properties of fibrils due to their special arrangement. Covalent bonds crosslinking type IX collagen with type II are unique. To consider these cross-links, Miles et al. [1] showed that COL2 and COL1 are anti-parallel. To assume the above features an array of 5 type II tropocollagens consisting of two periods with 67 nm lengths, first without collagen IX and then with collagen IX were designed (Figure 1). The persistence length of a 300 nm tropocollagen type II is 15 nm, and the number of its amino acids is known. Knowing the number of amino acids in COL1(IX), and COL2(IX), their corresponding persistence lengths and consequently their Young's moduli were calculated. By limiting the movement in one end along the fibre, a compressive force was slowly applied to the opposite end.

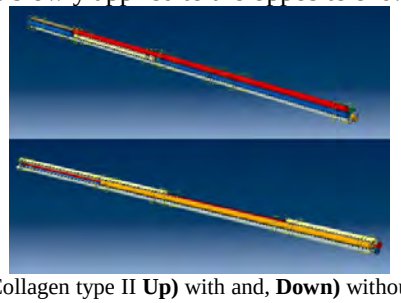

Figure 1 Collagen type II **Up)** with and, **Down)** without collagen IX models.

RESULTS AND DISCUSSION

The stress-strain curves are obtained for two opposite surfaces for each model (Figure 2). Two regions are observed: a primary region with a small Young's modulus, followed by a secondary region with a higher slope. The change in the slope is caused by a conformational change and the gradual growth in collagens' resistance against increasing tension. The primary Young's modulus with collagen IX (227 MPa) is approximately 30 percent stiffer than the model without (175 MPa). The secondary Young's modulus of the model with type IX collagen (315 MPa) is also 9 percent lower than the model without collagen IX (289 MPa). Since the molecular arrangement of collagens is asymmetrical, after applying the compressive load, it bends. Increasing the force makes the model buckle. The buckling load of the model with collagen IX (79 pN) is less than the model without collagen IX (87 pN). The results obtained for Young's moduli are consistent with previous investigations on collagens [2].

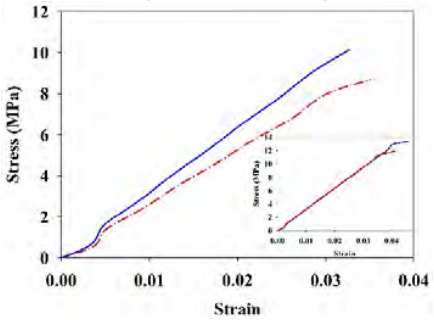

Figure 2 The stress-strain curve after applying pressure to the model results for the array with and, **Inset)** without collagen IX.

CONCLUSIONS

The presence of collagen IX can reduce the buckling force; hence we hypothesize that collagen IX acts as a barrier against collagen-degrading enzymes such as matrix metalloproteinases (MMPs) and delays the interaction of enzymes with fibrillar collagens. As a result of the remarkable effect of type IX collagen in the process of remodelling, growth, and destruction of collagen fibrils, it seems that this collagen can be used as a target molecule for the prevention and treatment of OA.

REFERENCES

[1] Miles, C.A., et al. *Journal of molecular biology* **277**(1): p. 135-144, 1998.

[2] Gachon, E. and P. Mesquida. *Acta Biomaterialia* **149**: p. 60-68, 2022.

AN INTEGRATED FINITE ELEMENT APPROACH TO SIMULATE INTERNAL BONE STRAIN IN RESPONSE TO JOINT LOADING

Timo van Leeuwen[1,2], Marco Schneider[3], Harry van Lenthe[4], Jonas Rubenson[5], Thor Besier[3], and Evie Vereecke[2]

[1] Research Foundation Flanders (FWO), Brussels, Belgium.
[2] Dep. of Development and Regeneration, KU Leuven, campus Kulak, Kortrijk, Belgium.
[3]Auckland Bioengineering Institute, University of Auckland, Auckland, New Zealand
[4]Dep. of Mechanical Engineering, KU Leuven, Leuven, Belgium.
[5]Dep. of Kinesiology, The Pennsylvania State University, USA.

Email : timo.vanleeuwen@kuleuven.be

INTRODUCTION

Bone is a complex and unique tissue that is capable of responding to its mechanical environment by adapting its own morphology in response to external loading. Exposing the direct relation between the mechanostimuli and the remodelling of bone that follows will be immensely valuable as it may facilitate both the prediction and prevention of bone strain issues and potential bone failure injuries. In order to understand this form-function relation between stimulus and response, accurate assessment of how the bone is loaded is crucial. To simulate both the external and the internal loading conditions of bone in response to the realistic joint loading, we present an integrated finite element (FE) – micro FE (µFE) approach to assess both external, articular bone stress and internal bone strain based on physiologically relevant boundary conditions.

METHODS

Our custom FE pre- and post- processing software suite is used to generate parametric FE models based on CT imaging of the joint in standardized loading positions. Joint loading conditions are used to simulate the inter-articular loading patterns during realistic joint interactions. Using our custom suite, these articular loading patterns are extracted and integrated in µCT based, whole bone µFE models that assess bone strain values at the level of the of the trabecular bone architecture. The disassociated bone models are aligned with ISB convention standards for intuitive interpretation. The approach was developed for the primate thumb joint, specifically the trapeziometacarpal joint, but is intended for broader implementations in other joints and taxa. In bonobos, gibbons, and macaques, various grasping types with different thumb positions were CT scanned as input joint positions. The FE approach yields articular loading patterns in which differences per position of the thumb can be identified. These loading patterns are then applied as boundary conditions to the trapezium bone and solved to assess internal bone strain using µFE. Bone strain values were evaluated in five bonobo thumb specimens and for five different types of grasping

RESULTS AND DISCUSSION

The µFE results indicate that strain distributions between different simulated grasps are highly similar, showing dissipation towards the proximo-ulnar cluster of trabeculae regardless of trapezial bone microarchitecture. Strain levels deviating from this pattern are shown to be likely related to the dissimilar, possibly pathological, external bone morphology rather than trabecular differences. The simulated bone strain values fall within realistic boundaries of a healthy response to habitual loading. The average mean strain value of 62.11 µε ± 18.05 µε and peak strain value of 578.36 µε found across all simulations do not exceed bone yield values based on even the lowest reported elasticity modulus (ε_{yield} = 3500 µε).

CONCLUSIONS

This approach offers a method to integrate realistic boundary parameters into the assessment of internal bone strain values. Our research collaboration is working on expanding, validating, and further developing the approach with the aim of addressing the relation between the stimulus and the response in bone functional adaptation. Currently, the project is being further developed into an open source software suite to study the fundamentals of bone functional adaptation in the bipedal model of Guinea Fowl.

ACKNOWLEDGEMENTS

This project was developed under the support of the KU Leuven and the FWO. Current and further developments are made possible by the FWO under the postdoctoral fellowship fundamental research grant awarded to dr. Timo van Leeuwen (grant no. 12B3523N).

Effusion-synovitis mediates the association between quadriceps weakness and worsening knee pain

Ze Gong [1], Jia Li [2], Di Ao [1] and Le Li [1]
[1] Institute of Medical Research, Northwestern Polytechnical University, Xi'an, China.
[2] Department of Orthopedics, Nanfang Hospital, Southern Medical University, Guangzhou, China.
Email: gongze0226@163.com

INTRODUCTION

Knee osteoarthritis (KOA) is a major cause of disability in older adults [1] , with more than 240 million adults suffering KOA [2]. However, approved therapies that modify the onset or progression of KOA remine elusive. Therefore, it is essential to identify the risk factors of KOA for early intervention. Quadriceps weakness has become an important predictor for knee pain, with strength training suggested as the first-line treatment by international guidelines. Nevertheless, it is noted that the mechanism underlying the association of quadriceps strength with knee pain is not clear.

In the knee, bone marrow and synovium are the source of pain due to their rich nociceptive innervation. Our team previously found that quadriceps weakness has the potential to cause the effusion-synovitis. An effect of quadriceps weakness on pain could be due to the intermediate effect of quadriceps weakness promoting effusion-synovitis which then cause pain. This is under urgent need to be investigated.

Using observational data acquired from the Osteoarthritis Initiative (OAI) cohort (an open-source database), we quantified the relation of muscle weakness and knee pain and then examined whether the association of muscle weakness with worsening pain was mediated by worsening effusion-synovitis.

METHODS

A longitudinal observational study was performed in 1050 participants (623 women and 427 men) included from the OAI, with complete records of quadriceps strength, effusion-synovitis, and knee pain at baseline, 1- and 2-year follow-ups. Quadriceps strength was measured at baseline, with subjects required to perform maximal voluntary isometric contraction. The highest value (Nm) was selected from three repetitions and normalized to body mass (Nm/kg). Effusion-synovitis was assessed in intercondylar region through Magnetic Resonance Imaging Osteoarthritis Knee Score (MOAKS) system based on MRI. Knee pain was evaluated according to Western Ontario and McMaster Universities Osteoarthritis Index (WOMAC) pain sub-scale. Other demographic characteristics and potential confounding factors were collected.

The relationship between WOMAC pain and quadriceps weakness was calculated by linear models, adjusted for age, sex, BMI, race, baseline WOMAC pain, Center for Epidemiologic Studies Depression Scale (CESD) score and Physical Activity Scale (PASE) score. Mediation models were used to assess the indirect effect of effusion-synovitis in the association of quadriceps weakness with worsening pain with adjustment for confounders. Given sex differences in strength, we further perform a sub-analysis stratified by sex.

RESULTS AND DISCUSSION

We found that the significantly negative association between baseline quadriceps strength and worsening pain in the primary and sub-group analyses at 1- and 2-year follow-ups (β: -0.87 - -0.26, $p<0.05$). These results were consistent with previous studies, indicating that quadriceps weakness was a critical risk factor for knee pain. In addition, mediation analyses showed that the association of quadriceps weakness with increased knee pain over 1 year was substantially mediated by the effusion-synovitis change in the whole population and females (**Figure 1**). We did not find similar results in males. This may be attributed to the lower quadriceps strength in females, which means that females are more prone to approach the strength threshold needed to protect the knee.

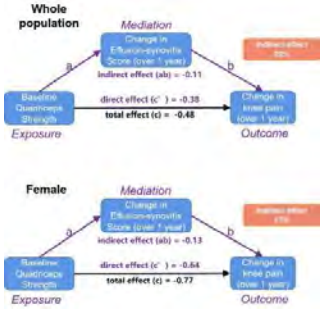

Figure 1. Schematic diagram of the mediating effect of effusion-synovitis changes on baseline quadriceps strength and knee pain changes.

CONCLUSIONS

In conclusion, quadriceps weakness is significantly associated knee pain worsening and this relation appears to be partially mediated by effusion-synovitis change, especially in females. These results remain to be verified in future interventional experiments.

ACKNOWLEDGEMENTS

This work was supported by the Education and Teaching Reform Funds for the Central Universities (22GZ230101).

REFERENCES

[1] Neogi T et al. *Osteoarthritis Cartilage* **21**: 1145-53, 2013.
[2] Losina E et al. *Arthritis Care Res (Hoboken)* **67**: 203-15, 201.

ULTRASONOGRAPHIC ASSESSMENT OF ACUTE FEMORAL CARTILAGE RESPONSE AFTER RUNNING AND CUTTING

Miyuki Hori[1], Masafumi Terada[1], Tadashi Suga[2] and Tadao Isaka[1]
[1] Faculty of Sport and Health Science, Ritsumeikan University / Shiga, Japan.
[2] Reserch Organization of Science and Technology, Ritsumeikan University / Shiga, Japan.
Email: gr0521se@ed.ritsumei.ac.jp

INTRODUCTION

Knee osteoarthritis (OA) is a significant chronic disease that leads to more years lived with disability and imposes a devasting health care burden [1]. Identifying deleterious changes in cartilage status and health are critical for developing effective strategies to reduce risk of progressive degradation of articular cartilage and knee OA development. Evaluating articular cartilage deformation following physical activities may provide valuable insight into early alterations of the articular cartilage before any declines occur in cartilage structure and health [2]. Researchers demonstrated that changes in the magnitude of knee joint loading affected the ability of the articular cartilage to absorb and redistribute biomechanical forces applied to the knee joint thought physical activities. Abrupt lateral movement, breaking, and accelerating have been theorized to contribute to joint degeneration [3], given that abnormal shear loading could adversely affect the deformational capability of the articular cartilage. In addition, it has been theorized that aberrant shear loading may lead to a shorter fatigue life of cartilage than compressive loading [4]. However, no authors have examined the association between types of mechanical joint loading and cartilage deformation. Understanding the influence of types of joint loading on cartilage deformation may help to develop comprehensive therapeutic strategies to decrease the risk of OA. Therefore, the purpose of this study was compared cartilage deformation in response to cutting and decelerating movement (shear loading), running (compressive loading) and control (no loading) using ultrasonography (US).

METHODS

A randomized order cross-over study was used to examine femoral articular cartilage thickness before and after three loading conditions. Nineteen healthy participants with no previous history of knee joint injury (age: 22.3 ± 2.4years, height:173.3 ± 5.1cm, body mass: 66.5±7.4kg) volunteered for this study. Participants completed three conditions, consisting of 1) 30 min-curing and breaking movement, 2) 30 min-running, and 3) control (30 min-rest in a supine position), during independent data collection sessions separated by at least 1 week at the same time of day. A femoral cartilage US examination was performed before (baseline), immediate after exercise (post0), 30 min (post30) and 60 min (post60) after each condition. For this study, 3 images were recorded of the dominant limb at each time point. Anterior femoral cartilage thickness was quantified and averaged from all 3 of the US images. A percentage change score from baseline to each post-test time point was calculated to represent the amount of acute cartilage deformation for each US measure following each condition. Repeated measures ANOVAs with Bonferroni post hoc analyses were used to compare cartilage deformation between loading conditions. Statistical significance was set at $p<0.05$.

RESULTS

There was a significantly greater intercondylar femoral cartilage deformation following the cutting condition at post0 ($p=0.03$), post30 ($p=0.02$), and post60 ($p=0.02$) compared to the running and control conditions (Figure 1). No differences were observed for other US measures between loading conditions ($p>0.05$).

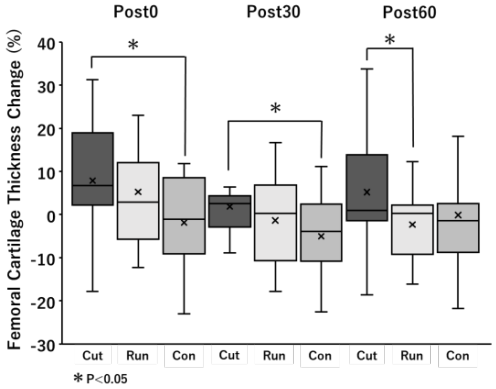

Figure 1. The amount of acute intercondylar femoral cartilage deformation following cutting (cut), running (run), and control (con).

CONCLUSIONS

We observed that cutting movements had a larger magnitude of acute intercondylar femoral cartilage deformation compared to running and control. Results from this study indicate that shear loading may have a larger influence on the magnitude of change in intercondylar femoral cartilage deformation. Future research may consider to use the cutting condition in pathological populations to monitor for early declines in cartilage health.

REFERENCES

[1] Hawker GA. *Clin Exp Rheumatol* **37**: S3-6, 2019.
[2] Harkey MS et al. *Ultrasound Med Biol* **44**: 311-20, 2018.
[3] Driban JB et al. *J Athl Train* **52**: 497-506, 2017.
[4] Miller RH. *Exerc Sport Sci Rev* **45**: 87-95, 2017

3D MR ANALYSIS REVEALS SEX-SPECIFIC CAM LOCATION DIFFERENCES IN FEMOROACETABULAR IMPINGMENENT PATIENTS

Jessica M. Bugeja[1], Ying Xia[1], Shekhar S. Chandra[2], Nicholas J. Murphy[3,4], Stuart Crozier[2], David J. Hunter[3,5], Jurgen Fripp[1] and Craig Engstrom[6]

[1]Australian e-Health Research Centre, Commonwealth Scientific and Industrial Research Organisation Health and Biosecurity, Herston, Australia.

[2]School of Information Technology and Electrical Engineering, University of Queensland, Brisbane, Australia.

[3]Kolling Institute of Medical Research, Sydney Musculoskeletal Health, University of Sydney, Australia.

[4]Department of Orthopaedic Surgery, John Hunter Hospital, Newcastle, Australia.

[5]Department of Rheumatology, Royal North Shore Hospital, St Leonards, Australia.

[6]School of Human Movement Studies, University of Queensland, Brisbane, Australia.

Email: jess.bugeja@csiro.au

INTRODUCTION

Cam femoroacetabular impingement (FAI) syndrome is a degenerative hip joint disorder, associated with severe hip pain during locomotion and the development of hip osteoarthritis. FAI syndrome is commonly assessed using the alpha angle on a radiological image plane between the 12:00 and 3:00 clockface positions, regardless of patient sex. Hip joint shape features, evaluated with statistical shape models (SSMs), are an important biomarker for osteoarthritis incidence, progression, and arthroplasty. However, to the best of our knowledge, no studies have investigated 3D SSM cam sex-based differences. This study investigated whether FAI syndrome differ with gender in respect to cam location as measured using focused shape modelling and partial least squares (PLS) regression.

METHODS

Hip MR images from 97 patients with FAI (56 male, 41 female, 16-63 years) were used [1]. CamMorph [2] was used to generate 3D surface models of the femur, and the latent variables (LVs) were derived from PLS regression to capture the sex-specific cam shape features. A two-way analysis of variance (ANOVA) assessed interactions between cam LVs, sex, and cam severity [2]. LVs with a significant sex effect (p<0.05) and a moderate to large Cohen's d effect size were analysed further. Additional exploratory analysis applied scatterplot and Pearson regression line analyses to assess the association of cam volume (generated using CamMorph [2]) and the alpha angle (measured at 1:00 and 3:00 o'clock by N.J.M.) on the LVs.

RESULTS AND DISCUSSION

LV 1 represented cam size and LV 2 characterised cam location (Figure 1). Cam volume significantly correlated with LV 1 (female r=0.83, male r=0.87: both p<0.001) and an alpha angle ratio $\left(\frac{\text{alpha angle at 1:00}}{\text{alpha angle at 3:00}}\right)$ was significantly correlated with LV 2 (r=0.47, p<0.001). The ANOVA indicated no significant interaction between the effects of sex and cam severity on the LVs. Moderate to large effect sizes were observed for sex and LVs 1 and 2 (p≤0.001, D≥0.75). Cam height data showed mean male and female patients presented with a superior- and anterior-focused cam, respectively. Male and female patients with a negligible, mild or moderate cam had a superior and anterior cam, respectively. Both male and female major cams had a global distribution. Although the current study findings are limited by a small cohort size, they suggest female alpha angle measurements should be made circumferentially (beyond 12:00 and 3:00). Additionally, female FAI prevalence data may be inadequate due to false negative FAI diagnoses. Future works are required to confirm current findings.

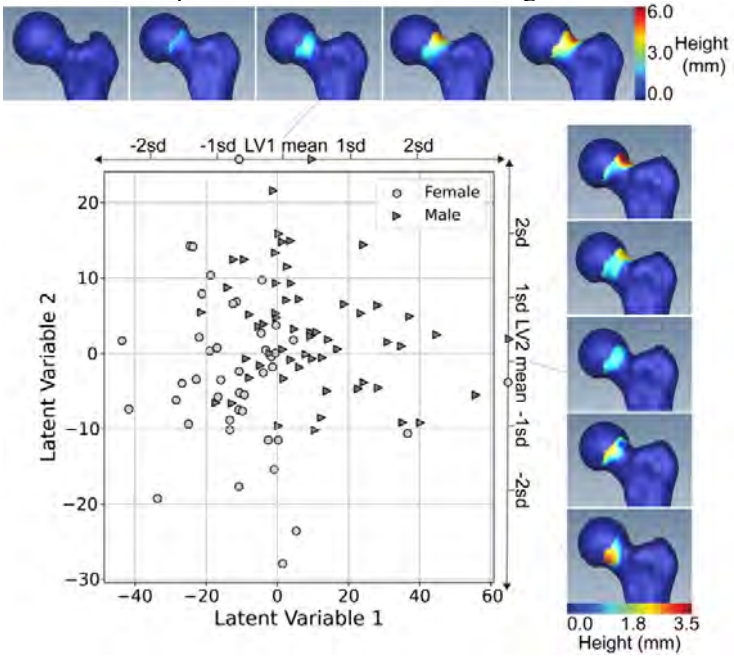

Figure 1 LV 1 and LV 2 scatterplot illustrating female and male cam size and location clustering. Light grey circle and dark grey arrowhead on axes represent the female and male group mean, respectively. LV = latent variable and sd = standard deviation.

CONCLUSIONS

In this study, LVs derived from PLS regression were associated with cam size and location, respectively. Male and female FAI patients with a negligible, mild or moderate cam volume exhibited a superior and anterior cam location, respectively. Major cam volumes occurred in similar locations irrespective of sex.

ACKOWLEDGEMENTS

We thank Mr James Williamson who helped progress the ideas of this work through our many conversations.

REFERENCES

[1] Murphy et al. *BMC Musculoskelet. Disord.* **18:** 406, 2017.
[2] Bugeja et al. *Quant. Imaging Med. Surg.* **2**: 4924-4941, 2022.

TIMING AND ACCURACY OF 3D PRINTED PELVIC FRACTURE PLATES

Dale Robinson[1], Peter Lee[1] and Andrew Bucknill[2]
[1] Department of Biomedical Engineering, University of Melbourne, Melbourne, Australia.
[2] Department of Surgery, Royal Melbourne Hospital, Melbourne, Australia.
Email: drobinson@unimelb.edu.au

INTRODUCTION

Pelvic fractures have a relatively rare incidence, representing 1.5% of all fracture cases, yet they are associated with high mortality (7-30%) [1]. These fractures are typically treated with fracture plates comprising a straight or slightly curving design which must be contoured intra-operatively, a process that is timely and imprecise. Plate fixation with screws is also challenging, as screws must stabilize the construct while avoiding injury to surrounding tissue. Patient-specific plates manufactured by 3D printing can potentially solve these issues; plates are created that conform to patient-specific anatomy, while controlling screw trajectories to remain within safe regions of the anatomy. The aim of this study was to evaluate the timing and accuracy involved in using 3D printed pelvic fracture plates, knowledge that will help identify improvements that may be needed to produce 3D printed pelvic fracture plates at scale.

METHODS

Five cadaveric pelvises were sourced from the University of Melbourne body donor program. A fracture was created by impaction of a ball-ended punch into the acetabulum. CT imaging was performed at clinical resolution, then all bony fragments were segmented to obtained their 3D geometry. Fracture reduction was achieved virtually be displacing each bony fragment until the surface of the bone appeared congruent. The outline of the fracture plate was drawn onto the bone, then cut from the bone with a boolean operation and finally extruded to a thickness of 3 mm (Fig. 1). Bicortical locking or non-locking screws (ϕ 3.5 mm) were used, with trajectories chosen to pass through the surgical window while avoiding sensitive anatomy. The plates were 3D printed in Ti6Al4V using a sintered laser melting (SLM) printer with 30 µm layers, followed by a stress relief anneal. Each plate was implanted and a post-op CT scan was obtained to measure print accuracy, implant positioning error and screw angulation error. The duration of each step was recorded.

RESULTS AND DISCUSSION

Each fracture plate was implanted in one hour or less. Apart from specimen 2, which was complicated by a pre-existing fracture plate (Fig. 1B), the design times were less than 10.0 hours, and print times varied from 27.0 to 32.5 hours (Table 1). 3D printing errors ranged from 0.10 to 0.49 mm, plates were mispositioned by 1.7 to 13.0 mm, and mean screw angulation errors ranged from 2.8 to 7.0°.

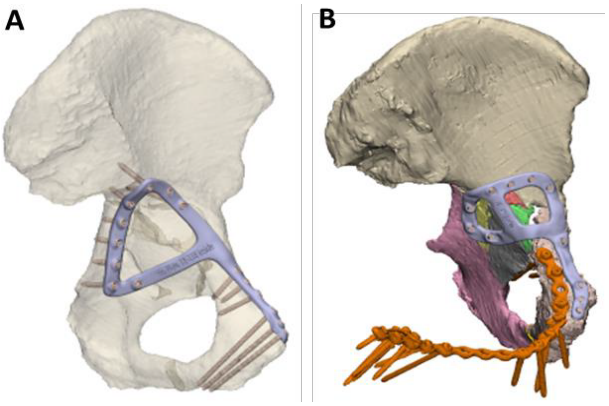

Figure 1 Example plate designs. **A)** Specimen 1. **B)** Specimen 2.

Table 1: Times and errors associated with design and manufacture of fracture plates.

Spec. no.	Design time (hrs)	Print time (hrs)	Print RMSE (mm)	Position error (mm)	Mean screw angle error (°)
1	3.5	32.0	0.37	1.7	6.2
2	17.2	32.0	0.49	5.7	7.0
3	3.0	32.5	0.10	7.5	2.8
4	9.5	32.0	0.13	13.0	6.3
5	7.5	27.0	0.26	5.1	7.3

CONCLUSIONS

A one-hour surgical time was an improvement compared to reported times for standard fracture plates (175-287 min [2]), thus, highlighting the benefit of using 3D printed fracture plates. For four specimens without a pre-existing plate, the total design and print time was less than 48 hours, a duration which would suggest that personalised plates are a clinically viable option. The print errors ranged from acceptable to large, which appeared to be related to the size of the plate. Hence, improved methods to better control the print accuracy of longer plates are needed, particularly regarding the build-up of thermal stresses that is typical of SLM printers. The errors in plate positioning and screw angulation were mostly affected by the limited surgical access available for the pelvic region. In future work, these errors must be reduced using tools such as surgical navigation or fluoroscopy in order for the benefits of subject-specific design to be fully realised.

REFERENCES

[1] Court-Brown C & Caesar B. Injury **37:**691-7, 2006.

[2] Lee AK et al. J Clin Med 11:5258, 2022

TROCHLEAR ORIENTATION OF TOTAL KNEE DESIGNS IS OPPOSITE TO THAT OF THE NATURAL FEMUR

Nikhil Gattu[1], Marriah Sutton[1], David B. Doherty[1], Sabir K. Ismaily[1],
David Rodriguez-Quintana[1], and Shuyang Han[1]
[1] Department of Orthopaedic Surgery, McGovern Medical School, UTHealth Houston, Texas, USA.
Email: shuyang.han@uth.tmc.edu

INTRODUCTION

Femoral component designs in total knee arthroplasty (TKA) have evolved to reflect the anatomy of the native knee, particularly the femoral condylar design. However, there is currently still a lack of consensus regarding the trochlear sulcus design, which is a major factor contributing to postoperative patellofemoral complications, such as patellofemoral maltracking, dislocation, and patellar component loosening [1]. The objective of this study was to compare the trochlear sulcus geometry of a broad range of prosthetic knee designs and that of the natural knee, thereby providing references for modification of femoral component designs.

METHODS

Three-dimensional computer models of 14 femoral component designs and 21 non-arthritic human femora (average age: 34.9±13.1) were reconstructed in this study. Each model was aligned in a standard reference coordinate system [2] and coaxial cutting planes were created in 15° increments around the trochlear groove axis (Figure 1). In each plane, the medial and lateral ridges, as well as the deepest point of the trochlear sulcus were marked. The mediolateral position of the sulcus, the sulcus angle (∠ABC), and the trochlear groove orientation θ were then measured (Figure 1). To facilitate comparison, the measurements of each model were normalized to a trochlear radius of 21.0mm.

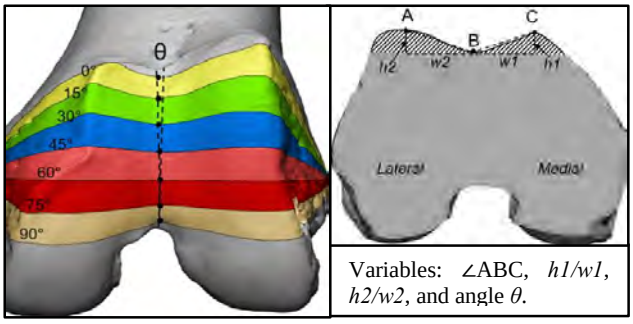

Figure 1. Measurement of the trochlear sulcus geometry

RESULTS AND DISCUSSION

Among the 14 components, nine were contemporary designs. Three (3/14) had a symmetrical geometry (Optetrack, Profix, and Klassic). The sulcus angle (∠ABC) of all components gradually decreased from 0° to 60° (Figure 2A), except AMK, Optetrak, and Profix, which remained fairly constant. All asymmetrical designs (11/14) had a laterally orientated sulcus (θ=7.1°±2.0°, range: 4.3°-10.5°, Figure 2B). Moreover, the height/width ratio of the medial and lateral ridges were nearly identical, and both increased with the planes.

In the natural femur, the sulcus angle (∠ABC) changed in a sine wave pattern from 0° to 120° and was 4°-13° lower than the prosthetic knees in different planes (Figure 2A). Moreover, contrary to the laterally oriented sulcus in prosthetic designs, the sulcus of the native knee was bilinear (0°-60° and 75°-90°) and had a medial orientation (Figure 2B) [3]. In addition, the height/width ratio of the native knee first increased from 0° to 30° and then decreased until 75° and increased slightly afterward, which was also different from the prosthetic designs (Figure 2C, 2D).

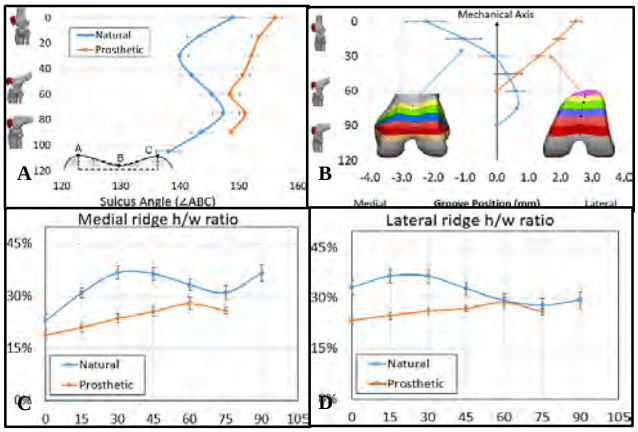

Figure 2. Comparison of the trochlear sulcus geometry of femoral component designs and the natural femur.

CONCLUSIONS

There are large variations in the trochlear sulcus design of contemporary TKA implants. Compared to the natural femur, the femoral components generally have a larger sulcus angle and lower height/weight ratio of the ridges, which could cause an increase in the risk of postoperative complications. Most importantly, although femoral components with a lateral sulcus orientation are often called 'anatomical', our finding demonstrated that the sulcus orientation of the natural femur was the opposite, i.e., a medial orientation. Therefore, it is worthwhile to revisit the rationale behind the lateral sulcus design of contemporary femoral components in TKA.

REFERENCES

[1] Chen S. et al. *Knee Surg Sports* **25**:3163-70, 2017
[2] Wu G. et al. *J Biomech* **35**:543-8, 2002
[3] Barink M. et al. *J Biomech* **39:** 1708-15, 2006

Accelerometer based assessment of upper extremity movement in patients with obstetric plexus palsy

Catherine Disselhorst-Klug[1], Ligia C S Fonseca[1], Jörg Bahm[2]
[1] Department of Rehabilitation and Prevention Engineering, Institute of Applied Medical Engineering, RWTH Aachen University, Aachen Germany.
[2] Clinic for Plastic, Hand and Burns Surgery, University Hospital Aachen, Aachen, Germany.
Email: disselhorst-klug@ame.rwth-aachen.de

INTRODUCTION

Obstetric Brachial Plexus Palsy (OBPP) occurs in approximately 0.5 to 0.77 out of 1000 newborns. In the case of OBPP the upper brachial plexus nerves are damaged and arm function is severely limited. Since the location and extend of the lesion of the Plexus Brachialis nerve are different in each child, the coping strategies of the patients are highly individual. OBPP patients' arm function has to be regularly examined in order to agree about new therapeutic goals. However, up to now this is done mainly through visual observations by physicians or therapists. In order to achieve at least some objectivity and to document functional changes the Mallet Scale (MS) is used. The MS distinguishes 5 different categories of severity. These categories are graded on a scale from I to V, with I being not testable and IV reaching the same endpoint as healthy subjects. MS V is reserved for health subjects only. However, since reaching a certain endpoint determines the membership to a particular category, coping strategies are not taken into consideration. The objective of this work is to present a new approach based on accelerometers in combination with a classification procedure, which allows the quantitative assessment of upper extremity movement performance of patients with OBPP.

METHODS

Experienced physiotherapists have evaluated the movement performance of 10 healthy children and 41 children suffering from OBPP. Each subject has been assigned to one of 5 categories of the MS. Three triaxial-accelerometers were placed at chest, upper arm and wrist of the subject. Acceleration signals have been recorded during repetitive "hand to mouth" tasks.

34 features were extracted from the acceleration signals. For each feature a linear correlation test between the feature value and the MS classification of the subjects was made. A feature was accepted as suitable if the correlation coefficient was higher than 0.5. In this way, a number of F relevant features was identified. Secondly, 6 weighting factors w_i = 0.5, 1, 1.5, 2, 3 or 4 were introduced and assigned to each relevant feature. Assignment was done with respect to the strength of the correlation between the MS score and the feature value.

To calculate a score quantifying the movement performance of each subject, 4 thresholds were identified for each of the F relevant features. The target for optimization of the thresholds was the best discrimination between the 5 MS categories. With respect to the thresholds, each feature value was assigned to a discrete number (N_i) with N_i = 0 representing a feature value within the feature specific thresholds of MS V (healthy subjects), N_i = 1 of MS IV, N_i = 2 of MS III, N_i = 3 of MS II and N_i = 4 of MS I.

An overall score (SC) quantifying the subjects' individual movement performance was calculated by adding the weighted discrete numbers of all relevant features according to:

$$SC = \sum_{i=1}^{F} w_i \cdot N_i$$

with F = number of relevant features, w_i = weighting factor and N_i = discrete number of each feature.

RESULTS AND DISCUSSION

F=13 features out of 34 features showed a correlation higher than 0.5 between the feature value and the MS category assigned to each subject. Figure 1 showed the resulting SC score as a function of the MS category. With the exception of MS I, there is a significant difference in SC score between all MS categories.

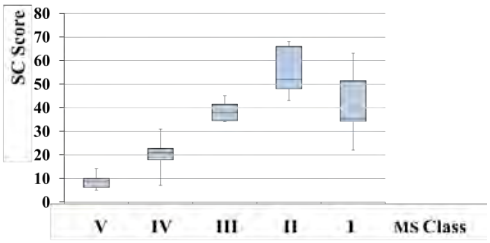

Figure 1 SC scores related to the categories of the MS.

The introduced procedure is designed to evaluate movement performance and to quantify the severity of compensational movement parts. Since MS I is just defined by not reaching a certain end-point, movement performance is more heterogenic in this category compared to the other MS categories.

CONCLUSIONS

The introduced approach demonstrated its ability to assess upper extremity movement performance in patients with OBPP quantitatively. Based on the SC score, direct feedback about the quality of movement performance can be given to patients, physicians and therapists. The quantitative and objective assessment of relevant movements for daily activities will enable an evidence-based, individualised treatment for OBPP patients.

DIFFERENCES IN TROCHLEAR SULCUS GEOMETRY OF TOTAL KNEE DESIGNS

Shuyang Han[1], Marriah Sutton[1], David B. Doherty[1], David Rodriguez-Quintana[1], and Philip C. Noble[1]
[1] Department of Orthopaedic Surgery, McGovern Medical School, UTHealth Houston, Texas, USA.
Email: shuyang.han@uth.tmc.edu

INTRODUCTION

The trochlear sulcus of the femoral component is a major factor contributing to maltracking of the patella following total knee arthroplasty (TKA). Although the femoral condylar design has evolved to reflect normal anatomy, consensus on the geometry of the trochlear sulcus has been lacking [1,2]. With newer data, more surgeons now frequently elect to leave the patella unsurfaced, heightening the importance to the limits of variations in trochlear morphology associated with satisfactory outcomes after TKA. The objective of the present study was to analyze the variation in the geometry of the trochlear sulcus of a broad range of contemporary TKA designs and compare with earlier generations of femoral components.

METHODS

Fourteen femoral components (9 contemporary, 5 legacy) from nine manufactures (Depuy, Exactech, Howmedica, Osteonics, Smith&Nephew, Stryker, Zimmer, Biomet, TJO) were obtained from a large retrieval collection. High resolution laser scans were performed for each component and 3D computer models were created and analysed using Geomagic Design X. Specifically, radial section planes were created in 15° increments for each component. In each section, the variables shown in Figure 1 were measured.

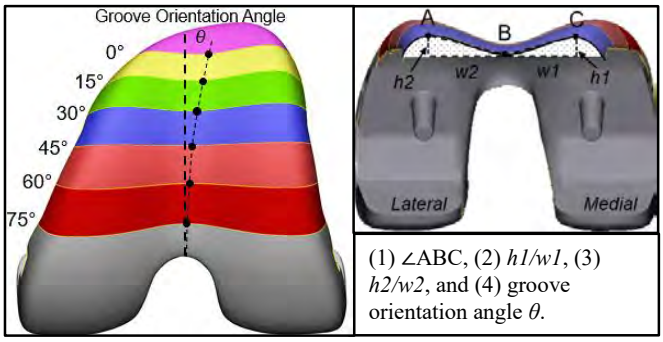

(1) ∠ABC, (2) *h1/w1*, (3) *h2/w2*, and (4) groove orientation angle *θ*.

Figure 1. Measurements of the trochlear sulcus geometry

RESULTS AND DISCUSSION

The sulcus angle (∠ABC) of all components gradually decreased from 156.2°±3.9° in the 0° plane to 148.5°±6.4° in the 60° plane, except for AMK (Depuy), Optetrack (Exatech), and Profix (S&N), which remained fairly constant. Excluding the three symmetrical designs (Optetrack, Profix, and Klassic), the deepest point of the sulcus gradually shifted medially towards the mechanical axis by 3.0±0.9mm (range: 1.9-4.8mm) from 0° to 60°, resulting in a groove orientation angle *θ* of 7.1°±2.0°. PFC Sigma had the largest groove orientation (10.5°), while ScorpioNRG had the lowest (4.3°). The lateral groove orientation was seen in each component and this was contrary to the anatomy of the natural knees [1]. However, the true deviation could be decreased as a result of femoral component positioning during TKA [2]. In addition, Optetrack (Exactech) and AMK (Depuy) demonstrated a high lateral ridge in the middle (30°-60°) of the component compared to other designs.

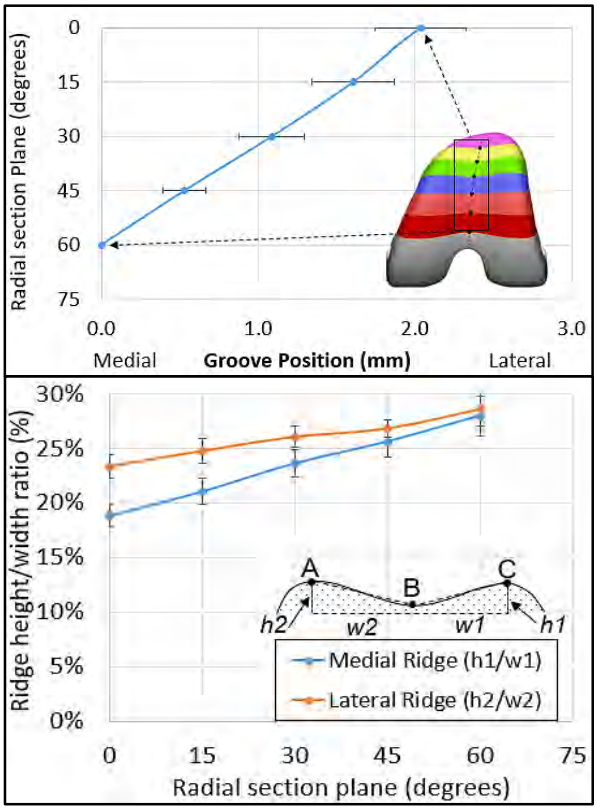

Figure 2. Average groove position of the 14 designs and the variation of the height/width ratio of the medial and lateral ridges.

CONCLUSIONS

The trochlear design of TKA implants does not always have clear anatomic parameters, a major factor in patellofemoral complications after TKA. Our study shows large variations in the geometry of the trochlear sulcus between different prosthetic designs. In the next step, we will compare these parameters to the trochlear geometry of the natural knee in an attempt to provide references for optimizing trochlear sulcus design of TKA implants.

REFERENCES

[1] Barink M et al. *J Biomech* **39**: 1708-15, 2006.
[2] Borukhov I et al. *Knee Surg Sports Traumatol Arthrosc*, 2021 (Online)

DESIGN AND EVALUATION OF A NOVEL PATIENT-SPECIFIC, UNLOADING KNEE BRACE

Jonas Steensgaard Stoltze[1], Anderson Oliveira[1], John Rasmussen[1], Michael Skipper Andersen[1,2]
[1]Department of Materials and Production, Aalborg University, Denmark.
[2] Center for Mathematical Modeling of Knee Osteoarthritis (MathKOA), Aalborg, Denmark.
Email: msa@mp.aau.dk

INTRODUCTION

Knee Osteoarthritis (KOA) is a degenerative joint disease and, combined with hip osteoarthritis, it is the most frequent cause of walking disability among elderly [1]. Multiple risk factors for the development of KOA, hereunder increased knee joint compressive forces (KJCF), have been identified. For this reason, unloading braces have been investigated, but their effect has not been clearly documented. Many brace designs have focused on reducing the Knee Adduction Moment (KAM) although it does not accurately predict the KJCF. The purpose of this study was, therefore, to develop a novel patient-specific knee brace concept to reduce the KJCF and evaluate its effect in a pilot patient study.

METHODS

The study was divided into three phases: 1) Unloading concept investigation. 2) Prototype development and 3) Evaluation of the brace concept.

Unloading concept investigation

To identify potential mechanisms to unload the knee joint, inverse dynamics-based musculoskeletal models (MSM) were created for ten healthy subjects during gait at self-selected pace in the AnyBody Modeling System (AnyBody Technology, Denmark). On these models, we applied idealized, support moments at the hip, knee and ankle and investigated how these alone and in combination affected the KJCF. The full details of the study can be found in in Stoltze et al. [2] and we found, among other measures, that a knee extension moment applied during early stance can reduce the first peak of the KJCF, whereas an applied ankle plantarflexion moment can reduce the second peak of the KJCF. Based on this, we decided to develop a knee brace prototype to unload the first peak as other studies have already developed a suitable ankle brace for the second peak [3].

Prototype development

Using a combination of strings, springs and a four-bar mechanism, a quasi-passive knee brace was designed to apply a knee extension moment during early stance (Figure 1, left). To apply the knee extension moment only during the early stance, a release mechanism was developed to control whether or not the strings were slack. For brace design details, see Stoltze et al. [4].

Evaluation of the brace concept

Gait data were collected for six KOA patients using motion capture and force plates without the brace.

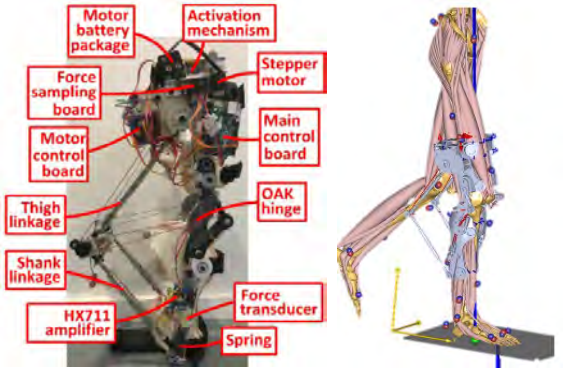

Figure 1 Left: Knee brace prototype. Right: MSM with brace.

For each patient, MSM were created, and an ideal brace model was implemented. Using the model, subject-specific brace parameters (spring stiffness, brace activation etc.) were determined to reduce the KJCF. Subsequently, the prototype brace was manufactured for one patient and the gait mechanics with and without the brace was measured using surface electromyography, marker-based motion capture and force plates. Lastly, the effect from the prototype brace was evaluated with MSM (Figure 1, right).

RESULTS AND DISCUSSION

The simulations with the ideal brace showed a varying reduction of the first peak KJCF between 3.5% to 34% across the six patients. The experiments with the prototype brace reduced the peak vastii muscle activation by 8% and the musculoskeletal models estimated an associated KJCF reduction of 26%. However, the impulse of the KJCF increased by 17%.

CONCLUSIONS

The results with the prototype brace shows promising results in terms of reducing the KJCF through the application of external moments to unload the muscles. However, further studies on large patient cohorts are required to determine the long-term effects on both pain, function and disease progression.

REFERENCES

[1] Bernad-Pineda M, et al. *Rev Esp Cir Ortop Traumatol* **58**: 283-289, 2019.
[2] Stoltze et al. *Int Biomech* **5**: 63-74, 2018.
[3] Kobayashi T et al. *J Biomech* **130**: 110845, 2022.
[4] Stoltze et al. *J Biomech Eng* **144**: 011007, 2022.

EXPERIMENTAL VALIDATION OF A KNEE IMPLANT DAMAGE PREDICTION FRAMEWORK

Michael Dreyer[1,2], Seyyed Hamed Hosseini Nasab[1], Bernhard Weisse[2] and William R. Taylor[1]
[1] Institute for Biomechanics, ETH Zürich, Zurich, Switzerland.
[2] Laboratory for Mechanical Systems Engineering, Empa, Dübendorf, Switzerland.
Email: michael.dreyer@hest.ethz.ch

INTRODUCTION

The gold standard for knee implant wear simulation, experiments according to ISO 14243, is too expensive and time consuming for large scale studies. Finite element simulation offers an alternative, but models need to be validated carefully. Moreover, the recent "Stan" dataset [1], containing representative in vivo joint level loads and kinematics based on data from load-sensing implants and video-fluoroscopy [2], presents an alternative set of boundary conditions for both force-controlled (FC) and displacement-controlled (DC) setups. In this study, we compared wear for the ISO and Stan conditions in both FC and DC configuration using simulation and laboratory testing, simultaneously validating a state-of-the-art finite element wear model.

METHODS

Here, we investigated the same knee implant Stan's data was obtained from (*Innex FIXUC*, Zimmer Biomet, Switzerland. To validate the wear model, two groups of three were tested on a six-station knee simulator for 5 million cycles (Mc). One group was subjected to the ISO FC boundary conditions and the other to Stan's kinematics in DC mode. The effective loads and kinematics of the implants were also recorded. Before and after the test, the specimens' 3D geometry was measured using a 3D scanner (Pro S3, HP Inc., USA) and surface deviation caused by wear and creep was visualized by comparison.

Finite-element models of these ISO FC and Stan DC implant wear tests were developed in Abaqus (Dassault Systemes, USA). However, differences in effective loads and kinematics in the joint models and test were expected. To control for this when evaluating wear, two additional models where the mean kinematics measured in each test group were applied in DC mode were run. For the four models in total, polyethylene inlay wear and creep was predicted for 5 Mc using a cross-shear and contact-pressure dependent wear model for the polyethylene inlay material [3] and a compressive creep model using custom software.

RESULTS AND DISCUSSION

Experimentally, wear of the DC Stan condition was 2.7 times higher than for the FC ISO condition (Figure 1, right). For the corresponding simulations (Figure 1, left), the DC CAMS model matched the experiment closely, while the FC ISO model drastically overpredicted wear. Rather than poor modelling of wear, this mismatch was due to a difference of several mm/degree of the predicted joint kinematics between the ISO FC model and bench test. Consequently, there was good agreement for the ISO model with measured kinematics (Fig. 1, middle) and for the Stan condition, which was always in DC mode.

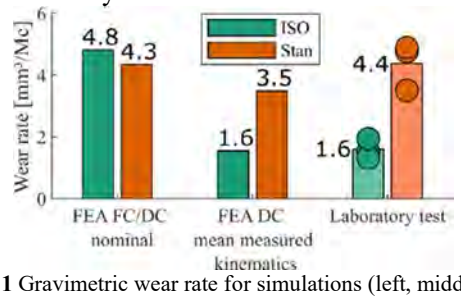

Figure 1 Gravimetric wear rate for simulations (left, middle) and laboratory wear test (right, circles represent each specimen).

The ISO FC model's surface damage (Table 1, top left) was significantly more anterior and covered a larger area than for the ISO model with effective kinematics applied in DC mode (Table 1, top middle), explaining the different wear volumes. For the Stan condition, both models agreed with the experiment (Table 1, bottom).

Table 1: Surface deviation caused by wear and creep after 5 million cycles for the four models and the test specimens

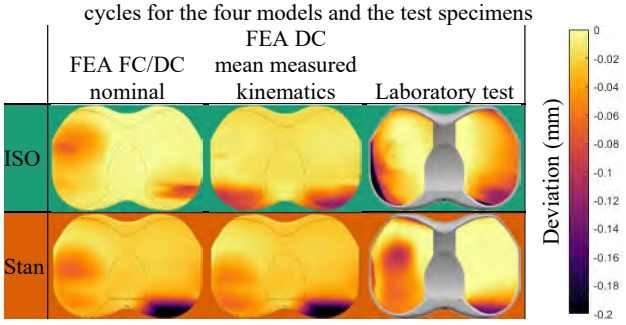

CONCLUSIONS

Overall, the comparison between the lab tests and the simulations using DC control served to validate our wear prediction algorithm. However, it appears sensitive to variations in contact mechanics. Still, our models are suitable for future investigations into wear and creep damage caused by different boundary conditions (e.g. Stan) or implants.

ACKNOWLEDGEMENTS

We thank Zimmer Biomet for access to data and performing the laboratory wear test.

REFERENCES

[1] Dreyer MJ et al. *J Biomech* **141**:111171, 2022.
[2] Taylor WR et al. *J Biomech* **65**:32-39, 2017.
[3] Dreyer MJ et al. *Tribol Lett* **70**(4):119, 2022

Evaluation of plantar pressure redistribution in novel footwear for people with diabetes

Sarah Hemler[1,2], Sofia Ntella[3], Kenny Jeanmonod[3], Yoan Civet[3], Yves Perriard[3], Zoltan Pataky[1,2,4]
[1] Faculty of Medicine, University of Geneva, Geneva, Switzerland
[2] Unit of Therapeutic Patient Education, WHO Collaborating Centre, Geneva University Hospitals, Geneva, Switzerland
[3] Integrated Actuators Laboratory, École Polytechnique Fédérale de Lausanne (EPFL), Neuchâtel, Switzerland
[4] Faculty Diabetes Centre, Faculty of Medicine, University of Geneva, Geneva, Switzerland
Email: sarah.hemler@unige.ch

INTRODUCTION

One of the main risk factors for ulcer formation and eventual lower limb amputation in people with diabetes is sustained high plantar pressure (PP). There is a need for off-loading footwear that actively adapts to the user's changing PP needs. To address this need, our team is developing intelligent footwear (IF) with an auto-contouring insole which will read PPs and automatically adapt the shape of the insole [1]. This pilot study tests the IF's mechanical ability to redistribute high PPs during gait by altering placement of fixed height modules (either full or deformed height).

METHODS

Four healthy participants walked 20m overground donning the PEDAR® system (Novel GmbH, Munich, Germany) in the IF (size EU43) with two comfort insole conditions: thin (TI) and medium-thickness (MI) insoles (Figure 1A). For each insole (TI or MI), baseline measures were collected followed by two to four adjustment conditions. The goal of these adjustments was to redistribute and reduce high PP via specific module replacement. To perform the adjustments, the researchers determined the location of the highest PP in the rearfoot and forefoot across both feet according to the PEDAR®. Then, under the area(s) of high PP, one to four of the 3D-printed full-height module replicas (30mm, Figure 1A-white modules) were replaced with a deformed-height module replica (27.5mm, Figure 1A-blue modules). The peak PPs for each of 99 PEDAR® cells per foot across two walking trials per condition were analysed. The peak PPs within a region (forefoot or rearfoot), around the module(s), and directly over a module were compared between the baseline and adjustment conditions for each insole.

RESULTS AND DISCUSSION

The average (SD) and range of baseline PPs were 392(102) and 273-603kPa, respectively. Across the 29 adjustment conditions, there was an average reduction within the region, around the module(s), and over the module(s) of 29(56), 34(54), and 60(39) kPa, respectively (Figure 1B). If the regional baseline PP was greater than 400 kPa, the adjustment reduced the pressure in that region by 55(66) or 129(19) kPa (11% or 21%) for the TI or MI. The baseline and adjustment PPs for the MI condition were lower than the TI.

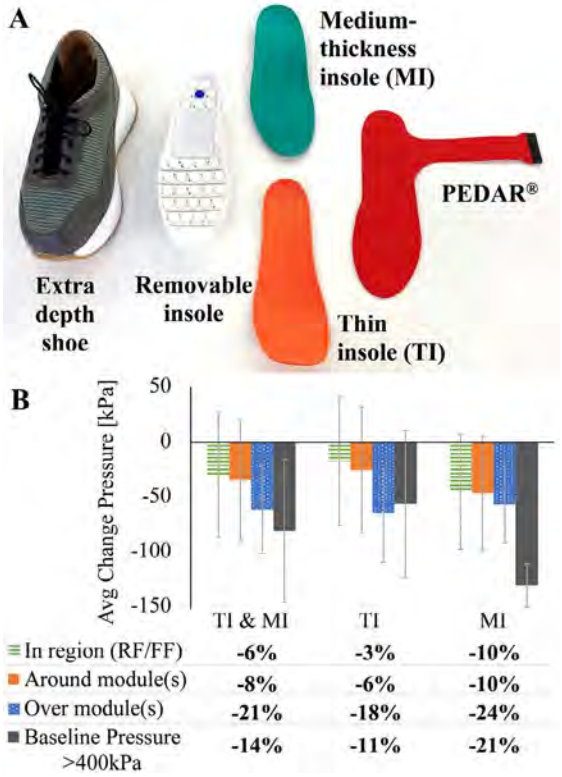

Figure 1 A) Footwear pieces used. B) Average PP reduction with the respective values of % change in pressure below.

CONCLUSIONS

Overall, the PPs in the adjusted conditions were lower than in the baseline condition and were most reduced when the starting baseline PP was above 400kPa. The largest PP reductions were close to the common clinical reduction goal of 25% [2]. This work shows that this novel footwear has promising potential to reduce high PPs and thus, reduce the risk of ulceration and amputation in people with diabetes. Future tests will use the electronic modules [1] and parts to assess the IF's redistribution algorithm, autonomy, human factors design, and thus, real-world application.

ACKNOWLEDGEMENTS

Funding was provided by the Switzerland National Science Foundation (Bridge Discovery Grant - 181020).

REFERENCES

[1] Pataky Z et al. *Rev Med Suisse*. **12**: 143-7, 2016.
[2] Bus S et al. *Diab Care*. **34**, 7: 1595-6000, 2011.

Quantifying Muscle Tone of Upper limb for stroke patients via an impedance-based Arm Circumference Motor Evaluation System (i-ACMES)

Chieh-Hsiang Hsu[1], Yu-Chen Lin[2], Hsiu-Yun Hsu[1,4], Fong-Chin Su[3,5] and Li-Chieh Kuo [1,3,5]

[1] Department of Occupational Therapy, National Cheng Kung University, Tainan, Taiwan.
[2] Department of Occupational Therapy, Da-Yeh University, Changhua, Taiwan.
[3] Department of Biomedical Engineering, National Cheng Kung University, Tainan, Taiwan.
[4] Department of Physical Medicine and Rehabilitation, National Cheng Kung University Hospital
[5]Medical Device Innovation Center, National Cheng Kung University, Tainan, Taiwan.
Email: jkkuo@mail.ncku.edu.twv

INTRODUCTION

Spasticity is abnormal muscle tone which often shows in patients with upper motor neuron syndrome. The Modified Ashworth Scale (MAS) is commonly used to classify abnormal muscle tone in clinical assessments. However, using the MAS to determine abnormal muscle tone heavily relies on experiences and judgments made by clinicians without using other objective tools or data. Robotic measurements can obtain more accurate muscle tone data. Only a few studies have described the muscle tone across multi-joints of upper limbs using robotic measurements. Therefore, this study aims to investigate the muscle tone patterns of stroke patients via a custom Arm Circumference Motor Evaluation System (ACMES) [1], which is a novel device using an indirect measure method to quantify human upper limbs endpoint impedance across multi-joints.

METHODS

The ACMES guides upper limbs in a circular motion via a rotation disk and handle and then measures the impedance of upper limbs during the rotation motion. Nine stroke patients (6 males, 3 females, mean age = 53.6 years) with different MAS scores were included in this study. Each participant was asked to sit in front of an adjustable chair and select an appropriate disc radius depending on the arm length. Next, each participant was asked to grasp the handle and place the forearm on the handrest with the hand stabilized on the handle using a bandage. Both the less-affected side and affected side were measured. The test conditions included three speeds (low/medium/high) and two rotation directions (ABD/ADD). The disk angle was defined using the shoulder horizontal adduction direction. The test was divided into two phases, the flexor stretched phase (FSP) and the extensor stretched phase (ESP). Two phases were divided by the elbow joint motion, as shown in Figure 1.

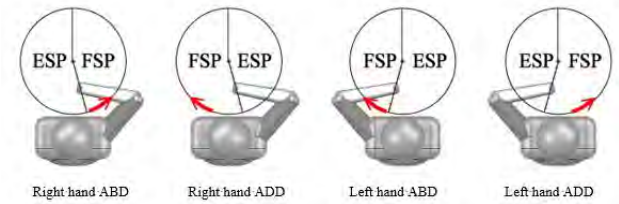

Figure 1 The definition of two rotation directions and two phases during the test.

The paired t-test was used to test the difference of the impedance between the less-affected side and affected side. All the data analysis and statistical analysis were performed using MATLAB R2020a.

RESULTS AND DISCUSSION

The result shows significant differences in all conditions except for the median speed and fast in ADD-ESP.

Table 1 The paired t-test of the peak value of impedance

Direction	Phase	Speed	Group	Mean	SD	*p*-value
ABD	FSP	Low	Less-Affected	0.01	0.01	0.03*
			Affected	0.06	0.07	
		Medium	Less-Affected	0.00	0.01	0.00**
			Affected	0.02	0.01	
		High	Less-Affected	0.00	0.00	0.01*
			Affected	0.02	0.01	
	ESP	Low	Less-Affected	0.01	0.01	0.00**
			Affected	0.05	0.02	
		Medium	Less-Affected	0.00	0.01	0.00**
			Affected	0.02	0.01	
		High	Less-Affected	0.00	0.00	0.01**
			Affected	0.02	0.01	
ADD	FSP	Low	Less-Affected	0.00	0.01	0.04*
			Affected	0.04	0.04	
		Medium	Less-Affected	0.01	0.00	0.02*
			Affected	0.02	0.01	
		High	Less-Affected	0.00	0.00	0.01*
			Affected	0.01	0.01	
	ESP	Low	Less-Affected	0.01	0.01	0.03*
			Affected	0.06	0.04	
		Medium	Less-Affected	0.01	0.00	0.05
			Affected	0.03	0.02	
		High	Less-Affected	0.00	0.00	0.07
			Affected	0.01	0.01	

*p<0.05, **p<0.01

Note. ABD: shoulder abduction first direction, ADD: shoulder adduction first direction, FSP: Flexor stretched phase, ESF direction: Extensor stretched phase, unit: Nms/deg

CONCLUSIONS

The result of this study shows the ACMES can indicate differences in spastic features between affected and less-affected sides of stroke patients. However, it will be necessary to recruit more participants with different demographic characteristics to collect more performance data to understand whether these physical or ergonomic issues would be potential significant factors influencing the impedance in the ACMES examinations.

ACKNOWLEDGEMENTS

This work was supported in part by the Medical Device Innovation Center, National Cheng Kung University from the Featured Areas Research Center Program within the framework of the Highest Education Sprout Project by the Ministry of Education in Taiwan.

REFERENCES

[1] C.H. Hsu et al. *JTEHM*.2021.3136754.

NOVEL ARTHROMETER PROVIDES QUANTITATIVE AND OBJECTIVE MEASURES OF UNIPLANAR AND MULTIPLANAR KNEE LAXITY

Carl Imhauser[1], Erin Berube[1], Akinola Oladimeji[1], David Shamritsky[1], Deborah Jones[1], Michael Parides[1], Danyal Nawabi[1], Andrew Pearle[1], Thomas Wickiewicz[1]
[1] Biomechanics Department, Hospital for Special Surgery, New York, NY, USA
Email: berubee@hss.edu

INTRODUCTION

Anterior cruciate ligament (ACL) rupture is a debilitating and costly knee injury that is common among young, active athletes and military personnel [1,2]. Both generalized joint hypermobility (GJH) and excessive laxity in one or multiple anatomic planes is related to increased risk of ACL injury [5]. However, the physical exams used to assess knee laxity, which include uniplanar tests of anterior-posterior (AP), varus-valgus (VV), and internal-external rotation (IER) laxities and the pivot shift exam, are subjective and are examiner dependent. Moreover, the relationship between GJH and knee laxity is not well understood. To address the lack of measurement instruments available to quantify uniplanar and multiplanar tests of knee laxity, we developed a novel arthrometer. This study had three goals: 1) to assess our device's safety; 2) to quantify its reliability and left-right symmetry in both uniplanar and multiplanar assessments; and 3) to relate GJH to uniplanar and multiplanar laxity exams.

METHODS

With IRB approval, 15 healthy, uninjured volunteers (8 males, 7 females; mean age: 28 ± 6 years) with no prior knee injuries were enrolled. The custom-designed knee arthrometer integrated an instrumented linkage with five degrees of freedom and measured translations and rotations in response to applied forces and moments (Fig. 1). The applied loads were measured using a six axis load cell (Mini58, ATI, Inc), which was fixed to the arthrometer. To conduct a test, the subject sat reclined in a chair, their leg was aligned and oriented at 20° of flexion, the femur was affixed to the chair, and the tibia was secured to the arthrometer. After 3 preconditioning cycles, the examiner manually applied AP forces (-50 N posterior to 135 N anterior), VV moments (±4 Nm), and IER moments (±2.5 Nm) to the tibia and the corresponding translations and rotations were recorded. The examiner performed a simulated pivot shift exam, consisting of the following loads applied in series: 2 Nm external rotation moment, 6 Nm valgus moment, 2 Nm internal rotation moment, and, finally, 50 N anterior force. Anterior tibial translation (ATT) was measured in response to these multiplanar loads. Two examiners conducted two independent tests on both left and right knees. Pain was assessed on a visual analog scale from 0 (no pain) to 10 (excruciating pain). Reliability within a single test and within (intra) and across (inter) examiners was characterized via intra-class correlation coefficients (ICC) and 95% confidence intervals (CI). Left and right leg symmetry was quantified via mean left-right difference in laxity. GJH was measured using the clinical Beighton score. The relationship between GJH and knee laxity was quanitified using linear regression ($\alpha = 0.05$).

RESULTS AND DISCUSSION

All volunteers completed the protocol. Pain across all tests was minimal (mean: 0.2 ± 0.1). Intra-trial reliability was excellent for all tests (≥0.92) while intra-examiner reliabilities ranged from good (0.66 in AP) to excellent (0.92 in VV). For all tests, inter-examiner reliabilities were good (all ICC's ≥ 0.62). Regarding left-right symmetry, in the AP, IER, and VV directions, and the simulated pivot shift, the mean difference was 0.4 ± 3.0 mm, 0.1 ± 4.1°, and 0.0 ± 0.5°, and 2.2 ± 2.0 mm, respectively. The mean Beighton score was 3.7 ± 1.2 ranging from 0 to 9. Regarding uniplanar laxities, the Beighton score was only associated with AP laxity ($R^2 = 0.43$, $p = 0.008$). In AP, a mean left-right difference of 2.6 mm will enable us to relate knee laxity and ACL injury risk [5]. In IER, a mean left-right difference of 3.1° will enable us to detect increased rotatory laxity and to indicate use of lateral augmentation surgery. For the simulated pivot shift, a mean left-right difference of 2.2 mm will enable more precise detection of ACL graft failure.

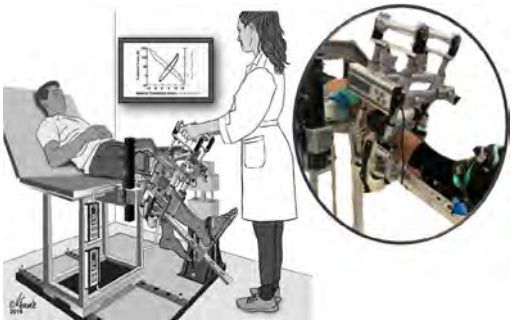

Figure 1: Knee Arthrometer

CONCLUSIONS

Our novel device was safe and showed promising reliability. The uncertainties in left-right symmetry were small enough to identify distinct, clinically relevant subgroups to stratify risk, diagnose injury, and indicate surgery. The Beighton score of GJH was not a surrogate for knee laxity in all anatomic planes.

REFERENCES

[1] Sanders 2016 AJSM [2] Owens 2007 Oxford [3] Webster 2016 AJSM [4] Lindanger 2019 AJSM [5] Magnussen 2016 Am J Sports Med [6] Opstelten 2007 Australian J of Physiotherapy [7] Lorbach 2009 KSSTA [8] Hull 1991 J Biomech Eng

HUMAN LOWER LEG MUSCLES GROW ASYNCHRONOUSLY

Brian V. Y. Chow[1,2], Robert D. Herbert[1,2], Bart Bolsterlee[1,3] and the MUGgLE Study investigators
[1] Neuroscience Research Australia (NeuRA), Sydney, NSW, Australia.
[2] School of Biomedical Sciences, University of New South Wales, Sydney, NSW, Australia.
[3] Graduate School of Biomedical Engineering, University of New South Wales, Sydney, NSW, Australia.
Email: b.chow@neura.edu.au

INTRODUCTION

Most studies of muscle growth in childhood have investigated only one or a few muscles. Consequently, little is known about the relative rates of growth in leg muscles. In this study, we sought to determine if leg muscles grow at proportionately different rates, or grow synchronously. The study is part of a large-scale longitudinal study on childhood muscle growth [1].

METHODS

Participants were 208 typically developing children (200 children 5-15 years and 8 infants <3 months; 121 boys and 87 girls; height: 54-180cm; weight: 4-82kg; tibia length: 9-43cm). Anatomical MRI images (mDixon or T1) of one leg from each child were obtained with a 3T MRI scanner. Each image was semi-automatically segmented [2] into ten 3D muscle surface models (Fig. 1A). Each model represented a muscle or a group of small muscles. Relative volume was calculated by dividing muscle volume by the child's total lower leg muscle volume. A small-sample test for isometry was used to test the hypothesis of synchronous muscle growth [3].

RESULTS AND DISCUSSION

If growth was synchronous, the volume of each muscle, expressed as a proportion of leg muscle volume, would be constant with age or leg length [i.e., lines in Figures 1B-C would be horizontal]. The lines were clearly not horizontal, so growth is asynchronous ($p < 0.001$). Before the age of 5, the two largest muscles of the triceps surae group (SOL and MG) grow disproportionately faster than other muscles. This may assist, or be caused by, the onset of weight bearing or ambulation. In contrast, the TA, EEP, TP and FHL muscles grow disproportionately slower than other muscles. Even in children > 5 years, growth is asynchronous ($p < 0.001$).

CONCLUSIONS

A large MRI dataset from a detailed investigation into human muscle growth was used to examine the synchronicity of muscle growth. Muscles in the lower extremity do not grow synchronously.

ACKNOWLEDGEMENTS

The study was supported by NHMRC grants (APP1156394, APP1117192). The authors acknowledge the facilities and scientific and technical assistance of the National Imaging Facility, a NCRIS capability, at the NeuRA Imaging, NeuRA, UNSW Node. BC is supported by UNSW Scientia and RTP scholarships.

REFERENCES

[1] Herbert RD et al. OSF: osf.io/scfxj, 2019.
[2] Zhu J et al. NMR Biomed **34**: e4609, 2021.
[3] Jolicoeur P. Biometrics **40**: 685-690, 19.

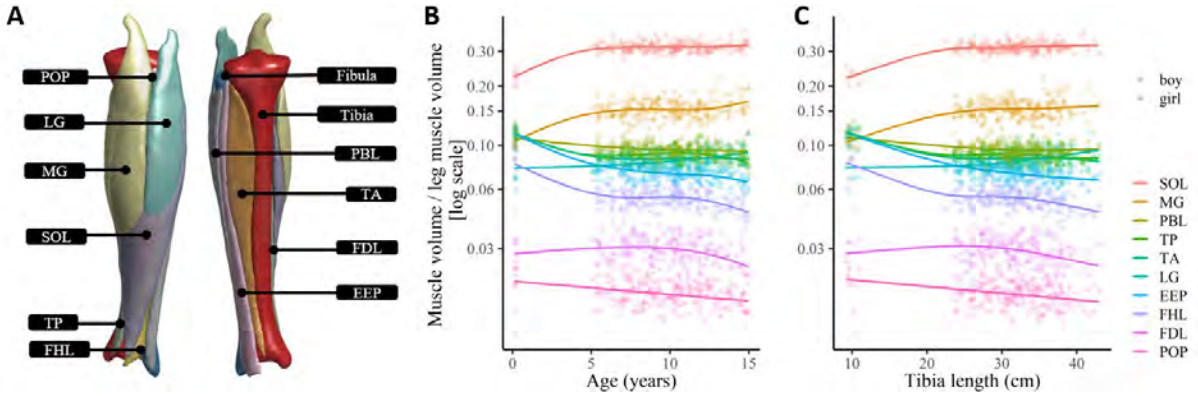

Figure 1: Ten 3D surface models (A): SOL = soleus, MG = medial gastrocnemius, PBL = peroneus brevis and peroneus longus, TP = tibialis posterior, TA = tibialis anterior, LG = lateral gastrocnemius, EEP = extensor digitorum longus, extensor hallucis longus and peroneus tertius, FHL = flexor hallucis longus, FDL = flexor digitorum longus, and POP = popliteus. Relationships between relative volume and age (B) and tibia length (C). Relative volume is plotted on a log scale. Lines are p-splines.

RESIDUAL FORCE DEPRESSION DURING SUBMAXIMAL VOLUNTARY CONTRACTIONS IS NOT SIMPLY RELATED TO THE PRECEDING POSITIVE MUSCLE WORK

Brent J Raiteri[1,2], Leon Lauret[1], and Daniel Hahn[1,2]

[1] Human Movement Science, Faculty of Sport Science, Ruhr University Bochum, Bochum, Germany
[2] School of Human Movement & Nutrition Sciences, The University of Queensland, Brisbane, Australia
Email: brent.raiteri@rub.de

INTRODUCTION

Residual force depression (rFD) and enhancement (rFE) describe the increase or decrease in force following active shortening or lengthening, respectively, relative to a reference steady-state isometric force [1]. rFD has been proposed to linearly increase with the amount of positive mechanical work [2], which means that limiting shortening under matched activation levels should theoretically reduce rFD. To test this hypothesis, the effective series elasticity of the tibialis anterior (TA) muscle-tendon unit (MTU) was reduced during ramp-and-hold contractions to reduce positive TA muscle work. Further, the amount of MTU lengthening (LEN) and shortening (SHO) to the same final MTU length was varied to alter the magnitude of TA net muscle work.

METHODS

Sixteen participants (23-33 yr, eight women) sat in a reclined posture (90° knee flexion, 110° hip flexion) with the plantar aspect of their right foot secured to the footplate attachment of a motorised dynamometer (IsoMed2000, Ferstl GmbH, DE) that measured net ankle joint torque (2000 Hz). After determining the ankle angle where maximum active dorsiflexion torque was produced (ANG_{Max}), participants matched the bipolar surface EMG signal recorded over TA (2000 Hz, NL905, Digitimer Ltd, UK) to within 30±5% of the maximum EMG amplitude recorded at ANG_{Max} for at least 21 contractions in seven conditions. Each condition consisted of two identical dynamic contractions and one fixed-end reference contraction (REF). The first two conditions involved TA MTU LEN from rest over a small (11-14°) and large amplitude (16-23°) during a 2-s ramp, which was followed by a 6-s hold phase at ANG_{Max}. The third condition involved a fixed-end preload phase during a 2-s ramp before MTU LEN over the large amplitude. The last four randomised conditions involved MTU SHO over similar small and large amplitudes without and with a preload.

TA's muscle fascicles were visualised with ultrasound at ~34 fps (ArtUs, TELEMED, LT). Fascicle lengths (doi.org/10.5281/zenodo.7411280) and fascicle forces were estimated post-processing [3]. Fascicle work from TA's superficial compartment was calculated as the area under the fascicle force-displacement curve. rFD or rFE were estimated as the mean difference in steady-state torque between the valid (≤10% difference in muscle activity level) dynamic and reference contractions.

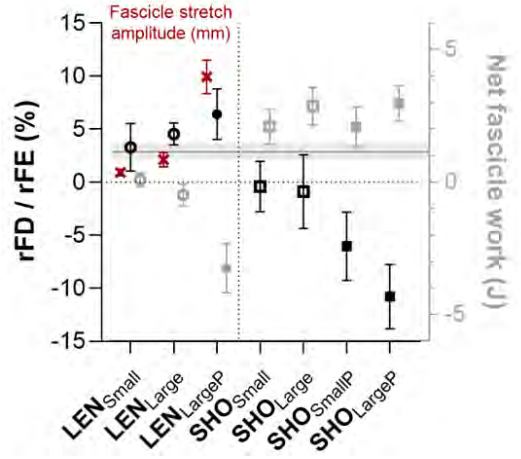

Figure 1. Mean (±95% confidence intervals, CIs) rFD and rFE magnitudes (black symbols), and TA net fascicle work magnitudes (grey symbols; REF: grey line and shaded area) during MTU LEN (circles) and SHO (squares) over small and large amplitudes without and with a preload (P: solid symbols). Red crosses (±95% CIs) indicate TA muscle fascicle stretch amplitudes during LEN.

RESULTS AND DISCUSSION

Reduced rFD and rFE was observed ($p \leq 0.024$) in the LEN conditions without and with a preload, respectively, but magnitudes were similar (3-6%, $p \geq 0.157$) despite different TA fascicle stretch amplitudes (0.9-9.9 mm, $p \leq 0.001$; Figure 1). No significant linear relation ($r_{11} = 0.33$, $p = 0.276$) was found between the reduction in TA positive fascicle work and rFD reduction in LEN conditions without a preload. rFD was similar (0-1%, $p \geq 0.935$) and increased (6-11%, $p \leq 0.007$) in SHO conditions without and with a preload, respectively. As work magnitudes were similar for SHO conditions without versus with a preload (Figure 1), rFD was not significantly related ($r_{41} = -0.24$, $p = 0.115$) to the positive muscle work during voluntary contractions.

CONCLUSIONS

rFD is only linearly related to the preceding positive muscle work for preloaded voluntary contractions.

ACKNOWLEDGEMENTS

This work (RA3308/1-1) was funded by the DFG.

REFERENCES

[1] Abbott BC et al. *J Physiol* **117**: 77-86, 1952.
[2] Herzog W et al. *J Biomech* **33**: 659-668, 2000.
[3] Maganaris CN et al. *J Appl Physiol* **90**: 865-872, 2001.

Post-activation potentiation does not contribute to *in vivo* residual force enhancement

Daniel Hahn[1,2], Lukas John[1], Brent J. Raiteri[1,2]
[1] Human Movement Science, Faculty of Sport Science, Ruhr University Bochum, Germany
[2] School of Human Movement and Nutrition Science, University of Queensland, Brisbane, Australia
Email: daniel.hahn@rub.de

INTRODUCTION

Residual force enhancement (rFE) refers to the phenomenon of increased muscle force output during an isometric contraction following active muscle stretch compared with an isometric contraction without prior stretch [1]. Although the exact mechanisms behind rFE remain unclear, it is thought that the enhanced force originates from increased cross bridge forces and passive contributions from the elastic element, titin.
Another physiological mechanism that is known to increase muscle force output is post-activation potentiation (PAP) [2]. PAP refers to the phenomenon of increased muscle twitch force following a conditioning contraction. Further, PAP increases with the force output of the conditioning contraction. Accordingly, PAP might contribute to rFE since the enhanced force output in the rFE state occurs following increased forces during active muscle stretch. Therefore, the aim of this research was to examine whether PAP contributes to rFE.

METHODS

Nineteen participants (4 females; mean age, height, and body mass: 25.7 years, 179.8 cm, and 78.3 kg, respectively) were lying prone on the bench of a motorised dynamometer (IsoMed2000, Ferstl GmbH, DE) that measured net ankle joint torque and crank arm angle. Supramaximal single pulse (200 µs) electrical stimulation (DS7AH, Digitimer, UK) of the tibial nerve was delivered to elicit plantar flexor muscle twitches and M-waves. M-waves and voluntary muscle activity of soleus (SOL), lateral (LG) and medial (MG) gastrocnemius were recorded by bipolar surface EMG (NL905, Digitimer Ltd., UK). All data were recorded at 2 kHz (16-bit Power-3 1401, CED, UK).
Participants performed four different conditioning contractions. 3 s before and after each contraction, participants received an electrical stimulation at 20° dorsiflexion to elicit unpotentiated and potentiated muscle twitches. The conditioning contractions included a SOL EMG-controlled fixed-end contraction (ISO_{50}) at 20° dorsiflexion (DF) and a stretch-hold contraction (ECC_{50}) from 0-20° DF at 40°/s with EMG control during the hold phases. Both contractions were performed at 50% of the maximal EMG amplitude recorded during maximal voluntary contractions at 20° DF. Before stretch, participants also needed to match a 50% EMG level determined for 0° DF. Participants also performed two torque-controlled fixed-end contractions at 20° DF; one condition required participants to match the torque level achieved following stretch of the stretch-hold contraction (ISO_{rFE}), and the other condition required participants to match the peak torque achieved during stretch of the stretch-hold contraction (ISO_{Peak}). All conditioning contractions lasted 6 s and visual feedback for control was provided on a screen in front of the participants. At least 3 min rest were provided between contractions. The sizes of M-waves and muscle twitches were determined as peak-to-peak amplitudes. rFE was determined as the normalised difference between the time-matched isometric torque 2.5-3s following stretch of the EMG-controlled stretch-hold contraction and fixed-end contraction.

RESULTS AND DISCUSSION

rFE following stretch was 8.5±2.8% (mean ± 95% confidence interval, CI). PAP following the conditioning contractions was 20.1±4.3%, 20.4±3.8%, 21.4±4.2%, and 33.7±5.7% for ISO_{50}, ECC_{50}, ISO_{rFE}, and ISO_{Peak}, respectively. PAP following ISO_{Peak} was significantly larger compared with PAP following all other conditioning contractions (Fig. 1). M-waves showed no significant differences.

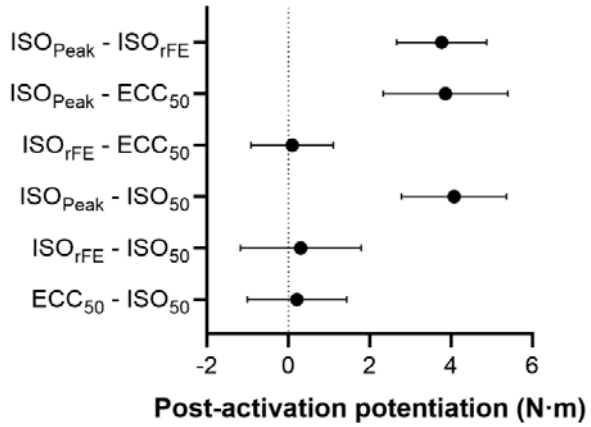

Figure 1 Mean differences±95% confidence intervals between PAP following the four conditioning contractions

CONCLUSIONS

As PAP following ECC_{50} was similar to PAP following ISO_{rFE} and ISO_{50}, PAP likely did not contribute to rFE. The larger PAP following ISO_{Peak} compared with ECC_{50} indicates that impulse rather than peak force output likely determines the potentiating effect.

REFERENCES

[1] Abbott & Aubert. *J Physiol* **117**: 77-86, 1952.
[2] Vandervoort A et al. *Exp Neurol* **81**: 141-152, 1983.

UNDERSTANDING AGING-RELATED SKELETAL MUSCLE WEAKNESS USING SHEAR WAVE ELASTOGRAPHY

Filiz Ates[1], Justus Marquetand[2], and Manuela Zimmer[1]
[1] Institute of Structural Mechanics and Dynamics, University of Stuttgart, Stuttgart, Germany.
[2] Department of Epileptology, Hertie-Institute for Clinical Brain Research, University of Tübingen, Tübingen, Germany.
Email: filiz.ates@isd.uni-stuttgart.de

INTRODUCTION

The force-generating capacity of skeletal muscles deteriorates with advancing age and in vivo monitoring of the mechanical adaptation of muscles would be invaluable for eliminating premature weakness. Ultrasound shear wave elastography (SWE) quantifies muscle mechanical properties by measuring the propagation velocity of the shear waves traveling within the tissue [e.g. 1,2]. Hence, SWE has the potential for early detection of muscle weakness. The objective of this study was to assess the mechanics of the biceps brachii muscle (BB) with the hypotheses that shear elastic modulus reflects (i) the increase in passive muscle stiffness imposed by length change, (ii) the activation-dependent mechanical changes in BB for older adults, and (iii) the differences between the mechanics of muscles of older and young adults.

METHODS

14 young (7 males, age: 28.07 ± 5.06 years) and 14 older (6 males, age: 68.71 ± 5.08 years) healthy volunteers participated. Elbow torque, BB SWE, and surface electromyography (sEMG) were measured at five elbow angles (60°-180°) from flexion to extension at rest, and during maximum voluntary contractions (MVC), and submaximal ramp contractions up to 25%, 50%, and 75% of MVC torque of elbow flexion. BB muscle length was also measured using ultrasound imaging.

RESULTS AND DISCUSSION

Even though the body height and weight of older adults were not significantly different compared to the younger group, their muscle length was 10.5% ± 2.0% shorter and the passive shear elastic modulus of BB was maximally 52.6% higher at 90º elbow angle for older adults (Fig. 1) ($p < 0.001$ for both). This indicates that muscle as a passive material becomes shorter and stiffer with age. The MVC torque was 23.67% less for older adults and it decreased from flexion to extension ($p < 0.0001$ for both). During MVC, the total shear elastic modulus of BB was found to be higher for older adults (by 11.21%, $p = 0.006$) with no significant effects of elbow angle. This could be due to increased passive stiffness even though force production capacity dropped with aging. However, the active shear elastic modulus did not show the effects of age during MVC either. On the other hand, the active shear elastic modulus changed with age ($p = 0.037$) at 25% MVC and elbow angle ($p < 0.001$ for all submaximal contractions) (Fig. 1). 16.18% lower active shear elastic modulus found for older adults at 25% of MVC aligns with the reduced force production in older ages.

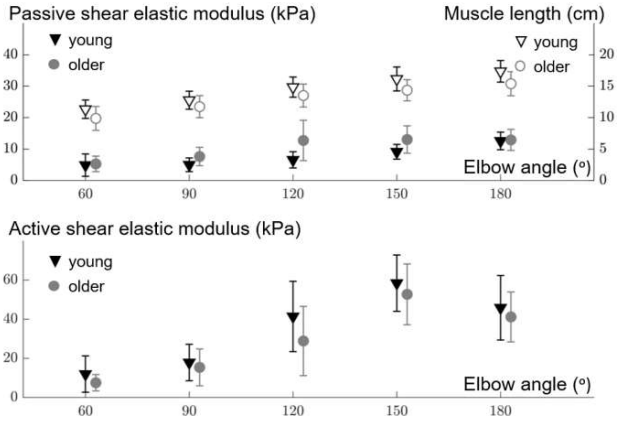

Fig. 1 Upper panel Muscle length, passive shear elastic modulus, and **Lower panel** Active shear elastic modulus during 25% of MVC with respect to elbow angle for young and older volunteers

CONCLUSIONS

The hypotheses were confirmed that shear elastic modulus reflected the changes led by muscle length, activations, and age. Present findings indicate that shear elastic modulus as a measure of muscle stiffness can be used to detect muscular alterations in passive state and during low-level activities (but not at MVCs). We conclude that SWE can be implemented as a muscle stiffness monitoring tool to be used in early muscle loss prevention, rehabilitation, and physiotherapy.

ACKNOWLEDGEMENTS

Bundesministerium für Bildung und Forschung (BMBF) the project ”3DFoot” (01EC1907B) and Deutsche Forschungsgemeinschaft (DFG) GRK 2198.

REFERENCES

[1] Ateş F et al. *Europ J Appl Physio* **118**:*585-593*, 2018
[2] Zimmer M et al. *J Mech Behav Biomed Mater* **137**: 105543, 2023.

SHEAR MODULUS DIFFERS BETWEEN REGIONS OF THE TIBIALIS ANTERIOR MUSCLE DURING CONTRACTION

Patricio Pincheira[1,2], Dean Mayfield[3], Sauro Salomoni[2], François Hug[4], Paul Hodges[2] and Glen Lichtwark[1]

[1] School of Human Movement and Nutrition Sciences, The University of Queensland, Brisbane, Australia.
[2]School of Health and Rehabilitation Sciences, The University of Queensland, Brisbane, Australia.
[3]Department of Evolution, Ecology, and Organismal Biology, University of California, Riverside, USA
[4] LAMHESS, Université Côte d'Azur, Nice, France
Email: uqppinch@uq.edu.au

INTRODUCTION

Changes in muscle stress and stiffness are important for development of force during contraction, but the distribution throughout a muscle is likely also important in terms of potential for muscle adaptation and injury. Surprisingly, little is known about the distribution of stress/stiffness in different regions of human muscles during contraction (in vivo). Because human muscles have complex structural and functional arrangements and are innervated by an intricate arrangement of motor neurons, it is difficult to predict/estimate the distribution of tissue stress/stiffness within muscle. Shear modulus (SM) estimated with supersonic shear imaging (SSI), has been demonstrated to be a reliable indicator of muscle stress and/or stiffness within a muscle [1]. The aim of this study was to quantify the distribution of SM in different regions of the human tibialis anterior (TA) muscle during contraction. We hypothesised that distinct regions of the muscle will present different SM values because of differences in architecture and microstructure (e.g., sarcomere length) across the muscle.

METHODS

Ten healthy participants performed voluntary, isometric contractions at 10, 20 and 30% of their maximum voluntary contraction (MVC), while SM was estimated using SSI (Aixplorer V9, transducer SL10-2 MHz, SuperSonic Imagine, France). SSI elastography maps were recorded at 0.7–1.3 Hz (resolution: 1x1mm) at 4 different locations within the TA muscle: proximal, mid medial, mid lateral, distal. From the same regions, fascicle lengths and pennation angles were estimated at the different force levels. A two-way ANOVA was used to evaluate the effect of factors "force" (MVC levels plus resting muscle) and "region" on SM, fascicle length and pennation angle ($p < 0.05$). Tukey's test was used for multiple comparisons between the different muscle regions.

RESULTS AND DISCUSSION

We found a main effect of "force" in all variables, and a main effect of "region" in SM and pennation angle. The multiple comparisons revealed differences in SM and pennation angle between the different muscle regions as denoted by "*" in Figure 1. These results suggest an heterogenous distribution of stress/stiffness within the TA, particularly, a smaller SM within the distal portion of the muscle. The smaller SM in the distal region is unlikely explained by the TA's smaller pennation angle in that region because we would have expected a decrease in SM with increased pennation angles (i.e., force levels).

Studies using passive movements [1] suggest that anatomical (e.g. smaller cross sectional area), mechanical (e.g. force-length relationship properties) or neural (e.g. intramuscular nerve/activation distribution) factors are likely candidates to explain heterogeneous distributions in SM. Animal models [2] suggest that contracting muscle may show differences in stress due to physiological factors such as sarcomere length, density of myofilaments, myofibrillar bundle diameter and/or intrinsic actin/myosin mechanical (cross-bridge) properties. Further studies are needed to elucidate how areas of higher relative stiffness within contracting muscle affect fascicle strain when external forces are applied to rapidly stretch the muscle.

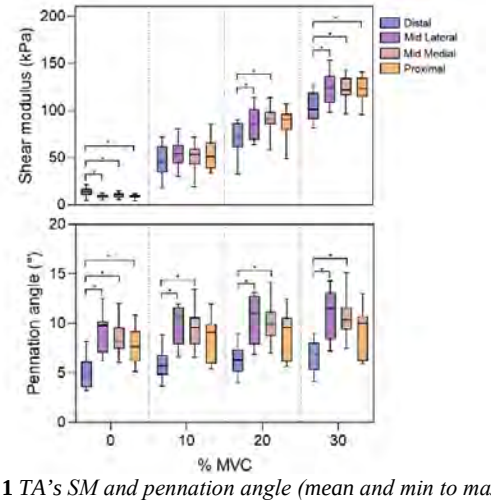

Figure 1 *TA's SM and pennation angle (mean and min to max) at different contraction levels.*

CONCLUSIONS

Distinct regions of the TA present different SM during contraction at different force levels. This may be because of a heterogenous distribution of anatomical, mechanical, neural and/or physiological factors.

REFERENCES

[1] Le Sant et al. J Anat **230**: 639-50, 2017
[2]Taylor G. *Proc Biol Sci* **267**: 1475-80, 20

Changes in Biceps Femoris Long Head Fascicle length during Sprinting

Dahua Ren [1], Shangjun Huang [2], Mianfang Ruan [1,3]
[1] College of Physical Education and Health, Wenzhou University, Wenzhou, China
[2]School of Medicine, Tongji University, Shanghai, China.
[3]Peak Sports Science Lab, Quzhou Peak Footwear Co., LTD, Xiamen, Fujian, China
Email: ruanmf@yahoo.com

INTRODUCTION

Hamstring muscle strain injury is the one of most prevalent injuries in sports. It occurs most often in the Biceps Femoris long head (BFlh). Due to lack of *in vivo* measurements of muscle fascicle length changes during springing, there are debates in the literature regarding the injury mechanisms. Yu et al.[1] proposed that excessive muscle strain is the direct, if not exclusive, cause of muscle strain injury during the late swing in sprinting when a lengthening of the hamstring muscles tendon unit (MTU) occurs. However, muscle fascicle may shorten or contract isometrically when muscle force increases[2]. The purpose of this study is to examine the muscle fascicle behavior of BFlh *in vivo* during sprinting using ultrasonography. The results of this study may bring insight to mechanisms of hamstring strain injury in sprinting.

METHODS

Seven male elite sprinters who had no lower extremity injuries within the past 12 months volunteered to participate in this study. 3D kinematics (200Hz; Vicon Motion Analysis, Oxford, United Kingdom) and ground reaction forces (1000Hz, Bertec Corporation, Columbus, OH) during steady-state at five discrete running speeds: 2m/s, 3m/s, 4m/s, 5m/s, and 6m/s on an instrumented treadmill were recorded simultaneously. Visual 3D (C-Motion, German- town, MD, USA) and OpenSim were used to compute MTU length. BFlh muscle fascicle length changes were recorded using a 128-element linear ultrasound transducer in B-mode, and Ultra-track software was used to track the muscle fascicle behavior.

RESULTS AND DISCUSSION

Regardless of running speed, BFlh fascicles lengthened <1cm during sprinting (Figure 1), which is consistent with fascicle length change magnitude during Nordic hamstring exercise [3]. The decoupling between MTU and muscle fascicle length change demonstrated that tendons are the main role in stretch. Since the amount of strain needed to cause a muscle strain injury is reduced when a muscle is maximally activated [4], excessive muscle strain could not be the direct cause of muscle strain injury during sprinting.

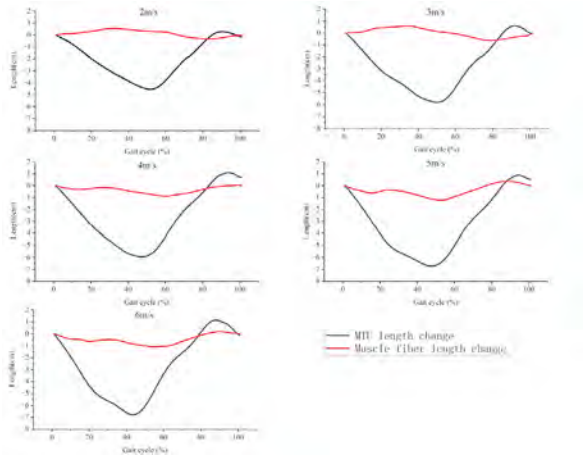

Figure 1 The length changes of BFlh fascicle and MTU

CONCLUSIONS

BFlh presents a nearly isometric fascicle behavior during late swing before foot strike, which suggests tendons are the main role in stretch and excessive muscle strain could not be the direct cause of muscle strain injury.

ACKNOWLEDGEMENTS

This study was support by the National Nature Science Foundation of China (31871204).

REFERENCES

[1] Yu, et al. J Sport Health Sci 6: 130-132, 2017
[2] De Brito Fontana et al. Eur j Appl physiol, 116: 1267-1277, 2016,
[3] Pincheira, et al. JSAMS 25: 684-689, 2022
[4] Brooks et al. J physiol, 488:459-69. 1995,

HOW DOES THE MEDIAL GASTROCNEMIUS AND ACHILLES TENDON INTERPLAY CONTRIBUTE TO THE MUSCLE-TENDON UNIT DURING GAIT IN CEREBRAL PALSY?

Francesco Cenni[1,2], Maria Sukanen[1], Afet Mustafaoglu[1], Zhongzheng Wang[2], Ruoli Wang[2] and Taija Finni[1]
[1] Faculty of Sport and Health Sciences, University of Jyväskylä, Jyväskylä, Finland.
[2] Department of Engineering Mechanics, KTH Royal Institute of Technology, Stockholm, Sweden.
Email: francesco.l.cenni@jyu.fi

INTRODUCTION

3D gait analysis can be enhanced by using portable ultrasound imaging (3DGAUS), thus allowing to assess muscle and tendon lengths during gait [1]. By focusing at the ankle joint, the interplay between medial gastrocnemius muscle (MG) and Achilles tendon (AT) is crucial for optimizing stability and propulsion during each gait cycle. In spastic cerebral palsy (CP), this interplay is altered with consequences to the overall function [2]. Despite the attempts of using musculoskeletal modelling, this interplay is still poorly understood in pathological conditions such as CP due to a lack of experimental data during gait. The goal of this study is to quantify the contribution of MG and AT length changes to the entire muscle-tendon unit (MTU) during gait in participants with CP and typically developed (TD) peers.

METHODS

3DGAUS data was acquired from 5 participants with CP (18.2±5.1 years, GMFCS I/III: 2/3) and 5 TD (18.4±4.7 years) during overground walking at preferred walking speed (average CP: 0.9 m/s, TD: 1.4 m/s). A 12-camera motion analysis system (Vicon Motion Systems Ltd.) operating at 200 Hz was used and synchronized with a portable ultrasound device (Telemed SmartUS), at 50 Hz. Lower-limb Plug-in-Gait model along with additional markers to define the local shank reference frame, were used. The ultrasound probe, within a probe holder instrumented with four reflective markers, was attached to the random (TD) or most-affected (CP) leg. Images were acquired first from the distal MG muscle-tendon junction (MTJ), and secondly from MG fascicles. The ultrasound image locations were mapped into the shank reference frame, allowing both whole muscle and tendon lengths to be estimated [1], and MTU length being their sum. Fascicle, MTU, whole muscle and tendon length patterns were averaged over at least 5 time-normalised gait cycles. Relative values are the length changes from the corresponding values at initial foot contact. Semi-automated software was used to track the MTJ [3] and fascicles [4]. Due to the small and heterogeneous sample, results are presented in a descriptive manner.

RESULTS AND DISCUSSION

Overall, relative length changes are more heterogeneous in CP than TD. On average, participants with CP showed reduced length changes for the MG muscle (2.5 mm in CP and 5.8 mm in TD), for the AT (7.3 and 15.1 mm) as well as for the MTU (9.3 and 15.6 mm), whilst fascicle changes were similar (9.0 and 10.2 mm) during the gait cycle (Figure 1A-B). An efficient behaviour for TD during the stance phase was observed, with the AT lengthening more than MG, whilst for CP, muscle and tendon contributed almost equally to the MTU lengthening at the stance phase (Figure 1C-D). At the final push-off, the contribution of MG to the MTU in TD and CP was 69.3% and 54.8%, and for AT 30.7% and 45.2%, respectively.

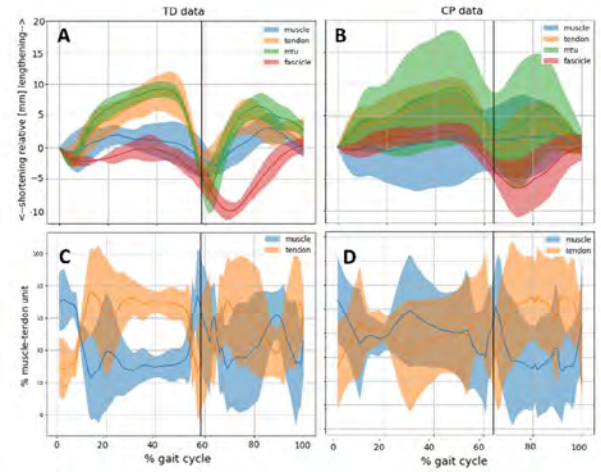

Figure 1. A-B: Relative length changes of muscle, tendon, MTU, and fascicle (mm); C-D: Contribution of the muscle and tendon (%) to the MTU for TD (left) and CP (right) participants. Vertical lines separate stance to swing phases.

CONCLUSIONS

Understanding the differential contributions of muscle and tendon to the overall MTU length in CP compared to TD is clinically relevant. In TD, MTU length changes at 10-50% of gait cycle were mostly due to the AT, whilst at the push-off phase the AT recoiled quicker than MG. This interplay seems impaired in CP, showing that the AT elastic mechanism is not properly exploited. This may be due to a more compliant AT as well as the inability of the MG to sustain an isometric contraction and contribute to the final push-off. These findings need to be confirmed once larger samples are processed.

ACKNOWLEDGEMENTS

F.C. is funded by the Marie Sklodowska-Curie, grant agreement No 101028724, and Promobilia No 20040.

REFERENCES

[1] Cenni F et al.Gait & Posture **90**: 464-67, 2021.
[2] Kalsi G et al. *J Biomech* **49**: 3194-99, 2016.
[3] Cenni F et al. *Exp Physio* **105**: 120-131, 2019.
[4] Farris DJ et al. *CMPD* **128**: 111-18, 2016.

Passive muscle stiffness does not change after eccentric-only resistance training at long muscle lengths with a long duration

Raki Kawama[1,2], Hironoshin Tozawa[1], Tatsuya Hojo[1,3], Taku Wakahara[3]
[1] Graduate School of Health and Sports Science, Doshisha University/Kyoto, Japan.
[2] Research Fellow of Japan Society for the Promotion of Science/Tokyo, Japan.
[3] Faculty of Health and Sports Science, Doshisha University/Kyoto, Japan.
Email: rkawama156413@gmail.com

INTRODUCTION

Resistance training is effective to enhance muscular strength and size, but has been empirically believed to increase passive muscle stiffness. The increase in the stiffness may negatively influence athletic performance and increase the risk of musculoskeletal injury through a limitation of joint range of motion [1]. Meanwhile, our recent study [2] showed that the passive stiffness of the semimembranosus (SM) acutely decreased after a session of resistance exercise with eccentric-only stiff-leg deadlift at long muscle lengths with a long duration. The acute change in muscle stiffness induced by stretching was suggested to correspond to its chronic change [3,4]. Thus, it is possible that resistance training at long muscle lengths with a long duration also chronically decreases muscle stiffness. However, this possibility has not been investigated yet. The present study aimed to investigate the chronic effects of resistance training at long muscle lengths with a long duration on passive stiffness of the individual hamstring muscles.

METHODS

Twenty-four healthy young males were randomly assigned into training (n = 12) and control (n = 12) groups. The participants in the training group performed three sets of 10 repetitions of eccentric-only stiff-leg deadlift at long muscle lengths ([50–100% of maximal exercise range of motion [0% = upright position]) with a long duration (5 s per repetition) for 10 weeks (two sessions per week). The training loads were 60%, 65%, and 70% of body mass at weeks 1–4, 5–7, and 8–10, respectively. Before and after the intervention period, the shear moduli of the individual hamstring muscles (the biceps femoris long head [BFlh], semitendinosus [ST], and SM), were measured using shear wave elastography. Additionally, maximal voluntary isometric torque of knee flexion and muscle volumes of the hamstring muscles (BFlh, the biceps femoris short head [BFsh], ST, and SM) were also measured. The changes in the measured variables during the intervention period were analysed by using the Wilcoxon signed-rank test.

RESULTS AND DISCUSSION

There were no significant changes in the shear moduli of BFlh, ST, or SM (p = 0.375 to 0.922) during the intervention period in both groups. Meanwhile, the maximal voluntary isometric torque (p = 0.004) and muscle volumes of BFlh, ST, and SM (p = 0.004–0.012) significantly increased after training intervention in the training group. The present results are consistent with the previous studies [5,6] that observed no changes in passive muscle stiffness after a period of resistance training. Thus, it may not be easy to change the passive muscle stiffness by resistance training. The lack of changes in the stiffness after resistance training may be related to low training frequency per week.

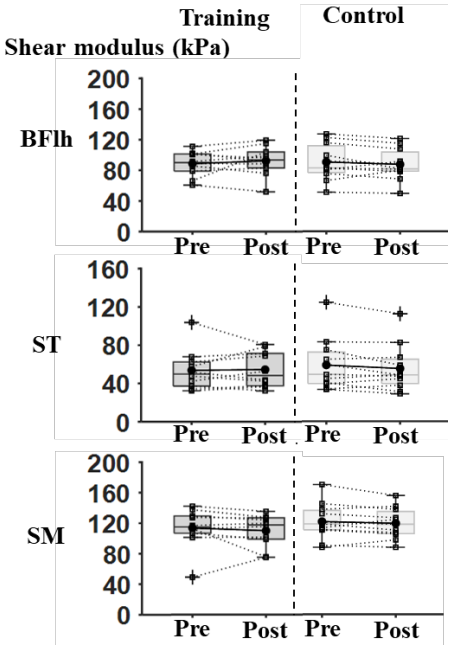

Figure 1 Changes in shear moduli of the individual hamstring muscles before and after intervention period.

CONCLUSIONS

Passive stiffness of the individual hamstring muscles does not change even after eccentric-only resistance training at long muscle lengths with a long duration.

ACKNOWLEDGEMENTS

This work was supported by a grant from the Japan Society for the Promotion of Science.

REFERENCES

[1] García-Pinillos et al. *J Sports Sci*, **33**: 1293-1297.
[2] Kawama R et al. *Eur J Appl Physiol,* Online ahead of print, 2022.
[3] Umegaki H et al. *Man Ther* **20**: 134-137, 2015.
[4] Ichihashi N et al. *J Sports Sci* **34**: 2155-2159, 2016.
[5] Seymore K et al. *Eur J Appl Physiol* **117**: 943-953, 2017.
[6] Vatovec R et al. *J Sports Sci* **39**: 2370-2377, 2021.

Constant force muscle stretching induces greater acute deformations and changes in passive mechanical properties compared to constant length stretching.

Guido Geusebroek[1], J.H. van Dieën[1], M.J.M. Hoozemans[1], W. Noort[1], H. Houdijk[2] and H. Maas[1]

[1] Dept. of Human Movement Sciences, Vrije Universiteit, Amsterdam

[2]Dept. of Human Movement Sciences, University Medical Center Groningen;

Email: G.M.Geusebroek@vu.nl

INTRODUCTION

Stretching is applied to lengthen shortened muscles in pathological conditions such as joint contractures. Different types of stretching, e.g. constant length (CL) and constant force (CF) stretching, can be used. It has, to our knowledge, not been investigated if the muscle-tendon unit's deformations and passive mechanics are affected differently by these stretch types. Impulse [1] and maximal strain [2] have been proposed to be determinants of the potential differences in the effect of stretching. We investigated (i) the acute effects of CL and CF stretching, on acute deformations and changes in passive mechanical properties of medial gastrocnemius muscle (MG) of the rat and (ii) the relationship between these effects and the impulse/maximal strain of stretching.

METHODS

Forty-eight hindlimbs from 13 male and 12 female Wistar rats (13 weeks old, respectively 424.6 ± 35.5 and 261.8 ± 15.6 grams) were divided into six groups (n=8 each). Three stretching intensities were applied for each stretch type; the MG was stretched to a length at which the force was 75%, 95%, or 115% of the force found at maximal dorsiflexion and held at either CF or CL for 30 min. Before and after stretching the passive muscle was lengthened to the length corresponding to maximal ankle dorsiflexion to assess MG peak force and peak stiffness. Also, muscle belly and tendon length were measured from displacement data and video. Linear mixed models were performed to assess the effects of stretch type/intensity on acute deformations and mechanical changes and to assess the relation of these outcomes with impulse/ maximal strain.

RESULTS AND DISCUSSION

CF stretching affected peak stiffness and muscle belly length more than CL stretching at similar stretch intensities ($p<0.01$) (Figure 1). This was also found for peak force and tendon length (data not shown). This is in line with previous findings in human subjects [3, 4]. Impulse was associated only with the decrease in peak force, while maximal strain was associated with the decrease in peak force, peak stiffness, and the increase in muscle belly length.

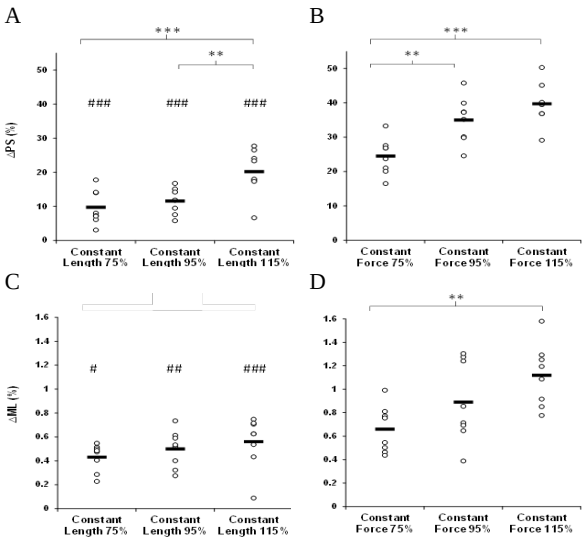

Figure 1 Individual (○) and mean (▬) values of changes in peak stiffness (ΔPS) [A,B] and muscle length (ΔML) [C,D] after 30 minutes of CL stretching [A,C] or CF stretching [B,D]. Significant differences between intensities ** $p<0.01$ and between stretch types # $p<0.05$, ## $p<0.01$, ### $p<0.001$.

CONCLUSIONS

We conclude that CF stretching results in greater acute deformations and changes in mechanical properties than CL stretching, which appears to be dependent predominantly on the differences in imposed maximal strain. Low-intensity CF stretching is equally effective as high-intensity CL stretching, while the latter is likely more painful.

ACKNOWLEDGEMENTS

This study was supported by 'de Heijne stichting'. The funding agency had no involvement in the study design; in the collection, analysis and interpretation of data.

REFERENCES

[1] Fukaya T et al. Sport Sci Health **17(1)**: 953–959 2021.
[2] Kruse A et al. Front Physiol **08** Oct 2021.
[3] Yeh C Y et al. J Electromyogr Kinesiol ***17*(4)**: 453–461 2007.
[4] Cabido C E T et al. J Strength Cond Res ***28*(4)**: 1050–1057 2014

Hamstring activation deficits during jumping and landing in athletes with hamstring strain injuries using time-frequency analysis method

Amornthep Jankaew[1], Ing-Shiou Hwang[1,2], Yih-Kuen Jan[3], and Cheng-Feng Lin[1,2]
[1] Institute of Allied Health Sciences, National Cheng Kung University, Tainan, Taiwan.
[2] Department of Physical therapy, National Cheng Kung University, Tainan, Taiwan.
[3] Department of Kinesiology and Community Health, University of Illinois at Urbana-Champaign, IL, USA.
Email: connie@mail.ncku.edu.tw

INTRODUCTION

Hamstring strains are the most common lower limb muscle injuries at all athletic levels. Previous studies have showed that athletes with hamstring injuries demonstrated activation deficits in either temporal characteristics or amplitudes during dynamic tasks [1]. However, it is not clear how the injured hamstrings respond to a jump-landing task which is an important activity central to hamstring injury rehabilitation. Also, no evidence of the function of the hamstrings by using time-frequency analysis during jumping which represents the stretch-shortening cycle (SSC) of the muscle has been explored. Thus, the study aims to investigate hamstring recruitment during vertical jumps in athletes with hamstring strains using wavelet analysis. Findings can be used to propose innovative rehabilitation methods regarding jumping training into the program for injured athletes.

METHODS

9 chronically injured athletes (22.3±1.9 years old with 7.6 months since injured) and 9 matched controls (21.3±1.9 years old) were recruited. Two surface EMG electrodes (Delsys Inc., USA) were attached to the middle belly of the lateral hamstring (LH) and medial hamstring (MH) on the injured leg and the matched leg. Three squat jumps (SJ) and countermovement jumps (CMJ) with maximum performance were performed on the force platforms. A 1D continuous wavelet transforms with the modulated Gaussian wavelet (Morlet) was used to analyse the EMG of the LH and MH during take-off (TO), Flight (FL), and landing (LD). Peak vertical ground reaction force during take-off and landing and loading rate (LR) were reported. Data were analysed in self-written code in MATLAB. A 2x2 repeated measures ANOVA was used to compare the differences between groups and jumps using the SPSS version 26 with the alpha level at 0.05.

RESULTS AND DISCUSSION

The injured group presented a lower mean frequency of both LH and MH in the TO ($p < 0.001$ and 0.049) and in the LD phases ($p < 0.001$ and 0.036; Table 1). In addition, the MH elicited greater activation in the CMJ than the SJ in the TO phase ($p = 0.015$). The statistical analysis of the kinetic outcomes demonstrated lower LD force ($p = 0.013$) and LR ($p = 0.018$) of the control group compared to the injured. While the CMJ could produce better TO force ($p < 0.001$) than the SJ (Figure 1).

In the discussion, a jump-landing activity requires a series of SSC components. Chronic hamstring strains contributed to a significant reduction in hamstring activation during the SSC movement. This deficit might be attributed to the deterioration of the stretch intensity and magnitude of the injured muscle leading to impairing the ability to store and utilization of elastic energy [2]. Also, decreased activation in the injured group may be associated with impaired stretch and tendon reflex of the prior hamstring injuries [3] leading to poor jumping and landing performance.

Table 1 Mean frequency of wavelet analysis of the LH and MH

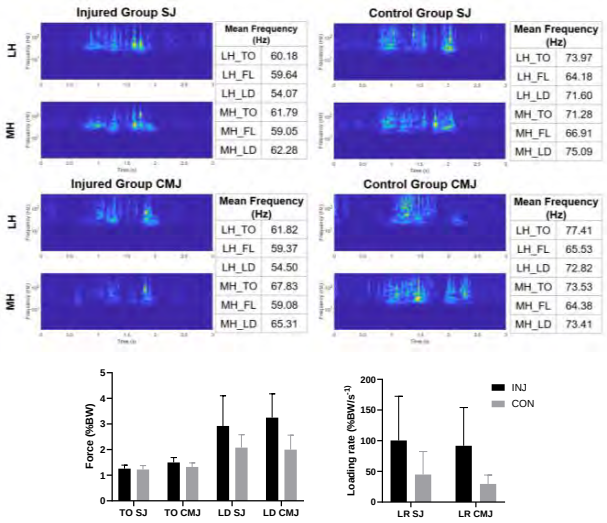

Figure 1 Kinetic outcomes of the SJ and CMJ

CONCLUSIONS

Athletes with prior hamstring strains displayed deficits in hamstring recruitment during the SJ and CMJ. The activation deficits influence the LD force and LR with no effects on the TO force. The findings could have a clinical implication that chronically injured athletes may need to resolve activation deficits in the SSC movement and the CMJ may be a useful tool to improve activation levels of the hamstrings.

REFERENCES

[1] Presland JD et al. *Sports Med* **51**: 2311-27, 2021.
[2] Van Hooren B & Zolotarjova J. *J Strength Cond Res* **31**:2011-20, 2017.
[3] Buhmann R et al. *Med Sci Sports Exerc* **52**: 1862-9, 2020.

THE RELATIONSHIP BETWEEN CENTER OF PRESSURE POSITION AND KNEE EXTENSOR MOMENT DURING DOUBLE-LEG SQUATTING

Tomoya Ishida[1], Ryo Ueno[1,2], Yu Kitamura[1], Yoshiki Yamakawa[1], Mina Samukawa[1] and Harukazu Tohyama[1]
[1] Faculty of Health Sciences, Hokkaido University, Sapporo, Japan.
[2] ORGO Inc., Sapporo, Japan.
Email: t.ishida@hs.hokudai.ac.jp

INTRODUCTION

Although the double-leg squat is a common rehabilitation exercise for strengthening lower limb muscles, coordination of the knee extensor moment is required to avoid exacerbation of symptoms such as patellofemoral pain. Recently, real-time feedback of the center of pressure (COP) position has been reported to be useful in modifying the knee extensor moment during double-leg squatting [1]. However, the evidence is limited to a 6% change in knee extensor moment for a 10% difference in foot length of the COP position [1]. The purpose of this study was to compare the knee extensor moment among the anterior, mid, and posterior COP positions.

METHODS

Sixteen male participants (22.9 ± 0.4 years, 173.6 ± 5.0 cm, 63.0 ± 6.6 kg) performed double-leg squatting under the following four conditions: anterior COP, middle COP, posterior COP, and natural conditions. The COP position target was set at the ball of the foot for the anterior condition, at the 1st tarsometatarsal joint for the middle condition, and at the navicular tuberosity for the posterior condition. Real-time feedback on the COP position during squatting was provided with the box indicating the range of target COP ± 10% foot length except for natural condition [1]. Double-leg squat was recorded using an optical three-dimensional motion analysis system (Cortex 5.0.1, Motion Analysis, USA) with seven cameras and two force plates (Type 9286, Kistler AG, Switzerland). Internal lower limb joint moment was calculated by inverse dynamics (Visual3D 6, C-motion, USA) and normalized to body mass. In addition to the peak moment, the mean COP position and moment were calculated for the phase in which the knee was flexed more than 60° [2]. Repeated measures ANOVA was used to compare the variables among conditions ($\alpha < 0.05$).

RESULTS AND DISCUSSION

The mean COP position was significantly different between the conditions except for between the natural and posterior COP conditions (Table 1). The peak knee extension moment in the anterior COP condition was 15% smaller than in the natural and posterior COP conditions and 11% smaller than in the middle condition (all $p < 0.001$). Peak hip and ankle extension moments were greater in the anterior COP condition than in the other conditions (Figure 1). The mean moment results showed a similar trend of difference in the peak moment analysis (Table 1).

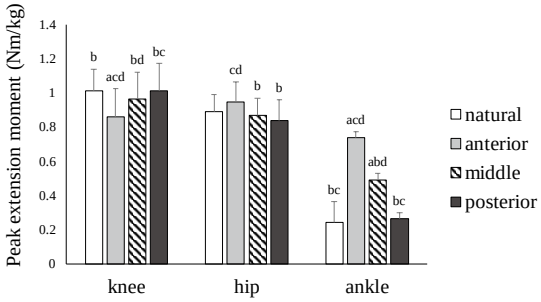

Figure 1. Comparisons of the peak extension moment aomong the four squatting conditions. Indexes indicate significant difference from natural (a), anterior (b), middle (c), and posterior conditions (d).

CONCLUSIONS

Real-time feedback of the COP position is useful for modifying the knee extensor moment, which can be increased or decreased by up to 15% of peak moment. To avoid an excessive patellofemoral loading, it may be useful to guide the COP anteriorly during double-leg squatting.

ACKNOWLEDGEMENTS

This work was supported by JPJS KAKENHI (JP20K19477).

REFERENCES

[1] Ishida T et al. *J Sports Sci Med* **21**: 341-6, 2022.
[2] Ishida T et al. *J Appl Biomech* **31**:62-8, 2023.

Table 1: Comparison of mean COP position and lower limb extension moments (mean [SD]).

	natural	anterior	middle	posterior	*p-value*
COP position, % foot length	35.8 (7.3)^{bc}	71.9 (2.3)^{acd}	53.9 (2.3)^{abd}	38.5 (2.1)^{bc}	< 0.001
Knee extension moment, Nm/kg	0.84 (0.10)^{bc}	0.67 (0.12)^{acd}	0.78 (0.12)^{abd}	0.85 (0.12)^{bc}	< 0.001
Hip extension moment, Nm/kg	0.70 (0.10)	0.72 (0.09)^{cd}	0.66 (0.10)^{b}	0.65 (0.13)^{b}	0.001
Ankle extension moment, Nm/kg	0.16 (0.10)^{bc}	0.64 (0.03)^{acd}	0.40 (0.04)^{abd}	0.19 (0.04)^{bc}	< 0.001

Indexes indicate significant difference from natural (a), anterior (b), mid (c), and posterior conditions (d).

INTER-SESSION RELIABILITY OF MARKERLESS LOWER LIMB KINEMATICS AND KINETICS IN RETURN-TO-SPORT TASKS OFTEN EVALUATED AFTER SERIOUS KNEE INJURY

Jiaming Xu[1], Zhishen Wen[1], Sylvia Augustine[2], Raihana Sharir[2,4], Camilla De Bleecker[1,3], Mark A. Robinson[2] and Jos Vanrenterghem[1]

[1] Department of Rehabilitation Sciences, KU Leuven, Leuven, Belgium.
[2] Research Institute for Sport and Exercise Sciences, Liverpool John Moores University, Liverpool, UK.
[3] Department of Rehabilitation Sciences, University of Ghent, Ghent, Belgium.
[4] Faculty of Sport Science and Recreation, Universiti Teknologi MARA, Shah Alam, Malaysia.
Email: jiaming.xu@student.kuleuven.be

INTRODUCTION

Criteria-based rehabilitation and return-to-sport (RTS) decision-making critically depends on a therapist's ability to assess movement quality of challenging activities [1]. Several approaches have been developing in recent years, no least the AI-driven markerless motion capturing solutions. The reliability and validity of these systems has been assessed in gait [2], but not in dynamic tasks such as hops, jumps or side stepping. Hence, the aim of this study was to assess reliability of markerless lower extremity joint kinematics and kinetics of dynamic RTS evaluation tasks.

METHODS

A single-group repeated-measures study of 4 healthy subjects (26±5 years) was conducted, with 2 sessions separated by 5±2 days. Five trials of six commonly used RTS evaluation tasks (see listed in Table 1) were recorded using 7 video cameras (Miqus, Qualisys, SE) and two 90x60cm force plates (9287C, Kistler, CH) at 180Hz and 2700Hz, respectively. Theia3D (v2022.1.0.2309, Theia Markerless Inc., CA) was used to compute inverse kinematic 3D pose estimations during all tasks. Analog signals were low-pass filtered at 18Hz, and joint angles and internal moments computed, using Visual3D (v2022.10.2, C-motion Inc., US). For this study we focused on sagittal and frontal plane outcome variables. Pointwise Interclass Correlation Coefficient (ICC) and Standard Error of Measurement (SEM) were calculated in R, and integrated for the observed duration of the task [3]. Integrated ICC values of ≥0.75, 0.50-0.74, and <0.50 were classified as 'good', 'moderate', and 'poor' reliability, respectively. SEM% were calculated from integrated SEM relative to the observed range of motion (joint angles) or highest joint moment value (positive or negative).

RESULTS AND DISCUSSION

Three out of six dynamic tasks had all integrated ICCs ≥0.50, when not accounting for frontal ankle moments (Table 1). ICCs in the other three tasks showed relatively poor inter-session reliability. Joint angular displacements were generally more reliable than joint moments, and had more stable pointwise ICC profiles throughout the movement (example shown in Figure 1). Overall, SEM did not vary much across planes or joints, yet SEM% was lowest in the sagittal plane.

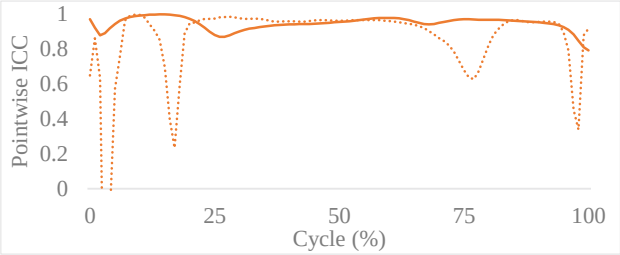

Figure 1 Pointwise ICC of sagittal knee angle (solid) and moment (dotted) in a crossover hop cycle (%) from initial contact to take-off.

CONCLUSIONS

Overall, joint kinematics were more reliable compared to joint kinetics, and the crossover hop and drop vertical jumps were more reliable than other tasks. The use of markerless motion capture for RTS evaluations shows considerable promise, yet further investigations, sample size expansions and/or developments are needed to overcome some joint or plane specific weaknesses.

REFERENCES

[1] Ardern C et al. *Br J Sports Med* **50**: 853-864, 2016.
[2] Kanko R et al. *J Biomech* **121**: 110422, 2021.
[3] Pini A et al. *Sports Biomech* **21(2)**: 179-200, 2022

Table 1 Test-retest reliability for joint angular displacements and moments of hip, knee and ankle in sagittal and frontal plane. Test-retest reliability is shown in colour based on ICC value. The actual values that are presented are SEM (SEM%).

ICC≥0.75	Joint Angle(°)						Joint Moment (Nm)					
ICC:0.50-0.74	Sagittal			Frontal			Sagittal			Frontal		
ICC<0.50	Hip	Knee	Ankle	Hip	Knee	Ankle	Hip	Knee	Ankle	Hip	Knee	Ankle
Countermovement Jump	11.0(15%)	11.2(12%)	4.0(6%)	1.9(20%)	2.3(30%)	2.9(52%)	16.4(14%)	13.6(11%)	11.2(13%)	8.0(15%)	3.8(20%)	4.9(54%)
Crossover Hop	4.2(14%)	1.9(5%)	1.6(4%)	2.3(15%)	2.2(23%)	2.2(32%)	22.0(8%)	18.5(9%)	21.0(14%)	19.6(13%)	10.3(15%)	10.3(28%)
Drop Vertical Jump	8.2(13%)	3.7(4%)	2.4(4%)	1.6(30%)	3.0(36%)	2.8(50%)	25.9(14%)	18.6(12%)	16.0(17%)	18.2(29%)	6.5(16%)	5.1(31%)
Single-leg Drop Vertical Jump	6.7(17%)	3.9(6%)	1.7(3%)	1.6(10%)	2.1(26%)	1.3(19%)	32.6(9%)	26.7(12%)	12.3(8%)	24.2(11%)	17.7(17%)	7.9(21%)
Single-leg Hop	9.4(55%)	3.7(9%)	2.6(12%)	2.5(34%)	3.8(79%)	2.9(50%)	27.4(10%)	20.7(10%)	15.7(19%)	18.6(9%)	9.6(9%)	8.3(24%)
Sidestep Cutting	3.5(6%)	3.6(8%)	8.9(23%)	1.9(10%)	4.5(58%)	1.6(16%)	54.1(10%)	54.8(24%)	36.4(20%)	19.8(20%)	26.4(31%)	18.9(26%)

EFFECT OF INCREASING WALKING CADENCE ON IMPACT LOADING IN ADULTS WITH KNEE OSTEOARTHRITIS

Khara A. James[1], Patrick Corrigan[2], Irene S. Davis[3], Joshua J. Stefanik[1]
[1] Dept of Physical Therapy, Movement, and Rehabilitation Science, Northeastern University, Boston, MA, USA
[2] Dept of Department of Physical Therapy and Athletic Training, Saint Louis University, St. Louis, MO, USA
[3] School of Physical Therapy and Rehabilitation Sciences, University of South Florida, Tampa, FL, USA
Email: james.k@northeastern.edu

INTRODUCTION

Knee osteoarthritis (OA) is a leading cause of disability worldwide. Because walking is recommended to manage symptoms, there is a critical need to develop treatment strategies that minimize the deleterious gait mechanics in adults with knee OA. Increasing cadence (i.e., number of steps taken per minute) may be a promising gait modification strategy because lower cadence is associated with higher knee joint loading [1] and risk of cartilage worsening [2]. In runners, increasing cadence reduces peak vertical ground reaction forces (vGRFs) [3]. However, it is unknown if cadence modifications during walking affect vGRFs in those with knee OA. The purpose of this study was to determine the effect of increasing walking cadence on impact loading in individuals with knee OA. It was hypothesized that the vertical impact peak and vertical load rates would be reduced with increasing cadence.

METHODS

22 participants with clinically defined knee OA were included (age = 61.8 ± 7.3; 81.8% female; BMI = 28.8 ± 6.6 kg/m^2). Baseline cadence was measured during a 5-minute walk at self-selected speed on an instrumented, split-belt treadmill. After the baseline condition, five experimental cadence conditions were completed in a random order. For each condition, participants were instructed to walk at 2%, 4%, 6%, 8%, or 10% over their baseline cadence for 2 minutes. A custom-written LabVIEW code was used to monitor and provide real-time visual feedback on cadence using GRF signals. Visual cues were supplemented with auditory cues from a metronome set to the target cadence. Participants were instructed to walk to the beat of the metronome, and to keep their cadence within ±1 step/minute of the target. GRFs were sampled (1200 Hz) for the duration of each condition. Measures of impact loading, i.e., vGRF impact peak (VIP), vertical average loading rate (VALR), and vertical instantaneous loading rate (VILR), were calculated for each step once the target cadence was met. Data were reduced by averaging the vGRF variables across 10 steps for each condition. A repeated measures analysis of covariance evaluated the effect of cadence on each vGRF variable while adjusting for gait speed.

RESULTS AND DISCUSSION

Preferred gait speed and baseline cadence ranged from 0.60 to 1.20 (mean ± SD = 0.87 ± 0.17) m/s and 83.6 to 124.0 (mean ± SD = 99.9 ± 11.8) steps/min, respectively. After adjusting for gait speed, there were no significant main effects of cadence on VIP (F=1.41, p=0.22), VALR (F=1.01, p=0.42), or VILR (F=1.61, p=0.16). Measures of impact loading did not reduce with increasing cadence as hypothesized; while insignificant, there was a gradual increase in these variables as cadence increased (Table). These increases may be partially attributed to the lack of time provided to learn a new motor pattern. Moreover, biofeedback via audible metronome may inadvertently stimulate participants to walk with punctuated steps, thereby increasing impact loading, though this was discouraged.

CONCLUSIONS

In adults with knee OA, increasing walking cadence by 2-10% at a constant speed has no immediate effect on impact loading when adjusting for gait speed. Future work may consider the effects of cadence modifications on more knee-specific measures of loading.

ACKNOWLEDGEMENTS

This research was supported by the ACSM Foundation Doctoral Student Research Grant and the Foundation for Physical Therapy Research.

REFERENCES

[1] Hart H et al. *Arthritis Care Res* **73**: 1667-1771, 2021.
[2] Hart H et al. *Arthritis Care Res* **70**: 107-113, 2020.
[3] Heiderscheit B et al. *Med Sci Sports Exerc* **43**: 296-302, 2011.

Table. Means ± SDs for impact loading variables for each cadence condition

	Baseline	+2%	+4%	+6%	+8%	+10%
VIP, BW/s	0.94 ± 0.01	0.98 ± 0.04	0.98 ± 0.03	0.98 ± 0.02	0.99 ± 0.04	1.01 ± 0.02
VALR, BW/s	6.78 ± 2.07	8.41 ± 1.01	7.99 ± 2.05	8.08 ± 1.42	8.12 ± 1.21	8.99 ± 0.92
VILR, BW/s	11.76 ± 1.60	11.52 ± 0.87	12.22 ± 1.61	11.87 ± 0.98	11.47 ± 1.41	12.26 ± 1.40

RELATIONSHIP BETWEEN COUNTERMOVEMENT JUMP AND FASTBALL VELOCITY IN ADOLESCENT BASEBALL PITCHERS

Hui-Wen Hsiao, Heng-Ju Lee
Department of Physical Education and Sport Sciences, National Taiwan Normal University, Taipei, Taiwan
Email: hjlee@ntnu.edu.tw

INTRODUCTION

Pitching performance in baseball requires transferring momentum from the lower extremity to the throwing arm. A significant and positive correlation was found between the lower extremity force output during the pitching cycle and pitching velocity, demonstrating the importance of lower limb strength in pitching [1]. Countermovement jump (CMJ) is one of the most common tests for assessing lower-limb strength. Previous studies have shown that lower-limb power performance during jump tests can predict pitching ball spinning velocity of professional baseball players [2]. However, most studies were focused on adult players, and more research needs to be conducted on the relationships between jump performance and baseball pitching performance among adolescent baseball pitchers. Therefore, this study aimed to determine the relationship between CMJ lower extremity power performance and fastball velocity and investigate the predictors of pitching velocity in adolescent baseball pitchers.

METHODS

A total of 18 teenage male baseball pitchers (age 14.1 ± 0.5 years; height 172.7 ± 6 cm; weight 67.5 ± 14.4 kg) from junior high school baseball teams participated in this study. They were asked to perform three CMJ and throw five fastballs on a custom-made pitching mound used for the indoor laboratory experiment after warm-up. CMJ tests were collected by a Kistler force plate (type 9260AA6, Kistler, Winterthur, Switzerland) with a sampling rate set at 2500 Hz. Ball velocity was measured with a pocket radar gun (Pocket Radar Ball Coach, PR1000-BC, Republic of South Korea). GRF data were smoothed using a Butterworth low-pass filter (4th Order Zero Lag) with a cut-off frequency of 12 Hz. CMJ's variables were collected and calculated from GRF data. Those data included braking force (BF), peak force (PF), braking rate of force development (RFD), braking impulse (BI), propulsive impulse (PI), peak power (PP), rate of power development (RPD), leg stiffness (LS), peak velocity, take off velocity, and jump height. We used the trial of CMJ data with the highest jump height and the average of the top three fastball velocities for the follow-up analysis. For Statistical analyses, the Pearson correlation coefficient examined the variable's relations with ball speed. Last, a stepwise multiple regression model determined the contribution of the overall CMJ variables that could predict fastball velocity in adolescent baseball pitchers.

RESULTS AND DISCUSSION

The 18 pitchers in the study had a mean fastball velocity of 111.85 ± 6.09 km/h. All variables normalized with weight show no significant associations. There are eight absolute forces-relate CMJ parameters with significant positive correlations between speed, including BF (r=.753, p<.001), PF (r=.638, p=.004), BI (r=.655, p=.003), PI (r=.62, p=.006), RFD (r=693, p=001), PP (r=548, p=.019), RPD (r=.672, p=.002), and LS (r=.689, p=.002)). We also discovered additional correlations between body height (r=.58, p=.012) and weight (r=.636, p=.005) with velocity. For the stepwise multiple regression analysis models, absolute BF (N) and body height (cm) combined to explain 62.5% of the variance in velocity (r=.818, p<.001). If only considered CMJ variables, absolute BF (N) can explain 54.1% of the variance (r=.753, p<.001). Researchers established a link between CMJ test performance and elbow injury risk in professional baseball pitchers, demonstrating the importance of the kinetic chain in pitching [3]. Pitchers with better CMJ power could likely transfer enough energy from the kinetic chain to improve their pitching performance and reduce injury risk. Other research using normalized CMJ variables found no significant relationships with ball velocity in professional players [2]. In contrast, our study showed that absolute strength might be more important than relative strength for adolescents, making body mass necessary in CMJ and pitching assessments.

CONCLUSIONS

Our study found that the CMJ's GRF variables and physical stature significantly correlate to pitchers' performance and would influence ball velocity among adolescent players. A pitcher with higher absolute braking force during CMJ and higher body height will have a greater chance to increase their fastball velocity. These characters can be a selection strategy for pitchers. Last, we recommend that pitchers in adolescence do lower limb strength training and gain lean body mass to enhance their potential fastball velocity.

REFERENCES

[1] Howenstein J et al. *J Biomech* **108**: 109909, 2020.
[2] Wong R et al. J Strength Cond Res **10**: 1519, 2022.
[3] Mayberry J et al. Am J Sports Med **48**: 1220–1225, 2020.

COMPARISON BETWEEN BACKWARD AND FORWARD PROPULSION IN WHEELCHAIR BADMINTON

Ilona Alberca[1], Bruno Watier[2], Félix Chénier[3] and Arnaud Faupin [1]
[1] Laboratoire IAPS, Université de Toulon, La Garde, France.
[2] LAAS-CNRS, Université de Toulouse, CNRS, UPS, Toulouse, France
[3] Mobility and Adaptive Sports Research Lab, Université du Québec à Montréal, Centre for Interdisciplinary Research in Rehabilitation of Greater Montreal, QC, Canada. Email: ilona.alberca@univ-tln.fr

INTRODUCTION

Wheelchair badminton is a recent sport that became a Paralympic discipline with the 2021 Tokyo games [1]. The peculiarity of this sport lies in the movements of the athletes which perform only successive forward and backward propulsion. Only four studies have investigated the differences between these two types of propulsion outside a sport setting [2-5]. However, backward propulsion modifies the kinematics of the propulsion of the athletes, which could thus act as a protective factor for the risk of injury [2][4]. However, these results relate to non-athletes and the results could differ in experienced athletes. Therefore, the objective of our study is to compare kinematics of forward and backward propulsion in experienced badminton athletes.

METHODS

18 French wheelchair badminton players (41.4±9.3 years; 64.9±11.1kg; 169.7±13.7cm) were recruited during the 2021 French Championships in Nueuil-les-Aubiers. The athletes did not have any injuries or pain affecting the propulsion of the wheelchair. They performed a consecutive forward and backward propulsion test for 1 min on a 3m straight line on a badminton court with a badminton racket. This test was created to reproduce the conditions encountered during the matches. The athletes used their own wheelchairs equipped with inertial measurement units (IMU) on the wheels. These tools allowed us to collect the following kinematic data: maximum first push velocity, maximum overall velocity, mean acceleration during the first push and mean deceleration from the last push. Fig. 1 illustrates the assessed variables.

RESULTS

Table 1: Comparison between backward and forward propulsion
*With * : $p < 0.01$, **: $p < 0.001$*

	Forward propulsion	Backward propulsion
	Mean (±sd)	**Mean (±sd)**
Maximum first push velocity (m/s)	4.57 (±0.69)	4.08 (±0.65)**
Maximum overall velocity (m/s)	3.47 (±0.71)	2.93 (±0.67)*
Mean acceleration (m/s^2)	6.08 (±1.60)	6.41 (±1.43)
Mean deceleration (m/s^2)	-10.19 (±4.26)	-9.52 (±3.45)

Significant differences between forward and backward propulsion were noted for all measured parameters.

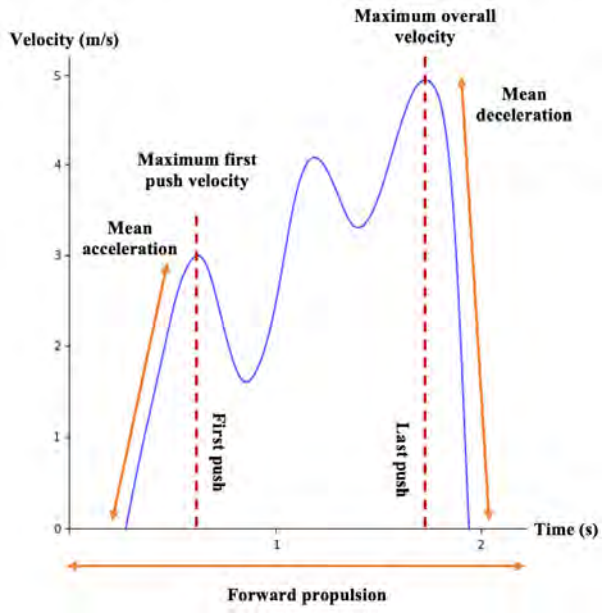

Fig 1: Propulsion velocity during forward propulsion

Maximum first push velocity, maximum overall velocity and mean deceleration were higher in forward propulsion than in backward propulsion, while **mean** acceleration was higher in backward propulsion *vs* forward propulsion.

CONCLUSION

The results are in the direction of a more efficient forward propulsion than backward. However, the mean acceleration is greater in backward propulsion without having a greater maximum first push and overall velocity. This may indicate that athletes have different propulsion kinematics depending on the chosen propulsion mode. These results are interesting for athletes and trainers who should promote training phases in backward propulsion and the transition from forward to backward propulsion to improve the performance of athletes.

[1] Janiaczyk. *Fizjoterapia* **23**(4): 66-72, 2015
[2] Haubert et al. *JSCM* **43**(5): 594-606, 2020
[3] Linden et al. *Med Sci Sports Exerc* **25**(11): 1265-8, 1993
[4] Mason et al.*J Spinal Cord Med* **38**(4): 476-84, 2015
[5] Salvi et al. *Arch Phys Med Rehabil* **79**(1): 36-40, 1998

ESTIMATING DISTRIBUTION OF MASS BETWEEN CASTOR- AND REAR WHEELS USING INERTIAL SENSORS DURING MANUAL WHEELCHAIR PROPULSION

Marit P. van Dijk[1], Louise Heringa[1], Marco Hoozemans[2], Monique Berger[3] and DirkJan Veeger[1]

[1]Department of BioMechanical Engineering, Delft University of Technology, Delft, The Netherlands
[2]Department of Human Movement Sciences, Vrije Universiteit Amsterdam, Amsterdam, The Netherlands
[3]Assistive technology for Mobility & Sports, The Hague University of Applied Sciences, The Hague, The Netherlands
Email: m.p.vandijk@tudelft.nl

INTRODUCTION

Mechanical power is an important performance determining factor in wheelchair sports. Recently, a method was proposed to estimate mean external power during hand rim wheelchair propulsion with data from inertial measurement units (IMUs) on the wheelchair [1]. With this method, mechanical power during wheelchair field sports can be estimated on court from power losses, i.e., rolling resistance (including internal resistance) and changes in kinetic energy. Although results show low errors when limited trunk motion was observed, power was significantly underestimated when considerable (within pushing cycle) variation in trunk inclination is involved during wheelchair propulsion. This under-estimation is due to a larger underestimation of rolling resistance caused by the trunk inclination-induced change in mass distribution between the front (castor) and rear wheels. Therefore, quantifying the dynamic relation between trunk inclination and mass distribution during wheelchair propulsion may improve power estimates. To that end, this study aims to estimate the mass distribution between the wheelchair's castor and rear wheels during hand rim wheelchair propulsion from IMU data with machine learning.

METHODS

In an experimental laboratory setup, 25 participants propelled a manual wheelchair on a large treadmill, with IMUs attached to their trunk (sternum), right wheel axle and wheelchair frame. Simultaneously, custom-made load pins in the castor wheel axes measured the instantaneous load on the castor wheels which was used as the gold standard. Subsequently, machine learning was applied to estimate the instantaneous load on the castor wheels from IMU data only, for which the best predictive set of IMU-based features and the best machine learning model were determined. The final model was evaluated by comparing the predicted with the observed load on the castor wheels. To ensure model robustness to different wheelchair and participant characteristics, the model was trained and tested on datasets with 0 kg, 5 kg and 15 kg of mass added at the seat or datasets in which the tire pressure of the rear tires was adapted to, respectively, 1.75, 3.5 and 5.25 bar. In addition, participants propelled the wheelchair using two different techniques: 1) while keeping the trunk static and 2) with full trunk motion. Of all data, the +5 kg data set of all participants, the 1.75 bar dataset of all participants and all six datasets of four participants were excluded in model training and were used to determine the accuracy of the final model. These 'excluded' data were referred to as test set.

RESULTS AND DISCUSSION

Results revealed that the best predictive feature set consisted of the linear velocity of the wheelchair, the linear acceleration of the wheelchair and the acceleration perpendicular to the sternum. Of the five machine learning models that were tested, a 'long short-term memory' (LSTM) model showed the most accurate predictions (see Figure 1). The mean absolute errors (MAE) for the wheelchair with no additional mass in the test set was 4.3±2.1%, with a root mean square error (RMSE) of 4.9±2.0% of the total mass, for the +5kg condition in the test set MAE was 3.0±1.4% and RMSE was 3.7±1.5% and for the 1.75 bar dataset in de test set MAE was 2.8±1.0% and RMSE was 3.7±1.4%. Similar results were found for the parts of the test set in which subjects were instructed to keep their trunk static compared with parts with full trunk motion.

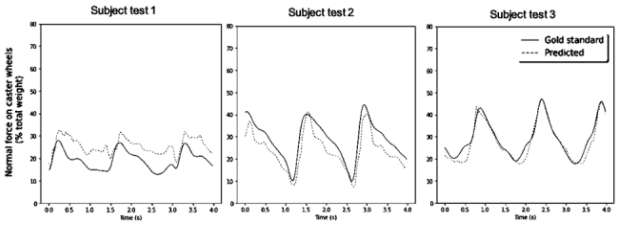

Figure 1 Results of LSTM model on test set with 0kg and 5.25 bar.

CONCLUSIONS

To conclude, instantaneous mass distribution between castor and rear wheels during hand rim wheelchair propulsion can be predicted relatively accurate from wheelchair and trunk-based IMU data. The machine learning model seems robust to different propulsion techniques, wheelchair and participant characteristics. When the predicted instantaneous castor load was used to calculate rolling resistance and, subsequently, power loss, a significantly better power estimation was found when compared with the power estimation based on 'non-varying' castor load. With the obtained model and input from IMUs on the wheelchair and trunk, mechanical power during wheelchair field sports can be estimated more accurately on the court.

REFERENCES

[1] van Dijk et al. *submitted to J Biomech*, 2023

Aerodynamics of dimple structure on soccer ball using 3D printer

S. Hong[1,2], S. Ito[2], T. Maruyama[3], K. Kimachi[1], M. Koido[1], M. Nakayama[1] & T. Asai[1]
[1] Faculty of Health and Sports Science, University of Tsukuba, Japan.
[2] Department of Mechanical Engineering, Kogakuin University, Japan.
[3] Institute for Liberal Arts, Tokyo Institute of Technology, Japan.
Email: hong.sungchan.fu@u.tsukuba.ac.jp

INTRODUCTION

The number of panels on the surface of a regular soccer ball has decreased from canonical 32 (Telstar and Fevernova, 1970 World Cup in Mexico to the 2002 World Cup in Korea and Japan) to 14 panels (Teamgeist, 2006 World Cup in Germany) to eight panels (Jabulani, 2010), and lastly, to six panels (Brazuca and Telstar18, 2014 and 2018). Moreover, during the UEFA Euro 2008, the Europass ball that was introduced had a prestressed concrete (PSC) creeps surface design; this ball was evidently rough due to the presence of various protrusions, such as squares, triangles, and hexagons [1]. As such, previous studies have reported on the effects of these changes in the ball's aerodynamic properties and flight trajectory [2]. studies have been conducted to evaluate and assess the changes on aerodynamic characteristics and flight properties due to the changes in the panel orientation that are attributed to the reduced number of panels. In this study, we created soccer balls (32-panels) with various surface shapes (differing dimple structures) using the same material (polyamide-12) using a 3D printer. After fabricating four types of soccer balls with different surface dimple shapes, we compared their aerodynamic characteristics in wind tunnel experiments along with an analysis of their flight trajectories. Further, we analyzed the effects of ball shapes on aerodynamics under constant conditions.

METHODS

In this experiment, we have fabricated soccer balls (with a diameter of 220 mm, 32 panels) from the same material (polyamide-12) on a 3D printer (HP Jet Fusion 3D 4200, HP), and the surfaces of the balls were coated with graphite. The weight of each soccer ball was set at approximately 450 g, which is similar to that of a regular soccer ball. The depth and width of the seams on the ball surface were manufactured at 2 and 1 mm, respectively. Furthermore, we have created the designs of the fabricated soccer balls using 3D CAD software (Autodesk Inventor Professional 2020, Autodesk Inc.). The wind tunnel experiment was conducted on the manufactured soccer balls. In this experiment, the wind speed (U) was set from 7 to 30 m/s, taking two measurements at 1 m/s intervals.

RESULTS AND DISCUSSION

The graphs below show the effects of various dimple shapes on aerodynamic properties of balls and show the correlation between four balls: smooth type, conical type, hemispherical type, and cylindrical type. These four soccer balls have the same seam structure, but each type has a different dimple structure. First, Figure 1A shows the correlation between the supercritical Reynolds number (Re_{crit}) and the proportion of dimples on the surface of the balls (ΣAd/Ab), and an extremely high correlation (R^2=0.91). Figure 2B shows the correlation between the supercritical Reynolds number of each of the four soccer balls and the proportion of the area of dimples and seams on the surfaces of the balls (ΣAd+ As/Ab), with an even higher correlation (R^2=0.92). These results suggest that the shape of the soccer ball surface, particularly the proportion of the dimple surface area, has a significant effect on soccer ball drag, including the ball's supercritical Reynolds number.

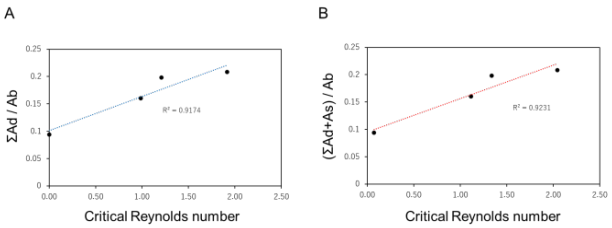

Figure 1 Correlation between the supercritical Reynolds number and dimple shape on the ball' surface of the soccer balls. A is the correlation between Re_{crit} and the dimple ratio (ΣAd/Ab), while B is the correlation between Re_{crit} and the dimple and seam ratio (ΣAd +As/ Ab).

CONCLUSIONS

In this study, we investigated the effects of the surface shape of soccer balls, which includes the dimple structure, that were fabricated using a 3D printer on their aerodynamic characteristics. The results demonstrate that the dimple structure characteristics on the surface of the soccer ball were strongly related to the aerodynamic forces applied to the soccer ball. Moreover, the shape and number of panels of the ball as well as the shape of the ball's surface are important factors in determining its aerodynamic characteristics.

ACKNOWLEDGEMENTS

This research was supported in part by a grant from Advanced Research Initiative for Human High Performance (ARIHHP), University of Tsukuba.

REFERENCES

[1] Hong et al. *J Sport Eng Technol.* **233**:67-74, 2019.
[2] Adrian & Derek. *Eur J Phys*. **39**: 034001, 2018.

THE LARGEST SEGMENTAL COMPONENTS OF ENERGY DIRECTLY CONTRIBUTING TO HEIGHT DO NOT EXPLAIN THE VARIANCE OF ITS TOTAL IN THE HIGH JUMP.

Natsuki Sado[1], Toshihide Fujimori [2] and Naoto Tobe[1]
[1] Faculty of Health and Sport Sciences, University of Tsukuba, Tsukuba, Japan.
[2] Graduate School of Comprehensive Human Sciences, University of Tsukuba., Tsukuba, Japan.
Email: sado.natsuki.gm@u.tsukuba.ac.jp

INTRODUCTION

The High Jump (HJ) is the most height-specific jumping mode for humans. Jumping higher means increasing the mechanical energy directly contributing to the centre of mass height (E_{vert}, the sum of vertical kinetic and gravitational potential energies) during take-off. E_{vert} in HJ is mainly induced by the stance-leg thigh and shank rotations [1]. The largest components are derived from the energy inflow to the segment due to proximal and distal joint work (thigh only) and from the conversion of horizontal kinetic energy (E_{horiz}) into E_{vert} (in thigh and shank) [2]. The curved approach further facilitates this conversion in HJ by altering the initial posture [1]. Meanwhile, from a performance perspective, jumpers can increase E_{vert} by increasing the components of the small contributors and/or decreasing the inhibition of the negative contributors, too. Thus, not only large but also small E_{vert} contributors can be related to the variance of the overall increase in E_{vert}. Here we show the discrepancy between the segment that generates the most E_{vert} and the segment that alone explains well the variance of the total E_{vert}.

METHODS

We analysed the kinematic and ground reaction force data of 16 male jumpers [22.3 ± 3.1 years, 1.801 ± 0.060 m, 66.60 ± 5.90 kg, personal and season best (PB, SB): 1.90–2.35 m, 1.80–2.30 m] who performed HJ with maximum effort with the bar set at 90% of each SB. We decomposed the change in E_{vert} during take-off into segmental components [2]. We used a simple regression to examine whether the E_{vert} component due to segment rotations explained the inter-individual variance of the total increase in E_{vert}. Prior to regression, we removed an outlier in the total increase in E_{vert} based on three times the median absolute deviation.

RESULTS AND DISCUSSION

The stance-leg thigh (4.20 ± 0.84 J/kg) and shank (3.93 ± 0.88 J/kg) rotations contributed the most to total E_{vert} (11.59 ± 0.81 J/kg); however, their variance alone did not explain the variance of total E_{vert} (Fig. 1B). Meanwhile, the variance of stance-leg foot and thoracic components significantly explained the variance of total E_{vert} (Fig. 1B). This supported our hypothesis. The thoracic and foot components are derived from the work of the thoraco-lumbar lateral flexors and ankle plantar flexors. Despite their relatively small E_{vert} inductions (Fig. 1A), we suggest their importance for performance.

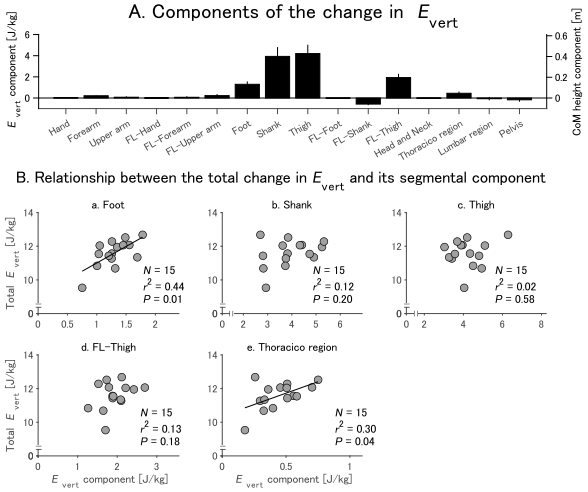

Figure 1 Segmental components of the change in E_{vert} (A) and their relationships to total change in E_{vert} (B) during the take-off.

E_{vert} components due to the stance-leg thigh and shank were negatively correlated (r^2 = 0.60, P < 0.01), and their sum was correlated with the total E_{vert} (r^2 = 0.57, P < 0.01). This suggests the existence of multiple strategies relating to the thigh and shank E_{vert} inductions to jump high in HJ. The shank component is only due to the conversion from E_{horiz} to E_{vert} while the thigh component invovles both the energy conversion and the energy inflow by the hip and knee work [2]. The knee exibits power pattern of absorption followed by generation, implying a strech-shortening action [2]. We suggest that the mechanical properties of knee extensors may be related to individual differences in jumping strategies, rather than the performance *per se*.

CONCLUSIONS

The variance of the largest E_{vert} components due to the thigh and shank does not explain well the inter-individual variance of the total increase in E_{vert}, whereas the variance of the thoracic and foot components each explain it. This suggests that larger components are not necessarily strong determinants of the performance variance. The thigh and shank results further suggest the existence of multiple strategies for jumping higher in HJ.

ACKNOWLEDGEMENTS

This study was supported by JSPS KAKENHI Grant-in-Aid for Young Scientists (21K17592) and Tateishi Fundation for Science and Technology (2221014).

REFERENCES

[1] Sado N et al. *Med Sci Sports Exerc* **54**: 120-8, 2022.
[2] Sado N et al. *J Biomech* **113**: 110082, 2020.

HAMSTRING MUSCLE KINEMATICS AND ACTIVATION DURING THE ACCELERATION PHASE IN SPRINTING OF SOCCER PLAYERS

Van Thiet Le[1], Yudai Kikuchi[1], Masayoshi Kubo[1]
[1] Department of Physical Therapy, Niigata University of Health and Welfare, Niigata, Japan.
Email: hwd22014@nuhw.ac.jp

INTRODUCTION

Hamstring strain injuries are the most common muscle injury in soccer that directly affects the performance of soccer players and the result of clubs. Sprinting was reported as the most common activity involving hamstring strain injuries. To define hamstring strain injury mechanisms, the hamstring kinematics and activation were investigated to predict the potential injury. However, the hamstring kinematics and activation in the acceleration phase of sprinting have not been clear, although this phase is crucial for sprinting performance. Therefore, the purpose of this study was to characterize the hamstring muscle kinematics and activation during the acceleration phase of sprinting in soccer players to define the potential hamstring strain injury mechanism.

METHODS

Ten male participants with no history of lower limb injuries in one recent year were recruited. The participant gave their written consent to participate. This study conformed to the recommendations of the Declaration of Helsinki and has been approved by the University Ethics Committee at Niigata University of Health and Welfare. Each participant was required to take at least three successful 15 m sprints. Full-body kinematics during the acceleration and the maximum-speed phases in sprinting of each participant was collected. The acceleration phase was defined as the three first steps. A full-body musculoskeletal model was used to make simulations based on the marker data from the experiment in the Opensim. Hamstring muscle kinematics was estimated based on the model's kinematics in simulations. Hamstring muscle activation was recorded using wireless electromyography. The raw EMG data were rectified before filtering to estimate linear envelope EMG data. We just analyzed three biarticular muscles of the hamstring.

RESULTS AND DISCUSSION

In the acceleration phase, the muscle length of all biarticular hamstring muscles was lengthened during the second half of the swing and the first half of the stance of the running gait cycle. The peak strain of biarticular hamstring muscles was reached at around 90 % of the running gait cycle. The biceps femoris long head was undergone significantly greater strain than two other hamstring muscles ($p<0.01$), with the peak strain approximately 10.4 ± 1.73 %, 8.35 ± 1.79 %, and 7.46 ± 1.65 % respectively at the late swing of the running gait cycle (Fig.1). This result contributed to the explanation of the higher rate of occurred injuries in the biceps femoris long head than in the semimembranosus and semitendinosus. The biarticular hamstring muscles were shortened during the stance, the first one-third and the last 10 % of the swing, while the positive elongation velocity occurred at approximately 60 to 90 % of the swing. Furthermore, the muscle activation of the biceps femoris long head and semitendinosus reached the highest point at approximately 90 % and the second peak at the foot-strike of the running gait cycle. In combination, the biarticular hamstring muscles undergo eccentric contraction and a high activation level on the late swing and initial stance.

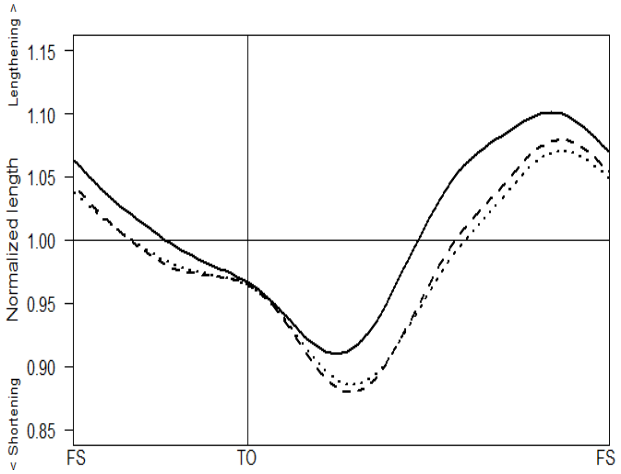

Figure 1 Biarticular hamstring muscle length during the running gait cycle in sprinting acceleration phase. The solid line (Biceps femoris long-head) dashed line (Semitendinosus), dotted line (Semimembranosus), TO (Toe-off), and FS (Foot-strike).

CONCLUSIONS

In conclusion, the mechanisms of potential hamstring injuries occurred at the late swing and foot-strike of the running gait cycle in the sprinting acceleration phase. The biceps femoris long head might be more susceptible to injuries than other hamstring muscles. The acceleration phase in sprinting should be gotten more attention to prevent hamstring strain in soccer players' sprinting.

REFERENCES

[1] Yu B et al. *J Biomech* **41**: 3121-3126, 2008.
[2] Kenneally-Dabrowski C J B T et al. *Scand J Med Sci Sports* **29**: 1083-1091, 2019.

SEX-SPECIFIC ANTHROPOMETRIC AND KINEMATIC PERFORMANCE DETERMINANTS IN NATIONAL ELITE JAVELIN ATHLETES

Chinedu Godwin Uzomba[1], Ezemagu Uchenna[1], Philip X. Fuchs[2]
[1]Department of Anatomy, Federal University Ndufu Alike, Ndufu-Alike Ikwo, Nigeria
[2]Department of Physical Education and Sport Sciences, National Taiwan Normal University, Taipei, Taiwan
Email: uzomba.godwin@funai.edu.ng

INTRODUCTION

Knowledge about the interaction of anthropometry and kinematics contributes to success in javelin throwing [1] and is important for sport scientists and coaches to assess performance determinants and adjust training regimes. The purpose of this study was to investigate the relationship of anthropometry and kinematics with javelin performance and to predict throwing distance based of anthropometric and kinematic parameters.

METHODS

Fifty javelin throwers (28 males and 22 females, age: 18-44 years) participated in this cross-sectional correlation study. Anthropometric data were collected via the direct standard anthropometric protocol [2]. During the 20th National Sports Festival, kinematic variables were obtained using two Vicon MX cameras at a sampling frequency of 200 Hz (Peak Performance Technologies, Inc., Oxford, UK) and the 2D kinematic video graphic technique. Paired sample t-test and multiple regression analysis were conducted via SPSS 23 (SPSS Inc. Chicago, IL) at a significance level of $p<0.05$.

RESULTS AND DISCUSSION

Differences in throwing distance (d=1.38, $p<0.001$) as well as in multiple anthropometric (d=0.864–2.252, $p<0.05$) and kinematic characteristics (d=0.704–1.115, $p<0.05$) between sexes suggested sex-specific analyses. Sex-specific correlation results can be found in Table 1. The 'stepwise forward' regression model for females achieved adjusted R^2=0.461, p=0.035 based on angle of trunk and body height. The model for males was based on chest girth and ankle angle (adjusted R^2=0.490, p=0.006). A model across sexes included sex, attitude angle, and arm girth as predictor criteria (adjusted R^2=0.549, p=0.012).

Table 1: Correlation of anthropometric and kinematic parameters with the javelin throwing distance.

Parameters	Male		Female	
	r	*p*	*r*	*p*
Age (years)	0.155	0.432	-0.049	0.829
Weight (kg)	0.344	0.073	**0.497**	**0.019**
Height (m)	0.084	0.671	**0.579**	**0.005**
BMI (kg/m^2)	0.361	0.059	0.199	0.376
Body fat (%)	0.324	0.093	0.142	0.528
Arm span (mm)	0.293	0.130	0.384	0.078
Arm girth (cm)	**0.575**	**0.001**	0.244	0.273
Chest girth (cm)	**0.595**	**0.001**	0.224	0.315
Thigh girth (cm)	**0.423**	**0.022**	-0.367	0.093
Attack angle (°)	-0.359	0.061	-0.044	0.846
Release angle (°)	**-0.495**	**0.007**	-0.154	0.494
Attitude angle (°)	**-0.495**	**0.007**	-0.271	0.222
Trunk angle (°)	-0.051	0.797	**0.617**	**0.002**
Ankle angle (°)	**-0.561**	**0.002**	-0.212	0.343
Throwing time (s)	**0.831**	**<0.001**	**0.485**	**0.022**
Release velocity (m/s)	**0.926**	**<0.001**	**0.897**	**<0.001**

CONCLUSIONS

The study outlined sex-specific performance determinants and predicted javelin throwing distance based on anthropometrics and kinematic movement characteristics. The findings can be used to establish performance profiles, assess performances, identify talented athletes, and adjust training protocols.

REFERENCES

[1] Manesh KM, Dhinu MR. *Kinesiol Slovenica* **22**(1):27-37, 2016.
[2] Alexandra A et al. *J Phy Edu Sport* **10**:329-37, 2012.

Classifying Punch Types and Ranges in Boxers: A Machine Learning Approach with IMU Sensor Data

Saravanan M[1], John Warburton [2], Ravi Hegde[3], Ranganathan Srinivasan[1] and Babji Srinivasan[1]
[1] Indian Institute of Technology Madras, Chennai, India.
[2] Liverpool John Moores University, Liverpool, United Kingdom
[3] Indian Institute of Technology Gandhinagar, Gandhinagar, India.
Email: babji.srinivasan@iitm.ac.in

INTRODUCTION

In competitive combat sports like boxing, boxer's performance evaluations, including the punch amount and its type, are a valuable source of data for coaching and performance improvement. Studies have shown that the use of machine learning (ML) techniques with IMU sensor data can accurately classify boxer's punch types, such as jab, hook, and uppercut [1]. However, to effectively evaluate the athlete's punch performance, it is crucial to classify the punch range. The ideal position for a boxer to engage in punching is when the weight of the athlete is evenly balanced over both legs, allowing for the body to rotate around a central axis. To achieve this position on engagement the boxer has to move their feet into range or distance, giving them the opportunity to punch. There are 3 main classifications of range, long, mid, and close. Punches will vary at these different ranges. At long range, most punches are straight with full extension of the arm. At mid and short range most punches will have a bend at the elbow and are termed as hooks or uppercuts. Therefore, in this work, we classify boxers' punch type and punch range using various ML techniques fed with IMU sensor data [2].

METHODS

We collected IMU sensor data (accelerometer and gyroscope; 200 Hz) and time-synchronized video recordings from eight elite boxers from the Inspire Institute of Sports (IIS), Karnataka, India. The boxers performed 320 punches for each of the 14 different punches, such as long-range lead jab, mid-range lead jab, long-range rear hook, etc. First, we performed time-frequency analysis of the IMU sensor data for each punch type to obtain Spatio-temporal features such as power spectral density in various frequency bands. Next, we employ several supervised ML techniques such as decision tree (Fine and coarse), random forest, linear discriminant, and quadratic discriminant to classify the punch type and punch range. The ground truth was obtained from the recorded video by visual inspection. Finally, we compared the accuracy obtained across these ML techniques.

RESULTS AND DISCUSSION

Initial results are demonstrated for classifying four different punch types and punch ranges (no punch, long-range rear jab to the head, mid-range rear hook to the head, and mid-range rear uppercut to the head). Fig. 1 shows the accelerometer data for different punch types. The classification result using various ML techniques is reported in Table 1. It can be seen that the random forest is more accurate than the other algorithms (96.5%). The confusion matrix revealed that all four punch types are classified accurately, except for the no punch and rear hook punch, where few instances are misclassified (Fig. 2).

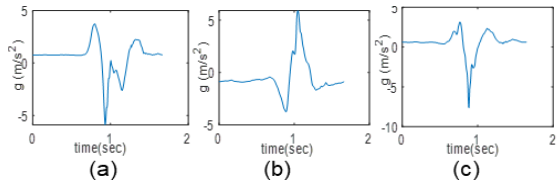

Figure 1. Accelerometer plot; (a) Jab (b) Hook (c) Uppercut

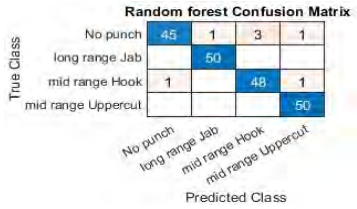

Figure 2. Confusion Matrix

CONCLUSION

The current study uses machine learning techniques to classify boxers' punch type and punch range using IMU sensor data. These classifications are important for improving the boxer's performance in aspects such as offense, defense, and overall control of the match. The results showed that the random forest algorithm performed better than other classification methods. Our future work aims to expand the algorithm to cover all 14 types of punches, their ranges, and to incorporate punch force in the classification. The ultimate goal is to create an IoT (internet of things) platform to aid coaches in evaluating athletes' performance remotely.

ACKNOWLEDGEMENTS

CoE for sports science and analytics for the funding.

REFERENCES

[1] Hanada Y et al. *Springer* 95-114, 2022.
[2] Stanley E et al. *open repository*, 2020.

Table 1: Classification results from various machine learning algorithms

Model	Accuracy	Precision	Recall	F1-score
Fine Decision Tree	90.5%	91.6%	91.65%	0.91
Coarse Decision Tree	69%	69.5%	76.04%	0.72
Linear Discriminant	89%	89%	90.1%	0.89
Quadratic Discriminant	63.7%	63%	78%	0.7
Random forest	**96.5%**	**96.5%**	**96.5%**	**0.96**

A SYSTEMATIC REVIEW AND EVALUATION OF OPEN-SOURCE TRANSTIBIAL AMPUTEE MUSCULOSKELETAL MODELS FOR USE ON FEMALE POPULATIONS

Misha Hasan[1], Tess M.R. Carswell[1], and Joshua W. Giles[1]
[1] Department of Mechanical Engineering, University of Victoria, Victoria, B.C., Canada.
Email: tmrc@uvic.ca

INTRODUCTION

Transtibial amputees (TTAs) have become a population of interest in the computational musculoskeletal (MSk) modeling community [1]. Most studies use a generic MSk model linearly scaled to match the subject's anthropometrics [2]. Despite their prevalence, generic models can neglect innate variations between distinct groups. For example, while sex differences exist in MSk geometry and musculotendon parameters [3], most generic models were developed using predominantly male data [4,5], affecting their validity to study female populations. Therefore, when choosing a model, it is important researchers are aware of the data used to develop and validate it. This work presents a systematic review of existing open-source TTA models, aiming to help guide researchers when choosing an MSk model. Existing models were also evaluated to determine the model most representative and capable of reproducing female TTA biomechanics. This model will be used in future work studying sex differences in amputees.

METHODS

A systematic search of 10 key terms was performed on three online databases (PubMed, Scopus, Web of Science). Eligible studies were retained for review if they presented an open-source, 3D, human MSk model representing a TTA with a generic non-osseointegrated (OI) prosthetic. A database was created based on data detailing the development and validation of the eligible models. The database was then used to evaluate the models on their capability of representing female TTAs based on predefined weighted criteria (Table 1) with scoring scales. Criterion 1 assesses how representative the model development data are of female TTAs. Criterion 2 determines how comprehensive the model's validation was as defined by the MSk Modelling Grand Challenge [6]. Criteria 3 and 5 assess the functionality and motions the model and its prosthesis can accommodate. Criterion 4 evaluates how transparent the model development process was in each study.

RESULTS AND DISCUSSION

The systematic search yielded 352 results. Upon consideration against eligibility criteria, three studies remained: LaPrè et al., Willson et al., and Miller & Esposito [1,7,8]. The database created compiles data for the three models, providing a detailed account of how and with what data each was developed and validated. However, through further investigation of the Miller & Esposito model, it was found to represent an OI prosthetic, making it ineligible for further analyses. Upon evaluation of the two remaining models, the Willson model scored higher against all criteria except Criterion 5. For this criterion, the LaPrè model was able to accommodate more motions than that of the Willson.

CONCLUSIONS

This work presents a systematic review and evaluation of existing open-source TTA models. Data on three models was compiled into a database resource for researchers in future modeling studies. Upon evaluating eligible models, the Willson model was determined the most representative and capable of reproducing female TTA biomechanics. This model will be used in future work studying sex differences in amputees.

ACKNOWLEDGEMENTS

Graduate funding for TMRC was provided by NSERC Canada Graduate Scholarships – Doctoral (CGSD).

REFERENCES

[1] Willson A et al. *Comp Meth Biomech Biomed Eng* :1-12 2022.
[2] Akhundov R et al. *PLos One* **17**: 1-16, 2022.
[3] Haizlip K et al. *Physiology* **30**: 30-39, 2015.
[4] Horsman M et al. *Clin Biomech* **22**: 239-247, 2007.
[5] Hoy M et al. *J Biomech* **23**: 157-169, 1990.
[6] Fregly B et al. *J Orthop Res* **30**: 503-513, 2012.
[7] LaPrè A et al. *Int J Num Meth Biomed Eng* **34**: e2936, 2018.
[8] Miller E, Esposito R *PLos One* **13**: e0191310, 2018.

Table 1: Criteria and weightings used to evaluate eligible models for selection.

Evaluation Criteria	Guiding Questions	Weight (%)
1. Representative of desired population	What were the demographics of subjects used to develop the model?	25
2. Experimentally validated	Was the model validated and if so, how?	25
3. Functionality of prosthesis model	What degrees of freedom and range of motion does the prosthetic accommodate?	12.5
4. Transparency of model development	Were the developers transparent in how they developed the model?	12.5
5. Functionality of overall model	What motion was the model validated for and what motions can it accommodate?	25

COMPLETE 3D KINEMATICS PARAMETERS OF THE TEMPORO-MANDIBULAR JOINTS USING IN VIVO DATA FUSION

Gaël Bescond[1], R. Glineur [1,2], V. Sholukha [1], S. Van Sint Jan [1].
[1] Laboratory of Anatomy, Biomechanics and Organogenesis (LABO), Université Libre de Bruxelles, Belgium.
[2] Department of Dentistry, Oral and Maxillo-facial Surgery, Orthodendistry and Stomatology, ULB, Belgium.
Email: gael.bescond@ulb.be

INTRODUCTION

The temporo-mandibular joint (TMJ) has implications in vital functions and its disorder prevalence is between 5% and 12% [1]. Quantitative motion analysis tools are of interest to better understand normal and abnormal TMJ behavior. The mandible shows morphologic and kinematic particularities: its motions rely on two joints where mandibular condyles are generally asymmetric and highly individual [2], they rotate during jaw opening and closing and translate vertically and anteroposteriorly [3]. Thus, we describe the detailed kinematic behavior of the TMJs through a 3D model, gathering the kinematic parameters contributing to the global movements of the mandible compared to the skull, as well as the local movements of the 2 condyles compared to their sockets and instantaneous helical axis analysis.

METHODS

Five healthy subjects fitted with a tailor-made dental cluster and a head cluster performed 10 mouth opening and closing cycles, 10 diductions and chewed for 20 seconds on a cork. An experimenter palpated with the A-Palp [4] 15 anatomical landmarks (ALs) on their skull and their mandible. The trajectory of the markers and ALs was recorded by opto-electronic cameras and stored in C3D files. Magnetic resonance imaging from the 5 subjects was processed through a segmentation procedure (Amira®) to obtain 3D models, imported into the lhpFusionBox, which is musculo-skeletal data processing software developed at ULB [5]. Virtual palpation was used to locate specific ALs and to build coordinate systems following the ISB recommendations [6]: a Jaw Global Frame (JGF) associated to a Skull Global Frame (SGF); a distal Right or Left Jaw Local Frame (RJLF, LJLF) associated to a Right or Left Skull Local Frame (RSLF, LSLF) (Fig.1). We then fused the ALs coordinates with the C3D motion files and the morphological model.

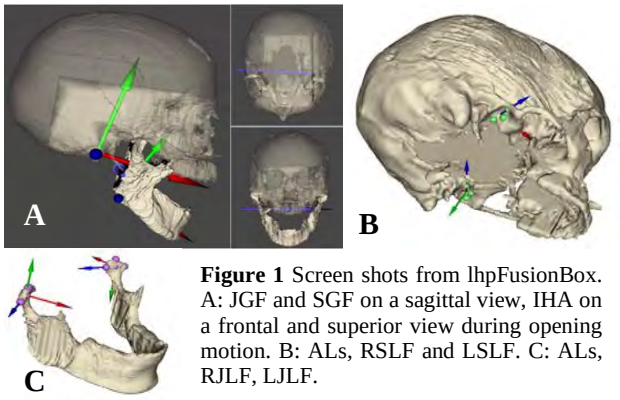

Figure 1 Screen shots from lhpFusionBox. A: JGF and SGF on a sagittal view, IHA on a frontal and superior view during opening motion. B: ALs, RSLF and LSLF. C: ALs, RJLF, LJLF.

RESULTS AND DISCUSSION

Motion cycles were normalized from 1 to 100% of rotations and translations duration in JGF and in the RJLF/LJLF, instantaneous helical axis (IHA) parameters (direction cosines, IHA rotation center coordinates, IHA rotations and translations) were computed for the 3 motions. The fusion residual error (Median RMSE = 8.0 mm) and data (Fig. 2) shows that our model is accurate enough and consistent with previous studies [7].

CONCLUSIONS

By providing complete 3D TMJ kinematics parameters, we hope to contribute to the development of engineers'own model. Also, the calculation of the IHA was made considering further anatomical studies including masticatory muscular lever arms.

REFERENCES

[1] Goulet JP et al. *J Dent Res* 74: 1738-44, 1995.
[2] Bescond G et al. *Morphologie* 105: 275-80, 2021.
[3] Jeanmart L et al. *Ann Radiol* 4: 575-89, 1961.
[4] Salvia P et al. *Gait & Posture* 29: 587–91, 2009.
[5] Chapman T et al. *M.S.* 29: 623–29, 2013.
[6] Wu G et al. *J Biomech* 28: 1257-61, 1995.
[7] Travers KH et al. *Arch Oral Biol* 45: 267–75, 2000.

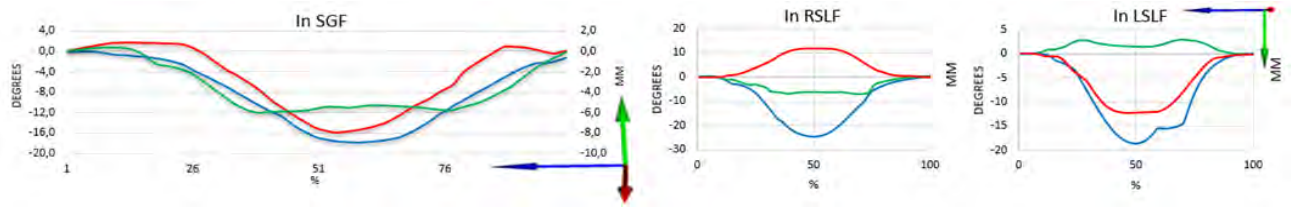

Figure 2: Median rotation around **Z-axis** and translations on **Y** and **X-axis** during mouth opening/closing motion. In LSLF, the motion frame has been oriented to have the Z-axis pointing in the same direction as on the right side, leading to an inversion of the other DOFs.

MUSCLE CONTRIBUTIONS TO THE BARBELL BACK SQUAT IN TRAINED FEMALES

William Goodman [1], Eric Helms[2], and David Graham [1]
[1] College of Education Health and Human Development, Montana State University, Bozeman, USA.
[2] Sports Performance Research Institute New Zealand, Auckland University of Technology, Auckland, NZ.
Email: wes@likeironstrong.com

INTRODUCTION

The barbell squat is used to enhance athletic performance and rehabilitate the lower body. Several studies describe muscle function during the squat [1,2] but in general most investigations to date ignore the ability of muscle forces to accelerate all joints, limb segments and the whole-body centre of mass (CoM) simultaneously [3]. The purpose of this study was to determine how lower extremity muscles contribute to the vertical acceleration of the CoM and to the flexion and extension accelerations of the ankle, knee and hip when squatting to parallel using 85% 1RM.

METHODS

Thirteen female participants with 6.00 ± 3.65 years of squatting experience completed the study. Participants completed 3 repetitions of the barbell squat at 85% of 1 repetition maximum to a depth where the thighs were parallel to the ground. Trajectories of 65 reflective markers attached to each participant and ground reaction forces under each foot were recorded simultaneously. Data analyses were performed using OpenSim (version 4.0). Muscle forces were estimated using static optimisation and the induced analysis algorithm was used to estimate each muscle's contribution to accelerations of the CoM and lower limb joints. Models were evaluated to ensure possible sources of error were within recommended tolerances [4].

RESULTS AND DISCUSSION

The soleus, vasti, gastrocnemius and gluteus maximus generated the largest upward accelerations of the CoM while the muscles that produced the largest downward acceleration about the CoM were the hamstrings, tibialis anterior, adductors and iliopsoas (Table 1). The muscles responsible for knee and hip extension acceleration were the vasti, adductors, hamstrings, and gluteus maximus while the muscle primarily responsible for knee and hip flexion acceleration was the soleus. The muscles responsible for ankle dorsiflexion acceleration were the vasti, adductors, hamstrings, and gluteus maximus. The main muscle responsible for plantar flexion acceleration was the soleus.

CONCLUSIONS

Overall, our findings indicate that during the squat exercise the muscles of the lower limb perform multiple roles to accelerate the joint they span, joints they do not span, and the CoM simultaneously. In some cases, biarticular muscles accelerated a joint opposite of its moment production. For example, the hamstrings produced a flexion moment at the knee but accelerated the knee into extension. These results corroborate prior findings [5] and demonstrate that considering only the anatomical function of a muscle may result in an incomplete assessment of a muscle's role [3,5]. Most importantly, a muscle's function is task specific, as it depends on both joint position and how an individual interacts with the environment, and this should be considered when prescribing compound exercises such as the barbell squat.

REFERENCES

[1] Bryanton M et al. *J Strength Cond Res* **26**:2820-2828, 2012.
[2] Wretenberg P et al. *Scand J Med Sci Sport* **3**:244-259, 1993.
[3] Zajac FE. *J Biomech* **35**: 1011-1018, 2002.
[4] Hicks J et al. *J Biomech Eng* **137**, 2015.
[5] Souza TR et al. *J Biomech* **130**, 2022.

Table 1: Mean Peak IAA of the CoM and Lower Extremity Joints (mean ± SD) Positive values are flexion and negative are extension.

Muscle Group	CoM Acc (m/s^2)	Ankle Acc (rad/s^2)	Knee Acc (rad/s^2)	Hip Acc (rad/s^2)
Soleus	3.05 ± .45	-823.97 ± 355.53	138.40 ± 60.02	286.97 ± 97.85
Vasti	2.34 ± .27	403.88 ± 123.05	-199.04 ± 86.07	-282.34 ± 133.17
Gastrocnemius	1.52 ± .76	-160.06 ± 161.53	78.25 ± 48.26	93.24 ± 60.05
Gluteus Maximus	0.61 ± .33	362.74 ± 97.77	-135.08 ± 41.45	-519.76 ± 122.34
Hamstrings	-0.51 ± .25	234.42 ± 95.82	-55.59 ± 38.83	-471.25 ± 153.88
Tibialis Anterior	-0.10 ± .13	18.91 ± 43.56	5.35 ± 8.81	5.03 ± 7.62
Adductors	-0.07 ± .04	139.98 ± 101.94	-47.15 ± 30.42	-157.74 ± 111.55

PREDICTING KNEE JOINT LOADING DURING DIFFERENT ACTIVITIES OF DAILY LIVING: A VALIDATION FRAMEWORK BASED ON THE CAMS-KNEE DATASET

Enrico De Pieri[1], Sara Sarabadani[1], Pascal Schütz[2], William R. Taylor[2], Philipp Damm[3], Jörn Seebeck[1] and Marc Bandi[1]

[1] Zimmer Biomet, Winterthur, Switzerland.
[2] Laboratory for Movement Biomechanics, Institute for Biomechanics, ETH Zürich, Switzerland.
[3] Julius Wolff Institute, Charité – Universitätsmedizin Berlin, Germany.
Email: enrico.depieri@zimmerbiomet.com

INTRODUCTION

Musculoskeletal modelling (MSKM) represents a powerful tool to assess internal body loads in a non-invasive manner, yet its use in product design and surgical planning is limited, mostly due to a lack of extensive validation. The CAMS-knee dataset [1], comprising kinematic and kinetic data from 6 subjects with instrumented total knee replacements during different activities of daily living (ADLs), represents the gold standard for MSKM validation. The aim of this study was to compare predicted knee contact forces (KCFs) against *in vivo* measurements across different ADLs, including level and downhill walking, stair descent, squatting, sitting, and rising from a chair.

METHODS

Motion capture data from the CAMS-knee dataset were used as input for an inverse dynamics analysis in the AnyBody Modeling System (AnyBody Technology A/S). The generic TLEM 2.1 lower-limb model [2] was scaled to match each subject's anthropometrics. The knee was modelled as a hinge joint and the muscles as Hill-type actuators. A muscle-volume-weighted 3rd-order polynomial criterion was used to solve the muscle recruitment problem [3]. Muscle contributions to the net joint moments and KCFs were computed to identify muscle-related errors, revealing necessary refinements in muscles' geometry [2]. KCFs were computed in an implant-based reference frame, derived from subject-specific implantation data from radiographic imaging, and normalized to body weight (BW). For each subject, five trials per ADL were analysed. Average root mean square error (RMSE) and coefficient of determination R^2 between predicted and measured KCF magnitudes were computed across trials for each subject and ADL.

RESULTS AND DISCUSSION

The gastrocnemii contributed to a large overprediction of KCFs during the push-off phase of downhill walking and stair descent, when the ankle is dorsiflexed and a large net plantar-flexion moment is required. The introduction of an anatomically realistic wrapping of the Achilles tendon around calcaneus and ankle shifted the plantar-flexing demand from the gastrocnemii to the soleus, reducing the error in the predicted KCFs. Following this refinement, the mean predicted KCF magnitudes showed good qualitative agreement with the measured data across all ADLs (Figure 1), although some variability between subjects persisted (Table 1).

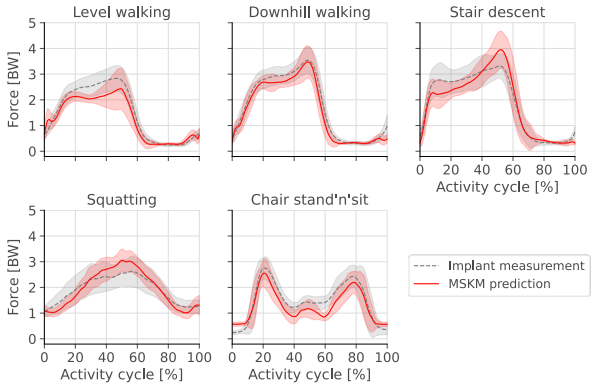

Figure 1 Mean (± SD) predicted (solid red) and measured (dashed grey) KCF magnitude for each ADL across all subjects.

CONCLUSIONS

The current study represents the most extensive MSKM quantitative validation for the prediction of knee loading to date. A strategy to identify errors associated with muscle geometry has been proposed, leading to the refinement of the Achilles tendon wrapping in the TLEM 2.1 model. The analysis of different ADLs enables to test MSK models across larger ranges of joint motion, revealing potential issues which may not be apparent when modelling level walking alone. The established validation framework will serve as a meaningful benchmark for future adaptations and improvements of both generic and personalized models.

REFERENCES

[1] Taylor WR et al. *J Biomech* **65**: 32-39, 2017.
[2] De Pieri E et al. *Plos One* **13(9)**: e0204109, 2018.
[3] Marra MA et al. *J Biomech Eng* **137**: 020904, 2015.

Table 1: Mean RMSE and R^2 between measured and predicted KCF magnitudes for each ADL (min–max range across subjects).

	Level walking	Downhill walking	Stair descent	Squatting	Chair stand and sit
RMSE [BW]	0.46 (0.25 – 0.77)	0.34 (0.19 – 0.42)	0.45 (0.32 – 0.58)	0.40 (0.20 – 0.60)	0.37 (0.20 – 0.56)
R^2	0.91 (0.88 – 0.95)	0.96 (0.93 – 0.98)	0.92 (0.90 – 0.95)	0.85 (0.66 – 0.96)	0.86 (0.75 – 0.96)

EFFECT OF THE LOADING DIRECTION ON THE PREDICTED LOCAL MECHANICAL PROPERTIES OF THE TIBIA IN THE OVARIECTOMISED MOUSE MODEL

Saira Mary Farage-O'Reilly[1,2,3], Vee San Cheong[2,4], Ilaria Bellantuono[1,2,3], Visakan Kadirkamanathan [2,5] and Enrico Dall'Ara[1,2,3]

[1] Department of Oncology and Metabolism, University of Sheffield, Sheffield, UK.
[2] INSIGNEO Institute for *in silico* Medicine, University of Sheffield, Sheffield, UK.
[3] Healthy Lifespan Institute, University of Sheffield, Sheffield, UK.
[4] Future Health Technologies, Singapore-ETH Centre, ETH Zürich, Singapore.
[5] Department of Automatic Controls and Systems Engineering, University of Sheffield, Sheffield, UK.
Email: smfarage-oreilly1@sheffield.ac.uk

INTRODUCTION

Understanding how bone responds to mechanical loading is fundamental for the development of new biomechanical treatments for musculoskeletal diseases [1,2]. Ovariectomy (OVX) is an accepted model for osteoporosis in mice. The *in vivo* tibial loading model is used to investigate the effect of passive mechanical loading on the mouse tibia [1,3]. While a nominal axial load is applied to the tibia through the knee and the ankle joints, the real loading direction in the experimental setup may induce out-of-axis loads on the tibia. These loads may dramatically alter the local strain distributions which affect the bone remodelling [4]. The aim of this study was to evaluate the effect of the loading direction on the predicted local mechanical properties of the tibia in the ovariectomised mouse model.

METHODS

Five female C57BL/6 mice were ovariectomised at week 14 of age. At weeks 18 and 20, the right tibiae were scanned using *in vivo* micro-computed tomography (micro-CT; 10.4µm/voxel). This data was acquired from a previous study [1].

Previously validated micro-CT based finite element models were generated from the segmented images (hexahedral elements; isotropic linear elastic material properties) for the mice at weeks 18 and 20 [5]. Three independent unitary loads cases were applied along the axial, medio-lateral or anterior-posterior direction for each mouse at each timepoint. The principal strains, principal stresses and strain energy density (SED) were recorded at the Gauss points.

A 12N axial load was applied to the finite element models using scaling and the superimposition of the effects to model the typical load applied in the *in vivo* tibial loading model.

The local properties for the different loading directions were calculated as a function of the angle from the inferior-superior axis (θ, 0-30° range, 5° steps), and the angle from the posterior-anterior axis (ϕ, 0°: anterior axis, positive anticlockwise, 0-355° range, 5° steps) (Figure 1).

RESULTS AND DISCUSSION

SED distributions were more sensitive to a change in θ compared to a change in ϕ at both timepoints (Figure 1). More values of lower SED were found for different loading directions at week 20 when compared against week 18, highlighting the importance of considering bone growth in the OVX mouse model. Differences in the variability between week 18 and 20 SED values may be due to the mice responding differently to the OVX.

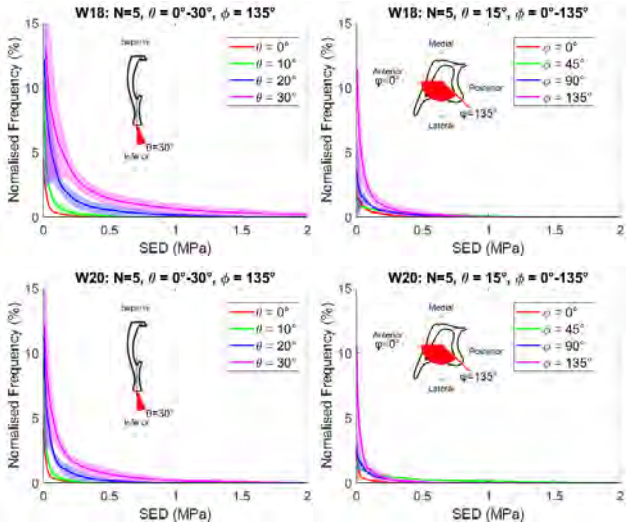

Figure 1 Frequency plots showing the mean and standard deviation for the SED for the group of five mice (N=5) for different loading directions with a 12N axial load, for (left) varying θ and fixed ϕ, (right) varying ϕ and fixed θ, (top) mice at week 18 of age, (bottom) mice at week 20 of age.

CONCLUSIONS

These results suggest that in studies which use the *in vivo* tibial loading model, repositioning of the tibia in the loading device may impact the distribution of local deformation and therefore of bone remodelling [3], and thus should be better controlled during the experiment.

ACKNOWLEDGEMENTS

This work was supported by the EPSRC (grants X/013991-12, EP/K03877X/1 and EP/S032940/1) and the NC3Rs (NC/R001073/1).

REFERENCES

[1] Roberts et al. *Sci Rep* **10(1)**: 8889, 2020.
[2] Sugiyama et al. *Bone* **43(2)**: 238-48, 2008.
[3] Giorgi and Dall'Ara *Med Eng Phys* **62:** 7-16, 2018.
[4] Cheong et al. *Front Bioeng Biotechnol* **9:** 676867, 2021.
[5] Cheong et al. *BMMB* **19(3):** 985-1001, 2020.

AUTOMATED TOOL FOR MUSCULOSKELETAL FINITE ELEMENT MODELING OF KNEE

Amir Esrafilian[1], Shakes Chandra[2], Anthony A. Gatti[3,4], Juha Töyräs[1,2,5], David J. Saxby[6], David G. Lloyd[6], and Rami K. Korhonen[1]

[1]Department of Technical Physics, University of Eastern Finland, Kuopio, Finland.
[2]School of Information Technology and Electrical Engineering, University of Queensland, Brisbane, Australia.
[3]Department of Radiology, Stanford University, Stanford, CA, USA
[4]NeuralSeg Ltd., Hamilton, ON, Canada
[5]Science Service Center, Kuopio University Hospital, Kuopio, Finland.
[6]Griffith Centre of Biomedical and Rehabilitation Engineering (GCORE), Menzies Health Institute Queensland and Advance Design and Prototyping Technologies Institute, Griffith University, Gold Coast, Australia.
Email: amir.esrafilian@uef.fi

INTRODUCTION

Abnormal knee mechanics is thought to be involved in the causal mechanisms that initiate and progress musculoskeletal (MSK) diseases, such as knee osteoarthritis. Multiscale musculoskeletal finite element (MSK-FE) models show promise in estimating personalized knee mechanics involved in these tissue degradation processes. However, creating such personalized models is cumbersome, with no automated methods existing. We developed and tested a fully automated tool to create personalized MSK-FE knee models with bones, cartilage, menisci, and ligaments.

METHODS

A 3D-nnUNet [1] network was trained using a total of 667 labeled knee MRIs [2,3] to auto-segment femoral, tibial, and patellar cartilages as well as bones, menisci, anterior and posterior cruciate ligaments, and patellar and quadriceps tendons (0.98≥DICE similarity coefficient≥0.82). A personalized MSK model was generated using auto-segmented geometries (Figure 1) and consisted of 12 degrees-of-freedom knee with elastic foundation tibiofemoral and patellofemoral contacts, and ligaments represented as non-linear springs [4]. Last, a modified hexahedral meshing algorithm [5] was used to create and then assemble personalized knee cartilage and menisci meshes. Depth-dependent fibril-reinforced material models with swelling were automatically assigned to cartilages and menisci [6]. Tool robustness (i.e., segmentation, models' assembly, and meshing) was investigated by creating 2,650 left and right knee MSK-FE models from datasets different than the training set. Using subject-specific motion data and MRIs, here we present one gait trial modeled using 1) the automated tool, 2) manual segmentation and meshing, assumed the gold standard, and 3) a previously developed atlas-based method [7].

RESULTS AND DISCUSSION

Creating one MSK-FE model from raw MRI took <6 minutes (single core, <4 GB VRAM). For tibial cartilage's maximum tensile stress during a gait cycle, root-mean-square-error between the manual and automated methods was 1.9 MPa, better than the 4.3 MPa between the manual and atlas-based methods.

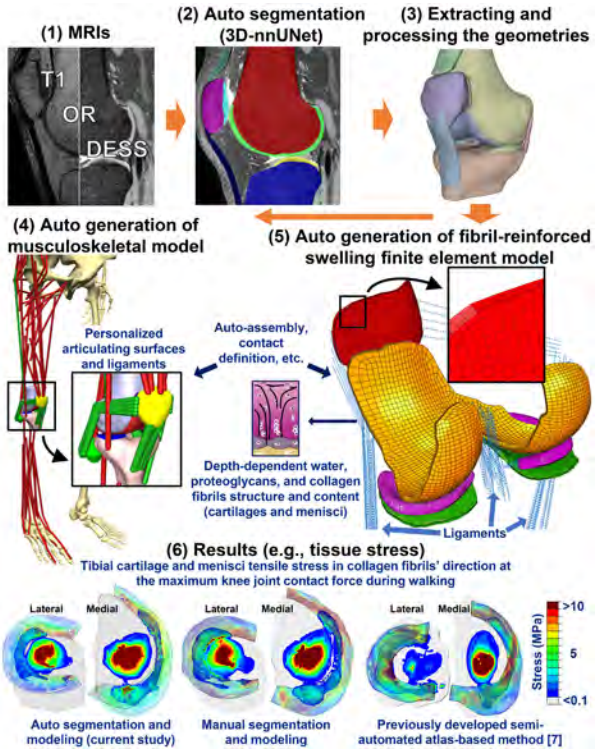

Figure 1. Illustration of the pipeline, created models, and results.

CONCLUSIONS

We presented a fully automated and robust tool for MSK-FE modeling of the knee. The tool provided more accurate modeling compared to the previous atlas-based method and was fast enough to enable the investigation of knee tissue mechanics in large cohorts and different functional activities.

ACKNOWLEDGEMENTS

Australian NHMRC Ideas Grant (APP2001734) and Saastamoinen Foundation.

REFERENCES

[1] Isensee F et al., *Nature Methods* **18**:203, 2021.
[2] Seim H et al., *Proc. MICCAI*: 215, 2010.
[3] Desai A et al., *arXiv*:2203.06823, 2022.
[4] Lenhart R et al., *Ann of Bio Eng* **43**:2675, 2015.
[5] Rodriguez B et al., *Comp Meth Biom* **20**:1543, 2017.
[6] Wilson W. et al., *J Biomech* **38**:1195,2005.
[7] Esrafilian A et al., *IEEE TBME* **69**:2860, 2022.

A CNN-based Approach to Classification of Parkinson's Disease Patients with and without Freezing of Gait during 360° Turning Task

Hwayoung Park[1], Changhong Youm[1,2*], Sang-Myung Cheon[3], Bohyun Kim[1,2], Hyejin Choi[1,2], Juseon Hwang[1,2], Minsoo Kim[1], and Young Jin Jeong[4]

[1]Biomechanics laboratory, Dong-A University / Busan, Republic of Korea

[2]Department of Health Sciences, Graduate School, Dong-A University / Busan, Republic of Korea

[3]Department of Neurology, School of Medicine, Dong-A University / Busan, Republic of Korea

[4]Department of Nuclear Medicine, Dong-A University Hospital / Busan, Republic of Korea

[*]Corresponding author email: chyoum@dau.ac.kr

INTRODUCTION

Parkinson's disease (PD) is one of the neurodegenerative diseases, and the cause is still unclear, so it is difficult to diagnose early, subjective diagnosis of severity according to degeneration of motor symptoms and disease progression, and objective and quantitative indicators for disease progression evaluation are insufficient. A classification modeling approach using visual images (Convolutional Neural Network, CNN algorithm) converted from time-series gait data will improve the accuracy of disease severity discrimination according to identifying more symptom-affected body segments in PD patients.

METHODS

The subjects of this study were each 30 PD patients with and without freezing of gait (freezers and non-freezers) and 30 healthy control group (controls) of the same age. PD patients performed the 360° turning tasks in the direction of the more affected side at the preferred speed in an off state of medication. Position and acceleration data of 40 body segments marker trajectories, including the center of mass, were used to analyze the time-series data of the turning phase. These position and acceleration time-series data were converted into new imaging and trained with a CNN algorithm technique (Figure 1). The performance of the three-group classification model was evaluated using accuracy.

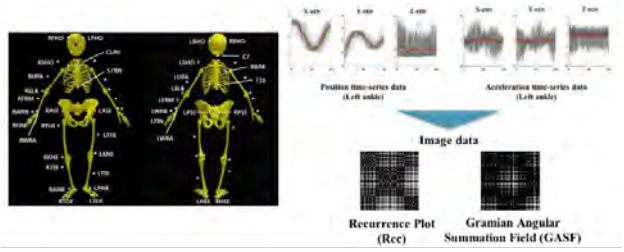

Figure 1 An example shows images converted from time-series data of position and acceleration using the body segments during 360° turning tasks.

RESULTS AND DISCUSSION

As a result, the body segments with the highest performance in classifying freezers, non-freezers, and controls were the left elbow at 61%, right tibia at 60%, and right ankle at 60% in the image-based position time-series data when using the Recurrence Plot (Rec) algorithm, and were the left upper arm at 60% and left knee at 60% when using the Gramian Angular Summation Field (GASF) algorithm. In addition, the left toe at 62% and right toe at 58% were found in the image-based acceleration time-series data when using the Rec algorithm. These results showed that freezers observed uncoordinated gait patterns between the left elbow and knee with more affected body segments and asymmetric steps to complete turning compared to non-freezers and controls [1]. Therefore, freezers may experience difficulty performing automatized movements without attention during turning [2].

CONCLUSIONS

The time-series gait pattern was confirmed using the whole body segments during 360° turning tasks on the affected side at the preferred speed in freezers and non-freezers. In addition, the CNN technique based on time-series gait data imaging may improve the availability as an objective indicator of disease severity in a clinical environment through early diagnosis of motor symptoms such as freezing of gait in PD patients.

ACKNOWLEDGEMENTS

This work was supported by the National Research Foundation of Korea(NRF) grant funded by the Korea government(MSIT) (No. 2022R1A2C100933711).
This research was supported by Basic Science Research Program through the National Research Foundation of Korea(NRF) funded by the Ministry of Education(No. 2022R1A6A3A0108756411).

REFERENCES

[1] Horak et al. *Mov. Disord.* **28**(11), 1544-1551, 2013.

[2] Holtzer et al. *J. Gerontol.* **69**(11), 1375-1388, 2014.

ROTARY SPINAL DYNAMICS IN GAIT – REFERENCE DATA AND FUNCTIONAL DESCRIPTIONS BASED ON SURFACE TOPOGRAPHY

Ulrich Betz [1], Janine Huthwelker [1], Jürgen Konradi [1], Claudia Wolf [1], Ruben Westphal [2], Irene Schmidtmann [2], Patric Schubert [3], Philipp Drees [4]
[1] Institute of Physical Therapy, Prevention and Rehabilitation, University Medical Center of the Johannes Gutenberg University (UMC) Mainz, Germany.
[2] Institute of Medical Biostatistics, Epidemiology and Informatics, UMC Mainz, Germany
[3] Institute of Complex Health Sciences, Hochschule Fresenius, University of Applied Sciences, Idstein, Germany
[4] Department of Orthopedics and Trauma Surgery, UMC Mainz, Germany
Email: ulrich.betz@unimedizin-mainz.de

INTRODUCTION

Back pain can lead to pathological movement patterns of the spine and vice versa. Therefore, motion analysis is a central component of prevention, diagnosis and therapy, which is, due to a lack of technical alternative, mainly based upon visual observations.
In the current functional model at initial contact the equilateral side of the pelvis is assumed to be maximally forward rotated while the shoulder girdle demonstrates a counter rotation. These opposing movements continue throughout the spine, resulting in a contrary rotation of the upper and the lower spine. T7 is considered to be a point of intersection that mediates between the different directions of movement resulting in no or at least reduced rotary motion. Due to technical progress today Surface Topography (ST) enables non-invasive gait analyses of the vertebral bodies (VB) from C7-L4 and the pelvis. In order to obtain so far lacking ST reference data for a standardized gait cycle (SGC) and to verify the functional model, we have carried out the present study.

METHODS

Three gait cycles of 201 healthy, pain free participants aged 18-70 years (mean 41.3; SD 13.4) have been examined. While walking on a treadmill at 5 km/h, participants were recorded using the DIERS Formetric III 4D. For each of 60 frames per second the rotational position of C7-L4 and the pelvis was calculated resulting in a continuous course of the individual VB and pelvis movement. A treadmill-integrated foot pressure measuring plate allowed for detections of the gait cycles. Using an interpolating spline function the observations were transformed into a SGC, in which the movements are related to 0-100% of SGC, starting with initial contact right foot.

RESULTS AND DISCUSSION

The mean curves of right- and leftside rotation of all investigated VB and the pelvis within the SGC are presented in the Figure. Instead of the expected symmetry, the oscillation is mainly slightly shifted to rightside rotation (negative values), as it is known from standing posture [1]. The averaged maximum of pelvic rotation to the left is 3.3° at 4% SGC and 1.8° at 55% SGC to the right. The amplitudes of rotary motion for pelvis and lumbar spine (LS) are almost identical, but reached their respective maximum shifted in relation to time. The thoracic spine (TS), however, demonstrated different amplitudes of rotary motion (T12-T8 ascending, T7-C7 descending), but all segments reached their maximum values almost contemporaneously. T7 revealed the largest averaged amplitude of rotary motion to the left 6.7° at 48% SGC and T8 to the right 8.2° at 98% SGC. We found large inter-individual differences in the movement in particular of pelvis and LS. There, the individual rotation maxima are time-spread over almost half SGC. This makes it difficult to interpret measurement data related to a pathology in question.

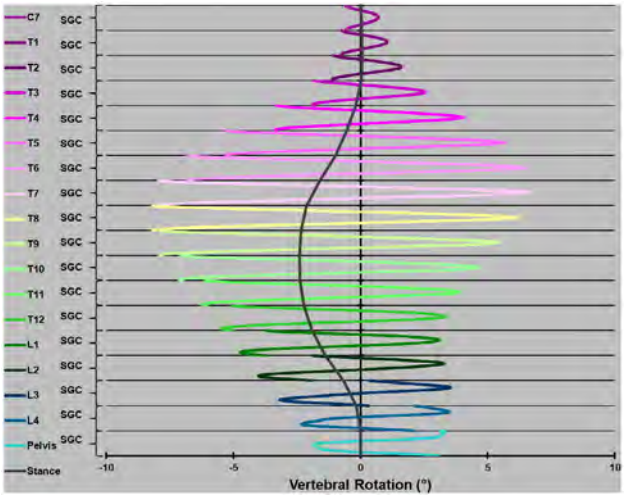

Figure: Mean rotation curves within a single SGC, displayed top down [1]. The beginning of the respective curve at the top indicates the position of VB/pelvis at the beginning of the SGC. A negative value means processus spinous to the left = rotation to the right, a positive value means rotation to the left.

CONCLUSIONS

Pelvis and LS as well as TS acted as a functional unit and demonstrated diametrically opposed, highly individual rotary movement patterns that are co-shaped by the standing posture. The results challenge the current functional model of spinal dynamics in gait.

REFERENCES

[1] Huthwelker J et al. *Hum Mov Sci* **88**: 103054, 2023

GAIT AND DYNAMIC POSTURAL STABILITY DURING OBSTACLE CROSSING IN THE INDIVIDUALS WITH EARLY-STAGE PARKINSON'S DISEASE

Nok-Yeung Law*, Jing Xian Li
School of Human Kinetics, University of Ottawa / Ottawa, Canada.
*Correspondence email: nlaw098@uottawa.ca

INTRODUCTION

Obstacle crossing is a challenge task for people with Parkinson's disease (PD) due to a higher propensity for falls. [1-2] Changes in gait and postural stability affect their ability to perform this task safely. [3-4] Limited understanding to dynamic postural stability exists in this population and findings from past studies were of PD participants with big variations in the condition's severity (mild-to-moderate to severe) and small sample size. This study aimed to examine the gait and dynamic postural stability during obstacle crossing in individuals with early-stage PD and compared with that in older healthy adults (HOA). It was hypothesized that the PD and HOA groups will show significant differences in gait speed, crossing length, pre- and post-horizontal distance, toe, and heel clearance distance; center of mass (COM) displacement and velocity, and COM-center of pressure (COP) separation distance; and maximum joint angles and range of motion of the hip, knee, and ankle. Moreover, single-leg stance (SLS) and timed up and go (TUG) test scores would be significantly different.

METHODS

Sixteen individuals diagnosed with idiopathic PD (7 F, 72 ± 7 years, 70 ± 17 kg, 171 ± 11 cm, UPDRS III 21 ± 9, H&Y 1 to 2), and sixteen age- and sex-matched HOA participated. The study was approved by the university's research ethics review board. Data was collected at the Human Movement Biomechanics Laboratory. The participants had no neuromuscular injuries in the last two years and able to stand and walk unassisted; written consent was obtained prior to participation. They were screened over the telephone. Their general cognitive function was assessed using the Montreal Cognitive Assessment (MoCA). The PD participants were tested in the ON-medication state, within 1 to 2.5 hours after their last medication dose.

Three-dimensional motion of obstacle crossing in the participants was captured using a ten-camera VICON system at 200 Hz. Ground reaction forces were recorded using four force plates at 2000 Hz embedded in the middle of the walkway. Thirty-nine reflective markers were attached to the skin or over the participants' clothing following the Plug-in-Gait marker set, as modified from the Helen Hayes marker set. The participants were asked to cross a 20-cm high obstacle that was setup in the middle of an 8-meter walkway at their self-selected comfortable pace. They were allowed to cross the obstacle with their self-select limb as the leading limb and with their comfortable shoes. Five successful trials of obstacle crossing were collected. SLS were collected three times with eyes open and three times with eyes closed; the best time of each condition was reported. A coin toss determined the order of the stance leg to use. TUG was recorded with a stopwatch over a 3-meter distance.

Differences in demographic variables between the two groups were tested using chi-square and independent-sample *t* tests depending on the variable's type after testing for normal distribution. Independent-sample *t* tests were used to examine any difference in the measures between the two groups. A *p*-value of ≤ 0.05 was considered significant. All statistical operations were performed using SPSS software v.20.

RESULTS AND DISCUSSION

The demographic characteristics of the PD and HOA groups were comparable. All participants completed the obstacle crossing trials successfully. The PD group had a shorter SLS time than the HOA group with eyes open (57.4 ± 41.7 s vs. 23.6 ± 20.9 s, $p = .009$) and eyes closed (11.3 ± 8.8 s vs. 3.9 ± 2.5 s, $p = .004$). TUG time was similar between the PD and HOA groups (12.7 ± 3.2 s vs. 11.4 ± 2.0 s, $p = .189$).

No significant difference in gait variables was found between the two groups, toe and heel clearance distance, and pre- and post-horizontal distance of the leading foot and trailing foot. The PD group crossed the obstacle with a slower gait speed and crossing speed, and slightly smaller crossing stride length of the leading foot compared to HOA group (1.35 ± 0.26 vs. 1.41 ± 0.17 cm). The PD group showed a smaller anterior-posterior COM displacement (35 ± 11 vs. 36 ± 8.6 cm) but a bigger medial-lateral COM displacement (9.5 ± 4.0 vs. 8.7 ± 3.9 cm) compared to the HOA group.

CONCLUSIONS

This study showed that individuals with early-stage PD crossed slowly with increased medial-lateral sway, indicating changed dynamic stability. The findings suggest that individuals in the early-stage PD can cross the 20-cm high obstacle but with altered gait and posture.

ACKNOWLEDGEMENTS

The researchers would like to thank the participants and *Parkinson's Canada* for their support of this study.

REFERENCES

[1] Paul S et al. *Neurorehabil* **28**: 282-290, 2014.
[2] Pelicioni P et al. *Int J Environ* **16**, 2019.
[3] Alcock L et al. *Gait Posture* **61**: 368-374, 2018.
[4] Liu Y et al. *J Med Biol Eng* **38**: 534-543, 2018.

Gait strategies identified by machine learning in older adults after spinal fixation

Naoto Mano[1], Kimihiko Mori[2], Ushikubo Tomohiro[3],
Takayuki konishi[1], Shun Ito[1], Jin Kuramoto[1] and Kimitaka Hase[4]
[1] Department of Physical Medicine and Rehabilitation, Kansai Medical University Hospital, Hirakata, Japan.
[2] Department of Physical Therapy, Faculty of Rehabilitation, Kansai Medical University, Hirakata, Japan.
[3] Department of AI Research and Development, Anima Corporation, Chofu, Japan.
[4] Department of Physical Medicine and Rehabilitation, Kansai Medical University, Hirakata, Japan.
Email: naotoman830@icloud.com

INTRODUCTION

Dynamic control of the center of mass (COM) and the center of pressure (COP) is crucial for gait performance. The COM in older adults with spinal deformity often shifts anteriorly during gait due to trunk flexion, which likely helps maintain velocity by expanding the anteroposterior COM-COP distance in the terminal stance. However, the trunk cannot flex during gait after spinal fixation. Thus, postoperative rehabilitation is needed to expand the COM–COP distance without trunk flexion. Machine learning can extract the essential characteristics of the gait strategy and may help suggest novel and optimal gait training for each cluster. We aimed to use machine learning to reveal the relationship between COM–COP distance and walking speed, and the gait characteristics related to COM–COP distance.

METHODS

One-hundred-and-five patients (mean age: 73.6 years) with spinal fixation from thoracic vertebrae to pelvis underwent three-dimensional gait analysis at 6 months postoperatively. First, Pearson's correlation coefficient between the COM–COP distance in the terminal stance and walking speed was calculated. Second, machine learning was applied. The gait characteristics related to the COM–COP distance were extracted by Mahalanobis distance [1] and Markov chain Monte Carlo sampling [2] of 116 gait parameters and were used to categorize gait patterns by hierarchical clustering. The feature extractions were repeated in each cluster. Path analysis was used to investigate whether the extracted gait characteristics affected the COM–COP distance and walking speed. All analyses were conducted by Python (3.8.1). The significance level was set at 0.05.

RESULTS AND DISCUSSION

The maximum COM–COP distance in the terminal stance was significantly correlated with walking speed (Figure 1). Gait patterns were categorized into Clusters A, B, and C in order of increasing COM–COP distance. Path analysis showed that knee extension moment in Cluster A, hip flexion angle in Cluster B, and minimum ankle power and hip flexion moment in Cluster C were significantly associated with the COM–COP distance (Table 1). Cluster C comprised the oldest, slowest walking patients with the most trunk flexion.

Our results suggest that the ability to carry the COM more anteriorly by knee extension moment in Cluster A and by larger hip flexion in Cluster B, and to place the COP more posteriorly by eccentric hip and ankle movement in Cluster C play a crucial role in walking.

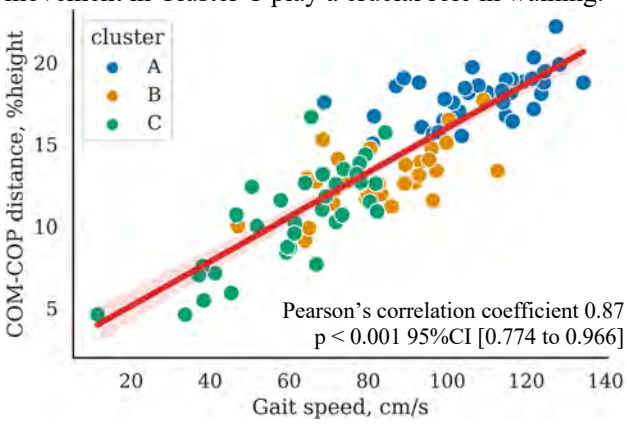

Figure 1: COM–COP distance and gait speed in each cluster.

CONCLUSIONS

More dynamic control of the COM and COP is likely required to improve gait speed in older adults after spinal fixation. Individuals with a small COM–COP distance can walk faster by moving the COP more posteriorly as a first step, then by preparing to move the COM more anteriorly by larger hip flexion, and finally by knee extension moments. The clinical application of machine learning may help offer optimal gait training for each cluster.

REFERENCES

[1] Ramakrishnan T et al. *Front Neurorobot* **12**:2,2018.
[2] Andrieu C et al. *Machine Learning* **50**:5-43, 2003.

Table 1: Relationship between the gait characteristics selected by machine learning and the COM–COP distance in each cluster.

Cluster	Independent Variables	β	p-Value	95%CI
A	Maximum knee extension moment	0.535	<0.001	0.250 to 0.821
B	Hip flexion angle at initial contact	0.583	<0.001	0.274 to 0.891
C	Minimum hip flexion moment	-0.547	<0.001	-0.809 to -0.285
C	Minimum ankle sagittal power	-0.333	0.014	-0.594 to -0.071

ARE ADAPTATIONS IN FALL PREDICTORS FOLLOWING A 12-WEEK MIXED POWER TRAINING RELATED TO GAIT PARAMETERS IN COMMUNITY-DWELLING OLDER MEN?

Aubertin-Leheudre Mylène[1,2], Richard Emma[2,3], Pion Charlotte[2,4], Hammad Rami[2,4], Gaudreau Pierrette[5], Morais José A[6], Bélanger Marc[1] & Gouelle Arnaud[3].

[1] Département de sciences de l'activité physique, Université du Québec à Montréal, Montréal (QC; Canada);
[2] Centre de recherche de l'institut universitaire de gériatrie de Montréal, Montréal (QC; Canada);
[3] UFR STAPS, Université de Reims Champagne Ardenne, Reims, France
[4] Département de biologie, Université du Québec à Montréal, Montréal, Canada.
[5] Département de médecine et CRCHUM, Université de Montréal, Canada.
[6] McGill University, Division of Geriatric Medicine, Montreal, Canada.
Email: aubertin-leheudre.mylene@uqam.ca

INTRODUCTION

During ageing, falls and mobility disorders are one of the main factors leading to loss of autonomy. Clinical functional assessments, such as the 3-m Timed Up and GO (TUG), are usually considered as fall predictors. On the other hand, gait impairment has been shown also to be an important fall predictor in older adults (OA). Among various factors, the loss of strength and muscle quality represent major independent variables which contribute to decrease gait performance, as it may underlie the motor control and balance impairments that lead to falls and adverse outcomes [1-3]. Improving muscle-related predictors of gait and functional performance [i.e. lean and fat masses, muscle strength (MS), quality (MQ) and power (MP)] seems to be a very important strategy to preserve the quality of life of OA. Exercise, especially power training (PT), is considered one of the best intervention to improve fall predictors such as gait parameters, kinematic measures of mobility or muscle function (MP, MS, MQ) [4-5]. Therefore, we aimed to assess whether improvement in muscle function after 12 weeks of mixed PT (MPT) would have an impact on both functional fall predictors and gait fall predictors in healthy older men.

METHODS

Participants: Twenty-one older (age:67±6years; BMI:25±3 kg/m^2; walking speed:1.45±0.23m/s) inactive community-dwelling men were recruited to participate in a 12-week MPT. *Intervention:* 12-week MPT (3sessions/wk.) Each session (1h) included 4 resistance (tempo: 1-0-2-0; 80% 1RM; set 8 to 12 repetitions) and 6 functional exercises. *Measures:* Spatio-temporal gait parameters (speed, stride length and width, stride rate, gait phases duration , GVI, walk ratio) were measured during a 6-min walk test using a Zeno® mat [6]. Fat-free mass (FFM; DXA©), muscle function [absolute and relative MS & MQ, estimated MP (Takaï [7])] and functional capacity [4-m walking speed, 3-m TUG, unipodal balance and stair test)] were also assessed. All measures were performed pre- and post-intervention. *Groups:* Participants were divided into 2 groups for selected fall/mobility predictors as responders (delta change Δ%>10%) *vs.* non-responders (Δ%<10%) Predictor parameters (TUG, MS, MQ & MP) were selected if: 1) correlated significantly with the gait parameters at baseline and; 2) changed significantly after the MPT intervention.

RESULTS AND DISCUSSION

Following the intervention, total FFM, MS (absolute and relative), MQ and MP (absolute and relative) increased ($p<0.05$). For functional parameters, only the stair test ($p=0.019$) and the 3-m TUG ($p=0.001$) improved. Finally, stride length, cadence, speed, duration of support and walk ratio changed significantly. First, there was no difference in Δ% gait parameters between TUG responders and non-responders. Regarding relative MS or MQ, a difference between responders & non-responders was observed for speed and stride length. Furthermore, when divided into absolute MP responders, only the walk ratio Δ% differed between the 2 groups. Finally, a difference was observed for single and double support duration between relative MS responders vs. non-responders.

CONCLUSIONS

A 12-week MPT improves muscle function as well as functional status and gait parameters. However, the adaptation of gait parameters appears unrelated to clinical improvement of fall/mobility predictors in healthy community-dwelling OA. Therefore, further studies investigating the effect of age or functional status are needed to better understand the interplay between muscle function and gait parameters.

ACKNOWLEDGEMENTS

MAL (salary award) and CP (scholarship award) are supported by the FRQS. This study is supported by 2 grants led by MAL from RQRV-FRQS & UQAM.

REFERENCES

[1] Martinikorena I et al. *JAMDA*, 17(11), 2016.
[2] Barbat-Artigas S et al. *JAMDA*, 14(11), 2013.
[3] Barbat-Artigas S et al. *JAMDA*, 17(11), 2016.
[4] de Vos NJ et al. *J Gerontol*, 60(5), 2005.
[5] Radaelli R et al. *Sports Med*, 2022.
[6] Balasubramanian et al. *Gait & Posture*, 41(4), 2015.
[7] Takai Y et al. *J Physiol Anthropol*, 28(3), 200

GAIT PROPULSION IN PATIENTS WITH UNILATERAL CEREBRAL PALSY WHEN WALKING WITH AND WITHOUT AN ANKLE FOOT ORTHOSIS

Jacqueline Romkes, Katrin Bracht-Schweizer, Elke Viehweger, and Morgan Sangeux
Neuro-Orthopaedic department, University of Basel Children's Hospital, Basel, Switzerland
Email: j.romkes@unibas.ch

INTRODUCTION

Gait propulsive force can be defined as the anterior component of the ground reaction force (aGRF) during gait. The ankle plantarflexion moment and the angle of the trailing limb (TLA) with the vertical during push-off are major contributors to increase the propulsive force generation [1]. Patients with unilateral cerebral palsy (uniCP) have an affected and non-affected body side. Therefore, a lower contribution of the affected side to propulsion can be expected, similar to post-stroke patients. One marked gait deviation in uniCP is an equinus gait pattern. An ankle foot orthosis (AFO) for the affected leg can improve the plantarflexed foot position during the swing phase of gait and improve the stability in stance (figure 1). Since little is known on gait propulsion in uniCP, the purpose of this study was to 1) explore the affected side's contribution to propulsion during gait in uniCP, and 2) explore the influence of walking with an AFO and footwear on the gait propulsive force generation.

Figure 1: Typical study patient with an AFO.

METHODS

Gait kinematics and GRFs of 83 uniCP patients (mean age: 11, range 5-47 years) walking barefoot and with an AFO and footwear at self-selected speed were investigated retrospectively. Propulsive impulse was defined as the integral of the aGRF over time during the stance phase of gait, normalised for the individual's body weight (BW) [2]. The contribution of the affected leg to propulsion, is the ratio between the affected side and the sum of both sides' propulsive impulse. Peak propulsive force, TLA (peak angle between vertical and vector from hip to ankle joint centre), peak plantarflexion moment, peak generating ankle power, step length, and walking speed were also calculated (MATLAB software, Mathworks Inc, Natrick (MA), USA). The Wilcoxon Signed Rank Test (α=0.05) and the effect size were used for statistical comparisons.

RESULTS AND DISCUSSION

Table 1 shows the results for the parameters of interest. When wearing an AFO and footwear compared to barefoot gait, the affected leg contributed less to gait propulsion than the non-affected leg. Therefore, gait became less symmetrical for the outcome measures in this study. Peak propulsive force, peak plantarflexion moment and peak generating ankle power during push-off were significantly lower for the affected compared to the non-affected leg. However, propulsive impulse of the two sides combined increased when an AFO was worn on the affected side.

CONCLUSIONS

This study focussed on gait propulsion and the influence of an AFO in patients with uniCP. On average, the contribution to propulsion of the affected leg decreased when walking with an AFO compared to barefoot walking. In addition, ankle power generation decreased and therefore did not modulate peak propulsive force. However, the TLA and plantarflexion moment were positively influenced when walking with an AFO leading to a higher walking speed and bilateral increased propulsive impulse.

REFERENCES

[1] Hsiao et al. *J Neuroeng Rehabilitation* 12:40, 2015.
[2] Deffeyes, Peters. *Gait Posture* 88:258-63, 2021.

Table 1: Parameter values and statistics (Wilcoxon Signed Rank Test (α=0.05), effect size: 0.3<r<0.5 (moderate), r>0.5 (large))

	values (median (interquartile range (Q3-Q1))				statistics (p-value / r-value for effect size (Z/sqrt(N))			
	barefoot		AFO and footwear		aff vs. non-aff		barefoot vs. AFO and footwear	
	aff	non-aff	aff	non-aff	barefoot	AFO	aff	non-aff
propulsion contribution (ratio)	0.496 (0.104)	0.504 (0.104)	0.474 (0.084)	0.526 (0.084)	0.124 / 0.169	**0.003 / 0.329**	0.3883 / 0.095	0.3883 / 0.095
propulsive impulse (%BW s)	2.82 (1.00)	2.99 (1.04)	3.09 (0.98)	3.35 (0.82)	0.140 / 0.162	**0.002 / 0.332**	**<0.001 / 0.387**	**<0.001 / 0.477**
peak propulsive force (%BW)	17.37 (6.78)	22.26 (6.84)	16.91 (5.63)	22.20 (8.58)	**<0.001 / 0.678**	**<0.001 / 0.715**	0.280 / 0.119	0.696 / 0.043
peak trailing limb angle (°)	31.3 (5.5)	29.9 (4.1)	33.2 (4.8)	31.1 (4.6)	**0.009 / 0.287**	**<0.001 / 0.433**	**<0.001 / 0.551**	**<0.001 / 0.567**
peak plantarflexion moment (Nm/kg)	1.05 (0.32)	1.26 (0.35)	1.09 (0.31)	1.39 (0.32)	**<0.001 / 0.689**	**<0.001 / 0.710**	**<0.001 / 0.394**	**0.001 / 0.354**
peak generating ankle power (W/kg)	2.05 (1.05)	3.99 (1.72)	1.34 (0.84)	3.07 (1.43)	**<0.001 / 0.761**	**<0.001 / 0.786**	**<0.001 / 0.683**	**<0.001 / 0.601**
step length (non-dimensional)	0.73 (0.11)	0.77 (0.13)	0.85 (0.12)	0.85 (0.16)	**0.006 / 0.300**	0.747 / 0.035	**<0.001 / 0.821**	**<0.001 / 0.749**
walking speed (non-dimensional)	0.41 (0.08)		0.44 (0.08)		NA	NA	**<0.001 / 0.591**	

Virtual Reality Skateboard Balance Training for Improving Balance Stability in the Elderly

Yi-Ching Tsai[1], Phunsuk Kantha[1], Dar-Ming Lai[2] and Wei-Li Hsu[1,3]

[1] School and Graduate Institute of Physical Therapy, National Taiwan University, Taipei, Taiwan.
[2] Division of Neurosurgery, Department of Surgery, National Taiwan University Hospital, Taipei, Taiwan.
[3] Physical Therapy Center, National Taiwan University Hospital, Taipei, Taiwan.
Email: wlhsu@ntu.edu.tw

INTRODUCTION

Postural balance is essential for daily activities. As aging leads to a decline in the ability to maintain upright stability, retraining postural balance is crucial for the elderly. Virtual reality (VR) training has been extensively used for specific clinical training [1]. To provide a realistic training environment, we designed an innovative virtual reality-based skateboard training system for balance training purposes. The aim of this study was to investigate the effects of this novel training system by comparing the kinematic and kinetic changes between pre- and post-training in the healthy elderly.

METHODS

A total of 19 healthy elderly (age: 62.21±7.23 years old) and 19 young participants (age: 27.21±2.90 years old) were recruited in this study. All participants completed two functional performance assessments: the Timed Up and Go test (TUG) and the Five Times Sit-to-Stand test (5STS). Moreover, participant also completed the single-leg-stance test. Elderly received 6 weeks of virtual reality skateboarding balance training (Figure 1), twice a week. This training system was integrated with the virtual reality environment and split-belt treadmill. The 3D motion-capture system (Vicon ver. 2.5, Oxford Metrics Ltd., OX, UK) and the force platform (AMTI OR6, Advanced Medical Technology Inc., MA, USA) were synchronized to collect the kinematics and kinetic data, respectively.

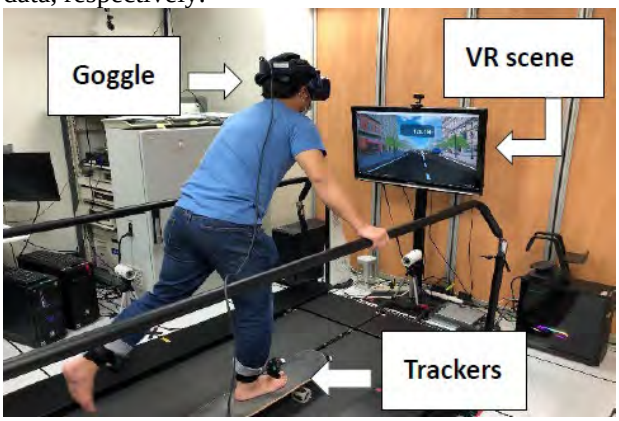

Figure 1 The VR skateboarding balance training system.

All statistical analyses were conducted using SPSS 18.0 software (SPSS, Inc., USA), with the α level of 0.05. The nonparametric Mann-Whitney U test and Wilcoxon signed-rank test were used to compare differences between groups (i.e., elderly and young) and within group (i.e., pre- and post-training), respectively.

RESULTS AND DISCUSSION

For differences between groups, the elderly had significantly decrease in scores on both 5STS and TUG tests, while showing significantly larger values of center of mass (COM) and center of pressure (COP) than young adults ($p < 0.05$). This suggests that decreased extremity power, high risk of fall, and postural instability should be of concern in the elderly population. After the training sessions, there was a significant improvement in functional performance and postural balance within the elderly group (Table 1). The elderly group had an improvement in the TUG test. Furthermore, the COM excursion in the anteroposterior direction and the COP mean distance in the elderly during the single-leg-stance test significantly decreased after training.

Table 1: Comparison of independent variables between pre- and post-training differences in the elderly group.

Independent variables	Pre-training	Post-training	*p*-value
Assessments			
TUG (sec)	9.14 ± 1.47	8.29 ± 1.13	**0.035***
5STS (sec)	7.74 ± 1.79	7.25 ± 1.72	0.446
Center of Mass			
Total excursion (cm)	25.75±27.78	19.76±9.21	0.099
AP excursion (cm)	18.92±5.95	17.61±4.89	**0.016***
ML excursion (cm)	27.83±31.13	21.88±11.47	0.136
Center of Pressure			
Mean distance (cm)	0.56±0.13	0.53±0.14	**0.040***
AP distance (cm)	0.59±0.15	0.59±0.16	0.421
ML distance (cm)	0.56±0.16	0.53±0.15	0.277

AP / ML, in the anteroposterior / mediolateral direction; *, $p < 0.05$.

CONCLUSIONS

This study confirmed the positive effectiveness of this virtual reality exergame on upright postural stability in the elderly population, and could reduce the risk of falls. For the implication in rehabilitation, this virtual reality might be a useful intervention in promoting the postural balance of various elderly with balance impairment.

ACKNOWLEDGEMENTS

This work was supported by the National Health Research Institutes (NHRI-EX112-11019EI) and National Science and Technology Council (MOST111-2223-E-002-004-MY3) awarded to Dr. Wei-Li Hsu.

REFERENCES

[1] Kantha P et al. *Frontn Bioeng Biotechnol* 11: 1136368, 2023.

EMG NORMALIZATION APPROACHES SHOW DIFFERING RESULTS IN OLDER ADULTS DURING A STEPPING TASK

Marcel B. Lanza*, Nathan Frakes, Vicki L. Gray
Department of Physical Therapy and Rehabilitation, School of Medicine, University of Maryland, Baltimore, United States. *mlanza@som.umaryland.edu

INTRODUCTION

To avoid a fall, taking a rapid step is a common strategy among older adults. In this sense, rapid activation of the muscles (e.g., rate of activation, RoA) appears to be important for stepping tasks, and surface electromyography (EMG) have been recorded during stepping tasks[1]. EMG normalization is often required during stepping tasks and allows researchers to compare EMG amplitude between different days and/or individuals[2] Yet, there is no consensus about how to normalize EMG amplitude during a voluntary stepping task. The previous research showed that EMG amplitude normalized by different EMG parameters present different values during a knee extension exercise[3]. Since researchers constantly put information from different studies together, understanding the impact of using different EMG parameters allows to decide which parameter should be used for EMG normnalization. Thus, the aim of the present study is to investigate the impact of using different EMG parameters as a reference to normalize the EMG amplitude of the gluteus medius muscle across different trials of a voluntary stepping task and its reliability.

METHODS

Fifteen health older adults (5 males / 10 females; age= 68.7 ± 3.6 years; height= 1.67 ± 0.1 m; mass= 81.8 ± 12.02 kg; BMI= 29.3 ± 4.87) were volunteers in this study. Ten voluntary choice reaction step test (CRST) were performed by standing on two adjacent force platforms. Surface EMG electrodes were placed on the gluteus medius (GM) accordingly to SENIAM guidelines. EMG signals were recorded at a frequency of 1500 Hz and filtered (4th-order Butterworth band-pass filter of 20–500 Hz) before calculating the EMG amplitude as the root mean square (RMS). The RoA was calculated from EMG onset to EMG peak for each CRST trial. Three EMG parameters were used as a reference for EMG normalization: 1) EMG peak during step ($EMG_{TrialMax}$); 2) EMG mean measured during the step ($EMG_{TrialMean}$), and 3) EMG measured at baseline ($EMG_{Baseline}$).

The statistical analysis was performed for the stance leg and stepping leg during the CRST. A repeated-measures one-way ANOVA test was performed followed by a Bonferroni post hoc test when necessary, and intraclass correlation coefficient for inter-trial reliability.

RESULTS AND DISCUSSION

When the right or left side is acting as stance leg or stepping leg, there was a difference in normalized EMG ($P< 0.0001$) with RoA normalized by $EMG_{Baseline}$ showing higher values than the others, and RoA normalized by $EMG_{TrialMean}$ showing higher values than $EMG_{TrialMax}$. Reliability was excellent with all ICC values above 0.839.

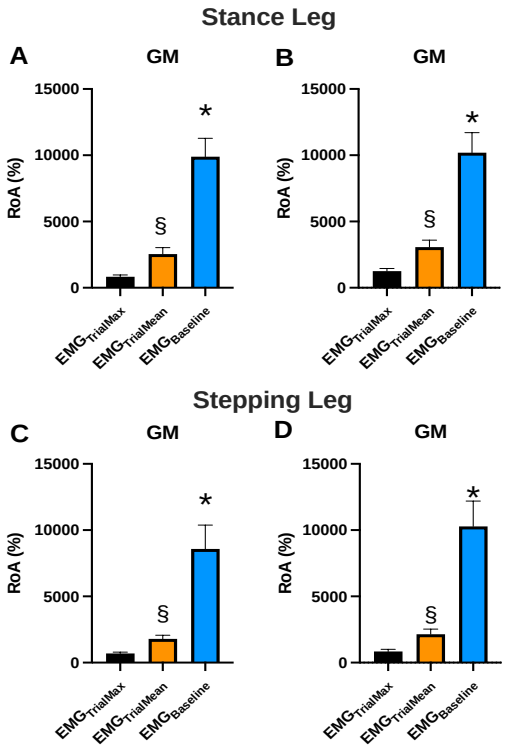

Figure 1 Likelihood of acceptance as a function of writing clarity. A and C are right and B and D are left EMG values.

CONCLUSIONS

The present study showed that the normalized RoA of the GM during a voluntary stepping task will be different depending on the EMG parameter used to normalize the signal, with excellent reliability for all EMG parameters. Therefore, comparisons between studies should be made with care between studies that use different EMG amplitude normalization procedures, even though all three EMG parameters present excellent reliability.

REFERENCES

[1] Lanza MB, *et al* JEK **55**, 102484, 2020.

[2] Besomi M *et al.* JEK, **53**,102438, 2021.

[3] Lanza MB, *et al* JEK **55**, 102724, 2023.

ADAPTATION IN REACTIVE BALANCE CONTROL OVER REPEATED STANDING SLIPS IN BALLET DANCERS

Caroline Simpkins[1] and Feng Yang[1]
[1] Department of Kinesiology and Health, Georgia State University, Atlanta, Georgia, United States of America.
Email: claubacher1@gsu.edu

INTRODUCTION

Ballet is being increasingly used to reduce fall risk in older adults [1]. Our recent work showed that ballet dancers react to a novel standing-slip more effectually than non-dancers through a more effective recovery step and a better trunk movement control [2]. This study aimed to test if the reactive responses to repeated slips would differ between ballet dancers and non-dancers. We hypothesized that dancers would exhibit a larger adaptation in reactive balance control than non-dancers.

METHODS

Twenty young adults were recruited: 10 ballet dancers (age: 24.5 ± 4.9 years) and 10 age/sex-matched non-dancers (22.6 ± 3.4 years). Participants wore a safety harness while undergoing the protocol on the ActiveStep treadmill (Simbex, NH). After three standing trials without a slip, participants were told a slip may or may not occur on any following trial. Then, three more standing trials were completed, followed by five unexpected standing-slips (S1-S5). The standardized slip was created by accelerating the belt forward to 1.2 m/s over 300 ms, and then reducing the belt speed to zero over 300 ms. The belt's slip distance was 36 cm. The S1 and S5 trials were analyzed.

Full-body kinematics were collected from 26 markers attached to the skin through a motion capture system (Vicon, UK). The belt's movement was measured by a marker attached to the belt. Locations of joint centers, heels, and toes were computed from filtered marker positions. Two time instants were obtained: the slip onset (ON) was calculated using the belt's movement and the recovery step liftoff (LO) was determined by the foot kinematics. Since LO occurred after ON, participants' performance at LO characterized the reactive control of balance after a slip. The body's center of mass (COM) kinematics were computed using the joint centers data. The two components of the COM motion state (position and velocity) were calculated relative to the base of support and normalized by foot length and $\sqrt{g \times bh}$, respectively, where g is the gravitational acceleration and bh represents the body height. Dynamic gait stability (a unitless variable) was calculated based on the COM motion state at LO. Step latency (sec) was the time elapsed from ON to LO and slip distance (normalized by bh) was the distance travelled by the belt marker from ON to LO. The primary outcome was the change in dynamic gait stability (as defined by the Feasible Stability Region (FSR) theory [3]) from S1 to S5. Secondary variables were S1-S5 changes in the step latency and slip distance. Independent t-tests (with the effect size of Cohen's d) or Mann-Whitney U tests (effect size: r) compared normally or non-normally distributed outcomes between groups, respectively. Statistical analyses were conducted using SPSS 28.0 (IBM, NY) and an α of 0.05.

RESULTS AND DISCUSSION

The results supported our hypothesis. Dancers showed larger adaptive changes in all outcome measures over the five slips than non-dancers. The dancers' improvement in stability at LO from S1-S5 was significantly greater than non-dancers (p = 0.003, Fig. 1a). This more rapid adaptation could be attributed to the improved reactive balance control involving a shortened step latency (p = 0.004, Fig. 1b) and reduced slip distance (p = 0.004, Fig. 1c).

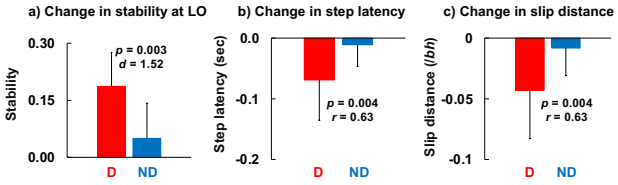

Fig. 1 Comparisons between dancers (D) and non-dancers (ND) of S1-S5 change in a) dynamic gait stability at LO, b) step latency, and c) slip distance. Also shown are p-values and effects sizes (Cohen's d or r).

CONCLUSIONS

Our study suggests that dancers can adapt their reactive balance control more quickly over repeated standing-slips than non-dancers primarily by initiating the recovery step much sooner. These findings could offer preliminary evidence for applying ballet to improve balance loss resilience and fall resistance for high fall risk populations. Studies with older ballet dancers are needed to investigate if they would exhibit similar adaptation as their young counterparts.

ACKNOWLEDGEMENTS

The authors thank Jiyun Ahn, Sangwon Shin, and Damario Wilcox for assisting with data collection.

REFERENCES

[1] Letton M et al. *JPAH* **17**: 566-574, 2020.
[2] Simpkins C et al. *J Biomech* **145**: 111366, 2022.
[3] Yang F et al. *J Biomech* **42**: 1903-1908, 2009.

CORTICAL INVOLVEMENT FOR POSTURAL CONTROL

Legrand T.[1], Mongold S.[1], Muller L.[1], Vander Ghinst M.[1], Naeije G.[1], and Bourguignon M.[1]
[1] UNI – ULB Neuroscience Institute, Université libre de Bruxelles (ULB), Belgium
Email: thomas.legrand@ulb.be

INTRODUCTION

The simplest tasks, such as maintaining upright stance, require the involvement of the cerebral cortex [1]. Sensory inputs from the visual, vestibular and somatosensory-proprioceptive systems are integrated by the cortex and are the basis for the development of a postural corrective strategy [2]. Our aim was to study postural maintenance through the lens of corticokinematic coherence (CKC), the coupling between brain activity and movement kinematics, to reveal how center of pressure fluctuations are encoded in the cortex. We also aimed to determine if such coupling reflects generated motor commands or proprioceptive integration at the cortical level for postural control.

METHODS

Thirty-six young healthy participants (age: 25 ± 3.5 years; weight: 71.7 ± 18.9 kg; 21 women) participated in this study. Participants completed a total of 8 recordings, in 4 standing conditions, each repeated 2 times, for a total of 10 minutes of recording per condition. The 4 conditions were bipedal quiet standing on a solid surface with eyes open (SEO) or closed (SEC) or on a foam mat under each foot with eyes open (FEO) or closed (FEC). Cortical activity was recorded during the balance tasks with a 64-channel EEG headcap (EEGO, ANT) and ground reaction forces and moments were recorded during each condition with a force plate (AccuSway, AMTI). Postural sways were quantified with the standard deviation of COP fluctuations (SD_{COP}). Coherence (i.e., CKC) was estimated between each EEG signal and COP fluctuations. For the electrode showing the maximal coherence between 0.5 Hz and 10 Hz, we derived the time delay from the phase slope of the cross-spectral density at frequencies where coherence was significant.

RESULTS AND DISCUSSION

Figure 1 presents COP traces, CKC topography and spectra, and estimated delays. An ANOVA confirmed CKC strength depends on balance condition ($F_{3,140} = 9.7$, $p < 0.0001$). Table 1 presents post-hoc tests. CKC strength was significantly increased in FEC compared to the other conditions. CKC in SEC was not significantly different from that in SEO. Estimated time delays from COP to EEG were significantly positive in FEC, supporting an afferent role to increased oscillations during situation of high postural demand. Finally, the percentage of change in SD_{COP} from a change in surface was correlated with CKC strength ($r = 0.267$, $p = 0.0236$).

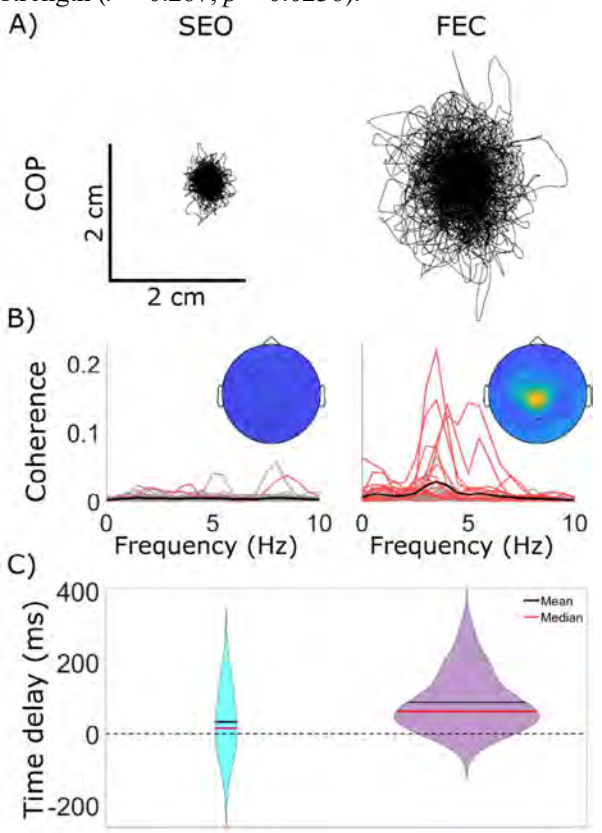

Figure 1 A) COP traces. B) Coherence spectra for each participant and corresponding average topography. Significant coherence is shown in red, and the grand average is shown in black. C) Estimated time delays from COP to EEG signals.

CONCLUSIONS

During challenging balance conditions, increased CKC may be indicative of less efficient balance control and increased need to monitor COP fluctuations. Such findings could help optimize the rehabilitation of patients with impaired balance.

REFERENCES

[1] Mierau A et al. *Brain Topogr* **30**: 434-446, 2017.
[2] Rasman B G et al. *Frontiers in Neurology* **9**: 899, 2018.

ACKNOWLEDGEMENTS

SM was supported by an Aspirant research fellowship awarded by the F.R.S.-FNRS (Belgium). SM, TL, and MB were supported by the F.R.S.-FNRS (Belgium; grant MIS F.4504.21).

Table 1: P-values and effect size of paired comparisons of CKC strength in different balance conditions.

	SEO vs. FEO	SEO vs. SEC	SEO vs. FEC	FEO vs. SEC	FEO vs. FEC	SEC vs. FEC
p-value	**0.0050**	0.1851	**< 0.0001**	0.5553	**< 0.0001**	**< 0.0001**
Effect size (*d*)	0.19	0.22	0.77	0.10	0.72	0.63

The Effect of Applying External Cutaneous Tension on Lower-limb Movement and Balance

Ning Tung [1], Kai-Chung Cheng[1], Bing-Shiang Yang[1,2,*]
[1] Department of Mechanical Engineering, National Yang Ming Chiao Tung University, Taiwan
[2] Mechanical and Mechatronics Systems Research Labs, Industrial Technology Research Institute, Taiwan
*Email: bsyang@nycu.edu.tw

INTRODUCTION

Increasing ankle stability has been a crucial topic to improve sports performance and avert sports injuries. In recent years, the number of athletes who use sports taping has gradually increased. Among many taping products, Dynamic tape® (DT) is believed to provide mechanical tension and boost sports performance [1]. Nonetheless, the effect of DT on lower-limb biomechanics and balance capability is still lacking scientific evidence. Therefore, the aim of this study was to investigate the effect of Dynamic tape® (DT) on the range of motion and balance of the lower limb.

METHODS

Eighteen healthy subjects (nine females; aged 22.6±1.9 years old) volunteered for this study. Static and dynamic balance, as well as ankle range of motion in the sagittal plane, were assessed in each subject under three different conditions in a randomized order: no taping (NT), dynamic taping (DT), and a placebo (PB) using MUELLER MWrap®. The tape was attached from the sole to the calf. In the static balance test, the subject stood by one foot in the center of a force plate (BMS400600, AMTI, USA) for 30 seconds on each leg. The center of pressure (COP) was used as the outcome measure. In the dynamic balance test, we employed the Y-balance test measurement [2] as our assessment tool. The subject stood with one leg on the center of a stance plate and used the other leg to touch three different directions three times each. The Y-balance test score was determined by calculating the average distance between the center of the stance plate and the maximum reach of the leg, normalized by the subject's leg length. We used an optical motion capture system (VantageV5, Vicon, UK) with Plug-in-Gait marker placement to determine the maximum range of motion (ROM) of the ankle joint in the sagittal plane during active movements. To test for significant differences between conditions, we employed the nonparametric Wilcoxon T-test (SPSS 22) and set the level of statistical significance at $p<0.05$.

RESULTS AND DISCUSSION

Table 1 shows the experimental results. The results of the DT condition were found to be lower than those of the NT and PB conditions in all COP parameters, indicating the efficacy of increasing stability. Additionally, the comparison between DT and NT conditions revealed that the COP area and anterioposterior sway were statistically significant ($p<0.05$).

In the Y-balance test, the score of the DT condition increased by 1.11 when compared to the NT condition. In addition, the Y-balance score difference in the DT condition was significantly different from those in the NT and PB conditions. This provides evidence that the use of DT is helpful in enhancing dynamic balance.

The maximum range of motion in the sagittal plane of the ankle joint during active movements was 1.16 degrees lower in the DT condition as compared to the NT condition, indicating that the DT condition still had an impact on the range of motion of the ankle joint.

Table 1. The result of static and dynamic balance test

	DT mean (SD)	NT mean (SD)	PB mean (SD)
COP path length (mm)	887.86 (203.57)	940.54 (248.73)	943.29 (296.09)
COP area (mm^2)	499.01 (138.22)	555.06* (172.15)	536.59 (229.68)
COP AP sway (mm)	36.24 (8.01)	41.69* (9.16)	40.76 (10.76)
COP ML sway (mm)	27.47 (3.91)	29.29 (4.75)	29.38 (5.25)
Y-balance score	90.79 (5.91)	89.68* (5.74)	89.36** (5.90)
ROM (degrees)	63.98 (4.02)	65.14** (3.49)	- -

DT: Dynamic tape; NT: No tape; PB: Placebo; COP path length: total path length of COP; COP area: the area including 95% of the COP data points; COP AP sway: maximum sway range of COP in anterioposterior direction; COP ML sway: maximum sway range of COP in mediolateral direction; Y-balance score: normalized Y-balance test score; ROM: range of motion, *p<.05 compared to DT, **p<.01 compared to DT.

CONCLUSIONS

According to the results of the dynamic test, the Y-balance score was significantly larger under the DT condition compared to both the NT and PB conditions. This suggests that the use of DT may increase balance ability, at least partially due to the restriction of ankle range of motion in the sagittal plane caused by the use of Dynamic tape®.

ACKNOWLEDGEMENTS

This study was partially supported by Taiwan National Science and Technology Council grant # MOST 109-2221-E-009-010-MY3.

REFERENCES

[1] McNeill, et.al. (2016) Dynamic tape. Is it all about controlling load. Journal of Bodywork and Movement Therapies 20.1
[2]. Coughlan, et al. (2012) A comparison between performance on selected directions of the star excursion balance test and the Y balance test. Journal of Athletic Training 47.4

PLANTAR TACTILE SENSATION, JOINT RANGE OF MOTION, AND PAIN ARE UNIQUE FALL RISK FACTORS FOR PEOPLE WITH KNEE OSTEOARTHRITIS

Peixin Shen[1], Li Li[2], Dewei Mao[1,3] and Qipeng Song[3]
[1] College of Human Movement Science, Beijing Sport University, Beijing, China.
[2] Department of Health Sciences and Kinesiology, Georgia Southern University, Georgia, USA.
[3]College of Sports and Health, Shandong Sport University, Jinan, China.
Email: 18323022054@163.com

INTRODUCTION

Falls among older adults result in injuries and even death. The incidence of falls is 33% among older adults aged over 65 and increases to 50% among same age with knee osteoarthritis (KOA)[1]. The impairment of postural control caused by KOA is one of the strongest risk factors and predictors for falls[1]. The Berg balance scale (BBS) is clinically used to assess postural control[2]. Poor proprioception (PPR) and plantar tactile sensation (PTS), pain, weak strength (ST), and limited range of motion (ROM) in the joints were detected in KOA patients[3], each of which alone can affect postural control. However, it is not clear how the combination of these factors affects postural control, the difference between people with and without KOA. Clarifying these issues can provide insight to facilitate the development of accurate KOA rehabilitation programmes. This study explored the relationship between the five factors and postural control in people with and without KOA.

METHODS

A total of 124 adults with KOA (age: 68.8±4.0 years; height: 160.55±7.7 cm; body mass: 69.3±10.1 kg) and 116 without KOA (age: 67.9±3.5 years; height: 162.4±7.7 cm; body mass: 64.5±9.8 kg) were recruited for the KOA and control (CON) groups. Postural control and pain were assessed by Berg Balance Scale (BBS) and Visual Analogue Scale (VAS). PPR, PTS, ROM, and ST were measured by Proprioception devices, Semmes-Weinstein monofilaments, goniometer, and IsoMed 2000 system, respectively. Partial correlations were used to test their relation to BBS, and factor analysis and multivariate regression were used to determine the degrees of correlation.

RESULTS AND DISCUSSION

In the KOA group, BBS was correlated with PPR, PTS, pain, ROM, and ST. In the control group, the BBS was correlated with PPR and ST. Regressions indicated the following equations: $BBS_{KOA}=54.41+(0.668*F_{ST})-(0.579*F_{PTS})-(1.141*F_{PPR})+(1.054*F_{ROM})-(0.339*F_{pain})$; $BBS_{CON}=53.85+(0.441*F_{ST})-(0.677*F_{PPR})$. In the KOA group, adjusted $r^2 = .612$, $p_{F1}=.003$, $p_{F2}=.008$, $p_{F3}<.001$, $p_{F4}<.001$, $p_{F5}=.009$, $\beta_{F1}=.218$, $\beta_{F2}=.189$, $\beta_{F3}=.374$, $\beta_{F4}=.343$, and $\beta_{F5}=.195$. In the CON group, adjusted $r^2=.464$, $p_{F1}=.004$, $p_{F3}<.001$, $\beta_{F1}=.248$, and $\beta_{F3}=.374$. Different factors related to postural control between those with and without KOA. Both proprioception and strength were associated with postural control in both groups since proprioception provides information of body position and strength is necessary to generate corrective torques for maintaining postural control[4]. PTS, ROM, and pain were only shown to be associated with BBS in KOA patients. The difference in correlations between PTS and postural control among people with and without KOA may be explained by sensory reweighting. Alternative sensory inputs can be used to compensate for the impairments of particular sensory inputs[2]. PTS might compensate for the deteriorated proprioception and provide useful information on postural control. Reduction Of pain has been linked to increased ROM in people with KOA[3], which could explain the correlation between pain/ROM and BBS was detected only in people with KOA. We have also observed that proprioception was correlated with postural control and ranked 1st among people with and without KOA. Previous research supports this view, reporting that proprioceptive afferents from the lower extremity was the primary source of information for postural control[5], and the influence of proprioception on postural control among older adults is greater than other sensory systems[6].

CONCLUSIONS

PTS, ROM, and pain are unique fall risk factors for people with KOA. Among older adults with KOA, postural control was correlated with the five factors at a sequence of proprioception, ROM, strength, pain, and PTS. Proprioceptive training should be prioritized in a KOA rehabilitation programme, as proprioception makes the greatest contribution to postural control.

ACKNOWLEDGEMENTS

Funding was provided by the International Society of Biomechanics Council (Student Matching Dissertation Grant) and the China Scholarship Council.

REFERENCES

[1] Ng & Tan. *AGE AGEING* **42**: 561-6, 2013.
[2] Song et al. *J SPORT HEALTH SCI* **10**: 585-93, 2021.
[3] Song et al. *SCAND J MED SCI SPOR* **30**: 1655-63, 2020.
[4] Shumway et al. *Lippincott Williams & Wilkins*, 2021.
[5] Hassan et al. *ANN RHEUM DIS* **60**: 612-8, 2001.
[6] Baert et al. *POSTURAL CONTROL* **32**: 1365-74, 2013.

SYNTHETIC SIMULATION OF STEPPING MANEUVER USING REINFORCEMENT LEARNING

Yoshimori Kiriyama[1] and Naoko Tamada [1]
[1] Department of Mechanical Systems Engineering, Kogakuin University, Tokyo, Japan.
Email: kiriyama@cc.kogakuin.ac.jp

INTRODUCTION

To avoid a falling down and to keep the upright posture, the foot is needed to step forward in a quite short duration. For this, the hip, knee, and ankle joints need to cooperate quickly. The cooperation of the joints to step the foot is based on the stepping strategy [1]. The stepping strategy seems to be induced by the neuro-musculoskeletal system of the human, but the principle or mechanism of the stepping strategy is not necessarily elucidated. In this study, to understand the stepping maneuver, the behaviors were searched using a reinforcement learning technique evaluating the relationship among the posture, the joint torque and disturbance loads.

METHODS

In this study, the human model consisted of seven rigid-body links including the upper body, and the bilateral feet, shanks, and thighs. The model was assumed to move in the sagittal plane, and all the joints rotate around the axes perpendicular in the sagittal plane. The physical parameters including weight, length and inertia moment were decided based on the averaged Japanese data [2]. Each joint was rotated by the joint torque $\tau = \alpha T_{joint}$, where α ($|\alpha| \leqq 1$) is a control activity, and T_{joint} is the maximum value of the torque by the muscles around the *joint* (= the hip, knee, and ankle). The positive or negative value of the torque corresponds to the rotatory direction of flexion or extension respectively. The control activity α needs to change itself to step forward. To obtain adequate α for time series, this study used a Deep Deterministic Policy Gradient (DDPG), which is a kind of a reinforcement learning technique. This method allows us to search an adequate policy to maximize a long-term reward, and then the model can keep the posture to step the foot. The reward R in this study was defined as following,

$$\begin{cases} R = \gamma_1 f(Y_U) + \gamma_2 f(\theta_u) + \gamma_3 f(X_A) + \gamma_4 f(Y_A) + \gamma_5 f(\|\boldsymbol{\tau}\|) + \gamma_6 T_{time} \\ f(x) = \frac{1}{x+\varepsilon} \qquad (\varepsilon = 1.0^{-7}) \end{cases} \tag{2},$$

where γ_i (i=1 to 6) is a weight factor, Y_U is the descent height of the upper body, θ_U is an inclination angle of the upper body, X_A and Y_A are the ankle position, $\boldsymbol{\tau}$ is a torque vector including all the torques at the time, and T_{time} is a duration time during which the model keeps upright. The function $f(x)$ was used to evaluate highly small values x. Some combinations of the weight factors were investigated to elucidate which terms of the reward equation were important to step the foot forward. To the model, forward loads (30 or 50 N) as disturbance were applied in duration of 0.4 or 0.01s.

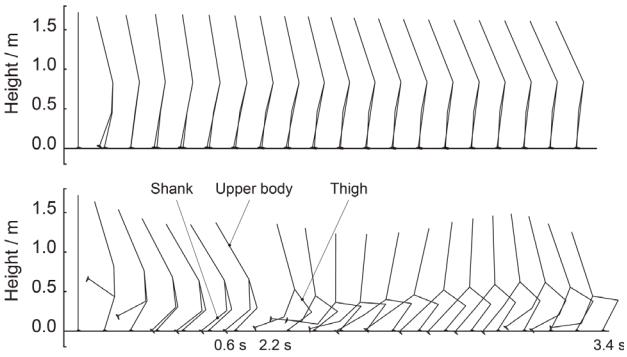

Figure 1 Stick pictures of simulated stepping maneuvers
Top: F = 30 N, t = 0.4 s, $\gamma_{i=1\sim6}$ = (4, 0, 2, 2, 1, 15)
Bottom: F = 30 N, t = 0.4 s, $\gamma_{i=1\sim6}$ = (0, 4, 2, 2, 2, 15)

RESULTS AND DISCUSSION

Figure 1 shows two typical results of the simulated maneuvers. In both simulations, the same value of the impulse of 12 Ns (= 30 N×0.4 s) was applied to the models. However, the different weight factors were used. The top figure does not show that the model steps the foot forward, and the bottom figure shows the stepping maneuver. In the top result, the torque generation could be suppressed (γ_5 = 1), and then the model could maintain the posture without the stepping maneuver. On the other hand, the bottom result shows the large joint motion and then the model steps the foot. The top result should maintain the height of the upper body, while the bottom simulation could show the change of the posture of the upper body due to the weight factors of γ_1 and γ_2. This means that the stepping maneuver should require an ease to generate joint torque and to tolerate the change of the posture. Thus, our method could be useful to understand the mechanism of the stepping maneuver.

CONCLUSIONS

Stepping maneuvers were simulated using Reinforcement learning. The maneuver seemed to require an ease of a generation of the joint torques.

ACKNOWLEDGEMENTS

A part of this study was supported financially by JKA through its promotion funds from KEIRIN RACE, and The Uehara Memorial Foundation.

REFERENCES

[1] Robert T et al. *J Biomech* **75**: 89-95, 2018.
[2] Digital Human Database, https://www.airc.aist.go.-jp/dhrt/dhdb.html, (accessed on 23 April, 2019)

Human Electrical Brain and Muscle Activity during Underwater Standing Balance

Seongmi Song[1] and Andrew D. Nordin[1,2,3]

[1] Division of Kinesiology, Texas A&M University, College Station, TX, USA, 77843
[2] Department of Biomedical Engineering, Texas A&M University, College Station, TX, USA, 77843
[3]Texas A&M Institute for Neuroscience, Texas A&M University, College Station, TX, USA, 77843
Email: nordina@tamu.edu

INTRODUCTION

Underwater gait and balance training is common during rehabilitation and is used for simulating reduced gravity environments due to the bodyweight unloading effects of buoyancy. Buoyancy provides vertical forces that oppose gravity in proportion to the degree of underwater immersion [1]. Greater external fluid resistance forces moving underwater compared to moving through air can also be used to strengthen muscles and increase energy expenditure during training [2, 3]. Although human biomechanics and electrical muscle activations have been studied during underwater gait and balance, we understand relatively little about how the human brain and body are interactively influenced by underwtaer bodyweight unloading. Here, we aim to identify changes in electrical brain and muscle activity during underwater standing balance, compared to standing on land, and in response to external balance perturbations. This knowledge can help to design personalized rehabilitation protocols using objective neural measures to assess postural control in conditions that were previously not possible.

METHODS

We instrumented ten healthy subjects with 64-channel wireless electroencephalography (EEG) and 14-channel electromyography (EMG) sensors on the left and right lower limbs during underwater standing balance. Here, we limited our analysis to the EEG data and EMG from the gastrocnemius and soleus muscles. We used customized pipelines and EEGLAB functions to analyse our EEG data [4] and calculated spectral power within frequency bands (θ: 4-8 Hz and α: 8-13 Hz) for each study condition. Study conditions included: (1) standing on land (ST), (2) standing underwater at chest-level (CST, ~50% unloading [2]), (3) standing underwater at waist-level (WST, ~30% unloading [2]), (4) standing underwater at waist-level water with low external fluid forces applied to the front of the body (WST+Low), and (5) standing underwater at waist-level with high external fluid forces applied to the front of the body (WST+High). We randomized condition order made comparisons using a one-way ANOVA with Bonferroni corrections for multiple comparisons ($\alpha = 0.05$).

RESULTS AND DISCUSSION

We identified greater alpha band spectral power from premotor cortex and reduced gastrocnemius and soleus muscle activity while standing underwater compared to standing on land; see **Figure**. In response to postural imbalance caused by high external underwater fluid forces applied to the front of the body, we identified reduced alpha band spectral power compared to standing on land or underwater at chest or waist-level. Taken together, greater premotor alpha band spectral power and reduced ankle plantarflexor muscle activity show that underwater bodyweight support reduced cortical engagement, while external balance perturbations increased electrocortical processing without affecting plantarflexor muscle activity.

CONCLUSIONS

Our findings provide insight into neuromotor changes in postural control during bodyweight unloading, which can provide biomarkers for developing rehabilitation protocols to restore and improve human balance.

REFERENCES

[1] R. Harrison et al. Physiotherapy Practice, 3: 2, 1987.
[2] N. P. Greene et al. Med Sci Sports Exerc, 41:9, 2009.
[3] H. Yokoyama et al. Scientific Reports, 11:1,2021.
[4] A. Delorme et al., Journal of neuroscience methods, 134: 1, 2004

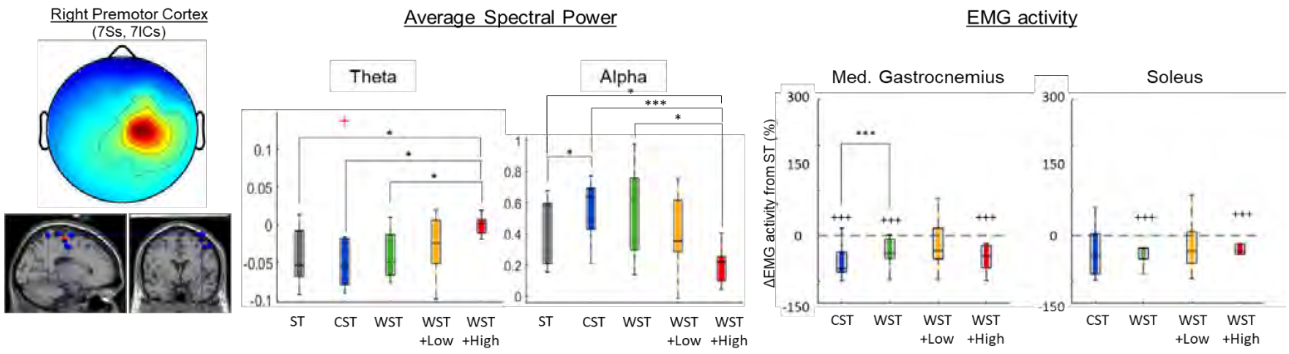

Figure: Average EEG spectral power results and percent changes in EMG activity compared to standing on land. (Left column) Mean EEG electrocortical topographic scalp map and dipole location (Middle) Average spectral power box plots by frequency bands and study conditions. (Right) Percent muscle activation changes in medial gastrocnemius and soleus muscles compared to standing on land.

MUSCLE POWER AND STRENGTH DEFICIENCIES IN FALLERS WITH LOWER LIMB LOSS

Lin, Isabel, Chang, Meghan, Chang, Kelvin, Lescas, Cali and Chen, Tzurei
Pacific University School of Physical Therapy and Athletic Training / Hillsboro, Oregon
Email: tchen@pacificu.edu

INTRODUCTION

Falls leading to injuries are prevalent in adults with lower limb loss, with a reported occurrence rate of 40-60% [1]. Limited literature examined the differences in power/torque between distinguished non-faller and faller groups in unilateral lower limb amputees compared to a control group [2,3]. Our research aims to investigate the differences in muscle power and torque in hip, knee and ankle joints under two different contraction speeds among three groups: control, non-faller and faller with lower limb loss.

METHODS

Eleven participants with lower limb loss (four transfemoral and seven transtibial; six with fall history in the past six months) and thirteen adults without lower limb loss participated in this study. Bilateral peak torque over bodyweight (Torque/BW) and average power were evaluated in hip extension/flexion, knee extension/flexion, and ankle dorsi/plantarflexion in isokinetic condition (60°/s and 120°/s) with a Biodex™ dynamometer [4]. A repeated measure mixed model ANOVA was used to identify group and speed effects on muscle power and torque. The significance level was set at 0.05.

RESULTS AND DISCUSSION

In measuring torque/BW, non-fallers were similar to control except for the affected limb knee extensors and flexors, and sound limb ankle plantar/dorsiflexors. Fallers' torque/BW were significantly smaller than control for all joint movements. In the control group, the torque/BW is significantly smaller in 120˚/s compared to 60˚/s in all joint movements. Speed affected torque/BW in faller and non-faller groups only for the sound and affected hip flexor, and for sound ankle plantar/dorsiflexors in non-fallers.

Control and non-faller groups were similar in all joint movements for power, except in affected knee extensors and flexors, where non-fallers' power values were significantly smaller than control. Fallers had smaller sound hip extensor muscle power compared to non-fallers. In addition, compared to control, fallers had smaller muscle power values in the following muscle groups: sound hip extensor/flexor, affected hip flexor, and affected knee extensor/flexors. No speed effect was found for fallers except for sound knee extensors, in contrast, significant speed effect was found in majority of the joint movements for control and non-fallers.

CONCLUSIONS

Non-fallers' sound limb performance is similar to control, while fallers' sound hip muscle power is smaller than the faller and control groups. Lack of propulsion strength during push off from the sound limb hip extensors may lead to compensations of hip flexors lifting the affected leg. With reduced hip flexor power in fallers' affected limb, foot clearance may decrease, causing the affected limb to catch during gait.

In addition, fallers are unable to generate larger muscle power during a higher speed contraction. The ability to generate fast and adequate movement to recover from loss of balance is critical for fall recovery. Power training emphasizing movement at higher velocities for the sound limb hip extensors and the affected limb hip flexors may be clinically important in improving physical function and reducing fall risk. Future intervention studies are needed to examine the effectiveness of power training for fall prevention in individuals with lower limb loss.

ACKNOWLEDGEMENTS

We would like to thank all the involved personnel from Pacific University for their assistance in data collection.

REFERENCES

[1] Hunter et al. *J PM&R* **9**:2, 2017
[2] Seroussi et al. *Arch Phys Med Rehabil.* **77**:11, 1996
[3] Vanicek et al. *Pros. and Orth. Int.* **34**:4, 2012
[4] Drounin et al. *J Applied Phyiol*. **22**:9, 2016.

Table 1: Sound limb hip extensor torque/BW and power for control, non-fallers, and fallers with lower limb loss

Torque/BW (%)	Control (n= 13) Mean (SD)		Non-faller (n= 6)		Faller (n= 5)		Group effect P values	Speed effect P value
Speed (˚/sec)	60	120	60	120	60	120		
Sound Hip Extensors	135.3 (65.2)	117.6 (70.0)	112.7 (35.3)	92.4 (25.7)	52.4 (32.7)	44.6 (34.1)	P= .034* P†= .366 P#= .010* P^= .104	P= .018* P_c= .027* P_{nf}= .078 P_f= .520
Power (Watts)								
Sound Hip Extensors	58.2 (21.2)	80.5 (41.3)	55.0 (11.0)	78.0 (22.0)	28.7 (20.4)	33.4 (29.1)	P= .038* P†= .828 P#= .013* P^= .041*	P= .007* P_c= .007* P_{nf}= .012* P_f= .535

P†= control and non-faller; P# = control and faller; P^ = faller and non-faller; P_c = within control; P_{nf} = within non-fallers; P_f = within fallers; * = p < .05

Initial Changes in Knee Loading from a Personalized Gait Modification are Associated with Changes in MRI Metrics of Cartilage Health after 1 Year

Kirsten Seagers, Scott D. Uhlrich, Julie A. Kolesar and Scott Delp
Mechanical Engineering, Stanford University, Stanford, CA, USA
Email: kseagers@stanford.edu

INTRODUCTION

Knee osteoarthritis affects 250 million people worldwide and is characterized by joint pain and cartilage degradation, where severe cases are treated with a total joint replacement [1]. Gait retraining is a non-invasive intervention for early-stage medial knee osteoarthritis that aims to reduce joint loads that are thought to contribute to pain and cartilage degradation [2]. Knee contact forces cannot be directly measured in the native knee, so surrogate metrics of knee loading have been used as targets for gait modifications. Yet, these surrogate metrics do not fully explain changes in knee contact forces [3]. It is unknown which joint loading metrics are most associated with cartilage degeneration. Quantitative MRI is sensitive to changes in cartilage composition and microstructure induced by changes in joint mechanics [4]. Here, we explore which changes in knee loading metrics, induced by a gait modification, are associated with changes in MRI-based estimates of cartilage microstructural health after one year.

METHODS

Twenty-five participants with medial knee osteoarthritis were trained to walk with a personalized foot progression angle modification over one year that reduced the peak knee adduction moment [5]. Using motion capture and force plate data from the initial visit, an OpenSim musculoskeletal modeling and simulation pipeline estimated changes, induced by the gait modification, in knee loading: external knee adduction moment, external knee flexion moment, vertical medial knee contact force, and shear medial knee contact force. MRI scans were conducted after the initial visit and after one year to calculate the change in $T_{1\rho}$ and T_2 relaxation times in the medial weight bearing compartment of the knee. Canonical correlation analysis was performed with leave-one-subject-out cross validation to find linear relationships between the knee loading and cartilage microstructure metrics which was evaluated using the Pearson correlation coefficient (α=0.05) [6]. Metrics that were statistically correlated with the identified canonical variates, called the Knee Loading Index and Cartilage Microstructure Index, were used to explore univariate correlations directly between knee loading and cartilage microstructure metrics.

RESULTS AND DISCUSSION

Reductions in the Knee Loading Index (i.e., reduced knee loading) and reductions in the Cartilage Microstructure Index (i.e., reduced $T_{1\rho}$ and T_2; improved cartilage microstructure) from canonical correlation analysis were correlated (r=0.84, p<0.001, Figure 1). Among the variables statistically correlated with the Cartilage Microstructure and Knee Loading Indices, the change in the T_2 relaxation time was positively correlated with the change in the late-stance peak vertical (r = 0.42, p = 0.04) and anteroposterior shear medial knee contact force (0.43, p= 0.03).

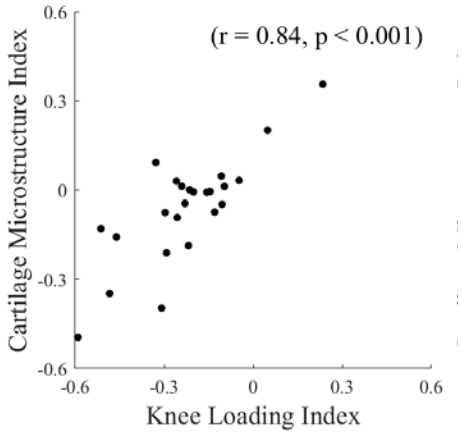

Figure 1. Canonical correlation analysis identified correlated Knee Loading and Cartilage Microstructure Indices.

CONCLUSIONS

Changes in knee loading from a personalized gait modification are associated with changes in the cartilage microstructure after one year. Reductions in late-stance peak anteroposterior shear and vertical medial knee contact force during initial training are associated with improved cartilage microstructural health after one year. Reducing peak medial compartment anteroposterior shear and vertical contact forces in late stance should be explored as targets for gait modifications.

ACKNOWLEDGEMENTS

This work was supported by the NSF Graduate Research Fellowship Program, The Mobilize Center, and the US Department of Veterans Affairs Rehabilitation R&D Service (I01 RX001811).

REFERENCES

[1] Murray, C et al. *Lancet* **380**: 2197-2223, 2010
[2] Andriacchi, T et al. *Ann of Biomed Eng.* **32**: 447-457, 2004
[3] Richards, R.E et al. *Osteoarthr. Cartil.* **26**: 1203-1214, 2018
[4] Monu, U.D. et al. *Osteoarthr. Cartil.* **25**: 513-520, 2016
[5] Uhlrich, S.D. et al. *J. of Biomech.* **144**:1-8, 2020
[6] Halilaj, E. et al. *Osteoarthr. Cartil.* **26**: 770-774, 2018

CHARACTERIZING MECHANICAL ADAPTATION OF MUSCLES AFFECTED BY MYASTHENIA GRAVIS USING SHEAR WAVE ELASTOGRAPHY

Manuela Zimmer[1], Benedict Kleiser[2], Justus Marquetand[2] and Filiz Ateş[1,2]

[1] Institute of Structural Mechanics and Dynamics, University of Stuttgart, Stuttgart, Germany.
[2] Hertie-Institute for Clinical Brain Research, University of Tübingen, Tübingen, Germany.
Email: manuela.zimmer@isd.uni-stuttgart.de

INTRODUCTION

Patients with myasthenia gravis (MG) show a post-synaptic defect of the neuromuscular transmission which often leads to muscle weakness. However, little is known about the mechanical adaptations of the muscles. Using ultrasound shear wave elastography (SWE), mechanical properties of skeletal muscles such as the shear elastic modulus as a measure of stiffness can be assessed assuming transverse isotropic and linear elastic material characteristics. Previously, SWE was shown to represent both passive [1,2] and active muscle mechanics [2,3] in vivo. Characterizing the muscle mechanics of MG patients, we hypothesized that muscle stiffness (i) demonstrates a muscle length-dependent characteristic both in passive and active states and (ii) increases with increasing contraction intensity. (iii) The muscle mechanics are altered compared to the healthy.

METHODS

11 patients (4 males, age: 47.64 ± 15.74 years) diagnosed with MG and 14 healthy volunteers (7 males, age: 28.07 ± 5.06 years) [2] participated in the study. SWE, surface electromyography (sEMG) of the biceps brachii muscle (BB), and elbow torque were measured at five elbow angles (60°-180°) at rest, during maximum voluntary contractions (MVC), and submaximal ramp contractions (up to 25%, 50%, and 75% of MVC torque) of elbow flexion. BB muscle length was determined by ultrasound imaging.

RESULTS AND DISCUSSION

MG Patients: The BB length increased with increasing elbow angle ($p < 0.001$). Normalized to the patients' individual maximum elbow torque, the MVC torque decreased from flexion to extension ($p < 0.001$) whereas the shear elastic modulus measured during MVC increased with increasing elbow angle ($p = 0.004$). Shear elastic modulus during rest also increased with increasing elbow angle ($p = 0.001$). The increase in muscle stiffness during MVC might be due to the increased muscle stiffness imposed by the extended joint positions and the resulting muscle length changes. sEMG amplitude during rest was above 3% in more than half of the trials. It might mean that the low-level muscle activity during rest is a symptom of MG showing the inability of MG patients to fully relax their muscles. Significant effects of elbow angle and contraction intensity ($p < 0.001$ for both) on shear elastic modulus were found during ramp contractions confirming the first two hypotheses posed.

Compared to the healthy group, MVC torque was 26.46% lower ($p < 0.001$). Shear elastic modulus during rest was greater by factor 2.1 ($p < 0.001$, Figure 1) for MG patients. The muscle weakness of the MG patients was quantified by the reduced torque production capability. SWE measurements reflected this at 75% MVC: During ramp contractions, the shear elastic modulus was 8.93% lower at 75% ($p = 0.044$, Figure 1) but not at 25% or 50% MVC ($p > 0.05$). The measured shear elastic modulus during muscle contraction represents the passive and active state combined. We conclude that at lower contraction intensities the increased shear elastic modulus during rest shadows the reduced shear elastic modulus imposed by the reduced torque outcome.

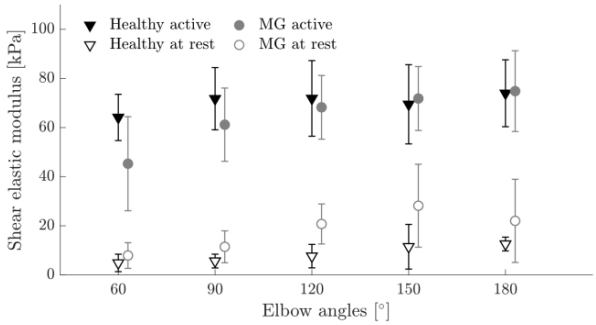

Figure 1 Shear elastic modulus at rest and during active state (submaximal ramp contractions at 75% of MVC torque) for Myasthenia Gravis (MG) patients and healthy volunteers

CONCLUSIONS

Mechanical properties of diseased muscle in MG were comprehensively studied and the hypotheses posed were confirmed. Muscle weakness of MG patients quantified as reduced torque production capability was partially reflected by the shear elastic modulus at submaximal contractions. Muscle stiffness being greater at rest in MG might be a promising diagnostic marker that needs to be further studied.

ACKNOWLEDGEMENTS

Funded by Deutsche Forschungsgemeinschaft (DFG, German Research Foundation) GRK 2198-277536708.

REFERENCES

[1] Ateş F et al. *Europ J Appl Physio* **118**:*585-593*, 2018
[2] Zimmer M et al. *J Mech Behav Biomed Mater* **137**: 105543, 2023
[3] Ateş F et al. *J Electromyo Kinesiol* **25**:*703-708*, 2015

Effects of Small and Normalized Q-Factor Changes on Knee Biomechanics in Stationary Cycling

Songning Zhang[1], Jacob Wilbert[1,2] and Sean Brown[1]
[1] Kinesiology, Recreation and Sport Studies, University of Tennessee, Knoxville, USA.
[2] Department of Prosthetics and Orthotics, Alabama State University, Montgomery, Alabama, USA.
Email: szhang@utk.edu

INTRODUCTION

Increased step width is a gait modification strategy that has been shown to reduce internal knee abduction moment (KAbM) in pateints with knee osteoarthritis (OA) [1]. However, increases in Q-Factor (QF, inter-pedal distance), have been shown to increase KAbM during stationary cycling, [2]. In the previous study [2], we used fixed and relatively large increases of QF. The purpose of the current study was to examine changes in KAbM with smaller and normalized increases in QF. It was hypothesized that KAbM would be greater with each normalized increase in QF.

METHODS

Fifteen healthy participants were included in this study (Age: 22.7±2.5 years, BMI: 23.95±3.21 kg/m2). They cycled in five different QF conditions. Each participant's QFs were achieved using a customized adjustable crank arm assembly (Figure 1). For all subjects, the narrowest QF was 160 mm and each subsequent QF was achieved by increasing from 160 mm by 2% of the participant's trochanteric leg length (L) in five QF conditions: Q1 (160 mm), Q2 (160 + 2%L mm), Q3 (160 + 4%L mm), Q4 (160 + 6%L mm), and Q5 (160 + 8%*L mm). A 13-camera motion capture system (240 Hz, Vicon) and a pair of custom instrumented pedals (1200 Hz, Kistler) were used to collect kinematic and pedal reaction force (PRF) data, respectively.

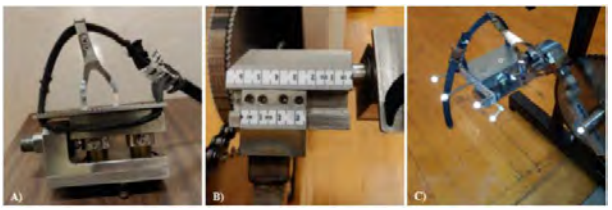

Figure 1. The custom pedal and crank arm assembly.

A mixed model analysis of variance was performed to detect differences between QF conditions ($\alpha = 0.05$).

RESULTS AND DISCUSSION

The peak KAbM was significantly greater in QF5 than QF1, QF2, QF3, and QF4 ($p \leq 0.004$ for all comparisons, Table 1). The KAbM was increased by at least 30% in Q5 from Q1, Q2, Q3, and Q4. The abduction ROM was reduced in QF4 and QF5 compared to QF1. Peak medial PRF was significantly greater (more negative) in QF5 than QF1, QF2, and QF3 ($p < 0.001$ for all comparisons). The peak PRF was increased by at least 20% in Q5 from Q1, Q2, and Q3. There was no significant change seen in knee extension moment.

Our hypothesis about the change of KAbM was partially supported. The mean QF difference (2%L) of 18 mm between conditions across all participants was smaller than the fixed QF change (42 mm) which induced a significant increase in KAbM in previous literature [2]. This study was the first to investigate the effects of small and normalized changes in QF.

CONCLUSIONS

The results of this study show that it is possible to detect a significant increase in KAbM with changes in QF as small as 2% of leg length at a high QF. Our data suggest that it is feasible to modify inter-pedal distance in cycling exercise prescription for the benefits of modulating medial compartment loading for patients with knee OA.

REFERENCES

[1] Bennett H et al. *Knee* **24**: 1326-1334, 2017.
[2] Thorsen et al. *J Sport Health Sci* **9**: 258-64, 2020.

Table 1: Mean peak PRF (N), peak knee angles and ROMs (°), and peak knee moments (Nm).

Variables	QF1	QF2	QF3	QF4	QF5	p values
Vertical PRF	233.5±34.8	217.4±32.6 [a]	222.2 ±29.2	217.2±27.0[a]	224.8±27.9	**0.010**
Medial PRF	-45.3±10.5	-45.7±7.8	-46.1±9.5	-50.1±10.2	-55.4±11.2 [a,b,c]	**<0.001**
Extension Moment	34.7±7.2	35.2±4.8	34.9±5.6	35.1±5.9	38.1±6.8	0.590
KAbM	-9.8±4.5	-9.6±4.1	-9.5±4.5	-10.6± 4.0	-12.9±4.6 [a,b,c,d]	**<0.001**
Abduction ROM	-5.7±2.6	-4.9±2.0	-5.2±2.5	-4.3±2.7 [a]	-3.8±2.5 [a,c]	**<0.001**

Significantly different compared to [a]QF1, [b]QF2, [c]QF3, [d]QF4.

Gait time series prediction using random forest model: A sensitivity analysis on IMU sensor location, window size, and number of features

Shima Mohammadi Moghadam[1], Ted Yeung[1] and Julie Choisne[1]
[1] The Auckland Bioengineering Institute, the University of Auckland, New Zealand
Email: smoh433@aucklanduni.ac.nz

INTRODUCTION

To date, a combination of Inertial Measurement Units (IMUs) and Machine Learning (ML) techniques has been used in many studies to predict some specific joint angles and moments. However, the optimal IMU sensor placement, number of features, and window size for predicting all gait time series (joint kinematics and kinetics) have yet to be determined. This study aimed to investigate how a random forest (RF) model's performance can be affected by different IMU combinations, the number of features it uses, and window sizes.

METHODS

Twenty healthy volunteers (11F, 27 ±5 yrs, 1.70 ±0.70 m, 66 ±10 kg) were asked to walk over-ground for a minimum of 16 trials. Marker trajectories from a 12-camera optical motion capture system (Vicon), 7 IMUs (Vicon IMeasureU), and 3 GR plates (Bertec) were synchronised. Pelvis, hip, knee, and ankle kinematics and kinetics were computed using a MAP-client [2] scaled OpenSim model (gait 2392) using marker trajectories and GRFs. Acceleration and angular velocity from IMUs in different locations (a combination of the pelvis, thigh, shank, and foot IMUs) were used for feature extraction by Tsfresh [3]. For each IMUs combination, we first extracted the top ten relevant features for each target (joint angles and moments); then, an RF model was trained using the most important features. Once the best IMU combination was determined, we changed the number of features from 10 to 50 with intervals of 10 and window sizes from 0.5 to 2s with intervals of 0.25 simultaneously to explore how it can affect the RF model's accuracy. To evaluate the performance of the RF model, a leave-one-out analysis was used in each step. Data analysis consisted of root mean square error (RMSE) calculation.

RESULTS AND DISCUSSION

Average RMSE was calculated between the OpenSim computed and RF-predicted joint angles and moments for each IMU combination (Figure 1). The average RMSEs for all IMU combinations were in the same range. In the case of using only one IMU, the lowest prediction errors were related to feet IMUs for both joints' kinematics and kinetics prediction. Therefore, we investigated the effect of the number of features and window size on the RF model's performance using only the feet IMUs. Regarding the optimal window size, 0.75s length of data provided the lowest prediction errors among all. By increasing the number of features from 10 to 50, we saw that RMSE converged to a constant value after 30 features, which means 30 is the optimal number of features to predict joint kinematics and kinetics.

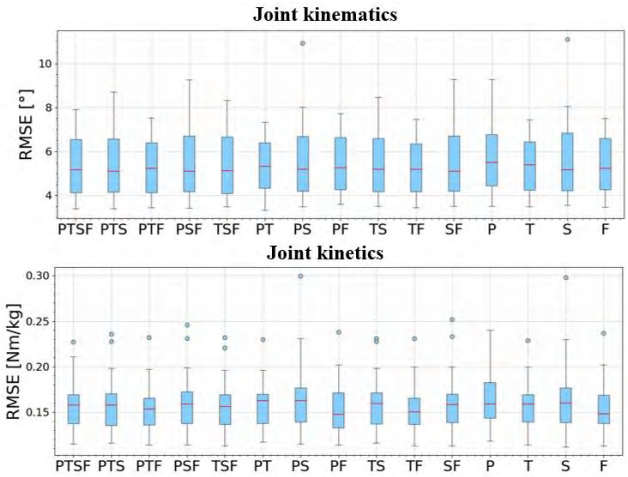

Figure 1 Joint kinematics and kinetics RMSE for different IMU placements. P stands for the pelvis, T for the thigh, S for the shank, and F for the foot.

CONCLUSIONS

This study suggests that using IMUs on each foot combined with an RF model is as accurate as using 7 IMUs with an average RMSE of 5.34 degrees for kinematics and 0.154 Nm/kg for joint moments' prediction. For future studies, it would be beneficial to explore how the IMU combination, number of features, and window size would affect the RF performance for muscle forces prediction. Moreover, determining a general optimal IMU sensor combination applicable to all functional movements would be of help to clinicians.

ACKNOWLEDGEMENTS

We would like to acknowledge the Health Research Council of NZ, the Science for Technological Innovation NZ, the Friedlander foundation, and the Aotearoa foundation for funding this study.

REFERENCES

[1] Gurchiek, R.D., Sensors, 2019. 19(23): p. 5227.
[2] Zhang,J., et al., International Symposium on Biomedical Simulation. 2014. Springer
[3] Christ M., et al. Neurocomputing, 2018. 307 p. 72-7

CAN COMPUTER VISION BE AS GOOD AS MULTI-CAMERA INFRA-RED SYSTEMS FOR MOTION ANALYSIS?

John Komar[1], Quah Jian Tan[1], Jit Ern Lim[1] and Corliss Zhi Yi Choo[1]
[1] Physical Education and Sport Science, National Institute of Education, Nanyang technological University, Singapore, Singapore.
Email: john.komar@nie.edu.sg

INTRODUCTION

Recent advancements in Computer Vision enables marker-less motion capture to potentially be a convenient and cost-effective alternative to conventional marker-based methods considered as the gold-standard. Marker-based motion capture is usually lab-based using multiple infrared cameras which requires extensive calibration and reflective markers attached on the human body. Marker-less motion capture drastically simplifies the requirements to just one or a few cameras from different angles [1]. Therefore, the purpose of this study was to quantify the accuracy of 2D and 3D marker-less motion capture through video processing from various camera angles and determine its feasibility.

METHODS

Two participants participated in this research, each of them were asked to perform simple fundamental movement skills: throwing a ball, catching a ball with different ball types (i.e., shapes, size, weight). Each participants performed 25 throws and 25 catches. Five cameras were used to video record the performance of those two participants and an infra-red motion capture system was used to collect kinematic data for those same trials (Qualisys, Sweden). Four video cameras were Qualisys cameras and positioned at various angles around the participant to test the optimal angle for kinematic detection: camera 1 in front (0 deg), camera 2 oblique (45 deg), camera 3 side (90 deg) and camera 4 oblique (135 deg). The camera 2 (oblique) camera was doubled with a 4k GoPro camera to test the effect of the camera resolution on the detection accuracy of the algorithm. The whole process was captured by the Qualisys system and video cameras simultaneously. 3D coordinates of the landmarks at a sampling frequency of 200Hz was exported from the Qualisys system. The videos recorded at 25Hz from Qualisys cameras and 59.94Hz from GoPro are processed using MediaPipe (https://google.github.io/mediapipe/) which predicts 3D coordinates of the landmarks frame by frame as demonstrated in Fig. 1.

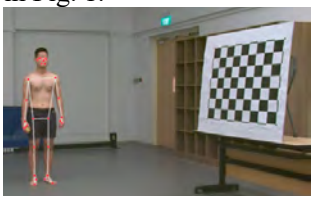

Figure 1 Sample of a camera view containing the calibration chessboard and the automatic detection of joints MediaPipe algorithm.

Accuracy and measurement error was therefore computed and compared between all the different views and camera types. Bland-Altman analysis, mean and standard deviation of absolute error was used to determine the validity of MediaPipe.

RESULTS AND DISCUSSION

Results were in accordance with similar set-up reported [2], while the % of measures outside the limit of agreement remains below 10% for all the conditions (average = 6.21%). While the frontal view showed the best results, the use of a higher resolution camera also shows better accuracy in the detection of the joints and kinematics (Table 1).

Table 1: Example of Bland & Altman results for a throwing movement

Camera View	Mean Bias (deg)	% Outside Limits of Agreement (+/- 1.96 SD)
1	12.44	6.44
2	15.97	5.62
3	15.37	6.71
4	14.42	8.16
2 (GoPro)	13.45	6.53

CONCLUSIONS

Computer vision algorithms seem to be a convenient tool for marker-less motion capture as they only require a single regular camera view to get 2D or 3D joint coordinates. While their accuracy in measuring raw angles is not perfect, they might be useful in detecting joint coordination, the occurrences of certain joint actions such as detecting the stroke frequency in swimming or running, or even to detect patterns of play in sport. Considering the continuous improvement in the algorithms, they represent a huge potential for movement analysis in the coming years.

ACKNOWLEDGEMENTS

This work was supported by a grant PG 09/22 KJ from the National institute of Education, Nanyang Technological university, Singapore.

REFERENCES

[1] S. Corazza, L. Mündermann, E. Gambaretto, G. Ferrigno, and T. P. Andriacchi. (2009). International Journal of Computer Vision, vol. 87, no. 1-2, pp. 156–169.

[2] S. L. Colyer, M. Evans, D. P. Cosker, and A. I. Salo. (2018). Sports Medicine - Open, vol. 4, no. 1.

Comparison of the validity of ground reaction forces from two different sets of body landmarks during sidestepping via artificial neural networks

Yulin Zhou[1], Hanjun Li[1], Hui Liu[2], Jianqiao Guo[3] and Tianqi Yao[4]
[1]School of Sport Science, Beijing Sport University, Beijing, China
[2]China Institute of Sports and Health, Beijing Sport University, Beijing, China
[3]School of Aerospace Engineering, Beijing Institute of Technology, Beijing, China
[4]Sports and Health Science Research Center National Institute of Sports Medicine, Beijing, China
Email: yulinzhou971020 @gamil.com

Introduction

Kinetics plays an important role in biomechanics, especially in sports injuries such as anterior cruciate ligament rupture (ACLR) which occurs during fast sidestepping. One of ACLR's risks is ground reaction forces (GRF) [1], however, it's hard to acquire in the field. Artificial neural network (ANN) is used to estimate GRF from kinematics such as body landmarks [2] which is easily obtained out of the laboratory. The performance of ANN mostly depends on inputs, but the effect of the number of body landmarks as inputs on the performance of ANN is not clear. This study aimed to determine the effect of landmarks setup on the validity of GRF estimated during sidestepping by ANN.

Methods

Four different sidestepping were executed by 71 male college soccer athletes, in total 12 trials per athlete. The motion was synchronously captured by infrared cameras and force plates (FP). The lower body landmarks included bilaterally hip centers, knee centers, ankle centers, heels, and toes, along with the mid-hip. Besides the landmarks above, whole body landmarks contained bilaterally centers of the shoulder, elbow, and wrist, plus the head's center. Whole body landmarks were obtained by transforming from anatomically relevant retroreflective markers. Coordinates of body landmarks and GRF normalized by body weight (BW) from the touch-down to the take-off of the sidestepping were extracted and normalized to 100 points.

The dataset was split subject-wise into training (61 athletes), validation (6 athletes), and test set (4 athletes). Two ANNs with whole (18*3*100) and lower body landmarks (11*3*100) as inputs separately were trained to estimate posterior-anterior (AP), lateral-medial (ML), and vertical (V) GRF (3*100) in the same dataset above. Pearson correlation coefficient (R) and root mean square error (RMSE) was used to evaluate the performance of ANN. Statistical parametric mapping was used to analyze significant differences in GRF curves between ANNs and the FP. The paired t-test determined the difference in the performance of ANNs with whole and lower body landmarks as inputs.

Results and Discussion

No significant difference was found in the performance of ANNs between the two inputs. There were few time points in the results of the whole (AP: 10-12% and 93-95%, V: 5-12%) and lower body landmarks ANN (AP: 10-12% and 96%, V: 5-15%) were significantly different with the FP. Both ANNs showed high correlations (R > 0.94) and low errors (RMSE: AP < 0.8BW, ML < 0.8BW, and V 0.27BW) with FP which proved that ANN could exextract useful information from landmarks to estimate GRF. The results indicated information provided by lower body landmarks was enough for ANN to accurately estimate GRF during sidestepping and the upper body landmarks may be meaningless because the main movement and the acceleration were from the lower body. Just a few time points in the outputs of two ANNs showed significant differences between the FP and the results of other time points were credible and useful.

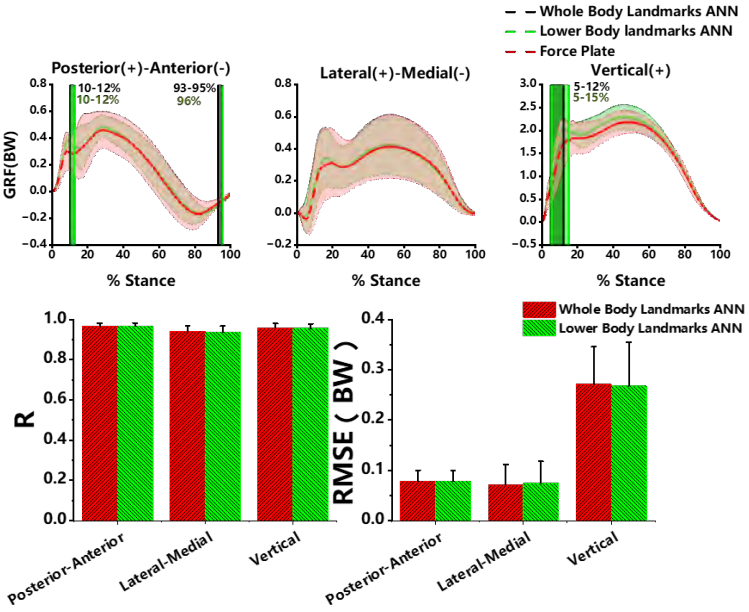

Figure 1: The performance of ANNs

Conclusions

The validity of ground reaction forces estimated by ANN during sidestepping wouldn't degrade with lower body landmarks as inputs compare to whole body landmarks. In practice, lower body landmarks are recommended as they could be used to obtain accurate ground reaction forces during sidestepping.

References

[1]Boyi, D. et al. (2012). *Res Sports Med,* 20(3-4): 180-197.
[2]Yulin, Z. et al. (2022). *ISBS Proceedings Archive,* 40(1): Article 196.

THE ESTIMATION OF GROUND REACTION FORCES DURING STAIR WALKING

Marion Mundt[1], Igor Komnik[2], Amar A. El-Sallam[3] and Jacqueline Alderson[1]
[1] Minderoo Tech & Policy Lab, Law School, The University of Western Australia, Crawley, WA 6009, Australia.
[2] Institute of Biomechanics and Orthopaedics, German Sport University Cologne, 50441 Cologne, Germany.
[3] School of Physics, Maths and Computing, Computer Science and Software Engineering, The University of Western Australia, Crawley, WA 6009, Australia.
Email: marion.mundt@uwa.edu.au

INTRODUCTION

Employing artificial neural networks (ANNs) to estimate parameters that cannot be directly or easily measured due to instrumentation limitations is a novel and feasible approach in biomechanics. One such application is stair walking; an important and physically demanding activity of daily living that is regularly studied to assess motor function in neurologic and orthopedic patients [1]. Three-dimensional (3D) ground reaction forces (GRF) provide input data for the determination of clinically relevant joint moments but in stair walking this generally relies on custom developed staircases with integrated force plates. A recently published ANN [2], trained to estimate 3D GRFs during stair walking using more than 3500 trials of 172 participants, reported correlations of 0.950-0.996 between ground-truth and predicted GRF signal. The significant size of the dataset, particularly from a biomechanics discipline perspective, suggests the trained ANN may be able to generalise when tested with new data inputs. However, it appears the training data in [2] was collected only by one research group that used a distinct data collection protocol, which may serve to restrict its generalisability to independent data from other laboratories and research groups.

In this study, we aim to investigate if Ma's [2] pre-published ANN can achieve similar GRF estimation accuracy as that achieved by the original source set, when independent test data inputs are used.

METHODS

The dataset provided by Ma [2] contains a trained ANN to estimate GRF for stair ascent and decent using 3D full-body joint angles as input data. The author further provides example data of a single participant. Independent test data collected by Komnik *et al.* [3] comprising 138 trials from 13 participants was used to test the accuracy of the proposed ANN. The stair setup in both studies was similar. Major differences between Ma's and Komnik's data were in the marker sets used which resulted in differences in joint angles [4]. To minimise differences, the accuracy of the model was evaluated using only 3D hip, knee, and ankle joint angles, which were more similar than upper body angles. First, we evaluated the accuracy of the pre-trained ANN, second, we applied transfer learning, and third, we fine-tuned the model using Komnik's data. The correlation coefficient (r) between the estimated and ground-truth GRF was determined for the stance phase of each step.

RESULTS AND DISCUSSION

The estimation accuracy of the base model was very good for Ma's provided sample data (r=0.976). However, the accuracy decreased using Komnik's data that was collected using a different marker set. The estimation of the GRF showed good accuracy for the anterior-posterior (r=0.868) and vertical (r=0.897) components, but not for the medio-lateral (r=0.640) component. The accuracy could be improved by 6.4% when applying transfer learning and another 4.1% when fine-tuning (Table 1) but it was still 9.0% lower than for the provided sample data of [2]. Since stair walking is a constrained movement, the variability in the training data is small. Hence, differences in joint angles due to the marker sets used cannot be covered.

CONCLUSIONS

This study shows that ANNs developed for biomechanics applications cannot be adopted easily to external datasets even when trained on a large dataset. Different experimental protocols, such as the use of different marker sets, can result in unknown patterns and larger variance in the input data. The ANN cannot handle unknown patterns and therefore estimate the desired output with low accuracy.

ACKNOWLEDGEMENTS

This work was partially funded by The University of Western Australia's Minderoo Tech and Policy Lab. We thank Ye Ma for providing his dataset, model and correspondence to enable this work.

REFERENCES

[1] Liu, D et al. Measurement **198**, 2022
[2] Ma, Y. *IEEE Dataport*, 2022
[3] Komnik I et al. *PLoS ONE* **13**(10), 2018
[4] Mantovani, G et al. *J Biomech Eng* **139**(4), 2017

Table 1: Correlation coefficient between the estimated and ground-truth GRF for the different models

	pre-trained ANN	transfer learning	fine-tuning	sample data
medio-lateral	0.640±0.100	0.746±0.069	0.798±0.059	0.962±0.018
anterior-posterior	0.868±0.038	0.895±0.039	0.924±0.032	0.980±0.018
vertical	0.897±0.029	0.919±0.028	0.942±0.016	0.987±0.006
mean	0.802±0.040	0.853±0.031	0.888±.024	0.976±0.014

Estimating knee arthroplasty patients' EQ-5D-5L VAS using IMUs and machine learning

Ted Yeung[1], Sabina Yang[1], Shasha Yeung[1], Faseeh Zaidi[2], Sebastian Weaver[1], Scott Bolam[2], Megan Lovatt[2], Thor Besier[1,4], Jacob Munro[3], Michael Hanlon[5], Paul Monk[1,3], Justin Fernandez[1,4]
[1] Auckland Bioengineering Institute, University of Auckland, New Zealand
[2] Faculty of Medical and Health Sciences, School of Medicine, New Zealand
[3] Faculty of Medical and Health Sciences, Surgery, New Zealand
[4] Department of Engineering Science, University of Auckland, New Zealand
[5] Domain Orthopaedic Surgeons, Auckland, New Zealand
Email: tyeu008@aucklanduni.ac.nz

INTRODUCTION

One in five patients experiences dissatisfaction with their knee replacement surgery not explained by existing outcome assessments used in the clinic, such as patient-reported outcome measures (PROMs) [1]. Biomechanical variables such as joint kinematics and forces can be used as objective measures of outcome assessment and could explain inconsistencies in patient satisfaction when coupled with PROMs. These measurements could be collected using cheap and accessible wearable sensors such as Inertial Measurement Units (IMUs) in-clinic and out-of-clinic. Using IMUs also have the benefit of not just relying on the patient answering a questionnaire. This removes subjectivity and the possibility of misinterpreting the questions. This study aimed to determine the best combination of PROMs and IMU-derived biomechanical measures for predicting postoperative patient satisfaction (EQ-5D-5L VAS).

METHODS

Synced Optical Motion Capture (OMC) and IMU data were collected from four healthy participants (two males, two females, 36 ± 9 years, 160 ± 9 cm, 68 ± 14 kg, during treadmill walking) and 28 patients (13 females and 15 males; 23 TKR and 5 UKR, age: 68.2 ± 6.2; height: 1.67 ± 0.11 m; body mass: 87.5 ± 19.4 kg; BMI: 31.3 ± 5.4 kg/m2, overground walking).

Knee contact forces (KCF) were calculated via biomechanical simulation in OpenSim [2] using the healthy participant's data. Next, regression models were built with the KCF as the target variable and relevant IMU features obtained through the python package tsfresh [3] as the predictor variables. These features are then used to train surrogate models for predicting patient satisfaction.

28 patient datasets (IMU + PROMs) were used to build patient satisfaction models at four time points: during physiotherapy, six weeks, six months, and one year after surgery. In addition, post-operative PROMs (Oxford knee score (OKS), OKS change score (pre- to post-operative OKS), forgotten joint score (FJS), EQ-5D-5L VAS and IMU measurements during physiotherapy sessions were collected from knee replacement patients.

RESULTS AND DISCUSSION

Selected features could accurately ($R^2 > 0.90$) predict the total KCF of seen participants across the stance phase 84% of the time. Using this result, a model to predict the EQ-5D-5L VAS score using OKS and IMU time-series features associated with knee kinematics and KCF during the patients' recovery period was created for the four time points. The most important combinations of variables for each time points were OKS, knee kinematics with OKS, KCF with OKS, and KCF only, respectively. The chosen models were able to predict EQ-5D-5L (VAS) scores within a mean difference of -0.070±4.33, 1.11±2.51, 0.29±1.85, and -0.23±1.58 units of the actual (95% confidence interval) for each time points (Figure 1).

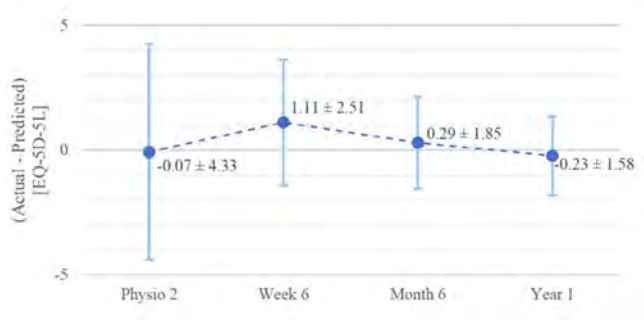

Figure 1 The mean difference and 95% confidence interval between the actual and predicted patient satisfaction across the four time points.

CONCLUSIONS

We have created a powerful predictor of satisfaction corresponding to knee contact force and OKS. In addition, due to the use of the same feature set biomechanics measures, we could estimate the patient's gait parameters if their score suggests that more information is needed to assess their joint function.

ACKNOWLEDGEMENTS

We want to acknowledge Science for Technological Innovation for funding this project, and we would also like to acknowledge VICON-IMeasureU for their technical support for this project.

REFERENCES

[1] D. Beverland, *Orthopedics* **33**: 9, 2010.
[2] S. L. Delp et al., *IEEE. Trans. Biomed. Eng*. 54: 11, 2007.
[3] M. Christ et al., *Neurocomputing* **307**, 2018.

USING DEEP LEARNING TO PERSONALIZE STROKE REHABILITATION

Sina David[1], Sonja Georgievska[3], Cunliang Geng[3], Yang Liu[3], Michiel Punt[2,3]
[1] Department of Human Movement Sciences, Vrije Universiteit Amsterdam, Amsterdam, The Netherlands
[2] Research Group Lifestyle and Health, Hogeschool Utrecht, Utrecht, The Netherlands
[3] Netherlands eScience Center, Amsterdam, The Netherlands
Email: s.david@vu.nl

INTRODUCTION

An impairment of gait due to a stroke results in a decline in quality of life and independence. Setting up efficient gait training requires an objective and wholesome assessment of the patient's movement pattern to target individual gait alterations. Current assessment tools are limited in their ability to capture the complexity of the movement and the amount of data acquired during gait analysis. This study aimed to investigate the ability of variational autoencoders (VAE) to recognize different gait patterns within both, pathologic and healthy gait.

METHODS

The 3D lower-limb joint angles of 29 stroke survivors [1] and 42 healthy participants [2] were used to train a VAE. All participants walked on a treadmill at preferred speed for several minutes. The data was acquired using optical motion capturing (see references for further details) and joint angles were calculated according to the ISB recommendations [3]. The foot contact events were used to segment one measurement of a participant into multiple epochs of four seconds of data (50 Hz) resulting in 5876 periods. These formed the input data for the VAE. The test set consisted of 2300 periods (35%). A 1D convolutional VAE was used as an unsupervised deep learning technique, containing 3 convolutional layers, a flatten and dense layer. The information from the encoder is represented in 3 latent variables which were used as the 3D coordinates to map each of the input files in the 3D space to further analyse the characteristics of a specific location. The decoder was used to reconstruct the input based on the latent space and is symmetrical to the encoder. The root mean squared error (RMSE), normalized RMSE (RMSE normalized to the joint's range of motion) and Pearson correlation coefficient r between the input and reconstructed signal was calculated to evaluate the reconstruction accuracy.

RESULTS AND DISCUSSION

The average RMSE and the nRMSE for the test set were 6.03° ± 2.71 and 23.02 % ± 4.05 respectively.
The correlation between the reconstructed and the raw data showed high (range 0.70 – 0.91) to moderate relationships (range 0.52 – 0.69) depending on the joint and plane.
The regional analysis revealed that the gait periods of one participant are located within the same region, apart from trials of another participant. Thus, supporting that the VAE can detect distinct gait patterns and also explaining the overall location of the stroke survivors versus the healthy participants (Fig. 1). Following the spiral structure of the latent space, an increase in the peak knee flexion angle and in the hip's sagittal plane amplitude was discovered. Also, a change from internally rotated to externally rotated ankle joint angles can be seen with an overall increase of transverse plane amplitude in the ankle while the frontal plane amplitude of ankle joint motion declines. Selected regions can be characterized by a higher asymmetry, reduced knee extension angles during the late swing as well as an altered plantar flexion angle, typically presented by stroke survivors. This opens a new opportunity to assess the gait quality of a patient purely based on the gait pattern. During the rehabilitation progress, the patient can be monitored by presenting the new gait data to the VAE and tracking a change of the patient's location within the latent space over time.

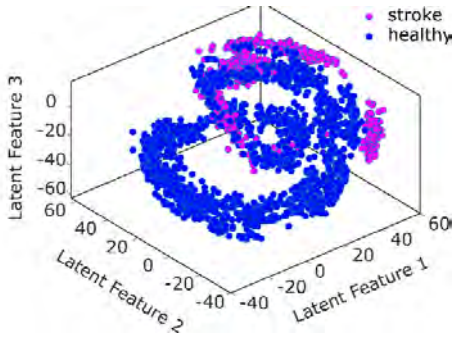

Figure 1 Representation of the test set within the 3D latent space.

CONCLUSIONS

The presented results highlight the promising nature of deep unsupervised learning algorithms to assess the movement pattern of an individual. By being able to recognize the smallest differences in gait patterns, VAEs could be utilized as an objective and data-driven tool to assess the holistic quality of movement in general and the gait alterations of patients more specifically. This is beneficial for the clinician to be efficient without loss of quality, and it is beneficial for the patient as therapy that focuses on individual needs will improve the rehabilitation outcome.

REFERENCES

[1] Punt M, et al. *J Biomech.* **55***:* 2017.
[2] Fukuchi CA, et al. *PeerJ*. **6**: 2018.
[3] Wu et al, *J Biomech.* **5**:543–548, 2002.

A MACHINE LEARNING APPROACH TO CHARACTERISING RUGBY HEAD IMPACTS FOR LABORATORY RECREATION

Danyon Stitt[1, 4], Natalia Kabaliuk[1, 4], Nicholas Ward[2], Keith Alexander[1], and Nick Draper[3, 4]
[1] Department of Mechanical Engineering, University of Canterbury, Christchurch, New Zealand.
[2] Department of Mathematics, University of Canterbury, Christchurch, New Zealand.
[3] Faculty of Health, University of Canterbury, Christchurch, New Zealand.
[4] Sports Health and Rehabilitation Research Center, University of Canterbury, Christchurch, New Zealand.
Email: natalia.kabaliuk@canterbury.ac.nz

INTRODUCTION

The incidence of head impacts in rugby has been a growing concern for player safety. While the use of headgear shows potential to mitigate head impact intensity [1,2], evaluating its on-field effectiveness is challenging. Rugby-specific laboratory testing methods, which involve the use of a steel headform and a steel impact surface [3], diverge from ecological validity. Head impact testing standards relevant to other collision sports (such as NOCSAE) have not been shown to represent unhelmeted rugby head impacts. This study aims to address this limitation by proposing a novel method for characterising head impacts for recreation in a laboratory drop test setting.

METHODS

The laboratory head impact dataset comprised 1,806 individual impacts using a drop test rig and a Hybrid III 50th percentile male headform with and without the accompanying HIII neck [1,2]. Linear and rotational accelerations, and rotational velocities, were measured for each impact and used to derive a feature set consisting of 73 single-value features. Four parameters were required to categorise a laboratory head impact: the impact location, impact surface angle, neck inclusion, and drop height. Assuming different kinematic features would better predict each of the four drop test parameters, separate k-nearest neighbours (KNN) models were developed for each. Data was split into training (70%) and testing (30%) datasets with each KNN model fit to the training data. The permutation feature importance algorithm identified the 10 most important features from which 10-fold cross-validation identified the optimal number of neighbours and subset of kinematic features. Accuracies and f1-scores were subsequently found using the hold out testing dataset.

RESULTS AND DISCUSSION

The KNN models predicting the impact location and impact surface angles achieved accuracies during testing of 97.6 and 93.0% respectively using the normalised peak linear and rotational accelerations in the x and z directions. The KNN model predicting neck involvement displayed an accuracy of 99.6% using only the log of the rotational velocity injury criteria (RVIC, algorithmically identical to the rotational injury, and head injury, criterion [4], but applied to the time-series rotational velocity), followed by the ratio of the PLA to the peak rotational velocity (PRV). This was in line with previous investigations that found the duration of the time-series rotational velocity peak to be most heavily affected by the presence of the HIII neck [1]. Finally, drop height was predicted with an accuracy of 96.0% using only the change in linear velocity during the impact. The f1-score for drop height predictions was lower than all other drop test parameters (Table 1). This resulted from the low precision and recall associated with the least common drop heights (7.5 and 22.5cm) with only 6 and 7 data points each compared to 130 – 133 for all others.

CONCLUSIONS

The present study proposed a method for categorising rugby head impacts for recreation in a laboratory setting. When combined with time series comparison and finite element simulated brain strain, this method may inform the development of improved headgear impact testing practices, providing more realistic assessments of the protective performance of new headgear.

ACKNOWLEDGEMENTS

None

REFERENCES

[1] Stitt D et al. *Ann Biomed Eng*: 1-15, 2022.
[2] Stitt D et al. *Ann Biomed Eng* **50**: 1546-64, 2022.
[3] World Rugby Handbook. 2014
[4] Kimpara et al. *Ann Biomed Eng* **40**: 114-126, 2012

Table 1: f1-scores and optimal number of neighbours from cross-validation and testing the KNN algorithm

	Impact location	Impact surface angle	Neck inclusion	Drop height
Macro-averaged f1-score	0.98	0.93	0.99	0.90
Number of neighbours	7	9	6	5

BRAIN TISSUE MECHANICS IN POSTMORTEM INTERVAL ESTIMATION

Natalia Kabaliuk[1,2], Pavithran Devananthan[1,2], Paul Docherty[1], Benjamin Ondruschka[3] and Johann Zwirner[3,4]
[1] Department of Mechanical Engineering, University of Canterbury, Christchurch, New Zealand.
[2] Bimolecular Interaction Centre, Christchurch, New Zealand.
[3] Institute of Legal Medicine, University Medical Center Hamburg-Eppendorf, Hamburg, Germany.
[4]Department of Oral Sciences, University of Otago, Dunedin, New Zealand.
Email: natalia.kabliuk@canterbury.ac.nz

INTRODUCTION

The post-mortem interval (PMI) estimation is a vital tool in forensic pathology focused on investigating the circumstances surrounding death. Routine methods include analyses of the rectal temperature [1], lividity [2], stiffness [3] and the electrical excitability of the facial muscles [4]. PMI is influenced by a number of factors and is reported as a suspected time since death period rather than a determined point in time [5]. Changes in the mechanical properties of biological tissues after death remain unexplored for forensic time since death estimations. Soft tissues, such as brain tissue, are of particular interest for improved PMI estimation due to rather fast decomposition which can occur in a matter of hours [6]. In this work, for the first time, the changes in the mechanical properties of ovine brain tissue were studied over four days post-mortem at different ambient conditions to probe the correlation between the tissue decomposition and PMI.

METHODS

Eight abattoir ovine brain tissue samples from frontal lobe, parietal lobe, anterior and posterior deep brain, superior colliculi, pons, medulla and cerebellum of 30 sheep were stored at an ambient temperature of 20°C ('warm') and further eight samples were refrigerated at 5°C ('cold'). The samples underwent rheological tests (MCR302; Anton Paar, Graz, Austria) on days zero to four after death. A 0.1 N preload was applied to the sample fully submerged in normal saline solution at 20 °C to ensure adhesion to the contact surfaces. The sample was given 100 seconds to recover before a total of 50 cycles of a rotational shear of 3% at 3Hz. The strain magnitude and strain rate were selected to prevent tissue slippage during testing and ascertain the strain rate independant tissue response. The storage modulus, loss modulus, complex shear modulus of the brain tissue were measured on a daily basis for four days.

RESULTS AND DISCUSSION

All brain tissue biomechanical rheological properties decreased for all brain regions investigated between 0 and 4 days as the tissue decomposed. The rate of tissue degradation was higher for the room temperature brain tissue compared to the refrigerated brain tissue. The day 4 moduli measured to be up to 20% and 40% lower than on day 0 for the cold and warm tissues respectively. Day 0 values of the storage modulus, loss modulus, complex shear modulus and torque revealed statistically significant decreases for all measured points in time after death. Additionally, the day 0 values comparison between the sampling brain regions showed no significant differences of the biomechanical properties within the cerebral samples. Some scatter was observed for the pons, medulla and cerebellum samples. The post-mortem tissue biomechanical properties over the subsequent four days revealed differences between the various brain regions. The samples from different regions exhibited varied rates of degradation over time reflected in the differences in the corresponding measured moduli. The storage moduli of the cerebral samples, for instance, were gradually decreasing over the four days of testing. While the medulla oblongata, being a part of the brainstem, storage moduli increased between days 3 and 4.

CONCLUSIONS

The biomechanical properties of brain tissue can discriminate between fresh and at least one-day-old samples with rheometry tests. Similar trends in brain tissue post-mortem mechanical moduli decrease between brain regions were observed but the sample retrieval sites was a major factor alongside with the tissue storage conditions. This evidences the value of biomechanical analyses for forensic time since death estimations.

ACKNOWLEDGEMENTS

The authors acknowledge funding provided for this research by the Bimolecular Interaction Centre.

REFERENCES

[1] Yang AS et al. *Fa Yi Xue Za Zhi*. **35**(6): 726, 2019.
[2] Suzutani T et al. *Hokkaido Igaku Zasshi*. **52**(6): 259, 1978.
[3] Anders S et al. *Int J Legal Med*. **127**(1): 127, 2013.
[4] Madea B et al. *Beitr Gerichtl Med*. **48**: 413, 1990.
[5] Hubig M et al. *Int J Legal Med*. **125**(4): 503, 2011.
[6] Sorg MH et al. *CRC Press*, 1997.

DEGRADING QUALITY OF PROTEOGLYCANS IN OSTEOARTHRITIC CARTILAGE

Eng Kuan Moo[1-3], Mohammadhossein Ebrahimi[2], Scott C. Sibole[3], Petri Tanska[2] and Rami K. Korhonen[2]
[1] Department of Mechanical and Aerospace Engineering, Carleton University, Ottawa, Canada.
[2] Department of Technical Physics, University of Eastern Finland, Kuopio, Finland.
[3] Human Performance Laboratory, University of Calgary, Calgary, Canada.
Email: engkuanmoo@cunet.carleton.ca

INTRODUCTION

Cartilage consists of proteoglycans (PGs), collagen fibres, interstitial fluid and ions. The main function of PGs is to provide compressive stiffness to cartilage by osmotic swelling [1]. In joint disease such as osteoarthritis (OA), PGs and/or collagens in cartilage degrade, causing functional deficit and joint pain. The PG degradation is generally construed as a loss of PG abundance [2]. It is unclear if the remaining PGs maintain the quality of generating osmotic pressure for load-bearing function. The purpose of this study was to estimate the osmotic pressure generating ability of PGs in cartilages at different OA stages using a geometrically, structurally and compositionally realistic Finite Element (FE) model. We hypothesised that the PG degradation in OA is related to abundance loss, but not to PG ability in generating osmotic pressure.

METHODS

18 cartilage-bone specimens harvested from tibias of 7 patients aged 68–79 years were measured for the depth-wise composition and structure of the cartilage [3]. PG abundance was measured in terms of optical densities of Safranin-O stained sections, which were converted numerically into fixed charge density (FCD). Collagenous organisation and content were measured by polarised light microscopy (PLM) and infrared spectroscopy, respectively. Based on OARSI scoring of the histological sections, the specimens were divided into healthy (0–1, n=5), early OA (2–3, n=6), and late OA (4–4.5, n=7) groups.

Cartilage was modelled as a multi-phasic material containing solid (collagens & PGs), water, and monovalent counterions (Na^+, Cl^-) [4]. PGs were modelled to contribute to tissue compressive stiffness by osmotic swelling resulting from the FCD and the configurational entropy. Collagenous network was represented by a continuous ellipsoidal distribution based on PLM data, with individual fibres modelled to only sustain tensile loads. Fluid flow is assumed to obey Darcy's law with an isotropic permeability.

The tissues were indented by four steps of 5% nominal tissue strain and stress-relaxed for 15-min at each step. The resulting indentation curves were used for FE modelling-informed numerical optimisation procedure to determine five material parameters, which include the fibre modulus (ξ) for collagens, as well as the attenuation of FCD (α_F), and the attenuation of configurational entropy (β_F) for PGs. A value of 0.0 and 1.0 for α_F or β_F indicates full and no attenuation, respectively.

RESULTS AND DISCUSSION

The optimization procedure produced a good fit to the experimental indentation data, with r^2 ranging from 0.87–0.95. PG abundance loss with OA was observed from densitometry data of unloaded tissues (Fig. 1B). We also found that the weight-bearing quality of PGs were severely degraded compared with healthy tissues (i.e., decrease of α_F and β_F values, Fig 1A), causing reduced osmotic pressure and, thus, decreased tissue compressive stiffness. Consequently, the superficial tissues of OA cartilage (top 10% depth) were deformed more than the healthy cartilage during indentation, leading to ~2x increase of the local FCD (Fig. 1B). Surprisingly, OA progression did not affect the moduli of individual fibres, with mean values ranging from 223 – 377 MPa for healthy, early OA and late OA tissues.

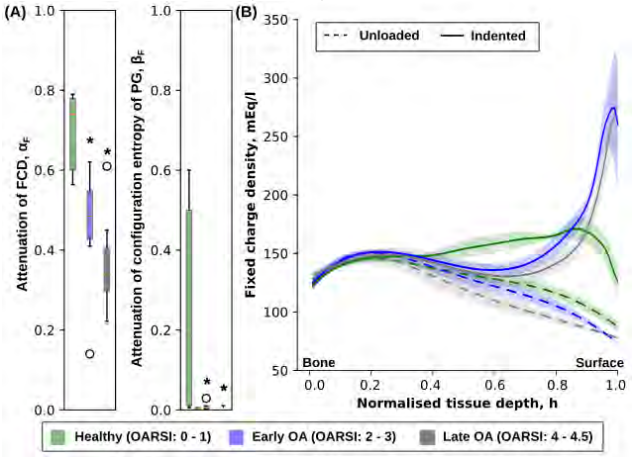

Fig. 1. (A) Fitted material properties of PGs, and (B) FCD distribution as a function of tissue depth for cartilage of different OA severity. * indicates statistical difference from healthy group.

CONCLUSIONS

Degradation of PGs involved a loss of their abundance and quality. This led to a doubling of FCD during physiological loading, which could cause additional metabolic stress to the cells and swelling tension to the embedded collagenous network. These findings highlight the significance of PG quality loss in OA pathogenesis.

REFERENCES

[1] Canal Guterl et al. *J Biomech* **43**: 1343-50, 2010.
[2] Mäkelä et al. *Osteoarth Cartilage* **22**: 869-78, 2014.
[3] Ebrahimi et al. *Ann Biomed Eng* **47**: 953-66, 2019.
[4] Ateshian et al. *J Biomech Eng* **135**: 1110011, 2013.

SKELETAL MUSCLE ANISOTROPIC MECHANICAL PROPERTIES QUANTIFICATION IN VIVO: COMBINING MAGNETIC RESONANCE ELASTOGRAPHY AND DIFFUSION TENSOR IMAGING

Zhongzheng Wang[1], Sven Petersson[2,3], Rodrigo Moreno[3] and Ruoli Wang[1]

[1] KTH MoveAbility Lab, Department of Engineering Mechanics, KTH Royal Institute of Technology, Stockholm, Sweden.
[2] Department of Clinical Neuroscience, Karolinska Institutet, Stockholm, Sweden.
[3] Department of Medical Radiation Physics and Nuclear Medicine, Karolinska University Hospital, Stockholm, Sweden
[4] Division of Biomedical Imaging, Department of Biomedical Engineering and Health Systems, KTH Royal Institute of Technology, Stockholm, Sweden
Email: zhowan@kth.se

INTRODUCTION

Due to its highly hierarchical structure, the mechanical properties of skeletal muscle are anisotropic. However, in the field of muscle biomechanics, most elastography methods assume the skeletal muscle as an isotropic material, which violates the anisotropy of skeletal muscle and cannot bring reliable insights into muscle function [1]. Recently, an increasing number of studies have proposed methods that consider the anisotropy of soft tissue in magnetic resonance elastography (MRE). Still, the use of anisotropic MRE in evaluating mechanical properties of skeletal muscles has been very limited due to the lack of a reliable methodology. This study aims to propose a direct MRE inversion approach with the combination of diffusion tensor imaging (DTI) for *in vivo* quantification of the anisotropic mechanical properties of two major ankle plantarflexors, gastrocnemius (GAS) and soleus (SOL).

METHODS

MRI data of 5 able-bodied subjects (3F/2M, 27.4±3.6 years) were analysed. All subjects gave written informed consent before participation. The study was approved by the Swedish Ethical Review Authority. The MRI scans were performed on a 3.0 Tesla MR scanner (Ingenia CX, Philips, Netherlands). All subjects were scanned in a supine position, with the thigh relaxing on a wedge and the foot fixed on a foot support while the GAS and SOL were assumed remaining relaxed. Anatomical scans, DTI, and multifrequency MRE were performed. The MRE scans were performed at three motion-encoding gradient directions at three frequencies (40, 50 and 60 Hz). The GAS and SOL were manually segmented into six sub-compartments according to the fascicle orientation. Tractography was performed using DSI studio for each muscle sub-compartment to identify the muscle fascicle coordinate system. The skeletal muscle was modelled as an incompressible transverse isotropy material. Laplacian unwrapping was used for phase unwrapping. Direct inversion of three complex-valued viscoelastic constants, shear modulus in the plane of isotropy μ_{12}^*, shear modulus in the plane of symmetry μ_{13}^*, and Young's modulus in the plane of isotropy E_3^*, were solved based on the curl-based wave equation [2]. The storage, loss, and magnitude moduli were calculated for each muscle sub-compartment. The performance of the proposed approach was evaluated as whether the characterization of anisotropy ($\mu_{12}^* \neq 1/3\,E_3^*$ and $\mu_{13}^* \neq 1/3\,E_3^*$) and frequency dispersion (different stiffness responses at various frequencies) can be determined in individual muscle sub-compartment.

RESULTS AND DISCUSSION

Anisotropy was found in all muscle sub-compartments at each frequency. Both $\mu_{12}^* \neq 1/3\,E_3^*$ and $\mu_{13}^* \neq 1/3\,E_3^*$ existed for all the storage, loss, and magnitude moduli, which was in line with previous research [2]. Frequency dispersion was also observed as stiffness increased with higher frequency (Figure 1). The major advantage of our proposed approach was the consideration of the complexity of fascicle orientation within GAS and SOL, as *in silico* experiments revealed that the accuracy of the MRE inversion decreased with an increase in the fascicle orientation complexity [3].

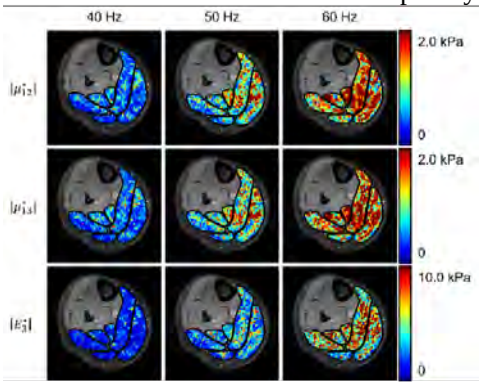

Figure 1 Elastograms of the three magnitude moduli at different MRE frequencies overlapped on the anatomical image.

CONCLUSIONS

We proposed a direct MRE inversion approach with the combination of DTI that can quantify the anisotropic mechanical properties of the skeletal muscle. The proposed approach has the potential to more accurately quantify muscle stiffness *in vivo* in related biomechanical and clinical research.

ACKNOWLEDGEMENTS

The study is funded by the Chinese Scholarship Council and Promobilia Foundation.

REFERENCES

[1] Bilston LE et al. *Ann Biomed Eng* **43**: 261-73, 2015.
[2] Guo J et al. *Magn Reson Med* **75(4)**: 1537-45, 2016.
[3] Babaei B et al. *Med Image Anal* **74**: 102212, 2021

BRAIN STRESS MEASUREMENTS DURING BIOFIDELIC HEAD SURROGATE IMPACTS

G. Zullo[1], E. Baldoin[1], M. Bäckström[2], A. Koptyug[2], and N. Petrone[1]
[1] Department of Industrial Engineering, University of Padova, Padova, Italy.
[2] Department of Engineering, Mathematics and Science Education, Mid Sweden University, Ostersund, Sweden
Email: giuseppe.zullo@phd.unipd.it

INTRODUCTION

Reducing head injuries is a priority since they represent one of the most likely cause of hospitalization and death after traumatic events. Skull and brain traumas could be mitigated by protective gear, and research is ongoing to improve its effectiveness. Indeed, evaluation of protective performance is carried out using rigid head forms and simple criteria based on linear and rotational kinematics [1,2], but is well known by numerical modeling that more factors such as strain/stress contribute to brain damage mainly during rotational impacts [3]. To address limitations of rigid head forms, some authors developed more biofidelic surrogates which account for soft tissues and other anatomical features [4,5]. Aim of the study is to improve an existing biofidelic head surrogate to investigate brain stress thanks to novel sensors [5,6], and test it in drop tests.

METHODS

Adult male MRI scans were obtained and simplified in a mesh manipulating software (MeshMixer, Autodesk, USA). Skull was divided into two halves and 3D printed in Polyamide with laser sintering technique. Brain and scalp models were used to create a set of dies to cast the two elements in PlatsilGel OO30 and PlatsilGel 10 silicone rubbers (Polytek, USA), respectively. During the casting of the brain: a tri-axial accelerometer, a tri-axial gyro meter, and a six-axis stress sensor [6] were embedded in its centre of mass. After completing the casting, the brain was covered with a 5 mm thick layer of open-cell foam to simulate the sub-arachnoid space of the meninges. Then, the brain was inserted in the skull which was closed and sealed. After closure, the cavity between skull and brain was filled with water to simulate the cerebral-spinal fluid, and the scalp was fit over the skull. Figure 1a shows the assembled head.
To test the surrogate, an anvil with a 44 kN load cell was prepared and preliminary drop tests from varying heights were performed. In these first trials, a Vega mountaineering helmet (Salewa, Italy) was fit on the head. Data were collected at 5 kHz and the 25 ms from first contact were analysed to compute injury criteria such as HIC [1] and peak Von Mises stress [3].

RESULTS AND DISCUSSION

Preliminary tests showed the response of the head as a function of energy and are reported in Table 1. Example of stress development inside the brain is showed in Figure 1b. Highest forces, acceleration, and stress were observed in the mid energy impact. Conversely, data from the head sensors better follow increases in load cell peak force, indicating a possible error in the test procedure that needs investigation. Nevertheless, tests with higher energy will be performed since injury criteria of HIC and Von Mises stress showed low values compared to hazardous thresholds [1,3].

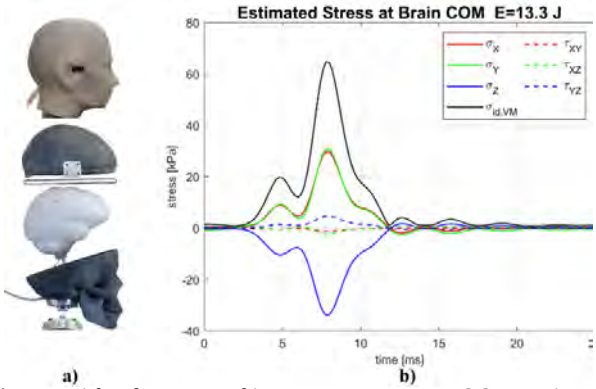

Figure 1 a) head surrogate; b) Von Mises stress in 13.3 J test (Z direction of impact; X, Y transversal directions).

CONCLUSIONS

The presented head surrogate includes several anatomical features which are rarely found in literature. Moreover, its sensors allow the experimental evaluation of injury criteria both based on global kinematics and on brain kinematics and stress/deformation. Further test will aim to increase impact energies and to validate the surrogate against numerical models and/or available cadaveric data under multi-directional impacts.

REFERENCES

[1] Hardy W. et al. *Stapp Car Crash J,* **51**: 17-80, 2007.
[2] Takhounts E. et al. *SAE Tech Pap,* 243-266, 2013.
[3] Sahoo D. et al. *Accid. Anal. Prev,* **92** 53-70, 2016.
[4] Ouellet S. et al. *Shock Waves,* **28** 19-36, 2018.
[5] Petrone N. et al. *J. Sci. Med. Sport,* 4-10, 2019.
[6] Zullo G. et al. *Sensors*, 2021.

Table 1: Results of preliminary drop tests.

Impact energy [J]	Peak force [N]	Peak linear acceleration [g]	HIC [g· s]	*Peak Von Mises [kPa]*
10	2352	55.6	39.6	37.5
13.3	3393	79.6	60.2	64.8
16.7	2750	76.0	68.0	47.7

A novel predict-update deep learning model for joint angle predictions from inertial measurement units

Vaibhav Shah[1,2], Philippe C .Dixon[1,2,3]
[1] Institute of Biomedical Engineering, Faculty of Medicine, University of Montreal, Canada
[2] Research Center of the Sainte-Justine University Hospital (CRCHUSJ), Canada
[2] School of Kinesiology and Physical Activity Sciences, Faculty of Medicine, University of Montreal, Canada
Email: vaibhav.shah@umontreal.ca

INTRODUCTION

Recent advances using deep learning to predict joint angles from inertial measurement units (IMUs) are promising [1], [2]. Nevertheless, current methods lack the accuracy of marker-based systems. Moreover, none of the prediction strategies have applied knowledge from pre-existing physical methods to guide model architecture. Here, we present a novel model with a "predict-update" block—based on the extended Kalman filter concept. We hypothesize that our approach will accurately predict sagittal plane knee joint kinematics.

METHODS

To demonstrate our approach, we used a database of IMU-based gait data from 30 participants [3]. First, ground truth was obtained by computing knee flexion/extension angles using a Complimentary filter (c.f. [4]). Next, trials were separated into two continuous gait cycles. A sliding window (window size = 60 and stride = 5) of acceleration and gyroscope data of thigh and shank sensors were used to predict knee flexion/extension angles. A subjectwise split with five repetitions (train/test: 80/20: 24/6 subject) validated model performance via the root mean squared error (RMSE). The model consisted of two blocks: the predict block, with three models (T1, T2, T3), and the update block, with two models (T4, T5). Blocks included Convolutional Neural Networks (CNNs), long short-term memory units (LSTMs), or combinations of the two (see Table 1). The predict block used the first 50 frames to predict the subsequent 10 frames, while the update block used the last 10 frames of present and predicted data to optimize results.

RESULTS AND DISCUSSION

The best configuration is a series of CNNs with a final LSTM block in T5 (Table 1). Average RMSE across all folds was 3.80 (mean) and 2.98 (median) (Fig. 1a). An example of predicted knee angles with predict block improving results is shown in Fig. 1b.

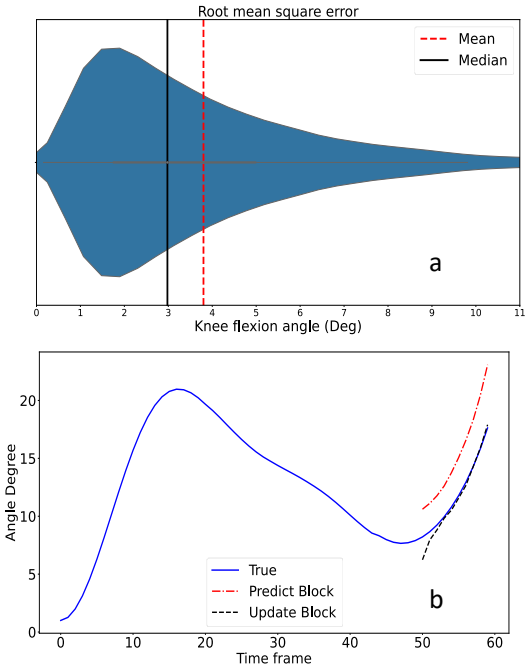

Figure 1 Prediction errors (a) and example predictions (b).

CONCLUSIONS

Results of the study show that a "predict-update" configuration optimizes predictions. Performance was improved compared to past studies where individual gait cycles were used as inputs [5]. Future work will optimize the model with motion capture data and extend to all lower-limb joints and planes. Our approach may facilitate real-time prediction scenarios.

ACKNOWLEDGEMENTS

First author is funded by TransMedTech & its funding partner, the Canada First Research Excellence Fund.

REFERENCES

[1] Gurchiek R. et al. Sensors **19**, 2019. [2] Weygers I. et al. Sensors **20**, 2020. [3] Luo Y. et al. Sci. Data **7**, 2020. [4] Ippersiel P. et al. Gait Posture, **91** 2022. [5] Sung. J et al. Sensors **22**, 2022.

Table 1: Information about the model combination used for predictions and the results of each model

Combinations	Predict Block (Uses past data)			Update block (present data)		Prediction
Model (input) (Output)	T1 (n,50,6) (n,10,6)	T2 (n,50,6) (n,10,6)	T3 (n,60,12) (n,10,1)	T4 (n,60,12) (n,10,1)	T5 (n,10,26) (n,10,1)	RMSE
Model Architecture	CNN	CNN	CNN	CNN	LSTM	3.80 ± 2.99

A method to estimate the kinetics of a collective load carrying in ants

J. Drapin[1], V. Fourcassié[1] and P. Moretto[1]
[1] Centre de Recherches sur la Cognition Animale (CRCA) - Centre de Biologie Intégrative (CBI), Toulouse, France.
Email: pierre.moretto@univ-tlse3.fr

INTRODUCTION

Social insect performances are inspiring robotics because of its remarkable cooperation in collective tasks. Yet, the phenomenon of collective transport among worker ants is often poorly understood, although it exists at least in 40 genera in different subfamilies of Formicidae [1]. Cooperative transport, occurs when a group of individuals work together to move an otherwise unmanageable object. However, analysing ant locomotion is challenging due to its scale. Current works are often reduced to one or few individuals and consider only the main joint locations [2]. To overcome this limitation, this study proposes to perform 2D kinematic analysis of a collective transport model: the long horn crazy ant *Paratrechina longicornis*. Our assumption is that the acceleration of the ant heads ($\vec{a}$) reveals their action forces on the load according to the fundamental physics principle (FPP, $\sum \vec{F} = \overrightarrow{mag}$) and explain the acceleration of the load centre of mass ($\overrightarrow{ag}$). The aim of this study is a first attempt to verify this assumption on the basis of the simplification of the forces to the accelerations measured thanks to the kinematics.

METHODS

In order to get the kinematic of a group of ants that collectively carry a load, we filmed from above a walkway (20 x 2,5 cm) (fig. 1a). Three infrared strobe spots, synchronised with the camera sampled at 300 Hz, were used to illuminate the walkway, allowing us to achieve a better contrast and reveal ant's joints. Then, the X, Y axes corresponding respectively to the antero-posterior and medio-lateral directions of the walkway, were defined by digitising the points of a control object (Lego® brick) of known dimensions. After a calibration, the location of the points on the ant's body and the load were tracked and specified in an external 2D coordinate frame calculated by Vicon Motus (v.10) software. This allows us to build a polyarticulated model comprising the four ant's heads and the load they transport.

RESULTS AND DISCUSSION

A set of 12 points of interest allowed digitizing the ant's necks and mandibles thus the corners of the load carried (fig. 1a). They were then used to define a 2D stick model system. The trajectories of the centre of mass of each ant's head and the one of the load in the XY frame can then be followed (fig. 1b). The acceleration of the load and of the ant's heads (fig1. c, d) calculated from these points have similar shapes during the 3 first seconds of the collective load transport (fig1. c, d). After this period, the shapes of the curves vary, which can sign the time of the beginning of the rotation of the load occurring at the end of the recording. Indeed, the load rotates due to the moment of force applied by the ants.

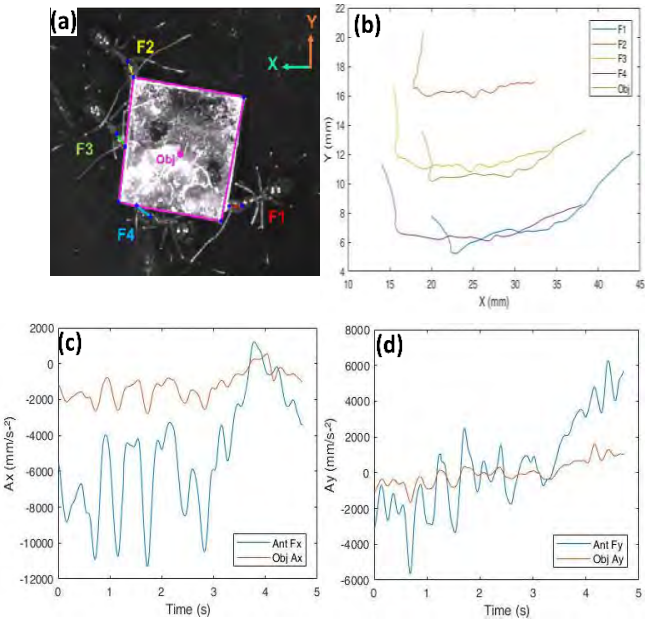

Figure 1: (a) Anatomic points locations: mandibles and ant's neck, and 4 points for the load. The nest was on the left of the image. **(b)** Ant's and load center of gravity trajectories. **(c, d)** Evolution of the acceleration (mm.s-2) of the ant's head (blue) and of the load carried (red) respectively on X and Y axis.

CONCLUSIONS

The purpose of this study was to test a method to estimate the forces applied by four ants on a load they collectively carry. The results demonstrate the accuracy of the method to discern the translations of the object due to the action force of the ants. Furthers investigations will enable us to precise the method to consider both translations and rotations in 3D to finally address the collaboration and the efficiency of the ants.

ACKNOWLEDGEMENTS

This work has been supported by the CNRS AO MITI Biomim. JD work was supported by a scholarship from the Collectivité Territoriale de Martinique.

REFERENCES

[1] Hölldobler B et al. *Springer-Verlag* **72**: 2, 1990.
[2] Reinhardt et al. *J.Exp Biology* **217**:13, 20.

Influences of Alteration in Running Foot Strike Angles on Internal Loading of the Tibia

Sanghyuk Han[1,2], Jeheon Moon[3], Jusung Lee[2], Sooji Han[4], Thorsten Sterzing[2], Dominic Farris[1], Hannah Rice[5]
[1] Public Health & Sport Sciences, University of Exeter, Exeter, UK.
[2] Human Performance Laboratory, Descente Innovation Studio Complex, Busan, Republic of Korea.
[3] Department of Physical Education, Korea National University of Education, Chungbuk, Republic of Korea.
[4] Motion Innovation Center, Korea National Sport University, Seoul, Republic of Korea.
[5] Department of Physical Performance, Norwegian School of Sport Sciences, Oslo, Norway.
Email: sh1024@exeter.ac.uk

INTRODUCTION

Different running landing patterns such as rearfoot striking (RFS) and forefoot striking (FFS) may affect kinematic and kinetic parameters associated with the risk of tibial stress fractures (TSF). Risk factors relating to TSF are not clear and it is important to quantify internal loading [1]. Foot strike is known to influence the work done at the ankle [2] which in turn may influence the loading of the tibia through muscular-tendinous forces. Thus, the aim of this study was to evaluate the influence of foot strike on tibial bending moments and stress.

METHODS

Nineteen recreational runners (9 males and 10 females) with a habitual RFS participated in this study. Participants were asked to run with their habitual running foot strike (HFS) pattern overground at 4.0 m/s (±5%). Participants were then asked to modify the landing patterns to a distinct RFS or FFS randomly. Participants were given verbal feedback regarding the landing patterns, defined as follows: a foot strike angle with a positive value represents toes higher than heel at the point of ground contact (HFS: 14.3 ± 6.4°; RFS: 29.0 ± 6.3°; FFS: -4.4 ± 3.9°; mean ± SD). Kinematic and kinetic data were recorded using 3D motion cameras and force plates. Tibial stresses in the sagittal plane were estimated at a cross section area at the distal 1/3rd of the tibia [2] using a customized Matlab script (Mathwork Inc.) [3]. Bending moments due to muscular forces was calculated using static optimization. One-way repeated measures ANOVA SPM analyses (www.spm1d.org) were conducted to compare time series throughout running stance ($p<0.05$). Post-hoc paired t-tests were performed with a Bonferroni correction.

RESULTS AND DISCUSSION

SPM indicated a main effect for the bending moment, anterior and posterior tibial stresses (Figure 1, $p<0.001$). Post hoc SPM paired t-test revealed that the bending due to muscular forces in FFS increased in comparison to both RFS and HFS (3-56% stance; 3-33% stance, respectively). The anterior stresses in FFS increased in comparison to both RFS and HFS (2-50% stance; 3-25% stance, respectively). The posterior stresses in FFS increased in comparison to both RFS and HFS (2-52% stance; 3-28% stance, respectively). There were no differences in anterior and posterior stresses between running with RFS and HFS. The greater bending due to muscular forces observed in FFS compared to other foot strikes may be the main explanation for the greater tibial stresses.

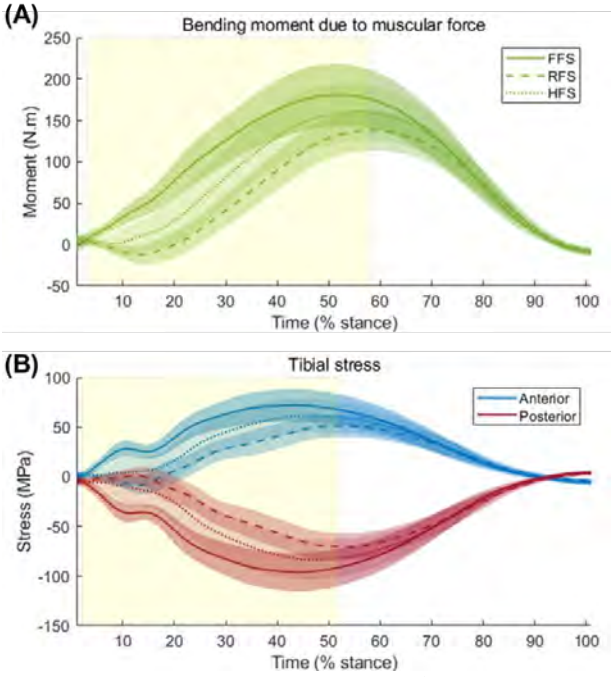

Figure 1 Bending moment due to muscular forces (A), and tibial stresses at the anterior and posterior peripheries (B). Vertical shaded areas indicate a main effect with a significant difference. Solid, dot, and dashed lines represent FFS, HFS and RFS, respectively.

CONCLUSIONS

Running with FFS could increase sagittal bending moments due to muscular forces at the distal 1/3rd of the tibia as a result of greater tibial stresses. This may have implications for the risk of TSF.

REFERENCES

[1] Matijevich E. S et al. *PloS one* **14(1)**: e0210000, 2019.
[2] Stearne S. M et al. *Med Sci Sports Exerc* **46(8)**: 1578-1587, 2014.
[3] Meardon S. A & Derrick T. R. *J Biomech* **47(11)**: 2738-2744, 2014.
[4] Rice H et al. *Med Sci Sports Exerc* **51(11)**: 2257-2264, 2019.

MUSCLE SHAPE CHANGES AND GEARING ARE MEDIATED BY INTERNAL MUSCLE PROPERTIES IN THE HUMAN GASTROCNEMII

Nicole Yvette Kelp[1], Sabrina Pinel[1], Christofer Clemente[2], Kylie Tucker[1], Francois Hug[1,3], and Taylor Dick[1]
[1] School of Biomedical Sciences, University of Queensland, St Lucia, Queensland, Australia.
[2] School of Engineering and Science, University of the Sunshine Coast, Sippy Downs, Queensland, Australia.
[3] Université Côte d'Azur, LAMHESS, Nice, France.
Email: n.kelp@uq.edu.eu

INTRODUCTION

Skeletal muscles bulge when they contract. These dynamic three-dimensional shape changes coupled with fibre rotation, influence a muscle's mechanical performance by uncoupling fibre velocity from muscle belly velocity in a process known as gearing [1]. Alterations in internal muscle properties, owing to aging [2] or disuse, may mediate the direction and degree to which a muscle bulges and gears during a contraction [3], but this remains unexplored during *in vivo* contractions. The aim of this study was to determine the influence of internal muscle properties on *in vivo* muscle shape change, fibre rotation, and gearing in the human gastrocnemii during isometric plantarflexion contractions.

METHODS

Twenty younger (24±3y) and 13 older (70±4y) adults participated in this study. Multi-modal imaging techniques including shear wave elastography, magnetic resonance imaging, and B-mode ultrasound were used to measure shear modulus (index of stiffness), intramuscular fat, and physiological cross-sectional area (PCSA), respectively. A dual probe ultrasound configuration was used to record synchronous changes in fascicle length, muscle thickness, and pennation angle during submaximal (30% MVC) and maximal isometric plantarflexion contractions in the MG and LG while participants laid prone with their ankle fixed at 90 deg. Gearing was calculated as the ratio of fascicle velocity to belly velocity (calculated with fascicle length multiplied by cosine pennation angle). Linear mixed effects models were used to determine the influence of Shear Modulus, Intramuscular Fat, and Fat-corrected PCSA on the change in pennation angle, muscle thickness and gearing. Significance was set to p=0.05.

RESULTS AND DISCUSSION

The MG had greater shear modulus (p<0.001), intramuscular fat (p=0.019), and fat-corrected PCSA (p<0.001) compared to the LG. The MG had higher gearing, greater fibre rotation, and less bulging in thickness at 100% MVC compared to the LG (all p<0.001). Fat-corrected PCSA was positively associated with fibre rotation, gearing, and changes in muscle thickness during submaximal contractions (all p<0.001), but negatively associated with changes in muscle thickness during maximum contractions (p<0.001). Increased muscle stiffness and intramuscular fat were related to limited muscle bulging in thickness (p=0.008) and reduced fibre rotation (p=0.014), respectively, but only at high forces (Fig. 1).

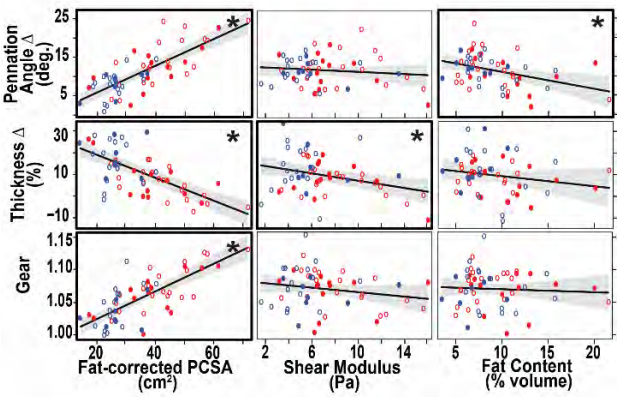

Figure 1 Effect of internal muscle properties on change in pennation angle, thickness, and gearing at 100% MVC. Data is shown for older (filled circle) and younger (open circle), medial gastrocnemius (red) and lateral gastrocnemius (blue). Darker lined boxes with an asterisk (*) indicates a significant relationship.

CONCLUSIONS

Our results highlight that internal muscle properties play an important role in modulating muscle shape change and gearing, particularly during high force contractions. Further, differences in internal properties between synergistic muscles may lead to differing mechanical behaviours. These findings improve our understanding of the factors that influence a muscle's mechanical response to force (i.e., gearing) which has future implications for preventing and treating muscle deficits associated with aging, disease or disuse.

ACKNOWLEDGEMENTS

We would like to acknowledge the UQ Centre for Advanced Imaging for assistance with MRI and Romain Feigean and India Lindemann for support data collection and processing.

REFERENCES

[1] Azizi et al. (2008). PNAS, 105:1745-1750.
[2] Holt et al. (2016). J Exp Biol, 219: 998-1003.
[3] Eng et al. (2018) Integr. Comp. Biol, 58:207-218.

FOOT AND ANKLE KINETICS ARE COUPLED DURING PROPULSION FOR WALKING AND RUNNING

Quinn Yetman[1], Lauren Welte[1,2], Aidan Shimizu[1], Michael Rainbow[1]
[1] Mechanical & Materials Engineering, Queen's University, Kingston, Canada.
[2] Mechanical Engineering, University of Wisconsin – Madison, Madison, USA.
quinn.yetman@queensu.ca

INTRODUCTION

The human ankle joint contributes up to 50% of the total mechanical power for walking and running [1], but it is unclear how the foot helps or hinders the ankle's ability to generate power. The unified deformable (UD) power approach is ideally suited for analyzing foot and ankle power, because it simplifies the foot's complexity by assuming that all structures distal to a proximal rigid body (bone) are massless and deformable [2].

We introduce a novel approach that applies the UD power model to highly accurate bone motion from biplanar videoradiography (BVR) and force plate measurements. This allows us to use the talus as the proximal rigid segment to compute foot power over the traditionally used calcaneus. The talus offers advantages over the calcaneus because it is the apex of the arch and all foot structures are distal to it. Our approach is advantageous because it allows us to characterize foot, ankle-foot, and talocrural (ankle) power.

Here, we seek to understand the kinetics underlying the previously observed coupling of medial longitudinal arch and ankle kinematics [3],[4]. We expect the foot and ankle will simultaneously begin generating power during propulsion.

METHODS

Six participants walked and ran in minimal shoes over split force plates while BVR data was captured. Models from CT scans were used to find the position and orientation of the foot bones over stance. Dorsiflexion of the first metatarsal with respect to the calcaneus defined arch deformation.

A UD segment analysis applied to the talus and tibia quantified the instantaneous power of the foot and ankle-foot complex, respectively. Ankle power was defined as the ankle-foot minus the foot power. The UD foot power was also calculated using the calcaneus to understand differences between using the talus and the calcaneus.

RESULTS AND DISCUSSION

The foot, ankle-foot, and ankle dissipate power in the first part of stance then generate power later in stance (Figure 1). Both the foot and ankle begin to produce power simultaneously (overlapping confidence intervals) at the point where the arch is maximally flattened, and the ankle is maximally dorsiflexed for both walking and running (72% ± 4% stance walking, 50% ± 2% stance running).

The foot power calculated using the calcaneus (not shown) agrees with the talus prior to toe strike. The calcaneus underestimates the positive power generated by the foot during propulsion for both walking and running.

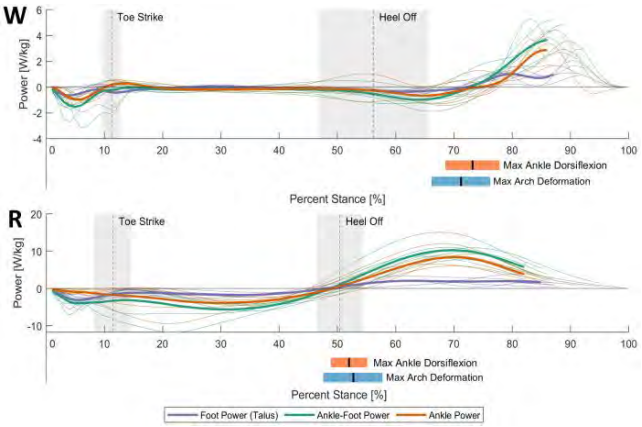

Figure 1. The UD foot, ankle-foot and ankle power plotted over stance for walking (W) and running (R). Thin lines represent each subject with the thick lines representing the mean (mean lines stop when data becomes unavailable for a single subject). Mean ± standard deviation of toe strike and heel off are indicated with dashed lines and gray shading. Orange and blue boxes represent mean ± standard deviation of maximum ankle dorsiflexion and arch deformation.

CONCLUSIONS

We found the ankle and foot simultaneously produce positive power during propulsion for both walking and running. This suggests the timing of arch and ankle mechanics, and their synchronization, is important for propulsion across locomotor modes. This supports the existence of a mechanism linking arch recoil and ankle plantarflexion.

We also found the UD power calculated using the talus was higher during propulsion than when calculated using the calcaneus. This suggests structures in the foot proximal to the calcaneus may be important for generating power during propulsion.

REFERENCES

[1] Farris et al. (2012). *J R Soc Interface,* **9**: 110-118.
[2] Takahashi et al. (2012). *J Biomech*, **45:** 2662-2667.
[3] Welte et al. (2021). *ISB 2021,* Stockholm (Abstract).
[4] Welte et al. (2022). *bioRxiv* (Preprint).

Inertial Measurement Unit calibration methods for the wrist joint: Which one should I use?

Alessandro Bonfiglio[123], Elisabetta Farella [3], David Tacconi[1], Raoul M. Bongers[4]
[1]Euleria Health, Rovereto, Italy; [2]University of Trento, Trento, Italy; [3] Fondazione Bruno Kessler, Trento, Italy.
[4] University of Groningen, University Medical Center Groningen, Groningen, Netherlands
email: abonfiglio@euleria.it

INTRODUCTION

Inertial Measurement Units (IMU) require complex calibration algorithms to convert orientation data expressed in their local reference frame into a clinically meaningful reference system. The algorithms require the wearer to perform a series of movements or poses. Several calibration methods have been developed to find the perfect trade-off between ease of use, accuracy and speed. Still, little work has been done to compare different calibration methods with each other and against a gold standard reference system [1,2]. Therefore, this paper contributes to covering this gap by assessing the accuracy and precision of a number of calibration techniques (static and dynamic) and comparing them against a gold-standard camera system.

METHODS

Seven healthy subjects with no signs of upper limb injury were recruited for this study. Five IMU sensors (Xsens DOT, Movella, The Netherlands) and five active 3-marker clusters (Optotrak Certus®, NDI, Canada), used as a gold standard reference system, were attached to the participants on the thorax, scapula, upper arm, forearm and wrist. The bony landmarks for the optical reference system presented in [3] were digitized after subjects were instrumented. Four IMU models were developed by employing different calibration techniques: 1) N-pose calibration (NP): the subject stands in neutral pose for three seconds; 2) Functional calibration (FC): the subject performs single plane movements for each joint to estimate individual rotation axes; 3) Manual alignment (MA): each sensor reference frame is manually aligned with the underlying bone frame; 4) One-Axis alignment (OA): one axis of the sensor is aligned with the long axis of the segment. The data acquisition protocol consisted of 1) Sensor calibration: a static N-pose and a series of controlled single-plane dynamic movements for shoulder, elbow and wrist; 2) Tasks: subjects were required to execute single-plane tasks for each upper limb joint and a series of multi-joint tasks that resemble common activities of daily living. A graph of an unconstrained wrist flexion/extension task at full range of motion is presented for one subject in the following paragraph.

RESULTS AND DISCUSSION

The four IMU models accurately estimated the wrist flexion/extension angle during a wrist flexion/extension task (Figure 1A). The maximum root mean squared error (RMSE) for the flexion/extension angle is 12.84±5.20° for NP, whereas the lowest RMSE is 8.76±4.16° for MA (Table 1). However, when performing the same task, the four models perform differently in estimating the radial/ulnar deviation angle (Figure 1B). In the same scenario, the highest RMSE is 34.76±9.53° for NP, whereas the lowest RMSE is 20.75±10.61° for FC.

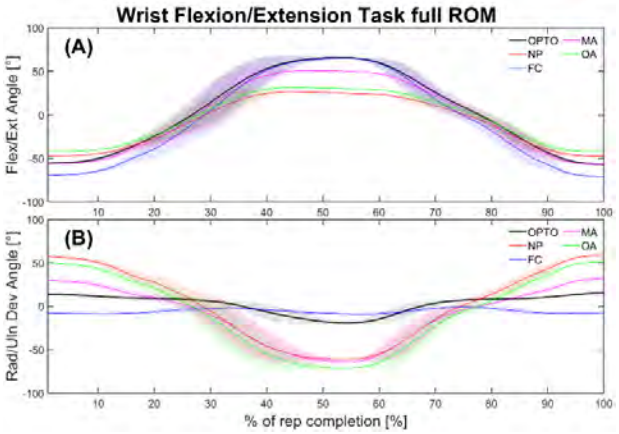

Figure 1: Plot of a wrist flexion/extension task starting from wrist fully flexed (0%) to fully extended (50%) and ending with full flexion (100%). Graph (A) displays the flexion/extension axis and graph (B) displays the radial/ulnar deviation axis.

CONCLUSIONS

All the four models presented perform rather similar in estimating the wrist flexion/extension angle, but their performance differs on the secondary rotation axis. Therefore, we advise a functional calibration approach for the best estimation of the overall wrist joint motion. However, for the highest accuracy possible on the flexion/extension axis, then we recommend the manual alignment (MA) method.

ACKNOWLEDGEMENTS

This project has received funding from the European Union's Horizon 2020 research and innovation programme under the Marie Skłodowska-Curie grant agreement No 956003.

REFERENCES

[1] Filippeschi et al. *Sensors*, **17**(6), 2017
[2] Bouvier et al. *Sensors*, **15**(8), 2015
[3] Wu et al. *J of Biomechanics*, **38**(5), 2006

Table 1: RMSE, correlation and offset (mean±standard deviation) of each IMU model calculated with respect to the optical reference system for both flexion/extension angle (FE) and radial/ulnar deviation angle (RUD) measured during a full ROM wrist flexion/extension movement.

Model	RMSE[°](FE)	RMSE[°](RUD)	R [-] (FE)	R [-] (RUD)	Offset[°](FE)	Offset[°] (RUD)
NP	12.842±5.200	34.762±9.526	0.997±0.004	0.188±0.823	7.396±5.574	10.958±11.460
FC	12.603±2.763	20.751±10.613	0.997±0.006	0.285±0.566	-6.121±8.188	-2.762±14.667
MA	8.760±4.158	26.131±10.245	0.997±0.002	0.782±0.446	1.409±6.105	15.48±10.229
OA	11.591±5.604	34.400±12.633	0.996±0.003	0.225±0.835	-1.226±7.764	8.846±15.820

Windlass Mechanism Engagement Influences Calcaneocuboid Joint Kinematics Within a Robotic-Driven Tibial Movement Envelope: A Preliminary Study

Anthony H. Le[1,2], Jordy A. Larrea Rodriguez[3], and Amy L. Lenz[1,2]

[1]Department of Orthopaedics, [2]Department of Biomedical Engineering, [3]Department of Electrical and Computer Engineering, University of Utah, Salt Lake City, UT, USA
Email: anthony.le@utah.edu

INTRODUCTION

Windlass mechanism describes how dorsiflexion of the metatarsophalangeal (MTP) joint tensions the plantar fascia around the metatarsal head during late-stance propulsion, pulling on the calcaneus, shortening, and raising the arch, and inverting the subtalar joint, configuring the foot into a stiff lever [1, 2]. However, this complex dynamic interaction and the basic functions of the windlass mechanism remain an understudied phenomenon. Particularly, individual hind- and midfoot joint kinematic compensations have not been thoroughly explored in the context of the windlass mechanism [3]. Therefore, the purpose of this preliminary study was to evaluate hind- and midfoot joint kinematics, specifically calcaneocuboid joint kinematics, during passive range of motion (ROM) testing with and without the windlass mechanism engaged using an *in vitro* robotic simulator approach.

METHODS

Two fresh-frozen tibia-to-toe tip cadaveric specimens (2 males; age = 60 ± 6 yrs old) with no history of injury or surgery were procured. Proximal tibia was affixed to a 6-axis robot manipulator end-effector via specimen-specific fixation. Infrared marker clusters were mounted to the tibia, fibula, talus, calcaneus, navicular, cuboid, 1st metatarsal, and 5th metatarsal and tracked using motion capture (Figure 1A). Weight-bearing computed tomography scans were acquired to determine transformations from marker clusters to bone local coordinate systems. Each specimen was tested with two underfoot conditions: motion on a flat surface and motion with a 45° toe-wedge to prescribe MTP joint dorsiflexion to engage the windlass mechanism. Specimens were loaded to 25% body weight in three poses, neutral, dorsiflexed, and plantarflexed, while prescribed dorsi-/plantarflexion, varus/valgus, and external/internal rotation (EIR) tibial motion. Tibiotalar, tibiofibular, subtalar (ST), talonavicular (TN), and calcaneocuboid (CC) joint angle rotations were calculated and normalized to percent activity. Statistical parametric mapping (SPM) analyses compared joint angle rotations between conditions ($\alpha = 0.05$).

RESULTS AND DISCUSSION

SPM analysis found increased CC joint external/internal rotations with the windlass mechanism engaged during peak prescribed tibial internal rotation in the neutral and plantarflexed poses (Figure 1B and D). CC joint external/internal rotations also increased with the windlass mechanism engaged during initial prescribed tibial internal rotation and during the transition between peak prescribed tibial internal and external rotation in the dorsiflexed pose (Figure 1C). Increased ST and TN joint ROMs with windlass mechanism engagement during prescribed EIR tibial motion were also observed, indicating changes in coupled motion.

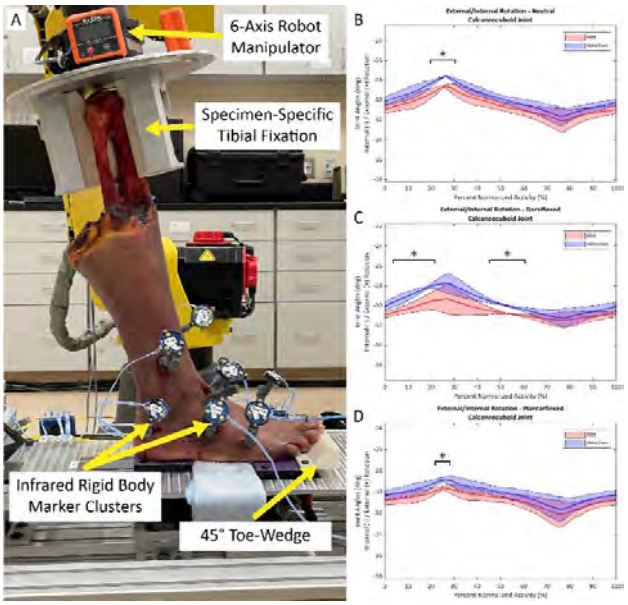

Figure 1. [A] Cadaveric specimen instrumented with marker clusters and affixed to end-effector of a 6-axis robot manipulator; Mean CC joint EIR motions during prescribed EIR in neutral pose [B], dorsiflexed pose [C], and plantarflexed pose [D] (* denotes $p<0.05$).

CONCLUSIONS

Windlass mechanism engagement increased CC joint kinematic compensations in the transverse plane. Altogether, windlass mechanism has subtle, but significant influences on midfoot kinematics. This preliminary study demonstrated a promising approach to exploring mechanistic influences of the windlass mechanism and future work will expand to include additional specimens and various foot postures.

ACKNOWLEDGEMENTS

This study was supported by Paragon 28.

REFERENCES

[1] Hicks. *J Anat* **88**:25-30, 1954.
[2] Bruening et al. *J Biomech* **73**:185-191, 2018.
[3] Welte et al. J R Soc Interface **15**:20180270, 2018.

VALIDATION OF EMG-DRIVEN MODEL-BASED ESTIMATIONS OF JOINT, MUSCLE, AND TENDON STIFFNESS

Christopher P. Cop[1], Kristen L. Jakubowski[2], Alfred C. Schouten[1,4], Bart Koopman[1], Eric J. Perreault[5,6,7] and Massimo Sartori [1]

[1] Department of Biomechanical Engineering, University of Twente, Enschede, the Netherlands.
[2] Wallace H. Coulter Department of Biomedical Engineering, Emory University & Georgia Institute of Technology, Atlanta, USA.
[4] Department of Biomechanical Engineering, Delft University of Technology, Delft, the Netherlands.
[5] Department of Biomedical Engineering, [6] Department of Physical Medicine and Rehabilitation, Northwestern University, Chicago, IL, USA.
[7] Shirley Ryan AbilityLab, Chicago, IL, USA.
Email: c.p.cop@utwente.nl

INTRODUCTION

Estimating muscle force and stiffness remains a challenge and current methods are often time-consuming and limited to controlled movements in laboratory setups. In this regard, electromyography (EMG)-driven musculoskeletal modeling is a promising method for the estimation of muscle force and stiffness during functional activities, which could eventually guide neurorehabilitation. Despite its potential, previous validations of EMG-driven model-based estimations of force and stiffness have been solely at the joint level [1], limited by a lack of *in vivo* muscle-level measurements of force and stiffness. This study presents the first attempts to validate EMG-driven model-based estimates of force and stiffness across spatial scales (i.e., joint, muscle and tendon) against experimental measurements of the same variables.

METHODS

An experimental approach was used to obtain reference ankle torques and ankle, muscle, and tendon stiffness [2]. Four healthy young adults completed two tasks using an instrumented rotatory motor to measure ankle torque and displacement. Participants performed a torque-tracking task and an EMG-tracking task, where they were instructed to produce voluntary plantarflexion torque or average triceps surae EMG at 15% of their maximum, respectively, with the aid of real-time visual feedback. The motor moved the participants' ankle through a 20-degree sinusoidal motion at 0.5 Hz. Small stochastic perturbations were superimposed on the large sinusoidal movement to quantify ankle impedance. B-mode ultrasound of the gastrocnemius medialis muscle-tendon junction was used to track muscle and tendon displacement. We estimated ankle, muscle, and tendon impedance from the collected data using time-varying system identification [3]. We evaluated the stiffness component of these impedances.

Experimental EMGs and joint angles were used to drive an EMG-driven model [1]. For each subject, reference joint torque and stiffness from the torque-tracking task were used to calibrate the EMG-driven model, while the EMG-tracking task was used for validation purposes.

RESULTS AND DISCUSSION

Preliminary results show that the EMG-driven model accurately characterized joint-level measures of torque and stiffness, as previously reported, but that predictions of muscle and tendon stiffness were less accurate (Table 1). In particular, estimated tendon stiffness was substantially higher than that measured experimentally.

Table 1: Fitting errors, normalized by experimental RMS. Mean values across all subjects.

Fitting error	Torque-tracking task	EMG-tracking task
Joint torque (%)	11	22
Joint stiffness (%)	13	34
Muscle stiffness (%)	58	55
Tendon stiffness (%)	213	179

CONCLUSIONS

Our results emphasize the importance of validating complex musculoskeletal models across different spatial scales. Future work will use muscle- and tendon-level measurements, in addition to joint-level measurements, to calibrate model parameters. We envision that our innovative approach, which combines expertise from different scientific communities, will eventually bridge the gap between precise measurements from constrained experiments and computational models able to simulate functional conditions relevant to neurorehabilitation.

ACKNOWLEDGEMENTS

Supported by ERC Starting Grant INTERACT (803035), NIH R01AR071162, F31AG069412, and ASB GIA.

REFERENCES

[1] Cop CP et al. *J Biomech* **145**: 111383, 2022.
[2] Jakubowski KL et al. *IEEE TBME* **69**: 12, 2022.
[3] Ludvig D et al. *IEEE TBME* **59**: 12, 2012.

Alterations of muscle activation to reduce knee loading for people with limb loss: a musculoskeletal simulation study

Jiayu Hu[1], Ziyun Ding[1]
[1]School of Engineering, University of Birmingham, Birmingham, United Kingdom
Email: j.hu.3@bham.ac.uk

INTRODUCTION

In England, over 42,000 major lower limb amputations (above the ankle) were performed during 10 years [1]. Among them, transtibial amputees could be at an increased risk of knee osteoarthritis (OA), thus reducing the quality of life [2]. Adverse biomechanic property is well accepted as the major risk factor of knee OA, especially for the medial compartment in the intact limb [3]. Studies have reported that knee adduction moment (KAM), as an important proxy for the medial contact force (MCF), was closely associated with clinical outcomes of medial knee OA [4]. It is also reported that a combination of KAM and knee flexion moment (KFM) leads to a better prediction of MCF [5]. Muscle coordination strategy altering muscle activation could be used to mitigate the development of knee OA. We used a musculoskeletal simulation to reduce the KAM or KAM&KFM of the intact limb to inform the muscle retraining strategy in people with limb loss.

METHODS

Motion data were collected from nine male subjects with unilateral transtibial amputation (age: 34 ± 2 yrs; weight: 86 ± 9 kg; height: 180 ± 3 cm). Marker trajectories and ground reaction forces (GRFs) were captured simultaneously using 10 cameras (Vicon, Oxford, UK) at 100 Hz and three force plates (Kistler, Winterthur, Switzerland) at 2000 Hz during walking gait and sit-to-stand activities. The OpenSim Moco, a software toolkit, was used to solve the optimal control problem of musculoskeletal simulation [6]. We conducted the musculoskeletal simulation of an amputation model developed from a generic full OpenSim musculoskeletal model, with the inputs of generalized coordinates and GRFs. Firstly, we only minimized the cost function of a combination of squared muscle controls and observed motion errors with the same weight factors. Secondly, we added another cost function to minimize the KAM. Thirdly, we combined the minimization of KAM and KFM based on the first step. Finally, we compared muscle activation solutions generated by the above-mentioned three steps.

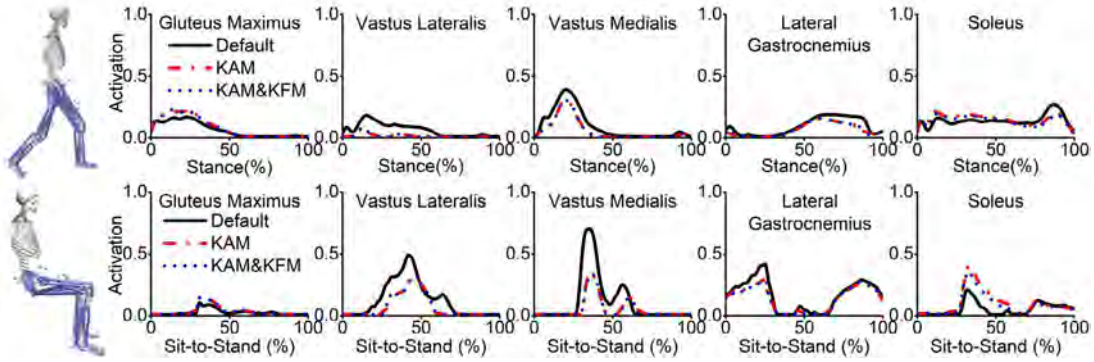

Figure 1 Muscle activations of default, minimised KAM and minimised KAM&KFM in walking and sit-to-stand for one representative.

RESULTS AND DISCUSSION

In the walking stance phase, muscle activations of the vastus lateralis and medialis, and lateral gastrocnemius, decreased by an average of 53%, 31% and 28% respectively after minimising KAM and KAM&KFM, and a similar pattern was observed in the sit-to-stand activity. In addition, muscle activations of the gluteus maximus and soleus increased in both two activities, especially for an average of two-fold increment in the soleus during sit-to-stand.

CONCLUSIONS

It was found that both gluteus maximus and soleus should be strengthened in these activities. This method could be used to develop promising treatment and rehabilitation for patients with knee disorders.

ACKNOWLEDGEMENTS

This work was supported by the Engineering and Physical Sciences Research Council (EPSRC) New Investigator Award (EP/V057138/1).

REFERENCES

[1] Ahmad N et al. *Diabetes Vasc Dis Res* **13**(5): 348-353, 2016.
[2] Norvell DC et al. *Arch Phys Med Rehabil* **86**(3): 487-93, 2005.
[3] Andriacchi TP et al. *Curr Opin Rheumatol* **18**(5): 514-8, 2006.
[4] Miyazaki T et al. *Ann Rheum Dis* **61**: 617-22, 2002.
[5] Meireles S et al. *Gait Posture* **45**: 115-20, 2016.
[6] Dembia CL et al. *PLoS Comput Biol* **16**(12): e1008493, 2020.

Creating subject-specific musculoskeletal models via morphometric transformation

Julia van Beesel[1,2], Adam Kewley[1], Philipp Gunz[2] and Ajay Seth[1]
[1] Biomechanical Engineering, TU Delft, Delft, Netherlands.
[2] Dept. of Human Origins, Max Plank Institute for Evolutionary Anthropology, Leipzig, Germany.
Email: j.v.b.vanbeesel@tudelft.nl

INTRODUCTION

Musculoskeletal models (MMs) are valuable tools to investigate biomechanical capabilities. To develop new MMs, researchers currently rely on collecting anatomical information from cadavers or multiple image sources (CT, MRI and Cryo). However, there is a growing need to develop specimen-specific musculoskeletal models for living patients, for example to predict the outcome of different surgical methods. Furthermore, studies have shown that MMs yield more accurate results when subject-specific musculoskeletal geometries are taken into account [1]. However, the development of subject-specific MMs entails a large amount of data collection and is time consuming. Our goal was to develop a new workflow for creating specimen-specific MMs that would reduce the amount of data collection and time investment required.

METHODS

In general, our workflow involves collecting patient skeletal data (for example through a CT scan), and transforming an existing MM to the subject-specific skeletal anatomy. We test this approach by transforming an existing shoulder MM [2] to the skeletal data provided by the visible human project (VHP) [3]. We use the thin-plate-spline interpolation based on correspondent anatomical landmarks to warp muscle attachment points and paths from the MM to the VHP skeletal data [4]. The muscle internal information (optimal fiber length, tendon slack length) is estimated using an optimisation algorithm [5]. The accuracy of the newly created model is evaluated through comparison to muscle path and muscle internal properties calculated from the 3D muscle volume information collected from the VHP Cryo scans, through comparison to an earlier created shoulder MM using the VHP data [6], and through comparison to adjusting model dimensions using the standard scaling tool of OpenSim.

RESULTS AND DISCUSSION

The newly estimated muscle path orientations fall within the VHP 3D muscle volumes (Figure 1). The similar muscle moment arms of the supraspinatus, middle and posterior deltoid, and subscapularis across arm abduction suggests that the transformed muscle geometry is also similar to the orientations used by Garner *et al*. [6]. Optimal fiber length and tendon slack length were comparable to the estimations of [6], but deviated somewhat from our 3D muscle volumes estimations, similarly as in [6]. Overall, the transformed MM was similar to the specimen-specific musculoskeletal geometry and yielded estimations of biomechanical capacities similar to a MM developed using traditional methods. Scaling the MM to the dimensions of the VHP skeleton shows deviating muscle moment arm and moment estimations compared to using the transformation method, suggesting the latter has a greater potential for representing the specimen-specific biomechanical capacities.

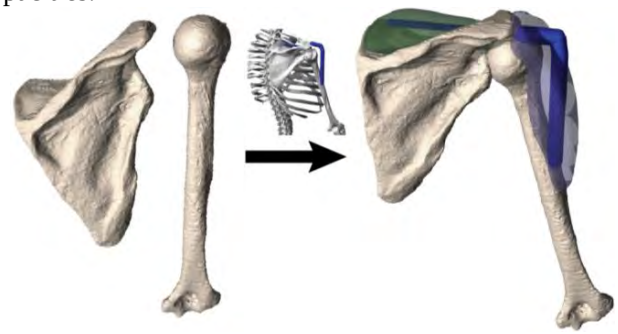

Figure 1 Creation of a subject specific model using the subject's skeletal geometry (left) and transforming a generic model (middle) to fit skeletal data. Estimated muscle attachment sites and paths fall within the patients 3D muscle volumes (right).

CONCLUSIONS

We developed a morphometric transformation workflow to create a new specimen-specific MM by transforming an existing MM. This show-case study focused on the transformation of a generic shoulder model to s specific subject, future studies will show if this method is equally successful for a greater number of subjects and a greater number of muscles and joints. The method is implemented in OpenSimCreator, an open-access software [7], which is free and easy to use.

ACKNOWLEDGEMENTS

NWO XS: OCENW.XS21.4.161
CZI EOSS2: 2020-218896
CZI EOSS5: 2022-252796
This project has been made possible in part by grant number 2020-218896 from the Chan Zuckerberg Initiative DAF, an advised fund of Silicon Valley Community Foundation.

REFERENCES

[1] Gerus P et al. *J Biomech* 46(16): 2778-86, 2013.
[2] Seth A et al. *Front Neurorobot* 13(90), 2019.
[3] Ackerman M J *Proc IEEE* 86(3): 504-11, 1998.
[4] Gunz P et al. *Hystrix It J Mamm* 24(1): 103-09, 2013.
[5] Modenese L et al. *J Biomech* 49(2): 141-48, 2016.
[6] Garner B A et al. *Comput Methods Biomech Biomed Eng* 4(2): 93-126, 2001.
[7] Kewley A. OpenSim Creator 0.3.2 *Zenodo*, 2023. https://doi.org/10.5281/zenodo.7575937

Video fluoroscopy and advanced musculoskeletal modelling unveil new insights into the mechanics of total knee arthroplasty during the golf swing

Seyyed Hamed Hosseini Nasab[1], Cédric Deguelle[1], Pascal Schütz[1], Nils Horn[3], Tomas Drobny[3], William R. Taylor[1], Stefan Preiss[3] and Renate List[2]

[1] Institute for Biomechanics, ETH Zürich, Zürich, Switzerland.
[2] Human Performance Lab., Schulthess Clinic, Zürich, Switzerland.
[3] Department of Orthopaedics/ Golf Medical Center, Schulthess Clinic, Zürich, Switzerland.
Email: seyyed.hosseini@hest.ethz.ch

INTRODUCTION

Golf remains popular in the elderly population even after total knee arthroplasty (TKA). However, considerable knee rotation with an almost fully extended knee during the club swing may expose implants to excessive loads that are conducive to mechanical failure and soft-tissue injury [1]. While the only study to measure *in vivo* knee contact forces during golf reported forces of up to 4.4 times body weight (BW) in the lead knee [2], our knowledge on the joint loading conditions remains limited to a small cohort with a specific implant design. Using video fluoroscopy and state-of-the-art musculoskeletal modelling, this study introduces a novel framework for non-invasive assessment of kinematics and loading of the knee during golf.

METHODS

Five experienced golf players (1f/4m, aged 73±6 years) with a fixed-bearing TKA (Persona®, Zimmer Biomet) were studied. Each subject performed three sets of 5 golf trials with the lead foot at a self-selected (ss), a 0° (0d), and a 30° (30d) externally rotated pose. In addition to the standard motion capture, the six degree of freedom (DoF) implant kinematics were measured using video fluoroscopy [3] (Fig. 1).

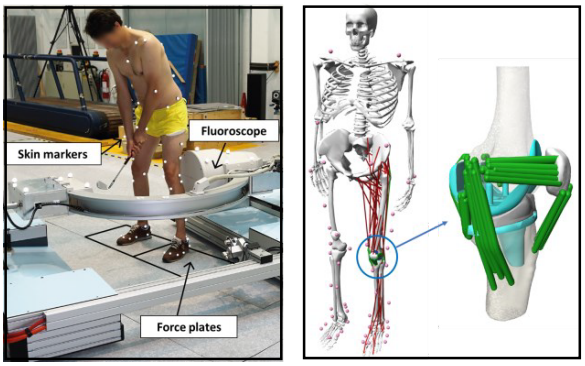

Figure 1: Measurement setup and musculoskeletal model.

A previously validated OpenSim model [4] with detailed knee structures was scaled to each subjects' anthropometry based on skin-marker locations in a standing trial. CAD models of the implant were placed within the bones based on postoperative X-ray images. Nonlinear springs representing knee ligaments and an elastic foundation contact model [4] were used to guide the 6 DoFs of the tibiofemoral and patellofemoral joint. The fluoroscopically assessed knee flexion angle together with skin-marker trajectories and ground reaction force data were used as inputs to the Concurrent Optimization of Muscle Activations and Kinematics (COMAK, [4]) algorithm. Translations and rotations of the tibiofemoral and patellofemoral joint were estimated using a cost function minimizing the sum of the squared muscle activations. Additionally, muscle, ligament, and knee contact forces were estimated throughout complete cycles of each golf swing.

RESULTS AND DISCUSSION

The very good agreement between model predictions and the fluoroscopic kinematics (Fig. 2) confirms validity of the modelling framework. Results indicated peak total tibiofemoral contact forces ranging from 1.9 to 3.9 BW, with no significant differences between 0d and 30d. These magnitudes are comparable to those measured during more challenging activities (e.g. jogging [2]). The peak patellofemoral contact force for 0d (2.1 BW) was larger than that of 30d (1.7 BW).

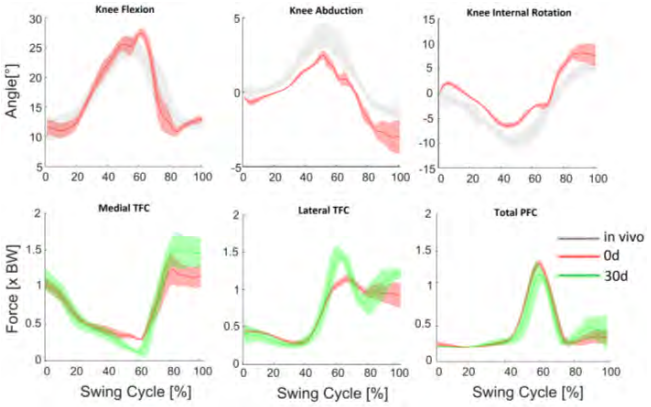

Figure 2: Fluoroscopically assessed kinematics and model predictions for an exemplary subject. TFC and PFC represent tibiofemoral and patellofemoral contact forces.

CONCLUSIONS

Clear variation across tibiofemoral and patellofemoral forces indicates that injury risk can be modulated through golfing stance and technique, and subjects should consider biomechanical optimisation of their own golfing approach according to their implant and soft-tissue status. This research continues towards elucidating the highest risk postures and techniques.

REFERENCES

[1] Baker et al. Sports Med. 47(12): 2621-2639, 2017.
[2] D'Lima et al. CORR 466(11): 2605-2611, 2008.
[3] List et al. PLoS One. 12(10): e0185952, 2017.
[4] Smith et al. J Biomech Eng. 138(2): 021017, 2016.
[5] https://github.com/clnsmith/opensim-jam

WEARABLE MOTION CAPTURE-DRIVEN MUSCULOSKELETAL FRAMEWORK FOR MULTISCALE ORTHOPEDIC BIOMECHANICS

Liming SHU[1*], Shihao LI[2], and Naohiko SUGITA[2]
[1] Department of mechanical engineering, Dalian University of Technology, Dalian, China.
[2] Department of mechanical engineering, University of Tokyo, Tokyo, Japan.
*Email: l.shu@dlut.edu.cn

INTRODUCTION

Musculoskeletal (MS) diseases, such as osteoarthritis and tendinopathy, impose a substantial burden on individuals and healthcare systems. We have a limited understanding of how physical behaviors, i.e., whole-body mechanics, influence the tissue state, which intensifies our failure to cure these prevalent and harmful diseases. MS modeling has been considered as an efficient approach to provide insights into the biomechanics of the MS system. However, the kinetics of the MS system and biomechanics of the joint tissues have been separately researched in most of previous numerical studies, which limites the understanding on interactive effects across scales.

The purpose of this research is to develop a wearable motion capture-driven multiscale MS framework to deterministically predict the individualized biofeedback and use it to link the physical behavior and tissue mechanobiology. It could be widely used in the orthopedic field, i.e., the design of rehabilitation and artificial prosthesis. This proposal provides a deterministic way to insights into the relationship between physical behaviors and tissue state, which will significantly provide a fundamental understanding of human biomechanics and help treat MS disease.

METHODS

In this study, a MS framework incorporating the wearable motion capture system and the physics-based finite-element MS human model was developed to provide the deterministic platform in multiscale orthopedic biomechanics, as shown in **Figure 1**. The wearable motion capture system included the inertia motion capture system (Xsens Awinda, Xsens Co. Ltd., Netherlands) and insole force sensor (Pedar system, Novel Co. Ltd., Germany), which was used to acquire the kinematics, axial ground reaction force, and foot-ground contact trajectory. It is known the foot-ground contact moments, lateral-medial contact force, and anterior-posterior contact force are essential inputs in the MS model, which cannot be measured by the insole force sensor. In this study, an optimization-based model was developed with the constraint of the measured foot-ground contact trajectory and axial ground reaction force [1]. Additionally, a whole-body finite element-based MS model was developed in finite element environment (Abaqus) with python-based program based on our previous studies [2]. The CAMS knee dataset [3] has been used to verify the proposed system.

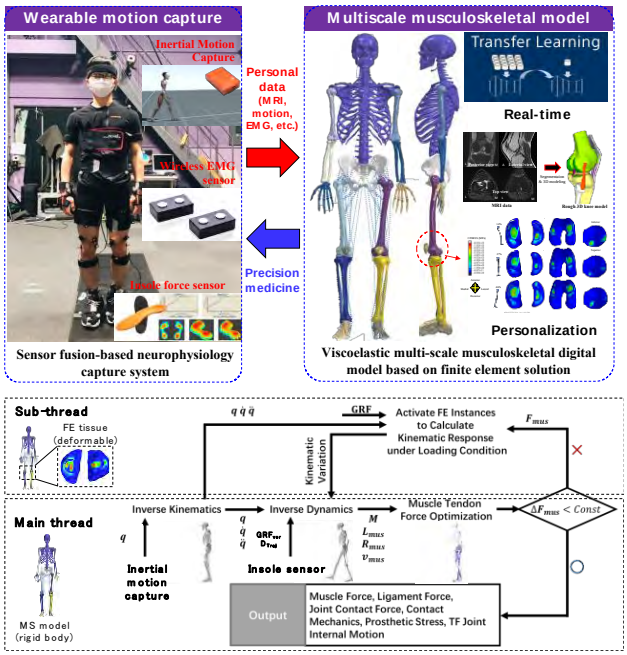

Figure 1 Framework of the proposed wearable motion capture-driven musculoskeletal model

RESULTS AND DISCUSSION

The predicted ground reaction forces and moments present good agreement (r^2>0.95) with experimental results during the gait cycle with different speeds. Additionally, the muscle activation, knee joint kinematics (r^2>0.85) and contact forces (RMSE: 0.28 body weight, r^2: 0.90) were compared with the data from CAMS knee dataset and presented a good agreement. The contact mechanics and stress were also simultaneously predicted during the simulation.

CONCLUSIONS

This study has presented an integral workflow for multiscale orthopedic biomechanics from the construction of wearable motion capture system and the subject-specific MS digital model, which can be widely used in the orthopedic field.

REFERENCES

[1] Jung Y et al. *J Biomech* **47**: 2693-2699, 2014.
[2] Shu L et al. *J Biomech* **77**: 146-154, 2018.
[3] Taylor W R et al. *J Biomech* **65**: 32-39, 2017.

AUTOMATED GENERATION OF PERSONALIZED FOOT-GROUND CONTACT MODELS

Spencer T. Williams, Claire V. Hammond, Marleny Vega, Geng Li, and Benjamin J. Fregly
Department of Mechanical Engineering, Rice University, Houston, TX, United States
Email: stwilliams@rice.edu

INTRODUCTION

One of the driving goals of musculoskeletal modeling is the optimization of treatments for individual patients with movement impairments [1-3]. For this to be possible, it must be feasible to create personalized musculoskeletal models. When predicting the effect of a treatment on walking, these models require an accurate representation of a patient's foot-ground contact mechanics to predict the ground reaction forces (GRFs) and moments produced by the new gait pattern [1,2]. Unfortunately, creating subject-specific foot-ground contact models is difficult and time-consuming, and most models do not account for ground reaction moments [1,2]. This study presents a new Matlab-based software tool for automatically generating subject-specific foot-ground contact models calibrated to experimental ground reaction force and moment data.

METHODS

The software isolates two-segment foot models from a full-body OpenSim [3] model and places linear viscoelastic elements in a grid on the bottom of the shoe. It uses MATLAB's nonlinear least squares optimization algorithm to optimize stiffness coefficients, a damping coefficient, a dynamic friction coefficient, a spring resting length, and deviations from spline-fitted experimental kinematics. The cost function penalizes kinematic changes, ground reaction errors, and each stiffness coefficient's deviation from a Gaussian weighted average of its neighbors to reduce discontinuities in stiffness profile. Users provide input data files and model settings through an XML file, which enables modification of included design variables, cost function terms, and allowable errors. To validate the method, we generated right-side personalized foot-ground contact models for one subject and varied the standard deviation of the Gaussian function (σ) used to penalize stiffness deviations.

RESULTS AND DISCUSSION

All models accurately reproduced experimental kinematics and ground reactions (Table 1). As expected, increasing σ decreased the standard deviation of stiffness coefficients. Mean stiffness also decreased, suggesting that a wider Gaussian more effectively reduces high outliers. Choosing σ for a model will depend on the properties of the subject's foot and shoe. For example, a shoe with a raised heel may require a lower σ than a more uniform shoe to allow for more variation in stiffness. Generating each of the models in Table 1 required 4 to 4.5 hours of CPU time.

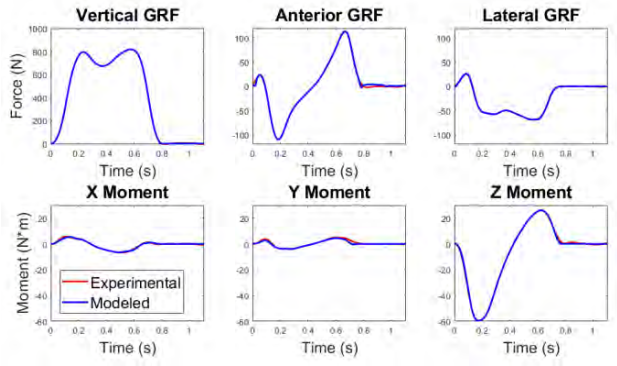

Figure 1: Modeled and experimental ground reactions for σ = 0.05.

CONCLUSIONS

This new tool automates the complex process of modeling foot-ground contact with a two-segment foot model, a critical step toward practical personalized musculoskeletal modeling. These results indicate that varying σ controls the stiffness distribution in the model without significantly impacting tracking of ground reactions and kinematics. Source code and tutorials for this tool will be available on SimTK.org as part of a model personalization pipeline plugin for OpenSim.

ACKNOWLEDGEMENTS

This research was funded by the U.S. National Institutes of Health (grant R01 EB030520 to B. J. Fregly).

REFERENCES

[1] Jackson J et al. J Biomech Eng 138,9, 2016
[2] Meyer A et al. Front Bioeng Biotech 4, 2016
[3] Seth A et al. PLoS Comput Biol 14(7), 2018

Table 1: RMS errors for ground reactions and kinematics with viscoelastic element stiffness distributions (mean ± standard deviation).

Gaussian σ	GRF RMSE (N)	Moment RMSE (N*m)	Rotation RMSE (°)	Translation RMSE (mm)	Stiffness (N/m)
0.05	1.813	0.564	1.983	5.195	3528.5 ± 1364.0
0.10	1.815	0.599	1.932	5.333	2789.4 ± 820.39
0.15	1.807	0.608	1.934	5.410	2664.9 ± 761.27

TOWARDS REHABILITATION OF UPPER LIMB DISORDERS VIA NEURO-MUSCULOSKELETAL MODELLING

Harnoor Saini[1], Oliver Röhrle[2], Thor Besier[1]
[1]Auckland Bioengineering Institute, University of Auckland, Auckland, New Zealand
[2]Institute of Modelling and Simulation of Biomechanical Systems, University of Stuttgart, Stuttgart, Germany
Email: h.saini@auckland.ac.nz

Introduction

The application of biomechanical simulation as a tool for the diagnosis and treatment of upper limb disorders, such as paralysis caused by stroke or rotator cuff injuries, is limited by the challenges in generating patient-specific anatomy and the complexity of the neuromuscular (NM) pathway. In this project, we utilize statistical shape models (SSMs) to efficiently generate anatomy from partial or sparse data of the upper limb. Additionally, we introduce a modelling framework for the NM pathway to provide a comprehensive neuro-musculoskeletal (NMSK) model. This model can be used to analyse the relationships between neural inputs and motor outputs, with the goal of improving diagnosis and treatment of NMSK pathologies.

Methods

To predict MSK geometry from limited data, we developed a proof-of-concept compound SSM for five bones of the left and right upper limb (total of 420 bone geometries) using the GIAS framework [1]. This SSM was used to investigate the interdependence of bone morphology in the upper limb. Furthermore, we applied the SSM to predict the forearm geometry from partial data of the upper limb.

Towards simulating the NM pathway, we developed a computational modelling framework that includes key components of the NM pathway from the motor cortex to muscle contraction (Figure 1) [2]. As a first step within this framework, a 3D MSK model with embedded motor units (MU) [3] was developed and used, for example, to measure the accuracy of MU twitch forces at the limb [4].

Results

The SSM results for the upper limb revealed, for example, that the inclination of the scapula is correlated with radial and ulnar twists, but inversely related to scapular version and humeral radius of curvature and torsion. Length scaling was generally consistent across bones, but bones in the forearm (radius and ulna) showed a greater proportional length change. The 3D MU embedded MSK model showed that MU twitch forces measured at the limb were underestimated due to force redistribution in the muscle, and that MU twitches do not linearly sum due to shear stresses in the muscle.

Conclusions

The preliminary results from the compound SSM analysis revealed the interconnection of shoulder girdle anatomy and has potential applications in surgical planning, such as shoulder arthroplasty, and in the generation of MSK models. The NM modelling results emphasized the importance of including MUs in MSK simulations. Accurate and personalized computer models can contribute to the effective diagnosis, treatment, and rehabilitation of NMSK pathologies.

ACKNOWLEDGEMENTS

This research was partially funded by the NZ MBIE Catalyst Strategic Fund ("12 Labours") and by the DFG (German Research Foundation) projects "Priority Program 2311" and "Soft Tissue Robotics".

REFERENCES

[1] Zhang J et al. *Biomed Sim*: 182-192, 2014.
[2] Haggie L et al. *Front Physiol*: under review.
[3] Saini H et al. *Biomech Model Mechanobiol*: 2022.
[4] Saini H and Röhrle O. *Twitch force*: 2023.

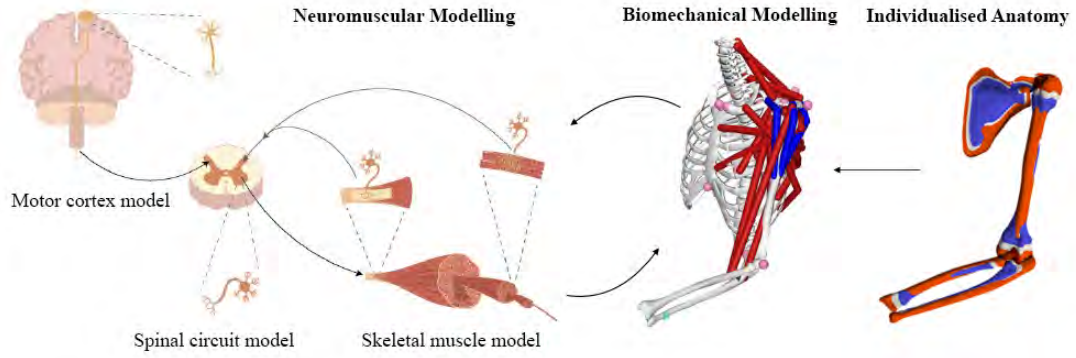

Figure 1: Modelling overview of the proposed neuro-musculoskeletal framework.

Validation of smartphone-based analysis of human kinematics during 45° changes of direction

Cameron H.N. Stephen, Ezio Preatoni[1]
[1]Department of Health, University of Bath, Bath, United Kingdom
Email: chns20@bath.ac.uk, ep314@bath.ac.uk

INTRODUCTION

Anterior Cruciate Ligament (ACL) injuries have significant injury burden and have long-term consequences such as osteoarthritis [1]. Changes of direction (CoD) are the most common mechanism of non-contact ACL injury and several kinematic quantities have been identified as risk factors during this task [2]. Therefore, assessment of CoD technique can be used to screen for ACL injury risk. To be applicable in regular practice, screening tools need to be reliable and simple to implement in-field. Novel open-source software (OpenCap) [3], allows for biomechanical field testing, using only 2 smartphones. OpenCap uses pose-estimation algorithms (OpenPose) and muscle driven simulations to compute kinematics and kinetics [3]. Currently, OpenCap has been validated for walking, squats, drop jumps, and sit-to-stands [3]. Further validation for different movements are necessary for its application in clincal and performance settings.

This study aims to validate OpenCap kinematics during 45° CoD with a 3-step run-up.

METHODS

Seven healthy participants performed ten 45° CoD with a 3-step approach, with their kinematics simultaneously captured by a 15-camera marker-based motion capture system (Qualisys, 200 Hz) and OpenCap (Version 1.6) using 3 smartphone-cameras (720p, 60 Hz). Twenty-three reflective markers were placed on the participants lower extremities and torso for Qualisys motion-capture. A single trigger was used to initiate both motion capture recordings and a LED light array. The LEDs were used to synchronise data between methods. Data were cropped from initial ground contact during the CoD to toe-off. Hip flexion angle, hip abdution angle, knee flexion angle, and ankle dorsi/plantar-flexion angle were computed on OpenSim for comparison.

Root mean square error (RMSE) and Statistical Parametric Mapping (SPM) were used to compare kinematics during the CoD (α=0.05).

RESULTS AND DISCUSSION

RMSE for hip flexion (11.94°), knee flexion (9.71°), and ankle flexion (7.82°) were greater than previously validated movements, which had a mean RMSE of 7.07° 5.69°, and 7.03°, respectively [3]. However, RMSE for hip abduction (2.50°) was lower than previously validated movements (5.69°) [3].

Over-estimation in hip flexion angles were observed for the entire duration of movement, with significant differences between methods at 0-20% and 60-90% (Figure 1). Greater knee flexion angle and plantar flexion angle is correlated with reduced knee joint moments during CoD lowering the risk of injury [2]. Therefore, underestimation in knee flexion angle from 20-80% and significant underestimation in plantar flexion angle at 20-50% of the CoD may result in falsely classifying individuals for higher injury risk (Figure 1). Finally, limited mean difference and small RMSE in hip abduction angles suggest that OpenCap can accurately measure frontal plane motion, previously not investigated.

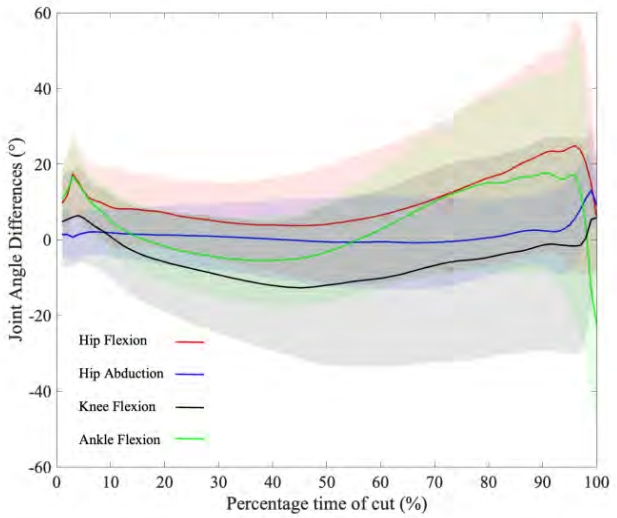

Figure 1: Mean joint angle difference between OpenCap and marker-based motion-capture. Shaded area shows standard deviation

CONCLUSIONS

OpenCap has several benefits over marker-based motion capture as it removes error from skin motion artefact and reduces time and costs of kinematic analysis. This study's results are promising for measuring frontal plane kinematics. However, further training of the pose-estimation algorithms or different experimental setup may be necessary for improving the system performance in estimating hip, knee, and ankle flexion angles, as the current outcomes may be not accurate enough to be used as an injury risk screening tool.

REFERENCES

[1] Lohmander et al. *Arthritis and Rheumatism* **50**: 3145-52, 2004
[2] Donelon et al. *Sports Medicine* **6**: 53, 2020
[3] Uhlrich S et al. *BioRxiv preprint* **86**: 34-9, 2022.

Estimating how sensorimotor impairments influence walking speed in persons with spinal cord injury with machine learning techniques

Minh T.N. Truong[1], Emelie Butler Forslund[2,3], Åke Seiger[2,3], and Elena M. Gutierrez Farewik[1,4]
[1] KTH MoveAbility Lab, KTH Royal Institute of Technology, Stockholm, Sweden.
[2] Aleris Rehab Station Stockholm, Stockholm, Sweden.
[3] Department of Neurobiology, Care Sciences and Society, Karolinska Institutet, Stockholm, Sweden.
[4] Department of Women's and Children's Health, Karolinska Institutet, Stockholm, Sweden.
Email: minht@kth.se

INTRODUCTION

People with spinal cord injury (SCI) often exhibit slow walking speed, a result of impairments in both motor and sensory functions. However, the precise causal effects of these impairments are not well understood due to the presence of various confounding factors such as level of injury, severity, time since injury, or age. To gain a deeper understanding of these effects, we propose using a combination of game theoretic approach, SHAP (SHapley Additive exPlainations) [1], and a gradient boosting machine learning model (XGBoost [2]) to study the causal impacts of motor and sensory impairments on walking speed in individuals with SCI.

METHODS

Nine individuals with SCI [5 men/4 women; age 56.2 years ± 11.4; level of injury from T4 to L4] and a control group without SCI [7 men/4 women; age 53.2 years ± 9.3] gave informed consent and participated. All participants underwent 3D motion analysis at a comfortable walking speed. Participants with SCI were assessed with manual muscle strength tests by an experienced clinician, and assigned a muscle strength score corresponding to the sum from 9 key lower extremity muscle groups. Sensory impairment was scored as a sum of the light touch scores as per the ASIA test according to international SCI guidelines. Non-impaired participants were assumed to have the maximum possible muscle strength (45) and sensory (56) scores. We created a model that incorporates a range of demographic and functional factors, including age, gender, BMI, motor level, sensory level, muscle strength score, light touch score, and assistive device, as inputs. The model output, walking speed, is intended to be indicative of walking performance. The model's goal is to map the complex relationship between performance outcomes and underlying demographic and functional factors. To ensure the validity of our results, we separated the dataset into training (90%) and testing (10%) sets. We trained our model using the XGBoost algorithm and analyzed its results using the SHAP package in Python.

RESULTS

Our model indicated that muscle strength score was the predominant factor influencing comfortable walking speed in individuals with SCI, followed by BMI and age (Figure 1A). The baseline value was the average walking speed among our training data set. For each participant, the model quantified how much each factor increased or decreased the baseline walking speed (Figure 1B).

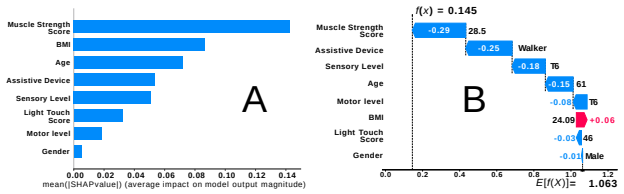

Figure 1: A. Average impact for each factor on model output; **B.** Contribution from each factor to push the model output from the base value in one participant with SCI. The numbers in each bar indicate how that factor contributes to a baseline walking speed of 1.063 m/s; for instance, muscle strength score of 28.5 (out of 45) results in a 0.29 m/s reduction in walking speed.

CONCLUSIONS

Our model has the potential to quantify how motor, sensory or other underlying factors can influence a given outcome performance measurement. In its current form, it describes how much each factor can decrease or increase a "baseline" walking speed, and has thus great potential in decoding the complex causal relationship between walking speed and sensorimotor sensory impairment, given other confounding factors such as BMI or the use of an assistive device. However, as the dataset is currently limited and the project is ongoing, it is possible that the model may be overfitted. As more data is collected in the future on this and on other patient populations, and as its ability to predict a larger set of performance outcome parameters is studied, the model has vast potential to provide clinically relevant insight into the complex factors that influence the motor performance.

ACKNOWLEDGEMENTS

We gratefully acknowledge the generous support by the Swedish Research Council and the Promobilia Foundation.

REFERENCES

[1] Scott L & Su-In L. *NIPS'17*: 4768–4777, 2017.
[2] Tianqi C & Carlos G. *KDD'16*: 785–794, 2016.

VALIDITY OF ARTIFICIAL INTELLIGENCE-BASED MOTION ANALYSIS SYSTEM ～ AI ANALYSIS VS. HUMAN ANALYSIS

Takumi Ino[1,3], Mina Samukawa[2], Tomoya Ishida[2],
Naofumi Wada[3], Yuta Koshino[2], Satoshi Kasahara[2], Harukazu Tohyama[2]
[1] Graduate School of Health Sciences, Hokkaido University, Sapporo, Japan.
[2] Faculty of Health Sciences, Hokkaido University, Sapporo, Japan.
[3] Faculty of Health Sciences, Hokkaido University of Science, Sapporo, Japan.
Email: ino-t@hus.ac.jp

INTRODUCTION

Artificial intelligence-based motion analysis (AI-MA) using convolutional neural networks and deep learning approaches have recently become an attractive tool for estimating motion data using human video analysis. Until recently, human visual inspection-based motion analysis (Human-MA) has been widely used for motion data analysis. However, this approach was time-consuming and had certain limitations in terms of validity. AI-MA has a potential to solve these problems. Therefore, the purpose of this study was to compare the accuracy of AI-MA with Human-MA and to clarify the validity of AI-MA.

METHODS

Twenty-one healthy young participants (10 males and 11 females, age: 20.7 ± 1.0 years, BMI: 21.6 ± 2.7 kg/m^2) participated in this study. Three successful drop vertical jump tests were set as the movement task. We used OpenPose [1] for the AI-MA base algorithm. As a conventional analysis, Human-MA based on human visual inspection was performed by a well-trained analyst with Frame-Dias V software (DKH, Japan). The knee abduction-adduction angle was calculated by AI-MA and Human-MA using the same single-plane video image. To confirm the validity, the same parameters were simultaneously recorded by a three-dimensional VICON motion analysis system (VICON: Vicon Nexus 2.10, Vicon Motion Systems Ltd., Oxford, England). Furthermore, video distortion was corrected with using spatial calibration information from the VICON three-dimensional motion analysis system to eliminate the effects of lens distortion from the video camera. Mean errors, mean absolute errors, and Pearson's correlation coefficient for waveform pattern evaluation were obtained (AI-MA vs. VICON, Human-MA vs. VICON).

RESULTS AND DISCUSSION

No significant difference was found between AI-MA and Human-MA for mean errors or mean absolute errors of knee abduction-adduction angles (Table 1). The Pearson correlation coefficients of AI-MA and Human-MA in comparison with VICON were 0.82 and 0.88, respectively. AI-MA showed good accuracy and did not differ from the conventional Human-MA. In addition, AI-MA had a strong correlation with VICON. Qualitatively, the waveform patterns obtained from AI-MA and VICON were fairly consistent (Fig. 1). Although certain measurement errors must be addressed, AI-MA should become a useful tool and has the advantage of saving costs and time for motion analysis.

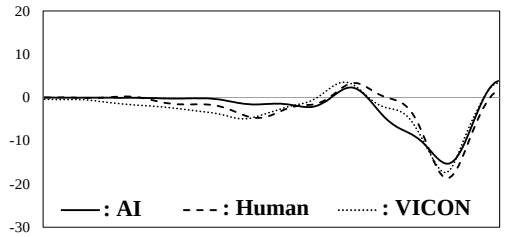

Figure 1 Example of the waveform pattern (one case)
Pearson's r vs. VICON: AI, 0.91, Human, 0.95

CONCLUSIONS

AI-MA was found a good accuracy compared to VICON and did not differ from conventional Human-MA. AI-MA has both cost-effective and time-saving advantages compared to conventional Human-MA.

REFERENCES

[1] Zhe Cao et al. IEEE Trans Pattern Anal Mach Intell. **43**: 172-186, 2021.

Table 1: Mean errors, mean absolute errors, and Pearson's correlation coefficients compared to the VICON 3D motion analysis system.

	AI	Human	*p-value*
Mean errors (95%CI)	1.3° (0.5° to 2.1°)	1.5° (0.7° to 2.2°)	0.763
Mean absolute errors (95%CI)	2.9° (2.4° to 3.4°)	2.6° (1.9° to 3.3°)	0.438
Pearson r (Max to Min)	0.82 (0.64 to 0.98)	0.88 (0.39 to 0.99)	0.120

AI: Artificial Intelligence-based motion analysis, Human: Conventional human visual inspection-based motion analysis

P-value: AI vs. Human by unpaired t-test

DEEP LEARNING SUCCESSFULLY CLASSIFIES ACOUSTIC EMISSION DATA FROM KNEE JOINTS

Ivan Vatolik [1], Chinedu Mbachu [1], Gordon Hunter [1], Nicola Swann [2], Michael Everington [1] and Andy T. Augousti [1]
[1] School of Engineering & Environment, Faculty of Engineering, Computing and the Environment, Kingston University London, UK.
[2] School of Biosciences & Medicine, Faculty of Health and Medical Sciences, University of Surrey, UK.
Email: k1465290@kingston.ac.uk

INTRODUCTION

The prevalence of injuries associated with dynamic physical activity has compelled scientists to study changes in body structures after exercise, with degenerative changes to tissues and implications of these of particular concern. The function of cartilage in joints is for bones in motion to evenly transmit loads from one body segment to another at very low friction. During these events it has been shown that cartilage undergoes changes in volume, thickness, and joint space narrowing [1]. In recent years much research has been conducted in developing novel ways of joint degeneration identification and joint health assessment using Acoustic Emission (AE) [2,3].

METHODS

32 adult volunteer participants took part in the study. The participants were assigned in one of the three age groups 18-34, 35-49 and 50+. To calculate kinematic and dynamic variables nine Qualisys Oqus 700+ cameras and a Kistler Force Plate were positioned around the capture area. 28 reflective markers were placed on specific body landmarks [4]. A sensitive condenser microphone connected to the Laryngograph DSP Unit [Laryngograph Ltd., London, UK] was attached on the lateral soft part of the knee. Each participant was asked to perform a set of three sit-stand-sit (S–S–S) cycles three times for each leg on five different days. A custom-made MATLAB code was developed to process and analyse collected data. Two different Deep Neural Networks (DNNs) were used to classify the AE signals. This research project and its methodology were granted ethical approval by the Ethics Committee of Kingston University London.

RESULTS AND DISCUSSION

This project aimed to analyse the AE signal data obtained from the knee joints of people performing an S-S-S cycle. The results indicate that. although no S-S-S cycle is the same, there is a correlation between the obtained AE and the associated kinematic data. The synchronized plot of the knee angle, angular velocity & accelaration, and AE signal shows that there is a relationship between them. The AE events can be seen to coincide with the peak velocities during ascent and descent for each of the three cycles. There are also smaller AE events occuring during a change in angular velocity.

The AE signal was explored in Time & Frequency domains. The findings show that amplitudes differ between participants and within sessions, however a unique AE pattern is evident. The frequency domain indicates that the signal is predominantly low frequency; signal with the most power >1kHz.

Two different Deep Neural Networks (DNNs) were used to categorise the AE signals. These were Recurrent Neural Network (RNN) and Convolutional Neural Network (CNN). CNN was applied to the spectrograms to try to predict the age group of each participant, and overall obtained the best testing accuracy with a score of 81.82% (see figure 1).

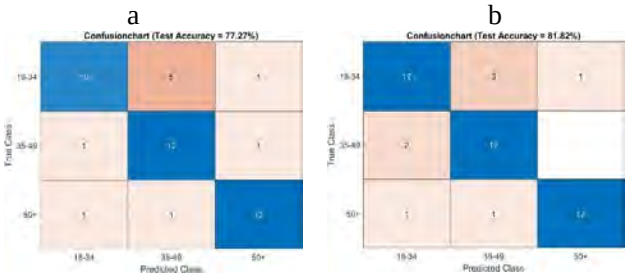

Figure 1 Best trained networks using spectrograms

CONCLUSION

The results of the experiment have shown that the characteristics of the AE signal can vary from one cycle to another, and even more so, from one day to another. However, the AE events appear to be directly correlated with the knee angular velocity. The use of DNNs shows that they can be used to categorise participants into age groups with good accuracy. To improve upon the accuracy of the model the inclusion and exploration of the kinematic features into the MATLAB model is the next step in our research.

REFERENCES

[1] Eckstein F et al. *Ann. Rheum. Dis.* **64** (2005)
[2] Mascaro B et al. *Med. Eng. Phys.* **31** (2009)
[3] Choi D et al. *Sensor. Mater.* **30** (2018)
[4] Vatolik I et al *Meas: Sens.* **24** (2022)

Evaluation of the estimated length of the plantar aponeurosis using a multi-segment foot model

Yuka Matsumoto[1,2], Naohiko Kanemura[2], and Naomichi Ogihara[1]
[1] Department of Biological Sciences, The University of Tokyo, Tokyo, Japan.
[2] Department of Health and Social Services, Saitama Prefectural University, Saitama, Japan.
Email: yuka-matsumoto@g.ecc.u-tokyo.ac.jp

INTRODUCTION

A multi-segment foot model incorporating the plantar aponeurosis (PA) was developed to estimate the pattern of stretch and tensile force generated by the PA during dynamic movements such as walking, running and jumping[1)]. This foot model comprised three segments (phalanx, forefoot, and hindfoot) and the PA was modeled as five linear springs connecting the origins and insertions via intermediate points (Fig . 1). The model defines the positions of these points with respect to the corresponding segment coordinate systems based on CT data of the foot of an adult male[1)]. Therefore, the lenghts of the PA during movements can be calculaetd based on the motion-caputured coordinates of the 14 markers attached to foot anatomical landmarks (Fig. 1). However, the validity of the length estimate of the PA using the multi-segment foot model has not been sufficiently investigated mainly due to the difficulty associated with measuring the true PA length during movements. The present study aimed to evaluate the accuracy of the length estimate of the PA by quantifying the true PA lengths in three different foot postures using computed tomography (CT).

METHODS

Three healthy adult males participated in the experiment. CT scans (SOMATOM go.Top 64; Siemens, Munich, Bavaria, Germany) of the foot with the attached 14 markers were performed in three different foot postures in the supine position: (1) non-weightbearing neutral posture, (2) simulated weightbearing posture with midfoot dorsiflexion and metatarsophalangeal (MP) joint plantarflexion, and (3) simulated weightbearing posture with midfoot plantarflexion and MP joint dorsiflexion (Fig. 2). The latter two postures were achieved by applying load to the foot using a loading device. The slice thickness and pixel size of the obtained images were 0.6 mm and 0.416 mm, respectively. To quantify the PA lengths of the foot from the CT scan data, semi-automatic segmentation and 3D reconstruction of the PA was performed using image analysis software Mimics 25.0 (Materialise, Leuven, Belgium). Each reconstructed 3D surface model of the PA was imported to Geomagic Design X 2020 (3D systems, Rock Hill, SC, USA) to quantify the true length of the PAs by digitizing the paths of the PA from the origins to insertions on the plantar surface of the PA. In addition, the PA lengths were estimated based on the 14 marker coordinates and the multi-segment foot model. The differences of the estimated and true PA lengths were calculated for each foot posture and subject, and expressed as the percentages of the PA lengths.

RESULTS AND DISCUSSION

The true lengths of the PA in the neutral position measured based on the CT data were 160 ± 3 mm, 165 ± 5 mm, 164 ± 4 mm, 155 ± 2 mm, and 148 ± 6 mm for PA1, PA2, PA3, PA4, and PA5, respectively (mean ± standard deviation). In the midfoot dorsiflexed, MP joint plantarflexed posture, the PAs were stretched by -2.1 ± 2.1 mm, -0.5 ± 4.3 mm, -3.3 ± 2.5 mm, -0.6 ± 0.5 mm, 0.7 ± 3.6 mm, respectively, and in the midfoot plantarflexed, MP joint dorsiflexed posture, they were stretched by 3.4 ± 4.7 mm, 0.5 ± 4.4 mm, -0.5 ± 2.5 mm, 1.5 ± 3.3 mm, 2.5 ± 3.8 mm, respectively. In the present experimental conditions, the PA lengths were maintained approximately constant regardless of variations in the foot posture possibly due to inability to stretch the PA in the simulated weightbearing postures. The differences between the PA lengths estimated based on the multi-segment model and the true values of PA lengths obtained from the CT data were less then 3 % of the PA length (Fig. 3), indicating that the estimated lengths of the PA based on the multi-segment foot model were reasonably accurate. However, further evaluation is necessary using the CT data of the foot with more stretched PAs using a weightbearing CT.

CONCLUSIONS

The estimation of the PA length using a multi-segment foot model may serve as a reliable tool to quantify the pattern of the PA stretch during dynamic movements.

REFERENCES

[1] Matsumoto Y et al. *Front Bioeng Biotechnol* **10**: 894731, 2022

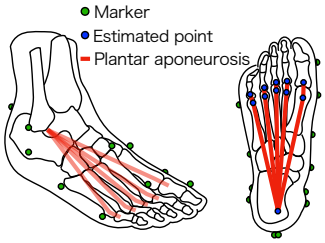

Figure 1 Multi-segment foot model incorporating plantar aponeurosis

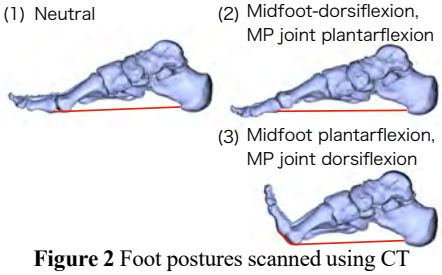

Figure 2 Foot postures scanned using CT

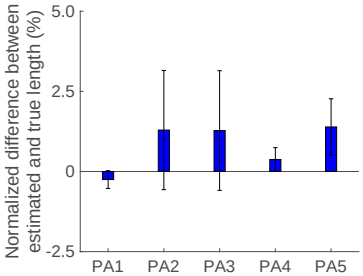

Figure 3 Normalized difference between estimated and true length

HELMET PERFORMANCE AND BODY EFFECTS IN HEAD IMPACTS IN E-SCOOTER FALLS

Wei WEI[1,2*], Nicolas Bailly[1,2], and Pierre-Jean Arnoux [1,2]
[1] Laboratoire de biomécanique appliquée, Aix-Marseille Univ & Univ Gustave Eiffel, Marseille, France.
[2] iLab-Spine, France & Canada.
*Email: wei.wei@univ-eiffel.fr

INTRODUCTION

Head injuries were reported as one of the most common injuries during electric scooter (or E-scooter) accidents [1]. Bicycle helmet was previously found efficient to reduce head impact loadings but not to prevent severe head injuries during E-scooter falls induced by collision with a curb [2]. However, the efficacy of a motorcycle helmet in reducing head injuries during these falls remains to be studied. In current testing standards, bicycle and motorcycle helmets are evaluated against drop tests using an isolated headform. In real accidents, other body parts besides the head can also interact with the ground and thus influence the impact responses of the head. Therefore, the objective of this study is to 1) study the performance of a motorcycle helmet in reducing head injuries 2) and the effect of the body in influencing head impact responses in E-scooter falls.

METHODS

The finite element (FE) model of E-scooter falls was previously developed to evaluate the efficacy of a bicycle helmet in reducing head injuries [2]. A total of 27 E-scooter falls due to the collision with a curb was previously simulated, representing different initial E-scooter speeds (10, 20, and 30 km/h), orientations of the curb (30, 60, and 90°), and orientations of the E-scooter (-15, 0 and 15°) [2]. This model was still used in this work to study the performance of a motorcycle helmet in head-ground impacts during these E-scooter falls. The helmet FE model was previously validated, optimized for better head protection [3], and evaluated in head-ground impacts during karting rollover accidents [4]. This helmet FE model was fit on the rider of the E-scooter fall FE model. A similar full-restart procedure was applied as was previously done [3] to inherit the body kinematics before the moment when the head hit the ground during E-scooter falls. Thus, the head-ground impact conditions were warranted the same among the E-scooter falls (or *full-body simulations*) without a helmet and with the bicycle or motorcycle helmet.

To study the body effects in influencing head impact responses, the head-neck joint was detached from the rider FE model also with the full-restart procedure at the moment of head-ground impact. Then the isolated head without a helmet and with the bicycle (Figure 1A) or motorcycle helmet would hit the ground with the same impact conditions as in the full-body simulations. Additionally, a virtually-added mass of 5kg and 10kg was respectively attached to the center of gravity of the head for the isolated head-ground impacts to study the effects of headform mass in influencing head impact responses. Finally, four series of E-scooter fall simulations without a helmet and with a bicycle or motorcycle helmet were performed: 1) full-body, 2) isolated head, 3) isolated head+5kg, and 4) isolated head+10kg.

RESULTS AND DISCUSSION

The HIC_36 (213.7~1746.8) and BrIC (0.23~1.18) predicted in full-body simulations with the motorcycle helmet were significantly ($p<0.01$) lower than those without a helmet (1780.0~42324.7 and 0.38~1.73) or with the bicycle helmet (337.9~30755.0 and 0.53~1.77) (Figure 1B and C). The HIC_36 was above the injury threshold (1000) in 24 (88.9%) and 14 (51.9%) E-scooter falls with a bicycle and motorcycle helmet respectively, with the BrIC above the injury threshold (1.0582) in 12 (44.4%) and 2 (7.4%) falls with a bicycle and motorcycle helmet respectively. The HIC_36 predicted in isolated (no added mass) head-ground impacts with the motorcycle helmet was significantly ($p<0.01$) higher than that predicted in full-body simulations. Otherwise, HIC_36 and BrIC predicted in isolated head-ground simulations were always significantly ($p<0.01$) lower than those predicted in full-body simulations, not depending on the helmet type or virtually-added mass to the head (Figure 1).

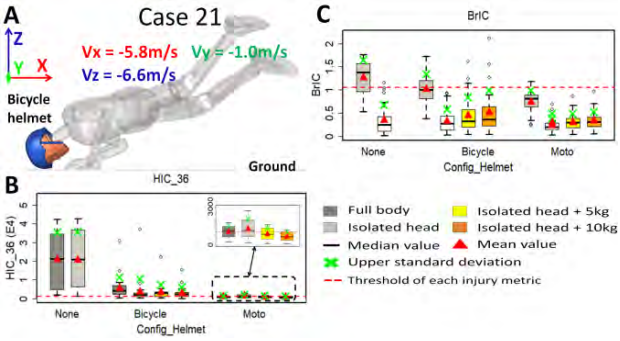

Figure 1 (A) An example of a full-body (transparent) E-scooter fall and an isolated (colored) head-ground impact simulation; (B) BrIC and (C) HIC_36 during E-scooter falls for full-body and isolated simulations with and without a helmet.

CONCLUSIONS

The motorcycle helmet was more protective than a bicycle helmet, but could not fully eliminate risks of severe head injuries during E-scooter falls. No matter the virtually-added mass, isolated head-ground impacts generally underestimated body effects in increasing head injury metrics and thus overestimated the helmets' efficacy in E-scooter falls.

REFERENCES

[1] Cicchino JB et al. *J Safety Res* **76**:256–261, 2021.
[2] Wei W et al. *Accid Anal Prev* **181**: 106935, 2023.
[3] Li et al, Int J Mech Sci, **199:** 106406, 2021.
[4] Wei W et al. 27th ESB, 2022

INFLUENCE OF MIDSOLE COMPRESSION ON ACCELERATION MAGNITUDE IN RUNNING

Robin Trama, John W. Wannop, Emily Smith, Darren J. Stefanyshyn
Human Performance Laboratory, Faculty of Kinesiology, University of Calgary, Calgary, AB, Canada
Email: robin.trama@ucalgary.ca

INTRODUCTION

Due to the repetitive movement of running, a large number of foot-ground impacts will be sustained over the course of a single run. From the repetitiveness of these impacts, the body is exposed to substantial impact-related mechanical stress [1]. Aside from the mechanical impact, runners will also experience mechanical vibrations in the bones and the soft tissues (i.e., muscle, tendon, fat, and skin) of the leg, which can lead to discomfort, fatigue, and muscle damage [2, 3]. A recent review found that shoes with thicker and more viscous midsoles were effective in limiting vibration magnitude [3], however, the actual compression of the midsole was not quantified. Only one study quantified the compression of the midsole during the stance phase of running, and found that when midsole compression was increased the foot, sacrum, and head accelerations were reduced [4]. However, the direct relationship between midsole compression and acceleration at different locations on the body has not been examined. Therefore, the purpose of this study was to investigate the influence of midsole vertical and horizontal compression on the magnitude and frequency of soft tissue vibrations and bone accelerations during running.

METHODS

Forty-eight individuals were instructed to run at their self-selected pace on an instrumented treadmill for four bouts of 5 minutes, wearing four different shoes. The different footwear conditions had identical uppers with only changes in the midsole construction via 3D printing. Vertical hardness of the midsole was quantified with mechanical testing, and the shoes were classified from soft to stiff (106 to 144 $N \cdot mm^{-1}$). A total of 7 reflective markers forming 3 clusters were glued on the lateral side of the midsole of the left shoes [4]. During the last minute of each run vertical and horizontal compression of the midsole over the stance phase was quantified by tracking the displacement of the markers at 200 Hz with optoelectronic cameras. In addition, ground reaction forces were recorded at 2000 Hz with force plates, and acceleration data at 6 locations (heel, tibia, calf, quadriceps, sacrum, head) was collected at 1600 Hz with tri-axial accelerometers. A continuous wavelet transform was used to analyze acceleration data and obtain the total energy of vibration at each frequency from 2 to 200 Hz. Non-parametric regressions with permutation tests were performed between the vibration energy and the maximal compression of the midsole.

RESULTS AND DISCUSSION

The midsole compression for the different shoes ranged from 1.0 to 8.2 mm (vertical) and 1.1 to 7.2 mm (horizontal), with greater compression occurring in the softer shoes. Regression analysis depicted that a more compressive midsole was significantly correlated with less vibration energy at each impact (Figure 1). Tibia and calf muscles were the locations where the greatest reduction occurred, especially with vertical compression. Energy at lower frequencies (4-15 Hz) of the sacrum and head was also reduced. A more compressive midsole can absorb more energy from the ground impact and lead to a less jerky running pattern, potentially increasing running comfort [2] and smoothness [4].

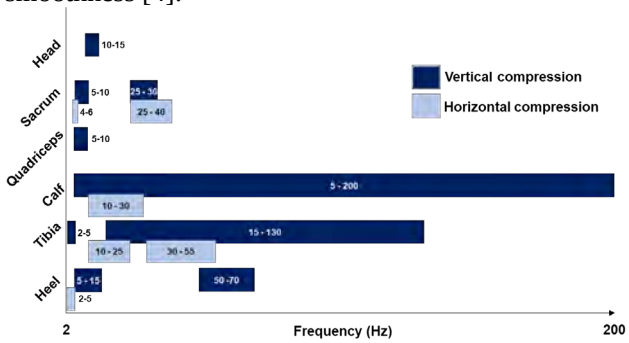

Figure 1 Summary of non-parametric correlations between midsole compression and vibration energy. Indicated are the frequencies where vibration energy was reduced when compression increased.

CONCLUSIONS

Alteration in midsole stiffness via 3D printing technology allowed the modification of midsole compression during running and reduced vibration exposure. Quantifying midsole compression and determining lower and higher bounds for optimal compression are yet to be done.

ACKNOWLEDGEMENTS

The authors would like to thank adidas for providing the shoes. This study was partially funded by the NSERC CREATE (We-TRAC No. CREATE/511166-2018), and the Eyes High program of the University of Calgary.

REFERENCES

[1] Zadpoor A and Nikooyan A. *Clinical Biomechanics* **26**: 1, 2011.
[2] Horvais N et al. *Footwear Science* **11**: 1, 2019.
[3] Play M-C, Trama R et al. *Sports Med – Open* **8**: 1, 2022.
[4] Clermont C et al. *Sports Biomechanics* **n/a:** n/a, 2022

Effect of slip anticipation on muscle activation pattern during walking down a slippery slope

Dain Shim [1], Yeon-Wook Seok[1], Joong-on Choi[1], Juntaek Hong[1], Yongjin Ahn[1], Dong-wook Rha[1]

[1] Department and Research Institute of Rehabilitation Medicine, Yonsei University College of Medicine, Seoul, Republic of Korea

Email: medicus@yonsei.ac.kr

INTRODUCTION

Falls and slips are serious trauma accidents and the leading cause of death every year, and reducing falls is important. Understanding reactive strategy for not slipping can be helpful in developing intervention techniques to reduce risk of falling. The reactive strategy can be confirmed by analyzing the activity of muscles during walking on slippery surface. Therefore, the aim of this study was to investigate the difference of muscle activation patterns when walking down a non-slip slope and slippery slope. Also, we analyzed the effect of prior notice for slippery slope as well.

METHODS

A total of 18 young healthy persons (14 males and 4 females; mean age 24.28±2.42 years) who could walk independently on a slope were recruited. The aprticipants walks on the wooden slope with an inclination angle of 15° was fabricated. The walking path was divided into 5 zones, and the slippery zone is 4th. (Figure 1) Participants conducted 3 gait trials: T1) walking down a non-slip slope, T2) walking down a slippery slope encountered unexpectedly, and T3) walking down a slippery slope with a prior notice The electromyographic (EMG) activity waw recorded from the muscles in the stance (right/slipping) leg, including the Vastus Lateralis (VL), Medial Hamstring (MH), Tibialis Anterior (TA) and Medial Gastrocnemius (MG) at 1111 Hz using Delsys Trigno wireless EMG (Boston, MA) with a bandpass filter (10–500 Hz). The raw EMG signal was time-normalized by dividing 1 stance phase into 10 equally spaced intervals and root mean square (RMS) values were calculated for individual muscles during each time interval. Maximum Voluntary Isomeric Contraction (MVIC) values for each muscle were expressed as a ratio of the maximum RMS value during walking down a non-slip slope. And the onset time was estimated as the first point when the smoothed signal exceeded the threshold (mean+15*standard deviation). In order to compare and analyze muscle activity during non-slip and slippery slope walking, the paired t-test was used.

RESULTS AND DISCUSSION

Explosive increases in the MVIC value were observed from all muscles in overall stance phase except for initial contact during T2 compared to T1. ($p<0.05$) (Fig.2)

And decreases in the MVIC value were also observed from all muscles in overall stance phase except for initial contact during T2 compared to T1 ($p<0.05$) There was no statistically significant difference in MVIC value During T3 compared to T1, and there was no significant difference in onset time as well. ($p<0.05$)

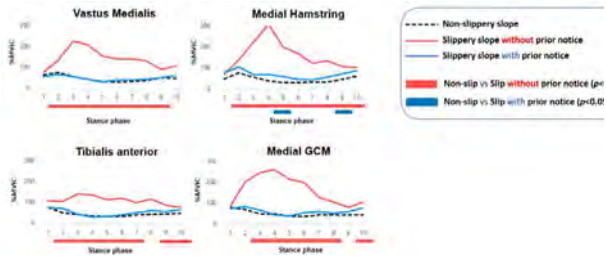

Figure 1 Comparison of Maximal Voluntary Isometric Contraction (MVIC) values of each of the muscles (Vastus Lateralis, Medial Hamstring, Tibialis Anterior and Medial Gastrocnemius) during walking down a non-slip slope

CONCLUSIONS

In all muscles, the magnitude of muscle activity was significantly increased about 260% during walking down on a slippery slope encountered unexpected compared to during walking down a non-slip slope.

In the presence of slip anticipation, it was expected that there would be a difference from walking on a non-slip slope due to non-slip compensation, but showed a similar muscle activation pattern as during walking a non-slip slope.

ACKNOWLEDGMENT

The research was supported by a grant (RS-2023-00215713) from ministry of food and drug safety in 2023

REFERENCES

[1] Chambers A et al. *Gait & Posture* **25**: 565-572, 2007.

[2] Cappellini G et al. *J neurophysiology* **103**: 746-760, 2010.

SIMULATION OF THE IMPACT PROCESS OF WATER CANNON ON CRANIO CEREBRAL INJURIES

Yinze Lei[1], Jing Xie[1,2,3], Pengwan Chen[1,2,3] and Daniel Rittel[4]

[1] State Key Laboratory of Explosion Science and Technology, Beijing Institute of Technology, China.
[2] Advanced Technology Research Institute, Beijing Institute of Technology, China.
[3] Explosion Protection and Emergency Disposal Technology Engineering Research Center of the Ministry of Education, China.
[4] Faculty of Mechanical Engineering, Technion - Israel Institute of Technology, Israel.
Email: 3277969453@qq.com

INTRODUCTION

The riot-control water cannon is a kind of large non-fatal weapon equipment that takes water as the main medium to control and disperse the crowds. However, the safety issues of the water cannon, especially the potential cranio-cerebral injury, is seldom reported. Therefore, the present work analysed numerically and theoretically the influence of riot-control water cannons on the cranio cerebral ensemble, and predicted the injury risk of the skull, cerebrum and neck under different impact situations.

METHODS

The spatial-temporal distribution of anti-riot water cannon pressure was studied by two-phase waterjet simulation and Vander Waals equation (Eq. 1).

$$p\left(V-m_{gas}b\right)^{\gamma}=p_0\left(V_0-m_{gas}b\right)^{\gamma} \qquad (1)$$

By considering the different working distances, different impact positions and different impact angles, the dynamic response of the human brain was systematically investigated. Combining four criteria (Skull Strength Criteria, Neck Injuries Criteria, Intracranial Stress Tolerance Criteria and WSTC/HIC Criteria), the injury risk was estimated and evaluated.

RESULTS AND DISCUSSION

The results showed that the peak value of equivalent pressure pulse decreased while the rising time of positive pressure shortened when the standoff distance becomes longer. (Fig. 1) Within a standoff distance of 7m, the dynamic response of the skull, brain and neck all exceeded the safety usage threshold(Table 1). When impacting different positions of the human brain at the same distance, the risk of injury of the frontal, temporal and occipital areas was 8.61%, 2.24% and 0.98%, which showed that When the oblique load was applied to the human brain, the neck injury coefficient increased by 160.2%, and the peak stress of the skull and cerebrum increased by 66.7% and 94.0%, respectively.

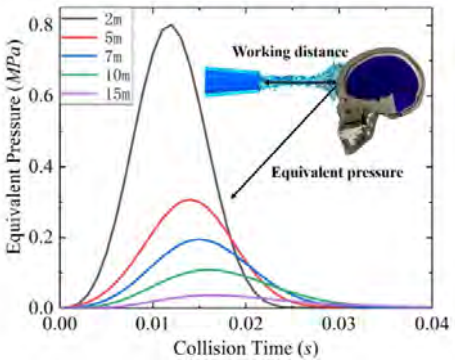

Figure 1 Equivalent pulse pressure curve of different working distances.

CONCLUSIONS

By using Skull Strength Criteria, Neck Injuries Criteria, Intracranial Stress Tolerance Criteria and WSTC/HIC Criteria injury criteria, cranio cerebral injuries can be described more accurately and comprehensively. The safe distance of this kind of riot-control water cannon should be greater than 7m. Compared with the normal impact, the oblique impact of the water cannon has a more severe influence. The frontal part was more susceptible to cause injury. The experimental verification and validation of the anti-riot water cannon impacting the brain model will be carried out in the future.

ACKNOWLEDGEMENTS

The project is supported by NSFC (Grant no: 12272053).

Table 1: The damage risk under different impact distance

Distance	Skull Strength Criteria	Neck Injuries Criteria	Intracranial Stress Tolerance Criteria	WSTC/HIC Criteria injury criteria
2m	Damage	Damage	Damage	High probability damage
5m	Damage	Safety	Damage	Small probability damage
7m	Damage	Safety	Safety	Safety
10m	Safety	Safety	Safety	Safety

SUBJECT-SPECIFIC FE ANALYSIS TO INVESTIGATE HOW DIFFERENT REHABILITATION EXERCISES INFLUENCE TENDON STRAINS IN ACHILLES TENDINOPATHY PATIENTS

Alessia Funaro[1], Vickie Shim[2], Ine Mylle[1] and Benedicte Vanwanseele[1]
[1] Human Movement Biomechanics Research Group, KU Leuven, Leuven, Belgium.
[2] Auckland Bioengineering Institute, University of Auckland, Auckland, New Zealand.
Email: alessia.funaro@kuleuven.be

INTRODUCTION

Achilles tendinopathy is characterized by altered tendon material properties and geometry, in particular decreased Young's modulus and tendon thickening [1]. Strain is a crucial factor for tendon adaptation and a strain dose of 5-6% has been shown to reverse early-stage pathological changes in Achilles tendinopathy patients [2]. However, it still remains unknown if current rehabilitation exercises provide this optimal strain dose in Achilles tendinopathy patients [3]. Finite element (FE) models of the Achilles tendon (AT) can be used to investigate the effects of tendinopathic material and geometrical changes [4] on regional tendon strain under load. The aim of this study was to develop subject-specific FE models of the AT with subject-specific material properties, geometry and muscle forces during common rehabilitation exercises to investigate their effect on AT strains.

METHODS

Six participants with mid-portion Achilles tendinopathy (4 males, 2 females; age: 58 ± 18 years; weight: 72 ± 10 kg; height: 176 ± 9 cm; VISA-A score: 76 ± 17) participated in the study. The subject-specific geometries of the free AT were obtained from 3D freehand ultrasound. Free form deformation method was used to develop subject-specific FE models. Our models also incorporated the twisted structure of AT subtendons [6]. Incompressible, transversely isotropic, hyperelastic material descriptions were used as in our previous study [5] with the subject-specific Young's modulus, which was calculated as the slope of the line fitted to the stress-strain data between 30% and 60% of the peak force for each patient (Young's modulus: 512.9 ± 145.7 MPa). Subject-specific muscles forces were obtained using a combination of 3D motion capture and musculoskeletal modelling of each patient. Five different rehabilitation exercises were measured: 1) unilateral heel rise, 2) unilateral heel drop with flexed knee and 3) with extended knee, 4) walking and 5) toe-walking. The muscle forces at the time of peak total muscle force were used as boundary conditions for the subject-specific FE analysis. The average of the maximum Lagrange strain, in the mid portion of the AT, was calculated to identify the differences between the rehabilitation exercises by using a repeated measures ANOVA. Statistical significance was accepted at $p<0.05$.

RESULTS AND DISCUSSION

Average strain in the mid-portion of the AT were significantly different between exercises (ToeWalk: 0.063 ± 0.021, UniDrop: 0.079 ± 0.022, Walk: 0.080 ± 0.018, UniRise: 0.081 ± 0.026, UniDrop Bent: 0.089 ± 0.026, mean ± SD). At the time of peak total muscle force, most of the exercises induce a strain higher than the reported optimal strain [3]. Even if walking is generally considered a safe form of exercise, average strains were also higher than the optimal. The average strain and the ranking of the rehabilitation exercises showed large variation across patients. The AT strains are not only task-dependent but also influenced by patients' material properties and geometry.

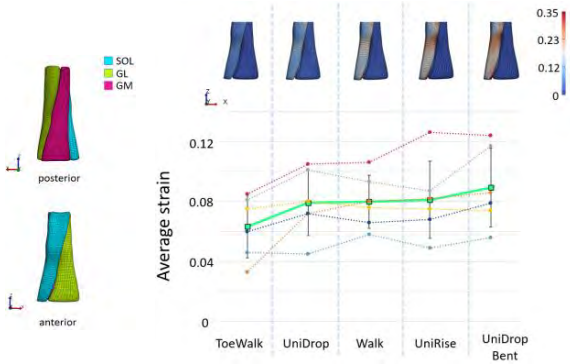

Figure 1 On the left, an example of FE model with the three twisted subtendons arising from Triceps Surae muscles. On the top right, a representative example of the distribution of the strain for the exercises. On the bottom right, the green line represents the mean and SD of the average strain for the exercises, in the mid-portion of the AT models. The dotted lines represent the average strain for the exercises for each participant, in the mid-portion of the AT models.

CONCLUSIONS

These FE models showed that the AT strains are influenced by subject-specific material properties, geometry and muscles forces, highlighting the need to develop personalized rehabilitation protocols. Future studies should investigate the influence of this large variability amongst patients with Achilles tendinopathy and the use of subject-specific analysis to design personalised rehabilitation protocol.

REFERENCES

[1] Arya and Kulig, *J Appl Physiol*, **108**:670–675, 2010
[2] Wang et al. *J. Orthop. Res*, **33**:1888–1896, 2015
[3] Pizzolato et al, *Br. J. Sports Med*, **53**:11-12, 2019
[4] Shim et al, *J. Biomech*, **82**:142-148, 2019
[5] Funaro et al, *Front. Bioeng. Biotechnol*, **10**:1207, 2022
[6] Pękala et al. *Scand J Med Sci Sports*, **27**:1705-1715, 2017

Effects of brace wearing and rehabilitation on foot muscle thickness and cross-sectional area after ankle inversion trauma

Rosemary Dubbeldam[1], Alexander Milstrey[2], Magdalena Sicher[1], and Sabine Ochman[2]
[1] Institute of Sport and Exercise Sciences, University of Münster, Münster, Germany
[2] Department of Trauma surgery, University Hospital Münster, Münster, Germany.
Email: r.dubbeldam@uni-muenster.de

INTRODUCTION

Patients suffering from chronic ankle instability (CAI) after ankle inversion trauma have lower intrinsic foot muscle volume compared to healthy controls [1]. These muscles are however progressively recruited in increasing postural demand [2], an activity which is impaired in CAI patients. While rehabilitation improves balance performance and extrinsic foot muscle strength in CAI [3], it is not clear if the intrinsic foot muscle strength also increases. Furthermore, little is known about the effect of brace wearing on intrinsic foot muscle strength after acute ankle inversion trauma. This study aims to analyse the effects of brace wearing and rehabilitation on intrinsic and extrinsic foot muscle thickness and cross sectional area (CSA) of patients suffering from acute and chronic ankle instability.

METHODS

Fourteen patients with a mean age of 24 (SD 6) years (7 males) suffering from acute (6) or chronic (8) ankle instability participated in a rehabilitation programme focussing on restoring functions and activities. The acute patients received an ultrasound assessment within one week of their injury (Philips Affiniti 50g). This was followed by a brace wearing period of 6 weeks, whereafter the rehabilitation started. An ultrasound assessment was performed of both limbs for all participants at the beginning and after 12 weeks of rehabilitation. The muscle thickness and CSA of the following 3 extrinsic and 3 intrinsic foot muscles were assessed: Tibialis anterior (TA), Peroneus longus (PL), Flexor digitorum longus (FDL), Hallux abductor (AbdH), Flexor hallucis brevis (FHB), and Flexor digitorum brevis (FDB). The muscles were analysed individually and as group of intrinsic or extrinsic muscles. A paired t-test was performed in SPSS to analyse the effects of the 6-week brace wearing in the acute patient group and the effects of 12-week training in both groups on the foot muscles. Also, the impaired and non-impaired limb were compared. Significant differences were reported for $p < 0.05$.

RESULTS AND DISCUSSION

There were no significant differences in muscle thickness or CSA between the impaired and non-impaired limbs, although the impaired limb's muscles tended to be smaller. The 6-week brace wearing caused a significant reduction in muscle thickness of the FDB from 0.76 (0.12) to 0.71 (0,12) cm and of the FHB from 1.35 (0.17) to 1.19 (0.10) cm (Figure 1). On the contrary, the TA thickness increased from 0.58 (0.12) cm to 0.70 (0.17) cm. During the 12-week rehabilitation training phase, a significant increase of the intrinsic foot muscles in thickness or CSA was observed (Table 1). The PL tended to increase in thickness after 12 weeks.

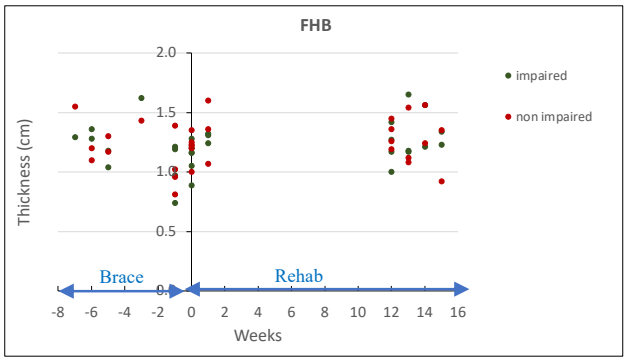

Figure 1 Decrease in FHB thickness during bracing phase (acute patients), followed by an increase in FHB thickness during rehabilitation phase (week 0 to week 12, all participants).

Table 1: Average (SD) thickness (cm) and CSA (cm^2) of the foot muscles for week 0 (start rehabilitation) and week 12.

Muscle	Week 0	Week 12	P
Sum intrinsic (cm)	2.86 (0.33)	3.18 (0.14)	0.04
Sum intrinsic (cm^2)	3.63 (0.69)	4.06 (1.03)	0.04
FDB (cm)	0.77 (0.13)	0.8 (0.14)	0.05
FHB (cm)	1.13 (0.17)	1.30 (0.17)	0.03
AbdH (cm^2)	1.93 (0.53)	2.09 (0.68)	0.05
PL (cm)	1.37 (0.29)	1.54 (0.27)	0.07

CONCLUSIONS

Brace wearing in the acute phase after injury is associated with up to 12% loss of intrinsic foot muscles and suggests the need to activate these muscles, e.g., isometrically and non-weight bearing, during this phase. During the rehabilitation phase, the intrinsic foot muscles recover with training. However, future studies should compare, if the muscle volume is able to fully recover to the level of healthy subjects.

REFERENCES

[1] Feger M et al. *Orth J Spo Med* **4(6)**: 1-8, 2016.
[2] Kelly L et al. *Clin Biomech* **27**: 46-51, 2012.
[3] Hou Z et al. *J Foot Ankle Res* **15(1)**: 9, 2022

IDENTIFYING MOVEMENT STRATEGIES TO OFFSET THE PERFORMANCE-INJURY RISK CONFLICT IN SIDE-STEP CUTTING VIA OPTIMAL CONTROL SIMULATIONS

Aaron Fox[1], Meghan Keast[1], Tess Rolley[1], Jason Bonacci[1], Richard Page[2,3] and Stephen Gill[2,3]
[1] School of Exercise and Nutrition Sciences, Deakin University, Geelong, Australia.
[2] Barwon Centre for Orthopaedic Research and Education, St John of God Hospital, Geelong, Australia.
[3] School of Medicine, Deakin University, Geelong, Australia.
Email: aaron.f@deakin.edu.au

INTRODUCTION

Side-step cutting manoeuvres are an important performance determinant in multi-directional sports, yet these manoeuvres are also linked to anterior cruciate ligament (ACL) injury [1]. Strategies for reducing ACL injury risk during side-step cutting have been developed, yet these often conflict with performance recommendations [2]. Identifying movement strategies that reduce hazardous knee loads during side-step cutting without affecting performance may enhance injury prevention uptake. We used a predictive simulation approach to identify biomechanical solutions that reduced potentially hazardous knee loads during side-step cutting without sacrificing performance.

METHODS

10 elite women's Australia Football players (25.0 ± 4.6 y; 1.71 ± 0.05 m; 67.9 ± 3.8 kg) participated. We used three-dimensional kinematic and kinetic data from an unanticipated 35-55º side-step cutting task. One successful trial from each participant was randomly selected to drive predictive simulations. A generic musculoskeletal model of the lower limbs and torso [3] was scaled to each participant and adapted to include: (i) a 3 DoF knee joint; (ii) idealised torque actuators at each joint; (iii) rolling-on-surface constraints at the feet to avoid ground penetration; and (iv) contact spheres on the cutting foot to estimate ground reaction forces (GRFs). We used the scaled musculoskeletal model with inverse kinematics and dynamics during the ground contact phase of the side-step cut to estimate joint angles and torques, respectively. A series of torque-driven simulations were conducted for each participant in OpenSim Moco [4]. First, a tracking simulation found the actuator signals that minimised errors in joint angles and torques, and GRFs estimated via the contact spheres versus experimental data – with this solution used as the initial guess for subsequent predictive simulations. Second, we generated a reference predictive simulation (i.e. '*reference*') of the side-step cut where only a lowly weighted goal tracking joint angles was used. Third, we repeated the prior simulation with an additional goal to minimise the frontal and transverse plane knee torques during the side-step cut (i.e. '*safer*'). In all simulations – the start and end point of the pelvis centre-of-mass (CoM), and time to complete the movement were constrained to match experimental data – to emulate performance. We compared full-body kinematics between the *reference* and *safer* simulations using one-dimensional statistical parametric mapping (SPM1D) paired t-tests ($\alpha = 0.05$ with Benjamini-Hochberg correction).

RESULTS AND DISCUSSION

Tracking and *reference* simulations had qualitatively similar joint angles and torques, and GRFs to experimental data. We observed large reductions in mean absolute frontal and transverse plane knee torques between the *reference* and *safer* simulations (0.41 ± 0.17 vs. 0.03 ± 0.01 Nm·kg^{-1} and 0.17 ± 0.10 vs. 0.02 ± 0.01 Nm·kg^{-1}, respectively), while achieving performance constraints (i.e. pelvis CoM and movement time). Visual inspection of *safer* simulations typically demonstrated better alignment of the GRF vector to the knee (i.e. reduced moment arm). Compared to *reference* simulations, *safer* simulations had increased ankle plantarflexion and reduced ankle dorsiflexion across the entire ground contact phase ($p = 0.034$). This demonstrates a shift to a fore-foot landing approach in *safer* simulations, in line with experimental [5] and simulation [6] works showing reduced knee loads with this approach. We identified no further statistically significant differences in kinematics between *reference* and *safer* simulations. The lack of differences alongside reductions in knee loads may be indicative of small kinematic changes having a large effect, or variable strategies being used across individuals.

CONCLUSIONS

A fore-foot landing approach to side-step cutting may be an effective global injury prevention recommendation that does not sacrifice performance. Further individualised kinematic changes may be necessary to minimise knee loads during side-step cuts.

ACKNOWLEDGEMENTS

We thank players and staff from the Geelong Cats Football Club for assisting with this research.

REFERENCES

[1] Olsen et al. *Am J Sports Med* **32**: 1002-12, 2004.
[2] Fox. *Sports Med* **48**: 1799-807, 2018.
[3] Lai et al. *Ann Biomed Eng* **45**: 2762-74, 2017.
[4] Dembia et al. *PLoS Comp Biol* **16**: e1008493, 2020.
[5] Donnelly et al. *J Sci Med Sport* **20**: 32-7, 2017.
[6] Donnelly et al. *J Biomech* **45**: 1491-7, 2012.

Electrical stimulation induced isometric muscle contraction can improve mechanical properties and reduce tendon adhesion followed adipose-derived stromal vascular fraction gel treatment in the rat Achilles tendinopathy

Ho-Yi Tuan-Mu[1,2], Kuan-Lin Liu[2,3], and Yu-Quan Ng[2]

[1] Department of Physical Therapy, Tzu Chi University, Hualien, Taiwan.
[2] Sports Medicine Center, Hualien Tzu Chi Hospital, Buddhist Tzu Chi Medical Foundation, Hualien, Taiwan
[3]Department of Orthopedic, Hualien Tzu Chi Hospital, Buddhist Tzu Chi Medical Foundation, Hualien, Taiwan
Email: hytuanmu@gms.tcu.edu.tw

INTRODUCTION

Tendinopathy, including tendinitis and tendinosis, is one of the most common soft tissue injury in the mordent society. Tendon is a poor self-limiting tissue, to overcome this shortage that many tissue engineering strategies were developed. Previous studies showed that loading to the injured tendon during healing is needed and many studies have shown that the passive loading could enhance the mechanical strength, however, the role of muscle contraction is missed in previous researches Moreover, the mechanical properties and most of all, adhesion, of the injured tendon after mechanical loading intervention post newly developed regenerative medical interventions are still missed [1]. The purpose of this study is to investigate the effects of isomatric muscle contraction post adipose-derived stromal vascular fraction (ADSVF) gel injection on the mechanical behavior and tendon adhesion in the rat Achilles tendinosis model.

METHODS

Thirty Sprague-Dawley male rats (~250g, 8 weeks old) were use and assigned to 2 treatment groups including ADSVF gel injection (SVF) and electrical stimulation induced isometric muscle contraction after ADSVF gel injection (SVF+IMC) groups. After skin shaved, all rats were anesthetized and injected with 0.1 μL collagenase type-I solution (0.1% w/v, CLS-1, Worthington, Lakewood, NJ) into the Achilles tendon on the both side under sonography guidance [2]. The treatment started after 2 weeks of injury induced. Rats were harvest at 7, 14, and 28 days after intervention. The ADSVF gel was conducted from donated rats' fat. The fat were cutting, centrifugation, and emulsification according to previous publication [3]. To induce the isometric muscle contraction, the rats were anesthetized and fixed on a customize loading frame with the ankle joint at 0° of plantar flexion. The gastrocnemius muscle was stimulated by a commercial electro therapy device (Dynaprog 527A, Dynaprog, Taiwan). A material testing system (MTS; Tension, Taiwan) with a 1000N load cell were used to evaluate the *in vitro* mechanical properties of the tendon, including tensile strength and tendon gliding. The Achilles tendon were cannulated to the loading frame of the system by the fixation of calf muscle and the calcaneal bone. After 10 times of preconditioning, the samples were pulled until failure. For the tendon gliding, all process was similar to mechanical strength except the insertion of the Achilles tendon were carefully dissected from the calcaneal bone. Two-way analysis of variance with Bonferroni post-hoc exam was used to compare the ultimate tensile strength and among groups. Statistic significant level was set at α=0.05.

RESULTS AND DISCUSSION

The ultimate tensile strength and tendon gliding were improved in both SVF and SVF+IMC group from 1-week post intervention to 4-week post intervention. The SVF+IMC group demonstrated significantly better ultimate tensile strength and lesser tendon adhesion comparing to SVF alone. That is, the isometric muscle contraction could improve mechanical strength and reduce adhesion. Our results indicated that the loading of the tendon is probably necessary after regenerative medicine treatment for the degenerative tendon.

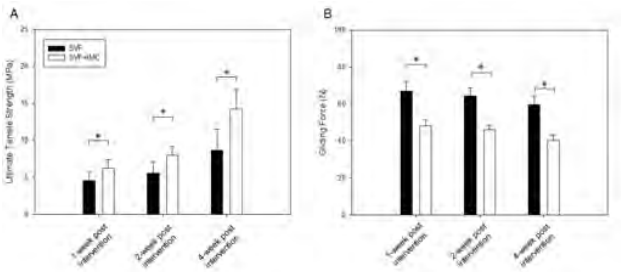

Figure 1. The ultimate tensile strength (A) and tendon gliding force (B) between different treatments and time duration. * denote $p < 0.05$. N=5 in each group and at each time point

CONCLUSIONS

In this study, we found that the tendon adhesion after ADSVF intervention might be reduced and the mechanical properties could be further improved with isometric muscle contraction.

ACKNOWLEDGEMENTS

Financial supports from the National Science and Technology Council at Taiwan (NSTC 110-2628-B-320 -002) is gratefully acknowledged.

REFERENCES

[1] Head PL. *Phys Med Rehabil Clin N Am* **27(4)**:1043-1054, 2016.
[2] Lee SY et al., *Sci Rep* **7(1)** 5100, 2017.
[3] Nakamura N et al., *Am J Sports Med* **48(2)**, 2020

Wearable Ultrasound Sensor for Lateral Epicondyle Tendinopathy Surveillance

Yeseop Park[1], Jihyun Lee[2] and Youkeun Oh[1]
[1] Department of Mechanical Engineering, Hongik University, Seoul, Republic of Korea.
[2] Department of Mechanical and Manufacturing Engineering, University of Calgary, Calgary, Canada.
Email: youkeun@hongik.ac.kr

INTRODUCTION

Lateral epicondyle tendinopathy (LET) or tennis elbow is an overuse injury caused by repetitive use of the forearm muscles [1]. It is a common cause of injury in various occupational groups who are exposed to repetitive use of the wrist and elbow. More than a million cases are diagnosed as LET each year in the United States [2,3]. Injuries to a tendon or ligament require a significant period of recovery and surgical or non-surgical treatment resulting in diminished quality of life [4,5]. It is thus critical to closely monitor the fatigue level of the fibrous connective tissues in order to prevent overuse of those tissues. This study aims to construct an ultrasonographic system that can quantitatively observe the morphological changes of the common extensor tendon (CET) and determine the fatigue state of CET during exercise.

METHODS

A total of 18 (10 males, 8 females) healthy university students participated in the study (IRB No: 7002340-202208-HR-019). To monitor the morphological changes as the fatigue was accumulated in the CET, a single-element ultrasound (US) transducer (2.25 MHz, Olympus, USA) was placed near the lateral epicondyle using a custom elbow brace. The US measurements were performed for the relaxed muscle condition, isometric maximum voluntary contractions (MVCs) at 0˚ forearm flexion, and isometric MVCs at 0˚ forearm pronation before and after the first and second fatigue exercises, respectively. To induce the CET fatigue, a gyroscopic hand exercise ball was used. Each subject was asked to maintain a minimum of 5000 rpm for 20 seconds and repeat three or five times. The CET thickness was calculated based on the time difference (Figure 1. red triangles on the left; t_2 -t_1), which correspond to the upper and lower layer of CET. The CET elevation was calculated using t_2, which corresponds to the lower layer of CET (Figure 1; red arrow). The nonparametric Wilcoxon Signed-Rank test was used to test the hypothesis (α=0.05).

RESULTS AND DISCUSSION

For the isometric forearm flexion condition, the mean CET thickness decreased by 26.6% (≈ -0.96 mm, p<0.001) and the mean CET elevation increased by 8.3% (≈ +1.04mm, p<0.001) (Figure 1). Similar results were observed for the isometric forearm pronation condition (Table 1). The results imply that the muscle-tendon unit was getting taut as the fatigue inducing exercise was repeated possibly due to the post activation potentiation. Even if it is partly due to the post activation potentiation, the morphological changes in the muscle-tendon unit during exercise can be still used as an indirect marker for injury prevention. Therefore, further studies are warranted to accurately quantify the accumulated fatigue level and correlate it to any morphological changes to prevent injury.

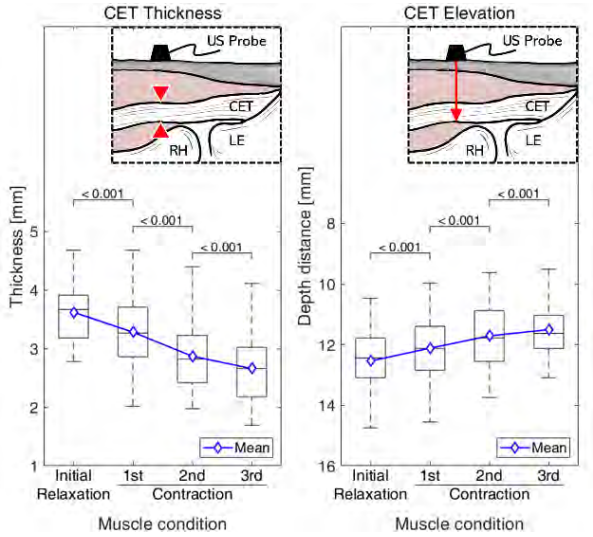

Figure 1 Morphological changes for the isometric forearm flexion

Table 1: CET changes in isometric forearm pronation

	Isometric forearm pronation
Mean CET thickness	-26.3% (≈ -0.90mm, p<0.001)
Mean CET elevation	+8.7% (≈ +1.09mm, p<0.001)

CONCLUSIONS

This study shows that the CET fatigue can be quantified by the changes in the CET thickness or elevation. This suggests that overuse-related Musculo-skeletal injury can be prevented by monitoring morphological changes in the muscle-tendon unit.

ACKNOWLEDGEMENTS

This research was supported by the MSIT (Ministry of Science, ICT), Korea, under the High-Potential Individuals Global Training Program) (2021-0-01568) supervised by the IITP (Institute for Information & Communications Technology Planning & Evaluation).

REFERENCES

[1] Scott A et al. *Br J Sports Med* **54**:260-262, 2020.
[2] Karanasios S et al. *Hand Ther.* **21**:00039-9, 2021.
[3] Walz D M et al. *Radiographics* **30**:167-184, 2010.
[4] Whaley A et al. *Clin Sports Med* **23**:677–691, 2004.
[5] Duncan J et al. *Br J Hosp Med* **80**:647–651, 2019.

DOES FEMALE HANDBALL PLAYERS WITH LOW HIP EXTERNAL ROTATION STRENGTH DISPLAY HIGHER KNEE ABDUCTION MOMENTS DURING SIDE-CUTTING THAN PLAYERS WITH HIGH STRENGTH?

Niels J. Nedergaard[1], Mette K. Zebis[2], Louise W. Nielsen[3], Andreas Henneberg[3], Jesper Lundbye-Jensen[4], Anke Karabanov[4] and Jesper Bencke[1]

[1] Human Movement Analysis Laboratory, Copenhagen University Hospital at Hvidovre, Copenhagen, Denmark.
[2] Department of Physiotherapy, University College Copenhagen, Copenhagen, Denmark.
[3] Department of Physiotherapy, University College Copenhagen, Campus North Zealand, Hillerød, Denmark.
[4] NEXS, University of Copenhagen, Copenhagen, Denmark

niels.jensby.nedergaard@regionh.dk

INTRODUCTION

The incidence of non-contact anterior cruciate ligament (ACL) injuries is high in womens team handball, particurlarly among young female players. During the early stance phase of side-cutting hip external rotator strength (HERS) is required to counteract the excessive hip internal rotation joint moments, which is contributing to the knee joint valgus position and thereby stressing the ACL. Thus, reduced HERS has been inditified as a risk factor of non-contact ACL injuries in handball [1] and other sports [2]. Therefore, the purpose of this study was to compare transverse hip and frontal plane knee angles and moments during side-cutting, and potential age-differences, between female handball players with low and high HERS.

METHODS

Sixty female handball players (32 children age: 12.5 ± 0.6 years and 28 adult's age: 23.8 ± 5.5 years) voluntarily participated in one test session. Maximum isometric HERS was measured with a handheld dynamometer. All players performed three maximum voluntary contractions in a seated position with the hip and knee in 90° flexion. HERS was normalised to body weight. Only the highest value was used for further analysis. Subsequently, players performed 5 side-cuts where peak hip internal rotation (IR) and knee abduction (Abd) angles and external moments for the dominant leg were recorded with a Vicon system and an AMTI force plate. Post data-collection, players were allocated to the low (≤ 2.0 N/kg BW) or high (> 2.0 N/kg BW) HERS group, respectively. A two-way ANOVA, with an alpha level of 0.05, was used to compare interactions effects and between groups and age differences.

RESULTS AND DISCUSSION

The low and high HERS groups had an average strength of 1.8 ± 0.2 N/kg BW and 2.3 ± 0.2 N/kg BW, respectively. The ANOVA showed no interaction effect (Table 1). The low HERS group displayed significantly lower peak hip IR moments during side-cutting (0.25 ± 0.13 Nm/kg BW, p = 0.045) compared to the high HERS group (0.33 ± 0.17 Nm/kg BW), and a tendency to higher peak hip IR angles (p = 0.070). Furthermore, the children displayed significantly higher external knee Abd moments (p = 0.034) than the adults , see Figure 1.

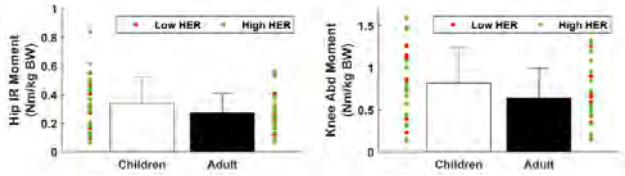

Figure 1. Mean ± SD external moments for children and adults, the individual players values are color-coded to their HERS score.

CONCLUSIONS

Regardless of age, female handball players with high HERS (>2.0 N/kg BW) was able to counteract higher hip IR moments during side-cutting, without greater peak IR angles, than players with low HERS. Moreover, low HERS was not associated with greater knee Abd angles or moments, but pre-teen players generally displayed higher knee Abd moments than adult players.

REFERENCES

[1] Zebis M et al. *Knee Surg Traumatol Arthrosc* **30**: 1341-51, 2022.

[2] Khayambashi K et al. *Am J Sports Med* **44**: 355-61, 2015.

Table 1. ANOVA analysis for peak hip IR and knee Abd angles and external moments.

	Low HERS		High HERS		Strength Effect	Age Effect	Interaction Effect
	Children *(N = 12)*	Adult *(N = 10)*	Children *(N = 20)*	Adult *(N = 18)*			
Hip IR Angle (°)	12.7 ± 6.2	16.5 ± 6.7	11.7 ± 10.4	9.9 ± 5.2	*p* = 0.070	*p* = 0.642	*p* = 0.181
Hip IR Moment (Nm/kg BW)	0.27 ± 0.15	0.22 ± 0.10	0.32 ± 0.19	0.35 ± 0.15	***p* = 0.045***	*p* = 0.878	*p* = 0.315
Knee Abd Angle (°)	6.2 ± 5.7	5.6 ± 4.5	4.0 ± 4.9	3.5 ± 4.6	*p* = 0.112	*p* = 0.665	*p* = 0.976
Knee Abd Moment (Nm/kg BW)	0.92 ± 0.37	0.59 ± 0.16	0.72 ± 0.43	0.56 ± 0.54	*p* = 0.307	***p* = 0.034***	*p* = 0.466

REDUCED TIBIAL LOADING DURING A 10KM RUN IN COMPETITIVE AND RECREATIONAL RUNNERS

Hannah Rice[1], Patrick Mai[2], Max Sanno[2] and Steffen Willwacher[2]

[1] Dept. of Physical Performance, Norwegian School of Sport Sciences, Oslo, Norway.
[2] Dept. of Mechanical and Process Engineering, Offenburg University of Applied Sciences, Offenburg, Germany.

Email: hannahr@nih.no

INTRODUCTION

Bone stress injuries particularly afflict runners. They occur as a result of microdamage accumulation alongside insufficient recovery. Loading magnitude is the most important contributor to bone damage accumulation [1], but loading quantity (e.g., number of steps) is also important. With increasing running speed, there is an increase in loading magnitude [2] but a decrease in the number of loading cycles to complete a given distance. Increased tibial loading as a result of running-induced fatigue accumulated over a run has been suggested to increase risk of stress injury [3]. The aims of this study were to 1) compare tibial loading between recreational (RR) and competitive runners (CR) throughout a demanding 10 km run; 2) quantify changes in tibial loading magnitude and rate of tibial damage accumulation throughout the duration of the run.

METHODS

Male runners who self-reported a 10 km season-best run slower than 47:30 min (RR) and faster than 37:30 min (CR) participated. The 10-km running protocol was performed at 105% of their season's-best time on a force-instrumented treadmill. Kinematics were synchronously collected, and data were obtained at 0km, 0.2km, 0.5km, 1 km and every km thereafter until 10km. Bending moments (M_{BE}) were estimated about the medial-lateral (ML) tibial axis at a distal 1/3rd centroid. Internal forces and moments were quantified by ensuring static equilibrium at each 1% of stance [4]. Muscular forces were estimated using static optimization with a cost function minimizing the sum of cubed muscle stresses. Peak M_{BE} was obtained, and cumulative damage was estimated using the following equation [5]:

$$\text{Cumulative damage} = \left[n \int_{t_i}^{t_f} (x_s)^b \, dt\right]^{\frac{1}{b}}$$

where n = number of steps, t_i,t_f = beginning and end of stance, respectively, x_s = ML M_{BE}, b = tissue-dependent weighting factor, 6.6 [6]. Two-way mixed ANOVAs (level of running x distance completed) were used to identify differences in ML M_{BE} and rate of damage accumulation per km.

RESULTS AND DISCUSSION

There were no interaction effects for peak M_{BE} or rate of damage accumulation. On average, peak M_{BE} was 31% higher in CR than RR, and decreased from the start to the end of the run by 5% (Figure 1A). There was a trend for greater rate of damage accumulation in the CR than RR ($p = 0.058$, $n_p^2 = 0.154$) and a decrease across both groups by 4% from the start to the end of the run (Figure 1B). Factors in addition to the loading experienced by the bone affect risk of bone stress injury – e.g. the tibiae of CR may be better adapted than RR to withstand loading.

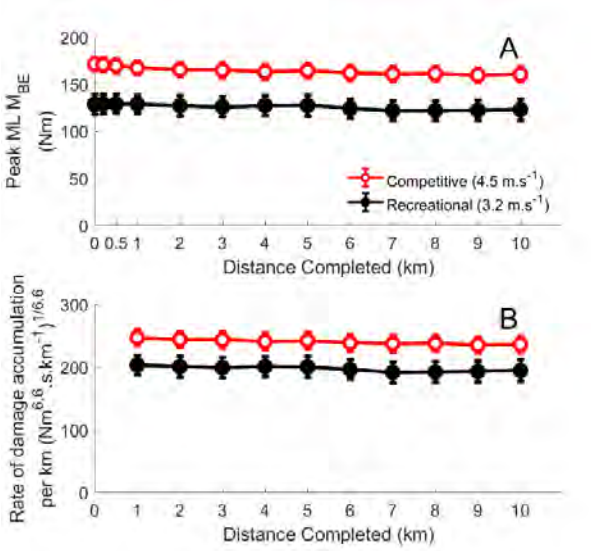

Figure 1: A) Peak ML M_{BE} in CR and RR throughout the 10km run; B) Rate of damage accumulation per km in CR and RR. Data points are mean values with standard error bars.

CONCLUSIONS

Competitive runners experience greater peak tibial loading than recreational runners when running 10km, due to the faster running speeds. There was also a trend for greater cumulative damage in CR than RR. Thus, completing a given running distance at a faster speed may increase the risk of a stress injury. Tibial loading decreases throughout a demanding 10km run suggesting that, in contrast to previous suggestions [3], running-induced fatigue-related changes in running mechanics may not be a primary mechanism for stress injury development.

REFERENCES

[1] Firminger et al. *MSSE* **52**: 1549-1556, 2020.
[2] Meardon et al. *AJSM* **49**: 2227-2237, 2021.
[3] Milgrom et al. *J Biomech* **40**: 845-50, 2007.
[4] Baggaley et al. *J Biomech. Eng* **144**, 2021.
[5] Firminger et al. *MSSE* **52**: 1549-56, 2020.
[6] Carter & Caler *J Orthop.Res* **3**: 84-90, 19

Effects of soft tissue artifacts on the calculated kinematics of the knee during gait

Wenjin Wang[1,2], Xiangming Li[2], Zhe Hu[3], Josef Viellehner[1], Igor Komnik[1], Shaobai Wang[2], Wolfgang Potthast[1]
[1] Institute of Biomechanics and Orthopedics, German Sport University Cologne, Cologne 50933, Germany.
[2] School of Kinesiology, Shanghai University of Sport, Shanghai 200438, China.
[3] Department of Physical Education, Jeonbuk National University, Jeonju 54896, Korea.
Email: wenjin.wang@stud.dshs-koeln.de (Wenjin Wang)

INTRODUCTION

Kinematics of the knee during gait has mostly been studied using optical motion capture systems (MCS). The presence of soft tissue artifacts (STA) between the skin markers and the underlying bone presents a major impediment to obtaining a reliable joint kinematics assessment[1,2]. In this study, we determined the effects of STA on the calculation of knee joint kinematics during walking and running, through the combination of high-speed dual fluoroscopic imaging system (DFIS) and magnetic resonance imaging technique.

METHODS

Ten male subjects walked and ran while data was collected simultaneously from MCS and high-speed DFIS. A paired t-test was used to compare the results obtained from MCS and high-speed DFIS. The error between the MCS and high-speed DFIS results was used to calculate knee joint rotation errors. The kinematic data obtained from the high-speed DFIS was considered as the "gold standard" of measurement. The statistical significance level was set at $*p < 0.05$.

RESULTS AND DISCUSSION

The average error values across all timepoints of skin markers-derived knee flexion, external, and varus rotations during walking were -3.2 ± 4.3°, 4.6 ± 3.1°, and 4.5 ± 3.2°, respectively (Table 1). At the before contact and initial contact of walking, knee external rotation and varus rotation calculated from skin markers were all significantly greater than the high-speed DFIS. At after contact, external and varus rotations calculated from skin markers were significantly greater than those from the high-speed DFIS (Fig. 1 and Table 1).

The average error values across all timepoints of skin markers-derived knee flexion, external, and varus rotations during running were -5.8 ± 5.4°, 6.6 ± 3.7°, and 4.8 ± 2.5° respectively (Table 1). A significant difference in knee internal-external and valgus-varus rotations was reported in skin markers-derived kinematics with respect to the high-speed DFIS, evidenced at the before contact during running. At initial contact and after contact, the external and varus rotations calculated from skin markers showed significantly greater rotations than the high-speed DFIS during running, however, the knee flexion was significantly smaller (Fig. 1 and Table 1).

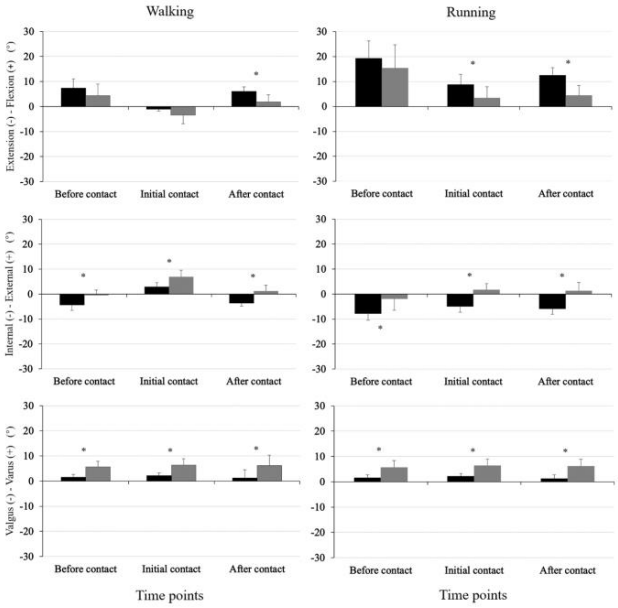

Figure 1 Means of knee joint rotations for walking and running were measured using MCS (grey) and high-speed DFIS (black).

CONCLUSIONS

The data indicated that STA will reduce the ability to accurately measure knee kinematics. The error values of knee kinematics obtained in this study offer a reference for differences between MCS and high-speed DFIS, and will be valuable in optimizing methods for analyzing knee kinematics during gait.

REFERENCES

[1] Cereatti A et al. *J Biomech* **62**: 5-13, 2017.

[2] Tsai T et al. *J Biomech* **44**: 1182-1188, 2011.

Table 1: Error values of skin markers-derived kinematics during walking and running of knee rotations.

	Walking			Running		
Average value during contact	Error, deg	Relative, %	Max, deg	Error, deg	Relative, %	Max, deg
Extension (-)- Flexion (+)	-3.2 ± 4.3	78	-11.4	-5.8 ± 5.4	43	-17.4
Internal (-)- External (+)	4.6 ± 3.1	271	11.6	6.6 ± 3.7	106	13.5
Valgus (-)-Varus (+)	4.5 ± 3.2	265	8.1	4.8 ± 2.5	200	9.2

ADAPTIVE BIOFEEDBACK GAIT RETRAINING ON SLOPES: A PROOF-OF-CONCEPT STUDY

Zoe Y.S. Chan[1,2], Roy T.H. Cheung[3], Sharon M.H. Tsang[2] and Reed Ferber[1,2]
[1] Faculty of Kinesiology, University of Calgary, Calgary, Canada.
[2] Department of Rehabilitation Sciences, the Hong Kong Polytechnic University, Hong Kong.
[3] School of Health Sciences, Western Sydney University, NSW, Australia.
Email: zoe.chan1@ucalgary.ca

INTRODUCTION

Incomplete translation of modified running biomechanics in untrained environment after gait retraining has been reported. [1] Theoretically, better retention and generalizability can be facilitated by introducing task variations during training, [2] such as changes in elevation. Gait retraining studies that reported success in reducing peak tibial acceleration (PTA) with the use of feedback, were conducted on level surfaces using a fixed training target. Runners demonstrate grade-specific biomechanical adaptations [3] which could affect PTA. Setting a single threshold based on running on a level surface may not be suitable for training on slopes. We propose the use of an adaptive feedback model for training along routes with elevation changes. To our knowledge, this is the first study to examine the effect of gait retraining on sloped conditions after completion of training along an outdoor running route with changes in elevations.

METHODS

An experienced female runner completed this exploratory study. Three identical in-field tests were conducted to obtain the baseline PTA value. Each test consisted of a five km run, with one 1600-m level, two 800-m uphill (3.2%) and two 800-m downhill (-3.2%) sections. An accelerometer (Blue Trident, Vicon, UK) was attached to the right leg of the runner to measure axial PTA and a GPS-enabled smartwatch (vívoactive HR, Garmin, US) was used to record elevation and speed. A treadmill test was conducted after the in-field tests. The treadmill test consisted of three sloped conditions (0%, 4% and -4%) at speeds that matched the corresponding sloped conditions during the in-field runs. The training consisted of six training sessions along the same route as the in-field tests. The training thresholds for each sloped condition were set at 80% of the baseline PTA values averaged across the corresponding sections of the in-field tests (Figure 1). An audio beep was provided through headphones when the training threshold was exceeded. The runner was instructed to land softer and avoid the beep. After the training, the runner repeated the in-field tests and six running bouts (two in each sloped condition) on the treadmill at the speed that matches the in-field tests at baseline and after the training. The reliable change index (RCI) between baseline and after training for each sloped condition was calculated, a value greater than 1.96 indicates a significant change in PTA with 95% confidence. [1]

RESULTS AND DISCUSSION

At baseline, the running speed for level, uphill and downhill conditions were 3.55, 3.46 and 3.83 m/s respectively. The running speeds for all sloped conditions were slower after the training, the adjusted speeds were 2.97, 3.00 and 3.09 m/s. Significant changes in PTA were observed in all sloped conditions, for both in-field (RCI>2.4) and treadmill (RCI>3.3) tests, when running at the adjusted speed. The largest change in PTA was observed during in-field downhill running, with a 59% (-10.3 g) reduction (Figure 1). However, when running on the treadmill at the same speed, no significant reduction was observed in the level and uphill conditions. A significant change was observed in the downhill condition (RCI=4.1) with a 15.7% (-1.8 g) reduction. In contrast to traditional treadmill-based training, running speed was not constrained in this study. Our findings suggested that speed adjustment may be a viable strategy for reducing PTA.

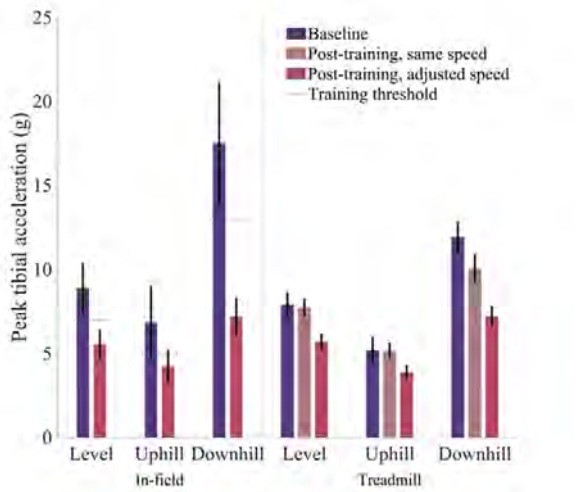

Figure 1 Peak tibial acceleration measured during in-field and treadmill tests. Bars and vertical lines indicate mean and SD respectively. Training thresholds are indicated by horizontal lines.

CONCLUSIONS

This exploratory study supports the use of adaptive feedback in gait retraining to reduce PTA. Among the sloped conditions, the training was most effective in reducing PTA during downhill running.

REFERENCES

[1] Zhang J et al. *Gait Posture* **69**: 8-12, 2019.
[2] Schmidt R et al. *Psychol Sci* **3(4)**: 207-218, 1992.
[3] Vernillo G et al. *Sports Med* **47**: 615-629, 2017.

TRAINED NOVICE RUNNERS INCREASE STEP FREQUENCY AND DECREASE FORCE APPLICATION

Janet H. Zhang-Lea[1,2], Zoe Y.S. Chan[1,3], Manish Sreenivasa[4], Roy T.H. Cheung[5] and Vincent C.K. Cheung[6]

[1] Department of Rehabilitation Sciences, The Hong Kong Polytechnic University, Hong Kong SAR. [2] Department of Human Physiology, Gonzaga University, Spokane, WA, USA. [3] Faculty of Kinesiology, University of Calgary, Calgary, Canada. [4] School of Mechanical, Materials, Mechatronic and Biomedical Engineering, University of Wollongong, NSW, Australia.[5] School of Health Sciences, Western Sydney University, NSW, Australia. [6] School of Biomedical Sciences and Choa Neuroscience Institute, Chinese University of Hong Kong, Hong Kong SAR.
Email: lea@gonzaga.edu

INTRODUCTION

In this study, we aimed to investigate how novice runners modulate running biomechanics while gaining experience in running. Our previous study from neural development perspective has reported that novice runners expressed a more efficient muscle activation pattern across 6 months of running [1]. Since running speed has been reported to equal to the multiplication of step frequency (SF), contact length, and stance averaged ground reaction force (avgGRF) [2], how these three variables varied in this group of novice runners across the 6 months of running remains unclear. We analysed the biomechanics data of the same group of novice runners, and hypothesized that SF would increase while avgGRF would reduce as the runners continued running.

METHODS

This study was a further analysis of the data published by Cheung et al., 2020 [1]. Eleven novice runners (<3 months of running experience) completed 3 treadmill running trials on a self-paced force-measuring treadmill before (baseline), 3-month, and 6-month after regular running training.

We recorded GRF at 1,000 Hz and filtered it using 4th order low-pass Butterworth filter with a cut-off frequency at 50 Hz. We then identified ground contact and toe-off using a 50 N threshold. We calculated SF based on ground contact information, and calculated contact length by multiplying contact time for the right leg with each participant's running speed. We calculated avgGRF as the average vertical force that was applied during the stance phase of running, and normalized it by body weight (BW). We constructed three linear mixed models to assess the effect of training on SF, contact length, and avgGRF, with each participant treated as a random factor. We set the level of significance at 0.05.

RESULTS & DISCUSSION

Training significantly affected SF ($F=4.62$, $p=0.04$), that SF increased by 3 steps/min for every 3-month interval (Fig. 1a). Participants did not significantly alter their contact length across the period that we tested ($F=0.26$, $p=0.61$, Fig. 1b). On average, changes in contact length between 3-moths, 6-months, and baseline are <1%. Training time significantly affected avgGRF ($F=13.5$, $p<0.001$), with 0.03 BW reduction in avgGRF for every 3-month interval (Fig. 1c).

After 3 months of running training, participants showed on average 7.6% increase in their SF in compared to baseline. After 6 months, 6 participants reduced their SF to a level that was comparable to baseline (< 3% difference), and the other 5 participants increased their SF on average by 10.7% compared to baseline. While our results are in line with previous findings, that a high SF has been considered to associate with better running economy [3], we also noticed large individual variance after 6 months of running. We previously reported that ~50% of novice runners presented with a merging muscle activation pattern, featuring a co-activation of ankle plantarflexors and knee extensors [1] after 3 months of running, but only ~30% of them still expressed such merging pattern after 6 months. We suggest studies with follow-ups longer than 6 months will be required to investigate changes in biomechanics and neuromuscular control for novice runners.

According to the equation that speed equals to the multiplication of SF, contact length, and avgGRF, while our participants increased their SF, they decreased avgGRF when running at the same speed after 3 and 6 months of running. When compared to baseline, all runners reduced their avgGRF on average by 4.8% after 6 months, which supports our hypothesis. Previous studies have suggested that avgGRF reflects the demand from the lower limb muscles to support the runner's weight during stance phase of running, and a reduced force application during stance phase of running has been associated with better running economy in distance runners [4].

Our previous study suggested that novice runners who expressed a more efficient muscle activation pattern ran with less mechanical energy loss [1], and our current results further support it from biomechanical perspective, that as novice runners continue to run, their running biomechanics also be modulated to benefit running economy.

CONCLUSIONS

Novice runners increased SF and reduced force applied after 6 months of running training. Such changes in running biomechanics could be a result from muscle activation pattern change as novice runners gained experience in running.

REFERENCES

[1] Cheung et al. *Nat Commun*, **11**, 4356, 2020
[2] Weyand et al., *J App Physiol*, **89**, 1991-1999, 2000
[3] Quinn et al., *J Strength Cond Res*, **35**, 2511, 2021
[4] Heise and Martin, *Eur J Appl Physiol*, **84**, 438-442, 2001

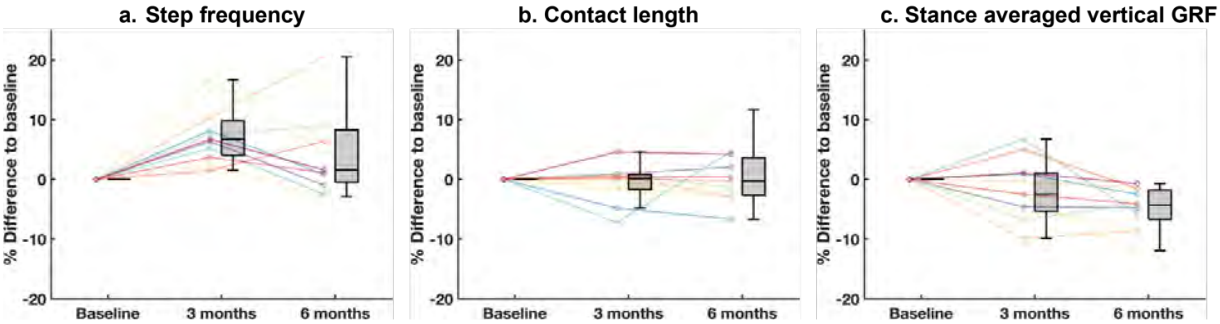

Figure 1 Changes (%) in step frequency (a), contact length (b), and stance-averaged vertical ground reaction force (c) measured after 3 and 6 months of running training compared to baseline. Each coloured individual line represents one participant.

Inter-individual differences in step length and step frequency change across running speeds

Masanori Sakaguchi[1], Nao Hirakawa[1], Kazunaga Nakayama[1], Ryo Matsunaga[1], Seigo Nakaya[1], and Norihiko Taniguchi[1]
[1] Institute of Sport Science, ASICS Corporation, Kobe, Japan.
Email: masanori.sakaguchi@asics.com

INTRODUCTION

The pacing behavior used by elite runners during a race is one of the most important tactics for success in distance running [1]. Humans change their running speed by altering a combination of step length and step frequency. Although faster running speeds can be achieved by increasing either step length or step frequency, changing these parameters independently is difficult because it is well-known that step length is inversely proportional to step frequency when running at a given speed [e.g. 2]. On the other hand, there exists inter-individual differences in step length and step frequency that have often been classified as aerial and terestrial runners [3]. Basically, the evaluation of the running style of athletes, whether they are aerial or terrestrial runners, is performed based on their running kinematics at a pre-defined speed. However, even though the running speed changes frequently as tactics during a race, no study has focused on the individual pattern of change in step length and step frequency as the running speed changes. Therefore, the purpose of this study was to elucidate the inter-individual differences in step length and step frequency changes across running speeds.

METHODS

Nineteen athletes, who compete in long distance running and whose best marathon record is less than 3 hours or equivalent, were recruited. A total of 68 reflective markers were attached to the athlete. Kinematic (250 Hz) and kinetic (1000 Hz) data were recorded simultaneously using a 24-camera motion capture system and three force plates. To minimize the influence of footwear, all athletes performed in a properly sized racing flat (Sortiemagic RP5, ASICS). All athletes were then asked to perform 15-30 straight running trials on a 50-m runway at various running speeds ranging from approximately 3.0 to 6.5 m/s. To encourage the athletes to run with their natural running styles, there was no restriction on the foot strike to a force plate; a trial was judged as successful if either of athlete's feet was in contact with any of the three force-plates with a natural running style.

Step length and step frequency were calculated for a single step for each trial. Step length was defined as the distance travelled by consecutive contralateral foot-strikes, calculated from the most-posterior heel markers of each foot. Step frequency was then calculated as the reciprocal of the time spent during a step cycle. Running speed was then calculated by multiplying step length and step frequency. The relationships between running speed and step length or step frequency were tested using Pearson's product moment correlation coefficient for each athlete. The association between the slopes of regression lines between running speed and step length (SL-Slope) and between running speed and step frequency (SF-Slope) were also tested. The significance level was set at $P < 0.05$.

RESULTS AND DISCUSSION

The significant positive correlations between running speed and step length were observed for all athletes ($r > 0.94$, $P < 0.01$). On the other hand, the correlations between running speed and step frequency were not always as strong as those between running speed and step length, only explaining 55% of the variance for the lowest case ($r = 0.74$, $P < 0.01$). The relationship between the regression slopes of the above relationships showed significantly negative correlation. This result indicates that every runner has a different ratio of step length changes and step frequency changes across running speeds.

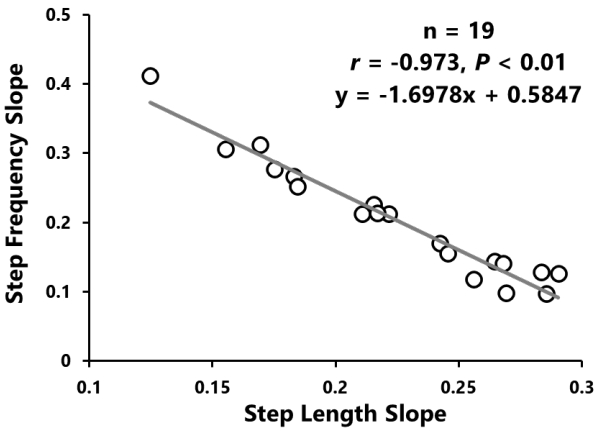

Figure 1 The association between the SL-Slope and SF-Slope

CONCLUSIONS

Judging running style, whether aerial or terrestrial, only by step length or step frequency at a given single speed is not necessarily sufficient to evaluate an individual's running style as it does not adequately capture the changes in step length and/or step frequency across running speeds. Instead, the combination of the SL-Slope and SF-Slope may be the possible method to assess the running style.

REFERENCES

[1] Casado A et al. *J Sport Health Sci* **10**: 537-49, 2021.
[2] Wayand P et al. *J Appl Physiol* **89**: 1991-9, 2000
[3] Gindre C et al. *Int J Sports Med* **37**: 25-29, 2016

Variation in tibia-fibular geometry is associated with strain-related changes during running.

Keast, M [1], Bonacci, J [1], Fox, A[1]
1. School of Exercise and Nutrition Science, Deakin University.
Email: mf.keast@gmail.com

INTRODUCTION

Naturally occurring variation in lower limb skeletal geometry has the potential to alter strain magnitude and distribution during locomotion. Tibial size is one geometric variation that has been cited for modifying the risk of developing tibial stress injuries [1]. Recent research using statistical shape models has identified several natural variations in tibia-fibula geometry. [2,3]. Some of these variations have been investigated using synthetic models that isolate individual geometries [3]. This methodology of isolating shape characteristics provides a clear way to isolate the effect of geometry on tibial strain. These methods, however, potentially represent an unrealistic tibia-fibula where concurrent shape variation is ignored. Estimating strain using participant specific bone models and finite element analysis provides the ability to examine the effects of geometric variations on strain in realistic skeletal geometry. We investigated the effect of tibia-fibula geometric variation on tibial strain magnitude during running at various speeds using participant-specific models.

METHODS

Participant specific three-dimensional models of the tibia-fibula were created using lower limb computed tomography (CT) scans from the right tibia and fibula of 30 cadavers (28.7± 6.7 years, 70.22 ± 11.36kg, 176.06 ± 11.61cm). Finite element (FE) models of the tibia-fibula were developed in FEBio. In each FE model: (i) generic joint reaction and muscle forces extracted from running at 3, 4 and 5m·s-1 [4] were applied to the tibia at the tibia-talus interface; (ii) the tibial plateau and medial malleoli were fixed; and (iii) the tibia-fibula interaction was modelled with tied contact and springs representing ligaments. Effective strain was then extracted from the tibial shaft (15 – 75% of tibial length). We used a non-parametric permutation method [5] to conduct classical hypothesis testing. We used this approach with linear regression models to evaluate the relationship between geometric characteristics (i.e. dependent variable) and effective strain along the tibial shaft (i.e. independent variable). Dependent variables were select principal component (PC) scores from three previously created statistical shape models [2], with 10 PC scores selected for statistical analyses. The principal component scores (i.e. dependent variables) were then input alongside the effective strain across the tibial shaft (i.e. independent variable) in separate linear regression models. An alpha level of 0.05 was used to calculate the critical t-value which denoted statistical significance.

RESULTS

We observed a statistically significant relationship between the thickness of the midshaft to upper tibia and condyle size to effective strain across areas of the tibial shaft. A higher score for this shape characteristic (i.e. increased thickness of the midshaft to upper tibia with increase in condyle size) was related to increases in effective strain at points along the distal anterolateral and proximal posterior regions of the tibial shaft at all three speeds. We also observed a statistically significant relationship between medulla cavity and midshaft cortical thickness to effective strain across areas of the tibial shaft. A higher score for this shape characteristic (i.e. decreased width of the medulla cavity and increased midshaft cortical thickness) was related to increases in effective strain across at specific points along the medial aspect at the distal end of the tibial shaft at a speed of 5 m/s.

CONCLUSIONS

Variations in tibial geometry can affect the magnitude of effective strain when running loads are applied to bone. Changes to thickness in the mid to upper portion of the tibia and to midshaft cortical thickness has the potential to increase strain in the distal portion of the tibia. It is possible that the increased thickness in the more proximal region caused the strain to be redistributed to the areas that are more susceptible to the applied loads (i.e. the distal end). An unbalanced degree of thickness between the upper and distal portions of the tibial shaft could potentially have a negative impact on tibial stress injury risk. Overall, our findings enhance understanding of the mechanisms underpinning tibial stress injury risk. However, it is still unknown the impact combinations of geometric variations have on tibial strain. Further investigation of the interactions between multiple shape characteristics is warranted.

REFERENCES

[1] Popp KL. *J Sci Med Sport*. 23(2), 2020.
[2] Keast M, *BioRxiv,* 90, 2021(Preprint)
[3] Bruce O, *Bone,* 161, 2022
[4] Hamner SR, *J Biomech*, 46(4), 2013
[5] Pataky T, *PeerJ Computer Science*, 2(11), 2016

Increasing step frequency reduces cumulated patellofemoral joint stress more at low running speed

Michiel Hagen[1], Anna Vanmechelen[1], Emile Cloet[1], Jan Sellicaerts[1], Kaat Van Welden[1], Jesper Verstraete[1], Danilo S. Catelli[1,2], Sabine Verschueren[1], Jos Vanrenterghem[1]
[1] Department of Rehabilitation Sciences, KU Leuven, Leuven, Belgium.
[2] Department of Movement Sciences, KU Leuven, Leuven, Belgium.
Email: michiel.hagen@kuleuven.be

INTRODUCTION

Patellofemoral pain syndrome is one of the most prevalent running-related injuries[1]. Interventions that are frequently used to reduce patellofemoral joint stress (PFJS) are alterations in running speed and step frequency. Remarkably, the combined effect of running speed and step frequency on PFJS parameters has not yet been investigated. The objective of this study was to investigate whether the load modifying effect of step frequency alterations was equally effective at different running speeds. More specifically, the peak PFJS and the cumulated PFJS per km were investigated.

METHODS

Twelve healthy recreational runners performed an incremental speed protocol on an instrumented treadmill. The protocol started at an initial running speed of 8km/h and increased by 2km/h every minute until 16km/h was reached. The protocol was completed three times: at habitual step frequency, 10% increased step frequency and 10% decreased step frequency. Kinematics data of the lower limbs and trunk were collected by 13 cameras of a passive marker-based motion capture system (100Hz, Vicon, UK). Markers were placed according to the Liverpool John Moores University model. Ground reaction forces were measured using two force plates embedded in the treadmill (1000Hz, Motek Medical, NL). Patellofemoral joint contact forces were calculated in OpenSim 3.3 using the Catelli model[2] and a standard modelling workflow[3]. The PFJS was then calculated by dividing the patellofemoral joint contact force by the angle-specific patellofemoral joint contact area, based on MRI data from the literature[4]. The cumulated PFJS was calculated by multiplying the PFJS impulse (PFJSi) per step by the number of strides per km. Main effects of running speed, step frequency and their interaction effect were evaluated using two-way repeated measures ANOVA's. In case of a significant effect, linear regression analyses were chosen as post-hoc analyses.

RESULTS AND DISCUSSION

For peak PFJS, significant main effects were confirmed for running speed and step frequency. Higher running speeds resulted in higher peak PFJS and increased step frequency resulting in lower peak PFJS (Table 1). There was no statistically significant interaction effect. The regression analysis of the peak PFJS showed separated parallel lines that increased similarly with increasing running speed (Figure 1). For the PFJSi per km, significant main effects for running speed and step frequency as well as a significant interaction effect were found. The regression analysis showed decreasing and converging lines as the running speed increased, suggesting that step frequency alteration was more effective at low running speed.

Table 1: P-values for the two-way repeated measures ANOVA's for peak PFJS and PFJSi per km.

	Running speed	Step frequency	Interaction
Peak PFJS	*p<0.001*	*p<0.001*	*p=0.338*
PFJSi per km	*p<0.001*	*p<0.001*	*p<0.001*

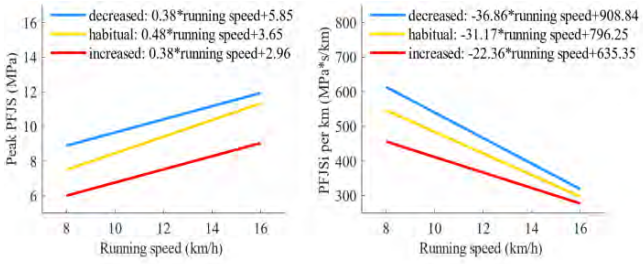

Figure 1: Regression lines for peak PFJS and PFJSi per km for each step frequency condition.

CONCLUSIONS

Whilst step frequency alterations are equally effective at low and high running speeds to change peak PFJS, the effectiveness on cumulated PFJS is higher at low running speeds. These findings are very relevant to optimise load management strategies for patients with patellofemoral pain syndrome.

ACKNOWLEDGEMENTS

Michiel Hagen is funded by a PhD fellowship fundamental research from FWO Flanders.

REFERENCES

[1] Kakouris N et al. *J Sport Health Sci.* **10**: 513-522, 2021.
[2] Catelli D et al. *Comp Meth Biomech. and Biomed Eng* **22**: 21-24, 2019.
[3] Lenhart R et al. *Med Sci Sport Exerc.* **46**: 557-564, 2014.
[4] Besier et al. *J Orthop Res.* **23**: 345-350, 2005

AN ADVANCED MODELLING FRAMEWORK FOR ASSESSING KNEE ARTICULAR MECHANICS AND SOFT TISSUE LOADING AFTER TOTAL KNEE ARTHROPLASTY

Ning Guo[1], Colin R. Smith[2], Adam Trepczynski [3], Philipp Damm[3], William R. Taylor[1] and Seyyed Hamed Hosseini Nasab [1]
[1] Department of Health Sciences and Technology, Institute for Biomechanics, ETH Zurich, Zurich, Switzerland.
[2] Department of Biomedical Engineering, Steadman Philippon Research Institute, Vail CO, USA.
[3] Julius Wolff Institute, Berlin Institute of Health at Charité-Universitätsmedizin Berlin, Berlin, Germany.
Email: bt@ethz.ch

INTRODUCTION

Generic musculoskeletal models often present substantial errors in the prediction of joint function after total knee arthroplasty (TKA) [1]. Therefore, subject-specific modelling is necessary to investigate knee mechanics and personalize surgeries. This study introduces an advanced modelling framework towards understanding the influence of different surgical parameters on the knee joint mechanics after TKA. The framework was validated using a detailed musculoskeletal model personalized to a subject measured within the CAMS-Knee project [2]. Loading and kinematics of the knee during level walking and squat from simulation results were accurately matched with data obtained from *in vivo* measurements.

METHODS

The subject-specific skeleton geometry was derived from CT images of a TKA patient in the CAMS-Knee datasets (K5R [2]). Bone segments were then linked to form a multibody model with hip, knee, and ankle joints. (Fig 1). Implant components were positioned within the subject-specific model based on their 3D pose within the CT images.

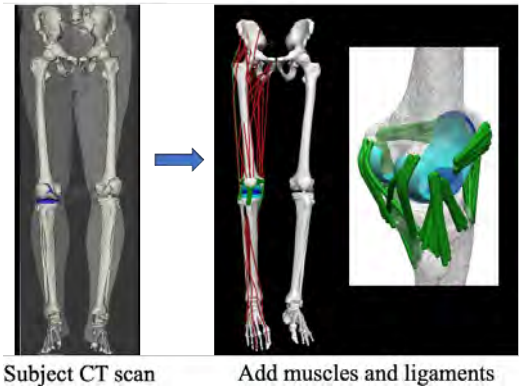

Figure 1 Model development framework.

Knee ligament footprints were identified based on anatomical literature. Ligaments were modelled using bundles of nonlinear spring elements connecting the ligament footprints. Ligament and muscle parameters were scaled and adjusted from previously developed models [3,4].

The tibiofemoral and patellofemoral joints were modelled with 12 degrees of freedom (DOFs) and guided by elastic foundation contact between the implant surfaces. Skin-marker trajectories and ground reaction force data were inputs to the COMAK tool [5] to estimate knee kinematics and loading during five trials of simulated level walking and squat. The outcomes were validated against *in vivo* measurements of contact force from an instrumented implant and tibiofemoral kinematics from fluoroscopy.

RESULTS AND DISCUSSION

Overall, the model was able to accurately predict tibiofemoral kinematics and loading patterns measured *in vivo* (Fig 2). Predicted knee contact forces reached 2.5 and 3.3 BW during walking and squatting, which indicate slight overestimation of the loads likely due to non-personalized parameters (e.g., muscle strength, ligament properties and muscle coordination strategy). Importantly, the framework also enables estimation of ligament and muscle forces as well as patellofemoral joint mechanics and thus allows further exploration towards understanding interrelationships between different joint structures and TKA surgical decisions.

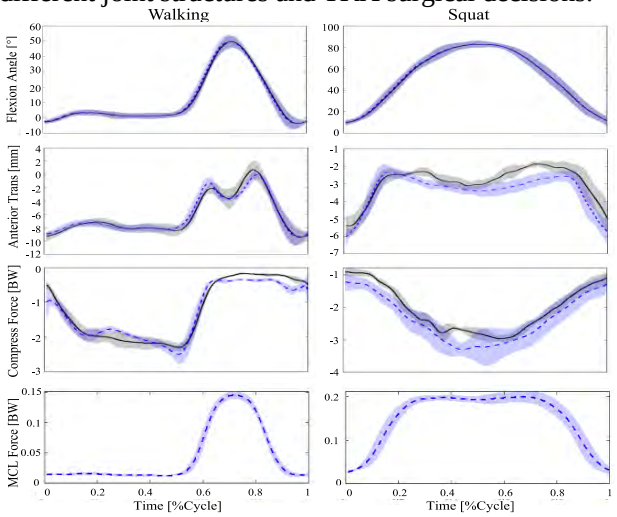

Figure 2 Forces and kinematics at knee during walking and squat (blue model, black experiment).

CONCLUSIONS

Our modelling framework enables reliable estimation of the knee joint mechanics during dynamic and quasi-static activities, thus providing a predictive tool for future investigations into the influence of surgical parameters (e.g., ligament release and implant alignment) on the joint function after TKA.

ACKNOWLEDGEMENTS

We would like to thank B. Braun Aesculap AG and the Chinese Scholarship Council for providing financial support to this project.

REFERENCES

[1] Nejad Z., et al. *Ann Biomed Eng*, 2020.
[2] Taylor W., et al. *J Biomech*, 2017.
[3] Arnold E., et al. *Ann Biomed Eng*, 2010.
[4] Smith C., et al. *J Biomech Eng*. 2016.
[5] Smith C. *https://github.com/clnsmith/opensim-jam*

DYNAMIC SIMULATION OF RUNNING USING A FULL-BODY MODEL WITH TRUNK MUSCLES

Harry G. Driscoll[1], Olga Panagiotopoulou[2], Marcus G. Pandy[1]
[1]Department of Mechanical Engineering, The University of Melbourne, Melbourne, Australia.
[2]Department of Anatomy and Evolutionary Biology, Monash University, Melbourne, Australia.
Email: hdriscoll@student.unimelb.edu.au

INTRODUCTION

A model of the human musculoskeletal system that includes a detailed representation of the torso has not previously been used to perform dynamic simulations of whole-body movement. Such a model would allow for a better understanding of trunk muscle function during dynamic activity by predicting the activations and forces of the deep and superficial muscle layers, thereby lending insight into the relationships between trunk muscle strength and athletic performance. The main aim of the present study was firstly, to create an anatomically-accurate and computationally-efficient full-body model that includes a detailed representation of the trunk musculature; and secondly, to implement this model in a dynamic simulation of medium-paced running.

METHODS

The model was created using OpenSim 3.3 [1] by combining the trunk muscles included in the model published by Raabe and Chaudhari [2] with the lower-limb model developed by Lai et al [3]. This was done because the lower-limb model developed by Lai et al. [3] is better suited to the higher hip and knee flexion angles present in maximum-effort activities such as running and jumping. The constraints controlling lumbar spine motion used by Raabe and Chaudhari [1] were replaced with a single-segment lumbar spine, yielding a two-segment trunk model. The specific tension of the trunk muscles was then modified to match that assumed for the lower limbs (60 N/cm^2) [3]. To enhance computational efficiency of the model, a simplified set of trunk muscles was created by grouping muscle-tendon units (MTUs) in the Raabe and Chaudhari trunk model [2] and replacing each group with a single MTU. MTUs were grouped to ensure that each major trunk muscle was still represented by at least one equivalent MTU. New origin and insertion sites and muscle fibre parameters were defined based on either a summation or average of values defined in the original set of MTUs. Muscle moment arms and muscle fibre parameters were then compared against literature data. The model was scaled in OpenSim 3.3 [1] and used to perform inverse kinematics, static optimization, and computed muscle control (CMC) for one subject running at 5.0 ms^{-1}.

RESULTS AND DISCUSSION

The final model consisted of 17 segments, 16 joints and 36 degrees of freedom, and was actuated by 116 MTUs. The model was used to perform a dynamic simulation of sprinting at 5.0 ms^{-1}, providing predicted muscle activations and muscle forces for 80 lower limb and 24 of the 36 trunk MTUs. Representing the lumbar spine as a single segment necessitated further modification of the remaining 12 MTUs to ensure the trunk segments could be adequately controlled. Model-predicted activations of the trunk muscles during medium-paced running (5 ms^{-1}) were consistent with those reported for running at 3.5 ms^{-1} derived using static optimization [2]. However, model-predicted activations obtained in the present study were typically higher and lasted for a longer duration due to the additional work that the trunk muscles must undertake to overcome larger ground reaction forces at higher running speeds. RMS errors for kinematic tracking vs. CMC predicted motion are given in Table 1 below. Future work will entail increasing the number of trunk muscles to 36 and performing simulations for both countermovement and squat jumps.

CONCLUSIONS

A full-body model incorporating 24 trunk muscles was used to perform a dynamic simulation of medium-paced running at 5.0 ms^{-1}. The model reproduced measured 3D joint motion using muscle activation patterns consistent with measured EMG.

REFERENCES

[1] Delp et al. *IEEE transactions on biomedical engineering* **54(11):** 1940-1950, 2007.
[2] Raabe M & Chaudhari A. *J Biomech* **49(7)**: 1238-1243, 2016.
[3] Lai et al. *Annals of biomedical engineering* **45(12)**: 2762-2774, 2017.

Table 1: Root-mean-squared errors between model-predicted and measured 3D joint motion for a dynamic simulation of running at 5.0 ms^{-1}.

	R-Hip Flex.	R-Hip Add.	R-Hip Rot.	R-Knee Angle	R-Ankle Angle	L5-S1 Flex.	L5-S1 Bend.	L5-S1 Rot.	T12-L1 Flex.	T12-L1 Bend.	T12-L1 Rot.
RMSE	9.741	3.574	2.878	18.21	9.954	2.396	3.285	2.261	5.642	2.003	1.961
Normalized	0.11	0.157	0.157	0.132	0.196	0.172	0.166	0.095	0.114	0.121	0.15

Unravelling adaptation strategies in sit-to-walk using predictive neuromuscular simulations: pain

Eline van der Kruk[1], Thomas Geijtenbeek[1]
[1] Biomechanical Engineering, Delft University of Technology, Delft, The Netherlands.
Email: e.vanderkruk@tudelft.nl

INTRODUCTION

Standing up from a chair is a key daily life activity (>60x per day) that is sensitive to functional limitations as we age. Most stand-up movements transfer directly into walking (sit-to-walk). Predictive neuromusculoskeletal models could possibly shed light on the interconnectivity and interdependency of neuromuscular capacity, reinforcement schemes, sensory integration, and adaptation strategies during stand up. The aim of this study was to develop and validate a planar neuromusculoskeletal model with reflex-based muscle control to simulate the sit-to-walk movement. The framework was used to simulated the sit-to-walk movement in different conditions (seat height, foot placement), reduced muscular capacity, reduced neural capacity, and altered movement objectives (pain). In this abstract we focus on the following hypothesis: “Altered trunk flexion strategies, which previously were shown to be related to muscle weakness, may also be related to pain avoidance” which was put forward in a recent review [1].

METHODS

In summary, a planar sit-to-walk musculoskeletal model (11 dof, 20 muscles) and controller were developed and optimized in SCONE [2] using a shooting-based optimization method. The sit-to-walk controllers consist of a two-phase stand-up controller (P1, P2) based on proprioceptive feedback from muscle length feedback (L), force feedback (F), velocity feedback (V), constant excitation (C), and vestibular feedback. The delayed feedback pathways were both monosynaptic an antagonistic. The free parameters were optimized to minimize the cubed muscle activation and gross cost of transport, at a prescribed minimum gait velocity, while avoiding falling, and ligament injury. We ran multiple parallel optimizations with the same initial guess and used the best set as start for the next set of optimizations. Final results were compared to a subset of recorded kinematics, ground reaction forces (GRF), and muscle activation (sEMG) from young (18-35 year) and older (>65 year) adults (n = 50), in which participants were asked to stand up and walk to a table at self-selected speed [3].

RESULTS AND DISCUSSION

The simulation resulted in altered trunk flexion when there was an increase of task demand (reduced seat height) or a decrease of muscular capacity (reduced VAS muscular strength). Pain avoidance, which we assumed would lead to an objective of reduced knee load, led to altered muscle recruitments (reduced ipsilateral activation of VAS and HAM, compensated by increased activation of the GMAX), and not to increased trunk flexion. The predictive simulations thus showed that increased trunk flexion is most likely the result of lack of muscular reserve rather than pain avoidance.

This is in line with the difference in kinematics and muscle activations that was found between moderate and severe knee osteoarthritis (OA) patients in experimental data. The increase of trunk flexion was only found in severe knee OA patients, whereas moderate knee OA patients maintained the same movement trajectory as healthy individuals but with altered muscle recruitment [1]. If we assume that severe OA patients have less muscular reserve than moderate OA patients as a result of reduced daily life activity, severe OA patients will employ increased trunk flexion in standing up to compensate for lack of strength. Over time, the unloading of the knee to avoid pain could be the cause of muscular weakness in specific muscles. In the simulations we saw that already in standing up, unloading the knee leads to reduced activation of the VAS muscle. Assuming this leads to reduced VAS strength this eventually results in a negative spiral. The compensation strategies increased the loading on ipsilateral and contralateral joints, likely leading to increased wear of other joints.

CONCLUSIONS

The simulation showed how increased trunk flexion, as observed in severe OA patients, is most likely the result of muscular weakness rather than pain avoidance. Whereas altered muscle recruitment is a way to reduce joint loading, like previously observed in moderate OA patients. Based on the results it might be beneficial to treat pain in knee OA patients early on to avoid compensatory muscle recruitments which lead to underuse of specific muscles.

ACKNOWLEDGEMENTS

NWO-TTW VENI Grant 18145(2021)

REFERENCES

[1] van der Kruk, et al. *J Biomech* **122**: 110411, 2021.
[2] Geijtenbeek, T JoOSS 38: 1421, 2019
[3] van der Kruk, E., et al. npj Aging, 8(1), 13, 2022

Towards a Musculoskeletal Shoulder Model Depicting Glenohumeral Translations Considering Bony, Ligamentous and Muscular Stability Constraints

Johanna Menze[1,2], Eleonora Croci[3,4], Michael Skipper Andersen[5], Hanspeter Hess[1], Stephen J.Ferguson[2], Andreas Marc Müller[3], Annegret Mündermann[3,4] and Kate Gerber [1]

[1] School of Biomedical and Precision Engineering , University of Bern, Bern, Switzerland.
[2]Institute for Biomechanics, ETH Zurich, Zurich, Switzerland.
[3] Department of Orthopaedics and Traumatology, University Hospital Basel, Basel, Switzerland.
[4] Department of Biomedical Engineering, University of Basel, Basel, Switzerland.
[5] Department of Materials and Production, Aalborg University, Aalborg, Denmark.
Email: johanna.menze@unibe.ch

INTRODUCTION

Glenohumeral (GH) stability is a delicate interplay between bony congruence, muscle contraction and ligamentous or capsular stability. The bony congruence confines the translational kinematics. While muscles provide stability to the humeral head in midrange motion, ligamentous and further connective tissue structures constrain the joint at endrange motion [1]. An imbalance can cause pathologies such as shoulder instability, osteoarthritis or rotator cuff tears, however, the underlying effect is not yet well understood.
The few shoulder models implementing GH translation define GH joint stiffness based on a reverse engineering approach of measured humeral head translations [2]. A musculoskeletal shoulder model applying biomechanical properties of bony, muscular and ligamentous structures would enable further investigation of pathological mechanisms.
We aimed to develop an advanced musculoskeletal shoulder model, considering bony contact forces, muscle active and passive stability and ligament mechanical properties, to calculate GH translations using force-dependent kinematics (FDK) [3].

METHODS

Motion capture data of 15 participants performing three 0° to 30° abduction-adduction cycles (VICON, UK) with 0 to 3kg handheld weight were incorporated into a musculoskeletal model of the right shoulder (Anybody 7.3, repository AMMR v.2.3.1) for subject scaling and to drive subject-specific motion [4]. Segmented glenoid, labrum and humeral head contact surfaces were developed from MRI images. GH and coracohumeral ligament stiffness, slack length and insertion sites were defined generically. The Hill muscle model was calibrated to subject size. Based on the acting joint forces and constraints, GH translations were calculated in each time step using FDK[3]. Resulting GH translations were compared between abduction-adduction cycles with different handheld weights and to existing measured inferior-superior translations from dynamic fluoroscopy imaging of the same subjects.

RESULTS

At 0kg handheld weight, seven shoulder models presented an anterosuperior GH escape and three an initial inferior drop. The remaining six models converged, and mean inferior-superior translations decreased from 3.5 to 1.8mm for 0 to 3kg handheld weight, however, did not match the 1.6mm and 0.8mm measured in patients with 0 and 2kg handheld weight, respectively (Figure 1).

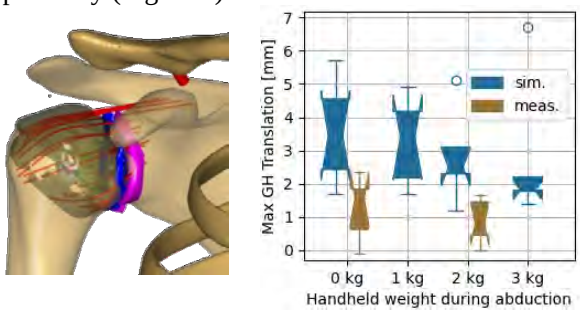

Figure 1 *(A) FDK Shoulder model and (b) Comparison of measured (meas.) and simulated (sim.)* inferior-superior GH translations

DISCUSSION AND CONCLUSIONS

This work presents a novel pipeline for more physiological shoulder modelling. GH translations calculated with this model are significantly higher than measured values especially at lighter handheld weights, indicating that muscular stabilisation is currently underrepresented. Enforced muscle recruitment with greater handheld weights led to the required stabilisation effect of the GH joint. Future work will focus on emphasizing the muscular recruitment for joint stability to subsequently further apply this model to assess pathological shoulders.

ACKNOWLEDGEMENTS

Funding from an ISB travel grant to visit Aalborg University and Anybody Technology, Aalborg, Denmark. Funding: Swiss National Science Foundation (SNF #189082).

REFERENCES

[1] Veeger H et al. *J Biomech* **40**: 2119-29, 2007.
[2] Auerbach M et al. *J Biomech* **106**: 19817, 2020
[3] Skipper Andersen M et al.*JBiomechEng* 139.9:,2017
[4] Croci E et al. *JMIR Res Protoc* **11.12**: e43769, 2022.

A DYNAMIC FOOT MODEL FOR PREDICTIVE SIMULATIONS OF GAIT

Lars D'Hondt[1], Friedl De Groote[1] and Maarten Afschrift[2]
[1]Department of Movement Sciences, KU Leuven, Leuven, Belgium.
[2]Department of Human Movement Sciences, Vrije Universiteit, Amsterdam, The Netherlands.
Email: lars.dhondt@kuleuven.be

INTRODUCTION

Predictive simulations that generate de novo gait patterns based on a musculoskeletal model (without using experimental gait data as input) are a powerful tool to explore causal relations between musculoskeletal properties and gait mechanics. State-of-the-art predictive simulations capture many features of human gait, yet generating realistic ankle mechanics remains a challenge [1]. Humans use their calf muscles and Achilles tendon to efficiently produce large positive ankle power at push-off. This strategy requires the foot to act as a stiff lever [2]. The human foot is compliant, but can be stiffened by muscle contraction and by tensioning the plantar fascia (an elastic structure that connects the heel and toes). This stiffening mechanism is associated with a 18±2° range of motion observed between hindfoot and forefoot [2]. State-of-the-art predictive simulations use a model with a 2-segment foot, thus do not account for midfoot motion. We present a 3-segment foot model that improves the realism of 3D predicitive simulations of gait.

METHODS

We adapted the musculoskeletal model used by Falisse et al. [1] to include a 3-segment foot model (hindfoot, midfoot-forefoot, toes) with a deformable longitudinal foot arch. Hindfoot and midfoot-forefoot segments are connected by a midtarsal joint with a single degree of freedom. We modelled ligaments with non-linear stiffness. We considered the plantar fascia as a single elastic element originating on the calcaneus, wrapping around the metatarsals, and inserting on the proximal phalange. We modelled plantar intrinsic muscles by a single Hill-type muscle with the same path as the plantar fascia. We reduced normalised Achilles tendon stiffness to 8 at 4 % strain, because this results in more realistic fibre lengths of the gastrocnemius medialis [1]. To model foot-ground contact, we placed five Hunt-Crossley spheres under each foot guided by foot anatomy and plantar pressure data: heel pad, lateral longitudinal arch, ball of the foot (2 spheres), and toes. Mechanical parameters were tuned to be consistent with heel pad properties from literature. Using our previously developed simulation workflow [1], we simulated walking at self-selecting speed based on a series of models to evaluate the effect of ankle and foot morphology on gait.

RESULTS AND DISCUSSION

Predictive simulations based on our 3-segment foot model better capture ankle kinematics and power than simulations based on a 2-segment foot model (Figure 1, thick lines). Simulated gait patterns were especially sensitive to heel pad, Achilles tendon, and arch stiffness (Figure 1, thin lines). (1) Stance knee flexion required a sufficiently stiff heel pad. (2) The Achilles tendon had to be sufficiently compliant to obtain ankle dorsiflexion and energy storage during mid stance. (3) Reduced ability to stiffen the foot (no plantar intrinsic muscle, very compliant plantar fascia, low arch height) resulted in exaggerated knee flexion during the second half of stance and reduced negative ankle power.

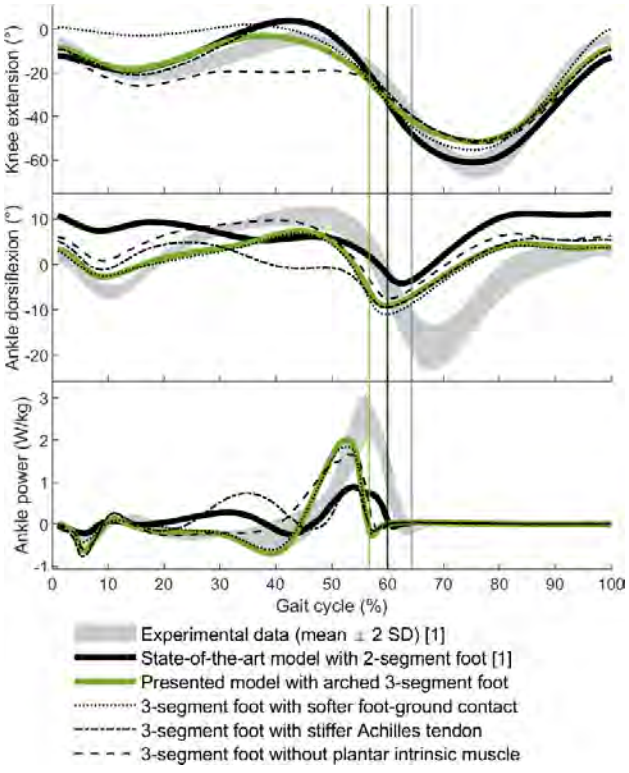

Figure 1 Predicted gait for different foot models.

CONCLUSIONS

Simulations can help elucidate how foot and ankle morphology shape whole body gait mechanics, which has implications for understanding foot pathologies and evolution, and for the design of bipedal robots.

ACKNOWLEDGEMENTS

KU Leuven internal funds C24M/19/064.

REFERENCES

[1] Falisse, A. et al. *PLOS ONE* **17**: e0256311, 2022.
[2] Holowka, N. B. et al. *J. Exp. Biol.* **221**: jeb174425, 2018

INSIGHTS INTO THE DIFFERENT STATE-OF-THE-ART OPTIMISATION APPROACHES FOR SOLVING THE SHOULDER MUSCLE REDUNDANCY PROBLEM

Maxence Lavaill[1], Saulo Martelli[1], and Peter Pivonka[1]

[1] School of Mechanical, Medical and Process Engineering, Queensland University of Technology, Brisbane, Australia.

Email: maxence.lavaill@qut.edu.au

INTRODUCTION

Estimating muscle forces *in vivo* is critical for understanding the internal biomechanics of shoulder motions. Current techniques solve the muscle redundancy problem either by static optimisation (SO), which assumes optimal control, by constraining the muscle forces to the available electromyography measurement (EMG-assisted methods) [1] or by stochastically sampling the entire spectum of possible muscle forces within admissible constraints [2]. This study aims to compare predictions of muscle and glenohumeral forces obtained using SO, EMG-assisted and stochastic methods to corresponding electromyography and glenohumeral contact force measurements reported in previous work [3].

METHODS

Data were previously obtained from a female participant (73 y.o., 168 cm, 72 kg) with an instrumented shoulder hemi-arthroplasty [3]. She was asked to perform a shoulder abduction-adduction task while fourteen bony landmark's locations (thorax, scapula, upper arm and forearm) were captured using an *Optotrack* system (Northern Digital Inc., Canada) at 50 Hz. Ten surface electrodes, placed on top of the Trapezius, Deltoideus, Pectoralis Major, Biceps and Triceps muscles, simultaneously recorded EMGs at a sampling rate of 1000 Hz. Filtered EMG envelopes were extracted. A previously developed upper-limb musculoskeletal model, consisting of 7 segments, 10 degrees-of-freedom and 91 muscle elements [4], was linearly scaled to match the anthropometry of the participant. Joint angles and moments were computed *via* inverse kinematics (IK) and inverse dynamics (ID) through *OpenSim 3.3*.

First, muscle recruitment was estimated using SO (*OpenSim 3.3* GUI) by minimising the sum of the muscle activation squared at each frame of the motion task. Second, a calibrated EMG-assisted method was adopted. This method consisted of 2 steps. Step one was calibrating the model's muscle parameters using the CEINMS toolbox [5] and data from a subsidiary shoulder abduction trial. Step two was running CEINMS on the main data in EMG-assisted mode. This mode combinedly minimised the glenohumeral joint torque errors, the muscle excitation errors for experimentally recorded muscles and the overall sum of the muscle excitations squared. Finally, a stochastic method, as presented in [2], was used. Based on the known moment arms, the method sampled 200000 muscle recruitment solutions satisfying the joint torques. Muscle forces were bound from 0 to 70% of their respective maximum force. Resultant glenohumeral joint forces were estimated using the muscle forces estimated from all three methods.

The experimental total glenohumeral joint force was compared against the stochastic range to determine whether the solution is part of the model. Then, each method was compared against the others in terms of muscle forces and resulting glenohumeral joint force and validated against the experimental EMG signals and instrumented glenohumeral joint force.

RESULTS AND DISCUSSION

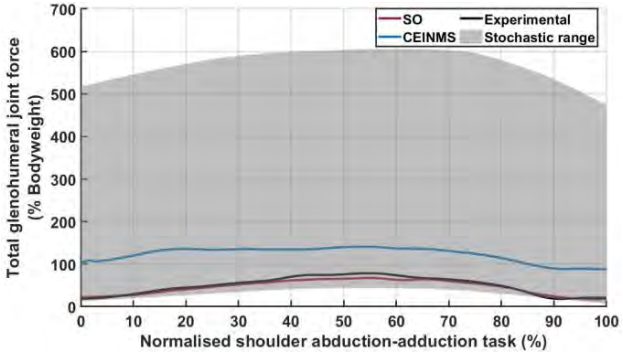

Figure 1 Normalised glenohumeral loads from the instrumented prosthesis (black) and from the estimated solutions using static optimisation (red) and EMG-assisted optimisation (blue).

The whole glenohumeral joint force measurement was within the stochastic range meaning that it represented a possible solution of the model (Fig. 1). Root mean square deviation (RMSd) between SO and experimental glenohumeral joint force was 41N. CEINMS overestimated the joint force (RMSd = 522N) due to higher co-contractions [1]. Moreover, SO expectedly stood close to the lower bound of the stochastic range (RMSd = 116N with lower bound). The whole stochastic range was 3800N wide on average.

CONCLUSIONS

The shoulder model's solutions included the joint measurements, as well as the CEINMS and SO solutions; the latter being the closest to the instrumented implant measurements. Future results including more patients and movements are currently being processed.

ACKNOWLEDGEMENTS

Dr. Nikooyan and Prof. Veeger are gratefully acknowledged for making the full dataset available. Moreover, the authors received support through the following ARC schemes: IC190100020 and FT180100338.

REFERENCES

[1] Kian et al., *J Biomech* **97**:109348, 2019.
[2] Martelli et al., *Interface Focus* **5(2)**:1-14.
[3] Bergmann et al., *J Biomech* **44(8)**:1543-1552, 2011.
[4] Nikooyan et al., *J Biomech* **43(15)**:3007-3014, 2010.
[5] Pizzolato et al., *J Biomech* **48(14)**:3929-3936, 2015

Three-dimensional training load of female university volleyball players during practice games

Chuan-Fang Hou[1], Fang-I Shih[2], En-Chung Chang[2] and Tzyy-Yuang Shiang[2]
[1] Department of Physical Education, National Taiwan Normal University, Taipei City, Taiwan.
[2] Department of Athletic Performance, National Taiwan Normal University, Taipei City, Taiwan.
Email: tyshiang@gmail.com

INTRODUCTION

Volleyball is a physically high demanding sport. Volleyball games contain different types of sprinting, change of direction, and jumping activities. Volleyball players often suffer from upper extremity, trunk, and lower extremity overuse injuries. Monitoring the training load of volleyball players is a great strategy to prevent injuries and improve sports performance. Training load derived from inertial measurement unit has been an indicator to monitor the athletes' activities during training and games [2,3]. Few studies investigated the percentage contributions of individual axis to training load of volleyball players. The purpose of this study was to investigate the percentage contribution of each individual axis to total training load of female university volleyball players during practice games.

METHODS

Thirteen female university volleyball players (173.5 ± 9.5 cm; 63.1 ± 4.2 kg; 22.1 ± 3.5 yrs.) were recruited in this study (3 outside hitters, 2 opposites, 4 middle blockers, 2 setters, 2 liberos). Inertial measurement unit (50Hz, Goalgo T1, Tromin, Taiwan) was placed on the players' left shoulder and used to collect the triaxial acceleration data of the players during practice game. The acceleration raw data was filtered at 10Hz using a low-pass Blackman filter (AcqKnowledge 4.1). The total training load was calculated as the sum of the squared instantaneous rate of change in acceleration of triaxial axes (Equation 1). The percentage contributions for the x (antero-posterior), y (medio-lateral), and z (vertical) axes were calculated by dividing sum of the squared instantaneous rate of change in acceleration of each axis by that of triaxial axes (Equation 2) [1,2,3]. One-way repeated ANOVA was used to reveal the differences among three axes percentage contributions. The significant level was set as $p < .05$.

Training Load
$= (a_{x1} - a_{x-1})^2 + (a_{y1} - a_{y-1})^2 + (a_{z1} - a_{z-1})^2$
Equation 1 Total Training Load.

Percentage contribution of each axis
$= (a_{x1} - a_{x-1})^2 / ((a_{x1} - a_{x-1})^2 + (a_{y1} - a_{y-1})^2 + (a_{z1} - a_{z-1})^2)$
Equation 2 Percentage contribution of each axis.

RESULTS AND DISCUSSION

The vertical training load reaches about 37.5% of total training load. Antero-posterior training load reaches about 32.3% of total training load. Medio-lateral training load reaches about 30.1% of total training load. The percentage contribution of vertical training load was significantly larger than those of antero-posterior and medio-lateral training load (Table 1). Previous study also revealed higher vertical load of soccer players in season games. However, the percentage contributions of antero-posterior and medio-lateral axes of volleyball players were higher than those of soccer players [1]. This result may be owing to more antero-posterior and medio-lateral axes of sports-specific movements in volleyball practice games.

CONCLUSIONS

Vertical training load contributes to significantly higher percentage of total training load in female university volleyball players during practice games. No significant differences exist among antero-posterior and medio-lateral training load. The injury prevention or strength and conditioning program of female university volleyball players should emphasize more on vertical axis of movements training to cope with the higher physical demands in vertical direction.

REFERENCES

[1] Clubb J et al. *PLoS One* **17**: e0262274, 2022.
[2] Randers M B et al. *Scand J Med Sci Sports* **24**: 130-137, 2014.
[3] Wylde M et al. *Int J Racket Sports Sci* **1**: 37-44, 2019.

Table 1: Percentage contributions of antero-posterior, medio-lateral, and vertical axes to total Training Load (AU).

TL_{AP} (%)	TL_{ML} (%)	TL_V (%)	*p-value*
32.3 ± 4.1*	30.1 ± 3.3*	37.5 ± 5.7	$p = 0.001$

*Significantly different from vertical Training Load; TL_{AP} (%) = % contribution to total Training Load in antero-posterior axis

TL_{ML} (%) = % contribution to total Training Load in medio-lateral axis; TL_V (%) = % contribution to total Training Load in vertical axis

SENSOR NUMBER-DEPENDENT ACCURACY OF GROUND REACTION FORCES AND CENTER OF PRESSURE IN SIMPLIFIED PRESSURE SENSOR INSOLES

Philip X. Fuchs[1,2], Wei-Han Chen[2], and Tzyy-Yuang Shiang[2]
[1] Department of Physical Education and Sports Science, National Taiwan Normal University, Taipei, Taiwan.
[2] Department of Athletic Performance, National Taiwan Normal University, Taipei, Taiwan.
Email: philip.fuchs@ntnu.edu.tw

INTRODUCTION

Measuring the center of pressure (CoP) and vertical ground reaction forces (vGRF) during gaits is integral for the assessment of balance performance and lower limb injuries. Pressure sensor insoles are very popular and practical tools for detection and monitoring in clinical context [1]. However, the large number of sensors in valid systems results in high product costs and limited accessibility in therapeutical settings [2]. Therefore, research attempted to simplify pressure sensor insoles by reducing the number of required sensors [2]. Since the required sensor number has been unclear, the purpose of this study was to compare multiple layouts with different sensor numbers and assess the accuracy of CoP and vGRF.

METHODS

Fifteen healthy participants performed two gaits (i.e., walking and jogging) at self-selected slow and fast speed. Kistler force plates (1000 Hz) and Pedar-X insoles (100 Hz) obtained CoP and vGRF. Based on anatomical points [1], eight different simplified insole sensor layouts were simulated, comprising 3–17 sensors. CoP and vGRF from simplified layouts were compared with force plate data to assess concurrent validity. Multivariable regression models estimated absolute vGRF for simplified sensor layouts. Pearson's Product-Moment correlation coefficient (r) and Lin's Concurrent Correlation Coefficient (CCC) were calculated for each participant over the entire time of ground contact of one step at $p<0.05$.

RESULTS AND DISCUSSION

Correlation and concordance between sensor layouts and force plates ranged between 0.71 and 0.97 (Table 1). Correlation and concordance differed between gaits for CoP ($\chi^2_{(7)}$: 0.70–0.83, $p<0.05$) and vGRF (η^2_p: 0.28–0.66, $p<.05$). Root mean square error (RMSE) of CoP was higher in walking (15±3 mm) than in jogging (10±6 mm). RMSE of vGRF (Figure 1) was calculated from absolute values that were estimated via a regression model for the sensor layout with the lowest sensor number with strong validity (>0.9) across gaits and speeds (i.e., 11-sensor layout).

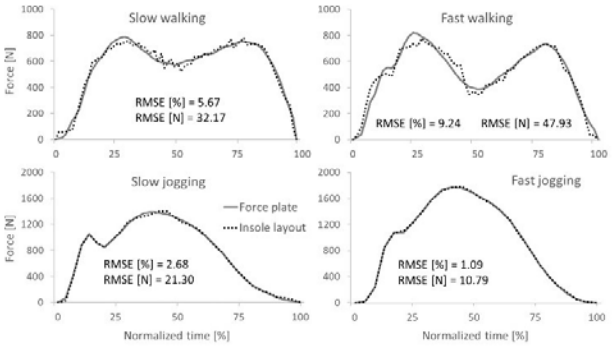

Figure 1 Representative absolute vGRF derived from the 11-sensor layout in comparison with force plate data; retrieved from [3].

CONCLUSIONS

The 11-sensor layout was identified as a promising compromise between sensor number and measurement accuracy across gaits and speeds. However, the observed differences in accuracy between gaits may suggest limited transferability of the current findings to other motor tasks. Future research is advised to optimize sensor layouts using 11 or more sensors, accounting for a wider range of common tasks.

REFERENCES

[1] Abdul Razak AH et al. *Sensors* **12**: 9884-9912, 2012.
[2] Saito M et al. *Med Eng Phys* **33**: 638-345, 2011.
[3] Fuchs PX et al. *Sports Biomech*, 2022.

Table 1: Mean±standard deviation of Pearson's Product-Moment correlation and Lin's Concordance Correlation Coefficient between sensor layouts and force plates across all participants for vertical ground reaction forces (vGRF) and center of pressure (CoP), respectively.

	Sensor layout (sensor number)							
	3	5	7	9	11	13	15	17
vGRF (walking)	0.75±0.11	0.71±0.13	0.81±0.08	0.87±0.06	0.92±0.04	0.93±0.04	0.92±0.05	0.91±0.05
vGRF (jogging)	0.82±0.15	0.84±0.11	0.92±0.07	0.94±0.06	0.96±0.05	0.96±0.05	0.95±0.06	0.95±0.07
CoP (walking)	0.75±0.25	0.78±0.16	0.83±0.26	0.88±0.12	0.91±0.11	0.91±0.11	0.86±0.28	0.92±0.11
CoP (jogging)	0.71±0.18	0.76±0.15	0.88±0.10	0.91±0.11	0.93±0.07	0.97±0.04	0.96±0.04	0.96±0.05

IMU METRICS ASSESSED DURING 2KM OF INDOOR TRACK VS SIDEWALK RUNNING

Hannah L. Dimmick[1], Andrew J. Pohl[1], Zoe Y.S. Chan[1] and Reed Ferber [1]

[1] Faculty of Kinesiology, University of Calgary, Calgary, Canada

Email: hannah.dimmick@ucalgary.ca

INTRODUCTION

Inertial measurement units (IMUs) are a popular tool to study running gait outside of a laboratory setting. However, for environmental control (i.e. interruptions, grade, surface/weather changes) and convenience, researchers frequently use indoor or outdoor track surfaces as a "real-world" condition. Despite previous studies demonstrating biomechanical differences between track surfaces and concrete/grass surfaces [1], it is often assumed that data collected on track surfaces will translate to other overground conditions. Therefore, the goal of this study was to determine the extent to which commonly-used IMU metrics differ between indoor track and outdoor sidewalk conditions.

METHODS

Twelve recreational runners (5F, 7M, age = 24.7 ± 4.3 yrs) completed 3 testing sessions on 3 separate days. Each session involved two experimental protocols. Following a 5-min warmup, two, 2km runs were performed in a randomized order: one on a 200m indoor track and one outdoors on a sidewalk route. Participants were encouraged to perform each run at the same self-selected speed. During each session, an IMU containing a tri-axial accelerometer (Shimmer3®; Shimmer Inc., Ireland: 200 Hz) was securely attached to the low back between L3-L5 vertebrae with axes X, Y and Z aligned in the mediolateral (ML), vertical (VT), and anteroposterior (AP) directions. The first and last 5% of each trial were excluded to reduce the effects of acceleration and deceleration. For each trial, individual steps were extracted using previously published methods [2]. Six features were derived from the acceleration signal: step time (ST), vertical oscillation (VO), braking speed (BR), and the peak acceleration of each axis ($PEAK_{ML}$, $PEAK_{VT}$, $PEAK_{AP}$). Because there was a significant difference between the track and sidewalk conditions for speed (indoor = 3.19 ± 0.33 m/s; outdoor = 3.31 ± 0.45 m/s; $p = 0.03$), each feature was corrected for speed by fitting a subject-specific polynomial model and using the residuals for further analysis. A multivariate Gaussian distribution was assumed to adequately model the variability of measures within each feature and fit to subjects' data via maximum likelihood estimation. For each testing session, the Hellinger distance (H), a distance measure describing the similarity between two probability distributions (0 = complete similarity, 1 = no similarity), was calculated to determine the similarity between the two conditions. A linear mixed model was used to detect differences in H between features.

RESULTS AND DISCUSSION

A visualization of distributions and calculated H is shown in Figure 1. When compared to all features, mean H of ST was significantly lower (0.19 ± 0.07, $p = 0.03$) and BR was significantly higher (0.41 ± 0.21, $p < 0.01$). The H for other features were not significantly different (VO = 0.24 ± 0.14, $PEAK_{ML}$ = 0.27 ± 0.09, $PEAK_{VT}$ = 0.28 ± 0.11, $PEAK_{AP}$ = 0.26 ± 0.10, $p > 0.05$). Although there is no standard H to determine a meaningful distance between distributions, these results imply there is some difference between biomechanical patterns on a track surface vs. sidewalk, most obviously in BR. Additionally, although H is directionally agnostic, further investigation indicated that the directionality of the individual variables was not consistent (i.e., some showed sidewalk > track, others opposite), indicating that there is likely not a straightforward bias from one condition to the other, but instead subject-specific functional differences in biomechanical gait patterns.

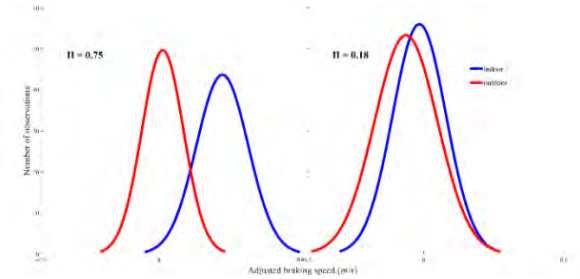

Figure 1. Example data for two subjects demonstrating large (left) and small (right) H for BR

CONCLUSIONS

Although researchers frequently use an indoor track to study overground, outdoor running, the large subject-specific H between probability measures observed in this study suggest that these conditions produce meaningfully different running gait biomechanical metrics. Thus, caution is warranted in assuming that IMU gait metrics from an indoor track can be effectively translated to other overground conditions.

ACKNOWLEDGEMENTS

This study was funded by the NSERC We-TRAC CREATE Training Program, an NSERC Discovery Grant, an NSERC Vanier CGS Award, and an Alberta Innovates Health Innovations Studentship.

REFERENCES

[1] Zhou W et al. *J Sports Sci.* **39**: 1822-1829, 2021.

[2] Benson LC et al. *Sensors*, **19**: 1483, 2019.

A hybrid machine learning model predicts ankle and knee moments in multiple tasks from a single IMU

Ting Long[1], Ted Yeung[1], Jereme Outerleys[3], Irene Davis[4], Justin Fernandez[1,2] and Thor F. Besier [1,2]

[1] Auckland Bioengineering Institute, University of Auckland / Auckland, New Zealand.
[2] Department of Engineering Science, University of Auckland / Auckland, New Zealand.
[3] Department of Mechanical and Materials Engineering, Queen's University / Canada
[4] School of Physical Therapy & Rehab Sciences, University of South Florida / USA
Email: tlon634@aucklanduni.ac.nz

INTRODUCTION

Monitoring ankle and knee joint moments in the field is important for assessing the risk of sports injury and monitoring rehabilitation. Inertial Measurement Units (IMUs) provide a low-cost and accessible opportunity to assess movement outside the laboratory, but it remains to be seen whether IMUs can predict joint moments across a wide range of sporting tasks. Here we present a hybrid machine learning (ML) model which first classifies each movement, then applies a task-specific regression model to predict time-series joint moments using a single ankle-mounted IMU as input.

METHODS

Four male collegiate basketball players performed repeated tasks (n), including walking (17), jogging (20), running (15), sidestep cutting (17), max-height jumping (17), and stop-jumping (16), resulting in a total of 102 movements. Optical motion capture, ground reaction forces and ankle-mounted IMU data were simultaneously collected (using VICON-IMeasureU and Bertec force plates). Scaled musculoskeletal models were created and flexion-extension ankle and knee joint moments estimated using the inverse dynamics (ID) tool within OpenSim [1]. ID results were considered the target for our ML model, using IMU data as input.

The hybrid ML model consisted of two stages. First, we classified each task used a Rocket classification model [2] (sktime). Second, a random forest regression model (sklearn) reconstructed the time series joint moments. IMU data were rolled into 0.1s time windows; then features were extracted from rolled time series (tsfresh). Finally, the selected features were fit to the regression model.

To verify the effect of this hybrid approach, we trained a generic model to predict all tasks and participants and compared this result as a baseline.

Leave-one-out cross-validation was performed and root mean square error (RMSE) and coefficient of determination (R^2) were used to compare the predicted joint moment to the ID joint moment. Accuracy score was used to measure the classification model accuracy.

RESULTS AND DISCUSSION

The accuracy score of the classification model was 0.99. Overall, the prediction effects of the hybrid model were better than the generic model (Table 1, Figure 1). This hybrid approach shows the potential to improve joints moment prediction effects in sports. However, the tasks in this study still cannot include all sports tasks, which limits the application scope of the model. The sample size of this study was not large, but additional participant data is being collected to test the approach across a larger cohort.

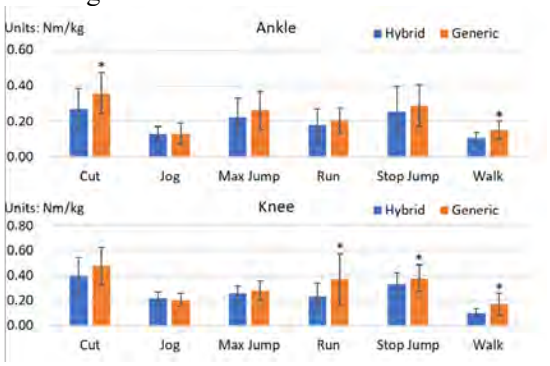

Figure 1 RMSE for cross-validations between predicted and ID joint flexion-extension moments.

CONCLUSIONS

A hybrid ML model can predict knee and ankle joint moments across a wide range of tasks using a single ankle-mounted IMU.

ACKNOWLEDGEMENTS

We acknowledge funding from GE Healthcare and the NBA for this investigation. The support provided by CSC during a study of Ting Long is acknowledged.

REFERENCES

[1] Delp S. L. et al. *IEEE Trans. Biomed. Eng* **54**: 1940-1950, 2007.

[2] Dempster A et al. *Data Mining and Knowledge Discovery* **34**: 1454-1495, 2020.

Table 1: R^2 for cross-validations between predicted and ID joint flexion-extension moments.

	Cut		Jog		Max Jump		Run		Stop Jump		Walk	
	Hybrid	Generic	Hybrid	Generic	Hybrid	Generic	Hybrid	Generic	Hybrid	Generic	Hybrid	Generic
Ankle	0.88±0.12	0.77±0.20	0.97±0.02	0.97±0.03	0.83±0.17	0.74±0.23	0.94±0.08	0.94±0.05	0.72±0.37	0.53±0.71	0.96±0.02	0.89±0.07
Knee	0.93±0.05	0.89±0.08	0.96±0.02	0.96±0.02	0.88±0.12	0.88±0.07	0.94±0.06	0.86±0.14	0.87±0.11	0.83±0.13	0.87±0.09	0.79±0.15

The relationship between "Hitting the Wall" phenomenon and gait changes during a full marathon

Nao Hirakawa[1], Yuki Ko[1], Masanori Sakaguchi[1]
[1] Institute of Sport Science, ASICS, Kobe, Japan.
Email: nao.hirakawa02@asics.com

INTRODUCTION

During a marathon, many runners experience "Hitting The Wall" (HTW), which is characterized by a significant slow-down in running pace. Although some studies have reported that gait changes occur even at moderate levels of fatigue that do not lead to HTW [1], such gait changes may not be a direct predictor of HTW [2], and no study has tracked the changes in runners prior to the onset of HTW. The purpose of this study was to investigate the differences in gait changes between runners who actually experienced HTW in a full marathon and those who did not, particularly prior to HTW.

METHODS

Ninety-three recreational runners were equipped with a GPS-integrated inertial measurement unit (CMT-S20R-AS, CASIO COMPUTER Co., Ltd.) at the waist; To investigate gait changes during the marathon race, parameters such as interval pace, cadence, step length, contact time, and vertical stiffness, and duty factor were calculated every 1 km or 0.25 km using a validated algorithm. We normalized the values by the ratio of the median value of each segment to the median value of a reference segment, which is the segment with the highest speed, for all variables of interest because the biomechanical variables are highly subject-specific [1]. In addition, each runner was asked to provide a pre-race expected record, an actual record, and a self-score (100-point scale). To investigate the effect of race progression on gait parameters between segments in each group of the runners who experienced HTW (HTW group) and those who did not experience HTW (non-HTW group), we applied the Friedman test, a nonparametric test using the median of each window in the eight segments from the start to 40 km. The Bonferroni test was used to compare the difference in each segment. Whether or not each runner experienced HTW during the race was defined as the group that experienced a slowdown of at least 25% at least 5 km, based on previously reported methods [3].

RESULTS AND DISCUSSION

Nineteen of 93 participants were labeled as the HTW, which is less than reported in previous studies. The HTW group had lower goal times (4:27:59 vs 3:30:00, $p<0.01$), a greater difference between expected and actual times (2084.4sec vs 259.9sec, $p<0.01$), and lower self-evaluations than the non-HTW group (56.8 vs 72.7, $p<0.01$). The section at which HTW began was 31.3 km ± 3.67 km, which was consistent reported in several previous studies. Two main effects of race progression on gait parameters were observed in this study. Changes in vertical stiffness after the start and remaining segments would indicate a global response of the spring-mass model to acute fatigue [1]; after 25km, a decrease in pace, shortening of step length, and prolongation of contact time and duty factor were significant. The difference between the HTW and non-HTW groups was that only the non-HTW group showed a change in vertical stiffness early in the race, it might be natural to assume that this is simply due to the larger sample size of the non-HTW group. Conversely, only the HTW group slowed down significantly even after 30 km; a decrease in cadence also occurred. Although runners tend to slow down probably due to induced-fatigue regardless of the occurrence of HTW, the decrease in cadence may indicate that they had reached a higher stage of fatigue.

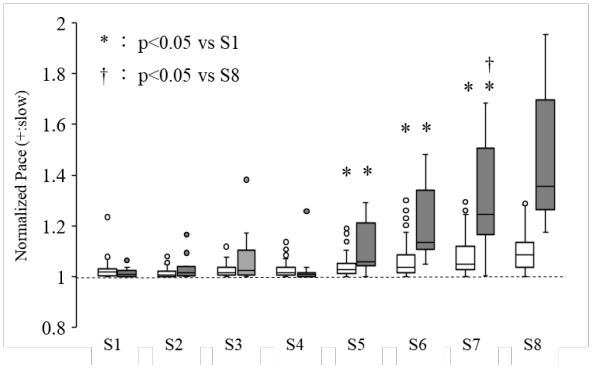

Figure 1. Normalized pace of the non-HTW group (white) and HTW group (grey)

CONCLUSIONS

While HTW has a significant impact on each runner's goal achievement and satisfaction, the gait changes measured in this study were not sufficient to predict the occurrence of HTW. When runners are fatigued, they may be more likely to make a decision to slow down before manipulating kinematic variables. Furthermore, of the kinematic variables that determine running speed, pace slow-down was found to result from shortened step length, with a small contribution from cadence for many runners. A decrease in cadence may be observed when the runner is in a high-fatigue state where HTW are more likely to occur.

REFERENCES

[1] Pirigent G et al. *Front Physiol.* **86**: 34-9, 2019.
[2] Buman P et al. *Psychology of Sport and Exercise* **9**: 177–190, 2008.
[3] Smyth B *PLoS One.* **16(5)**:e0251513.,2021

PROBABILITY OF CARDIAC-LOCOMOTOR COUPLING DURING DAILY ACTIVITIES

Aurora Rosato[1], Matilda Larsson[1], Eric Rullman[2] and Seraina A. Dual[1]
[1] Department of Biomedical Engineering, KTH Royal Institute of Technology, Stockholm, Sweden.
[2] Division of Clinical Physiology, Department of Laboratory Medicine, Karolinska Institutet, Stockholm, Sweden.
Email: seraina@kth.se

INTRODUCTION

Human locomotion is typically studied independently of the cardiovascular system, although the two are intrinsically linked. An example of their interaction is cardiac-locomotor coupling (CLC), which refers to the entrainment of heart rate (HR) and step rate (SR) during rhythmic exercise at a 1:1 ratio. Actively synchronizing the stepping with each diastole of the cardiac cycle, has been shown to provide improved cardiometabolic efficiency, demonstrated by a decrease in HR and in ventilation [1]. Active CLC can therefore be one way to improve hemodynamic efficiency, ensuring greater endurance performances. Previous studies investigated the presence of CLC in laboratory settings whereas observations during daily activities are still lacking. We do not know if and when CLC occurs physiologically. The aim of this study is to investigate the extent and the probability of CLC during unsupervised daily activities in contrast to random chance.

METHODS

We used a retrospectively acquired dataset, called PMData [2] (healthy, 13 men and 3 women, 34.85 ± 11.67 years of age). During five months, their HR and SR were recorded every minute by a Fitibit Versa 2 (Fitbit.Inc, San Francisco). We considered only SRs above 60 steps/min, indicative of physical activity [3]. Coupling is defined via the ratio between SR and HR as follows:

$$0.99 < \frac{\text{SR (steps/min)}}{\text{HR (beats/min)}} < 1.01$$

As HR and SR are correlated, observation of CLC may be attributed to chance. Thus, we compared the observed ratios to a random combination of SR and HR computed using Monte Carlo for each subject. A two-sample Kolmogorov-Smirnov test was used to test if the observed and random ratio distributions were different. All differences were tested with Wilcoxon signed rank.

RESULTS AND DISCUSSION

CLC occurs in every subject for 3 to 7% of the observed time. The median ratio per subject ranges from 0.87 to 1.00. In our cohort, CLC seems to be a spontaneous phenomenon during everyday activities.

The observed and random distributions are different ($p<0.001$ for every subject, Figure 1). In particular, the observed distribution has a median closer to the unity, it is more symmetric and less spread than the random. Hence, the result suggests that subjects tend to adapt their gait cycle to their cardiac cycle or vice versa, instead of these two systems being independent and random.

The probability of coupling is 34% higher for the observed distribution (0.042 vs 0.028, $p<0.001$, Figure 1), than for the random distribution. This shows that CLC could come from an active interaction rather than from chance.

Our findings raise new question whether there is a mechanism of interaction between the cardiovascular and the locomotor system. Our body's spontaneous predisposition to CLC indicates that we can actively achieve CLC and thereby improve our cardiac efficiency. This motivates new rehabilitation and training techniques to be investigated. A limitation of the present study is that such wrist-worn sensors are affected by artifacts in measuring HR.

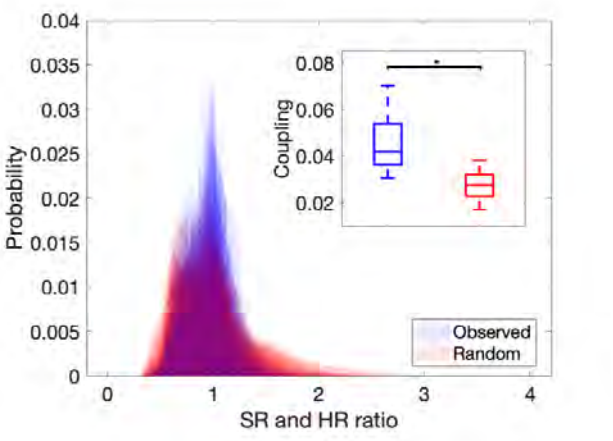

Figure 1 Ratio distribution curves of all subjects (N=16) and coupling probability. *Significant difference between conditions, P<0.001.

CONCLUSIONS

Spontaneous CLC occurs in every subject during unsupervised daily activities. Our small and healthy cohort supports that the incidence of CLC is not due to random chance. Future work will address the extent of diastolic CLC in a heterogeneous cohort through more robust chest-worn sensors.

ACKNOWLEDGEMENTS

Traveling Grant Karl Engvers foundation VT-2022-0066.

REFERENCES

[1] Constantini et al. *Med Sci Sports Exerc*,**50**(5):1046-1053,2018.
[2] Thambawita et al. In *Proceedings of the 11th ACM Multimedia Systems Conference*, 231-236.2020
[3] Tudor-Locke et al. *Preventive Medicine*, **53**(3): 178-181, 2011.

NEW PERSPECTIVE FROM OLD DATA: A CONTEMPORARY, QUANTITATIVE ANALYSIS OF THE FIRST REPORTED CERVICAL FACET DISLOCATION PRODUCED IN THE LABORATORY

Ryan Quarrington[1,2], Robert Bauze[3], and Claire Jones[1,2,3]

[1]Spinal Research Group, Centre for Orthopaedic & Trauma Research, The University of Adelaide, Australia.
[2]School of Mechanical Engineering, The University of Adelaide, Australia.
[3]Royal Adelaide Hospital, Adelaide, Australia
Email: ryan.quarrington@adelaide.edu.au

INTRODUCTION

Cervical facet dislocation (CFD) is frequently associated with spinal cord injury, yet the biomechanics underlying this devastating injury are not well understood [1]. In 1978, Adelaide Orthopaedic Surgeon Robert Bauze, working in Oxford in 1972/3, published the first study (of only two to date) to systematically produce CFD in cadaver spines [2]. The importance of this work is only now being fully realized [1]. Although the measurement techniques employed were innovative for the time, the manuscript was written in the narrative style of the day, and therefore didn't report quantitative kinematic or force data. A more nuanced analysis of this rich dataset may provide new insight regarding CFD mechanisms. The aim of this study was to re-examine in detail the cineradiograph films and strip charts of the Oxford study to determine the intervertebral rotations movements and axial forces that occurred during these simulated CFDs.

METHODS

In the original study, quasi-static axial loading was applied to fourteen cervical spines (occiput-T2) that were fixed caudally via a bone pin through the vertebral body and spindle within the canal (Fig A). Flexion-extension of the occiput was restricted but anterior translation was unconstrained. Sagittal cineradiograph films were available for ten spines; these were digitally scanned at high resolution, and global and intervertebral kinematics were determined at each frame (Fig B). Corresponding axial force charts were available for six specimens. These were scanned, and force data at each cineradiograph frame (indicated by synchronization pulses on the charts) were extracted (Fig C). Peak axial force and force at injury were determined. Descriptive statistics were obtained.

RESULTS AND DISCUSSION

Of the ten experiments with cineradiographs, anterior occiput translation (eccentricity) without rotation occurred for seven specimens, creating upper neck extension and lower neck flexion; CFD occurred at the level of transition from extension to flexion (1×C4/C5, 4×C5/C6, 2×C6/C7). The occiput detached from the loading platen during two experiments, permitting hyperflexion, and CFD was not observed. One specimen failed through the fixation spindle, so these data were omitted from analysis.

At the point of injury, the intervertebral angle (20.6±6.6°) and anterior shear displacement (4.1±2.9 mm) at the level of CFD were two- and four-times physiological limits [3], respectively. The upper cervical spine remained in extension, with 54.9±8.1 mm anterior eccentricity of the occiput. Four of the six specimens with force data underwent CFD at an axial load of 617±73 N, which was preceded by a peak axial force (1094±239 N) coinciding with posterior ligament rupture.

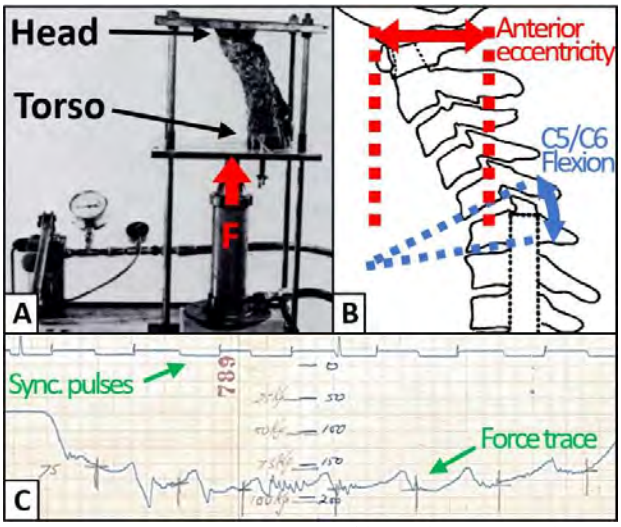

Figure 1 A) Bauze's test setup; B) kinematics measures from cineradiographs; and, C) annotated force chart.

CONCLUSIONS

This study provides new evidence supporting the contemporary hypothesis that the "ducking posture" (extended upper, flexed lower neck), not hyperflexion, is necessary for dislocation during axial loading. The kinematic and kinetic data may inform neck injury criteria specific to CFD to facilitate the development of novel safety devices.

ACKNOWLEDGEMENTS

Funding: ARC Discovery Project (DP190101209)

REFERENCES

[1] Nightingale, RW. *Clin Biomech* 64, 90-97, 2019.
[2] Bauze, RJ. *JBJS* 60-B(2), 239-245, 1978.
[3] Wu, SK. *Eur Spine J* 16, 1435-1444, 20

DIFFERENCES IN TRUNK ROTATION BETWEEN PEOPLE WITH AND WITHOUT LOW BACK PAIN DURING VARIOUS MOVEMENTS

Batbayar Khuyagbaatar[1], Batlkham Dambadarjaa[2], Ganbat Tumen-Ulzii[1] and Munkh-Erdene Bayartai[2]
[1]Department of Technical Mechanics, Mongolian University of Science and Technology, Ulaanbaatar, Mongolia
[2]Department of Physical Therapy, Mongolian National University of Medical Sciences, Ulaanbaatar, Mongolia
Email: batbayarkh@must.edu.mn

INTRODUCTION

In clinics, range of motion (ROM) during trunk rotations and functional tasks is commonly examined as part of musculoskeletal assessments to diagnose low back pain (LBP), and changes in the ROM are related to impairment or instability of the trunk [1]. Although there are many studies have identified movement abnormalities during either simple clinical tests or gait, the three-dimensional (3D) kinematics of the trunk has not been investigated for different functional tasks. In this study, we determined differences in 3D trunk kinematics during trunk rotations and functional tasks between people with and without non-specific LBP.

METHODS

We recruited 45 LBP patients (LBP group: 9 males and 36 females; age, 33±10 years; height, 162±8 cm; weight, 67±16 kg) and 45 healthy people (Control group: 14 males and 31 females; age, 24±8 years; height, 163±8 cm; weight, 59±10 kg). The full-body Xsens system (MVN, Xsens technologies, Netherlands) was used to record the 3D movements during the trunk rotations (flexion-extension, lateral bending, and axial rotation) and functional tasks (single-leg standing, walking, hurdle step, squad, and squat lifting). Each subject performed three times of each specific movement and functional task. The trunk ROM in the sagittal (SP), frontal (FP), and transversal plane (TP) were calculated using a relative orientation between pelvis and thorax segments and averaged for the LBP and control group.

RESULTS AND DISCUSSION

The LBP group exhibited smaller trunk ROMs than controls during the trunk rotations in three planes of motion. In contrast, trunk ROMs were larger in people with LBP during functional tasks except for rotation in TP during single-leg standing. But significant differences were observed during extension-flexion in FP and TP, bending in TP, rotation in FP and TP, single-leg standing in SP, walking in SP and FP, hurdle step in TP, and squat in FP, respectively ($p<0.05$) (Figure 1). These results were similar to previous studies, where they reported that patients with LBP exhibit smaller trunk rotations during clinical tests [2], and greater trunk ROM during functional tasks, which is possibly correlated with movement control impairment [3].

CONCLUSIONS

Our results showed differences in ROM during trunk rotation as well as functional tasks. People with LBP exhibited smaller trunk ROMs during trunk rotations, while it was larger during functional tests. Therefore, it is important to know which specific task is more useful to indicate the movement impairments due to the LBP.

ACKNOWLEDGEMENTS

This work was supported by the "Mongolia-Japan Engineering Education Development" project (J24C16) and the Mongolian University of Science and Technology (mfund-052022).

REFERENCES

[1] Papi E et al. *Clin Biomech* **55**: 53-64, 2018.
[2] Laird RA et al. *BMC Musculoskelet Disord* **15**: 229, 2014.
[3] Bayartai ME et al., *J Electromyogr Kinesiol* **69**: 102744, 2023.

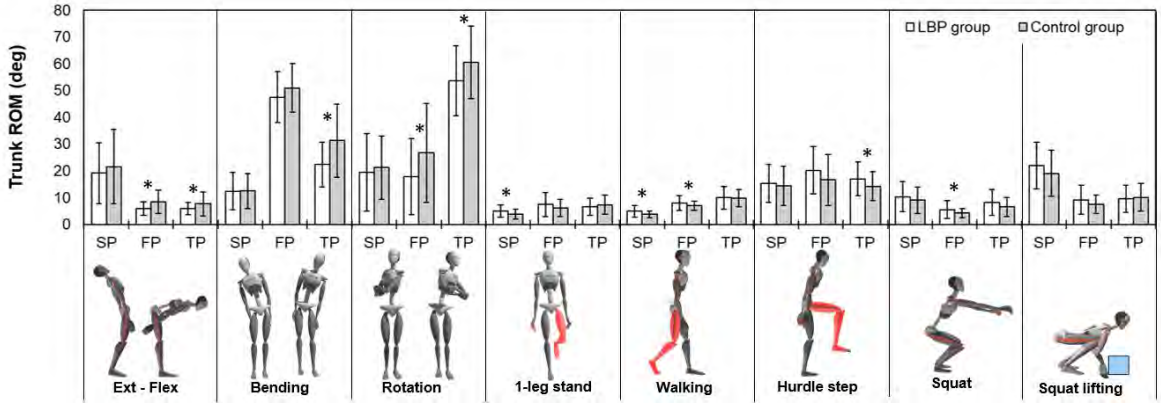

Figure 1 Trunk rotations in sagittal (SP), frontal (FP), and transverse plane (TP) for different movements. The * mark indicates $p<0.05$ between the two groups.

Effect of the draw-in maneuver on lumbar spine and hip motion during sit-to-stand for prevention of low back pain and urinary incontinence

J. Ishibashi[1], S. Ota[1,2]
[1]Graduate School of Health Care Studies, Seijoh University / Tokai, Aichi, Japan
[2] Department of Rehabilitation and Care, Seijoh University / Tokai, Aichi, Japan.
Email: jin.saku0120@gmail.com

INTRODUCTION

Sit-to-stand (STS) is frequently performed during daily life and may be associated with low back pain (LBP) and urinary incontinence (UI) due to lumbar kyphosis and contraction of the rectus abdominis muscle (RA), respectively. Exercises that contract the oblique and transversus abdominis (TrA) muscles and stabilize the spinal column are considered to be helpful against LBP. The draw-in maneuver (DI) selectively contracts the oblique and TrA muscles. We hypothesized that DI inhibits lumbar spine motion (lumbar kyphosis) and increases the hip flexion angle during STS, and could thus prevent LBP. UI is associated with dysfunction of the pelvic floor muscles (PFM), and therefore PFM training is recommended. Contraction of the trunk muscles influences the PFM, and contraction of the IO and TrA muscles leads to simultaneous PFM contraction. The PFM is less likely to contract, however, during contraction of the RA. We hypothesized that selective contraction of the oblique and TrA muscles without activation of the RA during STS by DI would prevent UI. Here, we investigated the effects of DI on the lumbar spine and hip joint angles, and trunk muscle activity during STS.

METHODS

Fifteen healthy adult males aged 18–22 years were included in the study. STS was measured 3 times. Subjects were then instructed on performing DI, and STS was measured another 3 times. The lumbar flexion and hip flexion angles, and activities of the RA, external oblique abdominis (EO), IO/TrA, and gluteus maximus muscles with and without DI were compared. The change from each joint angle in the sitting position to the peak angle during standing was measured. Electromyography was performed for 3 s from the start of the movement.

RESULTS AND DISCUSSION

DI during STS significantly decreased the maximum lumbar flexion angle (Table 1). In addition, EO and IO/TrA muscle activities were significantly increased (Figure 1), supporting the results of a previous study in which DI was shown to stabilize the lumbar spine by simultaneously contracting the EO and IO/TrA muscles [1] and demonstrating that DI had a stabilizing effect on the lumbar spine even during STS.

Furthermore, DI selectively activated the IO/TrA muscles without activating the RA even during STS, thereby allowing the PFM to contract more efficiently [2]. This finding suggests that DI might also have preventive effects against UI.

These comparisons in healthy subjects demonstrate the potential of DI during STS to prevent LBP and UI. Future intervention studies in patients with LBP or UI are thus warranted.

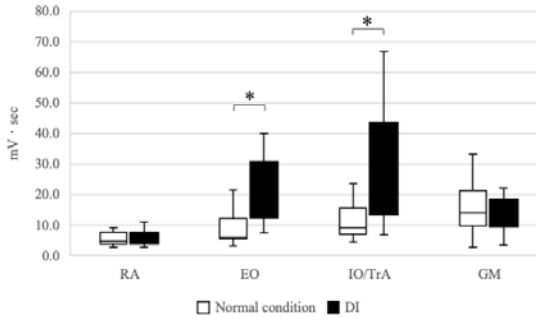

Figure 1: Muscle activity during STS (integral electromyography)

CONCLUSIONS

We demonstrated that DI during STS can decrease the maximum lumbar flexion angle and activate the EO and IO/TrA muscles without activating the RA. These results indicate that DI may be useful for preventing LBP and UI.

ACKNOWLEDGEMENTS

This work was supported by JSPS KAKENHI Grant Number 19H03970.

REFERENCES

[1] Gardner-Morse MG et al. *Spine (Phila Pa 1976)* **23(1)**:86-91, 1998.
[2] Arab AM et al. *Neurourol Urodyn* **30(1)**:117-120, 2011.

Table 1: Immediate effects of Draw-in Maneuver

	Without Draw-in Maneuver	With Draw-in Maneuver	P-value
Lumbar spine change (°)	5.5±4.2	6.8±4.1	0.85
Hip joint change (°)	21.1±3.3	19.3±4.5	0.89
Maximum lumbar flexion angle (°)	182.1±5.5	176.6±4.4	<0.001
Maximum hip flexion angle (°)	79.3±6.8	79.4±6.9	0.88

EFFECTS OF AGE AND GENDER ON BACK MUSCLE ACTIVATIONS DURING VARIOUS SPINAL MOVEMENTS

Chih-Hsiu Cheng[1], Asghar Rezaei[2], and Kenton Kaufman[2,*]

[1] School of Physical Therapy and Graduate Institute of Rehabilitation Science, Chang Gung University, Taoyuan, Taiwan
[2] Department of Orthopedic Surgery, Division of Orthopedic Research, Mayo Clinic, Rochester, MN, USA

Email: Kaufman.Kenton@mayo.edu

INTRODUCTION

Back muscles are the motors to drive spinal movements and responsible for stabilizing and supporting the trunk at the same time. Most back muscle studies have focused on sagittal flexion–extension tasks [1]. Comprehensive paraspinal muscle activity patterns during various spinal movements have not yet been fully investigated. Clarification of back muscle behaviors can reveal the underlying prerequisit control of spinal movements and understand its link to back disorders. Electromyography (EMG)-based measures of the trunk muscles have been used for the identification of biomechanical impairments in patients with low back pain, but the results are conflicting [2,3]. Potential confounding sources of variance, such as age and gender, could contribute to inconsistences. Accordingly, this study was performed to investigate the effects of age and gender on paraspinal muscle activation when performing different functional spinal movements.

METHODS

Thiry-one healthy participants (aged 66±10 years, 13 males and 18 females) over the age of 50 were recruited. Subjects who had difficulty performing daily living activities, or were with neuromuscular disorders, spinal pathologies, needing walking assistance, body mass index of greater than 35, and FRAIL score of 3 or greater were excluded. Surface EMG activities of bilateral paraspinal muscles at L3 level were measured (MA300; Motion Lab Systems, Inc.). Subjects were first instructed to perform quiet standing for 30 sec and then tasks including forward flexion (Flex), extension (Ext), maximal extension (MaxExt), object lifting (Lifting), sit-to-stand (S2S), level walking (Walking), right/left sidebending (SideB), right/left horizontal rotation (Rot), and right/left diagonal rotation (DRot) were performed. The quiescent level was set at 2.5 x standard deviation of EMG activity during the quiet standing task and used as the denominator of the normalized EMG for all tasks. Only dominant side muscle activations were used for analysis, with leg dominance being defined as the preferred leg for kicking a ball. A multiple linear regression model was used to access the association of the muscle activation with gender and age. Significance was set at 0.05 level.

RESULTS AND DISCUSSION

Twenty-three participants were right-dominant. The results showed a down trend of muscle activation with aging, especially in males (Figure 1). The muscle activations during the MaxExt, S2S and DRot-R tasks demonstrated the strongest relationship (adjusted R^2 = 0.17, 0.16 and 0.17, respectively) with marginal significance (p-value all smaller than 0.07).

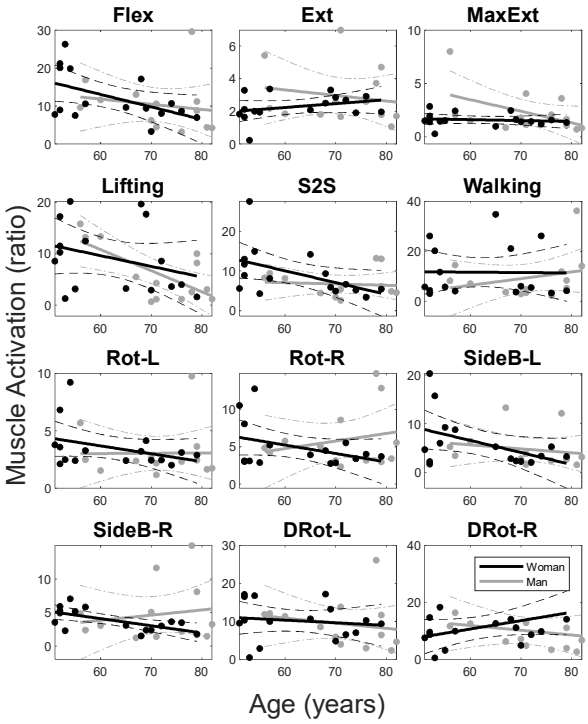

Figure 1 Regression plots of the paraspinal muscle activations for men (grey) and women (black) with their ages in different tasks.

CONCLUSIONS

This study quantified paraspinal muscle activations in a pain-free population of older adults. The results showed a down trend of muscle activation with aging. Such responses could lead to decreased trunk stiffness and may contribute to low back disorders. Further work is needed to incorporate a greater sample population to verify the trend.

ACKNOWLEDGEMENTS

We acknowledge the grant support from National Institutes of Health (NIH, K25AG068368).

REFERENCES

[1] Shin G et al. *J Electromyogr Kinesiol* **20**:742-9, 2010
[2] Lima M et al. *Gait Posture* **61**:250-6, 2018
[3] Serafino F et al. BMC *Musculoskelet Disord* **22**:432, 2021

BIOMECHANICAL INFLUENCE OF THE CAGE LORDOSIS IN AN ANTERIOR LUMBAR INTERBODY FUSION AT L4-L5 – A SIMULATION STUDY

Robin Remus[1], Marc Neumann[1], Andreas Lipphaus[2] and Beate Bender[1]
[1] Chair of Product Development, Dept. of Mechanical Engineering, Ruhr-University Bochum, Germany.
[2] Biomechanics Research Group, Dept. of Mechanical Engineering, Ruhr-University Bochum, Germany.
Email: remus@lpe.rub.de

INTRODUCTION

Low back pain is one of today's most common health problems. Fusion surgery may be considered when pain persists and conservative treatments fail to provide relief in a patient with degenerative disc disease [1]. One of the most successful fusion approaches, with success rates up to 97 %, is the anterior lumbar interbody fusion (ALIF) [2]. After removal of the affected intervertebral disc, an angle and height variable cage is placed between the cranial and caudal vertebral bodies. The global lumbar lordosis (LL) is patient-specific and affected by the cage lordosis (CL) choice. To reduce the probability of progress of adjacent segment diseases, the reconstruction of a physiological LL is essential in this regard [3]. In the light of customary discrete CL decisions of stand-alone ALIF, this simulative study investigates biomechanical effects of L4-L5 CL variances on adjacent spinal structures.

METHODS

We utilize a validated active hybrid model of the ligamentous lumbosacral spine [4] (Fig. 1A) built in ArtiSynth [5]. Unfused rigid vertebrae L1-S1 are interconnected with hyperelastic fibre-reinforced finite element (FE) intervertebral discs, ligaments, and facet joints. The intra-abdominal pressure is considered as a force on the thorax via muscle forces acting on the abdomen. Twelve sagittal symmetric muscle groups are implemented using 258 muscle fascicles with a Hill-type muscle model. The muscle redundancy problem is solved using an inverse-dynamic tracking controller which provides a solution of the forward dynamic simulation. Values of the cost function are the muscle activities squared as well as the target poses of the thorax and the lumbar vertebrae. Thus, all bones cranial to the stationary sacrum are free to move in space. For the stand-alone ALIF, L4 and L5 are rigidly connected with different CL of 14 ± 3°. Muscles and adjacent lumbar structures are undisturbed. Varying postures from extension to flexion (-10°, 0°, and +30°) with loads of up to 20 kg held in both hands are simulated.

RESULTS AND DISCUSSION

In relaxed upright standing (LC#1) pre-operative LL is 45° and a CL of 14° corresponds best to the unfused L4-L5 intervertebral angle (IVA). The post-operative LL change in LC#1 is maximal at CL = 17° with -1.3%. For all CL, the L5/S1 IVA increase, while L1/2 IVA decrease. Adjacent segments compensate for the L4/5 CL variances. A negative correlation between CL and IVA change is present in L3/4. Except in 30° flexion (LC#2), a significant increase in facet joint contact forces at larger CL is seen at L3/4. In LC#1 and LC#2 the intradiscal pressures (IDP) are lowest pre-operative. Large CL have the greatest influence on the IDP in LC#2. In percentage terms, the IDP increase at 11° CL is greatest in LC#1. In all postures without additional load and CL > 11°, the lumbar section of the M. longissimus exerts notably more force (9-125%) than in the pre-operative state. Except in extension, the M. multifidus is also more activated.

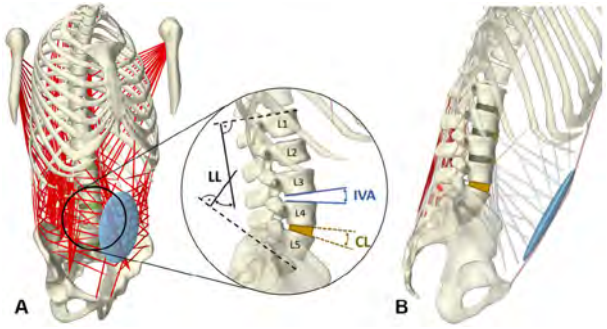

Figure 1 A) Active hybrid model and visualization of the sagittal spinal parameter in LC#1. B) LC#2 with right side muscles hidden.

CONCLUSIONS

From a biomechanical perspective, this simulation study confirms that replicating a physiological LL is important. For global sagittal balance, IVA changes are compensated by the musculoskeletal system, as in ALIF, which in turn leads to locally modified loads on adjacent lumbosacral structures. In upright standing with and without an additional load a L4-L5 CL larger than the pre-operative IAV, for example, reduces the IDP at all levels while decreasing cranial and increasing caudal the facet joint forces. In flexion, however, this results in more stress being placed on the cranial segments. Furthermore, other anatomies with diseases should be considered. Likewise, the hybrid approach may provide future opportunities to directly analyze the stresses between cage and FE bone for a faster fusion.

REFERENCES

[1] Udby P and Bech-Azeddine R, *Clin Neurol Neurosurg*, **133**: 64-69, 2015.
[2] Jackson K et al. *Asian Spine J*, **8**(5): 591-598, 2014.
[3] Szadkowski M et al. *Interdiscip Neurosurg*, **26**: 101312, 2021.
[4] Remus R et al. *PloS ONE*, **16**(4): e0250456, 2021.
[5] Lloyd J et al. 978-3-642-29014-5, 355-394, 2012.

DEEP PARASPINAL MUSCLE VOLUME ASYMMETRY IN ADOLESCENT IDIOPATHIC SCOLIOSIS

P. Duncombe[1], MT. Izatt[2,3], TJM. Dick[1], P. Pivonka[3], RD. Labrom[2,3], K. Tucker[1]
[1] School of Biomedical Sciences, The University of Queensland, Australia.
[2] Biomechanics and Spine Research Group, QUT at Centre for Children's Health Research and [3]School of Mechanical, Medical and Process Engineering, Queensland University of Technology, Australia.
Email: p.duncombe@uq.edu.au

INTRODUCTION

Adolescent Idiopathic Scoliosis (AIS) is characterised by a three-dimensional (3D) spine deformity that progresses between 10 and 18 years. An asymmetry in paraspinal muscle size and, therefore, force generating capacity may contribute to an asymmetry in the forces applied to the growing spine and leading to asymmetrical vertebral growth.[1] We have recently shown asymmetry in *grouped* deep (but not superficial) paraspinal muscles size at the level of the scoliotic curve apex, which is related to curve severity and skeletal maturity in those with AIS.[2] Here we aim to define *individual* paraspinal muscle volume (a)symmetry in the presence of AIS using magnetic resonance imaging (MRI) and segmentation techniques with far greater precision than has been previously possible.

METHODS

Data obtained from MRI's [T1-weighted 3D Gradient Echo sequence, voxel size: 0.2*0.2*5mm] is presented from: 11 female adolescents [all with right thoracic (Th) scoliotic curves (mean±SD); Cobb angle: 38±19°; curve apex: T7-10; age: 13.8±1.3 years; height:159±5 cm; Risser Grade for skeletal maturity: 0-4, who attended the Queensland Children's Hospital Spine Deformity Unit; and 11 control participants [with symmetrical spines (mean±SD); age: 13.7±1.9 years; height:163±6 cm; Risser Grade: 0-4].

At the level of the curve apex (and matched vertebral level for controls), the multifidus, spinalis, iliocostalis, and longissimus muscle cross-sectional areas (CSA; mm^2) were determined by manually delineating muscle boundaries from the MRIs. The CSA of consecutive slices, from the upper to the lower vertebral body boundaries, were multiplied by MRI slice thickness and summed, to calculate the muscle volume (mm^3) associated with the individual vertebral segment. A muscle volume asymmetry index [Ln(concave/convex volume)], was determined. When using this index, a value of 0.2 approximates a 20% larger volume on the convex side.[3]

RESULTS AND DISCUSSION

The multifidus volume was mean 28±18% greater on the concave than the convex side of the curve apex in AIS. This asymmetry was significantly larger ($p<0.01$) than that observed in the control group, mean -4±13% (Figure 1). No other between-group differences in asymmetry were observed (all $p>0.05$).

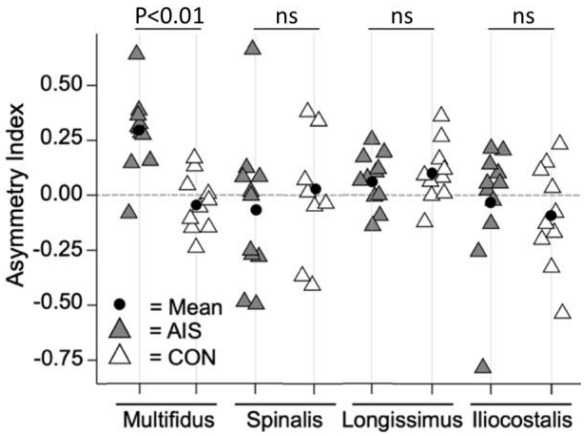

Figure 1 Muscle asymmetry at the scoliosis curve apex of adolescents with scoliosis (AIS: grey) and controls (CON: white). Individual (triangles) and group mean (circles) data shown, ns= not-significant.

CONCLUSIONS

The asymmetry found in AIS participants' deep paraspinal muscles, in particular the multifidus, lies outside the typical asymmetry range observed in adolescents with symmetrical spines. As scoliosis progresses, the vertebrae and spinous process rotate towards the curve's concavity with a decrease in the concave pedicle and vertebral body height.[4] Multifidus is intimately associated with these bony landmarks, spanning between the vertebral body, transverse and spinous processes, acting to stabilize, extend and rotate the spine. This supports the need for further work that considers the potential role of the multifidus in AIS presence and progression. Future outcomes from a larger dataset will quantify a greater number of anterior and posterior paraspinal muscle volume (a)symmetries (from vertebral levels T4-L4) and consider other factors that contribute to muscle force generation, including intramuscular fat, fascicle architecture, fibre composition and muscle activation.

ACKNOWLEDGEMENTS

This research is supported by the Scoliosis Research Society (#869283). PD is supported by a University of Queensland Postgraduate Scholarship.

REFERENCES

[1]Stokes, I. A.F. et al. *Spine*. **21**, 1161-1167, 1996.
[2]Duncombe, P. G. et al. *ISEK*. **24**, 131-132, 2022. *Currently in review.*
[3] Cole, T. J. et al. *Statistics in Medicine.* **19,** 3109-3125, 2017.
[4] Labrom FR. et al. *Eur Spine J*. **30**, 823-1834, 2021.

RELIABILITY OF ULTRASONOGRAPHY TO ASSESS SPINAL COMPRESSION DURING HEAVY LOAD CARRIAGE

Walters, SJ [1,2,3], Hoffman, BW [1], Coltman, CE [4] and Mills, DE [1]

[1] School of Health and Medical Sciences, University of Southern Queensland, QLD, Australia
[2] School of Medicine and Dentistry, Griffith University, QLD, Australia
[3]Martial Arts Research and Testing Laboratory, QLD, Australia
[4] Faculty of Health, University of Canberra Research Institute for Sport and Exercise, University of Canberra, ACT, Australia
Email: sherrilyn.walters@usq.edu.au

INTRODUCTION

Military personnel are often required to carry heavy equipment and supplies on their bodies. These loads place increased strain on the body and may lead to lower back injury [1]. Understanding the effects of heavy load carriage on spinal loading has implications for interventions aimed at reducing injury. Magnetic resonance imaging, the gold standard in spinal assessment, is costly and not practical for use during standing load carriage. Ultrasonography has been reliably used to estimate spinal loading via measurement of distances between vertebral processes with participants in a seated or recumbent position [2,3]. However, no studies have assessed its use during standing heavy load carriage. The aim of this study was to assess the test-retest reliability of ultrasonography to quantify spinal compression via measurement of distances between the transverse processes of the lumbar vertebrae in healthy adults during load carriage.

METHODS

5 males and 6 females (age: 33 ± 5 years; height: 155 ± 51 cm; mass: 75 ± 18 kg) attended the laboratory for two test sessions on two separate days. After 30 minutes of supine resting, ultrasound images were taken of the transverse processes of each lumbar vertebra (L1-L5) immediately on standing while unloaded, and after 30 minutes of standing while loaded with a 25 kg weighted vest. The same tasks were completed in both sessions.

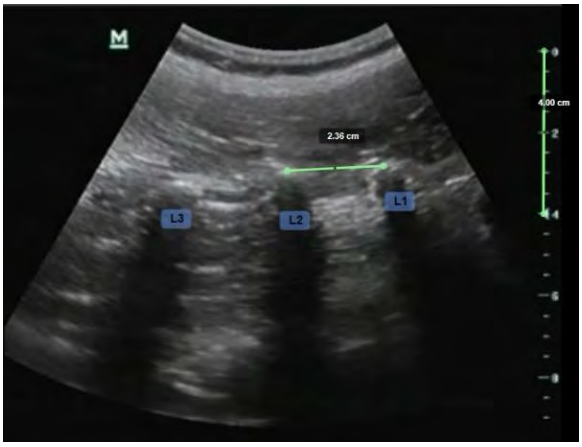

Figure 1 An example ultrasound image showing the measured distance (green horizontal line) between the L1 and L2 transverse processes.

Kinovea software (version 0.8.15, www.kinovea.org) was used to measure the intervertebral distances between transverse processes from L1-L5 (Figure 1). Within- and between- day reliability were assessed using coefficients of variation (ratio of standard deviation to mean; CV) and intraclass correlation coefficients (ICCs) with 95% upper and lower bound confidence intervals (95% CI). Intervertebral distances between loaded and unloaded conditions were compared using paired t-tests ($p<0.05$).

RESULTS AND DISCUSSION

Within- and between- day reliability was good to excellent with ICCs between 0.83 and 0.99 for all measurements. Within-visit between-participant CVs were between 7.1 and 12.1 for all measurements. The loaded condition resulted in significantly reduced inter-transverse process distances between L2-L3, L3-L4 and L4-L5 (Table 1).

Table 1: Distances between transverse processes for loaded and unloaded conditions and within-visit coefficients of variation (CV) from both visits. Results are presented as mean ± standard deviation.

Vertebra	Condition	Distance (mm)	CV (%)	P value
L1-L2	Unloaded	29.6 ± 3.41	12	0.190
	Loaded	29 ± 2.56	8.9	
L2-L3	Unloaded	32 ± 2.37	7.4	0.015
	Loaded	31.1 ± 2.54	8.2	
L3-L4	Unloaded	31.7 ± 3.21	10	<0.001
	Loaded	29.2 ± 2.19	7.5	
L4-L5	Unloaded	29.1 ± 2.56	8.8	0.003
	Loaded	27.3 ± 2.62	9.6	

CONCLUSIONS

These results indicate that ultrasonography may be a practical, cost effective, and reliable method for measuring the effects of heavy loads on the lumbar spine and assessing the effects of interventions aimed at reducing spinal compression during heavy load carriage.

REFERENCES

[1] Orr et al. *J Occup Rehabil,* **25(2)**: 316-322, 2015.
[2] Tozawa et al. *J Phys Ther Sci* **27(7)**: 2333-6, 2015.
[3] Poortmans et al. *J Manipulative Physiol Ther* **39(8)**: 586-93, 2016.

TARGETED MULTIFIDUS MUSCLE ACTIVATION REDUCES FIBROSIS OF MULTIFIDUS MUSCLE FOLLOWING INTERVERTEBRAL DISC INJURY

Hodges P[1], James G[1], Ahern BJ[2], Goss B

[1] 1NHMRC Centre of Clinical Research Excellence in Spinal Pain, Injury and Health, School of Health and Rehabilitation Sciences, The University of Queensland, Brisbane, QLD, Australia
[2]Faculty of Science, School of Veterinary Science, The University of Queensland, Gatton, QLD, Australia

INTRODUCTION

Low back pain and injury are associated with structural remodelling of the multifidus muscle including increased connective tissue (i.e., fibrosis). Experimental intervertebral disc (IVD) degeneration in animal studies induces fibrotic changes that include increased fibrogenic gene expression (Collagen I and III) and increased cross-sectional area of connective tissue across the multifidus muscle, as well as increased thickness of the epimysial layer of connective tissue that around the muscle [1]. These changes would impact the capacity of muscle to generate torque and regulate loading of the spine. Whole body aerobic exercise has been shown to partially attenuate these fibrotic changes but does not completely restore multifidus health [2]. More targeted exercise of the multifidus muscle might induce more complete resolution of fibrosis. This study aimed to investigate whether neurostimulation of the multifidus muscle could reduce fibrosis of the multifidus muscle in a model of IVD degeneration in sheep.

METHODS

IVD degeneration was surgically induced in 18 merino sheep via a partial thickness unilateral annulus fibrosus lesion to the right side of the L1/2 and L3/4 IVDs. All 18 sheep received an implantable neurostimulation device, that provides stimulation of the L2 medial branch of the dorsal ramus (ReActiv8, Mainstay Medical). Three months after surgery, the animals were divided into two separate groups, Non-Activated and Activated. The Activated animals received two 30-minute neurostimulation sessions per day for 3 months. The Non-Activated group received no stimulation. Six months after surgery, the multifidus muscle was harvested adjacent to the spinous process adjacent to L2 and L4 and. The muscle tissue underwent Van Gieson's and Sirius Red staining, and Collagen-I &-III immunostaining, examine tissue fibrosis. Expression of fibrotic genes was assessed using quantitative PCR.

RESULTS AND DISCUSSION

Targeted activation of the multifidus muscle reduced levels of fibrosis in the Activated group, compared to the Non-Activated group in the multifidus at L4 (which includes fascicles activated by the L2 nerve root stimulation). Connective tissue cross sectional area and Collagen-III expression were reduced across the whole multifidus muscle at L4 in the Activated group, but not at any individual region, suggesting the impact of the changes extends beyond the fascicle that is activated. No differences were detected to the cross-sectional area of muscle or adipose tissue, or Collagen-I expression at L4 between groups. The multifidus muscle adjacent to the L2 spinous process was not activated by neurostimulation of the L2 nerve root. No measures of the multifidus muscle at L2 differed between the Non-Activated and Activated groups.

CONCLUSIONS

These data reveal that targeted activation of the multifidus muscle reduces histological and genetic signs of muscle fibrosis induced by IVD degeneration.

ACKNOWLEDGEMENTS

This study was supported by a research grant from Mainstay Medical. PH is supported by a fellowship from the National Health and Medical Research Council of Australia (NHMRC).

REFERENCES

[1] Hodges PW, James G, et al. Spine 2015; 40(14):1057-71.
[2] James G, Klyne DM, Millecamps M, Stone LS, Hodges PW. Eur Spine J. 2019; 28(5):893-904.

CHANGES IN MUSCULAR COORDINATION PATTERNS OF THE ELDERLY POPULATION

Elisa Romero Avila[1], Hannah Lena Siebers[2], L. Cornelius Bollheimer[3], and Catherine Disselhorst-Klug[1]
[1] Department of Rehabilitation and Prevention Engineering, RWTH Aachen, Aachen, Germany.
[2] Department of Orthopedics, Trauma and Reconstructive Surgery, Uniklinik RWTH Aachen, Aachen, Germany.
[3] Department of Geriatric Medicine, Uniklinik RWTH Aachen, Aachen, Germany.
Email: romero@ame.rwth-aachen.de

INTRODUCTION

Movement velocity, joint position, and contraction type are not the only parameters that influence muscular activation but aging also has an effect on it. Research shows that in the elderly, increased coactivation of antagonist muscles and slower reaction times are observed, as well as a decrease in muscle force [1]. These changes lead to an increased risk of falls, as well as a reduced ability to independently perform Activities of Daily Living (ADL) [2]. The aim of this work is to analyse changes in muscular coordination patterns of upper extremity muscles with age as a function of angular velocity, joint angle and type of contraction.

METHODS

The muscular activation of the biceps (BI), brachioradialis (BRA) and triceps (TRI) was recorded from 20 healthy elderly (7♂, 13♀, avg. age 74.9 ± 5.8 years) by surface electromyography (sEMG) while performing flexion and extension of the elbow. The movement of the elbow joint, which was carried out at different angular velocities and with a constant load of 1kg over the entire range of motion, was as well recorded with a 3D motion capture system. Once the sEMG signals were processed according to SENIAM recommendations, the sEMG envelope of each muscle was further categorized into angular velocity (five intervals between 20 – 120°/s), elbow joint angle (five intervals between 25° - 125, where 0° represents full extension) and type of muscle contraction (concentric or eccentric). The results of these measurements were compared with data previously recorded under the same conditions in young healthy adults (7♂, 8♀, avg. age 26.2 ± 3.2 years) [3].

RESULTS AND DISCUSSION

In the flexion phase, an increase in the sEMG envelope was observed in all three muscles in the elderly group as angular velocity and joint angle increased. These results were consistent with those of the young adult group. However, the sEMG envelope in all three muscles was higher in the elderly group compared to young participants. Whereas in the young subjects the amount of activation was the same in all three muscles, in the elderly, muscular activation of BRA and TRI was higher than that of BI. This co-activation might be a strategy of the elderly to perform the movement at a controlled velocity and improve the stability of the elbow joint. Regarding the extension phase, the sEMG envelope of BI decreased with increasing angular velocity while sEMG envelope of BRA increased [3]. In contrast, in the elderly group, muscular activation of both BI and BRA increased with increasing angular velocity. As observed in the flexion movement, the sEMG envelope of TRI and BRA was higher than BI in the elderly group. Since in the young adults group, the increase in the muscular activation of BRA with increasing extension velocity cannot be explained by the force-velocity relationship, it has been assumed that BRA is mainly used to control velocity and position [3]. This seems to be different in the elderly, where age-related co-activation is observed, as the ability to generate force decreases with increasing angular velocity due to fewer, mostly large, functioning motor units. This goes along with a loss of fine motor skills in the elderly.

In contrast to the young subjects and to the force-length relationship, sEMG envelope of BRA and BI decreased with increasing extension angle. This may be due to two theories proposed in the literature on aging: 1) increased intramuscular connective tissue that would raise muscle force as it lengthens or 2) slower muscle contraction and fewer fast-twitch fibres that would reduce rate of torque development [1,2].

CONCLUSIONS

Muscular coordination patterns of the upper extremity muscles are altered in the elderly. This was proven by increased co-activation and different activation patterns of the BRA to execute the movement. However, this goes along with a loss of fine motor skills. Additionally, changes in the muscle characteristics and architecture seem to influence the changes in muscular coordination patterns in the elderly. This should be taken into account when implementing training routines that allow for an optimal physical activity and less dependency to perform ADLs.

ACKNOWLEDGEMENTS

The authors would like to thank Dr. Batista, Ms. Nagel and Ms. Fait for their support during the measurements and to CONACYT-DAAD (57649580) for the grant awarded to Elisa Romero Avila.

REFERENCES

[1] Callahan, D. M. and Kent-Braun, J. A., *J Appl Physio* **111**: 1345-1352, 2011.
[2] Raj, I. S., Bird, S. R. and Shield, A. J., *Exp Gerontol* **45**: 81-90, 2010.
[3] von Werder, S. C. F. A. and Disselhorst-Klug, C., *J Electromyogr Kinesiol* **28**: 67-75, 2016.

NATURAL KNEE BIOMECHANICS CAN BE RESTORED BY CUSTOMIZED HIGH-TIBIAL OSTEOTOMY: PRE/POST-OP FUNCTIONAL AND MORPHOLOGICAL EVALUATIONS

Belvedere C.[1], Gill H.S.[2], MacLeod A.[2], Grassi A.[3], Dal Fabbro G.[3], Zaffagnini S.[3], Leardini A[1].
[1] Movement Analysis Laboratory, IRCCS Istituto Ortopedico Rizzoli, Bologna, Italy
[2] CTI/Department of Mechanical Engineering, University of Bath, Bath, UK
[3] II Clinical Department, IRCCS Istituto Ortopedico Rizzoli, Bologna, Italy
Email: belvedere@ior.it

INTRODUCTION

Excessive knee varus results in altered tibio-femoral joint (TFJ) contacts and loading, and medial knee osteoarthritis onset [1]. High tibial osteotomy (HTO) is performed to delay end-stage osteoarthritis. This allows for tibial plateau realignment and medial condylar decompression [1], targeting normal knee function. Despite the good results achieved, issues concerning fixation plate design and implantation, and patient functional performance [2] still exist. To overcome these, a new customized HTO procedure has been developed [3]. Based on medical imaging, multiplanar deformities are addressed by 3D pre-operative (PRE) planning and implantation of a custom-designed 3D printed fixation plate, carefully placed by patient-specific instrumentation. To date, good preliminary post-operative (POST) results have been reported using an original multi-instrumental analysis [4]. The aim of this study is to corroborate the preliminary findings on the novel customized HTO procedure by extending the original method [4] to a larger patient group.

METHODS

25 patients (BMI<25; 40-65 years) with <20° knee varus underwent the new customized HTO procedure (3D Metal Printing Ltd, Bath, UK) [3,4]. PRE and POST (at 6 months) clinical and instrumental evaluations [4] were performed. Gait analysis (GA) was executed during level walking and stair climbing/descending using a 9-camera motion capture systems (Vicon®, UK), wireless EMG, ground-reaction-force (GRF) platforms, and an original protocol with additional markers on the tibial plateau rim for registration purposes. Patients also received weight-bearing computed tomography (WBCT, Carestream®, NY- USA) while still wearing the GA markers. CAD models for the femur, tibia, patella and markers were reconstituted from DICOM. 3D trajectories of markers collected during motion were then registered to the corresponding CAD models via SVD. Resulting transform matrices were used to register GRF data on the tibial CAD model and to calculate the GRF vector intersections with a virtual plane on the tibial plateau. Differences in PRE-vs-POST TFJ and patello-femoral joint (PFJ) contacts, and discrepancies in planned-vs-POST tibial plateau alignment and plate shape were performed via Distance-Map-Analysis (DMA, Geomagic®, SC-USA) based on relevant CAD models.

RESULTS AND DISCUSSION

After HTO, physiological knee function was assessed by clinical scoring and GA, showing POST joint kinematics and kinetics within the normality. Normal POST ab/adduction moments were observed, confirming reduced stress on the knee medial compartment. GRF registration on patient-specific tibial CAD was achieved with <2.4 mm error. POST GRF intersections with the tibial plateau were found to be significantly more lateral when compared to PRE ones (Figure 1a); in % of plateau width, this lateralization was 70.1±21.0 during walking and 79.4±30.0 in stair climbing/descending, and correlated well with POST kinetics. DMA showed: a) planned-vs-POST discrepancy (Figure 1b) in plate shape and plateau alignment <1.7 mm; b) POST plate-to-tibia adherence <2.4 mm, in line with that desired for proper bone healing; c) more homogeneous contacts between the two TFJ compartments and lateralized PFJ contacts, showing decompression at both TFJ and PFJ level.

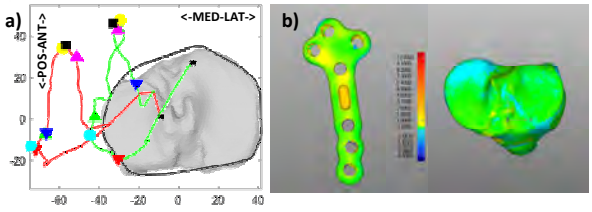

Figure 1 a) PRE (red) and POST (green) GRF-to-tibia intersection; b) Planned-vs-POST discrepancy as observed via DMA (green=0 mm) in plate shape and tibial plateau alignment.

CONCLUSIONS

The new customized HTO procedure restored normal knee biomechanics with concurrent reductions in reported pain. In detail, the study showed proper knee realignment, kinematics, kinetics and joint contacts after HTO, as well as consistency with pre-op plans. Preliminary results were confirmed here on a larger scale and with more evidence.

REFERENCES

[1] Zaffagnini S et al. *KSSTA*, **21**:934-941, 2013.
[2] Woodacre T et al. *Knee,* **23(2)**:276-82, 2016.
[3] MacLeod A et al. *Commun Med*, **1**:6, 2021.
[4] Ruggeri M et al. *Gait Posture*, **94**:144-152, 2022.

EFFECTS OF UNEXPECTED SLIP AND TRIP-INDUCED PERTURBATIONS ON DYNAMIC STABILITY AND SUPPORT MOMENT

Shabnam Shokouhi[1], Hossein Mokhtarzadeh[1], Lee Vee Sin Peter [1]
[1] Department of Biomedical Engineering, University of Melbourne, Melbourne, Australia.
Email: sshokouhi@student.unimelb.edu.au

INTRODUCTION

Injurious falls are predominantly caused by unexpected slips or trips during walking. In recent years, perturbation-based balance training (PBT) has been proven beneficial as a task-specific fall prevention intervention. However, the most effective perturbation type and intensity for fall prevention training is still an open question. In this study, we aimed to, first, identify which type of treadmill-induced perturbation, slip or trip, disturbs dynamic stability the most by using the perturbation response (PR) measure [1] ; and second, to investigate which type is more mechanically demanding by comparing support moment in the first recovery step post perturbation.

METHODS

Twenty-four healthy young adults (age=24.2±2.5, BMI=22.19±2.3) participated in our study. Trip and slip-like perturbations were administered using a split-belt treadmill by rapidly decelerating and accelerating the right belt, respectively. 3D Marker positions and ground reaction forces were recorded throughout the experiment. An inverse dynamic approach was used to find joint moments. The support moment was calculated as the summed ankle, knee, and hip extension moments for the first recovery step. Dynamic stability was measured using the margin of stability (MoS) [2]. The perturbation effect was then quantified using the Perturbation Response (PR) measure (Eq1) over six steps post-perturbation.

$$PR = \sqrt{\sum_{i=1}^{6}\left(\frac{MoS(i) - \overline{MoS^*}}{\sigma_{MoS^*}}\right)^2} \qquad (1)$$

where $\overline{MoS^*}$ and σ_{MoS^*} are mean and standard deviation of MoS at heel strike (HS) of 20 unperturbed gait cycles, and $MoS(i)$ represents MoS at the HS of the i^{th} cycle post-perturbation. Statistical Parametric Mapping (SPM) paired *t-test* was used to perform pairwise comparisons of support moment values and patterns between slip and trip recovery steps and Normal (unperturbed) walking. A paired-sample *t-test* was applied to compare PR between slip and trip.

RESULTS AND DISCUSSION

Trip-like perturbation resulted in a larger perturbation response (PR) on MoS compared to slip (Table 1), meaning that trip-like perturbation had a more destabilizing effect on MoS compared to slip perturbation. Moreover, participants used significantly greater support moments during the midstance (26-72%, $p<0.001$) of the recovery step following the trip-like perturbation compared to slip (Figure 1). This indicates that compared to slip, participants needed more extension moments from lower limb joints to prevent the centre of mass from collapsing following the trip perturbation.

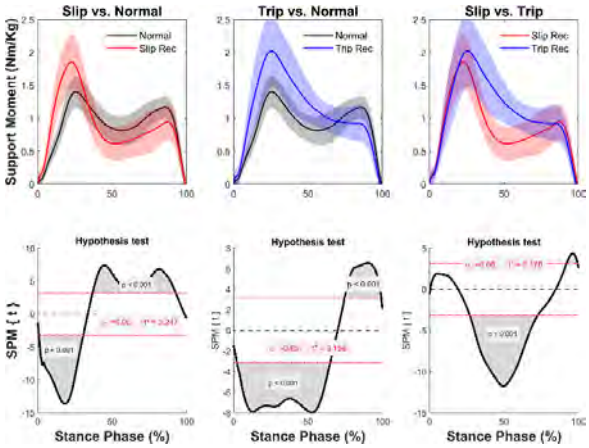

Figure 1 Support moment in Normal (black) vs slip-recovery (red), and vs trip-recovery (blue) with the statistical SPM results.

CONCLUSIONS

These findings indicate that trip-like perturbation was more challenging and had more destabilizing effects on gait stability and required a larger support moment from the lower-limb joints to keep the body upward and prevent collapsing. Therefore, it is more likely to result in falls and must be included in the PBT protocols. These findings could contribute to designing more efficient fall prevention interventions.

REFERENCES

[1] van den Noort, J.C., et al. J Biomech, 2017.
[2] Hof, A., M. et al. J Biomech, 2005

Table 1: Mean and standard deviation of Perturbation Response (PR) for MoS

	Perturbation Response (PR)		Slip vs. Trip		
	Slip	Trip	*P_value*	95% CI of difference	
MoS	5.18 (± 2.32)	12.11 (± 3.54)	<0.001	3.948	7.515

AN EXPERIMENTAL SETUP FOR ASSESSMENT OF TRACTION FORCE AND ASSOCIATED FETAL BRAIN DEFORMATION IN VACUUM-ASSISTED DELIVERY

Estelle Pitti[1,2], Annelies Severens[1], Maria Pop[1], Lotta Herling[2,3], Xiaogai Li[1], Gunilla Ajne[2,3] and Matilda Larsson[1]

[1] Biomedical Engineering and Health Systems, KTH Royal Institute of Technology, Stockholm, Sweden
[2] Clinical Science, Intervention and Technology – CLINTEC, Karolinska Institutet, Stockholm, Sweden
[3] Clinical Science Pregnancy Care & Delivery, Karolinska University Hospital, Stockholm, Sweden
Email: pitti@kth.se

INTRODUCTION

Vacuum-assisted delivery (VAD) can be performed during the second stage of labor to assist complicated vaginal deliveries. In VAD, a vacuum cup is placed on the scalp of the fetus and traction is applied during uterine contractions. Despite its common use worldwide, VAD is associated with higher neonatal morbidity compared with natural vaginal delivery. Furthermore, biomechanical evidence for safe VAD traction forces is still limited, although recent studies have shown that traction forces are often underestimated [2], and that high forces may lead to severe fetal delivery outcomes [3]. To date, accurate methods to evaluate VAD are lacking, which hinders development of VAD safety [1]. The aim of this study was to develop an experimental VAD testing setup and to investigate the impact of traction forces on fetal brain deformation.

METHODS

The experimental setup included three parts; a fetal head phantom, an assessment of traction forces and brain deformations, and a VAD device. A patient-specific fetal head phantom was developed based on segmentation of the brain, skull, fontanelles and sutures in CT scans of a newborn [4] using Slicer 3D 5.0.3. The brain phantom was cast in a 3D-printed mold using a composite hydrogel (6% PVA and 0.85% PHY in a 1:1 ratio) [5] (Figure 1a). The skull phantom was 3D printed using multi-material Polyjet technology so that the different skull lobes, fontanelles, and sutures could be printed together in one prototype using three different materials (RGD835, FLX-9870-DM, RGD 8510-DM, Stratasys) with realistic mechanical properties [6]. The skull phantom was printed in two parts, which were assembled by a screwing system (Figure 1b).

Before mounting the brain in the skull, nine 2-mm sonomicrometry crystals (Sonometrics) were manually inserted into the upper part of the brain (Figure 1a), while three crystals were fixed in the lower skull, to assess inter-crystal displacements and estimate brain deformation using trilateration. The fetal head phantom was attached to the bottom of a water tank and a metal Bird cup was placed on the skull using a vacuum pump. A digital force gauge (FH 1K, Sauter) was attached between the cup and the handle of the VAD system to record traction forces (Figure 1c). Sonomicrometry and force data were recorded during simulated VAD with a maximum force of 10-100N with increments of 10N.

RESULTS AND DISCUSSION

The experimental setup allowed simulated VAD testing up to traction forces of 100N. Crystals positioned 5.4 cm and 4.9 cm below the suction point showed a vertical brain tension that increased with the level of traction force, reaching a strain of 3.4% at 100N, 1.7% at 50N, and remaining close to zero at 10N (Figure 1d). The strain behavior varied in different directions, as well as with crystal position and the shape of the traction force curve. The relationship between traction force and fetal brain deformation needs to be further investigated; at higher forces closer to those used in clinical practice and when using a more controlled procedure for positioning the crystals. Further investigation is also needed to relate brain strain and adverse outcomes in VAD.

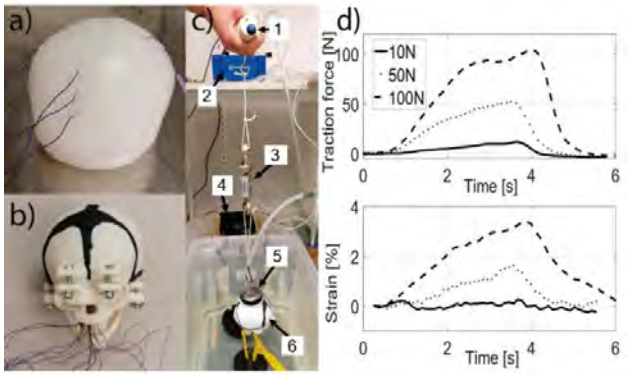

Figure 1 a) Fetal brain phantom (purple sonomicrometry crystal cables), b) Fetal head phantom, c) VAD setup, 1; VAD handle, 2; vacuum pump, 3; force gauge, 4; sonomicrometry, 5; VAD cup, 6; head phantom. d) Sample traction force and vertical strain curves.

CONCLUSIONS

The strain of the brain increased with increasing traction force, and at 100N a vertical strain of 3.4% was obtained. The experimental setup allows further investigation of the relationship between traction force and brain deformation to establish biomechanical evidence for safe VAD.

REFERENCES

[1] Goordyal D et al., *J. Med. Eng.* ***235*** (1):3-16, 2020.
[2] Pettersson K et al., *BJOG* **122**(13):1809-1816, 2015.
[3] Romero S et al., Acta Obstet Gynecol Scand, **101** (11):1238-1244, 2022.
[4] Edgar H.D.B et al., U.o.N.M., 2020.
[5] Forte A.E et al., Mater. Des. **112**: 227-238, 2016.
[6] Jones M et al., Forensic Sci. Int. **276**:111-119, 2017.

The BASMI limits patient specific examination compared to motion capture of a four-segment spine

Logan Wade[1], Raj Sengupta[2], James Bilzon[1] and Dario Cazzola [1]
[1]Department for Health, University of Bath, United Kingdom.
[2] Royal National Hospital for Rheumatic Diseases, Bath, UK.
Email: lw2175@bath.ac.uk

INTRODUCTION

Axial Spondyloarthritis (axSpA) is an inflammatory disease that mainly affects the spine, resulting in joint stiffness, entheseal inflammation and bone growth leading to vertebral fusion [1]. The widely used clinical Bath Ankylosing Spondylitis Metrology Index (BASMI) examines spinal mobility and is quick and easy to implement. However, this tool does not correlate well with radiographic disease progression [2], is highly subjective, and crucially, assumes mobility at specific points of the spine are indicitave of mobility across the spine. Each axSpA patient presents with highly variable symptoms, as regions of the spine may be selectively affected in some and not affected at all in others. Therefore, this study aimed to determine the effectiveness of the BASMI to examine whole and within spine mobility.

METHODS

In this ongoing study, fourteen (9M, 5F, 50 ± 9 years, 87 ± 22 kg, 175 ± 10 cm) of forty AS patients have had BASMI and 3D marker-based motion capture assessed. 3D motion capture (Qualisys) used marker clusters placed on six segments, head/neck, upper thoracic, lower thoracic, lumbar and pelvis, to examine an inverse kinematic segment-segment range of motion (RoM) in OpenSim [3]. RoM for each segment was calculated with respect to the inferior segment (e.g. lumbar RoM in respect to the pelvis). RoM is reported for maximal forward flexion, lateral bending, and axial rotation during standing. Movements were performed three times for each participant at their preferred speed and mean values reported. Whole spine RoM was the sum of all segment RoM's. Pearson r correlations are reported to describe the associations between the overall BASMI against overall spine RoM, and three of the five individual BASMI scores against comparable individual segment-segment ROM's. Correlation coefficients were classified as <0.2 (poor), 0.2-0.4 (weak), 0.4-0.6 (moderate), 0.6-0.8 (strong) and >0.8 (very strong).

RESULTS AND DISCUSSION

The overall BASMI score had moderate to strong negative correlations with whole spine RoM in forward flexion (r=-0.61), lateral bending (r=-0.69) and rotation (r=-0.57). Individual BASMI scores had strong negative correlations for forward lumbar flexion (r=-0.65) and lower thoracic lateral bending (r = -0.80), and moderate correlations for lumbar lateral bending (r = -0.42) and head/neck rotation (r = -0.45).

While some BASMI outcomes appeared to have strong negative correlations with patient mobility, other variables were only moderately associated. In addition, Figure 1 demonstrates how mobility at one region of the spine may vary wildly in three patients, while the same patients may be almost identical at another region. Therefore, segment-segment RoM is not indicative of mobility at neighbouring regions in axSpA patients. No BASMI correlations were above 0.8 (very strong) in magnitude, thus while some overall and individual BASMI scores represent strong associations to motion capture of a multi-segmented spine, all BASMI measures will likely be limited in their sensitivity of small changes required to monitor disease progression. As such, the BASMI does not provide sufficient detail to inform personalised treatment approaches and could potentially impede accurate monitoring of disease progression that present at multiple spinal levels.

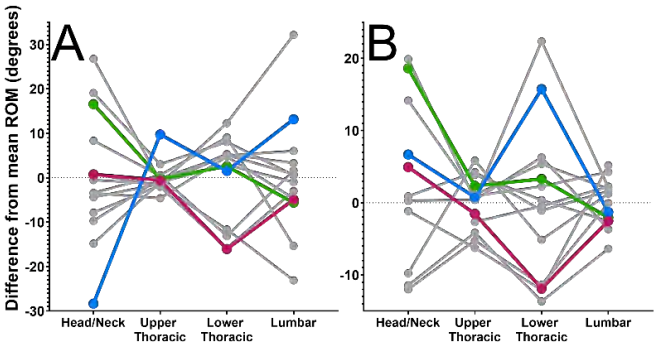

Figure 1: Forward flexion (A) and lateral bending (B), segment-segment ROM, normalised to the mean ROM across all participants. Three patients are highlighted to demonstrate the high variability across the spine.

CONCLUSIONS

To improve monitoring of spinal mobility and disease progression in axSpA, it is essential to focus on individual differences across the whole spine. Future work is needed to develop clinically applicable methods for obtaining reliable and sufficently detailed measures.

ACKNOWLEDGEMENTS

This research was funded by the Centre for Analysis of Motion, Entertainment Research and Applications (EP/M023281/1 and EP/T014865).

REFERENCES

[1] Hwang M et al. *Clin. Rheumatol.*, 40:3079-93. 2021
[2] Rezvani A et al. *Spine*, 37(19). 2012
[3] Bruno A et al. J Biomech Eng, 137(8). 2015

THE IMPORTANCE OF REPORTING PERFORMANCE-BASED OUTCOMES FOLLOWING INTRAMEDULLARY NAILING OF TIBIAL SHAFT FRACTURES

Simon Thwaites[1], Mark Rickman[1,2] and Dominic Thewlis[1,2]

[1] Centre for Orthopaedic & Trauma Research, University of Adelaide, Adelaide, Australia.
[2] Department of Orthopaedics & Trauma, Royal Adelaide Hospital, Adelaide, Australia.
Email: simon.thwaites@adelaide.edu.au

INTRODUCTION

No core outcome set exists for intramedullary (IM) nailing of tibial shaft fractures and the optimal nail insertion technique remains inconclusive. Studies commonly describe the presence of anterior knee pain (AKP) with various patient-reported outcome measures (PROMs) for pain and function. However, few studies [1] report objective, performance-based outcomes. This prospective study aimed to investigate differences in PROMs and performance-based outcomes following tibial nailing against a healthy reference group. It was hypothesised there may be differences in time taken for outcomes to reach equivalent levels to the healthy group, but all outcomes would be equivalent to the healthy group after 18 months follow-up.

METHODS

Patients were recruited through an ongoing randomised controlled trial comparing suprapatellar and infrapatellar nailing of extraarticular tibial shaft fractures [2]. Healthy volunteers were case-matched for age, sex, height, and body mass. PROMs included AKP (yes/no), visual analogue scale for knee pain ($VAS_{knee\ pain}{}_0^{10}$), and the Knee Injury and Osteoarthritis Outcome Score – Patellofemoral Subscale ($KOOS\text{-}PF_0^{100}$). Maximum isometric knee extension strength (IKE_{max}) was captured using a MicroFET2 dynamometer. Squatting kinematics were captured using a Vicon motion capture system. A Likert score of knee pain ([0 – 4] scale) was recorded following each activity. Data were processed using Matlab (vR2019b), OpenSim (v4.3), and R (v4.2.2). MAPClient informed scale factors for deep squat OpenSim models [3]. Unpaired Student t-tests or Wilcoxen tests were used for group differences following Shapiro tests for normality.

RESULTS AND DISCUSSION

Table 1 details participant outcomes at each time point grouped by AKP and no pain (NP). $VAS_{knee\ pain}{}_0^{10}$ and $KOOS\text{-}PF_0^{100}$ remained significantly different (p<0.05) to the healthy reference group up to 18 months. Whilst IKE_{max} was equivalent (p>0.05) to the healthy group at 6 months, and max squat hip and knee flexion were equivalent to healthy at 6 and 12 months, respectively (Figure 1). Max ankle dorsiflexion remained below (p=0.02) the healthy group at 18 months (Figure 1). There was no difference (p>0.05) in $VAS_{knee\ pain}{}_0^{10}$ between AKP and NP groups at any time point. Further analyses following increased recruitment and follow-up sessions, and inclusion of additional data is required (additional PROMs, functional tests, and sensor data).

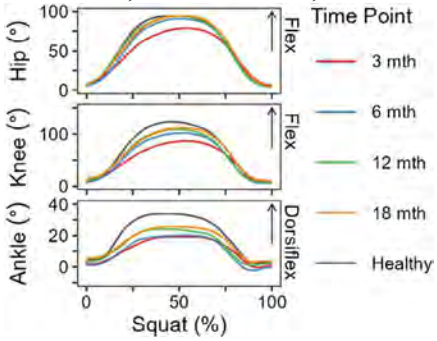

Figure 1 Mean squat flexion angles at the hip, knee, and ankle.

CONCLUSIONS

Performance-based outcomes may enhance reporting following IM nailing of tibial shaft fractures.

REFERENCES

[1] MacDonald D et al. *Eur J Tr Em Sur* **46**: 93-98, 2020
[2] Thwaites S et al. *Pilot Feas Stud* **8**: 110-122, 2022
[3] Catelli D et al. *CMBBE* **22**: 21-24, 2019

Table 1: Subgroup analysis of AKP and NP patients with the healthy cohort. ^ – p<0.5 between AKP and NP for that time point. * – p<0.5 with the healthy cohort. SQ – squat. $VAS_{knee\ pain}{}_0^{10}$ – 10 is high pain. $KOOS\text{-}PF_0^{100}$ – 100 is high function. $SQ\ likert_0^4$ – 4 is high pain.

	3 months		6 months		12 months		18 months		Healthy
	AKP (n = 10)	NP (n = 10)	AKP (n = 9)	NP (n = 7)	AKP (n = 8)	NP (n = 4)	AKP (n = 5)	NP (n = 6)	(n = 10)
$VAS_{knee\ pain}{}_0^{10}$	**3.8 (2.4)***	**2.9 (2.8)***	**2.6 (2.5)***	**1.5 (1.9)***	**1.7 (2.3)***	**3.6 (3.3)***	**2.9 (3.8)***	**1.6 (2.5)***	0.3 (0.9)
$KOOS\text{-}PF_0^{100}$	**48 (17)***	**49 (25)***	**63 (15)***	**75 (25)***	**66 (19)***	**58 (15)***	**65 (29)***	**81 (26)***	94 (16)
IKE_{maxcx} (N)	**223 (76)***	**170 (77)***	246 (100)	258 (84)	250 (54)	280 (123)	331 (96)	264 (87)	298 (70)
SQ $hip._{max}$ (°)	82 (30)	**78 (17)***	95 (22)	92 (15)	98 (10)	93 (13)	96 (16)	95 (15)	98 (18)
SQ $knee._{max}$ (°)	**100 (27)^***	**77 (15)^***	**104 (20)***	105 (21)	111 (15)	109 (26)	116 (19)	110 (23)	126 (19)
SQ $ankle._{max}$ (°)	**23 (8)***	**18 (6)***	**21 (7)***	**23 (7)***	**25 (4)***	26 (10)	30 (7)	**24 (9)***	35 (8)
$SQ\ likert_0^4$	**0.9 (0.6)***	**1.0 (1.3)***	**0.6 (0.5)^***	**0.0 (0.0)^**	0.1 (0.4)	0.5 (1.0)	0.3 (0.4)	0.5 (0.8)	0.0 (0.1)

FEMOROACETABULAR IMPINGEMENT PATIENTS SHOW ALTERED HIP KINEMATICS DURING LATERAL HOP AND DROP JUMP

Katrin Dätwyler[1,3], Enrico De Pieri[3], Nicola A. Maffiuletti[1], Michael Leunig[2], Stephen J. Ferguson[3] and Renate List[1]
[1] Human Performance Lab, [2] Hip Surgery Department, Schulthess Clinic, Zurich, Switzerland.
[3] Institute for Biomechanics, ETH Zurich, Zurich, Switzerland.
Email: katrin.daetwyler@kws.ch

INTRODUCTION

Patients with femoroacetabular impingement syndrome (FAIS) suffer from groin pain, functional limitations and an increased risk for early development of hip osteoarthritis [1]. FAIS is induced by an impingement of the femur and acetabulum, provoked by abnormal bone morphology, excessive hip movement or a combination of both [1]. Kinematics of FAIS patients were most often studied during walking, where sagittal hip range of motion (ROM) and peak hip extension were found to be lower than those of healthy controls [2]. In the current study, we investigated more demanding tasks, such as hopping and jumping, that could accentuate the FAIS-induced movement impairments. Thus, time-series 3D hip angles during different tasks were compared between FAIS patients and healthy controls.

METHODS

25 FAIS patients and 25 matched healthy controls of both sexes performed various tasks: walking, running, stepping up a two-step stair, stand up/sit down, single-leg squat, drop jump, lateral hop and pivot turn. For the three latter tasks, participants jumped or stepped down from a box of 30 cm. The loaded phase, from initial foot contact to take-off was considered to define the movement cycle, except for walking and running (heel strike to ipsilateral heel strike). Three-dimensional kinematic data was captured with 13 infrared cameras (Vicon, Oxford Metrics Ltd, UK) using a full-body marker set. Hip joint angles were calculated according to ISB recommendations. Time-series data of hip flexion, adduction and rotation angles of patients and controls were compared using vector-field statistical parametric mapping (SPM) with Hotelling's T2 statistic, followed by scalar post hoc SPM in case of significance.

RESULTS AND DISCUSSION

For walking, no significant differences in hip flexion, adduction and rotation were observed between FAIS patients and healthy controls. This is in contradiction with a recent review which, for continuous kinematic data, qualitatively concluded on reduced hip abduction of FAIS patients during terminal stance [2]. However, four of the 12 included studies did not report any difference for hip kinematics of patients and controls, and four studies reported differences for discrete kinematic variables only (ROM, peak angles).

During stand up/sit down, pivot turn, single-leg squat and running, no impairments in hip kinematics were observed. Also for stair climbing no group differences were observed, which is in agreement with Hammond et al. [3] but contradictory to the findings of Rylander et al. [4], who reported less hip sagittal ROM and peak hip internal rotation in patients.

When hopping laterally with the involved leg, FAIS patients showed more hip flexion at take-off (Figure 1). In contrast, less hip flexion was observed when landing for the drop jump (Figure 1). Reducing hip flexion during the drop jump might represent a strategy to avoid pain and decrease hip joint loading and has been previously observed in women with hip pain [5]. During take-off for the lateral hop, however, hip extensor weakness – which has previously been reported in FAIS patients [6] – might prevent full hip extension. Hip extensor weakness might take effect only during the unilateral hop, as the latter is more demanding than a bilateral drop jump.

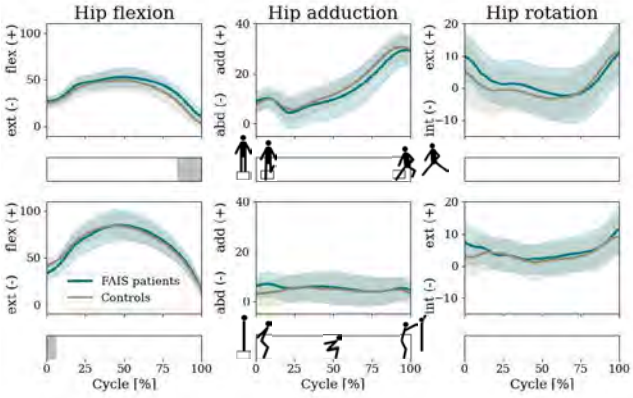

Figure 1 3D hip joint angles during lateral hop (top) and drop jump (bottom) of FAIS patients and healthy controls. Bars depict clusters of SPM significance in post hoc scalar-field t-tests.

CONCLUSIONS

These preliminary results show impaired hip kinematics of FAIS patients during lateral hop and drop jump, but not during walking and other studied tasks. Clinical assessments might therefore need to include demanding tasks, such as a hop, to reveal impairments. Next, musculoskeletal modelling could reveal the effect of altered kinematics on hip joint loading. In addition, patient stratification for different morphologies might improve the understanding of FAIS functional limitations.

REFERENCES

[1] Ganz R et al. *Clin Orthop Rel Res* **417**: 112-20, 2003.
[2] Yarwood W et al. *Arthroscopy* **38**: 174-89, 2022.
[3] Hammond CA et al. *Clin Biomech* **42**: 108-14, 2017.
[4] Rylander J et al. *J Orthop Res* **31**: 1461-8, 2013.
[5] Grosklos M et al. *Clin Biomech* **100**: 2022.
[6] Kivlan BR et al. *Int J Sports Phys Ther* **11**: 527-35, 2016.

POINCARÉ ANALYSIS DETECTS PATHOLOGICAL LOADING RATE VARIABILITY IN POST-ACLR INDIVIDUALS

Noah A. Davidson[1], Yannis K. Halkiadakis[1], Kristin D. Morgan[1]
[1] Department of Biomedical Engineering, University of Connecticut, Storrs, CT 06269, USA
Email: noah.davidson@uconn.edu

INTRODUCTION

Post-anterior cruciate ligament reconstruction (ACLR) individuals often suffer from impaired motor control that results in variable limb loading. Variable limb loading can present as loading rate variability (LRV) and can contribute to the development of knee osteoarthritis [1,2]. However, accurately quantifying LRV has proven challenging. Here, Poincaré analysis was used to quantitatively and graphically evaluate differences in short-term stride-to-stride and long-term limb LRV in healthy controls and post-ACLR individuals. We hypothesized that the post-ACLR individuals' overloaded limb would demonstrate greater short- and long-term limb LRV compared to healthy control and underloaded limbs. These findings would reveal how impaired motor control would alter individuals limb loading dynamics.

METHODS

Fourteen post-ACLR individuals and seventeen healthy controls completed a walking protocol on an instrumented treadmill. The post-ACLR participants performed initial walking baseline trials to define their underloaded and overloaded limbs based on their loading rate values. All participants then completed two five-minute walking trials at 1.0 m/s and 1.5 m/s. Poincaré analysis was performed to quantify short-term (SD1) and long-term (SD2) limb LRV in the post-ACLR underloaded and overloaded limbs and the right limb of healthy controls. An ANOVA was performed to compare differences in short-term and long-term LRV amongst the post-ACLR individuals' overloaded and underloaded limbs and the healthy controls right limb.

RESULTS AND DISCUSSION

Poincaré analyses revealed that post-ACLR individuals' overloaded limb exhibited greater short- and long-term limb LRV at the faster walking speed compared to healthy control and underloaded limbs ($p<0.05$) (Table 1). The post-ACLR individuals' overloaded limbs increased LRV was illustrated by a wide dispersion of loading rate values (Fig. 1). No differences were found at the slower walking speed.

These differences in short- and long-term limb LRV suggests that the post-ACLR individuals' overloaded limb suffers from impaired motor control that alters their ability to adopt and maintain healthy limb loading dynamics, which was masked at the slower speed. Thus, it is important for individuals to perform more demanding tasks that will challenge the neuromuscular system and uncover underlying neuromuscular dysfunction.

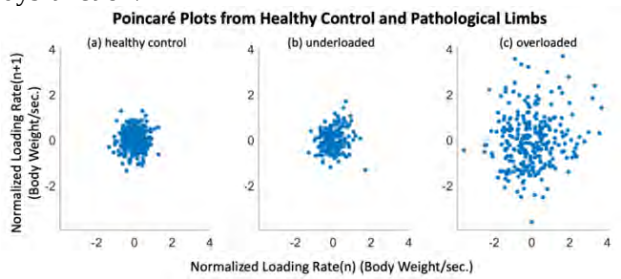

Figure 1 Poincaré plots of loading rate data for a healthy control participant's limb (a) and the underloaded and overloaded limbs for a post-ACLR participant (b, c) during the 1.5 m/s walking trials.

CONCLUSIONS

Poincaré analysis was successful in differentiating multiple facets of LRV between healthy and pathological populations. Furthermore, it revealed that post-ACLR individuals' overloaded limb continues to suffer from impaired motor control. These results suggest that Poincaré analysis could be a useful clinical tool to detect impaired motor control in pathological populations.

REFERENCES

[1] Noehren B et al. *Med. Sci. Sports Exerc.* **45**: 1340-1347, 2013.
[2] Moraiti CO et al. *J Arthrosc. Relat. Surg.* **25**: 742-749, 2009

Table 1: ANOVA comparison of loading rate standard deviation (SD), short-term variation (SD1), and long-term variation (SD2) from healthy control limbs and overloaded and underloaded limbs from post-ACLR participants during the 1.5 m/s trial (mean ± SD).

Variable	**Healthy** (n=17)	**Underloaded** (n=14)	**Overloaded** (n=14)	**p-value**
SD	0.59 ± 0.18^{a}	0.58 ± 0.19^{a}	0.85 ± 0.36^{b}	0.01^{*}
SD1	0.56 ± 0.17^{c}	0.54 ± 0.17^{c}	0.78 ± 0.31^{d}	0.01^{*}
SD2	0.62 ± 0.19^{e}	0.61 ± 0.22^{e}	0.90 ± 0.43^{f}	0.02^{*}

* significant difference (p-value < 0.5).

$^{a, b, c, \cdots}$ in each walking speed indicates significantly different means based on Tukey pairwise comparisons.

TEST-RETEST RELIABILITY OF MARKERLESS THREE-DIMENSIONAL GAIT KINEMATICS AND KINETICS, IN HEALTHY OLDER ADULTS

Andreia Carvalho[1,2], Jos Vanrenterghem[2], Sílvia Cabral[1], António P. Veloso[1] and Vera Moniz-Pereira[1]
[1]LBMF, CIPER, Fac Motricidade Humana, Universidade de Lisboa, Lisboa, Portugal.
[2] Research Group for Musculoskeletal Rehab, Fac. of Movement and Rehab Sciences, KU Leuven, Belgium.
Email: andreiafjcarvalho@gmail.com

INTRODUCTION

In older adults, alterations in biomechanics during common activities can be the early signs of various diseases. However, widespread use of motion analysis has been hampered by time and resource constraints of proven motion capture methods, i.e., marker-based optoelectronic systems. Recently, a method using a deep learning anatomical landmark prediction from video data has become commercially available. Prior studies have evaluated its validity and repeatability to assess gait in healthy young adults [1,2]. Since reliability can be population-specific, the aim of this study was to evaluate test-retest reliability of markerless gait kinematics and kinetics in healthy older adults.

METHODS

An intra-rater test-retest study was conducted, recruiting 11 healthy older adults (81±4 years). Gait analysis was performed twice (9±3 days' interval), using 8 Miqus video cameras (Qualysis, SE) synchronized with 2 force plates (Kistler, Instruments Ltd, SWI; BERTEC, Columbus, USA) at 85Hz and 850Hz, respectively. Participants walked in their everyday clothes and sports shoes at self-selected speed (20 gait cycles). Video data were processed with Theia3D (v2022.1.0.2309, Theia Markerless Inc, CA), using an Inverse Kinematics 3D pose estimation, filtered at 8Hz. The resulting 4x4 pose matrices were analyzed in Visual3D (v2022.03.3, C-Motion, USA). Analog signals were low-pass filtered at 8Hz. Lower limb joint angles (XYZ Cardan sequence) and moments (internal, normalized to subject's body mass) were computed. An integrated pointwise Interclass Correlation Coefficient (ICC) and measurement error (SEM) were computed for curve data (R-code) [3]. Minimal Detectable Change (MDC) was calculated from SEM. An integrated ICC value of 0.70 was considered acceptable.

RESULTS AND DISCUSSION

The average walking speed varied 0.03m/s between sessions. Kinematic ICCs were ≥ 0.70, and quite stable throughout the gait cycle (e.g. Figure 1), except for sagittal and transverse hip joint (Table 1). The SEM were < 2.0º and MDC ≤ 5º, with higher SEM% in the frontal and transverse plane. These SEM values were lower than those reported for discrete points [4]. Reliability for kinetics was similar, with ankle and knee parameters showing an ICC ≥ 0.75. ICCs during the swing phase fluctuated more though (e. g. Figure 1). Hip joint moments ICCs varied between 0.53-0.69; SEM were ≤ 0.05Nm/Kg and MDC ≤ 0.1 Nm/Kg.

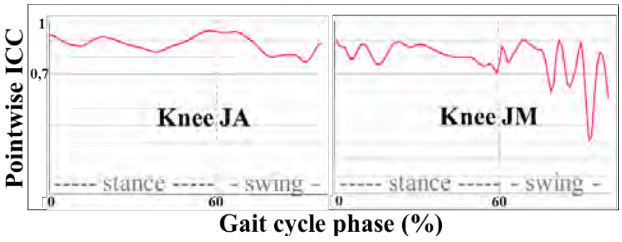

Figure 1 Pointwise ICCs for frontal knee joint angle/joint moment.

CONCLUSIONS

Our study revealed acceptable test-retest reliability for markerless gait kinematics and kinetics for the knee and the ankle, but not for the hip, in healthy older adults.

REFERENCES

[1,2] Kanko R et al. *Journal of Biomech* **121/7**: 2021.
[3] Pini A et al. *Sports Biomech* **21**: 179-200, 2022.
[4] Riazati S et al. *Front. Hum. Neurosci*. **16**: 2022.

Table 1: Integrated ICC, SEM and MDC of lower-limb joint angles (JA) and joint moments (JM): sagittal, frontal, transverse plane.

		Sagittal Plane			Frontal Plane			Transverse Plane		
		Hip	**Knee**	**Ankle**	**Hip**	**Knee**	**Ankle**	**Hip**	**Knee**	**Ankle**
JA	**ICC**	0.57	0.76	0.77	0.70	0.88	0.87	0.59	0.84	0.73
	SEM (°)|%	1.8|4%	1.3|2%	0.9|3%	0.9|19%	0.8|20%	0.6|6%	0.8|18%	1.3|12%	1.2|11%
	MDC (°)	5.0	3.5	2.6	2.6	2.2	1.6	2.2	3.6	3.2
JM	**ICC**	0.69	0.82	0.83	0.69	0.80	0.75	0.53	0.84	0.86
	SEM (Nm/Kg)|%	0.05|4%	0.03|3%	0.02|1%	0.04|3%	0.02|3%	0.01|3%	0.02|8%	0.01|3%	0.01|3%
	MDC (Nm/Kg)	0.15	0.07	0.06	0.11	0.06	0.03	0.05	0.02	0.02

DIFFERENCES IN FRONTAL JOINT KINETICS BETWEEN MARKERLESS AND MARKER-BASED MOTION CAPTURE SYSTEMS DURING TREADMILL RUNNING

Hui Tang[1], Jiahao Pan[2], Barry Munkasy[1], Li Li[1*]

[1] Department of Health Sciences and Kinesiology, Statesboro, Georgia Southern University, USA.

[2] Center for Orthopedic and Biomechanical Research, Boise, Boise State University, USA.

Correspondence Email: lili@georgiasouthern.edu

INTRODUCTION

The emergence of the Markerless motion capture systems (ML) has received increased attention due to its potential in the biomechanics field. Studies have supported the applicability of ML in gait analysis, particularly from the kinematic perspective (e.g., Kanko et al. 2021, [1]). Our previous study has shown the differences in lower extremity sagittal plane joint moments and powers between ML and marker-based (MB) systems during treadmill running [2]. Frontal plane motions are more subtle than those in the sagittal plane and muscles and ligaments that create them function primarily as stabilizers [3], to prevent injury. Therefore, the current study investigated the frontal plane lower extremity joint moments and powers estimated by MB and ML systems during treadmill running.

METHODS

Fifteen healthy, recreationally active young adults were recruited. Participants ran on a treadmill at 3.58 m/s for 2 minutes. The kinematic data were recorded simultaneously by eight infrared and eight high-resolution video cameras. An instrumented treadmill recorded the force data. The last ten strides of frontal plane moments and powers at the right hip, knee, and ankle were calculated from both MB and ML systems using inverse dynamics. The ensemble curves of mean and standard deviations of dependent variables were calculated based on individual measurements of each system. A two-tailed paired t-test was conducted using Spatial Parametric Mapping (SPM) analysis with an alpha level of .05.

RESULTS AND DISCUSSION

Ensembled curves of lower extremity frontal plane moments (left) and powers (right) estimated by MB and ML systems are presented in Figure 1. The SPM results showed significant differences in frontal plane joint kinetics estimated by MB and ML systems. Particular region of interest (ROIs) for ankle moments was between the 3%-30% and 86%-97% of the stride cycle. For ankle joint powers, the ROIs were during 15%-28% and 42%-55%. For the hip joint, the ROIs of the hip moments were during 85%-90%, whereas for the powers, ROIs were during 16%-23% of the stride cycle.

Noticeably, the significance of ankle joint kinetics estimated by MB and ML systems was mainly during the stance phase, where contacting the ground with an increased ankle inversion could indicate higher risks of ankle sprain [4]. Results indicated that ML might underestimate running injury risks. Given that frontal ankle kinetics are often used in investigating shoes and ankle-related injury studies (e.g., Lewinson et al. 2013, [5]), the salient differences from ML may induce more disputes. Additionally, the ML showed smaller magnitudes of hip production power but similar joint moments, which implied the ML might be less sensitive to hip abduction angular velocity during the early stance phase.

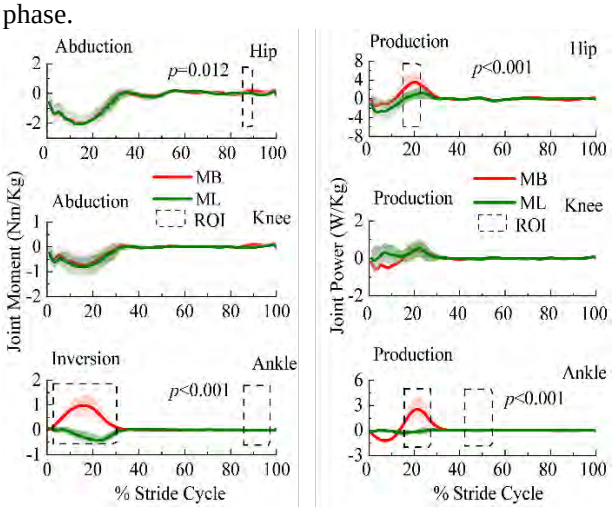

Figure 1. Ensembled curves of lower extremity joint moments (left) and powers (right) in the frontal plane between marker-based (red) and markerless (green) systems. The dotted rectangle regions represented the significant region of interests (ROIs) after Spatial Parameter Mapping (SPM) analysis.

CONCLUSION

Compared to the MB system, the ML demonstrated significant differences in the frontal plane ankle joint moments and powers. Despite the convenience of the ML system in biomechanical applications, the salient distinctions may better inform or complicate injury prevention and rehabilitation.

REFERENCES

[1] Kanko et al. *J Biomech* 127, 2021.
[2] Tang H et al., *Bioengineering* **9** (10), 2022.
[3] Novacheck, *Gait Posture*, 1998.
[4] Chinn et al., *Phys Ther Spor* (14), 2013.
[5] Lewinson R.T. et al., *J Spor Med* (23), 2013.

SIMPLE WALKING MODEL TO EXPLAIN HIP TORQUE COMPENSATION FOR REDUCED PROPULSIVE FORCE

Hajime Ohtsu[1,2], Kouta Sakoda[1] and Kazunori Hase[1]
[1] Department of Mechanical Systems Engineering, Tokyo Metropolitan University
1-1 Minami-Osawa, Hachioji, Japan.
[2] Japan Society for the Promotion of Science
5-3-1 Kojimachi, Chiyoda-ku, Japan.
Email: ohtsu-hajime1@ed.tmu.ac.jp

INTRODUCTION

In the elderly gait, the propulsive force generated by ankle plantar flexion is reduced due to aging, resulting in compensatory movements by the proximal muscles of the lower limb [1]. Specifically, the extension torque of the stance hip joint and flexion torque of the swing hip joint are increased during the push-off phase. Therefore, although reduced propulsive force and its compensations likely make gait unstable, the mechanism is not clear. The purpose of this study is to clarify the mechanisms by which propulsive force reduction and its compensation can make gait unstable using a simple walking model.

METHODS

The simple walking model consists of a point mass M at the hip, point mass m at the foot, massless legs of length l, and a massless trunk. The kinematics of this model are described by the stance leg angle θ relative to the vertical and the swing leg angle ϕ relative to the trunk (Fig. 1A). Note that the trunk was assumed to be always perpendicular to the ground. Therefore, the equations of motion for this model are expressed in dimensionless terms with the overall mass M, leg length l, and time $\sqrt{l/g}$ as the basic units as follows:

$$\begin{bmatrix} 1+\beta & \beta\cos(\theta+\phi) \\ \cos(\theta+\phi) & 1 \end{bmatrix}\begin{bmatrix} \ddot{\theta} \\ \ddot{\phi} \end{bmatrix} + \begin{bmatrix} -\beta\sin(\theta+\phi)\,\dot{\phi}^2 - (1+\beta)\sin\theta \\ -\sin(\theta+\phi)\,\dot{\theta}^2 + \sin\phi \end{bmatrix} = \begin{bmatrix} -k_1\theta \\ -k_2'\phi \end{bmatrix}, (1)$$

where $\beta = m/M$, $k_2' = k_2/\beta$ and k_1 and k_2 are the torque springs between the trunk and stance leg and between the trunk and swing leg, respectively. The step-to-step transition equation is expressed as follows (Fig. 1B):

$$\begin{bmatrix} \theta^+ \\ \dot{\theta}^+ \\ \phi^+ \\ \dot{\phi}^+ \end{bmatrix} + \begin{bmatrix} -\theta^- \\ \frac{\cos 2\theta^-}{B}\dot{\theta}^- \\ -\theta^- \\ -\frac{\cos^2 2\theta^-}{B}\dot{\theta}^- \end{bmatrix} + \begin{bmatrix} 0 \\ \frac{\sin 2\theta^-}{B} \\ 0 \\ -\frac{\sin 4\theta^-}{B} \end{bmatrix} I_{\mathrm{push}}, (2)$$

where $*^-$ and $*^+$ represent the pre- and post-collision states $*$, respectively, I_{push} represents the impulse generated by push-off, and $B = 1 + \beta\sin^2 2\theta^-$. The spring constant of the entire system is $k = k_1 = k_2'$, and the push-off impulse I_{push} was assumed to fully compensate for the energy loss due to the collision (i.e., $\dot{\theta}^- = \dot{\theta}^+$). Therefore, the periodic solution for increasing spring constant k is obtained by the Newton-Raphson method. Note that $\beta = 0.237$ was set with reference to the human body measurement data [2].

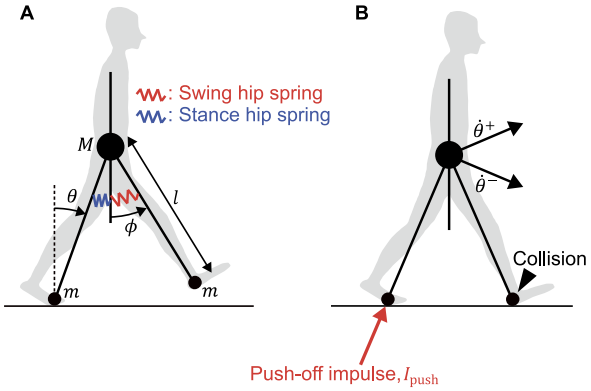

Figure 1 Simple walking model. (**A**) While the swing leg is lifted off the ground, the stance leg and the swing leg are adjusted by the torque springs. (**B**) The moment the swing leg collides with the ground, a push-off impulse is applied.

RESULTS AND DISCUSSION

We obtained a spring constant $k \approx 1.19$ corresponding to one initial condition $[\theta_0 \;\; \dot{\theta}_0] = [-0.4 \;\; 0.4]$. In the future, we aim to elucidate the mechanism of gait instability by calculating the periodic solution and the corresponding push-off impulse I_{push} when the spring constant k is changed.

CONCLUSIONS

We introduced a simple walking model that explains the reduction in propulsive force and its compensation. More detailed analysis to elucidate the mechanism of gait destabilization will be conducted in the future studies.

ACKNOWLEDGEMENTS

This work was supported by a Grant-in-Aid for Japan Society for the Promotion of Science fellows (grant number 21J10122).

REFERENCES

[1] Franz J R. *Exerc Sport Sci Rev* **44**: 129-136, 2016.
[2] Winter D A. *John Wiley & Sons*, 2009

Relationship between bicycle control and gaze behavior during a narrow-path ride

Takashi Kojima[1], Shunnosuke Anan[1], Katsuki Cho[1], and Masahiro Kokubu[2]
[1] Graduate School of Comprehensive Human Sciences, University of Tsukuba, Japan.
[2] Institute of Health and Sport Sciences, University of Tsukuba, Japan.
Email: takashi.kojima0120@gmail.com

INTRODUCTION

In recent years, bicycle use has been promoted because of its environmental and health benefits. In this context, knowledge that contributes to a stable ride is required. Based on comparisons between competitive cyclists and nonathletes[1], previous studies have demonstrated that small steering and leaning of bikes are important during a straight ride. Also, research has demonstrated that vision is important in bicycling and that competitive cyclists who practice more on road have a visual advantage in maintaining balance[2]. However, these were mostly cross-sectional studies, and longitudinal studies examining intraindividual changes are lacking. Therefore, this study aimed to examine the changes in movement and gaze behavior following two days of riding on straight and narrow paths.

METHODS

Nineteen university students with no previous competitive cycling experience wore an eye-tracking device and helmet and were asked to ride a bicycle motocross (BMX) bicycle on a board 12 cm in width and 30 m in length. The participants returned to the board and rode to the goal even if they deviated from the board. Motion sensors were attached to the helmets, shoulders, bicycle stems, and bicycle forks. Three trials were performed in the pre-test, and two sets of ten trials were performed in practice for two days. Within one week of practice, three trials were performed for the retention test. The following parameters were measured: the percentage of deviation from the lane (deviation rate); bicycle speed; head pitch angle (head pitch); eye position (eye); combined gaze angle (gaze); and optokinetic nystagmus (OKN) parameters (frequency, amplitude, duration, and speed) (Figure 1.a); stem yaw angle (stem); fork roll angle (folk), shoulder roll angle (lean); head roll angle (head roll) (Figure 1.b). The deviation rates obtained through the pre- and retention tests were compared using Wilcoxon's signed-rank test, with each parameter using a paired t-test. Multiple regression analysis was performed with the deviation rate as the objective variable and other parameters as the explanatory variables in the pre- and retention tests.

RESULTS AND DISCUSSION

The results of Wilcoxon's signed-rank sum test indicated that the deviation rate obtained through the retention test (median: 4.73%, IQR: 9.25%) was lower than that obtained through the pre-test (median: 10.97%, IQR: 7.58%). Paired t-tests indicated that the head pitch range, stem variability, range, root mean square (RMS) of velocity, fork variability, and range obtained via the retention test were smaller than those obtained via the pre-test. These results suggest that head stability, small steering, and bike leaning are important for ensuring cycling balance.

The results of the multiple regression analysis of the pre- and retention tests are summarized in Table 1. In the pre-test, three variables (i.e., stem variability, OKN frequency, and amplitude) were included in the regression equation, while in the retention test, seven variables (i.e., head roll range, head pitch range, quartiles, median, fork range, variability, and OKN frequency) were selected. These results suggest that small steering is important in the pre-test, whereas head stability and fine bike leaning are important in the retention test and that high-frequency OKNs is critical for maintaining the stability of the visual field, regardless of skill.

CONCLUSIONS

Through the two days of cycling on straight and narrow paths, the control strategy shifted from operating the steering wheel to stabilizing the head and leaning the bike. These results suggest that high-frequency OKNs, which maintain visual field stability, contribute to bicycle control.

REFERENCES

[1] Chain M et al. *PLoS ONE* **11**(2): 2016.
[2] Lion A et al. *Journal of Electromyography and Kinesiology* **19**: 623–630, 2009.

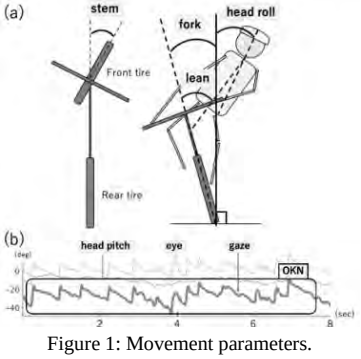

Figure 1: Movement parameters.

(a)eye and head (b)head and bicycle (BMX)

Table 1: Results of the multiple regression analysis of pre- and retention tests.

	Independent Variable	Dependent Variable	Adjusted R^2	DF	F	p	β	t	p	VIF
pre-test	deviation rate	stem (variable)					0.70	5.24	<.001	1.2
		OKN frequency	0.48	3,33	11.91	<.001	-0.45	-3.63	<.001	1.0
		OKN amplitude					-0.35	-2.68	.011	1.2
retention test	deviation rate	head roll (range)					0.18	2.45	.022	1.9
		OKN frequency					-0.21	-3.32	.003	1.3
		head pitch (range)					0.20	2.75	.011	1.9
		head pitch (median)	0.91	7,25	45.85	<.001	0.49	7.38	<.001	1.5
		fork (range)					1.18	7.17	<.001	9.4
		fork (variable)					-0.65	-4.38	<.001	7.7
		head pitch (IQR)					0.25	3.27	.003	2.0

EFFECT OF AIR RESISTANCE ON BRAKING AND PROPULSIVE IMPULSES DURING TREADMILL RUNNING

Jared Steele and Iain Hunter
Exercise Sciences, Brigham Young University, Provo, United States.
Email: Steelejared33@gmail.com

INTRODUCTION

Outdoor running can be perturbed from the slightest change in aerodynamic forces experienced by the body. These forces modify metabolic demand and change the ground reaction force profiles. Wind resistance acts as a resistive force that alters the anterior-posterior forces applied by the runner [1]. As headwind speeds increase, relative to running speed, aerodynamic drag is concomitantly increased. The increase in drag increases the metabolic demand of muscles working to maintain forward momentum and the necessary propulsive forces.

To date, studies investigating the relationship between running mechanics and wind resistance have either solely focused on the physiological changes [2] or used constructed apparatuses [3] to mimic wind resistance in lieu of generating wind. Therefore, the aim of this study was to examine the effect of generated air resistance on GRF profiles. Our secondary aim was to investigate if similar relative air resistances had different effects across running speeds.

METHODS

Twenty-four male subjects (age: 22.0 ± 6.4 years, mass: 65.3 ± 4.9 kg, height: 69 ± 2.1 inches) participated. Subjects ran continuously for five minutes at fast or slow treadmill speeds (4.46 and 3.35 m/s) before an additional 5-minutes at the other treadmill speed. During the five-minute bouts of running, four air resistance conditions, relative to treadmill speed, were applied: 1) Headwind (HW; +0.6m), 2) Tailwind (TW; -0.6 m/s), 3) No wind (NW; 0m/s), 4) No fan (NF; fan off).

A linear regression was used for each treadmill speed correlating horizontal impulse, braking impulse, propulsive impulse, stride rate, and ground time with fan velocity. These variables were measured during the final 30 seconds of each running speed.

RESULTS AND DISCUSSION

As air resistance was increased during fast treadmill running, there was an increase in horizontal impulse ($F=8.847$, $p<.001$, $R^2=0.097$) (Table 1).

Neither propulsive nor braking impulses were significantly different at the fast treadmill speed. It should be mentioned that propulsion during fast treadmill running was trending toward significance ($p=0.08$). Runners choose various approaches in overcoming air resistance in terms of how much braking and propulsion they generate. This is demonstrated by horizontal impulse showing significance, while propulsive and braking impulses did not.

During slow treadmill running, horizontal impulse demonstrated no significant difference across air resistance conditions. Matching with the squared velocity in a drag force equation, the faster the running, the more influential air resistance is upon application of horizontal force.

While horizontal impulse can be increased via an increase in propulsive forces or a decrease in braking forces, the trend of runners in this study opted to increase propulsion.

Ground time and stride rate were also analyzed with no significant differences during fast or slow treadmill conditions across all air resistance conditions.

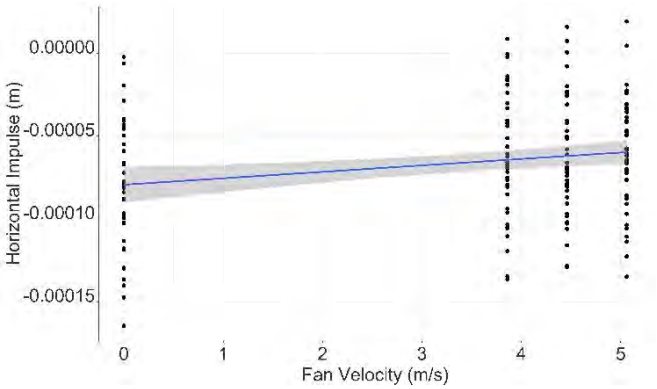

Figure 1 Linear regression of horizontal impulses during fast treadmill speed (4.46 m/s) in NF, TW, NW and HW conditions.

CONCLUSIONS

Horizontal impulse is significantly increased during faster treadmill running in the presence of air resistance. Running on a treadmill with no air resistance leads to differences in running mechanics compared with overground running. Future work will investigate other wind conditions (direction, velocities, and drafting) and its impact on running mechanics and metabolic factors.

REFERENCES

1. Chang, Y.H & Kram, R. *J. Appl. Physiol.* **86:** 1657-1662, 1999.
2. Pugh, L. G. E. *Physiol. J.* **213**: 255-276, 1971.
3. Da Silva et al. *J. Appl. Physiol.* **133:** 766-776, 2022

INFLUENCE OF NEGLECTING FREE MOMENT AND TRANSVERSE GROUND REACTION FORCES IN THE DETECTION OF THE INSTABILITY OF GAIT

Helene Pillet[1], Xavier Bonnet[1] and Bruno Watier[2,3]
[1] IBHGC, Arts et Metiers Institute of Technology, Paris, France
[2] LAAS-CNRS, CNRS, UPS, Université de Toulouse, France.
[3] CNRS-AIST JRL (Joint Robotics Laboratory), IRL, Tsukuba, Japan.
Email: helene.pillet@ensam.eu

INTRODUCTION

Monitoring the instability of gait is of great interest to detect and prevent falling risks. State of the art parameters such as the MMA-BCOM index, already evaluated in at risk population [1], basically requires the six components of ground reaction forces and moments or equivalently the position of the center of pressure and four components (i.e. the three components of the force and the vertical free moment). Unfortunatly, it is currently not possible to accuratly estimate the free moment from embedded sensors as well as the antero-posterior and mediolateral component of the force.
The aim of the study was to compare the estimation of the MMA-BCOM index when neglecting the free moment and/or the transverse components of the ground reaction forces with the estimation of the same index including all the components of the ground reaction forces and moments.

METHODS

Two groups of subjects (four with transfemoral amputation (TF) and eight non-amputee (NA)) performed a quantified gait analysis combining full body kinematics capture (200 Hz) with synchronised ground reaction forces and moments recording (1000 Hz). Three force plates were used to measure all the components during at least one entire gait cycle. Position of the center of mass was computed from a geometrical inertial model [2] and forces and moments components were filtered at 10 Hz prior to the computation of the MMA-COM index. This index is the distance between the Minimal Moment Axis and the Center Of Mass of the body and is obtained at each instant of time using:

$$\text{MMA} - \text{COM index} = \frac{\|\boldsymbol{F} \times \boldsymbol{M_{BCOM}}\|}{\|\boldsymbol{F}\|^2}$$

where $\boldsymbol{F} \times \boldsymbol{M_{BCoM}}$ is the cross product between the external forces and the external moment computed at the BCoM, $\boldsymbol{M_{BCoM}}$ [1]. The amplitude of the index was then retrieved and averaged over the gait cycle. Values were compared for the two groups and the three conditions: C1/ complete ground reaction forces and moments; C2/ neglecting the vertical free moment at the center of pressure; C3/ neglecting the free moment and the transverse components of the force.

RESULTS AND DISCUSSION

Average patterns of the MMA-BCOM index for both studied populations show that condition C3 differs from the reference condition C1 contrary to condition C2 which gives very close evolution compared to the reference.

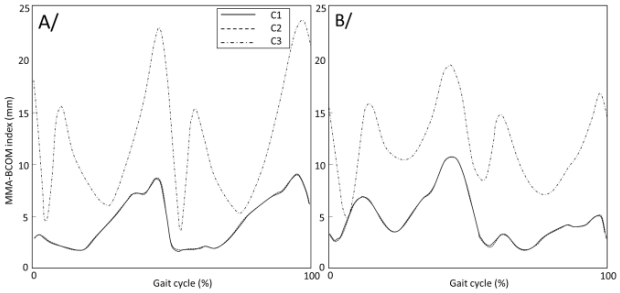

Figure 1 Average patterns of MMA-COM index for A/ NA group, B/ TF group and three conditions

The difference of amplitude of the index between condition C2 and condition C1 is 2 mm (+/-1.2 mm) on average for all the subjects. On the contrary this difference reaches 171 mm (+/-17 mm) between condition C3 and condition C1. In comparison, the difference of amplitude of the index is of in average 36 mm between NA and TF groups. Thus, contrary to condition C1 and C2, condition C3 is not accurate enough to differentiate the groups.

CONCLUSIONS

The results of this study show that the vertical free moment at the center of pressure can be neglected without hindering the capacity of the MMA-BCOM to discriminate the two populations. This conclusion makes realistic the quantification of the parameter by combining transverse forces estimated from inertial measurement units and location of the center of pressure estimated from pressure insoles.

ACKNOWLEDGEMENTS

Research supported by the Fondation de l'Avenir (grant number AP-RM-20-001) and ANR BAC2WALK (grant number 22-CE19-0003-01).

REFERENCES

[1] Al Abiad et al. *Appl. Sci.* **10**, 840, 2020.
[2] Pillet et al. *Gait and Posture* **31**: 147-152, 2010.

COMPARISON OF TWO HYPOMIMIA INDICATORS IN PARKINSON'S DISEASE

Elena Pegolo[1], Gloria Boldrini[1], Lucia Ricciardi[2] and Zimi Sawacha[1,3]
[1] Department of Information Engineering, University of Padova, Padova, Italy
[2] Molecular and Clinical Sciences Research Institute, St. George's University, London, UK
[3] Department of Medicine, University of Padova, Padova, Italy
Email: elena.pegolo@phd.unipd.it

INTRODUCTION

Parkinson's Disease (PD) is the second most prevalent neurodegenerative disorder affecting mostly the motor system. Among other symptoms, hypomimia is considered one of the clinical hallmarks of the disease. This feature causes impairment in face mobility leading to a reduction in patients' quality of life [1]. Even though face expression is one of the most important ways of communication, and this has been widely investigated. No objective measures of hypomimia are currently available. In order to describe face movements in relation to emotions, Ekman and Friesen developed the Facial Action Coding System (FACS) [2]. It encodes facial expressions by means of Action Units (AU) which are described by either single or group of muscles. One of the most used software that embeds AU detection is OpenFace [3].

In this regard, recently, the authors have developed a face mobility index (FMI) [4] with the aim to provide a quantitative measure of the symptom through an easy-to-interpret and intra-subject metric of face mobility applicable to PD.

The aim of this study is to compare the developed FMI against a measure of mobility based on AU with OF (AU_tot) on a cohort of PD and healthy control (HC) subjects. The FMI approach captures face mobility from a physiological point of view since landmarks are detected by muscle insertion points. Whereas AU_tot addresses emotion production from a cognitive point of view, being driven by AU detection. These different approaches could be crucial in understanding PD hypomimia etiology.

METHODS

17 HC (age = 65.8 ± 8.3 years) and 29 PD subjects (age = 68.5 ± 7.8 years) were enrolled in the study. Participants' videos of the basic emotions and the neutral expression were acquired. Frames corresponding to the peak of expressions were extracted and two indexes of face mobility were computed per emotion as follows:

1) FMI: a set of anatomical landmarks determined as the points of insertion of facial muscles was tracked; from these coordinates, 40 distances were calculated. FMI was determined as in [4] normalizing the obtained measures to the neutral expression and computing an overall measure of face mobility.
2) AU_tot: intensities of AUs were extracted through OF. OF is capable of detecting a set of 17 AUs and providing a scale of intensity per each AU from 0 to 5. AU_tot was computed as the summation of all the AUs intensities as a measure of AU-driven face mobility.

Comparison between the two indexes was performed by mean of Pearson correlation at $p<0.05$ significance level.

RESULTS AND DISCUSSION

Table 1 reports the results of the correlation between the two indexes (FMI and AU_tot). Significant correlations were found in the happiness emotion in HC and in the surprise one in PD. Only weak correlations were detected. Furthermore, as expected, values of ρ were lower in the PD population. Results of this study seem to indicate that the two indexes are capturing different facets of face expression. While FMI can be seen as an objective measure of face mobility, AU_tot is related to the cognitive aspects of emotion production.

Table 1: Correlation between the two indexes (FMI and AU_tot) per emotion in the two cohorts. Values in bold obtained a p-value <0.05.

ρ (FMI, AU_tot)	HC	PD
Anger	0.41	0.05
Disgust	0.38	0.19
Fear	0.21	0.19
Happiness	**0.62**	<0.01
Sadness	0.19	0.15
Surprise	0.37	**0.52**

CONCLUSIONS

In conclusion, the two approaches can be considered complementary since they depict different aspects of facial expression. Future developments are needed to validate these methodologies with surface electromyography.

REFERENCES

[1] Ricciardi et al., PLoS One, **12(1)**:e0169110, 2017
[2] Ekman et al., Consulting Psychologists Press, 1978
[3] Amos et al., CMU, **6(2)**: 20, 2016
[4] Pegolo et al., Sensors, **22(4)**: 1358, 2022

UNIQUE MASS DISTRIBUTION IN THE LOWER LIMBS OF DISTANCE RUNNERS AND ITS EFFECT ON MOMENT OF INERTIA .

Takeshi Edagawa [1], Toshihide Fujimori [1], Shogo Hashimoto [1],
Yoshikazu Okamoto [3], Takahito Nakajima [3] and Natsuki Sado [2]
[1] Graduate School of Health and Sport Sciences, University of Tsukuba, Tsukuba Japan.
[2] Faculty of Health and Sport Sciences, University of Tsukuba, Japan.
[3] Faculty of Medicine, University of Tsukuba, Japan.
Email: s2221436@s.tsukuba.ac.jp

INTRODUCTION

Morphological characteristics and distance running are theoretically well-related; a smaller lower limb moment of inertia around the hip ($I_{LowerLimb}$) can reduce the energy required to swing the lower limb, thereby improving running economy. Human morphology adapts to daily motor tasks, leading to the speculation that distance runners have smaller $I_{LowerLimb}$ than non-runners by smaller fat mass. Meanwhile, the individual variability in morphology is inhomogeneous, being greater in the proximal part [1]. Thus, the fat mass reduction might be limited at the distal part. The moment of inertia is proportional to the square of the radius of gyration ($I = mr^2$), and the relationship between $I_{LowerLimb}$ and lower-limb mass in distance runners may differ from that in normal individuals due to mass distribution. However, the inertial characteristics of long distance runners have not been fully examined.

We investigated the inertial characteristics of distance runners. We hypothesised that the relationship between $I_{LowerLimb}$ and body mass in distance runners differ from that in normal individuals.

METHODS

We analysed fat- and water-weighted MRI of the lower limbs of 20 distance runners and 18 untrained height-matched non-runners (age: 20 ± 1 years and 24 ± 3 years, height: 169.9 ± 5.6 cm and169.7 ± 4.0 m; body mass: 56.20 ± 4.12 kg and 68.93 ± 9.13 kg). We calculated the inertial properties by identifying the tissue (fat, lean or bone) of each voxel and combining the literature values for each tissue density [1]. We used the independent *t*-test and the analysis of covariance (ANCOVA) to compare the distance runners and non-runners.

RESULTS AND DISCUSSION

$I_{LowerLimb}$ was significantly smaller in runners (1.81 ± 0.29 kg.m^2) than in non-runners (2.08 ± 0.30 kg.m^2); however, the slope of the regression line of the relationship between $I_{LowerLimb}$ and lower-limb mass was significantly steeper in runners than in non-runners (Fig. 1). This suggests that the $I_{LowerLimb}$ is more sensitive to lower-limb mass in runners than in non-runners. The centre of mass (CoM) of the lower-limb was significantly more distal in runners than in non-runners (38.1 ± 0.8 vs. 36.8 ± 1.1%Lower limb length). Based on the mechanical relationship of $I = mr^2$, the difference in the slope resulted from the location of the lower-limb CoM.

All tissue masses of the whole lower limb were significantly lower in runners than in non-runners, with the effect size being largest for fat (d = 1.23). This suggests that the difference in lower-limb mass is mainly due to that in fat mass. Fat mass was lower in runners than in non-runners in all segments of the thigh, shank and foot, with the effect size being largest for the thigh (d = 1.07), implying that the difference in fat mass between runners and non-runners is greater proximally than distally. Taken together, we suggest that the fat distribution in runners, with the proximal-specific fat smallness, results in a more distal lower-limb CoM and a longer radius of gyration in runners than in non-runners.

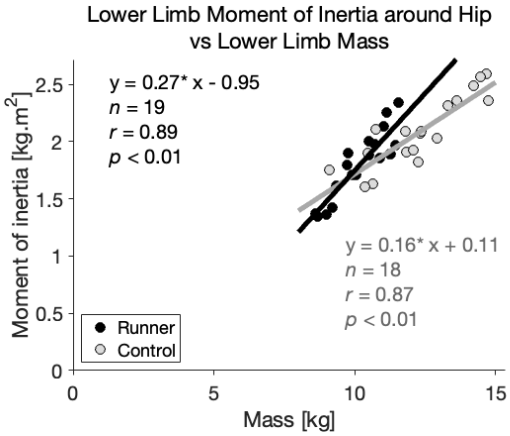

Figure 1 Relationship between lower-limb mass and moment of inertia around the hip.

CONCLUSIONS

We found that $I_{LowerLimb}$ was more sensitive to lower limb mass in runners than in non-runners. This difference was due to a difference in the mass distribution and location of the lower-limb CoM in runners, mainly attributed to a lower fat distribution in the proximal region.

REFERENCES

[1] Sado N et al. *Med Sci Sports Exerc* **55** (3): 590-600, 2023.

Mechanical interaction between Achilles tendon and plantar fascia during isometric ankle plantar flexion

Hiroto Shiotani[1], Katsuki Takahashi[2], Kazuki Tomari[2], Natsuki Sado[3] and Yasuo Kawakami[1]
[1] Faculty of Sport Sciences, Waseda University, Tokorozawa, Japan.
[2] Graduate School of Sport Sciences, Waseda University, Tokorozawa, Japan.
[3] Faculty of Health and Sport Sciences, University of Tsukuba, Tsukuba, Japan.
Email: h-shiotani@aoni.waseda.jp

INTRODUCTION

The Achilles tendon (AT) and plantar fascia (PF) are anatomically linked via the calcaneus in humans [1]. This indicates that the PF can serve as a pathway for transmitting passive tension of the AT to the forefoot. In an active state, AT compliance has been shown to modulate the operating length of the triceps surae muscle, thereby affecting its force-producing capacity [2]. Recently, we found that the AT and PF exhibit a balanced mechanical interaction upon passive ankle–foot dorsiflexion that modulates the passive range of motion of the human ankle-foot complex [3]. However, it remains unknown if the PF behaves as a simple in-series spring with the AT during muscle contraction, and its compliance influences preceding muscle–tendon behavior. Addressing this question will provide novel *in vivo* evidence for the muscle–tendon–fascia interaction that utilizes human-specific anatomical features in the ankle-foot complex. The purpose of this study was to investigate the interaction between the AT and PF during triceps surae muscle contraction and its impact on the force-producing capacity.

METHODS

Twenty-one healthy adults (12 males and 9 females, 23.0 ± 2.9 years) participated. Participants were reclined on the bed of a 3T magnetic resonance (MR) scanner (GE Healthcare, USA) with their dominant foot secured to a custom-made fixture (VINE, Japan) at the neutral position. Participants were requested to perform ramp isometric ankle plantar flexion (approx. 8 s to voluntary maximum, 5 s hold, 8 s to full relaxation; Figure 1A). During ramp contraction, oblique sagittal dynamic MR images were obtained with a 3D, fast gradient-recalled acquisition in the steady state sequence (TE: 3.0 ms, TR: 6.5 ms, FOV: 280 × 280 mm, matrix: 256 × 128, time resolution: 0.40 s [2.50 Hz], total phases: 70). A custom-built optical strain gauge (Shinko electric wire, Japan) was attached to the footplate of the fixture to obtain the strain data of footplate at a sampling rate of 100 Hz. The ankle plantar flexion torque was calculated by the strain and lever arm of the footplate.

At the time of submission, the length changes (ΔL) in AT and PF during ramp contraction have been measured with OsiriX MD software (Pixmeo, Switzerland) based on our previous study [3]. The onset of contraction was determined as the frame just before the beginning of action from the resting state. Due to the ongoing nature of this work, no statistical tests have been performed.

RESULTS AND DISCUSSION

Upon increasing and decreasing ankle plantar flexion torque during ramp contraction, the AT and PF were lengthened and shortened with their maximal elongation reaching up to 4.4 ± 2.5 mm and 3.0 ± 1.5 mm, respectively. The data confirm that the magnitude of AT and PF elongation is decoupled (Figure 1B) while showing individual variability. The results indicate that the PF is not a simple in-series spring with the AT.

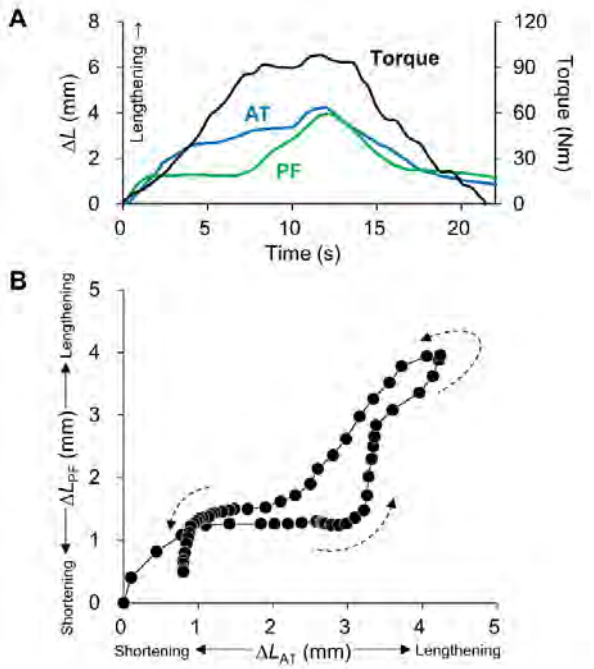

Figure 1 Exemplar of ΔL in AT and PF and joint torque (A), and relationship between ΔL in AT and PF for one participant (B).

CONCLUSIONS

Preliminary data provide novel evidence for the mechanical interaction between the AT and PF during fixed-end contraction of the triceps surae muscle in humans *in vivo*. Further data analyses will provide to examine its impact on the muscle operating length and force-producing capacity.

REFERENCES

[1] Stecco C et al. *J Anat* **223**: 665-676, 2013.
[2] Lichtwark G et al. *J Exp Biol* **109**: 4379-4388, 2006.
[3] Shiotani H et al. *Med Sci Sports Exerc* **55**: 66-73, 2023.
[4] Iwanuma S et al. *J Biomech* **44**: 2579-2583, 2011.

MARKERLESS SAGITTAL PLANE KINEMATIC ANALYSIS OF SPRINT RUNNING: COMPARISON BETWEEN A DEEP LEARNING ANALYSIS AND MANUAL DIGITIZATION

Hiroaki Noro[1], Shota Akahoshi[2], Keiichiro Hata[2,3], Yohei Yamazaki[2,3], Misato Ishikawa[2], Shuta Matsui[2], Lee Rou You[2], Kazuhiko Yamazaki[2], Toshio Yanagiya[1,2,3]

[1] Faculty of Health and Sports Science, Juntendo University, Chiba, Japan.
[2] Graduate school of Health and Sports Science, Juntendo University, Chiba, Japan.
[3]Institute of Health and Sports Science & Medicine, Juntendo University, Chiba, Japan
E-mail: hiroakinoro@gmail.com

INTRODUCTION

In sprint running, kinematic analysis is valuable in research and the sports biomechanics field. In recent years, markerless motion capture tools have been used to measure kinematic data because of several practical benefits. Most previous studies tested the markerless motion capture in indoor laboratory settings [1,2,3] and sprint competitions often held outdoors. Therefore, the test of the accuracy of the markerless motion capture system in the outdoor condition is needed to evaluate the motion of sprinters. Besides, DeepLabCut (DLC) is a markerless motion capture tool that utilizes deep learning. Therefore, this study aimed to examine the agreement of joint angles using markerless motion capture tools with manual digitization.

METHODS

To make trained data set in DLC, 159 sagittal plane view videos were used in which subjects performed 100-m or 400-m sprint running. In the DLC analysis, 18-20 pictures were selected automatically in each video. Then the shoulder, knee, ankle, and tip of the shoe were digitized manually on the DLC platform. In manual digitization analysis, a person who had experienced over a year digitized the same point. After that, six videos (these videos did not include the trained data set) were automatically digitized by the DLC with the trained data set.

The coordination data was smoothed in each analysis by a fourth-order Butterworth lowpass filter at 15 Hz, referencing Van Hooren et al. (2023) [4]. The hip, knee, and ankle joint angles were calculated, and the difference between DLC and manual digitization method was observed using one-dimensional statistical parametric mapping. All of the analysis was conducted using Python 3.8.

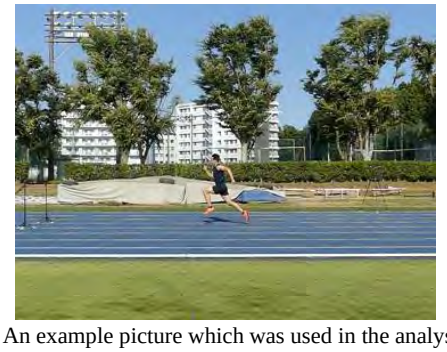

Fig1. An example picture which was used in the analysis.

RESULTS

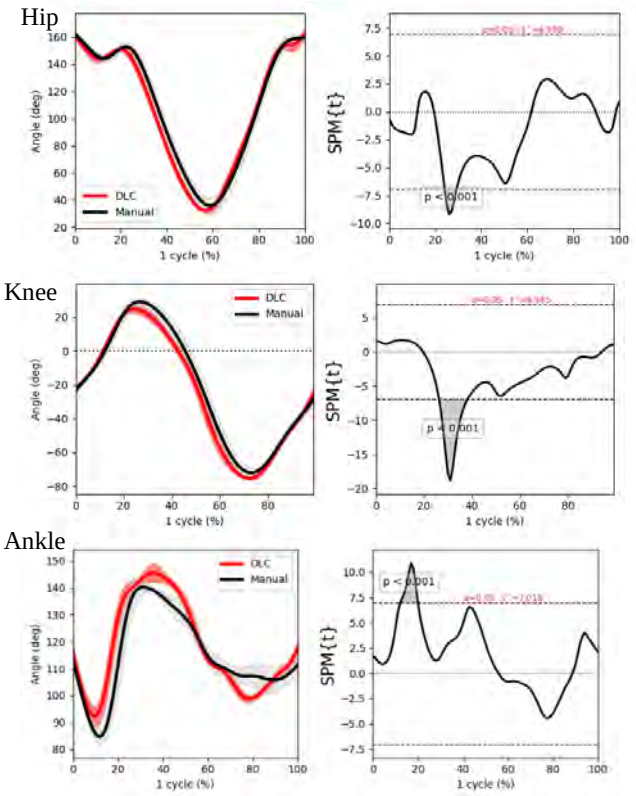

Fig2. Comparison between DeepLabCut (DLC) and Manual digitalization with statistical parametric mapping (paired t-test, $p < 0.05$).

The analysis was conducted in each hip, knee, and ankle joint angle, and significant differences were observed in the early stance phase (hip: 28%-39%, knee: 25%-29%, ankle: 13%-19%).

CONCLUSIONS

In outdoor sprint running, although Joint angles in the lower extremity in the DeepLabCut and manual digitization showed similar trends, a few differences were observed.

REFERENCES

[1] Cronin et al., Journal of Biomechanics, 2019
[2] Drazan et al., Journal of Biomechanics, 2021
[3] Johnson et al., Journal of Applied Biomechanics, 2022
[4] Van Hooren et al. *Scand J Med Sci Sports*, 20

Extreme elongation of triceps surae muscle-tendon unit was attributable to the elongation of the muscle rather than that of the tendon in rat

Satoru Hashizume[1], Atsuki Fukutani[1], Tadao Isaka[1] and Masaaki Mochimaru[2,3]

[1] Ritsumeikan University / Faculty of Sport and Health Sciences, Kusatsu shi, Japan.

[2] Ritsumeikan University / The Research Organization of Science and Technology, Kusatsu shi, Japan.

[3] National Institute of AIST / Human augmentation research center, Kashiwa shi, Japan.

Email: s-hashi@fc.ritsumei.ac.jp

INTRODUCTION

The stretch-shortening cycle (SSC) is known as the dynamic movement using muscle-tendon interactions. The SSC is the phenomenon in which the force exerted by the concentric contraction following the preceding eccentric contraction is enhancedcompared with the force exerted by the solely performed concentric contraction. Generally, tendon elongation is considered the primary mechanism of this force enhancement [1]. On the other hand, the recent study [2] reported that the magnitude of the SSC effect was not different between with and without the tendon. The fundamental reasons for this inconsistency across previous studies are thought to be attributable to the methods of data collections as follows; 1) direct or indirect determinations of the elongation of tissues, 2) number of muscles contracted during the SSC, 3) magnitude of the elongation of the muscle-tendon unit (MTU) during the preceding eccentric contraction. To resolve these discrepancies, this study aimed to determine the elongations of the rat triceps surae muscle and the Achilles tendon directly during extreme elongation of the MTU.

METHODS

Three male Sprague-Dawley rats were used in this study. The triceps surae MTU was surgically exposed, and then the surrounding tissues were carefully removed. The blood and nerve supplies were kept as intact. The distal end of the Achilles tendon was cut with a remnant piece of the calcaneus. The Achilles tendon with calcaneus was rigidly attached to a force transducer with a motor (Figure 1-A). The isometric tetanic contraction of the triceps surae muscle was evoked by electrical stimulation of the tibial nerve at the optimal length, and the triceps surae MTU was then elongated until the MTU was ruptured. During the above trial, the triceps surae MTU was imaged by using the high-spatial resolution camera. The pixel resolution of this system was approximately 0.015 mm.

RESULTS AND DISCUSSION

The ultimate elongation of the triceps surae MTU was 10.5 ± 0.4 mm. The elongations of the triceps surae muscle and the Achilles tendon were determined for each 10% of the ultimate elongation of the MTU (Figure 1-B). The elongation of the triceps surae muscle gradually increased from 0% to 90%, but not from 90% (8.4 ± 0.3 mm) to 100% (8.3 ± 0.4 mm). The elongation of the Achilles tendon slightly increased from 0% to 90%, whereas the corresponding elongation markedly increased 1.5 times from 90% (1.4 ± 0.1 mm) to 100% (2.2 ± 0.2 mm).

The current results revealed that the magnitude of elongation was markedly greater for the triceps surae muscle than for the Achilles tendon at each percentage of the ultimate elongation of the MTU. Further, the elongation of the Achilles tendon was seemed to be small despite the experimental conditions (the magnitude of stretch and the magnitude of force) of this study was far beyond the physiological range. These indicate that while the tendon elongation may contribute to the force enhancement during the SSC to some extent, this effect may not be the primary contributor.

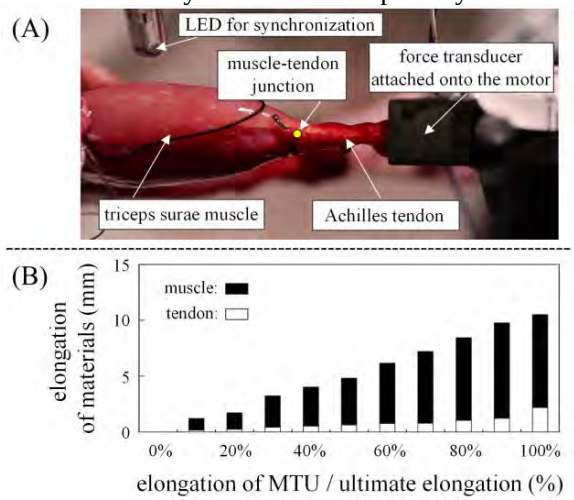

Figure 1 Experimental setting (A), the elongations of the triceps surae muscle and the Achilles tendon during the elongation of the corresponding MTU with tetanic contraction (B).

CONCLUSIONS

In conclusion, this study determine the elongations of triceps surae muscle and the Achilles tendon directly during extreme elongation of the correspoding MTU. As the results, the magnitude of elongation was markedly greater for the triceps surae muscle than for the Achilles tendon.

REFERENCES

[1] Kubo K et al. *J Appl Physiol* **87**: 2090-2096, 1999.

[2] Fukutani A et al. *J Exp Biol* **222**: jeb204032, 2019

Switch point of impact height of adjusting segments to reach ball heights during a two-handed backhand stroke at various impact heights

Sichao Zhang[1], Natsuki Sado[2], and Norihisa Fujii[2]
[1] Graduate School of Comprehensive Human Sciences, University of Tsukuba, Tsukuba, Japan.
[2] Faculty of Health and Sport Sciences, University of Tsukuba, Tsukuba, Japan.
Email: s2030468@s.tsukuba.ac.jp

INTRODUCTION

The two-handed backhand stroke has been most widely adopted by professional and amateur players but is less researched than the forehand strokes [1]. During a baseline rally, players have to hit the ball at various heights. A number of different patterns exist for reaching the ball height, such as adjustment of the lower/upper limb or trunk segment alone or in their combinations. However, it is unclear what solution that skilled tennis players use to adjust the lower and upper limbs and trunk to reach the various ball heights. Thus, we aimed to investigate the adjustment of segmental height according to the impact heights in highly skilled tennis players during a two-handed backhand stroke.

METHODS

Fifteen male university tennis players (right-handed) hit the incoming ball at various impact heights (72 ± 6 in total) to a 3 × 2 m target area cross-court with a two-handed backhand stroke behind the baseline. The impact height was presented in the ratio % of participant height. Segmental components that made up the racket height (segmental heights) were defined as the difference between the proximate joint and distal joint centers for the trunk and lower limbs, and as the difference between the distal joint and proximate joint centers for the racket and upper limbs (Figure 1). We used the piecewise linear regression method to determine the switch point of impact height at maximum R^2 for each segment.

RESULTS AND DISCUSSION

The switch point of impact height was found in right foot, right thigh, left shank, trunk, upper limbs from the distribution of segmental heights against impact height (Figure 1). The switch points of impact height [range of mean of each segment; 52.1−57.1%)] were around the ratio of leg length of the participants (50.9 ± 1.3%). This result indicates that tennis players switch the adjustment of the segments around the height of the pelvis. When impact height was lower than pelvis, the players mainly adjusted right thigh, left shank and trunk, which may facilitate keeping racket face angle by a similar posture of upper limbs. When the impact height was higher than pelvis, the players mainly adjusted right foot and both upper limbs. Before or when the supporting leg reaches its limited height, the players obtained the height from the ankle plantar flexion. Producing greater racket speed requires trunk rotation velocity. During the late forward swing, the extension of the frontal leg contributes to rotating the pelvis [2]. These findings suggest that players obtain the height by ankle plantar flexion to maintain the knee and hip in flexion that may facilitate rotating trunk at higher heights. Redundant degrees of freedom provide many solutions of combinations to reach the same racket outcomes. However, players consistently adopted a set of limited solutions that change the adjustment around an impact height. Players with higher accuracy also adopted a consistent adjustment of the velocity and angle of the racket according to the impact heights [3]. The present results suggest that a consistent strategy according to the ball conditions may facilitate controlling the velocity and angle of the racket.

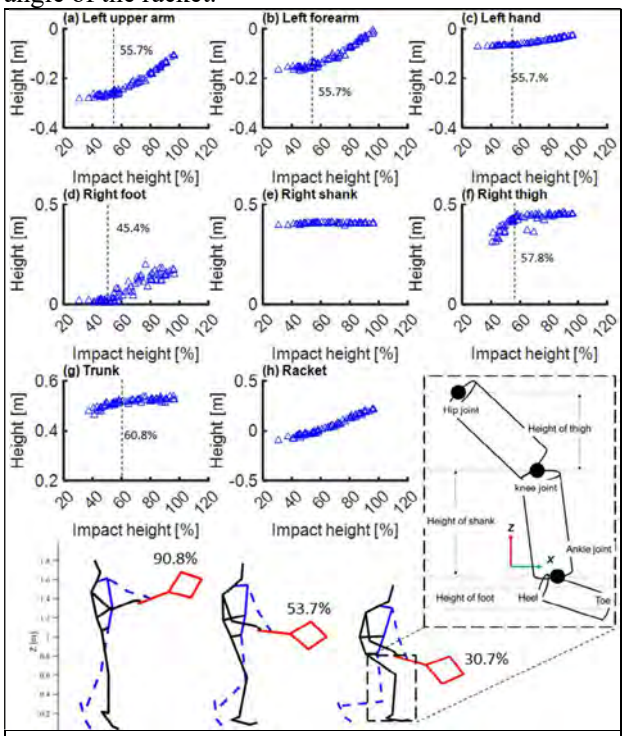

Figure 1 Relationships between impact heights and segmental heights. The switch point of this participant was 45.4−60.8%. Vertical dash lines represent the switch point for each segment.

CONCLUSIONS

Tennis players switch to using the upper and lower limbs to reach the impact heights around the pelvis. This suggests that beginners can refer to the pelvic height to determine the impact height. Below the pelvis, beginners can lower the body by the leg with same posture of upper limbs to hit the ball, while above the pelvis adjust upper limbs to obtain height.

REFERENCES

[1] Genevois et al. *J. Sports Sci. Med* **14**: 194-202, 2015
[2] Akutagawa et al. *J. Sports Sci.* **23**: 781-793,2007
[3] Zhang et al. *Sports Biomech* ***(online)***: 1-14, 2022

Reliability of ultrasound-based muscle cross-sectional area in lower-limb: A comparative analysis between Ultrasound and MRI

Yoko Kunimasa[1], Robin Macchi[2], Baptiste Corcelle[3], Constance P. Michel[4], Marc-Adrien Hostin[4], David Bendahan[4], Caroline Nicol[5]

[1]Niigata University, Niigata, Japan, [2] SEP-EA7370, INSEP, Paris, France, [3] LAMHESS (UPR 6312), University Côte d'Azur, Nice, France, [4] Aix-Marseille University, CNRS, CRMBM-UMR 7339, Marseille, France, [5] Aix-Marseille University, CNRS, ISM-UMR 7287 , Marseille, France.
Email: yoko.k@ed.niigata-u.ac.jp

INTRODUCTION

Muscle cross-sectional area (CSA) is an important and suitable parameter for estimating muscle function (e.g., strength and power) [1]. Since CSA is used for training or health monitoring, its reproducibility and validity are crucial issues. CSA assessment using ultrasonography (US) is considered as a convenient method, which is not time-consuming, expensive and not limited by location or target population, such as sports fields or children. In addition, the extended-field-of-view (EFOV or panoramic imaging) technique is a convenient technique for producing large cross-sectional images of the whole muscle that cannot be obtained with a single conventional US image [2]. However, the capture of some muscles may be difficult due to their specific size and shape [3]. This holds for large or curved muscles. Therefore, the purpose of this study was to quantify the reproducibility and validity of US-based CSA measurements of different lower limb muscles as compared to the "gold standard" MRI.

METHODS

Twenty-four healthy participants (12 men: 26.3 yr, 176.8 cm, 69.6 kg; 12 women: 24.8 yr, 165.8 cm, 59.7 kg) volunteered for the present study. The CSA of nine muscles of the dominant lower-limb was measured at the same location using ultrasonography (US) (MACH 30, SuperSonic Imagine, France) and MRI (3-T Vida, Siemens, Germany). During all measurements, the ankle and knee joints were positioned at 15-20° plantar flexion and 175-180° extension respectively. US measurements were performed in prone position for the calf and hamstrings, and in the supine position for the quadriceps and tibialis anterior muscles; MR acquisitions were performed in the supine position. Daily reproducibility of US and MRI measurements (n=16) was assessed using the intraclass correlation coefficient ($ICC_{1,1}$). Pearson product moment correlation and Bland-Altman analysis were used to analyze the relative and absolute validity, respectively, between US and MRI. Data are presented as mean ± SD with significance set at $p<0.05$.

RESULTS AND DISCUSSION

Reproducibility of CSA measurements was similar for US (0.994-0.999) and MRI (0.978-0.998) measurements.

The bias, lower and upper limits of agreement (LoA) and r^2 values are gathered in Table 1. The US-based CSA measurements were significantly and positively correlated with the corresponding MRI values with r^2 ranging from 0.54 to 0.90. The weakest correlation was found for the semimembranosus and the strongest for the rectus femoris muscle suggesting that the relative validity of US-based CSA versus MR-based CSA cannot be accepted equally for all muscles.

Bland-Altman analysis illustrated that US-based CSA measurements were systematically smaller than the corresponding MRI values for the whole set of muscles except tibialis anterior, for which US-based values were larger. Furthermore, larger muscles had larger absolute differences between US and MRI assessments, but curved muscles (e.g., gastrocnemius medialis) had unexpectedly similar absolute and relative errors to less-curved muscles (e.g., rectus femoris).

Table 1: Bias, lower and upper limits of agreement (LoA), and r^2 values by correlation analysis between US and MRI CSA.

Muscle	Bias (cm^2)	Upper LoA (cm^2)	Lower LoA (cm^2)	r^2
Biceps femoris long head	-2.01	0.29	-4.31	0.87***
Semitendinous	-1.18	1.14	-3.50	0.80***
Semimembranosus	-1.30	1.85	-4.46	0.54***
Rectus femoris	-2.06	-0.04	-4.08	0.90***
Vastus lateralis	-5.49	-0.74	-10.24	0.83***
Vastus medialis	-5.55	-0.86	-10.25	0.87***
Gastrocnemius medialis	-2.14	0.29	-4.57	0.89***
Gastrocnemius lateralis	-1.81	-0.40	-3.22	0.89***
Tibialis anterior	1.63	3.05	0.20	0.78***

Negative numbers indicate US values lower than MRI. ***$p<0.001$

CONCLUSIONS

The present comparative analysis indicates that using the EFOV algorithm, which may increase the risk of errors due to overlapping of successive images, the absolute error may be affected more by muscle size than by muscle curvature.

REFERENCES

[1] Ikai & Fukunaga. *Int Z Angew Physiol* **26**: 26-32, 1968.

[2] Ahtiainen et al. *Eur J Appl Physiol* **108**: 273-279, 2010.

[3] Noorkoiv et al. *Eur J Appl Physiol* **109**: 631-639, 2010.

THE RELATIONSHIP BETWEEN REACTION TIME AND LANDING MECHANICS ASSOCIATED WITH ANTERIOR CRUCIATE LIGAMENT INJURY DURING SINGLE-LEG LANDING

Yan-Long Chen[1], Tsung-Yeh Chou[2], Thomas Kaminski[2], Yu-Lun Huang[1]
[1] Department of Physical Education and Sport Science, National Taiwan Normal University, Taipei City, Taiwan.
[2] Department of Kinesiology and Applied Physiology, University of Delaware, Newark, USA.
Email: 81030018a@ntnu.edu.tw

INTRODUCTION

Poor neurocognitive function, including slow reaction time (RT), has been suggested as a potential risk factor for noncontact anterior cruciate ligament (ACL) injury by impacting judgment accuracy or movement coordination [1]. Improper sagittal plane lower extremity biomechanics, such as landing with greater kinetics while the knee is in near full extension, are associated with elevated ACL tension [2]. Understanding the relationship between neurocognitive performance and landing mechanics may provide insight into ACL injury prevention and return-to-play following ACL injury and reconstruction. However, limited study has examined this notion. Therefore, this study aimed to investigate the relationship between RT and sagittal plane landing mechanics associated with ACL injuries in healthy individuals during a single-leg task.

METHODS

Eight healthy participants (6 females, 2 males; age = 18.3±0.5 years, height=175.0±11.9 cm, mass = 65.9±10.7kg) participated in this study. Participants performed two touchscreen-based eye–hand coordination tasks, including direct and cognitive–motor integration (CMI) conditions [3]. RT in each condition was calculated as the time (in seconds) between the disappearance of the central target and movement onset. Additionally, participants completed three successful single-leg drop landing (SLJL) trials with their dominant limb. A 30 cm height box was placed at a distance equal to 25% of participants' height from the force plate. Lower extremity kinematics in sagittal plane and kinetics, including knee flexion angle (KFA) and internal knee extension moment (KEM) at initial contact (IC), peak KFA of the entire landing and peak KEM, peak vertical and posterior ground reaction forces (GRFs) between the initial 100 milliseconds after IC, during SLJL trials were calculated using data collected via an optical motion capture system interfaced with one force plate. GRFs and joint moments, were normalized by body weight and body weight*height, respectively. Pearson correlation coefficient (r) was used to examine the relationship between RT in direct and CMI conditions and sagittal plane landing mechanics ($\alpha<0.05$.) and were accordingly interpreted as negligible (<0.30), low (0.31-0.50), moderate (0.51-0.70), high (0.71-0.90), and strong (>0.90) correlation.

RESULTS AND DISCUSSION

Results of the correlational analyses are presented in Table 1., indicated that faster CMI RT, but not direct RT, was significantly correlated with less KEM at IC (greater knee flexion moment). The remaining landing mechanical variables were not correlated with RT under the direct and CMI conditions. Individuals who have faster CMI RT may engage hamstring pre-activation landing strategies to increase internal knee flexion moment at IC, thus co-contract with the quadriceps to stabilize the knee joint and potentially reduce the risk of ACL injury [4].

CONCLUSIONS

Faster RT during CMI condition explained 54.6% of variance in less KEM (greater knee flexion moment) at IC in healthy individuals. Our findings suggest that individuals with a better neurocognitive RT can utilize safer landing mechanics with respect to ACL injury risk potentially by engaging greater hamstring co-contraction, resulting in a decreased KEM during landing.

REFERENCES

[1] Swanik C B et al. *Am J Sports Med* **35**(6): 943-948, 2007.
[2] Kernozek T W et al. *Clin Biomech* **23**(10), 1279-1286, 2008.
[3] Dalecki M et al. *Eur J Sport Sci* **19**(9): 1257-1266, 2019.
[4] Ueno R et al. *Orthop J Sports Med* **9**(9): 23259671211034487, 2021.

Table 1: Pearson Correlation (r) coefficients between RT in two conditions and sagittal plane landing mechanics.

	KFA at IC	KEM at IC	peak KFA	peak KEM	peak vertical GRF	peak posterior GRF
Direct RT	-0.143 (p=0.736)	-0.333 (p=0.420)	0.405 (p=0.320)	-0.452 (p=0.260)	0.214 (p=0.610)	-0.476 (p=0.233)
CMI RT	-0.661 (p=0.074)	0.739* (p=0.036)	0.248 (p=0.553)	0.070 (p=0.869)	-0.222 (p=0.597)	-0.405 (p=0.319)

*Indicate statistical significance (p<.05).

The impulse of the lateral ground reaction force makes runners' lateral velocity change and their variability during the approach phase into the curved path in sprint running

Tatsuro Ishidzuka[1], Yuji Ohgi[1], Sam Gleadhill[2] Ryu Nagahara[3], and Tomohito Wada[3]
[1] Keio University, Kanagawa, Japan.
[2] University of South Australia, Adelaide, Australia.
[3] National Institute of Fitness and Sports in Kanoya, Kagoshima, Japan.
Email: tatsu1160@gmail.com

INTRODUCTION

The lateral ground reaction force (GRF) toward the centripetal direction acts on a runner who runs in a curved path. Previous research reported that the inward GRF impulse of the left foot contact phase was larger than that of the right foot contact phase in the curved path [1]. However, the lateral GRF acting on the runner during the approach phase into the curved path is unknown. Thus, this research aims to investigate the difference in the lateral velocity change between the right and left contact phases caused by the lateral GRF impulse in terms of participant variability.

METHODS

The authors conducted an experiment on a 50 m straight all-weather track with 50 force platforms (TF-90100, Tec Gihan, Uji, Japan; 500 Hz) embedded. We made a curved path (radius: 38.2 m) after 40 m of the straight path. Ten male collegiate sprinters performed five runs from straight into curved paths with their own 90-95% effort with their spiked shoes. We analyzed 18 trials (three trials of six participants) in which the ground reaction force could be measured for six steps (five steps on the straight path and one step on the curved path, Figure 1). The impulse of the lateral ground reaction force during each step was calculated and normalized by the participant's mass. The mean and standard deviation of three trials for each participant were calculated (Table 1).

RESULTS AND DISCUSSION

Only participant A had a larger lateral velocity change by the right foot contact phase than that by the left foot contact phase in the first, second, and third cycles. On the other hand, the other participants had a larger lateral velocity change by the left foot contact phase than that by the right foot contact phase in their second (except for participant F) and third cycles. Moreover, for participants B, D, and H, the difference in the lateral velocity change between the right and left foot contact phases was larger than those of participants F and G in their third running cycle. Therefore, these results suggested that the kinetics of the approach phase into the curved path can vary between individuals.

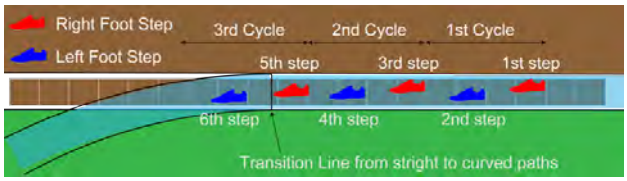

Figure 1 Definition of running cycles

CONCLUSIONS

This research suggests that the lateral velocity varied by the lateral GRF impulse on the left foot contact phase could be larger than that on the right foot contact phase during the approach phase into the curved path in sprint running. In addition, there was a variation between individuals in the difference of their lateral velocity change between the right and left foot contact phases.

REFERENCES

[1] Churchill S. M. et al. Scandinavian journal of medicine & science in sports **26 (10)** : 1171-1179, 2016.

Table 1: The lateral velocity change caused by the impulse of the lateral ground reaction force during each step (+: outward / -: inward)

	1st Cycle		2nd Cycle		3rd Cycle	
	Left (m/s)	Right (m/s)	Left (m/s)	Right (m/s)	Left (m/s)	Right (m/s)
Participant A	0.03 ± 0.06	-0.10 ± 0.02	-0.12 ± 0.08	-0.15 ± 0.07	-0.25 ± 0.10	-0.30 ± 0.05
Participant B	-0.06 ± 0.03	0.01 ± 0.02	-0.21 ± 0.06	0.04 ± 0.02	-0.45 ± 0.01	-0.19 ± 0.04
Participant D	-0.03 ± 0.01	0.01 ± 0.04	-0.12 ± 0.04	0.02 ± 0.01	-0.32 ± 0.04	-0.16 ± 0.09
Participant F	-0.02 ± 0.02	0.01 ± 0.02	-0.12 ± 0.05	-0.13 ± 0.07	-0.32 ± 0.02	-0.30 ± 0.02
Participant G	0.05 ± 0.05	-0.05 ± 0.06	-0.10 ± 0.13	-0.02 ± 0.02	-0.35 ± 0.11	-0.30 ± 0.03
Participant H	-0.12 ± 0.06	0.04 ± 0.06	-0.23 ± 0.06	-0.15 ± 0.05	-0.45 ± 0.11	-0.26 ± 0.07

PERFORMANCE STRATEGY IN THE HIGH JUMP VARIES BETWEEN INDIVIDUALS: MECHANICAL WORK EXERTION VS. ENERGY CONVERSION.

Toshihide Fujimori[1], Naoto Tobe[2] and Natsuki Sado[2]
[1] Graduate School of Comprehensive Human Sciences, University of Tsukuba., Tsukuba, Japan.
[2] Faculty of Health and Sport Sciences, University of Tsukuba, Tsukuba, Japan.
Email: fujimori.toshihid.sp@alumni.tsukuba.ac.jp

INTRODUCTION

Jumping is the most power-demanding tasks, of which the high jump is the extreme mode of jumping high for humans. Higher jumping can be translated as the acquisition of mechanical energy directly contributing to the raising of centre of body mass upwards (E_{vert}). In jumping modes from static conditions (e.g., squat and counter movement jump), since E_{vert} is mainly acquired by the lower-limb extensor work/power; the ability of mechanical work/power exertion is the major determinant of its performance. Meanwhile, in the jumping from a running approach, E_{vert} is also acuired by converting the energy due to the approach horizontal velocity into E_{vert} with non-extension movement [1].
In the high jump, athletes theoretically can increase the jump height either by increasing the effective work/power exertion and/or by increasing the converted energy; however, it is unclear which component determines performance. Inter-individual variance exists in the lower-limb joint movements during the take-off in the high jump even at similar levels of performance [2]. We hypothesised that jumpers may achieve their jump height from different E_{vert} acquisition components between individuals.

METHODS

Sixteen male high jumpers (22.6 ± 3.2 years, 1.80 ± 0.06 m, 68.2 ± 5.8 kg personal and season best record [PB and SB]: 1.90–2.35 m and 1.80–2.30 m) performed high jump trials with maximal effort with the bar setting to 90% of their SB. We analysed the kinematic and ground reaction force data. E_{vert} components during the take-off phase were decomposed into a component acquired via conversion from horizontal velocity ($E_{vert\_converted}$) and a component acquired via system work ($E_{vert\_syswork}$: net of effective joint work for moving the centre of mass). The mean of three trials was used as the representative value of the participant. Pearson's correlation coefficients were calculated to examine the relationship between the variables.

RESULTS AND DISCUSSION

$E_{vert\_converted}$ was 60.3 ± 3.9% (range 53.3–66.9%) of the total increase in E_{vert} during the take-off. Although both $E_{vert\_converted}$ and $E_{vert\_syswork}$ were significantly correlated with the total increase in E_{vert} (Figure1A-B), $E_{vert\_converted}$ and $E_{vert\_syswork}$ was not significantly correlated (Figure1D). Furthermore, the percentage of $E_{vert\_converted}$ in E_{vert} was not significantly correlated with the total increase in E_{vert} (Figure1C). These results indicate that the rate of E_{vert} acquisition components differs between individuals and is independent of the performance, supporting the hypotheses. This suggests that although jumping is the most power-demanding motor tasks, higher performance can be achieved not only by increasing the power/work exertion ability but also by improving $E_{vert\_converted}$ due to the non-extension movement in the high jump.

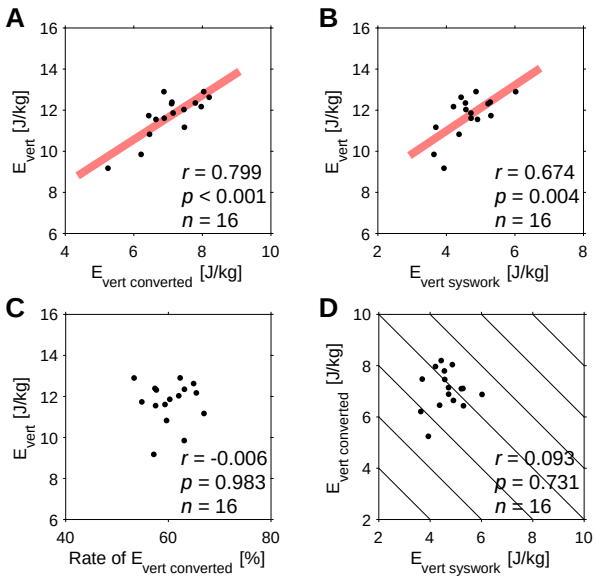

Figure 1 Correlations between E_{vert} and components of E_{vert}.

CONCLUSIONS

We found that performance is independent of whether greater lower-limb work exertion or greater conversion of the energy due to the approach horizontal velocity with non-extension movement. This suggests that to achieve higher performance in the high jump, athletes have the option of increasing either or both.

ACKNOWLEDGEMENTS

This study was supported by Tateishi Foundation for Science and Technology (2221014), and JSPS KAKENHI Grant- in-Aid for Young Scientists (21K17592).

REFERENCES

[1] Sado N et al. J Biomech 113: 110082, 2020.
[2] Ae M et al. New Stud Athl 23-3, 2008.

WHY ARE FORCE-VELOCITY PROFILES DETERMINED IN DYNAMOMETER EXPERIMENTS DIFFERENT FROM THOSE DETERMINED IN JUMPING EXPERIMENTS?

Maarten F. Bobbert[1], Kolbjørn Lindberg[2], Gøran Paulsen[2]
[1] Department of Human Movement Sciences, Vrije Universiteit, Amsterdam, The Netherlands.
[2] Department of Sport Science and Physical Education, University of Agder, Kristiansand, Norway.
Email: m.f.bobbert@vu.nl

INTRODUCTION

Force-velocity profiling has been proposed in the literature as a method to identify the overall mechanical characteristics of lower extremities [1]. A force-velocity profile is obtained by plotting for vertical jumps with different added loads the average push-off force as a function of the average push off velocity, fitting a straight line to the results, and extrapolating this line to find a theoretical maximum isometric force (F_0) and unloaded shortening velocity (v_0). Force-velocity profiles have also been determined using experiments with leg-press dynamometers, and these yielded values for F_0 and v_0 that were different from those obtained using loaded jumps [2, 3]. The purpose of the present study was to explain these differences by simulating loaded maximal squat jumps and leg extensions on an isokinetic leg press dynamometer over the same range of motion.

METHODS

Squat jumps with added loads of 0, 20, 40, 60 and 80% of body mass, as well as isokinetic leg extensions at velocities of 0.1 to 4 m/s, were simulated using a planar forward dynamic model of the musculoskeletal system [4]. The model had foot, shank and thigh segments and a head-arms-trunk segment, and was actuated by muscle-tendon complexes of SOLeus, GAStrocnemius, VASti, RECtus femoris, GLUtei and HAMstrings (Fig. 1). Each muscle-tendon complex was modeled as a Hill-type unit. The model calculated the segmental motions resulting from stimulation (STIM) input to the muscles. Initial STIM-levels were chosen such that equilibrium initial conditions were achieved. Subsequently, STIM of each muscle was allowed to switch 'on', and switching times were optimized using a parallel genetic algorithm to find maximum height for the loaded jumps, and maximum work on the leg press dynamometer for the different isokinetic velocities. Following [1], for each squat jump the gain in potential energy after take-off was divided by leg extension distance (formally, this yields the force averaged over distance, $\bar{F}^d$) and plotted as a function of half the take-off velocity to obtain the force-velocity profile. For each extension on the leg press, the work done on the dynamometer was divided by leg extension distance and plotted as a function of the isokinetic velocity.

RESULTS AND DISCUSSION

The force-velocity profiles for the two tasks were quite different (Fig. 1). The isokinetic leg press results demonstrate that the force-velocity relationship of the leg as a whole is nonlinear; it obviously depends on factors such as hip angle and preload. It is clearly not represented by the force-velocity relationship determined using loaded jumps, and the associated variables F_0 and v_0 have no physiological meaning. The reason is that the average push-off force is not determined by the average leg extension velocity; we should not be relating the average force during each jump to the average leg extension velocity during that jump, but to a higher velocity. The problem is, however, that this higher velocity is different for each loaded jump (see arrows for two jumps in Fig. 1) and it cannot be determined from measurements during a jump which velocity should be used. Hence, the force-velocity profile determined using loaded jumps does not represent the intrinsic force-velocity relationship of the leg as a whole. It is nothing other than what it is: a relationship between effective work per distance and half the take-off velocity in vertical jumps.

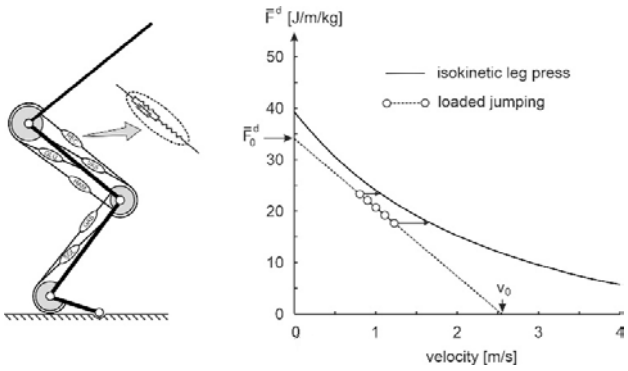

Figure 1 *Left*: Forward simulation model used in this study. *Right*: Force-velocity profiles determined for the model by simulating five squat jumps with added loads, and leg extensions on an isokinetic leg press dynamometer at different velocities.

CONCLUSIONS

To determine the intrinsic force-velocity relationship of the leg as a whole, different constant leg extension velocities should be imposed and the force or work done should be measured. This can only be achieved using isokinetic leg-press dynamometers; the force-velocity profiling approach based on loaded jumps is unsuitable for this purpose.

REFERENCES

[1] Samozino P et al. *J Theor Biol* **264**:11-8, 2010.
[2] Fessl I et al. *Int J Sports Physiol Perform* **17**: 1614-20, 2022.
[3] Lindberg K et al. PLoS ONE **16**(2):e0245791, 2021
[4] Bobbert M et al. *J Appl Physiol* **105**:1428-40, 2008.

ARE LOWER EXTREMITY JOINT KINETICS INFLUENCED BY SHOE COLLAR HEIGHT IN COLLEGIATE FEMALE VOLLEYBALL PLAYERS?

Tanner A. Thorsen[1], Lindsey G. Legg[1]
[1] School of Kinesiology and Nutrition, The University of Southern Mississippi
Email: tanner.thorsen@usm.edu

INTRODUCTION

Collegiate volleyball players commonly wear mid-cut (MC) shoes, with a collar height that rises just superior to the talocrual joint. Previous research has demonstrated that prophylactic restriction of ankle dorsiflexion range of motion (e.g., brace, tape, collar height) can alter lower extremity joint kinetics in both the sagittal and frontal planes. Increased joint moments have been linked with ankle and knee joint injury [1]. With the jumping and landing demands inherent in volleyball, risk for injuries such as ankle sprains and anterior cruciate ligamet rupture is increased, yet the effect of MC on lowe extremity jiont moments is unclear [2]. It is also unclear if collar height affects dominant (DL) and non-dominant limb (NDL) kinetics differently during unilateral landings. Thus, the purpose of this research was to elucidate the effects of a MC volleyball shoe compared to a standard low-top (LT) volleyball shoe on sagittal and frontal plane lower extremity joint moments, and between dominant and non-dominant limbs, during a landing task in collegiate female volleyball players.

METHODS

Seventeen female collegiate volleyball players (20.12 ± 1.32 years) performed unilateral forward drop landings on each limb in both MC and LT versions of the same shoe (Crazyflight, Adidas AG, Herzogenaurach, Germany). Participants landed from a 30 cm high box placed 40% of their height from the leading edge of a force plate. Limb dominance was defined as the limb used to kick a ball. GRF and lower extremity joint kinematics were collected using AMTI force plates (2400 Hz) and a 10-camera motion capture system (240 Hz), repectively. Sagittal and frontal plane internal joint moments were then computed using inverse dynamics for DL and NDL during each shoe conditon. A two-way repeated measures ANOVA was performed to compare shoe and limb conditions. Effect size was calculated as partial eta squared (n_p^2).

RESULTS AND DISCUSSION

Smaller peak plantarflexion moments were found with MC (Table 1). Greater peak knee abduction moments were found in DL (Table 1, Figure 1). At the hip, greater peak extension moment was observed in the DL, and greater hip abduction moment was observed in the dominant LT condition and in the NDL MC condition compared to the DL MC condition (Table 1).

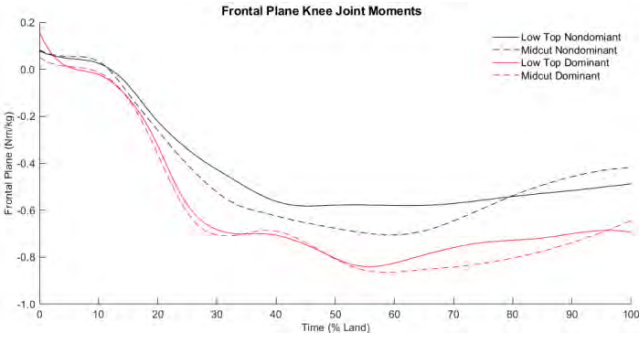

Figure 1 Frontal plane knee joint moments during the landing phase of a unilateral forward drop landing.

CONCLUSIONS

MC shoes promoted a reduced plantarflexion moment; however, this reduction was not sufficient to affect knee joint moments between shoes. Greater knee abduction moment was observed in the DL indicating players may have adopted more neutral landing mechanics on their NDL. This suggests that player preference may guide choice of shoe (MC vs. LT) and not prophylactic concern. Between limbs, however, improving landing mechanics on the DL may reduce knee injury risk (i.e., decreasing frontal plane joint moments) while playing volleyball, regardless of shoe [3].

REFERENCES

[1] Taylor et al. *Sports Health*. **14**: 328-35, 2022.
[2] Chandran et al. *J Athl Train.* **56**: 666-73, 2021.
[3] Hewett et al., *Am J Sports Med*. **33**:492-501, 2005.

Table 1: Joint moments of the lower extremity, presented as mean ± sd. Results of the two-way ANOVA are presented as p value ($\eta_p 2$). Bold indicates statistical signficance.

Joint Moment	ND LT	ND MC	D LT	D MC	Shoe	Limb	Interaction
Plantarflexion	-1.8 ± 0.34	-1.6 ± 0.24	-1.7 ± 0.45	-1.6 ± 0.34	**0.019 (0.298)**	0.689 (0.010)	0.079 (0.180)
Knee Abduction	-0.9 ± 0.24	-0.9 ± 0.28	-1.0 ± 0.25	-1.1 ± 0.30	0.280 (0.072)	**0.014 (0.323)**	0.068 (0.193)
Hip Extension	-2.0 ± 0.39	-2.0 ± 0.38	-2.2 ± 0.33	-2.2 ± 0.44	0.768 (0.006)	**0.001 (0.495)**	0.889(0.001)
Hip Abduction	-1.8 ± 0.28	-1.8 ± 0.22$^{\alpha}$	-1.9 ± 0.39$^{\alpha}$	-2.0 ± 0.36	0.552 (0.023)	0.178 (0.111)	**0.038 (0.242)**

$^{\alpha}$ = different from DMC

PECTRORALIS MAJOR AND DELTOID MUSCULARITY IN SHOT PUTTERS: REVERSAL OF WHETHER CROSS-SECTIONAL AREA OR VOLUME IS RELATED TO PERFORMANCE.

Shogo Hashimoto [1], Toshihide Fujimori [1], Takeshi Edagawa [1], Keigo Ohyama-Byun [2], Yoshikazu Okamoto [3], Takahito Nakajima [3], and Natsuki Sado [2]

[1] Graduate School of Health and Sport Sciences, University of Tsukuba, Tsukuba, Japan.
[2] Faculty of Health and Sport Sciences, University of Tsukuba, Japan.
[3] Faculty of Medicine, University of Tsukuba, Japan.
Email: hashimoto.shogo.qw@alumni.tsukuba.ac.jp

INTRODUCTION

A shot put is an event in which a heavy shot is 'put' forward and upwards. The muscles that cross the shoulder joint, which connects the trunk to the upper limb, are expected to be highly stressed during the shot put. It was suggested that maximal force and mechanical work/power exertion abilities of the shoulder muscles are important for performance [1]

The prime movers of the diagonal shoulder movement would be the pectoralis major (PM) and deltoid (DELT) muscles. The directions of action of these muscles are anatomically different and may have different effects on performance; however, to the best of our knowledge, shoulder muscularity in shot putters has not been examined. We assessed the PM and DELT morphology in shot putters using two indices: muscle cross-sectional area (CSA) and muscle volume, which reflect the potential for maximal force and mechanical work/power, respectively. We hypothesised that PM and DELT would be differentially related to shot put performance on the two measures.

METHODS

We collected the transverse water-weighted magnetic resonance images (MRIs) from the upper limbs (2 mm interval) and the trunk (5 mm interval) of 11 male shot-putters and 14 untrained males. From the MRIs, we calculated the maximum transverse CSAs and the volumes of PM and DELT. When calculating the volume of the DELT, one participant in both groups had missing MRI images and were excluded from this analysis. Welch's *t*-test was used for intergroup comparisons. Cohen's d was used for the effect size of each *t*-test. The relationship between each muscle index and the season's best were tested using Pearson product-moment correlation coefficient.

RESULTS AND DISCUSSION

CSA and volume in both muscles were significantly greater in shot putters than in untrained men ($p < 0.01$, $d > 1.40$), with the effect size in PM being larger for CSA and that in DELT being larger for volume, respectively. Season's best was strongly correlated with CSA and volume for both PM and DELT, with a stronger correlation in PM for CSA and that in DELT for volume, respectively (Figure 1). This inversion of volume and CSA supported our hypothesis. Athletes put a shot diagonally upward with the trunk almost vertical during the shot-put motion. Therefore, the mechanical demand of each muscle during the motion is considered as the large force exertion in PM to inhibit horizontal shoulder abduction due to the reaction force of the shot, and as the mechanical work/power exertion in DELT to increase the gravitational-potential energy of the upper limb and the shot. This study suggests that the morphology of the PM and DELT in shot putters and its relationship to performance are consistent with the mechanical demands of each muscle in the shot-put motion.

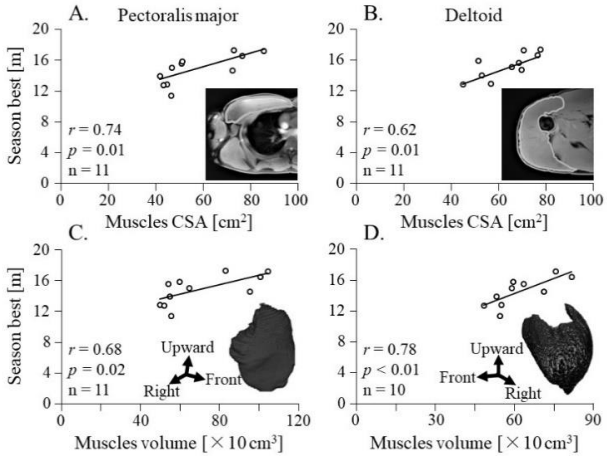

Figure 1 Relationship between muscle cross-sectional area (A, B) and muscle volume (C, D) of pectoralis major and deltoid muscles and season's best.

CONCLUSIONS

We find that CSA is more related to shot put performance in PM, whereas volume is more related to performance in DELT. The reversal of the relationship between these indices and performance is suggested to be consistent with the mechanical demands of the shot-put motion.

REFERENCES

[1] Terzis G et al. *J Sports Med Phys Fitness* **47**: 284-90, 2007.

FRONT KNEE CONTROL IN CRICKET FAST BOWLING

René E.D. Ferdinands[1], Peter Sinclair[1], Max Stuelcken[2] and Andy Greene [3]
[1] Faculty of Health and Medicine, University of Sydney, Sydney, Australia.
[2] School of Health, University of the Sunshine Coast, QLD, Australia.
Email: Edouard.ferdinands@sydney.edu.au

INTRODUCTION

Fast bowling is heavily reliant on the mechanics of the front leg, which acts as a quasi-rigid lever connecting the ground to the pelvis. There are four broad categories of front-leg technique: flexor, extender, flexor-extender, and constant brace [1]. However, coaches, tend to instruct fast bowlers to extend their front knee during delivery, claiming that this technique not only increases release height, but also generates faster ball speeds. A direct coaching intervention requires the bowler to actively engage the knee extensors during front foot contact, working on the premise that an independent increase in the knee extension angle will enhance the bowler's performance. This practice would conflict with research showing that joint angle is subject to non-local cumulative effects arising from distant parts of the kinetic link chain [2].

One method to determine the magnitude and type of knee muscle contribution to knee joint rotation is to calculate the angular work about the knee. Hence, the aim of this study was to analyse the knee angular work of a sample of young high performance fast bowlers during the arm-acceleration phase. We hypothesised that changes in knee extension-flexion angle are dependent on the effect of body segment motions occurring at locations in the kinetics link chain that are remote from the knee.

METHODS

A Cortex Motion Analysis System (Version 1.0, Motion Analysis Corporation Ltd., USA) was used to record three-dimensional (3D) motion and force plate data for 18 young fast bowlers during six bowling trials. Each bowler wore a full body marker set comprising fifty-one 25-mm spherical markers, which were attached to bony landmarks [3]. A recursive fourth-order low-pass Butterworth filter was sed to smooth the *xyz*-coordinates of the marker data. The smoothed motion analysis data of the markers were imported into a four-segment rigid-body 3D kinematics and kinetics model of the front leg designed using Visual3D software (Version 5, C-Motion, Germantown, MD). Local segment coordinate systems of the rigid-body model were defined for the pelvis and front leg. The normalised knee torque versus angular displacement data was interpolated by B-splines and then numerically integrated with the trapezoidal rule to calculate the normalised angular work at the knee using Mathematica (Wolfram Research, Inc., Version 12.0). Positive work indicates that the joint torque actively contributed to knee flexion-extension, whereas negative work indicates that knee flexion-extension was controlled.

RESULTS AND DISCUSSION

Most bowlers were flexors (61%), followed by flexor-extenders (28%), and then extenders (11%). Interestingly, the knee angular work for most of the arm-acceleration phase was negative, indicating the torque at the knee acted to control or resist the rate of knee flexion-extension. For instance, from 40-100% of the phase, the mean knee angular work for the bowlers in the knee flexor-extender group was negative, suggesting that the knee flexors were contracting to control the rate of knee extension from 60-100% of the phase (Figure 1). Similarly, negative knee angular work operated from 36-100% of the phase for the bowlers in the flexor group, and from 0-100% for the bowlers in the extender group.

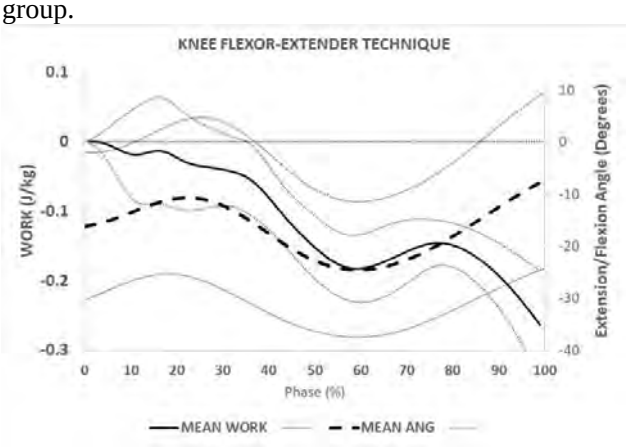

Figure 1 Mean normalised work at the knee and knee flexion-extension angle during the arm-acceleration phase for the flexor-extender technique.

CONCLUSIONS

The knee angular work at the front knee during the arm-acceleration phase of the fast-bowling action tended to be mostly negative for all front-leg techniques. Both knee flexion and extension were mostly controlled, suggesting that knee motion is influenced by non-local effects in the kinetic link chain. Coaching interventions that focus on increasing knee extension angle should consider the whole-body segment interactions on the knee.

REFERENCES

[1] Portus et al. *Sport Biomecch* **3**: 263-284, 2004.
[2] Hirashima et al. J Biomech **41**: 2874-2883, 2008.
[3] Beach et al. *J Sports Sci* **36**:1127-1134, 2018.

BIOMECHANICAL AND HISTOLOGICAL PROPERTIES OF DIFFERENT HUMAN TENDONS

Samantha Hefferan[1], Dylan Ashton[1], Carina Blaker[1], Christopher Little[1] and Elizabeth Clarke[1]

[1] Institute of Bone and Joint Research, Kolling Institute, Royal North Shore Hospital, Faculty of Medicine and Health, University of Sydney, Sydney, Australia.
Email: samantha.hefferan@sydney.edu.au

INTRODUCTION

Tendons play a major role in normal musculoskeletal functioning. Injury, pathology or disease of tendons can impair function and may require surgical repair or reconstruction. Characterisation of "normal" tendon structure and biomechanical properties is important for understanding mechanisms and progression of pathology and healing, and for understanding native properties to develop biomimetic grafts. This study aims to compare structural and functional characteristics of a range of different human tendons.

METHODS

Nine different tendons were retrieved from 39 fresh-frozen human cadaveric lower-limbs (35 donors; 22 male, 13 female; aged 49-99 years) including: Achilles tendon (AT), tibialis posterior and anterior (TP, TA), fibularis longus and brevis (FL, FB), flexor and extensor hallucis longus (FHL, EHL), plantaris (Plt) and flexor digitorum longus (FDL). The central length underwent tensile testing to failure, measuring maximum load at failure and ultimate tensile strength (UTS). Proximal and distal samples (1-3 sections per region) from the same 9 tendons were collected from a subset of 11 donors (5 male, 6 female; 68-99 years) for histological assessment using Haematoxylin and Eosin (HE), Toluidine Blue (TB) and Picrosirius Red (PSR) staining. A total of 936 region-matched images (312 per stain; 200x magnification) were included for analysis. Cell characteristics (cell density, and nuclear circularity and size) were quantified from HE images. A scoring system was developed assessing fibre architecture (HE, PSR), crimp wavelength (PSR), and proteoglycan content (TB). Biomechanics and cell characteristics were analysed using multivariate, mixed-effects linear regression, controlling for donor sex, age, height, weight, and tendon region. Semi-quantitative histology scores were analysed using Kruskal-Wallis and Dunn's test with proximal/distal regions analysed separately. Sidak's correction was used for multiple comparisons.

RESULTS AND DISCUSSION

There were no significant tendon-specific differences for UTS (Figure 1i) or maximum load when controlling for donor characteristics. Different tendons and tendon-regions exhibited different histological properties. Structural differences between tendons were more common in the distal versus proximal regions (Figure 1iii, iv). Distally, there were tendon-specific differences in crimp wavelength, and proteoglycan staining area and intensity, while only crimp wavelength varied between tendons in the proximal region. Regional variations in cell characteristics, crimp characteristics and proteoglycan content reflect different attributes associated with bone vs muscle ends of the tendon and different loading environments of the tendon/region.

Cell density was significantly influenced by the type of tendon ($p=0.0040$), with TA exhibiting significantly greater cell density compared to AT, TP, FB, Plt, and FDL; all $p<0.05$; Figure 1ii). Furthermore, the region of tendon (proximal/distal) was significantly related to cell density (distal = greater density; $p<0.0001$) as well as nuclear morphology (distal = more round; $p=0.0001$) and size (distal = smaller; $p=0.0007$). While greater cell density and morphology are often indicative of pathology [1,2], such variations may reflect different physiological or functional characteristics of the regional tissue. Interestingly, there were significant correlations between UTS of the central tendon and distal tendon cell characteristics: UTS decreased with increasing density ($p=0.0328$) and cirularity ($p=0.0009$), suggesting an overall altered structural capacity of tendons with greater cell numbers and rounding.

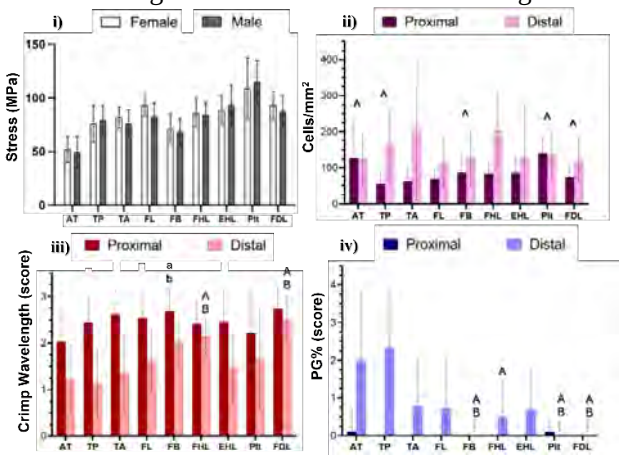

Figure 1. **i)** Ultimate tensile strength, **ii)** cell density, **iii)** crimp wavelength, and **iv)** proteoglycan staining area of nine different human lower leg tendons (see *methods* for abbreviations). Data as mean ± standard deviation, $p<0.05$ represented by symbols where applicable: ii) tendon different to TA (^); iii and iv) proximally different to AT(*a*) or TP (*b*); distally different to AT (*A*) or TP (*B*).

CONCLUSIONS

This study identifies unique histological properties of different tendons and variations associated with their mechanical properties. These relationships improve our understanding of tendon structure and function which has important clinical implications, particularly for the selection of grafts or the design of biomimetic materials based on specific native tissue properties.

REFERENCES

[1] Cook J et al. *J Orthop Res* **22**: 334-338, 2004.
[2] Movin T et al. *Acta Orthop Scand* **68**: 170-175, 1997.

Factors associated with good recovery from Achilles tendon rupture at 1-year post rupture

Ra'ad M. Khair [1], Lauri Stenroth [2], Neil J. Cronin [1,4], Ville Ponkilainen[3], Aleksi Reito [3] and Taija Finni [1]
[1] Faculty of Sport and Health Sciences, University of Jyväskylä, Jyväskylä, Finland
[2] Department of Technical Physics, University of Eastern Finland, Kuopio, Finland
[3] Central Finland Central Hospital Nova, Jyväskylä, Finland
[4] School of Sport and Exercise, University of Gloucestershire, UK.
Email: raad.m.khair@jyu.fi

INTRODUCTION

Tendon rupture leads to long-term functional, structural, and mechanical changes in the Achilles tendon (AT) and triceps surae (TS) muscles [1]. Despite many studies investigating the recovery of the AT after rupture, factors that are associated with good recovery are still poorly known. Thus, we aimed to explore interconnections between structural, mechanical, and neuromuscular parameters and their associations with markers of good recovery.

METHODS

A total of 35 patients with unilateral rupture (6 females) participated in this study. Muscle-tendon structural, mechanical, and neuromuscular parameters were measured 1-year after rupture. Mechanichal and structural parameteres were measured using ultrasonography. For detailed information on the measurements and calculations please refer to [2,3]. Surface electromyography (EMG) signals of soleus (SOL), MG, lateral gastrocnemius (LG) and flexor hallucis longus (FHL) were collected during 30% of maximal isometric ramp plantar flexion and normalized to root mean square (RMS) from a 1-sec window during maximum voluntary contraction. Total EMG activity of all plantarflexor muscles was also computed by summing the normalized SOL, MG, LG and FHL EMG activity. This cumulative value denoted 100% and was used to evaluate the relative contribution of each muscle to total plantarflexor activity.

Interconnections between the inter-limb differences (Δ) were explored using partial correlations controlled for age and sex, followed by multivariable linear regression to find associations between the measured factors and the following markers that indicate good recovery: 1) tendon length, 2) tendon non-uniform displacement, and 3) FHL normalized EMG amplitude difference between limbs. Covariates inclusion in the models was based on previous knowledge, considering the associations detected in the exploratory correlations. We also investigated the relative contribution of FHL to total triceps surae EMG activity during submaximal contraction between limbs.

RESULTS AND DISCUSSION

ΔMG (β=-0.12, [95%CI -0.20 – -0.03]) and ΔLG (β=-0.086, [95%CI -0.16 – -0.006]) subtendon lengths were associated with MG tendon Δstiffness. MG (β=11.56, [95%CI 4.22 – 18.90]) and soleus (β=2.18, [95%CI 0.10 – 4.05]) Δsubtendon lengths explained 48% of variance in FHL EMG amplitude (Figure 1). Regression models for tendon length and non-uniform displacement were not significant.

The relative contribution of MG on total plantarflexor EMG activity was lower in the injured limb with a mean difference of 0.061 (95%CI 0.02-1.0) and was accompanied by an increased FHL contribution to total EMG in the injured limb, with a mean inter-limb difference of -0.061 (95%CI -1.06 - -0.016).

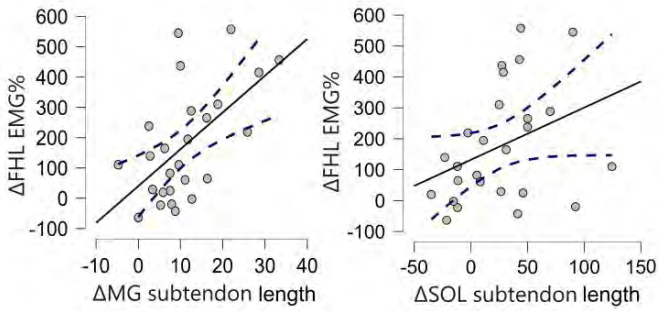

Figure 1 Scatter plots showing bivariate associations between the identified independent predictors of ΔFHL EMG% in the multivariate regression model.

CONCLUSIONS

Higher tendon stiffness may ameliorate the effects of tendon lengthening, so rehabilitative measures that promote MG muscle activation, and increase muscle strength along with tendon stiffness could improve functional outcomes. It is true that TS muscle weakness is partially compensated by FHL but FHL capacity to compensate for the loss of strength in the injured limb is limited due to relatively short plantarflexion moment arm. Thus, treatments and rehabilitation should not emphasize the role of FHL to allow recovery of the TS.

ACKNOWLEDGEMENTS

This work was supported by Academy of Finland (grants #323168 and #332915).

REFERENCES

[1]Svensson R et al. *Transl. SPORTS Med.* **2**, 316–324
[2]Khair R et al. *Clin Biomech* **92**, 105568
[3]Khair R et al. *Scand. J. Med. Sci. Sports* **31**, 1069

In-Vivo Patellar Tendon Strain Measured using Ultrasound Differs by Sex and Region of the Tendon

Naoaki Ito[1], Rodrigo Scattone Silva[2], and Karin Grävare Silbernagel[1]
[1] Department of Physical Therapy, University of Delaware, Newark, DE, USA.
[2] Postgraduate Program in Rehabilitation Sciences, Federal University of Rio Grande do Norte, Santa Cruz, RN, Brazil. Email: nito@udel.edu

INTRODUCTION

Patellar tendinopathy is a prevalent condition in young active individuals and is most common in males and in the medial region of the tendon [1,2]. In vitro tendon stiffness is known to differ by region (medial, lateral, central) [3], however studies in vivo are lacking. Males typically have stiffer tendons than females [4] and the variability in stiffness by region and sex may result in unbalanced loads within the patellar tendon during quadriceps contraction. Such unbalanced loads through the tendon may further explain the etiology of injury. The purpose of study was to investigate the differences in patellar tendon strain between regions and sex in healthy individuals.

METHODS

Healthy participants (10 male | 10 female, age: 26±4 years, body mass index: 25±3 kg/m^2) performed unilateral isometric knee extensions on a dynamometer at 60% of their maximal voluntary isometric contraction (MVIC) in 90° of knee flexion. Concurrent extended field of view ultrasound images of the patellar tendon were collected. Images were collected in the medial, lateral, and central regions of the patellar tendon. Resting images were also collected for each region. Patellar tendon strain was calculated by dividing the change in length at 60% MVIC by the resting length [5]. Linear mixed effects model using Satterthwaite's method was used to determine the fixed effects of region (medial, lateral, central), sex, and the interaction between sex and region on patellar tendon strain. Participants were included in the model as random effects. Pairwise comparisons were performed for significant findings (α=0.05).

RESULTS AND DISCUSSION

Main effects of sex ($p < 0.01$) and region ($p < 0.01$) were observed; however, no interaction effect ($p = 0.477$) was seen. Males had less strain than females (mean [95% confidence interval]: male strain = 8.3 [6.4 – 10.2] %, female strain = 13.8 [11.9 – 15.7] %). The central region (central strain = 6.9 [4.9 – 9.0] %) had less strain compared to both medial ($p < 0.01$, medial strain = 11.7 [9.7 – 13.7] %), and lateral ($p < 0.01$, lateral strain = 14.6 [12.6 – 16.6] %) regions. No statistically significant differences were observed between the medial and lateral regions ($p = 0.08$) (**Figure 1**).

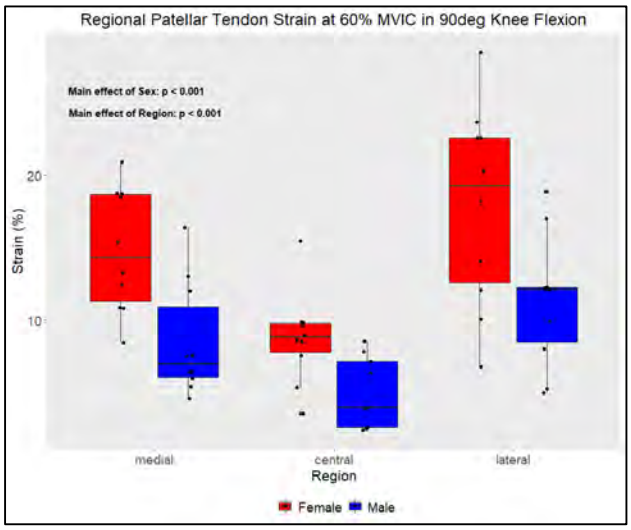

Figure 1. *Regional patellar tendon strain by sex. MVIC, maximal voluntary isometric contraction.*

Consistent with our previous knowledge about stiffer tendons in males compared to females [4], the patellar tendon in females experienced higher levels of strain at the same effort level compared to males. The medial and lateral regions of the tendon also experienced higher levels of strain compared to the central region. The high prevalence of patellar tendinopathy in the medial region [1] may be due to the medial region undergoing higher levels of strain at the same effort levels compared to the central region.

CONCLUSIONS

Patellar tendon strain differs by sex and region. The varying prevalence in sex and in location of patellar tendinopathy may in part be explained by the unbalanced loads observed. Tendon strain levels by sex and region may have to be considered as risk factors for injury and may guide interventions in rehabilitation when treating patellar tendon injuries.

ACKNOWLEDGEMENTS

Funding was provided by the National Institute of Health: R37-HD037985 and R01-AR072034.

REFERENCES

[1] Yu J et al. *Am J Roentgenol* **165**:115-118, 1995.
[2] Simpson M et al. *Sport Med* **46**: 545–557, 2016.
[3] Noyes F et al. *J Bone Joint Surg* **66**: 344-52, 1984.
[4] Taş S et al. *Acta Orthop Traumatol* **51**: 54-59, 2017.
[5] Edama M et al. *Clin Biomech* **61**: 52–57, 201

NEAR-INFRARED SPECTROSCOPIC ASSESSMENT OF PATELLAR TENDON MECHANICS

Adam Kositsky[1,2], Jari Torniainen[1,3], Lauri Stenroth[1], Ervin Nippolainen[1], Janne T.A. Mäkelä[1], Petri Paakkari[1], Heikki Kröger[4], Juha Töyräs[1,3,5], Rami K. Korhonen[1], Isaac O. Afara[1,3]

[1] Department of Technical Physics, University of Eastern Finland, Kuopio, Finland
[2] Menzies Health Institute Queensland, Griffith University, Gold Coast, Australia
[3] School of Information Technology and Electrical Engineering, University of Queensland, Brisbane, Australia
[4] Department of Orthopaedics, Traumatology and Hand Surgery, Kuopio University Hospital, Kuopio, Finland
[5] Science Service Center, Kuopio University Hospital, Kuopio, Finland
Email: adam.kositsky@uef.fi

INTRODUCTION

Near-infrared spectroscopy (NIRS) is a powerful bioanalytical technique that enables rapid, invasive but non-destructive assessment of human bone, cartilage, and meniscus properties [1]. NIRS has demonstrated great potential for estimating mechanical and compositional properties of bovine knee ligaments and patellar tendon (PT) when near-infrared spectra have been obtained from prepared testing samples [2,3]. However, estimating tendon properties with NIRS has not been performed with near-infrared spectra acquired with the tendon intact. Further, the viability of NIRS for characterizing human tendon material properties has yet to be assessed. Thus, the aim of this study was to investigate whether near-infrared spectra obtained from intact cadaveric PT can estimate its material properties.

METHODS

Eight fresh-frozen cadaver (5F; 65±8 yr; 1.72±0.15 m; 83±23 kg) knees were used. Near-infrared spectra were obtained from medial, central, and lateral PT regions via small incisions through the skin (Figure 1) using a Stellarnet spectrometer (DS-InGaAs-512). Each PT was harvested and split into three mediolateral pieces further divided at their approximate center width into anterior and posterior parts. Using a custom-made tool, each of the six pieces were cut into dumbbell-shaped samples at their approximate longitudinal center. Micro-computed tomography (SkyScan 1172, Bruker) was used to obtain sample cross-sectional area. After preconditioning, stress relaxation (one-step, 30 minutes at 8% strain) and sinusoidal (20 cycles of 0.5% strain amplitude from 8% strain at 0.1, 0.5, 1.0, 2.0, and 5.0 Hz) tests were performed in a mechanical testing device (Mach-1 v500css, Biomomentum; Figure 1). Then, samples were pulled to mechanical failure at 0.05%/s. Phase angle and dynamic modulus were obtained from the sinusoidal data, and parameters relating to toe and linear regions and yield and failure points were analyzed from stress-strain curves. Individual NIRS prediction models were constructed for each biomechanical variable and evaluated with five-fold cross validation. Depending on the output of the optimization process, regression was implemented as partial least squares or support vector machine [1–3]. As no systematic region-specific differences in PT material properties were found [4], data from each mediolateral region's anterior testing piece were used for the reference biomechanical data.

RESULTS AND DISCUSSION

Many biomechanical parameters obtained here could be predicted with reasonable error (i.e., $r_{CV} \geq 0.5$; $RMSE_{CV} \leq 20\%$) by NIRS spectra obtained directly on the patellar tendon. Model predictions of viscoelastic properties, which are important for the efficiency of movement, performed best.

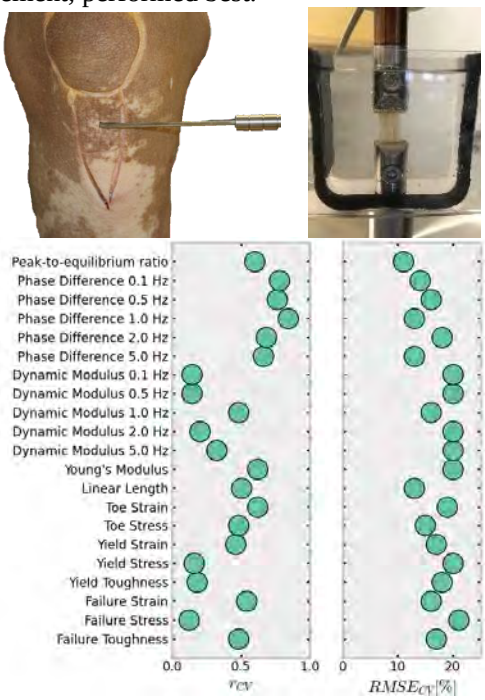

Figure 1. *Top*: *In situ* acquisition of near-infrared spectra (left) and *in vitro* mechanical testing (right). *Bottom*: Calibrated (r_{CV}) and cross-validated ($RMSE_{CV}$) comparisons between measured and predicted human patellar tendon material properties.

CONCLUSIONS

Further development of the NIRS probe and models of light-tendon and light-skin interactions may lead to the development of NIRS as a tool for non-invasive *in vivo* characterization of human tendon mechanics.

ACKNOWLEDGEMENTS

Academy of Finland (307932, 315820, 320135, 324529, 332915), Kuopio University Hospital (VTR 5063579, 5203118), Horizon 2020 H2020-ICT-2017-1 (780598).

REFERENCES

[1] Afara IO et al. *Nat Protoc* **16**:1297-329, 2021
[2] Torniainen J et al. *Ann Biomed Eng* **47**:213-22, 2019
[3] Torniainen J et al. *PLoS One* **17**:e0263280, 2022
[4] Kositsky A et al. *9th WCB* O-10078, 2022

EFFECT OF MINIMALIST SCHOOL SHOES ON INTRINSIC FOOT MUSCLE SIZE

Roy T.H. Cheung[1], Shayan Quinlan[2], Alycia Fong-Yan[2] and Irene S. Davis[3]
[1] School of Health Sciences, Western Sydney University, New South Wales, Australia
[2] Faculty of Medicine and Health, University of Sydney, New South Wales, Australia
[3] School of Physical Therapy and Rehabilitation Sciences, University of South Florida, Tampa, FL, USA
Email: Roy.Cheung@westernsydney.edu.au

INTRODUCTION

Walking in minimalist shoes has been reported to promote intrinsic foot muscle size and strength in active adults [1]. A recent investigation by our team, however found that minimalists did not result in larger or stronger intrinsic foot muscle among school aged children [2], which can be explained by the low minimalist index (46%) of their test shoes. Hence, we investigated the effect of true minimalist shoes on intrinsic foot muscle sizes and strength in school children.

METHODS

We recruited 28 healthy participants who aged between 9 to 12 from the same primary school which participated in our previous study [2]. Participants were excluded if they had any injury three months prior to recruitment, wore orthotics, or had general ligament laxity. After the baseline assessment, all participants were given a pair of minimalists (94% minimalist index, Softstar, OR, USA) as their regular school shoes for two school terms (i.e., February to September), followed by a re-assessment. The shoes were worn during school hours in accordance with strict uniform policy (6 hours/day, 3 days/week). The cross-sectional area (CSA) of abductor hallucis (AH) and flexor digitorum brevis (FDB) were measured by a portable ultrasound machine (VINNO Technology, Suzhou, China). The toe flexor strength (TFS) of the hallux and the lesser toes were measured by a customised dynamometer which demonstrated excellent reliability [3]. One-way ANCOVA were used to test differences in the dependent variables between minimalist and control groups (collected in [2]), using the pre-intervention measure as the covariate for the post-intervention measure analysed.

RESULTS AND DISCUSSION

Of 28 participants in the minimalist group, only 17 participants completed the study (attrition rate 39%). The demographics, including age, height, weight, and BMI between the two groups were comparable ($p>0.591$).

Significant greater CSA of FDB was found in the minimalist group ($p=0.026$, Figure 1), but not for other variables. When compared to moderate minimalist shoes [2], true minimalists resulted in a larger effect (Table 1). The absence of changes in the CSA of AH and TFS may be partly explained by the relatively short exposure (i.e., 3 days/week x 6 hours/day).

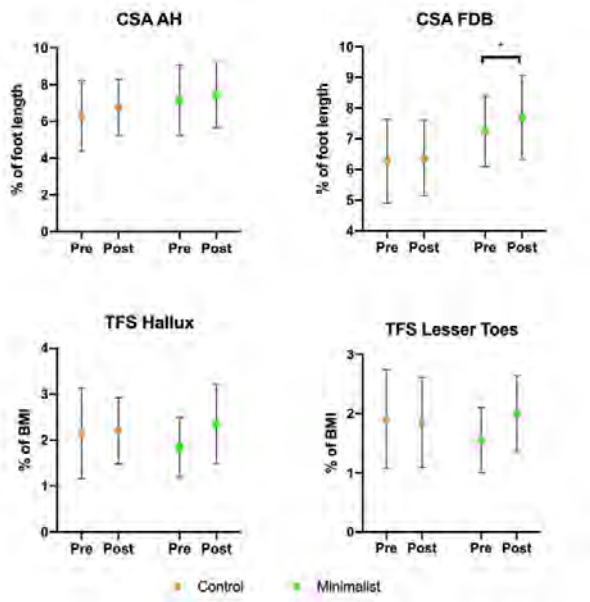

Figure 1 Cross-sectional area (CSA) and toe flexor strength (TFS) of selected intrinsic foot muscles before and after intervention.

CONCLUSIONS

Minimalist school shoes result in a greater FDB muscle size, but not AH. TFS was also unchanged over this 8-month period.

ACKNOWLEDGEMENTS

This study is supported by School of Health Sciences, Western Sydney University (Project number: 20840).

REFERENCES

[1] Ridge S et al. *MSSE* **51**: 104-13, 2019.
[2] Quinlan S et al. *Gait Posture* **92**: 371-7, 2022.
[3] Quinlan S et al. *Gait Posture* **85**: 20-4, 2021.

Table 1: Comparison of effect sizes (partial eta squared) between two minimalist school shoe studies. S=Small; M=Moderate; L=Large

	CSA AH	CSA FDB	TFS Hallux	TFS Lesser Toes
Cheung et al. (94% minimalist index)	0.01 (S-M)	0.10* (M-L)	0.02 (S-M)	0.03 (S-M)
Quinlan et al. (46% minimalist index)	0.04 (S-M)	0.05 (S-M)	0.05 (S-M)	0.04 (S-M)

Investigation of optimal perceived comfort in sports shoes with plantar pressure distribution

Wei-Ting Tu, Kuangyou B. Cheng
Institute of Physical Education, Health, and Leisure Studies, National Cheng Kung University, Tainan, Taiwan
Email: rb6101049@gs.ncku.edu.tw

INTRODUCTION

The comfort filter paradigm, allowing an athlete to select comfortable running shoes using his/her own comfort filter, has been proposed[1]. While adopting this paradigm would possibly reduce the injury risk and oxygen consumption, the perceived footware comfort may be influenced by multiple factors including anthropometry, skeletal alignment, foot sensitivity, and plantar pressure patterns. Footwear design features such as fit, torsional stiffness, cushioning, support, and stability have also been suggested to influence comfort[2].

Since the magnitude and distribution diagram of plantar pressure reveal force interaction between the foot and the ground, it might be reasonable to predict perceived comfort in shoes using the information of plantar pressure. For instance, compared with the least comfortable insole, significantly higher pressure and force magnitude in the midfoot area was found when wearing the most comfortable insole[3]. On the contrary, another study concluded that the perception of comfort of a running shoe cannot be predicted through impact and plantar pressure[4].

One possible reason for these contradictory results might be that while the plantar pressure data were under specific control in most studies, the perceived comfort varied with lots of physical and psychological characteristics. For example, individuals with a high foot arch prefer soft insert material. In contrast, those with a low foot arch favour hard insert material[5]. The perceived comfort might be different for each person, which explains the varied correspondence between plantar pressure and perceived comfort.

The purpose of this study was, (i) to demonstrate that similar individual comfort ratings in Visual Analogue Scale may result from two different kinds of plantar pressure distribution, and (ii) to identify the corresponding between plantar pressure and perceived comfort.

METHODS

Three heel-toe recreational runners with the foot size of US 7-9 were recruited in this study. The participants passed intra-rater reliability assessment with respect to the VAS (ICC $\geq$ 0.7)[2]. They were tested on 10 days with one session per day, only sessions four to six were used[5]. They performed 200m of walking on a treadmill at the speeds which they felt comfortable with, which was followed by indicating their comfort rating on the Visual Analogue Scale (0–150mm; '150' indicates the highest comfort level) in four different running shoes. An in-shoe plantar pressure measuring system (Industrial Technology Research Institute, Taiwan, sampling at 30 Hz, 89 sensors) was inserted to the shoe.

RESULTS AND DISCUSSION

Subject1 rated shoeA 120mm (Comfortable) and shoeB 113mm (Comfortable) in VAS, indicating two similar rating scores with different magnitude and distribution of plantar pressure. Around 20% more (Value of sensor: 0-255) pressure in the midfoot and heel regions was found (Table1). This may provide the reason for the previous contradictory results. It was also found that while some sensors showed positive correlation with comfort rating, some others did not.

CONCLUSIONS

Positive correlation in some sensors seemed to provide supporting evidence for the studies with consistent results. However, identifying relationship between plantar pressure and perceived comfort may in general be impractical due to the difficulty in finding a certain correlation which fits everyone. Furthermore, perceived comfort may vary with individual physical and psychological characteristics. With the plantar pressure data collected for the shoes regarded as comfortable in this study, a greater number of shoes tested in future research might provide data for optimal plantar pressure prediction based on machine learning algorithms.

REFERENCES

[1] Nigg Benno M., et al. *British journal of sports medicine* **49(20)**: 1290-1294, 2015.
[2] Hoerzer, S. et al. *J Footwear Science* **8(3)**: 155-163, 2016.
[3] Che, H., B. M. et al. *Clinical Biomechanics* **9(6)**: 335-341, 1994.
[4] Dinato, Roberto C., et al. *Journal of Science and Medicine in Sport* **18(1)**: 93-97, 2015.
[5] MÜNDERMANN, A., et al. *Medicine & Science in Sports & Exercise* **33(11)**: 1939-1945, 2001.

Table 1: The plantar pressure value of Subject 1 with shoe A and shoe B.

VAS Rate	Sensor4(Heel)	Sensor41(Heel)	Sensor52(Midfoot)	Sensor84(Midfoot)
120mm(Subject 1 with shoeA)	63.7	53.5	54.8	22.9
113mm(Subject 1 with shoeB)	92.2	102.1	109.3	65.0

Rate of knee flexion at the instant of landing during running can influence initial knee joint stiffness estimates due to running shoe cushioning.

Zhenyuan Zhang and Mark Lake
School of Sport and Exercise Science, Liverpool John Moores University, Liverpool, UK
Email: M.J.Lake@ljmu.ac.uk

INTRODUCTION

The setting of lower limb joint stiffness during running reflects the impact-moderating behaviour of the human neuromuscular system that is associated with both performance and injury risk. A joint torsional spring model is typically used to quantify stiffness by examining the initial slope of the joint moment-angle relationship. However, this approach may not be sensitive enough to reflect adaptations in the dynamics of landing that are linked with impact attenuation between different running shoe conditions [1]. An alternative joint stiffness calculation places more emphasis on the initial kinematic conditions of ground contact (kinematic-only method) [2], as the stiffness setting during early stance could elucidate the mechanics of impact attenuation which might contribute to reduced injury risk [3]. Therefore, this study aims to compare knee joint stiffness during the early impact phase of running with thin- and thick-cushioned shoes using the traditional moment-angle and the kinematic-only methods.

METHODS

Twelve experienced runners ran at 4.5 m/s on a runway with a force plate surrounded by an 8-camera motion capture system in the middle to record ground reaction force and marker trajectory data, respectively. They wore two pairs of running shoes constructed with either a thin (30mm) or thick (54mm) midsole. For the traditional calculation, knee joint stiffness at the early impact phase was represented as the slope of a regression line fitted to the knee joint moment-angle curve from initial contact (IC) to peak knee flexion velocity. The kinematic-only method for knee joint stiffness calculation (as detailed in Verheul et al. [2]) was determined over the same time period. A 2 x 2 repeated-measures ANOVA was performed to assess the influence of calculation methods on initial knee joint stiffness between shoe conditions.

RESULTS AND DISCUSSION

There was a significant interaction between calculation methods and shoe conditions ($F_{1,11}$=86.4, p=0.001). Figure 1 shows no significant difference in knee joint stiffness between the two shoe conditions using the traditional calculation method (p=0.774) which is in accordance with the literature [4]. When using the kinematic-only method, the thick shoe resulted in ~34% increase (p=0.001) in initial knee joint stiffness compared to that of the thinner midsole condition. The kinematic-only approach can be more influenced by the initial dynamics of landing, particularly the rate of knee flexion at the instant of ground contact. At this instant the knee was similarly flexed for the two shoe conditions, but the rate of knee flexion was significantly higher for the thinner midsole shoes (Table 1). This likely contributes to the lower initial knee stiffness during the impact phase for that shoe and can be partly explained by the notion of maintaining system stiffness. Adapting to more cushioning provided by a thick midsole, the body may increase initial knee joint stiffness to maintain the shod lower limb combined system stiffness. If the knee joint does not become stiffer with more cushioned shoes, the whole system will be less stiff and potentially detrimental to running economy [5].

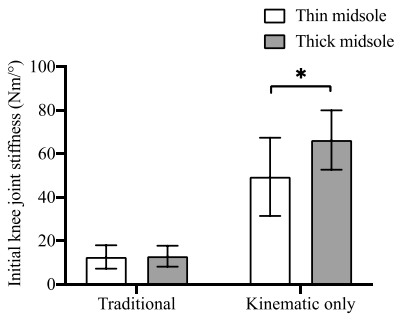

Figure 1 Initial knee joint stiffness in the two shoe conditions using the two calculation methods. * Significant at p<0.001.

Table 1 Knee flexion angle and angular velocity at initial contact (IC) during running in the two shoe conditions, * significant at p<0.001.

	Thin	Thick
Knee flexion angle at IC (°)	17.8 ± 5.9	18.6 ± 5.4
Knee flexion velocity at IC (°/s)	**241.1 ± 77.4***	201.4 ± 81.7

CONCLUSIONS

The moment-angle relationship for determining initial knee joint stiffness might be less sensitive to elicit the effect of different cushioned running shoes compared to kinematic-derived stiffness estimates that emphasise the initial dynamic conditions of foot strike during running.

REFERENCES

[1]Zhang and Lake. *Front. Sports Act. Living* **4**:824183, 2022.
[2]Verheul et al. *J. Appl. Physiol.* **122**(3):653-65, 2017.
[3]Johnson and Davis. *Gait Posture* **96**:149-53, 2022.
[4]Gruber et al. *J. Appl. Biomech.* **37**(5):408-14, 2021.
[5]Li et al. *J. Strength Cond. Res*. **35**(6):1491-99, 2021.

EFFECTS OF THE NIKE VAPORFLY 4% FEATURES ON MUSCLE ACTIVITY

Ashna Subramanium[1], Juan Aguero[1,2], Sandro R. Nigg[1] and Benno M. Nigg[1]
[1] Human Performance Laboratory, Faculty of Kinesiology, University of Calgary, Calgary, Canada.
[2] Universidad Iberoamericana Ciudad de Mexico, Mexico City, Mexico.
Email: ashna.subramanium@ucalgary.ca

INTRODUCTION

The Nike Vaporfly 4% (VP4) running shoe is often referred to as a game changer in improving running economy and performance. The substantial 4% energy savings observed have been attributed to a compliant and resilient midsole foam, curved carbon-fibre plate, and the shoe geometry [1]. Studies have tried to explain the observed results by comparing running mechanics in the VP4 shoe to previously established running shoes. One variable that is unexplored thus far, is the muscle activity while running in the VP4 shoes, even though muscle contractions are known to affect whole-body aerobic energy expenditure during locomotion [2]. Furthermore, almost all studies to date have compared the VP4 shoe to other running shoes (e.g., adidas Boost), which are substantially different in their construction This makes it challenging to explain the source of the observed improvements. Therefore, the purpose of this study was to investigate the effects of the VP4 shoe features on lower-limb muscle activity during running for three systematically changed construction features, the carbon fiber plate, the midsole material and the toe spring.

METHODS

Twelve healthy adult males participated in this study. All participants performed overground running at a constant speed of 3.9 m/s in four shoe conditions. The three test conditions were a prototype version of the VP4 shoe. These included “No Plate”, in which the carbon fibre plate had been removed from the midsole, “EVA”, in which the Nike PEBAX foam was replaced with a low-density EVA, and “Toe Wedge”, in which the toe spring was blocked by a foam wedge. The control condition was the original VP4. Muscle activity data were collected using a surface electromyography (EMG) system from four lower-leg muscles (tibialis anterior (TA), gastrocnemius medialis (GM), peroneus longus (PL), and the soleus (SOL)) at a sampling frequency of 2000 Hz. The overall EMG intensity was determined for each muscle in the four shoe conditions for each subject. Finally, the percent change in the overall EMG intensity was summarized (Fig. 1) to present the number of subjects that showed a higher versus lower intensity while running in the test shoes compared to the control shoe. A subject was considered to have a higher or lower intensity in the test shoe if they showed a change in intensity greater than ±5%.

RESULTS AND DISCUSSION

All three features (carbon plate, midsole material, and toe spring) tested in this study affected EMG intensity during running. Changes in EMG intensity were subject-specific, such that some subjects showed higher intensity, while some showed lower intensity in the test shoes compared to the control. Overall, subjects showed a relatively larger change of up to 100% when increasing the intensity, compared to a smaller change of up to 25% when decreasing the EMG intensity.

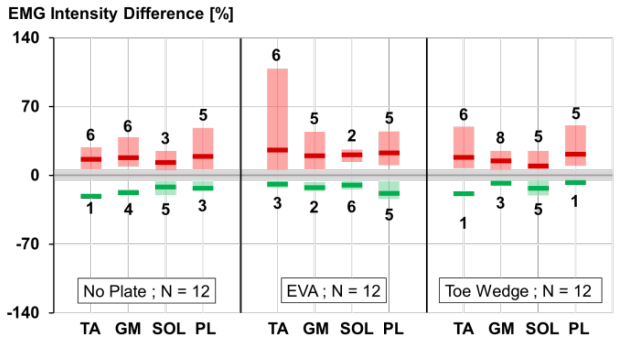

Figure 1. Changes in EMG intensity in the three test shoes (No Plate, EVA, and Toe Wedge) relative to the original Nike Vaporfly 4% (control) shoe in the four muscles (TA: Tibialis Anterior, GM: Gastrocnemius Medialis, SOL: Soleus, PL: Peroneus Longus). Positive values represent a higher EMG intensity, while negative values represented a lower EMG intensity in the test shoe compared to the control. The red and green shaded bars represent the percent change range observed in each test condition and each muscle, with the average presented by a solid red/green line within the shaded area. The numbers above and below the bars represent the number of subjects that showed an increase or decrease in the EMG intensity in the respective test shoes and muscles.

CONCLUSIONS

The Nike Vaporfly 4% shoe features such as the curved carbon fibre plate, PEBAX foam, and the forefoot geometry affect muscle activity during running. Differences in muscle activity adaptations in runners may help explain the large inter-runner variability in performance benefits achieved with advanced running shoes like the Nike Vaporfly 4%.

ACKNOWLEDGEMENTS

The prototype shoe modifications were done by *Orthotics in Motion, Calgary, Canada.*

REFERENCES

[1] Hoogkamer W et al. *Sports Med.* **49**: 133–43, 2019.
[2] Beck O N et al. *Scientific Reports.* **10**: 17154, 2020.

The effects of habitual foot strike pattern and footwear on running pattern and economy

Hyunji Kim[1,2], Jooeun Ahn[1,2,3]
[1] Department of Physical Education, Seoul National University, Seoul, South Korea.
[2] Soft Robotics Research Center, Seoul National University, Seoul, South Korea.
[3] Institute of Sport Science, Seoul National University, Seoul, South Korea.
Email: ahnjooeun@snu.ac.kr

INTRODUCTION

Minimalist shoes (MIN) have been known to induce barefoot running and enable runners to take more mechanical advantage than conventional cushioned running shoes (CON) [1] . Recently, racing shoes that boost the performance of long-distance runners with thick curved outsole and carbon-fiber plates (e.g. Alphafly; AF, Nike) have been additionally developed [2]. Multiple studies addressed the effects of MIN and CON on the running style [1], but they analyzed only the resultant pattern without considering the runner's original habitual pattern. Recent studies also compared the effects of AF and conventional shoes on running economy (RE) [2, 3], but there is still a lack of comprehensive understanding of the effect of shoe type on running pattern and RE. This study aims to investigate the hitherto unknown interaction between the habitual foot strike angle (FSA) and shoe conditions, and their effects on RE.

METHODS

Nine male recreational runners (Mean ± SD: age 29.0 ± 3.8 years; height 1.75 ± 0.04 m; body mass 73.7 ± 4.8 k) visited the laboratory on two separate days at least 48 hours apart and within a 2 week period. On the first visit, the participants performed an incremental test so that we could select the intensity of running on the next visit and measure their preferred FSA. Participants were divided into three groups based on their FSA: forefoot, midfoot and rearfoot strike runners. On the second visit, we provided the participants with 3 pairs of shoes: MIN (Asics SORTIEMAGIC RP5, average shoe mass: 160 g, offset: 0 mm), CON (Adidas UltraBoost 20, average shoe mass: 310 g, offset: 10 mm) and AF (Nike Air zoom α-fly next%, average shoe mass: 210 g, offset: 4 mm). The participants completed 3 sets of 7 min running (1 min at 70%, 1 min at 80%, and 5 min at 90% of maximal velocity) on a treadmill wearing one of the 3 different footwear during each set. The order of shoe conditions was randomized. We measured FSA and $\dot{V}O_2$ values at velocities below the ventilation threshold. We then performed multiple factor (3 shoe conditions × 3 habitual FSA groups) repeated measures ANOVA to identify their effects on FSA and RE.

RESULTS AND DISCUSSION

Depending on habitual FSA measured on the first visit, 3, 5, and 1 participants were categorized as rearfoot, midfoot, and forefoot group, respectively. The two- way ANOVA shows significant main effects of the group and significant interaction (group × shoe condition) on FSA. Additionally, we observed significant main effects of the group and shoe condition on RE. Compared with CON, AF and MIN improved RE by 4.96% and 3.08%, respectively with statistical significance. Post-hoc multiple comparisons additionally show that 1) FSA significantly decreased under AF and MIN conditions compared to CON condition for rearfoot group; 2) RE was significantly improved in midfoot and forefoot groups compared to rearfoot group; and 3) RE was significantly improved under AF condition compared to CON in midfoot and rearfoot groups (Figure 1). These findings demonstrate that AF with thick outsole saves metabolic cost by returning the energy effectively, but this merit is more noticeable in runners with habitual patterns of rearfoot and midfoot strike.

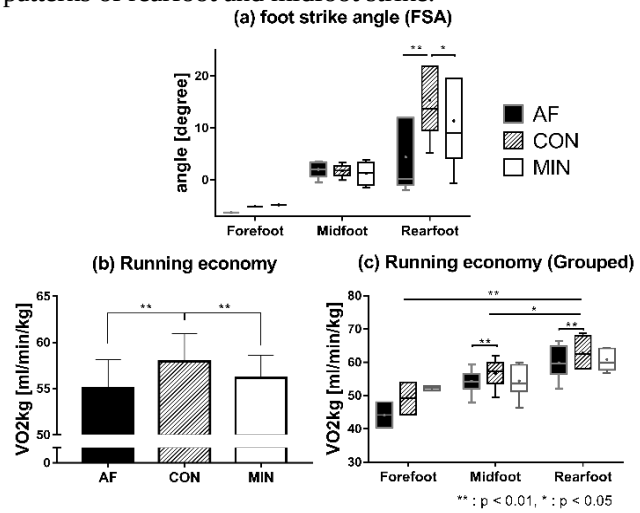

Figure 1. The outcome values for each group (forefoot, midfoot or rearfoot) and shoe condition (AF, CON or MIN). Dots and lines in the box indicate mean and median values, respectively.

CONCLUSIONS

Studies analysing the effect of footwear or other interventions should consider the habitual pattern of the runners as well as the designed intervention.

ACKNOWLEDGEMENTS

This research was supported by the National Research Foundation of Korea (NRF) Grants funded by the Korean Government (MSIT) (No. 2016R1A5A1938472).

REFERENCES

[1] Davis, I. S. et al. *Exer and Sports Sci Rev* **49(4)**: 228-243, 2021.
[2] Hoogkamer, W. et al. *Sports Med* **48(4)**:1009-1019, 2018.
[3] Sinclair, J et al. et al. *J of sports Sci* **34(11)**:1094-1098, 2016.

USING GAZE-TRACKING TO ASSESS COGNITIVE LOAD IN LOWER LIMB PROSTHETIC USERS

Sabina Manz[1,2], Michael Ernst[1], Thomas Schmalz[1], Strahinja Dosen[2] and Jose Gonzalez-Vargas[1]
[1] Ottobock SE & Co. KGaA, Duderstadt, Germany.
[2] Department of Health Science and Technology, Aalborg University, Aalborg, Denmark.
Email: sabina.manz@ottobock.de

INTRODUCTION

Clinical assessments of lower limb prosthetic users primarily focus on performance and psychological outcome measures [1]. The assessment of cognitive load, however, is often neglected.

It is known that lower limb prosthetic users have to deal with an increase in cognitive load (e.g., by focusing on the device during walking) [2,3], and research has shown that their gaze behavior, which indicates the focus of attention [4], indeed differs from the able-bodied population [5].

Therefore, gaze tracking might be an instrument to measure cognitive load while using a lower limb prosthesis, but this has not been investigated before. The aim of the present study was to test the feasibility of using gaze tracking for the assessment of cognitive load in lower limb prosthesis users.

METHODS

Two participants (P01 and P02) with unilateral transfemoral amputation (mobility level K3) participated in this pilot study. During the study, the participants wore a microprocessor-controlled prosthetic knee joint (GeniumX3, Ottobock). The participants were asked to perform a battery of tasks, including level walking (LW), walking on uneven ground (UW), obstacle avoidance (OB), a combination of stair ascent and ramp descent (SURD), as well as ramp ascent and stair descent (RUSD), in addition to a task outside of the laboratory (staircase climbing, SCUp/SCDown). For each task, the participants were asked to focus their visual attention on a target at the end of the walkway, unless they felt the need to look somewhere else (i.e., down on the pathway).

A mobile eye tracker (Tobii Pro Glasses 3) measured gaze location (i.e., focus of attention) during all tasks, and target fixation time expressed in % relative to total trial time was calculated. In addition, the participants were asked to rate the perceived cognitive demand of each task on an interval scale from 1 (very, very low) to 9 (very, very high).

Kinematic data were recorded from all laboratory-based tasks using an optical motion capture system.

Spearman's rank correlation coefficients were determined to describe the relationship between gaze data and perceived cognitive load.

RESULTS AND DISCUSSION

Figure 1 shows a significant negative correlation between target fixation time and subjective rating of cognitive load for P01 ($r = -0.91$, $p < 0.01$). Contrarily, P02 perceived all tasks as very easy (rated as 1) and the target fixation times did not decrease substantially (no correlation coefficients could be determined).

The results of P01 highlight the potential of a mobile eye tracker to measure cognitive load representative of perception.

Furthermore, the target fixation time was able to show that the tasks were not difficult enough for P02 to have an effect on cognitive load, leading to inconclusive results in this case (Figure 1).

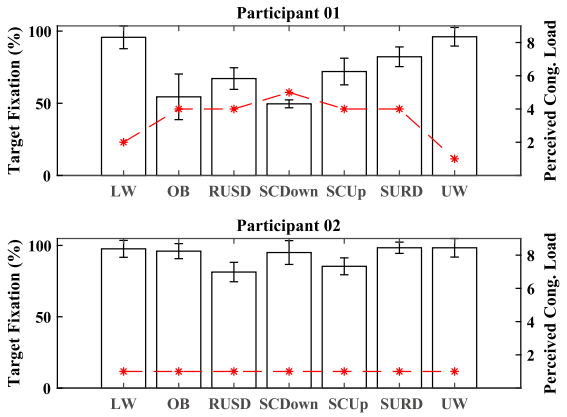

Figure 1 Target fixation times (in %, mean ± standard deviation) and perception of cognitive load (red dashed lines and asterisks) of all tasks for P01 and P02.

CONCLUSIONS

This pilot study has shown that using a mobile eye tracker could be an easy, objective measure for assessing the cognitive load of lower limb prosthetic users. Importantly, the approach of measuring cognitive load with a mobile eye tracker could be used outside of a laboratory environment, in the everyday lives of the users.

Future analyses of the kinematic data including more participants will be conducted to investigate if and how an increase in cognitive load affects performance.

ACKNOWLEDGEMENTS

This work is supported by the Marie Skłodowska-Curie Actions (MSCA) Innovative Training Networks (ITN) H2020-MSCA-ITN-2019 - 860850 – SimBionics.

REFERENCES

[1] Resnik L & Borgia M. *Phys Ther* **91**, 2011.
[2] Miller et al. *Arch Phys Med Rehabil* **82**, 2001.
[3] Möller S et al. *Prosthet Orthot Int* **43**, 2019.
[4] Eckstein M et al. *Dev Cogn Neurosci* **25**, 2017.
[5] Li M et al. *41st Ann Int Conf IEEE EMBC*, 2019.

Upper Extremity Kinematics are Affected by Socket Suspended Prostheses during Reaching Motions

Julia A. Dunn[1,2], Bob Wong[3], Sarina K. Sinclair[4], Heath B. Henninger[1,2], Kent N. Bachus[1,2,4], K. Bo Foreman[2,4,5]
[1]Department of Biomedical Engineering University of Utah, [2]Department of Orthopaedics University of Utah,
[3]College of Nursing University of Utah, [4]Department of Veterans Affairs, Salt Lake City, Utah,
[5]Department of Physical Therapy and Athletic Training University of Utah
Email: julia.dunn@utah.edu

INTRODUCTION

Individuals with transhumeral (TH) limb loss have the highest rate of prosthesis abandonment, up to 60%, often citing limited motion as the cause [1,2]. The conventional TH socket restricts movement, but there is a lack of literature regarding how TH prostheses impact kinematics during activities of daily living (ADLs). The present study aims to investigate the impact conventional socket-suspension systems have on a simple proprioceptive targeting motion in a cohort of individuals with TH amputation, specifically understanding how the use of a prosthesis affects body movement and positioning while reaching.

METHODS

Eight male subjects with TH limb loss and socket-suspended prostheses participated in the study (median age: 58 years (range 29-77). Four subjects used a body-powered hook, one a myoelectric hook, and three a myoelectric hand. The subjects had used their devices for a median of 5 years (range 2-12). Subjects completed a proprioceptive targeting task with their intact and prosthetic limb [3] under a 24-camera VICON Motion Analysis motion capture system (Vicon Motion Systems Ltd., Oxford, UK) at the Veterans Affairs Salt Lake City Gait Lab. A modified Plug-In Gait marker set was used to track the trunk, head, arms, forearms, and hands. The marker trajectory data were filtered in Visual3D (v6, C-Motion; Germantown, MD) with a fourth-order, low-pass Butterworth filter with a cut-off frequency of 6 Hz. Horizontal and vertical areas between the path of the targeting hand and the direct line between the start and end points of each trial were calculated. Motion smoothness was calculated from the number of velocity peaks, where an inverse relationship exists between motion smoothness and the number of velocity peaks [4]. Glenohumeral (GH) and trunk angular displacement were defined as the difference in joint angles at the start and end of each trial. Paired-Sample Wilcoxon Signed Ranks tests were used to compare the targeting conditions – intact versus prosthetic limb. Results are reported as mean (95% CI), $p \leq 0.05$ was significant.

RESULTS AND DISCUSSION

No significant difference was measurable in horizontal area when targeting with the intact limb v. the prosthesis, 14.56 cm^2 (0.60-28.52) vs. 15.32 cm^2 (7.99-22.64), respectively. No significant difference was measurable in vertical area when targeting with the intact limb v. the prosthetic limb, 25.37 cm^2 (3.27-47.47) vs. 63.83 cm^2 (0-127.69), respectively. The reaching motion was significantly more smooth when targeting with the intact limb compared to the prosthetic limb, 3.13 velocity peaks (1.78-4.47) vs. 2.25 velocity peaks (1.48-3.01), respectively, $p = 0.04$. This finding is consistent with the way distal joints are used for corrective movements in proprioceptive positioning, joints which are not actively repositioned when targeting with the prosthesis. GH flexion was significantly greater when subjects targeted with their intact limb than when they targeted with their prosthesis. In the three axes of trunk angular motion – flexion, lateral flexion, and rotation – there was significantly less angular displacement when targeting with the intact limb than the prosthesis (Table 1).

Table 1. Joint angular displacement during targeting. *p≤0.05

	Intact Limb	Prosthetic Limb
GH Flexion, mean (95% CI)	21°(16-26)	9°(2-15)*
Trunk Flexion, mean (95% CI)	1°(0-2)	12°(6-17)*
Trunk Lateral Flexion, mean (95% CI)	1°(0-2)	5°(3-6)*
Trunk Rotation, mean (95% CI)	3°(1-4)	9°(4-14)*

Our results identified significant impacts on kinematics when reaching with the prosthesis, as quantified by the differences in motion smoothness and joint angular displacements. These differences may effect how individuals use their prostheses: compensatory motions may impact neck and back pain and differences in smoothness could result in less reliable fine movements. Future studies will investigate the impact of TH prosthetics on body positioning and movement during a broader range of ADLs and other complex tasks.

CONCLUSIONS

This study aimed to quantify differences in kinematics between the intact limb and prosthetic limb in individuals using socket-suspended TH prostheses. Significant differences during a simple reaching task were identified. Understanding these impacts will enable future studies comparing socket-suspended systems to osseointegrated endoprosthetic systems for functional changes related to the suspension method.

ACKNOWLEDGEMENTS

This work was supported by the Department of Veterans Affairs Medical Research Funds (RX003071, RX002935) , resources at both the Salt Lake City VA Medical Center and the Orthopaedic Research Laboratory, University of Utah School of Medicine, Salt Lake City, Utah.

REFERENCES

[1] Wright T., et al. J Hand Sur, 20: 619-622, 1995.
[2] McFarland, L., et al. J Rehab Res & Dev, 47: 299, 2010.
[3] Dunn, J., et al. Arch Rehabil Res Clin Transl, 4:100202, 2022
[4] Schneiberg, S., et al. Dev Med Child Neuro, 52: 167-173, 2010

Straight-line walking on cross-slope in unilateral transfemoral prosthesis users

Genki Hisano[1,2,3], Xavier Bonnet[4], Lucas Sedran[4], and Helene Pillet[4]

[1] Tokyo Institute of Technology, Tokyo, Japan, [2] National Institute of AIST, Tokyo, Japan,
[3]Research Fellow of Japan Society for the Promotion of Science, Japan,
[4]Institut de Biomecanique Humaine Georges Charpak, Arts et Metiers Sciences et Technologies, Paris, France
email: hisano.g.aa@gmail.com

INTRODUCTION

Cross-slope walking is recognized as a daily encountered task and a greater biomechanical challenge than level walking in transfemoral prosthesis users (TFPUs) [1,2]. When walking on an inclined surface, the component of gravity along the slope always acts to pull the individual toward the bottom of the slope. To achieve the stable straight-line walking on the cross-slope, the individual is required to generate an equal amount of upward mediolateral ground reaction force (GRF) impulse to counteract this downward gravitational impulse. In particular, unilateral TFPUs have two different conditions; the prosthetic limb is either on the lower side or on the upper side. Thus, compared to able-bodied controls, they would have more difficulty in achieving the similar amount of mediolateral GRF impulse as gravitational impulse for both conditions. Therefore, the aim of this study was to compare the mediolateral GRF impulse and the gravitational impulse during cross-slope walking in unilateral TFPUs and able-bodied controls.

METHODS

Twelve unilateral TFPUs and fourteen able-bodied controls were asked to perform straight-line walking on a 6° (10%) inclined cross-slope surface at their self-selected walking speed. We recorded the GRF using two force platforms integrated in the cross slope for both limbs. At least four successful trials were selected for both the lower and upper prosthetic conditions. The upward mediolateral GRF impulse was calculated as the sum of the upward GRF impulses of the lower and upper side limbs. Further, the downward gravitational impulse during the gait cycle was calculated as the product of body weight, $\sin 6°$, and gait cycle time. All variables were normalized to the body weight of each participant. Finally, paired *t*-tests were performed to check the statistical differences in the upward ML GRF impulse and downward gravitational impulse for all conditions. Statistical significance was set at $p < 0.05$.

RESULTS AND DISCUSSION

Fig.1A&B shows the averaged mediolateral GRF for unilateral TFPUs and able-bodied controls during the stance phase of cross-slope walking. For the unilateral TFPUs, the upward mediolateral GRF impulse was significantly greater than that of the downward gravitational impulse for both the lower ($p < 0.001$) and the upper ($p < 0.001$) prosthetic conditions (Fig. 1C).

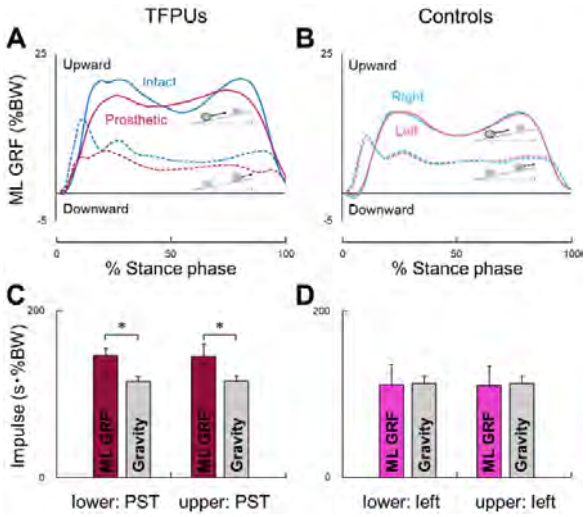

Figure 1 A, B) Averaged waveform of mediolateral (ML) GRF for TFPUs and able-bodied controls during the stance time of cross-slope walking. Positive GRF indicates the upward direction (from bottom to top side) along the cross-slope. Bold and dashed lines indicate lower and upper side conditions, respectively. **C, D)** Comparison between upward ML GRF impulse and downward gravitational impulse for TFPUs and able-bodied controls in both conditions: the prosthetic limb is on the lower side (lower: PST) and on the upper side (upper: PST). An asterisk (*) indicates a significant difference between ML GRF impulse and gravitational impulse.

However, no significant differences were observed between the two impulses for the able-bodied controls in either the lower and top left condition (Fig. 1D). These results suggest that the unilateral TFPUs in both conditions move upward rather than in a completely straight direction. This extra upward impulse could provide a margin of safety if the TFPUs encounter a disturbance that pushes them downward and causes them to fall.

CONCLUSIONS

TFPUs showed larger upward mediolateral GRF impulses than downward gravitational impulses during cross-slope walking, whereas able-bodied controls showed no significant differences between the two impulses. These results suggest that unilateral TFPUs have the specific mediolateral GRF control strategies compared to the able-bodied controls.

ACKNOWLEDGEMENTS

This work was supported by JSPS KAKENHI (20J20572), JST-Mirai Program (JPMJMI21H5), and ANR (ANR-292 2010-TECS-020).

REFERENCES

[1] Villa C et al., *Clin Biomech* **30:** 623-628, 2015
[2] Villa C et al., *Arch. Phy M* **98:** 1149-57, 2017

Unilateral transfemoral amputees might be at risk of lateral compartment degeneration of the knee joint

Diana Toderita[1], Clement D. Favier[1], David P. Henson[1], Vasiliki Vardakastani[1], and Anthony M.J. Bull[1]
[1] Department of Bioengineering / Imperial College, London, United Kingdom.
Email: diana.toderita15@imperial.ac.uk

INTRODUCTION

High-functioning unilateral transfemoral amputees (UTF) are susceptible to intact knee osteoarthritis (OA) [1], which is a mechanically-mediated condition. Unilateral transtibial amputees (UTT) are known to show medial intact knee compartment overload, which might explain the risk of OA for UTT [2], but little is known for UTF. This study aims to understand the mechanical indicators of the development and progression of knee OA in the UTF population.

METHODS

Gait motion capture and force plate data were collected from seven UTF with no known secondary conditions. All participants were fitted with microprocessor-controlled prosthetic knees and dynamic response feet and have been prosthesis users for a minimum of two years. Seven able-bodied people (AB) were group matched to the UTF cohort by sex, age, height, and mass. The control dataset is a subgroup of a previous dataset [3]. Musculoskeletal modelling was performed using Freebody to compute joint contact forces [4].

RESULTS AND DISCUSSION

Figure 1 and Table 1 present the knee loading characteristics for UTF and AB. Whilst the UTF lateral compartment of the knee presented higher loading rates, peaks, and impulse (area under the force curve) than AB, there were no significant differences in the medial knee loading between UTF and AB. These findings show that the higher knee loading for UTF is localized to the lateral compartment. As high and repetitive loading might lead to joint degeneration [5], the higher knee loading rate, lateral knee contact forces and impulse observed in this study indicate that UTF might be more susceptible to lateral knee OA as opposed to medial knee OA, as is the case for UTT [2].

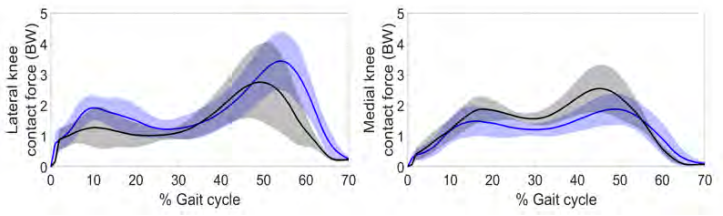

Figure 1. Lateral and medial intact knee joint contact forces. UTF – blue. AB - black.

CONCLUSIONS

Unexpectedly, this study's results indicate that the higher functional demand of the intact limb compared to AB may increase the risk of lateral knee OA in the UTF population, as opposed to UTT who might be more susceptible to medial knee OA [2]. Mitigation strategies could be explored through prosthesis adjustments, including alignment to shift the ground reaction force vector, or muscle strengthening to ensure optimal long-term musculoskeletal health.

ACKNOWLEDGEMENTS

The financial support from the Royal British Legion Centre for Blast Injury Studies is gratefully acknowledged.

REFERENCES

[1] Norvell D et al. *Arch. Phys. M.* **86**: 487-493, 2005.
[2] Ding Z et al. *J. Orthop.* **39**: 850-860, 2021.
[3] Long MJ et al. *Clin. Biomech.* **47**: 87-95, 2017.
[4] Cleather DJ et al. *R. Soc. Open Sci.* **2**: 140449, 2015.
[5] Ewers et al. *J. Orth. Res.* **19**: 779-784, 2001.

Table 1: Intact knee joint loading rate, contact forces and impulse.

	UTF	AB	*p-value*
Knee loading rate (Nm/(kg.s))	4.8 ± 1.7	3.4 ± 0.5	$p = 0.045$
1st peak lateral knee force (BW)	2.1 ± 0.4	1.6 ± 0.5	$p = 0.024$
2nd peak lateral knee force (BW)	3.5 ± 0.9	2.8 ± 1.3	$p = 0.322$
Lateral knee impulse (BW.s/m)	98.5 ± 17.0	77.1 ± 18.3	$p = 0.029$
1st peak medial knee force (BW)	1.6 ± 0.5	1.9 ± 0.4	$p = 0.164$
2nd peak medial knee force (BW)	2.0 ± 0.5	2.5 ± 0.7	$p = 0.131$
Medial knee impulse (BW.s/m)	63.7 ± 13.8	72.8 ± 14.7	$p = 0.108$

A non inferiority approach to investigate the influence of stem fixation and stem type on revision rates in elective THA procedures depending on patient age

Michael Morlock[1], Oliver Melsheimer[2]

[1] Institute of Biomechanics, Hamburg University of Technology (TUHH), Hamburg, Germany.
[2] German Arthroplasty Registry (EPRD Deutsches Endoprothesenregister gGmbH), Berlin, Germany.
Email: morlock@tuhh.de

INTRODUCTION

The overall early revision rate in elective Total Hip Arthroplasty (THA) three years after surgery is lower for cemented stems in the German Arthroplasty Register (EPRD): cemented 2.9% (2.8 - 3.0) vs. uncemented 3.4% (3.3 - 3.5). In elderly patients, however, the mortality rate is elevated for cemented fixation [1]. Consequently the outcome of uncemented stem fixation with increasing patient age has to be analysed in more detail to understand, how stem type and fixation affect the revision rate with increasing patient age.

METHODS

Elective primary THA cases for primary Coxarthrosis using uncemented cups without reconstruction shells were selected from the EPRD data base (n_0= 294,442). Five stem types were defined: cementless, cementless with collar, cementless short, cemented, and cemented with collar. Stems with at least 300 cases at risk three years after surgery were analysed individually. Revision rates of stem types were analysed in 4 age cohorts: below 60 years (“young”), between 60-70 (“mid-1”), between 70-80 (“mid-2”) and above 80 (“old”). The reference stem [2] for each cohort was determined as the stem with the lowest revision rate and at least 1000 cases under surveillance 3 years after surgery (n_3 = 151,035).

RESULTS AND DISCUSSION

No significant differences in revision rates between stem types and fixation were found for the “young” cohort (not shown). In the “mid-1” cohort, the revision rate for “cementless” stems was higher than for “cementless short” (p<0.001) and “cementless collared” stems (p< 0.001) (Table 1). In the “mid-2” cohort, “cementless stems” showed a higher revision rate as all other stem types (p<0.001; Table 1). “Cemented” and “uncemented collared” stems performed best in the “old” group with uncemented stems being inferior by 20% (Figure 1).

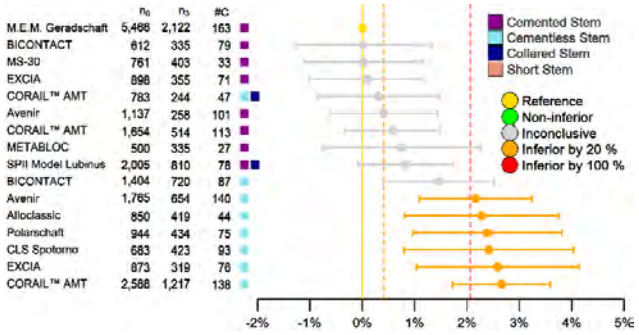

Figure 1: Non-inferiority plot for the investigated hip stems (type, fixation, design) in the “old” patient group.

CONCLUSIONS

“Cementless” and “cementless short” stems should not be used in patients older 80 years due to the higher risk of revision due to peri-prosthetic fracture [3]. The use of “cementless” stems in 70-80-year-old patients should be considered very carefully due to the increased revision risk shown in the EPRD. If cementing should be avoided, “cementless collared” stems seem to be a good alternative.

REFERENCES

[1] Della Valle A et al. JoA **37**: 1105-10, 2022
[2] Deere K et al. BMJ Open **9**: e026685
[3] Konow T et al. Bone&JointJ **103-B(4)**:650–658..

Table 1: Revision rates of the five stem types/fixation for the “mid-1” and “mid-2” age groups (n: number of stems implanted; age: median age; M/F: % male; BMI: body mass index; ASA: American Society of Anesthesiologists physical status classification; clinics: # of hospitals using the type; R_3: revision risk at 3 years; L_3/U_3: lower/upper confidence interval; n_3: number of stems under observation at 3 years.

Type	n_0 [#]	Age [years]	M/F [%]	BMI [kg/m²]	ASA [1 to 5]	Clinics [#]	R_3 [%]	L_3 [%]	U_3 [%]	n_3 [#]	Age group
cemented stem	3,904	68	26.0	28.4	2.3	431	**2.5**	2.0	3.1	2,045	mid-1
cemented collared stem	863	68	24.6	28.7	2.2	83	**3.4**	2.3	5.0	465	mid-1
cementless stem	70,747	66	40.3	28.7	2.1	683	**2.9**	2.8	3.1	37,329	mid-1
cementless collared stem	2,563	66	37.8	28.3	2.0	75	**1.5**	1.1	2.1	1,001	mid-1
cementless short stem	11,706	65	43.3	28.1	2.1	283	**2.2**	2.0	2.5	5,314	mid-1
cemented stem	23,194	77	24.1	27.0	2.3	572	**2.5**	2.3	2.7	12,466	mid-2
cemented collared stem	5,373	77	26.9	27.0	2.3	142	**2.3**	1.9	2.7	2,913	mid-2
cementless stem	71,969	75	36.6	27.5	2.3	686	**3.7**	3.5	3.8	39,644	mid-2
cementless collared stem	3,006	76	31.8	26.8	2.1	80	**2.3**	1.8	3.0	1,295	mid-2
cementless short stem	6,318	75	40.1	27.2	2.2	216	**2.6**	2.2	3.0	2,787	mid-2

CENTER OF MASS KINEMATICS ROBUSTLY PREDICT REACTIVE JOINT TORQUES AT THE ANKLE, KNEE, AND HIP DURING PERTURBED STANDING

Kristen Jakubowski[1*], Giovanni Martino[1], Gregory Sawicki[2], Lena Ting[1]

[1] Wallace H. Coulter Department of Biomedical Engineering, Emory University & Georgia Institute of Technology, Atlanta, USA [2] George W. Woodruff School of Mechanical Engineering, Georgia Institute of Technology, Atlanta, USA *Email: kjakubo@emory.edu

INTRODUCTION

Mimicking the healthy physiological response to postural perturbations may aid in developing robotic devices that augment human balance. Additionally, a *global* control scheme, where one control signal can be used for multiple joints, greatly simplifies the control of robotic devices compared to relying on an independent signal for each individual joint. Interestingly, the reactive muscle activity elicited in multiple leg muscles in response to postural perturbations is driven by *global* feedback of center of mass (CoM) kinematics [1]. Inspired by this physiological principle, Afschrift et al. [2] recently demonstrated that *global* feedback also drives the reactive torque at the ankle during standing and walking. However, it remains to be seen if this *global* feedback principle underlies the multi-joint torque response. Accordingly, we tested the feasibility of using *global* feedback of CoM kinematics to predict the reactive multi-joint torque response at the ankle, knee, and hip to perturbations during standing.

METHODS

We assessed reactive leg joint torques to backward support surface perturbations in 7 healthy young adults (25 ± 4 years). Participants maintained standing balance during randomized ramp and hold perturbations at 12 cm or 75%, 85%, and 95% of their step threshold, each tested four times. Whole-body kinetics and kinematics were used to estimate ankle, knee, and hip torques using the OpenSim Inverse Dynamics (ID) tool [3].

We used a modified version of the previously developed sensorimotor response model (SRM) [1] to estimate the reactive joint torques as a time-delayed linear combination of CoM kinematics. The previous SRM could only fit non-negative signals, such as electromyography (EMG). Thus, we modified it to predict negative signals, like joint torques (Fig 1A). Additionally, the previous SRM captured the direction-specific muscle-level responses (e.g., agonist muscles activated in response to CoM acceleration while antagonist muscles responded to CoM deceleration). Since we are examining the joint-level response, which is the net effect of the activation of individual muscles, we modified the model to predict the joint torque response to both CoM acceleration and deceleration. The goodness of fit between the ID and CoM estimated ankle, knee, and hip torques were assessed using R^2 (similarity in shape), and variability accounted for (VAF; similarity in magnitude). One-tailed t-tests were performed evaluating $R^2 \geq 0.75$ and VAF $\geq$ 75%.

RESULTS

For all joints and all perturbation magnitudes, the SRM reconstructed the ID torques well. The ID joint torques (Fig 1A, black) were similar in shape and magnitude to the CoM-derived joint torque (Fig 1A, green & yellow). Hip torque increased immediately following the perturbation, while ankle torque was delayed, which may be due to differences in tendon compliance between hip and ankle musculature that impact how muscle short-range stiffness is transferred to the joint. Across all participants, ankle (yellow), knee (blue), and hip (green) torque were reconstructed well for all perturbation magnitudes (all $p > 0.05$; Figure 1 B & C).

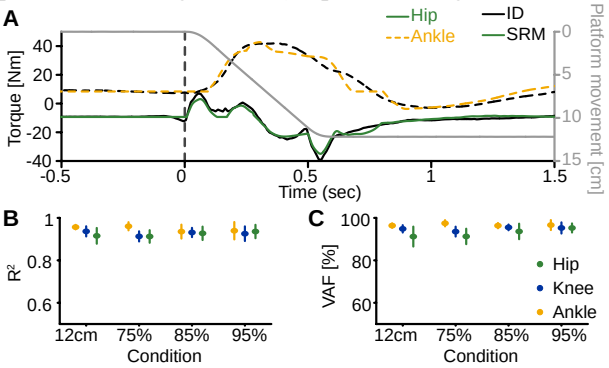

Figure 1 (A) Representative ID (black) and SRM-based reactive hip (solid, green) and ankle (dotted, yellow) torque to a 12 cm perturbation. The dotted grey line indicates the start of the perturbation, while the solid grey line is the movement of the platform. Positive torque indicates plantarflexion and hip flexion. (B & C) The R^2 and VAF across all participants during each perturbation condition (12 cm to 75%, 85%, and 95% of step threshold) for the ankle (yellow), knee (blue), and hip (green).

DISCUSSION & CONCLUSION

We found that a single control signal (CoM kinematics) can accurately predict the multi-joint torque response to standing perturbations of varying magnitude. These results provide important insights into the joint-level neuromechanical control of balance. Additionally, a physiologically-inspired *global* control scheme, with a one-to-many rather than one-to-one mapping, may simplify the control of lower-limb exoskeletons, prostheses, and bipedal robots.

ACKNOWLEDGEMENTS

Supported by NSF: ASEE #2127509

REFERENCES

[1] Welch & Ting. *J Neurophys* **101**: 6, 2009
[2] Afschrift et al. *PLOS Comput Biol* **17**: 6, 2021
[3] Delp et al. *IEEE T Bio-med Eng* **54**: 11, 2007

PERSONAL STANDING MOBILITY QOLO ENABLES PEOPLE WITH LOWER LIMB IMPAIRMENTS TO VOLUNTARILY STAND UP

Yukiyo Shimizu[1], Hideki Kadone[2], Yosuke Eguchi[3], Kai Sasaki[3], Yasushi Hada[1] and Kenji Suzuki[4]

[1] Department of Rehabilitation Medicine, Institute of Medicine, University of Tsukuba, Tsukuba, Japan.
[2] Center for Innovative Medicine and Engineering, University of Tsukuba Hospital, Tsukuba, Japan.
[3]Qolo Inc., Tsukuba, Japan.
[4]Center for Cybernics Research, University of Tsukuba, Tsukuba, Japan.

Email: shimiyukig@md.tsukuba.ac.jp

INTRODUCTION

Wheelchairs are crucial mobility devices for people with impairments in the trunk and lower limbs. However, when using a wheelchair, users are forced to maintain a prolonged sitting position. As a result, eye height differences, accessibility issues and complications related to sitting occur. We are developing Qolo, a mobility device that enables people with lower limb impairments to stand on their own and move in a standing position. When users bend their trunk forward, knee extension and standing motions are assisted by its gas springs (Fig 1). This device does not require any electricity during the sit-to-stand and stand-to-sit transitions [1]. Even people with lower limb disabilities can stand up in a few seconds, just as quickly as healthy people can. A powered wheelchair unit is attached to the device, enabling Qolo to move around. We performed a feasibility study of Qolo in people with spinal cord injuries (SCIs).

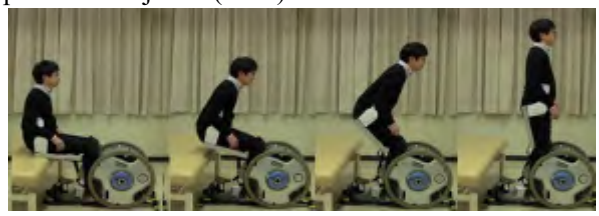

Fig.1

METHODS

In the first prototype, the participants were four SCI patients whose neurological levels of injury (NLI) ranged from T10 to L3, and the American Spinal Injury Association (ASIA) Impairment Scale (AIS) ranged from A to C. While the two individuals (L3C and T10C), whose Manual Muscle Test (MMT) for hip flexor was over one and knee extensor was over three, were able to perform both sit-to-stand and stand-to-sit transitions, the remaining two individuals (T10A and T11A) could only conduct stand-to-sit transitions. Thus, we modified Qolo to increase the spring tension. In the second prototype, we did experiments with 13 participants (ranging from C5 to L3, AIS A-C, Table 1).

RESULTS AND DISCUSSION

All 13 subjects were able to perform sit-to-stand and stand-to-sit transitions (Table 1). In addition, even a T4 SCI patient was able to conduct both movements using a hard trunk orthosis. As SCI patients higher than T6 level have a higher risk of autonomic disorders such as orthostatic hypotension and autonomic hyperreflexia, we think that the practical application of Qolo would be for SCI patients lower than T6 level. The advantages of being in a standing position are as follows: reduction of hip and knee joint contractures, prevention of pressure ulcers, alleviation of spasticity, as well as activation of the cardiovascular and digestive systems [2].

Moreover, using Qolo, people with SCIs may recreate their daily activities in a standing position; to enhance their quality of life (QOL).

Table 1

ID	Gender	Neurological Level	MMT Hip Ext.	MMT Knee Ext.	Qolo Stand-up	Qolo Sit-down
1	M	L3 C	1	3	✓	✓
2	M	T10 C	2/1	5/2	✓	✓
3	M	T12 A (acute)	0	0	✓	✓
4	F	T12 A	0	0	✓	✓
5	M	T11 A	0	1	✓	✓
6	F	T10 A	0	1	✓	✓
7	M	T9 A	0	0	✓	✓
8	M	T7 A	0	0	✓	✓
9	F	T6 A	0	0	✓	✓
10	M	T6 A	0	0	✓	✓
11	F	T4 A	0	0	✓	✓
12	M	C5 C	2/1	4/2	✓	✓
13	M	C6 C	1/2	2/4	✓	✓

CONCLUSIONS

Personal standing mobility Qolo enables people with lower limb impairments due to spinal cord injuries to stand up by themselves. Using Qolo has the potential to improve their trunk function and boost their QOL.

ACKNOWLEDGEMENTS

This research was supported by the Toyota Mobility Foundation and a grant-in-aid for scientific research.

REFERENCES

[1] Eguchi Y, et al. IEEE/ASME Transactions on Mechatronics 2018; 23: 1608-1618.

[2] Spinal Cord Injury Centre Physiotherapy Lead Clinicians: Clinical Guideline for Standing Adults Following Spinal Cord Injury, UK and Ireland. 2019

Effect of an Assistive Robotic System's Compliance on Subject's Muscular Activation and Comfort

Maximilian Siebert[1], Anna Wankum[1], and Catherine Disselhorst-Klug[1]
[1] Department of Rehabilitation and Prevention Engineering, Institute of Applied Medical Engineering, RWTH Aachen University, Aachen, Germany.
Email: siebert@ame.rwth-aachen.de

INTRODUCTION

In robotics, compliance refers to the amount a subject can move the end effector of a robot. Previous work showed a significant change in patients' muscular activation with different levels of robotic compliance during rehabilitation tasks, in which the patient actively supports the movement. In this application, a level of compliance similar to human therapist is suggested. [1]
To relieve the physical stress of caregivers during physical demanding tasks, assistive robotic systems are developed, which lift and hold patient's legs. In contrast to rehabilitation, patients do not perform active movements during these caregiving tasks. Even if there is no need to activate the muscles during such tasks, the degree of robotic compliance might affect the muscular activation, which, in turn, can influence the patient's comfort.
The objective of this work is to examine an appropriate level of compliance for assistive robotic systems in caregiving to ensure patients' comfort.

METHODS

In this study, a lightweight robotic arm (KUKA lbr med) held 30 healthy subject's (15 female, 15 male) legs for 60 seconds while a caregiver applied a decubitus bandage to the subject's foot. The task was performed in four different modes: 1) with low compliance of the robot (LC), 2) with medium compliance (MC), 3) with high compliance (HC), 4) with a second caregiver holding the leg without any influence of the robot (NR). The order of the different modes was randomized. After each mode subjects had a break for 60 seconds.
The amount of muscular activation of vastus lateralis, rectus femoris and gastrocnemius was recorded with surface electromyography (sEMG) according to SENIAM recommendations. The resulting sEMG envelope was calculated and the average of the envelope was used to characterize the amount of muscular activation. The average of the muscular activation was normalized to the corresponding human assisted mode (NR) of each subject.
Additionally, subjects made pair-by-pair comparisons of all four modes regarding their comfort and preference. The comparisons resulted in a score between -6 (preferred the human caregiver in all trials) and 6 (preferred the robotic assistance in all trials).

RESULTS AND DISCUSSION

The normalized muscular activation of vastus lateralis and rectus femoris did not show a significant change between the different levels of compliance. However, the sEMG was significantly lower compared to the human assisted mode (NR).
The normalized muscular activation of gastrocnemius showed a significant decrease from 1.12 (HC) to 1.05 (MC) and 0.91 (LC). However, in contrast to the knee extensors, no decrease in muscular activation compared to NR was found.
With an average score of 2.13, subjects showed a preference for the robotic assisted modes over the human assisted mode and mostly preferred LC.
Furthermore, the average muscular activation of all three muscles decreased for subjects with higher preference of robotic assistance (Fig. 1).

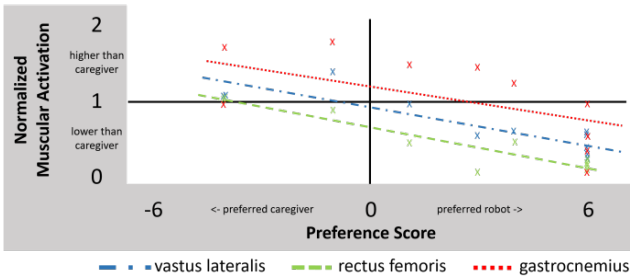

Figure 1: Comparison of robotic and human caregiver preference to muscular activation

It can be assumed, that the subjects higher preference of the LC mode led to higher trust and therefore to a general lower muscular activation compared to HC and MC modes. Additionally, the usage of an assistive robotic system seems to improve comfort in comparison to assistance of a second caregiver during the considered task.

CONCLUSIONS

These results confirm that, opposite to rehabilitation applications, a high, human-like amount of compliance of an assistive robotic system in caregiving seems not to be favorable and leads to higher muscular activation and lower acceptance of subjects than lower compliance.
While the study can prove the importance of robotic compliance on the subjects comfort and acceptance, the ideal amount depends on the use-case, in which the assistive system is used. It is highly recommended to consider compliance when designing assistive systems.

REFERENCES

[1] Becker S et al.; Comparison of Muscular Activity and Movement
Performance in Robot-Assisted and Freely
Performed Exercises; IEEE Transactions On Neural Systems And Rehabilitation Engineering 27-1, 2019.

FINDING ASSISTANCE STRATEGIES BASED ON MUSCULOSKELETAL SIMULATION AND MACHINE LEARNING

Xianyu Zhang, Shihao Li, Zhenzhi Ying, and Naohiko Sugita
Department of Mechanical Engineering, University of Tokyo, Tokyo, Japan.
Email: lsh@mfg.t.u-tokyo.ac.jp

INTRODUCTION

In recent years, many lower limb exoskeletons and other wearable assistive devices have been developed to assist human walking, particularly to reduce the metabolic cost of walking. However, this goal is difficult to achieve owing to the complexity of the human body and significant individual differences. To date, there is no consensus on the assistance strategy and no clear method to obtain a personalized assistance strategy. This has hindered the development and application of exoskeleton technology. In this study, we proposed an approach that combines musculoskeletal simulation (MS) with machine learning to obtain personalized effective and feasible assistance strategies for ankle-joint walking-assist exoskeletons (AWAEs) in real-time.

METHODS

The purpose of this study was to identify personalized assistance strategies applied to the ankle joint that could effectively and feasibly reduce the metabolic cost of walking at various speeds. To achieve this, the open-source software OpenSim was employed to conduct forward muscle-driven simulations. A publicly available gait dataset containing 22 subjects as reported by Camargo [1] was considered. Based on the approach of Uchida [2], an ideal actuator was added at the ankle joint of the musculoskeletal model. With MS, an ideal assistance (IA) strategy which could theoretically minimize the metabolic cost was obtained. To save simulation time and improve the feasibility and timeliness of the IA strategy, we modified its shape so that it provides assistance only in the plantarflexion direction and parameterized it with four features. Then a back propagation neural network was applied to predict the personalized assistance strategy in real-time by inputting physiological information that can reflect individual differences and real-time walking speed information. Finally, the prediction performance of our proposed approach was evaluated, and the performances of the IA and predicted assistance (PA) strategies in reducing metabolic costs were also evaluated through simulations.

RESULTS AND DISCUSSION

Through simulation verification, we found that our proposed method can predict personalized assistance strategies in real-time, and the obtained strategy has approximately 85% similarity in shape to the unilateral IA strategy. In terms of metabolic cost reduction, we found that the IA strategy reduced the total metabolic cost of calf muscles by 0.74 ± 0.18 w/kg (slow), 1.10 ± 0.25 w/kg (normal), and 1.37 ± 0.15 w/kg (fast) compared to the unassisted case, a relative reduction of approximately 60%. While the PA strategy effectively reduced the metabolic cost of calf muscles by 0.21 ± 0.11 w/kg (slow), 0.30 ± 0.12 w/kg (normal), and 0.50 ± 0.08 w/kg (fast), a relative reduction of approximately 20%. Although the PA strategy only achieves approximately 1/3 of the assistance effect of the IA strategy, our proposed method does not require laborious simulations and allows obtaining personalized assistance strategies for various speeds in real-time. Meanwhile, our approach yields a more feasible and practical strategy while maintaining the efficiency of reducing metabolic costs.

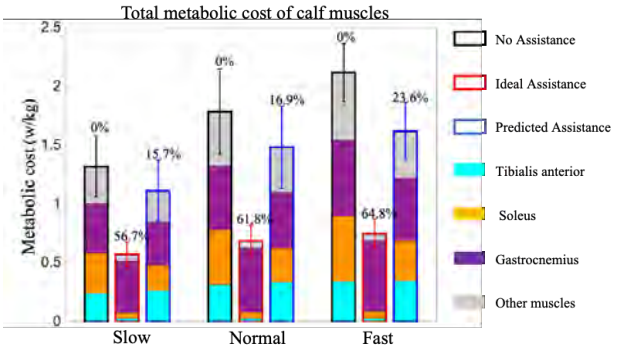

Figure 1 Metabolic costs of calf muscles with different strategies. The black, red, and blue borders indicate the three different strategies of no assistance, IA, and PA, respectively. And in each bar, different coloured areas represent the metabolic cost of different individual muscles: tibialis anterior (cyan), soleus (orange), gastrocnemius (purple), and others (gray).

CONCLUSIONS

In this study, we proposed a novel approach that combines musculoskeletal simulation with machine learning to obtain personalized effective and feasible assistance strategies for AWAEs in real-time. The obtained personalized assistance strategies are feasible and practical while maintaining efficiency in reducing metabolic costs. We expect our results to promote some consensus on assistance strategies for AWAEs. Further, we hope that this work can be used to guide the design of exoskeletons in the future.

REFERENCES

[1] Camargo J et al. *J. Biomech.,* 119: 110320, 2021.
[2] Uchida T et al. *PloS One*, 11.9: e0163417, 2016.

Neuromusculoskeletal Model-informed Bayesian Neural Networks-based control of a Knee Exoskeleton

Longbin Zhang[1], Xueyu Zhu[2], Ruoli Wang[1], and Elena M. Gutierrez Farewik[1,3]
[1]KTH MoveAbility Lab, Dept. Engineering Mechanics, KTH Royal Institute of Technology, Stockholm, Sweden
[2]Department of Mathematics, University of Iowa, Iowa City, Iowa
[3]Dept. Women's and Children's Health, Karolinska Institutet, Stockholm, Sweden
Email: longbin@kth.se

SUMMARY

In this study, an adaptive control framework was developed for a knee exoskeleton based on an EMG-driven neuromusculoskeletal (NMS) solver-informed Bayesian neural network (BNN) with uncertainty quantification. Knee flex/extension torque with uncertainty quantification was analysed. The assistance level of the knee torque determined by the uncertainty quantification was also investigated.

INTRODUCTION

Research interest in exoskeleton assistance strategies that integrate the user's torque capacity continues to grow exponentially. However, the predicted torque capacity from the users generally includes uncertainty from different sources, which may influence the next step of exoskeleton control where safety is a vital factor in the user-interface. The objective of this study is to develop an adaptive control framework for a knee exoskeleton based on an EMG-driven NMS solver-informed BNN. We aim to provide different assistance levels based on the uncertainty quantification of the user's estimated physiological torque.

METHODS

An adaptive control framework was developed for a knee exoskeleton based on an EMG-driven NMS solver-informed BNN model. The inputs of the NMS solver-informed BNN were two kinds of features: (1) experimental measurements -- muscle signals and joint angles, and (2) informative physical features extracted from the underlying NMS solver, such as individual muscle force and joint torque. The outputs were knee joint torque with uncertainty quantification represented by confidence bounds. The predicted knee torque with uncertainty confidence levels was then used to determine the assistance level of the knee exoskeleton through a TCP/IP data stream.

The input and output data for the EMG-driven NMS solver-informed BNN model was adopted from a previous study [1]. Eight able-bodied subjects performed ten types of daily activities, including fast walking, normal walking, slow walking, jump down from a stair, jump up to a stair, jump up, land, squat, sit to stand and stand to sit. Surface EMGs (Myon nano) of gastrocnemius medialis, gastrocnemius lateralis, rectus femoris, vastus medialis, vastus lateralis, biceps femoris, semitendinosus of one leg were recorded. Marker trajectories were recorded (Vicon V16, AMTI force plates), and kinematics and kinetics were computed based on the CGM2.3 model [2].

Knee flex/extension torque with uncertainty quantification was analysed. The assistance level of the knee torque determined by the uncertainty quantification was also investigated.

RESULTS AND DISCUSSION

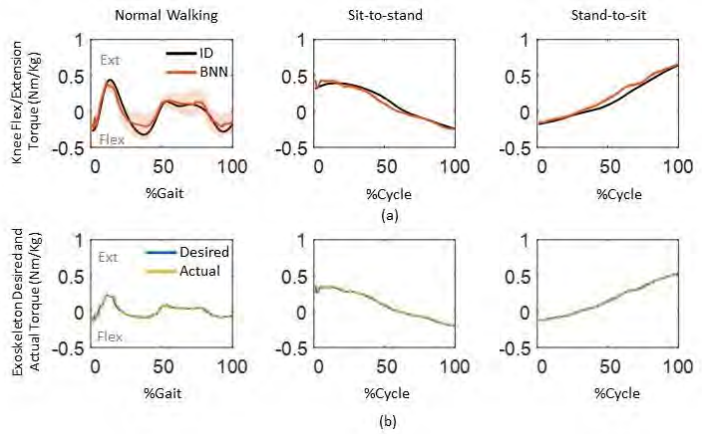

Figure 1: (a) One example of measured (by inverse dynamics (ID)) and predicted knee flex/extension torques (Nm/kg) by Bayesian neural networks (BNN, shown as mean ± std (uncertainty)) during normal walking, sit-to-stand and stand-to-sit. (b) One example of the desired and actual assistive torque from the knee exoskeleton.

BNN predicted knee torque accurately during sit-to-stand and stand-to-sit; however, slightly higher uncertainties of the predicted torque were observed around terminal stance and terminal swing (Fig. 1 (a)). This may be due to the transition between the stance and swing phases of gait. The adaptive control framework for the knee exoskeleton provided desired assistive torque with low error (Fig. 1 (b)). However, low assistive torques could be found during terminal stance and terminal swing because of the higher uncertainties.

CONCLUSIONS

The proposed BNN model was able to predict knee flex/extension torque with uncertainty quantification and transmit the prediction to the adaptive control framework to provide corresponding assistive torque. Further investigation is underway to develop an advanced assistive scheme based on the predicted torque and uncertainties using wearable sensors.

ACKNOWLEDGMENTS

We would like to acknowledge financial support from Promobilia Foundation (ref nr A22078, 18200 and 18014) and Swedish Research Council (2018-00750 and 2018-04902).

REFERENCES

[1] Zhang L. et al. (2022). *IEEE T NEUR SYS REH*, **30**: 600-609.
[2] Leboeuf F. et al. (2019). *Gait & Posture*, **69**: 235-241.

EVALUATION OF A PASSIVE UPPER-LIMB EXOSKELETON DURING A SIMULATED DYNAMIC WORK TASK OVER A LARGE SHOULDER WORKSPACE

Leon Lauret[1], Brent J. Raiteri[1,2], Paolo Tecchio[1] and Daniel Hahn [1,2]

[1] Human Movement Science, Faculty of Sport Science, Ruhr University Bochum, Bochum, Germany
[2] School of Human Movement & Nutrition Sciences, The University of Queensland, Brisbane, Australia
Email: leon.lauret@ruhr-uni-bochum.de

INTRODUCTION

Musculoskeletal disorders (MSDs) are a leading cause of work-related injuries in the industrial field and greatly affect worker well-being. Assistive devices, so-called exoskeletons, pose a promising solution for companies to reduce potential risk factors that lead to MSDs [1]. However, most upper limb exoskeleton studies [2,3] only examined exoskeleton support in overhead arm positions, which does not represent a realistic shoulder workspace [4]. Therefore, the aims of this study were to evaluate a passive exoskeleton over a large shoulder workspace and to construct an arm position-specific support profile to help inform how exoskeleton support should be adapted for different work tasks [4].

METHODS

Surface EMG recordings (1000 Hz) of the upper trapezius, anterior and middle deltoid, and biceps and triceps brachii were recorded from four participants (all male) and their upper body kinematics were captured using an eight-camera Vicon motion capture system. Data were recorded during three exoskeleton conditions: No support (NoExo), when the passive exoskeleton (Ottobock Paexo Shoulder) was not worn; optimal support (Exo_{opt}), which supported the participant's 90° abducted arm against gravity, and; maximal support (Exo_{max}), which applied double the support of Exo_{opt}. During these conditions, participants were required to complete two tasks with their right hand using a 1.5 kg cordless drill and their sternum aligned with the left column of screws: A pattern-task (PAT) that consisted of driving each screw of a 6x6 matrix for 10 s in a predefined pattern without a break in between screws, and; a mapping-task (MAP) that consisted of driving each screw of a 3x3 matrix for 10 s with a 30 s break in between screws. Mean EMG amplitudes (moving 500 ms root-mean-square amplitude) and shoulder and elbow angles were calculated post-processing. For PAT, the first and last 10 s from Exo_{opt} and Exo_{max} were compared with NoExo to investigate (1) immediate and (2) fatigue-dependent and/or learning-dependent effects of the exoskeleton, respectively. The MAP recordings were used to construct a heatmap to visualize differences in exoskeleton muscle support for different screw locations and arm positions. Differences were calculated as symmetrized percent differences.

RESULTS AND DISCUSSION

A reduction in mean (±SD) summed activity of the upper limb muscles was observed during the first 10 s of PAT (Exo_{opt}: -6.9±3.4%; Exo_{max}: -13.8±8.4%) that persisted until the end of PAT (Exo_{opt}: -6.0±3.1%; Exo_{max}: -12.3±12.8%). The heatmaps generated from MAP (Fig. 1) indicate that the reductions in mean summed muscle activity occurred in the overhead arm positions with either an abducted shoulder or an extended elbow. Conversely, the exoskeleton appeared to have a limited effect or even interfered with working positions close to the body.

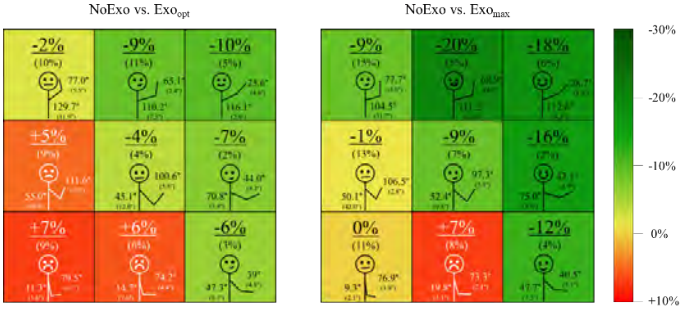

Figure 1. Heatmaps (n=4) of Exo_{opt} and Exo_{max} showing the mean (SD) shoulder abduction and elbow flexion angles and the mean (SD) differences in summed muscle activity at different screw locations with exoskeleton support.

CONCLUSIONS

The exoskeleton reduced overall upper limb muscle activity throughout the dynamic work task, with Exo_{opt} showing a more consistent effect than Exo_{max}, while Exo_{max} showed greater support. However, the mean reduction in muscle activity was not as large compared with previous studies that assessed a smaller shoulder workspace [2,3]. The heatmaps indicate that the system is only likely to be effective when working with an abducted shoulder and/or extended elbow.

REFERENCES

[1] De Looze et al. *Ergonomics* **59**: 671-681, 2016
[2] Maurice et al. *IEEE Transac* **28***:* 152-164, 2019
[3] Schmalz et al. *Int J of Env Research and Public Health* **16**: 4792, 2019
[4] De Vries et al. *IISE Transac* **7**: 311-321, 2019

LEG JOINT KINETIC DETERMINANTS OF SPRINT ACCELERATION RUNNING

Ryu Nagahara[1]
[1] National Institute of Fitness and Sports in Kanoya, Kanoya, Japan.
Email: nagahara@nifs-k.ac.jp

INTRODUCTION

Sprint acceleration ability is of great importance for many sports, particularly for 100-m races. Joint work and power are useful for understanding energy generation and absorption at joints during sprinting. Changes in joint work have been documented as the net work done at all three major leg joints linearly decreased with decreasing acceleration magnitude during sprint acceleration [1]. Although macroscopic changes in work done at each joint during sprint acceleration have been revealed, there is a lack of knowledge regarding the determinants of sprint performance in terms of waveform analysis using leg joint kinetic variables. Therefore, the purpose of this study was to demonstrate determinants of sprint performance during sprint acceleration in terms of step-to-step joint power waveform analysis.

METHODS

Sixteen male sprinters (mean ± SD: age, 20.4 ± 1.2 years; stature, 1.73 ± 0.04 m; body mass, 65.1 ± 3.7 kg; personal best 100-m time, 11.34 ± 0.41 s) participated in this study. Participants performed maximal effort 35- and 60-m sprints two or three times for each. A long (50 m) force platform system which was consisted of 54 force platforms (1000 Hz; TF-90100, TF-3055, TF-32120, Tec Gihan, Kyoto, Japan) measured GRF during sprinting from the start to the 27-m mark for the 35-m trials and from the start to 50-m mark for the 60-m trials. A motion capture system, which consisted of thirty-nine infrared cameras (250 Hz; Motion Analysis Corporation, Santa Rosa, CA, US), was used to measure three-dimensional coordinates of 47 retro-reflective markers affixed to the participant's body with a volume of approximately 30 m × 1.5 m × 2 m (length × width × height), covering the later 30-m of the force platform system. The participants started from the 23-m mark on the force platform system for 35-m trials and from the start (at the edge of the force platform system) for 60-m trials.

The thresholds to detect foot strike and toe-off were set at 20 N of vertical force. From the marker coordinate data, the endpoints of 15 segments of the whole body were determined [2]. The endpoint coordinates were smoothed with a fourth-order Butterworth low-pass digital filter with a cut-off frequency of 15 Hz. Joint moments at the hip, knee and ankle were calculated using a standard inverse dynamics analysis for both legs. Joint power was calculated by the dot product of the joint moment and angular velocity at each joint. Then, one-dimension statistical parametric mapping for correlation analysis was used to examine relationships between running speed and joint power signals during the support phase at each step.

RESULTS AND DISCUSSION

Statistical parametric mapping for correlation analysis revealed that mean running speed at each step was positively correlated with positive hip joint power at the 1st (45 to 61% of the support phase), 4th (26 to 32% of the support phase), 8th (15 to 41% of the support phase), 10th (23 to 37% of the support phase), and 12th step (25 to 30% of the support phase). Moreover, mean running speed was negatively correlated with positive hip joint power at the 4th (0 to 9% of the support phase) and 6th step (0 to 2% of the support phase). In addition, mean running speed was negatively correlated with negative hip joint power at the 15th (66 to 86% of the support phase) and 16th step (59 to 65% of the support phase). In terms of the knee joint, mean running speed was positively correlated with positive knee joint power at the 16th (66 to 78% of the support phase), 20th (61 to 72% of the support phase), and 22nd step (72 to 81% of the support phase). For the ankle joint, mean running speed was positively correlated with positive ankle joint power at the 4th (59 to 85% of the support phase), 6th (77 to 91% of the support phase), 8th (73 to 97% of the support phase), 16th (74 to 90% of the support phase), and 18th step (71 to 94% of the support phase). Moreover, mean running speed was negatively correlated with negative ankle joint power at the 4th (21 to 40% of the support phase) and 8th step (31 to 44% of the support phase).

CONCLUSIONS

The current results demonstrate that important joint kinetic variables could change during sprint acceleration. Particularly, positive power productions during the first half of the support phase were related to running speed in the early acceleration section, while negative power production (mainly produced by hip extension angular velocity and hip flexion moment) during the second half of the support phase could affect running speed during the later acceleration section. These findings can be useful for considering sprinting techniques and training programs for improving sprint performance.

REFERENCES

[1] Schache AG et al. *J Exp Biol* **222**: jeb209460, 2019.
[2] Nagahara R et al. *Biol Open* **3**: 689-99, 2014

BIOMECHANICAL ANALYSIS OF AN ELITE PARALYMPIC AMPUTEE SPRINTER IN STEADY STATE RUNNING ON TREADMILL AND TRACK

S. G. Breban[1], S. Barbacane[1], G. Fabris[1], M. Scapinello[1], G. Marcolin[2], V. Pelusi[1], A. G. Cutti[3], and N. Petrone[1]

[1] Department of Industrial Engineering, University of Padova, Padova, Italy.
[2] Department of Biomedical Sciences, University of Padova, Padova, Italy.
[3] INAIL Prosthetic Centre, Vigorso di Budrio, Bologna, Italy.
Email: samiragiuliana.breban@phd.unipd.it

INTRODUCTION

Running Prosthetic Feet (RPF) enable athletes with lower limb amputations to compete in high level track competitions [1]. However, their sprinting biomechanics is not fully understood [2]. Studying running kinematics (joint angles) and kinetics (Ground Reaction Forces-GRFs) aims to prevent injuries and enhance performance outcomes [1]. The aim of this work is to study kinematics and kinetics of an elite Paralympic sprinter in steady state running on both treadmill and track.

METHODS

A female gold medallist, unilateral transfemoral amputee Paralympic sprinter participated in this study. The athlete (55 kg, 1.60 m) used 1E91 standard RPF Cat. 3.5 and mono-axial 3S80 knee (Ottobock, Germany) with a specific alignment of the socket and the foot, equal to 15° [3]. Two sessions were performed: treadmill and indoor track (Palaindoor, Padova, Italy). During the treadmill session a SkillRun treadmill (Technogym, Italy) was placed on four P6000 force platforms (BTS, Italy; 1 kHz) and integrated with a DX-6000 motion capture system (BTS, Italy; 250 Hz). The athlete performed a steady state running test at 5 m/s for 7 s [4]. During the track session the athlete ran on a 60 m indoor athletic track and was captured by 28 infrared cameras (Vicon, UK; 300 Hz) covering the central 20 m of the track. RPF was instrumented with a 6-axis load cell mounted between the prosthetic knee and the clamp [5]. The load cell, whose pose was tracked via retro-reflective markers, was connected to a SLICE NANO compact acquisition system (DTS, USA; 2 kHz) placed in a running backpack. The athlete performed a sprint reaching an average steady state speed of 6.5 m/s. Kinematics and GRFs analyses of the Affected Limb (AL) were performed in both sessions. Cardan 'ZXY' angles of hip and knee joints and trunk were calculated, with Z being the medial-lateral axis. GRFs collected in the clamp Coordinate System (CS) were transformed into the ground CS after being low-pass filtered (4^{th} order Butterworth filter, cut-off: 15 Hz in treadmill and 52 Hz in track). Signals were segmented based on foot strike and foot off detection and averaged over 5 steps. Peak values and impulses of anterior-posterior (GRF_X) and vertical (GRF_Y) GRFs were calculated and normalized for the athlete's body weight (BW).

RESULTS AND DISCUSSION

Kinematics and GRFs analyses are reported in Figure 1. AL knee behaved similarly in both tests: fully extended during stance, while flexed during swing. AL hip ranges of motion were 60° and 89°, and average values were 30° and 49° for treadmill and track, respectively. These variations could be attributed to different test speeds (5 vs 6.5 m/s) and trunk inclination (0-10° vs 5-15°). Vertical GRF peaks were 2.61 N/BW in treadmill and 3.39 N/BW in track. Horizontal force had minima (braking) of -0.22 and -0.60 N/BW and maxima (propulsion) of 0.44 and 0.57 N/BW for treadmill and track, respectively. Net horizontal impulses were $9 \cdot 10^{-3}$ N·s/BW for treadmill (propulsion: $20 \cdot 10^{-3}$ N·s/BW, braking: $-11 \cdot 10^{-3}$ N·s/BW) and $5 \cdot 10^{-3}$ N·s/BW for track (propulsion: $26 \cdot 10^{-3}$ N·s/BW, braking: $-21 \cdot 10^{-3}$ N·s/BW). Differences could be related to athlete's speed [6] or confidence levels: further tests on an instrumented track would validate the wearable system.

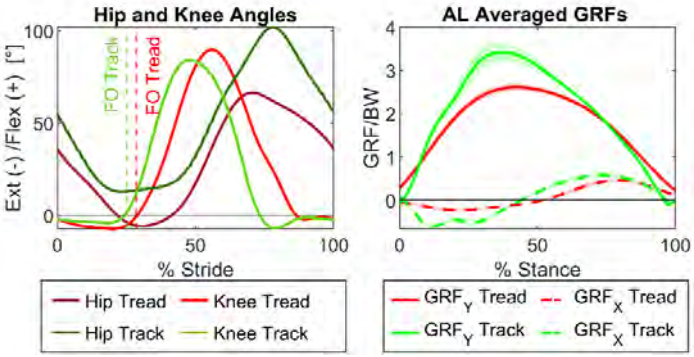

Figure 1 AL Hip and Knee joint angles in the sagittal plane (left) and AL averaged GRFs (right) for treadmill and track sessions

CONCLUSIONS

The aim of the present work was to report kinematic and kinetic data of an elite Paralympic sprinter running both on treadmill and on track. Results proved the feasibility of both test configurations and showed kinematic and kinetic differences, which open to further investigations.

ACKNOWLEDGEMENTS

Athlete and FISPES for their involvement in the study, INAIL for funding OLIMPIA project PR19-PAI-P4.

REFERENCES

[1] Hadj-Moussa F. et al. *Gait Posture* **92**: 83-95, 2022.
[2] Hobara H. et al. *Prosth Orthot Int,* 2022.
[3] Migliore G. et al. *Prosth Orthot Int* **45**: 46-53, 2021.
[4] Breban S. G. et al. *Proc. ISBS Conf.* **40**, 2022.
[5] Scapinello M. et al. *ISB,* 2023.
[6] Beck O. et al. *J Appl Physiol* **124**: 641-645, 2018.

THE INFLUENCE OF LATERAL WEDGED INSOLES ON THE PERFORMANCE OF A SHUFFLE MOVEMENT

Reyna C. Crawford[1,2], John W. Wannop[1], Darren J. Stefanyshyn[1,2]

[1]Human Performance Laboratory, Faculty of Kinesiology, University of Calgary, Calgary, Canada.
[2]Department of Biomedical Engineering, Schulich School of Engineering, University of Calgary, Calgary, Canada.
Email: reyna.crawford@ucalgary.ca

INTRODUCTION

In many sports, it is imperative to have the ability to quickly change directions, which can be facilitated through greater horizontal ground reaction forces (GRF) and greater ankle plantarflexor moments [1,2]. Research has shown that greater horizontal GRF and ankle moments during rapid change of direction movements have been achieved using a laterally banked surface [1]. During a lateral movement, the banked surface elicits a re-orientation of the GRF vector, and a frontal plane re-alignment of the ankle joint. Research suggests that as the ankle moves away from a neutral orientation, into greater ankle inversion, there is a decreased ability to produce sagittal plane ankle moments, that are key to sport performance [3]. To incorporate a laterally banked surface into a sport setting, lateral wedged insoles can be placed inside footwear, to mimic the structure of the banked surface. Therefore, the purpose of this study was to determine the influence of lateral wedged insoles on athletic performance during a shuffle movement.

METHODS

Eleven female (age: 21.9 ± 2.7 years, height: 1.71 ± 0.07 m, body mass: 65.3 ± 5.5 kg) and seven male (age: 22.7 ± 2.4 years, height: 1.83 ± 0.08 m, body mass: 83.6 ± 5.9 kg) collegiate basketball players participated in the study. The participants performed five successful trials of a shuffle drill in two shoe conditions. The conditions consisted of a Control condition, and a Lateral Wedge (LW) insole condition. The 3D printed insoles had a 5-degree incline on the lateral edge and tapered past the metatarsophalangeal joint for comfort. All participants wore Nike Kyrie Flytrap 5 basketball shoes, with both the natural insole (Control condition), and with the natural insole replaced with lateral wedged insoles (LW condition). During data collection, each participant performed maximal effort basketball-style shuffle movements where each trial consisted of shuffling between two endpoints that were 5 m apart on a straight line. The participants went between the endpoints twice while kinetic and kinematic data were collected during the stance phase of two changes of direction using a motion capture system (240Hz) and force platform (2400Hz). Timed athletic performance was measured with photocells. Statistical comparisons were made between the footwear conditions using a paired t-test at a significance level of $\alpha = 0.05$. The primary variables of interest were the timed performance, peak GRF in the direction of movement (horizontal GRF), GRF vector orientation, and ankle sagittal plane moment and power.

RESULTS AND DISCUSSION

Performance and biomechanical results of interest are shown in Table 1. While no difference in overall drill performance, there was a significant decrease in the change of direction stance time with the LW condition ($p=0.03$). A significantly greater horizontal GRF was observed with the LW condition ($p=0.02$), which led to a more horizontally oriented GRF vector ($p=0.03$). There were no differences observed at the ankle between the Control and Lateral Wedge conditions.

CONCLUSIONS

The use of lateral wedged insoles resulted in greater horizontal GRFs and a re-orientated GRF vector to a more favourable position for performance. These results led to a decrease in stance time, effectively reducing the amount of time needed for the participants to change direction.

ACKNOWLEDGEMENTS

This study was funded by the Natural Sciences and Engineering Research Council and We-TRAC (University of Calgary). Footwear was provided by Nike.

REFERENCES

[1] Wannop J. et al. *Hum Mov Sci* **33**: 97-107, 2014.
[2] Chen C. et al. *Gait Posture* **94**: 189-194, 2022.
[3] Stefanyshyn D. et al. *Sports Eng* **18**: 191-202, 2015

Table 1: Mean performance and biomechanical data during the shuffle movement. Bold values indicate a significant difference from control.

	Performance	Stance Time	Peak Horizontal GRF	Peak Vertical GRF	GRF Orientation (horizontal reference)	Peak Ankle Plantarflexion Moment	Peak Ankle Power
Control	5.06 s	0.446 s	1022 N	1410 N	54.3°	153 Nm	609 W
Lateral Wedge	4.99 s	**0.425 s**	**1074 N**	1446 N	**53.7°**	159 Nm	622 W

EFFECT OF CLEAT AND RIDER POSITIONING ON LEG JOINT FUNCTION

Colin R. Firminger[1], Michael J. Asmussen[1]
[1]Department of Biology, Mount Royal University, Calgary, Canada.
Email: cfirming@gmail.com

INTRODUCTION

Lower-limb joint torques and powers have been widely studied during cycling [1,2], yet the mechanical function of these joints remains unknown. Previous research has offered insight into how lower-limb joints function during walking and running by characterizing their behaviour relative to four basic mechanical components (i.e., strut, spring, motor, damper) [3]. Insight into the mechanical function of these joints could help elucidate how muscles function during cycling and inform how muscle tissue loading is affected by rider posture (i.e., seated versus standing) and foot placement (i.e., cleat positioning). We hypothesized that a standing posture would change the mechanical function of the joints such that strut function at the ankle would increase as it becomes more weightbearing and required to transfer energy, while a more posterior cleat positioning would decrease the motor function at the ankle as its external moment arm would decrease.

METHODS

Ten participants cycled on a stationary ergometer at 250W and at three cleat positions (neutral position, 2cm anterior, 2cm posterior). Centre of pressure and pedal reaction force data were collected with pressure insoles, while an 8-camera motion capture system collected marker data from the participant's right leg. Inverse kinematics and dynamics were performed in OpenSim to determine joint moments and powers. Previously-published equations [3] were modified to calculate normalized joint functional indices for the four aforementioned mechanical components during the entire pedal stroke. Changes in joint function with cleat and/or rider position were examined using a two-factor repeated measures ANOVA.

RESULTS AND DISCUSSION

During all forms of cycling, the hip and ankle functioned as motors while the knee functioned as a damper (Figure 1). The hip was significantly more of a damper when standing compared to seated ($p<0.001$). Descriptively, the ankle appeared to function more as a strut when in a standing position, although this difference was not significant. Cleat position did not significantly affect the mechanical function of the joints.

This study was the first to characterize the mechanical function of the lower-limb joints during seated and standing cycling. As motors, the hip and ankle tend to predominantly generate positive power throughout the majority of the pedal stroke. As a damper, the knee tends to absorb energy (negative work) throughout the majority of pedal stroke. Previous research from our group has noted changes to Achilles tendon strain with posterior cleat positioning, however it is interesting that the joint continues to function nearly identically regardless of cleat position. Similarly, while joint moment magnitudes have been shown to differ greatly between seated and standing postures [2], our research illustrates that joint function is relatively unchanged. This research points to a consistent function of the lower-limb joints during cycling, regardless of rider posture or cleat positioning. Future research should explore how the muscles crossing these joints enable this behaviour.

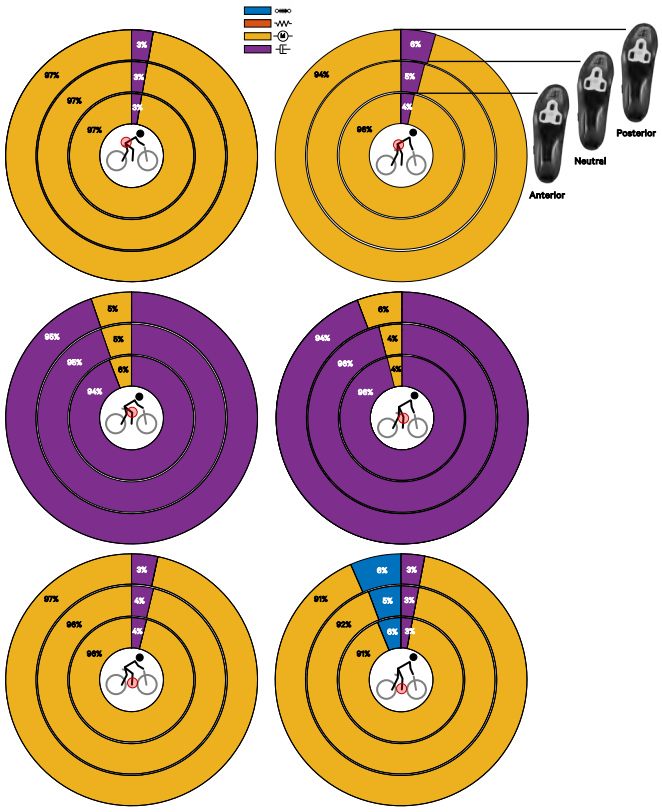

Figure 1 Normalized joint functional indices at the hip (top), knee (middle), and ankle (bottom) during seated (left) and standing (right) cycling at 250W. Inner to outer rings represent anterior, neutral, and posterior cleat position, respectively. Joint functions: blue = strut, red = spring, yellow = motor, purple = damper.

CONCLUSIONS

Cycling cleat and rider position appear to have little effect on lower-limb mechanical joint function during cycling, with the ankle and hip primarily functioning as motors and the knee largely functioning as a damper.

REFERENCES

[1] Gregor et al. *J. Biomech*. 18(5): 307-16, 1985.
[2] Caldwell et al. *J App Biomech*. **15**: 166-81, 1999.
[3] Qian et al. *J Biomech*. **49**:66-72, 2015.

IMPULSE GENERATION AND INITIAL VELOCITIES IN BASKETBALL TWO-FOOT RUNNING JUMPS

Jun Ming Liu[1], Antonia Zaferiou[1]
[1] Musculoskeletal Control and Dynamics Lab, Stevens Institute of Technology, Hoboken, NJ, USA
Email: jliu130@stevens.edu

INTRODUCTION

Jump height has performance implications for basketball [1]. However, two-foot running jumps (TFRJs) have not yet been studied in basketball. TFRJs involve the redirection of the body's momentum through application of linear impulse by each leg. In volleyball TFRJs, the first leg generated more vertical and less backward impulse than the second leg [2]. This study describes impulse generation by each leg in basketball TFRJs. Additionally, the initial velocities of the COM provide context for the impulse generated during the jump. In volleyball TFRJs, initial forward velocity correlated with jump height [2] and in stationary jumps, initial downward velocity correlated with jump height [3]. Thus, this study investigates if initial velocities and net impulse generated correlate with jump height. We hypothesize (1) that the first leg generates more vertical and less backward impulse than the second leg, (2) jump height correlates with initial forward velocity, initial downward velocity, and net vertical impulse.

METHODS

Nine male recreational to college-level basketball players volunteered for the study in accordance with the IRB. They performed five to ten TFRJs from NBA combine test distance (4.57m) to a basketball hoop while kinematic and kinetic data were collected (Bertec Force Plates 1000 Hz, Optitrack Motion Capture 250 fps). They performed self-selected warm up and were instructed to tap their preferred arm on the hoop as high as they could. Hoop height was selected during warm up for each participant to ensure max jump intent. The data were processed in MATLAB (Mathworks, MA). The forward axis was the average horizontal forward trajectory of the COM during flight, vertical axis was global vertical, and leftward axis is cross product of vertical and forward. The phase of interest starts from ground contact of first leg until final toe off (**Figure 1A**). Initial velocities of the COM were computed the frame before ground contact. Jump height is calculated from COM velocity at take-off. Linear impulse is the time integral of ground reaction force (GRF) of each leg through the phase of interest. Net vertical impulse is total vertical impulse from both legs minus downward impulse from bodyweight. Signed rank tests were used to compare impulse between legs ($p<0.05$). Pearson's correlation was calculated between jump height and initial velocities or impulses using the trial with median jump height for each participant ($p<0.05$).

RESULTS AND DISCUSSION

Compared to the second leg, the first leg generated more vertical impulse in all participants and more backward impulse in seven out of nine participants (**Figure 1**). There were non-significant positive correlations between jump height and initial forward velocity ($r=0.45$, $p=0.23$), initial downward velocity ($r = 0.18$, $p=0.63$), and net backward impulse ($r=-0.10$, $p = 0.79$). There was a significant positive correlation between jump height and net vertical impulse ($r=0.7$, $p=0.03$).

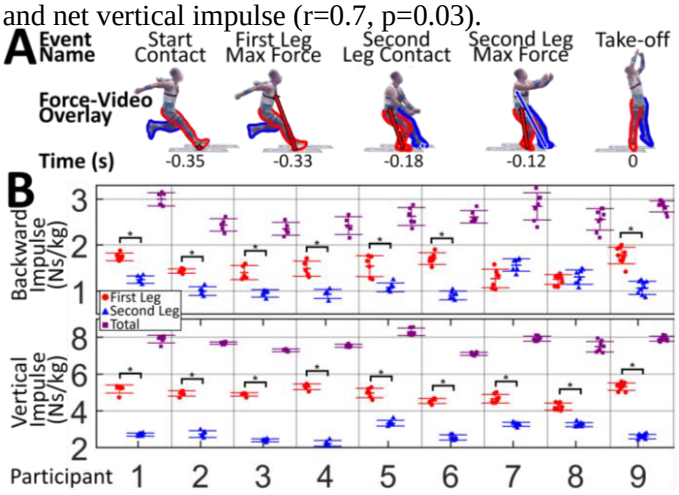

Figure 1: (A) Exemplar timeline and events in a jump (B) Backward (top) and vertical (bottom) impulse generated by the first (red) and second (blue) legs and total impulse from both legs (purple). *$p<0.05$

Compared to volleyball spike jumps, differences in impulse generation strategies may be due to greater initial forward velocity [2]. The non-significant correlations between jump height and initial velocities may indicate initial conditions play a small role in jump height, but more data are needed. The differences between basketball TFRJs and prior studies highlight importance for sports-specific jumping research. Differences in impulse may have performance and injury implications due to different movement strategies.

CONCLUSIONS

This study found that the first leg generated more backward and vertical impulse than the second leg in most participants. Jump height was only correlated with net vertical impulse. The findings differ from prior studies on volleyball spike jumps and stationary jumps, further encouraging sports-specific jumping research.

REFERENCES

[1] Ziv G. & Lidor R. (2009). *Sports Med.*, **39**(7)
[2] Fuchs P.X. et al (2019). *J. Sci. Med. Sport.* **22**(7)
[3] Gonzalez-Badillo & Marques (2010) *J. S.&C. Res.* **24**(12)

CENTRE OF PRESSURE AND ROLL OVER SHAPE FROM WEARABLE SENSORS DURING OVERGROUND RUNNING OF AN ELITE PARALYMPIC AMPUTEE SPRINTER

S. Barbacane[1], G. Fabris[1], S.G. Breban[1], M. Scapinello[1], R. Di Marco[2], A. G. Cutti[3] and N. Petrone[1]
[1] Department of Industrial Engineering, University of Padova, Padova, Italy.
[2] Department of Computer Science, University of Verona, Verona, Italy
[3] INAIL Prosthetic Centre, Vigorso di Budrio, Bologna, Italy.
Email: sarabarbacane.sb@gmail.com

INTRODUCTION

A comprehensive assessment of running performance of amputee sprinters requires the measurement of Ground Reaction Forces (GRFs) [1] and the estimation of joint moments [2]. An additional important parameter is the description of the trajectory of the Centre of Pressure (COP), which is usually expressed in the ground Coordinate System (CS). The projection of this trajectory onto a body-based CS is known as Roll Over Shape (ROS) [3]. ROS was introduced for walking, thus knowledge is limited in running and even more in amputee running. Aim of the work is to present a method to calculate the ROS of the affected limb in amputee sprinters using Running Prosthetic Foot (RPF).

METHODS

One elite Paralympic female sprinter (mass: 55 kg, height: 1.60 m) with unilateral transfemoral amputation participated in this study. She wore Runner 1E91 Cat. 3.5 RPF and 3S80 mono-axial prosthetic knee (Ottobock, Germany). She performed a series of sprints at a mean top speed of 6.5 m/s on a 60 m runway in an indoor athletic track (Palaindoor, Padova, Italy). Forces and torques were collected through a 6-axis load cell positioned at the RPF clamp and connected to a lightweight acquisition system (SLICE NANO, DTS, USA; 2 kHz). An inertial sensor (6DX, DTS, USA; 2 kHz) was used to measure the 3D acceleration and angular velocity of the RPF [4], while 28 infrared cameras (Vicon, UK; 300 Hz) captured the 65 retroreflective markers attached to the athlete's body and prosthesis. The trajectory of the COP was obtained combining the measured forces and torques with the absolute position and the sagittal inclination of the RPF. Load components were resolved in the ground CS, then the instantaneous horizontal anterior-posterior coordinate of the COP was calculated as the lever arm necessary to produce the torque measured at the clamp ($M_{z_{CL}}$). By analogy with a sound limb, where ROS describes the evolution of COP in a shank-based CS [3], ROS was here obtained by projecting the COP onto a clamp-based CS.

RESULTS AND DISCUSSION

The COP in Ground CS (Figure 1a) moves back from Foot Contact (FC) to Midstance (MS, i.e. hip joint centre vertically aligned with knee joint centre), due to the large deformation of the blade, then it moves again forward towards the foot tip up to its extremity at Foot Off (FO). In Clamp CS (Figure 1b), during the first phase of stance, large deflection of the RPF and the forward rotation of the proximal segments (clamp and pylon), causes the ROS to come quickly closer to the Clamp, reaching its maximum height at MS. In the second part of the stance, RPF recoils, recovering its initial shape, therefore ROS decreases. The resultant ROS is totally different from that of an intact foot, which has a convex circular trend instead, with a rocker radius depending on the running style (forefoot or rearfoot striking) [5]. It has been observed that in able-bodied people ROS shape remains unvaried when gait parameters change [3], but little is known about the variability of ROS in amputee athletes. Further studies will investigate this theme, including the relationship between ROS, running efficiency and usefulness in RPF bench testing.

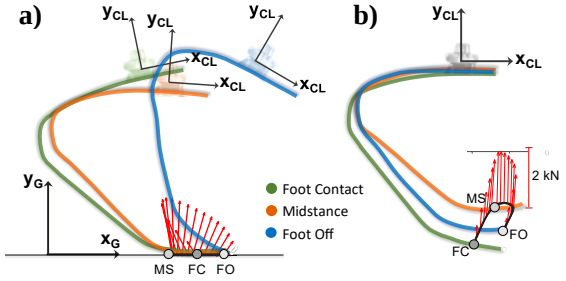

Figure 1 Schematic representation of RPF, GRF and COP/ROS trajectory (black line) at Foot Contact, Midstance and Foot Off. GRF are represented with red arrows for the whole stance phase. a) GRF and COP in Ground CS; b) GRF and ROS in Clamp CS.

CONCLUSIONS

The present study described a method to measure the ROS in an amputee sprinter running on track. This parameter, despite the lack of deep knowledge on this topic, is believed to have a crucial role in the alignment of prosthetic lower limb systems and also in the evaluation of athlete's performance.

ACKNOWLEDGEMENTS

Athlete and FISPES for their involvement in the study, INAIL for funding OLIMPIA project PR19-PAI-P4, Comune of Padova (Italy) for hosting the tests.

REFERENCES

[1] Makimoto A. et al. *J Appl Biomech* **33**:406-9, 2017.
[2] Namiki Y. et al. *Biol Open* **8**:bio039206, 2019.
[3] Hansen A.H. et al. *Disabl Rehab* **32**:2201-9, 2010.
[4] Scapinello M. et al. *ISB*, 2023.
[5] Kouwenhove L. et al. *Gait Posture* **86**:150-6, 2021.

Acceleration Transmission During Cricket Fast Bowling

Matthew Lamb[1], Stuart McErlain-Naylor[1], Paul Felton[2], Katherine Brooke-Wavell[1], Mark King[1]
School of Sport, Exercise and Health Sciences, Loughborough University, Loughborough, UK[1]
School of Science and Technology, Nottingham Trent University, Nottingham, UK[2]
Email: M.Lamb@lboro.ac.uk

INTRODUCTION

Lumbar stress fractures are the most time costly injury in professional cricket [1]. Research has shown greater ground reaction forces to be associated with greater stress fracture injury risk [2]. These forces cause accelerations that are transmitted through the tissues of the musculoskeletal system. Compliance such as tissue deformation extends the impact and reduces accelerations in a distal-to-proximal manner [3]. This study aimed to quantify the magnitude and frequency content of surface-measured accelerations at each major body segment during cricket fast bowling.

METHODS

Eleven male fast bowlers (19 ± 2 years, 80.5 ± 9.8 kg, 1.86 ± 0.06 m) participated in this study. Nine inertial measurement units (IMUs) (Vicon Blue Trident, Oxford, UK) recording at 1600 Hz were placed on: both distal tibia (5 cm superior to the lateral malleolus), both distal thighs (5 cm superior to the lateral femoral condyle), both greater trochanters, and L5, L1 and C7 vertebrae. Six maximum velocity deliveries were recorded in a laboratory environment allowing for a full-length run-up. Peak resultant acceleration in each position and its timing in relation to back foot contact (BFC), front foot contact (FFC) and follow-through contact (FT) were calculated, and the ground contacts were determined from synchronised high-speed video. Power spectral densities (PSD) of each distal tibia acceleration signal were visually inspected to identify common frequency ranges associated with the two main components of joint rotations and the elastic wave [3,4]. PSD integrals within the frequency range associated with the elastic wave component were determined for all signals. All parameters were averaged for the best three trials, determined by hitting the force plate at FFC and fastest delivery using a speed gun. Two-way (position x contact phase) repeated measures ANOVAs were performed in SPSS (Version 24, IBM SPSS Software) for each dependent variable, Bonferroni corrected to a significance threshold of $p < 0.017$. Post-hoc comparisons performed (not all reported for brevity) were again Bonferroni corrected.

RESULTS AND DISCUSSION

Both position ($F = 113$; $p < 0.001$) and phase ($F = 28.1$; $p < 0.001$) had significant effects on peak resultant acceleration (Figure 1). Accelerations decreased significantly with each step up the body until L5, and BFC accelerations were significantly less than FFC and FT. A significant interaction ($F = 10.1$; $p < 0.001$) indicated greater attenuation between positions following FFC and FT than BFC. Position ($F = 26.4$; $p < 0.001$) but not phase ($F = 4.45$; $p = 0.025$) or interaction ($F = 1.15$; $p = 0.331$) had a significant effect on time of peak acceleration (Figure 1). There was a general trend for greater delays at more superior positions. The 2–16 Hz and 16–58 Hz components were identified as encompassing the joint rotations and elastic wave, respectively. All main and interaction effects for elastic wave signal content were significant ($8.55 \leq F \leq 54.2$; $p < 0.001$). These results followed a similar pattern to those for peak resultant acceleration and are similar to previous findings in alternate high-impact activities [3]. Most of the distal tibia (peak) acceleration is attenuated before reaching the L5 region (91 ± 2%, 86 ± 5%, and 88 ± 4% following BFC, FFC, and FT, respectively), suggesting that the post-impact elastic wave may be unlikely to contribute to lumbar stress fracture risk. It is important to consider that surface accelerations do not represent internal bone loads, given the disregard of muscle forces [5]. Future research may quantify the attenuating effects of specific structures and effects on inverse and forward dynamic calculations. This is of particular relevance to experimental and theoretical attempts to understand lumbar stress fracture aetiology in cricket fast bowlers.

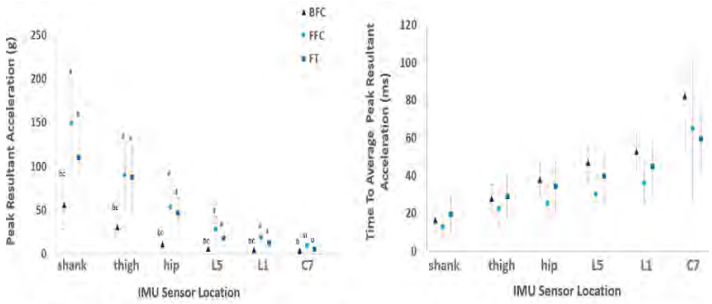

Figure 1. Peak (*left*) and time to peak (*right*) resultant acceleration (mean ± SD) at each position. a/b/c: significant difference ($p < 0.005$) between BFC-FFC / BFC-FT / FFC-FT, respectively.

CONCLUSIONS

Distal accelerations are greater during the FFC and FT phases, although the body remains capable of attenuating these. Mechanisms within the body prevent excessive accelerations from reaching the lumbar region. Results highlight the need to consider elastic wave attenuation within inverse and forward dynamics investigations of cricket fast-bowling.

REFERENCES

[1] Johnson et al. Phys Therapy in Sport. **13**: 45-52, 2012.
[2] Ranson et al. *J Sports Sci*. **26**: 267-76, 2008.
[3] McErlain-Naylor et al. *J Biomech*. **118**: 110269, 2021.
[4] Shorten and Winslow. *J Appl Biomech*. **8**(4): 288–304, 1992.
[5] Matijevich et al. *PLoS ONE*. **14**(1): e0210000, 2019.

Are sagittal plane leg alignment and the active peak force generated during running associated with medial tibial stress syndrome development?

Joshua PM. Mattock[1], Julie R. Steele[1], and Karen J. Mickle[2]
[1] Biomechanics Research Laboratory, University of Wollongong, Wollongong, Australia.
[2] School of Environmental and Life Sciences, University of Newcastle, Newcastle, Australia
Email: jmattock@uow.edu.au

INTRODUCTION

Medial tibial stress syndrome (MTSS) is an overuse injury that commonly affects female athletes [1]. MTSS is thought to be caused by tibial bone bending and a bone stress reaction above the tibia's remodeling capacity [1]. The sagittal plane tibial bending moment is reportedly associated with peak tensile strain at the site of MTSS pain and is influenced by an individual's leg alignment relative to the ground reaction force generated during the stance phase [2]. Despite MTSS commonly affecting females, no published study has assessed the sagittal plane leg alignment or peak vertical force generated by female long-distance runners with MTSS relative to their uninjured counterparts. Therefore, we aimed: (i) to determine whether sagittal plane leg alignment and the active peak force generated during running differed between female MTSS symptomatic and asymptomatic long-distance runners, and (ii) to present a prospective case study to determine the role of these variables in MTSS development.

METHODS

Eight MTSS symptomatic female long-distance runners (age = 32.1±10.9 years; mass = 65.9±6.2 kg; height = 1.69±4.6m) were matched on age, height, limb dominance and training load with 8 asymptomatic female controls (age = 32.4±10.4 years; mass = 62.9±3.2 kg; height = 1.68±6.8 m). All participants ran at least 30 km per week or were training for a long-distance event within the previous 6 months. Participants ran on a treadmill at a speed equivalent to their 10 km race time. 3D motion capture and plantar pressure-measuring insoles were used to determine each participant's sagittal plane hip, knee, ankle, and tibial alignment angles at the time of the active peak force generated during the stance phase. One female (P1; age = 47.5 years; mass = 71.8 kg; height = 1.59 m) developed bilateral MTSS symptoms during the study and is presented as a case study. A mixed-model linear regression and independent samples *t*-tests identified whether a significant difference existed between MTSS symptomatic and control limbs ($p<0.05$). Control group outcome variable means and standard deviations were used to calculate the minimally important difference to determine whether a substantial difference existed between the control group and P1 [3].

RESULTS AND DISCUSSION

MTSS symptomatic participants displayed a significantly slower running speed ($p=0.018$) and lower normalized active peak force ($p=0.002$) compared to control participants (see Figure 1). There was, however, no significant between-group difference in sagittal plane leg alignment. Compared to the control group, P1 displayed a substantially slower running speed, lower normalized active peak force, and a more vertical tibia (see Figure 1). We speculate that the slower running speed demonstrated by the symptomatic participants is to reduce pain and/or due to decreased plantar flexor strength and endurance [4]. Development of MTSS by P1 suggests that a slower running speed, lower active peak force, and more vertical tibia do not prevent individuals from developing MTSS.

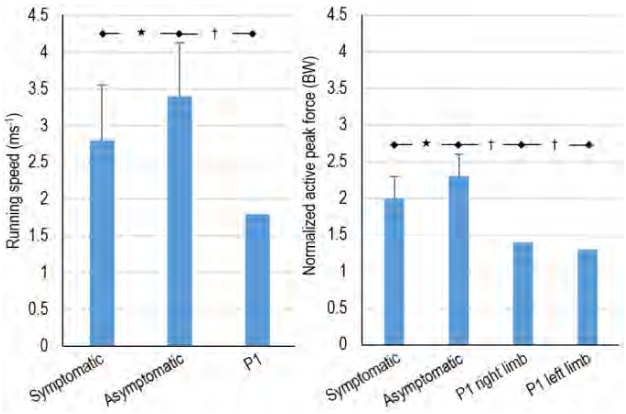

Figure 1 Mean running speed (+SD) and mean normalized active peak force (+SD) for 8 symptomatic, 8 asymptomatic controls and mean values at baseline for P1. ★ = significant difference between symptomatic and asymptomatic ($p<0.05$), † = substantial mean difference between asymptomatic and P1.

CONCLUSIONS

The slower running speed and lower active peak force displayed by participants with MTSS could be to reduce pain or an inability to maintain the same running speed as control participants over a prolonged duration. Developmet of MTSS by P1, despite a lower normalized active peak force and more vertical tibia, suggests the active peak force generated during running is of limited use as a screening tool to identify long-distance runners at risk of MTSS.

REFERENCES

[1] Moen MH et al. *Sports Med* **39**: 523-46. 2009.
[2] Phuah AH et al. *Gait Posture* **31**: 218-22, 2007.
[3] Norman GR et al. *Med Care* **41**: 582-92, 2003.
[4] Mattock J et al. J *Foot Ankle Res* **14**: 2021.

A CONSUMER-GRADE WEARABLE TECHNOLOGY IS VALID FOR THE ASSESSMENT OF WALKING GAIT "IN THE WILD"

Josh Carter[1], Grant Trewartha[1,2], and Ezio Preatoni[1]
[1] Department for Health, University of Bath, Bath, UK.
[2] NURVV Ltd, London, UK.
Email: jc2369@bath.ac.uk

INTRODUCTION

The clinical biomechanical analysis of gait can be an important tool for identifiaction of disease, physical deterioration, and gait abnormalities. Traditional gait analysis is typically lab-based, requires trained staff, and costly equipment, with single and sporadic assessments only showing a snapshot of the patient's gait. One approach that has been strongly advocated to overcome many of these limitations is the use of wearable sensors to perform in-field gait analysis for an extended period of time. Pressure-based insoles have been proposed as an effective method of portable gait analysis, typically targeting the calculation of spatiotemporal gait metrics. The purpose of this study was to evaluate whether the low cost and commercially available NURVV system is valid for the assessment of clinical gait parameters.

METHODS

Twelve healthy males (6) and females (6) walked on a split belt instrumented Bertec treadmill sampling at 1000 Hz. Participants wore a pair of NURVV run insoles inside modified Nike Free run trainers and a set of reflective markers were attached on both limbs (Figure 1). A 12-camera Qualisys motion capture system sampling at 250 Hz collected marker positions as participants completed a multi-stage walking protocol. Speeds ranged from 3-6 km/h, including trials where the participant was asked to imitate a limp on each leg. Using treadmill force data, initial foot contact and toe off events were taken when the vertical force exceeded and dropped below 40 N, respectively. Footstrike type was classified [1] from foot angles calculated in Visual3D using a modified version of the IOR foot model [2]. Timelines were synchronised and these results were compared to those output from the NURVV system that combines pressure data from 16 sensors with inertial measurement unit data to calculate real time metrics. Average Error, Limits of Agreement (LoA), Mean Absolute Percentage Error (MAPE), and Typical Error (TE) were calculated to compare lab-based and wearable systems.

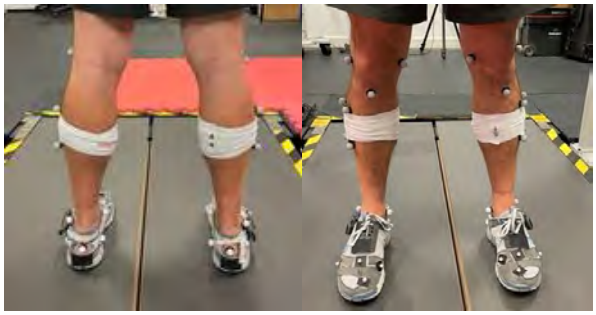

Figure 1 Experimental set-up and marker-set

RESULTS AND DISCUSSION

Identification of stride time and therefore cadence and stride time asymmetry by the NURVV system proved most accurate (Table 1). A small systematic error was seen in ground contact time, likely due to inaccurate identification of toe off timing, which in turn affected estimation of stance time (%) and swing time. These results are comparable to similar technologies previously tested. [3] On average the NURVV system overestimated walking speed in comparison to treadmill speed. However, participant positioning on the treadmill was not controlled for, which could limit the confidence in the comparison. Finally, the two systems had a 97.7% agreement on footstrike type with less than 0.1% of foot contacts being out by two classifications (i.e forefoot-heelstrike).

CONCLUSIONS

The NURVV system showed high agreement with the criterion lab-based measures. This system could be used as an effective tool to perform continuous and long-term gait analysis more easily on clinical populations in their daily life.

REFERENCES

[1] Altman et al. *Gait & Posture* **40**: 298-300.
[2] Leardini et al. *J Biomech* **40**: 554, 2007.
[3] Parati et al. *Sensors* **22**: 6392, 2022.

Table 1: Descriptive statistics evaluating the comparison of the NURVV system and criterion instrumented treadmill data. Positive values indicate larger NURVV system values

Metric	Average Error	LoA	MAPE range	TE range
Cadence (spm)	+ 0	[-3.7, 3.8]	1.0 – 1.9%	1.0 – 1.6
Ground Contact Time (ms)	- 22	[-83, 40]	3.2 – 6.1%	9.6 – 12.2
Stance Time (%)	- 1.9	[-8.0, 4.1]	3.4 – 6.2%	1.0 – 1.42
Stride Time Asymmetry (%)	+ 0	[-1.6, 1.7]	-	0.3 – 0.7
Stride Time (ms)	+ 0	[-9, 9]	0.2 – 0.5%	1.7 – 5.7
Swing Time (ms)	+ 21	[-40, 83]	4.8 – 10.5%	10.0 – 13.1
Walking Speed (m/s)	+ 0.28	[-0.20, 0.75]	-	0.08 – 0.22

Reduced number of motor modules recruited during stair descent in patients with knee osteoarthritis

Lasse Hansen, Jana Rogoschin, Igor Komnik and Wolfgang Potthast
Institute of Biomechanics and Orthopaedics, German Sport University Cologne, Cologne, Germany
Email: l.hansen@dshs-koeln.de

INTRODUCTION

Knee osteoarthritis (KOA) is a prevalent and severe condition with complex effects on human locomotion and activities of daily living (ADL). The concept of modular control focuses on underlying neuromuscular control strategies to identify groups of muscle synergies, referred to as 'motor modules'. Motor modules can be extracted from surface EMG data of multiple muscles using non-negative matrix factorization (NNMF), which is described as the most favorable method to identify muscle synergies in walking and running [1]. The number of motor modules is often used to describe the complexity of a movement, with a higher number being associated with more complex movements and improved motor performance [2]. Correspondingly, lower numbers of motor modules have been reported in connection with populations showing impaired motor performance, e.g. patients with dissatisfactory knee function after knee joint arthroplasty [3]. Since the effect of KOA on motor control strategies during locomotion has only been studied in level walking and results appear inconclusive [4, 5], the purpose of this study was to investigate neuromuscular organization in participants with KOA during level walking as well as stair climbing.

METHODS

Participants with diagnosed medial KOA (n = 12, 62 ± 7.7 years, 81 ± 10.3 kg, 6 female, 6 male) and an age-matched control group (n = 10, 64.1 ± 6.6 years, 68.1 ± 7.7 kg, 5 female, 5 male) carried out a minimum of 6 repetitions of level walking and stair climbing. Surface EMG of 8 lower limb muscles was recorded on each side, ground reaction forces and 3D kinematics were recorded and used for step detection. Subsequently, NNMF was performed on the EMG data. The appropriate number of motor modules was identified using a bootstrapping approach, whereby the variance in each bootstrapped sample of the original EMG accounted for (VAF) by the reconstructed EMG was calculated. The final number of motor modules was determined as the lowest number of modules which fulfilled the following criteria: Firtsly, the lower boundary of the 95% CI of the VAF in the sum of all muscles over all bootstrapped samples must be larger than 90%. Secondly, the VAF for each individual muscle must be larger than 70%, or the addition of another module does not raise the lower boundary of the 95% CI by a minimum of 5% [1, 6]. A two sample t-test was used to assess differences between the mean number of modules in the two groups. No outliers were excluded, test assumptions were examined and significance levels were set to .05 for all statistical tests. All calculations were carried out in MATLAB [R2022B, Natick, Massachusetts: The MathWorks Inc].

RESULTS AND DISCUSSION

In level walking and stair ascending, no difference in mean module count was observed between the two groups. During stair descending, the participants with KOA fulfilled the task with a significantly lower mean module count (M = 4.33, SD = 0.24) than the control group (M = 4.81, SD = 0.53); t(21) = -2.16, p = 0.049

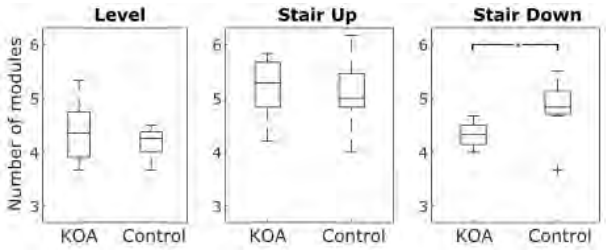

Figure 1 Mean number of modules in each condition. Asterisk indicates statistically significant difference at p < .05.

Descending a staircase is one of the physically most demanding ADL at knee joint level [7]. Therefore, it might more clearly point out existing differences in neuromuscular organization in patients with KOA. With further analysis of the recorded dataset, including more participants, incline walking, as well as kinematic and kinetic analysis, we aim to gain a deeper understanding of the effects of KOA on neuromuscular control.

CONCLUSIONS

The lower number of motor modules recruited in participants with KOA relative to healthy controls during stair descent indicates impaired motor performance in KOA patients during physically demanding ADL. To our knowledge, this has not been studied in a population with KOA for other tasks than level walking.

REFERENCES

[1] Rabbi M et al. Scientific Reports **10**: 8266, 2020.
[2] Allen J et al. *J Neurophysiol* **118**: 363-373, 2017.
[3] Ardestani M et al. *J Electromyo* **37**: 90-100, 2017.
[4] Roelker S et al. *PLoS One* **16(12)**: e0261862, 2021.
[5] Kubota K et al. *IEEE Neur. Sys.* **29**: 239-248, 2021.
[6] Koehn R et al. *PLoS One* **17(4)**: e0267340, 2022.
[7] Kutzner I et al. *J Biomech* **43**: 2164-2173, 2010

Achievement of bipedal locomotion in a two-dimensional neuromusculoskeletal model of unilateral transfemoral amputation

Daisuke Ichimura[1], Hiroaki Hobara[2], Genki Hisano[1,3,4], Tsubasa Maruyama[1] and Mitsunori Tada[1]
[1] Artificial Intelligence Research Center,
National Institute of Advanced Industrial Science and Technology, Tokyo, Japan.
[2] Faculty of Advanced Engineering, Tokyo University of Science, Tokyo, Japan.
[3] Department of Systems and Control Engineering, Tokyo Institute of Technology, Tokyo, Japan.
[4] Research Fellow of Japan Society for the Promotion of Science (JSPS), Tokyo, Japan.
Email: d.ichimura@aist.go.jp

INTRODUCTION

Adaptive locomotion is a prerequisite behavior of animals that helps increase its chances of survival. The central pattern generator in the spinal cord is responsible for the basic rhythm of locomotion through sensory feedback coordination, resulting in energy-efficient movement patterns [1]. Individuals with symmetrical lower limbs have energy-efficient symmetrical locomotion when on flat ground. In contrast, lower limb amputees with morphologically asymmetrical lower limbs exhibit asymmetrical locomotion patterns [2]. However, little is known about how the nervous system controls the lower limbs under these distinct conditions. Thus, we examined how individuals with unilateral transfemoral amputation (UTFA) control their intact and prosthetic limbs during locomotion using forward dynamics simulations of a neuromusculoskeletal model.

METHODS

We constructed a two-dimensional musculoskeletal model with 7 segments and 18 muscles as well as a neural model with a central pattern generator and sensory feedback systems (Figure 1A). The model included 51 free parameters that had to be determined to achieve stable locomotion. We employed a standard genetic algorithm (GA) to search for these parameters [3]. Then, we investigated two adaptation scenarios using a transfemoral prosthesis. In the first scenario, we re-searched 16 symmetric sensory feedback parameters for both lower limbs, which we called the "symmetric control model." This locomotion control strategy was the same as the normal model. The other scenario included 32 asymmetric sensory feedback parameters for both lower limbs, which we called the "asymmetric control model." We evaluated whether each model could acquire stable locomotion when walking for continuous 10 s periods.

RESULTS AND DISCUSSION

The tested models excluding the symmetric control model successfully acquired stable locomotion after 2000 generations of GA (Figure 1B). The locomotion pattern of the normal model qualitatively resembled that of human bipedal locomotion, while the asymmetric control model showed an asymmetric gait pattern (Figure 1C). These results suggest that individuals with UTFA acquire different control strategies from those of able-bodied individuals to achieve bipedal locomotion.

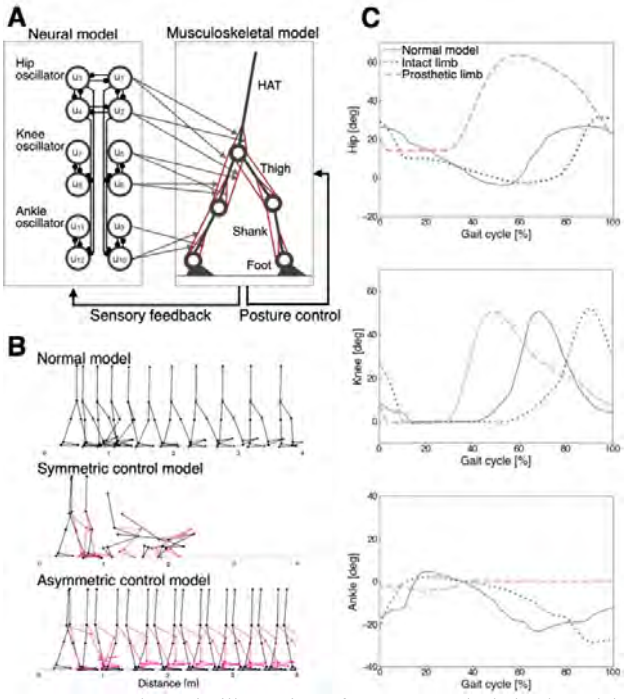

Figure 1 A: Schematic illustration of neuromusculoskeletal model. B: Stick pictures of normal, symmetric control, and asymmetric control models during walking. C: Joint angles during walking for the normal model and asymmetric control model.

CONCLUSIONS

We constructed a musculoskeletal model with UTFA. The results of the present study suggest that individuals with UTFA can re-acquire bipedal locomotion using modified neural control strategies. Moreover, our findings provide insight into effective gait assessment and clinical evaluation for gait rehabilitation.

ACKNOWLEDGEMENTS

This work was supported by JST-Mirai Program Grant Number JPMJMI21H5, Japan.

REFERENCES

[1] Stenum and Choi. *J Physiol* **593:** 3493-3511, 2020.
[2] Cutti et al. *J Neuroeng Rehabil* **15:** 2018
[3] Ichimura and Yamazaki. *Front Neurorobot* **13:** 2019

THE EFFECT OF EXERCISES DERIVED FROM CLINICAL GAIT ANALYSIS ON LOW BACK PAIN - A RANDOMIZED CONTROL TRIAL

Christina Kaltenbach[1], Markus Maier[1], Lena Tepohl[1] and Gert Krischak[2]
[1] Institute for Research in Rehabilitation Medicine, Ulm University, Bad Buchau, Germany.
[2] ZAR Friedrichshafen, Friedrichshafen, Germany.
Email: christina.kaltenbach@uni-ulm.de

INTRODUCTION

Musculoskeletal disorders rank as the number one cause of chronic pain worldwide, affect men and women of all ages, and have a major socioeconomic impact.
Research has shown that people suffering from low back pain exhibit limitations in motor control such as reduced mobility [1] or altered abdominal and back muscle activity [2]. Additionally, fear-avoidance behavior [3] can result in long term protective mechanisms [4]. Even though research has shown that low back pain affects gait (e.g. reduced stride length, increased asymmetry, and reduced spinal range of motion), research using clinical gait analysis as an assessment instrument to derivate exercises for rehabilitation is rare. Therefore, the aim of this study was to use clinical gait analysis to derive gait-specific exercises for patients with low back pain based on a randomized controlled trial.

METHODS

Patients (n=70) from a stationary rehabilitation centre suffering from low back pain were randomly assigned to an intervention (IG) or control group (CG). Clinical gait analysis was performed on an instrumented treadmill for 45 sec at a self-selected speed at the beginning (baseline) and after 3 weeks at the end of rehabilitation (follow-up 1). Subsequently, videos and graphically prepared abnormalities in the gait pattern were shown and explained to the IG. In addition, IG got specific and individual exercises, derived from the results, which were additionally performed during the next three weeks of rehabilitation. Main outcome was the present back pain, collected with the numerical rating scale (NRS) and spatio-temporal gait parameters were calculated with MyoResearch Software 3.14 (Noraxon Inc., Arizona, US). NRS was also examined three months after the rehabilitation (follow-up 2). A linear Mixed-Effect Modell was calculated for the NRS and a 2x2 rmANOVA was done for the gait parameters.

RESULTS AND DISCUSSION

After excluding dropouts, 30 patients (66.67% male, age: 55.1±7.2) and 28 (50% male, age: 52.3±8.3) remained in the IG and CG, respectively. The mean NRS at baseline was similar in both groups: IG (4.17±2.17) and CG (4.18±2.33). At the end of the rehabilitation the low back pain decreased 25% in the IG and 20% in the CG. 3 months after rehabilitation the IG continued to reduce low back pain by 18%, whereas in the CG the pain level increased by 0.6% (Figure 1). The linear mixed model examined the effect of the time and group (fixed effect) on NRS (predicted variable) and showed a significant effect for time ($F = 11.0$, $p = 0.004$), indicating that the time had a significant negative effect on low back pain. No interaction effects were found for gait parameters, but main effects were found for stride time ($F = 6.78$, $p = 0.010$), step time ($F = 6.78$, $p = 0.010$) and cadence ($F = 6.39$, $p = 0.013$).

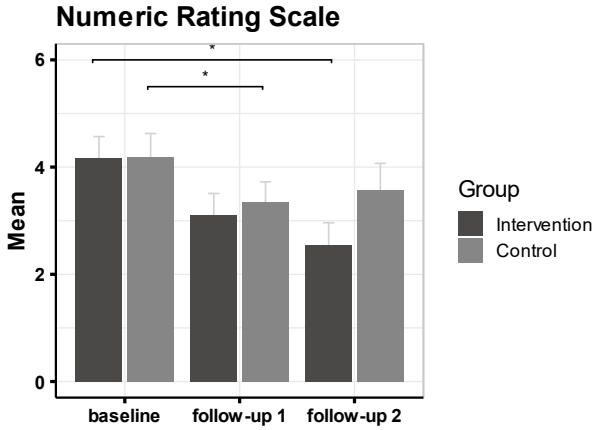

Figure 1: Present LBP on NRS at the beginning of rehabilitation (baseline), after 3 weeks of rehabilitation (follow-up 1), and three months after rehabilitation (follow-up 2). Mean + SEM is displayed.

CONCLUSIONS

The results showed that the individualized exercises for rehabilitation derived from gait analysis aided in reducing low back pain. Furthermore, low back pain in the intervention group reduced sustainably until follow up 2, whereas it worsened again in the control group after three months. The three-week rehabilitation had no effect on gait parameters in either group. However, further analysis with a healthy control group might reveal differences in gait parameters.

REFERENCES

[1] Laird RA et al. *BMC musculoskeletal disorders* **15**:1–13, 2014.
[2] Ghamkhar L, Kahlaee AH. *PM & R the journal of injury, function, and rehabilitation* **7**: 519–526, 2015.
[3] Pfingsten M, Schöps P. *Zeitschrift für Orthopädie und ihre Grenzgebiete* **142**:146–152, 2004
[4] Hodges PW, Tucker K.. *Pain* **152**: 90- 98, 2011

Altering foot orientation changes knee loading in people with and without knee osteoarthritis during three daily activities

Yi Wan[1], Polly Mcguigan[1], James Bilzon[1] and Logan Wade [1]
[1] Department for Health, University of Bath, Bath, United Kingdom.
Email: yw2984@bath.ac.uk

INTRODUCTION

Knee osteoarthritis (KOA) is a highly prevalent joint disease and a leading cause of disability, especially in the elderly population. Pathological changes such as bone spurs, cartilage loss and joint space narrowing generally occur in the medial compartment of the knee [1], where loading magnitude is commonly represented by knee adduction moment (KAM) [2]. Additionally, KAM impulse accounts for both the magnitude and duration of loading, which can provide insights into long-term wear. Foot orientation modifications have been found to reduce knee loading [3], although previous research has only examined KAM during walking and it remains unknown if KAM is similarly reduced during stair climbing and sit-to-stand activities. This study aimed to compare foot orientation modifications on knee loading in KOA and healthy participants, across several different daily activities.

METHODS

Twenty-seven KOA patients (67% female, 57 ± 5 years, 168 ± 10 cm, 78 ± 13 kg) and twenty-nine healthy participants (59% female, 56 ± 5 years, 170 ± 8 cm, 74 ± 14 kg) performed overground walking, sit-to-stand and stair ascent activities on force plates embedded in the ground or two-step stairs. Participants moved at their preferred speed during three, foot progression angle (FPA) conditions; 10˚ toe-in (I), 10˚ toe-out (O) and 0˚ neutral (N), with each condition repeated five times. Three-dimensional kinematic (200Hz) and kinetic data (1000 Hz) were recorded and processed to identify FPA using the frontal angle of the foot, and knee moments (normalised to body mass) using inverse dynamics (Visual 3D). Statistical analysis was performed using general linear mixed effect modelling (MATLAB) on FPA and 1st peak KAM.

RESULTS AND DISCUSSION

During all three activities, toe-in FPA led to a lower peak KAM in both KOA and healthy groups (Fig 1, $P < 0.001$). As FPA became more toe-in, there was a greater reduction in peak KAM for the healthy group, compared to the KOA group across all three activities ($P \leq 0.001$), despite the KOA group having a higher overall KAM. Toe-in FPA significantly reduced KAM impulse during stair ascent and sit-to-stand, in both healthy and KOA populations ($P < 0.05$), but was not significantly altered during walking ($P = 0.560$). Reducing KAM impulse, indicates less cumulative loading on the knee, which may slow the disease progression and reduce the rate of developing KOA in higher risk populations.

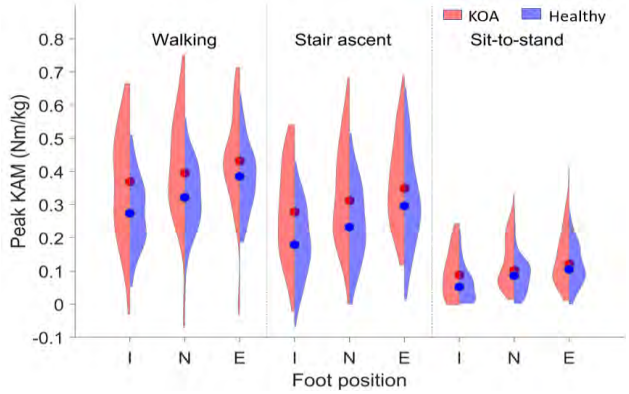

Figure 1 Violin plots of median peak KAM (range) during walking, stair ascent and sit-to-stand during toe-in, neutral and toe-out conditions for KOA and healthy population. I = toe-in, N = neutral, E = toe-out.

Toe-in FPA reduced KAM moment arm length, thus reducing the overall magnitude of KAM. This is consistent with previous literature that toe-in FPA can potentially migrate ground reaction force vector closer to the knee joint centre. In addition, toe-in FPA appeared to increase step width, which is an important factor to reduce knee loading.

All results showed a significant decrease in knee loading with toe-in FPA, indicating that toe-in gait can not only reduce knee loading during walking, but also in stair climbing and sit-to-stand, for both KOA and healthy populations. The results of this study suggest that gait modifications could assist in early clinical intervention and gait rehabilitation to slow the disease progression in KOA population, and could also be used as a preventive exercise strategy for people who are at increased risk of KOA. Future studies should consider the efficacy of long-term personalised gait retraining in patients with KOA, to assist with knee joint unloading and pain relief.

CONCLUSIONS

These results demonstrate the effectiveness of gait modification for clinical rehabilitation, which may also have substantial impact in preventive applications.

ACKNOWLEDGEMENTS

This project was funded by China Scholarship Council.

REFERENCES

[1] Ng et al. *Int J Behav Med* **19**:298-307, 2012.
[2] Vincent et al. *PM&R* **4**:S3-S9, 2012.
[3] Uhlrich et al. *J Biomech* **144**:11312, 2022.

IMPACT OF AGE ON MUSCLE ACTIVATION PATTERNS WITH A PROLONGED WALK

Athulya Simon, Skylar Holmes, Kiichi Ash, and Katherine A. Boyer
Department of Kinesiology, University of Massachusetts Amherst, USA
Email: kboyer@umass.edu

INTRODUCTION

Maintaining mobility is fundamental to extending our healthspan. Muscle weakness and neural changes with age that contribute to gait alterations in older adults may be compounded by muscle fatigue [1] exacerbating mobility deficits following activities of daily living. We have reported, in response to a 30-minute treadmill walk (30MTW) that induced knee extensor muscle fatigue, greater changes in gait mechanics for older as compared to younger adults [2]. The time course of changes in muscle activation patterns in response to this fatiguing walk are not known. The aim of this study was to quantify age-related differences in muscle activation patterns with a 30MTW. We hypothesize that older adults would experience increases in both proximal and antagonist electromyography (EMG) amplitude due to the 30MTW.

METHODS

EMG and foot kinematics were quantified for 7 younger (Y; 36.7 ± 3.4 years, 2 female) and 9 older (O; 71.4 ± 1.1 years, 5 female) healthy adults during a 30MTW at a preferred speed. At minutes (M) 7, 14, and 20 the treadmill was raised to a 3% incline for a 1-minute challenge period to mimic environmental challenges. The university IRB approved all procedures. EMG was recorded for 10 muscles (gluteus maximus-GM, biceps femoris-BF, semitendinosus-ST, vastus lateralis-VL, vastus medialis-VM, rectus femoris-RF, tibialis anterior-TA, gastrocnemius medialis-MG, gastrocnemius lateralis-LG, soleus-SO) every two minutes in the 30MTW. EMG were band-pass filtered (10-300HZ), rectified, and filtered using a 4th order lowpass Butterworth filter resulting in a linear envelope. EMG envelopes for each muscle were amplitude normalized to the maximum signal from an overground walk at 1.2m/s and time normalized to 100% of the gait cycle. Principal Component Analysis (PCA) was used to find variations in the dominant patterns of EMG activation for each muscle. PCs needed to describe >95% of the variation in the signals were retained for analysis resulting in 4-6 PCs for each muscle. PC scores were calculated by projecting participant waveforms onto the PCs. The PC scores for each muscle were compared between age groups and across time using repeated measures ANOVAs with $\alpha \leq 0.05$.

RESULTS AND DISCUSSION

Age related differences were seen in the LG, BF, and RF PC2 and VM PC3 scores with greater activation in older adults. Time differences, primarily increases in activation due to the incline, were seen in the ST and LG PC1 and MG and SO PC2 scores. Age x time interaction effects, showing age related differences in response to the 30MTW, were seen in the VL and BF PC3 and ST PC4 scores (Figure 1). VL and BF PC3 both represent variation in signal amplitude in mid and late stance and early swing. While VL PC3 scores were similar for the groups at M2, increases in score with time only for older adults indicate greater VL activation in mid stance and swing for older, but not younger, adults with the 30MTW. At M2, there were smaller BF PC3 scores for older adults indicating less BF activity at toe-off. However, at M30, the changes in BF PC3 scores indicate older adults increased BF activity around toe-off while younger adults decreased. ST PC4 represents variation in the signal amplitude and peak timing at heel-strike. While scores for ST PC4 in older were similar over time, a decrease in score with time for younger indicated there was an increase in peak ST EMG and delay in the timing of the peak for younger adults with exertion.

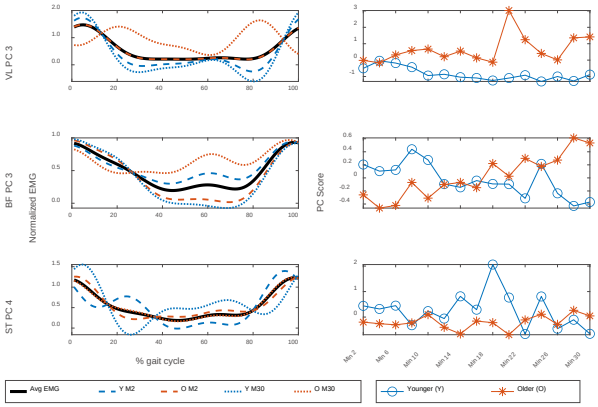

Figure 1 Left column: Average EMG activity throughout the gait cycle along with the PC*PC score from M2 and M30 added to the average EMG and multiplied by a factor of 5 for easier visualization. Right column: PC Scores over the 30MTW for each age group.

CONCLUSIONS

The EMG response to a 30MTW was not the same for younger and older adults. Older, but not younger, adults tended to shift to hip dominant activation patterns [3] while also increasing the co-activation of knee flexor and extensor muscles. These changes in activation patterns may lead to a more metabolically costly gait pattern with an increase in exertion for older adults.

ACKNOWLEDGEMENTS

NIH R01 AG068102

REFERENCES

[1] Kent-Braun et al. *Muscle Nerve* **49**: 209-17, 2014.
[2] Hafer J and Boyer K. *J App Biomech* **36**: 1-8, 2020.
[3] DeVita P et al. *J Appl Physiol* **88**: 1804–1811, 2000.

Predicted Ground Reaction Force Is Plausible to Use in Inverse Dynamics Based Musculoskeletal Simulation During Gait

Ryo Ueno[1,2], Ryotaro Numata[1] and Yasuaki Tsuyuki[1], Harukazu Tohyama[2]
[1] Department of Research and Development, ORGO Inc., Sapporo, Japan.
[2] Faculty of Health Sciences, Hokkaido University, Sapporo, Japan.
Email: ueno@orgo.co.jp

INTRODUCTION

The musculoskeletal simulation needs ground reaction forces (GRF) as an external force input to the multibody dynamics. Although measured GRF are often used to compute joint torques with the kinematics data, the residual forces and moments, which is the error between measured kinematics and forces, are observed and affect the inverse dynamics simulation [1]. A previous study reported that the GRF can be predicted from a kinematics data with lower residuals [2]. It helps clinicians to obtain the kinetics data without force plates. However, the validity of muscle forces/activations computed using the predicted GRF has remained unclear. Therefore, the purpose of this study was to determine the plausibility of predicted GRF for the estimation of muscle activation in the inverse dynamics based musculoskeletal simulation.

METHODS

An open-source motion capture dataset that contains gait data from 50 healthy subjects was used as the experimental data [3]. The data included marker trajectories, GRF and electromyography (EMG) from 8 lower limb muscles. CusToM [2] was used for the musculoskeletal simulations. Model calibration, inverse kinematics, external force prediction, inverse dynamics (ID) and static optimization (SO) were performed. In the prediction of GRF, forces on 14 contact points for each foot were optimized by minimizing forces on the contact points while satisfying multibody dynamics equations. Two sets of ID and SO were performed, one used predicted GRF (PRED) and another used experimentally measured GRF (EXP). Pearson's correlation was calculated to evaluate the similarity between EMG and estimated muscle activations for both PRED and EXP. To evaluate the differences between PRED and EXP, paired t-test was used to compare the trial-wise Pearson's R of the muscle activation similarity and root mean square of residual forces/torques. Additional Pearson's R between residuals and joint torques were computed to investigate how residuals affect computation of muscle activations.

RESULTS AND DISCUSSION

The mean value of the correlation between EMG and estimated muscle activation from the 8 muscles was significantly higher in PRED (R = 0.551) than EXP (R = 0.484) (P = 0.001 from t-test, Table 1). The residuals were 2-4 times higher in EXP compared to PRED (P < 0.001). In EXP, the highest correlation between residuals and joint torques was found between the hip extension moment and sagittal plane residual torque (R = 0.467). This would explain the lower muscle activation similarity from the hip extensors such as semitendinosus and gluteus maximus in EXP. Since the prediction of GRF eliminated the residuals during the optimization, the overall muscle activation similarity was better in PRED compared to EXP (Figure 1).

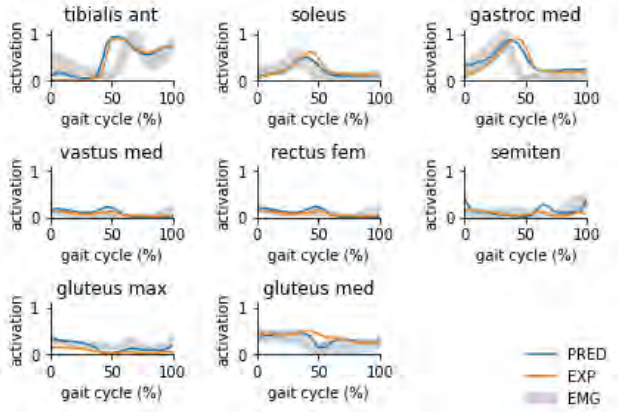

Figure 1 Estimated muscle activations using predicted GRF (PRED) and measured GRF (EXP) compared to EMG.

CONCLUSIONS

The muscle activations were plausibly and better estimated with predicted GRF than measured GRF in inverse dynamics based musculoskeletal simulation. Prediction of GRF helps to obtain kinetics data and muscle forces/activations in clinical applications.

REFERENCES

[1] Remy CD et al. *J Biomech Eng* **131**: 031005, 2009.
[2] Muller A et al. *J Open Source Softw* **4**: 927, 2019.
[3] Schreiber C et al. *Sci Data* **6**: 1-7, 2019.

Table 1: Pearson's correlation between EMG and estimated muscle activation when predicted (PRED) or measured (EXP) GRF was used.

The *P*-values shown are from the paired t-test that compared trial-wise *R*-values between PRED and EXP.

	tibialis ant	soleus	gastroc med	vastus med	rectus fem	semiten	gluteus max	gluteus med	**all**
PRED	0.412	0.621	0.650	-0.038	0.024	0.419	0.500	0.275	**0.551**
EXP	0.389	0.449	0.514	0.343	0.337	0.133	0.257	0.294	**0.484**
t-test P-value	0.001	< 0.001	< 0.001	< 0.001	< 0.001	< 0.001	< 0.001	0.005	**0.001**

PREDICTION OF GROUND REACTION FORCE AND MOMENT BY INERTIAL MEASUREMENT UNITS USING A 3D FORWARD DYNAMICS MODEL

Naoto Haraguchi[1] and Kazunori Hase[1]
[1] Department of Mechanical Systems Engineering, Tokyo Metropolitan University
1-1 Minami-Osawa, Hachioji, Japan.
Email: haraguchi-naoto1@ed.tmu.ac.jp

INTRODUCTION

Ground reaction force (GRF) and moment (GRM) are measured by force plates. While they measure GRF and GRM accurately, they have a limitation for the location of measurement. Previous studies have reported methods to predict GRF and GRM using inertial measurement units (IMUs) and a biomechanical model without the force plate [1]. While they predict GRF and GRM without a statistical model, they have a limitation for the prediction during the double support phase because of a closed-loop structure. Following the issue, recent studies have proposed methods for the prediction using a contact model [2,3]. However, there is still no method for the prediction based on a 3D biomechanical model with a simple system. Therefore, we developed a new method to predict GRF and GRM for application to clinical and use in sports. The present study aims to verify the validity and effectiveness of the new method.

METHODS

We developed a system for predicting GRF and GRM by a 3D forward dynamics model and experimental data recorded by IMUs. Firstly, to match the motion of the model and that of a participant, optimization determines the motion of the model that minimizes the cost function defined by physical loads and errors between the motion of the model and that of the participant recorded by IMUs. Then, the system computes GRF and GRM using a contact model between foot and ground based on the position of the contact points. We constructed the system using MATLAB 9.9 (MathWorks, Inc., USA).

18 participants volunteered for the walking experiment. 6 IMUs (TSND151; ATR-Promotions Inc., Japan) measured the motion of the whole body. For validation purposes, we recorded GRF and GRM by the force plate (TF-4060-D; Tec Gihan Co. Ltd., Japan) and motion capture system (OptiTrack Flex3; Natural Point Inc., USA). The IMUs data were input into the prediction system to compute the error with the motion of the model and predict GRF and GRM. We also calculated GRF and GRM about the projection of the ankle joint center using the force plate and motion capture data. The agreement between the measured and predicted data was derived from Pearson's correlation coefficients (ρ) and the relative root mean square error (rRMSE) [4].

RESULTS AND DISCUSSION

The vertical GRF and sagittal GRM throughout a gait cycle are shown in Figure 1. We succeeded in predicting them based on the present system. The system has an advantage in terms of versatility because it predicts GRF and GRM based on the 3D biomechanical model without a statistical model and complex system. Hence, the system might be applied for biomechanical analysis in various fields compared with previous methods.

The comparison of prediction accuracy with previous studies is shown in Table 1. The present method has a disadvantage in the lower accuracy than that of the previous studies which use a 2D biomechanical model or complex system.

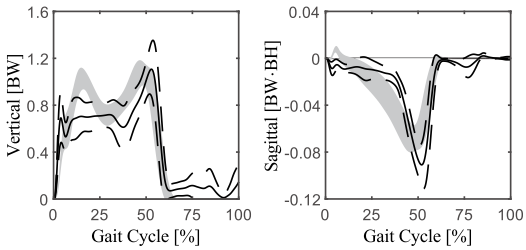

Figure 1 Vertical GRF normalized to body weight (BW) and sagittal GRM normalized to body weight (BW) times body height (BH). Solid and dashed lines represent the result predicted by the system and shaded area represents the result measured by the force plate.

Table 1: Pearson's correlation coefficients (ρ) and the relative root mean square error (rRMSE) observed in this study and reported by previous studies [2,3].

	Vertical GRF		Sagittal GRM	
	ρ	rRMSE	ρ	rRMSE
This study	0.884	18.2(3.9)	0.792	18.4(5.0)
Karatsidis et al., 2019	0.91	15.0(2.4)	0.91	17.5(6.8)
Dorschky et al., 2019	0.95	9.7(2.1)	-	-

CONCLUSIONS

We developed a new system for predicting GRF and GRM using IMUs and a 3D forward dynamics model. The present system might be applied for biomechanical analysis in various fields because the method does not require a statistical model and a complex system. In construct, the present method has a disadvantage in the lower accuracy than that of the previous studies.

ACKNOWLEDGEMENTS

This work was supported by JST SPRING, Grant Number JPMJSP2156.

REFERENCES

[1] Ancillao, A. et al., *Sensors* **18**: 2564, 2018.
[2] Karatsidis, A. et al., *Med Eng Phys* **65**: 68–77, 2019.
[3] Dorschky, E. et al., *J Biomech* **95**, 109278, 2019.
[4] Ren, L. et al., *J Biomech* **41**, 2750–2759, 2008.

Participant-informed models of the tibia-fibula complex: influence of geometry and density prediction errors on bone strain

Olivia L. Bruce[1,2,3], Jean Tu[2,3], and W. Brent Edwards[1,2,3]

[1] Department of Biomedical Engineering, University of Calgary, Calgary, Canada.
[2] Human Performance Laboratory, Faculty of Kinesiology, University of Calgary, Calgary, Canada.
[3] McCaig Institute for Bone and Joint Health, University of Calgary, Calgary, Canada
Email: olivia.bruce@ucalgary.ca

INTRODUCTION

Bone geometry and material properties greatly influence finite element (FE)-predicted bone strain [1, 2]. In the absence of subject-specific FE models based on computed tomography (CT) data, statistical appearance models (SAM) may provide a valuable tool to generate accurate, participant-informed models. The purpose of this study was to quantify errors in bone geometry, density, and FE-predicted bone strain of the tibia-fibula complex generated from a SAM and skin-mounted anatomical landmarks.

METHODS

Twelve markers were placed at palpable landmarks on the left lower leg of thirty (15 female, 15 male) young physically active participants. CT scans of the left lower leg and markers were subsequently obtained. The scans were used to generate participant-specific models and to determine mean offsets between the skin-mounted markers and corresponding landmarks on the bone surface. Landmark coordinates were also measured using a motion analysis system. Tibia-fibula geometry and density distribution were then predicted by morphing an existing SAM [1] along the first 1 through 5 cumulative principal components, minimizing the sum of squared distances between predicted and motion analysis-measured landmarks, accounting for soft tissue offsets.

Meshes predicted from landmarks and only the first principal component along with the CT-based meshes were used to generate finite element models. Muscle and ankle joint loads at the time of peak ankle joint contact force during running were calculated using an inverse dynamics-based static optimization using motion analysis data for each participant. Root-mean-square- error (RMSE) relative to the participant's CT-based model were calculated for geometry, density, and pressure-modified von Mises strain. Bland-Altman plots were created to evaluate agreement between models for strained volume, defined as the volume of elements experiencing strain above 4000 με; The acceptable limits of agreement were defined as ± 5%.

RESULTS AND DISCUSSION

RMSEs in geometry and density were not different between landmark-based predictions using 1 through 5 principal components ($p \geq 0.128$, median geometry RMSE = 4.4-4.8 mm, median density RMSE = 0.118-0.142 g/cm^3). The first principal component described isotropic scaling; the lack of improvement with additional principal components suggests that skin-mounted landmarks did not provide sufficient information to characterise variations in tibial geometry.

Geometry and density prediction errors led to large differences in strain and strained volume when compared to CT-based models. Median strain RMSE was 492 με. The agreement range for strained volume (-200% to 140%, Figure 1) when compared to the CT-based models far exceeded the acceptable limits.

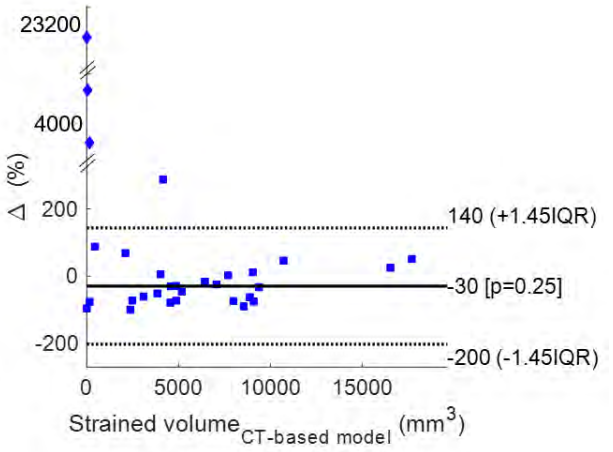

Figure 1 Bland-Altman plot showing percent differences in strained volume calculated from the landmark-predicted model and the CT-based (gold standard) model. Diamonds represent statistical outliers.

CONCLUSIONS

Skin-mounted landmarks were insufficient to capture tibial geometry and associated variations in density, leading to large errors in finite-element predicted bone strain. This approach for generating finite element models should not be used when making comparisons between groups to avoid possible errors in geometry. Some form of medical imaging is likely necessary to generate an accurate participant-informed tibia model.

ACKNOWLEDGEMENTS

Funding support was provided in part by NSERC (RGPIN 02404-2021 and CGS D – 534891 - 2019), and the NSERC CREATE We-TRAC program.

REFERENCES

[1] Bruce OL et al. *Bone* 161: 116443, 2022.
[2] Xu C et al. *IEEE. Trans. Biomed. Eng.* 67: 545 – 555, 2020

SENSORIMOTOR NOISE MIGHT EXPLAIN EFFORT IN AMPUTEE GAIT: A SIMULATION STUDY

Wouter Muijres[1], Maarten Afschrift[2], Renaud Ronsse[3], and Friedl De Groote[1]
[1]Department of Movement Sciences, KU Leuven, Leuven, Belgium.
[2]Department of Human Movement Sciences, Vrije Universiteit, Amsterdam, The Netherlands.
[3]Institute of Mechanics, Materials, and Civil Engineering, UCLouvain, Louvain-la-Neuve, Belgium.
Email: wouter.muijres@kuleuven.be

INTRODUCTION

Metabolic cost of walking is higher in transtibial amputees than in intact individuals due to reduced push-off from the prosthetic ankle. Although active ankle prostheses restore ankle push-off, improvements in metabolic cost of walking have been modest [1]. It has been hypothesized that this is because active prostheses do not restore balance control. Sensorimotor noise continuously disturbs locomotion and hence humans continuously control walking balance through sensorimotor feedback. The lack of both direct control of and sensory information from the ankle impairs balance control in amputees. Here, we used computer simulations of amputee walking to investigate whether the need to stabilize walking in the presence of sensorimotor noise might explain the increased metabolic effort in amputee as compared to intact walking. We hypothesized that effort would increase more with sensorimotor noise in transtibial amputees than in intact individuals due to impaired feedback control. We evaluated two types of prostheses: a passive and an active one. We expected that walking with an active prosthesis that provides a predetermined (optimal, see below) torque pattern would require similar effort as intact walking at low levels of sensorimotor noise due to the ability of the active prosthesis to generate push-off. At high levels of sensorimotor noise, we expected that walking with an active prosthesis requires similar effort to walking with a passive prosthesis.

METHODS

We simulated gait using a conceptual 2D torque driven model with 5 degrees of freedom [3], Fig. 1A. Torques consisted of a feed-forward component and linear, time-varying full state (angular positions and velocities) feedback. We solved for feed-forward torques and feedback gains that minimized expected effort for a full stride (imposed duration of 1.6s and length of 1m) in the presence of sensorimotor noise [2]. Effort was modelled as the squared sum of total (feed-forward and feedback) torques. We modelled walking with an active prosthesis by removing sensory information from the ankle and feedback control of the ankle on one side. We modelled walking with a passive prosthesis by additionally imposing zero ankle torque on one side (pin joint rather than spring as the conceptual model has no foot segment). We solved the stochastic optimal control problem using a previously proposed numerical approach [2] for different levels of sensory noise with constant motor noise.

RESULTS AND DISCUSSION

Differences in expected effort between amputee and intact gait increased with higher levels of sensorimotor noise mainly due to a larger increase in feedback torques (Fig. 1B-D). Walking with an active prosthesis reduced the biological feed-forward toque as compared to walking with a passive prosthesis and even intact walking at low levels of noise (Fig. 1C). However, the active prosthesis did not notably reduce the expected feedback effort explaining why it could not restore normal levels of effort.

CONCLUSIONS

Our simulations suggest that active prostheses should aim at supporting balance control in addition to providing push-off power to reduce the metabolic cost of amputee walking.

ACKNOWLEDGEMENTS

This project was support by FWO (1SF7322N).

REFERENCES

[**1**] Quesada RE et al. (2016) J. Biomech. 49: 3452–3459
[**2**] Van Wouwe T et al. (2022) PLoS Comput. Biol. 18: e1009338
[**3**] Kelly M. (2017) SIAM Rev. 59: 849–904

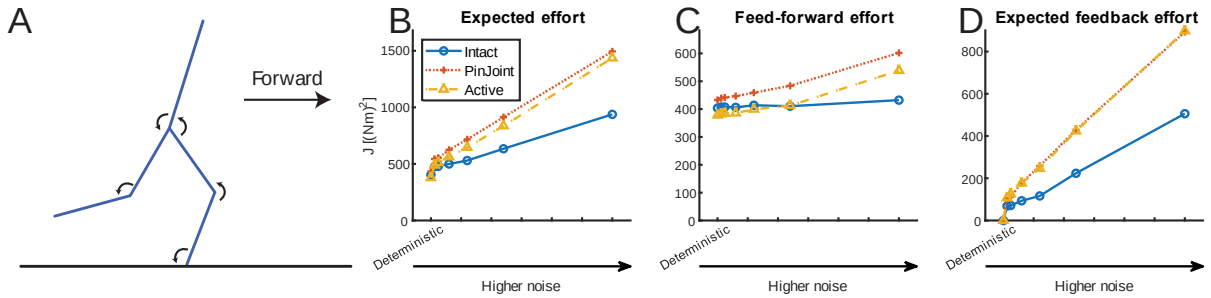

Figure 1. A. The model was driven by a torque actuator for each joint [3]. B. Expected effort of intact and amputee gait (pin joint and active prosthesis) for different levels of sensorimotor noise. C-D. Effort from feed-forward and feedback torques.

A CADAVERIC SHOULDER MOTION STUDY USING OPEN-LOOP CONTROL FOR SIMULATING IN-VIVO MUSCLE LOADING

David T. Axford[1,2], Robert Potra[2], Richard Appleyard[2], Janos Tomka[2], Antonio Arenas-Miquelez[2,3], David Hollo[2], Sumit Raniga[2], and Louis Ferreira[1]

[1] Department of Mechanical and Materials Engineering, Western University, London, Canada.
[2] Faculty of Medicine, Health, and Human Sciences, Macquarie University, Sydney, Australia.
[3] Hospital Quironsalud Valle del Henares, Madrid, Spain.
Email: daxford2@uwo.ca

INTRODUCTION

The shoulder is an unconstrained joint that relies on a delicate balance of soft tissue forces for joint stability and function. To better understand this balance, ex-vivo shoulder simulators are used to replicate in-vivo loading during simulated active motion. Existing simulators use control architectures that oversimplify muscle function by trivializing their effect on joint position or by neglecting to differentiate between functional groups within a muscle, namely the superior and inferior portions of the subscapularis. These architectures do not adequately represent the loading environment in the shoulder and are limited to performing simple planar motions within well defined regions. The objective of this study was to develop a control architecture that incorporates the complex function of each muscle to simulate multiple planes of motion.

METHODS

The developed shoulder motion simulator used an open-loop tendon excursion control architecture with iterative learning to simulate active motion by actuating eight muscles in the shoulder. The simulator performed scapular plane abduction (SPA), forward flexion (FF), internal/external rotation (IER), and circumduction (CIR) in eight cadaveric specimens (57 ± 6 years). Optical markers were used to track joint kinematics and a uniaxial load cell mounted onto each muscle actuator measured tendon load. For each motion, kinematic tracking accuracy was assessed using root mean square error (RMSE) and maximum absolute error (MAE).

RESULTS AND DISCUSSION

RMSE was less than 1.4 degrees and MAE was less than 6.3 degrees for all simulated motions and all three joint rotations (Table 1). Consistent with a previous EMG study [1], the anterior deltoid had more of a role in humeral elevation during FF (Figure 1) ($p < .001$), whereas the lateral deltoid contributed more to SPA ($p < .001$). Infraspinatus force was higher during FF than SPA ($p = .004$) indicating the infraspinatus has a role in elevation during FF. Superior subscapularis played a major role during both FF and SPA and was higher than the inferior subscapularis force ($p < .001$) supporting previous findings that the superior portion of the subscapularis contributes to arm elevation [2]. During IER, internal rotation was associated with an increase in inferior subscapularis force ($p < .001$). External rotation was associated with an increase in supraspinatus force ($p = .001$) providing biomechanical evidence for the external lag sign observed in patients with supraspinatus tears [3]. During circumduction, the anterior deltoid had the highest force when the arm moved anteriorly away from the scapular plane and the lateral deltoid force was greatest when the humerus moved posteriorly into the scapular plane.

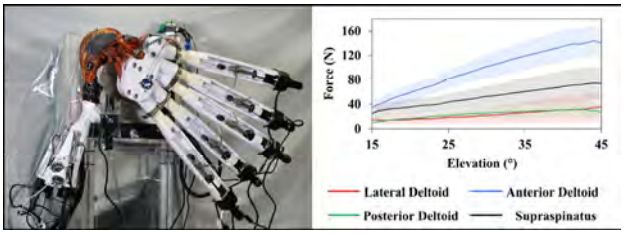

Figure 1 (Left) Cadaveric shoulder motion simulator. (Right) Average deltoid and supraspinatus forces vs. glenohumeral elevation during forward flexion.

Table 1: Root mean square error for all simulated motions.

	SPA	FF	IER	CIR
Elevation (°)	0.7	0.8	0.2	0.7
Plane of Elevation (°)	0.7	1.4	0.8	0.9
Axial Rotation (°)	0.7	1.2	0.9	1.2

CONCLUSIONS

This study presents the validation of a novel shoulder motion simulator that uses open-loop excursion control to achieve high accuracy when simulating multiplanar motions. The force relationships found in this study are consistent with those found in other biomechanical studies and can provide biomechanical evidence for clinical observations. This simulator is a valuable tool that will be used to improve our understanding of soft tissue forces in the shoulder.

REFERENCES

[1] Heuberer P et al. *Arch Orthop Trauma Surg* **135**: 549-563, 2015.
[2] Omi R et al. *J Anat* **216**: 643-649, 2010.
[3] Castoldi F et al. *J Shoulder Elbow Surg* **18**: 529-534, 2009.

Treadmill versus Overground Gait Characteristics in Autistic Individuals

Kevin A. Valenzuela[1], Melissa Bittner[1], Amanda Young[1] and Hunter J. Bennett[2]
[1] Department of Kinesiology, California State University Long Beach, Long Beach, CA, USA.
[2] Department of Human Movement Sciences, Old Dominion University, Norfolk, VA, USA.
Email: kevin.valenzuela@csulb.edu

INTRODUCTION

Current research evaluating gait utilize both overground walking and instrumented treadmills, depending on availability. Some variables have been shown to be statistically equivalent between modalities of measurement for healthy young adults [1]. However, certain populations with disorders, such as Parkinson's disease, have shown differences between the conditions [2]. It is currently unknown if young adult Autistic individuals currently show similarities or differences between these conditions. Therefore, the purpose of this research was to assess spatiotemporal gait characteristics in young adult Autistic individuals.

METHODS

Thirty-three Autistic individuals between the ages of 18-22 were recruited from local school districts to participate in this study. The inclusion criteria for the study included an educational diagnosis of Autism Spectrum Disorder and an ability to walk independently without assistance. A 15 camera Qualisys motion capture system (240Hz), Bertec force plates, and a Bertec instrumented treadmill (1200Hz) were used to collect raw marker and force data. On day one, subjects walked on a treadmill for three continuous minutes in order to establish a preferred gait speed. Subjects then had retroreflective markers attached bilaterally to their feet. Subjects performed three minutes of continuous walking at their self-selected speed. On day two, the same marker set was attached. Subjects performed ten overground walking trials on a 20m walkway. Data were imported into Visual3D. Spatiotemporal gait characteristics were calculated. A two-tailed paired samples t-test ($p<0.05$) was used to assess differences between the treadmill and overground gait conditions.

RESULTS AND DISCUSSION

Velocity, stride length, and step lengths were significantly increased during overground walking ($p<0.001$). Cycle time, double support time, stride width, and stance time were significantly decreased during overground walking (Table 1). While neurotypical adults have shown similar patterns between the two activities when gait velocity is matched [1], Autistic individuals showed reduced preferred gait velocity during overground walking, which altered spatiotemporal characteristics. Velocities were not matched in order to determine the differences in preferred velocity.

CONCLUSIONS

While research on the Autistic community continues to expand, the modality used to measure gait characteristics is important as the preferred velocity is different between the two tasks. Comparison of overground data to treadmill data should be interpreted cautiously.

REFERENCES

[1] Hollman, JH et al. *Gait & Posture* **43**: 204-9, 2016.
[2] Bello, O et al. *J Parkinson's* **4(1)**: 33-6, 2014.

Table 1: Spatiotemporal Gait Characteristics in Autistic Individuals on a Treadmill compared to Overground Walking

	Treadmill		Overground	
	Right Leg	Left Leg	Right Leg	Left Leg
Cycle Time (seconds)*	1.16 ± 0.18		1.03 ± 0.11	
Double Support Time (seconds)*	0.40 ± 0.11		0.28 ± 0.09	
Velocity (m/s)*	0.80 ± 0.19		1.41 ± 0.26	
Stride Length (m)*	0.91 ± 0.19		1.44 ± 0.18	
Stride Width (m)*	0.21 ± 0.05		0.14 ± 0.04	
Step Length (m)*	0.45 ± 0.10	0.45 ± 0.11	0.74 ± 0.14	0.68 ± 0.11
Stance Time (seconds)*	0.78 ± 0.15	0.78 ± 0.14	0.65 ± 0.09	0.63 ± 0.11
Swing Time (seconds)	0.39 ± 0.07	0.38 ± 0.06	0.38 ± 0.06	0.41 ± 0.07

*Significant difference between treadmill and overground conditions ($p<0.05$). Variables of different legs were compared against the same leg in the two conditions.

IN SITU VALIDATION OF POWER QUANTIFICATION FOR DYNAMIC WHEELCHAIR SPORTS

Mathieu Deves[1], Thibault Marsan[1], Arnaud Faupin[3] and Bruno Watier [1,2]
[1] LAAS-CNRS, CNRS, UPS, Université de Toulouse, France.
[2] CNRS-AIST JRL (Joint Robotics Laboratory), IRL, Tsukuba, Japan.
[3] IAPS, Université de Toulon, Toulon, France.
Email: mdeves@laas.fr

INTRODUCTION

Wheelchair racing is accessible to athletes who have impairments and are classified according to their level of impairment defined by the International Paralympic Committee (from T51 to T54). For such race, the acceleration phase is an important component of performance and has been directly linked to the ability of the athletes to apply high amounts of horizontal force and power [1]. This is well known to be the phase during which the maximum power is produced by the athletes. In Paralympics disciplines, it has been shown that more powerful athletes could achieve better results in speed tests [2]. A macroscopic method made it possible to calculate various biomechanical variables during able-bodied sprint running on the field [1]. Hence the objective of this study was to propose a protocol for estimating the power developed by the athletes during a wheelchair sprint.

METHODS

Five para-athletes of the national French para-athletics team and two former para-athletes volunteered for this study (EudraCT / IDRCB n° 2020-A02919-30). After a specific warm-up, the athletes performed two sprints of 50 m with 0 N, 10 N, 20 N and 30 N resistances. The 1080 Motion Sprint was used to apply in the field the resistances and collect horizontal velocity at 333 Hz. Photocells (WITTY, Microgate, USA) were used to measure time in the non-resistance sprints (0N). Using the 1080 Sprint and photocells raw data, maximal velocity (V_{max}), estimated time to 100 m, maximal horizontal force (F_{max}), and maximal power (P_{max}) were calculated (Table 1). Horizontal propulsion force (F_h) was calculated using the mass of the athletes and the wheelchair (m), the horizontal acceleration (a_h), the drag resistance (F_{aero}), the rolling resistance (F_{roll}), and the 1080 Sprint resistive force (F_{1080}):

$$F_h(t) = ma_h(t) + F_{aero} + F_{1080} + F_{roll}$$

RESULTS AND DISCUSSION

For all participants, increasing the resistance increased their estimated time to 100 m, while it decreased their maximal speed and power. Maximal force remained constant despite increasing resistance (Table 1). Force-velocity and power-velocity profiles differed between the subjects, and the highest maximal power was achieved by the S1, an athlete classified as T54, and the lowest was achieved by the athlete classified as T52 (Figure 1). Depending on the classification and sport specialty, the maximum power output varied, and the addition of resistance had different impact.

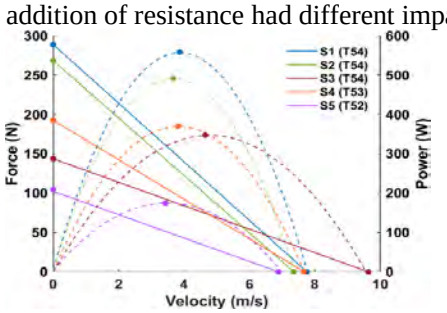

Figure 1 Force-velocity and power-velocity (dashed line) relationship of French para-athletes with 10 N resistance.

CONCLUSIONS

This study proposed a novel method to compute power developed by wheelchair athletes in the field. The protocol developed can be used by athletes for their training, as it can provide the power generated during a sprint and allow them to draw their force-velocity profile and track their progress. Both parameters are of great interest for both athletes and their coaches.

ACKNOWLEDGEMENTS

This work was funded by the ANR project PARAPERF (ANR--19-STHP-0005) and supported by French disabled sports federation (FFH) and Ministry of Sports.

REFERENCES

[1] Samozino P et al. *Scand J Med Sci Sport* **26**: 648-58, 2016.
[2] Loturco I et al. *Adap Phys Act Q.* **37**: 508-17, 2020

Table 1: Mean and standard deviation of the maximal values of each parameter for all conditions.

	0 N	10 N	20 N	30 N
Time 100 m (s)	16.6 ± 2.4	20.2 ± 3.4	23.5 ± 5.2	26.1 ± 5.8
V_{max} (m/s)	7.3 ± 0.9	6.5 ± 1.1	5.5 ± 1.0	4.9 ± 1.0
F_{max} (N)	187.1 ± 28.2	161.7 ± 72.7	162.3 ± 63.5	162 ± 56.9
P_{max} (W)	359.3 ± 81.7	321 ± 122.6	317 ± 124	300 ± 105.9

THE IMMEDIATE EFFECT OF A HOP-STABILIZATION PROGRAM ON GROUND REACTION FORCE DURING CUTTING MOVEMENTS IN INDIVIDUALS WITH CHRONIC ANKLE INSTABILITY

Teerapat Laddawong[1], Hiromi Saito[1], Toshiaki Soga[1] and Norikazu Hirose[2]
[1] Graduate School of Sport Sciences, Waseda University, Japan.
[2] Faculty of Sport Sciences, Waseda University, Japan.
Email: teerapat.l@fuji.waseda.jp

INTRODUCTION

Lateral ankle sprains (LASs) have been reported in 62.7% of soccer players, and up to 40% of first-time LASs patients suffer from chronic ankle instability (CAI). Prevention is essential since CAI causes 47% of recurrent ankle injuries. Cutting movement is a crucial dynamic motion in sports, and a change in biomechanical control may increase the risk of recurrent injury in individuals with CAI [1]. The hop-stabilization program may be implicated as a warm-up before engaging in the cutting movement to activate biomechanical patterns and is also effective for preventing recurring ankle sprains [2]. This study aimed to identify the effects of a hop-stabilization warm-up program on ground reaction force during cutting movement in individuals with CAI.

METHODS

Eight individuals with CAI and eight healthy subjects participated in this study. Each subject participated on two separate experiment days: a hop-stabilization and a control warm-up program, according to a crossover design. Before and after the warm-up program, the ground reaction force (GRF) during 45-degree cutting movements was administered. A two-way mixed-design ANOVA was used to find data differences between and within groups.

RESULTS AND DISCUSSION

The hop-stabilization warm-up programs reduced the peak posterior GRF in CAI subjects with mean differences of -0.052 ± 0.021, p=0.017 (Table1). The hop-stabilization warm-up programs had no influence on the GRF in the other direction and had no effect on the time to peak GRF. The peak posterior GRF could reduce ankle joint impact during cutting movement.

CONCLUSIONS

The hop-stabilization warm-up programs immediately reduced the peak posterior GRF in the CAI subjects during 45-degree cutting movements. The program might enhance the capacity to absorb GRF. These findings suggest that the program can benefit individuals with CAI by improving kinetic patterns prior to dynamic training.

REFERENCES

[1] Simpson JD, Stewart EM, Turner AJ, Macias DM, Chander H, Knight AC. Lower Limb Joint Kinetics During a Side-Cutting Task in Participants with or Without Chronic Ankle Instability. J Athl Train. 2020;55(2):169-75.

[2] Ardakani MK, Wikstrom EA, Minoonejad H, Rajabi R, Sharifnezhad A. Hop-Stabilization Training and Landing Biomechanics in Athletes with Chronic Ankle Instability: A Randomized Controlled Trial. J Athl Train. 2019;54(12):1296-303.

Table 1: Mean differences of the peak posterior ground reaction force (%body weight), p-value, and 95% confidence interval for the difference before and after the hop-stabilization and control warm-up program

Group	Mean difference (Pre-Post test) ± SE	p-value	95% confidence interval for difference
CAI with Hopping	-0.052 ± 0.021	0.017*	-0.094 to -0.01
CAI with Running	-0.058 ± 0.021	0.009*	-0.1 to -0.016
Healthy with Hopping	-0.002 ± 0.021	0.909	-0.045 to 0.04
Healthy with Running	-0.018 ± 0.021	0.395	-0.06 to 0.024

NEUROMUSCULAR ADAPTATIONS TO AERIAL LANDING PERFORMANCE FOLLOWING A SHARK BITE INJURY: A CASE-CONTROL STUDY

James R Forsyth[1], Christopher J Richards[1,2], Joshua PM Mattock[1], Deirdre E McGhee[1], Jonathan Shemmell[3] and Julie R Steele[1]

[1] Biomechanics Research Laboratory, University of Wollongong, Wollongong, Australia.
[2] Cenofex Innovations, Goulburn, Australia.
[3] Neuromotor Adaptation Laboratory, University of Wollongong, Wollongong, Australia
Email: jforsyth@uow.edu.au

INTRODUCTION

Aerials are highly complex manoeuvres in which surfers project a surfboard above the lip of a breaking wave before landing back on the wave's face. Executing such a difficult skill requires sophisticated neuromuscular coordination, particularly of the lower limbs [1]. Traumatic lower limb injury, however, can compromise an individual's ability to perform complex movements, unless they are able to make appropriate neuromuscular adaptations [2]. We present a case-control study of a highly skilled male surfer who, despite losing most of his left lateral quadriceps muscle during a shark bite, was able to return to performing aerials after extensive surgery and intensive rehabilitation. We investigate how this individual's lower limb muscles adapted following the loss of muscle mass to enable him to perform aerials. To control for time between experiments, we compared the surfer's data to a matched control.

METHODS

The participant who sustained the injury (P1, age: 26 years, height: 178.4 cm, mass: 67.3 kg) and the matched control (P2, age: 26 years, height: 176.2 cm, mass: 69.4 kg) both completed five repetitions of a surf-like simulated aerial task [1] in 2014 (pre-injury) and 2019 (post-injury). Medial gastrocnemius (MG), vastus medialis (VM), and semitendinosus (ST) muscle activity were collected for both limbs of each participant using Delsys Trigno wireless (1926 Hz; 2014) and Trigno IM systems (1111 Hz; 2019). We selected these muscles because they were not directly affected by the shark bite. Custom MATLAB scripts were used to process the data and align the EMG data with the landing impact markers [1]. Linear envelopes of the 500 ms before and after foot-surfboard contact in each trial were then evaluated using Statistical Parametric Mapping to compare muscle activation patterns [3]. The participants' trials were treated as independent. A 2x2 ANOVA was used to compare the EMG waveforms between participants (P1, P2) and limb (lead/uninjured, trail/injured). Where a main effect or interaction was found, we performed *post hoc* tests using a Bonferroni correction ($p < 0.05$).

RESULTS AND DISCUSSION

Pre-injury two-way ANOVA results suggested there were participant main effects for both MG and VM. Similarly, a main effect of limb was also present in VM and ST. However, following *post hoc* comparisons, only VM demonstrated significant differences.

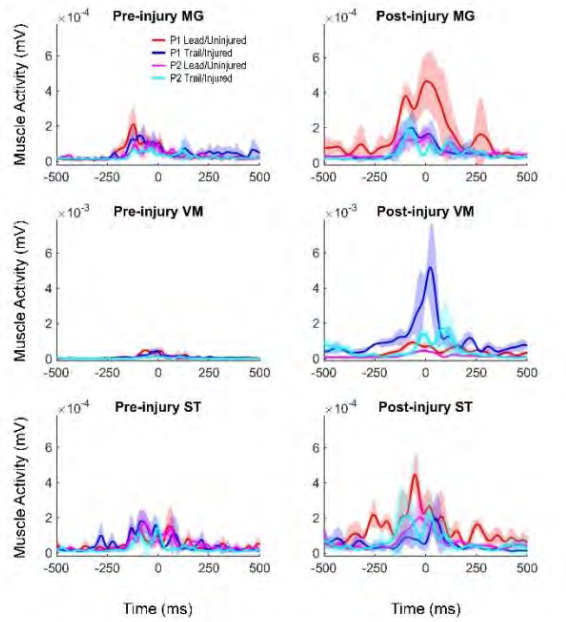

Figure 1 Mean ± SD waveforms of pre- and post-injury data for the lead/uninjured and trail/injured medial gastrocnemius (MG), vastus medialis (VM) and semitendinosus (ST).

Post-injury analyses revealed significant main effects of participant and limb for MG, VM and ST, with both VM and ST also showing significant interaction effects. Interestingly, only VM retained *post hoc* significance for participant and limb main effects, and interaction effects. Specifically, P1 displayed greater activation of the trail/injured VM compared to the lead/uninjured VM between 222-284 ms before landing ($p < 0.001$), as well as during landing (-3 to 13 ms; $p = 0.019$). This result suggests that P1 (the case) needed to contract the VM of his injured leg earlier, with increased EMG amplitude, to prepare for and dissipate the forces generated when landing an aerial. Although not significant in *post hoc* comparisons, additional adaptations to both MG and ST in the lead/uninjured limb may have occurred to accommodate P1's injury.

CONCLUSIONS

This unique study highlights that substantial adaptations to the neuromuscular control of landing a complex task, such as an aerial, can occur following traumatic injury.

REFERENCES

[1] Forsyth JR et al. *J Sports Sci* **30**: 1780-1788, 2021.
[2] Lindstrom et al. *Knee Surg Sports Traumatol Arthrosc* **18**: 106-114, 2010.
[3] Pataky T et al. *J Biomech* **48**: 1277-1285, 2015.

fMRI REVEALS FIDGETING MOTOR SKILLS IN ADHD IMPROVES PREFRONTAL CORTEX ACTIVATION DURING EXECUTIVE FUNCTIONING

X Zhao[1], G Waters[2], G Newburn[3], A Wang[1], V Shim[1], S Holdsworth[3], K Waldie[2] and J Fernandez [1,3]

[1] Auckland Bioengineering Institute, University of Auckland, New Zealand
[2] Department of Psychology, Faculty of Science, University of Auckland, New Zealand
[3] Mātai Medical Research Institute, Gisborne, New Zealand
Email: xzha365@aucklanduni.ac.nz

INTRODUCTION

A diagnosis of Attention Deficit Hyperactivity Disorder (ADHD) is typically established using a combination of several psychological assessments and occasionally surface electrophysiological mapping. Recently, MRI studies have shown the very real potential to establish useful ADHD biomarkers [1]. However, one clinical characteristic of ADHD that has yet to be explored using fMRI is fidgeting motor skills. In this pilot study, we investigated the potential for using fMRI integrated with a functional cognitive task to identify if fidgeting behaviour might modify medial prefrontal cortex (mPFC) activation.

METHODS

Ethical approval was received from the New Zealand Health and Disability Ethics Committee. The MRI setup used a 3T (GE Discovery Signa Premier) with a AIR™ 48-channel head coil. The lower limb was isolated with knee supports to prevent motion artifacts from influencing the head coil. Data collected when motion artifacts exceeded 3mm were removed from processing. Two volunteers (one diagnosed with ADHD and one neurotypical) participated in this pilot study. A fMRI sequence was used to evaluate the impact of fidgeting motor skills while performing an executive functioning assessment, the Flanker task [2]. The Flanker task consisted of each volunteer being asked to identify the direction of a central arrow symbol (using a clicking device) in an array of arrows. The default mode network (DMN) activations were contrasted using the standard network atlas Yeo2011[3] in the CONN toolbox [4].

RESULTS AND DISCUSSION

Activation in the mPFC increased by 94% in the ADHD participant while fidgeting and performing the Flanker task. In contrast, the neurotypical (NT) participant showed a decline of 82% in activation again under the same conditions (Figure 1 - top). This suggests that fidgeting might be a learned adaptive behaviour in the ADHD brain to improve higher executive functioning, whereas fidgeting might distract neurotypical participants and be perceived as a secondary loading task when it is not natural for them.

The ADHD participant showed a strong correlation between activity in the mPFC (circled area in Figure 1 - bottom) and the DMN during the Flanker task. Importantly, the ADHD volunteer's ability to shift away from the DMN during the Flanker task only improved while fidgeting. In contrast, the NT volunteer easily shifted from the DMN when performing the Flanker task without the need to fidget. Though it is known that those with ADHD have trouble transitioning from the DMN this is the first empirical MRI evidence that fidgeting activity assists this transition.

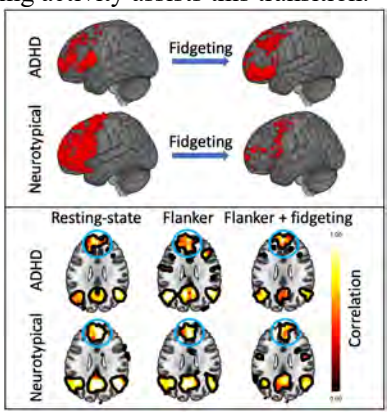

Figure 1 Top: brain activation (RED) for ADHD and NT participants with and without fidgeting. Bottom: Default mode network (DMN) correlation maps for ADHD and NT participants showing resting, Flanker task, and Flanker+fidgeting. The circled area is the mPFC seed point.

CONCLUSIONS

This study has revealed, for the first time, that fidgeting motor skills, may assist executive functioning in ADHD by increasing activation in the prefrontal cortex. This may assist those with ADHD shift from the DMN to other task-positive brain networks and offer clinicians an alternative to current medical interventions.

ACKNOWLEDGEMENTS

The authors acknowledge support from the Mātai Medical Research Institute and funding from the University of Auckland Ideation Grant awarded to J. Fernandez.

REFERENCES

[1] Albajara Sáenz et al. *Dev Med Child Neurol* **61(4)**: 399–405, 2019.
[2] Eriksen, B., & Eriksen, C. W. *Percept Psychophys* **16(1)**: 143–149, 1974.
[3] Thomas Yeo et al. *J Neurophysiol* **106(3)**: 1125–1165, 2011.
[4] Whitfield-Gabrieli, S., & Nieto-Castanon, A. *Brain Connect* **2(3)**: 125–141, 2012.

Breaking ground without breaking the bank - validation of a novel low-cost 3-axis force plate

Albertus Y[1,2], Stickells D[3] and Patel A[3],

[1] Human Biology, University of Cape Town, Cape Town, South Africa.
[2] Health, Physical Activity, Lifestyle and Sport Research Centre, Cape Town, South Africa.
[3]Department of Engineering, University of Cape Town, Cape Town, South Africa.

Email: Yumna.Albertus@uct.ac.za

INTRODUCTION

Force plates have a wide variety of uses in both high performance and rehabilitation [1,2], but their feasibility of use is limited by their large size, lack of portability, and high cost. Acino, a spinout company from the University of Cape Town, have developed a novel low-cost, light weight, 3-axis and portable force plate (NFP). The aim of this study was to validate kinetic and temporal variables of the NFP was assessed against the AMTI gold standard, during walking, vertical drop, and drop jump protocols; as well as to test the intra-session validity and reliability of the Acino force plates using these same protocols.

METHODS

The three-dimensional (3D) kinematic metrics were captured using a six camera Vicon Vantage motion analysis system capturing at 240 Hz, using CGM 2 model 40 marker-set. With temporal and kinetic variables measured with the NFP overlayed on top of AMTI force plates. 21 healthy physically active participants were recruited for this study (11 males and 10 females, height 172.7 ± 10.5 cm, weight 79.9 ± 20.9, age 25.3 ± 2.4 years).They performed eight walking trials, 6 vertical jump and drop jump trials over the force plates.

RESULTS AND DISCUSSION

Pearson's coefficient of correlation showed positive correlations between AMTI and Acino measurements across all variables with *r* values of exactly or very close to 1 for both force and time measurements during walking.

Table 1: Comparisons between temporal and kinetic variables measured on Acino and AMTI plates

Vertical Drop				
Variable	AMTI	NFP	Pearson's *r*	Cohen's *d*
Peak force (N)	2472.50 ± 388.49 *	2465.84 ± 386.22	r = 1.00	-0.60
Time to peak force (ms)	55.58 ± 14.75	56.58 ± 14.75	r = 1.00	†
Drop Jump				
Variable	AMTI	NFP	Pearson's *r*	Cohen's *d*
Peak force early stance (N)	2319.49 ± 407.44	2323.52 ± 414.36	r = 1.00	-0.09
Peak force late stance (N)	1380.84 ± 362.62	1386.74 ± 369.12	r = 1.00	-0.25
Stance time (ms)	475.62 ± 95.84	475.82 ± 95.95	r = 1.00	-0.10
Time to peak force: early stance (ms)	57.43 ± 10.31	57.92 ± 10.31	r = 0.97	-0.20
Time to peak force: late stance (ms)	329.55 ± 103.62	329.23 ± 101.89	r = 1.00	-0.06

There was no significant difference between AMTI and NFP for temporal or kinetic variables measured during vertical drop and drop jump trials (Table 1). Reliability, using coefficient of variation (CV) for AMTI and NFP was similar for temporal and kinetic variables. During walking trials, the CV for NFP was relatively low at 2.25 ± 1.05 and 3.34 ± 2.39 for peak force and stance time respectively; this was lower than that of the AMTI plates (3.76 ± 2.03 and 4.58 ± 3.28). The CV for the NFP was slightly higher with the peak force variable of the vertical drop trials at 4.88 ± 4.30%. The highest CV was for drop jump stance time (11.64 ± 5.73% ; 11.52 ± 5.65) for both NFP and AMTI respectively). Figure 1 highlights the agreement of measurement between NFP and AMTI plates during walking trials, with the large majority of points falling between the limits of agreement, similar results were found for the vertical drop and drop jump trials.

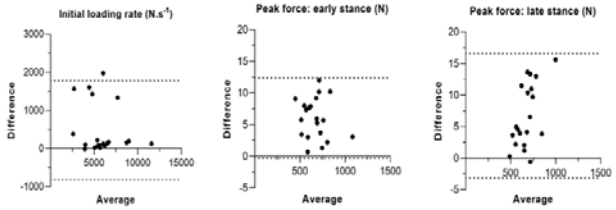

Figure 1. Bland-Altman plots for variables recorded during walking trials with 95% confidence intervals

CONCLUSIONS

The NFP showed high intra-session reliability, with low coefficients of variation and high intraclass correlation coefficients. The NFP was therefore found to be both valid and reliable in their measurements of kinetic and temporal variables in comparison to the AMTI plates, making them low-cost and portable alternatives to current industry standards.

REFERENCES

[1] Kumar, D et al. *Osteo and Cartil* **21(2):** 298–305, 2013.

[2] Mayberry, J. K et al. *J of Strength and Conditioning Res* **32(6):** 1619–1626, 2018.

TEXTURE ANALYSIS OF ULTRASOUND IMAGES TO EVALUATE MULTIFIDUS MUSCLE COMPOSITION: A COMPARISON BETWEEN HEALTHY SUBJECTS AND PATIENTS WITH LOW BACK PAIN

Jong Hun Kim[1], Patricio Pincheira[1,2], and Paul Hodges[2]

[1] School of Health and Rehabilitation Sciences, The University of Queensland, Brisbane, Australia
[2] School of Human Movement and Nutrition Sciences, The University of Queensland, Brisbane, Australia
Email: uqppinch@uq.edu.au

INTRODUCTION

Understanding how low back pain (LBP) affects back muscle composition is important because muscle performance and function are determined in part by muscle structure. Ultrasonography is extensively used as the first line of imaging for the evaluation of muscle composition because is safe, accessible, and provides real-time imaging. Most previous studies using ultrasound only consider muscle size. Analysis of muscle structure has largely been restricted to analysis of fat and muscle in MRI. Some studies have implementing ultrasound for analyses of structure, but with problems related to high inter-operator variability, dependence on echo-intensity and interpretation of structural features. New image processing approaches can overcome these limitations and provide measures of connective tissue content (which is challenging with MRI). Texture analysis characterises the spatial variation of pixel intensities within ultrasound images. These complex image processing features can provide surrogates of muscle composition and tissue characteristics. This study aimed to explore whether texture features of the multifidus muscle differ between individuals with and without LBP.

METHODS

Transverse ultrasound images from the right multifidus muscle at the fifth lumbar vertebrae were used. Texture features [1] (local binary patterns and histograms of oriented gradients) from the thoracolumbar fascia (i.e., region-of-interest with connective tissue texture) were used to train a support vector machine that was used to classify each pixel within the image area covered by the multifidus muscle (segmented by an evaluator with experience). The support vector machine model was trained with 1014 region-of-interests from 20 healthy participants. Images from twelve healthy participants and twelve with acute LBP (within 2 weeks of onset of pain) were used to calculate the percentage of pixels within the multifidus image presenting connective tissue-like texture. Values were compared between groups (t-test, significance < 0.05).

RESULTS AND DISCUSSION

The support vector machine resulted in an accuracy of 75.6(0.6)% for the local binary patterns and 85.3(3.6)% for the histograms of oriented gradients. Both texture measures suggest a lower number of pixels with connective tissue texture in the LBP group than the healthy group (Figure 1).

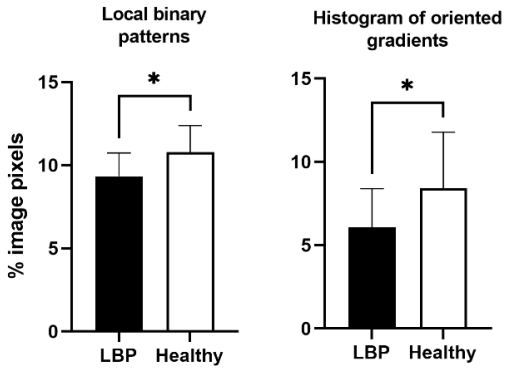

Figure 1 Percentage of pixels within the multifidus muscle image presenting connective tissue-like texture, comparison between groups.

This study shows for the first time the potential utility of texture features extracted from ultrasound images to characterise muscle composition in the multifidus muscle. Both textures utilised here detected differences in muscle composition between healthy and acute LBP participants. As both textures are different in nature [1], we are confident that the findings are not circumstantial to the texture used. Less connective tissue in the multifidus muscle in acute LBP could have several interpretations including a greater proportion of other tissue such as fat, differences in connective tissue prior to LBP, and so on. Further work is required to consider these possibilities. Our findings open the door for the use of more complex multiclass/multitexture classifiers for detailed quantification of fat and connective tissue infiltrations within the multifidus muscle. Future studies could explore the usefulness of other types of textures, combination of parameters (e.g., region region-of-interest size) and learning models (e.g., deep learning) to improve the accuracy of the classification models.

CONCLUSIONS

Ultrasound images of the multifidus muscle of individuals with acute LBP present a lower number of pixels with connective tissue texture in comparison with healthy subjects. This result suggests that texture analysis could be used to evaluate back muscles composition in patients with LBP.

REFERENCES

[1] Paris et al. *Ultrasound Med Biol* **47**: 880-895, 2021.

IMPROVING CYCLING FORCE SENSOR ACCURACY USING MULTILAYER PERCEPTRONS

Jonas Ebbecke[1], Josef Viellehner[1,2] and Wolfgang Potthast [1]

[1] Institute of Biomechanics and Orthopaedics, German Sport University Cologne, Germany
[2] Institute of Outdoor Sports and Environmental Science, German Sport University Cologne, Germany
Email: j.ebbecke@dshs-koeln.de

INTRODUCTION

To study musculo-skeletal loading in cycling, the accurate determination of pedal reaction forces is essential. Therefore a pedal including a three-axis piezoelectric sensor [9251A, Kistler, Winterthur, Switzerland] was developed. Pilot testing showed that with uniaxial force application, the inbedded sensor exhibits excelent linearities in all three spatial axes using a standard calibration matrix. However, with combined loading in multiple axes, as is common in cycling [1], linearity decreases and error values increase inacceptably. Here, there seem to be complex interactions between sensor and pedal body that cannot be solved by a linear calibration. Therefore, a neural network approach was chosen to increase accuracy. The aim of the present study was to validate the pedal sensor and its error correction.

METHODS

A multilayer perceptron (MLP), which is a fully connected class of feedforward artificial neural networks, was chosen for error correction. In order to provide a sufficient number of training data, a test rig was developed, allowing for standardized and combined loading cycles along the mediolateral (ML), anteroposterior (AP) and vertical (VERT) axis. The recorded data set included a total of 458700 data points with sinusoidal, multiaxial loadings in the range from 0 N to 500 N. This range was derived from typical force values of cycling [1, 3]. The data set was divided into two subsets to avoid overfitting (70% training set; 30% validation set). For the test data, a separate set was recorded to simulate cycling at a power of 300W and a cadence of ~70 rpm to test the MLP predictions with a cycling specific force pattern [1]. The sensor outputs were transformed to force values using a standard calibration matrix, normalized from 0 to 1 and then used as inputs for the MLP. The forces introduced to the pedal by the test rig served as target values.

For the configuration and training of the networks, the Scikit-learn library in Python was used [2]. Using the three data sets, a grid search was performed to find the optimal hyper parameter configuration. A stochastic gradient descent solver was used, the hyperbolic tangent activation function was assigned to each node of the hidden layers and an adaptive learning rate was applied. The number of hidden layers and nodes were systematically increased. Root mean squared error (RMSE), normalized RMSE (nRMSE), maximum absolute error (MAE) as well as the coefficient of determination R^2 were calculated for each prediction of the test data set. For each sensor axis, the MLP configuration with the lowest nRMSE in the test data set was selected afterwards.

RESULTS AND DISCUSSION

The grid search resulted in different MLP configurations for each sensor axis (ML: 44 nodes in 3 hidden layers; AP: 80 nodes in 3 hidden layers; VERT: 98 nodes in one hidden layer). The predictions of the best performing MLPs lead to substantial error reductions in all sensor axes ranging from -21.8% to -93.1% compared to the matrix calibration. The remaining RMSE was in the range of 0.21N to 1.69N, which corresponds to an nRMSE range of 0.10% to 3.21%. The maximum deviation between MLP predictions and target values was 8.87 N and occurred in the AP direction (Table 1). Further, R^2 could be increased from 0.973 to 0.999.

Using MLP corrections, the pedal shows lower error values than comparable pedal sensors [1, 3] as well as mobile force plates [4] and is at a comparable accuracy to permanently installed force plates [5]. Thus, the remaining error values can be classified as acceptable.

Table 1: MAE, RMSE and nRMSE values in all three spatial axes using the matrix calibration and the MLP predictions. Arrow indicates increase or decrease of error values with given relative difference.

	ML	AP	VERT
MAE [N]	3.52 $\downarrow^{-52.9\%}$	8.87 $\downarrow^{-52.7\%}$	3.07 $\downarrow^{-49.7\%}$
RMSE [N]	0.61 $\downarrow^{-21.8\%}$	1.69 $\downarrow^{-81.4\%}$	0.21 $\downarrow^{-92.7\%}$
nRMSE [%]	2.27 $\downarrow^{-22.5\%}$	3.21 $\downarrow^{-84.1\%}$	0.10 $\downarrow^{-93.1\%}$

Conclusion

Using a neural network approach, error values of the cycling pedal sensor could be reduced, and high accuracies could be achieved. Future work will evaluate the performance of the system *in situ*.

REFERENCES

[1] Alexander N et al. *J Sports Eng Technol* **229(4)**: 222-230, 2015.
[2] Pedregosa F et al. *JMLR* **12**: 2825-2830, 2011.
[3] Boyd T et al. *J Biomech* **29(8)**: 1105-1110, 1996.
[4] Peterson Silveira R et al. *Sports Biomech* **16(2)**: 177-186, 2017.
[5] Collins H S et al. *Gait Posture* **29(1)**: 59-64, 2009.

Estimation of ground reaction forces and center of pressure during stair walking using convolutional neural network based model

Ye Ma[1,2], Dongwei Liu[3], and Meijin Hou[2]
[1] Faculty of Sports Sciences, Ningbo University, Ningbo, China.
[2] Fujian University of Traditional Chinese Medicine, Fujian, China.
[3]Zhejiang University of Finance and Economics, Hangzhou, China
Email: maye@nbu.edu.cn

INTRODUCTION

Ground reaction forces (GRFs) and *center of pressure trajectories* (CoPs) are required for a comprehensive biomechanical analysis [1]. They are also important outcome measures in sports sciences or clinical areas [2,3]. GRFs and CoPs are usually measured by force plates settle in the center of a walkway. In the stair walking scenarios, staircases instrumented with at least two force plates are required to record a full gait cycle of both the left and right limb's GRFs and CoPs. However, such customized staircases are not the standard configuration of biomechanical labs and are also very difficult to fulfill in out-lab scenarios. Thus, it is desired to estimate GRFs or CoPs during stair walking without force plates.

METHODS

We developed a novel *convolutional neural network* (CNN) based model for estimating complete GRFs (include the vertical F_V, *anterior-posterior* (AP) F_{AP} and *medial-lateral* (ML) F_{ML} dimensions) and CoPs (include the AP C_{AP} and ML C_{ML} dimensions) during both stair descent and stair ascent scenarios using kinematics data as input. The CNN architecture, named V-Net is shown in Figure 1, top. The input of the network is a 260×42 tensor. The output scale is 260×10, where the second dimension stands for (F_V, F_{AP}, F_{ML}, C_{AP}, C_{ML}) of both left and right foot. This architecture involves five blocks. The inner structures of such blocks are shown in Figure 1, bottom. The scales of features passed among the blocks are labelled in blue. We built a relatively large dataset $D = \{K, F, C\}$ for training and validating our model, which includes 3782 stair walking trials collected from 172 subjects. The recruited subjects include healthy subjects and individuals with knee osteoarthritis or moderate-to-high risk of cardiovascular diseases. The dataset includes the whole-body kinematics K and their corresponding GRFs F and CoPs C recorded by force plates embedded in our customized staircase. The GRFs and CoPs are normalized to *body weight* (BW) and "foot length".

We used an inter-subject ten-fold cross validation to investigate the performance of our proposed model. The performance of our model is evaluated by comparing the predicted GRFs and CoPs of the entire gait cycle with those measured by force plates using normalized root-mean-squared error (nRMSE).

RESULTS AND DISCUSSION

Our model achieves the state-of-the art estimation performance with the nRMSE of 2.525%~7.518% and 5.012%~19.434% on the GRFs and CoPs estimation.

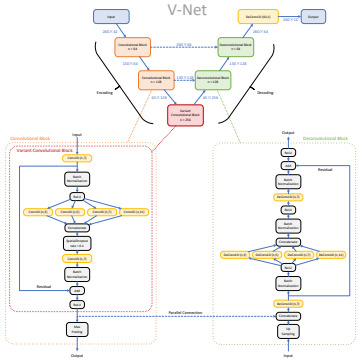

Figure 1 V-Net architecture

Table 1: Mean (standard deviation) of nRMSE (%) between our estimated GRFs and CoPs with their corresponding ground truth.

	Stair descent	Stair ascent
F_V	2.525 (1.165)	3.162 (1.382)
F_{AP}	3.220 (1.165)	7.130 (2.993)
F_{ML}	7.518 (3.595)	7.130 (2.993)
C_{AP}	11.298 (8.174)	19.434 (18.612)
C_{ML}	5.012 (2.121)	6.140 (2.324)

CONCLUSIONS

Our model achieved the state-of-the-art accuracy for estimating GRFs and CoPs during stair walking based on kinematic data. Such performance can meet the requirements of clinical use or sophisticated biomechanical study. Using our proposed model, GRFs and CoPs during stair walking can be estimated without force-plate-embedded staircases.

ACKNOWLEDGEMENTS

This study was funded by National Natural Science Foundation of China (Grant Number 61802338, 12002177).

REFERENCES

[1] Winter DA, Biomechanics and Motor Control of Human Movement. John Wiley & Sons, 2009.
[2] Winiarski S et al., Estimated ground reaction force in normal and pathological gait. Acta of Bioengineering Biomechanics, 11, 1, 2009.
[3] Winter DA et al., Assessment of balance control in humans, Medical Progress through Technology, vol. 16, 31–51, 1990.

Comparing the advantages and disadvantages of physics-based and neural network-based modeling for predicting cycling power

Patrick Mayerhofer[1], Ivan Bajić[2], and J. Maxwell Donelan[1]
[1] Department of Biomedical Physiology and Kinesiology, Simon Fraser University, Burnaby, Canada.
[2] Department of Engineering Science, Simon Fraser University, Burnaby, Canada.
Email: pmayerho@sfu.ca

INTRODUCTION

Mathematical models help us simulate real world behaviors in science and engineering. To develop these models, scientists can use their understanding of first principles to determine relationships between underlying variables. Depending on the complexity of the system, this can be a long process that requires extensive modeling expertise. Neural networks can optimize this process. They can approximate the input-output relationship, without explicitly knowing every detail, such as fixed parameters, of the system. Here, we test this premise by comparing how well a neural network model and a physics-based model predict mechanical power in cycling.

METHODS

First, we developed the physics-based model and the neural network model. For the physics-based model we used first principles to derive the power from the cadence, the gear ratio (defined as the ratio between the front bracket size and the rear bracket size), some fixed bike and participant parameters (such as weight and wheel diameters), and the drag [1]. For the neural network model, we used a recurrent neural network, consisting of one long-short-term-memory layer with eight nodes and a ReLU activation function.

To collect the required data for the models, we had nine participants cycle on a flat running track. Participants did two trials of 16 minutes, with one rear gear over, and one rear gear under their preferred gear ratio, respectively. A metronome commanded step changes in cadence of ±10% of their preferred cadence, and we measured the applied power from an SRM power meter (Dura-Ace, SRM GmbH).

Using this data, we trained and tested our models in predicting the measured power. For the physics-based model we used a Levenberg-Marquardt optimization algorithm to optimize for the only unknown, the drag number [2]. For the neural network model, we used an Adam optimization algorithm. To test the performance of the two models, we used k-fold cross-validation and split up the data into six sets, three per trial. We reserved one test set and trained the model on the remaining two of the same trial. We repeated this process for each test set and calculated the normalized root mean square error (NRMSE) as the respective test set's root mean square error's percentage of the mean of the measured power. To get the model's performance for a participant we averaged the six results. We then compared the mean NRMSE between the physics-based model and neural network model using a paired t-test.

RESULTS AND DISCUSSION

There were no significant differences between the physics-based model and the neural network model (Figure 1). The NRMSEs were 19.6±5.1% and 18.2±6.0% for the physics-based model and the neural network model, respectively ($p = 0.34$).

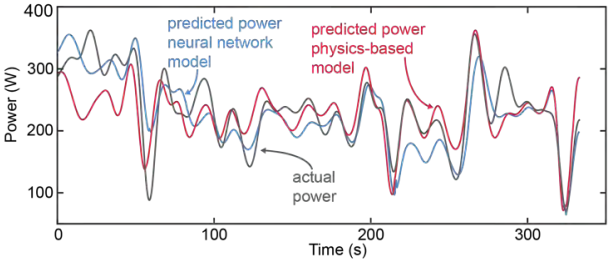

Figure 1 Neural network model (blue) prediction and physics-based model (red) prediction of the actual power (grey) in one representative participant's trial.

In our study, both models converged to similar, but not perfect, prediction accuracies. We expected this imperfect performance as there are many variables in cycling, such as continuous wind direction and speed, that affect the power output that we did not include in our models [3].

Adding more variables would be simpler with the neural network. With the physics-based model we would have to well understand the model to properly add a new variable. To add an additional variable to the neural network simply requires retraining the model with the added new variable in the input data.

CONCLUSIONS

If enough data is available, neural networks can help scientists to efficiently develop working models. If the goal is to properly understand a natural process, physics-based models remain the gold standard.

ACKNOWLEDGEMENTS

This work was funded by an NSERC Discovery Grant to JMD.

REFERENCES

[1] Mayerhofer P et al. *Proceed. ISEA Symp.* **49**, 2020
[2] Seber, GA & Wild CJ. *Nonlinear Regression*, 2003
[3] Martin CM et al. *J Applied Biomech* **14**, 1998

AI BASED AUTOMATED ERROR DETECTION FOR MEDICAL SKILLS TRAINING USING MARKERLESS BIOMECHANICS

Travis Eliason[1], Tylan Templin[1], Omar Medjaouri[2], David Chambers[2] and Daniel Nicolella [1]
[1] Musculoskeletal Biomechanics, Southwest Research Institute, San Antonio, USA.
[2] Intelligent Systems, Southwest Research Institute, San Antonio, USA.
Email: travis.eliason@swri.org

INTRODUCTION

Traditionally, practical medical skills have been taught through hands on training with an expert instructor available to evaluate performance and provide feedback. While successful, this approach provides inconsistencies in training quality as the feedback is qualitative, not all instructors are equally skilled, and they may have personal biases that affect their feedback. To address these issues, a new approach is needed in which unbiased, quantitative feedback can be provided to trainees to improve their skills. In this study, we utilized markerless biomechanics combined with machine learning technology to address these goals to build a prototype system that can automatically identify errors in a suturing skill.

METHODS

In order to develop a machine learning system capable of identifying errors in a medical skill, a training data set was needed. Utilizing a custom markerless biomechanics hand tracking system developed at SwRI, a training data set of 13 attendings, surgical residents, and medical students was collected. Each subject was asked to perform a 5 cm simple running suture on a reusable training surrogate (DAISE) while being recorded with four Sony RXO-II cameras placed around the table. Each subject performed the activity multiple times to increase the dataset size. Each individual was labelled as an expert (attendings, late year residents) or novice (medical students, new residents). Following data capture, each individual take was processed through the hand tracking system that outputs the kinematics of the subjects' hands during the motion.

Once processed through the markerless biomechanics system, the data from the experts was pre-processed to align each take in time and space to normalize variations in starting conditions. Next, each expert recording was broken up into 20 frame clips resulting in approximately 57,000 individual training samples of suturing kinematic data. This data was then used to train a Long Short Term Memory (LSTM) recurrent neural network autoencoder. This network is trained to predict an expert's future movement based on an input movement sequence. Once trained, this prediction can be compared to the actual measured movement to identify areas where subject movement deviated from expectation. Following training, each of the novice and withheld expert takes was processed forward through the network, and the reconstruction error was calculated to evaluate the networks performance.

RESULTS AND DISCUSSION

Figure 1 shows the normalized path prediction errors (difference between network predicted and measured movement) for both the novices and withheld expert takes. Novices had a higher proportion of their movements with larger errors compared to the experts, which can be used to identify thresholds for defining what prediction error level should be considered an error. For this study, any prediction error above 4 was labelled as a mistake, and each novice recording was evaluated to look for time regions with errors above this point. Once identified, the original videos were reviewed to verify that errors had in fact occurred and an interesting range of errors were identified. These included obvious errors, (needle driver slipping off the needle, retracting and reinserting the needle, etc.), as well as subtle errors that are not obvious to lay observers (e.g., grasping needle with wrong instrument).

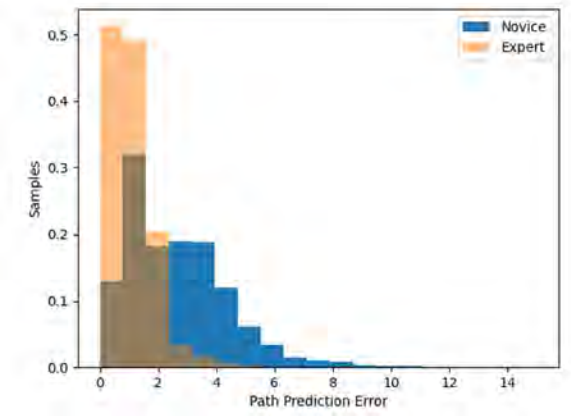

Figure 1 Normalized histograms of path prediction error for Novice and withheld Expert motions.

CONCLUSIONS

We have successfully shown that a prototype system that combines markerless biomechanical hand tracking and an LSTM autoencoder can accurately identify errors while trainees perform a suturing task. This system will lay the groundwork for building out a fully automated training tool which will allow trainees to receive unbiased, quantitative feedback while practicing key skills without the need for an expert instructor to be present.

ACKNOWLEDGEMENTS

This work was funded through the Medical Technology Enterprise Consortium (MTEC).

MyoSuite: Combining neuromusculoskeletal modelling with reinforcement learning to mimic motor control

Guillaume Durandau[1,2], Huawei Wang[2], Vittorio Cagiano[3] , Vikash Kumar[3] and Massimo Sartori [2]
[1] Department of Mechanical Engineering, McGill University, Montreal, Canada.
[2] Biomechanical Engineering Department, TechMed Centre, University of Twente, Enschede, The Netherlands.
[3] Meta AI Research, USA
Email: g.v.durandau@utwente.nl

INTRODUCTION

Musculoskeletal simulators have empowered biomechanical research in the last twenty years, with the most advanced one being the open-source simulator OpenSim [1]. OpenSim offers detailed models and precise simulation. The control of the complex model availble (neural control surrogate) offered in OpenSim is based on control theory which solves muscles redundancy based on pre-determined objective functions. This create the question on how human optimized movemen, whicht is still an open question but the current standard is based on reduction of muscle effort. Meanwhile, machine learning and the field of reinforcement learning (RL) have made impressive progress in the last couple of years. RL allows solving complex tasks and generalising to similar tasks family. This allows having policies, once trained, that can solve complex tasks from start to finish and that can adapt to non stationary condition. One of the well known limits of RL is the important number of training steps needed, requiring fast simulator which is currently not possible with OpenSim. This is why we developed MyoSuite [2], which allows the training and use of RL policy to control neuromusculoskeletal models. In this paper, we present available models and baseline policy in MyoSuite.

METHODS

MyoSuite is an open-source software[1] based on the Mujoco simulator and Gym AI library. We developed multiple upper-limb models based on the MOBL OpenSim model. Namely, a finger model (4 degrees of freedom (DOF) and 5 muscles), a wrist and hand model (23 DOFs and 39 muscles), an elbow model and an elbow and exoskeleton model (1 DOF and 6 muscles). We also integrated different conditions such as sarcopenia and muscle fatigue. Furthermore, we trained policy for tasks such as finger reaching, finger pose, elbow pose, hand reach, hand pose, turning a key, pen twirl and boading ball (Fig. 1).

RESULTS AND DISCUSSION

Results showed that MyoSuite was 60x to 4000x faster than OpenSim (depending on the number of muscles simulated) while having a difference in muscle force of only 4.1 ± 2.0%. Most tasks were able to be solved for a fixed target under 5 million steps except for the baoding ball task. When the target is randomized, only the finger pose and elbow pose are solved consistently (100% success rate). We also looked at the effect of conditions change in learned policy. Elbow pose policies (with and without exoskeleton assistance) were tested on different static (sarcopenia) and dynamics (fatigue) conditions without retraining. The exoskeleton assistance (percentage of elbow torque) was able to compensate for the induced weakness with an error of only a few degrees compared to 10 degrees error without exoskeleton for the sarcopenia conditions and the effect of fatigue reduced by half. Finally, to try to solve the problem of the generalization gap (fixed versus randomized), we organized the MyoChallenge[2] at the NeurIPS22 conference to solve the boading ball and a new task based on die rotation. The top teams were able to solve random die rotation with a success rate of 13% and baoding ball with a success rate of 55%. This show that human neural control and dexterity are still far superior to that of the latest AI algorithm and further research is needed both in AI and neural control to understand and solve this disparity. Our future work consist of implementing other model such as a lower-limb model to study locomotion or a bi-arm model to study complex manipulation.

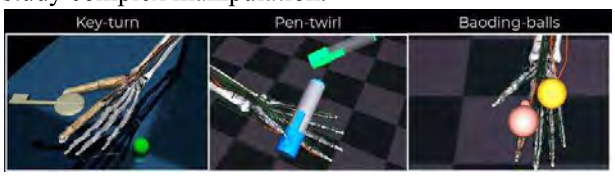

Figure 1 Task using the hand and wrist neuromusculoskeletal model for key-turn, pen-twirl and baoding ball.

CONCLUSIONS

MyoSuite opens new avenue to merge AI with neuromusculoskeletal modelling and provide in the future adaptative and fast biomechanical simulations. This will provide new solutions to advance rehabilitation, *in silico* study of neural control but as well in the field of AI with neural network advances.

REFERENCES

[1] Delp S. L., et al IEEE TBME 54.11, 2007
[2]Caggiano V., et al. arXiv preprint arXiv: 2205.13600, 202

[1] https://sites.google.com/view/myosuite

[2] https://sites.google.com/view/myochallenge

Estimation of Whole-body Posture during Walking in Unilateral Transfemoral Amputees Using Sparse Inertial Measurement Units and Deep Learning

Yuji Kumano[1,5], Suguru Kanoga[5], Genki Hisano[2,5], Masataka Yamamoto[1,3], Hiroaki Hobara[4], Hiroshi Takemura[1] and Mitsunori Tada[5]

[1] Tokyo University of Science, Chiba, Japan, [2] Tokyo Institute of Technology, Tokyo, Japan
[3] Hiroshima University, Hiroshima, Japan, [4] Tokyo University of Science, Tokyo, Japan,
[5] National Institute of Advanced Industrial Science and Technology (AIST), Tokyo, Japan
Email: 7522522@ed.tus.ac.jp

INTRODUCTION

Vaulting gait (plantar flexion in the intact limb during the single-limb support phase) is a typical gait pattern to increase toe clearance of the contralateral prosthetic limb in unilateral transfemoral amputees. Since the vaulting gait induces the secondary degenerative diseases in their intact limb [1,2], the whole-body posture estimation in their daily live could be an effective preventive strategy. In this study, we propose a deep-learning model to estimate the whole-body posture during walking with two inertial measurement units (IMUs) on the prosthetic shank and the heel of the intact limb in unilateral transfemoral amputees.

MATERISLS AND METHODS

First, we trained a deep-learning model with the gait data of able-bodied subjects. Then, we estimated the whole-body posture during walking in unilateral transfemoral amputees by re-training the pre-trained model with their gait data.

DhaibaWorks [3], a motion analysis software developed by AIST, was used to generate datasets from existing motion databases, the AIST Gait Database 2019 [4], and the datasets of the left-sided unilateral transfemoral amputees [5]. To obtain motion-related IMU data, we calculated the acceleration and angular velocity of the points on the left shank and right heel along their local coordinate.

After removing the abnormal data by visual inspection, the data on able-bodied subjects was 2741 trials of 290 subjects, while the data on left-sided transfemoral amputees was 40 trials of eight subjects (five trials per subject) which was divided into four trials for re-training and one trial for testing.

The network comprises two long short-term memory (LSTM) layers with 256 units and one dense layer with 51 units. It considers acceleration and angular velocity inputs from the previous 49 frames and the current frame (i.e., a total of 0.25 s) and estimates the three-axis joint angles of 17 bones. ReLU was used as the activation function in the LSTM layers, and a linear function was used in the dense layer. The loss function, learning rate, mini-batch size, number of epochs, and optimization algorithm were set to the mean squared error, 1e-3, 64, 30, and Adam, respectively. For re-training, we used fine-tuning. All layers were fine-tuned with the data of each subject. The hyperparameters used for fine-tuning were the same as those used for pre-training.

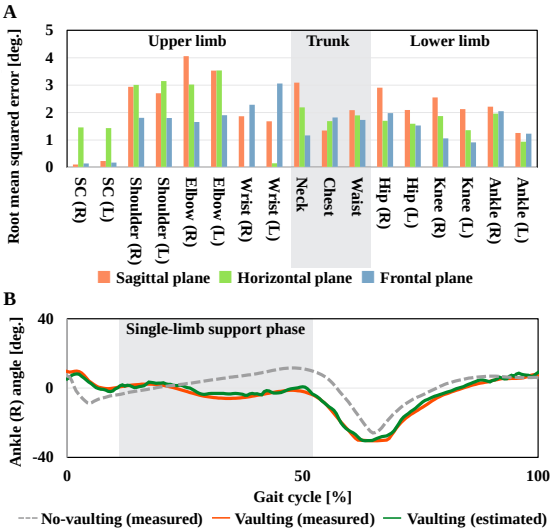

Figure 1 A: Average root mean squared errors of each joint angle. "SC" indicates sternoclavicular joint. B: Time sequences of the measured and estimated flexion-extension angle of the right ankle (intact limb) for the specific subject with vaulting gait.

RESULTS AND DISCUSSION

Average root mean squared errors of each joint angle for all subjects estimated from the proposed model are shown in Figure 1 A. It was less than 4.1 degrees. Time sequences of the measured and estimated flexion-extension angle of the right ankle (intact limb) for the specific subject with a vaulting gait are shown in Figure 1 B. It is clear from this figure that plantar flexion in the intact limb during the single-limb support phase, which characterizes a vaulting gait, can be estimated.

CONCLUSIONS

Our method would quantitatively measure the walking motion of unilateral transfemoral amputees in daily life, although it is necessary to fill the gap with real data.

ACKNOWLEDGEMENTS

This work was partially supported by the JST-Mirai Program Grant Number JPMJMI21H5, Japan.

REFERENCES

[1] Drevelle X et al. Clin Biomech **29**: 679-683, 2014
[2] Gailey R et al. Int J Rehab Res **45**: 15-30, 2008
[3] Endo Y et al. Proc. 3rd Int Digital Hum Modeling Symps 1-8, 2014
[4] Kobayashi Y et al. https://unit.aist.go.jp/harc/ExPART/GDB2019.html 2019
[5] Kobayashi T et al. Clin Biomech **80**, 2020

Fast bowling performance analysis using inertial sensors and machine learning

Shruti Bhandurge[1], Pete Alway[2], Matt Lamb[1], Sam Allen[1], Glen Blenkinsop[1], Andrew Lowe[3] and Mark King[1]
[1] School of Sport, Exercise and Health Sciences, Loughborough University, Loughborough, United Kingdom.
[2] England and Wales Cricket Board, Loughborough, United Kingdom.
[3]Institute of Biomedical Technologies, Auckland University of Technology, Auckland, New Zealand.
Email: s.bhandurge2@lboro.ac.uk

INTRODUCTION

The current state-of-the-art method to evaluate biomechanics of sport movements is through using 3D motion analysis and force plates. Such systems can be integrated with other acquisition devices and are accurate and reliable. However they are time-intensive, restricted to laboratories, expensive and require skilled operators [1]. Inertial measurement unit sensors (IMUs) have demonstrated high potential as an alternative in the mobility of conducting biomechanical testing in the field [1]. Traditional analysis includes correlations, linear regression and SPM, however for these complex datasets alternative techniques such as machine learning may offer new insights [2]. The aim of this research was to identify critical factors estimated using IMUs that best predict ball release speed (BRS) in cricket fast bowling with machine learning.

METHODS

Eight English County level bowlers (age 20 ± 2 years; height 1.80 ± 0.05 m and body mass 80 ± 5 kg) were recruited for the study with informed consent obtained in accordance with the Loughborough University Ethical Advisory Committee. Two Vicon blue trident inertial sensors (Vicon, Oxford, UK) sampling at 250 Hz were placed at the thorax and pelvis. Four high-speed Bonita cameras were positioned sagittal (ipsilateral), superior, posterior, and anterior of the bowler for qualitative reference. The testing protocol comprised a 2-over bowling spell performed with a 4-minute active rest period between each over in a laboratory environment that allowed for a full-length run-up. Sensor data of 64 deliveries (8 deliveries per bowler) were exported and analyzed in MATLAB and its Regression Learner App (Release 2022a, The MathWorks, Inc., Natick, Massachusetts, United States) with 5-fold cross validation. Regression models such as support vector machine (SVM) and Gaussian process regression (GPR) models were used to predict BRS. Statistical measures of root mean square error (RMSE), mean absolute error (MAE) and R-squared values were used to evaluate the performance (Table 1).

RESULTS AND DISCUSSION

Data showed a non-linear relationship between the performance variables and BRS. A GPR exponential model gave the best fit with five features explaining 82% of the variation in BRS with least error (Figure 1). The best predictors of BRS were change in linear velocity of the pelvis (lateral) from back foot contact (BFC) to front foot contact (FFC); change in linear velocity of the thorax (anterior) from BFC to FFC, and FFC to ball release (BR); change in thoracic angular velocity (transverse) from FFC to BR; and time duration from BFC to FFC. These variables add to the current knowledge of biomechanical variables linked to BRS.

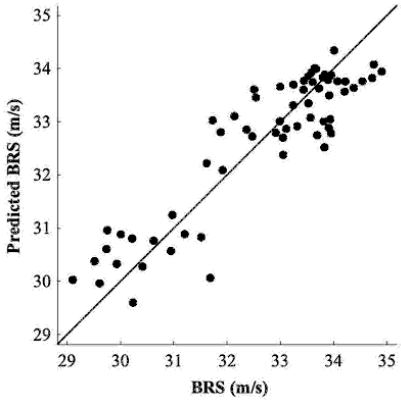

Figure 1: Non-linear GPR model predicted BRS vs true BRS.

CONCLUSIONS

In summary, non-linear regression models with five variables provided the best estimates of BRS with low errors. The methods used here may provide additional understanding of the performance variables linked to BRS that have not been identified with traditional analysis methods, aiding in advancing the current knowledge and understanding of cricket fast bowling.

REFERENCES

[1] Ancillao A et al. *Sensors* **18(8)**: 2564, 2018.
[2] Bunker R et al. *Applied Computing and Informatics*, **15(1):** 27-33, 2019.

Table 1: Linear and non-linear regression model performance

Features	Model	RMSE(m/s)	MAE(m/s)	R-squared
5	Linear SVM	1.11	0.94	0.51
5	Quadratic SVM	0.79	0.66	0.75
5	GPR exponential	0.66	0.55	0.82

A Novel method to measuring the slip of foot inside the shoes: Evaluation of socks friction using pressure sensors

Dongwook-Seo[1], Jinsu-Eun[1], Yeonwook-Yu[1], Sangsoo-Park[2] and Kikwang-Lee[1]
[1] College of Physical Education, Kookmin university, Seoul, Korea 02707
[2] College of Sports science, Korea university, Sejong, Republic of Korea 30019
Email: kklee@kookmin.ac.kr

INTRODUCTION

Slip of the foot inside the shoes affect the stability and stability of locomotion. Therefore, products with non-slip functions added to socks or insole are being released. However, it is difficult to evaluate the slip prevention performance because it is difficult to check the slip inside the invisible shoe due to the shoe upper. Hence, the purpose of this study is to propose a method to estimate the slip of foot inside the shoes in dynamic situation. Three pressure sensors were installed directly to the inner wall of the shoe, centered on the 5th metatarsal. The force values obtained from the pressure sensors were calculated to distinguish between the different friction characteristics of the socks.

METHODS

Fifteen participants were given three same sized socks with different friction characteristics and performed a shuttle run. The socks used in the experiment were characterized for friction by mechanical test in a previous study [1]: (1) Socks with polyurethane non-slip pad (US). (2) Socks with silicone non-slip pad (SS). (3) Socks without any non-slip pad (NS; Figure 1a). Three pressure sensors (SEEDTECH, Gyeonggi-do, Korea) were attached directly at sidewall inside the shoe (centered on the 5th metatarsal). All participants wore the same size shoe and performed the shuttle run task. The data obtained from the pressure sensor was analyzed into three events centered on the ON and OFF times: (E-A) when the pressure value started to increase continuously (window length more than 10 frames), (E-B) when the pressure value reached a maximum, and (E-C) when the pressure value reached a minimum.

RESULTS AND DISCUSSION

There were significant differences in peak force values and impulse values between sock types ($p < 0.001$; Figure 1b,1c). Bonferroni adjustments found the pairwise comparison results for all socks showed significant differences in peak force values and impulse values. ($p < 0.001$). There was no significant difference in slip time between sock types. ($p = 0.105$). The previous study suggested that there is a greater shift in foot displacement when performing a dynamic task while wearing low-friction socks [2], suggesting that the sidewalls of the shoe may detect greater contact forces with the shift in foot displacement. The pressure sensor installed in this study successfully measured the contact forces, and the data obtained from the sensors successfully distinguished the different frictional characteristics of socks In addition, the pressure value (peak, impulse) of the inner sidewall of shoes measured in this study was generally consistent with the friction coefficient difference pattern through static mechanical tests in previous studies. It was possible to estimate the slip inside the shoe through the force of pushing the inner sidewall of the shoe caught by the slip between the sock and the insole.

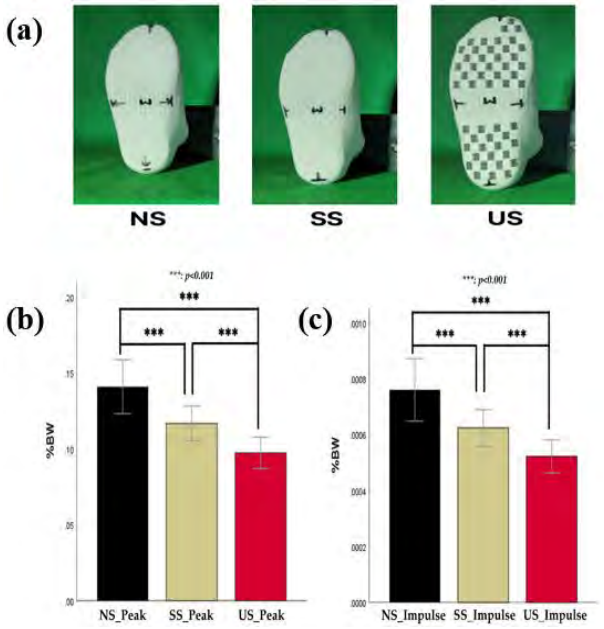

Figure 1 Figures of Socks and Statistical results of peak force values and impulse values. (a) types of socks. (b) peak force values. (c) impulse values.

CONCLUSIONS

The results of the static mechanical test conducted in the prior study [1] were consistent with the results of the dynamic condition task in this study. This suggests that static mechanical test in prior studies [1] can replace dynamic condition task that requires complex procedure.

ACKNOWLEDGEMENTS

This work was supported by the Ministry of Education of the Republic of Korea and the National Research Foundation of Korea(NRF-2021S1A5A2A03065436).

REFERENCES

[1] Eun J et al. Sensors. **22**(15), 5525, 2022.
[2] Apps C et al. *J Sports Sci.* **40** 1-9, 2022

INFLUENCE OF THE TYPE OF RUNNING SHOES IN THE LOWER LIMB MUSCULAR ACTIVITY

Gonçalo Marta[1], João Folgado[1], Carlos Quental[1] Francisco Guerra Pinto [1,2]
[1] IDMEC, Instituto Superior Técnico, Universidade de Lisboa, Portugal.
[2] FEBOT, NOVA Medical School, Portugal
Email: goncalo.marta@tecnico.ulisboa.pt

INTRODUCTION

Among other aspects, running footwear differs in the cushioning and support it provides to the stride of each practitioner, and the influence of these on muscle activity is still not well understood. The use of surface electromyography (EMG) along with the application of inverse dynamics using a multibody model, allows the development of a complete profile of muscle activity in the lower limbs during various movements. In this study, we aim to investigate the differences in muscle activation patterns for two distinct types of running shoes: neutral cushioning shoes and competition shoes without cushioning.

METHODS

EMG data from 8 different muscles - lateral and medial gastrocnemius, rectus femoris, biceps femoris, tibialis anterior, gluteus maximus, soleus and vastus medialis - were collected in the biomechanics laboratory of Lisbon (LBL). The volunteer's kinematic data were analyzed using the use of reflective markers and 14 infrared cameras. The volunteer ran at a self-selected speed, using the types of shoes under study, on force platforms embedded in the LBL's ground. The estimation of the internal reaction forces and muscle activations was achieved by combining the collected data with an inverse dynamics program. To do this, a whole-body musculoskeletal model with 18 rigid bodies and 80 muscle-tendon units was used. The muscle force sharing problem was solved through static optimization by minimizing muscle energy consumption while ensuring the fulfilment of the equations of motion and the bounds on the muscle activations between 0 and 1 [1]. The estimated muscle activations were validated by the laboratory-collected muscle activity.

RESULTS AND DISCUSSION

The preliminary results for the angles and reaction forces at the ankle, knee, and hip joints and muscular forces were analyzed. For the cushioned shoes, the results suggest increased plantar flexion at toe-off when compared with non-cushioned ones. The reaction forces at the hip, knee, and ankle joints appear to be higher for the non-cushioned shoes compared to the cushioned shoes, as shown in Figure 1(a) for the ankle joint. This result falls in line with what was found by Nigg et al., implying that cushioning reduces the reaction forces applied in the foot while raising the stance time [2] , as can be seen in Figure 1(a). Similarly, the estimated muscle activations had overall higher maximum values for the non-cushioned competition shoes, as illustrated in Figure 1(b) for the gastrocnemius lateral.

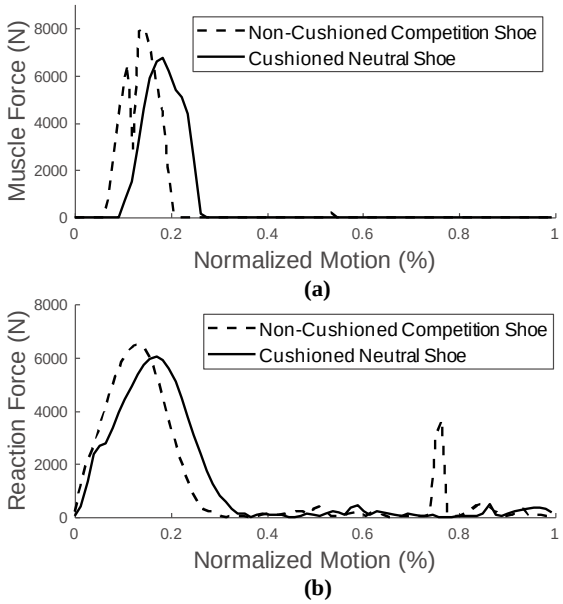

Figure 1. Depiction of estimated (a) ankle joint reaction forces and (b) muscular forces in the gastrocnemius lateral muscle for cushioned and non-cushioned running shoes.

CONCLUSIONS

A more comprehensive understanding of the impact that different types of running shoes have on the mechanisms of muscle or joint injury is necessary. The availability of such studies enables runners to have biomechanical knowledge to choose shoes that are suitable for their physical characteristics and goals.

ACKNOWLEDGEMENTS

This work was supported by Fundação para a Ciência e Tecnologia (FCT) through IDMEC, under LAETA, project UIDB/50022/2020, and the PhD scholarship SFRH/BD/145125/2019.

REFERENCES

[1] Quental C et al. “Influence of the Musculotendon Dynamics on the Muscle Force-Sharing Problem of the Shoulder—A Fully Inverse Dynamics Approach” *Journal of Biomechanical Engineering*, vol. 140, 2018
[2] Nigg B et al. “Influence of Heel Flare and Midsole Construction on Pronation Supination and Impact Forces for Heel-Toe Running” *International Journal of Sport Biomechanics*, vol. 4, 1988

INFLUENCE OF SHOE CUSHIONING ON PROXIMAL RUNNING KINEMATICS AND KINETICS

K. Reyes[1,2], C.D. Pollard[2,3] and J.J Hannigan[2,3]
[1]Program in Kinesiology, Oregon State University, Corvallis, OR
[2]Program in Physical Therapy, Oregon State University-Cascades, Bend, OR
[3]School of Biological and Population Health Sciences, Oregon State University, Corvallis, OR
Email: reyeskat@oregonstate.edu

INTRODUCTION

One of the most common injuries among runners is patellofemoral pain (PFP), which can be caused by excessive repeated loading of the patellofemoral joint (PFJ) [1]. The development of PFP in runners can potentially be influenced by footwear [2]. Footwear companies have designed variations in running shoe cushioning in an attempt to reduce injury risk, including reducing midsole cushioning (minimal shoes) and increasing midsole cushioning (maximal shoes). Current evidence on these shoes has focused on ankle biomechanics and ground reaction forces, with mixed evidence related to injury risk in both types of shoes [3]. Much less is known regarding the effect of varying midsole cushioning on proximal kinematics and kinetics at the knee and hip [4]. Therefore, the purpose of this study was to compare knee and hip kinematics and kinetics between traditional, maximal, and minimal shoes.

METHODS

Twenty-seven healthy experienced runners (8 men and 19 women) ranging from 18-45 years of age who ran a minimum of 10 miles per week with no major injuries for at least the previous 6 months and who have never trained in a minimal or maximal shoe were recruited to participate in this study. The maximal and minimal shoes for this study were custom designed by adding or removing cushioning from the traditional shoe (New Balance Fresh Foam Boracay) by the shoe manufacturer. Participants were asked to complete five running trials on their dominant leg while an 8-camera motion capture system and two embedded force plates were collected three-dimensional kinematic and kinetic data of the knee and hip in all three conditions. Quadriceps force, patellofemoral joint force (PFJF), contact area, and patellofemoral joint stress (PFJS) were estimated based on the methods outlined by Salem & Powers [5]. Peak knee and hip joint angles and moments and patellofemoral joint kinetics were compared between shoes using a repeated measures ANOVA ($\alpha = 0.05$).

RESULTS AND DISCUSSION

Knee moment data can be seen in Table 1. The peak knee extension moment (Figure 1) and peak knee internal rotation moment were significantly reduced in the minimal shoe. In addition, the peak hip adduction angle (trad: 11.28 ± 3.71°, max: 11.12 ± 3.85°, min: 10.33 ± 3.67°, $p = 0.035$), peak quadriceps force (trad: 66.07 ± 9.09 N/Kg, max: 67.78 ± 9.91 N/Kg, min: 61.43 ± 8.81 N/Kg, $p < 0.001$), PFJF (trad: 49.46 ± 6.7 N/Kg, max: 50.93 ± 7.68 N/Kg, min: 45.78 ± 7.08 N/Kg, $p = 0.001$) and PFJS (trad: 13.56 ± 2.53 MPa, max: 13.95 ± 2.99 MPa, min: 12.67 ± 2.48 MPa, $p < 0.001$) were all significantly lower in the minimal shoe compared to the other two shoes. No other significant differences were found between shoes for peak joint angles or moments at the knee and hip, $p > .05$.

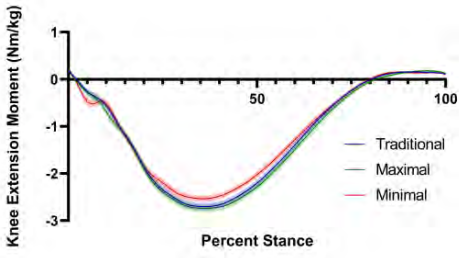

Figure 1: Ensemble curve for the knee extension moment in each shoe condition, (-) extension (+) flexion.

CONCLUSIONS

There were significant differences between minimal and both traditional and maximal footwear when analysing proximal running biomechanics. The decreases in peak knee extension moment, peak hip adduction, and PFJS supports previous research [2] that suggests minimal footwear may reduce the risk of injury to the knee.

REFERENCES

[1] Bonacci et al. *Br J Sports Med*. 2014.
[2] Esculier et al. *Gait & Posture*. 2017
[3] Becker & Borgia, *J Electromyogr Kines*. 2020.
[4] Hannigan & Pollard, *J Sci Med Sport*. 2020.
[5] Salem & Powers, *Clin Biomech*. 2001.

Table 1: Peak knee moments for each shoe condition.

	Traditional	Maximal	Minimal	*p*-value
Knee Extension (Nm/Kg)	-2.75 ± 0.38	-2.79 ± 0.40	-2.58 ± 0.35	< .001
Knee Valgus (Nm/Kg)	0.78 ± 0.28	0.74 ± 0.31	0.74 ± 0.32	.075
Knee Internal Rotation (Nm/kg)	0.42 ± 0.11	0.41 ± 0.13	0.38 ± 0.10	.028

A Pilot Study: Effects of an 8-week training intervention in carbon-plated running shoes

Justin Matties[1], K. Michael Rowley[1]
[1] Kinesiology, California State University East Bay, Hayward, United States.
Email: justin.matties@csueastbay.edu

INTRODUCTION

Lab testing with Nike Vaporflys (VP) has revealed running economy (RE) benefits of 2.5-4% [1,2]. With runners also anecdotally reporting less sore calf muscles and less "beat up" legs after hard workouts, use of VP may cause runners to undergo physiological adaptations since their muscles may be aided during training by the shoe's energy returning technology [1]. The purpose of this pilot study is to investigate the long-term effects of using VP in workouts by comparing training in VP vs in VP vs Nike Victory Waffle 5 flats (FL) on race performance and explore physiological and biomechanical adaptations.

METHODS

Collegiate cross country runners (n=8) completed pre- (PRE) and post-intervention (POST) lab testing in both VP and FL. They were assigned either VP or FL for an 8-week intervention. In PRE/POST, vertical jump (Vertec) and plantar flexion strength in knee flexed and extended positions were recorded (MicroFet2). Then runners were instrumented with EMG (Noraxon), a 6DoF lower body marker set (Vicon), and ran on an instrumented treadmill (Treadmetrix). Subjects ran 2 x 3-min trials at a self-selected race pace (7-10 min rest), followed by 4 x 5-min (5 min rest) at a submaximal pace (RER<1), in a randomized order. Metabolic (Cosmed) and biomechanical data were collected and compared. Trial paces were constant in PRE/POST. Using a forward selection technique, due to a large number of predictors and few observations using a full model was not possible, we tried to build an appropriate ANCOVA model to test main effects of intervention shoe assignment (VP/FL) and time point (PRE/POST).

RESULTS AND DISCUSSION

On average all participants' RE improved over the 8-week intervention, though FL group improved more than the VP group (FL: 5.61 ± 1.11%; VP: 0.97 ± 3.64%; p = 0.077, effect size (Hedges g) = 1.409). The FL group improved RE by 5.79 ± 1.02% when running in FL and by 5.43 ± 1.20% when running in VP. The VP group improved RE by 0.84 ± 4.64% when running in FL and by 1.11 ± 2.72% when running in VP. Computing a "VP % benefit" by comparing the RE when running in VP to running in FL shows that between PRE and POST, the VP intervention group increased their VP % benefit compared to FL (VP: 0.21 ± 2.23%; FL: -0.38 ± 0.24%; p = 0.433, effect size = 0.148), see Table 1. In this pilot phase there were no significant correlations between biomechanical measures and metabolic measures, though non-significant differences were observed in ankle angle (Figure 1), ankle moment, metatarsophalangeal joint angle, ankle power, vertical jump, plantar flexion strength, and the ratio of soleus and medial gastrocnemius muscle activation.

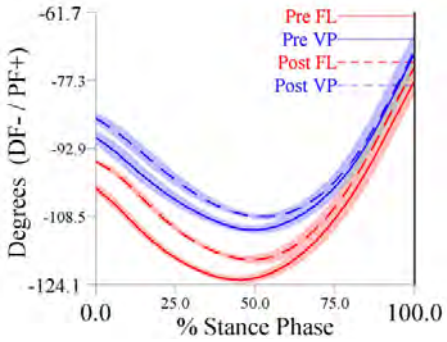

Figure 1 Representative graphs from a FL group subject showing ankle angle during stance phase during PRE & POST in VP & FL.

CONCLUSIONS

This pilot study suggests a specificity of training effect where participants improved relative RE more from PRE to POST when running in the shoe type they trained in. Overall, the FL group improved RE to a greater extent, suggesting that training in FL is more optimal for race performance despite decreasing the acute RE benefits incurred from super shoes. Heterogeneity of foot strike techniques likely prevented group biomechanical differences from being observed. We will use the effect sizes of these differences to power the next larger phase of the study.

ACKNOWLEDGEMENTS

We would like to thank the Nike Sports Research Lab (Beaverton, OR) for providing footwear for this study.

REFERENCES

[1] Hoogkamer W et al. *Sports Med* **48**:1009-1019, 2018.
[2] Joubert D & Garrett. *J Footwear Science* **14:2**: 71-83, 2022.

Table 1: Running economy (RE; VO2 in ml·kg^{-1}·min^{-1}) and VP % benefit within each intervention shoe group during PRE and POST.

	FL Group PRE	FL Group POST	VP Group PRE	VP Group POST
Average RE (VO2; ml·kg^{-1}·min^{-1})	52.35 ± 3.23	49.46 ± 4.11	55.18 ± 3.41	54.64 ± 3.96
VP % benefit (FL - VP RE as a % of FL RE)	1.55% ± 1.61	1.17% ± 1.37	0.67% ± 1.33	0.88% ± 1.38

MIDSOLE STACK HEIGHT, RUNNING ECONOMY AND STEP PARAMETERS

Montgomery Bertschy[1*], Herlandt Lino[1], Laura Healey[2], and Wouter Hoogkamer[1]
[1]Department of Kinesiology, University of Massachusetts, Amherst, Massachusetts, USA
[2]PUMA SE, Herzogenaurach, Germany
email: mbertschy@umass.edu

INTRODUCTION

Midsole cushioning is the foundation for all performance running shoes. In recent years, modernization of cushioning materials has allowed for an increase in midsole stack height while minimally compromising the mass of footwear. Researchers have suggested the regulation of this aspect of footwear design for competition [1]. Governing bodies have followed suit, implementing limitations to midsole thickness. However, the isolated effects of increasing midsole thickness are not well understood.

The purpose of this study was to measure the isolated effects of stack height on running economy and spatiotemporal step parameters.

METHODS

12 trained runners participated in this study. Sets of weight-matched footwear conditions were worn (30mm EVA, 40mm EVA, 60mm EVA, 60mm NITRO (a PEBA based material)) in size UK8/UK10 (m = 465g/515g). Subjects ran twice in each shoe condition in randomized, mirrored order (ABCDDCBA) for 5 minutes at 14 km/h with 5 minutes rest. We measured their oxygen uptake and carbon-dioxide production, and we calculated running economy as metabolic power for the final 2 minutes of the trial when aerobic steady state was achieved. Spatiotemporal variables were measured over 10 strides during the final minute of each running trial. One-way repeated measures ANOVA was used to evaluate the effects of shoe condition and Tukey's HSD analysis to evaluate shoe-by-shoe differences.

RESULTS AND DISCUSSION

Overall, there were significant effects of shoe condition on running economy and contact time. Within the firm EVA midsole material, larger stack height led to a non-significantly worse running economy. Post-hoc testing showed that 60 NITRO had a significantly lower metabolic power (16.09 ± 0.99 W/kg) than 60 EVA (16.52 ± 1.01 W/kg, -2.6%) and 40 EVA (16.44 ± 1.13 W/kg, -2.0%). 60 NITRO had a significantly longer contact time (0.212 ± 0.011s) than 40 EVA (0.209 ± 0.012s, +1.5%). Step frequency, step length, and peak vertical ground reaction force were similar between shoe conditions.

Overall, NITRO had better running economy than firm EVA. In real-world applications, this effect may be larger, as the NITRO shoes were lighter than EVA before weight-matching. Moreover, this reiterates the findings of Tung et al. that more cushioning is not always better [2,3]. However, the same may not be said for modern PEBA materials. While both materials seem to possess a capacity for reducing the "cost of cushioning" of the lower limbs, the mechanical properties of compliance and resilience in the PEBA midsoles may allow for an additional benefit from mechanical energy return, rather than dissipation.

This study has some limitations: the primary issues may be the mass at which the shoes were matched to (465g-515g), compared to typical mass of modern performance shoes (200g-250g). Additionally, longitudinal bending stiffness and rocker geometry cannot be identical between shoes due to their inherent link to stack height.

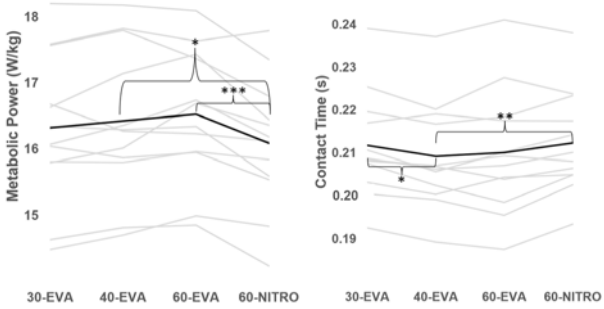

Figure 1 Metabolic power and contact time for all shoe conditions. Grey lines are individuals, and the black lines are group averages. Significance code: *P < 0.05, **P < 0.01, ***P < 0.001.

CONCLUSIONS

Increasing stack height alone does not lead to significant improvements in running economy. However, midsole materials with greater compliance and resilience can significantly improve performance. These findings aid in the future of performance footwear design and the rule creation of the governing bodies of performance running.

ACKNOWLEDGMENTS

This study was funded by PUMA; custom-made shoes were provided by PUMA.

REFERENCES

[1] Burns, G. T., & Tam, N. *British Journal of Sports Medicine*, *54*(8), 439–440, 2020.
[2] Tung, K. D. et al. *Medicine and Science in Sports and Exercise*, *46*(2), 324–329, 2014.
[3] Hoogkamer, W. *Footwear Science*, 12(2), 75–77. 2019.

The Effect of Initial Condition at the Onset of Stimulation on the Ratio of Muscle Stiffness to Force during Isometric Contraction

Siwoo Jeong[1] and Kiisa C. Nishikawa[2,*]

[1] Department of Physical Therapy, Jeonju University, Jeonju, Korea
[2] Department of Biological Sciences, Northern Arizona University, Flagstaff, AZ, USA
Email: *Kiisa.nishikawa@nau.edu

INTRODUCTION

Active shortening prior to isometric contraction affects the ratio of muscle stiffness to force (SFR) during isometric contraction [1]. Because this result cannot be solely explained by either the sliding filament theory or constant titin stiffness, it suggests that weakly-bound cross bridges or force-dependent titin stiffness may contribute to the varying SFR. However, it still remains unknown how SFR changes during isometric contraction.

To systemetically investigate which sarcomeric elements affect the SFR, we designed an experiment in which muscles develop force isometrically following two different conditions: 1) passive stretch, and 2) passive force enhancement.

METHODS

Maximal isometric force at $1.1L_0$ was established for whole soleus muscles isolated from wild-type mice (n=8). Two protocols were performed: 1) passive stretch (PS) from $0.9L_0$ to $1.1L_0$; and 2) active stretch from $0.9L_0$ to $1.1L_0$, rest for 10s (passive force enhancement, PFE), then held isometrically for four pause durations which allowed isometric force development (100, 200, 400 and 1000ms). Instantaneous muscle stiffness was measured at the four pause durations by a quick transient ($0.9\%L_0$ amplitude at a speed of $3L_0$/s). For comparison, muscle force and stiffness were also measured during isometric contractions (ISO) at $1.1L_0$ without passive or active stretch at the same pause durations after the onset of stimulation.

ANCOVA was used to compare muscle stiffness and force among different conditions (PS, PFE and ISO). Condition was the main effect, individual was a random effect nested within condition, and force was the covariate.

RESULTS AND DISCUSSION

The slopes (ANCOVA, $p < 0.05$) of the relationship between muscle stiffness and force differed significantly among conditions (PS, PFE and ISO). For the PFE condition, the slope was significantly smaller than PS (HSD, $p < 0.05$) and ISO (HSD, $p < 0.05$).

The different slopes of the relationship between muscle stiffness and force cannot be explained solely by cross bridge and/or constant titin stiffness. As isometric force increases, stiffness should increase equally regardless of initial condition given constant titin stiffness, since both muscle stiffness and force depend on the number of formed cross bridges. Therefore, the different slopes imply that titin stiffness changes during isometric force development.

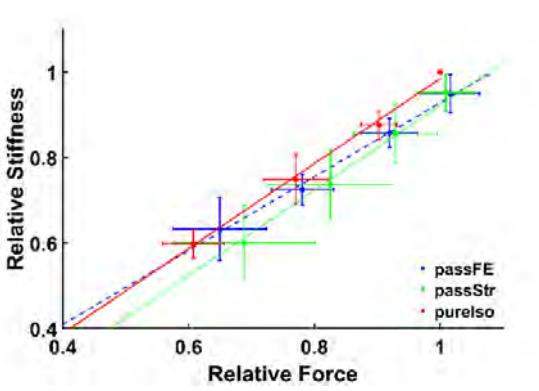

Figure 1. Force vs. Stiffness for PS, PFE and ISO (n=8).

Passive force enhancement is thought to be produced by increasing passive force developed by titin-actin binding [2]. We found that the PFE condition had a significantly different slope from both the PS and the ISO conditions, suggesting that the initial state of titin at the onset of isometric contraction produces a change in titin stiffness during isometric contraction.

CONCLUSIONS

This study shows that passive force enhancement induces different increasing rate of stiffness as muscle force increases. The sliding filament theory and constant titin stiffness are insufficient to explain the result. This finding suggests that titin stiffness changes during development of isometric force depending on the initial state at the onset of isometric contraction.

ACKNOWLEDGEMENTS: Supported by NSF IOS 2106049 and DBI-2021832

.

REFERENCES

[1] Jeong S & Nishikawa K. *Scientific Reports*, **13**:948, 2023.

[2] Herzog W. *J Appl Physiol*, **126**: 1782-1789, 2019.

Table 1. Muscle force at the onset of isometric stimulation in three conditions

	Passive FE	Passive stretch	Pure iso
Muscle force (mN)	43.2 ± 7.6[a,b]	75.8 ± 23.3[b]	37.41 ± 8.7

[a]significantly different from Passive stretch ($p < 0.001$); [b]significantly different from Pure iso ($p < 0.001$)

Preload affects muscle fascicle mechanics during maximal voluntary MTU lengthening actions

Paolo Tecchio[1], Brent J. Raiteri[1,2] and Daniel Hahn[1,2]
[1] Human Movement Science, Faculty of Sport Science, Ruhr University Bochum, Bochum, Germany
[2] School of Human Movement and Nutrition Sciences, University of Queensland, Brisbane, Australia
E-mail: paolo.tecchio@rub.de

INTRODUCTION

Muscle fascicle kinematics can be decoupled from muscle-tendon unit (MTU) kinematics due to MTU compliance, such that muscle fascicles can even shorten during MTU lengthening [1]. Understanding how preload (PL) affects decoupling during MTU lengthening actions is crucial to understand muscle mechanics and subsequent morphological and functional chronic adaptations to MTU-lengthening exercises. Therefore, this study aimed to evaluate how PL affects fascicle mechanics and force output during and following maximal voluntary MTU lengthening actions of the human tibialis anterior (TA).

METHODS

Twelve participants (five women; age (mean±SD): 25.6±2.7 yr) were in a reclined sitting position (~68° recline) with their right foot attached to a modified footplate that was connected to a dynamometer crank arm (~90° between footplate and tibia refers to a 0° ankle angle). The dynamometer (Isomed 2000, Ferstl, Germany) measured torque and crank arm angle. After a standardized warm-up, participants performed three maximal voluntary fixed-end reference contractions at ankle angles of 5° dorsiflexion (REF_S) and 35° plantarflexion (REF_L) in a randomized order. Three maximal voluntary MTU lengthening actions per randomized preload condition were then performed from REF_S to REF_L at 40°/s. PLs were 0% (PL_0), 50% (PL_{50}), and 95% (PL_{95}) of the REF_S peak torque. Participants received real-time visual feedback of their net ankle joint torque during each contraction, which they attempted to match within ±5% of two predefined torque ramps to reach PL levels of 50% and 95%. Participants were also instructed to contract as hard and fast as possible when the dynamometer crank arm started moving and to maintain each contraction for 5 s after MTU lengthening. Torque, crank arm angle, and TA muscle activity were recorded at 2 kHz using a 16-bit analog-digital converter (Power3 1401, CED, UK), and TA muscle fascicle kinematics were recorded at 33 fps using B-mode ultrasound (ArtUs, Telemed, Lithuania).

RESULTS AND DISCUSSION

For PL_0 and PL_{50}, fascicles actively shortened before they actively lengthened during MTU lengthening (Fig. 1). Fascicle lengthening amplitudes increased from 16.2±3.8 mm to 20±4.7 and 23.2±4.3mm for PL_0, PL_{50}, and PL_{95}, respectively. Similarly, negative fascicle work during MTU lengthening increased from -8.7±3.3 J to -11±4.7 J and -12.8 ± 4.7 J for the same respective conditions. Despite different fascicle kinematics, peak torque during MTU lengthening did not differ among conditions, but occurred at different fascicle lengths and ankle joint angles (14.8±4°, 10.9±5.4°, and 7±5.4° for PL_0, PL_{50}, and PL_{95}, respectively). Conversely, peak fascicle force, which was similar among conditions, occurred at similar fascicle lengths (~53.3±11.3 mm), fascicle velocities (~23.6±6.1 mm/s), and ankle angles (~17.5±4.7°). Residual force enhancement (rFE) of ~7% following MTU lengthening was similar among conditions, despite differences in stretch amplitude and in the amount of positive work (1.4±0.8 J, 1.4±1.1 J, and 1.9±1.0 J for PL_0, PL_{50}, and PL_{95}, respectively).

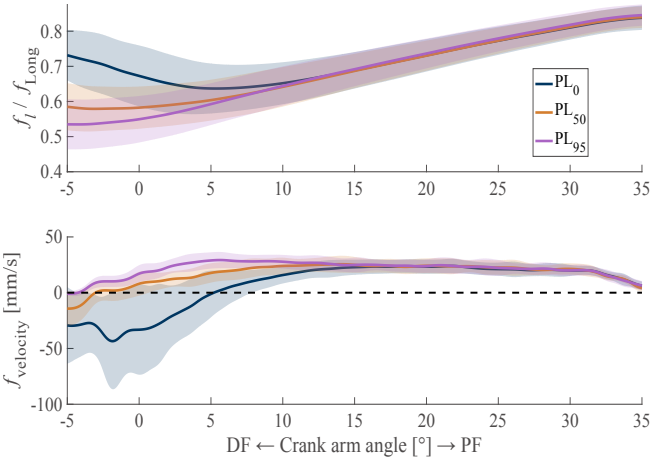

Figure 1: Normalized fascicle length changes (top panel) and fascicle velocities (bottom panel) during maximal voluntary MTU lengthening actions with different preloads (PLs).

CONCLUSIONS

Our results highlight that PL magnitude affects the decoupling of MTU and fascicle behavior, which leads to different fascicle mechanics despite identical joint kinematics. As altered fascicle mechanics during MTU lengthening might induce different chronic morphological and/or functional adaptations following MTU-lengthening exercises, decoupling needs to be considered when designing training programs. Further, rFE seems to be unaffected by positive work magnitudes and stretch amplitudes [2], suggesting that any force depression effect is abolished by the following stretch [3].

REFERENCES

[1] Griffith et al., *J Physiol, **436**: 219-236,*1991.
[2] Bakenecker et al., *eLife*, **11**: e77553, 2022.
[3] Herzog & Leonard, *J Biomech, **33**: 531-542,* 2000

MULTISCALE HAMSTRING MUSCLE ADAPTATIONS FOLLOWING A NINE WEEK ECCENTRIC TRAINING PROGRAM

Max H. Andrews[1,2], Anoosha Pai S[2], Reed D. Gurchiek[2], Patricio A. Pincheria[1,4], Akshay S. Chaudhari[3], Scott L. Delp[2], and Glen A. Lichtwark[1]

[1] School of Human Movement and Nutrition Sciences, The University of Queensland, Brisbane, Australia.
[2] Department of Bioengineering, Stanford University, Stanford, USA.
[3] Department of Radiology, Stanford University, Stanford, Stanford, USA.
[4] Faculty of Health and Behavioural Sciences, The University of Queensland, Brisbane, Australia.
Email: max.andrews@uq.edu.au

INTRODUCTION

Hamstring strains are one of the most prevalent injuries occurring in high-speed running sports, rising by as much as 4% annually [1]. Eccentric training has been proposed as a potential modality for preventing hamstring injury [2]. However, it is still unknown what muscle adaptations are facilitated by eccentric exercises over longer periods (>3 weeks) [3]. Therefore, we aim to quantify the multiscale hamstring muscle adaptations in response to 9 weeks of eccentric training.

METHODS

Four recreationally active participants (2 males, 2 females out of the 10 participants that are recruited for the ongoing study) completed 9 weeks of eccentric Nordic hamstring training. The training volume totalled 867 repetitions across the 9 weeks. Eccentric hamstring force was measured during the Nordic exercise from load cells measurements at the ankle. Sarcomere and fascicle lengths were measured in vivo using microendoscopy and 3D ultrasound. Resting fascicle length, sarcomere length, and serial sarcomere number (passive fascicle length divided by passive sarcomere length) in the biceps femoris long head muscle in central and distal region were compared before and after the training intervention.

RESULTS AND DISCUSSION

The pilot results (Fig. 1) show that Nordic eccentric training increased eccentric knee flexor force by 54% (p=0.040). Fascicle lengths increased by 19% in the central (p=0.007) and 36% in the distal region (p=0.004). The length of sarcomeres did not change significantly in either the central (p=0.324) or the distal region (p= 0.571). The estimated number of sarcomeres in series increased by 28% in the central (p=0.027) and 46% in the distal region (p=0.027). Overall, an addition of sarcomeres in-series appears to have enabled a conservation of sarcomere length.

CONCLUSIONS

Our study provides novel insights into multiscale hamstring muscle adaptations to eccentric training. Together with a report that showed that sarcomerogenesis is not detectable after 3-weeks of the same eccentric exercise [3], this preliminary work provides the first evidence that prolonged exercise is required to induce additions of sarcomeres in series within muscle fibres.

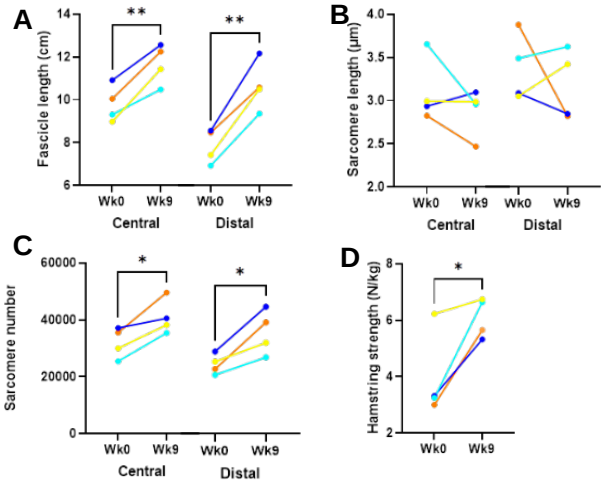

Figure 1. Multiscale Biceps Femoris Long Head muscle adaptations after 9-weeks of Nordic eccentric training. A) fascicle length, B) sarcomere length, C) sarcomere number, and D) eccentric strength. * and ** indicate statistically significant changes (p<0.05).

ACKNOWLEDGEMENTS

This work was supported by Australian Research Council Discovery Project (DP200101476), and in parts by NIH grants R01 AR077604, RO1 EB002524, RO1 AR079431, P41 EB02706, Stanford Graduate Fellowship, University of Queensland Graduate Scholarship, and Wu Tsai Human Performance Alliance at Stanford University and the Joe and Clara Tsai Foundation.

REFERENCES

[1] Ekstrand et al. *Br. J. Sports Med 50*: 731-737, 2016.
[2] Rudisill et al. *Am J Sports Med*, 2022.
[3] Pincheira at al. *J. Sports Health Sci 11:43-49, 2022.*

TYPICALLY DEVELOPING CHILDREN AND CHILDREN WITH CEREBRAL PALSY HAVE SIMILAR LEG MUSCLE MOMENT ARMS

Bart Bolsterlee[1,2], Brian V.Y. Chow[1,3], Robert D. Herbert[1,3] and the MUGgLE Study Investigators
[1] Neuroscience Research Australia (NeuRA), Sydney, NSW, Australia.
[2] Graduate School of Biomedical Engineering, University of New South Wales, Sydney, NSW, Australia.
[3] School of Medical Sciences, University of New South Wales, Sydney, NSW, Australia.
Email: b.bolsterlee@neura.edu.au

INTRODUCTION

Differences in moment arms between typically developing children and children with cerebral palsy could contribute to the frequently observed differences in joint strength and stiffness. Previous investigations of Achilles tendon moment arms in children with cerebral palsy have reached opposite conclusions, namely that their moment arms are smaller [1] or larger [2] than in typically developing children. These studies used relatively small samples of 8 [1] and 16 [2] children with cerebral palsy. Here, we compare Achilles tendon and tibialis anterior moment arms of 50 children with cerebral palsy and 200 typically developing children.

METHODS

Anatomical MRI scans (mDixon and/or T1-weighted scans) were obtained from the lower legs (including the talus) of 200 typically developing children (117 boys and 83 girls aged 5 to 15 years) and 50 children with cerebral palsy (30 boys and 20 girls, aged 5 to 15 years, 62% GMFCS1, 30% GMFCS2, 8% GMFCS3) while the ankle was in 15 degrees plantarflexion.

The tibia, talus, Achilles tendon and tibialis anterior tendon were semi-automatically segmented from the images. Tibia length was calculated as the maximum distance along the first principal component of the tibia surface model. The ankle joint axis of rotation was estimated as the axis of a cylinder fitted to the talar dome [3]. Moment arms of the Achilles tendon and tibialis anterior tendon were determined as the shortest distance from the joint axis of rotation to a 3rd-order polynomial fitted in 3D through points on the Achilles tendon and tibialis anterior tendon, respectively [3].

The effect of cerebral palsy on the relationship between tibia length and moment arm was examined using multiple linear regression.

RESULTS AND DISCUSSION

Moment arms of the Achilles tendon and tibialis anterior scale linearly with tibia length for both typically developing children and children with cerebral palsy (Fig. 1). In contrast to previous reports, we found no systematic difference in moment arms between children with cerebral palsy and typically developing children (likelihood ratio test p=0.08 for Achilles tendon; p=0.13 for tibialis anterior).

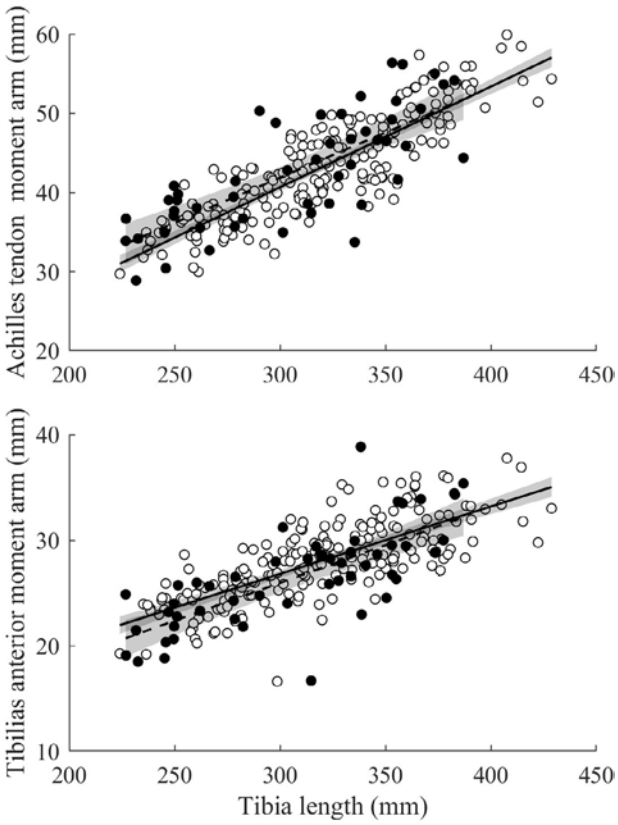

Figure 1 Achilles tendon moment arms (top) and tibialis anterior moment arms (bottom) vs. tibia length for children with cerebral palsy (n=50, black circles, dashed line) and typically developing children (n=200, white circles, solid line). Lines are regression lines and shaded areas are 95% confidence intervals.

CONCLUSIONS

Differences in moment arms around the ankle are unlikely to play a major role in group-level differences in strength and stiffness between typically developing children and children with cerebral palsy.

ACKNOWLEDGEMENTS

The study was supported by NHMRC grants (APP1156394, APP1117192). The authors acknowledge assistance of NeuRA Imaging (National Imaging Facility, a NCRIS capability). BC is supported by UNSW Scientia and RTP scholarships.

REFERENCES

[1] Kalkman et al. *J Biomech* **56**: 48-54, 2017.
[2] Alexander et al. *J Biomech* **82**: 307-12, 2019.
[3] Alexander et al. *J Biomech* **55**:134-38, 2017.

MUSCLE- AND SEX-SPECIFIC LEG MUSCLE VOLUMES IN CHILDREN WITH CEREBRAL PALSY

Jonathan Yu[1,2], Brian V.Y. Chow[1,2], Robert D. Herbert[1,2], Bart Bolsterlee[1,3] + MUGgLE Study Investigators
[1] Neuroscience Research Australia (NeuRA), Sydney, NSW, Australia.
[2] School of Biomedical Sciences, University of New South Wales, Sydney, NSW, Australia.
[3] Graduate School of Biomedical Engineering, University of New South Wales, Sydney, NSW, Australia.
Email: b.bolsterlee@neura.edu.au

INTRODUCTION

Children with cerebral palsy usually have much smaller leg muscles than typically developing children [1-3]. Previous investigations of muscle growth in children with cerebral palsy (CP) either evaluated only one muscle (usually the medial gastrocnemius muscle; e.g., [2]), or investigated multiple muscles on a small sample of children with cerebral palsy [3]. Therefore it is largely unknown if cerebral palsy impairs growth equally across muscles. In this study, we use muscle volume data from 208 typically developing children to develop reference distributions ('growth charts') of the relationship between age and muscle volume for typical lower leg muscle development. We then use the charts to determine where on those distributions the individual muscle volumes of 50 children with cerebral palsy lie.

METHODS

mDixon and T1-weighted MRI scans were acquired from the lower legs of 208 typically developing children (121 boys and 87 girls, including 8 infants aged 0.14 to 0.26 and 200 children aged 5 to 15 years) and 50 children with cerebral palsy (30 boys and 20 girls, age 5 to 15; 62% GMFCS1, 30% GMFCS2, 8% GMFCS3). Volumes of ten lower leg muscles/muscle groups were calculated from surface models which were constructed by semi-automatically segmenting MRI images [4].
Muscle volumes of typically developing children were regressed against age using quantile regression with B-spline basis functions [5]. The models were fitted separately for boys and girls. The regression models were used to create muscle growth charts specific to age, muscle, and sex. Muscle volumes of children with CP were expressed as percentiles from the distributions of typically developing children. For example, a percentile of 10 indicates 10% of typically developing children of the same age have smaller muscles.

RESULTS AND DISCUSSION

Muscle volumes were typically much smaller in children with cerebral palsy than in typically developing children (Fig. 1). The median percentile of total muscle volume for children with cerebral palsy was 11 for boys and 18 for girls. The lowest median percentiles were found for the tibialis anterior (boys: 1, girls: 2.5) and medial gastrocnemius muscles (boys: 1, girls: 10). The highest median percentile was found for the popliteus muscle (boys: 20, girls: 28). For all muscles except tibialis posterior, boys had lower median percentile scores than girls.

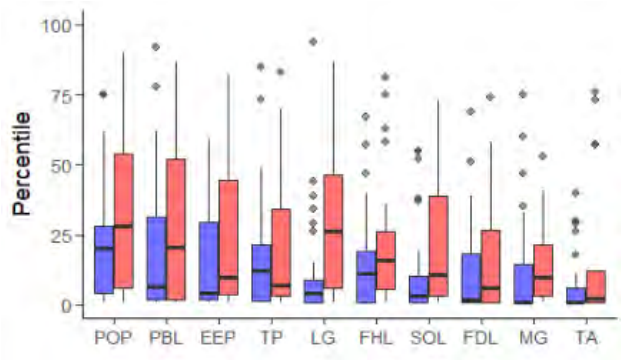

Figure 1 Boxplots of volumes of individual muscles in boys (blue, *n*=30) and girls (red, *n*=20) with cerebral palsy. Boxes span the 1st and 3rd quartile and whiskers span the full range excluding outliers, displayed as dots. POP=popliteus, PBL=peroneus brevis+longus, EEP=extensor digitorum longus, extensor hallucis longus, peroneus tertius, TP=tibialis posterior, LG=lateral gastrocnemius, FHL=flexor hallucis longus, SOL=soleus, FDL=flexor digitorum longus, MG=medial gastrocnemius, TA=tibialis anterior.

CONCLUSIONS

All lower leg muscles of children with CP are typically much smaller than those of typically developing children. While all leg muscles are affected, some muscles – particularly the medial gastrocnemius and tibialis anterior – appear to be more affected than others. Muscles appear to be more affected in boys than in girls.

ACKNOWLEDGEMENTS

The study was supported by NHMRC grants (APP1156394, APP1117192). The authors acknowledge the facilities and scientific and technical assistance of the National Imaging Facility, a NCRIS capability at the NeuRA Imaging (UNSW) Node. BC is supported by UNSW Scientia and RTP scholarships.

REFERENCES

[1] Barrett & Lichtwark, *DMCN* **52**, 784-801, 2010.
[2] Herskind A et al. *DMCN* **58**: 485-91, 2016.
[3] Handsfield GG et al. *Muscle Nerve* **53**:933-45, 2016.
[4] Zhu J et al. *NMR Biomed* **34**: e4609, 2021.
[5] Muggeo et al. *Stat Mod* **21**: p428-48, 2021.

A NEW MODEL FOR THE MOLECULAR MECHANISM OF MUSCLE CONTRACTION

Walter Herzog[1], Venus Joumaa[1], Shuyue Liu[1], Tim Leonard[1] and Heiliane de Brito Fontana[2]
[1] Human Performance Lab / University of Calgary, Calgary, Canada.
[2] Department of Morphological Sciences / Federal University of Santa Catarina / Florianopolis, Brazil.
Email: wherzog@ucalgary.ca

INTRODUCTION

For more than half a century, muscle contraction has been associated with the contractile proteins actin and myosin in sarcomeres [1]. Just over 20 years ago, we discovered a new mechanical property of skeletal muscle now referred to as "passive force enhancement" [2]. In the following decade, the structural protein titin was identified as the source of this passive force enhancement, and a role for titin in active muscle contraction emerged. However, the detailed molecular mechanims of the interplay between actin, myosin, and titin remain elusive. Here, we propose a new model of muscle contraction that fits current experimental observations. It involves actin and myosin in their traditional roles and adds titin-actin interactions that modulate titin's stiffness/force upon muscle activation.

METHODS

All results presented, and associated formulation of the new model for muscle contraction, were obtained from rabbit psoas single fibre, myofibril, and sarcomere experiments. Fibres, myofibrils, and sarcomeres are isolated and set up in a mechanical testing chamber that allows for controlled activation, controlled length changes and accurate force measurements [e.g., 3]. The results presented here are based on experiments in which preparations were stretched normally, with calcium activation but inhibition of cross-bridge attachment [e.g., 5], with fluorescent anti-body labelling of titin segments [4], and using strong/rapid (<1ms) stretching that caused "slippage" [6].

RESULTS AND DISCUSSION

Active stretching of single fibre, myofibril and sarcomere preparations resulted in an increase in steady-state force following stretching, i.e. "residual force enhancement" (rFE) (Fig. 1). rFE always occurs when preparations are stretched within the limits of their force generating capacity. We also observed that rFE was associated with an increase in titin stiffness and force up to four times its passive value [3], and that this increase in stiffness is associated with a stiffening of the proximal titin segment, likely caused by titin binding to actin [4]. However, this increase in titin-based force did not occur when cross-bridge formation was inhibited or was restricted to the weakly bound state [5]. Similarly, when active myofibrils were stretched rapidly producing slippage, no rFE or increase in titin stiffness/force was observed [6]. ***These results suggest that rFE and increased titin stiffness/force crucially depend on strong actin-myosin cross-bridge formation***. Based on these results we propose the following model for muscle contraction:

(i) When a muscle is activated cross-bridges engage, and titin binds its proximal segment rigidly to actin, thus increasing its stiffness and force.

(ii) Titin-actin interactions do not occur in the presence of activation (calcium) alone and do not occur when the strong cross-bridge state is inhibited chemically, mechanically, or by regulatory protein alteration.

(iii) Since the regulatory protein tropomyosin (TPM) controls cross-bridge attachment through a configurational change, and since further TPM configurational changes occur when cross-bridges go from weakly to strongly bound states, we propose that titin attachment to actin requires the configurational change of TPM when cross-bridges transit from weakly to strongly bound states.

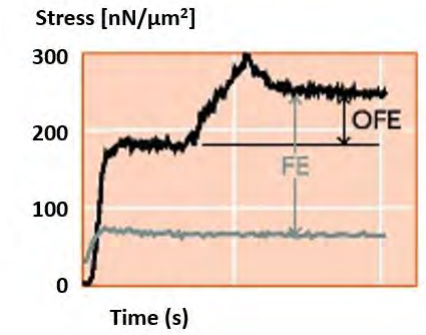

Figure 1 Force enhancement (FE) observed following active stretch (black) compared to a reference isometric contraction (grey) in a single sarcomere preparation.

CONCLUSIONS

Based on our experimental results, we propose that titin-actin interactions, responsible for the rFE property and active force production in skeletal muscle, are controlled by configurational changes of tropomyosin when cross-bridges go from the weakly to the strongly bound state.

ACKNOWLEDGEMENTS

CIHR, Killam Foundation, Nigg Chair, CRC Program

REFERENCES

[1] Huxley, AF (1957). Pro bio bioph chem, 256-319.
[2] Herzog, W et al. (2002). JEB 1275-1283.
[3] Leonard, TR et al. (2010). Am J Physiol C14-C20.
[4] DuVall, M et al (2017). JEB 220: 4418-4425.
[5] Joumaa, V et al. (2008). Proc Roy Soc B: 1411-1419.
[6] Liu, S et al. (2022). JEB 225(10).

IS THE APONEUROSIS PROTECTED FROM GREAT LENGTH CHANGES WHEN ACTIVE MUSCLE FORCES CHANGE DRAMATICALLY?

Fransiska M Bossuyt[1,3*], Sarah Abramovic[2], Tim Leonard[3], Andrew Sawatsky[3], Colin Smith[2], William R. Taylor[2], Walter Herzog[3]

[1]Neuromusculoskeletal Functioning and Mobility Group, Swiss Paraplegic Research, Nottwil, Switzerland, [2]Institute for Biomechanics, ETH Zurich, Switzerland, [3]Human Performance Lab, University of Calgary, Canada
Email: *Fransiska.bossuyt@paraplegie.ch

INTRODUCTION

Muscular aponeuoses consist of collagen fibres which transfer forces from the muscle to the tendon in a complex manner [1,2,3]. Given that isolated aponeuroses fail at forces below those observed during active muscle contraction [4], it can be hypothesised that aponeuroses require protection from large elongations when forces are high. The purpose of this study was to compare in-vivo aponeurosis length changes when the muscle forces are high with length changes when the muscle forces are low during locomotion in the Medial Gastrocnemius muscle (MG).

METHODS

In this abstract, we performed new analyses on data that has been published previously [1]. Specifically, sonomicrometry crystals were implanted in the MG of four sheep to measure proximal aponeurosis (i.e., continuation of the short, proximal tendon of the muscle) length changes at 496 Hz and a custom-built buckle-type transducer was implanted to measure muscle forces at 500 Hz. Data were collected while the sheep walked at 8 different combinations of speeds and inclination angles on a motorized treadmill. Force data were filtered using a fourth-order, low-pass (10 Hz), recursive Butterworth filter. Sonomicrometry data were pre-processed using SonoCleaner Software after which a low-pass (50 Hz), fourth-order, recursive Butterworth filter was applied. Absolute aponeurosis length changes were calculated when muscle forces exceeded and were below 30% of the peak force during the respective cycle (see Figure 1 left presenting the selected portion for 7 steps of one condition of one exemplary sheep). Length changes of the loading and unloading phase of at least five consecutive steps for each sheep and locomotion condition were averaged and statistically compared using non-parametric Wilcoxon signed rank test (SPSS Statistical Software with alpha = 0.05).

RESULTS AND DISCUSSION

Due to technical limitations and differences in walking ability between sheep, we focus on one walking speed where aponeurosis length changes were obtained for all four sheep (0.67 m/s). Aponeuroses length changes were about 3 times greater when forces were low (corresponding primarily to the swing phase of walking) compared to length changes when forces were high ($p=0.066$) (primarily stance phase - Figure 1, right). If we were to assume that all data points are truly independent observations, we would observe a highly significant difference in aponeuroses length changes between the high and low muscle force conditions ($p<0.001$). Regardless of sheep or treadmill condition, aponeuroses length changes were always greater when forces were low. We conclude from these results that the sheep MG aponeuroses is protected from large elongations when forces are high. The mechanisms underlying this protection remain unclear.

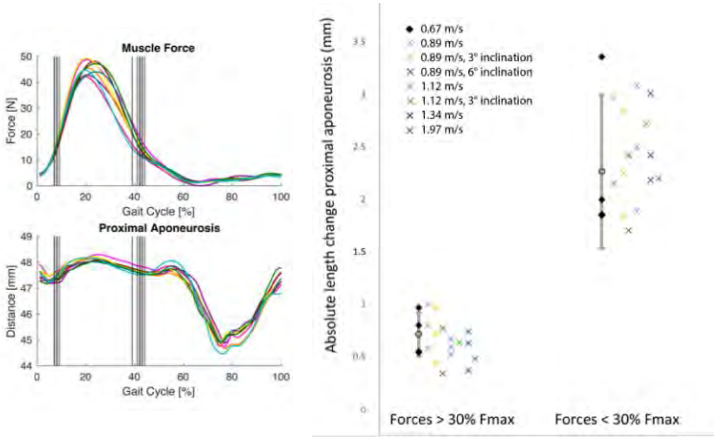

Figure 1: Left: Aponeurosis length and muscle forces of 7 steps of one sheep. Vertical black lines represent cut-off when forces are > or < 30%Fmax for each step. Right: Absolute length changes when forces > 30%Fmax and when forces < 30%Fmax for different conditions (see legend)

CONCLUSIONS

Aponeuroses length changes were small when muscle forces were high and aponeuroses length changes were large when muscle forces were small. High muscle forces were mainly found during the stance phase when the muscle actively produces force while low forces were mainly observed during the swing phase when the muscle only produces passive forces. This result supports the notion that aponeuroses are protected from high forces when muscles are activated. If confirmed in other muscles, it would be of interest to study how this aponeuroses protection works.

ACKNOWLEDGEMENTS

Swiss National Science Foundation (187793), Killiam Foundation, and the Canada Research Chair Program.

REFERENCES

[1] Bossuyt et al. *J Biomech*, 2023. [2] Epstein et al. *J Biomech,* **39**: 2020-2025, 2006. [3] Herzog. *BMC Biomed Eng*, 1-28, 2019. [4] Zuurbier et al. *J Biomech,* **27**: 445-453, 1994.

RELATHIONSHIP BETWEEN KNEE VALGUS ANGLE AND LATERAL TRUNK BENDING ANGLE DURING VOLLEYBALL SPIKE JUMP

Miki Kawai[1], Noriaki Maeda[1], Makoto Komiya[1], Shogo Tsutsumi[1], Tomoya Watanabe[1], and Yukio Urabe[1]
[1] Department of Sports Rehabilitation, Graduate School of Biomedical and Health Sciences, Hiroshima University, Hiroshima, Japan
Email: miki-kawai@hiroshima-u.ac.jp

INTRODUCTION

Anterior cruciate ligament (ACL) injuries often occur during jump landings. During jump landing, an increased lateral trunk bending angle increases the knee valgus angle of the bent trunk lateral side, which is a risk factor for ACL injuries. In volleyball, video analysis has shown that ACL injuries occur more commonly during spike jump landing of the nondominant leg, which is thought to be related to trunk movement [1]. However, it is unknown whether lateral trunk bending and the knee valgus angle are affected by ball position during spike jumps. Therefore, the purpose of this study was to investigate whether the relationship between the knee valgus angles and the lateral trunk bending during spike jump landing varies with ball position. We hope this study to provide basic information for the prevention of ACL injuries in volleyball.

METHODS

Fourteen female college volleyball players (20.5 ± 1.8 years) with at least 5 years of experience participated. Participants performed volleyball spike jumps in five trials. The ball positions during the spike jump were set at normal, dominant, and non-dominant positions. The normal position set a line perpendicular to the floor through the acromion. The measurement items were the knee valgus and lateral trunk bending angle at the initial contact (IC) of the spike jump landing using a three-dimensional motion analysis system (Vicon Motion Systems) with a sampling frequency of 100 Hz. The IC was defined as the point at which the ground reaction force exceeded 10 N. Outcomes were confirmed using Pearson correlations to examine the relationship between the knee valgus and lateral trunk bending angles. Statistical significance was set at $p < 0.05$.

RESULTS AND DISCUSSION

In the kinematic data, a positive correlation was observed between the knee valgus and lateral trunk bending angles in the non-dominant position ($r=0.60$, $p<0.05$). We also observed no association between the knee valgus and lateral trunk bending angles in the normal ($r=0.06$, $p=0.83$) and dominant positions ($r=0.08$, $p=0.77$) (Figure 1).

When the lateral trunk is bent, the center of gravity moves laterally, relative to the hip and knee. This causes an increase in the knee valgus angle [2]. In badminton, players must bend their lateral trunk to the non-dominant side when hitting the shuttle in the non-dominant position because the head interrupts the swing [3]. Volleyball has the similar situation when hitting the ball in a non-dominant position during the spike jump. Therefore, the lateral trunk was more bent to the non-dominant side, and the knee valgus angle increased when hitting the ball in the non-dominant position.

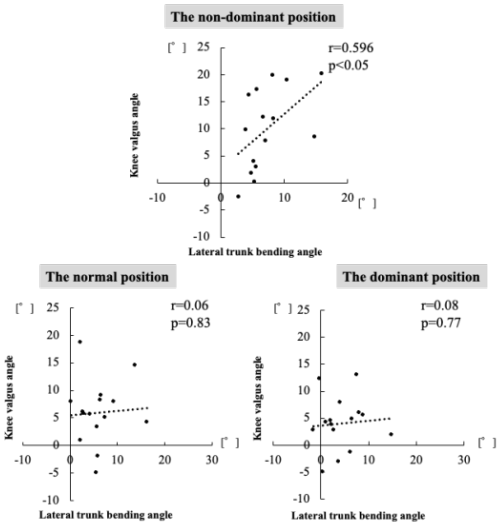

Figure 1 Relationship between the knee valgus angle and lateral trunk bending angle

CONCLUSIONS

This study showed that when the ball was in the non-dominant position, a positive correlation was observed between the knee valgus and lateral trunk bending angles, which may increase the risk of ACL injuries. It is very important that volleyball players and coaches understand the situation and posture that often cause ACL injuries in volleyball. This study might be helpful for the idea and fundamental information which is teaching players and coaches landing techniques and training methods to prevent ACL injuries.

REFERENCES

[1] Devetag F et al. *J Sports Med Phys Fitness* 58(1-2): 92-97, 2018.
[2] Hewett T et al. *Exerc. Sport Sci. Rev* 39(4): 161-166, 2011.
[3] Kimura Y et al. *Br J Sports Med* 46(1): 207-213, 2012.

FRAMEWORK TO SOLVE THE OPTIMUM ARMSTROKE IN CRAWL SWIMMING CONSIDERING SUBJECT-SPECIFIC SHOULDER JOINT TORQUE CHARACTERISTICS

Motomu Nakashima[1], Sotaro Tsuchiya[1], Ryosuke Toyoda[1], Akisue Kuramoto[1], Daiki Koga[1,2] and Hideki Takagi[2]
[1] Department of Systems and Control Engineering, Tokyo Institute of Technology, Tokyo, Japan.
[2] School of Health and Sport Sciences, University of Tsukuba, Tsukuba, Japan.
Email: motomu@sc.e.titech.ac.jp

INTRODUCTION

The armstroke in the crawl swimming is important since it mainly contributes to the thrust generation. The optimum armstrokes were solved by optimizating simulation for swimmers without any physical disability [1,2], with hemiplegia [3] and with unilateral transradial deficiency [4]. In those optimizaing simulations, the joint torque characteristics database, which was constructed based on experiments and musculoskeletal simulation [1], were always used as the constraints. However, since the joint torque characteristics vary according to individual, the optimum armstroke for each individual is also considered to vary. For this problem, a framework to solve the optimum armstroke considering subject-specific shoulder joint torque characteristics was proposed in this study.

METHODS

In the framework, the subject-specific shoulder joint torque has to be acquired to customize the database, which is used for the optimizing calculation. For this purpose, the specially customized swim ergometer was developed (Figure 1a). As the basic mechanism as a swim ergometer, paddles are attached to both hands of a participant, who pulls wires in the manner similar to the armstroke of the crawl swimming. The wires draw back automatically during the recovery stroke. The pulling speed of the wires is limited by a ratchet mechanism and an electric motor. The limit pulling speed can be changed by changing the rotational speed of the motor. When the pulling speed by a participant is slower than the designated one, no load acts on the paddles. However, if the pulling speed reaches the designated speed, it becomes very difficult for the participant to pull the wire at higher speed due to the ratchet mechanism. As a result, the pulling speed becomes constant for a certain period. The tension of the wire for the right hand is measured by a load cell. Using the developed ergometer, an experiment was conducted in which two male collegiate competitive swimmers participated. In addition to the measurement of the tension of the wire, an optical motion capture system (MAC3D, Motion Analysis Corp.) was used to measure the body motion. Nine infrared reflective markers were attached to the participants. The participants were asked to perform five armstrokes continuously on the ergometer for the three speeds of slow, medium and high and for the five styles of strokes (normal, horizontally flexed, horizontally extended, internally rotated, and externally rotated).

RESULTS AND DISCUSSION

As examples, the adduction angular velocity and joint torque at the shoulder in the case of medium speed and normal style of stroke are shown, respectively (Figure 1b,c). The averages for the five cycles were taken and two peak points are plotted in the graph for the peaks of the adduction angular velocity (green) and the joint torque (blue). The two values of joint torque at the two peak points were taken. Since such two joint torque values were obtained in one trial, 30 values (3 speeds times 5 stroke style) were obtained for one participant. These 30 values were used to modify the joint torque characteristics database.

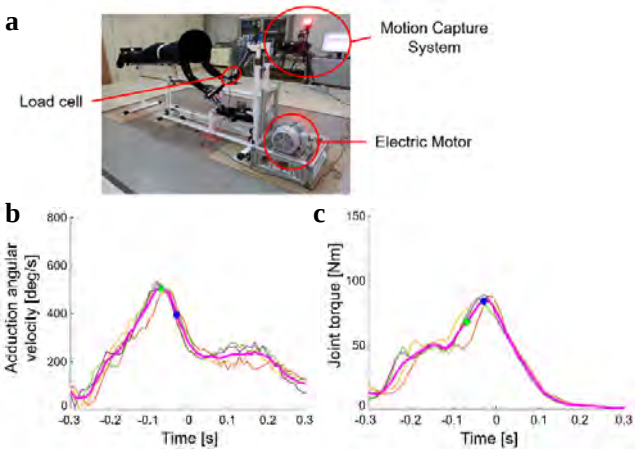

Figure 1 The specially customized swim ergometer (a), results of adduction angular velocity (b) and shoulder joint torque (c).

CONCLUSIONS

A framework to solve the optimum armstroke in crawl swimming considering subject specific shoulder joint torque characteristics was proposed. The shoulder joint torque characteristics database is next modified according to the acquired joint torque data. The optimizing simulation is finally conducted. The results of optimization are presented in the conference.

ACKNOWLEDGEMENTS

This work was supported by JSPS KAKENHI Grant Number JP20H04072.

REFERENCES

[1] Nakashima M et al. *J Biomech Sci Eng* **7**: 102-117, 2012.
[2] Nakashima M et al. *J Biomech Sci Eng* **9**: 1-9, 2014.
[3] Nakashima M et al. *Mech Eng J* **5**: 17-00377, 2018.
[4] Nakashima M et al. *J Biomech Sci Eng* **15**: 19-00467, 2020.

BARBELL SQUATS FOR CROSSFIT ATHLETES: EFFECT OF FOOTWEAR TYPE AND LOAD MAGNITUDE ON LOWER LIMB JOINT TORQUES

Eduardo Campos Martins[1], Daiani de Campos[1], Giorgio Poletto[1], Rodrigo Bini[2], Heiliane de Brito Fontana[1]
[1] Biomechanics Laboratory, Federal University of Santa Catarina, Florianópolis, Brazil.
[2] La Trobe Rural Health School, La Trobe University, Bendigo, Australia.
Email: martinseduardoc02@gmail.com

INTRODUCTION

In strength training practice, it is commonly assumed that increasing load during barbell squats results in a proportional increase in the magnitude of joint torques. However, kinematic changes resulting from larger loads may affect this assumption [1]. In some sports, such as CrossFit and Olympic weightlifting, the use of a footwear that elevate the heel in relation to forefoot (i.e., "lifter shoes") is very common. These shoes elicit changes in kinematics that help to overcome limitations on ankle dorsiflexion range of motion and may also affect the contributions of joint torques during squats [2]. In this study, we aimed to test the effects of the type of footwear and load magnitude on the hip, knee, and ankle torques during barbell squats.

METHODS

Sixteen (8M, 8W) professional CrossFit athletes had their three-repetition maximum (3RM) squat load and ankle range of motion assessed. With eight cameras (Vicon-Motion-Systems) and two force plates (AMTI), we conducted a three-dimensional analysis of three repetitions of barbell squat with a load of 50%, 70% and 90% of the 3RM, using a lifter shoe and a control non-lifter shoe (six randomized conditions). Through inverse dynamics, the resultant extensor (or plantar flexor) torques around the hip, knee and ankle were calculated. Torques were normalized to participants' mass and height. A two-factor (footwear and load) repeated measures ANOVA was used ($p<0.05$) to compare joint torques at the instant of maximum total lower limb extensor torque, i.e., when the sum of hip, knee and ankle torques reached its maximum. A statistical parametric mapping approach is being used to compare torque curves, but these results will only be available for presentation in the conference and therefore are not shown in this abstract.

RESULTS AND DISCUSSION

There were no interactions between the effects of load and footwear for the ankle ($p=0.59$), knee ($p=0.89$), and hip ($p=0.89$) torques. Additionally, no effect of footwear on joint torques was observed for hip ($p=0.94$), knee ($p=0.79$), and ankle ($p=0.82$) torques (Table 1). An increase in load resulted in a larger plantar flexor ($p<0.01$), and hip extensor ($p<0.01$) torques (Figure 1). No difference in knee extensor torque was observed across loads ($p=0.59$) (Figure 1). Contrary to what is often assumed, our experimental findings indicate that increasing load does not necessarily increase all lower limb joint torques and is not effective in increasing the demand on the knee extensor muscles during squats, regardless of the type of footwear. The absence of footwear effects might be related to the characteristics of the sample analyzed, such as a wide ankle dorsiflexion range of motion (54° ± 2.5°) and high-level competitive experience (3 years).

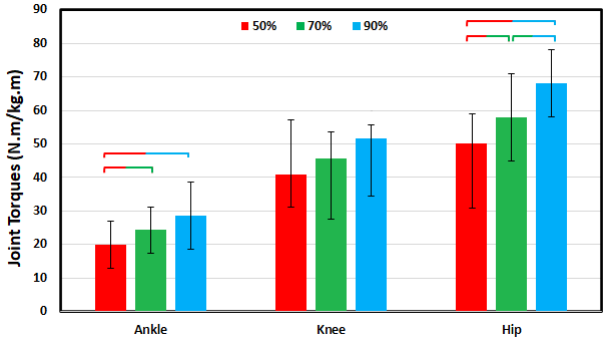

Figure 1 Normalized joint torques during barbell squats at different percentages of three-repetition maximum load. Results were pooled across footwear conditions and brackets show differences at $p<0.05$.

CONCLUSIONS

For professional CrossFit athletes, regardless of footwear, increasing external load from 50% to 90% of 3RM in the barbell squat seem to affect hip and ankle torques, but not knee torques. The analysis of torque curves using statistical parametric mapping will help to better understand these effects.

REFERENCES

[1] Kellis E et al. *J Sports Sci* **23**: 1045-55, 2005.
[2] Sato K et al. *J Strength Cond Res* **26**: 28-33, 2012.

Table 1: Mean (with standard deviation) joint torques (N.m/kg.m) for the two footwear type conditions.

	Control Shoe	Lifter Shoe	*p-value*
Ankle torques	24.2 ± 7.4	24.3 ± 8.2	0.82
Knee torques	44.8 ± 13.5	47.4 ± 13.8	0.79
Hip torques	58.4 ± 13.2	58.9 ± 12.6	0.94

SIMULATION OF RUNNING PROSTHETIC FEET GROUND REACTION FORCES USING A MULTI-AXIAL ROBOTIC WALKING SIMULATOR

G. Fabris[1], M. Scapinello[1], P. Mistretta[1], A.G. Cutti[2] and N. Petrone[1]
[1] Department of Industrial Engineering, University of Padova, Padova, Italy.
[2] INAIL Prosthetic Centre, Vigorso di Budrio (BO), Italy
Email: giacomo.fabris@unipd.it

INTRODUCTION

Running specific prostheses (RSPs) are assistive technologies specifically designed for elite athletes to reach their maximal performance in running competitions. RSPs comprise a custom-made socket, which hosts the residual limb, and a running prosthetic foot (RPF), a carbon-made curved blade. Depending on the amputation level, the RPF is directly clamped to the socket or linked via a knee or pylon to it. The selection of the appropriate RPF is essential to provide balance between flexibility and strength, allowing the athlete to express the maximum potential without putting the physical health at risk. A mechanical test bench was previously designed and constructed for evaluating ankle-foot prostheses [1], by reproducing the biomechanical patterns associated with gait related tasks on the prosthesis in an objective, repeatable, controllable and safe manner. Coming from this background, the aim of the work was the adaptation of such walking simulator into a running simulator for RPF.

METHODS

The test bench has three servo-pneumatic actuators that control simultaneously three degrees of freedom (DOFs) on the sagittal plane, namely the shank rotation around a fixed axis (θ_{shank}), the shank longitudinal displacement and the ground horizontal displacement. The composition of these two latter non-orthogonal DOFs allows to reproduce any relative translation of the shank in the sagittal plane and the corresponding ground reaction force (GRF), measured with a 6-axis load cell placed underneath the moving ground.

Actuators are controlled in position with the implementation of a two-level control architecture: on the low level a commercial controller, on the high level an iterative self-learning algorithm. The control method consists in performing a first iteration of the running simulation using tentative curves and generating new control curves for the following iteration, based on the difference between the simulated results and the reference data. This procedure is repeated until a target of difference between the signals is reached.

The reference data (θ_{shank}, GRF_x, and GRF_y) are retrieved from a previous *in-door* study of the research group [2]. The study involved a unilateral transfemoral medalist athlete (female, height $166cm$, mass $58kg$) running on a commercial treadmill placed over 4 force platforms, while 8 motion capture cameras captured the athlete's kinematics.

RESULTS AND DISCUSSION

The simulator stance duration was increased 8 times ($1.36s$) compared to the original stance duration ($0.17s$) since pneumatic actuators are not powerful enough to withstand the variable inertial loads generated by the rotating shank segment of the simulator at faster speed, leading to system instability. Moreover, pneumatic actuators suffer from internal frictions that resulted in disturbances and difficulties in achieving accurate position control.

However, the comparison between the averaged simulated (blue) and reference (red) signals overall proved that good results were achieved after 13 iterations of the process (Figure 1).

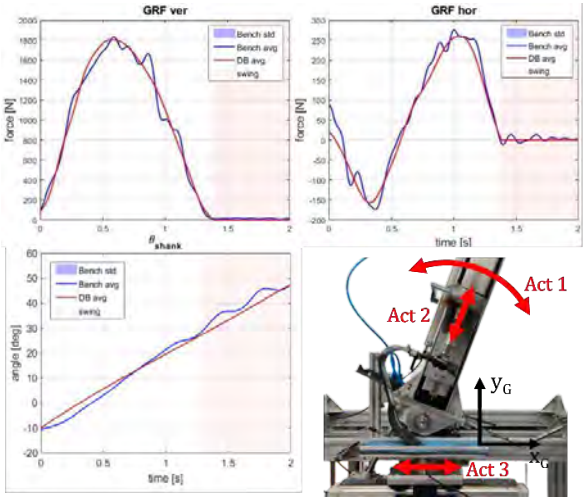

Figure 1 θ_{shank}, GRF_x, and GRF_y results at the 13th iteration of the process. The three DOFs and the Ground reference system are displayed with red and black arrows in the picture of the simulator.

CONCLUSIONS

A robotic walking simulator was adapted to simulate the running cycle of an elite athlete, reproducing collected biomechanical data (θ_{shank}, GRF_x, and GRF_y) with reference data. The agreement between test results validated the running simulator as an *in-vitro* testing scenario to replicate the running cycle and evaluate RPF performance in an objective, controllable and safe manner. Future work will be focused on the improvement of both the tracking performances and the automatic analysis capabilities.

REFERENCES

[1] Petrone N. et al. *Patent IT102021000006293, 2021.*
[2] Breban SG et al. *ISBS Proceedings Archive:* ***Vol. 40****: Iss.1, Article 22*, 2022.

KNEE BIOMECHANICAL DIFFERENCES DURING UNILATERAL LANDING BETWEEN SYMMETRICAL AND ASYMMETRICAL GROUPS CLASSIFIED BY HOP TESTS

Karine JV Stoelben[1,2], André G Andrade[3], Evangelos Pappas[4] and Felipe P Carpes[2]
[1] Childern Hospital of Eastern Ontario Research Institute, Ottawa, Canada.
[2] Federal University of Pampa, Uruguaiana, Brazil.
[3] Federal University of Minas Gerais, Belo Horizonte, Brazil.
[4] The University of Wollongong, Wollongong, Australia.
Email: karinestoelben@gmail.com

INTRODUCTION

Hop tests are used to stratify athletes for risk of injury, post-surgical recovery milestones and return to sport clearance [1]. A 10% performance criterion is broadly used to determine asymmetry in these tests, yet this is somewhat arbitrary [2]. In addition to performance criteria, we need to identify whether performance asymmetry translates into biomechanical differences. Therefore, we aimed to identify whether knee biomechanical differences exist during unilateral landings between symmetrical and asymmetrical groups as identified by hop test performance in male recreational athletes.

METHODS

Fourty-seven healthy men with a mean age (standard deviation) of 25 (3) years old, body mass of 81 (13) kg, height of 177 (7) cm, Tegner physical activity level of 5 (2), knee function in the Lysholm scale of 92 (7) were evaluated. Thirty-nine participants identified their right leg as their preferred leg to kick a ball. Participants performed single, triple and crossover hop tests for distance followed by unilateral drop jumps for biomechanical assessment. Maximal distance by each hop test and a mean of 3 trials of unilateral drop jumps were considered. Knee sagittal plane angle and moment were determined for the landing cycle of 2nd landing [101 points, from initial contact (threshold of 20 N) to the maximal knee flexion].

The participants were classified into symmetrical and asymmetrical groups according to their performance on the single, triple and crossover hops using the criteria of 10% (90 to 110% were considered symmetrical). The agreement between hop classification was assessed by Kappa coefficient. To determine group differences in the temporal series, a two-way functional analysis of variance for repeated measures was applied considering the factors leg (preferred vs . non-preferred) and group (symmetrical vs. asymmetrical) for each classification.

RESULTS AND DISCUSSION

The hop tests classification presented poor agreement among them (single vs. triple: 0.094; single vs. crossover: 0.097; triple vs. crossover: 0.109).

Considering the asymmetry classification during single and triple hop tests, no differences existed between groups or group*leg interaction for knee sagittal plane angles and moments. Knee sagittal angles did not present an effect of group or group*leg interaction considering the crossover hop test classification. However, there was a main group effect for knee sagittal moment. The symmetrical group presented a higher knee flexion moment from 34 to 71% of the landing cycle (Figure 1).

CONCLUSIONS

Asymmetry in the hop tests does not correspond to differences in biomechanical outcomes related to knee sagittal plane kinematics. However, crossover hop test asymmetry classifications can identify some differences in the unilateral landing kinetics; the asymmetrical group landed with lower knee flexion moment in the mid-phase of the landing cycle.

ACKNOWLEDGEMENTS

FPC and KJVS were supported by CNPq – Brazil.

REFERENCES

[1] Davies WT et al. *Sports Med* **50**(3): 485-95, 2020.
[2] Ebert JR et al. *Int J Sports Phys Ther* **16**(2): 393-403, 2021.

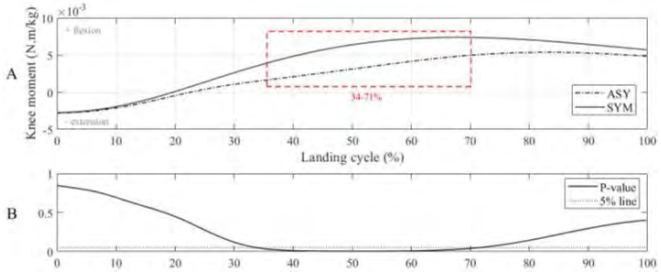

Figure 1. Group effect for knee sagittal plane joint moment considering triple hop test classification. A: group mean for knee sagittal moment, the red dotted line showed interval with differences between groups; B: p-value throughout landing cycle for group effect. ASY: asymmetrical group; SYM: symmetrical group.

Risk Factor Identification of Adductor Strain in Professional Soccer

Rebecca Davis[1], Benjamin Brewer, MS[2], Martha Hall, PhD[1,3], Jill Higginson, PhD[1,3]
[1] Biomechanics and Movement Science, University of Delaware, Newark, United States
[2]Epidemiology Department, University of Delaware, Newark, United States
[3]Mechanical Engineering Department, University of Delaware, Newark, United States
Email: davisrl@udel.edu

INTRODUCTION

Adductor injuries are among the most common hip and groin injuries that occur in soccer and have been found to account for up to 23% of all muscle injuries in a 15-year Union of European Football Associations study.[1,2] These types of injuries have been found to take a median of 14-22 days away from play but depending on the grade of strain can result in missing months.[3,4] This negatively impacts an athlete's playing exposure and career longevity as prior injury has been found to greatly increase the risk of getting a future adductor injury.[3] Determining injury risk factors allow us to understand the causal mechanisms of injury and can make staff aware of the most at-risk player groups. This will save players time and reduce the occurrence of future injuries.

METHODS

Injury data was collected from a professional soccer team from 2016-2021. This included 79 total male athletes (age 25±5.4 years); 17 experienced adductor strain (age 27±4.2 years). We identified the injury types, amount, and mechanism of injury (MOI) with a focus on adductor strain in this population. Position types included Goalkeepers, Forwards, Defenders, and Midfielders. Preseason adductor, abductor, and hamstring strength data were collected from the VALD Forceframe™ and Nordbord™. We assessed previous injury and >15% strength imbalances as risk factors for preventable lower extremity (LE) and adductor injuries. Preventable injuries are defined as any soft tissue injury due to non-contact mechanism that was reported by a player and recorded in the injury log by medical staff. Chi-squared tests, Generalized estimating equations (GEEs) and Random Forest algorithms were used to identify which variables are best able to predict injury outcomes.

RESULTS AND DISCUSSION

Hamstring strains, ankle sprains, and adductor strains accounted for the greatest amount of injuries. Adductor strains made up 15.8% of all preventable LE injuries (n=27). Of these injuries, change of direction, overuse, and running made up 70% of all mechanisms shown in Figure 1. Midfielders had the most amount of adductor injuries but also had the most amount of players in a position group. By position type, 25% of Goalkeepers 23% of Defenders, 18% of Midfielders, and 10% of Forwards had adductor strains during this time.

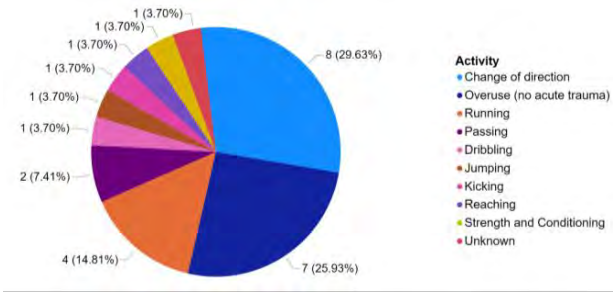

Fig 4. Adductor strain MOI (n=27) from 2016-2021

2021 preseason data showed athletes with >15% average adductor strength imbalance were more likely to experience a LE injury than individuals who did not have a >15% imbalance. No other significant differences in imbalance metrics were identified.
From the GEE, players who had a previous adductor strain were estimated to have 146 times the odds of adductor injury in a future half-season compared to a player who had no previous adductor strain ($p<0.0001$). Position type had no significant effect on an athlete's risk of future injury.

CONCLUSIONS

Our findings support that previous adductor strain is a risk factor for re-injury. Athletes with >15% average adductor strength were more likely to experience a LE injury. Greater evidence with the use of appropriate machine learning algorithms is needed to identify adductor strain risk factors. Further research will include identifying relationships between time since injury and utilizing metrics that can be linked to adductor strain etiology. Risk factor identification for adductor strains has the potential to create better preventative protocols and reduce the risk of injury. This will not only save players time away from play but also save teams money to rehab these athletes.

ACKNOWLEDGEMENTS

Funding: NSF GRFP, University of Delaware Mechanical Engineering Helwig Fellowship

REFERENCES

[1] Ekstrand, J., et al. *Br J Sports Med* **45**(7), 553–558, 2011.
[2] Werner, J., et al. *Br J Sports Med* **53**(9), 539–546, 2018.
[3] Lavoie-Gagne, O., et al. *Orthop J Sports Med*, **9**(9), 232596712110230, 2021.
[4] Werner, J., et al. *Br J Sports Med*, **43**(13), 1036–1040,2009.

INDIVIDUALIZED IMMEDIATE FEEDBACK ON SIDESTEP CUTTING TECHNIQUE REDUCES KNEE ABDUCTION MOMENTS IN FEMALE HANDBALL PLAYERS

Kevin Bill[1], Patrick Mai[1,2], Lasse Mausehund[3], Sigurd Solbakken[3], Uwe G. Kersting[1] and Tron Krosshaug[3]
[1] Institute of Biomechanics and Orthopaedics, German Sport University Cologne, Cologne, Germany.
[2] Department of Mechanical and Process Engineering, Offenburg University, Offenburg, Germany.
[3] Department of Sports Medicine, Norwegian School of Sport Sciences, Oslo, Norway.
Email: k.bill@dshs-koeln.de

INTRODUCTION

Landing heel first has been associated with elevated external knee abduction moments (KAM) [1], thereby potentially increasing the risk of sustaining a non-contact ACL injury [2]. Apart from the foot strike angle (FSA), knee valgus angle (VAL) and vertical center of mass velocity (vVEL) at initial ground contact (IC) have been associated with increased KAM in females across different sidestep cuts [3]. While real-time biofeedback training has been proven effective for gait retraining [4], the highly dynamic, non-cyclical nature of cutting maneuvers makes real-time feedback unsuitable and alternative approaches necessary. This study aimed at assessing the efficacy of immediate software-aided feedback on cutting technique in reducing KAM during handball-specific cutting maneuvers.

METHODS

Full-body kinematics (23 Qualisys cameras, 200 Hz) and ground reaction forces (two AMTI force platforms, 1000 Hz) of 50 female handball players (16.7 ± 0.9 years, 1.73 ± 0.07 m, 69.5 ± 9.9 kg) were captured during handball-specific sidestep cuts [5]. Players performed three baseline (PRE) cuts on each leg while peak KAM during early stance and technique variables at IC (FSA, VAL, and vVEL) were calculated immediately (< 3 seconds) upon completion using a custom-made MATLAB (The MathWorks, Inc., USA) application. Following PRE cuts, players received visual and verbal leg-specific feedback on KAM and technique. Critical thresholds for KAM and technique variable magnitudes were defined based on an existing dataset [3] and used for the systematic and organized feedback (Figure 1). Visual feedback was provided on a screen by means of bar graphs indicating KAM and technique variable magnitudes for each cut and a stick figure representing the posture at IC. Following each round of feedback, three more cuts on each leg were performed that were all preceded by combined internal and external cues to facilitate the desired changes in biomechanics. Data were checked for normality, and paired-samples *t*-tests (α = .05) were applied to compare PRE and POST KAM and technique independent of the degree to which the athletes adhered to the feedback. Effect sizes for normally and non-normally distributed data were calculated using Cohen's *d* and matched rank biserial correlation (r_{rb}), respectively.

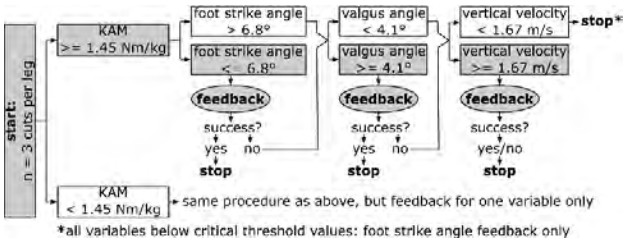

Figure 1 Procedure defining critical thresholds and feedback selection. Feedback was deemed successful if the mean post-feedback external knee abduction moment (KAM) of the three subsequent cuts fell below the predefined threshold of 1.45 Nm/kg.

RESULTS AND DISCUSSION

KAM significantly decreased after feedback (Table 1) aiming at adopting a forefoot strike (-14%, r_{rb} = .41, p < .001) and reducing VAL (-16%, d = .61, p = .019). FSA improved and VAL decreased, on average, by 10.7° (p < .001) and 1.4° (p = .020), respectively. No significant difference in KAM (8%, d = .23, p = .279) was found after feedback aiming at reducing vVEL (-16%, p = .006), however, this feedback was given seven times only as opposed to 79 and 18 times for feedback aiming at achieving a (more pronounced) forefoot strike and a reduction in VAL, respectively (Table 1).

CONCLUSIONS

Immediate individualized feedback on cutting technique shows great potential for reducing KAM and therefore ACL injury risk. Future studies are needed to assess if technique modifications can be retained.

REFERENCES

[1] David S et al. *J Sci Med Sport* **20:**1075-1080, 2017.
[2] Hewett TE et al. *Am J Sports Med* **33:**492-501, 2005.
[3] Bill K et al. *Front Sports Act Living* **4:**983889, 2022.
[4] Richards R et al. *Arch Phys Med Rehabil* **98:** 137-150, 2016.
[5] Kristianslund E et al. *Br J Sports Med* **48:**779-783, 2014.

Table 1: Results for each feedback given. Numbers in parentheses indicate the number of legs.

Feedback aimed at	KAM PRE [Nm/kg]	KAM POST [Nm/kg]	Effect size	*p*-value
Forefoot strike (n = 79)*	1.17 ± 0.51	1.01 ± 0.44	r_{rb} = .41	p < .001
Valgus reduction (n = 18)	1.58 ± 0.60	1.32 ± 0.45	d = .61	p = .019
Vertical velocity reduction (n = 7)	1.12 ± 0.56	1.03 ± 0.46	d = .23	p = .279

*denotes non-normal distribution

CORTICOKINEMATIC COHERECE: A PROPRIOCEPTIVE BIOMARKER FOR MOTOR PERFORMANCE

Scott Mongold[1], Christian Georgiev[1], Thomas Legrand[1] and Mathieu Bourguignon[1]
[1]Laboratory of Neurophysiology and Movement Biomechanics, Université libre de Bruxelles, Brussels, Belgium.
Email: scott.mongold@ulb.be

INTRODUCTION

Voluntary movement is made possible by a complex neural network spanning the brain, spinal cord, and muscles. Information propagates bidirectionally, as motor commands to the periphery, and as sensory information to the spinal cord and brain. Crucially, much of our understanding of motor performance and the coordination of muscles stems from the former. However, when the processing of proprioception is disrupted, efficient voluntary movement is compromised [1]. Corticokinematic coherence (CKC) is the coupling between brain and movement kinematics that occurs during repetitive movement and is thought to assess the cortical processing of somatosensory afferences [2,3]. Therefore, CKC could complement current assessments of physical performance by highlighting how the brain tracks sensory information. In light of this, we aim to explore whether CKC predicts motor performance.

METHODS

Thirty-seven healthy young adults (21 females) participated in the study. They were fit with an EEG cap (64 electrodes, ANT Neuro) and with EMG electrodes on first dorsal interosseous, biceps brachii, and anterior deltoid (Figure 1). Brain and muscle activity were recorded during 3 trials of the Box and Blocks test (BBT) (Figure 1A). Without brain/muscle recording, participants completed 5 trials of one subtest of the Purdue Pegboard Test (PPT), in which only the right hand was used. CKC was estimated as the coherence between EEG and rectified EMG amplitude. Cross-correlation and mutual information analyses, together with auto-correlation analysis were incorporated to assess coordination and regularity.

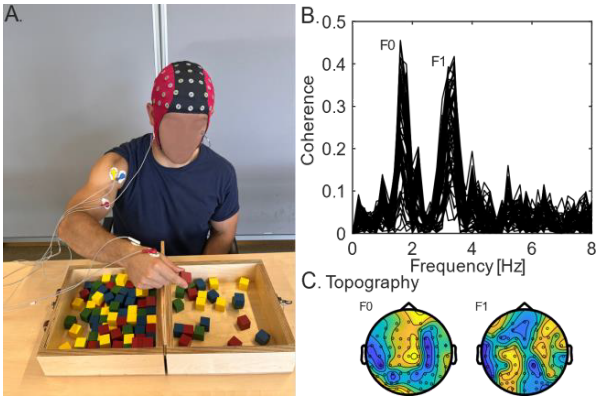

Figure 1. BBT recording set-up (A), and representative Coherence (B) and Topography (C) plots.

RESULTS AND DISCUSSION

In line with previous studies, CKC peaked at movement frequency (F0) and its first harmonic (F1; Figure 1B) with a topography compatible with a sensorimotor cortical origin (Figure 1C) [2,3], confirming that this method can be used in a more dynamic task, as compared to traditional finger tapping [4]. CKC at F1 (but not F0) correlated significantly with BBT scores and PPT scores (BBT, $r = 0.44$; $p = 0.005$; PPT, $r = 0.37$; $p = 0.022$), indicating a behavioral advantage of enhanced CKC, compatible with more effective proprioceptive processing. In addition, CKC at F1 showed no relationship with measures of coordination or regularity ($p > 0.05$). This lack of relationship suggests that CKC indeed captures meaningful information unique to cortical processing. Finally, BBT scores were not correlated with the measures of coordination and regularity ($p > 0.05$). There could be two main—and non-exclusive—reasons for this absence of relationship. First, it could be that regularity and coordination are not adequately captured by muscle activation pattern analyses only. Second, in a task where joint trajectories vary, other aspects of motor control such as flexibility and visuo-motor integration, are more important than coordination and regularity.

CONCLUSIONS

BBT and PPT scores are associated with the cortical processing of kinematic activity, in the form of CKC, indicating that efficient proprioceptive processing may be a functionally relevant contributor to motor performance. Future work should continue to develop CKC as a neuroimaging and biomechanical method to be used as a diagnostic, during clinical follow-ups, or in the sport setting, where risk and talent identification is increasingly quantified.

ACKNOWLEDGEMENTS

SM is supported by an Aspirant research fellowship awarded by the F.R.S.-FNRS (Belgium). SM, TL, and MB were supported by the F.R.S.-FNRS (Belgium; grant MIS F.4504.21).

REFERENCES

[1] Tuthill & Azim. *Current Biology* **28(5)**: 194-203, 2018.
[2] Bourguignon et al. *NeuroImage* **106**: 382-390, 2015.
[3] Piitulainen et al. *Frontiers in aging neuroscience* **10**: 147, 2018.
[4] Marty et al. *NeuroImage* **119**: 221-228, 2015.

EVALUATING THE MUSCULOSKELETAL IMPACT OF LOCAL MUSCLE VIBRATION

A Lowry[1], T Besier[1,2], M Alipour[1], A McMorland[1,3] and J Fernandez [1,2]
[1] Auckland Bioengineering Institute, University of Auckland, New Zealand
[2] Department of Engineering Science, University of Auckland, New Zealand
[3] Faculty of Science, Exercise Sciences, University of Auckland, New Zealand
Email: alow056@aucklanduni.ac.nz

INTRODUCTION

Spasticity and hypertonia are common symptoms of stroke and cerebral palsy. Literature has suggested that a hyperactive stretch reflex may bear some responsibility. Additionally, literature has suggested that spasticity and hypertonia can be ameliorated through the application of vibrations [1]. As such, the purpose of this pilot study was to investigate what effects local vibration therapy has on stretch reflex modulation. Effects were measured using the H-reflex, a technique which uses the same neural pathway as the stretch reflex [2], but is externally triggered electrically rather than through muscle spindles [3].

METHODS

Ethical approval was received from the New Zealand Health and Disability Ethics Committee. H-reflex was performed on five healthy typically developed adults. Subjects were tested while being seated on a chair, with knee joint angle of 120°, while remaining still with muscles relaxed throughout the experimentation.

The H-reflex setup and recruitment curve protocols were based on that found in the literature [4]. The following experiments were performed with stimulation levels of $H_{50\%}$ determined by the participants recruitment curve.

1. H-reflex during and post 1s of vibration applied to the lateral gastrocnemius and tendon.
2. H-reflex post 1min of continuous vibration to the lateral gastrocnemius and tendon.
3. H-reflex during 1s of vibration to the muscle belly, tendon, and proximal region of the rectus femoris, both ipsi- and contra-lateral.

Five H-reflex baseline and intervention trials were performed for each experiment. Data comparisons followed a within-subjects design.

RESULTS AND DISCUSSION

Subplot A in Figure 1 illustrates the impact 1s vibration has on the H-reflex. As can be seen, the H-reflex was reduced by ~80% during vibration applied to the lateral gastrocnemius muscle belly and tendon. Post 1s vibration, this dampening effect was reduced to ~30%. Effects were greater on the tendon.

Subplot B shows the response in the H-reflex following 1min of vibration applied to the muscle belly and tendon. As can be seen, the tendon appears to have a greater dampening effect on the H-reflex than the belly.

Subplot C illustrates the effect that vibration location has on the dampening effect of the H-reflex. Vibrations applied to the muscle belly and tendon resulted in the greatest dampening, approximately 80% and 75% respectively. The thigh has a smaller effect, this effect was greater with a higher frequency. Vibrations applied to the opposite thigh had the least effect, causing an H-reflex reduction of <%10.

Comparing subplots, the data indicates that the dampening effect persisted longer after 1min of vibration compared to 1s.

According to these findings, vibration has a dampening effect on the H-reflex, with this effect being heightened on the tendon. It can also be said that the effects of vibration persist beyond the time of vibration, albeit attenuating rapidly. Increasing the frequency also appears to prolong the attenuation, however, this can be lost depending on the distance from the target muscle.

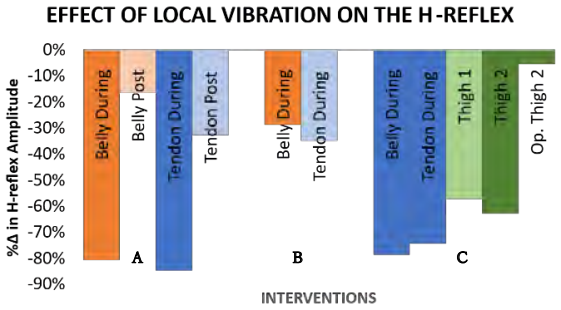

Figure 1 A: H-reflex during and post 1s vibration to muscle belly and tendon. B: H-reflex after 1min of vibration applied to the muscle belly and tendon. C: Influence of vibration location on H-reflex. Captured during 1s vibration

CONCLUSIONS

This study has found that local vibration does indeed have an impact on the H-reflex. Additionally, it has been confirmed that vibration location and duration influence the effect vibrations has on the H-reflex. Greatest effects were achieved by vibrating the muscle tendon.

ACKNOWLEDGEMENTS

The authors acknowledge support from the University of Auckland, and funding from the Auckland Bioengineering Institute, New Zealand.

REFERENCES

[1] R. Ritzmann et al. *Neuropsychiatr. Dis. Treat*, vol. 8, no. 14, pp. 1607-1625 2018
[2] S. Grosprêtre et al., J. *Neurophysiol.*, vol. 107, no. 6, pp. 1649–1654, 2012
[3] J. E. Misiaszek. *Muscle Nerve*, vol. 28, no. 2, pp. 144–160, 2003
[4] Q. Song et al., *Front. Aging Neurosci.*, vol. 14, no. March, pp. 1–10, 2022

COMPENSATORY COVARIATION OF BALL LAUNCH VARIABLES IN TENNIS STROKES

Yusuke Sudo[1,2], Yuta Kawamoto[2], Yoichi Iino[2] and Shinsuke Yoshioka[2]
[1] Department of Human and Engineered Environmental Studies, The University of Tokyo, Kashiwa City, Japan.
[2] Department of Life Sciences, The University of Tokyo, Meguro-Ku, Japan.
Email: sudo-yusuke@g.ecc.u-tokyo.ac.jp

INTRODUCTION

Accurate groundstrokes are crucial in tennis. To maintain the accuracy of the shots, there are two ways regarding the ball motion. One is to reduce the variability of the ball launch variables (initial position, velocity, and angular velocity), and the other is to use compensatory covariation of the variables. The compensatory covariation works to maintain the ball landing position regardless of the amount of variance in the launch variables. For example, an increase in launch angle with an increase in angular speed is considered compensatory covariation if the increase in ball flight distance due to the increase in launch angle is reduced by the increase in angular speed. In other words, the compensatory covariation stabilizes the results. In all ball launch variables, ball speed (BS), launch angle (LA), and angular speed (AS) have a considerable effect on the ball landing position, and these variables are determined by the racket motion. Therefore, this study investigates the compensatory covariation among these ball launch variables and their relationship to the racket motion in the tennis groundstrokes of skilled players.

METHODS

Nine collegiate tennis players (age: 19.9 ± 1.2 years, playing experience: 9.1 ± 3.2 years) participated in the experiment. They hit 43 forehand groundstrokes as accurately as possible towards the target on the opposite side of the court. Racket and ball movements were recorded using an optical motion capture system. Ball landing positions were calculated by integrating the equation of motion of a flying ball, taking into account drag and lift forces. The effect of covariation between specific launch variables can be evaluated by comparing hypothetical data sets in which covariation is broken with those in which it is maintained [1,2], as follows. One hypothetical data set was created from the original data set by shuffling all launch variables so that all shuffled variables have no covariation with the other variables (S_All). The other hypothetical data sets were created by shuffling all launch variables except two or three selected variables so that the selected variables retained covariation (S_Selected). The standard deviations of the ball landing position in the hitting direction were calculated from S_All (SD_{ALL}) and S_Selected ($SD_{Selected}$). The Covariation Index (CI) was defined as

$$CI = SD_{Selected}/SD_{ALL},$$

to evaluate the effect of covariation between/among the selected variables. CI statistically less than one indicates the existence of compensatory covariation due to the improvement of the stability of the ball landing position, while CI statistically greater than one indicates the existence of unfavorable covariation due to the deterioration of the stability of the ball landing position. The correlations between the racket swing kinematics just before the ball impact were also calculated to evaluate the effect of the swing motion on the covariation between the ball variables.

RESULTS AND DISCUSSION

The compensatory covariation existed between BS and LA but the compensatory covariation was not observed among BS, LA, and AS (Figure 1). This means that AS breaks the compensatory covariation between BS and LA. This break could be explained by the positive correlation (r = .43) between vertical swing angle and racket face angle (both upward positive). LA increases as the swing angle increases and AS decreases as the racket face angle increases. Both the increase in LA and the decrease in AS could lengthen the ball flight distance, therefore the positive correlation between the vertical swing angle and the racket face angle could break the compensation. The reason for this correlation would reflect the characteristics of the swing motion. Players could not freely adjust the direction of the racket face because they usually immobilize their arms near impact by co-contracting upper extremity muscles [3], which may be due to preparation for impact. When the wrist and elbow are immobilized, the change in shoulder angle affects both the direction of the swing and the face angle. Therefore, the face angle tends to deviate for the same direction for the swing angle.

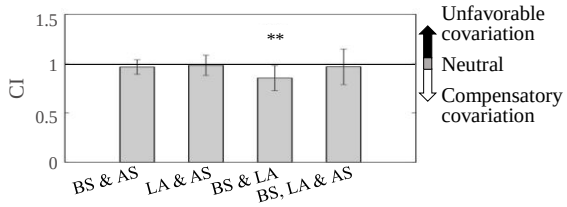

Figure 1 Covariation Index (CI) for all combinations of ball speed (BS), lunch angle (LA), and angular speed (AS). CI less than one indicates compensatory covariation. (**: $p < .01$)

CONCLUSIONS

In the tennis strokes of skilled players, although the ball speed and the launch angle showed compensatory covariation, the ball angular speed broke this compensation. This was due to the correlation between the vertical swing angle and the racket face angle. This correlation could be due to the immobilization of the arm just before impact.

REFERENCES

[1] Kudo K et al. *J Mot Behav* **32**: 337-345, 2000.
[2] Müller H et al. *Biol Cybern* **89**: 22-33, 2003.
[3] Sakurai S et al. *J Sports Sci* **18**: 901-914, 2000.

INVESTIGATION OF SENSOR-EMBEDDED KEY TO QUANTIFY DYNAMIC PINCH FORCE DURING KEY TURNING IN YOUNG VS OLDER HEALTHY ADULTS

Li Jing Soh, Jun Liang Lau, Lek Syn Lim, Eloise Lie and Phyllis Liang
Rehabilitation Research Institute of Singapore, Singapore.
Email: junliang.lau@ntu.edu.sg

INTRODUCTION

In rehabilitation, clinical assessments such as Wolf Motor Function Test (WMFT) that tracks motor recovery is essential. Sensor-based measurement can provide more quantifiable assessment in a precise, dynamic and unobstructed manner. Currently, it is known that load cell sensors can measure dynamic pinch force [1]. However, little is known about the dynamic pinch force of healthy adults. In addition, the influence of essential factors, such as key dimension, age and gender, should be carefully considered to allow systematic comparison across groups [2]. Hence, this study sought to provide a standardized instrumented key for systematic dynamic pinch force collection and present the preliminary data of young and older healthy adults.

METHODS

The data were collected from two groups of 10 healthy right-handed subjects from age-group 21-30 (M = 23.8, SD = 3.2, five females and five males) and 61-70 (M = 66.5, SD = 4.5, seven females and three males) to reflect the difference in dynamic pinch force produced between thumb and index finger among the groups. The key module was modified with a miniature load cell placed between a gap of 6.3mm to collect the dynamic pinch force and key turning angle (Fig. 1a). Participants were asked to grasp the sensor-embedded key and turn the key 180° clockwise and then counter-clockwise in a single action six times at the fastest speed. As a result, the right hand begins pronated to supinated, then back to pronated; the left-hand starts in the opposite order. For more information on the motion tasks and key module, kindly refer to the previous paper [3].

RESULTS AND DISCUSSION

The signals were sampled at 200Hz and post-processed with a 6 Hz low-pass filter (second order Butterworth) using R statistical language. During the execution motion of the key turning, the force profile displays a regular bimodal pattern and can be segmented into three phases based on turning angle (Fig. 1b). The force tends to peak at the end of the first and second phases, then drops to zero during the third phase. The older group exerts significantly higher force than the young group for both hands, with $p=0.0353$ for the right hand and $p=0.0224$ for the left hand *(p-value ≤ 0.05)* using t-test statistical method (Fig. 2). In addition, the older group displays significantly higher variance in force than young group for both hands with $p=0.0038$ for the right hand and $p=0.0021\ x10^{-3}$ for the left hand *(p-value ≤ 0.05)* using F-test statistical method (Fig. 2).

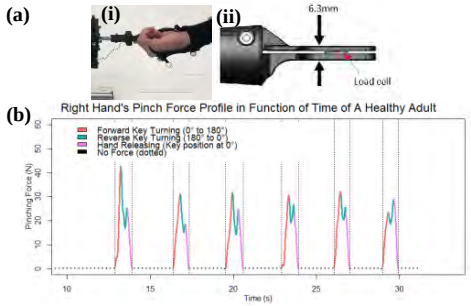

Figure 1 (a) (i) Actual instrumented key with embedded sensor, **(ii)** CAD model with the key module, **(b)** Right hand's dynamic pinch force profile of a representative participant across six repetitions of a key turning. Windows enclosed by every two vertical dotted lines represent one full cycle of the key turning movement.

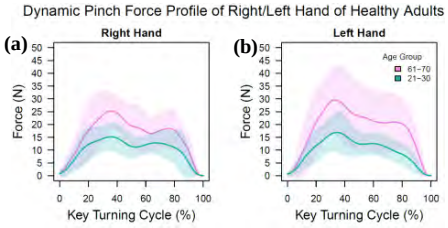

Figure 2 Mean force with the filled area of ± 1 standard deviation of the dynamic pinch force while turning the key.

CONCLUSIONS

This work demonstrated the valuable potential of a sensor-embedded instrumented key which draws preliminary insight that there is a difference in healthy dynamic pinch force profile, displayed in the manner of force modulated during different phases of the key turning motion in young and older age groups. Future work may consider testing on more subjects and exploring its motor recovery's tracking application.

ACKNOWLEDGEMENTS

The authors would like to thank the sponsorship of Nanyang Technological University (NTU), Agency for Science, Technology and Research (A*STAR) and National Healthcare Group (NHG).

REFERENCES

[1] Alberts, Jay L et al. *Neurorehabilitation and Neural Repair* **18.4**: 250-258, 2004.
[2] Smaby, Niels et al. *Journal of Rehabilitation Research & Development* **41.2**: 215-224, 2004.
[3] Liang, Phyllis et al. *Scientific Data* **7.1**: 290, 2020.

Calibrated muscle-synergies method for missing muscle excitations prediction during walking

Marco Romanato[1], Fabiola Spolaor[1], Zimi Sawacha[1,2]
[1] Department of Information Engineering, University of Padova, Padova, Italy.
[2] Department of Medicine, University of Padova, Padova, Italy.
Email: marco.romanato@unipd.it

INTRODUCTION

Despite the effectiveness of surface electromyography (sEMG)-driven models in personalized rehabilitation protocols, their use in out-of-the lab conditions is hampered due to the high number of required sEMG signals [1]. Muscle synergy analysis has been proposed in many fashions to predict unmeasured muscles excitations from the measured signals [2]. However, as best of authors knowledge, the reliability of a calibrated muscle-synergies approach to predict unmeasured muscles excitations, considering few sEMG recordings as muscle primitives, has not been previously investigated.

METHODS

The sEMG data of 4 healthy individuals (age = 60.0±2.1 years, BMI = 26.7±4.1 kg/m^2) have been recorded during walking. The electrical activity of the gluteus medius and maximus, adductor longus, tensor fasciae latae, sartorius, bicep femoris, semitendinosus, rectus femoris, vastus medialis and lateralis, gastrocnemius lateralis and medialis, soleus, peroneus longus and tibialis anterior was collected. Fifteen trials for each subject were divided into a calibration set (10 trials) and a test set (5 trials) after being filtered with standard procedures and normalised to the maximum value over all the trials [3]. Firstly, the calibration set trial was used to extract the 4-dimensional muscle synergies primitives ($W_{4,C}$) and weights matrix ($H_{4,C}$) through non-negative matrix factorization methods. The root mean squared difference (RMSD) between the experimental excitations and W_{4C} was used as metric to determine which subset of 4 sEMG better resembled $W_{4,C}$ ($\hat{W}_4$), while a scale factor was defined as S_f = mean($W_{4,C}$)/$\hat{W}_4$. The average of each H_{4C} of each calibration trial was considered as subject-specific weights matrix ($\hat{H}_4$). Then, per each test set trial, the same muscles defined in $\hat{W}_4$ were selected as "measured" sEMG signals ($\hat{W}_{4,T}$) while the others were treated as "unmeasured". $\hat{W}_{4,T}$ was then multiplied by C and $\hat{H}_4$ to reconstruct the complete set of muscle excitations ($\hat{W}_{4,T}$*C*$\hat{H}_4$). The actual trial-specific primitives ($W_{4,T}$) and vector of weights ($H_{4,T}$) have been extracted and used to predict the muscle excitations ($W_{4,T}$*$H_{4,T}$) with the one obtained with the proposed method. The RMSD, the coefficient of determination (r^2) and the variance accounted for (VAF) were used as metrics to compare the performance against the experimental excitations.

RESULTS AND DISCUSSION

In Figure 1 the considered experimental muscle excitations of a representative subject against the predicted ones are reported as example. Low values of RMSD and concomitantly high values of both r^2 and VAF are reported in Table 1 for both methods, suggesting an accurate prediction of the experimental measures.

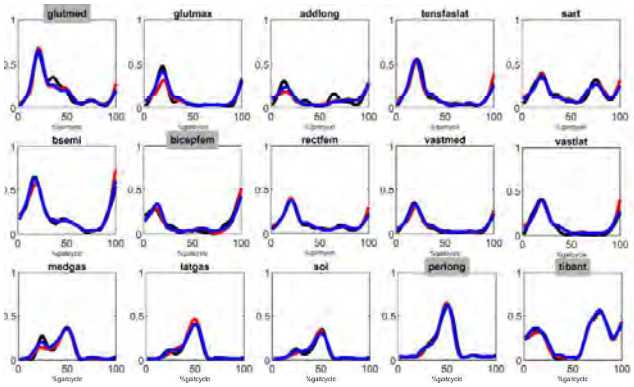

Figure 1 Considered muscle excitations of a representative subject (average of 5 test trials). In black the experimentally recorded excitations, in blue the excitations reconstructed via muscle synergy analysis (4 primitives), in red the excitations reconstructed via the proposed method (4 muscles excitations as primitives, chosen muscles are highlighted in grey).

CONCLUSIONS

The reliability of the proposed method to track "unmeasured" excitations was assessed. This could be pivotal in the creation of reliable sEMG-driven models considering a minimal experimental setup transferable in out-of-the-lab conditions (*i.e.,* home-based therapy, rehabilitation centres, gyms) where there is the need to cope with a reduced number of sensors while maintaining a reliable characterization of the research subject's neuromuscular status.

REFERENCES

[1] Kainz H et al. *Clin Biomech* **87**: 105402, 2021.
[2] Ao D et al. *Fncom* **14**: 588943, 2020.
[3] Mantoan A et al. *Source Cod Biol Med* **10**: 12, 2015.

Table 1: RMSD, r^2 and VAF as total of each considered muscle for the two different methods to reconstruct the experimental excitations.

Reconstruction method	**RMSD**	*p-value*	**r^2**	*p-value*	**VAF**	*p-value*
Actual synergies	0.037 ± 0.018	< 0.001	0.93 ± 0.07	< 0.001	0.996 ± 0.003	< 0.001
Proposed	0.063 ± 0.035		0.84 ± 0.14		0.978 ± 0.008	

IMPACT OF A HIGH-FAT HIGH-SUCROSE DIET ON JOINT AND MUSCLE INTEGRITY IN JUVENILE SPRAGUE DAWLEY RATS

Mauricio Delgado[1,2,3], Nada Abughazaleh[1,2], Ruth Seerattan[1], Raylene Reimer[1,2,4], David Hart[1,2] and Walter Herzog[1,2]

[1]Human Performance Laboratory, University of Calgary, AB, Calgary, Canada.
[2]McCaig Institute for Bone and Joint Health, University of Calgary, AB, Calgary, Canada.
[3]Departamento Ciencias de la Salud, Pontificia Universidad Católica de Chile, Santiago, Chile.
[4]Department of Biochemistry and Molecular Biology, University of Calgary, AB, Canada.
Email: mauricio.delgado@ucalgary.ca

INTRODUCTION

It has been reported that obesity and its comorbidities result in decreased mobility, leading to a sedentary lifestyle and musculoskeletal degeneration [1]. Previous studies have reported on the effects of consuming a high-fat/high-sucrose diet (HFS) on joint and muscle integrity in adult rats [2,3]. However, the effects of a HFS diet on Juvenile rats have not yet been explored. In view of the ever increasing obesity pandemic in children, it is important to understand the potential differential effects of HFS diets on adult and juvenile subjects. The aim of this study was to investigate the effects of consuming a HFS diet, for 14 weeks from weaning (3 weeks), on knee joint degeneration, and fat and collagen content in muscles of male Sprague Dawley rats.

METHODS

To assess joint degeneration twenty-nine male Sprague-Dawley rats were randomly assigned to either a high-fat/high-sucrose (HFS) diet (n = 15) or a standard chow control diet (CHOW; n = 14). Medial gastrocnemius (MG) muscles were collected from HFS group (n=10) and from the Chow group (n=8). Rats consumed the allocated diet for 14-weeks, starting immediately post-weaning at (3-weeks of age). At the end of the 14-week intervention period, body mass and body composition were analyzed using dual x-ray absorptiometry (DXA). Knee joints were harvested, processed in paraffin and sectioned at 10 µm. Two independent, blinded assessors scored the histological sections using a Modified Mankin scale. MG muscle was analyzed for fat and collagen content. Collagen content was determined using Picrosirius red staining and quantified as a percent of area fraction. Fat content was determined using an assay for triglycerides.

RESULTS

Rats consuming the HFS diet had a significantly greater body mass and percentage body fat ($p<0.001$, $p<0.001$, respectively, compared to rats in the Chow group. Rats in the HFS group had a significant increase in joint degeneration (Figure 1). MG muscle had a significant increase in collagen content compared to chow group rats ($p=0.002$). MG lipid content was similar between groups.

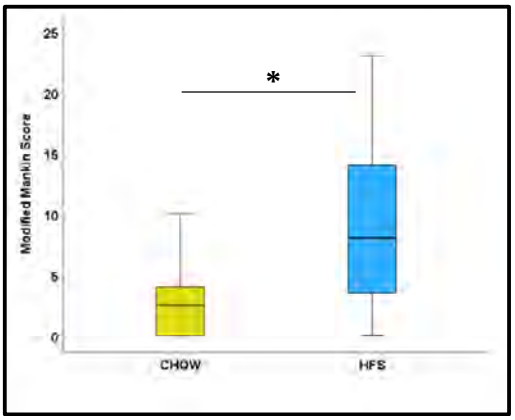

Figure 1: Modified Mankin Score of Knee Joint. (*) $p < 0.05$ (The total possible score for each joint is 68). Note, higher scores are associated with greater knee joint degeneration.

DISCUSSION

The increase in body mass and percent body fat in HFS group rats compared to control may indicate onset of metabolic syndrome that is associated with systemic inflammation [4], which may cause the observed structural changes in the knee and MG. It has been shown that feeding adult rats a HFS diet for 12 weeks caused a significant increase in fat infiltration in muscles [2]. The similarity in MG lipid content in the juvenile control and HFS group rats may indicate that the juvenile rats were better able to cope with the increase in fat in the HFS diet, thus preventing ectopic lipid storage in MG muscle.

CONCLUSIONS

A 14-week HFS diet intervention caused knee joint degeneration and increased muscle fibrosis in juvenile rats.

ACKNOWLEDGEMENTS

The Canadian Institutes of Health Research, The Canada Research Chair Programme, the Nigg Chair for Biomechanics, and the Killam Foundation.

REFERENCES

[1] Houmard et al., 2011. *J Obes.* 2011:250496.
[2] Collins et al., 2015. *Osteoarthr. Cartil.* **23**:957-965.
[3] Collins et al., 2016. *J. Orthop. Res.* **34,** 12:2069-2078.
[4] Collins et al., 2018. *Front. Physiol.* **9**:112.

SUBSTANTIAL REDUCTIONS IN ADULT PHYSICAL ACTIVITY FOLLOW AN EXERCISE-RESTRICTED GROWTH PERIOD IN GUINEA FOWL

Jurestovsky, DJ, Cox, SM, Salzano, MQ, Piazza, SJ, and Rubenson, J
Dept. of Kinesiology, The Pennsylvania State University, University Park, PA, USA.
Email: derek.jurestovsky@psu.edu

INTRODUCTION

Humans have become more sedentary in recent decades. One third of the global population fail to meet minimum exercise recommendations, and this figure rises to a staggering 81% for young people [1]. This decrease in activity has been linked to an increase in morbidity and mortality [2]. The determinants of adult inactivity, however, are poorly understood. While growth period behaviors have the potential to influence adult activity through psychological and physiological mechanisms, longitudinal studies linking growth-period conditions to adult activity levels are lacking. Here, we use an animal model amenable to controlled growth studies, guinea fowl, to test the hypothesis that inactivity during growth reduces adult activity levels. Birds were either permitted to exercise or had their activity limited both by restricting their access to movement and by the application of botulinum toxin type A (BTX-A) to temporarily limit leg muscle function [3,4].

METHODS

We obtained 13 one-day old guinea fowl keets from a regional breeder. At two weeks of age, animals were divided into two groups: an exercise control group (CON, n=7) and a BTX-A and restricted group (RES, n=6). Animals were pen-raised with food and water *ad libitum*. During growth (0-26 wks) CON birds were housed together in a large pen (3.14 m^2) with access to perch jumps and running, whereas RES birds were housed together in a smaller pen (1 m^2) with limited movement. BTX-A was injected into the gastrocnemius muscles at 7-8 wks of age and repeated at every 5 wks, with a total of four injections. After the injection period, when animals reached skeletal maturity (6 mo) all animals from both groups were housed individually in moderately-sized pens (1.49 m^2) with perches 35 cm above the floor. The birds were recorded with overhead cameras at regular intervals up to one year of age. These videos were then analysed to count the number of jumps to perch per minute (jumps/min) sampled randomly and clustered around 6 mo and 12 mo time points.

RESULTS AND DISCUSSION

The CON birds jumped to perch with greater frequency than the RES birds at both time points (Fig. 1). At 6 mo, CON birds jumped at a rate of 0.07±0.09 jumps/min, but not a single jump was recorded for RES birds ($p = 0.041$). The jump frequency for both groups increased at 12 mo, but was significantly higher for CON than for RES (0.16±0.11 versus 0.03±0.06 jumps/min; $p = 0.011$). There were no significant differences in jump frequency between the 6 mo and 12 mo time points within CON ($p = 0.056$) or RES ($p = 0.136$) groups.

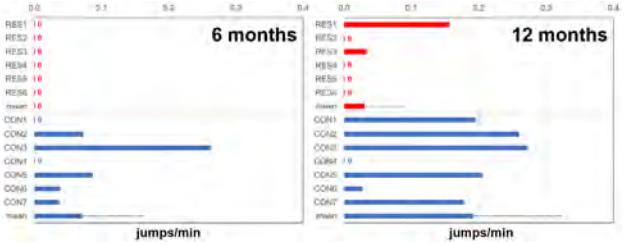

Figure 1. Jump frequency for exercise-restricted (RES) and control (CON) birds at 6 and 12 months with group means and standard deviations at each time point.

CONCLUSIONS

We found a significant reduction in voluntary adult exercise for birds whose growth-period exercise was limited by the dimensions of their living space and through pharmacological intervention. Later as adults, despite equal access to physical activity and the acute effects of BTX-A having been eliminated, the RES group showed a marked reduction in physical activity compared to the CON group. These differences were surprising given that jumping capacity (assessed by mechanical work), albeit lowered, is still substantial following growth-period disuse [5] and BTX-A treatment [Rubenson, unpublished data]. These results suggest that physical activity level during growth may influence adult physical activity levels. However, the present study cannot resolve the underlying mechanism of the activity reduction. It is possible that the RES birds failed to develop habitual jumping behaviours during the growth period. It may also be that RES birds adapted morphologically and physiologically to their growth period inactivity in ways that made jumping more effortful as adults.

ACKNOWLEDGMENTS

We would like to thank Justin Csaszar and the Animal Care Staff at the Centralized Biological Laboratory (PSU). Supported by NIH Grants R21AR071588 and R01AR080711.

REFERENCES

[1] Ozemek C et al. *PubMed* **62(2)**: 102-7, 2019.
[2] Penedo FJ et al. *PubMed* **18(2)**: 189-93, 2005.
[3] Longino D et al. *J.Ortho.Res.* **23**: 1411-8, 2005.
[4] Katugam K et al. *Fr. Bioe. Biot.* **8**: 1-15, 2020.
[5] Cox S et al. *J. Appl. Physiol.* **128(1)**: 50-8, 2020.

ISB·JSB FUKUOKA 2023

CONTINUUM MECHANICAL APPROACH TO RIGID BODY MECHANICS IN BIOMECHANICS

Salvatore Federico
Department of Mechanical and Manufacturing Engineering, The University of Calgary, Canada
Email: salvatore.federico@ucalgary.ca

INTRODUCTION

Since at least the works of the late Prof. Y.C. Fung, the tools of Continuum Mechanics proved to be fundamental in the biomechanics of tissues. However, also the biomechanics of motion, which is based on rigid body mechanics, can benefit from these same tools. Traditionally, rigid body mechanics has been considered as an independent branch of Mechanics. In a more modern approach, it can be considered as a particular case of Continuum Mechanics: a rigid body is represented by a continuum body subjected to the *kinematical constraint* of *rigid motion*. From a didactical perspective, this approach has the advantage of a unified mathematical framework [1]. The purpose of this work is to highlight some of the advantages that this more general presentation of rigid body mechanics can bring to biomechanics education.

METHODS

The *motion* of a continuum body is a time-dependent map

$$\phi(\cdot,t) : \mathcal{B} \to \mathcal{S} : X \mapsto x = \phi(X,t), \tag{1}$$

mapping, at every time t, *material* points X in the body $\mathcal{B}$ into *spatial* points x in the physical space $\mathcal{S}$ [2]. The motion ϕ is *rigid* if the distance between any two points X and X_P is invariant throughout, which implies

$$x = \phi(X,t) = x_P(t) + \boldsymbol{R}(t)\,\boldsymbol{\Xi}(X), \tag{2}$$

where (see Fig. 1) $x = \phi(X,t)$ and $x_P(t) = \phi(X_P,t)$ are the current positions of X and X_P, $\boldsymbol{\Xi}(X)$ is the material local position vector, $\boldsymbol{\xi}(x,t)$ is the spatial local position vector, and $\boldsymbol{R}(t)$ is an *orthogonal tensor*, which preserves distances and angles. The velocity field of the rigid body $\mathcal{B}$ is obtained by differentiating (2) with respect to time and by eliminating $\boldsymbol{\Xi}(X)$ by inverting (2), as

$$\boldsymbol{v}(x,t) = \boldsymbol{v}_P(t) + \boldsymbol{\Omega}(t)\,\boldsymbol{\xi}(x,t), \tag{3}$$

where $\boldsymbol{\Omega} = \dot{\boldsymbol{R}}\,\boldsymbol{R}^T$ is the *spin tensor* and coincides with the *velocity gradient* tensor $\boldsymbol{l} = \operatorname{grad}\boldsymbol{v}$.

RESULTS

One example of the convenience of the continuum mechanical approach is the term $\boldsymbol{\Omega}(t)\,\boldsymbol{\xi}(x,t)$ in (3). In classical rigid body mechanics, this is commonly written $\boldsymbol{\omega}(t)\times\boldsymbol{\xi}(x,t)$, in terms of the associated *angular velocity* $\boldsymbol{\omega}$. However, the spin tensor $\boldsymbol{\Omega}$ is a more fundamental object and indeed, in Biomechanics, it is the object obtained *directly* from motion analysis data.

In standard motion capture experiments, one acquires the positions of a body segment in a reference configuration (usually with the subject standing in anatomical posture) and evaluates the rotation tensor $\boldsymbol{R}(t)$ from the reference configuration to the current configuration at each time t [3]. Once $\boldsymbol{R}(t)$ is known, the spin tensor $\boldsymbol{\Omega} = \dot{\boldsymbol{R}}\,\boldsymbol{R}^T$ can be approximated by

$$\boldsymbol{\Omega}(t) \simeq \frac{\boldsymbol{R}(t+\Delta t) - \boldsymbol{R}(t)}{\Delta t}\,\boldsymbol{R}^T(t) = \frac{\boldsymbol{R}(t+\Delta t)\,\boldsymbol{R}^T(t) - \boldsymbol{i}}{\Delta t}. \tag{4}$$

where $1/\Delta t$ is the sampling rate of the motion analysis system and $\boldsymbol{i} = \boldsymbol{R}(t)\boldsymbol{R}^T(t)$ is the (spatial) identity tensor (the orthogonality of $\boldsymbol{R}$ implies $\boldsymbol{R}^T = \boldsymbol{R}^{-1}$). If needed, the angular velocity $\boldsymbol{\omega}$ can be obtained from the spin tensor $\boldsymbol{\Omega}$ as $\omega_i = \frac{1}{2}\,\epsilon_{ijk}\,\Omega_{kj}$, where ϵ_{ijk} is the Levi-Civita symbol (see, e.g., [1] for the definition).

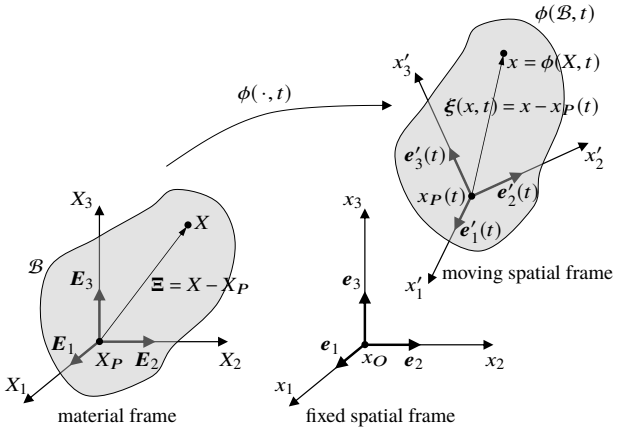

Figure 1: Continuum mechanical approach to rigid body kinematics

CONCLUSIONS

Biomechanics education can much benefit from an approach based on modern Continuum Mechanics. This work emphasised how a continuum mechanical approach to rigid body mechanics can facilitate the extraction of kinematical quantities, such as the spin tensor, from motion analysis data. Moreover, a basic education in modern Continuum Mechanics enables researchers in biomechanics of motion to more easily collaborate with researchers in biomechanics of tissues.

ACKNOWLEDGEMENTS

NSERC Discovery Grant RGPIN-2015-06027

REFERENCES

[1] Federico S, Alhasadi MF, *Theor Appl Mech* **49**: 157-181, 2022
[2] Marsden JE, Hughes TJR, *Mathematical Foundations of Elasticity*, Prentice-Hall, 1983
[3] Veldpaus FE et al., *J Biomech* **21**: 45-54, 1988

The Effects of 10 Weeks Movement Training for A Junior Student with Motor Impairment on Functional Mobility

Sheng-Yang Tso[1], Tien-Ni Wang[1], and Shu-Ting Kang[2]
[1] School of Occupational Therapy,National Taiwan University, Taipei, Taiwan.
[2] Gradate Institute of Sprots and Health, National ChangHua University of Education, ChangHua, Taiwan.
Email: d11429001@ntu.edu.tw

INTRODUCTION

Functional mobility means that a person moves independently in daily life to participate daily activities in a person's ecological environment, such as home, school, work, or community. While motor impairments affect students' daily functional activities, previous studies [1][2] reported that functional movement training is helpful for the children with motor impairments to improve their functional mobility. Thus, this study aimed to design a series of functional movement training to investigate its effectiveness on the child's functional mobility.

METHODS

This research was the A-B-M design, one of single-case study, that recruited a junior high school girl with motor impairment. The whole research was separated into three conditions. First, the baseline condition, the researcher used the measurement, the timed up and go (TUG), to evaluate the participant's functional mobility in each session until the data is stable (three consecutive points within one second). In the intervention condition, the special education teacher provided the functional movement training for the participant twice a week for ten weeks. After ten weeks, the condition entered into a maintenance condition. In the maintenance condition, the researcher only collected the score of motor abilities without providing any intervention four times a month to represent the performance of maintenance.

The functional movement training in this study aimed to improve a student's daily mobility in terms of fluent and stable gait. Two function movement activities, race walking and relay race, were provided. The TUG was used to represent a participant's functional mobility. The

In A-B-M design, the score of percentage Exceeding the Median, PEM common score was calculated to represent the effect size of the dependent variable.

$$PEM = \frac{the\ median(baseline) esceed\ the\ data\ point(intervetion)}{Total\ of\ data\ point\ in\ the\ intervention}$$

RESULTS AND DISCUSSION

Based on visual analysis, we produced the following results (figure 1). (a) In the baseline condition, the average second is 27.84, ranging from 27.1 to 29.3 seconds, and the level change is 1 second. (b) In the intervention condition, the average second is 25.7, ranging from 24.1 to 28.4 seconds, and the level change is 1.5 seconds. (c) In the maintenance condition, the average second is 25.8 seconds, ranging from 25.2 to 26.5 seconds, and the level change is 0.9 seconds. (d) Betweem baseline and intervention, we caculated immedicay of change and PEM. While the former score is 1.6 seconds, the seventh data was higher that the sitxth data. Thergfore, there are not existing the immediately result. However, as the intervention time incresased, the effect could be seen gradually in time. The later is 0.8, representing our intervention completely is high effect size. On the other hands, when the intervention withdrawed, we found the mean time in maintenance condtion was higher than time in intervention condition. It showed the effectiveness of maintenance was not good and participant couldn't effectively keep continously.

Figure 1 The result of functional mobility in three conditions.

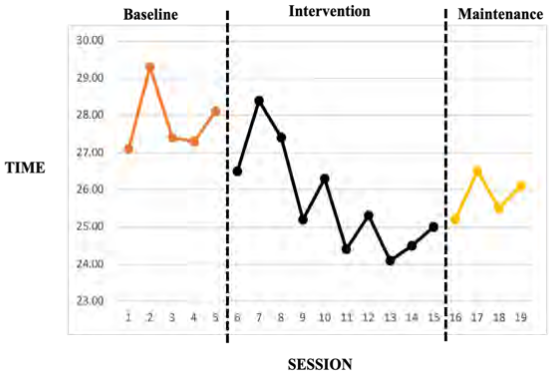

***Session 1 to 5 and 16-19, researchers collected the data directly before class**
***Session 6 to 10, researchers collected the data weekly at the end of the last class**

CONCLUSIONS

According to the result, we find that (a) it is effective that using functional movement training as intervention program to teach children with motor impairment. The result finally presents the time of functional mobility declines in the intervention condition. (b) The PEM score in our study is strong effect and can be demonstrated our outcome is significant. However, the maintenance effect can't retain continuously. Thus, we think providing functional movement interventions continuously for students with motor impairment is helpful for them to better their life equality.

REFERENCES

[1]Chang & Sher. *Special Education Quarterly* 155: 21-38, 2020.
[2]Yeh I C et al. *TheScientificWorldJournal* 686498, 2015
[3] Carey H et al. *The official publication of the Section on Pediatrics of the American Physical Therapy Association* 28: 401-408, 2016
[4] Christopher A et al. *Disability and rehabilitation* 43:1799-1813, 20

DOES A 100-DAY MENTORING PROGRAM CHANGE GIRLS' ATTITUDES & SELF-IDENTIFICATION IN SCIENCE, ENGINEERING & BIOMECHANICS?

Karen J. Mickle[1], Manuela Besomi[2], Celeste E. Coltman[3] Laura Diamond[4], Jayishni Maharaj[4], Martina Barzan[4], Michelle Hall[5], Crystal Kean[6] and Taylor Dick[2]

[1] College of Engineering, Science and Environment, University of Newcastle, Ourimbah, Australia; [2] School of Biomedical Sciences, University of Queensland, Brisbane, Australia; [3]University of Canberra Research Institute for Sport and Exercise, University of Canberra, Canberra, Australia; [4] Griffith Centre of Biomedical and Rehabilitation Engineering (GCORE), Griffith University, Australia; [5]Centre for Health Exercise and Sports Medicine, University of Melbourne, Melbourne, Australia; [6]School of Health, Medical and Applied Sciences, Central Queensland University, Mackay, Australia
Email: karen.mickle@newcastle.edu.au

INTRODUCTION

Of all STEM fields, engineering is the most underrepresented by women with enrollment statistics for engineering from Australian universities showing that engineering, has the lowest rate of female participation compared to other broad areas of study [1]. The Biomechanics Research and Innovation Challenge (BRInC) is a national program designed to engage high-school girls and early career biomechanists at two critical points when women traditionally disengage. BRInC focused on biomechanics research and/or innovation projects and includes workshops to expose high-school girls to the design thinking framework (empathy, definition, ideation, prototyping and evaluation) and entrepreneurial tools. Our aim was to evaluate the effect of BRInC on attitudes and self-identification in science, engineering, and biomechanics in Year 9-10 high-schoolgirls.

METHODS

Ninety-six Australian girls (Year 9 and 10) from 12 schools enrolled in BRInC. Over the 100-day program, girls were mentored by women early-career biomechanists and most teams met with their mentor(s) weekly to access resources and training, whereby they gained hands-on experience in biomechanics and the biomedical engineering fields.

Pre- and post-program surveys consisting of Likert scale items, assessed changes in three key areas: (i) self-identity as a scientist and engineer, (ii) attitudes toward engineering, and (iii) attitudes toward biomechanics. All survey data was collected online via Qualtrics. Data were downloaded and processed in STATA (StataCorp. 2013. Stata Statistical Software).

RESULTS AND DISCUSSION

Of 96 girls, 29 (30.2%) completed both pre- and post-surveys. We found improvements in all three areas after the girls participated in BRInC (Table 1). The mentees agreed more strongly with statements regarding whether they saw themselves as scientists and engineers, and they had significantly improved attitudes toward engineering and biomechanics specifically ($p \leq 0.01$). After the program, it was also more likely that mentees found:

- science more important, valuable, less confusing, more understandable, less boring, and less difficult and hard;
- maths more important, interesting, less dull, more valuable, less confusing, more exciting, less boring, and less difficult and less hard;
- biomechanics less dull, more valuable, less confusing, and more understandable.

CONCLUSIONS

The change towards positive attitudes could lead to more girls enrolling to study a variety of engineering or biomechanics-related disciplines, ultimately addressing the underrepresentation of women in STEM. These girls will be followed for 5 years to see if the positive shift in attitudes translates to university or career choices in the field.

ACKNOWLEDGEMENTS

This project was funded by a Women in STEM and Entrepreneurship Round 3 grant (WISEIII000051).

REFERENCES

[1] Franzway S et al. *Frontiers: A Journal of Women Studies* **30**: 89-106, 2009.

Table 1: Aggregated scores in scientist/engineer identity and attitudes toward engineering and biomechanics for pre and post BRInC program, where 1= strongly agree and 6= strongly disagree.

Scale	Example Questions	PRE	POST	*p-value*
Scientist/Engineer Identity	I see myself as a scientist	2.5 (2-3)	2.3 (1.8-2.8)	$p = 0.09$
Engineering Attitudes	Engineering is interesting	2.0 (1.7-2.3)	1.3 (1-2)	$p < 0.01$
Biomechanics Attitudes	I understand what biomechanics is	2.2 (1.8-2.8)	1.3 (1.8-2.2)	$p = 0.01$

Data presented are median scores (interquartile range). Pre-post measures were compared using Wilcoxon Signed Rank Test.

THE MECHANICAL ENERGETICS OF WALKING ON INCLINE SURFACES WITH PASSIVE ANKLE EXOSKELETON ASSISTANCE

James L. Williamson[1*], Glen A. Lichtwark[2] and Taylor J. M. Dick[1]
[1] School of Biomedical Sciences and [2] School of Human Movement & Nutrition Sciences
The University of Queensland, St Lucia, QLD, Australia
Email: james.williamson@uq.net.au

INTRODUCTION

The energetic benefits of passive ankle exoskeletons during level walking, via off-loading muscle force, are well-established [1]. For example, passive ankle exoskeletons mimic the catapult mechanism of the plantarflexors and Achilles tendon by storing and returning energy to the ankle via a spring-clutch mechanism. However, most exoskeleton studies have focused on human-device interactions during steady-state level walking. It remains unresolved how similar devices influence the biomechanics of movement under more variable gait conditions that would be expected in the real world. Investigation of the mechanics and energetics of unassisted walking on incline surfaces revealed a shift in the ankle, knee, and hip's relative contributions to positive and negative power [2]. Specifically, incline walking reduced the ankle's contribution to positive power which was offset by increased contributions from the knee and hip, compared to level walking. The aim of this study is to investigate the influence of varied levels of exoskeleton assistance on mechanical energetics of the lower limb during level and incline walking.

METHODS

Five participants (23±4 years, 64±7 kg) completed our ongoing study (with the aim to recruit 15 participants total). To familiarize the users with the device, participants walked on an instrumented treadmill (Bertec Corp., USA) at 1.25 ms^{-1} for five minutes at each exoskeleton stiffness (0, 50, 120, 220, 280 Nm rad^{-1}) on level and incline (+5°) surfaces. In a follow-up data-collection session, participants walked at 1.25 ms^{-1} with exoskeleton stiffness and grade pseudo-randomised. Device clutches and slack lengths were consistent with [1]. Exoskeleton moments were determined from dynamic spring displacements, as measured by reflective markers placed on the spring component of the device. Lower limb kinematics and kinetics were recorded using motion capture (120 Hz, Qualisys, Sweden) and force plates (1200 Hz) [3]. Biological ankle joint moments were calculated as the difference between the ankle moment, derived from inverse dynamics, and the exoskeleton moment. Time-varying joint powers were determined as the product of joint angular velocities and moments.

RESULTS AND DISCUSSION

As expected, during level walking, increases in assistance were associated with a more plantarflexed ankle, reduced biological ankle moments and ankle powers. Compared to level walking, incline walking with assistance provided more assistive torque, for all participants, due to larger spring excursions (Fig. 1A).

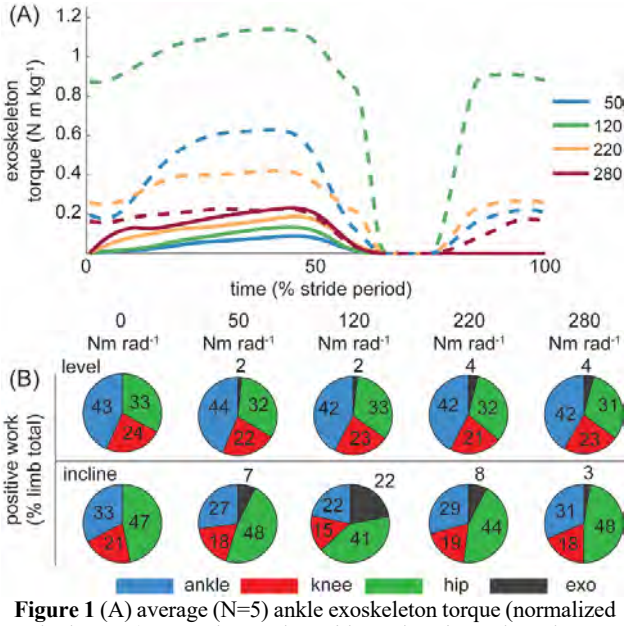

Figure 1 (A) average (N=5) ankle exoskeleton torque (normalized to body mass) exerted over the stride cycle. Line colour denotes device stiffness. Dashed lines represent the incline conditions. (B) relative contributions of the ankle, knee, and hip to positive lower limb work. Pie charts are not scaled to reflect positive work totals.

This behaviour was driven by exoskeleton clutch engagement during the swing phase of incline walking, unlike level walking. However, during incline walking, the largest peak torque did not occur at the high stiffness (280 Nm rad^{-1}) condition, as is the case during level walking, but rather at an intermediate stiffness (120 Nm rad^{-1}) (Fig. 1A). This difference appears to be driven by a reduction in ankle range of motion with increasing device stiffness. Specifically, at the 280 Nm rad^{-1} condition, ankle range of motion was reduced by 3.44°, compared to no assistance. Assisted incline walking led to a reduction in ankle net work at all stiffnesses, apart from the 280 Nm rad^{-1} condition. During incline walking, our preliminary analysis suggests that ankle exoskeletons influence the relative contribution of the knee and hip to total lower limb work (Fig. 1B). This is best evidenced by reduced knee and hip contributions to lower limb positive work at the incline 120 Nm rad^{-1} condition (Fig. 1B).

CONCLUSIONS

Our preliminary analysis suggests device operation should account for the environment (*e.g.,* slope) to best augment locomotion. Future efforts to determine whether these changes in work outputs correspond to improvements in movement economy during uphill locomotion will yield important insights.

REFERENCES

[1] Collins et al. *Nature* **522**: 212–215, 2015.
[2] Nuckols et al. *PLoS One* **15**: e0231996, 2020.
[3] Delp et al. *IEEE. Trans. Biomed. Eng.* **54**: 1940–1950, 2007.

PREDICTING INDIVIDUALIZED JOINT KINETICS OVER CONTINUOUS VARIATIONS OF WALKING AND RUNNING

Emma Reznick, Robert Gregg
Department of Robotics, University of Michigan, Ann Arbor, MI, USA
Email: reznick@umich.edu

INTRODUCTION

Gait is as individual as people, and taking this individuality into account in the design of assistive devices enables able-bodied and impaired people alike. In able-bodied individuals, the uniqueness allows powered devices to match the user's gait; tuning assistive devices for impaired populations goes further, enabling the user's ability while minimizing compensations. Kinematic individuality is well characterized and investigated, but cutting-edge assistive devices must also mimic the user's kinetic individuality. Previous studies [1] have shown that gait individuality is consistent within a type of motion, but not between ambulation modes (i.e., walking individuality is similar across inclines, but dissimilar to running). In this study, we investigate whether these kinematic trends apply to joint kinetics.

METHODS

From [2], kinetic individuality is isolated for each able-bodied participant ($n = 10$) at every task (χ): walking at different combinations of inclines ($\pm 0°$, 5°, and 10°) and speeds (0.8, 1, 1.2 m/s), and running at multiple speeds (1.8, 2, 2.2, and 2.4 m/s). The individual *kinetic* contribution (IKC) at each task is calculated by subtracting the individual's joint moments from the leave-one-out average (LOO) of the other participants. To determine how predictive one user's IKC is of their other tasks, we determine the *Modal* baselines for walking (χ_W: 1 m/s, 0°) and running (χ_R: 2 m/s, 0°). Then, we use an RMSE to quantify how well each baseline (and the LOO control) predict the experimental IKC, resulting in task-specific values for the *Walk*, and *Run*, and *LOO* methods. This protocol follows previous work for kinematics [1]. The resultant RMSEs are fed into N-way ANOVAS for each mode: considering subject, incline (walk only), velocity, joint, and method. The ANOVAS are then analyzed using post-hoc Tukey tests to determine significance.

RESULTS

For walking tasks, the Walk method was more predictive than the LOO for 76% of the all subjects, joints, showing improvements of 44%, 18%, and 31% at the ankle, knee, and hip, respectively (Figure 1, left). Similarly, the Run method gave a better estimate than LOO for 87% of running trials, improving fit by 51%, 60%, and 62% at the ankle, knee, and hip (Figure 1, right). Prediction of walking with χ_R showed significant decreases in fit for each joint, while prediction of running with χ_W showed incidental improvement.

The ANOVA for walking suggests that subject, incline, joint, and individualization method all significantly affected the results ($p \ll 0.05$), but velocity had no effect on the resulting RMSE. For the running ANOVA, all factors significantly affected the results. Post-hoc analysis shows that χ_W was a significantly better prediction of all joint IKCs than the LOO for walking, and χ_R was significantly better than the LOO for all running tasks. The inter-mode estimations showed no significant improvement for either mode.

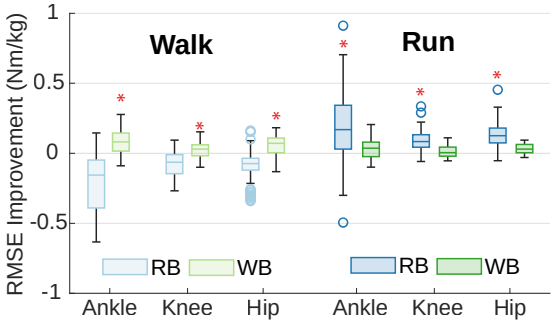

Figure 1: RMSE improvement (positive) over LOO average for walking (left) and running (right) kinetic trajectories. For each mode, we show prediction using both walking (WB) and running (RB) baselines. Red '*' indicate significant improvement.

CONCLUSIONS

Joint moments of an individual across a wide variety of speeds and inclines show significant similarity. Knowing this, we can simplify the individualization process of powered assistive devices by assuming that torque profiles are consistent across all tasks within a mode. For example, after tuning a device at level ground, walking individuality can be propagated to other speeds and inclines. Individualizing joint profiles is an important step towards biomimetic assistance from powered devices.

ACKNOWLEDGEMENTS

This work was supported by the National Institute of Child Health & Human Development of the NIH under Award Number R01HD09477.

REFERENCES

[1] Reznick E et al. *IEEE Open J. Eng. Med. Biol.* **3**: 211-7, 2022.
[2] Reznick E. et al. *Sci. Data* **8 (1)**: 1-12, 2021.

GAIT ADAPTATION ON REPEAT EXPOSURE TO A ROBOTIC HIP EXOSKELETON

Mark A. Price[1,2], Banu Abdikadirova[2], Jonaz Moreno Jaramillo[1], Meghan E. Huber[2], and Wouter Hoogkamer[1]
[1] Department of Kinesiology, University of Massachusetts, Amherst, USA.
[2] Department of Mechanical and Industrial Engineering, University of Massachusetts, Amherst, USA.
Email: mprice@umass.edu

INTRODUCTION

Robotic exoskeletons have strong potential to enable new paradigms in physio- and neurorehabilitation. Recently, we observed signatures of neural adaptation in participants wearing a portable robotic hip exoskeleton [1]. Asymmetric perturbations at the hip joints elicited adaptation and aftereffect patterns for step length asymmetry (SLA), propulsive and braking ground reaction force asymmetry (PGRFA and BGRFA, respectively), similar to typical responses to split belt treadmill walking [2]. To determine the suitability of this intervention for rehabilitation, it is necessary to evaluate the impact of repeated exposures on the user's behavior. Thus, we performed a study with two consecutive exposures to the intervention. We hypothesized that SLA, PGRFA, and BGRFA would be reduced from first to second exposure.

METHODS

We performed a gait adaptation protocol with six healthy young participants. Participants walked at 1.20 m/s on an instrumented dual-belt treadmill (Bertec Corporation) while wearing the exoskeleton for two 20-minute bouts, each consisting of a 5-minute baseline walking phase (motors off), a 10-minute perturbation phase (motors on), and a 5-minute washout phase (motors off). During the perturbation phase, the exoskeleton motors exerted repulsive and attractive torques about the left and right hip joints, respectively. Participants rested 5 minutes between bouts of walking. We recorded the 3D positions of reflective markers placed on each participant at 100Hz with an eight-camera motion capture system (Qualisys, Inc.), and calculated step length as the anteroposterior distance between heel markers at heel strike. We recorded ground reaction forces at 1000Hz with a pair of force plates located under the treadmill belts. We calculated asymmetry ratios for SL, PGRF, and BGRF for each stride as $(x_R - x_L)/(x_R + x_L) \times 100\%$, where x_R and x_L represent the dependent measure for the right and left leg, respectively. We averaged the first 10 strides of the perturbation and washout phases for each participant and compared the asymmetry magnitude between the first and second exposures to the exoskeleton protocol via paired t-tests.

RESULTS AND DISCUSSION

No significant difference was found between the two exposures for any measure, contradicting our hypothesis (Figure 1). This marks a distinct difference between behavioral effects elicited by the hip exoskeleton compared to split belt treadmill training, which has demonstrated significant savings upon second exposure on the same training day [3,4]. It is possible that adaptation to the initial exposure was simply so efficient that only marginal savings could be made, given the relatively minor torques exerted by the exoskeleton (<5 N-m). Performing this study with additional participants or with multiple, immediate exposures [4] may help to clarify whether adaptation to the exoskeleton changes on repeat exposure, with particular attention to PGRF aftereffect magnitude ($t(5) = -2.2$, $p = .08$). Encouragingly, the presence of an aftereffect remains clear upon repeat exposure, indicating that the exoskeleton may continue to cause aftereffects after wearers solidify a modified gait strategy from repeated use.

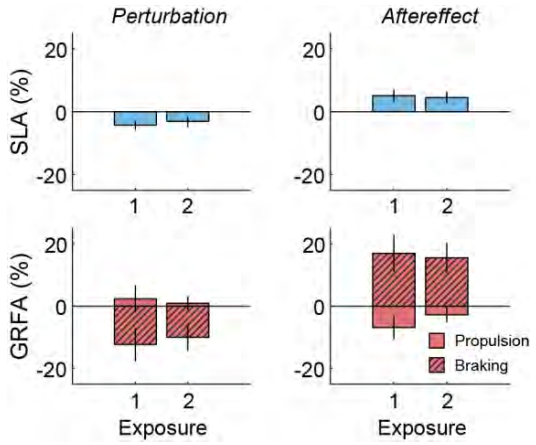

Figure 1 Group means for asymmetry measures between adaptation and readaptation conditions. Error bars reflect 2xSEM.

CONCLUSIONS

A second exposure to a hip exoskeleton asymmetry perturbation did not result in significant savings in the early perturbation or washout response. This may be due to small torques by the motors eliciting fast adaptation to begin with, causing marginal savings to be hidden in the variability between participants.

ACKNOWLEDGMENT

This work was funded by NIH Grant 1R21EB033450-01

REFERENCES

[1] B Abdikadirova et al. *BioRxiv* **2023***:* 527337, 2023.
[2] D Reisman et al. *Brain* **130**: 1861-1872, 2007.
[3] R Roemmich et al. *J Neurophys* **113**: 3459-3967, 2015.
[4] K Day et al. *J Neurophys* **119**: 2100-2113, 2018.

AN IMPROVED DESIGN OF AN UPPER LIMB EXOSKELETON FOR OVERHEAD TASKS

Georgios Aronis[1], Andrea Ancillao[1], Tommaso Del Grossi [2], Thomas Angeli [1], Margit Gföhler [1]
[1] Institute of Engineering Design and Product Development, TU Wien, Vienna, Austria.
[2] Department of Mechanical Engineering, Politecnico di Milano, Milan, Italy
Email: georgios.aronis@tuwien.ac.at

INTRODUCTION

Over the last years, assistive devices have been attractive to manufacturers as a means to improve the productivity of their workers. Among them, upper limb exoskeletons are considered of great interest since they can relieve the load from workers constantly involved in overhead tasks and activities that can cause severe work-related muscoloskeletal disorders which lead to multiple health leave days [1]. Extended research on the topic is still ongoing and major improvements are needed in terms of ergonomics, weight and efficiency. The aim of this work is to propose a novel upper-limb exoskeleton design and test its effects on the metabolic activity of a person while performing overhead work.

METHODS

The shoulder module of the exoskeleton was based on a previous design originally conceived for the rehabilitation of stroke survivors with limited residual muscle strength [2]. The new design is a passive, lightweight, and durable device aimed to provide the suitable torque to support both arms of the user at shoulder elevation angles larger than 90 deg. The new system was based on compression springs that were ad-hoc designed to provide the gravity compensation to the user while working overhead. The strength of the compensation can be adjusted by changing the tension and the initial position of the springs. More in detail, the spring was dimensioned via an optimization procedure aimed to reach a target support torque for the shoulder that was determined in a previous work [2]. A preliminary metabolic test was conducted on one subject performing an overhead task consisting of lifting a 1.5kg weight with and without the exoskeleton.

RESULTS AND DISCUSSION

The springs were located on the back of the user, parallel to the spine and embedded in the back support. The spring force was transferred to the arm via a cable embedded within the structure. This allowed an ergonomic weight distribution, not interfering with the arm brace. The dimensioning of the spring led to the activation curves shown in (Figure 1). A spring constant of 0.635 N/mm and length of 360mm was found to provide the best support for most of the users. The different coloured curves in (Figure 1) represent the theoretical required torques at different elbow positions; the dashed curve represents the torque provided by the spring. It was observed that the maximum torque is required when the arm is fully stretched. Thus, the spring was designed to provide a reasonable support at this case. The pretension design allowed to shift vertically the curves represented in (Figure 1).
The metabolic analysis showed that the use of exoskeleton led to a decrease in the main metabolic parameters. The respiratory frequency dropped from 20,2 (2,5) l/min to 14,5 (2,3) l/min, respiratory exchange ratio from 1,003 (0,068) to 0,950 (0,042) and heart rate from 85,3 (3,6) bpm to 80,2 (2,2) bpm.

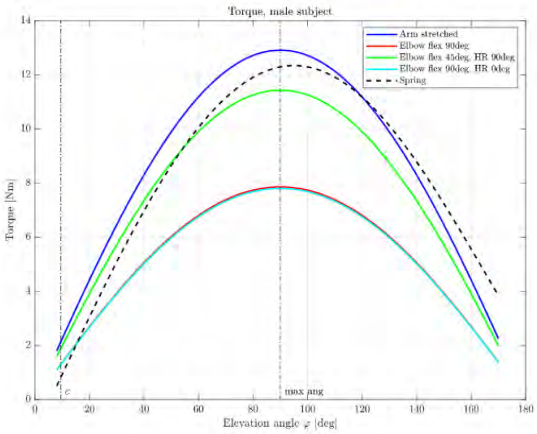

Figure 1 : Torque profiles at different elevation angles and possible use cases

CONCLUSIONS

From this preliminary study, it emerged that the new design was able to provide adequate support torque to help the subject during overhead tasks. Furthermore, the first prototype was able to reduce the metabolic cost of the task. Further studies will be required to assess the impact of the device on the muscular strategy and the effective energy expenditure over more subjects.

REFERENCES

[1] Bilancia et al. IJIDeM **15**, 525-539, 2021.
[2] Puchinger et al. IEEE BioRob **7**, 2018

WALKING WITH EXOSKELETONS: ESTABLISHING BIOMECHANICAL METRICS FOR QUANTIFYING ASSISTED-GAIT FAMILIARIZATION

Giorgos Marinou[1], Lizeth Sloot[1], Katja Mombaur[2]
[1]Institute of Computer Engineering (ZITI), Heidelberg University, Heidelberg, Germany
[2]Department of Systems Design Engineering and Mechanical and Mechatronics Engineering, University of Waterloo, Waterloo, Canada
Email: giorgos.marinou@ziti.uni-heidelberg.de

INTRODUCTION

Walking with exoskeletons has gradually evolved over the past two decades, from experimental setups to home use, establishing exoskeletons as well-facilitated devices for rehabilitated and assisted walking. Biomechanical evaluation of exoskeletons is a fundamental part of testing hardware and software modifications, but it can be quite challenging and inefficient since different users demonstrate different familiarization patterns and time windows. This study summarizes and extends previous work [1] on deriving and establishing a set of familiarization criteria based on biomechanical metrics, in order to *quantify the familiarization process* of young healthy adults walking with a lower-limb exoskeleton. Hence, the proposed method aims to improve exoskeleton-testing efficiency and accuracy of biomechanical measurements and data collection.

METHODS

Five able-bodied young male adults of 29.4 ± 4.9 years, 26 ± 1.4 BMI, walked with the lower-limb exoskeleton TWIN [2] over five bouts with a manual control mode and five more with a more automatic mode. Motion and muscle activity data were simultaneously collected using the Qualisys camera system (feet and sternum markers) and the Noraxon surface electromyography (EMG) system (triceps, biceps brachii, tibialis anterior and gastrocnemious medialis). Three spatiotemporal ((1) *stride duration*, (2) *mediolateral deviation from a straight path* and (3) *polygon of support*) and (4) *muscle activity* metrics are proposed as familiarization indicators, detailed in Marinou et al. [1]. Familiarization is defined as the reduction in magnitude of each of these four quantities. To assess an effect over time, Friedman's one-way analysis of variance (ANOVA) test was conducted separately for each mode (5 bouts), and a posthoc analysis was performed with a multiple comparisons test on the ten bout pairs with a significance value of $p < 0.05$. Results are reported in terms of median and interquartile range.

RESULTS

There were no significant changes in muscle activity for any of the examined arm or leg muscles, over both walking modes. Stride duration, mediolateral deviation, and polygon of support metrics indicated that participants start to show signs of familiarization to the exoskeleton after several walking bouts, and only in the automatic walking mode, as summarised in Figure 1. Stride duration decreased over bout 1 to 5 by 2.05 [2.61] s (average decrease: 16.9%, $p = 0.007$). Comparably, mediolateral deviations from straight-line walking decreased over time. There was an improved ability to walk in a straight-line path during the 5 bouts in the automatic mode, with a 63.8 [32.2] mm or 51.7% ($p = 0.014$) improvement between bout 1 and 5. The polygon of support area decreased similarly since participants did not show considerable changes during the first 5 bouts with the manual mode but the support area did decrease over bouts 2 to 5 of the automatic mode, by 0.0202 [0.0505] with an average decrease of 30.6% (p = 0.0316).

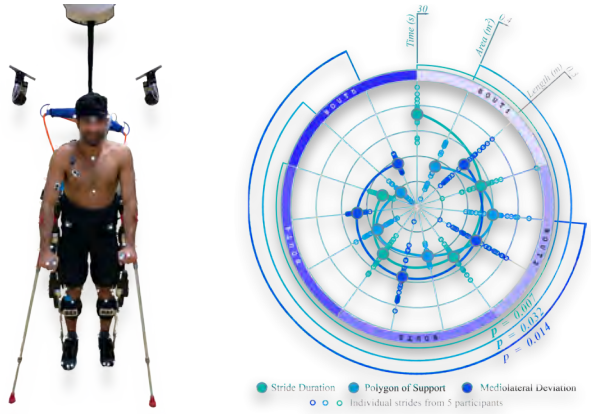

(A) (B)

Figure 1: (A) Experimental setup with exoskeleton and participant, (B) Summarized spatiotemporal metrics (1 - 3) results for automatic mode: large markers indicate median values and small markers individual participant values per stride. p-values reported concentrically.

CONCLUSIONS

Three biomechanical metrics have been established as familiarization indicators for lower-limb exoskeleton-assisted gait. Familiarization took place between bouts six and ten with the automatic walking mode. The presented approach of quantifying a user's familiarization allows to distinguish when familiarization begins and when we can start collecting meaningful data to evaluate these devices. Ongoing work to be included in conference presentation involves instrumented crutches and insoles that measure these metrics without the need of bulky laboratory equipment.

REFERENCES

[1] Marinou G et al. *IEEE RAS/EMBS* **9**: 9925360, 2022
[2] Laffranchi M et al. *Front Neurorob* **15**: 709731, 2021

Metabolic power response to added mass on the lower extremities during running .

Raziel Riemer*[1], Itay Coifman[1], Rodger Kram[2]

1. Industrial Engineering and Management Department, Ben-Gurion University of the Negev, Beer-Sheva, Israel
2. Integrative Physiology Department, University of Colorado, Boulder, CO, USA

* Corresponding author: rriemer@bgu.ac.il

INTRODUCTION

The use of wearable exoskeletal devices can enhance locomotor performance in various fields [1–4], but the added mass of such devices can cause a metabolic increase that needs to be overcome [3,5]. Previous studies have examined the effects of added mass, in forms such as shoes [6] , backpacks [7], and more. Notably, previous studies that have examined running metabolic power while loading the lower extreme have had very small sample sizes [8] or have not examined female runners and shank loading [9]. The present study aims to quantify the effects of adding mass to the thighs, shanks, and feet on the metabolic power required for running, using load magnitudes based on previous exoskeleton mass distributions. Furthermore, this study tests both women and men to determine any differences in effects between the sexes and develops numerical models to predict the effect of added mass on metabolic power for future assistive device design.

METHODS

Fifteen participants (7 females and 8 males) completed treadmill running trials ($3\ m \bullet s^{-1}$) normally and with lead mass (0.3–1.35 kg) attached bilaterally to the thighs, shanks, or feet. Using indirect colometry, metabolic power was measured and used to quantify the direct change and the relative changes due to added mass using linear models.

RESULTS AND DISCUSSION

For every kilogram of added mass per leg, gross metabolic power increased by approximately 16% (feet) and 11% (shanks) for females, which was slightly greater than the 11% and 8% increases for males, respectively. For thigh loading, metabolic power increased by 4% per 1000 g in both sexes (Figure 1). In the development of metabolic prediction equations, we found correction coefficients for Epstein-87 equations that were originally developed to predict a range of walking and running conditions with backpack weight (speed, incline, added mass, and terrain) [10]. The correction coefficients are a 9.8% addition for feet and a 6.4% addition for shanks per 1 kg compared to metabolic power calculated with the equations. This improved the prediction on walking and running with added mass on the lower extreme (compare [2,5]).

CONCLUSIONS

Adding mass more distally on the leg increases the metabolic cost of running to a greater degree. For the same absolute added mass on the feet or shanks, the metabolic rate increases more in females.

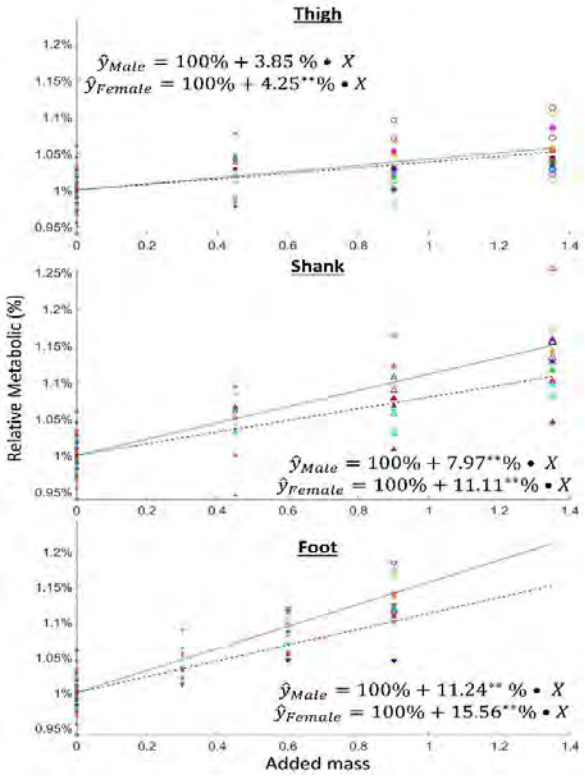

Figure 1 Relative increase in metabolic power due to added mass, as a function of the added mass at each location; female model = ... ; male model = – – –; ** = $p < .01$; * = $p < .05$.

ACKNOWLEDGEMENTS

This study was partially supported by the Israeli Ministry of Science and Technology and the Helmsley Charitable Trust through the Agricultural, Biological and Cognitive Robotics Initiative of Ben-Gurion University of the Negev.

REFERENCES

[1] J. Kim et al., Scientific Reports 12,1,1–13, 2022
[2] K. A. Witte et al., Sci Robot 5, 40,9108, 2020
[3] G. S. Sawicki et al., J Neuroeng Rehabil 17,1,1–9, 2020
[4] R. Nasiri et al. TNSRE 26,10,2026–2032, 2018
[5] E. Schertzer and R. Riemer, J Appl Ergon 45, 6,1422–1432, 2014
[6] J. R. Franz et al. Med Sci Sports Exerc 44, 8,1519-1525, 2012
[7] K. M. Simpson et al. Appl Ergon, 42, 3, 403–410, 2011
[8] M. J. Myers and K. Steudel, J Experimental Biology,116, 1, 363–373, 1985
[9] P. E. Martin, Med Sci Sports Exerc, 17, 4, 427–433, 1985
[10] Y. Epstein et al. J Appl Physiol Occup Physiol, 56,495–500, 1987

TIMING OF SHORTENING INFLUENCES FORCE DEPRESSION

Venus Joumaa[2], Eng Kuan Moo[1,2], and Walter Herzog[2]
[1] Department of Mechanical and Aerospace Engineering, Carleton University, Ottawa, Canada.
[2] Human Performance Laboratory, University of Calgary, Calgary, Canada.
Email: engkuanmoo@cunet.carleton.ca

INTRODUCTION

Residual force depression (rFD) is the loss of force following shortening of an activated muscle compared to the corresponding isometric contraction at the same final muscle length [1, 2]. In human, muscle contraction at a fixed joint angle is typically accompanied by fascicle shortening due to the compliant nature of the muscle-tendon unit (MTU), thereby causing rFD [3]. However, active shortening of muscle fascicles during fixed-end contraction of MTU occurs instantaneously with muscle activation, which is distinctly different from the classical way of rFD measurement whereby steady-state isometric force is achieved before any active shortening. As the rFD is thought to be caused by stress-induced inhibition of cross bridge formation [4], and is strongly associated with the work done [1], the rFD resulting from activation of compliant MTU may be lower than the classical rFD for the same amount of active shortening due to the rising active force, rather than the steadily high active force, during the early phase of muscle contraction. The purpose of this study was to determine the effect of timing of active shortening on the amount of rFD. We hypothesised that rFD is lower for active shortening that occurs instantaneously with muscle activation than for shortening that occurs following the attainment of steady-state active force.

METHODS

Intact tibialis anterior MTU of 8-10 week-old male C57/BL6 mice (N = 7) was set at resting length of ~10mm, and stretched by 3 mm (L1), 3.5 mm (L2) and 4 mm (L3) by a miniature dynamometer to lengths corresponding to the descending limb of the active force-length curve [5]. The MTU was activated isometrically by electrical stimulation of the sciatic nerve for 1.13s upon reaching the target length. For trials involving active shortening, MTU was stretched by 0.15 mm longer than the target length and activated. Active shortening of 0.15 mm at 0.5 mm/s was applied either instantaneously upon activation (INST) or delayed by 500ms following activation (DELAY). The MTU was allowed to recover at the resting length for 3 min between trials. The average steady-state force following active shortening was compared with that of the reference isometric contraction (ISO, Fig. 1A). The work done during active shortening was also calculated.

RESULTS AND DISCUSSION

MTUs stretched to L1 length had active force comparable to passive force, but the active forces of MTUs stretched to L2 and L3 lengths were lower than the passive force. Under this test protocol, activation-induced muscle shortening was minimised [5]. Force depression of the DELAY group was 5–9 %, and was significantly greater than the 1–5% force depression of the INST group (Fig. 1B). However, the work done during active shortening for the DELAY group was significantly lower than for the INST group at L2 and L3 lengths (Fig. 1C), which is against the general understanding of the positive correlation between work done and rFD [1]. We speculated that the manner in which rFD developed may be altered under high passive force seen at these MTU lengths.

CONCLUSIONS

We concluded that rFD depended on the timing of active shortening. rFD was lower in the INST group than in the DELAY group. However, the driving factor for this behaviour cannot be explained by work done during active shortening.

REFERENCES

[1] Herzog et al. *J Biomech* **33**: 659-68, 2000.
[2] Chen et al. *J Appl Physiol* **126**: 1066-73, 2019.
[3] Raiteri & Hahn Acta Physiol **225**: e13198, 2019.
[4] Joumaa et al. *Int J Mol Sci* **22**: 8526, 2021.
[5] Moo et al. J Exp Biol 223: jeb215020, 2020.

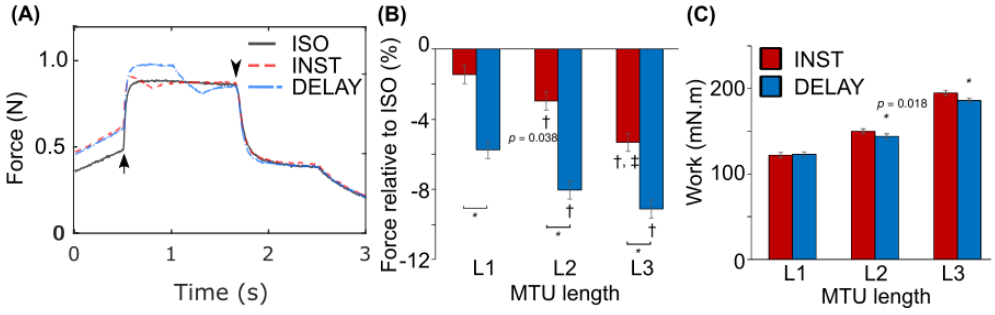

Fig 1: (A) Representative force trace, (B) magnitude of force depression, and (C) work done during active shortening for INST and DELAY conditions. The arrow and the arrowhead denote the start and end of muscle activation, respectively. * indicates statistical difference between INST and DELAY groups. † and ‡ represent statistical difference with L1 and L2, respectively.

THE EFFECTS OF GAIT RETRAINING ON THE BEHAVIOURS AND MECHANICAL PROPERTIES OF MEDIAL GASTROCNEMIUS-TENDON UNIT DURING RUNNING

Liqin Deng[1], Xini Zhang[2], Weijie Fu [1, *]

[1] Key Laboratory of Exercise and Health Sciences of Ministry of Education, Shanghai University of Sport, Shanghai, China; [2] Faculty of Sports Science, Ningbo University, Ningbo, China.
Email: fuweijie315@163.com

INTRODUCTION

The forefoot strike pattern (FFS) was always reported to be more economical and widely used by elite runners. The underlying reason includes the FFS allows greater storage and return of elastic energy from ankle tendons [1]. The previous studies verified this and reported the medial gastrocnemius (MG) contracted more slowly in FFS than in rearfoot strike pattern (RFS), which could be more energy-saving. Thus, gait retraining (GR) was highly recommended. However, few studies focused on the effects of GR at the MG-tendon unit (MTU) level. Thus, the aim of this study was to explore the effects of GR on MTU behaviour and mechanical properties.

METHODS

Twenty-four habitual RFS male runners were recruited and randomly divided into GR group and control group (CON). The participants in GR group were asked progressively transit to run with FFS in FiveFingers and those in CON were asked to keep their original running habits for 12 weeks. During tests, participants were asked to run at 9 km/h with traditional running shoes. An ultrasound system, motion capture system, and instrumented treadmill were used to capture the ultrasound image of MG, marker positions, and ground reaction forces (GRF) in real-time during running. The MG/MTU behaviour and mechanical properties were calculated. A 2x2 two-way repeated measures ANOVA was to analyze and the significance level α was 0.05.

RESULTS AND DISCUSSION

After 12 weeks, 10 participants in each group completed the training with nobody injured and eight in GR group transmitted to Non-RFS. These results illustrated the GR was safe and effective to transit foot strike pattern.

There was a significant interaction effect in the second peak GRF. Post hoc analysis revealed a significant increase after training in the GR group (Table 1).

There were no interactions but main time effects in MG fascicle shortening length and peak fascicle velocity. Specifically, both were significantly lower after 12 weeks (Figure 1). It was reported that the MG fascicle shortening length and peak fascicle velocity were negatively related to running economy [2], implying the MG could contract in a more efficient way after GR and long-term running.

Significant interaction effects were observed in MG force and MTU lengthening length. Post hoc analysis revealed significant increases in MG force in both groups and a significant increase in MTU lengthening length in GR group after training (Figure 1). It was inferred that the MG tendon was more compliant to make fuller use of stretch-shortening cycle, acting as compensation for MG to reduce higher force after GR.

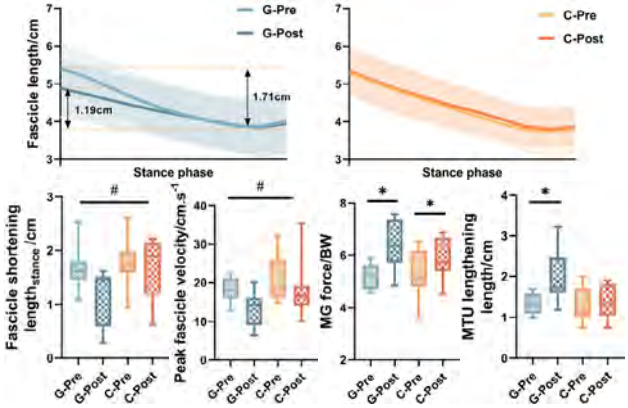

Figure 1 The effect of gait retraining on meidal gastrocnemius-tendon unit (MTU) behaviour and mechanical properties.
Note: G= gait retraining group, C= control group, *=significant difference, #=significant time main effect

CONCLUSIONS

The GR was safe and effective to transit FSP. After 12 weeks, the MTU lengthening length were greater in GR group, indicating GR helps enhance the elastic energy storage ability of MTU. Meanwhile, the MG fascicle shortening length and peak fascicle contractive velocity reduced after training but generated higher force in both groups, implying the MG could contract more efficiently after GR and long-term running.

ACKNOWLEDGEMENTS

This study was supported by NNSFC (12272238) and the "Outstanding Young Scholar" Program of Shanghai Municipal.

REFERENCES

[1] Anderson, L. M et al. *Sports Med* **50**: 885-917, 2020.
[2] Fletcher J R et al. *Front Physiol* **8**, 2017.

Table 1: The effect of gait retraining on foot strike angle and ground reaction force.

Variables	Gait retraining group（n=10）		Control group（n=10）		*P*-value		
	Pre	Post	Pre	Post	Time	Group	Interaction
Foot strike angle	13.19±3.84	3.69±6.91	15.44±4.05	15.79±3.65	**＜0.001**	**0.001**	**＜0.001**
The 2^{ed} ground reaction force	2.40±0.20	2.52±0.13	2.47±0.14	2.45±0.13	**0.041**	0.982	**0.011**

MUSCLE VOLUMES AND MOMENT ARMS OF HUMAN ROTATOR CUFF MUSCLES IN VIVO

Yilan Zhang[1,2], Lynne Bilston[2], Robert Herbert[2], and Bart Bolsterlee[1,2,3]
[1] University of New South Wales, Randwick NSW, Australia.
[2] NeuRA, Randwick NSW, Australia.
[3] Queensland University of Technology, Brisbane QLD, Australia.
Email: yilan.zhang@neura.edu.au

INTRODUCTION

Knowledge of muscle architecture and moment arms is crucial for understanding the functional morphology of the musculoskeletal system [1]. Traditionally, moment arms were measured in vitro. However, for the complex shoulder mechanism, it is difficult to determine the biomechanical effects of shoulder muscles on glenohumeral joint stablity and range of motion from cadaver measurements alone. This study investigates the feasibility of using magnetic resonance imaging (MRI) to quantify muscle volumes and moment arms of human rotator cuff muscles in vivo.

METHODS

Twelve healthy subjects (six males, six females; age 33 ± 6 years; height 170 ± 6 cm; weight 69 ± 10 kg; values are mean ± SD) with no symptoms or recent history of shoulder pathology were included in this study. mDixon anatomical scans of the right shoulders were acquired with a 3T MRI scanner (Philips Ingenia CX). Rotator cuff muscles were manually segmented on all slices of mDixon water images to create 3D surface models, from which muscle volumes were calculated. The glenohumeral joint centre of rotation was determined by fitting a sphere to the articular surface of the humeral head. A third-order polynomial curve was fit on each rotator cuff tendon in 3D to represent the muscle line of action. The moment arm was then estimated as the smallest perpendicular distance between the line of action and the centre of the fitted sphere (i.e., the centre of rotation).

RESULTS AND DISCUSSION

Muscle volumes and moment arms from this study were in good agreement with previously published [2] MRI-based measurements obtained in vivo (Table 1), suggesting our measurements were broadly accurate. Also, the variation in volumes between muscles is comparable with that reported by Juul-Kristensen et al. [2]. Minor differences in our values and those reported by Juul-Kristensen and colleagues could be attributed to inaccuracies in manual segmentation, differences in methods used to estimate centres of rotation and muscle lines of action, and differences in anatomical characteristics of participants between studies.

CONCLUSIONS

This study demonstrates the feasibility of using MRI to quantify the muscle sizes and moment arms of human rotator cuff muscles in vivo and provides preliminary evidence of validity. This study adds to the larger study conducted by Juul-Kristensen et al. [2] by measuring the properties of infraspinatus and teres minor separately. We also quantified moment arms in 3D, which overcomes limitations associated with 2D approaches [3].

These measurements could be used to explore skeletal muscle structure-function relationships non-invasively and to develop realistic computational models of the human shoulder for clinical and surgical applications.

We are currently working on complementing the dataset with other muscle architectural parameters (fibre length, physiological cross-sectional area and pennation angle) from diffusion tensor imaging data.

REFERENCES

[1] Channon et al. *J Anat* **216**: 446-462, 2010.
[2] Juul-Kristensen et al. *Cells Tissues Organs* **167**: 214-222, 2000.
[3] Hashizume et al. *J Biomech* **45**: 409-413, 2012.

Table 1: Comparison of muscle volume and moment arm of rotator cuff muscle between this study and a previously published in vivo study. Values are mean ± standard deviation across all participants.

Muscle	Muscle volume (cm^3)		Moment arm (cm)	
	This study (n = 12)	[2] (n = 20)[a]	This study (n = 12)	[2] (n = 20)[a]
Supraspinatus	53 ± 13	49 ± 8	2.4 ± 0.3	2.4 ± 0.1
Subscapularis	140 ± 37	154 ± 22	2.3 ± 0.2	2.3 ± 0.1
Infraspinatus	118 ± 31	124 ± 16	2.4 ± 0.2	2.3 ± 0.2
Teres minor	24 ± 7		2.5 ± 0.3	

[a] The infraspinatus and teres minor muscle were grouped together as one muscle [2].

CORRELATIONS BETWEEN ACHILLES TENDON MOMENT ARM AND PLANTARFLEXOR MUSCLE ARCHITECTURE

Logan K. Faux-Dugan and Stephen J. Piazza
Dept. of Kinesiology, The Pennsylvania State University, University Park, PA, USA.
Email: fauxdugan@psu.edu

INTRODUCTION

Because sufficient plantarflexor muscle moment is essential for locomotor function, its direct determinants are parameters of great interest in understanding the mechanics of locomotion. This moment is primarily the product of the Achilles tendon force and the plantarflexor moment arm of the Achilles tendon (ATMA), but the production of plantarflexor moment is complex because ATMA determines muscle length change and shortening velocity per unit change in ankle angle. A large moment arm has the potential to increase sarcomere shortening velocity and thus decrease force generating capacity during concentric contractions [1]. If, however, resting fascicle length scales with moment arm, then sarcomere operating range and force-generating capacity may be preserved [2].

Similarly, if muscles with larger physiological cross-sectional area (PCSA) also possess shorter moment arms, it might result in moment generating capacity being consistent across individuals. These relationships between ATMA and plantarflexor muscle architecture are thus important for understanding the roles played by muscles in producing locomotion. The purpose of this study was to investigate the relationship between ATMA and the architecture (fascicle length and PCSA) of the plantarflexor muscles lateral and medial gastrocnemius (LG and MG) in a young healthy population. We hypothesized that ATMA would correlate positively with fascicle length and negatively with PCSA in both muscles.

METHODS

Sixteen healthy young adults (9M/7F, age 27.64 ± 5.13 y, height 1.75 ± 0.03 m, mass 76.29 ± 4.36 kg) were recruited as participants in the study. Techniques integrating ultrasonography (US) and video-based motion analysis were used to quantify the architecture of LG and MG as well as the ATMA in each subject's right leg. With the participant in a prone position, transverse-plane 2D US images of the calf were collected in multiple sweeps. These images were used to create 3D models of LG and MG in Stradwin software from which muscle volumes were estimated. With the subject standing, static sagittal-plane US images were collected and analysed to estimate pennation angles and fascicle lengths. PCSA was computed by dividing the product of muscle volume and pennation angle by fascicle length. As the subject performed calf raises, markers on the foot and shank were tracked along with markers on an ultrasound probe placed over the Achilles tendon near the ankle [3]. Marker locations were processed to locate the ankle axis of rotation from the measured movement, while simultaneously locating the Achilles tendon from the US images. ATMA was estimated as component of the ankle moment due to a unit tendon force directed along the joint axis [3]. ATMAs reported below are those occurring when the ankle was in neutral position.

RESULTS AND DISCUSSION

For LG, a moderate significant correlation was found between ATMA and fascicle length (R = 0.53; p = 0.033) but no significant correlation between ATMA and PCSA (R = 0.38; p = 0.142) (Fig. 1). For MG, however, the opposite was found: A moderate significant correlation between ATMA and PCSA (R = 0.50; p = 0.048) and no significant correlation between ATMA and fascicle length (R = 0.37; p = 0.164).

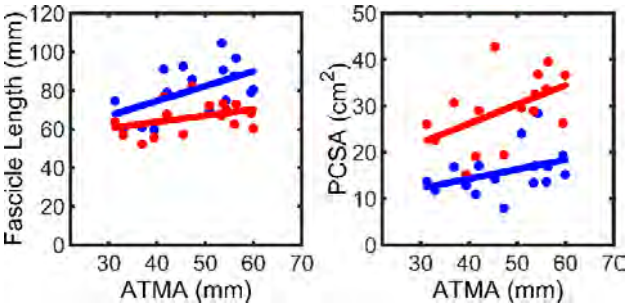

Figure 1 Correlations between ATMA and fascicle length (*left*) and PCSA (*right*). Results are shown for LG (*blue*) and MG (*red*).

CONCLUSIONS

These findings suggest that LG, a muscle with longer fascicles and smaller PCSA, is well suited for maintenance of force generation throughout the range of motion across individuals. But MG, a muscle with a larger PCSA and shorter fascicles, is more suited for static moment generation, and those individuals with the greatest force-generating capacity also benefit from having the best leverage in terms of their ATMA. Similar positive correlations between muscle size and moment arm have previously been attributed to muscle belly bulging altering the tendon line of action [4].

ACKNOWLEDGMENT

We wish to thank Rebecca Gonzalez for her assistance with the data collection.

REFERENCES

[1] Lieber R L and Ward S R *Philos Trans R Soc Lond B Siol Sci* **366**: 1466-76, 2011.
[2] Lieber R L *Acta Anat* **159**: 84-9, 1997.
[3] Wade et al. *J Biomech* **90**: 71-77, 2019.
[4] Sugisaki et al. *J Biomech* **43**: 2844-2847, 2010.

REGIONAL HAMSTRING HYPERTROPHIC ADAPTATION FOLLOWING A NINE-WEEK ECCENTRIC NORDIC HAMSTRING TRAINING PROGRAM

Anoosha Pai S[1], Max H. Andrews[1,2], Reed D. Gurchiek[1], Patricio A. Pincheira[2,3], Scott L. Delp[1], Glen A. Lichtwark[2], Valentina Mazzoli[4], and Akshay S. Chaudhari[4]

[1] Department of Bioengineering, Stanford University, Stanford, USA
[2] School of Human Movement and Nutrition Sciences, The University of Queensland, Brisbane, Australia.
[3] School of Health and Rehabilitation Sciences, The University of Queensland, Brisbane, Australia.
[4]Department of Radiology, Stanford University, Stanford, Stanford, USA.
Email: anoopai@stanford.edu

INTRODUCTION

Hamstring strains are the most common non-contact injuries, accounting for 37% of all muscle injuries in sports [1]. Although, eccentric Nordic hamstring exercise (NHE) induces hypertrophic adaptations in the hamstring muscle group, the training favourably develops biceps femoris short head and semitendinosus muscles [2]. However, the pattern of hypertrophy in different regions for different hamstring muscles is still unknown. Therefore, we aim to investigate the regional hamstring hypertrophic adaptations in response to 9 weeks of eccentric NHE training.

METHODS

Five recreationally active subjects (3 females, 2 males, 26.4±3.3 yrs., out of 10 recruited) completed a 9-week eccentric NHE intervention totalling 867 repetitions. Thigh region of all subjects were scanned in a 3.T MR scanner, (GE Healthcare) using IDEAL IQ (TR/TE=13.3/6.3ms, no. of echoes=6, flip angle 5°, matrix=252×252, FOV= 22.5-45cm, slice thickness= 6mm) before and after the intervention. Hamstring muscles, biceps femoris short head (BFSH), biceps femoris long head (BFLH), semitendinosus (ST), and semimembranosus (SM) were segmented in 3D Slicer blinded to pre/post intervention status. To keep measurements consistent across all subjects, hamstring volumes were measured from points of origin till the first appearance of patella on the MR slice. The hamstrings were divided into three equal regions: proximal, central, and distal. For each muscle, total and regional volumes were compared before and after the intervention using two-tailed paired sample T-test.

RESULTS AND DISCUSSION

The preliminary results showed that NHE increased overall hamstring volume in preferential order of ST (~22%, p=0.021), BFSH (~21%, p=0.027) BFLH, (~10%, p=0.001), and SM (~4%, 0.001). Regionally, NHE intervention increased BFSH volume mainly in central (~11%, p=0.006) and distal (~29%, p=0.035) regions (Fig. 1A). BFLH showed significant hypertrophy only in the distal (~10%, p=0.008) region (Fig. 1B). For ST, the increase in volume was significant only in the central region (~27%, p=0.015) (Fig. 1C). SM did not show any significant region-specific volume changes (Fig. 1D). Along with another study that showed increase in muscle fascicle length in the distal region of BFLH [5], our pilot results give novel insights into possible course of manifestation of these heterogeneous muscle adaptations.

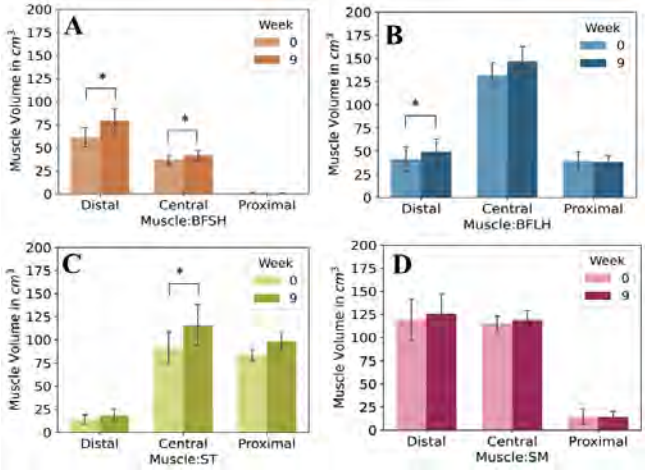

Figure 1. Hamstring muscle volume changes following 9-week eccentric NHE training program. Region-specific (distal, central, and proximal) muscle volumes for A) BFSH, B) BFLH, C) ST, D) and SM. * indicate statistically significant changes (p<0.05).

CONCLUSIONS

Overall, our results indicate that hamstring muscle adaptations to eccentric NHE are non-uniform and are muscle and region-specific.

ACKNOWLEDGEMENTS

This work was supported by ARC Discovery Project (DP200101476), and in parts by NIH grants R01 AR077604, RO1 EB002524, RO1 AR079431, P41 EB02706, Stanford Graduate Fellowship, University of Queensland Graduate Scholarship, and Wu Tsai Human Performance Alliance.

REFERENCES

[1] Oleksy et. al., Frontiers in Physiology. 12, 586624, 2021.
[2] Bourne et. al., J Sports Med. 51(5): 469-77, 2017.
[3] Pincheira et. al., J. Sports Health Sci. 11:43-49, 2022.

ULTRASOUND BASED MUSCLE QUALITY AND THE CONFOUNDING EFFECT OF SUBCUTANEOUS FAT LAYER IN INDIVIDUALS WITH OBESITY

Heiliane de Brito Fontana[1], Walter Herzog[2], Everson Nunes[3], Cinthia Correa[3]
[1] Morphological Sciences Department, Federal University of Santa Catarina, Florianopolis, Brazil.
[2] Human Performance Laboratory, Faculty of Kinesiology, University of Calgary, Calgary, Canada
[3] Laboratory of Investigation in Chronic Diseases, Federal University of Santa Catarina, Florianopolis, Brazil.
Email: heiliane.fontana@ufsc.br

INTRODUCTION

The role of obesity in the development of metabolic and cardiovascular diseases is well acknowledged and has been clinically examined. In contrast, little is still known on the effect of obesity on the musculoskeletal system , and diagnostic tools for monitoring changes in skeletal muscles are still poorly explored. Ultrasound imaging is a promising, non-invasive diagnostic tool to estimate muscle quality and fibrosis through echointensity (EI). However, subcutaneous fat between the utlrasound and the muscle region can result in reduced EI and therefore in overestimated muscle quality in individuals with obesity. Previous studies have tried to account for this confounding effect by applying pressure over the muscle in order to deform the layer of fat [1]. Here, we i) present an equation to correct for the independent effect of subcutaneous fat on ultrasound estimates of muscle quality, and ii) compare, for a sample of healthy adults with varying body composition, the differences between this newly developed correcting factor and the one available in the literature based on pressure [1].

METHODS

The independent effect of fat thickness on EI was verified using exogeneous layers of pork fat over the muscles in 10 participants. The regression between fat thickness and echointensity was verified and the slopes were averaged across individuals. Later, the rectus femoris and tibialis anterior EI were evaluated in 14 subjects ranging from lean to obese. Sonograms were obtained with a depth of 40 mm; general gain of 60 dB and TGC neutral. Focus position was adjusted to the muscle region of interest (ROI) [2]. EI was determined as the mean value of a gray-scale histogram function and was corrected for the confounding effect of subcutaneous fat using the correction factor developed by us and the one previously available in the literature.

RESULTS AND DISCUSSION

There is a significant error in the raw estimates of muscle quality (Table 1).

The analysis of the independent effect of fat resulted in the following correction equation: $EI_{corrected} = EI_{measured} + 39.2297 \times (adipose\ thickness\ in\ cm)$. Compared to the estimates corrected with the current equation, we observe a bias in muscle quality estimates using a pressure-based correction to account for the effect of subcutaneous fat thickness (Figure 1).

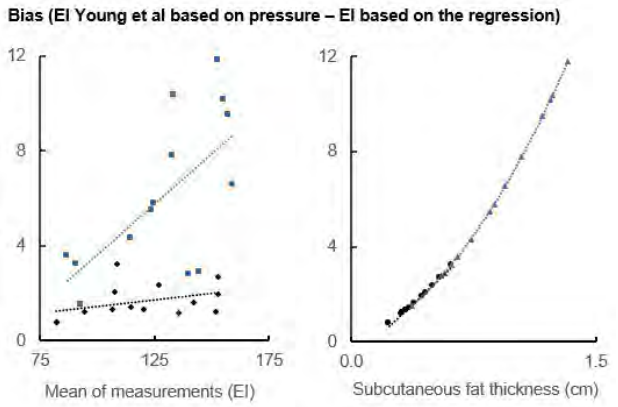

Figure 1 Left: bias in EI estimates corrected based on pressure applied on the probe (Young et al [1]) compared to estimates corrected by the independent effect of fat. Data for the TA are shown in black, and for RF, in blue. Right: Bias increases with increasing fat thickness.

CONCLUSIONS

EI estimates of muscle quality are significantly affected by the thickness of the subcutaneous fat. Using pressure to try to correct for the confounding effect of subcutaneous fat may introduce bias and lead to erroneous estimates of muscle quality in individuals with obesity. Here, we present an equation that was developed experimentally through the analysis of the independent effect of fat and suggest its use in future studies.

REFERENCES

[1] Young et al. *Muscle Nerve.* **52**(6): 963–971.
[2] Muller et al. *Appl.Physiol.Nutr.Metab.* **46**: 473–8

Table 1: Muscle quality estimates of the rectus femoris and tibialis anterior in healthy adults compared with ANOVA.

	Raw	Corrected	Corrected by pressure [1]	*p-value*
Rectus femoris	97 ± 20[a]	126 ± 24[b]	132 ± 26[c]	$p < 0.001$
Tibialis Anterior	105 ± 23	119 ± 25	120 ± 25	$p < 0.001$

ORTHOTROPIC BONE REMODELLING AROUND UNCEMENTED ACETABULAR COMPONENT

Sanjay Gupta, Ceby Mullakkara Saviour
Department of Mechanical Engineering, Indian Institute of Technology Kharagpur, Kharagpur, India.
Email: sangupta@mech.iitkgp.ac.in

INTRODUCTION

Aseptic loosening is often associated with adverse periprosthetic bone remodelling owing to stress/strain shielding. An earlier study proposed a thermodynamic-based model that could incorporate the coupling between the mechanical loading and biochemical reactions involved in bone adaptation [1]. Earlier studies which implemented the mechanobiochemical model in the intact and implanted femur ignored the anisotropic nature of bone and were limited to femur [1, 2]. The objectives of the study were to develop an improved mathematical framework orthotropic bone adaptation of a hemipelvis based on mechanobiochemical model and to compare the predictions with the orthotropic-strain-based bone adaptation.

METHODS

The patient-specific 3-D finite element (FE) models of intact and implanted hemipelvises were developed [3]. The newly developed framework considered thermodynamic-based bone adaptation along with the orthotropic material property determination based on the strains along the principal directions. The standard law of mass action was modified as Eqn. 1, to achieve the coupling between biochemical affinity of the reactions and the mechanical stimulus [1].

$$r_\alpha = k_{+\alpha} \prod_{i=1}^{n} [N_i]^{v_{\alpha i}} - k_{-\alpha} \prod_{i=1}^{n} [N_i]^{v'_{\alpha i}} + l_{\alpha v} d_{(1)} \quad (1)$$

Where r_α and A_α represents the rate and affinity of the α^{th} biochemical reaction (α = 1 to 5), l and k represents the phenomenological and reaction rate coefficients, respectively, $d_{(1)}$ represents the rate of dilatation (rate of volume variation). $v_{\alpha i}$ and $v'_{\alpha i}$ are the stoichiometric coefficients of the mixture of N_i entering and leaving the α^{th} reaction, respectively [1].

RESULTS AND DISCUSSION

The changes in bone density distribution, after equilibrium in bone remodeling, corresponding to orthotropic strain-based model (Figure 1b) and orthotropic MBC model (Figure 1c) were compared. The orthotropic strain-based model predicted an appreciable bone resorption (~75%) in the region of interest (ROI) 1, whereas the orthotropic MBC model predicted a slightly lesser reduction in average bone density (~50%) in the ROI 1. The sectional plots of figures 1b and 1c indicates similar high bone resorption (75-85%) predictions by both the models. However, orthotropic MBC model estimated more volume of bone elements (10-20%) to experience bone resorption. Similar bone apposition was observed near the acetabular rim (Figure 1) in the bone remodeling predictions of orthotropic strain-based model and the orthotropic MBC model. Despite the similarities within the bone density distributions (section 1-1, 2-2 of Figure 1 b, c) between the orthotropic strain based model and orthotropic MBC model, a clear distinction could be observed in the evolutionary bone density predictions.

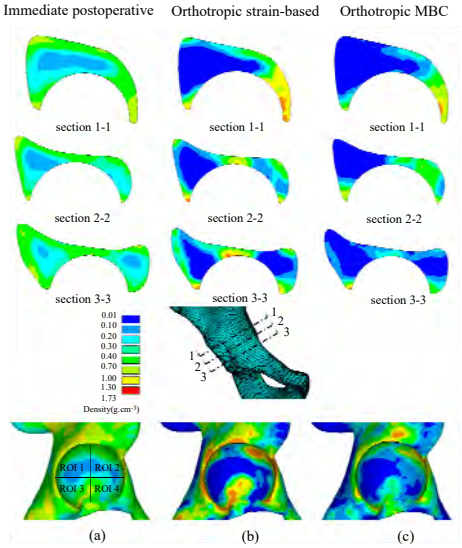

Figure 1: Changes in bone density distribution owing to implantation, sectional and lateral views: (a) immediate postoperative; (b) predicted by orthotropic strain-based model; (c) predicted by orthotropic MBC model.

CONCLUSIONS

The predictions of the orthotropic MBC model were agreed qualitatively with that of the orthotropic strain-based model. This novel framework of orthotropic MBC model implicitly incorporates the biochemical stimulus and the mechanical stimulus along with a detailed description of the bone anisotropy.

REFERENCES

[1] Bougherara et al., *J Biomed Mater Res A*. **95**(1):9-24. 2010.

[2] Tavakkoli Avval et al., *J Biomech Eng*, **136**(5): 051002, 2014.

[3] Saviour et al., *J Biomech Eng*, **145**(2):021009, 2023.

3D PERSONALIZED FOOT MODELS USING SURFACE-BASED STATISTICAL SHAPE MODELLING

Liangliang Xiang [1,2], Yaodong Gu [1,2], Vickie Shim [1], Ted Yeung [1], Alan Wang [1,3], and Justin Fernandez [1,2,4]
[1] Auckland Bioengineering Institute, The University of Auckland, Auckland, New Zealand.
[2] Faculty of Sports Science, Ningbo University, Ningbo, China.
[3] Center for Medical Imaging, Faculty of Medical and Health Sciences, The University of Auckland, Auckland, New Zealand.
[4] Department of Engineering Science, The University of Auckland, Auckland, New Zealand.
Email: lxia467@aucklanduni.ac.nz

INTRODUCTION

Personalized biomechanical models of the foot may assist in understanding form function relationships through techniques such as finite element (FE) analysis [1]. Foot geometric characteristics are usually obtained from medical images, which are considered the gold standard, primarily from computed tomography (CT) and magnetic resonance imaging (MRI). However, personalizing a foot and ankle joint model is highly time-consuming in terms of medical image collection and data processing. Statistical shape modelling (SSM) can represent a range of expected, evidence-based variations in a population and be used to intelligently scale a model to a subject with minimal information [2]. This study aimed to develop and validate a framework to rebuild a 3D foot including internal bones using SSM based on skin measurements.

METHODS

The 3D foot surface shape of 50 participants (age: 24.0±3.8 yrs; height: 1.75±0.06 m; mass: 67.6±7.8 kg) was scanned using an Easy-Foot-Scan machine to train a SSM following ethical approval. Model-based shape reconstruction was performed to generate foot surface geometry using a principal component analysis (PCA). Following this, free-form deformation (FFD) was performed to reconstruct internal bone meshes [3]. The pipeline for personalized foot model generation using surface-based SSM is shown in Figure 1. The model accuracy was established by comparing three reconstructed foot models (age: 24.3±2.5 yrs; height: 1.75±0.03 m; mass: 66.0±2.0 kg) to corresponding skin and bone geometries that were manually segmented and not part of the original training set.

RESULTS AND DISCUSSION

We used the top ten principal components representing 85% of the population variation. For prediction validation, the average Dice similarity coefficient (DSC), Hausdorff distance, and root mean square (RMS) error were 0.84±0.03, 1.83±0.10 mm, and 2.36±0.12 mm for bones, and 0.92±0.01, 2.2±0.19 mm, and 2.95±0.23 mm for the encapsulated tissue, respectively.

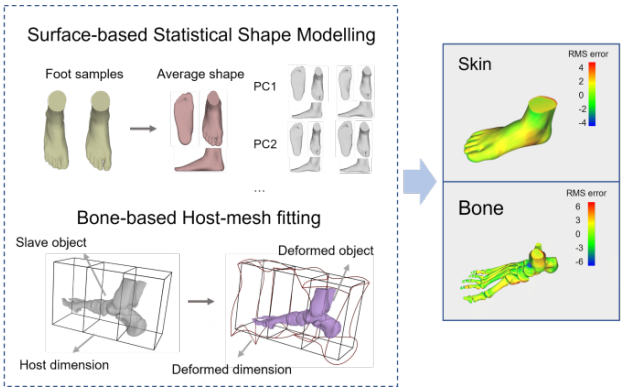

Figure 1 Illustration of the pipeline for 3D personalized foot model generation.

This study developed a personalized foot model reconstruction pipeline through a foot surface scan. Specifically, a PCA-based SSM coupled with FFD was used to rebuild the encapsulated skin and inner bones. We found that a 3D personalized foot model can be reconstructed using rapid surface scanning with minimal error. This approach eliminates the cost of medical imaging for reconstructing bone geometries and is time-saving. The proposed pipeline is an effective technique to rapidly personalize foot geometries for FE modelling and rigid body modelling such as with OpenSIM. This in turn will lead to more informed predictions with models especially in pathology.

CONCLUSIONS

This study presents a subject-specific foot model via SSM generation of the foot surface and bone reconstruction based on free-form deformation. The proposed workflow makes it possible to accurately generate foot models informed by population anatomy, which can be used in future anatomical and mechanical simulation investigations.

REFERENCES

[1] Xiang L et al. *J Biomech* **132**: 110941, 2022.
[2] Zhang J et al. *J Biomech* **49**: 3875-81, 2016.
[3] Fernandez J W et al. *Biomech Model Mechanobiol* **2**: 139-155, 2004.

Changes in hallux movement in people with chronic ankle instability during walking at different speeds

Tunpisith Jeamsupakorn[1,3], Chich-Haung Richard Yang[1,2,3], Kuan-Lin Liu[3,4]
[1] Institute of Medical Science, Tzu Chi University, Hualien, Taiwan.
[2] Department of Physical Therapy, Tzu Chi University, Hualien, Taiwan.
[3] Sport Medicine Center, Buddhist Hualien Tzu Chi Hospital, Hualien, Taiwan.
[4] Department of Orthopedic Surgery, Buddhist Hualien Tzu Chi Hospital, Hualien, Taiwan.
Email: 110353118@gms.tcu.edu.tw

INTRODUCTION

Lateral ankle sprain is one of the most common injuries during physical activities in the lower limb [1]. Previous studies have shown that 36% of lower limb injuries are associated with strains and sprains-related injuries, which often develop into chronic ankle instability (CAI). Hallux movement relates to foot function and posture, such as foot flat [2, 3], which is one cause of CAI. Previous research indicates that different walking speeds are associated with significant biomechanical changes in the movement pattern [4]; however, there are still inconclusive findings in relation to deficits in hallux movement as a functional activity, such as level walking at different speeds in individuals with CAI. Therefore, we aimed to explore hallux movement in CAI patients and healthy controls during walking at different speeds.

METHODS

We recruited 18 participants in both healthy and CAI groups (9 female and 9 male) with age- and BMI-matched. The participants of both groups are between 18-25 years old. Participants in the CAI group have suffered from ankle sprains for at least two episodes with recurrent ankle sprain within one year and did not have other lower-limb injuries over six months, and Cumberland Ankle Instability Tool (CAIT) score less than 21.5 scores. The healthy group did not have an ankle sprain, and other injuries in the lower limb within one year [5]. A Vicon Motion Analysis System (12 optoelectronic cameras) with Plug-in-Gait (PiG) and the Oxford Foot Model (OFM) were used to capture hallux kinematics in barefoot conditions during level-walking at fast speed (FS) (140 bpm), self-selected (NS), and slow speed (SS) (80bpm) during the stance phase. Comparisons were used between groups by using independent t-tests ($p<0.05$) and one-Dimensional Statistical Parametric Mapping (SPM-1D).

RESULTS AND DISCUSSION

Significant differences in hallux kinematics were found between the groups during level-walking at their FS, NS, and SS. Increases in hallux dorsiflexion were found in CAI group during mid-stance (MS) to terminal stance (TS) at FS and SS (mean difference (MD) 10.68 ° ; p=0.031, MD 10.01 ° ; p=0.003, respectively), and pre-swing (PS) at FS, NS, and SS (MD 8.67 ° ; p = 0.042,MD 6.79 ° ;p=0.049,MD 7.31 ° ;p=0.043, respectively), Then, CAI group showed increased hallux varus during MS at FS (MD -3.44 ° ; p=0.047), MS to TS at SS (MD -3.74 ° ; p=0.013) and PS at FS, NS, and SS (MD -3.44 ° ; p= 0.046, MD -3.45 ° ; p=0.049, MD -3.29 ° ; p= 0.048, respectively) when compared to the healthy group.

A previous study shows that increased hallux dorsiflexion is related to a decrease foot arch high, which can lead to foot flat problem [3]. In our study, the CAI group showed an increase hallux dorsiflexion and varus at three walking speeds, which relates to the hallux varus position. Nevertheless, Hallux Varus is related to foot intrinsic and extrinsic muscle imbalance such as flexor and extensor hallucis brevis and longus (FHB, EHB, FHL, EHL), abductor hallucis brevis and adductor hallucis[6]. More importantly, a recent study showed that EHL would be a pivotal muscle to improving CAI problems due to intramuscular angle change[7]. Consequently, an increase in hallux dorsiflexion and varus will cause CAI injury.

CONCLUSIONS

At different walking speeds, individuals with CAI may employ compensatory motor strategy in the hallux movement to adapt their functional movements by increased hallux dorsiflexion and varus during mid-stance to terminal stance (FS, SS) and pre-swing (FS, NS, and SS). These alterations in forefoot biomechanics during level walking may lead to structural adaptions, such as Hallux Varus, and flat foot deficits. Furthermore, these above changes in foot structures may be potential precursors to contribute to the recurrence rate of re-injury.

ACKNOWLEDGEMENTS

We would like to express our thanks to the financial supports from research grant (104-2410-H-320-004), National Science and Technology Council, Taiwan, and Intramural research grant (TCRD108-34), the Buddhist Tzu Chi Medical Foundation, Taiwan.

REFERENCES

[1]Herzog MM, et al. *J Athl Train* **54**:603-10. 2019.

[2]Kerr CM, et al. *Gait Posture* **67**:213-8. 2019.

[3]Shono H, et al. *Gait Posture* **92**:96-102. 2022.

[4]Fukuchi CA, et al. *Syst Rev* **8**:153. 2019.

[5]Gribble PA, et al. *J Orthop Sports Phys Ther* **43**:585-91. 2013.

[6]Mohan R, et al. *The Foot* **49**:101863. 2021.

[7]Negishi K, et al. *Foot Ankle Surg* **28**:1040-4. 2022.

PASSIVE PROPERTIES OF THE ACHILLES TENDON IN ATHLETES

Maria Sukanen[1], Ra'ad M. Khair[1], Iida Laatikainen-Raussi[1], Johanna K. Ihalainen[1], Pauline Eon[2], Antoine Nordez[2,3] and Taija Finni[1]

[1] Faculty of Sport and Health Sciences, University of Jyväskylä, Jyväskylä, Finland.
[2] Nantes Université, Movement-Interactions-Performance, MIP, UR 4334, F-44000 Nantes, France.
[3] Institut Universitaire de France, Paris, France.
Email: maria.e.sukanen@jyu.fi

INTRODUCTION

Different modes of mechanical loading lead to various adaptations in the mechanics of the Achilles tendon (AT) [1]. Despite these adaptations, AT is a common site of musculoskeletal conditions, usually due to sports activities [2,3]. Although AT has been frequently studied, knowledge of its' biomechanical organization and properties remains incomplete. Therefore, we exploratively investigated the internal AT displacement and passive AT shear wave velocity (SWV) of athletes. The aim was to investigate whether previous physical exercise, lower limb injury history, or individual characteristics influence internal AT displacement and AT SWV.

METHODS

A total of 131 athletes (48 men, 83 women; 19.5±3.8 years) from basketball (27), football (31), gymnastics (25), track and field (21) and ice hockey (27) were recruited from a local Sports academy. All subjects competed at the national level and actively trained in their sports. The study was approved by ethics committee and participants provided a signed informed consent.

Internal AT displacement was measured with cine B-mode ultrasonography and quantified offline using 2D speckle tracking [4]. Mean displacement (mm) was extracted for the overall tendon and for the anterior and posterior halves of the tendon. Maximum non-uniformity (mm), calculated as maximum-minimum displacement within the tendon cross-section, was also extracted. Shear wave elastography was used to measure resting AT SWV (m/s) from three distal locations longitudinally. SWV was extracted with a custom software (ElastoGUI). Participation in sport within two days before assessments, history of lower limb injuries, sport specialisation and leg dominance were asked. Significance of mean differences was tested using paired and independent samples *t* tests, and associations between outcome variables were tested using Pearson's correlation coefficient.

RESULTS AND DISCUSSION

Athletes without prior exercise exhibited greater AT non-uniformity (Figure 1) and mean displacement of the anterior half of the tendon, and lower SWV of the proximal AT measurement site (mean difference [95%CI]:1.768 mm [0.621–2.916], p=0.003; 1.556 mm [0.236–2.875], p=0.021; -0.887 m/s [-1.589- -0.185], p=0.014, respectively).

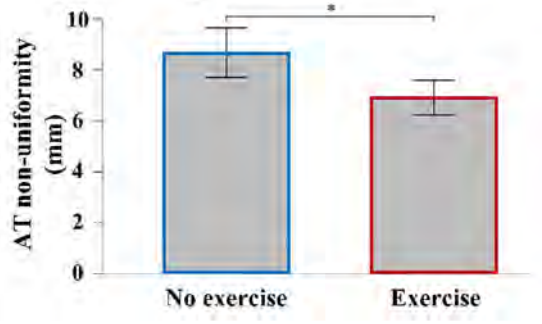

Figure 1. AT non-uniformity of athletes with or without exercise within two days before assessment.

Injury history or sex did not affect any of the outcomes measured. Sports differences were observed in men, with smaller AT mean displacement in basketball players compared to gymnasts (-3.741 mm [-6.938- -0.543], p=0.042), with the difference localizing in the anterior half of the tendon (-5.051 mm [-9.044- -1.058], p=0.022). The dominant leg showed a greater AT mean displacement in the posterior half of the tendon in gymnasts (1.2 mm [0.009–2.4], p=0.048), and in contrast, the displacement was greater for the non-dominant side (0.9 mm [0.05–1.8], p=0.039) in football players. In ice hockey players AT non-uniformity and SWV of the proximal AT measurement site were greater on the dominant side (1.2 mm [0.2–2.2], p=0.022; 0.8 m/s [0.1–1.5], p=0.031).

CONCLUSIONS

The internal displacement of the Achilles tendon was smaller if exercise was performed within two days before the assessment. This may reflect the necessary time course of tendon recovery in healthy individuals. The results suggest multifaceted differences in mechanical properties of Achilles tendon regarding sport-specific loading and leg dominance.

REFERENCES

[1] Obst et al. *Med Sci Sports Exerc.* **45(8)**:1534–44, 2013.
[2] Pedret et al. *Scand J Med Sci Sports* **30(12)**:2456–65, 2020.
[3] Leino et al. *Orthop. J. Sports Med.* **10(11)**: 23259671221131536, 2022.
[4] Slane & Thelen *J Biomech.* **47(12)**:2831-5, 2014.

Determining Torque-Angle Relationships of Human Toe Flexors

Samuel J Wisdish[1], Hannah Rice[1,2] Matthew A Ellison[1], and Dominic J Farris [1]
[1] Public Health & Sport Sciences, University of Exeter, Exeter, United Kingdom.
2 Department of Physical Performance, Norwegian School of Sport Sciences, Oslo, Norway.
Email: S.Wisdish@exeter.ac.uk

INTRODUCTION

We rely on the foot's muscles during tasks of movement, with the plantar intrisnic muscles (PIMs) actively facilitating propulsion during gait [1]. Weakness or atrophy of foot musculature is associated with reduced mobility, and strengthening of these muscles may help mitigate age-related mobility declines [2]. Understanding the force-generating capacity of the toe flexor muscles may therefore be a key to understanding healthy foot function. We aimed to establish toe flexion torque-angle relationships and improve *in-vivo* estimations of the parameters governing force production.

METHODS

Separate isometric hallux (HFT) and lesser digit (LDFT) flexion torque-angle data were twice collected from nine participants (age 28 ± 5 years) using a custom setup. Torque of twitch response to transcutaneous supramaximal stimuli applied at two tibial nerve sites (medial malleolus – MM; and popliteal fossa – PF) distinguished PIM, and PIM+extrinsic active contributions from passive contributions throughout MTP joint range, in four conditions (HFT_{MM}, $LDFT_{MM}$, HFT_{PF}, $LDFT_{PF}$). 3D kinematics were processed in OpenSim 4.3 using a multi-segment foot model. Active and passive torque-angle curves were computed within Matlab (Mathworks) using physiologically appropriate models [3] for each participant with curve coefficients of maximum torque (T_{max}), optimum angle (Θ_{opt}), passive stiffness (k) and slack angle (Θ_{slack}).

RESULTS AND DISCUSSION

HFT and LDFT torque-angle relationships and their coefficients showed good-excellent inter-day reliability (Table 1.). Greatest T_{max} occurred when innervating both the hallux flexors (3.04 ± 0.76 Nm) and lesser digit flexors (3.17 ± 1.05 Nm) from the PF. For all conditions T_{max} occurred at MTP joint angles (Θ_{opt}) that would be typically observed during the propulsive phase of gait (HFT_{PF} = 48 ± 14.6°; $LDFT_{PF}$ = 42.9 ± 14.9°) (Figure 1C), which suggests they may be optimised to contribute to propulsion. Furthermore, the peak total torque generated at the MTP joint was dominated by active, not passive, torques (Figure 1. A and B). Passive MTP joint torques are assumed largely to be generated by the plantar fascia (Figure 1. Panel A & B), and our results therefore question the functional importance of the windlass mechanism.

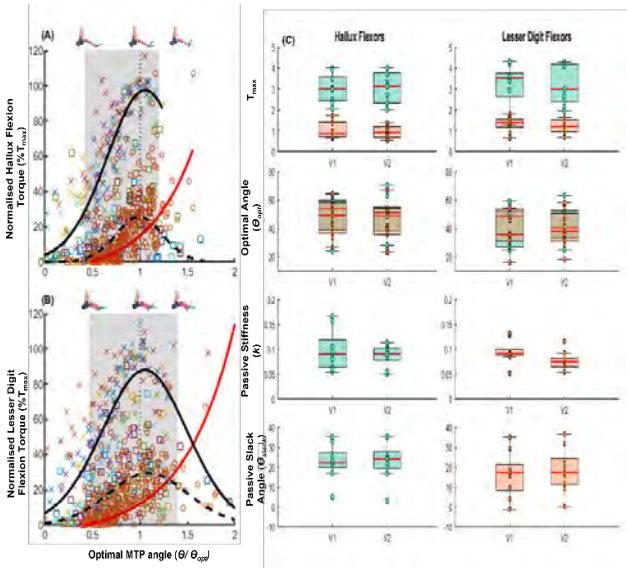

Figure 1. Comparison of mean toe flexor torque-angle relationships and coefficients. (A) and (B) plot mean normalised hallux flexor (A) and lesser digit flexor (B) torque-angle relationships from PIM only (dashed black), PIM + extrinsic (solid black) and passive torque (red) about the respective MTP joints. The shaded grey area represents typical range of MTP joint during propulsive phase of gait. (C) plots torque-angle relationship curve coefficients across Visit 1 & Visit 2 for each contraction condition (PIM only = orange; PIM + extrinsic = green).

CONCLUSIONS

Optimal force-generating angles of human toe flexors appears to be aligned with the typical MTP joint kinematics during propulsion, and are dominated by active muscle contraction. This may have implications for further understanding how active muscle contributions determine the foot's mechanical function in tasks such as walking.

ACKNOWLEDGEMENTS

S Wisdish is supported by the Engineering and Physical Sciences Research Council. EP/R513210/1.

REFERENCES

[1] Farris D et al. *J. R. Soc Interface* **17**: 20200208, 2020.
[2] Mickle K et al. *Clin Biomech* **40**: 14-19, 2016.
[3] Pincheira P et al. *Scand J Med Sci Sports* **28**: 2123-2134, 2018

Table 1. Analysis of reperated measures reliability of torque-angle curve coefficients determined using a custom-built setup and supramaximal stimulation protocol.

(n = 9)	HFT_{PF}				HFT_{MM}				$LDFT_{PF}$				$LDFT_{MM}$			
	T_{max} (Nm)	Θ_a (°)	k	Θ_{slack} (°)	T_{max} (Nm)	Θ_a (°)	k	Θ_{slack} (°)	T_{max} (Nm)	Θ_a (°)	k	Θ_{slack} (°)	T_{max} (Nm)	Θ_a (°)	k	Θ_{slack} (°)
ICC	0.81	0.82	0.72	0.97	-0.34	0.93	0.72	0.97	0.79	0.93	0.71	0.98	0.96	0.87	0.71	0.98
SEM	0.31	5.86	0.02	1.58	0.41	3.63	0.02	1.58	0.46	3.58	0.01	1.59	0.07	4.74	0.01	1.59
MDC	1.51	6.71	0.36	3.48	1.78	5.28	0.36	3.48	1.89	5.25	0.30	3.50	0.75	6.03	0.30	3.50

N.b (*ICC*, Intraclass correlation coefficients; *SEM*, Standard error of measurements; *MDC*, Minumum detectable change)

Individual rocker shoe parameters that reduce plantar peak pressure

Thomas Johnson[1], Frederico Klein[1], Juha M. Hijmans[2], Fredrik Olsson[1], Elena M. Gutierrez-Farewik[1,3]
[1]KTH MoveAbility Lab, Dept. Engineering Mechanics, KTH Royal Institute of Technology, Stockholm, Sweden
[2] University of Groningen, Univ. Medical Center Groningen, Dept. Rehabilitation Medicine, Groningen, the Netherlands
[3]Department of Women and Children's Health, Karolinska Institutet, Stockholm, Sweden

Introduction

Diabetes is an insulin deficient condition that is growing in many parts of the world (WHO [1]). One of the most common co-morbidities associated with diabetes is the loss of peripheral sensation. Increase in plantar pressure under the foot [2] contributes to development of diabetic foot ulcers (DFU), which can lead to amputation. Rocker shoes, or shoes with a curved midsole have been shown to decrease plantar pressure especially in the forefoot [3]. The aim of this study is to investigate the influence of a range of rocker shoe parameters in plantar pressure, with the specific goal of reducing to or maintaining peak pressure (PP) at all points of less than 200 kPa.

Methods

In this randomised crossover-controlled trial, twenty-four different rocker shoe conditions were tested on thirty-six able-bodied participants. Longitudinal bending stiffness (rigid (r) and flexible (f)), rocker radius (rr) - 60% and 70% of shoe length from heel, apex position (ap) - 55%, 60% and 65% of shoe length, and apex angle (aa) - 65° and 85° from the shoe longitudinal axis (from the heel to the 2nd toe) all varied in the different experimental shoe conditions. In-shoe plantar pressure insoles (Novel Pedar) were used to measure PP during ca. 12-15 gait cycles at 2 different speeds on a treadmill, with all shoe configurations and with participants' own everyday shoes (control). The speeds were height-, age- and gender-normalised preferrable walking speed [4], and slow walking (mean preferrable walking speed – 1 standard deviation). Sensors were grouped into 7 masks deemed clinically relevant to the development of DFU.

Results and Discussion

Stiffness, ap and rr all showed significant effects on the reduction of PP ($p<0.001$) in the forefoot. At the heel all rocker conditions lead to increased pressure relative to control ($p<0.001$). Stance phase was shown to be shorter in rocker shoes when compared to control.

Rocker shoes are effective in reducing PP distally [3] wherein a range of ap and rr can significantly reduce pressure in clinically relevant areas such as the hallux and the medial forefoot. However, all rocker conditions caused an increase in PP above the threshold value (200 kPa) at the heel in early stance phase. Increased PP at the heel may be associated with spatiotemporal gait changes in rocker shoes such as reduced double stance phase.

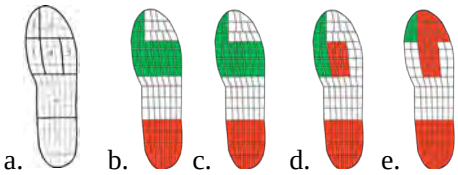

Figure 1. a. *Custom masks. Experimental rocker shoes compared to control, significant increase (green) and decrease (red).* ***b.*** *f- and* ***c.*** *r/ap55/aa65/rr60.* ***d.*** *f- and* ***e.*** *r/ap65/aa85/rr70*

Conclusion

Going forward it may be important to compensate for heightened pressure under the heel with some pressure redistributive material insole or midsole. These results indicate the importance of an individualised approach to the prescription of rocker shoes to reduce pressure at specific plantar areas of the foot.

ACKNOWLEDGMENTS

This project was funded by EIT Health (20250 IndiRock'nSole).

References

[1] World Health Organisation, "Diabetes." *World Health Organization (WHO)*, 2022.

[2] A. Veves, et al., *Diabetologia*: 35(7), 660-663, 1992.

[3] L. van Kouwenhove et al., *Gait Posture*: 86, 150–156, 2021.

[4] R. W. Bohannon, *Age Ageing*: 26(1), 15–19, 1997.

A SEGMENT FRAME OPTIMISATION METHOD TO STANDARDISE KINEMATIC SIGNALS

Ariana Ortigas Vásquez[1,2], William R. Taylor[3], Barbara Postolka[3], Pascal Schütz[3], Allan Maas[1,2], Michael Utz[1], Matthias Woiczinski[2], Thomas M. Grupp[1,2] and Adrian Sauer[1,2]

[1] Research and Development, Aesculap AG, Tuttlingen, Germany.
[2] Musculoskeletal University Centre Munich, LMU Munich, Munich, Germany.
[3] Laboratory for Movement Biomechanics, ETH Zurich, Switzerland.
Email: ariana.ortigas_vasquez@aesculap.de

INTRODUCTION

In motion analysis, kinematic signals are calculated from optical or inertial data to visually represent movement between joint segments. Despite ISB recommendations aiming to standardise the reporting of these signals [1], a lack of consensus around joint coordinate frame definitions remains. The influence of local segment frame position and orientation on the characteristics of kinematic signals has been shown to be a major limitation [2,3]. For consistent interpretation of joint motion to be possible, differences in frame alignments must therefore be addressed. Here, we assess the REference FRame Alignment MEthod (REFRAME) [3] on the knee kinematics of a cohort of 10 healthy subjects, investigating the method's ability to enable kinematic signal convergence in six degrees of freedom, despite the use of different frame definitions.

METHODS

REFRAME reorientates and repositions local segment frames such that the associated kinematic signals fulfil certain optimisation criteria. Here, *in vivo* knee kinematics captured using a moving videofluoroscope were used to validate REFRAME. While a common approach was used to define the tibial frame, three different femoral coordinate frames were defined using the following variations of the flexion/extension axis: cylindrical axis (CA), functional flexion axis (FFA), and transepicondylar axis (TEA) [2]. Flexion/extension, ab/adduction, and int/external rotation, as well as anteroposterior, mediolateral and proximodistal translation were calculated over five stair descent trials for 10 healthy subjects [4]. REFRAME then optimised the obtained kinematic signals to realign local frames such that root-mean-square errors (RMSEs) vs. 0 for ab/adduction and int/external rotation, as well as variances for all three translations, were minimised.

RESULTS AND DISCUSSION

Frame transformations induced by REFRAME led to noticeable changes in the magnitude and characteristics of the kinematic signals. In addition to evident convergence of the optimised signals (Fig. 1), pairwise comparisons of signals coming from different definitions led to a decrease in mean RMSE from 3.24mm±2.50mm to 0.24mm±0.05mm for translations, and from 2.62°±2.07° to 0.10°±0.16° for rotations. Changes in the orientation and position of local frames resulting from the implementation of REFRAME led to convergence of kinematic signals that originated from the same underlying movement but were calculated using different flexion/extension axis approaches.

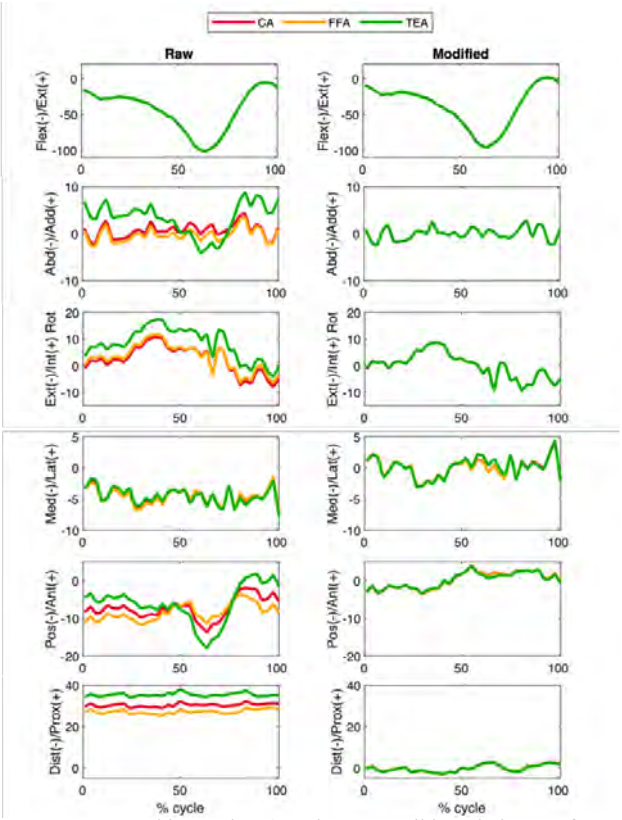

Figure 1 Knee kinematics (rotations [°]: tibia relative to femur; translations [mm]: femur relative to tibia) during a sample subject stair descent trial, using three different primary axes, before (raw) and after (modified) REFRAME. (CA and FFA partially covered by TEA)

CONCLUSIONS

REFRAME can enable the consistent interpretation and comparison of joint kinematics derived using different approaches.

REFERENCES

[1] Wu G & Cavanagh P *J Biomech* **28(10)**:1257, 1995.
[2] Postolka B et al. *J Biomech* **144**: 111306, 2022.
[3] Ortigas Vásquez et al. *In Review*, 2023.
[4] Postolka B et al. *J Biomech* **110:**109915, 2020

Is Peak Anterior Foot Position Related to Anterior Foot Position at Initial Contact during Gait Training with Visual Feedback?

Erik T. Hummer[1], Melvin Mejia[2,3], Xuan Liu[2,3] and Peter Barrance[2,3]

[1] Department of Kinesiology and Health, Rutgers University, New Brunswick, NJ, USA.
[2] Center for Mobility and Rehabilitation Engineering Research, Kessler Foundation, West Orange, NJ, USA
[3]Children's Specialized Hospital Research Center, New Brunswick, NJ, USA
Email: Erik.Hummer@Rutgers.edu

INTRODUCTION

Providing relevant and easy to interpret feedback stimuli is key for gait training paradigms utilizing augmented feedback. Anterior foot position at initial contact relative to the body (AFP_{IC}) provides insight into the severity of impairments in patient populations such as cerebral palsy (CP) [1], and hence could be a strong basis for a feedback retraining cue. During normative gait, the furthest anterior foot position (AFP_{Peak}) occurs simultaneously or close to initial contact, indicated by the "reversal" of the foot anterior/posterior velocity measured via motion capture [2]. AFP_{Peak} can be estimated purely through segmental kinematics as measured from wearable inertial measurement unit (IMU) orientations and does not require detection of initial contact which can be technically challenging, especially in pathological gait. We previously reported that a participant with CP responded to AFP_{Peak} feedback with increased knee extension at initial contact as anticipated [3]. In the current study we compared the relationships between AFP_{Peak} and AFP_{IC} during baseline (BAS) walking and AFP_{Peak} feedback exposure, to gain further insight into the adaptations to this visual cue.

METHODS

Results are presented from four participants (13.8 ± 5.1 yrs) diagnosed with CP and exhibiting increased knee flexion angle at initial contact. In all testing, participants walked on a treadmill at a self-selected speed with synchronized collection of lower extremity kinematics from four IMUs (60 Hz) and 3-dimensional motion capture (120 Hz). Participants first walked for one minute to obtain BAS gait kinematics. Participants then walked for six minutes with visual feedback followed by 3 minutes of rest, repeated three times. During feedback trials, a kinematic model utilizing 3D IMU orientations and segment lengths for the more involved side thigh and shank calculated relative foot position, displayed real-time as a red dot moving vertically [3]. The display incorporated scoring zones and awarded points in ascending order based on AFP_{Peak} for each step.

RESULTS AND DISCUSSION

During BAS, all participants displayed a strong correlation between AFP_{Peak} and AFP_{IC} (Figure 1). This supports the notion that, during gait, AFP_{Peak} could be considered a surrogate assessment of AFP_{IC}. When feedback was introduced, the observed correlations were maintained overall for 3 of the 4 subjects. Subject 2, however, displayed decoupling of the relationship. This subject adopted an unusual gait adaptation in which the time delay between the occurrence of AFP_{Peak} and initial contact was increased almost six-fold (Fig. 1). We observed adaptations including greater increases in AFP_{IC} among subjects 1, 3, and 4 (+13.5% - 853.2%) compared to subject 2 (+4.1%).

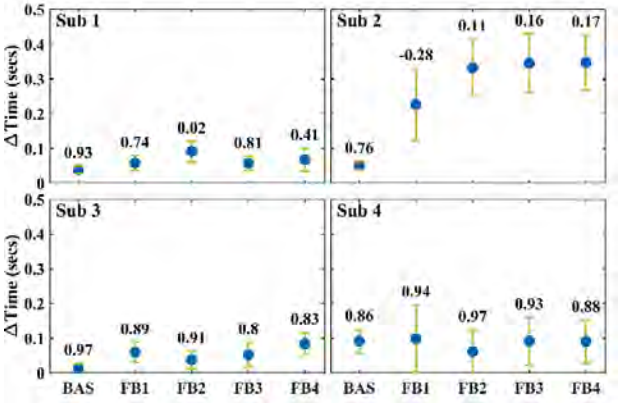

Figure 1. Time delays between AFP_{Peak} and AFP_{IC} (mean and S.D. bars) and AFP_{Peak}/AFP_{IC} correlation coefficients (numbers above S.D. bars) for baseline (BAS) and feedback (FB) trials.

CONCLUSIONS

With exceptions for some trials, three out of four subjects maintained high correlations between AFP_{Peak} and AFP_{IC} from BAS into AFP_{Peak} exposure. Hence, this feedback stimulus shows potential for gait training in paediatric CP when the intention is to target adaptations at initial contact. In this way, feedback systems such as this one can rely on IMU orientation only and avoid the need to detect foot contact in real-time. However, some individuals may respond to this feedback with unintended gait patterns in which AFP_{Peak} significantly precedes initial contact. For these circumstances, additional cueing from clinical staff may be adopted to model the type of adaptation to AFP_{Peak} visual feedback.

ACKNOWLEDGEMENTS

Funding for this study was provided by Children's Specialized Hospital and Kessler Foundation.

REFERENCES

[1] Balasubramanian et al. *Clin Biomech* **25:5**, 2010.
[2] Zeni et al. *Gait Posture* 27:4, 2008.
[3] Hummer et al. *NACOB*: Ottawa, CA, 2022.

Gait Kinematics for Severe Knee OA and Post-TKA from Markerless Motion Capture

Elise K. Laende[1], Jereme B. Outerleys[1], Vajra Keller[1], Anastasija Mihic[1], Kevin J. Deluzio[1]

[1]Queen's University, Kingston, Ontario, Canada

Email: elise.laende@queensu.ca

INTRODUCTION

The use of biomechanical data to inform clinical decision making in orthopaedics has been rare, largely due to practical limitations in obtaining motion capture data. Traditional marker-based motion capture systems are resource- and time-intensive with significant data collection burden for patients. Markerless motion capture technology using computer vision and machine learning approaches to obtain biomechanical data from standard video images offers significant advantages for ease of data collection, but must demonstrate the ability to produce relevant outcome metrics in a clinical population. The objectives of our pilot study were to (1) determine the feasibility of using markerless motion capture technology to record kinematics during a variety of tasks in an orthopaedic population recruited directly from clinic visits and (2) to compare gait waveform data collected on a severe knee osteoarthritis (OA) population to a control group, to replaced knee joints, and to historical marker-based data for similar groups.

METHODS

Orthopaedic patients with knee OA were recruited from an orthopaedic assessment clinic after referral to an orthopaedic surgeon for total knee arthroplasty. Participants wore the clothes and shoes they had worn that day. Severe OA patients (n=77) performed functional tasks during markerless motion capture: timed up-and-go (TUG), stair ascent and descent, quiet standing (balance), walking at self-selected speed, and fast walking. Previous knee replacements in the contralateral leg were analyzed separately (n=17). A control group consisted of members of the community over 50 years of age (n=29). Markerless motion capture was performed using 8 commercially available video cameras (Sony RX0-II) recorded at 60 Hz and processed using Theia3D (Theia Markerless Inc.). Historical data using a marker-based motion capture system for severe OA post-knee replacement, and control subjects were obtained from a previous publication [1].

RESULTS AND DISCUSSION

The markerless severe OA group was 56% female with mean age 69 years (SD 8). Kinematic data from the markerless system was calculated for all participants for all completed tasks with no discernable tracking issues. The markerless control group (59% female, mean age 58 years) had a self-selected walking speed of 1.3 m/s compared to 0.9 m/s for the severe OA group. Joint angle waveform data captured with the markerless system show similar patterns to historical data collected with marker-based motion capture for severe OA, post-knee replacement, and control groups (Figure 1).

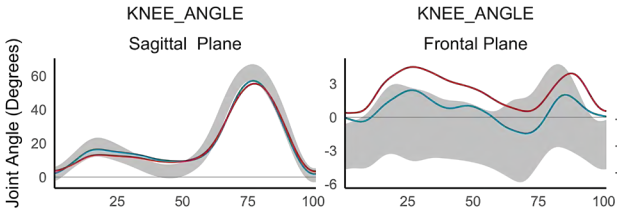

Figure 1 Joint kinematics from markerless motion capture in a cohort of severe knee OA patients (red) and post-total knee replacement (blue). Shaded regions represent +/- 1 standard deviation from age-matched control group means. Knee flexion in the sagittal plane and knee adduction angles in the frontal plane exhibit similar waveform pattern and magnitude characteristics as compared to historical maker-based data, specificially reduced flexion angles and greater varus alignment in the severe OA group. Replaced knees are closer to asymptomatic patterns.

CONCLUSIONS

This study demonstrates feasibility of using markerless motion capture for an orthopaedic population directly from a clinic visit with no restrictions on clothing. Kinematic data from markerless motion capture exhibited expected kinematic deviations based on historical marker-based gait data on similar populations. The ease of data collection and the standardized calculation of biomechanical metrics have important implications for clinical implementation as well as longitudinal and multi-centre studies.

ACKNOWLEDGEMENTS

REFERENCES

[1] Outerleys JB, et al., J Appl Biomech, 2021 37(2) 130-138.

GAIT CHARACTERISTICS OF OLDER ADULTS WITH SAGITTAL MALALIGNMENT PROGRESSION AFTER SPINAL FIXATION

Shun Ito[1], Naoto Mano[1], Kimihiko Mori[2],
Takayuki Konishi[1], Jin Kuramoto[1] and Kimitaka Hase[3]
[1] Department of Physical Medicine and Rehabilitation, Kansai Medical University Hospital, Hirakata, Japan.
[2] Department of Physical Therapy, Faculty of Rehabilitation, Kansai Medical University, Hirakata, Japan.
[3] Department of Physical Medicine and Rehabilitation, Kansai Medical University, Hirakata, Japan.
Email: itoshun@hirakata.kmu.ac.jp

INTRODUCTION

Spinal fixation for spinal deformity in adults corrects the alignment of the spine, both in static positions and during gait. However, mechanical complications occur in approximately 30% of cases postoperatively; sagittal malalignment is one of these factors. Gait characteristics are closely related to spinal alignment. Therefore, identifying gait characteristics in older adults with the progression of sagittal malalignment after spinal fixation aids decision-making in postoperative rehabilitation. Herein, we compared the gait characteristics of patients with and without sagittal malalignment after spinal fixation.

METHODS

Ninety-four patients (mean age: 74 years) who underwent spinal fixation from the thoracic to the pelvis were assessed by three-dimensional gait analysis six months postoperatively and by radiographic spinal alignment six months and one year postoperatively. Patients whose sagittal vertical axis (SVA) was > 0 at six months and increased from six months to one year postoperatively were defined as the sagittal malalignment group; the others were defined as the non-sagittal malalignment group. Inverse probability of treatment weighting (IPTW) was performed to adjust the covariates of the patients with and without sagittal malalignment. The covariates included were spinopelvic or radiographic parameters such as SVA, thoracic kyphosis, pelvic tilt, proximal junctional angle, lumbar lordosis, age, sex, knee extension strength, and ankle plantar flexion strength. To determine the characteristics of the individuals with the progression of sagittal malalignment, gait characteristics were compared using a generalized linear model between groups after IPTW. Then the coefficient of determination was calculated between the gait characteristics, which showed significant differences between groups, and other gait characteristics to reveal the gait pattern of the patients with the progression of spinal malalignment. Analyses were conducted using R software (version 4.0.3). $P < 0.05$ denoted statistical significance.

RESULTS AND DISCUSSION

The maximum trunk flexion angle during the gait cycle was significantly larger and the trailing limb angle (TLA) was smaller in patients with sagittal malalignment than those in patients without sagittal malalignment (Table 1, Figure 1). In patients with sagittal malalignment, the maximum trunk flexion angle was positively correlated with the maximum distance between C7 and the center of mass (COM) during the gait cycle ($r^2 = 0.61$, $p < 0.001$) and negatively correlated with TLA ($r^2 = 0.23$, $p < 0.001$), step length ($r^2 = 0.28$, $p < 0.001$), and hip extension angle at toe-off ($r^2 = 0.16$, $p = 0.01$). The results suggested that, despite adjusted radiographic parameters, patients who walked with trunk flexion and reduced step length may receive mechanical load by increasing the C7-COM distance.

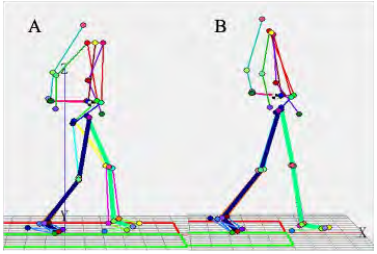

Figure 1 Gait pattern in patients with (A) and without (B) sagittal malalignment.

CONCLUSIONS

Although spinal alignment is corrected by spinal fixation, patients who cannot keep the trunk upright during gait may experience progression of sagittal malalignment. A rehabilitation strategy after spinal fixation aimed at keeping the trunk upright and carrying the lower limb posteriorly can effectively prevent the progression of sagittal malalignment.

Table 1: Comparison of gait characteristics of patients with and without sagittal malalignment.

Gait characteristics	With sagittal malalignment, n = 42	Without sagittal malalignment, n = 52	95%CI	*p-value*
Maximum trunk flexion, deg	12.2 ± 3.99	10.2 ± 3.91	0.318 to 3.76	0.021
Trailing limb angle, deg	16.1 ± 5.77	18.8 ± 4.17	0.381 to 4.92	*0.023*

ANALYSIS OF GAIT COORDINATION CHANGES AFTER TRAINING USING HAL IN PATIENTS WITH GAIT IMPAIRMENT DUE TO CENTRAL NERVOUS SYSTEM DISORDERS

Hideki Kadone[1], Yukiyo Shimizu[2], Seioh Ezaki[3], Sandra Puentes[4], Hiroki Watanabe[5], Shigeki Kubota[3], Aiki Marushima[5], Kenji Suzuki[1,4], Yasushi Hada[2] and Masashi Yamazaki[3]

[1] Center for Cybernics Research, University of Tsukuba, Tsukuba, Japan.
[2] Department of Rehabilitation Medicine, University of Tsukuba, Tsukuba, Japan.
[3] Department of Orthopaedic Surgery, University of Tsukuba, Tsukuba, Japan.
[4] Faculty of Engineering, Information and Systems, University of Tsukuba, Japan.
[5] Department of Neurosurgery, University of Tsukuba, Tsukuba, Japan.
Email: kadone@md.tsukuba.ac.jp

INTRODUCTION

Gait disturbance is commonly associated with disorders in the central nervous system such as stroke and spinal cord injury. Although there are reports on the effectiveness of robot-assisted gait training for these patients, they are often reported with clinical assessment, but not with biomechanical analysis of the gait changes. For this reason we aim to characterize the changes in gait control and lower limb muscle activity in these patients after robotic intervention, in terms of segmental coordination of the limbs and lower limb muscle synergies, by comparing between pre and post gait training using a bioelectrically controlled robot suit HAL (Hybrid Assistive Limb, Cyberdyne, Japan.), and between HAL and control groups, among patients with gait impairment due to stroke or spinal cord disorder.

METHODS

30 patients with disorders in the central nervous system (11: acute phase after stroke, 15: myelopathy and 4: spinal cord injury) underwent HAL treatment of 9-10 training sessions. 9 post stroke patients underwent conventional gait training of the same number of sessions. All-In-One walking trainer (Ropox A/S, Denmark) was used together. The training using HAL consisted 20 min of walking activity in a 25 m oval course at a comfortable pace using a single or double legged HAL to support the lower limb movement. Neuromuscular activity of the hip flexor, hip extensor, knee flexor, and knee extensor muscles of the affected side was detected through surface electrodes and processed to mechanically assist the patients' gait. Gait and lower limb muscle activity during 10m walking test was recorded using an optical motion capture (VICON, UK) and a wireless electromyography system (Trigno Lab, Delsys, USA).

RESULTS AND DISCUSSION

10m walking speed and the range of joint motion improved after the HAL sessions in both stroke and myelopathy patients [1,2]. As well, covariation analysis of sagittal elevation angle of the limb segments (thigh, shank, foot) showed closer to healthy segmental coordination after HAL, in terms of planarity and loop shape, in both stroke and myelopathy patients [2,3].

Muscle activity analysis showed improvement of symmetry of the lower limb muscle synergies in the stroke patients after HAL training [4], and when compared to the control group, improvement of timing synergies was observed in the HAL group [5]. A case analysis of a myelopathy patient suggested involvement of greater number of lower limb muscle synergies during HAL gait training [6].

Patients with complete paraplegia due to spinal cord injury used upper limbs to control HAL during training based on the symmetric coordination of upper and lower limbs during human gait. The patients showed activation of some of the lower limb muscles during and after HAL gait training [7].

Since HAL assists the lower limb joint motion by sensing the relevant neuro-muscular activity [8], we consider that actual achievement of the motion, and hence sensation of the motion, intended by the central nervous system during the robot-assisted gait training, helped to change the central nervous system's control of gait.

CONCLUSIONS

In this study, we analysed gait coordination changes after gait training using HAL in stroke patients and in patients with spinal cord disorders. The analyses showed improvement of coordinated control of the limbs and the muscles. The effect of HAL on the coordinated gait control by the central nervous system is discussed.

REFERENCES

[1] Puentes S, et al. Front. Neurosci. 12:719. 2018.
[2] Ezaki S, et al. Front. Neurorobot. 15:650118. 2021.
[3] Puentes S, et al. Front. Neurosci. 12:99. 2018.
[4] Tan CK, et al. Front. Neurosci. 12:276. 2018.
[5] Tan CK, et al. Front. Bioeng. Biotechnol. 8:770. 2020.
[6] Kadone H, et al. Front. Neurol. 11:102. 2020.
[7] Shimizu Y, et al. Front. Neurosci. 11:649. 2017.
[8] Sankai Y, et al. Science Robotics. 3:eaat3912. 2018.

EFFECTS OF POSTERIOR SPINAL FUSION SURGERY ON GAIT BIOMECHANICS IN PATIENTS WITH ADOLESCENT IDIOPATHIC SCOLIOSIS

Manish Gupta[1], Bhavuk Garg[1], Nishank Mehta[1], Rajesh Malhotra[1]
[1]Department of Orthopaedics, All India Institute of Medical Sciences, New Delhi, India
Email: manishgupta1307@gmail.com

INTRODUCTION

Scoliosis is a complex multidimensional spinal deformity which affects spinal anatomy, quality of movement and walking, and trunk symmetry. Posterior spinal fusion (PSF) is usually performed to stop curve progression, to reduce back pain and to restore asymmetric upper body [1]. Previous studies indicate that, there is an alteration of gait patterns in patients with Scoliosis and this gait pattern is substantially altered after surgical intervention. In India, these deformities are often neglected and present at a very late and much more deformed state (mean cobb angle $\geq 60^0$). So, we have planned a study to investigate the effects of posterior spinal fusion surgery on spatio-temporal, kinematics, kinetics and Electromyography (EMG) in severe Adolescent Idiopathic Scoliosis (AIS) patients during gait.

METHODS

This clinical prospective study after written informed consent included 60 AIS subjects and 20 healthy controls (mean age 16.3 Years) diagnosed with thoraco-lumbar/lumbar AIS (cobb angle MT 78.62 ± 8.10, TL/L 60.52 ± 7.42). Spatio-temporal parameters, kinematics, kinetics, & EMG were evaluated preoperatively and after 1 Year of surgery for AIS subjects and one time for healthy controls using instrumented 3D gait analysis (BTS, Italy) (Figure-1). Student T test, & two way annova were performed to find significant differences between pre and post operative AIS and healthy controls.

RESULTS AND DISCUSSION

Gait speed, cadence, step length were improved significantly after 1 Year of surgery. Trunk tiklt range, pelvis tilt range, gait profile score (GPS) and gait deviation index (GDI), were not changed significantly postoperatively. No significant changes in mean angle of spine flex extension, Peak during loading and propulsion, EMG activity of Erector spiane & gluteus medius were observed postoperatively (Table-1). A comprehensive study involving long-term post-operative follow-up is needed to draw decisive conclusions regarding alteration in gait of scoliosis patients postoperatively.

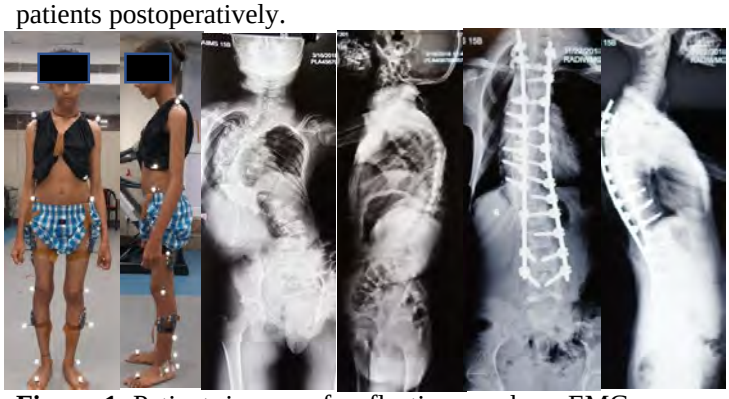

Figure-1 Patient image of reflective marker, EMG placement and pre & post operative x ray of AIS subject

CONCLUSIONS

The results of our study suggested that Surgical intervention did not cause any significant changes in the upper and lower limb kinematics during gait, despite of large part of spinal fusion. Postoperative significant improvements in spatio-temporal parameters explain the well functioning in daily life of subjects with Adolescent Idiopathic Scoliosis.

REFERENCES

[1] de Kleuver M, et al, Optimal surgical care for adolescent idiopathic scoliosis: an international consensus. Eur Spine J, 2014, 23(12):2603–2618.

Table 1: Comparisons of spatio-temporal, kinematics, kinetics, &EMG of healthy controls, AIS preoperatively & after 1 year of surgery: Values are in Mean (SD)

Variables	Healthy Control	AIS Preoperative	p value	AIS Postoperative (1 Year)	p value
Gait Speed (m/s)	1.17 (0.12)	0.96 (0.12)	**0.009**	1.06 (0.11)	**0.01**
Cadence (Steps/min)	116.42 (6.60)	106 (3.11)	**0.001**	112.93 (5.11)	**0.001**
Step Length (m)	0.60 (0.68)	0.55 (0.04)	**0.01**	0.59 (0.09)	**0.05**
Trunk tilt range (angle in degree)	2.7 (0.85)	3.6 (0.76)	**0.05**	3.3 (0.88)	0.53
Pelvis tilt range (angle in degree)	4.6 (0.67)	3.2 (0.63)	**0.05**	3.4 (0.55)	0.79
Spine Flex-Extension (angle in degree)	20.12 (6.32)	18.32 (6.68)	0.78	19.14 (6.23)	0.78
Gait Profile Score	5.54 (1.71)	7.57 (1.82)	**0.05**	7.82 (1.12)	0.56
Gait Deviation Index	99.98 (4.89)	90.12 (7.91)	**0.001**	92.29 (8.11)	0.89
Peak During Loading (V GRF)	101.53 (5.12)	96.76 (8.93)	**0.05**	99.88 (6.12)	0.18
Peak During Propulsion (V GRF)	109.71 (3.12)	103.47 (8.60)	**0.05**	105.65 (6.34)	0.72
Wt Load (%)	50.66 (4.02)	55.6 (6.86)	**0.01**	53.43 (4.32)	0.87
Erector Spinae (mV)	0.07 (0.05)	0.035 (0.02)	**0.001**	0.039 (0.03)	0.14
Gluteus Medius (mV)	0.05 (0.03)	0.031(0.03)	**0.001**	0.35 (0.04)	0.15

THREE-DIMENSIONAL VECTOR ANALYSIS OF GROUND REACTION FORCE MOMENT ARMS: CONCEPTUAL CONSIDERATIONS AND EXPERIMENTAL VERIFICATION

Shinichi Kawamoto, Momoko Nagai-Tanima, Tomoki Aoyama
Department of Human Health Science, Graduate School of Medicine, Kyoto University, Japan.
Email: kawamoto.shinichi.26m@st.kyoto-u.ac.jp

INTRODUCTION

Various geometric algorithms are used in the calculation of three-dimensional moment arms (3D-MA) in vivo. Inappropriate use of vector equations for 3D-MA in the context of purpose may occur without comprehension of its meaning. This research attempted to classify various research publications for 3D-MA and identify geometrical differences among the algorithms theoretically and experimentally.

METHODS

3D-MA were classified geometrically into three major categories and renamed based on conceptual considerations. The vector equations of the algorithms were collectively reinterpreted using 3D vector analysis. Additionally, these vector algorithms were verified experimentally. The moment arms of the ground reaction force about the knee in a deep squat position were determined in 31 healthy subjects using an optoelectronic motion capture system. MA with a fixed axis were calculated in four algorithms including three 3D-MA and one two-dimensional (2D-) MA.

RESULTS AND DISCUSSION

3D-MA were classified by definition: MA about a Point, Conversion MA, and Medical MA (Table 1). Figure 1 represents a schematic showing various 3D vectors, 3D-MA, and mutual relationships. Medical MA [1] is:

$$d_3(=d_4)=\overrightarrow{CG}\cdot\frac{\hat{\mathbb{F}}\times\hat{\mathbb{u}}}{|\hat{\mathbb{F}}\times\hat{\mathbb{u}}|}\ (=\mathbb{B}\cdot(\hat{\mathbb{A}}\times\hat{\mathbb{u}})) \quad (1)$$

Where $\cdot$ denotes dot product and $\times$ denotes cross product of vectors. Conversion MA [2] is:

$$d_3\sin\alpha=\overrightarrow{CG}\cdot(\hat{\mathbb{F}}\times\hat{\mathbb{u}}) \quad (2)$$

where α denotes twist angle between the line of action and the axis of rotation. To keep the moment-force relation universal in 3D also, the Medical MA algorithm imposes a component resolution on the force side, whereas the Conversion MA algorithm does on the MA side. MA about a point [3,4] is:

$$d_1=|\mathbb{P}\times\hat{\mathbb{F}}| \quad (3)$$

$$\text{or}\ \ d_2=|\mathbb{P}-(\mathbb{P}\cdot\hat{\mathbb{A}})\hat{\mathbb{A}}| \quad (4)$$

The following inequality holds geometrically as long as the identical axis (whether fixed or moving) is in use:

$$d_3\sin\alpha\le d_3(=d_4)\le d_1,d_2 \quad (5)$$

Regarding verification, Conversion MA was 2% shorter ($P<0.001$), 2D-MA was 10% shorter ($P<0.001$), whereas MA about a point was 3% longer ($P<0.001$) than Medical MA, which agreed with the geometrical deduction.

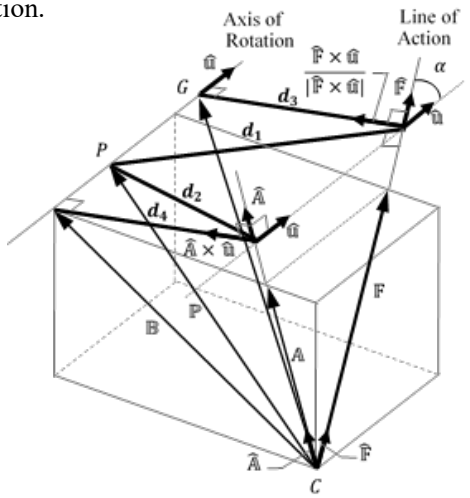

Figure 1 Schematic showing the vectors and the moment arms in three dimensions. d_1, d_2: Moment arm about a point, d_3, d_4: Medical moment arm, C: the origin of force, G: the foot of the perpendicular from the line of action to the axis of rotation, P: the joint center, $\mathbb{F}$: the force vector, $\hat{\mathbb{F}}$: the unit force vector, $\hat{\mathbb{u}}$: the unit vector along the line of action, $\mathbb{A}$: the projection of $\mathbb{F}$ into the plane perpendicular to the axis of rotation, $\hat{\mathbb{A}}$: the unit vector of $\mathbb{A}$, $\mathbb{B}$: the vector from C to the point perpendicular to the axis of rotation, $\mathbb{P}$: the vector from C to the joint center.

CONCLUSIONS

For the three-dimensional moment arm, there exist three major groups of definitions with discrete values, therefore researchers should choose the appropriate one to match concepts with individual purposes.

REFERENCES

[1] Sheehan FT et al. *J Biomech* **40**: 1968-1974, 2007.
[2] Pandy MG et al. *Exerc Sport Sci Rev* **27**(1):79-118, 1999
[3] Dostal and Andrews. *J Biomech* **14**: 803-812, 1981.
[4] Hunt M et al. *J Biomech* **39**: 2213-2220, 2006.

Table 1: Geometrical classification of three-dimensional moment arms

Classification name	Definition	Concept
Moment arm about a point	Perpendicular distance from a joint center to the line of action	Applicable to ball-and-socket joint
Conversion moment arm	Perpendicular distance between the axis to the line of action multiplied by the sine of the angle between these two lines	Coefficient converting scalar force into scalar moment
Medical moment arm	Perpendicular (shortest) distance between the axis of rotation and the line of action	Focusing solely on force component which contributes to rotation

AUTOMATED GENERATION OF PATIENT-SPECIFIC INTERVERTEBRAL DISC FEM MODELS BASED ON CT IMAGES

Kati Nispel[1,2], Gabriel Gruber[1], Tanja Lerchl[1,2], Veit Senner[1] and Jan Kirschke[2]

[1] Associate Professorship of Sport Equipment and Sport Materials, School of Engineering and Design, Technical University of Munich, Munich, Germany.

[2] Department of Diagnostic and Interventional Neuroradiology, School of Medicine, Klinikum rechts der Isar, Technical University of Munich, Munich, Germany.

Email: kati.nispel@tum.de

INTRODUCTION

Patient-specific numerical models of the spine offer a great potential for analyzing personalized biomechanics and may help to find individual back pain treatments. [1] Automated segmentation pipelines are used for modelling bony tissue like vertebrae, but the automated model creation of soft tissue, such as intervertebral discs (IVD), still includes time-consuming manual steps. We implemented an algorithm that uses patient-specific CT images to interpolate IVDs between adjacent vertebrae and generates FEM-ready, meshed volume bodies.

METHODS

An automated image segmentation based on artificial intelligence [2] was used to segment and register vertebrae from a CT image. A projection method then determined the endplates of the 3D vertebrae, which were supplemented by IVD border points using interpolated polynomials (Figure **1**). That done, two distinct approaches were investigated to create a 3D volume mesh: surface-based and volume-based. As surface-based approaches, a Ball-Pivoting algorithm (1) and a Poisson surface reconstruction (2) were implemented using different parameters. The resulting 3D surface mesh was subjected to three different smoothing methods: Laplace, HC and Taubin. Subsequently, the mesh was converted to a 3D volume mesh using surface reconstruction techniques. Instead of generating a 3D surface of the IVD border point cloud, volume-based approaches filled the inside of the IVD with a point cloud volume. To create an FEM model, it was further processed with a 3D Delaunay triangulation (3) and voxel-based methods (4). The most promising approaches were determined by evaluating and comparing mesh quality measures. The resulting meshes were smoothed using Laplace, HC and Taubin algorithms with varying parameters to determine the most suitable one. A python script was implemented to convert the final model into an Abaqus input format. For validation, the geometry of the automatically created bodies was compared to respective, manually segmented disc models. To allow comparability, smoothing steps were temporarily undone for the algorithms' validation.

RESULTS AND DISCUSSION

The surface-based Poisson reconstruction method (b) with a linear fit and a depth parameter of 10 proved to be most accurate in creating a 3D volume mesh of the IVD. With α=1, the 3D Delauney triangulation (3) resulted a marginally lower overall mesh quality and a lower geometric consistency. The Ball-Pivoting algorithm (1) resulted in bad mesh quality. Voxel-based methods (4) failed to represent the original IVD geometry in this study, but the straightforward use of hex elements could be advantageous in future studies.

For the surface-based Poisson reconstruction (2), Taubin smoothing resulted in the least change of geometry using a parameter combination of n=200/ λ=0.9 or n=1000/ λ=0.5. Comparison of the manually segmented geometries and the automatically created IVDs of (2) showed good agreement. To sum up, the implemented algorithm successfully created 3D volume models of intervertebral discs based on the segmentation of vertebrae in CT images.

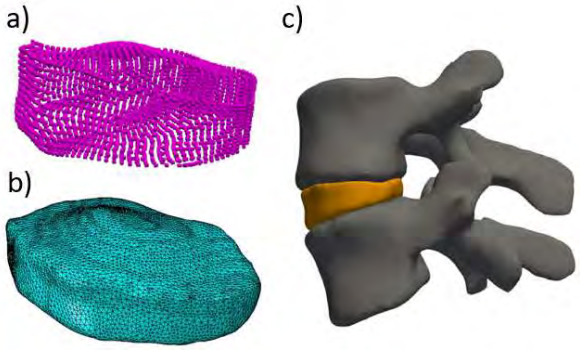

Figure 1 a) IVD border point cloud. b) 3D volume mesh after smoothing was applied. c) Integrated model of a functional spinal unit containing one IVD and two vertebrae.

CONCLUSIONS

The proposed algorithm generates FEM models of the IVD with decent quality. It contributes to the automated implementation of patient-specific spine models by reducing manual intervention and improving efficiency.

ACKNOWLEDGEMENTS

This research was funded by the European Research Council (ERC) under the European 530 Union's Horizon 2020 research and innovation program. Grant-Nr.: 101045128 — iBack-epic — 531 ERC-2021-COG.

REFERENCES

[1] Lerchl, T et al. *Bioengineering* **10(2)**, 202, 2023

[2] Sekuboyina A et al. *Med Image Anal* **73**: 102166, 2021

BACKPACK CARRYING: A COMPARISON BETWEEN MARKER-BASED AND MARKERLESS SYSTEMS

Heredia-Jimenez, J[1]

[1] Department of Physical Education and Sports. Human Behaviour & Motion Analysis Lab (HubemaLab), University of Granada. Spain
Email: herediaj@ugr.es

INTRODUCTION

3D analysis can be performed utilising marker-based capture systems that are considered the gold standard method for movement analysis [1]. The occlusion of reflective markers on the back and pelvis preclude the use of traditional marker-sets during gait analysis when the subject is carrying equipment on their back (i.e. backpacks or exoskeletons)[2]. An alternative that can solve back occlusion and the limitations of marker-based systems is markerless technology. The aim of this study is to compare the trunk-pelvis models between marker-based and markerless systems while carrying a backpack.

METHODS

16 healthy adults (9 males) participated in this study. The average (SD) age was 35.4 (10) years, their height was 1.71 (0.09) m and weight was 67.2 (12.3) kg. Participants walked at a self-selected walking speed in two randomized experimental conditions: loadless walking and walking with a 10 kg-backpack. The trials were recorded with two different motion capture systems (marked-based (Qualisys AB, Sweden) and markerless (Theia, Canada)). The marker set model used was previously validated in backpack carriage studies [3]. An SPM-1 dimension Anova [4]. was used to compare between systems and conditions.

RESULTS AND DISCUSSION

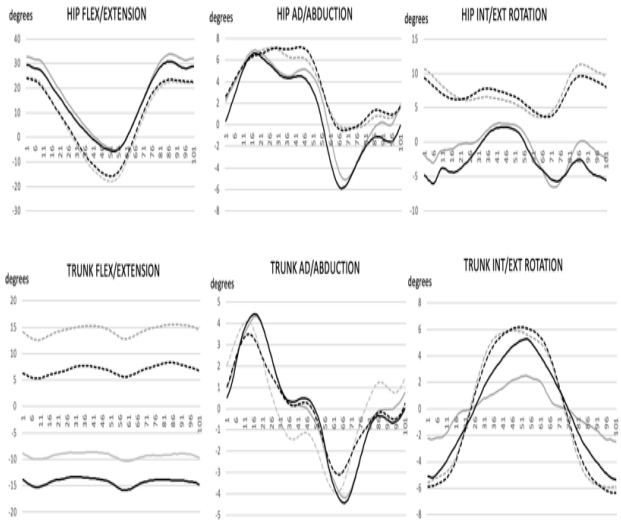

Figure 1. Comparison of kinematic waveforms under four experimental conditions. Black solid: loadless markerbased- black dotted: loadless markerless; grey solid: backpack markerbased, grey dotted: backpack markerless

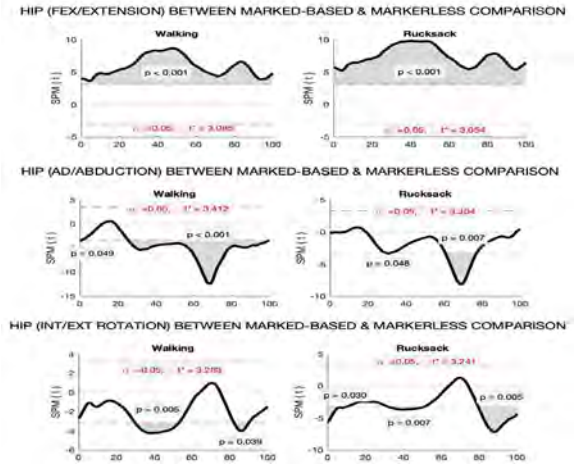

Figure 1. Hip kinematics with marker-based and markerless systems compared during loadless and backpack conditions.

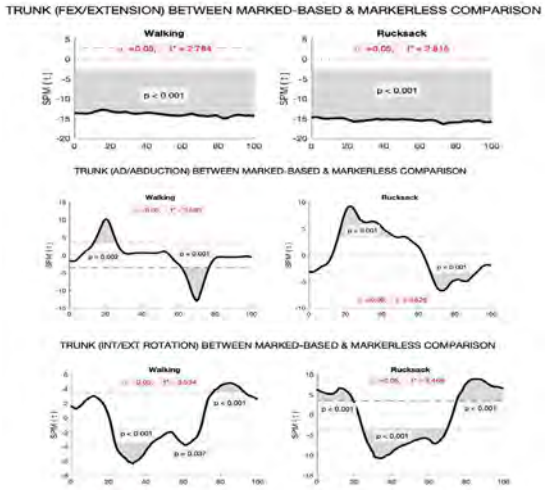

Figure 2. Trunk kinematics with marker-based and markerless systems compared during loadless and backpack conditions.

CONCLUSIONS

Kinematics of the sagittal plane did show an offset between marker-based and markerless models and partial significant differences during the gait cycle in the frontal and transverse planes across both conditions (loadless and rucksack). The markerless model showed an overestimation of the thorax angle and underestimation of the hip angle in the sagittal plane compared to the Hubemalab marker-based model. For this reason, the author advises to take into consideration the offset between different models.

REFERENCES

[1] Sinclair J et al. Sports *Biomech* **11**: 430-7, 2012.
[2] Wu G et al. *J Biomech* **38**: 981-92, 2005
[3] Orantes E et al.. *J Biomech Eng* **143 (4)**, 2021.
[4] Pataky TC et al. *J Biomech* **48**: 1277-85, 2015.

ADAPTIVE P-SPLINES FOR CHALLENGING FILTERING PROBLEMS IN BIOMECHANICS

Andrew J. Pohl[1], Matthew R. Schofield[2], W. Brent Edwards[1], Reed Ferber[1]
[1]Faculty of Kinesiology, University of Calgary, Calgary, Canada
[2]Department of Mathematics and Statistics, University of Otago, Dunedin, New Zealand
Email: andrew.pohl@ucalgary.ca

INTRODUCTION

For signals with rapidly changing derivatives, such as those involving impacts, determining a filter cutoff frequency [1], or smoothing penalty [2], able to capture signal peaks during periods of rapid change while also removing noise from less volatile regions is problematic without over smoothing the peaks or under smoothing periods of low volatility. A potential solution is an adaptive p-spline [3] where the amount of penalization of spline coefficients is allowed to vary across the time domain of the signal. It is hypothesized that an adaptive p-spline will outperform traditional filtering and non adaptive approaches.

METHODS

Adaptive p-splines extend standard p-splines and are best understood as a hierarchical statistical model. Observations y_t for recorded samples $t = 1,\dots T$ are modelled via a spline of order d.

$$y_t = [\boldsymbol{B}\boldsymbol{\theta}]_t + \varepsilon_t \qquad (1)$$

where $\boldsymbol{B}$ is a $T \times (K+d)$ B-spline basis matrix defined over K equally spaced interior knot points spanning the range of observed times and ε_t is additive white noise. We let $K = 100$ and consider quintic splines $(d = 5)$. A p-spline is achieved via incorporation of a penalty on the integrated second derivative of the modelled function. With equally spaced knots this is approximated by a random walk prior on the second finite difference of spline coefficients $\boldsymbol{\theta}$ with variance of the random walk τ^2 determining the smoothness of the fit:

$$\theta_k = 2\theta_{k-1} - \theta_{k-2} + \upsilon_k, \qquad \upsilon_k \sim \mathrm{N}(0,\tau^2) \qquad (2)$$

Adaptive p-splines allow τ^2 to vary over the time domain. We examine two candidate models: one in which variation in τ^2 is described by an AR(1) process $(\mathrm{APS_{AR}})$ and when the variation in τ^2 is described by a cubic B-Spline $(\mathrm{APS_{cubic}})$. We choose the Dowling dataset[1] as a benchmark, which describes the angular displacement and acceleration of a rigid body impacting a barrier. The percentage root mean squared difference (RMSD) for each model when estimating the angular acceleration from the noisy angular displacement signal was computed and compared to that obtained from a Butterworth filtering approach with cutoff frequency determined via an autocorrelation procedure [1]. Bayesian inference with regularizing priors was used to estimate coefficients for each adaptive p-spline model.

RESULTS

A standard p-spline approach outperformed Butterworth filtering and was further improved when the degree of penalization was allowed to vary (Table 1). Acceleration estimates from each approach are outlined in Fig. 1 A Butterworth filter does a poor job when estimating peaks in acceleration and periods where the rigid body is stationary (0.35-0.6s) both of which are well described by an adaptive p-spline with the acceleration peak at impact best described by via the $\mathrm{APS_{AR}}$ model.

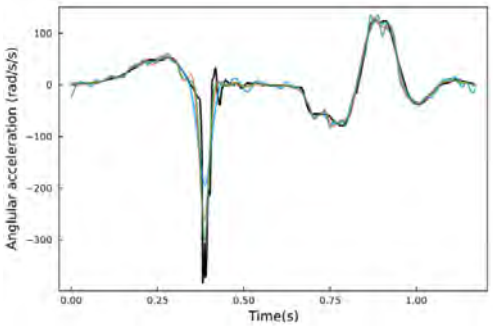

Figure 1: Estimated angular acceleration derived after Butterworth filtering (blue), $\mathrm{APS_{cubic}}$ (orange) and $\mathrm{APS_{AR}}$ (green). Ground truth acceleration in black.

CONCLUSIONS

When examining signals with rapidly changing derivatives adaptive p-splines outperform traditional filtering and non-adaptive spline methods. Biomechanists should consider adaptive p-splines especially if features such as the magnitude of impact peaks, loading rates or periods of negligible acceleration are of interest.

ACKNOWLEDGEMENTS

This study was funded by the NSERC CREATE WeTRAC Training Program.

REFERENCES

[1] Challis J. *J. Appl. Biomech* **15**: 303-317, 1999.
[2] Woltring. H. *Adv. Eng. Soft* **8**: 104-113, 1986.
[3] Rodríguez-Álvarez et al. *Stat Comp* **29**: 483-500, 2019.

Table 1: Root mean squared difference(%) for each model when applied to the Dowling dataset.

Signal	Butterworth filter	P-Spline	$\mathrm{APS_{AR}}$	$\mathrm{APS_{cubic}}$
Angular displacement	0.74	0.72	**0.71**	**0.71**
Angular acceleration	40.63	37.03	**26.74**	32.29

[1]Avaliable from: https://isbweb.org/resources/data-resources

SHAPE OPTIMIZATION OF DENTAL IMPLANT THREAD GEOMETRY

Andi Isra Mahyuddin[1], Satrio Wicaksono[1], Hakim Dwi Ananda[1], Pramudita Satria Palar[1] and Tatacipta Dirgantara[1]

[1] Faculty of Mechanical and Aerospace Engineering, Institut Teknologi Bandung, Bandung, Indonesia.
Email: aim@itb.ac.id

INTRODUCTION

Denture implantation is a popular remedy to overcome the adverse impacts of tooth loss. However, mechanical failures such as fixture fractures are still reported [1]. To the best of our knowledge, existing dental implant-related studies focused on evaluating commercially available implant components or optimizing the geometry for volume reduction. In this study, optimization of the fixture thread geometry was performed to obtain a better thread geometry that produces a better stress distribution on the mandibular bone.

METHODS

Twenty fixture samples with different thread angle combinations were generated using the Latin hypercube sampling method. Each sample satisfies four boundary conditions including $55.68° \leq \theta_1 \leq 90°$, $55.68° \leq \theta_2 \leq 90°$, $\theta_1 \geq \tan^{-1}(\frac{0.63tan\theta_2}{0.43\tan\theta_2 - 0.63})$, and $\theta_2 \geq \tan^{-1}(\frac{0.63tan\theta_1}{0.43\tan\theta_1 - 0.63})$, which is derived according to Figure 1 by keeping the value of D and T constant, 0.63 and 0.43 mm, respectively.

Finite element analysis using Ansys ® was implemented to compare the performance of each sample. The simulated 3D model consists of four components: first molar tooth prosthesis, sectioned cortical and trabecular bone, and implant assembly. Interactions between each component were assumed to be perfectly fit and osseointegrated. Furthermore, each component was assumed to have isotropic, linear elastic, and homogeneous behavior. Zirconia and Ti-6Al-4V were chosen to represent the prosthesis and implant. Around 140000 tetrahedral elements were used for discretization. The type of simulation was static structural. Fixed supports on the mandible mesial and distal sides were defined for the boundary condition, and an axial load of 720N was defined on the enamel surface as the loading condition.

RESULTS AND DISCUSSION

The averaged maximum and minimum principal stresses in cortical and trabecular bone produced by each sample are shown in Figure 2. In cortical bone, the safe maximum principal stress was found in only four samples and the safe minimum principal stress in only six. In trabecular bone, the safe minimum principal stress was found in all samples. However, the safe maximum principal stress was only in two samples. Sample with $\theta_1 = 58.38°$ and $\theta_2 = 72.88°$ was the only one that produced a safe maximum and minimum principal stress on both cortical and trabecular bone.

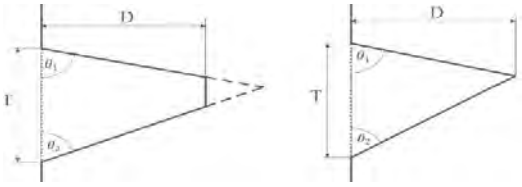

Figure 1 Simplified cross-section of fixture thread.

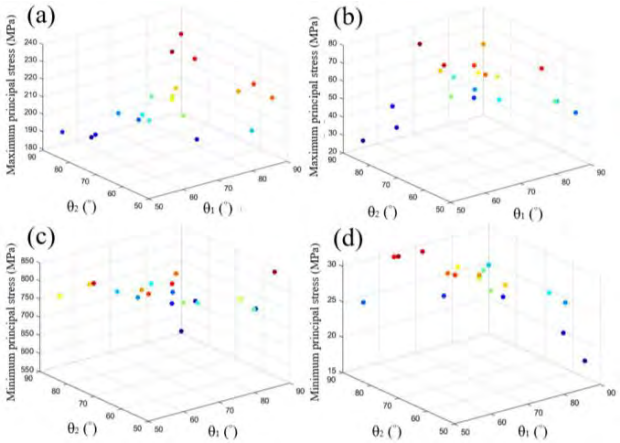

Figure 2 Produced maximum principal stress: (a) cortical, (b) trabecular; Produced minimum principal stress: (c) cortical, (b) trabecular.

The best sample is equivalent to the commercially available reversed buttress thread [2]. The other samples that performed well were equivalent to square, buttress, and V-shaped thread.

CONCLUSIONS

The optimization of the fixture thread angle generated using the Latin hypercube sampling method and assessed using finite element analysis reveals that the sample equivalent to reversed buttress thread is the best. Future studies will consider more geometric parameters, tooth regions, and loading cases.

ACKNOWLEDGEMENTS

Funding from: UKICIS, PDUPT, and P2MI.

REFERENCES

[1] Yu HC & Kim YK. *Maxillofac Plast Reconstr Surg* **42(1)**: 1-3, 2020.

[2] Kong L et al. *Int J Oral Maxillofac Implants* **23(1)**: 65-74, 2008.

Thermal assessment of an ankle-foot orthosis for varied climatic conditions

Nishit C. Pachpande[1] and Ganesh M. Bapat [1]
[1] Department of Mechanical Engineering, BITS Pilani K.K. Birla Goa Campus, Goa, India.
Email: ganeshm@goa.bits-pilani.ac.in

INTRODUCTION

An Ankle-Foot Orthosis (AFO) is a commonly prescribed wearable orthotic device to assist patients with neuromuscular disorders during walking. However, recent studies show that the patient compliance with AFOs is often poor [1], mainly due to improper fit, discomfort issues and resulting skin problems. An orthosis limits the contact of the skin with air which in turn restricts the convective and radiative heat transfer from the limb. Hence, we hypothesize that similar to lower-limb prosthesis wearers, lower-limb orthosis users also experience thermal discomfort. This thermal discomfort and sweating can potentially cause health issues like skin irritation, skin maceration, bacterial infections, and unpleasant odour [2]. Therefore, the aim of this research is to investigate the temperature distribution in an AFO-limb assembly for varied climatic conditions using a generic, 3D finite element (FE) model of a lower leg braced with an AFO.

METHODS

A simplified CAD model of the lower leg was developed using SolidWorks software, with the shank modelled as a solid cylinder and the foot as a triangular wedge. The cylindrical shank was concentrically divided into layers of skin, fat, muscle, and bone. The solid-ankle AFO was modelled using thermoplastic with an Ethaflex cushion. The AFO-limb assembly was imported in ANSYS Mechanical 18.1 for the FE simulations. The sweep meshing method was used on the cylindrical shank, with Hex20 elements on the shank and Tet10 elements on the orthosis and foot. The mesh size (0.005 mm) was finalized using a mesh convergence study. The FE model was validated using boundary conditions similar to previous studies [3] and then further applied considering temperate and tropical climatic conditions. Metabolic volumetric heat generation values for muscle, skin, fat and foot were referred from [4] for resting condition. Convection and radiation boundary conditions were applied to the exposed skin and outer orthosis shell. The ambient temperature for temperate climate (typical in Europe and North America) was considered to be average 20 ºC while for the tropical region (typical in South-East Asia) was considered to be average 42 ºC. and fat was 36.67 ºC. For skin, temperature was set to 30ºC and 36ºC, corresponding to ambient temperatures of 20ºC, and 42ºC respectively [5].

RESULTS AND DISCUSSION

The temperature distribution on the skin of the anterior and posterior portion of the leg was recorded after 1 and 2 hours of wearing the AFO under varied climatic conditions (Table 1). Thermoplastic AFO keeps posterior skin covered with AFO hotter in temperate climate and cooler in tropical climate as compared to anterior skin exposed to ambient weather conditions. Figure 1 shows the temperature contours after wearing the orthosis for 2 hours in two climatic conditions.

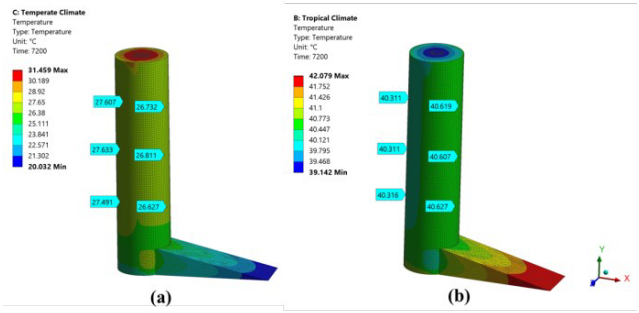

Figure 1: Skin surface temperature contours in (a) temperate and (b) tropical climatic conditions after 2 hours of no activity

CONCLUSIONS

The FE analysis showed that the temperature variation of the skin was found to be dependent on the climatic conditions and resting time duration. Thermoplastic AFO shell acts as insulator obstructing the heat transfer. These findings provide insights to design and select appropriate liner materials for an orthosis considering varied climatic conditions. The study suggests the need for designing AFOs that allow better heat transfer to improve the comfort of the wearer. Future studies need to be conducted considering perspiration mode of heat transfer.

REFERENCES

[1] Bashir AZ et al. *J Manipulative Physiol. Ther*. **45:**114-126, 2022.
[2] Roniger L. *LER Magazine*, 2016.
[3] McCorkle et al. *Prosthet Orthot Int* **46**:432-436, 2022.
[4] Peery et al. *IEEE Trans Neural Syst Rehabil Eng.* **14**:336-43, 2006.
[5] Liu Y et al. *J. Therm Biol.* **38**:440-448, 2013.

Table 1: Average skin surface temperature of the leg after 1 and 2 hours of no activity for temperate and tropical climatic conditions

	Temperate climate (Ambient T= 20 ºC)		Tropical climate (Ambient T= 42 ºC)	
	After 1 hour	After 2 hours	After 1 hour	After 2 hours
Mean anterior skin temperature (ºC)	28.8	26.7	31.6	40.6
Mean posterior orthosis-skin interface temperature (ºC)	29.2	27.6	39.4	40.3

GAIT ANALYSIS AND ENERGETICS OF A NOVEL PASSIVE DYNAMIC CUSTOM FOOT AND ANKLE ORTHOSIS IN A POPULATION OF FOOT-DROP PATIENTS

Paolo Caravaggi[1], Giulia Rogati[1], Alessandro Zomparelli[2], Franco Cevolini[3], Luca Zamagni[1], Massimiliano Baleani[1], Roberta Fognani[1], Luca Boriani[1], Alberto Arceri[1], Maurizio Ortolani[1], Lisa Berti[1], and Alberto Leardini[1]

[1] Movement Analysis Laboratory, IRCCS Istituto Ortopedico Rizzoli, Bologna, Italy.
[2] Department of Technology and Innovation, University of Southern Denmark, Odense, Denmark.
[3] CRP Technology, Modena, Italy.
Email: paolo.caravaggi@ior.it

INTRODUCTION

Ankle-foot Orthoses (AFOs) are orthopedic devices commonly prescribed to support the foot during the swing phase of gait in individuals with foot-drop. Off-the-shelf AFOs are a cost-effective option and widely utilized, but they may not adequately address the variations in foot and leg morphology and the degree of deficit present in each individual. As such, custom-made AFOs are often necessary. The purpose of this study was to to evaluate the kinematic and energetic characteristics of a new passive-dynamic, custom-made AFO in a sample of 10 individuals with foot-drop.

METHODS

Ten unilateral foot-drop patients were enrolled in the study (8M, 2F; age 65 ± 11 years). Custom AFOs were designed and modelled as to match the shape of the foot and leg of each patient in weightbearing. AFOs were produced via selective-laser-sintering of a fiberglass-reinforced polyamide powder (Windform GT®, CRP Technology). Patients were fitted with skin-markers according to a validated lower-limb kinematic protocol [1]. Five walking trials were recorded for each patient in each of the three conditions: wearing the custom AFO; wearing a standard Codivilla spring, and shod (no-AFO). Temporal profiles of hip, knee and ankle joints rotations were calculated via the joint coordinate system [2]. sEMG was used to detect activation of the gastrocnemius and tibialis anterior muscles in the affected and non-affected limb. Three reflective markers were attached to the posterior aspect of the custom AFO to measure the relative flexion-extension motion of the calf-shell with respect to the foot plate. The angle/resisting-moment relationship established for each AFO using an ad-hoc experimental setup [3] were used to estimate the work done by the custom AFO during the stance phase. Friedman test was used to detect statistically significant differences in kinematics and spatio-temporal parameters between shod and the two AFO conditions.

RESULTS AND DISCUSSION

Patients walked at faster normalized gait speed (%height/s) wearing the custom AFO (53.9±12.6) with respect to the Codivilla (53.4±14.0) and shod (51.0±13.5) conditions ($p<0.05$). All patients showed larger ankle dorsiflexion in the swing phase wearing the AFOs with respect to the no-AFO condition (Figure). In terms of energetics, negative work is done at midstance to flex the calf-shell of the custom AFO, which is released to the ankle in the push-off phase. Custom AFOs were rated significantly more comfortable than the Codivilla spring.

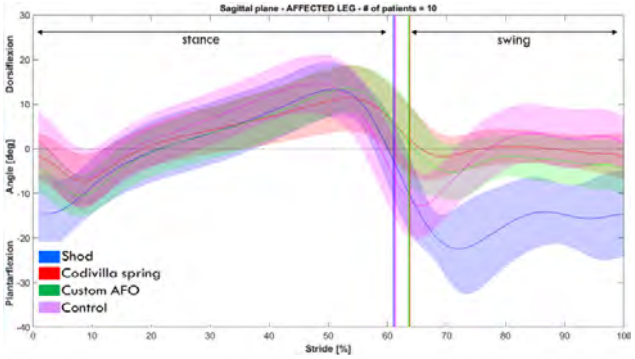

Figure 1 Inter-subject mean (±1SD bands) sagittal-plane rotations of the ankle joint during normalized gait duration in the control population, and in the foot-drop patients in the three conditions: shod (no-AFO); wearing the Codivilla spring and wearing the custom AFO.

CONCLUSIONS

Patients suffering from foot-drop and with other foot postural and morphological alterations or ailments, are usually not fully satisfied with standard AFOs. According to the outcome of this study, a passive-dynamic custom AFO, designed to comply with the shape of the leg and foot in weightbearing, provides foot-drop patients with better comfort and results in improved functional parameters with respect to a widely used standard AFO.

ACKNOWLEDGEMENTS

The authors would like to thank the Italian Ministry of Health 5x1000 program for partially funding this study.

REFERENCES

[1] Leardini A et al., *Gait&Posture* **86**: 34-9, 2007.
[2] Grood & Suntay, *J Biomech Eng* **105(2)**: 136-44, 1983
[3] Rogati G et al., *J Biomech* **142**: 111239, 2

SIMULATING PROSTHESIS CONDITIONS IN CYCLING: A COMPARATIVE STUDY

Heloísa SERATIUK FLORES[1], Wen Liang YEOH[2], Kyosuke MORINAGA[3] and Satoshi MURAKI[4]
[1] Graduate School of Design, Kyushu University, Fukuoka, Japan.
[2] Faculty of Science and Engineering, Saga University, Saga, Japan.
[3]Faculty of Rehabilitation, Hiroshima International University, Higashi-Hiroshima, Japan.
[4] Faculty of Design, Kyushu University, Fukuoka, Japan.
Email: heloisasflores@gmail.com

INTRODUCTION

Cycling is a low impact activity that is becoming increasingly popular amongst amputees [1] and can benefit the recovery process, aside from just being a step towards regaining the ability to walk [2]. However, the study of amputee cycling can be complicated, given that depending on the nature of the procedure, amputations are carried out at different levels, making it difficult to generalise the results. Therefore, the objective of this study is to evaluate the use of custom-made orthoses as an option to simulate and investigate the biomechanics of cycling by transtibial amputees. This was carried out by comparing the range of movement (ROM) during the use of orthoses that simulate amputee cycling, to data presented in the paper "The Biomechanics of Cycling with Transtibial Prosthesis: A Case Study of a Professional Cyclist" by Koutny et al. [3], which collected biomechanics data for the cycling movement of a professional amputee cyclist.

METHODS

Female (n = 5; age: 22–29 years; height:157–164 cm) and male (n = 3; age: 20–24 years; height: 164–183 cm) able-bodied participants were recruited, and custom-made orthoses for cycling (Arizono Orthopaedic Supplies Co. Ltd., Fukuoka, Japan) were manufactured to fit the right leg of each participant, in order to prevent direct contact between the biological foot and the pedal.

For the biomechanics assessment of the cycling practice, participants cycled on an AeroBike 75XL (Konami, Japan) ergometer. Trials lasted 1 minute each, which consisted of cycling at different cadences, 40 rpm and 50 rpm, under two different resistance settings, 40 W and 60 W respectively, which are compatible with recreational cycling. Conditions were set as intact cycling (IC) and simulated amputee cycling (SAC).

The assessment of ROM was accomplished through capturing video footage, using a Panasonic HC-300M (Panasonic, Japan) camera, placed at the right side of the participant. The participants were fitted with seven auto-adhesive markers, placed at anatomical landmarks on the right side of the body to enable motion tracking.

RESULTS AND DISCUSSION

IC and SAC conditions for this study were measured on the same participant, while the participant in the comparable case study had his biomechanical data compared to a control study [4], carried out at similar professional loads and cadences with 6 participants; data for all of which are shown in Table 1. Minimum knee angles showed a decrease of 22° ± 1.0°, similarly, maximum knee angles also showed a decrease of 13° ± 0.5° between intact and simulated amputee cycling under both loads in the present study, and between the intact and amputee cycling in the comparative data. ROM presented an increase of 8° ± 1.1° between intact and simulated or amputee conditions for all comparable data.

Table 1: ROM for the knee for the present and comparative studies.

	MIN	MAX	ROM
IC 60W	45°	118°	73°
SAC 60W	24°	105°	81°
Increase	**-21°**	**-13°**	**8°**
IC 40W	49°	119°	70°
SAC 40W	26°	106°	80°
Increase	**-23°**	**-13°**	**10°**
Control Study*	46°	112°	66°
Amputated Limb*	24°	98°	74°
Increase	**-22°**	**-14°**	**8°**

* Data for the comparative studies.

CONCLUSIONS

Minimum and maximum knee angles decreased, while ROM showed increase between the intact cycling conditions, and the comparable amputee or simulated amputee cycling conditions. The evaluation presented here indicates a possible successful emulation of prosthetic conditions for the practice of cycling through the use of orthoses. However, future studies should collect more data, for more amputee cyclists at more appropriate recreational levels.

REFERENCES

[1] Poonsiri, J., et al. (2018). Bicycling partcipaton in people with a lower limb amputaton: A scoping review. *BMC Musculoskeletal Disorders:* **19(1)**.

[2] Fonda, B., & Sarabon, N. (2012). Biomechanics of Cycling. *Sport Science Review*: **19(1–2)**, 187–210.

[3] Koutny, D., et al. (2013). The Biomechanics of Cycling with a Transtibial Prosthesis: A Case Study of a Professional Cyclist. *International Journal of Medical, Health, Biomedical, Bioengineering and Pharmaceutical Engineering:* **7**.

[4] Ercison, M.O., et al. (1988). Joint Motions of the Lower Limb during Ergometer Cycling. *J Orthop Sports Phys Ther:* **9(8)**, 273-8.

3D PRINTED CUSTOMIZED INSOLES: A FEM AND GAIT ANALYSIS COMBINED APPROACH

Zimi Sawacha[1,2], Mariaelisa Crosato[1], Elisa Bertoncello [3] and Annamaria Guiotto[1]
[1] Department of Information Engineering, University of Padua, Padua, Italy.
[2] Department of Medicine, University of Padua, Padua, Italy.
[3] Orthomedica S.r.l., Padova, Italy.
Email: zimi.sawacha@unipd.it

INTRODUCTION

Foot musculoskeletal disorders are usually treated with plantar customized insoles (CI), which provide healing aid by direct mechanical effects on the lower extremities [1]. Tipically CI are designed and produced based on plaster casting and vacuum forming techniques, with a high level of the subjective knowledge required by practitioners and lab technicians. Lately, the CI design benefited from computer aided technologies; however the subjectivity has not been removed yet [2]. However, the success of these two approaches is based on the need to let the patient try the CI prior to purchasing it [2]. This work describes a new methodology for the design and the check of the effectiveness of CI finite element modeling (FEM) combined with gait analysis and 3D printing.

METHODS

A healthy subject with flatfoot was used as a case study and proof of the methodology. The foot geometry was acquired with a 3D scanner (Structure 3D), in unloaded position, to scale a previously developed foot FEM (Abaqus) [3]. Plantar pressure data and foot-floor angle were acquired respectively by pressure insoles (PedarX, Novel) and a markerless technique [4] while the subject was walking at self-selected speed at the manufacturer site. An stl surface was generated from pressure data and processed through Blender, Simplify 3D and PrusaSlicer: three insoles with different infills or inserts were designed and one was 3D printed (Bioflex, straight filling, 90% infill, 3D-DELTA WASP-4070). The shapes of the designed insoles were included in the FEM and tested by FEM simulation with the subject-specific loads (from the plantar pressures) and kinematics acquired during gait [3] as boundary conditions. The results of the simulations with and without the three insoles were validated through the comparison with the experimental plantar pressure data. Simulated pressures and internal stresses in the plantar soft tissues were compared across the three insoles.

RESULTS

Table 1 shows no considerable difference between peak Von Mises stresses obtained with the Cad Cam and straight infill insoles, in correspondence of the heel plantar aspect of the foot, even though a higher peak pressure was recorded (Figure 1).

Table 1: Pressure and Von Mises stresses on the foot with the

PI	Peak Pressure	Peak Von Mises
Cad Cam solid infill	144 kPa	227 kPa
Straight infill with 2 inserts honeycomb	209 kPa	230 kPa
Infill 15% Full honeycomb	734 kPa	450 kPa

3 PIs: peak values. Infill 15% Full honeycomb

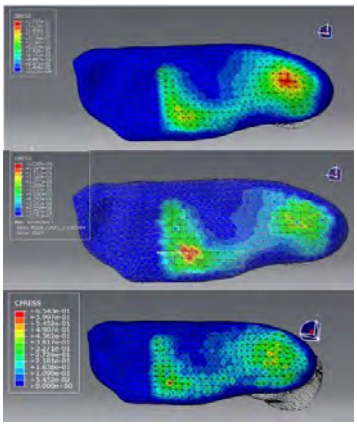

Figure 1: Simulated plantar pressures with the three CIs. From the top: Cad Cam, Straight infill with 2 inserts honeycomb and Infill 15% Full honeycomb.

CONCLUSIONS

The proposed method can be used to predict the effect of the CI before its production, and to use the simulated pressure and internal stress for its optimization. This approach can overcome the limit of the traditional long trial-and-error procedures as well as removing the subjectivity associated with the technician. Future developments will include trying different filling materials, slicing, inserts, and filling distribution.

REFERENCES

[1] Moisan et al. *Clinical Biomechanics* 95:105641, 2022 .
[2] Lochner S. et al. *Comput Aided Des Appl* **9**: 1-11, 2012.
[3] Guiotto A. et al. *J biomech* **47**(12): 3064-3071, 2014.
[4] Sawacha Z et al. *Sensors* **21**: 4746, 2021.

BIOMECHANICAL INVESTIGATION OF A NOVEL PLATE FOR POSTERIOR TIBIAL PLATEAU FRACTURE WITH POSTERIOR CRUCIATE LIGAMENT AVULSION FRACTURE

Peter Andreas Timotius[1], Dean Chou[1,2,3,4], and Tai-Hua Yang[1,2,5]

[1] Department of Biomedical Engineering, National Cheng Kung University, Tainan, Taiwan.
[2] Medical Device Innovation Center, National Cheng Kung University, Tainan, Taiwan.
[3] Miin Wu School of Computing, National Cheng Kung University, Tainan, Taiwan.
[4] National Center for High-performance Computing, Hsinchu, Taiwan
[5] Department of Orthopaedic Surgery, National Cheng Kung University Hospital, Tainan, Taiwan.
Email: p88097034@gs.ncku.edu.tw

INTRODUCTION

Posterior tibial plateau fracture is an uncommon injury with 28.8% of all tibial plateau fracture cases [1]. A concomitant posterior cruciate ligament (PCL) avulsion fracture might also appear as a result of high-energy injuries such as dashboard injuries from motorcycle accidents in which a posterior directed force is applied to the proximal tibia when the knee is flexed [2, 3].
Common implant designs used for treating posterior tibial plateau fracture are T-shaped buttres plate and dual plate [4], while toothed plate and hollow lag screw have been stated as reliable approach for treating PCL avulsion fracture [5]. However, there remains a lack of an optimal fixation design for posterior tibial plateau fracture along with concomitant PCL avulsion fracture.
Therefore, the purpose of this study is to analyze the stability provided by newly designed plate for treating such fractures, by using finite element analysis (FEA).

METHODS

The 3-dimensional (3D) tibia was obtained from scanning a synthetic tibia using 3D scanner, followed by geometry cleaning. The cortical and cancellous bone were prepared based on rough measurement of CT scan image of bone, thus representing the heterogeneity of the bone better [6]. The plate and screws were prepared using computer aided design software. The PCL avulsion fracture was designed in similar fashion with average anatomic PCL tibial insertion [7].
FEA software was utilized for pre-processing where mesh generation, material properties, and boundary conditions were set. Absolute displacement and von Mises stress were interpreted in post-processing software to evaluate the stability of novel design implant.

RESULTS AND DISCUSSION

Figure 1 showed the results of simulation, where smooth transition of displacement over the fracture border indicates greater mechanical stability [8]. The displacement value happened on the tibial plateau region was 0.04 to 0.08 mm. This result was lower than the assumed failure displacement threshold of 3 mm [4]. The maximum von Mises stress were around 63 MPa, happening in the most distal screw. The value is below its destruction value of 2800 MPa [6], implying the implant would not fail within the given the loading condition representing a person in standing mode [4].
Such convincing stability provided by the implant can be caused by the novel part of the plate which lies in its screw positioning, where it has a subarticular raft construct with a compression screw placed through the pre-contoured proximal end.
This can give more stability from the superior side of PCL avulsion fracture compared to screw placed independently of a buttress plate.

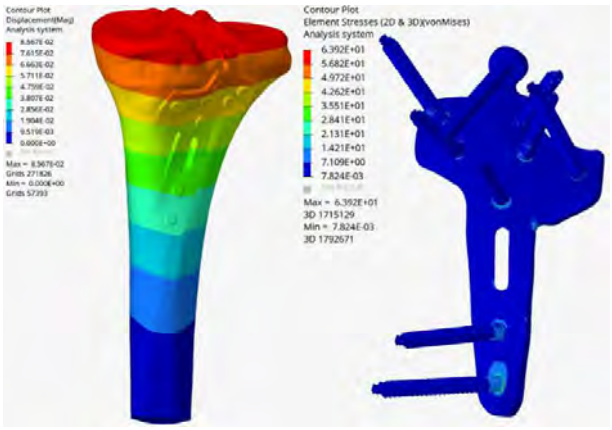

Figure 1 Absolute displacement (left) and stress distribution on the implant (right) of novel design implant

CONCLUSIONS

This study investigated the stability provided by the novel design implant. Additionally, the model used in this study considers the heterogeneity of the bone. With the satisfactory result of stress and displacement distribution, it is implied that this implant might give promising stability, thus making it safe to be used in treating posterior tibial plateau fracture, especially the one with concomitant PCL avulsion fracture.

REFERENCES

[1] Alpert JM et al. *J Knee Surg* **21(1)**: 50-4, 2008.
[2] Lee T-C et al. *Kaohsiung J Med Sci* **29(10)**: 568-77, 2013.
[3] Katsman A et al. *Curr Rev Musculoskelet Med* **11(3)**: 503-509, 2018.
[4] Zeng ZM et al. *Knee* **18(1)**:51-4, 2011.
[5] Chen W et al. *Singapore Med J* **57(1)**:39-44
[6] Wang Y et al. *Sci Rep* **11(1)**:1781, 2021.
[7] Sasaki SU et al. *Arthroscopy* **23(11)**:1226-50, 2007.
[8] Ferre LS et al. *J Mech Behav Biomed Mater* **134**:105392, 20

PREDICTING THE MECHANICAL PROPERTIES OF ATHEROSCLEROTIC CORONARY ARTERIES

Ricardo Caballero[1], Miguel Ángel Martínez[1,2], Estefanía Peña[1,2]
[1] Aragón Institute of Engineering Research (I3A), University of Zaragoza, Zaragoza, Spain.
[2] Biomedical Research Networking Center in Bioengineering, Biomaterials and Nanomedicine (CIBER-BNN), Zaragoza, Spain.
Email: rcaballero@unizar.es

INTRODUCTION

Cardiovascular diseases are the first cause of death worldwide and, in particular, atherosclerosis affects 50% of cardiopathic patients [1]. Mechanical characterization of atherosclerotic arteries is crucial for accurate risk assessment of heart attack. However, existing methods have a common issue: a long waiting time incompatible with today's hospital day care exams [2]. The presented study explores a methodoloy to provide an accurate real-time estimation of mechanical properties of atherosclerotic coronary ateries.

METHODS

An Artificial Neural Network (ANN) has been developed to accurately estimate Young's moduli of necrotic core (E_core) and fibrotic tissue (E_plaque). First, we built a large and idealized database by conducting Finite Element Analyses (FEA) of 540 2D idealized geometries of atherosclerotic coronary arteries with varying stenosis ratios (SR), fibrous cap thickness and core thickness. A statistical analysis to pre-process the data and determine the most influential variables was performed to select the inputs for the ANN. The ANN was based on Multilayer Perceptron (MLP) architecture and was trained and tested using the developed database. Then, the ANN was applied to a realistic database, previously build throughout FEA. To improve the predictions, the ANN was fine-tuned using the transfer-learning technique, where the last four layers were re-trained using the realistic dataset.

RESULTS AND DISCUSSION

The statistical analysis showed a quadratic pattern in the behaviour between the candidate variables and the response variables. The most influential variables in the prediction of Young's moduli of the necrotic core and plaque were the SR (%), and the strains of the core and the fibrous cap with an accuracy of 92.8% and 97.67% respectively. The ANN trained with the large and idealized database presented relative errors in the prediction of E_core and E_plaque lower than 4% both during the training and the testing step. However, when applied to a realistic dataset, the ANN struggled to accurately predict the mechanical properties. To improve its performance, a fine-tuning process was performed, utilizing the 50% of the realistic dataset to re-train the last four layers of the ANN. The result was a relative error lower than 3% both in E_core and E_plaque when predicting the remaining 50% of the realistic dataset.

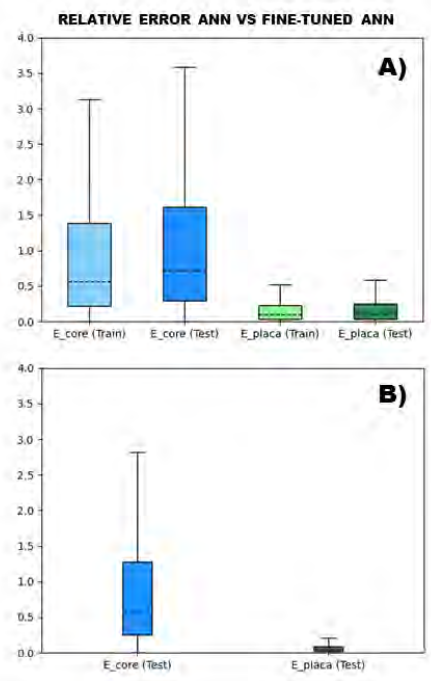

Figure 1 Relative error in the predictions of E_core and E_plaque. A) Original ANN. B) Fine-tuned ANN.

CONCLUSIONS

This study provides a novel perspective on the estimation of material properties in coronary arteries through a large and representative database that takes into account different core sizes, fibrous cap thicknesses, and stenosis ratio values. The promising achieved results set a path for the application of neural networks in the estimation of mechanical properties of patient-specific coronary arteries.

ACKNOWLEDGEMENTS

The authors gratefully acknowledge the research support of the Spanish Ministry of Science and Technology through project PID2019-107517RB-I00, and its funding through grant PRE2020-095671.

REFERENCES

[1] Roth G. Et al., The Lancet, 10159, 2018
[2] Thim T., Danish Medical Bulletin, 57, 2010

MECHANICAL CHARACTERIZATION OF PASSIVE MYOCARDIAL RESPONSE AT DIFFERENT ANIMAL AGES IN PORCINE HEARTS

Nicolás Laita[1], Alejandro Aparici[1], Miguel Ángel Martinez[1,2], Manuel Doblaré[1,2] and Estefanía Peña[1,2]
[1] Aragón Institute of Engineering Research (I3A), University of Zaragoza, Zaragoza, Spain.
[2] Biomedical Research Networking Center in Bioengineering Biomaterials and Nanomedicine (CIBER-BBN), Spain
Email: nlaita@unizar.es

INTRODUCTION

Cardiac tissue presents a complex mechanical response that is essential to understand to develop innovative therapies for cardiac pathologies. It is widely accepted that cardiac tissue presents an orthotropic behaviour, undergoing diverse loading conditions during cardiac cycle [1,2]. Hence, to ensure a complete three-dimensional characterization, considering different loading scenarios is required. Following this line, several mechanical tests were performed into porcine specimens. We considered two groups of animals of two different ages to assess the influence of age on the mechanical response of cardiac tissue.

METHODS

Porcine left ventricular transmural biopsy specimens were obtained from 12 white pigs. 7 animals were used at 3 months of age (3MA) and the rest at 6 months of age (6MA), when they had already doubled their weight. Following the experimental procedures observed at the literature [1-3], cyclic biaxial extension tests, triaxial shear tests and confined compression testing were performed at different areas of the left ventricle free wall (LVFW). Two different types of confined compression tests were made, the first one allowed the fluid to flow out of the sample and the other did not. The former allows to assess the permeability of the tissue and the latter its compressibility. Biaxial samples were obtained at the medial anterior (MA) region of the LVFW for 3MA and at the apical anterior (AA) region of the LVFW for 6MA. Shear samples as well as compression samples were obtained at the medial posterior (MP) region of the LVFW. All samples were obtained following the cardiac tissue muscular fiber directions. A total of 33 biaxial tests, 104 shear tests and 67 compression tests were performed.

RESULTS AND DISCUSSION

Mean results are shown for every test (Figure 1). Biaxial and shear results show an hyperelastic and orthotropic behaviour consistent to the literature, with a stiffer response at fiber direction. At both tests, we observe a more rigid response for the 6MA animals, suggesting that the stiffness of cardiac tissue increases with animal age. We also observe a more isotropic response at the biaxial results of 6MA. However, this may be due to regional differences between MA and AA areas, as fiber alignment is weaker at AA region. Confined compression results show a compressible response, with a 10% volume reduction. No significant differences were obtained at confined compression without fluid output and greater values of pressure were obtained at 6MA respect to 3MA when fluid output was allowed. This suggests that tissue compressibility remains the same, but its permeability decreases with animal age.

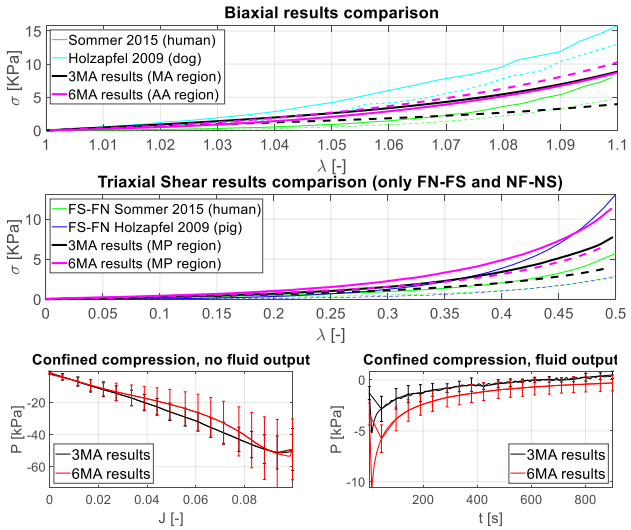

Figure 1. Results from biaxial (top), shear (middle) and confined compression tests (bottom). For biaxial and shear results, continuous line represents fiber direction and dotted line normal to fiber direction

CONCLUSIONS

A complete three dimensional characterization including biaxial, triaxial shear and confined compression tests has been performed at porcine cardiac tissue considering animals of two different ages. We obtained a compressible, hyperelastic and orthotropic behaviour, which is consistent to literature. Our results suggest that the behaviour of cardiac tissue becomes stiffer with increasing age of the animal, as well as experiencing a reduction in its permeability.

ACKNOWLEDGEMENTS

European Economic Community (project BRAV3, C1-BHC-07-2019/H2020) and Spanish Ministry of Economy (project PID2019-107517RB-I003)

REFERENCES

[1] Dokos S. et al, Am. J. Physio. **283:** 2650-2659, 2002.
[2] Sommer G. et al, Acta Biomat. **24:** 172-192, 2005.
[3] McEvoy, E. et al, **140:** J. of Biomech. Eng. 8, 2018.

EVALUATION OF BIOMECHANICAL EFFICIENCY OF DUAL MOBILITY TOTAL HIP ARTHROPLASTY: MULTIBODY DYNAMIC ANALYSIS

DaeHyeon Wee[1,3], JeongAh Pak[1], TaeJin Shin[3], JungSung Kim[3] and Dohyung Lim[1,2]
[1] Department of Mechanical Engineering, Sejong University / Seoul, South Korea.
[2] RNX.Ltd / Seoul, South Korea.
[3] Corentec.Inc/ Seoul, South Korea.
Email: dli349@sejong.ac.kr

INTRODUCTION

Total hip arthroplasty (THA) is well known as a highly successful procedure and can significantly improve quality of life and restore mobility for people with severe hip pain and disability [1]. However, as with any surgical procedure, there are still risks and potential complications [1]. Dual mobility THA has been recently applied clinically, as one of several alternatives to overcome the risks and potential complications [2]. However, a little information is available on bio-mechanical efficiency of dual mobility THA. Therefore, the aim of the current study is to evaluate the bio-mechanical efficiency of dual mobility THA, particular in squat motion.

METHODS

Full body musculoskeletal models with/without a traditional or dual mobility THA were developed based on a musculoskeletal model in AnyBody Managed Model Repository (AMS version 7.4.0., Anybody Technology Aalborg, Denmark) provided by the AnyBody Research Group (Figure 1). To evaluate the biomechanical efficiency of dual mobility THA, squat motion was applied to the full body musculoskeletal models. Then 10 – 100° hip flexion and no rotation ankle flexion were applied to the models. Validation of the full body musculoskeletal models were performed by comparing the joint reaction forces computed by the models with them reported by Layton et al. [1].

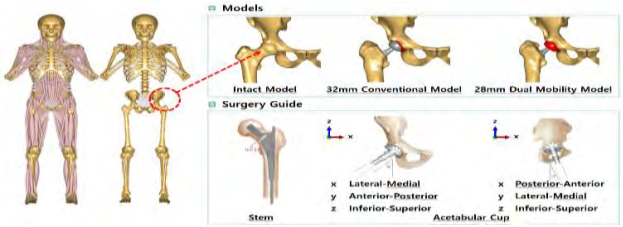

Figure 1. Full body musculoskeletal models: A) without THA, b) with traditional THA (considered a 32mm head size of femoral component, c) with dual mobility THA (considered a 28mm head size of femoral component and a 36mm mobile linear thickness)

RESULTS AND DISCUSSION

The results of the validation showed a reliability level of approximately 82% compared with them reported by Layton et al. [1] and Koyanagi et al. [3]. The joint reaction forces showed similar tendency in all full body musculoskeletal models with/without a traditional or dual mobility THA during the squat motion (Figure 2). However, full body musculoskeletal model with dual mobility THA showed no dislocation of the femoral head for hyper-flexion of the hip joint, relative to the model with a traditional THA. The major muscle forces surrounding the hip, knee and ankle joints were similar in all models with/without a traditional or dual mobility THA (Figure 3).

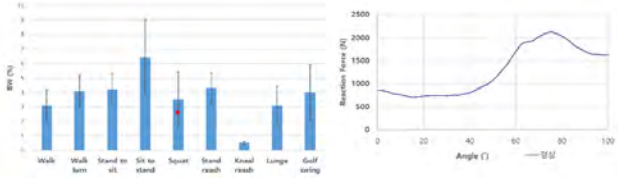

Figure 2. Validation of Joint reaction forces during the squat motion in the conditions

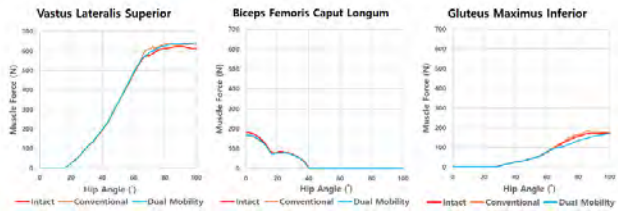

Figure 3. Muscle forces in a) vastus lateralis superior, b) biceps femoris caput longum, c) gluteus maximus interior for the squat motion in the conditions with/without a traditional or dual mobility THA

CONCLUSIONS

In conclusion, Dual mobility THA may have an effective benefit in maintaining biomechanical stability in terms of reducing the risk of dislocation. However, it is necessary to conduct additionally comprehensive research considering various biomechanical and clinical conditions.

ACKNOWLEDGEMENTS

This work was supported by the Korea Medical Device Development Fund grant funded by the Korea government (Project Number: 1711134998, RS-2020-KD000038).

REFERENCES

[1] LAYTON, Robin; MESSENGER, Neil; STEWART, Todd., *Medical Engineering & Physics*, 2022, 108: 103894.
[2] JEWETT, Brian A.; COLLIS, Dennis K. High complication rate with anterior total hip arthroplasties on a fracture table. *Clinical Orthopaedics and Related Research®*, 2011, 469: 503-507.
[3] KOYANAGI, Junichiro, et al. In vivo kinematic analysis of squatting after total hip arthroplasty. *Clinical Biomechanics*, 2011, 26.5: 477-483

IMPROVING PROSTHETIC FEET WITH POLYMER MATERIALS: A STUDY OF MECHANICAL PROPERTIES

Agus Setyo Nugroho[1,2], Muhammad Nouman[1], Sirirat Seng-iad[1]

[1] Sirindhorn School of Prosthetics and Orthotics, Faculty of Medicine Siriraj Hospital, Mahidol University, Bangkok, Thailand.

[2] Prosthetic and Orthotic Department, Polytechnic of Health Sciences, Surakarta, Indonesia.

Email: [1] agussetyo.nug@student.mahidol.edu, [1]muhammad.nou@mahidol.edu, [1]sirirat.sen@mahidol.edu

INTRODUCTION

Lower limb prosthesis must meet the core requirements including tensile strength, density, corrosion resistance, shear strength, flexibility, durability, and cost efficiency. These considerations depend on the nature of the material being used including foot design, and applied manufacturing process [1]. This study proposed three common materials to manufacture the prosthetic foot; including Acrylonitrile Butadiene Styrene (ABS), Polyethylene Terephthalate Polyester (PETG), Polylactic Acid (PLA), High Density Polyethylene (HDPE) and, Polypropylene (PP). The proposed materials are intended to have high mechanical properties and suitable for this application. Also, to compare these materials to select the best material for manufacturing prosthetic legs. Mechanical properties of materials proposed for use in the manufacture of prosthetic legs were tested.

METHODS

In testing the mechanical properties of the five materials, specimens were made for each material in accordance with the ASTM guidelines in accordance with the tests to be carried out, for tensile tests using a guide ASTM D638 Type 1 [2], for bending tests using a guide ASTM D790 [3] and for impact tests using ASTM D256 [4] guidelines (Figure 1).

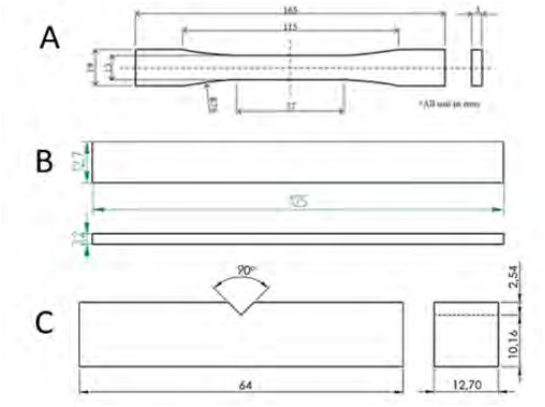

Figure 1. Dimension specimens **(A)** ASTM D638 Type1, **(B)** ASTM D790, **(C)** ASTM D256-03

RESULTS AND DISCUSSION

The results of testing the mechanical properties of the polymer material showed better mechanical properties with HDPE than the other polymer materials used in this study with the results of tensile strength 33.55 MPa. Bending test having a compression strength of 83.74 MPa and impact test have impact value 0.0777 j/mm² (Table1).

Table 1: Mechanical properties polymer materials.

Material	Tensile Strength (MPa)	Compression Strength (MPa)	value impact (J/mm2)
ABS	31,147	108,90	0,0150
PLA	20,357	65,63	0,0037
PETG	23,867	83,57	0,0030
HDPE	33,553	132,93	0,0777
PP	33,040	101,77	0,0137

CONCLUSIONS

The tensile, bending, and impact tests performed on the five types of polymer materials revealed that HDPE materials had the best resistance to tensile, pressure, and sudden loading/shock compared to the other types of polymer materials used in this research. As a result, it was determined that HDPE is the best choice for the manufacture of prosthetic legs due to its high mechanical properties and light weight compared to prosthetic legs made from other polymeric materials such as ABS, PETG, PLA, and PP.

REFERENCES

[1] J. K. Oleiwi and A. N. Hadi, *IOP Conf. Ser. Mater. Sci. Eng.*, vol. 1094, no. 1, p. 012151, 2021, doi: 10.1088/1757-899x/1094/1/012151.

[2] M. Ast, “D638, Standard test method for tensile properties of plastics,” *TF_~ VFING HOOP TENSILE l’REN …*, no. C, pp. 1–16, 2013, doi: 10.1520/D0638-10.1.

[3] ASTM D790, “Standard Test Methods for Flexural Properties of Unreinforced and Reinforced Plastics and Electrical Insulating Materials. D790,” *Annu. B. ASTM Stand.*, vol. i, pp. 1–12, 2017, doi: 10.1520/D0790-17.2.

[4] ASTM, “D256-10E1,” *Methods*, no. January, pp. 1–20, 2004, doi: 10.1520/D0256-10.

PILOT STUDY OF CARTILAGE CREEP AND RECOVERY DETERMINED WITH NONINVASIVE MAGNETIC RESONANCE IMAGING AND CLASSICAL MECHANICAL TESTING

Bo Eitel Seiferheld[1], Kenneth Krogh Jensen[2], Jens Brøndum Frøkjær[2,3], Jan Schjødt-Thomsen[1] and Michael Skipper Andersen[1]

[1] Department of Materials and Production, Aalborg University, Aalborg, Denmark.
[2] Department of Radiology, Imaging Research Unit, Aalborg University Hospital, Aalborg, Denmark.
[3] Department of Clinical Medicine, Aalborg University, Aalborg, Denmark.
Email: bes@mp.aau.dk

INTRODUCTION

Knee osteoarthritis (KOA) is commonly diagnosed by pain and radiographic findings, but these may not be present in the early stages [1,2]. Alternatively, tissue response to mechanical loading has been suggested as a potential biomarker for early OA [2]. Recently, a magnetic resonance imaging (MRI) stress test was proposed to measure cartilage creep [3]. However, the accuracy of this approach has not been tested. Therefore, this study aimed to develop and test a fast-imaging sequence to quantify *ex vivo* creep and recovery response and compare it to a classical mechanical test performed in a controlled environment.

METHODS

A 4.5% weight/volume agarose plug (9 mm diameter) was prepared and underwent unconfined creep and recovery test using MRI and classical mechanical testing. For the MRI test the sample was loaded in a custom-made MRI-compatible device within a knee coil. Sagittal plane images were generated using a multiphase FIESTA sequence (FOV: 12 cm; resolution: 160x200; slice thickness: 4 mm; flip angle: 45°; TR: 4.3 ms; TE: 1.8 ms) with a 3T scanner sampling at 1.62 Hz. After 5 minutes of preloading (0.01N), the initial thickness was determined from reference images. Subsequently, a compression creep load (0.982N) and recovery load (0.01N) were applied, and both imaged for 5 minutes, respectively. Thickness changes were manually segmented from selected MRI images in both phases, and a power fit was performed separately in each phase. Finally, the sample underwent an identical loading scenario using a DMA850 sampling at 3Hz.

RESULTS AND DISCUSSION

Mechanically loading the sample resulted in a time-dependent creep and recovery response (Figure 1), but differences were observed between the response. The initial elastic contribution showed great agreement, but the creep strain was overestimated with the MRI (Table 1). Strain calculations based on sub-millimetre changes of voxels are highly sensitive, and one voxel difference would result in an average error of 3.47%. Thus, accounting for partial volume artifacts and limited spatial resolution is necessary for accurate estimations.

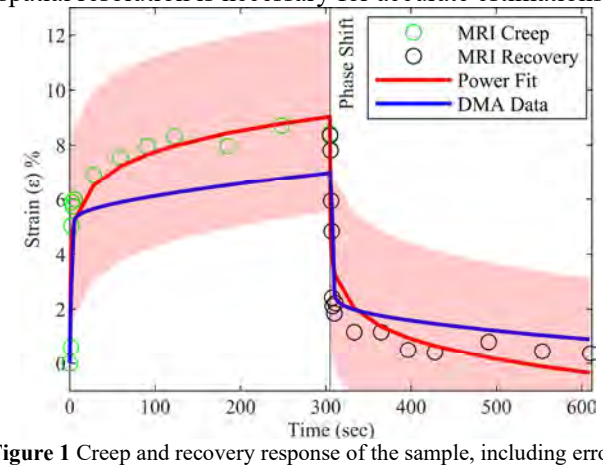

Figure 1 Creep and recovery response of the sample, including error estimates of one voxel.

CONCLUSIONS

The agarose gel sample showed a time-dependent creep and recovery behaviour during compressive loading, indicating that fast imaging MRI sequences may pose as a tool to determine *in vivo* creep and recovery response. Nevertheless, future work is needed to validate the accuracy and reliability of this approach.

ACKNOWLEDGEMENTS

Center for Mathematical Modelling of Knee Osteoarthritis (MathKOA) is funded by the Novo Nordisk Foundation (grant no. NNF21OC0065373).

REFERENCES

[1] Glyn-Jones et al. *The Lancet* **386**: 376-387, 2015.
[2] Cutcliffe et al. *Sci Rep* **10**: 1547, 2020.
[3] Paranjape et al. *Sci Rep* **9**: 2283, 2019.

Table 1: Comparison of the equilibrium and initial strains for the creep and recovery response of the sample with the MRI and DMA.

	Initial sample thickness	Creep strain after 4 min	Initial loading strain after 5 sec	Recovery strain after 4 min	Initial unloading strain after 5 sec
MRI-measurements	6.62 mm	0.58 mm (8.7%)	5.14% (1.02%/s)	0.0 mm (0.0%)	5.65% (1.13%/s)
DMA-measurements	6.68 mm	0.45 mm (6.8%)	5.20% (1.04%/s)	0.07 mm (1.08%)	4.4% (0.88%/s)

FINGER PALPATION ON AN ARTERY AS GAUSSIAN SPACE FILTER

Debadutta Subudhi[1], M Manivannan[2], K. K. Deepak[3]

[1]Touch Lab, Department of Applied Mechanics, IIT Madras, Chennai, India
[2]Touch Lab, Department of Applied Mechanics, IIT Madras, Chennai, India
[3]Dept of Physiology, All India Institute of Medical Sciences (AIIMS), New Delhi, India
Email: dev.subudhi49@gmail.com, mitmani@gmail.com, kkdeepak@gmail.com

INTRODUCTION

Artery palpation is a standard method to touch and feel cardiovascular functionality. Modern science assesses three parameters such as rate, amplitude, and rhythm in general. In ancient science, radial artery palpation is used for disease diagnosis. In both cases, the force field transmitted to the fingertip from the artery is a crucial factor. The palpation involves fingertip interaction with the forces from the arterial wall. The current work studies the force distribution with a constant force palpation at a single location on the arteries with various elastic moduli.

METHODS

The pressure distribution across the curvature due to palpation on the artery is investigated using fluid-structure interaction (FSI) modeling in COMSOL 5.5 to a non-pulsatile and pulsatile flow. The constriction of palpated arteries is assumed at both sides of the artery. The non-pulsatile flow is with a velocity inlet of 0.23m/sec and 80 mm Hg outlet condition for 1 second in 100-time steps. The study includes three elastic arteries($E = 0.3MPa, 0.6MPa, 0.9MPa$) with corresponding intima-media thickness ($0.4mm, 0.45mm, 0.5mm$) as shown in Figure 1.

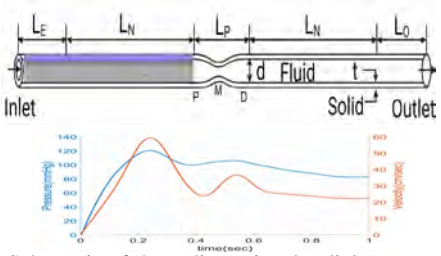

Figure 1: Schematic of three-dimensional radial artery model with the velocity and pressure boundary conditions [1] at the inlet and outlet

RESULTS AND DISCUSSION

A higher elasticity zone captures high-frequency components in the pulse, whereas a lower elasticity zone captures very low frequency. The intermediate elastic zone between them captures the low-frequency component of the pulse as evident from the root locus plot 2. Along the length of the artery, the distal (D) sites on the artery contain very low-frequency components of pressure pulse whereas proximal (P) sites on the artery contain high-frequency components of the pulse. The palpation amplifies the deviations in the pulse profile and in the spectral distribution of the pulse waves at P, and D locations for various arteries during pulsatile flow. The palpation can make the artery operate in passive or active modes [2] to result in pressure change along the length of the artery.

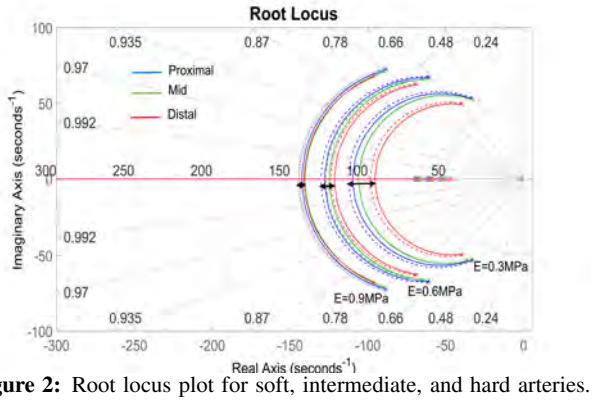

Figure 2: Root locus plot for soft, intermediate, and hard arteries. The solid line is during palpation, and the dashed line is without palpation).

CONCLUSIONS

The palpation aids in separating the powers under various frequency bands in the spatial domain within one single pulse in the pulsatile response of the artery. The step response shows the spatial filtering property of the Gaussian loading that acts as a Gaussian Space Filter. The experimental validation of this study will be analyzed further in the future.

REFERENCES

[1] Saeid Khalafv et al. Journal of Biomechanical Engineering, 137(6).
[2] Belousov et al. Medical Biological Engineering Computing, 59(9), 1785-1794.

Deformable headform design choices: An evaluation of brain simulant stiffness influence on intracranial displacements and strain

Sheng Xu[1], Jean-Jacques Demiannay[1], Simon Ouellet[2], Austin Azar[2], Oren Petel[1]
[1] Department of Mechanical and Aerospace Engineering, Carleton University, Ottawa, ON, Canada, K1S 5B6
[2] Defence Research and Development Canada Valcartier, Quebec City, QC, Canada, G3J 1X5
Email: oren.petel@carleton.ca

INTRODUCTION

Deformable polymeric headforms are being developed as new tool for helmet performance evaluation [1]. These headforms often contain elastomeric brain tissue simulants to model the response of the human head to impact and/or blast wave loading events. Sylgard 527 has been commonly used to represent brain tissue, but has been shown to be stiffer than brain tissue under quasi-static conditions [2]. However, brain tissue has presented a strong strain-rate dependence, making it stiffer than Sylgard 527 at strain rates relevant to mild traumatic brain injury (i.e., 10^2-10^3 s^{-1}) [3]. This difference will cause elevated intracranial strain measurements in these deformable headforms. In the present work, we investigate different brain tissue simulant formulations that possess varied stiffness properties to determine their strain response for comparison to cadaveric datasets.

METHODS

The tunable stiffness of brain simulants was achieved by mixing two commercially available polydimethylsiloxan (PDMS), Sylgard 527 and Sylgard 184, with different ratios, from soft to stiff, which were pure 527, 40:1, 20:1 and 10:1. The brain simulants with differnet stiffness were used to prepare four different deformable closed headforms, based on the BIPED Mk2 [1]. These headforms were subjected to a series of impacts from a linear impactor at speeds ranging from 2.5 m/s to 4.5 m/s. Two impactor caps were used in testing, a 75 mm vinyl nitrile end cap and a Neoprene rubber end cap. Numerous radiopaque markers were embedded within the same parasagittal plane of the headform brains. Marker motions were tracked using a high-speed X-ray imaging system (5,000 fps). A digitial image correlation analysis was used to calculate the displacement and intracranial strain fields within the headform.

RESULTS

A direct comparison of the resultant displacements of a single point in the frontal region across brain simulant formulations is shown in Figure 1a, for the same impact conditions (4.5 m/s). This comparison showed that the stiffer material, had a greater resistance to motion, lower strains, and a shorter response time. The 95th percentile true strain response in the same frontal region shows that increasing tissue simulant stiffness changed both the peak strain and strain patterns during the impact (Figure 1b).

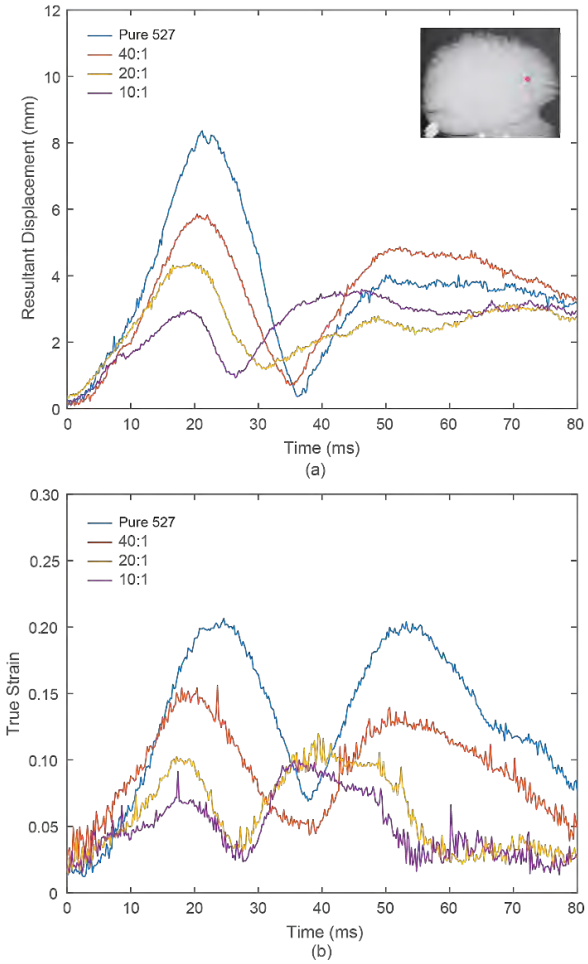

Figure 1 The response comparison of different brain simulants formations in frontal region at impact velocity 4.5 m/s. (a) Resultant Displacement at a single point; (b) 95th percentile true strain.

CONCLUSIONS

The investigation of several brain simulant formations demonstrated that stiffness of the brain simulants can be used to optimize brain simulant selection. This approach could also improve the biofidelity of future headform design through a validation with cadaveric data.

REFERENCES

[1] S. Ouellet and M. Philippens, Shock Waves, 28:19-36, 2017.
[2] D. Singh, et al. J Biomech, 92: 84-91, 2019.
[3] B. Rashid, et al. *J Mech Behav Biomed Mater*, *33*:43–54, 2014.

THE INFLUENCE OF THE TERTIARY BRONCHI ON STRAIN-INDUCED PULMONARY INJURY

MacKenzie Brannen[1], Gia Kang[1], Rohan Banton[2], John D. Clayton[2] and Oren E. Petel[1]
[1] Department of Mechanical and Aerospace Engineering, Carleton University, Ottawa, Canada.
[2] U.S. Army Research Laboratory, Aberdeen Proving Ground, Aberdeen, USA.
Email: oren.petel@carleton.ca

INTRODUCTION

Pulmonary contusion is a prevalent injury related to thoracic trauma events, however it currently lacks both reliable mechanistic understanding and predictive criteria [1]. Finite element (FE) models have have been used to study the response of the body to blunt-impact trauma, in which the lungs are often assumed both homogeneous and isotropic, almagamating the alveoli and bronchi structures into a monolithic mass. These models typically predict peak strains at the surface of the impact site, which is qualitatively validated against tissue damage imparted on the surface of animal surrogate lungs [2]. We have shown that these approximations are unable to resolve local maxima in the dynamic strain fields that occur within the interbronchial regions [3]. This suggests that the current finite models may be underestimating and mislocating strain-induced injuries, such as contusion.

METHODS

Fixed porcine lungs, preserved using a Bioflex process to maintain tissue flexibility (NASCO, Fort Atkinson, WI), were instrumented with a 2D array of elastomeric radiopaque markers outlining the surfaces of the lung parenchyma in the plane of the tertiary bronchi. Additional radiopaque markers, encapsulated within flexible heat shrink tubing, were inserted within the tertiary bronchi. The instrumented lungs were suspended from a custom impact fixture and inflated to a physiologic expiratory pressure. A pneumatic cannon was used to launch a 53.5 g plastic sphere towards the lungs at speeds ranging from 7.1-14.60 m/s, inducing a direct deformation of the lung surface characteristic of thoracic trauma. The dynamic deformation of the lungs was captured using a high-speed x-ray imaging system at 7500 fps, and the displacements of the markers were used to quantify the trans-lobe, interbronchial, and superficial parenchymal true strains through the definition of quadrilateral elements (Fig. 1). Strain fields measured in fresh porcine lung specimens were also compared to the severity of resultant regional tissue damage to validate strain as a mechanism of injury.

RESULTS AND DISCUSSION

The difference in peak strains measured in the parenchymal surface elements and within overlapping trans-lobe elements are consistent with the results seen in current isotropic FE models, whereby peak strain is observed at the surface of the impact site. However, when the interbronchial strains in regions adjacent to the surface elements are considered, the effect of the inhomogeneity of the bronchial structures is evident. Due to the increased stiffness, the bronchi are displaced upon impact, generating localized measures of maximum principal, minimum principal, and maximum shear true strains (MPS, mPS and MSS) that exceed both the trans-lobe and surface strains (Fig. 1).

CONCLUSIONS

These results show that the inclusion of the bronchial structures is necessary in biofidelic lung models. Furthermore, model validation efforts relying on measures of physical tissue damage should not be limited to surface pulmonary contusion and must be expanded to include regions adjacent to inhomogeneities such as the bronchial network.

REFERENCES

[1] Eaton et al., *J Biomech Eng,* 144:090801, 2022.
[2] Gibbons et al., *J Biomech Eng,* 137:041002, 2015.
[3] Brannen et al. *J Mech Behav Biomed Mater,* 130: 105181, 2022.

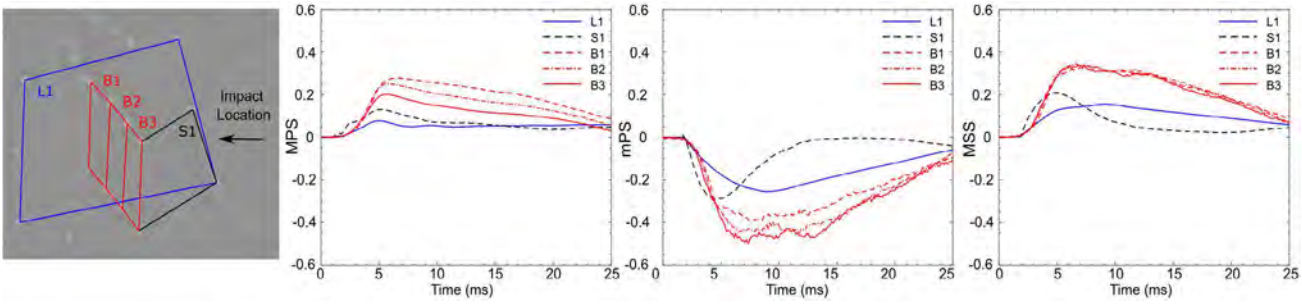

Figure 1: Quadrilateral strain element locations and resultant true principal strains for a 7.1 ± 0.1 m/s direct impact.

Identification of joint motions affected knee valgus after multi-directional single-legged drop landing by principal component analysis

Takayuki Koike[1,2], Koudai Ozaki[2], and Masaaki Okauchi[1,2]
[1] Science and Technology, Oita University, Oita, Japan.
[2] Graduate school of Engineering, Oita University, Oita, Japan.
Email: t-koike@oita-u.ac.jp

INTRODUCTION

ACL rupture or injury frequently occurs in the early phase of single–legged landing from a jump toward the front, back, left, and right directions and is due to the knee valgus during the landing. Knee and hip flexor displacement are reduced during lateral landing rather than forward landing [1]. However, no studies have investigated which lower limb joint movements are associated with the knee valgus. This study aims to investigate which joints in the lower limb are involved in the knee valgus that occurs after single–legged drop landing (SLDL) from multiple directions.

METHODS

Ten male students with no previous ACL injury or rupture performed the SLDL from a 30 cm height box with each leg. We instructed the subjects to drop from the box to a Force–platform (Sports Sensing inc., 1000Hz) placed in the frontal direction (0 degrees) and at 30, 60, and 90 degrees lateral to the landing leg, and to land with the entire sole of the foot. The subjects' whole-body kinematics was captured by four high-speed cameras (For-A inc. and Ditect inc., 250 fps), and the coordinated reflective markers attached on the body were digitized (Dipp-Motion V/3D, Ditect inc.). The coordinates were used to calculate joint angles in lower limbs using the Euler method. We calculated the touchdown angle and the angular displacement up to the time when the vertical ground reaction force (Fz) reached its maximum value after landing. We calculated the correlation coefficient (CC) between these variables and the knee valgus/varus angular displacement in each landing task. These angles were further converted to principal component (PC) scores using PC analysis up to the fifth PC, where the cumulative contribution ratio first reached 0.8 or greater. Then we extracted the labels of the angles constituting the PC scores using factor loadings.

RESULTS AND DISCUSSION

We found individual difference in the mean and standard deviation value of angular displacement of knee valgus/varus. Meanwhile, we found high CC values between knee valgus/varus displacement and several kinematic variables, for example, hip internal rotation (Fig.1). Table 1 shows the main variables, factor loadings, and PC scores of the 1st PC for the dominant and non–dominant leg obtained by PCA. These scores included the knee valgus/varus and hip internal rotation shown in Figure 1 for both legs, indicating that an increase in the PC score not only means an increase in the valgus and internal rotation but also means that the joint displacements in both directions are related. These findings suggest that inhibiting knee valgus after landing, which is a risk factor for ACL injury, requires decreasing internal rotation of the hip joint after landing, and furthermore, utilizing the muscular strength of the external rotation muscles, gluteus maximus and six deep external rotators, that antagonize the internal rotation may reduce the risk of this injury.

Table 1. PC scores, factor loadings and contribution rate obtained from PC1.

	Dominant leg 1st PC		Non–dominant leg 1st PC	
Factor loadings	Knee Valgus/Varus	0.929	Knee Internal/External rotation	0.864
	Anke Spination/Pronation	0.894	Knee Valgus/Varus	0.834
	Hip Internal/External rotation	-0.876	Hip Internal/External rotation	-0.809
	Knee Internal/External rotation	0.866	Hip Abduction/Adduction	0.785
	Knee Flexion/Extension (Touchdown)	-0.816	Hip Flexion/Extension	0.745
Contribution rate	0.396		0.375	

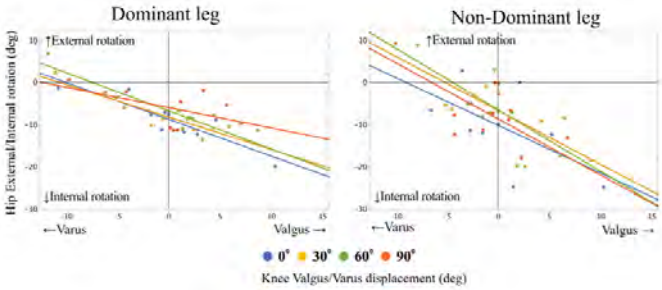

Figure 1. Scatter plot of knee valgus and hip internal rotation displacements.

CONCLUSIONS

Correlation analysis and PCA of the kinematic variables revealed that hip internal rotation and other movements related to the knee valgus movement that occurs after a SLDL are involved. This suggests that the external rotator muscles at the hip can be an important muscle in inhibiting the external rotation.

REFERENCES

[1] Komsac et al. *J Phys. Ther. Sci.*, **25**: 1109-1113, 2013.

VINYL SPORTS FLOOR CUSHIONING THICKNESS AFFECTS SHOE-SURFACE TRACTION IN FUTSAL BUT NOT MECHANICALLY EVALUATED ANKLE INVERSION MOMENT

Filip Gertz Lysdal[1,2,3], Lasse Jakobsen[3], Katrine Okholm Kryger[1], Timo Bagehorn[2],
Shariman Ismadi Ismail[4], Uwe G. Kersting[2,5] and Ion Marius Sivebæk[4]
[1]Sport, Allied Health and Performance Science, St. Mary's University, Twickenham, United Kingdom
[2]Department of Health Science and Technology, Aalborg University, Aalborg, Denmark
[3]Department of Civil and Mechanical Engineering, Technical University of Denmark, Lyngby, Denmark
[4]Faculty of Sports Science and Recreation, Universiti Teknologi MARA, Shah Alam, Malaysia
[5]Institute of Biomechanics and Orthopaedics, German Sport University Cologne, Cologne, Germany
Email: filipgertz.lysdal@stmarys.ac.uk

INTRODUCTION

Point elastic artificial sports flooring is largely preferred by Futsal players, who also complete futsal-specific agility course faster on this surface, compared to hardwood flooring [1]. These artificial floors come in various designs with varying levels of shock absorption, and it is believed that the improvements found in performance might be due to the higher traction [1], which could be facilitated by a greater local deformation of the floor against the shoe sole [2]. Excessive traction might also come with a downside, as greater horizontal forces would arguably lead to increases in lower extremity joint loading, and a potentially increased risk of ankle sprain injury [3].

It is still unknown, however, whether shoe-surface friction is actually affected by the thickness of the underlying cushioning layer under artificial sports floors, and whether a further thickening would lead to further increases in traction – and whether this would be reflected by an increase in inversion moment.

METHODS

In this mechanical study, three different thicknesses of Taraflex™ indoor sports floor (Gerflor, Villeurbanne, France) was tested. All conditions had similar 2.1 mm vinyl top layer (Shore A: 91.0±0.9) but varied in thickness (0mm, 4.9mm, 9.8mm) of the underlying cushioning layer (Shore A: 26.0±0.6).

The additional floor was installed onto a force platform (AMTI OR6-7-1000, Watertown MA, USA) prior to calibrations, and the varying heights were adjusted for.

A Puma futsal shoe (Invicto II, Puma GmbH, Herzogenaurach, Germany; outsole Shore A: 72.2±1.2) was attached onto an artificial foot at the end of a custom build enlarged British pendulum, that was fixated to the floor above the force plate.

Ten trials were recorded for each floor condition using eight infrared highspeed cameras sampling at 500 Hz (Oqus 300+, Qualisys AB, Gothenburg, Sweden) to capture the kinematics of 13 retroreflective markers via Qualisys Track Manager (v. 2021.2). Force plate data was sampled at 1000 Hz. Both kinematic and kinetic data was filtered at 35 Hz using a 4th-order low-pass Butterworth filter. Early contact friction coefficient and mechanical ankle joint kinetics was analysed in Visual 3D v6 (C-Motion Inc., Maryland, USA) between 10 and 200 N in vertical ground reaction force.

RESULTS AND DISCUSSION

The coefficient of friction (COF) was similar at initial contact and decreased as the normal force increased. At the 200N cut-off, the 9.8 mm cushioning layer had a 6% and 3.5% higher COF than the zero and 4.9 mm cushioning thicknesses, respectively (Table 1).

Table 1 Friction coefficient (COF) at 10N and 200N normal force.

Cushioning thickness	COF at 10N (SD)	COF at 200N (SD)
0.0 mm	0.90 (0.02)	0.83 (0.01)
4.9 mm	0.90 (0.02)	0.85 (0.00)
9.8 mm	0.92 (0.02)	0.88 (0.01)

To our surprise, there was no measurable difference in mechanical inversion moment about the ankle joint (Figure 1), despite the increase in COF with the added cushioning layers.

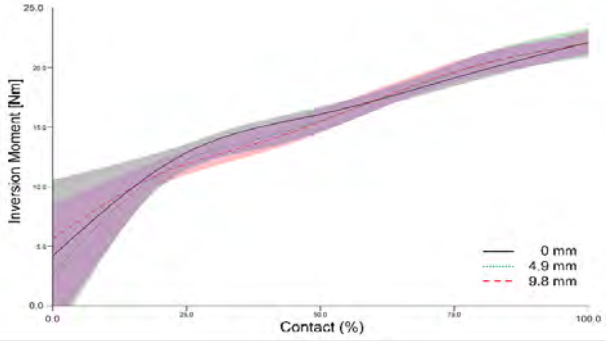

Figure 1 Inversion moment between 10 and 200 N normal force.

The change in thickness as the surfaces would compress was not adjusted for, which might affect the centre of pressure – and the inversion moment calculated.

CONCLUSIONS

The thickness of the cushioning layer under indoor vinyl sports floors affects mechanical impact friction in futsal. However, this is not reflected by a similar increase in mechanical joint moments.

REFERENCES

[1] Ismail SI et al. *Sports Biomech* **23**: 1-12, 2022.
[2] Moriyasu K et al. *Tribol Int* **136**: 548-555, 2019.
[3] Lysdal FG et al. MEDNTD **16**: 100141, 2022.

IN VIVO INVESTIGATION OF MICROSTRUCTURAL BRAIN CHANGES FOLLOWING FOOTBALL HEADING

Hugh McCloskey[1,2], Rhosslyn Adams[1], Carolyn McNabb[2], Megan Barnes-Wood[1], Bethany Keenan[1,2], John Evans[2], Derek Jones[2], Peter Theobald[1]
[1] School of Engineering, Cardiff University, Cardiff, UK.
[2]Cardiff University Brain Research Imaging Centre, Cardiff University, Cardiff, UK. Email: TheobaldPS@Cardiff.ac.uk

INTRODUCTION

Repeated football heading may be a cause of the increasing incidence of neurodegenerative disease in former elite players [1]. Correlating head impact exposure and disease incidence is hindered by conclusive diagnosis relying on post-mortem examination. An alternative route to predict injury risk correlates head kinematic data to metrics including head and rotational injury risk (HIC, RIC respectively). These are, however, intended for single, high-magnitude collisions and so prevent meaningful investigation of cause-and-effect. This pre-post study increases the sensitivity of such comparisons, investigating whether repeated heading causes changes in microstructural neuroanatomy and assesses whether changes correlate with injury scores.

METHODS

Six male university-level footballers (21 – 23 years) volunteered for a baseline brain scan (t = 0 hrs), using a 3 Tesla Connectom MRI scanner (Siemens), capable of gradient strengths of 300mT/m. Scans followed a high angular resolution diffusion imaging (HARDI) protocol. Participants then performed 10 headers, with controlled deliveries and instructions to attempt neck flexion-extension only (t = 2hrs). All wore personalised, instrumented mouthguards to capture head kinematics in 6 degrees of freedom (SWA; Swansea, UK). HIC and RIC scores were calculated for each header. A follow-up HARDI scan (t = 24 hrs) then allowed derivation of change in mean diffusivity (MD), for 50 white matter tracts (derived using TractSeg) in each participant. Increased MD has been shown to correspond to increased water content, edema and inflammation [2]. A linear mixed-effects model was then used to assess the effect of peak HIC and RIC on changes in MD.

RESULTS

Peak HIC [mean = 33.17, ± 14.52] was not significantly associated with any change in MD. Peak RIC [mean = 1230440, ± 724713.7] was significantly correlated with MD increase in the left inferior fronto-occipital fascicle (IFO) This is consistent with observations of acute traumatic brain injury in other sports [3]. However this result became non-significant after correction for multiple comparisons (Figure 1, Table 1).

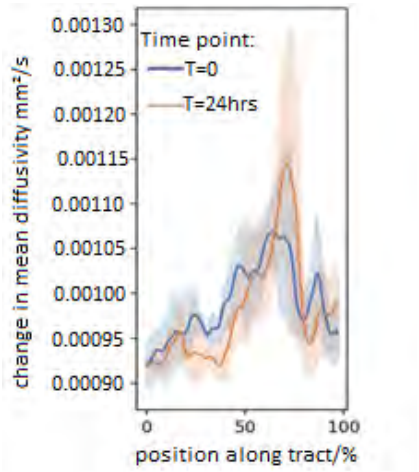

Figure 1: Group mean MD along the IFO left tract at T=0 and T=24.

CONCLUSIONS

Peak RIC scores initially appeared to correlate significant to an increase in MD in the IFO. This became non-significant after corrections for multiple comparisons.

ACKNOWLEDGEMENTS

HM and MBW received funding from Charles Owen. HM is also funded by KESS. CM was supported by DJ' Wellcome Trust Strategic Award. The study was sponsored by the Cardiff University Impact Accelerator Account, KESS, and the Football Association of Wales.

REFERENCES

[1] Mackay D.F. et al. N Engl J Med 381:1801-1808, 2019.
[2] Hetherington H. et al. H Clin Neuro 127: 309-318, 2015.
[3] Gajawelli, N et al. World Neurosurg 80:824-828, 2013. **80**:824-828, 2013.

Table 1: Tables that extend across both columns should be placed at the bottom of the abstract.

Tract	$\Delta MD(x10^{-5})$	T-value	p-value	p-value after corrections for multiple comparisons
IFO left	+1.112867	−3.096	$p = 0.03$	$p =>0.05$

INFLUENCE OF SPORT SURFACE PROPERTIES ON UTILIZED TRACTION AND LOWER EXTREMITY BIOMECHANICS OF AMERICAN FOOTBALL PLAYERS

John W. Wannop[1], Shaylyn Kowalchuk[1], Emily Smith[1], Philipe Aldahir[2], E. Meade Spratley[2], Cody M. O'Cain[2], Gwansik Park[2], Darren Stefanyshyn[1]

[1] Human Performance Lab, Faculty of Kinesiology, University of Calgary, Canada
[2] Biomechanics Consulting and Research (Biocore), LLC, Charlottesville, United States
Email: b.wannop@ucalgary.ca

INTRODUCTION

Synthetic turf holds a distinct advantage over natural grass, due to the ability to alter the different components of artificial turf. While changes in sport surface components can alter performance [1], insight into how these changes in performance are achieved is absent. Therefore, the purpose of this study was to investigate the biomechanical differences on artificial turf associated with changes in athletic agility performance.

METHODS

Eighteen University grid-iron football players (nine speed players and seven power players) performed three modified football specific movements (agility drill, vcut, 3 cone drill) on three artificial turf surfaces: i) Control, commonly installed artificial turf surface for sporting activities, ii) Shockpad (SP), identical to the Control, except for the addition of an underlying shockpad, iii) Low Faceweight (LW), with identical infill composition to the Control, but reduced carpet area density. These surfaces have previously been shown to alter agility performance [1]. All surfaces were installed in the lab over a force platform (2400Hz) to quantify utilized traction while using a motion capture system (240Hz) to quantify changes in the lower extremity movement patterns of the athletes. Data was compared between the different surfaces using a repeated measures ANOVA (α=0.10) with within participant factors of surface and between participants factors of player position.

RESULTS AND DISCUSSION

During all movements there was a significant effect of surface on utilized traction at take-off (vcut, p=0.061; agility, p=0.058; cone, p=0.005) and the frontal plane ankle angle (vcut, p=0.076; agility, p=0.002; cone, p=0.011) with players utilizing a lower amount of traction and having a lower peak frontal plane ankle angle on the low traction surface (LW). During the agility drill and vcut movement, a significant effect of surface was seen for the peak frontal plane rearfoot-floor angle (vcut, p<0.001; agility, p<0.001), with players having a flatter foot orientation on the high traction surfaces (Control and SP).

CONCLUSIONS

When on a high traction surface football players have a flatter foot orientation, which may increase cleat engagement and allow players to generate a greater utilized traction at take-off. Players additionally increase their ankle angle to maintain upper body orientation while increasing shoe-surface interaction.

ACKNOWLEDGEMENTS

Football cleats were provided by Nike and the surfaces were provided by FieldTurf. Funding for this study was provided by a National Football League (NFL) grant.

REFERENCES

[1] Wannop et al. *Life*, 10(12) 2023.

Table 1: Utilized traction and frontal plane foot and ankle angles on the different surfaces. Data represent the mean±SD of all participants.

		Influence of Surface				Influence of Position		
		Control	LW	SP	p-value	Speed	Power	p-value
Utilized Translational Traction at Takeoff	Vcut	1.56±0.39	1.34±0.27	1.61±0.37	**0.061**	1.54±0.22	1.46±0.28	0.526
	Agility	1.65±0.30	1.45±0.43	1.56±0.34	**0.058**	1.61±0.13	1.49±0.39	0.379
	Cone	1.53±0.43	1.23±0.24	1.34±0.39	**0.005**	1.47±0.26	1.23±0.34	0.130
Minimum Rearfoot Eversion Angle [deg]	Vcut	14.4±5.6	16.6±6.1	11.8±8.2	**< 0.001**	15.2±6.0	13.2±6.7	0.782
	Agility	17.2±8.5	21.3±8.0	13.9±7.7	**<0.001**	19.1±7.1	15.5±10.1	0.539
	Cone	-8.6±9.0	-9.2±9.6	-7.4±6.1	0.262	-9.3±6.5	-7.4±8.7	-0.876
Peak Ankle Inversion Angle [deg]	Vcut	21.8±7.5	18.2±6.8	23.9±8.1	**0.076**	21.4±7.4	21.1±6.7	0.778
	Agility	27.8±9.3	24.1±9.2	30.0±9.2	**0.002**	26.5±9.9	28.3±9.5	0.851
	Cone	28.2±5.5	27.1±5.9	29.5±4.6	**0.011**	30.2±5.4	26.0±3.9	**0.081**

Exploring the acute neuromuscular effect of accentuated eccentric loading during unconstrained vertical jump with different loading locations on the body

Eric Yung-Sheng Su[1], Timothy Carroll[1], Dominic Farris[1,2] and Glen Lichtwark[1]
[1] School of Human Movement and Nutrition Sciences, Faculty of Health and Behavioural Sciences, The University of Queensland, Brisbane, Australia
[2] Public Health and Sports Sciences, Faculty of Health and Life Sciences, University of Exeter, Exeter, UK.
Email: yungsheng.su@uq.edu.au

INTRODUCTION

Accentuated eccentric loading (AEL) is an exercise where additional load is added to the body during the eccentric phase of a movement and then immediately decoupled during the concentric phase. It has been suggested that applying AEL during countermovement jump may increase jump height and power output [1, 2]. However, there is conflicting evidence for this effect [3, 4], and it remains unclear whether this increased performance is due to mechanical reasons, such as increased energy stored in the tendon, or just a more effective movement coordination strategy. This study aimed to examine how applying AEL loads at different locations on the body impacts the jump height and power output of a maximal countermovement jump.

METHODS

We collected data from 2 healthy adult participants, but ongoing data collection aims to collect 13 participants (aged 18-45). In session 1, the participant selected a preferred countermovement depth (CMD) for non-weighted condition and practiced AEL jumps (20% body mass) to the same depth with two different conditions (loading from pelvis and trunk). Each jump was performed on a customised pulley system with an electromagnet attached, which allowed adding weights during the jump and automatically releasing weights at the bottom of the countermovement. We monitored and controlled CMD in these conditions using a linear potentiometer transducer via a waist belt (GymAware, Kinetic Performance Technology, Canberra, Australia) to provide instant feedback after each jump. Two more conditions were used without CMD constraint: AEL from hand-held dumbbells (20% body mass) and free countermovement jump without arm swing. In session 2, the participant performed three successful maximal jumps for each condition. We randomized the order for conditions with and without constrained CMD. Two AMTI force plates were used to collect ground reaction forces synchronously with 8 high speed video cameras (FLIR) through a 3D motion capture system (Vicon). Markerless motion analysis software (Theia Markerless) was used to analyse whole body three-dimensional kinematics, including the location of the body centre of mass. Surface EMG of 8 lower limb muscles were also collected. Only the trial with the highest jump height for each condition was analysed.

RESULTS AND DISCUSSION

We found decreased jump height with AEL conditions in pelvis and trunk loading compared to non-AEL conditions. CMD was constrained in pelvis and trunk loading conditions (<3 cm difference), and hence the hip and knee angles at the bottom of the jump did not differ meaningfully between AEL and non-AEL conditions. However, both participants increased jump height with AEL in dumbbell loading. The mechanism for increased jump height requires more consideration, as kinematics and CMD varied substantially despite both participants improving jump height. Data are reported in Table 1.

CONCLUSIONS

Our preliminary data suggests that when CMD was constrained (<3 cm between conditions), AEL did not increase maximal jump height. However, when CMD was not constrained and AEL was loaded from both hands, participant increased jump height. This performance-enhancing effect could be explained by adopting a deeper squat depth or through shifts in the position of the centre of pressure related to arm movement, but further investigation is needed.

REFERENCES

[1] Aboodarda S J et al. *Int J Sports Physiol Perform* **8**: 181-187, 2013.
[2] Sheppard J et al. *Int J Sports Sci Coach* **2**: 267-273, 2007.
[3] Aboodarda S J et al. *J Strength Cond Res* **28**: 2314-2323, 2014.
[4] Wagle J et al. *Sports Med* **47**: 2473-2495, 2017.

Table 1: Differences in jump height, CMD, hip and knee angles at the bottom of the jump at different loading conditions.

	Dumbbell Loading		Pelvis Loading		Trunk Loading	
	Participant 1	Participant 2	Participant 1	Participant 2	Participant 1	Participant 2
Δ Jump Height (cm)	+2.6948	+3.5948	-3.8005	-3.8269	-1.1652	-2.1011
Δ CMD (cm)	-3.2076	+7.5533	+2.6026	+1.4267	-1.0269	-0.3592
Δ Hip Angle (°)	-2.8720	+10.4325	-1.3614	-0.7306	+0.8572	+2.2671
Δ Knee Angle (°)	-8.8966	+11.3011	+3.2441	1.0560	-3.2030	-1.7312

Dynamic Sagittal Plane Joint Loading Biomechanics in Individuals with ACL Reconstruction with and without a History of Ankle Sprains Compared to Healthy Controls

Sugimoto YA[1], Garrison JC[2], Hannon JP[3], Goto S[4], Singleton SB[5], Dewald JPA[1]

[1]Department of Physical Therapy & Human Movement Sciences, Feinberg School of Medicine, Northwestern University, Chicago, USA

[2] Memorial Hermann | Rockets Sports Medicine Institute, Houston, TX, USA

[3]St. Louis Children's Hospital: Young Athlete Center, St. Louis, MO

[4]Texas Health Sports Medicine, Fort Worth, TX

[5]UT Southwestern, Fort Worth, TX

Email: yuki.sugimoto@northwestern.edu

INTRODUCTION

55% of athletes who have had an ACL reconstruction (ACLR) return to competitive levels of sports [1]. 30% of these athletes suffer another ACL injury in the contralateral or ipsilateral limb within 24 months of return-to-sport (RTS) which may eventually result in knee osteoarthritis within ten years [1]. One of the potential risks for a repeat ACL injury is sagittal plane knee loading abnormalities [2]. Individuals with ACLR avoid loading the surgical knee by shifting the load to the ipsilateral hip [2]. It is known there is a significant association between ACL injury and a history of prior ankle sprains [3]. However, little is known about how a history of ankle sprains impacts sagittal plane joint loading biomechanics during simple bilateral and more complex unilateral tasks at RTS in individuals with ACLR. Therefore, the purpose of this study was to evaluate if sagittal plane loading biomechanics between lower extremity joints (i.e., ankle, knee, hip) changes across tasks at RTS in individuals with ACLR with a history of ankle sprains (ACLR-AS) compared to individuals with ACLR and healthy controls.

METHODS

Thirty-nine athletes, who were matched by sex, height, weight, and limb dominance, performed five trials of double-limb squats (DLS) and then single-limb squats (SLS) followed by a 30-second rest between trials and 1-minute rest between tasks. The kinematics and ground reaction force data were recorded at 120 Hz (Qualisys) and 1200 Hz (AMTI), respectively. In order to assess the integrated biomechanics of the lower extremity joints during squatting, energy absorption contribution (EAC) from separate joints was used. EAC was computed by averaging the middle three trials' negative joint work during the decelerating phase of DLS and SLS relative to total EAC. This negative joint work represents the muscle-tendon unit at individual joints and was normalized by athletes' height and weight. Athletes' surgical limbs were identified as the limb with ACLR and ACLR-AS, and healthy controls were given a surgical limb based on matched athletes. Nonsurgical limbs were defined as contralateral to the surgical limb. 3 (group) × 3 (joints) × 2 (tasks) repeated measures analysis of variance were conducted to examine differences between groups and within joints and tasks in EAC during DLS and SLS in the surgical limb. Alpha was set a priori at 0.05.

RESULTS AND DISCUSSION

Significant group × joints × task interactions were found in the surgical limb ($F_{4,72}$=7.543; P=.011). Tukey post hoc comparisons revealed ACLR-AS and ACLR groups displayed greater EAC at the hip (ACLR-AS: 38.91±3.09%, P=.01; ACLR: 44.09±3.09%, P<.001) and lower EAC at the knee (ACLR-AS: 38.91±3.09%, P=.010; ACLR: 44.09±3.09%, P<.001) during SLS compared to healthy controls (Hip: 28.13 ± 3.09%; Knee: 56.58±2.82%). All three groups significantly loaded the knee the most, followed by the hip and ankle during DLS (P-range:<.001-.038) and SLS (P-range: .009-.038), with the exception of the ACLR group, which displayed a load-sharing strategy between the hip (44.09±3.06%) and knee (41.70±2.82%) during SLS.

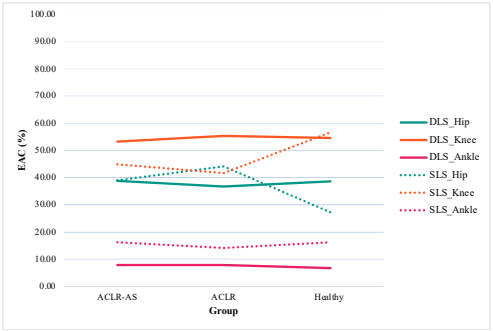

Figure 1 Significant interactions of Group by Joints by Task for EAC in the Surgical Limb

CONCLUSIONS

Group differences in loading biomechanics depended on joints and tasks. The ACLR-AS and ACLR group increased loading at the hip during more complex SLS in the surgical limb compared to healthy controls at RTS. The sagittal plane joint loading biomechanics used by the ACLR-AS and ACLR groups did not differ based on a history of ankle sprains. To comprehend load-sharing strategies employed by the ACLR group, further research on proprioceptive characteristics and potential deficits, in the case of ACLR, especially at the knee joint, may be required to better understand mechanisms that may explain differences in loading biomechanics.

REFERENCES

[1] Arderno CL et al. *BJ Sports* **48**: 1543-1552, 2014
[2] Robinson et al. *Orthop J Sports Med* **10**: 1, 2022
[3] Theisen et al. Int J Exerc Sci **12**: 24-33, 2019

Use of a novel mobile application to assess calf muscle function in sport

Kim Hebert-Losier[1], Te Manawa Ngawhika[1,2], Nicholas Gill[1,3] and Carlso Balsalobre-Fernandez[4]
[1] Te Huataki Waiora School of Health, University of Waikato, Tauranga, New Zealand
[2] Bay of Plenty Steamers, Bay of Plenty Rugby Union, Tauranga, New Zealand
[3] New Zealand Rugby Union, Wellington, New Zealand
[4] Applied Biomechanics and Sport Technology Research Group, Universidad Autónoma de Madrid, Spain
Email: kim.hebert-losier@waikato.ac.nz

INTRODUCTION

Over 60% of practitioners in sport and exercise science use mobile appications to collect data [1]. Mobile applications are an appealing and affordable alternative to laboratory systems. These applications are useful in field-settings to inform practice when valid and reliable. The Calf Raise application (CR_{app}) was developed to facilitate testing of the triceps surae (i.e., calf) muscles in a clinical or field-based context. Given that these muscles are key for many sport-related activities, included maximal-effort accelerated sprints, testing calf muscle function is likely to inform on athletic ability. We aimed to establish the validity and reliability of the CR_{app} in a cohort of Rugby Union players, and explore the potential association between 10-m sprint times and calf muscle strength-endurance and power metrics.

METHODS

Cohorts of professional male Rugby Union players participated in the validity (n = 20; 35% backs), test-retest reliability (n = 18, 61% backs), or correlation (n = 16, 63% backs) portions of this project. In all studies, players completed three single-leg tests once on both legs: (1) bodyweight power; (2) 35 kg weighted power; and (3) endurance. The CR_{app} was used to track the vertical displacement of a marker placed below the lateral malleolus using computer-vision algorithms. The vertical displacement was used to extract peak power from the power tests and total repetitions, peak height, total displacement, and total work from the endurance test. Three-dimensional motion capture and force plates were used to extract the same metrics for validation purposes. Players were tested twice a week apart to assess test-retest reliability. The 10-m sprint times of players were tested 3-4 days after calf muscle testing using single-beam timing lights in the correlation study.

Two-way mixed effects single measurement intraclass correlation coefficients ($ICC_{3,1}$) and typical errors expressed as coefficient of variations (CV) with 95% confidence intervals (CI) were calculated to quantify relative and absolute concurrent validity and test-retest reliability. Relative validity and reliability were considered *fair*, *good*, and *excellent* when ICC values reached 0.40, 0.75, and 0.90, and *poor* when <0.40. Absolute validity and reliability were deemed acceptable when CV was < 10%. Pearson correlations and 95% CI between sprint times (average and best trial) and calf muscle metrics were computed using estimates based on Fisher's z transformation with bias adjustment. Correlations were considered *small*, *moderate*, and *large* when reaching 0.10, 0.30, and 0.50, and *trivial* when <0.10. Statistical significance was set to $p < 0.05$.

RESULTS AND DISCUSSION

The relative validity of CR_{app} metrics was *good* to *excellent* and absolute validity of CR_{app} metrics was acceptable compared to 3D motion capture and force plate data (ICC 0.84–1.00, CV ≤ 6.6%). Test-retest reliability of CR_{app} metrics was *good* with acceptable retest errors (ICC 0.83–0.88, CV≤ 9.8%) across metrics.

There were *large* significant correlations between 10-m average sprint times and calf muscle bodyweight power, weighted power, and total displacement and total work during endurance testing ($|r|$ = 0.51–0.63). There were *large* significant correlations between 10-m best sprint times and calf muscle weighted power, and total displacement, total work, and peak height during endurance testing ($|r|$ = 0.50–0.53).

CONCLUSIONS

The metrics from the calf muscle testing procedures extracted using the CR_{app} were valid and reliable in male Rugby Union players. These metrics were largely correlated to their 10-m sprint times, an indicator of their acceleration ability. Other than being used as a performance indicator and monitoring tool, the CR_{app} may prove useful in injury prevention efforts, rehabilitation, and return-to-play decision making for calf muscle and Achilles tendon injury, a prevalent concern in Rugby Union players.

ACKNOWLEDGEMENTS

Two authors (KHL and CBS) are developers of the free-to-use CR_{app}. A researcher (TN) not related to app development collected all data.

REFERENCES

[1] Shaw MP et al. *JMIR mHealth and uHealth* **9**: e21763.
[2] Hebert-Losier et al. *Calf Raise* (v.1.5.1) [Mobile application software].

Influence of Immediate Dry Needling Therapy for Hamstring Muscle Fatigue on Standing Balance Control

Shih-Wun Hong[1,2], Tsung-Jung Ho[2], Christopher Lo[1] and Keng-Chang Kuo[2]
[1] Department of Physical Therapy, Tzu Chi University, Hualien, Taiwan.
[2] Department of Chinese Medicine, Hualien Tzu Chi Hospital, Hualien, Taiwan.
Email: swhong0624@gms.tcu.edu.tw

INTRODUCTION

Muscle fatigue is described as a reduction of maximal force or power that the involved muscles can produce, and it can develop gradually after onset of sustained physical activity. Among all the muscle in the lower limbs, hamstring injury is often associated as a risk factor leading to hamstring strain during sports activities. Dry needling (DN) has been a common intervention for the treatment of muscle fatigue because it induce immediate analgesia of the myofascial trigger point without hyperaesthesia for patients with myofascial pain. Variables describing the movement of the centre of pressure (COP) are useful for the evaluation of balance behaviors such as body postural sway. The purpose of the current study was to investigate the effect of dry needling on standing balance in terms of COP sway variables.

METHODS

Nine young and healthy subjects from Hualien community aged from 20-35 years old participated in the current study. In a gait laboratory, each subject was guided to perform static balance test, namely standing with feet close up with eyes closed for 60 seconds before and after induced muscle fatigue exercise (Control and Fatigue Conditions) and after dry needling therapy for fatigue (DN Condition). The induced muscle fatigue exercise is defined as fifty active flexion of the knee with resistance of the therabands while prone on the treatment bed. The dry needling therapy was delivered by an experienced and qualified Chinese medicine doctor (Keng Chang Kuo) using disposable sterilized stainless steel needles. The dry needles were located at myofascial trigger points of the biceps femoris, semitendinosus and semimembranosus muscles. Each trigger point was needled with 1 minute of fast in-out cone-shaped technique. The time-varying COP positions were calculated from the ground reaction force data using the forceplate. The sway area of the COP (ACOP) was described by an equivalent ellipse covering 95% of the samples along each axis obtained by principal component analysis. The ratio of the lengths of the major axis and minor axis was also calculated to describe the distribution of the COP positions. A one-way analysis of variance with block design of each subject was used to compare the differences of ACOP and ratio of axis lengths between conditions.

RESULTS AND DISCUSSION

There were no significant differences of ACOP between Control and Fatigue Conditions. After dry needling therapy for fatigue (DN), the subjects showed greater ACOP compared with those in Control and Fatigue Conditions. Moreover, there were no significant differences of ratio of axis lengths between conditions.

Hamstring fatigue might not affect the strategy of co-contraction of knee extensor and flexor muscles for maintenance static standing balance. However, relaxation of the hamstring muscle using dry needling therapy may cause greater posture sway (i.e. ACOP) of the body during quiet standing. Dry needling may be an effective treatment for relaxation of the muscle leading to compromise the strategy of co-contraction of the agonist and antagonist muscles for static balance control. Moreover, no significant differences of the ratio of axis lengths between conditions indicates that fatigue or dry needle therapy might not affect the unity of posture sway during standing.

CONCLUSIONS

Dry needling may be an effective treatment for relaxation of the muscle leading to compromise the strategy of co-contraction of the agonist and antagonist muscles. It is suggested that dry needling therapy might not suitable for decreasing posture sway of static balance control.

ACKNOWLEDGEMENTS

The authors gratefully acknowledge the financial support from National Science and Technology Council (Grant No.: MOST 110-2221-E-320 -003).

Table 1: The sway area (ACOP) and ratio of the lengths of the major axis and minor axis (L_{major} / L_{minor}) of the COP in subjects before and after induced hamstring fatigue exercise (Control and Fatigue) and after dry needling therapy (DN) for 60-second quiet standing.

	Control	Fatigue	DN	*p-value*
ACOP (mm^2)	432.9 ± 212.3	405.5 ± 159.1	586.3 ± 232.5	$p = 0.001$
L_{major} / L_{minor} (mm/mm)	1.4 ± 0.2	1.4 ± 0.1	1.3± 0.2	$p = 0.231$

CONTRIBUTION TO THE RACKET HEAD VELOCITY IN THE TENNIS FOREHAND DRIVE BETWEEN INTERMEDIATE AND HIGH-PERFORMANCE PLAYERS

Bruno Pedro[1], Sílvia Cabral[1], Jerusa P. R. Lara[2] and António P. Veloso[1]

[1] Universidade de Lisboa, CIPER, Faculdade de Motricidade Humana, Laboratório de Biomecânica e Morfologia Funcional, Cruz Quebrada, Portugal

[2]Reference Center in Sports Sciences—SESI, 05303-902 São Paulo, Brazil

Email: bmpedro@fmh.ulisboa.pt

INTRODUCTION

The tennis forehand drive is the first technique usually learned by beginners [1] and is considered the second most important technique in tennis just behind the serve [2]. Given that ball velocity depends highly on the velocity of the racket head, many researchers have attempted to determine the most efficient mechanics for higher racket velocity [3]. Based on the method developed in previous studies [4], researchers have identified the upper limb rotations that most contribute to the racket head velocity between different type of forehand shots [5]. Despite the importance of the latter studies comparing different techniques, no study used this method to compare the contributions of upper limb rotations to the racket head velocity between different levels of expertise. Thus, the aim of this study was to compare the contributions of the upper limb segments rotations to the racket head velocity in the tennis forehand drive between intermediate (INT) and high-performance (HP) tennis players.

METHODS

Twenty-seven tennis players Participated in this study, 12 intermediate and 15 high-performance. The tennis forehand strokes were performed inside the laboratory (Figure 1). Athletes were asked to hit the ball like in a real situation. Kinematic data were collected at 240Hz with an optical system with fifteen infrared high-speed cameras using the Qualisys Track Manager (version 2.17, Qualisys AB, Gothenburg, Sweden) software. The contribution of the upper limb segment's rotations to the racket head velocity was calculated using the method developed in a previous study [4].

RESULTS AND DISCUSSION

The results showed significant differences between INT and HP tennis players (Table 1) in the contribution of the shoulder (representing the contribution of the trunk and lower limbs) to the racket head velocity. No other significant differences were found between both levels. The results of this study differ from a previous study [5] which referred the internal rotation of the upper arm as the most important rotation to the racket head velocity.

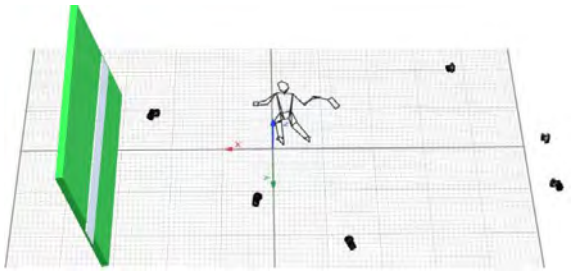

Figure 1 Laboratory test environment with fifteen infrared high-speed cameras during forehand drive performance.

CONCLUSIONS

The horizontal shoulder velocity represents a key factor that might distinguish intermediate from high-performance tennis players. Tennis coaches and athletes should focus in developing higher velocities of the shoulder to achieve a higher performance.

ACKNOWLEDGEMENTS

This work was supported by the Fundação para a Ciência e Tecnologia, under Grant UIDB/00447/2020 to CIPER - Centro Interdisciplinar para o Estudo da Performance Humana (unit 447).

REFERENCES

[1] Seeley MK et al. *Sports Biomech* 10: 415–26, 2011.

[2] Reid M et al. JSS Medicine 12: 225–231, 2013.

[3] Landlinger J et al. *JSSci Med*; 9: 643–651, 2010.

[4] Sprigings E et al. *J Biomec*; 27: 245–254, 1994.

[5] Elliott B et al. *J Appl Biomech*; 13: 182–196,1997.

Table 1: Contribution of the upper limb rotations to the racket head velocity between INT and HO tennis players.

Segments	Intermediate		High-Performance			
	Mean ±SD (m/s)	Contribution (%)	Mean ±SD (m/s)	Contribution (%)	p	d
Shoulder (Trunk and lower limbs)	1.6 ± 0.7	7,9	2.2 ± 0.6 (m/s)	11,9	0.012*	-1,0
Upper Arm – Flex / Ext	8.0 ± 2.3	40,0	8.7 ± 1.7	41,5	0.855	0,1

VSIMULATORS TO EXPLORE HUMAN STATIC AND DYNAMIC BALANCE CONTROL

Genevieve Williams [1,*], Naser Taleshi [1], Sarah E. Lamb[1] and James M. W. Brownjohn [2]
[1] Faculty of Health and Life Sciences, University of Exeter, Exeter, UK.
[2] Vibration Engineering Section, Department of Engineering, University of Exeter, Exeter, UK
*Email: g.k.r.williams@exeter.ac.uk

INTRODUCTION

At the University of Exeter, UK we are adressing a range of research topics to further understand static and dynamic balance control in healthy and clinical populations using our state-of-the-art VSimulators facility. VSimulators has a 3.7 m^2 platform, that can be programmed to move precisely in 6 degrees of freedom with an amplitude of up to 4cm, where frequency of motion can range between 0.4 and 40 Hz. The floor of the platform is covered with an array of 9 AMTI force plates (Fig. 1a), the area is surrounded by a Motive motion capture system. In addition, VSimulators is integrated with 9 virtual reality headsets and we have synchronised add ons; FNIRS, EMG, IMUs, eye tracking, and gas analysis technologies.
Here we demonstrate the system through a study which aims to identify critical frequencies of floor motion that results in transitions in balance control stratergy. Previous work in this area has focussed on large amplitudes of platform motion (9-23 cm at 0-3 Hz) in the anterio-posterior (AP) direction, and defined ankle to hip dominant strategies with transition from in-phase to anti-phase centre of pressure-centre of mass (COP-COM) relation occuring at around 0.5 Hz [1-3]. Here we use smaller amplitude platform motion reflective of real life to investigate how the postural system regulates hip, knee and ankle strategies to govern the COP-COM coordination.

METHODS

Nine young healthy participants stood on the VSimulators platform as it sinusoidally translated in the AP direction. Platform frequency was linearly scaled from 0.4 Hz to 6 Hz and then back down to 0.4 Hz with amplitude of 2 mm peak, resulting in platform acceleration between 0 to 2.5 m/s^2 (Fig. 1c). Full body motion capture and force plate data were collected. Using a 4-segment model, hip, knee and ankle joint torques were calculated via inverse dynamic analysis. Coordination between the joint torques, and COP-COM relative motion were quantified by vector coding. Ankle, knee and hip postural strategies were defined based on the phase relationship between hip-knee and knee-ankle joint torque couples [4].

RESULTS AND DISCUSSION

There was a significant effect of platform frequency on knee-ankle torque and COP-COM phase relationship. At frequencies below 2.27 Hz, an ankle strategy was used (in-phase knee-ankle torque), which resulted in in-phase COP-COM motion with the COP being dominant. As the frequency of the platform increased beyond 2.27 Hz, COM motion became dominant. At this point, a knee strategy was used, which involved anti-phase knee-ankle torque and allowed the COP to regain dominance over the COM.

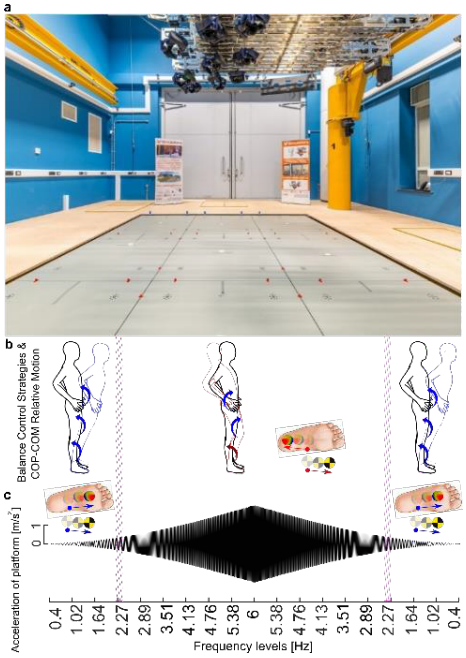

Figure 1 (a) VSimulators facility, (b) Balance strategy as defined by hip-knee and knee-ankle torque phase relation, (c) and COM-COP phase relation during changes in platform frequency.

CONCLUSIONS

The study identified the knee strategy as a new and relevant strategy used with small amplitude platform motion, that are more representative of real-world settings. We show evidence that the transition between ankle and knee strategies underpins the transition between COP-COM relative motion.
Work of our group in the VSimulators facility is focussing on health related (ageing, Parkinson's disease) and basic science research to understand mechanisms of human balance control.

ACKNOWLEDGEMENTS

EPSRC EP/P020690/1 University of Exeter, UK.

REFERENCES

[1] Ko et al., *J Hum. Mov. Sci.*: **20**, 737-764, 2001.
[2] Ko et al., *J Hum. Mov. Sci.*: **38**, 1-14, 2014.
[3] Dutt-Muzumder et al., *J Hum. Mov. Sci.*: **52**, 24-35, 2017.
[4] Taleshi N et al. *J Nature Scientifc Reports* **12(1)**: 21030, 2022.

A MODEL PREDICTIVE CONTROL SCHEME FOR HUMAN BALANCE RECOVERY IN RESPONSE TO A CONTINUOUS TIME-VARYING PLATFORM MOTION.

Naser Taleshi[1,*], Amid Kheirandish[2], James M. W. Brownjohn[3], Sarah E. Lamb[1] and Genevieve K. R. Williams[1]
[1] Faculty of Health and Life Sciences, University of Exeter, Exeter, UK.
[2] Department of Electrical Engineering, Khaje Nasir Toosi University of Technology, Tehran, Iran.
[3] Department of Engineering, University of Exeter, Exeter, UK
*Email: nt420@exeter.ac.uk

INTRODUCTION

Many researchers have attempted to understand the fundamental properties of the human balance control system by quantifying recovery strategies in response to an external perturbation. For example, continuously scaling platform frequency has revealed a number of different transitions between adaptive balance strategies. Model predictive control (MPC) is an emerging advanced method applied to understand and predict human postural responses as it is able to represent characteristics of the human motor system such as prediction, adaptation, multi-joint control, and optimization. Building on previous MPC models that simulated postural response to sudden and short floor motions [2], here we aim to propose and test an MPC based scheme of human balance control in response to more demanding and continuous translational perturbations shown in (Figure 1g).

METHODS

The model was tested using data from our previous study [1] that analysed balance recovery in response to small amplitude underfloor movement where frequency was scaled from 0.4-6 Hz in the AP direction. The model consists of a four-segment biomechanical model with sensory feedback that maps joint recovery motion to the neural controller (MPC). Then, the MPC generates corrective torques through an optimization process, to maintain an upright standing position. Biomechanical constraints and optimization criteria in the MPC scheme were set to achieve human-like recovery behaviour and investigate effective regulation of postural strategies. Postural strategies are identified by the phase relationship between corrective output joint torques, as described in more detail in our previous work [1].

RESULTS AND DISCUSSION

Simulation results using the proposed MPC scheme, as shown in (Figure 1c-d, f) are well aligned with our experimental results [1]. Model results show a transition from in-phase to anti-phase (blue to red bars) for knee-ankle torque and COP-COM relative motion at a frequency of 3.5 Hz, while hip-knee torque remained in-phase at all frequencies. It seems that to deal with the loss of stability caused by scaling platform frequency, MPC controller can regulate adaptive postural responses and transit between them and change coordination between COP-COM motion accordingly.

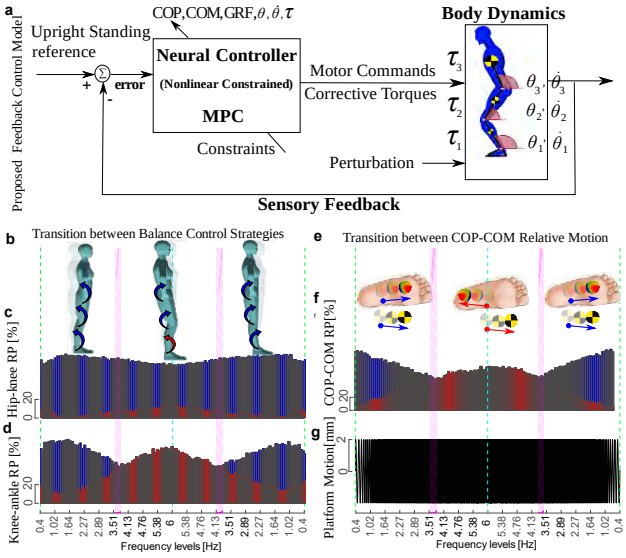

Figure 1 (a) Model schematic, (b) balance strategy as defined by (c) hip-knee and (d) knee-ankle torque phase relation, and (e, f) COM-COP phase relation during changes in platform frequency (g).

CONCLUSIONS

The facility of MPC to continually update predictions and control actions based on anticipated future events, while adhering to biomechanical constraints, makes it well-suited for handling complex and unpredictable dynamic behaviours, such as transition between postural strategies under effect of scaling platform frequency. Future work aims to apply this model to explore the landscape of postural strategies that emerge across a wide range of platform amplitudes and frequencies. By taking into account specific constraints or limitations associated with different population groups, such as the elderly or those with Parkinson's Disease, this model can also be refined to predict or simulate their behaviour.

ACKNOWLEDGEMENTS

This work was supported by EPSRC DTP and College of Life and Environmental Sciences at University of Exeter.

REFERENCES

[1] Taleshi N et al. *J Nature Scientifc Reports* **12(1)**: 21030, 2022.
[2] Shen K et al. *J IEEE Access* **8**: 92050-92060, 2020

INFLUENCE OF SPRING-LOADED ANKLE EXOSKELETONS ON GASTROCNEMIUS FASCICLE BEHAVIOUR DURING BALANCE TASKS

Jemima Po[1], James Williamson[1], Jordan Yee[1], Dominic Farris[2,3] and Taylor Dick[1]
[1]School of Biomedical Sciences, University of Queensland, Brisbane, Australia
[2]Sport & Health Sciences, University of Exeter, Exeter, United Kingdom
[3]School of Human Movement & Nutrition Sciences, University of Queensland, Australia
Email: j.po@uq.net.au

INTRODUCTION

Wearable assistive devices have wide-ranging applications in human augmentation and rehabilitation. Spring-loaded exoskeletons provide mechanical assistance at the ankle joint by storing and returning energy, mimicking the behaviour of the Achilles tendon and plantarflexors. Previous studies have shown that passive devices reduce the energetic demands of locomotion [1]. However, wearing lower limb exoskeletons alters patterns of fascicle length changes and muscle activation [2]. This may complicate balance control which requires constant monitoring and adjustment of ankle muscle function. Balance is further challenged by manipulating the support base and sensory inputs. Increasing postural demand changes balance strategies and the neuromuscular behaviour of the plantarflexors [3,4]. As such, the influence of exoskeletons may extend beyond locomotor economy to affect postural control in a task-dependent manner. The aim of this study was to assess the influence of passive ankle exoskeletons on muscle fascicle behaviour during balance tasks of varied difficulty.

METHODS

Thirteen participants performed four balance tasks: (i) quiet standing with eyes open (EO), (ii) eyes closed (EC), (iii) active sway (AS), and (iv) reduced base of support (RBOS). Tasks were performed for 60s on a force plate (Bertec Corp., USA) at three exoskeleton spring stiffnesses: 0, 42, and 85 Nm rad^{-1}. Medial gastrocnemius (MG) fascicle lengths were measured using B-mode ultrasound (ArtUS, Telemed), and processed using a semi-automated algorithm (UltraTrack v4.2). Linear mixed-effects models determined the influence of exoskeleton assistance and balance condition on the mean and standard deviation (SD) of fascicle length during the task. Tukey's post hoc tests were performed to identify significant differences between conditions. Significance was set to $p<0.05$.

RESULTS AND DISCUSSION

There were significant main effects of exoskeleton stiffness ($p=0.002$) and balance condition ($p=0.012$) on mean MG fascicle length, but no stiffness*condition interaction (Fig.1A,C). Post hoc analyses revealed that during AS with low exoskeleton assistance (42 Nm rad^{-1}), MG fascicles operated at 4.3% longer lengths compared to no assistance ($p=0.032$), but there were no differences with the highest level of assistance (85 Nm rad^{-1}). During the EC balance condition with low assistance (42 Nm rad^{-1}), MG fascicle lengths increased by 4.9% and 5.2% compared to no assistance ($p=0.031$) and the stiffest assistance (85 Nm rad^{-1}) ($p=0.02$), respectively. Fascicle lengths did not differ between exoskeleton stiffnesses for EO or RBOS. There was a main effect of condition ($p<0.001$) and a stiffness*condition interaction ($p=0.003$) on the variability (SD) in MG fascicle operating lengths, but no effect of exoskeleton stiffness. This meant that fascicles operated at shorter lengths (Fig.1C) and tended to vary more (Fig.1D) during more challenging postural tasks (AS and RBOS) than quiet standing (EO and EC).

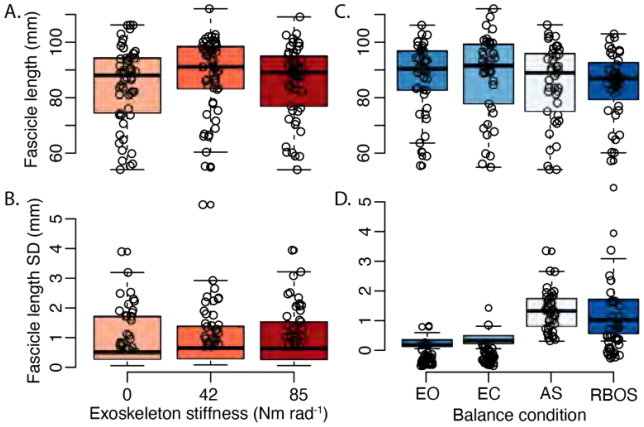

Figure 1 Mean MG fascicle length (A,C) and standard deviation (B,D) for three exoskeleton spring stiffnesses and four balance conditions (eyes open (EO), eyes closed (EC), active sway (AS), reduced base of support (RBOS)).

CONCLUSIONS

When balancing with passive ankle exoskeletons, changes in plantarflexor fascicle dynamics are dependent on the level of exoskeleton assistance and the difficulty of the balance task. Future investigations into the influence of these wearable devices on neuromuscular control in populations with balance deficits (e.g., ageing) will provide insights into the restorative potential of passive devices.

REFERENCES

[1] Collins, SH et al. *Nature* **522**: 212-215, 2015.
[2] Farris, DJ et al. *J Appl Physiol* **115**: 579-85, 2013.
[3] Donath, L et al. *Maturitas* **91**: 60-68, 2016.
[4] Gebel, A et al. *Front Physiol* **10**: 1135, 2019.

A SINGLE SESSION TREADMILL PERTURBATION-BASED BALANCE TRAINING FOR FALL PREVENTION: EFFICACY AND MECHANISMS

Deepak Ravi[1], Friederike Schulte[2], William Taylor[1], Navrag Singh[1], Chris Awai[3], and Raphael Schweri[1]
[1]Laboratory for Movement Biomechanics, ETH Zurich, Switzerland
[2]SturzZentrum Schweiz, Switzerland [3]cereneo Foundation, Switzerland
Email: deepak.ravi@hest.ethz.ch

INTRODUCTION

Perturbation-based balance training (PBT) has been demonstrated to be an effective and feasible task-specific approach for reducing fall incidence in older adults. Previous studies have shown that a single session of PBT can impart fall-resistance skills, which can be retained for up to a year [1]. However, most of these single-session studies focus on overground slip perturbation training, even though treadmill setup seems to enable greater perturbation loads and clinical feasibility. The goal of our study was to establish the efficacy of such a treadmill protocol with respect to balance outcomes and mechanisms underlying the intervention's effect, in order to gain acceptance in clinical practice.

METHODS

In this pilot study, 20 older adults without neurological or orthopaedic conditions were recruited. The participants were randomly and equally divided into an intervention group (50% female, with a mean age of 67.1±2.7 years) and a control group (50% female, 72.8±4.9 years). The control group received treadmill walking training in a single session consisting of three blocks of 8 minutes each. For the participants in the intervention group, the training additionally included antero-posterior perturbations (32 in total) by sudden acceleration or deceleration of the treadmill belt (increments of 0.25 m/s^2, from 0.5 m/s^2 up to a maximum of 2.25 m/s^2). Training efficacy was evaluated by analysing 4-minute assessment blocks, which feature a single deceleration perturbation at 2.25 m/s^2, before (Pre) and after (Post) training. We measured the individual's resilience to perturbations through the maximum center of mass (COM) deviation from pre-perturbation, steady-state movement patterns, and the time taken to recover [2]. The mechanisms were evaluated by determining the degree of coordination between the COM and foot placement [3].

RESULTS AND DISCUSSION

The control group had a decrease in maximum deviation of COM of 12.3±17 millimetres, while the intervention group showed a decrease of 24.2±28 millimetres. Additionally, the control group saw an average increase in recovery time of 2.3±3.2 seconds, while the intervention group experienced a decrease of 2.5±6.9 seconds. The degree of coordination between COM and foot placement increased in both the control (3.7±11.3%) and the intervention (2.8±5.4%) groups. Both groups exhibited a relatively high foot placement control before training, which may have limited their ability to improve it further.

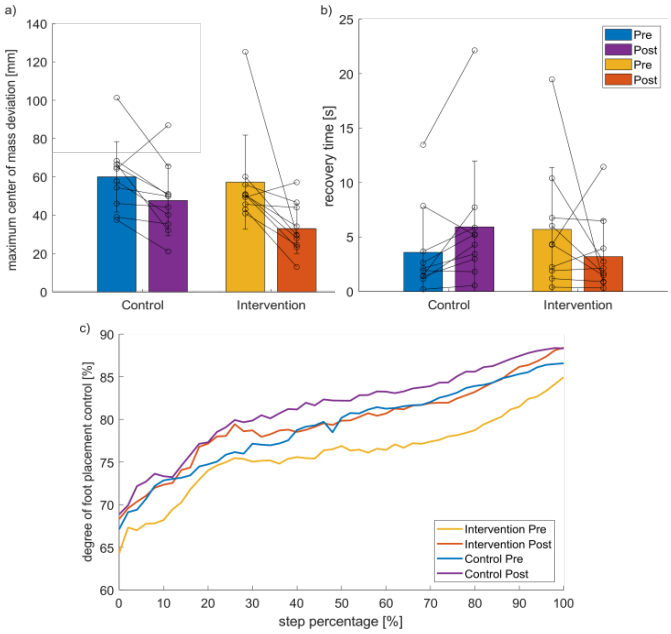

Figure 1 Effects of PBT on a) maximum center of mass deviation b) recovery time c) degree of foot placement control for the swing phase from toe off (0%) to heel strike (100%) - quantified as the relative explained variance of a regression model linking mediolateral foot placement to mediolateral position and velocity of CoM [3].

CONCLUSIONS

Our results indicate that a single session of treadmill PBT may yield greater within-session benefits in improving balance in comparison to conventional treadmill walking training. The significance of these findings remain to be investigated in a more in-depth analysis of mechanistic changes to e.g., base of support or step length and its relationship to maximum COM deviation and recovery time.

ACKNOWLEDGEMENTS

Funding: Innosuisse - Swiss Innovation Agency (52519.1 INNO-LS). **Research Staff:** Leonie Wunderli and Livia Rätzo.

REFERENCES

[1] McCrum C et al. *Front. S A Living* **4**:1015394, 2022
[2] Ravi DK, et al. *J E Biology* **224**:5, 2021
[3] Bruijn SM et al. *J R Soc Interface* **5**:20170816, 2018

Emulating human postural control adjustment with perturbation using quadratic objective function

Seongwoong Hong, Sukyung Park
Department of Mechanical Engineering, KAIST, Daejeon, Republic of Korea.
Email: sw.hong@kaist.ac.kr

INTRODUCTION

Human postural control refers to the mechanisms that allow people to generate motions in response to external perturbations while maintaining an upright posture. Previous research that have attempted to explain these mechanisms based on control theories gave a suitable analysis using simple controllers. However, in a study explaining the postural control as a trade-off between stability and control effort [1], the controller has low reproducibility with respect to human data. In contrast, research that accurately duplicates human postural control using a feedback controller [2] has not identified objectives that could be useful for interpreting human movement. This study therefore quantified the contribution of postural stability and control effort that can reproduce human movement. Specifically, we determined the objective function of a linear feedback controller that reproduces postural response adjustments with external perturbation.

METHODS

To examine the relative contribution between stability and control effort in postural control, a quadratic cost function of the stable linear feedback controller was identified. The response of human postural control was collected in the same way with the previous study [2]. Angles, angular velocities, and torques were collected and calculated.

A linear feedback controller for the angles and angular velocities of two joints was introduced to reproduce the human data. The controller gain was determined to minimize the discrepancy between human data and simulation data for external perturbations, while stabilizing the closed-loop system.

A quadratic cost function for the angles, angular velocities and torques of two joints was formed to reflect the trade-off between postural stability and control effort. In order to quantify objectives, the parameter matrix was determined to obtain the optimal gain for the linear feedback controller that reproduces human data.

RESULTS AND DISCUSSION

The linear feedback controller reasonably well reproduced the human postural data in response various perturbation magnitudes. It replicates human trajectories well in time trajectories and ankle-hip trajectories graphs, as shown in Figure 1-A,B, and exhibited a gradual decrease in ankle torque as perturbation magnitude increased.

In addition, the penalization factor of ankle angle within the objective function was gradually scaled with perturbation. Among the eigenvectors of the cost function matrix that reproduces human data, the eigenvalue of the vector dominated by ankle angle declines gradually as the magnitude of perturbations increases, as shown in Figure 1-C. This indicates that the objective function changed in the direction of reducing the control effort to move ankle as the magnitude of perturbations increased.

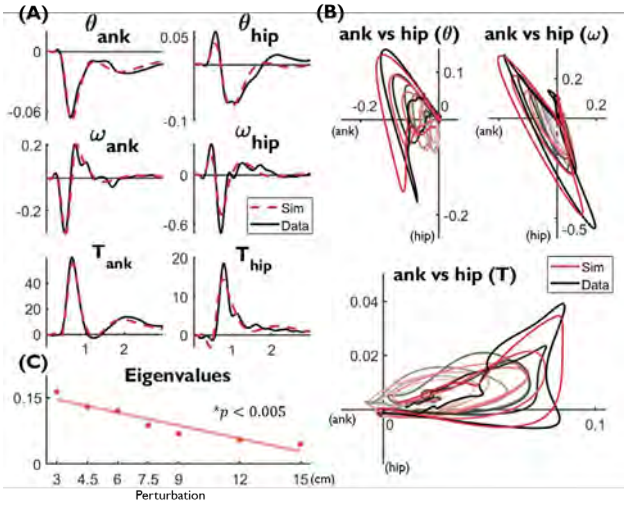

Figure 1 (A) Time trajectories and **(B)** the change in ankle versus hip trajectories in response to the change in perturbations of the linear feedback controller that imitate human data, and **(C)** increased perturbation decreases ankle angle dominated eigenvalue

CONCLUSIONS

This study identified the objective function of a controller that replicates human postural control, and showed that stabilization of ankle movement control decreases with perturbation. This result is consistent with previous studies that the human postural control strategy gradually reduces the contribution of ankle torque in response to increasing perturbations due to the influence of biomechanical constraints [2]. The outcomes demonstrated that the trade-offs between stability and the expense of human movement control could be quantified using the quadratic cost function.

ACKNOWLEDGEMENTS

This work was supported by the Faculty Basic Research Funds for 2022.

REFERENCES

[1] Kuo, A. D. *IEEE Trans. bioed. eng.*, *42*(1), 87-101 1995
[2] Park, S. et. al. *Experi. brain res.*, *154*(4), 417-427. 2004

Motor performance after treatment of pilocytic astrocytoma in childhood

Fredrik Öhberg[1], Gunilla Elmgren Frykberg[2], Artin Omar[1], Jens Lundin[1], and Ingela Kristiansen[3]
[1] Dep. of Radiation Sciences, Umeå University, Umeå, Sweden.
[2] Dep of Medical Sciences, Uppsala University, Uppsala, Sweden
[3] Dep. of Women's and Children's Health, Uppsala University, Uppsala, Sweden
Email: Fredrik.Ohberg@umu.se

INTRODUCTION

Low grade astrocytoma is the most common central nervous tumour in childhood and pilocytic astrocytoma (PA) the most common tumour type in this group. These tumors can be located in different parts of the brain but are mostly found in the posterior fossa [1]. The cerebellum, located in the posterior fossa, plays an important role in the acquisition of new motor skills, coordination, and quality of movement as well as being involved in cognition [2]. Treatment of a tumor in the posterior fossa can lead to future neurocognitive complications for the patient [3].
Studies (e.g. [4]) have described motoric, and cognitive complications for treated patients with pilocytic astrocytoma, but there is still a lack of knowledge on the full extent of said complications.
The goal was therefore to analyse motor performance in children and young adults with treated PA when performing a dual task compared to a matched control group without disability.

METHODS

The study was conducted as a cross-sectional case control study at Uppsala University Hospital, Sweden and 8 children (ages 9-17) and 12 young adults (ages 21-33) participated. All the patients had been surgically treated for PA in the posterior fossa between 1995-2011. One young adult patient was excluded due to factors affecting motoric functions. A total of 19 patients were included in the final analysis. The controls were population-based and were matched for age, gender, height, and weight. Each patient was matched to two controls. In total, 16 children and 22 young adults gave their informed consent and data from these were included in the final analysis.
Data collection of the motor performance was performed during some of the tests included in the Mini-BESTest (e.g., the test Timed Up and Go (TUG)). Both the study and the control group performed a TUG test and repeated the same test as they solved a cognitive task.
The data come from 5 inertial measurement sensors placed on both thighs and shanks and one around the waist, where each sensor contained a three-dimensional gyroscope (16-bit, range ±2000°/s), accelerometer (16-bit, range ±16 g), and magnetometer (13-bit, range ±1200 µT). Each sensor sent data wireless to a laptop equipped with the software MoLab regarding their orientation in a global space during the performed tests.
Several outcome variables (both temporal and spatial) were calculated offline and split into separate datasets (i.e., children and young adults). A linear mixed model analysis was then performed on each outcome variable set as dependent with the independent factors set to patient/control and single/dual task. The estimation method used was restricted maximum likelihood and alpha value was set to 0.05 with confidence interval adjustment LSD(none) for all statistical tests.

RESULTS

The statistical analysis was conducted separately for the different datasets and the interaction between the addition of a cognitive task and the patient- and control group were examined. Statistically significant interactions were found for children dataset regarding absolute time, but not for younger adults (Figure 1).

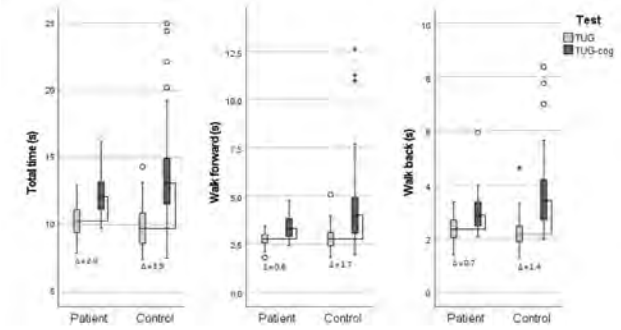

Figure 1 *Boxplots illustrating total time, and time to complete the walk forward and walk back subphase during a Timed Up and Go (TUG) and a Timed Up and Go-cognitive (TUG-cog) for the child patient- and control group. Mean difference between TUG and TUG-cog for patients and controls is shown. s: seconds; Δ: mean difference; o: outside value; ∗: far out value.*

CONCLUSIONS

Children in the control group performed worse than patients regarding total time and time to complete two subphases. No statistically significant differences were found for young adults. The patients were therefore not more impaired than controls with the addition of a cognitive task to a TUG-test.

REFERENCES

[1] Gupta N et al. Pediatric CNS Tumours. 3:d ed, 2017.
[2] Koziol LF et al. *Cerebellum*. **13**(1): 151-77 2014.
[3] Mulhern R et al. *The Lancet Oncology* **5**(7): 399-408 2004.
[4] Kristiansen I et al. *Cancer Reports* **5**: e1548, 2022

ACCURACY OF A 2D CAMERA FOR OBTAINING 3D DATA IN RUNNING

Iain Hunter, John Hedengren, McGyver Clark, and Luke Vankeersbilck
Exercise Sciences, Brigham Young University Provo, United States of America.
Email: iain_hunter@byu.edu

INTRODUCTION

In the past, three-dimensional motion capture data required multiple cameras. Utilizing machine learning, a framework called MediaPipe (Google Corp) generates three-dimensional data of 33 body landmarks [1,2]. This is different than other machine learning frameworks such as OpenPose that only provide two-dimensional data. Running mechanics are of specific interest to us. Thus, we set out to determine which camera views would provide the greatest accuracy for sagittal plan hip, knee, and ankle angles.

METHODS

Eight subjects ran on a treadmill while being recorded with a traditional 12 camera motion capture system (Qualisys with Visual3D) and a single cell phone camera (iPhone SE 2020, Apple Corp) at 240 Hz. The iPhone was placed behind the runner, then rotated to a front view in 30 deg increments allowing for 30-s clips at -90, -60, -30, 0, 30, 60, and 90-deg camera positions. MediaPipe Pose produced 3D positions of hip, knee, ankle, and shoulder that were used to calculate sagittal plane angles for comparison with the output from Visual 3D.

Pearson-r correlations were computed for the hip, knee, and ankle calculations for each camera view between MediaPipe and motion capture data. ANOVA compared these correlations between camera views for each angle with Bonferroni post-hoc tests with alpha set at 0.05.

RESULTS AND DISCUSSION

Correlations between MediaPipe and motion capture were excellent statistically speaking for the knee (Figure 1 and Table 1). However, there were some notable differences between the two methods when looking at peak flexion and extension angles. Ankle and hip angles were not predicted well by MediaPipe. Camera views in the frontal plane produced very low accuracy from MediaPipe for all joint angles. This is likely due to the feet and sometimes knees becoming hidden from view. All other camera views were much more similar.

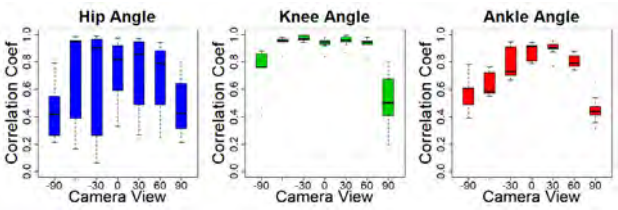

Figure 1 Boxplots of correlation coefficients. -90 represents a front view of the subject, 0 is a side view, and +90 is a rear view.

Motion capture data calculated hip angles from the thigh relative to vertical while for MediaPipe, hip angles were calculated with a vertex of hip and endpoints of the matched knee and the average of the two shoulders. This explains some of the low correlations observed for hip angles.

MediaPipe has a nice advantage of other methods such as OpenPose due to providing three-dimensional data allowing for sagittal, frontal, and transverse joint angles, but needs accuracy improvements especially for certain body parts.

We are interested in how other frameworks accuracy compares to motion capture when using just a side view as most other frameworks utilize.

CONCLUSIONS

MediaPipe provides three-dimensional data for 33 body landmarks. These landmarks can be used to produce joint angles, but have some limitations from certain camera views when body parts become obscured. The hip is especially inaccurate due to not knowing pelvis orientation for obtaining hip angles.

REFERENCES

[1] Garg S et al. *J Ambient Intell Human Comput* **13**: 2022.

[2] Singh AK. *Advances in Intelligent Systems and Computing* **1413**: 2021.

Table 1: Correlation coefficients comparing MediaPipe (single camera) to Qualisys with Visual3D (motion capture 12-camera system).

	-90	-60	-30	0	30	60	90
Hip (corr coef)	0.42±0.19	0.67±0.35	0.63±0.40	0.74±0.22	0.73±0.27	0.69±0.25	0.48±0.21
Knee (corr coef)	0.73±0.18	0.95±0.04	0.98±0.02	0.93±0.04	0.96±0.04	0.92±0.06	0.50±0.20
Ankle (corr coef)	0.58±0.13	0.63±0.09	0.78±0.11	0.85±0.13	0.90±0.06	0.81±0.05	0.45±0.10

Improving estimation accuracy of energy expenditure during running from a single IMU by estimating mechanical power via estimating ground reaction force.

Bumjoon Kim[1], Sukyung Park[1*]

[1] Department of Mechanical Engineering, Korea Advanced Institute of Science & Technologies , Daejeon, Korea

Email: bumjoon.kim@kaist.ac.kr[1], sukyungp@kaist.ac.kr[1*]

INTRODUCTION

Energy expenditure (EE) during running is a key metric for health management and runner motivation. Although several wearable devices, such as smart watches, provide EE information, it is known that estimation error is substantial (NRMSE 2793%). [1] Using biomechanical criteria such as mechanical work, recent research in the field of biomechanics has attempted to quantify EE at different running speeds with great precision. [2] However, since mechanical work can only be measured in a laboratory setting, if it is estimated via a basic wearable device and then employed, the estimation accuracy of the wearable device might be enhanced. Therefore, in this study, we estimate mechanical power(P_{mech}) when running from a single inertial measurement unit (IMU) by using running biomechanics and use it to increase the accuracy of EE estimates while maintaining convenience.

METHODS

For estimating EE using a single wearable sensor, we estimated P_{mech} from estimated ground reaction force (GRF) from a single IMU and use it to estimate EE. In detail, we GRF from sacrum-mounted IMU data based on our previous work [3] that estimated GRF during walking using an artificial neural network model (ANN) derived from a spring-loaded inverted pendulum model (Figure 1. (B)). P_{mech} was calculated from mechanical power done to centre of mass (P_{com})derived from estimated GRF and estimated centre of mass velocity (v_{com})(Figure 1. (B)) EE was estimated by an ANN using P_{mech} and running speed (V_{run}) as inputs. (Figure 1. (B)) Through the whole EE estimation process, leave-one-subject-out cross validation was used to verify the proposed method.

Ten young male subjects were participated in this study. They ran for 10 minutes on the treadmill at three kinds of speed; high (>75%$VO2_{max}$), moderate (50~75%$VO2_{max}$), and light intensity (<50%$VO2_{max}$). EE, GRF, and kinematic data from a sacrum-mounted IMU were measured.

Table 1: Validation of EE estimation result.

Intensities	RMSE (W/kg)	NRMSE (%)	R^2
Low	1.05	27.5	0.18
Moderate	1.05	28.4	0.01
High	1.58	24.4	0.03
Overall	1.38	18.6	0.48

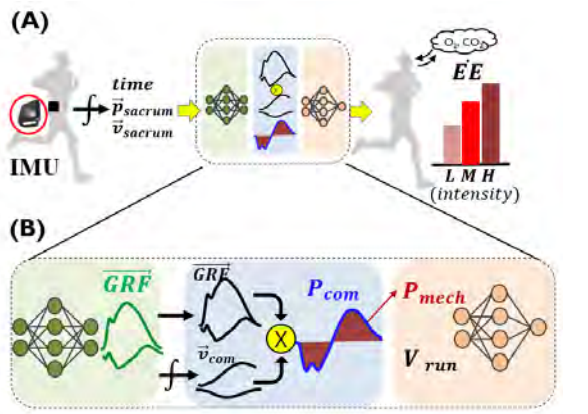

Figure 1. (A) Schema of whole EE estimation process (B) Details of inner process. 1) Estimating GRF using neural network. 2) Deriving v_{com} P_{com} and P_{mech} from estimated GRF 3) estimating EE using P_{mech} and V_{run}

RESULTS

Using a single IMU, we estimate EE during running through estimating GRF and P_{mech} from a single IMU. GRF, v_{com} and P_{mech} were estimated with normalized root means square error (NRMSE) 13.0%, 12.6% and 9.0%, respectively. The NRMSE of EE estimation in case of low, moderate and high intensity was 27.5% 28.4% and 24.4% respectively. (Table 1.) The overall EE was estimated with NRMSE about 18.6% and R^2= 0.48. The proposed method improves the accuracy of EE estimation with an error less than 20% that was reported error of smart watches.

CONCLUSIONS

In this study, we estimated mechanical power from a single IMU in order to enhance the accuracy of the EE estimation during running from the wearable device. Ultimately, we could estimate EE with NRMSE 18.6% and R^2=0.48, which is more accurate than smartwatch. It was demonstrated that the accuracy of the information provided could be enhanced while keeping the practicality of wearable devices by using biomechanical knowledge.

ACKNOWLEDGEMENTS

This research project was supported by the sports promotion fund of Korea sports promotion foundation (KSPO) from Ministry of Culture, Sports and Tourism

REFERENCES

[1] Slade P et al. *Nature Com.* **12(1)**: 1-11, 2021.

[2] Riddick R.C.& Kuo A. D. *Sci. Rep.* **12(1)**: 1-11, 2022

[3] Lim H et al. *Sensors* **20**: 130,

Groucho running reveals disparate results between ground reaction force and tibial bone strain: a finite element analysis

Arash khassetarash[1*], Benno M. Nigg[1], W. Brent Edwards[1,2]

[1] Human Performance Laboratory, Faculty of Kinesiology, University of Calgary, Calgary, Canada.
[2] McCaig Institute for Bone and Joint Health, University of Calgary, Calgary, Canada.

Email: arash.khassetarash@gmail.com

INTRODUCTION

Several studies have examined the relationship between ground reaction forces and stress fractures in running [1]; however, the majority of the load borne by bone stems from muscular contraction [2], and even then, the relationship between applied load and bone strain is often complex and nonintuitive. Groucho running [3], i.e., running with increased stanced-leg knee flexion, is characterized by reduced ground reaction force and increased muscular work. The purpose of this study was to determine if reductions in ground reaction force associated with Groucho running were associated with corresponding reductions in bone strain.

METHODS

Twelve physically active males ran on an instrumented treadmill (Bertec Corps., Columbus, OH) for 5 minutes in each of three conditions: Preferred, Groucho, and Exaggerated Groucho. The latter two conditions were accomplished by having participants reduce their peak vertical ground reaction force to 85% and 75% of the Preferred condition, respectively by exaggerating knee flexion in stance. Inverse-dynamic-based musculoskeletal modelling was used to calculate lower extremity muscle and joint contact forces. These forces served as inputs to a participant-specific finite element model of the tibia-fibula complex [4], which was created from computed tomography images of each participants lower-limb. The 90th percentile pressure-modified von Misses strain (peak strain) and volume of bone experiencing strains over 3000 με (strained volume) were calculated for the main outcomes.

RESULTS AND DISCUSSION

On average, there was 15.6% and 22.6% reduction in peak vertical ground reaction force during Grouch and Exaggerated Grouch running compared to Preferred condition. To date, finite element analysis has been completed for a single participant. Compared to Preferred running, peak vertical ground reaction force for this participant was reduced by 14.6% and 27.1% during Groucho and Exaggerated Groucho running, respectively. Proportional reductions in ground reaction forces were not observed in tibial bone strain metrics (Table 1). Although, peak strain and strained volume in Groucho decreased by 9.7% and 19.6%, respectively, corresponding changes in Exaggerated Groucho running were negligible (-1.5%) or considerably higher (+19.1%). In this scenario, the increased strained volume of 19.1% in the Exaggerated Groucho conditions would be expected to cause bone failure much sooner than the Preferred condition [5].

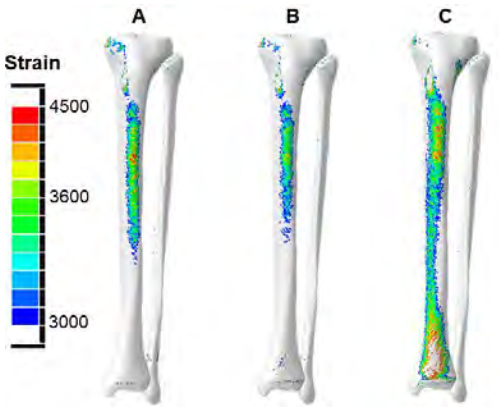

Figure 1 Tibial-fibular strain distribution for the three running techniques. A) Preferred, B) Grouch, and C) Exaggerated Groucho Only high strain parts (>3000 με) are shown in colormap.

CONCLUSIONS

This study used Groucho running as a model to reduce ground reaction forces and increase muscle work. These preliminary findings, to be confirmed with additional participants, suggest that running conditions that reduce ground reaction forces are not necessarily associated with corresponding reductions in bone strain. Interventions aimed at decreasing stress fracture risk through ground reaction force modification should be interpreted with caution.

REFERENCES

[1]Zadpoor et al. *Clin Biomech* **26**: 23-28, 2010.
[2]Scott et al. *Appl Sci* **22:** 357-369, 1989
[3]McMahon et al. *J Appl Physiol* **62**: 2326-2337, 1987.
[4]Khassetarash et al. *J Biomech Eng* **145**: 041007, 2023.
[5]Haider et al. *J Biomech* **122**: 110434, 2021.

Table 1: External and internal loading variables during different running techniques (N=1)

	Preferred	Groucho	Exaggerated Groucho
Peak vertical ground reaction force (N)	1887	1611	1376
90th percentile strain (με)	3951	3567	3893
Strained volume (mm^3)	7934	6382	9447

EFFECT OF RUNNING SPEED AND INCLINATION ON BIOMECHANICAL RISK FACTORS FOR MEDIAL TIBIAL STRESS SYNDROME

Leon Robertz[1], Kevin Bill[1], Uwe G. Kersting[1,3], Markus Kurz[3], Wolfgang Potthast[1], Patrick Mai[1,2] and Steffen Willwacher[2]

[1] Institute of Biomechanics and Orthopaedics, German Sport University, Cologne, Germany
[2] Institute for Advanced Biomechanics and Motion Studies, Offenburg University, Offenburg, Germany
[3] Sports Tech Research Centre, Mid Sweden University, Östersund, Sweden
Email: l.robertz@dshs-koeln.de

INTRODUCTION

The popularity of running as a regular exercise may be explained because it allows for self-organized training in nearly any environment leading to variations in running speed and inclination (which have rarely been included in biomechanics analyses of runners). The sport has also been associated with a considerable amount of overuse injuries (OIs) resulting in around 2.5 to 33.0 OIs per 1000 h of practice [1]. Medial tibial stress syndrome (MTSS) is one of the most common OIs. The development of OIs is multifactorial while the types of injuries are likely related to exceeding a tissue-specific stress threshold. Direct measurements of tissue stress are difficult. Recently researchers have linked specific OIs to biomechanical risk factors (BRFs) [2]. As the effect of altered running speed and inclination on BRFs for MTSS has not yet been investigated, the purpose of this study was to assess the previously identified BRFs during varied running conditions.

METHODS

We collected 30s trials of full-body motion (17 cameras, 200 Hz, Qualisys) and ground reaction force (GRFs) data (2000 Hz, Gaitway 3D) from 21 recreational runners (8 female, 13 male, 176 ± 6.55 cm, 68.6 ± 9.20 kg, 25 ± 4 years). They ran in their own shoes on uphill (+5%, +10%, +15%), downhill (-5%, -10%, -15%), and level (0%) conditions, each at 2.5 m/s, 3 m/s, and 3.5 m/s in a semi-randomized order. We calculated BRFs for MTSS [2] (peak rearfoot eversion - PRE, rearfoot eversion duration - RED, peak contralateral pelvic drop - PCPD) using a custom-build Matlab script (R2022a) averaged over at least 20 steps. A 20 N threshold of raw vertical GRF defined the stance phase. Two-way repeated measures ANOVAs on BRFs (inclination x running speed) were used for testing significant (sig.) main and interaction effects (JASP 0.16). We further conducted Bonferroni-corrected post hoc tests and calculated effect sizes (partial eta squared - η_p^2, small: 0.01 - 0.059, medium: 0.06 - 0.139, large > 0.14 [3]). Data were checked for normality and sphericity.

RESULTS AND DISCUSSION

We found sig. main effects for running speed (PRE: p_{Speed} = .02, η_p^2 = .20; PCPD: p_{Speed} = .002, η_p^2 = 0.34), for inclination (PCPD: $p_{Incline}$ = .023, $\eta_p 2$ = 0.16), but no sig. interaction effects. Post hoc results are summarized in (Figure 1) with effect sizes being small (speed) and medium (inclination) at most. Although no differences were found compared to level running, a sig. trend towards reduced PCPD for downhill running was found. While PRE was affected by speed, RED was not, suggesting that the underlying structures had less time to get into greater eversion with increasing running speed. This may result in higher stress on the tissue and may progress MTSS development [4]. While sig. trends for the BRFs exist absolute changes in angles are small.

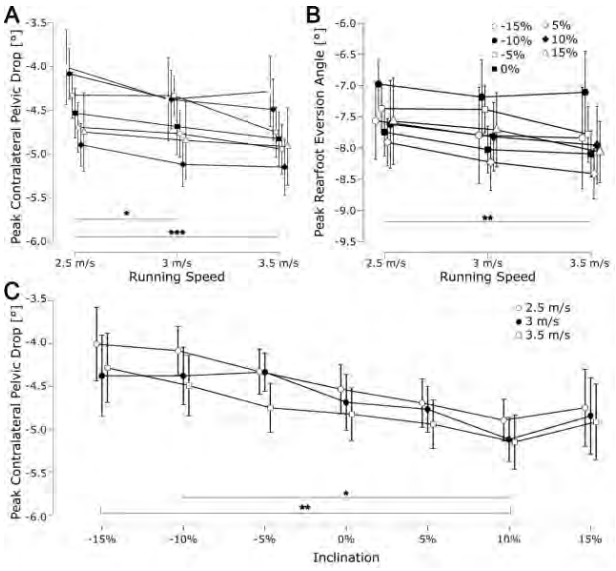

Figure 1 Descriptive plots for post hoc tests with significant differences indicated by asterisks (* p < .05, ** p < .01, *** p < .001). Bars display confidence intervals (95%).

CONCLUSIONS

Running at higher speed increases BRFs (PRE and PCPD) for MTSS. In combination with the inclination effect, this emphasizes that a combination of downhill running and reduced running speed is to be preferred when recovering from MTSS.

REFERENCES

[1] Videbæk et al. *Sports Med* **45**: 1017–1026, 2015.
[2] Willwacher et al. Sports Med **52**: 1863–1877, 2022.
[3] Cohen J. *Routledge* **2**: 274-357, 1988.
[4] Bouché and Johnson. *J Am Podiatr Med Assoc* **97(1)**: 31–36, 2007.

INFLUENCE OF WALKING AND RUNNING SPEEDS ON TIBIA IMPACT STRESS

Qichang Mei[1,2], Justin Fernandez[1,2], Yaodong Gu[1,2]
[1] Faculty of Sports Science, Ningbo University, Ningbo, China.
[2] Auckland Bioengineering Institute, The University of Auckland, Auckland, New Zealand.
Email: meiqichang@outlook.com

INTRODUCTION

Tibia pain has been one of commonly documented injury among distance runners, which was primarily due to the accumulation of repetitive impact[1]. The realigned mechanical axis in the lower extremity may redistribute the impact loading[2], thus leading to micro-damage in the bone structure. Once the remodeling failed, the tibia pain was presented, or even stress fracture.

This study was aimed to evaluate the loading patterns in the tibia using a musculoskeletal-driven Finite Element simulation approach.

METHODS

This study included two sections. Participants joint a motion captue experiment in a lab in the first section. Runners performed walking (at 1.0m/s and 1.4m/s) and running (at 2.7m/s, 3.3m/s and 4.0m/s) tests on a forceplate instrumented treadmill with synchronously collection of marker trajectories. Marker positions and ground reaction forces were used to calculate joint angles, moments, muscle forces and joint reaction forces following an established musculoskeletal (MSK) modelling workflow[2].

During the second section, participants attended a MRI scanning to collect the medical imaging of the lower extremity, which were then segmented to obtain the 3D geometries in '*stl*' files. The geometries were meshed in HyperMesh, and then extracted as '*inp*' files for post-process the material properties assignment and assembly in ABAQUS. The joint angles, muscle forces and joint reaction forces were loaded as boundary conditions for Finite Element (FE) simulation using a standard explicit static solver.

RESULTS AND DISCUSSION

As in the **Table 1**, the ankle reaction forces in the axial directions were presented during landing impact for walking and running. The specific knee angles in the sagittal plane were showed as well, that knee flexion angles are 13.1° (1.0m/s), 14.9° (1.4m/s), 32.4° (2.7m/s), 34.5° (3.3m/s) and 38° (4.0m/s). The knee flexion angles were employed to position the tibia model, and axial ankle forces were loaded to run FE simulation in ABAQUS (**Figure 1**).

As observed from the MSK-driven FE simulation, the main stress was focalised at the distal one-third region in the anterior facet of tibia (cortial layer). The peak stresses across the incremental speeds were between the magnitude of 3.3-5.1GPa in the cortial bone, and 0.2-1.8GPa in the trabeculae bone.

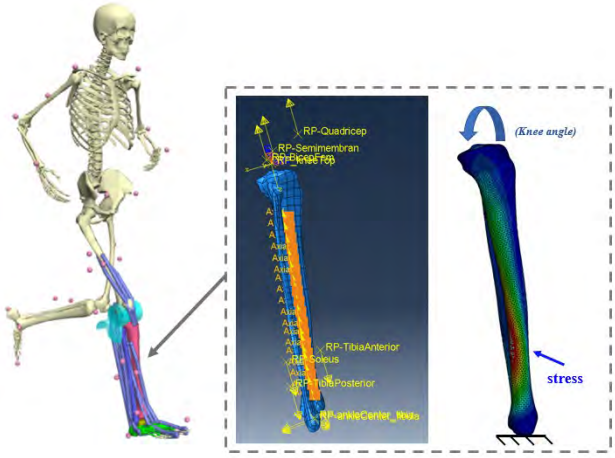

Figure 1. Outline of MSK-driven FE simulation approach.

CONCLUSIONS

The influence of walking and running speeds on the biomechanical loadings and tibia stress were reported. Findings may provide implications for the monitoring of tibia stress and loading accumulation, and prevention of tibia pain related running related injuries.

ACKNOWLEDGEMENTS

This study was supported by the National Natural Science Foundation of China (No. 12202216).

REFERENCES

[1] Hoenig T et al. *Nature Reviews Disease Primers* 8(1): 26, 2022.
[2] Mei Q et al. *Frontiers in Physiology* **10**: 573, 2019.

Table 1. Axial ankle reaction forces at incremental speeds during walking and running

	Speed at 1.0m/s	Speed at 1.4m/s	Speed at 2.7m/s	Speed at 3.3m/s	Speed at 4.0m/s
Walking	1390N	1542N	-	-	-
Running	-	-	2392N	3418N	4633N

How does the inclusion of glenohumeral joint stability affect the estimates of individual muscle forces during shoulder movements?

Italo Belli[1,2], Sagar Joshi[1,2], J. Micah Prendergast[1], Irene Beck[1,2], Cosimo Della Santina[1], Luka Peternel[1] and Ajay Seth[2]
[1] Cognitive Robotics, Technische Universiteit Delft, Delft, The Neterlands.
[2] Biomechanical Engineering, Technische Universiteit Delft, Delft, The Netherlands.
Email: i.belli@tudelft.nl

INTRODUCTION

The shoulder is one of the most complex structures in the human musculoskeletal system due to its many degrees of freedom, the numerous muscles spanning it, and its inherent instability. Shoulder movements are generated by a synergy of large superficial muscles and deeper stabilizing ones, where musculoskeletal simulations are necessary to gain an in-depth understanding of the actions of individual muscles. The effect of glenohumeral (GH) stability on the estimated actions of individual muscles, however, remains widely unknown. In this study we aim to quantify the effect of GH stability.

METHODS

To estimate individual muscle forces, we developed a Rapid Muscle Redundancy (RMR) solver, that leverages the OpenSim API to compute estimates of muscle activations and joint reaction forces (JRFs) from a musculoskeletal model through optimization, given recorded motions. The RMR solver introduces two innovations that enable it to solve for muscle activations efficiently. First, we enforce first-order dynamic feasibility of the activation values through linear constraints, and second, we formulate JRFs as linear functions of the predicted muscle activation. The latter consists in the following expression, evaluated at each time-step:

$$JRF = Ax + JRF_0$$

where x is a vector containing the activations of each muscle, JRF_0 is the force produced in the current state when all of the muscles are de-activated, and A represents the effect of maximum (1.0) activation of each muscle on the joint reaction force. This simple formulation allows for efficient inclusion of the GH stability constraint in the optimization, formulated as a directional constraint on the JRF at the glenoid (similarly to Chadwick et al. [1]). We compared the RMR solver's estimates against the computed muscle control (CMC) algorithm and EMG measurements. To analyse how the GH constraint affects muscle activations, we used RMR to estimate activations with and without inclusion of the GH constraint. The shoulder model, as well as the dataset (motions and filtered EMG signals) were obtained from a previous study [2].

RESULTS

The comparison between the RMR solver and CMC for shoulder movements resulted in virtually the same estimates of muscle activations, but in a fraction of the time: while CMC needed a computation-to-real-time ratio of over 200 to complete the analysis, the RMR solver required only 40. The effect of the GH stability constraint on muscle activations (Table 1) indicates that stability does not affect the activations of most superficial muscles, but significantly affects the activations of the rotator cuff muscles (first four rows of the table, where shaded cells represent high difference).

Muscle	Flexion+	Abduction+	Shrugging+
Teres minor	0.02	0.03	0.07
Infraspinatus	0.07	0.08	0.11
Subscapularis	0.05	0.13	0.11
Supraspinatus	0.04	0.03	0.00
Trapezius	0.01	0.00	0.01
Serratus Anterior	0.00	0.00	0.02
Deltoids	0.04	0.02	0.01
Lats dorsi	0.00	0.00	0.00
Teres major	0.03	0.05	0.12
Pectoralis major	0.03	0.00	0.02

Table 1: Maximum RMS difference between the activations of various muscles predicted by the RMR solver, with and without the inclusion of the GH constraint. Tasks considered are shoulder flexion, abduction and shrugging performed holding a 2-kg load.

DISCUSSION AND CONCLUSIONS

We introduced a RMR solver that estimated muscle forces of a shoulder model in agreement with CMC but more than 5 times faster. The RMR solver formulation shows promise for real-time or human-in-the-loop applications. Moreover, the novel way in which the JRFs are handled makes it easy and quick to consider additional constraints as we demonstrated with the GH stability constraint. Our findings show that stabilizing the GH joint can have substantial effects when estimating muscle activations of the rotator cuff muscles, while having little effect on other shoulder muscles. Our results indicate that comparing superficial muscle activations to EMG is a necessary but insufficient condition to validate estimates of shoulder muscle activation.

REFERENCES

[1] Chadwick et al. "Real-Time simulation of three-dimensional shoulder girdle and arm dynamics" *IEEE. Trans. Biomed. Eng.* **61**(7):1947-1956, 2014.
[2] Seth al. "Muscle contributions to upper-extremity movement and work from a musculoskeletal model of the human shoulder", *Front Neurorobot* 13:90, 2019.

THE EFFECT OF TOUCHDOWN CONFIGURATION ON TOP SPRINTING SPEED: A SIMULATION STUDY

Nicos Haralabidis[1], Jennifer Hicks[1], Scott Delp[1,2]
[1] Department of Bioengineering, Stanford University, Stanford, USA.
[2] Department of Mechanical Engineering, Stanford University, Stanford, USA.
Email: nicos.haralabidis@stanford.edu

INTRODUCTION

Increasing sprint speed is a priority for coaches and athletes in many sports. Numerous biomechanical investigations have explored how the kinematics at touchdown affect top sprinting speed (e.g., [1,2]); however, the conclusions from these studies differ, potentially because observational experimental approaches make assessing cause-effect relationships difficult. We used a predictive simulation approach to determine how changes in touchdown kinematics affect top sprinting speed. We also explored how simuation results compare with previous studies and coaching principles.

METHODS

We scaled a three-dimensional musculoskeletal model [3] to an international caliber male sprinter, and used a direct collocation optimal control framework to generate two predictive simulations of maximal speed sprinting. In the first simulation ('nominal') we constrained the model's positional kinematics at touchdown to closely match (within ± 1.5°) previous experimental sprinting kinematics data. In the second predictive simulation ('widened') we widened the permissible bounds of the model's positional kinematics at touchdown (permitted to vary by ± 15°). The simulations were formulated in MATLAB (2022b; MathWorks Inc., Natick, MA, USA) using CasADi [4] and solved using IPOPT [5]. Horizontal touchdown distance (the horizontal distance between whole-body center of mass and foot at touchdown) and inter-knee touchdown distance (the horizontal distance between the knees at touchdown), important coaching parameters, were also extracted from both simulations.

RESULTS AND DISCUSSION

The simulation with widened bounds resulted in a 7.1% increase in speed compared to the nominal simulation (12.1 vs. 11.3 m/s). In addition, the widened simulation was characterized by a 6.5% increase in the horizontal distance between the whole-body center of mass and foot at touchdown (0.33 vs. 0.31 m) and a 95% increase in the inter-knee distance at touchdown (0.13 vs. 0.06 m). Interestingly, the changes we observed in the altered touchdown simulation, despite the improvement in speed, did not align with current coaching theory or prior literature. Previous studies have suggested that reducing the horizontal touchdown distance enhances speed, by reducing the horizontal braking force. Instead, increasing the horizontal touchdown distance may allow the ankle plantarflexor muscles to generate greater force through operating eccentrically and thus contribute to the sharp rising-edge of the vertical ground force, which is critical to attaining greater top speeds. This is supported by the greater peak force we observed in the gastrocnemii in the widened simulation. A reduced inter-knee touchdown distance is also advocated in sprinting, as the non-stance limb is thought to be more favourably positioned to contribute to the generation of vertical momentum and force. However, the increased inter-knee touchdown distance we observed, through the non-stance limb being positioned further behind, may have resulted in the non-stance limb being positioned in a more advantageous configuration at touchdown from which to be accelerated and contribute to vertical force production.

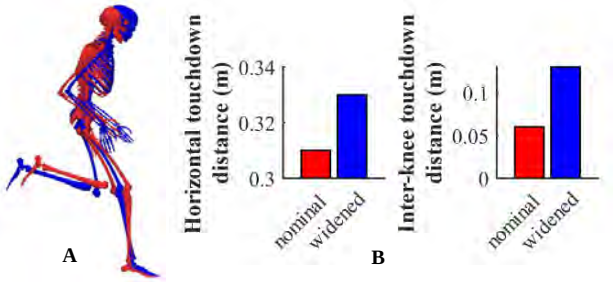

Figure 1 Touchdown configuration of the nominal (red) and widened (blue) simulations (A) and changes in coaching parameters (B).

CONCLUSIONS

Enabling changes in kinematics at touchdown led to an increase in top speed, although the changes in technique variables differed from current coaching ideologies. Future work will further explore the mechanisms responsible for the technique variable changes we observed.

ACKNOWLEDGEMENTS

Supported by the Joe and Clara Tsai Foundation through the Wu Tsai Human Performance Alliance.

REFERENCES

[1] Haugen T et al. *IJSPP* **13**: 420-427, 2018.
[2] Kunz H et al. *BJSM* **15**: 177-181, 1981.
[3] Hamner S et al. *J. Biomech.* **43**: 2709-2716, 2010.
[4] Andersson J et al. *Math Prog Comp* **11**: 1-36, 2019.
[5] Wächter et al. *Math Prog* **106**: 25-57, 2006.

DESIGN AND SIMULATION OF FLOW FIELD FOR SINUSOIDAL SCAFFOLD USING COMPUTATIONAL FLUID DYNAMICS

Theresia Baumgartner[1], Markus Bösenhofer[2,3], Olivier Guillaume[4,5], Aleksandr Ovsianikov[4,5], Michael Harasek[2,3] and Margit Gföhler[1]

[1] Faculty of Mechanical and Industrial Engineering, TU Wien / Institute of Engineering Design and Product Development, Vienna, Austria.
[2] Faculty of Technical Chemistry, TU Wien / Institute of Chemical Engineering, Environmental and Bioscience Engineering, Vienna, Austria.
[3] K1-MET GmbH, Area 4 – Simulation and Analyses, Linz, Austria.
[4] Faculty of Mechanical and Industrial Engineering, TU Wien / Institute of Materials Science and Technology, Vienna, Austria.
[5] Austrian Cluster for Tissue Regeneration (https://www.tissue-regeneration.at), Vienna, Austria
Email: theresia.baumgartner@tuwien.ac.at

INTRODUCTION

Bone can heal small defects by itself but fails to do so in case of severe bone damage. A common treatment for severe damage is grafting bone. Approximately 1.6 million bone grafts are performed in the United States per year [1]. Unfortunately, this treatment has several serious drawbacks, such as a high risk of infections or even donor site morbidities. Tissue Engineering and regenerative medicine is a promising biomedical alternative to cure severe bone damage. Scaffolds can be used to re-build the bone structure since they can support seeded cells and provide an optimal environment for cell growth [2]. The scaffold's geometry design influences flow characteristics, mass transfer rates, and wall shear stress (WSS). The WSS is an important parameter to investigate because it affects the differentiation and bioactivity of cells inside the scaffold. In this work, we investigate the influence of the scaffold geometry on the flow field, WSS and mass transport using computational fluid dynamics (CFD). The reliability of the numerical results is evaluated using the µ-particle image velocimetry (PIV) method.

METHODS

Scaffold geometries, which have a sinusoidal channel featuring different amplitudes and frequencies, are designed and meshed using SALOME®. The CFD simulations are performed using the open-source software OpenFOAM®. The evaluation of the nutrient distribution is investigated using the *scalarTransportFoam* solver. This solver is a steady-state laminar flow solver with a superimposed diffusive-advective mass transport equation. The fluid flow is described by the three-dimensional Navier-Stokes equation. For the µ-PIV validation experiments, scaffolds are printed inside a micro-channel using the Two-Photon polymerization method. A cross-linking photosensitive polymer called ethoxylated trimethylolpropane triacrylate, trimethylolpropane triacrylate (ETA:TTA) is used and polymerized using a femtosecond pulsed laser. Polystyrene fluorescent tracer particles with a diameter of 2 µm are excited at two points in time induced by a synchronized laser in the µ-PIV system to visualize the flow fields.

RESULTS

The numerical results indicate that increasing the frequency or amplitude affects the flow velocity in the sine cavity. Secondary vortexes are formed exceeding the threshold frequency of 3.5 mm^{-1} for an amplitude of 0.1 mm. The CFD simulations indicate that WSS depends on the flow rate and scaffold design and decreases by increasing frequencies. For an inlet flow rate of 5 mm/s, the WSS inside the sine cavities is below 0.1 Pa, whereas the highest WSS is at the negative peaks of the sine wave. The CFD results for the mass transport of the nutrient are unsymmetrically distributed inside the sinusoidal cavities. The concentration decreases over the length of the scaffold. The µ-PIV experiments validate the flow behaviour of the CFD results, and they reveal the formation of vortexes at the same frequencies.

CONCLUSIONS

The results confirm the potential of CFD to easily pre—evaluate and optimize geometric variations before printing the scaffolds for experimental evaluation. The numerical results show that the WSS and the mass transfer depend on the geometry and the flow rate. The sinusoidal texture decreases the WSS and is at least 75 % lower compared to the channel wall. The µ-PIV results confirmed the numerical results, but the experimental evaluation is still a challenging technique and depends on several factors as the seeding concentration of the tracer particles.

REFERENCES

[1] O'Keefe et al., Tissue Eng. **Part B, Rev**.: 389-392, 2011.
[2] Campos Marin et al, Interface Focus, **5(2)**: 20140097, 2015.

DEVELOPMENT OF A WORKFLOW TO MORPH VOLUMETRIC MESHES CONSISTENTLY ACROSS A POPULATION OF PEDIATRIC FEMURS

Yidan Xu[1], Julie Choisne[1] and Thor Besier[1]
[1] Auckland Bioengineering Institute, The University of Auckland, Auckland, New Zealand.
Email: yxu356@aucklanduni.ac.nz

INTRODUCTION

Finite element (FE) analysis has been proven to be effective for gaining a better understanding of bone mechanics and improving implant design [1]. However, FE models are mostly developed based on a generic template which is not representative of the diverse population. To address this issue, statistical shape models have been recently used to capture anatomical variations in bones and incorporated these variations into FE analysis. The statistical shape and density modeling requires point-to-point and element correspondences between each model through manual or semi-automatic placement of landmarks on the surface and volumetric mesh morphing [2]. A previous study have looked at the variation in shape of lower limb bones in children [3]. Now, we would like to create volumetric meshes that are consistent with the shape variation of that population. Therefore, the aim of our study was to develop an algorithm capable to automatically morph a volumetric mesh from a femur template to 663 femurs from a paediatric population aged 4 to 18 years.

METHODS

A previous study [3] developed a template mesh for the femur and fitted it to 663 femurs from 333 children aged 4 to 18 years old, with heights from 96 to 192 cm [3]. We decided to convert this femur template mesh into a 4-noded tetrahedral volumetric mesh using TetGen (WIAS, Berlin, Germany). Due to the large variation in height from our dataset (148 cm ±24 [min: 96, max: 192]), each femur surface mesh was first scaled isometrically to the template surface mesh before morphing to lower down the potential deformations during the morphing step. Second, the volumetric template mesh was fitted into each scaled model using "host-mesh" fitting described in a previous study [4]. Then the morphed models in scaled sizes were linearly scaled back to their original size. Finally, the scaled-back models were fitted again into their corresponding original surface mesh to minimize the error between the shape of the morphed mesh and their original shape. Volumetric mesh quality was computed for each femur using the radius ratio [5]. The radius ratio is determined as the normalized ratio of the radius of the inscribed sphere to the radius of the circumsphere.

RESULTS AND DISCUSSION

The morphed meshes were found to be within an acceptable range of 1-3, with values closer to 1 considered as being an equilateral tetrahedron (figure 1). However, the standard deviation was a bit high for some femurs which was not related to size (figure 2). The mesh quality was maintained throughout the automatic morphing process. This study agreed to the conclusion in a previous study of automatic mesh generation in adult femurs [2].

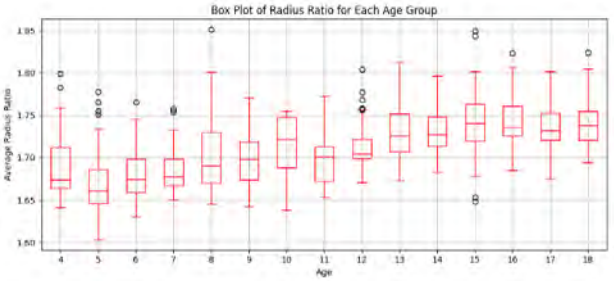

Figure 1: Average of radius ratio of morphed meshes.

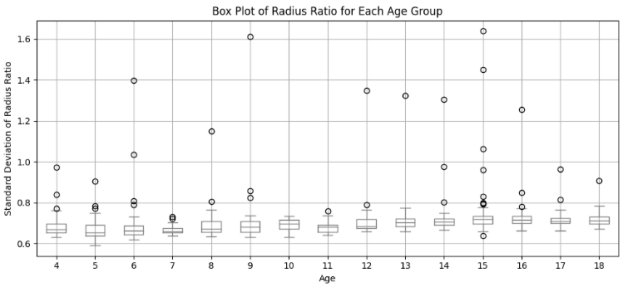

Figure 2: Standard Deviations of radius ratio of morphed meshes.

CONCLUSIONS

Based on the quality values, we can conclude that our morphed meshes are suitable for the next step of our modeling framework which is building a statistical density model and personalized FE. In the future, we will expand our work to include the tibia, fibula and pelvis of our dataset. This workflow will be used to create personalised (bone geometry and material properties) FE models for a population of children and adolescent aged from 4 to 18 years. This model will provide a better understanding of bone biomechanics for a paediatric population.

ACKNOWLEDGEMENTS

The authors would like to acknowledge the Aotearoa foundation in NZ for funding this study.

REFERENCES

[1] Altai Z etl al. *Biomech Model Mechanobiol* **17**(4):1001-1009, 2018
[2] Bryan R et al. *Med Eng Phys* **32**(1):57-65, 2010.
[3] Carman, L et al. *Sci Rep* **12**, 3251, 2022.
[4] Fernandez JW et al. *Biomech Model Mechanobiol* **2**(3):139-155, 2004
[5] V. N. Parthasarathy et al. *Finite Elem Anal Des* **15**:255–261, 1993

PHYSICS-BASED FEATURES IMPROVE THE GENERALIZABILITY OF A NEURAL NETWORK PREDICTING GROUND REACTION FORCES

Janelle M. Kaneda[1], Scott D. Uhlrich[1], and Scott L. Delp[1,2,3]
[1] Dept. of Bioengineering, [2] Mechanical Engineering, [3] Orthopaedic Surgery, Stanford University, Stanford, USA.
Email: jkaneda@stanford.edu

INTRODUCTION

While wearable and video-based technologies have enabled out-of-lab estimation of kinematics [1], additionally estimating ground reaction forces (GRFs) for kinetics would enable estimation of loading measures related to musculoskeletal injury and disease [2]. Deep learning models have predicted GRFs for specific tasks such as running and walking [3,4]. However, a task-independent model to predict GRFs would be more generally useful. Physics-based measures, like center-of-mass (COM) accelerations, are directly related to GRFs [5,6]. Using these terms as inputs to a machine learning model may improve accuracy for tasks within [6] and outside of the training set, improving generalizability. We hypothesized that including physics-based features in a deep learning model trained on walking and jumping will improve GRF predictions for a cutting task not included in the training set (i.e., unseen task).

METHODS

We used marker-based inverse kinematics and GRFs from 68 individuals (40 women, 46–80 years) with medial knee osteoarthritis walking at different foot progression angles (100 trials/subject) [7], and from 76 female soccer athletes (10–18 years) performing cutting and double- and single-legged jumping (15 trials/subject) [8]. We trained a bidirectional long short-term memory (LSTM) model [3] to predict bodyweight-normalized GRFs from 42 time series features derived from OpenSim models [9–11]: joint angles, COM position and acceleration × subject mass, and foot velocity. We split our data by subject 80:10:10 across the training, development, and test sets, resulting in 5,949 training and 805 test examples. The development set was used for hyperparameter tuning, and the test set was held out for model evaluation. The training set had walking and jumping, and development and test sets had all tasks. We calculated root mean square error (RMSE) and Pearson's *r* for test set predictions from stance limbs.

RESULTS AND DISCUSSION

For the unseen cutting task, adding physics-based features reduced RMSE for vertical GRF from 1.38 to 0.69 body weights (BW, Figure 1B). The inclusion of physics-based features did not substantially change performance for antero-posterior or medio-lateral GRFs during cutting (Figure 1B), nor for vertical GRFs for tasks in the training set (Figure 1A).

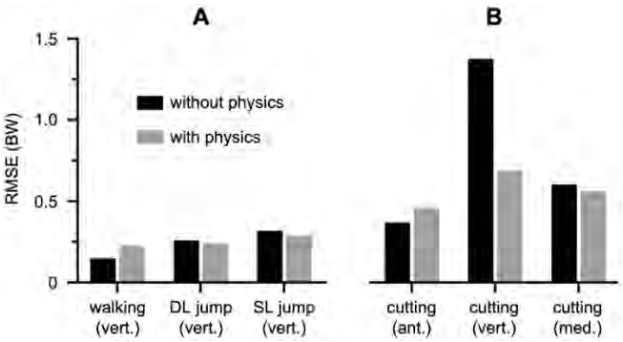

Figure 1 GRF RMSE in body weights (BW) for tasks within (A) and outside of (B) the training set, with (grey) and without (black) physics-based features. Vertical GRF is shown for training set tasks (A), and antero-posterior and medio-lateral components are also shown for cutting (B). DL: double-legged; SL: single-legged.

Adding physics-based features resulted in the largest accuracy improvement for vertical GRF in the unseen cutting task, while accuracy did not substantially change for the other GRF directions. This could be improved by adding tasks with more medio-lateral acceleration to the training set. Additionally, a generalized model trained on multiple tasks may reduce accuracy for a single task. An LSTM model trained solely on walking achieved *r* values of 0.98, 0.93, and 0.88 for antero-posterior, vertical, and medio-lateral GRF [4], while our comparable values are 0.91, 0.86, and 0.94.

CONCLUSIONS

Including whole-body COM features as inputs to a neural network predicting GRFs reduced vertical GRF error for the unseen cutting task. Physics-based features may make GRF prediction models more generalizable, but a more diverse training set is needed to train a useful generalized model.

REFERENCES

[1] Halilaj E et al. *J Biomech* **129**: 110650, 2021.
[2] Uhlrich S et al. *bioRxiv* 2022.07.07.499061, 2022.
[3] Alcantara R et al. *PeerJ* **10**: e12752, 2022.
[4] Mundt M et al. *Med Eng Phys* **86**: 29-34, 2020.
[5] Cavagna G et al. *Physiol J* **217**: 709-21, 1971.
[6] Alcantara R et al. *PeerJ* **9**: e11199, 2021.
[7] Uhlrich S et al. *J Biomech* **144**: 111312, 2022.
[8] Thompson J et al. *Am J Sports Med* **45**: 294-301, 2017.
[9] Seth A et al. *PLoS Comput Bio* **14**: e1006223, 2018.
[10] Rajagopal A et al. *IEEE Trans Biomed Eng* **63**: 2068-79, 2016.
[11] Caruthers E et al. *J Appl Biomech* **32**: 487-503, 2016.

GAIT ABNORMALITY DETECTION BY INERTIAL MEASUREMENT UNIT AND MACHINE LEARNING

F. Ferryanto[1], Raymond Angsetya[2], Pramudita Satria Palar[3] and Andi Isra Mahyuddin [1]
[1] Mechanical Engineering Research Group
[2] Mechanical Engineering Study Program
[3] Flight Physics Research Group
Faculty of Mechanical and Aerospace Engineering, Institut Teknologi Bandung, Bandung, Indonesia
Email: f.ferryanto@itb.ac.id

INTRODUCTION

A study conducted on 101 patients with Parkinson's found that 48% of patients had experienced a fall, and 24% of them had fallen more than once [1]. The number of Parkinson's disease patients continues to grow and is predicted to reach 6.17 million in 2030 [2]. Therefore, early and automatic detection of the symptoms of this disease is important to avoid the risk of falling and death. One way of early detection is to use the IMU sensor which is often found on smartphones. With the current developments in computer and machine learning science, gait abnormalities can be classified automatically. Thus, the purpose of this research is to develop a method which can detect gait abnormalities in general.

METHODS

In this study, there were 35 subjects who participated in which there were 25 healthy subjects and 10 subjects with movement disorders. Healthy subjects are subjects who have never fractured a bone and have no nervous disorders. Subjects with impaired gait were patients at the Department of Physical Medicine and Rehabilitation Hasan Sadikin Hospital, Bandung. The subject's walking motion data was taken using the IMU MPU9250 which has six degrees of freedom. This IMU is placed on the thigh, lower leg and sole of the foot as shown in Figure 1.

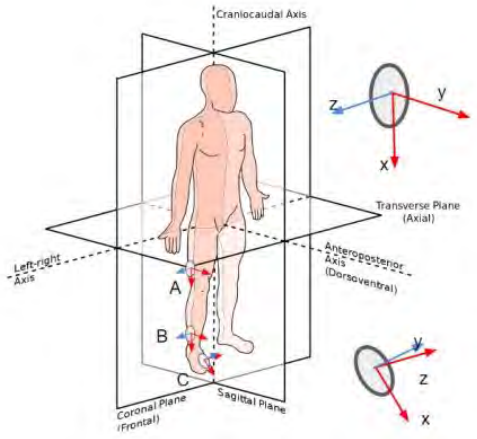

Figure 1 Location of placement of IMU sensors

The sensor output data is then filtered with a low-pass filter with a cut-off frequency of 5 Hz. Alignment of data is done to classify one cycle of walking motion. Each data cycle is calculated the value of the lower control limit (LCL), the average and the upper control limit (UCL). Anomaly calculations are performed using two methods: (1) the frequency of the signal crossing the UCL/LCL boundary, and (2) the sum of each signal difference that crosses the UCL/LCL boundary against that boundary. The determination of LCL and UCL is carried out by decision trees and random forests. Accuracy, precision, and recall values are calculated for each method.

RESULTS AND DISCUSSION

The performance of the anomaly detection test using a decision tree (DT) and random forest (RF) is shown in Table 1.

Table 1: Performance of decision tree and random forest in detecting gait abnormality.

Sensor	Accuracy (%)		Precision (%)		Recall (%)	
	DT	RF	DT	RF	DT	RF
1st Method						
A	79.21	84.03	79.27	84.86	84.06	86.26
B	81.92	94.03	81.70	85.63	86.26	85.16
C	90.66	93.97	94.15	96.02	88.46	92.85
ABC	93.07	96.38	91.62	98.29	96.15	95.05
2nd Method						
A	83.43	85.24	84.32	85.12	85.71	88.46
B	83.43	86.74	87.13	90.11	81.86	85.16
C	90.96	92.77	90.42	94.88	93.40	91.75
ABC	91.56	95.48	90.95	97.71	93.95	93.95

CONCLUSIONS

The best method for detecting walking motion anomalies is the random forest method. In addition, the sensor placement position that produces optimal detection is in the foot (metatarsal).

ACKNOWLEDGEMENTS

The authors gratefully acknowledge the support from ITB who have made this work possible through *Penelitian, Pengabdian Masyarakat, dan Inovasi* (P2MI) scheme research grant for year 2022.

REFERENCES

[1] Kerret al. *Neurology* **75**:2, 116-124, 2010.
[2] Tan. *Neurology Asia,* Neurology Asia, p. 8, 2013

USING IMU TO PREDICT THE EFFECT OF PROSTHETIC ALLIGMENT ON KNEE MOMENTS

Gilmar F. Santos[1], Carina Gempfer[1], Marco Gustav[1], Christof Hurschler[1], Henning Windhagen[2] and Eike Jakubowitz[1]

[1] Laboratory for Biomechanics and Biomaterials, Hannover Medical School, Hannover, Germany.
[2] Orthopaedic Clinic in Diakovere Annastift, Hannover Medical School, Hannover, Germany.
Email: FernandesdosSantos.Gilmar@mh-hannover.de

INTRODUCTION

The gait of transtibial amputees is dependent on prosthetic alignment. Inappropriate position of the prosthetic foot relative to the socket could lead to osteoarthritis or low back pain [1]. However, the interpretation of optimal prosthetic alignment is subjective [2]. The use of inertial measurement unit (IMU) in conjunction with machine learning (ML) allows the measurement outside the gait laboratory and could assist the prosthetist in finding the optimal prosthetic alignment. The aim of this study is to use IMU measurements and ML to predict changes in knee moment caused by altered prosthetic alignment.

METHODS

Motion capture and IMU data of 13 unilateral transtibial amputees and 13 controls were collected. The amputees walked with optimized prosthetic alignment defined by a prosthetist and with a standardized exceeding plantarflexion (PF) of prosthetic foot. 3D knee moments were calculated using inverse dynamics. A Long Short-Term Memory neural network (NN) was trained using the control (NN1) and amputee (NN2) data. The knee moments of both sides for a control (only NN1) and of the prosthetic side for the optimized and PF conditions of a patient (NN1 and NN2) were predicted using unseen IMU data as input. Normalized Root Mean Square Error (nRMSE) by range of the knee moment was calculated between inverse dynamics and prediction.

RESULTS AND DISCUSSION

We were able to predict knee abduction moment (KAM) for the control. NN1 could predict the reduced KAM of the patient in comparison to the control (Figure 1). Furthermore, the prediction of all knee moment components for the patient was improved using NN2 in comparison to NN1, especially for the knee rotation moment, where the nRMSE was reduced from 44.76% to 17.57% (Table 1). PF condition increased the first peak of KAM, which was predicted in both NNs (Figure 1).

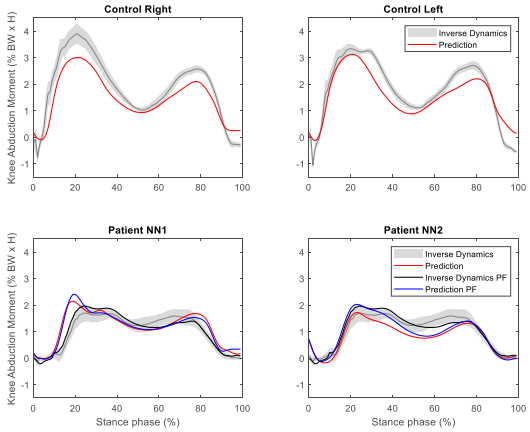

Figure 1 Knee abduction moment for the control and patient.

CONCLUSIONS

Even using control data as training, the differences between control and amputee patient and prosthetic alignments were predicted. Using patient data as training improved the predictions. However, the inter-individual variability of patients and a relatively small number of individuals may affect the NN training. The results indicate that the IMU can be used to predict altered knee moments in transtibial amputees as a function of improper prosthetic alignments. Future work will focus on introducing a classification model to identify prosthetic gait with different perturbations regarding the alignment.

ACKNOWLEDGEMENTS

The work was funded by the Bundesministerium für Wirtschaft und Energie (Germany) (“VarioFit” no. 16KN089720).

REFERENCES

[1] Zhang T et al. *Gait Posture* **76**: 85-91, 2020.
[2] Jonkergouw N et al. *PLoS One* **11(12)**: e0167466, 2016.

Table 1: nRMSE (%) of knee flexion moment (KFM), knee abduction moment (KAM) and knee rotation moment (KRM).

	KFM right / NN1	KFM left / NN2	KAM right / NN1	KAM left / NN2	KRM right / NN1	KRM left / NN2
Control	7.55 ± 2.49	5.55 ± 1.41	10.48 ± 2.35	9.57 ± 1.49	11.07 ± 2.34	9.16 ± 2.26
Patient	13.65 ± 1.53	10.84 ± 1.83	16.91 ± 4.77	14.46 ± 3.73	44.76 ± 6.40	17.57 ± 4.39
Patient PF	15.88 ± 0.15	11.20 ± 3.18	12.28 ± 2.78	10.09 ± 2.69	26.51 ± 4.50	13.98 ± 6.52

The approach chosen for data dimensionality reduction affects the results of running technique clustering

Adrian R. Rivadulla[1], Xi Chen[2], Dario Cazzola[1], Grant Trewartha[1], Ezio Preatoni[1]
[1]Department for Health, University of Bath, Bath, UK
[2]Department of Computer Science, University of Bath, Bath, UK
Email: arr43@bath.ac.uk

Introduction

Clustering to find patterns in high dimensional human biomechanics datasets, such as those collected by modern motion capture systems, is gaining popularity. For example, it has been shown that runners clustered based on their technique react differently to different footwear [1] and rehabilitation interventions [2]. Dimensionality reduction (DR) is a critical step prior to clustering to prevent data from becoming sparse as the number of dimensions increases [4]. It is common practice in general machine learning research to test several DR techniques to choose the most optimal solution for a specific problem [4]. Researchers in human biomechanics on the other hand seem to have defaulted to using Principal Component Analysis (PCA) to perform DR [2, 3], which may not always be the optimal choice, especially if nonlinear relationships are present in the data. Furthermore, it is unclear how the DR approach affects the clustering output and, therefore, whether studies are comparable.

We used three different DR techniques combined with hierarchical clustering to group runners based on their technique and compared the resulting cluster partitions.

Methods

Ninety-eight long-distance runners (48 females, 50 males; age: 34±10 years; height: 1.73±0.09 m; body mass: 65.74±9.9 kg) completed a four-minute run at 12 km/h on a treadmill at 1% gradient. Full body kinematics were collected using motion capture (Oqus, Qualysis, Gothenberg, Sweden). Mean trunk-to-pelvis, hip, knee and ankle sagittal plane angles, centre of mass vertical displacement normalised by leg length (time-continuous variables, 1D), stride frequency and duty factor (discrete variables, 0D) were calculated to characterise running technique. The three DR techniques tested were:

Fourier + PCA. 1D variables were modelled as Fourier series with the minimum number of harmonics required to reconstruct angular and translational signals with an error <2° and <5 mm, respectively. The Fourier coefficients and 0D variables were then concatenated and PCA was applied.

Direct PCA. 1D and 0D variables were concatenated and PCA was applied.

Autoencoder. 1D and 0D variables were concatenated and a fully connected neural network autoencoder was trained and tested using all the individual curves from every participant (70/30, train/test). Hyperparameter optimisation (number of hidden layers and units per layer) was performed using a grid search and a 5-fold cross validation scheme on the training data. The encoder part of the network was then used for DR.

For PCA methods, the number of components explaining 95% of the variance in the data were kept. For the autoencoder, the number of latent dimensions (encoder output) was selected experimentally based on reconstruction error.

Hierarchical agglomerative clustering (similarity metric: Euclidean distance, linkage criteria: Ward) was then implemented. Our objective was to find clusters as separable as possible, so we calculated Silhouette scores for different numbers of clusters and chose the largest Silhouette score. The optimal number of clusters was two regardless of the DR technique used. The Adjusted Mutual Information (AMI [0-1] random-perfect agreement) score was calculated between the clustering partitions resulting from each DR technique.

Results

The Silhouette scores (Table 1) were low regardless of the DR technique, indicating low separability of our dataset. The autoencoder resulted in marginally more separable clusters. There were differences in cluster assignments when comparing direct PCA to the autoencoder and especially when comparing Fourier + PCA to the autoencoder.

Table 1: Silhouette and AMI scores compared to autoencoder.

DR	Silhouette score	AMI score
Autoencoder	0.19	
Direct PCA	0.16	0.42
Fourier + PCA	0.15	0.03

Discussion

Our analysis indicates that clustering results obtained with different DR techniques may not be comparable as DR methods can capture different aspects of the data. The autoencoder seemed to result in slightly better separability of the data in our dataset. However, it requires more development and computing resources compared with direct PCA for marginal improvements in our case. Researchers using clustering algorithms are advised to select their DR techniques carefully according to their objective when conducting a clustering analysis.

References

[1] Hoerzer et al. (2015). *J Biomech,* **48**: 2072-2079.
[2] Watari et al. (2021). *Front Bioeng*, **9**: 645710.
[3] Phinyomark et al. (2015) *J Biomech,* **48**: 3897-3904.
[4] Fournier et al. (2019) *IEEE AIKE,* **2**: 211-214.

Conditional Generative Deep Learning in Biomechanics: Generating Synthetic Motion Capture Datasets by Controlling Subject Anthropometrics

Metin Bicer[1,2], Andrew TM Phillips[1], Alessandro Melis[3], Alison McGregor[4], Luca Modenese[1, 5]
[1] Department of Civil and Environmental Engineering, Imperial College London, UK.
[2] Faculty of Sport Sciences, Hacettepe University, Ankara, Türkiye
[3] VivacityLabs, London, UK.
[4] Department of Surgery and Cancer, Imperial College London, London, UK.
[5] Graduate School of Biomedical Engineering, University of New South Wales, Sydney, Australia.
Email: m.bicer19@imperial.ac.uk

INTRODUCTION

Data collection and sharing in biomechanics is often limited by lack of access to participants, time, ethical and financial constraints. In a previous study, we developed a workflow to augment existing datasets by synthetic trials using generative adversarial networks (GANs) [1] and an app [2] to generate synthetic data was shared with the community. A limitation of that study was the impossibility of controlling the generation of synthetic data, for example based on subject anthrophometrics. Thus, this study aims to extend our initial approach and generate mocap data, marker trajectories and ground reaction forces (GRFs) of synthetic walking trials based on subject leg length and mass.

METHODS

A small gait dataset (real dataset) collected from 8 healthy subjects (mass: 68.4±11.5 kg, leg length: 91.5±7.5 cm, height: 1.74±0.13 m) was divided into two classes based on subject mass and leg length, with conditions set at 60 kg and 91 cm (corresponding to a height of around 1.71 m), respectively. The classes were labeled as "low mass" and "high mass" for subject mass, and "short" and "tall" for subject leg length. The same optimized GAN architecture as in [1] was used to train the data, with separate networks trained for subject mass (M-GAN) and subject leg length (LL-GAN). During training, a single number (0 or 1) was used to inform the network of the subject's condition (mass or leg length). For example, a "short" subject's data was labelled with 0, while a "tall" subject's data was labelled with 1. After proper training, synthetic gait data was generated using the conditions specified by M-GAN and LL-GAN.

RESULTS AND DISCUSSION

The two models were able to generate mocap data based on their corresponding conditions (50 trials for each condition). Our M-GAN generated two subject mass ranges, with "low mass" subjects weighing 55.4±3 kg and "high mass" subjects weighing 69.9±3 kg (Figure 1.a). Additionaly, LL-GAN generated "short" subjects having 84.6±4.6 cm leg lengths, and "tall" subjects having 96.5±3.3 leg lengths (Figure 1.b).

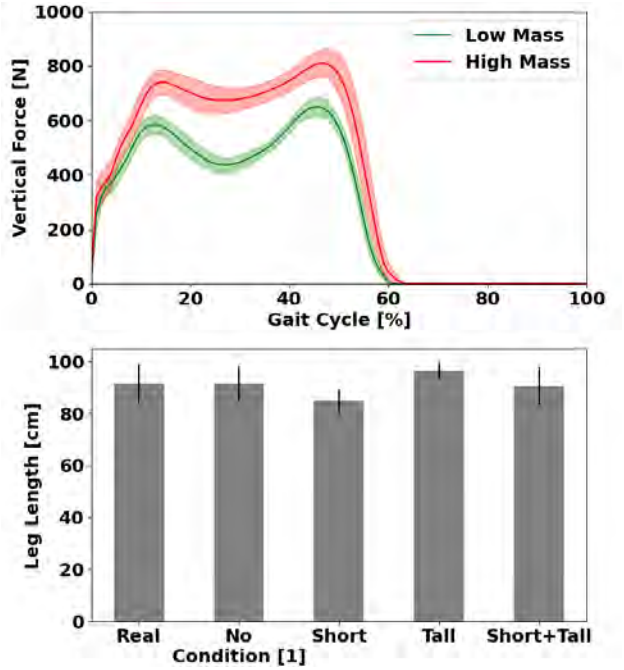

Figure 1. a) Distribution of generated vertical forces with mass conditions (M-GAN), b) Comparison of generated subject leg lengths (LL-GAN) to the real subject leg lengths.

CONCLUSIONS

With the intention of extending our previous generative approach [1], we developed two separate models to generate synthetic mocap data based on two classes of subject mass and height. M-GAN model could generate data based on subject mass, while LL-GAN achieved data generation by conditioning on leg lengths. Both models will be deployed into our web app [2] for conditional mocap data generation. A limitation of this approach is that the data generation conditioning had to be done separately for only two conditions. The main reason behind our adopted strategy was that the real dataset does not contain a wide range of subject anthrophometrics. Thus, future work will adress this limitation by incorporating publicly available datasets into our framework to generate synthetic mocap data for a wide range of subject anthropohometrics using walking speed as an additional condition.

REFERENCES

[1] Bicer et al. J. Biomech. 144, 111301, 2022.
[2] https://thisgaitdoesnotexist.streamlitapp.com

Gait-based person re-identification across force platform datasets from different countries

Kayne A. Duncanson[1], Simon Thwaites[1], Fabian Horst[2], Gary Hanly[3], William S.P. Robertson[4], Ehsan Abbasnejad[5] and Dominic Thewlis[1]

[1] Adelaide Medical School, University of Adelaide, Adelaide, Australia; [2] Department of Training and Movement Science, Johannes Gutenberg-University, Mainz, Germany; [3] Defence Science and Technology Group, Department of Defence, Edinburgh, Australia; [4] School of Mechanical Engineering, University of Adelaide, Adelaide, Australia; [5] Australian Institute for Machine Learning, University of Adelaide, Adelaide, Australia.
Email: kayne.duncanson@adelaide.edu.au

INTRODUCTION

Person re-identification (re-ID) involves matching biometrics (i.e., biological cues to identity) over time to re-establish identity. There is great interest in using walking gait for person re-ID in security applications (e.g., threat detection) as it can be measured discreetly in dynamic environments. Using machine learning (ML), studies have shown that features encoded in one set of ground reaction force (GRF) data are effective for distinguishing between another set of previously unseen GRF data for re-ID, provided that the latter is acquired from the same group of individuals under the same experimental conditions [1]. This study aimed to determine the extent to which features encoded in GRF data from one set of IDs can be used to distinguish between GRF data from another set of IDs with different demographics under different experimental conditions.

METHODS

The aim was achieved by training and testing a ML model on separate force platform datasets. Four public datasets containing GRFs and centres of pressure from healthy individuals were utilised: ForceID A (number of IDs (N)=193), a subset of GaitRec (GaitRec (shod) (N=208)), Gutenberg (N=350), and AIST (N=300) [2-5]. Each dataset was constrained to contain 185 IDs × 10 samples to control for the effects of dataset size and distribution on model performance. Scenario I involved training (N=148) and validating (N=37) a fully-connected neural network model on one dataset and then testing it on another (N=185). Scenario II was the same as Scenario I except a second dataset was included for training (N=296) and validation (N=74) to see if this changed test performance. Five-fold cross validation (5-CV) was conducted on training and validation sets, with the test set constant on each fold. All possible training and validation vs. test combinations of the four datasets were implemented. Predictions were generated based on a challenging evaluation setting where there was only one random prior sample per ID to match with a given query sample. Mean rank-1 re-ID accuracy over 5-CV was reported.

RESULTS AND DISCUSSION

In scenario I, accuracy was above 90% when a barefoot (B), preferred speed (PS) dataset (AIST or Gutenberg) was used for testing, regardless of the dataset used for training and validation (Figure 1). Accuracy was 79-88% when a shod (S), multi-speed (MS) dataset (ForceID A or Gaitrec (shod)) was used for testing and the remaining S, MS dataset was used for training and validation. Finally, accuracy was 54-57% when a S, MS dataset was used for testing and a B, PS dataset was used for training and validation. In scenario II, accuracy increased by 26-31% when the test set was a S, MS dataset and a S, MS was included with a B, PF dataset for training and validation (Figure 1 – right). Findings suggest that S, MS data are more challenging and more generally applicable for person re-ID than B, PS data. Perhaps models trained on S, MS data must learn features that are robust to increased gait variability due to complex interactions between walking speed and footwear. This could explain why models trained on B, PS data were relatively ineffective at distinguishing between S, MS data for re-ID.

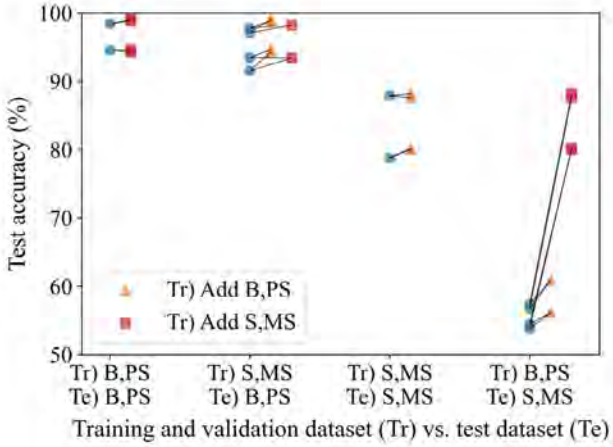

Figure 1 Test accuracy according to dataset configuration in terms of footwear and walking speed characteristics. B=barefoot, S=shod, PS=preferred speed, MS=multi-speed.

CONCLUSIONS

A simple ML model can encode features of GRF data from one set of IDs and then use these to distinguish between GRF data from another set of IDs with different demographics under different experimental conditions with 80+% accuracy.

REFERENCES

[1] Horst F et al. *Sci. Rep* **9**: 1-13, 2019.
[2] Duncanson et al. *ForceID Dataset A*; Figshare; DOI:10.25909/14482980.
[3] Horsak B et al. *Sci. Data* **7**: 143, 2020.
[4] Horst F et al. *Sci. Data* **8**: 232, 2021.
[5] Kobayashi Y et al. *AIST Gait Database*; https://unit.aist.go.jp/harc/ExPART/GDB2019_e.html, 2019.

Deep Learning-based Vertical Ground Reaction Force Estimation during Walking with Inertial Measurement Units of the Left Wrist and Both Heels

Yuta Takanobu[1,3], Yuji Kumano[1,3], Suguru Kanoga[3], Masataka Yamamoto[1,2], Hiroshi Takemura[1], and Mitsunori Tada[3]

[1] Tokyo University of Science, Chiba, Japan, [2] Hiroshima University, Hiroshima, Japan, [3] National Institute of Advanced Industrial Science and Technology (AIST), Tokyo, Japan.
Email: 7519056@ed.tus.ac.jp

INTRODUCTION

Vertical ground reaction force (vGRF) is important information in gait analysis and is typically measured with a force plate. Thus, the gait analysis is usually conducted in specific indoor environments such as in a laboratory. To overcome this limitation, previous studies have estimated vGRFs using one inertial measurement unit (IMU) of the left shank [1] and three IMU of the left thigh, shank, and foot [2]. In this study, we construct a deep learning model and estimate vGRFs during walking from three IMUs, one each on the left wrist and both heels to realize daily gait analysis with a smartwatch and smart shoes and compare the accuracy of estimation with other sensor positions employed in the previous studies [1, 2].

MATERIALS AND METHODS

A motion analysis software [3] was used to generate IMU data from the AIST Gait Database 2019 [4], which contains motion and vGRF data. The vGRF data were normalized by the body weight of each subject and used to extract the stance phase to construct a dataset of IMU data and normalized vGRF data while the foot was in contact with the floor. The dataset was then divided into those for the left or right foot to ensure better estimation accuracy.

After removing the abnormal data by visual inspection, the dataset of the left stance phase was 2999 trials of 350 subjects, while the dataset of the right stance phase was 3003 trials in total. Five subjects for the left (493 trials) and for the right stance phase (495 trials) randomly sampled from each age group, 20s to 70s in 10 years increment, were used to test the estimation accuracy.

Our model comprises two long short-term memory layers with 256 units and one dense layer with one unit. It considers three-axis acceleration and angular velocity inputs from the previous 19 frames and the current frame (i.e., a total of 0.1 s) and estimates the current vGRF. To evaluate the influence of the IMU position on the estimation accuracy, we trained the models for the left and right vGRFs separately with three different IMU position sets as follows.

- IMUs on the left wrist and both heels (our proposal)
- An IMU on the left shank (same as [1])
- IMUs on the left thigh, shank, and foot (same as [2])

RESULTS AND DISCUSSION

Figure 1 (a) shows the measured and estimated vGRFs of one trial when the IMUs were attached to the left wrist and both heels. It is clear from this subfigure that our proposed model can estimate the overall waveform of the vGRFs except for the first 19 frames shown in the dotted line. Figure 1 (b) summarizes the accuracy of estimation for different IMU position sets. We compared the accuracy using normalized root mean squared errors (NRMSEs) for three cases: (1) the overall waveform, (2) the amplitude of the first peak, and (3) the time of the first peak. As can be seen from this subfigure that our proposed model was comparable to the most accurate estimation result of the overall waveform achieved by three IMUs on the left thigh, shank, and foot. In terms of the peak amplitude and peak time, our proposed model was the most accurate. It is necessary to estimate the stance phase only from the IMU data when this system is in actual use. Our proposed model is advantageous in this respect since having IMUs of both heels makes phase estimation easy.

(a)

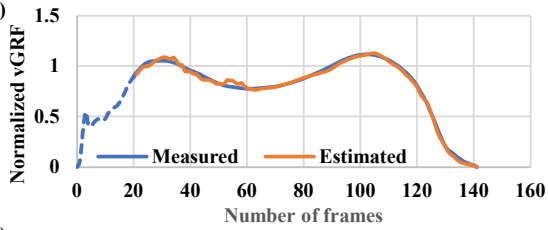

(b)

IMU position	Waveform	Peak amplitude	Peak time
Left wrist and both heels	6.70 %	7.12 %	4.38 %
Left shank	8.02 %	8.68 %	4.81 %
Left thigh, shank and foot	6.26 %	7.32 %	4.41 %

Figure 1 (a) Measured and estimated vGRFs of one trial. (b) NMRSEs for different IMU position sets

CONCLUSIONS

We estimated vGRF during walking with only three IMUs. While the model should be verified with real data, it could be used in daily life.

ACKNOWLEDGEMENTS

This work was partially supported by the JST-Mirai Program Grant Number JPMJMI21H5, Japan.

REFERENCES

[1] Jiang X et al. Sensors **20**: 4345, 2020
[2] Md Sanzid Bin H et al. TechRxiv, 2022
[3] Endo Y et al. Proc. 3rd Int Digital Hum Modeling Symps, 2014
[4] Kobayashi Y et al. https://unit.aist.go.jp/harc/ExPART/GDB2019.html 2019

INVESTIGATING THE EFFECTS OF TRANSFEMORAL AMPUTEE ANATOMY ON STRESS AND STRAIN DISTRIBUTION IN OSSEOINTEGRATED IMPLANTS USING A 3D FE MODEL

Tiereny McGuire[1] and Anthony M J Bull[1]
[1] Bioengineering, Imperial College London, London, UK.
Email: t.mcguire19@imperial.ac.uk

INTRODUCTION

Osseointegrated prostheses (OIP) for transfemoral amputees represent a solution to the array of complications caused by sockets. Bypassing the soft-tissues, loads are transferred directly through the musculoskeletal (MSK) system. Mechanical complications such as bone fracture, loosening, and implant failure represent a barrier to OIP success [1]; it is important to identify how the human anatomy affects the biomechanical profile of these OIPs so that clinicians can feel confident in their recommendations. The aim of the study is to assess the effects of gender and amputation length on stress/strain distribution across the bone-implant interface through utilisation of a 3D finite element (FE) model. The overarching goal is to improve patient outcomes by producing hypotheses on biomechanical failure to inform surgical intervention and implant design.

METHODS

Four healthy adult CT scans (2 female) were used to generate 12 femur models of different lengths. Each bone was amputated at 30, 40 and 50% of the original lengths and the surgical procedure of implantation simulated to create bone-implant assemblies. The assemblies were meshed (minimum element size of 3mm) and material properties applied (using grey scale values for bone) forming 3D FE models. The femurs were subdivided into seven Gruen Zones (GZ) and fixed proximally. Representative loads [2] were applied to the distal face of the device in a static structural analysis with assumed full osseointegration contact. Data were cleaned and statistical analyses ($p < 0.05$) performed using non-parametric tests to understand the effects of anatomy on stress and strain distribution across the system.

RESULTS AND DISCUSSION

Median stresses and strains in the system were found to be similar amongst the different bone lengths (Table 1). More detailed bone analysis, however, showed there were significantly different strains experienced in GZ3&5 ($p = 0.022$ and $p = 0.029$) and stresses in GZ4 ($p = 0.018$) (Figure 1). As femur length decreases, the implant is located higher up the medullary canal, closer to the increased proportion of trabecular bone that is less dense and more fragile than cortical bone. The results also showed a statistical difference ($p = 0.004$) between genders, with female bones experiencing higher strains (F:0.0068 and M:0.0002).

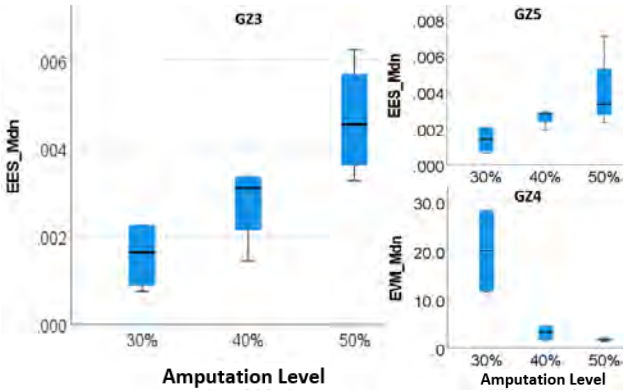

Figure 1 Volume of stress and strain due to level of amputation.

CONCLUSIONS

This model facilitates quantification of stress and strain distribution, allowing predictions of mechanical complications associated with anatomical differences. Results indicate the importance of prescribed implant geometric specification in directing load transmission through the MSK system to optimise this stress/strain distribution and improve the probability of implant success.

ACKNOWLEDGEMENTS

This work was supported by the UK Engineering and Physical Science Research Council (EPSRC) grant EP/S02249X/1 for the Centre of Doctoral Training in Prosthetics and Orthotics.

REFERENCES

[1] Hagberg et al. *JOT* **38**: 56-64, 2023.
[2] Niswander et al. *Med Eng Phys* **84**: 56-64, 2020.

Table 1: Summary data for median Equivalent Elastic Strain (EES) and Equivalent von Mises Stress (EVM) for different amputation levels.

Amputated length	Bone		Implant		Adapter	
	EES	EVM (MPa)	EES	EVM (MPa)	EES	EVM (MPa)
30%	0.00306	5.92	0.00004	4.72	0.00248	2.70
40%	0.00412	4.15	0.00005	5.67	0.00179	2.63
50%	0.00332	2.76	0.00003	5.40	0.00140	2.62

Relationship between time since amputation and gait asymmetry in unilateral transfemoral amputees

Takeshi Hara[1], Genki Hisano[2,3], Toshiki Kobayashi[4], Hiroaki Hobara[5]
[1] Graduate School of Advanced Engineering, Tokyo University of Science, Tokyo, Japan
[2] Systems and Control Engineering, Tokyo Institute of Technology, Tokyo, Japan
[3]Research Fellow of Japan Society for the Promotion of Science, Japan
[4] Department of Biomedical Engineering, The Hong Kong Polytechnic University, Hong Kong, China
[5]Faculty of Advanced Engineering, Tokyo University of Science, Tokyo, Japan
Email: 8218066@ed.tus.ac.jp

INTRODUCTION

Time since amputation (TSAmp) is one of the factors that affect the walking ability and social reintegration among lower limb amputees. For example, it was found that gait outcome and mobility score were improved with longer TSAmp [1,2]. However, little is known about how the TSAmp affects gait mechanics in lower limb amputees. Therefore, the aim of this study was to investigate the relationship between TSAmp and the asymmetry of spatiotemporal parameters in unilateral transfemoral amputees over a wide range of walking speeds.

METHODS

We recruited 26 individuals with transfemoral amputation (7 females and 19 males, K-3 or K-4 levels, average TSAmp 12 ± 8.7 years). All participants were asked to walk on an instrumented treadmill (FTMH-1244WA, Tec Gihan, Kyoto, Japan) at 8 speeds from 2.0 to 5.5 km/h in 0.5 km/h increments. We determined spatiotemporal gait parameters, such as stance phase, swing phase, double support time, cadence, step time, and step length were calculated for their intact and prosthetic limb, respectively. The asymmetry ratio was calculated by prosthetic value/intact value [3]. If the asymmetry ratio equals 1, it indicates perfect symmetry. If the asymmetry ratio is greater than 1, it means a smaller value on the intact limb compared to the prosthetic limb and if it is less than 1, it means a greater value on the intact limb compared to the prosthetic limb. After that, Pearson correlation or Spearman's rank correlation was conducted at each speed to determine if there were any linear correlations of the spatiotemporal asymmetry ratio in response to TSAmp. Statical significance was set at $p < 0.05$.

RESULTS AND DISCUSSION

As shown in Figure 1, there were no significant correlations between the TSAmp and asymmetry of spatiotemporal gait parameters (except for double support time at 5.0 km/h). Current results agree with a previous study, which demonstrated that TSAmp had little impact on mobility score [2]. These results suggest that the association between TSAmp and asymmetry of spatiotemporal gait parameters would be weak. In other words, while gait outcome and self-reported mobility score showed improvement with longer TSAmp [1,2], TSAmp may not be necessarily correlated with the asymmetry of gait parameters in unilateral transfemoral amputees.

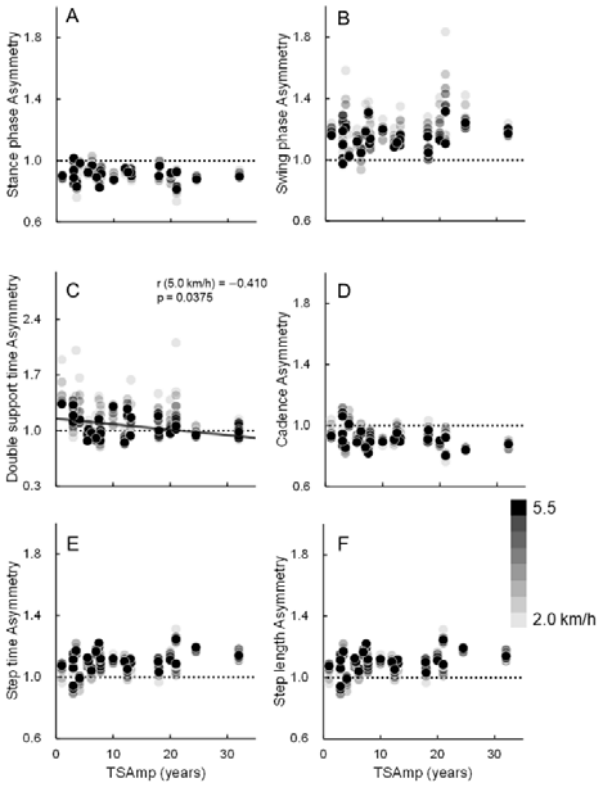

Figure 1 Scatter plots of time since amputation (TSAmp), and asymmetry of spatiotemporal gait parameters at eight speeds (A: stance phase, B: swing phase, C: double support time, D: cadence, E: step time, F: step length).

CONCLUSIONS

The results of the present study suggest that the association between TSAmp and the asymmetry of spatiotemporal gait parameters may be weak.

ACKNOWLEDGEMENTS

This work was partly supported by JSPS KAKENHI (19K11338) and JST-Mirai Program (JPMJMI21H5).

REFERENCES

[1] Puhalski et al., *J Prosth Orth,* **20**: 53-60, 2008.
[2] Seth et al., *Am J Phys Med Rehab,* **101**: 32-39, 2022.
[3] Patterson et al., *Arch Phys Med Rehab,* **89**: 304-310, 2008.

METABOLIC COST AND MUSCULOSKELETAL METABOLIC QUANTIFICATION OF WALKING WITH AN ABOVE KNEE PROSTHESIS SIMULATOR

Bonnet X.[1], Bonnet-Lebrun A.[1], Boos A.[1], Sedran L.[1], Heidsieck C. [1], Thomas-Pohl M.[2] and Pillet H.[1]
[1] IBHGC, Arts et Métiers, Paris, France.
[2] Service de Médecine et de réadaptation, Hôpital d'Instruction des Armées, France, Paris, France.
Email: xavier.bonnet@ensam.eu

INTRODUCTION

Above-knee amputees show an increase in metabolic consumption of nearly 50% compared to asymptomatic subjects [1]. Walking with a prosthesis alters joint moments and powers and there is an increase in work at the residual hip and at the contralateral limb. COM work has also been quantified using the Individual Limb Method, again showing a severe decrease in propulsion of the prosthetic limb and significant compensation on the contralateral limb [2]. However, this increase in mechanical work remains far more lower than the increase in metabolic cost. In order to take into account the action of the bi-articular muscles, the cost associated with isometric muscle work and the elastic part of the muscle work [3], the objective of this study is to quantify the energy cost of walking using a simple 2D musculoskeletal model including the 8 main muscles of the lower limb and to compare these results with the metabolic consumption estimated from gas exchanges.

METHODS

Six asymptomatic subjects (AS) walked first without a prosthesis and then equipped with a knee prosthesis associated with an energy restitution foot (Above Knee prosthesis Simulator: AKS). Kinematics, kinetics, and gas exchanges were collected. A musculoskeletal model composed of 8 muscles per leg was used to quantify the metabolic cost of each muscle with the muscle metabolic model of Minetti et al [4].

RESULTS AND DISCUSSION

The measured metabolic cost is doubled between walking without versus with a simulator (3.6 (0.4) J.kg^{-1}.m^{-1} vs. 7.6 (1.1) J.kg^{-1}.m^{-1}). The model, consistent with the results of Koelewijn et al [3], shows an asymmetry of hip muscle recruitment between the two legs, with an overall increase in muscle effort during simulated amputation (Table 1).

Despite greater efforts at the ankle than at the hip, the metabolic cost is about 40% of the total cost for these two joints in healthy subjects. When subjects are fitted with the prosthesis simulator, native ankle and knee are replaced by prosthetic joints and therefore do not induce any metabolic cost anymore. The increased metabolic costs of the hip muscles on the prosthetic side and of the muscles of the contralateral limb do not compensate for this reduction. (Table 1).

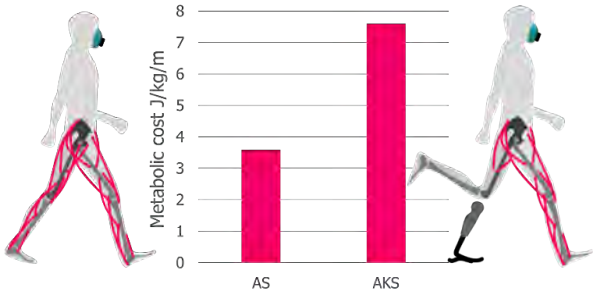

Figure 1 Metabolic cost measured for asymptomatic (AS) walking and with the above knee prosthesis simulator (AKS).

CONCLUSIONS

The current model does show an increase in muscle work related to the use of the femoral prosthesis, but this very simple model (2D, 8 muscles) does not explain the additional metabolic cost observed in amputees. Two ways of improving the model could be to integrate the muscles of the abdominal and lumbar spine and to take into account the frontal plane.

ACKNOWLEDGEMENTS

This study was made possible by the funding support and of the Direction Générale de l'Armement (DGA).

REFERENCES

[1] van Schaik L et al. *PLoS One* **14(3):** e0213256, 2019.
[2] Bonnet X et al. *J Biomech* **129**: 110843, 2021.
[3] Koelewijn A et al. *PLoS One* ***14(9)****:e022203, 2019.*
[4] Minetti A et al. *J theor Biol.* **4**: 1997.0407, 1997.

Table 1: Individual muscles metabolic cost in J.kg/m, mean (sd).

Muscle cost (J/kg/m)	Gluteus	Ilio Psoas	Biceps Fem	Rectus Fem	Vastus	Gastroc	Soleus	Tib. Ant
AS walking	*0.05 (0.02)*	*0.22 (0.04)*	*0.06 (0.03)*	*0.08 (0.02)*	*0.07 (0.04)*	*0.24 (0.05)*	*0.17 (0.03)*	*0.09 (0.03)*
TFS contralateral side	*0.18 (0.03)*	*0.19 (0.02)*	*0.19 (0.03)*	*0.05 (0.01)*	*0.04 (0.02)*	*0.28 (0.05)*	*0.17 (0.06)*	*0.09 (0.02)*
TFS Fitted side	*0.07 (0.02)*	*0.16 (0.02)*	*0.06 (0.01)*	*0.14 (0.04)*				

INFLUENCE OF HIP FLEXION CONTRACTURE ON GAIT PARAMETERS OF TRANSFEMORAL AMPUTEES: A PRELIMINARY STUDY

ARRIBART Kevin[1,2], KANIEWSKI Anton[1], DECHARTE Florian[2], BONNET Xavier[2] and PILLET Helene[2]
[1] Institut Robert Merle d'Aubigné, Valenton, France.
[2] Arts et Metiers Sciences et Technologies, Institut de Biomecanique Humaine Georges Charpak, Paris, France.
Email: kevinarribart@gmail.com

INTRODUCTION

52% of above knee amputees are affected at least once by low back pain, but the influent parameters are far to be fully understood. In the same time, above knee amputation can result in hip flexion contracture (HFC) characterized by a persistant hip flexion. HFC therefore limits the extension capacity and decreases the hip range of motion (ROM). The recommandation of prosthesis fitting is to align the socket with 5° of flexion in the absence of HFC and to the value of the measured HFC otherwise [1]. Previous studies have found pelvic compensations during gait as consequence of HFC in different populations such as patients with neurological disease or osteoarthritis [2]. The main objective of the study is to quantify sagittal pelvic and spinal ROM of above knee amputees with and without HFC during gait. Secondary objectives concern frontal and transverse plane and general gait parameters.

METHODS

An observational study was conducted, including above knee amputees, with healthy contralateral limb, walking with a prosthesis since at least 1 month without walking aids. Hip ROM, socket flexion and HFC were measured with a goniometer. Gait analysis was performed using Vicon® with 27 reflective markers. Data were analysed with Excel® and Matlab® softwares.

RESULTS AND DISCUSSION

12 patients were included and classified in two groups: with HFC (7 persons), and without HFC (5 persons). Differences were observed between groups with and without HFC (Figure 1). A t-test highlighted significant differences in the sagittal plane at pelvis and thoracic level during gait (Table 1). Regarding secondary judgement criteria, patients with HFC had a significantly lower stance phase time (p = 0.036), and a higher swing phase time than patients without HFC (p = 0.036), a decrease in the sagittal hip ROM on the amputated side (p = 0.001) as well as a significant increase in pelvic ROM in the transverse plane (p = 0.011). A decrease of the amputated limb hip ROM seems to be correlated with an increase of sagittal pelvis and thoracic ROM (respectively r = -0.525, p = 0.04; r = -0.578, p = 0.024). These results suggest that further studies should be focused on parameters that can be modified to increase the hip ROM and decrease spinopelvic ROM during gait. Other studies are needed to understand the link between spinopelvic conditions of above-knees amputees during gait and complications such as low back pain.

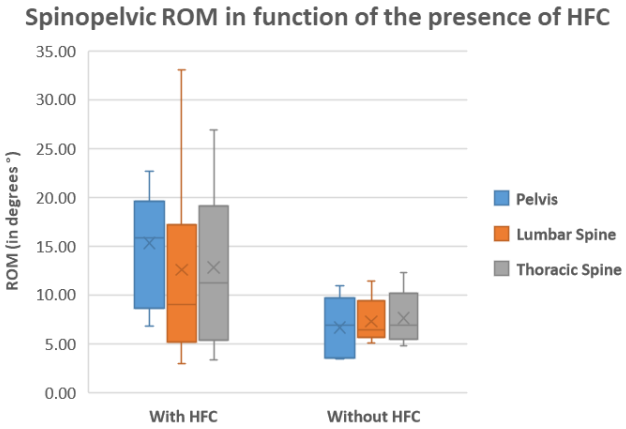

Figure 1: ROM of spinopelvic level in transfemoral amputees with and without HFC.

CONCLUSIONS

Spinopelvic ROM seem to be more important at the pelvic and thoracic spine level for above knee amputees with HFC and correlated with the hip ROM on the amputated side during gait. A larger number of patients is needed to confirm our initial finding.

REFERENCES

[1] Poonsiri J et al. *Disability and Rehabilitation* 44: 3749-59, 2022
[2] Lee Laura W et al. *American Journal of Physical Medicine and Rehabilitation* **76**: 502-8, 1997

Table 1: Sagittal Spinopelvic ROM in function of the presence of HFC

	With HFC	Without HFC	*p-value*
Pelvis ROM (Degrees °)	15.05 ± 5.75	6.73 ± 3.23	p = 0.008
Lumbar Spine ROM (Degrees °)	12.69 ± 10.35	7.27 ± 2.5	p = 0.142
Thoracic Spine ROM (Degrees °)	9.95 ± 8.28	2.56 ± 0.69	p = 0.039

Bilateral asymmetry of ground reaction forces during running in unilateral transfemoral amputees

Mai Watanabe[1], Hiroaki Hobara[2]
[1]Graduate School of Advanced Engineering, Tokyo University of Science
[2]Faculty of Advanced Engineering, Tokyo University of Science
E-mail: 8219124@ed.tus.ac.jp

INTRODUCTION

The development of running-specific prostheses (RSP) contributed to the sports and exercise opportunity for unilateral transfemoral amputees (UTFAs). However, due to the morphological and functional asymmetric feature of the running biomechanics in UTFAs, running-related injuries frequently occur in the intact limb of UTFAs [1]. Previous studies investigated the kinetic features, such as peak value and the initial slope of the ground reaction forces (GRFs), and compared the feature between intact and prosthetic limbs [1,2]. However, little is known about how the bilateral differences in the GRFs exist during the entire stance phase. Therefore, the purpose of this study was to clarify the differences in GRFs between intact and prosthetic limbs in UTFAs at various running speeds during the entire stance phase.

METHODS

Ten runners with unilateral transfemoral amputation (7 males and 3 females) participated in this study. Each participant performed running trials on an instrumented split-belt treadmill at incremental speeds of 30, 40, 50, 60, 70, and 80% of their maximum running speeds. GRFs were measured from both prosthetic and intact limbs over 16 consecutive steps at each running speed. Then, Statistical Parametric Mapping (SPM) was applied to the acquired time series of GRFs to quantitatively evaluate the differences in ground reaction forces between both limbs.

RESULTS AND DISCUSSION

The anteroposterior and vertical GRF of the intact limb was significantly greater than those of the prosthetic limb in the early stance phase in a range of running speeds (Fig. 1). These results were consistent with a previous study which showed that the intact limb had a significantly greater anteroposterior and vertical first peak during sprinting in UTFAs [2]. A potential explanation of the between limb differences in the early and midstance GRF may be the foot strike pattern, which would be caused by the different foot shapes and leg lengths between limbs [3]. On the other hand, in the late stance phase, the prosthetic limb showed significantly larger vertical GRF than the intact limb. One reason may be suggested that the prosthetic limb does not have active plantar flexion of the ankle joint.

CONCLUSIONS

This study revealed that differences in GRF between the prosthetic and intact limbs in UTFA were distributed throughout the stance phase. These differences may be related to leg length, foot shape, mechanical properties, and functional anatomy of ankle joint motion.

ACKNOWLEDGEMENTS

We thank all the athletes who participated in this study.

REFERENCES

[1] Hobara et al., *Clin Biomech*, 2020.
[2] Makimoto et al., *J Appl Biomech*, 2017.
[3] Andrada et al., *J Exp Biol*, 2013

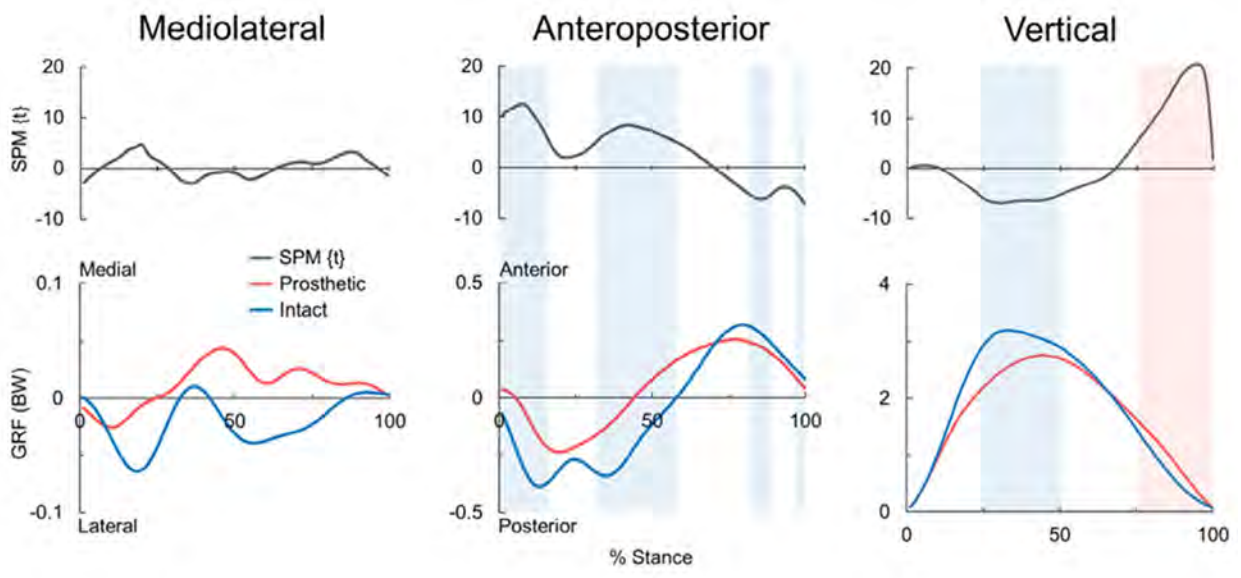

Figure 1 Statistical *t*-value of SPM (gray) and GRF profiles of prosthetic (red) and intact (blue) limbs at 60% of running speed of participants' 100-m personal record. The pale red and blue range indicate that the prosthetic and intact limb is significantly larger, respectively.

THE EFFECT OF A 6-WEEK INTRINSIC FOOT MUSCLE TRAINING INTERVENTION ON STATIC AND DYNAMIC BALANCE IN TEAM SPORTS PLAYERS

Matthew Stoner[1], Stephanie Grady[1], Tom Drayton[1], Wing-Kai Lam[2] and Charlotte Apps[1]
[1] School of Science and Technology, Nottingham Trent University, Nottingham, UK
[2] Sports Information and External Affairs Centre, Hong Kong Sports Institute, Hong Kong, China
Email: matt.stoner@ntu.ac.uk

INTRODUCTION

The intrinsic foot muscles (IFM) support the foot arches and are proposed to enhance plantar proprioception and thus aid dynamic balance [1]. Strengthening the IFM using the short foot exercise (SFE) technique has been shown to be more effective in enhancing dynamic balance than foot/ lower leg exercises that also activate the extrinsic foot muscles [2]. Despite this, team sports players currently lack training aimed at strengthening the IFM. Moreover, previous foot strengthening research has mostly assessed barefoot balance, but sports players often wear athletic footwear during training practice which diminishes stimulation of the plantar mechanoreceptors. The effect of IFM training to improve shod balance is currently unknown. Therefore, the aim of this study was to compare the effect of footwear in a 6-week IFM training programme on static and dynamic balance ability in team sports players.

METHODS

Twenty-six team sports players were randomly assigned to an intervention group (n=13) or a control group (n=13). All participants completed a familiarisation, a pre and post-test sessions. Participants in the intervention group completed a 6-week IFM training intervention between the pre and post-testing sessions, which involved 100 repetitions of the SFE on each foot, every day [2]. During pre and post-tests, static balance was determined using a standard 30 second single-leg stance test [3] while ground reaction forces (AMTI, BP400600) were recorded. The standard deviation of the medial lateral (ML) centre of pressure velocity was calculated. Dynamic balance was assessed using an 8-direction star excursion balance test (SEBT) and a single leg, 10-second wobble board task. Reach distances from the SEBT were averaged across directions and normalised to the participants' leg lengths. ML stability index was computed from the wobble board data [4]. The mean of three trials per test were calculated on the dominant leg in both barefoot and a standardised athletic shoe for control and intervention groups respectively. Pre-test results were subtracted from post-test results and compared statistically using a 2-way mixed ANOVA ($p<0.05$).

RESULTS AND DISCUSSION

The 2-way mixed ANOVA revealed no significant main effects of group or shod condition in the static and dynamic balance tasks (Table 1). Individual differences from the single-leg wobble board task in the intervention group revealed the 6 participants with the highest ML stability index score (>4.0) at pre-test whilst barefoot had improved balance at post-test (≥1.0). No trends were observed in the shod condition in the intervention group or either footwear condition in the control group. This implies that the wobble board task could detect barefoot balance improvement after SFE training in team sports players with worse balance. In the single-leg static balance task, no such individual improvements were observed. This balance test may have not been challenging enough to reveal balance ability differences in this sports population. The SEBT revealed similar results, with no observable improvements in both groups, regardless of shod condition. SEBT performance varies due to sport, playing ability experience and so this could have had a factor in this current multi-sport study [5].

Table 1. The difference in the pre and post-test results for the balance test across groups and shod condition. Data is presented as mean (S.D.); a positive value represents an improvement in the SD ML velocity of and SEBT reach distance. A negative value represents an improvement in the stability index

	Barefoot		Shod	
	Control	Intervention	Control	Intervention
ML Velocity SD	1.37 (2.40)	1.42 (12.9)	0.39 (4.64)	4.94 (19.6)
Normalised Reach Distance - (%)	3.05 (8.72)	3.56 (8.04)	1.76 (5.77)	2.96 (6.79)
ML Stability Index – (au)	-0.16 (1.05)	-0.99 (1.15)	-0.34 (1.38)	-0.07 (1.74)

CONCLUSIONS

Short foot IFM training did not elicit improvements in barefoot or shod balance performance in healthy, team sports players after a 6-week intervention. Future research should consider the use of more sensitive metrics, a progressive overload approach to the training and focus on individuals with poor balance.

REFERENCES

[1] McKeon P et al. *B. J. Spor. Med*. **49**: 290-299, 2015.
[2] Lynn S et al. *J. Spor. Rehab*. **21**: 327-333, 2012.
[3] Jakobsen M et al. *Eur. J. Appl. Physiol.* **111** : 521-530, 2011.
[4] Arnold B et al. *J. Athl. Train*. **33**: 323-327, 2021.
[5] Stiffler M et al. *J. Orth. & Spor. Phys*. Ther. **45**: 772-780, 2015.

Lumbar and Pelvis Movement Comparison between Cross-court and Long-line Topspin Forehand Stroke: Based on Musculoskeletal Model

Yuqi He[1,2,3], Zixiang Gao[1,2,3], Gusztáv Fekete[2], András Kovács[3], Aleksandar Nedeljkovic[4], Dusan Mitic[4], and Yaodong Gu[1]

[1] Faculty of Sports Science, Ningbo University, Ningbo, China.
[2] Savaria Institute of Technology, Eötvös Loránd University, Szombathely, Hungary.
[3] Faculty of Engineering, University of Pannonia, Veszprém, Hungary.
[4] Faculty of Sport and Physical Education, University of Belgrade, Serbia.
Email: heyuqi0809@outlook.com

INTRODUCTION

Due to the critical role of lumbar and pelvis movement on the axial rotation of the trunk rotation and hitting speed, pelvis movement plays a crucial role in powerful hitting sports, such as table tennis, tennis, and baseball [1]. Players need to increase the acceleration of their playing hand by optimizing their stroke skill and the efficiency of the power chain transmission, which brings gains to the spin effect and flight speed of the ball during the topspin forehand [2]. The cross-court (CC) and long-line (LL) topspin forehand, as the basic strokes in racket sports, have been widely studied not only in table tennis but also in tennis. The purpose of this study was simulation the musculoskeletal model in the OpenSim software to investigate the difference in lumbar and pelvis movements between CC and LL topspin forehand strokes in table tennis.

METHODS

Sixteen male table tennis athletes (Height: 1.73±0.03 m; Age: 22.89±2.03 y; BMI: 23.45±0.69 kg/m^2; Experience: 8.33±0.71 y) performed CC and LL topspin forehand to return the ball from the coach. The kinematics and kinetics of the trunk and lower limb were recorded by the Vicon motion capture and Kistler force platform. Input the data to OpenSim and establish the Giat2392 musculoskeletal model for simulation. The one-dimensional statistical parametric mapping (SPM1d) and independent samples t-test was performed in MATLAB and SPSS to analyze the kinematics and kinetics. LAR indicates lumbar axial rotation, LLB indicates lumbar left lateral bending, LF indicates lumbar flexion, and PAR indicates pelvis axial rotation.

RESULTS AND DISCUSSION

As shown in Figure 1 and Figure 2, the key finding of this study was (1) the main difference between CC and LL topspin forehand in the lumbar movement was found in the LLB and LF, the Rom, peak moment, and maximum angle of the LLB and LF in CC were significantly higher than LL; (2) the Rom, peak moment, and maximum angle of PAR in CC were significantly higher than LL; (3) the moment of LL in the LF and LLB was significantly higher than CC in the early stroke phase.

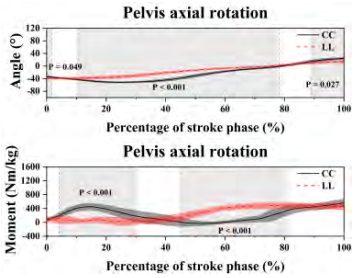

Figure 1 Illustration of the angle and moment of the PAR between the CC and LL topspin forehand. Grey-shaded areas indicate significant differences ($p < 0.05$).

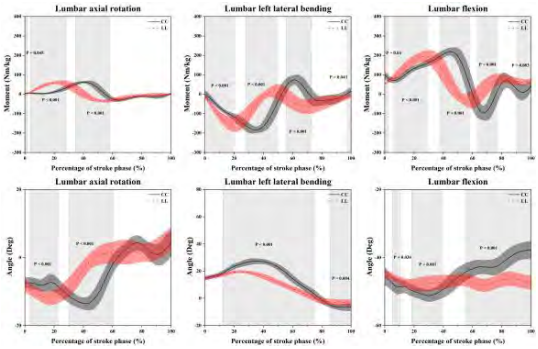

Figure 2 Illustration of the angle and moment in the lumbar and pelvis between the CC and LL. Grey-shaded areas indicate significant differences ($p < 0.05$).

CONCLUSIONS

Players could enhance the motor control of lumbar and pelvis movements, either by enhancing core strength to improve the explosive power of lumbar and pelvis movements or by flexibility training to enhance lumbar and pelvis synergy, as these modalities are able to enhance the level of energy transfer in the power chain and improve performance. Beginners could quickly understand the role and contribution of the lumbar and pelvis in topspin forehand skills based on the results of this study, thus making it easier to master CC and LL topspin forehand skills.

ACKNOWLEDGEMENTS

This study was sponsored by the China Scholarship Council (CSC NO.202108330001).

REFERENCES

[1] Akutagawa S et al. *J Sports Sci* **23**: 781-93, 2005.
[2] He Y et al. *J Sports Sci Med* **19**: 522-8, 2020.

Influence of Release Positions on Optimal Release Conditions in Basketball

Yuki Inaba[1], Noriko Hakamada[1], and Munenori Murata[2]
[1] Department of Sport Science and Research, Japan Institute of Sport Science, Tokyo, Japan.
[2] Faculty of Sports and Life Science, National Institute of Fitness and Sports in KANOYA, Kagoshima, Japan.
Email: yuki.inaba@jpnsport.go.jp

INTRODUCTION

In recent National Basketball Association (NBA) games, the number of mid-range two-point shots and three-point shots have reversed; the percentage of mid-range shots decreased from 31% in the 2010-11 season to 13% in the 2020-21 season while those of three-point shots increased from 22% to 39% [1]. Furthermore, although the three-point shot distance for NBA is set at 7.24 m, many shots are currently attempted far behind the three-point line. However, release conditions such as the release speed and release angle that are required for making those shots from long distances have not been reported elsewhere. Additionally, the influence of release height on release conditions for different shot distances is of our interest because each player's body size and physical fitness varies. Although it has been reported that a higher release height is advantageous in terms of shot probability in free-throw shots [2,3], the influence of release height in long shots has not been investigated. Therefore, the purpose of this study is to investigate optimal release conditions by assuming shooting distances in line with recent basketball trends and release heights that consider various physical characteristics of players. Specifically, the influences of the release height and shot distance on the optimal release angle and release speed were quantified.

METHODS

The ball trajectories after release from different heights and distances were simulated using the fourth order Runge-Kutta algorithm. The equation of motion of the ball in air was formulated by considering the air drag and lift force. The spin rate, coefficient of air drag, and coefficient of lift force were fixed at 117 rpm, 0.20, and 0.16, respectively, based on the experimental data obtained by motion analysis of three-point shots by ten male collegiate basketball players. Release height, position, speed, and angles varied from 1.5 m to 3.5 m, from 2.0 m to 12.0 m, from 3.0 m/s to 15.0 m/s, and from 30.0 deg to 65.0 deg, respectively. The shot success was judged based on the ball arrival position at the height of the goal ring, or 3.05 m from the floor; if the position was where it could go through the ring without touching the rim, it was regarded as a success. The minimum-speed angle [2] and the average release speed at the minimum-speed angle were calculated for each condition of release height and distance, and regarded as the optimal release condition.

RESULTS AND DISCUSSION

The influence of the release height and shot distance on the minimum-speed angle and the release speed at the minimum-speed angle were observed. In the three-point shot (7.24 m distance) condition, for example, as the release height increased from 1.5 m to 3.5 m, both minimum-speed angle and the release speed at the minimum-speed angle decreased (Figure 1). In addition, the area of successful shot combination of the release speed and release angle was larger at higher release heights, especially at a lower release angle and release speed.

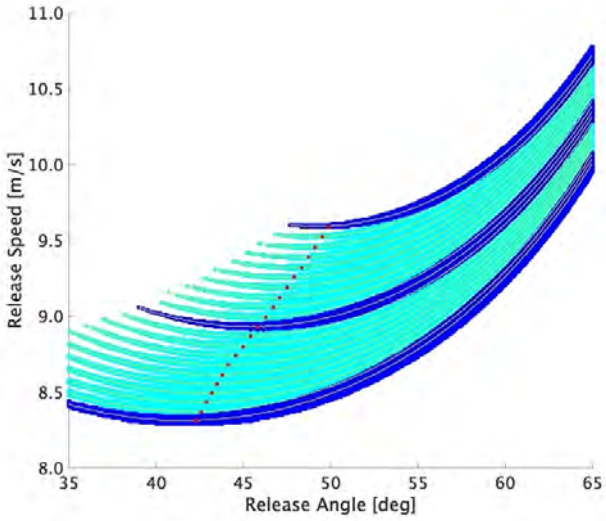

Figure 1 The combination of release angle and speed which results in successful shots from various release height from 1.5 m to 3.5 m in shots from 7.24 m distance are shown in blue (dark blue at the top is the one from the lowest release height 1.5 m, in the middle is from 2.5 m, at the bottom is from 3.5 m, and the ones between those release height are shown in light blue). The red dots show the minimum-speed release angle for each condition.

CONCLUSIONS

The optimal release speed and angle differ depending on the release height and shot distance, which should be considered for efficient coaching and practice.

ACKNOWLEDGEMENTS

This work was supported by JSPS KAKENHI (grant number 18K17848).

REFERENCES

[1] Schuhmann J. *https://www.nba.com/news/3-point-era-nba-75,* 2021.
[2] Brancazio P. *Am J Phys* **49(4)**,1981.
[3] Tran C et al. *J Sport Sci* **26(11)**, 2008.

THE INFLUENCE OF POCKET CHARACTERISTICS ON LACROSSE SHOT PERFORMANCE

Scott Dominey, Dean C. Hay
School of Physical and Health Education, Nipissing University, North Bay, Canada.
Email: deanh@nipissingu.ca

INTRODUCTION

The effect of pocket design on ball accuracy and velocity in lacrosse is not well researched. Ball velocity is greater than estimated using a rigid body stick model [1], suggesting the shape of the pocket can affect performance. Whip, defined as the pocket shape responsible for changing the resistance of the ball as it releases, can be altered by adjusting the pocket strings. Anecdotally, higher whip holds the ball in the pocket longer, resulting in greater throwing velocity. Conversely, lower whip is thought to release the ball earlier in the throwing motion [2]. In this study, the effect of whip on ball accuracy and velocity was tested using two overhand throwing techniques.

METHODS

Fourteen varsity male lacrosse players (21.6 yr ± 3.0; 180 cm ± 8.7; 84.1 kg ± 14.0; mean ± SD) gave their informed consent to participate in this study (NUREB102710). Ball, stick, and participant kinematics were recorded at 300 Hz with a 15 camera passive-marker system (Qualisys, Sweden).

Evo Warp Pro 2 sticks (Warrior, USA) with Whip 1, Whip 2, and Whip 3 heads, along with each participant's personal stick were used in counterbalanced order for the static (throwing motion with limited lower body movement) and dynamic (throwing motion with a stepping sequence) throws. Three trials were completed for each condition, resulting in 24 total trials per participant. Participants were instructed to throw the ball as hard and as accurately as possible at a target located ≈ 2.5 m in front of the participant at a height of 1.02 m.

Repeated-measures ANOVAs (type of throw x whip) were used to test for significant (α = .05) differences in ball velocity and accuracy. The mean values of the three throws for each condition were used in the analyses.

RESULTS AND DISCUSSION

For throwing velocity, significant main effects for type of throw (p < .001, $\eta 2$ = .479) and whip (p < .001, $\eta 2$ = .849) were found. Significant (p < .05) differences were found between Whip 1 and Whip 3; Whip 2 and Whip 3; and Whip 1 and Personal Stick (Table 1). For throwing accuracy, a significant main effect of whip on mean resultant error (p < .001, $\eta 2$ = .557) was found. Significant differences were identified between Whip 1 and Whip 2; Whip 1 and Whip 3; and Whip 1 and Personal Stick (Figure 1).

Higher whip resulted in increased throwing velocity and accuracy. These trends were consistent between the dynamic and static throwing techniques and suggest that pocket design can significantly impact throwing performance [1].

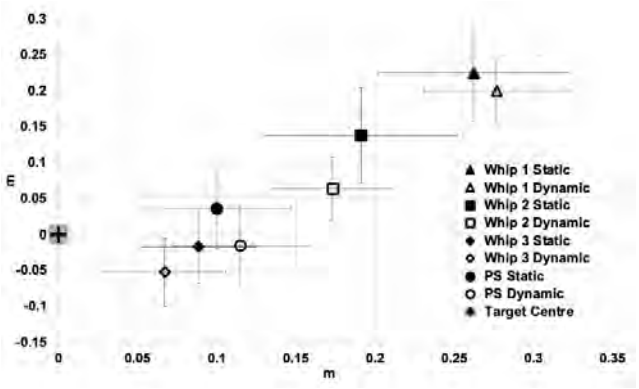

Figure 1 Throwing accuracy of different whips for static and dynamic lacrosse shots (means ± 95% CI).

CONCLUSIONS

Lacrosse sticks with a higher whip pocket produced greater ball velocity and greater accuracy. As experienced players tend to use a relatively high whip level in their personal stick, it was likely that they were able to match their release point for accurate throws with the Whip 3 stick. Conversely, with a low whip stick, the players had difficulty adjusting their release point, resulting in shots landing high and right of the target. An analysis of stick angle at release found significant differences between conditions that support our conclusions. These trends were consistent between throwing techniques.

REFERENCES

[1] Crisco JJ et al. *J Appl Biomech* **25**: 184-191, 2009.
[2] Warrior.com, retrieved 2022.

Table 1: Throwing velocity of different whips for static and dynamic lacrosse shots (means ± 95% CI).

Type of Throw	Whip 1	Whip 2	Whip 3	Personal Stick
Static	28.8 ± 1.9	29.4 ± 1.8	31.1 ± 2.3	30.5 ± 1.9
Dynamic	30.2 ± 1.8	31.3 ± 1.6	32.5 ± 2.0	32.2 ± 2.2

SIMULATED KNEE MECHANICS DURING A MAXIMAL FORWARD BRAKING AND BACKWARD ACCELERATION IN ELITE ATHLETES

Rodrigo B. Mateus[1], Colin R. Smith[2], Ventura Ferrer-Roca[3], António P. Veloso[1]
[1] CIPER, Faculty of Human Kinetics, University of Lisbon, Cruz Quebrada, Portugal
[2] Steadman Philippon Research Institute, Vail, Colorado, USA
[3] High Performance Center (CAR), Sant Cugat del Valles, Spain
Email: rodrigomateus@fmh.ulisboa.pt

INTRODUCTION

In professional sports, when deceleration tasks are inappropriately performed, the resulting mechanical loads at the knee joint can increase risk of injury. Greater insight into soft tissue loading mechanisms is therefore essential for investigating the causes of injuries in elite sports. To this end, the goal of this work is the study of knee mechanics whilst performing maximal forward braking and backward acceleration in elite athletes.

METHODS

Fourteen injury-free elite male team-sports athletes participated in this study (age:22 ± 4 years, height:185 ± 4 cm, mass:77 ± 11 kg). Biomechanical data were collected using 8 infrared cameras (Qualisys) at a frequency of 300Hz and 2 force plates (Kistler). Musculoskeletal modelling was performed using a scaled version of the model from Lenhart [1]. The motion analysis measurements were input to the COMAK algorithm to predict muscle forces, secondary knee kinematics, ligament forces and cartilage contact pressures [2].

RESULTS AND DISCUSSION

The *vasti* produced the largest forces, with an early peak while absorbing impact during braking and a late peak while propelling the body to through the backward acceleration phase of the movement (Figure 1-(A)). Patellar Tendon (PT) loading demonstrates a similar double peak, whereas, the ACL is loaded during the backward acceleration phase of the movement, peaking slightly below 2160N, the ultimate failure load of an intact ACL (Figure 1-(B)) [3]. These findings can be explained by the presence of a posteriorly directed ground reaction force during this task, which fixes the foot and tibia to the floor and thus the inertia of the body causes the femur to translate anteriorly and protect the ACL by counteracting the strain produced by the eccentric contraction of the *vasti* [4]. Also, when the knee is flexed beyond 60º, the PT is oriented posteriorly relative to tibia, so the PT force would off-load ACL. During the second phase, the loading of the ACL may occur due to trunk and knee extension. Contact forces of the tibiofemoral (TF) and patellofemoral (PF) joints (Figure 1- (C);(D)) reflect the GRF and *vasti* force profiles. Two peaks in the TF joint were measured during the braking phase, with the majority of the first peak occurring on the lateral compartment, and the second on the medial compartment.

CONCLUSIONS

This work leveraged musculoskeletal simulation to gain a comprehensive understanding of knee mechanics during maximal forward braking and backward acceleration. The lack of ACL loading during braking is an interesting finding and can inform rehabilitation programs.

ACKNOWLEDGEMENTS

This work was supported by CIPER-FCT (I&D unit 447, project reference UIDB / 00447/2020), and FCT (Ph.D. grant reference DFA/BD/7356/2020).

REFERENCES

[1] Lenhart, *Ann. Biomed. Eng* **43**:2675–2685, 2015.
[2] https://simtk.org/projects/opensim-jam
[3] Dargel et al. *Strat. Trau Limb Reconstr* **2**:1–12, 2007
[4] Shin et al. *J Biomech* **40**: 1145-1152, 2007.

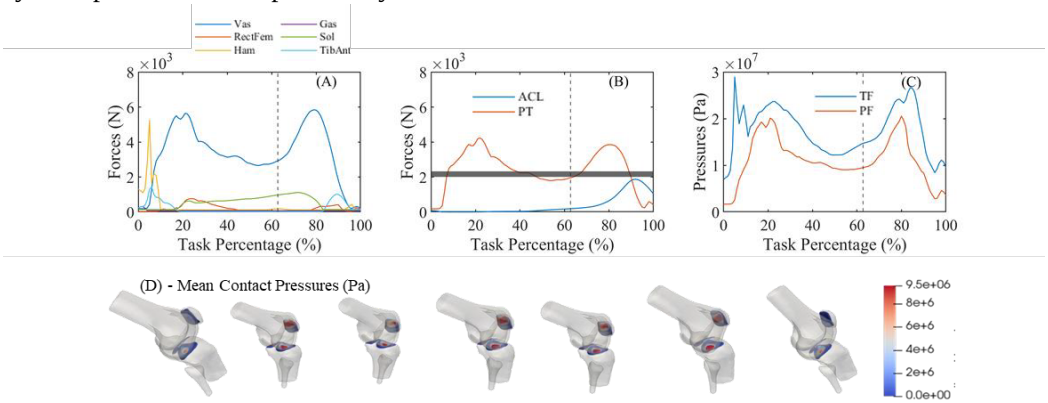

Figure 1. Simulated knee mechanics during a maximal forward braking and backward acceleration task, of one subject (mass = 80.9 Kg).

NEUROMUSCULAR EFFECT OF WARM-UP ON REGULATION OF MOTOR UNIT PROPERTIES DURING ISOMETRIC TORQUE PRODUCTION TASKS

Jiseop Lee[1], Dawon Park[1], Joo-Young Lee[3,5], Byung Hee Hong[4,5], and Jaebum Park [1,2,5]

[1] Department of Physical Education, Seoul National University, Seoul, South Korea.
[2] Institute for Sports Science, Seoul National University, Seoul, South Korea.
[3]Department of Textiles, Merchandising and Fashion Design, Seoul, South Korea
[4]Department of Chemistry, Seoul, South Korea
[5]Advanced Institute of Convergence Technology, Seoul National University, Seoul, South Korea
Email: auburnjiseop@snu.ac.kr; parkpe95@snu.ac.kr

INTRODUCTION

The warm-up exercise is assumed to be a well-discovered and applied methodology for enhancing muscle force generation. Remarkably, little is known about the neuromuscular mechanism of the warm-up exercise at the level of the motor unit within a muscle. The activation components of motor units are assumed to be regulated by the central nervous system (CNS), including the firing rate and recruitment threshold (i.e., order of the recruitment) [1]. The current experiment attempted to observe the changes in the two components of motor units after the established protocol of the warm-up exercise in an isometric condition of muscle force generation.

METHODS

Fifteen healthy subjects were recruited, and they performed isometric maximal voluntary torque (MVT) production by the elbow joint. The experimental conditions included elbow flexion and extension with two joint angles, 10° and 90°. The trajectories followed a ramp contraction. They increased at a rate of 10% MVT/s and were sustained at 100% MVT for 4 s. The same experiments were done before and after the warm-up exercise. The warm-up protocol for the muscle of the elbow flexor and extensor complied with the ACSM guideline. In particular, the index of the warm-up effect was the gross body temperature (i.e., the increment by about 6%). The decomposition EMG system was employed to identify multiple motor units using a specialized surface EMG electrode and placed on the biceps brachill (BB) and triceps brachii (TB) muscles. Further, the isometric machine was used to record biomechanical signals (i.e., torque and joint angle).

RESULTS AND DISCUSSION

Isometric elbow flexion and extension torques were increased significantly after the warm-up exercise for both 10° and 90° of elbow angle ($p < 0.001$), which were associated with the recruitments of higher threshold motor units after the warm-up exercise (Figure 1). Also, the firing rates of motor units observed in the same threshold were larger with the warm-up exercise (i.e., scaled-up and elongated regression line after the warm-up exercise in Figure 1) [2].

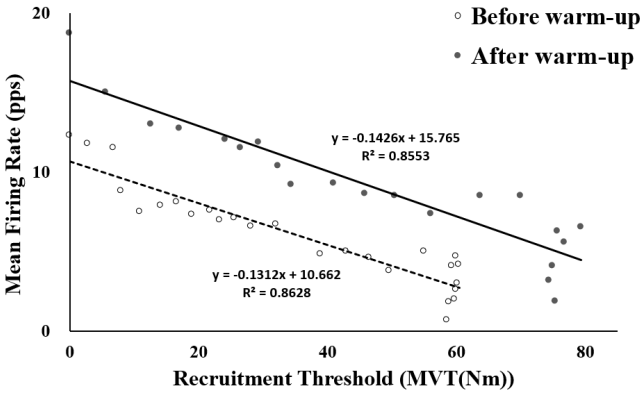

Figure 1. Linear regression line showing the relationship between the mean firing rate and the recruitment threshold for a representative subject.

These results were further associated with significant increments of power spectral densities of the gamma band (35-60 Hz), especially in the relatively large motor units ($p < 0.0001$).

CONCLUSIONS

The current results confirmed the fact that the warm-up exercise causes changes in the neuromuscular components of the motor units within muscles in such a way that the firing rate of the recruited motor unit was increased. In addition, the warm-up exercise seemed to be associated with the recruitment of large motor units (e.g., Type II, fast-twitch motor units) with larger spectra power at the frequency band of the voluntary contraction (35~60Hz).

ACKNOWLEDGEMENTS

This research was supported in part by the Basic Research Program through the National Research Foundation of Korea (NRF), funded by the MSIT (2022R1A4A503404611), and Basic Science Research Program through the National Research Foundation of Korea (NRF) funded by the Ministry of Education (2022R1A6A3A13073107)

REFERENCES

[1] De Luca & Contessa. *J Biomech* **48**: 195-203, 2015.
[2] De Luca & Contessa. *J Neurophysiol* **107**.1: 178-195, 2012.

Effects of Speeds on Ground Reaction Forces during Skipping Gait

Genki Tokuda[1], Toshiki Uchiyama[1] and Hiroaki Hobara[2]
[1] Graduate School of Advanced Engineering, Tokyo University of Science, Tokyo, Japan.
[2] Faculty of Advanced Engineering, Tokyo University of Science, Tokyo, Japan.
Email: 8219080@ed.tus.ac.jp

INTRODUCTION

Skipping has a double support phase as displayed during walking but it also incorporates a flight phase as observed in running. Although a simulation study demonstrated that skipping gait was stable over a wide speed range [1], very few studies have experimentally verified the effects of speed on skipping gait mechanics. Especially, the ground reaction forces (GRFs), which are defined as the force exerted by the ground on a body in contact with it, are known as fundamental gait parameters used in biomechanics. Thus, the aim of the present study was to investigate the effects of speeds on the GRF parameters during skipping gait.

METHODS

Ten healthy male subjects without musculoskeletal impairments performed bilateral skipping gait on an instrumented treadmill (FTMH-1244WA, Tec Gihan, Kyoto, Japan) at 10 speeds (2.0–11.0 km/h with increments of 1.0 km/h). We collected ground reaction forces (GRFs) from the instrumented treadmill at 1000 Hz. We determined four peak values of anteroposterior GRF, and two peak values of vertical GRF (Fig. 1-A). Negative peak values of anteroposterior GRFs (F_{Y1}, F_{Y3}) were defined as the minimum GRF in the range of 0% to 30% and 30% to 70% stance, respectively. Positive peak values of anteroposterior GRF (F_{Y2}, F_{Y4}) were defined as the maximum GRF in the range of 30% to 70% and 70% to 100% stance, respectively. The peak values of vertical GRF (F_{Z1}, F_{Z2}) were defined as the maximum ground reaction force in the range of 0% to 50% and 50% to 100% stance, respectively. The Shapiro–Wilk test was used to confirm data normality. Then, we used one-way repeated measures ANOVA (10 levels) and a post-hoc comparison when the data were normally distributed. If the data were not normally distributed, the Friedman test (10 levels) and a Wilcoxon signed rank test were used. Statistical significance was set at $p < 0.05$.

RESULTS AND DISCUSSION

Initial peak braking GRF (F_{Y1}) increased with increasing belt speed (Fig. 1-B), but midstance braking GRF (F_{Y3}) decreased from 2.0 km/h to 6.0 km/h and kept constant afterward (Fig. 1-B). Initial propulsive GRF (F_{Y2}) increased from 2.0 km/h to 7.0 km/h but it kept similar values until the top speeds (Fig. 1-C). Propulsive GRF at the terminal stance (F_{Y4}) was nearly zero until 6.0 km/h, but it significantly increased from 7.0 km/h to 11.0 km/h (Fig. 1-C). The peak vertical GRF (F_{Z1} and F_{Z2}) increased with increasing belt speeds, respectively (Fig. 1-D). A previous study approximated the skipping gait using a simple bipedal spring-loaded inverted pendulum model [1]. The GRF patterns in their study were similar to the current results. Further, the previous study suggests that anteroposterior GRFs at the earlier (F_{Y1} and F_{Y2}) and later half (F_{Y3} and F_{Y4}) of the stance were related to the trailing limb, and the leading limb, respectively. Thus, the main propulsive force of the skip is provided by the trailing limb, and the leading limb also exerts a propulsive force from 7.0 km/h to adapt to speed increments. The increase in peak vertical GRF (F_{Z1} and F_{Z2}) can be attributed to the decrease in stance time and the increase in flight time.

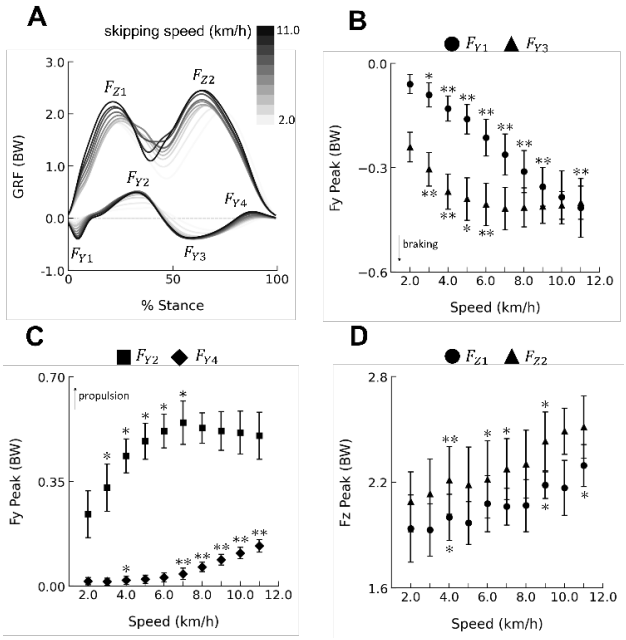

Figure 1. A) Averaged trace of vertical and anteroposterior GRFs of all speeds. B) Peaks of anteroposterior GRF (braking function, F_{Y1} and F_{Y3}). C) Peaks of anteroposterior GRF (propulsive function, F_{Y2} and F_{Y4}). D) Peaks of GRF (F_{Z1} and F_{Z2}). Asterisks (*, **) indicate significant differences from previous speeds at $p < 0.05$, and 0.01, respectively.

CONCLUSIONS

The results of the present study suggest that the skipping GRFs vary according to changes in speeds.

ACKNOWLEDGEMENTS

We appreciate all subjects who participated in the study.

REFERENCES

[1] Andrada et al. *R Soc opensci* **3**: 160602, 2016.

NEUROMUSCULAR RESPONSES TO UNEXPECTED SLIPS DURING HUMAN WALKING

India Lindemann[1], Taylor Dick[1]
[1] School of Biomedical Sciences, Faculty of Medicine, University of Queensland, Australia
Email: uqilinde@uq.edu.au

INTRODUCTION

Falls result in over 680,000 deaths worldwide each year [1]. Understanding how humans maintain balance to stay upright during movement in the face of unpredictable environments is thus of critical importance to public health. Perturbation experiments largely extrapolate muscle dynamics from joint kinematics, rather than through *in vivo* measurements. Previous results from perturbed hopping showed that co-activation of the ankle plantarflexors and dorsiflexors enables favourable plantarflexor muscle dynamics for perturbation recovery [2]. However, measures of how both agonist and antagonist muscles behave *in vivo* during unexpected perturbations remains unknown. The aim of this study is to determine how neuromuscular control and muscle–tendon dynamics are modulated in the ankle plantarflexors and dorsiflexors to maintain stability during unexpected slip-induced perturbations to human walking.

METHODS

Fifteen young adults (23.3±3.5 yrs; 8 males, 7 females) participated in the study. Slip perturbations were delivered by rapidly accelerating and decelerating the right belt of a split-belt instrumented treadmill over 50% of the stance phase duration to 0.7 m s^{-1} above their preferred walking speed (Fig 1B). During the perturbations, lower limb kinematics and kinetics were obtained using 3D motion capture (Qualisys) and force plates (Bertec); muscle activity in the triceps surae and tibialis anterior (TA) using surface electromyography (Trigno Delsys); and fascicle lengths in the medial gastrocnemius (MG) and TA using dual probe B-mode ultrasound (ArtUS, Telemed). Comparisons in muscle activation and fascicle dynamics were made between normal walking, the perturbation, and the recovery step (one step after perturbation). Preliminary analysis (n=3) is presented here.

RESULTS AND DISCUSSION

The perturbation led to a reduction in stance time of the perturbed limb and an increase in peak ground reaction force (GRF) in the second half of stance after belt velocity had peaked. Stance time also decreased in the non-perturbed limb in the recovery step following the perturbation. Plantarflexor (MG, LG, SOL) and dorsiflexor (TA) muscle activity increased during the perturbation compared to normal walking (Fig. 1A). During the perturbation, TA fascicles underwent a brief period of lengthening, followed by active shortening whilst the MG fascicles shortened for the duration of the perturbation (Fig. 1B). This coactivation of the ankle plantarflexors and dorsiflexors enabled fascicle length changes to behave 'in phase' (i.e. both shortening) as opposed to out of phase behaviour present during normal walking. Stretch reflexes in the TA may be responsible for altered muscle behaviour during the initial phase of the slip to enable successful balance recovery.

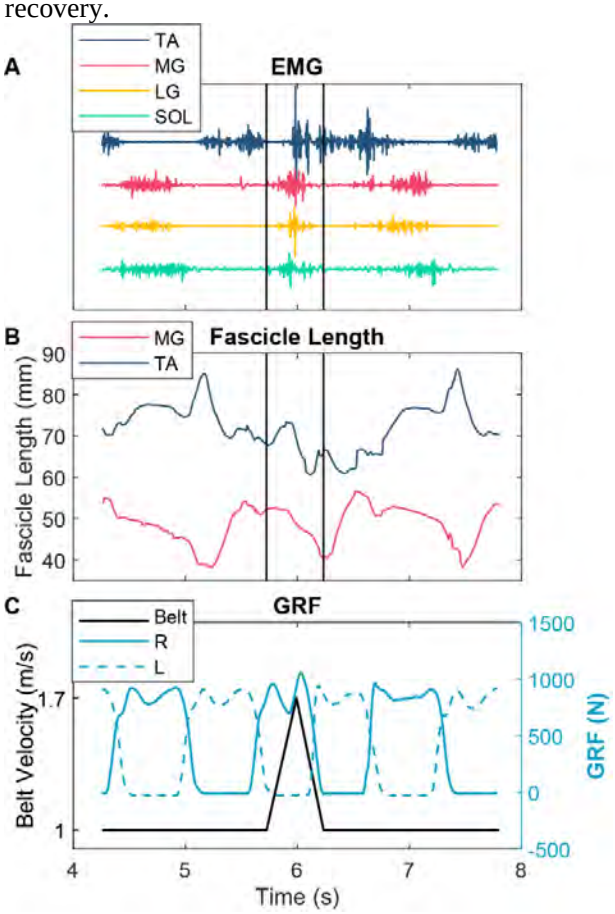

Figure 1 Measures for the perturbed step and one step either side are presented from one slip trial. EMG traces are shown for the tibialis anterior (TA), medial (MG) and lateral gastrocnemius (LG), and soleus (SOL) (A), as are fascicle lengths of the MG and TA (B). GRFs are shown with the belt velocity, illustrating the timing and strength of the slip perturbation (C)

CONCLUSIONS

Our preliminary results suggest that a muscle-based latch mechanism may mediate the perturbation response via sensory feedback. Further analysis will determine the generality of these results in the larger sample of participants for which we have collected data (n=15).

REFERENCES

[1] World Health Organization, 2021
[2] Dick et al. *Proc Royal Soc B* **288**(1947): 20210201, 2021

The differences in the characteristics of the body part angular momentum in the frontal plane during walking between young and older adults

Kodai Kawase[1], Shoma Kudo[2], Takahiko Sato[3], and Akinori Nagano[4]
[1] Graduate School of Sport and Health Science, Ritsumeikan / Shiga, Japan.
[2] National Institute of Advanced Industrial Science and Technology / Chiba, Japan.
[3] Faculty of Rehabilitation, Biwako Professional University of Rehabilitation / Shiga, Japan.
[4] Faculty of Sport and Health Science, Ritsumeikan / Shiga, Japan.
Email: gr0469ih@ed.ritsumei.ac.jp

INTRODUCTION

Whole-body angular momentum (WBAM) about the whole-body center of mass has often been used to investigate dynamic balance during walking [1]. WBAM on the frontal plane changes periodically during walking, and its amplitude is larger in older adults than younger adults [2]. The larger amplitude suggests that older adults walk with a larger postural sway in the mediolateral direction. However, it remains unclear which body parts mostly affect the age-related difference in WBAM during walking. Such knowledge can provide a better understanding of the underlying mechanisms of dynamic balance regulation in older adults during walking. Therefore, the purpose of this study was to investigate the age-related differences in the body part angular momentum (BPAM) during walking between young and older adults.

METHODS

Kinematic data in AIST Gait Database 2019 provided by National Institute of Advanced Industrial Science and Technology in Japan were used for data analysis in this study [3]. 50 young (Age: 26.8±5.4) and 78 older adults (Age: 67.7±3.3) were randomly chosen from the database, and five separate walking data from each of them were utilized for the analysis.

The whole body of the participant was modelled with 15 linked rigid-body segments based on the coordinate data of 42 markers. BPAM and WBAM on the frontal plane during walking were calculated. The postural sway during walking was evaluated by the maximum WBAM about the whole-body center of mass during a stride cycle. The angular momentum of each segment was categorized into five BPAMs: the right and left legs (foot, shank, and thigh), right and left arms (hand, forearm, and upper arm), and torso (head, thorax, and pelvis). The frame in which the WBAM was maximum during the stride cycle was used to calculate the five BPAMs. WBAM and BPAMs were normalized by a square of body height and the whole-body mass.

WBAM and BPAMs over five strides of each participant were used to calculate the average of WBAM and BPAMs of each participant. An independent sample t-test was used to compare the average values of WBAM and BPAMs between young and older adults. The significance level was set at 0.05.

RESULTS AND DISCUSSION

The maximum WBAM in older adults was significantly larger than that in young adults ($p<0.001$, Figure1). This result indicates that older adults walked with a larger postural sway in the mediolateral direction, and this result was consistent with the previous study [2]. BPAM of the left leg, left arm, and torso in older adults were significantly larger than those in young adults ($p=0.014$, $p=0.004$, $p<0.001$, Figure 1). These results indicate that the age-related difference in WBAM during walking is caused by the larger angular momentum of the left leg, left arm, and torso in older adults. A previous study reported that the hip abductor muscle was important for the regulation of WBAM, and this muscle torque was a deficit in older adults [4] [5]. The age-related difference in BPAMs during walking could be caused by age-related deficits in joint torque especially of the hip.

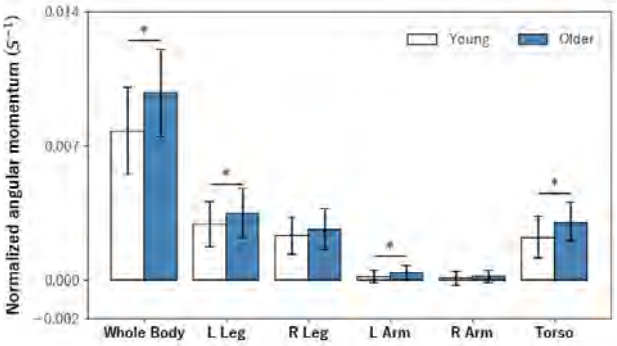

Figure 1 The maximum WBAM and five BPAMs (*: $p<0.05$)

CONCLUSIONS

The age-related difference in WBAM during walking was caused by the large angular momentum of the left leg, left arm, and torso in order adults. The findings in this research would be useful to program an effective intervention for improving the dynamic balance during walking in older adults.

ACKNOWLEDGEMENTS

This work was supported by JST SPRING, Grant Number JPMJSP2101.

REFERENCES

[1] Vistamehr A et al. *J Biomech* **49**: 396-400, 2016.
[2] Vistamehr A et al. *J Biomech* **128**: 110717, 2021.
[3] Kobayashi Y et al. AIST Gait Database 2019, 2019.
[4] Neptune RR et al., *J Biomech* **49**: 2975-2981, 2016
[5] Inacio M et al., *J Biomech* **82**: 244-250, 2019

Pendular energy exchange at very slow walking speeds reveal positive work shift from double support to single stance

Timothy K. Byles-Ho[1] and Amy R. Wu [1]

[1] Department of Mechanical and Materials Engineering, Queen's University, Kingston, Canada.
Email: 16tkbh@queensu.ca, amy.wu@queensu.ca

INTRODUCTION

Humans need to expend energy to walk. Previous research has found that taking advantage of the energy transfer between kinetic and gravitational potential energy could reduce the amount of mechanical energy expended during gait. By calculating the phase shifts between kinetic and potential energy curves, Cavagna et al. (2020) demonstrated that the optimal speed is 1.6 m/s, which was the speed that required the least mechanical energy to maintain steady-state gait [1].

Aging, neurological deficits, or lower limb injuries can lead to walking at slower speeds [2]. Investigations of energy exchange could help improve our understanding of the mechanics of walking, such as whether dynamic walking breaks down at very slow speeds. Prior research has captured energy phase shifts at normal speeds, however it is unclear how the phase shift behaves at slower speeds. We aimed to measure the phase shift between kinetic and gravitational potential energy at very slow speeds (<0.5 m/s). We hypothesized that as speed decreased, the kinetic and gravitational potential energy would move further out of phase.

METHODS

We used slow walking data from a public dataset [2]. Eight subjects walked on an instrumented treadmill at prescribed speeds of 0.4, 1.2, 1.8, 2.2 km/h (denoted here as 0.11, 0.33, 0.50, and 0.61 m/s) and at a self-selected speed. The position and velocity of the body centre of mass (BCOM) was determined using a double integration of force platform data [3]. From the BCOM position and velocity data, kinetic energy and gravitational potential energy were calculated per stride.

We determined the phase shifts for each speed using the method proposed by Cavagna et al. (2020) [1]. Ground reaction forces were used to separate each stride into single stance and double support phases. The α phase shift was measured during double support (Equation 1):

$$\alpha = 360 * \frac{t_{pk+}}{\tau} \qquad (1)$$

where τ is step time and t_{pk+} is the time between maximum kinetic energy and minimum gravitational potential energy. The β phase shift was measured during single stance (Equation 2):

$$\beta = 360 * \frac{t_{pk-}}{\tau} \qquad (2)$$

where t_{pk-} is the time between maximum potential energy and minimum kinetic energy during single stance [1]. We performed a t-test on the mean values of α and β across all subjects to determine if the mean values were significantly different from zero.

RESULTS AND DISCUSSION

As speed decreased, α remained positive until the slowest speed of 0.11 m/s (Figure 1). The β values followed a similar trend, changing from positive to negative at the slowest speed. All shifts were significantly different from zero ($p<0.05$). The α and β values at the fastest two speeds (0.61 m/s and self-selected) were comparable to Cavagna et al. (2020) [1].

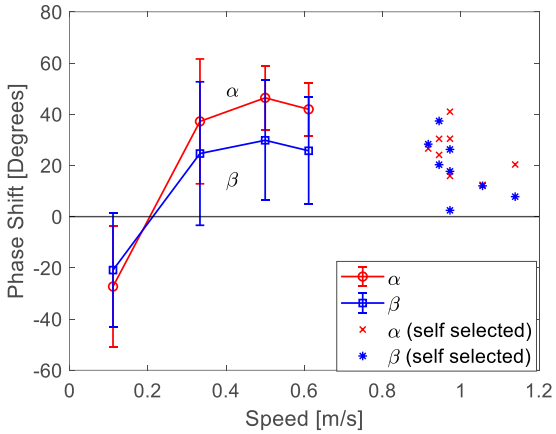

Figure 1 Phase shifts α and β as a function of speed. Average α (circles), β (squares), and s.d. bars shown for each speed except for self-selected, where individual subject means are shown.

A positive α indicates that positive work was done during double support to accelerate the body while a positive β indicates that negative work was being performed during single stance [1]. At very low speeds (~0.2 m/s), both phase shifts become negative. Our finding suggests that at extremely slow speeds, positive work is required during single stance, possibly due to a reduction in pendular dynamics. In contrast, less positive work is required during single stance at faster speeds due to the pendular exchange of energy [1]. One limitation that necessitates further research is the increased variability observed in both phase shift values as speed decreased, likely derived from varying methods of walking very slowly among subjects.

CONCLUSIONS

At very slow speeds, humans seem less able to take advantage of pendular dynamics and need to rely more on mechanical energy added during single stance to maintain steady-state gait.

ACKNOWLEDGEMENTS

NSERC Discovery Grant, Ingenuity Labs

REFERENCES

[1] Cavagna GA and Legramandi MA. *J Exp Biol* **223** (21), 2020
[2] Wu AR et al. *Sci Rep* **9**: 18079-10, 2019
[3] Gard S et al. *Hum Mov. Sci,* **22:**597-610, 2004

The effect of knee extensor fatigue on metabolic cost in running

Key Nahan[1], Martin Héroux[1,2], John Kerr[1], Davide Bastia[1], Harrison Finn[1,2], Kirsty A. McDonald[1]
[1]University of New South Wales, Sydney, NSW, Australia
[2]Neuroscience Research Australia, Sydney, NSW, Australia
Email: k.nahan@unsw.edu.au

INTRODUCTION

Whole-body energy expenditure and muscle fatigue minimization are important criteria dictating human locomotor performance [1,2]. In running, these criteria are closely related—more motor units are recruited when a fatigued muscle must maintain its pre-fatigued force contribution [3], and the volume of active muscle affects the total metabolic expenditure observed during running [4]. The current study aims to explore this relationship further by considering the effect of localized knee extensor (KE) muscle fatigue. It is hypothesized that running in presence of KE fatigue will increase the metabolic cost of locomotion when compared to an unfatigued run.

METHODS

Two male recreational runners participated. They first completed a warm up, which was followed by a baseline run (BR) on a standard treadmill at 10 km h^{-1}. Participants then performed a maximum voluntary contraction (MVC) on a dynamometer (Humac, USA) and completed a fatigue protocol on a leg extension machine (three sets of repetitions to failure). Their MVC was assessed to ensure fatigue had reached the study's target value of 75-85% [5] ('pre' MVC). When this occurred, participants completed a fatigued run (FR) on the treadmill at 10 km h^{-1}, before their MVC was captured for a final time ('post' MVC).

Net metabolic cost of transport was computed from gaseous exchange data (Cosmed, Italy). Integrated electromyography (iEMG; Delsys, USA) was computed from the linear envelope of the raw vastus lateralis (VL) and biceps femoris (BF) signals, normalized to the mean peak value in the BR, parsed into strides and integrated. Preliminary results are presented for both participants; however it is expected that a full dataset will be prepared ahead of the conference.

RESULTS AND DISCUSSION

KE peak torque reduced to 75.4% and 83.7% of pre-baseline run MVC values after the fatiguing protocol for Participants 1 and 2, respectively. Post-FR values were 67.3% and 81.7% of the pre-baseline run MVC for Participant 1 and Participant 2, respectively. Thus, fatigue recovery did not occur during the run. Net metabolic cost responses to localised KE fatigue were variable. Participant 1's metabolic cost of transport was reduced between the BR and FR (5.02 vs. 4.67 J kg^{-1} m^{-1}, respectively), however, Participant 2 did not demonstrate a noteworthy change (4.85 vs. 4.95 J kg^{-1} m^{-1}, respectively). The complete dataset is required to understand whether an overall trend can be established for this population, or whether large variability in responses will exist. Interestingly, iEMG data indicate that while VL (agonist) muscle activity increases, BF (antagonist) muscle activity decreases when fatigued (Fig. 1). This observation conflicts with previous data showing a rise in antagonist muscle contributions with increased agonist fatigue [6]. However, this is the first study to consider localized fatigue in relation to a highly metabolically demanding task: running.

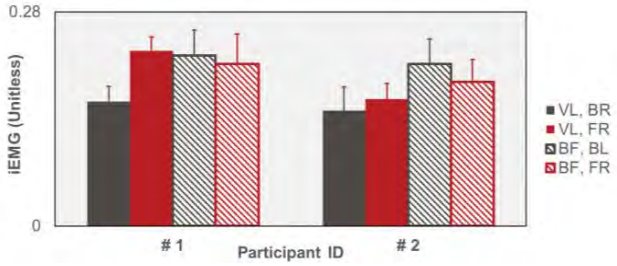

Figure 1 iEMG for the vastus lateralis (VL) and biceps femoris (BF) during the baseline (BR) and fatigued (FR) runs.

CONCLUSIONS

Our results may indicate that recreational runners can avoid substantial metabolic cost penalties—that may otherwise be invoked by fatiguing the knee extensors—through a reduction in knee flexor muscle activity. Data collection and analysis is ongoing.

ACKNOWLEDGEMENTS

This work was supported by ASICS Oceania.

REFERENCES

[1] Ralston HJ. Eur. J. Appl. Physiol. Occup. Physiol. 17: 277-83, 1958

[2] McDonald K et al., Proc. R. Soc. B. 289: 20221189, 2022

[3] Contessa P et al. Journal of Neurophysiology. 116(4): 1579–1585, 2016

[4] Fletcher, J. R., & MacIntosh, B. R. Journal of Applied Physiology. 118(2): 193–199, 2015

[5] Nicol C et al. Scandinavian Journal of Medicine & Science in Sports. 1(4):195–204, 1991

[6] Psek, J. A., & Cafarelli, E. Journal of Applied Physiology. 74(1): 170–175, 1985

THE ACHILLES SUBTENDONS EXHIBIT DISTINCT LOADING PATTERNS DURING WALKING

Lauren Welte[1], Darryl G Thelen[1,2]
[1] Department of Mechanical Engineering, University of Wisconsin, Madison, WI, USA
[2] Department of Biomedical Engineering, University of Wisconsin, Madison, WI, USA
Email: lwelte@wisc.edu

INTRODUCTION

Propulsive energy generated at the ankle during locomotion is primarily contributed by the Achilles tendon (AT) [1]. The morphologically complex AT is composed of three subtendons, one from each of the three triceps surae muscles. Relative motion between the subtendons has been well-documented at various slow walking speeds [2], [3], and reduction in relative motion is linked to propulsive deficits in older adults [4]. However, understanding how subtendon loading changes during gait has been limited by challenges in measuring depth-dependent differences in *in vivo* load. Here, we use novel depth-dependent tensiometry to investigate subtendon loading at faster walking speeds.

METHODS

One participant (F, 25, 173 cm, 60 kg) gave informed consent to participate in this study (University of Wisconsin IRB: 2018-0487-CP019). They walked on a treadmill at three speeds (1.25, 1.50 and 1.75 m/s). A shear wave tensiometer, composed of an electrodynamic tapper and a high-speed linear ultrasound transducer (Phillips CL 15-7, 22mm, centre frequency 8.92 MHz, used with 64LE Vantage, Verasonics), were attached to the participant's ankle, at the level of the free tendon (Figure 1). The induced taps' (50 Hz) shear wave propagation speed along the tendon, as a surrogate for tendon loading [5], was measured by a custom algorithm and averaged over 0.5mm depths of the AT. Time synchronized electromyography data of the soleus (SOL), medial gastrocnemius (MG) and lateral gastrocnemius measured muscle activations.

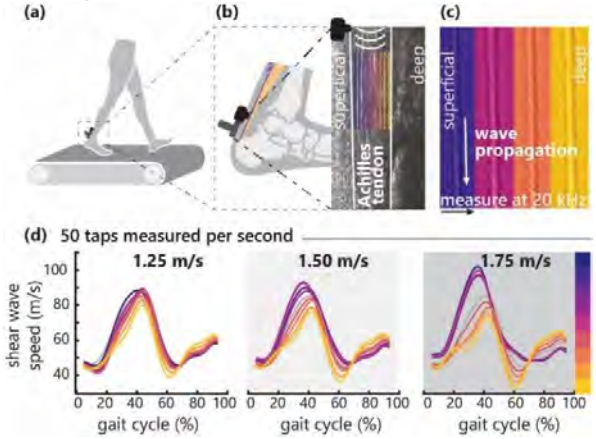

Figure 1: (a) Participants walked on a treadmill at 1.25, 1.50 and 1.75 m/s while (b) ultrasound images were captured at 20,000Hz for each tap at 9 tendon depths. (c) The wave speed is measured at each tap. (d) Shear wave speed, as a surrogate for tendon loading, and derived from the first two principal components, is shown over stance for each depth and walking speed.

Principal component (PC) analysis was conducted on the wave speed during each stride (~2 per trial) at each depth (9). PCs 1-3 were tested for linear correlation with depth and walking speed. PCs 1 and 2 explained 54% of the variance in the shear wave speed waveforms and were linearly related to both tendon depth and walking speed ($p < 0.01$, $R^2 = [0.07, 0.53]$). Based on the results of the regression, discriminant analysis classified the first two PC scores as a function of depth and walking speed. Waveforms were reconstructed from the mean PC scores for each classified walking speed and depth.

RESULTS AND DISCUSSION

Tendon depth was one of the primary sources of variability in the wave speed time series (Figure 1d). The reconstructed waveforms for each depth clustered in two distinct groups, strongly suggesting that we imaged two independent sub-tendons (likely MG and SOL). The shear wave speed was generally faster in the superficial tendon than in the deep tendon and increased with walking speed. Simultaneous increase in MG muscle activation with walking speed suggests that the gastrocnemius supports increased demand for forward propulsion, and therefore likely makes up the superficial tendon [6].

The deep tendon showed a plateau effect in wave speed in mid-stance, whose effect increased with walking speed. A quicker increase in tension between 10-20% of the gait cycle drove this plateau effect, suggesting the deeper tendon requires tension earlier in stance when walking faster. During swing phase, consistent with passive loading from ankle dorsiflexion in late swing, the AT had increased tension, with higher wave speeds occurring in the SOL subtendon. AT tension resulting from passive stretch may be more easily redistributed across the bi-articular MG than the uni-articular SOL.

CONCLUSION

Load-sharing strategies in the AT subtendons are task-dependent. Measurement of these loading patterns are critical to understanding propulsive deficits in older adults and improving treatment for AT injury.

ACKNOWLEDGEMENTS

Funding from NIH (R01AG051748) and NSERC PDF.

REFERENCES

[1] Arndt, A. et al. *Clin. Biomech.* **13**: 532–541, 1998.
[2] Franz, J. et al. *J. Appl. Physiol.* **119**: 242–249, 2015.
[3] Franz, J. et al. *Gait Posture* **41:** 192–197, 2015.
[4] Clark, W et al. *Sci. Rep.* **11**: 21264, 2021.
[5] Martin, J. A. et al. *Nat. Commun.* **9**: 1592, 2018.
[6] Clark, W et al. *Ann. Biomed. Eng.* **49**, 703–715, 2021.

PATELLOFEMORAL KINETICS WALKING IN MAXIMAL, MINIMAL AND TRADITIONAL SHOES

JJ Hannigan[1,2] and Christine D. Pollard[1,2]
[1] Program in Physical Therapy, Oregon State University – Cascades, Bend, OR, USA
[2] School of Biological and Population Health Sciences, Corvallis, OR, USA
Email: jj.hannigan@osucascades.edu

INTRODUCTION

Maximal and minimal shoes, characterized by the amount of midsole cushioning, have both become popular in older populations for activities of daily living, such as walking. However, previous gait research has suggested that the external knee adduction moment (KAM) may increase in maximal shoes, while the knee flexion angle at initial contact as well as the peak knee flexion angle may increase in minimal shoes compared to traditional footwear [1]. Together, this may indicate an increased risk of developing knee osteoarthritis (OA) over time in these shoes [2-3]. However, it is currently unknown how minimal and maximal shoes affect patellofemoral kinetics, and thus patellofemoral OA risk [4], during gait. Therefore, the purpose of this study was to compare patellofemoral joint kinetics between maximal, minimal, and traditional shoes during gait.

METHODS

After signing an informed consent document, twenty-one reflective markers and six marker clusters were placed 16 healthy females (age: 59.0 ± 3.6 years). All participants performed 5 successful walking trials in three shoe conditions: maximal (Hoka Bondi), traditional (New Balance 880) and minimal (Merrell Trail Glove) shoes. Lower extremity biomechanics were measured with a 3D motion capture system (Vicon Motion Systems) collecting at 250 Hz, and two force plates (AMTI) collecting at 1000 Hz.

Angular kinematics and kinetics were calculated using Visual3D software (C-Motion). Quadriceps force, patellofemoral joint reaction force, patellofemoral contact area, and patellofemoral joint stress were estimated using the formulas described in Brechter & Powers [5]. Patellofemoral joint kinetics were then compared using a repeated measures ANOVA ($\alpha = .05$).

RESULTS AND DISCUSSION

The peak knee flexion angle was significantly larger in the minimal shoe compared to the maximal and traditional shoes ($p < .001$). No significant differences were noted for the peak knee extension moment, peak quadriceps force, peak patellofemoral joint reaction force, and peak patellofemoral joint stress, $p > .05$ (Table 1).

CONCLUSIONS

Despite differences in sagittal plane knee kinematics, no significant differences between shoes were noted for any measure of patellofemoral joint kinetics, most notably patellofemoral joint stress. Previous research suggested that maximal shoes may increase the external knee adduction moment [1], which has been correlated with increased medial compartment contact forces and knee OA disease progression [2-3]. However, the results of this study suggest that altering shoe cushioning may not affect patellofemoral joint kinetics. Thus, based on these findings, walking in maximal or minimal shoes may not alter patellofemoral knee OA risk [4]. More research is needed on the effect of footwear in individuals currently suffering from knee osteoarthritis.

ACKNOWLEDGEMENTS

The authors would like to acknowledge Sherri Dean, Bella Krevitz, and Pete Haglund for their assistance with data collection and analysis.

REFERENCES

[1] Hannigan & Pollard. *Gait Posture* **83**: 245-9, 2021.
[2] Marriott et al. *J Biomech* **94**: 123-9, 2019.
[3] Miyazaki et al. *Ann Rheum Dis* **61**: 617-622, 2002.
[4] Teng et al. *Clin Biomech* **30**: 383-390, 2015.
[5] Brechter & Powers. *Med Sci Sport Exer* **34**: 1582-93, 2002.

Table 1: Variables of interest in each shoe condition.

	Traditional Shoe	Maximal Shoe	Minimal Shoe	*p-value*
Peak Knee Flexion (°)	39.6 ± 4.1	41.0 ± 4.3	42.7 ± 4.3	< 0.001
Peak Knee Extension Moment (Nm/kg)	0.77 ± 0.33	0.80 ± 0.35	0.77 ± 0.32	0.529
Peak Quadriceps Force (N/kg)	16.4 ± 7.2	17.2 ± 7.6	16.4 ± 7.1	0.554
Peak Patellofemoral Joint Force (N/kg)	10.6 ± 5.0	11.3 ± 5.3	10.7 ± 5.1	0.506
Peak Patellofemoral Joint Stress (MPa)	4.1 ± 1.6	4.2 ± 1.7	4.1 ± 1.6	0.746

HOW WELL DO MACHINE LEARNING MODELS TRAINED ON TREADMILL WALKING DATA PERFORM ON OVERGROUND DATA?

Sailee Sansgiri, Krista Vohlakari, Taija Finni, Timo Rantalainen and Neil J. Cronin
Faculty of Sport and Health Sciences, University of Jyväskylä, Jyväskylä, Finland
Email: ssansgir@jyu.fi

INTRODUCTION

In gait analysis, accurate estimation of ground contact timings (time between initial contact and toe-off of the same foot) is essential for determining spatio-temporal parameters. While using treadmills for gait analysis increases the number of strides that can be analysed per measurement, some gait characteristics differ between treadmill and overground walking, which hinders the translation of treadmill walking to overground conditions [1].

Machine learning (ML) based assessments have high accuracy in determining spatio-temporal parameters for healthy adults in overground and treadmill walking using kinematic data [2]. However, they are tuned to specific features of their training datasets and hence may not make accurate predictions on unseen datasets.

In this study, we examine how 4 common ML models trained to identify ground contact timings for treadmill walking perform on overground walking data from different individuals. By doing so, we aim to comment on the generalization of these ML models to different gait conditions.

METHODS

3-D kinematic and kinetic data were collected from 27 healthy adults (26 ± 2.6 years). 3-D raw IMU signals (input) from sensors placed at the waist, left foot and right foot were sampled at 120 Hz. Ground contact sampled at 100 Hz (ground truth) was determined using pressure insoles in the shoes of the participants. Approximately 400 steps (overground walking; self-selected speeds) and 600 steps (treadmill walking; 3.5 to 6 km/h at increments of 0.5 km/h) were collected from each participant.

4 supervised ML models- K-nearest neighbour (KNN), Random Forest (RF), Support Vector Machine (SVM) and a multilayer feed-forward Neural Network (NN)- were implemented using treadmill walking data from 21 participants (Figure 1). A 5-fold cross validation was performed to check for overfitting. Algorithm performance was tested on treadmill and overground walking from the remaining 6 participants. The results were also compared to a kinematic method of gait event detection [3]. RMSE was calculated on the difference between the true ground contact timings (from insoles) and the timings predicted by the algorithm in milliseconds (ms).

RESULTS AND DISCUSSION

On treadmill data, RMSE (±SD) values of 8.1 ± 3.3 ms (KNN), 9.2 ± 3.8 ms (RF), 8.4 ± 4.3 ms (SVM) and 6.9 ± 3.8 ms (NN) were observed. As expected, the performance on overground walking was considerably worse, with the respective values being 14.3 ± 5.7 ms (KNN), 18.2 ± 7.2 ms (RF), 15.3 ± 4.6 ms (SVM) and 16.7 ± 6.3 ms (NN). All ML approaches surpassed the performance of the kinematic algorithm which reported values of 23.3 ± 10.8 ms (overground) and 28.4 ± 12.6 ms (treadmill). This was expected as kinematic algorithms generally rely on certain heuristics which may be difficult to generalize across different individuals and gait conditions.

The KNN and SVM methods outperformed the NN approach when testing on overground data. Overall, the KNN approach performed best on unseen data.

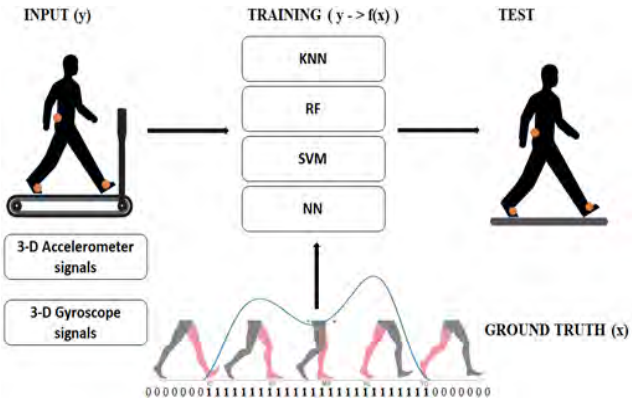

Figure 1 Schematic diagram of the methodology. 4 ML approaches were used to approximate target function f that mapped 3-D accelerometer and gyroscope signals from the waist and foot IMUs (y) to ground contact timings obtained from vertical ground reaction force data (x). KNN- K-nearest neighbour; RF- Random Forest; SVM- Support Vector Machine; NN- Neural Network.

CONCLUSIONS

The results indicate that while all ML approaches outperformed the kinematic approach in both treadmill and overground walking, there is not a “one-model-fits-all” approach due to the inability of ML approaches to generalize to unseen gait conditions. Evidence suggests that simpler ML algorithms may have an advantage over NN approaches in this regard. However, this experiment should be replicated in other gait conditions (e.g. jogging and stair-climbing) and compared to deep learning approaches before drawing this conclusion.

REFERENCES

[1] Hollman J. H. et al. *Gait Posture* **43**: 204-9, 2016.
[2] Khera P. et al. *J Med Eng Technol* **44**: 441-67, 2020.
[3] Zijlstra W. et al. *Gait Posture* **18**: 1-10, 2003.

Timed-up-and-go test segmentation algorithm based on a wearable sensor technology: a technical validation in people with multiple sclerosis

Arash Atrsaei[1], Frederic Meyer[2], Pål Berg-Hansen[3], Trine M. Seeberg[4], Elisabeth Gulowsen Celius[3], Andreas Austeng[2], Fabien Massé[1]

[1] Digital Motion Analytics, MindMaze, Lausanne, Switzerland.
[2] Department of Informatics, University of Oslo, Oslo, Norway.
[3] Department of Neurology, Oslo University Hospital, Oslo, Norway.
[4] SINTEF Digital, Smart Sensor Systems, Oslo, Norway.
Email: arash.atrsaei@mindmaze.ch

INTRODUCTION

Due to different phases, the timed-up-and-go (TUG) test requires a complex coordination of the lower and upper limbs. Wearable sensor technology can provide detailed evaluation of the biomechanics of the movements during this test. Previous studies have shown high reliability and sensitivity of the instrumented TUG (iTUG) test in several patient populations, but little validation has been performed, especially in people with multiple sclerosis (pwMS) and only on the total duration of the test [1]. Therefore, in this study we validated an algorithm that extracted different subphases of the TUG test based on wearable sensors.

METHODS

Forty-one pwMS and 15 age-matched controls were recruited for the study (AutoActive project, number 270791, a research project in the IKTPLUSS program financed by the Norwegian Research Council). Participants were equipped with three Physilog® 5 (MindMaze SA, CH) sensors on sacrum and feet. Accelerometer and gyroscope data was used with 128 Hz sampling frequency. Moreover, two GoPro 7 (GoPro Inc, US) cameras were recording videos with 50 fps. Participants performed the TUG test in two sessions. Based on signal processing methods, the total duration of the test, sit-to-walk, turning, and turn-to-sit durations were extracted from the wearable sensors (IMUs). One observer annotated the videos for each subphase of the TUG test. The difference between the IMU-based results and the observer's annotation as the reference was calculated. Pearson's correlation coefficient was also obtained to determine the degree of agreement between the two systems. Finally, pwMS were grouped into moderately and severely disabled groups based on their disability score. Wilcoxon rank-sum test was used to determine if the error of the IMU-based results were significantly different between control, moderate, and severe groups. Finally, to assess the inter-rater variability, a group of pwMS were randomly chosen for which a second observer annotated the videos.

RESULTS AND DISCUSSION

The difference as well as the correlation coefficient between the reference and IMU-based results were shown on Table 1. High agreements exist between the IMU-based measures and the reference values except for the sit-to-walk duration. The reason can be due to the difficulty of marking the end of this transition. The limits of agreement (mean ± 1.96SD) for the total duration of the test was (-1.3 , 1.1) seconds which is less than the minimal detectable change reported for pwMS [2]. Therefore, the IMU-based algorithm can reliably estimate the duration of different subphases of the TUG test and discriminate different stages of the MS. The Wilcoxon rank-sum test showed no significant difference in the errors between the control, moderate, and severe groups except for the turn-to-sit duration. This can be due to the difficulty of this complex transition for the severe group of the patients. The inter-rater variability and the absolute error of the IMU-based results have been shown in Figure 1. The latter was either in the same range or significantly lower than the difference between two observers which implies that IMUs can provide an objective measure of the TUG test.

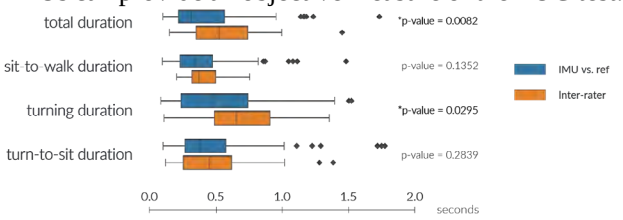

Figure 1 IMU error vs. inter-rater variability

CONCLUSIONS

The findings indicate that the IMUs along with the dedicated algorithm could estimate the duration of the subphases of the test in a reliable and objective manner.

REFERENCES

[1] Flachenecker F et al. *Multiple sclerosis & related disors* 39: 101903, 2020
[2] Valet M et al. *J Phys Rehabil Med* **55**: 450-455, 2019

Table 1: Difference and correlation between IMU-based results and reference

	Total duration	Sit-to-walk duration	Turning duration	Turn-to-sit duration
Reference values (s): mean ± SD	10.21 ± 2.17	1.33 ± 0.51	1.81 ± 0.48	2.57 ± 0.58
Difference (s): mean ± SD	-0.13 ± 0.62	0.08 ± 0.46	0.36 ± 0.46	0.29 ± 0.38
Pearson's correlation coefficient	0.95	0.55	0.71	0.78

Detecting the Progression of Gait Impairments in Parkinson's Disease using Wi-Fi

Tzu-Yang Weng, Chi-Lun Lin
Mechanical Engineering, National Cheng Kung University, Tainan, Taiwan.
Email: n16101905@gs.ncku.edu.tw
10408019@gs.ncku.edu.tw

INTRODUCTION

The Parkinson's disease (PD) can causes difficulties during gait, such as imbalance, decreased speed and stride length, and shuffling steps [1]. These issues may increase the risk of falls and further limit mobility in individuals with PD. The diagnosis of PD can be challenging because it has a gradual onset, making it important to continuously monitor the progression of the patient's condition.

Channel state information (CSI) represents the combined effect during the propagation of Wi-Fi signals from the transmitter to the receiver. Wi-Fi-based sensing has the advantages of being passive, contactless, and privacy-preserving. For gait detection, studies have used CSI to collect gait information to achieve human regonition. [2]. Therefore, this paper proposes a method to detect abnormality during gait and extract quantitative information for assessing the severity of PD.

METHODS

CSI data was collected when a healthy person walked in different levels of abnormality, including normal gait, short-stepped gait, one leg dragging [3] and shuffling gait.

Our computer algorithm processed a CSI sequence of magnitude and quantitatively extracted walking speed, cadence, and step length. The data processing included Butterworth band-pass filtering, principal component analysis and short-time Fourier transform. We superposed the output spectrograms of the first ten principal components to enhance the features of motion, and the maximum energy zone (torso contour [2]) in the resulted plot was used to extract walking speed. Next, the weighted average of the spectrogram was used to smooth out the torso contour curve for more accurate estimation of walking steps. Finally, the step length can be calculated from the walking speed and number of steps.

RESULTS AND DISCUSSION

The results indicated that the proposed method could distinguish different levels of abnormality (Figure 1). The variation in frequency during gait, which represented walking speed, was used to quantitatively differentiate between these cases. The torso contour (red zone) in a spectrogram contained oscillations, which illustrated acceleration and deceleration phases of steps caused by initial swing and terminal swing (Figures 1a – 1d). The normal gait and the other three abnormal ones performed by the same person were clearly distinguishable by showing different patterns and magnitudes of oscillation. The walking speeds were extracted from the data in time-frequency domain, and the number of steps could be identified by finding the peaks in the torso contour plot (Figure 1e). Therefore, the cadence and step length of these cases could be estimated. Special features could also be depicted by these plots. For example, the torso was nearly static during the period of dragging one leg during, leading to a flat area with relatively lower frequencies in the spectrogram (Figure 1c).

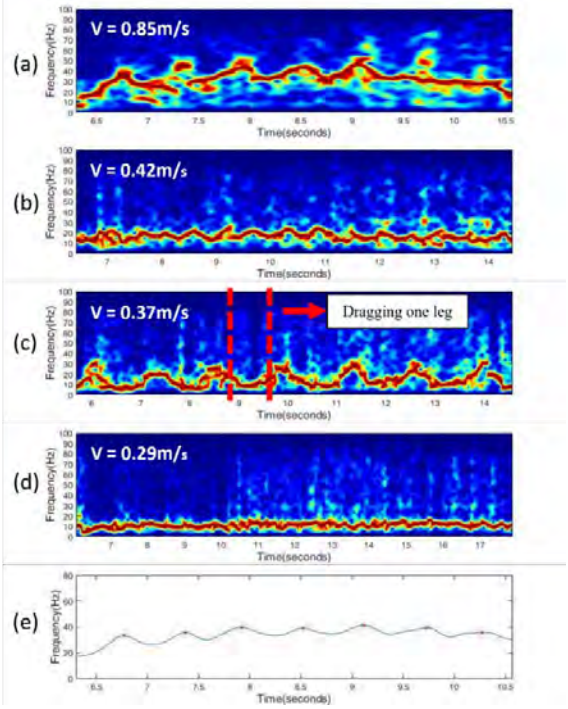

Figure 1 Spectrograms of (a) normal gait, (b) short-stepped gait, (c) one leg dragging, and (d) shuffling gait. (e) The profile curve of torso contour converted from (a) for counting steps.

CONCLUSIONS

The proposed method successfully detected gait impairments that would present in different stages of PD. Important gait parameters, such as walking speed, cadence, and step length, were quantified. With continuous detection, the patient's daily condition can be tracked to understand the disease progression and drug efficacy, which help the doctor prescribe more accurately.

REFERENCES

[1] M. E. Morris, F. Huxham, J. McGinley *et al.*, "The biomechanics and motor control of gait in Parkinson disease," Clinical Biomechanics, 16(6), 459-470 (2001).

[2] W. Wang, A. X. Liu, and M. Shahzad, "Gait recognition using wifi signals." 363-373.

[3] E. Tolosa, A. Garrido, S. W. Scholz *et al.*, "Challenges in the diagnosis of Parkinson's disease," Lancet Neurol, 20(5), 385-397 (2021).

CAPACITIVE SENSING FOR NATURAL ENVIRONMENT REHABILITATION MONITORING

Owen Pearl[1], Nataliya Rokhmanova[1], Louis Dankovich[2], Sarah Bergbreiter[1], & Eni Halilaj[1]
[1] Mechanical Engineering, Carnegie Mellon University, Pittsburgh, USA
[2] University of Maryland College Park, College Park, USA
Email: owen.pearl@cmu.edu

INTRODUCTION

Capacitive sensing (CS) is a mature technology that enables versatile, cost-effective, power efficient, flexible, robust to noise, and lightweight portable technologies like touch screens and promixity sensors [1]. However, previous use of CS on humans has only emphasized gesture recognition or activity classification [2]. Here we characterize capacitive touch sensing as a gait rehabilitation monitoring technology and show that it captures clinically relevant gait modifications in natural environments with the fidelity of laboratory tools. We hypothesized that CS would perform better than electromyography (EMG) and muscle-driven simulations (SIM) [3] at detecting adherence to therapeutic gait retraining prescriptions.

METHODS

We developed an affordable CS-based circumferential sleeve and benchmarked it against EMG and SIM muscle forces using marker-based motion capture (Figure 1). Our $35 (USD) custom-built CS sleeve measures circumferential capacitive profiles of the shank, which are primarily governed by bulging of the gastrocnemius, soleus, and tibialis anterior. Expansion in cross-sectional area decreases the distance between four copper tape electrodes in the CS sleeve and the subject's skin, which results in an increase in their capacitive coupling. We benchmarked the CS sleeve on 20 adults (12 males, 8 females; 25.2 mean ± 2.2 std years of age), both indoor and outdoor. A Freidman test was used to compare the ability of CS, EMG, and SIM to detect changes between baseline walking gait at a subject's preferred speed and a modified 5° toe-in gait, which has been shown to help slow knee osteoarthritus progression [4].

RESULTS AND DISCUSSION

Our results indicate that the CS sleeve can distinguish between baseline and toe-in gait as well as, or better than, existing laboratory benchmarks of muscle activity. The CS sleeve detected a higher root-mean-square difference (RMSD) between the baseline and toe-in gaits than EMG, both inside ($p < 0.0001$) and outside ($p = 0.0156$) of the lab. CS also detected a similar RMSD to simulations performed inside the lab ($p = 0.4076$). These findings indicate that CS matches or surpasses the ability of current state-of-the-art laboratory tools at detecting adherence to gait retraining prescriptions. Because CS uses circumferential electrodes, it likely captured additional information about the gait modification reflected in parts of the musculotendon complex that EMG and SIM were unable to capture (e.g., tendons and ligaments near the ankle). By synthesizing information from multiple muscles and tendons automatically, CS alleviates the need to select specific muscles for monitoring a priori.

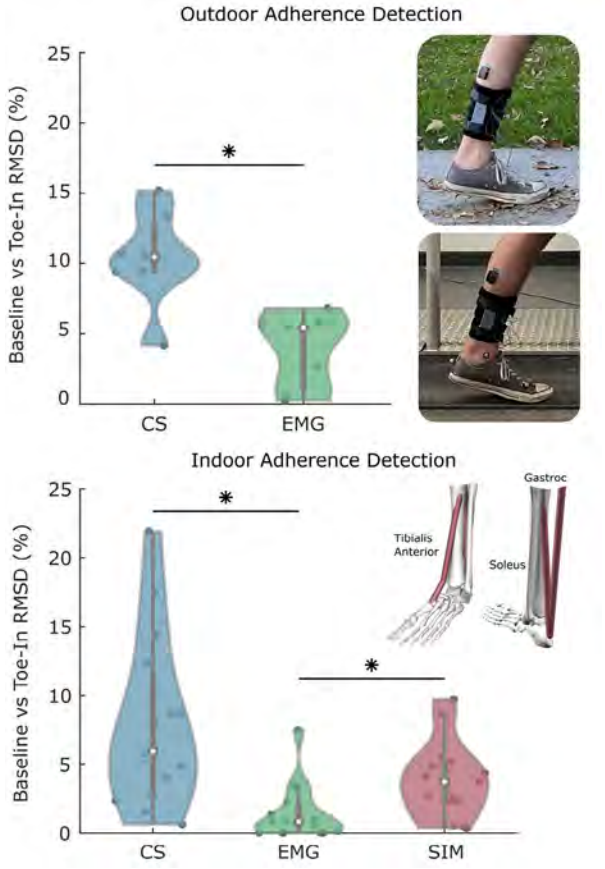

Figure 1. Capacitive sensing wearable detects larger physiological changes in muscle activity resulting from a therapeutic gait modification than EMG and musculoskeletal simulations.

CONCLUSIONS

CS has rich potential for democratizing rehabilitation monitoring with wearable sensors and smart garments of different form factors, given its flexibility, low cost, and sensitivity to even small changes in gait (i.e., 5°).

ACKNOWLEDGEMENTS

Supported by NSF DGE1745016 and DGE2140739.

REFERENCES

[1] Grosse-Puppendahl, T., et al. *CHI*. 2017.
[2] Cheng, J., et al. *Pervasive Computing*. 2010.
[3] Delp, S., et al. *IEEE Trans*. 2007.
[4] Uhlrich, S., et al. *J. Biomech.* 2018.

ESTIMATING ENERGY EXPENDITURE USING WEARABLE SENSORS DURING INDOOR AND OUTDOOR LOCOMOTION

Mohammad Mohammad[1], Abed Abu Hijleh[1], Gillian Phillips[1], Megan McAllister[1] and Jessica Selinger[1]
[1] School of Kinesiology and Health Studies, Queen's University, Kingston, Canada.
Email: 16mm126@queensu.ca

INTRODUCTION

Measures of metabolic energy expenditure can provide valuable insight into healthy and impaired gait, the design and control of assistive devices, and rehabilitation progress [1,2]. Currently, the gold standard for estimating energy expenditure is indirect calorimetry, where oxygen use is captured via a gas mask [3]. Although accurate, indirect calorimetry systems are expensive, cumbersome, and often limited to lab settings. Therefore, our aim is to develop a cheap, lightweight method for accurately and continuously estimating energy expenditure during outdoor locomotion using wearable sensors.

METHODS

Participants. We recruited healthy adults who are recreational runners with no known musculoskeletal or cardiopulmonary impairments (n = 22, 11 F). *Equipment*. Each participant was instrumented with a portable indirect calorimetry system to measure energy expenditure, as well as the following wearable sensors to estimate energy expenditure: accelerometers at the pelvis and foot, a heart rate monitor, and a respiratory belt. *Protocol*. During indoor testing participants walked and ran on a treadmill (~4.6 km) at varying speeds (1.25-2.5 m/s), inclines (0% and 5%) and added weight conditions (0 and 3% body weight at the ankle). During outdoor testing participants walked and ran, with and without the added weight, on a predefined outdoor route (~4.8 km) that included sections with distinct average inclines (~0% and 5%). *Analysis*. We used multiple regression (MLR) analysis, as well as long short-term memory (LSTM) recursive neural network (NN), with a leave-one-out cross-validation design to predict energy expenditure using custom metrics derived from wearable sensors and participant anthropometric data. Participant sensor data was binned using an estimation time interval of 10s. Due to equipment malfunction, only data from 18 participants (n = 18, 9 F) was included in the final analysis.

RESULTS AND DISCUSSION

We found that we could estimate energy expenditure in real-world settings with relatively high levels of accuracy across changing terrain and variable conditions. We found that our NN method has an average absolute error of 14%, which is among the most accurate wearable sensor methods reported to date [2,3]. We were also able to maintain relatively low error rates using a model that only used data available from a typical consumer smartwatch (SW model). The correlation (R^2) between measured and predicted energy expenditure was above 0.9 for all participants in all models (Figure 1a). Average absolute errors in estimated energy expenditure, across all conditions, were typically ~0.9 W/kg. This resulted in lower percent errors for higher work rate tasks, such as running, and higher percent errors for lower work rate tasks, such as standing (Figure 1b).

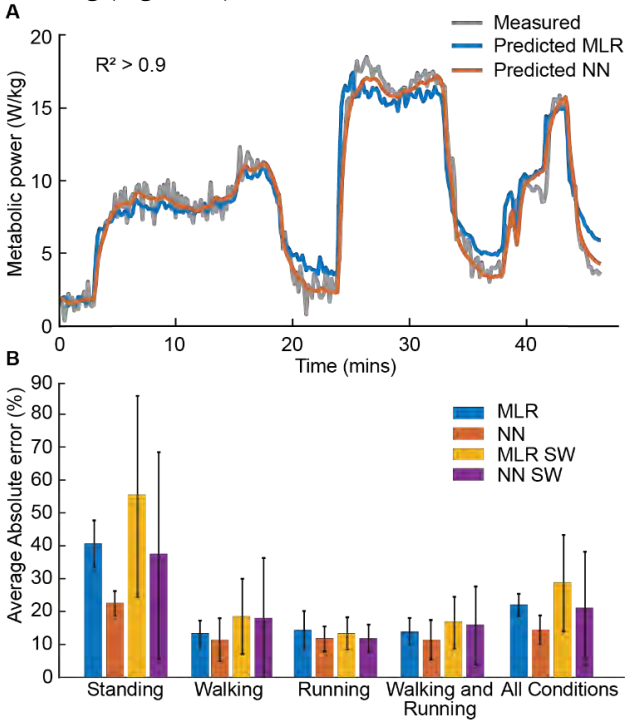

Figure 1. *A*: Measured and predicted metabolic power timeseries for a representative outdoor participant using full MLR and NN models. *B*: Across participant average absolute percent error between measured and predicted metabolic power for various outdoor conditions using full MLR and NN models, as well as smartwatch (SW) models.

CONCLUSIONS

Development of a cheap, lightweight method for accurately estimating energy expenditure could allow researchers and clinicians to predict energy expenditure outside lab settings, for extended periods, and in diverse populations [4]. This could have applications in the design and control of assistive aids, gait rehabilitation, weight-loss programs, and sport and recreation.

REFERENCES

[1] Benson L et al. *Gait Postur* **63**: 124-38, 2018.
[2] Ingraham K et al. *J Appl Physiol* **126**: 717-29, 2019.
[3] Slade P et al. *Nat Commu* **12**: 4312, 2021.
[4] Caron N et al. *Eur J Appl Physiol* **118**: 381-8, 2018.

Validation of the Lower Limb Joint Kinematics in the Sagittal and Frontal Planes Calculated by a Self-Developed Dual Kinect Azure Sensors System

Kun-Chun Lin[1], Hsuan-Lun Lu [1]

[1] Department of Biomedical Engineering, Da-Yeh University, Changhua, Taiwan (R.O.C.)
Email: hllu@mail.dyu.edu.tw

INTRODUCTION

Human movement analysis is widely used in the fields of clinical diagnosis, treatment evaluation, sport science, cinema/game industry. Infrared stereophotography motion analysis system is most used to be implemented owing to its high accuracy and reliability. However, it requires experienced operators, sufficient space for system setup, expensive cost of the system, complicated experimental setup. These not only decrease the will of the target subjects but also limit the widespread implementation in the current clinical practices. Machine learning based depth-RGB camera system, i.e., Kinect azure, gave an opportunity to estimate the three-dimension positions of the body joints. Studies on evaluation capability, measurement accuracy and usages in clinical practices using Kinect Azure based measured system have increasing trend recently. However, the accuracy of the joint kinematics was not investigated in the previous studies. Therefore, the current study aimed to evaluate the accuracy of the joint kinematics in the lower limbs during gait determined using dual Kinect azure sensors by conducting with VICON system.

METHODS

Twelve young subjects were participated in the current study. Each subject wore Plug-In-Gait marker set and was asked to walk at his/her preferred walking speed, under surveillance of six-camera stereophotography system (VICON, Vero 2.2). At the same time, two Kinect azure sensors were positioned alongside to the walking direction, the camera focal axis was set to around 30 degrees faced to the subject. Two Kinect Azure were both calibrated following the procedure instructed by OpenCV [1]. The relative coordinate systems of the two Kinect sensors were then determined. Each joint position was calculated as the mean position when transformed the coordinates from slave Kinect sensor to master Kinect sensor. The definition of the sagittal and frontal planes was then determined by adjusting the walking direction of the whole gait cycle and vertical direction. The joint angles were obtained by connecting the target joint position to adjacent joints and then projected to sagittal and frontal planes, to derive flexion/extension and abduction/adduction angles of each lower-limb joint. Each joint angle in the complete gait cycle was then extracted from both systems. Following with a linear interpolation procedure, 101-point data will be determined for each joint angle in a gait cycle. Root-mean-square errors (RMSE) were then calculated by dividing two set of 101-point data. The larger the RMSE value, the less accurate the joint kinematics determined by Kinect system.

RESULTS AND DISCUSSION

The joint kinematics of the ankle had higher accuracy when compared to the knee joint (Fig. 1). The higher RMSE values of the knee joint could be caused by the noisy estimation of the hip joint. The machine-learning based joint position tracking kernel has been reported that lower measuring accuracy for the estimation of the hip joint. Therefore, the linkage represented of thigh that defined by knee and hip joint positions could thus be affected [2].

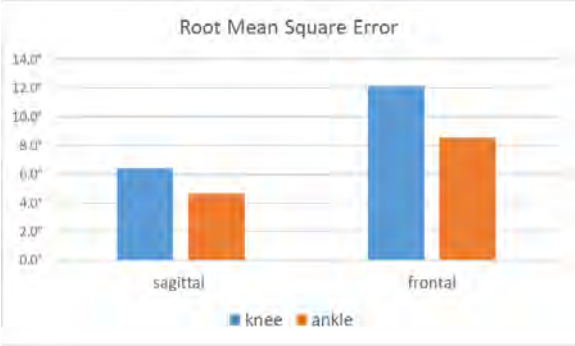

Figure 1 The root-mean-square error (RMSE) determined by dual Kinect Azure Sensor, which were compared to VICON system. The RMSE values of the knee (6.4° and 12.2°) and ankle (4.7° and 8.5°) in the sagittal and frontal planes, respectively.

CONCLUSIONS

The current study has successfully investigated the accuracy of the calculation of the joint kinematics determined by a dual Kinect Azure sensors system, when compared to the Vicon system. The current study could provide useful information for the implementations using Kinect Azure and the descriptions of error distribution for the further studies.

ACKNOWLEDGEMENTS

This project was supported by the National Science and Technology Council, Taiwan. (111-2813-C-212-026-E)

REFERENCES

[1] Bradski, G. and A. Kaehler (2008) *O'Reilly Media, Inc*.

[2] Ma, Y., *et. al.*, (2020) *IEEE*. p. 1201-1206.

CHANGES IN FOOT PRESSURE DURING DOWNHILL WALKING AFTER USING A BIOFEEDBACK WHICH REDUCES ACCELERATION

Alexandra Giraldo-Pedroza, Winson Chiu-Chun Lee
School of Mechanical, Materials, Mechatronic and Biomedical Engineering, University of Wollongong, Wollongong, Australia
Email: ccwlee@uow.edu.au

INTRODUCTION

Maintaining stability during gait is a challenge for the postural control system, which increases with ageing and inclined surfaces. Older adults have greater landing vertical accelerations than younger adults [1]. Walking downhill can further increase acceleration and produce faster forward body movement [2], which affects postural stability. This increases the risk of falls outdoors [3]. Whilst wearable devices that provide customized biofeedback have been used to improve gait performance in older adults, there is a limited attempt in using biofeedback to improve stability during a downhill walk. Landing acceleration during walking reflects how well the centre of mass (COM) moves to disperse the force of the body as it lands. In this pilot study, we investigate the changes in stability after using biofeedback which aims to reduce landing acceleration. Stability was studied through the analysis of the plantar pressure distribution (PP) and the displacement of the COP.

METHODS

To measure landing acceleration (LA), a 2.4cmx2.4cm 9DoF IMU Breakout (SparkFun 9DoF IMU Breakout – ICM20948) was firmly taped to the anteromedial distal aspect of the tibia. The IMU was aligned with the tibia's longitudinal axis and LA was measured. The IMU communicated with a wireless biofeedback unit. It included a board ATmega32U4 (SparkFun Qwiic Pro Micro) and two vibrating motors (1027 Flat Coreless Vibrating Motor, Baolong Electronic Group) placed in the back of the pelvis. A customized Arduino (1.8.19) and MATLAB (20018b) program were built to analyse based on stride segmentation the peak acceleration during heel strike and provide a 3.5v signal noise indicating the exceed of the target acceleration.
The experiment involved a healthy 67-year-old female volunteer. Her initial LA was measured as she walked downhill on a 10° slope and 18.2 meters ramp. She then underwent a gait retraining walking for 15 minutes at the same downhill condition. The training involved the use of biofeedback, which vibrated unless 20% reduction in LA was achieved. The participant was instructed to move the pelvis' weight backwards as a strategy to reduce the acceleration.

The participant walked over the standardised pressure floor mat GaitRite to collect measurements of the COP and COM measurements. A total of 94 steps were analysed. To analyse the PP, the foot was divided into six areas: rearfoot (A1, A2), midfoot (A3, A4), and forefoot (A5, A6). LA was recorded by the IMU device and filtered using a weighted average low-pass filter at 8.3 Hz.

RESULTS AND DISCUSSION

Analysis showed that biofeedback has reduced the LA by approximated 20.4%. The total anteroposterior displacement of the COM increased by 2.7%. While its velocity increased by 3% at heel strike, it decreased by 27% at the end of the midstance phase.
The impulse was reduced at the heel and midfoot by more than 10% (A1, A2, A3) while it increased by 15% at the distal midfoot. The peak pressure decreased at the heel between 5-10% (A1, A2) while increased in the distal midfoot and toes (A4, A5, A6 >10%). The area of contact increased by more than 10% at the distal midfoot (A4).
Based on these results, a slower velocity in the COM at the mid stance suggests locomotion adjustments that may influence reductions in forward momentum during the propulsion phase and in agreement with the literature, it could promote stability [4]. It may be possible that due to the reduction of load at the heel and midfoot, there is a greater shock absorption, which is required for stabilising the walk. This pilot study found increments in the impulse at midfoot and toes. The push-off requires impulse to increase the swing capacity and further stabilise the heel during heel strike.

CONCLUSIONS

In this pilot study, it was observed that after using biofeedback which reduces landing acceleration, there was a reduction in the velocity of the COP, a reduction in the load and a greater impulse in the forefoot. This may imply evidence of strategies to promote stability, however further studies need to be completed with greater samples size.

REFERENCES

[1] Scaglioni-Solano et al. J Gaitpost **41**: 153-8, 2015.
[2] Vieira et al. J Biomech **56**: 10-18, 2017.
[3] Hong et al. Gait Posture **42**: 523-8, 2015.
[4] Hong et al. Appl Bionics Biomech **2018**:2028638, 2018

Automated gait event detection using wearables/ IMU for data acquisition and deep learning for placement classification

Yong Kuk Kim[1], Joong-on Choi[1,2], Sai Ganesh Sarvotham Pai[1,3], William R Taylor[1], Navrag B Singh[1,3]
[1] *Laboratory for Movement Biomechanics, Institute for Biomechanics, ETH Zürich, Switzerland*
[2] *Department and Research Institute of Rehabilitation Medicine, Yonsei University College of Medicine, South Korea*
[3] *Singapore-ETH Centre, Future Health Technologies, CREATE campus, 1 CREATE Way, #06-01 CREATE Tower, Singapore 138602*

SUMMARY

Gait events such as heel strike (HS) and toe-off (TO) are detected using inertial measurement unit (IMU) data, i.e., from a 3D accelerometer or 3D gyroscope, or both. IMU algorithms require sensor orientation and threshold tuning, which are operator-dependent and necessitate substantial expert user intervention. Deep learning (DL) offers a data-driven alternative for detecting gait events in an automated manner. However, little is known about how sensor placement affects DL's ability to detect gait events. Therefore, this study examined the usability of DL to classify sensor placement and then detect gait events by using a variety of IMU placement combinations as input. **Our approach was able to classify the placement of sensors with an F1 score of 98.9% using an accelerometer. Over 99% of the test set, all sensors detected HS within 15ms. TO detection decreased from Ankle (97.3%), Wrist (89.1%), Head (87.3%) to Trunk (65.2%).** As seen, the detection of TO compared to HS detection remained challenging, especially in Trunk. Thus, depending on the task, different sensor sets should be considered to detect gait events in a repeatable and fully automated manner.

INTRODUCTION

Neuromotor impairments in diseases like Parkinson's Disease are identified through clinical gait analysis. Accurate gait event detection is necessary for this study, especially for IC and TO. Experts must currently manually identify these occurrences in clinical practice using kinetic (which requires force plates) or kinematic data, which is time consuming, expensive, and operator dependent. Applications of Dl and IMUs have shown their ease of us and potential for detecting gait events[1], allowing extensive use cases in remote conditions, i.e., home monitoring. Little is known about how sensor placement affects DL's ability to detect gait events. Additionally, it is yet unclear how different combinations would affect the detection outputs of algorithms. This has substantial practical relevance because the number of sensors and their positions can vary greatly. Such evaluations would make it possible to choose the best placement of IMUs for screening and monitoring operations.

Therefore, this study aims to investigate a) how well DL can classify the sensor placement from IMU data and b) what sensor placement provides the most optimal performance for gait event detection.

METHODS

3-D kinematic and IMU data were collected from **22 participants** (Age: 26 ± 2.6 years) who performed barefoot walking on a treadmill for 6 minutes. The true events were found using a 3-D kinematic marker-based foot velocity algorithm. We assigned 80% of the data to the training set, 10% to the validation set, and 10% to the test set to avoid overfitting. The total dataset includes 25200 events (12600 IC and TO events each). The network utilized a Convolutional Neural Network (CNN) consisting of a **6-layer of conv1D (**specialized for capturing data that have long-range dependencies) **followed by BatchNorm1d and SiLU,** a fully connected output layer, and a sigmoid activation function. Tri-axial acceleration and angular velocity time series were cut to a length of 256 frames around the true event with a random offset and used as inputs to train the model with an Adam optimizer (learning rate=0.001) and a weighted binary cross-entropy loss to balance the occurrence of gait events within the data input (1HS and 255 no event).

RESULTS AND DISCUSSION

Table 1: An overview of performance for HS and TO evaluated recall, precision, and F1 score. TP: Detection rate of annotated events, FP: Detection of events that are not annotated, FN: No detection

Sensor Placement	Ankle						Wrist					
Matrix	TP	FN	FP	Recall	Precision	F1	TP	FN	FP	Recall	Precision	F1
HS	3596	0	0	100	100	100	3586	0	11	100	99.7	99.85
TO	3409	0	186	100	94.8	97.33	2733	165	505	94.3	84.4	89.076
Sensor Placement	Head						Trunk					
Matrix	TP	FN	FP	Recall	Precision	F1	TP	FN	FP	Recall	Precision	F1
LHS	1785	0	17	99.1	99.1	99.1	1798	0	2	100	99.9	99.95
RTO	1361	111	226	92.5	85.8	89.02	612	448	117	57.7	84	68.409
RHS	1791	1	8	99.9	99.6	99.75	1804	0	0	100	100	100
LTO	1328	24	427	98.2	75.7	85.49	725	164	726	81.6	50	62.006

The model successfully detects the placement of the sensor with an accuracy of 99.2%, using 3D acceleration. Overall, HS detection scored an average of 99.75%, and TO providing 81.8% using both the 3D acceleration and gyroscope. Despite the general acceptance of TO detection being more challenging, it is interesting to observe a substantial deterioration of performance at the trunk level. Our results were based on a primitive DL model; thus, more advanced models, such as Temporal Convolutional Network and Attention Transformer, could improve the overall performance. The robustness of the DL model can be improved by training on a different population group, such as the elderly, thus ultimately providing optimal gait event detection in a repeatable and fully automated manner to ease clinical gait analysis.

REFERENCES

1. Greve C et al Sensors 22: 4957, 2022;

Evaluation of hip joint kinetics in rehabilitation exercises for children with cerebral palsy

Jasper Kwasny[1], Uwe Kersting[1], Ibrahim Duran[2], Eckhard Schönau[2] and Cynthia Fantini Pagani[1]
[1] Institute for Biomechanics and Orthopaedics, German Sport University Cologne, Cologne, Germany
[2]Pediatrics and Adolescent Medicine, University Hospital Cologne, Cologne, Germany
Email: j.kwasny@dshs-koeln.de

INTRODUCTION

Children with cerebral palsy (CP) are often prescribed strength training exercises to improve independent gait and avoid or delay the necesity of orthopaedic intervention. However, strategies for preventing hip dysplasia in children with cerebral palsy lacks clinical consensus. Exercises which maximize hip extensors have been suggested as a possible target group [1]. Attempts to identify these exercises have been done from an EMG perspective, however, exercises which generate maximal hip extension moments in children with CP remains unknown.

METHODS

Four typically developing children (13.75±0.4 years, 60.3 ±15.1kg) and four (12.8±2.6 years, 44.5±11.9kg) children with CP participated in one kinematic and kinetic data collection session in a motion capture lab with 18 infrared cameras at 200 Hz (Qualysis) and in-ground and stairway instrumented force plates at 1000 Hz (Kistler). Subjects completed five repetitions of three typical rehabilitation exercises prescribed to children with CP: Bilateral squats, lunges, hip extension step up-and-down, as well as gait. The children with CP were permitted to use a rail for balance during squat and lunge. A generic musculoskeletal model [2] was scaled to static trials, and kinematics and kinetics were calculated for the exercises using OpenSim 4.4. Inverse kinematics and inverse dynamics were used to compute hip extension moments. Trials were time normalized to 100 percent and to subject body mass and mean moment curves were generated over all trials and subjects. Descriptive statistics and qualitative assessments were used to analyse the peak hip extension moments and mean hip extension moment curves due to the small sample size at this stage.

RESULTS AND DISCUSSION

Preliminary results indicate that the hip extension step up-and-down exercise generated the maximal hip extension moment in the children with CP (1.075 Nm/kg ±0.401), whereas in the control group, maximal extension moment occurred in the lunge exercise (1.408 Nm/kg ± 0.227) (Figure 1). Peak normalized hip extension moments decreased in the lunge and squat exercise relative to gait in the children with CP as they unloaded their hips while using the support rail.

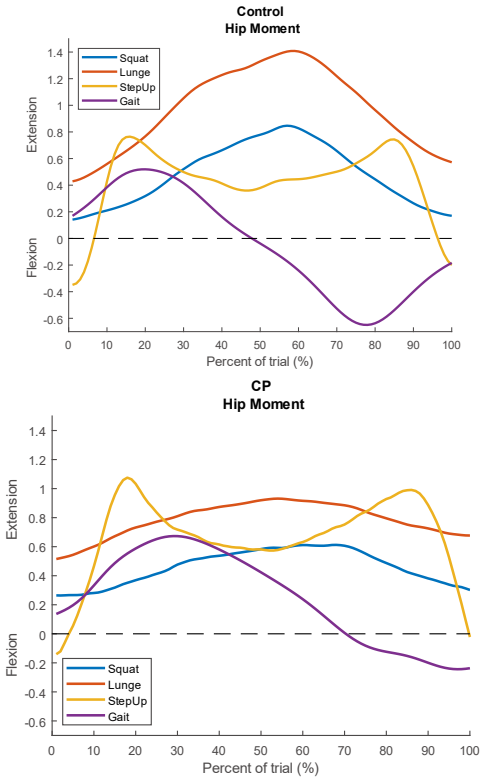

Figure 1 Normalized hip flexion and extension moments (nm/kg) of various exercises in children with CP and healthy controls.

CONCLUSIONS

Early results suggest hip extension step up-and-down exercise maximizes hip extension moments in children with CP. Future aims to evaluate the exercise protocols include increasing the sample size, and calculating the magnitude and orientation of the hip joint contact force, using subject specific musculoskeletal modelling.

ACKNOWLEDGEMENTS

Funding: German Sport University Cologne. Subject recruitment in cooperation with UniReha Köln.

REFERENCES

[1] Daly C. et al. *Gait and Posture* 70: 270-274, 2019.
[2] Rajagopal A et al. *IEEE Trans Biomed Eng* **63**:2068-79, 2016.

Longitudinal changes in Kinematics of the lumbopelvic hip complex and their association with the onset of CAM deformity: a two-year follow-up of high risk adolescent elite football players.

Dalia Al Otti[1,3], Stijn Ghijselings[1,3], Filip Staes[2], Lennart Scheys[1,3]

[1]*Institute for Orthopaedic Research and Training, University Hospitals Leuven, Belgium;* [2]*Department of Rehabilitation Sciences, KU Leuven, Belgium;* [3]*Department of Development and Regeneration, KU Leuven, Belgium.*

Corresponding author: Dalia.alotti@kuleuven.be

INTRODUCTION

Cam deformity of the proximal femur leads to a loss in the naturally concave head-neck junction. It has been linked to the development of intra-articular damage, femoroacetabular Impingement and ultimately to the early onset of hip osteoarthritis. Compelling evidence has identified adolescent males with high levels of physical activity to be at greater risk of developing CAM.

Recent longitudinal studies have shown that adolescents who develop CAM have distinct morphological features of the femur on radiological scans.[1] However, findings were primarily extracted from static imaging thus neglecting the highly dynamic nature of the etiology. Therefore a multidimensional kinematic exploration of movement execution and its association with the longitiudnal changes of radiological spine-pelvic-femoral parameters is highly warranted in this population.

METHODS

26 elite football players were included for baseline measurements and 2-year-follow-up measures are currently ongoing (6/26 completed). Players were initially included if they trained for a minimum of 12 hrs/week and underwent physical screening to rule out current pain or injury. Both at baseline and follow-up, participants underwent a hip radiographic examination consisting of a modified Dunn view scan and a full body bi-planar radiography scan (EOS imaging, Paris, FR): Table 1. Based hereon (alpha angle > 60°), participants were divided in a CAM and no-CAM group at follow-up. In addition, 3D kinematics (Vicon, UK) were collected during a range of motor tasks, including unconstrained deep squats. Resulting data was exported to Visual3D software (C-motion, USA) to analyse peak joint angles of pelvis and hip in the dominant leg.

	Age (years)	Weight (kg)	Height (cm)	Alpha angle (°)	Neck Shaft Angle (°)	Pelvic Incidence (°)
CAM (n=3)						
Baseline	14.3±1	54±9.5	162.2±6.7	52.0±4.4	133.1±2.9	49.4±7.0
Follow-up	16.6±1.5	65.6±6.5	173.2±5.2	63.2±2.8	134.3±1.7	49±3.0
No CAM (n=3)						
Baseline	13.4±0.2	52.0±11.4	168.0±10.6	51±2.7	129.0±5.1	45.9±3.0
Follow-up	15.5±0.2	65.3±7.6	179.9±3.2	53.2±2.2	130.6±3.7	46.3±5.8

Table 1: Descriptive statistics and femoro-spinoplevic angles for the two measurement points.

RESULTS AND DISCUSSION

Statistical significance was set to p <0.05 and a non-parametric approach was used. Kinematics at baseline vs. Follow-up showed significant differences in pelvis anteversion and hip abduction within the CAM group. Pelvic anteversion also significantly differed between the CAM and no CAM groups at follow-up. A Spearman correlation revealed a significant positive correlation between alpha angle and pelvic anteversion (r=0.92) as well as pelvic incidence (PI) (r=0.84) at follow-up.

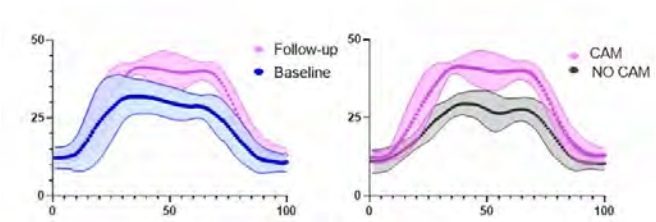

Figure 1: Y-axis represents Sagittal Pelvis range of motion in degrees (anteversion +) and X-axis represents 1 deep squat cycle.

CONCLUSIONS

Our preliminary results show that adolescents who develop CAM exhibit peak pelvic anteversion values that are higher than their baseline values as well as higher than peers with no CAM at follow-up. Such movement pattern has been linked to excessive anterior femoral head coverage which can lead to impingement.[2] This seems to be associated with an increase in PI values. A higher PI has been identified in adults with CAM as a predictor of symptom development in femoroacetabular Impingement.[3] Hence longitudinal analysis of dynamic spinopelvic characteristics has potential to identify adolescents that are at high risk of developing CAM as well as recognize charaterstics linked to symptom development in adulthood.These findings can be relevant in establishing clinical screening protcols.

REFERENCES

[1] P van Klij et al.,(2021), *Knee Surg Sports Traumatol Arthrosc.*;**29**(5):1401-1410

[2]M. Lamontagne et al., (2009) *Clin. Orthop. Relat. Res*, **467**(3): 645–650

[3] K.C.Ng et al.,(2018), *The American Journal of Sports Medicine*; **46**, 1331:1342

Validity and Reliability of Bodiometer Mobile App for Postural Analysis

Nesa Keshavarz Moghadam[1], Victor R. A. Cossich[1], Larry Katz[1]
[1]Sport Technology Research Laboratory, Faculty of Kinesiology, University of Calgary, Calgary, Canada
Email: nesa.keshavarzmoghad@ucalgary.ca

INTRODUCTION

Postural abnormalities are widespread in developed countries that can contribute to musculoskeletal disorders, pains, and diseases [2]. Although some advanced postural screening technologies exist, they are typically only available at specialized clinics [1]. Bodiometer is an innovative and accessible solution for mobile devices, offering a non-invasive, user-friendly, and cost-effective postural screening technology. This study aimed to evaluate the validity and reliability of the Bodiometer mobile app for 2D postural analysis in the sagittal plane.

METHODS

Step 1 – Validity: Bodiometer scans (using an iPad 8th) were compared to the data generated from a Vicon Motion System (6 Cameras, Vero, 100Hz), the reference gold standard. To conduct the tests, we used a mannequin. This approach helped eliminate the variability in individual participants. It enabled a clear understanding of the instrument's functionality and the potential for operator measurement errors without the interference of posture variability. To ensure consistency with Bodiometer's automatic virtual marker set, we placed reflexive markers on specific landmarks, including the right ear, shoulder and hip joint, lateral knee, and ankle. Then, we measured the angles of body parts – head, shoulder, hip, and knee – relative to the vertical line using the reflexive markers placed on specific landmarks, following the Bodiometer's approach (Figure 1). A total of 15 trials were collected using a tripod. The data was analyzed using one-sample t-test (Vicon's mean angle vs. Bodiometer), Intraclass Correlation Coefficient (ICC), and Root Mean Square Error (RMSE). Step 2 – Reliability: To assess the inter-rater reliability, five raters used iPads to screen posture, replicating the process used in clinical settings. To determine the intra-rater reliability, each rater repeated the tests three times within a single session, with a 3-minute. The app automatically calculated the angles of the body parts. To evaluate both the inter-rater and intra-rater reliability, we used the Intraclass Correlation Coefficient (ICC).

RESULTS AND DISCUSSION

Table 1 shows significant differences between Bodiometer and Vicon. The ICC was 0.95 for the validity data. For the reliability we observed excellent inter-rater reliability with an ICC of 0.99. Additionally, all evaluators exhibited excellent intra-rater reliability, with ICC values raging from 0.97 to 0.99.

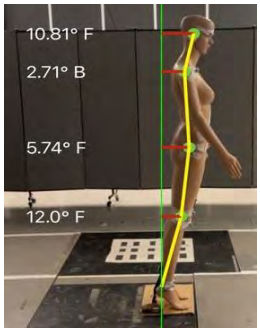

Figure 1 Virtual markers and body part angles generated using Bodiometer's mobile app for postural analysis.

CONCLUSIONS

Our study demonstrates that Bodiometer's mobile app is a valid and reliable tool for 2D postural analysis in the sagittal plane.

ACKNOWLEDGEMENTS

This research is supported by a MITACS postdoctoral grant cosponsored by Animation Leader Technology Inc., developers of Bodiometer.

REFERENCES

[1] Roggio F et al. *WJ Orthopedics,* **12(7):** 467-484, 2021.

[2] Kuo Y et al. *J Gait & posture*, **67:** 187-193, 2019.

Table 1: Bodiometer vs. Vicon Body Part Angles Sagittal Plane: comparison and Root Mean Square Error (RMSE)

Angles	Vicon	Bodiometer	p-value	RMSE
Head (°)	16.7 ± 0.0	17.5 ± 6.1	0.77	4.9°
Shoulder (°)	-6.9 ± 0.0	-5.5 ± 2.6	**0.05**	2.1°
Hip (°)	11.4 ± 0.0	8.0 ± 2.3	**<0.01**	3.1°
Knee (°)	10.0 ± 0.0	11.8 ± 2.4	**0.01**	2.2°

A MACHINE LEARNING APPROACH TO DIFFERENTIATE STABLE FROM UNSTABLE TOTAL KNEES FOR DATA MINING

Erica M. Ramirez [1], Kathrin Ebinger [1], Christopher Ferrigno [1], Denis Nam [1], and Markus A. Wimmer [1]
[1] Department of Orthopedic Surgery, Rush University Medical Center, Chicago, USA.
Email: markus_a_wimmer@rush.edu

INTRODUCTION

Joint instability after total knee arthroplasty (TKA) is a common observation and has been associated with activity limitations, pain and poor quality of life. From a mechanical perspective, joint stability is preserved when the joint can recover from subtle perturbations. However, establishing objective measurements for knee stability has been difficult [1]. Here, we propose a semi-supervised approach using clustering techniques to separate stable from unstable knee joints based on gait pattern and to subsequently data mining of the kinematic, kinetice and electromyographic (EMG) features. For the purpose of this abstract, we focus on EMG features and hypothesized that co-contractiction indices may differ.

METHODS

TKA subjects with occasional or frequent instability of the knee joint during daily activity underwent gait analysis in the Human Motion Lab. All subjects were evaluated with a point cluster (PCT) marker set and EMG surface electrodes. The ratio of mean EMG rectus femoris and biceps femoris was determined for each of the eight phases of the gait cycle according to Perry. Additional TKA subjects, who were tested under identical protocols, were added from an IRB approved data repository. As a comparator group, a healthy, elderly subject group, whose gait features should be different from those with self-reported and/or suspected TKA instability, was included as well.

Fourteen different gait variables, previously discussed as potential objective knee instability parameters [2], were applied to cluster subjects. Each combination was processed through a self-organizing map (SOM) with the neurons distributed in a two-dimensional grid. The SOM was tuned to different topographies, learning rates, and epochs; then each SOM output was used as input for the k-means. In our approach, the optimal number of clusters was investigated (between 2 and10). The solution reliability was evaluated through the Fleiss' Kappa index, and the clusters' consistency was assessed with the Silhouette coefficient. To identify differences between groups, one-way ANOVAs were performed. Post-hoc tests between groups were done using Bonferroni or Games-Howell.

RESULTS AND DISCUSSION

The final cohort comprised 91 TKA subjects and 34 healthy control subjects. Several combinations reached an almost perfect agreement, suggesting that clustering did not occur by chance. However, regarding the clusters' consistency, only two combinations gave reasonable results with one seemingly addressing 'instability'. A split based on dynamic joint stiffness (DJS) lead to a 'high stiffness' group with a minority population (12%) that included all but one of the known unstable subjects. The remaining TKA subjects showed a lower stiffness that was comparable with that of the healthy group. Hence, data mining was conducted on the DJS based clustering.

The EMG coactivity ratios throughout the gait cycle are shown in Figure 1. During the periods of initial contact, loading response and terminal swing the biceps femoris was dominant. During the remaining periods, for both the 'low stiffness' and 'healthy' subjects, the rectus femoris had a relatively higher activity than the biceps femoris, with a peak during initial swing. In contrast, for the 'high stiffness' subjects, biceps femoris activity was dominant ($p=0.033$ during initial swing).

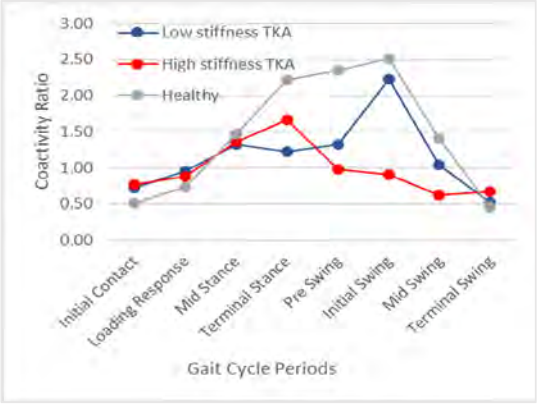

Figure 1 EMG Rectus Femoris to Biceps Femoris coactivity ratio.

CONCLUSIONS

Gait analysis in conjunction with machine learning provides a rich resource for discovery. Using a clustering approach that split the TKA cohort, we found differences in co-contraction indices between stable and unstable total knee joints.

ACKNOWLEDGEMENTS

Searle Pilot Award, Rush University

REFERENCES

[1] Baker PN et al. *Bone Joint J* **95-B(10)**: 1359, 2013.
[2] Schrijvers JC et al. *Gait Posture* **70**: 235-253, 2019

ENGAGEMENT OF THE CRUCIATES AND MEDIAL MENISCUS IS RELATED TO ANTERIOR-POSTERIOR KNEE LAXITY BUT NOT CRUCIATE LIGAMENT VOLUME

Erin Berube[1], Brian Frondorf[1], Joseph Manzi[1], Jacob Hirth[1], Swithin Razu[1], Danyal Nawabi[1], Andrew Pearle[1], Thomas Wickiewicz[1], Carl Imhauser[1]

[1] Biomechanics Department, Hospital for Special Surgery, New York, NY, USA
Email: berubee@hss.edu

INTRODUCTION

Rupture of the anterior cruciate ligament (ACL) is a debilitating injury with increased prevalence among young, active individuals[1]. Clinical studies have identified intrinsic factors that are associated with increased risk of non-contact ACL injury to guide interventions in these high-risk groups, including ligament properties and joint kinematics[2]. In particular, heightened anterior-posterior (AP) laxity is a risk factor for first time non-contact ACL injury, especially in females[3]. The anterior and posterior cruciate ligaments (ACL and PCL) are the primary ligamentous restraints to anterior and posterior tibial translation. Moreover, the ACL and medial meniscus (MM) work in concert to resist applied anterior tibial loads[4,5]. However, biomechanical factors that explain heightened AP laxity in the native knee are poorly understood. It is also not well understood how these parameters of tissue engagement relate to tissue geometry. The purpose of this biomechanical study was two-fold: to determine 1) whether AP laxity of the native knee is related to the biomechanical function of the ACL, PCL, and the menisci as quantified by the parameters of tissue engagement and 2) whether ACL and PCL volume is related to these tissue level properties of engagement.

METHODS

Thirteen, unpaired, fresh-frozen human cadaveric knees were acquired for testing (age: 37 ± 9, range: 25-54; 7 female) and MR scanned. Specimens were mounted to a robotic manipulator (Kawasaki ZX165U). Using the robot, AP forces of ±100 N were applied at 30° of flexion to simulate a clinical test of AP laxity. The force carried by the cruciates and menisci as a function of the applied AP loads was calculated via the principle of superposition. Subsequently, engagement parameters of the ACL, PCL, MM, and lateral meniscus (LM) were quantified. These parameters were: (1) in situ slack, (2) in situ stiffness, (3) tissue force at the peak applied anterior and posterior loads[5]. Subsequently, net in situ slack, defined as the difference between in situ slack of the ACL and PCL and of the PCL and MM was calculated. Finally, we measured cruciate volume using manual segmentation of the MR scans (Fig. 2). To address our goals, simple linear regressions were performed to identify correlations between (1) AP laxity and net in situ slack (mm) of the ACL/PCL, the PCL/MM and (2) AP laxity and in situ stiffness (N/mm) for each structure and (3) ACL/PCL volume and the parameters of tissue enagement. Finally, ACL and PCL volume were related to net in situ slack via multiple linear regression.

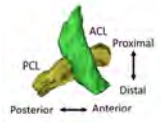

Figure 2: Representative segmentation of the ACL and PCL.

RESULTS AND DISCUSSION

The net in situ slack of the PCL/ACL and PCL/MM averaged 4.2 ± 2.2 ranging from 0.1 to 7.6 and 4.9 ± 2.7 mm ranging from 0.1 to 8.0, respectively (Fig. 1). AP laxity was positively correlated with the net in situ slack of both the ACL/PCL and the PCL/MM ($p \leq 0.008$) and to in situ stiffness of the ACL and the PCL ($p \leq 0.001$). ACL and PCL volume averaged 2430 ± 586 and 2670 ± 502 mm^3, respectively. ACL and PCL volume did not correlate with any parameters of engagement ($p>0.6$).

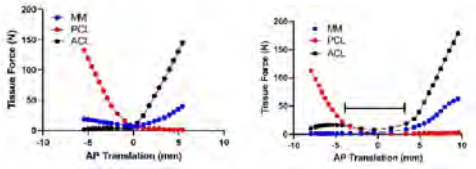

Figure 1: Representative plots of two knees with the least (left) and greatest (right) net in situ slack of the PCL and ACL. The black bar indicates net in situ slack.

We introduced a novel biomechanical measure, net in situ slack, which describes how force is passed between the major AP stabilizers as the knee undergoes AP translation. Our findings suggest those with heightened AP laxity may require specialized neuromuscular training to ensure their muscles effectively resist AP loads. This novel relationship may also inform surgeons how to tension ACL and PCL grafts intraoperatively. In knees with elevated AP laxity, the cruciates and medial meniscus provide minimal restraint to AP loads over a substantial range of AP translation. Therefore, individuals with highly lax knees must be more reliant on the muscular and articular anatomy to maintain joint stability, which may leave them at elevated risk of injury.

CONCLUSIONS

The net engagement of the PCL and ACL and the PCL and MM provide a framework for understanding why those with heightened AP laxity are at elevated risk of non-contact ACL injury. This framework provides the underpinnings for more focused injury prevention algorithms targeting muscular stabilizing mechanisms to compensate in the AP direction.

REFERENCES

1. Beynnon 2014 AJSM. 2. Wang 2021 Jorthop Sports Med 3. Uhorchak 2003 AJSM. 4. Kent 2020 AJSM. 5. Watanabe JOrthop Sci 2004 6. Imhauser 2017 Jbiomech

Investigating the Influence of Different Foot Positions during the Golf Swing on the Skin-Marker-Based Kinematics after Total Knee Arthroplasty

N. Horn[1], A. Ortigas Vásquez[2], P. Bänteli[3], S. Stulz3, P. Schütz[2], S. Ferguson[2], T. Drobny[1], R. List[3], S. Preiss[1]
[1] Department of Orthopaedics/ Golf Medical Center, Schulthess Clinic, Zurich, Switzerland.
[2] Institute for Biomechanics, ETH Zürich, Zürich, Switzerland.
[3] Human Performance Lab., Schulthess Clinic, Zürich, Switzerland.
Email: horn.nils@gmail.com

INTRODUCTION

Despite leading to joint discomfort in up to a third of players with total knee arthroplasty (TKA) [1], golf remains one of the most recommended sports by orthopaedic surgeons after knee replacement [2]. Among the potential solutions proposed to address this problem is the recommendation to modify a golfer's stance. This investigation therefore aims to assess rotational knee kinematics during the golf swing in three different foot positions of the leading leg. Our approach differs from that of previous research primarily in its focus on elderly TKA patients over young healthy participants, thereby serving as a better representation of the affected population.

METHODS

Eleven recreational golfers (age 69.6 ± 8.8 years; 2 females; weight 83.6 ±15.5 kg; height 1.78 ± 0.08 m; BMI 26.3 ± 3.8; months post-op 43.7 ± 11.9) with TKA in the lead leg were analysed at least two years post-operatively. Six subjects had Fixed-Bearing Persona TKA (Zimmer Biomet), while five had Mobile-Bearing Attune™ TKA (DePuy Synthes) implants. The golf swing using an 7 iron golf club was evaluated for three different foot positions of the lead leg: 1) self-selected, 2) 0° external rotation, and 3) 30° external rotation from stance set up to the end of follow-through. Motion capture used a marker-based optical system and the IfB marker set [3]. Rotational knee kinematics were evaluated using a linear mixed model analysis of variance ($p<0.0005$), with different foot positions as fixed effects (self-selected condition excluded), and implant design and subject as random effects.

RESULTS AND DISCUSSION

For the left knee, an angled lead foot significantly increased maximum tibial external rotation, while decreasing maximum internal rotation. Overall range of motion (ROM) in this plane was increased by a 30° foot position. In the frontal plane, ROM was not significantly affected, although maximum abduction decreased, and maximum adduction increased. For the right knee, an angled foot decreased ROM in the sagittal plane, while in the transverse plane maximum internal rotation decreased.

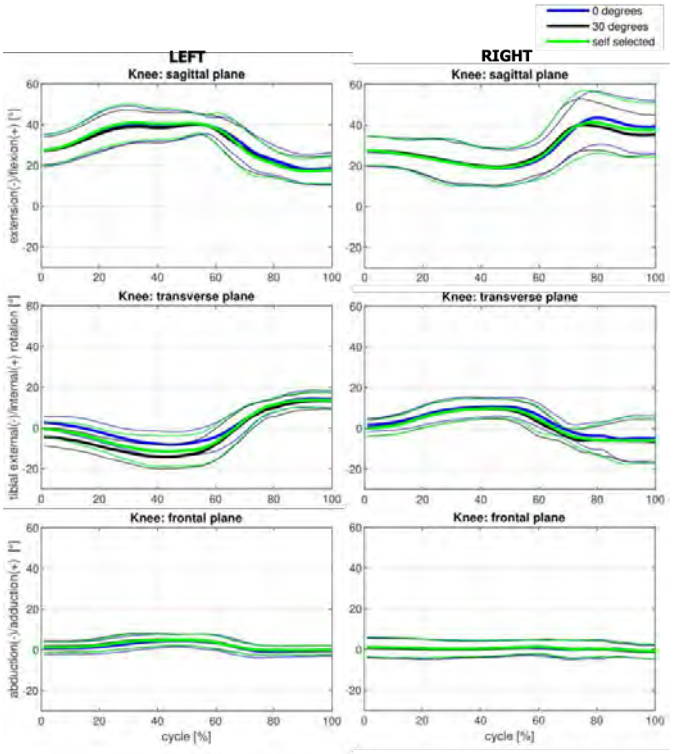

Figure 1 Angle progressions in three planes for left and right knees normalised to the golf swing cycle. Results presented as the mean (thick line) ± 1 SD (thin lines) over the subjects (n = 11).

CONCLUSIONS

Varying the position of the lead foot in the golf stance influences knee kinematics during the golf swing.

REFERENCES

[1] Mallon and Callaghan *J Arthroplasty* **8**(3*)*, 1993
[2] Oljaca et al. *Acta Orthop Belg* **84**(4), 2018
[3] List et al. *J Strength Cond Res* **27**(6), 2013

Table 1: Mean ± 1 SD of min, max and ROM values for knee angles in three planes (n = 11).

	Angle (°)								
	Sagittal			Transverse			Frontal		
	max	min	ROM	max	min	ROM	max	min	ROM
Left									
0	46.8 ± 5.3	16.5 ± 5.9	30.3 ± 8.1	14.9 ± 4.0	-9.5 ± 6.0	24.4 ± 8.0	5.2 ± 3.3	-1.7 ± 3.0	7.0 ± 1.7
30	46.2 ± 4.3	16.0 ± 6.1	30.2 ± 8.2	13.9 ± 4.0	-15.3 ± 5.8	29.2 ± 8.0	6.1 ± 3.0	-1.2 ± 2.6	7.3 ± 1.8
self-selected	47.5 ± 5.2	16.1 ± 5.6	31.4 ± 8.0	14.5 ± 3.6	-13.1 ± 6.8	27.6 ± 9.2	6.0 ± 2.8	-1.2 ± 2.7	7.2 ± 1.6
Right									
0	46.0 ± 12.4	16.4 ± 8.4	29.5 ± 14.8	12.2 ± 5.5	-9.8 ± 7.3	22.0 ± 7.6	2.5 ± 4.2	-2.5 ± 3.9	5.1 ± 2.0
30	43.4 ± 10.7	16.8 ± 8.7	26.6 ± 10.8	10.7 ± 5.5	-11.3 ± 6.7	21.9 ± 7.1	2.4 ± 4.1	-2.4 ± 4.0	4.8 ± 1.0
self-selected	45.6 ± 11.9	16.7 ± 8.8	28.9 ± 11.0	11.4 ± 5.7	-11.1 ± 7.5	22.5 ± 6.2	2.6 ± 3.9	-2.4 ± 4.1	5.0 ± 1.8

INCLUSION OF DISTAL FIBULAR TRANSLATIONS IN MULTI-SEGMENTED FOOT MODELING FOR LATERAL ANKLE LIGAMENT STRAINS

Renee Alexander[1], Rui Ding[1], and Tim Derrick[1]
[1] Department of Kinesiology, Iowa State University / Ames, Iowa, United States.
Email: rma24601@iastate.edu

INTRODUCTION

Ankle sprains account for over 80% of ankle injuries in sports with ankle injuries reported as 10-30% of all sports injuries [2]. Musculoskeletal models can be used to assess the strain in individual ligaments if the kinematics of the relevant bones are known. Input to these models are typically segment or joint angles, however, the distal fibula is known to translate relative to the tibia during plantar flexion and dorsiflexion [5]. It is unknown how these translations will affect the resulting ligament strain. Damage to the anterior talofibular (ATFL), posterior talofibular (PTFL), and calcaneofibular (CFL) ligaments characterize a lateral inversion ankle sprain. Thus, any movement of the fibula may impact the lateral ankle ligament strains and, therefore, the potential for an ankle sprain. The purpose of this research was to use a musculoskeletal model to estimate the effects of fibular translation on resulting lateral ankle ligament strain during plantar flexion and dorsiflexion at the tibiotalar joint.

METHODS

A musculoskeletal model of the foot [4] was implemented in MATLAB. The vertical and mediolateral translation of the distal fibula relative to the distal tibia were estimated from [3] for a typical range of motion during slow running of -20° plantar flexion to 20° dorsiflexion [1]. Anteroposterior translations were small and inconsistent and therefore not modelled. Anatomical position strains were estimated to be 3, 8, and 7% for the ATFL, PTFL, and CFL ligaments respectively [6]. Two models were developed, one without and one with tibiofibular translations.

RESULTS AND DISCUSSION

In both models, as the tibiotalar joint became more plantar flexed, strain increased in the stretched ATFL, decreased in the relaxed PTFL and remained relatively constant in the CFL (Figure 1). Fibular translations increased strain in the ATFL and the CFL at -20° plantar flexion. PTFL strains decreased. However, PTFL and CFL strains increased at 20° dorsiflexion (Table 1). Between the models, the inclusion of fibular translations increased the ATFL and PTFL's strain change per degree of plantar flexion/dorsiflexion at the tibiotalar joint, and hence increased their maximum strain and laxity at the ends of the tested range of motion. The strain in the CFL, however, did not change much between the models.

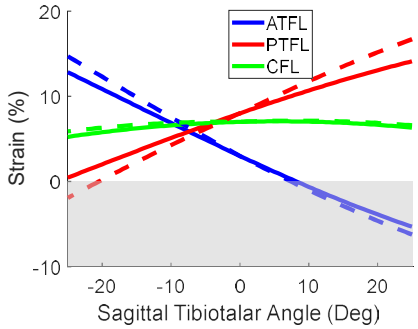

Figure 1 Ligament strain estimates for the ATFL (blue), PTFL (red), and CFL (green). Dashed lines represent the model including fibular translations as compared to the model without (solid lines).

CONCLUSIONS

Fibular translations were included in a musculoskeletal model to estimate their effect on resulting lateral ankle ligament strains during plantar flexion and dorsiflexion. Ligament laxity and strains increased based on the ankle position within the range of motion. Our musculoskeletal model can become more accurate by including fibular translations; however, it is not clear if these small values can be estimated in vivo when skin marker movement is included.

REFERENCES

[1] Arndt A et al. *J Biomech.* **40(12)**: 2672-2678, 2007.
[2] Fong D et al. *Sports Med.* **37**: 73-94, 2007.
[3] Huber T et al. *Foot Ankle Surg.* **18**: 203-209, 2012.
[4] Malaquias T et al. *Comput Method Biomec.* **20**: 153-159, 2016.
[5] Novak A et al. *Foot Ankle Int.* **35**: 178-191, 2014.
[6] Purevsuren T et al. *Proc Inst Mech Eng H: J Eng Med.* **232(5)**: 458-467, 2018.

Table 1: Estimated ligament strains for slow running range of motion. Model without (1) and with (2) fibular translations.

Ligament	-20° PF (1)	-20° PF (2)	0°	20° DF (1)	20° DF (2)
Anterior Talofibular (ATFL)	10.84	12.29	3	-3.88	-4.62
Posterior Talofibular (PTFL)	2.02	0.21	8	13.05	15.16
Calcaneofibular (CFL)	5.78	6.32	7	6.65	6.86

IDENTIFYING THE SLACK POSTURES OF HUMAN SKELETAL MUSCLE ACROSS THREE-DIMENSIONAL JOINT

Jun Umehara[1,2], Norio Fukuda[2], Shoji Konda[2,3] and Masaya Hirashima[2]
[1] Faculty of Rehabilitation, Kansai Medical University, Hirakata, Japan.
[2] Center for Information and Neural Networks, Advanced ICT Research Institute, NICT, Suita, Japan.
[3] Department of Health and Sport Sciences, Osaka University Graduate School of Medicine, Toyonaka, Japan.
Email: umeharaj@makino.kmu.ac.jp

INTRODUCTION

The elasticity of skeletal muscle is defined as the length-tension relationship for modeling the muscle [1]. The length-tension relationship should be biomechanically accurate for every muscle because it substantially influences the simulation of musculoskeletal model. However, prior models are limited in muscles on the two-dimensional (2D) joints, such as the ankle and knee, unable to address the muscle across the three-dimensional (3D) joint, such as the shoulder. The reason behind this is an ill-posed problem as formulating many-to-one correspondence between joint postures and muscle tension. Here we demonstrate a novel method to model the 3D posture-tension relationship of the human skeletal muscle by identifying the passive properties.

METHODS

Data were obtained from five healthy men. The posture of upper limb and the shear modulus of pectoralis major muscle passing across the shoulder joint were simultaneously measured using motion capture system and ultrasound elastography respectively, while the upper limb was passively and slowly moved to the horizontal extension direction by a dynamometer (2 degree/s) to lengthen the pectoralis major muscle. These measurements were systematically performed on nine movement planes at 10 to 90° abduction, and consequently a large amount of data on the shear modulus and its corresponding postures was obtained (Figure 1 A).

The shear modulus corresponding to postures was represented in the polar coordinates. Subsequently, we performed the dimensionality reduction to transform the data points of shear modulus from the polar coordinates into a one-dimensional space by minimizing the area enclosed by the boundary of data points of shear modulus (Figure1 B). Finally, the conventional linear and exponential function previously used to model the passive muscle properties in the 2D joint [2] was fitted to the experimental data on the low-dimensional space using a least square method. The fitting accuracy was assessed by calculating the coefficient determination (R^2).

RESULTS AND DISCUSSION

Interestingly, the shear modulus corresponding to 3D postures in the polar coordinates presented an analogical geometric distribution to that in the 2D joint. Consequently, the R^2 in terms of fitting accuracy ranged from 0.75 to 0.93 in all participants, indicating the conventional linear and exponential model can be accurately fitted to the experimental data (Figure1 C). Figure1D shows the modeled relationship between 3D postures and shear modulus in Cartesian space. In this figure, as a representative of the many-to-one correspondence between postures and shear modulus, the dashed red line indicates the so-called muscle slack postures on which the passive tension begins to increase.

In this study, we hypothesized that the 3D posture-tension relationship could be represented in the low-dimensional space by the conventional model, given the comparable biomechanical properties of muscle between 2D and 3D joints. Our results showed that this analogy between 2D and 3D joints holds.

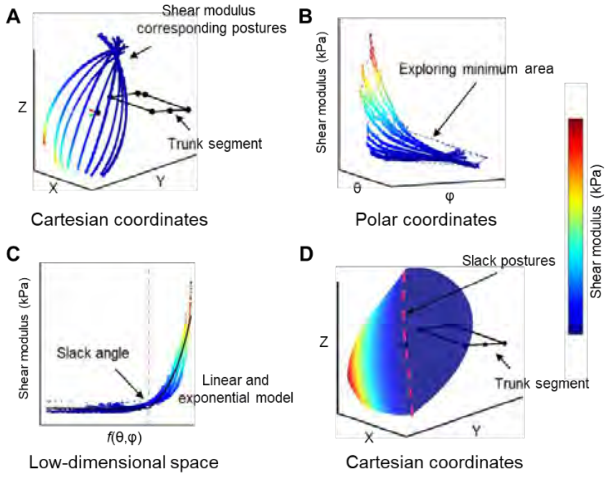

Figure 1 Modeling of 3D posture-tension relationship.

CONCLUSIONS

This study demonstrated that the 3D posture-tension relationship of skeletal muscle could be represented using the conventional model by identifying the passive properties in the low-dimensional space.

ACKNOWLEDGEMENTS

This work was supported by a Grant-in-Aid for Early-Career Scientists (22K17765).

REFERENCES

[1] Zajac FE. Crit Rev Biomed Eng **17**: 359-411, 1989.
[2] Nordez A et al. *J Biomech* **43**: 379-82, 2010.

EASY-TO-USE MATLAB SOFTWARE FOR PERSONALIZING OPENSIM NEUROMUSCULOSKELETAL MODELS

Claire V. Hammond[1], Marleny M. Vega[1], Di Ao[1], Geng Li[1], Spencer T. Williams[1], Mohammad S. Shourijeh[1], Ayman Habib[2], Carolynn Patten[3] and Benjamin J. Fregly[1]

[1]Department of Mechanical Engineering, Rice University, Houston, United States.
[2]Department of Bioengineering, Stanford University, Stanford, United States.
[3]Department of Physical Medicine and Rehabilitation, UC Davis School of Medicine, Sacramento, United States.
Email: cvhammond@rice.edu

INTRODUCTION

Scaled generic musculoskeletal models are commonly used to analyze the movement of human subjects. However, such models do not represent the unique characteristics of individual subjects. To maximize model fidelity, one can use personalization techniques to minimize the errors between experimental measurements and model predictions. This study describes an easy-to-use software toolset for personalizing joint, muscle-tendon, neural control, and ground contact model properties for OpenSim [1,2] musculoskeletal model.

METHODS

We have developed four model personalization tools and a data preprocessing tool to integrate with the OpenSim GUI and run from XML settings files similar to other OpenSim tools [1, 2]. Running a tool starts a Matlab process that performs the actual calculations. The toolset accepts a scaled OpenSim model along with marker motion, ground reaction, and EMG data collected during gait and/or other movements and calculates personalized joint, muscle-tendon, neural control, and ground contact model parameter values. The tools in typical order of use are:

1) Joint Model Personalization (JMP) – personalizes parameters defining joint positions/orientations within bodies and, optionally, body scaling and marker locations within bodies in a scaled OpenSim model.

2) Data Preprocessing - organizes OpenSim inverse kinematics, inverse dynamics, and muscle analysis results calculated after JMP, as well as EMG data, into trial- and data-specific formats to facilitate faster computation and organization for subsequent tools.

3) Muscle-tendon Model Personalization (MTP) - personalizes parameters defining Hill-type muscle-tendon models and estimates muscle activations and forces for muscles with EMG data.

4) Neural Control Model Personalization (NCP) - personalizes parameters defining muscle synergy control models for all muscles and personalizes parameters defining Hill-type muscle-tendon models and estimates muscle activations and forces for muscles without EMG data.

5) Ground Contact Model Personalization (GCP) - personalizes parameters defining deformable foot-ground contact models.

The flow of data and parameter values through the toolset is outlined in Figure 1.

RESULTS AND DISCUSSION

The Matlab-based Model Personalization toolset for OpenSim is freely available on SimTK at https://simtk.org/projects/nmsm. The project includes tutorials that demonstrate how to use each tool based on sample video motion capture, ground reaction, and EMG data collected from an individual post-stroke walking on an instrumented treadmill.

CONCLUSIONS

The Model Personalization toolset described here will make it easier for the research community to develop personalized neuromusculoskeletal models of individual subjects or patients and may eventually help facilitate the design of optimized personalized interventions for various movement impairments.

ACKNOWLEDGMENTS

This work was funded by the National Institutes of Health under award number R01 EB030520.

REFERENCES

[1] Delp SL et al. (2007). IEEE, 55: 1940-50.
[2] Seth A et al. (2018). PLoS, 14(7): e1006223.

Figure 1: The flow of data and parameter values through the toolset.

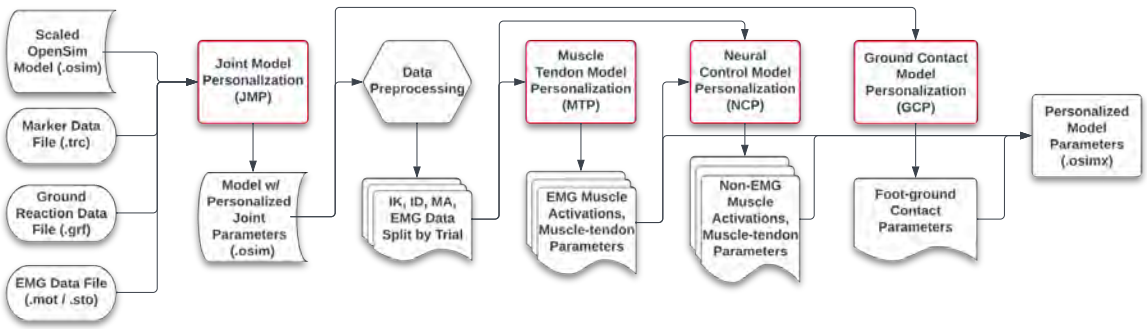

COMBINED STATISTICAL SHAPE MODEL CAN PREDICT LOWER LIMB BONE SHAPE VARIATION IN A PAEDIATRIC POPULATION

Julie Choisne[1], Laura Carman[1] and Thor Besier [1]

[1] Auckland Bioengineering Institute, The University of Auckland, Auckland, New Zealand
Email: j.choisne@auckland.ac.nz

INTRODUCTION

The skeletal anatomy of children differs significantly from adults, yet musculoskeletal models were mainly developed from adult datasets. Subject-specific models from medical imaging are costly and time-consuming [1]. Ideally, we would scale musculoskeletal models using an atlas built from a population of paediatric bones that captures morphological variation of the growing skeleton. The aims of this study were to: 1) characterise lower limb bone shape variation in a typically developed paediatric population aged 4 to 18 years old and 2) evaluate bone shape prediction error using a combined shape model.

METHODS

Post-mortem CT scans of 333 children (137 F, Age: 12 ± 5 Y, H: 148 ± 24cm, M: 49 ± 22kg) [2] were obtained from the Victorian Institute of Forensic Medicine (VIFM, Australia). The pelvis, femurs, and tibias/fibulas were segmented. Each bone was non-rigidly registered and fitted to a template mesh, using radial basis functions to achieve nodal correspondence. Each pelvis, femur, and tibia/fibula were then rigidly aligned to a selected template case with a neutral pose. The bones were then combined and the shape model was characterized using principal component analysis [2]. The predictive power of the combined statistical shape model was assessed with a leave one out (LOO) analysis using height, ASIS width, femur length, and tibial length, which were found to be the best predictive factors. Further optional inputs to the model can include partial medical imaging and motion capture marker location.

RESULTS AND DISCUSSION

The first 3 principal components (PCs) captured 92.5%, 2.07%, and 0.53% of the variation in the dataset (Figure 1). The first PC described combined size and shape variation and the second and third PCs described shape variation and the aspect ratio of the long bones. The results from the LOO analysis gave an average RMSE of 2.94 ± 0.83mm and a Dice score of 0.8.

CONCLUSIONS

This unique dataset characterises morphological variation in lower limb bones in a paediatric population aged from 4 to 18 years. It allows for prediction of new bone shapes with lower errors than typical scaling for use in clinical settings and musculoskeletal modelling. Future work will add articulation to the model for incorporation into the MAP client for building personalised OpenSim models.

ACKNOWLEDGEMENTS

Data from the VIFM made this research possible. The authors would like to thank the University of Auckland doctoral scholarship, the Health Research Council of NZ, the Friedlander Foundation and the Aotearoa Foundation for providing financial support to this project.

REFERENCES

[1] Scheys L. et al. *Gait Posture* **33**: 158-64, 2011.

[2] Carman L. et al. *Sci. Report.* **12**: 3251, 2022

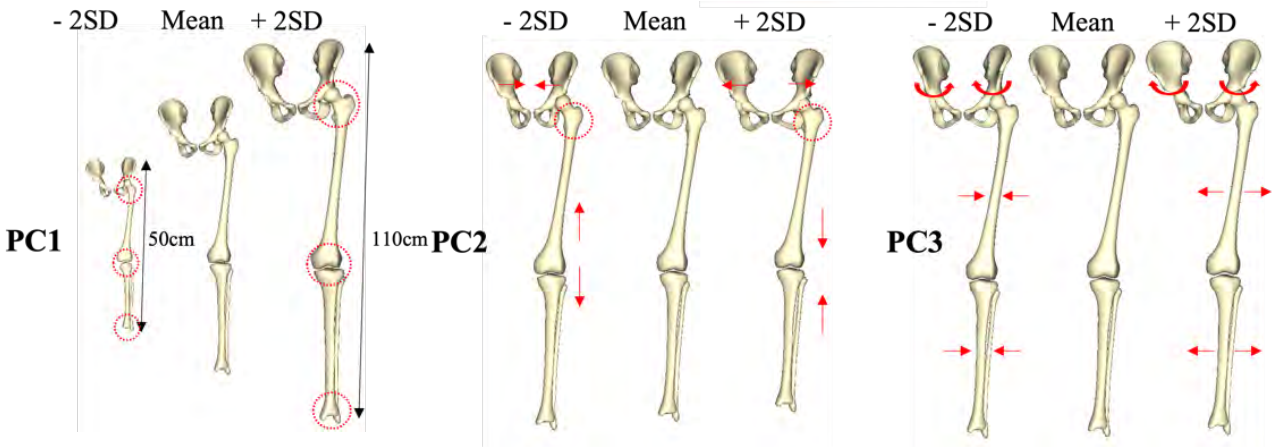

Figure 1: First 3 PCs of the combined statistical shape model. Red annotation indicate main changes in shape

Muscle Force Estimation Based on Angle–EMG–Force Relationship and Electromechanical Delay

Takuya Mitani[1] and Koh Inoue[2,3]
[1] Graduate School of Engineering, Kagawa University, Takamatsu, Japan.
[2] Area of Mechanical Systems Engineering, Kagawa University, Takamatsu, Japan.
[3] National Institute of Advanced Industrial Science and Technology (AIST), Takamatsu, Japan.
Email: s22d502@kagawa-u.ac.jp

INTRODUCTION

Measuring muscle force during gait can provide critical knowledge in the field of gait biomechanics; however, noninvasive measurement of muscle force is difficult. Muscle force is estimated using a musculoskeletal model. In previous studies, muscle force estimation was assisted by electromyography (EMG), such as %MVC [1]. However, the effect of the electrophysiological characteristics of muscle force exertion, such as changes in joint angle, on the EMG amplitude [2] and electromechanical delay (EMD) of muscles [3] still have not been considered for muscle force estimation using EMG. The purpose of this study was to estimate muscle forces during gait using the angle–EMG–force (muscle activity level) relationship (a.-E.-f. relationship) and EMD of muscles.

METHODS

One healthy adult (male, 21 years old, 169 cm, 59.2 kg) participated. Gait kinematic, kinetic, and EMG data were measured by a motion capture system, force plates, and wireless surface EMG sensors, respectively.

To obtain the a.-E.-f. relationship of the leg muscles, a static force measurement task was conducted for each muscle with a custom-made measurement device. The knee and ankle joint angles were set under five conditions for the tasks. The participant adjusted the EMG amplitude of each muscle to target values (0–150% of the maximum values during gait, every 30%) with visual feedback. The muscle activity level during the task was estimated using a musculoskeletal model (AnyBody Technology). A regression model (a.-E.-f. relationship, quadric surface fitting) under a static condition was constructed.

The EMD was calculated using the estimated muscle force and the EMG signals. The EMD time was calculated with a cross-correlation function [3] using all the data from contraction to relaxation during the task (*ccEMD*). Another EMD time was calculated using the intervals of the EMG and muscle force onsets (*onsetEMD*) and offsets [4] (*offsetEMD*).

The muscle force during gait was estimated using the musculoskeletal model and a Hill-type muscle model with and without the a.-E.-f. relationship and the EMD.

RESULTS AND DISCUSSION

The EMG–force relationship changed with the joint angle. Figure 1 shows the estimated muscle force during gait. The rectus femoris and the tibialis anterior did not generate muscle force during the stance phase in the estimation without EMG but were activated with the a.-E.-f. relationship. These results suggest that muscle force estimation with EMG can include agonist and antagonist muscle co-activation. In addition, the a.-E.-f. relationship provides more accurate estimation compared with previous studies using EMG.

The timing of the estimated muscle activation differed with and without the EMD. Moreover, the onset of *ccEMD* was approximately 7% of the gait cycle later than *onset–offsetEMD,* on average, through the muscles. The peak force difference with and without the EMD was 138 N for the tibialis anterior. The contraction velocity affected the force estimation values.

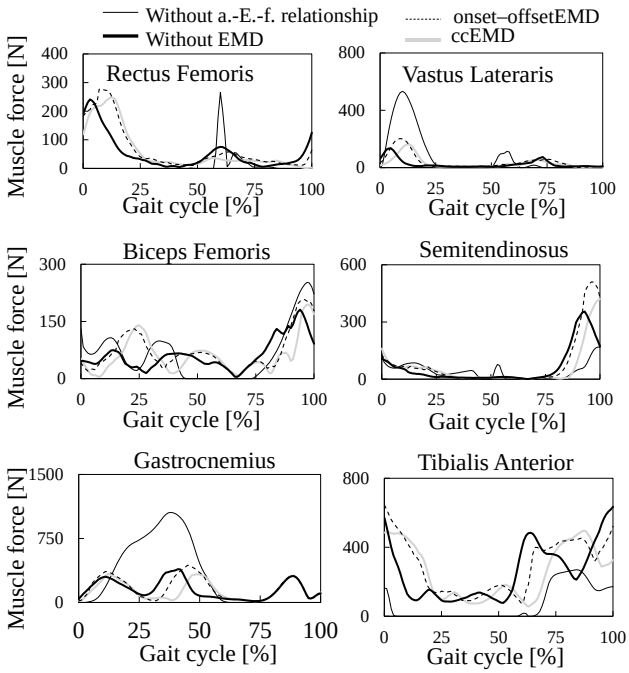

Figure 1 Estimated muscle force

CONCLUSIONS

The muscle force during gait was estimated with and without the a.-E.-f. relationship and EMD of leg muscles. The results showed differences in the activation timing and peak force values. The present method using the a.-E.-f. relationship and the EMD provides more accurate estimation for individuals compared with the methods used in previous studies.

REFERENCES

[1] Lloyd D et al. *J Biomech* **36**: 6, 2003.
[2] Doheny E et al. *J Electromyogr Kinesiol* **18**: 5, 2008.
[3] Vos E. et al. *Eur. J. Appl. Physiol* **60**: 60, 1990.
[4] Chavanagh P R et al. *Eur. J. Appl. Physiol* **42**: 1979.

RELATIVE ENERGY COST OF THE GAIT PHASES ACROSS WALKING SPEEDS

Israel Luis[1], Maarten Afschrift[2], Friedl De Groote[3] and Elena M. Gutierrez-Farewik[1,4]
[1] KTH MoveAbility Lab, Dept. Eng. Mechanics, KTH Royal Institute of Technology, Stockholm, Sweden.
[2] Faculty of Behavioural and Movement Sciences, Vrije Universiteit Amsterdam, Amsterdam, Netherlands.
[3] Department of Movement Sciences, KU Leuven, Leuven, Belgium.
[4] Department of Women's and Children's Health, Karolinska Institutet, Stockholm, Sweden.
Email: ailp@kth.se

INTRODUCTION

The swing phase was estimated to account for 29% of the total metabolic cost at a preferable walking speed, which lies within the experimental inferences that suggest a relative cost from 10% up to 33% [1]. Yet, little is known about the relative cost of the swing phase across walking speeds. Energy expenditure may be estimated using metabolic cost models, which consist of equations describing the relationship between muscle-tendon mechanics and heat dissipation at various contraction conditions. A comprehensive understanding of the relative cost of the gait phases might support rehabilitation programs and the design of assistive devices. In this study, we performed inverse dynamics musculoskeletal simulations informed with EMGs to estimate the relative energy cost of muscle activity during stance and swing phases across walking speeds.

METHODS

Eight able-bodied adults were asked to walk at 100%, +/-15%, 30%, and 45% of their preferred walking speed, during which gait kinematics (Vicon V16, CGM2.4), ground reaction forces (AMTI), and EMGs in one leg were recorded in biceps femoris long head, semitendinosus, vastus lateralis and medialis, tibialis anterior, gastrocnemius lateralis and medialis and soleus, using bipolar surface wireless electrodes (myon/Cometa). Vastus intermedius excitation was estimated as the average of vastus lateralis and medialis excitations. A musculoskeletal model [2] was scaled to each subject's dimensions, and maximum muscle force was scaled according to muscle volume, estimated based on body weight and height [3]. Inverse kinematics and inverse dynamics were computed for all trials using OpenSim 4.1. The passive force-length characteristics of the muscle actuators were calibrated to match experimental passive torque-angle relationships reported by Silder et al. [4]. An algorithm based on direct collocation was used to solve the muscle redundancy [5]. Recorded time-series EMG data were used to constrain the excitations of the corresponding muscles in the musculoskeletal model. Remaining muscle excitations were computed by minimizing muscle excitations squared assuming optimal motor control. Achilles and patellar tendon stiffness were optimized so that the muscle-tendon actuators' torque better reproduces the inverse dynamics solution. The energy expenditure was computed using a metabolic cost model proposed by Uchida et al. [6], and repeated measure correlation was used to compute the relationship between the relative energy cost of gait phases and walking trials.

RESULTS AND DISCUSSION

Of the total energy cost at self-selected speed, 31.5% occurs during the swing. The major contributor to energy cost in the stance was the plantarflexors during push-off, and in the swing, the hip flexors during initial and mid-swing. Relative energy cost during gait phases correlated with walking speed ($p<0.05$); proportionally, more energy was consumed during stance than during swing as walking speed increased.

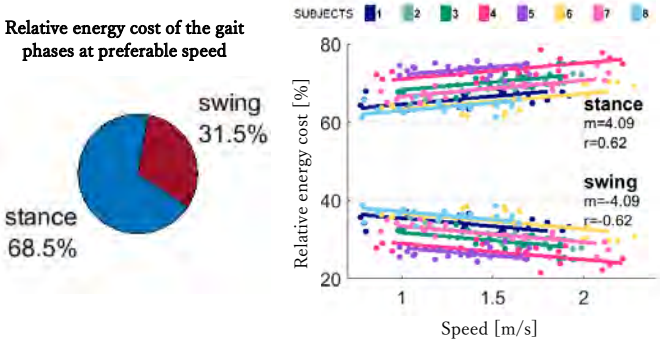

Figure 1 Average relative energy cost of the gait phases among all subjects at the preferable speed [left] and repeated measure correlation of the relative energy cost of the gait phases at each subject across walking trials [right].

CONCLUSIONS

Almost 1/3 of the total metabolic cost during normal walking occurs in the swing phase, and this proportion decreases as speed increases. It is suggested that an increase in the walking economy might be achieved by supporting primarily the plantarflexors during the stance phase and hip flexors during the swing phase.

ACKNOWLEDGMENTS

The authors would like to acknowledge the Swedish Research Council (nr 2018-00750) and the Promobilia Foundation (nr 18200) for their generous support.

REFERENCES

[1] Umberger, J. R. Soc. Interface, **7**, 1329-1340, 2010.
[2] Rajagopal et al, *IEEE Biomed*, **63**, 2068-2079, 2016
[3] Handsfield et al. *J. Biomech*, **47**, 631-638, 2014
[4] Silder et al. *J. Biomech*, **40**, 2628-2635, 2007
[5] De Groote et al, *Ann. Biomed. Eng.*, **44**, 2922–2936, 2016
[6] Uchida et al, *PLOS ONE*, **11**, e0150378, 2016

TOWARDS AUTOMATIC GENERATION OF SUBJECT-SPECIFIC KNEE JOINT KINEMATIC MODELS FROM MEDICAL IMAGING

Beichen Shi[1], Martina Barzan[1], Azadeh Nasseri[1], Jayishni Maharaj[1], Laura Diamond[1], David Saxby[1]

[1]Griffith Centre of Biomedical and Rehabilitation Engineering, Menzies Health Institute Queensland, Griffith University, Gold Coast, Australia

Email: beichen.shi@griffithuni.edu.au

INTRODUCTION

The passive 6 degree-of-freedom tibiofemoral joint (TFJ) kinematics can be predicted via parallel mechanisms, which are composed of rigid analytic representations of articular contact surfaces and ligamentous constraints [1]. Medical imaging can be used to personalized these mechanisms, but requires extensive manual processing thus limitting widespread use. Automatic identification of feduciary antomy via geometric analysis or atlas deformation has been proposed. However these approaches do not include ligamentous attachments, and thus cannot be used for automatic generation of personalized knee kinematic models. This study aimed to: (1) automatically identify geometrical parameters required to generate personalized TFJ kinematic models and compare them against manually identified equivalent; (2) compare TFJ kinematics from automatically and manually generated models; and (3) validate these models using *in vivo* knee kinematics from medical imaging.

METHODS

Three-dimensional models of lower limb bones as well as TFJ ligaments and cartilages were created using magnetic resonance imaging (MRI) of 8 healthy youths (4 females; 14.0±2.6 years) taken at ~0° TFJ flexion. Thirty geometric parameters (e.g., TFJ articular surface centres, ligament attachments) were both manually and automatically identified. Anatomic landmarks and articular surfaces were estimated via geometric analysis (e.g., principal inertia axis, cross-sectional area, primitive shape fitting) using the STAPLE toolbox (https://github.com/modenaxe/msk-STAPLE) [2]. Ligament attachments were embedded into an anatomic atlas (i.e., median-size bone) and non-rigidly registered to novel bones, thus approximating their ligament attachments [3]. Automatically and manually identified geometric parameters were compared using Euclidean distance (mm) for landmarks and ligament attachments (centroid), and root mean square error (mm) (RMSE) of vertices for articular surfaces.

RESULTS AND DISCUSSION

Compared to manual identification, automatic approach identified bone landmarks and joint articular surfaces with mean (SD) error of 5.6 (3.7) and RMSE of 3.4 (1.0) mm, respectively (Table 1). Compared to manual identification, ligament attachment centroids were automatically identified with mean (SD) error of 6.9 (4.0) mm (Table 1). Manually identified ligament attachment surfaces from MRI were 4.7 mm in average radii when approximated as circular.

Table 1. Tibiofemoral joint geometric parameter error (Euclidean distance (mm) for landmarks and ligaments centroid; RMSE for articular surfaces).

Estimation method	Mean (SD) error	Range
Landmarks	5.6 (3.7)	1.9, 12.9
Articular surfaces	3.4 (1.0)	1.5, 5.4
Ligament attachments	6.9 (4.0)	2.6, 19.5

SD-standard deviation; RMSE-Root mean square error.

Ligament attachments estimations using atlas registration had lower accuracy than bone landmark estimations which were computed via geometric analysis (Table 1). Ligament centroids were 6.9 mm from manual identification, or ~1.5 times average radius of ligament attachment surfaces (4.7 mm). Identification of ligament attachments might be improved by adjusting bone atlas (e.g., averaging multiple atlantes) or directly deriving from segmentation of ligaments on MRI. Knee articular surfaces were estimated with low error (Table 1). The worst-case estimate the articular surface on femoral condyle had RMSE of 5.2mm when compared to manual identification. The resulting approximated spheres based on the articular surfaces had radii of 17 (manually identified) and 19 (automatically identified) mm and a minor difference of 1.2 mm between sphere centres. The effect of the parameter estimation errors on the predicted TFJ kinematics is unknown and will be investigated further.

CONCLUSIONS

Geometric parameters required to construct TFJ kinematic model can be estimated from subject-specific bone geometry. At the conference, aims (2) and (3) will be fulfilled by constructing the TFJ mechanism from the auto- and manual-generated geometrical parameters and comparing their predicted TFJ kinematics.

REFERENCE

[1] Wilson, D. R. et al. *Gait Posture* **5(2)**: 108-115, 1997.
[2] Modenese, L. et al. *J Biomech*: 110186, 2020.
[3] Zhang, J., et al. *Comput Methods Biomech Biomed Engin* **21(7)**: 498-502, 2018.

ADVANCED SIGNAL PROCESSING TECHNIQUES INTEGRATED INTO A TEXTILE-EMBEDDED EMG GARMENT FOR ANKLE TORQUE ESTIMATION IN POST-STROKE INDIVIDUALS

Donatella Simonetti[1], Maartje Hendriks[2], Joost Herijgers[3], Carmen Cuerdo del Río[1], Bart Koopman[1], Noel Keijsers[2] and Massimo Sartori[1]

[1] Biomechanical engineering, University of Twente, Enschede, Netherlands.
[2] Sint Maartenskliniek, Ubbergen, Netherlands.
[3] Twente Medical Systems Int. (TMSi), Oldenzaal, Netherlands
Email: d.simonetti@utwente.nl

INTRODUCTION

Post-stroke gait recovery is one of the primary rehabilitation goals. In clinics, observational gait assessments and instrumented 3D gait analysis are the standards for functional assessments of residual motor capacity. While the first is limited to its subjectivity, the second requires a fully equipped laboratory with pricey instrumentation and time-consuming setup and data processing. Moreover, current clinical assessments do not give quantitative metrics on muscle strength and how it affects gait performance throughout the rehabilitation. In this regard, equipped gait laboratories together with neuromusculoskeletal (NMS) modeling techniques can provide objective evidence of the patient's musculoskeletal function. However, this technology is not compliant with the restricted time limit in clinical practice. We developed a unique pipeline that integrated a fast-to-wear modular 64 textile-embedded EMG leg garment, a generalized and automated EMG clustering algorithm for the fast localization of leg muscles, and an EMG-driven NMS model for the estimation of muscle-specific activation, ankle muscle-tendon forces and resulting torques during walking in post-stroke individuals.

METHODS

Seven hemiparetic stroke participants (age = 57 ± 8.7 years, height = 179 ± 5.1 cm, weight = 88.9 ± 16.5 kg) were recruited by the Sint Maartenskliniek (Ubbergen, The Netherlands). EMG, kinetic and kinematic data were recorded during two main tasks: walking at comfortable and faster speeds. A 64-channel EMG grid embedded in a stretchable garment was applied on the paretic leg. The 64-electrode space was reduced in a few muscle-specific clusters by applying two non-negative matrix factorization (NNMF)-based steps. Afterward, averaged muscle activations were computed for both speeds, and input to EMG-driven NMS model to estimate ankle torque. The automatically derived EMG-driven ankle torque estimation was compared with respect to experimental torque and manually derived EMG- driven torque estimates.

RESULTS AND DISCUSSION

The results showed the ability of NNMF-based EMG clustering to extract the position of the main muscles by using 64-electrode activations during a few gait cycles of slow walking speeds. We used the automatically derived muscle-specific clusters and obtained electrophysiologically consistent muscle-specific envelopes during both walking speeds. Finally, the EMG clustering algorithm provided muscle-specific EMG envelopes with the accuracy needed to drive an NMS modeling framework and estimate dynamically consistent ankle torques. This was visible for the unseen tasks (i.e., not used for the NMS model calibration, such as fast walking) and when using abnormal muscle activations from post-stroke individuals. We show the results of automatically derived EMG (Figure 1.A) and estimated torque (Figure 1.B) for one subject walking at a comfortable speed.

CONCLUSIONS

We show how to go from a multi-channel EMG-embedded leg garment to ankle plantar-dorsi flexion torque by means of automatic NNMF-based EMG clustering and NMS modeling techniques. The developments made in this study open new avenues for fast and quantitative musculoskeletal function assessment in post-stroke individuals and potentially for any injured population.

ACKNOWLEDGEMENTS

The work was supported by EFRO OP Oost GUTs (20913301). The smart garment was developed in collaboration with TMSi (Oldenzaal, Netherlands) and Bard.zo Proad (Ommen, Netherlands).

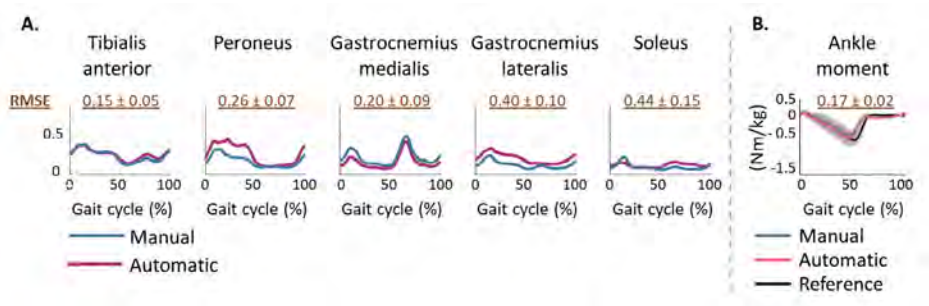

Figure 1: (A) Manually (blue) and automatically (red) derived EMG envelopes. The mean over all gait cycles, for one subject, comfortable walking speed and muscles are plotted; (B) Experimental ankle torques (black) and estimated via EMG-driven NMS modeling using both automatically (red) and manually (blue) derived EMG envelopes.

DIGITAL SOLUTION: A 3-DIMENSIONAL KINEMATIC RATING ALGORITHM FOR SINGLE-LIMB STANCE TEST

Yu Yuan Lee[1], Lena Fennen[1], Rosemary Dubbeldam[1]

[1] Institute of Sport and Exercise Sciences, University of Münster, Münster, Germany

INTRODUCTION

Single Limb Stance Test (SLST) is a reliable movement test to assess fall risk and balance [1]. Our aim is to automate the SLST performance assessment by developing a marker-based rating algorithm using the Balance Error Scoring System (BESS) [2].

METHODS

19 healthy young adults (25 ± 5 years, 10 males, 9 females) and 9 young adults with chronic ankle instability (25 ± 6 years, 6 males, 3 females) were included. The Qualisys motion capture system was used to record full body segment motions. The participants performed the SLST with eyes-closed and eyes-open for 60 seconds. Each participant performed two trials of each condition on each limb. Only the second non-dominant (healthy) or impaired (patients) limb SLST trial was analysed. The BESS (Table 1) was evaluated for each trial by 3 people and the balance of each participant was classified as good, moderate, or bad. *MATLAB*® was used to build the rating algorithm based on the BESS items. The algorithm used the marker positions of the toe, fore foot, hind foot, thigh, trunk, and wrist segments to calculate the balance errors in the BESS items. A paired t-test was used to study the relationship between human and digital BESS assessment.

Table 1: Balance Error Scoring System (BESS)

1.	Lifting forefoot or heel from the ground
2.	Pelvis movement more than 30 degrees of flexion or abduction
3.	Stepping, stumbling, or falling
4.	Arm movement
5.	Remaining out of the test position for more than 5 seconds
6.	Eye close count (not applicable in 3D segment motion capture system)

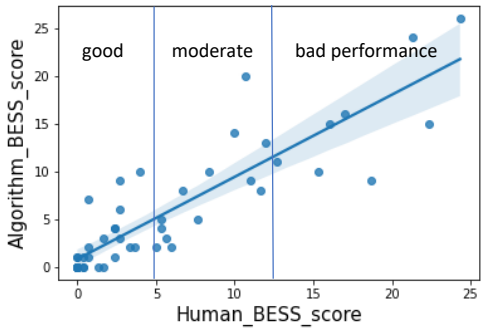

Figure 1: The comparison of the BESS score between the rating algorithm and human assessors.

RESULTS

49 trials including 26 eyes-closed and 23 eye-open SLSTs were analysed. Among them, 60% demonstrated good, 24% moderate, and 16% bad performance, which corresponded to a BESS of <5, 5-12 or >12 respectively. The BESS score assessed by the algorithm is highly correlated to the human assessed BESS score ($r = 0.88$, $p = 0.001$) (Figure 1). The Root Mean Square Error between the assessments is 2.1.

DISCUSSION AND CONCLUSIONS

The marker-based rating algorithm can efficiently and objectively assess SLST performance. The algorithm is repeatable and more accurate in small movement assessment than the subjective human observations. Furthermore, the algorithm can be further deployed in a 2-dimensional video-based motion capture system to provide a low-cost solution for the assessment of fall risk and balance.

ACKNOWLEDGEMENTS

We would like to thank V. Lima, A. Radetzky and O. Ojomo for their assessment of the BESS.

REFERENCES

[1] Drusini A et al. *Aging Clin Exp Res* **14**(1): 42-46, 2002
[2] Rienmann B et al. *J Spo Rehab* **8**(2): 71-82, 1999

NOVEL ANALYSIS OF CENTRE OF PRESSURE IN TEXTURED SHOES: A PILOT STUDY

Helen Branthwaite[1], Wendy Carswell[1] Shin Hirai[2], Andrew Greenhalgh[3,1], Ben Hunter[4] and Nachiappan Chockalingam [1]

[1] Centre for Biomechanics and Rehabilitation, Staffordshire University, Stoke on Trent, UK
[2] Mizuno Corporation, Osaka, Japan.
[3] School of Life and Medical Sciences, University of Hertfordshire, Hatfield, UK
[4] School of Human Sciences, London Metropolitan University, London, UK
Email: n.chockalingam@staffs.ac.uk

INTRODUCTION

Falls are a growing health concern in older adults. Interventions for fall prevention include exercises and sensory stimulation with textured surfaces [1]. Clinical monitoring of falls is a multipurpose task that is subjectively measured. Balance, related to unexplained falls, measured in gait labs, utilises centre of pressure (COP) excursion analysis on pressure or force plates. Traditional methods focus on evaluating stability through posture variability or magnitude of sway. However, recent research using non-linear analyses has led to a better understanding of the underlying physiology. Indeed, fractal analyses are considered useful tools to analyse postural control. Different frequency ranges can be analysed, revealing the role of proprioception and the visuo-vestibular system in neural control [2]. This paper focuses on a novel fractal analysis to extend the knowledge in this area and to aid the development of evidence-based insole interventions to reduce the incidence of falls.

METHODS

Twenty-one healthy females (age: 62.2 ± 3.7 yr; body mass: 73.0 ± 23.8 kg; stature: 1.58 ± 0.19 m) were recruited. Footwear grouping was randomly assigned in a single blinded manner. Shoe types included: a control with no texture (C; n = 6); full length texture with a dimpled midsole (T1, n = 7); and forefoot only texture with dimple in forefoot only (T2; n = 8) [Figure 1]. Participants were instructed on use of the shoe which included wearing for a minimum of 45 minutes, 3 times a week over a six-week period. Baseline COP data were recorded for 30 sec during quiet barefoot standing on a Footscan pressure mat (RScan International, Olen, Belgium) recording at 250 Hz pre- and post-intervention. Linear measures of COP included: anteroposterior (AP) range and mediolateral (ML) ranges. Fractal scaling of the COP velocity and positional data in AP and ML directions was quantified using frequency specific fractal analysis (FsFA; [2]) Frequency bands for proprioceptive and visuo-vestibular neural control were set at 20-2 Hz ($FsFA_{High}$) and 0.5-0Hz ($FsFA_{Low}$), respectively. A two-way repeated measures ANOVA (time x group) was used to test for differences in each of the dependent variables. Effect sizes were described in terms of partial eta-squared (ηp^2, with $\eta p^2 \geq 0.06$ representing a moderate effect and $\eta p^2 \geq 0.14$ a large effect).

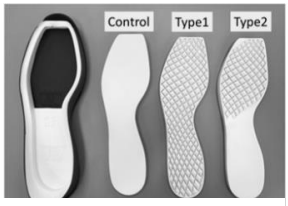

Figure 1. Construction of intervention footwear for each condition midsole.

RESULTS AND DISCUSSION

No time x group interaction effects were shown. A significant main effect for group was evident in AP COP range ($p = 0.034$, $\eta p^2 = 0.492$). A significant main effect was also demonstrated for time in $FsFA_{High}$ of the velocity in the ML direction ($p = 0.010$, $\eta p^2 = 0.763$). No further differences were identified between groups for fractal scaling measures. $FsFA_{High}$ and $FsFA_{Low}$ of COP velocities were closer to white noise ($1/f^0$). Conversely, FSFA of COP positional data was between Brownian ($1/f^2$) and pink (1/f) noise, values are in accordance with previous work [2].

Table 1: Tables that extend across both columns should be placed at the bottom of the abstract.

	Control (C)		Full-length (T1)		Forefoot (T2)	
	Pre	Post	Pre	Post	Pre	Post
COP Position						
$FsFA_{High}$ ML	1.16 ± 0.22	1.28 ± 0.64	1.38 ± 0.36	1.25 ± 0.30	1.22 ± 0.34	1.34 ± 0.29
$FsFA_{High}$ AP	1.48 ± 0.34	1.65 ± 0.35	1.65 ± 0.33	1.64 ± 0.24	1.63 ± 0.26	1.53 ± 0.38
$FsFA_{Low}$ ML	1.26 ± 0.97	1.28 ± 0.99	1.22 ± 0.16	1.27 ± 0.30	1.22 ± 0.16	1.21 ± 0.17
$FsFA_{Low}$ AP	1.22 ± 0.08	1.23 ± 0.10	1.43 ± 0.14	1.29 ± 0.17	1.31 ± 0.07	1.28 ± 0.11
COP Velocity						
$FsFA_{High}$ ML *	0.64 ± 0.39	0.47 ± 0.32	0.87 ± 0.54	0.47 ± 0.16	0.44 ± 0.22	0.45 ± 0.22
$FsFA_{High}$ AP	0.41 ± 0.25	0.41 ± 0.28	0.46 ± 0.34	0.31 ± 0.12	0.39 ± 0.29	0.29 ± 0.11
$FsFA_{Low}$ ML	0.49 ± 0.09	0.47 ± 0.12	0.53 ± 0.19	0.47 ± 0.19	0.58 ± 0.14	0.53 ± 0.21
$FsFA_{Low}$ AP	0.39 ± 0.12	0.43 ± 0.20	0.35 ± 0.10	0.44 ± 0.14	0.52 ± 0.18	0.43 ± 0.17

Values are expressed as Mean ± SD. ML, mediolateral; AP, anteroposterior. * denotes a significant main effect for time ($p < 0.05$).

This work demonstrated a significant decrease over time in $FsFA_{High}$, representing a shift towards white noise. $FsFA_{High}$ is indicative of how movement is regulated by somatosensory feedback mechanisms [2]. In the linear measures, a significant group effect was noted between the midsole conditions, with AP COP range greatest in the two experimental groups (T1 and T2). This could render the user of the midsole more adaptable over time.

CONCLUSIONS

The marked decrease in scaling exponent in the novel midsole over time, shows the potential utility of this intervention to alter short-loop postural regulation.

REFERENCES

[1] Collings R et al., *Foot* **25**(3)159-163, 2015
[2] Gilfriche P et al., Front. Physiol. **9**:293;2

DYNAMIC OPTIMIZATION OF HUMAN GAIT TO SOLVE KINEMATIC-KINETIC MISMATCH

Zuming Xiao[1], Xinyue Wang[1], Jianqiao Guo[1], Qiang Tian[1]
[1] Key Laboratory of Dynamics and Control of Flight Vehicle, School of Aerospace Engineering, Beijing Institute of Technology, Beijing, China
Email: guojianqiao@bit.edu.cn (J. Guo)

INTRODUCTION

Dynamic modelling of human gait has been widely used to investigate the biomechanical alternations due to musculoskeletal pathology. However, numerous factors, including the measurement errors of the spinal curve flexions, the inertial differences between the musculoskeletal model and the corresponding subject, etc., can cause a mismatch between the kinetic and kinematic measurements. Therefore, using the measured joint kinematics as model inputs, the human gait model cannot keep upper body balance. This study proposed a dynamic optimization method to eliminate this mismatch by introducing an interpolation function to rectify the measured errors of spinal kinematics.

METHODS

The study has been approved by the ethics committee of Beijing Institute of Technology. A healthy male subject (29 years, 175 cm, 59 kg) was recruited and instructed to walk at a certain speed. Nineteen reflective markers were placed on the following anatomical landmarks: the left/right anterior superior iliac crest, the midpoint of the posterior superior iliac spine, the front side of the left/right thigh, the left/right lateral femoral condyle, the left/right medial femoral condyle, the left/right tibial trochanter, the left/right lateral malleolus of the fibula, the left/right medial malleolus of the tibia, the left/right toe, and the left/right heel.

A multibody musculoskeletal model with a detailed lumbar structure was developed using our in-house code [1]. During the simulation, the lower limb joint movements were constrained based on the measured data, and only the pelvic sagittal posture was calculated via forward dynamics. Foot-ground reaction forces were determined using a contact model for soft tissues [1].

To rectify the mismatch between kinematic and kinetic data, a three-order Fourier series was used to define the lumbar spine flexion angle in the sagittal plane, and the range for Fourier coefficients was determined based on the measured spinal curve in literature [2-3]. The posture of L1-L5 vertebrates was distributed according to the lumbopelvic rhythm [4]. The Fourier coefficients were then obtained through dynamic optimization. The cost function minimized the errors of the sagittal pelvic posture along with the spinal flexion angle during a gait cycle. The periodicity constraint was also utilized to decrease the deviation between each gait cycle. The optimization process was implemented in MATLAB using the fmincon function. A total of ten local optimizations were performed since the model parameter optimization was sensitive to the initial guess.

RESULTS AND DISCUSSION

As shown in Fig. 1, the predicted gait can keep balance without falling. Increasing the weight of the spinal flexion in the cost function can reduce its variations. The optimized spinal movements were in qualitative agreement with the literature. However, the predicted range of spinal bending (43 deg) was slightly larger than that in the literature [2] (40 deg). Moreover, the predicted spinal bending curve obtained still performed a deviation of 12 deg between the beginning and end of the gait cycle, which could be related to the form of the interpolation function or the failure to find the global optimum. Further investigations would extend the proposed method to three-dimensional cases.

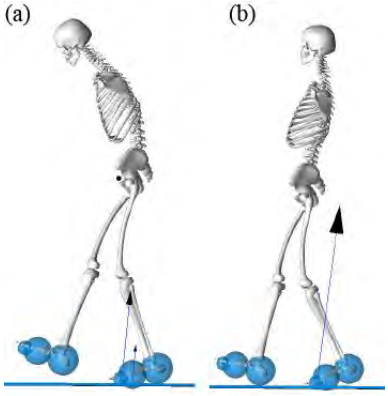

Figure 1 Comparison of the predicted spine flexion before (a) and after (b) dynamic optimization.

CONCLUSIONS

The proposed method successfully predicted feasible solutions of a two-dimensional spinal curve without falling, highlighting the possibility of quantifying the patient-specific spinal motions without attaching infrared reflective markers.

ACKNOWLEDGEMENTS

This work was supported in part by the China National Natural Science Foundations of China (12102035).

REFERENCES

[1] Wang X et al. *Acta Mech Sin*, **38**: 522140, 2022.
[2] Preece SJ et al. *Hum Mov Sci* **45**: 110-118, 2016.
[3] Seay JF et al. *J Spine* **36**: E1070-E1079, 2011.
[4] Christophy M et al. *Biomech Model Mechanobiol*, **11**: 19-34, 2012.

Markerless motion capture is sensitive to postural balance parameters in a clinical stroke population.

Anastasija D. Mihic[1], Jereme B. Outerleys[1], Sachitha R.B.A. Wijekoon[2], Stephen H. Scott [2], Kevin J. Deluzio[1], Elise K. Laende[1]

[1] Mechanical and Materials Engineering, Queen's University, Kingston, Ontario.
[2] Centre for Neuroscience Studies, Queen's University, Kingston, Ontario.
Email: Anastasija.mihic@queensu.ca

INTRODUCTION

The centre of mass (COM) is widely used to evaluate postural control, as it provides a measure of the distribution of body mass in relation to the base of support. Postural control is a critical aspect of balance and stability, and its assessment is crucial in evaluating the functional abilities of individuals. The measurement of postural sway has widely been studied in individuals following stroke to understand the effects of neurological impairment on balance[1][2]. COM however, cannot be directly measured and is estimated through stereophotogrammetric methods such as motion capture or centre of pressure (COP) measurement using force plates. Traditional marker-based motion capture methods are cumbersome due marker placement and thus, a more straight forward approach using COP from force plates has been adopted[3]. Although force plates are less time consuming and require less technical expertise than marker-based methods, their use poses a barrier to clinical integration as they are expensive, non-portable, and require special installation. Markerless motion capture is a novel solution that utilizes a deep learning approach to estimate anatomical landmarks and calculates 3D pose from video, allowing for estimation of COM from a full body model. The markerless solution removes the need for specialized labs, minimizes technical requirements, and is more portable allowing easier integration into clinical settings. The objective of this study was to determine if COM derived from markerless motion capture is sensitive enough to detect differences in postural control between stroke and healthy age matched controls.

METHODS

Inpatient stroke participants were introduced to the study by physiotherapists. Each participant performed a quiet standing balance task with the instructions of standing with their toes pointed forward, arms by their side, eyes open looking straight ahead. Participants with no known history of neurological or musculoskeletal impairments served as a control group. Each participant preformed a quiet stand with the same instructions as above. All participants wore the shoes and clothing they came in with that day. The trials were recorded at 60 Hz using eight commercially available time-synchronized Sony RX0II (Sony Corporation, Minato Japan) video cameras. Video data were processed using Theia3D (Theia Markerless, Kingston, ON) to obtain COM kinematics. Data were filtered at 5 Hz using a low pass Butterworth filter in Visual3D (C-motion, Germantown, MD). All data were normalized by COM height[4] and the range of COM excursion was calculated. Group differences in the medio-lateral (ML) range were compared using a Mann-Whitney-Wilcoxon test. Significance was set at 0.05. All statistical analyses were performed in R (v.4.2.2, R Core Team).

RESULTS AND DISCUSSION

16 participants were include in the analysis, 8 stroke (2 female, 6 male; mean(SD) age 77(13), range 58-93) and 8 healthy controls (4 female, 4 male; mean(SD) age 68(8.1), range 60-83). Compared with healthy controls, participants who had a stroke had higher postural sway in the ML direction (median(IQR) excursion (mm): stroke 29.2(12.6), controls 18.0(5.4), p = 0.01, Figure 1). These findings are consistent with the literature[1] where individuals with stroke where shown to have a larger sway in the ML direction.

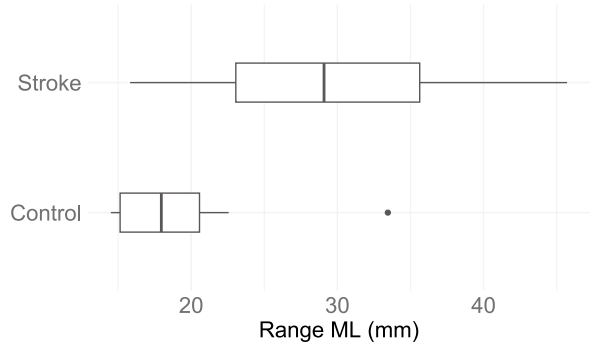

Figure 1 Range of COM excursion in the ML direction of a stroke population versus an age matched control.

CONCLUSIONS

Markerless motion capture is sensitive to differences in postural sway characteristics between individuals following stroke and healthy age matched controls. The increased accessibility of the technology compared to historical methods make it a promising tool for clinical integration.

REFERENCES

[1] Dickstein R. et al. *Arch Phys Med Rehabil* **81**: 364-67, 2000.
[2] Yu W. et al. *Arch Phys Med Rehabil* **89**: 1133-9, 2008.
[3] Winter D. et al. *J. Neurophisol* **80**: 1211-1221, 1998.
[4] Chiari L. et al. *Clin. Biomech* **17**: 666-667, 2022.

AGE-RELATED CHANGES IN ANKLE PROPRIOCEPTION AND THEIR RELATIONSHIP TO POSTURAL CONTROL

Chrysostomos Sahinis[1], Anastasia Papavasileiou[1], Anastasia Theodosiadou[2], Marie Fabre[3], Thomas Lapole[3], Baudry Stephane[2], Dimitrios A Patikas[1], and Ioannis G Amiridis[1]

[1] School of Physical Education & Sport Science, Aristotle University of Thessaloniki, Laboratory of Neuromechanics, Serres, Greece
[2] ULB Neuroscience Institute, Université Libre de Bruxelles, Laboratory of Applied Biology and Research Unit in Applied Neurophysiology, Brussels, Belgium
[3] Université Jean Monnet Saint-Etienne, Lyon 1, Université Savoie Mont-Blanc, Laboratoire Interuniversitaire de Biologie de la Motricité, F-42023, Saint-Etienne, France
Email: sachinic@phed-sr.auth.gr

INTRODUCTION

Proprioception enables the conscious and unconscious perception of the spatial and mechanical status of the musculoskeletal system, providing essential information for the production of coordinated movements and to control balance. However, as people age, the proprioceptive sensors and their neural pathways undergo alterations that lead to a decreased sensitivity, acuity, and integration [1]. These alterations reduce efficiency of balance control, leading to an increased reliance on visual inputs and increased agonist-antagonist coactivation [2]. Our study aimed to investigate the relationship between proprioceptive function at the ankle level and postural control across lifespan.

METHODS

Thirty participants divided into three groups of age: Group 1: < 18 years, Group 2: 18-40 years and Group 3: > 40 years. The evaluation of postural control was performed on a force platform to compute the center of pressure (CoP) displacement in four different sensory conditions: open eyes and close eyes, stable and unstable surface (foam). The mean velocity of the CoP excursion in antero-posterior and medio-lateral direction was computed to quantify the postural sway.
The evaluation of ankle proprioception was performed using unilateral and contralateral tests of sense of position during both plantar flexion and dorsiflexion. The ipsilateral test consisted in placing for 15 s the ankle in a target position that the participant had to retain and subsequently reproduce, while the referenced contralateral test involved placing one ankle in a reference position that the participant had to reproduce with the contralateral ankle. The mean absolute error was used to provide an index of the real difference between the performance produced and the target.

RESULTS AND DISCUSSION

Among the different groups, Group 2 presented the lesser CoP velocity while Group 1 exhibited the greatest CoP velocity ($p < 0.05$). Similarly, the Group 2 displayed less mean absolute error (greater proprioception), only in the contralateral test of plantar flexors while the Group 1 presented the greatest mean absolute error ($p < 0.05$). Additionally, a significant correlation was observed between contralateral test of plantar flexors only with the eyes-open condition in stable surface (the greater the error, the greater the postural displacement).

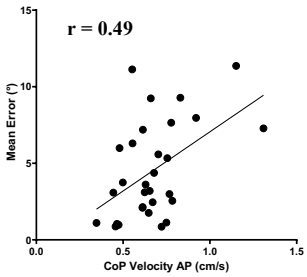

Figure 1 Relationship between contralateral plantar flexion sense of position test with Center of Pressure velocity in the anterior-posterior axis.

CONCLUSIONS

A better proprioceptive acuity is associated with lower CoP displacement during postural control tasks. Our study highlights the importance of proprioception in maintaining postural stability throughout lifespan. This has important implications for the development of interventions aimed at improving balance control, particularly in populations with compromised proprioceptive function, such as older adults or individuals with neurological disorders.

ACKNOWLEDGEMENTS

This research was funded by the Greek General Secretariat for Research and Technology (ERA-NET NEURON JTC 2020, 271 T12EPA5-00018)

REFERENCES

[1] Henry & Baudry *J Neurophysiol* **122**:525-38, 2019.
[2] Craig et al. *Neuroscience* **332**: 251-261, 2016.

PROPRIOCEPTIVE INTERFERENCE VIA TENDON VIBRATION DURING STANDING IN CHILDREN WITH CEREBRAL PALSY

Patikas D.[1], Fabre M.[2], Sahinis C.[1], Theodosiadou A.[3], Lapole T.[2], Amiridis I.G.[1], Baudry S.[3], Papavasileiou A.[1]

[1] Laboratory of Neuromechanics, School of Physical Education and Sports Science at Serres, Aristotle University of Thessaloniki, Serres, Greece.

[2] Université Jean Monnet Saint-Etienne, Lyon 1, Université Savoie Mont-Blanc, Laboratoire Interuniversitaire de Biologie de la Motricité, F-42023, SAINT-ETIENNE, FRANCE

[3] Laboratory of Applied Biology and Research Unit in Applied Neurophysiology, ULB Neuroscience Institute, Université Libre de Bruxelles, Brussels, Belgium.

Email: dpatikas@auth.gr

INTRODUCTION

Cerebral palsy (CP) is a permanent movement disorder that affects muscle tone, with symptoms such as poor coordination, tremors, muscle stiffness and muscle weakness. Impaired balance contributes to gait deficits and earlier studies have documented that children with CP are less stable when performing static tasks with and without visual feedback [1]. This suggests that children with CP are likely to present deficits in integrating sensory inputs from other sources such as proprioception. Local tendon vibration (LTV) is a means of increasing muscle spindle afferents activity, distorting the proprioceptive signal [2]. Perturbations induced by LTV during standing are compensated by postural adjustments, as reflected in muscle activity. However, whether CP leads to specific postural compensation in response to LTV remains unknown. The purpose of this study was to examine the stability and leg muscle activation through electromyography (EMG) of children with CP and typically developed (TD) children, before, during, and after LTV, when standing with eyes closed.

METHODS

Ten children with CP (13.0±1.7 yrs, 147.3±0.5 cm, 48.1±0.9 kg) and 16 TD children (14.0±3.8 yrs, 161.2±1.2 cm, 54.8±0.9 kg) were asked to stand with eyes closed for 60 s (three trials), while bilateral LTV was applied over the Achilles tendon for 15 s. The velocity of the center of pressure [CoP; on the anterior-posterior (AP) and mediolateral (ML) direction] and trunk (Tr) were calculated with data from a force platform and an accelerometer respectively. EMG responses from the soleus (SOL), gastrocnemius medialis (MG) and tibialis anterior (TA) muscles were measured. All data were analyzed in 5-s windows before LTV (pre-LTV), after the LTV onset, during LTV (i.e., last 5 s of LTV) and after the end of LTV (post-LTV). The rate of change of the variables after the onset, during and after the offset of LTV was expressed as the $\log_2$ ratio relative to values before LTV onset. A linear mixed model was used to compare the differences between the LTV conditions, groups, and their interaction.

RESULTS AND DISCUSSION

Both groups increased their CoP-AP, CoP-ML and Tr velocity, when LTV was introduced, with greater increase for the CP than TD group in Tr velocity ($p=0.005$). This shows that although LTV was applied distally, on the Achilles tendon, its effects were more pronounced over the trunk for children with CP, indicating a more general destabilization. EMG amplitude increased in all muscles at the onset and during LTV in children with CP ($p<0.001$) but not TD children, except for TA at the onset and during LTV (Figure 1).

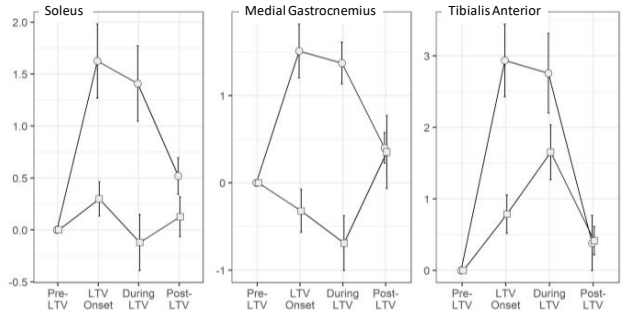

Figure 1 Change in EMG activity for children with CP (circles) and TD children (squares) relative to the values before LTV.

CONCLUSIONS

The main finding of this study is that in the presence of LTV, children with CP have different neuromuscular response compared to TD children, by activating both plantar- and dorsiflexors and resulting greater destabilization at trunk level. This indicates greater dependency from proprioceptive feedback in CP and illustrates one possible underlying cause of their motor disability. This dictates the need to implement interventions that promote somatosensory integration.

ACKNOWLEDGEMENTS

This research was funded by the Greek General Secretariat for Research and Technology (ERA-NET NEURON JTC 2020, 271 T12EPA5-00018)

REFERENCES

[1] Rose J et al. *Dev Med Child Neurol* **44**: 58-63, 2002.

[2] Roll JP et al. *Exp Brain Res* **76**: 213-22, 1989

Relative importance of the visual system for balance control is reflected in the continuous margins of stability while walking

Saskia Neumann[1], Cyrille Mvomo[1], Deepak Ravi[3], Friederike Schulte[2], Lorenz Assländer[4], Chris Awai[1]
[1] cereneo Foundation, Switzerland
[2]SturzZentrum Schweiz, Switzerland [3]Laboratory for Movement Biomechanics, ETH Zürich, Switzerland
[4]Department of Sport Science, University of Constance, Germany
Email: saskia.neumann@cereneo.foundation

INTRODUCTION

The adaptability of the locomoter system to respond to environmental changes such as perturbations during walking is based on the interaction of the muskuloskeletal and central nervous system. Aging is associated with a degradation of these systems and overreliance on visual feedback, which diminishes the capability to react to challenges to stability during walking, leading to balance deficits and falls. Perturbation-based balance training (PBT) mimics the accidental and unpredictable nature of slips and trips in daily life in a safe environment and allows reactive gait adjustments. While PBT demonstrates efficacy in reducing fall risk, the underlying mechanisms is unclear. One candidate mechanism is a recalibration of the sensory weights away from latency- and attention-heavy processes such as vision. We here investigate the interaction between visual contribution to balance control and margin of stability (MoS) during walking.

METHODS

Within this study, we investigate 20 healthy adults over 60 years of age who receive three blocks of eight minutes of multidirectional perturbation training on a Computer Assisted Rehabilitation Environment (CAREN). Prior and after the training, a virtual Sensory Integration Test (vSIT) [1] is administered to assess visual contribution to balance control. Within the training, a total of 32 perturbations are applied in medio-lateral (2.25-18cm displacement) and anteroposterior (0.5-2.25 m/s^2 acceleration) direction while walking at a comfortable walking speed. Perturbation magnitude is personalized based on the maximal perturbation successfully resisted during standing. For this analysis, the MoS are calculated for all steps within block 1 of the training and is compared to the visual weights from the vSIT taken just prior.

RESULTS AND DISCUSSION

Of the currently analysed elderly population (n=8), there is a slightly increased visual weight compared to young healthy controls (0.42% vs 0.39%). More strikingly, the elderly participants converge into two discrete clusters. The MoS analysis shows that participants with greater visual weight are the ones with smaller MoS. This also correspond to greater temporal variability and more variability in foot motion patterns (Figure 1).

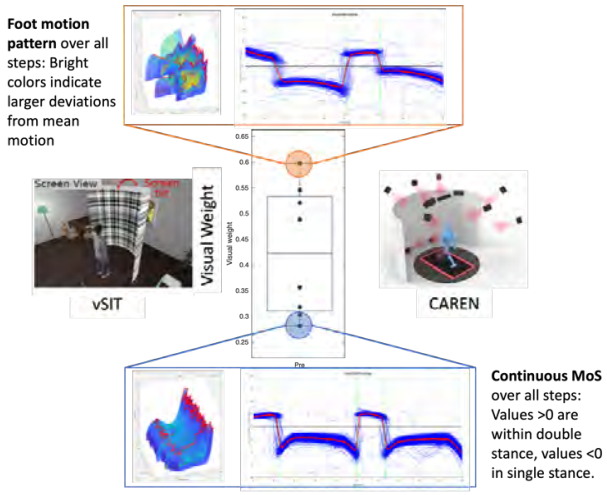

Figure 1 Visual weights and representative continuous margins of stability for two elderly participants. Note the difference in MoS at initial single stance and the difference in foot trajectory consistency. vSIT depicted on the left, CAREN on the right (credit: Stefan Schneller).

CONCLUSIONS

This preliminary analysis supports our expectation that there is an interaction between visual contribution to balance and MoS during walking. We are currently extending the analysis to include all 20 elderly and contrast steady walking with individual responses to single perturbations. In a next step we will evaluate how the MoS change throughout all three training blocks and whether this is equally reflected by a change in visual weight and perturbation resilience. This approach may provide some insight into the underlying mechanisms of PBT and will hopefully contribute to the field of fall prevention.

REFERENCES

[1] Assländer L et al. *Scientific Reports*, 2023
[2] Kobayashi T et al. *J Biomech* **130**: 110845, 2022

Joint kinematic and kinetic responses to added mass on the lower extremities during running.

Itay Coifman[1], Rodger Kram[2], Raziel Riemer*[1]

1. Industrial Engineering and Management Department, Ben-Gurion University of the Negev, Beer-Sheva, Israel
2. Integrative Physiology Department, University of Colorado, Boulder, CO, USA

* Corresponding author: rriemer@bgu.ac.il

INTRODUCTION

Recent advances in leg exoskeleton technology have allowed for the augmentation of human locomotion by reducing metabolic power during walking and running [1,2]. However, the additional mass of these devices can increase metabolic power and alter joint kinematics and kinetics, necessitating consideration of the effects of added mass magnitude and distribution in exoskeleton design. The effects of added foot and leg mass on metabolic power during running have been extensively studied, but the effects on joint kinematics and kinetics have yet to be investigated. The present study analyzes the kinematic and kinetic effects of running with added mass on the feet, shanks, and thighs. This analysis is important for the design of wearable assistive devices and for gaining a better understanding of locomotion.

METHODS

Fifteen participants (7 females and 8 males) completed treadmill running trials ($3\ m \bullet s^{-1}$) normally and with lead mass (300–1350 g) attached bilaterally to the thighs, shanks, or feet. We quantified the lower limb biomechanics with motion capture and ground reaction force data using standard inverse dynamics analysis.

RESULTS AND DISCUSSION

Only moderate kinematic changes occurred in response to the distal added limb mass. Maximum hip flexion and maximum knee flexion angles during the swing phase increased by approximately 9% and 6%, respectively, for each kilogram added to each foot. However, adding even small masses to the legs caused dramatic changes in joint moment and power, particularly during the swing phase. For example, adding 1 kg to each foot increased maximum joint moment by as much as 42% (knee extension in late swing) and maximum joint power by as much as 50% (hip generation in late swing) (Figure 1). These changes have implications for shoe design, for people who run with added mass on their legs for sport or strength training, and for the design of wearable devices. These effects might be leverageable when designing particular exoskeletons—such as energy harvesters [3–8], which heavily rely on negative work (which increased at swing) with regenerative braking to generate electricity.

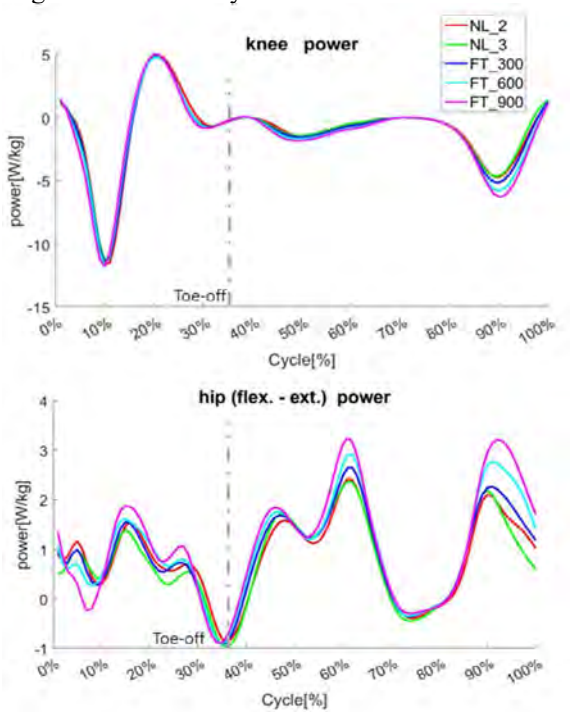

Figure 1 Participants' average power profiles under different loading conditions of the feet; 0% of the gait cycle is defined as the initial foot–ground contact; FT_300, FT_600, and FT_900 represent the added mass at each foot of 300 g, 600 g, and 900g, respectively; NL_2 and NL_3 represent no load running at 3 $m \bullet s^{-1}$.

CONCLUSIONS

Leg joint kinematics were largely conserved in response to adding mass to the legs. Adding mass to the legs more distally increased joint power mainly at the knee and hip joints during the swing phase, whereas proximal loading mainly affected the ankle joint mechanics during the stance phase.

ACKNOWLEDGEMENTS

The study was partially supported by the Israeli Ministry of Science and Technology and the Helmsley Charitable Trust through the Agricultural, Biological and Cognitive Robotics Initiative of Ben-Gurion University of the Negev.

REFERENCES

[1] R. Nasiri et al. TNSRE 26,10,2026–2032, 2018
[2]J. Kim *et al. Science (1979) 365,6454,668-672,2019*
[3]A. Cervera et al. *J Emerg Sel Top Power Electron 4,1,293,302,2016*
[4]M. Shepertycky et al. *Science (1979)*, 372, 6545,957-960, 2021
[5]J. M. Donelan et al. *Science (1979)* 319,5864,807–810,2008
[6]R. Riemer et al. *Science (1979)* 372, 6545,909–911,2021
[7]M. Gad et al. *Front Robot AI, 9 ,2022*
[8]J. Fan et al. *Energy Conversion and Management* 195, 641-649,2019

EFFECTS OF GAIT VARIABILITY AND ENCOURAGED EXPLORATION ON ADAPTATION TO ANKLE EXOSKELETONS

Gillian Phillips[1], Anthony Chen[1], Megan J. McAllister[1] and Jessica C. Selinger[1]
[1] School of Kinesiology and Health Studies, Queen's University, Kingston, Canada
Email: 17gp@queensu.ca

INTRODUCTION

Exoskeletons have potential applications in the rehabilitation and enhancement of human gait. In the past decade, numerous exoskeletons have reduced the energetic cost of walking[1], potentially allowing users to walk for longer durations before fatiguing. However, acheiving these benefits often requires hours of walking time, during which the user must adapt to the novel and complex dynamics created by the assistive device[2,3]. This is a nontrivial feat, as gross characteristics, joint level kinematics and kinetics, and individual muscle activities may all need to be adjusted to optimally move in concert with the device. Recent work by our group[4] and others[3] suggests that high gait variability may facilitate this adaptation process by providing experience with different-cost gaits. Here, our purpose is to test how gait variabilty, whether naturally occuring or created through encouraged exploration, effects the rate and magnitude of a users' adaptation to ankle exoskeletons. We hypothesize that individuals who display high natural (implict) gait variability will more readily adapt to the device and that verbal (explict) encouraged exploration will expedite adaptation.

METHODS

We will test 10 healthy adults with no prior experience walking in an exoskeleton and no lower limb impairments. To date, we have tested 2 participants. We instrumented participants with bilateral ankle exoskeletons (Humotech) that provide assistive plantar flexion torques. We controlled the timing and magnitude of the assistive torques using a custom real-time angle-based controller. We also instrumented participants with 22 reflective markers for optical motion capture (Qualisys), 9 dominant limb EMG sensors (Delsys) to measure muscle activity, and a portable indirect calorimetry system to measure metabolic energy expenditure (Cosmed). All walking occurred on a fully instrumented split-belt treadmill (Bertec). Participants completed a total of 102 minutes of walking on a single testing day. During a baseline trial the exoskeletons were unpowered, allowing participant habituation and qualification of natural gait variability. Next, the exoskeletons were turned on and we assessed the level of adaptation both before and after an exploration trial where we incited high gait variability by encouraging participants to explore different ways of walking using verbal prompts.

RESULTS AND DISCUSSION

Our preliminary findings suggest that encouraged exploration may facilitate adaptation toward more energy optimal gaits. In one example participant, net metabolic cost reductions of 12% were achieved pre-exploration, but these savings more than doubled post-exploration to 30%. These cost savings were accompanied by a 20% reduction in soleus average integrated EMG, a 15% reduction in ankle angle range of motion, and no change in step frequency. Next steps include collecting data from the remaining participants and evaluating the relationship between an individual's implicit and explicit variability and their adaptation.

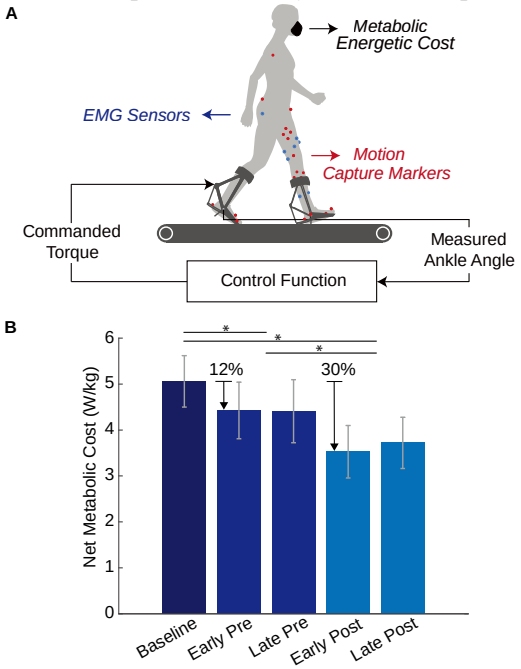

Figure 1 A) Schematic of participant instrumentation. **B)** Metabolic cost reductions from one example participant. Cost reductions, compared to the unpowered condition (Baseline), were evident prior to the encouraged exploration trial (Early Pre and Late Pre), but more than doubled afterward (Early Post and Late Post).

CONCLUSIONS

Our work will help elucidate the role of implicit and explicit gait variability during adaptation to lower limb exoskeletons. This may provide insight into how we can best facilitate and expedite the adaptation process when a user is learning to walk with a novel assistive device.

REFERENCES

[1] Sawicki et al. *J NeuroEng Rehabil* **17**: 25
[2] Abram J et al. *Curr Biol* **32**: 2222-2232.e5
[3] Poggensee K et al. *Sci Robot* **6**: eabf1078
[4] Selinger J et al. *J Exp Biol* **222**: jeb198234

Design of a 2-DoF Soft Ankle Exoskeleton for People with Dropfoot and Excessive Inversion

Xiaochen Zhang [1], Yi-Xing Liu [1], Ruoli Wang [1] and Elena M. Gutierrez-Farewik [1,2]
[1] KTH MoveAbility Lab, KTH Royal Institute of Technology, Stockholm, Sweden.
[2] Department of Women's and Children's Health, Karolinska Institutet, Stockholm, Sweden
Email: xiaocz@kth.se

INTRODUCTION

Dropfoot, or inability to lift the foot due to muscle weakness and/or atypical motor control, is a common secondary gait disorder after a stroke or other neurological injury. Dropfoot can negatively impact one's walking independence and confidence [1], and make daily activities less convenient and more challenging. Ankle-foot orthoses are frequently prescribed to assist in daily life [1]; they passively supplement for deficient dorsiflexor strength, but they also disrupt natural ankle motion and muscle recruitment. Exoskeletons made of soft and/or compliant components to compensate for atypical motor control have been frequently explored in the past decade [2]. The purpose of this study is to design a lightweight, soft 2-DoF active ankle exoskeleton specially intended to compensate for dropfoot and excessive inversion and test its performance and feasibility in simple ankle movements.

METHODS

The design consists of four components: waist belt, calf wrap, a pair of shoes, and sensors (EMG sensors and load cells). A controller with two different control modes was designed to assist ankle joint motion in sagittal and frontal planes: 1) position control to track the desired ankle joint angles; 2) forcefree control [2] to compensate for the device's intrinsic friction during ankle plantarflexion by extracting the cable tensile force. The device's feasibility was preliminarily evaluated on two able-bodied subjects (1 male: 25 y/o, 54.9 kg; 1 female: 30 y/o, 53.0 kg). Ankle joint angle was computed based on the 3D movement analysis (Vicon V16, markers as per CGM2.4). Each subject conducted three case studies, from a seated position and relaxed ankle joint muscles (verified by EMG signals): Case 1: position control of the foot, from a plantarflexed and inverted position: the foot first rested on two wedges in different angles and directions and moved to a neutral position (target angle = 0°) during a 0.75s duration; Case 2: position control during plantarflexion: the foot moved from the neutral position to a plantarflexion position in a 0.3s duration (target angle = 9° by using wedge); Case 3: forcefree control during plantarflexion, from the neutral position to a plantarflexed position.

Tracking errors between the measured and the target ankle angles were determined in the first two cases. In case 3, the duration of plantarflexion from 0° to 20° was measured as an index to evaluate the restriction in the condition of Forcefree control, Free (no restriction by removing cables) and Friction (with passive exoskeleton).

RESULTS AND DISCUSSION

With position control, the exoskeleton assisted the ankle to reach the target angle with an error of 1.6° in the sagittal plane and 0.6° in frontal plane in case 1 (Fig. 1a) and with an error of 0.8° in the sagittal plane in case 2 (Fig. 1b). The Forcefree controller decreased the movement duration by 0.31s, which is 43% less than with the Friction condition (Fig. 1c).

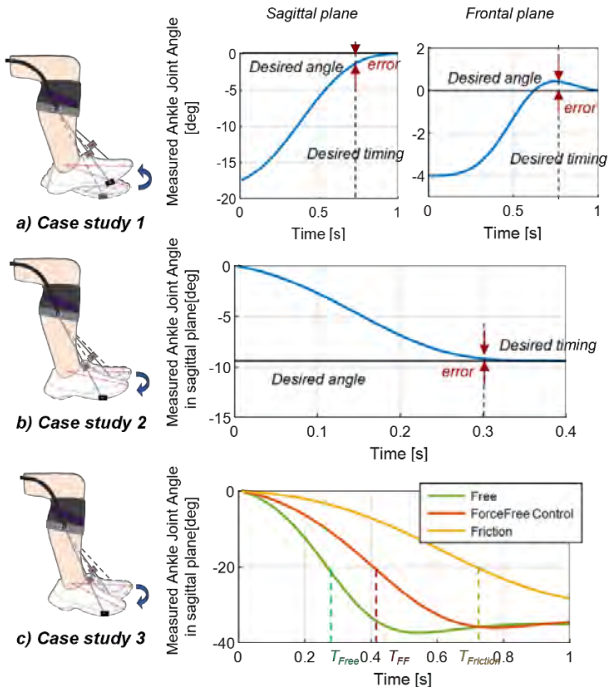

Figure 1 The measured ankle joint angles during three case studies from a representative subject.

CONCLUSION

In this study, we evaluated the performance of our 2-DoF active ankle exoskeleton on subjects' ankle joint response. Our preliminary results revealed that the use of a two-mode controller led to a good tracking performance and less restriction than passive exoskeleton, which supports its potential for assisting gait in persons with with dropfoot and excessive inversion. Our future work will t investigate the device's effect when subjects are not in a relaxed state.

ACKNOWLEDGEMENTS

We gratefully acknowledge the generous support from the Promobilia Foundation (ref nr 22000, 18200).

REFERENCES

[1] Awad L et al. *Sci. Transl. Med.*, **9(400)**, p.eaai9084, 2017
[2] Lerner, Z F et al. *IEEE Trans. Neural Syst. Rehabilitation Eng.*, **26(10)**,1985-1993, 2018

GREEN EXOSKELETON BASED ON BIOMECHANICAL ENERGY HARVESTER

Yakir Knafo[1, 3], Yinjie Zhuo[2], Avi Manor[3], Alon Osovizky[3,4] and Raziel Riemer[2]*
[1]Mechanical Eng. School, Tel-Aviv University, Israel; [2]Industrial Eng. and Mgmt., Ben-Gurion University of the Negev, Israel, * rriemer@bgu.ac.il; [3]NRCN, and [4]Rotem Industries, Ltd., Israel

INTRODUCTION

Exoskeletons are designed to augment their users. There are two main types of exoskeletons, passive devices, which rely on elements such as springs and clutches to provide assistance and are limited to a single type of activity (e.g., walking) [1], and active exoskeletons, which use motors to provide assistance. Active exoskeletons typically use batteries as their energy source. Thus, the exoskeleton's operating time between charges is limited. This study presents a novel active exoskeleton without the need for a continuous external power source.

METHODS

The exoskeleton is based on harvesting biomechanical energy, which captures energy from the wearer's negative work movements (during which muscles act as brakes) and stores it in a battery or super-capacitor for later use. It returns the harvested energy when the joint is required to perform positive work (muscles working as a motor). Thus, provides assistance without the need for an external power source. To do this, an electronic circuit board with the active control of a brushless DC (BLDC) motor was developed and implemented on a knee exoskeleton. The main parts of the electronic circuit board are a low-power microprocessor, a digital logic circuit, an H-bridge, and super-capacitors. The control algorithms use three signals: rotation direction, desired operating mode (motoring or regenerating), and control signal (pulse-width modulation).

RESULTS AND DISCUSSION

We tested this technology on a Sit-To-Stand (STS) motion assistance task [2], which required the motion of going down from a standing to a sitting position. The exoskeleton aided in moving downward, while charging the super-capacitors (~10 Joules). Next, while the user was moving from a sitting to a standing position, the energy from the capacitors was used to drive the motor for assistance. In an experiment, a participant performed the STS motion (Fig. 1) while the torque applied by the device to the knee was measured using a torque meter (mini45, ATI Industrial Automation), and the participant's kinematics and kinetics were recorded using a motion capture system (Qualisys, Gothenburg, Sweden) with a force plate (Bertec, Columbus, Ohio). The joint angle and torques were calculated using Visual 3D. The results showed that the total knee torque was 65–70 Nm and the torque applied by the device ranged from 7–10 Nm.

CONCLUSIONS

The device's ability was demonstrated with the STS motion, yet with further development of the control system, it could also assist with movements such as walking.

ACKNOWLEDGEMENTS

The study was partially supported by the Israel Ministry of Science and Technology and the Helmsley Charitable Trust through the Agricultural, Biological and Cognitive Robotics Initiative of the Ben-Gurion University of the Negev.

REFERENCES

[1] Tiboni et al., "Sensors and Actuation Technologies in Exoskeletons: A Review," 2022.
[2] Shepherd and Rouse, "Design and Validation of a Torque-Controllable Knee Exoskeleton for Sit-to-Stand Assistance," 2017.

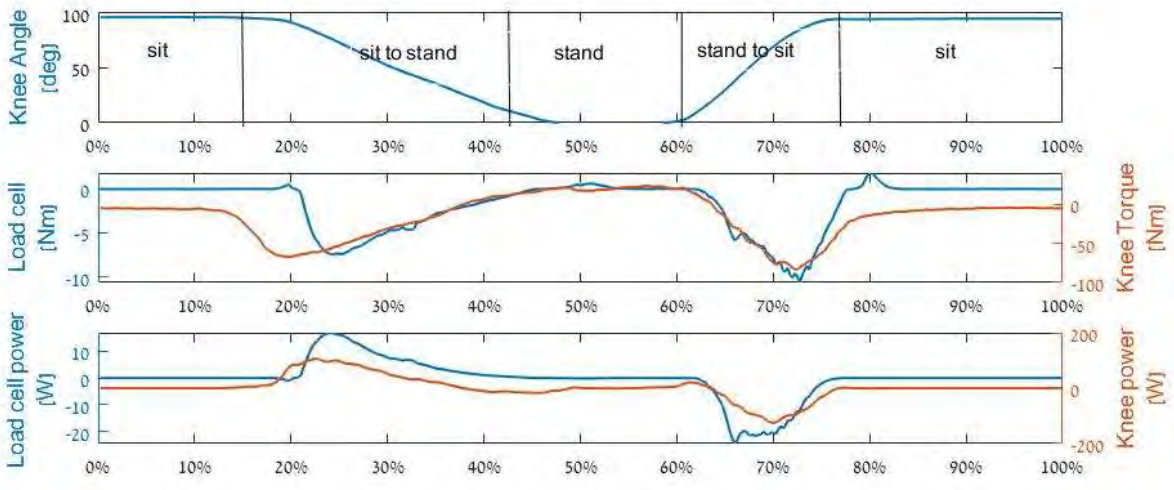

Figure 1. Knee angle, torque, and power during STS. Left y-axis label refers to the knee exoskeleton assistance (blue). Right y-axis label refers to the knee motion (orange).

BIOLOGICALLY INSPIRED TRAJECTORIES FOR ACTIVE ASSISTANCE OF STANDING UP AND SITTING DOWN BY ROBOTIC ROLLATORS

Marko Ackermann[1,2], Lizeth H. Sloot[1] and Katja Mombaur[3]
[1] Institute of Computer Engineering, Heidelberg University, Heidelberg, Germany.
[2] Dept. of Mechanical Engineering, FEI University Center, São Bernardo do Campo, Brazil.
[3] Dept. Systs. Design Eng., Dept. Mech. and Mechatronics Eng., University of Waterloo, Waterloo, Canada.
E-mail: marko.ackermann@ziti.uni-heidelberg.de

INTRODUCTION

Difficulty in standing up and sitting down affects about two thirds of older persons in long-term care [1]. Effective robotic assistance can help this population lift out and into the chair, providing a more independent living. Investigations on robotic assistance in STS provide useful insights [2,3], but generally accepted, effective assistance trajectories are still unknown and its effects on biomechanical performance and stability are poorly understood. We propose a set of parametrized trajectories for sit-to-stand and stand-to-sit assistance, whose velocity profiles are based on experimental shoulder trajectories, and that can be scaled by subjects antropometry and motion duration. These trajectories will be investigated experimentally using a robotic lab device (Fig.1, bottom) in a ongoing study.

METHODS

Acromion marker trajectories were collected during 3-5 repetitions of standing up and sitting down for 10 younger (Yng, 28±5 yrs) and 7 older adults (Eld, 78±9 yrs). Data was filtered, divided by subject's thigh length (L), and scaled by motion duration T (seat off to stance on in sit to stand; stance off to seat on in stand to sit), resulting in normalized velocities in L/T, which were averaged resulting in an inverted C-shaped trajectory (Exp. Avg, Fig.1). Horizontal (i=x) and vertical (i=z) average velocities for sit to stand and stand to sit and for the younger and older adult groups were approximated by 2 gaussian curves according to

$$v_{i,n}(\tau) = a_{1i}\, e^{-[(\tau-b_{1i})/c_{1i}]^2} + a_{2i}\, e^{-[(\tau-b_{2i})/c_{2i}]^2}, \quad (1)$$

with τ=0/τ=1 *(seat off/stance on* or *stance off/seat on* for sit-stand and stand-sit) (iC-shape, Fig.1). This trajectory reproduces shoulder trajectory on the handles, providing natural support with arms stretched vertically. Shape variations to be investigated were obtained by slight manipulation of the parameters in (1): *i*) monotonically forwards and upwards motion with a_{2i}=0 (iL-shape, Fig.1); *ii*) simple straight trajectory by shifting velocities (b_{1i}) in x and z in time (Straight, Fig.1); *iii*) S-shape trajectory by manipulating c_{1z} for velocity in z.

RESULTS AND DISCUSSION

The average measured durations (T) are 0.91±0.01 s (sit-stand Yng); 1.02 ± 0.03 s (stand-sit Yng); 1.52 ± 0.21 s (sit-stand Eld); 2.31 ± 0.26 s (stand-sit Eld). Coefficients in (1) were obtained by optimization. The profiles for sitting up of younger adults are illustrated in Fig.1.

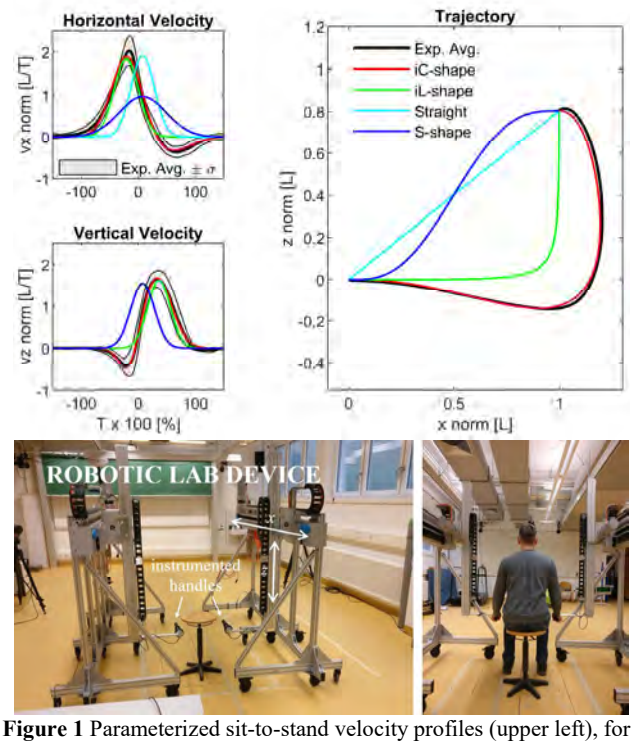

Figure 1 Parameterized sit-to-stand velocity profiles (upper left), for the corresponding different trajectory types (upper right), inverted C-shape (iC-shape), inverted L-shape (iL-shape), Straight and S-shape. Robotic lab device to impose handle trajectories (bottom).

CONCLUSIONS

This is the first study that proposes and systematically compares biologically inspired trajectories for robotic assistance of standing up as well as sitting down. From shoulder trajectories of younger and older adults, we determined straightforward parameterized assistance velocity profiles scaled by anthropometry and duration, which can be used as reference in future investigations. Results on the ongoing investigations on the biomechanics and stability effects of these trajectories with a robotic lab device will be reported in the congress.

ACKNOWLEDGEMENTS

Carl Zeiss Foundation, Germany, HeiAge project.

REFERENCES

[1] Jeyasurya J et al. *J Reh Res Dev* **50**: 835-44, 2013.
[2] Geravand M et al. *Auton Robot* **41**: 575-92, 2017.
[3] Mombaur K et al. *J Biomech* **58**: 131-38, 20.

EFFECTS OF FINGER FLEXION FORCE ON MEDIAN NERVE COMPRESSION

Shengwei Li[1], Ping Yeap Loh[2]
[1] Graduate School of Design, Kyushu University, Fukuoka, Japan.
[2] Department of Human Life Design and Science, Faculty of Design, Kyushu University, Fukuoka, Japan.
Email: li.shengwei.652@s.kyushu-u.ac.jp

INTRODUCTION

Work-related biomechanical stress on median nerve compression is critically relevant to carpal tunnel syndrome. Ultrasound imaging on the median nerve is useful for ergonomics intervention and prevention. Finger flexion force exertion causes gliding and displacement of the flexor tendons and compress the median nerve. [1] Previous study have shown that grip force leads to morphological changes in the median nerve and affects the cross-sectional area of the medial nerve (MNCSA). [2] The main objective of this study is to investigate the effect of individual finger flexion force exertion on the MNCSA.

METHODS

Five healthy right-handed young adults (3 males and 2 females; age = 26.8 ± 6.1 years old; height 167.5 ± 13.9 cm; weight = 72.3 ± 7.7 kg; BMI = 26.1 ± 3.7 kg/m^2) were recruited. Ultrasound examination of the median nerve was performed using a Toshiba Viamo Portable ultrasound system. The median nerve of the dominant wrist was examined in the proximal transverse plane. Four finger conditions were examined, including index finger (IF) only, middle finger (MF) only, ring finger (RF) only and total finger (TF, index, middle, and ring fingers together), while three finger flexion force levels were examined, namely, no force (Control), 50% force and 100% flexion force. Finger flexion force was measured by load cells (LTMS-25, Toyo Sokki, Japan) with PowerLab (ADInstruments, Australia) and ultrasound image was synchronized with LabChart (v7.3.8, ADInstruments, Australia). The load cells were connected to the second phalange of the volunteers through iron wires and soft webbings, while the angle of the proximal interphalangeal joints of the volunteers was approximately 65°. Ultrasound images were then exported for MNCSA measurement by a tracing method with ImageJ. The independent variable is the flexion force level and the dependent variable is the MNCSA at different flexion force levels. One-way repeated ANOVA and post hoc pairwise Bonferroni-corrected comparisons were conducted with flexion force levels as factors to examine the changes of MNCSA.

RESULTS AND DISCUSSION

The mean values of MNCSA for Control, IF50, IF100, MF50, MF100, RF50, RF100, TF50, and TF100 were summarized in Figure 1, and the corresponding flexion force were listed in Table 1. For IF, MF, and TF, the MNCSA at 50% flexion force showed no significant changes compared to Control condition, while MNCSA decreased significantly as TF flexion force changed from 50% to 100% flexion force ($p<0.05$). However, from Control to 100% flexion force, the MNCSA of RF increased significantly.

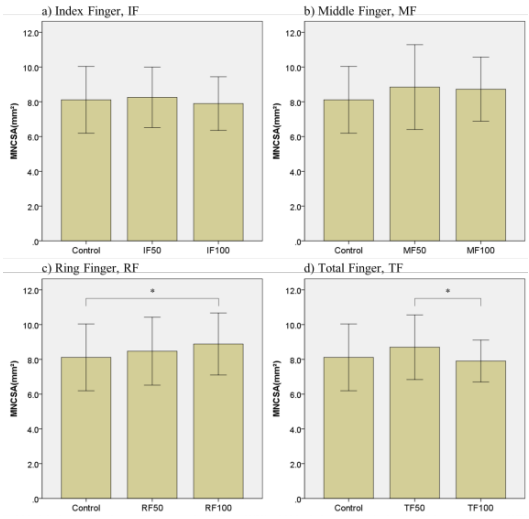

Figure 1 MNCSA changes with IF, MF, RF, and TF flexion force. (*, $p<0.05$)

CONCLUSIONS

In this study, both individual finger and total finger flexion force exertion cause differ compression stress to the median nerve, and results in MNCSA changes among young adults.

ACKNOWLEDGEMENTS

This work was supported by JSPS KAKENHI, Grant Number 21K17686.

REFERENCES

[1] Li ZM et al. *Human Movement Science* **87**: 103044, 2023.
[2] Loh PY et al. *PeerJ* **4**: e2510, 2016.

Table 1: Finger flexion force of different finger flexion force conditions.

Finger flexion force	IF	MF	RF	TF
50% force (N)	27.8 ± 10.6	32.1 ± 13.2	27.2 ± 13.7	56.0 ± 23.8
100% force (N)	55.5 ± 21.3	64.2 ± 26.3	54.3 ± 27.5	112.0 ± 47.5

Energy transfer during a collective stretcher transport

Nour Sghaier[1], Nadim Fakhry[1], Nicolas Turpin[2], and Pierre Moretto [1]
[1] CRCA, Université Paul Sabatier, Toulouse, France,[2] IRISSE, Université La Réunion, La Réunion, France.
Email: Pierre.moretto@univ-tlse3.fr

INTRODUCTION

Power flow has widely been investigated for gait analysis and sport movements such as baseball throw or tennis service. Such analysis provides insights about how much energy is flowing in or out of a segment and how energy transfers between adjacent segments [1]. However, only very few studies focused on energy transfer during a collective load transport. In our previous researches we showed a global alteration of the CoM pendular behaviour of the Poly-Articulated Collective System –composed of all the individuals acting together –and an increase of the cost of their movement (sum of joint moments) when increasing the load transported [2] that suggested change in power flow. In the present research we investigated the energy transfer occurring in the upper limbs of two participants carrying a stretcher-like object, with a particular focus on the differences between the right and left sides.

METHODS

Seven groups of two matched-participants (mean ± s.d.: age = 23,9 ± 2,2 year; height = 1,72m ± 0,09m; mass = 65,5 kg ± 8,3kg) performed three transports of a strecher-like object while looking at each other so that participant P1 performed a forward walking with a visual feedback of the external environment and participant P2 performed a backward walking with no visual feedback. Each was equipped with 42 spherical reflective markers. The 3-D kinematics of the upper limb and trunk was then recorded using 19 Vicon cameras sampled at 200 Hz. The carried object was equipped with four handles each including 6-axis force sensors (Sensix©, France) to record the external forces applied by the participants. The handles were synchronised and sampled at 2000 Hz. An inverse dynamic method enabled us to estimate the forces and moments at each joint of the upper limb [3]. Power flow analysis was then conducted following references 1 and 4:

$$Eq.\ 1:\ JFP = joint\ reaction\ force\ .\ \ linear\ joint\ velocity$$

$$Eq.\ 2:\ STP = segment\ torque\ .\ \ joint\ angular\ velocity$$

$$Eq.\ 3:\ SP_{seg} = JFP_{prox} + JFP_{dist} + STP_{prox} + STP_{dist}$$

Segment power: SP_{seg}, joint force power: JFP, segment torque power: STP , *prox* and *dist*: proximal and distal ends of each segments, i.e. C7, shoulder, elbow and, wrist [1, 4]. Energy transfer was computed as the difference between the time-integral of SP_{seg} for 2 adjacent segments (proximal-distal). Wilcoxon test was then performed to compare the means of right and left energy transfer.

RESULTS AND DISCUSSION

Figure 1 represent the energy flow of each of the four joints of the left and right sides of both participants.

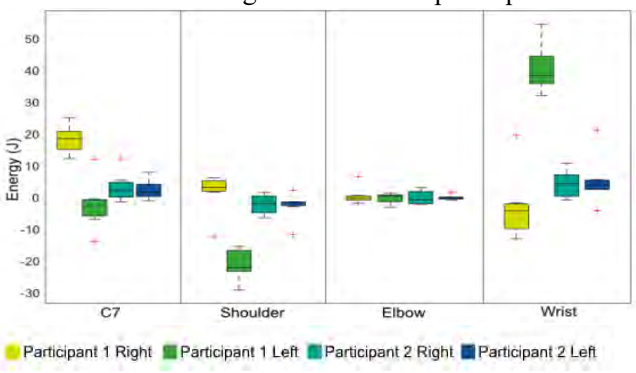

Figure 1 Boxplot of the average of delta energy transfer of participants 1 and 2. $p<0.05$

The results showed significant differences across the participants. Except at wrist, P1 created energy flow using his right side and counterbalance with his left side. P1 wrist acted in a contralateral and opposite direction. P2 energy flows were close to zero meaning it never created or dissipated energy but managed to be neutral. Moreover, a null delta energy around the elbow joint of both participants supports the idea of a locked joint with a very few degree of freedom. Therefore, the articulation being fixed can neither supply nor dissipate but transmits energy. P1 seeing in the direction of the displacement, he guided. P2 going backward was assisting well staying neutral and may be fixing all his joints. These results confirm [2] who observed that the sighted participant also guided and controlled when his partner only lifted and followed the movement.

CONCLUSIONS

This research gives insight into the energy transfer occurring during a collective stretcher transport, and confirm the guider-follower duality to be reproduced in collaborative robot.

ACKNOWLEDGEMENTS

This work is supported by the ANR as part of the project Collaborative Robot (Cobot) project (Projet-ANR-18-CE10-0003).

REFERENCES

[1] Winter DA et al. *Biol Cybern* 1978; 29: 137–142.

[2] Fumery G et al. *Sci Rep* 2021; 11: 4346.

[3] Cahouët V et al. *J Biomech* 2002; 35: 1507–1513.

[4] Zatsiorsky et al. Human Kinetics, 2002.

Biomechanical changes associated with heavy load carriage using differing rucksack designs

Matthew Ellison[1], Brett Still[2], Bethany Canty[2], David Mullineaux and Franky Mulloy[2]
[1] Public Health and Sports Science, University of Exeter, Exeter, UK.
[2] Sport and Exercise Science, University of Lincoln, Lincoln, UK.
Email: m.ellison3@exeter.ac.uk

INTRODUCTION

Military personal carry operational heavy loads, often consisting of a rucksack and body armour [1]. Heavy load carriage has been shown to change biomechanical variables during walking, standing and running e.g. [2]. There is limited understanding of the effects of rucksack design on these changes despite numerous commercial designs issued to service personnel worldwide. The effects of wearing a rucksack over armour as opposed to integrated armour are also unknown. The aim of this study was to quantify the effects of common rucksack features such as hip and chest strapping on the biomechanical changes associated with loaded running. The interaction of body armour and rucksack was also investigated.

METHODS

15 males who participated in regular resistance and cardiovascular training were recruited. Participants undertook four 1 km runs consisting of 50 x 20 m shuttles. Four loaded conditions were investigated: PC (5 kg plate carrier); LF (plate carrier + litefighter rucksack); BFMout (plate carrier + Camelbak BFM rucksack); BFMin (plate carrier + Camelbak BFM rucksack, rear plate moved from plate carrier to rucksack). The litefighter rucksack did not have any hip or chest strapping whilst the BFM had both; the litefighter had fixed shoulder straps whilst the BFM had back length adjustment. Rucksack loads were set at 20 kg such that total load was always 25 kg when wearing a rucksack and plate carrier. Retroreflective markers were used to identify the segments of the right lower limb, torso and head. Kinematic data was collected for one stace phase during each shuttle run using 15 Raptor cameras and Cortex software (version 7.02 Motion Analysis Corporation, CA). Peak knee flexion, peak forward torso lean and peak lateral torso lean timing were calculated for analysis, timings of peaks were also calculated. Variables were compared using a one-way repeated measures ANOVA. Bonferroni adjusted post-hoc t-tests were used where significant effects were identified.

RESULTS AND DISCUSSION

Discrete statistics and p values for all analysies can be seen in Table 1. Peak knee flexion timing was found to be different between conditions. Post hoc tests showed that peak knee flexion occurred significantly later in stance in the BFM_{out} condition compared to PC ($p = 0.024$). Peak forward torso lean during stance was found to be different between conditions. Post hoc tests showed that all three rucksack conditions had greater forward lean than PC (LF $p \leq 0.001$; BFM_{out} $p \leq 0.001$; BFM_{in} $p \leq 0.001$). Additionally, the BFM_{in} condition had significantly greater lean than the LF condition ($P = 0.004$). Peak forward torso lean timing occurred significantly later in stance for PC compared with the three rucksack conditions (LF $p = 0.009$; BFM_{out} $p \leq 0.001$; BFM_{in} $p \leq 0.001$). All three rucksack conditions had earlier peak lateral lean than PC (LF $p = 0.002$; BFM_{out} $p \leq 0.001$; BFM_{in} $p \leq 0.001$).

CONCLUSIONS

Results demonstrate that rucksack design has a significant effect on the biomechanics of heavy loaded carriage. Integration of body armour and rucksack can have significant effects on torso lean during stance and should be considered when combining these two pieces of equipment.

REFERENCES

[1] Andersen et al. *S Medicine* **22**, 2016.
[2] Birrell et al. *Ergonomics* **52**: 1298-1304, 2009.

Table 1: Mean, standard deviations and p values for all discrete variables analysed

Variable	Mean ± SD				p	F
	PC	LF	BFMin	BFMout		
Peak knee flexion (deg)	45.80 ± 5.10	44.00 ± 4.47	44.95 ± 3.36	45.22 ± 5.26	0.329	1.17
Peak knee flexion timing (% stance)	29.79 ± 3.35	39.05 ± 16.07	40.20 ± 20.59	45.99 ± 19.45	0.023	3.824
Peak forward torso lean (deg)	6.32 ± 4.60	13.16 ± 4.12	15.76 ± 4.05	14.88 ± 3.97	≤0.001	50.216
Peak forward torso lean timing (% stance)	63.12 ± 13.72	45.46 ± 13.40	45.26 ± 11.72	42.99 ± 8.79	≤0.001	14.957
Peak lateral torso lean (deg)	2.45 ± 1.15	4.67 ± 6.68	2.86 ± 1.40	3.09 ± 1.22	0.335	1.165
Peak lateral torso lean timing (% stance)	63.27 ± 20.36	33.83 ± 20.00	30.59 ± 11.69	30.59 ± 10.11	≤0.001	17.211

SUBJECTIVE AND OBJECTIVE EVALUATION OF SITTING-INDUCED SUSTAINED LOW-INTENSITY MUSCLE FATIGUE

Hui Lyu[1*], Jian Wang[2], Xiaoyan Dong[3]
[1] Ningbo Research Institute, Zhejiang University, Ningbo, China.
[2] Department of Sport Science, Zhejiang University, Hangzhou, China.
[3] School of Qixin, NingboTech University, Ningbo, China.
Email: lvhui@zju.edu.cn

INTRODUCTION

Muscle fatigue is defined as an exercise-induced reduction in the capacity to generate the required force or power output (Vollestad, 1997). Muscle fatigue is task-dependent (Enoka, 1995), and the mechanisms behind it partly depend on exercise intensity. In today's workplace, heavy-labor work is becoming rare and replaced mainly by sustained low-intensity work. However, the knowledge of sustained low-intensity muscle fatigue and its evaluations is still limited.

METHODS

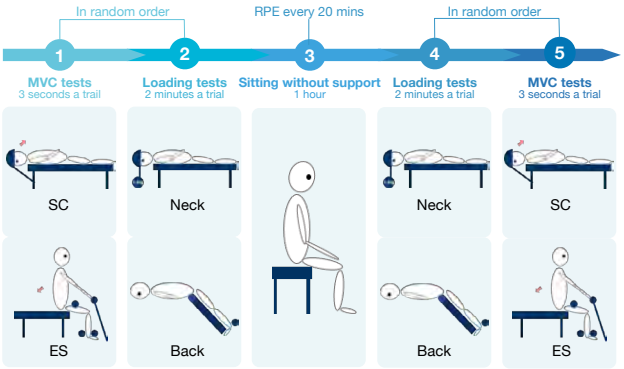

Figure 1 Experimental procedure

Ten male (20.6 ± 3.2 years) and ten female (19.3 ± 0.8 years) self-reported healthy students volunteered for the study. After outfitting and familiarization, subjects completed maximal voluntary isometric contractions (MVCs) of neck and back extension; loading tests of prone with neck loaded (1.5 kg) and Biering-Sorenson test on the roman chair. After 1-hour unsupported sitting, all the tests were repeated immediately (Figure 1). RPE was reported every 20 minutes during 1-hour sitting.
The right splenius capitis (SC) and erect spinea (ES) were recorded with the sEMG system (Delsys, USA). Root mean squared value (RMS), mean power frequency (MPF), entropy (EN), and DET% extracted from recurrence quantification analysis were computed during MVC and loading tests.

RESULTS AND DISCUSSION

RPE increased significantly during 1-hour sitting without muscle differences at any time point. As shown in Figure 2 (left, MVC tests), entropy decreased significantly after 1-hour sitting in SC and ES. Figure 2 (right, loading tests) found that for SC, RMS displayed a fatigue effect from 100 seconds in the females, and MPF showed a time effect from 60s post-sitting. For ES, there was no significant fatigue effect.

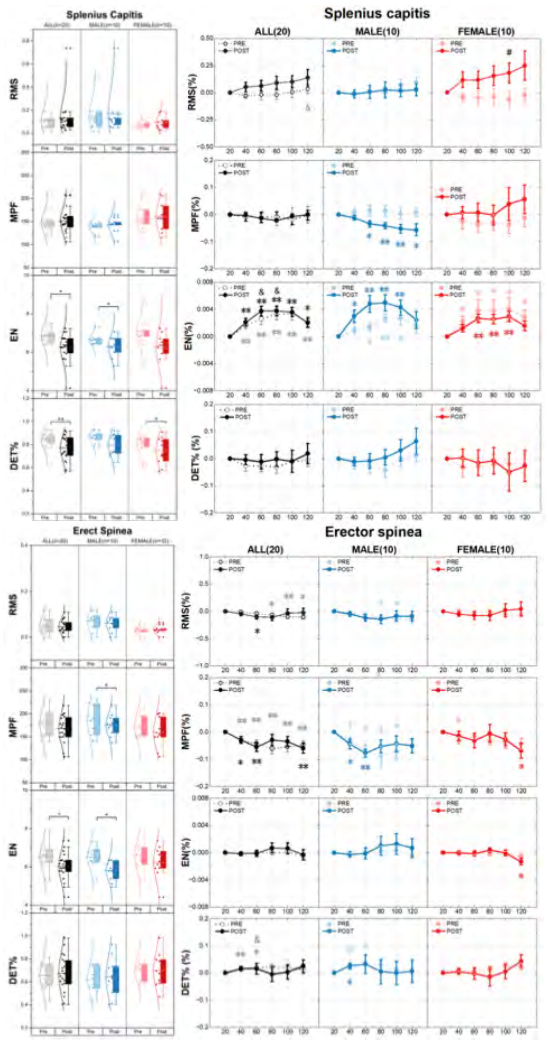

Figure 2 sEMG indexes during MVC (left) and loading test (right). Left: */** significant fatigue effect(<0.05, 0.01). Right: # significant fatigue effect (<0.05), & significant gender difference (<0.05), */** significant time effect (<0.05, 0.01).

CONCLUSIONS

For sitting-induced sustained low-intensity muscle fatigue: 1) females displayed higher subjective fatigue in the upper and lower back than males; 2) entropy of EMG from MVCs was effective in detecting fatigue in the neck and lower back muscles; 3) RMS and MPF were more sensitive than non-linear indexes from loading tests in detecting fatigue; 4) a better design of loading tests may serve as a new method to evaluate sustained low-intensity muscle fatigue.

REFERENCES

[1] Vollestad N. *J Neurosci Methods,* **74**: 219-27, 1997.
[2] Enoka RM. *J Electromyogr Kinesiol,* **5**: 141-9, 1995.

INFLUENCE OF WALKING SPEED AND LOAD ON SPINAL CURVATURE AND PELVIC ORIENTATION DURING PUSHING TASKS

Daniel Körner[1] and Catherine Disselhorst-Klug[1]
[1]Department of Rehabilitation and Prevention Engineering, Institute of Applied Medical Engineering, RWTH Aachen University, Aachen, Germany.
Email: koerner@ame.rwth-aachen.de

INTRODUCTION

Manual pushing and pulling of heavy loads or equipment takes up a large part of the working day in many occupations in manifold sectors. Although often considered as trivial and common tasks, their non-ergonomic repetition can pose a biomechanical risk for the spine[1]. Despite ergonomic guidelines limiting load, task duration and frequency for manual handling tasks, the favourable stable and balanced posture of the upper body is often not maintained in everyday work. Although there are indicators that changes in spine curvature are related to excessive tissue stress and vertebral loading[2], so far the spinal curvature during pushing and pulling tasks is only sparsely explored. Marker-based optical measurement systems and inertial measurement units allow measurement of the trunk posture, but the accurate assessment of the spinal posture still poses a challenge. Scanning stereography provides a non-invasive, non-contact method to detect the position and pose of the spinal cord under static and dynamic conditions[3].
Therefore, the aim of this work is to study the effect of load and walking speed during pushing tasks on the spinal curvature for loads and walking speeds that are common in everyday occupational scenarios.

METHODS

The experimental set-up reproduces the pushing a load on a straight track (fig. 1). The subjects are walking on a treadmill at a selectable constant speed. They push a handle that is at individual hip height (60% of body height). The handle is mounted in such a way that it can only be moved back or forth. An exchangeable weight is attached to a cable that is redirected by a pulley and connected to the handle. This way the gravitational force acting on the weight is acting in the opposite direction of the subjects walking direction. The test subjects are pushing with different randomized combinations of load (*0N*, *80N* and *160N* force) and walking speed (*3km/h* and *5km/h*) that are adjusted between measurements.
The subjects are asked to lift the weight and hold it at a stable position while walking on the treadmill. Small fluctuations of the position are acceptable since this reflects a real pushing scenario. The subjects get about 30 seconds time to adapt to the conditions. When a uniform movement is established, the spinal posture as well as pelvic and trunk orientation are recorded over the course of five seconds. Afterwards the treadmill slows down and the weight can be dropped. The subjects get three minutes resting time between measurements.
The spinal posture of 15 healthy subjects pushing a load in a continuous and straight manner is measured. The mean values of kyphosis angle, lordosis angle, pelvic inclination and trunk inclination over three gait cycles are evaluated.

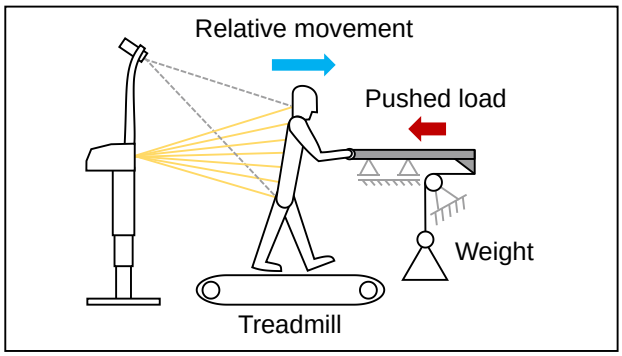

Figure 1: Experimental setup reproducing a pushing task

RESULTS AND DISCUSSION

Mean values of kyphosis angle and lordosis angle did not show a significant change with increasing load while pelvis and trunk inclination increased. This indicates an anterior tilt of the upper body with no significant signs of deformation of the spine in the sagittal plane. Since an anterior tilt of the upper body gives better support during pushing, an anterior tilt of the trunk could be expected with increasing pushing load while it is surprising that spine curvature is not affected.
Both kyphosis angle and lordosis angle decrease when walking speed increases. Trunk and pelvic inclination also increase with increasing walking speed. In contrast to higher pushing loads, higher walking speeds result in an alteration of the spinal curvature, resulting in a more excessive tissue stress and vertebral loading.

CONCLUSIONS

Results show that load and walking speed affect pelvis and trunk inclination while spine curvature is only affected by walking speed. The results suggest that walking speed should be considered when assessing the risk of pushing tasks if moving high loads.

REFERENCES

[1] Vukicevic A et al. *J ESWA* **183**: 115371, 2021.
[2] Keller T et al. *The spine J* **5**: 297-309, 2005.
[3] Schulte T et al. *J Spinal Disord* Tech **21**: 1, 2008.

CORRELATION BETWEEN PSYCHOSOCIAL FACTORS AND PHYSICAL LOAD OF WORKERS IN THE ELECTRONIC COMPONENTS INDUSTRY

Jansen Atier Estrázulas[1], Fernando José Herkrath[1,2], Mario Sobral[3]
[1] Biomechanics laboratory, Amazonas State University, Manaus, Brazil.
[2] Fiocruz Amazônia, Oswaldo Cruz Foundation, Manaus, Brazil.
[3] Federal Institute of Education, Science and Technology of Amazonas, Manaus, Brazil.
Email: jestrazulas@uea.edu.br

INTRODUCTION

Work-related musculoskeletal disorders have been a major concern as they are the most common occupational diseases worldwide [1]. The literature indicates that psychosocial risk factors are related to MSD. They do not act in isolation, their effect combines (and often exacerbates) the effects of physical load factors [2,3]. This negative relationship goes both ways, that is, just as psychosocial risk factors can contribute to increasing the consequences of physical workload, physical workload can also enhance the perception of some psychosocial factors [3]. Thus, this study aimed to evaluate the correlation between psychosocial factors and the physical load of workers in an electronic components industry.

METHODS

This cross-sectional study evaluated 115 workers at a company in the electronics sector in the city of Manaus, Amazonas, Brazil. The jobs included in the study were manual activities in assembly, soldering, packaging and revision of electronic components. The assessment instruments used were: 1) the HSE Indicator Tool (HSE-IT) questionnaire, which assesses the worker's psychosocial risks through 35 items and seven dimensions, and 2) Strain Index, an ergonomic tool focused on physical load on hands and wrists, evaluating six parameters. Initially, a descriptive analysis of the instruments domains was performed. Then, the associations between the HSE-IT and Strain Index items were analysed using Spearman's correlation coefficient. All analyses were performed using Stata SE, version 15.0. The significance level adopted was 0.05. This research obtained ethical approval under CAAE number 58380122.6.0000.5016, Amazonas State University.

RESULTS AND DISCUSSION

The mean values of the dimensions of the HSE-IT and Strain Index are shown in Table 1. A significant association was identified between the intensity of effort and demands (r_s=0.25; p=0.006), managers support (r_s=0.22; p=0.021) and relationships (r_s=0.25; p=0.006). Associations were also identified between duration of effort and changes (r_s=-0.20; p=0.031), as well as the total score of the Strain Index instrument with the control dimension of the HSE-IT (r_s=-0.19; p=0.045).

Table 1 Descriptive analysis of the assessed instruments (n=115).

Variable	Mean	±SD
Strain Index		
Intensity of exertion	1.36	0.76
Duration of exertion	1.21	0.55
Exertion per minute	1.34	0.65
Hand/wrist posture	1.51	0.36
Speed of work	1.10	0.21
Duration of task per day	1.00	-
Total	3.34	2.97
HSE-IT		
Demands	3.28	0.42
Control	1.70	0.17
Managers support	4.53	0.16
Peers support	4.50	0.02
Relationships	3.68	0.16
Role	5.00	-
Change	3.57	0.32

The Strain Index total score was moderate. The control dimension of the HSE-IT, which assesses the autonomy of workers performing their activities, was the most critical. Although no significant correlation was observed between control and Strain Index parameters, an association with the total score was identified. The results showed that SI items correlated with different dimensions of the HSE-IT. Therefore, when using both tools, we can prioritize the workstations that require control for upper limb problems and also be indicative of the need to address psychosocial risks [2,3].

CONCLUSIONS

A relationship was found between physical load factors on hands and wrists and psychosocial factors, evidenced by the association of effort intensity with demands, managers support and relationships dimensions. The possibility of interaction between these aspects, potentializing the consequences through a bidirectional path, indicates the need for ergonomic analyses with holistic approaches in the assessment of occupational risks, since the recognition and interventions only in the physical load or psychosocial risks may not be enough to prevent future impairments to workers' health.

REFERENCES

[1] Hassani M et al. *Int J Ind Ergon* **88**: 103275, 2022.
[2] Yves R et al. *Bull Acad Natle Méd* **201**: 1149-60, 2017.
[3] EU-OSHA. https://osha.europa.eu/en/themes/musculoskeletal-disorders

THE CHANGES IN BALANCE, LOWER EXTREMITY STRENGTH AND POWER OF COLLEGE TENNIS PLAYERS AFTER AGILITY TRAINING

Mu-Tzu Su[1], Anne Dixie M. Lim[1], Shih-Wun Hong[1] and Ho-Yi Tuan-Mu[1,2]
[1] Department of Physical Therapy, Tzu Chi University / Hualien, Taiwan
[2] Department of Sports Medicine Center, Hualien Tzu Chi Hospital, Buddhist Tzu Chi Medical Foundation / Hualien, Taiwan
Email: mandy880902@gmail.com, annedixielim@gmail.com, swhong0624@mail.tcu.edu.tw, hytuanmu@mail.tcu.edu.tw

INTRODUCTION

Tennis, a quick-moving explosive sport, requires a combination of strength, flexibility, agility, and tennis-specific skills to excel in a single game. Tennis players must serve, receive, or hit the ball several times. This process includes multiple sprints in different directions, rapid stops, sudden changes in direction, and vertical jumps, among other things. They need to maintain balance during the hitting process and effectively return the ball. The stability, coordination and sensitivity of the lower body are very important to them. Agility, or the ability to sprint and change directions quickly while running, is thought to benefit lower extremity function. However, agility training was sometimes skipped in the training protocol by student-athletes due to time-consuming and unclear effects on physical ability. The aims of this study are to determine whether agility training can improve the balance, muscle strength, and muscle power of local college tennis players or not.

METHODS

Thirteen college tennis players from Tzu Chi University were recruited in this study. Each participant underwent 30 minutes training protocols from the International Tennis Federation and/or United States Tennis Association twice a week. Outcome measurements, including the vertical jump test and the single hop test for power, the Y-balance test for balance, and the wall squat test for strength, were evaluated. The Wilcoxon Signed Rank Test was used to compare the differences before and after six weeks of the training program by using the Statistical Package for the Social Sciences software. A significant level of p-value < 0.05 was set.

RESULTS AND DISCUSSION

After six weeks of agility training, significant improvements were found in the Y-balance tests posterolateral reach with right leg standing (95% interval changes = 63.7~117.4 to 82.02~112.05) and the Y-balance test anterior reach with left leg standing (95% interval changes = 45.00~69.9 to 43.1~81.59). The Y-balance tests is related to lower extremity stability and postural control. In this study, two Y-balance test directions were found to be improved[1], which are movements that resemble the foot's position when striking a tennis backhand. The improvement in this findings may be explained by the fact that the subjects are student-athletes, who may not have trained their non-dominant side adequately[2]. This also applies to the backhand, which performs comparatively poorly as compared to the forehand. Foot dominance also affects support strategies. The dominant foot is usually related to stability and non-dominant foot related to mobility. The stability of the lower limbs will directly affect the power of hitting the ball and the accuracy of the hitting process. If agility training can improve the balance of the lower limbs in this direction, it may also improve sports performance. However, there were no statistically significant changes in muscle power or strength after six weeks of training(Table1). The overload principle suggests that agility training may not have significantly improved these players' muscle adaption.

Table 1: Y-balance tests Posterolateral reach and Anterior reach

	Pre-test	Post-test	*p-value*
Posterolateral reach (right leg stand)	90.54 ± 13.70	97.04 ± 7.66	$p = 0.036$
Anterior reach (left leg stand)	57.46± 6.36	62.35 ± 9.82	$p = 0.016$
vertical jump test	39.23±10.76	41.54±10.75	*P=0.248*
wall squat test(right)	37.23±17.82	37.33±9.34	*P=0.972*
wall squat test(left)	47.25±24.36	40.22±12.11	*P=0.552*

CONCLUSIONS

Six weeks of agility training may improve balance but not muscle strength and muscle power for college tennis players. Our results suggest that the six weeks of agility training may improve the balance ability, especially in posterolateral reach with right leg standing and anterior reach with left leg standing, which should be incorporated into the training protocol for tennis players.

REFERENCES

[1] Kovacs, M. S. Sports medicine, 37(3):189-198, 2007.
[2] Kozinc, Ž., & Šarabon, N. PLoS One, 16(11), 2021

PERFORMANCE DIFFERENCES AMONG U-15 AND U-18 SOCCER PLAYERS: A STUDY OF SPEED, CHANGE OF DIRECTION, AND EXPLOSIVE POWER.

Muhammad Iftiqar Ahmad Termizi[1], Raja Mohammed Firhad Raja Azidin[1,3] and Raihana Sharir[1,2]
[1]Faculty of Sports Science and Recreation, Universiti Teknologi MARA, Shah Alam, Malaysia.
[2]School of Sport and Exercise Sciences, Liverpool John Moores University, United Kingdom.
[3]Faculty of Sport Science, Malang State University, Indonesia
Email: iftiqar_termizi95@yahoo.com

INTRODUCTION

Changes in muscle metabolism due to sex, age, and maturation can impact youth sport performance [1]. While age-related changes have been well documented, the specific effects of maturation on muscle and sport performance are not well understood [1][2]. More studies are needed to compare performance differences between different age groups, especially in young athletes [4]. This current study aims to determine the differences in speed, change of direction, and explosive power between U-15 and U-18 soccer players.

METHODS

Thirty secondary school soccer players (n=30) participated in this study. The participants were divided into two groups: U-15 (n=15; aged 13-15 years) and U-18 (n=15; aged 16-18 years). Each participant underwent three physical tests: 20 m sprint test, arrowhead agility test, and counter-movement jump (CMJ) test. A speed timing gate system was utilized to record the time of the sprint for the 20 m sprint test and the arrowhead test in order to minimize any potential biases in the testing. The Counter-Movement Jump Test was conducted using the "My Jump 2" application on a smart mobile phone.

RESULTS AND DISCUSSION

An independent T-test revealed a significant difference ($p<0.05$, $p=0.043$) in explosive power performance between the U-15 and U-18 soccer players (Table 1). In addition, a trend towards significant in speed performance ($p=0.05$) was also observed. This can be attributed to the difference in age, as the U-18 soccer players are older and therefore capable of producing greater muscular power. As the individual transitions from childhood to adulthood, numerous physiological changes occur in the neuro-muscular system, including muscle-tendon development, muscle activation, circulation of androgens, and motor unit recruitment [5]. Additionally, as players mature, they tend to display increased maximal force production and improved muscle capabilities, specifically regarding their muscle's stretch-shortening cycle (SSC) and the strength of the lower limb muscles crucial for executing jumps [3].

	U-15	U-18			
	Mean ±Std	Mean ± Std	df	t	p
20 m sprint test	3.23 ± 0.09	3.16 ± 0.11	27.43	2.01	0.05
Arrowhead test (right)	8.45 ± 0.30	8.28 ± 0.29	27.98	1.51	0.14
arrowhead Test (left)	8.49 ± 0.30	8.39 ± 0.30	28.00	0.95	0.35
CMJ Test	36.66 ± 4.48	40.37 ± 5.10	27.54	-2.12	0.04*

Table 1. Performance test comparison between U-15 and U-18.
*Indicate significant difference.

CONCLUSIONS

The findings of this study demonstrate a faster speed and higher power performance in U-18 players compared to U-15 players. These findings may suggest that in youth players, differences in age and maturity may have a significant impact on sport-related performance. This is due to the interplay of various physical and physiological variables that are related to age, growth, maturation, and sex. Typically, earlier-maturing players are taller, heavier, and more muscular than later-maturing players. However, these differences may be altered by specific training interventions.

ACKNOWLEDGEMENTS

The author expresses appreciation to Sultan Idris Shah II Secondary School, Malaysia for allowing the recruitment of participants for this study. The author also thanks all those who helped in the completion of this project with their invaluable contributions and cooperation.

REFERENCES

[1] Armstrong, N., et al. "British J Sports Medicine." 860–864, 2015.
[2] Rodriguez-Rosell, David, et al. "J Strength and Conditioning Research." 196-206, 2016.
[3] Kurihara T et al. *PLoS ONE*, 2021
[4] Peitz M et al. *PLoS ONE*, 2018
[5] Kumar N, Tumkur Anil. "Sports." 59, 2021.

Influence of Penn State University on the International Society of Biomechanics

Brian L. Davis, Ph.D[1]
[1] Department of Mechanical Engineering, Cleveland State University, Cleveland, Ohio, 44115, USA
Email: B.L.Davis@csuohio.edu

INTRODUCTION

The International Society of Biomechanics (ISB) was founded in 1973, with its first president being Dr. Jurg Wartenweiler from Switzerland. The creation of the ISB was on the campus of Penn State University, where Dr. Richard (Dick) Nelson had established a lab in 1967, initially focusing on sport biomechanics. This humble beginning in a circular water tower would later result in groundbreaking research into human gait, ergonomics, muscle mechanics and biomechanical instrumentation.

METHODS

This historical review is based on published literature, ISB archives, and communication with ISB pioneers.

RESULTS AND DISCUSSION

In is first 50 years, the ISB has had 23 presidents, with the first two (Wartenweiler and Nelson) each serving 4 years. Of these presidents, 7 (Table 1) have had close ties with Penn State (three as faculty members, and four who obtained doctorates, two advised by Nelson, and two by Cavanagh). Nelson's first doctoral graduate was Doris Miller, who was a member of the first Executive Council and the first woman to serve on ISB's Council. The next woman elected to the Executive Council (Micheline Gagnon) was also one of Nelson's students. Her research on sprinting was completed in 1976, 13 years before she became an ISB Council member.

The ISB organization depends on multiple volunteers. Dewey Morehouse and Nelson served as Treasurers for 9 years, and other Penn State alumni have served multiple terms as Secretary General or Newsletter Editor. Challis is the current archivist who oversees the collection of ISB documents at Penn State.

Figure 1. A historical marker on the campus of Penn State University. It highlights the formation of the Biomechanics Lab in 1967, and the founding of the ISB 6 years later. https://hhd.psu.edu/news/2010/biomechanics.html

CONCLUSIONS

Students and faculty such as Nelson and Cavanagh and others associated with Penn State have played key roles in both the initial development of the ISB as well as the continued growth around the world.

ACKNOWLEDGEMENTS

The author acknowledges the role of Penn State in his own professional growth, and the network of colleagues that is the hallmark of ISB.

REFERENCES

[1] Miller, D. I., 2021. *J of Appl. Biomech* 37, 585-6.

Table 1: Seven presidents in ISB's first 50 years have close connections with Penn State. Their terms cover 16 years.

President	Years	Connection to PSU	Dissertation title (or in the case of faculty, other
R.C. Nelson	1977-81	Faculty	
Paavo Komi	1981-83	PhD student ('70)	Effect of ecc. and conc muscle conditioning on tension and electrical activity of human muscle
R. Norman	1989-91	PhD student ('77)	The use of electromyography in the calculation of dynamic joint torque
P. Cavanagh	1985-87	Faculty	
M. Rodgers	2003-05	PhD student ('85)	Plantar pressure distribution measurement during barefoot walking
B. Davis	2005-07	PhD student ('91)	A biomechanical investigation of simulated zero-gravity locomotion
J. Challis	2013-15	Faculty	

KINEMATIC ANALYSIS OF CHINESE HANDWRITING IN ADULTS WITH MILD COGNITIVE IMPAIRMENT

Tsai-Yu Shih[1], Wen-Feng Huang[1], Mai-Yi Wu[1], Chien-Liang Liu[2], Tien-Ni Wang[1] and Hao-Ling Chen[1]
[1] School of Occupational Therapy, College of Medicine, National Taiwan University, Taipei, Taiwan
[2]Department of Neurology, Taipei City Hospital, Taipei, Taiwan
Email: hlchen@ntu.edu.tw

INTRODUCTION

Early detection of cognitive decline in older adults has become increasingly important. Cognitive and motor dysfunction were found in patients with mild cognitive impairments (MCI). The kinematic features of alphabetical handwriting have been reported as a potential indicator for discriminating between adults with and without MCI [1]. In Chinese handwriting, the spatial arrangement of characters was more diverse than words in alphabetic writing. Exploring kinematic features of copying characters with 1 to multiple components may reflect different cognitive and motor dysfunction in patients with MCI [2]. Thus, this study aimed to investigate the Chinese handwriting performance of adults with and without MCI.

METHODS

Fourteen participants with MCI (5 males, mean age: 76.0) and 14 healthy controls (HC) (5 males, mean age: 73.3) were recruited to copy Chinese characters with 1 to 5 components (Figure 1(A)). The stylus trajectories were collected by a digitalized tablet and pen (Figure 1 (B)). The kinematic parameters calculated in this study include: (1) The sill time during each stroke, (2) the ratio of in-air to on-paper trajectory length (length ratio) and (3) the ratio of in-air to on-paper time (time ratio). The generalized estimated equations were conducted to confirm the kinematic differences in handwriting between the MCI and HC groups.

(A)

1	井、正
2	困、的
3	你、原
4	落、能
5	影、偷

(B) 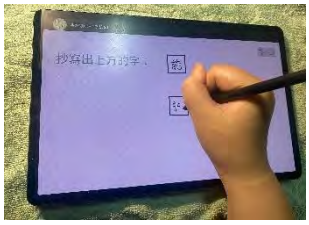

Figure 1 Experimental equipment and task. (A) Copying material of 1 to 5 components. (B) Digitalized tablet and pen.

RESULTS AND DISCUSSION

Table 1 summarizes the results for kinematic parameters. Significant interactions were found in length ratio (p=.015), time ratio (p=.023) and still time (p<.001). The MCI group showed a significantly larger time ratio than the HC group in all copying tasks (p=.001-.013). Furthermore, the MCI group showed a significantly larger length ratio (p=.004-.022) and a longer still time (p=.004-.017) than the HC group when copying characters with more than one component. Patients with MCI wrote strokes with more redundant trajectories and longer pauses, indicating difficulties in processing writing movements with complex spatial configurations. Those results indicate patients with MCI performed writing movements less efficiently than those in the HC group. Copying characters with more than one component may exhibit that patients with MCI have impaired visuospatial skills.

CONCLUSIONS

Patients with MCI showed more characteristics of impairments when copying characters with the increased number of components. Using Chinese characters with complex spatial arrangements as copying material is necessary to detect both motor and visuospatial dysfunction.

ACKNOWLEDGEMENTS

This study was funded by the Ministry of Science and Technology (MOST 110-2628-E-002-004).

REFERENCES

[1] Werner et al. *J Gerontol B Psychol Sci Soc Sci* **61B**: 228-236, 2006
[2] Yu NY et al. *Hum Mov Sci* **65**: 71-79, 2019.

Table 1: Kinematic analysis of copying Chinese characters with 1 to 5 components. (mean ± standard deviation)

Number of	Length ratio		Time ratio		Still time (per stroke)	
Components	MCI	HC	MCI	HC	MCI	HC
1	0.570 ± 0.259	0.434 ± 0.153	0.490 ± 0.300	0.278 ± 0.127	0.182 ± 0.342	0.047 ± 0.013
2	0.440 ± 0.148	0.336 ± 0.098	0.340 ± 0.136	0.192 ± 0.075	0.132 ± 0.116	0.058 ± 0.013
3	0.577 ± 0.190	0.435 ± 0.107	0.557 ± 0.479	0.238 ± 0.086	0.233 ± 0.264	0.071 ± 0.019
4	0.643 ± 0.427	0.327 ± 0.089	0.628 ± 0.675	0.194 ± 0.059	0.200 ± 0.160	0.080 ± 0.029
5	0.756 ± 0.530	0.360 ± 0.104	0.643 ± 0.526	0.175 ± 0.069	0.308 ± 0.350	0.087 ± 0.032

Abbreviations: MCI, mild cognitive impairment; HC, healthy control.

Novel Spring Cleat Testing with Custom-Built Shoe Test Device Yields Null Result

Gregory Chingas, MS[1], Andrew Kraszewski, PhD[1], and Howard Hillstrom, PhD[1]
[1] Leon Root, MD Motion Analysis Laboratory, Hospital for Special Surgery, New York, USA.
Email: chingasgreg@gmail.com

INTRODUCTION

The player-shoe-surface interface is a complex, variable system [1]. Though traction at the shoe-surface interface is implicated in lower extremity injury, studies suggest flexible cleat components lessen rotational stiffness, affecting injury type and risk [2-4]. A deformable, dual spring-loaded cleat (Cleat Assembly, or CA; Patent No.: US 11,213,101 B2) could affect lower extremity injury similarly through coupled compression and bending. The purpose of this study was to quantify repeatability of a custom-built shoe test device in producing torsional friction parameters (TFPs) and differentiate between CAs with stiff and soft compression and bending springs. Barring strong test device reliability, it was hypothesized that TFPs would decrease from standard cleats to stiff CAs, and from stiff to soft CAs.

METHODS

Test device reliability testing

Ten cleats with rigid spikes were rotated by two testers (GC and AK). Cleat, tester, and test options (test-retest and remove-replace) orders were randomized. Cleats were rotated 10 times for each of three test options, and each cleat was rotated 30 times per tester, or 60 total times. Rotations were performed using prosthetic feet over artificial turf adhered to a force plate. Cleats were positioned in foot flat prior to rotations, and turf position was consistently changed to reduce wear. Rotations were performed with a compressive force and rotational pressure of about 50 lbf and 70 psi, respectively.

Cleat Assembly testing

Soft and stiff CAs were prepared using commercially available springs matching CA specifications. Seven cleats were tested by one tester (author GC), and each cleat was rotated 20 times – 10 times per CA type (soft or stiff). Otherwise, procedures from test device reliability testing were followed.

Motion analysis

An eight-camera motion capture system and one force plate were used. Reflective markers were placed on all cleats at toes, heel, and proximal and distal lateral and medial locations.

Statistical analysis

Rotations 4 through 10 from all tests were analyzed. Stiffness (torque linear regression from 0 to 5° rotation), peak torque (torque taken at 15°), and release coefficient (moment-to-vertical force ratio) were computed from test device reliability (control) and CA testing. Cronbach's alpha (α) values were computed to quantify test device internal consistency. Wilcoxon signed-rank tests were used to compare TFPs produced in control, soft CA, and stiff CA conditions, and p values less than 0.05 were considered significant.

RESULTS AND DISCUSSION

The test device was excellent ($\alpha \geq 0.875$) at consistently producing TFPs (Table 1). For CA testing, data from one cleat were omitted from analyses given outlier behavior in soft and stiff conditions. There were no significant differences for stiffness and peak torque between all conditions ($p > 0.05$). Though a decrease in release coefficient from control through soft CA was expected, a significant increase in this TFP from control to stiff CA ($p = 0.018$) and stiff CA to soft CA ($p = 0.047$) was observed (Figure 1).

Table 1: Cronbach's alpha values for TFPs. Internal consistency was assessed as excellent ($1.0 > \alpha \geq 0.8$), good ($0.8 > \alpha \geq 0.6$), and moderate ($0.6 > \alpha \geq 0.3$).

	Stiffness	Peak torque	Release coefficient
Cronbach's Alpha	0.875	0.898	0.899

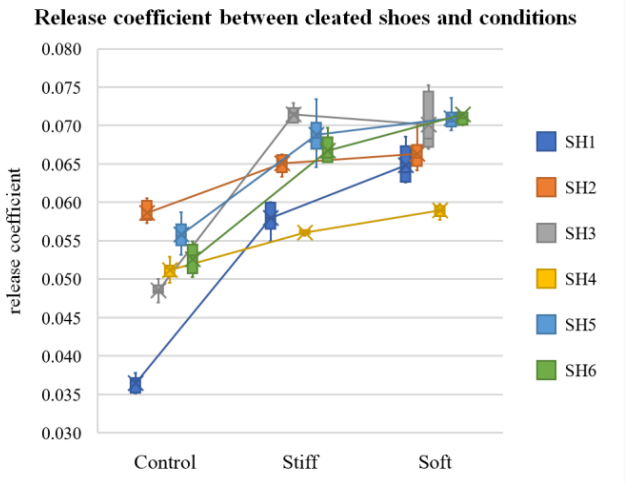

Figure 1: "X" marks indicate mean values, which are connected between condition for all shoes by lines.

CONCLUSIONS

Despite the test device's reliability in producing TFPs, CA testing yielded a null result, which necessitates vetting the current CA design. Understanding the test device's static response (i.e., peak torque timing and magnitude given a specific input) would be ideal for future testing to better define and assess TFPs. Lastly, future tests with the test device should be conducted using real-world forces and moments.

REFERENCES

[1] O'Conner et al. *Foot Ankle Clin* **18**: 369-80, 2013.
[2] Torg et al. *Am J Sports Med* **2**: 261-9, 1974.
[3] Villwock et al. *Am J Sports Med* **37**: 518-25, 2009.
[4] Button et al. *J Biomech Eng* **137**: 061004, 2015.

Tracking golf swing trajectory using a single IMU by applying biomechanics and machine learning

Myeongsub Kim and Sukyung Park
Department of Mechanical Engineering, Korea Advanced Institute of Science and Technology, Daejeon, Korea.
Email: myeongsub@kaist.ac.kr

INTRODUCTION

Human motion monitoring services using wearable devices are becoming popular, but the information from most golf-related devices is limited to operation-related and club kinematics. Recently, golf wearable devices have shown a trend to provide kinematic details on the body, but the amount of information and accuracy is still limited. Therefore, in this study, we applied biomechanics and machine learning to improve the tracking accuracy of the upper limb's trajectory using a single IMU.

METHODS

Three technical issues should be addressed in order to enhance the swing tracking accuracy: segmentation, orientation calibration, and trajectory calibration.

Before addressing the issues, to collect the golf swing data, nine professionals and eleven amateur golfers with an average handicap of 15.3 were recruited. A 6-axis IMU was attached to the wrist, and data was collected from the IMU and the motion capture system, swinging 10 times each with a driver and a 7-iron.

First, we segmented the golf swing data from the IMU signal into swing phases using a heuristic approach [1]. The indicators of minimum, maximum, or zero-crossing of the IMU signal were manually selected to segment the address (ADD), backswing top (BST), impact (IMP), and finish (FIN) points.

Then we applied a convolutional neural network (CNN) to calibrate the initial sensor orientation. The sensor orientation during the entire swing was calculated using the angular velocity from the IMU.

Finally, we calibrated and estimated upper limb trajectories. The wrist speed was calibrated with the traits that the speed comes to 0 at ADD, BST, and FIN. The wrist trajectory was calibrated to approximate a circle. The elbow and shoulder trajectories were estimated from the wrist trajectory by modeling the elbow flexion using trigonometric functions.

RESULTS AND DISCUSSION

Tracking accuracy using the methods at each step described above was calculated and compared.

Using a heuristic method, we segmented the golf swing phases with a mean absolute error (MAE) of approximately 60ms on average (Figure 1A).

Without using any additional calibration motion, the suggested CNN-based method calibrated the initial sensor orientation with a MAE of about 7.5 degrees (Figure 1B). This result shows higher accuracy than the baseline obtained using the averaging method and the N-pose and T-pose methods currently in use [2], which revealed errors of between 6 to 40 degrees.

The proposed method reduced the MAE by 70%, compared to the naïve integration, calibrating the wrist trajectory from the IMU with a MAE of about 0.15m. With a MAE of 0.11 m and 0.13 m, respectively, the proposed method estimated the trajectory of the unmeasured elbow and shoulder joints during the backswing and downswing phases (Figure 1C).

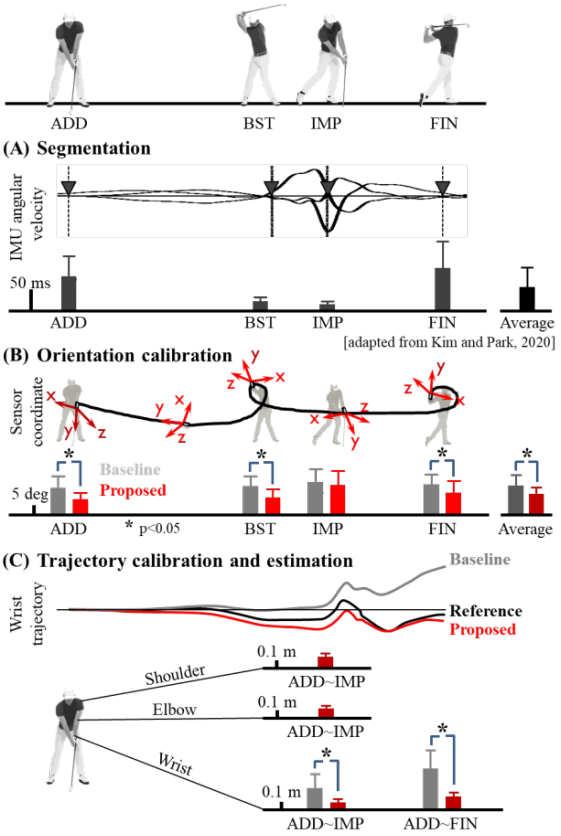

Figure 1 MAE of the (A) segmentation, (B) orientation calibration, and (C) trajectory calibration and estimation.

CONCLUSIONS

In this study, we enhanced the tracking accuracy of the upper limb kinematics from a single IMU by applying biomechanics and machine learning. It implies that we might be able to overcome the wearable devices' motion tracking limitations by comprehending the biomechanical characteristics of the movement.

ACKNOWLEDGEMENTS

This research project was supported by the sports promotion fund of Korea sports promotion foundation (KSPO) from Ministry of Culture, Sports and Tourism.

REFERENCES

[1] Kim and Park. *Sensors* **20(16)**: 4466, 2020.
[2] Robert-Lachaine et al. *G&P* **54**: 80-86, 2017.

SEMI-AUTOMATIC DEFINITION OF SUBJECT-SPECIFIC MUSCLE PARAMETERS FOR MUSCULOSKELETAL MODELS OF ADULT SPINAL DEFORMITY PATIENTS

Birgitt Peeters[1], Erica Beaucage-Gauvreau[2], Lieven Moke[3], Friedl De Groote[4], Ilse Jonkers[2,4], Lennart Scheys[1,2,3]
[1] Institute for Orthopaedic Research and Training (IORT), KU Leuven, Leuven, Belgium. [2] Institute of Physics-based Modeling for in silico Health (iSi Health), Leuven, Belgium. [3] Division of Orthopaedics, University Hospitals Leuven, Leuven, Belgium. [4] Department of Movement Sciences, KU Leuven, Leuven, Belgium.
Email: birgitt.peeters@kuleuven.be

INTRODUCTION

Adult spinal deformity (ASD) is a degenerative disorder resulting in three-dimensional (3D) spinal deformities [1]. ASD is known to alter spinal biomechanical parameters, like muscle geometry and physiology, yet these are still neglected by current treatment decision-making [2]. Musculoskeletal models (MSKM) are increasingly used to evaluate these parameters in many other musculoskeletal disorders. However, existing generic MSKM fail to account for the altered spinal biomechanical parameters in ASD [3] and to date, no biofidelic MSKM for ASD patients exist. The aim of this research is to develop an efficient image-based workflow for the definition of subject-specific muscle parameters in MSKM of ASD patients.

METHODS

MKSM of one representative ASD patient with subject-specific muscle parameters was defined in a workflow, using Mimics and 3-Matic, with python interface (Materialise, Belgium): 1) Semi-automatic multi-atlas segmentation of muscles in magnetic resonance imaging (MRI); 2) Landmark-based registration of previously developed OpenSim [4] spine MSKM, with personalized geometry and spinal alignment [5], to MRI; 3) Muscle parameter definition: attachment points and wrapping surfaces. Attachment points are defined automatically with a closest-point algorithm. Wrapping surfaces are used to prevent bone penetration and ensure a realistic anatomical muscle representation. These surfaces are defined with three different methods; Method 1: manual cylinders and spheres definition, Method 2: automated tori definition using an optimal fit to the vertebral geometry, Method 3: manual adjustment of the dimensions, 3D orientation, and position of the tori from Method 2 to visually correct for discontinuities in moment arms (MA). For all methods, the MA at the lumbar intervertebral joints spanned by respectively 22, 48, and 18 fascicles of the psoas, multifidus, and erector spinae muscles in the resulting personalized MSKM are compared to the MA of a generic MSKM [5] scaled to the anthropometry of the same ASD subject for the following range of motion: flexion-extension and lateral bending: -8° to +8°, axial rotation: -5° to +5°.

RESULTS AND DISCUSSION

The generic MSKM resulted in unphysiological behaviour with many fascicles penetrating bone, thus resulting in smaller MAs (Fig. 1). In addition, some fascicles had the opposite action compared to the personalized MSKM, highlighting the inability of generic MSKM to account for the 3D malignment. However, the wrapping surfaces in the personalized MSKM introduced small discontinuities in MA, compared to the generic MSKM (Fig. 1). Method 1 usually resulted in the least and smallest discontinuities, but required almost twice as many wrapping surfaces as Methods 2 and 3, thus increasing the computational cost. Method 2 generally resulted in the largest discontinuities, albeit still relatively minor. Method 3 often reduced and even removed these discontinuities.

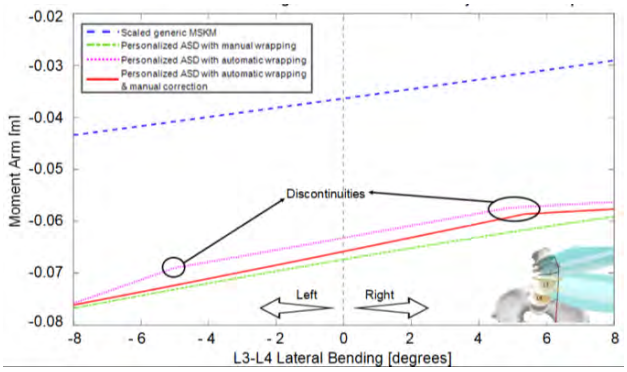

Figure 1 Moment arms at the L3-L4 intervertebral joint during lateral bending for fascicles of the left psoas muscle.

CONCLUSIONS

This novel workflow is the first to allow for an efficient definition of realistic subject-specific muscle parameters in MSKM of ASD patients, with an anatomically correct muscle geometry, while preventing bone penetration during the representative range of motions. The workflow will be validated for a larger set of patients, but is already promising to provide accurate biomechanical analyses of ASD.

ACKNOWLEDGEMENTS

The authors thank Flanders' Fund for Scientific Research (1SE6223N) for financial support.

REFERENCES

[1] Ailon et al, *Neurosurgery* **77**: S75-S91, 2015.
[2] Joshi et al, *Neurospine* **16**: 686-694, 2019.
[3] Haddas et al, *Spine J.* **21**: 1193-1204, 2021.
[5] Overbergh et al, *J. Biomech.* **110**: 109946, 2020.
[6] Delp et al, *IEEE Trans. Biomed. Eng.* **54**: 1940-1950, 2007.

The Role of Spinal Muscles for Lumbar Loads during Static Loading Tasks in Large Patient Cohorts: A Musculoskeletal Modeling Study

Tanja Lerchl[1,2], Kati Nispel[1,2], Veit Senner[1], and Jan S. Kirschke[2]

[1] Associate Professorship of Sport Equipment and Sport Materials, School of Engineering and Design Technical University of Munich, Munich, Germany

[2] Department of Diagnostic and Interventional Neuroradiology, School of Medicine Klinikum rechts der Isar, Technical University of Munich, Munich, Germany

Email: tanja.lerchl@tum.de

INTRODUCTION

Numerical models of the musculoskeletal system are an integral part of biomechanical and clinical research. Multibody modeling allows the consideration of biomechanical systems from a holistic perspective, and thus, takes into account multiple influencing factors of mechanical loads. Being the source of major health issues worldwide, the human spine is subject to a variety of studies using these models to investigate and understand healthy and pathological biomechanics of the upper body. Models usually consider muscle mophology from cadaver studies or imaging data from a single individual. However, muscle morphology is highly individual, depending on various factors, such as age, fitness, genome, or pathological changes of the musculoskeletal system of the respective subject. To this date, only few studies exist, that systematically investigate the effects of altering muscle morphology on spinal loading[1].

METHODS

We used our validated pipeline for automated generation of individualized models of the torso with detailed lumbar spine[2] to assess the influence of altering muscle physiological cross sectional area (PCSA) on spinal loading in 93 patients. For abdominal muscle force estimation, we used a combination of inverse dynamics and static optimization (*global search, fmincon, Matlab*). The cost function was defined as the sum of cubed muscle stress and maximum muscle stress was set to 1MPa. We simulated static upright standing, 30° flexion, and symmetric lifting of 10kg close to the chest and with stretched arms. The PCSA of single fascicles of erector spinae (ES) and multifidus muscle (MF) were each set to 0%, 30%, and 50%. Resulting spinal loads were compared to results from simulations with full muscle architecture considering the patient's individual upper body weight and spinal alignment.

RESULTS AND DISCUSSION

Depending on individual lumbar alignment, effects were most evident in upper (T12/L1) and lower levels of the lumbar spine (L5/S1) in loading tasks with a 10 kg weight lifted with stretched arms. Normalized anterior-posterior shear loads increased to 128 % on average, with a maximum of 208 % at T12/L1 for ES PCSA reduced to 30%. Simultaneously, compression forces were increased up to 120% (Figure 1).

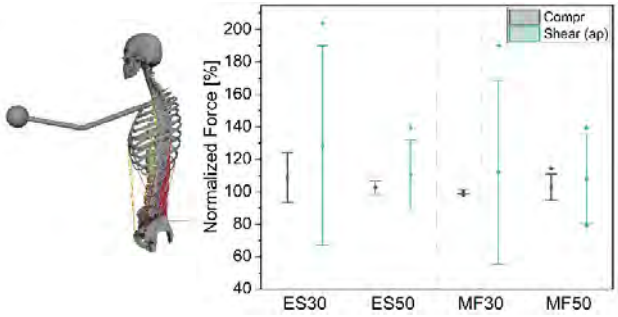

Figure 1 Normalized anterior-posterior shear and compression forces in T12/L1 during lifting of 10 kg with stretched arms under consideration of individual anthropometry and spinal alignment.

Static equilibrium conditions could not be met for the vast majority of models with disabled ES or MF. With increasing body weight or lumbar malalignment, models with reduced MF were less likely to meet static equilibrium conditions for challenging loading tasks.

CONCLUSIONS

Our results indicate that the loss of functional muscle cross sectional area, e.g. due to muscle atrophy or intramuscular fat, leads to increased spinal loading with a pronounced effect on anterior-posterior shear forces. Furthermore, our study emphasizes the relevance of paraspinal musculature for spinal stability and associated malalignment[3] to prevent potentially pathological overload.

ACKNOWLEDGEMENTS

This research was funded by the European Research Council (ERC) (European Union's Horizon 2020). Grant no.: 101045128—iBack-epic—ERC-2021-COG.

REFERENCES

[1] Wang K et al, *Bioengineering (Basel)*. **10**(1):67, 2023.

[2] Lerchl T et al, *Front Bioeng Biotechnol.* **10**:862804, 2022.

[3] Muellner M et al, *Spine J.* **22**(12):2006-2016, 2022

Quantifying Spinal Parameters for Scoliosis Using A Low-Cost 3-Dimensional Motion Capture System

Pitchaya Rayothee[1,2] and Professor Philip Rowe[1]
[1] Department of Biomedical Engineering, University of Strathclyde, Glasgow, Scotland.
[2] Faculty of Medicine Siriraj Hospital, Mahidol University, Bangkok, Thailand.
Email: Philip.rowe@strath.ac.uk

INTRODUCTION

A lateral deviation of the spine of more than 10° is considered scoliosis [1]. Adolescent idiopathic scoliosis accounts for 80% of cases and is more common in girls than boys [2]. Scoliosis treatment options include non-surgical and surgical correction. Spinal orthosis is recommended as a treatment option to delay the curve progression [1]. Radiography is a standard method for quantifying outcomes [1]; however, it can be harmful and cannot be described in three dimensions (3D). A motion capture system is another option; however, current systems are expensive and not available in clinics [3]. Therefore, the study objective was to develop an alternative method to quantify the spinal parameters (SP) for scoliosis using a low-cost 3D motion capture system.

METHODS

We developed a low-cost 3D motion capture system. Which utilised eight Raspberry Pis (3B+) each with a camera which streamed to a local network real time images wirelessly. A central, windows based computer running a purpose written C++ programme in Visual Studio 2019 collected and analysed the video frames from the cameras. White markers were used to track key anatomical landmarks. Twenty-five passive markers were attached using double sided wig tape to the spinous processes of C7/T7/T12/L2/L5; acromion processes; axilla level; inferior angle of scapula; waist level; at the same level as T12/L2/L5; PSIS; xyphoid process; umbilicus; middle distance between xyphoid and umbilicus; and middle distance between ASIS.
In the initial test phase, a scoliotic manikin was used to quantify relevant spinal parameters and check for accuracy and precision. After calibrating the camera and attaching the marker, the manikin was positioned in the center of the camera frame (Figure 1.a). The developing software then determined the locations of the markers prior to calculating the SP during the data processing method. The system was then used to measure before and after orthotic casting in a series of patients to determine the amount of change produced in spinal curvature during casting.

RESULTS AND DISCUSSION

The graphical user interface (GUI) displayed fourteen SP, including the level of shoulder, axilla, and waist; distance between left and right side to the central line at the axilla and waist level; thoracic kyphosis; lumbar lordosis; Cobb angle at T7 and L2; trunk horizontal rotation at T7, T12, L2 and L5 level; and coronal decompensation (Figure 1.b). Moreover, there were another sixteen SP for further evaluation, including upper and lower thoracic, upper and lower lumbar in sagittal, coronal, and 3D angles with respect to the horizontal plan. The results displayed on the GUI were the most common SP observed by clinicians during the assessment process. Additionally, another set of SP were previously studied by Jane [3] and included in this study for further analysis.

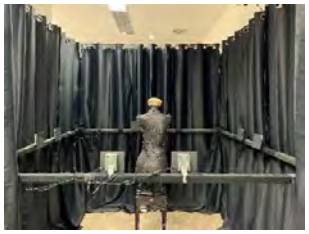

a)

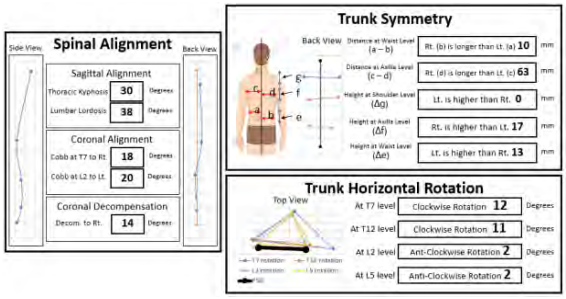

b)

Figure 1 a) A low-cost 3D motion capture system and b) Results of spinal parameters and a graphical representation of the trunk.

CONCLUSIONS

A low-cost 3D motion capture system technique can be developed to quantify appropriate SP in clinics. In a clinical situation, the clinician normally observes by eye; however, the motion system developed could assist in quantifying and reporting the result and hence provide a scientific basis on which to develop future practice.

ACKNOWLEDGEMENTS

I would like to thank the University of Strathclyde for my Ph.D. study and thank the Faculty of Medicine Siriraj Hospital, Mahidol University, for my PhD scholarship.

REFERENCES

[1] Negrini S et al. *J Scoliosis* 10:8, 2015.
[2] Negrini S et al. *J Scoliosis and Spinal Disorders* 13:3, 2016.
[3] Jang SH. *Thesis [Ph.D.]*

Passive neck stiffness and range of motion in 80 adults up to 80 years of age

Liu M[1,2], Quarrington RD[1,2], Sandoz B[3], Robertson WSP[1], Jones CF[1,2]

[1] School of Electrical and Mechanical Engineering, The University of Adelaide, Adelaide, Australia

[2] Adelaide Spinal Research Group, The University of Adelaide, Adelaide, Australia

[3] Arts et Métiers Institute of Technology, IBHGC, Paris, France

Email: mingyue.liu@adelaide.edu.au

INTRODUCTION

Human neck range of motion (ROM) during researcher-initiated movements reduces with age [1], but neck behaviour when the muscles are relaxed (i.e. passive) has only been reported for young and mid-age adults [2, 3]. Passive ROM and stiffness data is needed for computational modelling and surrogate neck design. Therefore, the aim of this study was to measure passive neck stiffness and ROM in flexion, extension, lateral bending and axial rotation, and to examine if these outcomes were dependent on age and sex.

METHODS

Two custom low-friction testing apparatus were used for bending (flexion/extension, lateral bending) and axial rotation tests. Participants were strapped to each apparatus lying in the prone or lateral position, and their head was slowly rotated by the researcher to their maximum ROM. An electromyography system (Trigno, Delsys, USA; 2 kHz) with real-time audio feedback was used to alert participants if they exceeded a "passive" muscle activation threshold. Reflective markers were placed on the participants' head, neck, and upper torso to provide instantaneous moment arm and head/neck kinematic data, via a 13-camera motion capture system (Vantage, Vicon, UK; 100 Hz). Bending moments were calculated by multiplying the tangential pulling force (9327C, Kistler, SUI; 2 kHz) by its instantaneous moment arm. Axial rotation moments were recorded by a six-axis load cell (MC3A, AMTI, USA; 2 kHz). Three trials were performed for each motion. Moment-angle plots were generated for each trial, and divided into three zones via an automated cubic and tri-linear fit process. Neck stiffness was calculated as the gradient of the moment-angle data in each zone. The effect of age, sex, and their interaction, on ROM and stiffness were examined with linear regression models (flexion, extension) and linear mixed models (lateral bending, axial rotation; fixed effect: left/right side, random effect: participant). Post-hoc tests were completed if the age-sex interaction was significant (SPSS, IBM, USA; $p < 0.05$). For brevity, stiffness and ROM for lateral bending and axial rotation are reported as the mean of left and right.

RESULTS AND DISCUSSION

40 males and 40 females participated (age: 20 – 80 years). ROM for flexion, extension, lateral bending and axial rotation were 46 ± 11, 63 ± 14, 37 ± 11 and 66 ± 17 degrees, respectively, and were not dependent on age ($0.05 < p < 0.49$) or sex ($0.21 < p < 0.97$). Age effects on extension (zone 3) and lateral bending (zone 1-2) stiffness were sex dependent ($p < 0.01$), with 3.16, 4.56 and 9.08 Nmm/deg/yr increase for males and 1.10, 2.13 and 3.94 Nmm/deg/yr increase for females (Figure 1). Stiffness increased with age, independent of sex, in extension (zone 2: 1.32 Nmm/deg/yr, $p < 0.01$), lateral bending (zone 1: 0.37 Nmm/deg/yr, $p < 0.01$) and axial rotation (zone 1-3: 0.19, 0.58, 1.11 Nmm/deg/yr, zone 1: $p = 0.045$, others $p < 0.01$).

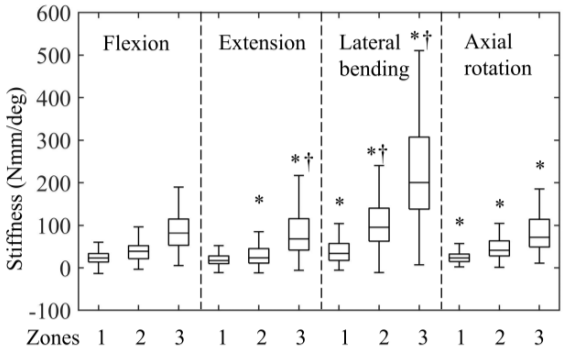

Figure 1: Neck stiffness in each zone, for all motions. All ages and both sexes are presented together for brevity. *Significant age effect ($p < 0.05$). †Significant age-gender interaction ($p < 0.05$). Box: median, 1st and 3rd quartile. Whiskers: indicate minimum and maximum data points that are within 1.5 interquartile range from the box.

CONCLUSIONS

Unlike seated researcher-initiated neck ROM reported previously [1], passive lying neck ROM was not dependent on age or sex. Passive neck stiffness generally increased with age in extension, lateral bending, and axial rotation, and the "rate" of this increase was sometimes sex dependent. Stiffness in flexion was not age dependent in this cohort. These data enhance understanding of the effects of age and sex on cervical spine mechanics and provide data for computational and surrogate neck modelling.

ACKNOWLEDGEMENTS

Funding: The Hospital Research Foundation.

REFERENCES

[1] Dvorak, J et al. *Spine* **17**: 393-398, 1992.
[2] McGill, S. Clin Biomech 9, 193-198, 1994.
[3] Dugailly, P. Clin Biomech 53, 65-71, 2018.

VALIDITY AND RELIABILITY OF NECK RANGE OF MOTION AND REPOSITIONING ERROR MEASURED BY A VIRTUAL REALITY SYSTEM

Imane Boukhalfa[1], Clara Leyh[1], Gaetan Schleich[1], Mathieu Tits[2] and Veronique Feipel[1]
[1] Laboratory of Functional Anatomy, Laboratory of Anatomy, Biomechanics and Organogenesis, Université Libre de Bruxelles, Brussels, Belgium.
[2] Department of Physiotherapy, Brussels University Hospital, Brussels, Belgium.
Email: imane.boukhalfa@ulb.be

INTRODUCTION

Virtual reality systems constitute a new and interesting approach to the assessment and treatment of musculoskeletal musculoskeletal disorders, particularly chronic neck pain [1, 2]. The objective of this work was to evaluate the concurrent validity and test-retest reliability of the measurements of neck range of motion (ROM) and cephalic repositioning (CR) using a commercial virtual reality system, the Virtualis®, in order to be able to integrate it in clinical routine.

METHODS

Thirty healthy subjects (aged 18-70 years) volunteered to participate in our study. Each subject performed two measurement sessions, 5 to 7 days apart. During the first session, the Virtualis® system, via a virtual reality headset (VIVE Cosmos Elite), and a 14-camera VICON® system tracking reflective markers were placed on anatomical landmarks were used simultaneously to evaluate the validity of the measurement. During the second session, only the virtual reality system was used. The sessions, in standardized seated position, consisted of measurements of cervical ROM in the three planes followed by a neutral CR test after right and left rotation. Six trials were executed for each task and the average value was computed. ICC(2,k) and Bland & Altman method were used to compare systems and sessions.

RESULTS AND DISCUSSION

Reliability: The ICC(2,k) for the ROM analysis ranged from 0.74 to 0.92, corresponding to levels of agreement ranging from moderate to excellent [3]. Mean differences (MD) between sessions did not exceed 3.2°. The ICC(2,k) for CR was 0.35 corresponding to a poor level of agreement (MD = 0.2°, Figure 1).

Validity: The results obtained in the analysis of ROM showed a moderate to excellent agreement (ICC(2,k) >0.67) for flexion/extension ROM with a MD between instruments of 1° for flexion and 7° for extension.
Validity was poor for left/right rotation with a mean difference larger than 24° (ICC(2,k) >0.19), and fair for left/right lateral bending (mean difference > 7°; (ICC(2,k) >0.52). Larger ROM was measured by the Virtualis system for axial rotation and lateral bending.

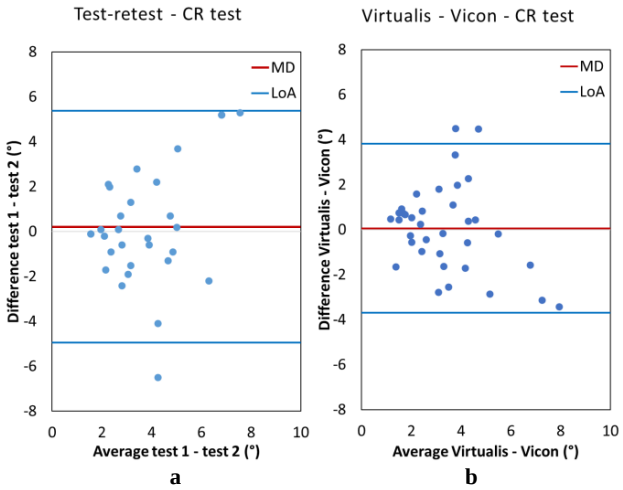

Figure 1 Bland & Altman plots for CR. a) reliability; b) validity.

Regarding the CR test, validity of the Virtualis® was found to be moderate with a mean difference between systems of 0.1° and an ICC(2,k) of 0.67 (Figure 1).

CONCLUSIONS

Virtualis® was shown to have a good reliability for cervical ROM measurements. Concerning concurrent validity, the results indicate acceptable agreement for sagittal plane motion. However, for lateral bending and especially axial rotation, Virtualis overestimated ROM significantly. This bias is linked to the contribution of the upper thoracic spine. Work is in progress to propose a resolution of this source of bias.
On the other hand, cervical repositioning errors measured by Virtualis® displayed negligible differences between repeated sessions and compared to Vicon reference measurements, pointing at a good reliability [4] and validity of Virtualis, despite low ICC values, probably linked to the low dispersion of measurements [5].

REFERENCES

[1] Gumaa M et al. *Phys Ther* **99**: 1304-25, 2019.
[2] Kiper P et al. *J Electromyogr Kinesiol* **51**: 102397, 2020.
[3] Portney LG et al. *Foundations of Clinical Research*. Pearson/Prentice Hall, 2009.
[4] Kramer M et al. *J Electromyogr Kinesiol* **19**: 353-61, 2009.
[5] Goodwin LD et al. *J Exp Educ* **74**: 251-66, 2006.

NEUROMUSCULAR ADAPTATIONS IN ANKLE DORSIFLEXOR IN PERSONS WITH SPINAL CORD INJURY

Asta Kizyte[1], Haocheng Zhang[1], Emelie Butler Forslund[2], Elena Gutierrez Farewik[1,3], and Ruoli Wang [1]
[1] KTH MoveAbility Lab, KTH Royal Institute of Technology, Stockholm, Sweden.
[2] Rehab Station Stockholm, Research and Development Unit, Stockholm, Sweden.
[3]Department of Women's and Children's Health, Karolinska Institutet, Stockholm, Sweden.
Email: astad@kth.se

INTRODUCTION

Spinal cord injury (SCI) may lead to sensory-motor impairment, including diminished muscle control, muscle weakness, and paralysis. Lower leg muscles, crucial for daily activities like walking and maintaining balance, are often affected due to their innervation in the lumbar and sacral segments of the spine. There is potential for partial recovery during the acute phase of SCI due to numerous neurophysiological changes [1] that may persist during the sub-acute and chronic SCI. However, the knowledge of these neurophysiological adaptations in the dorsiflexor muscles is still limited. High-density electromyography (HD-EMG) allows non-invasive observation of muscle activation and motor unit behavior *in vivo*, helping to understand these adaptations and aid in developing effective treatment and rehabilitation strategies for individuals with SCI.

METHODS

HD-EMG data (64 channels) were collected from the *tibialis anterior* of eleven participants (7 male, age: 56.0 ± 10.8 yrs., BMI: 25.9 ± 3.1) with sub-acute or chronic (> 7 months) SCI and ten age-matched control participants (4 male, age: 55.5 ± 9.4 yrs., BMI: 29.1 ± 4.6). The subjects were asked to perform four repetitions of isometric dorsiflexion at 20% and 50% of their maximum voluntary contraction (MVC) while seated on a chair, with their hip and knee fixed at 90º and ankle fixed in the neutral position. Participants were given visual feedback to guide the contraction intensity. The torque was measured simultaneously using an ankle dynamometer. The HD-EMG data was decomposed into separate motor unit firing events using convolutional kernel compensation [2]. Parameters, such as maximal torque (normalized to body weight), variability of sustained torque (CoV_{TRQ}), normalized EMG amplitude ($NRMS_{EMG}$), motor unit discharge rate and variability (CoV_{ISI}), and motor unit recruitment thresholds were calculated for each person. Between-group comparisons were made, and the statistical significance was determined with independent samples t-test (normally distributed data, $p < 0.05$) or the Man-Whitney U test (non-normal distribution, $p < 0.05$).

RESULTS AND DISCUSSION

The preliminary results showed a slightly decreased dorsiflexor strength (SCI: 0.49 ± 0.14 Nm/ kg; control: 0.57 ± 0.08 Nm/kg; p = 0.105) in the SCI group. We found that participants in both groups could maintain the torque with similar variability (at 20% MVC SCI: 0.06 ± 0.06, control: 0.05 ± 0.03, p = 0.81; at 50% MVC SCI: 0.05 ± 0.05, control: 0.05 ± 0.03, p = 0.61). However, the SCI participants needed a higher $NRMS_{EMG}$ to achieve the same level of torque as the control participants (Fig. 1A), indicating an altered strategy in force generation. At 50% MVC, the motor units were recruited at lower torque thresholds (Fig. 1D) and continued firing at lower discharge rates (Fig. 1C) in individuals with SCI, but with similar variability as in the control group (Fig. 1B). These alterations in motor unit behavior observed in persons with SCI may contribute to their muscle weakness and reflect altered force modulation strategies after the impairment.

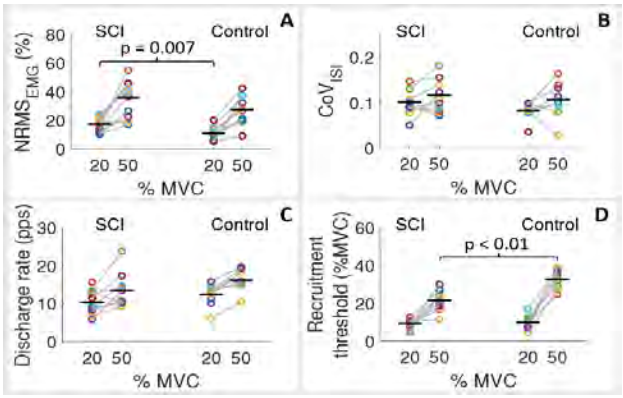

Figure 1 (A) EMG amplitudes, (B) variation of motor unit firings, (C) motor unit discharge rates and (D) recruitment thresholds. The horizontal bars indicated the group means, and the brackets with p values indicated statistical significance.

CONCLUSIONS

Torque, EMG, and motor unit parameters were observed in SCI and control groups. Most notably, we found increased EMG activation and decreased motor unit recruitment thresholds following SCI. The results indicated altered neural control strategies for force generation and gradation in individuals with SCI. Knowledge of these neuromuscular adaptations may aid the future research in SCI rehabilitation and treatment.

ACKNOWLEDGEMENTS

This work was supported by the Swedish Research Council (Starting Grant, 2018-04902) and Promobila Foundation (grant ref. 18200, 20039, and 21025).

REFERENCES

[1] McKay W et al. *Spinal Cord* **49**: 421–429, 2011
[2] Holobar A et al. *IEEE Trans. Signal Process.* **55**: 4487–4496, 2007

PATIENT-SPECIFIC MODELING OF MANDIBULAR MUSCULOSKELETAL SYSTEM AND ITS APPLICATIONS IN TRISMUS ESTIMATION

Jianqiao Guo[1], Junpeng Chen[2], Xinyue Wang[1], Jing Wang[2] and Qiang Tian[1]

[1] MOE Key Laboratory of Dynamics and Control of Flight Vehicle, School of Aerospace Engineering, Beijing Institute of Technology, Beijing, China.

[2] Department of Oral and Maxillofacial Surgery, Peking University School and Hospital of Stomatology, Beijing, China.

Email: guojianqiao@bit.edu.cn (J.Guo)

INTRODUCTION

The oral and maxillofacial tumor has become one of the ten most common tumors worldwide. Most patients can recover their mandibular bone anatomy with the help of digital surgical planning; however, nearly half of them cannot open their mouths wide (i.e., trismus) after six months of recovery. Musculoskeletal modeling provides a systematic way to estimate jaw opening functions [1]. This study proposed a patient-specific modeling framework of the mandibular musculoskeletal system based on medical imaging and jaw kinematics measurement. It was utilized in jaw opening predictions and validated by postoperative measurements.

METHODS

This study's protocol was approved by the Institutional Research Board of Peking University School and Hospital of Stomatology (PKUSSIRB-201942015). Ten preoperative patients with unilateral mandibular tumors were included. As shown in Figure 1, subject-specific mandibular geometry was measured and reconstructed based on CBCT data, and the bone-cutting regions were prescribed by ProPlan software. Mandibular muscles were discretized by a flexible cable element with a typical Hill-type model [2]. Their insertions were registered based on the nonlinear iterative closest point method. The patients were required to perform three repetitive cycles of maximal jaw opening-closing movements, and their mandibular kinematics were measured by the WinJaw system. The desired fiber length of each muscle was calculated via inverse dynamics simulations. Their activations before the surgery were then obtained by a proportional-integral-derivative controller considering the differences in muscle cross-sectional area. The changes in muscle biomechanical parameters in the postoperative stage were estimated based on the average value of spiral CT data. These values were used to predict the postoperative jaw opening functions, validated by the six-month follow-up measurements of the mandibular kinematic data.

RESULTS AND DISCUSSION

As a validation, the average root-mean-square error (RMSE) of the predicted mandibular opening magnitude averaged by the recruited patients was 3.5mm. The predicted mandibular incisor trajectories were highly correlated with the postoperative measurement of each patient (R^2=0.95 ± 0.05). Using 25mm of maximal jaw opening as the inclusion criteria of severe trismus [3], the proposed framework successfully predicted the jaw opening functions of 80% of recruited patients. The sensitivity in predicting severe trismus was 66.7%, and the prediction specificity was 85.7%. The performance of estimating trismus was influenced by the patient's age, tumor classification, and tumor-involved regions. The current modeling approach did not consider the biomechanical influence of the scar tissue, potentially reducing the active force generation. The activation patterns of the masticatory muscles were assumed unchanged after the surgery since the observed EMG data were patient-specific and could not be averaged. Moreover, the proposed model performed poor accuracy in estimating jaw deviations. Further investigations should include a more detailed model of the temporomandibular joint.

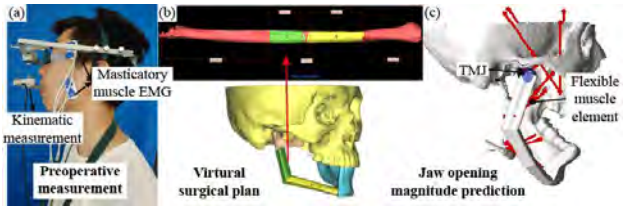

Figure 1 Schematics of the jaw opening function predictions. (a) Preoperative measurement of jaw kinematics & EMG data; (b) Virtual surgical planning based on jawbone anatomy; (c) Predictions of jaw opening magnitude based on patient-specific modeling.

CONCLUSIONS

The proposed musculoskeletal modeling framework successfully predicted the sagittal jaw opening functions before mandibular reconstruction surgery, highlighting its potential use in surgical planning.

ACKNOWLEDGEMENTS

This work was supported in part by the China National Natural Science Foundations of China (12102035).

REFERENCES

[1] Guo J et al. *J Biomech* **139**: 111143, 2022.
[2] Guo J et al. *Multibody Syst. Dyn.* Accepted, 2023.
[3] Dijkstra P et al. *Oral Oncol*, **40**: 879-889, 2004.

A musculoskeletal modelling framework for evaluating instability after reverse total shoulder arthroplasty

Yichen Huang[1], Dale L. Robinson[1], Lukas Ernstbrunner[1,2], Rami M. A. Al-Dirini[3], Mark Taylor[3], Peter Vee Sin Lee[1] and David C. Ackland[1]

[1] Department of Biomedical Engineering, University of Melbourne, Parkville, VIC 3010, Australia.
[2] Department of Orthopaedic Surgery, Royal Melbourne Hospital, Parkville, VIC 3050, Australia.
[3] Medical Device Research Institute (MDRI), Flinders University, Clovelly Park, Adelaide 5043, Australia.
Email: yichenh2@student.unimelb.edu.au

INTRODUCTION

Reverse total shoulder arthroplasty (RSA) is an established treatment for irreparable rotator cuff tears of the glenohumeral (GH) joint. However, this procedure can be associated with a relatively high complication rate, with joint instability being the most common complication. Scapula anatomy and a deficient rotator cuff are known to affect the inherent stability of RSA, but there have been few studies exploring this topic. The aims of this study were twofold. Firstly, to develop a virtual clinical trials modelling framework for the GH joint after RSA; and second, to use this framework to quantify the effects of scapula size, glenoid version, and rotator cuff tears on joint stability after RSA.

METHODS

A previously published statistical shape model (SSM) was used to generate an average 50th percentile adult scapula and a 98th percentile scapula [1]. This was achieved by applying the mode of variation for size to the mean shape with 0 standard deviation and +2 standard deviation, respectively. Similarly, four glenoid versions (6° anteversion, neutral, 6° retroversion and 16° retroversion) were generated for each scapula size. The mean geometry of an age-matched humerus was also generated using a published SSM [1].

For each anatomy, RSA was virtually performed in an automated manner using Zimmer Biomet components according to the recommended surgical technique.

A previously published rigid-body model was modified to match each post-operative joint anatomy and used to calculate joint reaction forces for 45° arm abduction with an (i) intact rotator cuff (ii) supraspinatus tear (iii) combined supraspinatus and infraspinatus tear (iv) combined supraspinatus and subscapularis tear [2].

Finite element (FE) models (Figure 1a) were then developed for each post-operative joint anatomy. For each anatomy, joint reaction force calculated from the rigid-body model was applied as joint compressive load in the FE model, and then the joint was anteriorly dislocated in the FE simulation. Dislocation force, the force required to dislocate the joint anteriorly, was calculated for each post-operative joint anatomy and used as a proxy for joint stability (Figure 1b).

RESULTS AND DISCUSSION

Larger scapula size led to increased dislocation force (1105N vs 730N as peak dislocation force for each size), thus higher GH joint stability. Larger retroversion of glenoid also yielded higher dislocation force and joint stability. Rotator cuff muscle tears significantly reduced dislocation force, especially when two muscles were torn. For example, a tear to the supraspinatus and infraspinatus resulted in an average 84% drop in dislocation force relative to that in the intact rotator cuff.

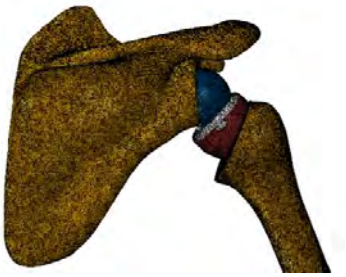

(a)

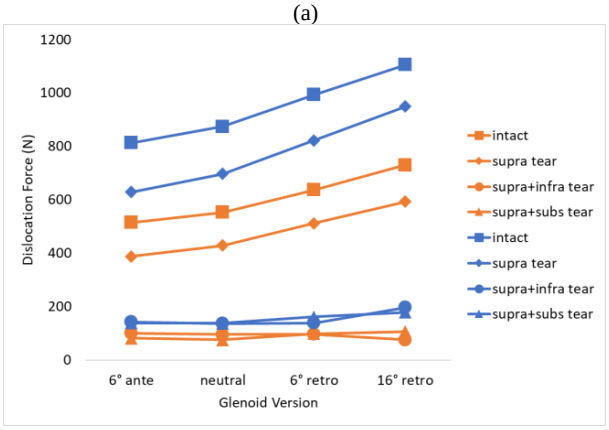

(b)

Figure 1 FE model (a) and calculated joint dislocation force (b) for shoulder joint after RSA. Orange lines represent 50th percentile anatomy while blue lines represent 98th percentile anatomy. Acronyms are as follows: anteversion (ante), retroversion (retro), supraspinatus (supra), infraspinatus (infra) and subscapularis (subs).

CONCLUSIONS

This study developed a virtual clinical trials modelling framework to investigate shoulder joint instability after RSA. The results show that a combined supraspinatus and infraspinatus (or subscapularis) tear significantly reduced joint stability after RSA, while larger scapula size yielded a more stable joint. The findings may help to guide surgical planning and rehabilitation to patients with rotator cuff tear to avoid early joint dislocation.

REFERENCES

[1] Huang Y et al. *BMMB* **21**: 249–259, 2022.
[2] Wu W et al. *J Biomech* **49**: 3623-3634, 2016.

A pipeline to morph the finite element model of lumbar spine and generate personalised spinal implant

Yihang Yu[1], Dale Robinson[1], David Ackland[1] and Peter Vee Sin Lee[1]
[1] Department of Biomedical Engineering, University of Melbourne, Melbourne, Australia.
Email: yihangy@student.unimelb.edu.au

INTRODUCTION

Lumbar interbody fusion (LIF) with interbody cages is an established treatment for degenerative disc disease, however, generic cages comprising standardised shapes and sizes still encounter complications such as cage migration and subsidence. Preoperative planning of LIF surgery incorporating biomechanical analysis provides the possibility to address post-operative complications by optimising implant positioning and customising its 3D geometry to suit a specific patient. However, current customisation processes involve excessive time and expense to develop patient-specific finite element (FE) models to validate bespoke implant designs [1]. Therefore, our project aims to build an automated pipeline to generate patient-specific FE model and interbody cage for the lumbar spine.

METHODS

A template lumbar spine FE model was established in ABAQUS 2017 based on an average-sized healthy male. The surface mesh of the FE model was non-rigidly aligned to a training set of 46 lumbar spines, from which a principal component analysis was performed [2]. By choosing the weightings of these principal components, the FE model surface mesh could be fit to a new spine. The full FE model could then be generated by the following: (a) generation of solid meshes based on the updated surface mesh, (b) assigning bone material properties using computed tomographic scans for the new subject, (c) removing overclosures between facet joints, and updating facet joint ligaments, and (d) since all boundary conditions, constraints and interactions were defined by the surface mesh, hence, these were automatically updated when the surface mesh was fit to the new subject. Once the spine mesh was fitted to the new subject, a customised cage was created by extruding a 2D cage template in the axial direction then trimming it via a boolean function with the adjacent endplates. Adjustment of cage material, type, size, position and orientation was set as built-in functions of the pipeline.

RESULTS AND DISCUSSION

To evaluate the performance of intact lumbar FE models, the flexion-extension range of motion (ROM) was simulated for the template model, morphed models for four patients, and a morphed model with a customised cage (Figure 1A). The facet joint forces (FJF) of intact spine models under extension and torsion were also computed (Table 1). The predicted ROM for each model compared well with published data [3], while the addition of the cage reduced the total ROM (Figure 1B). Overall, the FJF appeared to be at the lower range of that reported in the literature, which is likely due to modelling differences affecting the facet joint contact stiffness such as their initial contact area, their assumed thickness or the orientation/properties of surrounding ligaments.

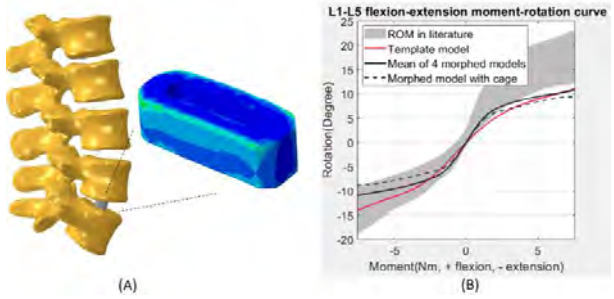

Figure 1. (A) Morphed lumbar FE model with cage. von Mises stress contours for the cage in flexion is indicated. (B) ROM of morphed and template models compared to models in literature [3].

CONCLUSIONS

In conclusion, the pipeline can generate FE models and customized spinal cages with predictive outputs that compare well to reported data. The pipeline's automatic capability reduces the manual effort involved in FE model development, making it viable for use in spinal surgery planning and interbody cage customisation. In future work the pipeline will be verified with more subjects, and expanded to incorporate optimisation of cage material properties.

REFERENCES

[1] Tong Y et al. *The Spine Journal* **20**(6): 833-846, 2020.
[2] Zhang J et al. *Comput Methods Biomech Biomed Engin* **2**(3): 176-185, 2014.
[3] Dreischarf M et al. *J Biomech* **47**(8): 1757-1766, 2014.

Table 1: Facet joint force compared to experimental data in literature.

Loading type	Lumbar level	Facet joint force (N)		
		Literature range	Template model	Morphed models
Extension	L1 - L2	13.0 – 91.0	25.7 ± 1.3	9.4 ± 5.5
	L3 - L4	4.0 – 50.0	20.7 ± 2.2	21.6 ± 1.0
Torsion	L1 - L2	27.0 – 113.0	42.0 ± 0.1	18.2 ± 8.5
	L3 - L4	38.0 – 110.0	29.7 ± 1.6	32.2 ± 3.9

EFFECT OF PELVIC TILT ON FEMORAL HEAD COVERAGE AFTER PERIACETABULAR OSTEOTOMY

Ryan D. Blackwell[1], Nicholas J. Dunbar[2], Stephen Parlamas[2], Sabir K. Ismaily[2], David Rodriguez-Quintana[2], Alfred A. Mansour[2], Shuyang Han[2]

[1] John Sealy School of Medicine, Galveston, USA.
[2] Department of Orthopedic Surgery, McGovern Medical School, UTHealth Houston, USA.
Email: shuyang.han@uth.tmc.edu

INTRODUCTION

Developmental dysplasia of the hip (DDH) leads to early-onset of hip osteoarthritis due to the presence of a shallow acetabula and poor femoral coverage. It causes structural instability, decreased load-transferring area, and abnormal joint stress distribution on articular cartilage. Periacetabular osteotomy (PAO) has been a successful procedure to correct these morphological abnormalities and subsequently improve hip biomechanics, delaying or even preventing the development of osteoarthritis. Success of the operation is dependent on optimal positioning of the acetabular fragment, so surgeons frequently plan for these operations using 2D parameters derived from radiographs to estimate joint coverage, yet it is unclear if these are reliable metrics. Additionally, previous studies investigating hip joint biomechanics evaluated the joints in a standardized position, which does not apply to most patients given the inherent and positional variability of pelvic tilt, which has a significant effect on acetabulum orientation [1-2]. Therefore, the objective of this study was to quantify the effect of pelvic tilt on femoral head coverage after PAO.

METHODS

Hip models of 22 patients (25 hips) with DDH were created using pre-operative CT images (Materialise Mimics, Materialise, Belgium). The pelvic tilt was measured in pre-op standing X-ray using the method proposed by Tannast et al. [3]. Then, each model was positioned in the ISB coordinate system and the pelvic tilt was adjusted to the pre-op neutral position. Next, a simulated PAO was carried out by laterally rotating the acetabular fragment until the lateral center edge angle (LCEA) reached 35°, followed by 10° anterior rotation of the fragment. A custom MATLAB program was built to measure the femoral head coverage under different pelvic tilt conditions (Figure 1). Specifically, the measurements were repeated at 0°, ±5°, ±10°, and ±15° pelvic tilt. At each position, the 2D projection of the lunate surface on the transverse plane was measured and divided into four quadrants. Statistical significance was evaluated through a paired, two-tailed Student's t-test ($p=0.05$).

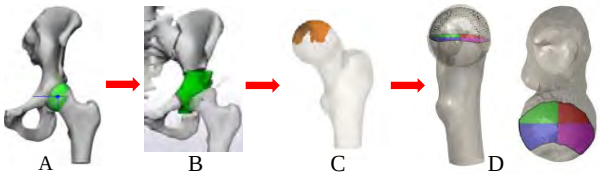

Figure 1 Measurement of load-bearing coverage. A) 3D hip models from CT scans. B) Simulated PAO. C) 3D coverage. D) 2D projection of femoral coverage on the transverse plane.

RESULTS AND DISCUSSION

As the pelvic tilt increased from neutral (i.e., 0°) to 15° anteriorly, there was a significant increase in the coverage in the anterolateral (AL) quadrant and a significant decrease in the posterolateral (PL) coverage ($p<0.0001$). On the other hand, posterior pelvic tilt led to a significant decrease in total coverage ($p<0.04$). Moreover, there was a significant decrease in the AL coverage ($p<0.0001$) and a significant increase in the PL coverage ($p<0.0001$). No significant differences were detected in the posteromedial (PM) or anteromedial (AM) coverage across all levels of pelvic tilt.

CONCLUSIONS

The findings of this study demonstrated the effect of pelvic tilt on femoral head coverage after PAO. More anterior tilt results in increased load-bearing coverage, and more posterior tilt results in decreased load-bearing coverage. These findings indicate that natural pelvic tilt should be considered when planning a PAO.

REFERENCES

[1] Henak C et al. *Osteo Cart* **22**: 210-7, 2014.
[2] Pullen W et al. *Am J Sports Med* **42**: 2643-8, 2014.
[3] Tannast M et al. *Skeletal Radiol* **35**: 149-55, 2006.

Table 1: Average coverage area in the four quadrants, and in total, under different levels of pelvic tilt.

	15° Posterior	10° Posterior	5° Posterior	0° (Neutral)	5° Anterior	10° Anterior	15° Anterior
AL	150.85±42.56	167.79±41.00	184.65±39.16	199.65±37.89	212.59±35.05	223.36±32.63	232.77±30.66
PL	220.58±33.85	208.71±37.81	201.02±33.93	188.93±35.87	174.07±35.08	160.39±37.28	145.81±37.85
PM	282.94±70.39	274.90±62.80	290.61±59.99	291.88±61.74	297.82±55.22	301.28±47.86	304.60±50.87
AM	258.49±62.27	259.42±60.88	271.58±61.21	267.82±69.45	266.33±66.71	268.85±60.93	264.09±65.77
Total	912.87±149.68	910.82±147.65	947.86±140.94	948.28±154.73	950.81±145.21	953.88±132.01	947.26±140.37

Differentiating activity of forearm finger flexors and extensors for SEMG biofeedback training

Christian Sure[1], Sascha Selkmann[1], Marc Neumann[1] and Beate Bender[1]
[1] Chair of Product Development, Dept. of Mechanical Engineering, Ruhr-University Bochum, Germany.
Email: sure@lpe.rub.de

INTRODUCTION

Surface electromyography (SEMG) based biofeedback training is a common approach in the therapy of motor dysfunctions of the hand. Usually, methods for SEMG-Biofeedback rely on simple measurement setups, where only a few large and roughly positioned electrodes are used to discriminate combined hand and finger flexor from extensor activity [1]. For the training of complex hand movements like grips however, a finer degree of muscular differentiation could be beneficial. In our efforts to develop new strategies for differentiating muscle activity in the forearm during SEMG biofeedback training, we are currently evaluating the feasibility of analyzing and comparing the SEMG amplitude measured at small, strategically placed electrodes to estimate the activation state of individual finger flexors and extensors. The goal of the presented study was to identify suitable electrode sites and assess the correlation as well as the selectivity of the respective SEMG amplitude to the activity of individual muscles for finger movement.

METHODS

Subjects performed isolated, as well as combined isometric finger flexions and extensions while incrementally increasing the applied finger force. During contractions. SEMG signals were recorded across a wide area of the forearm. Finger forces were measured using a custom hand force meter (Fig 1a, bottom). Applied finger forces, as well as force targets, were visualized to the subjects. In a first session, isolated finger extensions and flexions were performed while subjects were instructed to increase finger force in steps of 0.5 N from 0 to 8 N. In a second session, an additional constant force of 3 N in the same direction was to be applied to an adjacent finger. The monopolar SEMG signal was recorded at 96 electrode sites with a measuring system from DeMeTec. Electrodes were applied with the help of a custom forearm sleeve equipped with 6 electrode rings, each containing 16 equally spaced dry electrodes (Fig. 1a). Measurement sites were prepared according to common standards. The signal was recorded with a sample rate of 1024 S/s and filtered using a high pass at 10 Hz and a notch at 50 Hz. SEMG amplitude was evaluated by calculating root-mean-square (RMS) within a time window of 1 s.

RESULTS AND DISCUSSION

During isolated finger activation, characteristic signal hotspots formed at specific areas across the forearm (Fig. 1b). Based on these hotspots, sites with potentially high correlation to individual finger muscle activity could be identified (Fig. 1c). Signal amplitude at these sites show the typical [2], approximately linear correlation to the applied finger force. Gradients differ between fingers and muscle groups, with gradients of extensors being generally lower than flexors (Fig. 1d). During combined movements, selectivity at the sites varied depending on the distance between hotspots of the active muscles. Electrode sites in non-overlapping hotspots, like e.g. the extensors of fingers IV and V, show a high degree of selectivity, with RMS amplitude being nearly constant on one site and incrementally increasing in the other. In the case of overlapping hotspots, such as the extensors of fingers III and IV, an increase of amplitude due to crosstalk can be observed on the site of the stationary finger.

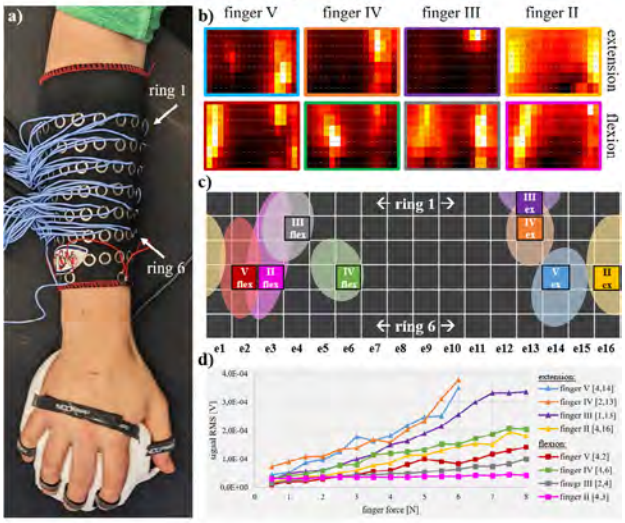

Figure 1 a) SEMG-sleeve with hand force meter. b) SEMG amplitude (RMS) across electrode matrix in heatmap view. c) identified hotspots with high correlation to isolated finger activation d) relationship between finger force and RMS amplitude at chosen electrode sites during isolated finger activation

CONCLUSIONS

The study reinforces our assumption, that evaluating and comparing SEMG amplitude measured at small, strategically placed electrodes might be a suitable approach for estimating activity of individual finger flexors and extensors. Further strategies for differentiating activity of muscles with overlapping hotspots must be developed though.

REFERENCES

[1] Sturma A et al. *Front Neurosci* **12**: 906, 2018.
[2] Ricard M. D. *Int J Sports Med* **26**: 66, 2005

LOWER LIMB AMPUTEES HAVE SIMILAR UPPER LIMB FUNCTION 8Y POST INJURY AS UNINJURED GROUP: THE ADVANCE COHORT STUDY

Fraje Watson[1], Angela E Kedgley[1], Alexander Bennett[2] and Anthony M J Bull[1]
[1] Department of Bioengineering, Imperial College London, London, UK.
[2] Defence Medical Rehabilitation Centre, Loughborough, UK.
Email: f.watson@imperial.ac.uk

INTRODUCTION

Increased biomechanical load on the upper limb (UL), and subsequent injury has been identified in wheelchair users [1]. We hypothesised that lower limb (LL) amputees make similar biomechanical compensations with their ULs through crutch use, balance and coordination needs, transfer activities and UL bodyweight loading.

ADVANCE is a 20yr prospective cohort study collecting medical and psychosocial data from 1145 military servicemen, half of whom sustain combat injury [2]. The aims of this study are to compare UL disability at baseline assessment (a mean of 8yrs post-injury) in (1) LL amputees and the uninjured comparison group, and (2) the full cohort.

METHODS

Disability of the Arm, Shoulder, and Hand (DASH) questionnaire data was collected from injured and uninjured ADVANCE participants frequency matched for deployment, age, and rank. DASH scores range from 0-100, with a higher score denoting more UL disability.

DASH data was non-parametric, and appropriate statistical tests were used with an alpha level of 0.05.

RESULTS AND DISCUSSION

DASH data was available and valid for 1092 participants (mean age: 34yrs).

DASH was higher for the injured group compared to the uninjured group (p<0.001). Major and partial UL amputees (p<0.002), triple amputees with a unilateral major UL amputation (p<0.002), and LL amputees with partial UL amputation (p<0.002) all had higher DASH scores than the uninjured group (Table 1, Figure 1).

DASH was not significantly different between unilateral LL amputees, bilateral LL amputees, and the uninjured group. This finding suggests minimal UL disability 8yrs post-injury that we hypothesised might result from high reliance on the ULs. Similarly, DASH was not significantly different for triple amputees (with a unilateral major UL amputation) compared to unilateral major and partial UL amputees only. This further supports the finding that LL amputation did not increase UL disability (Table 1, Figure 1).

Injury type	n	DASH (SD)
Uninjured[abcd]	562	3.6 (8.3)
Injured	530	9.7 (14.2)
Non-amputee[ae]	363	9.8 (14.1)
Unilat LL amputee[fgh]	70	4.4 (7.0)
Bilat LL amputee[i]	38	5.9 (11.0)
UL amputee (major + partial)[befi]	14	21.7 (19.5)
Triple amput. (unilat major UL)[cg]	12	13.5 (13.7)
LL amputee + partial UL amp[dh]	32	17.6 (20.3)

Table 1: DASH scores for ADVANCE participants. [a-i]p<0.002 per Bonferroni correction

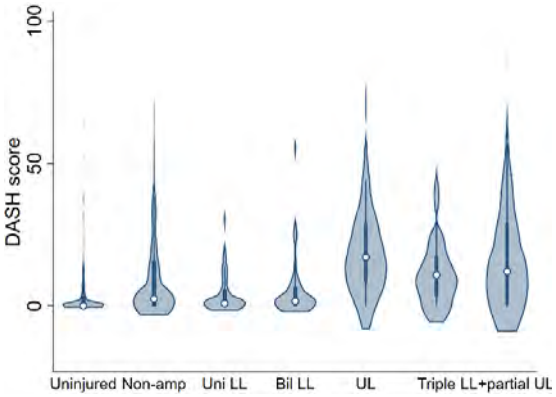

Figure 1: Violin plots for DASH scores of ADVANCE participants (LL=lower limb, UL=upper limb, uni=unilateral, bil=bilateral).

CONCLUSIONS

Contrary to our hypothesis, unilateral and bilateral LL amputees had similar DASH scores to the uninjured population, and triple amputees had similar DASH scores to UL amputees. These results suggest that assumed biomechanical compensations resulting from LL amputation did not increase UL disability, 8yrs post-injury.

Overall, the ADVANCE cohort have lower DASH scores than equivalent military and civilian populations [3,4]. The ADVANCE cohort is currently young, so longitudinal study of their UL disability will be of great interest, particularly for the LL amputees.

ACKNOWLEDGEMENTS

We thank the whole ADVANCE team and participants, and the ADVANCE charity for funding.

REFERENCES

1. Tsai et al, *Clin Biomech*, **55**: 79-85, 2018
2. Bennett et al, *BMJ Open*, **10**:e037850, 2020
3. Pfister et al, *BMJ Mil Health*, **6**:393-397, 2021
4. Pet et al, *Injury*, **47**:2783-2788, 2016

VALIDATION OF A MARKER CLUSTER-BASED APPROACH TO ESTIMATE SCAPULA MOTION

Jennifer Maier[1], Julie Muccini[2], Ellen Kuhl[1], and Scott L. Delp[1,2]
[1] Department of Mechanical Engineering, Stanford University, Stanford, California, USA.
[2] Department of Bioengineering, Stanford University, Stanford, California, USA.
Email: jenmaier@stanford.edu

INTRODUCTION

Fast and dynamic motions of overhead athletes like volleyball hitters can lead to shoulder injuries. Measuring the in-vivo shoulder kinematics is necessary to analyze the biomechanics leading to injuries. The main challenge when recording shoulder motions with marker-based motion capture is the scapula, as it moves subcutaneously and its motion cannot be recorded with skin-mounted markers. Current approaches to measure scapula motion have mostly been validated on small ranges of motion and/or static poses [1, 2]. We present results of initial experiments that evaluate the accuracy of a method that uses an acromion marker cluster (AMC) to estimate scapula motions during large range of motion trials.

METHODS

Our proposed method is an extension of an approach presented in [1] and uses five instead of two calibration shoulder poses, see Fig. 1. In all five poses, at 0° abduction/flexion, 180° abduction, 180° flexion, and maximal horizontal adduction and abduction, we locate the scapula by palpation to define the relation to the AMC. We use this information to compute the scapula position in a new trial by interpolation in the three body planes based on the humeral elevation angle. The estimates in the three body planes are weighted by the length of the upper arm projected onto the respective body plane and summed to form the final scapula estimate. Using the measured AMC, we register the estimate to the subject's current position.

We evaluated the method on three subjects at static poses of different angles of shoulder abduction, flexion, and horizontal abduction, and on static poses of scapula elevation and depression, by comparing the estimated scapula positions to palpated measurements of the scapula. Furthermore, subjects performed dynamic full range of motion trials of abduction, flexion, and horizontal abduction, and we extracted frames of similar humeral angles as the static measurements and compared them to the palpated scapula positions of the corresponding static measurements.

RESULTS AND DISCUSSION

Results on the static trials show an average rotation RMSE of 4° and translation RMSE of 11 mm compared to palpation. Our method requires more calibration poses than the existing double calibration approach [1], but shows reproducible, accurate results over a larger range of motions, see Table 1. The deviations between static measurements and poses extracted from the dynamic trials are higher (6° and 27 mm), but within the acceptable range for most studies.

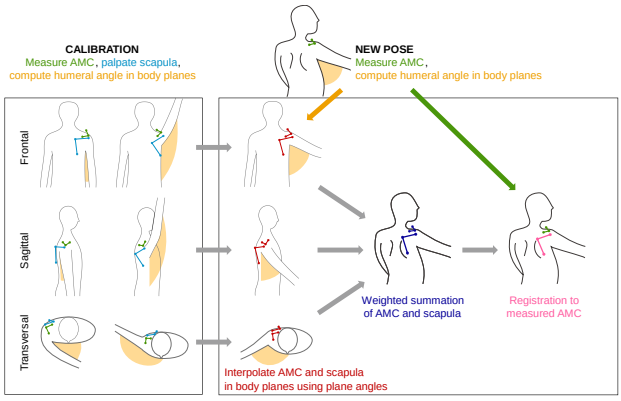

Figure 1 Schematic description of the scapula estimation method.

CONCLUSIONS

Our method for AMC-based scapula estimation shows promising results for an application in large range dynamic motions. Our next step is to combine this technique with a physically constrained biomechanical model to enable analyses of shoulder motions and provide guidelines to prevent shoulder injuries in overhead athletes.

ACKNOWLEDGEMENTS

This work was supported by the Joe and Clara Tsai Foundation through the Wu Tsai Human Performance Alliance.

REFERENCES

[1] Brochard S et al. *J Biomech* **44**: 751–754, 2011.
[2] Rapp E et al. *J Biomech* **61**: 269–274, 2017.

Table 1: Average root mean squared error (RMSE) over all subjects for rotation and translation in the scapula coordinate system.

	Average rotation RMSE	Average translation RMSE
Small range of motion (0° < humeral angle < 120°)	4°	10 mm
Large range of motion (humeral angle < 0° or humeral angle > 120°)	4°	12 mm

Investigating the Torque-Velocity Relationship Within the Human Shoulder During High-Demand Tasks

Kayla D.L. Lee, Erin C.S. Lee, Annabel Vrba, and Michael J. Rainbow
Mechanical and Materials Engineering, Queen's University, Kingston, ON, Canada.
Email: lee.kayla@queensu.ca

INTRODUCTION

The shoulder complex may have evolved to produce high torques across a range of speeds – facilitating tasks with different torque-velocity requirements like carrying heavy loads and high-speed throwing [1]. In lower extremity joints, such as the knee, torque decreases as velocity increases, which is reflective of the force-velocity relationship in muscles [2]. We question whether the shoulder's complex architecture allows it to maintain high torque during low and high speeds, which is consistent with its functional requirements. While previous studies have provided insight into the shoulder's ability to produce torque under static conditions, unloaded tasks, or uni-planar motions [3], there is little research regarding loaded and dynamic functional tasks.

This study aims to address this gap by introducing a novel approach to perform inverse dynamics in the upper extremity to assess three-dimensional shoulder joint motion and torque. Here, we examine a loaded functional task performed across a range of speeds. We tested the prediction that shoulder torque would decrease as angular velocity increased.

METHODS

Five participants (1F/4M, Average age = 22) performed an isokinetic shoulder task. Participants started with their right arm overhead and pulled a cable across their body, ending the task at their left hip. They were tasked with applying maximal force at a prescribed cable speed and were allowed to execute the task in a manner that felt most natural to them. A motion capture system (Qualisys, Goteborg, Sweden) collected their 3D motion, and a controllable cable resistance machine (1080 Quantum) collected their force output. The cable machine was set to a maximum speed of 0.5 m/s and was increased by 0.5 m/s with each trial until the participant could no longer achieve the speed. Participants were allowed self-selected rest time between trials. The 1080 applied the resistance required to prevent the participant from exceeding the set speed. We computed the position and orientation (poses) for the pelvis, trunk, right upper arm, right forearm, and right hand in Visual 3D (C-Motion). The shoulder joint was modelled by computing the functional joint centre from a low-abduction circumduction task. We used inverse dynamics to compute the shoulder moment and angular velocity (Figure 1). For each participant, linear regression was performed on the peak moment at the shoulder as a function of peak angular velocity across cable speeds.

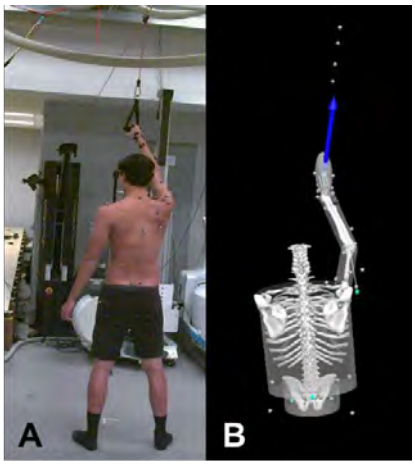

Figure 1 (A) Participant performing isokinetic task with 1080 Quantum cable machine. **(B)** The force vector was tracked with markers on the cable and applied to the hand. Inverse dynamics was performed on a link-segment model (Visual 3D, C-Motion).

RESULTS AND DISCUSSION

The slowest and fastest participants achieved angular velocities of 484 and 670 deg/s, respectively. Across participants, peak moments ranged from 18 to 92 Nm. Across cable speeds, participants achieved a wide range of angular velocities (min range: 216, max range: 466 deg/s). However, within each participant, peak shoulder torque remained relatively constant where slopes were not statistically different than zero ($p > 0.2$) and ranged from -0.1 to 0.02 Nm/deg/s. These results are consistent with the idea that the shoulder complex can maintain high torque over a wide range of speeds.

CONCLUSIONS

We found peak shoulder torque to be statistically independent of angular velocity during the tested unconstrained task. We do not doubt the shoulder muscles follow typical force-velocity constraints, but speculate that high-torque may be maintained through a combination of dynamically changing muscle moment arms, differential contributions of the scapulothoracic and glenohumeral joints, and/or differential activation of the complex muscle architecture. A future biplanar videoradiography study examining both constrained and unconstrained shoulder motion may allow us to tease out these potential factors. This approach may allow us to better understand how differences in person-specific anatomy influence shoulder function and dysfuntion.

REFERENCES

[1] Larson et al. *Evolution of the Hom. Shoulder*, 2009.
[2] Taylor et al. *J Appl. Physiol.* **63:** 116-121, 1991.
[3] Häberle et al. *BMC Sports Sci. Med. Rehabil.* **10:** 22-35, 2018.

Post-operative kinematics of Coracobrachialis and Short Head of Biceps after Reverse Total Shoulder Arthroplasty

Roopam Dey[1*], Jonathan Glenday[2], Jean-Pierre du Plessis[1], Sudesh Sivarasu[1], and Stephen Roche[1]
[1] Faculty of Health Sciences, University of Cape Town, Cape Town, South Africa.
[2] Hospital for Special Surgery, New York, USA.
*Email: roopam.dey@uct.ac.za

INTRODUCTION

Reverse total shoulder arthroplasty (RTSA) alters biomechanics of muscles around the glenohumeral joint (GHJ). These changes are well documented for muscles like deltoids[1], but limited research has been performed on post-RTSA biomechanics of coracobrachialis (CBR) and short head of biceps (SHB). In this study, using computational models, we compared muscle moment arms and lengths of CBR and SHB between native and RTSA shoulders.

METHODS

The Newcastle Shoulder Model (NSM)[2], a pre-validated upper extremity musculoskeletal model was used for this study. The NSM was modified with bone geometries obtained from 3D reconstructions of 15 non-diseased shoulders, constituting the native shoulder group. Delta XTEND prosthesis, with a glenosphere diameter of 38mm and polyethylene thickness of 6mm, was virtually implanted in all the models creating the RTSA group. Moment arms were measured using the tendon excursion method and muscle lengths were calculated as the distance between the muscles' origin and insertion points. These values were measured during 0°-150° of abduction, forward flexion, scapular plane elevation, and -90 to 60° of external-internal rotation with the arm at 20° and 90° of abduction. Statistical comparison between native and RTSA group was analysed using spm1D.

RESULTS AND DISCUSSION

Forward flexion moment arms (Figure 1) had the greatest increase between RTSA (CBR:25.3±4.7 mm; SHB:24.7±4.5 mm) and native groups (CBR:9.6±5.2 mm; SHB:10.2±5.2 mm). CBR and SHB were longer in the RTSA group by a maximum value of 15% and 7% respectively. Both muscles had larger abduction (Figure 2) moment arms (CBR: 20.9±4.3 mm; SHB: 21.9±4.3 mm) in RTSA compared to the native group (CBR: 19.6±6.6 mm; SHB: 20.0±5.7 mm). Abduction moment arms were observed earlier in RTSA (CBR: 50º; SHB: 45º) compared to the native group (CBR: 90º; SHB: 85º). In the RTSA group, both muscles had elevation moment arms until 25° of scapular plane elevation motion, whereas in the native group the muscles only had depression moment arms. Both muscles had small rotational moment arms which were significantly different between RTSA and native shoulders during different stages of the motion.

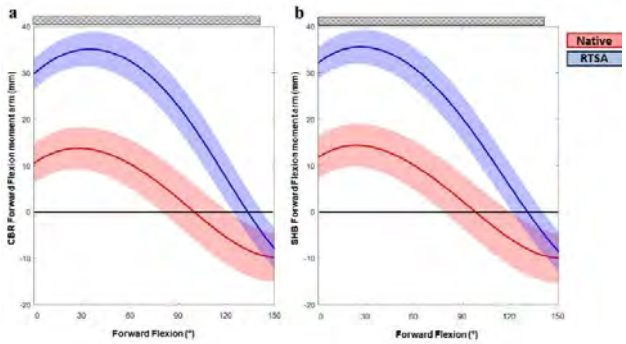

Figure 1: Forward flexion moment arms in RTSA and native shoulders for a) CBR and b) SHB. Statistically significant difference was observed for most of the motion.

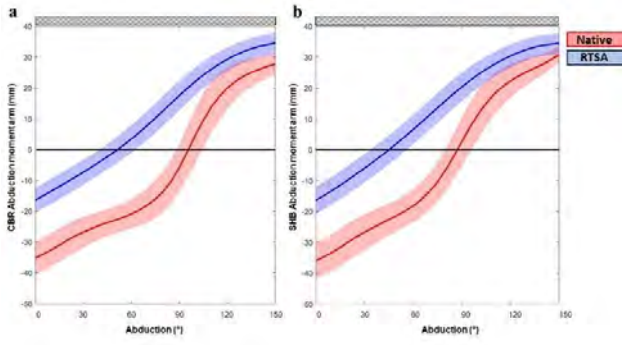

Figure 2: Abduction moment arms in RTSA and native shoulders for a) CBR and b) SHB. Statistically significant difference was observed for the complete motion.

CONCLUSIONS

RTSA makes CBR and SHB early abductors and stronger forward flexors. The surgery increases their length which might increase tension on the conjoint tendon.

REFERENCES

[1] A. Kontaxis and G. R. Johnson, "The biomechanics of reverse anatomy shoulder replacement – A modelling study," *Clin. Biomech.*, vol. 24, pp. 254–260, 2009, doi: 10.1016/j.clinbiomech.2008.12.004.

[2] I. W. Charlton and G. R. Johnson, "A model for the prediction of the forces at the glenohumeral joint," *Proc. Inst. Mech. Eng. Part H J. Eng. Med.* , vol. 220, no. 8, pp. 801–812, 2006, doi: 10.1243/09544119JEIM147.

.

Investigating Shoulder Muscle Coactivation Ratio Changes Following and Overhead Fatigue Task

Matthew S. Russell, Sam Vasilounis, Janessa D.M. Drake, and Jaclyn N. Chopp-Hurley
Kinesiology and Health Science, York University, Toronto, Ontario, Canada.
Email: msr@yorku.ca

INTRODUCTION

Subacromial Impingement Syndrome (SAIS) and rotator cuff tears account for 30-45% of all clinically presenting shoulder conditions [1, 2]. Mechanically, reduction of the subacromial space can be the result of alterations in shoulder muscle activation and subsequent kinematics, leading to SAIS [3, 4]. The effect of muscle fatigue on kinematics has yielded highly variable outcomes, with differential effects on the subacromial space. It is unclear whether fatigue leads to changes in scapular and rotator cuff muscle co-activity, which may provide insight into kinematic variability [4]. This study investigated fatigue-related changes in shoulder muscle coactivation following an overhead drilling task.

METHODS

18 healthy, right-handed adults (19-35yr; BMI 23.7 ± 3.2 kg/m^2) have initially participated in this research. Participants were instrumented with surface (sEMG) and fine-wire intramuscular (iEMG) electromyography (Delsys Trigno, Natick, MA), as well as right thoracal, scapular, and upper limb kinematics (Vicon MX, Hauppauge, NY). Participants completed a series of maximum voluntary contractions (MVC) to allow for EMG normalization [5-7]. In a standing position, participants were tasked with using a simulated drill to approximate overhead targets until volitional fatigue. This protocol has been previously validated in literature to effectively fatigue the rotator cuff muscles [8, 9]. Submaximal (15%) shoulder abduction and adduction exertions at 90° were completed after every 5 minutes of the fatigue task and immediately following failure. EMG signal time-varying normalization was implemented to remove the muscle fatigue-related amplitude artefact, making EMG amplitude comparisons between pre-fatigue and post-fatigue possible [10]. Scapular, rotator cuff, and deltoid-rotator cuff coactivation ratios for submaximal 90° abduction and adduction were compared at pre-, mid-, and post-fatigue using one-way ANOVAs. A chi-squared model evaluated the change in rotator cuff muscle dominance at pre-, mid-, and post fatigue.

RESULTS AND DISCUSSION

Preliminary results show coactivation changes between middle deltoid and supraspinatus consequent of global upper limb fatigue from overhead work. The ANOVA model between middle deltoid and supraspinatus ($F_{(2,48)}$ = 4.29; p = 0.02) revealed a significant LSD post hoc comparison between the pre-fatigue (μ = 28.3, σ = 22.3) and post-fatigue (μ = 33.5, σ = 72.8) state; p = 0.007 (Figure 1). Chi-squared model comparing muscle activity between supraspinatus and infraspinatus ($X^2_{(2,N = 36)}$ = 7.33; p = 0.026) indicated an increase in infraspinatus activity relative to supraspinatus activity associated with fatigue.

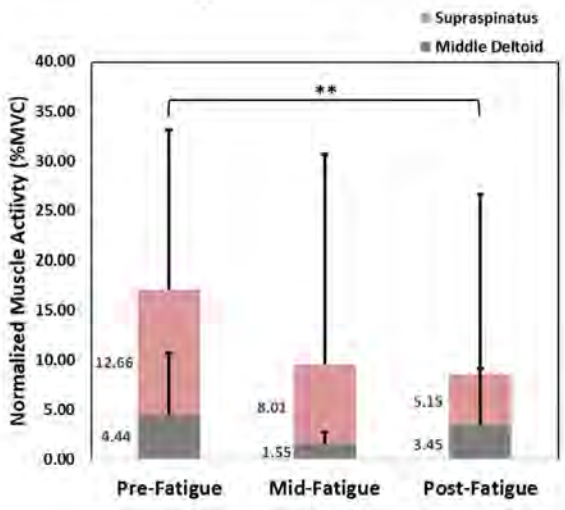

Figure 1 Middle Deltoid-Supraspinatus Muscle Coactivation Changes with Fatigue. ** denotes p<0.01.

CONCLUSIONS

Initial results of this research provide evidence to suggest that muscle fatigue consequent of occupationally relevant overhead work may produce transient changes to the coactivation ratio between middle deltoid and supraspinatus. Increases in middle deltoid activity relative to supraspinatus activity increase superior humeral head translation and are a known risk factor for SAIS and rotator cuff impingement [4, 11]. Relationships between these changes in muscle co-activation and kinematics are forthcoming.

ACKNOWLEDGEMENTS

We acknowledge the support of the Centre of Research Expertise for the Prevention of Musculoskeletal Disorders (CRE-MSD) and Natural Sciences and Engineering Research Council of Canada (NSERC).

REFERENCES

[1] Van der Windt D et al. *ARD* **54**: 959-64, 1995
[2] Van Rijn R et al. *SJWEH* **36**: 189-201, 2010
[3] Cools A et al. *AJSM* **35**: 1744-51, 2007
[4] Chopp-Hurley J et al. *JEK* **29**: 55-63, 2016
[5] Boettcher C et al. *JOR* **26**: 1591-97, 2008
[6] Ginn K et al. *JOR* **29**: 1846-49, 2011
[7] McDonald A et al. *Int Biomech* **4**: 9-16, 2017
[8] Sood D et al. *Ergonomics* **50**: 497-513, 2007
[9] Sood D et al. *Ergonomics* **60:** 1405-14, 2017
[10] McDonald A et al. *JEK* **39**: 58-69, 2018
[11] Myers J et al. *JSAMS* **12**: 603-8, 2009

Disentangling Allometry and Sex-Based Differences in Scapula Shape

Erin Lee[1], Rebekah Lawrence[2], and Michael Rainbow[1]
[1] Department of Mechanical and Materials Engineering, Queen's University, Kingston, Canada.
[2] Program in Physical Therapy, Washington University in St. Louis School of Medicine, St. Louis, USA.
Email: erin.lee@queensu.ca

INTRODUCTION

Sex is often a key determinant of musculoskeletal disease and can influence treatment. For example, sex-based differences in knee shape have inspired sex-specific implants [1]. It is unknown whether sex-based differences in scapula shape play a role in the pathomechanics of shoulder disease or injury. However, scapula shape features are strongly associated with soft-tissue injury [2]; thus, it is important to understand the role of sex in the scapula's highly variable morphology.

A caveat of measuring sex-based shape differences is that the male skeleton is, on average, larger than the female skeleton. Even after scaling structures to a common size, *allometry* (shape changes as a function of size) may persist as a source of morphological variation. While previous studies have reported sex-differences in scapula shape [3], they did not account for allometry; thus, apparent sex-based differences could instead reflect inherent differences in body size. If sex-based treatments are developed for the shoulder, this would disadvantage females and males whose body size is above or below their respective group means. Here, we used a geometric morphometrics approach to disentangle allometry from sex-based differences. We tested the null hypotheses that male and female scapulae would not exhibit different allometric relationships, and that shape changes due to allometry would not differ from shape differences associated with sex (Fig. 1).

METHODS

We acquired scapula surface meshes for 45 male (age=54±11) and 80 female (age=56±10) individuals [1,4]. The 3D coordinates of 29 anatomical landmarks were scaled and aligned via Procrustes superimposition, yielding $3 \times 29 = 87$ shape variables. We computed scapula centroid size as a proxy for body size.

We quantified directions of shape variation – called *shape vectors* – associated with sex (sex-distinction) and size (allometry). Allometry vectors were composed of the slopes calculated by regressing each of the 87 shape variables on centroid size. The sex-distinction vector was oriented from the mean female to mean male shape variables. Goodall's F-tests assessed the statistical significance of the vectors.

To disentangle allometric shape variation from sex-based variation, we computed within-sex allometry vectors and compared their directions to the sex-distinction vector by calculating the angle between vectors. Parallel vectors indicating identical shape changes would yield an angle of θ=0°. For visualization, we projected the vectors onto a lower-dimensional shape space via Principal Component Analysis (PCA).

RESULTS AND DISCUSSION

Scapula shape differed significantly between sexes ($F=6.62$, $p<0.0001$, Fig 1). While allometry explained a small amount of total shape variation (1.8% in males, 3.2% in females), the relationship was strong in female scapulae ($p=0.0013$). Contrary to the null hypotheses, male and female allometry vectors were distinct from each other (θ=86°), and from the sex-distinction vector (θ=88° for males, θ=128° for females, Fig. 1).

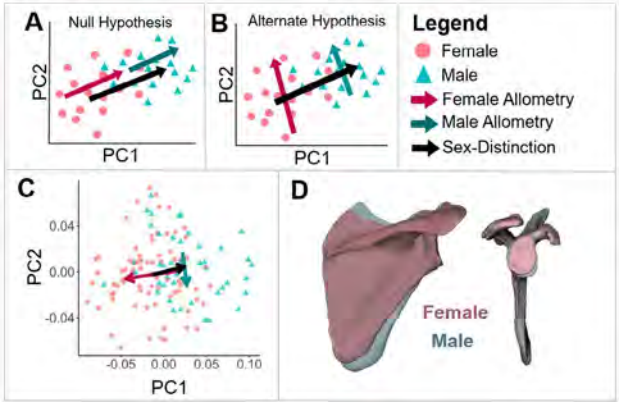

Figure 1 (A) Null hypothesis: allometry vectors align with sex-distinction vector, indicating sex-differences due to allometry. **(B)** Alternative hypothesis: allometry vectors are orthogonal to sex-distinction vector, indicating non-allometric sex differences. **(C)** Results: Individuals and shape vectors projected onto PC1-PC2 space. **(D)** Mean mesh warped along sex-distinction vector, with the magnitude of shape change doubled for visualization. Relative to the mean female scapula, the mean male scapula is more superior-inferiorly broad, has a less superiorly-inclined and more retroverted glenoid, and exhibits a wider supraspinatus attachment site.

CONCLUSIONS

Our findings suggest that sex differences in scapula shape cannot be attributed to inherent differences in body size. While future work is required to investigate the biomechanical effects, these shape differences have the potential to alter normal joint mechanics and contribute to sex-specific differences in mechanisms of injury.

ACKNOWLEDGEMENTS

We thank M. Bey and H. Henninger for providing access to scapula surface meshes.

REFERENCES

[1] Asseln et al. *The Knee* **25**: 545-558, 2018.
[2] Lee et al. *Clin Biomech* **78**: 105091, 2020
[3] Maranho et al. *Forensic Sci* **2**: 780-294, 2022.
[4] Kolz et al. *J Biomech* **117**: 110266, 2021.

A Study of Suitable Takeoff Motion of a Ski Jumper Using Principal Component Analysis and Computational Fluid Dynamics

Shin Ikeda[1], Keizo Yamamoto [2], Rahul Bale[3], Tokimasa Shimada [3], and Makoto Tsubokura[1,3]

[1] Graduate school of system informatics, Kobe University, Kobe, Japan.
[2] School of Lifelong Sport of Department of Sport Education, Hokusho University, Ebetsu, Japan
[3] RIKEN-Center for Computational Science, Kobe, Japan.
Email: 1895022t@stu.kobe-u.ac.jp

INTRODUCTION

The motions of ski jumping is often divided into four parts: in-run, takeoff, flight, and landing. Of these motions, the takeoff motion in which largely change jumpers' posture in a short time of about 0.2~0.3 seconds is considered to strongly affect the flight distance. However, there is no consensus as to what an optimal take-off posture ought to be. Therefore, the purpose of this study is to analyse a large, markerless motion capture based, dataset of trials using principal component analysis (PCA) to find an optimal takeoff posture.

METHODS

First step of the obtaining trial data involves capturing the takeoff motions in the trial jumps from 10 directions. Using the video data with Theia3D, which is a markerless motion capture system with deep learning, we measure the takeoff motion data. Next, using the motion data with Visual3D, we calculate the jumper's trunk angles of attack at takeoff (TAKEOFF), 0.1 seconds after takeoff (AFT100), and 0.2 seconds after takeoff (AFT200). Using PCA with the time series data of the trunk angle of attack, the principal component scores of all trials are plotted on a scatter diagram to find the skilled group, and the takeoff motion representative of the skilled group is confirmed in Visual3D. Finally, we use Computational Fluid Dynamics (CFD) to analyse the aerodynamic characteristics of the takeoff motion. The CFD analysis was conducted using a framework developed by Nishino et al [1].

RESULTS AND DISCUSSION

The scatter diagram of the principal component scores of all the trials obtained by PCA is shown below (Figure 1). Skilled is defined as a trial jump with a distance of 90m or more, and normal as a trial jump with a distance of 80m to 90m, and unskilled as a trial jump with a distance of less than 80m.

From the scatter diagram, it is found that there are two types of good takeoff motions. The two types of good takeoff motions are defined as Type A and Type B, and the takeoff motions representing each type were checked in Visual3D. The results show that Type A gradually increases the trunk angle of attack from TAKEOFF to AFT200, while Type B increases the angle of attack from TAKEOFF to AFT100 and tilted forward from AFT100. And, the aerodynamic characteristics of Type A and B are confirmed by using CFD.

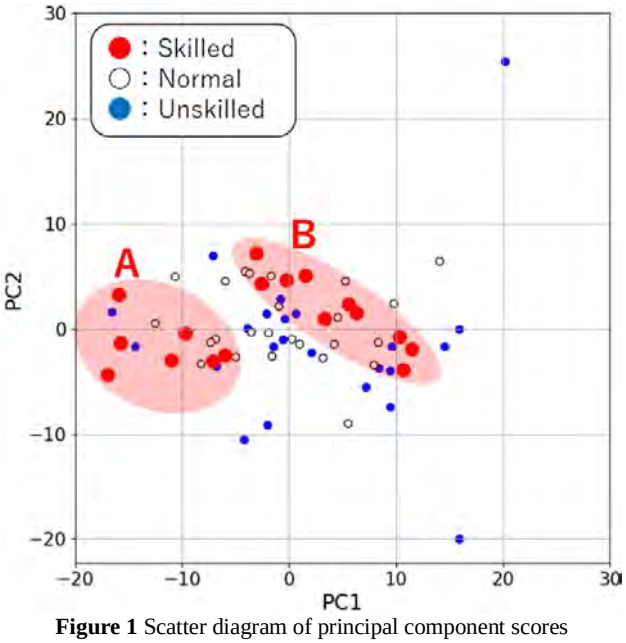

Figure 1 Scatter diagram of principal component scores

CONCLUSIONS

Through this study, we conclude that there are two types of appropriate takeoff motions in ski jumping. Furthermore, the aerodynamic characteristics of the two takeoff motions were analysed by using CFD.

REFERENCES

[1] Takahiro N. *Numerical study on the transient aerodynamic forces acting on a ski jumper*: 2022

FLEXIBLE MULTIBODY MODELING OF THE SKIER MUSCULOSKELETAL SYSTEM AND ITS APPLICATIONS IN ALPINE SKIING

Nan Gao[1], Huitong Jin[1], Jianqiao Guo[2], Gexue Ren[1] and Chun Yang[1]
[1] Department of Engineering Mechanics, Tsinghua University, Beijing, China.
[2] MOE Key Laboratory of Dynamics and Control of Flight Vehicle, School of Aerospace Engineering, Beijing Institute of Technology, Beijing, China.
Email: yangchun@mail.tsinghua.edu.cn

INTRODUCTION

The performance of alpine skiing, a risky winter sport, has been benefited from mechanical simulation and analysis. The quantitative measurement and analysis on turning maneuvers is crucial to skill advancement of skiers in both training and match. Kinematics characteristics analysis was thus provided for alpine skiers[1]. The kinetic features, such as joint moments and muscle forces, however, are crucial and urgent for to improving training outcomes, the mechanical simulation model of alpine skiing is yet to be improve.

In the present study, a custom-designed wearable system was adapted to harvest the kinematic signals at each turning of the skiers. Based on these data, we built a skier's musculoskeletal model (Figure 1A) and successfully simulated the trajectory of the body mass center, the joint moments, the muscle activation patterns of the skier, and the friction between the ski and snow surface during the ski movements. The ski-turning technique of skiers were then evaluate quantitatively.

METHODS

Two ski volunteers (a coach and a beginner) were recruited to complete the ski turns under the same conditions. Seventeen inertial sensors were attached to the volunteers limbs to capture their posture and movement during each ski turning (Figure 1B); Ski geometry and dynamical parameters were detected by three-dimensional scanning and vibration tests and used to describe the ski-snow interaction behaviors in a dissipative contact model; Windward area of the skier was calculated by the projected area of the human body in the coronal plane to estimate the air resistance[2]. Upon using posture data as input, we coupled the ski-snow contact model and musculoskeletal model to simulate the mass center trajectory, the snow reaction forces, the joint moments and the muscle activation patterns of the skiers[3].

A global positioning system (GPS) collecting the skier's motion trajectory, a pair of plantar pressure measurement insoles measuring the ground reaction forces were adapted to evaluate the accuracy of the simulation results of the skier's musculoskeletal model.

With this model, the skiers' speed, body mass center trajectory, joint angle and moments, ski angle and position, and muscle activation at each time point were determined. The turning technology was thus evaluated based on these parameters.

RESULTS AND DISCUSSION

The simulation results of the skier's center of mass trajectories were consistent with the measurements, with a correlation coefficient of r=0.97. The normalized ski-snow contact forces were also compatible with the measured plantar pressure, with a correlation coefficient of r=0.94 (Figure 1C). Comparison between the coach and the beginner further demonstrated the technical errors of beginners (Figure 1D): The adductor magnus of the beginner was continuously activated during the turning maneuver, resulting in hip adduction. The unnecessary adduction posture increased the friction between the ski board and its underlying snow surface. The force of the hip extensor muscle group of the beginner was too small, resulting in a slight hip flexion angle. The center of mass tended to move backward of the pelvis, and led to a wrong ski posture.

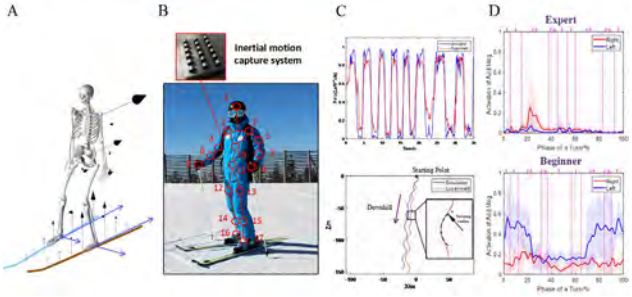

Figure 1 A Skier's musculoskeletal model; B Inertial sensors; C Validation of the model; D Activation of adductor magnus.

CONCLUSIONS

The proposed wearable measurement system successfully measured the kinematics and ski-snow interaction data during the alpine skiing maneuver. The skier's musculoskeletal model has been proved feasible to evaluate the performances of each skier, which shed a light to elevating the training outcomes with quantitative biomechanical data.

REFERENCES

[1] Heinrich D. *et al. Front Bioeng Biotechnol* **10**: 894568, 2022
[2] Sequeira M *et al. Comput Methods Biomech Biomed Engin* **Sep 10**: 1-9, 2022
[3] Wang X *et al. Acta Mech Sin* **38**: 522140, 2022.

SEX DIFFERENCES IN NETBALL PLAYERS' FOOT SHAPE: IMPLICATIONS FOR SHOE DESIGN

Maddison M. Kirk[1], Joshua P.M. Mattock[1], Celeste E. Coltman[2] and Julie R. Steele[1]
[1] Biomechanics Research Laboratory, School of Medical, Indigenous & Health Sciences, University of Wollongong, Australia
[2] University of Canberra Research Institute for Sport & Exercise, University of Canberra, Australia
Email: mkirk@uow.edu.au

INTRODUCTION

With the increasing professionalisation and popularity of men's netball, integrating males into a historically female-centric sport has raised important questions about the design and fit of footwear. Although there is a wide range of netball shoe models based on the foot dimensions of women, there is currently only one netball-specific shoe exclusively marketed for men [1]. This men's netball-specific shoe, however, is a hybrid-court shoe with design compromises so it can be used for both netball and volleyball [1]. Given the limited choice of netball-specific footwear for men, nearly 30% of male netball players have reported wearing female netball-specific shoes, and 70% wear shoes not designed for the sport [1]. Footwear designed using foot dimensions unrelated to the individuals likely to wear the shoes can lead to ill-fitting footwear. Of concern, 80% of male netball players have reported foot-related problems and pain in their last netball season [1]. Developing netball-specific footwear for males based on the foot dimensions of men is necessary to ensure proper shoe fit and to prevent foot-related problems. Therefore, we aimed to establish any differences in the dimensions and shape of the feet of male and female netball players to help inform netball shoe design recommendations for men.

METHODS

The feet of 251 representative male netball players (age: 26.1±8.3 yrs; height: 183.3±8.5 cm; mass: 87.7±21.5 kg) and the feet of 251 representative female netball players (age: 22.1±6.9 yrs; height: 172.5±13.8 cm; mass: 75.5±14.1 kg) were scanned using a Tiger full foot 3D scanner. The 3D foot scans were then analysed using a custom MATLAB script to derive eight measurements that characterised foot shape. Independent samples *t*-tests were then used to determine whether there were any significant differences in the foot dimensions derived for the left feet of the male compared to the female netball players ($p < 0.05$). We compared both the absolute foot dimensions and the foot dimensions normalised to foot length.

RESULTS AND DISCUSSION

The male netball players had significantly larger foot dimensions than the females, particularly at the ball of the foot, heel and instep (Figure 1). The foot dimensions normalised to foot length also significantly differed between the men and women, highlighting that men's feet are not simply a scaled-up version of females' feet; instead, the men and women's feet differed in several critical shape dimensions. This finding is consistent with previous findings in other cohorts, such as firefighters and young adults, which revealed that compared to women, men have much longer and broader feet that are different in shape, especially at the angle formed by the axis of the metatarsal heads and dimensions of the arch [2,3]. The sex differences in foot shape may explain the high prevalence of foot-related problems reported by male netball players and their dissatisfaction with the fit and comfort of the current shoes they wear during netball activity [4].

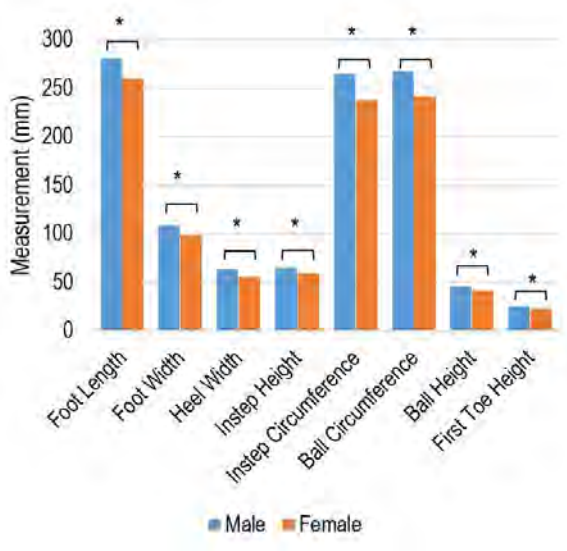

Figure 1 Differences in absolute foot dimensions, grouped by sex. * = $p < 0.001$.

CONCLUSIONS

The fit and functionality of netball-specific shoes must be improved to better cater for male foot dimensions. In addition, the sex differences in foot dimensions and shape must be considered when designing netball-specific footwear for men. Such improvements will help optimise shoe fit and comfort while minimising foot-related problems and pain associated with wearing ill-fitting footwear.

REFERENCES

[1] Kirk et al. *Sports Med - Open* **8**:103-114, 2022.
[2] Wunderlich et al. *Med Sci Sports Exerc* **33**:605-11, 2001.
[3] Jeyeon et al. *Appl Ergon*. **102**:103753. 2022.
[4] Kirk et al. *Footwear Sci.* 2023.

OPTIMAL ATTITUDE REORIENTATION OF FREE-FLOATING HUMANS BY RECTILINEAR JOINT ACTUATION

Yuki Kubo[1] and Junichiro Kawaguchi[2]

[1] Institute of Space and Astronautical Science, Japan Aerospace Exploration Agency, Sagamihara, Japan.
[2] College of Engineering & Computer Science, The Australian National University, Canberra, Australia.
Email: kubo.yuki@jaxa.jp

INTRODUCTION

Rotational dynamics (attitude dynamics) of a free-floating multibody has been investigated for a long time. It is known that the attitude motion of the multibody exhibits nonholonomic properties in which final orientation depends on its joint actuation procedure. Thus, properly designed body actuation process can generate arbitrary attitude reorientation even when total angular momentum of the system is kept zero. The typical research topics on this field are a righting reflex of falling cats [1] and reorientation of free-floating astronauts or aerial sports player [2,3]. In these systems, resulting attitude motion during joint actuation can be solved by numerical integration, but on the other hand, it is difficult to solve its inverse problem in which joint actuation process is designed to obtain arbitrary atititude reorientation. Previous studies have not generally solved the inverse problem, but instead, constrained most degree-of-freedom of control input to largely reduce exploration space for the solution. Thus, conventional methods have not made the most of potential attitude reorientation capability.

METHODS

This research proposes a novel method to solve the inverse problem of the attitude reorientation of a free-floating multibody. We refer to the proposed method as *rectilinear joint actuation* in which all m joints of the multibody are actuated along rectilinear path in m-dimensional joint angle space. The rectilinear path that connects starting and final joint configurations is iteratively modified to achieve target final attitude and self-collision-free constraints while optimizing total amount of joint angle displacement. The proposed method can handle large number of control degree-of-freedom and make the most of potential attitude reorientation capability of the free-floating multibody. In addition, each stroke of the rectilinear path results in concise attitude solution whereas the successive rectilinear stroke can yield sufficiently complicated attitude maneuver. In particular, this rectilinear joint stroke is suitable for humans because they can accomplish desired attitude maneuver simply by sequential posing of their body, not following complicated torque histories.

RESULTS AND DISCUSSION

The proposed motion planning method is validated by numerical simulation of free-floating human model. We used average physical properties of human body in this simulation. In the example simulation shown below, the target attitude rotation is set to be -30 degrees around x-axis (Figure 1). The human sequentially switches body poses and achieves target attitude after 5 strokes of joint actuation. The entire body actuation process does not cause self-collision and satisfies joint angle limit constraints. The resulting attitude maneuver is agile and efficient due to optimization.

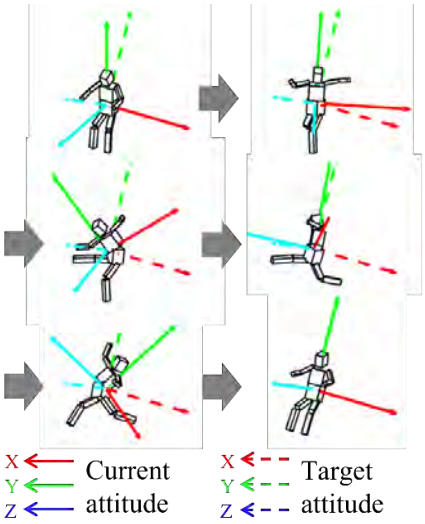

Figure 1 Example of optimized attitude reorientation of a human.

CONCLUSIONS

This research proposed a novel method for free-floating humans to achieve target body reconfiguration and attitude reorientation simultaneously. The proposed method greatly enhances attitude reorientation capability of large degree-of-freedom systems that conventional methods cannot make the most of its potential capability. Numerical simulation validated the proposed motion planning method effectively achieves agile attitude reorientation.

REFERENCES

[1] Kane TR et al. *Int J Sol & Str* **5(7)**: 663-670, 1969.
[2] Kane TR et al. *J Biomech* **3.1**: 39-49, 1970.
[3] Yeadon MR, *J Biomech* **46.5**: 1008-1013, 2013

IMPACT OF MENSTRUAL CYCLE ON ANAEROBIC POWER AMONG YOUTH CRICKETERS

Vijay Dhamodharan[1], Shanmugapriyanka Ilangovan[1], Rajinikumar Palaniyappan[1]
[1] Center of Excallence in Biomechanics, TNPESU, Chennai, India.
Email: vijaydhamu5@gmail.com

INTRODUCTION

The single most difficult challenge for athletes, particularly female athletes, is avoiding low energy availability due to its known effects on menstrual function and bone health – as evidenced by the Female Athlete Triad. Many aspects of athletic performance may suffer as a result of these changes in physical functioning [1]. There is a general lack of understanding regarding the relationship between menstrual cycle (MC) phases and performance in elite athletes. The purpose of the study is to investigate whether the menstrual cycle phase influences the anaerobic power in young female cricketers.

METHODS

This study was formulated as a homogenous group design. For the purpose of this study twenty young female cricketers (n=20) who represented the district and state teams were selected as subjects purposely (purposive sampling). This is a two-group comparative study as shown in Figure 1. To collect necessary data, the following variables were measured namely Menstrual Phase, Follicular phase, Ovulation phase, Luteal phase using Clue App and the Peak take-off Ground Reaction Force (GRF) during the Counter Movement Jump (CMJ), Standing Broad Jump (SBJ) GRF and Plyometric Pushup (PP) were measured through Kistler Force plate model 9287CA with dimension 1200x600x100 and analysed using MARS software. Subjects were asked to perform 3 trials with 1min rest between them. Best of the 3 trials was chosen for the research. Since only the anaerobic power of the athlete was studied, the take-off force was chosen as the variable of study [2].

RESULTS AND DISCUSSION

The athletes were categorised into group 1 and group 2 based on the bleeding phase of the individual. 63.2% athlete's mensural phase length was between 1-4 days, 21.1% was between 1-6 days, and 15.8% was 7 days or more.78.9% athletes prefer moderate intensity workout during the menstrual phase.26.3% athletes agreed that they feel strong during menstrual phase. 52.6% athletes prefer to train or compete during follicular phase of the menstrual cycle. Among twenty athletes 84.2% were comfortable competing during bleeding phase. The results from the table I shows that the obtained 't' values of 3.277, 2.269 and 2.879 were smaller than the table 't' value of 2.101. It is obviously shown that there was a significant difference between Counter Movement Jump (CMJ) GRF, Standing Broad Jump (SBJ) GRF and Plyometric Push-up (PP) GRF among bleeding and non-bleeding group of young female athletes.

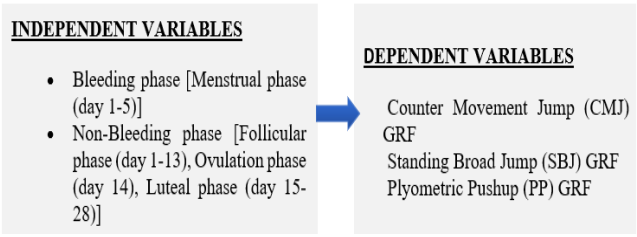

Figure 1 Research Design- Two Group Comparative study.

CONCLUSIONS

These results show that there is difference in the peak force generation between bleeding [Menstrual phase (day 1-7)] group and non-bleeding [Follicular phase (day 1-13), Ovulation phase (day 14), and Luteal phase (day 15-28)] group of female athletes. Further studies in the same area with static group comparation by repeated design to study the anaerobic power during different phases of MC might provide more insights.

REFERENCES

[1] Elliott and Pitchers. Professional Strength & Conditioning, 55, pp. 19-30, 2019.

[2] García-Pinillos et al. Int J Environ Res Public Health, *18*(9), 4830, 2021.

Table 1: Tables that extend across both columns should be placed at the bottom of the abstract.

	Non-Bleeding Group (n=10)	Bleeding Group (n=10)	t - value	*Sig (2-tailed)*
CMJ - GRF (N)	1235.20 ± 114.657	1068.80 ± 112.396	3.277	0.004
SBJ - GRF (N)	1194.31 ± 202.79	1002.53 ± 175.102	2.263	0.036
PP - GRF (N)	1235.20 ± 114.65	530.31 ± 1776.156	2.877	*0.010*

Gravel Bike Ground Reaction Forces

Josef Viellehner[1,2], Wolfgang Potthast[1],
[1] Institute of Biomechanics and Orthopaedics, German Sport University Cologne, Germany.
[2] Institute of Outdoor Sports and Environmental Science, German Sport University Cologne, Germany.
Email: j.viellehner@dshs-koeln.de

INTRODUCTION

Gravel biking is a recent trend in cycling. The profiled and wider tires of gravel bikes allow for a more variable use than traditional road bikes and also allow riding off paved roads. For the design of the bikes, the loads that occur during typical riding maneuvers, such as hitting a small obstacle, are of interest.Noteworthy, data on ground reaction forces in cycling is rare.
Therefore, this pilot study aims to provide metrics on the bike-ground interaction for biking over a small obstacle.

METHODS

Ground reaction forces (GRF) when riding over a 40 mm x 40 mm obstacle were recorded by three riders (BM: 75.3 ± 9.5 kg, BH: 1.83 ± 0.04 m). Each participant completed three attempts at 6 m/s approach speed in a seated position. The Gravel-Bike (Addict Gravel 10 2022, Scott, CH) included carbon rims (Capital 1.0 X40, Syncross, CH) and 700x45c tires (G-One Bite performance, Schwalbe, GER) at 1.5 bar tire pressure. GRF (Kistler, Winterthur, CH) were recorded at 1000 Hz and lowpass filtered (Butterworth, 2nd order, recursive, 300 Hz).
The front wheel and rear wheel impacts on the obstacle were detected via the anterior-posterior GRF. Extracted discrete variables are the vertical and longitudinal peak forces and the momentum of force along the driving direction to quantify the amount of braking. Signal processing and descriptive statistics are done using Matlab (Matlab R2021B, The MathWorks, USA).

RESULTS AND DISCUSSION

Figure 1 illustrates vertical and longitudinal GRF for the front-and-rear wheel during a single impact. Vertical peaks occurred up to 904.8 ± 194.7 N at the front wheel and 1311.0 ± 349.2 N at the rear wheel. Backward-oriented peaks reached up to -293.2 ± 19.7 N (front) and 402.4 ± 50.9 N (rear). Discrete variables are summarized in table 1.

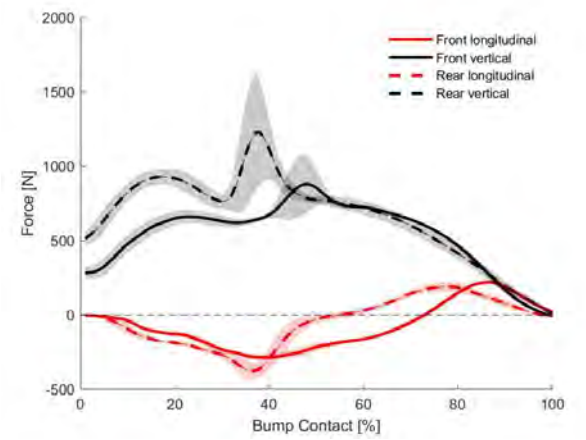

Figure 1: Vertical (black) and driving direction (red) GRF for front and rear wheel impact. Negative longitudinal GRF is orientated against the driving direction (backward).

CONCLUSIONS

The results suggest, following previous research, that rear-wheel loading is higher than front-wheel loading [1]. Horizontal peak forces at 30% of the vertical peak force demonstrate, that the loading scenario is not purely vertical but a 2D phenomenon. To the best of our knowledge, this study is the first to provide GRF time histories for typical loading scenarios as single impacts in (gravel) biking. The methodological approach might help future research to understand the systematic effects of e.g., speed, obstacle size, or technical interventions such as damping systems on bicycle loading.

REFERENCES

[1] De Lorenzo, D. & Hull, M. (1999), *Journal of Biomechanical Engineering,* 121(4),399-405.

Table 1: Peak forces in vertical and driving direction and momentum of force in driving direction for front and rear wheel (mean ± sd)

	Peak Force [N]			Momentum of force [Ns]	
	forward	backward	vertical	forward	backward
Front Wheel	221.3 ± 13.5	-293.2 ± 19.7	904.8 ± 194.7	1.7 ± 0.1	-5.5 ± 0.2
Rear Wheel	193.0 ± 31.4	-402.4 ± 50.9	1311.0 ± 349.2	2.7 ± 0.4	-5.5 ± 0.3

Performing both resisted and non-resisted trunk extension in prone are recommended to elicit maximum voluntary contraction of the spinal extensors in adolescents with idiopathic scoliosis and controls

Phoebe Ng[1,2], Phoebe Duncombe[2], Wolbert van den Hoorn[3], Andrew Claus[4], Maree Izatt[5,6], and Kylie Tucker[2]

[1]KK Women's and Children's Hospital, Singapore, [2]School of Biomedical Sciences, The University of Queensland, Australia,[3]ARC Training Centre for Joint Biomechanics, Queensland University of Technology (QUT), Australia, [4]Royal Brisbane and Women's Hospital, Australia, [5]Biomechanics and Spine Research Group, QUT at Centre for Children's Health Research, Australia, [6]Queensland Children's Hospital, Australia

Email: phoebe.ng@uq.edu.au

INTRODUCTION

Adolescent idiopathic scoliosis (AIS) is a three-dimensional deformity of the spine, diagnosed between the ages 10-18 years. It is associated with morphological and physiological differences in paraspinal muscles. Paraspinal muscle activation, recorded using electromyography (EMG), may also differ between convex and concave sides of the spine in those with AIS. The greatest evidence for asymmetrical paraspinal muscle activity is in those with progressive, right-thoracic curves, recorded during static postural tasks [1]. However, inconsistent EMG electrode placement, data processing, reporting of methods, and normalisation methods prevents clear interpretation of current evidence. Normalisation of EMG is important when comparing amplitude of activation during submaximal tasks between individuals, groups and/or muscles [2]. The development of standardised EMG recording and normalisation procedures will assist comparison of paraspinal muscle activation amplitude between sides and participants with and without AIS.

The aim of this study was to identify the spinal extension task that achieves peak amplitude of activation above, at and below the primary scoliosis curve in adolescents with AIS, and the same spinal levels in controls. We first compared five tasks during pilot testing: maximal trunk extension in i) prone and ii) sitting, both resisted with multiple straps; iii) a modified biering-sorenson test; iv) manually *resisted* trunk extension in prone (Fig 1A), and v) the *superwoman* with no resistance (Fig 1B). From these, the *resisted* and *superwoman* tasks consistently provided the greatest activation amplitude of paraspinal muscles, and were chosen for further study.

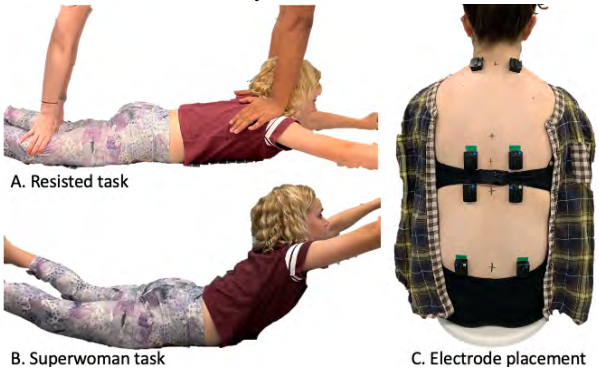

Figure 1 The (A) resisted and (B) superwoman tasks performed to obtain maximal activation of paraspinal muscles, measured using bilaterally placed surface electromyography electrodes (C).

METHODS

Adolescent females with primary right thoracic AIS (n=11, mean[SD] age: 13.8[1.3] years) and without AIS (n=11, 13.8[1.9] years) were recruited through a Spine outpatient clinic at the Queensland Childrens' Hospital, and community. Bipolar surface electrodes were placed bilaterally at vertebral levels: C7,T9,T12, & L5 (Fig 1C).

Participants were provided with training of the maximal voluntary activation tasks, during which they were provided with visual feedback of their muscle activation. Once familiar with the tasks, participants were verbally encouraged to increase their contraction over 3 seconds, then *contract as hard as possible* for ~ 3 seconds before returning to rest. Both tasks were repeated 3 times, with at least 1 minute rest between contractions. Data were sampled at 2000sps, then filtered (50-500Hz, 4th order Butterworth band pass), and rectified and low pass filtered at 2Hz. The maximum amplitude obtained for each contraction was obtained, and all data were then normalised to the maximum obtained across all contractions for each muscle independently.

RESULTS AND DISCUSSION

On a group level, there was neither a difference in the normalised EMG amplitude between tasks (*superwoman* and *resisted;* main effect task: p=0.71), nor group (AIS and control; main effect group: p=0.22). Peak activation was achieved with the *superwoman* task in 45%, and in the *resisted* task in 55%, of the activation measurements [considering activation was measured on 2 sides x4 muscles x2 tasks x22 participants]. For individual participants, the difference in maximum amplitude between tasks was up to 46% (mean [SD]: 20 [15]%). This means that if only one of these tests were performed the maximum amplitude could be underestimated by up to 46%, which severely impacts the ability to interpret normalised activation data.

CONCLUSIONS

We recommend using resisted and non-resisted trunk extension in prone as an optimal approach to determine peak voluntary activation.

ACKNOWLEDGEMENTS

This study is funded by the Scoliosis Research Society.

REFERENCES

[1] Ng et al. *J Electromyogr Kinesiol* **63**, 1-11, 2022
[2] Besomi et al. *J Electromyogr Kinesiol* **53**, 1-17, 2020

Greater asymmetrical spinal muscle activity during submaximal trunk extension in adolescents with idiopathic scoliosis than those without

Kylie Tucker[1], PTT Ng[1,2], P Duncombe[1], A Claus[3], MT Izatt[4,5], P Pivonka[6], R Labrom[4,5] and W van den Hoorn[6]

[1]School of Biomedical Sciences, The University of Queensland, Australia, [2]KK Women's and Children's Hospital, Singapore,[3]Royal Brisbane and Women's Hospital, Australia, [4]Biomechanics and Spine Research Group, Queensland University of Technology at Centre for Children's Health Research, Australia, [5]Queensland Children's Hospital, [6]ARC Training Centre for Joint Biomechanics, Queensland University of Technology.

Email: k.tucker1@uq.edu.au

INTRODUCTION

Adolescent idiopathic scoliosis (AIS) is a three-dimensional deformity of the spine, diagnosed between the ages 10-18 years. Curve progression is associated with three-dimensional wedging of spinal vertebrae and discs. It is well known that muscle activity and morphology influence muscle force generation, and that the forces applied to bones and discs are substantial moderators of growth and adaptation [1]. To date, the greatest evidence for asymmetrical paraspinal muscle activity is in those with progressive, right-thoracic curves, recorded during static postural tasks [2]. However, data varies greatly between studies, and previous outcomes are highly dependent on the methodological approaches taken [2].

The aim of this study was to determine if the symmetry of paraspinal muscle activation amplitude differs in adolescents with AIS compared to controls, during a voluntarily driven, symmetrical, submaximal task.

METHODS

Adolescent females with AIS (primary right thoracic curves, n=11, mean[SD] age: 13.8[1.3] years) and without AIS (n=11, 13.8[1.9] years) were recruited through a Spine outpatient clinic at the Queensland Children's Hospital and the local community.

Participants first performed a series of six maximal back extensions. Three of these were conducted in an unresisted *superwoman* pose, and three were manually *resisted* at the shoulders and thighs. The maximum activation recorded in any trial, for each muscle separately, was used for normalisation. Participants then performed a series of five (20-40s) submaximal *superwoman* contractions (Fig 1A). Visual and verbal feedback was provided to encourage participants to maintain a level of activation at T9, which was between 10-30% of their maximal activation (i.e. 10-30% MVC, from T9 left + right).

Muscle activity was recorded using bipolar surface electrodes placed bilaterally at vertebral levels: C7, T9, T12 & L5 (Fig 1B). Data were sampled at 2000sps, then filtered (50-500Hz, 4th order Butterworth band pass), and rectified and further low pass filtered at 10Hz. The *symmetry index of muscle activity was determined using* Ln (Right/Left), which equates to Ln (Convex/Concave) in the AIS cohort. The symmetry index, for each muscle separately, was compared using independent t-tests.

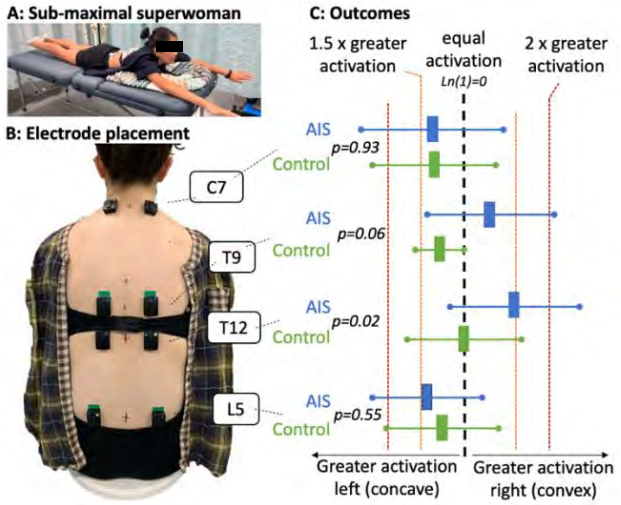

Figure 1A) Submaximal superwoman pose; B) electrode placement, C) symmetry index of muscle activation in adolescent idiopathic scoliosis (AIS) and controls. Data right of the line of equality = greater activation on the right (convex in AIS) side.

RESULTS AND DISCUSSION

The symmetry index was different between groups at T12 (p=0.02; Fig 1C). Greater activity was observed on the convex side of the curve at T12 in all but one participant with AIS. Individual variability in this measure will be further explored. The difference in asymmetry between AIS and controls was also close to significant at T9 (p=0.06). Our work supports previous studies, that use a variety of tasks and normalisation methods, and demonstrate the greatest evidence for convex>concave paraspinal muscle activation asymetry at the level of the apex and lower end vertebral level of the curve (~T9 and T12 respectively for our study) [5].

CONCLUSIONS

Compared to control participants, adolescents with AIS display greater asymmetry in paraspinal muscle activation at T12 during submaximal trunk extensions. This asymmetry was not observed in the cervical or lumbar spine regions. The origins and consequences of this asymmetry are important to consider further.

ACKNOWLEDGEMENTS

This study is funded by the Scoliosis Research Society.

REFERENCES

[1] LeVeau et al. *Phys Ther*, **64**: 1874-82, 1984.
[2] Ng et al. *J Electromyogr Kinesiol* **63**: 1-11, 2022.

Ankle power in gait is more relevant to the maximum instance firing rate of soleus than gastrocnemius

Hayase Funakoshi[1], Takanori Kokubun[1]
[1] Department of Health and Social Services, Graduate School of Saitama Prefectural University / Saitama, Japan.
Email: Funakoshi-hayase@spu.ac.jp

INTRODUCTION

Gait speed is a crucial health indicator that is closely associated with mortality and a primary focus of rehabilitation interventions. Ankle plantar flexion plays a significant role in generating the propulsive force required for faster gait, accomplished by pushing off with the toes. This movement is driven by the triceps surae muscles, which comprise the Soleus and Gastrocnemius. The force generated by these muscles is determined by structural and neural factors, including the firing patterns of motor units. Previous study has established that the Impulse is closely linked to the maximum instance discharge rate (IDRmax) of motor units during isometric contraction tasks[1)]. And ankle power has been shown to be related to gait speed[2)]. So we hypothesizesd that ankle peak power in gait is also contributed by IDRmax of triceps surae. We used decomposition algorithms capable of tracking the firing behavior of individual MUs during dynamic tasks to investigate the relationship between MU firing and ankle power (NeuroMap software; Delsys Inc.; De Luca et al., 2015).

METHODS

Subject was 12 healthy young adult (6 male and 6 female). They are provided written informed consent, following a detailed explanation of the study's purpose and risks according to the Declaration of Helsinki. The 4 channel Electromyography (EMG) (Delsys.inc) was putted on soleus (SOL), medial (MG) and lateral (LG) gastrocnemius. Task was 3-minute gait at 6 different speed including the maximum and minimum speed on the treadmill with force plate surrounded by the 3-dimensional motion capture system. Each speed was determined with self-awareness. MU firing times were extracted from the EMG signals from each sensor separately using decomposition algorithms. Only MUs with accuracy estimates of 85% or higher were included into further analysis. The correlation coefficient was calculated between IDRmax (maximum value of reciprocal of inter spike interval in a 150 msec interval before the ankle moment peak) of MU and ankle power, and maximum gait speed.

RESULTS AND DISCUSSION

High MU maximum firing rate contributes generating ballistic force. So, we expected that ankle plantar flexion that is related to the gait speed in faster gait is related to the higher IDRmax. Consistent with previous research, there was a significant positive correlation between ankle peak power and maximum walking speed (r=0.72, p>0.00). The correlation coefficient between IDRmax of SOL and ankle power was 0.71 (p>0.00), IDRmax of MG was -0.19 (p=0.10), IDRmax of LG was 0.17 (p=0.16). In addition, IDRmax of SOL has significant positive correlation with the maximum gait speed (r=0.61, p>0.00). Only SOL had significant positive correlation, but because previous study indicates that triceps surae doesn't completely receive the same neural drive, this study supports this phenomenon. And the factor for difference between SOL and MG, LG can be related to the MU twitch properties and size principle. MUs of soleus are recruited early for 90% slow-twitch fibers, so the firing rate is related to the subsequent increase in force. On the other hands, gastrocnemius has a 1:1 ratio of slow-twitch and fast-twitch fibers. Since recruitment and firing were mixed in gastrocnemius, IDRmax of MG and LG didn't have significant correlation with ankle peak power.

CONCLUSIONS

We conclude that instance firing rate of SOL can contribute to the gait speed via ankle peak power. But further studies are needed to completely confirm this hypothesis.

ACKNOWLEDGEMENTS

This work was supported by the Sasakawa Scientific Research Grant from The Japan Science Society [2022-6043].

REFERENCES

[1] Del vecchio et al. *J Physiol* **597**: 2445-56, 2019.
[2] Da Silva et al. *Sci. Rep.* **10**: 202

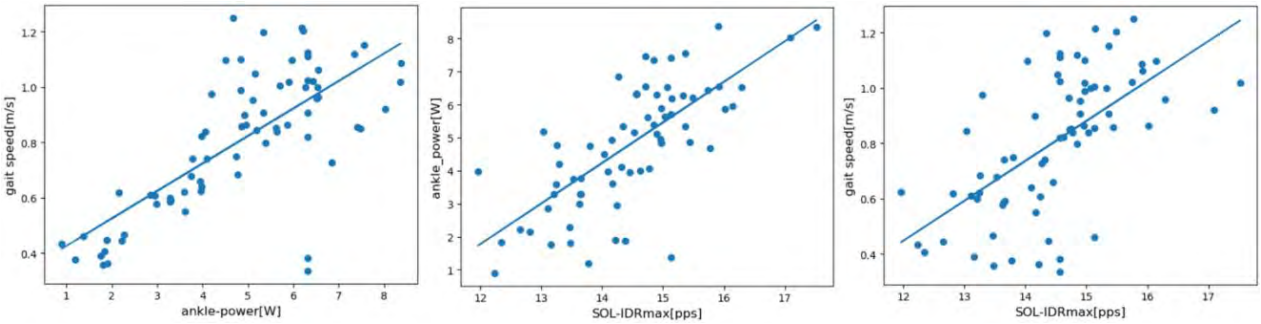

Supraspinal integration of proprioception is crucial for locomotor robustness

Alessandro Santuz[1,2], Olivier Laflamme[2] and Turgay Akay[2]

[1] Development and function of neural circuits, Max Delbrück Center for Molecular Medicine, Berlin, Germany.
[2] Atlantic Mobility Action Project, Brain Repair Centre, Department of Medical Neuroscience, Dalhousie University, Halifax, NS, Canada.

Email: alessandro.santuz@mdc-berlin.de

INTRODUCTION

Animals constantly move in complex environments. In vertebrates, locomotor activity is generated in part by central pattern generators in the spinal cord [1]. When somatosensory feedback is removed and supraspinal pathways are left intact, central pattern generators alone are not sufficient to ensure robust locomotion in the presence of external perturbations [2]. In mammals, information about the position of the body in space and relative to the body itself (i.e. proprioception) is conveyed to the central nervous system by mechanosensory neurons that carry signals from muscle spindles, Golgi tendon organs and joint receptors. Feedback from muscle spindles and Golgi tendon organs plays a central role in locomotion [2], [3]. Part of the proprioceptive information is processed in the spinal cord and three main pathways convey the rest to brain structures: the dorsal and ventral spinocerebellar tracts and the dorsal column-medial lemniscus (DCML) pathway. While the sensory circuitry in the dorsal column is relatively well investigated, the role of higher centres in integrating proprioceptive information during locomotion is still unclear. Here, we set out to explore the relevance of supraspinal integration of proprioceptive feedback via the DCML pathway during mouse locomotion. We hypothesised that not only spinal but also supraspinal processing of proprioception must be involved in the tuning of locomotor output in challenging environments. We show that supraspinal processing of proprioceptive feedback becomes critical when locomotion is challenged by external perturbations.

METHODS

Recordings were conducted on 18 adult (age 89 ± 20 days; mass 25.9 ± 3.9 g) male mice with C57BL/6 background: 5 wild-type for DCML lesion, 5 muscle spindle-deficient *Egr3*$^{-/-}$ [4], 5 *PV*^{Cre}*::Avil*^{iDTR} for acute ablation of muscle spindles and Golgi tendon organs triggered by diphtheria toxin injection [5] and 3 *PV*^{Cre}*::Rosa*^{EGFP} for the sham experiments. Eight bipolar EMG electrodes were surgically implanted in as many muscles of the right hind limb. Muscle synergies were extracted from EMG activity using the R package "musclesyneRgies" [6] v0.7.1-alpha. The DCML pathway was surgically lesioned using micro scissors. Animals walked on a custom-built perturbation treadmill (University of Cologne, Germany), capable of administering sudden mediolateral displacements or accelerations of the belt at random time intervals. For markerless body part tracking we processed high-speed videos of the sagittal plane in DeepLabCut [7] v2.1.10.

RESULTS AND DISCUSSION

The effects of perturbations on kinematics were visible only in the wild type, as an increased variability of the hip joint angle at touchdown. In *Egr3*$^{-/-}$ and *PV*^{Cre}*::Avil*^{iDTR} mice, the lack of proprioceptors made the kinematic variability increase, independently on the presence of perturbations. After lesion, wild-type mice showed overall low kinematic variability, comparable to that observed before surgery in unperturbed locomotion. Similar to kinematics, the complexity or "accuracy" of muscle activation patterns was lowered in response to perturbations only in wld-type animals. Proprioceptive-deficient mutants always showed low complexity of activation patterns, a sign of constant internal perturbation. Lesioned wild-type mice often halted locomotion in the presence of perturbations, showing no modulations of complexity, which remained high.

CONCLUSIONS

We showed that animals lacking proprioceptors locomoted in a constantly perturbed state, irrespective of the administration of mechanical perturbations. This was not the case in wild-type mice, in which we surgically interrupted the flow of proprioceptive feedback to the brain through the dorsal column. After the lesion, the lesioned animals behaved similarly to pre-lesion unperturbed walking, both in the absence and presence of external perturbations. This translates into two main conclusions: i) the removal of proprioceptors in mice impairs locomotion proportionally to the level of ablation and ii) supraspinal integration of proprioceptive information is crucial to ensure robust locomotion. Taken together, our results show a clear involvement of supraspinal proprioceptive structures in the production of robust, continuous locomotion.

REFERENCES

[1] Brown TG *Proc. Royal Soc. B* **84**: 308-319, 1911

[2] Grillner S & El Manira A *Physiol Rev* **100**: 271-320, 2020

[3] Pearson KG *Curr Opin Neurobiol* **5**: 786–791, 1995

[4] Tourtellotte WG & Milbrandt J *Nat Gen* **20**: 87–91, 1998

[5] Takeoka A & Arber S *Cell Rep* **27**: 71-85, 2019

[6] Santuz A *JOSS* **7**: p. 4439, 2022

[7] Mathis A et al. *Nature Neurosci* **21**: 1281–1289, 2018

GAIT KINEMATICS AND SURFACE EMG ALTERATIONS ASSOCIATED TO DIFFERENT MOSAICISM TYPE IN CHILDREN WITH FRAGILE X SYNDROME

Fabiola Spolaor[1], Annamaria Guiotto[1], W. Piatkowska[1], Elisa DiGiorgio[2], Valentina Liani[2], Roberta Polli[2], Alessandra Murgia[2], Zimi Sawacha[1,3]
[1] Department of Information Engineering, University of Padua, Padua, Italy
[2] Dept of Women's and Children's Health - University of Padova, Italy
[3] Dept of Medicine - University of Padova, Italy

Email: fabiola.spolaor@unipd.it

INTRODUCTION

Gene Fragile X Messenger Ribonucleoprotein 1 (FMR1) encodes an RNA binding protein that is implicated in a multitude of crucial neurodevelopmental processes, including early embryonic motor circuits [1]; transcriptional silencing of the FMR1 is the main cause of inherited intellectual disability and autism spectrum disorder called Fragile X Syndrome (FXS). "Premutation" and "full mutation" are the two main categories of FMR1 mutations associated with different clinical phenotypes; somatic mosaicism can represent a strong FXS phenotype modulator [2]. Mosaicism in FXS refers to two different FMR1 allele variations: size mosaicism (i.e. different numbers of CGG repeats between the two alleles), methylation mosaicism (i.e. full-mutation allele is fully or partially methylated) [3]. The present study explored the differences between healthy subjects, full mutation and both methylation and size mosaicism in terms of musculoskeletal alterations during gait.

METHODS

After appropriate informed consent by the parents, the gait of 36 FXS children ((FX) mean(±SD) age of 10 (±3.6) years, BMI of 19.4 (±3.6) Kg/m2) and 10 controls ((CS), mean(±SD) age of 10 (±3.07) years, BMI of 20.4 (±4.5) Kg/m2) was assessed at the BiomovLab (CS) and at the Paediatric Department of the University of Padua. Within the FXS group of 28 children with full mutation ((FX-FM), 3 children with methylation mosaicism (FX-MET) and 5 with size mosaicism (FX-DYM) were detected . Kinematics in terms of joint angles and surface electromyographic data (sEMG) were simultaneously acquired through four synchronized cameras (GoPro Hero3, 30fps) and an sEMG system (FreeEmg, BTS, 1000Hz) that collected the activity of Tibialis Anterior, Gastrocnemius Lateralis, Rectus Femoris and Biceps Femoris. At least three left and right gait trials per subject were processed. From sEMG parameters, envelope peak and its occurrence within the gait cycle were computed, sagittal plane kinematics was assessed from video recordings [2].

RESULTS AND DISCUSSION

In terms of joint angles both FM-MET and FM-DYM showed a statistically significant reduction of the knee flexion and an increase of the ankle extension; meanwhile only FX-MET showed an increase in hip flexion angle during the whole gait cycle. Concerning with sEMG, FX-MET showed a decrease in Tibialis Anterior activity during midstance and terminal swing, accompanied by an increase in terminal stance; a decrease in Gastrocnemius Lateralis activity during midstance, and finally an increase in Biceps Femoris activity during terminal stance. In the comparison between both FX-MET and FX-DYM with CS, even though no statistically significant differences were detected, the envelope shapes of all muscles showed an altered pattern.

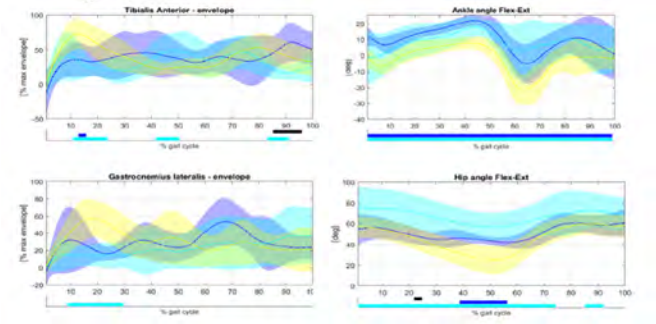

Figure 1 On the right column Tibialis Anterior and Gastrocnemius Lateralis envelope shaper, on the left column knee and hi angles in degree. Mean and standard deviations are represented as bands according to the colour reported in the legend.

CONCLUSIONS

These results seem to suggest that FX-DYM and FX-FM presented similar differences in the sEMG pattern when compared with CS, while FX-MET displayed a pattern more similar to CS. -M eanwhile, in terms of kinematics, the data showed similar alterations in FX-MET and FX-DYM with respect to CS.

REFERENCES

[1] Barker CM et al Front. Neurosci. Nov **3**;16:962901 2022
[2] Piatkowska W et al Appl. Sci. **12**(3), 1612, 2022
[3] Meng et al. Am J Med Genet.**188**A:858–866,

Lower extremity muscle activity in case of slipping during 90-degree change of direction tasks with and without an ankle brace

Uwe G. Kersting[1,4], Anna Lingner[1], Priscila.B. Silva[2] , Natalie Mrachacz-Kersting[3] and Anderson S.C. Oliveira[4]
[1] Institute of Biomechanics and Orthopaedics, German Sport University Cologne, Cologne, Germany
[2] UCN School of Physiotherapy, Aalborg, Denmark
[3] Department of Sport and Sport Sciences, Albert-Ludwigs-University Freiburg, Germany
[4] Departments of HST and MP, Aalborg University, Denmark
Email: u.kersting@dshs-koeln.de

INTRODUCTION

Ankle sprains have been reported as the most common injuries during sport games. They may occur during landing or fast cutting movements either with or without interference of an object or opponent. Often considered to be a minor injury an unrecognized high proportion of complications and associated costs were reported by Larsen et al. [1]. In a recent review [2], it has been stressed that the underlying injury mechanism may vary between cases while many studies assessed the general benefits of interventions, such as bracing or training, The goal of this study was to assess the effect of bracing on muscle activity of lower extremity muscles during side cuting on normal and simulated slippery surfaces.

METHODS

Sixteen team sports athletes volunteered in this study (28.2 +/- 3.7 y, 72.9 +/- 7.0 kg, 175 +/- 7 cm). Full-body kinematics (Qualisys, 240 Hz) and ground reaction forces (AMTI, 1000 Hz) were recorded. The force plate rested on a 4-DoF robotic actuator [3] which moved horizontally in approach direction by 0, 4 or 8 cm in a randomized order, 25 ms after touch-down. Cutting was performed in two sets with eight trials per condition, when wearing a semi-rigid ankle brace (AirCast) or no brace. Electromyographic (EMG) signals were recorded from nine leg and thigh muscles of the cutting leg and rectus femoris and gluteus maximus of the contralateral side (1200 Hz, Biovision). Kinematic data were analysed in Visual3D (C-motion) and EMG data using a customized script in MatLab (The Mathworks).
Joint angles, moments and corrected GRF values were determined at touch-down and during the stance phase. From the EMG data, average rectified values (ARV) were calculated in three time-intervals, i.e., the last 50 ms prior to touch-down (PRE), the first 70 ms after initial ground contact (EARLY) and 70-120 ms after touch-down (LATE). A two-factor repeated measures ANOVA on the factors BRACE and SLIP condition was employed for statistical analysis using a Bonferroni post-hoc test. Significance was attested if $p<0.05$.

RESULTS AND DISCUSSION

The kinematics showed marginal differences between slip conditions while the main effect for BRACE was a more dorsiflexed ankle at touch-down and a slightly increased range of knee flexion during ground contact, confirming [4]. Different SLIP conditions did not alter the muscle activity in the PRE and EARLY intervals but a reduced activity for VM during LATE (not shown). There was a significantly increased RF_C activity during LATE for the BRACE condition (shown for 0 cm slip in Fig. 1) indicating that the use of a brace affects muscle action of the contralateral hip.

CONCLUSIONS

Wearing a brace affects not only the ankle and knee kinematics of during cutting but also the muscle activity of the muscle of the contralateral hip during a cutting task. This may have implications for long term use of ankle braces.

REFERENCES

[1] Larsen E et al. *Scand J Med Sci Sports* 9(5):285-9, 1999.
[2] Lysdal FG et al. *Sports Biomech21(4):***33.** 492-501, 2022.
[3] van Doornik J et al. *IEEE Trans Biomed Eng* 54(9):1696-702, 2007.
[4] Kersting UG *Proc of 7th WCB*, Pres. 9-20, 2014.

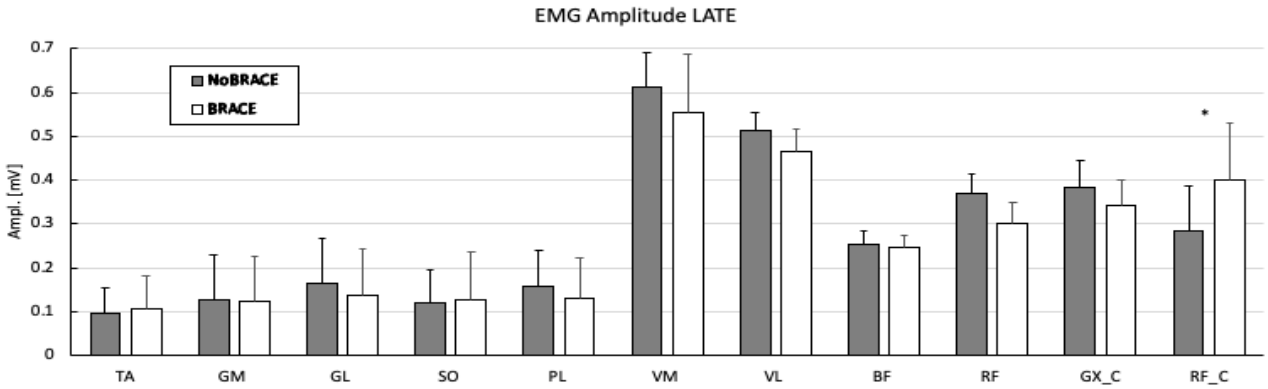

Figure 1. ARV values for LATE time interval at NoSLIP comparing BRACE and NoBRACE conditions. TA: tibialis ant., GM: gastrocnemius med., GL: gastrocnemius lat., SO: soleus, PL: peroneus long. VM: vastus med., VL: vastus lat., BF: biceps femoris, RF: rectus femoris, GX_C: gluteus max. contralateral side, RF_C: rectus femoris contralateral side.
* Denotes significant difference.

REGIONAL NEUROMUSCULAR CONTROL OF THE HUMAN HAMSTRING MUSCLES

Patrick Smart[1], Patricio Pincheira[1,2], Yuyao Ma[2], Eduardo Martinez-Valdes[3], Francesco Negro[4], Glen Lichtwark[1] and Andrew Cresswell[1]

[1] School of Human Movement and Nutrition Sciences, The University of Queensland, Brisbane, Australia
[2] School of Health and Rehabilitation Sciences, The University of Queensland, Brisbane, Australia
[3] School of Sport, Exercise and Rehabilitation Sciences, University of Birmingham, Birmingham, UK
[4] Department of Clinical and Experimental Sciences, Università degli Studi di Brescia, Brescia, Italy
Email: uqppinch@uq.edu.au

INTRODUCTION

The hamstring muscles are biarticular; that is they span two joints. Biarticular muscles in the thigh control the distribution of force and torque around the hip and knee joints. They are often considered to have well-defined actions and function based on their anatomy. However, recent evidence suggests that some biarticular muscles have region-specific activations that can be interpreted as regional differences in function within the muscle [1]. For instance, in the medial gastrocnemius, motor units (MU) can show different behaviour across distinct muscle regions, suggesting that a single muscle could have areas that are controlled selectively by the nervous system. Surprisingly, little is known about the representation of this phenomenon in the hamstring muscles. The aim of this study was to determine regional variation in hamstring muscle MU firing properties during voluntary contractions performed at different muscle lengths (hip and knee joint configurations).

METHODS

Twelve recreationally active male volunteers, aged between 18-30 years, participated in the study. With the participants laying in the prone position, four different joint configurations were used to manipulate hamstrings muscle length (Hip 0° – Knee 0°; Hip 0° – Knee 90°; Hip 70° – Knee 0°; Hip 70° – Knee 90°). At each position, participants performed isometric contractions at 40% of a previously determined maximal voluntary isometric contraction. High-density electromyography (HD-EMG) signals were recorded from the biceps femoris long head (BFlh) using two 2-D adhesive grids of 32 channels (8 rows x 4 columns, 10 mm inter electrode distance). Electrodes were placed in the mid and distal regions of the muscle. Signals were sampled using a wireless analogue to digital converter (Sessantaquattro, OT Bioelettronica, Torino, Italy). Knee flexion torque was quantified using an isokinetic dynamometer (Humac Norm, Stoughton, USA). HD-EMG signals were decomposed [2] to identify the following MU properties: mean discharge rate, recruitment threshold and coefficient of variation of the inter-spike interval (CoVisi). A mixed-effects model was used to evaluate the effect of 'joint configuration' (four levels) and 'region' (two levels) on motor unit properties ($p \leq 0.05$).

RESULTS AND DISCUSSION

The mixed-effects analysis revealed no main effects or interactions (joint configuration x region) for any of the variables analysed (Figure 1).

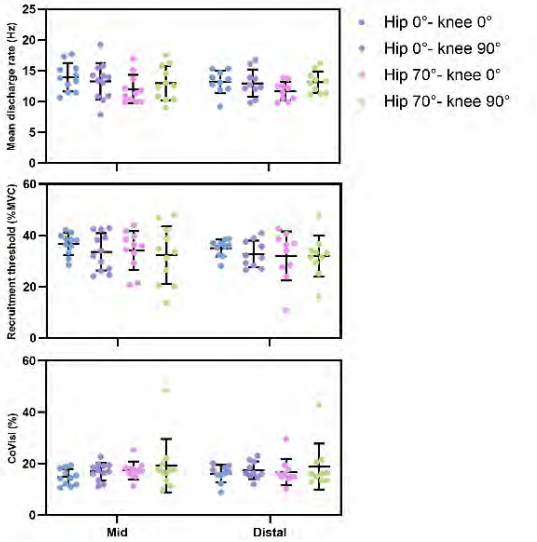

Figure 1 MU properties at different joint configurations and BFlh regions.

These results show no regional variation in BFlh muscle neural control during isometric contractions performed at different joint configurations. This may suggest that MUs are uniformly recruited througout the BFlh when the muscle activates at maintained muscle lengths. However, since previous evidence suggests regional changes in BFlh EMG amplitude during concentric/eccentric tasks [3], it may be plausible that the change in muscle length rather than the muscle length itself is a key factor leading to regional changes in neural control. Further, it is still possible that regional differences in MU firings are more evident in the proximal end of the muscle (closer to the hip).

CONCLUSIONS

The BFlh muscle does present regional variation in neural control during voluntary isometric contractions performed at different muscle lengths. Further studies are needed to elucidate if the same treand is maintained during shortening/lengthening contractions.

REFERENCES

[1] Watanabe K et al. *Ex Sport Sci Rev* **49**: 179-87, 2021.
[2] Negro et al. *J Neural Eng* **13**: 02627, 2016.
[3] Hegyi A et al. *Med Sci Sport Ex* **51**: 2274-85, 2019.

New approach for calculating a functional subtalar joint axis

Anja Seeger[1], Sascha Schlechtweg[2] Wilfried Alt[1]
[1] Institute of Sport and Movement Science, University of Stuttgart, Stuttgart, Germany.
[2] Stryker Leibinger GmbH & Co. KG, Freiburg im Breisgau, Germany.
Email: anja.seeger@inspo.uni-stuttgart.de

INTRODUCTION

The orientation of the subtalar axis (STA) might be associated with various overload and injury mechanisms of ankle and knee joints [1]. Methods of axis determination mostly concentrate on a anatomical STA and are often expensive and time-consuming (e.g. imaging methods) and therefore an obstacle to large-scale studies. Antother possibility is the analysis of a ***functional axis*** of eversion and inversion movement (fSTA). Schlechtweg [2] describes an approach to calculate the the deviation and inclination angle of the fSTA using two Intertial Meausurment Units (IMU) and a kinematic model based on Seel and Schauer 2012 [3] in reference to an anatomic coordinate system defined by Manter in 1941 [4]. In this study a measurement procedure was used that only needs a single IMU for estimation of the orientation of a fSTA.

METHODS

The IMU is attached dorsal to the calcaneus, using a fixing clamp with the yaw axis of the IMU (aktos-mini, myon AG, Schwarzenberg, Switzerland) in line with the longitudinal axis of the foot (Figure 1a). To indentify the sensors pitch and roll orientation a static acceleration measurement was conducted while the subjects' foot stood flat on the ground. By calculating the angles between the acceleration vector and the frontal and transverse planes the orientation of the IMU in the anatomical coordinate system could be fully defined. The gyroscope signals from eversion and inversion movement were captured with the foot in max. dorsiflexion to lock the talocrural joint within the mortise. The algorithm calculates the rotation axis of the IMU by using a principal component analysis (PCA) of the gyroscope signals based on the assumption that the IMUs connection to the heel bone is quasi-rigid and on the definition of the fSTA as an finite non helical axis.

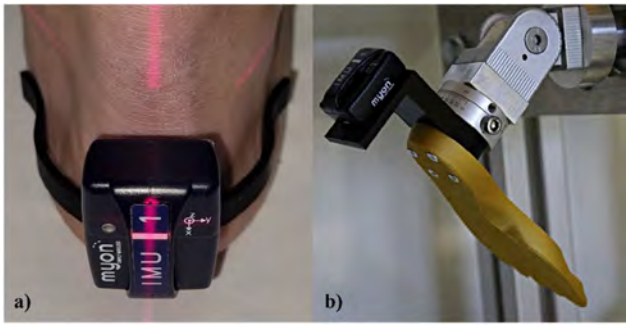

Figure 1: a) Fixing clamp with IMU, b) Testing machine with IMU.

Validity was tested with a mechanical testing machine (Figure 1b), simulating the movement of the subtalar joint for different predefined deviation and inclination angles. The measurement settings included a range from 10° lateral to 40° medial deviation and an inclination range from 15° to 60°. The mean difference between the values pre-set on the testing machine and the measured IMU values and the RSME are shown in Table 1.
In order to test the reliability of the system, the procedure was repeated 10 times with one male subjects right foot. The average of inclination and deviation and the CV (coefficient of variation) are shown in Table 1.

RESULTS AND DISCUSSION

In this study we tested a new method to determine a functional axis of rotation of the subtalar joint. With a CV of 0.07 for the deviation and 0.01 for the inclination angle, the subject measurements show acceptable reliability of the method. The validity of the method has been proved within a mechanical testing machine. The results show a small RSME for the deviation (0.5) as well as for the inclination angle (0.6). Thus the angles calculated by the algorithm describe the orientation of a fSTA.

Table 1: Results for testing machine and subject measurements.

	Testing machine		Subject	
	Difference	RSME	Angles	CV
Deviation °	0.25 ± 0.4	0.5	14 ± 0.1	0.07
Inclination °	0.4 ± 0.6	0.6	39 ± 0.5	0.01

CONCLUSIONS

The algorithm is valid for calculation an axis of rotation between inversion and eversion movements of the foot. This functional axis might be highly determined by the anatomical STA. The position is assumed based on the paper from Piazza et al. [5]. Therefore, this described procedure could be a huge benefit especially for large-scale studies.

REFERENCES

[1] McClay I et al. *Foot Ankle Int* **17**: 499-502, 1996.
[2] Schlechtweg S *Dissertation*, 2020.
[3] Seel T et al. *IEEE MSC*: 0-4, 2012.
[4] Manter J et al. *The Anat. Rec.* **80**: 397-409, 1941.
[5] Piazza S *Foot and Ankle Clinics*, *10*, 425–442, 2005

Acute Effects of High-Definition Transcranial Direct Current Stimulation on Ankle Force Sense and Cortical Activation

Chuyi Zhang[1], Bin Shen[1], Songlin Xiao[1] and Weijie Fu[1,*]

[1] Key Laboratory of Exercise and Health Sciences of Ministry of Education, Shanghai University of Sport, Shanghai, China.

Email: fuweijie315@163.com

INTRODUCTION

Force sense is a conscious proprioception that assesses an individual's ability to detect muscle tension [1]. The ankle is positioned close to the body's base of support, and its force sense plays an important role in maintaining human balance and motor control [2]. Transcranial direct current stimulation (tDCS), a neuro-biomechanical ergogenic technology that can effectively modulate cortical excitability and enhance physical performance, has recently been introduced into the field of sports science [3]. However, little is known regarding the central modulation mechanism of tDCS in terms of foot and ankle sensorimotor function. Therefore, the purpose of this study was to explore the acute effects of high-definition tDCS (HD-tDCS) on the ankle force sense and activation of the sensorimotor cortex in healthy adults, in order to provide new ideas for improving ankle proprioception at the level of the central nervous system.

METHODS

Sixteen healthy adults (8 males and 8 females; age: 25.5 ± 1.8 yrs; height: 170.8 ± 10.9 cm; weight: 63.9 ± 11.9 kg) were recruited. Participants were randomized to receive 2 mA HD-tDCS or sham stimulation over the primary motor cortex (M1) for 20 minutes in two sessions (3-7 days apart). Both before and after the intervention, the plantarflexion force sense of the right ankle was obtained by the Contrex Isokinetic dynamometer, and the activation of the sensorimotor cortex was monitored by the functional near-infrared spectroscopy (fNIRS) in 23 channels during the plantarflexion force control task. A two-way repeated measures ANOVA (tDCS condition × time) was performed on all test variables.

RESULTS AND DISCUSSION

The root mean square error (RMSE) of the ankle force sense test had a main effect of time ($F_{(1,30)} = 5.880$, $p = 0.022$, and $\eta_p^2 = 0.164$, Figure 1). Specifically, RMSE decreased by 19.97% after real stimulation and by 10.23% after sham stimulation. This suggested that HD-tDCS has the potential to enhance ankle force sense, which may contribute to improving ankle stability. The maximum voluntary isometric contraction (MVIC) of ankle plantarflexion had no significant interaction or main effect. The cortical activation of channel 2, which is located in the supplementary motor area, had a significant interaction between tDCS condition and time ($F_{(1,30)} = 9.899$, $p = 0.004$, and $\eta_p^2 = 0.248$, Figure 1). Post-hoc analysis showed that the activation of this channel was significantly greater after real stimulation than before ($p = 0.02$, Cohen's $d = 0.91$), while there was no significant difference in the activation of the channel after sham stimulation. It indicated that the modulation of cortical excitability by HD-tDCS may have an impact on ankle force sense. No significant interaction or main effects were found for other channel activations.

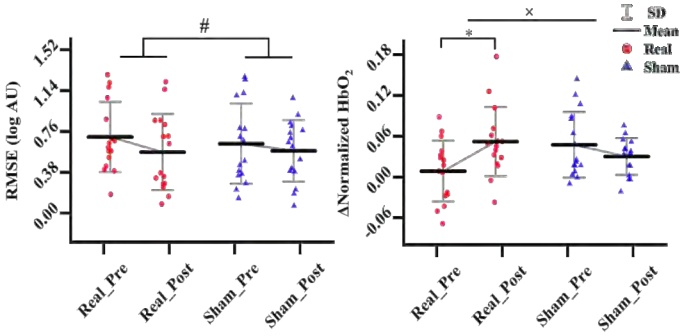

Figure 1 Effects of tDCS on the right ankle force sense and the cortical activation of channel 2.
Notes: # indicates a significant time main effect; × indicates a significant interaction; * indicates a significant difference before and after the intervention.

CONCLUSIONS

This study found that anodal HD-tDCS over M1 can increase the activation of the sensorimotor cortex during the ankle force sense test in healthy adults, suggesting that HD-tDCS is a potential intervention to improve the ankle force sense at the level of the central nervous system.

ACKNOWLEDGEMENTS

This research was funded by the National Natural Science Foundation of China (12272238, 11932013) and the "Outstanding Young Scholar" Program of Shanghai Municipal.

REFERENCES

[1] Smith B et al. *J Athl Train* **47**: 282-288, 2012.
[2] Smajla D et al. *PLoS One* **14**: e0210881, 2019.
[3] Wang B et al. *Front Neurosci* **15**: 648354, 2021.

How do bones of the sub-talar joint complex cope with size?

Paige Treherne[1], Dr Michael Rainbow[2], Dr Luke Kelly[1]
[1]Human Movement and Nutrition Sciences, The University of Queensland, Brisbane, Australia
[2]Department of Engineering, Queen's University, Kingston, Canada
Email: p.treherne@uq.edu.au

INTRODUCTION

Despite the wide variation in the size and shape of humans and their feet, less is known about how our feet change shape with increasing size. This may have important consequences for how we contend with increased body weight associated with size and the large muscular forces that are applied across the joints. The square-cube law states that if a bone grows isometrically, the surface area (SA) will grow at a slower rate than the volume ($SA = volume^{2/3}$). Under isometric scaling conditions, as bone and body mass increase in volume joint contact stress increases more rapidly, since stress = force/SA. Some terrestrial taxa scale allometrically across a range of interspecific sizes - meaning the shape of their skeleton changes as they get larger such that joint contact stress remains relatively constant across a wide range of sizes [1]. Within humans, the calcaneus and talus are the largest bones in the foot and form the sub-talar joint, which experiences high forces during locomotion. This study aimed to determine if the calcaneus, talus and the sub-talar joint surface areas (JSA) scale isometrically or allometrically across individuals.

METHODS

3D bone models of the talus and calcaneus were generated from computed tomography scans of the right foot in 36 individuals (mass: 73.4 ± 13.9 kg; height: 171.2 ± 8.1 cm; 21M, 15F) using Mimics. Calcaneus and talus bone models were centred then aligned using their inertial coordinate systems and an iterative closest point approach. Correspondence was obtained using a non-rigid coherent point drift (CPD) algorithm to a reference bone. The bones were scaled with a Procrustes analysis, and final correspondence was found using non-rigid CPD to the mean bone of the sample. For sub-talar joint complex analysis (calcaneus and talus combined) the bones were aligned to their respective inertial coordinate systems. Two different analyses were completed: principal component (PC) analysis of the individual bones and PC analysis of the sub-talar joint complex. Each principal component is a quantitative measure of shape variation, with each individual bone, or joint in the sample given a PC score (dependent on individual bone or joint complex PC analysis). To evaluate allometry, log-log plots were calculated for the bone volume and surface area of the talus and calcaneus, and surface area of their articular surfaces (Figure 1, A and B). A slope of 0.67 means the surface scales isometrically, with values either side of this termed allometry. To determine the relationship between size and shape, the PC scores for each mode of variation at a bone level were plotted against bone volume, and at a joint level against the combined bone volume.

RESULTS AND DISCUSSION

The calcaneus scales with negative allometry (slope = 0.62) meaning the surface area grows even slower than would be expected for isometric scaling. Similarly, the calcaneus' anterior medial facet scales with negative allometry (slope = 0.65), while the posterior facet scales with strong positive allometry (slope = 0.72) where the surface area grows faster than the isometric function. The talus scales isometrically (slope = 0.67). The talar dome and sub-talar surface scales with positive allometry (slope = 0.71 and 0.71). The first PC of calcaneus shape variation (15.6% of variation, $p<0.05$) was associated with bone volume. Here, the tuberosity becomes larger, the cuboid facet gets longer, and the bone grows taller relative to its length as the bone gets larger (Figure 1 C, top). No PCs of the talus showed any relationship with size. At a joint complex level, the second mode of variation (12.5% of variation, $p<0.05$) was linked to total bone volume. The calcaneus showed similar shape variations as the single bone analysis (larger tuberosity, longer cuboid facet, taller). On the talus, the talar head widened and the posterior process shortened as the sub-talar joint complex volume increased (Figure 1 C, bottom).

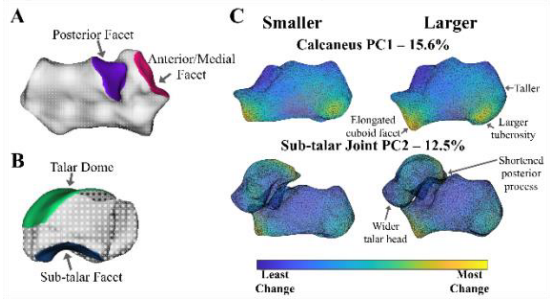

Figure 1 (A) Joint surface areas (JSA) on the right calcaneus. **(B)** JSAs on the right talus. **(C)** Anatomical shape variations at ±2SD from mean shape of calcaneus PC1 and sub-talar joint PC2 modes of variation. Heatmap shows where the most change is occurring.

CONCLUSIONS

We have shown the presence of distinct patterns of shape and scaling variance in the two largest bones of the foot. Interestingly, at a bone level the calcaneus scales allometrically and appears to become more robust (cube-like) as it gets larger. Additionally, the joint surfaces areas on both bones (except for the anterior/medial facet on the calcaneus) scale with positive allometry, potentially assisting with offsetting joint contact stresses as humans become larger. Whether these changes are present at birth or are the result of plasticity is an open question. Further analysis is required to determine if these scaling and shape variances are related to function.

REFERENCES

[1]Dick & Clemente, *PLoS Biol.* **15**(1): 2000473, 2017

The mechanism of leg stiffness adjustment during hopping with different hop frequencies

Kazuki Kuriyama[1], Daisuke Takeshita[1]
[1] Department of Life Sciences, The University of Tokyo, Tokyo, Japan
Email: k-kuriyama@g.ecc.u-tokyo.ac.jp

INTRODUCTION

The spring-like property of muscle-tendon complexes (MTC) plays an important role in movements with stretch-shortening cycle. A simple spring-mass model can express the characteristics of hopping and running [1]. In this model, the leg stiffness can be determined by the center of mass (CoM) movement and ground reaction force. Nagano et al. determined the leg stiffness for hopping with different hop frequencies based on the spring-mass model [2]. They found that the leg stiffness is higher for a higher hop frequency and speculated that the leg stiffness was adjusted by the contraction of triceps surae muscle fibers. However, the details of the mechanism for the adjustment of leg stiffness remain ambiguous. Therefore, we aimed to clarify the mechanism of the leg stiffness adjustment during hopping with different hop frequencies, from the viewpoint of the behavior of triceps surae MTC.

METHODS

Nine healthy adult men who exercise regularly participated as subjects. They conducted hopping at seven different frequencies (from 2.0 Hz to 3.5 Hz) controlled by a metronome. They were instructed to place their hands on the opposite shoulders and keep their knees as extended as possible. The coordinates of anatomical landmarks of the whole body were recorded with a motion capture system. The ground reaction force was recorded with force plates embedded in the ground. In addition, longitudinal images of the medial gastrocnemius muscle (MG) of the right leg were obtained by a real-time B-mode ultrasound apparatus. The MTC length of MG was calculated from the ankle and knee joint angles [3]. The fascicle length of MG was determined by manually digitizing the ultrasound images. The leg stiffness (k_{leg}) was determined by the vertical displacement of the CoM of the subject and the ground reaction force. The stiffness of MTC (k_{MTC}) was determined by the MTC length change and the load on the Achilles tendon, which was calculated from the ankle joint torque and the moment arm of the Achilles tendon.

RESULTS AND DISCUSSION

k_{leg} increased with increasing hop frequencies. This result is consistent with the previous study [2]. k_{MTC} also increased with increasing hop frequencies, and there was a strong correlation (r=0.88, p<0.001) between these two stiffness values. At hop frequencies used in the present study, ankle joint stiffness is the major determinant of k_{leg} rather than knee or hip [4]. Therefore, k_{MTC} appeared to mainly determine k_{leg}.

While the MTC length change showed similar patterns for all the hop frequencies, the fascicle length change showed different patterns for different hop frequencies (Figure 1). The fascicle almost kept its length at low hop frequencies. On the other hand, the fascicle shortened throughout the entire ground contact phase at high hop frequencies.

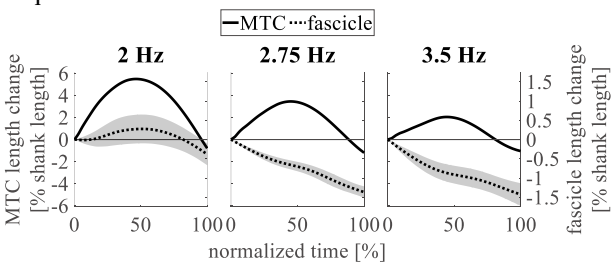

Figure 1: the length changes of the MTC and the fascicle of MG during the ground contact phase

To understand how the length change of the MG fascicle affected k_{MTC}, a simulation with a model consisting of contractile component (CC) and series elastic component (SEC) was performed. The result showed that the shortening and lengthening of CC increases and decreases k_{MTC}, respectively. This can be interpreted from the viewpoint of the equivalent spring of CC and SEC connected in series. Using the stiffness of CC (k_{CC}) and that of SEC (k_{SEC}), k_{MTC} can be determined based on the formula for two springs in series:

$$1/k_{MTC} = 1/k_{CC} + 1/k_{SEC}.$$

When CC lengthens under increasing load, CC is considered to have positive stiffness, making k_{MTC} smaller than k_{SEC}. In contrast, when CC shortens against load, CC is considered to have "negative stiffness", making k_{MTC} larger than k_{SEC}. MG fascicle shortening appeared to contribute to the large leg stiffness, which is required to realize high hop frequencies, by increasing k_{MTC}.

CONCLUSIONS

Large k_{leg} at a high hop frequency was associated with large k_{MTC}. The large k_{MTC} was presumably caused by the MG fascicle shortening during the ground contact phase. The fascicle shortening can be interpreted as negative stiffness, increasing k_{MTC}. It was suggested that humans can adjust their leg stiffness to realize a certain hop frequency during hopping, by changing the dynamics of triceps surae muscle fibers.

REFERENCES

[1] Blickhan R, *J Biomech*, **22**: 11-12, 1989
[2] Nagano A et al., *Japan J Phys Educ Hlth Sport Sci*, **46**, 2001
[3] Hawkins D et al., *J Biomech*, **23**: 5, 1990
[4] Hobara H et al., *Eur J Appl Phisiol*, **111**: 9, 2011

EFFECTS OF COMPRESSION GARMENTS ON LOWER LIMB BIOMECHANICS DURING RUNNING UNDER FATIGUE

Jichao Wang, Yang Yang, Yongxin Xu, Weijie Fu*
Key Laboratory of Exercise and Health Sciences of Ministry of Education, Shanghai University of Sport, Shanghai 200438, China
Email: fuweijie@sus.edu.cn

INTRODUCTION

Compression garments are widely used in sports, and it has a certain promotion effect on athletes' abilities such as endurance, strength, speed and fatigue recovery. Exercise fatigue increases the risk of injury and is one of the applications for compression garments. Earlier research found that the efficacy of compression garments could be more effectively tested through fatigue intervention. This study aimed to investigate the role of compression garments in running and to provide a theoretical basis for improving performance.

METHODS

Twelve healthy male subjects (age: 23.3±2.1, height: 177.2±6.6, weight: 73.3±5.7) were randomly selected to wear compression garments and control shorts for two running fatigue sessions. Each test was conducted before and after the fatigue induction program, and data were collected for 15 s after the subjects' movements were stabilized. The kinematic and kinetic data of the hip, knee and ankle joints during exercise were collected synchronously using a Vicon motion capture system and a Bertec three-dimensional treadmill. One-way ANOVA was used to analyze joint angle, moment, vertical work and other parameters.

RESULTS AND DISCUSSION

After fatigue, during the stance phase, the maximum flexion angle of the knee was significantly increased (p=0.029), the minimum flexion angle of the knee (p=0.013) and the maximum flexion angle of the hip (p<0.001) was significantly decreased in the compression garments condition. The peak value of the pedal-extension moment of the knee was significantly increased (p=0.035) in the compression garments condition (Table 1); in addition, after fatigue, the subjects had greater vertical work (p=0.016) in the compression garments condition. Compression garments can significantly increase the peak moment of the knee (Figure 1), Duffield et al. [1] showed that there was no change in peak contraction force or force production rate in fatigued muscles when wearing compression garments, thus compression garments do not directly increase muscle power, but rather improve mechanical efficiency. Therefore, we believe that the increased moment of the knee in this study may be an increase in the overall mechanical efficiency of the muscle movement. Therefore, we believe that compression garments can have some anti-fatigue effects through their mechanical advantages.

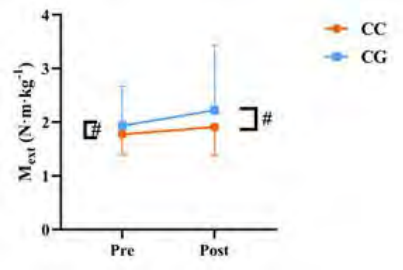

Figure 1 Pedal-extension moment of the knee joint.

CONCLUSIONS

When wearing compression garments, knee and hip flexion angles decreased, knee moments increased, and lower limb work capacity improved. These changes are the opposite of the effects caused by exercise fatigue, thus suggesting that compression garments may help to delay fatigue, and improve muscle control.

ACKNOWLEDGEMENTS

This study was supported by NNSFC (12272238) and the "Dawn" Program of Shanghai Education Commission (19SG47).

REFERENCES

[1] Duffield R et al. Journal of ence & Medicine in Sport **13(1)**: 136-140, 2010.

Table 1: Kinematic and kinetic data of the lower limbs. (M_{ext}: peak value of the pedal-extension moment.)

		Control Condition		Compression Garments		
Joint		Pre	Post	Pre	Post	*p-value*
Knee	M_{ext} (N·m·kg^{-1})	1.77±0.38*	1.91±0.53	1.93±0.74	2.22±1.20	p = 0.035
	θ_{min} (deg)	-13.59±4.52*	-14.96±5.32	-10.70±4.98	-11.97±3.56	p = 0.029
	θ_{max} (deg)	-39.06±4.22*	-42.19±3.82	-37.64±3.68	-39.33±3.76	p = 0.013
Hip	θ_{max} (deg)	41.26±9.24*	39.07±13.25	35.32±4.74	37.65±5.45	p < 0.001
Leg	W (J/kg)	0.20±0.07*	0.10±0.05	0.21±0.08	0.14±0.04	p = 0.016

Effects of HD-tDCS on the Changes of EEG-sEMG Coherence after Running-Induced Fatigue

Jianglong Zhan[1], Changxiao Yu[1], Weijie Fu[1]
[1] School of Exercise and Health, Shanghai University of Sport, Shanghai, China.
Email: fuweijie@sus.edu.cn

INTRODUCTION

High-definition transcranial direct current stimulation (HD-tDCS) can cause changes in the local excitability of cerebral cortex and has been used to explore the effect on fatigue. However, most studies evaluating the effects of HD-tDCS have focused on changes in extrinsic exercise performance (e.g., exercise duration, muscle strength)[1,2], while ignoring to some extent the intrinsic connection between the central nervous system and peripheral muscles. The purpose of this study was to investigate the effect of HD-tDCS on corticalmuscular coherence (CMC) between central electroencephalography (EEG) signals and peripheral muscle surface electromyography (sEMG) signals in beta (16-30 Hz) and gamma (31-50 Hz) bands after running-induced fatigue.

METHODS

A total of 24 healthy male college students were enrolled in this study. Subjects were randomly assigned to real and sham HD-tDCS groups and received real (2 mA stimulation for 20 minutes on M1) and sham stimulation (30 seconds of active stimulation only at the beginning) for five consecutive days, respectively. After the subjects wore EEG caps and wireless sEMG electrodes and warmed up sufficiently, the running-induced fatigue test was performed. Immediately after the fatigue test, continuous maximum force is performed in an ankle plantar flexion-dorsiflexion exercise (this process simultaneously acquires EEG signals and sEMG signals). After the first trial, HD-tDCS intervention was performed. On the first day after the end of the intervention, a second trial was conducted: the procedure and duration of the run were the same as above.

EEG data selection: Based on previous related study[3], 5 regions of interest (FC1, FCz, C1, Cz, CP1) related to lower limb movement were selected in this study.

sEMG data selection: The tibial anterior muscle (TA), lateral head of gastrocnemius (LG), medial head of gastrocnemius (MG), and soleus muscle (SOL) of the subject's right lower limb were selected as test muscles. A two-way ANOVA (Stimulus condition×Time) was performed on all tested variables (21.0, SPSS Inc., USA).

RESULTS AND DISCUSSION

In the beta band: After the intervention of the real stimulation group, the coherence coefficients between EEG of C1 Cz and TA were increased significantly during the ankle joint dorsiflexion phase as compared to the sham group (Table 1).

In the gamma band: After the intervention of the real stimulation group, the coherence coefficients between EEG of C1 CP1 Cz FC1 and TA were increased significantly during the ankle joint dorsiflexion phase as compared to the sham group (Table 1).

CONCLUSIONS

HD-tDCS can increase the synchronization of bio-electric activity between peripheral muscles and contralateral motor cortex in beta and gamma bands after running-induced fatigue, and the central nervous system regulated motor cortex and peripheral muscle activity, resulting in increased coupling between contralateral motor cortex and peripheral muscle activity.

ACKNOWLEDGEMENTS

This research was funded by the National Natural Science Foundation of China (12272238, 11932013) and the “Outstanding Young Scholar” Program of Shanghai Municipal.

REFERENCES

[1] Hazime F A et al. J Sports Phys Ther **12**: 402, 2017.
[2] Wachter D et al. Exp Neurol **227**: 322, 2011.
[3] Jacobs J V et al. Neuron **298**: 1-11, 2015.

Table 1: The coherence coefficients under different stimulus conditions

	Beta-TA					Gamma-TA				
	Real		Sham			Real		Sham		
ROIs	Pre	Post	Pre	Post	*P* value	Pre	Post	Pre	Post	*P* value
C1	0.199 ± 0.023	0.225 ± 0.033*	0.235 ± 0.037	0.217 ± 0.037	0.042	0.198 ± 0.026	0.226 ± 0.038*	0.233 ± 0.038	0.209 ± 0.036	0.028
CP1	0.204 ± 0.023	0.217 ± 0.031	0.231 ± 0.035	0.208 ± 0.041	0.101	0.199 ± 0.018	0.224 ± 0.029*	0.231 ± 0.038	0.210 ± 0.040	0.028
Cz	0.201 ± 0.031	0.233 ± 0.037*	0.237 ± 0.037	0.215 ± 0.038	0.024	0.200 ± 0.024	0.226 ± 0.030*	0.230 ± 0.037	0.210 ± 0.035	0.036
FC1	0.207 ± 0.025	0.223 ± 0.034	0.229 ± 0.036	0.215 ± 0.040	0.165	0.203 ± 0.024	0.227 ± 0.031*	0.232 ± 0.036	0.209 ± 0.034	0.045
FCz	0.206 ± 0.026	0.223 ± 0.033	0.233 ± 0.041	0.212 ± 0.040	0.097	0.204 ± 0.026	0.219 ± 0.032	0.235 ± 0.038	0.210 ± 0.039	0.098

*: $P<0.05$; *P* value: Interaction effect *P* value

Tibial-tuberosity trochlear-groove distance in healthy subjects and patients with patellofemoral pain syndrome: a weight-bearing 4DCT study

L. Buzzatti[1,3], B. Keelson[1,2], T. Scheerlinck[2], S. Héréus[1], G. Van Gompel[2], T. Verstraten[1,4], J. Vandemeulebroucke[1], J. De Mey[2], N. Buls[2], E. Cattrysse[1]
[1]Vrije Universiteit Brussel (VUB), Brussels, Belgium. [2] Universitair Ziekenhuis Brussel (UZ Brussel), Brussels, Belgium. [3]School of Allied Health, Anglia Ruskin University (ARU), Cambridge, UK. [4]Flanders Make, Brussels, Belgium.
Email: Luca.Buzzatti@vub.be

INTRODUCTION

In medical imaging, weight-bearing dynamic analysis could provide more valuable information on the kinematics of the lower limb than unloaded static images. Dynamic CT (4DCT) is an image acquisition method that allows capturing motion with good temporal resolution and excellent morphological details. However, the performed movements have always been investigated in non-weight-bearing conditions due to the supine position required by the CT scanner design. TTTG is an orthopaedic metric that is used to estimate whether there is an indication for surgical correction (i.e. distal realignment procedures). This study aims to provide reference data on normal tibial tuberosity-trochlear groove distance (TTTG) values observed in healthy subjects during weight-bearing dynamic CT acquisition. In addition, we compared data from patients with patellofemoral pain syndrome (PFPS) to their contralateral asymptomatic side and the reference values of healthy subjects.

METHODS

21 healthy adults and 3 patients with PFPS volunteered for this study. The study was approved by the local Ethics Committee. In order to simulate constant gravitational force during horizontal dynamic CT acquisition, a novel weight-bearing device compatible with a 256-slice wide beam CT was used. The device had a platform to position the feet, a moving component to support the subject, and a loading system that provides constant resistance. Each subject performed consecutive cycles from full knee extension to flexion and back to full extension. A dynamic CT scan protocol (16x50cm FOV, 80kvp, 50mA, 6.7s) was used to acquire images of both knees at the same time, while the subject was performing the task. Using automatic multi-atlas segmentation and rigid registration, a transformation matrix was computed for each time point representing the movement of each bone (Tibia, Femur). TTTG was calculated, and its change during 0° and 30° of knee flexion was evaluated. TTTG values of the PFPS knees were compared to their contralateral asymptomatic side and healthy subjects.

RESULTS AND DISCUSSION

Going from full extension to 30° of knee flexion, the TTTG decreased gradually by 6.8 mm from 12.2 mm of full extension in healthy subjects (Figure 1a). A similar decreasing pattern was seen in patients. However, the symptomatic side (S-red) presented higher values than both the asymptomatic side (AS-blue) and knees of healthy controls (green). TTTG of the asymptomatic side aligned with the values from the healthy control group after the first 10-15 degrees of flexion (Figure 1b).

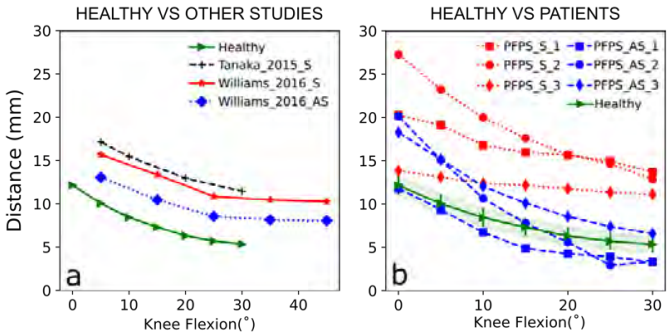

Figure 1 a: TTTG comparison between healthy subjects and published studies [1,2] on patients with patella dislocation; b: TTTG comparison between healthy subjects and patients with PFPS; S: symptomatic; AS: asymptomatic

Overall, TTTG distances in healthy subjects were lower compared to those measured in other studies [1,2] on symptomatic knees but these studies did not have a weight-bearing condition and included patients with patella dislocation (Figure 1a).

CONCLUSIONS

Our study shows the possibility to describe orthopaedic metrics, such as TTTG, in a dynamic weight-bearing mode in healthy subjects and patients using dynamic CT images.
Compared to both healthy subjects and the contralateral asymptomatic side, patients suffering from PFPS show more lateralized tibial tuberosity in the first 30° of knee flexion during a weight-bearing dynamic flexion-extension movement. This was observed during the whole motion trajectory.
The results from healthy participants can be used as preliminary normative values when comparing patients suffering from patella motion related conditions.

REFERENCES

[1] Tanaka MJ et al. (2015). *Arthroscopy*, **31**(9):1748-55.
[2] Williams AA et al. (2016). *Arthroscopy*, **32**(1):55-61

CONCURRENT VALIDITY AND RELIABILITY OF A MOBILE iOS APPLICATION USED TO ASSESS CALF RAISE TEST KINEMATICS

Ma. Roxanne Fernandez[1,2*], Josie Athens, PhD[3], Carlos Balsalobre-Fernandez, PhD, CSCS-D[4], Masayoshi Kubo, RPT, ScD[5] and Kim Hébert-Losier, PT, PhD[1]

[1]Division of Health, Engineering, Computing and Science, Te Huataki Waiora School of Health, University of Waikato, New Zealand. [2]Department of Physical Therapy, College of Rehabilitation Sciences, University of Santo Tomas, Philippines / [3]Department of Preventive and Social Medicine, University of Otago, PO Box 56, Dunedin 9054, New Zealand./ [4]Applied Biomechanics and Sport Technology Research Group, Universidad Autónoma de Madrid, Spain/ [5]Department of Physical Therapy, Niigata University of Health and Welfare, Japan.
*Email: mf182@students.waikato.ac.nz

INTRODUCTION

The calf raise test (CRT) is used in rehabilitation and sports medicine to evaluate calf muscle function [1]. The novel Calf Raise application (CR_{app}) for iOS uses computer-vision algorithms to objectively measure CRT outcomes (i.e., repetitions, positive work, total height, peak height, fatigue index, and peak power) and replicate laboratory-based metrics that are difficult to measure clinically [2]. We aimed to validate the CR_{app} by examining its concurrent validity and agreement levels against laboratory-based equipment. We also assessed its intra-rater and inter-rater reliability.

METHODS

CRT outcomes (i.e., repetitions, positive work, total height, peak height, fatigue index, and peak power) were assessed in thirteen individuals (6 males,7 females) on three occasions on both legs using the CR_{app}, 3D motion capture, and force plate simultaneously. Data were extracted from two markers: below the w lateral malleolus (n=77) and on the heel (n=77). Concurrent validity and agreement were determined from 154 data files using intraclass correlation coefficients ($ICC_{3,k}$), typical errors expressed as coefficient variations (CV), and Bland-Altman plots to assess biases and precision. Reliability was assessed using $ICC_{3,1}$ and CV values. (See Figure 1 for the test experiment set-up).

Figure 1 Marker placement below the lateral malleolus (left image) and on the heel (middle image). The back round sticker of 24 mm in diameter and retroreflective marker of 12.5 mm in diameter enabled tracking within the Calf Raise application and Qualisys SD motion capture system, respectively. The placement of two-iPad devices positioned 30 cm from the markers is also shown (right image).

RESULTS AND DISCUSSION

The validity of CR_{app} outcomes was good to excellent across measures for both markers (mean ICC ≥0.878), with precision plots showing good agreement and precision. CV ranged from 0% (repetitions) to 33.3% (fatigue index) and were on average better for the lateral malleolus marker. Inter and intra-rater reliability were excellent (ICC≥0.949, CV≤5.6%). Due to the lack of tools to objectively quantify CRT performance, repetition is the primary outcome used in clinics. Lab-based equipment is not suitable for clinical use due to its expensive price, time commitment, expertise requirements, and portability. Furthermore, studies suggest that measuring calf raise height and total work alongside the repetitions are crucial in measuring plantar flexion endurance using CRT in both healthy and clinical populations [3, 4].

CONCLUSIONS

CR_{app} is valid and reliable within and between users for measuring CRT outcomes in research and practice, aligning with recent advances in mobile technologies and their increased use in healthcare.

REFERENCES

[1] Hébert-Losier, K, et al., Raising the standards of the calf raise test: A systematic review. J Sci Med Sport 2009; 12(6): 594-602. https://doi.org/10.1016/j.jsams.2008.12.628

[2] Hébert-Losier, K and C Balsalobre-Fernández, Calf raise mobile application software. 2020.

[3] Silbernagel, KG, et al., A new measurement of heel-rise endurance with the ability to detect functional deficits in patients with Achilles tendon rupture. Knee Surg Sports Traumatol Arthrosc 2010; 18(2): 258-264.

[4] Byrne, C, et al., Intrarater reliability and agreement of linear encoder derived heel-rise endurance test outcomes measures in healthy adults. J Electromyogr Kinesiol 2017; 36: 34-39. https://doi.org/10.1016/j.jelekin.2017.07.004.

EFFECTS OF TASK DIFFICULTIES ON FIRST-GRADE CHILDREN'S HANDWRITING PERFORMANCE IN COPY ACTIVITIES

Yu-An Tsai[1], Pin-Chen Hung[1], Po-Ya Chuang[1], Wen-Feng Huang[1], Tien-Ni Wang[1] and Hao-Ling Chen[1]
[1] Department of Occupational Therapy, National Taiwan University, Taipei, Taiwan.
Email: r11429010@ntu.edu.tw

INTRODUCTION

Handwriting is a fundamental academic skill for children. In general, children start learning handwriting skills in the first grade by copying characters. The structure of Chinese characters is varied, some of them with complicated geometric features and strokes [1], which causes different difficulty levels in copying, and may affect handwriting performance. A previous study suggested that the number of strokes may affect handwriting fluency in first-grade children [2], however, the effects on handwriting legibility remained unclear. In addition, the materials used in the study were alphabetic letters. Given the uniqueness of spatial arrangement in Chinese characters, the generalizability of the above result was constrained. Hence, this study aims to investigate the influence of copy task complexity on handwriting performance in first-grade children using Chinese characters.

METHODS

17 typically developing children in first grade were recruited in the study. Subjects were required to complete 2 copy tasks on a Wacom tablet: (1) easy task characterized by fewer strokes; (2) difficult task characterized by more strokes. All tasks used high-frequency Chinese characters selected from the mainstream textbooks in Taiwan. In addition, the kinetic and kinematic data would be collected by the tablet to record the writing process. A computerized program was implied to evaluate the legibility of writing products in 4 aspects: Size, Position, Orientation, and Deformation [3]. The larger value of each aspect indicated poor legibility. Pair t-test was examined for the differences between two copy tasks from the same subjects.

RESULTS AND DISCUSSIONS

All the kinematic and kinetic variables demonstrated significant differences (Table.1). Subjects showed greater tip force and writing speed, along with less length and time ratio (in-air/ on-paper) in the easy task, representing higher efficiency. In addition, less coefficient of variation (CV) of tip force and stroke velocity was found in the easy task, representing higher consistency and fluency. Regarding legibility, significant differences were only found in orientation and deformation (Table.1). The results suggested orientation and deformation were the main reasons caused the decline of legibility in the difficult task, not size or position.

CONCLUSIONS

The present study suggests the number of strokes is one of the critical reasons affecting the handwriting performance (especially in orientation and deformation aspects) of first-grade children. The findings may support clinicians and educators to modify the content of handwriting tasks and develop intervention principles.

REFERENCES

[1]Yeh et al. *J Exp Psychol Hum Percept Perform* **28**, 933–947, 2002
[2]Thibon et al. *Acta Psychol* **182**, 200–211, 2018
[3]Huang et al. *Journal of Taiwan Occupational Therapy Association* **38**, 36-55, 2020

Table 1: Pair t-test of Kinetics, Kinematics, and Legibility results between Difficult and Easy copy tasks

	Difficult task	Easy task			Difficult task	Easy task	
Kinetics	Mean (SD)	Mean (SD)	*p*	***Kinematics***	Mean (SD)	Mean (SD)	*p*
Max TF	.57 (.13)	.71 (.14)	.00**	Length ratio	1.04 (0.23)	.55 (.09)	.00**
Mean TF	.44 (.10)	.57 (.13)	.00**	Time ratio	.49 (.06)	.29 (.05)	.00**
CV of TF	.32 (.02)	.30 (.03)	.00**	Mean SV	99.12 (30.05)	117.36 (33.90)	.00**
Legibility	Mean (SD)	Mean (SD)	*p*	CV of SV	.34 (.04)	.25 (.05)	.00**
Size	.73 (.09)	.71 (.08)	.42	Mean character time	7.09 (1.82)	2.57 (.76)	.00**
Orientation	-1.14 (1.30)	.26 (2.24)	.05*				
Position	23.06 (5.52)	22.51 (6.50)	.72				
Deformation	6.12 (.58)	5.42 (1.29)	.02*				

TF: tip force; CV: coefficient of variation; SV: stroke velocity; * Significant at the 0.05 alpha level; ** Significant at the 0.01 alpha level

INVESTIGATION OF THE ACTIVATION IN UPPER LIMB MUSCLES WHILE USING AUGMENTED REALITY MIRROR THERAPY

Tsai-Yu Chen[1], Che-Wei Lin[2], Yu-Chen Lin[3], Chieh-Hsiang Hsu[1], Hsiu-Yun Hsu[4] and Li-Chieh Kuo [1,2]

[1] Department of Occupational Therapy, College of Medicine, National Cheng Kung University, Tainan, Taiwan.
[2]Department of Biomedical Engineering, College of Engineering, National Cheng Kung University, Tainan, Taiwan.
[3]Department of Occupational Therapy, College of Nursing and Health Sciences, Dayeh University, Changhua, Taiwan.
[4]Department of Physical Medicine and Rehabilitation, National Cheng Kung University Hospital, College of Medicine, National Cheng Kung University, Tainan, Taiwan.
Email: jkkuo@mail.ncku.edu.tw

INTRODUCTION

Mirror neurons (MN) are activated in action observation and execution, which are involved in motor learning [1]. Mirror therapy (MT) is one typical strategy for dealing with upper limb motor impairment in stroke rehabilitation. Patients perform simple tasks with the unaffected arm, and the mirror reflects movements like the affected arm. When they focus on mirror reflection, MN activities are observed to facilitate neuroplasticity in the brain [2]. In this study, we instructed healthy adults to execute three tasks via augmented reality mirror therapy (ARMT). Simultaneously, surface electromyographic signals (sEMG) were recorded from the abductor pollicis brevis (APB), extensor digitorum communis (EDC) and flexor digitorum superficialis (FDS) in the upper extremities. The study aims to investigate muscle activities in the non-dominant hand, which keeps static during the ARMT. We hypothesize that muscle activation in the non-dominant hand will be detected during tasks.

METHODS

We developed a mobile application which is deployable on iOS operating systems. Subjects were asked to sit in front of a table with a virtual reality headset (https://apps.apple.com/tw/app/armt/id1637540862). The software captured image data and mirrored these movements when they performed tasks with the dominant hand. Thus, bilateral hand movements would be shown through the ARMT headset to the real world. Because we recorded muscle activities in healthy subjects to examine whether MN was activated during ARMT, we considered the non-dominant hand to be affected [3,4]. We used Trigno Wireless EMG System, (Delsys Inc., Natick, USA), EMGworks® Analysis 4.7.3.0 (Delsys Inc.), and MATLAB® (The MathWorks, Natick, Massachusetts, USA) to collect then analyze muscle activation in APB, EDC and FDS in both hands during the ARMT. There were three tasks in the study. Task 1: Sequential finger touching. Task 2: Wrist extension. Task 3: Wrist flexion. APB was detected in task 1. Both EDC and FDS were detected in task 2 and task 3. During ARMT, subjects followed instructions to do tasks 30 times respectively with their dominant hand and kept their non-dominant hand static. The descriptive analysis would be used to inspect the muscle activation in the non-dominant hand during ARMT in different tasks.

RESULTS AND DISCUSSION

We recruited five healthy adults for this study by convenience sampling. The participants (3 females and two males) ranged from 22 to 25 years old (mean age of 23.8 years; 0.98 standard deviations). All of them were right-handed. From the results, the muscle activation in EDC of the non-dominant hand (Figure 1) in task 2 in subject No.4 was activated remarkably. The other trials could not find similar muscle activities. There were two possible explanations: (1) The motor control ability of subject No.4 was worse than other subjects, so muscle activation in the non-dominant hand was not inhibited completely only in task 2; and (2) MN were activated successfully during task 2.

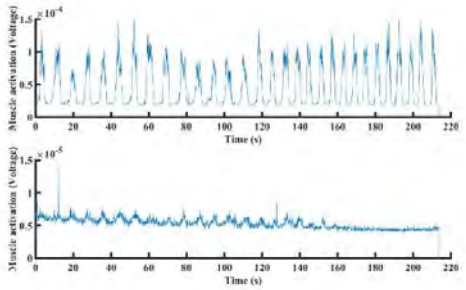

Figure 1 Muscle activation in EDC of task 2 in subject No.4 (Upper: Dominant hand; lower: Non-dominant hand).

CONCLUSIONS

This study provides preliminary outcomes about MN activities via sEMG. Additional research is needed to support the MN activation during ARMT. Future work should recruit a larger sample of subjects and collect brain activity during ARMT to clarify the MN activation in the brain and muscles.

REFERENCES

[1] Gatti R et al. *Brain Imaging Behav* **11**(2): 565-576, 2017.
[2] Nogueira N et al. *Brain Res Bull* **177**: 217-238, 2021.
[3] Stewart J.C et al. *Exp Brain Res* **232**: 2407-19, 2014.
[4] Schaefer S.Y. et al. *Neuropsychologia* **47**(13): 2953-66, 2009

Effectiveness of the Low-Dose Camp-Based Bilateral Intensive Training on Motor Function in Children with Unilateral Cerebral Palsy

Zhi-Chi Weng[1], Kai-Jie Liang[1], Jia-Le Pong[1], Hao-Ling Chen[1,2] and Tien-Ni Wang [1,2]
[1] Department of Occupational Therapy, National Taiwan University, Taipei, Taiwan.
[2] Department of Physical Medicine and Rehabilitation, National Taiwan University Hospital, Taipei, Taiwan.
Email: r11429001@ntu.edu.tw

INTRODUCTION

Upper limb dysfunction is a typical impairment in children with unilateral cerebral palsy (UCP), which causes difficulties in their daily lives. To deal with these deficits, bilateral intensive training (BIT), one of the most promising evidence-based neurorehabilitation programs, has been frequently applicated to children with UCP. This approach is based on the neuroplasticity and motor learning theories that emphasizing on the use of bimanual hands in daily participation. BIT was reported to be benefited for children's motor function in affected hand, and further transfer these motor skills to daily activities [1]. Owing to the repetitive practice, the intensive protocol often challenges the participants' motivation [2]. Thus, a child-friendly and group-formed camp, with relatively low dosage as 36 intervention hours within one week, was proposed to fit their busy schedules. The aim of this study is to estimate the efficacy of the low-dose camp-based BIT for UCP children on the motor function including upper limb movements of the affected hand and the performance of daily bimanual activities.

METHODS

Sixteen children with UCP were recruited. Participants received the BIT intervention program for 36 hours during a one-week summer camp. Outcome measures included the Melbourne Assessment-2 (MA-2), the ABILHAND-Kids, and the Observation Test of Capacity, Performance, and Developmental Disregard Questionnaire (OTCPDDQ), which were conducted at pre-intervention and post-intervention. The MA-2 was used to examine movement quality of unilateral upper limb including 4 subtests: active range of motion (AROM), accuracy, dexterity, and fluency. Moreover, the ABILHAND-Kids and the OTCPDDQ were used to represent a child's daily bimanual motor performance. Paired t-test was used to examine the difference between pre- and post-intervention.

RESULTS AND DISCUSSION

Table 1 reveals the scores of each outcome measure. The upper limb movements measured by the MA-2 showed significant improvement in AROM (t=3.873, p=0.002), dexterity (t=2.711, p=0.016), and fluency (t=4.069, p=0.001) after the intervention, while accuracy (t=-1.472, p=0.162) was no evidence for increase. Regarding bimanual performance, there was a significant increase in the quality of OTCPDDQ (t=3.419, p=0.004), but not in the frequency of OTCPDDQ (t=1.602, p=0.130) or ABILHAND-Kids (t=1.7466, p=0.101). Additionally, the effect size of this intervention (d=0.11-0.46, small to moderate effect) was lower than a previous program (η^2=0.21-0.58, large effect), which was a 60-hours BIT treatment for the hand function of UCP children [3]. The results demonstrated that the intesive intervention with the total of 36 hours, which was near half of 60 hours, could obtain small to moderate effectiveness.

CONCLUSIONS

This study indicates that the camp-based BIT intervention with low dosage has the potential to be a feasible and effective approach for children with UCP. It benefits the affected hand function and the quality of daily bimanual motor performance. Future research for different measurement domains, such as kinematic or psychosocial outcomes, is recommended to vairified our study findings.

REFERENCES

[1] Facchin P et al. *J Phys Med Rehabil*. **90(7)**:539-553, 2011.
[2] Chen YL et al. *J Physical & Occupational Therapy in Pediatrics*. **39(2)**: 139-150, 2019.
[3] Gordon AM et al. *J Dev Med Child Neurol.* **49(11)**:830-838, 2007.

Table 1: Results of MA-2, ABILHAND-Kids, and OTCPDDQ.

	MA-2				ABILHAND-	OTCPDDQ	
	AROM	accuracy	dexterity	fluency	Kids	quality	frequency
pre- (mean±SD)	78.9 ± 18.6	91.8 ± 17.0	57.6 ± 17.8	61.0 ± 16.3	31.6 ± 3.8	29.3 ± 7.5	30.1 ± 8.7
post- (mean±SD)	83.6 ± 16.0	85.0 ± 12.2	61.2 ± 14.5	66.7 ± 14.7	33.3 ± 4.3	31.2 ± 7.0	31.1 ± 8.9
Cohen's d	0.266*	0.46	0.22*	0.36*	0.43	0.26*	0.11

*p < .05

MOTOR PLANNING IN CHILDREN WITH UNILATERAL CEREBRAL PALSY

Cherng-I Chou[1], Chiao-Yu Yang[1], Kai-Jie Liang[1], Hao-Ling Chen[1] and Tien-Ni Wang [1]
[1] Department of Occupational Therapy, National Taiwan University, Taipei, Taiwan.
Email: caflys8697@gmail.com

INTRODUCTION

Motor planning is the process of managing a sequence of movement to perform a task [1]. The end-state-comfort (ESC), which describes the tendency to reach comfortable position at the end of motion, has often been used to represent motor planning skills. Moreover, as Surkar et al (2018) suggested, reaction time (RT), the time interval between presentation of task stimuli with onset of motor execution, is aslo an important parameter in motor planning [2]. Previous study indicated that individuals with unilateral cerebral palsy (UCP) may have problems in motor planning skills, leading to daily living dysfunctions [3]. Given the motor planning in children with UCP remains unclear, this study aims to compare motor planning skills for children with UCP. Besides, predictors of motor planning skills in children with UCP were also investgiated.

METHODS

Fifteen children with UCP and eighteen TD children aged 5 to 13 years old were recruited in this study. The motor planning skills were assessed with a cup-grasping task, in which the ESC and RT (modified to the time lag between presentation of task stimuli with the onset of manipulating the target object) were collected. The motor quality and the motor proficiency were assessed by the Melbourne Assessment-2 (MA2) and subtests of the Bruininks-Oseretsky Test of Motor Proficiency-2 (BOT-2), respectively. Independent t-test was examined for the group differences, and stepwise regression was performed for exploring the predictors of motor planning skills.

RESULTS AND DISCUSSIONS

The result showed that children with UCP demonstrate significantly less ESC ($t = 3.258$, $p = 0.004$) and more RT ($p = -5.555$, $p < 0.001$) while using their nondominant hand compared to TD children. The MA2 is a significant predictor for the ESC ($F = 7.550$, $R^2_{adj} = 0.319$, $p = 0.017$, Table 1), and MA2 and BOT-2 are important factors for the RT ($F = 8.442$, $R^2_{adj} = 0.515$, $p = 0.005$). The results inferred that the motor quality may affect the motor planning accuracy, and the poor motor quality and proficiency may lead to increased RT in UCP children. Different predictors were identified for various motor planning parameters (ESC and RT) which highlights the importance to include both aspects into measurement.

CONCLUSIONS

In summary, impaired motor planning skills were observed in children with UCP. Motor planning accuracy could be predicted by their motor quality, while motor planning RT could be predicted by both motor quality and proficiency. These results would benefit for the clinicians to provide adequate activities while targeting on the specific outcome.

REFERENCES

[1] Martinie O et al. *Brain sciences* ***11.7***: 920, 2021.
[2] Surkar SM et al. Res Dev Disabil 80: 64–73, 2018.
[3] Steenbergen B et al. *DMCN* ***48.9***: 780–783, 2006.

Table 1: Predictors of Motor Planning Accuracy and Motor Planning Reaction Time in Children with Unilateral Cerebral Palsy

Parameters	B (SE)	β	t	R^2_{adj}
ESC				
Model 1				0.319*
MA2	0.423 ± 0.154	0.606	2.748*	
RT				
Model 1				0.308*
MA2	-228.793 ± 85.068	-0.598	-2.690*	
Model 2				0.515**
MA2	-255.371 ± 71.950	-0.667	-3.549**	
BOT-2	-25.744 ± 10.053	-0.482	-2.561*	

MA2: Melbourne Assessment-2; BOT-2: Bruininks-Oseretsky Test of Motor Proficiency-2

* Significant at the 0.05 alpha level

** Significant at the 0.01 alpha level

PREDICTING FACTORS OF HANDWRITING LEGIBILITY IN CHILDREN AT PRESCHOOL AND FIRST GRADE

Pin-Chen Hung[1], Wen-Feng Huang[1], Po-Ya Chuang[1], Tien-Ni Wang[1], Hao-Ling Chen [1]
[1]School of Occupational Therapy, National Taiwan University, Taipei, Taiwan, R.O.C
Email: hlchen@ntu.edu.tw

INTRODUCTION

Handwriting is considered a critical functional skill for children. Poor handwriting might affect their academic achievement and learning motivation, especially for handwriting beginners. Understanding factors that influence beginners' handwriting is essential in formulating effective strategies and interventions. Various factors related to handwriting legibility have been demonstrated in some research[1], such as visual perception, motor coordination, and visual motor integration. Previous studies have revealed that lower-grade and middle, upper-grade children respond to handwriting demands via different related skills. However, few studies explored which related skills contributed to beginners' handwriting legibility. Therefore, this study aimed to investigate which visual perceptual motor skills had potential contributions to handwriting legibility for children in the beginning stage, that is, kindergarten and first grade.

METHODS

20 children were recruited respectively in preschool (5-6 years old) and first grade in Taipei, Taiwan. Children were instructed to copy Chinese characters which were high-frequency characters they often contacted with. In addition, a computerized program developed by our research team was adopted to analyze written legibility in four aspects: *Size, Position, Orientation,* and *Deformation.* The larger the value of each aspect, the worse the performance of legibility[2]. The visual perceptual motor skills were assessed by the following evaluation tools: (1) Test of Visual Perceptual Skills, 4th Edition (TVPS-4) for understanding visual perception (VP) ability of children; (2) Beery-Buktenica Developmental Test of Visual-Motor Integration (Beery VMI) for assessing visual motor integration (VMI) of children, and (3) Computerized Perceptual Motor Skills Assessment developed by our team for exploring motor coordination ability in which the higher score represents poorer motor coordination (MC) performance[3]. Pearson correlation coefficients and step-wise regression were completed to investigate the significant predictors of each handwriting legibility aspect.

RESULTS AND DISCUSSION

The results showed a medium level of correlation between MC ability and handwriting deformation in preschoolers (r=.539, p=.017). Regression analysis indicated that MC was the only significant contributor to deformation for preschoolers accounting for 29.1% of the variance. Preschoolers with satisfactory MC seemed to have efficient pen control, which would in turn influence their handwriting legibility. On the other hand, a medium negative relationship was found between VMI and handwriting deformation in the first grade (r=-.478, p=.039). Regression analysis demonstrated that VMI was the only significant predictor of deformation for first graders contributing 22.9%. First graders with acceptable VMI seemed to have fine copy skills, which was regarded as a fundamental function in writing.

CONCLUSIONS

This study identified the predicting factors associated with legible handwriting in kindergarten and first grade. The handwriting legibility of the preschoolers seemed to heavily depend on motor coordination, whereas that of the first graders was visual-motor based. The findings may assist clinicians and educators in developing intervention guidelines, preventing children from handwriting deficiency.

REFERENCE

[1] Lee et al. *The American journal of occupational therapy,* 70(6),2016
[2]Huang et al. *Journal of Taiwan Occupational Therapy Association, 38*(1), 36-55, 2020
[3] Liu et al. *Journal of Taiwan Occupational Therapy Association, 37*(1), 41-54, 2019

Table 1: The correlation coefficient between handwriting legibility and visual perceptual motor skills in preschool and first grade

Preschool	Size	Orientation	Position	Deformation
Visual motor integration	.194	.101	.075	.110
Visual perception	-.048	-.143	-.184	-.122
Motor coordination	.345	.002	.181	.539*
First grade	Size	Orientation	Position	Deformation
Visual motor integration	.341	.288	.241	-.478*
Visual perception	.112	-.336	.349	-.108
Motor coordination	-.278	-.119	.054	.167

The static method of computing leg stiffness in running measures a smaller value than the dynamic method.

Seungjoo Noh[1] and Sukyung Park[2]
[1] Department of Mechanical Engineering, Seoul National University, Seoul, Republic of Korea.
[2] Department of Mechanical Engineering, KAIST, Daejeon, Republic of Korea.
Email: istack0309@snu.ac.kr

INTRODUCTION

Elastic energy stored momentarily during running is closely related to energy consumption and serves as a key indicator of energy stored in muscle fibers and tendons. Leg stiffness(k_{leg}) is used when estimating elastic energy. Thus, when k_{leg} varies by the computing methods, it can potentially affect the analysis of energy storage characteristics in muscle fibers and tendons. In general, k_{leg} is computed by calculating the ratio of the maximum vertical ground reaction force(F_{peak}) to the maximum contraction length of the leg(ΔL_{peak}) based on the spring loaded inverted pendulum(SLIP) model [1,2] (Figure 1A). Alternatively, it can be computed as a parameter of the SLIP model that best predicts the entire ground reaction force(GRF) data [3,4]. Therefore, this study will compare the differences in k_{leg}, ΔL, and elastic energy values resulting from the two different methods of computing k_{leg}.

METHODS

In this study, we computed the k_{leg} value in two ways base on SLIP model: a static method based on peak values and a dynamic method based on generated GRF value. The static method uses the $-F_{peak}/\Delta L_{peak}$ formula, with ΔL_{peak} calculated by the method of Farley et al. [1]. The dynamic method computes k_{leg} as a parameter of the SLIP model that minimizes the sum of the mean square error between the vertical and horizontal GRF data and the model's GRF. The value of k_{leg} was determined using fmincon function of MATLAB®, with k_{leg}, touchdown angle, and touchdown velocity as input parameters. For the model's GRF, we used the GRF value from the 30th step of the model that guaranteed at least 50 steps. The vertical displacement of the center of mass (CoM) was calculated by double integration of the vertical acceleration. The length of the subject's leg was modelled as 0.53 times the subject's height [5]. The elastic energy was calculated as half of k_{leg} times ΔL_{peak} squared, according to the formula for elastic energy.

Ten male participants (age: 24.80 ± 2.10 years, mass: 72.60 ± 4.50 kg, height: 1.75 ± 0.05 m) were recruited for the study. The participants performed running on a treadmill at a fixed speed of 3.1 m/s. The GRF data for 29 consecutive steps were collected for each participant.

RESULTS AND DISCUSSION

Both k_{leg} and ΔL_{peak}, and elastic energy, showed statistically significant differences between the static and dynamic methods (Figure 1C). For k_{leg}, the static method produced a lower value. For the magnitude of ΔL_{peak} and elastic energy, the dynamic method produced a smaller value.

When calculating leg length change(ΔL) using the calculation method employed in the static method and examining the GRF values according to ΔL, the values do not follow linearity throughout the entire phase (Figure 1B). Therefore, the difference in k_{leg} values between the two methods can be explained by the point that the static method relies solely on information from the moment of maximum contraction, whereas the dynamic method includes and represents information of the entire contact phase.

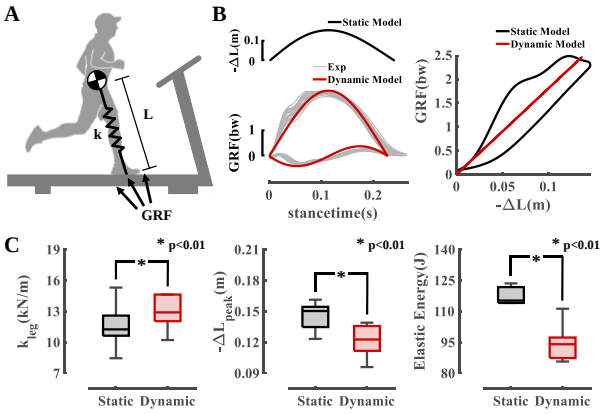

Figure 1 (A) SLIP model in running (B) GRF and $-\Delta L$ during contact phase. (C) k_{leg}, $-\Delta L_{peak}$, and stored elastic energy values obtained by two methods.

CONCLUSIONS

In this study, we confirmed that the k_{leg} value varies significantly depending on the computing method used in running, leading to a difference in the estimated elastic energy. This indicates that the computing method of k_{leg} affects the analysis of energy consumption, as well as the energy storage characteristics of muscle fibers and tendons in running. Furthermore, it is necessary to determine a more appropriate method for estimating elastic energy in future studies.

ACKNOWLEDGEMENTS

The authors would like to thank Jongbin Kim (Professor, Division of Kinesiology, Silla University) and Sang-Kyoon Park (Professor, Motion Innovation Center, Korea National Sport University) for providing experiment data.

REFERENCES

[1] Farley C T et al. *J Exp Biol* **185(1)**: 71-86, 1993.
[2] Blum Y et al. *J Biomech* **42(14)**: 2400-2405, 2009.
[3] Geyer H et al. *Proc. Royal Soc. B P ROY SOC B-BIOL SCI* **273(1603)**: 2861-2867, 2006.
[4] Kim S & Park S *J Biomech* **44(7):** 1253-1258, 2011.

SIDESTEP CUTTING MANOEUVRES DURING HUMAN RUNNING EXHIBIT SPRING-MASS BEHAVIOUR

Kat Daniels [1,2] and J F Burn [2]
[1] Department of Sport and Exercise Sciences, Manchester Metropolitan University, Manchester, UK
[2] Department of Mechanical Engineering, University of Bristol, Bristol, UK
Email: k.daniels@mmu.ac.uk

INTRODUCTION

Sidestep cutting manoeuvres are used by running bipeds for rapid changes of direction [1]. In humans, these manoeuvres are commonly studied in the context of athletic performance and injury. The spring-mass model is a simple mathematical model of bouncing gait that has been used to gain insight into the mechanics and control of locomotion in 2D and, more recently, in 3D [2-3]. Here, we show that many features of human sidestep cutting dynamics can be captured by a simple 3D spring-mass model. We then use the model to explain previous empirical observations relating cutting dynamics to running speed and angle.

METHODS

Whole-body optical motion capture and ground reaction force data were collected from 63 human participants (male; aged 18-35; no self-reported musculoskeletal or neurological impairments) during the change-of-direction stance phase of a running cut manoeuvre. Participants performed three maximum-effort 90° sidestep cuts from each leg. The location of the centre of mass (CoM) was estimated from segment positions and published inertial data. Individual spring-mass model simulations for each trial were generated using input parameters initial velocity (v_x, v_y, v_z,), leg stiffness (k; estimated as average leg stiffness from initial contact to the instant of maximum leg shortening), body mass (m), initial leg length (L_0) and leg angle from the vertical (θ_{xy}, θ_{xz}) (Figure 1A). The equations of motion for the model were solved numerically (MATLAB 2020a, The MathWorks, Inc., USA) and simulations were compared to measured kinematics and ground reaction forces.

RESULTS

Average model prediction errors were <10% for stance time, mediolateral impulse, braking impulse and CoM-foot displacements (stance time results presented as an example in Figure 1B). The model also predicted leg angle at foot-off to within 5° of the measured angles. Model simulations explained (a) the relationship between running speed and key kinematic and kinetic variables during the change-of-direction stance phase; and (b) the non-linear relationships with cutting angle that have previously been reported (e.g. [4]) for horizontal plane ground reaction forces and CoM stance phase kinematics.

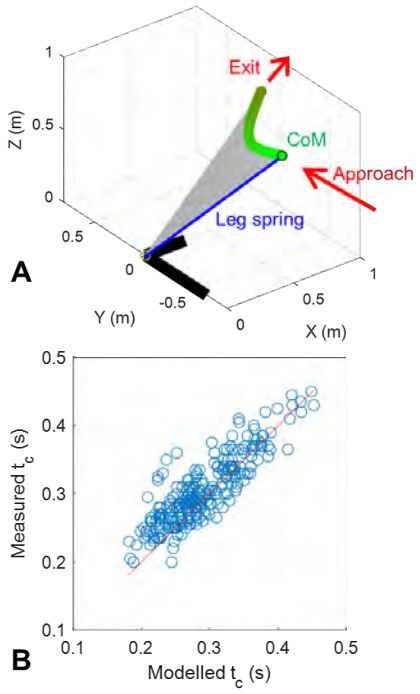

Figure 1. 3D spring-mass model schematic (A) and relationship between modelled and measured sidestep cut stance time (t_c) for all participants (B; r = 0.84; p<0.001).

CONCLUSIONS

Our findings suggest that several key aspects of sidestep cutting dynamics are governed by a relatively small number of parameters and can be explained by a simple 3D spring-mass model. Further exploration and development of this model may provide insight into performance limits and optimisation of turning manoeuvres in humans and other bipedal species.

REFERENCES

[1] Jindrich and Qiao (2009), *Chaos*, **19**(2):026105
[2] Blickhan (1989), J *Biomech.*, 22:1217-27
[3] Wu and Geyer (2013), *IEEE Trans. Robot.*, **29**(5):1114-24
[4] Havens and Sigward (2015), *Gait Posture*, **42**(3):240-45

HOW CONNECTING THE LEGS WITH A SPRING IMPROVES HUMAN RUNNING ECONOMY

Jon P. Stingel [1], Jennifer L. Hicks[2], Scott L. Delp[1,2]
Departments of [1]Mechanical Engineering and [2]Bioengineering, Stanford University, Stanford, CA, USA.
Email: stingjp@stanford.edu (J.P. Stingel), jenhicks@stanford.edu (J.L. Hicks), delp@stanford.edu (S.L. Delp)

INTRODUCTION

Connecting the legs with a spring attached to the shoelaces reduces energy expenditure during steady-state running [1]. While experiments have shown that this spring can reduce the joint moments generated by muscles, it is unknown which muscles are able to save energy. We used muscle-driven simulations to discern which muscles were saving energy and how.

METHODS

We collected experimental data of 7 subjects running on a treadmill at 2.67ms^{-1}, with and without the spring connecting their legs [1]. We scaled a full-body musculoskeletal model to each subject and used direct collocation to create muscle-driven simulations that tracked kinematics and solved for the muscle activity required to generate the movement [2,3]. We simulated four gait cycles per subject-condition and computed the rate of energy expenditure for each muscle, ensuring the summed full-body rates were similar to those measured experimentally [4].

RESULTS AND DISCUSSION

Simulations showed savings in both stance (1.5±0.2 W/kg, P<3x10-4) and swing (0.3±0.1 W/kg, P<0.05), though savings in stance were larger, with savings occurring in the gluteal muscles (-0.14±0.03 W/kg, P<0.004), quadriceps (-0.14±0.04 W/kg, P<0.03), hip flexors (-0.11±0.02 W/kg, P<0.003), hamstrings (-0.09±0.03 W/kg, P<0.04), and hip adductors (-0.06±0.01 W/kg, P<0.002) in each leg. Interestingly, the muscles that saved the most energy, did so during stance when the spring does not have any tension. The savings were facilitated by participants adopting a higher stride frequency with less hip, knee and ankle flexion. With this gait, supporting and redirecting the body center of mass became less costly, as seen in muscles such as the gluteus medius and the vastus lateralis. The gluteus medius saved the greatest amount of energy of the muscles in the model, and did so by reducing its muscle fiber velocity, force, and activation (Figure 1). Similar changes occurred in the quadriceps, which led to a reduction in heat production by the muscle, as well as the mechanical work that it performed. These results show that the simple spring device reduced the energy cost of running at the same speed by supplying an external force to users, allowing them to take advantage of a more efficient gait pattern.

CONCLUSIONS

Musculoskeletal simulations revealed that the gluteal, quadriceps, hip flexor, hamstrings, and hip adductor muscle groups saved energy while running with a spring connecting the legs. We dissected the muscle state changes that contributed to the reductions in energy expenditure. Further, this understanding could be used to aid the design of devices that can assist runners at different speeds or that provide alternative benefits to users such as offloading a tendon or joint.

REFERENCES

[1] Simpson et al. *J. Exp. Biology* **222**(17) (2019)
[2] Rajagopal et al. *IEEE T.Biomed.Eng.* **63**(10) (2016)
[3] Dembia et al. *PLOS Comp.Biology* **16**(12) (2020)
[4] Uchida et al. *PLOS ONE* **11**(3) (2016)

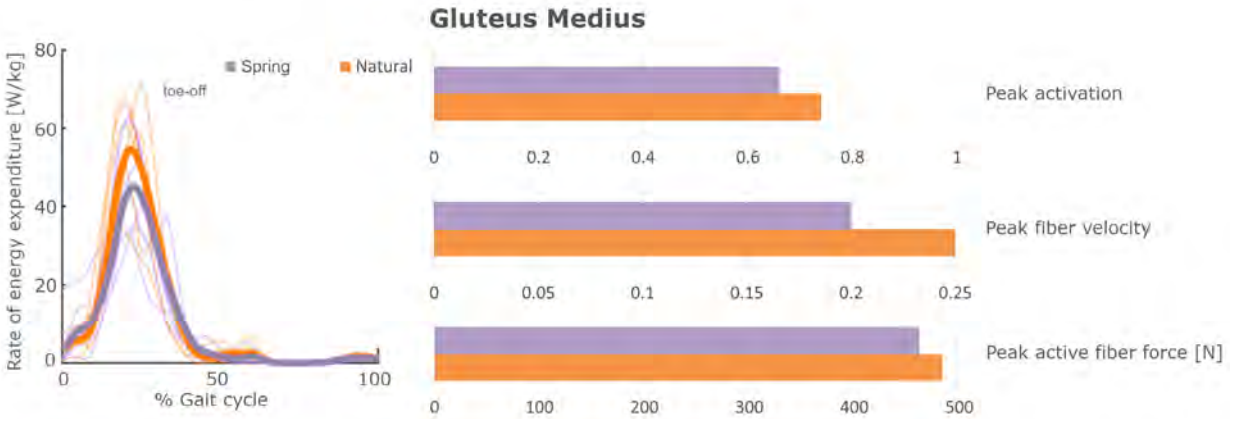

Figure 1: Gluteus medius changes in rate of energy expenditure throughout the gait cycle and the corresponding muscle state changes that contribute to the reduction. On the left, the average of all subjects (thick line) and individual subject averages (thin dotted line) for the gluteus medius muscle rate of energy expenditure are plotted throughout the gait cycle. Orange lines represent the natural runs and purple shows the runs with the spring. The bar plots on the right show the peak muscle activation (range from 0-1), fiber velocity (in normalized units of number of optimal fiber lengths per second), and active fiber force averaged across all subjects at the time of highest energy expenditure for both natural (orange) and spring (purple) running.

Changes in Leg Stiffness as a Result of Differences in Leg BMD in Various Age Groups During Running

Jinsung Jung[1], Jongbin Kim[2], Sang-Kyoon Park[3] and Sukyung Park [1]
[1] Department of Mechanical Engineering, KAIST, Daejeon, Republic of Korea
[2] Division of Kinesiology, Silla University, Busan, Republic of Korea
[3] Motion Innovation Center, Korea National Sport University, Seoul, Republic of Korea
Email: jinsungjung@kaist.ac.kr

INTRODUCTION

One of the biological characteristics that often decreases with aging is bone mineral density(BMD), which indicates the strength of the bones. Meanwhile osteoporosis and other bone-related disorders, as well as decreased physical performance, are mostly brought on by a decline in BMD. A decrease in BMD has been linked to cases of decreased physical performance[1]. The fact that kinematic characteristics during running change according to differences in BMD, while kinetic characteristics do not, has been reported[2]. And kinematics and kinetics are not independent but together determine the dynamics of running. Therefore, in this study, through a correlation analysis between BMD and leg stiffness during running, we set out to investigate and quantify the relationship between BMD and running biomechanics.

METHODS

We measured leg BMD, and by applying ground reaction force(GRF) and kinematic data from running experiments to a model from a prior study, we were able to obtain leg stiffness. 19 male subjects, ranging in age from 20 to 70, participated in the experiment (43.7±16.9yrs, 171.5±5.1cm, 70.2±8.1kg). Dual Energy X-ray Absorptiometry(Hologic, USA) was used to measure the subjects' leg joints' BMD. After that, the subjects ran on a treadmill with a force plate embedded in it for 5 minutes at a self-selected speed while the GRF and motion capture data were collected(Bertec, USA; Qualisys, Sweden) (Fig.1 A). The running SLIP model by Geyer et al. was used for data analysis[3]. The leg stiffness(k) and strike angle (α_0) were determined through a non-linear optimization process that minimizes the objective function defined by the RMSE between the measured GRF and the simulation values. The model's numerical solution was calculated using the ode45 function in MATLAB® (Fig.1 B). We ran enough optimization processes with random initial conditions to prevent local minima of the variables, and k was normalized by initial leg length(l_0) and mass.

RESULTS AND DISCUSSION

The correlation between the subjects' characteristics and their leg BMD revealed that there were significant variables that displayed noteworthy relationships. With regard to leg BMD, we looked at age, GRF peak, running speed, and normalized leg stiffness K (Fig.1 C). These variables indicated R^2 of 0.206, 0.010, 0.045, 0.376, respectively, and *p-values* of 0.051, 0.684, 0.385, and 0.005. Particularly, a strong correlation between leg stiffness and leg BMD is indicated by the comparatively high R^2 and low *p-value* of K. The running SLIP model assumes that the leg behaves as a single spring. So the range of motion (ROM) of the leg joint influences the displacement of the spring. The kinematic characteristics such as the ROM of knee during running are known to considerably decline with age[2], and from the data of this study, there are no relationship between the leg BMD and GRF. As a result, it could be inferred that the GRF, which is unrelated to leg BMD, causes the leg stiffness to increase if the leg joint's ROM decrease as a result of older age and low leg BMD.

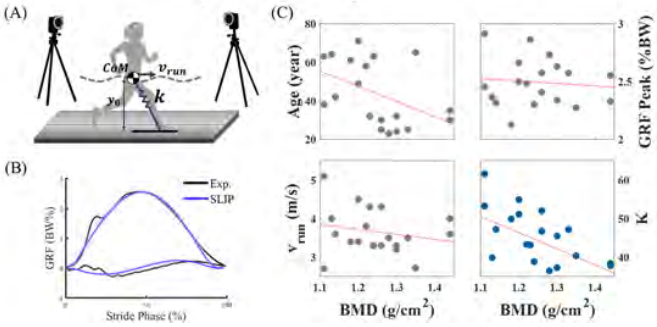

Figure 1 (A) Experimental setup and SLIP model for finding leg stiffness (B) Measured results of vertical and horizontal GRF and simulation results of the SLIP model (C) The correlation between BMD and age, GRF peak, running speed, normalized leg stiffness

CONCLUSIONS

This study identified a link between leg stiffness and leg BMD during running. This is assumed to be the outcome of changes in leg BMD and leg joint movement, as reported in previous study. These findings relating leg stiffness, which is an indicator of physical condition and the capacity to store and release energy during running, may help future studies understand the characteristics of running in the elderly.

ACKNOWLEDGEMENTS

This study was supported by the Faculty Basic Research Funds for 2022 (A0601003029) of KAIST.

REFERENCES

[1] Valdimarsson Ö et al. *J Bone Miner Res* **20**: 906-12, 2005.
[2] Kim J, Park S-K. *Int J Environ Res Public Health* **19**, 2022.
[3] Geyer H et al. *J Theor Biol* **232**: 315-28, 2005.

INFLUENCE OF SYNERGY CONTROL ASSUMPTIONS ON PREDICTED WALKING FUNCTION FOLLOWING PELVIC SARCOMA SURGERY

Marleny M. Vega[1], Geng Li[1], Payam Zandiyeh[2], Valerae O. Lewis[3], Benjamin J. Fregly[1]
[1]Department of Mechanical Engineering, Rice University, Houston, TX, United States
[2]Department of Orthopaedic Surgery, University of Texas Health Science Center, Houston, TX, United States
[7]Department of Orthopaedic Oncology, University of Texas MD Anderson Cancer Center, Houston, TX, United States
Email: ma86@rice.edu

INTRODUCTION

A recent study predicted the impact of operated side psoas muscle retention on walking function following pelvic sarcoma surgery [1]. While the predicted post-surgery walking motions were generally consistent with clinical observations, an unrealistically large lateral trunk lean to the operated side was observed. These walking predictions were generated using a synergy control structure to define lower body muscle activations, where time-invariant synergy vectors (minus muscles removed during surgery) were assumed to remain unchanged post-surgery while time-varying synergy activations were allowed to change to achieve a periodic walking motion. In this study, we investigate whether allowing the time-invariant synergy vectors to change while keeping the time-varying synergy activations constant would produce post-surgery walking predictions more consistent with clinical observations.

METHODS

Video motion capture, ground reaction, and EMG data collected previously from a healthy male subject walking at his self-selected speed were used for this study [1]. A neuromusculoskeletal model of the subject was created in OpenSim [2] by personalizing four model elements: joint models, muscle-tendon models, foot-ground contact models, and a neural control model using muscle synergies (see [1] for details). The most common surgical scenario encountered at MD Anderson Cancer Center in Houston, which involves removing multiple hip (including gluteus medius) and lower back muscles on the operated side, was applied to the model assuming the simulated patient received a custom pelvic prosthesis with artificial hip joint.

The modified model was used in two direct collocation optimal control problems formulated in GPOPS-II [3] to investigate the influence of lower body synergy control assumptions on predicted post-surgery walking function. The first problem allowed synergy activations to change freely while the corresponding synergy vectors (minus muscles removed during surgery) remained unchanged, while the second problem allowed synergy vectors to change freely while the corresponding synergy activations remained unchanged. Both problems included light tracking of the original joint motions. Pre- and post-surgery walking data collected from an actual pelvic sarcoma patient whose surgical decisions were similar to the most common scenario were visualized for comparison.

RESULTS AND DISCUSSION

Both optimization problems produced physically realistic walking motions. However, the formulation that allowed synergy vectors to chage freely (Fig. 1c) produced a lateral trunk lean that was the most consistent with clinical observations (Fig. 1b). Thus, individuals who receive pelvic sarcoma surgery may change their coordination strategy (as indicated by synergy vectors) more than their coordination timing (as indicated by synergy activations) to achieve a post-surgery walking motion with minimal lateral trunk lean.

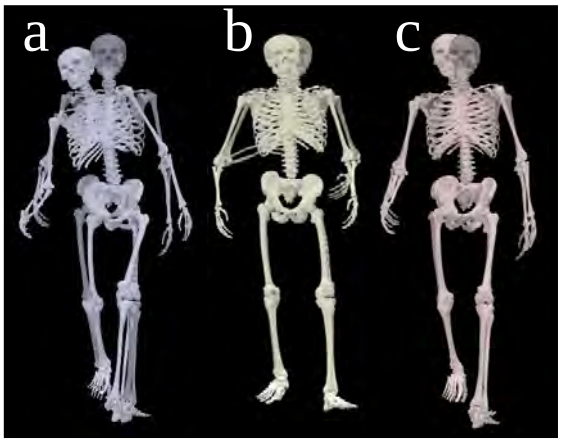

Figure 1: Comparison of pre-surgery (translucent skeleton) and post-surgery (opaque skeleton) walking motions. a) Experimental vs. predicted post-surgery with changeable synergy activations for healthy subject. b) Experimental pre-surgery vs. experimental post-surgery for pelvic sarcoma patient. c) Experimental vs. predicted post-surgery with changeable synergy vectors for healthy subject.

CONCLUSIONS

The goal of this research is to predict post-surgery walking function given a pre-surgery personalized walking model and the implemented surgical decisions. Once such predictions can be generated reliably, this computational approach may help inform surgical, rehabilitation, and custom pelvic implant design decisions for this unique patient population.

ACKNOWLEDGMENTS

This work was funded by the Cancer Prevention and Research Institute of Texas (grant RR170026) and by the National Institues of Health (grant R01 EB030520).

REFERENCES

[1] Vega M et al. *Frontiers Bioeng* 10**:** 855870.
[2] Seth A et al. *PloS Comp Biology* 14(7): e1006223.
[3] Patterson M et al. *ACM Trans Math Softw* 10: 2558904.

PREDICTING KNEE ADDUCTION MOMENT DURING WALKING BY LOWER LIMB ALIGNMENT USING FORWARD DYNAMICS SIMULATION

JongHyeon Park[1], Seungbum Koo[1]
[1] Department of Mechanical Engineering, Korea Advanced Institute of Science and Technology, Daejeon, Republic of Korea.
Email: skoo@kaist.ac.kr

INTRODUCTION

Varus and valgus lower limb alignments affect knee adduction moment [1], which is closely associated with symptoms in the knee [2]. It has been reported that medial knee osteoarthritis is associated with higher knee adduction moment [3]. The quantitative relationship between lower limb alignment angle and knee adduction moment could be calculated using a simple statics calculation for a standing pose, but it has yet to be well investigated during dynamic walking. Recently, gait controllers for forward dynamics simulation could be made of artificial neural networks and trained using deep reinforcement learning. The study's objective was to quantify the association between the knee alignment angles and knee adduction moment during walking using the forward dynamics simulation.

METHODS

The RaiSim dynamics solver [4] and a custom skeletal model with 27 degrees-of-freedom were used for forward dynamics simulation (Figure 1). A two-layer perceptron was trained for the skeletal model to track a measured normal walking motion of a healthy subject using deep reinforcement learning [5]. Reference gait motions with varus and valgus lower limb alignments were generated by adjusting the knee angle in the normal walking data. A total of five gait controllers were trained, including two valgus (-5° and -10°), two varus (5° and 10°), and a normal lower limb alignment (0°). The knee adduction moment (KAM) was measured through the torque applied to the knee of the skeletal model for the five lower limb alignment cases. The moment arm of the ground reaction force for the knee joint was calculated using the center of pressure of the sole and the center of mass of the skeletal model in each frame.

RESULTS AND DISCUSSION

The KAMs were affected by the lower limb alignment. KAM and moment arm increased as the lower limb alignment angle increased toward the varus. In the varus lower limb alignment (10°), the average and peak value of the KAMs were 43.5 Nm and 122 Nm. In the valgus lower limb alignment (-10°), the average and peak value of the KAMs were -7.69 Nm and 54.9 Nm (Table 1). The knee adduction moment (y, Nm) and lower limb alignment angle (x, degree) were associated with $y = 2.449 x + 18.20$, $p<0.001$.

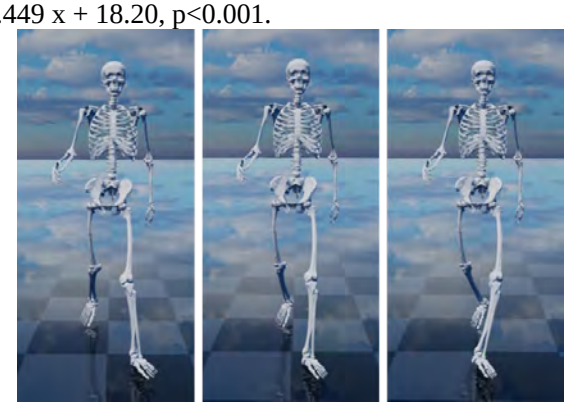

Figure 1 The valgus (left), normal (middle), and varus (right) lower limb alignment for forward dynamic simulation

CONCLUSIONS

Our forward dynamics simulation could generate walking motions with arbitrary lower limb alignments and be used to calculate knee adduction moment. The knee adduction moment angle increased by about 2.5 Nm with the increase of lower limb alignment toward the varus by 1°. Larger varus lower limb alignment causes higher KAM during walking.

ACKNOWLEDGEMENTS

This research was supported by the NRF (MSIT Project No. 2022M3C1A3080598) and by IITP (MSIT Project No. 2022-0-00025) funded by the Korea government.

REFERENCES

[1] Kristyn M. et al. *J Biomech* **46**: 1408-1412, 2013.
[2] Sharma L et al. *Annals of the rheumatic diseases* **69**: 1940-1945, 2010.
[3] Foroughi N et al. *The Knee* **16**: 303-309, 2009.
[4] Hwangbo J et al. *IEEE RA-L* **3**: 895-902, 2018.
[5] Peng X et al. *ACM ToG* **37**: 1-14, 2018.

Table 1: Mean and peak of KAM and moment arm in normal, varus, valgus lower limb alignment. (negative values indicate abduction)

Lower limb alignment angle		Valgus (-10°)	Valgus (-5°)	Normal (0°)	Varus (5°)	Varus (10°)
KAM (Nm)	Mean	-7.69	7.60	20.0	27.6	43.5
	Peak	54.9	59.9	77.7	117	122
Mean moment arm (mm)		6	17	31	49	65

THE FOOT'S MIDTARSAL JOINT ALTERS THE METABOLIC COST OF WALKING

Daniel J. Davis and John H. Challis
The Biomechanics Laboratory, The Pennsylvania State University, University Park, PA, USA.
Email: DanielJDavis@psu.edu

INTRODUCTION

Researchers have used computational musculoskeletal models to investigate the mechanisms underlying changes in the metabolic cost of locomotion. However, the midtarsal joint (i.e., the arch) is frequently ignored. The function of the foot's arch is thought to influence the energetics of locomotion [1], but most current musculoskeletal models are unable to capture this influence.

The aim of the present study was therefore to examine the differences in the metabolic cost of the stance phase of walking due to modelling the midtarsal joint. To do so, a whole-body musculoskeletal model with a three-segment foot that could produce stance phase midtarsal joint angles, moments, and powers similar to those estimated *in vivo* was developed.

METHODS

A two-dimensional musculoskeletal model was developed in OpenSim [v4.4; 2]. The model comprised two three-segment feet along with shanks, thighs, and a pelvis, head, arms, and trunk segment. Twenty-six muscles actuated the model's joints. The plantar aponeurosis was modelled using a path spring along the plantar surface of the foot, and a torsional spring at the midtarsal joint represented other passive structures.

Walking data from 14 participants was collected [3], and the generic model was scaled to a representative subset of three participants (2M/1F, 65.8 ± 10.6 kg, 1.72 ± 0.11 m) for which bilateral marker data was available. Simulations which minimized the sum of muscle excitations squared, and the discrepancies with experimental joint angles, joint angular velocities, and ground reaction forces during the stance phase of walking gait were then performed using OpenSim Moco [4]. The torsional spring stiffness at the midtarsal joint was treated as a parameter which was varied between simulations. The metabolic cost of the stance phase was estimated used modelled muscle behavior [5].

To explore the influence of modelling the foot without the arch, the midtarsal joint was converted to a weld joint which permitted no angular displacement. The stance phase of walking gait was then simulated again.

RESULTS AND DISCUSSION

The inclusion of the midtarsal joint reduced the metabolic cost of the stance phase of gait by 0.3%, 3.0%, and 1.4% for each participant, respectively. The largest difference in the net metabolic rate between the two conditions occurred near the time of push-off, when the ankle joint angles were also the most different (Figure 1). Both the gastrocnemius and soleus muscles consumed more energy at this time as well (Figure 1), indicating that ignoring the mechanics of the midtarsal joint alters the extent to which the triceps surae function in a metabolically favorable manner.

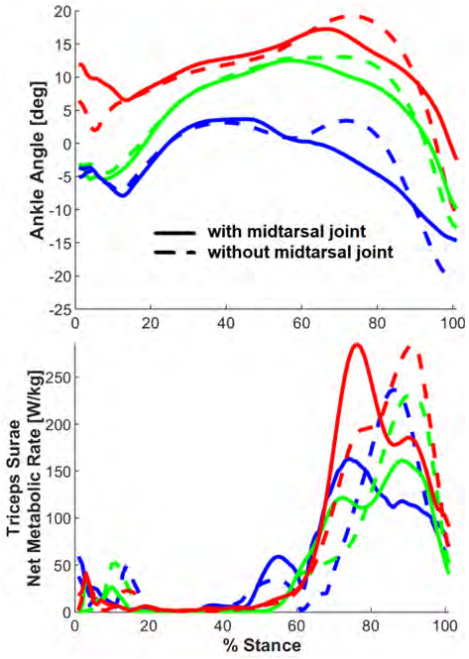

Figure 1 Ankle joint angle and triceps surae net metabolic rate differences between simulations with and without a midtarsal joint.

CONCLUSIONS

Including the midtarsal joint (i.e., the arch) in a whole-body musculoskeletal model decreased the metabolic cost of the stance phase of walking. This was primarily due to a reduction in metabolic energy required for push-off. More appropriately modelling the foot therefore allows for an enhanced understanding of locomotor propulsive energetics, which has important implications for studies of human performance, disease, and/or aging.

REFERENCES

[1] Hicks JH *J Anat* **88**: 25-34, 1954.
[2] Delp SL et al. *IEE Trans Biomed Eng* **54**: 1940-50, 2007.
[3] Davis DJ & Challis JH *PLoS ONE* **17:** e0274141, 2022.
[4] Dembia CL et al. *PLoS Comput Biol* **16**: e1008493, 2020.
[5] Koelewijn AD et al. *Comput Methods Biomech Biomed Engin* **21**: 521-531, 2018.

4D Shape and Growth modelling in Cerebral Palsy Paediatrics

Salim G. Bin Ghouth [1], Thor F. Besier [1,2], and Geoffrey G. Handsfield [1]

[1] Auckland Bioengineering Institute, University of Auckland, Auckland, New Zealand.
[2] Department of Engineering Science, University of Auckland, Auckland, New Zealand.
Email: sbin088@aucklanduni.ac.nz

INTRODUCTION

Cerebral palsy (CP) is neurodevelopmental disorder arising from a brain lesion during the neonatal period and is a common cause of disability in children and adolescents [1], [2]. Although the brain lesion is single-stage, non-progressive neural damage, CP musculoskeletal movement impairments worsen progressively with age [1]. In this research, we investigate the shape, fibre architecture, and growth of the soleus muscle which is an important muscle for gait and has been shown to be commonly affected by CP [3]. Conventional structural and architectural properties of the soleus muscle have been extensively investigated previously. However, quantitative shape descriptions of the soleus muscle have only recently been reported by our group in children and adolescents with CP [4]. Here, we conduct a 4-dimentional (longitudinal) statistical shape model and fibre architecture assessment of the soleus muscle to investigate the shape progression and growth in a cohort of children and adolescents with CP and a typically developing (TD) cohort. This *de novo* approach utilizes recent advancements in anatomical and diffusion MRI (aMRI and dMRI) to offer an *in vivo* assessment of the spatial and temporal variations of the soleus in children and adolescents with CP to better understand growth, shape change, and associated altered biomechanics.

METHODS

We acquired aMRI and dMRI at three discrete time points over a period of 15 months for a cohort of children and adolescents with CP and a TD cohort. We generated 3-dimensional volumetric meshes and vector fields of fibre orientation (input data) of the data representing the 3-dimentional architecture of the soleus muscle of both cohorts. The input data was normalized and size was removed. Then, the 3-dimensional volumetric meshes were registered against a reference mesh and vector fields were registered accordingly. Vector field data were interpolated to reduce computational cost using a nearest neighbour algorithm. Principal component analysis was applied and dominant shape and fibre tracts arrangements (i.e., principal components) were extracted. The means and variations of model output were quantified and compared between the two cohorts.

RESULTS

The 4-dimensional models of the children and adolescents with CP cohort and TD cohort can extract the dominant features and their variance in each cohort with a few principal components depending on the discrete time points of data collection. In our research, we were able to capture a maximum of two dominant features that distinguish each cohort given that we conducted three discrete time points of this longitudinal study.

CONCLUSIONS

We generated 4-dimentional shape and vector field models of the soleus muscle in cohorts of children with CP and TD children. The 4-dimentional shape and vector field models can describe shape progression and growth variations within and between the two cohorts. Future studies will include more longitudinal and cross-sectional data to extract more distinguishable dominant features of the soleus muscle between both cohorts and use finite element modelling to interpret the functional impairment of the soleus muscle in children and adolescents with CP.

REFERENCES

[1] H. K. Graham et al. *Nat. Rev. Dis. Prim.*: 2, 2016.

[2] M. Oskoui et al. *Dev. Med. Child Neurol.*: 55, no. 6, 509–519, 2013.

[3] G. G. Handsfield et al. *Muscle and Nerve*: 53, no. 6, 933–945, 2016.

[4] S. G. Bin Ghouth et al. *Scientific Reports*: 12, no. 1, 7711, 2022.

Estimation of musculoskeletal parameter values using hindlimb rat models

Gil Serrancolí[1], Matthew C. Tresch[2]
[1] Department of Mechanical Engineering, Universitat Politècnica de Catalunya, Barcelona, Spain.
[2] Departments of Biomedical Engineering, Physical Medicine and Rehabilitation, and Neuroscience Northwestern University, Chicago, United States of America.
Email: gil.serancoli@upc.edu, m-tresch@northwestern.edu

INTRODUCTION

The estimation of neuromusculotendon parameter values can be highly influenced by the type of movements used during the estimation process [1]. Moreover, the choice of human movements to accurately reproduce the kinematics and dynamics is not obvious. Tests in animals allow measuring data that in humans would be more difficult. In this study, we estimated neuromusculotendon parameter values of a rat hindlimb, such that they are able to reproduce the kinematics of trajectories produced from stimulation of a single muscle.

METHODS

The experimental data used for the estimation contained marker trajectories (Vicon, Oxford, UK) of six trials in which a single muscle of a rat hindlimb was stimulated at a time. The rat was anesthetized with the pelvis fixed, and at each trial one muscle was stimulated through intramuscular electrodes while the others remained passive. The six muscles stimulated were iliopsoas, gluteus superficialis, semitendinosus, vastus lateralis, biceps femoris posterior, and biceps femoris anterior. Each stimulation consisted of a step function with a duration of 0.5 seconds. A rat hindlimb model with 13 degrees of freedom was used [2] to obtain joint angles in OpenSim and represent the skeletal dynamics. Absolute degrees of freedom of the pelvis with respect to the ground and secondary degrees of freedom of the ankle were prescribed. The other degrees of freedom of the model (three at hip, one at knee and one at ankle) were driven by 38 muscles, represented with compliant muscle-tendon Hill-type actuators [3]. The system included fibre and tendon damping properties to analyse their impact on the prediction results. A tracking optimal control problem (OCP) was formulated [4] to optimize optimal fibre and tendon slack lengths of all muscles, and fibre and tendon damping parameters, such that the predicted kinematics during muscle stimulation replicated the experimental kinematics. Time activation and deactivation constants, and the maximum activation value were also calibrated for the stimulated muscle. The state variables included joint coordinates and their velocities, and normalized tendon forces, while joint accelerations, and the derivative of normalized tendon force served as control variables. The OCP was formulated using a direct collocation method, imposing Hill-equilibrium equations for all muscles, muscle activation dynamics equations for the muscle activated, and equations of motion for all degrees of freedom in an implicit form. Deviations of optimal fibre length values from the reference [2] were penalized.

RESULTS AND DISCUSSION

The calibrated set of optimal fibre and tendon slack lengths led to overall accurate results for all five degrees of freedom (Table 1), as illustrated by the example of stimulating gluteus superficialis shown in Figure 1. Once muscle parameters are optimized, this framework can also be used to predict other movements.

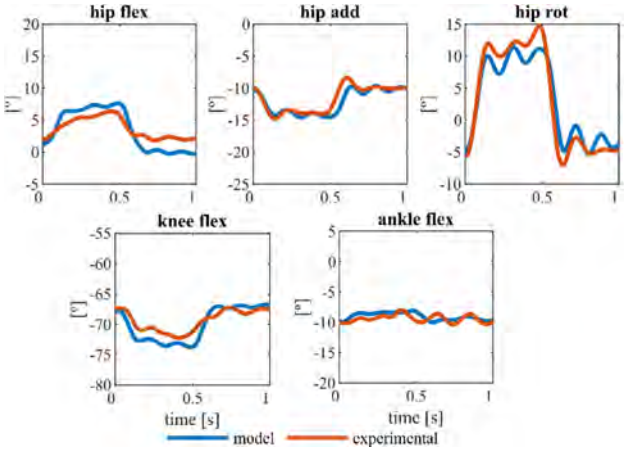

Figure 1 Example of kinematics tracking, stimulating gluteus superficialis.

CONCLUSIONS

The presented model can reproduce experimental data accurately. This framework allows the study of the influence of damping parameter values and level of stimulation on the estimated musculotendon parameter values.

REFERENCES

[1] Serrancolí, G et al. *Med. Eng. Phys.* **85**: 35-47, 2020.
[2] Johnson, WL et al. *J Biomech* **41**: 610-619, 2018.
[3] De Groote, F et al. *Ann Biomed Eng* **44**: 2922-36, 2016
[4] Falisse, A et al. PloS One **14**: e0217730, 2019

Table 1. Mean and standard deviation of root mean square errors (RMSE) for the five tracked degrees of freedom across all six trials.

	Hip flexion	Hip adduction	Hip rotation	Knee flexion	Ankle flexion
RMSE q [deg]	1.5 ± 0.6	1.4 ± 0.8	1.7 ± 1.1	1.9 ± 0.6	1.1 ± 0.5
RMSE $\dot{q}$ [deg/s]	2.0 ± 0.9	1.7 ± 1.0	2.3 ± 1.2	3.5 ± 2.2	1.7 ± 0.7

Musculoskeletal simulations integrating a smooth knee pressure contact model

Mohanad Harba[1], Joan Badia[1], Gil Serrancolí[1]
[1] Department of Mechanical Engineering, Universitat Politècnica de Catalunya, Barcelona, Spain
Email: mohanad.harba@upc.edu, joan.badia.torres@estudiantat.upc.edu, gil.serrancoli@upc.edu

INTRODUCTION

One of the benefits of biomechanics modelling is that we can compute variables that are usually not directly measurable, like joint contact forces or pressures. Computational efficiency and level of personalization are two terms that could seem contradictory. While we would need to know the contact pressure values to study joint degeneration, the computation of these variables within a musculoskeletal simulation, which is already computing muscle and contact forces and kinematics, might be quite time consuming. Moreover, collision detection algorithms are typically not continuous. Gradient-based optimizations using automatic differentiation tools have been shown to be the most efficient when formulating musculoskeletal simulations [1]. However, the cost function and constraints need to be continuous to avoid issues with the convergence.

METHODS

In this study, we developed a smooth collision-detection algorithm to compute joint pressures within musculoskeletal simulations, and this was applied to a knee joint wearing a prosthesis [2]. An optimal control problem (OCP) was formulated to track experimental data while satisfying dynamic, path, boundary, and continuity constraints. The OCP was solved using CasADi, calling the equations of motion (from OpenSim/Simbody). We formulated a smoothed pressure contact model based on elastic foundation theory in a C++ code, which was embedded into a .dll file. As indirect validation, we ensured that knee contact forces were reasonably well tracked with respect to experimental ones using data from the Knee Grand Challenge to Predict In Vivo Knee Contact Loads [3], while joint kinematics and ground-reaction forces can be tracked closely. Skeletal dynamics were represented using an OpenSim model with 34 degrees of freedom driven by 94 muscles. A visualization framework developed in Blender was created to visualize the results.

RESULTS AND DISCUSSION

An optimal solution is obtained tracking knee contact forces with RMSE = 56.0 N (r = 0.99) for the medial side and RMSE = 45.2 N (r = 0.98) for the lateral (Figure 1), and joint angles with RMSE = 1.62 ± 3.24º (r = 0.94 ± 0.20). Simultaneously, muscle forces and foot-ground contact forces were estimated. The computational time was 8.16 hours without parallelization in an Intel Xeon W2123 CPU at 3.6 Hz. This model provides the pressure values in each mesh face for both the tibial and femoral components of the prosthesis. One of the main advantages of this model is that pressure values could be minimized during predictive simulations to obtain patterns which avoid joint degeneration. So far, the pressure contact model is based on an elastic-foundation contact model. The integration of tangential contact forces is assessed to model the interaction more closely.

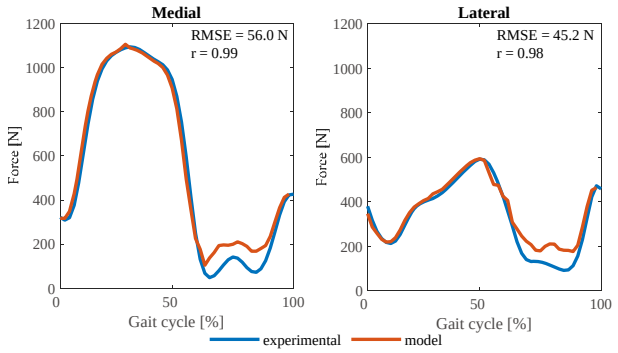

Figure 1 Experimental and model knee contact forces (medial – left, and lateral – right), with root mean square errors (RMSE) and correlation coefficients (r).

CONCLUSIONS

The validation in natural knees (without instrumented prosthesis) is challenging, though the possibility to simultaneously predict kinematics and dynamics data is promising to validate the results indirectly. This will allow studying how joint pressure distribution and muscle activation change after an orthopaedic injury or a neuromuscular disorder. This model could also be applied in other applications, such as in human-device interactions, and open the door to perform simulations of musculoskeletal simulations at the level of pressure data.

ACKNOWLEDGEMENTS

G. Serrancolí acknowledges the support from Serra Húnter Program.

REFERENCES

[1] Falisse et al. *Plos One* **14**: e0217730, 2019.
[2] Serrancolí et al. *Comput. Methods Biomech. Biomed. Eng.: Imaging Vis. Lect. Notes Comput. Vis. Biomech.* **38**, 2022.
[3] Fregly et al. *J. Orthop. Res*. **30**: 503-513, 2012.

Quadriceps Adaptation in Response to Split-Belt Asymmetric Walking in Long-Term Post-ACLR Patients

Yannis K. Halkiadakis[1], Noah A. Davidson[1], Kristin D. Morgan[1]
[1]Department of Biomedical Engineering, University of Connecticut, Storrs, CT 06269, USA
Email: yannis.halkiadakis@uconn.edu

INTRODUCTION

Lingering neuromuscular dysfunction often continue to plague post anterior cruciate ligament reconstruction (ACLR) individuals long after rehabilitation and their return-to-sport. These deficits commonly present as quadriceps inhibition resulting in decreased muscle activation and strength [1,2]. This quadriceps inhibition can have detrimental consequences including the initiation and progression of knee osteoarthritis and increased secondary ACL injury risks. Thus, post-ACLR rehabilitation protocols that increase quadricep muscle strength and engagement are needed to combat these harmful consequences.

Purposely induced asymmetric walking is a promising rehabilitation protocol that can override inhibitory muscle activation to restore healthy gait dynamics in pathological populations. Here, purposely induced asymmetric walking perturbations was used to increase quadriceps function and promote positive gait adaptations in post-ACLR individuals. We hypothesize that asymmetric walking trial will result in increased quadriceps activation that will be maintained after the asymmetric walking trial.

METHODS

Fifteen post-ACLR individuals (>1 year from surgery) participated in an asymmetric walking protocol. The protocol was performed on a Bertec split-belt instrumented treadmill, with marker data collected using a 12-camera Vicon motion capture system. Participants completed an asymmetric walking protocol that consisted of three trials: baseline symmetric 1.0 m/s trial, an asymmetric walking trial with the reconstructed limb at 1.0 m/s and contralateral limb at 1.5 m/s, and a de-adaptation symmetric trial at 1.0 m/s.

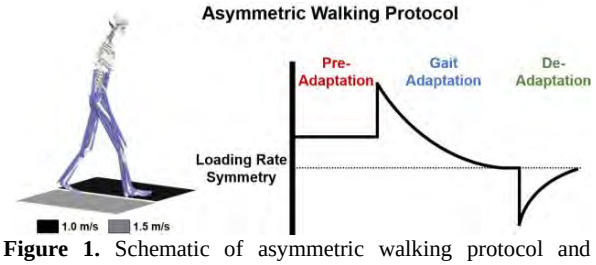

Figure 1. Schematic of asymmetric walking protocol and the reduction in between-limb loading rate asymmetry.

OpenSim musculoskeletal software was used to generate patient-specific simulations of the participants to evaluate changes in muscle function in response to the asymmetric walking protocol (Fig. 1). First, participants anthropometrics were scaled to OpenSims' 23 degree-of-freedom, 92 musculotendon actuator model. Next inverse kinematics was performed to compute the joint angles. Residual reduction algorithm tool was run to ensure that the gait simulations were dynamically consistent. Lastly, computed muscle control (CMC) was used to estimate individuals' lower extremity muscle forces during the loading phase of each gait cycle for each trial. The muscle groups of interest include the quadriceps, hamstrings, gastrocnemius, and gluteal groups. Peak lower extremity muscle force was during the loading phase was extracted from the CMC results. A repeated measures ANOVA was run to determine if there was a significant difference (p = 0.05) in muscle force production between trials for any muscle group.

RESULTS AND DISCUSSION

The percent change in muscle activity was calculated for each muscle group using the baseline 1.0 m/s results as the initial condition (Fig. 2). The results demonstrated that there was a significant increase in force production in the quadriceps, hamstrings, and gluteal muscles during the asymmetric walking trial (Fig. 2). Moreover, it was shown that the quadriceps, hamstrings, and gluteal muscles all maintained elevated muscle force production, compared to the baseline trial, during the symmetric de-adaptation walking session. These results are significant because it indicates that the asymmetric walking trial not only can induce positive muscle force production, but lead to short-term sustained elevated muscle force production. Between-limb loading rate asymmetry also decreased in response to the protocol (Fig. 2).

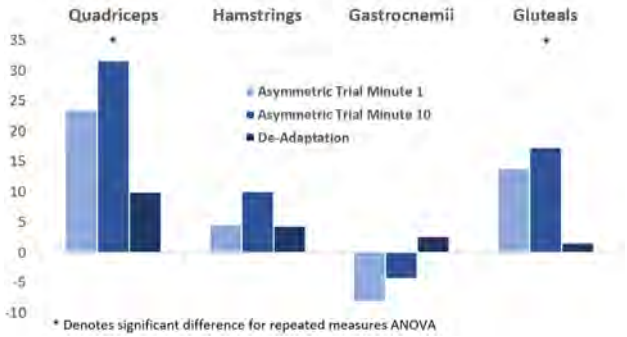

Figure 2. The percent change in muscle output for each of the muscle groups of interest when compared to the baseline symmetric trial at 1.0 m/s.

CONCLUSIONS

This study demonstrated that a purposely induced asymmetric walking protocol has the potential to promote healthy quadriceps function in post-ACLR individuals.

REFERENCES

[1] Palmieri-Smith, R. et al. *Clin Sports Med,* **27(3)**, 405-424, 2008
[2] Pietrosimone B et al. *J. Athl. Train.* **56(9)**, 960-966, 2021

ACHILLES TENDON FORCE DURING WALKING CAN BE PREDICTED USING TWO SMARTPHONE CAMERAS

Zhengliang Xia, Daniel Devaprakash, Bradley Cornish, Rodney S. Barrett,
David G. Lloyd, Andrea Hams, and Claudio Pizzolato
Griffith Centre of Biomedical and Rehabilitation Engineering (GCORE), Menzies Health Institute Queensland, Griffith University, Queensland, Australia
Email: zhengliang.xia@griffithuni.edu.au

INTRODUCTION

Achilles tendon (AT) adaptation can be modulated by strain, a mechanical variable modifiable via biofeedback [1]. Achilles tendon force, predicted using neuromusculoskeletal (NMSK) modelling [2], can be used to estimate AT strain. However, NMSK methods require high-quality data from specialised laboratory equipment and extensive data processing. Combining computer vision with deep learning is an alternative solution for obtaining AT force in ecologically valid settings. Pose estimation methods (e.g., OpenPose) enable automatic detection of human keypoints (e.g., joint centres and anatomical landmarks) from videos, facilitating real-world application. Deep learning models (e.g., long short-term neural network (LSTM)) have shown promise in predicting biomechanical variables (e.g., joint angles and moments) and may be trained to map the complex relationship between human motion and AT force. Therefore, this study aimed to develop a LSTM model to predict AT force from keypoints synthesised from laboratory based NMSK data and test the developed model using new videos recorded by two smartphones.

METHODS

The training dataset of LSTM model consisted of 3D motion capture (MOCAP), ground reaction forces, electromyography (EMG) of 16 participants (male:10; female:6) performing over-ground walking tasks. A calibrated EMG-informed NMSK model (CEINMS) estimated AT force time-series during the stance phase [3]. For the LSTM model training ten pose-estimated keypoints were synthesised (bilateral hip, knee, ankle, toe; midpoints hip joint centres, and midpoint of acromia) from 3D MOCAP marker trajectories. Synthesised keypoints data were augmented using a per-trial [4] and per-frame Gaussian noise. The final training data comprised 910 trials including the ten 3D keypoints position data, and the height and mass of each participant, used as LSTM model inputs to predict the AT force. Model hyperparameters were optimised using hyperband tuning with a train-test split of 7:1. Leave-one-out cross validation was used to evaluate model performance using coefficient of determination (r^2) and root mean square error (RMSE) between the NMSK and LSTM estimates of AT force. A final LSTM model was then retrained using the fully available training dataset. The final LSTM model was then verified using new outdoor video data of three participants (two males) not previously included in the training dataset. The slow-motion videos (sample rate: 240Hz; resolution: 1080×1920) were recorded from two smartphones (iPhone 8 and iPhone 13, Apple) and cropped to the right leg's stance phase, using OpenPose (v1.7.0) to automatically obtain pose keypoints [5]. Keypoints were triangulated and transformed to the world coordinates, consistent with the training data, and used as input to the final LSTM model to predict AT force.

RESULTS AND DISCUSSION

Leave-one-out cross validation showed that AT force could be predicted using the LSTM model with low error compared to NMSK modelling (RMSE = 200.44±69.86N; r^2 = 0.92±0.05). When using the pose estimation data of new participants extracted from the smartphone videos, the model estimated AT forces comparable to ground truth data (Figure 1).

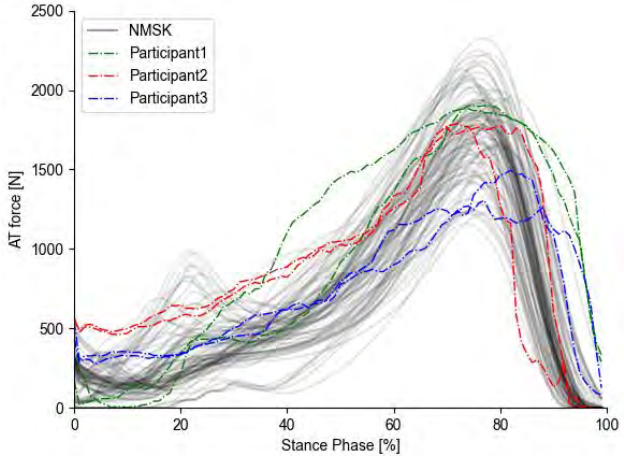

Figure 1 The comparison of ground-truth AT force from NMSK modelling pipeline and predicted AT force using real pose estimation data as input for the LSTM model.

CONCLUSIONS

Achilles tendon force during walking can be well predicted by LSTM model using videos recorded from two smartphones. These predictions are within the expected range of AT force established via NMSK modelling of the training dataset. Future refinement and application of this technology may see biofeedback approaches being developed to inform AT training and rehabilitation programs.

REFERENCES

[1] Pizzolato C et al. *Br J Sports Med* **53**: 11-12, 2019
[2] Pizzolato C et al. *Front Bioeng Biotechnol* **8**: 878, 2020
[3] Needham L et al. *Sci Rep* **11**: 20673, 2021
[4] Devaprakash D et al. *J Appl Physiol* **132**: 956-965, 2022
[5] Cao Z et al. *IEEE Trans Pattern Anal Mach Intell* **43**: 172-186, 2021

Explaining Deep Learning Models for Age-related Gait Classification Based on Time-series Acceleration

Xiaoping Zheng[1], Michiel Reneman[2], Bert Otten[1] and Claudine Lamoth[1]
[1] Department of Human Movement Sciences, University of Groningen, Groningen, The Netherlands.
[2] Department of Rehabilitation Medicine, University of Groningen, Groningen, The Netherlands.
Email: X.Zheng@umcg.nl

INTRODUCTION

Gait pattern classification is important in healthcare for age and pathology related gait changes monitoring and classification [1]. To improved the gait classification performance, conventional machine learning (CML) has been widely used, which is based on handcrafted gait features extracted from accelerometer data. However, the extraction of handcrafted features is laborious, requires expert knowledge, and may lead to suboptimal classification performance. In contrast, end-to-end deep learning approaches such as convolutional neural networks (CNN) integrate feature extraction and classification within the neural network model, eliminating the need for handcrafted features and potentially leading to improved performance. While DL approaches may provide promising classification performance, their black-box character limits their use in healthcare decision-making [2].

Therefore, this study aims: 1) to compare the classification performance of 4 CML approaches (based on handcrafted gait features) with a CNN to classify age groups (adult vs. older adult) based on raw accelerometer data. 2) to increase the transparency in gait classification process for CNN by using Explainable Artificial Intelligence approach (XAI, e.g. layer-wise relevance propagation (LRP)).

METHODS

A total of 267 healthy adults were involved and divided into two groups: adult (18-65, n=130) and older adults (>65, n=137). Participants completed a 3-minute walking with a 3D-accelerometer (100 Hz) attached near the L3 lumbar segment. 36 gait features were extracted and used to train CML (Support Vector Machine (SVM), Naive Bayes, K-Nearest Neighbourhood, and Random Forest). The raw signal data were fed to CNN with 256-sample window size. The classification performance comparison of CNN and CML was evaluated by commonly used evaluation metrics (e.g. the area under the receiver operating characteristic curves (AUC)). The CNN classifier model was explained by LRP. Higher absolute LRP values mean more relevant to the classification.

RESULTS AND DISCUSSION

Table 1 Classification performance comparison.

	Accuracy	AUC	Precision	Recall	F-score
CNN	0.88	0.93	0.83	0.96	0.89
SVM	0.74	0.83	0.74	0.74	0.74

Table 1 shows the classification performance of CNN and SVM (the best performing CML). CNN outperformed SVM in all accuracy metrics by a significant margin. This supports that CNN is more effective than CML and eliminates the need for handcrafted features. In Figure 1, the absolute LRP values visualized the key signal regions for classification. The figure shows that the signals during heel-strike play a significant role in distinguishing between the adult and older adult groups. Higher LRP values in these regions may indicate distinct movement patterns and aid in age group differentiation.

CONCLUSIONS

DL such as CNN outperformed CML in gait pattern classification and does not need handcrafted features. The use of XAI techniques, such as LRP, increases the transparency of DL and holds great potential for applicating in clinical gait analysis to support medical decision-making in the future.

REFERENCES

[1] Liu X et al. *J Front. Comput. Sci.* **3**: 661676.
[2] Zhang Z et al. *Ann. Transl. Med.* **6**: 11.

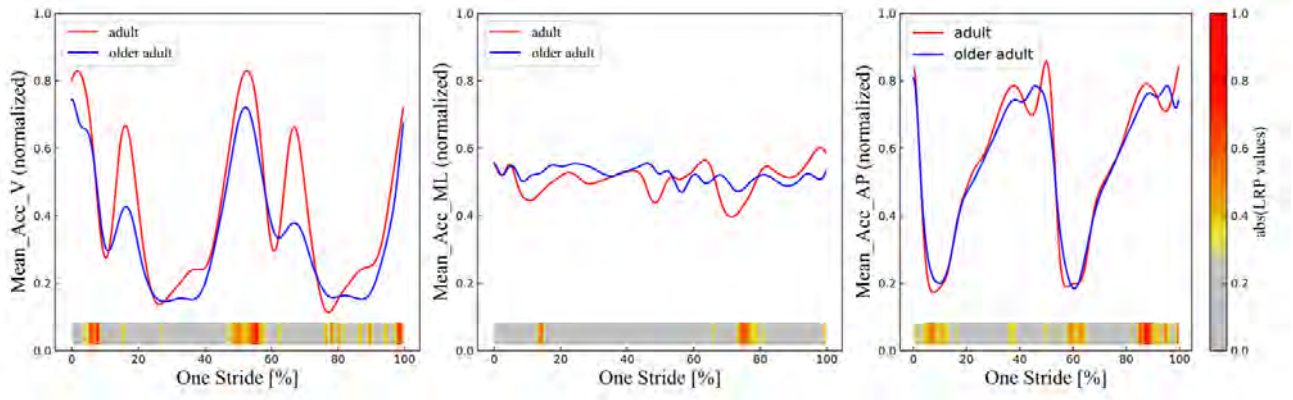

Figure 1: absolute layer-wise relevance propagation values for one stride acceleration. Acc: acceleration; V: vertical (pointed to ground); ML: medio-lateral (pointed from left to right); AP: Anterior-posterior (pointed to walking direction)

Transfer Learning with Simulated and Recorded Data Improves Predictions of Upper Extremity Biomechanics

Kalyn M. Kearney[1], Tamara Ordonez Diaz[1], Joel B. Harley[2], Jennifer A. Nichols[1]
[1] J. Crayton Pruitt Family Department of Biomedical Engineering, University of Florida, Gainesville, United States
[2] Department of Electrical and Computer Engineering, University of Florida, Gainesville, United States
Email: kalynkearney@ufl.edu

INTRODUCTION

Machine learning is a powerful tool for modeling complex human movements. However, the high cost of acquiring biomechanical data often limits observations and therefore the generalizability of these models. Meanwhile, there is untapped utility in musculoskeletal models for informing machine learning predictions. Transfer learning, the process of training a machine learning model on one task (e.g. simulated data) and re-purposing this knowledge for another task (e.g. measured data), has therefore emerged as a potential tool for predicting human movement [1,2].

Our objective was to create and validate transfer learning frameworks that use artificial neural networks to model complex upper extremity movements. Specifically, we modeled lateral pinch, a task involving the combined, redundant effort of muscles acting about the wrist and thumb. Our results elucidate the impact of transfer learning on machine learning model accuracy and exemplify how this technique may be used to improve predictive models of human movement.

METHODS

We developed feedforward (FF) and long short-term memory (LSTM) neural networks to regress three-component lateral pinch thumb-tip forces from eight muscle activations. We trained and tested two versions of each neural network. The first was trained solely on recorded data. The second was a transfer-learning model that was pre-trained with simulated data and fine-tuned on recorded data (Fig. 1, left).

To provide observations to the transfer learning models, we generated 6,594 lateral pinch simulations using a thumb model [3] and OpenSim v. 4.1. Each simulation included a unique combination of scaling (young adults [4]) and target force (40 to 80 N). Simulation-derived muscle activations were neural network inputs and thumb-tip forces were outputs.

To train and test the neural networks, we recorded experimental data. These data were recorded from five female and three male, right-handed, young adults (IRB#202202263). Muscle activity was recorded using fine-wire electromyography (EMG) collected at 3000 Hz from eight muscles. Simultaneously, lateral pinch force was collected using a 6-axis force sensor. During data collections, subjects performed three 5-second maximum voluntary contractions of lateral pinch with 30 seconds of rest between each. Each neural network was trained on the same seven subjects' data, with one subject's data used for testing.

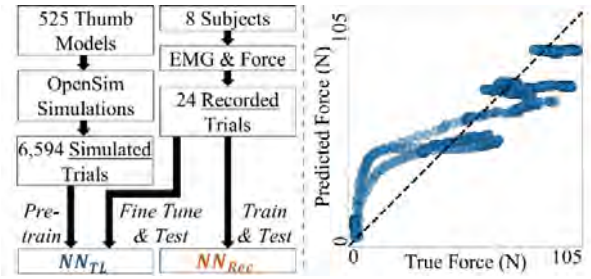

Figure 1: Framework used to develop neural networks informed via recorded data and transfer learning, denoted NN_{Rec} and NN_{TL}, respectively (left). Parity plot for LSTM developed via transfer learning when predicting on the test subject's data (right). The forces displayed represent thumb-tip force magnitude.

RESULTS AND DISCUSSION

Neural networks trained on recorded data alone underperformed relative to their transfer learning counterparts. Test predictions of FF and LSTM models trained only on recorded data had mean absolute errors (MAEs) of 6.9 N and 5.9 N, respectively. By comparison, FF and LSTM models developed via transfer learning achieved MAEs of 6.0 N and 5.6 N. The LSTM developed via transfer learning (Fig. 1, right) outperformed every other model and maintained generalizability to distal and palmar thumb-tip forces. These results indicate that pre-training neural networks on simulation data enhances model generalizability. Furthermore, our approach can be easily adapted and applied to predict other movements.

CONCLUSIONS

Our work suggests that machine learning models of human movement can benefit from the knowledge contained in musculoskeletal simulations. Through continued efforts, models with greater generalizability to real-world conditions may be achieved.

ACKNOWLEDGEMENTS

Funding from National Science Foundation Graduate Research Fellowship (DGE-1842473) and National Institutes of Health (NIBIB R21 EB030068).

REFERENCES

[1] Park et al. 2020. IEEE Robot Autom Lett.5.2: 3525-3532 [2] Dao, TT. 2019. Med Biol Eng Comput. 57: 1049-1058. [3] Nichols et al. 2017. J Biomech. 58: 97-104. [4] Fryar et al. 2016. Vital Health Stat 3. 39: 1-46.

Validity and reliability of 3D markerless motion capture using low-cost cameras

Victor Cossich[1], Conrado Laett[2], Andressa Lemos[3], Inaê Marcelo[3], Frederico Brasil[3], Felipe P Carpes[3]

[1] Sport Technology Research Laboratory, Faculty of Kinesiology / University of Calgary, Calgary, Canada.
[2] Neuromuscular Research Laboratory / INTO, Rio de Janeiro, Brazil.
[3] Laboratory of Neuromechanics, Federal University of Pampa / Uruguaiana, Brazil.
Email: victor.cossich@ucalgary.ca

INTRODUCTION

3D motion capture is widely used to evaluate human biomechanics [1]. Innovative markerless systems have emerged as an alternative to expensive and time-consuming reflexive marker-based methods using computer vision and machine learning to track motion without physical markers [2]. Here we set out to determine the validity and reliability of lower limb angular kinematics and centre of mass (CoM) displacement obtained using a markerless system using low-cost webcams compared to a gold standard system.

METHODS

Eighteen participants (26.2 ± 6.3 years) performed a countermovement akimbo protocol, consisting of 10 trials (30 seconds rest) in a test-retest design. Data were collected with a Vicon Motion System (15 cameras, Bonita B10, sampling at 100 Hz, 21 reference markers, Plug-in Gait model) and a markerless system using pre-trained artificial intelligence model and a custom-built triangulation algorithm using Python (2 cameras, Logitech C270, sampling at 30 Hz) operating simultaneously. Signals Position data were filtered (low-pass, 2nd order, Butterworth, 5 Hz cut-off). The right hip and knee sagittal plane angular movements were calculated. Validity was assessed using Statistical Parametrical Metrics (SPM) 1D and reliability was assessed using paired t-test and intraclass correlation (ICC) using take-off peak angles and the maximal jump height.

RESULTS AND DISCUSSION

SPM revealed a consistent signal pattern between both systems (Figure 1). We did not observe significant test-rest differences, and good to very good ICC values were found (Table 1). Further analysis should include the ankle joint and the analysis of bilateral asymmetries.

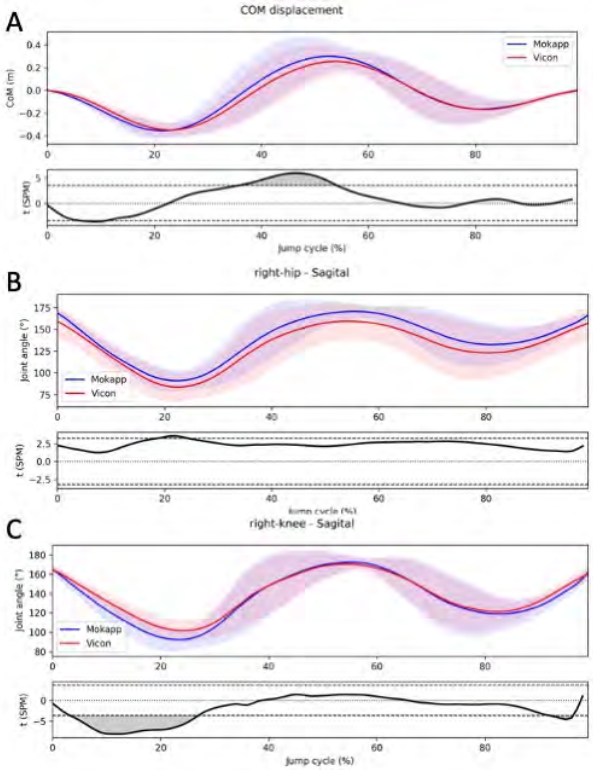

Figure 1. CoM displacement (A), hip (B), and knee (C) kinematics plotted with mean signal represented by lines and standard deviation represented by a shaded area. Markerless data are shown in blue and Vicon data are shown in red. The bottom panel showed the SPM outcomes with the grey-shaded area indicating a significant difference.

CONCLUSIONS

3D markerless motion capture using off-the-shelf, low-cost cameras accurately tracked hip, knee, and CoM kinematics during a countermovement jump.

REFERENCES

[1] Drazan et al. *J Biomech* **125**: 110547, 2021.
[2] Kanko et al. *J Biomech* **127**: 110665, 2021.

Table 1: Test-retest Reliability for Key Measures of Maximum Vertical Height, Hip and Knee kinematic during a Countermovement Jump

	Test	Retest	p-value	ICC
Maximum Vertical Height (m)	0.37 ± 0.09	0.37 ± 0.08	0.27	**0.96**
Hip Take-off (°)	86.3 ± 12.3	89.1 ± 12.5	0.29	**0.80**
Knee Take-off (°)	88.2 ± 10.7	89.5 ± 12.6	0.58	**0.80**

AUTOMATIC MULTI-STRUCTURE PEDIATRIC KNEE BONE SEGMENTATION USING OPTIMAL MULTI-LEVEL OTSU THRESHOLDING TECHNIQUE

Nandhini K[1], Guess T[2], Stylianou A[3], Duren D[2], Pacicca D[4], Mutsvangwa T[5], Bhushan Borotikar[1]

[1] Symbiosis Centre for Medical Image Analysis (SCMIA), Symbiosis International University, Pune, India.
[2] School of Medicine, University of Missouri, Columbia, MO, USA.
[3] School of Science and Engineering, University of Missouri Kansas City, Kansas City, MO, USA.
[4] Department of Orthopedics, Connecticut Children's Medical Center, Connecticut, CT, USA.
[5] Division of Biomedical Engineering, University of Cape Town, Cape Town, South Africa.
Email: Bhushan.borotikar@gmail.com

INTRODUCTION

Radiologists find MRI interpretations of pediatric knee joints challenging, especially the ones with growth plates [1], [2]. Pediatric MRI's low-level information on thin structures such as cortical bone or growth plate create complexity. In such cases, thresholding-based methods (including binary or multilevel thresholding) are typically used to uncover the intensity profile ranges of different classes [3]. However, current automatic segmentation methods do not use any thresholding techniques. The main contribution of this study was to introduce a new multilevel thresholding-based training framework as a separate input channel to a deep learning 3D-UNet model to improve the performance of the segmentation.

METHODS

The proposed framework involved following steps: 1) The MR image dataset was passed to the Multi-level Otsu algorithm which divided it into different classes and for each class, number of thresholds were estimated. 2) For each class, optimal thresholds were identified by the multi-Otsu algorithm and threshold images were reconstructed. 3) The images were then used in the UNet training model as an input channel. 4) After training, a post-processing algorithm (removal of small objects, largely connected components etc.) was performed to enhance the quality of the segmented outputs.

Retrospectively acquired pediatric knee MRI datasets (n = 20) of girls (age 13 to 16 years) were used in this study (3.0T scanner, 3D GRE sequence). Each dataset was manually segmented for training using 3D Slicer toolbox. Labels considered for this study are Trabecular (femur proximal, fibula distal, tibia distal), cortical (femur, tibia, fibula) and others (Femur distal, fibula proximal, tibia proximal. For Multi-Otsu algorithm the number of classes assigned for each individual label were three. The proposed method was compared with existing meta-heuristic thresholding method and Baseline 3D-UNet model using metrics of DICE (similarity index), Hausdorff distance (HD), Root Mean Square Error (RMSE), and Mean Absolute Error (MAE). The AdamW optimizer was used with 600 epochs and the channel size of 16, 32, 64, 256.

RESULTS AND DISCUSSION

Histogram thresholding method performed poorly and failed to identify the homogeneity intensity issue (Table 1). Baseline 3D-UNet model performed better for labels with larger spatial size such as trabecular region, but performance declines with smaller spatial size such as cortical regions (Table 1). The proposed framework performed better than the other two algorithms in all the regions except for cortical femur (Table 1). This could be due to fuzzy intensity ranges that may have failed to fit within defined class of multi-Otsu.

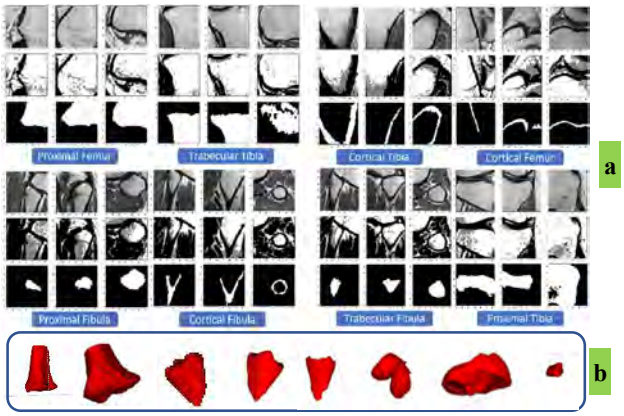

Figure 1 (a) Threshold images generated based on optimal Multi-Otsu algorithm. (b) Segmentation output using proposed model

CONCLUSIONS

This study focused on eliminating the issue of intensity homogeneity in pediatric MRI and proposed a Muti-level thresholding approach to be integrated with a deep learning model for training. This work is limited with bone segmentation application. Future research can be directed towards combining multi tissue and bone structures for pediatric knee segmentation.

REFERENCES

[1] Pai DR et al., AJR, 1019-1027,2011.
[2] Kuwabara A et al., Cur. Rev. Msk. Med., 2021
[3] Ping-Sung L et al., J. Inf. Sci. Eng. 17(5), 2001.

Table 1: Comparative analysis of Proposed framework of Multi-level Otsu+ 3D UNet with other models.

Performance	Baseline 3D-Unet				Histogram + 3D-UNET				Proposed Multi-OTSU + 3D-UNET			
	Dice	***HD***	***RMSE***	***MAE***	***Dice***	***HD***	***RMSE***	***MAE***	***Dice***	***HD***	***RMSE***	***MAE***
Mean	**0.82**	179.61	0.072	0.008	**0.35**	172.94	0.146	0.030	**0.85**	109.81	0.059	0.005

A METHOD OF DETECTING HUMAN MOVEMENT INTENTIONS IN REAL ENVIRONMENTS

Yi-Xing Liu[1], Zhaoyuan Wan[1], Ruoli Wang[1], and Elena M.Gutierrez-Farewik[1,2]

[1]KTH MoveAbility Lab, KTH Royal Institute of Technology, Stockholm, Sweden.

[2]Department of Women's and Children's Health, Karolinska Institutet, Stockholm, Sweden.

Email: lyixing@kth.se

INTRODUCTION

Accurate and timely movement intention prediction can facilitate exoskeleton control during transitions between different locomotion modes [1]. Detecting movement intentions in real-environments remains a challenge due to unavoidable environment uncertainties [2]. False movement intention detection may also induce risks of falling and general danger for exoskeleton users. To this end, in this study, we aimed to develop a method for detecting human movement intentions in real environments. The proposed method is capable of self-correcting by implementing decision fusion and deep Bayesian neural network [2].

METHODS

Data was collected on 2 able-bodied subjects, including environment images and 3D gaze points from a portable eye tracker (Pupil Core), and linear accelerations and angular velocities from IMU sensors (Cometa System) during level ground walking, ramp ascent, ramp descent, stair ascent, and stair descent were used to preliminarily evaluate the feasibility of the proposed method. In total seven IMU sensors were placed on lower limbs and pelvis of the participants. All data were segmented and labelled as different locomotion modes. Eighty percent of the total data were used for training: four temporal features extracted from all gaze points and IMU sensor signals within an analysis window of 150 ms were concatenated and used as inputs to train the prediction model for movement intention detection with a deep Bayesian neural network [2]. Images from the scene camera on the eye tracker were used to train the prediction model for identifying terrains with a deep convolutional neural network [3]. All neural network models were trained carefully to avoid overfitting. During the testing process, the remaining 20% of gaze points and IMU signals were used for movement intention detection and the images for terrain identifications. Decision fusions were then made based on the detected movement intentions and the identified terrains (Figure 1).

RESULTS AND DISCUSSION

Based on our preliminary test, fusing gaze points and IMU signals achieved higher prediction accuracy than only using IMUs for movement intention detections. Fusions at the decision level further improved the prediction accuracies by correcting partial false detections from the previous step (Table 1). For instance, we found that the intentions from walking to ramp ascent which were incorrectly detected as from walking to walking were corrected by the identified terrain, i.e., the next terrain was ramp instead of level ground. Data collection and method evaluation in real environments are currently. underway. More locomotion modes, participants, and complex terrains, for instance, mud, concrete, and grass will be investigated.

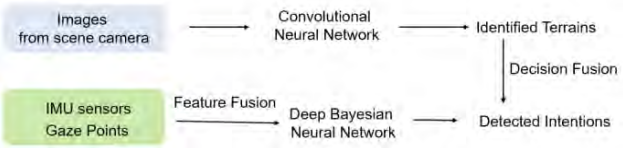

Figure 1 Framework of the proposed method

Table 1 Overall prediction accuracy (%) among locomotion modes, with and without feature fusion and decision fusion

	Without Decision Fusion	With Decision Fusion
Pure IMUs	87.7	–
IMUs+Gaze Points	90.2	96.4

CONCLUSIONS

This study proposed a new method of detecting human movement intentions using and eye tracker and IMU sensors. The overall prediction accuracy was increased by fusions at two levels: 1) at the feature level, fusing gaze points with IMU sensor signals for detecting movement intention; 2) at the decision level, fusing decisions of identifying terrains from images with the previously detected movement intentions from gaze points and IMUs. We believed that the proposed method could potentially improve the robustness of movement intention detection in real environments.

ACKNOWLEDGEMENTS

This project was generously funded by the Promobilia Foundation (ref nr 18200 and A22083).

REFERENCES

[1] Tucker et al., *J. Neuroeng. Rehabili.*, 2015.
[2] Zhong et al., *IEEE Trans. Autom. Sci. Eng.*, 2021.
[3] Al-dabbagh et al., *Robot. Auton. Syst.,* 2020.

DIFFERENCES IN JOINT KINEMATICS BETWEEN SNATCH AND CLEAN LIFTS IN WEIGHTLIFTING

Ganbat Tumen-Ulzii[1], Munkhbat Tumurbaatar[1], Khosbayar Tsenkherjav[2] and Batbayar Khuyagbaatar[1]
[1]Department of Technical Mechanics, Mongolian University of Science and Technology, Ulaanbaatar, Mongolia
[2] Mongolian Weightlifting Federation, Ulaanbaatar, Mongolia
Email: batbayarkh@must.edu.mn

INTRODUCTION

The snatch and clean and jerk are the main lifting techniques involved in the competition. Both techniques start with the same movements until the second pull phase, then the body movement is differentiated during the turnover, catch, and recovery phases [1]. Few studies have studied the bilateral comparison of kinematic parameters between the snatch and clean techniques. In this study, we have investigated the kinematic difference between the two techniques using wearable inertial sensors.

METHODS

In this study, seven female Mongolian weightlifters participated. Two test sessions were carried out to record body movements using the wearable inertial sensors (Wearnotch, Notch Interface Inc), which were attached to the chest, waist, arm, forearm, thigh, and shank using the straps. The first tests were snatch followed by clean. Each participant performed three snatch and clean lifts at 70 % of the one-repetition maximum. The shoulder, elbow, hip, knee, and trunk joint angles were calculated, normalized, and averaged for two different techniques using Matlab® [2]. The lifting phases were defined for the snatch and clean [1,3]. The barbell velocity at the 2nd pull phase was estimated using the sensor on the forearm. An independent sample t-test was used to compare the mean values of joint angles during the snatch and clean with a significant level of 0.05.

RESULTS AND DISCUSSION

The maximum shoulder abduction, shoulder flexion, elbow extension, knee extension, hip extension, and trunk extension were 82°/56°, 164°/87°, 185°/172°, 127°/154°, 137°/166°, 161°/164° in the snatch/clean, respectively (Figure 1). The joint movements were significantly different except for the hip and knee joints ($p<0.05$). Arm movements are different in two techniques; such as lifters moving the barbell from the floor to overhead in the snatch and the shoulder in the clean. Similar hip and knee angles were observed which is known to elicit the greatest amount of power output during the pulling phases. The barbell velocity was higher in the snatch (1.14 ± 0.51 m/sec) than in clean (1.07 ± 0.66 m/sec) ($p=0.68$), which was similar to the previous studies, where they reported that 1.65–2.28 m/sec during the snatch and 0.88–1.78 m/sec during the clean [1,3].

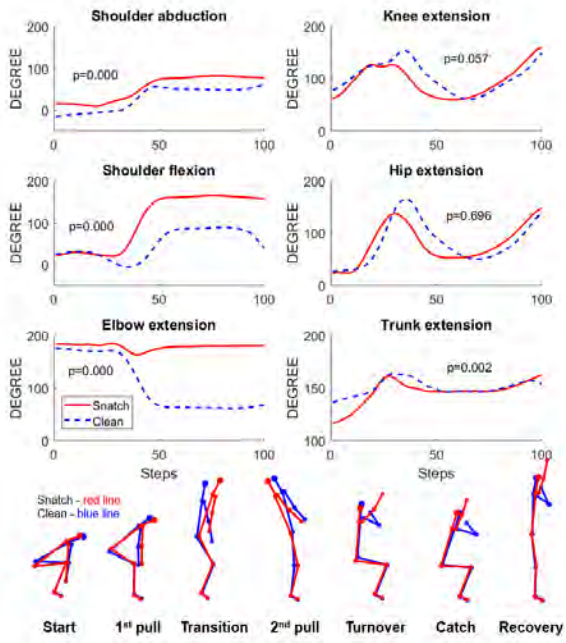

Figure 1 Joint angles during the snatch and clean with p-value

CONCLUSIONS

We investigated the joint angles and barbell velocity to find the difference between the snatch and clean technique using wearable inertial sensors. Although some of the information is known to coaches and athletes, it is better to be aware of the detailed body segment movements. This study provides a kinematic comparison between the snatch and clean lifts, which may help to understand the similarities between the two techniques and enable us to best prescribe the appropriate exercises.

ACKNOWLEDGEMENTS

This work was supported by the "Mongolia-Japan Engineering Education Development" project (J24C16) and the Mongolian University of Science and Technology (mfund-052022).

REFERENCES

[1] Werner I et al. *Front. Psychol.* **11**:606070, 2021.
[2] Choi YC et al. *Int J Precis Eng Manuf*, **22**:1105-12, 2021.
[3] Ho LKW et al., *J. Strength Cond Res,* **28**:574–586, 2014.

Comparison of ballistic training and complex training on explosive performance in upper limbs

Hsiang-Hsin Wang[1], Jia-Zhen Li[2], Yan-Hao Chen[2] and Yun-Cheng Lin [3*]
[1]Department of Sports Training Science-Combats, National Taiwan Sports University, Taoyuan City, Taiwan.
[2] Graduate Institute of Physical Education, National Taiwan Sports University, Taoyuan City, Taiwan.
[3] Center of Sports Development and University Social Responsibility, National Taiwan Sports University, Taoyuan City, Taiwan.
Email: yuncheng@ntsu.edu.tw

INTRODUCTION

Ballistic training (BT) allows the athlete to accelerate a light load as fast as possible with no deceleration phase, which improves neural factors, including motor-unit recruitment, and to develop explosive strength. Complex training (CT) is a resistance training that comprision of heavy load resistance training to induce post-activation potentiation (PAP), followed by a matched light load and higher velocity training. Both types of training have been proved to improve velocity and explosive performance, but which is the best training method to enhance velocity and explosive power has attracted the attention of coaches and athletes. Hence, this study aimed to compare the training effects between BT and CT. Secondly, this study could provide practical support and sugesstion to strength and conditioning professionals/coaches working in competitive environments to aid in strength development of their athelets.

METHODS

Twenty-four health college students were recruited and divided into a ballistic training group (BTG, n=12) and a complex training group (CTG, n=12).

Two training groups completed an 8-week resistance training program that included 3 training sessions per week. The subjects of BTG performed bench throw (figure 1) with 40% 1RM. The subjects of CTG performed bench press with 85% 1RM at first set, then completed the final two sets of bench throw training with 40% 1RM.

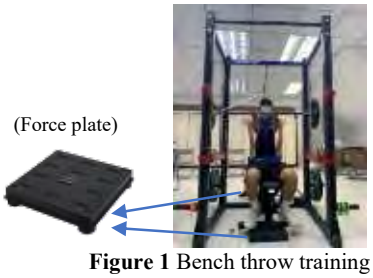

Figure 1 Bench throw training and test.

Before and after the resistance training, two force plates (force plate, PASCO, California, USA) be used to test the maximum voluntary contraction and the height of push-ups (PH), then calculate the rate of force development during the bench press. (RFD_{50ms}, RFD_{100ms}, RFD_{max}). Data of baseline and enhancement percentage of training effects between both groups were analyzed using Independent-Sample t-Test. The Paired Samples t-test was used to compare the difference between pre-test and post-test. $\alpha = .05$.

Figure 2 The height of push-up test.

RESULTS AND DISCUSSION

Both groups have significant improvements in explosive power (RFD_{50ms}, RFD_{100ms}, RFD_{max}), and height of push-up ($p<.01$). However, the enhancement percentage of RFD_{max} in CT was significantly higher than BT ($p<.01$).

Table 1: Comparison of dependent variables between pre and post test.

	G	Pre-test *M (SD)*		Post-test *M (SD)*		*t-value*
RFD_{50ms}	BT	966.37	(223.4)	1219.59	(355.4)	-5.518**
(Ns^{-1})	CT	975.44	(246.4)	1195.99	(249.6)	-7.269**
RFD_{100ms}	BT	1852.12	(438.2)	2307.97	(471.3)	-12.013**
(Ns^{-1})	CT	1846.41	(447.9)	2360.06	(513.5)	-9.945**
RFD_{max}	BT	2257.79	(550.2)	2621.78	(566.3)	-8.456**
(Ns^{-1})	CT	2243.35	(640.2)	2783.30	(735.1)	-8.196**
PH	BT	14.96	(2.53)	17.57	(3.44)	-3.558**
(cm)	CT	14.91	(2.17)	17.15	(3.59)	-4.939**

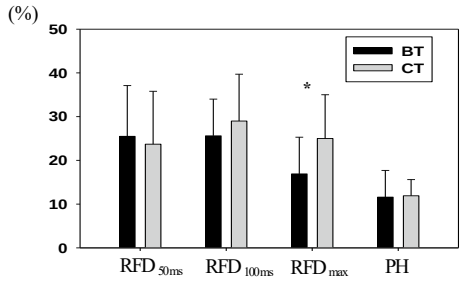

Figure 1 The percentage of enhancement of the two groups

Ballistic training could induce specific changes in the force-velocity relationship to improve the athlete's initial force rate performance [1]. However, complex training trigger post-activation potentiation and produce a better explosive power enhancement effect [2].

CONCLUSIONS

Both BT and CT are effective training methods for developing explosive strength and contraction speed. Probably because of PAP, the enhancement percentage of RFD_{max} in CT is significantly better than that of BT.

ACKNOWLEDGEMENTS

The experiment is supported by the National Science and Technology Council, Taiwan. (110WFA9810029_BASE).

REFERENCES

[1] Cormie P et al. *SC Journal* **30:** 67-69, 2008.
[2] Ju´arez D et al. *IE Science* **17:** 233-241, 2009.

USING LANDING ERROR SCORING SYSTEM WITH AUTOMATED JOINT ANGLE TRACKING AS A SCREENING TOOL TO PREDICATING LOWER EXTREMITY SPORTS INJURIES FOR ATHLETES: A PROSPECTIVE STUDY

Hsiao-Yun Chang[1,*], Chun-Wen Chiu[2], Yun-Cheng Lin[1], Hung-Chueh Chen[3], and Chu-Ling Lo[4]
[1] Department of Athletic Training and Health, National Taiwan Sport University, Taoyuan, Taiwan
[2] Department of Sport Training Science - Ball, National Taiwan Sport University, Taoyuan, Taiwan
[3]College of Exercise and Health Sciences, National Taiwan Sport University, Taoyuan, Taiwan
[4]Department of Physical Medicine, Cheng Ching General Hospital, Taichung, Taiwan
Email: yun1130@ntsu.edu.tw

INTRODUCTION

Landing Error Scoring System (LESS) is one of the movement detection methods, that are often used on the sports sideline to predict risk of lower limbs injuries [1]. It can be used to evaluate the good or fail mechanism of jump-landing technique. Although LESS is a convenient way to manually assess the risk of lower limb injury, the agreement and validity of individual scoring items are still incomparable with the 3D motion analysis system in the laboratory[2,3]. The system of this study was using image recognition and automatic joint angle tracking method. It can track the joint range of motion (ROM) and between-limb distance on individual scoring items, so it can understand the details of jump-landing technique for individual scoring items. Therefore, the purpose of this study was to use the image recognition and automatic joint angle tracking to assessed LESS score and prospectively tracking the injury rate of lower limb of athletes for half-year as a predictor of the risk of lower limb sports injuries.

METHODS

Twenty-six collegiate athletes (10 women and 16 men, age= 20.4 ± 0.72 years, height= 169.5 ± 7.9 cm, weight= 65.4 ± 9.7 kg) performed 3 jump-landing trials that were recorded by 2 web cameras (Logitech C920 Full HD Pro web cam) in the front and lateral side of the participates (Figure 1). For the jump-landing assessment, participants jumped from a 30-cm-tall box to a designated area in front of the box. We instructed them to complete a maximal vertical jump immediately after landing in the designated area. The web cameras were controlled by a laptop computer with a self-written ROM tracking software (written with Labview VISION module). The values obtained from 3 trials were averaged to obtain a participant's LESS score. After data collection, one researcher (H.Y.C.) evaluated the recorded video data and scored the LESS. After jump-landing assessment, all participants were followed half-year by one researcher (H. C. C.) at each week by using telephone tracking to identify those who subsequently suffered any sports injury. IBM SPSS Statistics for Windows was used for data analysis. The participants according to their LESS scores divided into the Good group (LESS score ≦5) and Poor group (LESS score >5). The Chi-square test was used to compare of the differences in the manual grading LESS scores and injury rate between Good and Poor groups. The independent T-test was used to compare of the ROM differences in each item of the LESS assessment (17 items). Significance was set at $P < .05$.

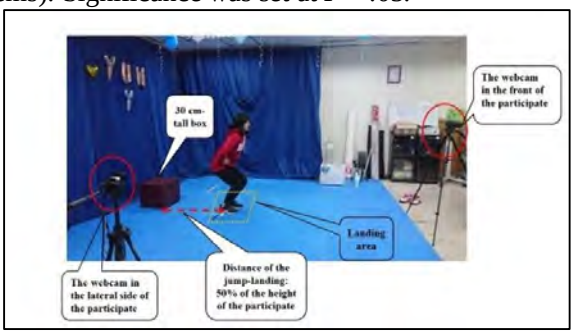

Figure 1 Experiment setup.

RESULTS AND DISCUSSION

The results indicated that significant better in LESS score for the Good group (3.92±0.9) than the Poor group (6.6±1.0) (p=.00); However, there was no significant difference between both groups for lower extremity sports injuries (Good group: injury rate=35.70%, Poor group: injury rate=40%, $\chi^2_{(df=1,\ N=24)}$=0.046, p=.831). Among the joint ROM, the mean hip ROM in maximum knee flexion (p=.011), hip joint displacement (p=.02), mean maximum knee flexion ROM (p=.025), knee joint displacement (p= .018) and the hip joint displacement greater than 45 degrees in the maximum knee flexion (p=.001) were reached a significant difference, and the rest of the items did not reach a significant difference. In total, the joint ROMs in the Good group were better than that of the Poor group; there is no significant difference between the lower limb sports injury rate and the ROM in each LESS items.

CONCLUSIONS

The Good group had better joint ROM and displacement than the Poor group; However, there was no significant difference between both groups for lower extremity sports injuries rate. It may need more tracking period and more participates to clarity the results.

ACKNOWLEDGEMENTS

The funding was supports by National Science and Technology Council, Taiwan (No.: MOST 111-2410-H-179-006)

REFERENCES

[1] Padua DA et al. *Am J Sports Med* **37**: 1996-2002, 2009.
[2] Smith HC et al. *Am J Sports Med* **40**: 521-6, 2012.
[3] Mauntel TC et al. *J Athl Train* **52**: 1002-9, 2017.

PROFILE OF HIP ROTATIONAL RANGE OF MOTION FOR THE HEALTHY COLLEGIATE BASEBALL PLAYERS

Chun-Wen Chiu[1, *], Hsin-Min Wang[2], Cheng-Hsun Hsieh[2] and Hsiao-Yun Chang[3]
[1] Department of Sport Training Science - Ball, National Taiwan Sport University, Taoyuan, Taiwan
[2] Bachelor Program of Athletic Performance, National Taitung University, Taitung, Taiwan
[3]Department of Athletic Training and Health, National Taiwan Sport University, Taoyuan, Taiwan
Email: cjw19800310@ntsu.edu.tw

INTRODUCTION

Adequate flexibility is an essential factors for athletes performance, neither for baseball players. Repeative loading in lower extremities during throwing for baseball players may lead to hip and groin injuries [1]. Limitation of hip range of motion (ROM) may alter throwing or hiting kinetmatics and affect the transfer of energy form lower to upper extremities, eventually influence the players' performance[2]. Hence, it is necessary to understand the hip ROM of the baseball players. Therefore, the purpose of this study was to examine the hip rotational ROM and to compare the difference between dominant and non-dominant hip for the healthy collegiate baseball players.

METHODS

Fifteen healthy collegiate male baseball players were recruited to participate this study (Height: 178.9±7.8 cm, weight: 81.0±13.4, age: 18.1±0.4). The demography of the participates are list in Table 1. The hip rotational ROMs were taken in sitting position with using plastic goniometer, included internal and external rotation (IR and ER) (Figure 1). Total rotation ROM was obtained by summing the internal and external rotation measures from each limb. Both of limb were measured randomly. All of the hip ROM measurement were tested by one researcher (C. W. C.). The hip IR or ER ROM deficit were calculated by the following formula:

*Hip IR or ER deficit (%) = [(dominant hip ROM-nondominant hip ROM)/nondominant hip total rotation]*100*

IBM SPSS Statistics for Windows (version 20.0; Armonk, NY: IBM Corp.) was used for analysis the results. The Paired t-test was used to analyse and compare the difference of hip IR, ER, and total rotation between dominant and non-dominant side. An α-value set at .05.

RESULTS AND DISCUSSION

Tables 1 show the descriptive values for hip IR, ER, and total rotation from the collegiate baseball players. No significant side-to-side differences ($p > .05$) were found in hip IR or ER in the collegiate baseball players. Additionally, total rotation ROM did not differ between extremities in the collegiate baseball players. The result of the hip IR deficit was presented with 3.04±7.86% and the hip ER deficit was 0.77±8.05%. The hip IR deficit was more than the hip ER deficit. It was indicated that we need to pay attention to hip IR deficit.

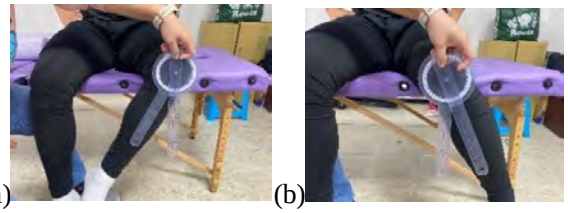

(a) (b)

Figure 1 The hip rotational ROM assessment. (a) external rotation (ER), (b) internal rotation (IR).

RESULTS

Tables 1 show the descriptive values for hip IR, ER, and total rotation from the collegiate baseball players. No significant side-to-side differences ($p > .05$) were found between the dominant and non-dominant hip in IR or ER in the collegiate baseball players. Additionally, total rotation ROM did not differ between extremities in the collegiate baseball players. The result of the hip IR deficit was presented with 3.04±7.86% and the hip ER deficit was 0.77±8.05%. The hip IR deficit was more than the hip ER deficit. It was indicated that we need to pay attention to hip IR deficit.

CONCLUSIONS

In summarize, the healthy collegiate baseball players were no side-to-side differences in hip IR, ER, and total rotation ROM. But, the hip IR deficit was more than the hip ER deficit. It was indicated that we need to pay attention to hip IR deficit for healthy baseball players.

REFERENCES

[1] Mlynarek RA et al. *Curr Rev Musculoskelet Med* **11**: 19-25, 2018.

[2] Plummer HA et al. *Int J Sports Phys Ther* **16**: 1323-9, 2021.

Table 1: Hip Rotation Range of Motion for the collegiate baseball players

Range of Motion	Dominant	Non-dominant	*t*	*p*	Cohen's *d*#
Hip ER, deg	44.5± 8.7	44.2±11.7	.168	.869	0.03
Hip IR, deg	50.7±14.7	48.1±11.9	1.365	.194	0.2
Total Rotation, deg	95.3±14.7	92.3±14.4	1.071	.302	0.21

Note: ER: External Rotation; IR: Internal Rotation; deg, degrees

BIOMECHANICAL PATTERNS ASSOCIATED WITH KNEE INJURY IN FEMALE FUTSAL PLAYERS DIAGNOSTIC WITH THE CHANGE OF DIRECTION AND ACCELERATION TEST (CODAT): A CROSS-SECTIONAL ANALYTICAL STUDY

Ferrandez-Laliena, L[1], Vicente-Pina, LP[1], Sanchez-Rodriguez, R[1], Heredia-Jimenez, J[2], Orantes-Gonzalez, E[3]
Lucha-Lopez, MO[1], Hidalgo-Garcia, C[1], Tricas-Moreno, JM[1]

[1] Physiotherapy Research unit, Faculty of Health Science, University of Zaragoza, Zaragoza, Spain
[2] Department of Physical Education and Sports. Human Behaviour & Motion Analysis Lab (HubemaLab), University of Granada, Ceuta, Spain
[3]Department of Sports and Computer Science, Faculty of Physical Education and Sports, University of Pablo de Olavide, Sevilla, Spain
Email: lferrandez@unizar.es

INTRODUCTION

Anterior cruciate ligament (ACL) is the most common knee ligament injury. Its incidence is 3 times higher in female soccer players than males, and usually it is caused by a non-contact mechanism[1]. This is due to a failure in biomechanical pattern. Studies showed a compilation of the main biomechanical risk factors thresholds which explain the "perfect loading storm" that defines the ACL injury mechanism, being the valgus collapse the main biomechanical risk factor related to ACL injury [1,2]. Latest researches have studied the incidence ratio by limb dominance condition, because in futsal the ball determinates the biomechanics pattern. The primary aim of this study was to identify kinematic differences at initial contact between female futsal players with and without previous knee injury, in a functional motor pattern test. The secondary aim was to determine kinematic differences between dominant limb (DL) and non-dominant limb (NDL) in the hole group, in the same test.

METHODS

Sixteen futsal female players volunteered to participate in the study, aged 23.4 + 5.03 years. Allocation depended on clinical history: previous knee injury (KI), by valgus collapse mechanism without surgical intervention, or no injury, that conformed the control group. The evaluation protocol included the functional test change of direction an acceler-ation test (CODAT) which was recorded ones with DL and NDL. A 3D motion capture system (Qualisys AB, Göteborg, Sweden) was used to analyze the kinematics of change of direction. Twenty-six reflective markers were placed. Visual3D software (C-Motion Inc., Germantown, USA) was used to analyze the change of direction task. Mean and standard deviation (in degrees) of the flexion/extension, adduction/abduction and internal/external rotation of the trunk, pelvis, hip and knee were computed, for the DL and the NDL.

RESULTS AND DISCUSSION

Knee valgus was significantly higher in the DL (9.02 ± 7.31 degrees) than in the NDL (1.27 ± 9.05 degrees) (p= 0.049), in the hole group. Our results showed a higher ACL injury risk motor pattern in DL than in NDL. "Valgus collapse" defined was the combination of hip adduction, hip internal rotation and knee abduction. In this study, in the DL, the limb which had a quantity of knee valgus near to injury risk threshold, KI players had more hip adduction than control players at the change of direction task (Cohen's d: 0.82). Therefore, KI group performing a kinematic pattern like the ACL injury pattern. Hip and knee internal rotation are involved in knee valgus definition [1,3]. In this study, both groups had knee internal rotation at the evaluation moment, but KI players had hip internal rotation in contrast to control players who developed hip external rotation (*Cohen's d:* 0.88). Nobody has studied the influence of the pelvic rotation yet. In our study, KI players made a contralateral pelvic rotation, following trunk motion direction. In contrast to control group, in which contralateral trunk rotation existed, combined with ipsilateral pelvic rotation to the DL (*Cohen's d:* 1.06). This might be a balance mechanism to counteract the opposite trunk rotation, and to decelerate medial velocities suffered by the knee because of the trunk rotation movement[4].

CONCLUSIONS

Our study found kinematic differences at initial contact between female futsal players with and without previous knee injury, in a motor pattern test. The players with no previous history of knee injury had more kinematic patterns to avoid the valgus collapse mechanism in the hip adduction and internal rotation and in the pelvis rotation in the DL. All the players showed more knee valgus in DL, which is the limb with more risk of injury, revealing the clinical relevance of the neuromuscular stabilization training for this limb.

KEY WORDS

Knee Injury; Kinematics; Soccer; Sports; Anterior Cruciate Ligament; Prevention; Physiotherapy; CODAT

REFERENCES

[1] Lucarno S et al. *Am J Sports Med* **49**: 1794-802, 2021.
[2] Di Paolo S at al. *Sport Biomech*, 2022.
[3] Della Villa F et al. *Br J Sports Med* **54**:1423–32, 2020.
[4] Critchley ML et al. *Sport Biomech* **19**: 421-437, 202

Reducing variability may not increase the success rate of motor task: Toward a proper interpretation of function

Arata Kimura [1], Hirotaka Nakashima [1]
[1] Department of Sport Science and Research, Japan Institute of Sports Sciences, Tokyo, Japan.
Email: arata.kimura@jpnsport.go.jp

INTRODUCTION

In darts or ball throwing, the release positions and velocities of the darts or ball (release parameters) may be systematically related so that deviations in one parameter are canceled out by compensatory changes in the other parameters [1,2]. The systematic relationship between release parameters reduces the variability of the ball or darts arrival position. However, it should be noted that such a systematic relationship between parameters does not always increase the success rate of the motor tasks (e.g. hitting rate to the target during the darts or ball throwing). Without recognizing this point, we might incorrectly conclude that the systematic relationship between parameters always has the function of increasing the success rate of motor tasks. Here our study will experimentally illustrate that the systematic relationship between release parameters may not increase the hitting rate to the target during ball throwing. Given the results of this experiment, our study attempts to discuss the proper interpretation of function.

METHODS

Twelve right-handed college baseball players participated in the study. Each participant threw 30 baseballs at two different-sized targets (small and large targets) aiming at a target 10 m away from the participants, for a total of 60 balls. Furthermore, the participants threw alternately with an overhand and a sidearm throwing. Therefore, the participants threw 15 balls with overhead throwing and 15 balls with sidearm throwing to a large target out of the 30 balls and did the same to a small target.

We identified the systematic relationship between the release parameters to reduce the variability of the ball arrival position and to increase the hitting rate to the target by using the method of the previous study [3]. The method identifies a systematic relationship by comparing the variability of the ball arrival position between measured and decorrelated surrogate data. The surrogate data can be produced by randomly reordering all release parameters across trials to remove all possible correlations among them. Then, the surrogate data are substituted into a forward dynamics model to determine the variability of the ball arrival position. A systematic relationship is present when the variability of the ball arrival position with surrogate data is higher than with measured data. Whether the systematic relationship increases the hitting rate to the target was examined by comparing the hitting rate of the surrogate and measured data.

RESULTS AND DISCUSSION

The variability of the ball arrival position with surrogate data was higher than with measured data in the small target (Figures 1A and 1B). It showed that the release parameters were systematically related to reducing the variability of the ball arrival position (Figures 1A and 1B). In other words, the release parameters had the function of reducing the variability of the ball arrival position. Furthermore, the systematic relationship between release parameters increased the hitting rate to the target (Figures 1A and 1B), indicating that the release parameters also had the function of increasing the hitting rate to the target. For the large target, the variability of the ball arrival position with surrogate data is higher than with measured data (Figures 1C and 1D). The result indicated that the release parameters had the function of reducing the variability of the ball arrival position. On the other hand, in contrast to the small target condition, the release parameters did not have the function of increasing the hitting rate to the target (Figure 1C and 1D). Our study revealed that the function of the release parameters may be altered depending on the target size, task constraints in abstract terms.

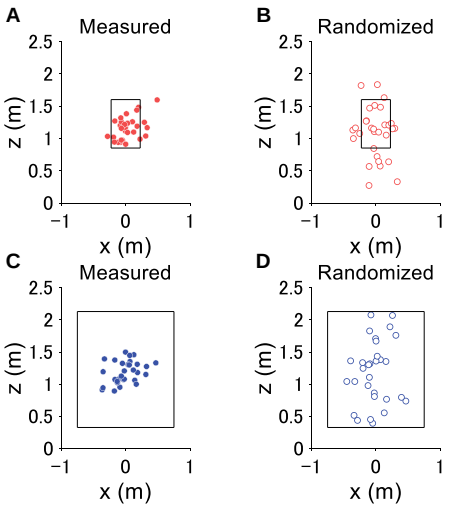

Figure 1 The ball arrival position with the measured and surrogate data in small and large target sizes.

CONCLUSIONS

Our study concluded that the proper interpretation of the function requires the consideration of the task constraints.

REFERENCES

[1] Müller H et al. *J Hum Mov Stud* **36**: 103-126, 1999.
[2] Dupuy et al. *J Sports Sci* **18**: 375-382, 2000.
[3] Kimura et al. Hum Mov Sci **77**: 102799, 2021.

EFFECT OF A PHYSIOTHERAPY PROGRAM ON THE REVERSAL OF RISK FACTORS FOR PATELLAR TENDINOPATHY IN AMATEUR FEMALE SOCCER PLAYERS. CLINICAL TRIAL

Vicente Pina, L[1], Dobon Reus, I[1], Ferrández Laliena, Loreto[1], Sanchez Rodriguez, R [1], Heredia-Jimenez, J [2], Orantes-Gonzalez, E[3], Lucha Lopez, MO [1], and Tricas Moreno, JM [1].

[1] Physiotherapy Research unit, Faculty of Health Science, University of Zaragoza, Zaragoza, Spain
[2] Department of Physical Education and Sports. Human Behaviour & Motion Analysis Lab (HubemaLab), University of Granada, Ceuta, Spain
[3] Department of Sports and Computer Science, Faculty of Physical Education and Sports, University of Pablo de Olavide, Sevilla, Spain

Email: herediaj@ugr.es

INTRODUCTION

Patellar tendinopathy has an incidence of 49.2% among knee injuries (1) This incidence could be conditioned by the neuromuscular deficit in single-leg stabilization actions (2). Being potentially preventable through intervention on modifiable risk factors such as neuromuscular control deficit and muscular imbalances between quadriceps and hamstrings in sagittal plane, and between vastus medialis (VM) and vastus lateralis (VL) in frontal plane.

The objective is to determine whether the use of a dynamic physiotherapy active program focused on improving muscle control of the knee stabilizers is effective in the reversal of neuromuscular risk factors in knee tendinopathies in amateur female soccer players.

METHODS

A sample of 20 amateur female soccer players from C.D. Fuensport (EG) and C.D. Valdefierro (CG) was selected, with an allocation ratio of [1:1]. Initially, muscle activation in the dominant leg (DL) and non-dominant leg (NDL) was assessed by surface electromyography (Trigno Avanty Delsys, Natick, USA). Peak activation of the rectus femoris (RF), vastus medialis, vastus lateralis and biceps femoris (BF) was recorded in two functional tests, Single leg CMJ and the Go-Back test. Gait muscular activation was used for data normalization. After the initial evaluation a physiotherapeutic intervention of specific dynamic exercises was performed on GE for 6 weeks followed by a final re-evaluation. For the statistical analysis, a contrast of variables between independent samples (T-student) and related variables (independent samples t-test) was performed. Finally, the effect size was analyzed using Cohen's d. A confidence level of 95% was established.

RESULTS AND DISCUSSION

Nine EG and eight EC players were analyzed. Significant differences were achieved ($p<0.05$) between groups in both legs in BF activation time. EG recruited all the NDL musculature and BF muscle in DL before braking, which is considered a protective factor of knee injury (3). In contras the CG activated the RF first in DL and VM in NDL, this quadriceps activation could be a risk factor for anterior instability of the knee favoring anterior translation of the tibia (4) and increasing the tension supported by the patellar tendon. Both groups presented a H/Q risky co-contraction ratio both in PD and PND, but GC presented a higher risk ($d>0.8$).

CONCLUSION

Intervention through a physiotherapy program improves neuromuscular control in amateur soccer players. Achieving BF activation prior to braking and H/Q co-contraction close to braking, reducing the risk of patellar tendinopathy injury and knee injury.

KEY WORDS

Electromyography, Patellofemoral Pain Syndrome, Physical Education and Training.

BIBLIOGRAPHY

[1] Martín-San Agustín R et al. Environ Res Public Heal Artic Public Heal 18, 2021.
[2] Trojan JD et al. Orthop J Sport Med 7(4), 2019.
[3] Damavandi M et al. Hum Mov Sci 70: 102596, 2020.
[4] Behrens M et al. *PLoS One* 8(2):e56988, 2013.

THE SCAPULOHUMERAL RHYTHM OF JAVELIN THROWERS

Tang-Yun Lo[1,2], Wei-Rong Chen [2] and Jia-Hao Chang[2]
[1] Office of Physical Education / Tamkang University, New Taipei, Taiwan.
[2] Department of Physical Education and Sport Science / National Taiwan Normal University, Taipei, Taiwan.
Email: 159760@o365.tku.edu.tw

INTRODUCTION

The scapula plays an important role in kinetic chain during overhead throwing. Because of high intensity training, bone and tissue adaptations were changed in the overhead throwers. It might change the scapular and humeral motion during shoulder abduction. The purpose of this study was to understand the scapulohumeral rhythm difference between javelin throwers and healthy university students.

METHODS

Six division 1 college javelin throwers and six healthy college students were recruited in this study. The elbow should be placed in a brace at 90° of flexion with the forearm in supination, and special stand was used to made shoulder move on the scapular plane[1]. Electromagnetic motion capture system (Fastrak, Polhemus, 100Hz) was used to capture the shoulder abduction every 10 degrees from 0° to end range. Because of muscle hypertrophy, some javelin throwers test from 10° of shoulder abdction. The trunk, scapular and humerus were defined by 9 points: C7, T8, SN (suprasternal notch), PX(xiphoid process), AA (acromial angle), IA(inferior angle of the scapula), RS (root of the spine of the scapula), EL(lateral epicondyle) 、EM(medial epicondyle)[3] . The scapulohumeral rhythm were analyzed after calculating the angle between humerus and trunk (A_{HT}), the angle between humerus and scapula (A_{HS}) and the angle between scapula and trunk (A_{ST}).

RESULTS AND DISCUSSION

The end range of dominant side was 70.6±5.7 degree in the javelin throwers, 84.8±5.2 in the healthy college students. The scapulohumeral rhythm of dominant side in javelin throwers was 1:5.7 (A_{ST}: A_{HS} =1:5.7), in healthy strudents was 1:4.6 (A_{ST}: A_{HS}= 1:4.6). The relationship between A_{HS} and A_{HT} were shown in figer 1 and figer 2.

CONCLUSIONS

The pattern of scapula and humerus might changed in javelin throwers. The scapula moved less and humerus move more of dominant side during shoulder abduction in javelin throwers. It might increase the loading of glenohumeral joint and over stretched the muscle between scapular and humerus. This change might increase the risk of shoulder injury in javelin throwers.

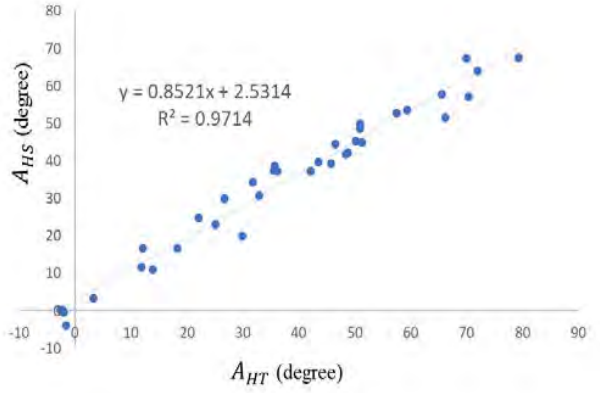

Figure 1 The relationship between A_{HS} and A_{HT} of dominant side in javelin throwers.

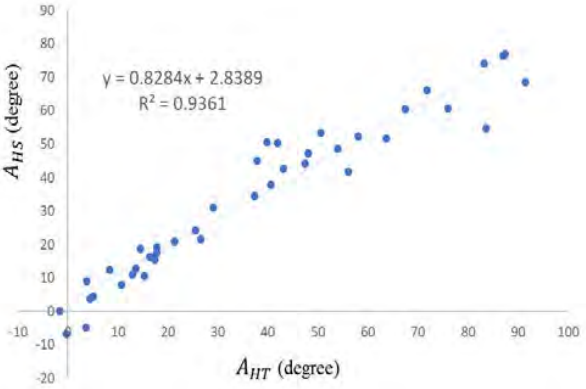

Figure 2 The relationship between A_{HS} and A_{HT} of dominant side in healthy college students.

ACKNOWLEDGEMENTS

This research is supported by the National Science and Technology Council, Taiwan. (MOST106-2410-H003-097 and MOST 111-2410-H-032-073)

REFERENCES

[1] Karduna, A. R., McClure, P. W., Michener, L. A., & Sennett, B. (2000). Dynamic Measurements of Three-Dimensional Scapular Kinematics: A Validation Study. Journal of Biomechanical Engineering, 123(2), 184-190. doi:10.1115/1.1351892
[2] H. T., Lin, A. T., Hsu, G. L., Chang, J. C., Chien, K. N., An, F. C., Su. (2007) Determining the Resting Position of the Glenohumeral Joint in Subjects Who Are Healthy. *Physical Therapy*, 87 (12), 1669–1682.

RELATIONSHIPS BETWEEN THE LOWER EXTREMITY BIOMECHANICS AND FORWARD PROPULSION IN THE PREPARATORY MOTION FOR AN EFFECTIVE JUDO THROW

Takanori Ishii[1], Sentaro Koshida[2]
[1] Centre of Liberal Arts Education, Ryotokuji University, Urayasu, Japan
[2] Faculty of Health Sciences, Ryotokuji University, Urayasu, Japan
Email: ishii@ryotokuji-u.ac.jp

INTRODUCTION

To provide appropriate coaching of throwing skills to athletes, it is necessary to fully understand the kinematic characteristics of throwing skills. Therefore, we sought to elucidate the biomechanical characteristics that differentiate skill levels so that coaches can improve their observational skills to appropriately assess their performance. Ishii et al. (2018)[1] reported that elite athletes landed the pivot foot with a more flexed knee, whereas college athletes landed the pivot foot with a more extended and stiff knee, suggesting that the landing biomechanics of the pivot side may be important in determining the skill level of seoi-nage, one of the most frequently used judo throwing techniques. The study also showed that the elite athletes were able to maintain higher forward propulsion during the preparatory motion, resulting in larger angular momentum generation for an effective throw. Although the authors speculated that the 'soft' landing may be associated with the effective seoi-nage, there are no reports that show whether lower extremity biomechanics during the pivot foot landing are related to forward propulsion in seoi-nage. Therefore, we aimed to identify kinematic variables of the lower extremity associated with the seoi-nage skill by identifying differences in the landing kinematics of the pivot side, forward propulsion, and their relationship between the judo athletes with different seoi-nage skills.

METHODS

The participants were 19 male judo athletes including 3 medallists at the World Judo Championships. Three-dimensional coordinate data for 94 reflective markers on the participants' bodies were captured with 18 cameras of a VICON-MX system at 250 Hz for the tori (the person throwing an opponent) and the uke (the person being thrown by the tori) during seoi-nage movement[1]. The centre of mass (COM) of the tori was estimated using body segment parameters for the Japanese athletes. In addition, we calculated the predetermined kinematic parameters of the whole-body COM and knee of the tori. Finally, the uke's COM angular momentum was calculated, and the top six participants were assigned to the high-skilled group and the bottom six to the skilled group.

A Mann-Whitney U test was performed to test differences between the two groups in the COM acceleration in the anterior-posterior (A-P) and vertical directions, and in the joint angle and angular velocity of knee flexion of the tori's pivot side during the turning phase. In addition, the Pearson's correlation coefficients were calculated between the horizontal knee orientation angle of the tori's pivot side and the COM velocity in the A-P and vertical direction during the turning phase. MATLAB R2022b was used for all the calculations ($p \leqq 0.05$).

RESULTS AND DISCUSSION

In the contrast to the skilled judo athletes, the highly skilled athletes showed little forward or downward COM deceleration during the turning phase. This suggests that the highly-skilled athletes were not exposed to the braking component of the reaction force during the pivot foot landing. There was no significant difference in the knee kinematics during the pivot foot landing. However, we found significant correlations between the knee projection angle at the moment of pivot foot landing and both the A-P ($r = -0.58$, $p < 0.001$) and vertical ($r = 0.84$, $p < 0.001$) components of the whole-body COM velocity at the end of the turning phase. This suggests that the knee orientation at the pivot foot landing is related to the forward propulsion in the turning phase of seoi-nage.

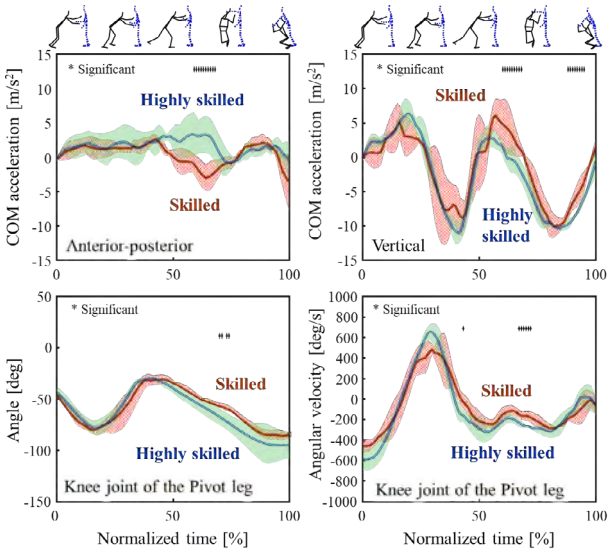

Figure 1 The kinematic variables of highly skilled and skilled judo athletes.

CONCLUSIONS

The highly skilled judo athletes were not subjected to the braking force during the pivot leg landing phase. Although there was no significant group difference in knee kinematics, we found a significant correlation between the deviation angle of hip rotation and the whole-body COM velocity. Coaches may be better to observe foot orientation rather than knee joint angle during the pivot foot landing when coaching seoi-nage.

REFERENCES

[1] Ishii T et al. *Sport Biomech* 17(2): 238-250,2018.

THE EFFECT OF DECREASING COR OF BASEBALL ON BATTING STATS AND BATTING PERFORMANCE: IN A CASE OF PROFESSIONAL BASEBALL LEAGUE

Shu-Wei Chen[1,3] and Jyh-How Huang[2,3]

[1] Graduate Institute of Athletics and Coaching Science, National Taiwan Sport University / Taoyuan, Taiwan
[2] Sport Information and Communication Department, National Taiwan University of Sport / Taichung, Taiwan
[3] Taiwan Society of Baseball and Softball Science / Taipei, Taiwan

Email: hsuwei0922@gmail.com

INTRODUCTION

The coefficient of restitution (COR) indicates the ability of an object to return to its original shape after being deformed by an outside force. The higher COR of baseball affects the greater exit velocity and flight distance of batted balls [1]. The Nippon Professional Baseball (NPB) used a "unified ball," which has been manufactured with a COR as close as possible to the lower limit for baseballs from 2011 season. It caused that the overall performance of pitchers improved, and the performance of batters dropped a lot [2]. The Chinese Professional Baseball League (CPBL) in Taiwan also reduced the COR of baseball for the unusual high batting stats and long game times. In 2020, the CPBL changed the COR requirement from 0.560 ± 0.200 to 0.550 ± 0.100 before the second half period started. The purpose of this study was to understand the effects of decreasing COR of baseball on batting stats (included hitting average, slugging percentage, and home runs), and batting performances (included exit velocity of batted balls and flight distance of batted balls) in 2 half periods of the 2020 CPBL season. To our knowledge, this is the first study of the effect of the COR of baseball on in-game performance.

METHODS

The data were produced by totally 12 batters who played in the CPBL 2020 season, and all reach on the leaderboard of hitting average, whom had 186 plate appearances per half period at least. At the moment of 2020 season ended, the mean height of these batters was 180.08 ± 3.34 cm, their mean weight was 81.17 ± 10.26 kg, and their mean age was 28.08 ± 4.74 years old. The data of batting stats were obtained from the official CPBL website. The data of batting performance were collected by TrackMan radar tracking system. The study was also approved by the Institutional Review Board (TSMH IRB No. 19-024-B). Due to minimize the ballpark factor, all data of batting performance were collected by a standard TrackMan radar tracking system at the same stadium. The paired-t test were performed to compare the difference of batting stats and batting performances between 2 different half period with different COR of baseball by using SPSS v28.0, and statistical significance was indicated by $p < 0.05$.

RESULTS AND DISCUSSION

The batting stats and batting performences of 2 half periods were presented in Table 1. The hitting avarage, slugging percentage, home runs, and exit velocity of batted ball were significantly lower in the 2nd half period of 2020 CPBL season. The result showed that the batting states and batting performances decreased followed by the decreasing of COR of baseballs. And the unchanged flight distances of batted ball might hinted that the batter adjusted their strategy to adapt the changing of COR of baseball.

CONCLUSIONS

The COR of baseball effect the batting stats and batting performance, and the batters could also adapt by the adjustment of hitting strategy.

ACKNOWLEDGEMENTS

The authors give their heartfelt thanks for the partial financial support by the Ministry of Science and Technology, Taiwan (110-2627-H-028-002). The authors also appreciate the CPBL and Wei-Chuan Dragons to provide the batting stats and batting performance data we analysed in current study.

REFERENCES

[1] Kagan DT. *Am. J. Phys.* **58**: 151, 1990.
[2] Chen SW et al. *Sports Coaching Sci.* **27**: 45, 2012.

Table 1: The batting stats and battng performences of 2 half periods of 2020 CPBL season.

	COR required	AVG	SLG	HR	Exit velocity (m/s)	Flight distance (m)
2020 1st half period	0.560±0.020	0.34±0.03	0.55±0.10	10.33±6.91	38.80±1.10	53.22±11.54
2020 2nd half period	0.550±0.010	0.29±0.03	0.43±0.07	5.25±4.71	37.25±1.41	50.63± 6.42
p-value	--	*p=0.002**	*p<0.001**	*p<0.001**	*p=0.005**	*p=0.287*

*: $p<0.05$. COR: coefficient of restitution; AVG: hitting average; SLG: slugging percentage; HR: home runs.

EVALUATION OF THE MUSCLE WORK IN GYM EXERCISES WITH A "WATER BALL" COMPARED WITH A MEDICINE BALL

Alexis Herbaut[1] and Aurore Valgalier[1]
[1] Human Factors & Ergonomics, Decathlon SportsLab, Lille, France.
Email: alexis.herbaut@decathlon.com

INTRODUCTION

Medicine ball is a useful equipment for both physical conditioning and rehabilitation. Studies showed that regular training with a medicine ball during several weeks allowed to improve functional performance and to gain in muscle power [1, 2]. Also, instability resistance training with unstable surfaces or devices is popular in fitness training facilities to enhance balance, increase core activation and improve motor control [3].

The objective of this study was to evaluate the differences in terms of muscle activities when performing different gym exercises with a Water Ball compared with a Medicine Ball.

METHODS

Twenty-five women participated in the study (age: 27.1 ±4.3 years old, height: 1.68 ±0.07 m, weight: 61.5 ±7.6 kg). Inclusion criteria were to practice a gym activity at least once a week and being injury-free for 6 months.

They tested 2 conditions: control condition was a 3-kg Medicine Ball (MB) and experimental condition was a 3-kg Water Ball (WB). WB was a plastic ball half-filled with water. They performed 3 different exercises during 30 seconds: squat shaking (SS), abdo twist (AT) and backward lunge-vertical raise with dominant hand (LR).

Muscle activities of 14 muscles were recorded with EMG (®DelSys Inc, Boston, Massachusetts, 2000 Hz): Biceps Brachii, Triceps Brachii, Flexor Carpi Radialis, Extensor Carpi Radialis, Trapezius Descendant, Deltoideus Medius, Erector Spinae Longissimus, Rectus Abdominis, Obliquus Internus Abdominis, Gluteus Medius, Biceps Femoris, Rectus Femoris, Vastus Medialis and Vastus Lateralis.

EMG data were processed using Visual 3D software (®C-Motion, Rockville, MD). First, EMG signals of each muscle were filtered with a Butterworth filter (bandpass, 4th order, zero phase lag, bandwidth 20–400 Hz). After rectifying the signal, the EMG root-mean-square value was computed. For each trial, the integrals over time during the 30 sec of exercise were computed to assess the muscle activity.

Statistical analyses were done using XLStat (©Addinsoft Inc, NY, USA). A paired Student *t*-test was used to compare WB and MB. Significant threshold was set at $p<0.05$.

RESULTS AND DISCUSSION

No significant differences were found between WB and MB for SS and AT movements. Significant larger muscle activities were observed for 11 out of 14 muscles in WB compared to MB for LR movement ($p<0.05$, Figure 1).

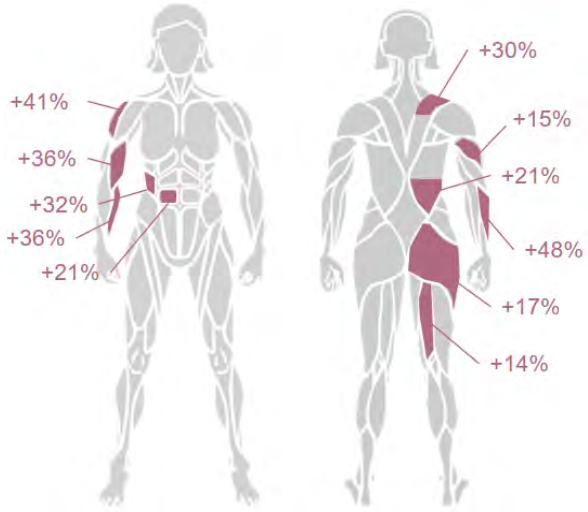

Figure 1 Differences in muscle activities (%) with Water Ball (WB) compared with Medicine Ball (MB) for the backward lunge-vertical raise exercise. Only significant differences ($p<0.05$) are presented.

The main difference between LR and the 2 other movements is that LR was performed with the ball held with only one hand while SS and AT were executed with the ball held with 2 hands. It seems that using the WB with only one hand is the necessary condition to generate the instability and as a consequence to increase the muscle work in order to compensate for it.

CONCLUSIONS

Using the Waterball allowed an increased muscle work compared with a Medicine Ball for exercise performed with one hand.

ACKNOWLEDGEMENTS

The authors would like to thank Decathlon for providing the products to test.

REFERENCES

[1] Szymanski DJ et al. *J Strength Cond Res* **21(3)**: 894-901, 2007.
[2] Raeder C et al. *J Strength Cond Res* **29(7)**: 1904-14, 2015.
[3] Behm C et al. *Sports Health* **5(6)**: 500-3, 2013.

Narrow stance width during the bar twist exercise decreases the trunk twist torque

Kazutaka Takahashi[1], Hidenori Shinohara[2]
[1] Faculty of Human Science and Design, Japan Women's University, Tokyo, Japan.
[2] Faculty of Sport Science, Nippon Sport Science University, Kanagawa, Japan.
Email: takahashikaz@fc.jwu.ac.jp

INTRODUCTION

Training the trunk twist muscles with stretch-shortening cycle movements is important in various sports, including throwing and hitting. Bar twist exercises are recognized as plyometrics in trunk-twisting muscles. This exercise is performed in an upright position, and trunk twist is thought to be caused by the rotation of the pelvis. However, only a few studies have examined the role of the lower limbs in exerting trunk twist kinetics. In various sports, the torque that causes the lower limb to rotate the pelvis is increased in the hip abduction position [1]. We hypothesized that changing the hip abduction angle by changing the foot width during bar twist exercises would also change the pelvic rotation and trunk twist torque. This study aimed to investigate the influence of the stance width on trunk twisting in bar twist exercises.

METHODS

The study included 13 male athletes who regularly performed strength and power training (age, 19.69 ± 0.85 years; height, 1.75 ± 0.05 m; mass, 67.91 ± 6.07 kg, mean ± SD). All participants performed the bar twist exercise in Normal (the stance width is wider than the shoulder width) and Narrow (the shoulder width is wider than the stance width) postures. Each trial was performed at least three times. The trial with the highest bar angular velocity was analyzed. The three-dimensional coordinates of the retro-reflective markers fixed on the body (47 points) and the outer ends of the bar (two points) were recorded using eight infrared cameras (200 Hz). The ground reaction force was measured using two Kistler force platforms (1000 Hz). A paired t-test was used to detect differences in the means of each variable. Effect sizes were calculated using Cohen's d and interpreted using the following scale: 0.2–0.5, small; 0.5–0.8, medium; >0.8, large. The alpha level was set at 0.05.

RESULTS AND DISCUSSION

The maximal angular velocity of the bar and trunk twist and the maximal trunk twist torque during the Narrow were significantly smaller than that during the Normal. These variables have large effect sizes. Therefore, the narrow posture may be a less trunk explosive force- and power-developing exercise in bar twist exercises than the normal posture. The pelvic rotation torque defined as the torque exerted by the hip joint torque, and the force around the superior–inferior axis of the pelvis through the left and right hip joints was not significantly different between the narrow and normal postures. Moreover, these variables have small effect sizes. Although lower limb flexion–extension movements contribute to the pelvic rotation torque [1], the lower limb joints were not restricted in this study. The results suggested that the narrow and normal postures have different lower extremity kinematics that affects the pelvic torque.

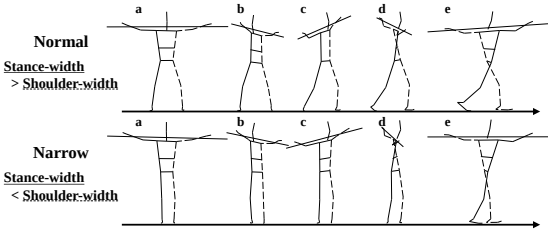

Figure 1 Difference in foot placement during the bar twist exercise. Participants rotate the bar clockwise from a to b and then rotate counter-clockwise (b to e).

CONCLUSIONS

In bar twist exercises, a narrow stance width decreases the trunk twisting torque.

ACKNOWLEDGEMENTS

This work was supported by JSPS KAKENHI Grant Number 21K17591.

REFERENCES

[1] Iino and Kojima. *J Hum Mov Sci* **45**: 133-152 2003.

Table 1: Kinetic and kinematic variables during the bar twist exercise in the normal and narrow postures.

	Normal	Narrow	Effect size	*p-value*
Maximal bar angular velocity (deg/s)	404.29 ± 55.42	318.73 ± 26.09	1.98	$p < 0.001$
Maximal trunk twist angular velocity (deg/s)	232.23 ± 51.87	158.58 ± 30.55	1.73	$p < 0.001$
Maximal trunk twist torque (Nm/kg)	3.19 ± 0.90	2.10 ± 0.67	1.38	$p < 0.001$
Maximal pelvic rotation torque (Nm/kg)	2.60 ± 1.24	2.21 ± 0.98	0.35	$p = 0.061$

ACUTE: CHRONIC WORKLOAD RATIO AND ACCUMULATED NEUROMUSCULAR FATIGUE IN COLLEGE MALE RUGBY SEVENS ATHLETES: A PILOT STUDY

Qianhui Sun [1], Heng-Ju Lee [1]
[1] Department of Physical Education and Sport Sciences,
National Taiwan Normal University, Taipei, Taiwan
Email: hjlee@ntnu.edu.tw

INTRODUCTION

The relationship between training load and sports injury has recently received intense attention and discussion. The acute and chronic workload ratio (ACWR) is considered an influential factor in monitoring sports injuries. Rugby league athletes with ACWR between 0.85 and 1.35 are more resistant to injury [1]. However, the relationship between ACWR and accumulated neuromuscular fatigue is not clear. At the same time, single-point variables like jumping height or peak force and power are not sensitive enough to neuromuscular fatigue [2]. The countermovement jump (CMJ) test is the gold standard for neuromuscular fatigue monitoring. Therefore, Twenty CMJ variables with ACWR in different intervals for college male rugby sevens athletes have been compared in this study.

METHODS

Data were collected from five male college rugby sevens athletes (18.6±1.2 years, 1.73±0.02m, 74.1±7.37Kg) in 4 weeks. The workload was estimated by multiplying the session rating of perceived exertion with the CR-10 scale by the session duration in minutes after every training session. One-week data (acute workload) and four-week rolling average data (chronic workload) were used to calculate ACWR. Athletes whose ACWR was either below 0.85 or over 1.35 would be classified as a non-ideal group (NIG), and the others would be the ideal group (IG). Force plate sampling at 1000Hz was used to collect data on CMJ performance for everyone at the beginning of the first week as the baseline and the end of the fourth week and the changes were examined through the differences between two weeks divided by the baseline data multiplied by 100%. Twenty CMJ variables were assessed, including velocity, power, force, and time during concentric and eccentric jump phases calculated by MATLAB. An unpaired t-test ($\alpha<0.05$) was applied to compare the CMJ performance between NIG and IG.

RESULTS AND DISCUSSION

There are two athletes in NIG whose ACWRs were 0.84 and 0.78, respectively. Three athletes in IG (ACWR: 1.12, 1.01, and 1.08). 2 variables, duration in unweighting phase and time to peak force, among 20 have shown significant differences between the two groups shown in Table 1, which may reflect the importance of variables exposing CMJ mechanics instead of single-point variables or jumping output. Time to peak force in IG has increased but decreased in NIG, which may show that different ACWR reflecting different training loads and accumulation of training stress have led to different alterations in CMJ mechanics. In a previous study, a longer time to peak force was also found after a 6-week progressively increased training load for elite female rugby sevens athletes [3]. Because of the limited sample size, further investigation into the relationship between ACWR and CMJ performance should be conducted.

CONCLUSIONS

Male rugby sevens athletes with different levels of ACWR may have different accumulated neuromuscular fatigue reflected by CMJ performance. Moreover, a thorough analytical approach to CMJ performance is advised for practitioners.

REFERENCES

[1] Hulin B et al. *Br J Sports Med* **50**: 231-236, 2016.
[2] Alba-Jiménez C. et al. *Sports (Basel)* **10**, 2022.
[3] Gathercole R et al. *Int J Sports Med* **36**: 722-728, 2015.

Table 1: The change of CMJ variables compared with baseline for NIG and IG

	NIG (N=2)	IG NIG (N=3)	*p-value*
Duration in unweighting phase (%)	-10.27 ± 5.68	23.08±11.42	0.034
Time to peak force (%)	-5.02 ± 10.04	22.13±1.68	0.016

Estimation of Time Consistency in Taekwondo Group Poomsae with Inertial Measurement Unit

He Minyan[1], Wei-Han Chen[2,3,4], and Tzyy-Yuang Shiang[2]
[1] Department of Physical Education and Sport Science, National Taiwan Normal University, Taipei, Taiwan.
[2] Department of Athletic Performance, National Taiwan Normal University, Taipei, Taiwan.
[3] Department of Physical Education and Kinesiology, National Dong Hwa University, Hualien, Taiwan.
[4] Graduate Institute of Sports Equipment Technology, University of Taipei, Taipei City, Taiwan.
Email: tyshiang@ntnu.edu.tw

INTRODUCTION

Taekwondo Poomsae is recognized as a combination of postures, kicks, and hand techniques, but it was not scored as an official Olympic event because the scoring process was too subjective. Especially in the three-person team posture, the estimation of time consistency cannot be discerned by the eye, so how to quantify it becomes very important. In this study, a method was proposed to obtain motion signals through a wearable inertial measurement unit (IMU) to achieve the estimation of time consistency in Taekwondo Poomsae performance (Koryo-type), and then to assess the level of the group of athletes. It is expected to reduce the subjective scoring of group character judges.

METHODS

The subjects in this study were two groups of Taekwondo athletes. One group was composed of three 2022 World Championship champions (age: 20.5 ± 0.5 years, height: 175 ± 10 cm, mass: 66 ± 8 kg) and the other one was composed three sparring athletes (age: 24 ± 2 years, height: 171 ± 4 cm, mass: 65 ± 7 kg). All athletes wore inertial measurement unites (DOT, XSENS, USA) on their right wrists and left and right ankles, and performed a group exercise in a Koryo-type.

The sampling rate of IMU was 120Hz. A 40Hz low-pass filter was employed to eliminate the noise in acceleration data. The time consistency was evaluated by calculating the sum of the absolute differences in time to resultant acceleration peak between the three athletes.

RESULTS AND DISCUSSION

The world champion group has better movement consistency because of less time difference in peak acceleration occurrence (Table 1). The IMU can effectively obtain acceleration data during training and competition. It can also effectively tell the different levels of Taekwondo athletes by measuring the acceleration peak and its time of occurrence. Wearable devices are easier to implement and non-invasive, it can be placed on the athlete's body to capture their movement information [1]. IMU usually obtains the quantization criteria in motion by detecting the measured acceleration or angular velocity signals: maximum value, minimum value, or slope change [2]. With the use of IMU in Taekwondo Poomsae, the temporal and spatial characteristics of the athletes' practice of the three different postures were also effectively monitored and evaluated [3]. The IMU is easy to use and allows for effective monitoring and acquisition of athletes' time parameters in group pins, in line with previous studies.

CONCLUSIONS

IMU can evaluate athletes' time consistency in Taekwondo Poomsae, and the collection of these data can compensate for the lack of quantitative data in previous training and competitions.

REFERENCES

[1] Pueo, B., & Jimenez-Olmedo, J. M. *Retos* **32**: 241-247, 2017.
[2] Camomilla, V., Bergamini, E., Fantozzi, S., & Vannozzi, G. *Sensors* **18**: 873, 2018.
[3] Kim, Y. K. *Korean J Sport Biomech* **31**: 199-204, 2021.

Table 1: The time consistency of movements among athletes in different sensor location and action (n = 6).

	Right wrist	Right ankle	Left ankle	Total
Action name	TJ1/ TJ2/ TJ3 / TJ4	(SKT) / HFK1 / HFK2 / HSK	(SKT) / HFK1 / HFK2 / HSK	
Sparring group (sec.)	0.09 / 0.17 / 0.12 / 0.23	(0.75, 0.56) / 1.69 / 1.21 / 1.67	(1.21, 0.05) / 0.17 / 0.15 / 0.06	8.13
World champ group (sec.)	0.06 / 0.08 / 0.07 / 0.11	(0.37, 0.08) / 0.14 / 0.23 / 0.20	(0.07, 0.28) / 0.13 / 0.01 / 0.12	1.95

TJ = tiger jab; SKT = side kick; HFK = high front kick; HSK = high side kick

INFLUENCE OF TURF FIBRES ON MECHANICAL TRACTION OF ARTIFICIAL TURF SURFACES

Michael J. S. Esposito[1,2], Shaylyn Kowalchuk[1], Emily Smith[1], Darren J. Stefanyshyn [1,2] and John W. Wannop[1]
[1] Human Performance Lab, Faculty of Kinesiology, University of Calgary, Calgary, Canada.
[2] Department of Biomedical Engineering, Schulich School of Engineering, University of Calgary, Calgary, Canada.
Email: michael.esposito@ucalgary.ca

INTRODUCTION

Components of artifical turf, such as infill material and fibre density, can be manipulated to alter the mechanical properities of the playing surface. Previous research has shown infill material [1,2] and fiber density [2] can influence rotational traction and athlete biomechanics. However, the influence of fibre components of an artificial surface remain unknown; therefore, the purpose of this study was to determine the influence of fibre parameters on surface traction.

METHODS

Twelve different artificial turf surfaces were mechanically tested on a robotic testing machine. The surfaces had systematic changes in fibre pile height (length of fibres), face weight (weight of the fibre pile), thatch ('root zone' of artificial turf), gauge (distance between two adjacent artificial fibre yarns), stich rate (number of stitches per 10cm), and denier (linear density of the fibre yarn).

The testing machine consisted of a six degree of freedom P2000 servo-driven parallel link robot (Mikrolar Inc., Hampton, USA) utilizing a movable platform stationed under a rigid steel frame. The turf to be tested was rigidly attached to the movable platform of the robotic testing machine and a right prosthetic foot, which was used to simulate a physiological foot, was fitted with a size 10 shoe (adidas 16.4 FXG cleat). The shoe and foot were attached to the frame of the robotic testing machine at 20° of plantarflexion in series with a triaxial load cell (AMTI, model MC5, Waterton, USA) to measure the forces and moments in all three orthogonal directions during testing.

Rotational traction testing was performed by raising the platform to apply a 650 N normal load to the shoe, after which the platform was internally rotated 20° at a speed of 75°/second. Force and moment data were recorded by the load cell at 1000 Hz throughout the duration of each test. Rotational traction between the shoe and each surface was defined as the peak moment about the vertical axis. A total of five trials were performed at different locations on each surface condition.

Linear traction testing was performed by raising the platform to apply a 650 N normal load to the shoe, after which the platform was moved linearly. It was moved forward to simulate acceleration forces and backwards to simulate braking forces for five trials of each. All trials were performed at different locations on each surface condition to account for surface wear. Linear translational traction was measured in two orientations: i) parallel to the fibre stitching and ii) perpendicular to the fibre stitching.

RESULTS AND DISCUSSION

Changes of translational and rotational traction from each fibre parameter are shown in Table 1. For both translational and rotational traction, all variables had a moderate effect on traction, with the exception of thatch. Stitch rate and gauge had the largest effect on both translational and rotational traction, with increasing stitch rate and gauge lowering traction.

Table 1. Largest percentage change in traction for each parameter.

Fibre Parameter	Translational Traction	Rotational Traction
Pile Height	10.4 %	6.5 %
Face Weight	13.6 %	6.8 %
Thatch	1.4 %	2.7 %
Gauge	22.6 %	8.9 %
Stitch Rate	22.5 %	10.5 %
Denier	17.1 %	4.3 %
Orientation	8.8 %	-

CONCLUSIONS

The results of the current study indicate that artificial turf fibres can influence traction, with stitch rate and gauge having the largest effect. Future work can create an optimal surface from combining these results with previous literature and determine its influence on athlete biomechanics and injury risk.

ACKNOWLEDGEMENTS

This study was funded by a Natural Sciences and Engineering Research Council of Canada Collaborative Research and Development Grant

REFERENCES

[1] Villwock M R et al. *P I MECH ENG P-J SPO* **223(1)**: 11-19, 2009.
[2] Wannop JW et al. *J SPORT SCI* **37(16)**: 1849-1856, 2019

CLUB HEAD PARAMETER OF EFFECTING AMATEUR GOLFER'S SMASH FACTOR IN REAL GOLF COURSE SITUATIONS

Tsung-Yu Huang[1], Yu-Wei Chan[1], Chia-Yu Jih[2] and Wen-Tzu Tang[1*]
[1] Department of Athletic Training and Healthy, National Taiwan Sport University, Taoyuan, Taiwan
[2] Software Technology Institute, Institute for Information Industry, Taipei, Taiwan
Email: wttang@ntsu.edu.tw

INTRODUCTION

Smash factor is an important indicator of golf performance (Kim & Ridgel, 2019; Lynn et al., 2013; Tilley & Macfarlane, 2012). Smash Factor is ball speed divided by club speed. For example, a smash factor of 1.3 means that when the club speed of 100 mph, the ball speed is 130 mph. The better golf swing has a smash factor of 1.50 means that when club speed of 100 mph and. ball speed is 150 mph. Improving smash factor will help increase the amount of energy transferred from the club head to the golf ball, even with the same club swing speed. From clubhead related parameters such as club speed, dynamic loft, attack angle, face angle, and club path at impact ball, there are several factors that contribute to smash factor. However, it is unclear which parameters are critical factor related to Improve smash factor. Therefore, the purpose of this study is to explore the correlation analysis between smash factor and club head parameters and find out the important factors that affect hitting efficiency. Providing coach or player related information will help improve swing performance.

METHODS

Five amateur handicap golfers participated in this study (mean handicap of 91±6.51; mean height of 175±4 cm; mean weight of 77±8.80 kg). The golfer had at least years' experience. Before performing the experiment, all participants signed an informed consent form to confirm their understanding of the experimental process. Participants were informed of the benefits and risks of the investigation prior to signing an institutionally approved informed consent document to participate in the study. This study uses the trackman instrument to measure the smash factor and other swing data of players' swings. Participants were instructed to warm up for ten minutes before entering the stand-by experimental swing position. Each golfer must swing with a 9 iron on the tee. Participants were asked to perform a exert maximum effort in performing every swing. Each participant performed 12 swings with a break of one minute between each swing. Pearson product moment correlation coefficients were calculated between the smash factor and club delivery/ ball launch. All statistical analyses were performed with SPSS version 20.0 (SPSS Inc., Chicago, IL, USA).

RESULTS AND DISCUSSION

The results of this study showed that each player could observe a significant relationship between smash factor and face angle. And other parameters were not significantly correlated (table 1). When the face angle is larger, the club face is more open, and the ball will be shot to the right. The swing speed cannot transfer effectively form club to ball. Therefore, the face angle is larger, it will reduce the smash factor.

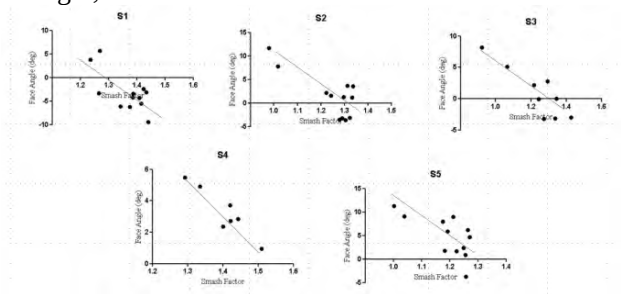

Figure 1 The correlation coefficients between the smash factor and face angle for all participants; S: Subject.

CONCLUSIONS

Our research found that the face angle error was primary factor that cause decreasing smash factor at the amateur level. This also means accuracy control the face angle is important to help improve their smash factor at the amateur level.

ACKNOWLEDGEMENTS

We thank Ministry of Economic Affairs (DOIT), Institute for Information Industry (III), Taiwan Golf Course Association (TGCA) and Taipei Golf Club (TPGC) for the financial support (Project 111-EC-17-D-11-1832).

REFERENCES

[1] Kim J H et al. *Int. J. Sports Sci. Coach* **14(6), 786-797**, 2019.

[2] Lynn, Scott K et al. *Int. J. Golf Sci* **2(2), 116-125**, 2013

Table 1: The correlation coefficients between the smash factor and club delivery for subject (S1).

Club delivery	Pearson r	*p-value*		Pearson r	*p-value*
Attack Angle (deg)	0.374	0.320	Club Speed (mph)	-0.662	0.019*
Club Path (deg)	0.374	0.320	Low Point (in)	-0.358	0.343
Face Angle (deg)	-0.712	0.009**	Swing Plane (deg)	0.271	0.393

BIOMECHANICAL FACTORS AFFECTING LONG JUMP DISTANCE IN JAPANESE MALE UNIVERSITY ATHLETES

Yamato Takayama [1,2], Masaki Morinaga [1], Taiki Komatsu [1], Yuzo Koyama [1] and Kentaro Yamanaka [2]

[1] College of Sports Sciences, Nihon University, Tokyo, Japan.
[2] Graduate School of Life Sciences, Showa Women's University, Tokyo, Japan.
Email: takayama.yamato@nihon-u.ac.jp

INTRODUCTION

A number of studies have investigated the factors that affect jumping distance in the long jump. Using a multiple regression approach, Graham-Smith & Lees [1] demonstrated the regression equation for long jump distance in UK male national-level long jumpers: jump distance (m) = 1.396 + 0.485 S_{TD} (Speed of the CM at touch-down) [m/s] + 5.836 $H_{TD\text{-}TO}$ (Change in Height from touch-down to take-off) [m] – 0.655 $S_{TD\text{-}TO}$ (Change in Speed from touch-down to take-off) [m/s]. However, no study has clarified the factors that affect the long jump distance in Japanese male university athletes with different skeletal structures, muscle strength, and performance level. In this study, therefore, we investigated the factors affecting long jump distance in Japanese male university athletes using a method similar to that of Graham-Smith & Lees [1].

METHODS

Four male university athletes who signed a consent form (21 ± 1.2 years old, 174.7 ± 0.8 cm, 67.0 ± 3.39 kg) participated in this study. For a total of eight trials during Men's Long Jump in Nihon University Competition, three-dimensional (3-D) coordinates of fourteen retro-reflective spherical markers were measured by an 8-camera motion capture system (VICON) at a sample rate of 200 Hz. The markers were fixed to anatomical landmarks on the right and left side of the athlete's toe, ankle, knee, hip, shoulder, elbow and wrist. The jumping distance was measured using a measuring tape. Using by the 3-D kinematic data around the long jump take-off, we conducted a multiple regression analysis and identified factors contributing to long jump distance. Following the results of Graham-Smith & Lees [1], we chose long jump distance as the dependent variable and S_{TD}, $H_{TD\text{-}TO}$, and $S_{TD\text{-}TO}$ as explanatory variables (Figure 1).

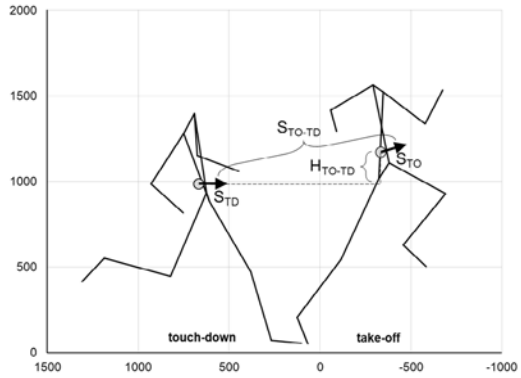

Figure 1 Stick figure representation of biomechanical parameters used as explanatory variables in multiple regression analysis.

RESULTS AND DISCUSSION

Table 1 shows the results of multiple regression analysis. The multiple regression equation of two explanatory variables in S_{TD} and $H_{TO\text{-}TD}$ significantly explained the jumping distance in Japanese male university athletes.

CONCLUSIONS

By multiple regression analysis using biomechanical parameters, we could clarify the factors that affect the long jump distance in Japanese male university athletes. It is expected that such data will be applied to sports coaching to improve performance.

ACKNOWLEDGEMENTS

The authors are grateful to all of the athletes who participated in this study.

REFERENCES

[1] Graham-Smith & Lees *J. Sports Sci.* **23**: 891-903, 2005

Table 1: Result of multiple regression analysis for long jump distances in Japanese male university athletes

Dependent variable: long jump distance [m]

Model	*R*	R^2	Adjusted R^2	*F*	*p*	Explanatory variable	*B*	*SE*	*β*	*t*	*p*
Model 1	0.813	0.660	0.604	11.669	0.014*	Intercept	1.873	1.493		1.255	0.256
						S_{TD}	0.558	0.163	0.813	3.416	0.014
Model 2	0.880	0.775	0.685	8.621	0.024*	Intercept	-2.836	3.234		-0.877	0.421
						S_{TD}	0.857	0.237	1.248	3.615	0.015
						$H_{TD\text{-}TO}$	9.875	6.180	0.551	1.598	0.171
Model 3	0.902	0.813	0.673	5.799	0.061	Intercept	-2.257	3.359		-0.672	0.539
						S_{TD}	0.762	0.264	1.110	2.893	0.044
						$H_{TD\text{-}TO}$	10.240	6.314	0.572	1.622	0.180
						$S_{TD\text{-}TO}$	0.453	0.453	0.248	0.900	0.419

*: P < 0.05

RELATIONSHIP BETWEEN THE POSITION OF HIP JOINT AND RANGE OF MOTION OF LOWER LIMB JOINT DURING CYCLING

Hayato Seki[1], Shigetada Kudo[2], Katumasa Tanaka[3], Shigehiro Hashimoto[3] and Yoshimori Kiriyama[4]
[1] Graduate School of Mechanical Engineering, Kogakuin University, Tokyo, Japan
[2] School of Transdisciplinary Science and Design, University of Tsukuba, Kuala Lumpur, Malaysia.
[3] Department of Mechanical Engineering, Kogakuin University, Tokyo, Japan.
[4] Department of Mechanical Systems Engineering, Kogakuin University, Tokyo, Japan.
Email: ad20501@ns.kogakuin.ac.jp

INTRODUCTION

In pedaling movements, an appropriate saddle height is important to achieve efficient performance and prevent the lower limb injuries. Even though many conventional saddle height adjustments seem to assume that the pelvis does not move, recent studies have implied that the pelvis vertically moved in pedaling movements[1]. This means that the position of the hip joint also moves during pedaling motion, and then the lower extremities change based on the pelvic motion. Therefore, the purpose of this study is to clarify the relationship between the hip joint position and the joint angles of the lower extremity in pedaling movements.

METHODS

Ten healthy male volunteers (23±2 y/o, 1.70±0.05 m, 60 ±7 kg) were recruited for this study. They had no prior cycling training experience. Each subject performed pedaling motion at a comfortable saddle height. The subjects were asked to perform pedaling motion at 90 rpm and the workload of 80, 90, 100, 110 and 120 W. Three-dimensional kinematic data were recorded using an optical motion capture system (200 Hz). Using the reflective markers placed on the anatomical characteristic points of the lower limb, the joint position and the joint angles of the hip, knee and ankle were evaluated. In this study, the significance level was set to $p < 0.05$. Also, the significance level was evaluated using Mann-Whitney-U-test.

RESULTS AND DISCUSSION

Figure 1(a) shows the relationship between the ranges of motion (ROM) of the hip and knee joint angles. The subjects were divided into two groups; the Large group has the large ROM of both joints and the Small group has the small ROM. The Large group significantly shows that the length of the lower extremity is shorter than the Small group (803.2±14.7 < 842.5±20.0 mm). Figure 1(b) shows the averaged trajectories of the joint position of the greater trochanter (GRT) as the hip and knee, ankle and the 5th metatarsal joint as the toe. In the Large group, the hip and knee positions show larger trajectories than the Small group. Especially, the Large group moved the hip and knee joint positions more downward around the bottom dead center (BDC) than the Small group. On the other hand, the ankle and toe

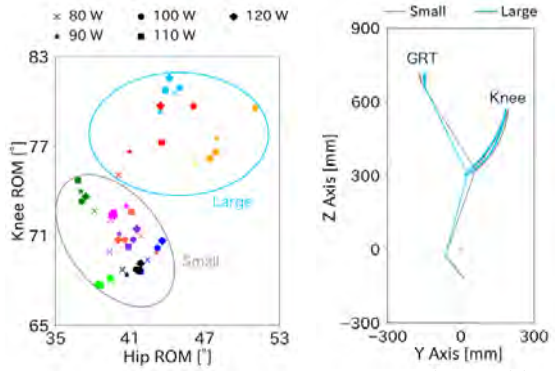

(a) ROMs of the hip and knee joints. Each color expresses one subject. **(b)** Trajectory of the joint positions.

Figure 1 ROM and trajectory of Large and Small groups

positions show similar trajectory shapes, and the joint positions do not show a large difference around BDC. The Large group has shorter lower extremities, and then the group should had needed to make the length long from the hip to the toe around BDC. Therefore, the group should extend both of the hip and knee joints around BDC. Of course, the Large group had been potentially able to move the joints to the lower positions, because all the subjects adjusted the saddle height to pedal comfortably in this study. However, in the low position, the Large group should have required to flex more the hip and knee joint angles because the crank length is large relative to the saddle height compared with the Small group. To avoid excessive flexion, the Large groups could be prefer to a high saddle position. Thus, the Large group moved the hip and knee positions downward, and the trajectory was different from the Small group.

CONCLUSIONS

In a pedaling movement, the subjects were divided into the two groups based on the range of the hip and knee joint angles. The Large group significantly moved the positions of the hip and knee joints around BDC.

ACKNOWLEDGEMENTS

A part of this study was supported financially by JKA through its promotion funds from KEIRIN RACE, and The Uehara Memorial Foundation.

REFERENCES

[1] Costes A et al. *J Biomech* **48**: 2998-3003, 2015.

INVESTIGATION OF ARCHERY EXPERIENCE ON SHOULDER GIRDLE MOTION AND ACROMIOHUMERAL DISTANCE AT FULL DRAW

Takeru Abekura[1], Noriaki Maeda[1], Makoto Komiya[1], Mitsuhiro Yoshimi[1], Satoshi Arima[1], Shogo Tsutsumi[1], Yoshihiro Shigekuni[1], Yukio Urabe[1]

[1] Department of Sports Rehabilitation, Graduate School of Biomedical and Health Sciences, Hiroshima University, Hiroshima, Japan.
Email: tabekura1124@gmail.com

INTRODUCTION

In archery, shoulder pain is likely occur during the full draw phase. One of the factors for shoulder pain is subacromial impingement syndrome (SIS). SIS is primarily caused by collision of the humeral head and the acromion, with the acromiohumeral distance (AHD) between the humeral head and the acromion being smallest in abduction, internal rotation, and horizontal adduction positions of the glenohumeral (GH) joint. Beginners and non-experienced archers tend to have a large horizontal GH adduction angle by the string tensions at full draw [1]. However, the effect of archery experience on kinematics of the shoulder girdle and AHD at full draw is unknown. This study aimed to compare the AHD , additionally the angle of the GH and scapulothoracic (ST) joint in the frontal, sagittal, and horizontal planes during full drawing between experienced and non-experienced archers and to prevent SIS in beginner archers.

METHODS

Twenty-two healthy men participated in this study. Those with at least 1 year of archery experience were included in the archer group and those with no archery experience in the control group. Kinematic data of the ST and the GH joint were obtained using an electromagnetic tracking device (Liberty; Polhemus, Inc., USA) from all participants (archer group: 7, control group: 15) during drawing motion with and without the bow string. Full draw was as the period from 1 second before the release of the string (release) to the release. The AHD was measured under three conditions at the standing (the shoulder in 0 degrees of abduction and the humerus in a neutral position) and full draw positions (with and without the bowstring) using B-mode ultrasound (SONIMAGE MX1; Konica Minolta, Inc., Japan). The probe was fixed at the midpoint of the acromion on the bow string side in all conditions. Three images of the subacromial space were acquired for each condition, and the AHD (mm) was defined as the distance from the most lateral side of the acromion to the superior margin of the humeral head [2]. The statistical analysis used two-way ANOVA by the archery experience and the conditions ($p<0.05$).

RESULTS AND DISCUSSION

In the kinematic data, only the GH horizontal adduction angle showed an interaction effect on archery experience and the use of bow string ($\eta^2=0.074$, $p<0.05$). The main effect of archery experience was observed in ST internal rotation, posterior tilt, and GH abduction angle ($p<0.05$). There was a significant interaction effect of AHD on archery experience and conditions ($\eta^2=0.346$, $p<0.001$). No significant differences were observed between groups in the without-bow-string condition ($p=0.652$). A significant difference shows between groups in the bow string condition ($p<0.05$); the AHD was larger in the archer group than that for the control group (**Figure 1**).

Archers have greater shoulder extensor strength because they resist horizontal adduction moments in every drawing motion. In this study, the difference in shoulder extensor strength in each group may have also led to intergroup differences in the ST joint internal rotation and GH joint horizontal adduction angle. In previous studies, archers maintained a full draw position due to lower trapezius and latissimus dorsi muscle activity and string tension to reduce shoulder fatigue from the drawing motion [3]. About the archer group, contraction of the lower trapezius muscle produced higher ST joint posterior tilt and GH joint abduction, and the force of the latissimus dorsi muscle pulling the humeral head downward may have caused an increase in the AHD at full draw with the bow string.

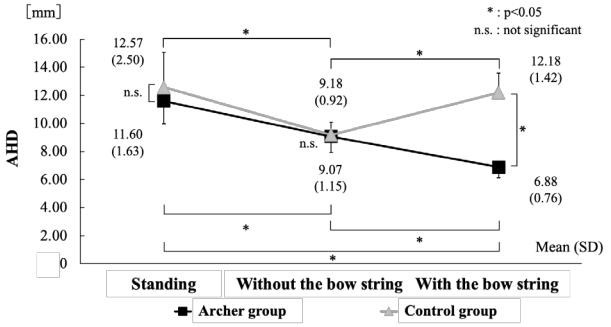

Figure 1 AHD at the standing and full draw positions.

CONCLUSIONS

This study suggested that the reducing the horizontal abduction angle at the full draw may help contain the decrease in AHD due to string tension and prevent SIS for beginner archers.

REFERENCES

[1] Shinohara H et al. *J Sports Med Phys Fitness* **58**: 1752-1758, 2018.
[2] Longo S et al. *Phys Ther Sport* **23**: 105-112, 2017.
[3] Kim R et al. *Clin Shoulder Elb* **21**: 145-150, 2018.

Differences of maximum inclination and center of mass accelerations between professional and amateur ballet dancers during pirouette in classical ballet

Yurina Tsubaki[1], Yui Kawano[2], and Mayumi Kuno-Mizumura[1]
[1] Graduate School of Humanities and Science, Ochanomizu University, Tokyo, Japan.
[2] Japan Institute of Sports Sciences, Tokyo, Japan.
Email: y.tubaki.1@gmail.com

INTRODUCTION

The pirouette is a fundamental turn in classical ballet and it is crucial to keep the body stable. Previous studies focus on the inclination angle between the vertical axis and the line from the center of pressure (COP) to the center of mass (COM). Previous research has indicated that less experienced dancers have greater difficulty in keeping the line straight compared to experienced dancers while performing in flat shoes [1,2]. However, pirouettes are typically performed while wearing pointe shoes on stage. Thus, it is vital to delve deeper into the movement characteristics associated with pointe shoes, which are more challenging than flat shoes. Therefore, the current study determined differences between professional and experienced amateur ballet dancers regarding the pirouette.

METHODS

A total of seven professional and nine experienced amateur ballet dancers participated in this study. Retroreflective markers were applied to 35 body sites based on the Plug-In Gait full-body model. An 8-camera motion-capture system (Vicon MX, 250 Hz) and two force plates (Kistler, 1,000 Hz) were used for data collection. The subjects wore their pointe shoes and performed the right single pirouettes from the 4th position and finished in the 5th position (Fig. 1) until they achieved three successful trials. All participants preferred to perform right pirouettes. The motion was divided into four phases (Phase 1: turn initiation, Phase 2: single leg initiation, Phase 3: single leg support, and Phase 4: ending) following a previous study (as outlined in Figure 1). The analysis items were the maximum anterior-posterior and gesture-supported leg-side inclination between the straight-line connecting COP and COM (COP-COM) and the vertical axis in each phase. Furthermore, the maximum anterior-posterior and gesture-supported leg-side COM acceleration were calculated. The average of the three trials was used for statistical analysis. Unpaired t-tests or Mann-Whitney U tests were employed to evaluate differences between the two groups, depending on the regularity of the data. Statistical significance was set at $p<0.05$.

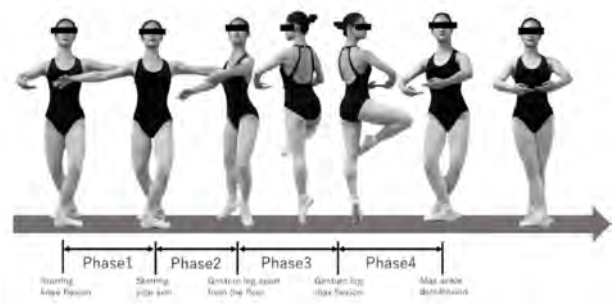

Figure 1 Task and phase division

RESULTS AND DISCUSSION

For the COP-COM inclination, there were no significant differences across Phases 1 to 3. Table1 presents the result of maximum COP-COM inclination and COM accelerations in phase 4. Professional ballet dancers exhibited significant fewer posterior inclinations than amateur dancers ($P<0.05$). Additionally, professional dancers demonstrated lower maximum accelerations for both posterior and support leg side in Phase4, when compared to amateur dancers ($p<0.05$). These findings suggested that, compared to amateur experienced dancers, professional dancers possess a greater ability to control the acceleration of their COM and maintain a less forward inclination during the ending phase.

CONCLUSIONS

In this study, we compared professionals and experienced amateurs regarding the inclination of the COP-COM and the acceleration of the COM in Pirouette. The difference between professionals and experienced amateurs was observed only in Phase4, which is the ending of the motion This fact contributes to a deeper understanding of the sophisticated movement patterns of pirouettes with pointe shoes.

REFERENCES

[1] Lin CW et al. *Res Q Exerc Sport* **85** : 330-340, 2014.
[2] Lin CW et al et al. *Front. Bioeng. Biotechnol* **7**:290, 2022

Table 1: Maximum COP-COM inclination and COM accelerations in phase4

	professional	amateur	Effect size	*p-value*
COP-COM inclination (anterior/posterior) (°)	0.10 ± 0.01 / 0.04 ± 0.02	0.10 ± 0.02 / 0.07 ± 0.03	0.04 / 1.18	0.94 / 0.02
COP-COM inclination (gesture / support) (°)	0.03 ± 0.02 / 0.06 ± 0.01	0.06 ± 0.04 / 0.06 ± 0.01	0.95/ 0.23	0.15 / 0.30
COM accelerations (anterior/posterior) (m/s^2)	1.70 ± 0.70 / 1.80 ± 0.40	2.20 ± 0.50 / 2.40 ± 0.30	0.82/ 1.70	0.19 /0.01
COM accelerations (gesture / support) (m/s^2)	1.30 ± 0.20 / 2.10 ± 0.50	1.70 ± 0.50 / 2.70 ± 0.30	1.05/ 1.46	0.07 /0.04

EVALUATION OF TRUNK MUSCLE ACTIVITIES DURING THE ARABESQUE

Kanae Ouchi[1], Yoshihide Tokuda[2], and Yoshiyuki Kokubun [3]

[1] Department of Judo Physical Therapy, Teikyo heisei University, Tokyo, Japan.
[2] Department of Physical Therapy, Teikyo heisei University, Tokyo, Japan.
[3] Department of Judo Physical Therapy, Teikyo heisei University, Chiba, Japan.

Email: k.ouchi@thu.ac.jp

INTRODUCTION

Arabesque, which is known as a basic pose in classical ballet. Several kinematic studies have reported that skilled dancers showed more pelvic motion in performing arbesque than novice dancers [1,2]. In addition, abdominal muscles have been known to play important roles for postural support before limb movements [3]. However, trunk muscle activitiy for performing arabesque has not been fully elucided.
Thus, we investigated the role of trunk muscles during arabesque.

METHODS

Five experienced contemporary dancers [age: 27 to 44 years old, 2 men and 3 women (height: 161.6±4.6 cm, weight: 50.0 ± 3.7 kg)] volunteered for this study. Participants were recruited from professional dance companies and signed written consent forms prior to participation. This study was approved by the ethical committee of Teikyo Heisei University (Approval No.2021-066). Thirty-nine reflective body markers were applied to each subject. A Three-dimensional motion analysis system (Vicon Nexus 2.5, sampling frequency: 100 Hz) and force plate (Kistler, sampling frequency: 1,000 Hz) were used to quantify the pelvis and the right leg motions. Furthermore, surface EMG (DELSYS, sampling frequency: 1,000 Hz) was used to analyse the trunk muscle activities. EMG electrodes were placed on the following muscles: rectus abdomins (RA) and lumber erector spinae (ES). The average root mean square of EMG amplitude with Butterworth filter (20 to 400 Hz passed) were using each trial. Participants practiced the movement sequence – standing position, passe, attitude, arabesque, to standing position. Each posture was held for two seconds. The right leg was the gesture leg for all participants. Medians and interquartile ranges (IQR) were calculated.

RESULTS AND DISCUSSION

During the arabesque phase, the median anterior pelvic tilt was 46.7 (IQR 39.7 to 57.2)° , the median obliquity angle toward the left leg was -1.9 (IQR -2.5 to -1.9)° , and the median transverse rotation angle toward the right leg was 33.5 (IQR 29.9 to 38.3)° (Figure 1). Furthermore, the median ES and RA activities were 19.3 (IQR 7.1 to 22.5) times and 1.4 (IQR 1.4 to 1.7) times, respectively (Figure 2).
In the current study, it is thought that the contribution of the pelvis to gesture leg motion in various ballet movements [4]. Therefore, we confirmed the pelvic rotation and anterior tilt during arabesque using Three-dimensional motion analysis system. Additionally, EMG of ES was increased during arabesque.

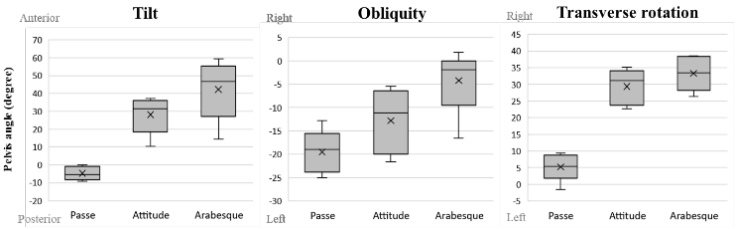

Figure 1 Angular change (pelvis).

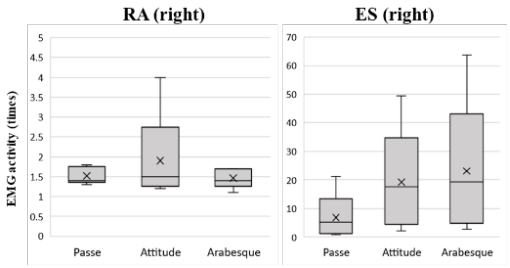

Figure 2 The activities of trunk muscles.

CONCLUSIONS

In conclusion, our study suggests that ES regulate the trunk extension during arabesque. On the other hand, the RA are not directly involved in performing arabesque.
Further investigation is required to elucidate the trunk stabilities of arabesque.

ACKNOWLEDGEMENTS

We thank the dancers who donated their time to participate in this study.

REFERENCES

[1] Shaw B. *J Dance Med Sci* **16**: 1, 2012.
[2] Margaret W et al. *J Dance Med Sci* **11**: 4, 2007
[3] Tesh K et al. *Spine* **12**, 1987
[4] Patterson R et al. *J Biomech Eng* **142**, 2020

THE INVESTIGATION OF THE MOBILITY IN THE FIRST TARSOMETATARSAL JOINT IN FORCED TURNOUT OF BALLET DANCERS

Honoka Ishihara[1], Noriaki Maeda[1], Makoto Komiya[1], Tsubasa Tashiro[1], Shogo Tsutsumi[1], Satoshi Arima[1], Miki Kawai[1], Yuki Tamura[1], Yukio Urabe[1]

[1] Department of Sports Rehabilitation, Graduate School of Biomedical and Health Sciences, Hiroshima University, Hiroshima, Japan
Email: ishihono0810@gmail.com

INTRODUCTION

Turnout (TO), which is the external rotation of the lower extremities mainly accomplished by the hip joint, is a major component of ballet movements. While, recent studies have pointed out the possibility that inappropriate TO, which is often called the forced TO, may be involved in the hallux valgus (HV) development of dancers [1]. The forced TO is formed with an excessed turnout angle over the possible external rotation at the hip joint, and it is an apparent turnout created with compensation by the foot hyperpronation and the floor friction. HV is a serious concern to be prevented for dancers because of its pain and deformity which affect their performance. The forced TO is pointed out as the risk factor of HV, however, the effect of forced TO on dancers' HV is unclear [1]. This study focused on the hypermobility of the first tarsometatarsal (TMT) joint which affected the HV development [2] and aimed to examine whether the first TMT mobility is different depending on the forced TO.

METHODS

In total 16 female dancers without HV deformity of pain (32 feet, average age: 18.1 ± 2.3 years old.) participated in this study. Participants performed a plié, the most fundamental ballet movement like a squat, in 3 conditions: Control, Reasonable TO (RTO), and Forced TO (FTO). Participants stood in the neutral position at hip joint internal/external rotation for Control, and The TO angle for RTO was at which each participant could create a maximum active hip joint external rotation. FTO was made as the maximum apparent TO position and it was allowed to use foot pronation or floor friction. Ultrasonography (US) was used to measure the gap of location between the first metatarsal (FM) and the medial cuneiform (MC). US system was synchronized with a 3-dimensional motion capture analysis system to detect a plié duration from the start of knee joint flexion to the end of the extension and calculated the maximum ankle joint dorsiflexion and the average foot pronation angles. The gap in the first TMT joint was represented by the vertical distance of FM minus that of MC. The comparison among 3 conditions for each parameter was performed with repeated measures ANOVA and the Bonferroni method as post-hoc test.

RESULTS AND DISCUSSION

The foot during *plié* in FTO was more pronated compared with in Control and RTO ($p<0.05$). The displacing to the plantar direction in the vertical location of MC and the changes in the gap of the first TMT joint in the FTO were greater than in the other 2 conditions (**Figure 1**).

This study showed that greater displaces to the plantar in MC and change in the gap of the first TMT joint were found with FTO. The forced TO created an apparent TO greater than the angle of external rotation possible at the hip joint is accomplished with the foot hyperpronation. Such inappropriate compensation results in the overload of the midfoot and collapsing of the medial longitudinal arch [3]. Since the lowering of the medial longitudinal arch relates to the hypermobility of the first TMT joint [3], reduction of the midfoot stability and greater valgus force on the first ray of the foot that occurred with the forced TO were considered to relate to the change in the alignment of the first TMT joint. This finding suggests that the forcing of TO may lead to compounds the hypermobility of the first TMT joint and it will be in the negative chain of increased mobility in the first TMT joint and midfoot collapse.

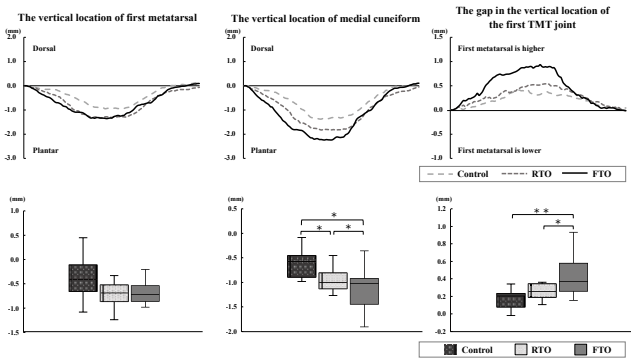

Figure 1 Comparison of the first TMT joint mobility (Upper: temporal data, Lower: moving average) during a plié in 3 conditions. *p<0.05.

CONCLUSIONS

The present study indicated that *plié* in FTO occurs the greater mobility of the first TMT joint. The results suggest that repetitive movements with the forced TO possibly compound the hypermobility of the first TMT joint and lead to HV deformity.

REFERENCES

[1] Seki H et al. *Plos ONE* **15**: e0231015, 2020.
[2] Clasoe WM et al. *Phys Ther* **90**: 110-120, 2010.
[3] Biz C et al. *Muscles Ligaments Tendons J press limited* **2**:282-288, 2013.

REGULATE VELOCITY ON COMBINED TRAINING IMPROVING THE COLLEGE BASKETBALL PLAYERS JUMPING PERFORMANCE

Chen-Fu Huang, Bo-Ying Chen
Department of Physical Education and Sports Science, National Taiwan Normal University, Taipei, Taiwan.
Email: huangchenfu@gmail.com

INTRODUCTION

Resistance training intensity could be quantified by collecting barbell mean velocity data during the concentric phase (González-Badillo et al., 2010) and using percentage velocity loss (%VL) to determine each set's repetition (Pareja-Blanco et al., 2017). Due to a lack of training time during the season, two training methods (strength and power training) combined into the same training session, Faude et al. (2013) found that combined training improved athletes' muscular strength and jumping ability. However, proper training load to avoid fatigue was critical. Thus, this study aimed to investigate the effect of velocity regulation of combined training on basketball players jumping performance.

METHODS

This study recruited eleven basketball players and divided them into velocity-based training (VBT) (n=7) and percentage-based training (PBT)(n=4). The four-week training program included session one: half squat (HS) and high pull (HP), and session two: trap-bar deadlift (TDL) and power clean (PC), which were performed on different days, three times a week. In addition to combined training, there were another three days of high-intensity technical training a week. Forty-eight hours before combined training, executed the 1 RM test and established the load-velocity relationship profile (LVRP). In the PBT training program, the first two weeks did 80%1RM HS and TDL 4 sets x 8reps and 80%1RM HP and PC 4 sets x 5 reps; the last two weeks executed 85%1RM HS and TDL 4 sets x 6reps and 85%1RM HP and PC 4sets x 3 reps. In the VBT training program, we used LVRP to determine the training load (Table 1), and we used 30%VL in the first two weeks and 20%VL in the last two weeks to regulate repetition. GymAware linear position transducer (50 Hz) was used to collect the barbell velocity, and one Kistler force plate (1000 Hz) collected CMJ parameters, including peak vertical ground reaction force (PGRF), rate of force development (RFD) and jump height (JH). Descriptive statistics were used to explain the results of the study.

RESULTS AND DISCUSSION

The main finding was that PGRF, RFD, and JH increased after four-week training in the VBT group, while the PBT group's PGRF and RFD had a slightly decreased trend (Table 2). The load was fixed for the PTB group; the intensity of the combined training might generate excessive neuromuscular fatigue that reduces the jumping performance. However, the VBT group's load was variable, and the training load would be adjusted according to the prescribed velocity. Table 1 showed that the target velocity was maintained in the first two weeks or the last two weeks, and the training load gradually increased, indicating a trend of increasing muscle strength.

Table 1: VBT group load and velocity training program

	W1	W2	W3	W4
HS	119.4±7.0	122.5±12.6	133.9±6.1	137.0±8.0
	0.54±0.07	0.52±0.04	0.50±0.03	0.49±0.01
TDL	142.1±0.6	154.0±0.6	159.6±0.6	169.5±0.5
	0.64±0.05	0.59±0.05	0.56±0.05	0.54±0.03
HP	67.1±6.7	70.3±7.3	72.2±10.5	77.6±10.8
	1.32±0.14	1.28±0.13	1.21±0.10	1.19±0.07
PC	57.7±8.1	65.1±7.5	64.8±11.7	69.8±10.9
	1.34±0.17	1.30±0.09	1.27±0.05	1.28±0.03

Note: The upper column unit was kg; the lower was m/s.

Table 2: The differences between pre-and post-training CMJ

	VBT	PBT
PGRF(BW)	0.06±0.13	-0.16±0.23
RFD (BW/s)	1.22±1.79	-0.42±0.83
JH (cm)	2.08±1.35	0.77±1.19

CONCLUSIONS

This study aimed to achieve the best training stimulation by regulating the velocity zone during combined training. The results indicated that the VBT group's jumping performance and muscle strength improved because the variable load could avoid excessive fatigue and low-stimulation training. This study recommended that coaches and strength and conditioning trainers can monitor the players' fatigue by adjusting the training velocity and %VL to avoid injuries during training and increase sports performance improvement.

REFERENCES

[1] González-Badillo JJ et al. Int. J. Sports Med **31**:347-352, 2010
[2] Pareja-Blanco F et al. Scand J Med Sci Sports **27**:724-735, 2017
[3] Faude O et al. J. Sports Sci **31**:1460-1467, 2013

ANTEROPOSTERIOR HAND POSITION AT SET POSTURE AFFECTS THE SUBSEQUENT BLOCK START PERFORMANCE

Takuma Hayashi[1], Yuta Yamaguchi[1], Tetsunari Nishiyama[1,2], Masanori Nagashima[2], Masuhiko Mizuno[2] and Mitsuo Otsuka[1,2]

[1] Graduate School of Health and Sport Science, Nippon Sport Science University, Yokohama, Japan.
[2]Faculty of Sport Science, Nippon Sport Science University, Yokohama, Japan.
Email: 22sma22@nittai.ac.jp

INTRODUCTION

During a sprinter's acceleration, the starting motion can be divided into reaction and pushing phases. The high performance in both phases has been investigated using the reaction time and external horizontal power [1,2]. Recently, it was found that trunk kinetics is a determinant of block performance [3]. Since skeletal muscles have an optimal length at which the muscle tension maximises [4], there would be an optimal starting posture at which both trunk and lower-limb muscle groups can generate the maximised force. Trunk muscle lengths can be simply adjusted by changing the space between the hand and foot positions. Therefore, the purpose of this study was to examine the effects of changing the anteroposterior distance from the hands to the forefoot at a set posture on various starting performances in the reaction and pushing phases.

METHODS

The participants were 16 male collegiate sprinters (age: 20.5 ± 1.2 years old; height: 174.5 ± 3.6 cm; body mass: 67.6 ± 5.6 kg; 100-m personal record: 10.64 ± 0.16 s). Participants were instructed to perform two block-start trials with five different hand-and-foot spaces (preferred distance [forefoot position from the start line: 45.5 ± 6.0 cm; rearfoot position from the start line: 74.1 ± 7.2 cm], ± 7.2 cm, and ± 14.4 cm) at the set posture. The starting blocks were fixed on two force plates (TFP-404011B, Technology Service, Nagano, Japan) using double-sided tape. The ground reaction forces (GRFs) were sampled at 1000 Hz. To familiarise the participants with the dashes from the five set postures, they performed these trials on another day. The external horizontal power was calculated by the average value of external power in an anterior direction to translate the whole-body centre of mass.

RESULTS AND DISCUSSION

Many previous studies have reported that start performances are affected by the set posture, which is especially adjusted by the block space [5]. In contrast, we first clarified the effect of changes in anteroposterior distance from the hands to the forefoot block.

It was found that the longer the hand-and-foot space, the higher the external horizontal power (Figure 1). Compared to the external horizontal power in the trial with the athlete's preferred posture, it increased by 15% in the +14.4-cm trial; in contrast, it decreased by 13% in the −14.4-cm trial. Interestingly, in the longer hand-and-foot space trials, the horizontal GRF impulses, especially the rear-foot impulses, significantly decreased. In contrast, the pushing time was significantly shorter in the longer hand-and-foot space trials. The higher external horizontal power is directly contributed by both the high horizontal GRF impulse and the short pushing time. Therefore, it was suggested that a shorter pushing time remarkably contributes to achieving higher external horizontal power when the hand-and-foot space is lengthened at the set posture.

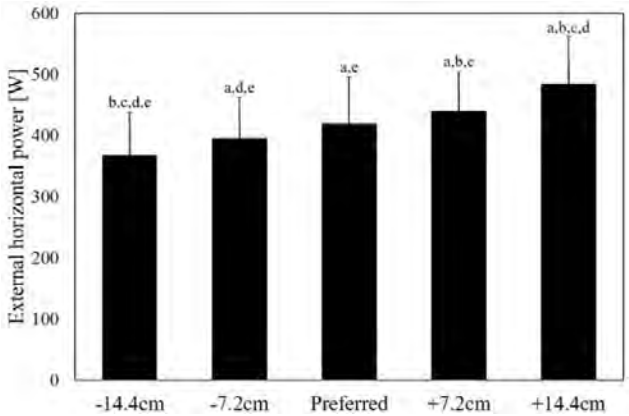

Figure 1. External horizontal power in the five trials. Significant differences between the −14.4-cm, −7.2-cm, preferred distance, +7.2-cm and +14.4-cm trials are denoted by a, b, c, d, and e, respectively ($p < 0.05$).

CONCLUSIONS

We first examined the effects of changing the hand-and-foot space at the starting posture on the subsequent starting performances. It was found that a higher external horizontal power was significantly enhanced when the hands were positioned further away from the feet in the set posture compared to that in the preferred posture. The long length of "bridge" at the set posture may allow sprinters to accelerate more largely. Conversely, in the athletic sprint event, the longer hand-and-foot space increased the running distance from the forefoot. Therefore, sprinters should select a balanced set posture considering the negative effect of increasing the subsequent running distance.

REFERENCES

[1] Martin DE et al. *New Stud Athletic* **10**: 67-79,1995.
[2] Willwacher S et al. *PLoS ONE* **11**:18,2016.
[3] Sado N et al. *PLoS ONE* **15**(3): e0230145,2020.
[4] Gordon A et al. *J Physiol* **184**:170192,1966.
[5] Schot PK et al. *Res Q Exerc Sport* **63**:137-47,1992.

VALIDITY OF APPROACH-RUN SPEED IN POLE VAULTING USING LASER DISPLACEMENT METER OR BODY-ONLY MODEL

Atsuto Noro[1], Fumiaki Kobayashi[1,2], Shigeo Hatakeyama[2] Yasuo Shinohara[3] and Mitsuo Otsuka[1,2]
[1] Graduate School of Health and Sport Science, Nippon Sport Science University, Yokohama, Japan.
[2] Faculty of Sport Science, Nippon Sport Science University, Yokohama, Japan.
[3] Faculty of Management, Josai University, Sakado, Japan.
Email: 22sma19@nittai.ac.jp

INTRODUCTION

A pole vault event is a competition in which athletes compete in the maximal height of an upward leap, following an approach run using an approximately 2 kg bar (pole). Previous studies reported that the higher the peak approach-run speed, the higher the maximal height of centre of mass (COM) during a leap [1]. The most common measurement device for analysing approach-run speed uses a laser displacement meter or high-speed camera to obtain the position of the jumper's body [1,2]. During the approach run until the pole plant, the vaulter not merely runs with holding the pole but also immediately tilts it forward before plunging into the box. Therefore, the mass and forward-leaning motion of the pole should be considered in the rigid-body model as a whole system when analysing the approach-run speed. Therefore, the purpose of this study was to test the agreement between the approach-run speeds of pole vaulters calculated using three different methods: 1. using the COM position of the body-only model (body-only method), 2. using the COM position of the whole-system (body + pole) model (whole-system method), and 3. using the position of the jumper's back position obtained using a laser displacement meter (laser method).

METHODS

The participants were 15 male collegiate athletes (height: 1.72 ± 0.05 m; mass: 66.6 ± 5.4 kg; personal record: 4.20 ± 1.03 m) with adequate experience in pole vault competition. A high-speed camera (RX IV, SONY, Tokyo, Japan) was placed at approximately 90 m from the right side of the running course to capture all trials during the competition. The sampling frequency of the high-speed camera was 240 Hz. A Laser displacement meter (LDM301S, Jenoptik, Germany) was placed on a 1.2-m tripod 48 m behind the vault box. The sampling frequency of the lase displacement meter was 100 Hz. A total of 19 trials were used for further analysis. The body-only model was created with a 14-segment rigid-body model. The mass of the pole and its centre position were measured directly before the trials and used for the whole-system model. The two-dimensional positions of the whole body and poles were obtained in the sagittal plane using a digitising software (Frame-DIAS 5, Q'sfix, Tokyo, Japan). Approach-run speeds in the body-only and whole-system methods were calculated using the first-time derivatives of the COM and pole position. To quantify the agreement between the methods, Bland–Altman tests were used between the whole-system and the other two methods for several variables of approach-run speed.

RESULTS AND DISCUSSION

A large proportional bias was observed in the peak approach-run speed when the laser method was used (r = 0.75; Figure 1). By the laser method, the peak approach-run speed of over 8.0 m/s was overestimated; in contrast, that of less than 8.0 m/s was underestimated. The great record in the pole vault is related to the approach-run speed [1]; therefore, it is suggested that comparing approach-run speeds between different record groups should be avoided because overestimated differences are largely observed. In addition, a random error of ± 0.44 m/s was found in peak approach-run speed in the laser method (Figure 1). Koyama et al. (2019) found that the difference of 0.10 m jump height is related to the difference of approach-run speed of 0.09 m/s by its regression equation [3]. Hence, changes in the approach-run speed of an athlete should be carefully assessed using the laser method.
As the other result, there was a fixed bias of −0.06 m/s in decreases in approach-run speed at the pole plant in the body-only method.

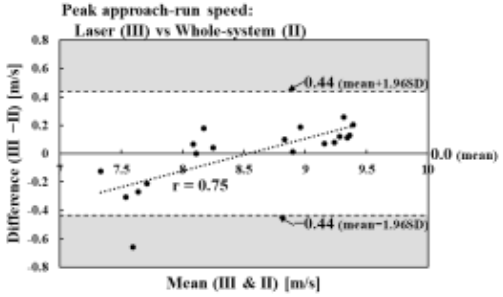

Figure 1 The degree of agreement between the two methods for the peak approach-run speed according to the Bland-Altman analysis.

CONCLUSIONS

Bland-Altman analysis revealed that a proportional bias or fixed bias was involved in the laser and body-only methods, indicating that these methods should be carefully used when assessing the differences between groups or changes within athletes.

REFERENCES

[1] Linthorne NP and Weetman AHG. *J Sports Sci Med* **11**: 245-54, 2012.
[2] Yang MH et al. *J Hum Sport Exerc* **16**: 273–83, 2021.
[3] Koyama H et al. *Bull Stud Athl JAAF*. **15**: 243–50, 2019 (in Japanese).

Does the lower limb muscularity relate to long-sprint performance in 400-m sprinters?

Keishi Kuroki[1], Tadashi Suga[1], Masafumi Terada[1], Yuki Kusagawa[1], Haruto Arai[1], Takahiro Tanaka[1], Mitsuo Otsuka[2], Akinori Nagano[1], and Tadao Isaka[1]

[1] Faculty of Sport and Health Sciences, Ritsumeikan University / Shiga, Kusatsu, Japan.

[2] Faculty of Sports Science, Nippon Sports Science University / Kanagawa, Yokohama, Japan.

Email: sh0247hx@ed.ritsumei.ac.jp

INTRODUCTION

The generation of large torques by muscles crossing the lower limb joints is necessary for superior sprint performance in sprinters. The joint torque is largely determined by the size of agonist muscle group. We and others previously determined that larger sizes of specific muscles, particularly the hip extensor and flexor muscles (gluteus maximus [GM] and psoas major [PM]), of the lower limb are related to better 100-m sprint performance in sprinters [1-3]. Thus, the lower limb muscularity plays an important role in achieving superior 100-m sprint performance in sprinters. Despite the close relationship between lower limb muscularity and 100-m sprint performance, it is unknown whether the lower limb muscularity plays an important role in achieving superior long-sprint performance in sprinters. In this study, we examined the relationships between lower limb muscle sizes and long-sprint performance in 400-m sprinters.

METHODS

The cross-sectional areas (CSA) of seven muscles of the lower limb in 30 male 100-m specialized sprinters and 30 male 400-m specialized sprinters were measured using magnetic resonance imaging. The seven lower limb muscles included the GM, PM, adductors, quadriceps femoris, hamstrings, dorsiflexors, and plantar flexors. To minimize the effect of difference in body size among individuals, the relative CSA normalized to body mass was also used for analyses of this study. The International Amateur Athletic Federation (IAAF) score was used as a parameter for 100-m or 400-m sprint performance based on the personal best time of the sprinter in each group. Comparisons of the lower limb muscle CSA variables between the 100-m and 400-m groups were performed using an unpaired *t*-test or Mann–Whitney U test. Relationships between lower limb muscle CSA variables and IAAF score in each group were evaluated using a Pearson's product moment correlation coefficient.

RESULTS AND DISCUSSION

Absolute and relative CSAs of all seven lower limb muscles did not differ significantly between 100-m and 400-m sprinters (all *P*s > 0.05). The absolute and relative CSAs of the GM and PM of 100-m sprinters were significantly correlated with the corresponding IAAF scores (Figure 1A: r = 0.455 to 0.538, all *P*s < 0.05). This result is consistent with those of previous studies [1-3]. In contrast, there were no significant correlations between the absolute and relative CSAs of all seven lower limb muscles, including the PM and GM (Figure 1B), of 400-m sprinters and the corresponding IAAF scores (r = –0.303 to 0.337, all *P*s > 0.05). A series of our studies reported that favorable morphological variables of the lower limb bones (e.g., longer forefoot bones) and joints (e.g., greater knee extensor moment arm) were related to better long-sprint performance in 400-m sprinters [4, 5]. Therefore, the bone and joint structures rather than the muscle size of the lower limb may be important morphological factors contributing to superior long-sprint performance in 400-m sprinters.

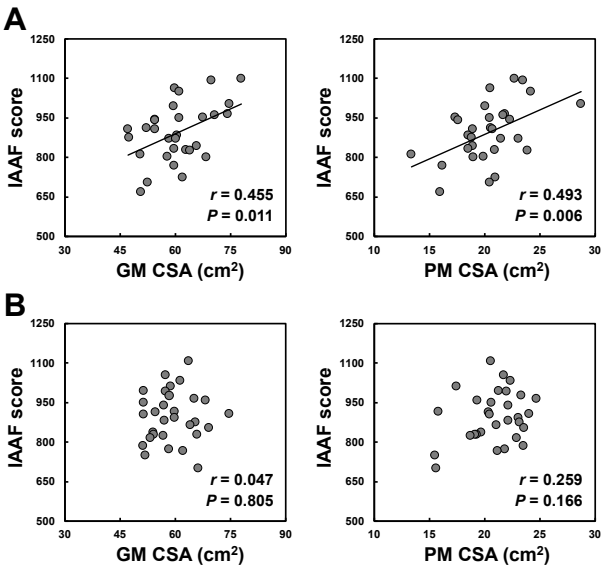

Figure 1. Relationships between CSAs of the GM and PM and the IAAF scores in 100-m (A) and 400-m (B) sprinters

CONCLUSIONS

We found that the lower limb muscularity may not play an important role in achieving superior long-sprint performance in 400-m sprinters. Therefore, the present findings suggest that specific morphological factors contributing to superior sprint performance may differ between 100-m and 400-m specialized sprinters.

REFERENCES

[1] Miller R et al. *Med Sci Sports Exerc* **53**: 804-815, 2021.
[2] Sugisaki N et al. *Int J Sports Physiol Perform* **13**: 214-219, 2018.
[3] Tottori N et al. *BMC Res Notes* **14**: 74, 2021.
[4] Tomita D et al. *BMC Res Notes* **11**: 583, 2018.
[5] Tomita D et al. *BMC Res Notes* **13**: 297, 2020.

AGE-RELATED DIFFERENCES IN ELECTROMYOGRAPHIC LATENCIES OF THE LOWER LIMB MUSCLES IN STANDING SPRINT INITIATION THROUGHOUT CHILDHOOD AND ADOLESCENCE

Mizuki Kitamura[1], Tadao Isaka[2] and Mitsuo Otsuka[1]
[1] Faculty of Sport Science, Nippon Sport Science University, Kanagawa, Japan.
[2] Faculty of Sport and Health Science, Ritsumeikan University, Shiga, Japan.
Email: 20aa378@nittai.ac.jp

INTRODUCTION

Short reaction time to external stimuli is an important ability in various sports involving sprint running. In childhood and adolescence, muscles and nerves develop with age [1]. Therefore, the reaction time and related electromyographic (EMG) latencies of the lower limb muscles would change based on growth. This study aimed to elucidate age-related differences in whole-body reaction time and EMG latencies of the lower limb muscles during sprint initiation.

METHODS

Fifty-four boys aged 5 to 18 years (age, 14.5 ± 5 years; mass, 44.8 ± 22.2 kg; height, 156.6 ± 20.9 cm) participated in this study. The participants performed five sprint starts of 2.0 m on the experimental track. They were instructed to perform sprints, starting from their preferred standing postures. The timing and intensity of the go signal were fixed at 2.0 s and 80 dB, respectively, to reduce the standard deviation of the reaction time [2].

The ground reaction force (GRF) data for both feet were recorded separately using two force plates (9281CA, Kistler Holding AG, Winterthur, Switzerland). Surface EMG activities of the rectus femoris (RF), longer head of the biceps femoris (BF), and lateral head of the gastrocnemius (GS) muscles from both legs were recorded using a wireless surface EMG system (WEB-7000, Nihon Kohden, Tokyo, Japan). The sampling rates of the GRF and EMG data were set to 1000 Hz.

The reaction time of each foot and EMG latency of each muscle were determined by using the onset when the signal first rose above the value of the mean plus four times the standard deviation during the baseline zone (from −0.500 s to 0 s of the go signal; Figure 1).

RESULTS AND DISCUSSION

Chronological age was significantly related to the rear-leg reaction time ($r = -0.64$, $P < 0.05$) and EMG latencies of the rear-leg BF muscle ($r = -0.49$, $P < 0.05$). In contrast, chronological age was not significantly related to the other EMG latencies or reaction time of the front leg. In standing sprint start, the reaction time needed to react to a go signal can be divided into four durations: (1) that taken for the input information to reach the auditory receptors, (2) that taken for the brain to process the information and issue commands to the periphery, (3) that taken for the commands to pass through the spine and peripheral nerves, and (4) that taken for the muscles to exert force towards the ground following the onset of muscle contractions. Therefore, at the sprint initiation, older boys seem to shorten the rear-leg reaction time by shortening all or part of the processing durations in the central and peripheral nerves above-mentioned in the (1)-(3).

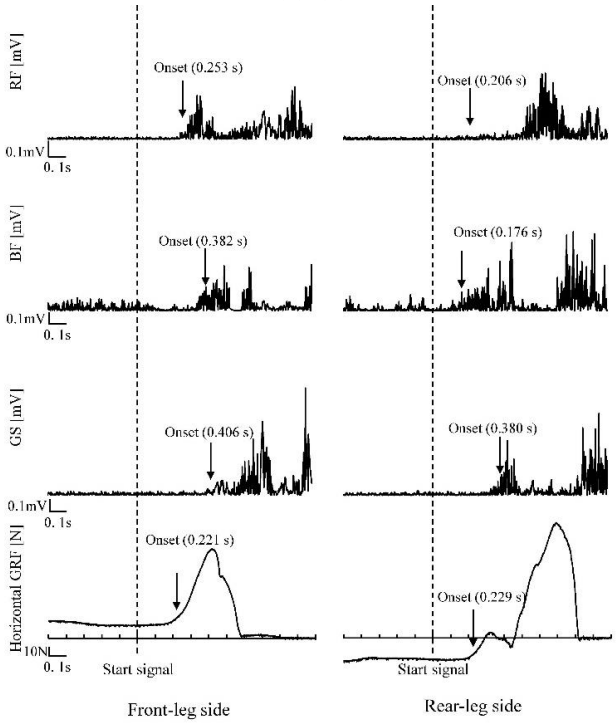

Figure 1. Example of a typical time-series data of the horizontal GRF and EMG signals of the RF, BF and GS muscles at sprint initiation in a boy aged 5 years. Vertical lines represent the timing of the go signal.

CONCLUSION

The findings from this study suggest that the growth and development of speed in sprint initiation is likely caused by shorter muscular latencies of the rear-leg BF. These findings may deepen our understanding of the development of sprint initiation in childhood and adolescence.

ACKNOWLEDGEMENTS

This work was supported by the Ministry of Education, Culture, Sports, Science and Technology Grant-in-Aid for Young Scientists (18K17906).

REFERENCES

[1] Scammon RE. *Measurement Man*, 1930.
[2] Otsuka M et al. *New Stud Athl*, **32**: 87-95, 2017.

CORRELATION BETWEEN CUE TIP SPEED AND KINEMATICS OF 9-BALL BREAK SHOT

Pui Wah Kong[1], Jing Wen Pan[1], John Komar[1] and Chen Yang[2]
[1] Physical Education and Sports Science Academic Group, National Institute of Education, Nanyang Technological University, Singapore.
[2] Max Nader Lab for Rehabilitation Technologies and Outcomes Research, Shirley Ryan AbilityLab, Chicago, USA
Email: puiwah.kong@nie.edu.sg

INTRODUCTION

Break shot is the first shot in cue sports, serving to separate the racked object balls in games. A break shot requires a high cue tip speed, as confirmed by a previous study which revealed that the break shot had a greater acceleration at impact than other types of shots (e.g., top spin shot, back spin shot) [1]. In the literature, there is generally a lack of biomechanical investigations of the human movements while performing cue sports shots. Previous work examined the kinematics of the upper body movements such as joint range of motion (ROM) and peak angular velocity without considering the temporal characteristics associated with these variables [2]. Since temporal characteristics may provide useful information regarding joint movement sequences, it could help researchers and practitioners better understand the cueing movement. Therefore, this study aimed to incorporate temporal aspect to analyze the upper body kinematics that could be related to cue tip speed during 9-ball break shots.

METHODS

This present study was approved by the Nanyang Technological University Institutional Review Board (Protocol Number: IRB-2019-06-37). Twenty-two male, active cue sports players [mean (standard deviation); age 25.2 (5.5) years old; playing experience 5.8 (4.9) years; height 171.8 (5.2) cm; body mass 68.4 (10.2) kg] were recruited. All participants had at least one-year playing experience at the time of the study.

After warm-up, each participant performed 8 break shots with the cue ball remaining on the pool table after the shot. To facilitate kinematic analysis, a 3D motion capture system with 8 infrared cameras (250 Hz, Vicon MX, Oxford Metrics Ltd., Oxford, UK) was used. Retro-reflective markers were placed on the upper body landmarks of the participants and the cue stick.

Kinematic data were analyzed using the Visual3D software (v2021.09.1, C-Motion, Germantown, MD, USA). Data during the movement phase were extracted from the start of forward swing to the end of follow-through. Joint ROM was obtained for negative humeral elevation, elbow flexion/extension, and wrist abduction/adduction. In addition, time to peak angle was determined and time normalized to the movement phase (100%). A Pearson correlation coefficient was computed to examine the linear relationship between cue tip speed and each upper body kinematic variable using JASP (version 0.16.4).

RESULTS AND DISCUSSION

The mean (SD) cue tip speed at impact was 4.7 (0.5) m/s across all 22 participants. There was a significant and positive correlation between the cue tip speed and time to peak elbow flexion/extension angles (Table 1, r = 0.447, p = 0.037).

Table 1: Correlations between cue tip speed at impact and each upper body kinematic variable.

	Mean (SD)	r	p
Range of motion (deg)			
Shoulder	21.2 (13.3)	-0.307	0.165
Elbow	107.2 (43.4)	0.300	0.176
Wrist	28.6 (11.9)	0.217	0.332
Normalized time to peak angle (%)			
Shoulder	74.5 (24.1)	0.014	0.952
Elbow	79.0 (19.2)	0.447	**0.037***
Wrist	78.3 (26.5)	0.063	0.779

Shoulder denotes negative humeral elevation; Elbow denotes elbow flexion/extension; Wrist denotes wrist abduction/adduction.

CONCLUSIONS

This study found that time to peak angle may play a more important role than joint ROM in contributing to cue tip speed at impact in 9-ball break shot. Reaching peak elbow flexion at a later phase of the cueing movement might indicate a greater utilization of the momentum generated from shoulder. This, in turn, can increase the cue tip speed and enhance break shot performance.

ACKNOWLEDGEMENTS

National Institute of Education Academic Research Fund (NIE AcRF, RI 1/19 KPW), Nanyang Technological University, Singapore.

REFERENCES

[1] Kornfeind P et al. *Procedia Eng* **112**: 540-5, 2015.
[2] Pan J W et al. *Front Psychol* **130**: 691043, 2021

Potential injury mechanisms in ulnar collateral ligament injuries; magnitude and variability of elbow load in repetitive baseball pitching

Bart van Trigt[1,1], Thomas van Hogerwou[2,1], Ton (A.J.R) Leenen[3,2], Marco (M.J.M.) Hoozemans[4,2], Frans (F.C.T) van der Helm[5,1], DirkJan (H.E.J.) Veeger[6,1]
[1]Department of Biomechanical Engineering, Delft University of Technology, Delft, The Netherlands
[2] Department of Human Movement Sciences, Vrije Universiteit Amsterdam, Amsterdam, the Netherlands.
Email: b.vantrigt@tudelft.nl

INTRODUCTION

High performance in sports is closely related to overuse injuries. A common overuse injury in baseball pitching is the Ulnar Collateral Ligament (UCL) injury, this is due to high and repetitive loads on the medial side of the elbow [1]. To be able to prevent UCL overuse injuries, it is important to understand the effect of repetitive pitching on the UCL load magnitude and variability [2]. We investigated if repetitive pitching influences the elbow load magnitude and variability and if a relationship is present between repetitive pitching and elbow muscle activation.

METHODS

Fifteen asymptomatic male baseball pitchers threw 60 to 110 fastballs until reporting fatigue. Body kinematics were recorded with a motion capture system at 400 Hz. The peak external valgus torque was calculated for every pitch with an inverse dynamical model. Electromyography of three elbow muscles (flexor pronator muscle group (FPM), biceps, and triceps) was recorded at 2000Hz during every pitch. The area under the curve (AUC) of the rectified EMG signal was calculated over a window of 150ms before maximal external shoulder rotation. Co-contraction index (CCI) was calculated for the biceps-triceps muscle pair. A moving window of ten pitches was applied to all variables and moved over a single subsequent pitch. Linear mixed models were used to investigate the relationships between repetitive pitching and the following four outcome variables: (1) within-individual peak external valgus torque magnitude and (2) valgus torque magnitude variation, (3) flexor pronator muscle group activity and (4) biceps-triceps co-contraction index.

RESULTS AND DISCUSSION

The results of the linear mixed models (table 1) showed no significant relationship between the external values torque magnitude and within-individual variability with repetitive pitching on a group level; but both variables showed significant variance in the association across participants (Figure 1, colored lines). On a group level, the FPM activity was not significantly related to repetitive pitching. In addition, the biceps-triceps co-contraction index showed a trend but was not significant in relation to repetitive pitching. The FPM activity and the biceps-triceps co-contraction index showed significant variance in the association across participants. The results indicate the importance of individuality in association with repetitive pitching.

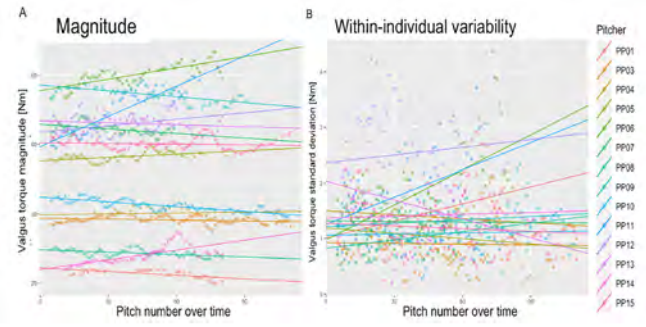

Figure 1 *peak external valgus torque magnitude (A) and variability (B) for each participant associated with repetitive pitching.*

CONCLUSIONS

Significant large differences exist between pitchers in their individual courses in elbow valgus torque and muscle activity with repetitive pitching. This shows the importance of individuality in relation to repetitive pitching. To arrive at effective elbow injury prevention in baseball pitching, individual characteristics of changes in elbow load magnitude and variability and muscle activity in relation to the development of UCL injuries should be investigated.

ACKNOWLEDGEMENTS

This work was supported by the NWO Domain Applied and Engineering Sciences (AES) under project number [R/003635].

REFERENCES

[1] Anz A.W. et al. *AMJSM.* ***38****(7),1368, 2010*
[2] van Trigt B et al. *Appl. Sci.* ***12****(13), 6549*, 2022

Table 1: Linear mixed model analysis results of the predictor variable window number in association with the four outcome variables. ß is the slope of the linear relationship of the fixed effect. CI is the confidence interval with the lower and upper limits at respectively 2.5% and 97.5%. * p<0.05

Outcome variable	ß		CI	t	significance
Elbow load magnitude	0.0129	-0.0108	0.0366	1.065	0.286
Elbow load variability	0.0029	-0.0018	0.0077	1.21	0.223
FPM (AUC)	$-1.3*10^{-4}$	$-4.5*10^{-4}$	$1.7*10^{-4}$	-0.84	0.39
CCI Triceps-Biceps	$-5.1*10^{-4}$	$-10*10^{-4}$	$-0.7*10^{-5}$	-1.93	0.053

SEX-SPECIFIC EFFECTS OF FATIGUE ON MUSCLE ACTIVATION DURING A SINGLE-LEG LATERAL JUMP LANDING TASK

Davine Yang, Tailynn Chang, Samuel Lamanuzzi and Julie N. Côté
Department of Kinesiology and Physical Education, McGill University, Montreal, Canada.
Email: davine.yang@mail.mcgill.ca

INTRODUCTION

Knee injuries are common in direction-changing sports, with injury risk increasing with fatigue [1]. Females exhibit around 3 times greater risk of injury than males [2], despite showing similar levels of central fatigue [3]. Imbalances in muscle activation can contribute to injury. Females are known to have greater quadriceps (Q) to hamstring (H) activation [4], as well as lower activation of the lateral H under fatigue [5]. These factors may contribute to dynamic knee instability. However, sex and fatigue effects on muscle activation during typical tasks involved in direction-changing sports are unclear. The objectives of the study were to examine the effects of sex and fatigue on activation amplitude of the Q and H muscles during a single-leg jump landing. We hypothesized that with fatigue, both sexes would have similar decreases in activation amplitude, but that females would have greater increase in muscle coordination ratios.

METHODS

Twenty-five participants (15F; age 21.7 ± 1.8 yrs) were included in the study. Participants were recruited from university varsity sports involving running and/or cutting. Surface electromyography (EMG; Trigno, Delsys) readings were collected from the vastus lateralis (VL), rectus femoris (RF), vastus medialis (VM), biceps femoris (BF), and semitendinosus (ST) muscles of the dominant leg at 2000Hz (Vicon Nexus, UK). Maximal voluntary isometric contractions (MVIC) were conducted for the Q and H muscles. Participants performed the jump landing task before and after a fatiguing cycling protocol of 9 x 30s sets of high-intensity cycling, interspersed by 90s of rest. Three successful jump trials (i.e. when the participant could land on 1 foot and stay for 5s) were taken in each fatigue condition (before, after) for data processing. EMG data were collected for the duration of each jump trial.

All data were processed using custom written Matlab script. Raw EMG data were bandpass filtered and normalized to MVICs. The root mean square (RMS) was calculated during the landing phase of each jump. The group average EMG RMS value across the successful trials was taken for statistical analysis. Effects of sex and fatigue on EMG data were assessed using General Estimating Equations in SPSS.

RESULTS AND DISCUSSION

Significant sex x fatigue interactions on Q activation (P=0.001) and Q:H activation ratio (P=0.002) were found. Females had a decrease in Q activation amplitude and Q:H activation ratio with fatigue, whereas males experienced insignificant changes (Figure 1). No significant effects were found for hamstring activation. Main effects of sex and fatigue were observed on VM and VL activation ratio. Females had a higher VM:VL activation than males (P=0.021) and VM:VL showed an increase in fatigue (P=0.001).

A decrease in Q:H activation towards a 1:1 ratio suggests that muscle coordination imbalances that contribute to knee injury risk may be more related to mediolateral differences. Higher VM:VL activation may contribute to increased medial pull of the knee when landing.

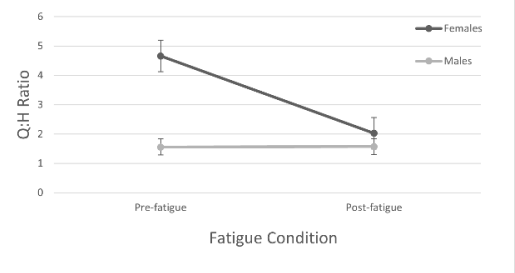

Figure 1 Q:H activation ratio across fatigue conditions, where Q = $\bar{x}$ VL, RF, VM and H = $\bar{x}$ BF and ST EMGRMS.

CONCLUSIONS

The current findings show that females' muscular patterns of knee stabilisation when landing are affected differently by fatigue than males, particularly in Q activation. Decreases in muscle activation may lead to loss of control and instability of the knee joint. Different fatigue protocols, paired with lower extremity kinematics and sideways sporting manoeuvres are worth examining to further understand how changes in muscle activation contribute to knee injury risk in sport.

ACKNOWLEDGEMENTS

The authors thank Sylvan Adams Sports Science Institute for providing funding for the project.

REFERENCES

[1] Hiemstra LA. *J Orthopaedic & Sports Physical Therapy,* **31**(10): 598-605, 2001.
[2] Montalvo AM et al. *J Ath Train* **54**: 472-82, 2019.
[3] Temesi J et al. *Med and Sci in Sports and Exercise*, **47**(4): 1372-82, 2015.
[4] Chappell JD et al. *Am J Sports Med* **35**: 235-41, 2007.
[5] Daniusevičiūtė L et al. *Clin Biomech* **24**: 82-7, 2013.

Effect of taping on muscle activity during squatting exercise

Mao Zeniya[1], Mayumi Mizumura-Kuno[1]
[1] Humanities and Science, Ochanomizu University / Graduate School, Tokyo, Japan.
Email: ma0.zeniya@gmail.com

INTRODUCTION

In squat exercises, the hip, knee, and ankle joints are involved. In this motion, each joint affects the ROM of the other joints [1]. Taping stabilizes joints, however, it can lead to joint restriction. Therefore, squatting with restricted ROM by taping may restrict muscle activity and may not provide sufficient benefits from training. Previous studies on landing motion have reported that ankle dorsiflexion ROM restriction due to taping may decrease muscle activity in the soleus and other muscles [2]. This study aimed to examine the effect of taping on the muscle activity involved in the movement of the three lower extremity joints during squatting.

METHODS

Ten healthy adult women without lower extremity pain participated in this study. They were asked to perform squats while sitting back until their thighs were parallel to the floor. The speed of the movements was standardized using a metronome to achieve a rhythm of 60 beats per minute. They performed descending, stopping, and ascending phases, each lasting for 4 s. Two conditions were compared: a control condition (SQ) and taped condition (TSQ) in which ankle joint restrictions were applied using taping.

The three lower extremity joint angles were calculated using the Frame-Dias system (DKH) with markers affixed to the acromion, greater trochanter, head of the fibula, lateral malleolus, and fifth metatarsal. The subject muscles were the tibialis anterior (TA), rectus femoris (RF), and soleus (SOL) muscles. Muscle activity was measured using surface electromyography. The analyzed section was divided into 12 phases, 1–4, 5–8, and 9–12 for descending, posing, and ascending, respectively. In the descending and ascending phases, normalization was performed with the hip ROM from phases 1–4 reflected as 100%, increasing by 25% in each phase of the ROM. The root mean square value for the muscle in each phase was calculated and normalized using the maximum voluntary muscle contraction.

RESULTS AND DISCUSSION

During the descending phase 4, only muscle activity in the RF was significantly higher in the TSQ condition than in the SQ. No significant differences were observed in the TA and SOL muscles during any of the phases.

In this study, the maximum knee joint angle in the SQ condition was higher than that in the TSQ. This result is consistent with previous studies in which ankle dorsiflexion restriction affected knee flexion [3]. In addition, previous studies have shown that during squatting, quadriceps muscle activity peaks when the knee joint reaches 80°–90° and then stabilizes [4]. It is possible, therefore, that the muscle activity of the RF reached a higher value during the SQ muscle activity because of the difference in knee ROM between the two conditions during phase 4. However, significant differences were only found in the RF muscles, suggesting that muscle activity of the three lower limb joints during squatting may be slightly affected by the presence or absence of taping.

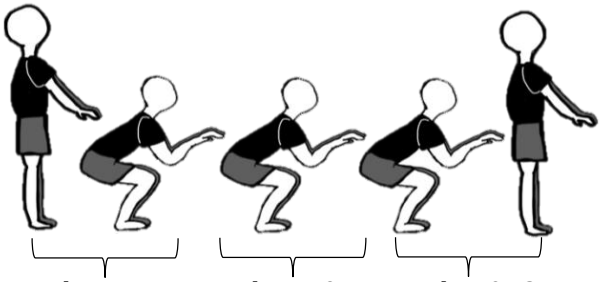

Figure 1 The analyzed section

CONCLUSIONS

The results of this study suggest that ankle dorsiflexion restriction by taping may not affect the amount of muscle activity during squatting.

REFERENCES

[1] Shimizu, J Jpn Health Sci **18**:200-209, 2016
[2] Chung-Hwi, J. Phys. Ther. Sci **15**:81-85, 2003
[3] Karli, J Athl Train **49**:723-732,2014
[4] Schoenfeld, Squatting Kinematics and Kinetics **24**: 3497-3506, 2010

Table 1: Three joints angle of lower extremities (mean±SD)

joint angle	Hip	Knee	Ankle
SQ	89.0±13.0	74.8±10.8*	35.7±6.8*
TSQ	89.3±13.0	70.8±9.5	42.4±7.5

Table 2: %MVC of the RF in the descending phase (mean±SD)

RF	Phase 1	Phase 2	Phase 3	Phase 4
SQ	11.8±4.3	18.7±7.6	31.4±16.3	39.6±15.5*
TSQ	10.1±2.7	15.4±4.7	23.5±8.6	31.2±14.1

* $p<0.05$

Effects of the incline board on discus throwing motion

Shota Kikuchi[1], Keitaro Seki[2], Kazumichi Ae[3] and Kiyohide Aoyama [2]
[1] Graduate School of Literature and Social Sciences, Nihon University, Tokyo, Japan
[2] College of Humanities and Sciences, Nihon University, Tokyo, Japan
[3] Nippon Sport Science University, Tokyo, Japan
Email: chsh22008@g.nihon-u.ac.jp

INTRODUCTION

Discus throw is a track and field event in which athletes throw a discus of a specified weight and compete over a distance. Discus throwing motion is highly complex and intricate, comprising both rotational and translational movements. The delivery phase is the most important phase of the discus throwing motion, as the discus velocity is primarily gained during this phase. Internal rotation of the right lower limb is a crucial movement for acceleration of the body–discus system in this phase [1]. An inclined board, which is placed under the right foot, is employed as a training method to learn the body's acceleration during the delivery phase. The right foot plays a crucial role in the acceleration and rotation of the body during discus throw. However, there is a lack of conclusive evidence regarding this training method. By contrast, an inclined board is also utilized in the training of the take-off technique in long jump [2]. This approach can alter movement naturally and lead to the acquisition of better techniques. Thus, the present study aims to clarify the effects of an inclined board on body acceleration and rotation in a standing discus throw drill that imitates the delivery phase of discus throw.

METHODS

The participants were 15 male right-handed discus throwers (height: 1.77 ± 0.05 m, weight: 82.6 ± 11.0 kg). They were asked to perform the standing throw motion without a discus, which is one of the technical drills of the discus throw, under four different inclined board conditions: 0°, 4°, 8°, and 12°. To avoid the influence of the order of the tests, they were performed in a random order. In three inclined conditions (4°, 8°, and 12°), the right foot was placed on the incline board, which was fixed on the force plate. The ground reaction forces (GRF) of both feet were measured using a force plate (9281 B, Kistler, Switzerland) at 1 kHz. The coordinate data of the anatomical landmarks of the body were captured using a motion capture system (Vicon Vero v2.2, Vicon Motion Systems, UK) at 250 Hz. The moment of the GRF about the vertical axis through the body's center of mass (CoM) was calculated as the cross product of the position vector from the CoM to the center of pressure and the GRF. A one-way analysis of variance for repeated measurements was conducted to test the main effect of the inclined board (SPSS Ver.29, IBM, USA).

RESULTS AND DISCUSSION

Figure 1-a demonstrates that the impulse of the throwing direction component of the GRF was significantly greater in the 12° condition than in the 4° and 0° conditions and in the 8° condition than in the 0° condition, but no significant difference was found between the 12° and 8° conditions and between the 4° and 0° conditions. This result suggests that the effect of using an inclined board may accelerate the body in the throwing direction. The maximal moment of the GRF about the vertical axis through the CoM was significantly greater in the 12° and 8° conditions than in the 4° and 0° conditions, but no significant difference was found between the 4° and 0° conditions (Figure 1-b). This result suggests that a steeper inclined board generates a moment about the vertical axis. In baseball batting, the internal rotation of the right lower limb generates the moment of GRF about the vertical axis through the CoM, and it contributes to the rotation of the lower trunk [3]. Even in discus throw, when the right lower limb generates a moment, it accelerates the body during the delivery phase.

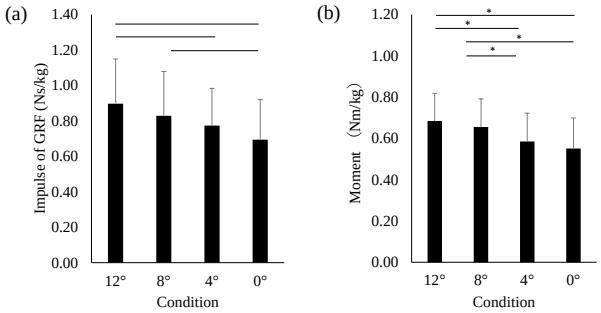

Figure 1 (a) Impulse of the throwing direction component of the GRF (right) and (b) the maximal moment of the GRF (right) about the vertical axis through the CoM.

CONCLUSIONS

The results revealed that the inclined board increased the throwing direction component of the GRF impulse and the moment of the GRF about the vertical axis through the CoM. Therefore, the inclined board improves the body–discus system acceleration, which might be attributable to the right lower limb motion.

REFERENCES

[1] Maeda et al. (2019). Jpn J. Phys. Educ. Health Sport Sci, 64(1):21–36.
[2] Koyama et al. (2015). Sports Biomechanics, 4(2):113–129.
[3] Ae et al. (2019). Jpn J. Phys. Educ. Health Sport Sci, 64:135–149.

Relation between throwing arm angle and trajectory of the pitched ball in baseball

Hirotaka Nakashima[1]*, Arata Kimura[1]*, Yuma Tsukamoto[2], Shuntaro Kuroyanagi[3], Yuka Ando[3], and Shinji Sakurai[3]

[1] Department of Sport Science and Research, Japan Institute of Sports Sciences, Tokyo, Japan.
[2] School of General Education Health and Sports Education Program, Chubu University, Aichi, Japan
[3] School of Health and Sport Sciences, Chukyo University, Aichi, Japan.
* These two authors contributed equally to this work.
Email: hirotaka.nakashima@jpnsport.go.jp

INTRODUCTION

The baseball batters can estimate the trajectories of the fastballs from the pitching forms. This is because the pitching form was strongly correlated with the orientation of spin axis [1] and the orientaiton generally determines the trajectories of the fastball [2]. Then, can baseball batters estimate the trajectory of the breaking balls from the pitching form? We aimed to investigate the relation between the pitching forms and the trajectories of each pitch type.

METHODS

Fifteen male collegiate baseball pitchers, who used an overhand, three-quarter, and side-hand throw style, participated in this study. They threw all the pitch types they would normally throw in a game. This study focused on the fastballs, curveballs, sliders, changeups, and cutters. Three high-speed cameras were used to record the pitching motion and pitched ball. The relation between the pitching forms and the trajectories of each pitch type was quantified by the correlations between the throwing arm angle (Figure 1) and the angle of each pitch (θ). The throwing arm angle was defined as the angle between the vector from shoulder to wrist at ball release and the horizontal plane from the viewpoint of second base (Figure 1). The angle of each pitch was calculated as the angle between the X-axis and the line from the origin to the deviation of each pitch in the vertical and horizontal deviation plane (Figure 1). The vertical and horizontal deviations were simulated as the differences between the coordinates at the ball arrival position with and without considering ball spin.

RESULTS AND DISCUSSION

The angles of fastballs ($\theta_{fastballs}$) and curveballs ($\theta_{curveballs}$) were significantly correlated with the throwing arm angle. This means that the fastballs and curveballs pitched by overhand pitchers had less horizontal and more vertical deviation. On the other hand, the fastballs and curveballs pitched by side-hand pitchers had more horizontal and less vertical deviation. The results indicated that the batters can estimate the trajectories of these pitch types from pitching forms. However, the angles of sliders ($\theta_{sliders}$), changeups ($\theta_{changeups}$), and cutters ($\theta_{cutters}$) were not significantly correlated with the throwing arm angle. This is because the deviations of these pitch types varied regardless of the pitching forms. The deviations of these pitch types were across multiple quadrants in Figure 1 whereas those of fastballs and curveballs were almost within a single quadrant. Therefore, it was thought that the sliders, changeups, and cutters were difficult to estimate the trajectories from the pitching forms.

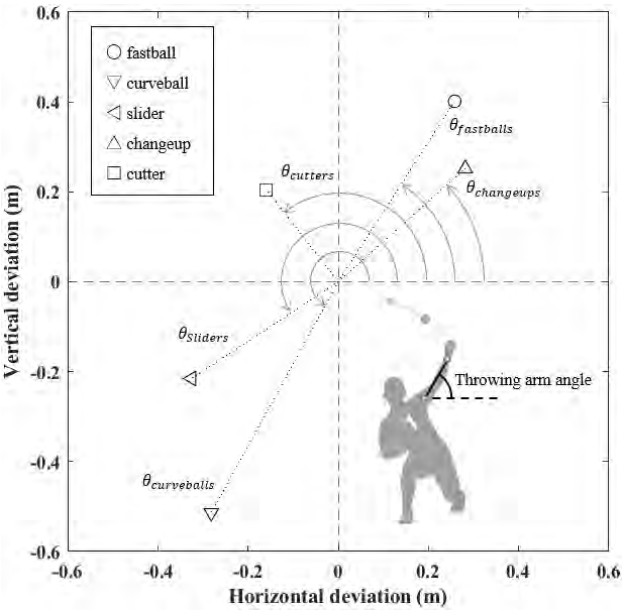

Figure 1 Definitions of the angle of the pitch (θ) and throwing arm angle.

CONCLUSIONS

We found that the directions of the deviations in fastballs and curveballs were correlated with the throwing arm angle. This result indicated that batters can estimate the trajectories of fastballs and curveballs from pitching forms.

REFERENCES

[1] Jinji et al. *J Sports Sci* **29**: 761-767, 2011.
[2] Jinji and Sakurai. *Sports Biomech* **5**: 197-214, 2006.

Table 1: Correlation coefficient of the throwing arm angle and the angle of the pitch (θ)

$\theta_{fastalls}$ (n = 15)	$\theta_{Curveballs}$ (n = 12)	$\theta_{Sliders}$ (n = 11)	$\theta_{Changeups}$ (n = 9)	$\theta_{Cutters}$ (n = 7)
r=0.91, p<0.01	r=0.61, p<0.05	r=0.39, n.s.	r=0.16, n.s.	r=-0.18, n.s.

Biomechanical analysis of the golf swing in one-length and conventional irons

Yu Kashiwagi[1], Tomoya Hirano[2], Tadashi Wada[3], Seiji Shimatani[4] and Kazuo Funato[2]
[1] Senshu university institute of sport, Kanagawa, Japan.
[2] Graduate School of Sport System, Kokushikan University, Tokyo, Japan.
[3] School of Science and Engineering, Kokushikan University, Tokyo, Japan.
[4] Faculty of Business Administration, Kanagawa University, Kanagawa, Japan.
Email:thc0961@isc.senshu-u.ac.jp

INTRODUCTION

Modern golf statistics indicate that the putter accounts for only 15% of a player's score while the remaining 85% is attributed to shot accuracy [1], so the importance of shot precision in determining one's score cannot be overstated. The function of iron clubs is to effectively strike the ball over a desired distance with a high degree of accuracy. The adjustment of the horizontal ground reaction force of the target leg has been identified as a crucial factor in attaining the desired distance when using the same iron club [2]. While simulations suggest that club length accounts for 20% and loft angle for 80% ball distance [3], their exact contribution to human players remains unclear. This study aimed to assess the impact of club differences on ball distance through a comparative analysis of the swinging motion of a one-length iron club and a conventional iron club.

METHODS

Eighteen male collegiate golfers (age: 20.7 ± 1.4 years; height: 174.3 ± 4.0 cm; body mass: 69.6 ± 9.4 kg; Best score: 70.1 ± 3.9) participated in this study. The subjects performed swings on two Kistler force plates (operated at 1 kHz) using their iron clubs and a custom-made one-length iron club. The experimental trials comprised five swings per club, with three swings selected for analysis based on a content report scale rated four or higher. The one-length club used was a set of irons with lofts ranging from 46 degrees (Pitching Wedge) to 26 degrees (No.5), all adjusted to a length of 37 inches (Fig.1 A). The kinematics of the swings were captured through motion capture (VCION, Oxford, operated at 200Hz), with the analysis period defined as the time frame from address to impact. The swing data, including distance, number of revolutions, and swing speed, were recorded using a distance trajectory measurement system (Trackman).

The swing data, including distance, number of revolutions, and swing speed, were recorded using a distance trajectory measurement system (Trackman).

RESULTS AND DISCUSSION

Figure 2 shows the correlation between loft angle and carry for both a one-length and a conventional iron club. As the loft angle decreases, the distance for both types of clubs increases. Conversely, the disparity in distance between the one-length and conventional iron clubs elevates from 4.5 to 8.4 yards as the loft angle decreases, yet the average overall distance difference was only about 4.2%, which was not statistically significant. Previous research has reported that the horizontal component of the ground reaction force at the target leg affects distance control when iron clubs of the same number are used [2]. However, in this study, no disparities were detected in the peak ground reaction force resulting from the different club structures. The fact that distance remained constant, despite variations in club length, suggests that the participants adjusted the distance by accommodating the clubs to their preferred equipment.

CONCLUSIONS

The findings of this research imply that one-length iron clubs, capable of decreasing length-induced swing errors, are a viable option, particularly for amateur golfers seeking to attain consistent distance control.

REFERENCES

[1] Broadie M. *Avery*, 2014.
[2] McNitt-Gray JL et al. *Sport Biomech* **12**: 121-131, 2013
[3] Tutelman D. URL: https://www.tutelman.com/golf/clubs/singleLength1.php, 2016.

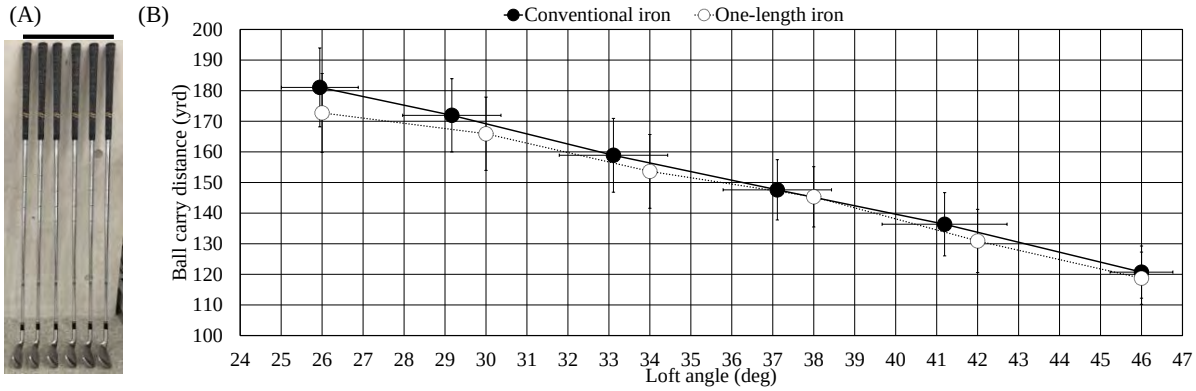

Figure 1 Photo of custom-made one-length iron (A). Relationship between loft angle and ball carry distance in conventional and one-length irons (B).

QUANTITATIVE ESTIMATION OF THE FOREARM PERFORMANCE FATIGABILITY IN A SCREWING MODEL

Yen-Wei Chiu[1,3], Hao-Yuan Hsiao[2], Zhi-Yan Wang[2], Wen-Fan Chen[3], Yuan-Kun Tu[2], Yi-Jung Tsai[1], Chih-Kun Hsiao[1]*
[1] Medical Research Department, E-Da Hospital / Kaohsiung 824, Taiwan
[2] Department of Orthopedics, E-Da Hospital / Kaohsiung 824, Taiwan
[3] Institute of Medical Science and Technology, National Sun Yat-Sen University / Kaohsiung, 80424, Taiwan
Email: shiaujk@gmail.com

PURPOSE

In this study, quantitative methods were used to assess forearm muscle strength and fatigue characteristics during a screw-driving task to understand whether screw-driving-related operations increase the potential risk of forearm muscle fatigue.

MATERIALS AND METHODS

1. Participants

A total of 12 healthy adults (10 males and 2 females; age range: 21–38, mean age: 26.2 ± 6.5 years), participated in this experiment. The body height and the weight of the subjects were 170.5 ± 8.6 cm and 67.5 ±13.2 kg (mean ± SD), respectively.

2. Methods

Twisting a screwdriver involves a combination of grip force (GF), driving torque (DT) or torsional moment, and push force (PF). The torsional moment is generated from the driver's handle through a handgrip force and friction from the screwdriver. A wooden specimen was installed on the experimental platform, and both ends of the specimen were clipped on the experimental platform for the driving test. The surface electrodes were placed on the BB, BR, and extensor carpi ulnaris (ECU) of the subject. The maximal isometric grip force, isometric driving torque, isometric push force, EMG amplitude, and insertion forces during cycling were measured

3 Statistics

The paired t-test to investigate differences in the maximum isometric forces (MIGF, MIDT, MIPF) data and EMG amplitudes between the pre-fatigue and poet-fatigue conditions were conducted. One-way ANOVA and LSD post-hoc comparison tests were conducted to identify the EMG difference between BB, BR, and ECU.

RESULTS AND DISCUSSION

Figure 1 (A), showed significant differences between the 1-st (MIDT=13.6%, MIPF=14.8%) and 8-th (MIDT=6.7%, MIPF=7%) and 4-th (MIDT=12.1%, MIPF=11.6%) and 8-th screw-driving maneuvers in terms of the amount of change in MIDT and MIPF. Figure 1 (B) shows the EMG amplitudes for the BB, BR, and ECU relative to the change in maximal isometric grip force (ΔEMG %) before the screw insertion operation, with values of 17.4%, 28.1%, and 29.7%, respectively. The percentage variation in the EMG for these three muscles was 16.7%, 39.3%, and 37.3%, respectively, for the MDT test [Figure 1 (C)].

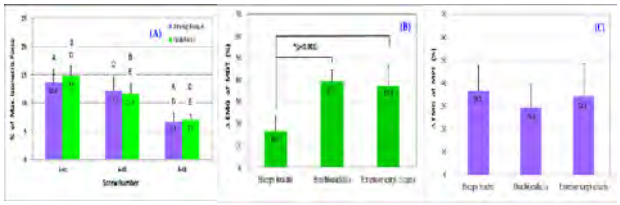

Figure 1 (A) MGF; (B) EMG-MGF; (C) EMG-MDT

Figure 2 (A)&(B) shows the DT and PF generated per minute for the insertion of each screw. A linear relationship was detected between the DT insertion rate (IR) and the screw number (R2 = 0.9791). Similar results were also observed for the IR of PF with screw number (R2 = 0.9669). The fourth screw had a significantly decreased IR compared with the first screw.

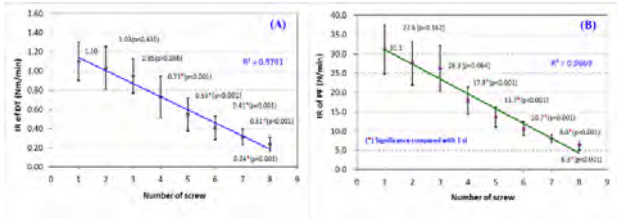

Figure 2 (A) Insertion rate of DT; (B) Insertion rate of PF

CONCLUSIONS

The major findings of this study emphasize the influence of forearm muscle strength and fatigue when screw driving. (1) Our investigation shows that the DT and PF decreased with an increase in the number of screws inserted; the screw insertion rate decreased linearly with the number of screws. (2) Both the brachioradialis and the extensor carpi ulnaris have a greater percentage of muscle loss in grip strength and torque than the biceps and are more likely to fatigue than the biceps. (3) This study presents a potential risk for muscle fatigue due to exposure to repetitive driving tasks. The risk of upper limb muscle injury to clinicians from screw-in operation still needs more clinical confirmation.

ACKNOWLEDGEMENTS

Partial support for this work was provided by E-Da Hospital (Grant no. EDAHI-107001). All authors express great acknowledgments.

REFERENCES

[1] De Luca et al. *Critical reviews in biomedical engineering.* **11** 251-279, 1984.
[2] Merletti R et al. *Journal of applied physiology.* **69** 1810-1820, 1990.

EFFECT OF INSERTION SPEED ON THE INSERTION TORQUE VALUE AND INITIAL STABILITY QUOTIENT OF DENTAL IMPLANT

Jui-Ting Hsu[1,2]*, Yuan-Yang Hsu[2], Ming-Tzu Tsai[3], Heng-Li Huang[1,2]
[1] Department of Biomedical Engineering, China Medical University, Taichung, Taiwan
[2] School of Dentistry, China Medical University, Taichung, Taiwan
[3] Department of Biomedical Engineering, Hungkuang University, Taichung, Taiwan
Email: jthsu@mail.cmu.edu.tw

INTRODUCTION

For dental implant surgery, the osseointegration is the important factor in determining the success rate [1]. The previous researchers indicated that the primary stability of an dental implant is a good indicator of osseointegration quality. Generally, the maximum insertion torque value (ITV) and initial stability quotient (ISQ) were commonly used as the indexes of the primary stability of dental implant. Seceral researchers have evaluated the implant shape, surface treatment, and bone quality on the primary stability of dental implant. Howver, only few studies have reported on the effects of the insertion speed on primary stability. According to the American Society for Testing and Materials regulation, the implant should be inserted at a speed between 1 to 5 rpm [2]. However, in clinical surgery, the common insertion speeds used are 10, 20, and 30 rpm [3]. Therefore, the purpose of this study was to investigated the effects of insertion speed on the insertion torque value and initial stability quotient of dental implants.

METHODS

The dental implants were inserted at four speeds: 4, 10, 20, and 30 rpm, into artificial bone specimens (Figure 1). During and after the insertion process, the maximum ITV and ISQ were measured. For the statistical analysis, the Kruskal–Wallis tests were used to determine the three evaluated indexes among the four insertion speed.

Figure 1 Artificial bone specimens and dental implant used in this study.

RESULTS AND DISCUSSION

The ITV and ISQ values were 39–60.2 N·cm and 70–77 (Table 1 and Figure 2), respectively. For the insertion speed on implant primary stability, significant differences in ITVs were observed among the four insertion speeds. In general, the higher the insertion speed, the lower the ITV; especially for the ITVs for implants inserted at 4 rpm were significantly higher than which measured at 20 and 30 rpm. In addition, the ISQs differed significantly differences among the four insertion speeds.

Table 1: ITV and ISQ of dental implant at the four insertion speeds.

Stability indicator	Statistical parameters	Insertion speed (rpm) 4	10	20	30	*P*†
ITV	Median	54.5[a]	50.0[ac]	46.0[bc]	44.0[b]	0.004
	IQR	6.7	4.0	4.0	4.5	
	Max	60.2	53.0	48.0	45.0	
	Min	50.9	46.0	42.0	39.0	
ISQ	Median	72.0[a]	75.0[b]	75.0[b]	73.0[ab]	0.016
	IQR	2.0	2.0	0.5	1.5	
	Max	73.0	77.0	75.0	75.0	
	Min	70.0	74.0	74.0	73.0	

rpm: revolutions per minute; ITV: insertion torque value; ISQ: implant stability quotient; IQR: interquartile range; Max: Maximum; Min: Minimum; *P*†: Kruskal–Wallis test, Post hoc pairwise comparisons were conducted using Mann–Whitney exact tests with Bonferroni adjustment; medians with the same letter (a, b, c) do not differ significantly at the 0.00833 (0.05/6) level.

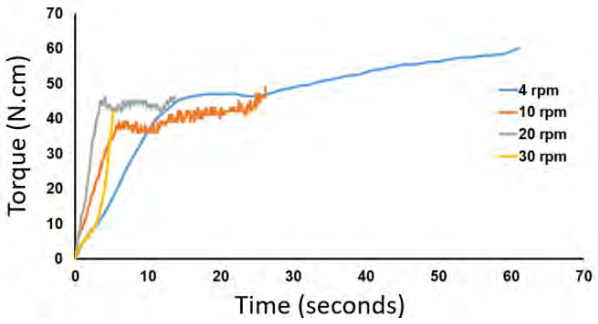

Figure 2 Torque-time curves during implant insertion.

CONCLUSIONS

The ITV and ISQ differed significantly among the four insertion speeds. The results indicated that a lower insertion speed resulting in higher primary stability.

REFERENCES

[1] F. Javed, et al. *Interventional Medicine and Applied Science*, **5**: 162-167, 2013.
[2] ASTM F543-17 standard specification and test methods for metallic medical bone screws. American Society for Testing and Materials, West Conshohocken.
[3] G. E. Romanos, et al. *Clinical implant dentistry and related research*, **16**: 89-95, 2014.

DEVELOPMENT OF AN ADVANCED PROTOTYPE SIMULATOR FOR DENTAL EDUCATION

Mi-El Kim[1], Jaehoon Sim[2], Jaeheung Park[2], Ho-Beom Kwon[3], Young-Seok Park[1]
[1]Dental Research Institute and Department of Oral Anatomy, School of Dentistry, Seoul National University, Seoul, Republic of Korea.
[2]Department of Transdisciplinary Studies, Graduate School of Convergence Science and Technology, Seoul National University, Seoul, Republic of Korea
[3]Dental Research Institute and Department of Prosthodontics, School of Dentistry, Seoul National University, Seoul, Republic of Korea.
Email: ayoayo7@snu.ac.kr

INTRODUCTION

In the field of dental education, clinical practice education is important for students as an essential part of the core curriculum. However, most patients are reluctant to receive dental treatment from inexperienced students. Hence, to address this issue, many simulators have been introduced to the dental industry. The purpose of the study was to fabricate an upper-body prototype simulator for dental education, to try it whether it can simulate the mandibular movement and to test the possibility of the stimulator responding to stimuli during dental practice.

METHODS

A computer model was developed based on segmentation of the hard and soft tissues using CT and MRI DICOM data, and virtual muscles were also created to simulate the primary movements of the mandible. After that, the simulator was 3D printed using the PLA material for the hard tissue and the rubber material for the soft tissue. An actuator was used to generate the motion of the simulator that mimics the human temporomandibular joint (TMJ), and the response to dental treatment was controlled by water level and pressure sensors. Then, the computer simulation of the mandibular motion of the simulator was performed in a 3D simulation program. The maximum mouth opening of the actual simulator was measured with a digital vernier caliper to compare the mandibular range of motion of a human.

RESULTS AND DISCUSSION

The upper-body simulator consisted of an operational unit, an upper body with an electric device, a head with a TMJ and dentiforms (Figure 1A). The TMJ of the simulator was capable of driving two degrees of freedom, implementing rotational and translational movements, which are the most important movements in the opening and closing of the mandible (Figure 1B). The mandibular range of motion of the simulator was 50 mm, which is within the normal range of maximum mouth opening for an adult. The head of the simulator was equipped with an LED sensor that displays the state and water level of each joint. A buzzer was also used to convey the status of the simulator audibly.

Additionally, articulators are used to reproduce or simulate mandibular movements during prosthetic treatment or clinical education [1]. This simulator, as compared to commonly-used semi-adjustable articulators, have similar rotational and translational movements, with differences found in their respective degrees of freedom. The reason is that if the two actuators were located on both sides of the mandibular joint, significant vibrations due to the elasticity of linear motion could be observed. To minimize this, the actuators were located separately in the skull and mandible.

Unlike the articulator, the human upper body simulator had the advantage of directly reproducing the mandibular motion simulation comparable to a real patient and thus simulating the human body by reacting similarly using various sensors [2]. Therefore, using simulator heads can be particularly useful for presenting students about the fundamentals of mandibular movements and for providing dental clinical practice training.

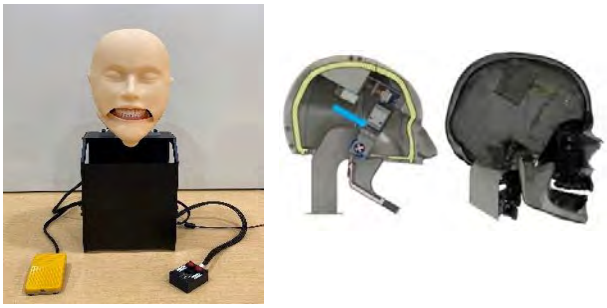

Figure 1 The upper-body prototype simulator (A) and internal structure of simulator head (B)

CONCLUSIONS

Although the prototype simulator was able to achieve the objectives, further advancements are still required to improve its efficiency and stability. Through continuous improvement and development, the simulation of the human body becomes more realistic, and it is expected to develop into a future-oriented dental education that improves student concentration and encourages them to consider how to communicate with patients.

ACKNOWLEDGEMENTS

This work was supported by SNU Brain Fusion Program of the Seoul National University in 2019(490-20190048).

REFERENCES

[1] Mohamed SE et al. *J Prosthet Dent* **36**: 319-25, 1976.
[2] Abe S et al. *Eur J Dent Educ* **22**: e327-36, 2017.

Computational Model Verifying Effects of Ultrasound Settings on Temperature Changes in Nitinol Implants

Shaye Tiell[1], Brian Davis[1] and Josiah Owusu-Danquah[1]
[1] Center for Human-Machine Systems, Cleveland State University, Cleveland, United States.
Email: s.tiell@vikes.csuohio.edu

INTRODUCTION

A longstanding orthopedics/biomechanics issue relates to the use of metal fixation devices to stabilize fractures in pediatric patients. There are contradictory demands, namely rigidity to maintain skeletal alignment versus the need to accommodate bone growth.

Shape memory alloys (SMAs) such as nitinol are well-known for their unique ability to undergo a shape change in response to a thermal stimulus. Minimally invasive nitinol implants which can reconfigure or adjust their shape across several temperature points could provide pediatric fixation devices that allow bone growth [1-4]. In the context of orthopaedic implants, this feature would ideally require an external (non-invasive) heating stimulus. One option is therapeutic ultrasound. Ultrasound's ability to quickly raise temperatures, and transcutaneously activate shape changes in nitinol implants could represent a novel approach for eliciting a thermoelastic transformation [5].

The purpose of this study was to investigate the features of therapeutic ultrasound that correspond with temperature changes in nitinol specimens via a computational model along with experimental data.

METHODS

This study used multibody dynamic simulations [6] to assess the relative heating effects caused by ultrasound magnitude versus frequency (Table 1). The model included spring-mass elements in series as well as viscous elements to represent damping properties. The dependent variable of interest was the kinetic energy of the mass that represented nitinol.

For validation pursposes, nitinol specimens were submerged in water to a depth of about 5 cm. Two ultrasound machines (the Sonicator 750 and Dynatron 150) were separately placed on the surface of the water. Ultrasound was applied to each specimen for 2 minutes. Specimen temperatures were recorded before ultrasound was applied and after each 30 second period. Trials were performed with low and high frequency and power settings (Table 1). All analyses were done in R [7]. An analysis of covariance (ANCOVA) was used to assess differences in mean temperatures due to power and frequency parameters (Figure 1).

Table 1 Therapeutic ultrasound machines and corresponding frequency and power settings.

	Frequency (MHz)		Power (W/cm^2)	
Therapeutic Ultrasound Machine	Low	High	Low	High
Sonicator 740	1	3	1	2
Dynatron 150	1	3	1	3

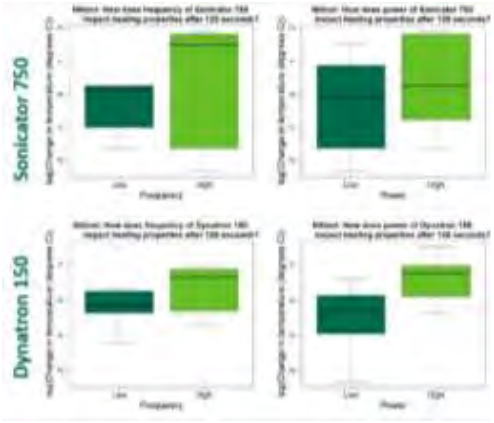

Figure 1 Four boxplots show every combination of factors (frequency and power) for the mean change in temperature after 120 seconds of heating by therapeutic ultrasound.

RESULTS AND DISCUSSION

There is a significant difference between low and high power settings on mean temperature change using the Dynatron 150 (3-way ANOVA; p=0.013). The model's predictions matched the benchtop testing data. Thus, the model verified significant effect on mean temperature due to high amplitude settings with no significant effect on mean kinetic energy at different frequency settings.

CONCLUSIONS

Nitinol implants can quickly and easily increase in temperature when applying therapeutic ultrasound. These findings could dramatically impact the design of metal implants that need to accommodate growth. Therapeutic ultrasound power settings rather than frequency settings are key to obtaining the thermal affects needed to allow nitinol implants to change shape.

ACKNOWLEDGEMENTS

The authors would like to acknowledge Dr. Deborah Espy who provided the therapeutic ultrasound equipment and Dave Dudzinski at the Cleveland Clinic for the nitinol specimens. Funding from the National Science Foundation (Award 2131894) is also acknowledged.

REFERENCES

[1] Currenton TL et al. *Injury* 52(10), 2820-2826, 2021.
[2] Holman H et al. *Artif. Organs* 45(5), 454-463, 2020.
[3] Barney MM et al. *J Mech Behav Biomed Mater* 4(7), 1431-1439, 2011.
[4] Wadood A. *Adv Mater Sci Eng* 2016, 1-9, 2016.
[5] Dewhirst M et al. *SPIE Proceedings* 2003.
[6] Hexagon AB. *MSC ADAMS View*. 20
[7] R Core Team. *R Found Stat Comp* 2021.

Gait Event Detection Using the Single IMU on the Unilateral Electromechanical KAFO

Sumin Yang[1], Jongman Kim[1], Bummo Koo[1], Seunghee Lee[1] and Youngho Kim[1*]
[1] Biomedical Engineering, Yonsei University, Wonju, South Korea
[*]Email: younghokim@yonsei.ac.kr

INTRODUCTION

Gait parameters are one of the important evaluating factors in gait analysis and can be defined by gait events. Patients with sarcopenia or paraplegia use orthosis for assisting their gaits. A knee-ankle-foot orthosis (KAFO) helps patients to be stable during gait and embedded sensors in the orthosis measure gait signals to control[1]. Various data provided from the orthosis allow for evaluating the gait pattern of patients. In this study, a gait event detection algorithm for an electromechanical KAFO was developed using a single IMU sensor on the single-sided leg. The developed algorithm will be applied to the developing KAFO, and used for monitoring gait patterns. Four events (initial contact(IC), opposite initial contact(OIC), toe off(TO), and opposite toe off(OTO)) were determined by the single IMU on the thigh.

METHODS

Fourteen healthy adults (9 males, 5 females, 22.3±1.4yrs, 167.2±9.2cm, 65.2±13.0kg) participated in the experiment. Two IMUs (Xsens Technologies BV, Netherlands; 60Hz) were attached to both thighs. Force plates (AMTI, USA; Kistler, Switzerland; 1000Hz) and a 3D motion capture system (Vicon Motion System Ltd, Oxford, UK; 200Hz) were used for the reference.

Accelerations of the vertical axis(Z) and the mediolateral axis(Y) and the pitch angular velocity (GyroY) were used to detect gait events. AccZBP and AccLSA [2] were obtained by filtering the acceleration data using a 1.9~2.1Hz band-pass filter and a least square acceleration (LSA) filter, respectively. AccYBP was also obtained using a 0.95~1.05Hz band-pass filter. Two local minima in AccYBP represented one gait cycle. AccRB was calculated by subtracting AccZBP from the raw acceleration data. Then, peakLSA was determined by the peak point of AccLSA between two local minimums of AccZBP. The local maximum point of AccRB within a certain section based on peakLSA was defined as an IC. GyroY3 and GyroY12 were obtained using 3Hz and 12Hz low-pass filter from GyroY, respectively. TO was defined by the minimum point in GyroY12, and OTO the first local maximum point after IC. OIC was defined by finding the zero-crossing after OTO in GyroY3. The error rate was defined by dividing the difference between the detected events and the reference data by one gait cycle. In addition, stance and swing phases were determined.

RESULTS AND DISCUSSION

The errors in detecting gait events were 0.65±1.02%, 5.32±3.73%, 1.45±1.20%, and 2.35±1.96% for IC, OTO, OIC, and TO respectively (Figure 1). Stance and swing phases were 61.02±4.67% and 38.98±4.67% respectively based on our algorithm, which showed errors of approximately 2.40% in both phases compared with the reference data (Table 1). These errors would be originated from the errors detecting OTO.

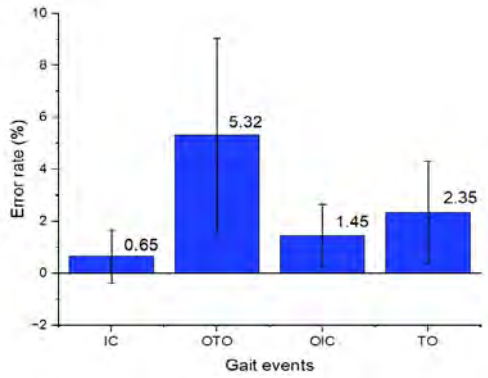

Figure 1: Errors in gait event detection of the present study

CONCLUSIONS

The gait event detection algorithm was developed using a single IMU on the thigh. The error rates of the gait event detection were 0.65±1.02%, 5.32±3.73%, 1.45±1.20%, and 2.35±1.96% for IC, OTO, OIC, and TO respectively. In the future, the present algorithm will be implemented to the electromechanical KAFO and validated in the real-world situation.

ACKNOWLEDGEMENTS

This research was financially supported by the Institute of Civil Military Technology Cooperation funded by the Defense Acquisition Program Administration and Ministry of Trade, Industry and Energy of Korean government under grant No.21-SF-GU-07.

REFERENCES

[1] Felix P. et al. *ICARSC 2017*. 110-115, 2017.
[2] Lee H. et al. *J. Biomed. Eng. Res.* **30.3**: 213-220, 2009.

Table 1: Stance and swing phases in a gait cycle

	Reference		Detected	
	Stance	Swing	Stance	Swing
Mean±SD(%)	58.62±1.58	41.38±5.53	61.02±4.67	39.98±4.67

KINEMATICAL DIFFERENCES BETWEEN WATER SURFACE AND UNDERWATER CONDITIONS IN FLUTTER KICK SWIMMING

Ichikawa H[1], Taba S[2], Mori S[3], Shimojo H[4] and Shimoyama Y[4]

[1] Department of Sports Health and Welfare, Nishikyushu University, Kanzaki, Japan.
[2] Faculty of Sports and Health Science, Fukuoka University, Fukuoka, Japan.
[3] Department of Sports Science, Kyushu Kyoritsu University, Kitakyushu, Japan.
[4] Department of Health and Sports, Niigata University of Health and Welfare, Niigata, Japan.
Email: ichikawahi@nisikyu-u.ac.jp

INTRODUCTION

In front crawl swimming, the upper limbs play a role to exert the propulsive force. On the other hand, the motion of lower limbs is known as flutter kicks, and their conbributions and importance in swimming performance has been discussed. Ichikawa et al. (2020) reported that the propulsive force exerted by the flutter kick on the water surface and in the underwater conditions differently depending on swimming speed [1]. There are no reports or literature that mention the differences in the motion of the flutter kick. The purpose of the study is to clarify the kinematical differences of the flutter kick between the surface and the underwater conditions.

METHODS

The subjects were six male university swimmers with competitive experience. The trial consisted of a 25 m flutter kick with the maximal effort. The swimmers performed the trials under the conditions of the surface and the underwater with high-intensity LED markers attached to the swimmers' right wrist, shoulder, greater trochanter, knee, ankle and 5th MP-joint. Swimming movements were recorded from the swimmer's right side using an underwater camera with 60Hz as sampling frequency. The coordinates of the body markers during the 10m-15m section in trials were calculated using the two-dimensional DLT method. The angles of the four segments, such as the trunk, thigh, shank and foot with respect to the horizontal plane were calculated. The angles of the hip, knee and ankle joints were also calculated respectively. Swimming speed was calculated as the time derivative of the horizontal displacement of the hip joint. The kinematic data for the five cycles with the smallest variance in swimming speed were extracted and compared between the surface and underwater conditions.

RESULTS AND DISCUSSION

The mean (standard deviation) value of the swimming speed were 1.37 (0.13) m/s in the underwater condition and 1.21 (0.07) m/s in the surface condition, with the underwater condition being significantly faster ($p<0.05$). The angle of shoulder, hip, knee and ankle joint on the sagittal plane showed the similar patterns between the conditions. The trunk had a maximum, minimum and mean angle that was greater on the water surface than in the water ($p<0.05$). The minimum and mean angles for the thigh were greater under the surface condition than the underwater ($p<0.05$). Statistical comparisons of the shank and the foot were not performed because the foot markers moved above the water surface and were not visible, so complete one-period kinematics data could not be obtained under the surface condition. It was observed that each segment maintained a horizontal posture in the underwater, whereas the head side was higher and the foot side was in a deeper position in the surface condition (Fig. 1). The inclination of the segments in the surface condition increases the frontal projected area during the flutter kick, resulting in larger resistance. Therefore, the swimming speed would be lower in the surface condition than in the underwater condition.

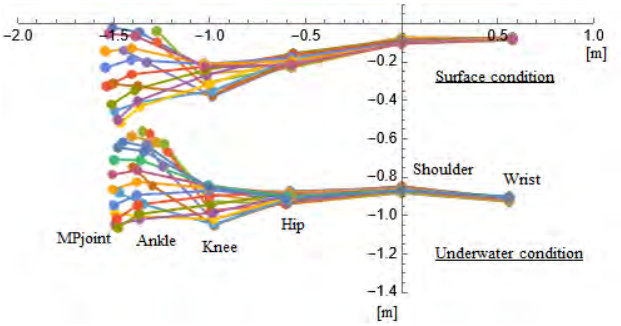

Figure 1 Stick pictures of flutter kick swimming on the sagittal plane under the surface and the underwater conditions.

CONCLUSIONS

Kinematical differences in flutter kick swimming between surface and underwater conditions were attributed to whole-body inclination, which would affect swimming speed. The differences in swimming speed between the conditions may be different from those expected by swimmers and coaches.

ACKNOWLEDGEMENTS

This work was supported by JSPS KAKENHI Grant Number JP22K11590.

REFERENCES

[1] Ichikawa H et al. *Proceedings of The 13th Conference of the International Sports Engineering Association* **49**(1): 167, 2020.

RELATIONSHIP BETWEEN sEMG AMPLITUDE AND MUSCLE FIBER CONDUCTION VELOCITY EACH SHORT-TERM WAVEFORM WITH MUSCLE FATIGUE

Aya Shirai [1,2], Kazuyuki Mito[3] and Genci Capi[2]

[1] Department of Electrical Engineering and Electronics, Aoyama Gakuin University, Tokyo, Japan.
[2] Department of Mechanical Engine, Hosei University, Tokyo, Japan.
[3] Department of Informatics, The University of Electro-Communications, Tokyo, Japan.
Email: a.shirai@aoyamagakuin.jp

INTRODUCTION

Surface electromyogram (sEMG) is one of the non-invasive and objective method to evaluate muscle function, and applications in the fields of sports training and rehabilitation are expected. Some researchers reported sEMG amplitude values increase, frequency values decrease, and muscle fiber conduction velocity (MFCV) decrease with muscle fatigue [1]. However, the values of these indicators also change depending on the difference in force of muscle contraction, and there are individual differences in the values and change rate of values. Hence, levels of assessment in muscle fatigue have not yet been reached. sEMG signals are interference pattern of the activity of individual motor units, and the value of amplitude or MFCV different depend on motor unit. Therefore, this study examined the relationship the amplitude and MFCV each waveform in short section with muscle fatigue.

METHODS

Ten healthy males participated in this study. The subjects were seated in a chair and sustained isometric contractions of the right elbow at the elbow joint angle of 90 degrees during 40 % of maximum voluntary contraction. sEMG was recorded from the right biceps brachii muscle and the electrode that composed of eleven silver wires (diameter of 1 mm, length of 10 mm) attached on the muscle belly. The distance between the electrodes was 5 mm. Ten signals were derived bipolarly from adjacent wires filtered by band-pass from 5 Hz to 1 kHz and were digitized with sampling frequency of 10 kHz. In the data, the signals were sampled 5 seconds every 10 % between 0-100 % of endurance time and the root mean square (RMS) of the amplitude and MFCV were calculated each waveform that exceeds 0.05 mV in maximum value during 8ms. In addition, the distributions of RMS and the inverse number of MFCV were calculated to examine the relationship between RMS and MFCV with muscle fatigue. It consists of 126 classes, and RMS was divided into 14 classes (0 to 0.7 mV) and the inverse number of MFCV was 9 classes (0.05-0.5).

RESULTS AND DISCUSSION

The mean of RMS and SD for all subjects increased from 0.07 ±0.03 (0%time) to 0.15±0.08 (100%time) mV, and the reciprocals of MFCV also increased from 0.17±0.06 to 0.21±0.06. A paired t-test for the results were conducted and found a significant difference between RMS ($p<0.01$). The results match past study, and these are supposed to be caused by increasing the number of active moto units and shifting active muscle fibers from fast twitch to slow twitch with muscle fatigue [2]. However there are individual differences were great for the values and it was difficult to estimate the limit state of muscle fatigue using previous method. Figure 1 shows heatmaps of the ratio of the number of waveforms each %time in one subject as a representative result. As the results, It was confirmed that the distribution was concentrated along certain area that has the characteristics of low RMS and the reciprocals of MFCV at early stage of muscle fatigue. After that the distribution was quite variable with muscle fatigue. The coefficient of variation (CV) of ratio over all classes decreased from 3.67 (0 %time) to 1.47 (100%time), and the maximum ratio decreased from 24.6 % to 5.73 %. The results provide the evidence that motor unit recruitment of various sizes were required with muscle fatigue.

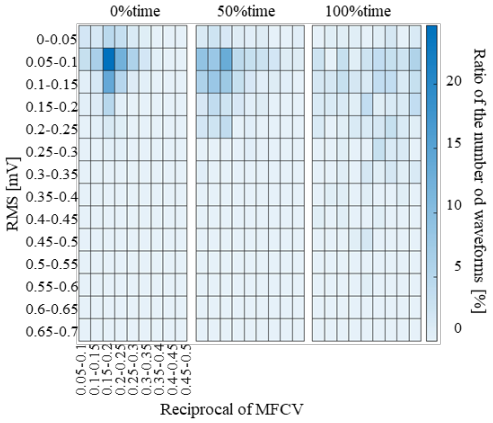

Figure 1 Heatmap of the ratio of waveforms.

CONCLUSIONS

In this study, we examined the relationship between MFCV and RMS with muscle fatigue and MFCV and RMS were calculated each waveform in short section. As the results, the indicators were remarkably different depend on waveform and it is necessary to consider the relationship between MFCV and RMS each waveform in addition to the mean values with muscle fatigue.

REFERENCES

[1] Marco G et al. *physiol Meas* **38**: 27-60, 2017.
[2] Linnamo V et al. *J Electromyogr Kinesiol* **10**: 293-300, 2000.

Development of a Statistical Shape Model of the Knee for Predicting Bone/Cartilage Morphology and Articular Contact Trajectories During Activities

Kuan-Hsien Wu[1], Hsuan-Yu Lu[1], Mei-Ying Kuo[2], Cheng-Chung Lin[3], Horng-Chaung Hsu[4], Tung-Wu Lu[1,5]
[1] Department of Biomedical Engineering, National Taiwan University, Taiwan, R.O.C.
[2] Department of Physical Therapy, China Medical University, Taiwan, R.O.C.
[3] Department of Electrical Engineering, Fu Jen Catholic University, Taiwan, R.O.C.
[4] Department of Orthopaedic Surgery, China Medical University, Taiwan, R.O.C.
[5] Department of Orthopedic Surgery, School of Medicine, National Taiwan University, Taiwan, R.O.C.
Email: **twlu@ntu.edu.tw**

INTRODUCTION

Computerized tomography (CT) based 2D/3D registration techniques using bi-plane fluoroscopy is a non-invasive method for accurately measuring *in-vivo* knee joint kinematics. Magnetic resonance imaging (MRI) is needed to create further a subject-specific cartilage model for measuring arthrokinematics. However, MRI alone is expensive, time-consuming and often fails to accurately produce bone models. Therefore, many studies have been devoted to developing methods for calculating knee arthrokinematics based solely on computerized tomography (CT) bone information. The purposes of this study were to develop a statistical shape model (SSM) of the knee bones using datasets of CT and MR images and, together with CT images and knee flexion/extension kinematic data, to reconstruct three-dimensional (3D) subject-specific knee bone/cartilage models for calculating the arthrokinematics of the joint during functional activities.

METHODS

To build the knee SSM model, this study collected 35 models of the bone and cartilage of knee joints from Asian young adults as the training models. This study also developed a method by using this SSM model for reconstructing subject-specific cartilages of the knee joint via the CT bone mode and flexion-extension kinematics. To verify the feasibility of this method, 3D knee joint kinematics during cycling were measured *in vivo* in nine healthy young males (age: 23.4±1.7 years, height: 1.7±0.04 m, weight: 69.6±12.2 kg, body mass index: 23.0±3.7) without any neuromusculoskeletal diseases of the lower limbs. The left knee of each subject was imaged by CT (voxel size: 0.586 × 0.586 × 0.625 mm^3; GE, Lightspeed 16 MDCT, USA) and MRI (3-Tesla, Verio, Siemens, Germany) for the reconstruction of subject-specific volumetric models of the knee. Each subject also performed isolated left knee flexion/extension and cycling while a biplane fluoroscopy system imaged the knee joint. Their subject-specific knee models were reconstructed using MRI and CT, and the arthrokinematics during cycling were calculated [1] and considered the gold standard to verify the accuracy of SSM and the contact obtained. The reconstruction error of the 3D cartilage model, namely femoral, medial and lateral tibial cartilage, and the root-mean-square error (RMSE) of the contact points on the medial and lateral tibial compartments was then obtained as a measure of the performance of the proposed method.

RESULTS AND DISCUSSION

The cartilages of each subject were reconstructed (Figure 1), and the shape error of the SSM reconstructed cartilage was 1.88 ± 0.74mm on the femoral cartilage, 1.18 ± 0.29mm on the medial tibial cartilage, and 1.55 ± 0.44mm on the lateral tibial cartilage. Moreover, the contact point error calculated on the medial side of the knee joint was 1.33 ± 0.71mm in the anterior-posterior (AP) direction, and 2.64 ± 1.48mm in the medial-lateral (ML) direction. The contact point error calculated on the lateral side of the knee joint was 0.77 ± 0.37mm in the AP direction, and 2.26 ± 1.48mm in the ML direction.

Figure 1 The reconstructed cartilage of a typical subject.

CONCLUSIONS

The current results demonstrated that the proposed SSM-based method is a feasible and acceptable technique for reconstructing the cartilage morphology and contact patterns without MR imaging, as proven by the comparative analysis of contact points against the reconstruction of the knee joint based on flexion-extension kinematics and the CT bone model.

REFERENCES

[1]. Lin C-C et al. *Med Phys* 45.8: 3637-3649, 2018.

A biomechanical study of novel Braided PET artificial Ligament for ACL Reconstruction

Shenglin Li[1,2], Shuhan Wang[2], Wenliang Liu[2], Chao Zhang[1] and Jian Song[1,3,*]
[1] School of Biomedical Engineering, Shenzhen Campus of Sun Yat-sen University, Shenzhen, China.
[2] Shenzhen Institute for Drug Control, Shenzhen Testing Center of Medical Devices, Shenzhen, China
[3] State Key Laboratory of Tribology, Tsinghua University, Beijing, China.
Email: songj67@mail.sysu.edu.cn

INTRODUCTION

Inspired by the histological characterization of cortical bones, in this study, we developed a novel braiding strategy for mechanical and fatigue properties improvement of artificial ligament by using two different kinds of PET threads to mimic overlapping bone lamellas layers consisting of soft collagen fibrils and hard hydroxyapatite [1,2].

METHODS

The artificial ligaments were composed of a shell and core. The shell part was designated as a hollow tubular braided structure with three independent layers. Threads consisting of fibers with a density of 150 D (denoted as “stiff fibers”) for tensile strength to meet clinical demands, while the ones consisting of fibers with a diameter of 0.3 mm (denoted as “hard fibers”) are adopted to resist fatigue failures. The core part was braided by stiff fibers, while the shell part was by a combination of stiff and hard fibers with three different amount ratios. Mechanical and fatigue tests were used and conducted after heat treatment of different durations to compose a sample matrix (Table 1).

RESULTS AND DISCUSSION

Tensile test results confirmed adequate tensile strength for short-term clinical recovery, among which H1S1 attained up to a maximum tensile force of 3776N, while friction tests indicated a proportional decrease in the COF with a quantity increase of hard threads (Figure 1). Besides, longer heat treatment duration contributed to stabilizing texture constructs under different friction conditions as seen from the error bars.

CONCLUSIONS

A novel method to improve biomechanical performance of artificial ligaments was proposed in this work. We successfully improved the tribological performance of braided ligament by 25% compared to the control group on the guarantee of adequate mechanical strength for short-term clinical recovery. This work provides an alternative for biomechanically accountable scaffold design and basis of potential bioactivity improvements, which is on the list of our future work.

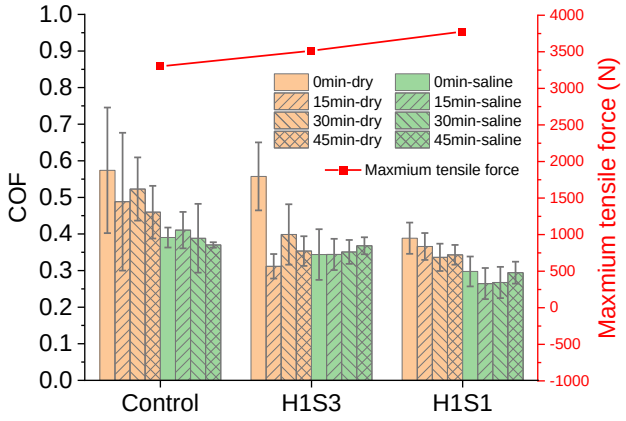

Figure 1: Tensile test results and friction test results of artificial ligament samples with different braiding strategies.

ACKNOWLEDGEMENTS

This work is financially supported by the Shenzhen Science and Technology Program (Grant No. RCBS20210706092410021), the Tribology Science Fund of State Key Laboratory of Tribology in Advanced Equipment (Grant No. SKLTKF22B13) and the Start-up Funding to Prof. J. Song from Sun Yat-sen University.

REFERENCES

[1] Shenglin L et al. *J Orthop Translat* **36**: 205-15, 2022.
[2] Nwachukwu BU et al. *Arthroscopy* **35**: 2233-47, 2019.

Table 1: Sample matrix of artificial ligament samples.

Friction test conditions	Braiding strategy	Heat treatment duration			
		0 min	15 min	30 min	45 min
Dry	H:S = 0	Control-0	Control-15	Control-30	Control-45
	H:S = 1:3	H1S3-0	H1S3-15	H1S3-30	H1S3-45
	H:S = 1:1	H1S1-0	H1S1-15	H1S1-30	H1S1-45
Saline	H:S = 0	Control-0s	Control-15s	Control-30s	Control-45s
	H:S = 1:3	H1S3-0s	H1S3-15s	H1S3-30s	H1S3-45s
	H:S = 1:1	H1S1-0s	H1S1-15s	H1S1-30s	H1S1-45s

PRE-IMPACT FALL DETECTION DURING ELECTRIC SCOOTER RIDING

Seunghee Lee[1], Bummo Koo[1], Sumin Yang[1], Jongman Kim[1], Dongkwon Kim[1] and Youngho Kim[1]
[1] Department of Biomedical Engineering, Yonsei University, Wonju, Korea.
Email: younghokim@yonsei.ac.kr

INTRODUCTION

Electric scooters (e-scooters) have been widely used as the personal mobility because it is easy to drive and has a reasonable price. The number of serious e-scooter accidents in Korea was 900 in 2021 and has been doubled annually [1]. Wearable devices such as an airbag system have been under development to protect the rider from the serious impact injury during e-scooter riding. A pre-impact fall detection algorithm for e-scooter riders was developed using an IMU sensor in this study.

METHODS

20 healthy adults (23.3 ± 1.7 years old, 173.0 ± 6.7 cm, 74.5 ± 13.2 kg) were recruited from Yonsei University for the study. Four normal drivings and one fall movement were performed by subjects with an e-scooter (Ninebot Segway ES2, Xiaomi, China). An IMU sensor (Xsens Dot, Xsens Technologies B.V., Netherlands) was attached to T7 position of the subject to measure three-axis acceleration and three-axis angular velocity with 60Hz sampling frequency. The data obtained from the IMU sensor was filtered to remove noise using a second-order Butterworth low-pass filter (cutoff frequency: 5 Hz). Sum vector magnitudes of acceleration and angular velocity (A_{SVM} and G_{SVM}), and roll angles were calculated from the IMU sensor data. Algorithm 1 used threshold values of both A_{SVM} and G_{SVM}. On the other hand, Algorithm 2 also used roll angles as well as A_{SVM} and G_{SVM}. Grid search was applied to determine the thresholds for the algorithm from 16 subjects, and the test was made from the rest 4 subjects.

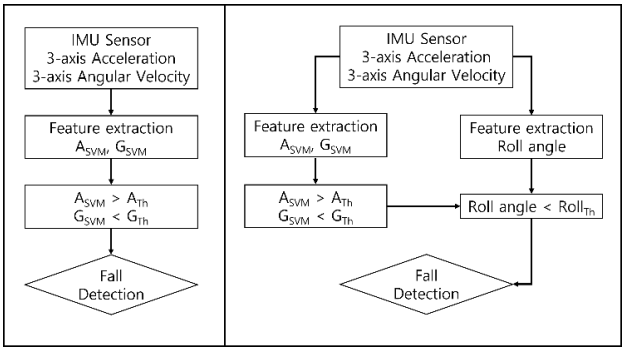

Figure 1. Flow chart of the algorithm (left: Algorithm1, right: Algorithm2).

RESULTS AND DISCUSSION

Table 1 showed the performances of algorithms. The specificity of both algorithms was 100%. Algorithm 2 that considered roll angles as well as A_{SVM} and G_{SVM} showed higher specificity and accuracy than Algorithm 1. In addition, Algorithm 2 resulted in smaller lead-time than Algorithm 1. Although the lead-time slightly decreased in Algorithm 2, it was sufficient for airbag deployment. Algorithm 1 showed 100% sensitivity, being widely accepted in detecting falls in a motorcycle [2], but revealed only 90% specificity in e-scooter riding. Algorithm 2 failed to detect only one normal e-scooter riding. A significant improvement in the specificity was obtained, as roll angles were additionally used in Algorithm 2. In the future, machine learning-based pre-impact detection algorithm will be studied to improve the performance.

CONCLUSIONS

Two different threshold-based algorithms were applied to detect pre-impact falls during e-scooter riding. Both algorithms showed 100% sensitivity in detecting falls during e-scooter riding. Algorithm 2 using A_{SVM}, G_{SVM}, and roll angles showed better specificity than Algorithm 1 using only A_{SVM} and G_{SVM}. This study successfully detected e-scooter falls using threshold-based algorithms.

ACKNOWLEDGEMENTS

This research was partly supported by the Institute of Civil Military Technology Cooperation funded by the Defense Acquisition Program Administration and Ministry of Trade, Industry and Energy of Korean Government under grant No.21-SF-GU-07 and project for Cooperative R&D between Industry, Academy, and Research Institute (S3104657) funded by the Ministry of SMEs and Startups (MSS, Korea).

REFERENCES

[1] Traffic Accident Analysis System, *Traffic accident statistical analysis report*; 2021
[2] Boubezoul A et al. *Control Engineering Practice* **21.3**: 286-297, 2013.

Table 1: Performances of algorithms.

	Sensitivity (%)	Specificity (%)	Accuracy (%)	*Lead-time (ms)*
Algorithm 1	100.0	90.0	92.0	433.3±135.8
Algorithm 2	100.0	98.7	99.0	380.0±103.2

HEAD IMPACTS DURING JUDO PRACTICE IN COLLEGE JUDOKAS: A PRELIMINARY STUDY

Sentaro Koshida[1], Takanori Ishii[2], Hiroshi Churei[3], Hiroshi Kubota[4]
[1] Faculty of Health Sciences, Ryotokuji University, Urayasu, Japan
[2] Centre of Liberal Arts Education, Ryotokuji University, Urayasu, Japan
[3] Graduate School of Medical and Dental Sciences, Tokyo Medical and Dental University, Bunkyo-ku, Japan
[4] Faculty of Education, Tokyo Gakugei University, Koganei, Japan
Email: koshida@ryotokuji-u.ac.jp

INTRODUCTION

Previous epidemiological studies have shown that the risk of head injury in judo is relatively high, particularly when being thrown backwards with osoto gari [1]. In addition, the biomechanical studies have suggested that the magnitude of the impact on the head when thrown is greater when thrown with the osoto gari than with other judo throwing techniques [2]. However, the previous biomechanical studies have only estimated the biomechanical quantities applied to the head during throwing in a laboratory setting. Therefore, it is unclear whether the previous results accurately reflect the head impact during being thrown in actual judo situations. The aim of this study was to quantify the head impact caused by different judo throwing techniques during actual judo sparring practice.

METHODS

Participants were four male collegiate judokas belonging to the same university judo club. A mouthguard-type inertial sensor (The Nexus A9 Smart Mouthguard, HitIQ Ltd., VIC, Australia) was placed in the mouth to obtain linear (*g*) and angular (rad/s^2) head accelerations as an indicator of the head impact during judo practice. Video images of each participant during judo sparring practice were also recorded with date and time stamps. The head impact data were then matched to the video images to time-synchronise the head impact in the situation in which the participant was thrown.

RESULTS AND DISCUSSION

There were no definite or suspected cases of head concussion among the participants during the study period.

After analysis of a total of 39 training sessions, 377 throwing situations were identified from the video footage, of which 11.4% (43/377) resulted in head impacts with accelerations of 10 *g* or greater.

The median [95th percentile] peak linear and rotational head accelerations were 16.1 [25.7]*g* and 1219.6 [2435.6] rad/s^2 respectively. The result also showed that most of the head impacts were distributed in the relatively low impact range of linear acceleration below 15*g* and/or angular acceleration below 1500rad/s^2 (Figure 1).

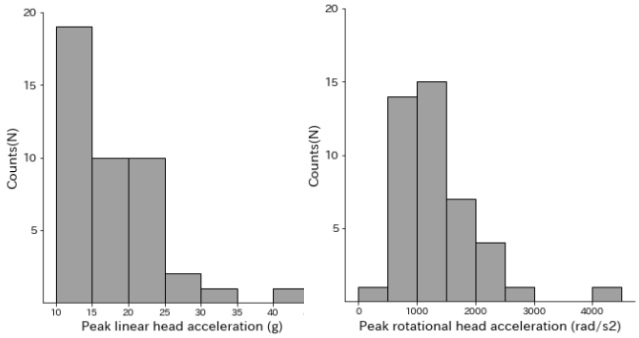

Figure 1 Distribution of head impact magnitude in 43 cases.

Of the 377 scenes, the most common situation was thrown with seoi-nage(58/382,15.2%) and uchimata (58/382, 15.2%), followed by osoto-gari (47/382, 12.3%), and the most common head impact situation exceeding the 10*g* threshold was when thrown with uchimata (13 cases), followed by seoi-nage (9 cases) and kosoto-gari(including kosoto-gake) (6 cases).

Previous studies have suggested that being thrown with osoto-gari may put judokas at high risk of head injury. However, we did not find any situation in which the participants were thrown with osoto-gari exceeding 10*g* impact during the recorded session, although the osoto-gari was the third highest throwing technique observed across all throwing situations. Our findings suggest that careful consideration should be given to the relationship between the risk of head injury and the judo throwing techniques.

CONCLUSIONS

We quantified the head impact applied to the head in actual judo situation. About 10% of the head impacts above the threshold were identified in the being thrown situation, and most were considered to be in the low impact range. The results of laboratory studies may differ from actual situations as to whether the risk of head impact differs between different techniques.

ACKNOWLEDGEMENTS

The work was supported by the JSPS KAKENHI [number 19K11471].

REFERENCES

[1]Kamitani T et al. *Am J Sport med* **41**: 1915-21, 2013.
[2]Koshida S et al. *Eur J Sport Sci* **17**: 417-24.

INJURY-RELATED GAIT VARIABLES DURING RUNNING AND LOADED WALKING IN U.S. ARMY TRAINEES DIFFER BY SEX, BUT NOT PHYSICAL ACTIVITY LEVEL

Caleb D. Johnson[1], Lauren K. Sara[2], Molly M. Bradach[2], Katelyn I. Guerriere[1], Leila A. Walker[1], Stephen A. Foulis[1], Julie M. Hughes[1], David R. Mullineaux, Irene S. Davis[3]
[1] Military Performance Division, U.S. Army Research Institute for Environmental Medicine, Natick, MA, USA
[2] Spaulding National Running Center, Spaulding Rehabilitation Hospital, Cambridge, MA, USA
[3]School of Physical Therapy and Rehab Sciences, University of South Florida, Tampa, FL, USA
Email: caleb.d.johnson24.civ@health.mil

INTRODUCTION

Low levels of physical activity (PA) and fitness are associated with increased rates of lower-extremity musculoskeletal injury during U.S. Army Basic Combat Training (BCT).[1] A large proportion of these injuries result from running and walking with load carriage (loaded walking) activities. While less is known about loaded walking, early stance ground reaction forces (GRFs) and peak tibial accelerations (TAs) have been associated with injury in runners.[2] Further, runners have shown differences in gait mechanics and injury rates based on training volume and experience.[3-4] Finally, injury rates have been shown to be higher in female vs male trainees.[1] Therefore, our purpose was to compare running and loaded walking GRFs and TAs across PA and running experience levels, as well as sexes, in Army trainees. We hypothesized that females and those with lower PA and no running experience would show higher GRF and TA metrics.

METHODS

Data from 306 Army trainees (179 male, 117 female) were collected in the first week of BCT. An inertial measurement unit was attached to the distal tibia. Participants ran (2.68-2.90m/s) and walked with an 18.1kg pack (1.21-1.34m/s) on an instrumented treadmill. For both, 7 strides of data were collected after a 3-minute warm-up. Early stance peak vertical and resultant TAs (VTA/RTA) and vertical instantaneous GRF loading rates (VILR) for the dominant leg were calculated for both tasks and averaged across strides. Vertical stiffness for running and the first peak vertical force for loaded walking were also calculated. Participants were grouped based on self-reported exercise habits in the 2 months prior to BCT as: low (0-2x/wk), medium (3-4x/wk) and high (>4x/wk) PA. Participants who reported substantial changes in exercise prior to BCT were excluded (n=105). Groups were also formed based on competitive running experience at the high school level or higher. ANOVAs were used to test for the effects of PA grouping and sex on GRFs and TAs. T-tests were used to assess the effects of running experience on running variables only.

RESULTS AND DISCUSSION

There were no significant main effects of PA grouping (F=0.087-1.188, p=0.31-0.92) or interactions with sex (F=0.439-2.013, p=0.14-0.65). There were significant main effects of sex, with females having higher VTA and RTA during running, and higher VTA, RTA, and VILR during loaded walking (Table 1). No significant differences were found between trainees with competitive running experience compared to without (t=0.045-0.466, p=0.65-0.96).

Our hypotheses were not supported for PA levels or running experience. This may be partially due to the need for more detailed data to accurately group trainees, such as the exercise types and intensity for PA and training volume for running experience. For example, Paquette [3] demonstrated significant differences in gait mechanics between active runners, solely based on training volume. We did find higher peak TAs and GRF loading rates in females vs males during both tasks, with small to moderate effect sizes.

CONCLUSIONS

Our results demonstrate significantly higher loading in females during running and walking with load carriage. Further work is needed to confirm whether these differences are a contributing factor to the higher injury rates seen in female vs male trainees during BCT.

ACKNOWLEDGEMENTS

Supported by US DoD award W81XWH-20-C-0123 P0001. The opinions/assertions herein are the private views of the authors, not to be construed as official policy or reflecting views of the US Army.

REFERENCES

[1] Kaufman, *Am J Prev Med* **18**: 54-63, 2000.
[2] Van der Worp, *Br J Sports Med*, **50**: 450-57, 2016.
[3] Paquette, *Scand J Med Sci Sports*, **31**: 380-87, 2021.
[4] Damsted, J Sci Med Sport, **22**: 281-87, 2019

Table 1. Main effects of sex on GRFs and TAs during running and walking with load carriage (BW, body weights)

	Men (Mean ± SD)	Women (Mean ± SD)	F	p-value	Cohen's d
Running	N= 120	N= 69			
VTA (g)	9.73 ± 3.69	11.15 ± 4.33	8.159	<0.01	0.35
RTA (g)	12.22 ± 4.45	13.98 ± 4.52	8.958	<0.01	0.39
Walking	N= 123	N= 79			
VTA (g)	2.26 ± 0.45	2.52 ± 0.58	10.995	<0.01	0.50
RTA (g)	2.99 ± 0.59	3.39 ± 0.80	16.731	<0.01	0.56
VILR (BW/s)	20.89 ± 5.19	23.93 ± 6.21	11.666	<0.01	0.53

ESTABLISHING SCIENTIFICALLY MEANINGFUL EFFECT SIZES FOR KNEE ABDUCTION MOMENT CURVE REDUCTIONS IN SIDESTEPPING USING 1D POWER ANALYSIS

Hazel Tucker[1], Todd C. Pataky[2], Jos Vanrenterghem[3] and Mark A. Robinson[1]
[1] Research Institute for Sport and Exercise Sciences, Liverpool John Moores University, UK
[2] Department of Human Health Sciences, Kyoto University, Japan
[3] Department of Rehabilitation Sciences, KU Leuven, Belgium
Email: m.a.robinson@ljmu.ac.uk

INTRODUCTION

The knee abduction moment (KAM) is often used as a primary outcome measure in biomechanics. In the context of knee injury risk, high KAMs are undesirable and can be reduced through training interventions [1]. Although researchers often focus on reducing the peak KAM, knee loading is also cumulative so a reduction in the moment curve may be desired.

An empirical aim of altering the KAM curve requires a 1D effect of interest (i.e. the shape of the curve) and an effect size, both required for 1D (curve-based) power analysis [2].

The aim of this study was to (1) establish a scientifically meaningul KAM curve and effect size for 1D power analysis, and to (2) contrast sample size estimation results using 0D and 1D power analyses.

METHODS

A systematic search of Scopus and Web of Science was performed to extract papers assessing the KAM during sidestep cutting. To determine KAM effect sizes, we identified studies reporting a pre to post change in peak KAM following a training intervention (>4 weeks).

To establish a typical KAM curve, a second group of papers were selected from the initial search that visually reported a 1D KAM curve. These studies had to have tested healthy participants, used an approach run, clearly labelling of direction, use clear units over 100% stance and other criteria. Where data were not directly available KAM curves were digitized using WebPlotDigitizer.

Using the resulting 1D curve and an informed range of effect sizes [0.2, 0.4, 0.6, 0.8, 1.0] literature-informed reduced KAM signals were created using a negative Gaussian pulse applied to the 1D effect signal closest to the mean curve from all studies. 1D sample size estimation was conducted using power1d (v.0.1.1, https://github.com/power1d) in Python [3].

Omnibus power (i.e., power associated with effect detection anywhere in time) was calculated and the minimum sample size where power>0.8 was estimated across the range of effect sizes. For comparison, 1D sample sizes were compared to 0D sample sizes using the same effect sizes with alpha at 0.05 and a power of 0.8.

RESULTS AND DISCUSSION

Effect size: Eleven papers reported sidestepping pre-post peak KAM changes following a training intervention. Effect sizes ranged from 0.06-0.77 (equivalent to 0.03-0.14 Nm/kg). The most successful intervention was a 6-weeks of technique training [1]. Whilst a range of effect sizes might be expected for different interventions it makes choosing literature informed effect sizes challenging. Interestingly, the effect sizes chosen for power analysis in the intervention studies were all >0.65 or not explicitly reported.

Effect curve: Twenty papers had visually reported a KAM curve (figure 1). There was some surprising dissimilarity between curves with respect to KAM curve shape, magnitudes, direction and key features.

Power analysis: 1D sample sizes ranged from 310 (effect size of 0.2) to 18 (effect size of 1.0). In comparison 0D sample sizes ranged from 8-148. Differences between 0D and 1D sample sizes ranged from 10-162 samples, similar to previous work [2].

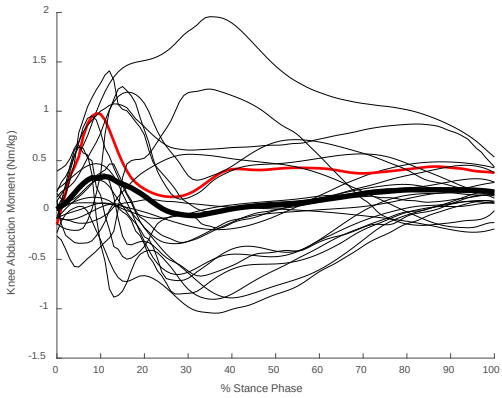

Figure 1. KAM curves during sidestepping (mean curve – bold; closest to the mean curve – red). The red "effect" curve was used for subsequent 1D power analysis.

CONCLUSIONS

Conducting robustly powered interventions to reduce KAM curves is challenging due to inconsistent effect sizes and profiles. Critical reflection on the suitability of the KAM as a primary outcome measure is required, e.g. concerning inter-lab (in)consistencies.

REFERENCES

[1] Dempsey A et al. AJSM 37: 1765-73, 2009.
[2] Robinson MA et al. J Biomech 122: 110451, 2021.
[3] Pataky TC. PeerJ Comp Sci 3: e125, 2017.

LONGITUDINAL RECOVERY OF LATERALITY IN THE UPPER EXTREMITY ACTIVITY AFTER DISTAL RADIUS FRACTURES

Terufumi Iitsuka[1], Hiroshi Kurumadani[2], Yoshiyuki Inagaki[3] and Hideyuki Ota[4]
[1] Department of Rehabilitation, NARAGAKUEN University, Nara, Japan.
[2] Graduate School of Biomedical & Health Sciences, Hiroshima University, Hiroshima, Japan.
3Nagoya Ekisaikai
Email: iitsuka@naragakuen-u.jp

INTRODUCTION

Distal radius fractures are the most common upper extremity fractures. They are often the subject of rehabilitation, and the primary outcomes are joint range of motion and muscle strength. On the other hand, there are some cases in which recovery of these outcomes does not necessarily lead to use of the disabled upper limb in daily life. Recently, monitoring with accelerometers has attracted attention as a method to objectively measure impaired upper limb activity in daily life [1,2]. For distal radius fractures, the affected side of the fracture is one of the factors that affect the use of the disabled upper limb in daily life. The human hand has a laterality, with the dominant hand generally performing the primary movement and the non-dominant hand performing complementary. Therefore, it is thought that a dominant hand fracture affects the use of the disabled upper limb more than a non-dominant hand fracture, and that symmetrical upper limb activity is less likely to occur, but this is still unclear.

METHODS

Subjects were recruited that aged 65 years or older with a diagnosis of distal radius fracture who visited the Nagoya Ekisaikai Hospital, between May 1, 2019 and September 30, 2021. This study was conducted after approved from the institutional review board of the affiliated institution.

Accelerometer: The Actigraph GT-3XBT (Actigraph, Pensacola, FL) is a compact and lightweight 3-axis solid-state accelerometer (46 mm × 33 mm × 15 mm, 19 g) with a sampling rate of 30 Hz and a ±8 G range. In this study, measurements were taken by attaching the accelerometer to the wrist using a wristband. The data was measured continuously for 24 hours.

Data processing: The activity count (0.001664 g/count), a unit unique to the acceleration, was calculated after applying a bandpass filter from 0.25 to 2.5 Hz and setting the epoch time to 1 second. The values of the three axes (x,y,z) were combined by the root-mean-square process to obtain a vector value (VM; Vector magnitude) as data.

Laterality index (LI): Laterality in upper limb activity was calculated using the laterality index (19, 20, 21) with the following formula;

$$LI = VM(Rt)-VM(Lt) / VM(Rt)+M(Lt)$$

RESULTS AND DISCUSSION

There were 42 subjects, all of whom were right-handed. Of the 42 subjects, 19 had injuries to the dominant hand (right) and 23 to the non-dominant hand (left). There were no significant differences in age, gender, fracture type, time from injury to surgery, and start of rehabilitation between dominant and non-dominant hand injuries group ($p<0.05$). Regarding longitudinal recovery, LI quickly approached 0 (bilaterally symmetrical) at 4 weeks postoperatively in the dominant hand injured patients, while LI was significantly higher than the dominant hand injured group in the non-dominant hand injured group even at 12 weeks postoperatively ($p<0.05$, split-plot design ANOVA) (Figure 1).

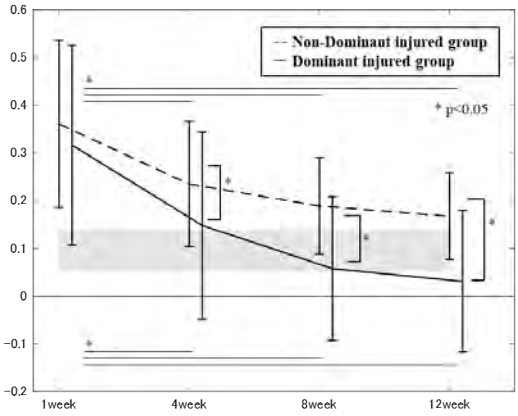

Figure 1

Recovery of laterality index in the distal radius fracture patients.

・X-axis; postoperative weeks, Y-axis; laterality index. 0" indicates bilateral symmetry. For the dominant injury group, the laterality index is multiplied by "-1". Thus, a positive value indicates "use on the non-fracture side" and a negative value indicates "use on the fracture side".

・Gray areas indicate LI averages for healthy subjects.

CONCLUSIONS

The injured side affected the longitudinal recovery of upper limb activity; especially, the recovery tends to be delayed in the upper limb use for non-dominant injured patients. Further rehabilitation methods should be considered.

REFERENCES

[1] Lemmens RJ, et al. *PLoS One.* **10**: e0118642, 2015.
[2] Hurd WJ, et al. *J Electromyogr Kinesiol.* **23**: 924-9, 2013.

Relationship Between Plantar Foot Pressure and High-Risk and Early Knee Osteoarthritis

Teng PSP[1], Wu T-L[2], Chok E[2], Tan SY[3], and Ang WT[2]
[1] Physical Education and Sports Science Academic Group, National Institute of Education, Nanyang Technological University, Singapore
[2] Rehabilitation Research Institute of Singapore, Nanyang Technological University, Singapore
[3] Clinical Research Unit, National Healthcare Group Polyclinics, Singapore
Email: phillis.teng@nie.edu.sg

INTRODUCTION

Knee osteoarthritis (OA) is common, and incidence will rise with the aging Asian population in countries like Singapore and as obesity rates increase [1]. However, there is currently a lack of understanding of the biomechanical factors that predate knee OA [1]. Also, the ankle and foot biomechanics have potential influences on knee OA development [2,3]. Plantar pressure distribution changed with knee OA [2][3] but data for people at high-risk knee OA are lacking. Having foot/ankle symptoms increased risk of developing knee OA but plantar insole pressure was not collected [4]. This research therefore aimed to address the current knowledge gap in how plantar pressure influences the onset of knee OA. We evaluate the plantar pressure differences among normal, high-risk and early knee OA Asian participants.

METHODS

Twenty-one normal (age: mean 49.8 (SD 12.2) years old, height: mean 1.59 (SD 0.11) m, weight: mean 52.3 (SD 9.5) kg)), 13 high-risk (age: mean 46.9 (SD 12.4) years old, height: mean 1.63 (SD 0.10) m, weight: mean 62.8 (SD 15.5) kg)) and 5 early knee OA (age: mean 59.4 (SD 7.5) years old, height: mean 1.61 (SD 0.05) m, weight: mean 67.5 (SD 8.6) kg) participants were recruited. Normal participants were defined as: BMI < 23; waist circumference < 80cm for females and < 90cm for males; had no pain in the past six months; no occupation history of high-risk activities of prolong loading of the knees and no family history of OA. Rest of participants were sent for Xray and graded using the Kellgren/Lawrence (KL) method. Only participants with KL grading of 2 and below were recruited and were sent for a doctor evaluation to further categorize these participants into 'normal', 'high-risk' or 'early OA'. The Knee injury and Osteoarthritis Outcome Score (KOOS), Singapore English and Chinese versions LK 1.0 was also collected. Participants walked at a self-selected fastest velocity over a flat 10m walkway in provided shoes (Adults Aquashoes 100, Decathlon, France). Plantar insole measures were measured using the Moticon insole sensors (Moticon ReGo AG, Munich, Germany).

RESULTS AND DISCUSSION

Overall average KOOs score was 97 (SD 4), 95 (SD 5) and 84 (SD 13) for normal, high-risk and early OA participants respectively. Figure 1 shows a representative of the differences in average peak pressure among normal, high-risk and early OA participants. A Mann-Whitney U test ($\alpha = 0.05$) showed that high-risk and early OA participants (combined as one group) exhibited significantly higher maximum pressure ($p = 0.01$ to $p = 0.02$) than normal participants at sensors in the boxed area (Figure 1). As compared to high-risk participants, early OA participants exhibited higher mean peak planter pressure especially at the lateral side of the mid and forefoot (Figure 1D). This is the first study that recruit high-risk participants and results suggest that high-risk or early knee OA participants might be identified through plantar pressure differences. A bigger sample size should be used to further validate this result.

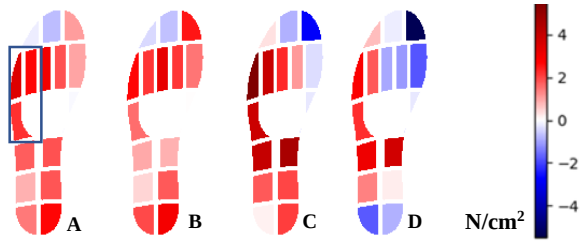

Figure 1 Plantar pressure differences between (A) combined high-risk-early OA minus normal, (B) high-risk minus normal, (C) early OA minus normal and (D) early OA minus high-risk. Boxed region was significantly higher in maximum plantar pressure for high-risk and early knee OA participants as compared to normal participants.

CONCLUSIONS

High-risk and early OA participants combined exhibited significantly higher plantar pressure than normal participants at the lateral aspect of the mid and forefoot during walking. This could provide a method of identification of high risk and early OA participants.

ACKNOWLEDGEMENTS

This research is supported by the Rehabilitation Research Institute of Singapore (RRIS) through RFP/19004.

REFERENCES

[1] Leung Y et al. *Proc Singapore Health* **22(1)**: 31–39, 2012.
[2] Saito L et al. *Arch Phys M* **94(12)**: 2502–2508, 2013.
[3] Lidtke R H et al. *J Am Podiatr Med Assoc* **100(3)**: 178–184, 2010.
[4] Peterson K L et al. *Osteoarthr Cartil* **25(5)**: 639–646, 2017.

SIMULATED TUNNEL VISION AND LOWER LIMB KINEMATICS DURING GAP CROSS-OVER

Tadashi Uno[1], Taihei Matsuo[2], Ping Yeap Loh[3]
[1] Center of Liberal Arts and Science, Sanyo-Onoda City University, Yamaguchi, Japan.
[2] Graduate School of Design, Kyushu University, Fukuoka, Japan.
[3] Faculty of Design, Kyushu University, Fukuoka, Japan.
Email: t-uno@rs.socu.ac.jp

INTRODUCTION

As the number of people with low vision is increasing worldwide [1], their safe mobility is an urgent issue. These challenges are long-lasting in progressive eye diseases such as retinitis pigmentosa. Patients with ocular disease present not only with visual impairment but also with visual field disturbances and reduced contrast sensitivity [2]. Therefore, a different movement strategy is required when straddling a gap than when walking on level ground. This study aimed to clarify the effect of afferent tunnel vision on lower limb movements when straddling a gap.

METHODS

Eight healthy young adults with normal vision were recruited from the university community (male, n = 2: age 22.5 ± 0.7 years; female, n = 6: age 23.3 ± 1.9 years). Participants were instructed to walk and cross over platforms with a gap at the same level (0 cm) and raised platform (+15 cm) under two vision conditions: normal or corrected eyesight and tunnel vision (10°) simulation goggles (M. TAKATAOPTICAL Co., Ltd, Japan). The dimension of the origin platform was 1.1 m (L) × 1.1 m (W) × 0.3 m (H), and two target platforms namely the same level and raised were 1.1 m × 1.1 m × 0.3 m and 1.1 m × 1.1 m × 0.45 m, respectively. A 10 cm gap was designated between the platforms.

Cortex™ 3D motion analysis software, consisting of 8 infrared cameras (Motion Analysis Corporation, Santa Rosa, CA, USA) and 9.5 mm diameter reflective markers, was used to record the participants' motion using the Helen Hayes marker set. Gait kinematic parameters of the leading foot (LF), such as the ROM of the hip, knee and ankle joints and the highest point of toe clearance were calculated using the KineAnalyzer software (Kissei Comtec Co., Ltd, Japan).

RESULTS AND DISCUSSION

Two-way repeated-measure ANOVA was used to analyze the effects of vision and platform conditions. For D2, the main effects of vision and platform are not significant. However, the vision × platform showed significant interaction ($p < 0.05$). Post hoc analysis showed participants exhibit a higher D2 at platform 45 cm compared to platform 30 cm ($p<0.05$) at tunnel vision condition (Figure 1a). The ROM of the hip and ankle joints up to LF ground contact was characterized differently depending on the visual condition (Figure 1b, c, d).

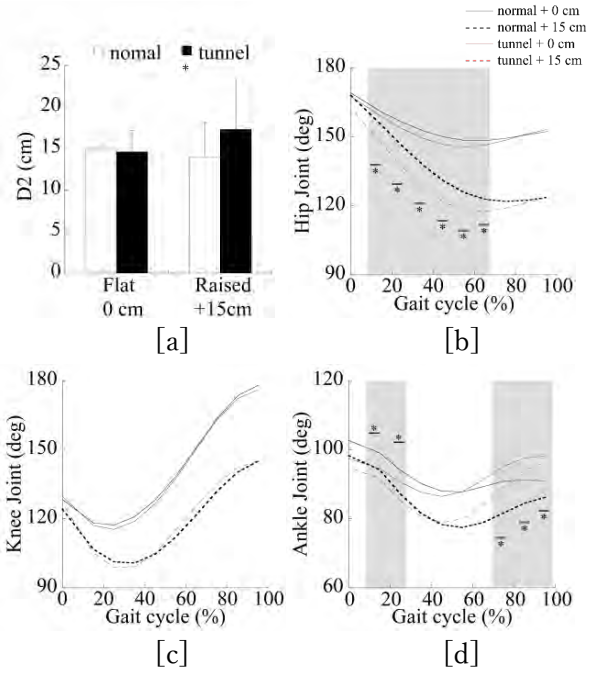

Figure 1 [a]Highest points of the LF(D2), ROM Joint [b; Hip], [c; Knee], [d; Ankle] Changes during gap cross-over. *: $p<0.05$

CONCLUSIONS

At raised 15 cm platform, participants with tunnel vision condition lifted their legs higher to perform the movement than those in the normal or corrected vision condition. These results suggested that participants employ adjustment with the hip and knee flexion-extension movement to complete the cross-over movement under reduced visual field conditions. Generally, when visual sensory input is reduced due to visual field impairment, participants will experience difficulties with object perception and postural control occur [3]. Therefore, in order to reduce the risk of tripping and falling on steps with tunnel vision condition, participants attempted to straddle with higher feet raise.

ACKNOWLEDGEMENTS

This work was supported by JSPS KAKENHI Grant Number JP22K11530.

REFERENCES

[1] GBD 2019 Blindness and Vision Impairment Collaborators. *The Lancet. Global Health* **2**: e144-160, 2021.
[2] Haymes S et al. *Optometry and Vision Science* **10**: 621-637, 1996.
[3] Peterka R et al. *J Neurophysiology* **88**: 1097-1118, 2002.

COMPARISON OF THE EFFECTS OF VIBRATION THERAPY WITH STRETCHING EXERCISE IN SCHOOL TEACHERS WITH MYOFASCIAL PAIN SYNDROME OF THE TRAPEZIUS

Chia-Lin Chen[1], Chun-Wen Chiu [2], Yun-Cheng Lin [3] , Yu-Tun Lin[4] and Hsiao-Yun Chang [3]
[1] Department of Physical Therapy, Hung Kuang University, Taichung, Taiwan
[2] Department of Sport Training Science - Ball, National Taiwan Sport University, Taoyuan, Taiwan
[3] Department of Athletic Training and Health, National Taiwan Sport University, Taoyuan, Taiwan
[4] College of Sports and Health Sciences, National Taiwan Sport University, Taoyuan, Taiwan
Email: chialin@hk.edu.tw

INTRODUCTION

The prevalence of self-reported musculoskeletal disorders (MSD) among school teachers ranges between 39% and 95%.[1,2] Neck pain was the most common teaching-related musculoskeletal disorders.[2] A recent survey from patients with chronic non-specific neck pain showing myofascial pain syndrome (MPS) were prevalent (93.75%) in the upper trapezius.[3] Self-management strategies are considered essential to the management of persistent musculoskeletal disorders. Although studies examined vibration therapy (VT) and stretching exercise (SE) in myofascial pain syndrome (MPS),[4,5] no study has yet compared these two treatments. The purpose of this study was to comparite the effect of self-administered vibration therapy and stretching exercise in the upper trapezius on teachers with myofascial pain syndrome.

METHODS

30 teachers with upper trapezius myofascial pain were enrolled into two treatment groups: vibration therapy group and stretching exercise group. All participates received the treatments for 2 weeks, and 3 times a week. Visual Analog Scale (VAS) of Pain, VAS of Pain threshold with a force of 2 kg/cm2 (VAS $_{2KG}$), Pressure Pain Threshold (PPT), and the range of motion (ROM) of neck sidebending to the opposite side were assessed at baseline and intermittent after the first, and final treatment sessions.

RESULTS AND DISCUSSION

In the vibration massage group, the VAS of Pain ($p<.001$), the VAS of Pain threshold with a force of 2 kg/cm2 ($p=.01$), the PPT ($p=.02$), the side bend ROM of the neck ($p<.001$) had significant improvement after intervention. In the stretching exercise group, the VAS of Pain ($p<.001$) and the side bend ROM of the neck ($p=.02$) had significant improvement as well. (Figure 1)..

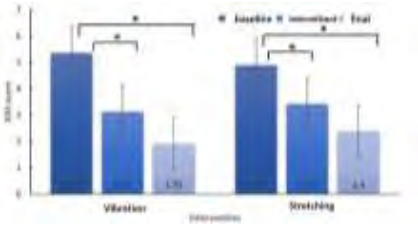

(A) VAS score

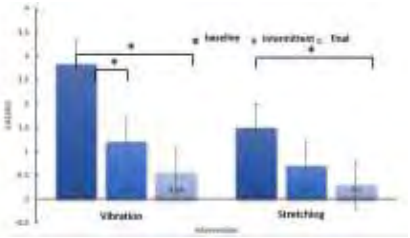

(B) VAS$_{2KG}$

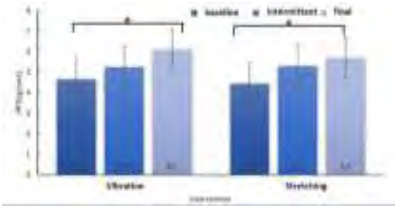

(C) PPT

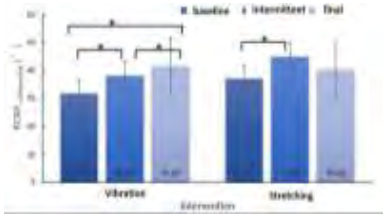

(D) ROM$_{sidebending}$

Figure 1 Differences in related parameters before, intermittent, and after intervention. (A) VAS score (B) VAS $_{2KG}$ score (C) Pressure Pain Threshold (D) Neck ROM of sidebending

CONCLUSIONS

Either vibration massage or stretching exercise had an immediate improvement in relieving pain. The vibration therapy is slightly better than the stretching exercise. Therefore, it is recommended that teachers with upper trapezius myofascial pain can apply vibration therapy or stretching exercises to relieve the pain and improve the joint function.

REFERENCES

[1] Erick PN et al. *BMC Musculoskelet Disord.* **12**: 260, 2011.
[2] Chiu TW et al. *Public Health.* **120**: 563-565, 2006.
[3] Cerezo-Téllez E et al. *Pain Med.***17**:2369-2377, 2016.
[4] Dueñas L et al. *Clin Biomech*. **78**:105071, 2020.
[5] Buranruk O. *J Bodyw Mov Ther*. **32**:29-35, 2022.

Influence of pelvic and lower limb joint kinematics on hamstring muscle-tendon strain during the late swing phase of maximal speed sprinting

Teumitsu Miyazaki[1] and Norihisa Fujii
[1] National Institute of Fitness and Sports in Kanoya, Kanoya, Kagoshima, Japan.
[2] Faculty of Sports and Health Sciences, University of Tsukuba, Tsukuba, Ibaraki, Japan.
Email: t-miyazaki@nifs-k.ac.jp

INTRODUCTION

Hamstring strain injuries would occur during the late swing phase of high-speed running [1]. The biceps femoris long head (BFlh) has a higher incidence rate of strain injuries than the other hamstring muscles. Although a previous study have investigated differences in sprint kinematics between lower limbs with and without hamstring strain injuries [2], the pelvic and lower limb joint kinematics that affect hamstring muscle-tendon unit (MTU) strain during maximal speed sprinting remain unclear. Thus, we aimed to identify the pelvis and lower limb joint kinematics which has a greater impact on the hamstring MTU strains during the late swing phase of maximal speed sprinting using an angle-driven simulation.

METHODS

Forty male collegiate athletes (age, 20.1 ± 1.2 years; height, 170.5 ± 5.5 cm; body mass, 70.5 ± 7.4 kg) participated in this study. All participants performed several 50 m sprinting trials with their maximal effort (sprint velocity, 8.95 ± 0.6 m/s). A three-dimensional motion capture system sampling at 250Hz (VICON-MX, Vicon Motion Systems Ltd., UK) was used to record three-dimensional marker trajectories attached to the whole body. We simulated sprint motion, which increases the BFlh MTU length during the late swing phase from experimental sprint motion, using a single averaged musculoskeletal model consisting of the pelvis and right lower limbs [3]. The optimization was performed by minimizing an objective function with a constraint that the simulated sprint motion was equal to the targeted BFlh MTU length. The targeted BFlh MTU length was increased from the MTU length of the experimental sprint motion. To minimize the differences in the sprint kinematics and kinetics between simulated and experimental sprint motions, the objective function was the sum of three components with weighting factors: squared error between the experimental and simulated (1) angular acceleration, (2) joint torque, and (3) residual force and moment exerted to the pelvis for each degree of freedom. We calculated the change ratios of pelvic anterior/posterior tilt, and hip and knee flexion/extension joint angles at the simulated sprint motion from the experimental sprint motion. These change ratios were compared between the pelvis, hip, and knee joints using one-way analysis of variance with repeated measures. If the main effect was significant, pairwise comparisons were conducted for all pairs using a paired two-tailed t-test with Bonferroni correction. Statistical significance was set at $p < 0.05$.

RESULTS AND DISCUSSION

The peak BFlh MTU length of the simulated sprint increased compared to that of the experimental sprint (Figure 1a). The pelvic anterior tilt, hip flexion, and knee extension angles of the simulated sprint were greater than those of the experimental sprint. Additionally, the change ratio of pelvic anterior/posterior tilt angle was larger than those of hip and knee flexion/extension angles (Figure 1b; $p < 0.001$). The results indicate that the pelvic anterior tilt would have a more significant impact on BFlh MTU length during the late swing phase, compared to hip and knee flexion/extension angles. Pelvic anterior tilt might be a biomechanical factor associated with the risk of hamstring strain injuries [3]. Thus, the findings of this study imply that training strategies aimed at decreasing pelvic anterior tilt during the late swing phase of maximal speed sprinting could be effective in preventing hamstring strain injuries.

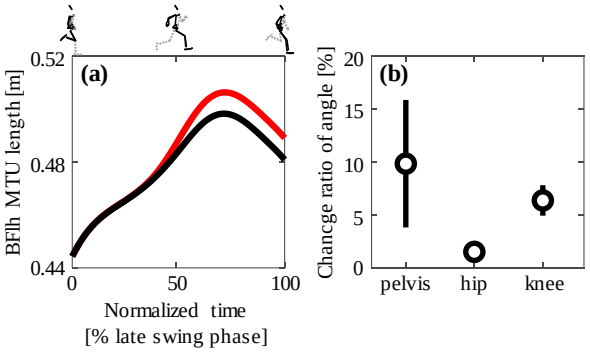

Figure 1 (a) Mean simulated (red line) and experimental (black line) BFlh MTU length during the late swing phase of maximal speed sprinting. (b) Mean values (open circle) and standard deviation (vertical line) of change ratios of pelvis, hip, and knee joint angles.

CONCLUSIONS

This study simulated sprint motion that increases BFlh MTU length during the late swing phase of maximal speed sprinting using an angle-driven simulation. Our results demonstrate that an increase in pelvic anterior tilt angle has the greatest impact on an increase in BFlh MTU length during the late swing phase of maximal speed sprinting compared to hip and knee joint angles.

REFERENCES

[1] Woods C et al. *Br J Sports Med* **38**: 36-41, 2004.
[2] Higashihara A et al. *J Sports Sci* **37**: 2744-2740, 2019.
[3] Miyazaki T and Fujii N, *Sports Biomech*, in press.
[4] Schuermans J et al. Gait Posture **57**: 270-277, 2017.

KINEMATIC COMPARISON OF LOWER EXTREMITY BEFORE AND AFTER TOTAL HIP REPLACEMENT FOR HIP DYSPLASIA: A CASE REPORT

Tserenchimed Purevsuren[1], Enkhtaivan Narangerel[2], Ganbat Danaa[1], Bayarsaikhan Barizad[1], Batbayar Khuyagbaatar[1]and Otgonbayar Maidar[2]
[1]Department of Technical Mechanics, Mongolian University of Science and Technology, Ulaanbaatar, Mongolia
[2]Joint center, The First Central Hospital, Ulaanbaatar, Mongolia.
Email: tserenchimed.p@must.edu.mn

INTRODUCTION

Total hip replacement (THR) is an alternative surgical option for chronic hip injuries including severe hip osteoarthritis and dysplasia [1]. It has been stated that Mongolian national hospitals have been performing THR since 1998. Domestic clinical studies have utilized patient-reported surveys and qualitative approaches to evaluate the outcome of THR, and it is favorable in Mongolia. However, from a biomechanical viewpoint, there is no quantitative evidence of THR on recovering functional motion and improving hip joint mobility for patients with hip dysplasia. Therefore, the current study was purposed to quantitatively investigate hip joint motion before and after THR for patients with hip dysplasia using a wearable motion capture system.

METHODS

Two male subjects with chronic hip dysplasia participated in this study. For patient 1 (32 years old, male), the right-sided THR surgery was performed and for patient 2 (47 years old, male), bilateral THR was performed with a single experienced surgeon (15 years of experience). A conventional posterior approach was used to perform THR surgeries with commercial hip implants (K-Implant, Germany) [2]. The wearable motion capture system (MVN, Xsens technologies, Netherlands) was utilized to capture hip joint motion during walking and squatting before and after THR [3]. Three-dimensional hip range of motion (ROMs) was recorded during clinical tests conducted by an experienced surgeon. Also, the pre-operative and post-operative hip joint kinematics were compared to the control group (10 healthy male subjects).

Table 1: Comparison of hip ROM during clinical tests before and after THR

		Flex	Int	Ext	Abd	Add
Patient 1	Before	44º	8º	8º	10º	7º
(right hip)	After	59º	22º	32º	27º	16º
Patient 2	Before	50º	9º	8º	10º	11º
(right hip)	After	42º	12º	22º	11º	4º
Patient 2	Before	58º	7º	9º	8 º	6º
(left hip)	After	64º	25º	8º	20 º	7º

RESULTS AND DISCUSSION

The results of clinical tests relieved that post-operative ROM in hip flexion, internal and external rotation, abduction, and adduction were mainly increased after THR (Table 1). However, a decrease in hip flexion and adduction was observed in the right hip of patient 2. Such a result may be related to the consequence of the bilateral THR procedure. Although post-operative hip kinematics were improved during walking and squat, it was not fully recovered as normal subject data (Figure 1).

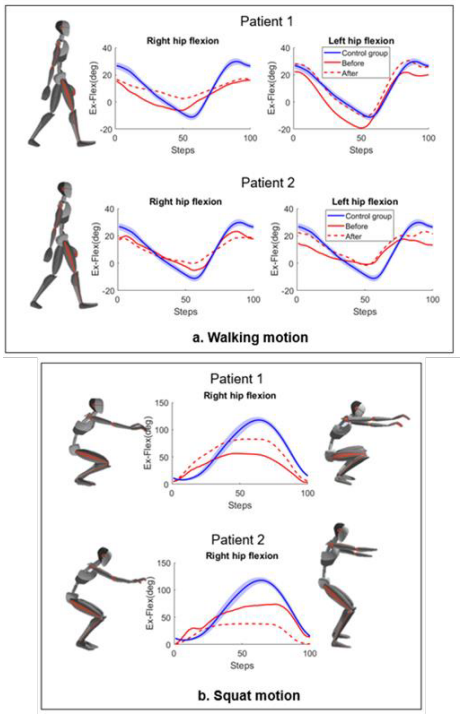

Figure 1 Hip flexion-extension during walking and squat before and after THR

CONCLUSIONS

This is the first quantitate report of the kinematic comparison before and after THR surgery in Mongolia. The result could provide new insight to the surgeons to assess joint functionality, and surgical outcomes and to improve rehabilitation protocol.

ACKNOWLEDGEMENTS

This work was supported by the “Mongolia-Japan Engineering Education Development” project (J24C16) and the Mongolian University of Science and Technology (mfund-052022).

REFERENCES

[1] Du Y et al. *Clin Biomech* **15**: 504-515, 2000.
[2] Prill R et al. *Sensors* **21**: 8221, 2021.
[3] Ilchmann T et al. *Hip International* **24**: 2-6, 2014.

Stair Ambulation Reveals Greater Medial Meniscus Extrusion in Healthy Young Volunteers

Takato Hashizume[1], Yosuke Ishii[1], Yuko Nakashima[2], Saeko Okamoto[1], Riko Okinaka[1], Yoshitaka Iwamoto[1], Kaoru Okada[3], Kazuya Takagi[3], Nobuo Adachi[4] and Makoto Takahashi[1]

[1] Department of Biomechanics, Graduate School of Biomedical and Health Sciences, Hiroshima University / Hiroshima, Japan.

[2] Department of Musculoskeletal, Ultrasound in Medicine, Graduate School of Biomedical and Health Sciences, Hiroshima University / Hiroshima, Japan.

[3] Ultrasound Business Operations, Healthcare Business Headquarters, KONICA MINOLTA, INC / Tokyo, Japan.

[4] Department of Orthopedic Surgery, Graduate School of Biomedical and Health Sciences, Hiroshima University / Hiroshima, Japan.

Email: bad0206tkt@gmail.com

INTRODUCTION

Medial meniscus extrusion (MME) expands with greater mechanical stress. Increase in MME during gait was correlated with mechanical stress [1] whereas it is still unknown the dynamics of MME during stair ambulation. The mechanical stress is known to be higher in stair ambulation than that in gait, and the increase in MME might expand according to the greater mechanical stress. Then, the aim of this study is to investigate the effect of mechanical stress during stair ambulation on increase in MME.

METHODS

Twenty healthy participants (females: 10, age: 22.3 ± 0.9 years) were recruited in this study. They were asked to perform in three tasks of gait, stair ascent and descent. The vertical grand reaction force (GRFz) as the representative mechanical stress and knee flexion angle during stance phase were obtained by three-dimensional motion analysis system. The MME was evaluated by ultrasonography. A prototype transducer with a flat-shaped linear-array was placed longitudinally on the medial joint space and recorded the dynamics of meniscus during task on video mode. The value of MME was shown as the distance from the medial tibial plateau cortex to the outermost edge of the medial meniscus. Moreover, the increase in MME was identified as the difference in MME at the maximum and the initial contact during task.

RESULTS AND DISCUSSION

The GRFz and increase in MME during stair ascent and descent were higher than that during gait (Table1). Moreover, there were no correlation between the GRFz and the increase in MME for three tasks. Although a previous study reported that a mechanical stress was correlated with the increase in MME [2], our result including task of the stair ambulation did not support it. Stair ambulation requires motion with deep knee flexion compared with gait. The medial meniscus has the feature of movement to posterior and lateral direction during knee flexion, and it raise concern about masking the effect of mechanical stress on the increase in MME. Therefore, the increase in MME during stair ambulation could occur by a combination of the mechanical stress and knee flexion motion. These results may contribute to understand the dynamics of medial meniscus during motion with deep knee flexion on the knee.

CONCLUSIONS

Stair ambulation revealed the greater increase in MME.

REFERENCES

[1] Ishii Y et al. *Knee* **38**: 82-90, 2022.
[2] Achtnlch A et al. *Knee Surg Sports Traumatol Arthrosc* **26**: 2282-8, 2018.

Table 1: The Increase in MME and GRFz.

	Gait	Stair ascent	Stair descent
Increase in MME (mm)	0.68 ± 0.20	1.01 ± 0.39*	0.89 ± 0.26*
GRFz first peak (N)	591.41 ± 129.87	594.98 ± 112.12	759.21 ± 153.08*
GRFz second peak (N)	613.76 ± 118.66	672.31 ± 111.80*	562.68 ± 114.59

Note: * indicates a significant difference from gait condition, $p < 0.05$

Numerical Simulation of Bone Metabolism Over time with Aging

Teppei Mano[1], Shigehiro Hashimoto[2], Katsumasa Tanaka[2], Masafumi Machida[3] and Yoshimori Kiriyama[4]
[1] Course of Mechanical Engineering, Kogakuin University, Tokyo, Japan.
[2] Department of Mechanical Engineering, Kogakuin University, Tokyo, Japan.
[3] Department of Orthopedic Surgery, Saitama Children's Medical Center, Saitama, Japan.
[4] Department of Mechanical Systems Engineering, Kogakuin University, Tokyo, Japan.
Email: manoteppei.k@gmail.com

INTRODUCTION

Bone mineral density (BMD) generally increases until the age of 20 to 44 y/o, but BMD of 2 to 18% decreases during from 35 to 59 y/o [1]. It has been reported that the decrease of BMD is cased by the shorter bone metabolism period and longer bone formation period [2]. To understand the mechanism of the bone metabolism, in this study, we calculated the bone metabolic step and reproduced the change of BMD due to aging.

METHODS

In this study, we conducted bone remodelling simulation to reproduce the bone metabolism. To obtain the distribution of the bone mineral, we took Multi-detector row computed tomography (MDCT) images, which is higher resolution than a single-detector row CT and allows us to take images for the human. MDCT is lower resolution than μCT, and one pixel of the image includes the bone trabecular structure and cavity. Therefore, the CT value expresses an average between the brightness of the bone and cavity. In this study, we divided one pixel size of MDCT into subpixel sizes of μCT, and estimated the ratio among the bone, cavity, and calcification. In this study, the brightness of the bone was assumed white, the cavity was black, and the calcification was gray respectively, and the averaged brightness corresponded to the brightness of the MDCT. The subdivided pixels for μCT had one of the characteristics of the bone, calcification, and cavity, but they did not assume to reflect the microstructure of the trabecular bone. In this study, the subdivided pixels of the bone and calcification were metabolized, and then the brightness was changed. The metabolism consisted of the resorption, formation and rest as shown in Figure 1 (a). After the step of the metabolic calculation, the averaged brightness was calculated for the size of MDCT pixel. The changes of BMD were evaluated through the cycle [1][3].

In this study, to reproduce young age, the resorption, the formation, and the rest were assumed as 4, 16, 80% respectively, while to reproduce elderly age, they were 12, 48, 40%.

Also, to reproduce the bone porosis, the maximum brightness of each subdivided pixel was reduced by 10%. This reduction was applied after 100th step, and more 100 steps were calculated.

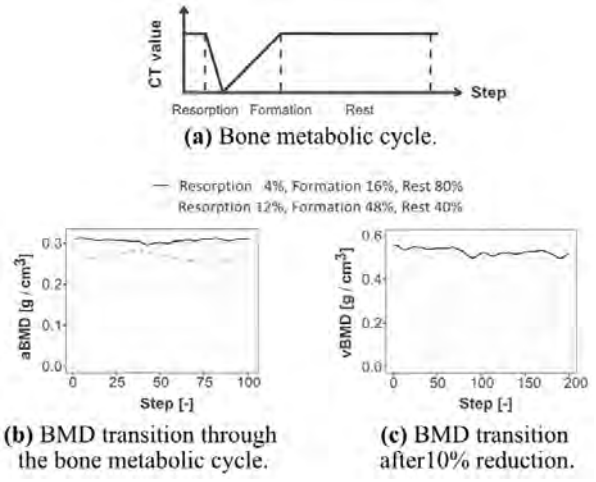

Figure 1 Bone metabolic cycle and BMD transition.

RESULTS AND DISCUSSION

As shown in Figure 1 (b), the elderly age shows low areal BMD (aBMD) value through the cycle, with compared to the young age. In the simulation of the elderly age, 60% of the bone and calcification was metabolized, and then the many of the subdivided pixels were in the process of the calcification duration. This should result in the low aBMD value. Figure 1 (c) shows a change of volumetric BMD (vBMD) through two metabolic cycles. After one cycle of the bone metabolism (100th step later), the vBMD decreases by 3.5%, with a maximum reduction of 10.9% through the later cycle. After the 10% reduction, the subdivided pixels become the maximum values sequentially. Therefore, the vBMD could show uneven waveforms, not flat waveforms. Thus, the two conditions in this study could reproduce the process of the osteoporosis caused by age.

CONCLUSIONS

The bone metabolism simulation considering the ratio of the resorption, formation and rest, and the changes of baseline of BMD could allow us to reflect the BMD due to aging.

ACKNOWLEDGEMENTS

A part of this study was supported financially by JKA through its promotion funds from KEIRIN RACE, and The Uehara Memorial Foundation.

REFERENCES

[1] Orimo H. Osteoporo Jpn 4: 643-53, 1996.
[2] Erik F.E. et al. Metab Bone Dis Relat Res. 5: 243-52, 1984.
[3] Ikeda Y. et al. Japanese Society of Gerodontology. 13: 8-22, 1998

MORPHOLOGICAL CHARACTERISTICS OF THE FEMORAL CARTILAGE IN TRAINED AND UNTRAINED INDIVIDUALS

Junhyeong Lim, Sanghyup Park, Jinwoo Lee, Dongkyun Seo, Sungkyu Jeon, Seunghun Lee, Jaewon Kim, and Jihong Park

Athletic Training Laboratory, Kyung Hee University, Yongin, Korea.
Email: jihong.park@khu.ac.kr

INTRODUCTION

High frequency and intensity and long duration of exercises with insufficient recovery can deteriorate the structural integrity of articular cartilage, which may lead to joint degeneration such as osteoarthritis [1]. Cross-sectional comparisons between athletes with different types of mechanical loading (e.g., compressive vs compressive with rotational) and untrained individuals of the morphological characteristics of the femoral cartilage could suggest cartilage health in response to a long-term adaptation of physical activity in terms of volume and type. Therefore, this study compared the cross-sectional area (CSA) and thickness (medial, lateral, and intercondylar) of the femoral cartilage between archery and badminton players to non-athlete individuals.

METHODS

Thirty-four male archery players (20.2 years, 173.9 cm, 76.4 kg, career: 10.2 years), 37 male badminton players (20.2 years, 177.5 cm, 72.1 kg, career: 11.3 years), and 36 non-athlete males (21.5 years, 174.9 cm, 71.3 kg, ≥150 min of exercise per week) participated in this study. Individuals with a history of musculoskeletal surgery were excluded. After giving informed consent, subjects were seated with their knees fully extended for 20 min to remove the effect of preceding weight-bearing activities. Afterwards, the testing knee was flexed to 140°, and a 10.0 MHz linear probe (30 fps with a depth of 3.0 cm) was placed between the medial and lateral femoral condyles and then rotated to visualise the clear view of the cartilage. Three images on each leg were obtained (dominant: the leg to kick a ball). The CSA and thickness (medial, lateral, and intercondylar) were then calculated using ImageJ software. Values on three images from each dependent measurement on each side were averaged and analysed using two-way (side × group) analysis of variances; and Tukey tests were performed. Cohen's d effect sizes (d) were calculated for the statistical significances.

RESULTS AND DISCUSSION

There were no statistical interactions on any of the dependent measurements ($F_{5,210}$≥28.03, p≥0.46, Table 1). Regardless of side, the femoral cartilage CSA ($F_{2,208}$=35.87, p<0.0001) and medial ($F_{2.208}$=26.76, p<0.0001), lateral ($F_{2,208}$=31.43, p<0.0001), and intercondylar thicknesses ($F_{2,208}$=69.05, p<0.0001) were different between groups. Specifically, the badminton players showed greater femoral cartilage CSA compared with the archery players (18%, p<0.0001, d=1.07) or non-athlete individuals (19%, p<0.0001, d=1.33). The same pattern was observed with thicknesses: badminton players showed thicker medial (≥13%, p≤0.0011, d≥0.54), lateral (≥18%, both p<0.0001, d≥0.89), and intercondylar (≥29%, both p<0.0001, d≥1.55) thickness compared with archery players and non-athlete individuals. Greater CSA and thickness may have been due to cartilage enlargement and hypertrophy [2] as a long-term adaptation of sport-specific movements in badminton.

CONCLUSIONS

Badminton players showed greater CSA and thicker femoral cartilage than archery players and non-athlete individuals. Our data suggest that rotational force could be the primary contributing factor on articular cartilage health.

ACKNOWLEDGEMENTS

This work was supported by the National Research Foundation of Korea (NRF-2021S1A5A2A01062062).

REFERENCES

[1] Pfeiffer S et al. *J Ultrasound Med* **39**: 957-65, 2020.
[2] Harkey M et al. *J Athl Train* **53**: 1082-88, 2018.

Table 1: The femoral cartilage cross-sectional area (mm^2) and thickness (mm).

Mean (95% CI)	Cross-sectional area		Medial thickness		Lateral thickness		Intercondylar thickness	
	Dominant	ND	Dominant	ND	Dominant	ND	Dominant	ND
Archery	75.6 (5.4)	75.5 (5.2)	2.1 (0.2)	2.1 (0.2)	2.0 (0.2)	2.1 (0.2)	2.0 (0.1)	2.0 (0.1)
Badminton	94.7 (5.1)	89.6 (4.7)	2.4 (0.2)	2.4 (0.2)	2.6 (0.2)	2.4 (0.2)	2.8 (0.2)	2.7 (0.2)
Non-athlete	74.3 (3.2)	74.5 (4.1)	1.8 (0.1)	1.8 (0.1)	1.9 (0.1)	2.0 (0.1)	2.0 (0.1)	1.9 (0.1)

CI: confidence interval, ND: nondominant

THE FATIGUE LIFE OF CORTICAL BONE DOES NOT INCREASE WITH TEST INTERRUPTIONS

Tudor Muresan[1,2], Ifaz T. Haider[1,2], Andrew Sawatsky[1,2] and W. Brent Edwards[1,2,3]
[1] Human Performance Lab, Faculty of Kinesiology, University of Calgary, Calgary, Canada.
[2] McCaig Institute for Bone and Joint Health, University of Calgary, Calgary, Canada.
[3] Department of Biomedical Engineering, University of Calgary, Calgary, Canada.
Email: wbedward@ucalgary.ca

INTRODUCTION

Mechanical fatigue of load bearing bone is an inevitable consequence of physical activity. Over time, cyclic loading of the skeletal system causes microdamage accumulation that reduces the overall quality of bone and leads to an accumulation of residual strain with continuous loading. In life, however, people do not cyclically load their bones continuously; rather, physical activity bouts are interrupted by periods of inactivity. It has been illustrated that residual strains in bone are recoverable when periods of unloading are provided [1,2], but whether or not this may serve as a self-healing function that extends the fatigue-life (i.e., number of cycles to failure) of bone has never been tested. The purpose of this project is to quantify the influence of test interruptions on fatigue life measurements of cortical bone.

METHODS

Twenty cortical bone specimens were extracted from bovine tibiae and machined into prismatic beams (20 x 3 x 3 mm). The samples were evenly allocated (n = 5 each) to two loading groups (continuous or interrupted) and two loading levels (140 or 150 MPa) balanced by bone apparent density. All samples were cyclically loaded in a 4-point bending configuration on an E3000 (Instron) while submerged in phosphate-buffered saline at room temperature. Cyclic tests were conducted in load control to the prescribed peak magnitude with a load ratio (i.e., minimum-to-maximum stress) of 0.1 and a frequency of 2 Hz. The continuous load group was tested without rest until failure or a predefined runout of 500,000 cycles. The interrupted group was loaded for 1 hour, followed by 2 hours of rest, and this order was repeated until failure or runout. A survival analysis was conducted to examine differences in log cycles to failure between groups with a criterion alpha level of 0.05.

RESULTS AND DISCUSSION

Fatigue-life measurements varied several orders of magnitude, which is in line with previous cyclic tests of cortical bone. Bones loaded at 150 MPa did not have a significantly lower fatigue-life than bones loaded at 140 MPa (p=0.073), and no differences between continuous and interrupted loading groups was observed (p=0.581).

During cyclic tests of this nature, bone may accumulate damage as a function of loading cycles (fatigue damage) and/or loading duration (creep damage). Creep strain recovery has previously been demonstrated *in vitro* [1,2], and we wondered if a similar phenomenon may delay damage accumulation and increase fatigue-life measurements when rest was incorporated into fatigue tests. Although we did not detect a significant effect of continuous vs. interrupted loading, our sample size was relatively small. In the future, we plan to test additional samples at lower load levels, which may better demonstrate difference between groups, as viscous strain may be more recoverable at low loads. It is important to remember that this study focused on understanding mechanical mechanisms that influence fatigue life in vitro. *In vivo*, bone remodeling and adaptation have an important influence on fatigue life.

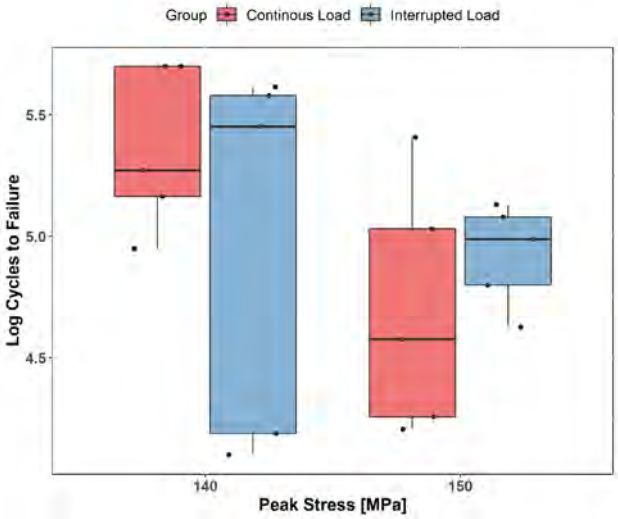

Figure 1 Fatigue life of continuous and interrupted groups.

CONCLUSIONS

Cyclic loading interruption did not have a significant effect on the fatigue life of bovine cortical bone, but a larger samples size and additional load levels may be needed to confirm this finding.

ACKNOWLEDGEMENTS

This work was supported in part by the Natural Science and Engineering Research Council of Canada (NSERC; 02404-2021, and RTI 00013–2016).

REFERENCES

[1] Currey *J Exp Bio* **43**: 279-92, 1965.
[2] Lakes & Saha *J Biomech Eng* **178**: 178-80.

DEPTH DEPENDENT TENSILE PROPERTIES OF ARTICULAR CARTILAGE

Francesca de Vecchi [1,2], Spencer Fullam[1], Federica Boschetti[2] and Markus Wimmer [1]
[1] Department of Orthopedic Surgery, Rush University Medical Center, Chicago (IL), USA.
[2] Department of Chemistry, Materials, and Chemical Engineering, Politecnico di Milano, Milan, Italy.
Email: francesca_devecchi@rush.edu

INTRODUCTION

Articular cartilage is responsible for load transmission, shock absorption and allows smoothness of articulation. It is composed of a dense extracellular matrix with mainly proteoglycans and collagen fibers, and cells. The distribution of these components defines three main zones: a superficial zone in which the collagen fibers are packed and parallel to the articular surface, a transitional zone where the collagen fibers are less packed and obliquely oriented, and a deep zone characterized by collagen fibers perpendicularly oriented. These differences define an anisotropic and inhomogeneus behavior and the characterization of the resulting variation of mechanical properties is a critical challenge due to the microscopical scale. Methods have been developed to investigate the depth dependent compressive and shear properties of cartilage [1]. Work has also been performed to capture tensile properties throughout depth [2], but the study was limited by the thickness of the slices that excluded the superficial zone. The aim of this study was to characterize the tissue in terms of tensile properties, with a sufficient spatial resolution that included all zones of cartilage. We hypothesized that cartilage shows depth dependent tensile properties.

METHODS

N=8 cartilage explants from four 8 months old bovine stifle joints were used. The explants were obtained from the medial side of the joint parallel to the antero-posterior line and were washed in $CaCl_2$ solution for 1h. Dogbone shaped samples were cut from each explant according to ASTM D638 for tensile testing type IV. The samples were then frozen in OCT and after 2 days they were cut into 9 slices of 80µm thickness each using a cryostat. In order to obtain flat dogbones, from each sample an average of 30µm depth was removed from the surface. Additionally, 20µm were discarded between each of the following slices until 900µm depth were reached. Each slice was moved into a well plate with PBS solution to avoid dehydration. Tensile tests were then run at a strain rate of 1% strain per second until rupture of the sample. During testing the sample was kept hydrated by constantly dropping PBS solution onto the tissue. Stress-strain curves were obtained from each slice and 4 parameters were identified for analysis: Ultimate tensile stress (UTStress), Ultimate tensile strain (UTStrain), Elastic modulus (EM), Toe modulus (TM). A repeated measures ANOVA was performed on the above parameters to investigate whether cartilage depth influences tensile properties.

RESULTS AND DISCUSSION

UTStress, EM and TM demonstrated similar tendencies (Fig. 1). All three parameters had their minima at approximately 200µm. Also, intermediate values were found in the most superficial layer, and the highest values were found in the deep layers. The repeated measures ANOVA indicated a significant effect (Tab 1). In contrast, UTStrain showed similar values throughout depth.

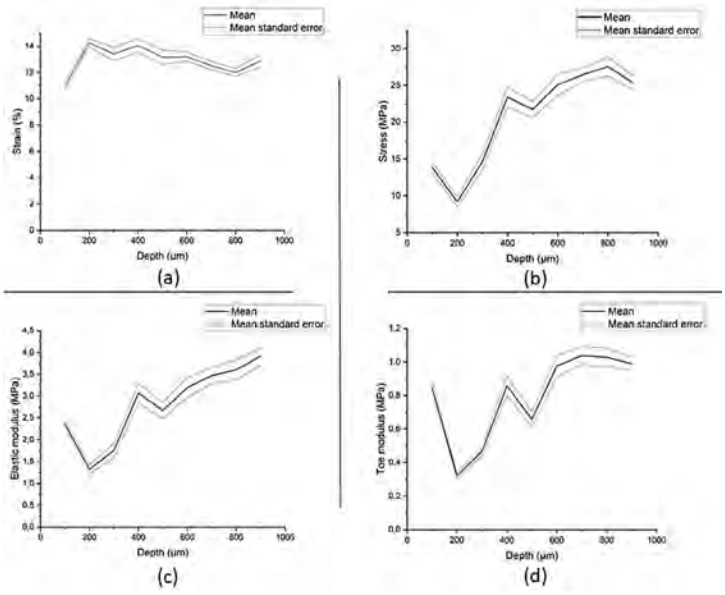

Figure 1 (a) UTStrain, (b) UTStress, (c) Elastic modulus, (d) Toe modulus for 80µm thickness slices from 30µm to 900µm depth.

Parameter	*p-value*
UTStrain (%)	$p = 0.246$
UTStress (MPa)	$\mathbf{p < 0.001}$
Elastic modulus (MPa)	$\mathbf{p < 0.001}$
Toe modulus (MPa)	$\mathbf{p = 0.028}$

Table 1: p-values of the repeated measures ANOVA.

CONCLUSIONS

Most tensile properties of articular cartilage are dependent on cartilage depth. A spatial resolution of smaller than 100 µm was necessary to capture this effect.

REFERENCES

[1] Wang CC et al. *J Biomech* **124**(5):557-567, 2002
[2] Woo SL et al. *J Biomech*. **9**(12):785-791, 1976

Effects of High Tibial Osteotomy on Three-dimensional Knee Kinematics in Patients with Knee Osteoarthritis during Isolated Knee Flexion Measured Using Bi-plane Fluoroscopy

Kao-Shang Shih[1], Pei-Ling Weng[2], Chia-Ling Fan[2], Yi-Ching Wang[2], Yi-Chen Wu[2], Cheng-Chung Lin[3], and Tung-Wu Lu[2,4]
[1] Department of Orthopedic Surgery, Shin Kong Wu Ho Su Memorial Hospital, Taiwan, R.O.C.
[2] Department of Biomedical Engineering, National Taiwan University, Taiwan, R.O.C.
[3] Department of Electrical Engineering, Fu Jen Catholic University, Taiwan, R.O.C.
[4] Department of Orthopedic Surgery, School of Medicine, National Taiwan University, Taiwan, R.O.C.
Email: twlu@ntu.edu.tw

INTRODUCTION

Knee osteoarthritis (OA) is one of the most common diseases caused by articular cartilage degeneration, which affects the movement of the joint and leading to joint pain and stiffness. **High tibial osteotomy** (HTO) surgery, a joint-preserving surgery, is a widely used surgical method for patients with medial compartment OA [1] and with the inter-articular distance being one of the decisive index for predicting post-surgery prognosis. However, no study has investigated the effects of pre- and post-HTO surgery during functional activities and measured the *in vivo* inter-articular distances. Current study aimed to measure the *in vivo* three-dimensional kinematics of the knee joint pre- and post-HTO surgery during functional activities using biplane fluoroscopy.

METHODS

Fifteen subjects with OA (age: 58.07 ± 9.51 years; BMI: 28.56 ± 5.27 kg/m^2) performed isolated knee flexion pre and post-HTO surgery with the motions of bones measured by a bi-plane fluoroscopy system. Three-dimensional bone geometric models of the femur and tibia were then reconstructed from computed tomography images. The 3D fluoroscopy method [2] was used to determine the motions of the bones overall image frames, which were used to calculate the angles of the tibiofemoral joints against the motion. The data were then used to calculate the inter-articular distances of the medial and lateral compartment of the joint during motions to quantify the effects of HTO on the joint during isolated knee flexion. Paired-T test was used for comparisons between pre and post data with α=0.05.

RESULTS AND DISCUSSION

The pre-surgery inter-articular distance in both the medial and lateral compartments of the joint were compared with the post-surgery inter-articular distance (Figure 1 (a), (b)) and the results indicated that subjects who underwent HTO surgery showed significantly greater inter-articular distance in the medial compartment during isolated knee flexion at 35° to 65° but there was no significant difference in the lateral compartment throughout the whole motion. The current results showed that after the HTO surgery, the change of the tibial alignment lead to medial condylar lift-off, which increased the distance between the medial compartment and may stop the progression of medial compartment osteoarthritis of the knee. The current results suggested that patients with medial compartment knee OA can expect improvement in clinical outcomes after HTO surgery.

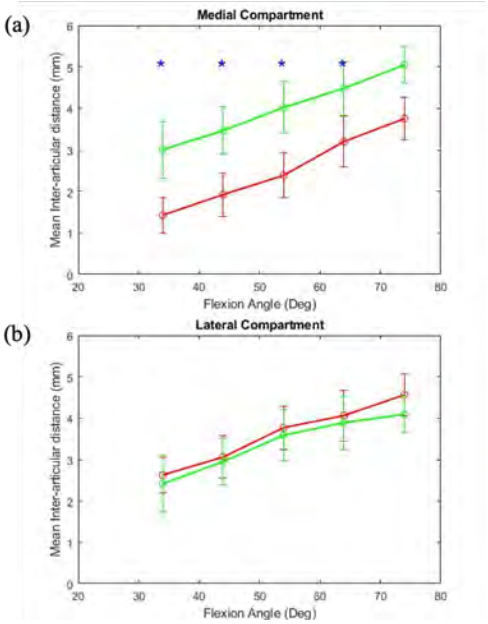

Figure 1 (a) Mean values (standard deviations) of the inter-articular distances of the pre (red) and post (green) HTO operation of the medial and (b) lateral compartment of the tibiofemoral joint.
* Significant difference between pre-OP and post-OP group.

CONCLUSIONS

The mean inter-articular distance in the medial compartment was found to increase after HTO surgery, and the medial condylar liftoff is likely to unload the involved joint compartment. The current findings may contribute to a better understanding of the underlying mechanism for the treatment of medial compartment arthritis.

ACKNOWLEDGEMENTS

Financial support: Ministry of Science and Technology of Taiwan (MOST 107-2221-E-341 -001 -MY3)

REFERENCES

[1] Robert F. LaPrade., et al. *The Journal of Arthroscopic & Related Surgery* **28(3)**: 354-364, 2012.
[2] Lin, C.-C., et al. *Applied Sciences* **10(23)**: 8426, 2020.

ADAPTING THE PROSTHESIS EVALUATION QUESTIONNAIRE TO ASSESS SEX DIFFERENCES IN THE PROSTHETIC NEEDS AND PRIORITIES OF LOWER LIMB AMPUTEES

Tess M.R. Carswell[1], Helen Monkman[2] and Joshua W. Giles[1]
[1] Department of Mechanical Engineering, University of Victoria, Victoria, B.C., Canada.
[2] School of Health Information Science, University of Victoria, Victoria, B.C., Canada.
Email: tmrc@uvic.ca

INTRODUCTION

Despite ~30% of lower limb amputees (LLAs) being female [1], the majority of LLA and prosthetics research is focused on males [2]. Female LLAs also experience different challenges than males, including having a higher risk of osteoarthritis, lower functional abilities, higher prosthesis rejection rates, and greater overall dissatisfaction [3]. A key aspect of early-stage medical device research is consulting with users to understand their specific needs [4]. Therefore, studying sex differences in the prosthetic priorities of LLAs through survey methods may improve understanding of female-specific needs as well as inform the design of sex-specific prosthetics. However, as females have been historically underrepresentated or overlooked, most prosthesis questionnaires neglect what may make them different. To this end, we took a user-centered design (UCD) approach to adapting the Prosthesis Evaluation Questionnaire (PEQ) [5] to better capture and assess sex differences in LLA prosthetic needs and priorities.

METHODS

A committee of 5 female LLAs (i.e., prosthesis users) was formed to engage them in developing a modified questionnaire. We met with these users to assess and adapt the original PEQ. In doing so, they contributed to the creation of a modified instrument targeting technical and personal aspects of a user's prosthesis, and sex and gender related topics. In the adapted questionnaire, 7 of the 9 validated PEQ subscales were retained and new questions were added to better target the study's objectives. Closed questions were scored on Likert scales from 1 (negative) to 10 (positive). Results were analysed using Mann-Whitney U tests in SPSS.

RESULTS AND DISCUSSION

The questionnaire was completed by 18 LLAs (9 female, 9 male). No statistically significant sex differences (i.e., $p < 0.05$) were found in participant demographics, making these good comparative groups. Although no significant sex differences were found in the validated PEQ subscales, differences were found in individual questions on mobility and psychosocial factors (Table 1). Females expressed a significantly poorer ability to ambulate up or down a steep hill, potentially linking to their prosthetic and functional challenges presented in literature [3]. As well, sex-specific challenges related to mobility have major implications for the design of sex-specific prosthetics. Such challenges can also further impact psychosocial aspects of an amputee's life. For instance, female participants were significantly less interested in having children because of their amputation. However, this had no effect on men's interest. We plan to explore links between such psychosocial aspects and mobility challenges by triangulating questionnaire findings with those from planned follow-up interviews.

CONCLUSIONS

A UCD approach was taken to modify the PEQ and assess sex differences in LLA prosthetic needs. Female participants expressed poorer ambulation capabilities with their prosthetic compared with males. Sex-specific challenges with LLA mobility emphasize the need for further research addressing sex differences in physical and psychosocial aspects. Such differences have major implications for and can ultimately guide design of sex-specific prosthetics.

ACKNOWLEDGEMENTS

Graduate funding for TMRC was provided by NSERC Canada Graduate Scholarships – Doctoral (CGSD).

REFERENCES

[1] Imam B et al. *Can J Pub Heal* **108**: e374-e380, 2017.
[2] Sagawa Y et al. *Gait Posture* **33**: 511-526, 2011.
[3] Randolph B et al. *Mil Med* **181**: 66-68, 2016.
[4] Gherardini F et al. *Int J Adv Man Tech* **91**: 5-8, 2017.
[5] Legro M et al. *Arch Phy Med Reh* **79**: 931-938, 1998.

Table 1: Selection of questionnaire results for male and female participants showing 25th percentile, median, and 75th percentile values.

Source	Subscale/Question	Female (n = 9)			Male (n = 9)			*p-value*
		P25	Median	P75	P25	Median	P75	
PEQ	Ambulation Subscale – overall ambulation ability	4.9	6.0	7.9	6.0	7.6	8.6	$p = 0.171$
PEQ	Ambulation ability up steep hill using prosthetic	2.0	5.0	7.0	5.0	8.0	9.5	$p = 0.033$
PEQ	Ambulation ability down steep hill using prosthetic	1.5	3.0	6.5	4.5	5.0	8.0	$p = 0.045$
New	Effect of amputation on interest in having children	4.0	8.0	10	10	10	10	$p = 0.012$

KINEMATICS OF DOWNHILL SKIING WITH LOWER LIMB PROSTHESIS ON TWO SKIS

Filip Hrusa[1], Karel Jelen[1], Petr Kubovy[1] and Vaclav Bittner[2]

[1] Sport Sciences-Biomedical Department, Charles University / Faculty of Physical Education and Sport, Prague, Czech Republic.

[2] Department of Physical Education and Sports, Technical University of Liberec / Faculty of Science, Liberec, Czech Republic.

Email: filiphrusa@gmail.com

INTRODUCTION

The most common technique for amputee (amp.) skiers is three-track skiing, where the amp. skis on one ski with the help of so-called stabilizers, or crutches with small skis [1]. In this technique, the amputee skier loads the axial system by unilaterally overloading the healthy leg. Theory suggests that amp. skiers can extremely overload the healthy limb during a ski turn, resulting in the same overload as non-amp. skiers on both legs, which is 6g [2]. Based on the development of prosthetics, skiers with lower limb amputation have been given a new opportunity to ski on two skis with active involvement of the amputated limb through the prosthesis. Our aim is to compare the kinematics of movement during the skiing turn of skiers with and without amputation (WA), this is pilot research in laboratory conditions, which will be followed by field research on the ski slope.

METHODS

We analyzed the kinematics of lower limb movement using the Qualisys opto-electrical system (figure 1 left) on the SkyTech Interactiv ski trainer (figure 1 right). The toe and little toe of the foot (prosthesis), the ankle joint axis, the outer epicondyle of the knee joint, and the lateral side of mid-thigh were identified. The following parameters were monitored during the 6 left and right ski turns: thigh motion relative to the mat in the frontal and sagittal planes, tibia motion relative to the mat in the frontal and sagittal planes, and knee joint angle during the ski turns. Individual parameters were recorded at the apex of the turn and in the transition between turns. The following groups were observed: skier with transfemoral amputation (TFA), skier with transtibial amputation (TTA), and skier WA. Amputee skiers were equipped with a special ski prosthesis ProCarve, Otto Bock, Germany. The results were analyzed using statistical method: variance of movement with 95% probability, maximum range of motion, and mean angle of each parameter.

RESULTS AND DISCUSSION

While the prosthetic ski was internal results showed maximum values of 27° in the frontal plane of the thigh in a skier with a TFA, in the skier with TTA this parameter was 19°, and for the non-amputee skier at 17° for the nondominant leg. It indicates that the TFA skier relies more on the healthy leg during the turns. Another selected parameter was the average angle of the knee joint, which was 140° for the non-amputee skier at the non-dominant leg (inner ski), 147° for the skier with TTA, at the leg with prosthesis (inner) and 144° for the TFA leg with prosthesis (inner ski) indicating a very similar biomechanical movement to the non-amputee.

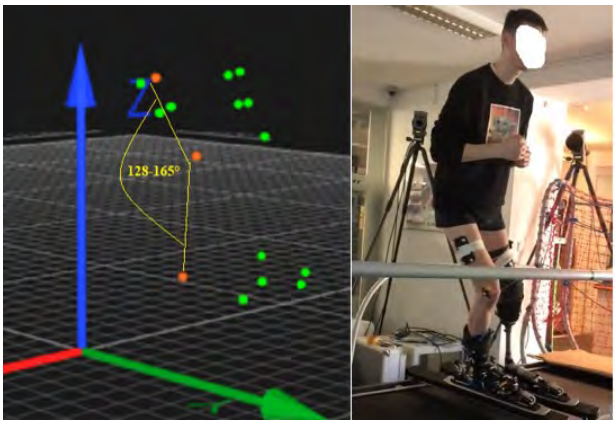

Figure 1 Qualisys software(left) and skier with TT amputation on SkyTech Interactiv ski trainer during messurement (right).

CONCLUSIONS

According to the results, the pneumatic-hydraulic prosthesis is suitable for downhill skiing even for skiers with transfemoral amputation. The adjustment of the prosthesis corresponds to the basic position of the skier WA. Future studies should consider targeting distribution of the load equally on both skies to avoid overloading of the healthy limb.

ACKNOWLEDGEMENTS

This project was supported by grant agency of the Charles University number: 430222.

REFERENCES

[1] Hrusa F *Downhill skiing technique with unilateral above-knee amputation on two skis.* 2017.

[2] Haugen P et al. *Science and skiing*, **4**, 419-429, 2009.

NON-LINEAR FINITE ELEMENT APPROACH FOR A PRIORI MODAL ANALYSIS OF PROSTHETIC FOOT

T M Balaramakrishnan[1], Alexander Joseph V. Paul[1], S. Natarajan[1], S. Sujatha[1*]
[1]TTK Center for Rehabilitation Research and Device Development (R2D2), Machine Design Section
Department of Mechanical Engineering, Indian Institute of Technology Madras, Chennai 600036, India
[*]Corresponding author: sujsree@iitm.ac.in

INTRODUCTION

A prosthetic foot is an artificial device designed to reproduce the functionality of the foot-ankle complex absent in a person post amputation. A passive foot does not use any motors or active mechanical components. Energy storage and return (ESAR) feet (a type of passive feet) store strain energy during mid-stance and terminal stance and return it during the pre-swing phase to assist in forward progression. The usage of this energy for push-off will be most effective when the natural frequency of the prosthetic foot corresponding to the bending of the foot in the sagittal plane matches the walking step frequency [1]. Hence, the objective is to develop a methodology for a-priori evaluation of the natural frequencies and mode shapes of an ESAR foot design.

METHODS

The modal analysis is done using a finite element model of the foot at the terminal stance. A mass (that represents the mass of the human body) attached to a pylon is added to the foot (see Figure 1).

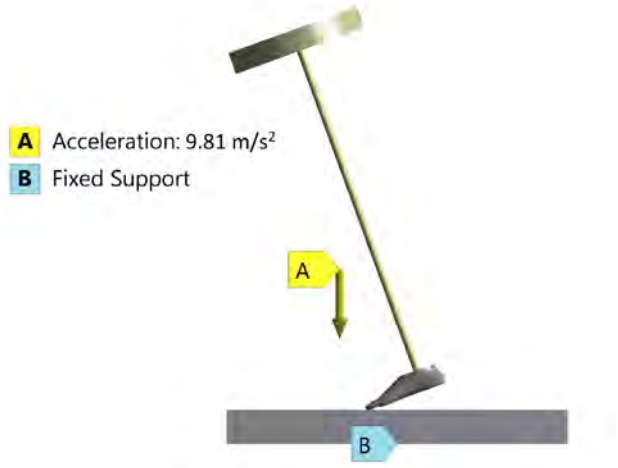

Figure 1: The complete model with the boundary conditions.

The computational model is discretized with tetrahedral elements. The neo-Hookean material model is assigned to the foot shell (to account for the non-linearity) and the contact between the foot and the ground is assumed to be frictional to replicate the conditions during walking on level ground. An acceleration field (that represents the acceleration due to gravity) creates the required ground reaction force that loads the foot. This load deforms the foot and generates a prestress in the foot. Modal analysis is then carried out on the prestressed foot to evaluate the natural frequencies and mode shapes of the system.

RESULTS AND DISCUSSION

The first mode of vibration is of concern in the case of an ESAR foot design. The mode shape for the first mode of vibration of a preliminary in-house design is shown in Figure 2.

Figure 2: The mode shape of the first mode of vibration of an ESAR foot design.

The first natural frequency of this design is evaluated to be 5.01 Hz.

CONCLUSIONS

Using analytical methods for modal analysis is very difficult with nonlinear material models and complex geometries. The finite element methodology developed by this group [2] is capable of handling these challenges. This novel approach of using finite element formulation for evaluating modal parameters of a foot from a computer-aided design model enables multiple iterations without the need for the fabrication of prototypes in the initial design phase.

ACKNOWLEDGEMENTS

The authors would like to thank Prof. C. Sujatha of the Department of Mechanical Engineering, Indian Institute of Technology Madras for her technical advice.

REFERENCES

[1] Noroozi Siamak et al, J Sports Engineering and Technology **227**: 39-48, 2012.
[2] T.M. Balaramakrishnan et al, Medical Engineering & Physics **92:** 64-70, 2021.

Unilateral above-knee amputees gait analysis with a statistical parametric mapping

Jin-Joo Yang[1,2], Ha-Eun Jo[1], Cheon-Seok Oh[1], Tae-Hee Kim[1] and Oen-Jei Woo[1]

[1] VHS Medical Center, Prostehtics & Orthotics Center, Seoul, Korea.
[2] Korea National Sport University, Seoul, Korea.
Email: dndjswp@gamil.com

INTRODUCTION

Gait is an evaluation tool and basic movement that identifies differences according to the type of disease, the characteristics of rehabilitation, or intervention with assistive device. Biomechanical studies often evaluate the mean, maximum, and minimum values of major events and sections, but data on continuous curves over time is very important in analyzing gait characteristics. In particular, utilizing time-continuous analysis such as statistical parametric mapping (SPM) has become common in human biomechanical studies and plays an important role in identifying undiscovered differences in walking cycles[1]. In particular, it is important to achieve bilateral ambulatory symmetry during walking despite morphological and musculoskeletal asymmetry due to limb loss for individuals with uneven thigh amputation. In the case of thigh amputation patients, it is important to understand the walking cycle pattern and affected and intact limbs balance through SPM.

METHODS

The subjects were approved by VHS' Bioethics Committee (IRB) for nine men (age: 62.5±9.0 height: 170.5±5.0cm, weight: 65.7±7.7 kg) who had no illusory pain at the femur terminal, and all participants participated with written consent. After warming up, the participants walked along the 12-meter sidewalk. A preference speed walking of each object person is performed, and three walking data out of a total of 10 walking data are collected and used for analysis. 44 markers were attached to the subject's body using eight Motion Analysis units operated by Cortex software for 3D motion analysis. To reduce marker noise, a secondary low pass Butterworth filter was filtered at a cutoff frequency of 6 Hz. One stride of lower limb joint angle and stance phase of vertical ground reaction force (VGRF) analyzed in Visual 3D and Cortex were normalized as a percentage. For statistical analysis, SPM was performed using MATLAB, and the significant level was set to α=0.05.

RESULTS AND DISCUSSION

There was no significant difference in the hip joint. Knee joint angle showed a significant difference in 6-18% corresponding to loading response and terminal stance and 87-92% corresponding to terminal swing, and the affected limb showed small movement. The ankle joint angle showed a significant difference in 68-75% corresponding to the initial swing, and the affected limb showed small movement. In the case of the VGRF, the difference was shown in 2-15% of the stance phase corresponding to loading response and terminal stance, and the affected limb showed small movements.

The results of this study show that the affected limb shows a small knee movement in the early stage, the VGRF is also small, and the ankle movement of the flexor forms a small VGRF. In addition, it can be seen that there is a difference in walking due to the small curvature of the knee joint during the swing phase.

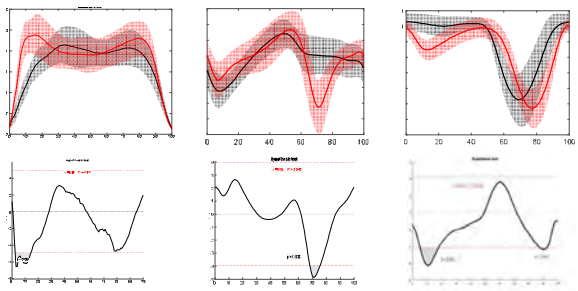

Figure 1 SPM in gait(from the left : VGRF, ankle, knee angle).

CONCLUSIONS

Gait evaluation of unilateral aboce-knee amputees through SPM is needed because differences not found in general gait evaluation can be confirmed. Since there are many type of knee device, in later study, it is necessary to examine differences according to various knee devices by studying multiple subjects.

ACKNOWLEDGEMENTS

This research was supported by a grant of the Korea Health Technology R&D Project through the Korea Health Industry Development Institute (KHIDI), funded by the Ministry of Health & Welfare, Republic of Korea (grant number : HJ22C0003)

REFERENCES

[1] Eric C., & Todd C. Pataky. J Biomech 119: 110329, 2021.
[2] Hisano G et al. J Biomech 15: 110201, 2021.

EFFECT OF SILANIZED ZrO2 ADDITION ON THE PHYSICAL PROPERTIES OF 3D PRINTING RESIN

Jinkyung Park[1], Hoon Kim[2] and Ho Beom Kwon[1]
[1]Dental Research Institute and Department of Prosthodontics, School of Dentistry, Seoul National University, Seoul, Republic of Korea.
[2] Technical Institute, Graphy,Inc., Seoul, Korea.
Email: congsim25@snu.ac.kr

INTRODUCTION

3D printed materials for removable prostheses showed lower flexural, bond, and impact strengths compared to heat-polymerized PMMA [1]. Therefore, some clinicians recommend 3D printed denture fabrication for interim or immediate dentures; however, there are no available 3D printed definitive dentures yet [2]. For this purpose, a filler such as silanized ZrO2 was added to the resin matrix in order to improve the physical properties of 3D printed dentures. The aim of this study was to evaluate the effect of adding ZrO2 filler in different concentrations on the physical properties of the 3D printing resin. The null hypothesis is that the addition of silanized ZrO2 to matrix resin will not increase the physical strength of the 3D printing resin.

METHODS

Double-cross-linked urethane dimethacylate resin (TC-80, Graphy Inc., Seoul, Republic of Korea) was used as a matrix component for 3D printed dentures and artificial teeth fabrication. And then, monomer and oligomer were added to ensure the low viscosity of the material. Moreover, photo-initiator composed of Bis(2,6dichlorobenzoyl)-(4-propylphenyl)-phosphine oxide (Iragacure 819, BASF, Germany) was also prepared. Silanized ZrO2 was added as a filler to composite resin in amounts of 0, 0.1, 0.2, 0.3, 0.5, 0.7, 1.0, and 1.5g, respectively, for 100g resin matrix samples. Specimens were designed with CAD software and 3D printed using the DLP method. For each specimen, flexural strength and tensile strength tests were conducted with UTM, and flexural and tensile modulus were also calculated. Flexural strength test specimens were prepared in accordance with ISO 10477, and three-point bending tests were conducted. Tensile strength test specimens were prepared in accordance with ASTM D638.

RESULTS AND DISCUSSION

The results of the material properties according to the respective concentrations of the silanized ZrO2 filler are presented in Table 1 and Figure 1. The 0.50% silanized ZrO2 added group had the highest flexural strength and modulus, with a value of 161.53 MPa. However, the 0.10% silanized ZrO2 added group showed a decrease in flexural strength and modulus compared to the control group (0%). The reason could be that the filler particles hindered the polymerization of the resin matrix when the silane ZrO2 filler concentration was increased from 0.00 to 0.20% [3]. Moreover, the tensile strength and modulus of the materials added with silanized ZrO2 peaked at a concentration of 0.50%; however, the trend of the flexural strength and modulus graph was not inconsistent. Although filler particles can strengthen the physical properties of the resin by deflecting cracks and absorbing stress [4], they can also hinder the resin matrix. It stands to reason that the tensile strength of the resin will decrease when the filler concentration exceeds 0.50%.

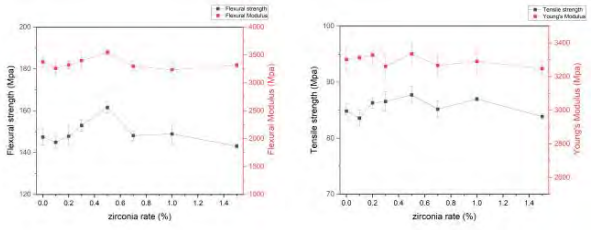

Figure 1. Flexural strength and flexural modulus (right) and tensile strength and Young's modulus (left) of composited resin with different concentration of silanized ZrO2.

CONCLUSIONS

This study evaluated the effect of adding silanized ZrO2 filler on the flexural and tensile strengths and modulus of the 3D printing resin. Flexural strength and tensile strength were the highest when 0.50% of filler concentration was added.

REFERENCES

[1] Dimitrova M et al. *J. Compos. Sci*. **6**: 87, 2022.
[2] Anadioti E et al. *BMC Oral Health* **20**: 343, 2020.
[3] Rodríguez, HA et al. *Mater. Sci. Eng. C* **101**: 274-282, 2019.
[4] Niu H et al. *Dent Mater* **38**:1801-1811, 2022.

Table 1: Flexural strength and tensile strength (MPa) depending on silanized ZrO2 filler concentration added to the resin matrix.

ZrO2/resin matrix (w/w%)	0.00%(control)	0.10%	0.20%	0.30%	0.50%	0.99%	1.48%	*p-value*
Flexural strength (MPa)	147.43	144.90	147.83	152.91	161.53	148.14	143.10	$p = 0.007$
Tensile strength (MPa)	84.83	83.58	86.31	86.55	87.71	85.18	86.99	$p = 0.00$

FUNCTIONAL EFFECTIVENESS OF CUSTOM ACL BRACING: A FINITE ELEMENT ANALYSIS

Alexandria Mallinos[1], Brian Davis[2], and Kerwyn Jones[3]
[1] Department of Chemical and Biomedical Engineering, Cleveland State University, Cleveland, Ohio, USA.
[2] Department of Mechanical Engineering, Cleveland State University, Cleveland, Ohio, USA.
[3] Department of Orthopaedic Surgery, Akron Children's Hospital, Akron, Ohio, USA.
Email: a.mallinos@vikes.csuohio.edu

INTRODUCTION

Functional Anterior Cruciate Ligament (ACL) orthoses are prescribed to patients with the goal of preventing anterior tibial translation (ATT) and valgus moments at the joint. The limited and inconsistent data available on knee orthoses (KO) biomechanics make it difficult to assess the effectiveness of functional ACL bracing. Advancements in finite element technology have opened the possibility for accurate and quantitative assessments of subject-specific knee orthoses.

The purpose of this study was to determine how effective custom ACL bracing is in preventing ATT. The contact pressures of custom ACL orthoses obtained by Ghadikolaee et al. [1] were replicated in the patient-specific finite element models. Our previously developed baseline knee models [2] were utilized to determine how effective this orthosis design is in preventing ATT when subject to Lachman and pivot shift tests.

METHODS

22 CT images of juvenile knees were utilized (ages: 9-18). FEBio was used to construct each tibiofemoral joint. Following data established by Ghadikolaee et al. [1], two sensor pads (C1 = 5.08 kPa; C2 = 6.75 kPa) were placed along the tibial crest (Figure 1). To replicate the Lachman test, anteriorly directed forces of 67 N, 89 N, and 133 N were applied to the tibia. To simulate the pivot shift test, an anteriorly directed force of 133 N was applied to the tibia in addition to a combined rotatory load of 4 Nm internal tibial torque and 10 Nm valgus [3]. A 95% confidence interval (CI) was used to determine statistical significance between the bracing and non-bracing groups for each loading condition.

Figure 1 FEBio model of juvenile knee with pad placement.

RESULTS AND DISCUSSION

As expected, the custom ACL orthosis simulation resulted in less ATT than the non-bracing models for both loading conditions (Table 1). The 95% CIs demonstrate that the custom ACL knee orthosis provides a significant ($p<0.05$) resistance to ATT compared to the non-bracing models.

The finite element simulations showed that custom KO designs statistically minimize ATT when subject to loading conditions that can harm the healing graft. The custom KO design resulted in approximately 1 mm less ATT than the non-bracing options. This highlights the importance of accurately fitting a KO to a patient. If the fit of the orthosis is not sufficient, it is likely that the device will not be effective in preventing ATT. This is especially significant if there is a gap of 1 mm between the orthosis and the tibia as this might result in minimal resistance to ATT.

Future studies will utilize this methodology to assess the biomechanical effectiveness of the different KO designs (four-point force system vs total contact; custom vs custom-fit/off-the-shelf) to determine which offers the greatest protection to an ACL-deficient knee.

CONCLUSIONS

Utilizing finite element technology makes it possible to assess knee orthosis biomechanics in manner that cannot be assessed in a clinical setting. Custom functional ACL knee orthosis provide a significant resistance to anterior tibial displacement.

ACKNOWLEDGEMENTS

This project is funded by Cleveland State University's Cellular and Molecular Medicine fellowship.

REFERENCES

[1] Ghadikolaee, M.S. *JPO* **32**: 142-148, 2020.
[2] Mallinos, A.D. *J. Biomech* **136:** 1-7, 2022.
[3] Wan, C. *Med. Biol. Eng. Comput.* **55**: 2097-2106, 2017.

Table 1: Descriptive statistics of FEBio simulations for the Lachman and pivot shift tests.

FEBio - Lachman Test (mm)					FEBio - Pivot Shift Test (mm)			
Mallinos et al. - Without Bracing			*Ghadikolaee et al. - Custom KO*		*Mallinos et al. - Without Bracing*		*Ghadikolaee et al. - Custom KO*	
	Mean	SD	Mean	SD	Mean	SD	Mean	SD
67 N	5.53	0.35	4.82	0.39	4.38	0.78	3.64	0.18
89 N	6.53	0.28	5.60	0.30				
133 N	7.54	0.34	6.58	0.42				

DYNAMIC FINITE ELEMENT ANALYSIS FOR THE METAMATERIAL PROSTHETIC LINER OPTIMIZATION

Vasja Plesec[1], Gregor Harih[1]
[1] Laboratory for Intelligent CAD Systems, Faculty of Mechanical Engineering, University of Maribor, Slovenia.
Email: vasja.plesec@um.si

INTRODUCTION

Lower limb prosthetic liners are mostly made of solid elastomers or foam-like polymers, providing limited customisation and often a costly solution. Previous authors have proposed 3D-printed metamaterials to address this problem and improve limb-prosthesis interaction [1]. Instead of a lengthy and costly trial-error approach of physically testing different designs to optimise liners, this study proposed an explicit finite element method to analyse and optimise metamaterial liners in a virtual environment. Various unit cells were numerically evaluated, and based on the results, specimens were 3D-printed and tested to validate the numerical model. The explicit finite element method allows effective simulation of complex time-domain problems by solving second-order differential equations directly. This enables a cost-efficient and rapid evaluation of complex structures and helps optimise metamaterial liners by reducing the contact pressure on the limb surface while maintaining the stability of the prosthesis.

METHODS

To prove the applicability of the newly developed metamaterial liner, a numerical analysis was performed using a recently developed generic transtibial model and the results were analysed in terms of contact pressure, stress-strain and deformation [2]. The metamaterial structures were evaluated both numerically using the explicit dynamic method and experimentally by a uniaxial compression test of 3D-printed flexible thermoplastic polyurethane samples. The stress-strain results from the uniaxial compression test were used to validate the numerical model results and to design a homogeneous material model of the metamaterial structure, which was used in the following simulation of the transtibial limb-prosthesis system. The generic transtibial model with definitive patellar tendon bearing prosthesis was used to simulate the newly designed liner for three loading scenarios, namely: donning of the socket, heel strike and push-off loading cases according to ISO 10328.

RESULTS AND DISCUSSION

The results regarding the contact pressure at the limb-liner interface as well as liner deformation, were analysed to assess the applicability of the newly developed metamaterial liner. The criterion for socket optimisation was to minimise contact pressure while maintaining the prescribed deformation of the liner. The relative comparison with the frequently used silicone liners shows that the customisable metamaterial liners can further reduce contact pressure while preserving adequate deformation, thus improving comfort, and maintaining stability.

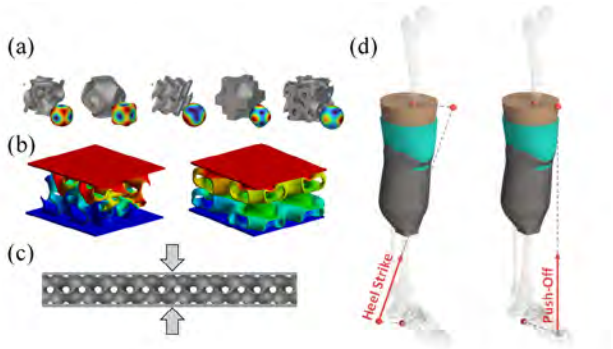

Figure 1 (a) Metamaterial unit cell evaluation, (b) explicit dynamic finite element simulation of the metamaterial samples, (c) uniaxial compression test, (d) generic transtibial limb-prosthesis model for liner evaluation.

CONCLUSIONS

In this study, a novel approach was adopted to investigate the 3D-printed metamaterial prosthetic liners in a virtual environment by using explicit dynamic finite element methods. The proposed low-cost and rapid numerical solution assists in developing optimised metamaterial liners that improve comfort by reducing contact pressure while providing adequate stability for the prosthesis wearer. Advanced 3D-printing technologies combined with nonlinear dynamic simulation could deliver an improved customisable socket-liner system faster and at lower cost.

ACKNOWLEDGEMENTS

The authors acknowledge the financial support from the Slovenian Research Agency (research core funding No. P2-0063).

REFERENCES

[1] Brown N et al. *J Biomech Eng* **143(5)**: 051001, 2021.
[2] Plesec V et al. *WCB 2022 Taipei,* 2022.

AN AFFORDABLE SOFT ROBOTICS PROSTHETIC HAND WITH RIGID STRUCTURES

Vani Virdyawan[1], Akmal Reza Ahkam[2], F Ferryanto[3], Andi Isra Mahyuddin[3] and Sandro Mihradi*[3]
[1] Mechanical Production Engineering Research Group
[2]Graduate Student, Mechanical Engineering Study Program
[3] Mechanical Design Research Group
Faculty of Mechanical and Aerospace Engineering, Institut Teknologi Bandung, Bandung, West Java, Indonesia
Email: sandro@itb.ac.id

INTRODUCTION

There are more than 3 million upper extremity amputees in the world, of which 80% live in Low-Middle Income Countries (LMIC) [1]. In LMIC, where most of the jobs are mainly labour intensive, the upper extremities amputees face socio-economic problems. Even though there are several commercially available prosthetic hands, they usually cost more than 20,000 USD and are designed based on rigid links. This high price makes them unaffordable for most amputees living in LMIC [2]. Various research have been conducted to develop affordable prosthetic hands based on soft robots made from compliant materials that could be actuated using pressurised fluid. This reduces the need for a complex mechanical system and makes the prosthetic cheaper and also lighter. This paper discussed a new type of soft robot that is designed with stiffening structures to mimic the kinematics of human fingers. The grasping ability of this soft prosthetic design is then discussed and compared with the human hand and a prosthetic hand with rigid links.

METHODS

The soft fingers were manufactured using EcoFlex™ 00-30 (Smooth-On, Inc. USA). Two strain-limiting layers were employed to achieve optimum bending motion: 1) helical winding to limit radial expansion and 2) a cloth to limit the axial expansion on one side of the chamber. Simulations were performed to determine the rigid structures' parameters to optimise the soft finger's kinematics. The fingers were then attached to a 3D-printed palm covered with silicon to improve friction during the grasping (Figure 1a). All fingers were controlled using a single 3/2-way pneumatic valve to reduce the number of components. The fingers were then tested to grip several objects, i.e. a cube, a bottle, a mug, a tennis ball, and a table tennis ball. The pressure on each finger was measured using Force Sensitive Resistors (FRS).

RESULTS AND DISCUSSION

To achieve a 240° bending, the pressure of the finger is 0.5 bar (Figure 1b). The bending shape mimics the kinematic of the human finger. It requires only an on-off control to grasp the objects due to the compliant nature of the fingers. The soft prosthetic hand can grasp all four objects. Compared to the rigid prosthetic hand, all fingers on the soft prosthetic hand have a similar pressure (Figure 1c). It means that the tip of the soft hand can still touch and provides enough pressure. Finally, the weight of the prototype is 270 g, and the manufacturing cost for the whole system is below 500 USD, which is suitable for LMIC

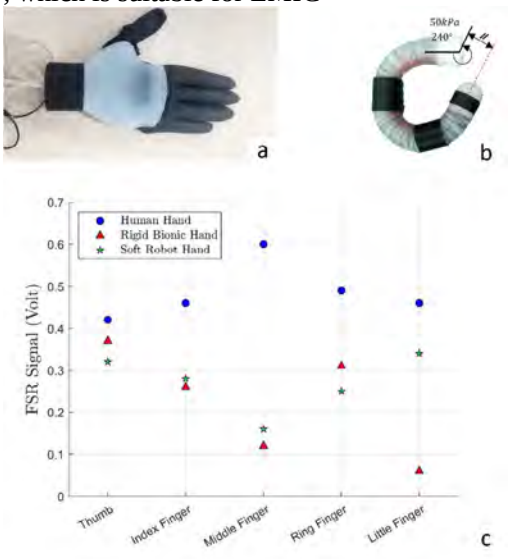

Figure 1 a) The prototype of the soft robot hand; b); the bending of the soft robotic finger; c) the pressure measurements of the fingertips while grasping a tennis ball.

CONCLUSIONS

This paper discusses the design and performance of an affordable soft robot prosthetic hand with rigid structures. The rigid structures generate a similar kinematic of the finger to that of human fingers. Grasping experiments show that the soft robot prosthetic hand could properly grasp objects with various shapes. The compliant nature of the robot also shows that there are more surface contacts between the fingers of the soft robot compared to its rigid counterpart.

ACKNOWLEDGEMENTS

This work was supported by a NFIL, ID 623531377 and Kemdikbudristek, Republic of Indonesia, contract no: 083/E5/PG.02.00.PT/2022.

REFERENCES

[1] Phillips B, et.al., *Proc. GHTC 2015*, pp. 52–58, 2015.
[2] Basumatary H, et.al., *IEEE Trans. Human-Machine Syst.* 50, no. 2, pp. 116–130, 2020

ACCURACY OF INERTIAL MEASUREMENT UNITS (IMUS) TO MEASURE ANKLE RANGE OF MOTION: APPLICATION IN TRANSTIBIAL PROSTHESIS USER

Jutima Rattanakoch[1], Manunchaya Samala[1,*], Weerawat Limroongreungrat[2], Gary Guerra[3], Kittichai Tharawadeepimuk[2], Ampika Nanbancha[2], Wisavaporn Niamsang[1], Pichitpol Kerdsomnuek[4] and Sarit Suwanmana[2]

1 Sirindhorn School of Prosthetics and Orthotics, Faculty of Medicine Siriraj Hospital, Mahidol University, Thailand; jutima.rat@mahidol.edu; manunchaya.saa@mahidol.edu; wisavaporn.nia@mahidol.edu
2 College of Sports Science and Technology, Mahidol University, Thailand; weerawat.lim@mahidol.edu; kittichai.tha@mahidol.edu; ampika.nan@mahidol.edu; sarit.suwanmana@gmail.com
3 Exercise and Sport Science Department, St. Mary's University, San Antonio, Texas, USA; gguerra5@stmarytx.edu
4 Department of Orthopaedic Surgery, Faculty of Medicine Siriraj Hospital, Mahidol University, Bangkok, Thailand; pkerdsomnuek@gmail.com
* Correspondence: manunchaya.saa@mahidol.edu

This abstract is one part of paper which published open access: https://doi.org/10.3390/s23031738

INTRODUCTION

IMUs are an option for motion analysis due to their low cost and ability to evaluate the kinematics of free-living environments. [1]. Suggestions from previous research [2] show that validation studies for groups of prosthesis wearers must look at the optical (motion capture (OMC) for gold-standard comparisons with IMUs. So, this study aimed to assess the IMU accuracy of IMU measures of the walking ankle joint angle of transtibial amputees (TTA) compared to OMC.

METHODS

The Siriraj Ethical Review Board approved the study. Thirty TTA's were recruited and underwent simultaneous motion capture from two systems. The key kinematic parameters were compared. To compare the IMU and OMC protocols, a paired t-test with a significance level of = 0.05 was used, followed by Bonferroni-corrected t-tests (= 0.005).

RESULTS AND DISCUSSION

Table 1 shows typical gait parameters and their SD over 30 TTAs. The highest standard deviation values were observed for Ankle ROM Ab/Adduction calculated by the IMU (17.1°). Statistic significant differences in joint parameters caused by a change in the protocol were evident in the out-of-sagittal plane ($p < 0.05$) on the amputated side.

Table1: Ankle ROM by the IMU and OMC

Parameters	IMU (SD)	D3 (SD)	Value-p	P< 0.05	P<0.001
Sound Ankle ROM					
Plantar/dorsiflexion	(7.8)28.1	(6.0)29.9	0.6587		
Ab/Adduction	(17.1)11.0	(2.7)8.7	0.0628		
Inv/Eversion	(6.4)16.0	(5.1)14.0	0.0477	*	
Amputated Ankle ROM					
Plantar/dorsiflexion	(14.0)17.0	(6.7)11.7	0.1931		
Ab/Adduction	(16.8)10.9	(2.3)2.5	0.0295	*	
Inv/Eversion	(6.5)16.0	(2.2)1.7	0.0000	*	**

CONCLUSIONS

All comparisons of ankle ROM between the IMU and OMC systems support the idea that the IMU and OMC give similar kinematic results. The IMU can provide accurate motion data in the sagittal plane for a transtibial prosthetic gait study, showing that it is valid. Nonetheless, this study's results revealed that, compared to the typical OMC system, the IMU may produce accurate results and is a feasible device for evaluating the gait of amputees.

ACKNOWLEDGEMENTS

This project is supported by Mahidol University.

REFERENCES

[1] Marion M et al. *J Biomechanics,* 84: 81 -86, 2019.
[2] Samala M et al.Sensors 20(5):1-10, 2022

Biomechanical Analysis based on the Skull Model to derive the Optimal Screw Configuration of the 3D Printing Patient-Specific Reconstruction Plate used for Maxillofacial Bone Defects

Dong-Young Je[1], Won-Hyeon Kim[1], Ho-Joon Shin[1], Jisung Kim[1], Youjeong Son[1], Seoyoung Won[1], Sung-Ho Lee[1], Jungwon Lee[2], Young-Jun Lim[2] and Bongju Kim[1]

[1] Dental Life Science Research Institute, Seoul National University Dental Hospital, Seoul, Korea
[2] Department of Prosthodontics, Seoul National University Dental Hospital, Seoul, Korea
Email: bjkim016@gmail.com

INTRODUCTION

Bone defects of mandible caused by factors such as tumors and traumatic injuries was primarily treated with reconstruction plates[1-3]. Conventionally, the widely used mini and reconstruction plates have weak strength and aesthetic issues [2-3]. Although, patient-specific reconstruction plates with Three-dimensional (3D) printing technology have been used in recent years, previous studies analyzing biomechanical properties in reconstructive design were inadequate. Therefore, in this study, we compared various designs and tried to derive the optimal plate.

METHODS

The 3D bone models were constructed using the mimics innovation program based on the cone beam computed tomography (CBCT) images of a Korean male. In order to distinguish between the cortical and cancellous bones, the cortical bone was set a constant thickness of 2 mm. The surgical models of mandibular bone defect were assumed a frequently occurring class 2 fracture type, and the number of screws of the anterior and posterior plates was set to 6 each. In order to derive the optimum screw configuration, a total of 72 models were constructed considering the anterior 8 and the posterior 9 (Fig 1). Three load conditions of the incisor, canine, molar teeth were applied to analysis the stress distribution of the plate and screw.

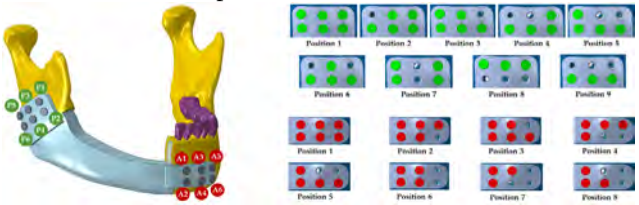

Figure 1 Surgical model and anterior-posterior screw configuration.

RESULTS AND DISCUSSION

It was confirmed that the stress distributions of the plate and screw showed similar tendencies in all models (Fig 2). In the incisor loading, the stress distribution of the plate and screw showed the highest value in the anterior 6 and 7 positions and the posterior 2 and 7 positions (Fig 2). On the other hand, the anterior 5 and 8 positions and the posterior 7 position showed the lowest values (Fig 2). In the canine loading, the stress distribution of the plate and screw showed the highest value in the posterior 8 position (Fig 2). However, the Peak von Mises stress (PVMS) was no difference in the anterior screw configurations (Fig 2). On the other hand, the posterior 2, 4 and 7 positions showed the lowest values (Fig 2). In the molar loading, the stress distribution of the plate and screw showed the highest value in the posterior 8 position (Fig 2). While, the anterior 8 position was showed the lowest value. In the posterior region, the 4 position of screw and the 3 position of plate were showed the lowest value (Fig 2). The 8 position of the posterior plate was high at all three loads, so it is predicted that there is a high failure risk after surgery. On the other hand, the screw configuration of the posterior plate showed lower stress in 4 and 7 positions compared to other screw configurations, and in the 8 position of the anterior plate showed lower stress than the other screw configurations. Therefore, it is expected that the reconstruction plate should be designed in consideration of the anterior 8 position and the posterior 4 and 7 positions for the initial stability after surgery.

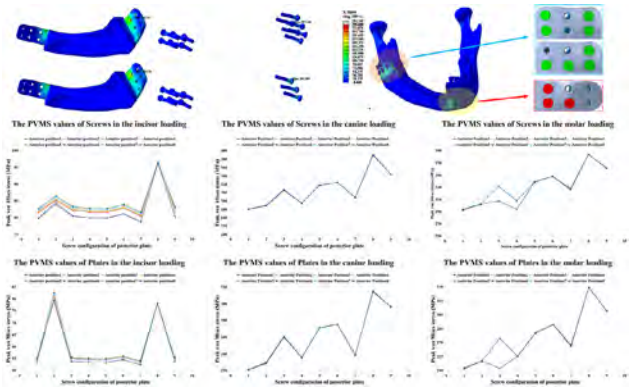

Figure 2. The PVMS results for 3 loads and screw configurations.

CONCLUSIONS

Based on our study, the posterior screw configuration was considered as a factor that significantly influences the stress distribution. As for the posterior screw configuration. The posterior 4 and 7 positions and the anterior 8 position are considered to have a high initial stability because the stress distribution was lower than those of the other configurations. Therefore, in the future manufacturing of patient-customized reconstructive plates, it is proposed to consider the anterior 7 position and the posterior 4 and 7 positions.

ACKNOWLEDGEMENTS

This work was supported by the research project of the Seoul National University Dental Hospital.

REFERENCES

[1] Erdmann D et al. *Der Chirurg* **75**: 799-809, 2004.
[2] Wallace CG et al. *Plast Reconstr Surg* **125**: 305-14, 2010.
[3] Kumar BP et al. *J Maxillofac Oral Surg* **15**: 425-41, 2015

DEVELOPMENT OF A FINITE ELEMENT MODEL FOR SIMULATIONS OF COLD FLOW AND NECK-LINER IMPINGEMENT IN HIP PROSTHESIS

Lu Shen[1], Changhee Cho[2]
[1] Graduate School of Environmental Engineering, The University of Kitakyushu, Kitakyushu, Japan.
[2] Faculty of Environmental Engineering, The University of Kitakyushu, Kitakyushu, Japan.
Email: d2mba015@eng.kitakyu-u.ac.jp

INTRODUCTION

Wear and failure of the ultra-high-molecular-weight polyethylene (UHMWPE) component after total joint replacement cause serious clinical and biomechanical reactions [1], thus restricting the longevity of artificial joints. In retrieved UHMWPE acetabular cup liners of hip prostheses, catastrophic wear and failure are frequently observed as shown in Figure 1 [2]. It appears that cold flow and neck-liner impingement in hip prosthesis contribute to significant increases in wear and failure of the UHMWPE acetabular cup liner.

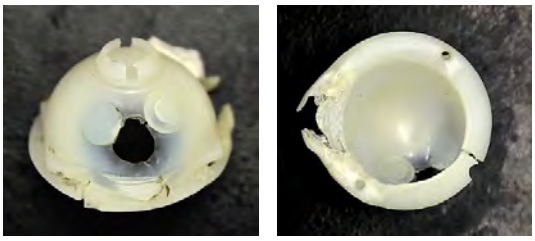

Figure 1 Retrieved UHMWPE acetabular cup liner of hip prosthesis showing catastrophic wear and failure (290 months in vivo).

METHODS

The main purpose of this study is to investigate the influences of cold flow and neck-liner impingement in hip prosthesis on the wear and failure of the UHMWPE acetabular cup liner. Development of a finite element model for simulations of cold flow and neck-liner impingement in hip prosthesis, and finite element simulations of these phenomena were performed.

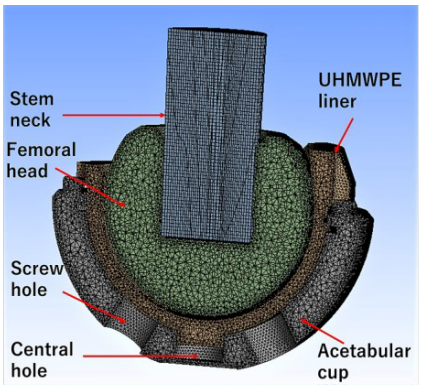

Figure 2 Finite element model of hip prosthesis for simulations of cold flow and neck-liner impingement.

Finite element model of the hip prosthesis developed in this study is shown in Figure 2. Metallic components were modelled as rigid bodies. UHMWPE acetabular cup liner was modelled as an elasto-plastic body. 3D solid modelling was performed by using the SolidWorks. The finite element simulation was performed by using the Ansys Workbench.

RESULTS AND DISCUSSION

An example of the finite element simulation results is shown in Figure 3. In the simulation of cold flow, it was found that stress concentrations near the edge of screw holes have significant influence on the states of contact stresses and plastic deformations in the surface and backside of the UHMWPE acetabular cup liner. In the simulation of neck-liner impingement, it was found that high contact stresses which exceed the yield stress of UHMWPE and considerable plastic deformations occurred in the rim of the liner.

The results of this analytical study suggest that change in mechanical states due to the occurrence of cold flow and neck-liner impingement in hip prosthesis is the cause of catastrophic wear and failure of the UHMWPE acetabular cup liner.

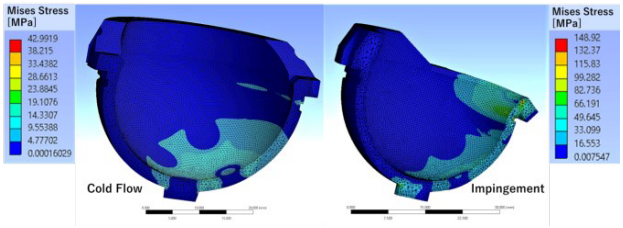

Figure 3 Contour plot of contact stress (von Mises stress) of the UHMWPE acetabular cup liner shown in Figure 2.

CONCLUSIONS

It is necessary to improve resistance to the occurrence of cold flow and neck-liner impingement in order to decrease the wear and failure of the UHMWPE acetabular cup liner and to increase the longevity of hip prosthesis.

ACKNOWLEDGEMENTS

This work was supported by JSPS KAKENHI Grant Number JP21K12689. The authors would like to thank the Dept. of Orthop Surg, UOEH for providing the retrieved artificial hip joints.

REFERENCES

[1] Ingham E et al. *Proc Instn Mech Engrs* **214** (Part H): 21-37, 2000.
[2] Cho C et al. *CMBBE 2019 Conference Proceedings*: 539-549, 2020.

Reliability Analysis of Two Stability Measurement Methods depending on Dental Implant Length and Bone Density

Jungwon Lee[1], Won-Hyeon Kim[2], Myeongkwan Kang[2], Youjeong Son[2], Jisung Kim[2], Sung-Ho Lee[2], Seoyoung Won[1], Ho-Joon Shin[2], Bong-Ju Kim[2] and Young-Jun Lim[1]

[1] Department of Prosthodontics, Graduate School of Dentistry, Seoul National University, Seoul, Korea
[2] Dental Life Science Research Institute, Seoul National University Dental Hospital, Seoul, Korea
Email: leejungwon95@naver.com

INTRODUCTION

Implant stability is an important factor in implant success, including promotion of bone formation and load sharing[1-2]. In order to measure the implant stability, two measurements have been used, such as the resonance frequency analysis and percussion method[3]. However, the initial stability was affected by various factors such as measurement method, equipment, and angle etc. Therefore, in this study, we aimed to analyze the reliability of the two measurement methods and analyze the correlation according to factors such as bone densities and implant lengths.

METHODS

Two composite bones with low density(15 pcf) and high density(30 pcf) were used to compare the measurement reliability by normal and osteoporotic bones. The ten implants each having a length of 7.3 mm, 10 mm and 13 mm were inserted in the two different bones, for a total of 60 implants. Using Osstell Beacon (resonance frequency method) and Anycheck (percussion method), the measurements were repeated five times per implant by three observers. In order to compare the differences between Osstell Beacon and Anycheck, we analyzed the intra- and inter-observer reliability. In addition, the effects of changes in bone density and implant length on stability were analyzed. The intra- and inter- observer reliability was analysed using Cronbach's alpha. Correlation analysis was performed using Pearson's correlation coefficient.

RESULTS AND DISCUSSION

In the intra- and inter-observer reliability, the results were identified that Cronbach's alpha coefficients were all 0.8 over, confirming that the measurements of observers showed high reliability (Table 1). In order to compare the stability according to the change of the implant length, the ISQ(Osstell Beacon) and the IST(Anycheck) values were measured. In the low density, it was confirmed that increasing the length of the implants showed higher stability(Fig 1). On the other hand, the stability values of the high density tended to be similar with changes in implant length(Fig 1). The ISQ and IST values with changes in bone density showed a trend of increasing stability for the two measurement methods with increasing bone density for all implant length types(Fig 2). In the low bone density, the stability was confirmed to be higher with longer implant length(Fig 1). Furthermore, the stability was confirmed to be higher with higher bone density regardless of change in the length of the implants(Fig 2).

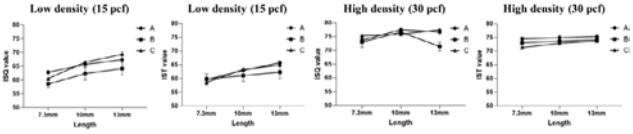

Figure 1. The ISQ and IST values depending on the implant lengths.

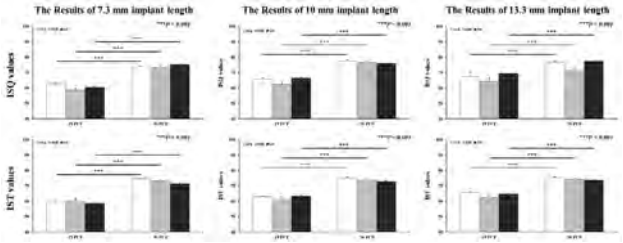

Figure 2. The ISQ and IST values depending on bone quality in the three implant lengths.

CONCLUSIONS

Based on our results, both Osstell Beacon and Anycheck showed the similar trend according to the change in implant lengths and bone densities. Therefore, it considered that the stability measurements between the Osstell Beacon and Anycheck show comparable levels of reliability with respect to various factors (bone density and implant length). Additionally, the results of our study is expected that the stability measure does not affect the change of implant length at high bone densities, whereas it may affect the stability measure at low bone densities.

ACKNOWLEDGEMENTS

This work was supported by the research project of the Seoul National University Dental Hospital.

REFERENCES

[1] Ivanova V et al. *Int J Environ Res Public Health* **18**: 6994, 2021.
[2] Farzad P et al. *Clin Implant Dent Relat Res* **6**: 24-32, 2004
[3] Bilhan H et al. *J Oral Implantol* **41**: e90-e95, 2015

Table 1: The Reliability results of the intra- and inter-observer for two different method (Osstell Beacon and Anycheck).

	Intraobserver Reliability			Interobserver Reliability
	Observer A	Observer B	Observer C	
ISQ values (Osstell Beacon)	0.996	0.996	0.998	0.971
IST values (Anycheck)	0.998	0.998	0.998	0.984

Influence of Prosthetic ankle-angle and walking speed on Pylon moments in the Two Axis aDaptable Ankle

Kieran Nichols, Rebecca Roembke, Sofya Akhetova and Peter Adamczyk
Mechanical Engineering Department, University of Wisconsin Madison, Madison, WI, U.S.A.
Email: knichols@wisc.edu

INTRODUCTION

Persons with lower-limb amputations can replace their lost limbs using passive, active, or semi-active prostheses. Semi-active prostheses attempt to recover more of the biological ankle mechanics and can give functional benefits of prosthetic adaptability, low cost, and low weight compared to passive and active devices [1]. The Two Axis aDaptable Ankle (TADA) [1] is a novel semi-active prosthetic ankle that allows for independent modulation of sagittal and frontal ankle angle (±10 degrees).

Boone et al. (2013) found that sagittal and frontal misalignment of transtibial prostheses at the pylon joint significantly affects pylon (socket) moments around 75% of stance, compared to nominal alignment (clinically-based) [2]. The TADA allows more biomimetic ankle angle control that can give users influence over their joint mechanics.

This study aims to investigate the influence of various TADA angles and walking speeds on prosthetic pylon moments while users walk over flat ground. The main hypothesis is that the peak averages of sagittal and frontal pylon moments will be higher at non-neutral TADA angles and larger walking speeds.

METHODS

Ten participants with no amputations will be chosen for this study, approved by the UW-Madison IRB. This abstract presents preliminary data for one participant (n=1). The participant walked on flat ground at three consistent self-selected speeds (slow, medium, fast) while wearing a full-body set of Xsens motion sensors. The TADA was mounted laterally to the participant's right foot using a custom-made ankle bypass orthosis.

The participant walked with various TADA stance angles including neutral (90° ankle dorsiflexion and no eversion), Plantarflexion (PF), Dorsiflexion (DF), Eversion (EV), and Inversion (IV). Three successful strides were collected for each TADA angle and speed totaling 45 strides. The peak pylon moments (sagittal and frontal) of the successful trials were averaged for each speed.

The TADA controller uses the Robotic Operating System (ROS) programs (C++/Python), involving dual motor control with hall sensor feedback, load cell between the TADA and pylon, shank IMU motion reconstruction, data collection, and a user interface. In addition, the Xsens suit will give a secondary source of validation for the kinematic data of the ankle/foot, lower and upper legs, and center of mass.

Table 1: a partial set showing the typical anatomical ankle angles, polar coordinates, and their respective average peak sagittal and frontal pylon moments for the medium speed.

TADA Ankle angles	Polar coordinates (PF, EV)	Average Peak Sagittal Pylon moments (Nm)	Average Peak Frontal Pylon moments (Nm)
Plantarflexion	(10, 0)	1374	543.7
Dorsiflexion	(-10, 0)	1400	355.3
Neutral	(0, 0)	1235	433.3
Eversion	(0, 10)	1315	289.0
Inversion	(0, -10)	1206	496.0

RESULTS AND DISCUSSION

These results show the average peak sagittal pylon moments decrease with increasing walking speed and that the frontal pylon moments than sagittal pylon moments are more sensitive to changes in TADA angles. The hypotheses were not supported, but the results can be used to create a moment-targeting controller to accommodate for walking speed and attempt to lower peak pylon moments by adjusting the TADA angles. For example, at a medium speed, moving a neutral foot (peak of 433Nm) to a more dorsiflexed angle would lower the peak frontal moment (peak of 355Nm).

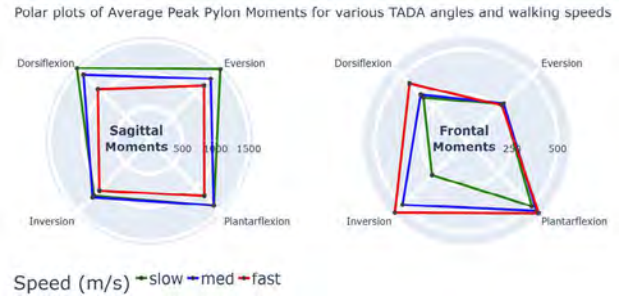

Figure 1 Polar graphs showing average peak sagittal and frontal pylon moments for various TADA angles and walking speeds. The background grid represents the TADA angles, and the line colors represent the peak pylon moment for a given walking speed.

CONCLUSIONS

The TADA could enable modulation of lower-body mechanical outcomes by controlling the 2D TADA angles due to its systematic relationship with ankle angle, walking speed, and pylon moment. Automated, real-time moment-targeting control could allow users to adapt to terrain conditions such as stairs and ramps, or to alter biomechanical loads such as undesirable knee moments.

REFERENCES

[1] Adamczyk P. *Powered Prostheses*: 201-259, 2020.
[2] Boone D et al. *Gait & Posture* **37**: 626-30, (2013).

PATIENT-SPECIFIC OPTIMISATION OF CUSHIONING STIFFNESS IN DIABETIC FOOTWEAR

Panagiotis Chatzistergos[1], Alfred Gatt[2,1], Cynthia Formosa[2,1], Jonathan Sinclair[3,1] and Nachiappan Chockalingam[1,2,3]

[1] Centre for Biomechanics and Rehabilitation Technologies, Staffordshire University, Stoke-on-Trent, UK
[2] Faculty of Health Sciences, University of Malta, Msida, Malta
[3]Faculty of Allied Health and Wellbeing, University of Central Lancashire, Preston, UK
Email: Panagiotis.chatzistergos@staffs.ac.uk

INTRODUCTION

The use of appropriate cushioning materials in diabetic footwear or orthoses is very important for their capacity to offload the foot-at-risk [1] and therefore for their ability to protect against diabetic foot ulceration (DFU). Previous research has shown that optimum cushioning is strongly affected by the magnitude of plantar loading [2,3]. Indeed, people who load their feet more heavily appear to need stiffer cushioning materials for optimum offloading. As a first step towards clinically applicable optimisation of cushioning in diabetic footwear/ orthoses, this study explores whether optimum cushioning stiffness can be predicted using simple demographic and anthropometric parameters that are linked, in the literature, to the magnitude of plantar loading.

METHODS

Sixty-nine adults with diabetes at risk of developing a DFU were recruited from the population attending diabetic foot clinics at the main general hospital of Malta (age= 67y ± 11y, BMI= 26.8kg/m^2 ± 5.7kg/m^2). Shod plantar pressure (PP) and pressure time integral (PTI) were measured during walking (Pedar®, Novel®) without any additional cushioning material (baseline), and after adding flat 10mm thick footbeds. Seven bespoke cushioning materials [3] were used with stiffness ranging from very soft to very stiff (Figure 1). The materials that minimised PP (PP optimum) or PTI (PTI optimum) across the surface of the foot were identified for each participant. Multinomial regression was used to test whether optimum cushioning stiffness could be predicted based on demographic/ anthropometric parameters known to affect plantar loading (i.e. gender, age, weight, height, shoe size).

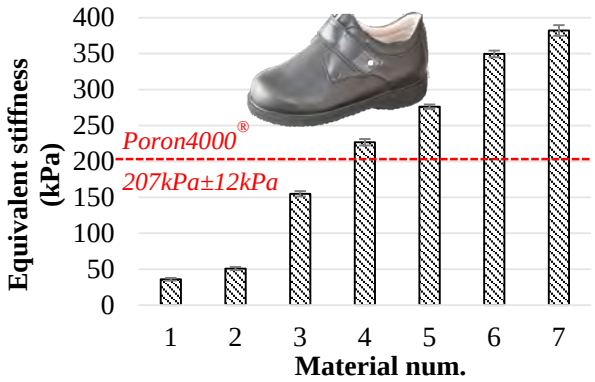

Figure 1: The diabetic shoe and the range of stiffness of the bespoke footbeds[3] (materials 1 to 7) that were used in this study. The stiffness of a cushioning material commonly used in diabetic footwear/ orthoses (Poron4000®) is also shown as reference.

RESULTS AND DISCUSSION

Comparing the materials that minimised PP against those that minimised PTI (Figure 2) showed that PTI optimum materials were significantly softer than PP optimum (Wilcoxon signed rank test,2-tailed, p<0.001).

Using simple demographic/anthropometric parameters as predictors enabled the correct prediction of optimum stiffness level in 70% of participants. The predicting capacity of this regression model was statistically significantly better than an intercept-only model (X^2(df)= 27.646(10), Sig.=0.002). In this case an intercept-only model can be interpreted as providing everyone with the same cushioning stiffness.

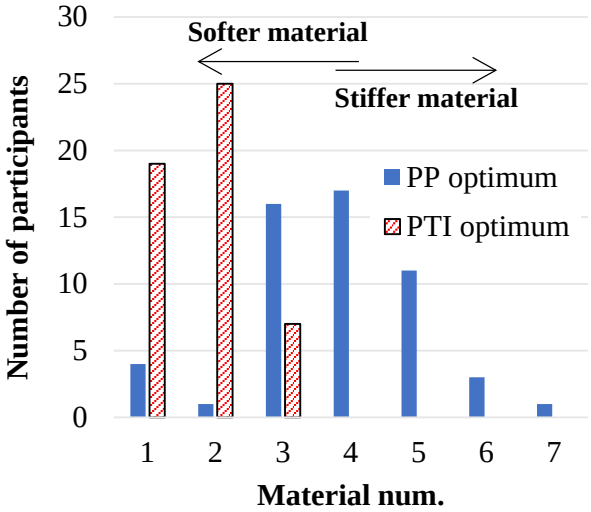

Figure 2: The frequency with which each bespoke footbed material achieved maximum PP reduction and maximum PTI reduction.

CONCLUSIONS

Patient-specific PP optimum cushioning stiffness can be predicted using five simple demographic/ anthropometric parameters. These results open the way for integrating patient-specific optimisation of cushioning stiffness into everyday clinical practice for the design of effective diabetic footwear/ orthoses.

ACKNOWLEDGEMENTS

We would like to thank Kyle Cassar for his role in recruitment, data collection and data extraction.

REFERENCES

[1] Chatzistergos et al. Gait Posture 79: 244–50, 2020.
[2] Chatzistergos et al. Med Eng Phys 37:531–8, 2015.
[3] Chatzistergos et al. Ann Biomed Eng 45:1929–40, 2017.

A Simple Method to Overcome Weakness in FDM 3D Printed Parts for Stronger Prosthetic Sockets

Mukul Talaty[1,2], Jacob Hillegass[1], Robert Chiccarine[1], Juan Arias Sanz [3], Renaijah Purvis[1] and Marcus Besser[1]
[1] Penn State University, Abington PA, USA,
[2] Gait & Motion Analysis Laboratory, MossRehab, Elkins Park, PA, USA,
[3] Brick Labware, Dallas, TX, USA.
Email: mxt103@psu.edu

INTRODUCTION

Digitally designed and 3D printed prosthetic sockets show much promise including advantages such as being inexpensive, light, and strong, while also being cleaner, faster, more repeatable and requiring potentially less skill of the fabricator. Socket mechanical properties must consistently meet or exceed those of conventionally fabricated sockets to realize these advantages. Preliminary work has shown high variability in socket strength including some that are not sufficiently strong to be used clinically (Gershutz, 2012; Pousset 2019). Ongoing testing by our group has shown material choice and print parameters to have a large effect on socket strength. Failure almost always consisted of cracks running predominantly along layers of the print in and near the shuttle region of the socket. Due to the multidirectional loading of a socket during actual use, this directional weakness, characteristic of a 3DP part, cannot be overcome by judicious print orientation. Methods like 3D fill compositing have recently been introduced (Nickel 2020) and are proprietary approaches that require additional materials, adhesive(s) and possibly specialized equipment to produce the composite structure (US Patent Application No.: US 2018 / 0243111 A1). We evaluated a simpler method to overcome the inherent weakness in FDM 3D printed objects that required no special equipment.

METHODS

Special samples were 3D printed for tensile strength testing (Figure 1). The *test* sample was printed with a central channel in which the insert was installed. A small 3D printed rod (6mm square cross-sectional) was manually inserted into a square hole in the test sample. When assembled, the print directions of the main part and that of the insert were orthogonal. There was interference between insert and channel into which it was designed to fit (i.e. pressure held the insert in place). Three methods were used to install the insert: 1) Press - the insert was pressed into the test specimen with a moderate manual effort (estimated 10-25lbs of downward force), 2) the insert was hammered into the specimen, and 3) combination of press and hammer. Test and reference samples were identical in all other ways (geometries, print specifications [material, infill, layer height) etc.). We explored whether insert tolerance (i.e. overlap in dimensions of insert and channel), insertion method, and insert density (15%, 30%, 50%, 75% and 100%) affected insert-strengthened parts.

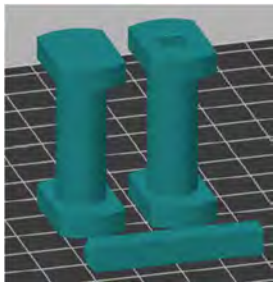

Figure 1 Tensile test samples. Reference sample (left), test sample (right) with a vertical channel in which the reinforcing insert was placed, and the rod (front) inserted into the channel; all parts were printed in the orientation shown.

RESULTS AND DISCUSSION

Composite parts utilizing orthogonal print orientations (i.e. the reinforcing insert) significantly increased part strength (Table 1). In tension, non-reinforced samples failed catastrophically at 84 pounds, on average. The reinforced samples failed at 229 pounds, on average. On preliminary analysis, insert interference had a modest effect whereas insert infill and insertion method did not have an effect. Bending tests were also run but those data have not yet been formally analyzed. Initially, it seems that reinforced parts also appear to be stronger in bending and did not fail catastrophically as did reference specimen. We developed a preliminary means to implement the insert into a socket and have prototyped that design but have not yet tested them. We also explored variable infill and layer height to strengthen without increasing weight and possibly to shorten fabrication times. Testing and data analysis is ongoing.

Table 1: The effect of insert and interference on ultimate strength.

	Strength (lbf)	#Samples
Without Insert	84 ± 45	23
With Insert	229 ± 77	94
Insert Interference		
Low x mod.	230 ± 75	15
Low x high	229 ± 81	44
Mod. x high	257 ± 29	22
Mod. x v.high	257 ± 36	6

Notes. Strength reported as mean ± standard deviation. Insert interference reported w/rt cross sectional dimensions.

CONCLUSIONS

The described approach considerably strengthens FDM based parts and warrants further study for both prosthetic sockets and any other 3D printed parts which have complex loading requirements that may not be met using judicious part orientation during printing.

REFERENCES

[1] Gershutz et al. *JRRD* **49**: 405-26, 2012.
[2] Pousett et al. *CPOJ* **2**: 1-10, 2019.
[3] Nickel et al. *JPO* **32**: 295-300; 2020

ENERGETICS OF A NOVEL PASSIVE DYNAMIC CUSTOM AFO IN GAIT: ANALYSIS IN A SAMPLE OF FOOT-DROP PATIENTS

Luca Zamagni[1], Giulia Rogati[1], Alessandro Zomparelli[2], Franco Cevolini[3], Massimiliano Baleani[4], Roberta Fognani[4], Maurizio Ortolani[1], Zimi Sawacha[5], Alberto Leardini[1] and Paolo Caravaggi[1]
[1]Movement Analysis Laboratory, IRCCS Istituto Ortopedico Rizzoli, Bologna, Italy
[2]Department of Technology and Innovation, University of Southern Denmark, Odense, Denmark
[3]CRP Technology, Modena, Italy
[4]Medical Technology Laboratory, IRCCS Istituto Ortopedico Rizzoli, Bologna, Italy
[5] BioMov Lab, Dep. of Information Engineering, University of Padova, Italy
Email: paolo.caravaggi@ior.it

INTRODUCTION

Passive Dynamic Ankle Foot Orthoses (PD-AFOs) are orthopedic devices prescribed to patients with mild foot-drop condition. These patients are often affected by weakness of the ankle plantar-flexors, in addition to a deficit of the ankle dorsiflexor muscles. While the main requirement of AFOs is to support the foot in the swing phase of gait, the flexibility of PD-AFOS enables both energy storage and releasing during the stance phase. This study aimed at estimating the energy expenditure of a novel custom PD-AFO in a sample of mild foot-drop patients.

METHODS

Eight custom PD-AFOs were designed and modelled as to match the shape of the foot and leg of 8 patients with unilateral foot-drop condition (3F, 5M; age 62.0 ± 13.1 years, BMI 25.8 ± 2.5 kg/m^2). AFOs were produced via selective-laser-sintering of a fiberglass-reinforced polyamide powder (Windform GT®, CRP Technology). Patients were instrumented with skin markers according to a validated lower-limb kinematic protocol [1] and an 8-camera motion capture system (Vicon) recorded the markers' trajectories during walking at self-selected comfortable speed. Three reflective markers were attached to the flexible component of the AFO to establish a local reference frame for the AFO calf-shell (Figure 1, left). The relationship between the calf-shell flexion angle with respect to the foot plate, and the resisting moment to flexion due to the AFO stiffness, was determined for each AFO via an ad-hoc experimental setup [2]. The temporal profiles of flexion angles in stance were determined for each patient as the relative rotation between calf-shell and foot-plate which was assumed to move rigidly with the footwear. For each patient, the work done by the AFO was calculated as the dot product of the calf-shell resisting moment and rotation angle (Figure 1) across five walking trials. AFO power was calculated as the time derivative of the work.

RESULTS AND DISCUSSION

The estimated work done by the custom AFO during normalized stance phase was largely consistent across patients/AFOs (Figure 1). Negative work is done during ankle dorsiflexion (~40-80% of stance in Figure 1) to flex the calf-shell and this energy (positive work) is released to the ankle at foot-off (~80-100% stance in Figure 1). The average maximum energy stored by the calf-shell across all AFOs was 0.013 ± 0.005 J/kg. Some energy is also exchanged due to the bending of the anterior part of the foot-plate, but this was not accounted for in the present study.

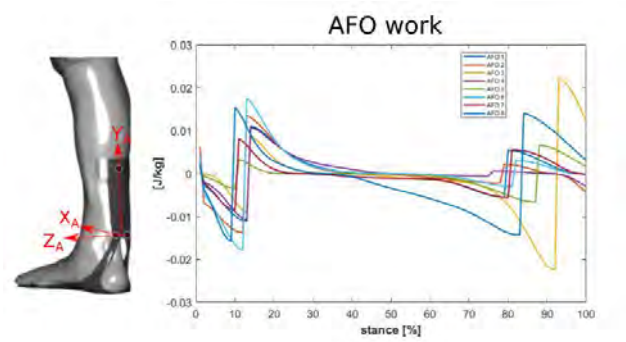

Figure 1 Left, 3D render of one of the custom AFOs made for one of the 8 foot-drop patients. Three reflective markers attached to the posterior side of the calf-shell were used to establish a local reference frame with axes Xa, Ya, and Za. Right, temporal profile of the average work normalized by body weight [J/kg] done by each of the 8 AFOs calf-shell over normalized stance phase.

CONCLUSIONS

The energy expenditure of a novel passive dynamic custom AFO has been estimated in a population of mild foot-drop patients. According to this study, the present custom AFO can store some energy at midstance, and this is released to the ankle at foot-off. This energy could be beneficial to assist those patients with weakness of the ankle plantarflexor muscles.

ACKNOWLEDGEMENTS

This study was partially funded by the Italian Ministry of Health 5x1000 funding scheme.

REFERENCES

[1] Leardini A. et al., *Gait&Posture* **86**: 34-9, 2007.
[2] Rogati G. et al., *J Biomech* **142**: 111239, 2022.

Footwear comfort and the effect of customised foot orthotic insoles and BMI

Lloyd Reed[1], Matthew Triggs[1,2]
[1] FootMotion Australia, Brisbane, Australia.
[2] School of Clinical Science, Queensland University of Technology, Brisbane, Australia.
Email: lreed@footmotion.com.au

INTRODUCTION

Foot orthoses have been shown to have immediate and short term sustained effects on comfort and functional biomechanics in running [1]. Mills et al [2] examined foot orthoses worn in walking and running and reported that a 10.2mm change in comfort rating, on a 100mm visual analogue scale (VAS) was clinically important. Zin et al [3] determined that there was little difference in comfort ratings of basketball footwear by subjects with either 'heavy' or 'light' BMI. This study aims were to examine the effects of customised foot orthoses on 'overall comfort' and examine if this was influenced by BMI.

METHODS

Subjects were recruited through a podiatry practice and footwear store and fifty three adults (27 females, 26 males, age 47.2 ± 15.7 yrs) completed the study. Subjects were screened for medical, foot health and footwear history to ensure there were no contraindications to treadmill walking or use of customised orthoses. Subjects were categorised as 'underweight/normal' (Group 1, BMI ≤ 24.9) and 'overweight/ obese' (Group 2, BMI ≥ 25.0) and fitted with customised orthotic insoles - 'Medical Green Insoles (MGI)' (Footbalance Systems Ltd, Vantaa, Finland). The same insoles with additional arch support (MGI+) were given to Group 3, overweight/obese subjects only. Overall comfort was assessed on a 150mm VAS after walking on an instrumented treadmill (Zebris GmbH) at comfortable walking speed for three minutes, wearing; usual footwear (including usual insoles /orthoses), usual footwear with MGI or MGI+ and usual footwear again. Subjects wore the orthoses for 4 weeks in their daily activities, then the testing was repeated. Not all completed the sixth comfort rating and it was excluded from analysis. Differences in overall comfort measures were assessed using a mixed factors ANOVA model (SPSS version 28.01 (IBM, New York, USA)), with GROUP as a between subjects factor and TIME as a within subject factor. Tukey post hoc tests were performed. Demographic characteristics of the three subject groups were assessed using ANOVA models. Alpha was 0.05 for all tests.

RESULTS AND DISCUSSION

There were no differences in mean age or height for the three groups and no difference in weight or BMI for the two overweight/obese groups 2 and 3. There was a significant GROUPxTIME interaction (F2.7, P=0.008) and Figure 1 shows the means and standard errors of comfort ratings for each group. At 4 weeks, overall comfort when wearing orthotic insoles was significantly higher than in usual shoes for Group 1 (difference 37.0±5.8 mm) and Group 3 (difference 25.7±5.9mm) and higher than the limits of agreement of ± 20mm from a Bland and Altman analysis [4]. Overweight/obese individuals with standard MGI insoles (Group 2) showed no difference in any overall comfort measures.

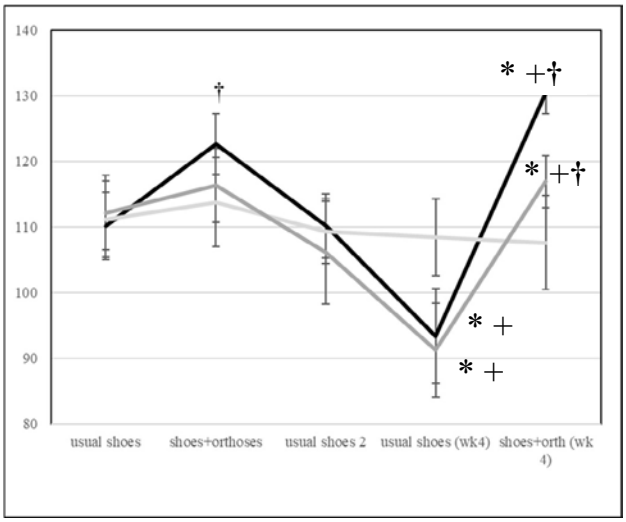

Figure 1 Mean & SEM of ratings of 'Overall comfort' (mm)
Group 1, Group 2, Group 3, * significant difference to usual shoe time 1, + significant difference to usual shoe time 2 † significant difference to usual shoes week 4

CONCLUSIONS

Footwear comfort can be increased with customised orthotic insoles. However, comfort improvements may be dependent on BMI and orthotic design. More research is needed to establish optimal design features for customised orthotic insoles for people across BMI groups.

ACKNOWLEDGEMENTS

Footbalance Systems Ltd, Vantaa, Finland for donating orthotic insoles.

REFERENCES

[1] Műndermann A et al. *J Appl Biomech* **20**:71-84, 2004.
[2] Mills K et al. *Med Sc Sports Exerc* **42**:1966-71, 2010.
[3] Zin et al. *J Sports Sci* **34**:756-765, 2016.
[4] Bland JM, Altman DG. *Lancet* **1**:307-310,1986.

REMOTE TECHNOLOGIES FOR TESTING PHYSICAL FUNCTION

Neil J. Cronin[1,2], Maedeh Mansoubi[3], Erin Hannink[4], Benjamin Waller[5,6], Helen Dawes[3,4,7]

[1] Faculty of Sport & Health Sciences, University of Jyväskylä, Finland; [2] School of Natural, Social and Sport Sciences, University of Gloucestershire, UK; [3] Intersect@Exeter, College of Medicine and Health, University of Exeter; [4] Centre for Movement, Occupational and Rehabilitation Science (MOReS), Oxford Brookes University; [5] Physical Activity, Physical Education, Sport and Health Research Centre (PAPESH), Sports Science Department, School of Science and Engineering, Reykjavik University, Reykjavik, Iceland; [6] Good Boost Wellbeing limited; [7] Oxford Health, Biomedical Research Centre, University of Oxford
Email: neil.cronin@jyu.fi

INTRODUCTION

Clinical testing of body function is important in diagnosis and rehabilitation of common musculoskeletal conditions and is usually performed in dedicated facilities (hospitals, community clinics). Recent developments in artificial intelligence, particularly computer vision, could make it possible to perform clinical testing remotely, freeing up resources. We examined accuracy and concurrent validity of a semi-automated computer vision system for estimating distance and angle parameters from common functional tests recorded with a mobile phone or webcam.

METHODS

The test protocol included two stages. Firstly, the accuracy of the computer vision system was tested using different camera positions and objects with known dimensions. The second stage involved concurrent validity testing in two participant groups. The results generated by our computer vision system were compared to those of a trained clinician. A total of 62 participants (31 healthy, age 35±8; 31 with axial spondyloarthropathy, age 53±12) performed a series of functional tests whilst standing or sitting 1.5m from the camera. They repeated the movement a second time while an experienced certified physiotherapist manually measured variables of interest so that these values could be compared to the results obtained with computer vision. For a description of how the tasks were performed see [1]. A modified version of OpenPose [2] was used to detect the x,y coordinates of body keypoints, and these coordinates were used to compute angles/distances. Manual and computer vision-derived scores were compared using Bland-Altman plots and 95% confidence intervals. One-sample t-tests were used to determine whether differences between methods were significantly different to 0. Pearson's correlations between the two methods were also computed. For the sit-to-stand test, Mann-Whitney U was used to compare the number of repetitions.

RESULTS AND DISCUSSION

Our approach estimated known object dimensions to within 2% for objects of different sizes, different object-camera distances, and different angles relative to the camera. Mean differences between computer vision and manual estimates are shown in Table 1. For all tests, the correlations between the estimates of the two methods represented large effect sizes ($r^2 > 0.25$). For the sit-to-stand test, there was no statistical difference between methods in the number of repetitions performed (Mann Whitney U [n=60] = 3601, z = -0.432, p = 0.666).

Table 1: Mean differences between computer vision and manual estimates for each test.

Test (unit)	Mean difference	SD of difference	95% CI	*t* statistic	*p* value
Tragus to wall (cm)	1.4	2.5	0.6 - 2.3	4.52	< 0.001
Cervical rotation (cm)	2.5	1.2	2.1 - 3.0	16.81	< 0.001
Shoulder flexion, left (°)	2	14	−3 – 7	0.99	0.33
Shoulder flexion, right (°)	3	15	−2 – 9	1.57	0.12
Side flexion, left (cm)	−0.5	3.1	−1.6 - 0.6	−1.34	0.19
Side flexion, right (cm)	0.5	3.4	−0.7 - 1.7	1.05	0.30
Lumbar flexion (cm)	−1.1	8.2	−4.0 - 1.8	−1.05	0.30
Hip abduction, left (°)	−10	10	−13 - −6	−7.51	< 0.001
Hip abduction, right (°)	−10	10	−13 - −6	−7.26	< 0.001
Hip internal rotation (cm)	−2.1	6.0	−4.2 - 0.0	−2.78	0.007

CONCLUSIONS

Our markerless computer vision approach provided estimates of distance and angle measures that were generally statistically comparable to manual measures performed by a trained clinician. In the future, this kind of approach could be used to monitor functional capacity and to manage physical therapy remotely. Our approach is built on top of an open-source algorithm, and thus lowers potential barriers to implementing accurate movement analysis outside of a lab environment.

REFERENCES

[1] Hannink E et al. *OSF*. https://osf.io/hsv7p/, 2021.
[2] Cao Z et al. *IEEE TPAMI*, 2019.

Development of a Neural Network for Prediction of Ovine Hip Joint Centers

Aaron Henry[1], Dana Gaddy[2], Larry Suva[2], Michael R. Moreno[1,4], Andrew B. Robbins[1,3]
[1] College of Engineering, Texas A&M University, College Station, TX.
[2] College of Veterinary Medicine & Biomedical Sciences, Texas A&M University, College Station, TX.
Email: ahenry@tamu.edu

INTRODUCTION

Estimation of the hip joint center (HJC) is a vital component of motion capture and subsequent kinematic and kinetic analyses. Errors in estimation of the HJC can propagate through these analyses resulting in additional error [1]. As such, accurate estimation of the HJC is critical for biomechanical calculations.

Various functional and predictive methods for estimating the location of the HJC have been developed in humans, and to a much lesser extent quadrupeds [2]. Functional methods require subjects to voluntarily move their joints through a large range of motion, which is challenging, and in some cases impossible to achieve in animal models. Alternatively, predictive methods use anatomical measurements to determine the HJC in reference to particular anatomical landmarks [3].

Since functional measurement of the HJC is not feasible in ovines, it is typically assumed to be at the geometric center of the femoral head as measured from tomographic imaging. While this has been done, it has not been applied generally to multiple animals to generate a predictive model as measured from tomographic imaging. While this has been done, it has not been applied generally to multiple animals to generate a predictive model [4]. Other estimations of the HJC in quadrupeds have utilized a marker placed on the greater trochanter of the femur, and assume this is at the HJC, and assume this is at the HJC [5]. Calculation of hip joint kinematics using this method have shown to be highly susceptible to error due to more pronounced soft tissue coverage over the joint [6]. Development of a predictive model of ovine HJC based on multiple animals would enable superior estimation of HJC, increasing accuracy of biomechanical measurements.

METHODS

Full body ovine CT scans (Siemens Biograph mCT) were segmented in 3DSlicer. Segmented bones were then exported as STL files. HJCs were estimated by fitting a sphere to the articulating surface of the femoral head, excluding the iliofemoral ligament using AutoDesk MeshMixer. 14mm spheres were then placed on anatomical landmarks of the pelvis, femur, and tibia to replicate motion capture markers (although soft tissue thickness was not accounted for) and were used to define a pelvic coordinate system.

A neural network was trained on the data from each animal. Sixteen Rambouillet sheep were used; 10 were used for training the network and 6 were used for testing and tuning the network. For each animal, CT scans were available at either ages 2 months, 7 months, or 14 months, with many having multiple time points. The test set was chosen such that there was sufficient diversity in age, sex, and phenotype among the test data. This resulted in a total of 48 training data points and 20 testing data points, with each animal being present in the data set up to three times (at the three ages noted above).

A neural network was created using Tensorflow Keras in Python, with inputs that included the age, sex, phenotype, pelvic and femur measurements, and marker positions from the CT reconstructions. Sex and phenotype data were one hot encoded while age and weight were scaled using the SKLearn standard scaler. The network consisted of an input layer, 2 hidden layers, and an output layer. The number of neurons per layer was initially chosen at random and later tuned by finding the minimum Euclidean distance between the predicted HJC and actual HJC. Rectified linear unit activation functions were used for each layer while mean squared error was used for the loss. The adam optimizer was used for the model.

RESULTS AND DISCUSSION

The neural network performed exceptionally well with mean Euclidian distance error between the actual and predicted HJC of 3.53±1.67mm. This error is much smaller than current predictive methods in humans which range from 10-40mm, despite (or perhaps because of) the relatively small set of training data [2]. Further work will be done to assess the models performance on input data containing measurement errors to more closely replicate sources of error such as the placement of markers above soft tissue, movement artifacts, and potentially erroneous marker placement.

CONCLUSIONS

A neural network was successfully created and trained that was able to accurately predict the location of the HJC in ovines using categorical and marker location data. This neural network can be used to improve kinematic and kinetic analysis of ovine gait.

REFERENCES

[1] Stagni R. et al. *J Biomech*, 33(11), 1479–1487, 2000.
[2] Kainz H. et al. *Clin Biomech*, 30(4), 319–329, 2015.
[3] Harrington et al. *J Biomech*, 40(3), 595–602, 2007.
[4] Duda G. N. et al. *J Biomech*, 31(3), 201–210, 1997.
[5] Faria, L. G. et al. *BMC Veterinary Research*, 10(1), 294, 2014.
[6] Kim et al. *Vet Comp Orthop Traumatol*, 24(05), 326–332, 2011.

THE INFLUENCE OF PROTECTIVE EQUIPMENT ON PERFORMANCE IN ICE HOCKEY

Rebecca Lennartz[1,2], Arash Khassetarash[1], Evangelos Spyrou[3], Aiden Hallihan[3], Bjoern Eskofier[2] and Benno Nigg [1]
[1] Human Performance Lab, University of Calgary, Calgary, Canada.
[2] Machine Learning and Data Analytics Lab, Department Artificial Intelligence in Biomechanical Engineering, Friedrich-Alexander-Universität Erlangen-Nürnberg, Erlangen, Germany
[3] CCM Hockey, Montreal, QC, Canada
Email: Rebecca.lennartz@fau.de

INTRODUCTION

Understanding an ice hockey player's movements and the restrictions incurred by the protective equipment is crucial for improving the equipment and subsequently, player's performance. The optimum design of the protective equiment is specially challenging given the complexity of the movements and manuevers in ice hockey. This complexity arises from the multitude of possible variables that describe player's motion and therefore complex analysis methods are required to help direct the researcher's attention toward the right variables. The purpose of this work was to utilize artificial neural network (ANN) and layer-wise relevance propagation (LRP) [1] to understand how complex drills in ice hockey were affected by the presence of protective equipment.

METHODS

Seventeen male ice hockey players (age: 26.4 ± 7.0 years; mass: 86.4 ± 6.5 kg; height:183.8 ± 6.5 cm) skated the long axis of the ice rink as fast as possible. The sprint time over 30 meters was recorded (Brower TCi Timing system) and the movement data was captured by inertial measurements units integrated into the Xsens MVN Awinda System. The sprints were performed twice in either with (Equipment) or without protective equipment (No Equipment) conditions in a randomized order. Individual strides were defined from one ice contact to the subsequent ice contact of the same foot. A total of 24 strides were extracted for each of the participants. The trajectories of 12 joint angles (Figure 1) were extracted and normalized. All trajectories for one movement were concatenated into one single feature vector. A shallow ANN was trained to distinguish whether the sprint stride was performed in Equipment or No Equipment condition. Using LRP, the contribution of each variable to the classification result of the ANN was determined.

RESULTS AND DISCUSSION

On average, the participants performed the sprint drill 1.64 % faster in No Equipment compared to Equipment condition ($p = 0.0037$). The model was trained 17 times while leaving one participant out each time for testing, reaching an average accuracy of 99.3 %. The average relevance scores that were derived from the ANN model are depicted in Figure 1. Each row corresponds to one rotational degree of freedom, while each column depicts one percent of the stride cycle. The histograms at the top and right part of the figure show the vertical, and horizontal summation of the heatmap respectively.
The results show that the ANN can distinguish between the two conditions while observing differences in performance. Thus, it appears that protective equipment impairs performance. The presented data indicate that rotations around the medial-lateral axis (in sagittal plane) and movements associated to the shoulder, knee, and hip joint contributed the most to the classification result.

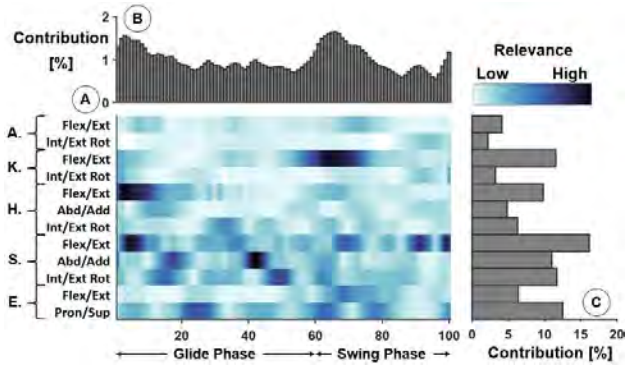

Figure 1 Averaged relevance scores per variable (A) over one sprint stride and contributions within a step cycle (B) and joint trajectories (C) using A. = ankle, K. = knee, H. = hip, S. = shoulder, E. = elbow.

CONCLUSIONS

The proposed methodology based on ANN and LRP was able to highlight the variables and time points that differ between Equipment and No Equipment conditions. We were able to distinguish the important movements that the protective equipment restricts, and future design can leverage this information. In general, this approach allows researchers to investigate a question from a holistic point of view and therefore make informed decisions in complex, multivariate problems.

ACKNOWLEDGEMENTS

This work was supported by a fellowship of the German Academic Exchange Service (DAAD).

REFERENCES

[1] Bach S et al. *PLOS ONE* **10(7),** 2015

MODELING HEALTHY AND IMPAIRED GAIT DYNAMICS USING RECURRENT NEURAL NETWORKS

Taniel S. Winner[1], Michael C. Rosenberg[1], Trisha M. Kesar[2], Lena H Ting[1] and Gordon J. Berman[3]
[1] W.H. Coulter Dept. Biomedical Engineering, Emory University & Georgia Tech, Atlanta, GA, USA.
[2] Department of Rehabilitation Medicine, Division of Physical Therapy, Emory University, Atlanta, GA, USA.
[3] Department of Biology, Emory University, Atlanta, GA USA.
Email: twinner@emory.edu

INTRODUCTION

Modeling the neuromechanics of walking, particularly in neurological disorders, is challenging because current biomechanical simulations lack appropriate neural control mechanisms and constraints [1][2]. These challenges suggest the need for a more holistic approach to capturing the neuromechanical constraints of walking derived from data. Here we use a Recurrent Neural Network (RNN) model to recapitulate the dynamical features of gait in a common latent space by capturing spatiotemporal dependencies between sagittal plane lower-limb joint angles during treadmill walking in healthy and impaired individuals. Individual-specific, low-dimensional representations of the model parameters define individuals' gait dynamics (**gait signatures**), enabling direct comparison between individual and group dynamics across speeds, interpretation of inter- and intra-limb coordination patterns, and prediction of the time evolution of joint coordination across speeds. This framework may facilitate the development of future tailored gait interventions and track meaningful changes in the fundamental neuromechanical mechanism of walking.

METHODS

To capture the underlying dynamics of gait using machine learning, 15 seconds of sagittal plane kinematic data from able-bodied (AB) (N=5) and post-stroke (N=7, > 6 months after stroke) participants walking at six different treadmill speeds were input to a sequence-to-sequence RNN model trained to predict a one-step time-shifted version of the kinematic input data [3]. The RNN architecture consisted of an input layer, a hidden layer, and an output layer. To compare dynamics between individuals, individual-specific gait signatures were computed by first projecting the RNN internal activations for all individuals into a common basis using principal components (PC) analysis. The PC weights were then phase averaged over the gait cycles at each speed, producing the '**gait signature**'. Gait signatures were visualized as multidimensional trajectories over a gait cycle in 3D or projected into a coordinate map using multi-dimensional scaling (MDS).

RESULTS AND DISCUSSION

Our model's ability to predict at least one gait cycle of individuals' future kinematics supports that it encodes the neuromechanical dynamics governing gait kinematics. Resulting gait signatures revealed dynamic similarity in AB vs. heterogeneity in stroke individuals (Figure 1, A). Individuals' gait signatures were speed independent; their 6 speed gait signatures clustered together rather than with other individuals' signatures at similar speeds (Figure 1, B). The gait signatures of more impaired stroke survivors who walked at slower speeds, were located further away from AB signatures.

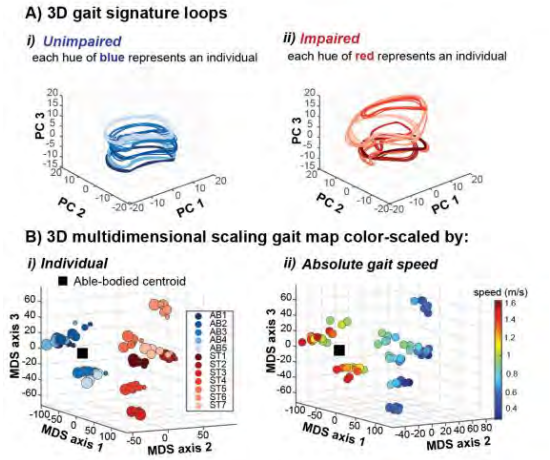

Figure 1 A) 3D unimpaired (i) and impaired (ii) individual gait signatures. B) 3D MDS map of all gait signatures coloured according to individual (i) and absolute gait speed (ii).

Further, subcomponents of the gait signature reveal biomechanically interpretable coordination (e.g., PC1 encoded hip flexion and extension) [3]. Gait signatures uncovered that 2 stroke survivors with similar Fugl-Meyer scores and self-selected walking speeds, had different gait signature components, showing promise for its use to tailor gait rehabilitation.

CONCLUSIONS

Gait signatures capture individual-specific gait differences irrespective of walking speed. This framework provides a generalizable, holistic method for characterizing and predicting cyclic, dynamical motor behaviour.

ACKNOWLEDGEMENTS

Emory Synergy/Nexus II Award, NSF: M3X CMMI1762211, Sloan Scholarship: G-2019-11435, NSFGRFP 1937971, NICHD: F31HD107968-01 and NICHD F32HD108927.

REFERENCES

[1] Falisse et al. *J Royal Soc. Interface* **16**, 2019.
[2] Meyer et al. *Front Bioeng Biotechnol* **4**: 77, 2016
[3] Winner et al. *BioRxiv*, 2022

HIGH EFFICENCY BARBELL RECOGNITION MODEL BY CONSIDERING CONVOLUTIONAL NEURAL NETWORK

Jin-Yi Lin, Ching-Ting Hsu*, Wei-Hua Ho and Pao-Hung Chung
Graduate Institute of Sports Equipment Technology, University of Taipei, Taipei, Taiwan R.O.C.
Email: jingting@utaipei.edu.tw

INTRODUCTION

The barbell trajectories is an important factor for Olympic weightlifting while including much kinematic parameters to indicate the sport performance. Trajectories can be used to achieve a successful lift [1]. Furthermore, the barbell trajectory can be indicated the snatch movement successful by excellent male lifter [2]. As mentioned, barbell trajectory containing many important kinematic parameters, however, it needs scientist or experts utilizing kinematic analysis tools to obtain it. But difficultly operation makes real-time kinematic analysis difficultly utilizing in daily training or competition. Convolutional neural network (CNN) is one distribution of AI which exports for image recognition. Many pre-trained CNN models such as VGG19 provide image recognition architecture [3]. In this paper, we want to build a high efficiency barbell recognition model based on VGG19 to find the barbell from video frame and further connect as its trajectory.

METHODS

We consider pre-trained convolutional neural network, VGG19, as our barbell recognition model. VGG19 can find barbell from video frame in high efficiently and archive high performance with less model training consumption. There are two steps for creating our model. First step is sampling gathering. We collect video sequence from public competitions, the barbells are captured from each frames. We have positive and negative samples. Positive sample means that full and complete barbell. Since the colour of barbell denotes weight on the bar, thus, barbells of various colours are considered. We collect pieces of barbell, background equipment and people's body as the negative samples to make barbell recognition model learning. The second step follow by sample collected is model training. All training samples from first step will separate into three groups, and they are 80% training samples, 15% validation samples and 5% testing samples, respectively. All samples are both including positive and negative sample. After training samples are ready, we adjust model's parameters such like batch size, freeze layers and epoch for both considering training and validation results. Our proposed VGG19 barbell recognition model are 10 and 80, respectively.

When we fine trained the VGG19 barbell recognition, this model will be connected by our previous work [4] to fast track in feature frames of the video sequence.

RESULTS AND DISCUSSION

Results of our VGG19 barbell recognition model archives 95%, 100% and 87.5% for recognition accuracy, precision and recall, respectively. From the confusion matrix in Table 1, our model can both archive recognition performance and efficiency.

Table 1 Confusion matrix

		Predict class	
		True	False
True class	True	100%	0
	False	14.29%	85.71%

In this paper, we propose a VGG19 barbell recognition model combined with our previous semi-automatic barbell tracking algorithm which obtains high accuracy barbell trajectory and kinematic parameters.

Our barbell recognition model obtains barbell without reflective dots, this improvement reduces the operation procedure and makes sport biomechanics easily utilized in daily training life. In the past, since kinematic analysis software is difficult to use, thus, coaches observe athlete's gesture by their eyes with their experience. From this research, our VGG19 barbell recognition model provide both efficiency and accuracy barbell position to further provide barbell kinematic parameters from video sequence. This results not only provide the efficiently and easily gathering barbell trajectory, but also show the machine learning technique aiding the weightlifting training.

CONCLUSIONS

We propose a VGG19 barbell recognition model provides an efficiently and easily tool for kinematic analysis and indicate the machine learning technique can be suit for sport science.

ACKNOWLEDGEMENTS

This research is supported by National Science and Technology Council, Taiwan, R.O.C. The project number is NSTC 112-2425-H-845-002-.

REFERENCES

[1] Chiu, H., & Liang, J. BCH angles of young female weightlifters during snatch movement. In:*ISBS-Conference Proceedings Archive*, 2019.

[2] Nagao, H., Kubo, Y., Tsuno, T., Kurosaka, S., & Muto, M.. A biomechanical comparison of successful and unsuccessful snatch attempts among elite male weightlifters. *Sports,* **7(6)**: 151, 2019.

[3] Bansal, M., Kumar, M., Sachdeva, M., & Mittal, A. Transfer learning for image classification using VGG19: Caltech-101 image data set. *Journal of Ambient Intelligence and Humanized Computing,* 1-12, 2021.

[4]. Hsu, C. T., Ho, W. H., & Chen, J. S. High Efficient Weightlifting Barbell Tracking Algorithm Based on Diamond Search Strategy. Advances in Intelligent Systems and Computing **831**: 252-262, 2019.

Prediction of GRF and joint moments from different combinations of kinematic data

Juan Cordero-Sánchez[1], Bruno Bazuelo-Ruiz[2], Pedro Pérez-Soriano[2] and Gil Serrancolí[3]
[1] Department of Physiotherapy, University of Alcalá, Alcalá de Henares, Spain.
[2] Department of Physical Education and Sports, Universitat de València, Valencia, Spain.
[3] Department of Mechanical Engineering, Universitat Politècnica de Catalunya, Barcelona, Spain.

Email: j.cordero@edu.uah.es

INTRODUCTION

Ground reaction forces (GRF) are necessary to understand the cause of any movement [1], and joint moments provide key information to gain insight into the net muscle contribution at each joint [2]. Artificial neural networks (ANN) can facilitate the computation of these variables outside laboratories. However, most studies focused on dynamic data estimations from kinematic variables are applied to gait [3]. Joint coordinates and their derivatives might play a different role when predicting dynamic data. Therefore, the aim of this investigation was to explore the combinations of lower limb joint coordinates and their derivatives that best predict GRF and joint moments using ANN during running. Besides, the capability of the ANN to predict dynamic data from kinematics obtained using different motion capture systems was also analysed.

METHODS

The ANN training-set comprises data collected from sixteen participants using an inertial motion capture system (Xsens Technologies B.V.) and a force plate (Dinascan/IBV). Each participant performed ten running trials on a ten metres walkway at 3.3 ± 0.33 m/s. Kinematics variables and GRF were filtered using a zero-lag four-order low-pass Butterworth filter with a cut-off frequency of 10 and 15 Hz, respectively. Joint moments were computed using OpenSim. Four sets of input variables were tested to predict anteroposterior and vertical GRF as well as ankle, knee and hip flexion moments, with combinations of joint coordinates, velocities and accelerations. Thus, 20 ANN were trained finding their best structures by GridSearch hyperparameter tunning and 5-fold cross-validation. One layer and 300 neurons with a dropout rate of 5% were the hyperparameters that best performed. A leave-one-out cross-validation was performed to evaluate how well the ANN predicted unknown data. The used test-set data came from the study of Hammer and Delp [4], captured with an optical camera system and subjects running on an instrumented treadmill at 3 m/s. Finally, a repeated measures ANOVA with a pairwise comparison was performed to determine the significance of the correlation and normalized root mean square error (nRMSE) differences among the predictions using different kinematic variable combinations.

RESULTS AND DISCUSSION

Moderate-to-strong mean correlations values (r = 0.6-0.9) were obtained for the GRF and ankle and knee moment predictions (Figure 1). Hip moment correlations were low (0.1-0.4). Mean nRMSE values for the anteroposterior and vertical GRF range between 1.3-1.8 and 4.7-5.7 N/kg, respectively. Joint moment nRMSE values range between 0.8-1.2, 0.5-0.9 and 1.2-1.7 Nm/kg for the knee, ankle and hip. Knee flexion moment nRMSE ranges has similar magnitude as those found by Stetter et al. [5] while our correlation was higher.

Overall, the nRMSE showed that the use of joint coordinates alone as input to the ANN could predict the data accurately, and in some cases with significant differences ($p<.05$) with respect to adding joint coordinate derivatives as input.

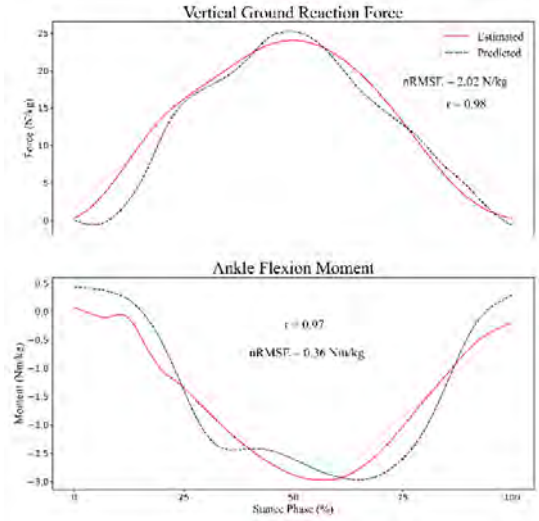

Figure 1. Estimated vs predicted vGRF and ankle flexion moment.

CONCLUSIONS

Joint angles seem to have all the information necessary to predict GRF and joint moments with good accuracy when running. This study also shows the feasibility of using the same ANN to predict GRF and joint moments with data that come from different datasets and experimental techniques.

REFERENCES

[1] Nüesch C et al. *Gait & Posture* **62**: 117-123, 2018.
[2] Winter D. *Biomech and Motor control*, 2009.
[3] Anciallo H et al. *Sensors* **18(8)**: 2564, 2018.
[4] Hammer S et al. *J Biomech* **46(4)**: 780-787, 2013.
[5] Stetter B et al. *Front. Bioeng. Biotechnol* **8**:9, 2020.

Evaluation of deep neural networks-based frame interpolation of X-ray fluoroscopic images of dynamic knee motions

Yu-Chien Chen[1], Cheng-Chung Lin[1], Tung-Wu Lu[2], Mei-Ying Kuo[3], and Horng-Chaung Hsu[4]
[1] Department of Electrical Engineering, Fu Jen Catholic University, New Taipei City, Taiwan
[2]Department of Biomedical Engineering, National Taiwan University, Taipei, Taiwan
[3]Department of Physical Therapy, China Medical University, Taichung, Taiwan
[4]Department of Orthopaedic Surgery, China Medical University Hospital, Taichung, Taiwan
Email: 129787@mail.fju.edu.tw

INTRODUCTION

Clinical biplane X-ray imaging system can be utilized to acquire fluoroscopic images of the joint motion in a budge-efficient way, beneficial to translate motion analysis to clinical practice. However, asynchronous images captured from two x-ray units affect the accuracy of the reconstructed skeletal kinematics using 3D/2D image registration [1]. To address the issue, synthesizing a realistic middle image between two consecutive X-ray frames may help create a virtual synchronous biplane X-ray configuration. The study aimed to implement, train and evaluate state-of-art deep convolutional neural networks (CNN)-based RGB video frame interpolation techniques [2]–[4] for the synthesis of intermediate X-ray fluoroscopic images.

METHODS

Four frame interpolation CNNs namely, Softsplat[2], RRIN[3], XVFI[4] and IFR[5] were implemented. To train frame interpolation CNNs specific to the fluoroscopic image interpolation, a new x-ray dataset containing 38312 quintuplets of consecutive fluoroscopic frames at a resolution of 512×512 was first established. The 1st and 5th frames in the quintuplets were taken as the inputs, and the middle 3 frames served as the ground truth frames. Each network was trained for 300 epochs using Adam optimizer. The trained networks were utilized to generate intermediate fluoroscopic frames on the testing set comprising 1600 frames recoding the cadaveric knee motions at various speeds [1].

RESULTS AND DISCUSSION

The peak signal-to-noise ratio (PSNR) of the generated intermediate frames with the frame interpolation CNNs were shown in Fig.1. In general, the implemented CNNs enabled generating visually satisfactory images with median PSNR >31 dB. The performances of the four CNNs were degraded with the higher speeds of the skeletal motion in consecutive frames. Among the four CNNs, RRIN gave slightly higher median values of PSNR (Fig. 1) at the expense of the parameters used in the network (Table 1). While Softsplat possesses fewer parameters, it requires the highest number of flops to synthesize an image due to the use of grid network. This feature may favor dealing with difficult cases, especially in higher-speed motion scenarios. The XVFI and IFR were advantageous in lower network complexity with a slight compromise on the quality of interpolated images.

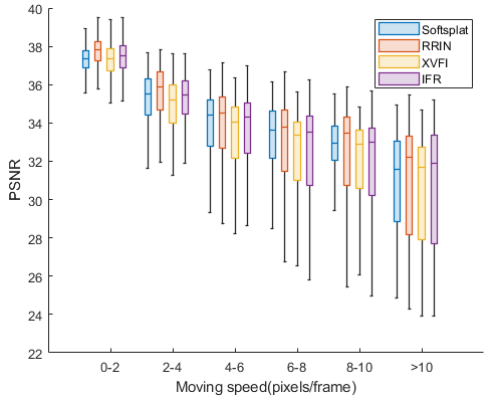

Figure 1 Boxplots show the distribution of PSNR for each net at different moving speeds of bones (pixels/frame).

CONCLUSIONS

The four frame interpolation CNNs were demonstrated to yield visually satisfactory intermediate fluoroscopic frames with median values of PSNR >32 dB after proper model training. Further studies are warranted to validate their use in the 3D joint kinematics tracking with 3D/2D image registration.

REFERENCES

[1] C.-C. Lin et al. Med. Phys 3637–3649, 2018
[2] S. Niklaus et al. In Proceedings of the IEEE/CVF Conference on Computer Vision and Pattern Recognition 5437-5446, 2020
[3] H. Li et al. ICASSP 2020-2020 IEEE International Conference on Acoustics, Speech and Signal Processing (ICASSP) 2613–2617, 2020
[4] H. Sim et al. In Proceedings of the IEEE/CVF international conference on computer vision 14489–14498, 2021
[5] L. Kong et al. In Proceedings of the IEEE/CVF Conference on Computer Vision and Pattern Recognition 1959–1968, 2022

Table 1: Flops and parameters of each frame interpolation CNN.

	Softsplat	RRIN	XVFI	IFR
Flops (G) / Time (S)	219.436 / 1.4	211.459 / 0.8	53.286 / 0.3	57.511 / 0.4
Parameters (MB)	14.332	18.299	5.272	4.729

JOINT ANGLE CALCULATION AND PREDICTION VIA OPENPOSE ESTIMATION AND MACHINE LEARNING MODEL FOR RIDING POSE ADJUSTMENT IN CYCLING

Yun-Ju Lee[1*] and Yi-Jie Chen[1]

[1] Department of Industrial Engineering and Engineering Management, National Tsing Hua University, Hsinchu, Taiwan.

Email: yunjulee@ie.nthu.edu.tw

INTRODUCTION

Bike fitting aims to match the bike size and individual riding posture in cycling, which is a long-term process. It requires a lot of back-and-forth testing and fine-tuning to determine the best sweet spot of comfort and riding speed. Most importantly, great bike fitting can avoid musculoskeletal injuries. However, the current bike fitting uses anthropometric information in a standing or static riding posture without considering individuals' differences and dynamic effects.

The present study proposed a dynamic approach of joint angle calculations via the OpenPose outputs to simulate riding poses with seat height adjustments during cycling.

METHODS

Ten healthy adults (age = 24.4±0.84 years, height = 167.96±9.41 cm, body weight = 61.30±14.08 kg) participated in the experiment. The protocol was approved by the Institutional Review Board of National Tsing Hua University (REC #: 11003HE021). The participants were instructed to ride for six minutes and maintain the cycling cadence at 80~90 revolutions per minute (RPM). The RGB images of one minute (6000 frames) were taken as inputs to OpenPose and used to determine the coordination of the left and right key joint points. The toe and hip are (green points in Fig. 1) the centre of the circles, and the foot and thigh segments are the radius to make two red circles (Fig. 1). The shank segment length determines the distance between these two red circles. The segment lengths were assumed to be constant. The equations and calculations are in Fig.1, conducted in the model with ReLU and Adam to determine the seat height with the minimized violated frames of joint angles.

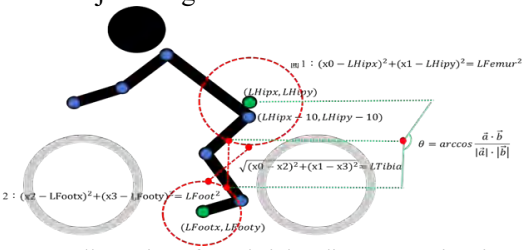

Figure 1 Illustration of seat height adjustment estimation with the coordination and the equations.

RESULTS AND DISCUSSION

The riding cadence was 84.00±1.41 RPM and 83.70±1.25 RPM (t(9)=0.709, p=0.496), and the seat height was 64.99±4.88 cm and 66.09±4.47 cm (t(9)=1.557, p=0.154) before and after the adjustment.

For the riding posture comparisons (Fig. 2), the OpenPose simulated skeletons showed an average of 9.12 degrees across all joints throughout the one-minute riding. The mean per joint position error (MPJPE) was not significantly different from the training and non-training sets in the simulated skeleton. After adjusting, the number of violated angle frames significantly decreased in the ground truth skeletons (t(9)=2.968, p=0.016).

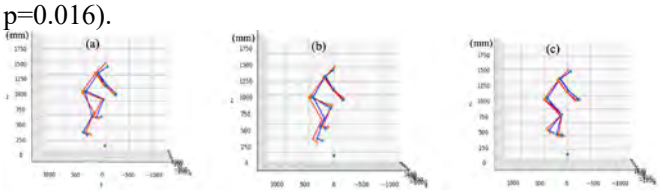

Figure 2 Illustration of the OpenPose simulated skeletons (blue) and the group truth skeletons (orange) when the right foot at (a) 6 o'clock, (b) 3 o'clock, and (c) 9 o'clock.

The similar MPJPE suggested that the model could work functionally in both situations regardless of the training set or seat heights [1]. The violated frames of joint angle showed the reduction pattern in both the OpenPose and ground truth skeletons. However, the definitions of joint centre resulted in the different number of frames between OpenPose and the group truth [2]. Finally, seven participants were suggested to increase the seat height from 2 to 4 cm, and three participants were to decrease the seat height by 2 cm. The variation indicated that our approach considered the individual joint angles and segment length instead of recommending increases or decreases in seat height.

CONCLUSIONS

The present study combined the coordination from OpenPose for constant segment length and moving joint centre with seat height in the machine learning models. The improvement of bike fitting successfully reduced the violated period of joint angle and specific adjustments for the individual during cycling.

ACKNOWLEDGEMENTS

The work was financially supported by National Science and Technology Council in Taiwan, under Grant MOST-110-2636-E-007-021.

REFERENCES

[1] Martinez J et al. *IEEE International Conference on Computer Vision*, 2017.

[2] Haberkamp LD et al. *J Biomech* **144**: 111333, 2022

ESTIMATING HAND REACTION FORCES FROM ARM SEGMENT ACCELERATIONS DURING HANDCYCLE PROPULSION USING MACHINE LEARNING

Griffin C. Sipes[1], Kellie M. Halloran[1], Sanmi Koyejo[2], Ian Rice[3], Mariana E. Kersh[1,4]
[1]Dept. of Mechanical Science and Engineering, University of Illinois Urbana-Champaign, Urbana, IL, USA
[2]Department of Computer Science, Stanford University, Stanford, CA, USA
[3]Department of Kinesiology, University of Illinois Urbana-Champaign
[4]Beckman Institute for Advanced Science and Technology, University of Illinois Urbana-Champaign
Email: gsipes2@illinois.edu

INTRODUCTION

Up to 78% of wheelchair users experience shoulder pain or injury [1], but few data are available on shoulder loads during everyday propulsion. Quantifying shoulder torques and muscle forces could help identify the biomechanical sources of increased injury risk. Unfortunately, there are currently no commercially available instrumented handrims that can measure the hand reaction forces and moments (HRFM). Recently, machine learning has been used to predict ground reaction forces during walking gait from segment accelerations measured by inertial sensors. Thus, our objective was to evaluate whether this same approach could be used during propulsion.

METHODS

Data from a larger study evaluating exercise intensity during recumbent handcycling was used. A benefit of handcycling is the prescribed movements resulting in continuous kinetic cycles. Subjects (n=20) from the UIUC wheelchair team performed high and moderate intensity propulsion cycles. An instrumented custom handle was used to collect HRFM data along with motion capture data [2]. An upper limb musculoskeletal model was scaled to each subject and linear and angular accelerations of the hand, radius, and humerus were calculated using inverse kinematics. The resulting dataframes (n=240 cycles) were shuffled and split into training (70%), validation (15%), and test (15%) sets. Each set was standardized by subtracting its mean and dividing by its standard deviation.

Four two-layer, bi-directional long short-term memory (biLSTM) networks (200 nodes/layer, dropout of 0.4 after each layer) were created (TensorFlow 2.10.0). Model input was accelerations for a complete propulsion cycle (n=356 timesteps) and the task was to predict cycle kinetics (three forces, three moments). Models were trained for 500 epochs with each batch containing the entire training set. Mean squared error was used as the training loss function and Adam optimization algorithm was used as the optimizer (learning rate 0.0003). Models 1-3 were trained on the hand, radius, and humerus segments, respectively, and model 4 was trained on all three segments. Models were evaluated using the normalized mean absolute error (NMAE) (Eq. 1) (MATLAB R2021b and R 4.2.2).

$$NMAE = \frac{\frac{1}{N}\sum_{i=1}^{N}\left|y_{actual,i} - y_{predicted,i}\right|}{\frac{1}{N}\sum_{i=1}^{N}\left|y_{actual,i}\right|} \quad (1)$$

RESULTS

The model trained on the radius performed the best with a mean NMAE across all predictions of 0.60 (Table 1). The combined, humerus, and hand models had mean NMAEs of 0.62, 0.66 and 0.71, respectively. No model performed significantly better than any other for any prediction variable. Considering a representative cycle (median error for output F_z), our model predictions follow the temporal trends of the ground truth loads, but the magnitude of predicted values tend to be lower (Fig. 1).

Table 1: Normalized mean absolute error for each model compared across each prediction variable. Errors are expressed as Mean(SD).

Model	F_x	F_y	F_z	T_x	T_y	T_z
Hand	0.8(1.8)	0.6(1.1)	1.1(0.5)	0.5(0.2)	0.5(0.2)	0.6(0.3)
Radius	0.5(0.2)	0.5(0.2)	1.0(0.4)	0.5(0.2)	0.5(0.2)	0.6(0.4)
Humerus	0.6(0.3)	0.5(0.2)	1.0(0.5)	0.5(0.2)	0.6(0.2	0.7(0.4)
Combined	0.6(0.2)	0.4(0.2)	1.1(0.6)	0.5(0.2)	0.5(2)	0.6(0.3)

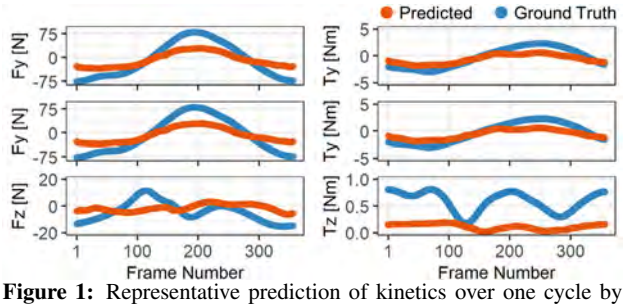

Figure 1: Representative prediction of kinetics over one cycle by model trained on hand acceleration data.

CONCLUSIONS

As there were no significant differences in model performance, a single IMU placed on the wrist (or a smartwatch) could provide enough data to predict the propulsion kinetics during handcycling. Next steps include retraining and validating the model on experimentally collected IMU data and adapting the model for more complex tasks, such as manual wheelchair propulsion.

ACKNOWLEDGEMENTS

Funding provided by the National Science Foundation.

REFERENCES

[1] Curtis, K.A. et al. *Arch. Phys. M.*, 1999.
[2] Halloran, K.M. et al. (Preprint), 2022.

VALIDITY AND RELIABILITY OF DEEP LEARNING METHODS TO ANALYSE KNEE OSTEOARTHRITIS USING MAGNETIC RESONANCE IMAGING: A SYSTEMATIC REVIEW

Surabhi Thatte[1], Sachin Tapasvi[2], Bhushan Borotikar[1],
[1] Symbiosis Centre for Medical Image Analysis, Symbiosis International University, Pune, MH, India
[2] Director, The Orthopaedic Speciality Clinic, Pune, MH, India
Email: bhushan.borotikar@gmail.com

INTRODUCTION

Recently deep learning (DL) based algorithms have emerged as best performing methods for solving classical medical image analysis problems such as image segmentation, classification, registration, and synthesis [1, 2]. Management of knee osteoarthritis (OA) routinely involves tackling image analysis problems listed above. The purpose of this paper is to report validity and reliability of DL-based methods to analyse knee OA using Magnetic Resonance Imaging (MRI) modality.

METHODS

The search was conducted on articles published in three databases (Web of Science, PubMed and Scopus) between 1990 and August 2022. Search string consisted of keywords "knee", "osteoarthritis", "deep learning", automatic" and "MRI". The study was registered in PROSPERO – an international prospective register for systematic reviews. Results of the study were categorized based on the validity and reliability of the problem area addressed. Any studies not focused on the knee joint, any review articles, studies based on imaging other than MRI, and studies not in English were excluded from this review. Selected studies were analysed based on the reported validity and reliability of DL methods to assess knee OA problems on MRI [3]

RESULTS AND DISCUSSION

A total of 431 studies were identified through database search. After removing duplicates and applying inclusion/exclusion criteria, 45 studies were found suitable for this systematic review. Selected studies were assessed based on the problems associated with Knee OA. Segmentation for OA analysis was reported by 29 studies, classification was reported by 12 studies, registration was reported by 1 study, synthesis was reported by 4 studies, and outlier detection was reported by none. There were 2 studies which addressed both segmentation and classification problems. Performance of any DL framework includes validity and reliability metrics as a part of its testing protocol. Therefore, we analysed these studies as per the reported performance measurement metrices (Figure 1). For segmentation problem, the most common metric reported is Dice Similarity Coefficient (DSC), followed Volume Overlap Error (VOE), Volume difference (VD), Average symmetric surface distance (ASSD), Root Mean Square Surface Distance (RMSD), Average Hausdorff Distance (Avg HD). For classification problems metrics of Receiver Operating Characteristic curve (ROC), Area under Curve (AUC), Sensitivity and Specificity are reported.

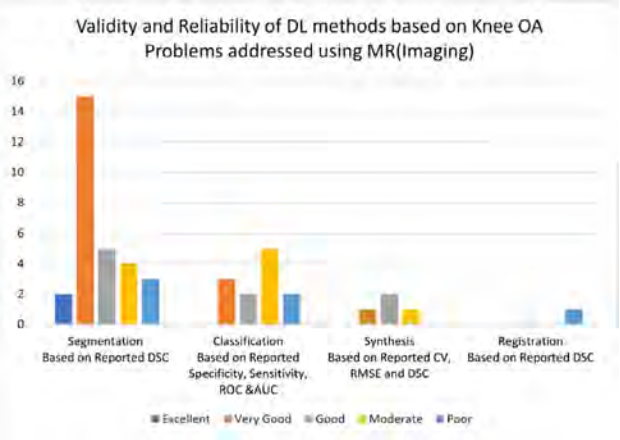

Figure 1 Systematic Review Outcome

Registration problem used DSC metric. Studies on synthesis problem used DL for synthesising super-resolution in the context of OA MRI biomarkers. They used DSC, VOE, VD, coefficients of variation (CV), concordance correlation coefficients (CCC), Root Mean Square Error (RMSE), Pearson Correlation (PC), Structural Similarity Index (SSI), Peak Signal to Noise Ratio (PSNR) and Normalized Mean-Squared Error (NMSE). After scrutinizing the studies based on the dataset used, it was evident that only OAI dataset is publicly available and has become a standard for comparing research outcomes [4]. Most of the studies addressed knee OA problems using a specific MR sequence, focusing on cartilage and tissue information only, making these DL methods highly data agnostic. A multi-tasking problem solving DL method is lacking in the literature. Current literature lacks interpretable and explainable DL models.

CONCLUSIONS

Segmentation remains the majorly studied problem area followed by classification. Standardization in validity and reliability measures is needed.

REFERENCES

[1] Latif et al. *AI in Med*, 122, 102213, 2021.
[2] Panfilov E et al. *JOR*, 40(5), 2022.
[3] Pedoia V. et al. J *MRI*, 49(2), 2019.
[4] https://nda.nih.gov/oai/

CLASSIFICATION OF EMG SIGNALS DURING CONTRA-LATERAL ARM MOVEMENT

Azmin Sham Rambely[1], Abu Bakar Yahya[1], and Nur Syahirah Izzati Zaidi[1]
[1] Faculty of Science & Technology, Universiti Kebangsaan Malaysia Bangi, Selangor, Malaysia
Email: asr@ukm.edu.my

INTRODUCTION

Characterization of EMG signals in human movements using machine learning algorithms has attracted many researches in clinical [1] and robotic applications [2]. The aim of the paper is to determine the best method among four machine learning models, which are Naïve-Bayes (NB), random forest (RF), k-Nearest Neighbor (KNN) and Support Vector Machine (SVM) in classification of EMG signals during a daily activity of touching a contra-lateral shoulder. The process consists of three parts: time division of data according to phases of movement, the EMG feature extraction based on time domain, and four machine learning models.

METHODS

The participants consisted of 20 healthy normal subjects (five male and 15 females, with mean age of 39.1 years (SD 10.3, range 24-56 yo), mean weight 72.9 kg, mean height 160.7 cm, mean right arm length 57.9 cm. All participants were free from any injury and written consent were obtained. The study was approved by research Ethics committee UKM (NN-2016-045). Arm movement of touching contra-lateral shoulder activities were recorded using a Vicon motion analysis system with a recording rate of 100 Hz. The EMG signals from deltoid, biceps, and palmaris longus muscles on the right arm were recorded using a Delsys EMG system.

The arm moved from ipsilateral thigh to the contralateral shoulder, rested on the shoulder and returned to its initial position. Three phases of arm movement were identified (lifting, static and returning the arm) and data were classified based on these phases. The data of arm movements were divided according to the arm movement angles, Figure 1.

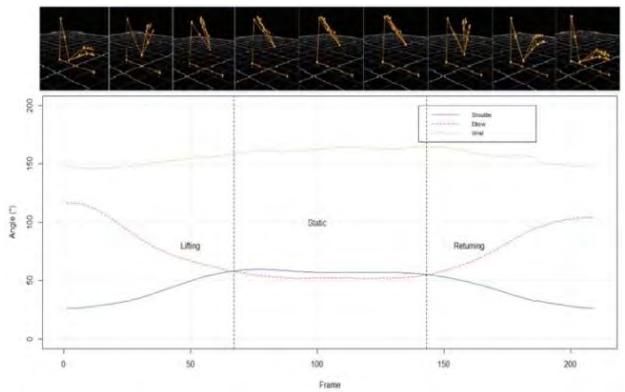

Figure 1 Angles for shoulder, elbow and wrist joints during touching contralateral shoulde

In the classification phase, three time-domain features were extracted which were maximum amplitude, mean absolute value, and root mean squared value, using supervised machine learning models. The data were divided into 80% training and 20% testing. The training data were classified using the four models.

RESULTS AND DISCUSSION

A comparison of the average percentage accuracy of algorithm classification for each time domain against the three phases of arm movement showed MVS produced the highest values. To evaluate the performance of the classification models, confusion matrices of different parameters for each model, such as accuracy, precision, recall and F-measure were obtained. The MVS model showed the best performance in all parameters with values in accuracy, precision, recall and F-score rates at 94.88, 95.10, 94.90, and 94.80, respectively, Table 1.

Table 1: Comparison of percentage evaluation of machine learning model metric scores.

	Confusion matrices (%)			
Model	Accuracy	Precision	Recall	F-measure
NB	94.02	94.00	94.00	94.00
MVS	94.88	95.10	94.90	94.80
RF	91.45	91.70	91.50	91.30
KNN	76.90	79.40	76.90	76.40

CONCLUSIONS

The results showed that all the classification models achieved accuracies ranging between 76–95%. Moreover, it was found that the MVS model had the best performance among the four tested models. However, confusion matrices of different parameters can be improved.

ACKNOWLEDGEMENTS

The first author is grateful for the grant from UKM with code GP-2021-K007147.

REFERENCES

[1] Chen PW et al. *Int. J. of Env. Res. and Public Health* **18(4)**: 1-16, 2021.
[2] Laksono PW et al. *Machines* **9(3)**: 56, 2021

ESTIMATING L5/S1 FLEXION-EXTENSION MOMENT WITH AN ARTIFICIAL NEURAL NETWORK METHOD IN MANUAL LIFTING TASKS: A PRELIMINARY VALIDATION STUDY

Chien-Chi Chang[1,*] and Pin-Ling Liu[1]

[1] Department of Industrial Engineering and Engineering Management, National Tsing Hua University, Hsinchu, Taiwan

Email: max.chang@ie.nthu.edu.tw

INTRODUCTION

Manual lifting activity is one of the most commonly reported risk factors for low back pain (LBP) in the workplace. L5/S1 moment estimated by biomechanical models allows ergonomists to evaluate if the lifting tasks carried by the workers could potentially cause overexertion injuries. Conventional measurements to perform such analyses mostly require the use of laboratory-based optical motion tracking systems (OMTSs) and force plates (FPs). However, these advanced types of equipments are usually expensive and bulky. In addition, it could be a challenge to use them outside a well-controlled lab environment. Researchers had proposed alternative motion tracking methods of using the markerless skeletal model driven by joint data obtained from portable depth cameras such as Kinect (Microsoft, USA). However, the use of Kinect-identified joint location as a counterpart for the L5/S1 joint position had been found to yield significant error between 16.8 to 33.7 cm during standing [1]. In our previous study [2], we proposed the use of an artificial neural network (ANN) method to improve the accuracy of a markerless skeletal model for L5/S1 position identification. In the current study, we further investigated the accuracy of L5/S1 moment estimations based on our previously proposed work. The measurement results of the L5/S1 flexion-extension moment during symmetrical lifting are reported.

METHODS

A lifting database comprising the postural data output from the Kinect skeletal model and OMTS during various symmetrical lifting motions was collected simultaneously with the corresponding ground reaction forces measured by FPs. A total of twenty participants' data was extracted from the database and was divided into the training dataset (15 out of 20) and the validation dataset (5 out of 20). The training dataset was used to develop the ANN model for improving the L5/S1 position prediction based on the joint coordinate data output from the Kinect skeletal model as reported in the previous study [2]. Once the ANN model was developed, it was then applied to predict the L5/S1 positions for each participant in the group of validation dataset. An inverse dynamics model [3] was utilized to estimate the flexion-extension moments at the L5/S1 joint through a top-down biomechanical modelling approach based on the ANN-predicted L5/S1 positions. The flexion-extension moments at the L5/S1 joint based on the data output from OMTS and FPs for the same validation dataset group were also calculated through a bottom-up biomechanical modelling approach and were treated as the gold standard. The difference between the ANN method and the gold standard in estimating the L5/S1 flexion-extension moment was examined.

RESULTS AND DISCUSSION

The mean (SD) of the errors for estimating the L5/S1 flexion-extension moments from the ANN method during the entire duration of various liftings with respect to the validation dataset was 16.76 (8.33) Nm. A randomly selected example of the L5/S1 moment during a symmetrical lifting trial comparing the estimation based on the ANN method against the gold standard is illustrated (Figure 1).

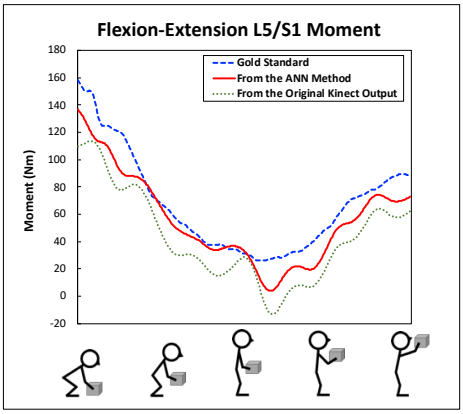

Figure 1 The ANN method estimated flexion-extension L5/S1 moments vs. the gold standard measurement

CONCLUSIONS

Applying the ANN method to obtain a more accurate L5/S1 position from the Kinect markerless skeletal model output shows the accuracy in estimating the L5/S1 moment can be improved. If a portable depth camera system such as Kinect is needed for the applications of field assessment, the ANN-based method can provide a more accurate evaluation of the L5/S1 moment in manual lifting tasks.

ACKNOWLEDGEMENTS

This work was supported by the Ministry of Science and Technology, Taiwan. (MOST 109-2221-E-007-062-MY3).

REFERENCES

[1] Xu X et al. *Applied Ergo* **49**: 47-54, 2015.
[2] Pin-Ling L et al. *J Biomech* **130**: 100844, 2022.
[3] At L. Hof. *J Biomech* **25(10)**: 1209-1211, 1992.

THE EFFECT OF SLANTED COMPUTER MOUSE IN A QUICK CLICK TASK: A PILOT STUDY

Kuang-Wei Lin[1], Yu-Lin Chen[1,2] and Winny Chang[1]
[1]User Research Department, BenQ Corporation, Taipei City, Taiwan.
[2] Graduate Institute of Athletics and Coaching Science, National Taiwan Sport University, Taoyuan City, Taiwan.
Email: Wade.KW.Lin@BenQ.com

INTRODUCTION

Online first-person shooter (FPS) games have grown in popularity, such as Counter-Strike: Global Offensive (CS: GO), Valorant, and Fortnite. In these FPS games, the ability to shoot accurately and quickly with a computer mouse is essential. Ergonomic computer mice promote a more neutral wrist and forearm position and avoid applying external pressure to the palmar wrist region. A previous study, however, discovered that ergonomic devices did not reduce carpal tunnel pressure [1]. Although an ergonomic mouse may not reduce the risk of carpal tunnel syndrome, the different shapes of computer mouse might alter the forearm muscle activation patterns. To the best of our knowledge, no studies on the effect of computer mouse slanted angles on clicking movement have been conducted. Therefore, the purpose of this study was to compare the effects of two different computer mouse slanted angles (0° and 5°) in a quick click task.

METHODS

Eight male esports gamers volunteered to participate in this study. The CS: GO was used for this study. The gamers were asked to click left button of computer mouse as fast as possible until an enemy was killed. Hand motion data were recorded with an eight-camera Motion Analysis Corporation Kestrel motion capture system. The muscle activities of the extensor carpi radialis longus, extensor carpi ulnaris, 1st dorsal interossei, 4th dorsal interossei, abductor digiti minimi and extensor indicis muscle were recorded by the Delsys EMG system during the task. Figure 1 showed two prototype computer mice with different slanted angles. The Wilcoxon signed-rank test was used to determine whether there was a significant difference between the slanted mouse and the non-slanted mouse. The statistical significance level was set at $\alpha = 0.05$.

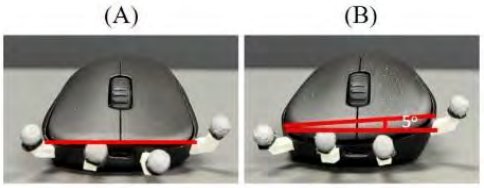

Figure 1 The computer mice with 0° (A) and 5° (B) slanted angles.

RESULTS AND DISCUSSION

The results revealed that when participants used the computer mouse with slanted angle of 5°, the index finger MCP joint angle was significantly greater. However, the click velocities and activation levels of all the muscles did not differ significantly between the two slanted angles of the computer mouse (Table 1). A previous study found that the slanted angles (0°-30°) of computer mice influenced forearm muscle activation [2]. The reason for this disparity could be that the slanted angle in this study was only 5°. Future studies are needed to determine whether greater slanted angles can affect gamers' performances.

CONCLUSIONS

In conclusion, the computer mouse with a 5° slanted angle had no effect on the muscles or performance in the quick click task.

REFERENCES

[1] Annina S et al. *Appl Ergon* **47**: 151-156, 2015.
[2] Chen H-M et al. *Clin Biomech* **22**: 518-523, 2007.

Table 1: Average and standard deviation values for index finger kinematics and muscle activation in quick click task.

Variables	0°	5°	*p-value*
Click velocity (mm/s)	-19.77 ± 4.36	-20.78 ± 4.76	0.64
Index finger MCP joint angle (°)	143.58 ± 8.99	148.19 ± 8.43	0.01*
Extensor carpi radialis longus activity (%)	6.57 ± 2.86	5.85 ± 2.39	0.31
Extensor carip ulnaris activity (%)	9.61 ± 5.45	9.16 ± 4.51	0.64
1st dorsal interossei activity (%)	11.26 ± 9.47	11.39 ± 9.16	0.95
4th dorsal interossei activity (%)	6.00 ± 2.07	6.08 ± 2.01	0.95
Abductor digiti minimi activity (%)	3.24 ± 1.23	3.13 ± 1.30	0.74
Extensor indicis muscle activity (%)	15.52 ± 9.20	14.36 ± 9.07	0.25

MUSCLE FATIGUE COMPARISON BETWEEN SLANTED AND NON-SLANTED GAMING MICE

Winny Chang[1], Kuang-Wei Lin[1], and Yu-Lin Chen[1,2]
[1] User Research Department, BenQ Corporation, Taipei City, Taiwan.
[2] Graduate Institute of Athletics and Coaching Science, National Taiwan Sport University, Taoyuan City, Taiwan.
Email: Winny.TY.Chang@BenQ.com

INTRODUCTION

The gaming mouse is crucial to professional gamers' performances. It comes in different designs, contributing to various effects on maneuvering the mouse. Some studies have investigated the effects of slanted angles during general computer tasks. A prior study discovered that performances in pointing and dragging tasks worsened as the slanted angle increased [1]. Another study found that slanted angles would affect surface electromyography (EMG) levels in a text-editing task [2]. However, the effects of slanted angles in esports have not been explored. Thus, this study examined the upper limb muscle fatigue difference between slanted and non-slanted gaming mice in an intensive shooting task.

METHODS

Eight right-handed male esports gamers participated in this study. Their ages ranged from 19 to 27 years old, and the average age was 24.3 (SD: 2.9). The shooting task required the gamers to kill 200 enemies as fast as possible in the Counter-Strike: Global Offensive "Aim Botz - Training" Workshop. The enemies appeared in random positions within a designated range. Gaming mice with slanted angles of 0° and 5° were tested (Figure 1). Six upper limb muscles were assessed: the first dorsal interosseous (1st DI), the fourth dorsal interosseous (4th DI), extensor indicis (EI), abductor digiti minimi (ADM), extensor carpi ulnaris (ECU), and extensor carpi radialis (ECR) muscles. EMG signals were collected from the start to the end of the shooting task using the Delsys Trigno system. The raw EMG signals were bandpass-filtered between 20 and 450 Hz and then divided at 3-second intervals. In each interval, the median frequency was calculated with fast Fourier transforms using Matlab. Finally, linear regression analyses were conducted on the calculated median frequencies as a function of time, and the median frequency slopes in the six muscles were determined as the slopes of the regression lines. The Wilcoxon signed-rank test was used to determine whether there was a significant difference between the slanted and non-slanted gaming mice. The statistical significance level was set at $\alpha = 0.05$.

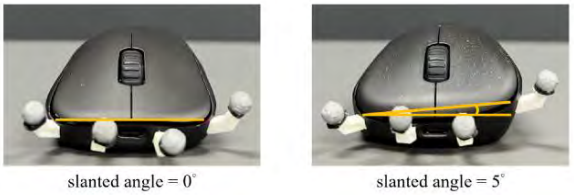

Figure 1 Gaming mice tested in the experiment.

RESULTS AND DISCUSSION

The median frequency slopes of the two gaming mice were not significantly different from each other in all six upper limb muscles (Table 1). However, there was a relatively larger difference in the ADM muscle. The median frequency when using the non-slanted mouse dropped more compared to that when using the slanted mouse, indicating that non-slanted mice might be more prone to fatigue in this muscle when performing an intensive shooting task.

Table 1: Median frequency slopes in the six upper limb muscles.

	slanted angle = 0°	slanted angle = 5°	*p-value*
1st DI	-0.051 ± 0.039	-0.032 ± 0.042	0.742
4th DI	-0.022 ± 0.087	-0.030 ± 0.051	1.000
EI	-0.027 ± 0.031	-0.024 ± 0.095	0.148
ADM	-0.085 ± 0.151	-0.025 ± 0.132	0.078
ECU	-0.015 ± 0.041	-0.023 ± 0.034	0.313
ECR	-0.001 ± 0.020	-0.009 ± 0.033	0.547

A previous study found that an increase in slanted angle (30° vs. 0°) caused lower muscle activity in the ECU muscle in a 30-minute task of highlighting, copying, and pasting text [2]. This suggests the fatigue of the ECU muscle may also be different. In this study, however, there was no significant difference between the two mice in this muscle. Possible reasons may be the smaller angle difference (5°) and the shorter task time (around 2 minutes). Therefore, it is recommended that future studies should: (1) include more slanted angles that cover a larger range; and (2) lengthen the task time. That way, the effects of slanted angles in esports might become more prominent, which could help design new gaming mice that benefit gamers.

CONCLUSIONS

This study shows that a five-degree difference in the gaming mouse slanted angle does not significantly affect fatigue during the shooting task in the 1st DI, 4th DI, EI, ADM, ECU, and ECR muscles. The fatigue difference between the slanted and non-slanted mice was relatively larger for the ADM muscle.

REFERENCES

[1] Jung K. *Appl Ergon* **45(3)**: 450-5, 2014.
[2] Chen H-M et al. *Clin Biomech* **22(5)**: 518-523, 2007.

MUSCULOSKELETAL ANALYSIS OF UPPER LIMB MOTION DURING REPETITIVE TASKS

Akisue Kuramoto[1], Masaya Noguchi[1] and Motomu Nakashima[1]
[1] Department of Systems and Control Engineering, Tokyo Institute of Technology, Tokyo, Japan.
Email: akisuekura@sc.e.titech.ac.jp

INTRODUCTION

From the viewpoint of occupational safety and health, it is important to manage worker fatigue. Muscle fatigue can cause work-related musculoskeletal disorders [1]. In other words, some method to assess muscle fatigue in working conditions is important. One of the strategy of such methods is perforimg musculoskeletal simulation of work motions measured in actual work environment. It is expected that the measurement of work motions in the actual work environment will become easier in the future. This is because the method of estimating the 3D posture of the human body from moving images, which has been actively developed in recent years [2], can be applied to the moving images of surveillance cameras installed in the work environment. On the other hand, few studies have discussed on the changes of work motion and physical fatigue during repetitive task. Therefore, as a preliminary step to the discussion, this study aims to confirm whether changes in work motions in repetitive tasks are related to changes in muscle activity.

METHODS

By the IMU-based motion capture system Perception Neuron Studio (Noitom Inc, Florida), three-dimensional human body motion was measured while a healthy male participant performed a simulated occupational task to lift a bottle (500 g) from elbow height to shoulder height. This task was repeated 100 times in a row at the frequency of once per 2 seconds. Both start and end points of the task were set at 80 % of the upper limb length in the midsagittal plane in the natural standing position. For muscle activity simulation, the measured motion data was applied to musculoskeletal model of human body using the commercial software Anybody (Anybody Technology, Aalborg, Denmark). The human body model was adjusted to the body height and weight of the participant.

RESULTS AND DISCUSSION

During the period when the participant was lifting a bottle, the flexion and abduction angles of the shoulder joint were about 70 degrees and 30 degrees in the first ten times, whereas were about 60 degrees and 20 degrees in the last ten times, respectively. In addition, the elbow flexion angle was about 50 degrees in the first ten times, whereas was about 70 degrees in the last ten times. In other words, in the last ten times, the participant performed work motion around a posture that kept their upper arms closer to his body with his elbow extending than in the first ten times. Results of musculoskeletal analysis show that the activity of the middle deltoid works on shoulder abduction decreased in the last ten times, whereas the activity of the biceps brachii works on elbow flexion was similar through the experiment (Figure 1). These results indicate that the participant changed work motion to reduce shoulder workload without increasing elbow workload.

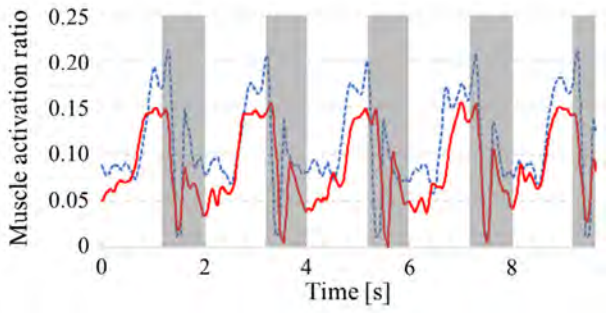

(a) middle deltoid

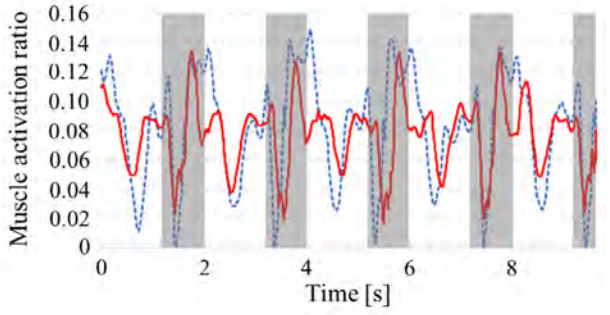

(b) biceps brachii

Figure 1. Simulation results of muscle activation ratio. Blue dashed line and red solid line show results from the 5th to 9th and from 89th to 93rd times, respectively. Areas with a grey background indicate time periods when the participant did not have a bottle.

CONCLUSIONS

This study analysed time changes of body motion and muscle activity in a repetitive lifting task. Musculoskeletal simulation results indicate that body motion at the ends requires less activity of shoulder muscles with similar activity level of elbow muscles compared to that at the beginnings. This shows the applicability of the musculoskeletal simulation in quantitative evaluation of the muscle activity change along with the work motion change.

REFERENCES

[1] Hu B and Ning X. *Annals of biomedical engineering* **43**: 2112-2119, 2019.

[2] Kuramoto A et al. *J of Biomechanical Science and Engineering*, https://doi.org/10.1299/jbse.22-00305, 2023.

Effect of superficial tissue and intermuscular connections on the shear modulus distribution within the rectus femoris muscle

Taiki Kodesho[1], Takuya Kato[1], Gakuto Nakao[1], Yu Yokoyama[1], Yuhei Saito[1], Kota Watanabe[2], Yuki Ohsaki[3], Masaki Katayose[2] and Keigo Taniguchi[2]

[1] Graduate School of Health Sciences, Sapporo Medical University / Hokkaido, Sapporo, Japan.
[2] Department of Physical Therapy, School of Health Sciences, Sapporo Medical University / Hokkaido, Sapporo, Japan.
[3]First Division of Anatomy, School of Medicine, Sapporo Medical University / Hokkaido, Sapporo, Japan.
Email: kodesho@sapmed.ac.jp

INTRODUCTION

Intramuscular heterogeneity exists in the shear modulus of the rectus femoris (RF) muscle [1]. However, the underlying heterogeneity mechanisms are not entirely understood. Previous research has reported that detachment of superficial tissues reduces the shear modulus by 50% [2]. However, the effect of superficial tissues on the shear modulus has only previously been examined at one site and its involvement in heterogeneity is unknown. Additionally, changes in shear modulus distribution have not been investigated when inter-tissue connections are disconnected so that fascial force transmission does not occur. The aim of this study was to examine the effects of the skin, deep fascia, and intermuscular connections on the shear modulus of the RF at multiple sites.

METHODS

Eleven donors were fixed using the Thiel method. The mean age at death was 84.8 years (ranging 60–98 years). Measurements were performed at 0°, 60°, and 120° knee flexion in a neutral hip position. Tissue processing was performed under four conditions: superficial tissue (CONT), skin off (SKIN), deep fascia detachment (FASC), and intermuscular connections detachment (ALL). The shear modulus of RF muscle was measured using ultrasound shear wave elastography (Aixplorer Ver. 12. MSK mode; Hologic, Marlborough, USA). The measurement sites were the proximal (25% of the length of the RF), central (50%), and distal (75%). The study was approved by the Sapporo Medical University Ethical Committee (approval number: 30-2-26).

RESULTS AND DISCUSSION

Three-way ANOVA revealed no significant interaction between treatment, site, and angle (P = .156), treatment and angle (P=.067), or site and angle (P=.441). There was a significant effect of treatment (P<.001), site (P=.010), and angle (P<.001) and interaction between treatment and site (P<.001). Figure 1 shows a graph of RF shear modulus measurements based on treatment and site interactions. Post-hoc test results showed that the shear modulus in the CONT and SKIN conditions were greater than those in the FASC (vs. CONT: p = .010, vs SKIN: p = .030) and ALL (vs. CONT: p < .001, vs SKIN: p < .001) conditions. Proximal region measurements in the FASC condition were greater than that in the ALL condition (p = .019). In the central region, the shear modulus in the CONT and SKIN conditions were greater than that of the ALL condition (vs. CONT: p = .023, vs SKIN: p = .003). There were no significant differences among the shear modulus of the distal region between any of the treatment conditions. The proximal shear modulus was greater than that of the central (p = .048) for the CONT condition. There were no significant differences between the SKIN condition measurement sites. The distal shear modulus was greater than that of the proximal (p = .004) in the FASC condition, and the distal shear modulus was greater than that of the proximal (p = .002) and central (p = .006) in the ALL condition.

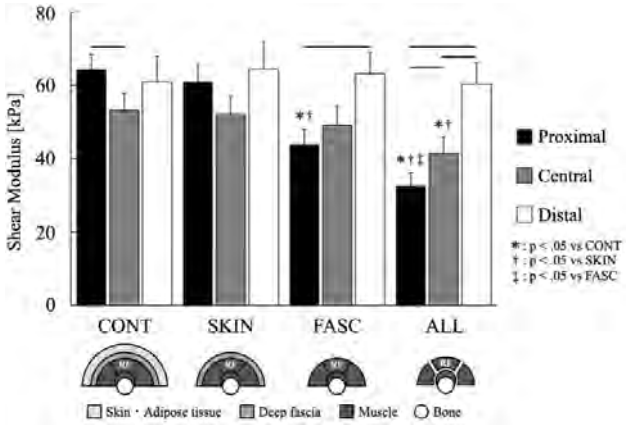

Figure 1 Rectus femoris shear modulus based on treatment at each site.

CONCLUSIONS

The shear modulus decreased in the RF's proximal and central regions due to the detachment of the deep fascia and inter-tissue connections. Regional dependence may exist in the effects of superficial tissues and interstitial connections on the shear modulus of the RF. These results suggest that the superficial fascia and inter-tissue connections should be considered during muscle evaluation and clinical treatment.

REFERENCES

[1] Kodesho T et al. *Eur J Appl Physiol* **121**: 1441-9, 2021.
[2] Yoshitake Y et al. *Ultrasound Med Biol* **42**: 674-82, 2016.

Short-Term Impact of Basketball Workout on Knee Medial Meniscus

Hsin-Min Wang[1], Jen-Chieh Lai[2], Yin-Chou Lin[3], Chin-Chih Chiou[4]
[1] Graduate Institute of Sports and Health, National Changhua University of Education, Changhua, Taiwan.
[2] Department of Orthopedic Surgery, Taichung Armed Forces General Hospital, Taichung, Taiwan.
[3] Department of Physical Medicine and Rehabilitation, Chang Gung Memorial Hospital, Taoyuan, Taiwan.
[4] Department of Sports, National Changhua University of Education, Changhua, Taiwan.
Email: hmwangat@gmail.com

INTRODUCTION

Knee meniscus injury is common injuries on basketball with high surgery rate and long-term impact on knee cartilage health [1]. Dynamic extrusion of the meniscus was associated with meniscal injuries which could be used to examine the meniscal health [2]. While acute structural response of medial meniscus from non-weight bearing to weight bearing position are widely reported, how knee medial meniscus responses to specific sports workout are not well understood. The purpose of this study was to determine the degree of displacement on knee medial meniscus in response to 30 minutes of basketball-specific workout.

METHODS

Twenty division I high school male basketball athletes (1.77 ± 0.07 m, 73.4 ± 12.2 kg, 16.1 ± 0.9 yrs) without lower extremity injury within 6 months, previous knee surgery, or serious knee injury history were recruited. All participants underwent ultrasound imaging of the knee medial meniscus on both limbs during non-weight bearing, weight bearing position, immediately after, and one hour after a 30 minute basketball workout. The 30 minutes basketball workout included 8 minutes of dynamic warm-up exercise, 8 minutes various defense drills, 8 minutes interleaving layup and pull-up jumper. Meniscal extrusion was measured via ultrasound imaging which was defined as peripheral medial meniscal margin exceeding the tibiofemoral compartment of the knee. Two-way repeated measures ANOVA examined the differences in right and left knees meniscal extrusion during non-weight bearing, weight bearing position, immediately after, and one hour after a 30 minute basketball workout.

RESULTS AND DISCUSSION

There was no significant main effect of limb on knee medial meniscal extrusion ($F(1,19) = 0.242$, $p = .628$). The left knee meniscus extrusion was similar with right limb (2.5 ± 0.1 mm Vs 2.5 ± 0.1 mm). There was significant main effect of time points on knee meniscus extrusion ($F(3,17) = 8.772$, $p = .001$). Post hoc tests using the Bonferroni correction revealed that knee meniscus extrusion increased from non-weight bearing to weight bearing position (2.2 ± 0.1 mm Vs 2.5 ± 0.1 mm, $p = .022$) and was increased from weight bearing position to immediately post-workout (2.5 ± 0.1 mm Vs 2.6 ± 0.1 mm, $p = .049$). There was no significant difference between immediately post-workout and an hour post-workout (2.6 ± 0.1 mm Vs 2.6 ± 0.1 mm, $p = 1.000$). There was no interaction between limb and time points on knee meniscus extrusion ($F(3,17) = 0.690$, $p = .570$).

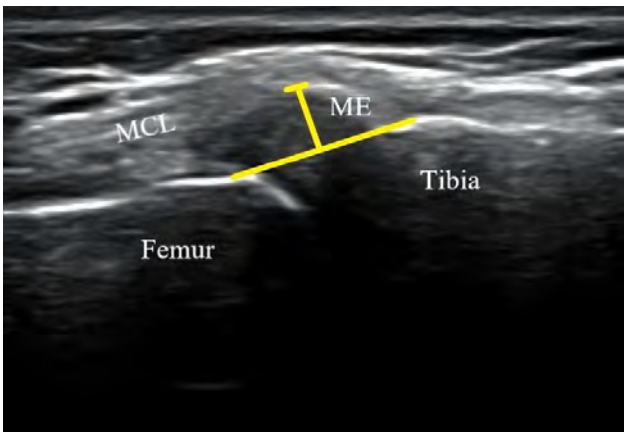

Figure 1. Ultrasound examination of medial meniscal extrusion. ME, meniscal extrusion; MCL, medial collateral ligament.

CONCLUSIONS

After 30 minutes basketball workout, the displacement of knee medial meniscus was higher than non-weight bearing and weight bearing position and was similar with an hour later after workout. This work suggests that basketball workout induced short-term structural displacement in knee medial meniscus and could not recover after an hour rest. Future research should focus on how knee meniscus responses to long-term sports activities and the association with meniscus injury.

ACKNOWLEDGEMENTS

This work is funded by National Science and Technology Council, Taiwan. (MOST 111-2410-H-018-034)

REFERENCES

[1] Kim S et al. *J Bone Joint Surg* **93(11)**: 994-1000, 2011.

[2] Karpinski K et al. *Knee Surg Sports Traumatol Arthrosc* **27(10)**: 3311-3317, 2019.

THE EFFECT OF DIFFERENT FILE TYPES AND DXA PROTOCOLS ON AN IMAGE PROCESSING FRACTURE RISK PREDICTION TOOL

Ali Ammar[1], Fatemeh Jazinizadeh[2], Jonathan D. Adachi[3] and Cheryl E. Quenneville[1,2]
[1] School of Biomedical Engineering, McMaster University, Hamilton, ON, Canada.
[2] Department of Mechanical Engineering, McMaster University, Hamilton, ON, Canada.
[3]Department of Medicine, McMaster University, Hamilton, ON, Canada
Email: ammara@mcmaster.ca

INTRODUCTION

A recently developed image processing technique uses 2-D statistical shape and appearance modelling (SSAM), which analyzes the shape and density of the femur to predict hip fracture risk accurately [1,2]. A dual-energy X-ray absorptiometry (DXA) scanner has many imaging protocols clinicians may use, with a standard protocol typical for hip DXA scans. The IVA-HD imaging protocol provides a high-definition image typically used on the lateral spine, yet may provide a more accurate fracture risk prediction if applied to the hip. In addition, the present algorithms [1,2] were developed using JPGs, so theoretically, performance could be enhanced by using a file type with a higher resolution (e.g., DICOM). The main concern is JPG images are low-resolution images as this image type does not preserve each original pixel. DICOM images are considered high-performance images that can be converted to high-resolution images like PNG while maintaining the actual pixel values of the image [3]. The goal of this study was to quantify any differences in the SSAM fracture risk tool by comparing each DXA protocol (standard hip & IVA-HD) in JPG & DICOM format (i.e., four total image types).

METHODS

Cadavers and patients were used in this study to test further the sensitivity of the SSAM fracture risk algorithm (i.e., with femur and pelvis, and femur only). A device was designed and built to support cadaveric femurs in a DXA scanner. A 15 cm clear bucket filled with water simulated the attenuation of muscle and fat [4]. Seven isolated cadaveric femurs (5M/2F, age 59.9±11.9 years) were DXA scanned at a neutral position (parallel to the DXA table) using a Hologic Discover A system. Each femur was scanned using two main imaging protocols from the DXA scanner: a standard hip and an IVA-HD. Similarly, six patients (1M/5F, age 69.5±7.74 years) were also recruited from the Hamilton Osteoporosis Diagnostic Clinic to receive an additional scan using the IVA-HD imaging protocol, in addition to their regular scheduled hip DXA scan (standard hip) (Fig 1.). Each hip scan for all subjects (patients & cadavers) from each protocol was exported to two different file types: DICOM and JPG (52 total images). To use the SSAM algorithm and apply landmarks along the femur [2], the DICOM images were converted to PNG. Each image was assessed using the SSAM algorithm [1]. Briefly, the SSAM algorithm applies principal component analysis (PCA) to obtain the main modes of variation. Logistic regression is then used, applying the modes, age, and bone mineral density values to find the probability of sustaining a fracture [2]. The probability fracture was outputted for each image/file type. A two-way repeated measures ANOVA (α=0.05) with a Bonferroni post-hoc test was used to determine the effect of the protocols and file types on fracture probability and compare the impact on different subjects.

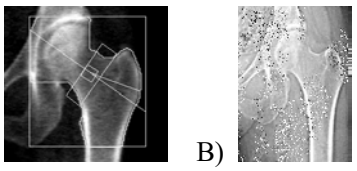

Figure 1 Hip DXA scan using (A) clinical standard (B) IVA-HD

RESULTS AND DISCUSSION

The degree of freedom was corrected using Greenhouse-Geisser (ε<0.75) due to violating the assumption of sphericity. When examining the four image types, no significant differences (p=0.254) were found in the probability of sustaining a fracture. This demonstrates that the fracture risk prediction tool's output was unaffected by the protocol or file type selection. This is important to assess because IVA-HD is not regularly used for a hip assessment. Since it provides a higher-quality image, this comparison ensured that the current hip protocol used clinically could remain utilized for diagnosis and fracture risk assessment. Also, using DICOM and JPG (regardless of DXA protocol) did not alter the results of the fracture risk prediction tool, which can enable this tool to be used in a clinical setting, irrespective of the file type used. Finally, the fracture probability while using the four image types was not significantly impacted (p=0.254) by the interaction between cadavers and patients. This further supports the sensitivity of the tool as regardless of the subjects (either cadaver or patient) and image types used, the tool's output remains unaffected.

CONCLUSIONS

Novel fracture prediction tools rely on high-quality images for accurate performance. This study's results indicate that the present tool performs equally well on DXA scans regardless of file type or scan protocol, showing potential for clinical integration.

REFERENCES

[1] Jazinizadeh, Quenneville. 2020. *Med Eng Phys.*, **78**
[2] Jazinizadeh, F *et al*., 2020. *Osteo. Int.*, **31**
[3] Varma D., 2012. *Indian J Radiol & Imaging*, **22**
[4] Wahnert D., 2009. *BMC Musculoskeletal Disord*. **10**

MRI-based spine models for patient specific surgical planning

Megan Kenny[1], Cathy Holt[1], Valerie Sparkes[2], Dionne Shillabeer[1], Alisdair MacLeod[3], Alberto Casonato[3], Sashin Ahuja[4] and David Williams[1]

[1] Musculoskeletal Biomechanics Research Facility, School of Engineering, Cardiff University, Cardiff, UK.
[2] School of Healthcare, Cardiff University, Cardiff, UK.
[3] Orthoscape, 3D Metal Printing LTD, Bath, UK.
[4] Welsh Centre for Spinal Surgery & Trauma, UHW Cardiff &Vale UHB, Cardiff, UK.
Email: williamsd37@cardiff.ac.uk

INTRODUCTION

Scoliosis is an abnormal spine curvature mainly affecting children, progressing rapidly as they grow. If conservative treatment fails, surgery can prevent progression and improve spinal alignment. Implanting screws in a deformed spine can be challenging, risking spinal cord and nerve root injury, causing neurological issues. To address this, surgical planning tools can create patient specific guides. CT scans used to generate 3D models for surgical planning come with a high ionising radiation dose which is problematic for children, as it increases risk of radiation induced cancer, and it is not a clinical standard in the UK. Improvements in Magnetic Resonance (MR) imaging allow better bone-tissue delineation, with no radiation risk. It is safe for clinical pre-operative investigation and performed routinely in scoliosis surgery. This study aims to validate MR generated spine models compared with CT generated models.

METHODS

Porcine spine specimens (n=6) were acquired and imaged using a Somatom go.Sim CT scanner (Siemens) and a 3T Magnetom Prisma MR scanner (Siemens). A series of different sequences were performed to determine the best imaging parameters. Individual vertebrae were segmented in Simpleware Scan IP (Synopsys) using semiautomated threshold techniques from the two imaging modalities. 3D models were then exported and the MR and CT models were registered using an iterative closest point technique and then compared using a 3D deviation map (Artec Studio 13). Initial pilot was performed comparing MR derived model (T1 VIBE) with CT for one spine specimen.

RESULTS AND DISCUSSION

Visual differences between the two imaging modalities can be seen in Figure 1. 3D Deviation results can be seen in Table 1. Initial results show that the overall difference between MR derived bone models vs gold standard CT models is approximately a single voxel of the MRI (0.6mm^3). This suggests that MRI is a suitable and accurate alternative to CT imaging. The main limitation of MR imaging is the increased scan time and processing time required for generating models. Future work will quantify the difference between imaging modalities further, using 2D measurements such as pedicle width and height [1,2] and carrying out clinical MR imaging (1.5T) as an additional comparator.

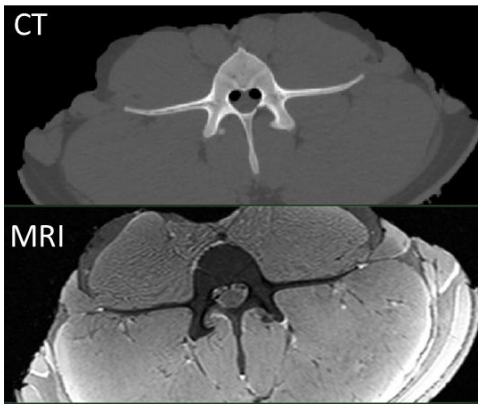

Figure 1 Representative axial slice of vertebra showing visual difference between CT and MR imaging

CONCLUSIONS

MR imaging is a viable and accurate alternative to CT imaging for the application of surgical planning of the spine. Future work will advise on which clinical MR sequence is most appropriate for incorporating into future surgical planning software.

ACKNOWLEDGEMENTS

This project is funded by the Medical Research Council Confidence in Concept Scheme.

REFERENCES

[1] Pacha H et al. *IJSSurgery* **14(5)**:671-680, 2020.
[2] Morita K et al. *Surg and Rad Anat* **43**:833-842, 2021

Table 1: Three dimensional differences between MRI and CT derived vertebra models for one porcine spine.

Vertebra	Root Mean Squared Deviation (mm)	Mean Absolute Difference (mm)
L1	0.61	0.48
L2	0.54	0.40
L3	0.68	0.65
L4	0.62	0.61
T16	0.63	0.68
T15	0.72	0.85

The Association of Normalized Cross-Correlation with Biplanar Videoradiography Tracking Error

Kaito Lee[1], Amy Morton[2], Beatriz Paniagua[3], Anthony Lombardi[3], Joseph J Crisco[2], Michael J Rainbow[1]
[1] Mechanical & Materials Engineering, Queen's University, Kingston, Canada.
[2]Department of Orthopaedics, Brown University, Providence, USA.
[3]Medical Computing, Kitware Inc., Carrboro, North Carolina 27510, USA.
kaito.lee@queensu.ca

INTRODUCTION

Biplanar Video radiography (BVR) is an essential approach for measuring *in vivo* bone motion during dynamic activities. It is well established for tracking larger joints, such as the knee; however, tracking complex joints such as the foot and the wrist, where there are many small, occluded bones, remains challenging. Autoscoper (Brown University) is an open-source software solution designed to facilitate bone tracking. Here, a 3D bone volume is projected as a digitally reconstructed radiograph (DRR) onto the two radiographs captured by BVR. The partial volume is rotated and translated until the DRRs best match the radiographs. This process is repeated for each bone across time, yielding 6dof bone and joint motion.

While manual or semi-manual tracking approaches can yield accuracies on the order of 1 mm and 1 degree in the foot [1], the process is time consuming. Optimization algorithms promise to automate tracking. Autoscoper uses a particle swarm optimization to minimize normalized cross-correlation values (NCCs) between the DRR and the radiographs. Bones with minimal occlusion from neighbouring bones have strong correlation between low NCCs and accurate pose estimation [2]. In multiarticular joints, the NCC values of a DRR representing a single bone may not be at a minimum when the pose is correct because a DRR derived from a single bone may not match well with radiographs containing multiple, occluding bones.

The purpose of this study was to determine whether the optimized NCCs yield accurate pose estimation for bones in the foot joint. We took advantage of a rare, *in vivo* dataset where the participant had tantalum beads implanted into their tibia, talus, and calcaneus.

METHODS

The partial volume talus was generated from a CT scan (0.39x0.39x0.625mm). The pose of the partial volume was initialized by applying 6dof transformation matrices from the bead tracking (Figure 1A). The NCCs for the bead poses were evaluated before optimization. Then, the particle swarm optimizer altered the pose at each frame such that the NCCs were minimized. This process was repeated across 20 frames with three optimizer search limits of -0.1, -1, and 3 (+/- mm and degrees). Rotational errors were quantified using the angle swept by the rotation axis between the bead-based transforms and the optimized transforms. A repeated measures ANOVA and post-hoc t-tests evaluated whether the NCC values differed.

RESULTS AND DISCUSSION

The optimizer found NCC values between 9 and 11% lower than the correct bead-based pose ($p<0.05$). There were differences among the NCCs across the search limits ($p > 0.05$); however, the angular error differed by 0.8°, 1.1°, and 1.3° degrees for the 0.1, 1, and 3 search limits, respectively. The maximum error was 6° (Figure 1 C,D). This suggests the optimizer is indeed minimizing the NCC value but low NCC is not strongly correlated with correct pose.

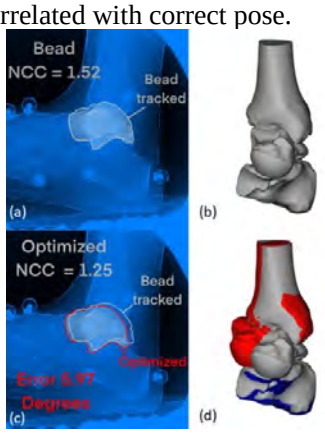

Figure 1 (a) The bead tracked talus (grey outline). (b) Bead tracked calcaneus, talus, and tibia. (c) Autoscoper image of the optimized (red) and bead tracked (grey) talus. (d) The bead tracked (grey) overlayed with the optimized (red) bones.

CONCLUSIONS

These results suggest that a semi-manual approach with manual rotoscoping is still the best-practice for tracking foot bones using Autoscoper, and the optimizer should be used with caution. Errors using a semi-manual method are on the order of 1 mm and 1 degree [1]. Multi-bone tracking, where the pose is optimized for all occluding bones at once may provide better correspondence between NCC and the correct pose. Collision detection may also yield more accurate automated tracking. These limitations are planned to be addressed in the next iteration of Autoscoper, which will also entail porting it into the 3D Slicer computing environment (SlicerAutoscoper[M]).

ACKNOWLEDGEMENTS Supported in part by NIH/NIAMS under award number R01AR078924.

REFERENCES

[1] Welte L et al. 2022
[2] Miranda et al. 2011

Towards dynamic CT imaging in revalidation tracking of jaw movements: An experimental phantom study

Benyameen Keelson[1], Stijn Huys[2], Yannick De Brucker[1] , Gert Van Gompel[1] Johan De Mey[1] and Nico Buls[1]
[1] Department of Radiology, Universitair Ziekenhuis Brussel (UZ Brussel), Vrije Universiteit Brussel, Brussel, Belgium.
[2] Engineering Science, section of Biomechanics, Catholic University of Leuven, Leuven, Belgium.
Email: benyameen.keelson@vub.be

INTRODUCTION

Jaw functions such as biting, chewing, swallowing, and speech are facilitated by the temporomandibular joint (TMJ). Disoders that impact TMJ function can hence cause social dysfunction and discomfort to patents[1].

The aim of this experimental phantom study was therefore to investigate the feasibility of using dynamic CT scans to evaluate TMJ motion. We established a scanning protocol and a realistic mock-up phantom with detailed mandibular anatomical representation.

In addition, the complete image processing workflow was set in place and the radiation dose to the patient was simulated using a humanoid virtual phantom. Preliminary results of mandibular motion in a patient that had undergone joint replacement surgery was evaluated.

METHODS

A 3D printed phantom (created by segmenting DICOM files of CT data of a male jaw) mounted on a six degrees of freedom stewart platform was developed to simulate mandibular movements with variable speeds.

Dynamic CT acquisition was achieved using a clinical 256-slice Apex Revolution CT (GE Healthcare, Waukesha, Wisconsin, USA). Continuous volume scans were obtained without table motion during the movement of the phantom. A series of rigid transformation matrices were estimated using a pairwise volume-based image registration workflow. This allowed to describe motion of the phantom for each time point from the computation of Cardan angles.

RESULTS AND DISCUSSION

From the phantom experiments, the 3D trajectory of the condyles could be successfully traced and represented in 3D plots (figure 1). Average 95% confidence interval for the displacement was 0.41mm, 0.61mm and 0.20mm for the X, Y and Z axis respectively. In terms of rotations, results were 1.39°, 0.31° and 1.29° for the X, Y and Z axis respectively. CTDIvol was 63.95mGy and a DLP of 1023mGycm corresponding to an effective dose of 1.3mSv.

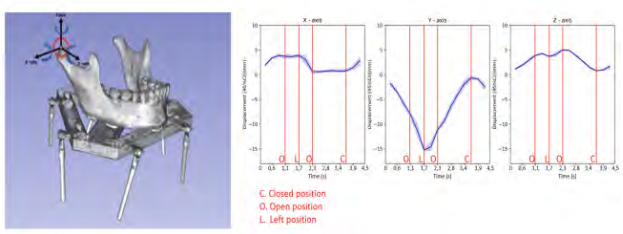

Figure 1 Plots showing the displacement of a point of interest on the mandibular phantom along X,Y and Z axis. Markings on the plot indicate the different motion of the mandibular phantom

CONCLUSIONS

This preliminary study showed reproducible results. Future applications could be in pre-operative planning or potential patient follow-up from combining the visual and 3D graphical mandibular motion kinematics.

ACKNOWLEDGEMENTS

Acknowledgments are optional and may specify research funding and resources including organisation name and reference numbers (if applicable).

REFERENCES

[1] D. de M. Trize, M. P. Calabria, S. de O. B. Franzolin, C. O. Cunha, and S. N. Marta, “Is quality of life affected by temporomandibular disorders?,” Einstein, vol. 16, no. 4, p. eAO4339, Nov. 2018, doi: 10.31744/EINSTEIN_JOURNAL/2018AO4339.

EFFECTS OF PHYSICAL ACTIVITY LEVEL AND MOTOR FUNCTION ON HIPPOCAMPAL VOLUME IN THE OLDER ADULTS

Kota Anjiki[1], Soichi Ando[1], Rie Tomiga[2], Kento Ishimura[1], Yujiro Kose[2], Kosuke Kano[1], Mizuki Sudo[3],

Yosuke Yamada[4], Naoyuki Ebine[5], Yasuki Higaki[2], Hiroaki Tanaka[2], and Yoichi Hatamoto[2,4]

The Fukuoka Island City Study Group

[1] Graduate School of Informatics, University of Electro-Communications, Chofu, Japan.
[2] Faculty of Sports and Health Science, Fukuoka University, Fukuoka, Japan.
[3] Physical Fitness Research Institute, Meiji Yasuda Life Foundation of Health and Welfare, Tokyo, Japan.
[4] National Institute of Biomedical Innovation, Health and Nutrition, Osaka, Japan.
[5] Faculty of Health and Sports Science, Doshisha University, Kyoto, Japan.
Email: kota.anjiki@uec.ac.jp.

INTRODUCTION

Regular physical exercise increases hippocampal volume and has beneficial effects on brain function such as memory function in the older adults [1]. However, it remains unclear to what extent physical activity level (PAL) and/or motor function is linked with hippocampal volume in the older adults. The purpose of this study was to examine whether hippocampal volume is associated with PAL and/or motor function in the older adults. Based on previous studies, we predicted that both PAL and motor function affect hippocampal volume.

METHODS

We analyzed data from thirty-nine older adults (27 females) (age: 70.9 ± 7.1 yr.). Structural MRI was collected on a 3.0 Tesla scanner (Magnetom Skyra, Siemens). Gray matter volume of the hippocampus and total intracranial volume were assessed using voxel-based morphometry, and hippocampal volume was divided by total intracranial volume. Total energy expenditure for 16 days was measured using the doubly labelled water method [2]. Basal metabolic rate was predicted using the Ganpule equations for adult men and women [3]. Then, PAL was calculated by dividing the total energy expenditure by basal metabolic rate. Total metabolic equivalents (METs) were calculated from accelerometers data. Timed-Up and Go test (TUG) and one-leg standing time test with eyes open were performed to evaluate motor function. Multiple regression analyses were conducted to analyze the relationship between hippocampal volume and independent variables (age, sex, PAL, METs, TUG, and one-leg standing time). Data are expressed mean ± SD.

RESULTS AND DISCUSSION

Hippocampal volume was 7,322 ± 824 mm^3, and normalized value was 0.56 ± 0.06 %. Normalized hippocampal volume was greater in the female older adults as compared with male older adults ($p < 0.001$). Female older adults also exhibited greater total METs ($p < 0.01$) and PAL ($p < 0.001$) than male older adults. Multiple regression analysis revealed that hippocampal volume was associated with sex ($p = 0.001$) and tended to be associated with TUG ($p = 0.099$) (adjusted $R^2 = 0.445$, $p < 0.001$). PAL and METs reflect temporal trends in, but not regular, physical activity level. In the current cohort, regular physical activity was presumably greater in females than males. Hence, we can assume that sex, but not PAL and METS, was associated with hippocampal volume in the present study.

CONCLUSIONS

The present study suggests that regular physical activity and, to a lesser extent, motor function are associated with hippocampal volume in the older adults.

ACKNOWLEDGEMENTS

This study was supported by was supported by the JSPS KAKENHI Grant number 22H03493 to S.A.

REFERENCES

[1] Ericksen KI et al. *Proc Natl Acad Sci U S A* **108**:3017-3022, 2011.
[2] Takae R et al. *J Nutr Helath Aging* **24**:1023-1030, 2020.
[3] Ganpule AA et al. *Eur J Clin Nutr* **61**:1256-61, 2007.

Table 1: Physical activity level, total (METs*min/day), timed up and go test, and one-leg standing time test.

Physical activity level	Total METs*min/day	Timed up and go test (sec)	One-leg standing test (sec)
1.80 ± 0.26	874 ± 243	6.53 ± 1.73	41.8 ± 38.1

TASK-ORIENTED WHOLE BODY REACHING IMPROVES POSTURAL PERFORMANCE IN HEMIPARESIS PATIENTS AFTER STROKE

Jen-Suh Chern[1], Yi-Rou Chen[2] , and Yi-Ching Tsai[1]
[1] Graduate Institute of Rehabilitation Counseling, National Taiwan Normal University, Taipei, Taiwan.
[2] Power & Health Rehabilitation Clinic, Taipei, Taiwan.
Email: chern8616@gmail.com (J-S Chern)

INTRODUCTION

Stroke is the primary cause of disability globally. Postural control deficits following stroke increase risk of fall and functional dependence [1]. Bean-bag activity (BBA) is a frequent used task-oriented whole body reaching activity uses in rehabilitation clinics routinly to improve stroke patients' postural control performance. Changes in postural control performance was reflected in functional mobility, stability limit, balance, and center of pressure sway total path length [2]. The purpose of this study is to investigate the effects of BBA on postural control performance in hemiparesis patients after stroke.

METHODS

This is an experimental-control, pre-posttest experimental design study. 21 hemiparesis patients, 11 in experimental (A) and 10 in control (B) group, who fulfilled the inclusion and exclusion participated in this study. Participarnts in group A underwent BBA training for twelve weeks, twice a week for 60 minutes each time, while those in group B underwent routine occupational therapy which was comprised mainly sedentary activities. Participants in both group underwent similar physical theray programs at the same time. Postural control performance was measured by Timed-Up and Go Test (TUG) , Functional Reach Test (FRT), center of pressure travel path (COPTPL) in three stance postures (bilateral feet shoulder width v.s. close together v.s. heel-toe stance) and two vision conditions (eyes open v.s. close). All the variable was measured at one week before and 6 and 12 weeks after training. Descriptive and repeated measure two-way analysis of variance were used and effect sized was calculated. SPSS 23.0 statistical soft-ware package was used.

RESULTS AND DISCUSSION

The results showed no significants difference ($p > 0.05$) between groups in demographic characteristics. The interaction of group and test times was significant ($p < 0.05$) indicating the difference between groups was affected by the measurement time points. The simple main effects of group showed that the group A performed significantly better than the group B in TUG ($p = 0.022$), FRT ($p = 0.010$) and BBS ($p = 0.034$). The calculated effect size showed that the training in group A improved the postural control performance mediumly to largely in terms TUG ($\eta p^2 = 0.182$), FRT ($\eta p^2 = 0.252$), and BBS ($\eta p^2 = 0.206$). The improvement of COPTPL during stance was not signivicant, while the effect size showed that BBA training induced COPTPL change mediumly to largely($\eta p^2 = 0.69$-0.109) in stance posture demanding high control effort, such as stance in eyes closed condition. Finally, 6 weeks of training in group A with BBA was able to improve the postural control performance and another 6 weeks of training was able to improve those performance further. The training in group B was not able to improve but deteriorate the postural control performance of the participants. It is necessary to monitor the risk of fall of after BBA training.

Table 1: Summery of repeated measure two-way ANOVA.

	Time	Group A (n = 11)	Group B (n=10)	Effect size	*p-value*
TUG	T1	22.13±14.91	39.00±40.67	0.182#	0.022*
	T2	19.99±14.05	37.89±41.395		
	T3	17.06±10.50	38.10±40.34		
FRT	T1	27.36 ±6.87	29.60± 2.72	0.252#	0.010*
	T2	29.82± 7.01	30.40 ±4.93		
	T3	33.18 ±6.19	31.10 ±5.15		
BBS	T1	43.09± 8.13	38.80 ±12.86	0.206#	0.034*
	T2	47.18 ±7.52	40.80±12.94		
	T3	48.00 ±7.24	41.00 ±23.23		

CONCLUSIONS

Task-oriented whole body reaching activity required the performer to control their posture according to the goal of the task and was efficient in improving the postural control performance not only during dynamic but also static context. Interventions focus on sedentary activities might deteriorate patients postural control This effects of BBA on lowering the risk of fall in hemiparesis patients after stroke should be further investigated.

REFERENCES

[1] Chern J-S et al. *AJPMR* **85**: 201-8, 2006.
[2] Persson CU et al. *J Neuroeng Rehabil* **11**: 83, 2014.

The Effects of Internal Perturbations on Balance for the Fallers and Non-fallers with Parkinson's Disease: a preliminary study

Yu-Chuan, Tsai[1], Chiung-Yu, Cho[1,2], Jeng-Feng Yang[1,2]
[1] Department of Physical Therapy, National Cheng Kung University, Tainan, Taiwan.
[2] Physical Therapy Center, National Cheng Kung University Hospital, Tainan, Taiwan.
Email: t66104089@gs.ncku.edu.tw

INTRODUCTION

Parkinson disease (PD) is a progressive neurodegenerative disorder of the central nervous system. The most critical disability as disease progression is postural instability, which is a main motor deficit associated with balance ability and fall risks. Falling is very common in PD, which occurs in sixty-eight percent of patients with PD each year. However, not all of the patients with PD are at risk of falls, some of them only have some functional declines or minimal impairment in balance. Thus, it is critical to distinguish the fallers (PD-F) from non-fallers (PD-NF) of PD and provide fall prevention program as soon as possible.

Patients with PD could be distinguished from normal individuals under the visual deprivation and dual task condition by using static posturography [1][2]. However, whether using visual deprivation and dual task paradigm can distinguish PD-F from PD-NF is unclear. As a result, this study aimed to compare the performance of postural control under different internal perturbation conditions between PD-F and PD-NF by using static posturography.

METHODS

The participants were allocated to PD-F and PD-NF according to their previous fall history. The participants were allocated to PD-F if the falls history greater than or equal to one time in past one year [1]. All participants were tested during the on-medication state [2] The participants were instructed to stand barefoot on the force plate (Qoppa, Taiwan). They were asked to perform three balance tasks randomly, including eye open (EO), eye closed (EC) and performing dual task, color judgement task (DT) while standing [2]. The sampling rate for force plate was set at 120 Hz for seventy seconds. The participants were performed two times in each condition and the means was be calculated.

RESULTS AND DISCUSSION

All participants increased the path length, velocity, and instability ratio in EC and DT as compared with EO, except for PD-NF in DT. The PD-F had longer path length and higher velocity in DT compared with EC, but the opposite was found in PD-NF. In contrast, all participants showed less instability ratio in DT as compared to EC (Figure 1). The executive and sensory function deficits might affect the postural control. The increasing mediolateral (ML) range and decreasing anteroposterior (AP) range were observed in PD-NF, it might be due to the axial rigidity, and their balance was compensated by ML sway. The PD-F increased the sway in both directions in order to maintan the posture stability [2] [3].

For group difference, there were diffrences for velocity and length in DT, and for instability ratio in EC and DT (Figure 1). The postural control deficits was detected in EC because their condition might induce inhibition on the visual adaptive strategy. In addtion, the invisible posture control deficits could be detected by inhibiting attention strategy to compensate the basal ganglia circuit deficits [1] [2] [3]. Using internal perturbations might be suitable to distinguish PD-F from PD-NF.

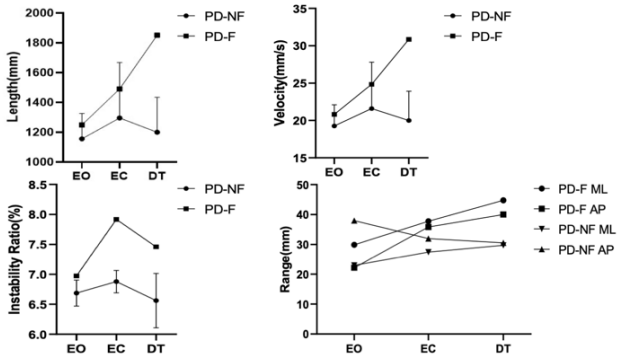

Figure 1 Comparison of the postural control parameters between groups and among conditions

CONCLUSIONS

Using internal perturbations, especially DT might be suitable to distinguish PD-F from PD-NF. Early identifying faller and providing preventive intervention is crucial for PD. All questions about the conference should be addressed to isb-jsb2023-ab@congre.co.jp.

REFERENCES

[1] Johnson, L. et al. Movement Disorders, 28(9), 2013.
[2] Morris, M. et al. Gait & posture, 12(3), 2000.
[3] Morenilla, L. et al. Frontiers in Psychology, 11, 2020.

Table 1 The characteristic of center of pressure parameters between PD-F and PD-NF in different conditions

	PD-NF (N=3, Age=63)			PD-F (N=1, Age=78)		
	EO	EC	DT	EO	EC	DT
Path length (mm)	1155.80	1295.10	1199.71	1248.8	1490.5	1851.3
Velocity (mm/s)	19.26	21.58	20.00	20.81	24.84	30.85
Instability ratio (%)	6.69	6.88	6.56	6.9732	7.92	7.46
Range in AP/ML (mm)	23.02/37.98	27.43/31.98	29.74/30.54	29.90/22.18	37.79/35.84	44.77/40.03

Plantar pressure distribution response to various gait speeds and its relationship with gait balance in overweight adults

Kim, Hyun Kyung[1], Qu, Hang[2], and Chou, Li-Shan[2]
[1] Depart School of Kinesiology, Louisiana State University, Baton Rouge, Louisiana, USA.
[2] Department of Kinesiology, Iowa State University, Ames, Iowa, USA.
Email: hkkim@lsu.edu

INTRODUCTION

Overweight individuals often report gait imbalance issues, which can further impair mobility and increase the risk of falls. [1]. Becauase the foot is the first body part to interacts with the external surroundings during walking, assessing plantar pressure can provide important information regarding gait balance control. Therefore, this study aimed to investigate the difference in plantar pressure between overweight and non-overweight during walking at different speeds.

METHODS

Eleven overweight individuals (Female 4/Male 7; 27.2±8.1 years; BMI: 29.4±2.8kg/m^2) and 13 non-overweight individuals (Female 7/Male 5; 23.3±7.9 years; BMI: 22 kg/m^2) walked on a 10-meter walkway at three controlled speeds (80%-120% of preferred). The degree of gait imbalance was quantified by calculating the extent of the mediolateral whole-body center of mass (COM). Wireless pressure sensing insoles (Xsensor®) was used to measure plantar pressure data. All participants wore the same traditional running shoes (New Balance, prototype). An analysis of variance model was conducted to investigate the effect of body size, gait speeds, or their interactions on the peak mediolateral COM (including displacement (m), velocity (m/s), and acceleration (m/s^2) and peak plantar pressure (kPa) from hallux (T1), second-fifth toes (T2-5), metatarsal 1-2 (M1-2), metatarsals 3-5 (M3-5), lateral midfoot (LM), medial midfoot (MM), lateral heel (LH), and medial heel (MH) during walking.

RESULTS AND DISCUSSION

Significant group effects of peak plantar pressure under the later forefoot (P = 0.03), lateral midfoot (P = 0.02), and medial heel (P = 0.02) were observed (Table 1). The peak pressure was transmitted from the medial heel during the mid-stance phase to the lateral forefoot during the pre-swing, which was more prominent in overweight gait (Fig 1). However, only mediolateral COM displacement (P = 0.02) and acceleration (P = 0.04) revealed significant speed effects. At a slower walking speed, both groups seem to have a greater range of COM displacement, indicating a slower walking speed may induce gait imbalance.

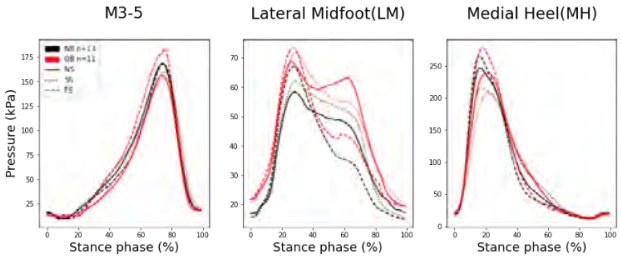

Figure 1 Plantar pressure under the M3-5, LH, and MH during the stance phase of the gait cycle. This figure reports only three anatomical regions that revealed significant group effects.

CONCLUSIONS

This study was the first to document the effect of body size and gait speeds on plantar pressure distribution and COM during walking. Different gait speeds altered mediolateral COM motion during walking. Only the plantar pressure distribution responded differently across the body size group during walking. Based on the current results, overweight individuals appear to have increased pressure on the lateral side of the foot for stable walking.

REFERENCES

[1] Neri Silvia G et al. *A Biol.Sci. Med. Sci* **75**: 952-60, 2019.

Table 1: Two-way ANOVA analysis for body size effect, gait speed effect, and their interaction on peak plantar pressure.

	Group effect	Speed effect	Group × Speed	Effect size
M3-5	**.03**	.49	.77	0.08€
LM	**.02**	.62	.95	0.1€
LH	.51	**.002**	.93	0.21¥
MH	**.02**	**.001**	.93	0.1€, 0.2¥

Reducing fall risk using 12-weeks of online dance classes for women aged 65 and above.

Emma H Chen MSc(c), Andreas Bergdahl PhD, Mary Roberts PhD
Department of Health, Kinesiology and Applied Physiology, Concordia University, Montréal, Canada.
Email: emma.chen@outlook.com

INTRODUCTION

Falls cause 85% of injury-related hosptializations and 95% of hip fractures among Canadian older adults [1]. These injuries disporportionately affect women across all age classifications of older adults [2]. Postural stability decreases with age due to deterioration of sensory systems, muscular strength and mobility [3]. It is well-known that physical activty can improve postural stability [3], however traditional exercise programs lack adherence for older women and can be difficult to access for those living in remote areas or affected by social distancing guidelines [4]. The aim of this study was to determine if 12-weeks of online dance classes could provide an engaging and accessible method for older women to improve their postural stability.

METHODS

22 women (74.7 years ± 5.8) completed two, 1-hour long integrative ballet-modern dance classes per week, for 12-weeks over Zoom. Postural stability, dynamic balance and functional strength were assessed at pre (week 0), mid (week 6) and post (week 12). Postural sway was analysed during 30-seconds of quiet standing on force plates, dynamic balance was assessed using a modified Star Excursion Balance Test and knee and ankle strength were assessed using the 30-Second Sit-to-Stand test and the Calf Raise Senior test. Significance was evaluated using one-way repeated measures ANOVA and nonparametric Friedman test ($p<.05$).

RESULTS AND DISCUSSION

17 participants completed the 12 weeks of online dance classes, with a strong adherence rate of 80.4%. Significant improvements were found in knee and ankle strength through the intervention (Figure 1). Participants performed a higher number of repetitions on the 30-second Sit-to-Stand from pre to mid ($p=.015$) and pre to post ($p=0.011$), while they performed an increased number of calf-raises from mid-post ($p=.012$) and pre-post ($p=.005$). Clinical significance was also demonstrated during the Calf Raise Senior test from mid-post and pre-post. Significant improvements in dynamic balance were found in the distanced reached during the Star Excursion Balance Test from pre-post in lateral ($p=.010$) and posterior-lateral directions ($p=.004$). A lack of findings regarding postural sway may be due to the insufficient intensity of online dance classes, as the online medium necessitates lower intensity to ensure the participants' safety.

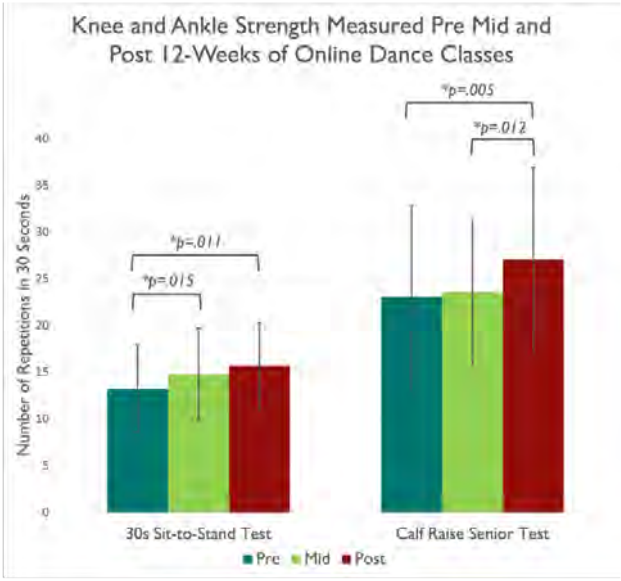

Figure 1. Increases in strength over 12-weeks of online dance classes with error bars illustrating standard deviation

CONCLUSIONS

Our findings demonstrate that 12-weeks of online dance classes may serve as a fun and engaging way for older women to improve their strength and dynamic balance, thereby reducing their fall risk. As the online medium was shown to be safe while lacking in sufficient intensity to induce improvements in postural sway, current studies are exploring the addition of blood flow restriction. Online dance classes demonstrate great potential as fall prevention programming for older women who may otherwise face barriers to participate in exercise. With the increased accessibility of online classes, more women may have opportunities increase their independence and quality of life as they age.

ACKNOWLEDGEMENTS

Canadian Graduate Scholarship – Master's Program Canadian Institutes of Health Research/Instituts de recherche en santé du Canada; Fonds de Rechereche Santé Quebéc – Formation de Maîtrise

REFERENCES

[1] PHAC. *Seniors' Falls in Canada,* 2014
[2] Stevens JA et al. *J Aging Phys Act* **17**: 167-180, 2014.
[3] Carter ND et al. *Sports Med* **31**: 427-438, 2001.
[4] Bethancourt HJ et al. *J Clin Med* **12**: 10-20, 20

DEVELOPMENT OF THE TWO-DIMENSIONAL MECHANICAL MODEL OF HUMAN STABILITY

Martyna Sopa[1], Grażyna Sypniewska-Kamińska[1], Tomasz Walczak[1], Henryk Kamiński[1]
[1] Institute of Applied Mechanics, Poznan University of Technology, Poznan, Poland.
email: martyna.sopa@doctorate.put.poznan.pl

INTRODUCTION

Human movement analysis is an increasingly popular topic. However, there is still a need to develop knowledge about estimating the forces and moments of forces acting in the joints, since they cannot be measured unequivocally. Another difficulty is the appearance of an external force acting on a human in the model of motion. For this reason, the authors propose a model of human motion treated as a semi-closed chain, defined by the Euler-Newton equations [1]. This model was tested on the example of a fall caused by an external force, i.e. a fall that may occur during a sudden braking of a public transport vehicle. The input data were obtained with the use of an optoelectronic motion capture system, dynamometric plates and a dynamometer. The proposed model can be later on applied in devices for monitoring and assessing human movement.

METHODS

In this study, participants were asked to backward fall. The movement was captured with the use of the optoelectronic motion capture system (sampling frequency of 250 Hz and spatial measurement resolution of 0.001 m) complemented by two AMTI force plates with a sampling frequency of 500 Hz and measurement resolution of 0.001 N. With the use of platforms, the ground reaction forces (GRF) and the centre of pressure (COP) trajectory were captured. Additionally, the external random force was applied to the participants' body to cause a backward fall. The time course of the external force was registered with the use of a dynamometer (sampling frequency and measurement resolution are equal to 500 Hz and 0.5 N, respectively). The participants were standing with each leg on a separate platform.

The mechanical model of human was described as a semi-closed chain of symmetrical non-deformable rigid bodies connected by rotational joints. Because the inertial and mass parameters of segments were taken from David Winter's description, the placement of markers on the subjects' body was determined [2].

To make the collected data applicable to Newton-Euler equations the necessary accelerations were calculated and smoothed using the Taylor series.

The input variables on the model are inertial and mass parameters of the body, accelerations of centres of masses and angular accelerations of segments, GRF and COP of the right lower limb. The output of the model are COP and GRF given by the left lower limb on its force plate. The output variable allows for the assessment of the accuracy of the model.

RESULTS AND DISCUSSION

The presented method allowed for acquisition of a mechanical model of human motion in two-dimensional space. The comparison of vertical and horizontal GRF during the performance of external force-caused fall, obtained with the use of the model and measured by the platform is shown in Figure 1. One can notice, that the waveform representations of the GRF in time are less accurate when the system is perturbated by an external disturbance – while accelerations and inertial parameters have a more significant impact on the performance of the model.

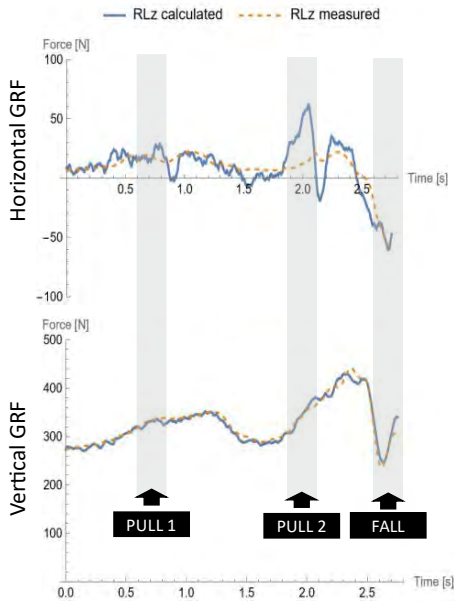

Figure 1 Comparison of the vertical ground reaction force measured by force plate and obtained by the model.

CONCLUSIONS

The proposed model can be considered sufficient for biomechanical studies. The inertial parameters of segments of the body have a crucial impact on the performance of the model, especially when studying fast-changing movements.

REFERENCES

[1] Dasgupta B et al. *A general strategy based on the Newton-Euler approach for the dynamic formulation of parallel manipulators*, Mechanism and Machine Theory **34**: 801-824, 1999.

[2] Winter D.A, *Biomechanics and Motor Control of Human Movement*, John Wiley & Sons; Waterloo, Ontario, Canada, 2009

Leg Muscle Activities during Single Leg Stance

Jooyeon Ko[1,2], Hyun Kyoon Lim[3,4]
[1] Department of Physical Therapy, Daegu Health College / Daegu, South Korea.
[2] Korean Balance Ability Data Center, University / Daegu, South Korea.
[3] Medical Measurement Team, Korea Research Institutes of Standards and Science / Daejeon, South Korea.
[4] Department of Medical Physics, University of Science and Technology / Daejeon, South Korea.
Email: julie0202@dhc.ac.kr (J.K.); hlim@kriss.re.kr (H.K.L.)

INTRODUCTION

Postural stability during standing could be an important index for elderly people. Especially, postural stability on a single leg stance (SLS) may reveal the overal and general systematic information of the central nervous system failure, atheletes injury, and other motor control abilities [1]. It may also be used as a good index to evaluate sports injury and performance, stroke, etc. To date, single leg stance is usually assessed by the total time not by quantitative physiological measurement such as surface electromyography (sEMG). In this study, authors recorded multi- channel sEMG from six muscles of each leg during SLS and evaluated the muscle activity patterns.

METHODS

All subjects signed consent forms before participation (IRB no. DHCIRB-2022-06-0008). Total of 20 neurologically intact subjects (3 males, 17 females, and average age=68.9±4 years) were asked to follow the standard protocol for SLS made by the Korean Balance Ability Data Center. Total of 12 surface EMG (sEMG) electrodes were attached to both legs for SLS test. sEMG recording was made from rectus femoris, tibialis anterior, peroneus, biceps femoris, gastrocnemius, and soleus for right and left leg. We made prototype sEMG profile using sEMG data from 18 subjects as the control group and later sEMG data from two subjects who were chosen arbitrarily among 20 subjects were compared as the test group. sEMG recording system was (Ultium, Noraxon, USA) with a bandwidth of 10-500 Hz and 2000 s/s/channel. A root mean square (RMS) algorithm was used and then total data were integrated for the test window. The sEMG was recorded up to 30 seconds for SLS for each subject. We normalized the integrated sEMG data using the sampling rate. Multi-channel sEMG patterns were compared during SLS. The whole process for EMG assessment followed the Brain Motor Control Assessment Protocol (BMCA) [2]. In short, a prototype vector was made using 18 subjects using six response elements of one side. Finally, similarity index and total EMG activity were calculated

RESULTS AND DISCUSSION

Average EMG amplitude was 114.7±25.5 μV for right SLS (range 50.4~152 μV) and 119.4±18.5 μV for left SLS (range 86.5~151.8 μV). Similarity index was 0.96±0.04 for right side (range 0.8~1.0), and 0.98±0.02 for left side (range 0.9~1.0) (Fig. 1). Time duration could give us only one dimensional information regardless of various motor control patterns of elderly people. In this point, similarity index and EMG total activity during SLS could give us new additional information because neurologically intact subjects showed the similar motor control pattern during SLS. It may be an useful index to screen elderly people who possibly have motor control difficulties on a single leg stance even though they could stand on one leg for acceptable amount of time comparing to people who has no difficulties for SLS.

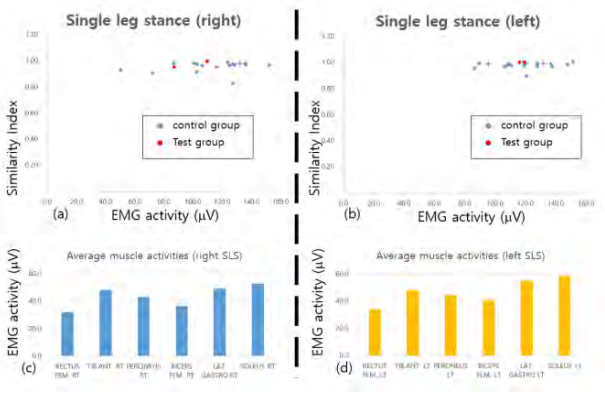

Figure 1 Similarity index and EMG activities during single leg stance for right (a) and left side (b). Multi- channel sEMG are showing the similar activities during SLS for right (c) and left side (d).

CONCLUSIONS

In this study, we applied BMCA protocol to see whether multi-channel sEMG among subjects are showing consistent and similar activities during SLS test. Results showed similarity index and total magnitude of sEMG may be a good screening tool for elderly people who may have difficulties in maintaining for SLS.

ACKNOWLEDGEMENTS

This study was financially supported by the Ministry of Trade, Industry, and Energy (MOTIE), Korea, under the Korean Reference Data Center Program supervised by the Korea Research Institute of Standards and Science (KRISS).

REFERENCES

[1] Quarmby A et al. *Front Sports Act Living* **4**: 1012471, 2022.
[2] Lim HK et al. *J Rehabbil Res Dev* **42**: 413-22, 2005.

Alteration of Inter-joint Interaction during Standing due to Spinal Cord Injury

Kimiya Fujio[1], Kenta Takeda[1], and Noritaka Kawashima[1]
[1] Department of Rehabilitation for movement function, Research Institute of National Rehabilitation Center for Person with Disabilities, Saitama, Japan.
Email: fujiokimiya@yahoo.co.jp

INTRODUCTION

Inter-joint interaction in lower limb is one of the essential mechanisms for human standing. There are, at least, two types of interactions: for whole body center of mass (COM) kinematics and for local joint kinematics [1]. Those interactions work for counteracting to decrease the objective (COM and joint angular) acceleration. Our previous research indicated that aging deteriorates the former interaction, but it does not affect the later. It implies that control mechanisms are separated for each interaction, and if the central nervous system (CNS) contributes to the later, the inter-joint interactions for local joint kimematics could be impared in patiants who have a disfunction of the CNS. Thus, we focused on the inter-joint interaction in patients with spinal cord injury (SCI). The purpose of this study was to clarify whether inter-joint interaction, especially that for local joint kinematics, would be impared in SCI patients.

METHODS

We utilized database in our laboratory for the analysis. Sixteen healthy and Sixteen people with SCI were allocated into 2 groups respectively (desired power: 0.85, effect size: 0.25, alpha: 0.05). The dataset included kinematic signals recorded by a motion capture system (8 infrared cameras on Mac3D system, Helen Hayes-marker set, 200Hz) during standing without any aid. Every trial was measured for 30 seconds. In order to analyse inter-joint interaction, standing posture was modelled by a double inverted pendrum with lower and head-and-trunk segments. After calculating hip/ankle joint angular accelerations, COM acceleration and gravitational/muscle/velocity-dependent torques, we applied induced-acceleration analysis [2] to separate contribution of each torque for the net angular acceleration in ankle/hip joint. In this method, the components of joint angular acceleration were distinguished by origin that from homonymous and that from remote joints (e.g. ankle joint angular acceleration was composed with not only component from ankle but also that from hip joint). Finally, uncontrolled manifold (UCM) approach was applied to quantify the above 2 types of inter-joint interactions (joint angular acceleration for COM, and the components of angular acceleration for local joint kineamtics; $UCM_{ankle/hip}$). Statistical test (Mann-Whitney test) was applied at α=0.05.

RESULTS AND DISCUSSION

We found that both COM acceleration and angular acceleration in ankle/hip joints were significantly increased in SCI patients. It indicated postural sway and joint kinematics during standing were larger and faster in SCI. Nevertheless, UCM_{ankle} was higher in SCI group ($p=0.016$, $r=0.596$), while UCM_{hip} was not different between healthy and SCI groups, indicating not deteriorated inter-joint interaction in SCI. Statistical test further showed that both components of ankle and hip angular accelerations were significantly larger in SCI patients (Figure1, lower). Those results suggested that inter-joint interaction for local joint kinematics was preserved even when the CNS (spinal cord) was damaged. Instead, we suspect that larger accelerations of all components from homonymous and remote joints cause the increased joint angular acceleration.

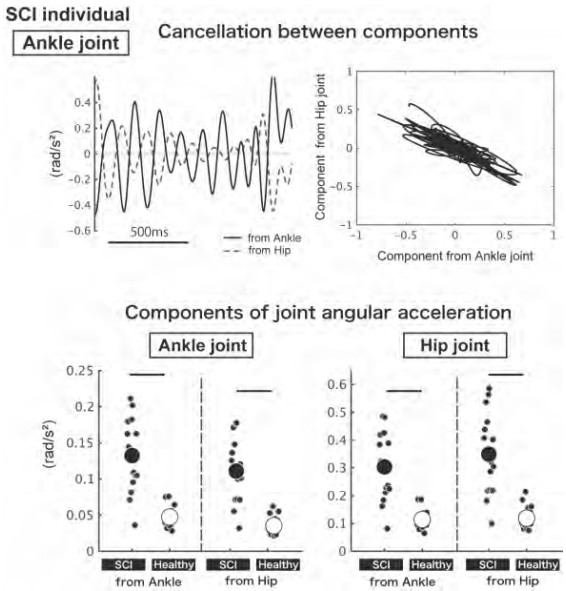

Figure 1 Inter-joint interaction for local joint kinematics.

CONCLUSIONS

Our results demonstrated that inter-joint interaction for local joint kinematics is not always impaired in people with SCI. It could rather be caused by a larger acceleration effect of each component from homonymous and remote joints. Further studies are expected to clarify the details of mechanisms for inter-joint interaction by using a multi-link pendrum model.

ACKNOWLEDGEMENTS

We thank to all alumni/alumnae and collaborators who contributed to building our database.

REFERENCES

[1] Sasagawa et al. *J Neurophysiol* **111**: 313, 2014.
[2] Zajac et al. *Gait Pos* **16**: 215, 2002

Research on the balance ability of freestyle skiing aerial skills athletes based on specific frequency band EEG

Youcai Guo[1], Xin Wang[2] and Tianyu Zhao[3]

[1] School of Exercise and Health, Shenyang Sport University, Shenyang, China.

[2] School of Exercise and Health, Shenyang Sport University, Shenyang, China.

[3] College of Sciences, Northeastern University, Shenyang, China.

Email:13840334069@163.com

INTRODUCTION

To explore the relationship between specific frequency band EEG and balance performance of freestyle skiers aerial skills during balance control tasks with different difficulty.

METHODS

Select 17 freestyle skiers of the national team as the research object. The subjects used the HUMAC portable balance instrument to perform the standing continuous balance test (CBT) of the dominant leg and the non-dominant leg on the soft and hard support surfaces respectively, and recorded the center of pressure (COP) of the body during the subject's standing balance process.

The 64-lead EEG recorder (ANT Neuro) was used to simultaneously collect the EEG signals of the subjects during the balance task. Each test is performed for 30s, with an interval of 1min. After the collected signals are processed by segmentation, downsampling, and artifact removal, frontal lobe (F3, Fz, F4), frontal lobe-central (FC1, FCz, FC2, C3) are selected. , C1, Cz, C2, C4), central-parietal lobe (CP1, CPz, CP2, P3, Pz, P4) and other three regions to the θ (4-8Hz) frequency band Fast Fourier transform (FFT) and then After natural logarithmic transformation, the average value of electrode power was taken for each region.A 2 × 2 × 3 three-way repeated measures analysis of variance (ANOVA) was designed, and the independent variables were: support surface (2 levels: hard and soft support surface) × standing leg (2 levels: dominant leg, non-dominant leg) × brain Sensory cortical areas (3 levels: frontal, frontal-central, central-parietal).

RESULTS AND DISCUSSION

(1) Compared with both feet, the average amplitude of Cop on one foot was significantly higher than that on both feet , and there was no significant difference in the average amplitude of Cop in the dominant leg and the non-dominant leg ; (2) In unstable surface, during the balancing process of standing on the support surface, the swing degree of the COP of the left leg standing and the right leg standing was significantly greater than that of the subjects with a hard support surfaceswing ($P<0.001$);(3) The energy values of theta waves in the three sensory cortex areas were significantly higher than those in the hard support condition ($P<0.05$), and the non-dominant leg was higher than the dominant leg ($p<0.05$). (4) The ANOVA results of cortical activity in the theta frequency region showed that different support legs had significant effects in frontal ($p<0.001$), frontal-central ($p<0.01$) and centro-parietal ($p<0.001$) regions .

CONCLUSIONS

(1) Freestyle skiing aerial skills athletes' balance control ability on the soft support plane is weaker than the hard support surface balance ability; (2) The left and right balance ability of freestyle skiing aerial skills athletes is stronger than the front and rear balance ability; (3) Balance task As the difficulty increased, theta activity in the frontal, fronto-central, and central-parietal regions of the cerebral cortex increased. In addition, frontal-central and central-parietal Theta power was associated with balance performance.

A STATIC MODEL PREDICTS ROOF-TO-LADDER TRANSITION FRICTION REQUIREMENTS

Sarah C. Griffin[1] and Kurt E. Beschorner[1]
[1] Bioengineering, University of Pittsburgh, Pittsburgh, USA
Email: scg57@pitt.edu

INTRODUCTION

Ladder-related injuries create a severe burden on the working population. Specifically, transitioning across support surfaces and lateral leaning lead to more than 20% of fatal ladder-related incidents [1]. Previously, a relationship has been found between the lateral lean angle (defined by the relationship between the center of mass and the base of support in the frontal plane) and the medial/lateral (ML) directed required coefficient of friction (RCOF) in walking [2]. An inclined beam model is often used to determine friction and normal reaction forces. The goal of this work is to determine the predictive ability of a simple static model on friction requirements in the ML direction.

METHODS

Seventeen healthy participants who regularly climb ladders completed six trial replicates for two ladder conditions: a traditional extension ladder that requires climbers to step around the ladder when transitioning to a roof and a modified extension ladder that allows the user to step through the top. Kinetics were collected from the rung and passive reflective markers quantified body kinematics. ML RCOF was calculated as the ratio of ML shear force to the normal force in a coordinate system relative to the shoe's contact plane. The ML body angle was the angle between vertical and the frontal plane projection of a vector from the toe to the trunk center of mass.

A static model based on an inclined beam was utilized to predict the ML RCOF. The model was based on a point mass (i.e., the climber's trunk) located at the top of a massless beam (the segment connecting the trunk to the foot). The beam's orientation was defined by the body angle (θ) measured from vertical. The predicted ratio of the friction and normal force at the ground was found to be: $ML\ RCOF = \tan(\theta)$.

Model fit was determined via the root mean squared error (RMSE) and a bivariate correlation analysis with the experimental values as the outcome variable and predicted values as the regressor. Better models would correspond to a linear fit with a slope nearer to one, a y-intercept of zero, and low variance around the fit line.

RESULTS AND DISCUSSION

Acceptable agreement was found between the predictions and experimental data (**Figure 1**). The regression analysis resulted in a significant linear relationship ($t = 12.49$, $p < 0.001$) with a slope of 0.758 and an R^2 value of 0.722, indicating that the model explained most of the variance in the data. The low RMSE (0.046) also supports the strength of this model.

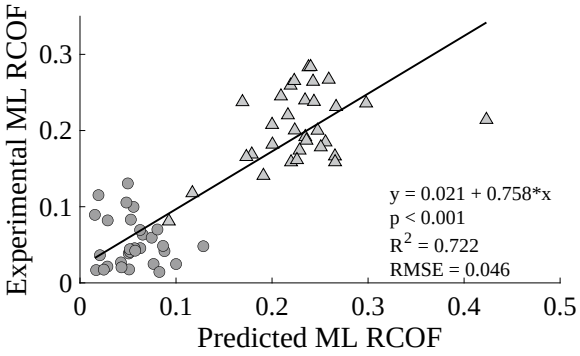

Figure 1: Bivariate relationship between the predicted ML RCOF and the experimental ML RCOF where circles correspond to a walk-through ladder and triangles correspond to a traditional ladder top.

These results demonstrate that the relationship between the ML friction requirements and frontal plane body angle is well explained by a static model. This simple relationship between kinetics and kinematics is advantageous for applications of ladder safety research. Kinetic data is difficult to collect and requires modifying a ladder structure and using expensive and non-portable force plates. Kinematic data, on the other hand, can be collected in the field through use of wearable technology or camera-based methods. Results of this model suggest that individuals should attempt to minimize their ML body angle during roof-to-ladder transitions, keeping their center as closely aligned with their foot as possible. Researchers can use this to develop both individual- and context-specific feedback which can be delivered to ladder users in real time, thus minimizing the number of lateral slips that occur during roof-to-ladder transitions.

CONCLUSIONS

The predicted values correlated with the experimental ML friction requirements during roof-to-ladder transitions. The existence of a mechanistic model to explain previous experimental work strengthens safety recommendations and allows researchers to provide subject- and context-specific feedback to improve ladder safety.

ACKNOWLEDGEMENTS

The authors would like to thank the lab manager Jenna Trout and students Bridget Cahir, Chris Deschler, and Claire Tushak for their help. This research was funded by NIOSH R01OH011799 and NSF GRFP 2139321.

REFERENCES

[1] Shepherd, G. et al. *Ergo*. **49**(3): 221-234, 2006.
[2] Yamaguchi, T. et al., *J Biomech.* **74**: 163-170, 2018.

EVIDENCE FOR MODIFYING EXTENSION LADDER DESIGN TO REDUCE SLIPPING RISK

Violet Williams[1], Sarah Griffin[1], and Kurt Beschorner[1]
[1] Department of Bioengineering, University of Pittsburgh, Pittsburgh, PA, USA.
Email: Violet.Williams@pitt.edu

INTRODUCTION

Falls threaten safety in both occupational and non-occupational settings. Ladder falls are the second most common cause of falls, accounting for 8% of all occupational falls [1]. A quarter of falls resulting in an emergency department visit involved extension ladders [2]. One challenge in extension ladder climbing is the transition between the fly or upper section and the base or lower section. The fly is stacked on top of the base but minimal justification exists for this design choice. This study examined the effect of the extension ladder fly configuration on an individual's slip risk quantified by required coefficient of friction (RCOF).

METHODS

The testing apparatus consisted of two extension ladders, each oriented at 75° from horizontal. One configuration was a traditional fly ladder. The other configuration was a reversed extension ladder with the fly section underneath the base section (Figure 1). The transition between the fly and base sections occurred at the 3rd and 4th ladder rungs where anterior/posterior foot placement must change. Participants were asked to ascend and descend the ladder to the 5th rung at a comfortable but urgent pace for three trials of each configuration. The 3rd rung of each configuration was attached to a force plate and 12 motion tracking cameras (Vicon) collected kinematic data. Only descent trials were included in this analysis. RCOF was calculated as the ratio of the resultant shear and normal forces on the shoe in its local coordinate system. The RCOF values were split into two halves of stance with the bounds of initial foot contact, toe off, and the midpoint between these times. The root mean squared (RMS) values were found for each half of stance and averaged between the replicates of a participant's descents in each configuration. 16 participants (10 male, 6 female; 34.50 ± 15.37 years) were analysed. Paired t-tests were conducted with ladder configuration as the independent variable and RMS RCOF as the dependent variable.

RESULTS AND DISCUSSION

There was no significant difference found between the traditional and reversed configurations for RMS RCOF ($t_{15} = 0.798$; $p = 0.438$) in the 1st half of stance. In the 2nd half of stance higher RMS RCOF values occurred in the traditional fly configuration than the reverse ($t_{15} = 3.008$; $p = 0.009$) (Figure 1). These values indicate an increased risk of backwards slip in the traditional fly ladder as the individual prepares for toe off. This difference is likely because while transitioning from the fly to the base section of the traditional configuration, the plane of the rungs moves forward. One possibility is that the shift results in a more anterior foot placement, and the increased horizontal distance between the participant's foot and center of mass could increase the friction force required. The relationship between this lateral distance and force direction is commonly explained by an articulated strut model. Another possibility is that climbers unaware of the forward shift contact the rung closer to their toes as they don't fully shift their foot forwards. This difference in position could increase the moment arm from the ankle, rotating the foot and increasing RCOF [3].

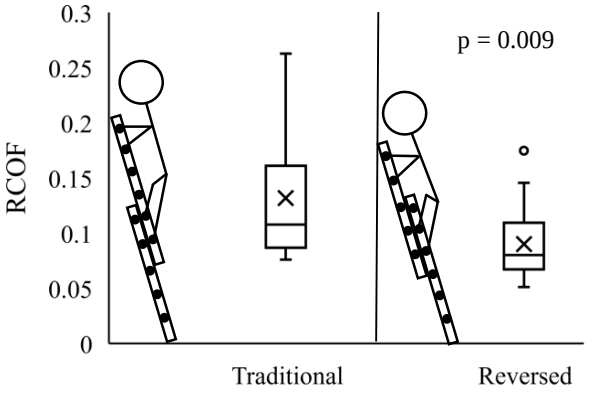

Figure 1: RMS RCOF values for traditional and reversed fly configurations in the 2nd half of stance where X signifies the mean, and the lines signify the median and interquartile range.

CONCLUSIONS

The reversed fly configuration was found to have significantly lower values of RCOF during ladder descent. These results indicate that there may be a higher slip risk during late stance for traditional fly ladders. An opportunity may exist to improve extension ladder safety by reversing the fly configuration.

ACKNOWLEDGEMENTS

The authors would like to acknowledge the assistance of Jenna Trout, Bridget Cahir, Chris Deschler, and Claire Tushak. This work was supported by NIOSH R01OH011799 and NSF GRFP 2139321.

REFERENCES

[1] Webster T. Workplace Falls. *Compensation and Working Conditions*, 2000.
[2] Cabilan C et al. *Emergency Medicine Australasia* **30(1)**: 95-102, 2018.
[3] Martin E et al. *J Biomech* **99:** 109507, 2020.

Decompose centre of pressure component affecting centre of mass acceleration in quiet standing

Taku Miyazawa[1,2], Hiroki Hanawa[1], Keisuke Hirata[3], Keisuke Kubota[4] and Naohiko Kanemura [2]

[1] Department of Rehabilitation, University of Human Arts and Sciences, Saitama, Japan.
[2] Graduate Course of Health and Social Services, Saitama Prefectural University, Saitama, Japan
[3] Department of Rehabilitation, Tokyo Kasei University, Saitama, Japan.
[4] Research Development Centre, Saitama Prefectural University, Saitama, Japan.
Email: taku_miyazawa@human.ac.jp

INTRODUCTION

In human bipedal standing, centre of mass (COM) is the controlled variable and centre of pressure (COP), representative point of the ground reaction force, is controlling variable. Several studies found COM acceleration (COMacc) is regulated to be minimum in quiet standing and sensitive to age-related changes in the postural control [1,2]. Since COMacc is equal to the horizontal ground reaction force, it is expected to be related to the behavior of the COP. A few studies revealed COP velocity reflects whole body COMacc [3], but the relationship between them is not clear. We divided the COP into low and high frequency components and analysed which COP behavior leads to COM acceleration.

METHODS

The subjects were 18 young adults and 9 health elderly. They held a static standing on a force platform (Type9281B, Kistler, Switzerland) for 30s with their eyes open or eyes closed. Four trials were performed for each visual condition. COP position and horizontal ground reaction force were obtained from a force plate, sampled at 1000 Hz. COP was decomposed into low frequency components (rambling) and high frequency components (trembling) [4]. COP velocity was calculated differentiated by COP displacement.

RESULTS AND DISCUSSION

Trembling had a larger coefficient of determination with COMacc than rambling (Fig.1). Multiple regression analysis showed that rambling had the largest coefficient(β) to COMacc in the anterior-posterior (AP) direction, while COPvel had the largest coefficient in the medio-lateral (ML) direction (Table.1).

Rambling reflect migration of the reference point from one instant equilibrium point and trembling is oscillation respect to the moving equilibrium reference [4]. The latter is related to the intrinsic mechanical properties of postural muscle. Human standing is unstable in AP direction, approximated by an inverted pendulum. The COMacc in AP direction is related mainly to the fast and small oscillation generated by muscle. In the ML direction, on the other hand, no relationship between trembling was observed. We presume load/unload mechanism in the ML direction led to these results. These trends were observed regardless of age, suggesting that the increase in COMacc, especially elderly, is influenced by the increase in oscillation around the equilibrium reference rather than by the migration of the reference point.

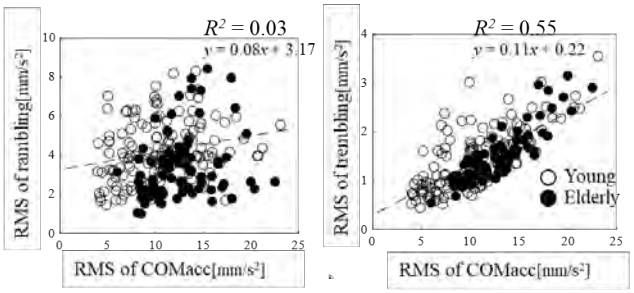

Figure 1 Linear regression for COM acceleration and rambling/trembling in anterior-posterior direction

CONCLUSIONS

COM acceleration is influenced by trembling in the AP direction and not rambling. This relationship may be a factor in the increase in COM acceleration due to aging and disease.

REFERENCES

[1] Masani et al. *Neurosci Lett* **422**: 202-206, 2007
[2] Yu et al. *Arch Phys Med Rehabil* **89**: 113-1139, 2008
[3] Masani et al. *Gait & Posture* **39**: 946-952, 2017
[4] Zatsiorsky et al. *Motor Control* **3**: 28-38, 1999.

Table 1: Multiple linear regression analysis for COM acceleration in quiet standing.

	Anterior-posterior			Medio-lateral		
	β	t	*p-value*	β	t	*p-value*
Constant	12.44	78.80	*<0.0001*	8.00	62.41	*<0.0001*
Rambling	-0.17	-1.02	*0.30*	0.55	3.84	*<0.001*
Trembling	2.46	14.40	*<0.0001*	0.34	2.11	*0.03*
COP velocity	1.10	6.46	*<0.0001*	1.71	10.90	*<0.0001*

THE EFFECTIVENESS OF ARTIFICIAL INTELLIGENCESPORT TRAINING MIRROR COMBINE WITH CHINESE MARTIAL ARTS FOR LOWER EXTREMITIES BALANCE

Cheng-Wei Chen, Ching-Ting Hsu*, Wei-Hua Ho and Pao-Hung Chung
Institute of Sports Equipment Technology, University of Taipei
*E-mail: jingting@utaipei.edu.tw

INTRODUCTION

Chinese martial arts is an exercise that improves the balance and lower limbs stability, but not restricted by all age groups thus very suit for the general public. Human balance ability can be separated to static balance and dynamic balance [1]. Chinese martial arts movements mainly depend on hand shape, step shape, body shape, strength coordination, clear movement and stillness. Mirror image training is one of the main methods of martial arts training. The mirror is a very important tool in sports training, because the mirror reflects learners image for learners to observe and adjust own movements.In this paper, we improve the traditional mirror training to artificial intelligence sports training mirror which not only provide reflection image but also both real time and play back video with skelet combined with Chinese martial arts training to observe the balance ability improvement.

METHODS

Exercise procedure:In this study, we recruit10 young female participants for a 6-week balance training. In this paper, we arrange a set of basic lower limbs actions from Chinese martial arts to improve lower limbs stability. These actions are horse step, lunge, single step, frontal kick and side kick. Participants do each action for 30 seconds, 5 sets in each exercise and 2 times exercises for a week. Balance ability evaluation:In this study, we utilize Y-balance to evaluate participants' balance ability [2]. Statistical method:SPSS Statistics 20.0 is utilized to test statistical data. And, paired sample *t* test evaluates the balance ability difference between before and after our balance exercise. The level of statistically significant difference is set as $p < 0.05$.

RESULTS AND DISCUSSION

Table 1 and Table 2 shows the results of 6-week balance exercise for artificial intelligence sport training mirror and traditional mirror, respectively. From these tables,we can observe that after 6-week exercise, the dynamic balance ability of the expermental group has significantly improvement. However, from Table 1, we can observer that AT of the experimental group also improves after our artificial intelligence sport mirror balance exercise. On the other hand, there is no significant difference in the dynamic balance ability between the pre-test and post-test in the control group (Table 2). These results denotes that after 6-week of artificial intelligence sports training mirror combined with step exercises can improve the dynamic balance ability of young females.

Table 1: Experimental group dynamic balance pre-test and post-test

		(SD)	(Mean)	(*P*)
AT	Pre	82.40	7.69	0.129
	Post	97.56	14.66	
PM	Pre	84.20	15.87	0.010 *
	Post	104.50	19.31	
PL	Pre	97.00	21.57	0.036 *
	Post	113.23	16.69	

*$p < 0.05$

Table 2: Control group dynamic balance pre-test and post-test

		(SD)	(Mean)	(*P*)
AT	Pre	83.40	6.87	0.215
	Post	81.20	7.87	
PM	Pre	95.53	21.71	0.399
	Post	97.10	19.22	
PL	Pre	105.06	22.78	0.261
	Post	107.23	21.41	

*$p < 0.05$

CONCLUSIONS

This study shows the effect of dynamic balance ability and lower limbs stability improvement by utilizing artificial intelligence sports training mirror combined with Chinese martial arts. The results show that the artificial intelligence sports training mirror can efficiently and significantly improve the balance ability and the lower limbs stability.

ACKNOWLEDGEMENTS

This research is supported by Ministry of Science and Technology, Taiwan, R.O.C. The project number is

REFERENCES

[1]Hatzitaki,V.,Zlsi,V., Kollias, I. & Kioumourtzoglou, E. (2002). Perceptual-motor contributions to static and dynamic balance control in children. *Journal of motor behavior*, 34(2), 161-170.

[2]Smith, C. A., Chimera, N. J., & Warren, M. (2015). Association of y balance test reach asymmetry and injury in division I athletes. *Medicine and science in sport and exercise*, 47(1), 136-141.

GAIT STABILITY RESTRICTIONS DID NOT ELICIT COMPENSATION FROM REMAINING STRATEGIES

Aaron N. Best[1], Mark Vlutters[2] and Amy R. Wu[1]
[1] Mechanical and Materials Engineering, Queen's University, Kingston, Canada
[2] Department of Biomechanical Engineering, University of Twente, Enschede, Netherlands
Email: aaron.best@queensu.ca

INTRODUCTION

Healthy humans are proficient at overcoming everyday perturbations to avoid falls, but the underlying mechanisms that allow for stable gait are still unclear. Humans primarily utilize three stability strategies: corrective stepping (stepping strategy), centre of pressure (CoP) modulation (ankle strategy), and upper body momentum modulation (trunk strategy) [1]. Previous studies found that stepping is the predominant strategy for maintaining stability [1]. However, it is unclear if the strategies will compensate for one another when one is restricted. Focused on mediolateral behaviour, we aimed to investigate strategy restrictions, hypothesizing that when one strategy is limited, the remaining strategies will provide compensation.

METHODS

Ten healthy subjects (2F/8M, 27.9 ± 3.8 years, 173.4 ± 11.2 cm, 70.4 ± 10.3 kg) walked on a treadmill with randomized mediolateral perturbations applied to the pelvis at right toe-off. Subjects walked in four different randomized conditions – three restricted and one unrestricted. The ankle strategy was restricted using shoes with a narrow strip of rubber (2 cm) on the bottom, limiting mediolateral CoP modulation [2]. The trunk strategy was restricted using a brace that restrained spine bending. The stepping strategy restriction was imposed by laser lines projected onto the ground at a fixed step width.

Trunk strategy was assessed by changes in trunk angular acceleration, ankle strategy by CoP changes during single support, and stepping strategy by step width changes. For the former two measures, the deviation area between the mean trajectory of the unperturbed strides and a perturbed stride was calculated, and then linear fits were created between the deviation area and perturbation magnitude (Figure 1). For step width, the percent change in step width between an unperturbed stride and a perturbed stride was calculated. Similar linear fits were created between the percent change in step width and the perturbation magnitudes. The slopes and intercepts of the linear fits were compared to the no restriction condition using repeated-measures ANOVA and post-hoc t-tests with a Holm-Sidak correction ($\alpha = 0.05$).

RESULTS AND DISCUSSION

The restrictions were successful in reducing the effectiveness of the intended strategy, with reduced slopes for trunk angular acceleration and stance CoP, and reduced intercept for step width change for the respective restriction conditions (Table 1). Contrary to our hypothesis, the investigated measures did not suggest compensatory behaviour. However, the rate at which swing time decreased as a function of perturbation magnitude was 22% greater for the stepping restriction compared to the no restriction (p = 0.007), suggesting other gait changes may have allowed for stability to be maintained.

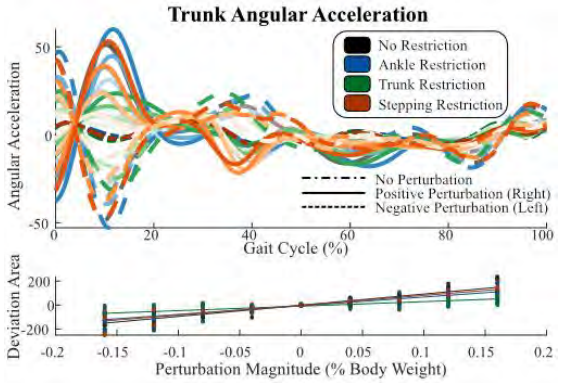

Figure 1: Exemplar analysis to compare restriction conditions. Darker shading indicates a stronger perturbation.

CONCLUSIONS

Despite restrictions, healthy humans overcame perturbations without exhibiting compensation. Stricter restrictions may elicit compensatory behaviour.

ACKNOWLEDGEMENTS

NSERC CGS-D, NSERC MSFSS, Ingenuity Labs

REFERENCES

[1] Bruijn S et al. *J R Soc Interface*, 2017.
[2] van Leeuwen A et al. *PLOS ONE*, 2020.

Table 1: Summary of the linear fits and statistical comparisons. Asterisks accompanying the slope or intercept (non-dimensional) indicate statistically significant difference from No Restriction. Asterisks on the *p-value* indicate significance from repeated measures ANOVA.

		No Restriction	Ankle Restriction	Trunk Restriction	Stepping Restriction	p-value
Trunk Angular Acceleration	Slope	934 ± 368	725 ± 333	375 ± 262*	819 ± 281	2.96*e*-7*
	Intercept	-1.5 ± 14.1	-5.7 ± 14.2	-9.0 ± 9.8	-1.2 ± 12.6	0.282
Stance CoP	Slope	13.0 ± 3.9	8.6 ± 4.4*	12.5 ± 3.7	13.6 ± 3.9	0.001*
	Intercept	-0.5 ± 0.2	-0.4 ± 0.2	-0.5 ± 0.2	-0.5 ± 0.2	0.079
Percent Change in Step Width	Slope	259 ± 187	271 ± 165	257 ± 158	202 ± 217	0.075
	Intercept	5.4 ± 10.5	8.3 ± 7.1	3.2 ± 7.7	-2.2 ± 7.2*	0.004*

EFFECTS OF BILATERAL SUBTHALAMIC DEEP BRAIN STIMULATION ON BALANCE CONTROL DURING SIT-TO-STAND IN PATIENTS WITH ADVANCED PARKINSON'S DISEASE

Ya-Hung Wang[1], Chi-Chung Kuo[2,3], Pei-Yeh Chiang[4], Chin-Hua Fu[2], Yun-Chen Hsu[1], Mei-Ying Kuo[1*]
[1]Department of Physical Therapy, China Medical University, Taichung, Taiwan.
[2]Department of Neurology, Taichung Tzu Chi Hospital, Taichung, Taiwan.
[3]School of Post-Baccalaureate Chinese Medicine, Tzu Chi University
[4]Department of Neurosurgery, Taichung Tzu Chi Hospital, Taichung, Taiwan
Email: mykuo@mail.cmu.edu.tw

INTRODUCTION

Parkinson's disease (PD) is a neurodegenerative disorder that impairs postural and balance control. Postural and balance disabilities during functional transitional activities, such as rising from a chair, are highly correlated to falls. The sit-to-stand (STS) movement is a complex transitional activity that requires sufficient propulsive force to accelerate the body forward and then upward. Deep brain stimulation (DBS) has been shown to be an effective surgical procedure to improve the motor performance of PD. However, the influence of subthalamic DBS on STS remains unclear. The study aims to investigate the dynamic balance in patients with advanced PD during STS before and following bilateral subthalamic DBS.

METHODS

Five patients with advanced PD (63±8y/o, 63±17kg, 1.6±0.7m) (Hoehn and Yahr stage III to IV when off medication) participated in the current study with written informed consent. All patients had undergone medication and received bilateral subthalamic DBS surgery. All PD participants were recruited from the Movement Disorders Outpatient Clinic at the Department of Neurologists, Taichung Tzu Chi Hospital. An 8-camera motion capture system with a sampling rate of 120Hz (Vicon Vantage System, Oxford Metrics Ltd., UK) and two force plates (AMTI, USA) were used. Each subject performed sit-to-stand (STS) with knee flexion of 80 degrees (STS-80) and 110 degrees (STS-110) at a self-selected pace. All PD subjects were tested under two conditions: (1) medication on before DBS surgery (pre-DBS) and (2) medication on and 3-4 months after DBS surgery (post-DBS). Three successful trials for each condition were collected and analyzed. A chair was placed on one force plate, and two feet stepped on another force plate. A 13-body-segment model of the whole body was used to calculate the position of the body's center of mass (COM) as the weighted sum of the segmental COMs of all body segments [1]. The segmental inertial properties were determined using Dempster coefficients. The center of pressure (COP) positions were calculated from the force plate. The anterior and posterior (A/P) positions and medial and lateral (M/L) positions of the COM and COP were analyzed. The STS was composed of three phases: phase I (flexion-momentum phase), phase II (momentum-transfer phase), and phase III (extension phase) [2]. The balance control capability is represented by the peak displacement distances of COM and COP in the A/P and M/L directions. Parameters before and after DBS were compared using the Mann-Whitney U test, with statistical significance set at 0.05.

RESULTS AND DISCUSSION

Comparing pre- and post-DBS, the results showed that the peak displacement distance of A/P and M/L of the COM and COP become smaller during phases II and III of STS-80 and STS-110 (Table 1).

Table 1. Mean values of peak displacement (mm) of the COM and COP at phase I, II, and III during STS with knee of 80 and 110 degrees.

		STS-80			STS -110		
		Pre-DBS	Post- DBS	P value	Pre-DBS	Post- DBS	P value
COM A/P	Phase I	35.60 (20.39)	72.77 (13.56)	0.67	31.04 (19.76)	64.12 (18.88)	0.41
	Phase II	138.07 (38.65)	83.40 (0.26)	0.06	132.69 (34.71)	67.81 (27.62)	0.06
	Phase III	143.87(12.89)	123.78 (7.51)	0.08	130.15 (7.73)	111.06 (12.28)	0.08
COM M/L	Phase I	4.33 (2.95)	2.48 (0.87)	0.25	1.63 (0.57)	2.47 (0.33)	0.51
	Phase II	18.71 (2.50)	3.38 (1.96)	0.06	20.36 (11.38)	3.21 (2.48)	0.06
	Phase III	22.27(3.60)	22.39 (5.14)	0.27	20.03 (3.10)	22.32 (1.01)	0.40
COP A/P	Phase I	2.25 (0.55)	1.19 (0.18)	0.39	1.77 (0.34)	1.24 (0.09)	0.44
	Phase II	14.76 (10.95)	2.90 (3.03)	0.05*	5.36 (2.864)	2.95 (3.14)	0.05*
	Phase III	17.44 (5.50)	10.18 (12.26)	0.00*	16.75 (2.22)	10.90 (11.53)	0.05*
COP M/L	Phase I	1.05 (0.11)	0.63 (0.16)	0.74	0.66 (0.29)	0.64 (0.13)	1.00
	Phase II	4.20 (1.81)	1.31 (1.47)	0.03*	3.71 (1.64)	1.32 (1.49)	0.03*
	Phase III	7.89 (3.35)	1.69 (0.67)	0.05*	4.92 (2.71)	1.79 (0.81)	0.01*

*Significant difference between pre-DBS and post-DBS

CONCLUSIONS

After DBS surgery, it is helpful for PD patients to achieve balanced control during sit-to-stand standing. From sitting to standing, phase II and phase III are the most challenging to maintaining balance control. Because Phase II is at the largest angle of the knee joint, sufficient muscle strength of the lower extremity is required to stand up. Phase III needs the trunk to erect again and sufficient muscle strength. For PD patients after DBS, it is recommended to strengthen and maintain lower limb strength training and exercise.

ACKNOWLEDGEMENTS

Financial Support: Ministry of Science and Technology Taiwan (110WFD2410354) and Taichung Tzu-Chi Hospital (TCCRD-I-110-38-1).

REFERENCES

[1] Chen, SC *et al*. Gait Posture 33: 695- 700.
[2] Seven YB et al. *Hum Mov Sci* 27: 65-79, 2008.

Effect of small perturbation balance training using wearable device on muscle activity related to reactive postural control

Taku Washida[1], Masataka Yamamoto[1,2] and Hiroshi Takemura [1]
[1] Tokyo University of Science, Chiba, Japan
[2] Hiroshima University, Hiroshima, Japan
Email: 7519108@tus.ac.ed.jp

INTRODUCTION

Reactive postural control is important for fall prevention. Perturbation-based balance training using medical device is effective for fall prevention. However, this training requires large therapeutic instruments or medical expert guidance. Recently, we developed wearable balance training device (WBTD : Figure 1), which is allowed users to perform perturbation-based balance training at home. Although the WBTD improve static postural control [1], the effect of WBTD on reactive postural control is still unclear. The purpose of this study was to investigate the effect of WBTD on muscles activity related to reactive postural control.

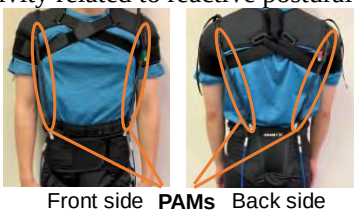

Figure 1 Wearable balance training device (WBTD) which can generate unexpected small perturbation by pneumatic artificial muscles (PAMs).

METHODS

Twelve healthy adult males participated in this study (age: 23 ± 0.9 years; dominant leg: right). Subjects were separated into a device group and a sham group equally. At the training session, all subjects were asked to perform a tandem stance with wearing the WBTD (in total 16 times of 1 minute trial). In device group, WBTD perturbated subjects laterally in random timing and direction for a minute, while WBTD didn't perturb subjects in the sham group. Before and after training session, pre-test and post-test session were conducted using air cylinders as assessment for reactive postural control. The air cylinders were placed on each side of the subjects and perturbed the subjects' pelvis laterally at random timing and direction. During test session, subjects were evaluated their reactive balance function by center of pressure (COP) and electromyography (EMG). EMGs were obtained from both side gluteus medius (GM) and adductor longus (LM). After the perturbation occurred (0 ms), time series COP data of the test session was separated into epochs as follows: 100 to 250 ms (epoch c1), 250 to 400 ms (epoch c2), and 400 to 550 (epoch c3) ms. While EMG data was separated as follows: 50 to 200 ms (epoch e1), 200 to 350 ms (epoch e2), and 350 to 500 (epoch e3) ms. Lateral maximum displacement (LMD) and sway area (SA) were calculated in each epoch. Co-contraction index (CCI) was calculated in each epoch. CCI combination was right-leg (right-GM and right-LM). The amount of change obtained by subtracting the pre-test from the post-test in each index was conducted at a t-test in the device group and the sham group. Statistical significance was set at $p < 0.05$.

RESULTS AND DISCUSSION

Showing some of the results. Figures 2A and 2B show the device group significantly decreased, compared to those in the sham group of the LMD in epoch c1, c2 and SA in epoch c2 ($p < 0.05$). This result suggests the training by WBTD was effective in the improvement of reactive balance function. Figure 2C shows the device group significantly decreased, compared to those in the sham group of right-leg CCI in epoch e3 ($p < 0.05$). Higher rates of CCI are associated with a higher risk of falls [2]. Right-leg CCI in epoch e3 was decreased, possibly improving the balance of using GM and LM to maintain posture. Training with WBTD may contribute to fall prevention.

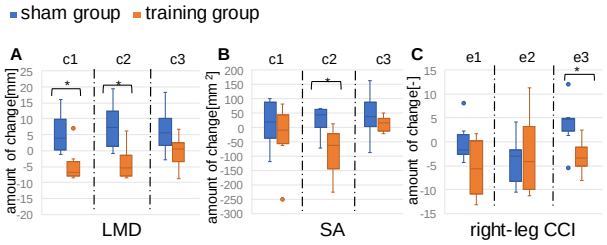

Figure 2 A-C : Amount of change obtained by subtracted pre-test from post-test in each time interval of evaluation index of COP and EMG (c1 means epoch c1, e1 means epoch e1).

CONCLUSIONS

Training with WBTD seemly improvement reactive balance function immediately. To find out the mechanism of improvement in more detail, we should investigate older adults with a larger sample size.

ACKNOWLEDGEMENTS

This work was supported in part by JSPS KAKENHI under Grant 22K18240.

REFERENCES

[1] Yamamo M et al. Appl Sci **9**:15 2019
[2] Nelson W et al. Eur J Appl Physiol **112**:1379-1389 2012

The Effect of suspensory Strategy on Postural Control under Lateral Perturbations: A Study on COM Height and Balance Performance

Linjing Jiang[1], Satoshi Kasahara[1], Tomoya Ishida[2], Yuta Koshino[1], Mina Samukawa[1], and Harukazu Tohyama[1]
[1] Faculty of Health Sciences, Hokkaido University, Sapporo, Japan
Email: jlinjing@eis.hokudai.ac.jp

INTRODUCTION

Postural control under lateral perturbations is essential for maintaining balance and stability during various daily activities. At the same time, the suspensory strategy of bending the knees or squatting is a recognized strategy for stabilizing and maintaining balance by lowering the center of mass (COM) [1]. Although this study investigated the contribution of the suspensory strategy to voluntary postural stability in the anterior-posterior direction, it is unclear whether the suspensory strategy affects postural stability under lateral perturbations. This study aims to investigate whether the suspensory strategy (lowering the COM height) affects balance performance when subjected to unpredictable lateral perturbation.

METHODS

Eighteen healthy young adults (10 males, 8 females; mean age 24.4 ± 2.2 years; weight 62.0 ± 13.9 kg; height 168.8 ± 5.3 cm) participated in this study. This study was to adjust the COM height by having participants assume three different postures: standing, semi-squatting, and squatting. External lateral perturbation was produced with the platform moved in the rectilinear direction, and participants did not know its onset and motion direction. The displacement of the participants' center of mass (COM) and the perturbation generator were measured using a 3D motion capture system. We calculated the initial time and reversal times of the COM movement, as well as the minimum margin of stability (mini-MOS), which is the distance between the predicted displacement of the COM and the edge of the base of support in the frontal plane (Figure 1). We used one-way repeated ANOVA to analyze the data for initial time, reversal time, and mini-MOS, and post-hoc Bonferroni tests to compare differences between postures. The significance level was set at $p < 0.05$.

RESULTS AND DISCUSSION

From one-way repeated ANOVA, there were significant differences in reversal time and mini-MOS at different COM heights, but no significant differences in initial time (Table 1). Post-hoc analyses showed that reversal time was longer in the standing posture compared to both the semi-squatting and squatting postures ($p < .05$). This supports that the suspensory strategy benefits the temporal parameters of postural stability response to unpredictable lateral perturbation. Post-hoc analyses revealed that the mini-MOS was significantly shorter in the squatting posture compared to both the semi-squatting and standing postures ($p < .05$). This indicates that excessive knee flexion or deeper squat decreases postural stability in external lateral perturbation.

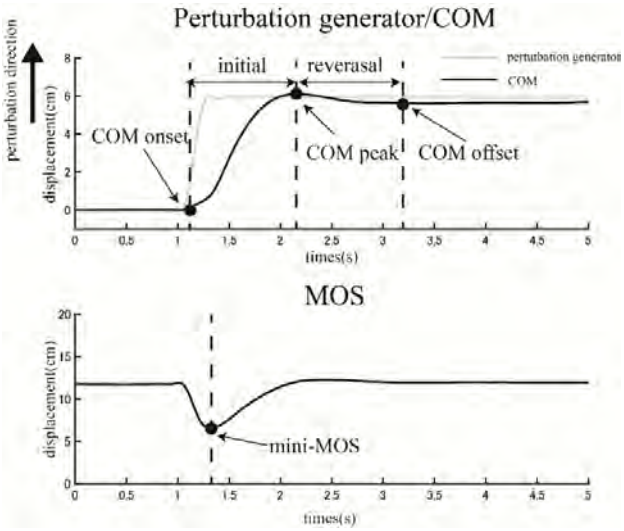

Figure 1 Raw data sample from an experiment.

CONCLUSIONS

These findings suggest that while lowering the COM height through the suspensory strategy may improve balance ability, caution should be exercised to avoid lowering it too much, as this could indicate potential risks for postural control, as shown in the case of the squatting posture.

REFERENCES

[1] Kasahara S et al. Gait Posture 42(4):448-54. 2015.

Table 1: Results from the one-way repeated ANOVA for outcome measures.

	Standing	Semi-squatting	squatting	η2	*p-value*
Initial time (s)	1.29 ± 0.32	1.30 ± 0.32	1.25 ± 0.24	0.01	$p = 0.781$
Reversal time (s)	0.73 ± 0.51	0.46 ± 0.42*	0.25 ± 0.29*	0.45	$p < 0.001$
mini-MOS (cm)	7.70 ± 2.00	7.33 ± 2.13	6.5 ± 1.52*#	0.30	$p = 0.002$

mini-MOS: minimum margin of stability; p-value: one-way ANOVA's p value; * means this data have significant difference with standing $p < 0.05$; # means this data have significant difference with semi-squatting $p < 0.05$

AGE-INDUCED MODIFICATIONS IN POSTURAL SWAY AND FORCE STEADINESS DURING PLANTAR AND DORSIFLEXION

Ioannis G Amiridis[1], Chrysostomos Sahinis[1], Anastasia Papavasileiou [1] Theodosiadou Anastasia[2], Marie Fabre[3], Thomas Lapole[3], Baudry Stephane[2], and Dimitrios A Patikas[1]

[1]School of Physical Education & Sport Science, Aristotle University of Thessaloniki, Laboratory of Neuromechanics, Serres, Greece.

[2]ULB Neuroscience Institute, Université Libre de Bruxelles, Laboratory of Applied Biology and Research Unit in Applied Neurophysiology, Brussels, Belgium.

[3]Université Jean Monnet Saint-Etienne, Lyon 1, Université Savoie Mont-Blanc, F-42023, Laboratoire Interuniversitaire de Biologie de la Motricité, Saint-Etienne, France.

Email: jamoirid@auth.gr

INTRODUCTION

Postural control plays an essential role in daily activities throughout lifespan. Muscles acting around the ankle, knee and hip joint are of great relevance for maintaining posture [1]. Dynapenia (poverty of strength) is often associated with reduced performance in daily living activities, decreased mobility, impaired standing balance, expanded hospitalization and less protection from falling in old age [2]. The age-related deterioration in strength is not uniform between lower extremity muscles as the rate of decline in plantar flexors force is the largest compared with other muscle groups [3] and the relation between muscle strength and postural control is age-dependent [4]. Recently, it was demonstrated that the most consistent explanatory variable for the variance in sway-area rate was force control of the hip abductors and ankle dorsiflexors as indicated by the magnitude of the normalized force fluctuations (force steadiness) during a submaximal (5% and 15%) isometric contraction [5]. Therefore, the aim of this study is to examine the postural control across life span, associated with force steadiness of the plantar flexors and dorsiflexors.

METHODS

All participants (range of age: 7 – 70 years) were physically active, healthy and free from any disease or impairment. The postural sway was evaluated by employing the NIH Toolbox test of standing balance (Kistler, 1000 Hz), which requires individuals to stand on a rigid or foam surface with eyes open or closed for 60 s. The average CoP velocity, the peak-to-peak amplitude, the standard deviation of CoP displacement, the root mean square (mm) of CoP in anterior-posterior (A/P) and medio-lateral (M/L) axis were used.

The force steadiness during plantar flexion and dorsiflexion at 5% and 15% MVC was evaluated in an isometric dynamometer. Visual feedback of the applied force was provided. The force fluctuations were expressed as the coefficient of variation (CoV: standard deviation/mean*100) during the 5 steadiest seconds of the submaximal contraction (average of 3 trials).

RESULTS AND DISCUSSION

All CoP variables had a U-shaped distribution by age, with those who are very young or very old having the highest values. Similarly, the CoV for force during plantar flexion and dorsiflexion was high for the participants before puberty, it decreases in adolescent and then increases again with age. Pearson's test showed strong positive correlation between CoV for force during plantar flexion at 5% and 15% and CoP velocity in M/L axis during standing on a rigid surface with eyes closed (Figure 1). However, the correlations did not reach always the significance, especially for the dorsiflexors and the standing task on a foam surface.

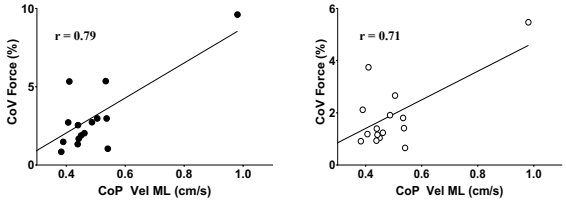

Figure 1 Correlation between the Coefficient of Variance for force during plantar flexion at 5 and 15% MVC and Centre of Pressure velocity in medio-lateral axis during standing on a rigid surface with eyes closed.

CONCLUSIONS

Children and older adults presented poorer postural control during standing and poorer force steadiness with the ankle muscles compared to young and middle-aged adults. The postural control was correlated with the force fluctuations depending on the standing task and the muscles involved.

ACKNOWLEDGEMENTS

This research was funded by the Greek General Secretariat for Research and Technology (ERA-NET NEURON JTC 2020, 271 T12EPA5-00018).

REFERENCES

[1] Amiridis et al. *Neurosci Lett* **350**: 137-140, 2003.
[2] Clark & Manini. *J Gerontol A Biol Sci Med Sci* **63**: 829-834, 2008.
[3] Danneskiold-Samsøe et al. *Acta Physiol* **197**: 1-68, 2009.
[4] Svoboda et al. *Plos One* **14**: 1-10, 2019.
[5] Davis et al. *Exp Brain Res* **238**: 487-497, 2020.

Effects of Eye Dominance on Whole-Body Balance Control During Level Walking in The Elderly

Ju Yang Tiong[1], Yi-Ling Lu[1,2], Cheng-Hao Yu[1], Yu-Lin Tsai[1,3],
Kuan-Wen Wu[3,4] Ting-Ming Wang[3,4] and Tung-Wu Lu[1,4]
[1] Department of Biomedical Engineering, National Taiwan University, Taiwan
[2] Department of Ophthalmology, Cheng Hsin General Hospital, Taiwan
[3] Department of Orthopaedic Surgery, National Taiwan University Hospital, Taiwan
[4] Department of Orthopaedic Surgery, School of Medicine, National Taiwan University, Taiwan
Email: twlu@ntu.edu.tw

INTRODUCTION

Vision plays a significant role in the maintenance of stability. The laterality of the eye, so-called "eye dominance", have shown to be related to visual acuity, speed of information processing and even postural control [1]. With compromised vestibular and proprioceptive systems, the importance of visual information in gait are further highlighted in older people, while visual field deficits caused by ageing lead to an inability to recover balance with subsequent increased risk of falls. Therefore, the study aimed to identify the effects of eye dominance on whole-body balance control during level walking in the elderly.

METHODS

Thirteen older adults without neuromusculoskeletal and ocular disorders participated in this study. Each subject walked at a self-selected pace on an 8-m walkway with three visual field conditions, namely dominant vision (DV), non-dominant vision (N-DV) and full vision (FV), while the balance control was quantified by inclination angles (IA) of the line joining the body's centre of mass (COM) and centre of pressure (COP), and the rate of change of IA (RCIA) [2]. Spatial-temporal parameters, namely walking speed, cadence, step length, stride length and stride width, were also calculated. Comparisons of all the calculated variables between test conditions were performed using paired t-tests with a significance level of 0.05.

RESULTS AND DISCUSSION

Compared to the FV condition, the elderly walked with increased step length, step width and cadence for the DV condition (Table 1). Similar gait patterns were found for the N-DV condition, except for increased walking speed but decreased stride length (Table 1).

Table 1: Means (standard deviations) of the temporal-spatial parameters in the elderly for all vision conditions. P_{DV} = DV vs. Control; $P_{N\text{-}DV}$ = N-DV vs. Control; P_S = DV vs. N-DV; *: $p < 0.05$.

Parameters (unit)	Conditions			P-Value
	DV	N-DV	Control	P_{DV}, $P_{N\text{-}DV}$, P_S
Walking Speed (mm/s)	1071.4 (62.0)	987.1 (103.6)	958.8 (106.4)	0.29, 0.01*, 0.01*
Stride Length (mm)	1090.6 (30.0)	1033.0 (34.3)	1047.4 (39.3)	0.09, 0.01*, 0.01*
Step Length (mm)	545.5 (15.5)	543.8 (16.1)	526.6 (20.7)	0.01*, 0.01*, 0.36
Step Width (mm)	95.0 (25.8)	92.7 (25.3)	77.8 (27.6)	0.01*, 0.02*, 0.33
Cadence (step/min)	117.2 (5.2)	117.2 (5.1)	109.8 (10.0)	0.01*, 0.01*, 0.95

For the IA-related and RCIA-related variables, differences in between-condition comparisons were found in the sagittal plane but not in the frontal plane (Fig. 1). The elderly showed increased sagittal IA during single limb support (SLS) but decreased sagittal RCIA at contralateral heel-strike (CHS) and the first peak value during terminal double limb support (tDLS) for the N-DV condition when compared to the FV condition (Fig. 1A and B). Compared to the DV condition, the elderly increased sagittal RCIA during tDLS for the N-DV condition (Fig. 1A and B).

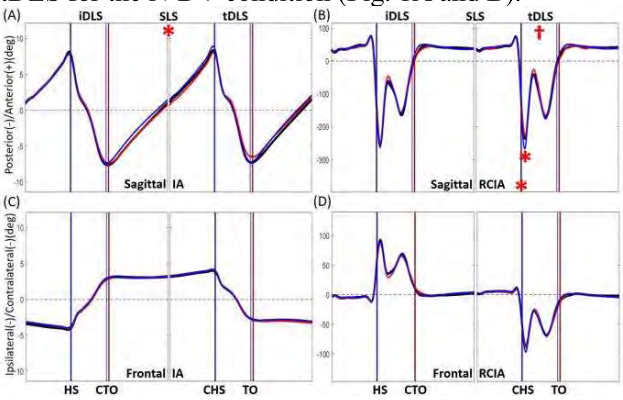

Fig. 1 Ensemble-averaged curves of COM-COP inclination angle (IA) and rate of change of IA (RCIA) in the sagittal plane and the frontal plane. TO: toe-off; HS: heel-strike; CTO: contralateral toe-off; CHS: contralateral heel-strike; iDLS: initial double limb support; SLS: single limb support; tDLS: terminal double limb support. Black line: Control; Red line: DV; Blue line: N-DV. *: N-DV significantly different from the Control; †: N-DV significantly different from DV.

CONCLUSIONS

The current study was the first in the literature to identify the effects of eye dominance on balance control in the elderly during walking. The results suggested that the elderly with non-dominant vision showed significantly compromised whole-body balance control strategies with altered COM-COP control – especially in the sagittal plane – that may lead to an increased risk of falling [2].

ACKNOWLEDGEMENTS

Financial support from the Cheng Hsin General Hospital, Taiwan (CHGH112-(N)09) is greatly appreciated.

REFERENCES

[1] Coren, S. *Percept Mot Skills* **88(2)**: 424-426, 1999.
[2] Lee, H. J., & Chou, L. S. *Arch. Phys. M.* **87(4)**: 569-575, 2006.

EFFECTS OF SCOLIOSIS ON UPPER BODY BALANCE CONTROL IN MIDDLE-AGE ADULTS DURING OBSTACLE CROSSING

Wen-Horng Lo[1,2], Ju Yang Tiong[1], Kuan-Wen Wu[3,4] , Ting-Ming Wang[3,4] and Tung-Wu Lu [1,3]
[1] Department of Biomedical Engineering, National Taiwan University, Taipei, Taiwan.
[2] Division of orthopedic surgery, Fu Jen Catholic university hospital, New Taipei City, Taiwan.
[3]Department of Orthopaedic Surgery, School of Medicine, National Taiwan University, Taipei, Taiwan.
[4]Department of Orthopaedic Surgery, National Taiwan University Hospital, Taipei, Taiwan.
Email: twlu@ntu.edu.tw

INTRODUCTION

Scoliosis affects physiological functions and appearance perception, which can cause pain and further deterioration in adolescent patients with severe deformities. Although it is common for the adult population to have some form of spinal deformity, only less than 10% of them are symptomatic [1]. This study aimed to identify the dynamic pattern of trunk and pelvis kinematics during obstacle-crossing in the asymptomatic scoliosis middle-aged population to further our understanding of the potential biomechanical changes which may assist in their clinical management to avoid surgery in later life.

METHODS

Eight middle-aged patients with asymptomatic scoliosis (SBC group) and eight healthy age-matched controls (Control group) participated in the current study with informed written consent as approved by the Institutional Research Board. Each subject walked at their preferred walking speed and crossed a height-adjustable obstacle (i.e., 10%, 20% and 30% of the subject's leg length). A counterbalanced measures design was used, while the sequence of the obstacle conditions was decided by a random number table. Three-dimensional marker trajectories were measured using an eight-camera motion capture system (Vicon 512, Oxford Metrics Group, UK) at 120 Hz, and the ground reaction forces (GRF) and the center of pressure (COP) were measured at 1080 Hz using two forceplates (AMTI, USA) placed on either side of the obstacle [2]. Angular motions of the trunk and pelvis during obstacle crossing were calculated. The crossing speed, cadence, stride length, and angular position of the trunk and pelvis were analyzed using a two-way mixed-design analysis of variance (ANOVA) with one between-subject factor (group) and one within-subject factor (obstacle height). Whenever a height effect was found, a polynomial test was used to determine the trend. All statistical analyses were performed using SPSS version 20 (SPSS Inc., Chicago, IL, USA).

RESULTS AND DISCUSSION

Compared to the Control group, the SBC group showed significantly slower crossing speed, shorter stride length, and lower cadence during obstacle-crossing (Table 1). In addition, the SBC group showed significantly increased pelvic and trunk posterior tilt during obstacle-crossing. With increasing obstacle height, both SBC and Control groups linearly increased their upper-body posterior tilt (Figure 1).

Table 1: Means (standard deviations, SD) of the crossing speed, stride length, and toe-obstacle and heel-obstacle distances in the patients with asymptomatic scoliosis (SBC) and healthy adults (Control) when crossing obstacles of 20% leg length (LL).

	SBC	Control	Group effect
Crossing speed (m/s)	1.03 (0.16)	1.33 (0.11)	p = 0.01*
Stride length (m)	1.27 (0.07)	1.41 (0.04)	p = 0.01*
Cadence (step/min)	76.38 (8.9)	93.21 (5.9)	p = 0.01*

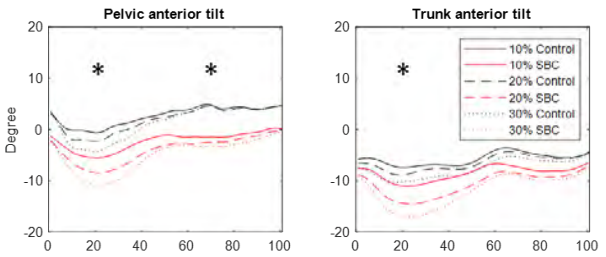

Figure 1: The mean curves of the angles of the pelvic and trunk in the sagittal plane in the SBC (red) and Control (black) groups when crossing obstacles of 10%, 20% and 30% of the leg length. * Significant linearly increasing trend.

CONCLUSIONS

Patients with asymptomatic scoliosis were found to develop a more conservative obstacle-crossing technique, i.e., with significantly greater posteriorly tilted upper body position. Further studies on the joint kinematics and kinetics of the locomotor system will be helpful for a better understanding of the different adopted mechanisms between the groups.

ACKNOWLEDGEMENTS

Financial support from the Fu Jen Catholic university hospital, Taiwan (PL-202108006-V) is greatly appreciated.

REFERENCES

[1] Stokes IA et al. Spine. 21(10), 1162-7. 1996.
[2] Wu KW et al. PLoS One. 15(2), e0228752. 2020.

NEUROMUSCULAR RESPONSES DURING STANDING WITH SENSORY RESTRICTIONS ARE NOT RELATED TO FIELD TEST PERFORMANCE IN CHILDREN WITH CEREBRAL PALSY

Papavasileiou A.[1], Sahinis C.[1], Fabre M.[2], Theodosiadou A.[3], Baudry S.[3], Lapole T.[2], Amiridis I.G.[1], Patikas D.[1]

[1]Laboratory of Neuromechanics, School of Physical Education and Sports Science at Serres, Aristotle University of Thessaloniki, Serres, Greece.

[2]Université Jean Monnet Saint-Etienne, Lyon 1, Université Savoie Mont-Blanc, Laboratoire Interuniversitaire de Biologie de la Motricité, F-42023, Saint-Etienne, France.

[3]Laboratory of Applied Biology and Research Unit in Applied Neurophysiology, ULB Neuroscience Institute, Université Libre de Bruxelles, Brussels, Belgium.

Email: anastapt@auth.gr

INTRODUCTION

In cerebral palsy (CP), neuromuscular function is abnormally developed, causing gait and postural impairments [1]. Reduced postural control and the resulting increased risk of falling might be caused by the inadequate interaction between sensory feedback and motor command when standing upright. The significance of sensory feedback can be tested by manipulating sensory sources and assessing their consequences on motor responses. [2]. A correlation between these responses and the extent of motor capacities, depicted from field tests, might give an insight into the causes of the impairment. This might refine diagnostic tests and treatments. Therefore, the purpose of this study was to investigate the neuromuscular responses while standing with sensory restrictions and to test if these responses are correlated with performance in field tests in children with CP and typically developed (TD) children.

METHODS

Nine children with CP (12.5±1.7 yrs, 147.3±0.5 cm, 46.1±0.8 kg) and 16 TD children (14.0±3.8 yrs, 161.2±1.2 cm, 54.8±0.9 kg) were evaluated in the field tests of 10 m walking at comfortable and maximum speed, 2- or 6-minutes walking (for CP or TD, respectively), and the time up and go test. Children with CP had 1.73±0.98 [mean±standard deviation (SD)] level of ankle spasticity, as evaluated using the average of the plantar and dorsiflexors score, based on the modified Ashworth's scale. All participants were asked to stand comfortably on a force platform, in four different sensory conditions: eyes open (EO) or eyes closed (EC), on a rigid (R) or foam (F) surface. The SD and velocity of the center of pressure (CoP) on the anterior-posterior and mediolateral direction, the trunk acceleration (TrA), as well as the root mean square of the soleus (SOL), gastrocnemius medialis (MG) and tibialis anterior (TA) muscles electromyogram (EMG), were recorded in three, 60-s trials, in each balance condition. The rate of change for ECR, EOF and ECF was expressed as the $\log_2$ ratio relative to EOR. A linear mixed model was used to compare the differences between conditions, groups, and interaction. The correlation between the variables was examined with the Pearson's r, whereas Spearman's rho was calculated when normal distribution was not granted.

RESULTS AND DISCUSSION

Children with CP demonstrated overall lower performance in all field tests compared to TD children. Both SD and velocity of CoP and TrA demonstrated greater values for the children with CP than TD children, in all four conditions. However, the rate of change was greater in TD children, indicating a ceiling effect for the values of children with CP, probably because they demonstrated great values even at EOR condition. However, no variable regarding CoP and TrA or the rate of changed compared to EOR was correlated to any of the field tests. Regarding the EMG, although GM and SOL increased in ECR, EOF and ECF conditions compared to EOR in both groups, the extent of these changes did not correlate with the performance in any of the field tests.

CONCLUSIONS

The current findings indicate that the adaptations during sensory restrictions from visual (i.e., eyes closed) and proprioceptive (i.e., foam) sources may not reflect motor capacity of children with CP and TD children in complex balance tasks, characterized by changes in sensory flow during the completion of the task. Accordingly, changing the input from other sensory sources (e.g., vestibular) or in a different manner than in the current study (e.g., changing the proprioceptive input by means of local tendon vibration), may highlight possible links between physical performance and sensory feedback in CP.

ACKNOWLEDGEMENTS

This research was funded by the Greek General Secretariat for Research and Technology (ERA-NET NEURON JTC 2020, 271 T12EPA5-00018).

REFERENCES

[1] Zhou et al. *Front Hum Neurosci* **2015**:891390, 2015.

[2] Paillard et al. *BioMed Res Int* **2015**:891390, 2015

A Bi-Planar Inverted Pendulum Model for Evaluating the Dynamic Stability in Patients with Duchenne Muscular Dystrophy During Level Walking

Shu-Jiun Lin[1], Yu-Lin Tsai[1,2], Shiuan-Huei Lu[1], Cheng-Hao Yu[1],
Tsan-Yang Chen[1], Kuan-Wen Wu[2,3], Ting-Ming Wang[2] and Tung-Wu Lu[1,3]
[1] Department of Biomedical Engineering, National Taiwan University, Taiwan, R.O.C.
[2] Department of Orthopaedic Surgery, National Taiwan University Hospital, Taiwan, R.O.C.
[3] Department of Orthopaedic Surgery, School of Medicine, National Taiwan University, Taiwan, R.O.C.
Email: twlu@ntu.edu.tw

INTRODUCTION

Duchenne muscular dystrophy (DMD) is a genetically defective and lethal neuromuscular disorder characterized by severe and progressive muscular weakness. Muscular weakness in the lower limbs contributes to altered kinematic patterns and with ~~unstable~~ balance disturbances during gait ~~in patients with DMthatD~~ subsequently leading to increased risk of falls ~~, increasing the risk of falls~~ [1]. However, difficulties still exist in synthesizing this kinematic and kinetic information to reveal the underlying dynamic stability control in patients with DMD during gait. Therefore, this study aimed to develop a novel balance evaluation method based on a bi-planar inverted pendulum model with measured gait data to quantify the dynamic stability in patients with DMD during the single limb support (SLS) phase.

METHODS

Fifteen patients with DMD and fifteen healthy controls were recruited in this study. Each subject walked at a self-selected pace on an 8-m walkway while the kinematic and kinetic data were measured. A bi-planar inverted pendulum model based on Pai and Patton [2] was used to determine the feasible stability region on the phase portrait between the joint angle and angular velocity of the stance ankle. The magnitude of the stability margin index (SMI) was defined as the Euclidean distance between the measured gait data and the edge of the corresponding feasible stability region. The negative sign of SMI signified that the feasible stability region was violated, meaning that the subject was dynamically unstable at the corresponding instant. A segmented least squares regression fitted between the joint angle of the stance ankle and SMI during SLS was used to estimate the joint angle of the stance ankle and corresponding SMI at the initial instant, the intersection instant and the terminal instant, and the change in SMI between each two instant (Figure 1). Comparisons of all the calculated variables between patients with DMD and healthy controls were performed using independent t-tests with a significance level of 0.05.

RESULTS AND DISCUSSION

For all calculated variables, differences in between-group comparisons were found in the frontal plane but not in the sagittal plane (Figure 1). Compared to the healthy controls, patients with DMD walked with significantly decreased frontal SMI at the initial and intersection instant (Figure 1B) but similarly at the terminal instant. These results suggested that patients with DMD showed significantly compromised whole-body balance control strategies with altered COM-ankle control in the frontal plane which may ~~lead to an~~partially contribute to increased risk of falling.

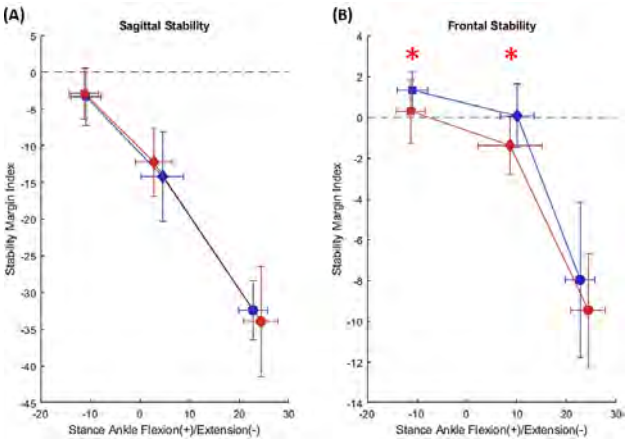

Figure 1 Comparisons of the joint angle of the stance ankle and corresponding SMI at the initial instant, the intersection instant and the terminal instant in (A) the sagittal plane and (B) the frontal plane during level walking with the corresponding standard deviations shown as error bars. ■: initial instant; ◆: intersection instant; ●: terminal instant (red: DMD; blue: Control). *: DMD significantly different from Control.

CONCLUSIONS

This study was the first in the literature to develop a quantifiable~~ied~~ balance evaluation method based on an inverted pendulum model to evaluate the dynamic stability control in patients with DMD during SLS. The current results showed that patients with DMD have a higher risk of falling in the medial-lateral direction during the early stage of SLS due to altered COM-ankle control in the frontal plane.

ACKNOWLEDGEMENTS

The authors are grateful for the financial support from the National Science and Technology Council, Taiwan (MOST110-2221-E002-027-MY3).

REFERENCES

[1]Armand, S., et al. *Gait Posture* 21: 369-78, 2005.
[2]Pai, Y.C., et al. *J Biomech* 30: 347-54, 1997.

MUSCLE-TENDON BIOMECHANICS AND DAILY STEPS IN PATIENTS RECOVERING FROM ACHILLES TENDON RUPTURE

Taija Finni, Maria Sukanen, Iida Laatikainen-Raussi and Raad Khair
[1] Faculty of Sport and Health Sciences University of Jyväskylä, Finland.
Email:taija.finni@jyu.fi

INTRODUCTION

Achilles tendon rupture (ATR) results in long term functional deficits characterized by longer and thicker tendon, muscle atrophy and weakness, and decreased heel-rise performance in the injured limb [1]. Rehabilitation exercises are important for recovery, but in addition to spesific rehabilitative measures also daily physical activity may be relevant for the time course of recovery. We examined and expected to find associations between the daily steps at 2, 6 and 12 months, and biomechanical factors at 12 months post rupture.

METHODS

Data was extracted from a clinical cohort study "non-operative treatment of Achilles tendon Rupture in Central Finland: a prospective cohort study – NoARC" (trail registration: NCT03704532) Recruitment and treatments are described in detail in [2]. The number of patients measured at 12 months (m) was 45, but due to missing data, 15 is the minimum number of participants in some correlations.

At 12m, bilateral measures of isometric plantarflexion strength (MVC), medial gastrocnemius (MG), lateral gastrocnemius (LG) and soleus (SOL) subtendon lengths, MG fascicle length, MG and LG muscle cross-sectional area, tendon stiffness and ankle joint resting angle were assessed as described in [2]. MG fascicle operating range during heel rise was assessed. From all variables, limb asymmetry was calculated as ((healthy-injured)/healthy)*100 and used in analysis.

At 2m (N=24), 6m (N=22) and 12m (N=35), the patients were given 3D accelerometers (RM42, UKK Institute, Finland) that were to be worn on hip on 7 consecutive days. Wear time was to be marked on a diary. Step counts were analyzed based on algorithms of Actilife-software. Recordings with at least 3 days and 10 hours of good data were included in the analysis. Mean daily steps from the recording period and daily minimum and maximum step counts were extracted.

Repeated measures ANOVA was used to check the differences in daily steps across time and two-tailed Pearson's correlations were calculated between step variables and biomechanical variables at 12m.

RESULTS AND DISCUSSION

Mean daily step count (N=15) increased ($p<0.001$) from 4824±1331 at 2m to 8389±2706 at 6m and remained similar at 12m being 8240±2902. Maximum step count at 2m correlated with average step count at 6m ($r=0.651$, $p=0.006$) and maximum step count at 6m correlated with average step count at 12m ($r=0.507$, $p=0.022$).

Associations between step data and biomechanical variables at 12m were found only between LG subtendon length asymmetry and mean daily steps at 2m ($r=-0.529$, $p=0.024$, N=18, Figure 1).

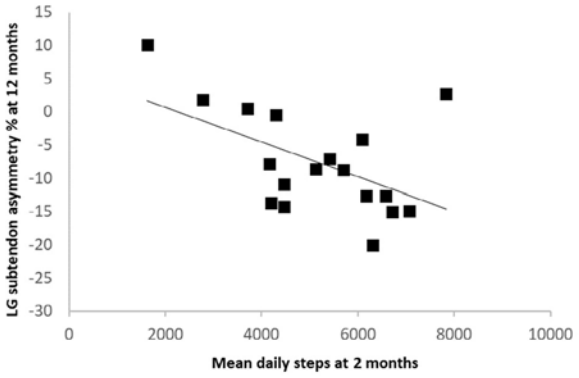

Figure 1 The only significant association found between daily steps and biomechanical variables examined at 12m.

CONCLUSIONS

Maximum daily step count associates with average step count at a later time point suggesting that step count of the most active day may reflect future potential for increased physical activity. The one association found between biomechanical variables and step counts should be interpreted carefully since it may be a chance finding. However, the observation warrants for further studies whether too much daily steps in the early rehabilitation phase could have negative influence on tendon elongation.

ACKNOWLEDGEMENTS

Funded by Academy of Finland grant #323168, UNderstanding REStoration of Achilles Tendon function after rupture (UNRESAT)

REFERENCES

[1] Silbernagel KG et al. *Am J Sports Med* **40**:1564-71
[2] Khair R et al. *Clin Biomech, **92**, 105568.*

Effect of isometric quadriceps exercise on stiffness and hemoglobin concentration of the infrapatellar fat pad in knee osteoarthritis.

Syoya Nakanishi[1,2], Masashi Kitano[2,3], Masahiro Tsutsumi[4], Makoto Wada[1], and Shintarou Kudo [2,4,5]
[1] Wada Orthopaedic Clinic / Osaka, Japan.
[2] Graduate School of Health Sciences, MORINOMIYA University of Medical Sciences / Osaka, Japan.
[3]mediVR, Inc / Tokyo, Japan.
[4]Inclusive Medical Science Research Institute, MORINOMIYA University of Medical Sciences / Osaka, Japan.
[5]AR-Ex Medical Research Center / Tokyo, Japan.
Email: n.syoya.pt@gmail.com

INTRODUCTION

Knee osteoarthritis (KOA), one of the most common degenerative knee diseases, is related to the fibrosis of the infrapatellar fat pad (IFP) in its pathomechanism [1]. Recently, it has been suggested that the IFP fibrosis involves HIF-1α activation induced by hypoxia [2]. In young healthy subjects, the IFP stiffness changes occurred during the isometric quadriceps exercise (IQE) and the close relationships between this change and the oxygenation in the IFP was suggested [3]. However, it is unclear whether similar results can be obtained in the KOA. This study aimed to elucidate the characteristics of KOA patients with respect to IQE-induced changes in IFP stiffness and hemoglobin concentration.

METHODS

Eighteen knees of 9 patients with a bilateral KOA were included in the KOA group (mean age, 70.3±7.6 years; 9 females). The control group consisted of 18 knees of 9 healthy volunteers without a history of surgical treatment, trauma, or neurological disorder (mean age, 31.1±7.1 years; 4 males, 5 females). The IFP stiffness was measured during the IQE and then hemoglobin concentration in the IFP before, during, and after the IQE. The measurement limb position is the long sitting position, and the IQE is performed by pressing the manchette of the sphygmomanometer pressurized to 100 mmHg placed in the popliteal space. Exercise intensity was set at 10% of the maximum IQE. The IFP stiffness was measured based on the shear wave velocity at using ultrasound scanner with a 18 MHz linear transducer. The region of interest was set within the IFP, and measured at rest and 10% IQE. The hemoglobin concentration was measured using near-infrared spectroscopy. The modified Beer-Lambert method was used to calculate oxygenated hemoglobin (O2Hb) and deoxygenated hemoglobin (HHb), and the sum of the two, total hemoglobin (cHb). The exercise task was performed 10 times with one set of 10% IQE for 10 seconds and a 3-second rest. Measurement value before the IQE (Pre) was recorded as the mean resting value at 1 min before the IQE, those during, the mean minimum value of 10 times, and those after the IQE (Post), the mean resting value 3–4 min after the IQE. Two-way ANOVA was performed for the IFP stiffness in Group (KOA, control) and exercise task (rest, IQE), and repeated measure ANOVA for hemoglobin concentration in Group (KOA, control) and timing of measurement (pre, IQE-t, post). Multiple comparison procedures were used for post hoc comparisons. All significance level was set at $p<0.05$.

RESULTS AND DISCUSSION

The IFP stiffness significantly increased during the IQE in control (Table 1, Pre vs IQE; 1.3±0.2 m/s vs 3.4±0.5 m/s, $p<0.001$), but did not significantly change in the KOA (Table 1, Pre vs IQE; 2.3±0.6 m/s vs 2.9±1.1 m/s, $p=0.23$). With regard to the hemoglobin concentration in IFP, the O2Hb significantly increased after the IQE compared to pre-IQE in both group, but the O2Hb after the IQE was significantly higher in the control than in the KOA (Table 1, Control vs KOA; 3.4±1.6 mol/dl vs 0.8±1.6 mol/dl, $p<0.001$). Repeated changes in the IFP stiffness by the IQE may improve the IFP hypoxia through capillary compression and release. Therefore, it was suggested that the KOA obtained oxygenation by the IQE, but to a lesser degree than the control due to the insufficient increase of the IFP stiffness by the IQE.

CONCLUSIONS

The KOA showed less change in IFP stiffness and hemoglobin concentration during IQE than the control .

REFERENCES

[1] Belluzzi E et al. Biomed Res Int 2019
[2] Kitagawa T et al. Biomedical Reports 17: 79, 2022
[3] Katayama N et al. J Phys Ther Sci 33: 722-723, 2021

Table 1: Change in the IFP stiffness and each hemoglobin index in each period.

	IFP stiffness(m/s)		O2Hb(mol/dl)			HHb(mol/dl)			cHB(mol/dl)		
	Rest	IQE	Pre	IQE	Post	Pre	IQE	Post	Pre	IQE	Post
Control	1.3±0.2	3.4±0.5*	0.2±0.6	-3.1±4.0*	3.4±1.6*	0.3±0.5	-2.0±1.3*	0.0±0.8	0.0±0.8	-5.1±4.8*	3.3±1.7*
KOA	2.3±0.6†	2.9±1.1	0.1±0.5	-1.2±2.4*	0.8±1.6*†	0.0±0.9	-0.1±1.9	0.0±1.5	0.1±1.1	-1.3±4.0†	0.7±2.5†

Asterisks (*) indicate data that are significantly different from Pre ($P<0.05$). Daggers (†) denote data when OA group differs significantly from control group ($P<0.05$)

Effect of creep after twenty minutes of full lumbar flexion on subsequent lifting

Mitsuhiro Ota[1,2], Yoshitaka Iwamoto[1,3], Wataru Kawakami[1] ,Yosuke Ishii[1,3] and Makoto Takahashi[1,3]
[1] Department of Biomechanics, Graduate School of Biomedical and Health Sciences, Hiroshima University, Hiroshima, Japan.
[2] Department of Physical Therapy, Hiroshima College of Rehabilitation, Hiroshima, Japan.
[3] Center for Advanced Practice and Research of Rehabilitation, Graduate School of Biomedical and Health Sciences, Hiroshima University, Hiroshima, Japan.
Email: mitsuhiro081225@gmail.com

INTRODUCTION

Prolonged lumbar flexion is thought to cause creep of the passive tissues of the spine [1]. As a result, spinal stability is reduced, which may make the lumbar region more vulnerable to external stress when high exertion is required immediately after prolonged bending postures such as lifting loads. However, it is unclear whether the creep of spinal passive tissues due to prolonged lumbar flexion affects lifting.

Previous studies have suggested that the upper and lower lumbar spine move differently, and understanding spinal kinematics requires analysis of multiple segments [2]. Additionally, increased flexion angles lead to increased shear forces [3]. Therefore, understanding the spinal flexion angle changes due to spinal passive tissue creep during lifting in multiple segments is important for low back pain (LBP) prevention.

Therefore, this study, the effect of twenty minutes of full lumbar flexion on lifting was examined in multiple segments.

METHODS

The subjects were 10 healthy men with no history of LBP and a body mass index below 25.

The creep protocol consisted of sitting on a platform and performing lumbar forward bending for twenty minutes. Lifting movements were performed in knee joint extension (Stoop method), and the weight of the box to be lifted was 10% of the body weight. Measurements were taken from the time the box was grasped until the patient stood completely upright.

The data measurement method used was a 3D motion capture system and a force plate to obtain kinetics and kinematics data. Spinal markers were affixed 4 cm lateral to Th7 and L1, and L4, and on the spinous processes of Th3, L3, and L5 to define segments. The flexion angle was defined based on the position of the upper segment relative to the lower segment (Figure 1). The distributions of all continuous variables were examined using the Shapiro-Wilk test. Paired t-tests were performed for continuous values following a normal distribution and Wilcoxon rank sum tests for non-normally distributed data variables. The null hypothesis was rejected at $p < 0.05$.

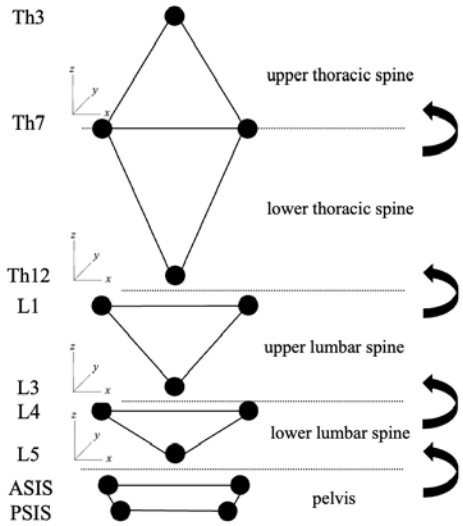

Figure 1 The position of the spinal marker position and the definition of the segment

RESULTS AND DISCUSSION

The spinal flexion angle during lifting after creep was found to increase predominantly in the lower lumbar spine and upper lumbar spine (before creep protocol: 15.87 ± 6.27°, after creep protocol: 16.76 ± 6.32, $p < 0.05$) and upper lumbar spine and lower thoracic spine (before creep: 18.39 ± 7.16°, after creep: 19.04 ± 7.19 °, $p < 0.05$). Spinal passive tissue creep from twenty minutes of lumbar flexion was found to increase the maximum flexion angles of the lower lumbar spine and upper lumbar spine and upper lumbar spine and lower thoracic spine during lifting.

CONCLUSIONS

Attention should this indicates that attention should be paid to the movements between the lower lumbar spine and upper lumbar spine and between the upper lumbar spine and lower thoracic spine when considering the prevention of LBD by creep.

REFERENCES

[1] Solomonow M et al. *J Electromyogr Kinesiol* **14**: 49-60, 2004.
[2] Leardini A et al. *Clin Biomec* **26**: 562-571, 2011.
[3] Skrzypiec D et al. *Clin Biomec* **27**: 646-651, 2012

Computer simulation on obturator prosthesis for velopharyngeal defect

Hobeom Kwon[1], Aein Mon[1], and Mi-El Kim[2]
[1]Dental Research Institute and Department of Prosthodontics, School of Dentistry, Seoul National University, Seoul, Republic of Korea.
[2]Dental Research Institute and Department of Oral Anatomy, School of Dentistry, Seoul National University, Seoul, Republic of Korea.
Email: proskwon@snu.ac.kr

INTRODUCTION

Velopharyngeal closure plays a crucial role in oral and maxillofacial functions including speech and swallowing. It is known to be a complicated coordination of the muscles in the soft palate and pharynx. Although velopharyngeal closure patterns varied based on individuals, it was reported that normal velopharyngeal closure for speech can be classified into four distinct patterns. The reported typical 4 patterns are coronal, circular, circular closure with the Passavant ridge, and sagittal closure. However, it is not clearly reported whether one of the patterns can be changed into other patterns when the anatomic or physiologic changes occurs through practice or prosthetic treatment, although it was suggested that several factors such as learning capability and anatomical variations can have influence on that.

As velopharyngeal closure is three-dimensional mechanism and occurs in the area that is hard to be observed, current methods evaluating velopharyngeal closure can have limitations. Using three-dimensional computer simulation, the whole velopharyngeal mechanism can be easily observed and it is possible to investigate exact muscle coordination for normal swallowing. In addition, it can be found that the necessary change of muscle activation after morphologic alteration, the influence of different levels of muscle activation with same anatomical structures, and the possibility of changing closure patterns.

The purpose of the study was to analyse the action of muscles related to velopharyngeal closure and the influence of the muscle activation during velopharyngeal closure.

METHODS

A three-dimensional model for computer simulation was developed. The images from Visible Korean Human Project were used for the development of the model. The data were made of a Korean male in his sixties. The segmentation for the model was done using a segmentation software. The mandible, masticatory muscles, hyoid bone, soft palate and pharynx were included. After segmentation, the morphological data were sent to ArtiSynth which is a three-dimensional biomechanical modelling platform.

In Artisynth model, bones were regarded as rigid bodies and soft tissues were made of finite element materials. The directions of muscles based on the anatomy were defined and set in the artisynth model.

Data on muscle activations and material properties of the structures from the previous studies were used. After normal velopharyngeal closure was performed by muscle activations, alterations of velopharyngeal pattern were tried by changing activation level of muscles without morphological change in the muscles.

The changes in the muscle activation were as follow.

Table1: muscle activation changes during simulation

Situation\muscle activation	Levator Veli Palatatini muslce	Uvular muscle	Superior pharyngeal constrictor muscle	Palatoglossus muscle	Palatopharyngeal muscle
Normal closure	0.3 N	0.3	0.3	0.3	0.3
Soft Palate Defect	0	0	0.3	0.3	0.3
Soft palate defect muscle control	0	0	0.6	0.3	0.3

RESULTS AND DISCUSSION

With computer models velophayngeal closure could be performed. When there is a soft palate defect situation, by increasing force of superior pharyngeal constrictor muscle, the velophagyngeal closure was enhanced.

Continuation of the use of obturator prosthesis would strengthen the muscles of pharyngeal muscles including superior pharyngeal constrictor and it would contribute the velopharyngeal closure.

CONCLUSIONS

The impact of muscle activation on velopharyngeal closure was analyzed using computer simulation. It was revealed that enhancing the force of the superior pharyngeal constrictor muscle can improve velopharyngeal closure, and that continue use of obturator prosthesis may further improve the defect situation.

ACKNOWLEDGEMENTS

This study was supported by grant no 04-2018-0097 from the SNUDH Research Fund.

REFERENCES

[1] Sanguineti V et al. J Acoust Soc Am 103: 1615-27, 1998
[2] Skolnick ML et al. Cleft Palate J 12: 369-76, 1975

BIOMECHANICAL EFFECTS OF AN ARAMANY CLASS VI OBTURATOR PROSTHESIS: A 3D FINITE ELEMENT ANALYSIS

Aein Mon[1], Mi-El Kim[2] and Ho-Beom Kwon[1]

[1]Dental Research Institute and Department of Prosthodontics, School of Dentistry, Seoul National University, Seoul, Republic of Korea.

[2]Dental Research Institute and Department of Oral Anatomy, School of Dentistry, Seoul National University, Seoul, Republic of Korea.

Email: proskwon@snu.ac.kr

INTRODUCTION

Maxillary defects are very common in clinical practice due to the surgical management of oral and maxillofacial lesions, trauma, and congenital malformations. Prosthetic rehabilitation can enhance the quality of life of maxillary defect patients with the fulfillment of their functional, speech, and aesthetic needs as well. However, partially edentulous maxillectomy dental arches are quite different from normal partially edentulous dental arches in terms of support and stabilization [1]. Moreover, massive maxillary defects have a negative impact on both the biomechanics of the obturator prostheses and the biomechanical response of the supporting tissues [2]. Aramany class VI defect is a defect that lies anterior to the remaining abutment teeth, and the prosthetic management of this kind of defect is quite difficult. To the best of our knowledge, there are no studies about the biomechanical analysis of obturator prostheses in class VI maxillary defects. The purpose of the study was to evaluate the biomechanical effects of an Aramany Class VI obturator prosthesis in comparison to a removable partial denture (RPD) prosthesis.

METHODS

A basic 3D geometric skull model, including the maxilla and teeth, was developed based on the CBCT data of a female volunteer using modeling software. An Aramany class VI defect extending from the right first premolar to the left first premolar was created with this basic model. A partially edentulous maxillary model with the same missing teeth but without a bone defect was also created as a control model. For the virtual fabrication of splinted surveyed crowns, remaining abutment teeth were prepared after 3D printing. A maxillary obturator prosthesis and a RPD prosthesis were virtually constructed for respective models in a similar framework design. Tetrahedral meshes of all the components in each model were generated using the Visual-mesh program. A static load of 100 N was applied to the marginal ridges of incisors and canines as well as the triangular ridges of the buccal and palatal cusps of the premolars of the prosthesis in a 45° oblique direction to stimulate masticatory forces. The analysis was processed using the Visual-Crash software. The maximum von-Mises stress and displacement values were analyzed and compared for each component of the models.

RESULTS AND DISCUSSION

Concerning biomechanical stresses on the prostheses, the metal framework of the obturator prosthesis did not exhibit greater maximum von-Mises stress values than that of the RPD prosthesis, showing the values of 216.3 MPa for the obturator model and 315.9 MPa for the RPD model. The maximum stress values of the PMMA resin surface were presented at 4.3 MPa, similarly, for both models. Moreover, the maximum stresses on the surveyed crowns of each model were almost the same (149.4 MPa on the right side and 93 MPa on the left side in the obturator model, and 154.2 MPa and 99.4 MPa, respectively, in the RPD model). Regarding the biomechanical response of the supporting tissues, the maximum von-Mises stresses on the periodontal ligament of the remaining teeth were significantly greater in the obturator model (about 20 times) compared to the RPD model. In addition, the obturator model showed greater maximum displacement values of the remaining abutment teeth than that of the RPD model. Moreover, the prosthesis displacement distribution pattern of each model was also significantly different (Figure 1). However, the stresses on the remaining bone were not greater in the obturator model than in the RPD model.

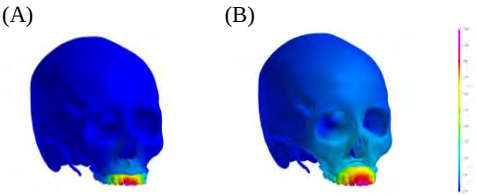

Figure 1: Prosthesis displacement distribution pattern of (A) RPD model (control model); (B) obturator model (experimental model).

CONCLUSIONS

Within the limitations of the study, it can be concluded that the Aramany Class VI obturator prosthesis had a significant biomechanical impact on the remaining abutment teeth rather than on the bone or the prosthesis itself. Therefore, special attention should be paid to the prosthesis framework design and the maintenance of the supporting dental tissues for the long-term prognosis of the obturator prostheses in the prosthetic rehabilitation of maxillary defect patients.

REFERENCES

[1] Hase et al. *Dent Mater J* **33**: 383-8, 2014.
[2] Desjardins. *J Prosthet Dent* **39**: 424-35, 1978.

BIOMECHANICAL ANALYSIS OF THE EFFECTS OF POST & CORE IN SHORT CLINICAL CROWN

Jae-Bok Lee[1], Mi-El Kim[2] and Ho-Beom Kwon[1]
[1]Dental Research Institute and Department of Prosthodontics, School of Dentistry, Seoul National University, Seoul, Republic of Korea.
[2]Dental Research Institute and Department of Oral Anatomy, School of Dentistry, Seoul National University, Seoul, Republic of Korea.
Email: proskwon@snu.ac.kr

INTRODUCTION

Many patients who come to dental hospital has short clinical crown due to physical trauma or severe attrition. Even the clinical crown length of targeted tooth is short, dentist have to make the definitive prosthesis as its original state for esthetic and functional reason. Therefore, after finishing the endodontic treatment, clinician has to decide whether to do the post & crown before the definitive prosthesis, or not. The aim of this study is to evaluate the effect of post and core in maxillary lateral incisor with short clinical crown. The null hypothesis is that the post and core treatment will increase the physical strength and retention of the definitive prosthesis.

METHODS

Two three-dimensional finite element models of maxilla, lateral incisor and the adjacent teeth were developed. RCT(root canal treatment) model was composed of the maxillary bone, endo-treated maxillary lateral incisor with definitive prosthesis. Post & crown model was composed of the maxillary bone, endo-treated maxillary lateral incisor with post & core and definitive prosthesis. PDL spaces, and cement spaces were also developed.

Figure 1. configuration of RCT model(left), and Post & core model (right)

Oblique loading of 50N that simulated occlusal force was applied to the definitive prosthesis of each model. The stress distribution patterns and the maximum von-Mises stress value(MPa), maximum displacement values(μm) of the individual components were compared.

RESULTS AND DISCUSSION

In the supporting alveolar bones, stress was concentrated in the cortical bone at the labial of cervical area of #12. The highest von-Mises stress in the cortical bone for RCT model was 14.1, MPa and 7.2 MPa for post & core model.

In tooth #12, the highest von-Mises stress in ceramic crown turned out to be 8.4 MPa in RCT model, and 8.2 MPa in post & core model, and both at the mesial of the marginal ridge of incisors. The highest von-Mises stress for dentin were 5.2 MPa for RCT model, and 3.6 MPa for post & core model, and both at the labial cervical area. In the PDL space around tooth #12, the highest von-Mises stress turned out to be 0.1 MPa for RCT model at the apex, and 0.2 MPa for post & core model at the palatal or cervical area. Additionally, for ceramic cement layer, the highest von-Mises stress was 5.7 MPa for RCT model, and 4.3 for post & core model at the labial of cervical area. The highest von-Mises stress of resin part of tooth #12 for RCT model was 2.2 MPa at the bottom. The highest von-Mises stress of post cement layer and post & core of tooth #12 for post & core model were 2.2 at the middle of the post, and 0.9 at the palatal of middle of the post, retrospectively.

Displacement value of ceramic crown for RCT model (11.9μm) was higher than that of post & core model (6.7μm), also for cortical bone(3.2μm, 1.6μm) and GP cone(10.3μm, 0.6μm).

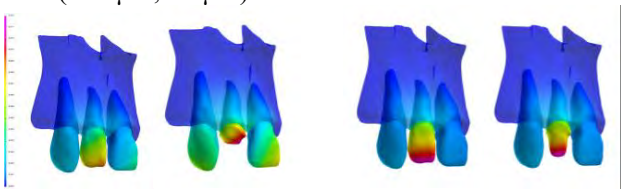

(A) (B)

Figure 2. Displacement pattern of RCT model(A), and post & core model(B)

CONCLUSIONS

This study evaluated the effect of post & core in short clinical crown on the maximum von-Mises stress value and maximum displacement value. Generally, both value was higher in RCT model.

REFERENCES

[1] Chuang SF et al. *JPD*, **104(6)**: 379-88,2010
[2] I. Krejci et al. *J Dent Res,* **73(6)**: 1228-1232, 1994
[3] Lugwisha et al. *IJDR*, **4(11)**: 2260-2265, 2014

Table 1: Maximum von-mises stress value (MPa) in the individual component of tooth #12 with oblique load (50N)

Component	Cortical bone	ceramic crown	dentin	PDL	GP cone	ceramic cement layer	post cement layer	resin	post & core
RCT model	14.1	8.4	5.2	0.1	0.02	5.7	-	2.2	-
Post & core model	7.2	8.2	3.6	0.2	0.004	4.3	2.2	-	0.9

STRESS ANALYSIS IN THE MANDIBLE OF COMPLETE DENTURE PROSTHESIS WEARERS – A BIOMECHANICS PERSPECTIVE

Mary Delia Z. Bondoc[1], Aein Mon[1], Mi-El Kim[2], Ho-Beom Kwon[1]

[1]Dental Research Institute and Department of Prosthodontics, School of Dentistry, Seoul National University, Seoul, Republic of Korea.

[2]Dental Research Institute and Department of Oral Anatomy, School of Dentistry, Seoul National University, Seoul, Republic of Korea.

Email: proskwon@snu.ac.kr

INTRODUCTION

The number of edentulous patients have been continuously increasing. This is due to a globally upward trend in the elderly population, likewise resulting to considerably increasing demands for prosthodontic treatments [1]. Dental clinics have commonly used complete and partial denture prostheses in order to restore patients' oral health, mastication, and improve their quality of life. In mastication, these complete dentures play a critical role in distributing occlusal loads to the underlying mucosa and residual ridge over a large denture-tissue supporting interface [2]. The purpose of this study was to analyse the stresses generated in the mandible of complete denture prosthesis wearers and their corresponding effects.

METHODS

Three-dimensional finite element models were made of the mandible, mucosa, denture base and denture teeth using CT, DICOM and STL data. The models were fabricated via a mesh generation software (Visual-Mesh; ESI Group). Six models were developed with differing load directions [vertical and oblique (45°)] and static loads (50 N, 100 N and 150 N) respectively. The loads were distributed to the posterior teeth: the buccal slope of the buccal cusp, the lingual slope of the buccal cusp, and the buccal slope of the lingual cusp, respectively [1]. Maximum von Mises stress and displacement values were then compared and analyzed. All materials used were assumed to be linear, homogeneous, and isotropic. Finite element analysis was done with a modelling software (Visual-Crash for PAM, Visual-Viewer; ESI Group) (Figure 1). In order to prevent dislodgement of models during simulation, all nodes of bone surfaces in the models were bounded in all directions: condylar head, insertions of temporalis, masseter, and medial pterygoid muscles.

RESULTS AND DISCUSSION

The maximum von Mises stress (mPa) results of the six models are summarized at Table 1. It can be observed that stress load towards the residual ridge is directly proportional to the maximum stress values (MPa) received. Conversely, no significant differences were found in the mucosa, denture teeth and denture base respectively, except for 50 N with vertical loading at 1.30 MPa. These positive stress values can be correlated to alveolar bone resorption based on several previous studies. In addition, the maximum displacement values (μm) on mucosa at vertical - 100 N and 150 N were 20.10 and 36.90; oblique - 100N and 150 N were 37.6, 41.7 respectively. The results showed that stress load is directly proportional to the extent of mucosal displacement. These values are significant for further assessment of denture stability and pain perception.

Table 1: Maximum von Mises stress values (MPa) of different components of the models.

Part	Load Direction	50 N Load (MPa)	100 N Load (MPa)	150 N Load (MPa)
Cortical bone	Vertical	0.40	3.80	8.10
	45°	0.10	4.40	4.50
Mucosa	Vertical	0.05	0.05	0.05
	45°	0.05	0.05	0.05
Denture teeth	Vertical	4.20	4.30	4.30
	45°	4.30	4.30	4.30
Denture base	Vertical	1.30	4.19	4.30
	45°	3.70	4.30	4.30

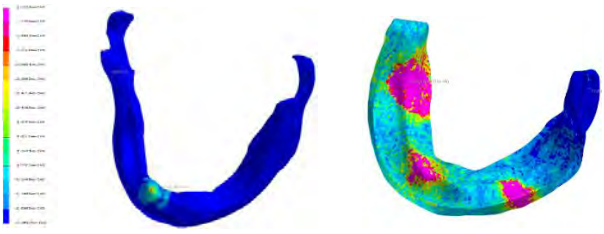

Figure 1 Stress concentration areas on the mandibular cortical bone and mucosa with 150 N vertical load.

CONCLUSIONS

The present study demonstrated that complete denture prostheses may translate mucosal displacement and induce stresses to the bone which may lead to resorption. This represents the first phase of research to evaluate the stress loading in the mandible that can help further studies to expand and consider anisotropic properties of tissues, and accuracy of denture teeth models and masticatory behaviors.

REFERENCES

[1] Dejak B et al. *J Prosthet Dent* ***90***: 591-7, 2003.

[2] Żmudzki, J et al. *Biomech. Model. Mechanobiol.***14**: 679-91, 2014.

Diagnosis of Anterior Cruciate Ligament Deficiency Using a Composite Index Calculated from the Knee Flexion and Muscle Force

Haoran Li[1], Shuang Ren[2], Hongshi Huang[2], Yingfang Ao[2], Qiguo Rong[1]

[1] Department of Mechanics and Engineering Science, College of Engineering, Peking University, Beijing, China
[2]Department of Sports Medicine, Peking University Third Hospital, Institute of Sports Medicine of Peking University, Beijing Key Laboratory of Sports Injuries, Beijing, China
Email: 2001111706@pku.edu.cn

INTRODUCTION

Anterior cruciate ligament (ACL) deficiency (ACLD) is a common injury in the sports crowd. The ACL plays an important role in maintaining the stability of the knee joint. The clinical diagnosis of ACLD is complex and expensive, and the diagnostic process requires the subjective judgment of clinicians. For auxiliary diagnosis, many studies have used statistics to study the gait in ACLD [1]. Regardless of the statistical method used, feature selection is the most important variable. With the help of musculoskeletal models, the kinematics and dynamics in ACLD-affected knees can be used as statistical features [2]. This study was performed to identify patients with ACLD through a composite index that combined kinematics and muscle forces.

METHODS

Twenty-five male patients with unilateral chronic ACLD (the contralateral side was intact) were recruited before ACL reconstruction (ACLD group). A control group comprising nine healthy male volunteers with no history of musculoskeletal injury or surgery in the lower extremities was selected (Control group). The experimental 3D data were collected while the patient was jogging using an optical motion capture system. For each participant, five successful jogging trials were recorded, and these results were imported into multi-body dynamics software, AnyBody Modeling System. A composite index containing the data of the knee flexion and muscle forces' characteristic points, which were the time points in the gait cycle when the most significant difference was observed between the two groups, was used in this study. The selection method of the characteristic points is shown in Figure 1 (using the vastus as an example). Comparing the ACLD and Control groups based on knee flexion and muscle force data for all participants, t-tests were performed at each point during a 0–100% gait cycle. The data of the characteristic points ($p < 0.05$ and p values were minimal) were finally filtered out as a matrix to calculate the composite index. Finally, the matrix was processed using principal component analysis to select features.

RESULTS AND DISCUSSION

A multivariable linear regression model using the composite index was developed to predict, with 79.1% accuracy, whether participants had ACLD. The positivity determined the grouping. Both of the features were significant at the $p = 0.001$ level by the t-test. The

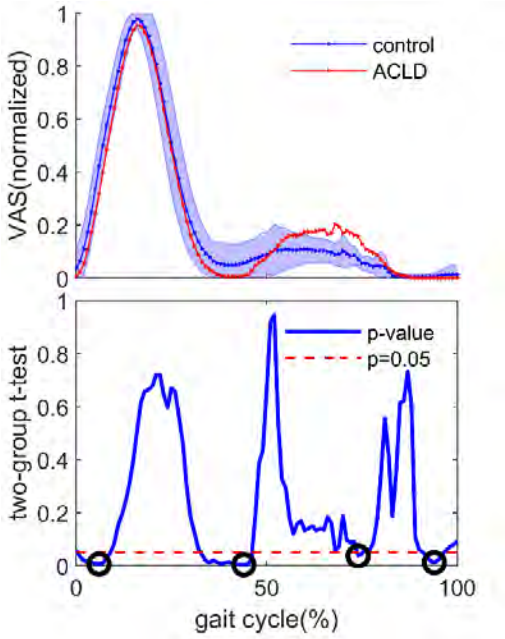

Figure 1 Extraction method of characteristic points (taking the muscle force of vastus as an example). Average force and error band of muscles are shown on the top. P values are shown on the bottom. The black circle is the selected characteristic point.

coefficients for the two features were −1.5504 and −1.6218, respectively. Two hypothetical subjects from the ACLD and Control groups had feature values close to the mean of their respective groups. Their expected final regression results were 0.5458 and −0.3690, which were clearly classified into the two groups. The subject values from the features generated by the composite index were −0.1490, −0.0937 for the ACLD group and 0.2069, 0.1301 for the Control group. It was noteworthy that the subject values of the two groups also differed in the positivity and negativity, verifying the validity of the composite index in the regression model and proving that using only the composite index is also a successful evaluation index.

CONCLUSIONS

The composite index and characteristic points can be used to extract effective information more quickly and conveniently for diagnosis.

ACKNOWLEDGEMENTS

This research was funded by the Natural Science Foundation of China Grant (Grant No: 11872074).

REFERENCES

[1] Christian J et al. *Clin Biomech* **33**: 55-60, 2016.
[2] Kokkotis C et al. *Sci Rep-Uk* **12**: 6647, 2022

Degree of Association between Knee Health with Pelvis Mobility and Plantar Pressure

Arnab Sarmah[1,2], Lipika Boruah[3], Satoshi Ito[4], Subramani Kanagaraj[1,3]
[1] Department of Mechanical Engineering, IIT Guwahati, Assam, India [2] Graduate School of Engineering, Gifu University, Gifu, Japan. [3]Center for Intelligent Cyber-Physical Systems, IIT Guwahati, Assam, India. [4]Faculty of Engineering, Gifu University, Gifu, Japan
Email: sarmah18@iitg.ac.in

INTRODUCTION

Degenerative musculoskeletal disorders account for large proportion of the adult population with several cases of work inability, temporary disability and probable early retirement. OA is a degenerative joint disease that leads to chronic pain and disability thus restricting physical functioning and their ability to perform activities of daily life[1]. Among the activities of daily life, walking is considered to the most important one[2]. This study, thus attempts to quantify the degree of association between the knee joint health and the kinematics of pelvis and plantarpressure variables.

METHODS

The Study includes 3 healthy subjects and 3 OA subjects. The healthy subjects have mean age of 27 and the OA patients are of a mean age of 66.33. All three subjects are suffering from bilateral advanced knee OA and are of grade 2 or higher as per the Kellgren-Lawrence (K/L) system. The healthy subjects have no history of musculoskeletal disorders. The study is approved by the Institute Human Ethical Committee (IHEC), IIT Guwahati. Gait of the subjects is recorded using a wearable sensor and a Pressure Mat in Gait & Motion Analysis Lab, IITG as shown in Figure 1(a).

Figure 1 Data collection in (a) Gait & Motion Analysis Lab using (a)Wearable Sensor (b) Pressure Mat.

The wearable sensor captures the right and left pelvis angles in three directions during normal walking as shown in Figure 1 (b) and the trunk flexion extension angle during Timed Up and Go (TUG) experiment. In addition, the plantar pressure of the subject while walking has been captured using the Pressure Mat as shown in Figure 1(c). The parameters obtained from the experiment includes the time from TUG test, pelvis angle in three planes and the trunk flexion extension as kinematic variables and gait line length, plantar pressure data of the foot divided in three sections namely forefoot, midfoot and heel as kinetic variables.

RESULTS AND DISCUSSION

The pelvis and trunk angles were recorded with respect to the gait cycle percentage. Thus, mean, and standard deviation (SD) of the pelvis angle and trunk angle were used for comparative analysis along with the kinetic variables for the distinction between healthy subjects and subjects with knee OA. The degree of correlation between the knee health and the kinematic and kinetic variables are quantified using the Point biserial correlation (r_{pb}) as shown in Table 1. It can be observed that except for mean values of Pelvis Obliquity left and Pelvis rotation right, all the mean and SD parameters have negative r_{pb}. The negative r_{pb} for the SD parameters indicates the reduced mobility in all the directions. The kinetic variables also have negative correlation which is supported by the negative r_{pb} value of Gait line, thus indicating reduced foot contact time.

Table 1: r_{pb} relating health status and gait variables.

Variables		r_{pb}	
		Left	Right
Pelvis Tilt	Mean	-0.66	-0.66
	SD	-0.62	-0.61
Pelvis Obliquity	Mean	0.87	-0.67
	SD	-0.46	-0.54
Pelvis Rotation	Mean	-0.43	0.16
	SD	-0.82	-0.87
Gait Line		-0.49	-0.4
TUG		0.78	
Forefoot	Force	-0.73	-0.59
	Pressure	-0.37	-0.42
Mid Foot	Force	-0.44	-0.52
	Pressure	-0.56	-0.53
Heel	Force	-0.81	-0.53
	Pressure	-0.59	0.09

CONCLUSIONS

The negative r_{pb} of the SD of kinematic variables is a direct indication of the reduced mobility in the pelvis due to degradation in the knee health. This has also reduced the load taken by the foot as evident by the negative r_{pb} for both the force variables and gait line. Thus, it can be inferred that knee health greatly affects the kinematic of the pelvis and the plantar pressure parameters and thus have a high degree of association. Thus, these parameters can act as biomarkers of assessing knee health.

ACKNOWLEDGEMENTS

The authors acknowledge the support provided by NECBH through a Department of Biotechnology, Govt. of India sponsored project (BT/COE/34/SP28408/2018), IIT Guwahati.

REFERENCES

[1] Gikaro et al., "Activity limitation and participation restriction in Osteoarthritis and Rheumatoid arthritis: findings based on the National Health and Nutritional Examination Survey," *BMC Musculoskelet. Disord.*, vol. 23, no. 1, pp. 1–8, 2022.
[2] C.E. Tudor- Locke and A. M. Myers, "Challenges and opportunities for measuring physical activity in

Knee Joint Moments Calculated Using Markerless Motion Capture Can Distinguish Osteoarthritis Severity During Walking Gait

Jereme Outerleys[1], Anastasija Mihic[1], Jacob Calderone[1], Vajra Keller[1], Elise Laende[1] and Kevin Deluzio [1]
[1] Mechanical and Materials Engineering, Queen's University, Canada.
Email: Jereme.Outerleys@Queensu.ca

INTRODUCTION

Joint loading patterns of the knee in the frontal and sagittal planes can discriminate knee osteoarthritis (OA) severity[1,2], have been linked to disease progression[3], and are targets for treatment. Joint moments are typically calculated using inverse dynamics with kinematic inputs from marker-based motion capture. Recent advances in markerless motion capture technology can measure kinematics that show high agreement with marker-based data with improved inter-session repeatabilty[4]. Reduced clothing constraints and shorter collection times associated with markerless methods are clear advantages for large-scale and longitudinal clinical investigations. The objective of this study was to investigate whether knee joint moments calculated using kinematic inputs from markerless motion capture can distinguish knee OA severity.

METHODS

Subjects were recruited from an orthopaedic clinic. Knee OA severity was determined clinically by advanced practice physiotherapists. Subjects with severe and moderate medial knee OA were included, yand a group of asymptomatic controls. Subjects walked back and forth across a 10m-walkway embedded with 4 force plates (AMTI, 1200 Hz) for 60s at self-selected walking speed in their own clothing and footwear. Video data were captured by 8 cameras (OptiTrack, 1080p, 60 Hz) digitally synchronized with force data. A calibration chessboard placed in a known location relative to each force plate aligned video and force coordinate systems. Video data were processed using Theia3D (Theia Markerless, v2021.3.02047) to obtain 3D kinematics from an inverse kinematics model with 3 degrees of freedom at the ankle, knee, and hip. The data were lowpass filtered at 8 Hz for kinematics and 50 Hz for force. Inverse dynamics was used (Visual3D, v2023.02.1) to obtain internal knee flexion and adduction moments resolved in the joint coordinate system and normalized by body mass. Moments were time normalized to stance phase and ensemble averaged over at least 3 strides. Principal component analysis extracted the first two modes of waveform variability[1] (PCs), and ANOVAs with post-hoc comparisons (Tukey HSD) were used to test for differences across severity in PCs and gait speed ($\alpha < 0.05$).

RESULTS AND DISCUSSION

Forty-two subjects were included in the analysis (24 severe, 10 moderate, 8 control). Groups were well matched in age (Table 1). PC1 captured overall waveform magnitudes while PC2 captured the difference between early and late stance. A severity effect was detected in PC2 for both the knee flexion and adduction moments (Table 1). The severe and moderate groups had stiffer flexion moment patterns compared to controls (Figure 1). The severe group also displayed a more sustained adduction moment pattern compared to moderates and controls. Gait speed decreased with severity and contributes to differences in kinetic outcomes in these populations. These data agree with previous work[1,2] that report decreased sagittal moments and more sustained loading patterns in the frontal plane, with increasing levels of knee OA severity.

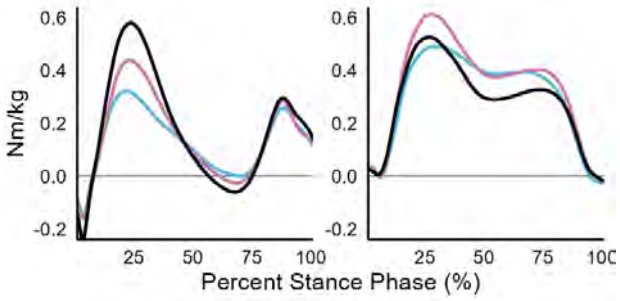

Figure 1 Group mean knee flexion (left) and adduction (right) moments of controls (black), moderate (purple), severe (blue).

CONCLUSIONS

Kinematics from markerless motion capture produce joint loading outcomes that can distinguish between knee OA severities. This demonstrates the clinical utility of markerless motion capture by replicating clinical findings reported in the literature and more globally provides additional validity of the technology.

REFERENCES

[1] Deluzio and Astephen. Gait Posture. 25:86-93, 2007.
[2] Outerleys et al. J Appl Biomech. 37:130–8, 2021.
[3] Davis et al. Clin Biomech. 61: 233-9, 2019.
[4] Kanko et al. J Biomech. 121:110422, 2021.

Table 1: Mean (SD) age, gait speed and knee moment PC scores for each severity group. F = female, M = male.

	Control (N=8,5F,3M)	Moderate (N=10,4F,6M)	Severe (N=24,9F,15M)	p_{ANOVA}
Age (years)	68(8)	63(11)	68(8)	0.322
Gait Speed (m/s)	1.34 (0.10)	1.13 (0.13)	1.05 (0.13)	< 0.001
Flexion Moment PC1 Score	0.74 (1.00)	0.04 (1.20)	-0.26 (1.41)	0.181
Flexion Moment PC2 Score	0.91 (0.57)	0.06 (0.88)	-0.34 (0.55)	0.011
Adduction Moment PC1 Score	0.10 (0.96)	-0.53 (0.84)	0.08 (1.09)	0.218
Adduction Moment PC2 Score	0.35 (0.30)	0.14 (0.46)	-0.24 (0.33)	0.003

In Vivo Kinematics of Total Ankle Prosthesis with Different Talar Implant Shapes

Rea Ikeda[1], Naruyuki Hayashi[1], Hiroaki Kurokawa[2], Shinichi Kosugi[3], Yasuhito Tanaka[2], Masataka Yamamoto[1,4] and Hiroshi Takemura[1]

[1] Tokyo University of Science, Chiba, Japan. [2] Orthopaedic Surgery, Nara Medical University, Nara, Japan. [3] Kosugi Orthopaedic & Rheumatology Clinic, Osaka, Japan. [4] Hiroshima University, Hiroshima, Japan.
Email: 7519009@ed.tus.ac.jp

INTRODUCTION

Total ankle arthroplasty (TAA) is one of the surgical treatments for end-stage ankle osteoarthritis. The two-component type implant models that replaced the upper surface of the talus (standard TAA) are commonly used. On the other hand, the standard TAA has problems like talar component subsidence. Another model that uses talar body prosthesis (combined TAA) is expected as an effective strategy for the problems and was reported to improve objective foot scores, subjective pain assessments, and range of motion [1]. However, little is known about in vivo kinematics of the talar prosthesis and the differences between standard TAA and combined TAA. The purpose of this study is to measure in vivo three-dimensional kinematics of the standard TAA and the combined TAA during ankle dorsiflexion-plantarflexion and investigate differences in kinematics due to different shapes of the talar implants.

METHODS

The study included 19 participants (9 standard TAA, 10 combined TAA) who underwent total ankle arthroplasty. First, the 3D implant models of ankle dorsiflexion and plantarflexion were created from Computed Tomography (CT) images by using ITK-SNAP. To define the standard position of the implants, a global coordinate system was made on the model data of the tibial implants. Then, tibial implants of dorsiflexion and plantarflexion were aligned with it by Go-ICP [2,3] algorithm. Next, the middle position of talar implants was defined with the model data of aligned tibia implants and talar implants of standard TAA, and a talar reference system was created on the model data of talar implants. In the case of standard TAA, talar implants of dorsiflexion and plantarflexion were aligned with the referent system by Go-ICP algorithm. In the case of combined TAA, the underside of the talar implants was cut off and the remaining upper side was aligned with the model data of the talar implant by the same method as the standard TAA. The combined TAA implants were designed to have the same diameter of the talar surface as the standard TAA implants. The cutting process was done manually ten times per each subject's implant data. For the evaluation of 3D kinematics during dorsiflexion and plantarflexion, the rotation angles and the displacements for the alignment are calculated by using the Go-ICP results. In the case of combined TAA, the averages of ten times were used as the results. Both reference systems in this study are defined in the same way as in previous research [4].

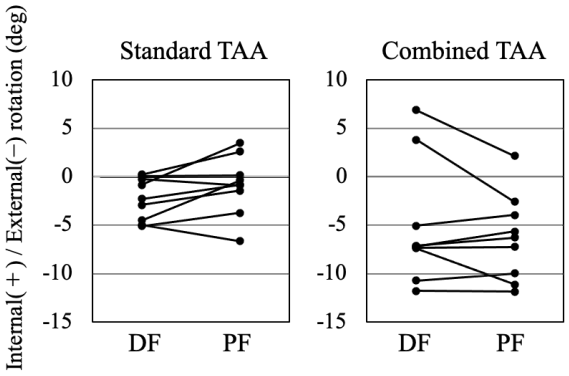

Figure 1 Internal/external rotation angle of standard TAA and combined TAA during dorsiflexion and plantarflexion.
DF: dorsiflexion; PF: plantarflexion.

RESULTS AND DISCUSSION

The internal/external rotation angles of implants during dorsiflexion and plantarflexion are shown in Figure 1. From dorsiflexion to plantarflexion, the implants of the standard TAA group rotated internally. This is a similar movement to a normal ankle joint [5]. On the other hand, some of the implants of the combined TAA group rotated externally. There was a significant difference between them in external rotation in plantarflexion. The rotation angle of the combined TAA group varied greatly among individuals. From dorsiflexion to plantarflexion, the implants of the combined TAA group translated medially and posteriorly. These implant translation patterns were not seen with the standard TAA group, and they tend to translate only posteriorly.

CONCLUSIONS

There were differences in the internal/external rotation angle and the direction of implant movement between the standard TAA group and the combined TAA group. The results may provide useful data for selecting the optimal implant shape.

REFERENCES

[1] Morita S et al. *J Bone and Joint Surgery* **5**: 4, 2020.
[2] Yang J et al. *IEEE Transactions on Pattern Analysis and Machine Intelligence* **38(11)**: 2241-2254, 2016.
[3] J. Yang et al. *IEEE International Conference on Computer Vision*, 1457-1464, 2013.
[4] Yamaguchi S et al. *J Biomech* **44**: 995-1000, 2011.
[5] Fukuno M et al. *J Biomech* **101**: 109651, 2020.

ASYMMETRY ON FOREARM ROTATION MOVEMENT IN PATIENTS WITH PARKINSON'S DISEASE AND SWEDD

Ji-Won Kim[1,2], Yuri Kwon[1,2], Minseung Kim[1] and Do-Young Kwon [3]

[1] Department of Biomedical Engineering, Konkuk University, Chungju, Republic of KOREA
[2] Institute of Biomedical Engineering, Konkuk University, Chungju, Republic of KOREA
[3] Department of Neurology, Korea University College of Medicine, Ansan-city, Korea University
Email: kjw802@kku.ac.kr

INTRODUCTION

Asymmetric symptoms of bradykinesia is one of the representative moto symptoms in Parkinson's disease (PD). Recently, 4%–14.7% of patients diagnosed with PD have been showed normal dopamine transporter imaging and they have been referred to as having scans without evidence of dopaminergic deficit (SWEDD) [1]. The clinical characteristics of SWEDD is similar to that of PD. Also, SWEDD is difficut to describe its phenomenology. It is important to understand clinical characteritics of SWEDD and to distinguish patients with SWEDD from patients with PD for accurate and effective interventions. Therefore, the aim of this study was to investigate motor symptom asymmetry on forearm rotation performance using gyro sensor in patients with PD and SWEDD.

METHODS

Twenty-three patients with SWEDD, 23 patients with PD and 23 controls participated in our study. Patients with normal dopamine transporter imaging and normal brain MRI among patients diagnosed with PD were determined as the SWEDD patients [2]. For quantitative measures of forearm rotation movement, a custom-made angular velocity measurement system based on gyro sensor (CG-L53, NEC/Tokin, Japan) was used. In our study, forearm rotation categories were selected as the same tasks for investigation from the UPDRS part III (motor examination). All participants were asked to perform forearm rotation task for 15 s as rapidly as possible and with as large an amplitude as possible. The sensor signals were recorded in both right and left forearms at 250 Hz sampling frequency. Butterworth digital low pass filter with 50 Hz cutoff frequency was used. To evaluate asymmetry of forearm rotation performance, ratio of root mean squared (RMS) angular velocity between both forearms was calculated. Analysis of variance (ANOVA) and post-hoc (Tukey) test were performed to compare control, PD and SWED groups.

RESULTS AND DISCUSSION

Figure 1 shows results of asymmetry on forearm rotation speed among control, PD and SWEDD groups. There were significant group differences ($P<0.001$). Asymmetry of PD patients was significantly greater than that of SWEDD patients ($P < 0.001$). Expectedly, PD patients exhibited greater asymmetry compared to control group. In contrast, no significant difference was observed between SWEDD and control group ($P >0.05$) These results indicate that PD patients show asymmetric bradykinesia in forearm rotation movement, whereas SWEDD patients have less asymmetric forearm speed.

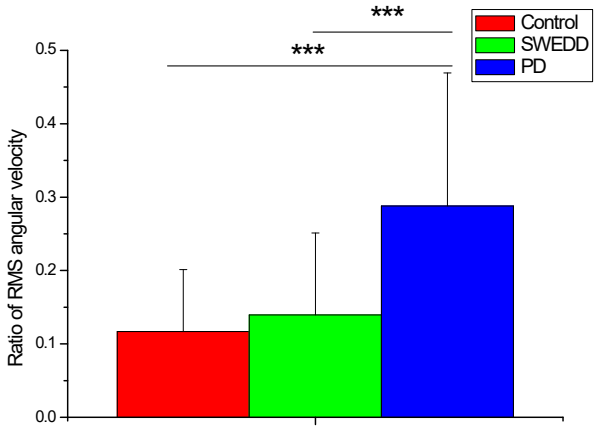

Figure 1 Comparison of asymmetry of forearm rotation in control, PD and SWEDD groups.

CONCLUSIONS

This study investigated asymmetry of forearm rotation speed in PD and SWEDD patients. PD patients had asymmetric bradykinesia while SWEDD patients had normal ratio of forearm speed. These findings could aid clinicians in identifying potential SWEDD patients among PD patients.

ACKNOWLEDGEMENTS

This research was supported by the National Research Foundation of Korea (NRF) funded by the Ministry of Education (No. 2018R1C1B6008083 and 2022R1I1A3065537)

REFERENCES

[1] Whone AL, et al. Slower progression of Parkinson's disease with ropinirole versus levodopa: The REAL-PET study, *Ann Neurol*, **54**:93-101, 2003.
[2] Jennings DL, et al. (123I) beta-CIT and single-photon emission computed tomographic imaging vs clinical evaluation in Parkinsonian syndrome: unmasking an early diagnosis, *Arch Neurol*, **61**:1224-1229, 2004

IMU-instrumented Timed-Up and Go test identified task-specific mobility declines in older adults

Yu-Pin Liang, Gregory Welk and Li-Shan Chou
Department of Kinesiology, Iowa State University, Ames, Iowa, USA.
Email: yupinl@iastate.edu

INTRODUCTION

Each year, in the US, one out of four older people falls, and one out of five falls results in a severe injury, such as hip fractures or traumatic brain injuries [1,2]. Declined gait balance control has been identified as a leading risk factor for falls [3]. Gait variability or altered center of mass (COM) motion may indicate gait imbalance [4]. The Timed-Up and Go test (TUG) is a commonly utilized clinical assessment for examining mobility, balance, and fall risk in older adults [5]. TUG measures the time taken by an individual to complete the tasks, which include rising from a chair, walking a distance of three meters, turning, walking back to the chair, and sitting down. An older adult who takes more than 12 seconds to complete the TUG is considered at risk for falling. While the TUG test has demonstrated utility for screening elderly with impaired gait balance [6] the overall time measure provides limited information for identifying the factors that contribute to an elevated risk of falling. The purpose of this study was to employ IMU-instrumented TUG to enhance our screening of individual task performance and quantification of body movement, which, taken together, could better guide clinicians in detecting mobility impairment and developing intervention plans.

METHODS

Seven male and five female older adults (>65y/o) were recruited for this ongoing study. All participants performed the TUG test with one IMU placed at the fifth lumbar vertebra (L5) as the proxy location of whole-body COM. Participants who took more than 12 seconds to complete the TUG test were classified as at-risk for falling (RF), and those who took less than 12 seconds were coded as non-risk for falling (NRF). TUG test was further divided into 6 task phases, including the sit-to-walk (STW), walking out (W1), turning around (TUA), walking back (W2), turning in place (TIP), and sitting down (SD) (Figure1). The time duration for each of the six TUG phases was identified with the IMU data and compared between two groups by independent t-test statistical approaches with $\alpha = 0.05$.

RESULTS AND DISCUSSION

Seven participants were classified as NRF and five participants as RF. Mean absolute time measured for each of the six task phases were 1.35, 2.38, 1.68, 2.29, 1.31 and 1.21 seconds for NRF, and 2.07, 3.04, 2.51, 2.94, 2.33, and 1.28 seconds for RF (Figure 2). Mean percentages of the overall time for the six phases were 13, 23, 16, 22, 13 and 18 percent for NRF, and 14, 21, 18, 21, 16, and 10 percent for RF. Participants in the RF group spent significantly more time in STW, TUA, and TIP ($p<0.05$). Individuals in the RF group allocated a significantly greater proportion of time to TIP ($p<0.05$) and a trend in a greater proportion of time to STW ($p=0.089$). There were no significant time-related differences between the two groups in W1, W2, and SD. The turning-related activities in the TUG were the major feature distinguishing the RF and NRF groups.

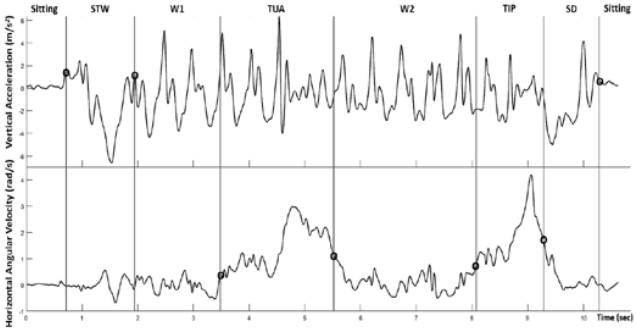

Figure 1 Representative data points to differentiate six phases of Timed Up & Go

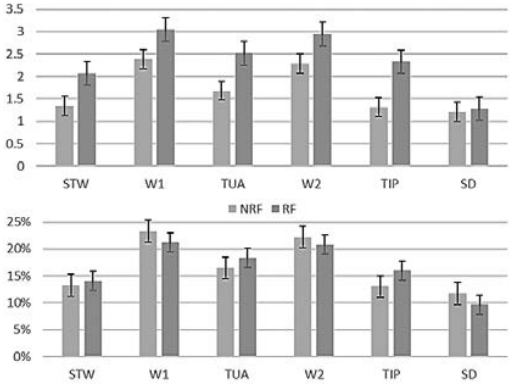

Figure 2 The raw (y-axis: seconds) and proportional (y-axis: 1=100%) time spending distribution in six phases of Timed Up & Go between NRF and RF groups.

CONCLUSIONS

Result of this study indicates that the IMU-instrumented TUG test could quantify each segment of the TUG and identify specific segments that contribute to risks or poor overall performance. Our next steps are to examine the kinematic data obtained from the IMU to better understand the mechanisms underlying the prolonged task performance. Such information would enhance the specificity in the clinician's screening of mobility impairment and the development of interventions for fall prevention.

REFERENCES

[1]Bergen G et al. *Morb Mortal Wkly Rep*, **65**(37), 993-998, 2016.
[2] Sterling DA et al. *J Trauma, **50**(1), 116-119.*, 2001.
[3] Salzman B. *Am Fam Physician*, **82**(1), 61-68, 2010.
[4] Howell DR et al. *Arch Phys Med Rehabil, **94**(8), 1513-20*, 2013.
[5] Podsiadlo & Richardson. J Am Geriatr Soc, **39**(2):142-8,1991.
[6] Nightingale CJ et al. *J Aging Phys Act*, **27**(2), 230-233, 20

A Statistical Analysis of the Shape and Density Distribution of the Talus

Jordan Stolle[1], Christine M. Harper[2], Kristyn K. Voegele[3] and Sorin Siegler[1]
[1] Drexel University, Philadelphia, Pennsylvania, United States.
[2] Cooper Medical School of Rowan University, Camden, New Jersey, United States.
[3] Rowan University School of Earth and Environment, Glassboro, New Jersey, United States.
Email: jts376@drexel.edu

INTRODUCTION

Understanding talar morphology is critical to the effective design and implantation of total ankle replacements. The success of an implant, however, is dependent not only on talar shape, but also on the local density of the underlying cancellous bone. Computed tomography (CT) can be used to extract the density of the cancellous bone for analysis and use in various applications. The purpose of this study is to observe and quantify the external shape and internal density of the talus. [1]

METHODS

Sixty non-pathological subjects were selected for this study. Weight-bearing CT scans of the leg were collected in bilateral standing posture. Three-dimensional models of the talus of each subject were generated, and local density values corresponding to the Hounsfield Unit of each CT voxel were extracted. A weighted spherical harmonic (SPHARM) analysis was performed to quantify talar external shape, and an average talus model was created. [2] One hundred seventy-nine volumes of interest were placed in the average talus and warped into the same relative positions in all other subjects using the thin plate spline interpolation function established using the output of the SPHARM analysis. [3] Separate principal component analyses (PCA) were run to summarize variation in both external shape and cancellous density respectively. Non-parametric statistics were run to test for significant differences between males and females and among different age brackets (young ≤35, middle 36-54, older ≥55) for both the shape and density data, as well as among different bone regions for density data.

RESULTS AND DISCUSSION

No significant differences in shape exist between males and females or among different age groups. In density, however, there are significant differences between males and females, as well as between the old group and both the young and middle groups. (Table 1).

The first PC (71% of variance) of density data corresponds to overall bone density, with high- and low-density specimens at the positive and negative extremes of PC1 (Figure 1).

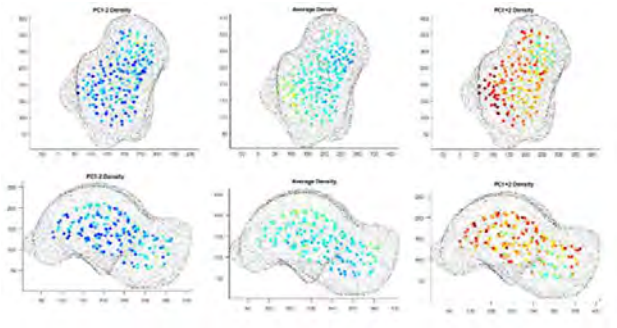

Figure 1 Axial (Top) and Medial (Bottom) Views of the First Principal Component of Density Variance, with Negative Extreme (Left), Average (Middle), and Positive Extreme (Right) (+/-2 sd)

The talar dome, head, and lateral process are significantly denser than the other regions of the talus. ($p<0.05$ for all three regions)

CONCLUSIONS

This study shows that while there is no significant difference in talar shape between male and female or among different age groups, there is significant variation in talar density both between and among these groups. Knowledge of variation in shape and internal density among humans is an important factor to consider for fixation at the bone-implant interface. This process can also be generalized to other bones, allowing for insights throughout the body.

REFERENCES

[1] Shiota, Momma, D et al, *Orthopaedic Journal of Sports Medicine*, **8(11)**, 2020. https://doi.org/10.1177/2325967120963085
[2] Harper, C. M. Et al, *Journal of Anatomy* **240(4)**, 678–687, 2022.
[3] Sylvester, & Terhune, C. E. et al. *Anthropology* **163(3)**, 553–569, 2017.

Table 1: Statistical Significance of Shape and Density Differences Between Categories

	Female vs. Male	Young vs. Older	Young vs. Middle	Middle vs. Older
Shape p-value	0.35	0.77	0.78	0.41
Density p-value	**0.001**	**0.003**	0.618	**0.002**

Kinematic and Kinetic Analysis of Upper Limb Elevation Exercises in Baduanjin

Geonhui Kang[1,3], Cheol-hyun Kim[1,2], and Sangkwan Lee[1,2,3]
[1] Stroke Korean Medicine Research Center / Wonkwang University, Gwangju, Korea.
[2] Department of Internal Medicine and Neuroscience / Wonkwang University, Gwangju, Korea.
[3] Hanbang Cardio-Renal Syndrome Research Center / Wonkwang University, Iksan, Korea.
Email: sya0474@naver.com

INTRODUCTION

Habitual physical activity is attracting more important attention in the aging modern society.[1] Asians have emphasized habitual exercises such as Taichi and Yoga from ancient times to the present.

Baduanjin is one of the physical activities that Asians have performed. Baduanjin consists of eight movements and is known as a very simple, easy-to-learn, and effective exercise for preventing various diseases.

Focusing on two of Baduanjin's eight movements, the exercises lifting the upper extremity, we conducted kinetic and kinematic analysis by dividing the subjects into skilled and unskilled groups.

METHODS

We recruited six skilled people who regularly trained Baduanjin and six beginners who did not learn it. IRB (Investigational Review Board) deliberation was obtained (WKIRB 2019-3) and this study was registered to CRIS (KCT0003840).

Eight infrared cameras and six force plates were installed in the motion analysis room. After measuring the height and weight of the study subject, anthropometric measurement was performed. After that, the subject performed the first and third movements of Baudanjin on force plates installed in the center of the motion analysis room with 22 retroreflective markers attached to the body of the study subject.

The collected marker data were modeled with our model and preprocessed for analysis. Kinematic analysis was conducted on the right glenohumeral (GH) joint, the most movable joint in upper limb movement. Local coordinate systems representing the shoulder and upper arm each were created, and the angle between the two coordinate systems was calculated by quaternions. Finally, the GH joint angle was represented as the Euler angle.

As a statistical method to investigate the difference between the two groups, the Shapiro-Wilk test and F test were performed first. An unpaired two-sample t-test was performed when normality and homoscedasticity were satisfied, and the Mann-Whitney U test was performed when normality was not satisfied. All statistics were performed by Rstudio.

RESULTS AND DISCUSSION

The key point of Baduanjin's first movement "Two Hands Supporting the Sky – Regulates All Internal Organs" is holding both arms up. In this motion, the flexion angle of the GH joint was 144.37(±1.94)° for the unskilled and 128.47(±1.51)° for the skilled group. This result was contrary to the expectation that the flexion angle of the skilled group would be greater.

The difference in the left and right ground reaction forces (GRF) between the two groups was investigated to confirm whether the forces were distributed in a balance between both feet when performing the Baduanjin first and third movements.

When performing the first movement, the difference in GRF was 0.912(±0.675)% of the weight for the skilled and 2.743(±0.794)% of that for the unskilled group ($p=2.2e-16$, $W=9705$). When performing the third movent "Single Hand Pushing Up – Helps the Spleen and Stomach," the difference in GRF was 0.992(±0.763)% of the weight for the skilled and 2.638(±1.079)% for that of the unskilled group ($p=2.2-16$, $W=9050$).

These differences are noteworthy as an indicator of the proficiency of the skilled group because the weight of the body should be evenly distributed on both feet to secure stability when exercising to widen the upper extremity, which is a characteristic of the above two movements.

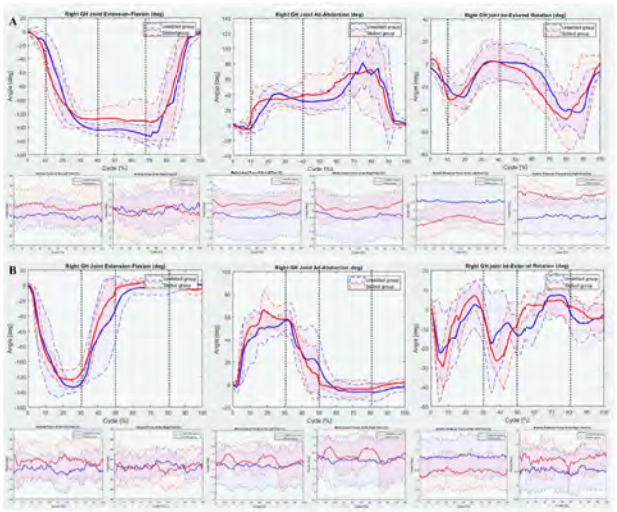

Figure 1 Kinematic and Kinetic Analysis Results of Baduanjin's first and third movements. A: "Two Hands Supporting the Sky – Regulates All Internal Organs"; B: "Single Hand Pushing Up – Helps the Spleen and Stomach"

CONCLUSIONS

The difference between the two groups could be confirmed when performing Baduanjin's upper limb elevation exercises. This difference is expected to be used as an indicator of proficiency evaluation of these exercises.

REFERENCES

[1] Loprinzi PD et al. *Med Sci Sports Exerc* **47(11)**: 2347-52, 2015.

BIOMECHANICAL EFFECT OF FLOOR SIT-TO-STAND MOVEMENT ON THE OPTIMAL SURGICAL SITE IN ACLR SURGERY: A COMPUTATIONAL ANALYSIS

Jaewoong Han[1], Byeongchan Cho[1], Bowon Jeong[1], Tae Soo Bae[1]
[1] Department of Biomedical Engineering, Jungwon University, Chungbuk, Korea.
Email: bmebae@jwu.ac.kr

INTRODUCTION

ACL reconstruction (ACLR) surgery is performed for damaged ACL and the selection of an appropriate surgical site for the implanted graft is very important to determine the success of the ACLR surgery. However, there are insufficient studies on the selection of the optimal surgical site considering the floor sit-to-stand (FSTS) motion of Asians during ACL reconstruction, and the biomechanical evidence for improving the technique is insufficient. Therefore, the purpose of this study is to find a biomechanical basis for determining the optimal surgical site of the ACL allograft tendon considering the continuous FSTS movement during Outside-in ACLR surgery.

METHODS

A 3D knee joint was reconstructed through an image processing program (Mimics 20, Materialize Inc., Belgium) from CT images. To match the bone shape of the knee and the FSTS movement of the knee, motion analyses (Cortex 8, Motion analysis Inc., USA) were performed after attaching the reflective markers following Helen Hayes's markerset on the same position during knee FSTS motion to get the continuous kinematic data of the FSTS movement. A total of 24 cases were simulated at 24 surgical sites in at the starting point of the femoral tunnel at a radius of 5 mm, 10 mm, and 15 mm based on the femoral epicondyle. Through MFBD analyses, von-mises stresses on the implanted graft were calculated during continuous knee FSTS motions. The FSTS motion was divided into four phases, and we tried to find the optimal surgical site by calculating the stress applied to the implanted graft through MFBD analysis and then performing comparative analysis (Figure. 1).

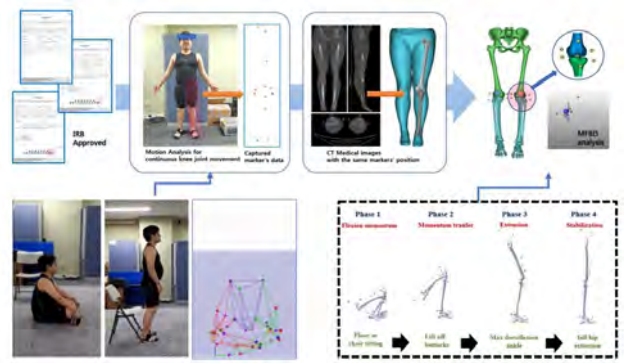

Figure 1 Flowchart of MFDB analysis for four phases of floor sit-to-stand using a three-dimensional knee joint model from CT images and knee joint movement from motion analysis with same reflective markers.

RESULTS AND DISCUSSION

In phases 1, 2, 3, and 4, the average stress for each surgical site was 47.52 MPa, 55.30 MPa, 52.25 MPa, and 12.41 MPa. The stress of the graft was the smallest at the proximo-posterior surgical site with a radius of 15 mm, and the stress of the graft was 23.30 MPa, 29.30 MPa, 27.28 MPa, and 7.09 MPa in phases 1, 2, 3, and 4 in order. Conversely, the stress of the graft was the greatest at the distal anterior surgical site with a radius of 15 mm, and the stress of the graft was 67.09 MPa, 72.78 MPa, 66.08 MPa, and 16.35 MPa in phases 1, 2, 3, and 4. In phase 2, the average stress of the graft at each surgical site was 55.36 MPa, which was larger than in other phases. When the surgical site was posterior or proximal, the stress of graft decreased as the radius increased, and when the surgical site was anterior or distal, the stress of graft decreased as the radius decreased.

In the floor sitting culture of Asians, it is common to maintain the Phase 1 posture for the longest time. At this time, the stress of the implanted ACL graft was higher than the yield stress (25.5 MPa) of ACL graft except for the proximal and posterior surgical site with a radius of 15 mm. Therefore, it is recommended that clinicians avoid setting the femoral tunnel start point towards the distal and anterior areas as much as possible during ACLR surgery. In this study, the finite element model was applied to the graft tendon, but femur and tibia were applied rigid bodies, it is expected that some errors will occur when comparing the results with the implanted graft in actual clinical practice.

CONCLUSIONS

Unlike the chair STS culture of Westerners, when outside-in ACLR surgery is performed on Asians exposed to FSTS culture, it will help to increase the success rate of ACLR surgery by not setting the starting point of the femoral tunnel near the anterior distal part.

ACKNOWLEDGEMENTS

This research was supported by Basic Science Research Program through the National Research Foundation of Korea (NRF) funded by the Ministry of Education (NRF2017R1D1A3B04033410)

OPTIMAL HINGE POSITIONS ON TIBIAL WEDGE IN BIPLANE OPEN-WEDGE HIGH TIBIAL OSTEOTOMY AS VARUS DEFORMITY ANGLE

Tae Soo Bae[1], Hyeongho Baek[1], Bowon Jeong[1], Jaewoong Han[1]
[1] Department of Biomedical Engineering, Jungwon University, Chungbuk, Korea.
Email: bmebae@jwu.ac.kr

INTRODUCTION

It is well known that biplane open wedge high tibial osteotomy is one of effective surgical techniques which relieve tibial varus and pain in patients with osteoarthritis. However, it is still difficult to determine an appropriate hinge position to prevent fracture in the lateral cortex of tibia in the process of making an open wedge or after applying a bone plate and body weight. Nevertheless, the optimal hinge position related to risk of fracture is still controversial. Therefore, in this study, we tried to present a biomechanical basis for determining the hinge position by using a heterogeneous model.

METHODS

Three-dimensional lower extremity models were constructed using Mimics (Figure 1a). The tibial wedge started at 40 mm distal to the medial tibial plateau, and osteotomy for three hinge positions was performed toward the head of the fibula (mid position), 5 mm proximal from the head of the fibula (proximal position), and 5 mm distal from the head of the fibula (distal position). Finally, tibial wedges were ended at 5mm far from tibial lateral cortex. The three tibial models for biplane open wedge high tibial osteotomy were made with varus deformity of 5, 10, 15 degrees with 3-matic software. The material properties of tibial bone in each model were set to heterogeneous material properties which converted from Hounsfield's unit to Young's modulus by applying empirical equation in existing studies. For a loading condition, displacement at the posterior cut plane was applied referring to Hernigou's table considering varus deformity angle. All computational analyses were performed by using FE commercial software (Figure 1b).

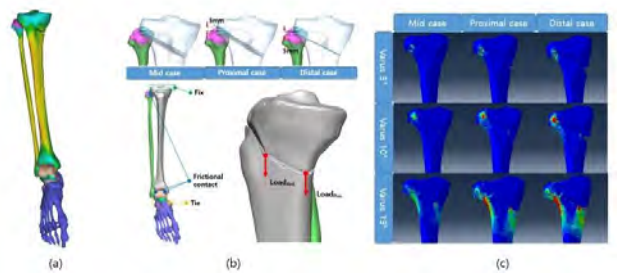

Figure 1 Computational analysis model for biplane OWHTO surgery (a)Heterogeneous tibia model, (b) Three hinge positions, loading & boundary condition in FE model, and (c)Von-mises stress contours as hinge positions and varus deformity angles.

RESULTS AND DISCUSSION

In To estimate the risk of fracture in the lateral cortex of tibia, von-mises stresses on the tibial wedge were calculated for three hinge positions considering varus deformity angles. The maximum stress increased to an average of 213±9% when the varus angle was 10 degrees compared to 5 degrees and increased to an average of 154±8.9% when the varus angle was 15 degrees compared to 10 degrees. In addition, the maximum stress of the distal position was 19 times higher than that of the mid position and 5 times higher than that of the proximal position on average (Figure 1c). For varus deformity angles, the maximum stress of the tibial wedge tended to increase as the varus deformity angle increased. For hinge position of tibial wedge, maximum stress was the lowest in the mid position, while the highest in the distal position.

CONCLUSIONS

These results suggest that the risk of fracture would be low in the order of mid, proximal, and distal hinge position and the distributed stress tends to increase as the varus angle increases.

ACKNOWLEDGEMENTS

This work was supported by the National Research Foundation of Korea (NRF) grant funded by the Korea government (NRF-2022R1A2C1009995)

Ground reaction forces during the full driver shot of Japanese male professional golfers

Tomoya Hirano[1], Yu Kashiwagi[2], Seiji Shimatani[3] and Kazuo Funato [1]
[1] Graduate School of Sport System, Kokushikan University, Tokyo, Japan.
[2] Senshu University Institute of Sport, Kanagawa, Japan.
[3] Faculty of Business Administration, Kanagawa University, Kanagawa, Japan.
Email: tohirano@kokushikan.ac.jp

INTRODUCTION

In recent years, the cost of force plates and similar devices for measuring vertical ground reaction force (GRF) has been reduced; thus, obtaining biofeedback on force information in golf practice has become feasible [1]. Therefore, the exertion of GRFs for achieving maximum shot distance by skilled golfers can be helpful information for recreational golfers. Nonetheless, the detailed GRFs changes during a full driver shot in skilled golfers have not been shown previously. The current study investigated the GRFs of Japanese male professional golfers during a full driver shot.

METHODS

Eight Japanese male professional golfers (age: 35.5 ± 1.7 years; height: 1.74 ± 7.7 m; body mass: 75.1 ± 9.4 kg) and 19 male collegiate golfers (age: 19.3 ± 1.2 years; height: 1.73 ± 4.7 m; body mass: 68.4 ± 7.4 kg) participated in this study. The experimental challenge involved a driver executing a full shot and achieving the greatest possible distance. The experiment was conducted in an indoor experimental facility. The GRFs of the front and rear legs were measured using two force plates (9287, Kistler; operated at 1000 Hz). Based on the address posture, the GRF was defined with the x-axis pointing forward (anteroposterior), the y-axis pointing from the tee to the target (mediolateral), and the z-axis pointing vertically upward (vertical). Time-series data for anteroposterior, mediolateral, and vertical GRFs were normalized to 100% for the downswing phase. A two-sample t-test using statistical parametric mapping (SPM) was used to compare groups of averaged GRFs [2].

RESULTS AND DISCUSSION

Compared to amateur golfers, professional golfers showed a trend toward greater maximum clubhead velocity during full driver shots (49.3 ± 2.1 vs. 51.7 ± 3.8 m/s, respectively, p = 0.13, n.s., effect size = 2.69). According to SPM, professional golfers produced a greater vertical GRF component in their front legs during 75%–91% of the downswing than amateur golfers (Figure 1). Other GRF components showed no differences between groups. In a research, it was found that the large vertical GRFs of the leading foot during downswing acceleration and 40 ms prior to impact were major predictors of driven ball velocity [3]. A greater vertical GRF of the front leg during the downswing may accelerate the body's center of mass vertically, increasing clubhead velocity. These results suggest that the push movement with the front leg during the downswing is crucial for the shot's quality.

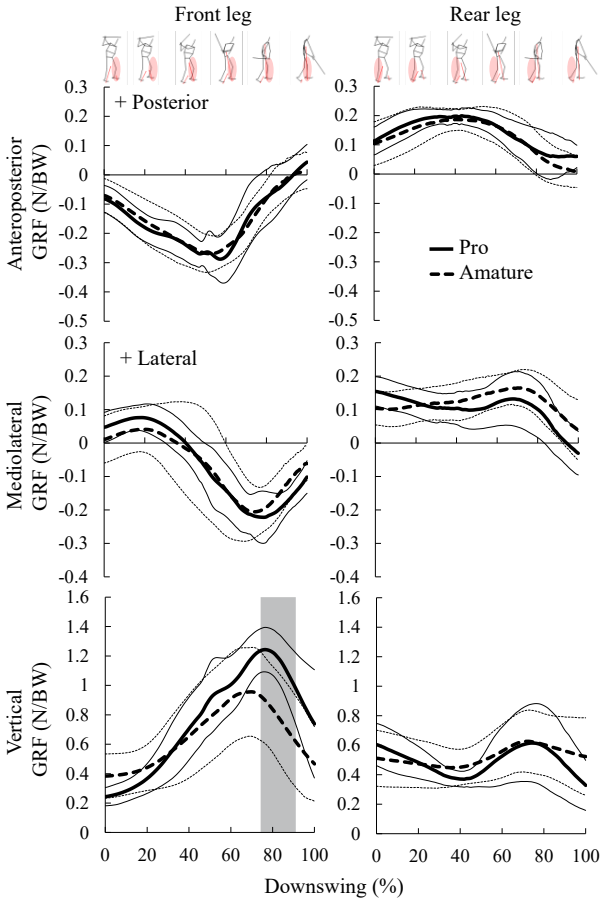

Figure 1 Waveforms of the GRF during the downswing of professional golfers, and amateur golfers. The mean and standard deviation are indicated by bold and thin lines, respectively. The shaded area indicates differences in curves between groups based on SPM results.

CONCLUSIONS

We examined the GRFs of Japanese professional and amateur golfers during full driver shots. The results showed that the front leg of the professional golfers had a greater vertical GRF during the late downswing. These results provide insights into the magnitude and timing of the forces required to increase the distance of driver shots during golf practice.

REFERENCES

[1] Queen RM et al. *JSCR* **27**: 2481-2486, 2013.
[2] Pataky TC. *CMBBE* **15**: 295-301, 2012
[3] Chu Y et al. *J Sports Sci* **28**: 1251-1259, 2010

IS THERE A LINEAR RELATIONSHIP BETWEEN SWIMMING VELOCITY AND VERTICAL BODY POSITION IN FRONT CRAWL FOR EACH STROKE PHASE?

Sohei Washino[1], Yasuhide Yoshitake[2], Hirotoshi Mankyu[3] and Akihiko Murai[1]
[1] Human Augmentation Research Center, National Institute of Advanced Industrial Science and Technology, Chiba, Japan. [2] Graduate School of Science and Technology, Shinshu University, Nagano, Japan. [3] Department of Coaching of Sports and Budo, National Institute of Fitness and Sports in Kanoya, Kagoshima, Japan.
Email: s.washino@aist.go.jp

INTRODUCTION

It is well-known that keeping the swimmer's body position as high as possible is a crucial way of reducing drag and thus improving swimming performance. Coaches visually inspect the swimmer's vertical body position to evaluate the swimmer's ability or condition. Therefore, it is important for swimmers and their coaches to understand the factors determining a swimmer's vertical position. Swimming velocity is one of the factors associated with the vertical body position during swimming [1,2], and vertical body position increased linearly with swimming velocity over a wider velocity range during front crawl [2]. However, since this relationship was established for the average over a complete stroke cycle [2], coaches are required to observe the swimmers for the entire stroke cycle to evaluate their vertical body position fully. Focusing on specific phases within the stroke cycle rather than averages for a stroke cycle may provide practical information for swimmers and their coaches to easily detect changes in a swimmer's vertical body position. Despite this potential benefit, it remains uncertain whether a linear relationship between swimming velocity and vertical body position holds for each stroke phase (e.g., pull, recovery). This study aimed to investigate whether the linear relationship between swimming velocity and vertical body position establishes for each stroke phase in front crawl.

METHODS

Eleven college-level male swimmers (21.5 ± 2.3 y) performed a 15 m front crawl at various swimming velocities ranged from 0.8 to 1.6 m/s with sustained forced maximal inspiration to control for lung volume effects [3]. The three-dimensional positions of 36 reflective markers attached to the swimmer's body were captured at 100 Hz using an underwater motion-capture system (Qualisys). The body's center of mass (CoM) was estimated from individual digital human models with inertial parameters using inverse kinematics [2,3]. The horizontal CoM velocity and vertical CoM position relative to the water surface as an index of vertical body position were calculated for one stroke cycle and divided into five stroke phases (i.e., entry, pull, push, release, and recovery) [1]. We used a linear mixed-effects model with random intercepts and slopes to test whether there was a positive trend between mean swimming velocity and mean vertical CoM position for one stroke cycle and for each stroke phase. It was constructed with the swimmers as a random effect and swimming velocity as a fixed effect. Marginal R^2 (R^2m; variance explained by fixed effects) and the conditional R^2 (R^2c; variance explained by both fixed and random effects) of the linear mixed-effects models were calculated.

RESULTS AND DISCUSSION

There was a positive trend between mean swimming velocity and mean vertical CoM position for one stroke cycle (β = 0.037, p < 0.001, Figure 1). There was a positive trend between mean swimming velocity and mean vertical CoM position for the entry (β = 0.041, p < 0.001), pull (β = 0.055, p < 0.001), push (β = 0.048, p < 0.001), release (β = 0.030, p < 0.001), and recovery (β = 0.024, p < 0.001) phases, respectively (Figure 1). These results indicate that a linear relationship between swimming velocity and vertical body position during front crawl can be established for one stroke cycle as well as for any stroke phases.

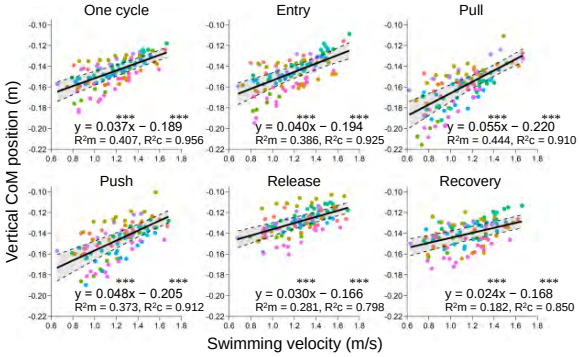

Figure 1 Swimming velocity plotted against the vertical CoM position across swimmers for one stroke cycle and for each stroke phase. Point colour corresponds to each swimmer of the data point.

CONCLUSIONS

The linear relationship between swimming velocity and vertical body position during front crawl was established for each phase of the stroke cycle. This finding provides practical information for swimmers and their coaches to easily detect changes in swimmer's vertical body position by focusing on specific stroke phases.

ACKNOWLEDGEMENTS

This work was partly supported by JSPS KAKENHI Grant Number JP20K14686.

REFERENCES

[1] Gonjo T et al. *Sports Biomech*: 1-12, 2021.
[2] Washino S et al. *Sports Biomech*: 1-13, 2022.
[3] Washino S et al. *Scand J Med Sci Sports* **32**(12): 1724-1737, 2022.

EVALUATION OF MUSCLE ACTIVATIONS OF UPPER ARM IN COLLEGIATE ATHLETE DURING 200-M FRONT CRAWL: A PILOT STUDY

Jia-Hao Chang*, Ying-Wei Lee, Chien Huang, Chia-Chuan Chang, I-Cheng Huang
Department of Physical Education and Sport Sciences, National Taiwan Normal University, Taipei, Taiwan.
*Email: jhchang@ntnu.edu.tw

INTRODUCTION

Muscle activations of upper arm during swimming could be measured and recorded by electromyography (EMG) to understand what the muscle did while swimmer swam. Monitoring the changes of the muscle activation in each stroke during swimming provided the information for the coach to know the muscle condition of the swimmer. Therefore, it is important to identify the stroke cycle of swimming correctly and quickly in the swimming poor. The wearable inertial measurement unit (IMU) is easy to be used for special event detecting to define the stroke cycle of swimming [1]. Using electromyography combined with wearable IMU to record the muscle activations during swimming could provide the exact information whether the muscle fatigue or not. The purpose of this study was to evaluate the muscle activations of the upper extremity in each stroke cycle during 200-m front crawl.

METHODS

Six front crawl male swimmer in college division I were recruited as participant in this study. No shoulder pain and any musculoskeletal injury in past 6 months were reported. The experimental procedure has been explained to swimmers and the participant gave informed consent. Three wearable IMU (Blue Trident, VICON), sampling @ 120 Hz, attached on the sternum and both forearm, and four water proof EMG electrodes (Mini Wave, COMETA), sampling @ 2400 Hz, placed on the muscle belly of pectoralis major, latissimus dorsi, triceps, and deltoid in dominant side, were used to collect and record the kinematics and muscle activities of swimmer, separately, in the 200-m front crawl. Each swimmer performed a 200-m front crawl trial at their maximal in a 50-m indoor swimming pool. Swimming stroke cycle was calculated from the IMU data based on the method modified from the report by James et al. [2] Raw EMG signal was filtered with a 4th order band-pass Butterworth filter with cut-off frequencies of 20 and 400 Hz. Then, linear envelope was found by full-wave rectified and smoothed with a 4th order low pass Butterworth filter of 10 Hz. Ten swimming stroke cycles from 15~45 meter in each swimming trip, totally 40 swimming stroke cycles, were used to understand the changes of muscle activation during 200-m front crawl. Mean values of the processed EMG amplitude relative to each respective maximal voluntary isometric contractions (MVIC) in each swimming stroke cycles were considered as outcomes for descriptive statistics.

RESULTS AND DISCUSSION

The muscle activations of pectoralis major, latissimus dorsi, triceps, and deltoid are showed in table 1 and on figure 1. The values of mean EMG were lower in the 2nd and 3rd 50-m trips. Using IMU to identify the swimming stroke cycle during front crawl is feasible, and the muscle activations could be calculated in each swimming stroke cycle to know the muscle condition.

Table 1: Muscle activations in each swimming trip during 200-m front crawl (Mean ± Standard deviation)

(%MVIC)	1st 50-m	2nd 50-m	3rd 50-m	4th 50-m
Pectoralis Major	28.8 ± 18.2	25.5 ± 15.1	24.9 ± 11.1	26.2 ± 10.1
Latissimus Dorsi	19.7 ± 8.0	21.9 ± 10.6	22.7 ± 11.1	25.8 ± 12.5
Triceps	62.4 ± 23.1	58.0 ± 24.8	64.6 ± 32.8	60.8 ± 30.2
Deltoid	30.5 ± 22.8	28.2 ± 18.9	29.9 ± 21.7	33.7 ± 25.9

CONCLUSIONS

The results supported using EMG device combined with wearable IMU to explain the muscle activation correctly and quickly is feasible in the indoor swimming poor.

ACKNOWLEDGEMENTS

Funded by National Science and Technology Council, Taiwan (MOST 110-2410-H-003-092).

REFERENCES

[1] Dadashi F et al. *J Sport Sci* **34**: 1405–1412, 2016.

[2] James D A et al. *Sports Technol* **4**: 141-150, 2011.

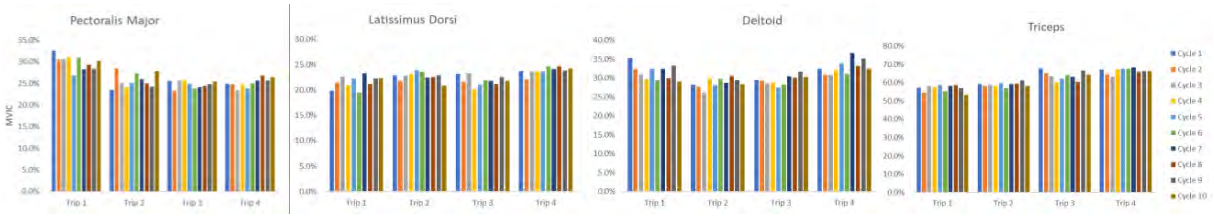

Figure 1 Muscle activations in each swimming stroke cycles during 200-m front crawl.

The Effects of Two-Step Golf Swing Drills on Swing Rhythm and Clubhead Speed in Competitive Juniors

Kanji Mori[1], Taylor North[1], Kai-Jen Cheng[1], Seungho Baek[1], Hunter Alvis[1] and Young-Hoo Kwon[1]
[1] Biomechanics & Motor behavior Laboratory, Texas Woman's University, Denton, Texas, USA.
Email: kmori1@twu.edu

INTRODUCTION

The two-step swing drills (TSSD) are designed to promote a good swing rhythm by enhancing the golfer-ground interaction [1] through repeated rhythmic unloading/loading of each leg (i.e., stepping-like leg actions). The purpose of this study was to assess the effects of single TSSD session on swing rhythm and the clubhead speed. It was hypothesized that the TSSD would increase the clubhead speed, motion ranges, ground reaction force (GRF) peaks, and the angular velocity peaks of the axle-chain system [2].

METHODS

Ten competitive right-handed junior golfers (15-18 years old; mean age = 16.1 years; 9 males and 1 female) participated in this study and performed seven maximal effort drives with their own drivers before (pre-test) and after (post-test) a TSSD session each. The TSSD session (< 45 minutes) mainly consisted of 4 stages (Figure 1). Each stage started with a trigger motion either by swinging the club toward the target (club trigger) or by moving the body slightly (body trigger). Up to two steps (trail-side and lead-side) were taken in the stages. Correct timings of the steps along with rhythmic leg actions and speedy backswing were emphasized throughout the stages. The drill swings were repeated in each stage until the golfer exhibited correct step timing and/or reasonably fluent motion flow judged by the investigators.

Stage 1	Stage 2	Stage 3	Stage 4
Club trigger	Club trigger	Club trigger	Body trigger
Feet together	Narrow stance	Normal stance	Normal stance
Both steps	Lead-side step	No step	No step

Figure 1. Trigger type, stance, and steps used in the TSSD stages

A 10-camera optical motion capture system (500 Hz) and two force plates were used in acquiring the swing trials. The clubhead speed at impact, motion ranges of the body/pelvis, vertical GRF peaks (maximum and unweighting), and the angular velocity peaks of the axle-chain system were obtained. The pre- and post-test values were compared by using paired *t*-tests ($p < .05$).

RESULTS AND DISCUSSION

As a result of participation in single TSSD session, the clubhead speed increased significantly (Table 1) All participant revealed increases in the clubhead speed: +1.0 to +5.3%. Among the vertical GRF peaks, the unweighting peak significantly decreased, meaning more unweighting was induced by the stepping-like leg actions between the trail-side (right leg) push in the backswing and the lead-side (left leg) push in the downswing. The horizontal motion ranges (away from and toward the target) were characterized by consistent increases, while the vertical motion ranges (upward and downward) of the body CM partially increased significantly. Increases in the angular velocity peaks were observed across the board in both the backswing and the downswing with minor exceptions.

CONCLUSIONS

The findings show that the TSSD can be used as natural means to develop a rhythmic and dynamic golf swing. The stepping-like leg actions facilitate horizontal motions more than the vertical, and unweighting more than loading in terms of interaction with the ground.

REFERENCES

[1] Han, K. H. et al. *S Biomech* **18**(2): 115-134, 2019.
[2] Han, K. H. et al. S Biomech **18**(6): 663-685, 2019.

Table 1: Summary of the changes in the kinematic and kinetic parameters

Parameter		Before	After	Parameter		Before	After
Clubhead speed (m/s)**		44.60 (3.53)	45.93 (3.41)	BS angular velocity peak (°/s)	Hip line**	-126 (31)	-151 (24)
Vertical GRF (BW)	Max	1.67 (0.36)	1.71 (0.34)		Thorax**	-226 (48)	-263 (35)
	Unweighting**	0.83 (0.10)	0.79 (0.10)		Shoulder line**	-285 (59)	-323 (49)
	Lead-foot	1.28 (0.27)	1.30 (0.25)		Upper lever**	-353 (78)	-389 (61)
CM motion range (cm)	Away*	-6.5 (4.6)	-8.1 (4.2)		Club**	-556 (121)	-617 (92)
	Toward**	13.8 (4.1)	18.1 (4.1)		Wrist	-262 (59)	-280 (46)
	Upward-BS*	1.1 (0.8)	2.2 (1.8)	DS angular velocity peak (°/s)	Hip line*	491 (75)	518 (82)
	Downward*	-3.7 (1.6)	-4.9 (2.2)		Thorax	658 (77)	692 (84)
	Upward-DS	4.2 (1.8)	4.6 (2.4)		Shoulder line*	807 (68)	841 (83)
Pelvis motion range (cm)	Away*	-4.3 (4.3)	-5.9 (3.9)		Upper lever**	1,063 (115)	1,102 (116)
	Toward**	15.9 (3.7)	20.9 (4.1)		Club**	2,100 (180)	2,170 (173)
	Downward	-6.3 (1.6)	-6.6 (1.6)		Wrist**	1,317 (222)	1,389 (235)
	Upward	8.4 (2.7)	8.7 (3.2)				

Values in *M* (*SD*); * p< .05; ** p<.01; BW – body weight; CM – center of mass; BS – backswing; DS – downswing

CONSERVED BIOMECHANICAL STRATEGIES FOR STANDING AND WALKING BALANCE IN THE UPRIGHT AND INVERTED POSTURE

Charlotte Le Mouel[1,2]

[1] Department of Movement Science, Institute of Sport and Exercise Science, University of Münster, Germany.
[2] Centre Borelli, Université Paris Cité, Université Paris Saclay, ENS Paris Saclay, CNRS, Paris, France
Email: charlotte.lemouel@normale.fr

INTRODUCTION

Balance during upright standing and walking requires controlling the ground reaction force (GRF, purple arrow in Figure 1) and center of pressure (CoP, red dot in Figure 1) according to the position of the whole body center of mass (CoM, green dot in Figure 1). This is achieved through a combination of muscle synergies and sensory feedback [1]. Maintaining balance in the inverted posture follows the same biomechanical requirements as in upright stance. This study shows that learning this novel skill allows the emergence of novel sensory feedback and muscle synergies which implement conserved biomechanical strategies.

METHODS

Sixteen gymnasts performed standing and walking both in the upright and inverted posture. GRF and CoP were recorded using force plates (Kistler). The positions of 38 markers placed on the body were recorded (Qualysis) and used to estimate the position of the CoM [2].

RESULTS AND DISCUSSION

During stance in both the upright (Figure 1, B) and inverted posture (Figure 1, C), subjects control the position of their CoP (Figure 1, A – C, red) according to delayed feedback control of the position and speed of the CoM [1] (Figure 1, B, C, prediction in black).
During walking in both the upright (Figure 1, E) and inverted posture (Figure 1, F), subjects maintain balance by aligning the GRF angle (Figure 1, D – F purple) with the angle of line connecting the CoM to the CoP (Figure 1, D – F, blue). This strategy minimises rotation around the CoM.

DISCUSSION

Although they must rely on different sensory information and muscle synergies, gymnasts nevertheless use conserved biomechanical strategies to maintain balance in the upright and inverted postures, both during standing and walking. Future work will address how this strategy emerges in gymnasts learning to walk on their hands.

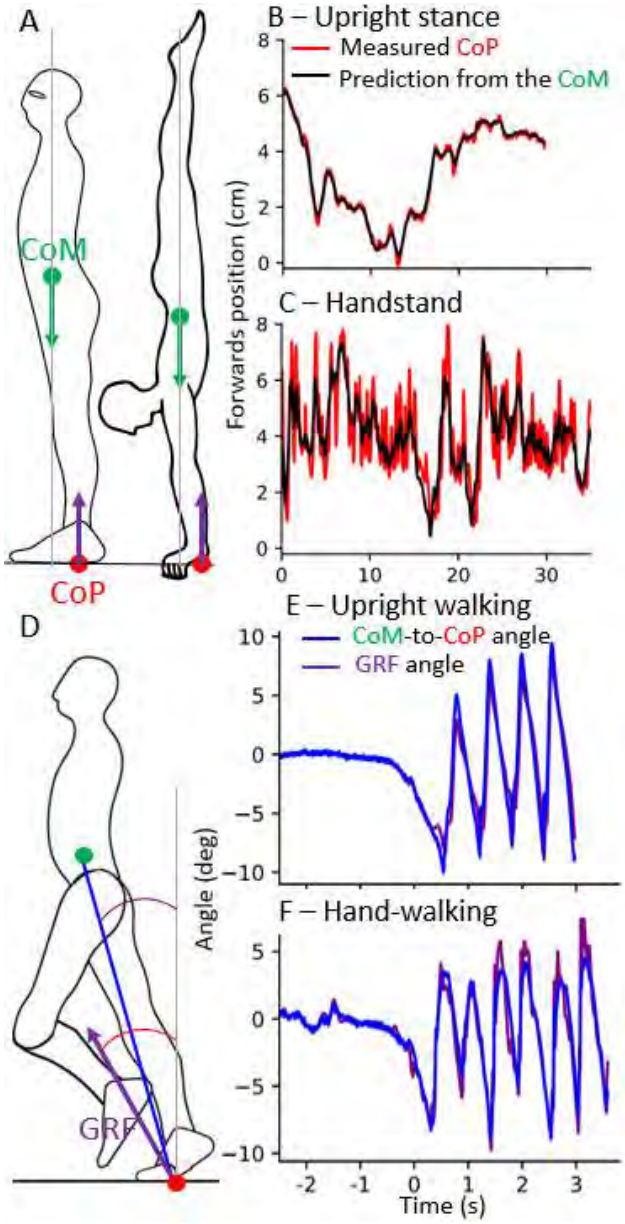

Figure 1 Standing and walking balance. During stance (A – C), the measured position of the CoP (red) can be predicted from the position and speed of the CoM (prediction in black) at previous timepoints, both in upright stance (B) and handstand (C). During walking (D – F), subjects control the angle of the GRF (purple) to keep it aligned with the line from the CoP to the CoM (blue) during both upright walking (B) and hand-walking (C).

REFERENCES

[1] Le Mouel C et al. *PLoS Comput. Biol.* **15**(11): e1007463, 2019.

[2] Dumas R et al. *J Biomech* **40**(3): 543–553, 2007

International Society of Biomechanics (ISB) 2023

SHOULDER, SCAPULOTHORACIC, AND GLENOHUMERAL JOINT MOVEMENTS DURING BADMINTON OVERHEAD SWING MOTION IN STANDING VERSUS WHEELCHAIR SITTING POSITIONS

Yuki Tamura[1], Noriaki Maeda[1], Makoto Komiya[1], Kazuki Fukui[2], Mitsuhiro Yoshimi[1], Koki Tsuchida[1], Takeru Abekura[1], Yukio Urabe[1]

[1] Department of Sports Rehabilitation, Graduate School of Biomedical and health Sciences, Hiroshima University, Hiroshima, Japan.

[2] Japan Para Badminton Federation, Tokyo, Japan.

Email: yuki-tamura0309@hiroshima-u.ac.jp

INTRODUCTION

Wheelchair badminton players develop shoulder joint pain (Shoulder pain) more frequently than standing badminton players [1]. Shoulder pain occurs in the section from the shoulder joint in maximum external rotation (MER) to impact during the overhead swing motion. Shoulder joint movement is performed by interlocking movements of the scapulothoracic and glenohumeral joints. Therefore, it is necessary to analyze each to understand the mechanism of shoulder pain onset. However, no studies have investigated the movement of each joint during the swing motion in wheelchair badminton. This study aimed to compare the shoulder, scapulothoracic, and glenohumeral joint movements at the MER during overhead swing motion between standing (ST) and wheelchair sitting (WC) positions to elucidate the factors contributing to shoulder pain in wheelchair badminton players.

METHODS

Ten healthy male college students (Mean age, 22.3 ± 1.9 years) with at least 3 years of standing badminton experience participated in this study. Kinematic data were obtained using an electromagnetic tracking device (240 Hz, Liberty; Polhemus) from all participants during the overhead swing motion in ST and WC positions. Participants were instructed to perform the swing motion with maximum effort five times in each condition. The measurement items were shoulder joint angle in external rotation, scapulothoracic joint in posterior tilt, and glenohumeral joint in external rotation at the MER during the motion. For the statistical analysis, a paired t-test was used to compare items between the two conditions. Statistical significance was set at $p<0.05$.

RESULTS AND DISCUSSION

In the WC versus ST position, the shoulder joint angle in external rotation and the scapulothoracic joint angle in posterior tilt were significantly smaller by 3.6° and 2.2°, respectively. No significant difference was observed in the glenohumeral joint angle of external rotation in each condition (**Table 1**). The movement of the shoulder joint in external rotation involves a combination of the scapulothoracic joint in posterior tilt, glenohumeral joint in external rotation, and trunk extension movements. Among them, scapulothoracic joint movement contributes the most to the shoulder joint in external rotation movement [2]. However, sitting position in a wheelchair may limit the movement of the scapulothoracic joint in posterior tilt due to thoracic kyphosis, which may result in a smaller angle of the shoulder joint during external rotation. In contrast, a stronger swing motion requires a greater shoulder joint angle during external rotation [3]. Thus, in the WC position, which involves a smaller scapulothoracic joint angle in posterior tilt, an excessive glenohumeral joint in external rotation movement may have been induced to increase the shoulder joint angle in external rotation. This finding may be related to the occurrence of shoulder pain among wheelchair badminton players.

CONCLUSIONS

This study showed that the swing motion in the WC position involves less scapulothoracic joint movement than that in the ST position and may induce excessive compensatory glenohumeral joint movement. This may account for the predilection of shoulder pain among wheelchair badminton players.

REFERENCES

[1] Mohd J et al. *The Physician and Sportsmedicine* **50(4)**: 316-322, 2022

[2] Miyashita K et al. *The American Journal of Sports Medicine* **38(2)**: 363-368, 2010.

[3] King M et al. *Applied Sciences* **10(4)**: 1248, 2020.

Table 1. Joint angles at the MER during the motion in the WC versus ST positions

	ST	WC	*p-value*
Shoulder joint in external rotation (°)	93.0 ± 12.1	89.4 ± 13.1	**0.038**
Scapulothoracic joint in posterior tilt (°)	8.4 ± 9.2	6.2 ± 9.3	**0.040**
Glenohumeral joint in external rotation (°)	89.5 ± 10.8	87.3 ± 11.5	0.320

Data are expressed as means ± SD.

Mass-spring characteristics explain the temporal step parameters but are not specific to individuals across phases in accelerated sprinting.

Arata Tatsumi[1], Toshihide Fujimori[2], Takeshi Edagawa[2], and Natsuki Sado[3]
[1] School of Physical Education, Health and Sport Sciences, University of Tsukuba / Tsukuba, Japan.
[2] Graduate School of Comprehensive Human Sciences, University of Tsukuba / Tsukuba, Japan
[3] Faculty of Health and Sport Sciences, University of Tsukuba / Tsukuba, Japan.
Email: tatsumi.arata.ay@alumni.tsukuba.ac.jp

INTRODUCTION

Sprinting is a periodic motion in which the support phase and the flight phase are repeated. Numerous spatiotemporal patterns exist even at the same speed, and inter-individual variability has been observed [1]; however, its determinants have not been fully clarified. During sprinting, the lower limb behaves like a spring. Its properties can be evaluated by the mass-spring model with leg and vertical stiffness (k_{leg} and k_{vert}: the ratio of maximum force to leg compression and vertical displacement, respectively), which can be estimated as a function of spatiotemporal variables and body size parameters [2]. Thus, the stiffness properties might determine the inter-individual spatiotemporal variability. The trends of k_{leg} and k_{vert} for multiple sprinters were also reported to be constant over a range of phases in the 100 m sprint [2]. However, the joint stiffness, which determines overall spring-mass stiffness, is influenced by several factors, such as neuromuscular control and mechanical muscle-tendon properties [3]. Thus, it is unclear whether the stiffness is individual specific (i.e., whether the same individuals always exhibit stiff/compliant behaviour) across a range of phases.
We investigated the relationship of spring-mass behaviour to spatiotemporal variables, and its individual specificity across a wide range of phases within the acceleration phase of the 100 m race.

METHODS

Three high-speed cameras (480 fps) recorded the 0-45 m of sanctioned 100 m races. The toes of 19 male sprinters were digitized. Contact and flight duration and contact position were obtained. Sprint speed was calculated as the product of step length and frequency. We calculated k_{leg} and k_{vert} from these spatiotemporal variables [2].
We divided the 0-40 m into four sections of 10 m each, and the average values of each section were used in the analysis. We examined the relationship of k_{vert} and k_{leg} to the spatiotemporal variables by using a single regression analysis. Prior to regression, we excluded the outliers in the explanatory variables and in the residuals from the regression equation based on three times the median absolute deviation. To evaluate the individual specificity, the agreement in each variable among the four sections was assessed by the intraclass correlation coefficient (ICC).

RESULTS AND DISCUSSION

In all sections, both k_{vert} and k_{leg} were not significantly correlated with maximal sprint speed ($r \leq 0.28$), but were significantly correlated with the contact duration and to the ratio of contact duration to flight duration ($r \geq 0.52$), except for the 0-10 m for k_{vert}. The results suggest that spring-mass behaviour explains intra-individual temporal variability rather than sprint performance. Meanwhile, the agreement of each k_{vert} and k_{leg} between phases was fair (Figure 1, ICC $\leq$ 0.338), suggesting that the spring-like behaviour was not individually specific across a wide range of the phases in the acceleration. The spring-mass stiffness is determined by multiple factors, such as neuromuscular control and muscle-tendon mechanical properties [3]. Therefore, we suggest that the effects of these factors on the spring-mass behaviour differ from phase to phase within the acceleration phase of the 100 m race.

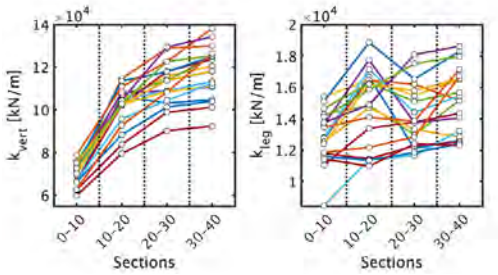

Figure 1: Intra-individual variation in k_{vert} and k_{leg}

CONCLUSIONS

We found that intra-individual variability in the spring-mass behaviour determined the temporal step parameters during each phase within the acceleration phase of the 100 m race. Meanwhile, the spring-mass behaviour was not individually specific throughout the entire acceleration phase. Therefore, we suggest that although the temporal step parameters for each phase are determined by the spring-mass behaviour, the determinants of this behaviour differ from phase to phase.

REFERENCES

[1] Salo et al., Med Sci Sports Exerc **43**, 1055-1062, 2011.
[2] Morin et al., Int J Sports Med **27**, 158-165, 2006
[3] Hortobagyi and De Vita, J Electromyogr Kinesiol **10**, 117-126, 2000.

ACCURACY OF THE CENTRE OF MASS ESTIMATION BASED ON PICTURES AMONG IQFOIL WINDSURFING ATHLETES

Martyna Białecka[1], Aleksander Błażkiewicz[2,3], Martyna Sopa[1], Agata Mrozek[1], Tomasz Walczak[1], Jakub Grabski[1], Monika Grygorowicz[4,2]

[1] Institute of Applied Mechanics, Faculty of Mechanical Engineering, Poznan University of Technology, Poland.
[2] Rehasport Clinic FIFA Medical Centre of Excellence, Department of Sport Science, Poland.
[3] Polish Yachting Association, Warsaw, Poland.
[4] Department of Physiotherapy, Poznan University of Medical Sciences, Poland.
Email: martyna.bialecka@put.poznan.pl

INTRODUCTION

Windsurfing hydrofoil is a lifting surface located horizontally at the tip of a board vertical fin submerged in water. As the windsurfing board gains speed, the foil lifts it above the water surface, reducing its drag and allowing the board to sail at higher speeds in less wind conditions. This change of sailing mode (board in the water vs. board in the air) creates completely new demands on the position of the athlete's body. Studying the body position in real iQFOiL sailing conditions is not easy due to the low availability and high cost of waterproof motion analysis systems. However, estimating the position of the center of mass (COM) of the body can be approximated on the basis of image analysis and basic anthropometric data of the competitor. The right position of the athlete's COM may be the key to better performance.

The aims of the study were as follows: (1) development of the algorithm that will calculate the location of the iQFOiL's athlete COM, based only on the two pictures taken in perpendicular planes and anthropometric data, (2) calculate the accuracy of the algorithm compared to the motion capture system, (3) development of the characteristics that describe the location of the COM regardless of the rake angle of the mast.

METHODS

Three athletes who trained in iQFOiL for at least one year participated in the study. Each of them performed five repetitions of three positions of the body: with high hips, low hips, and with one hand supported on an uphaul rope attached to the mast (Figure 1). Every repetition was recorded with the BTS Smart DX motion capture system and two mobile phone cameras. COM was estimated according to the method described in [1]. We developed the algorithm that calculates the location of the main joints based on photos and lengths of the body segments (*iQFOiL_photo*). The accuracy of the *iQFOiL_photo* algorithm was calculated as the absolute difference between the COM location calculated based on the motion capture system and with the use of *iQFOiL_photo*. COM was calculated separately for the upper limbs, lower limbs, and entire body and expressed as a perpendicular and parallel distance from the plane passing through the wrists and ankle joints (WA plane) of the athlete in the sagittal plane.

RESULTS AND DISCUSSION

The best accuracy of the COM estimate based on photos was observed for the lower limbs as a parallel distance to the WA plane (5,7 ± 4,7 mm). The worst accuracy was observed for the upper limbs as a parallel distance to the WA plane (25,6 ± 14,2 mm). This result seems reasonable as the algorithm was calculating the position of the adjacent joint, starting from the ankle joint. The accuracy of the overall COM estimate was 6,8 ± 5,3 mm for the perpendicular distance and 16,9 ± 10,2 mm for the parallel distance from the WA plane.

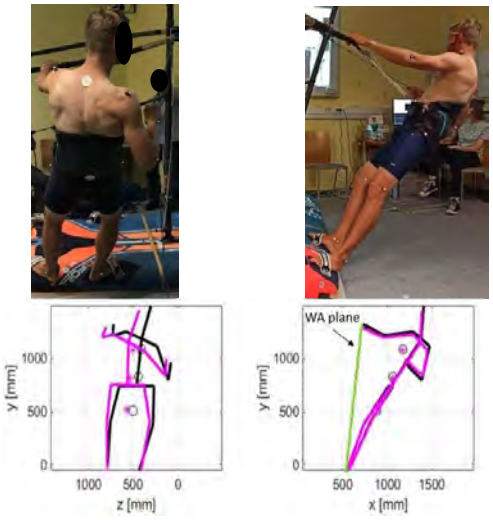

Figure 1 An example of photo input data and body position reconstruction with the *iQFOiL_photo* algorithm in the form of stick biomechanical model and determined COM.

CONCLUSIONS

The *iQFOiL_photo* successfully reconstructed body position and location of COM although addressing the question whether its accuracy is sufficient to observe the change in athlete's performance, demands further study.

ACKNOWLEDGEMENTS

We would like to thank Mr Mariusz Goliński and Polish Yachting Association for participation in the study. The project was supported by the Ministry of Sport and Tourism in Poland (grant for supporting scientific projects in the field of competitive sport in 2022.).

REFERENCES

[1] C. Clauser, T. J. McConville, and T. Young, "Weight, volume, and centre of mass of segments of the human body," Ohio, 1969.

ASSESSING THE LIKELIHOOD OF ACL INJURY IN VOLLEYBALL PLAYERS AT UITM BY UTILIZING THE LANDING ERROR SCORING SYSTEM

Muhammad Hidayat Jamaludin[1], Ezhan Iqbal Zulkiflie[1], Radin Rafeeuddin Radin Dzulfakar[1] and Raihana Sharir[1,2]
[1]Faculty of Sports Science and Recreation, Universiti Teknologi MARA, Malaysia.
[2] School of Sport and Exercise Sciences, Liverpool John Moores University, United Kingdom.
Email: raihanasharir@uitm.edu.my

INTRODUCTION

Anterior cruciate ligament (ACL) injuries are common in dynamic sports, with high loading to the knee being a risk factor [1,2]. Screening is crucial in identifying individuals with high injury risk. The gold standard laboratory-based screening is costly, so field-based screening methods have emerged, including the Landing Error Scoring System (LESS). LESS, developed in 2009, is a simple and reliable kinematic assessment tool that evaluates 17 items during a jump-landing task and is commonly used in studies [3]. Volleyball is a sport prone to ACL injuries, with players requiring jumps for attacking and defending [4,5]. This study aims to determine the LESS score of volleyball players and explore gender differences.

METHODS

22 injury-free UiTM volleyball players were tested in a laboratory. 11 male (mean ± SD: age 21.18 ± 1.54 years, height 172.68 ± 7.75 cm, mass 69.41 ± 11.58 kg) and 11 female (mean ± SD: 22.27 ± 1.10 years, height 155.55 ± 4.23 cm, mass 53.88 ± 6.80 kg) participants were tested in the UiTM lab using 2 video cameras to record 3 trials of the jump landing task. Kinematic assessments were made using the LESS and analyzed with 2D-motion analysis software (Kinovea v0.8.25).

RESULTS AND DISCUSSION

This study's findings showed no significant differences in the mean LESS scores between genders ($t(20) = -.909$, $p > 0.05$). However, individual LESS scores revealed that one male and one female player had moderate scores ($5 < \text{LESS score} \leq 6$) and two female players scored poorly (LESS score > 6) in their jump landing biomechanics. Male players tended to land with a more upright body position compared to female players, and most female players scored lower in overall impression compared to males. Both male and female players demonstrated narrow stance width (5/11 males, 7/11 females) and knee valgus displacement (5/11 males, 10/11 females). Although the overall LESS scores suggest low injury risk for both male and female volleyball players, attention should be paid to the individual items in the LESS protocol. Poor scores in specific items may increase their risk of future ACL injury.

CONCLUSIONS

The results suggest that the use of LESS scores did not reveal significant differences between genders in this study. It is possible that individual assessments may provide more valuable information for injury risk screening and classification, rather than relying solely on group data. Further research may be necessary to confirm these findings and to investigate the utility of individual assessments in injury prevention.

ACKNOWLEDGEMENTS

The authors extend their thanks to the UiTM volleyball players and Miss Farah Afiqah Mohamed Razali for their collaboration and help during the process of collecting data

REFERENCES

[1] Sandon, A. et al. *Knee surgery, sports traumatology, arthroscopy* **30**: 1380-1387, 2021.
[2] Wetters, N. et al. *Operative Techniques in Sports Medicine* **24**: 2-6, 2016.
[3] Padua, D.A. et al. *The American Journal of Sports Medicine* **37**: 1996-2002, 2009.
[4] Borràs, X. et al. *The Journal of Strength & Conditioning Research* **25**: 1686-1694, 2011.
[5] Sattler, T. et al. *The Journal of Strength & Conditioning Research* **26:** 1532-1538, 2012.

Table 1: Independent sample T-test for total score of Landing Error Scoring System.

	Gender	Mean (SD)	Levene's Test	t	Df	p-value
Landing Error Scoring System score	Male	3.43 (±1.49)	.086	-.909	20	.374
	Female	4.06 (±1.77)				

*significance level, $p<0.05$

MEASUREMENT OF HORIZONTAL GROUND REACTION FORCE MOMENT IN THE GOLF SWING

Sung Eun Kim[1,2*], Amy L. Ladd[1]
[1] Department of Orthopaedic Surgery, Stanford University / Stanford, CA, USA.
[2] Motion & Gait Analysis Laboratory, Stanford University / Palo Alto, CA, USA.
Email: cjsekim@stanford.edu

INTRODUCTION

The mechanics of each sport differ, yet the same calculation is used to determine the human-ground interaction. Horizontal ground reaction force moment (*GRFM*) is commonly used to define human-ground interaction generating body rotation, in which the length of the moment arm is measured between the horizontal ground reaction force vector and either position of the combined center of pressure (COP), the position relative to the proportions of each vertical ground reaction force, or center of mass. *GRFM* is used across rotation-related sports, such as golf swing [1], baseball (pitchers) [2], and dance (turns) [3]. The measurement interprets the combined COP as the axis of rotation while one foot is applying forces to rotate the body. The mechanics of each rotation-related sport is different. For instance, the transition phase during the golf swing, both feet push the ground simultaneously [1]. In contrast, the baseball pitcher's lead foot (i.e., the left foot for right-handed player and vice versa) is up in the air when the trail foot pushes the ground toward the target [2]. The measurement of the length of the moment arm should differ in the golf swing, specifically between the ground reaction force vectors of each foot, which interprets one foot is the axis of rotation while the other foot applies forces. We proposed the suggested measurement is more associated with body rotation than the combined COP measurement. This study aimed to compare the two measurements of the length of the moment arm in calculating the horiozontal *GRFM* during the golf swing. We hypothesize that peak horizontal *GRFM* with the suggested measurement is more associated with peak pelvis angular velocities than the combined COP measurement during the golf swing.

METHODS

Professional male golfers (n = 13) participated in this study. The thirty-five reflective markers placed on the Plug-in-Gait model and ground reaction force were collected using 8-infrared cameras (Vicon, 250Hz) and force platforms (AMTI, 2000Hz). *GRFM* was defined by cross product between the horizontal ground reaction force and length of the moment arm, in which Method 1. *CC* uses the combined COP, and Method 2. *CL* and *CT* use the COP of the lead and trail foot, respectively, as the axis of rotation. We have eliminated the next step of summing the free moments of each foot as not affecting the result of comparison between measurements. The angular velocity of the pelvis in the horizontal plane ($AV_{P,Z}$) and *GRFM* were calculated at its peaks. Pearson correlation coefficients were performed between the *GRFM* and $AV_{P,Z}$. The critical significance was set at $p < 0.01$.

RESULTS AND DISCUSSION

Peak *GRFM* from Method 1 showed small but non-significant association with peak $AV_{P,Z}$ (lead foot: r = 0.67, p = 0.013, trail foot: r = 0.66, p = 0.014) (Figure 1a and 1c, respectively), whereas peak *GRFM* from Method 2 was associated with peak $AV_{P,Z}$ (lead foot: r = 0.82, p < 0.001, trail foot: r = 0.84, p < 0.001) (Figure 1b and 1d, respectively). Method 1 was not considered significant due to an extremely conservative adjustment of the Type II error rate. All peaks occurred during the early downswing. Our results demonstrate Method 2 might be more accurate way to calculate horizontal *GRFM* during the golf swing.

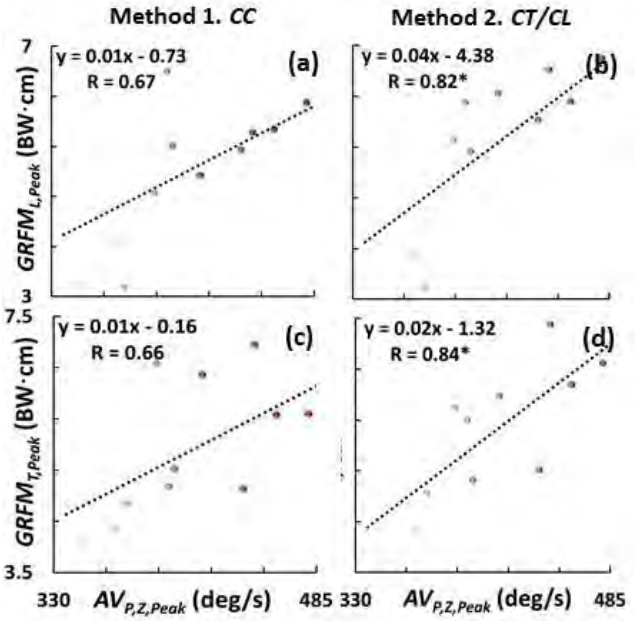

Figure 1. Pearson correlations between the peak horizontal ground reaction force moment, *GRFM*, from the combined COP (Method 1) and suggested measurements (Method 2) of the lead (a, b) and trail (c, d) foot and peak pelvis angular velocity, $AV_{P,Z}$.

CONCLUSIONS

Different methodologies should be considered in investigating human-ground interaction mechanics across a variety of rotationally based sports. Future research is needed to identify clear classification criteria for using different methodologies.

REFERENCES

[1] Han KH et al. *Sport Biomech* **18**: 116-34, 2019.
[2] Liu JM et al. *Sport Biomech* **21**: 1-16, 2022
[3] Zaferiou AM et al. *J App Biomech* **32**: 425-43 2016

ASSOCIATIONS AMONG LAND-JUMP BIOMECHANICS AND IMAGING OF THE PATELLAR TENDON IN MALE BASKETBALL PLAYERS DURING THE PRESEASON

Erin Argentieri[2], Andrew Kraszewski[1], O. Kenechi Nwawka[1]
[1] Hospital for Special Surgery, New York, USA.
[2] University of California Berkeley, Berkeley, California, USA.
Email: KraszewskiA@hss.edu

INTRODUCTION

Patellar tendinopathy (PT) or "jumper's knee" is a common degenerative condition that affects jumping athletes. Symptoms may be subtle or non-existent at preseason, but structural abnormalities may be present. Imaging PT prevalence via conventional and quantitative MRI and ultrasound (US) may provide useful insights if combined with biomechanics. [1]

Objective: Explore how clinically pertinent PT affects biomechanical land-jump patterns and predictive classsification using biomechanical and advanced imaging measurements.

METHODS

26 NCAA Division I and II male basketball players were recruited during preseason. Player VISA-P scores were collected. We measured lower extremity sagittal joint kinematics and kinetics from dual force platforms during a land-jump test. Clinical variables were: presence of radiologic PT (rPT: no/yes) as seen on conventional US and MRI, positive symptoms (no/yes: VISA-P≤80), and presence of Doppler hyperemia (no/yes). Tendons were imaged proximally and distally with quantitative UTE-MRI acquisitions; short proton density fraction PS and T2*S and T2*L decay constants (ms) were taken from a bi-exponential fit to the time echo signal. Quantitative tendon ultrasound shear wave velocity (SWV) was measured at proximal, mid, and distal tendon regions.

Statistics: Each limb was an observation (N=52). Effect of biomechanics with rPT (no/yes), symptoms (no/yes: VISA-P≤80), and hyperemia (HYP) (no/yes) was tested with multivariate models. Logistic regression fit biomechanical and imaging variables to classify VISA-P, rPT, and HYP observations.

RESULTS AND DISCUSSION

We identified 8 limbs that were symptomatic, 13 limbs with rPT, and 11 limbs with hyperemia. MANOVA tests (Table 1) saw increased joint flexion velocity and decreased maximum vertical limb associated with rPT.

Per outcome a sample of 278,256 five-variable models were fit from a 34-variable pool. From these, the best models in terms of 95th percentile AICc and accuracy (Figure 1) had these most frequent variables: 1) Max Hip FlexVel, 2) Max VGRF, 3) Hip Flex IC, 4) Time to max VGRF, 5) Knee Flex IC, and 6) SWV Proximal. Accuracy ranged above 90%.

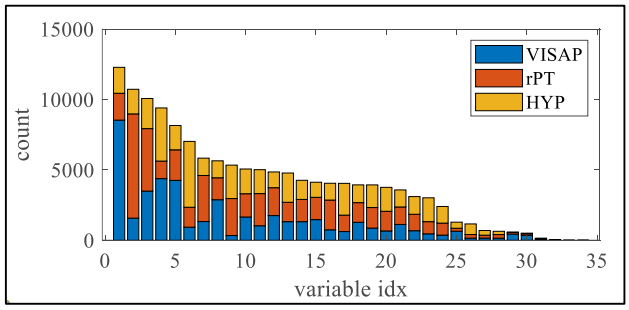

Figure 1. Stacked cumulative frequencies of best model variables.

CONCLUSIONS

This study links clinical, imaging, and functional metrics that may benefit a multi-modal screening tool for athletic populations at risk for PT.

Future work should focus on pre- to post-season changes and development of better statistical power.

ACKNOWLEDGEMENTS

Supported by an NBA/GE Healthcare grant.

REFERENCES

[1] Tayfur A et al. *Sports Medicine* **52**: 123-137, 2022.

Table 1: Results from significant 1-way MANOVA tests. IC = initial contact; FlexVel = flexion angular velocity; VGRF = vertical ground reaction force; %BW = percentage body weight.

Ind. variable	Dep. variables	joint	yes	no	MANOVA p-value	Post-hoc p-value
rPT	Max VGRF (%BW)	--	159 ± 24	188 ± 33	0.048	0.005
	FlexVel IC (deg/s)	Hip	133 ± 72	72 ± 80	0.028	0.024
		Knee	169 ± 90	162 ± 116		--
		Ankle	10 ± 105	14 ± 105		--
VISA-P	FlexVel IC (deg/s)	Hip	161 ± 61	74 ± 82	0.042	0.007
		Knee	240 ± 67	150 ± 110		0.031
		Ankle	88 ± 141	-1 ± 91		0.025
	FlexVel VGRF (deg/s)	Hip	478 ± 66	367 ± 114	0.022	0.011
		Knee	555 ± 60	491 ± 145		--
		Ankle	259 ± 81	287 ± 130		--

BIOMECHANICAL KNOW-HOW OF LEARNING BICYCLE KICK AND JUMPING SIDE VOLLEY IN SOCCER

Gongbing Shan
Department of Kinesiology, University Lethbridge, Lethbridge, Canada.
Email: g.shan@uleth.ca

INTRODUCTION

In soccer, both bicycle kick and jumping side volley have provided viewers breathtaking moments that seem virtuosic in scope. Since the establishment of FIFA Puskás Award (the aesthetically significant goal of the year) in 2009, goals achieved by the two soccer socoring techniques (SSTs) have been nominated 31 times by FIFA nomination committee, 21.7% of all nominees [1]. Yet, the two kicks are biomechanically under-studied and, even worse, there is a dearth of biomechanical approach on their learning and training. Relying on the talent of athletes to improvise on the kicks can hardly be considered as a viable learning method [2]. The current study aims to provide biomechanical know-how of learning the two acrobatic SSTs.

METHODS

Using 3D motion capture technology and full-body biomechanical modelling, key features of the two SSTs were quantified, and hereafter, their motor sequencing were identified. The identified motor control uniqueness was applied to design a training program for learning the two SSTs at college-level players.

RESULTS AND DISCUSSION

Bicycle kick is a back-facing-goal, overhead kick performed in the sagittal plane [3]; whereas jumping side volley is a side-facing-goal, side kick performed in the transversal plane [4]. Both SSTs can be divided into three phases: jumping, airborne and landing (Figure 1).

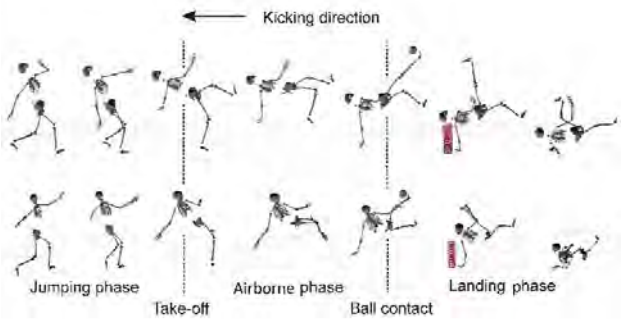

Figure 1 3D quantification of bicycle kick (top) and jumping side volley (bottom).

The 3D kinematics revealed the following features. **For bicycle kick**: 1) Just before take-off, non-kick side leg moved up toward the athlete's chest, as the trunk reached a horizontal position. 2) In airborne phase, two control characteristics – bicycle-like legs' control and whip-like kick-leg control – were identified. 3) During landing, damping the impact force during falling was achieved through an arm-hip landing, i.e. sharing the load using a sequence of partial landings (Figure 1, top). **For side volley**: 1) Before jumping, athletes' trunk and hips rotated away from the goal, and during the take-off, the non-kick leg was raised while the trunk and hip reversed rotational directions and came to twist toward the goal; at the same time, the trunk approached a more horizontal position. 2) While airborne, the kicking foot followed a smooth rainbow-like trajectory accompanied by continuous body rolling towards the goal. 3) Dispersion of landing impact is accomplished through an arm-hip landing strategy (Figure 1, bottom).

Based on the biomechanical quantification, we designed a reversed training method (i.e. landing training first) and applied successfully in college-level training. Eleven students mastered the two SSTs (Figure 2).

Figure 2 Repetitive kick training (top: bicycle kick, bottom: jumping side volley) with biomechanically proper landing technique.

CONCLUSIONS

Due to the fact that repetitive practice will not happen without a proper landing technique to prevent injuries, the learning of the two SSTs should begin with the last phase – landing. Mastering a safe landing technique is the foundation that can ensure repetitive practice to improve kick quality.

ACKNOWLEDGEMENTS

The study was supported by the National Sciences and Engineering Research Council of Canada (NSERC).

REFERENCES

[1] Shan G. *Appl Sci* **12(21)**: 10886, 2022.
[2] Shan G et al. *Bioengineering* **9(8)**: 333, 2022.
[3] Shan G et al. *Sci Bull* **60(8)**: 819–821, 2015.
[4] Zhang X et al. *Appl Sci* **10(14)**: 4785, 202, 2020.

A NINE-WEEK ACL INJURY PREVENTION PROGRAM FOR FEMALE HANDBALL PLAYERS: EFFECT ON KNEE JOINT LOADING, CUTTING TECHNIQUE AND PERFORMANCE

Patrick Mai[1,2], Kevin Bill[2], Lasse Mausehund[3], Sigurd Solbakken[3], Steffen Willwacher[1], Uwe G. Kersting[2] Ola Eriksrud[4] and Tron Krosshaug[3]
[1] Institute for Advanced Biomechanics and Motion Studies, Offenburg University, Offenburg, Germany
[2] Institute of Biomechanics and Orthopaedics, German Sport University Cologne, Cologne, Germany
[3] Department of Sports Medicine, Norwegian School of Sport Sciences, Oslo, Norway
[4] Department of Physical Performance, Norwegian School of Sport Sciences, Oslo, Norway
Email: patrick.mai@hs-offenburg.de

INTRODUCTION

Compared to males, females have a higher risk for suffering a non-contact anterior cruciate ligament (ACL) injury [1]. ACL injury prevention programs appear to lack game specificity, and relationships between knee loading, technique, and performance have rarely been reported. This study aimed to determine if a handball-specific ACL injury prevention program can lower knee joint loading while enhancing performance and optimizing cutting techniques in females.

METHODS

Full-body kinematics (Qualisys, 200 Hz), ground reaction forces (AMTI, 1000 Hz), and sprint performance (1080 Motion, 333 Hz) of 51 female handball players performing a 180° change of direction task (CoD) were captured at baseline (T0). Athletes approached from 5 m, performed a 180° turn, and returned with game-like intensity. Following baseline testing, 23 athletes (INT) (17 ± 1 years, 1.71 ± 0.06 m, 69.9 ± 10.6 kg) returned for post-testing (T1). INT were assigned to a nine-week intervention program, including hip and calf muscle strength and cutting technique training, focusing on forefoot landing and avoiding knee valgus. The remaining 28 athletes (CON) continued their regular training. After nine weeks, 20 INT (17 ± 1 years, 1.76 ± 0.06 m, 70.8 ± 8.3 kg) and 20 CON athletes returned. The external peak knee abduction moment (KAM) within the first 60 ms after touchdown was used as an injury risk metric. Changes in cutting technique were determined using the center of mass velocity and knee valgus angle at touchdown and ground contact time. CoD performance of the athletes was assessed using the average approach (start to 180° turn) and exit (180° turn to start) speed and the total time. Mixed-rANOVAs (group x time) were used (α = .05) to assess differences between the time points, groups, and their interaction.

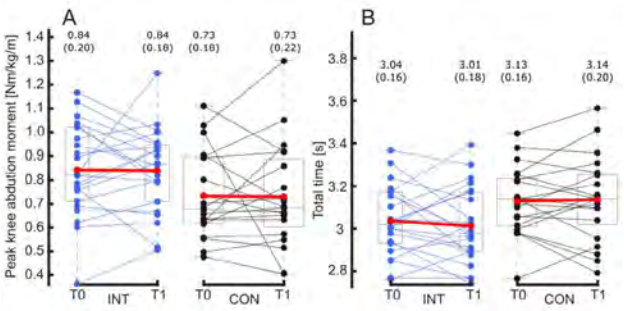

Figure 1: Peak external knee abduction moment (A) and total time (B) for the control and intervention group at T0 and T1.

RESULTS AND DISCUSSION

No KAM changes were observed in either group over time. In the INT group, half of the athletes reduced KAM while the other half increased KAM, resulting in no changes on average. INT had significantly greater KAM (T0 and T1) than CON (Fig.1A, Tab.1). Changes in cutting technique were similar in both groups. From T0 to T1, the average approach speed significantly increased in INT (2%) and decreased (-2%) in CON ($p_{interaction}$ = .03). Both groups showed lower exit speeds at T1 than at T0 (p_{time} < .001). No improvements in the total time (Fig.1B) were observed for either group (p_{time} and $p_{interaction}$ > .05) .

CONCLUSIONS

The handball-specific ACL prevention program tends to improve technique and performance without affecting KAM during CoD. A longer intervention period might be required to induce reductions in KAM and further improve technique and performance.

REFERENCES

[1] Chia L. et al. *Sports Med* **52:**2447–2467, 2022.

Table 1: Mean ± SD for the selected parameters at baseline (T0) and after nine weeks (T1) for the control (CON) and intervention group (INT). Non-significant p-values (p>0.05) on group, time, or interaction effects are not reported.

	Ex. knee abduction moment [Nm/kg/m]		CoM velocity at touchdown [m/s]		Knee valgus at touchdown [°]		Ground contact time [ms]		Average approach speed [m/s]		Average exit speed [m/s]	
	T0	T1	T0	T1	T0	T1	T0	T1	T0	T1	T0	T1
INT	0.84±0.20	0.84±0.18	2.23±0.28	2.30±0.25	-7±5	-4±3	460±40	420±50	2.84±0.15	2.90±0.20	3.05±0.09	3.10±0.09
CON	0.73±0.18	0.73±0.22	2.36±0.30	2.25±0.29	-4±3	-3±-3	490±70	480±90	2.71±0.15	2.66±0.17	2.90±0.17	2.97±0.16
p -value	p_{Group} = .04				p_{Time} = .002		p_{Time} = .02		$p_{Interaction}$ = .03		p_{Group} < .001; p_{Time} < .001	

REFERENCE VALUES OF JUMP TESTS STRATIFIED BY SEX USING AN INSOLE-EMBEDDED IMU

Meihui Li[1], Minju Kim[1], Lauren Fridman[2], Nicholas Tran[2], Christopher Napier[1]
[1]SFU Run Lab, Department of Biomedical Physiology and Kinesiology, Simon Fraser University, Burnaby, Canada
[2]Plantiga Technologies Inc., Vancouver, British Columbia, Canada
Email: meihui_li@sfu.ca

INTRODUCTION

Jumping is one of the most fundamental lower body movements among sports [1]. Jump tests can also be used to assess lower body performance for athletes and patients. The identification of reference values for jump tests may help clinicians to evaluate the risk of lower extremity injuries or readiness to return to sport after injury. For example, single-leg jump tests can be prognostic for future knee-related outcomes in individuals after ACL injury [2]. To date, no reference values for spatiotemporal variables in healthy people are available in the scientific literature. Our study aimed to present sex-stratified reference values for spatiotemporal variables in healthy adults via insole-embedded inertial measurement units (IMUs).

METHODS

One-hundred and eighty-seven healthy participants wore insole-embedded IMUs and performed the following jump tests: consecutive countermovement jump (CCMJ), cyclic jump (CJ), single-leg jump for distance (SLJD), and single-leg jump for height (SLJH). Outcomes included: relative strength index (RSI), average jump height (AJH), maximum jump height (MJH), and maximum jump distance (MJD). Statistical differences between sexes were tested using an independent samples t-test.

RESULTS AND DISCUSSION

Eighty-nine females (age: 42.3±11.6 y; height: 1.68±0.06 m; mass: 62.4±9.2 kg) and ninety-eight males (age: 41.4±12.5 y; height: 1.81±0.06 m; mass: 76.7±8.9 kg) completed all jump tests and were included in the analysis. The reference values for all participants are presented in Table 1, stratified by sex. There were significant differences between males and females in all jump outcomes (p<0.05). Specifically, the maximum and average jump height and distance of males were significantly greater than females. There was no statistical difference in asymmetry values of SLJD and SLJH between sexes (p>0.05).

CONCLUSIONS

Our study presents reference values for healthy males and females for the most common jump tests. These values can be used to assist clinicians to screen for lower body sports injuries and assess athletes for return to sport following injury. We found that Males demonstrated greater average and maximum jump heights and distances compared to females. Our results agree with previous studies, which found that absolute force and power measurements were higher in males compared with females [3]. Interestingly, the previous study stated that females might be more prone to producing forces asymmetrically than males in countermovement-jump and squat-jump tasks [4]. However, our outcomes show that males and females did not differ in asymmetry values of single-leg jumps for height and distance. This inconsistency might be because previous findings were based on double-legged hops, but our asymmetric conclusions were based on single-legged hops.

Table 1. Outcomes for all jump tests stratified by sex (n=187).

Jump Test	Outcome	Limb	Female	Male	p
SLJD	MJD	L	1.07±0.22	1.33±0.25	<0.01*
		R	1.11±0.22	1.34±0.26	<0.01*
		A(%)	7.03±5.62	5.8±4.56	0.10
SLJH	MJH	L	9.44±3.13	12.85±3.78	<0.01*
		R	9.53±2.81	13.35±4.28	<0.01*
		A(%)	10.68±9.71	11.31±9.79	0.66
CCMJ	MJH		25.5±22.46	30.55±11.88	= 0.05*
	AJH		19.91±4.77	26.47±6.48	<0.01*
	RSI		0.74±0.21	0.9±0.34	<0.01*
CJ	MJH		17.94±5.81	26.48±24.64	<0.01*
	AJH		15.74±5.29	19.66±5.19	<0.01*
	RSI		1.57±0.44	1.86±0.42	<0.01*

L=left; R=right; A=asymmetry; SLJD=Single leg jump for distance; SLJH= Single leg jump for height; CCMJ=Consecutive countermovement jump; CJ= Cyclic jump; MJD=maximum jump distance; MJH=maximum jump height; AJH= Average jump height; RSI= Relative strength index; *=$p \leq 0.05$

REFERENCES

[1] R Ramirez-Campillo et al. *J Sport and Health Science.* 2022;**11**:656-670.
[2] West TJ et al. *Br J Sports Med.* Epub ahead of print: 20 Jan 2023.
[3] Rice PE et al. *European J of Sport Science*. 2017; **3**: 286-293.
[4] Bailey CA et al. *Int J Sports Physiol Perform*. 2015; **10**:504-50.

ASSOCIATIONS OF ROTATIONAL RANGE AND STRENGTH OF SHOULDER WITH REGARD TO ELBOW VALGUS STRESS DURING PITCHING IN YOUTH BASEBALL PLAYERS

Yu-Chun Lin[1], Yang-Hua Lin[1], Chih-Hao Chiu [2], Hsiao-Yun Chang[3], Cheng-Yu Chen[4], Po-Tsun Chen*[1,2]
[1] School of Physical Therapy and Graduate Institute of Rehabilitation Sciences, College of Medicine, Chang Gung University, Taoyuan, Taiwan
[2] Department of Orthopedic Surgery, Linkou Chang Gung Memorial Hospital, Taoyuan, Taiwan
[3]Department of Athletic Training and Health, National Taiwan Sport University, Taoyuan, Taiwan
[4]Graduate Institute of Athletics and Coaching Science, National Taiwan Sport University, Taoyuan, Taiwan
Email: ptchen@mail.cgu.edu.tw

INTRODUCTION

Medial elbow pain occurs frequently in youth baseball players[1]. The injured elbow demonstrates instability when bearing high stress during pitching [2], which may be related to the unbalanced strength of rotator cuff and periscapular muscles and the restriction of range of motion (ROM) in shoulder [3]. However, there was no study to show the changes of medial elbow after improving restricted ROM and imbalanced strength of the shoulder in youth baseball players. This study aimed to analyze the effects of twelve-week conditioning exercise for shoulder on the stress of medial elbow during pitching in youth baseball players.

METHODS

Sixteen male youth baseball players (mean age 10.4±0.7 years) were recruited. All the participants received the evaluations before and after the conditioning exercise, including ROM and strength of shoulder external and internal rotation (ER and IR), the strength of periscapular muscles, ball speed, and elbow valgus torque (Nm), arm speed (rpm), and arm slot (°) during pitching. The twelve-week conditioning exercise included scapular stabilization training, rotator cuff resistance training, and stretching exercises for shoulder. Pair-t test was used to compare the outcomes before and after twelve-exercise. The level of statistical significance was set at $p < 0.05$.

RESULTS AND DISCUSSION

After exercise, both ROM and strength of ER and IR were increased significantly. The increases in strength of middle deltoid and lower trapezius were noticed. The ball speed after exercise was faster significantly than before exercise. A significant increase in arm speed and a decrease in arm slot were also found during pitching, while elbow valgus torque was not altered after exercise. Although the less am slot may lead to the risk of an elbow injury, the normal arm slot was reported between 43-49°[4]. The increases in shoulder strength and ROM after twelve-week exercise may allow players to pitch with bearing higher stress.

CONCLUSIONS

Conditioning exercise for shoulder can improve the imbalance in ROM and strength of shoulder in youth baseball players. The elbow valgus stress is not only affected by shoulder movement, but the correctness of movement chain during pitching also plays a critical role. For reducing valgus, the components of pitching technique may also be integrated into training exercise to correct the pitching mechanics.

REFERENCES

[1] Matsuura, T., et al. Phys Sportsmed, 2016. **44**(2): p. 97-100.
[2] Hattori, H., et al. J Shoulder Elbow Surg, 2022. **31**(12): p. 2602-2610
[3] Mine, K., et al. Orthop J Sports Med, 2021. **9**(12): p. 23259671211064645.
[4] Garner, S., et al. Sports Biomech, 2021. **20**(1): p. 86-95.

Table 1: The pre and post value for the conditioning exercise

	Pre-evaluation	Post-evaluation	*p-value*
Shoulder ER ROM, deg	91.8±13.2	105.9 ±9.6	p =0.01**
Shoulder IR ROM, deg	38.4±11.6	65.6 ±12.8	p =0.01**
Shoulder ER strength, kg	6.4±2.2	7.6±2.8	p =0.01**
Shoulder IR strength, kg	8.5±2.0	9.5±2.3	p =0.01**
Elbow valgus torque, Nm	27.2±9.7	32.8±5.6	p =0.06
Arm speed, rpm	870.5±90.6	917.9±115.3	p =0.05*
Arm slot, deg	61.1±12.3	51.6±12.2	p =0.05*

Data are expressed as mean ±standard deviation
*: Statistically significant: $p < 0.05$ ； **: Statistically significant: $p < 0.01$

IMPACT OF COLD EXPOSURE AND WARM-UP ON MUSCLE TEMPERATURE AND COUNTERMOVEMENT JUMP VARIABLES

Itaru Chiba[1], Mina Samukawa[2], Tomoya Ishida[2], Satoshi Kasahara[2], Harukazu Tohyama[2]
[1] Sports Training Center, Nippon Sport Science University, Tokyo, Japan
[2] Faculty of Health Sciences, Hokkaido University, Hokkaido, Japan
Email: i-chiba@nittai.ac.jp

INTRODUCTION

In cold environments, heat dissipation from the body surface decreases the muscle temperature (Tm), which inhibits muscle contraction and reduces jump performance [1]. Warm-up (WUP) is important to avoid Tm reduction and improve performance. However, there have been no reports on the effects of cold exposure and subsequent WUP on jump performance using ground reaction force (GRF). Therefore, this study aimed to examine the effects of cold exposure and subsequent WUP on Tm and jump performance.

METHODS

Thirteen healthy male college students (age: 21.4 ± 1.2 years) participated in this randomised crossover design study. This experiment was conducted in a laboratory and the temperature was set at 10°C or 24°C. The participants sat and rested for 30 min. The Tm of the vastus lateralis and CMJ were measured on a portable force plate (Ex-jumper, DKH Inc., Tokyo, Japan) before and after the WUP. The WUP intensity was set at 60% of maximum oxygen uptake. The GRF data before and after the WUP with the maximum jump height were used for further analysis. CMJ phases were attributed to the following three phases: unloading, eccentric, and concentric phases using GRF data and centre of mass (COM) velocity obtained by the time integral of acceleration [2]. Jump height was calculated using the following formula:

$$(\text{Jump height}) = (\text{Takeoff velocity})^2 / (2 \times 9.81)$$

The peak, braking, and unloading GRF were defined as follows: maximum GRF during CMJ, GRF at the end of the eccentric phase, and minimum GRF during CMJ, respectively. Peak power was defined as the maximum power during CMJ (GRF×COM velocity). The net eccentric and concentric impulses were calculated using the time integral of the GRF above the system weight during the eccentric and concentric phases. The duration of each jump phase was calculated as the time spent in the jump phase. A two-way repeated ANOVA or Friedman test with Bonferroni correction as a post hoc test was conducted. A p-value < 0.05 was considered statistically significant.

RESULTS AND DISCUSSION

Muscle temperature significantly increased after the WUP in both conditions ($p < 0.05$), although there was no significant difference between the conditions. Jump height, peak GRF, peak power, and net concentric impulse increased after WUP in 24°C conditions, and jump height, net eccentric, and concentric impulse increased after WUP in 10°C condition ($p < 0.05$). Peak GRF after WUP in 24°C was significantly higher than that after WUP in 10°C ($p < 0.05$). The unloading and braking GRF did not change after WUP or between conditions. However, the phase times did not change significantly. Cold exposure and WUP may affect Tm, jump height, and GRF-related variables in the concentric phase (i.e. concentric muscle contraction). Hence, cold exposure and WUP may not affect certain GRF-related metrics during the unloading and eccentric phases of eccentric muscle contraction or the jump phase time.

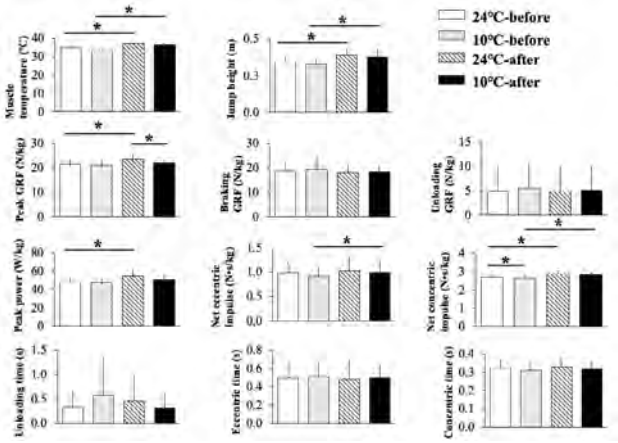

Figure 1. Comparisons between ambient temperature conditions and before and after WUP; * significance less than 0.05

CONCLUSIONS

Cold exposure and WUP may affect force output during jumps but not kinematics. Cold exposure may decrease the effects of WUP on jump performance. Further research is necessary to clarify the relationship between ambient temperature and athletic performance enhancement after the WUP.

REFERENCES

[1] Racinais S et al. *Scand J Med Sci Sports* **20**: 1-18, 2010
[2] Harry J et al. *Med Sci Sports Exerc* **52**: 993-1000, 2020

TOWARDS A CONTACT MODEL OF THE RUGBY UNION SCRUM

Zak Sheehy[1,2], James Cowburn[1,2], Andrea Braschi[1,2,3], Josh Carter[1], Grant Trewartha[4], Ezio Preatoni[1, 2], and Dario Cazzola[1,2,3]

[1] Department for Health, University of Bath, Bath, UK.

[2] Centre for Health and Injury and Illness Prevention in Sport (CHi2PS), University of Bath, Bath, UK

[3] Centre for the Analysis of Motion, Entertainment Research & Applications University of Bath, Bath, UK

[4]NURVV Ltd, London, UK

Email: zjms20@bath.ac.uk

INTRODUCTION

The scrum is a rugby union set piece used to restart play after a rule infringement or stoppage. Whilst scrum injury incidence appears to be less than that of other rugby activities, the mean severity of injury appears to be relatively high [1], with the front-row players being most susceptible [2]. Experimental investigation with risk of injury to participants is unethical but insilico methods allow for simulation of injurious scenarios without fear of harm. Investigation of the forces acting on players within the scrum may allow researchers to better understand the mechanisms of injury. However, directly measuring forces in-field is currently impossible. Thus, the aim of this study was to create a scrum-based contact model of the shoulder to investigate forces experienced by the front-row.

METHODS

Coordinate data [3] of live scrums was used to inform the kinematics of an OpenSim 5-sphere contact model (Figure 1) representing the shoulders of front-row players. Contact forces were described via Hunt-Crossley formulations. Data from five different shoulder-to-shoulder impacts were used to optimise for stiffness, dissipation, and 3D sphere positions, minimising the error in simulated peak forces. Forces were compared to live force data [3] from Tekscan pressure sensors (model 3005) placed on the front row players' shoulders. Median parameter values across trials became the final model. For preliminary evaluation of the model, forward dynamic simulations were constructed with only the pelvis x-translation. Initial states (positions and velocities) and controls (accelerations) were derived from the 5 original trials (training set), and 3 new trials (test set). The mean absolute peak error between the live and simulated force across trials was calculated.

RESULTS AND DISCUSSION

All data sets produced mean absolute peak force errors comparable to those of Tekscan pressure sensors during impact events [4] (Table 1). However, an error of 254N is considerable and the data exhibited a large mean time to peak error (12% of simulation duration). Although the sensors' sampling frequency (500Hz) may be limiting, a major limitation of this study is potential errors in transcribing kinematics to the model. Exact points of reference for the coordinates were unknown so these were approximated to anatomical landmarks, potentially affecting penetrations of the contact spheres, and generating aberrant forces.

Table 1. Comparison of mean Absolute Peak Error and Absolute Time to Peak Error between Data Sets and TekScan Sensors [4]

	Peak Error (N)	Time to Peak Error (s)
Training Data (n = 5)	207 ± 90.8	0.170 ± 0.307
Test Data (n = 3)	331 ± 285	0.0991 ± 0.0384
All Data (n = 8)	254 ± 179	0.143 ± 0.236
Tekscan Sensor	320 ± 228	N/A

Moreover, pressure data provides the sum of absolute forces applied to the sensor in the normal direction (direction of travel). Thus, only simulated forces acting along this axis can be used. Furthermore, forces applied to the sensor are assumed to be evenly distributed in each direction of application, so the current model can only be used when acceleration is zero (initial impact). The model also lacks ground reaction forces, limiting predictions of the scrum's 'sustained push' phase. Next, more data and relatable kinematics with net forces may improve the model.

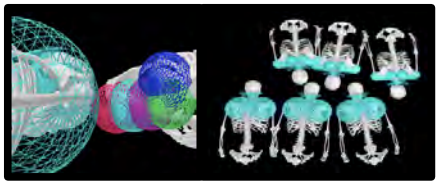

Figure 1: The Contact Model and Full Model

CONCLUSIONS

This study is a first step, supporting the possibility of replicating peak force to the standard of wearable technology. However, it is the hope of the authors to strive for a model encapsulating all force characteristics of the scrum with implications for acute and chronic injuries.

REFERENCES

[1] West S et al. *Br J Sports Med* **55**: 676-682, 2021.
[2] Trewartha G et al. *Br J Sports Med* **49**:425-433, 2015.
[3] Cazzola D et al. *Br J Sports Med* **49**: 541-546, 2015.
[4] Cazzola D et al. *J Sports Eng and Technol* **228**: 147-151, 2014.

EFFECT OF DIFFERENT SPEED IN ECCENTRIC PHASE IN SQUAT PROTOCOLS ON HIP FLEXORS AND EXTENSORS ACTIVATION

Anna Pisz[1], Dominik Kolinger[1], Michal Wilk[1,2], Michal Krzysztofik[1,2] and Petr Stastny[1]
[1] Faculty of Physical Education and Sport, Charles University, Prague, Czech Republic.
[2] Academy of Physical Education in Katowice, Poland.
Email: piszan@gmail.com

INTRODUCTION

Many studies have used the squat as a trigger to induce post activation potentiation and evaluated its effect on strength and power performance due to its wide application by practitioners and researches [1]. However, different movement speed during squat might affect the results [4]. Although there are studies supporting the use of eccentric loading as a conditioning activity [2], there is still missing evidence supporting its effect on the hip flexors/extensors with manipulation of time under tension.

METHODS

16 professional male handball players (age 16.5 ± 1.2 years; body mass 79.8 ± 9.9 kg; height 184 ± 6.5 cm; personal body fat 10.3 ± 5.2 %; 3RM 74.1 ± 19.1 kg) participated in the study. During familiarization session, each subject underwent a 3RM front squat assessment and was introduced to the experimental protocols. After the first visit, subjects returned to the laboratory on 2 occasions separated from each other by 2 to 5 days. In one session, 90% 1RM front squats at a maximum speed with plyometric effect were used as a conditioning activity, where subjects performed the exercise individually. In the other session, an eccentric load of 120% 1RM in the front squat was used as conditioning activity, where the downward movement lasted 2 seconds, and assistants helped lift the weight to the starting position. In both protocols, the total number of repetitions of the conditioning activity was 3. The order of the protocols was randomly selected. Each session began with a standardized warm up protocol, after which subjects performed 3 repetitions of hip flexion/extension with 180°/s speed on Biodex Isokinetic Dynamometer laying in supine position, that served as baseline (Pre). Two minutes after the baseline measurement, the subjects started conditioning exercise according to the chosen protocol. Post measurements, the same as Pre, were recorded respectively at 5th, 7th and 9th minute after the end of the conditioning activity.

RESULTS AND DISCUSSION

Significant improvement in peak torque for concentric hip flexion (Flex_Con) ($p = 0.02$), eccentric hip extension (Ext_Ecc) ($p = 0.04$) and for concentric hip extension (Ext_Con) ($p < 0.01$) were detected compared to baseline in both groups, only in eccentric hip flexion (Flex_Con) there was not significant improvement observed after conditioning activity in both protocols ($p = 0.43$) (Table 1). No significant differences were detected between the protocols.

CONCLUSIONS

Based on the results it can be concluded that both eccentric loading front squat and front squat perfomed at a maximum pace shows similar improvements in concentric hip flexion/ extension and eccentric hip extension. Therefore, practitioners can use both protocols interchangeably as a tool to induce post activation potentiation with the purpose to enhance hip strength.

ACKNOWLEDGEMENTS

This research was funded by Programme for Development of Fields of Study at Charles University under Grant PRIMUS 22/HUM/019, and by Cooperatio Sport Sciences – Biomedical & Rehabilitation Medicine.

REFERENCES

[1] Bauer P et al. *J Strength Cond Res* **33**: 995-1000, 2019.
[2] Cuenca-Fernández F et al. *J Sports Sci* **37**: 443-51, 2019.
[4] Hughes J et al. *J Strength Cond Res* **30**: 3450-5, 2016.

Table 1: Changes in peak torque (Nm) between baseline (Pre) and maximum result (POST) after conditioning activity in both protocols.

* Significant change, XXX- front squats at a maximum speed with plyometric effect, R200- front squad with eccentric loading

	Flex_Con		Flex_Ecc		Ext_Con		Ext_Ecc	
	XXX	R200	XXX	R200	XXX	R200	XXX	R200
Pre (Nm)	160.8 ± 10.1	157.5 ± 10.4	196.3 ± 10.9	202 ± 11.3	227.3 ± 14	213 ± 14.4	349.5 ± 24.9	329.3 ± 25.8
Post (Nm)	164.2 ± 8.5*	177.1 ± 8.8*	203.1 ± 10.9	208.2 ± 11.3	254.5 ± 12.1*	244 ± 12.6*	374.9 ± 24.4*	383.6 ± 25.3*

SAGITTAL PLANE LOWER EXTREMITY BIOMECHANICAL RESPONSE TO SOCCER CLEAT STUD LENGTH DURING A CUTTING TASK

Emily Karolidis[1], Michael E. Hahn[1]
[1] Department of Human Physiology, University of Oregon, Eugene, USA.
Email: ekarolid@uoregon.edu

INTRODUCTION

In the sport of soccer, anterior cruciate ligament (ACL) injury incidence is 3x higher in female athletes than male [1]. Unique to females, dynamic control patterns of the knee joint demonstrate quadriceps dominance, where developmental imbalances tend towards greater knee extensor strength, recruitment, and coordination [2]. This unmatched strength ratio in the knee joint stabilizers tends towards altered sagittal plane mechanics, subjecting the female knee to greater ACL loading and overall injury susceptibility. Despite mechanical differences between sex, soccer footwear is designed for males. High traction footwear may exceed ligament loading capacity, exacerbating female risk of ACL injury [3]. Due to body mass differences between sex, traction may be unsuitably high due to excess stud length. The purpose of this study is to determine the effect of soccer cleat stud length on female athlete knee mechanics and muscle activity. It is hypothesized that there is an ideal zone of stud length (50-75% original length) that produces more favourable knee mechanics.

METHODS

Four pairs of Nike Mercurial soccer cleats (women's 7.5) were tested, three pairs of which were abraded to a stud length of 25%, 50% and 75% of the original (control). Contact surface area matched the control condition. Seven competitive female soccer athletes, age 21 ± 1.3, weight: 58.4 ± 4.3 kg, height 166.8 ± 3.2 cm performed cutting tasks in an indoor turfed facility in accordance with IRB approval. Consenting athletes performed 6 cuts (80% maximum speed to 120° cut, 3 trials each direction) in each condition. Cut direction and footwear condition order were randomized.

Trajectories of 18 retroreflective markers were collected with an 18-camera system (Vicon, 100 Hz), and ground reaction force data were collected using 4 force platforms (AMTI, 1500 Hz). Surface electromyography (sEMG) (Noraxon DTS, 1500 Hz) recorded biceps femoris (BF) and vastus lateralis (VL) activity on the right limb. The sEMG signals were bandpass filtered (3-500 Hz, 4th order Butterworth), full-wave rectified, linear enveloped (6 Hz) and normalized to maximum dynamic contraction magnitude (control shoe). Integrated EMG (iEMG) analysis was performed from initial foot contact until peak flexion, standardized to 0.5 s. The ratio between VL and BF iEMG was compared, representing knee stabilizing muscle involvement. Peak knee flexion and internal knee extensor moment at peak flexion were calculated using the Plug-in-Gait model. Repeated measure ANOVAs were used to detect differences in knee flexion, extensor moment, individual iEMGs and ratios across conditions (α=0.05).

RESULTS AND DISCUSSION

Table 1 presents descriptive statistics of knee mechanics and muscle activity, with green colour fill denoting preferred mechanical landing strategy [3]. No statistically significant differences in knee flexion, extensor moment, iEMG muscle summation of VL or BF nor iEMG ratio were found across conditions. However, preferred mechanics were most often found in the 50 and 75% stud length conditions, encouraging greater knee flexion, reduced extensor moment, reduced quadriceps and increased hamstring contributions, and a preferential ratio of knee stabilizer muscle activity in favour of the hamstring muscle.

CONCLUSIONS

While this research does not provide definitive conclusions on the relationship between stud length and female knee mechanics, it does offer suggestive evidence that a reduction of stud length holds potential in reducing knee loading during cutting tasks.

ACKNOWLEDGEMENTS

This work was supported by the Wu Tsai Human Performance Alliance and the Joe and Clara Tsai Foundation.

REFERENCES

[1] Waldén et al. *Knee Surg Sport Tr A*, **19**: 3-10, 2010.
[2] Myer et al. *J Athl Training*, **39**: 352-364, 2004.
[3] Butler et al. *Scan J Med Sci Sport*, **24:** 129-135, 2012.

Table 1. Knee mechanics, integrated muscle activity, and muscle activity ratios across cleated conditions

	Peak Knee Flexion (°)	*Peak Internal Extensor Moment (Nm/kg)*	*Vastus Lateralis iEMG Summation*	*Biceps Femoris iEMG Summation*	*iEMG ratio (VL:BF)*
25%	50.34 ± 2.41	4.44 ± 1.07	26.70 ± 7.81	29.40 ± 13.55	1 : 1.09
50%	48.56 ± 4.82	4.34 ± 0.98	22.11 ± 6.05	32.07 ± 10.81	1 : 1.55
75%	51.40 ± 3.65	4.25 ± 0.87	28.04 ± 11.33	37.29 ± 25.34	1 : 1.41
100%	48.93 ± 4.60	4.35 ± 1.05	25.00 ± 5.57	31.05 ± 9.13	1 : 1.36
p-value	*0.093*	*0.878*	0.648	0.992	0.595

Biomechanical analysis of the take-off phase in Japanese male pole vaulters

Tomoki Yamamoto[1], Tomoya Hirano[1], Fumiaki Kobayashi[2] and Kazuo Funato[1]
[1] Graduate School of Sport System, Kokushikan University, Tokyo, Japan.
[2] Faculty of Sport Science, Nippon Sport Science University, Kanagawa, Japan.
Email:nittaidai16@gmail.com

INTRODUCTION

The take-off phases of the pole vault are final touchdown (TD), pole plant (PP), and final take-off (TO) [1,2]. The purpose of the take-off phase of the pole vault is to reduce the decrease in horizontal velocity; the impact that occurs during PP has been found to decrease horizontal velocity. In addition, a study of elite athletes reported that they exhibited PP in the late ground phase [1].In the take off posture, it has been reported that the upper grip, during PP, can be raised higher overhead to increase the bend of the pole [3].From these results, PP appears in the late ground contact phase in pole vault take off, and it is important to reduce the deceleration of horizontal velocity and increase pole bending by increasing the grip height during PP.
However, there are no studies on the timing of PP and take-off posture in Japanese pole vaulters, nor are they explicitly stated in the guidelines[4]. This study aims to clarify kinematic and kinetic characteristics during the Take-off Phase, for Japanese pole vaulters including top-class Japanese athletes.

METHODS

This study was conducted with seven male pole vaulters (PB: 5.46 ± 0.23 m, height: 178 ± 4.7 cm, weight: 70 ± 5.2 kg). Athletes ranged from those who had competed in World Championships to those who had competed in regional competitions. Participants performed five trial runs, each with the same number of preparatory strides as in an actual competition. The trials were captured using a three-dimensional motion analysis system (VICON) to acquire three-dimensional kinematic data. Ground reaction forces (GRF) during the Take-off Phase were recorded using a force plate (KISTLER) situated underneath the runway and box. The three-dimensional kinematic data were filtered at 10-12 Hz using a fourth-order Butterworth low-pass filter after determining the optimal cut-off frequency. The analysis was performed from the crossing (TD) to the height of peak gravity (HP), as determined from the best trial run in the subjective evaluation. The GRFs were defined as anterior/posterior (Fy), mediolateral (Fx), and vertical (Fz).

RESULTS AND DISCUSSION

Ground contact time showed a similar trend among subjects.Vertical GRF at TO was high (13.2 N/BW) at the beginning of contact and then decreased toward TO. Athlete A considered the top performer, exhibited the greatest propulsive GRF (0.5 N/BW) compared to other athletes. The time of TD to PP varied among subjects, but athlete A arrived at PP when the peak propulsion GRF of the stance leg was achieved (as indicated in Table 1). Athlete A had a higher grip height and center of mass height at PP compared to other athletes and was nearly at the same height as at TO, but the horizontal distance between their toes and the upper grip at PP tended to be shorter than that of other athletes (Table 1). Athlete A demonstrated a propensity to have a higher horizontal velocity of the center of mass at TO, with PP appearing later in the contact phase, consistent with previous research. Nonetheless, some athletes, such as Athlete E, exhibited a high horizontal velocity of the center of gravity at the time of release from the ground even though their PP appeared in the first half of the ground contact, suggesting an exceptional ability to bring the PP forward in the initial half of contact phase to enhance the horizontal velocity of the center of mass at TO.

Table 1: Comparison of variables for each subject (n=7)

Variables	Unit	A	B	C	D	E	F	G
HP	(m)	5.38	5.26	5.19	5.11	4.99	4.94	4.78
Contact	(s)	0.11	0.12	0.11	0.13	0.12	0.11	0.12
TD-PP	(s)	0.088	0.088	0.036	0.076	0.12	0.084	0.068
Fy@PP	(N/BW)	0.5	-1.3	-1.3	0.2	0.0	0.1	-0.7
Fy@Propulsive peak	(N/BW)	0.5	0.2	0.3	0.4	0.3	0.3	0.3
Grip height@PP	(m)	2.20	2.11	2.02	2.09	2.16	2.08	2.17
COM height@PP	(m)	1.18	1.12	1.07	1.16	1.23	1.14	1.17
Grip height@TO	(m)	2.22	2.16	2.11	2.15	2.17	2.13	2.24
COM height@TO	(m)	1.22	1.29	1.21	1.24	1.24	1.21	1.30
Grip height(TO-PP)	(m)	0.02	0.05	0.09	0.07	0.01	0.05	0.08
COM height(TO-PP)	(m)	0.04	0.17	0.14	0.08	0.01	0.07	0.13
Horizontal velocity@TO	(m/s)	8.02	6.86	7.19	6.88	7.49	6.85	6.64

CONCLUSIONS

Most of the Japanese pole vaulters' times at PP appeared in the braking phase. Top athlete A's time at PP was near the maximum value of propulsive ground reaction force at take off. It was also considered that a shorter horizontal distance between the upper grip and toe during PP would result in a higher grip height.
From these results, it was considered that reaching the time of PP at the point of maximum propulsive ground reaction force would reduce the deceleration of the horizontal velocity of the center of gravity, and that the higher the grip height at PP, the greater the pole bend

REFERENCES

[1] Frère Julien et al. *Sports Biomech* **9**: 123-138, 2010.
[2] Launder A et al. *Track Tech* **112**: 3991-3995,1990.
[3]McGinnis P M. *U.S.A. Track and Field* 1-4, 2007.
[4]JAAF. *Taishukan* **112**: 65-71, 2007.

A new approach to evaluate the ACL risk of re-injury after reconstruction

Sahar Ostadrahimi[1], Siavash Kazemirad[1, *]
[1] School of Mechanical Engineering, Iran University of Science and Technology / Tehran, 16846-13114, Iran.
[*]Email: skazemirad@iust.ac.ir

INTRODUCTION

The second anterior cruciate ligament (ACL) injury is very propable in professional football players in both the ipsilateral and contralateral legs [1]. In order to enhance the injury prevention and rehabilitation programs, different test procedures have been proposed to determine whether or not an athlete is ready to return to sport after the ACLR. These test procedures, however, typically lack validation [2]. Therefore, there remains a need to develop effective screening test procedures to identify athletes at the risk of a secondary ACL injury. The aim of this study was to propose a return-to-sport procedure to prevent the athletes from a second ACL injury.

METHODS

Six professional football players which three of them experienced the ACL reconstruction (ACLR) performed the gait test. It is worth mentioning that all three ACLR subjects experienced the ACL injury in their dominant leg. All subjects performed the gait test in the Gait Analysis Laboratory. The muscle activation force, knee joint kinetic and kinematic parameters, and ACL loading were obtained by the Opensim musculoskeletal analysis. Then we present an index for assessing the risk of the second ACL injury in professional football players after the reconstruction by comparing the maximum ACL graft force during the gait cycle and the intact ACL ultimate tensile load were used. The suggested criterion for the classification of the ACL health status for the injured and non-injured leg was called the ACL injury risk index (IRI).

RESULTS AND DISCUSSION

The possibility of the ACL re-injury of the subjects tested was obtained through the proposed IRI. Figure1 illustrates the mean value and standard division of the IRI for both aACL and pACL bundles for the dominant and non-dominant legs in the ACLR and control groups. According to Figure 1, it was observed that the IRI value was significantly higher in the ACLR group compared to the control group for both aACL (p=0.015, 99%) and pACL (p=0.006, 99.8%) bundles. The increase in the ACL force of the ACLR group may be explained by the changes in the muscle activation force and the knee contact force after the ACLR. It was also noted that the mean IRI was higher for the non-dominant (contralateral) leg in both the control and ACLR groups, which may be due to higher knee contact forces that caused higher ACL loading. Using the proposed IRI and observations made on the ACLR and control football players, the observations of other researches that indicated an increase in the ACL injury risk for both the dominant and non-dominant legs after the ACLR was confirmed [3].

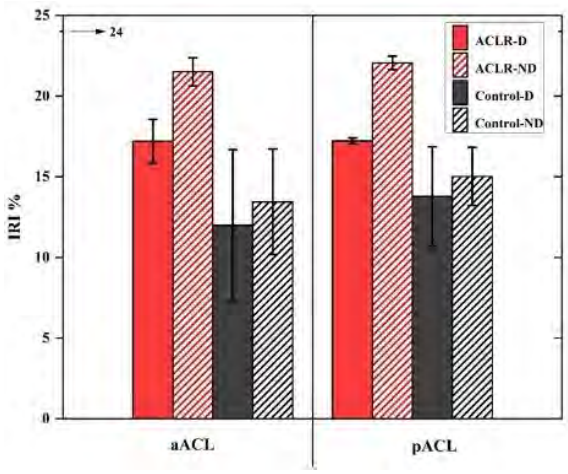

Figure 1 The mean value of IRI for the ACLR and control groups.

CONCLUSIONS

An injury risk index which was proposed in this study based on the maximum ACL force during the walking gait cycle to identify the football players under the re-injury risk. The results of this study in the comparison of the ACL bundles loading during the gait tests in football players control and ACLR groups indicated the lack of proper rehabilitation of the lower limbs rehabilitation in the recovery programs after the reconstruction. The new approach can be used in a new return-to-sport procedure which takes into account the ACL loading for both the injured and contralateral legs. It may help physicians to prescribe specific recovery programs for both legs of football players and reduce the risk of re-injury. The obtained results also suggested that the proper rehabilitation of quadriceps and gastrocnemius muscles is required in the recovery programs after the ACLR for reducing limb asymmetries.

REFERENCES

[1] Clark et al. *Physical Therapy in Sport*, **35**, 2018.
[2] Bates et al. *Clinical Biomechanics, **61***, 2019.
[3] Sharifi et al, *J of Biomechanics*, **117**: 110258, 2021.

Effect of resin on ball velocity of the step-shooting in female handball players

Aoi Fujimoto[1] , Tsuyoshi Iitake[1], and Hiroyuki Nunome[2]
Graduate School of Sports and Health Science, Fukuoka University, Fukuoka, Japan[1],
Faculty of Sports and Health Science, Fukuoka University, Fukuoka, Japan[2]

INTRODUCTION

In handball, the use of resin as an non-slip material has been permitted by the rules and has become the standard in national and international games (International Handball Federation [IHF], 2022; rule3:2). To date, only a few studies have focused on the effect of resin on handball shooting. Sasakura et al (1982) reported that the use of resin had an apparent effect to increase initial ball velocity in handball jump shooting of male players. However, it is still unknow whether the use of resin enhances the resultant shooting velocity in female players. Although female players allowed using a smaller size of the ball by the rules, their relatively weaker grip strength might disturb a firm gripping of the ball (Japan Sports Agency, Physical Fitness and Athletic Performance Survey, 2021). We hypothesed that the use of resin would provide famele players a better grip of the ball, thereby inducing a faster resultant shooting velocity. The purpose of the presenty study was, therefore, to assess the effectiveness of resin on the resultant shooting velocity of female handball players.

METHODS

Nine university-level female handball players (age:20 ± 1.3 years, height: 160.6 ± 3.6 cm, weight: 58.0 ± 4.8 kg) participated in the present study. The participants were asked to perform five step-shootings with and without resin, respectively.

The three-dimensional coordinates of the shooting arm (prefered side) were captured by a 12 camera optoelectronic motion capture system (Vicon, VANTAGE) at 500 Hz. Geometric center of the ball was estimated from five markers attached on ball surface using the least square technique. The ball velocity was obtained from the first derivative of the raw trajectory of the ball center in the anterior-posterior direction.

Statististical comparison was conducted for the initial ball velocity between the two conditions using a paired t-test ($p < 0.05$) and Cohen's d was used to calculate the effect size and evaluated as trivial (0–0.19), small (0.20–0.49), medium (0.50–0.79) and large (0.80 and greater) .

RESULTS AND DISCUSSION

The initial ball velocity of with resin (19.4 ± 1.0 m/s) was significantly higher than that of the condition without resin (18.5 ± 0.9 m/s) with a larger effect size ($p = 0.001$, $d = 0.84$). Figure 1 shows the average (± SD) changes in the ball velocities with and without resin. The difference in the ball velocities between the two conditions was not appreciable until 80% of the normalized time, and then, the difference became apparent in the latter half of the shooting motion (80–100% of the normalized time). It can be seen that the use of resin may increase resultant shooting velocity of female handball players. In addition, the relative linear velocity between ball and third metacarpal head at ball release with resin (4.4 ± 0.5 m/s vs. 4.8 ± 0.6 m/s) was significantly larger than that of without resin with a large effect size ($p = 0.02$, $d = 0.9$). This finding suggested that the use of resin made some differences regarding the contribution of wrist and/or finger movements to increase ball velocity.

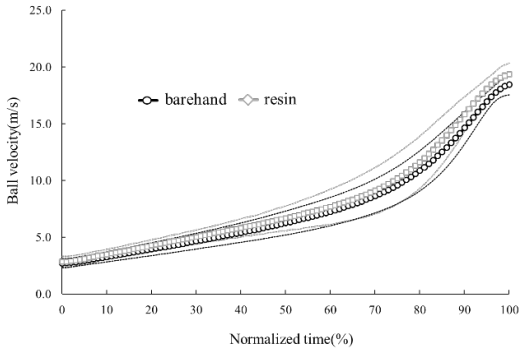

Figure 1: Average ball velocity changes with and without resin.

CONCLUSIONS

In handball, the use of resin as an non-slip material demonstrated a significant effect to increase resultant shooting velocity of female players. The use of resin most likely enchances the contribution of hand motion to ball velocity during the final phase of shooting.

REFERENCES

[1] International Handball Federation. (2022). IX. Rules of the Game: a) Indoor Handball. Edition 1 July 2022. 09A - Rules of the Game_Indoor Handball_E.pdf (ihf.info)
[2] Japan Sports Agency, Physical Fitness and Athletic Performance Survey, 2021 (in Japanese). https://www.mext.go.jp/sports/b_menu/toukei/chousa04/tairyoku/kekka/k_detail/1421920_00005.htm
[3] Sasakura et al (1982). The effect of resin in handball games, in the case of jump shoots (in Japanese). Japan Society of Physical Education Conference Issue 33-167.

Head Striking Patterns of Japanese Kendo between elite traditional Kendokas and elite tournament players

Ting-Cheng Chou [1], Tsung-Yu Huang[1], Wen-Tzu Tang [1]
[1] Graduate Institute of Athletics and Coaching Science, National Taiwan Sport University, Taoyuan, Taiwan.
Email: wttang@gmail.com

INTRODUCTION

Japanese Shinai kendo evolved into an athletic-centered sport in the 1950s from its mid 16th century origin. Unlike traditional kendo, which focuses on defeating enemies, athletic kendo focuses on acquiring valid strikes. This difference in purpose may lead to the development of differentiated striking movements in athletic kendo and also, the formation of "atekko kendo" [1]. This study aim to investigate the difference between the kendo movements of elite Kendokas (who practices traditional kendo), and elite tournament players (who practices athletic kendo). Focusing on the trajectory of the Shinai(bamboo sword), Shinai tip, and hilt, and the speed of the Shinai tip during the “men” strike (head strike), as it is the major wining area in athletic kendo.

METHODS

Four elite Kendo participants were recruited and grouped: two traditional Kendokas (learned kendo in Japan, 6th and 8th Dan, aged 60 and 70) as the “KR” group, and two tournament players (learned kendo in Taiwan, 3rd and 6th Dan, aged 24 and 34, one a 6th year national player, the other an national champion) as the “TR” group. This study was approved by the Ethics Committee, and all participants signed the consent form. Eight trials are collected after warm up and practice. The KR group performed Head Strike using traditional movements, and the TR group used athletic movements in tournaments. The striking movement is divided into 4 phases: preparation (Ph1), backswing (Ph2), acceleration I (Ph3), and acceleration II (Ph4) by 5 events: initiation with ground reaction force (T1), initiate of the shinai tip’s backswing (T2), end of the backswing (T3), the top of tip (T4), first contact on target (T5). Rear foot force was measured using AMTI triaxial force plate. Motion data are collected through the Motion Analysis System with 11 high-speed cameras (200Hz) and data processed through Cortex7.1. Forty nine reflective markers on the participant and 5 markers on the Shinai are attached according to manual. Motion trajectory were drew using Excel. Independent t tests was used and equality of variance was verified using the *Levene* test in SPSS 20.0 to compare shinai tip speed of the two groups.

RESULTS AND DISCUSSION

Regarding the movements of the Shinai tip, the results showed that in Ph1 (Figure1), only TR had a downward movement. Furthermore, in Ph2, the tip’s backswing distance of TR is smaller than KR. Then, in ph3 and ph4, the tip moved forward for both groups but only KR integrated an upward movement in ph3. For the Shinai hilt, the hilt moved forward for both group similarly in ph2~4. However, only TR have a similar downward movement in ph1 as the tip. These results illustrated TR tendency to initiate the striking movement by lowering the whole shinai, and with a smaller backswing in the ph1. KR however, did not initiate with the shinai, but with ground propulsion while holding the shinai still. Inferring that KR initiate the attack in a less prominent way, while TR initiate the attack with a forestall movement, conforming to the hypothesis. Table 1 showed the difference in the tip velocity of the two groups. KR has higher tip velocity at T1(V) and T4 (Vx, V), and TR had higher tip velocity at T2(Vz,V) and T3 (Vx, V). Yet, both groups have a similar tip velocity at T5. Table 1 also showed that tip velocity at T1 and T2 share a similar value for KR, while TR showed a increase in tip velocity from T1 to T2. Both groups showed the rise in tip velocity mainly from T3 to T4, demonstrating two different speed patterns contributing to the tip’s striking speed.

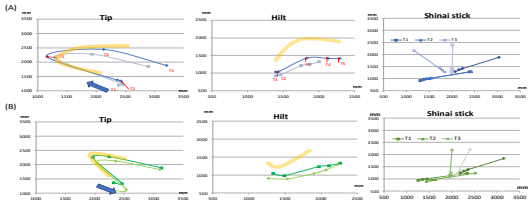

Figure 1. Tip, hilt trajectory and Shinai at 5 events (a) KR and (b) TR group.

CONCLUSIONS

Elite tournament players tend to lower the hilt first then up during preparation, followed by a small backswing of the tip, while traditional Kendokas tend to initiate with only foot propulsion and without moving the shinai to be less prominent. And despite the slower initiation and backswing speed, traditional Kendokas are capable of, through greater acceleration, reach striking speeds similar to that of elite tournament players on impact. Results testifies that traditional kendokas (averagely aged 65) are capable of reaching same striking speed as elite tournament players (averagely aged 30) using traditional kendo skill. Therefore, despite harder to master, more emphasis should be focused on traditional kendo skills in teaching.

ACKNOWLEDGEMENTS

Thanks to Mr. Hiroshi Ozawa, eight-dan Kendo Kyoshi, Emeritus Professor of Tokyo University of Science.

REFERENCES

[1] Koya Sato スポーツ人類學研究 第 21 号：1 - 16. 2019

Table 1: KR AVG±SD : TR AVG±SD in T1~T5 Shinai tip movement speed.

mm/sec	T1			T2			T3			T4			T5		
	T1x	T1z	T1 V	T2x	T2z	T2 V	T3x	T3z	T3 V	T4x	T4z	T4 V	T5x	T5z	T5 V
KR	400.6 ± 116.2	-276.9 ± 337.0	533.3 ± 278.3	-268.6 ± 122.0	4316.3 ± 1248.0	4343.1 ± 1267.2	700.1 ± 581.5	-206.2 ± 461.1	903.7 ± 499.0	17876.9 ± 2041.7	-825.2 ± 1168.5	17927.8 ± 2062.3	15369.6 ± 1768.3	-12821.5 ± 6006.1	20603.7 ± 3377.2
TR	239.5 ± 171.2	-23.2 ± 107.5	266.8 ± 167.6	-437.9 ± 230.0	5851.5 ± 1352.5	5880.3 ± 1363.7	1530.5 ± 481.6	1602.7 ± 707.3	2306.8 ± 641.9	15231.3 ± 2024.0	-1100.8 ± 527.9	15313.8 ± 2065.1	15845.7 ± 532.1	-11901.5 ± 1354.2	19882.8 ± 1019.5
p-value	0.066	0.052	0.037 *	0.125	0.045 *	0.047 *	0.010 *	<0.000 *	0.001 *	0.028 *	0.542	0.032 *	0.455	0.660	0.552

* P <0.05
* V：Resultant Velocity

Effect of different knee angles on hamstring muscle activity during Nordic hamstring exercise with a sloped platform

Taspol Keerasomboon[1], Toshiaki Soga[2] and Norikazu Hirose[3]
[1]College of Sports Science and Technology, Mahidol University, Bangkok, Thailand.
[2] Graduate School of Sport Science, Waseda University, Tokyo, Japan
[3] Faculty of Sport Science, Waseda University, Tokyo, Japan
Email: taspol.kee@mahidol.edu

INTRODUCTION

Nordic hamstring exercise (NHE) is commonly prescribed for preventing hamstring injury [1]. Performing NHE on the incline slope of the lower leg support at 20° and 40° allows the participants to perform the movement through an entire knee angle [2,3]. Alteration of the knee and hip angle affects hamstring activity during hamstring exercise [2,3,4]. However, the magnitude of hamstring activity with changing knee and hip angle during NHE on incline slope planform is still unknown. Therefore, this study aimed to investigate an electromyographic (EMG) activity in the hamstring during NHE on incline slope planform with a variation of the knee and hip angle at isometric contraction to identify a preferable exercise for recruiting hamstring activity.

METHODS

Thirteen male volunteers performed NHE with three different knee extension (120°, 130°, and 150°) and three different hip flexion angles (0°, 30°, and 45°) goniometer was used to monitor the knee and hip joint angle for maintaining NHE at isometric contraction for 5 seconds. The electromyographic data obtained during each condition was normalized with the values collected during maximal voluntary isometric contraction of each muscle (nEMG). A multivariate analysis of variance with repeated measures using syntax was used to compare the normalized electromyography of each muscle across the different knee and hip angles. Significant main effects were followed up by Turkey post-hoc procedures. Significance was set at $P<0.05$.

RESULTS AND DISCUSSION

There was a significant main effect among the knee and hip angles for the BFl and ST ($p < 0.05$). There was an interaction between knee and hip angle for the BFl and ST ($p < 0.05$). The nEMG activity values during hip 0° for the BFl and ST at knee extension at 150° and hip 0° were significantly higher compared to the knee extension at 120°and hip 0° and knee extension at 130°and hip 0°($p < 0.05$). This might be explained by the fact that when the knee is extended to a greater extent with spine angle relative to the horizontal is increased and, hence, the force gravity moves away from the center of rotation of the trunk leading to an increase in gravity force.

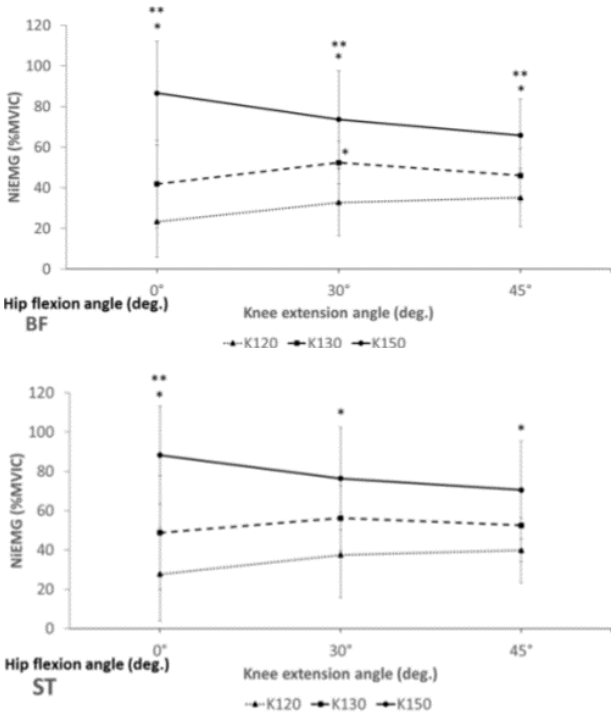

Figure 1 Differences in nEMG (%MVIC) activity during knee extension (120°, 130°, 150°) and hip flexion angles (0°, 30°, 45°) in the BF and ST muscles during isometric NHE on a sloped platform inclined at 30° The symbol * indicates a statistically significant difference between 120°and other angles. The symbol ** indicates a statistically significant difference between 130°and other angles.

CONCLUSIONS

The finding of this study showed that BFl and ST EMG activities during isometric NHE on the incline slop planform at 30° at knee 150° and hip 0° might be better for recruiting hamstring activity. However, it is still unclear in other degrees of incline slope planform.

REFERENCES

[1] van Dyk N et al. Br J Sports Med. 53(21):1362-1370, 2019.
[2] Šarabon N et al. PLoS One. 14(10), 2019.
[3] Soga T et al. J Sports Sci Med. 20(2):216-221,2021.
[4] Keerasomboon T et al. J Sports Sci Med. 19(4):630-636,2020.

ANGULATION OF HANDLE FORCE APPLICATION FROM THE CABLE DIRECTION IN ACHIEVING A TURN IN THE HAMMER THROW.

Eri Nonaka[1], Norihisa Fujii[2], Natsuki Sado[2], Sekiya Koike[2]
[1] Graduate School of Comprehensive Human Sciences, University of Tsukuba, Tsukuba, Japan.
[2] Faculty of Health and Sport Sciences, University of Tsukuba, Tsukuba, Japan.
Email: s2030463@s.tsukuba.ac.jp

INTRODUCTION

Hammer throw is a continuous high-speed rotational motion that requires a large handle force application to accelerate the hammer head. The hammer acceleration is largely determined by the cable force [1], even with its small directional component to the hammer velocity [2] (Figure 1A). A hammer consists of a series of three segments: a handle, a cable (about 0.95 m long), and a hammer head (4.00 kg for females and 7.26 kg for males), with two torque-free ball joints. Under these structural constraints, the hammer head is driven only by the cable force in the cable direction, while throwers can control its magnitude and direction by exerting the handle force angled from the cable direction with couple of forces applied by their hands. Previous studies [1-5] have provided valuable insights into the cable force to accelerate the hammer head, while none of the insight into the handle force with angulation. Thus, we examined the angulation of the handle force and investigated its effect on the hammer movement during a turn that alternates hammer deceleration and acceleration. We hypothesized that hammer throwers exert the handle force with angulation to control the hammer movement.

METHODS

We analysed motion data of indoor hammer throwing from four male and four female throwers collected by a motion capture system (VICON-MX, 29 cameras, 250 Hz). The handle force–cable angle ($\theta_{H\text{-}C}$) was calculated from the motion data during the third turn and its significant difference from zero was assessed by a one-dimensional statistical parametric mapping (SPM1D) two-tailed one-sample *t*-test ($\alpha = 0.05$).

We simulated the hammer movement with and without $\theta_{H\text{-}C}$ to investigate its effect using a three-segment force-driven computer simulation, with its initial conditions matched with the experimental data.

RESULTS AND DISCUSSION

Hammer throwers exerted the handle force significantly angled opposite to the hammer velocity during the 59–68% time-segment of the turn, when the hammer was accelerated, with peak and mean $\theta_{H\text{-}C}$ of -0.83±0.33 and -0.12±0.073 deg (Figure 1B). This result supported our hypothesis. Brice et al. [2] showed that the cable direction relative to the hammer velocity determines whether the hammer accelerates or decelerates. We further added that the cable direction is controlled by the handle force with angulation. This finding expanded our understanding of possible options for hammer throwers to accelerate the hammer head with the cable force.

Despite the small $\theta_{H\text{-}C}$ (about 1 deg, Figure 1B), our simulation revealed that the handle force without angulation led to the hammer head moving out of the throwing circle (Figure 1C). This indicated that observed $\theta_{H\text{-}C}$ was small, and in the negative direction for the hammer acceleration, but essential to achieve the turn in the hammer throw inside a throwing circle with 2.13 m diameter. Theoretically, a small mass of the cable and handle means a small inertial resistance when controlling them toward the direction perpendicular to the cable. We suggest that hammer throwers achieve a continuous high-speed rotational motion under the highly directional sensitivity of a large handle force.

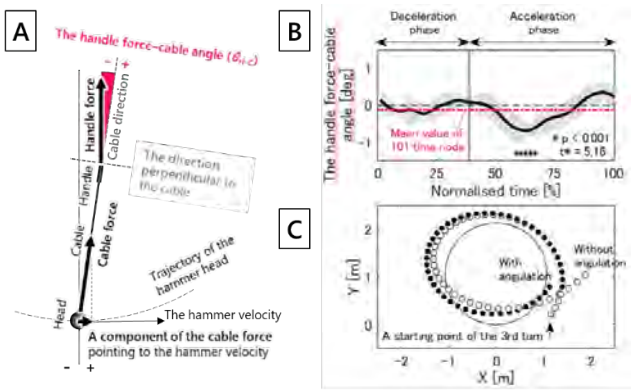

Figure 1 (A) Factors involved in hammer acceleration. (B) The handle force–cable angle $\theta_{H\text{-}C}$. The vertical line is a starting point of the hammer acceleration. (C) The hammer movements with and without angulation of the handle force (Blacked and whited circles, respectively).

CONCLUSIONS

Hammer throwers exerted the handle force with angulation, especially when the hammer accelerated. Despite its small value of around 1 deg, the simulated removal of the angulation moved the hammer head significantly outside the throwing circle. Hammer throwers may achieve a high-speed rotational motion under the highly directional sensitivity of handle force.

REFERENCES

[1] Dapena J. *J Biomech* **17**: 553-559, 1984.
[2] Brice SM et al. *Sports Biomech* **10**: 174-184, 2011.
[3] Dapena J and Feltner ME. *J Biomech* **22**: 565-575, 1989.
[4] Murofushi K et al. *Sports Biomech* **6**: 301-314, 2007.
[5] Fujii N. 26th ISBS Conference, 2008.

A BIOMECHANICAL ANALYSIS ON THE STRAIGHT JUMP OF GYMNASTICS TRAMPOLINE

Yuji OHGI[1], Ginga Munetomo[2], Hiroki Ozaki[3] and Tokio Takagi[3]
[1] Graduate School of Media and Governance, Keio University, Fujisawa, Japan.
[2] Graduate School of Comprehensive Human Sciences, University of Tsukuba, Tokyo, Japan.
[3] Japan Institute of Sports Sciences, Tokyo, Japan.
Email: ohgi@sfc.keio.ac.jp

INTRODUCTION

Trampoline gymnastics requires athltes to performa 10 different acrobatic rouines in their flight phase. While difficulty and execution scores are resulted in their performance, flight height is prerequite of the higher scored somersaults. Therefore, the straight jump is the basic skill of trampoline gymnastics. From the view point of the conservation of energy, since their jumps are sometimes over 8m, it is easily assumed that large amount of reaction force acts to the athlete during his landing and pushing phases on the trampolin bed. This heavy reaction force might cause the great physical load to the athlete's lower extremities and their spine. The purpose of this study was to investigate and the quantify the kinematics and kinetics of the trampoline straight jump motion during the landing phase.

METHODS

The subjects were four top-level athletes who had been certified as S-rank designated athletes in trampoline competitions set by the Japan Gymnastics Association. The experiment was conducted in the Trampoline facility in Japan Institute of Sports Science. Twenty optical motion capture cameras (Vicon MX-T20 , 200Hz) were settle up around the trampoline target areas viewed from ground to 2nd/3rd floored catwalks. Fifty reflective markers were attached onto the subject's whole body. The inertial parameters of the subject were calculated using Ae's estimation equations [1].

RESULTS AND DISCUSSION

The authors hypothesized that trampoline jump is 2-dimensional motion on the sagittal plane, the whole-body joint forces and torques were solved by the inverse dynamics method using Newton-Euler equations from the distal end of the upper extremity and head during the landing phase. The bed reaction force (BRF) acting at the COP was estimated. For this calculation, the authors hypothesized COP location was at the middle of ankle and MP3 joint. BRF was also validated by using conservation of energy of subject's kinetic and potential energy on the trampoline bed. As the results, the stiffness of the trampoline bed might have a non-linear characteristic. The estimation of the reaction force at the ground contact point was tested using inverse dynamics and the conservation of energy law, but the results showed good agreement at low jumping heights, but not at high jumping heights and large reaction forces, suggesting a nonlinear spring. During leg extension on the bed, the body's center of gravity was always located in front of the ground point, and during the latter half of the jump, the body tilted backward due to the increased hip torque exerted, which was predicted to place a large burden on the lumbar spine.

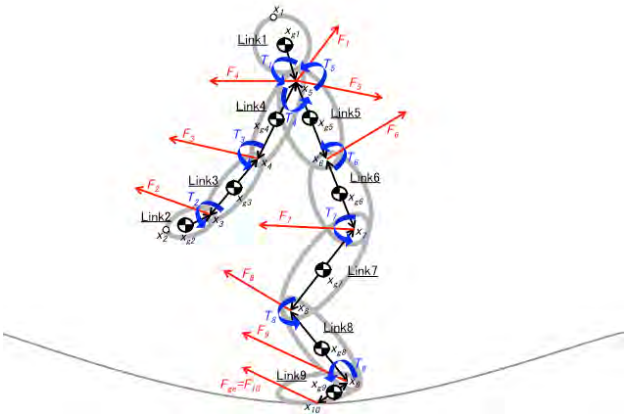

Figure 1 Two dimensional linked segment model of the trampoline athlete.

CONCLUSIONS

This study clarified the kinematics and kinetics acting on the lower limbs during straight jumps on the trampoline bed. It was suggested that the very large force acting on the lumbar spine during hip torque exertion in the latter half of the jumping motion may contribute to the low back pain observed in trampolinists.

REFERENCES

[1] Ae, et al. *Biomechanism,* **11**:23-33, 1993.

Table 1: Example of estimation results of the maximum reaction force acting to the athlete's feet.

Num of Jump	by linear mass/spring model with Energy conservation law	by Inverse Dynamics model
1st/3rd/6th/12th	3702.8/5244.7/6321.3/6862.8N	3381.4/5808.5/7741.1/8614.4 N

THE EFFECTS OF FOOTWEAR ON THE PLANTAR PRESSURE UNDER THE METATARSAL HEADS DURING ROPE SKIPPING

Kaicheng Wu[1], Jun Li[1], Dongqiang Ye[2], Baoren Cao[2], Liqin Deng[1], Songlin Xiao[1], Weijie Fu[1,*]
[1]Key Laboratory of Exercise and Health Sciences of Ministry of Education, Shanghai University of Sport, Shanghai, China
[2]Warrior Sports & Science Research lab, Shanghai Warrior Shoes Co.Ltd, Shanghai, China
Email: fuweijie@sus.edu.cn

INTRODUCTION

Rope skipping has grown in popularity recently as a simple and practical at-home exercise due to the gradual rise of the "home exercise" concept. Previous research has indicated that the peak pressure mainly occurred in the metatarsal heads during jump rope exercises [1]. Prolonged high plantar pressure during rope skipping may increase the risk of metatarsalgia and metatarsal stress fractures and lead to soft tissue degeneration [2]. Footwear serves as an interface between the foot and the ground to protect the plantar surface and modify the plantar pressure distribution. A shoe with thicker midsoles would reduce ground reaction forces during drop landing, as would a specially designed shoe. Therefore, the purpose of this study was to investigate the effects of footwear on the plantar pressure under the metatarsal heads during rope skipping.

METHODS

Sixteen healthy male college students with more than six years of physical activity (age: 25 ± 2.7 years, height: 175.77 ± 3.7 cm, body mass: 72.3 ± 6.49 kg) were recruited. The Novel Pedar-X (50 Hz) was used to collect plantar pressure of the dominant leg. Three regions (medial forefoot, MedFF; middle forefoot, MidFF; and lateral forefoot, LatFF) of the collected data were evaluated, crossing from the first to fifth metatarsals. During the test, the participants were randomly assigned to perform a two-legged jump rope trail at a fixed frequency (2.2 Hz) in two footwear conditions: Asics GT-2000-10 running shoes (24mm forefoot, 32mm rearfoot) with an upturned forefoot design and a gel insert under the first metatarsal area; Health 2255 rope skipping shoes (9mm forefoot, 15mm rearfoot) with a flat forefoot design and no inserts in the midsole. Paired *t*-tests were used to determine the differences in all variables. The 95% confidence intervals and effect size (Cohen's d) of each parameter was calculated. The significance level α was set at 0.05.

RESULTS AND DISCUSSION

The plantar pressure results show that the peak fore of MedFF area and MidFF area; peak pressure of MedFF area and MidFF area; pressure–time integral of MedFF area and MidFF area were significantly lower in Asics brand shoes ($p < 0.05$, Table 1). This may have been affected by the cushioning materials (gel) and midsole thickness in the forefoot of the footwear. There was no statistically significant difference found in the LatFF area for peak force, peak pressure, and pressure–time integral between the two footwear conditions (Table 1). The above suggests that choosing the Asics running shoe may prevent plantar injuries by lessening the force and pressure on the 1st to 4th metatarsal heads during rope skipping.

CONCLUSIONS

The thicker midsole with a particularly cushioned forefoot design helped to reduce plantar pressure in the metatarsophalangeal joint, which may have beneficial effects on the plantar injury during jump rope exercise. Thus, the Asics shoe may be more suitable for long-term jumping exercise.

ACKNOWLEDGEMENTS

This research is supported by the Shanghai Warrior Shoes Co. Ltd.

REFERENCES

[1] Yu, H B et al. *Bioengineering (Basel)* **4**, 2022.z
[2] Chuckpaiwong, B et al. *Br J Sports Med* **41(8)**, 2007.

Table 1: Descriptive statistics and statistical results of plantar pressure of the forefoot during the jump rope test.

Variables	*Health*	*Asics*	*P-value*	*95% CI*	*Cohen's d*
P_{force} MedFF (N)	272.95±85.6	235±70.51	**＜0.001**	[19.645;56.263]	0.796
P_{force} MidFF (N)	301.36±57.9	267.15±68.74	**0.003**	[14.05;54.365]	1.444
P_{force} LatFF (N)	127.77±38.88	121.98±39.45	0.329	[-6.445;18.025]	0.175
$P_{pressure}$ MedFF (kpa)	305.94±119.09	257.53±79.13	**0.001**	[12.009;39.122]	0.685
$P_{pressure}$ MidFF (kpa)	213.38±39.43	192.28±46.94	**0.003**	[6.506;25.673]	1.151
$P_{pressure}$ LatFF (kpa)	143.03±38.28	136.69±44.18	0.088	[-1.158;15.089]	0.198
P•T MedFF (kpa•s)	44.55±16.59	36.28±10.93	**0.001**	[3.949;12.596]	0.994
P•T MidFF (kpa•s)	33.57±6.34	28.82±4.84	**0.003**	[1.878;7.619]	2.987
P•T LatFF (kpa•s)	21.27±4.03	21.24±4.41	0.976	[-2.429;2.499]	0.008

MedFF: medial forefoot; MidFF: middle forefoot; LatFF: lateral forefoot; P_{force}: peak force; $P_{pressure}$: peak pressure; P•T: pressure–time integral.

REDUCED MEDIAL-LATERAL DISPLACEMENT OF THE BODY'S CENTER OF MASS DURING WALKING IN STARTING SOCCER PLAYERS IN HIGH SCHOOL FOOTBALL LEAGUE

Anne Dixie M. Lim[1], Shih-Wun Hong[1,3], Chun-Chung Tan[2], Tsung-Jung Ho[3]
[1] Department of Physical Therapy, Tzu Chi University, Hualien, Taiwan
[2] Department of Rehabilitation Medicine, Hualien Tzu Chi Hospital, Hualien, Taiwan
[3] Department of Chinese Medicine, Hualien Tzu Chi Hospital, Hualien, Taiwan
Email: annedixielim@gmail.com, swhong0624@mail.tcu.edu.tw

INTRODUCTION

The ability to maintain balance is critical to a soccer player's performance. Good balance gives stability during diverse motions such as dribbling, shooting, and defending, allowing players to control the ball more efficiently and with more accuracy. These specific adaptations or techniques are believed to result from soccer players' experience in a competitive environment. The current study aims to investigate the differences of dynamic balance in terms of medial-lateral (M/L) and vertical displacements of the body's center of mass (COM) during level walking between the starting and non-starting lineup of a high school soccer team which is in the High School Football League of Taiwan.

METHODS

Eight starting and eight non-starting soccer players from National Hualien Senior High School participated in the current study with informed written consent, as approved by the Institutional Research Board. Each subject walked at a self-selected pace on an 8-meter walkway. Thirty-nine infrared retro-reflected markers were placed on specific landmarks of the body to track the motion of the segments. The kinematic and kinetic data were measured with a 7-camera motion analysis system (Vicon, Oxford Metrics, U.K.) and two force plates (AMTI, U.S.A.). A 13-body-segment model of the whole body was used to calculate the position of the body's COM as the weighted sum of the segmental COMs of all body segments. Body segmental inertial properties were obtained using the Dempster's coefficient. The M/L and vertical displacements of the COM are described as the differences of the maximum and minimum values in the medial-lateral and superior-inferior axis of a gait cycle respectively. All the calculated COM displacements were normalized to leg length. An independent t-test was applied to compare the variables (M/L and vertical COM displacements) between the starting and non-starting groups. All significance levels were set at α=0.05.

RESULTS AND DISCUSSION

The starting soccer players showed significantly decreased M/L COM displacement during walking compared with the non-starting ones (p=0.01, Table 1). On the other hand, no significant differences of the vertical displacement of the COM were found between groups (p=0.49, Table 1). The results of the study found that the starting soccer player have better balance performance in M/L direction in terms of decreased COM displacement. The level of competition for soccer players was positively linked to their postural stability. Studies have shown that there is a positive correlation between M/L displacement and energy expenditure, suggesting that the starting group may have a lower rate of fatigue, leading to better performance on the field. The advantage of balance ability in the starting players may be caused by different training program or innate superior characteristics of their body. On the other hand, previous studies have shown a lack of correlation between vertical COM displacement and metabolic cost, suggesting that minimizing displacement doesn't necessarily minimize metabolic cost. This is likely why no significant differences of vertical COM displacement between groups were observed in the current study. It is suggested that the training regimen for the control of COM in the M/L direction may be necessary for the soccer players.

CONCLUSIONS

Overall, the study's findings indicated that the starting soccer players demonstrated better postural performance in the M/L direction, as seen by a reduced rate of COM displacement, when compared to the non-starting players.

ACKNOWLEDGEMENTS

The authors gratefully acknowledge the financial support from National Science and Technology Council (Grant No.: MOST 110-2221-E-320 -003).

Table 1: Medial-lateral (M/L) and vertical displacements of the body's center of mass (COM) in the starting and non-starting soccer players

	Starting	Non-starting	*p-value*
M/L COM displacement (%LL)	1.70 ± 0.58	3.08 ± 1.24	p = 0.01
Vertical COM displacement (%LL)	2.61 ± 0.31	2.45 ± 0.12	p = 0.49

*LL: leg length

THROWING PERFORMANCE AND KINEMATIC ANALYSIS OF OVERHEAD THROWING IN MALE ELITE AND VARSITY CUP CRICKETERS

Leondiris, J[1], Dutton, M[1], Albertus, A[1] and Gray, J [1]
[1] Physiological Department, University of Cape Town
Email: jordanleondiris@gmail.com

INTRODUCTION

Throwing is one of the most dynamic movements performed, requiring significant segmental co-ordination and rhythmical muscle activation to execute. Most available research of the overhead throw pertains to baseball, with distinctly less in cricket. Throwing performance represents the combination of throwing speed (TS) and throwing accuracy (TA). These are both critical to performance but cannot be optimized simultaneously [1]. This phenomenon is referred to as the speed-accuracy trade-off. It describes that any increases in velocity results in improved accuracy until a threshold is reached. Any further increases above this threshold velocity produces decrements in throwing accuracy. From the distinction of the phases of throwing, three critical points can be identified. These are considered crucial for injury prevention and include the following: Maximal External Rotation (MER), Ball Release (BR), Maximal Internal Rotation (MIR).

METHODS

The three-dimensional (3D) kinematic metrics were analysed using a six camera Vicon Vantage motion analysis system capturing at 240 Hz. A custom 78-piece marker set was applied to participants (N=12). Each participant threw 26 throwing trials, 13 static and 13 dynamic with the following objective breakdown: three maximal efforts to establish maximal throwing speed (MTS), five >75% MTS, five Self-Paced (SP) per throwing approach. Throwing velocity was measured using a radar gun. Participants threw towards an accuracy target, which was placed 20 meters away. The target illustrated ICC regulation stumps that had colour coded surrounding areas that denoted the point system. Three points for stump contact, two points for the white area, one point for the green area and zero for missing the target completely.

RESULTS AND DISCUSSION

Originally, the speed-accuracy trade-off began as a hypothesis that was accepted after being supported with ample evidence. The highest throwing speeds were achieved during the dynamic approach. Accuracy scores were highest (50% greater than during Max) during the static approach and when participants selected their pace (SP). Along with an almost 15% drop off in throwing velocity when throwing SP compared to Maximal. The highest throwing arm shoulder rotational velocity at BR in deg/s was achieved during the maximal throws of each respective approach, as expected. However, the static approach exhibited a higher velocity, which makes us consider the effect of the run-up on the throw. The players potentially recorded faster throwing speeds without the expected increases in shoulder rotational velocities due to the force being generated during the forward motion of the run up and not entirely by the upper limb, like during static throwing. Specifically, up to 55% of the energy required to pitch can be attributed to lower body force contributions [2].

CONCLUSIONS

The speed-accuracy trade off tends to persist in elite male cricketers. Throwing kinematics illustrate that this cohort shows higher shoulder rotational velocities at BR during static throwing versus dynamic throwing (Max & >75% MTS), alluding to the lower body force contribution during a run-up for force generation at the shoulder. Throwing from a dynamic position could provide a protective role on the shoulder in the long run.

ACKNOWLEDGEMENTS

Acknowledgments are reserved for the National Research Fund (NRF), South Africa.

REFERENCES

[1] Freeston J et al. *Percep & Mot Skill* **118**: 637-6550, 2014.
[2] Sundaram B et al. *Int J Sp Phys Ther* **7**: 576-585, 2012.

Table 1: Shoulder rotational velocities at BR between static and dynamic approaches (deg/s). Bold values expressed in median & [IQR]

	Static		Dynamic		
Objective	BR	SD/IQR	BR	SD	*p-value*
Maximal	5808.04	1164.58	5650.79	1387.17	$p = 0.593$
75% MTS	**5532.20**	**[1682.6]**	5167.45	1278.68	$p = 0.077$
Self-Paced	4420.24	816.14	4862.31	801.93	$p = 0.002$*

*Significant difference is set at $p \leq 0.05$.

Case Study: Can Tensiomyography Predict Sports Performance?

Kyoungkyu Jeon[1,2,3,4,5], Hojun Joo[1,5], Sangwon Lee[6] and Hyungwoo Lee [1,2,5]
[1] Division of Sports Science, Incheon National University, Incheon, South Korea
[2] Department of Human Movement Science, Incheon National University, Incheon, South Korea
[3] Sport Science Institute, Incheon National University, Incheon, South Korea
[4] Health Promotion Center, Incheon National University, Incheon, South Korea
[5] Functional Rehabilitation Biomechanics Laboratory, Incheon National University, Incheon, South Korea
[6] Sports Conditioning Center, Incheon Sports Council, Incheon, South Korea
Email: guddn318@inu.ac.kr

INTRODUCTION

Tensiomyography (TMG) is one of the mechanomyographic evaluation methods and is a device that evaluates the static contractile properties of skeletal muscle in response to a single electrical stimulus of 0 to 100 mA for 1 ms [1-3]. Because it does not involve motivation or volitional effort, it is possible to objectively evaluate the muscle contractile properties, and it has been used to characterize the muscle contractile properties of specific sports athletes and to establish the relationship between sports performance abilities [4,5]. As such, it is necessary to obtain functional information that can predict the athletic performance of athletes with measurement variables derived from TMG. Therefore, the purpose of this study is to compare the static contractile properties of skeletal muscle in major leaguers, second-team players, and ordinary person.

METHODS

This study was conducted with 1 major leaguer, 1 2nd team player, and 1 normal person each from the general public. TMG (TMG-100 System electrostimulator, Slovenia) was used to compare and analyze the static contractile properties of erector spinae muscles. To compare and analyze the contractile properties of the measured muscle, measure-remeasurement and intra-rater reliability index (ICC) were the highest variable, maximum radial displacement (Dm, 0.91-0.99), a variable that records the maximum contractile displacement of the muscle, and 10 to 10 of the maximum contractile displacement. A contraction time (Tc, 0.70-0.98), a time variable required to contract to 90%, was used [3].

RESULTS AND DISCUSSION

As a result of comparing the contractile properties of the erector spinae muscle, the major leaguers had the lowest results in all variables <Table 1>.

A previous study comparing power and endurance athletes showed lower Tc and Dm in power athletes. In addition, since the major leaguers had the lowest results in Tc, which has a significant positive correlation with Type I, it is judged that the ratio of Type II is higher in the erector spinae muscles of major leaguers than other groups [6]. In addition, reduced Dm would have been shown due to improvement in passive stiffness, such as increased muscle tone and stiffness due to muscle hypertrophy, which can be suggested to contribute to improved muscle performance [7].

CONCLUSIONS

As a result of analyzing the static contractile properties of the erector spinae muscle, the Tc and Dm of the major leaguers were lower than the other groups due to the type of muscle fiber and the characteristics of muscle hypertrophy, and it was judged that the muscle performance was the best.

ACKNOWLEDGEMENTS

This study was supported by the University Innovation Support Project of Incheon National University.

REFERENCES

[1] Ditroilo, M et al. *J Electromyogr Kinesiol* **23**: 558-563, 2013.
[2] Rey, E et al. *J Electromyogr Kinesiol* **22**: 866-872, 2012.
[3] Martín-Rodríguez, S et al. *J Strength Cond Res* **31**: 3524-3536, 2017.
[4] García-García, O et al. *Open Access J Sports Med* **10**: 49-69, 2019.
[5] Paravlic, A. H et al. *J Musculoskelet Neuronal Interact* **22**: 179, 2022.
[6] Park, S. *J Exerc Rehabil* **16**: 325, 2020.
[7] Kojić, F et al. *Eur J Appl Physiol* **122**: 2223-2231, 2022.

Table 1: Result of tensiomyography to erector spinae of the participants

Variables	Major leaguer	2nd team player	Normal
Tc (ms)	6.58	15.31	17.34
Dm (mm)	0.16	3.89	4.65

Abbreviation. Tc, contraction time; Dm, maximum radial displacement

Comparison of differences in muscle activity according to the types of conventional deadlifts

Seungho An[1,2,5], Seungwon Lee[1,2,5], and Kyoungkyu Jeon[1,2,3,4,5]
[1] Division of Sports Science, Incheon National University, Incheon, South Korea
[2] Department of Human Movement Science, Incheon National University, Incheon, South Korea
[3] Sport Science Institute, Incheon National University, Incheon, South Korea
[4] Health Promotion Center, Incheon National University, Incheon, South Korea
[5] Functional Rehabilitation Biomechanics Laboratory, Incheon National University, Incheon, South Korea
Email: jeonkay@gmail.com

INTRODUCTION

Deadlift is one of the basic resistance exercises performed to improve and evaluate muscle strength, and it is used in exercise programs by effectively inducing muscle strength and neuromuscular development using the muscles of the whole body [1-3]. Deadlift performed by move the hip joint, knee and ankle joints with maintaining a neutral spine during the movement, and conventional deadlift is one of the most widely performed [4,5]. Among the conventional deadlift movements, the powerlifting deadlift (PD) exhibits a high hip position and horizontal trunk angle to the ground, in contrast, the weightlifting deadlift (WD) exhibits a lower hip position and vertical trunk angle [6]. Previous studies have reported that muscle activation patterns in the lumbar spine and lower extremities may vary between PD and WD, but analysis of muscle overuse or risk of sprains was not performed because muscle activity was not measured during motion [7]. Therefore, the purpose of this study is to analyze muscle activity by comparing EMG between PD and WD.

METHODS

For this study, 9 adult males under the age of 30 with more of weight training experience were recruited (age; 20.78±1.09 years, height; 176.11±4.22 cm, weight; 71.58±4.01kg). The subjects repeated both PD and WD 5 times each with 70% of 1 repetition maximum for this experiment. PD placed the barbell on a straight line from the inferior angle of the scapular to the ground and performed the motion in a high hip and horizontal body position. WD placed the barbell on a straight line from the collarbone to the ground, allowing the movement to be performed at a lower hip and a near-vertical trunk position. For muscle activity analysis, 8-channel wireless EMG equipment (Ultium^{TM}, Noraxon, USA) was used, and EMG sensors were attached to the erector spinae (ES), gluteus maximus (GM), biceps femoris (BF), and vastus lateral muscle (VL) based on previous studies. For statistical analysis, a paired *t*-test was used for the SPSS 26.0 (IBM, USA), and all variables were calculated as mean and standard deviation. The statistical significance level was set at $P < 0.05$.

RESULTS AND DISCUSSION

A result of this study, the EMG values of ES, GM, and VL were significantly high than during WD operation than PD (p=0.000). According to previous studies, since WD increases horizontal distance between the center of gravity and the barbell compared to PD, it can exhibit higher ES activity by increasing torque and external shear force of the lumbar spine, and it can also exhibit higher VL activity by increasing knee extension moment [6]. The difference between the results of previous studies and this study is that the activity of GM was significantly higher in WD than in PD. Based on previous studies showing that the activity of GM increases as lower pelvis position is shown during squats, it is thought that lower pelvis position, greater extension moment of the hip joint [8].

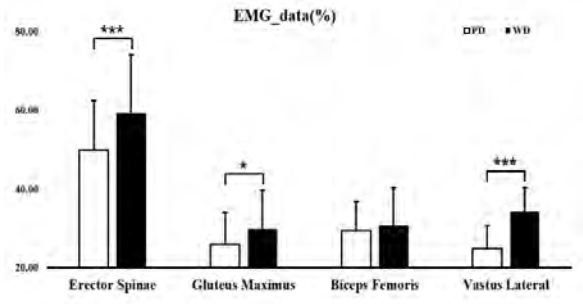

Figure 1. EMG comparison between PD and WD

CONCLUSIONS

As a result of this study, greater muscle activity was shown in the ES, GM, and VL muscles during the WD compared to the PD, and there was no significant difference in the BF.

ACKNOWLEDGEMENTS

This study was supported by the University Innovation Support Project of Incheon National University.

REFERENCES

[1] Ferland P et al. *Int J Exerc Sci* **13(4)**: 281-297, 2020.
[2] Ji Y et al. *Korean J Sport Sci* **30(3)**: 275-283, 2020.
[3] Suchomel T et al. *Sports med* **48**: 765-785, 2018.
[4] Ronai P et al. *ACSM's Health Fit J* **24(2)**: 31-36, 2020.
[5] Holmes C et al. *ACSM's Health Fit J* **24(3)**: 17-23, 2020.
[6] Edington C et al. *Sports* **6(3)**: 90, 2018.
[7] Aasa U et al. *Sports biomech* **21(6)**: 701-717, 2022.
[8] Caterisano A et al. *J Strength Cond Res* **16(3)**: 428-432, 2002.

Kinetic determinants of acceleration performance in sideward sprint start from standing position

Takahiko Sato[1,2], Yusuke Fukuhara[3], Yuto Kobayashi[3] and Tadao Isaka[4]
[1] Faculty of Rehabilitation, Biwako Professional University of Rehabilitation, Shiga, Japan.
[2] Ritsumeikan Global Innovation Research Organization, Ritsumeikan University, Shiga, Japan.
[3] Graduate School of Sport and Health Science Ritsumeikan University, Shiga, Japan.
[4] Faculty of Sport and Health Science, Ritsumeikan University, Shiga, Japan.
Email: t-satou@fc.ritsumei.ac.jp

INTRODUCTION

In many ball games, an ability to travel a given distance in a shorter time is advantageous for getting a loose ball or evading opponents. Hence, superiority of starting techniques and an effectiveness of training methods have widely been discussed [1-2]. Although the sprinting direction depends on the game situation, most previous studies focused on the forward sprint start and the following sprint. Our previous study demonstrated that soccer players use the forward step and false step techniques with similar frequency when they start sprinting in a sideward direction from a standing position [3]. However, effective training methods for improving the acceleration performance in the sideward sprint starts are still unclear. Therefore, to obtain an insight on improvement of the sprint performance, this study aimed to identify key variables influencing the acceleration performance in a sideward sprint starts by using the forward step and false step techniques.

METHODS

Ten male soccer players and ten male lacrosse players participated to this study. They started 5-m sprints in the right direction from a stationary standing position with a parallel stance. After a ready signal, each participant self-initiated sprinting by using either the forward step or false step technique according to the instruction. Reflective markers were attached on their anatomical landmarks, and the three-dimensional coordinates data were recorded by a motion capture system sampling at 200 Hz. Fifteen force plates sampling at 1000 Hz were used to measure the ground reaction force (GRF) from the ready signal to the second step in the springing direction. Frame at the movement initiation was detected based on the change in the vertical components of the GRFs. Velocity of the participant's center of mass was calculated at the movement initiation and the flight phase after the second step in the sprinting direction (v_i and v_f). Body mass data of each participant was adjusted based on the impulse-momentum relationship between v_i, v_f, and GRF impulse. Correlation analyses on the deterministic models were utilized to identify the key variables influencing the performance outcome in each sprint start technique [4]. v_f was set as the outcome measure, and factors producing that were v_i and the change of the velocity (Δv) generated by each of the following step events: initial push-off by the right and left foot, false step (only in the false step technique), and the first and second step in the sprinting direction (1st and 2nd step).

RESULTS AND DISCUSSION

In the deterministic model of the forward step technique, v_f correlated to Δv of the initial push-off of the left foot and the 1st step significantly (Figure1). Since a significant correlation between v_f and Δv of the 2nd step was not found, it is suggested that enhancements of accelerating before the 2nd step can improve the acceleration performance.

In the deterministic model of the false step technique, v_f correlated to Δv of the initial push-off of the right foot, the false step, and the 2nd step significantly. Although the false step and the 2nd step accelerate the COM, the initial push-off of the right foot generated deceleration (Figure1). These results suggest that the acceleration performance can be improved by not only enhancements of accelerating but minimization of decelerating.

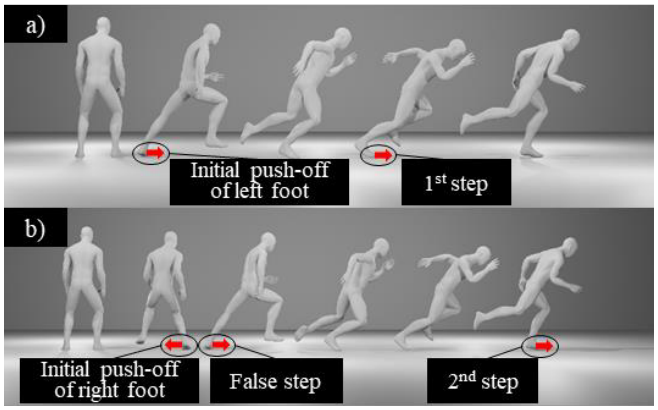

Figure 1 Step sequences and directions of Δv significantly correlated to v_f in a) forward step and b) false step techniques.

CONCLUSIONS

This study demonstrated the key variables influencing the acceleration performance in sideward sprint start by using the forward step and false step techniques. These findings can be useful knowledge for establishing the training methods to improve the performance of acceleration in a sideward sprint start and the following sprint.

REFERENCES

[1] Haugen T et al. *Spo Med - Open* **5**: Article No. 44, 2019.
[2] Schwenzfeier A et al. *Spo Biomech* **21**: 958-965, 2022
[3] Sato T et al. *Heliyon* **7**: e07333, 2021.
[4] Hay J et al. *Biomechanics* **V**: 13-19, 1976.

ANGULAR MOMENTUM ANALYSIS OF FOUR STYLES OF BASEBALL PITCHING

Tomohisa Miyanishi[1], Kazushi Shimada[2], Takashi Kawamura[3],
Daisaku Hirayama[3], Keizo Takahashi[4] and Ryu Nagahara[5]
[1] Faculty of Sports Science, Sendai University, Miyagi, Japan.
[2] Faculty of Human Sciences, Kanazawa Seiryo University, Kanazawa, Japan.
[3] Faculty of Health and Sport Sciences, University of Tsukuba, Ibaraki, Japan.
[4] Faculty of Sports Study, Biwako Seikei Sport College, Shiga, Japan.
[5] National Institute of Fitness and Sports in Kanoya, Kagoshima, Japan.
Email: tm-miyanishi@sendai-u.ac.jp

INTRODUCTION

The aim of this study was to compare the angular momentum (H) values of five groups of body segments during an entire throwing cycle in the overhand (OS), three-quarter (TS), sidearm (SS), and underhand (US) styles of the baseball pitching motion.

METHODS

Ninety-one male amateur pitchers (25 high school, 62 collegiate, 4 post-collegiate) participated in this study. Ninety-five maximum-effort fastball pitches from the pitcher's mound to the catcher were videotaped with two cameras at 240 Hz at a baseball stadium. The 3D coordinates of body landmarks and ball were calculated using the DLT method. After discarding seven pitches that fell within the buffer zones that overlap between TS and SS, the remaining 88 pitches by 84 participants were classified into the four delivery styles (30 OS, 26 TS, 20 SS and 12 US) using the arm slot angle criteria reported in a previous study [1]. Landmark coordinates were expressed in a right-handed reference frame in which the X axis pointed toward the right, the Y axis pointed forward in the direction of the pitch, and the Z axis pointed upward. The landmark coordinates of the left-handed participants in the sample (eight) were subjected to a symmetrical transformation to make them appear right-handed. The 16 body segments and the ball were combined into five segment groups: trunk-head, left leg, right leg, left arm, and right arm and ball. Their angular momentum components (HX, HY and HZ) were calculated during the wind-up (P1), stride (P2), right arm-cocking (P3) and right arm-acceleration (P4) phases using the methods of a previous study [2], and were standardized for the standing height and body mass of each participant. All times were expressed as percentages of the total duration of the throw. ANOVA was performed to assess the differences in the physical characteristics of the participants (age, standing height, body mass and throwing experience) and in the ball velocity between the styles with a multiple comparison using Bonferroni corrections. Statistical parametric mapping (SPM) analysis was performed to detect differences among the styles in the time-dependent curves of the H components [3]. Significance level was set at 5% (p<0.05) in all statistical analyses.

RESULTS AND DISCUSSION

No significant differences between the styles were found in the physical characteristics of the participants. Significant differences in ball velocity (34.9±1.9 m/s for OS; 35.3±1.9 m/s for TS; 33.8±1.9 m/s for SS; 32.0±1.9 m/s for US) were found between the OS and US styles and between the TS and US styles (both p<0.001).

In the latter half of P3 and in P4, the HY of trunk-head, right leg, and left arm had counterclockwise angular momentum in the view from the back, while those of the right arm and ball and of the left leg had clockwise angular momentum. Overall, these segment groups cancelled the angular momentum values of each other and kept the body in balance.

Significant differences between the styles were found in all three H components of the five segment groups. The differences were concentrated in the late P2 phase and in the P3 and P4 phases for HX and HZ, and in the middle of the P2 phase and in the P3 and P4 phases for HY. The exception was the right leg HX, which showed almost no differences between the styles. In the P3 and P4 phases, the increase in the HX of the right arm and ball, which contributes to increase the ball velocity, was progressively smaller for OS, TS, SS and US. Conversely, the increase in the HZ of the right arm and ball was progressively larger for OS, TS, and SS and US, although there was no difference between the last two. It was suggested that the HX of the five segment groups (especially the right arm and ball and the trunk-head) in the OS, TS and SS from the late part of the P2 phase to the end of the P4 phase contributed to increase ball velocity, but it was not enough to cause significant differences in ball velocity between these three styles.

CONCLUSIONS

This study revealed the time-dependent patterns of angular momentum of the five body segment groups, as well as differences in the angular momentum values of those body segment groups, during an entire throwing cycle in the four styles of baseball pitching motion.

REFERENCES

[1] Miyanishi T et al. *Int J Sports Sci Coach*, 2022. https://doi.org/10.1177/17479541221128355
[2] Dapena J. *J Appl Biomech* **13**: 239-53, 1997.
[3] Pataky TC. *CMBBE* **15**: 295-301, 2012.

AN INTERACTION BETWEEN LANDING HEIGHT AND GROUND CONDITION IN GROUND REACTION FORCE DURING TWO-LEG LANDING

Jeongeun Moon[1], Geon-Tak Kim[2], Jae-Kyun Ryu[2], and Jihong Park[1]
[1]Athletic Training Laboratory, Kyung Hee University, Yongin, Korea.
[2] Biomechanics Laboratory, Kyung Hee University, Yongin, Korea.
Email: jihong.park@khu.ac.kr

INTRODUCTION

Athletes who frequently perform high jumps and acrobatic movements such as Taekwondo (TKD) Shibum are susceptible to injuries [1]. Vertical ground reaction force (vGRF) is one of the primary contributing factors known to increase the risk of injury, which is associated with landing height [2] and ground conditions [3]. For example, the magnitude of vGRF is attenuated when landing on a cushioned ground (e.g., sponge mats). However, the relationship between the landing height and ground condition remains unknown. Hence, this study examined the interaction between landing heights and ground conditions in peak vGRF (PvGRF) and time to PvGRF (TTPvGRF).

METHODS

Nineteen healthy, collegiate male Taekwondo Shibum athletes (20.7 years, 172.6 cm, 65.5 kg) volunteered. Participants visited the laboratory once and performed two-leg landings from three different heights (0.45 m, 0.90 m, and 1.35 m) on three different ground conditions (ground—force plate, TKD mat—2 cm thick, and sponge mat—14 cm thick) in a counterbalanced order. Five successful trials for each height and ground condition were recorded. A successful trial was defined when each foot completely landed on each force plate (960 Hz). The PvGRF (body weight: BW) and TTPvGRF (ms) during the stance phase (initial contact >25 N to peak knee flexion—not reported in this abstract) of each side (dominant vs. nondominant) were separately compared using a two-way mixed model analysis of variances and Tukey tests (p<0.05). Cohen's d effect size (ES) was calculated for the statistical significances.

RESULTS AND DISCUSSION

The PvGRF on the dominant side was different (height × condition: $F_{4,144}$=11.71, p<0.0001, Table 1). Specifically, on the ground (force plate), as the landing height increased, vGRF also increased (0.45 m: ×2.4 BW, 0.90 m: ×3.7 BW, 1.35 m: ×6.3 BW, p<0.0001, ES>3.66). When landing on the TKD and sponge mat from a height of 1.35 m, vGRF was attenuated to ×5.2 BW (p=0.0002, ES=0.76) and ×3.3 BW (p<0.0001, ES=3.11), respectively. The vGRF on the nondominant side (height × condition: $F_{4,144}$=8.91, p<0.0001) showed a similar pattern to the dominant side. TTPvGRF on the dominant side was different (height × condition: $F_{4,144}$=7.62, p<0.0001). Specifically, on the ground, (force plate) TTPvGRF was decreased from a landing height of 0.45 m (44.4 ms) to 0.90 m (36.9 ms, p<0.05, ES=0.85). When landing from a height of 1.35 m, using the sponge mat can increase the time to reach PvGRF by 19.1 ms, compared with landing on the ground (p<0.0001, ES=3.91). The non-dominant side (height × condition: $F_{4,144}$=4.78, p=0.001) also showed similar patterns to the dominant side.

CONCLUSIONS

The vGRF increases as the landing height increases. Using the TKD mat does not seem to be beneficial for a height <0.90 m. While the landing impact goes up to ×6 BW when landing from 1.35 m, the sponge mat should be used in order to reduce vGRF by 52 %.

REFERENCES

[1] Doo H et al. *Res Sports Med* **In Press:** 2021.
[2] Yeow CH et al. *The Knee* **16:** 381-6, 2009.
[3] Lee J et al. *Asian J Kinesiol* **15:** 93-104, 2013.

Table 1: Changes in PvGRF and TTPvGRF during drop landing

		Dominant			Nondominant		
		0.45 m	0.90 m	1.35 m	0.45 m	0.90 m	1.35 m
Ground	PvGRF (BW)	2.4 (0.9)	3.7 (1.0)	6.3 (1.9)	2.2 (0.9)	3.6 (1.2)	6.1 (2.0)
	TTPvGRF (ms)	44.4 (11.6)	36.9 (4.7)	30.9 (3.9)	45.2 (9.5)	37.9 (4.9)	31.9 (4.8)
TKD mat	PvGRF (BW)	2.5 (0.8)	4.0 (0.7)	5.2 (1.1)	2.3 (0.7)	3.6 (0.8)	5.1 (1.1)
	TTPvGRF (ms)	39.8 (12.8)	34.4 (4.1)	32.3 (4.6)	40.5 (10.7)	36.7 (5.9)	32.3 (3.8)
Sponge mat	PvGRF (BW)	1.4 (0.3)	2.3 (0.4)	3.3 (0.7)	1.2 (0.2)	2.0 (0.4)	3.0 (0.8)
	TTPvGRF (ms)	73.9 (14.2)	54.4 (3.2)	50.0 (5.2)	68.3 (10.2)	53.4 (4.0)	50.0 (4.9)

Values are mean (standard deviation); BW: body weight; TTPvGRF: time to peak vertical ground reaction force

DIFFERENCES IN LOWER EXTREMITY MUSCLE ACTIVATION PATTERNS DURING ANTICIPATED OR UNANTICIPATED SINGLE-LEG DROP JUMP TASKS

Jaewook Lee[1], Hyunji Doo[2], Jihyun Kim[2], Jong-Chul Park[3], Eonho Kim[4] and Jihong Park[1]
[1]Athletic Training Laboratory, Kyung Hee University, Yongin, Korea
[2] Department of Sports Science, Korea Institute of Sports Science, Seoul, Korea
[3] Department of Marine Sports, Pukyong National University, Busan, Korea
[4] Department of Physical Education, Dongguk University, Seoul, Korea
Email: jihong.park@khu.ac.kr

INTRODUCTION

A single-leg landing from a jump or a single-leg landing followed by immediate jumping is frequent athletic movements that have the potential to cause injuries. If the movement task is performed under an unanticipated situation (e.g., the task after landing is not preplanned), the injury risk could be greater [1]. Appropriate muscle activation (e.g., timing and magnitude) is essential for dynamic stabilisation of the lower extremity joints. Therefore, the purpose of our study was to examine the lower extremity muscle activation patterns during the anticipated and unanticipated single-leg drop jump tasks. Subjects under the unanticipated condition would have less activation before and after initial contact when compared with those under the anticipated condition.

METHODS

Surface electromyography (EMG, 1,500 Hz) was collected from 17 healthy young male subjects (24 years; 173 cm; 72 kg) and included measurements from the gluteus medius (GM), rectus femoris (RF), vastus medialis (VM), semitendinosus (ST), biceps femoris (BF), tibialis anterior (TA), and medial gastrocnemius (MG) on the dominant leg. Subjects were asked to drop down from a wooden box 40 cm high with their dominant leg (landing), then immediately jump with their dominant leg as high as possible (jumping). For the anticipated condition, subjects were informed of the drop jump task prior to the initial drop. For the unanticipated condition, the specific task was visually shown on a light-emitting diode screen with an upward or downward arrow for jumping or landing, respectively, which was triggered by the infrared sensor when a subject's foot was sensed prior to initial contact. Three successful trials on each condition were averaged for analysis. Muscle activation patterns were identified during the drop phase (200-ms prior to initial contact to initial contact) and the weight acceptance phase (initial contact to peak knee flexion); normalised by the peak amplitude recorded on each trial; smoothed (a 4th order zero-phase-shift Butterworth high- and low-pass with a cutoff freqency of 15 and 20 Hz, respectively); then compared using functional linear models [2] to detect differences between conditions (p<0.05) and Cohens' d effect sizes (d).

RESULTS AND DISCUSSION

During the drop phase (0% being 200 ms prior to initial contact, and 100% being initial contact), activation of the VM (75%) and ST (73 to 82%) were less (VM: < 32%, d=0.48; ST: < 34.2%, d=0.52), but activation of the TA (1 to 6%) was greater (< 43%, d=0.60) for the unanticipated condition relative to the anticipated condition. During the weight acceptance phase (0% being initial contact, and 100% being peak knee flexion), activation of the GM (66 to 77%, and 85 to 98%), RF (55 to 97%; Figure 1), VM (71 to 97%), ST (44 to 53% and 72 to 73%), BF (92 to 100%), and TA (63 to 94%) were less (GM: < 34%, d=0.60; RF: < 45%, d=0.85; VM: < 38%, d=0.71; ST: < 36%, d=0.69; BF: < 44%, d=0.70; TA: < 34%, d=0.64) for the unanticipated condition relative to the anticipated condition.

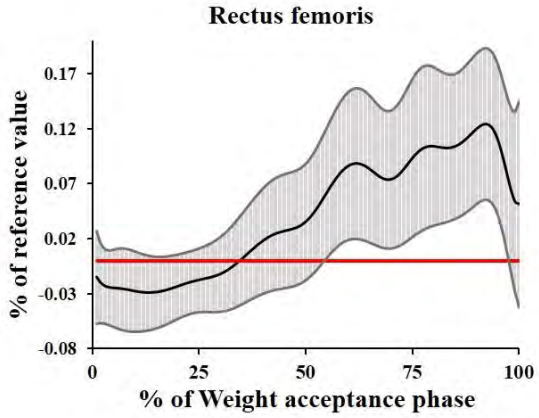

Figure 1. Result for the rectus femoris during the weight acceptance phase. The black line represents the mean difference between conditions (anticipated – unanticipated), and the grey band represents the 95% confidence intervals. When the grey band does not pass the red zero line, a statistical difference between the conditions exists.

CONCLUSIONS

Overall, less muscle activation in the lower extremity was observed when the movement task (e.g., landing or jumping) was not preplanned. These neuromuscular changes could alter joint kinematics and stability in the lower extremity, which may increase the injury risk [3]. Therefore, practitioners or coaches in open-skill sports should be aware of these aspects and establish the appropriate injury prevention strategies.

REFERENCES

[1] Simpson JD et al. *Hum Mov Sci* **64**: 133-41, 2019.
[2] Park J et al. *J Hum Kinet* **60**: 39-49, 2017.
[3] Palmieri-Smith RM et al. *J Electromyogr Kinesiol* **18**: 973-9, 2008.

NEUROMUSCULAR FATIGUE OF VASTUS LATERALIS DURING FATIGUING SQUAT EXERCISES IN TRAINED AND UNTRAINED PEOPLE: TIME-FREQUENCY ANALYSIS

Jihong Park[1], Hoon Kim[2], Dongkyun Seo[1], Sungkyu Jeon[1], Seunghun Lee[1]
[1] Athletic Training Laboratory, Kyung Hee University, Yongin, Korea
[2] Department of Sports Medicine, Soonchunhyang University, Asan, South Korea
Email: jihong.park@khu.ac.kr

INTRODUCTION

Exercise-induced fatigue affects neuromuscular functions such as muscle force and muscle activation. Because these neuromuscular fucntions affect movement alterations such as joint kinematics and kinetics, which may increase injury risks, it is important to understand neuromuscular patterns during fatiguing exercises. Many previous studies have reported neuromuscular fatigue during exercises, but single-joint exercises such as ankle dorsiflexion, thumb adduction, knee extension, and elbow flexion were traditionally investigated using electromyography (EMG) amplitude analysis [1]. Although the existing data are valuable, further investigation is needed because single-joint movements do not occur in daily activities and because frequency contents are also affected by fatigue, not only EMG amplitude. Additionally, experiences of specific exercises may affect neuromuscular responses under fatiguing status. Therefore, the purpose of the current study was to examine the effects of the set and repetition on muscle activation of the vastus lateralis during fatiguing squat exercises in trained and untrained people.

METHODS

Eighteen trained and 16 untrained people participated in this study. Participants performed five sets of multiple repetitions of squats with a fatiguing protocol. One video camera and an EMG electrode on the vastus lateralis of the dominant leg were used to collect motion and muscle activation data, respetively. Concentric and eccentric phases were identified using bar trajectories in video data with Kinovea software. Muscle activation data were analysed with wavelet transformation with 30 non-linearly scaled wavelets, then we summed the intensities across all time points for each wavelet [2]. We extracted Principal Components (PCs) and PC scores using Principal Component Analysis (PCA). Then, we performed three-way analysis of variances ($p<0.05$). Independent variables were set (1–5 sets), and repetition (initial vs. end), group (trained vs. untrained). Dependent variables were their PC scores. In the current abstract, we report differences in PC2 scores, which captured frequency contents because our main interest was EMG frequency response in muscle activation.

RESULTS AND DISCUSSION

There are significant main effects for the repetition (Figure 1B, $p=0.001$) and set (Figure 1C, $p=0.03$) in the PC2 score measured during the concentric phase of the squat. There was a significant main effect for repetition (Figure 1E, $p=0.003$) in the PC2 score measured during the eccentric phase of the squat.

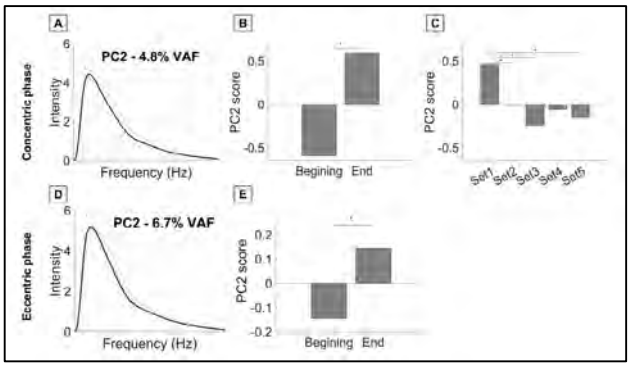

Figure 1. Effects of ±1SD of PC scores in PC2 of vastus lateralis EMG data during concentric (A) and eccentric (B) phases of squats. PC2 scores patterns depending on repetition (B and E) and set (C). VAF: variance accounted for.

Our results showed that the accumulated repetitions shifted EMG frequency toward the low frequency ranges during the concentric phase. Conversely, EMG intensity was shifted more toward the high frequency ranges as sets were accumulated, compared to the first set during the concentric phase. In the eccentric phase, the EMG intensity was shifted toward the low frequency ranges as repetitions were accumulated.

CONCLUSIONS

The training status did not affect the fatiguing responses of the vastus lateralis. However, the accumulated repetitions and sets were factors that influenced the frequency contents of activation of the vastus lateralis. Importantly, the direction of frequency shift was the opposite between accumulated repetition and sets. Our results suggest that trainers should consider repetitions and sets as different factors on neuromuscular fatiguie during squats. For example, the fatiguing squat exercises should increase repetitions and sets depending on frequency ranges that are targeted for training.

ACKNOWLEDGEMENTS

The results were parts of data collected as a class project (SM32602) in the Department of Sports Medicine at Kyung Hee University.

REFERENCES

[1] Hunter SK. et al. *Exerc Sport Sci Rev* **32**, 44-9, 2004.
[2] von Tscharner V. *J Electromyogr Kinesiol* **10**, 433-45, 2000.

Track GRFs from an elite transfemoral paralympic sprinter using a wearable clamp dynamometer

Mattia Scapinello[1], Giacomo Fabris[1], Andrea G. Cutti[2] and Nicola Petrone [1]
[1] Department of industrial engineering, University of Padova, Padova, Italy.
[2] INAIL Prosthetic Centre, Vigorso di Budrio, Bologna, Italy.
Email: mattia.scapinello@phd.unipd.it

INTRODUCTION

Knowledge of ground reaction forces (GRF) between the foot and the ground is essential for Paralympic athletes with lower limb amputees who practice running and jumping in order to analyse and optimize the biomechanics of the sporting gesture, to improve safety and reduce the likelihood of injury. Different approaches can be found in literature for the measurement of GRF; a large number of force platforms embedded in the track [1] involve dedicated expensive installations, running on instrumented treadmills [2] or treadmills placed on 4 force platforms [3] requires specific training and limits high acceleration sprinting, direct sensing from instrumented and calibrated RPF using strain gauges [4] limits the study to pre-instrumented RPF. Aim of the present work was the design, installation and track testing of a wearable load acquisition system capable of acquiring six load components at the RPF enabling the quick evaluation of different RPF or different alignments.

METHODS

The wearable load acquisition system consists of a commercial thin six-axis load cell (diameter 65mm, thickness 9mm, mass 0.19kg) equipped with two custom made titanium plates designed and built to connect mechanically with the pyramid adapters present in the RPS for athletes with TF amputation. The load cell calibration was bench validated applying known masses and torques. The device was installed between the Ottobock 1E91 Runner Std. Cat. 3.5 C-shaped foot clamp and the Ottobock 3S80 SPORT sports knee of the prosthesis of an elite female athlete of the Italian Paralympic national team (55 Kg, 1.60 m). The system was connected to a wearable data logger (DTS SLICE NANO, DTS, USA) placed in the backpack worn by the athlete during test sessions, together with its Lithium-Polymer battery, while a six degree of freedom inertial sensor (6DX PRO-A, DTS, USA) was placed under the clamp on the RPF (Figure 1a). The Palaindoor athletics track located in Padova was covered with a total of 28 motion capture cameras (Vicon Motion System, Oxford, UK), 22 mounted on tripods placed all along the runway, covering approximately 20-metres-long acquisition volume, and 6 cameras installed on a double portal structure, placed in the centre of the runway. Indoor test sessions consisted in six sprint trials: in the first three the start occurred in the calibrated volume, in other three the athlete reached the calibrated volume at constant speed around 6.5 m/s (approximately 60% of personal maximal speed). Clamp Reaction Forces acquired in the load cell reference system (X_{LC}, Y_{LC}) were filtered using a 4th order, low pass Butterworth filter (cut-off 52 Hz) while GRFs in the Ground reference frame (X_{GR}, Y_{GR}) were computed using the clamp orientation matrix (sagittal angle θ_{LC}), obtained from Motion Capture data.

RESULTS AND DISCUSSION

GRFs from steady state running are in agreement with literature findings [2], GRFs during start show clear differences with steady running and represent an original result for transfemoral paralympic elite athletes. The delayed vertical peak and the positive horizontal component confirm the need of track testing for the appropriate evaluation of running biomechanics.

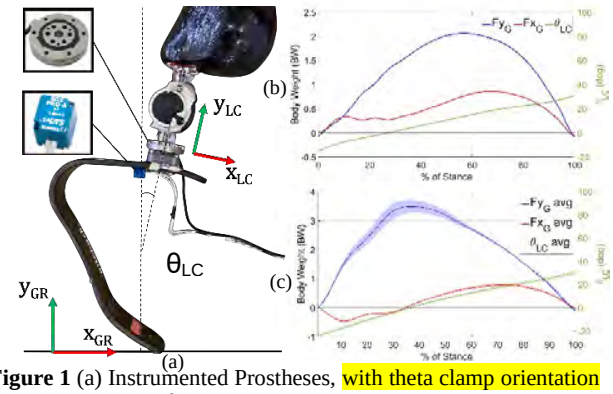

Figure 1 (a) Instrumented Prostheses, with theta clamp orientation (b) GRF from the 4th step in a START event. (c) GRF mean curves

CONCLUSIONS

A wearable system for RPF clamp load collection was developed and applied to a transfemoral elite paralympic sprinters to measure GRFs. The system will give insight into sprinting biomechanics and allow investigating the effect of RPF stiffness and alignment.

ACKNOWLEDGEMENTS

Athlete and FISPES for their involvement in the study. INAIL for funding the OLIMPIA project PR19-PAI-P4.

REFERENCES

[1] Nagahara R et al. *J Appl. Biomech.* **34**, 104–110, 2018.
[2] Ueda et al. *J Sports Med* **37**, 1087–1090, 2016.
[3] Breban SG et al. *ISBS Proceedings Archive:* ***Vol. 40****: Iss.1. Article 22*, 2022.
[4] Petrone N. et al. *Sensors* **20**(20): 5758, 2020.

COMPARISON BETWEEN ROTATIONAL SHOT PUT TECHNIQUE AND DISCUS THROW

Tadahiko Kato [1], Kei Maeda [2] and Jun Mizushima [3]
[1] Department of Materials and Human Environmental Sciences, Shonan Institute of Technology, Fujisawa, Japan.
[2] Department of Health and Sports Sciences, Kyoto University of Advance Sciences, Kameoka, Japan.
[3] Department of Health and Sports Sciences, Toyo University, Tokyo, Japan
Email: kato@mate.shonan-it.ac.jp

INTRODUCTION

The rotational technique is becoming the mainstream technique in recent shot put competitions (Dinsdale et al., 2017). This technique involves rotating the body in a similar way to the discus throw, which is also a throwing event in athletics, during the preparatory phase before delivering the throwing material. There are many similarities between the rotational shot put technique and the discus throw, with several athletes having competed in both events at the international level. However, threr is limited knowledge available on biomechanical comparisons between the shot put and discus throw.

Therefore, the aim of this study was to clarify the biomechanical similarities and differences between the rotational shot put technique and the disucs throw.

METHODS

Sixteen male shot putters (stature: 1.77 ± 0.06 m, body mass: 111.38 ± 9.78 kg, shot put record: 15.31 ± 1.38 m) and 16 male discus throwers (stature: 1.79 ± 0.05 m, body mass: 92.63 ± 9.92 kg, discus throw record: 48.29 ± 4.07 m) participated this study. Both groups were comparable in WA scoring tables of Athletics 2022 (shot put: 841.81 ± 81.74, discus throw: 845.88 ± 74.35). Their throwing motions during athletic competitions were recorded using two or three DV cameras at 60 fps with a shutter speed of 1/1500 s for the shot put (HDR-CX675, Sony, Tokyo, Japan) and at 300 fps with a shutter speed of 1/3000 s for the discus throw (EX-F1, Casio, Tokyo, Japan). The throwing material and 25 end points of each body segment were manually digitized at 60 Hz for the shot put and at 100 Hz for the discus throw, and three-dimensional DLT method was applied to collect coordinate data. A Butter worth digital filter with the cut-off frequencies ranging from 3 to 9 Hz was used to smooth the coordinate data. Smoothed coordinate of the shot put motion was converted to a 100 Hz equivalent time axis using a spline function.

The initial velocity of the throwing material at the moment of release (RV) was obtained. The throwing material and the athletes's body were assumed to be a system. The velocity of centre of gravity of the system (CGV), the linear momentum of the system (LM), the angular momentum of the system (AM) and the impulse of the throwing material were calculated.

The Pearson product-moment correlation coefficient was used to understand the relationship between the RV and other variables. The Welch t-test was used to compare the variables between shot put and discus throw. All significant level was set at 0.05.

RESULTS AND DISCUSSION

A significant positive correlation was found between the RV and total CGV at release in the discus throw (r = .634). However, only the shot put showed a significant positive correlation between RV and LM just before the release (r = .583).

Figure 1 illustrates the total CGV and toral LM throughout the throwing motion (initiation-release of the throwing material) with the normalized time as 100% of whole motion. The discus throw had significantly higher CGV than shot put in almost all phases of the throwing motion (25-97% time, $p < 0.05$). In contrast, shot put and discus throw generally showed comparable values of LM during the entire throwing motion, although there were significant differences in some phases (36-48, 71-76, 82-89 and 95-100 % time, $p < 0.05$). One of the critical differences between the shot put and discus throw is the size of the space available for the throwing motion. These differences between the shot put and discus throw represent the characteristics of each event.

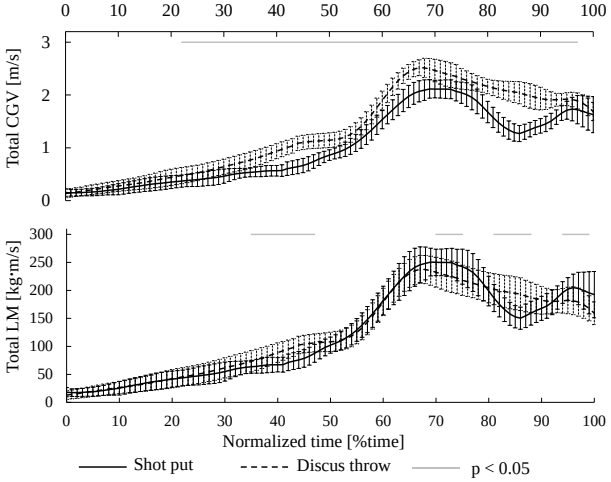

Figure 1: Comparison the Total CGV and total LM between the shot put and the discus throw during the whole throwing motion.

CONCLUSIONS

Based on these findings, discus throwers utilize the available space to accelerate the system, whereas shot putters control the system within a restricted space and increase the linear momentum of the system, resulting in higher throwing records.

REFERENCES

[1] Dinsdale et al. (2017). Biomechanical Report for the IAAF World Championships London 2017.

THE EFFECT OF SINGLE-LEG ROTATIONAL LANDING ON KNEE KINEMATICS

Weerawat Limroongreungrat[1], Nuttaput Phuvachaivivate[1], Jim Richards[2], Parunchaya Jamkrajang[1]
[1]College of Sports Science and Technology, Mahidol University, Nakorn Pathom, Thailand.
[2]Allied Health Research Unit, University of Central Lancashire, UK
Email: Parunchaya.jam@mahidol.edu

INTRODUCTION

High or repeated single-leg landing, particularly unpredictable landings, can lead to a high load to the lower extremities. A previous study showed that the risk of lower limb injury increases when the direction of the landing task changes from forward to lateral due to a stiff landing strategy [1]. However, while most research has focused on knee biomechanics with forward-directed landing tasks, the impact of landing orientations on knee kinematics in other planes still needs to be determined. Moreover, little research has been conducted investigating rotational landings in different directions. Therefore, this study aimed to investigate the effect of single-leg rotational landing on knee kinematics between altered landing locations. We hypothesized that the knee kinematics of the dominant leg would significantly differ between the rotational landing directions.

METHODS

Fifteen healthy male basketball players volunteered for this study. Single-leg landing tasks were recorded using 44 reflective markers attached to the participant's trunk and lower limbs following a previously published model [2] using a 3D motion analysis system and a force platform. Prior to data collection, participants warmed-up for 10 minutes. For the landing tasks, participants were asked to stand on their dominant leg with the knee extended and hands on the side of the body, then jump from a 30-cm high box and then land on the dominant leg in three directions; forward landing (FL), right rotational landing (RRL) and left rotational landing (LRL), using their dominant leg (DL. Participants were instructed to look forward and balance as quickly as possible and hold the single limb stance for 5 seconds on landing. The order of landing directions was randomized using a ballot method. A 30-second rest was provided between each trial. Three successful landing trials in each direction were analyzed. Knee joint kinematics at the initial contact (IC) and maximum knee flexion (MKF) were calculated using Visual 3D. All data were normally distributed and differences between the directions were explored using Repeated Measure ANOVA tests ($p<0.05$) and significant main effects were explored using post-hoc Tukey tests.

RESULTS AND DISCUSSION

There was a significant difference in knee joint internal rotation among the three conditions at MKF (Table 1). The post-hoc test further revealed significantly greater internal rotation in RRL compared with FL. Landing with the knee internally rotated may have increased the load on the ACL [3], which may be considered risky and could lead to ACL injury.

CONCLUSIONS

When performing different single-leg rotational landing directions, there are differences in knee joint angles, particularly knee internal rotation at the MKF. Changes in this angle may lead to an increase in the risk of ACL injury. Using such tasks needs to be carefully considered when being used in individuals who may be at a higher risk of such injuries and during the rehabilitation of ACL injuries.

REFERENCES

[1] Sinsurin K et al. *Journal of physical therapy science,* ***25***(9): 1109-1113, 2013.
[2] Vanrenterghem J et al. *Gait & posture*, **31**(4): 517-521, 2010.
[3] Shinde T et al. *Physical Therapy in Sport*, **58**: 87-92, 2022.

Table 1: Knee joint angle during different rotational drop landing positions

Knee Joint angle (deg)	FL	LRL	RRL	*p-value*
Initial contact				
Flex (-)/Ext (+)	-18.4 ± 7.46	-25.9 ± 28.2	-24.9 ± 28.1	$p = 0.721$
Abd (-)/Add (+)	-1.69 ± 6.52	-1.65 ± 7.78	-1.03 ± 7.51	$p = 0.421$
IR (-)/ER (+)	-5.99 ± 21.1	-7.23 ± 21.2	-5.99 ± 20.4	$p = 0.537$
Maximum knee flexion				
Flex (-)/Ext (+)	-59.8 ± 8.28	-69.3 ± 25.4	-67.6 ±25.7	$p = 0.144$
Abd (-)/Add (+)	-0.02±11.1	-0.01±9.97	-2.81±10.9	$p = 0.276$
IR (-)/ER (+)	-2.33±0.63	-3.31±11.3	-4.24±11.8*	$p = 0.045$

*Significant difference between front landing (FL) and right rotational landing (RRL)

BONE-REMODELLING IN THE FOOT: APPLICATION TO EXERCISE DURING THE COVID-19 LOCKDOWN

J Kim[1], L Xiang[1], P Kelly[2], Q Mei[1,3,4], S Gusso[5,6], T Besier[1,2] and J Fernandez [1,2,4]

[1] Auckland Bioengineering Institute, University of Auckland, Auckland, New Zealand.
[2] Department of Engineering Science, University of Auckland, Auckland, New Zealand.
[3] Faculty of Sports Science, Ningbo University, Ningbo, China.
[4] Research Academy of Grand Health, Ningbo University, Ningbo, China
[5] Department of Exercise Sciences, University of Auckland, Auckland, New Zealand.
[6] Liggins Institute, University of Auckland, Auckland, New Zealand.
Email: hkim375@aucklanduni.ac.nz

INTRODUCTION

Inspired by Wolff's law, many bone remodelling algorithms have been developed and evaluated, but their application has not been explored in the foot. This study aims to extend the application further, evaluating numerically predicted osteogenic responses at the foot against experimental hopping data collected during the COVID-19 lockdown in New Zealand. Two different subject-specific finite element (FE) models were developed to investigate the spectral (Model A) and temporal (Model B) modelling behaviour.

METHODS

Following ethical approval participants attended scanning sessions on a SIEMENS scanner (Model A) and a 1.5T Avanto Fit scanner (Model B). Their feet were segmented in Mimics and meshed in HyperMesh to provide a finite element geometry that was solved in Abaqus. A linear elastic lumped soft tissue model was used with Young's modulus of 1.15 MPa, and Poisson's ratio of 0.49. Plantar fascia was represented by linearly elastic connectors whose stiffness was 200N/mm. Plantar pressure measured during gait, and Achilles tendon force were applied to load the foot. Model A considered walking to reproduce morphogenesis induced by the most dominant daily activity, where the subject's bone mineral density (BMD) distribution was measured by computed tomography (CT). Model B replicated an experimental study where a subject performed a hopping exercise on the allocated exercise leg while the other leg served as a control. The exercise lasted one year, with the COVID-19 pandemic lockdown happening during the first eight months. BMD changes at the foot were measured by dual X-ray absorptiometry (DEXA). A continuum damage mechanics based anisotropic bone remodelling model [1] with an ability to evolve the setpoint value following the cellular accommodation theory [2] was employed to predict the osteogenic responses.

RESULTS AND DISCUSSION

A cortical bone layer of similar thickness as the measurement was predicted in Model A by the bone remodelling algorithm around the outer edges of the calcaneus (Figure 1A), denoted by the representative density value of cortices. Density changes predicted in Model B also shared a similar trend with the measured data (Figure 1B); both legs showed subtle density changes during the lockdown interval, but they gained densities after the lockdown, with more increase happening at the exercise leg. Both models showed good agreement between the numerical prediction and the measured data, demonstrating a reliable performance of the bone remodelling algorithm in temporal and spectral aspects.

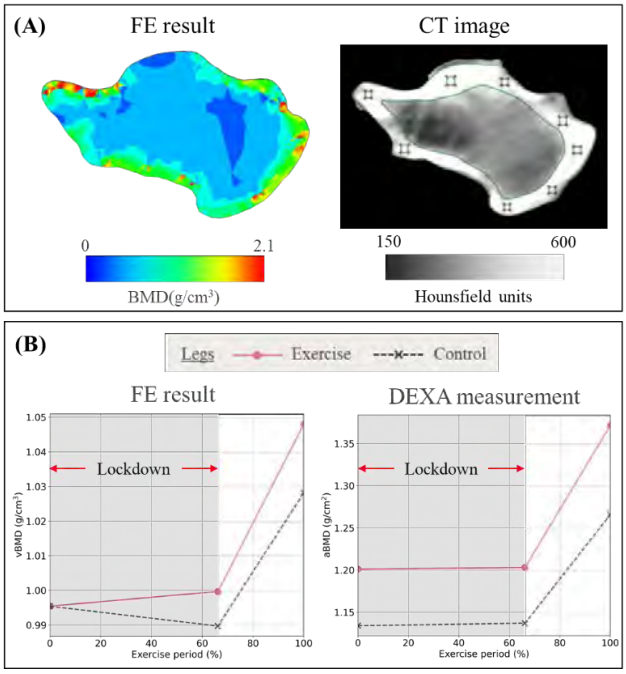

Figure 1 (A) Density distribution predicted by the bone remodelling algorithm in Model A, and CT showing relative Hounsfield units at the calcaneus. (B) Predicted and measured density changes during the hopping exercise.

CONCLUSIONS

This study showed that a widely used bone remodelling algorithm can be successfully extended to the foot and reproduce morphological features of a relatively thick cortical bone layer, and how the frequency and the intensity of daily loading influence density changes.

REFERENCES

[1] Doblaré M & García J M. *J Biomech* **35**: 1-17, 2002.

[2] Turner C H. *Calcified Tissue International* **65**: 466-471, 1999.

VALIDATION OF MARKERLESS MOTION CAPTURE FOR THE ASSESSMENT OF JOINT REACTION FORCES UNDER VARYING BODY-BORNE LOADS

Isabel Coll[1], Matthew P. Mavor[2], Allison Clouthier[2] and Ryan B. Graham[1, 2]

[1] Ottawa-Carleton Institute for Biomedical Engineering (OCIBME), Ottawa, ON, Canada.
[2] School of Human Kinetics, Faculty of Health Sciences, University of Ottawa, Ottawa, ON, Canada.
Email: icoll077@uottawa.ca

INTRODUCTION

As a mission's success relies on its troop's ease and speed of travel, it is crucial to objectively evaluate a soldier's movement pattern and joint stress under different equipment configurations [1]. Traditional optical motion capture involves the time-consuming process of placing reflective markers directly on the skin, which is challenging when wearing clothing and bulky body-borne loads. An emerging option is markerless motion capture (e.g. Theia3D, Theia Markerless Inc., Canada) which uses deep neural networks to track the position of anatomical landmarks from an array of synchronized RGB video cameras. The aim of this study is to determine whether a markerless motion capture system can accurately capture the joint loading of heavily equipped participants, compared to an optical motion capture system.

METHODS

Data were collected simultaneously from 7 video cameras recording at 60 Hz (Vue, Vicon, UK) and 11 infrared optical motion capture cameras recording at 120 Hz (Vantage V5, Vicon, UK). 16 participants (8 females; 8 males; height = 1.7 ± 0.1 m; weight = 72.8 ± 10.0 kg) performed a series of three walking and running trials over a 6-metre distance and under four different equipment configurations: C1 = 5 kg, C2 = 21 kg, C3 = 35 kg (C2 + 14 kg small pack), and C4 = 41 kg (C2 + 20 kg rucksack) [2]. Data from the video cameras were processed using the Theia3D software. Resultant joint angles and joint centres were used to perform subject-specific scaling and inverse kinematics (IK) in OpenSim v4.3 (SimTK, USA) using the Rajagopal full-body musculoskeletal model [3]. Residual reduction analyses (RRA) and static optimization (SO) were also conducted to estimate muscle forces and subsequently compute lower limb joint loading. For the optical data, marker coordinates were used to perform these same steps in OpenSim v4.3, again with the Rajagopal model. Both joint angles and contact forces were compared between the systems via root mean square error (RMSE) and Pearson's correlation coefficients.

RESULTS AND DISCUSSION

Overall, kinematic results show good agreement between the optical and markerless motion capture systems for the lower body joint angles. Results of joint loading RMSEs for the heaviest configuration (C4) at the ankle, knee, and hip joints were found to be 0.53 ± 0.14 xBW, 0.44 ± 0.13 xBW, and 0.49 ± 0.19 xBW, respectively. These results are presented in (Figure 1) for walking trials only. The results from both systems were very highly correlated during both walking and running at all joints (r > 0.90). RMSE between systems systematically increased as body-borne load increased, which may have been caused by optical data quality during trials with bulkier equipment.

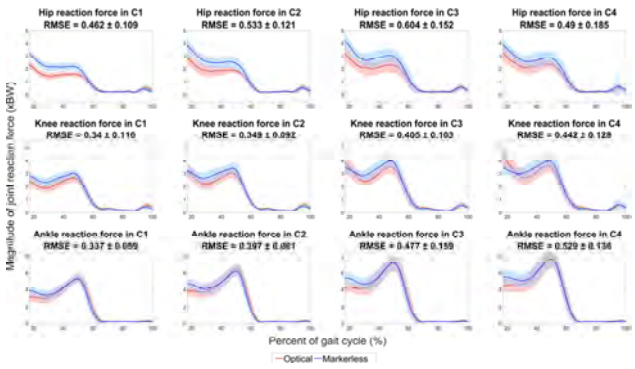

Figure 1. Plots of lower limb joint reaction forces through gait under all loading conditions for walking trials.

Although there is an offset between the joint loading estimated from both motion capture systems, they both predict similar changes in peak joint loading through the equipment configurations. Future work will aim at evaluating the cause of this joint loading offset, probably related to coordinate system alignment issues.

CONCLUSIONS

Markerless motion capture appears to be a feasible alternative to measure soldier joint loading of the lower limbs, even when carrying bulky equipment. In a military context, it could potentially facilitate in-field assessment of soldiers' biomechanics in different equipment configurations to contribute to their safety.

ACKNOWLEDGEMENTS

This study is funded by the Master's Research Scholarship from the *Fonds de recherche du Québec en nature et technologies.*

REFERENCES

[1] Boffey et al., 2019. Mil. Med., 184(1–2).
[2] Mavor et al., 2019. DRDC-RDDC-2020-C001.
[3] Rajagopal et al., 2016. IEEE Trans. Biomed. Eng., 63(10)

The effect of subscapularis repair following posterosuperior rotator cuff tear severities on superior joint shear force during abduction in reverse shoulder arthroplasty

Donghwan Lee [1] and Choongsoo S. Shin [1]
[1] Department of Mechanical Engineering, Sogang University / Seoul, Republic of Korea.
Email: cshin@sogang.ac.kr

INTRODUCTION

Reverse shoulder arthroplasty (RSA) is a surgical procedure to treat pain and provide functional improvement in patients with severe rotator cuff tear arthropathy [1]. Previous clinical studies reported that severe rotator cuff tears in RSA may increase the risk of postoperative dislocation [1,2]. For this reason, subscapularis repair in RSA has been considered to improve glenohumeral joint stability [2].
Increased superior joint shear force in RSA may contribute to joint instability in the superior-inferior (SI) direction during abduction [3]. However, the effect of subscapularis repair in RSA following posterosuperior rotator cuff (supraspinatus and infraspinatus) tear severities on the superior joint shear force is unclear. Therefore, the purpose of this study was to examine the effect of subscapularis repair following posterosuperior rotator cuff tear severities on the superior joint shear force during abduction in RSA.

METHODS

7 male subjects (age: 24.7±2.4 years, mass: 74.2±6.2 kg, height: 176±5.7 cm) participated in experiments. The subjects were instructed to take 3-seconds to perform 120° abduction in the coronal plane. Motion capture data were recorded for each subject using a motion capture system with 10 infrared cameras (9 Eagle, 1 Raptor; Motion Analysis Corp., Santa Rosa, CA, USA). A 3-dimensional musculoskeletal shoulder model was implemented using the AnyBody Modeling System (V7.3.4., AnyBody Tech., Aalborg, Denmark). The musculoskeletal model of RSA was then developed using the Equinoxe Reverse Shoulder System (Exactech, Gainesville, FL, USA). Posterosuperior rotator cuff tear severities were modelled into 4 types (Figure 1).
The superior joint shear force of both subscapularis torn and repaired RSA models was compared with that of the intact rotator cuff RSA model, respectively. The effective rate of subscapularis repair in the superior joint shear force was calculated as the number of effective cases divided by the number of all cases (8 cases).

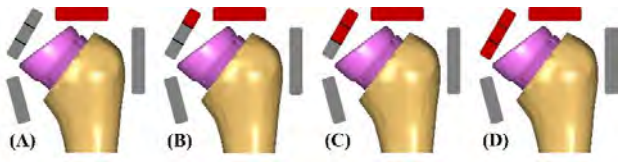

Figure 1 Rotator cuff configuration in the RSA model: (A) type A, isolated bundle tear of the supraspinatus; (B) type B, superior bundle tear of the infraspinatus; (C) type C, middle bundle tear of the infraspinatus; (D) type D, entire bundle tear of the infraspinatus.

RESULTS AND DISCUSSION

Table 1 The effect of subscapularis repair on the superior joint shear force in comparison with 3 models.

			(n = 7)
Type A	E[a]	4 (75°/90°/105°/120°)	Effective rate
	IE[a,b]	4 (15°/30°/45°/60°)	50%
Type B	E[a]	5 (60°/75°/90°/105°/120°)	Effective rate
	IE[a,b]	3 (15°/30°/45°)	62.5%
Type C	E[a]	4 (75°/90°/105°/120°)	Effective rate
	IE[a,b]	4 (15°/30°/45°/60°)	50%
Type D	E[a]	3 (90°/105°/120°)	Effective rate
	IE[a,b]	5 (15°/30°/45°/60°/75°)	37.5%

E, effective; IE, ineffective.
[a]Significant differences between the intact rotator cuff RSA model and subscapularis torn RSA model ($P < .05$).
[b]Significant differences between the intact rotator cuff RSA model and subscapularis repaired RSA model ($P < .05$).

In the type A, B, and C conditions (isolated bundle tear of the supraspinatus to the middle bundle tear of the infraspinatus), the effective rate of subscapularis repair in the superior joint shear force was greater than or equal to 50% (Table 1). In the type D condition (entire bundle tear of the infraspinatus), the effective rate was 37.5% (Table 1). A previous simulation study reported that posterosuperior rotator cuff tears in RSA increased the superior joint shear force and may reduce joint stability in the SI direction during abduction [4]. Our results suggest that the subscapularis repair in RSA could improve joint stability in the SI direction by sufficiently decreasing the superior joint shear force during abduction.

CONCLUSIONS

Patients who underwent RSA may require subscapularis repairing to sufficiently decrease the superior joint shear force during abduction.

ACKNOWLEDGEMENTS

The research was supported by KIAT (Korea Institute for Advancement of Technology) grant funded by the Korea Government (MOTIE: Ministry of Trade Industry and Energy) (P0013646).

REFERENCES

[1] Boileau P et al. *J Shoulder Elbow Surg* **14(1 Suppl S)**: 147-61S, 2005.
[2] Edwards TB et al. *J Shoulder Elbow Surg* **18(6)**: 892-6, 2009.
[3] Ackland DC et al. *J Orthop Res* **29(12)**: 1850-8, 2011.
[4] Ackland DC et al. *J Orthop Res* **37(1)**: 211-9, 2019.

Morphological musculoskeletal database of upper extremity using homologous modeling

Shoji Konda[1,2], Norio Fukuda[2], Jun Umehara[2,3] and Masaya Hirashima[2]
[1] Department of Health and Sport Sciences, Osaka University Graduate School of Medicine, Toyonaka, Japan.
[2] Center for Information and Neural Networks, Advanced ICT Research Institute, NICT, Suita, Japan.
[3] Faculty of Rehabilitation, Kansai Medical University, Hirakata, Japan.
Email: skond.med@osaka-u.ac.jp

INTRODUCTION

Musculoskeletal simulation models have been widely used in field of biomechanics. In this model, muscles have been generally simplified as wires, but volumetric muscle models have been developed in recent years [1,2]. The volumetric data of the bone and muscle were created from cadaver [1] or medical imaging data [2]. There is a database that publishes three-dimensional shape models of organs of the whole body, but the shape is limited to certain standard shape [3]. There is no database which has an average shape and its variation of the bones and muscles. For the use of muscle skeletal simulation, the bone and muscles should be represented by homologous models. The homologous model is a model in which the data of any subject is reconstructed to consist of the same number of grids of the same topology, and each grid is defined to have the same anatomical meaning. Thus, we aimed to develop a morphological musculoskeletal database using homologous modeling.

METHODS

Eighty-nine male young adults were asked to participate in this study. This study was approved by the institutional review board, and the participants provided written informed consent. Magnetic resonance (MR) images of left upper extremity from shoulder joint to wrist joint were acquired by a 3-Tesra MR system (MAGNETOM Vida, Siemens, Erlangen, Germany). The participants were asked to lie on the spine position so that the left upper extremity was positioned in the center of bed. The left upper extremity was covered by three coils (two Body-coils and a flexible-coil). We acquired three images for covering the entire left upper extremity on the coronal plane by 3D image acquisition sequence (T1-wighted VIVE Dixon sequence, FOV: 480 mm × 480 mm, resolution: 1.0 mm × 1.0 mm × 1.5 mm, scan time: 6 minutes). Three images were composed to acquire image of the entire upper extremity. For an automatic extraction of bone and muscle region of the left upper arm, a learning dataset was constructed by manual segmentation for a part of subject. Then, the bone and muscle regions were automatically extracted from the MR image of all subjects by the trained deep neural network (U-Net).

A template model which has a regularly arranged grids was created from bone and muscle regions extracted from one subject (Figure 1-a and -b). The origin and insertion of the muscle cannot be identified on the MR image, and these points were determined on the bone based on the anatomical knowledge. Thus, the template model has entire path of the muscle from origin to insertion. To create homologous models for eighty-eight subjects, the template model was fitted to the bone and muscle regions extracted from each subject's MR image by the initial pose alignment and following free-form deformation technique.

RESULTS AND DISCUSSION

Figure 1-c shows the fitted homologous models of two subject with different physiques and postures. The subject on the left had the well-developed muscles and the scanned posture was in abduction. In contrast, the subject on the right had slim muscles and the scanned posture was in neutral compared with subject on the left. The homologous modeling enabled to represent the bone and muscles in different physiques and postures between subjects.

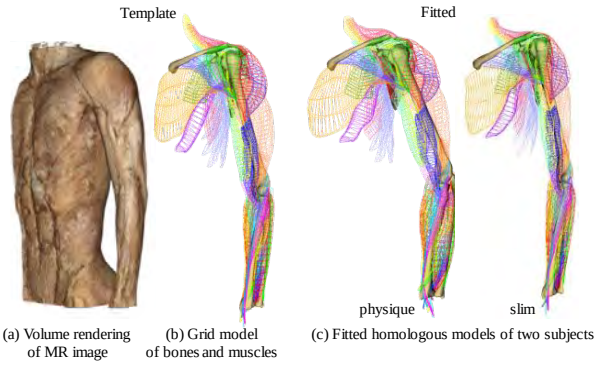

Figure 1 Homologous modeling of upper extremity.

CONCLUSIONS

We developed the morphological musculoskeletal database of left upper extremity using the automatic extraction from MR image and the homologous modeling. The homologous modeling enables the statistical shape analysis. In future study, musculoskeletal database of whole body may be created, and it is expected to be used in the simulation studies.

ACKNOWLEDGEMENTS

This study was supported by JSPS KAKENHI Grant Numbers JP18H03149 and JP21H03320.

REFERENCES

[1] Teran J et al. *IEEE Trans Vis Comput Graph* **11**: 317-328, 2005.
[2] Blemker S et al. *Ann Biomed Eng* **33**: 661-673, 2005.
[3] Mitsuhashi N et al. *Nucleic Acids Res.* **137**: 782-785, 200

EFFECTS OF CHRONIC ANKLE INSTABILITY ON ANKLE JOINT ANGLES AND LIGAMENT STRAINS DURING UNANTICIPATED CUTTING TASKS

Hoon Kim[1], Kristof Kipp[2]

[1] Department of Sports Medicine, Soonchunhyang University, Asan, South Korea.
[2] Department of Physical Therapy, Marquette University, Milwaukee, USA.
Email: hkim0625@sch.ac.kr

INTRODUCTION

Chronic ankle instability (CAI) is one of the most common injuries for active people [1]. Previous studies reported that people with CAI have greater risks of recurrent ankle sprains by reporting differences in talocrural and subtalar joint angles separately between people with and without CAI. However, risks of the sprain in anterior talofibular (ATFL), posterior talofibular (PTFL), and calcaneofibular (CFL) ligament may not be simply estimated with a joint angle because the ligament length is not only affected by joint angles but also other factors (geometry). Hence, it is important to study ligament strain as well as joint angles to better understand risks of ankle sprain. Therefore, the purpose of this study was to compare ankle joint angles and ligament strains between people with and without CAI.

METHODS

Eleven healthy people and 11 people with CAI participated in this study. Participants performed unanticipated cutting tasks while motion data were collected with motion capture cameras. We scaled a generic OpenSim [2] model to create a subject-specific model which includes ATFL, PTFL, and CFL (Fig. 1F). We used Inverse Kinematics to calculate ankle joint angles and Point Kinematics to calculate ligament lengths (L) during the task and a neutral position (L_o). Ligament strain was then calculated as $(L - L_o)/ L_o$. The talocrural and subtalar joint angles and ligament strains were trimmed to the ground contact phase. Statistical Parametric Mapping was used to compare joint angles and ligament strains. The alpha value was set to 0.05. In addition, we used Curve Fitting to show how CFL strain varies with ankle joint angles (Fig. 1E).

RESULTS AND DISCUSSION

There was a significant difference in subtalar joint angle between people with and without CAI during 14-15% of the ground contact period of an unanticipated cutting (Fig. 1A) ($p = 0.049$). However, there were no significant differences in ankle ligament strains (Fig. 1BCD) between people with and without CAI during an unanticipated cutting ($p > 0.05$). These results suggest that studying mechanics related to injury risk of lateral ankle sprain should include analysis of ligament strains in addition to ankle joint angles.

CONCLUSIONS

Although people with CAI exhibited different subtalar joint angle compared to healthy controls, the estimated ankle ligament strains were not different. Therefore, the current study suggests that biomechanical studies should include not only ankle kinematics but also ligament strains as dependent variables when investigating risks of ankle sprains in people with CAI.

ACKNOWLEDGEMENTS

We would like to acknowledge assistance from the National Institutes of Health (T32 HD007422-20) and a Research Stipend from the NIDRR. This work was supported by the National Research Foundation of Korea Grant funded by the Korean Government (NRF-RS-2022-00165979).

REFERENCES

[1] Gribble A. et al. *Br J Sports Med*, 50(24), 1496-1505
[2] Delp L. et al. *IEEE Trans Biomed Eng*, 54(11), 1940.

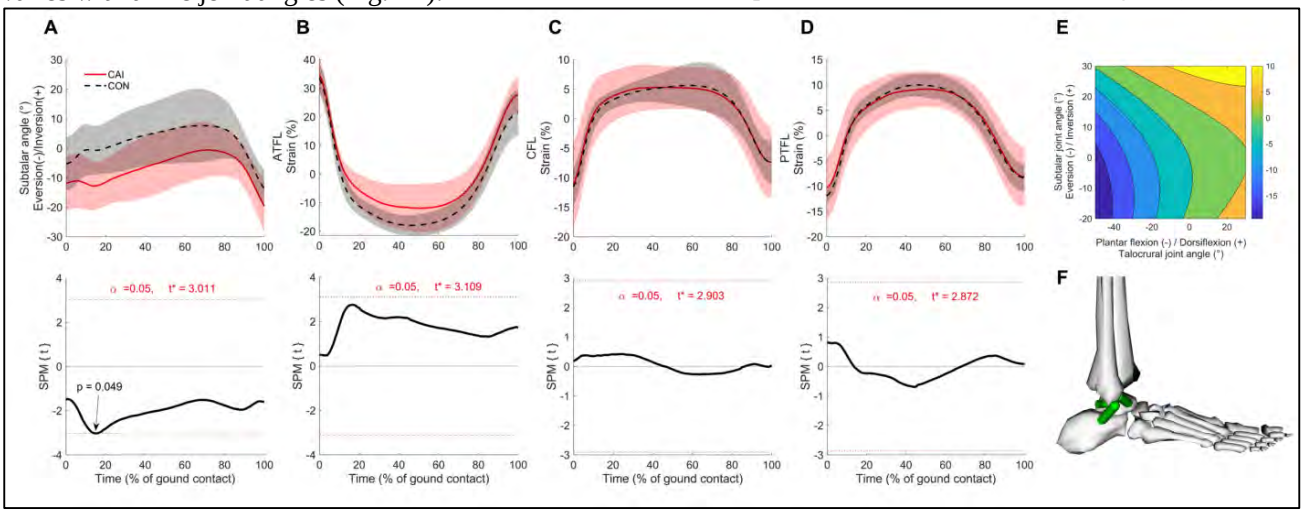

Figure 1: Mean and standard deviation and statistical parametric mapping of subtalar joint angle (A), ATFL (B), PTFL (C), and CFL strain (D). A contour figure of CFL strain depending on ankle joint angle (E). A generic model with ATFL, PTFL, and CFL (F).

Comparison of Synergy Extrapolation and Static Optimization for Estimating Multiple Unmeasured Muscle Activations during Walking

Di Ao[1,2], Benjamin J. Fregly[1]
[1] Department of Mechanical Engineering, Rice University, Houston, USA
[2] Institute of Medical Research, Northwestern Polytechnical University, Xi'an, China
Email: aodi0422@gmail.com

INTRODUCTION

Electromyography (EMG)-driven musculoskeletal modeling and static optimization (SO) are two primary computational approaches used for estimating muscle forces. EMG-driven modeling method depends on reliable EMG signals to bypass the muscle redundancy problem while simultaneously allowing for calibration of musculotendon properties, while SO is typically used when EMG data are missing from important muscles. Synergy extrapolation (SynX) has been developed recently for estimating unmeasured muscle excitations within EMG-driven modeling [1][2], which can resolve the difficulties caused by technical gaps in experimental EMG measurement, such as inaccessibility of deep muscles using surface electrodes or an insufficient number of EMG channels. However, SynX was validated in cases where EMG data from only one important hip muscle group (iliopsoas) was assumed to be missing at a time [1], and how well multiple missing muscle excitations can be predicted concurrenly using SynX ramains unkonwn. Furthermore, it would also be worthwhile to compare SynX and SO for estimating muscle activations when only eight channels of EMG signals (typically provided by a EMG-recording device) are experimentally available.

METHODS

A generic full-body OpenSim musculoskeletal model [3] was scaled to match each subject's anthropometry using OpenSim 4.0 [4]. Each leg of the model possessed six degrees of freedom (DOFs). SynX and SO were evaluated using gait datasets collected from two subjects post-stroke performing treadmill walking at self-selected and fastest-comfortable speeds, which include sixteen channels of measured EMG (collected using surface and fine wire electrodes) per leg. Eight EMG signals measured either using fine-wire electrodes or associated with muscles making small contributions to joint moments were treated as "unmeasured" and used to evaluate the reliability of SynX and SO quantitatively. SynX used nonlinear optimization to calibrate model parameters, synergy vector weights and average values for constructing unmeasured excitations and for constructing residual excitations simultaneously [1], while SO solved a time frame of muscle activation at a time while incorporating generic model parameter values. To evaluate the performance of both approaches, we also performed EMG-driven calibration using the full set of EMG signals, where no EMG signals were treated as "unmeasured" ((henceforth referred to as "experimental"). Root mean square error (RMSE) and Pearson correlation coefficient r between experimental and estimated muscle activations for unmeasured muscles were computed to quantify matching of magnitude and shape, respectively.

RESULTS AND DISCUSSION

Overall, SynX estimated unmeasured muscle activations with reasonable accuracy (r=0.55±0.13 and RMSE=0.08±0.06) (figure 1). Comparing to standard SO (r=0.11 ±0.30and RMSE=0.15±0.15), SynX made significantly more accurate predictions of unmeasured muscle activations in terms of similarity of both magnitude (p for RMSE=0.021) and shape (p for r<0.01).

CONCLUSIONS

SynX outperformed SO for a large number of estimating muscle activations, which broadens the possibilities for EMG-driven calibration of muscle-tendon properties and may eventually contribute to the design of personalized treatments for mobility impairments, when difficulties exist with collecting EMG signals from important muscles.

ACKNOWLEDGEMENTS

Cancer Prevention Research Institute of Texas (CPRIT) funding RR170026.

REFERENCES

[1] Di A. et al. *Front. Bioeng. Biotechnol.*: 1533, 2022.
[2] Di A. et al. *Front. Comput. Neurosci.*: 588943, 2020.
[3] Rajagopal, A. et al. *IEEE Trans. Biomed. Eng. 63, 2068–2079,* 2016.
[4] Delp, S. L. et al. *IEEE Trans. Biomed. Eng. 54, 1940–1950,* 2007.

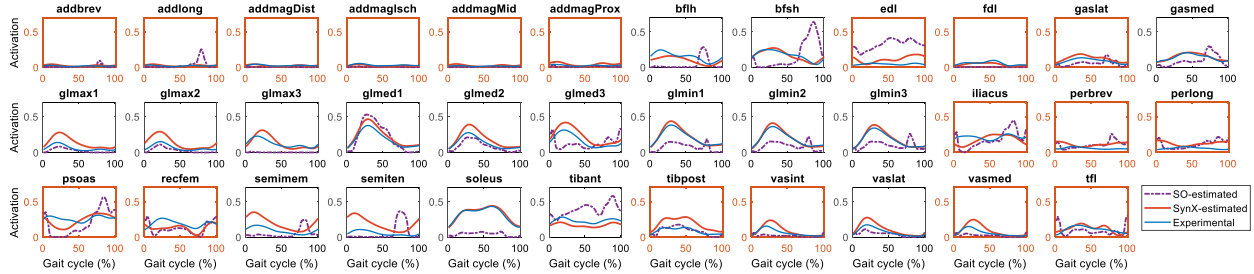

Figure 1 Average SynX-estimated (red solid curves), SO-estimated (purple dash curves) and experimental (blue solid curves) muscle activations across calibration trials, legs and subjects. Data are reported for the complete gait cycle, where 0% indicates initial heel-strike and 100% indicates subsequent heel-strike. The subplots with orange axes indicate the muscles that were associated with unmeasured EMGs.

PELVIS STABILIZING MUSCLES ACTIVITY AND FORCES IN HIP FLEXION RESISTANCE TRAINING ANYBODY MODELING

Dobrochna Fryc[1], Michael Skipper Andersen[2], Katarzyna Jochymczyk-Woźniak[1], Katarzyna Nowakowska-Lipiec[1], Hanna Zadoń[1] and Robert Michnik[1]

[1] Department of Biomechatronics, Silesian University of Technology, Zabrze, Poland.
[2] Department of Materials and Production, Aalborg University, Aalborg, Denmark.
Email: dobrochna.fryc@polsl.pl

INTRODUCTION

One of the most important aspects of physiotherapy is the problem of muscle balance in the pelvis girdle region. The typical observed scheme include hip flexors shortening and hypertension and hip extensors weakening and elongation. The scheme is present both in typical posture defects [2] and low back pain [1]. The idea of the hip flexion resistance training arised basing on muscle resistance training morpho-physiological adaptation mechanisms [3,4]. Since typical daily activities include a variety of hip extension resistance and endurance training, the oposite exercise was selected as a potential sollution to the pelvis stabilizing muscles inbalance.

METHODS

The movement of the resistance hip flexion was recorded with the BTS Smart system for one healthy individual (woman, age 29, weight 49 kg, height 168 cm). There were 28 movement cycles recorded. Each trial contains the exercise performed with both legs in the order: 1) right leg, 2) left leg. Equipment used in the exercise was a free weight machine constructed according to the patent P.435615 (Figure 1B). The exercise was performed with the use of the device weight only. Strain gauges were placed under the feet platforms (separately for the front foot and the back foot) and in the bindings (placed on the back of the feet). A motion capture-driven Musculoskeletal Model (MS) (Figure 1A) was created in the AnyBody Modeling System (AnyBody Technology A/S, Denmark) with the measured forces applied as boundary conditions.

RESULTS AND DISCUSSION

The MS model inverse dynamics study showed that all crucial hip flexors and abductors were highly activated in the exercise. The force generated by each muscle (Figure 1C) was determined by its size and function and did not reflect the muscle activity level. The exercise was designed as a multijoint opposite equivalent of the squat exercise. The resistance application in the movement was therefore untypical for human motor system anatomy. The obtained training conditions showed that the most active muscles generate unproportionally low forces. The disproportion suggests a potential for hypertrophy in long term training [5].

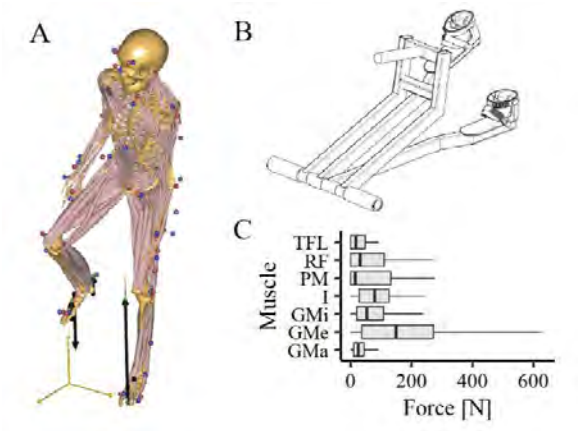

Figure 1A MS model of the exercise, **1B** training equipment construction scheme, **1C** Selected muscles forces in hip flexion resistance training, GMa – Gluteus maximus, GMe – Gluteus medius, GMi – Gluteus minimus, I – Iliacus, PM – Psoas major, RF – Rectus femoris, TFL – Tensor fasciae latae.

CONCLUSIONS

The results show that the proposed exercise activates targeted muscles (hip flexors and abductors) and has a potential to build hypertrophy in muscle groups that present the scheme of shortening in individuals diagnosed with posture defects or chronic low back pain. The exercise requires further validation as a candidate for posture and pain kinesitherapy.

ACKNOWLEDGEMENTS

This research was partially funded by polish Ministry of Education and Science as part of the Excellence Initiative - Research University program. Funding was awarded as a grant in an internal pro-quality competition for funding ground-breaking research (project number: 32/041/SDU/10-21-07).

REFERENCES

[1] Geisser ME et al. *J. Pain* **6**:711-26, 2005.
[2] Hrysomallis C et al. *J. Strength Cond. Res* **15**:385-90, 2001.
[3] Joanisse S et al. *F1000Res* **24**, 2020.
[4] Jones DA et al. *Q. J. Exp. Physiol* **74**:233-56, 1989.
[5] Lim C et al. *Med Sci Sports Exerc* **54**:1546-59, 2022.

THE EFFECT OF MULTIPLE MEASUREMENT ANGLES ON THE PREDICTION OF JOINT TORQUE-ANGLE PARAMETERS

Amy O. Parkinson[1], Paul J Felton[1], Martin G.C. Lewis [2] and Charlotte Apps[1]
[1] School of Science and Technology, Nottingham Trent University, Nottingham, UK.
[2] Qualisys AB, Gothenburg, Sweden.
Email: amy.parkinson@ntu.ac.uk

INTRODUCTION

The joint torque-angle relationship exhibits a bell-shaped curve, where peak isometric torque occurs in the mid-range. This relationship has previously been modelled using a quadratic function where parameters are optimised to best fit experimental data [1]. Experimental joint torque is typically measured at multiple joint angles throughout the joint range of motion using an isokinetic dynamometer [1,2]. Despite this, it is currently unknown how the number and location of these measurement angles affects prediction of the torque-angle relationship. The purpose of this study was, therefore, to investigate the effect of multiple measurement angles on the prediction of the torque-angle relationship for knee flexors and knee extensors.

METHODS

A two-parameter quadratic was used to model torque production as a function of joint angle for the knee flexors and knee extensors (Equation 1):

$$T_\theta = \left(1 - k_2\left(\theta - \theta_{opt}\right)^2\right).T_0 \qquad \text{Eq1.}$$

where optimal angle (θ_{opt}), width (k_2) and peak isometric torque (T_0) were extracted from literature and used to calculate isometric torque production (T_θ) at 10° intervals throughout the joint range of motion (flexion: 90°; extension: 85°). To simulate submaximal torque production, random noise (0-10Nm) was subtracted from the torque data at each measurement site to create 100 torque-angle curves for each joint action. The effect of the number and location of multiple measurement angles was determined for all possible measurement combinations for a minimum of three joint angles up to the maximum available in the joint range (flexion: 10, extension: 9). Simulated annealing was used to optimise parameters θ_{opt}, k_2 and T_0 and minimise the unweighted unbiased RMS difference [1] between the simulated torque data and the joint torques calculated by the quadratic function. The percentage error between the original parameters derived from the literature and optimised parameter values was calculated for all joint torque-angle curves.

RESULTS AND DISCUSSION

The percentage error between optimised and original parameter values for θ_{opt}, k_2 and T_0 decreased as the number of measurement sites increased for both the knee flexors and knee extensors (Table 1). Larger percentage errors for knee flexion may be explained by the nature of the torque-angle profile, which is predominately ascending and flat, compared to that of the knee extensors which demonstrates a more acute ascending-descending curve. The shape of the torque-angle curve may also explain observably larger percentage errors in k_2, particularly for the knee flexors. Generally, smaller percentage errors were observed for combinations that included a measurement site nearest to the optimal angle, which was close to full extension for the knee flexors (0°) and near the mid-range for the knee extensors (60°). For the knee flexors, combinations consisting of measurement sites closest to the optimal angle (e.g., [0°, 10°, 20°]) resulted in small errors in T_0 and θ_{opt}. Such combinations, however, resulted in larger errors in k_2 compared to combinations which spanned more of the joint range (e.g., [0°, 50°, 80°]). For the knee extensors, combinations consisting of measurement sites closest to the optimal angle (e.g., [60°, 70°, 80°]), or of purely ascending (e.g., [20°, 30°, 40°]) or descending (e.g., [80°, 90° ,100°]) sites exhibited larger errors across all parameters.

Table 1. Mean (±SD) percentage error between optimised and original parameter values across measurement combinations

	Number of measurement sites			
	3	**5**	**7**	**Max**
Knee Flexion				
T_0	6.1 ± 3	4.5 ± 1.1	3.9 ± 0.7	3.9
θ_{opt}	7.9 ± 2	4.9 ± 1.4	3.7 ± 0.7	3.4
k_2	57 ± 31	23 ± 7.7	16 ± 3.5	14
Knee Extension				
T_0	3.0 ± 1.3	2.1 ± 0.4	2.1 ± 0.2	1.9
θ_{opt}	0.7 ± 0.9	0.1 ± 0.1	0.1 ± 0.0	0.1
k_2	8.7 ± 7.9	2.6 ± 1.2	2.0 ± 0.4	2.4

T_0 = peak isometric torque (Nm), θ_{opt} = optimal angle (°) and k_2 = width

CONCLUSIONS

More accurate predictions of the torque-angle relationship should be expected for protocols with more measurement sites. The magnitude of this effect, however, decreases exponentially such that measuring all available sites may not be necessary. Furthermore, the strategy of measurement site selection can increase measurement accuracy. Practitioners should, therefore, consider the research question, muscle group under investigation and practical constraints when formulating an experimental protocol.

REFERENCES

[1] King MA, Lewis MG, & Yeadon MR. *Int J Multiscale Comput Eng* **10**(2): 117-130, 2012.
[2] Lewis MG, Yeadon MR, & King MA. *Hum Mov Sci*, 57: 388-399, 2018.

3D MODELING OF LEVER ARM AND MOMENT-GENERATING CAPACITY OF STERNOCLEIDOMASTOID AND SCALENUS MUSCLES IN RESPIRATORY MOVEMENT

David Biteau [1], Véronique Feipel [1,2], Serge Van Sint Jan [1], Benoit Beyer [2]

[1] Laboratoire d'Anatomie, Biomécanique et Organogénèse, Université Libre de Bruxelles, Brussels, Belgium

[2] Laboratoire d'Anatomie Fonctionnelle, Université Libre de Bruxelles, Brussels, Belgium

Email: david.biteau@ulb.be

INTRODUCTION

Sternocleidomastoid and scalenus muscles may be involved in musculoskeletal and/or respiratory disorders. Moment generating capacity of these muscles were previously explored during cervical movements [1] but their respiratory motion lever arm and moment generating capacity are still to be determined. Therefore, the aim of the present study was to determine lever arm and moment generating capacity of the muscles of interest using 3D modelling approach.

METHODS

Previously published kinematic data [2] computed from CTscan performed at three lung volumes (TLC: total lung capacity, MIC: middle of inspiratory capacity and FRC: functional residual capacity) were used in the present study.

3D thorax bone models and breathing kinematic data (ranges of motion, mean helical axis (HA) location and orientation) were combined to a generic cervical spine model (GCSM). With LHPFusionBox software (http://lhpfusionbox.org), anatomical landmarks (AL) were positioned on each model for further registration and at the insertion sites of scalenus anterior (Sant), medius (SMed) and sternocleidomastoid (SM). The GCMS was then registered on the first thoracic vertebra of each subject using similarity transformation. (Figure 1A). Length and LA were computed according to the HA of the first costovertebral joint (Figure 1B) using the direct method (shortest distance between muscle line of action and HA). Force and isometric moment generating capacity (MGC) at different lung volumes was computed using data from [1]. The relative variations were calculated as a percentage of the FRC reference position.

RESULTS AND DISCUSSION

Globally, all muscles displayed an increase of LA and MGC from FRC to TLC.

The relative LA variations ranged between 22 ± 18.3% and 35 ± 38.7% for SAnt and SMed respectively.

Relative MGC variations at TLC compared to FRC ranged from 17 to 33 % for SMed and SM, respectively. (table 1). Note that the greatest variations of both LA and MGC occurred between FRC and MIC (i.e. under 50% of the inspiratory capacity) and can be explained by the greater range of rib motion during this phase [2]. Prior work [1] reported scalene muscles maximal LA close to 20 mm for cervical spine lateral bending while the present study showed a minimum LA of 25.1 mm for respiratory contribution. The present minimal LA of SM (32.5 mm) represents approximately 50% of the value obtained for cervical spine lateral bending (55 mm) and 200 % of the value reported for axial rotation (15 mm).

Considering the MGC, for SC, minimal respiratory contribution represents around twice the value reported to generate the flexion and almost the same as for axial rotation.

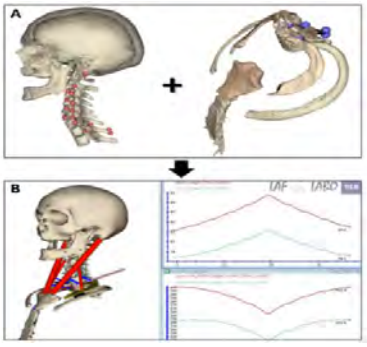

Figure 1: A: Left: GCSM with AL on insertion sites and Th1; Right: Upper thorax model with AL on Th1. B: 3D visualization of SAnt and SM with results of length and LA over

Table 1: Lever arm (mm) force capacity (N) and Moment generating capacity (N.m) for each muscle at different lung volume.

Muscle	Respiratory Position	Lever arm (mm)	Force capacity (N)	MGC (N.m)
SAnt	FRC	29,5	45,4	1,3
	MIC	33,9	49,4	1,7
	TLC	35,0	50,4	1,8
SMed	FRC	25,1	72,0	1,8
	MIC	29,2	70,9	2,1
	TLC	30,2	69,9	2,1
SM	FRC	32,5	65,6	2,1
	MIC	39,3	68,2	2,7
	TLC	41,3	68,4	2,8

CONCLUSIONS

Absolute and relative SAnt, SMed, and SM muscle LA and MGC during respiratory movement were quantified using a modelling approach. For all muscles, LA and MGC increased during inspiration. Respiratory contribution could be compared to cervical movement capacity. Further research will explore interaction of respiratory mechanics in clinical conditions.

REFERENCES

[1] Vasavada, A. N. et al. (1998). *Spine*, **23**(4) : 412–422.
[2] Beyer, B. et al. (2016). *Resp. Phys.Neurobiol.**232** :57-65*
[3] Hughes, R. et al. (1998). *J Biomech*, **31**(2): 157–160.

A modelling approach to determine femoroacetabular impingement in badminton-specific motions

Dominic Bachmann[1], Lukas Beringer[2], Igor Komnik[1], Oliver Steimer[3], Diana Hell[4], Stefan Zachow[5], Günther Schneider[4], Karen aus der Fünten[2] and Wolfgang Potthast[1]
[1] Institute of Biomechanics and Orthopaedics, German Sport University Cologne [2] Institute of Sport and Preventive Medicine, Saarland University [3] Clinic of Orthopaedics, Saarland University Medical Centre
[4] Clinic for Diagnostic and Interventional Radiology, Saarland University Medical Centre
[5] Zuse Institute, Berlin, Germany
Email: d.bachmann@dshs-koeln.de

INTRODUCTION

Femoroacetabular impingement (FAI) syndrome is an increasingly recognized impairment in high-impact sports athletes. Mostly, an abnormal morphology of the femoral neck (CAM) is present. Coupled with high-impact movements and a high range of motion it can lead to degeneration of the labrum and ultimately to osteoarthritis [1]. In badminton, movements such as the lunge, which involve extreme hip flexion, internal rotation, and partly adduction, are likely to cause FAI. The purpose of this study was to use a subject-specific modeling approach to define the femoroacetabular clearance (FAC) and the pathomechanics of a badminton player with FAI syndrom.

METHODS

One subject (age: 27, height: 1.94 m, weight: 94 kg, CAM-deformity: left) was positioned in supine recumbency in a 3 T Tesla MRI. Sequences were taken in sagittal, transverse and dorsal plane with isotropic voxels (1x1x1 mm^3). The subject then moved through six steps to the maximum flexion, adduction & internal rotation (FADIR) position, with quasi-static pauses between each step for further MRI captures. Afterwards, motion capture data was recorded with 12 cameras (250 Hz). The subject performed three badminton movements (chasse step, back lunge and ready position) and a supposed FAI inducing (FADIR) movement. To create the subject-specific hip model, the neutral position of the subject in the MRI was segmented using 3D Slicer. Due to incomplete capture of the distal femur on the MRI, a statistical shape model (MapClient) was fitted to the subject's anatomical landmarks and merged with the segmentation using the host mesh fitting Plugin in MapClient [2]. Hip Joint Centre (HJC) was calculated using the best spherical fit method. OpenSimCreator was utilized to embed the segmentations with the Gait2392 Model settings, resulting in a subject-specific hip model for calculating minimal FAC. The MRI of the maximum FADIR position visualized the impingement and served to validate the OpenSim model. FAC was defined as the minimal Euclidean distance between the CAM-deformity and superior edge of the acetabulum.

RESULTS AND DISCUSSION

The FAI inducing motion result showed a FAC of 2.14 mm (Tab. 1). The subject reported a stabbing pain during the final position, indicating that an impingement may have occurred. Further analysis of badminton-specific motions revealed similar FAC levels, providing further indication of an impingement. Despite the limitations in determining the exact location of the HJC during high-impact movements due to soft tissue compression, the labrum was likely impinged upon, given its average height of 6 to 7 mm [3] and the small FAC observed. Also, the model allows the analysis of the biomechanics, enabling the identification of potential compensatory movements, such as pelvic list, which may assist to an increased FAC (Fig. 1).

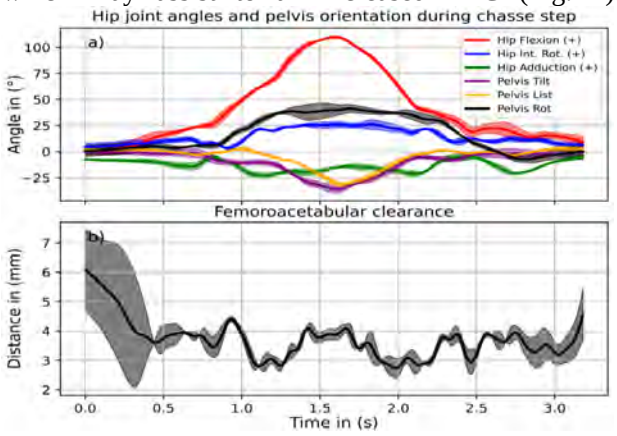

Figure 1 a) Hip joint angles and pelvic orientation according to ISB coordinate system b) FAC between Cam-def. and acetabulum.

CONCLUSIONS

The hip model enables the analysis of FAC of the athlete coupled with its biomechanics. Badminton specific movements demonstrated a potential FAI risk throughout several intervals of the motion but more subjects are needed to define patterns.

REFERENCES

[1] Ganz R et al. *Clin Orthop Res* **417**: 112-120, 2003.
[2] Zhang J et al. ISBMS **8789**: 182-192 2014.
[3] Won YY et al. *Yonsei Med J.* **44**: 855-862, 2003.

Table 1: Results of the FAC for the different badminton-specific and FAI inducing motions.

	FAI inducing	Chasse step	Ready position	Lunge back
FAC in (mm)	2.14 ± 0.11	2.38 ± 0.02	2.35 ± 0.38	2.41 ± 0.00

Analysis of Force Characteristics and Muscular Activity of Temporomandibular Joint in Three Masticatory Motions: Multibody Dynamics Simulation

Sung-Ho Lee[1], Won-Hyeon Kim[1], Myeongkwan Kang[1], Ho-Joon Shin[1], Jisung Kim[1], Youjeong Son[1], Seoyoung Won[1], Jungwon Lee[2], Young-Jun Lim[2] and Bongju Kim[1]

[1] Dental Life Science Research Institute/Innovation Research & Support Center for Dental Science, Seoul National University Dental Hospital, Seoul, Korea
[2] Department of Prosthodontics, Seoul National University Dental Hospital, Seoul, Korea
Email: bjkim016@gmail.com

INTRODUCTION

Temporomandibular joint disorder(TMD) is a complex disease caused by various factors such as trauma, malocclusion, and many studies on treatment methods were conducted. The TMD was an area that can be recovered through proper diagnosis at an early stage, but in vivo analysis of the temporomandibular joint(TMJ) is difficult to perform in a clinical situation. In order to overcome this problems, biomechanical characteristics were analyzed through electromyography and mandibular movement trajectory[1-3]. however, it is only applied as an supported methods because it is difficult to analysis the muscles of the TMJ in vivo. Therefore, to improve the diagnosis and treatment of the TMD, this study analyzed the muscle characteristics of the TMJ according to the movement of the TMJ using motion capture analysis techniques and a inverse dynamics-based musculoskeletal model.

METHODS

In order to conduct this study, 4 healthy adult women who did not have the TMD or missing teeth and were able to perform normal masticatory movements was selected. The maxillary and mandibular tooth shapes for each subject were extracted through an oral scanner, and a customized mouthpiece was designed through a CAD program and outputted through a 3D printer. The TMJ movements was defined as three main movements such as open-close, side-to-side, protrusion-retraction. The open-close was subdivided into two operations, the max and half open-close. Using a three-dimensional motion capture system based on 8 infrared cameras, motion analysis was performed by repeating movements 3 times for 3 movements, and changes in chewing characteristics were measured. At this time, EMG sensors were attached to both cheeks to verify the inverse dynamics model. Through motion analysis, subjects with representative masticatory characteristics were selected among 4 subjects, and analysis of the inverse dynamics-based musculoskeletal TMJ model was performed by applying representative motion data. In the inverse dynamics model, three movements (half open-close, side-to-side, protrusion-retraction) were considered. The reaction force of the TMJ and the muscle characteristics of the joint periphery were measured according to each movement.

RESULTS AND DISCUSSION

The reaction force of the TMJ for the three movements tended to be highest in the upward and medial directions (Fig 1). In the lateral movement, it was confirmed that the reaction force was high in the anterior direction only (Fig 1). Regarding the muscle characteristics around the TMJ, it was confirmed that the superior lateral pterygoid had the highest contractile force in common in the three movements (Fig 1). This muscle was involved in the forward movement, anterior-inferior rotation, lateral rotation and movement of the mandible. In addition, it was confirmed that the temporal muscle was activated to stabilize the joint during the three movements of the TMJ. It was confirmed that the activated muscles appeared differently as the occlusal and non-occlusal states occurred during one mastication cycle for three movements (Fig 1).

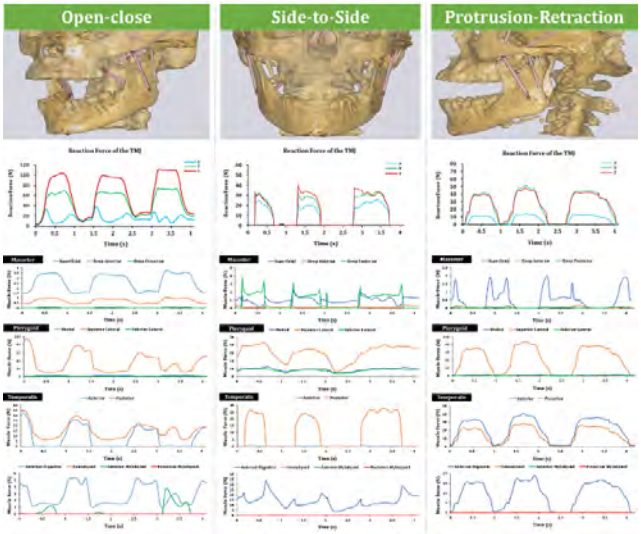

Figure 1 Results of temporomandibular joint reaction force and four major muscle activity for three masticatory movements.

CONCLUSIONS

Based on our results, the correlation between movements and muscles of the TMJ can be analyzed, and it is thought that a more appropriate diagnosis can be made by analyzing the in vivo muscle characteristics of the TMD.

ACKNOWLEDGEMENTS

This work was supported by the National Research Foundation of Korea(NRF) grant funded by the Korea government(MSIT) (No. 2022R1F1A1076344).

REFERENCES

[1] Andersen MS et al. *J Biomech Eng* **139**:091001, 2017.
[2] Thelen DG et al. *J Biomech* **39**:1107-1115, 2006
[3] de Zee M et al. *J Biomech* **40**: 1192-1201, 2007

IMPACT OF ACROMIOCLAVICULAR AND CORACOCLAVICULAR LIGAMENT IMPLEMENTATION ON THE SHOULDER MUSCULOSKELETAL SIMULATION

Takayuki Aimi[1,2], Atsushi Ueda[3], Yasuo Nakamura[1]
[1] Doshisha University, Kyoto, Japan. [2] Japan Society for the Promotion of Science, Tokyo, Japan.
[3] Hankai Hospital, Osaka, Japan.
Email: aimibiomechanics@gmail.com

INTRODUCTION

In shoulder musculoskeletal (MSK) simulations, the acromioclavicular (AC) and coracoclavicular (CC) ligaments have not been considered in numerous studies. Additionally, posterior rotation of the sternoclavicular (SC) joint has often been estimated through the motion of the scapula and clavicle [1] or constrained. Therefore, the availability of ligaments, which are significant force generators, and the extent of the SC posterior rotation can affect the validity of simulation outcomes. The purpose of this study is to determine the effects of ligament and degree of freedom (DoF) for SC posterior rotation on the accuracy of muscle activity estimation.

METHODS

We conducted synchronous motion capture (Motion Analysis, USA) and surface electromyography (EMG; Delsys, USA) measurements on two male participants (A:24 years, 165 cm, 60 kg; B:23 years, 169 cm, 57 kg) during arm elevation in the coronal, scapular, and sagittal planes. Joint angles were calculated using inverse kinematics from marker trajectories. EMG was recorded for the 12 muscles of the shoulder and arm. Using OpenSim 4.4 [2], based on an existing shoulder model [3], the ligaments were incorporated as nonlinear springs. In addition, the SC posterior rotation DoF was added and the rotation was estimated [1]. Muscle activation was estimated using a computed muscle control algorithm under four conditions: combinations of SC posterior rotation input (NR: no rotation; ER: estimated rotation) and absence (NoLig) or presence (Lig) of ligaments. To evaluate the validity of simulation, the time-normalized (201 points) EMG and estimated muscle activation under each condition were compared using Spearman's correlation coefficient (r); waveforms deemed similar if $r \geq 0.5$.

RESULTS AND DISCUSSION

In both participants and for all tasks, the validity was higher for Lig than for NoLig. This can be attributed to the disregard of the role of ligaments and the reliance on muscle activity alone to elevate the arm. Furthermore, for Lig across most tasks, the validity was higher for the upper trapezius, serratus anterior, and latissimus dorsi for NR and for the middle trapezius and anterior deltoid for ER (Table 1). Since neither SC posterior rotation inputs showed high validity for all muscles, the treatment of SC posterior rotation should be carefully considered by the muscle of interest. Furthermore, there may be other SC posterior rotation input besides NR and ER that yield more valid simulation results.

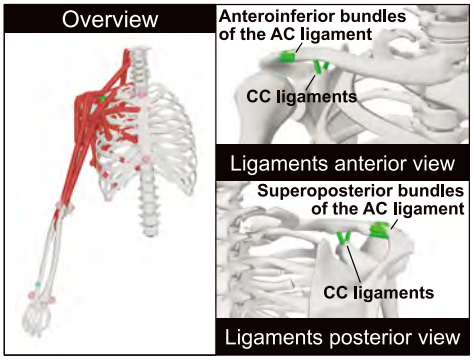

Figure 1 MSK model developed by OpenSim 4.4.

Table 1 Correlation coefficient between measured EMG and estimated muscle activities during scapular plane elevation in participant A ($r \geq 0.7$ for red and $r \geq 0.5$ for pink).

Muscle		NoLig		Lig	
		NR	ER	NR	ER
Trapezius	Upper	0.46	**0.58**	**0.82**	**0.59**
	Middle	**0.69**	**0.70**	0.40	**0.71**
	Lower	**0.68**	**0.71**	**0.81**	**0.71**
Deltoid	Anterior	0.28	**0.82**	0.44	**0.87**
	Middle	**0.66**	**0.64**	**0.69**	**0.63**
	Posterior	0.50	0.45	**0.56**	**0.61**
Pectoralis Major	Clavicle	-0.17	0.25	-0.24	**0.54**
	Sternum	-0.04	-0.72	-0.31	-0.70
Infraspinatus		**0.54**	**0.53**	**0.58**	**0.56**
Serratus Anterior		0.28	0.26	**0.88**	0.28
Teres Minor		0.45	0.46	0.49	**0.51**
Latissimus Dorsi		**0.61**	0.43	**0.90**	**0.62**

CONCLUSIONS

In shoulder MSK simulation, incorporating the AC and CC ligaments leads to more accurate muscle activity estimations. Further refinement of SC posterior rotation input may allow for more valid simulations.

ACKNOWLEDGEMENTS

This work was supported by JSPS KAKENHI [grant number JP21J20038].

REFERENCES

[1] van der Helm F and Pronk G. *J Biomech Eng* **117**: 27–40, 1995.
[2] Seth A et al. *PLoS Comput Biol* **14(7)**: e1006223, 2018.
[3] Seth A et al. *Front Neurorobot* **13**: 90, 2019.

DIFFERENCES OF MUSCLE BEHAVIORS BY MUSCLE ACTIVATION MINIMIZATION AND METABOLIC ENERGY MINIMIZATION IN MUSCULOSKELETAL DYNAMICS SIMULATION

Young-Jun Koo[1], Seungwoo Yoon[1], and Seungbum Koo[1,]

[1] Department of Mechanical Engineering, Korea Advanced Institute of Science and Technology, Daejeon, Republic of Korea
Email: skoo@kaist.ac.kr

INTRODUCTION

Energy-optimal human movement theories are widely accepted to understand human behaviors [1]. Minimizing the sum of squared muscle activations has been frequently used to determine muscle recruitment during musculoskeletal simulation due to the benefit of computational cost [1, 2]. A previous study reported that minimizing squared activations and metabolic energy consumption had practically similar results in muscle forces [2]. However, minimization of energy consumption affected muscle kinematics, which is important to pathologic gaits of cerebral palsy [3]. The objective of this study was to quantify the effect of optimization criteria that minimized squared activations or energy consumption on muscle length and velocity.

METHODS

The study was approved by the IRB of KAIST. Full-body motion capture data of a healthy subject (23 years, 65.4 kg, 171.2 cm) was obtained during normal walking. A reference gait kinematics was prepared using the motion data.

A full-body musculoskeletal model with 150 muscles was constructed (Figure 1A). The metabolic energy consumption was estimated based on maintenance heat rates, shortening heat rates, and mechanical works of muscles along with a basal metabolic energy rate [4].

Two neural-network-based gait controllers were trained using a deep reinforcement learning method [5]. One gait controller pursued minimization of the sum of squared muscle activations along with motion tracking to the measured gait kinematics. The other pursued minimization of metabolic energy consumption.

Forward dynamics gait simulations were performed for 20 gait cycles. For statistical analysis, gait kinematics, ranges of normalized muscle length (RNML), and peak normalized muscle velocity (PNMV) of rectus femoris, soleus, and tibialis anterior were calculated. The differences in RNML and PNMV between the two controllers were statistically tested via student t-test.

Table 1: RNML, eccentric PNMV, and concentric PNMV for rectus femoris, soleus, and tibialis anterior of the activation and energy minimization controllers (*significant difference with $p<0.05$)

	Rectus femoris		Soleus		Tibialis anterior	
	activation	energy	activation	energy	activation	energy
RNML	0.30 (0.00)	0.30 (0.01)	0.50* (0.01)	0.45* (0.02)	0.16* (0.00)	0.15* (0.01)
PNMV (eccentric)	0.95* (0.07)	0.51* (0.04)	0.86* (0.04)	0.11* (0.07)	0.42* (0.06)	0.28* (0.03)
PNMV (concentric)	0.45 (0.06)	0.47 (0.04)	0.55* (0.06)	0.13* (0.01)	0.46* (0.04)	0.34* (0.02)

RESULTS AND DISCUSSION

Full-body kinematics generated by the activation controller and energy controller were similar (Figure 1B). Root-mean-squared (RMS) differences of lower limb kinematics were less than 2.0°.

RNMLs of the soleus and tibialis anterior were significantly smaller in the energy controller than in the activation controller. Eccentric PNMV and concentric PNMV were also significantly smaller in the energy controller than in the activation controller. The RNML and PNMV results are summarized in Table 1.

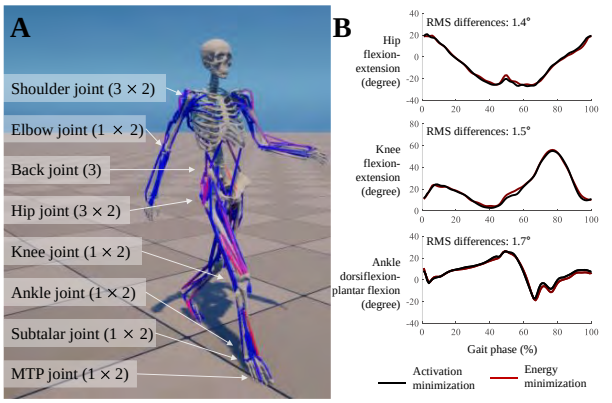

Figure 1 (A) a full-body musculoskeletal model with 150 muscles and (B) lower limb kinematics during gait simulation

CONCLUSIONS

The results of the study showed that muscle kinematics such as RNML and PNMV generated by the energy controller were significantly smaller than those of the activation controller. The differences in muscle kinematics might be caused by shortening heat rates and mechanical works of muscles [4]. The implementation of energy minimization would represent muscle kinematics behavioral characteristics to optimize muscle metabolic energy.

ACKNOWLEDGEMENTS

This research was supported by the NRF (MSIT Project No. 2022M3C1A3080598) and by IITP (MSIT Project No. 2022-0-00025) funded by the Korea government.

REFERENCES

[1] Delp et al. *Ieee T Bio-Med Eng* **54**: 1940-50, 2007.
[2] Anderson and Pandy. *J Biomech* **34**: 153-61, 2001.
[3] Van der Krogt et al. *Gait Posture* **26**: 532-8, 2007.
[4] Umberger. *J. R. Soc. Interface* **7**: 1329-40, 2010.
[5] Jung and Koo. *Front. Bioeng. Biotechnol*, 1504, 2022.

OPTIMAL CONTROL SIMULATIONS USING WEARABLE SENSORS AND PERSONALIZED MUSCULOSKELETAL MODELS - A NOVEL APPROACH TO MODELLING GAIT

Grace McConnochie[1], Dominic Thewlis[1], Aaron Fox[2], Clint Bellenger[3]
[1]Adelaide Medical School, University of Adelaide, Australia; [2]School of Exercise and Nutrition Sciences, Deakin University, Geelong, Australia; [3]Alliance for Research in Exercise, Nutrition and Activity (ARENA); Allied Health and Human Performance unit; University of South Australia, Australia
Email: grace.mcconnochie@adelaide.edu.au

INTRODUCTION

Inertial measurement units (IMUs) are an increasingly popular modality for biomechanical data collection outside the constraints of the laboratory environment. IMU-based joint kinematics are subject to errors from signal noise and drift, soft tissue artefacts, device calibration, and model scaling [1]. Hence, data collection has been predominately limited to controlled laboratory environments or involved few isolated outcome measures. Optimal control simulations can combine a predictive and tracking approach to modelling gait - including physiologically based objectives of locomotion, and having less reliance on experimental data [2]. The aim of this study was to pilot a more holistic and dynamically consistent approach to biomechanical modelling with wearables, using optimal control simulations to track IMU signals with subject-specific musculoskeletal models.

METHODS

Gait data were collected on a subject running on a treadmill at 12, 14 and 16 km/h. Eight Blue Trident IMUs were attached to the torso and lower limbs. Optimal marker-based motion capture was collected simultaneously in Vicon as a data reference standard. Accelerometer, gyroscope and magnetometer signals were fused offline to obtain sensor quaternions [3]. Sensor orientations on the subject were calculated from two static poses [4]. The 3D torque-driven OpenSim model was scaled using statistical shape modelling (MAP Client), via anatomical landmarks on a skeletal mesh fitted to the LiDAR point cloud of the subject [5]. Ground contact was modelled using eleven Hill-Crossly contact spheres attached to the model's feet. Optimal control simulations were performed in OpenSim Moco (V4.4, SimTK, USA). System dynamical equations governing the model states and controls were solved for implictly on a discretized mesh of 100 nodes. As the primary objective, IMU accelerations, angular velocities and orientations were tracked with virtual IMUs at analogous positions on the OpenSim model. Lowly weighted objectives to minimize effort, maintain symmetry and track generic running kinematics and ground contact forces were included. An initial guess was generated from a tracking simulation of generic running kinematics.

RESULTS

The LiDAR scan and marker-based model scaling factors were congruent. In comparison with optical motion capture, mean RMSE errors of 8°, 16°and 14°were seen at the hip, knee and ankle respectively (Figure 1).

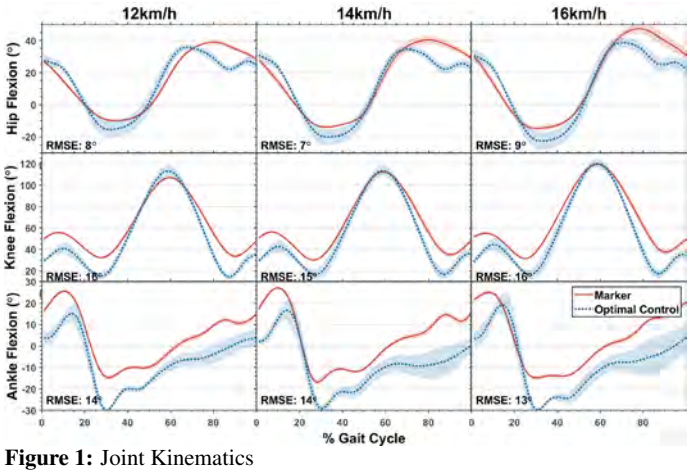

Figure 1: Joint Kinematics

CONCLUSIONS

This work employs IMU sensors within an optimal control framework to model running gait. An appropriately scaled musculoskeletal model with a hybrid objective function combining IMU tracking and effort terms, produced dynamically consistent, kinetic and kinematic measures. Further tuning of the simulation can improve agreement with optical motion capture data. Future work will involve a larger cohort and use muscle-driven models to estimate internal forces and the cost of locomotion. Applications range from modelling experimental data captured outside the laboratory setting, to predicting intervention outcomes in areas such as rehabilitation and sports performance.

REFERENCES

[1] Weygers I et al. *Sensors* **20(3)**: 673, 2020
[2] Dembia C et al. *Comput. Biol.***16(12)**: 2020
[3] Laidig D et al. *Inf Fusion* **91**: 187-204, 2023
[4] Palermo E et al. *Measurement* **52**: 144-5, 2014
[5] Keller M et al. *CVPR* **6**: "Osso: Obtaining Skeletal Shape from Outside," 2022.

CREATION OF A HEAD-GROUND CONTACT MODEL FOR EQUESTIAN FALL IMPACTS

James Cowburn[1,2], M. Polly McGuigan[1,2,3], Keith Stokes[1,2,4], and Dario Cazzola[1,2,3]
[1] Department for Health, University of Bath, Bath, UK.
[2] Centre for Health and Injury and Illness Prevention in Sport (CHi2PS), University of Bath, Bath, UK.
[3] Centre for the Analysis of Motion, Entertainment Research and Applications, University of Bath, Bath, UK.
[4]Rugby Football Union, Twickenham, UK.
Email: j.cowburn@bath.ac.uk

INTRODUCTION

Due to the high velocity nature of horse racing, when jockeys fall it can result in career-ending and life-altering injuries [1]. Musculoskeletal simulations provide a controlled, non-invaisive method for studying injury mechanisms of falling jockeys. Estimating forces experienced by the jockey when impacting the ground is necessary to correctly identify injury mechanisms and design preventative interventions. The aim of this study was to estimate paramaters of an equestrian helmet-head-ground contact model, which is a key element to perform realsitic predictive simulations in horse racing.

METHODS

Forward dynamic simulations were performed to replicate a monorail drop rig test [2]. The resultant acclerations were digigisted for 6 conditions: 3 head orientations (front, front boss, and rear boss) and 2 anvil orientations (flat and 45°). An OpenSim model of the skull, using masses of a Hybrid III head form (4.54kg) and a commercial helmet (0.65kg). A single-sphere contact model was used with a Hunt-Crossley force. The initial model positions and velocities were set to match the drop test immediately before impact, and the accelerations were set to zero. The simulation time was 0.03s, to match the digitised data (Figure 1). A bounded optimisation was performed using the SciPy library (v1.9.0) in Python (v3.8.10) to find the best sphere radius, and Hunt-Crossley stiffness, dissipation, transition velocity and friction (static, dynamic and viscous) parameters. The goal was to minimise the sum of squared error between the digitised and simulated data. The optimised kinematics from each trial was used as reference data. An additional forward dynamic simulation was performed per trial with the median optimised parameter values. The RMSE was calculated between the new simulated and reference coordinates.

RESULTS AND DISCUSSION

Digitised accelerations were tracked to within an RMSE of 40 $m \cdot s^{-2}$ (4.01 BW expressed as a force). The error eminates from the inability to accurately replicate the monrail test rig. The rig constrained the dummy head after impact which cannot be simulated without external force information. When using the median values (Table 1), rotational and translational coordinates were within 4° and 1.4cm, repectively, of the optimised reference data. The stiffness value exceeded that reported for racing turfs ($5e^4$-$1.5e^5$ [3]) but was less than that of common helmet materials (e.g. ~$8e^9$ [4]), which reflected the interaction between the softer turf and stiffer helmet-head. Therefore, dissipation coefficient and sphere radius were sufficient to provide appropriate damping and depth and rate of deformation. Given the model aimed to estimate forces and not to describe the nature of the colliding bodies, these values were deemed appropriate. Similarly, the remaining friction coefficients dictate the shape of the friction model, and could be viewed as adequate within this model. Future work will aim to further scrutinise the model paramaters under different racing turf (going rating) conditions.

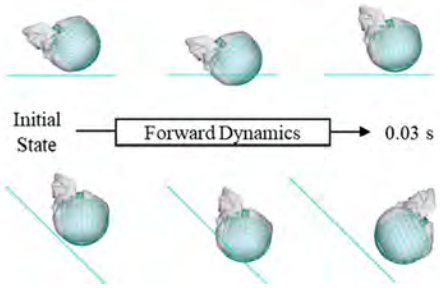

Figure 1 Visual progression of the model state during forward dynamic simulations.

CONCLUSIONS

The contact parameters derived in this study are in-line with realistic values. This allows the contact model to be integrated with predictive simulations of jockey falls, enabling the identification of injury mechanisms and the development of safe fall techniques and protective garments to mitigate against injury risk.

ACKNOWLEDGEMENTS

The authors would like to acknowledge the Racing Foundation for funding this work.

REFERENCES

[1] Balendra G et al. *Br J Sports Med* **42**: 22-24, 2008.
[2] Clarke M et al. *Ann Biomed Eng* **48**: 2247-67, 2020.
[3] Clarke M et al. *J Biomech Eng* **142**: 061006.
[4] Forero Rueda & Gilchrist. *J Sports Eng and Technol* **226**: 208-19

Table 1: Median parameters calculated from optimised values from each condition

	Stiffness (N/m)	Dissipation	Static Friction	Dynamic Friction	Viscous Friction	Transition Velocity ($m \cdot s^{-1}$)	Sphere Radius (m)
Median	$3.283e^6$	0.066	0.011	0.638	0.100	0.914	0.091

THE PROSTHETIC METATARSOPHALANGEAL JOINT STIFFNESS DURING WALKING ON VARIOUS ENVIRONMENTS: A SIMULATION STUDY

Pankwon Kim[1] and Choongsoo S. Shin[1]
[1] Department of Mechanical Engineering, Sogang University, Seoul, Korea.
Email: cshin@sogang.ac.kr

INTRODUCTION

The metatarsophalangeal (MTP) joint is one of the important factors in lower limb prosthetic design. The MTP joint supports over 30% of the body mass during the push-off phase [1]. MTP joint stiffness affects the ankle moment and power consumption [2]. Several studies attempted to mimic human motion by implementing the MTP joint in the prosthesis design [2,3]. However, these studies focused on the MTP joint mechanics during flat-ground walking. Therefore, the purpose of this study is to propose the stiffness of the prosthetic MTP joint during walking on flat ground, upstairs, downstairs, uphill, and downhill.

METHODS

One male participated in this pilot study. The experimental tasks were walking on flat ground, uphill, downhill, upstairs, and downstairs. The participant was instructed to walk at a self-selected speed during the experiments. A 3-dimensional motion capture system equipped with 10 infrared cameras was used to record the motion of the knee, ankle, and MTP joint at a sampling rate of 400 Hz. The ground reaction force (GRF) data were recorded using a force plate at a sampling rate of 1200 Hz.

A prosthetic model with an MTP joint was developed using OpenSim. The foot was divided into two objects: a prosthetic keel and a prosthetic forefoot section [4]. Then the MTP joint between the prosthetic keel and forefoot section was modeled as a hinge joint. A path actuator composed of a single spring was added 0.05 m below the center of rotation of the MTP joint. A cylindrical wrapping object was inserted into the MTP joint (Figure 1).

To determine the stiffness, simulations were performed in three steps. The first step was to compute the MTP flexion moment through inverse dynamics (ID) with the gait2392 model in OpenSim. The second step was to compute the MTP flexion moment through Computed Muscle Control (CMC) with the prosthetic model in OpenSim. The third step was to match the peak MTP flexion moment calculated in the second step with that calculated in the first step by changing the actuator stiffness repeatedly.

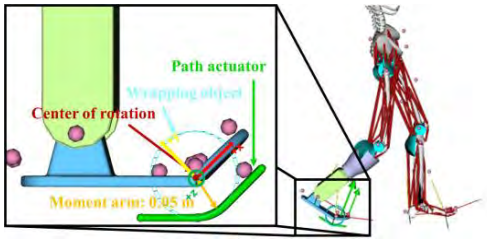

Figure 1 An actuator modelling of metatarsophalangeal joint

RESULTS AND DISCUSSION

Compared with the peak MTP flexion moments calculated through inverse dynamics, the moments calculated using CMC were matched within the error rate of 0.5%. (Table 1). The path actuator stiffness was the highest at 5.00 N/mm during stair ascent (Table 1). Since there is a difference in the MTP joint stiffness according to each walking environment, further study is needed to develop a prosthetic control algorithm to implement variable stiffness based on our results.

CONCLUSIONS

In conclusion, the MTP joint's stiffness could be determined through the developed prosthesis model using OpenSim during walking on flat ground, upstairs, downstairs, uphill, and downhill.

ACKNOWLEDGEMENTS

This work was supported by the National Research Foundation of Korea (NRF-2019R1A2C1089522).

REFERENCES

[1] Hayafune N et al. *Foot.* **9**: 88-92, 1999.
[2] Zhu J et al. *Mechatronics* **24**: 1254-61, 2014.
[3] Patrick S et al. *Front Neurorobot.* **16**: 809380, 2022
[4] McDonald KA et al. *Sci. Rep.* **11**(1): 1924, 2021

Table 1: Peak MTP flexion moment and MTP joint stiffness during flat-ground, stair ascent, stair descent, uphill, and downhill walking.

	Flat-ground	Stair ascent	Stair descent	Uphill	Downhill
Peak flexion moment calculated by ID (Nm)	5.07	5.83	1.88	3.02	5.91
Peak flexion moment calculated by CMC (Nm)	5.08	5.83	1.89	3.01	5.91
Stiffness (N/mm)	2.95	5.00	0.83	1.40	2.77

Validity evaluation of muscle force and muscle activity estimated using two-dimensional vertical GRF

Zeming JIN[1], Takeo MARUYAMA[1]
[1] Social and human science, Tokyo Institute of Technology, Tokyo, Japan.
Email: jin.z.aa@m.titech.ac.jp ; maruyama@ila.titech.ac.jp

INTRODUCTION

The musculoskeletal simulation can calculate the muscle activity and can reproduce muscle damage that cannot be reproduced by measurement experiments [1]. It is possible to investigate how changes in muscle force, which are difficult to measure directly, affect movements such as jumping.So far, the evaluation of muscle activity is mainly electromyography (EMG). In another study, we performed a jump experiment with 4EMGs attached on lower limbs . 3D ground reaction force (3DGRF) and coordinate data measured by MotionCapture system were used as input data for Opensim's Gait2392 simulation model, and EMG was calculated. The calculated EMG was compared with the EMG measured in the experiment to evaluate the validity of the simulation model. The EMG and muscle force calculated using the Gait2392 simulation model can be taken as a standard reference. Jeffrey reported that sagittal plane jump landing can screening high-risk motion patterns [2]. It is necessary to verify the validity of EMG and muscle force estimated using a simple two-dimensional vertical GRF (vGRF) in order to apply it to motion analysis using two-dimensional image while actual sports and daily living scenes. Therefore, in this study, we analyzed the four muscles of the lower limbs during the countermovement jump (CMJ), and compared the EMG and muscle force estimated using the vGRF and the 3DGRF. Then, the validity of the muscle force and muscle EMG estimated using only the vGRF is verified.

METHODS

The experimental subject of this study is a single healthy male (age:31, height:178cm, weight:85kg). Before conducting this experiment, the content of the trial was explained to the subject in advance, and consent was obtained from the subject. In this experiment, CMJ from a standing posture were performed three times, and the attempt that reached the highest jump height was adopted for analysis. Subject was instructed to take off as quickly as possible and jump as high as possible with maximum effort, with hands on hips. Markers were affixed to 32 locations on the whole body, and images were taken using eight MotionCapture cameras (manufactured by Motion Analysis), and the sampling frequency was set to 200Hz. Using a force plate (Kistler, 600mm x 900mm) to measure the GRF of the right foot during jumping at a sampling frequency of 1000Hz. Analysis was performed using the Opensim Gita2392 model. Simulation 1 used 3DGRF data and Simulation 2 used only vGRF data. Static optimization was performed to improve the long head of the biceps femoris (BF), rectus femoris (RF), lateral gastrocnemius (LG) and tibialis anterior (TA) EMG and muscle force were compared, and validity was evaluated by Root mean square (RMS).

RESULTS AND DISCUSSION

Table 1 shows the estimated maximum EMG, muscle force, and RMS (Table 1). It was observed that EMG and muscle force estimated using vGRF only were smaller than those estimated using 3DGRF. There was a tendency to underestimate the EMG and muscle force of all the lower limbs estimated using only the vGRF, but the time to reach the maximum muscle force and the maximum EMG coincided, and the change curve are almost the same. In addition, the EMG of BF, RF, LG, and TA during the CMJ by simulation model showed similar results to the muscle force exertion patterns of previous studies [3].Since the simulation model was calculated based on the Hill model, when only the vGRF is used, muscle length and muscle contraction speed are not affected, and only the force is considered to be affected. Since the simulation model agrees qualitatively and quantitatively, it is considered to be valid, and we believe that EMG and muscle force during jumping can be predicted using only the vGRF. However, it is thought that it is necessary to clarify how large the estimated value is evaluated in future research.

CONCLUSIONS

The purpose of this study is to verify the validity of estimation of lower limbs EMG and muscle force during CMJ by a musculoskeletal simulation model using only vGRF. The results underestimated the EMG and muscle force estimated using vGRF only, but showed similar change curves. It is considered to have sufficient validity.

REFERENCES

[1] Dumitru I. Caruntu et al. *J Computational and Nonlinear Dynamics* **14 (10)**: 101005, 2019.
[2] Jeffrey B. Taylor et al. *J Sports Medicine* **4(6)**: 1177, 2016.
[3] Bence Kopper et al. *J Electromyogtaphy and Kinesiology* **23**:132, 2013

Table 1: Mean value and RMS of estimated EMG (au) and muscle force (N) during CMJ

Mean value (RMS)	BF	RF	LG	TA
EMG (3DGRF)	0.08 (0.14)	0.10 (0.20)	0.05 (0.06)	0.09 (0.13)
EMG (vGRF)	0.07 (0.12)	0.08 (0.16)	0.05 (0.06)	0.08 (0.10)
Muscle Force (3DGRF)	66.93 (111.69)	110.51 (227.16)	31.15 (38.43)	61.90 (84.04)
Muscle Force (vGRF)	61.16 (98.04)	96.36 (178.73)	29.04 (35.28)	54.07 (71.60)

HINDFOOT ARTICULAR JOINT LOADING DURING WALKING: A COMBINED *IN VIVO* AND *IN SILICO* STUDY

Barbara Postolka[1], Bryce A Killen[1], Hannelore Boey[1,2], Jos Vander Sloten[2] and Ilse Jonkers[1]
[1] Human Movement Biomechanics Research Group, KU Leuven, Leuven, Belgium
[2] Biomechanics Section, KU Leuven, Leuven, Belgium
Email: barbara.postolka@kuleuven.be

INTRODUCTION

Increased joint contact stresses, can lead to cartilage degeneration and thus the development of osteoarthritis. Analysis of cartilage contact mechanics using musculoskeletal model-based simulations provides insights into subject-specific articular joint loading and can provide an estimation of disease risk. While articular joint loading has been well studied in the knee, less is known about loading of the ankle and subtalar joints. Therefore, the aim of this study was to combine state of the art *in vivo* kinematics with novel *in silico* musculoskeletal simulations to estimate ankle and subtalar articular joint mechanics in healthy subjects.

METHODS

12 healthy subjects (29 ± 10 years) with no history of foot-ankle injuries provided written informed consent to participate in this study. Foot-ankle kinematics during a simulated stance phase were acquired using 4D CT imaging [1]. Individual ankle and subtalar 3D kinematics were calculated based on bone specific anatomical coordinate systems [2]. For *in silico* assessment of the hindfoot articular joint mechanics, cartilage contact for the ankle (tibia/talus) and subtalar (talus/calcaneus) joints were added to a foot-ankle model [3]. Contact components were modelled using an elastic foundation formulation based on cartilage stiffness and mesh penetration [4]. Models were then used in a forward simulation whereby ankle and subtalar rotations were prescribed based on the 4D CT measurement. Articular joint mechanics were then estimated using the OpenSim joint and articular mechanics (JAM) tool [4]. To investigate articular joint loading, the contact area as well as mean and peak pressure of the ankle and subtalar joint were analysed.

RESULTS AND DISCUSSION

The ankle joint showed a larger contact area compared to the subtalar joint while mean and peak pressure were higher for the subtalar joint (Table 1). Throughout the stance phase, tibio-talar contact occurred predominantly lateral whereas talo-calcaneal contact occurred at the medio-anterior part of the subtalar joint (Figure 1). For both joints, peak pressure and maximum contact area were found during mid stance.

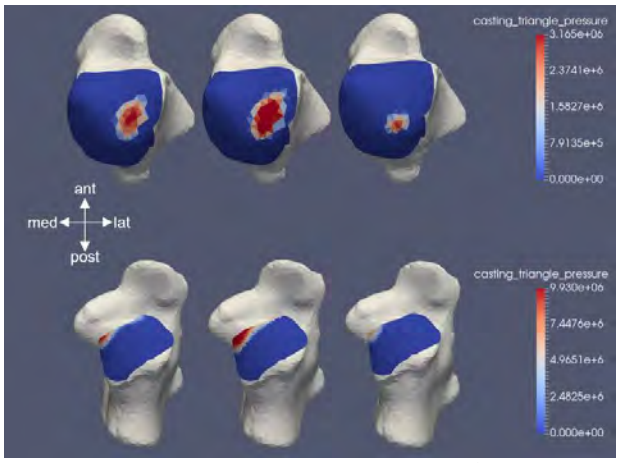

Figure 1: Cartilage contact pressure distribution of the ankle joint projected on the talus (top row), and subtalar joint projected on the calcaneus (bottom row) at initial loading, mid stance, and push off for one subject.

CONCLUSIONS

This study showed a first analysis of articular joint mechanics of the ankle and subtalar joint during simulated gait. Using a musculoskeletal foot-ankle model combined with recently developed methods to estimate cartilage contact mechanics, this study allowed novel insights on the location and magnitude of articular joint loading. While this study provided important findings in a controlled loading situation, further developments are needed to enable the use for functional analysis during other dynamic *in vivo* activities. Furthermore, analysis of pathological cohorts such as subjects with chronic ankle instability can help to understand changes in articular joint mechanics and how they are related to joint degeneration.

ACKNOWLEDGEMENTS

This work was partially funded by the Berghmans – Dereymaeker research chair on foot and ankle biomechanics.

REFERENCES

[1] Postolka et al. *8th iFAB Congress*, 2023
[2] Conconi et al. *J Foot Ankle Res* **14**(1):1-13, 2021
[3] Malaquias et al. *CMBBE* **20**(2):153-159, 2017
[4] Smith et al. *CMBBE Imaging Vis* **6**:491-498, 2018

Table 1: Contact area, mean pressure, and peak pressure during a simulated stance phase of walking. Mean ± standard deviation across all 12 subjects are presented.

	contact area	mean pressure	peak pressure
ankle joint	1.11 ± 0.12 cm^2	1.90 ± 0.09 MPa	4.25 ± 0.30 MPa
subtalar joint	0.64 ± 0.12 cm^2	4.49 ± 0.84 MPa	13.80 ± 2.19 MPa

Control Strategy of the Locomotor System for Obstacle-Crossing in Adolescents with Severe Idiopathic Thoracic Scoliosis: Trade-offs Between Mechanical Energy Expenditure and Foot Clearance

Cheng-Hao Yu[1], Tse-Hua Huang[2], Shiuan-Huei Lu[1], Hsuan-Yu Lu[1], Chia-Han Hu[1], Kuan-Wen Wu[3,4], Ting-Ming Wang[3,4] and Tung-Wu Lu[1,4]

[1] Department of Biomedical Engineering, National Taiwan University, Taipei, Taiwan
[2] Department of Mechanical Engineering, National Taiwan University, Taipei, Taiwan
[3] Department of Orthopaedic Surgery, National Taiwan University Hospital, Taipei, Taiwan
[4] Department of Orthopaedic Surgery, School of Medicine, National Taiwan University, Taipei, Taiwan
Email: twlu@ntu.edu.tw

INTRODUCTION

Adolescent idiopathic scoliosis (AIS) is the most common type of three-dimensional spinal deformity. Patients with AIS have been found to adopt a bilateral asymmetric joint-to-end-point kinematic strategies with an increased risk of falls during obstacle-crossing [1]. However, it remains unclear of the overall control strategies of the locomotor system for obstacle negotiation in patients with AIS based on the currently known individual kinematic variables. Therefore, the purpose of the current study was to use multi-objective optimal control (MOOC) techniques [2] to identify the overall control strategy in adolescents with AIS when crossing obstacles of three different heights.

METHODS

Twelve adolescents with Lenke 1 thoracic AIS and twelve healthy controls participated in this study. Each subject walked and crossed an obstacle of three heights (i.e., 10%, 20%, and 30% of the subject's leg length) with either the concave- (AIS-A) or convex-side (AIS-V) limb leading while the kinematics and kinetics were measured. A MOOC technique was used to evaluate the control strategies during leading crossing [2], formulated as the best-compromise weighting sets for the conflicting objectives of minimizing mechanical energy expenditure and maximizing the toe-obstacle and heel-obstacle clearances. Mechanical energy expenditure, toe-obstacle and heel-obstacle clearances of the swing-limb were also calculated. Two-way ANOVA were used to study between-subject (group) and within-subject (AIS-V vs. AIS-A or obstacle height) effects on all calculated variables.

RESULTS AND DISCUSSION

Compared to the healthy controls, patients with AIS increased energy expenditure weighting for both AIS-A and AIS-V conditions (Figure 1A). Nevertheless, the mechanical energy expenditure increased under the AIS-A condition but decreased in AIS-V (Figure 1B). Patients with AIS only showed decreased toe-obstacle clearance for AIS-A but there were no any other significant differences in end-point variables in tested conditions (Figures 1C and D). With increasing obstacle height, both AIS and Control groups showed significantly increased mechanical energy expenditure (Figure 1B). These results suggested that patients with AIS were inclined to reduce energy costs compared to the healthy controls. Lower-limb joint work under AIS-A was emphasized to reduce mechanical energy expenditure at the expense of decreased toe-obstacle clearance with an increased risk of falls. The normal toe-obstacle clearance during AIS-V appeared to be a compensation for increased mechanical energy expenditure requirements, which may be affected by the geometric asymmetry of the spine in lateral deformation.

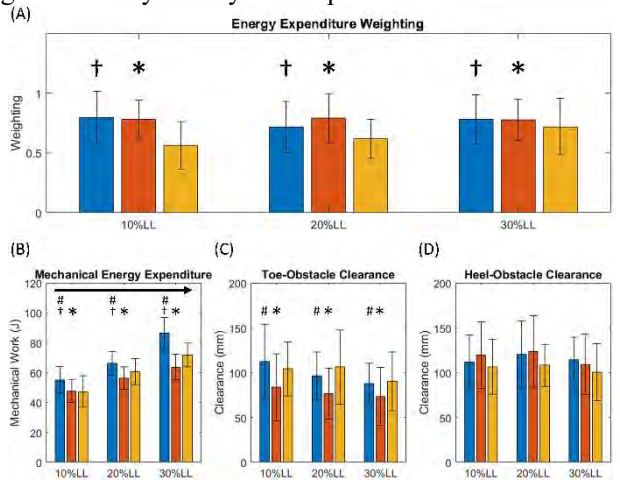

Figure 1 Comparisons of the mean (A) energy expenditure weighting, (B) mechanical energy expenditure and (C) toe-obstacle clearance and (D) heel-obstacle clearance above the obstacle during leading crossing with the corresponding standard deviations shown as error bars. *: AIS-A significantly different from Control. †: AIS-V significantly different from Control. #: AIS-V significantly different from AIS-A. With increasing obstacle height, a right arrow indicates a linearly increasing trend (blue bar: AIS-V; red bar: AIS-A; yellow bar: Control).

CONCLUSIONS

This study identified the overall control strategy in patients with AIS during obstacles crossing. Based on the current results, it is speculated that patients with AIS adopted an altered energy-efficient strategy with bilateral symmetry but showed asymmetric changes in mechanical energy expenditure and end-point control.

ACKNOWLEDGEMENTS

The authors are grateful for the financial support from the National Science and Technology Council, Taiwan (MOST 110-2813-C-002-364-E).

REFERENCES

[1] Wu, K.W., et al. *Gait Posture* **71**: 211-218, 2019.
[2] Lu, T.W., et al. *Gait Posture* **36(3)**: 552-556, 2012.

MUSCLE FATIGUE: EXPERIMENT AND SIMULATION

Zeinab Saghaei Nooshabadi[1], MohammadReza Zakerzadeh[1], MohammadAli Nazari[1]
[1] School of Mechanical Engineering, College of Engineering, University of Tehran, Tehran, Iran.
Email: zeynab.saghaee@ut.ac.ir

INTRODUCTION

Fatigue is one of the major causes of muscle and ligament injuries during many tasks and exercises. One of the most common definitions of fatigue is “failure to maintain the required force to continue performing a task” [1]. This process is described by the decline of muscle Maximal Voluntary Contraction (MVC) force [2]. Previous studies on over-training in athletes show that fatigue often occurs before muscle injuries, where muscles are very vulnerable. These injuries can lead to loss of muscle strength [1]. The role of muscle fatigue in sports performance and rehabilitation makes it necessary to investigate its influence [3]**.** The purpose of this reserch is to detect fatigue level during a physical activity in synergic muscles. The activity history of the selected muscles is obtained via simulation in OpenSim.

METHOD

A healthy 23 years old man (mass:64 kg, height:189 cm) participated in this study. A set of reflective markers were positioned on anatomical landmarks and motion capture system was used to measure the 3D markers displacement. Ground reaction forces were recorded by force plates. The subject was asked to walk continuously for 2 minutes at a constant speed 1 m/s. Therefore, each gait cycle takes about one second. Before starting the exercise, the Maximal Voluntary Contraction (MVC) of each selected muscle was recorded. Using marker trajectories muscle forces were calculated. After importing markers data in OpenSim, using inverse dynamics, muscles’ control data were obtained. In the following the computed muscle controls are used to find muscle activations.

RESULTS AND DISCUSSION

To analyse the results of two gait cycles, one at second 2 and the other at second 120, are used as starting position and terminal positions respectively. As shown in figure 1, the force produced, for example, in soleus muscle in seconds 2 and 120 is compared with each other in the corresponding gait cycle. The active forces are calculated for the other muscles in these two gait cycles. The initial and final maximum force produced in the selected muscles are shown in table 1. As it is given in table 1, the most reduction is happened in the vastus lateralis muscle.

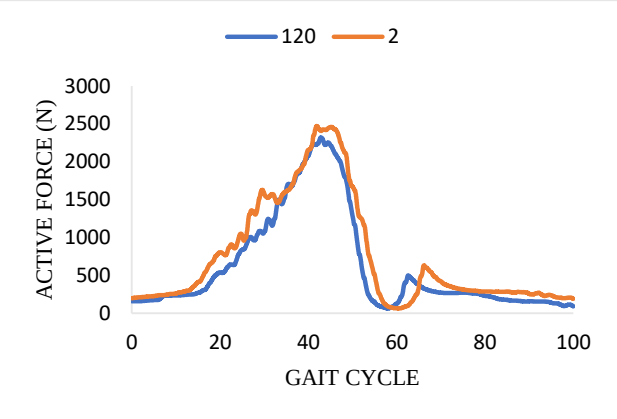

Figure 1 Force produced in soleus during gait cycle in seconds 2 and 120

CONCLUSIONS

According to the simulation data, the maximum reduction in muscle capability is seen in vastus lateralis muscle which is the largest muscle of quadriceps muscles. This muscle directly opposes vastus medialis on the inner portion of thigh. The vastus medialis muscle is the most affected muscle in contusion. This shows the fatigue in vastus lateralis decrease its supporting action and hence leaves the other muscles more susceptible to injuries.

REFERENCES

[1] Elshafei, M. and E. Shihab. Sensors (Basel)21(3).2021.
[2] Jing, C., et al. *Digital Human Modeling and Applications in Health, Safety, Ergonomics and Risk Management. Human Body, Motion and Behavior* 978-3-030- 77816-3. ffhal-03173264f. 2021.
[3] Rampichini, S., et al. Entropy (Basel) **2**(5), 2020

Table 1: percentage reduction of maximum produced force (N) in selected muscles in seconds 2 and 120

Time(s)/muscle	soleus	gluteus medius	Vastus lateralis	Gastrocnemius (med)	Gastrocnemius (lat)
120	2320.76	434.99	152.03	1047.15	303.88
2	2471.30	468.59	208.37	1097.15	335.15
Decrease (%)	6.1	7.2	27.0	4.6	9.3

Lower limb mechanical load in ballet jumps with turnout and neutral positions (work in progress)

Filipa João[1], Rodrigo Mateus[1], Luis Xarez[2] and António Veloso [1]
[1], Biomechanics and Functional Morphology Laboratory, University of Lisbon / Faculty of Human Kinetics, Lisbon, Portugal.
[2] Faculty of Human Kinetics, Lisbon, Portugal.
Email: filipajoao@fmh.ulisboa.pt

INTRODUCTION

In classical dance (ballet), most of the vertical and horizontal jumps are performed with an increased external rotation position of the lower limb (turnout). To obtain the amount of turnout that is considered to be aesthetically acceptable in theory, which is about 140 degrees, some ballet dancers use the knee, ankle and feet to increase the amplitude between both feet. These compensation mechanisms have been reported as risk factors for the increased incidence of knee, ankle and foot musculoskeletal injuries in dancers [1]. Vertical jumps are constant motor actions that take part in dance choreographies. Jumps occur with different initial conditions and lower limb positions, being the tournout position a recurrent one. The purpose of the present study was to investigate the effect of turn out position on the lower limb muscle forces during vertical jumps performed by classical ballet dancers from the Portuguese National Ballet Company.

METHODS

As a work in progress, one professional classical ballet dancer from the Portuguese National Ballet Company was recruited to perform this pilot study. An informed consent was previously signed by the participant. Motion capture was performed using a markerless camera system (8 Qualisys Miqus, 3-megapixel resolution video cameras), sampling at 85 Hz. Two Bertec Force Plates collected the ground reaction force (GRF) data with a frequency of 1000 Hz. The subject performed a sequence of vertical jumps starting from the following lower limb initial conditions: 1st position (A- with an externally rotated hip joint position and B- with both feet parallel in neutral position), 2nd position (A and B) and 4th position (A and B).
Markerless motion capture video data were processed using Theia3D (v2021.1.0.1450), from which 4x4 pose matrices of each body segment were exported for analysis in Visual3D (C-Motion, USA). An Opensim generic musculoskeletal model with 19 degrees of freedom and actuated by 92 Hill-type muscle-tendon units was scaled to match the anthropometric characteristics of the subject [2]. Residuals reduction was performed to compensate for dynamic inconsistencies between the measured kinematics and GRF. Individual muscle forces were estimated using computed muscle control algorithm during the braking and propulsion phases of the jump.

RESULTS AND DISCUSSION

For this preliminary analysis, data from two jumps (one in neutral position and the other in turnout position) are presented. The subject was a female with 50kg of mass and 1.62m of height.

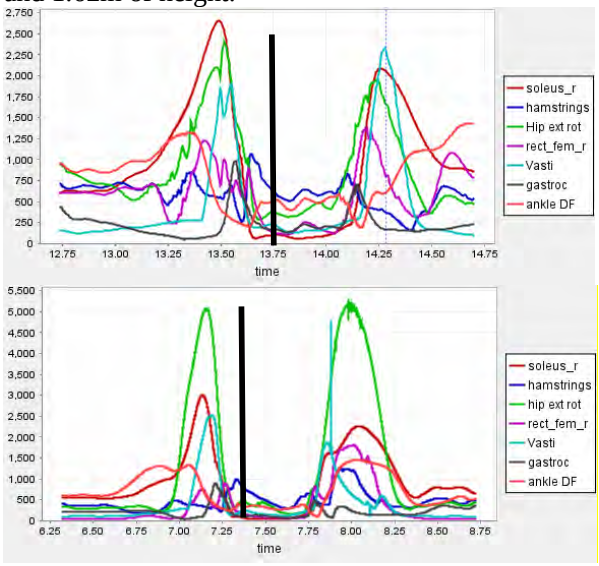

Figure 1 Muscle forces during 1st position (top) and 1st parallel position (bottom) vertical jumps. Vertical line is the take off instant

CONCLUSIONS

In the parallel jump, the subject uses more the hip external rotator muscles when compared with the regular 1st position. Both soleus and vasti muscles are the main force producers but with greater intensity in the parallel jump. Probably due to the different and less used technique.

ACKNOWLEDGEMENTS

This work was supported by CIPER-FCT (projects: UIDB/00447/2020 and PTDC/EMD-EMD/5804/2020).

REFERENCES

[2] van Merkensteijn, G. G., & Quin, E. (2015). J Dance Med Sci, 19(2), 57–62.
[3] Delp SL et al., IEEE Trans Biomed Eng, 54(11): 1940-1950, 20

CONSEQUENCES OF LIMITING ELECTROMYOGRAPHY AND GROUND REACTION FORCES ON MODELLED ANTERIOR CRUCIATE LIGAMENT FORCES

Azadeh Nasseri[1], Riad Akhundov[1], Adam Bryant[2], David Lloyd[1] and David John Saxby[1]
[1]Griffith Centre of Biomedical and Rehabilitation Engineering, Menzies Health Institute Queensland / Griffith University, Gold Coast, Australia.
[2]Centre for Health, Exercise & Sports Medicine / University of Melbourne, Melbourne, Australia.
Email: a.nasseri@griffith.edu.au

INTRODUCTION

Modern computational models can accurately quantify anterior cruciate ligament (ACL) loads during dynamic tasks in the laboratory [1,2]. These models use body motion, ground reaction forces (GRF), and electromyograms (EMG). However, acquiring EMG and GRF outside the laboratory, i.e., sports fields or medical clinic, is challenging due to instrument costs, setup time, and skills to acquire and interpret data. Limiting EMG and GRF data, while maintaining model prediction accuracy, would be practically valuable for translation of ACL modelling technology outside the laboratory. We examined the consequences of limiting EMG and GRF on fidelity of model-predicted ACL loads.

METHODS

Twenty-three healthy females (mean (±standard deviation) age, mass, and height of 19.7 (±4.0) years, 59.7 (±9.5) kg, and 1.65 (±0.06) m, respectively) performed a standardized drop-land-jump task, while body motion, GRF, and surface EMG were acquired. Data were used in four neuromuscular models: EMG-informed and static optimization, each with three dimensional (3D) and exclusively vertical GRF. For each model, external biomechanics, lower limb muscle forces, and knee contact forces were computed, and subsequently used to estimate ACL force [1,2]. The ACL force across stance and rank-order of participants based on their peak ACL force were compared across models using one-way repeated measures ANOVA and *post hoc* t-tests via statistical parametric mapping and Kendall's rank correlation, respectively.

RESULTS AND DISCUSSION

Compared to EMG-informed + 3D GRF, both EMG-informed and static optimization methods using only vertical GRF generated significantly higher ACL force (mean differences, 205.5 N and 253.8 N, respectively) for most of stance. When 3D GRF were used, differences between EMG-informed and static optimization were observed only within the final 20% of stance (mean differences, 116.4 N). Compared with static optimization + 3D GRF, both EMG-informed and static optimization combined with only vertical GRF generated significantly higher ACL force (mean differences, 89.1 N and 137.4 N, respectively) for most of stance (Figure 1). No statistically significant correlations in rank-order of participants were found between EMG-informed + 3D GRF and the other models (Table 1), meaning model configuration affects both absolute and relative magnitude of ACL forces. Although, vertical GRF is readily measured in-field using commercially available instruments, this study demonstrated using only vertical GRF substantially overestimated ACL loads. Simplifying the neural model to static optimization overestimated ACL loading even when modelling used 3D GRF.

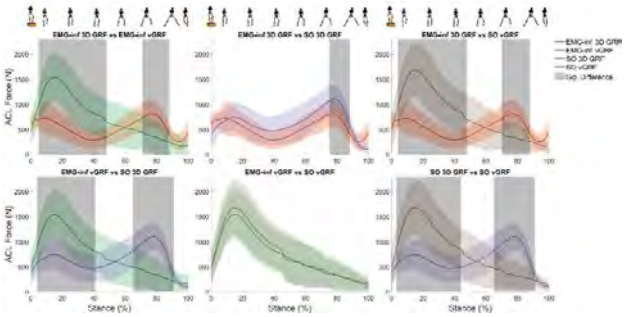

Figure 1. Pairwise comparisons of ACL force (±1 standard deviation) over stance of drop-land-jump estimated via four modelling approaches.

CONCLUSIONS

Simplifying requirement for experimental measures of muscle activation patterns via static optimization and/or reducing GRF from 3D to only vertical force resulted in spurious model estimates of ACL loading. Compared to modelling with 3D GRF, using only vertical GRF resulted in much larger ACL forces due to a lack of a posteriorly directed GRF during landing. The consequence of neglecting EMG in favour of static optimization was more complex. Individual responses were highly variable, but resulted in a small but significant increase in ACL loading for the cohort studied. Finally, rank order of participants based on their peak ACL loading could not be preserved under any simplified modelling approach used in this study. Findings indicate both EMG and 3D GRF should be included to model ACL loading during dynamic tasks.

REFERENCES

[1] Nasseri A et al. *Comput Meth Prog Bio* **184**, 2020.
[2] Nasseri A et al. *Med Sci Sports Exerc* **53(6)**, 2021.

Table 1. Kendall's rank correlation of peak ACL force between different modelling approaches during drop-land-jumping.

	SO + vGRF	SO + 3D GRF	EMG-inf + vGRF
Correlation	-0.028	-0.012	0.067
p-value	0.876	0.958	0.676

ACTIVITY OF SUPERFICIAL TRUNK MUSCLES IN PATIENTS WITH STROKE DURING GAIT: A CASE SERIES

Cruz, Christopher[1], Chiong-Maya, Arlene[1], Tiuseco, Archelle Jane[1], Alcantara, Loraine[1], Bieren, Arieane Christie[1], Javier, Victorio Luis Gabriel[1], Maban, Marissa, Joanna[1], Partin, Dorothy Gayl[1]e, Sison, Krizia Mariel[1], Velez, Jacinto III[1], and Young, Har-li[1]

[1] College of Rehabilitation Sciences, University of Santo Tomas, Manila, Philippines.
Email: cgcruz@ust.edu.ph

INTRODUCTION

One of the common sequelae of stroke is difficulty walking, which is strongly attributed to the affectation of the activity of the lower extremity and trunk muscles [1]. Rectus abdominis (RA) and external obliques (EO) muscles provide pelvic stabilization needed for proper leg movements to occur during walking [2]. Most of the studies available have analyzed different activities of the lower extremity muscles [3] and no studies have been found to analyze the activity of RA and EO or the superficial trunk muscles as a whole. The aim of this study is to describe the activity of superficial trunk muscles in terms of peak amplitude and duration using EMG in the gait of patients with stroke.

METHODS

This descriptive case series study will utilize an electromyogram to measure the amplitude of superficial trunk muscle activation during the gait of patients who have had a stroke for the first time and are in Brunnstrom Stage 3 of motor recovery.

RESULTS AND DISCUSSION

Observation made with the use of EMG showed that both the right and left RA and EO of all participants were active all throughout the gait cycle with their peak activity variably seen during loading response, midstance, and terminal stance of the reference leg (right leg), with 70% observed to peak in activity during midstance.

The pattern of muscle activity of RA and EO in the study may be caused by the demands of gait in maintaining minimal displacement of the center of gravity (COG) in relation to positional changes undergone by the body, as well as by the compensations made by the RA and EO for the loss of function of the lower extremities brought about by stroke. This may be taken into account in planning rehabilitation for patients with stroke, which may focus on these muscles when addressing ambulation ability.

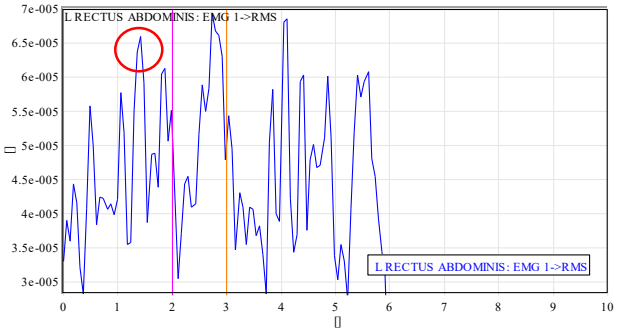

Figure 1 Muscle activity of left rectus abdominis during gait of participant 1. The peak muscle activity of this muscle was obtained during the midstance of the reference leg.

CONCLUSIONS

The superficial trunk muscles- RA and EO- assessed in this study were active all throughout the gait of the participants, with 70% observed to peak in activity during midstance. These observations are assumed to have been brought by the high work demand to the superficial trunk muscles in maintaining minimal displacement of the COG during midstance and/or to be a manifestation of compensation for the weakness of the lower extremity muscles directly brought about by stroke. Further studies are needed to provide concrete evidence of such assumptions.

REFERENCES

[1] Vasileva, D. et al. *Open Access Macedonian Journal of Medical Sciences* **53**: 2017
[2] Pereira, LM. et al. *Journal of Electromyography and Kinesiology* **21**: 2010.
[3] Marsden, J. et al. *Journal of Electromyography and Kinesiology* **23(4)**: 2013

Table 1: The phases of gait in which the peak muscle activity of the left rectus abdominis (RA) obtained for participant 1.

		Peak Activity (Volts)		
Participant	Muscles	Loading Response	Midstance	Terminal Stance
1	Left RA		6.60E-05	

Classification of People with Parkinson's Disease Based on Images Converted from Time-Series Data during 360° Turning Task

Hyejin Choi[1,2], Changhong Youm[1,2*], Sang-Myung Cheon[3], Hwayoung Park[1], Bohyun Kim[1,2], Juseon Hwang[1,2], Minsoo Kim[1], Byungjoo Noh[4], and Young Jin Jeong[5]

[1] Biomechanics laboratory, Dong-A University / Busan, Republic of Korea
[2] Department of Health Sciences, Graduate School, Dong-A University / Busan, Republic of Korea
[3] Department of Neurology, School of Medicine, Dong-A University / Busan, Republic of Korea
[4] Department of Kinesiology, College of Natural Sciences, Jeju National University / Jeju, Republic of Korea
[5] Department of Nuclear Medicine, Dong-A University Hospital / Busan, Republic of Korea
Email: chyoum@dau.ac.kr

INTRODUCTION

Parkinson's disease (PD) is one of the neurodegenerative diseases; motor impairments of people with PD start on the unilateral predominance throughout the progression of the disease and present bilateral impairments at a later stage. However, determining the severity of motor symptoms in people with PD relies on subjective diagnosis by neurologists. Furthermore, objective measurement needs to be studied to identify and classify body segments according to disease severity in people with PD. Therefore, this study aims to classify people with PD and healthy controls based on imaging of time-series data using objective and in-depth turning tasks for directions toward the more affected side of people with PD. In addition, there is to present objective factors that may determine the severity of the disease, and its accuracy is to confirm.

METHODS

The participants were 30 people with PD and 30 age-matched healthy controls. People with PD performed the 360° turning task at their preferred speed toward the directions of the inner step of the more affected side in the "Off" state of medication, and the healthy controls performed the task toward the left side. To analyze the time-series data, the position and acceleration data of a total of 40 body segments marker trajectories, including the center of mass, were used, which were converted into new imaging and then trained with a convolutional neural network (CNN) algorithm technique (Figure 1). The performance of the two-group classification model was evaluated using accuracy.

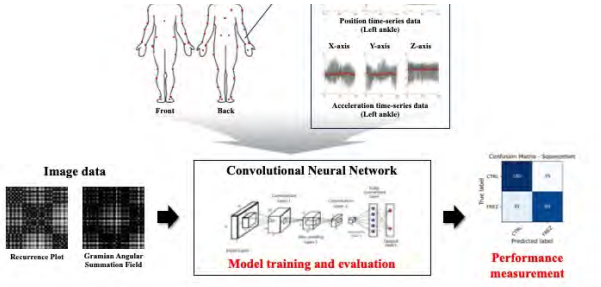

Figure 1 Flow chart for the proposed method.

RESULTS AND DISCUSSION

The body segments classified in the people with PD and the healthy controls were the left (82%) and right (81%) elbows and the left (80%) and right (80%) shoulders in the position time-series data. In addition, they were left (84%) and right (81%) heels, right toe (81%), left ankle (81%), left posterior superior iliac spine (84%), and left wrist (83%) in the acceleration time-series data. In previous studies, the classification accuracy of people with PD and healthy controls during straight gait using wearable sensors was reported to be 87.2% through the distal segments' upper and lower limbs symmetry [1]. The asymmetric characteristics of upper and lower limb segments are most pronounced during disease progression [2]. Therefore, our results identified body segments with bilateral coordination problems of the upper and lower limbs of people with PD based on whole-body segments during turning.

CONCLUSIONS

We identified symptom-affected body segments using full body segments during 360° turning for directions toward the more affected side of people with PD, and suggest that the CNN technique, a deep learning algorithm analysis based on time-series data imaging of identified body segments, may contribute to improving disease severity discrimination and classification of people with PD in the clinical environment.

ACKNOWLEDGEMENTS

This work was supported by the National Research Foundation of Korea (NRF) grant funded by the Korea government (MSIT) (No. 2022R1A2C100933711). This research was supported by Basic Science Research Program through the National Research Foundation of Korea (NRF) funded by the Ministry of Education (No. 2022R1A6A3A0108756411).

REFERENCES

[1] Sant'Anna et al. *IEEE Trans. Biomed. Eng.* **58**(7), 2127-2135, 2011.
[2] Troisi Lopez et al. *Ann. N.Y. Acad. Sci.* **1516**(1), 247-261, 2022.

STRETCH STRAIN SENSOR FOR ABDUCTION OF THE TALONAVICULAR JOINT

Shintarou Kudo[1,2], Keisuke Hirakawa[2], Masahiro Tsutsumi[1,2] and Isao Yamaguchi [1,3]
[1] Inclusive medical sciences research institute, Morinomiya University of medical sciences, Osaka, Japan.
[2] Graduate school of health sciences, Morinomiya University of medical sciences, Osaka, Japan.
[3] Department of radiological sciences, Morinomiya University of medical sciences, Osaka, Japan.
Email: kudo@morinomiya-u.ac.jp

INTRODUCTION

Foot biomechanics studies in relation to flatfoot deformity have shown that peritalar subluxation at the transverse tarsal joints, particularly increasing abduction of the talonavicular joints, needs to be assessed in the clinical setting. However, the foot movement assess without footwear such as socks and shoes, although the footwear influences for foot movement. Sakamoto and Kudo had shown that the stretch strain sensor (STR) could assess forefoot inversion and dorsiflexion in relation to the hindfoot with footwear[1], however, abduction of the talonavicular joint could not be assessed. The purpose of this study was to develop assessment methods using the STR for abduction of the talonavicular joint.

METHODS

The 14 feet of 14 normal male volunteers (age 44.6±8.0 years old, height 1.72±0.06 m, weight 73.4±13.4 kg) participated in this study. This study was performed after obtaining ethical review approval from our institution.

The difference in talonavicular coverage angle using radiographs between sitting and quiet standing was defined as talonavicular coverage angle excursion (TNCA-E) as the abduction of the talonavicular joint. Foot strain in both sitting and quiet standing was assessed using the STR sensor attached to the medial side of the foot in four patterns. Pattern 1 positioned between the navicular and the sustentaculum tali, pattern 2 between the medial cuneiform and the sustentaculum tali, pattern 3 between the navicular and the medial malleolus and pattern 4 between the medial cuneiform and the medial malleolus. In addition, the STR sensor is inclined for as long as possible to rotate approximately 40 degrees upward from the transverse plane in patterns 1 and 2 and approximately 50 degrees downward from the transverse plane in patterns 3 and 4 (Figure 1).

The change in foot strain between quiet standing and sitting was calculated from four patterns. The difference between four patterns was evaluated using Freedman's test with Bonferroni test. And the correlation coefficient between four patterns of strain change and TNCA-E was assessed using Spearman's coefficient.

RESULTS AND DISCUSSION

The foot strain using pattern3 (median;1.05 (25%-75%;1.04-1.07)) was significantly greater than that using pattern1 (1.03 (1.01-1.06)) and pattern2 (1.03 (1.01-1.04)), and the foot strain using pattern4 (1.05 (1.03-1.06)) was significantly greater than that using pattern1. In addition, the TNCA-E have a significant correlation coefficient with the medial side of the foot strain in pattern3 (r=0.60, p=0.02, power=0.73), and other patterns did not show the significant correlation coefficient.

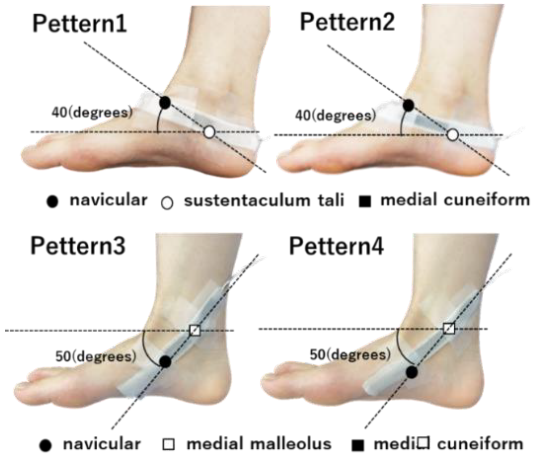

Figure 1 Four mounted patterns of STR sensor

The axis of motion of the talonavicular joint is inclined dorsally by approximately 40 degrees from the transverse plane [2]. The STR in pattern3 and 4 were mounted on the skin perpendicular to this axis, therefore the STR mounted on pattern3 could reflect the abduction of the navicular relative to the talus. And pattern4 was mounted from the medial malleolus to the medial cuneiform, so it might not be difficult to maintain it perpendicular to the axis of motion of the talonavicular joint. The STR in Pattern3 may have the capability to assess the abduction/adduction of the talonavicular joint with footwear conditions.

CONCLUSIONS

The abduction of the talonavicular joint with footwear can be assessed using STR mounted between medial malleolus and navicular.

ACKNOWLEDGEMENTS

This study has been supported by the Descente and Ishimoto memorial foundation for the promotion of sports science.

REFERENCES

[1] Sakamoto K, et al. *Gait Posture* **86**: 180-185, 2021.
[2] Nester C, et al. *JAPMA* **92**(2):77-8

Time series for the whole-body synergy of the hip angle during gait in patients with hip osteoarthritis

Takuya Ibara[1], Koji Fujita[1], Naoto Watanabe[2], Ryohei Takada[2], Kazumasa Miyatake[2] Akimoto Nimura[1], Keiichi Akita[3]

[1] Department of Functional Joint Anatomy / Tokyo Medical and Dental University, Tokyo, Japan
[2] Department of Orthopaedic Surgery / Tokyo Medical and Dental University, Tokyo, Japan
[3] Department of Clinical Anatomy / Tokyo Medical and Dental University, Tokyo, Japan
Email: ibara.fana@tmd.ac.jp

INTRODUCTION

For patients with hip osteoarthritis (OA), the hip extension limitation is considered a risk factor for disease progression [1]. When considering a rehabilitation approach to prevent disease progression, it is important to know whether the hip flexion-extension movement can be controlled. Recently, researchers have focused on the inter-trial variability of the task variable formed by whole-body movements as an index of the task-specific stability [2]. If the hip angle is sufficiently controlled, the inter-trial variability is reduced and the hip angle is stabilized. This study aimed to investigate a hip movement strategy during gait at the point where the inter-trial variability is produced by whole-body movements.

METHODS

A public gait dataset comprising 106 patients with unilateral hip OA (hip OA group) and 80 asymptomatic participants (asymptomatic group) [3-6] was used. Data were recorded using a motion capture instrument, and twelve stance phase data were extracted from each participant. Using the joint position, the head, neck, upper trunk, lower trunk, knee, and shank angles (supported leg) in the sagittal plane (elemental variables) were calculated, as well as the hip joint angle formed from the elemental variables (task variable). An uncontrolled manifold analysis (which quantifies the contribution of the elementary variables in the stabilization of the task variable) was then performed, and the synergy index ΔV was calculated. The variances of the elemental variables that did not affect the task variable (V_{UCM}) and those that affected (V_{ORT}) them were also calculated, along with the value of the task variable (angle) and its standard deviation (std). Subsequently, statistical parametric mapping (SPM) was performed using a one-sample t-test if the ΔV was more than 0 (whether stabilizing), followed by two-sample t-test to compare the group differences in all variables.

RESULTS AND DISCUSSION

The ΔV in both groups is significantly higher than 0 throughout the stance phase ($p < 0.001$), indicating that the hip angle is stabilized throughout the stance phase. The degree of synergy for stabilization is similar in both groups with respect to the ΔV and V_{UCM} (Figure 1 A, B). However, the V_{ORT} and std beyond 70% of the stance phase (Figure 1 C, E) are slightly higher. Prior to this, the hip angle beyond 20% of the stance phase (Figure 1 D) varies, and the hip angle in the hip OA group is slowly extended within a limited range. This indicates that the gait strategy in the hip OA group can be changed earlier in the stance phase to avoid the need for external stabilization in the sagittal plane during gait.

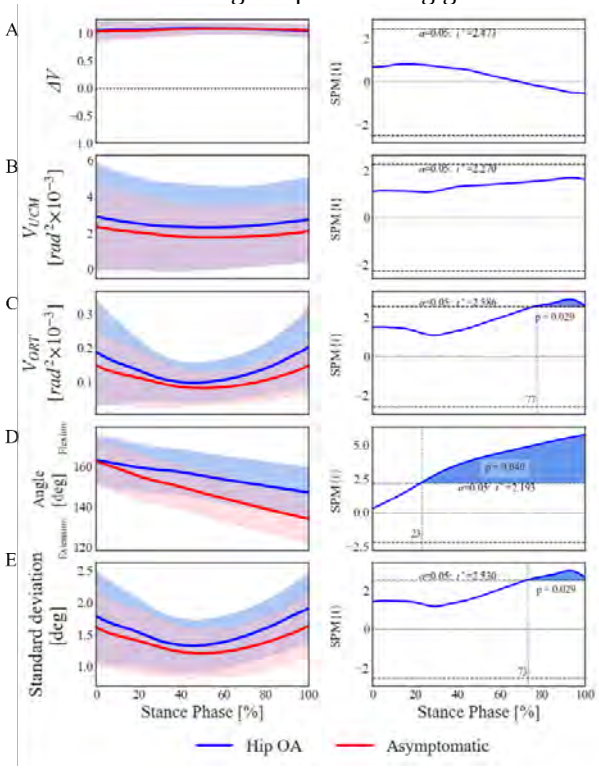

Figure 1 Results of the SPM two-sample t-test of the ΔV, V_{UCM}, V_{ORT}, angle, and std. The mean, standard deviation (left panel), and t value calculated from the SPM (right panel) are shown.

CONCLUSIONS

In this study, patients with hip OA were able to sufficiently stabilize their hip angles during the stance phase by changing their strategy in the early stance phase. Therefore, it is important to consider the reasons for changing the strategy during rehabilitation.

ACKNOWLEDGEMENTS

This study was supported by JSPS KAKENHI (Grant No. JP 21K21250).

REFERENCES

[1] Lievense AM et al. *Arthritis Rheum* 57: 1368-74, 2007.
[2] Latash ML et al. *Phys Ther Res* **25**: 1-11, 2022
[3] Bertaux A et al. *Scientific Data* **9**: 399, 2022.
[4] Laroche D et al. *Figshare* 14420645: v2, 2021.
[5] Laroche D et al. *Figshare* 14420756: v2, 2021.
[6] Laroche D et al. *Figshare* 13655975: v10, 2022

Biomechanical Analysis of Contralateral Cane Use

Hyeoun-Soo Shin[1], Min-Jae Kim[1], Gwang-Moon Eom[1]
[1] Biomedical Engineering, Konkuk University, Chungju , Korea.
Email: kkurehab@naver.com

INTRODUCTION

Osteoarthritis (OA) in knee, especially at the medial tibiofemoral compartment, is a leading cause of disability in elderly people [1,2]. Increase in the knee adduction moment (KAM) was associated with the risk of progression of medial knee osteoarthritis and chronic knee pain [3,4]. Contralateral cane use, but not the ipsilateral one, resulted in significant reduction of KAM [5-7]. However, the mechanism how the contralateral cane use reduces KAM is still unclear. Therefore, the purpose of this study was to identify the mechanism of the reduction.

METHODS

Sixteen healthy young male subjects with no history of lower limbs disease were included in this study. A T-shape cane was used by the right hand which is contralateral to the left (ipsilateral) leg. Subjects were instructed to make the tapping timing of the contralateral cane close to that of the ipsilateral foot contact.

Subjects walked on a 5 m walkway, in the middle of which three force plates were instrumented. Two plates along the progression of subjects were used for legs and the other for the cane. Seven motion capture cameras (Motion Analysis Inc., CA.) were used for kinematic measurement with Helen-Hayes full marker set. Subjects wore tight Mocap suits, hat, and foot covers on barefoot exclusively designed for motion capture, on which reflective markers were placed. No-cane and two cane loading conditions (5 and 10 % Body Weight(BW)) were designed. For the cane loading practice, subjects were requested to match the peak cane load presented by a force platform with the designated loading. Three measurements were made for each loading condition after enough practice.

Kinetic data (KAM, ground reaction force: GRF, and its lever arm) and kinematic data (knee joint center, center of mass: COM, and center of pressure: COP) on the frontal plane during stance phase of ipsilateral leg were extracted from the measured data by using Cortex 8 program (Motion Analysis Inc.) and custom-made Matlab program. The lever arm was calculated on the frontal plane of the knee joint axis. From the GRF on the frontal plane, two instants of peaks in the first and second half of stance phase (1st and 2nd peak instants hereafter) were determined. Kinetic and kinematic data at peak instants were designated as variables for further analysis.

RESULTS AND DISCUSSION

The reduction of KAM in response to the cane loading was correlated far more with the lever arm than with the magnitude of GRF.

Fig.1 shows how the lever arm is altered by cane loadings, i.e., how COM, knee joint center, and GRF change their location and direction. It is noted that the medial shift in response to the increase in cane loading was dramatic for the knee joint center, however the change in GRF direction was not significant. The results suggest that the reduction of KAM was mainly due to the medical shift of knee joint center rather than the change of GRF direction.

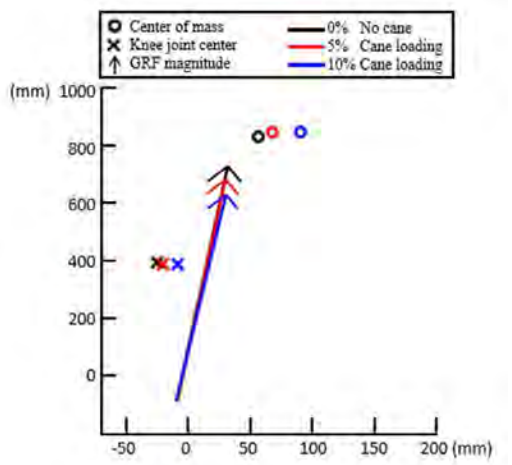

Figure 1 GRF, knee joint center, and COM on the frontal plane at the 1st peak of GRF. For the comparison of different cane loadings, the ankle joint position was set to be at the origin.

CONCLUSIONS

Lever arm had dramatic effect in reducing knee adduction moment rather than GRF magnitude. Lever arm was reduced by medial shift of knee joint center rather than tilting of GRF.

ACKNOWLEDGEMENTS

This work was supported by Korea Research Foundation with the funding of the Ministry of Education in 2022. (2021R1I1A3050968)

REFERENCES

[1] Felson DT, et al. *Ann Intern Med* **133**: 635-46, 2000.
[2] Ledingham J, et al. *Ann Rheum Dis* **52**: 520-6, 1993.
[3] Miyazaki T, et al. *Ann Rheum Dis* **61**: 617-22, 2002.
[4] Thorp LE, et al. *Arthritis Rheum* **57**: 1254-60, 2007.
[5] Chan GN, et al. *Clinical Biomechanics* **20**: 396-404, 2005.
[6] Kemp G, et al. *Arthritis Rheum* **59**: 609-614, 2008.
[7] Simic M, et al. *Arthritis Care Res*. **63**: 405-26, 2011.

Relationship between leg muscle co-contraction and jerk during gait.

Toshinori Miyashita [1,2], Shintarou Kudo [1,3]
[1] Inclusive medical science research institute, Morinomiya University of Medical Sciences / Osaka, Japan.
[2] Osaka Bay Clinic, Morinomiya University of Medical Sciences/ Osaka, Japan.
[3] AR-Ex medical research center / Tokyo, Japan.
Email: toshinori_miyashita@morinomiya-u.ac.jp

INTRODUCTION

It is known that the co-contraction of dynamic and antagonist muscles increases during gait in the elderly, limiting smooth locomotion[1]. Miyashita et al. estimated ankle power using an IMU sensor, and the establishment of a gait analysis method using an IMU sensor is highly needed in gait analysis research[2]. Therefore, the aim of this study is to investigate whether the co-contraction rate can be estimated using IMU sensors.

METHODS

The participants were 11 outpatients orthopaedic clinic (73.7 ± 6.8 yrs,1.56 ± 0.9 m, 53.3 ± 9.7 kg). An IMU (Cometa, Milano, Italia, 143Hz) was attached to the fibular head of the lower leg (three axes; Ax: vertical, Ay: anterior-posterior, Az: mediolateral axes). Surface electromyography (EMG) was measured from the anterior tibialis (TA: area A), lateral gastrocnemius muscles (GL: area B) using the Wave COMETA EMG system (2000Hz). EMG signals were processed using a Butterworth bandpass fourth order filter of 20 – 400Hz, full-wave rectification, and then a Butterworth lowpass fourth order filter of 6Hz. The muscle co-contraction uses formula (1). (Figure 1) [2]. The measurement task performed comfortable and maximum gait speed. The calculated jerk in each direction was reported as Ax', Ay', Az', and the jerk in the three-axis direction was condensed into one value as the instantaneous magnitude of the vector using the formula (2) [3]. The calculated percent co-contraction and jerk for one gait cycle was divided into stance phase, loading response (LR), mid stance (MSt), terminal stance (TSt), and pre-swing (PSw). The peak jerk value was calculated for each phase and the mean value was calculated from five gait cycles. The variables were investigated age, sex, height, weight, gait speed (comfortable, maximum), percent co-contraction (%), jerk, and estimated ankle joint power (formula (3)). The Spearman's rank correlation coefficient were used to examine the correlation between percent co-contraction and jerk.

・$Percent\ contraction(\%) = 2 \times \frac{common\ area\ A\&B}{area\ A + area\ B} \times 100$ (1)

・$m = \sqrt{Ax'^2 + Ay'^2 + Az'^2}$ (2)

・$Estimated\ ankle\ power(W) = -4.869 + 0.269 \times Ay + 0.104 \times Body\ Weight$ (3)

RESULTS AND DISCUSSION

The dorsiflexors of the ankle are activated during LR, however, an insufficient response to the load occurs with increasing activity of the plantarflexors. The jerk, which represents the instantaneous change in acceleration, is also greater when the change in force is greater. Therefore, jerk is expected to increase when the load responding is sufficient. The negative correlation between the co-contraction and the jerk of the LR in the current study indicates that the changes in force during the load response phase were less due to the co-contraction.

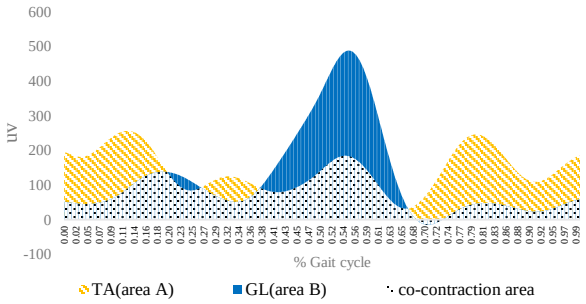

Figure 1 lower leg muscle co-contraction in the gait cycle.

CONCLUSIONS

There is possibility that an IMU can be reflect muscle co-contraction of lower leg muscle from jerk of lower leg during LR phase.

ACKNOWLEDGEMENTS

This work was supported by JSPS KAKENHI (grant number JP22K17622)).

REFERENCES

[1] Lo, J. et al. Gait Posture. 53: 110-114, 2017.T
[2] Miyashita, et al. J Phys Ther Sci. Apr;31(4):354-359. 2019.
[3] Na, A., et al. Hum. Mov. Sci. 64, 409–419, 2019.

Table 1: Correlation coefficients between percent co-contraction and jerk in each stance phase.

	LR		MSt		TSt		PSw	
Comfortable gait speed	r=-0.28	p=0.40	r=-0.2	p=0.55	r=0.05	p=0.91	r=0.31	p=0.36
Maximum gait speed	**r=-0.67**	**p=0.04**	r=-0.53	p=0.12	r=-0.6	p=0.07	r=-0.21	p=0.56

(The Spearman's rank correlation coefficient, p<0.05)

TOWARDS PRECISION ASSESSMENT OF GAIT IMPAIRMENTS IN STROKE SURVIVORS

Jun Liang Lau[1], Ananda Sidarta[1], Wu Tsung-Lin[1], Phyllis Liang[1], and Karen Chua Sui Geok [1,2,3,]
[1] Rehabilitation Research Institute of Singapore, Nanyang Technological University, Singapore.
[2] Department of Rehabilitation Medicine, Tan Tock Seng Hospital Rehabilitation Centre,
[3]Institute of Rehabilitation Excellence, Singapore
Email: junliang.lau@ntu.edu.sg

INTRODUCTION

Mobility impairments remain a major concern for people with stroke, impacting their quality of life and limiting community participation. Clinical interventions for gait impairments aim to improve gait quality and reduce compensatory movements. Current clinical practice in gait analysis relies heavily on visual observation which is subjective and dependent on clinical experience. Hence, there is a need to objectively measure gait abnormality and identify its precise location within the gait cycle. We proposed an innovative precision measurement method to assess post-stroke gait impairment clinically using movement analytics powered by SPM1D [1], while at the same time studying the feasibility and patient tolerance.

METHODS

A total of 15 stroke participants (*M* age = 53.73 years old, *SD* = 12.20, 4 females) who fulfilled the following criteria were recruited: (1) unilateral hemiparesis, (2) > 6 months post-stroke; (3) ambulant with at most contact guard/standby supervision with/without walking aid during the study, (4) 10m Walk Test score ≥ 0.2m/s; (5) distance of ≥ 50m for the 6 min Walk Test without rest stop; (6) with Functional Ambulation Category of ≥4 and AMT>6/10. They were excluded if they had psychological and cognitive problems and uncontrolled or unstable medical conditions. The participants were asked to perform a list of lower-limb tasks as outlined in our previous work [2]. All movements were recorded with a 2-megapixel Miqus M3 motion capture system (Qualisys AB, Sweden) using a modified CAST marker set. The markers datasets were first preprocessed and joint angle trajectories (hip, knee, and ankle) were modelled and extracted using Visual3D (C-Motion Inc., USA). Gait cycle segmentation was done using a custom-made code in Python. Time-normalised joint trajectories for each participant during walking were averaged across different repetitions to obtain the subject-level dataset. Joint trajectories of the affected and unaffected lower limbs were compared using a paired *t*-test function in SPM1d.

RESULTS AND DISCUSSION

All stroke participants successfully completed the tasks. Only the results of the walking task are reported. Compared to the normal hip (Figure 1), the affected hip shows reduced flexion during initial contact and terminal swing. During the swing phase, the paretic knee is more extended, and with increased ankle adduction.

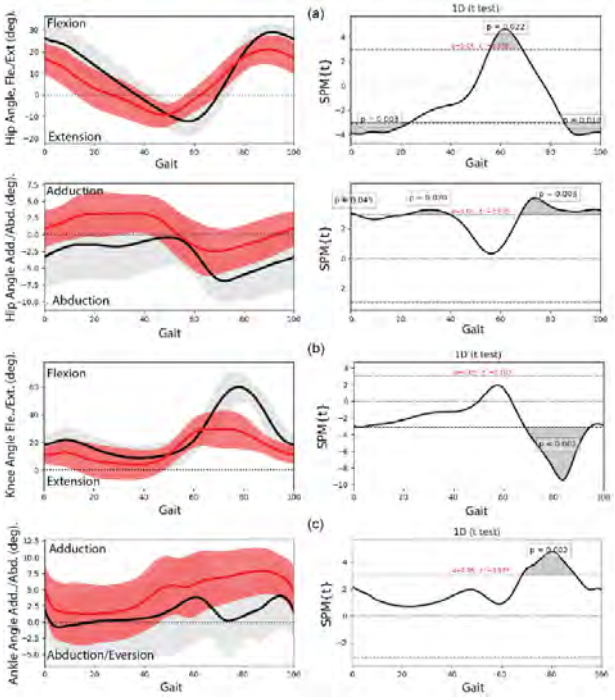

Figure 1. Outputs from the SPM1d analysis comparing affected (**red**) and unaffected (**black**), (a) hip joints, (b) knee joints, and (c) ankle joints during walking. The X-axis represents the full gait cycle. Data are taken from all 15 participants. Significant deviations ($p < 0.05$) are indicated in shaded grey.

CONCLUSIONS

This study shows that SPM1d can specifically identify asymmetry in the gait cycle during walking, where significant abnormalities lie. Future analyses will examine stroke-induced compensatory patterns during walking. This method will potentially be useful clinically as an objective tool to add precision to treatment evaluation.

ACKNOWLEDGEMENTS

The authors thank the Nanyang Technological University (NTU), Agency for Science, Technology and Research (A*STAR) and the National Healthcare Group (NHG) for funding the study.

REFERENCES

[1] Pataky, T. *J Biomech* **43**: 1976, 2010.
[2] Liang P, et al. *Scientific Data* **7**:290, 2020.

Oxygen consumption and center of foot pressure trajectory changes with a 3D-printed insole based on the 3D-scanned individual soleprint

Mizuki Kondo[1], Tatsuro Ishidzuka[2], Yuji Ohgi[2] and Masahiro Okuno[2]
[1] NEC Corp., Minato, Japan.
[2] Graduate School of Media and Governance, Keio University, Fujisawa, Japan.
[2] Rapithela Corp., Seto, Japan.
Email: kondomizuki0726@gmail.com

INTRODUCTION

A medical use of insoles aims to treat, reduce pains and improve the function of those who have disability or abnormality with their lower limbs. In comparison, healthy people use insoles to prevent injuries and pain in the lower limbs and to improve feeling of walking [1]. People use insoles made of different materials depending on their purposes. For the variety of foot shapes of individuals, the author hypothesized that 3D scanning and 3D printers would be beneficial for fabricating insoles for each demand. This research aimed to investigate the effectiveness of the 3D scanned/printed insoles for normal gait for healthy adults.

METHODS

Twenty adult males with normal feet with an arch height ratio of 11-15 % were recruited for our study. The insoles were fabricated using eLabo (Rapithela Corp.) based on digital data of the 3D-scanned participant's soleprint. The insoles were made of EPU41, a UV-curable urethane elastomer. The thickness of the insole was 5 mm. We conducted the experiment under three conditions: bare feet, experimental shoes, and experimental shoes with the 3D-printed insole. Participants walked on the circular path in the following procedure : (1st) walking two laps, (2nd) walking 5 minutes, (3rd) walking 1 minute, (4th) walking two laps. We measured the center of pressure (COP) trajectory using a 9.042m large-scaled foot pressure sensor mat (Nissha Corp.) during (1st) and (4th). Also, expired gas was obtained during (3rd) with douglas bag. Then, the oxygen consumption ($\dot{V}O_2$) was calculated. The maximum lateral amplitude of the COP trajectory of 16 participants was identified, except for participants whose expired gas was leaked.

RESULTS AND DISCUSSION

The median of the $\dot{V}O_2$ for 16 participants with 3D-printed insole condition was smaller than those of the experimental shoes condition (Table 1). Fig. 1 shows the boxplot of the maximum lateral amplitude of the COP related to the foot width for 16 participants with barefoot, experimental shoes, and 3D-printed insoles. The median of the maximum amplitude of the COP trajectory with the 3D-printed insole condition was the smallest for those of the other conditions (Fig. 1). However, the maximum amplitude of the COP trajectory with the 3D-printed insole condition for some participants was not smaller than those of the experimental shoes condition. The maximum amplitude of the COP trajectory was reported to be a barometer of gait stability [2]. Therefore, it was suggested that 3D-printed insoles reduced COP fluctuations for some participants and improved gait stability.

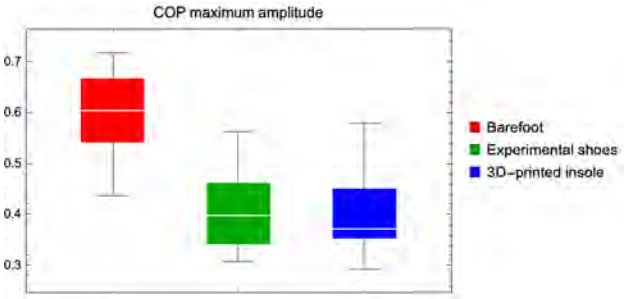

Figure 1 Ratio of COP maximum amplitude related to the foot width with barefoot, experimental shoes, and 3D-printed insoles.

CONCLUSIONS

The results of improved gait stability due to decreased COP maximum fluctuations and reduced oxygen consumption with 3D-printed insole condition suggested that the 3D-printed insole based on the 3D-scanned participant's soleprint could reduce the physical load in a walking motion. However, there were still variations between individuals in the effect of the 3D-printed insole based on the 3D-scanned participants' soleprints.

REFERENCES

[1] Maryam Hajizadeh et al. , The Foot, **42**: 101646, 2020.
[2] H Chang, D E Krebs, Arch Phys Med Rehabil, **80**, 5: 490-494, 1999.

Table 1: $\dot{V}O_2$ results for 16 Participants

	Barefoot	Experimental shoes	3D-printed insole
$\dot{V}O_2$[ml/kg/min]	0.01024	0.01169	0.0112

COMPARISONS OF ENERGY EXPENDITURES AMONG CHILDREN DIAGNOSED WITH IDIOPATHIC TOE WALKING AND TYPICAL CHILDREN USING INERTIAL SENSORS

Rahul Soangra[1,2], Dylan Normandin[4] and Marybeth Grant-Beuttler [4,5]
[1] Crean College of Health and Behavioural Sciences, Chapman University, Orange, USA.
[2] Fowler School of Engineering, Chapman University, Orange, USA.
[4]Oregon Institute of Technology, Klamath Falls, USA
[5]Oregon Health & Science University, Portland, USA
Email: soangra@chapman.edu

INTRODUCTION

Children diagnosed with Idiopathic Toe Walking (ITW) walk on their toes and are liable to leg pain and fall injuries. It is crucial to understand how toe walking affects energy expenditure in these children compared to typical children of the same age. In this study, we utilized an inertial measurement unit (IMU) attached at the low back to evaluate the number of steps and energy expenditure in the child's natural setting for three days. Twenty participants were instructed to wear a sensor on their low back for three days, and their activities of daily living (ADL) were objectively quantified during weekdays and weekends in their natural settings. We found energy expenditure was higher among children diagnosed with ITW compared to typical controls. We also found the children diagnosed with ITW took shorter and more steps than age-matched controls. A future investigation into biomechanics and new gait interventions is needed to improve gait efficiency and energy expenditure among children diagnosed with ITW.

METHODS

Ten healthy controls and ten children diagnosed with ITW were recruited in this study. The participants were age matched and consisted of 15 males and 5 females (Age: 8.85 ± 3.45 years, Height:52.96 ± 9.52 cm, Weight: 75.28 ± 40.52 lbs). The study was approved by Chapman University Institutional Review Board (IRB 20-219). To understand energy expenditure in natural settings McRoberts sensor (Dynaport, McRoberts, The Netherlands) was wore by children at their low back for three days after their initial visit to the lab.

RESULTS AND DISCUSSION

For total energy expenditure, ITW subjects took 73.7% more steps on weekdays and 36.8% more steps on weekends than healthy subjects. For the relative total energy expenditure lying percentage, ITW subjects had a 14.3% higher value than healthy subjects on weekdays and a 2.8% higher value than healthy subjects on weekends. For the relative total energy expenditure sitting percentage, ITW subjects had a 4.3% higher value than healthy subjects on weekdays and a 6.4% higher value than healthy subjects on weekends. For the relative total energy expenditure walking percentage, ITW subjects had a 30% higher value than healthy subjects on weekdays and a 7.2% lower value than healthy subjects on weekends. Idiopathic toe walking (ITW) certainly affects daily activities and the quality of life.

Previously researchers have reported that children with cerebral palsy had lower physical activity levels and, as a result, lower total energy expenditure (TEE) values [1]. An investigation on children treated with home parenteral nutrition reported that children undergoing home parenteral nutrition programs had similar levels of TEE as the healthy control children analyzed in the study [2]. As per our knowledge, there has been no investigation on energy expenditure and activities of daily living in children diagnosed with ITW. Our preliminary data shows that ITW children took more steps than healthy children on both weekends and weekdays. This may be due to their shorter step lengths compared to controls. Additionally, children diagnosed with ITW had a more significant relative TEE percentage for lying, sitting, walking, and stair walking on weekends and weekdays.

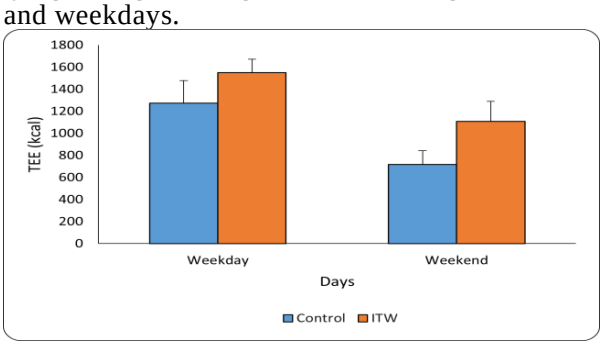

Figure 1 Total Energy Expenditure (TEE) for healthy controls and ITW participants during weekdays and weekends.

CONCLUSIONS

Using advanced technologies like accelerometers our team collected data that could reveal some of the adverse effects of ITW on daily activities and energy expenditures. All questions about the conference should be addressed to soangra@chapman.edu.

ACKNOWLEDGEMENTS

We thank CHOC, Kay Family Foundations and NSF (Award # 2224325).

REFERENCES

[1] Beghin L et al. *Pediatric Research* **53(4)**: 684-690, 2003.

[2] Martin-Martin J et al. *Sensors* **22(7)**: 2552, 2022.

Relationship between gait kinematics and fall risk in patients with Parkinson's disease.

Ryo Yamasaki[1,2], Yu Inoue[1,2,3], Haruki Toda[4]
[1] Department of Rehabilitation, Kurashiki Heisei Hospital, Kurashiki, Japan.
[2] Graduate School of Humanities and Social Sciences, Hiroshima University, Higashi-Hiroshima, Japan.
[3] Research Institute of Health and Welfare, Kibi International University, Takahashi, Japan.
[4] Robot Rehabilitation Center, The Hyogo Institute of Assistive Technology, Kobe, Japan.
Email: ryo.yama.20.1@gmail.com

INTRODUCTION

Patients with Parkinson's disease (PD) are at high fall risk. Falls prevention requires an easily accessible and objective tool to screen for fall risk. Recently, marker-less motion capture systems have been used for convenient assessment of gait kinematics. We hypothesized that differences in the fall risk would reflect in the gait kinematics in patients with PD. This study aimed to investigate whether gait kinematics obtained with marker-less motion capture are associated with fall risk.

METHODS

Patients with PD hospitalized at the Center for Neuromodulation at Kurashiki Heisei Hospital from January to February 2023, who were able to walk without physical assistance or aids, were included in this study. The Microsoft Kinect V2 sensor (Microsoft Corp.) was used as a marker-less motion capture system. Data obtained from measurements were processed using Mobile Motion Visualizer AKIRA (MMV AKIRA, System Friend Inc.). Participants walked along a 5m path toward the Kinect sensor at a comfortable and fast gait, each once. Using the skeletal coordinate data recorded by MMV AKIRA, walking speed, stride length and time, cadence, and step width were calculated as spatiotemporal variables of gait. The maximum trunk forward lean, bilateral shoulder flexion, extension and abduction, hip flexion and extension, and knee flexion and extension angles during one gait cycle were also calculated. These variables were calculated using MATLAB R2022b (MathWorks Inc.). The fall risk for participants was evaluated using the Mini-Balance Evaluation Systems test (Mini-BESTest). We defined the Mini-BESTest score <19 points as a high-risk group and ≥19 points as a low-risk group, based on a cut-off for high fall risk [1]. Spatiotemporal and joint angle variables of gait were compared between the high-risk and low-risk groups using the Mann-Whitney U test. Statistical analysis was performed using R ver. 4.1.2, with a significance level of 5%. Additionally, *r*-values were calculated as effect size.

RESULTS AND DISCUSSION

A total of 9 patients (5 in the high-risk group and 4 in the low-risk group) were included in the study. In the comfortable gait, there were no significant differences between the high-risk and low-risk groups in all variables. However, the high-risk group tended to have a larger trunk forward lean and left hip flexion angle ($p = 0.111$, $r = 0.531$). In the fast gait, the stride length was significantly shorter in the high-risk group (Table 1). Furthermore, bilateral hip flexion angles were larger, and walking speed tended to be lower in the high-risk group (Table 1).

CONCLUSIONS

The feature of gait kinematics obtained with the marker-less motion capture system differed between the high-risk and low-risk groups for falls. Those differences in fast gait were greater than comfortable gait.

REFERENCES

[1] Mak MKY et al. *J Rehabil Med* **45**: 565-571, 2013.

Table 1: Comparison of spatiotemporal variables and trunk and hip angles during fast gait.

	high-risk group	low-risk group	*p*-value	*r*-value
Trunk forward lean (°)	6.9 (6.0 - 30.9)	7.8 (5.5 - 10.3)	0.730	0.115
Right hip flexion (°)	37.7 (31.5 - 46.6)	30.9 (29.6 - 31.3)	0.064	0.619
Left hip flexion (°)	31.2 (29.7 - 31.5)	24.5 (22.8 - 26.8)	0.064	0.619
Right hip extension (°)	13.4 (1.9 - 19.3)	19.1 (14.1 - 24.6)	0.286	0.356
Left hip extension (°)	16.0 (6.5 - 24.1)	22.4 (19.0 - 25.5)	0.190	0.436
Cadence (steps/min)	142.3 (139.0 - 146.2)	136.8 (135.2 - 139.4)	0.323	0.329
Stride length (cm)	108.4 (101.0 - 109.1)	127.0 (121.1 - 135.7)	0.032	0.716
Walking Speed (m/sec)	1.2 (1.2 - 1.2)	1.4 (1.3 - 1.6)	0.111	0.531

Values represent medians and interquartile ranges.

TRUNK MOVEMENT DURING NORDIC WALKING EVALUATED USING A GYROSCOPE IN PATIENTS WITH HIP OSTEOARTHRITIS

Chiho Fukusaki[1,2], Taisuke Nakamichi[2]
[1] School of Health and Sport Sciences, Chukyo University, Toyota, Japan.
[2] Graduate School of Frontier Sciences, The University of Tokyo, Kashiwa, Japan.
Email: fukusaki@sass.chukyo-u.ac.jp

INTRODUCTION

Patients with hip osteoarthritis (hip OA) frequently show a large movement of the trunk during walking, which has found to be a major risk factor for falling [1]. Nordic walking (NW), which is walking with two poles, is one of the exercises for patients with hip OA [2] and acts as a walking aid in their daily life. It has been observed that NW reduces the vertical contact force in patients with knee OA [3] and improves gait asymmetry in patients with knee and hip OA [4]. This study aimed to investigate whether NW reduced trunk movement during walking in patients with hip OA.

Inertial sensors are used for gait analysis, especially in clinical settings, as they can easily measure gait parameters and do not disturb the patients' usual walking. This study used a gyroscope to evaluate the trunk movements during walking.

METHODS

Participants: Twelve female patients with hip OA who were familiar with NW participated in this study. This study was approved by the Research Ethics Committee of the University of Tokyo and written informed consent was obtained from all participants prior to participation.
Protocol: Participants were instructed to walk along a 15-m level walkway first without poles (normal walking) and then with poles (NW) at a preferred speed. They wore a triaxial gyroscope at the level of the xiphoid process to evaluate the trunk movement. Two triaxial gyroscopes were positioned above the lateral malleolus of each leg to determine the heel contact. The sampling rate of the gyroscopes was 100 Hz.
Signal analysis: Ten steps in the middle of the 15-m walkway were determined and cadence (steps/s) during the interval was calculated. The root mean square (RMS) of the angular velocity around each of the three axes at the xiphoid process was calculated during the 10 steps.
Statistical analysis: Changes in cadence affect the angular velocity of the trunk. To evaluate trunk movement without the effect of cadence, we calculated and compared the following two parameters:
RMS ratio = RMS of angular velocity during NW / RMS of angular velocity during normal walking.
Cadence ratio = Cadence during NW / Cadence during normal walking.

A paired *t*-test was used to compare RMS ratio to cadence ratio. P-values less than 0.05 were considered to be statistically significant.

RESULTS AND DISCUSSION

Table 1 shows the cadence and RMS values of triaxial angular velocity during normal walking and NW. The RMS ratio of the yaw angular velocity was significantly larger than the cadence ratio ($p < 0.01$). There was no significant difference between the RMS ratio of the pitch angular velocity and the cadence ratio. The RMS ratio of the roll angular velocity was significantly smaller than the cadence ratio ($p < 0.001$).

These results suggest that patients with hip OA showed larger yaw rotation and smaller roll rotation of the trunk during NW than during normal walking. A smaller roll rotation implies a smaller lateral sway, indicating a reduced risk of falling during NW. A large yaw rotation during NW would relate to the arm movements needed to move the poles forward and backward.

Table 1 Cadence and RMS values during normal waking and NW.

	Normal walking	NW	Cadence ratio RMS ratio
Cadence (step/s)	1.82 ± 0.12	1.66 ± 0.14	0.916 ± 0.074
RMS-yaw (dps)	20.1 ± 5.7	21.9 ± 6.4	1.099 ± 0.197 *
RMS-pitch (dps)	18.0 ± 7.9	16.3 ± 7.3	0.906 ± 0.111
RMS-roll (dps)	11.5 ± 3.5	8.6 ± 2.5	0.759 ± 0.104 *

*Significant difference between cadence ratio and RMS ratio.

CONCLUSIONS

Using a gyroscope, this study showed that NW reduced lateral trunk movement and increased horizontal trunk rotation during walking in patients with hip OA.

REFERENCES

[1] Lin XB et al. *Clin Biomech* **30**: 874-880, 2015.
[2] Fukusaki C et al. *J Nov Physiother* **8**: 1000383, 2019.
[3] Bechard DJ et al. *Osteoarthr Cartil* **20**: 1500-1506, 2012.
[4] Kato N et al. *J Phys Fitness Sports Med* **9**: 65-73, 2020.

EFFECTS OF THE MONOCULAR VISION IN ENDPOINTS CONTROL DURING OBSTRUCTED GAIT

Yi-Ling Lu[1,2], Ju Yang Tiong[1], Kuan-Wen Wu[3,4], Ting-Ming Wang[3,4] and Tung-Wu Lu [1,3]
[1] Department of Biomedical Engineering, National Taiwan University, Taipei, Taiwan.
[2] Department of Ophthalmology, Cheng Hsin General Hospital, Taipei, Taiwan.
[3]Department of Orthopaedic Surgery, School of Medicine, National Taiwan University, Taipei, Taiwan.
[4]Department of Orthopaedic Surgery, National Taiwan University Hospital, Taipei, Taiwan.
Email: twlu@ntu.edu.tw

INTRODUCTION

Vision is known as the most important sensory input system for the interpretation of the inner body state and outer environmental circumstances. Aging and its related ocular diseases may cause rapid or chronic descent of the vision, with cataract being one of the most common eye diseases in the elderly, accounting for about 88% of the elderly suffering from vaired degrees of cataract [1]. However, there is no research to date that have investigated how decreased vision affect the whole-body balance control during obstructed gait. This study aimed to quantify the visual impact on the end-point control in healthy elders when performing obstacle-crossing with monocular or binocular vision.

METHODS

Sixteen healthy older adults walked at a self-selected pace on an 8-meter walkway and performed obstacle-crossing with three different obstacle heights (i.e., 10%, 20% and 30% of the subject's leg length) under two visual conditions (i.e., binocular and monocular vision) (Fig. 1). Thirty-nine infrared retroreflective markers placed on anatomical landmarks commonly used in human motion analysis were used to track the motions of the body segments using an 8-camera motion analysis system. For the three obstacle-crossing heights and two visual conditions, a counterbalanced measures design was used, while the sequence of the obstacle and visual conditions were based on a pre-generated random number table.

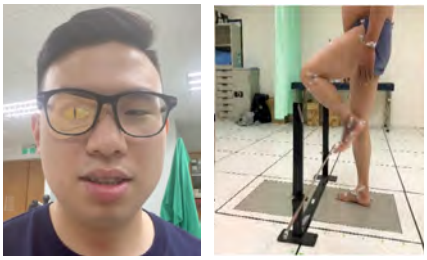

Fig. 1 Subjects crossed a height-adjustable obstacle with binocular and monocular visions.

The marker data were used to calculate endpoint variables. Crossing speed was calculated as the average speed of the whole body's center of mass in the direction of progression over the crossing cycle [2]. A two-way mixed-design analysis of variance (ANOVA) with one between-subject factor (vision) and one within-subject factor (obstacle height) was performed to analyse the spatiotemporal parameters, namely crossing speed, stride length, toe-obstacle distance, heel-obstacle distance, and toe-obstacle clearance.

RESULTS AND DISCUSSION

Subjects showed significantly greater leading and trailing toe-obstacle clearances but lower crossing speed with monocular vision during obstacle-crossing when compared to those with binocular vision (Table 1). No significant between-vision differences were found in stride length, toe-obstacle and heel-obstacle distances (Table 1). No significant height effects were found for any spatiotemporal parameters.

Table 1: Means (standard deviations, SD) of the crossing speed, stride length, and toe-obstacle and heel-obstacle distances with the binocular and monocular visions when crossing obstacles at 20% leg length (LL).

	monocular	binocular	Vision effect
Crossing speed (m/s)	0.78 (0.09)	0.76 (0.09)	$p = 0.01$*
Stride length (%LL)	132.6 (6.9)	132.1 (9.4)	$p = 0.06$
Horizontal distance (%LL)			
Toe-obstacle	27.68 (4.5)	26.50 (3.7)	$p = 0.67$
Heel-obstacle	18.46 (4.7)	19.10 (6.1)	$p = 0.53$
Vertical clearance (%LL)			
Leading-toe	28.93 (5.9)	24.37 (4.6)	$p = 0.01$*
Trailing-toe	25.88 (5.6)	21.62 (8.2)	$p = 0.01$*

CONCLUSIONS

Healthy older adults with monocular vision displayed an obstacle-crossing technique that aimed to produce a lesser risk of tripping control. More studies are needed to assess the fall risk in subjects with visual impairment in older adults.

ACKNOWLEDGEMENTS

Financial support from the Cheng Hsin General Hospital, Taiwan (CHGH112-(N)09) is greatly appreciated.

REFERENCES

[1] Hugosson M et al. *Ups. J. Med. Sci.* **125**: 311-5, 2020.
[2] Kuo CC et al. *Scientific reports* **12**: 1-10, 2022

ALIGNING LOCAL SEGMENT FRAMES BASED ON DIFFERENT OPTIMISATION CRITERIA TO STANDARDISE KINEMATIC SIGNALS

Adrian Sauer[1,2], Ariana Ortigas Vásquez[1,2], Barbara Postolka[3], Pascal Schütz[3], Allan Maas[1,2], Michael Utz[1], Matthias Woiczinski[2], Thomas M. Grupp[1,2], William R. Taylor[3]

[1] Research and Development, Aesculap AG, Tuttlingen, Germany.
[2] Musculoskeletal University Centre Munich, LMU Munich, Munich, Germany.
[3] Laboratory for Movement Biomechanics, ETH Zurich, Switzerland.
Email: adrian.sauer@aesculap.de

INTRODUCTION

Clinical gait analysis involves deriving signals from raw kinematic data to characterise the movement between joint segments. In spite of previous attempts to ensure the reporting of kinematics is standardised, disagreement among the approaches used to define joint coordinate frames and thereby determine kinematic signals prevails. The exact alignment of segment frames has been clearly demonstrated to considerably affect the estimated values of joint kinematics [1,2]. Consequently, tackling these differences in local coordinate frames is essential to allowing the consistent interpretation of joint movement patterns. The REference FRame Alignment MEthod, an extension of the Frame Orientation Optimisation Method [2], specifically accounts for these differences by optimising a selected parameter characterising the studied signal. Here, we investigate the effects of using different statistical parameters to define the underlying objective function to be optimised.

METHODS

REFRAME realigns local segment frames to minimise the values of user-selected optimisation criteria. This study considered a healthy subject's rotational knee kinematics (based on a transepicondylar flexion axis approach), previously captured *in vivo* using dynamic videofluoroscopy during a stair descent trial [1]. Five different REFRAME implementations were applied to the flexion/extension, ab/adduction and int/external rotation signals, where each implementation minimised one of the following statistical parameters of ab/adduction: sum of absolute values, root-mean-square error (RMSE) vs. 0, variance, maximum absolute value, range of motion, and RMSE vs. a reference curve.

RESULTS AND DISCUSSION

Frame transformations produced by REFRAME led to noticeable changes in the magnitude and characteristics of the optimised kinematic signals, both in ab/adduction, as well as flexion/extension and int/external rotation. Changes in ab/adduction were visibly associated with the underlying statistical parameter used to formulate the objective function (Fig. 1). Although previous work demonstrated consistent frame alignment across datasets could be achieved using different implementations of REFRAME [2], the results presented here clearly highlight the importance of considering the exact objective function being optimised before attempting to make any clinical interpretations of the optimised kinematic signals.

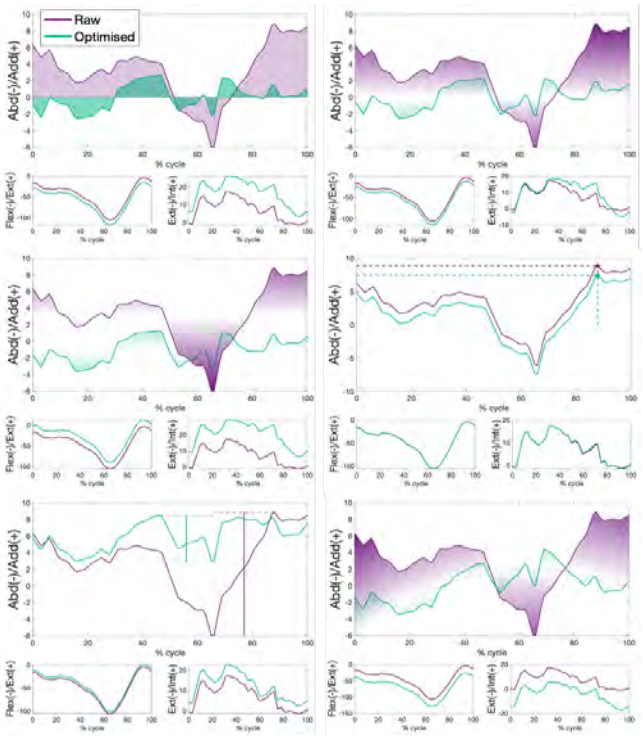

Figure 1 Knee kinematics [°] (tibia relative to femur) for a sample subject stair descent trial before (raw) and after (optimised) REFRAME implementations with different objective criteria (from top to bottom, left: sum of absolute values, variance, range of motion; right: RMSE vs. 0, maximum absolute value, and RMSE vs. a reference curve).

CONCLUSIONS

While REFRAME has the potential to address differences in the local frame alignment of kinematic datasets, the implications of the underlying objective function should be critically considered, especially when attempting to interpret the clinical significance of the optimised kinematic signals.

REFERENCES

[1] Postolka et al. *J Biomech* **144**: 111306, 2022.
[2] Ortigas Vásquez et al. *in review*, 2023

CENTRE OF PRESSURE DISPLACEMENT AND VELOCITY DURING GAIT IN SUBJECTS WITH LOW BACK PAIN

Clara Leyh[1,2,3] and Véronique Feipel[1,2]

[1] Laboratory of Functional Anatomy (LAF), Université Libre de Bruxelles (ULB), Belgium.
[2] Laboratory of Anatomy, Biomechanics and Organogenesis (LABO), Université Libre de Bruxelles (ULB), Belgium.
[3] UPHF, LAMIH, Valenciennes, France
Email: clara.leyh@ulb.be

INTRODUCTION

Few studies have investigated the excursion and velocity of the center of pressure (COP) during gait in subjects with low back pain [1-2] although postural instability [3], modified ground reaction forces and plantar pressures [4,5] as well as planus feet [2,6] have been observed in these patients.
The aim of this study was therefore to study center of pressure displacement and velocity during gait at different velocities in patients with low back pain and to compare those with healthy subjects.

METHODS

78 healthy controls (CG) and 146 subjects with low back pain (LBP) walked barefoot three times at three different self-selected speeds (slow, preferred, fast) over a 6-m long walkway, the GAITRite (CIR Systems) or the ZENO (ProtoKinetics). The order of gait speeds was randomized. A 2-m lead-up and follow-through distance was completed to avoid acceleration and deceleration bias. From GAITRite raw contact data and extracted ZENO COP parameters, average values over three trials were computed for posterior-anterior, medial–lateral and resultant displacements (COP*x*, COP*y*, COP*xy*) and velocities (V*x*COP, V*y*COP, V*xy*COP).
Normality, homoscedasticity and linearity assumptions of COP data as well as covariate (age) and independent variable (group) independency were verified to explore differences in COP parameters between three gait velocities (dependant variable) after controlling for age (mixed-model ANCOVA). Mauchly tests explored sphericity assumptions and, where necessary, adjusted p-values were assessed. Tukey HSD test were computed to explore interactions between velocities and independent variables (group).

RESULTS AND DISCUSSION

Mixed-model ANCOVA assumptions (homoscedasticity, linearity, independency covariable-independent factor and homogeneity of regression slopes) were met.
Except for COP*y* that was not influenced by gait velocity after controlling for age (p=0.15), COP*x* as well as all COP velocity parameters increased with increasing gait speed (adj. p<0.001). COP*xy* presented instead a concave U-shaped variation from slow to fast speed (adj. p<0.001).
Between groups, V*x*COP and V*xy*COP did not differ at slow and preferred speeds (p≥0.11) but, at fast speed, subjects with LBP presented significantly lower V*x*COP and V*xy*COP than controls (p<0.001) (figure 1). Moreover, in subjects with LBP, COP velocity differences between gait speeds tended to be smaller than in controls (|Preferred-Slow|=5.5±2.5 cm/s versus 7.0±3.2 cm/s and |Fast-Preferred|=7.3±3.4 cm/s versus 9.1±3.7 cm/s, respectively), reflecting potentially the increased gait velocity of controls, especially at fast speed. Indeed, at fast velocity, controls walked significantly faster with a greater cadence than subjects with LBP (185±0.29 cm/s and 0.21±0.31 steps/s versus 166±0.30 cm/s and 2.10±0.31 steps/s, respectively). In contrast, no differences between groups in COP displacements and V*y*COP were observed after controlling for age.

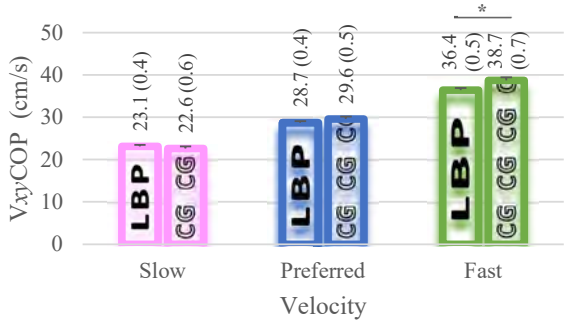

Figure 1 Group-Velocity Interaction for total COP velocity (VxyCOP) at slow (pink), preferred (blue) and fast (green) speeds in subjects with low back pain (LBP) and controls (CG). Adjusted averages and standard errors (vertical bars) are reported for their covariates at their means (Age=38.1 yrs). Asterisks denote the statistically significant differences between groups within gait velocities.

CONCLUSIONS

This study indicates an effect of velocity on mean posterior-anterior and total COP displacement, in agreement with reported anteriorization and posteriorization of the COP at fast speed at 65-90% of stance phase and at heel strike, respectively [7]. The effect of low back pain on mean posterior-anterior and total COP velocities was present only at fast speed but further studies should deepen this finding by controlling gait speed between groups.

REFERENCES

[1] Lee J et al. *J. Phys. Ther. Sci* **23**: 923-26, 2011
[2] Menz H et al. *Rheumatology* **52**: 2275-82, 2013.
[3] Ruhe A et al. *BMC Musculoskelet Disord* **12**: 162, 2011.
[4] Koch C et Hänsel F *Front Psychol.* **9**: 2236, 2018.
[5] Fayez E et Elsayed E *Med. J. Cairo Univ.* **80**: 7-10, 2012
[6] Brantingham J and al. *J Chiropr Med* **5**: 123-7, 2006.
[7] Pataky T et al. *Gait Posture* **40**: 255-8, 2014.

A COMPARISON OF TWO MULTI-SEGMENT SPINE MODELS TO ASSESS MOVEMENT DURING GAIT IN ADOLESCENT IDIOPATHIC SCOLIOSIS

Robert A. Needham[1], Aoife Healy[1], Filip Lazic[2], Nikola Jevtic[2], and Nachiappan Chockalingam[1]
[1] Centre for Biomechanics and Rehabilitation Technologies, Staffordshire University, Stoke on Trent, UK.
[2] Scolio Centar, Novi Sad, Serbia.
Email: r.needham@staffs.ac.uk

INTRODUCTION

A multi-segment spine modelling approach offers a detailed understanding on the complex movement of the scoliotic spine during gait. However, there are several models proposed that utilise difference kinematic modeling approaches [1,2]. Therefore, it is important to compare the segment angles from these models if the associated data will inform clinical management strategies. This study compared the angle outputs from two multi-segment spine models during gait in patients with AIS.

METHODS

Following ethical approval, eight participants (6 female; 15±2 years, 1.7±5.7 m, 59.2±8.7 kg) with scoliosis (S) and four (3 female; 15±1.3 years, 1.64±6.4 m, 55.6±8.8 kg) non-pathological participants (NP) were recruited. Marker trajectory data was collected at 100 Hz using a 10-camera motion capture system (Vicon, Oxford, UK). Reflective markers were attached to the spine and back in accordance with Model 1 (M1) [1] and Model 2 (M2) [2]. Participants were required to walk barefoot at their preferred walking speed (S: 1.08±0.15 m/s; NP: 1.22±0.06 m/s) and fast walking speed (S: 1.44±0.12 m/s; NP: 1.49±0.13 m/s). Segment angle data from 5 trials were time scaled and normalised to 100% of the gait cycle. Upper thoracic, lower thoracic, upper lumbar and lower lumbar segment angles were analysed using ROM and time-series waveforms.

RESULTS AND DISCUSSION

Differences in the ROM and time-series waveforms for the spine segments were apparent both between and within the participant groups, and across kinematic modelling approaches at different walking speeds. For example, the mean lower lumbar segment transverse plane ROM in general was greater for M1 in comparison to M2 (Figure A, B, C, and D). Greater ROM for M1 could be attributed to greater relative movement between reflective markers on the back surface and those attached over the spinous processes. This contrasts with M2 that utilises a 3D cluster approach which negates relative movement between markers, since they are in a fixed position.

Opposing ROM findings were seen across participants, with ROM increasing for some and decreasing for others for both models across different walking speeds. Potentially, both modelling approaches may be influenced by surface topography and lumbar morphology characteristics such as soft tissue artefact, muscle definition, skin elasticity and body composition which affect angle outputs [3].

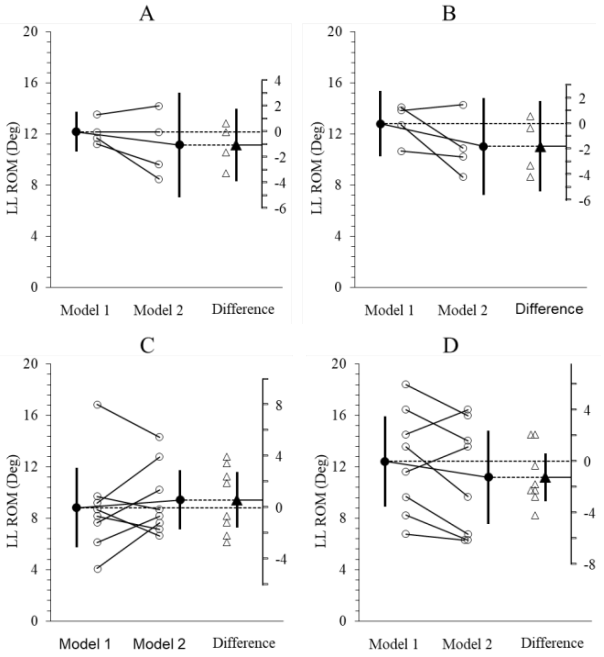

Figure 1 Mean (black circle) and individual (white circle) gait cycle range of motion (A non-pathological PWS and B non-pathological FWS / C scoliosis PWS and D scoliosis FWS) for lower lumbar segment transverse plane angle for Model 1 and Model 2.

CONCLUSIONS

Understanding back surface topography and morphological factors combined with single-subject analysis is vital for understanding and interpreting reported angles from different kinematic modelling approaches. This will contribute to effective clinical management.

ACKNOWLEDGEMENTS

This research was part-funded by the British Scoliosis Research Foundation.

REFERENCES

[1] Christe G et al. *J Biomech* **49**: 2060-2067, 2016.
[2] Needham RA et al. *Prosthet Orthot Int* **40**: 624-635, 2016.
[3] Needham RA et al. *J Med Eng Technol* **40**: 172-185. 2016.

MULTI-SEGMENT SPINE MOVEMENT IN ADOLESCENCE IDIOPATHIC SCOLIOSIS AND EFFECT OF WALKING SPEED

Aoife Healy[1], Robert Needham[1], Filip Lazic[2], Nikola Jevtic[2], and Nachiappan Chockalingam[1]
[1] Centre for Biomechanics and Rehabilitation Technologies, Staffordshire University, Stoke on Trent, UK.
[2] Scolio Centar, Novi Sad, Serbia.
Email: a.healy@staffs.ac.uk

INTRODUCTION

Research has shown that walking speed affects the amplitude of lower limb joint kinematics in non-pathological children, with most values decreasing at slower speeds and increasing at faster speeds [1]. An understanding of the effect of walking speed on multi-segment spine movement and in children with scoliosis is required. This study aims to evaluate the impact of scoliosis and walking speed on joint range of motion (ROM) and time-series waveforms.

METHODS

Following ethical approval, eight participants (6 female; 15±2 years, 1.7±5.7 m, 59.2±8.7 kg) with scoliosis (S) and five (4 female; 15±1 years, 1.62±7.0 m, 52.6±10.0 kg) non-pathological participants (NP) were recruited. A 10-camera motion capture system (Vicon, Oxford, UK) collected marker trajectory data at 100 Hz. Reflective markers were attached to the spine, back, pelvis and lower limbs [2,3]. Participants were required to walk barefoot at their preferred walking speed (S: 1.08±0.15 m/s; NP: 1.22±0.06 m/s) and fast walking speed (S: 1.44±0.12 m/s; NP: 1.49±0.13 m/s). Data from 5 trials were time-scaled and normalised to 100% of the gait cycle. Upper thoracic, lower thoracic, upper lumbar and lower lumbar segment angles were analysed using time-series waveforms and ROM.

RESULTS AND DISCUSSION

In line with previous findings for lower limb joint kinematics an increase in the mean amplitude of spinal kinematics was seen at the faster walking speed in both groups. However, differences in ROM and time-series waveforms for the spine segments were evident both between and within the participant groups, and across the different walking speeds. For example, the mean lower lumbar segment transverse plane ROM was higher for NP than S, but differences were evident between individuals within the groups (Figure 1A and B). There was greater variability in the time-series waveforms across S (Figure 1C, D, E and F). These observations highlight differences between the groups and that at different walking speeds participants utilised individual compensatory movements. The variability across S may be attributed to variations in Schroth classifications within the group [4].

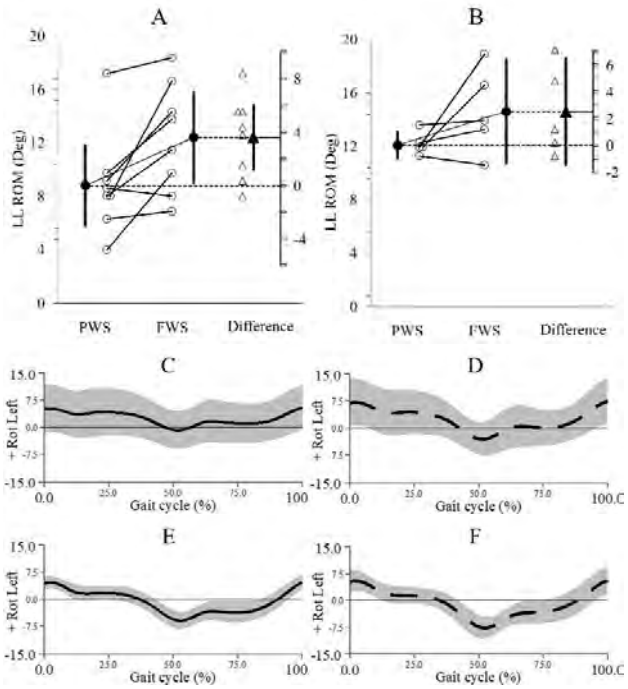

Figure 1 Mean (black circle) and individual (white circle) gait cycle range of motion (A scoliosis and B non-pathological) for lower lumbar segment transverse plane angle for preferred walking speed (PWS) and fast walking speed (FWS). Lower lumbar segment transverse plane angle for PWS (C scoliosis and E non-pathological) and FWS (D scoliosis and F non-pathological).

CONCLUSIONS

Both having scoliosis and walking at varying speeds were found to impact spine segment ROM and time-series waveforms. Results highlight that single-subject analysis should accompany group analysis to aid understanding and support the development of effective patient-specific treatment interventions.

ACKNOWLEDGEMENTS

This research was part-funded by the British Scoliosis Research Foundation.

REFERENCES

[1] Fukuchi CA et al. *Syst Rev* **8**: 153, 2019.
[2] Christe G et al. *J Biomech* **49**: 2060-2067, 2016.
[3] Leardini A et al. *Gait Posture* **26**: 560-71, 2007
[4] Needham et al. *Presented to British Scoliosis Society Annual Conference*, 2022

Instrumented Assessment of Falls Risk in Subjects with Mild Parkinson's Disease

Yen-Chun Lin, Sai-Wei Yang
Department of Biomedical Engineering
National YangMing ChiaoTung University, Taipei, Taiwan
Email: swyang@nycu.edu.tw

INTRODUCTION

Parkinson's disease (PD) mainly affects the motor nervous system, and common clinical symptoms include resting tremors, muscle stiffness, motor impairment, slow movement, poor posture control, and unstable gait. Motion disorders lead to an increased risk of falls in patients with Parkinson's disease (Galna etal., 2010; Stegemoller etal., 2012). Clinical scales are mostly used to evaluate the risk of falls, such as: The unified Parkinson's disease rating scale (The unified Parkinson's disease rating scale, MDS-UPDRS) part 3 - motor examination, Berger scale (Berg Balance Scale (BBS), Tinetti Performance Oriented Mobility Assessment (POMA), but most of the assessment methods are based on observation (Kegelmeyer et al., 2007). The purpose of this study was to investigate the characteristic differences in muscle activation and gait ability between PD patients with Hoehn & Yahr grading stage (H & Y Stage) 2 ~ 3 and healthy elderly people of the same age, and using instrumented biomechanical parameters, to score each item of the POMA scale, and comparing the instrumental score and the observation scale score.

METHODS

The experiment recruited 4 PD patients, all onset on the left side, age: 63.5±4.72; H & Y Stage: 2.25 ± 0.25; POMA: 21.00 ± 3.96; MDS-UPDRS - motor function test: 19.5 ± 8.20; BBS: 51.00 ± 2.94 and 6 normal subjects, age: 66.16±3.3; POMA: 28.00±0.00; BBS: 55.00±0.82. After explaining the purpose and procedure of the experiment, and asking the subjects to fill out the consent form, a basic measurement and questionnaires were performed. CTSIB balance tests were conducted.

RESULTS AND DISCUSSION

The results showed that in the PD sit-to-stand test, because the lower activation of the left lower limb muscles, the ability to adjust the postural balance during the sit-to-stand process was low. In the walking test, it was found that the left footstep width of PD was 14% wider, the stride frequency was 28% smaller, and the pace was 18% slower than that of the healthy elderly of the same age(Fig 1). When crossing obstacles, due to the lack of muscle strength of the left lower limb, the center of pressure (CoP) showed larger excursion, and affected the center of mass (CoM)sloshing and significant changes in the CoM-CoP incline angle. The Sensory Integration and Balance Clinical Test (CTSIB) found that the vestibular and proprioceptive balance of PM was low. There are differences between POMA scale observation and instrumental scoring, particularly significant difference in the balance evaluation, but, there is no statistically significant difference between the balance observation scores but the gait assessment in comparison with normal subjects. Although there is no statistical difference between the PD gait and the total score and the instrumental evaluation, compared with normal people who had a full score of 16 for balance and a full score of 12 for gait, the instrumental evaluation can better reveal the stability and prediction of PD dynamic posture the likelihood of its fall occurring.

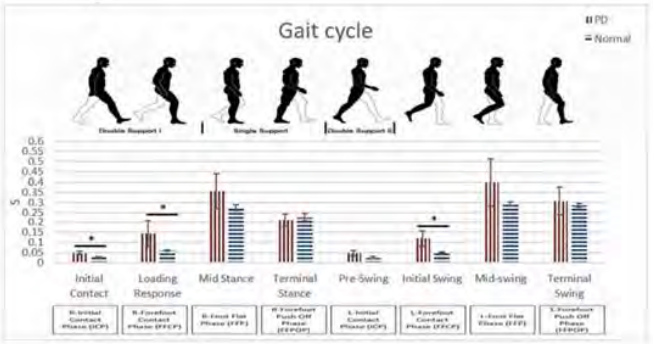

Figure 1 *Time spent on each gait cycle phase*

CONCLUSIONS

Based on the four PD participants who had a consistent left limb onset symptom occurring, the study concluded that due to the lack of strength of the left lower limbs, and the degradation of the vestibular and body balance mechanisms, resulted in unstable posture balance ability in sitting to standing, walking, crossing obstacles, and static balance tests. The instrumental evaluation of POMA scale can scientifically predict the risk factors of falls in patients with mild PD by using biomechanical parameters.

ACKNOWLEDGEMENTS

This study is supported by National Science and Technology Council, ROC.,through the grant MOST 111-2221-E-A49-058

REFERENCES

[1] Galna B et al. *Hum Mov Sci.,29:843-852, 2010.*
[2] Kegelmeyer DA et al. Phys Ther. ;87(10):1369-78, 2007
[3] Stegemoller EL et al., Arch Phys Med Rehab 93, 2012

MACHINE LEARNING CLASSIFICATION OF GAIT IN LEPROSY PATIENTS WITH FOOT DROP

Adriane Mara de Souza Muniz[1,2], Jose Carlos Cohen[3], Henrique Lelis Clemente de Oliveira[1], Maria Katia Gomes[3], Luciano Menegaldo[1]

[1] Programa de Engenharia Biomédica (PEB/COPPE), Universidade Federal do Rio de Janeiro, Rio de Janeiro, Brazil, [2] Escola de Educação Física do Exército (EsEFEx), Rio de Janeiro, Brazil, [3]Hospital Universitário – Universidade Federal do Rio de Janeiro, Rio de Janeiro, Brazil.
Email: lmeneg@peb.ufrj.br

INTRODUCTION

Leprosy (Hansen's disease) is a neglected tropical chronic infectious condition, with around 200,000 new cases reported yearly worldwide. Common peroneal nerve injury frequently occurs, causing foot drop [1]. The resulting altered gait pattern has not been previously described using 3D gait analysis or classified with machine learning. This study uses logistic regression (LR) and random forest (RF) techniques for discriminating normal gait from foot drop gait caused by leprosy.

METHODS

Gait kinematics and dynamics were analyzed from 12 patients with unilateral drop foot caused by leprosy (8 men; 44.7±10.8 years; 1.7±8.2 m; 82.6±20kg) and 15 healthy controls (12 men; 37.6±15.6 years; 1.7±6.1 m; 74.5±18.6kg). Each subject could walk independently at their self-selected speed along a 10 m walkway for five successful trials. Helen Hayes markers protocol was used to reconstruct gait using the hardware (8 cameras, two force platforms) and software from a BTS (Milan, Italy) system. Fifteen parametric gait variables were evaluated from the patient's affected limb and control's dominant limb and used as classifiers' independent variables: Stance: ankle at initial contact (A_IC); maximal plantar flexion (PFA); maximal knee flexion (KFA); maximal knee adduction (HAA); ground reaction force first (FPF) and second peak (SPF) of force; maximal plantarflexion torque (PFT); maximal knee extension torque (KET); maximal hip flexion (HFT) and extension (HET) torque. Balance: maximal dorsiflexion (Dorsi_B); maximal knee flexion (KFB); maximal hip flexion (HF_B). Gait cycle: pelvic tilt range (PTR) and gait speed. The outcome binary variable was to belong to the patients' (1) or controls' group (0), with a 0.5 cutting point.

For the LR model, the stepwise approach based on the Akaike information criterion (AIC) was used for variables selection, followed by the χ^2 test to contrast with a complete model or with subsets of variables. The selection of variables is made automatically in the RF.

The classifiers' performance was assessed using k-fold cross-validation because our sample size is small. Performance metrics (accuracy, sensitivity, specificity and AUC) were averaged from 5 folds. Class balance was performed in the training group using a bootstrap-based technique (random over-sampling examples - ROSE) with 100 samples. Processing was made in R 4.2.1(R Core Team, 2022).

RESULTS AND DISCUSSION

RF performed better than LR, although not statistically significant (Table 1), similar to [2]. The LR stepwise selection identified A_IC, PFA, Dorsi_B, KFA, HAA and HET as relevant variables. For RF, the most relevant variables were Dorsi_B, PTR, A_IC and HFT (Figure 1).

Table 1: Models performance metrics.

	Accuracy	Sensitivity	Specificity	AUR
LR	0.73 ± 0.19	0.62 ± 0.44	0.81 ± 0.37	0.86 ± 0.22
RF	0.86 ± 0.20	0.81 ± 0.37	0.87 ± 0.35	0.95 ± 0.22
p-value	0.084	0.260	0.500	0.207

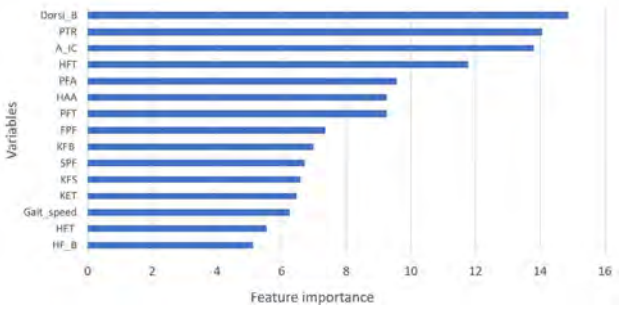

Figure 1 RF feature importance.

CONCLUSIONS

Random forest outperformed logistic regression. For both classifiers, sagittal ankle motion and hip torque were the more important features that classify gait with leprosy foot drop. These results might help guide patients' treatments and follow-up of rehabilitation programs.

ACKNOWLEDGEMENTS

CNPq, CAPES, FINEP and FAPERJ

REFERENCES

[1] Ooi W et al. *Muscle Nerve* **30**: 393-409, 2004.

[2] Gupta A et al. Comput Gr Image Process, **1155**, Springer: Singapore, 2020.

MULTI-SCALE ENTROPY CAN BE USED TO DISTINGUISH BETWEEN FALLERS AND NON-FALLERS

Arezoo Amirpourabasi[1], Sallie Lamb[2], Jia Yi Chow[3] and Genevieve Williams [1]
[1] Sport and Health Sciences, University of Exeter/ Exeter, UK.
[2] Medical School, University of Exeter/ Exeter, UK.
[3]Physical Education and Sports Science, Nanyang Technological University, Singapore
Email: a.amirpourabasi@exeter.ac.uk

INTRODUCTION

The chance and extent of gait instability increases with age [1]. More recently, nonlinear dynamic analysis (NLD) has been used to understand changes in gait as a function of ageing [2]. NLD methods provide the opportunity to study inner structure, regularity, complexity and stability of gait represented by a recorded time series in a more direct way and has presented strong evidence of identifying risk of falling [3]. A recent systematic review indicated that Lyapunov Exponent and Multiscale Entropy are the most commonly used nonlinear dynamic analysis methods in the study of falls in older adults [4]. However, further investigation is needed to determine which method is better suited for distinguishing fallers from non-fallers.

METHODS

The study included 34 healthy female participants aged over 60 years (17 with history of falling and 17 without history of falling in the last year) with a mean age of 73 years (SD = 5.3) and a mean body mass index of 23.4 kg/m2 (SD = 2.7). Whole-body marker trajectories were recorded at 220Hz using an automated 3D motion capture system with a 12 camera motion capture system (Miqus M3, Qualisys AB, Gothenburg, Sweden). Each participant completed four trials of 2-minute treadmill walking at preferred speed (PS), as well as at -20% (slow) and +20% (fast) of PS. The first 2 minutes of each experimental session was used as a warm-up/treadmill adaptation period. The collected data were filtered using a 4th-order Butterworth 14Hz low-pass filter. Short- (SLyE) and long-term (LLyE) LyE using Rosenstein's method, largest LyE (LyE) using Wolf's method and Multiscale Entropy (MSE) using were calculated for joint angles in Sagittal (S), Frontal (F) and Transvers (T) planes, and CoM position in three Medio lateral (ML), Anterior posterior (AP) and Vertical (V) directions. Principal component regressions (PCR) analysis and multiple t-test performed to analysis data.

RESULTS AND DISCUSSION

Results from the stepwise logistic regression on rotated principal components revealed that, across all three different speeds, the Multiscale Entropy (MSE) of the ankle joint in the frontal plane was a significant predictor for distinguishing fallers from non-fallers among the study participants. Specifically, a one-unit increase in MSE of the ankle angle in the frontal plane was associated with a 0.36 decrease in the odds of falling at preferred walking speed (OR = 0.64, 95% CI [0.45-0.92], p <0.001), a 0.26 decrease in the odds of falling at slow speed (OR = 0.74, 95% CI [0.49-0.92], p <0.001), and a 0.38 decrease in the odds of falling at fast speed (OR = 0.62, 95% CI [0.45-0.92], p <0.001). Table 1 presents the p-values of multiple t-test obtained from the output of PCR at three different speeds. These results suggest that MSE of the ankle angle in the frontal plane can be a useful tool for predicting fall risk in older adults at different walking speeds. Further research is needed to determine the effectiveness of MSE in other populations and settings, and to explore the potential of other NLD methods for fall risk assessment.

CONCLUSIONS

In conclusion, our findings suggest that analysing the Multiscale Entropy (MSE) of the ankle angle in the frontal plane may provide valuable information for assessing fall risk in older adults. Specifically, higher MSE values in the frontal plane of the ankle joint were found to be associated with a decreased risk of falling, even after controlling for other variables. These results were consistent across all three different walking speeds and the four different nonlinear dynamic (NLD) methods mostly used in the literature. Therefore, clinicians and researchers may consider using MSE of the ankle angle in the frontal plane as a simple and effective tool for fall risk assessment in older adults.

REFERENCES

[1] Bizovska, L. et al. Acta of bioengineering and biomechanics, 2018.
[2] Stergiou, N. Human Kinetics Publishers, 2004.
[3] Mehdizadeh, S. Gait & posture, 2018.
[4] Amirpourabasi, A., et al., Sensors, 2022.

Table 1: The p-values of multiple t-test obtained from the output of Principal component regressions (PCR) at three different speeds.

Variable	Preferred Speed	Slow speed	Fast speed
Ankle-F plane-MSE	<0.001	<0.001	<0.001
Knee-S plane-SLyE	0.08		
CoM-AP-MSE	0.02		

Measurements of tibial rotational range of motion and healthy adult characteristics

Shingo Kawakami[1], Hiroyuki Fujisawa[2], Naoki Igarashi[1]
[1] Department of Rehabilitation, Sendai Rehabilitation Hospital, Tomiya-shi, Japan.
[2] Department of Rehabilitation, Tohoku Bunka Gakuen University, Sendai-shi, Japan.
Email: kawakami.shingo8@gmail.com

INTRODUCTION

In clinical practice, the evaluation and treatment of tibial rotation function is performed in patients with osteoarthritis and ACL injuries. There are numerous opportunities to focus on the tibial rotation function during step movements associated with the change of direction, particulary in high performers, including patients with ACL injuries (crossover step, side step, etc.). Alternatively, when driving a car (automatic transmission) with a paralyzed lower limb, there is an opportunity to focus on the pedaling motion by tibial rotation. Despite its importance in evaluating tibial rotation function, the development of a simple measurement method and a reference range of motion are yet to be established. [2]

The goal of this study was to determine the intrarater reliability and range-of-motion (ROM) characteristics of a tibial rotation ROM instrument that was made by the author (Figure 1).

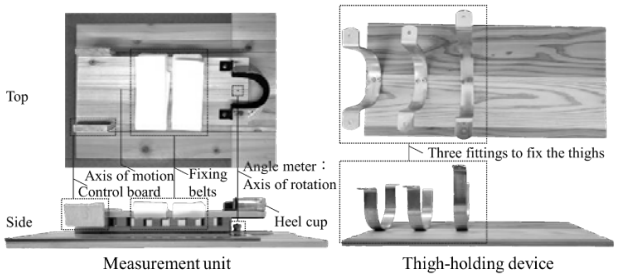

Figure 1 Instrument to measure tibial rotation range of motion.

METHODS

This study included forty healthy adults (23 males, mean age 20.7 ± 1.9 years, 80 legs). None of them had a history of knee problems. The measuring instrument was self-made and comprised a measuring unit and a thigh-holding device. A protractor and a control board that applies force and guides motion compromise the measuring unit. The structure is intended to fix the plate on which the sole of the foot is placed (plantar plate) on the protractor's axis of movement and allow it to rotate freely. The thigh-holding device is made up of three U-shaped metal fittings that are fastened to a board and can be adjusted.

The passive tibial rotation ROM was measured in a sitting position with knee flexion 90° using a self-made instrument. Other movements were used to measure ROM, with the second toe as the axis of movement. The μTas-MT1 (ANIMA) control board was fixed and loaded with the previously discovered resistance value of 4.8 Nm. [3] For the lower extremity, the measurement conditions were two conditions (left/right) and three measurement repetitions.

R software, version 4.0.4 was used for statistical analysis. This was a one-tester intrarater reliability study. The values of the ICC can range from 0 to 1, with a higher value indicating better reliability. ICC less than 0.20 was considered as slight; 0.41-0.60 as moderate; 0.61-0.80 as substantial, and 0.81-1.00 as almost perfect. Normality distribution was confirmed with a prior Shapero–Wilk test for intrarater reliability on the measurements. Furthermore, gender differences in tibial internal and external rotation ROM were examined. A t-test was performed following the Shapiro–Wilk test. Furthermore, the level of significance was set at 5%.

RESULTS

In the estimation of intrarater reliability in tibial internal rotation ROM, high values were obtained ($ICC_{1,3}$= 0.996; 95%CI = 0.994-0.997). Similarly, high values in tibial external rotation ROM ($ICC_{1,3}$ = 0.997; 95%CI = 0.995-0.998) were obtained. Male tibia of external and internal rotation ranges were 50.5 ± 7.6° and 34.1 ± 9.6°, respectively. Females, alternatively, had a range of external and internal rotation of the tibia of 61.1 ± 7.8° and 43.4 ± 8.9°, respectively. Females had a considerably greater range of tibial external and internal rotation motion in than male ($p < 0.001$).

CONCLUSIONS

In measuring tibial external and internal rotation ROM, self-made instrumentation demonstrated high reliability. The measurement is done while sitting, and the structure allows for the application of objective resistance values, indicating the possibility of high versatility for use in clinical practices. There may be gender differences in tibial rotational ROM, and basic data on tibial rotation ROM is necessary for developing a scientifically based physical therapy evaluation and treatment program.

REFERENCES

[1] Kawakami S et al. Ann Rep Tohoku Phy Ther **33**: 12-18, 2021.
[2] Kawakami S et al. J Phys Ther Sci **28**: 2430-2433, 2016.
[3] Kawakami S et al. Ann Rep Tohoku Phy Ther **32**: 1-6, 2020.

DOES THE LOWER EXTREMITY MUSCULAR FUNCTION SYMMETRY EXIST IN ATHLETES WITH ACLR?

Ning Chu[1], Yin-Ju Chen[1], Yu-Ting Tzeng[1] and Heng-Ju Lee [1]
[1] Department of Physical Education and Sport Sciences, National Taiwan Normal University, Taipei, Taiwan
Email: hjlee@ntnu.edu.tw

INTRODUCTION

The secondary injury of the anterior cruciate ligament (ACL) has attracted more attention in many studies. The incidence of ACL injury on the non-injury side is even twice that of the ACL injury on the injured side (Grassi, 2020). Lower limb asymmetry is one of the risks of injuries. The functional Y-Balance Test (YBT) composite value <94% bilateral symmetry is associated with a greater risk of injury (Plisky, 2006). In muscle strength, a lower H:Q ratio was associated with an increased risk of recurrent ACL graft rupture. Studies also showed that after passing the return to sport tests, the asymmetry of the limbs still exists or gradually develops toward the trend of asymmetry, which leads to secondary ACL injuries. Therefore, this study aims to assess the asymmetry in YBT and bilateral muscle strength after ACL reconstruction.

METHODS

Participants: Ten ACLR and five healthy athletes were recruited to participate in this study. The conditions of ACLR acceptance were: unilateral and one ACL reconstructed surgery; all athletes have completed the rehabilitation and returned to sports. All participants were without lower limbs musculoskeletal injury within six months.

Procedures: Participants performed the function test with the method of YBT. Both legs were tested separately in 3 directions (anterior, posteromedial, and posterolateral). The maximal reach distance of 3 trials was recorded for analysis. The concentric strength of the quadriceps (Qcon), the concentric strength of the hamstring (Hcon) and the eccentric strength of the hamstring (Hecc) of the participants were measured by Biodex isokinetic dynamometer, and the angular velocity was set at 60°/s. One set of 3 repetitions with maximum effort was executed. Both legs were tested separately, and each trial was initiated with the non-injured limb.

Statistics: All the variables were compared between groups using independent-sample *t*-tests. The symmetry index = injury side/non-injury side*100% for ACLR group, and the symmetry index = L side/R side*100% for the healthy group. Significant level was set at $\alpha \leq .05$.

RESULTS AND DISCUSSION

The participants' characteristic data are in Table 1. The reconstructed grafts were all semitendinosus for ACLR. The symmetry index of all the variables (Figure 1.) showed that ACLR's hamstring concentric and eccentric strength symmetry indexes were lower than the healthy group. These variables of the injury leg were lower than the non-injury leg in the ACLR group. The role of the hamstring is to counteract the forward shear force exerted by the quadriceps on the tibia to reduce the stimulation of ligaments and joints. It is important to reduce and prevent secondary ACL injuries. The YBT index, quadriceps concentric strength, and traditional and functional H:Q ratio were not significantly different

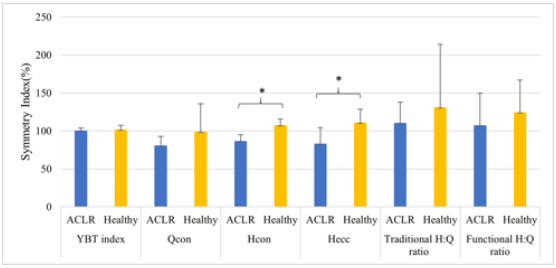

Figure 1 The symmetry index of variables, *p<.05

CONCLUSIONS

Although the athletes have returned to sport over two years, and the results of their YBT are symmetrical, the hamstring's concentric and eccentric strength may still be asymmetry. This might lead to a higher risk of secondary ACL injury.

REFERENCES

[1] Plisky, P et al. *J Orthopaedic and Sports Physical Therapy 36*: 911–919, 2006.
[2] Grassi, A et al. *The American Journal of Sports Medicine 48*: 310–317, 2020.

Table 1: Participants characteristics

Group	Age(yrs)	Height(cm)	Weight(kg)	Post-surgery(month)	Return to Sport(month)
ACLR (n=10)	22.3 ± 3.5	163.9 ± 8.3	66.8 ± 13	39.4 ± 25.9	33.8 ± 22.4
Health (n=5)	20.8 ± 3.3	166.6 ± 7.2	68 ± 16		

Analyses of Lower Limb Asymmetry in Division I Women Basketball Players: A Pilot Study

Pin-Chun Tseng, Hui-Wen Hsiao, Heng-Ju Lee
Department of Physical Education and Sport Sciences, National Taiwan Normal University, Taipei, Taiwan
Email: hjlee@ntnu.edu.tw

INTRODUCTION

In basketball, lower limb injuries are the most likely to occur. More than 60% of lower limb injuries occur during practice or competition, and the proportion of injuries to female athletes is more significant than that of male athletes [1]. Since basketball is a sport with unilateral dominance, it may cause asymmetry of lower limb balance and strength between the dominant and non-dominant sides. In jumping and landing tasks, if the difference between the two sides of the lower limbs is too significant, it will increase the incidence of non-contact lower limb injuries, such as injury of the anterior cruciate ligament (ACL). For sports that use the single leg, single leg drop jump is more suitable as an assessment method [2]. Therefore, this study aimed to analyze the Reactive Strength Index (RSI) and Dynamic Postural Stability Index (DPSI) differences between the dominant and non-dominant sides of female basketball players through single-leg drop jumps.

METHODS

Seven Division I female basketball athletes were recruited in this study (age:23.86 ± 1.46 years old; height:174 ± 5.95 cm; weight:67.71 ± 8.48 kg). Subjects had no severe head and lower extremity injuries or surgery within half a year. Within three months before the start of the experiment, subjects are without acute lower extremity injuries. This study defines the dominant side, which players subjectively think of as the foot they use to kick the ball.

In the experiment, a force plate (Kistler, 9260AA6, Winterthur, Switzerland, 1000Hz) was used to collect the ground reaction force parameters for data analysis during the single leg drop jump, including Jump height, RSI, Impact force, and DPSI. Using paired t-test to compare the differences between RSI, Jump height, landing impact force, and DPSI of the dominant and non-dominant side.

RESULTS AND DISCUSSION

The results of this study show (Table 1) that the dominant side is significantly larger than the non-dominant side in the RSI of single-leg drop jump, but there were no significant differences in jumping height, impact force, and DPSI. All seven subjects in this study's dominant side are right sides. However, there was no significant difference in jumping height between the dominant and non-dominant sides. The difference in RSI showed that the dominant side could reach the same jump height with a shorter movement time, which may be related to specific movements of basketball pattern to explain, such as unilateral jumping. Jumping injuries are common in basketball, especially when landing on a single leg. Past research has also shown that jumping and landing in an asymmetric pattern has a higher probability of non-contact injuries [3].

CONCLUSIONS

The symmetry of the lower limbs helps improve and reduce the risk of injury [4]. The difference in the RSI between the dominant and non-dominant side of the women's basketball players in Division I may be one of the potential injury risks. It is still needed to determine whether the RSI can be used as an effective indicator for predicting athletes' lower limb injuries. There are currently only seven subjects in this study, and the experiment will continue in the future. After enough subjects, the results will be more convincing.

REFERENCES

[1]. Agel, J et al. *J Athl Train,* ***42***: 202, 2007.
[2]. Taylor, J B et al. *Orthop J Sports Med,* **4**: 2325967116655158, 2019.
[3]. Yu, B et al. *Br J Sports Med*, ***41***(1), 47-i51,2007.
[4]. Niksic, S. R et al. *Int J Res Ex Phys,* ***15***(1)*, 50-63,*2019.

Table 1: Single leg drop jump parameters

	Dominant	Non-Dominant	*p-value*
Jump height (m)	0.11 ± 0.02	0.10 ± 0.01	$p = .121$
RSI (m/s)	0.29 ± 0.05	0.24 ± 0.04	$p = .046^{*}$
First impact force (%BW)	3.13 ± 0.32	3.07 ± 0.30	$p = .636$
Second impact force (%BW)	2.81 ± 0.55	2.76 ± 0.51	$p = .850$
DPSI	0.30 ± 0.14	0.21 ± 0.13	$p = .316$

* Significant at $p < .05$

GENDER DIFFERENCES IN KINEMATICS AND MUSCLE ACTIVITY DURING THE PREPARATION PHASE OF THE SINGLE-LEG LANDING TASK IN BADMINTON

Zhe Hu[1], Wenjin Wang[2], Lihao Guan[1], Maolin Dong[1], Yanjia Xu[1], Sukwon Kim[1], *
[1]Department of Physical Education, Jeonbuk National University, Jeonju, Jeollabukdo, 54896, South Korea
[2]Institute of Biomechanics and Orthopedics, German Sport University Cologne, Cologne 50933, Germany
Email: huzhe0710@jbnu.ac.kr

INTRODUCTION

Anterior cruciate ligament (ACL) injuries usually occur in non-contact sports that require repeated jumps, landings, and postural changes, and previous studies have shown that the incidence of ACL injuries is higher in female athletes, about 2-6 times higher than in males. In another epidemiological study on ACL injury in badminton, female badminton players had a higher incidence of ACL than males [1]. Investigating gender differences in muscle activity in badminton players during the pre-landing preparation phase of high-risk single-leg landing tasks and incorporating gender differences in kinematic data would better help badminton coaches, players, and rehabilitators understand the potential risk mechanisms that may contribute to the high incidence of non-contact ACL injuries in females.

METHODS

Sixteen badminton players (8 male, 8 female) performed a single-legged badminton landing task, and kinematic data and muscle activity data of the lower extremity were recorded for each subject. Gender differences in lower limb kinematic data, mean values of lower limb muscle activity, and co-contraction values during the landing preparation phase were compared using an independent samples t-test.

RESULTS AND DISCUSSION

In the badminton landing task, the knee valgus angle was greater in females than in males (6.27 ± 2.75 vs. 1.72 ± 3.20) in the pre-landing preparation position （Table 1）. During the pre-landing preparation phase (100mms before initial contact). prospective studies in athletes have shown that a large knee valgus angle predicts a potentially high risk of subsequent ACL injury. The mean and standard deviation of lower limb muscle activity during the landing preparation phase of a single leg landing task after a backhand side overhead stroke in badminton, as shown in Figure 2.

Compared to male badminton players, females exhibited greater gluteus maximus (44.92±18.00 vs 20.34±11.64), rectus femoris (41.56±9.84 vs 26.14±10.46), and medial gastrocnemius (37.39±17.31 vs 19.11±11.17) lateral gastrocnemius (36.86±17.82 vs 13.59±2.71) muscle activity. This may be due to the large gluteus maximus, rectus femoris, and gastrocnemius muscles associated with large ACL loads [2].

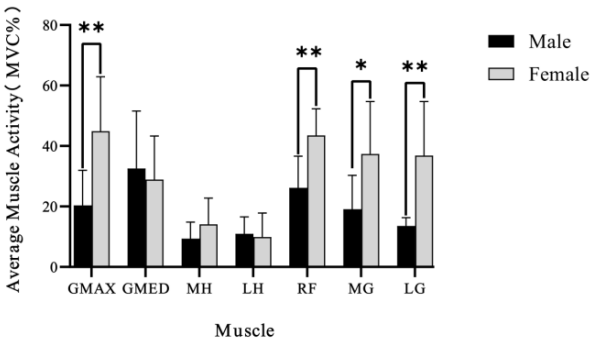

Figure 1 Mean and standard deviation of lower limb muscle activity during the preparation phase before landing for the single-leg landing task in badminton. * and ** represent statistically significant differences ($p<0.05$) and highly significant differences ($p<0.01$), respectively.

CONCLUSIONS

During the landing preparation phase of the badminton single-leg landing task, there were significant gender differences in neuromuscular control (muscle activity patterns, movement patterns) between badminton players. Female badminton players exhibit neuromuscular control strategies that may be inadequate for ACL protection and a potential risk factor for a high incidence of ACL injury. In the future, when developing programs to prevent ACL injuries in female badminton players could consider targeting the optimization of neuromuscular control during the pre-landing preparation phase.

REFERENCES

[1] Kimura, Y., et al., *Mechanisms for anterior cruciate ligament injuries in badminton.* Br J Sports Med, 2010. **44**(15): p. 1124-7.

[2] Otsuki, R., M.J. Del Bel, and D.L. Benoit, *Sex differences in muscle activation patterns associated with anterior cruciate ligament injury during landing and cutting tasks: A systematic review.* J Electromyogr Kinesiol, 2021. **60**: p. 102583

Table 1: Means and standard deviations (degrees) of knee joint angles during the landing preparation phase of the single-leg landing task in badminton. ** represents highly significant differences.

	Male	Female	p Value
Flexion（+）/extension（-）	19.47±6.42	18.08±7.33	0.6924
Valgus（+）/varus（-）	1.72±3.20	6.27±2.75	0.0087**
External（+）/internal rotation（-）	-4.39±4.67	0.15±4.29	0.0622

Predicting Post-surgery Muscle Activations following Internal Hemipelvectomy Surgery

Geng Li[1], Di Ao[1], Marleny M Vega[1], Payam Zandiyeh[2], Shuo-Hsiu Chang[3], Alexander N Penny[4], Valerae O Lewis[4], and Benjamin J Fregly [1]

[1] Department of Mechanical Engineering, Rice University, Houston, USA.
[2] Department of Orthopaedic Surgery, UT Health, Houston, USA.
[3] Department of Physical Medicine and Rehabilitation, UT Health, Houston, USA.
[4] Department of Orthopaedic Oncology, UT MD Anderson Cancer Center, Houston, USA.
Email: Geng.Li@rice,edu

INTRODUCTION

Reliably predicting post-surgery walking function can help inform better designs of surgical treatments and reconstructive implants for pelvic sarcoma patients. One key task is to predict the muscle activations during post-surgery walking. Muscle synergies have been used to represent muscle activations in lower dimensionality via the combination of time-varying synergy activations and vectors of muscle weightings, defined as the synergy vectors [1]. A previous study predicted post-surgery walking while assuming synergy vectors remain constant pre and post surgery [2]. We explore in this study the methods of using pre-surgery muscle synergies to predict post-surgery muscle activations.

METHODS

Experimental gait data of a pelvic sarcoma patient were collected before the internal hemipelvectomy surgery and 12 months after the surgery. A subject-specific musculoskeletal model was developed in OpenSim, to simulate and analyze the gait motions of each sessions [3]. We calibrated an EMG-driven model using 15-16 channels of EMG data for each of the operated and the non-operated leg pre and post-surgery and obtained muscle activations [4]. The pre-surgery muscle activations of each leg were decomposed into muscle synergies using non-negative matrix factorization from which the synergy vectors were set constant while synergy activations varied cycle-to-cycle. We subsequently investigated: 1). if the pre-surgery muscle synergy vectors, or 2). if the pre-surgery muscle synergy activations (mean), can reconstruct the post-surgery activations at a high level of "variability accounted for" (VAF). The post-surgery synergy parameters were solved via a non-negative least square problem of the pre-surgery muscle synergy parameters and post-surgery muscle activations. The percent variability accounted for (VAF) was used to evaluate both cases.

RESULTS AND DISCUSSION

The reconstruction of post-surgery muscle activations was at VAF<20% in Case 1, whereas at VAF>90% when ≥6 synergies were used in Case 2 (Figure1).

CONCLUSIONS

Using pre-surgery synergy activations combined with minimally changed synergy vectors may be the more reliable way to predict post-surgery walking given the high VAF in reconstructing muscle activations.

ACKNOWLEDGEMENTS

This work was supported by Cancer Prevention Research Institute of Texas funding RR170026.

REFERENCES

[1] Banks C et al. *Front.Comput.Neurosci* **11**: 78, 2017.
[2] Vega M et al. *Front.Bioeng.Biotechnol.***10**: 1, 2022.
[3] Li G et al. *Front.Bioeng.Biotechnol.***10**:964359, 2022.
[4]Ao D et al.*Front.Bioeng.Biotechnol.***10**:962959, 2022.

Figure 1: % VAF of the reconstructed post-surgery activations from Case 1) and 2) using n = 4, 5, 6, and 7 muscle synergies

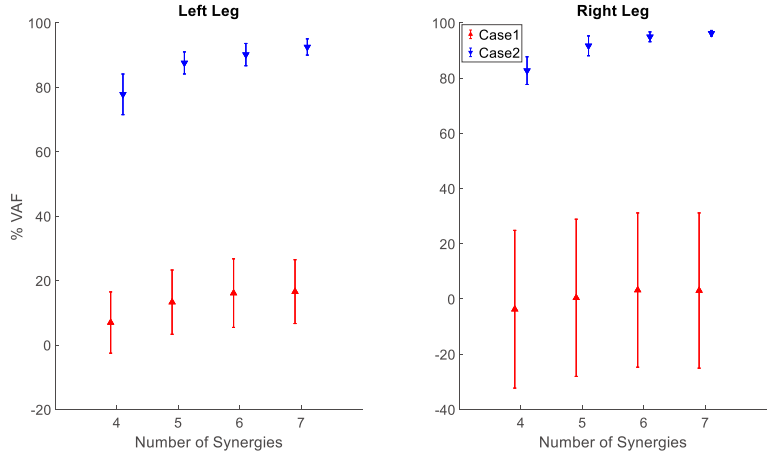

EFFECT OF SHOE SOLE THICKNESS ON THE EXTERNAL ANKLE JOINT INVERSION MOMENT DURING DROP LANDINGS ON A TILTED SURFACE

Nahoko Sato[1], Yasuo Ikegami[2]
[1] Faculty of Rehabilitation Science, Nagoya Gakuin University, Nagoya, Japan.
[2] Research Centre of Health, Physical Fitness and Sports, Nagoya University, Nagoya, Japan.
Email: nsato@ngu.ac.jp

INTRODUCTION

Many shoe companies utilise damping materials, such as gel, air, or springs, in the midsole to prevent injuries and improve performance, resulting in the development of many shoes with thicker midsoles, particularly for running. Thick-soled shoes have also been developed for other sports, such as basketball, where the foot is often exposed to horizontal ground reaction force (GRF), such as cutting movements. When the foot is exposed to horizontal forces during landing, the external ankle inversion/eversion moments that the foot undergoes depend on the positions of the centre of pressure and ankle joint centre [1]. Thus, if the position of the ankle joint centre become higher because of thick soles, these moments generated by the horizontal GRF would become larger. Although there have been many studies on the effect of shoe sole thickness on running movement, the effect of sole thickness on foot kinetics exposed to horizontal GRF has not been clarified.

This study aimed to investigate the effect of different sole thicknesses on foot kinetics during landing movements on a tilted surface exerting horizontal inward GRF on the foot. It was hypothesised that the thickness of the sole increases the distance between the ground and centre of the ankle joint, resulting in a larger moment arm of the horizontal GRF, which generates a larger inversion moment.

METHODS

Twenty healthy men (age: 20.6 [standard deviation (SD) 1.7] years; height: 171.1 [SD 1.8] cm; and mass: 63.0 [SD 8.6] kg). The Nagoya Gakuin University Research Ethics Committee approved the experimental procedure, and written informed consent was obtained from each participant before commencement of the experiment.

In this study, three conditions with different shoe midsole thicknesses were used; the same shoe model (Stan Smith, Adidas) was used for all three conditions, and the thickness of the midsole was adjusted to provide 25 mm (control condition), 35 mm (+10 mm condition), and 45 mm (+20 mm condition) from the outsole to the insole, respectively. The shoes used in each condition had the same upper cup, heel cup, and outsole.

Spherical markers were attached to nine landmarks on the right lower leg and foot. Participants were asked to drop land with right leg onto a tilted force platform (Kistler instruments) at 25° from 0.3 m above the force platform for the aim of exerting a constant horizontal inward force on the foot. Their motions were captured using a 10-camera motion capture system (Vicon Motion Capture Systems), sampling at 500 Hz. This motion capture system was electronically synchronised to the force platform, which was sampled at 1,000 Hz. The three conditions were randomised, and five trials were conducted for each condition.

The time from the toe contact to the first peak of the horizontal component of the GRF (Fy) was defined as the initial landing phase. During the initial landing phase, the external ankle inversion moment due to Fy and its moment arm were calculated. All the parameters were averaged over five trials for each participant. Variables from the three conditions were analysed using one-way repeated-measures analysis of variance, followed by the Tukey's post hoc test for multiple comparisons. Statistical significance was set at $p < 0.05$.

RESULTS AND DISCUSSION

The inversion moment at the time of peak Fy was largest in the +20 mm condition (0.20 [SD 0.03] Nm/BW), followed by the +10 mm (0.18 [SD 0.03] Nm/BW), and then the control (0.16 [SD 0.02] Nm/BW), with significant differences among the three conditions ($p < 0.05$). The moment arm of inversion moment at that time also showed the largest value in the +20 mm condition, although there was no significant difference in the value of Fy among the three conditions. These results support our hypotheses.

Although materials with poor cushioning were used to adjust the midsole thickness in this study, it has been reported that a shoe with high cushioning reduces the peak value of the GRF during running [2]. Thus, a material with higher shock absorption should be used in the thick-soled shoes to minimise the disadvantage of the increased moment arm owing to thick-soled shoes.

CONCLUSIONS

When the foot is exposed to horizontal GRF, the external ankle inversion moment would increase with a thicker sole. This is caused by the thicker sole increasing the moment arm of the horizontal GRF. Cutting movements with thick-soled shoes are considered to increase the risk of ankle sprains.

REFERENCES

[1] Sato et al. *Sports Biomech* **18**: 28-38, 2019.
[2] O'Leary et al. *J Am Podiatr Med Assoc* **98**: 36-41, 2008.

AGING EFFECTS ON HIP POWER DURING SLOPE WALKING

Zihan Yang[1,2], Zhiqi Liu[2], Songhua Yan[2], Jizhou Zeng[2] and Kuan Zhang[2]
[1] Fashion Accessory Art and Engineering College, Beijing Institute of Fashion Technology, China.
[2] Beijing Key Laboratory of Fundamental Research on Biomechanics in Clinical Application, Capital Medical University, China.
Email: 226909999@qq.com

INTRODUCTION

Slope walking is inevitable activity during daily life, and the risk of falling in the elderly is increased due to increased challenges to balance control during slope walking [1]. Up to 453% hip powers increase required in young adults when incline walking [2], but little is known about the elderly, even though muscle strength decreases with aging [3]. Therefore, this abstract aims to quantify the total work done in the 3D hip joint.

METHODS

Twenty healthy male adults (Ten young: 23.7±1.1yrs, 67.5±5.0kg, 174.8±4.6cm. Ten elderly: 64.8±2.4yrs, 68.1±7.4kg, 170.4±5.6cm) were fitted with 29 retroreflective markers (Helen Hayes Marker Set). Participants were habituated to the walkway area and then performed at least three walking trials at each of the three grades (+6°, 0°, -6°). Each participant walked at a self-selected speed. Each subject took at least two steps on the slope before and after contacting the force platform. The GRF data and kinematic data were captured with a mounted force platform (Kistler 9286B, Switzerland) and a 6-camera 3D Optical Capture system (Motion Analysis Raptor-4, USA). Each foot's major gait events (heel strike and toe-off) were visually identified. GRF data were filtered using a fourth-order zero-lag Butterworth filter of 15 Hz. Positive (P) and negative (N) work were calculated in each trial by integrating the power curves over one stride. Two-way repeated measures ANOVA($\alpha \geqslant 0.05$) was used to assess slope effect, with Tukey post hoc tests.

RESULTS AND DISCUSSION

Significant changes in 3D hip joint work are presented in Figure 1. Positive and negative work were compared with 0° in the top and middle planes. Elderly hip work was compared with the young at the bottom. In the sagittal plane, a significant interaction effect of aging and gradient was found on the positive work ($p<0.01$), a significant interaction effect of aging and gradient was found on the negative work ($p<0.01$). In the frontal plane, aging significantly affected positive work ($p<0.01$), a significant interaction effect of aging and gradient was found on the negative work ($p<0.01$). In the transverse plane, aging significantly affected positive work ($p<0.01$). Negative work was affected by aging ($p<0.01$) and gradient ($p=0.01$) (Figure 1). For the young, the largest changes were observed in the frontal plane with up to 198% increase in work relative to level gait. For the elderly, the largest changes were observed in the sagittal plane with up to 197% increase in work relative to level gait. Compared with the young group, aging has led to more than five times power increase in the transverse plane.

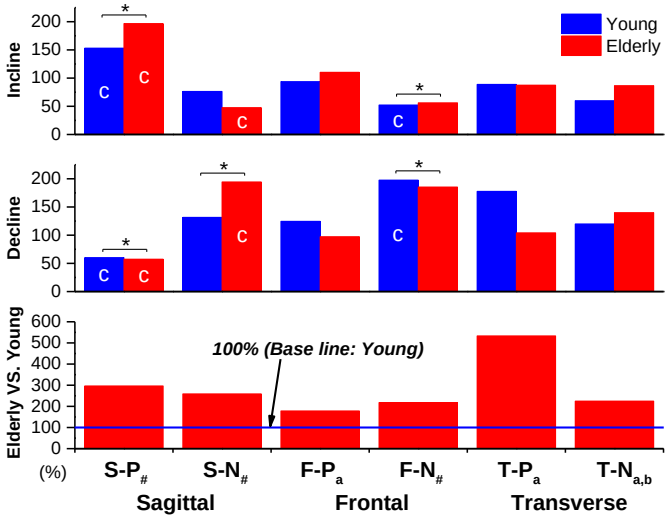

Figure 1 Hip joint work percentage during incline walking (top), decline walking (middle) relative to level walking, and the elderly hip joint work relative to the young during level walking(bottom). P=positive work, N=negative work, S=sagittal, F=frontal, T=transverse. Blue bars indicate young participants, red bars indicate elderly participants. Pound (#) indicates significant interaction of aging and slope. a and b indicate significant main effects of aging and slope, respectively. c indicates a significant slope effect with level walking, and asterisk (*) indicates a significant aging effect.

CONCLUSIONS

During slope walking, older people generate more positive and negative work than young people to accommodate inclines and declines. It required up to five times work increased. These results provide insight into the reasons for environmental barriers [4] and may shed light on a higher risk of falls for slope walking.

REFERENCES

[1] Honeycutt PH et al. *Geriatr Nurs*. **23(5)**: 250-7, 2002.
[2] Yang Z et al. *J Biomech* **92**: 35-44, 2019.
[3] Prince F et al. *Gait & Posture* **5(2)**: 128-35, 1997.
[4] Merja R et al. *BMJ open* **7(6)**: e012826, 2017.

ACUTE EFFECTS OF PROPRIOCEPTIVE NEUROMUSCULAR FACILITATION STRETCHING ON LOWER LIMB MUSCLE ACTIVATION IN OLDER AND YOUNGER ADULTS

Fiona Higgs[1,3] and Samantha L. Winter[2,3]
[1] Department of Sport and Nutrition, University College Birmingham, Birmingham, UK.
[2] School of Sport, Exercise and Health Sciences, Loughborough University, Loughborough, UK.
[3] Department of Sport and Exercise Science, Aberystwyth University, Aberystwyth, UK.
Email: f.higgs@ucb.ac.uk

INTRODUCTION

The effects of proprioceptive neuromuscular facilitation stretching (PNF) on falls risk factors in older adults is unknown due to insufficient and low quality data. While flexibility training is recommended to older adults with a history of falling, static stretching has been associated with diminished lower limb voluntary activation (VA) [1,2] - a factor detrimental to balance [3]. Caution regarding pre-exercise static stretching has been advised [4]. Suitability of PNF for older adult populations remains unknown, yet some chronic strength gains are reported in young adults [5]. The purpose of this study was to compare acute effects of PNF on percentage VA (%VA) of the plantarflexor muscles between older and younger healthy adults. It was hypothesised that reductions in %VA would be reported after PNF, with greater effect in older adults.

METHODS

Two age groups: older group (3 females and 5 males (mean ± SD): age, 63 ± 2 years; height, 1721 ± 85 mm; weight, 74 ± 10 kg) and younger group (5 females and 4 males (mean ± SD): age, 26 ± 2 years; height, 1746 ± 86 mm; weight, 45 ± 13 kg). Cross-over design, all participants completed three laboratory visits in 10-14 days. Visit 1: familiarisation, Visits 2 and 3: randomised experimental condition - PNF (3 repetitions of a 10 second (s) isometric contraction at ~65% self-reported effort followed by 5-10 s rest) or control (active ankle ROM). Isometric maximal voluntary contractions (MVC) of plantar-flexor muscles followed each condition, with ≧1 minute rest. All participants completed both conditions (right leg only). Six MVC trials immediately followed experimental conditions, alternating between MVC *with* and MVC *without* doublet using the interpolated twitch technique (ITT) (1.5 s into MVC (superimposed) and 5 s after MVC (potentiated)) via two cutaneous electrodes (one each over the proximal and distal ends of the gastrocnemius muscle). During each trial participants viewed visual feedback of isometric plantarflexor torque data collected via Biodex III dynamometer, Biodex Medical Systems, Shirley, NY; 85° hip, and 0° knee flexion, with ankle 0° plantarflexion). %VA was calculated as:

$$\left[1 - \left(\frac{\text{superimposed doublet}}{\text{potentiated doublet}}\right)\right] \times 100.$$

RESULTS AND DISCUSSION

Paired t-tests and three-way repeated measures analysis of variance (ANOVA) showed no significant effect for age or condition in %VA: (mean ± SD) younger group: control = 82 (0.2)% and PNF = 75% (0.2); older group: control = 87 (0.1)% and PNF = 87 (0.2)%, where $p > 0.05$ (see Figure 1).

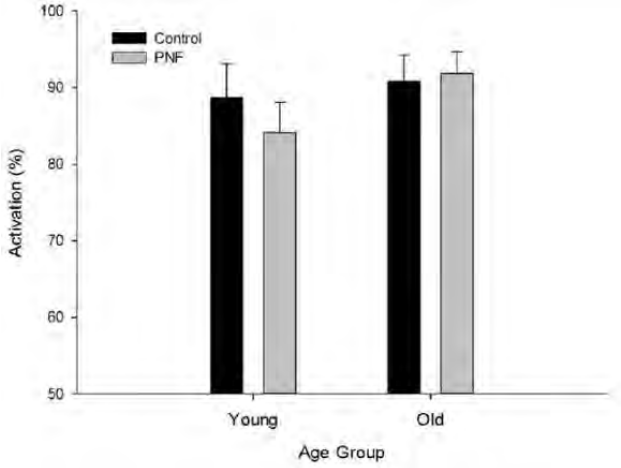

Figure 1 No significant effect for age or experimental conditions was found b three-way repeated measures ANOVA.

CONCLUSIONS

PNF showed no significant reduction in plantarflexor %VA or MVC torque in older adults. It may be a suitable alternative to static stretching. Future studies should investigate chronic effect on flexibility and %VA.

ACKNOWLEDGEMENTS

Data collected at Aberystwyth University (AU), UK. Funded by AU Departmental PhD Scholarship.

REFERENCES

[1] Trajano et al. J Appl Physiol, **115**(2): 212-218, 2013.
[2] Fowles JR et al. J Appl Physiol **89**(3):1179-88, 2000.
[3] Onambélé-Pearson, G et al. J Appl Physiol **100**(6): 2048–2056, 2006.
[4] Kay AD et al. Med Sci Sports Exerc, **44**(1):154-64, 2012.
[5] Rees S et al. J Strength Cond Res, **21**(2): 572-7, 2007.

SAGITTAL RANGE OF MOTION CHANGES IN CYCLING WITH ASYMMETRIC CRANK ARMS

Sean A. Brown[1], Jacob Wilbert[1], Jim Martin[2], and Songning Zhang[1]
[1] Kinesiology, Recreation, and Sport Studies, University of Tennessee, Knoxville, TN, USA
[2] Department of Nutrition and Integrative Physiology, The University of Utah, Salt Lake City, Utah, USA.
Email: sbrow159@vols.utk.edu

INTRODUCTION

Multiple studies have examined biomechanical changes to crank arm length in healthy adult athletes [1,2,3]. However, these studies only implemented symmetric and bilateral changes of crank arm length. Asymmetric crank arms may have clinical applications in individuals with physiologic asymmetries. The purpose of this pilot study was to examine the kinematic changes during cycling with asymmetric crank arm lengths in a healthy population. It was hypothesized that sagittal plane range of motion (ROM) in lower extremity joints would decrease as the crank arm length decreased.

METHODS

Seven recreationally active and healthy young adults (4 males, Age: 25.0±4.0 years, BMI: 24.4±3.4 kg/m^2) were included in this study. They cycled on a cycle ergometer (Excalibur Sport, Lode, Groningen, Netherlands) at seven different crank arm lengths on the right limb while the left crank arm was fixed at 170 mm (standard crank arm length). The participants started with the standard 170 mm crank arm length on both sides. In the remaining six test conditions, the right crank arm length was randomly adjusted from 130 – 190 mm at 10 mm increments using a custom adjustable crank arm. The workrate was fixed at 100 Watts and the cadence at 80 revolutions per minute. A 13-camera motion analysis system (240 Hz; Vicon Motion Analysis Inc., Oxford, UK) was used for 3-dimensional kinematic data collection. A 2 (side) x 7 (crank length) mixed model analysis of variance was performed to detect differences of ROMs between the two sides and crank arm length conditions for the hip, knee, and ankle ROMs ($\alpha = 0.05$).

RESULTS AND DISCUSSION

There were significant interactions for all ROMs ($p < 0.001$). The post hoc comparison results for the right side with different crank arm lengths showed that hip extension ROM decreased with each decrease of crank arm length from 190 mm (all $p \leq 0.017$), except for the comparison of 180 vs. 190 mm (Table 1). The knee extension ROM also decreased with each decrease of crank arm length from 190 mm (all $p \leq 0.002$). This pattern continued at the ankle with decreased ankle plantarflexion ROM with each decrease of crank arm length from 190 mm (all $p \leq 0.031$), except for the comparison of 180 vs. 190 mm, 160 vs. 170 mm, and the 140 vs. 150 mm conditions. As expected, there were no significant differences on the left side (the fixed crank arm length) between all comparisons. There were no significant differences from the left and the right limb during the symmetric crank arm condition.

Our hypothesis that sagittal plane ROM of hip, knee, and ankle joints would decrease as the crank arm decreased was mostly supported. Crank arm length has the greatest impact on the knee joint with 4 –6° of change for every 10 mm change in crank arm length while the hip and the ankle joints showed a 2 – 4° change for the same adjustments to the crank arm length.

CONCLUSIONS

The results of this study provide the first evidence of lower extremity joint ROM changes with asymmetric adjustments to crank arm lengths. It is still unknown of joint kinetic changes with such adjustments. Future research should investigate the impact of crank asymmetry in individuals with a physical asymmetry.

REFERENCES

[1] Ferrer-Roca V et al. *J Sprt Sci* **35**: 1328-1335, 2017.
[2] Too, D. et al. J Sprt Sci, **18** (3): 153-161, 2000.
[3] Barratt, P. et al. Med Sci Sprt Exer, **48** (4): 705-713, 2016.

Table 1: Sagittal plane joint range of motion (°) across different crank length conditions: Mean ± STD.

		130 mm	140 mm	150 mm	160 mm	170 mm	180 mm	190 mm
Hip ROM	Left	49.1±6.2	48.7±7.3	49.0±6.2	49.2±6.0	49.2±6.5	48.7±6.6	47.7±6.5
	Right	38.7±6.2	40.7±6.9[a]	43.6±6.6[a,b]	46.2±6.4[a,b,c]	48.5±7.1[a,b,c,d]	50.7±6.8[a,b,c,d,e]	53.5±6.1[a,b,c,d,e]
Knee ROM	Left	77.3±9.8	77.6±10.5	77.5±9.9	77.6±9.5	77.6±10.3	77.4±10.5	77.9±9.7
	Right	58.9±9.4	63.3±10.5[a]	68.4±9.8[a,b]	72.3±11.4[a,b,c]	76.6±11.7[a,b,c,d]	80.6±11.0[a,b,c,d,e]	85.4±11.0[a,b,c,d,e,f]
Ankle ROM	Left	19.2±7.2	20.3±6.7	18.8±6.0	19.2±5.8	18.9±6.6	21.2±8.3	20.3±6.9
	Right	5.8±5.2	9.0±4.8[a]	11.8±7.0[a]	14.6±8.9[a,b,c]	17.0±10.6[a,b,c]	21.7±13.1[a,b,c,d,e]	27.1±11.6[a,b,c,d,e]

Significantly different compared to [a]130mm, [b]140mm, [c]150mm, [d]160mm, [e]170mm, [f]180mm.

Effect of calf electrical stimulation training on sprint and jump performance

Sheng-Wei Jia[1], Zhao-Wei Chu[1], San-Jun Yang[2], Feng-Qin Fu[1], and Fan Yang [1,2]
[1] Li Ning Sports Science Research Center, Li Ning (China) Sports Goods Company Limited, Beijing, China.
[2] Department of Physical Education and Research, China University of Mining and Technology-Beijing, Beijing, China.
Email: yangfan6@li-ning.com.cn; jiashengwei@li-ning.com.cn

INTRODUCTION

Electrical muscle stimulation (EMS) training is often used in sports rehabilitation and strength training, most of the EMS training to the quadriceps as the main target, but the calf muscle electrical stimulation training is often ignored, it is one of the main power muscles of sprint and jump. The purpose of this study was to examine whether the addition of EMS to a regular calf muscle training regimen resulted in changes in muscle strength that resulted in greater benefits for sprint and jump performance.

METHODS

Twenty healthy athletes were divided into two groups (regular calf training and calf training combined with EMS). The main training target are calf gastrocnemius muscles. All athletes train for 4 weeks. 30m sprint time, jump height and muscle activation characteristics were assessed before and after training. Bidirectional (group x time) factorial analysis of variance was performed for repeated measurements, with $\alpha = 0.05$ to determine whether there was a significant effect.

RESULTS AND DISCUSSION

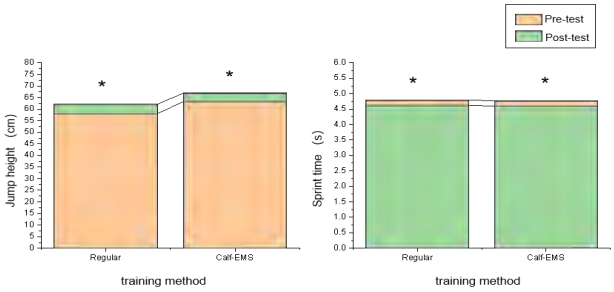

Figure 1 Comparison of pre-test and post-test exercise performance results (* represents a significant difference between Pre- and Post-test)

Both regular and Calf-EMS groups showed increased jump height and faster sprint time after training ($P < 0.001$). Compared with calf training with or without the assistance of EMS, there was no improvement in the results of training and EMG (Figure 1, Table 1).

The current findings do not support our original hypothesis, which suggested that electrical muscle stimulation (EMS) has been recognized as an effective method leading to significant improvements in explosive strength and athletic performances [1]. One plausible explanation would be due to the short training duration (a total of 11 sessions in four weeks) and constant EMS intensity over the training sessions. Previous studies found that EMS training can significantly improve countermovement jump performance by 17% (8 weeks) and drop jump by 6.6% (12 week) [2], respectively, while only increment of 5.5% was evident in our four-week training.

CONCLUSIONS

Calf-EMS training can significantly improve sprint and jump performance, but there is no obvious advantage over conventional training. Future training should consider electrical stimulation of different muscles or longer training sessions.

REFERENCES

[1] Bax L, Staes F, Verhagen A. Does neuromuscular electrical stimulation strengthen the quadriceps femoris? A systematic review of randomised controlled trials. Sports Med. 2005;35(3):191-212.
[2] Babault N CG, Bernardin M, Pousson M, Chatard JC. Effects of electromyostimulation training on muscle strength and power of elite rugby players. J Strength Cond Res. 2007 May;21(2):431-7.

Table 1: Tables that extend across both columns should be placed at the bottom of the abstract.

	Pre-test		Post-test		*p-value*		
	Calf-EMS	Regular	Calf-EMS	Regular	Interaction	Group	Time
Jump height (cm)	63.2±2.2	58.1±2.2	66.9±2.4	62.1±2.4	.832	.140	<.001
Sprint time (s)	4.76±0.10	4.80±0.10	4.60±0.09	4.62±0.09	.825	.851	.001
Integrated EMG – medial	155.9±22.7	105.4±22.7	144.8±19.4	136.7±19.4	.159	.277	.492
Integrated EMG – lateral	180.1±28.7	132.5±28.7	186.6±25.5	148.3±25.5	.846	.174	.641
RMS EMG – medial	80.5±8.0	76.7±8.0	79.3±10.2	93.4±10.2	.361	.566	.425
RMS EMG – lateral	82.5±8.8	94.3±8.8	88.8±15.1	129.2±15.1	.209	.071	.076

Middle-aged adults altered the joint strategy but not muscle-tendon interaction during gait

Iseul Jo[1,3], Yoon-Hyung Cho[1,3], Hae-dong Lee[2,3]
[1]Department of Physical Education, Graduate School of Yonsei University, Seoul, Korea
[2]Department of Physical Education, College of Educational Sciences, Yonsei University, Seoul, Korea
[3]Frontier Research Institute of Convergence Sports Science, College of Educational Sciences, Yonsei University, Seoul, Korea
Email: whdltmf53@yonsei.ac.kr

INTRODUCTION

The tendon transfers the force generated by the muscle and stores and reuses the elastic energy through the muscle-tendon unit (MTU) interaction. Aging changes tendon compliance and the capacity to reuse elastic energy. Elderly individuals showed shorter fascicle length behavior and less tendon shortening during locomotion, which led to increased muscle activity and less elastic energy reusability [1].
It was noted that the Achilles tendon (AT)'s mechanical characteristics changed dramatically with age at around 46 years, but that the 40s and 20s were similar [2]. Therefore, we aimed to investigate the mechanical property of the AT and its behavior during walking in the 50s.

METHODS

Eight healthy males with middle-aged (50s, height: 174.9 ± 6.8cm, weight: 74.0 ± 10.7kg, age: 55.9 ± 2.2yr, walking speed: 1.18 ± 0.2) and eight young adults (20s, height: 175.6 ± 5.8cm, weight: 79.0 ± 9.8kg, age: 27.1 ± 1.2yr, walking speed: 1.15 ± 0.2) were recruited.
An isometric plantar flexion was conducted using a dynamometer to measure muscular force and AT elasticity. Muscle-tendon junction (MTJ) in medial gastrocnemius (MG) was captured using B-mode ultrasound. Also, their walking at the preferred speed was captured with motion capture systems, ground reaction force (GRF), Electromyography (EMG), and ultrasound.

RESULTS AND DISCUSSION

The 50s showed lower muscle force and compliant characteristics in AT. Reduced mechanical properties were similar to an aged tendon in the elder.
Furthermore, the 50s walked with flexed joints of their lower extremities. However, they do not differ in MTU behavior. Although the 50s had less capacity to use AT, their joint strategy might permit them to perform MTU interaction like the 20s [3].

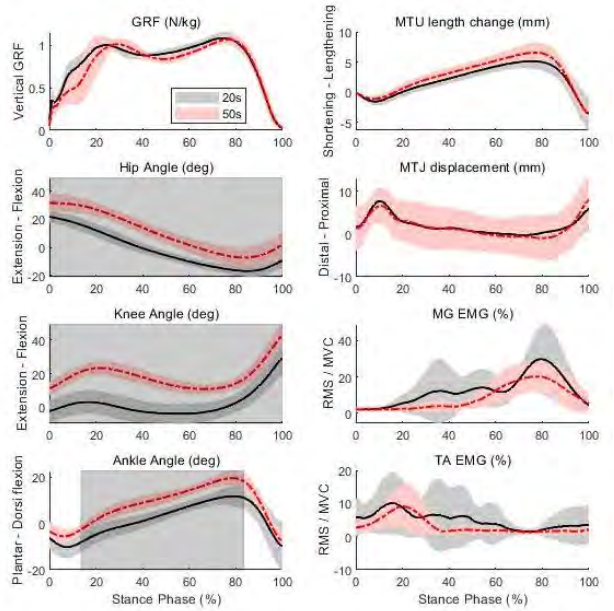

Figure 1 Joint angles and MTJ displacement during the stance phase. The movement was compared using SPM1D, and the shaded area shows a significant difference.

CONCLUSIONS

Middle-aged people demonstrated the deteriorated mechanical characteristics of the AT, which were less effective in transferring force and reusing elastic energy. Our results showed that the changed joints' strategy seems to enable MTU behavior in the 50s. In conclusion, aging impacts the gait and architecture of the 50s; they need to train for health and prepare for aging.

REFERENCES

[1] Mian, Omar S., et al. *Acta physiological* **189.1**: 57-65, 2007.
[2] Kubo et al. *Scientific Reports*, **12.1**: 1702, 2022
[3] Panizzolo, Fausto A., et al. Gait & posture **38.4**: 764-769, 2013

Table 1: Mechanical tendon properties and muscle torque in the 20s and 50s.

Variables	MG Peak Torque (Nm)	MG Force (N)	Maximal elongation (mm)	Stiffness ($N \cdot mm^{-1}$)	Hysteresis (%)	Tendon CSA (mm^2)	Strain (%)	Stress (Mpa)
50s	114.4 ± 31.6*	376.5 ± 104.0*	15.0 ± 5.4*	32.1 ± 10.4*	26.1 ± 12.0*	64.1 ± 16.4*	7.8 ± 2.8*	6.0 ± 1.5*
20s	156.7 ± 28.3	515.6 ± 93.0	21.5 ± 4.2	51.7 ± 19.3	14.1 ± 6.5	50.2 ± 9.4	11.1 ± 2.3	10.5 ± 2.3
Effect size	1.41	1.41	1.33	1.26	1.24	1.04	1.30	2.33
p-value	*0.014*	*0.014*	*0.018*	*0.024*	*0.027*	*0.057*	*0.021*	*0.000*

* Significantly different at $p < .05$ between groups

Comparison of Differences in Lower Extremity EMG According to Foot Angle during Self-Weight Squat in Adult Women with Genu Valgum

Chanki Kim[2,5], Jiyoung Kim[2,5], Haeryang Jo[1,5] and Kyoungkyu Jeon[1,2,3,4,5]

[1] Division of Sports Science, Incheon National University, Incheon, South Korea
[2] Department of Human Movement Science, Incheon National University, Incheon, South Korea
[3] Sport Science Institute, Incheon National University, Incheon, South Korea
[4] Health Promotion Center, Incheon National University, Incheon, South Korea
[5] Functional Rehabilitation Biomechanics Laboratory, Incheon National University, Incheon, South Korea
Email: kimchangi96@inu.ac.kr

INTRODUCTION

Genu valgum is a condition in which one or both knees are deviated toward the centerline [1]. As the TFA (tibiofemoral angle) increases, the pressure applied to the patellofemoral joint increases and anterior knee pain occurs, which tends to increase knee instability [2]. As such, physical malalignment is a major cause of musculoskeletal injury [3]. It was reported that the squat with medial knee displacement showed a decrease in the vastus lateralis muscle EMG and an increase in the gastrocnemius EMG compared to a squat in which the knee was correctly aligned [4-5]. Therefore, the purpose of this study is to compare and analyse whether there is a difference in muscle activity according to the condition of the foot angle during self-weight squat in adult women with genu valgum.

METHODS

15 adult women in their twenties with genu valgum participated in this study. In order to measure EMG of the lower extremities according to foot angle during self-weight squat, two-foot angle (0º, 30º) were performed. A paired *t*-test was used to compare and analyse the difference between the two-foot angle conditions. All statistical analysis was performed using SPSS 26.0 (IBM, USA), and all variables were calculated as mean and standard deviation. The statistical significance level was set at $P < 0.05$.

RESULTS AND DISCUSSION

As a result of this study, there was a significant difference in lower limb EMG between the two conditions (0º, 30º) in the left VMO (t_{14}=2.344, p=.034), right VLO (t_{14}=2.303, p=.037), left VLO (t_{14}=2.488, p=.026), left RF (t_{14}=2.704, p=.017), right GAS (t_{14}=-3.595, p=.003), left GAS (t_{14}=-2.871, p=.012) during self-weight squat. In the case of medial knee deviation during squats, a pattern of decreased vastus lateralis muscle activity and increased gastrocnemius activity appears [5-7]. According to the results of this study, compared to the case where the EMG is 0º, when the foot angle is 30º, when the vastus lateralis muscle decreases and the gastrocnemius muscle increases, from the EMG point of view, and when the angle is set to 30º during self-weight squats, medial knee deviation may occur.

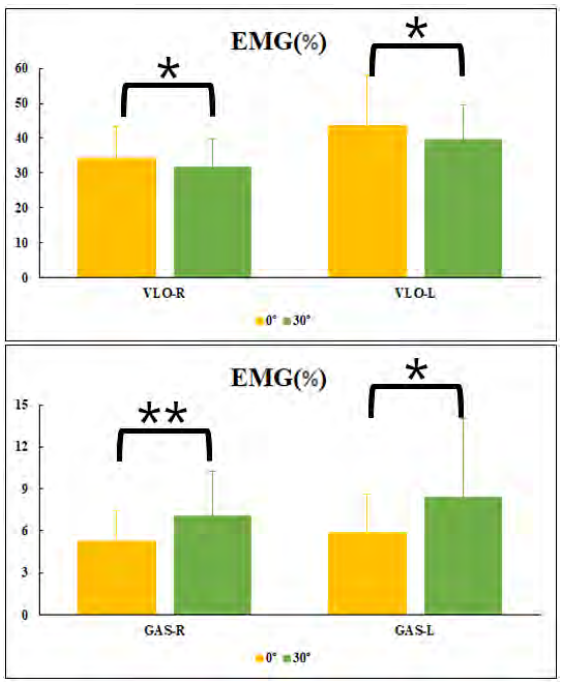

Figure 1. Results of lower extremity EMG according to foot angle during self-weight squat.
Note: data are mean ± standard deviation. *p<.05, **p<.01.
Abbreviation: EMG: electromyography; VLO: vastus lateralis; GAS: gastrocnemius R: right leg; L: left leg

CONCLUSIONS

The results of this study showed a decrease in the activity of the vastus lateralis muscle and an increase in the activity of the gastrocnemius muscle compared to the foot angle of 30º to 0º, which means medial knee deviation may occur during self-weight squats. Therefore, it is thought that adult women with genu valgum will be able to perform squats with a less risk of injury than when the foot angle is 0º during self-weight squats.

ACKNOWLEDGEMENTS

This study was supported by the University Innovation Support Project of Incheon National University.

REFERENCES

[1] Kwon, J et al. *Orthopedics*, **36(6)**: 840-843, 2013.
[2] Hewett, T et al. *Am J Sports Med* **33(4)**: 492-501, 2005.
[3] Dohee, K et al. (2010). *J Exerc Rehabil* **6(2)**: 125-134. 2010.
[4] Powers, C et al. *Foot Ankle Int*, **23(7)**, 634-640. 2002.
[5] Macrum, E et al. *J Sport Rehabil*, **21(2)**, 144-150, 2012.
[6] Padua, D et al. *J Athl Train* **47(5)**: 526-36, 2012.
[7] Bell, D. et al. *J Athl Train* **4(3)**: 117-125, 2012.

ECCENTRIC PRELOAD INCREASES WORK DURING SHORTENING BY COUNTERACTING RESIDUAL FORCE DEPRESSION

Tobias Göcking[1], Denis Holzer[2] and Wolfgang Seiberl[1]
[1] Department of Human Sciences, Bundeswehr University Munich, Neubiberg, Germany.
[2] Technische Universität München, Munich, Germany.
Email: wolfgang.seiberl@unibe.de

INTRODUCTION

Residual Force depression (rFD) is defined as a decrease in steady-state isometric force following active shortening compared to a purely isometric contraction at identical muscle length and activation. It is generally accepted that the magnitude of rFD depends on the amount of work performed during the active shortening phase. Despite this, Seiberl et al. [1] showed that the work performed during the shortening phase of stretch-shortening cycles (SSC) was greater compared to pure shortening controls, yet the resulting rFD was smaller. This contradicts some accepted ideas about rFD mechanisms related to stress-induced inhibition of cross-bridge attachments associated with the amount of work performed during the shortening [2]. This study aimed to add understanding about the influence of stretch-induced performance enhancement on shortening work and rFD after SSCs. By controlling the amount of eccentric and isometric preload prior to shortening, we focused on shortening work, rFD and the rate of force-redevelopment after shortening.

METHODS

Electrically stimulated ankle plantar flexor torque was measured during preloaded shortening and SSC contractions (range 25° at 40°/s). Three different protocols were used: 1) preloaded shortening with constant low intensity (*SHO*); 2) shortening with high stimulation intensity during preload and low stimulation intensity during the shortening phase (*SHO-matched*); 3) SSC with constant low intensity (SSC). Low intensity was referred to stimulations evoking ~30% of the maximum voluntary torque. The second stimulation intensity (high) is used to reach identical preload torque values as measured at the end of stretch in SSCs in order to match identical preload before shortening. Repeated-measures ANOVA was used to analyze parameters of interest (force/torque, work, rFD, rate of force redevelopment (RFrD) across conditions during and after shortening (α=.05).

RESULTS AND DISCUSSION

Despite identical preload (p=1.00), shortening work during *SSC* was 1.2 ± 0.2 times higher than during *SHO-matched. SSC* and *SHO-matched* showed 1.8 ± 0.5 and 1.6 ± 0.4 times higher work compared to *SHO,* respectively. During steady-states after shortening, *SHO-matched* resulted in greatest rFD (23.9 ± 11,8%), compared to *SHO* (16.3 ± 13.4%) and *SSC* (8.2 ± 10.1%). RFrD was comparable after *SSC* and *SHO-matched,* and *SHO*.

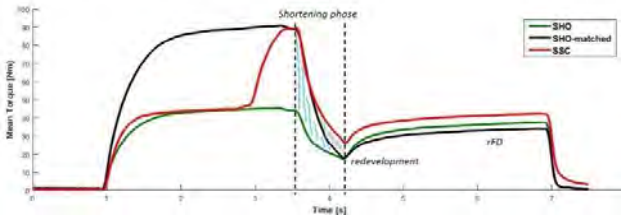

Figure 1 Torque for shortening (*SHO*) *vs* shortening with high preload (*SHO-matched*) *vs* SSC with constant low intensity (SSC).

CONCLUSIONS

Data of *SHO-machted* and *SSC* clearly show that the amount of preload makes the primary contribution to performance enhancement in muscle shortening. However, the type of preload still makes a difference, and eccentric preload outperforms torque-matched isometric preload especially towards the end of the shortening, resulting in less depressed torque/force. Therefore, eccentric preload in SSCs also positively influences force generating readiness of muscles after the shortening phase by reducing the amount of rFD during and after shortening. Interestingly, the rate of force redevelopment was not different after the shortening; yet redevelopment started from a higher level after *SSC* condition (Figure 1). Recent theories favor titin related mechanisms responsible for increased forces during stretch and reduced force depression during shortening [3]. Thus, the increased force generating readiness for following muscle actions after SSCs might also be explained by titin related mechanisms. Further research on different structural levels should focus also on the phase of force redevelopment after SSCs.

ACKNOWLEDGEMENTS

This project is funded by the German Research Foundation (DFG) - project number 354863464.

REFERENCES

[1] Seiberl et al., *Physiol Rep* **3 (5)**, 2015.
[2] Granzier and Pollack, *J. Physiol.* **415**, 1989.
[3] Tomalka et al., *Front Physiol*, **11**, 921, 2020.

The Impact of Spring Tension on Muscles Activation in The Lower Limbs during Footwork Movements in Pilates

Yongseok-Park[1], Jongho-Yang[1], Hyeongwook-Joo[1], Kwangmin-Choi[1] and Kikwang-Lee[1*]
[1] College of Physical Education, Kookmin University, Seoul, Korea 02707
Email: kklee@kookmin.ac.kr

INTRODUCTION

Pilates is one of the most popular exercise. For increased pilates populations, it's important to know bionmechanical functions of Pilates, which muscles are used. Through this learning, people can be informed of the purpose of exercise. However, there are not enough researches on Pilates. In other words, It needs additional studies in terms of biomechanics. In this study, we focused on analyzing footwork, one of the most representative exercises of Pilates. The purpose of this study was to analyze the impact of spring tensions on muscle activities of the lower limbs during footwork motion.

METHODS

Eight female Pilates instructors participated this experiment. All participants performed footwork movements on the reformer. There were three types of movement intensity: Low (L), Mid (M) and High (H). Each movement was performed 6 times at the same speed (15bpm) at each intensity. Five surface EMG sensors (Delsys, Massachusetts, USA) were utilized to obtain muscle activity signals, and the sensors were attached to the biceps femoris (BF), semitendinosus (ST), rectus femoris (RF), vastus lateralis (VL) and vastus medialis (VM). The measured EMG signals were normalized to the resting state (%RVC). The footwork movement was divided into extension phase and flexion phase. The iEMG was used to calculate muscle usage, and time was normalised to each phase to analyze the pattern of muscle activity affected by knee angle.

RESULTS AND DISCUSSION

During footwork movements, a pattern of increasing muscle activity was observed as knee angle increased in BF, ST, VL and VM (Figure 1). These results suggest that the load on the spring influenced the muscle activity pattern. Spring is a form of elastic resistance. These results are consistent with Hooke's law, which states that the elastic resistance of a spring increases as the spring length increases [1]. In the iEMG data (Table 1), VL and VM showed statistically significant differences in spring loads ($p < 0.000$). In contrast, there were no significant differences in BF, ST and RF. The VL and VM are monoarticular muscles, while the other muscles are biarticular muscles. According to the previous research, monoarticular muscles acted as mobilizers, whereas biarticular muscles acted as stabilizers [2]. And footwork motion has a consistent trajectory of movement, and it is less affected by gravity due to the reformer carriage. These reasons seem the latent considerations of the iEMG results. The iEMG results suggest that the footwork movement affects the monoarticular muscles more.

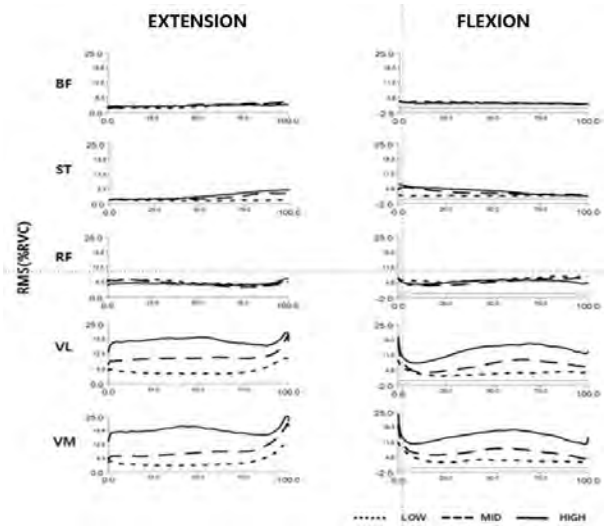

Figure 1 Muscle activation pattern according to the knee angle.

CONCLUSIONS

The EMG results showed that as spring tension increased, iEMG of the VL and VM also increased during footwork movements. However, there were no differences in BF, ST and RF. As a result, this suggests that the footwork motion may be better consideration to training monoarticular muscles rather than biarticular muscles.

ACKNOWLEDGEMENTS

This is work was supported by the National Research Foundation of Korea (NRF) grant funded by the Korea government (MSIT) (No. 2021M3I2A107741313).

REFERENCES

[1] Rychlewski J. J A. Math&Mech **48**; 303-314, 1984
[2] Robertson D et al. *J A. biomech* **24**: 333-339, 2008.

Table 1: The results of iEMG (average ± SD)

	LOW	MID	HIGH	*p-value*
VL	18.35 ± 6.82	38.88 ± 7.85	68.26 ± 18.66	$p = 0.000$
VM	17.2 ± 10.23	34.6 ± 6.93	66.72 ± 18.09	$p = 0.000$

Comparative analysis on lower extremities kinematic of adult women during stair ascend according to heel height

Sangha Park[1], Sabin Chun[1], Duhyun Kim[1] and Jongchul Park[2]
[1] Department of Physical Education, Pukyong National University / Busan, Republic of Korea.
[2] Major of Marine-Sports, Division of Smart Healthcare, Pukyong National University / Republic of Korea.
Email: jcpark@pknu.ac.kr

INTRODUCTION

Modern shoes are used not only for functional purposes but also as an element of fashion. Women wear high heels to emphasize their individuality and fashion, but choose low heels for comfort. However, the higher the heel of the shoe, the higher the probability of falling when walking on stairs, which can be a risk factor for injury (Tencer et al., 2004). Therefore, in this study, we compared and analyzed the kinematic variables of the lower extremities according to the height of the heel when an adult woman ascended stairs wearing three types of shoes with different heel heights.

METHODS

The subjects of this study were 24 healthy adult women who had no lower extremities injury within 3 months (age: 22.08±1.28, height: 160.43±4.30, weight: 54.10±6.39, foot size : 232.29±2.54). In this study, the model staircase consisted of 9 infrared cameras (sampling rate: 200fps) and 3 layers, and the ground reaction force measuring machine (sampling rate: 1000Hz) was built in the middle layer.
The subjects wore shoes (1cm, 5cm, 7cm) in random order, and collected variables for the range of motion(ROM) of the lower extremities in the stance phase by distinguishing the initial contact (IC) and toe off (TO) times when the dominant foot landed on the measuring instrument. All data were analyzed by calculating the average value of three stair ascends.

RESULTS AND DISCUSSION

For both shoe conditions, the main differences in ROM between the three types of shoes occur at the hip and ankle joints (Table 1). In addition, the lower the heel, the greater the ROM of the ankle joint in the sagittal, frontal, and lateral planes than the higher heel.
These results are judged to be for limiting excessive movement of the ankle, as the higher the heel, the more plantar flexion of the ankle (Gu et al., 2013). However, there was no difference in heel height in the ROM in the three planes of the knee joint. Finally, a higher heel at the hip joint has a smaller anterior plane ROM than a lower heel. This is confirmed by the fact that the variability according to the gait style among the subjects was not controlled because the speed was not controlled(Opila-Correia, 1990).

CONCLUSIONS

As a result of this study, the lower the heel, the greater the range of motion of the ankle joint, and the ROM the hip joint in the frontal plane than high the heel. These results indicate that the lower the heel was more stable and resulting in a greater ROM. However, It was confirmed that the difference in gait pattern between the subjects due to not controlling the speed.
Thus, follow-up research is needed to derive accurate results on the effect of heel height differences on the body by controlling the speed so that subjects can measure at a constant speed in the future.

REFERENCES

[1] Gu Y et al. *J Biomedical Engineering and Technology*, **12**(3), 240-251, 2013.
[2] Opila-Correia K A. *A physical medicine and rehabilitation*, **71**(11), 905-909, 1990.
[3] Tencer A F et al. *J the american geriatrics society*, **52**(11), 1840-1846, 2004

Table 1: Lower extremities range of motion in three planes according to heel height when ascending stairs.

		Heel height			*F*(*p*) / *Z*(*p*)	Post hoc
		1cm[a]	5cm[b]	7cm[c]		
Ankle	SP	25.59±4.25	23.94±5.01	24.01±3.94	4.557(.016)	a>b,c
	FP	12.76±3.43	11.23±3.17	10.98±2.39	5.317(.008)	a>b,c
	TP	7.370±2.29	6.329±1.56	6.638±1.27	3.497(.039)	a>b
Knee	SP	47.67±4.81	48.66±5.11	48.85±4.30	2.275(.114)	-
	FP	19.65±5.50	19.47±5.21	19.49±4.51	0.116(.891)	-
	TP	14.55±5.81	14.47±6.28	14.17±5.25	0.333[v] (.846)	-
Hip	SP	59.65±4.23	59.09±4.87	59.35±3.67	0.811(.451)	-
	FP	18.69±4.12	18.00±4.07	16.18±3.14	12.500(.001)	a,b>c
	TP	11.36±3.08	10.49±2.95	10.52±2.97	3.049(.057)	-

Values express as mean ± standard deviation, v: non-parametric statistics, a: 1cm, b: 5cm, c: 7cm, SP: Sagittal plane, FP: Frontal plane, TP: Transverse plane

Kinematic analysis of metatarsophalangeal joint during level and slope walking

Sang Woo Jung[1], Pankwon Kim[1], Jiyoung Jeong[1] and Choongsoo Shin [1]
[1] Department of Mechanical Engineering, Sogang University, Seoul, Republic of Korea.
Email: cshin@sogang.ac.kr

INTRODUCTION

Powered prosthesis can improve the walking performance of the amputees [1]. Although metatarsophalangeal (MTP) joint contributes important roles in push off and double support phase during walking [2,3], few studies on powered prostheses including MTP joint have been performed [4]. In addition, previous studies have reported the MTP joint kinematics during level walking [5-7] but kinematic data during slope walking have not been reported. Actual outdoor ground surfaces often include uphill or downhill. Therefore, the aim of this study was to investigate the MTP joint sagittal kinematics during uphill/downhill walking and compare them with during level walking.

METHODS

Nine healthy male subjects (age: 23.3±0.78 years, height: 171.8±3.92 cm, mass: 69.7±6.12 kg) participated in this study. To measure the MTP joint kinematics, 30 retro-reflective markers were placed on the lower limb. The kinematic data were recorded at 400Hz using a motion analysis system equipped with ten infrared cameras. Each gait cycle was defined as the period between the initial heel strike and subsequent heel strike of the same foot. Since the obtained data were not normally distributed, Mann-Whiney U-test was performed at a significance level of 0.05.

RESULTS AND DISCUSSION

Both initial contact and maximum value of MTP joint angle in downhill walking was significantly smaller than level walking ($P<.05$, $P<.01$) (Table 1). Additionally, MTP joint maximum dorsiflexion was significantly greater in uphill than downhill walking ($P<.01$ Table 1). The maximum MTP dorsiflexion appeared in the late stance phase in all three conditions (Figure 1, Table 1). There were no kinematic parameters indicate significant difference between during level and uphill walking.

Maximum MTP joint dorsiflexion was 40.4° and stance phase covered 60% of one gait cycle during level walking, which are similar with previously reported values as 45° and 63% [5,7]. In addition, MTP joint maximum dorsiflexion condition was 42.9° during 15° slope uphill walking. Our results can be utilized as a design guideline for powered prosthesis with MTP joint.

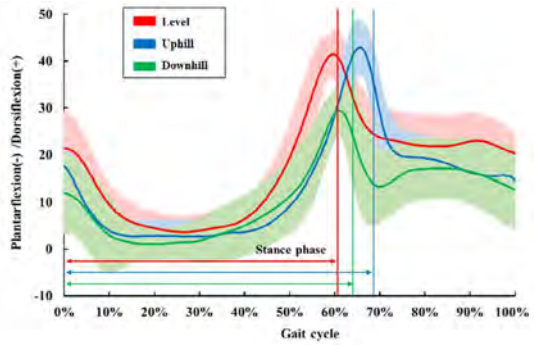

Figure 1 MTP joint kinematics during level, uphill, and downhill walking

CONCLUSIONS

Both initial contact angle and maximum MTP dorsiflexion in downhill walking were smaller than in level walking, whereas no differences were found in uphill walking compared to level walking.

ACKNOWLEDGEMENTS

This work was supported by the National Research Foundation of Korea (NRF-2019R1A2C1089522).

REFERENCES

[1] Samuel A et al. *IEEE Trans Robot* **25**: 51-66, 2009.
[2] Hayafune N et al. *The Foot* **9**: 88-92, 1999.
[3] Miyazaki S & Yamanoto S. *Gait Posture* **1**: 133-40, 1991.
[4] She H et al. *Advanced Robotics* **34**: 689-97, 2020.
[5] Bovi G et al. *Gait Posture* **33**: 6-13, 2011.
[6] Khazzam M et al. *J. Orthop. Res.* **25**: 319-29, 2007.
[7] Allan J et al. *J Foot Ankle Res.* **13**: 33, 2020.

Table 1 Kinematics of MTP joint during level, uphill, and downhill walking

	Dorsiflexion at initial contact (deg)	Maximum dorsiflexion		Stance, % of gait cycle
		Angle (deg)	% of gait cycle	
Level	21.4±7.8	40.4±5.2	59.7	60.5
Uphill	17.4±3.6	42.9±5.9	65.5	68.4
Downhill	11.9±8.6 [a]	29.4±5.0 [a,b]	61.1	64.6

[a] *P<0.05, significant difference between level and downhill*
[b] *P<0.05, significant difference between uphill and downhill*

BIOMECHAMICAL EVALUATION OF A HYBRID SUTURE ANCHOR WITH EXPANDABLE BARBED IN OSTEOPOROTIC SWINE BONE BLOCK

Yu-San Chen[1], Sai -Wei Yang[2], Yu-Ting Yo[2], Shao-Fu Huang[2], Chun-Li Lin[1]
[1] Department of Biomechanical Engineering, National Yang Ming Chiao Tung University, Taipei, Taiwan
[2]Medical Device Innovation and Translation Centre, National Yang Ming Chiao Tung University, Taipei, Taiwan
Email: xw9672gi24@gmail.com

INTRODUCTION

The main challenge of bone anchoring devices is early pull-out of implant, causing loosening of tightened suture. This phenomenon is especially found in osteoporotic patient, due to decreased bone content to cling on.[1] The aim of this study was to propose a hybrid suture anchor with axis-symmetry expandable barbs that can outspread to enhance holding power inside osteoporotic bone. Biomechanical evaluation of anchor stability was performed by static/dynamic pull-out test inside normal/osteoporotic bone samples.

METHODS

A 5.5mm in diameter hybrid suture anchor with axis-symmetry barb mechanism at middle was designed and manufactured to compare the biomechanical stability with a standard suture anchor (control group). The barb mechanism of the hybrid suture anchor can expand by pushing down the inner core to according to enhance the holding power of the surrounding bone according to the situation of bone osteoporosis (Figure 1) [2]. Total of 20 blocks of proximal swine humerus were prepared, and randomly divided into 10 normal and 10 osteoporotic samples which were decalcified with 0.5M EDTA solution for 8 weeks [3]. Hybrid and standard anchors were inserted into the bone blocks at 45°angle to mimic the real clinical situation (received horizontal and vertical pull-out forces). The barbed mechanism was pressed to full-expand in osteoporotic group to enhance the holding power but not in the normal bone. Each bone block was clamped onto the testing machine and the suture was hooked through a SMC knot at the other end (Figure 1C) Static pullout and after dynamic 150-cyclic load pullout tests were performed (n=5). The pull out forces in dynamic tests were set at 150N and 70.2N for normal and osteoporotic bone, respectively, and the frequency was set at 0.5Hz.

RESULTS AND DISCUSSION

The result of all pull out strength tests were shown in Table 1. One barbed anchor in normal bone and two in osteoporotic bone failed during dynamic loading. All the fiber-wires were torn during dynamic tests of control group anchor inside normal bone, indicating strength value surpass its average tensile strength, which lies around 265N in our previous tests. The results have shown 1.66 fold increase in strength of barbed anchor inside osteoporotic bone after dynamic loading. This could result from the barb mechanism tightening up surrounding bone matrix during dynamic cycling. The hybrid anchor without barbs expand showed no difference (p=0.81) with control group in static strength inside normal bone. Although there is a 1.55 fold difference in static strength inside osteoporotic group, no significant difference was found (p=0.02).

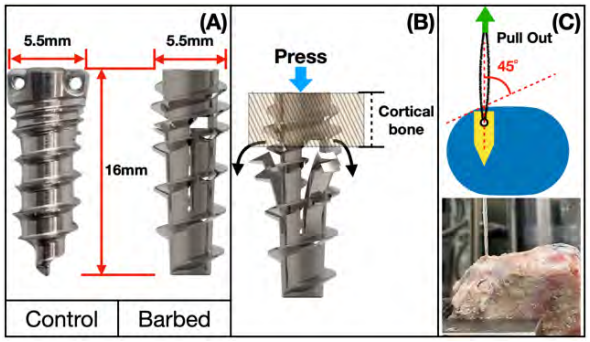

Figure 1 (A)Design parameter of hybrid anchors, (B)Expanding mechanism; (C)Setup of pull-out strength test

CONCLUSIONS

The new hybrid suture anchor with barbed design can improve the stability after dynamic cyclic loading.

REFERENCES

[1] Matthias F.P. et al. *Arch Orthop Trauma Surg* **129(3)**:379-9, 2009.
[2] Chih-Hwa C. et al. *Int J Bioprint,* 8(4):608, 2022.
[3] Ching-yi L. et al. *J Neurosurg Spine* **14**: 789-798, 2011.

Table 1: Pull-out strength in static strength test and after 150 cycles of dynamic loading

	Static strength test			After dynamic fatigue		
	Barbed (N)	Control (N)	*p*	Barbed (N)	Control (N)	*p*
Normal bone	246.93(±28.0)	241.38(±42.2)	0.81	266.69(±68.1)	Nil	N/A
Osteoporotic bone	150.75(±37.8)	234.6(±52.8)	0.02	249.83(±31.7)	218.83(±27.3)	0.19

BIOMECHANICAL EVALUATION OF A 3D PRINTED ADJUSTABLE ASSEMBLY THIN BONE PLATES FOR TRANSVERSE PATELLA FRACTURE

Chiao-Min Chang [1,2], Shao-Fu Huang [1,2], Chi-Yang Liao [3], Wei-Che Tsai [1] and Chun-Li Lin [1,2]
[1] Department of Biomedical Engineering, National Yang Ming Chiao Tung University, Taipei, Taiwan.
[2] Medical Device Innovation and Translation Center, National Yang Ming Chiao Tung University, Taipei, Taiwan.
[3] Department of Orthopedics, Tri-Service General Hospital Songshan Branch, National Defense Medical Center, Taipei, Taiwan
Email: cherryamigo.be10@nycu.edu.tw

INTRODUCTION

Surgical treatment with anterior tension band wiring (used K-wires directly or cannulated lag screws) for the transverse patella fracture usually rises clinical complications included failure of fixation, migration and skin irritation. Although bilateral fixed-angle plate was introduced to provide greater stiffness and lower fracture gap dehiscence for transverse patella fractures [1]. However, problems were emerged with inaccurate pre-bending and alignment, interference of bone screws, and lack of holding power for bone fragments. The aim of this study was to develop a titanium 3D printed anatomical contour bone plate with hook mechanisms and size adjustable assembly thin bone plates (AATBP) for patella fracture fixation. Cyclic loading test was performed to evaluate the biomechanical stability between this osteosynthesis system specifically designed and tradition anterior tension band wiring for use on the transverse patella fracture.

METHODS

Two thin bone plates were contoured anatomically and can be assembled by ratchet to adjust the assembled plate size to fit the corresponding patella anterior surface. Two-pair hooks on the proximal and distal edges of the assembled plate that can grip the fractured fragments of the patella were also designed. The thin bone plates were fabricated by a metal 3D printer (AM400, Renishaw, Gloucestershire, UK) using titanium alloy powder and cleaned using ultrasonic oscillations. Six identical left patellae made from 3D printed ABS material (ABS-P430; Stratasys, Ltd., Minnesota, USA) with transverse fractures for fixation with anterior tension band wiring approach featured two stainless steel K-wires and AATBP securing with 2.4mm inter-crossing locking screws were prepared for biomechanical testing. The specimens were mounted on the a specially designed testing platform to simulate 90 ° angle knee flexion using an artificial femur condyle as a pivot point [2]. The medial, lateral fracture gaps and maximum pull force detected by load cell were measured using digital ruler after cyclic test with 300 cycles under 150N applied on the model.

RESULTS AND DISCUSSION

The AATBP can effectively fine-tune the proper fixing position according to the transverse patella fracture situation through the ratchet design and the superior and inferior hooks can grip on the proximal and distal edges of the patella to generate holding power to tighten the fracture fragments. However, thin bone plates with complex geometry needed to take a lot of efforts and time consuming by using traditional manufacturing processes and desired to adopt the metal 3D printing manufacturing. The maximum patellofemoral forces during knee flexion tests were found at 60 degrees and consistent with the physiologic locomotion and indicated the rationality of the testing platform. The cyclic loading tests showed that the average maximum patellofemoral force of using AATBP was lower than that of tension band wiring. The fracture gap at the medial and lateral sides of the assemble thin-plates were 0.027±0.06mm and 0.067±0.03mm and significantly smaller than those of the tension band wiring were 1.965±0.63mm and 2.343±0.32mm, respectively.

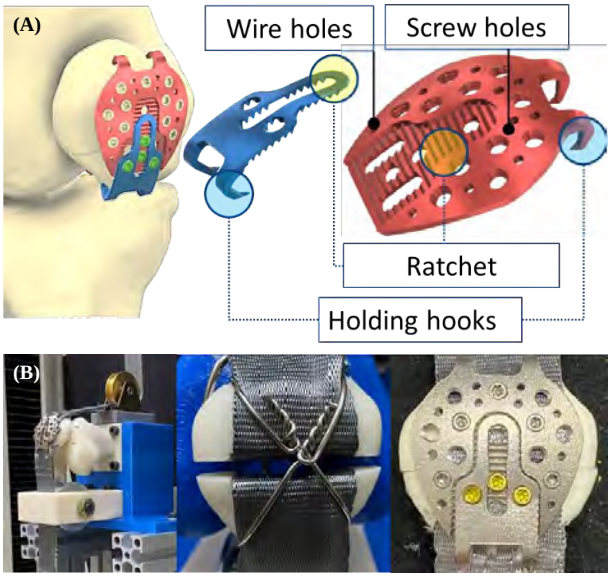

Figure 1 (A)CAD model of AATBP; (B)Testing platform and specimens (middle: tension band wiring and right: AATBP).

CONCLUSIONS

This in vitro biomechanical cyclic loading test implied that used of the titanium 3D printed AATBP can effectively maintain stability for transverse patella fracture.

REFERENCES

[1] Wild H. et al. *Clin Biomech* **25**: 341-7, 2010.
[2] Thelen S et al. *Injury* **43**: 1290-5, 2012.

PULLOUT EVALUATION OF A NOVEL PEDICLE SCREW WITH A PROXIMAL PEDICLE SLEEVE AUGMENTATION

Ting-Shuo Hsu[1,2], Hsuan-Wen Wang[1] and Chun-Li Lin[1]

[1] Biomechanical Engineering, National Yang Ming Chiao Tung University, Taipei City, Taiwan.
[2] Department of Orthopaedic Surgery, Shuang Ho Hospital, Taipei Medical University, New Taipei City, Taiwan
Email: B101093048@tmu.edu.tw

INTRODUCTION

Pedicle screw fixation is the mainstay technique for lumbar spine stabilization in various spine disorder. However, insufficient fixation strength wound cause screw loosening which caused failure of pedicle screw fixation. Previous study has shown the cortical bone of pedicle provides almost 60% of the pullout strength and provides more than 80% of the cranio-caudal stiffness [1]. The stabilizing effect over the vertebral body is relative not as important.

The geometry of the pedicle isthmus is an ovoid cross-section, we designed a novel pedicle screw with an elliptical pedicle sleeve to enhance the squeezing (compact pedicle) effect within the pedicle isthmus area. We hypothesized the pedicle screw fixation strength could be enhanced by the novel pedicle screw.

METHODS

Determining the pullout out strength of designed screws is essential. In this study, geometry of pedicle screws for the novel screw have been modified to improve their pull-out performance. The geometric feature of the novel screw was showed (Figure 1). The different pitches between the pedicle isthmus(proximal) and vertebral core(distal) provided a advancing and compression effect of pedicle sleeve during screw insertion. The novel screw with a size of 6.0 mm X 45 mm were used. In conventional screw group, the polyaxial screws (Baui Biotech, Co., Ltd., Taiwan) with a size of 6.0 mm × 45 mm were inserted.

Pullout strength test have been conducted in accordance with ASTM F543 Annex 3. A pilot hole with a diameter of 5.0mm was predrilled. The screw was inserted to 60% and 100% length in each group, respectively. A commercially available synthetic bone with a density of 0.32 g/cm3 (20PCF, Pacific Research Laboratory, Inc., Vashon Island, WA, USA) was used. Axial tensile force was applied at a rate of 5mm/min until the screw pullout out of block or fails. Load versus displacement curve with max load was recorded. These experiments were conducted in three trials for each group. The independent t-test was employed to analyze the data of the two groups.

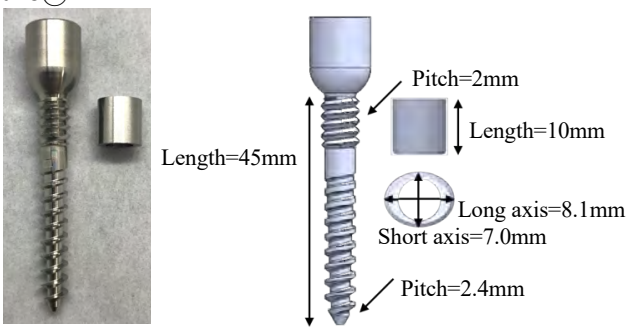

Figure 1 The novel pedicle screw with a proximal pedicle sleeve augmentation (left). The geometric feature of the novel screw (right).

RESULTS AND DISCUSSION

The results of pullout strength were showed (Table 1). In the condition of full-length insertion, the pullout strength of the novel pedicle screws was 1865.7 ± 97.6 N, whereas the pullout strength of the conventional screws was 1723.3 ± 13.9 N. The pullout force of the novel screw was significant increased.

Previous study also reported the similar findings. Tsuang et al [2] found that proximal 1/3 unthreaded screws provide higher pullout strength compared to full threaded screws. We suggested that the effect of squeezing (compact cancellous bone) within proximal pedicle isthmus portion increased the fixation strength. Further study is necessary to evaluate the biomechanical properties of the novel screw in the animal and human spine models.

CONCLUSIONS

A modified geometry of pedicle part of the pedicle screw influences the stability of pedicle screw fixation strength. This study concludes the novel pedicle screw augmented with a proximal pedicle sleeve leads to a significant increased pullout strength compared to a standard pedicle screw.

REFERENCES

[1] Hirano T et al. *Spine (Phila Pa)* **22**: 2504-2509, 1997.
[2] Fon-Yih Tsuang et al. *Clinical Biomechanics* **39**: 71-76, 2016.

Table 1: Results of pull-out strength with 60% and 100% insertion length of pedicle screws.

Insertion length	Conventional screw	Novel screw augmented with pedicle sleeve	*p-value*
60% length (N)	708.2 ± 9.1	767.8 ± 38.1	0.029
100% length (N)	1723.3 ± 13.9	1865.7 ± 97.6	0.034

Lateral trunk muscles thickness change during seated virtual reality-guided exercise

Masashi Kitano[1,2], Masami Nakamoto[1,3], Kengo Kawanishi[3,4], Takashi Kitagawa[1] and Shintarou Kudo [1,3,5]
[1] Graduate School of Health Sciences, MORINOMIYA University of Medical Sciences / Osaka, Japan.
[2]mediVR, Inc / Tokyo, Japan.
[3]Inclusive Medical Science Research Institute, MORINOMIYA University of Medical Sciences / Osaka, Japan.
[4]Department of Rehabilitation, Kano General Hospital / Osaka, Japan.
[5]AR-Ex Medical Research Center / Tokyo, Japan.
Email: 2021dms001@s.morinomiya-u.ac.jp

INTRODUCTION

The lateral abdominal muscles play a role in stabilizing the trunk during anticipatory postural control [1]. It has been suggested that mediVR Kagura (mediVR, Inc., Japan), which performs virtual reality-guided reaching exercises in a seated position, may improve trunk movement during walking [2]. We hypothesized that one of the factors by which Kagura improves gait function may be the activation of the lateral abdominal muscles by the reaching motion. Therefore, the purpose of this study was to clarify the changes in muscle thickness of the lateral abdominal muscles that occur during virtual reality-guided and normal reaching exercises.

METHODS

Twenty-two healthy adults (mean height,170.2 ± 4.6 cm; mean weight, 59.7 ± 5.9 kg; mean age, 21.2 ± 2.3 years) were randomly assigned to the Kagura group, which performed the reaching exercise in a seated position using Kagura, and the Control group, which performed reaching without VR, 11 subjects each. In both groups, six directions of reaching were used.
The target point of reaching in each direction was 90% of the maximum reaching position. The reaching exercise was performed for 20 minutes. The muscle thickness of the right lateral abdominal muscles (external oblique (EO), internal oblique (IO), and transversus abdominis (TrA)) were measured before and after each intervention using an ultrasound imaging system (US) in a resting sitting position and in six reaching position (reaching with the right upper limb; 1. ipsilateral forward, 2. ipsilateral diagonally forward, 3. ipsilateral lateral, reaching with the left upper limb; 4. contralateral forward, 5.contralateral diagonally forward, 6. contralateral lateral). The probe was placed 3 cm medial to the intersection of the perpendicular line from the right axilla and the height of the umbilicus, and EO, IO, and TrA were imaged. The change in muscle thickness was calculated by subtracting the thickness of the muscle when reaching from the thickness of the muscle in the resting sitting posture. Differences in the amount of change in muscle thickness in the above six postures between groups were tested using either an unpaired t-test or a Mann-Whitney u-test. The significance level was set at less than 5%.

RESULTS

No significant differences were found between groups before the intervention for all muscle thickness changes. After intervention, the muscle thickness changes of TrA was significantly greater in the Kagura group than in the Control group in ipsilateral 3-way reaching position (Figure 1).

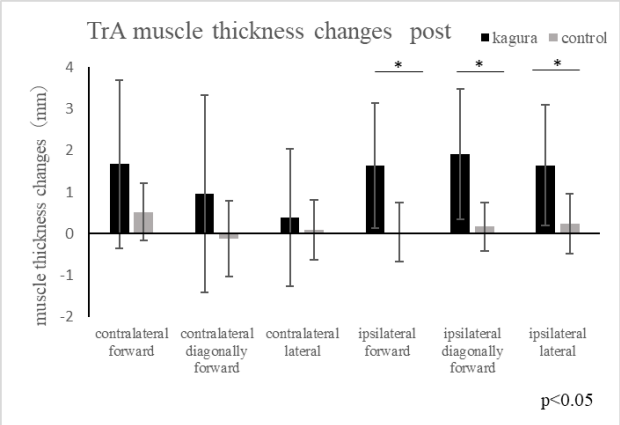

Figure 1 Change in the thickness of transversus abdominis muscle after intervention.

In this study, TrA, one of the lateral abdominal muscles, was activated in the VR reach exercise compared to the normal reach exercise.
In the normal reaching exercise, the positional information of the target point and his/her own body are perceived using visual and proprioceptive feedback [3]. On the other hand, the virtual reality-guided reaching exercises may have trained postural control based on prediction, since the subject could not visually perceive his/her own body on the VR.

CONCLUSIONS

The results suggest that Kagura may have an effect to activate TrA during the reaching motion.

REFERENCES

[1] Hodges PW et al. *Neurosci Lett.* **16**: 265(2):91-4.1999.
[2] Nakamoto M et al. *Int J Environ Res Public Health.* **16**;18(24):13267.2021.
[3] Sarlegna FR et al. *Adv Exp Med Biol*. **629**:317-35. 2009.

OPTIMISATION OF THE ELECTRODE CONFIGURATION OF A SEMG SENSOR SYSTEM TO BE USED IN REHABILITATION SETTINGS

Elmar Junker[1], Elisa Romero Avila[1], Catherine Disselhorst-Klug[1]
[1] Department of Rehabilitation and Prevention Engineering, RWTH-Aachen, Aachen, Germany.
Email: junker@ame.rwth-aachen.de

INTRODUCTION

The use of wearable devices to monitor a person's movement performance has increased in recent years in the field of rehabilitation. These devices provide healthcare professionals with information regarding the status of the patient and considerations for their therapy [1]. If the recording of the muscular activation through surface electromyography (sEMG) were considered in these devices, a more reliable monitoring and a greater understanding about the patient's condition would be obtained. To this end, a 16-channel sEMG sensor system has been developed with a design that allows an autonomous use by the user [2]. However, to ensure an adequate and reliable recording of sEMG signal quality, the material, type, and configuration of the electrodes should be considered according to the purpose of the sEMG sensor system and the guidelines for sEMG recording [3]. The aim of this work is to stablish an appropriate dry electrode arrangement by analyzing the effect of inter-electrode distance (IED) and electrode diameter on the sEMG signal energy and quality and to incorporated the findings into the sEMG sensor system which is to be used during dynamic tasks.

METHODS

Optimization of electrode-size and IED

For this, two linear electrode arrays with a 10 mm IED were considered. Each array consisted of six, dome-shaped gold-plated electrodes with a diameter of either 5 mm or 8 mm. The electrode arrays were assessed during isometric contraction of the biceps brachii. Influence of electrode size and IED on signal energy, signal-to-noise-ratio and reproducibility were analysed.
When using dry electrodes in a bipolar configuration IEDs between 10 and 20 mm are the best compromise between high signal energy, a high reproducibility and with a small risk of crosstalk. Regarding the electrode size, no effect between both sizes was observed during long-term measurements. However, it was found that the 8 mm diameter electrode required more time to stabilize and provide less consistent measurements compared to the 5 mm-diameter electrode.

Integration into the sEMG sensor system

Based on the previous results, 5 mm dome-shaped gold-plated electrodes were incorporated in the sEMG sensor system. Seven electrodes were used to form an electrode array with an IED of 15 mm (Figure 1). Three electrodes formed a bipolar configuration to minimise the potential for incorrect localisation of the electrodes in the longitudinal direction of the muscle. Four electrodes arranged in a rectangular way were configured as reference electrode. To minimize transversal misalignment eight of these electrode arrays were arranged in the shape of an armband to form 16 sEMG channels (Figure 1). Additionally, in this way, the orientation of the bipolar leads was parallel to the muscle fibres. To evaluate the system during dynamic tasks with respect to the risk of crosstalk and movement artefacts, muscular activation of the biceps was recorded while performing flexion and extension of the elbow. Signal-to-noise ratio (SNR) and root mean square (RMS) values were computed.

RESULTS AND DISCUSSION

No motion artefacts were observed during the dynamic tasks. Furthermore, despite the fact that dry electrodes were considered, the sEMG signal was obtained with low noise as a result of the shape and size of the electrodes that allowed a constant contact with the skin surface. The selection of a bipolar configuration and IED of 20 mm ensured that a low SNR (28 dB) was obtained. The design of the sEMG sensor system allowed a parallel orientation of the electrode array to the muscle fibre. Moreover, it also prevented misplacement, regardless of the user's experience in locating the muscle. Ultimately, the sEMG sensor system enabled non-invasive recording of muscular activation with little assistance required or discomfort.

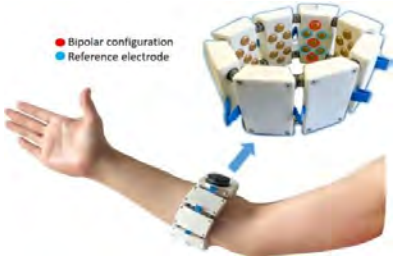

Figure 1 Design of the electrode array for an sEMG-sensor system

CONCLUSIONS

The proposed electrode array integrated in a user-friendly sEMG sensor system allowed the achievement of adequate and reliable sEMG signal quality with a low risk of crosstalk and movement artefacts even during dynamic tasks. Moreover, the design of the sEMG sensor system allows for positioning on the lower limbs, making it a device that can be easily and reliably used in a rehabilitation setting due to its design and features.

ACKNOWLEDGEMENTS

Elisa Romero Avila would like to thank CONACYT-DAAD (57649580) for the grant awarded.

REFERENCES

[1] Patel et al. *J Neuroeng. Rehabil* **9**: 21, 2012.
[2] Romero Avila et al. *Sensors* **20**: 7348, 2020.
[3] Besomi et al. *J Electromyogr Kinesiol* **48**: 128-144, 2019.

DEVELOPING AND VERIFICATION OF THE INNOVATIVE BLOOD FLOW RESTRICTION TRAINING DEVICE

Lu-Hwa Lu[1], Yu-Lin You[2], Chia-Chi Yang[3], Bing-Shiang Yang[4] and Lan-Yuen Guo[1,3*]
[1]Department of Sports Medicine, Kaohsiung Medical University, Kaohsiung, Taiwan.
[2]Department of Sports Medicine, China Medical University, Taichung, Taiwan.
[3]The Master Program of Long-Term Care in Aging, Kaohsiung Medical University, Kaohsiung, Taiwan.
[4]Department of Mechanical Engineering, National Yang Ming Chiao Tung University, Hsinchu, Taiwan
Email: yuen@kmu.edu.tw

INTRODUCTION

The progression of blood flow restriction (BFR) training include the design of tourniquet cuffs with lower pressure gradients and the use of limb occlusion pressure (LOP). It is recommended that when using BFR equipment for training, the personal tourniquet pressure can be set according to the personalized LOP, which can reduce the risk of nerve damage and avoid the use of BFR potential complications[1].

Although there are currently commercially available instruments that can automatically measure personalized LOP based on measured LOP and set the degree of blood flow restriction during training, the cost of using the commercial instrument is expensive. On the other hand, the palm style aneroid sphygmomanometer is cheaper, it cannot determine the LOP so it is difficult to make personalized design blood flow restriction training program.

The purpose of our study will aim to overcome these problems by developing the innovative BFR training device. We use innovative BFR training device with a palm style aneroid sphygmomanometer and a commercially available BFR system, using Laser Doppler Flowmetry (LDF) as the gold standard. And we use palm style aneroid sphygmomanometer and a commercially available BFR system, PTS for BFR to conduct the reliability test and establish Intraclass correlation (ICC)[10].

METHODS

A total of 43 subjects participated in this study, 26 males and 17 females.The LDF probe was placed on the subject's index fingertip. Our study used two kinds of blood flow restriction, palm style aneroid sphygmomanometer (manual pressurization) and PTS for BFR (electrical pressurization). Two blood flow restriction systems were placed on the subject's left upper arm, and the order in which the systems are used is randomized.

Palm style aneroid sphygmomanometer (innovative BFR training device)

Skin blood perfusion was measured, we manually increased cuff pressure in 20-mmHg stepwise increments until the skin blood perfusion was no longer measured by LDF.

PTS for BFR (commercially available BFR system)

Easi-Fit BFR tourniquet cuffs (Delfi Medical, Vancouver, VC, Canada) and the instrument containing LOP calculation sensors and software werer used. The tourniquet cuff increases cuff pressure in 10-mmHg stepwise increments.

RESULTS AND DISCUSSION

Reliability test outcome

The ICC of PTS for BFR is 0.770 representing high correlation. And the ICC of palm style aneroid sphygmomanometer is 0.882 presenting high correlation.

Statical difference of LOP obtained by three different measurement methods

LOP obtained from three different measurement methods was showned in Table 1.

CONCLUSIONS

Both innovative BFR training device and commercially available BFR system were reliable, our innovative BFR training device seems to be more reliable. Using LDF as the gold standard, our innovative BFR training device is as accuraccy as commercially available BFR system.

ACKNOWLEDGEMENTS

This work was supported by the National Yang Ming Chiao Tung University and Kaohsiung Medical University Joint Project [NYCUKMU-111-I006] and Ministry of Science and Technology in Taiwan [MOST 111-2622-E-037-002 and MOST111-2410-H-037-025-MY2].

REFERENCES

[1] Masri BA et al. J Med Biol Eng **36**: 644-650, 2016

Table 1: LOP obtained from three different measurement methods

Conditios	LOP_electronic (commercially BFR)	LOP_electronic based on LDF	LOP_manual (innovative BFR)	P-value
Mean±SD (mmHg)	121.91±9.99	114.07±11.95	112.02±11.13	0.001

The Validity of Inverse Dynamics Calculations for Lower Limbs During Gait Using a Markerless Motion System

Huang Tianchen[1], Linda Fan[2], and Mianfang Ruan[2]
[1] Department of Life Sciences, University of Tokyo, Tokyo, Japan
[2]Peak Sports Science Lab, Quzhou Peak Footwear Co., LTD, Xiamen, Fujian, China

Email: ruanmf@yahoo.com

INTRODUCTION

Marker-based motion capture is the "gold standard" method for acquiring the accurate 3D human motion. Recently, a markerless motion capture system was developed as an alternative method to overcome the shortcomings of the marker-based system, such as high price, time-consuming, et al. Markerless motion capture system estimated body joint centers and other anatomical landmark positions by a deep learning algorithm based on a training dataset[1], which overcomes the drawbacks of traditional systems and improved the efficiency of data collection. The previous study[2] tested the validation of kinematic measurements captured by markerless systems. As far as we know, no studies have tested the validation of inverse dynamics calculations using a markerless system. Devita[3] found that the kinematics of gait were not different in patients recovering from anterior cruciate ligament (ACL) injury and reconstruction surgery compared with healthy people, but joint moments are different. Certainly, it is crucial to acquire joint moments data from inverse dynamics calculations for gait analysis. This study aims to test the validation of inverse dynamics calculations for lower limbs during gait using a markerless motion capture system.

METHODS

16 healthy volunteers (28.2 ± 8.2 years age, 174.0 ± 6.2cm height, 69.3 ± 13.2kg weight) participated in this study. Participants wore tight-fitting, minimal clothes and the same type of running shoes. A 13-camera marker-based system (1200-megapixel, Nokov, China) and an 8-cameras markerless camera system (800-megapixel, Tsing-I, China) were positioned around a runway. Both systems recorded at 120 Hz. A force platform (Kistler, Switzerland) was embedded under the middle of the runway, which recorded the data at 1200Hz. 39 retroreflective markers were placed on each subject. The force platform and two motion capture systems collected data simultaneously.

RESULTS AND DISCUSSION

Compared with the marker-based system, the coefficient of multiple correlations (CMC) for the lower limb in the sagittal was $\geqslant 0.82$, and in the transverse planes was $\geqslant 0.75$ (Figure 1). We observed large inter-individual differences in joint moments between the two systems. Cation should be given when subjects' anthropometry data have a large deviation from that of the dataset. Increasing the size of the dataset or adding a manual correction procedure can help improve the accuracy of the joint center positions and further improve the validity of the joint moments calculation using the markerless motion capture system.

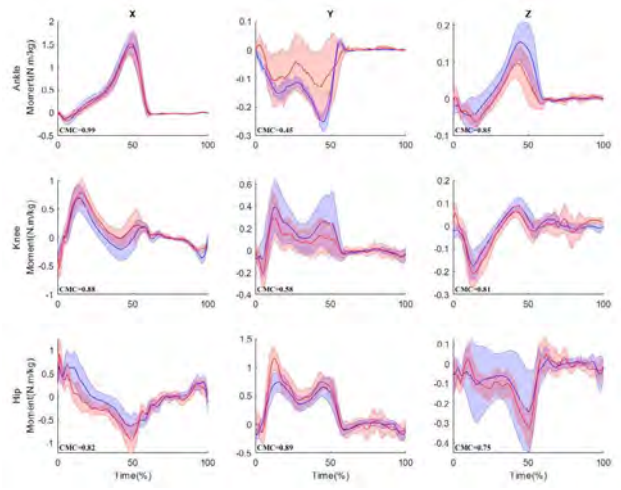

Figure 1: Lower limbs joint moment (Mean±SD) and CMC (blue: marker-based, red: markerless)

CONCLUSIONS

The markerless motion capture system can be used for lower limbs inverse dynamics calculations in the sagittal and transverse planes during gait.

ACKNOWLEDGEMENTS

This study was supported by TsingDe Intelligence Technology Co., Ltd China.

REFERENCES

[1] DRAZAN J F et al. *J Biomech* **125**: 110547, 2021.
[2] KANKO R M et al. *J Biomech* **127**: 110665, 2021.
[3] DEVITA P et al. *MED SCI SPORT EXER* **30**: 1481-1488, 1998.

Reliability of OpenCap with smartphone videos to measure hip and knee angle during two-step test

Ono I[1], Iwamoto Y[1,2], Ishii Y[1,2], Toyoda Y[1], Mizutani M[1] and Takahashi M[1,2]
[1] Department of biomechanics, Graduate School of Biomedical and Health Sciences, Hiroshima University, Hiroshima, Japan
[2] Center for Advanced Practice and Research of Rehabilitation, Graduate School of Biomedical and Health Sciences, Hiroshima University, Hiroshima, Japan
Email: m226719@hiroshima-u.ac.jp

INTRODUCTION

The Two-Step test is an index of gait ability in locomotive syndrome, evaluated by the distance travelled during the two steps [1]. The current two-step test only focuses on distance traveled, but obtaining kinematic data in the two-step test will allow us to understand the cause of gait ability decline. Three-dimension (3D) opto-electronic motion capture is considered the gold standard of kinematic analysis [2] , are seldom used in clinical settings. Then, smartphone based 3D movement analysis system, the OpenCap (Stanford University, CA, USA) , is proposed to be easily used in clinical settings to assess kinematics. The aim of this study is to confirm the reliability of kinematic measurements during the two-step test using OpenCap.

METHODS

We included 8 young, injury-free participants (age 21.5 ± 0.5 years; height 165.0 ± 0.1 cm; weight 54.5 ± 7.9 kg; male 3). Participants performed three trials of each two-step test from the right foot. OpenCap data were acquired at 60 Hz using two iPhones (Apple, CA, USA). The two iPhones were placed on a tripod 0.9 m positioned at a 40° angle to the participants. Three-dimensional motion analysis system data were acquired at 100 Hz using a ten-camera Vicon MX (Vicon Motion Systems, Oxford, UK). The reflective markers were attached to 35 landmarks according to the plug in gait model. The sagittal plane joint angles of the hip and knee joints were calculated from the acquired kinematic data, from which two peak values were extracted for each joint (Figure 1). To determine the OpenCap validity, the mean difference and 95% limits of agreement (LoA) between the OpenCap and Vicon were calculated for each angle peak using the Bland-Altman method. The 95% LoA were defined as the average difference ± 1.96 times the standard deviation of the difference. The correlation coefficient was obtained from the Bland-Altman plot, and the significance level was set at 5%. All data analysis was performed using Matlab (Mathworks, Inc. Natick, MA, USA).

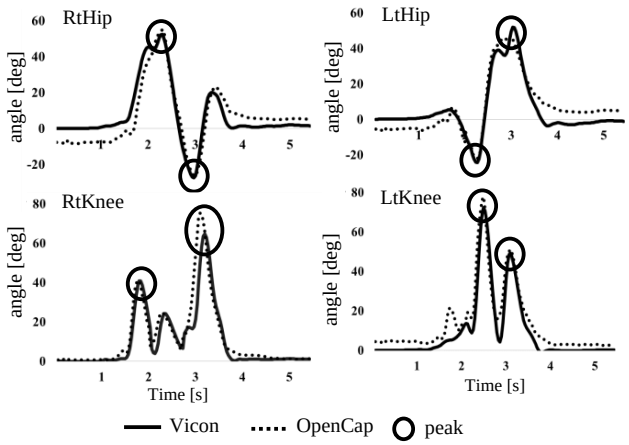

Figure 1: Joint angles of hip and knee in the sagittal plane

RESULTS AND DISCUSSION

The 95% LoA results indicated that OpenCap tended to underestimate hip and knee angles (Table 1). There were no significant errors in the RtHip 2nd peak and LtHip 1st peak, but these peak values were for movements with small angular changes. Furthermore, the correlation coefficient values suggest that OpenCap can measure movements with small angular changes with high accuracy, but the accuracy may decrease as the angular change increases.

CONCLUSIONS

OpenCap can be a reliable evaluation tool in the two-step test, but it is imperative to understand its characteristics of measurement accuracy of joint motions.

REFERENCES

[1] Ishibashi H et al. *Osteoporos Sarcopenia* **4**: 86-94, 2018
[2] Barker S et al. *Med Eng Phys* **28**: 460-467, 2006

Table 1: Results of statistical analysis on peak joint angle values. *Indicate model p<0.05

joint	RtHip		LtHip		RtKnee		LtKnee	
peak	1st		2nd		1st		2nd	
difference	6.54	1.35	1.87	6.34	5.95	-7.31	-3.48	2.75
95% LoA	(3.81 9.29)	(-0.83 3.54)	(-0.07 3.81)	(2.56 10.12)	(3.58 8.32)	(-10.42 -4.20)	(-5.68 -1.28)	(0.95 4.55)
r	0.57*	0.87*	0.59*	0.85*	0.13	0.44*	0.11	0.55*

ACCURACY EVALUATION OF LOWER LIMB JOINT ANGLES WITH MARKERLESS MOTION CAPTURE DURING SPIN TURN

Takuya Kikuchi[1], Katumasa Tanaka[2], Shigehiro Hashimoto[2] and Yoshimori Kiriyama[3]
[1] Graduate School of Mechanical Engineering, Kogakuin University, Tokyo, Japan
[2] Department of Mechanical Engineering, Kogakuin University, Tokyo, Japan.
[3] Department of Mechanical Systems Engineering, Kogakuin University, Tokyo, Japan.
Email: ad21002@ns.kogakuin.ac.jp

INTRODUCTION

Motion measurement is a fundamental biomechanical technique to understand the principle of the human movements. Especially, it is quite important to measure sports movements for improvement of performance and avoidance of sports injury. A markerless motion capture (MMC) technique is one of most useful method. Recently, an image recognition with a deep neural network or distance measurement with LiDAR have been used widely to capture human motion. On the other hand, MMC through visual hull (MMC-VH) [1] needs optical images only, and allows us to measure sports motion in many situations. However, the accuracy of the method depends strongly on camera resolution, and then it is difficult to measure minor or complicated joint motion, such as the knee axial rotation or adduction/abduction, with high accuracy. In this study, we have improved the accuracy, and compared with marker-based system.

METHODS

In this study, spin turn maneuver was measured for a healthy subject (1.74 m, 68 kg, 26 y/o). Motion images were captured using calibrated nine VGA (640 × 480 pixels) cameras at 120Hz. In MMC-VH, the accuracy of a visual hull expressing the three-dimensional subject volume decides the error of measurement. To improve the accuracy, in this study, silhouette images are extracted by k-nearest neighbor background subtraction. To make the contour clearly, accurate subpixel edge location was calculated at subpixel points [2]. Here, the contour line was expressed with point cloud data, and some point cloud data from all images were combined. The three-dimensional point cloud was used to construct the visual hull with ball-pivoting algorithm. The subject surface shape was obtained with a body scanner, and the body segments were matched to the visual hull. The relative postures between the matched segments were calculated as the joint angles. In this study, the joint angles were based on the ISB definition.
To validate and confirm the accuracy, in this study, optical marker-based motion capture (OMC) system was used simultaneously.

RESULTS AND DISCUSSION

Figure 1 shows the three-dimensional knee angles. In the Flexion, the double knee action is confirmed, and this study and OMC show a good agreement. The knee flexion is larger than the other knee motions, and then the shape around the knee joint should deform largely

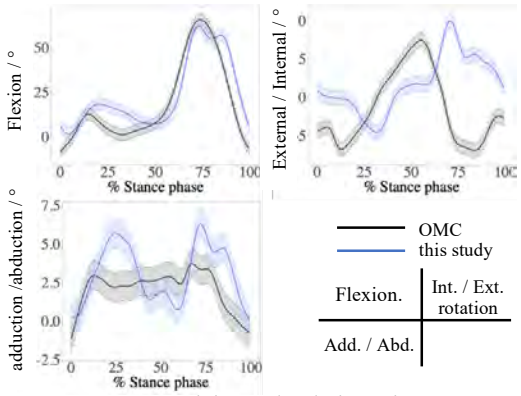

Figure 1 Knee joint angles during spin turn.

and the visual hull could agree with the actual deformation. In the adduction /abduction, this study and OMC have a moderate agreement less than 5°, but they are apart a little at 25 and 75% stance phase. At the time, the shank of swing phase approached to the other shank of the stance phase, and then the visual hull showed the shanks crossed. In the Internal/External rotation, this study and OMC were apart from each other after 75% stance phase. The I/E rotation is quite small compared with flexion. Also, the axial rotation does not make the distal end of the shank move largely or deform the surface of the knee joint. Thus, this study and OMC could not have a good agreement. Generally, the knee joint angles other than flexion are not large. Therefore, a special technique such as a point cluster method is required to measure small joint angles with high accuracy [3]. Even though our method did not completely correspond to OMC, the difference was quite small. Therefore, our method could be useful to improve the accuracy of MMC-VH.

CONCLUSIONS

We proposed a new method to improve MMC-VH, and measured spin turn maneuver with MMC-VH. For the three-dimensional knee movements, our method almost showed a good agreement with OMC.

ACKNOWLEDGEMENTS

A part of this study was supported financially by JKA through its promotion funds from KEIRIN RACE, and The Uehara Memorial Foundation.

REFERENCES

[1] Corazza S et al. *Int J Comput Vis* **87**: 156-169, 2010.
[2] Trujillo-Pino et al. *Image and Vision Computing* **31**: 72-90, 2013.
[3] Andriacchi et al. *J Biomed Eng* **120**: 743-749, 1998.

Investigating the relationship between local and global gait stability

Ann-Kathrin Harsch[1], Daniel Koska[1] and Christian Maiwald[1]
[1] University of Technology Chemnitz, Institute of Human Movement Science and Health, Chemnitz, Germany
Email: ann-kathrin.harsch@hsw.tu-chemnitz.de

INTRODUCTION

Gait stability is differentiated between local dynamic and global stability. Local dynamic gait stability can be determined using the short-term maximal Lyapunov Exponent λ_s from the field of nonlinear dynamic methods and describes the sensitivity to small intrinsic perturbations. An increasing λ_s indicates greater instability [1]. The Margin of Stability (MOS) as a dynamic global stability parameter describes the response to external perturbations in gait. A negative MOS is associated with instability [2]. Both measures can distinguish different interventions (e.g., perturbations), but there is a lack of research evaluating whether there is a relationship between local and global stability [1].

METHODS

This study analyzed the data from Kopiske et al. [3]. 19 young adults participated in 5-minute walks on a split-belt treadmill. The first trial involved normal (unperturbed) walking at 1 m/s, while the second trial included a randomly occurring acceleration at one side of the split-belt treadmill to provoke slip-like events. Motion capture data was used to determine the respective foot position at ground contact, as well as the center of mass (COM) taken from the hip markers. $\lambda_{s,com}$ was calculated from the COM position in anterior-posterior direction, in which the perturbation occurs. $\lambda_{s,com}$ was taken from the middle 150 strides of the trial. The embedding dimension was set to 3, with a participant-specific time delay. $\lambda_{s,com}$ was then calculated as mean logarithmic short-term divergence from start to the first half stride. To quantify global stability, the continuous MOS was calculated by determining the shortest distance between the extrapolated position of the center of mass and the anterior Base of Support, calculated from current ground contact marker [4]. For perturbed gait, the differences between minimum and maximum MOS excursion within five strides after each slip event were averaged across all slips of one trial (MOS_{range}). MOS_{range} indicates more instability when increased.

RESULTS AND DISCUSSION

Both, MOS_{range} and $\lambda_{s,com}$ indicated more instability during perturbed gait vs. unperturbed gait. However, a consistent increase in MOS_{range} for perturbed gait is shown in Figure 1A, while $\lambda_{s,com}$ showed more interindividual variation (Figure 1B). Figure 1C suggests a negative correlation between the $\lambda_{s,com}$ from unperturbed gait and the MOS_{range} in response to perturbations. Hence, a more locally stable gait was associated with less global stability.

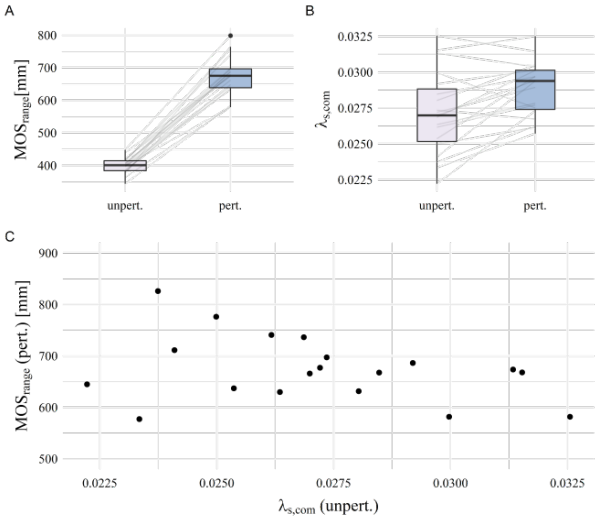

Figure 1. Effect of gait perturbations on **A:** global stability and **B:** local dynamic stability. **C:** Correlation of MOS_{range} and $\lambda_{s,com}$

These findings are contrary to the common assumption that less stable normal gait (higher $\lambda_{s,com}$) leads to a more pronounced response to external perturbations. However, this study design does not allow any causal inference. Furthermore, results need to be replicated, since they also may be attributed to the complex and abstract methodology of the parameters used. In particular, calculating $\lambda_{s,com}$ is intricate, with no established procedure, input signal or clear-cut outcome.

CONCLUSIONS

Our results indicate that individuals with less stable gait ($\lambda_{s,com}$) have a smaller response to external perturbations. Further research is needed to fully understand the underlying causes of these observations.

REFERENCES

[1] van Emmerik et al. *J Sport Health Sci* **5**: 3-13, 2016.
[2] Watson et al. *BMC Muskoloskelet Disord* 22:1-29, 2021.
[3] Kopiske et al. *J Vis* **21**: 1-20, 2021
[4] Hof et al. *J Biomech* **38**: 1-8, 2004

UNCOVERING CLUSTER STRUCTURES WITHIN EMG SIGNATURES OF GESTURES

Jonas Große Sundrup[1], Katja Mombaur[1]
[1]Canada Excellence Research Chair Human-Centred Robotics and Machine Intelligence, Systems Design Engineering and Mechanical & Mechatronics Engineering, University of Waterloo, Waterloo, Canada
Email: jonas.grosse-sundrup@uwaterloo.ca, katja.mombaur@uwaterloo.ca

INTRODUCTION

Gesture recognition systems have gained traction and popularity for quite some time. However, often times the focus on pure performance leads to choosing methods with limited understandability. We investigate a gesture recognition approach based on muscle signatures that provides both competitive performance as well as intuitive functional understanding, allowing for applications both in application as well as in reseach and an informed extension to new applications and research questions. This both highly accurate gesture recognition as well as foundational insight into cluster structures.

METHODS

We used the Myo Armband, an 8-channel sEMG recording device surrounding the forearm, to obtain muscle signatures for 7 different gestures. 700 recordings over 7 gestures (snap, fist, conunt, open, wave, wave out, point) were obtained after instructing 2 participants in how to do them. The actual recordings, however, were unsupervised, using instructional software, close to a real-world application. We employ Dynamic Time Warping (DTW) [2] to account for the naturally emerging time variability in humen motion when assessing the similarity of different recorded muscle signatures of these gestures. Based on the distance measure this establishes, we also assess the relative distribution of signature clusters their separability relative to each other.

Based on this we implement a simple k-Nearest-Neighbours with DTW, similar to [1], and extend on this by establishing bounds on the need of reference data, rejection approaches to make this classifier suitable for arbitrary, non-gesture data, and explore condensing techniques based on barycenter averaging [3] to improve both performance and stability.

RESULTS

When employing this procedure, we find classification accuracies at 97% - 99%, depending on subject. To understand how this emerges, we compute the distribution of DTW-distances within a cluster, i.e. every element of that cluster to every other element in the same cluster, and the distribution of each element of one cluster to each element of another cluster, depicted in Figure 1), with bold depicting the pointwise distances within a cluster. We find a clear separation pattern between most of the gestures with exceptions only for “point” and “wave out”, which explains the strong accuracy results.

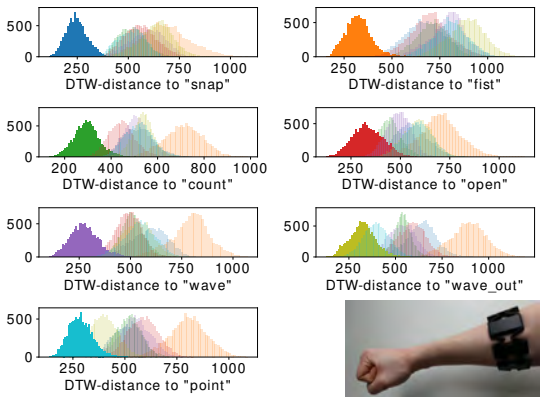

Figure 1: Pointwise cluster distance distributions for one subject.

It further shows the clustering structure of the underlying data, which in turn explains why the condensation techniques in play perform equally strong at lower computational cost as the exploit this clustering structure. The same structural findings can be exploited for an informed selection of gestures that favor cluster separability and as a consequence high classification accuracy. Based on this, we can show that three reference recordings over four days is enough for peak accuracy and we can also establish that d being the 50th percentile of the within-cluster distance distribution yields strong accuracy again above 97% - 99% while rejecting less than 10% of classifyable samples.

CONCLUSIONS

We have established a procedure to understand cluster distributions of EMG signals, allowing intuitive understanding of classification approaches, for which we established an bound on necessary data as an approach for live datastream classification. This insight allows to build onto this in a simple fashion to answer both emerging questions of research as well as practical challenges.

ACKNOWLEDGEMENTS

We acknowledge financial support by the German Federal Ministry of Education and Research (grant number 16SV7772) and the Canada Excellence Research Chairs Program.

REFERENCES

[1] Benalcázar, M. et al., *IEEE ETCM*, 2017
[2] Müller, M., *Information Retrieval for Music and Motion - Dynamic Time Warping*, 2007
[3] Petitjean, F. et al., *Pattern Recognition*, 2017

Prediction of the hip joint center position using statistical geometric transformation: validation in canine models

Cheng-Chung Lin[1], Hung-Ju Sun[2], and Ching-Ho Wu[2]
[1] Department of Electrical Engineering, Fu Jen Catholic University, New Taipei City, Taiwan.
[2] Institute of Veterinary Clinical Science, National Taiwan University, Taipei, Taiwan.
Email: lin.chengung@gmail.com

INTRODUCTION

The hip joint center (HJC) position, often utilized for determining the femoral anatomical reference frame, is crucial for musculoskeletal modeling and kinematics and kinetics analysis. In scenarios where medical images are not available, predictive methods using linear regressions were commonly used, but none of them was universally acknowledged to outperform others. The functional methods were shown to surpass predictive methods in prediction accuracy and reliability [1] at the expense of additionally specific motion tasks for subjects. The study aimed to propose a new predictive method for HJC position via statistical geometric transformation. The new approach was trained/evaluated with a leave-one-out cross-validation scheme; and compared to those obtained from linear and nonlinear regressions.

METHODS

Twenty-six mature Taiwan dogs without detectable musculoskeletal abnormalities were recruited. Computed tomography (CT) scans were taken for each dog, from which the CT-derived pelvic and femoral models were reconstructed. Bilateral iliac crests and ischial tuberosities on the pelvic models and the greater trochanter, lateral femoral condyle, and HJC (taken as the femoral head centroid) on the femoral models were manually digitized. A deformable template of the above-mentioned bony landmarks was constructed in reference to the building process of the statistical shape model [2]. As a result, a new bony landmark configuration can be generated by superposing controllable deformations onto the averaged landmark configuration, and meanwhile, the template allows free rotation of the femoral landmarks about the HJC. The geometric transformation of the template was carried out by best-fitting the generated landmark configuration to landmarks (except for HJC) extracted from the target subject's bone models. The final landmark configuration gave the predicted HJC position. On the other hand, linear regression models and the nonlinear random forest regression were also built for HJC prediction, in which the inter-landmark distances were computed and taken as the model predictors. A leave-one-out cross-validation scheme was employed to train/evaluate the model performances.

RESULTS AND DISCUSSION

For the linear regression models, the most representative predictors in the prediction of HJC position in cranial/caudal (Cr/Cd), dorsal/ventral (D/V), and lateral/medial (L/M) directions were pelvic length (PL), iliac crests width (ICW), and both ICW and ischial tuberosities width (ITW), respectively. Both the linear and nonlinear regressions as well as the statistical geometric transformation procedure could yield predictions of HJC positions within the area of the acetabulum (Fig. 1). Among the three approaches, the statistical geometric transformation gave the most reliable HJC prediction as the correlation coefficients between the predicted and ground truth HJC positions were 0.96, 0.78 and 0.77 in C/C, D/V and L/M directions, respectively. The corresponding values for regressions were lower than 0.94, 0.29, and 0.67. The geometric transformation method also yielded predictions of HJC position with the lowest absolute errors in C/C and D/V directions. The means (standard deviations) of the absolute errors were 1.18 (1.19) mm and 1.96 (1.67) mm, respectively. The corresponding mean values for regressions were greater than 1.66 mm and 2.40 mm.

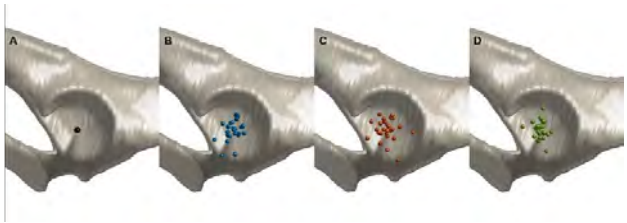

Figure 1 Schematic representation of (A) a ground truth HJC position and the predicted HJC position using (B) linear regression (C) random forest regression and (D) geometric transformation methods.

CONCLUSIONS

The present study developed a new geometric transformation method in conjunction with the deformable template of the bony landmarks for determining the HJC position. Instead of relying on limited geometric features of the bone as utilized in regression models, the new approach takes associated modes of deformation of bony landmark configuration on the pelvis and femur into account, which was demonstrated to yield a more accurate prediction of HJC position.

REFERENCES

[1] H. Kainz, et al., Clinical Biomechanics, vol. 30, no. 4, pp. 319-329.
[2] H.-Y. Lu et al., Frontiers in bioengineering and biotechnology, vol. 9, p. 736420

AUTOMATED GAP-FILLING ALGORITHM FOR KINETIC DATA OF FINGER MOVEMENT: PIANIST HAND MOTION CLEANING USING SPATIO-TEMPORAL IMPUTATION

Taegyun Kwon[1], Dawon Park[2], Joonhyung Bae[1], Jonghwa Park[3], Jaebum Park[2,4] and Juhan Nam[1]
[1]Graduate School of Culture Technology, KAIST, Daejeon, Republic of Korea.
{[2]Department of Physical Education, [3]College of Music, [4]Institute of Sport Science}, Seoul National University, Seoul, South Korea
Email: juhan.nam@kaist.ac.kr

INTRODUCTION

Notably, kinematic data are essential to examine various aspects of the piano performance as "art," including the levels of individualized techniques by a professional pianist, etc. For relatively accurate data acquisition, the approach of marker-based capture is employed. However, missing data points during capturing and incorrect embedment of pre-defined body models during data processing seems to be inevitable drawbacks due to the nature of finger movements of piano performance. Therefore, we propose a specialized framework for cleaning hand motion data without an explicit hand model by applying general imputation and interpolation techniques.

METHODS

We captured 86 trials (about *20sec* each) of performances of a pianist. We attached 54 (4mm diameter) reflective markers to both hands and fingers (Figure 1). We used eight infrared cameras to record kinematic data at 120Hz. We separated 9 trials and randomly erased 10% of the data for the test. In addition, the velocity of each key depression is recorded with the recordable piano (Yamaha Disklavier C7). The average missing ratio was 19.6% for the fingertips and 14.6% for all data points. The imputation procedure consisted of four steps: 1) Points on the back of the hand are imputed with iterative linear imputation (MICE) [1], and we transform the all points according to the back of the local hand coordinate (Figure 1). 2) Outlier detection was performed. Points with longer or smaller than 20% of segment length or points with large covariance in Elliptic Envelope [2] were removed. 3) Spatial interpolation: For fingers, we iteratively applied radial basis function interpolation. We interpolated a point per step, and the orders were determined by considering the degree of freedom of the finger movement. 4) Temporal interpolation: Temporal cubic split interpolation were used to smooth the unwanted fluctuation.

We evaluated the reconstruction error of the missing points in mean square error (MSE) and the Pearson correlation between the vertical velocity of fingers and the recorded note velocity. The maximum velocity for 0.3*sec* before the key depression was used.

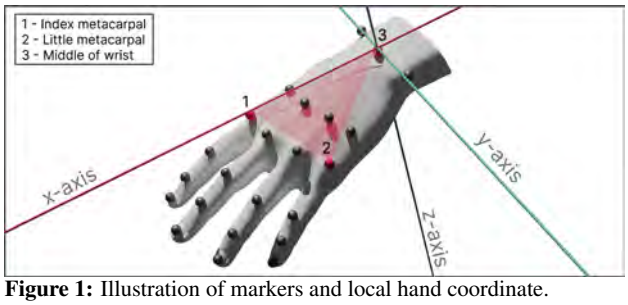

Figure 1: Illustration of markers and local hand coordinate.

RESULTS AND CONCLUSIONS

Our framework not only imputes all missing points, but also reduces reconstruction errors significantly as shown in Table 1. Although the velocity correlation in our framework is somewhat lower than that in the raw data, the imputed data preserve the natural movement of the keystrokes welgiven that it contains significantly more imputed keystrokes (260 additional imputed keystrokes). Our framework is generally applicable because it operates without a prior model and requires only a very small data set.

ACKNOWLEDGEMENTS

This work was supported by Seoul National University Research Grant in 2021

REFERENCES

[1] Rousseeuw, et al. *Technometrics* **41.3**: 1999.
[2] Fasshauer, Gregory E. *World Scientific* **Vol. 6**: 2007.

Table 1: Evaluation Results. The unit of MSE is *cm*

	Reconstruction Errors				Key Depression Velocity Corr.		
	Average MSE	Backhand MSE	Finger MSE	FingerTip MSE	Correlation	p-value	#N note
RAW	-	-	-	-	.622	1.43e-7	1224
MICE (Baseline)	1.904	1.160	2.595	2.531	.270	.0296	1484
Spatial Interpolation	2.007	1.160	2.793	2.157	.156	.214	1484
+Temporal Interpolation	0.698	0.437	0.941	0.761	.553	1.76e-6	1484

Steadiness of isometric plantarflexion is reduced when changing posture from supine to prone position

Moeka Samoto[1], Momoka Nakamura[1], Yasuhide Yoshitake[1]
[1] Graduate School of Science and Technology, Shinshu University, Ueda, Japan.
Email: 12mok27@gmail.com

INTRODUCTION

When skeletal muscle is exposed to an artificial external loading, the force-generating capacity of muscle is mostly reduced due to the deformation of muscle [1]. As gravitational force, to which humans are regularly and unconsciously exposed, can also deform the soft tissues in humans [2], it is possible that muscle is deformed and consequently the force-generating capacity of muscle is affected by gravity. If this is true, muscle (motor unit) activity during contractions at a given force level would be altered by gravity, because motor unit (MU) activity is determined by its force-generating capacity.

The ability to perform a steady isometric contraction, so-called steadiness is determined by the variability of MU discharge frequency [3]. The purpose of the current study was to examine the effect of change in the orientation of the muscle relative to gravity on the steadiness of isometric contractions and the variability of MU discharge frequency, and whether these changes were dependent on contraction intensity.

METHODS

Healthy young men (n = 11) participated in this study. To change the orientation of the muscle with respect to gravity, participants lay in the prone and supine positions. Participants performed steady isometric plantarflexion at 20% and 40% of their maximal voluntary contraction (MVC) for 20 s with visual guidance with the right knee extended and the ankle in the 15° plantarflexion for both positions. To quantify the steadiness of the plantarflexion (amount of torque fluctuations), SD and CV of torque were calculated for the middle 8 s of the contraction.

High-density surface EMG was recorded from the medial gastrocnemius muscle during steady contractions according to standard procedures. High-density EMG signals were then decomposed with a convolutive kernel compensation method [4]. A single experienced investigator manually inspected all decomposition results with the specifically designed software for the decomposition of motor unit discharge (DEMUSE), retaining only those that were characterized based on a pulse-to-noise ratio [5]. To examine the effect of muscle orientation on motor unit activity, a motor unit successively discharging for both positions was extracted based on a cross-correlation analysis of the motor unit action potential extracted by spike-triggered averaging from high-density surface EMG. The mean, SD, and CV of discharge frequency of the extracted MUs were then calculated.

RESULTS AND DISCUSSION

In the steady contraction at 20% MVC, SD and CV of torque were 42% and 46% greater in the prone compared with the supine position ($P < 0.05$). The mean discharge frequency of ninety-nine trackable MUs across positions did not change, but SD and CV of discharge frequency were greater in prone than supine ($P < 0.05$).

In the steady contraction at 40% MVC, for the seven participants who had at least one MU tracked across positions, there was no difference in SD and CV of torque between positions. The mean discharge frequency of sixty-six trackable MUs was significantly ($P < 0.05$) but slightly greater (3.5%) in the prone position compared with the supine position, while SD and CV of MU discharge frequency were not different ($P > 0.05$). These results suggest that torque fluctuations during steady contractions at 20% MVC were greater in the prone position, accompanied by greater variability in MU discharge frequency.

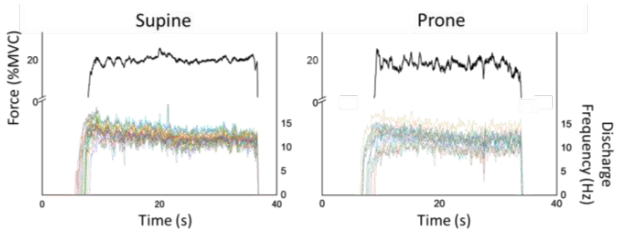

Figure 1 Representative signals of force and instantaneous discharge frequency of trackable MUs across supine (left) and prone (right) positions of a participant during steady contractions at 20% MVC.

CONCLUSION

Our results indicate that change in the orientation of the muscle with respect to gravity induced alterations in both the steadiness of isometric plantarflexion and variability of MU discharge frequency during steady contractions only at lower contraction intensities.

ACKNOWLEDGEMENTS

Supported in part by Grant-in-Aid for Scientific Research (B) in Japan to YY.

REFERENCES

[1] Monte. *Exp. Physiol* **106**: 486-495, 2021.
[2] Flament et al. *Int J Cosmet Sci* **37**: 291, 2015.
[3] Enoka and Farina. *Physiology* **36**: 114-130, 2021.
[4] Holobar & Zazula. *IEEE Transactions on Signal Processing* **55**: 4487-4496, 2007.
[5] Holobar et al. *J Neural Eng* **11**: 1741-2560, 2014.

ENERGETICS, MECHANICS, AND MUSCLE: LOCOMOTOR ADAPTATIONS TO CHRONIC LIMB LOADING DURING DEVELOPMENT

Kavya Katugam-Dechene[1], Talayah A. Johnson[1,2], Ian Dechene[1], Suzanne M. Cox[1,3], Stephen J. Piazza[1], and Jonas Rubenson[1]

[1]Biomechanics Laboratory, Dept. of Kinesiology, The Pennsylvania State University, University Park, PA, USA.
[2]McKay Orthopaedic Research Laboratory, Dept. of Bioengineering, University of Pennsylvania, Philadelphia, PA, USA.
[3]Dept. of Biology, Duke University, Durham, NC, USA.
Email: kavya@psu.edu

INTRODUCTION

Humans and other animals adapt to expend the least amount of metabolic energy to complete a movement task, both over acute [1-3] and evolutionary timeframes [1,4]. Whether adaptations in locomotor economy occur in response to altered life history, especially during development (e.g. environmental fluctuations, or training in humans) remains less clear. Further, the mechanical underpinning to adaptations in locomotor economy that may occure during development have not been well explored.

We have previously demonstrated that chronic limb loading during development substantially alters locomotor economy; it was found that chronically limb-loaded animals (LL) cary additional limb mass remarkably more economically than control animal (CON) [5]. Here we test the hypothesis that a reduction in mechanical limb work contributes to the observed lower metabolic cost of carrying externally applied limb mass after chronic limb loading. Specifically, we hypothesize that (1) LL animals locomote with added limb mass using less mechanical power than CON animals, and (2) the increase in mechanical power between unweighted and weighted conditions will be smaller for LL animals than CON animals.

METHODS

To study the effect of load stimulus during development on locomotor mechanics, we applied an average load of 3.5% body mass unilaterally to the lower right limb of a group of guinea fowl, continuously from 1-16 weeks of age (limb-loaded group, LL; n = 10). CON birds were raised in the same conditions but with no external limb loading (n = 10). At 16 weeks old, half of the birds (N = 5 per group) were video recorded (100 Hz) walking on a treadmill in both unilaterally loaded and non-loaded conditions. An inverse dynamic formulation was used to analyse swing-phase kinetics. We compared mechanical data to previously collected metabolic data on the same animals in the same conditions [5].

RESULTS AND DISCUSSION

At 16-weeks old, LL animals used 24% less metabolic energy than CON animals to walk with 3.5% BM loading [5]. Our hypothesis that LL had lower mechanical power than CON was, however, refuted. Surprisingly, our data is suggestive of LL animals having even greater mechanical power than CON animals, although this difference was not statistically significant at an alpha of 0.05 ($p = 0.12$, ES = 1.18; figure 1).

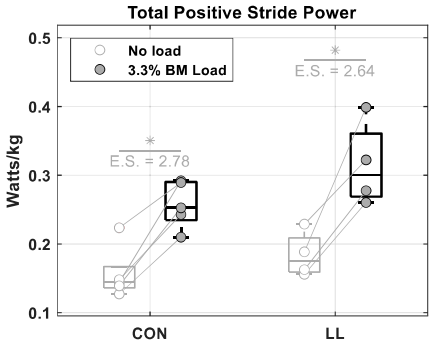

Figure 1 Total positive stride power (watts/kg) for both CON and LL animals. *significant difference due to loading ($p < 0.05$).

CONCLUSIONS

LL animals required no less limb power to carry additional mass compared to CON, despite the observed large reduction in metabolic energy consumption [5]. Increases in limb power in LL animals were isolated to the right (chronically loaded) limb, specifically driven by a larger increase in power at the ankle from unloaded to loaded walking. We propose that muscle-level adaptations may explain the improved locomotor economy in LL animals compared to CON animals. Further work is being conducted to investigate whether adaptations to muscular architecture explain how animals were able to achieve improvements in locomotor economy after growth-period loading. Preliminary findings indicate adaptations not only in muscle mass, but also in sarcomere properties after limb loading.

ACKNOWLEDGEMENTS

Supported by NIH Grants R21AR071588 and R01AR080711.

REFERENCES

[1] Alexander *Prin Animal Loc*, 2003.
[2] Barnes & Kilding *Sports Med* **45**: 37-56, 2015.
[3] McCann & Higginson *Sports Med* **7**: 158-162, 2008.
[4] Dawson & Taylor *Nature* **246**: 313-314, 1973.
[5] Johnson *PSU KINES Master's Thesis,* 2021.

EFFECTS OF DIFFERENCES IN FRICTION CONDITIONS OF FINGERTIPS ON UPPER LIMB MOVEMENT DURING FASTBALL PITCHING IN BASEBALL

Souta Suzuki[1], Takeshi Yamaguchi[1,2], Daiki Nasu[3] and Takehiro Fukuda[3,4]

[1] Department of Finemechanics, Graduate School of Engineering, Tohoku University, Sendai, Japan.
[2] Graduate School of Biomedical Engineering, Tohoku University, Sendai, Japan.
[3] Kashino Diverse Brain Research Laboratory, NTT Communication Science Laboratories, Kanagawa, Japan
[4] Graduate School of Arts and Sciences, Tokyo University, Tokyo, Japan
Email: souta.suzuki.r6@dc.tohoku.ac.jp

INTRODUCTION

In baseball pitching, friction between fingertips and ball is an important factor in pitching performance. Our previous study showed that in fastball pitching, the application of rosin powder to the fingertips increased ball spin rate and improved ball control [1]. On the other hand, under wet conditions, the ball spin rate and ball speed decreased and ball control got worse [1]. These results are thought to be caused by the change in the friction between fingertips and the ball as well as the resulting upper limb motion during pitching.

In this study, we estimated the coefficient of friction (COF) between the fingertips and the ball and investigate the effects of the difference in the COF on upper limb motion during fastball pitching.

METHODS

The subjects were six experienced male pitchers who threw overhand. The pitch was a four-seam fastball. The friction conditions between the fingertips and the ball were as follows: no application between the fingertips and the ball (unapplied condition), water applied condition, rosin powder applied condition, and pine resin applied condition.

We measured whole-body kinematics during pitching using a motion capture system. We also captured videos of the ball and fingers during the release process from the side of the subject using a high-speed camera. The translational and angular velocities of the ball were estimated from the trajectories of multiple marks drawn on the ball.

Based on the study of Fuss et al.[2], we estimated the COF between the fingertips and the ball using the translational and angular velocities of the ball. We calculated the external rotation angle of the shoulder during pitching based on the study by Miyashita et al.[3]. The centrifugal force acting on the hand was calculated using the hand velocity v_{hand}, the pitching radius R and the mass of the ball m. We used v_{hand}^2/R as the index for the centrifugal force acting on the ball during pitching.

RESULTS AND DISCUSSION

The mean COF under the water-applied condition (0.91±0.20) was 29.3% lower ($p < 0.01$) than that under the unapplied condition (1.28±0.24). On the other hand, the COF under the rosin powder applied condition (1.41±0.23) was 10.0% higher than that under the unapplied condition ($p < 0.01$). There were no significant differences in COF between unapplied and pine resin applied conditions ($p > 0.05$).

The maximum external rotational (MER) angle of the shoulder decreased by 1.4° ($p < 0.05$) in the water applied condition and increased by 0.2° ($p < 0.01$) in the rosin powder applied condition compared to the unapplied condition. The velocity of the hand at release timing decreased by 2.6% ($p < 0.01$) in the water applied condition and increased by 1.2% ($p < 0.05$) in the rosin powder applied condition compared to the unapplied condition.

The value of v_{hand}^2/R from the MER to the release time tended to be smaller in the water applied condition than in the other conditions (Fig. 1). This trend was observed in all subjects. The pitcher was not able to obtain sufficient friction force under the water applied condition and may behave to reduce the centrifugal force acting on the ball by reducing the hand velocity and increasing the radius of the circular path of the hand during pitching.

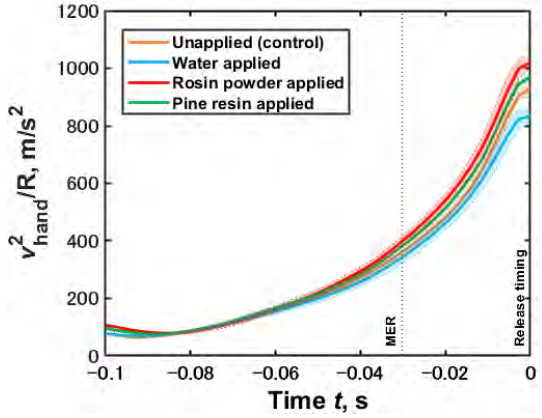

Figure 1 Representative time series of the index of centrifugal force index acting on the ball during the pitching motion.

CONCLUSIONS

The reduction of COF between fingertips and a ball resulted in decreased MER angle and decreased centrifugal force due to the decreased hand velocity and increased radius of the circular path of the hand to prevent the ball from slipping out of the hand.

REFERENCES

[1] Yamaguchi T et al. *Proc. SOBIM2021*: C1-1, 2021.
[2] Fuss FK et al. *J Sports Eng Tech*: 1-15, 2022.
[3] Miyashita K et al. *J Sports Sci Med* **7**: 47-53, 2008.

BIOMECHANICS OF HANDCYCLING HIGH INTENSITY INTERVAL TRAINING

Kellie M. Halloran[1], Joseph Peters[2,3], Michael Focht[1], Ian Rice[4], Mariana E. Kersh[1,3,5]
[1]Mechanical Science and Engineering, University of Illinois Urbana-Champaign, Urbana IL, USA
[2]Disability Resources and Educational Services, University of Illinois Urbana-Champaign
[3]Beckman Institute for Advanced Science and Technology, University of Illinois Urbana-Champaign
[4]Kinesiology, University of Illinois Urbana-Champaign
[5]Carle Illinois College of Medicine, University of Illinois Urbana-Champaign
Email: kellie2@illinois.edu

INTRODUCTION

Up to 68% of people with spinal cord injuries (PwSCI) report shoulder pain[1] which makes exercise challenging for this population. High intensity interval training (HIIT) has been recommended to improve cardiovascular health safely because it incorporates periods of active rest[2]. However, it is unclear how the increased intensity of HIIT affects shoulder loading compared to moderate intensity continuous training (MICT). Therefore, the aim of this study was to **quantify shoulder joint angles and torques during recumbent handcycling HIIT and MICT**. We used a musculoskeletal model[3] to evaluate shoulder plane, shoulder elevation, and shoulder rotation angles and torques during exercise.

METHODS

Following IRB approval, wheelchair users with SCI (n=20, 9 females) age 22(2.73) with 16.8(4.09) years of wheelchair use were recruited. Participants engaged in three recumbent handcycling protocols 2-7 days apart[4]: (1) Baseline to determine peak power output (PPO); (2) HIIT: 10x1 min 90% PPO, 1 min 10% PPO; (3) MICT: 45% PPO until equivalent workload to HIIT reached. Handle loads were collected using a handle instrumented with a six-axis load cell (ATI). Segment kinematics (23 markers) were recorded using a 10-camera system (Vicon). We used an acromion marker cluster to determine scapular motion[5]. Kinematic and hand force/moment data were collected at six workload-matched timepoints in HIIT and MICT.

Kinematic data was smoothed with a moving average filter (Matlab vR2021a). Both kinetic and motion data were filtered (2nd-order Butterworth, cutoff frequency = 10 Hz and 8Hz, respectively). The first 10 propulsion cycles were averaged at each timepoint. A musculoskeletal model of the shoulder[3] was scaled to each subject (OpenSim v3.4) and used to calculate joint angles and torques using inverse kinematics and inverse dynamics. Angle range of motion (RoM) and mean torque magnitude were averaged over all timepoints. Normally distributed datasets were compared using paired t-tests (R v4.1.2); non-normal using Wilcoxon signed ranks tests (α = 0.05). RoM and torques were compared between HIIT and MICT at each timepoint and are reported as median (median absolute deviation).

RESULTS

There were no differences in joint angle RoM between HIIT and MICT (Table 1). HIIT torques were 38.3% higher than MICT on average (Fig. 1B, $p<0.001$).

Table 1: Angle RoM and Torque (τ). Bold values indicate significant difference ($p<0.001$) between HIIT and MICT.

		Plane	Elevation	Rotation
RoM	MICT	73.9(16.7)	22.2(9.6)	78.2(20.9)
(°)	HIIT	77.9(20.2)	24.1(8.0)	74.9(20.5)
τ	MICT	10.7(3.5)	7.4(2.7)	10.4(2.8)
(Nm)	HIIT	**14.3(6.0)**	**10.2(4.4)**	**14.9(5.3)**

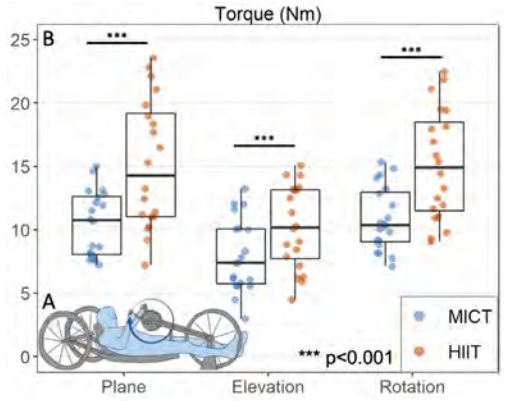

Figure 1: A) Recumbent handcycle. B) Joint torque magnitude.

CONCLUSIONS

The consistency of kinematics during HIIT and MICT is likely due to the uniform nature of handcycling. Higher torques in HIIT are therefore attributed to increased forces[4]. While increased torques are related to shoulder pain[6], it remains unclear if the torques during HIIT would contribute to shoulder tendinopathy. The cardiovascular and enjoyment benefits of HIIT[7] may warrant the increased shoulder exertion. More work is needed to determine the effect of HIIT on muscle and tendon loads to evaluate the risk of injury.

ACKNOWLEDGEMENTS

Assistance from Prof. David Ackland. Funding: NSF.

REFERENCES

[1] Subbarao J et al. *J Spinal Cord Med* **18**:1, 1995. [2] Nightingale T et al. *Arch Phys Med Rehab* **98**:8, 2017. [3] Wu W et al., *J Biomech* **49**:15, 2016. [4] Halloran KM et al., *SSRN*, preprint, 2022. [5] Warner MB et al., *Hum Mov Sci*, **31**:2, 2012. [6] Chang L et al., *J Appl Biomech*, **38**:6, 2022. [7] Astorino T and Thum J. *J Spinal Cord Med*, **41**:1, 2018. **Fig. 1**: Biorender.com

CHARACTERISTIC OF THIGH MUSCLE HYPERTROPHY INDUCED BY ELECTRICAL MUSCLE STIMULATION TRAINING

Kosuke Kano[1], Ryota Akagi[2], Yuto Hashimoto[3], Yusuke Miyokawa[2], Daigo Shiozaki[2], Yoshinari Yajima[2], Koki Yamada[2], Sari Kanbayashi[1], Kota Anjiki[1], Itsuki Kanno[1], Mizuki Sudo[4], Takanobu Okamoto[3] and Soichi Ando[1]

[1] Graduate School of Informatics, University of Electro-Communications, Chofu, Japan.
[2] Department of Bioscience and Engineering, Shibaura Institute of Technology, Saitama, Japan.
[3] Department of Exercise Physiology, Nippon Sport Science University, Tokyo, Japan.
[4] Physical Fitness Research Institute, Meiji Yasuda Life Foundation of Health and Welfare, Tokyo, Japan.
Email: kano061901141010@gmail.com

INTRODUCTION

Several studies suggest that electrical muscle stimulation (EMS) can be used as an alternative modality to voluntary exercise. EMS training improves muscle strength and prevents muscle atrophy after surgery [1]. Nevertheless, the effects of EMS training on thigh muscle mass are less understood. Therefore, this study aimed to characterize the effects of EMS training on the quadriceps and biceps femoris muscles hypertrophy.

METHODS

Thirty-five heathy male participants were divided into EMS training (n = 19) and control (n = 16) groups. In the EMS group, the participants performed EMS (Myoelectoric Medicine EMS) three times per week for 8 weeks. The EMS system was designed to simulate motor unit activities during strong voluntary muscle contraction, and stimulation frequencies gradually increased from 12 to 60 Hz. Before and after the training, maximal isometric knee extension torque was measured. The quadriceps muscle cross-sectional area (CSA) was assessed at mid-thigh (50% of the femur) and the biceps femoris muscles (long head and short head) CSA were assessed at distal (70% of the femur) regions using magnetic resonance imaging. We performed a two-way analysis of variance (ANOVA) with group (between) and time (within) as factors.

RESULTS AND DISCUSSION

We observed a significant interaction on the quadriceps femoris muscle CSA ($p = 0.016$). In the EMS group, the quadriceps femoris muscle CSA increased (Figure 1 upper, Pre: 62.0 ± 8.3 cm^2 vs. Post: 64.2 ± 8.6 cm^2, $p < 0.001$). In the Control group, the quadriceps femoris muscle CSA did not change (Pre: 63.5 ± 7.7 cm^2 vs. Post: 63.8 ± 8.9 cm^2, $p = 0.93$).

We also observed a significant interaction on the short head of the biceps femoris muscle ($p = 0.016$). The short head of the biceps femoris muscle increased in the EMS group (Figure 1 lower, Pre: 4.4 ± 1.0 cm^2 vs. Post: 4.9 ± 0.9 cm^2, $p < 0.001$), but not in the Control group (Pre: 4.2 ± 0.9 cm^2 vs. Post: 4.3 ± 1.0 cm^2, $p = 0.79$). Conversely, neither main effects nor an interaction was found on the long head of the biceps femoris muscle ($p > 0.05$) (EMS group, Pre: 7.6 ± 2.2 cm^2 vs. Post: 7.8 ± 2.0 cm^2; Control group, Pre: 6.7 ± 1.7 cm^2 vs. Post: 6.5 ± 1.6 cm^2). The present results indicate that EMS training induced muscle hypertrophy of the thigh muscle. Since the short head of the biceps femoris is a deep muscle, these results suggest that the present EMS system stimulated both superficial and deep muscles adequately.

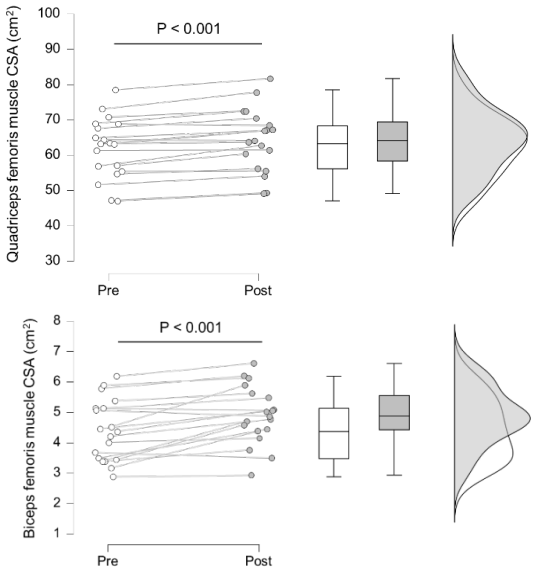

Figure 1 Changes in quadriceps femoris muscle CSA (upper) and short head of biceps femoris muscle CSA (lower) before and after EMS training. (open: Pre; filled: Post)

CONCLUSIONS

EMS training of the thigh muscles induces muscle hypertrophy of the quadriceps femoris and biceps femoris muscles, including deep muscle.

ACKNOWLEDGEMENTS

This study was supported by the JSPS KAKENHI Grant number 22H03493 to S.A and Grant number 17KK0174 to R.A.

REFERENCES

[1] Moritani T. Electrical muscle stimulation: Application and potential role in aging society. *J Electromyg Kinesiol* **61**: 102598, 2021

Advent of carbon thick shoe changes morphological advantages for long-distance running ability

NOBUE Ayaka[1], SANO Kanae[1] and ISHIKAWA Masaki[2]

[1] Morinomiya University of Medical Science, Osaka, Japan.
[2] Osaka University of Health and Sport Sciences, Osaka, Japan.
Email: ayaka_nobue@morinomiya-u.ac.jp

INTRODUCTION

The technological intervention of the sport items can change the movement skill and morphological characteristics as well as enhance athletic performance. For example, the slap skate shoes and LZR Racer swimwear can enhance athletic performance but also bring important movement skills and morphological characteristics of musculotendons which have not been considered advantageous previously.

In track and field events, the advent of thick-soled carbon shoes (**Carbon Thick Shoe**) in 2017, as opposed to the traditional thin-soled light shoes (**Traditional Shoe**), has dramatically enhanced long-distance running performance. Until the advent of Carbon Thick Shoe, Achilles tendon length ($\mathbf{L_{AT}}$) was a crucial advantage for long-distance running performance [5,7]. However, it is uncertain whether the morphological advantages of $\mathbf{L_{AT}}$ for long-distance runners would be effective with the advent of Carbon Thick Shoe.

Therefore, the purpose of the present study was to examine musculoskeletal characteristics related to long-distance running performance before and after the advent of Carbon Thick Shoe. It was hypothesized that $\mathbf{L_{AT}}$ can be related to the running performance of the distance runners who wore Traditional Shoe. However, these relationships will become irrelevant with the distance runners who wore Carbon Thick Shoe. Instead, the psoas major muscle size can be crucially related to the running performance of the distance runners who wore Carbon Thick Shoe.

METHODS

Table 1 shows the physical characteristics of participating long-distance runners. The Traditional Shoe group was measured from 2014 to 2019. The Carbon Thick Shoe group who had worn them for more than 2 years was measured from 2020 to 2022.

The $\mathbf{L_{AT}}$ and the cross-sectional area (CSA) of the psoas major muscles at the Jacobi line were measured by musculoskeletal ultrasonography (Noblus, Hitachi-Aloka Inc.). The relationships between these parameters and their athletic performance (the season records of 5000 m, 10000 m and half marathon) were calculated for each group using Pearson's correlation coefficient.

Table 1. Physical characteristics of the participants

	Age (years)	Height (cm)	Body mass (kg)	Half marathon time
Traditional Shoe (n=59)	23.2±4.2	171.6±5.2	57.4±4.4	1:03:14±0:01:38
Carbon Thick Shoe (n=58)	21.5±3.6	170.8±4.8	55.8±4.6	1:03:58±0:01:51

RESULTS

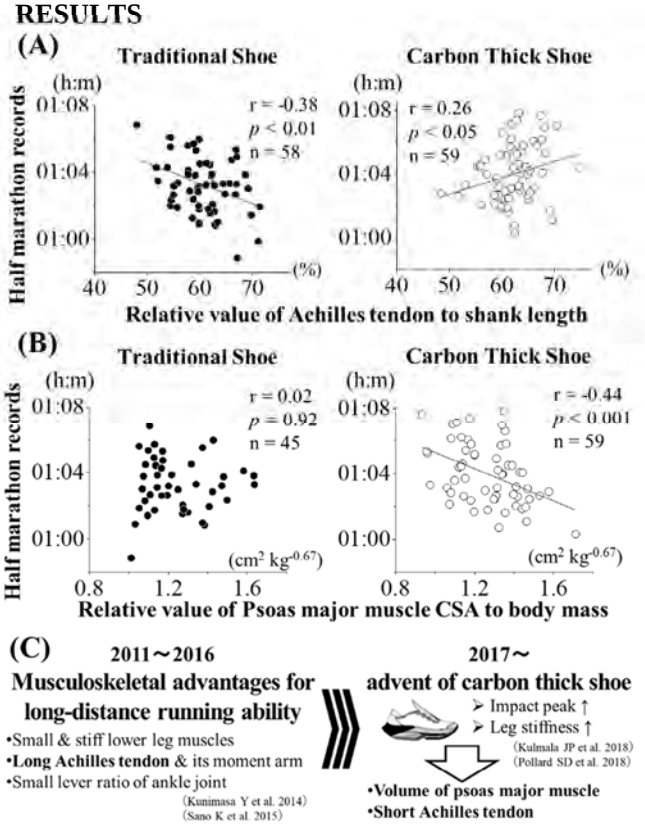

Figure 1. Relationships (A) between L_{AT} and half marathon records and (B) between psoas major muscle and half marathon records for different shoe groups and (C) schema of functional and morphological changes due to the advent of Carbon Thick Shoe.

DISCUSSION

- ✓ The increased stride due to the increased leg length of the thick soles (Stack height) can increase the hip joint [1] and psoas major muscle works.
- ✓ Carbon Thick Shoe can increase foot mechanical work and power [3], but to its detriment, may not utilize the elastic energy of AT. Consequently, the use of Carbon Thick Shoe may lead distance runners to improve postural control due to muscle-tendon modulation such as competitive trampoline athletes who have long soleus muscle length and short $\mathbf{L_{AT}}$ [2].

REFERENCES

[1] Agresta C et al. *Front Sports Act Living*. **4**:815675, 2022.
[2] Baba T et al. 66th *J Physical Fitness Sports Med*, 196, 2011.
[3] Hoogkamer W et al. *Sports Med* **49**:133-43, 2019.
[4] Kulmala JP et al. *Sci Rep*. **8**:17496, 2018.
[5] Kunimasa Y et al. *Scand J Med Sci Sports*.**24**:e269, 2014.
[6] Pollard SD et al. *Orthop J Sports Med* **6**:1-5, 2018.
[7] Sano K et al. *Eur J Appl Physiol* **115**:849-59, 2015.

Different effects of a single ingestion of quercetin on motor unit recruitment in upper and lower limbs.

Taichi Nishikawa[1,2], Masamichi Okudaira[2], Ryosuke Takeda[2], Tetsuya Hirono[2,3], Toshiyuki Ohya[2] and Kohei Watanabe[2]

[1] Graduate School of Health and Sport Sciences, Chukyo University, Toyota, Japan
[2] School of Health and Sport Sciences, Chukyo University, Toyota, Japan
[3] Research Fellow of Japan Society for the Promotion of Science
Email: kyanonnisikawa@gmail.com

INTRODUCTION

Quercetin, a polyphenolic flavonoid found in onions and tea, has garnered attention as an ergogenic aid for enhancing human physical performance [1]. It exhibits high affinity for adenosine receptors and functions as an antagonist of adenosine [2], thereby promoting the release of neurotransmitters such as acetylcholine and dopamine [3]. Our previous research has demonstrated that a single ingestion of quercetin can decrease the recruitment threshold of motor units [4]. This suggests that quercetin ingestion may augment the number of motor unit activations in muscle performance (e.g. muscle endurance) and have implications for exercise and strength training. Although the previous study was investigated on the lower limb (vastus lateralis, VL), it is uncertain if similar effects would be observed in the upper limb. Caffeine, which bears structural resemblance to quercetin and functions as an antagonist of adenosine, has been reported to elicit different effects in the upper and lower limbs [5]. The present study, therefore, sought to compare the effects of quercetin ingestion on the recruitment thresholds of motor units in the biceps brachii (BB) and VL.

METHODS

In a double-blind, counterbalanced, randomized and crossover design, five adults underwent isometric elbow flexion and knee extension exercises before (PRE) and 60 minutes after (POST) ingesting quercetin glycosides 200mg (QUE) or a placebo (PLA). Each condition was separated 72hours. Four types of submaximal isometric exercises were performed using ramp contractions that incrementally applied torque from 0% to 15%, 30%, 50%, and 70% of MVC. High-density surface electromyography (HD-sEMG) was recorded from the BB and VL during ramp contractions. Individual motor units of the BB and VL were identified from HD-sEMG and changes in recruitment thresholds were examined by tracking motor units from PRE to POST.

RESULTS AND DISCUSSION

A total of 122 motor units were detected in the BB and 423 in the VL. Figure 1 indicates the different effects of quercetin and placebo ingestion on the recruitment threshold of motor units. The results show an interaction between muscle group and quercetin ingestion at 30% and 50%MVC ramp, indicating that quercetin ingestion may differently affect the recruitment thresholds of BB and VL motor units (Figure 1). The findings of this study suggest that quercetin ingestion may decrease the recruitment threshold of upper limbs motor units than lower limbs. Previous research, focused different effect of caffeine ingestion on upper and lower limbs, has been suggested that these differences may be attributed to variations in motor unit recruitment patterns and / or muscle size between the upper and lower limbs [5]. While quercetin has been shown to enhance muscle performance in both the upper and lower extremities, the extent of these effects may vary between the two muscles.

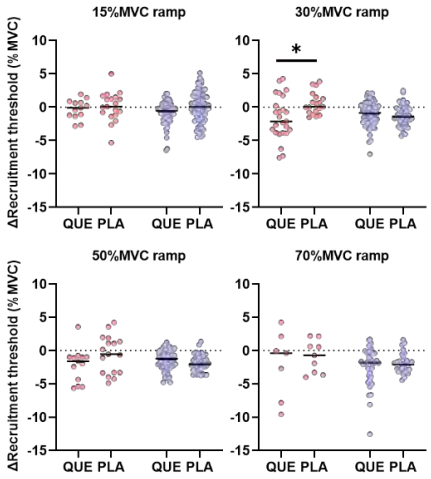

Figure 1 Difference of recruitment threshold of motor unit during ramp contractions from PRE to POST. Red and Blue dots represent difference of recruitment threshold of BB and VL motor units. * $p < 0.05$ QUE vs. PLA

CONCLUSIONS

This study assessed the effects of a single dose of quercetin on the recruitment thresholds of motor units in the BB and VL muscles using HD-sEMG. Results indicate different effects of quercetin ingestion on the recruitment threshold of upper and lower limbs motor units. Present study suggested that the ergogenic effects of quercetin may vary between upper and lower limbs.

REFERENCES

[1] Kressler J et al. Med Sci Sports Exerc, 43: 2396-2404, 2011.
[2] Alexander S. P. Phytother Res, 20: 1009-1012, 2006
[3] Cheuvront S. N. et al. Am J Physiol Regul Integr Comp Physiol, 296: R394-401, 2009.
[4] Watanabe K et al. Exp Brain Res, 239: 1567-1579, 2021.
[5] Black C. D. et al. Med Sci Sports Exerc, 47: 1145-1158, 2015.

DIFFERENCES IN VISCO-ELASTIC PROPERITES OF MUSCLE AND TENDON BETWEEN 100M AND 400M SPRINTERS

Toshiaki Oda[1], Takeru Matsumoto[1], Satoshi Mikata[1], Soma Saito[1], and Hiroyasu Tsuchie [2]
[1] Life and Health Sciences, Hyogo University of Education, Kato, Japan.
[2] Toyo University, Kawagoe, Japan.
Email: toda@hyogo-u.ac.jp

INTRODUCTION

During the contact phase of running, the visco-elastic properties of the muscle-tendon complex (MTC) play a crucial role in functional muscle-tendon interaction and the recycling of elastic energy [1]. In sprint events of track race, the 100m and 400m athletes have different determinants of athletic performance, such as muscular endurance. Therefore, it is likely that the viscoelastic properties of the MTC also differ in these events. The aim of this study was to investigate the viscoelastic properties of the lower leg MTC in track and field athletes of100m (short sprint) and 400m (long sprint) .

METHODS

A total of 38 male subjects (n=25;100m and n=13; 400m) participated in the study. The viscoelastic properties of the MTC were measured using the vibration method under multiple load settings (similar to Fukashiro et al. [2]). The subject was placed in a seated position (ankle and knee joints 90deg), with the ball of the foot on a force plate edge. A weight was placed on the knee, and with the posture maintained by isometric contraction (the muscle force exerted was varied), the damped oscillation of the triceps surae muscle was induced. The waveforms were regressed by the least-squares method on the following equation (1) to calculate the unknowns, gamma (γ), omega(ω), a_c, a_s and M.

$$F(t)=e^{-\gamma t}(a_c cos\omega t+a_s sin\omega t)+\mathrm{Mg} \quad (1)$$

where F is force, t is time, e is Napier number, γ is damping factor, a is amplitude, ω is angular frequency, M is effective mass, and g is gravitational acceleration. Then, after consideration of the moment arm of muscle, the elastic and viscous coefficients (k and b) of MTC were calculated.

$$k = M(\omega^2+\gamma^2) \quad (2)$$
$$b=2M\gamma \quad (3)$$

From the experimental results obtained, the coefficients were calculated for every 100N up to 700N. In addition, the elasticity of MTC was separated into muscle and tendon components, based on the assumption that they are arranged in series. The calculated parameters were compared between 100m and 400m.

RESULTS AND DISCUSSION

The study found that 100m athletes had higher elastic coefficients of muscle-tendon complex (MTC) under force exertion conditions of 100-400 N. However, no difference was observed under higher force conditions or in viscous coefficients between groups. When comparing muscle and tendon separately, the elastic coefficients were significantly higher for the 100m group in muscle (**Fig 1A**) and the 400m group in tendon (**Fig 1B**). However, no significant correlation was observed between athletic performance and each coefficient in both groups. These results suggest that the 100m athletes use an increased elasticity due to increased muscle contraction, while the 400m athletes may use the higher intrinsic elasticity of tendons to achieve the overall elasticity required during sprinting, such as acceleration and maximal speed phases.

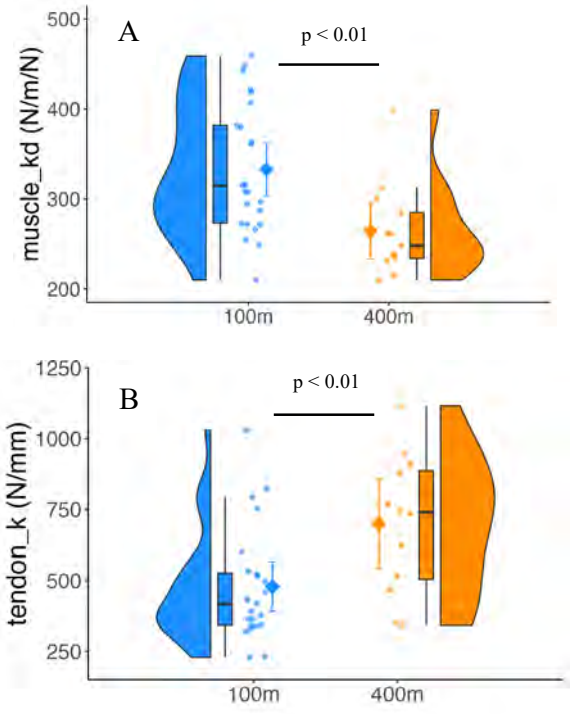

Fig 1 Individual values and their distribution. Diamond marks indicate average values. A: elastic rate of muscle, B: elastic coefficient of tendon.

REFERENCES

[1] Roberts and Azizi. *J Exp Biol.* **214**: 353-61, 2011.
[2] Fukashiro et al. *Acta Physiol Scand.* **175**, 183-87, 2002.

Effect of restricted thoracic expansion during shoulder external rotation on scapulothoracic and glenohumeral joint motion

Mitsuhiro Yoshimi[1], Noriaki Maeda[1], Makoto Komiya[1], Tsubasa Tashiro[1], Kazuki Kaneda[1], Satoshi Arima[1], Shogo Tsutsumi[1], Takeru Abekura[1], Yukio Urabe[1]

[1] Department of Sports Rehabilitation, Graduate School of Biomedical and Health Sciences, Hiroshima University, Hiroshima, Japan

Email: mitsuhiroyoshimi0116@hiroshima-u.ac.jp

INTRODUCTION

Throwing injuries of the shoulder are caused by repeated throwing motions in overhead sports such as baseball. Shoulder external rotation in the throwing motion involves movement of the scapulothoracic (ST) and glenohumeral (GH) joints, thoracic spine, and thorax. Restriction of thoracic expansion may decrease ST joint motion and compensate by excessive GH joint motion. However, it is unclear how restricting the expansion of the thorax alters shoulder motion. This study aimed to elucidate changes in ST and GH joint movements caused by restricted thoracic expansion during shoulder external rotation.

METHODS

Eighteen right-handed healthy males (mean ± SD: age, 21.9 ± 1.8 years; BMI, 21.4 ± 2.0 kg/m²) participated in this study. The participants performed shoulder external rotation in two conditions: with and without restriction of the thorax. The thoracic expansion was restricted by taping, which was applied to the fifth and tenth rib positions. The participant sat and performed shoulder external rotation from 90° abduction and 75° external rotation to the maximum external rotation (MER) angle [1]. Kinematic data were measured using an electromagnetic tracking device (Liberty, Polhemus, Inc., USA). The joint kinematics data were measured based on the relative positions of the thorax, scapula, and humerus: internal rotation, upward rotation, and posterior tilt angle of the scapula relative to the thorax (ST joint), and external rotation angle of the humerus relative to the scapula (GH joint). The angles at 75° of external rotation and MER angle for each variable were measured respectively, and the difference was calculated as the angular displacement. The Wilcoxon signed-rank test was used to compare each variable in the two conditions. Additionally, the difference between with and without restricted conditions for angular displacements (displacement in the "with restriction condition" - displacement in the "without restriction condition") was calculated, and the relationship between each variable was examined using Spearman's rank correlation coefficient. The statistical significance level was set at $p<0.05$.

RESULTS AND DISCUSSION

In with restriction condition, ST posterior tilt decreased ($r=0.50$, $p<0.05$) and GH external rotation increased ($r=0.67$, $p<0.01$) in the MER angle. A decrease in displacement of ST posterior tilt ($r=0.74$, $p<0.01$) and an increase in displacement of GH external rotation ($r=0.66$, $p<0.01$) were also observed. On the other hand, no significant differences occurred in MER angle and ST internal rotation and upward rotation angles. A significant negative correlation existed between the difference in the displacement of ST posterior tilt and GH external rotation with a correlation coefficient of -0.54 ($p<0.05$, Figure 1).

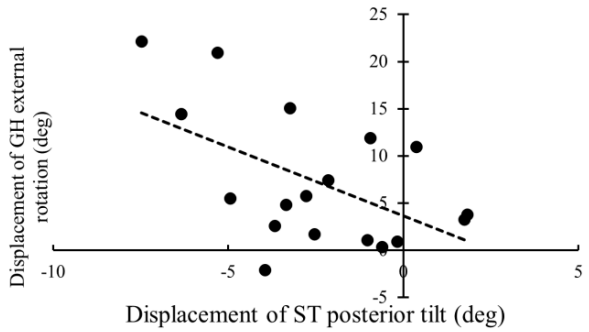

Figure 1: Correlation between displacement of ST posterior tilt and displacement of GH external rotation.

A previous study reported that a decrease in ST joint motion resulted in a decrease in MER angle [1]. However, in the present study, MER angle did not change with restriction. This was because the excessive GH external rotation compensated for the decreased motion of the ST joint. It has been reported that malfunctioning of one of the joints directly affected the other joint [2]. Restriction of thoracic expansion limited ST joint motion but may have resulted in greater GH motion to prevent a decrease in shoulder external rotation. Restriction of thoracic expansion was suggested to increase dependence on GH joint motion and possibly lead to shoulder injuries.

CONCLUSIONS

The present study indicated that restriction of thoracic expansion causes changes in ST and GH joint movements. Improvement of thoracic expansion exercises may be important in the prevention of throwing injuries of the shoulder.

REFERENCES

[1] Suzuki Y et al. *Gait Posture* **67**: 207-212, 2009.
[2] Paine R et al. *Int J Sports Phys Ther* **8**: 617-629, 2013.

Motor unit firing properties of tibialis anterior during peripheral nerve stretching

Tetsuya Hirono[1,2], Taian M Vieira[3], Alberto Botter[3] and Kohei Watanabe [1]
[1] School of Health and Sport Sciences, Chukyo University, Toyota, Japan.
[2] Research Fellow of Japan Society for the Promotion of Science, Japan.
[3] Laboratory for Engineering of the Neuromuscular System (LISiN), Politecnico di Torino, Turin, Italy
Email: hirono.tetsuya.56x@kyoto-u.jp

INTRODUCTION

Peripheral nerves are subjected to length changes with joint movement [1, 2], possibly affecting the firing and recruitment properties of motor units. This notion stems from changes in stiffness of peripheral nerves observed in patients with neuropathologies, such as nerve compression [3] and diabites neuropathy [4]. Patients with such peripheral nerve pathologies were reported to have low motor unit firing rate [5], suggesting attenuated cortocomotor excitability. It seems therefore plausible to ask whether nerve stiffness may affect motor unit firing patterns. The purpose of this study was to investigate motor unit firing patterns during peripheral nerve stretching.

METHODS

Eighteen healthy young adults participated in this study (age: 30.3±6.0 yrs, 1.8±0.1 m, 68.8±11.3 kg, 4 females). They sat in different two hip positions. One was hip flexion position (FLEX) where sciatic nerve was stretched, whereas the other was hip extension position (EXT) where the nerve was not stretched. Peripheral nerve conduction time was measured to confirm whether the nerve was stretched. Specifically, peroneal nerve was electrically stimulated below the fibular head, and the action potential of extensor digitorum brevis was detected using electromyography (EMG). The delay between stimulation onset and the maximum of the compound muscle action potential was used to measure the conduction time. To investigate motor unit firing properties of tibialis anterior during dorsiflexion, the participants performed ramp-up isometric contractions with a 10-s ascending phase to 20% of maximum voluntary contraction (MVC) and 20-s sustain phase at 20%MVC. High density surface EMG signals was collected from tibialis anterior during the ramp-up contraction tasks during each position. Recorded monopolar surface EMG signals were analyzed and individual motor units were identified. Additionally, detected motor units were tracked between two conditions. Recruitment thresholds and firing rate at 10-20 %MVC and during 20%MVC sustain phase were calculated and compared between two conditions.

RESULTS AND DISCUSSION

The number of detected motor units was 181. Conduction time of peroneal nerve during FLEX was significantly shorter than that during EXT (FLEX: 14.9±1.4ms, H-EXT: 15.0±1.3ms, p=0.016), suggesting that peripheral nerve was stretched during hip flexion position. Motor unit recruitment thresholds was significantly higher during FLEX than during EXT ($p < 0.01$). Additionally, motor unit firing rate at 10-20%MVC during FLEX was significantly lower than during EXT ($p < 0.01$). Those results suggested a possibility that peripheral nerve stretching might affect the motor unit firing properties.

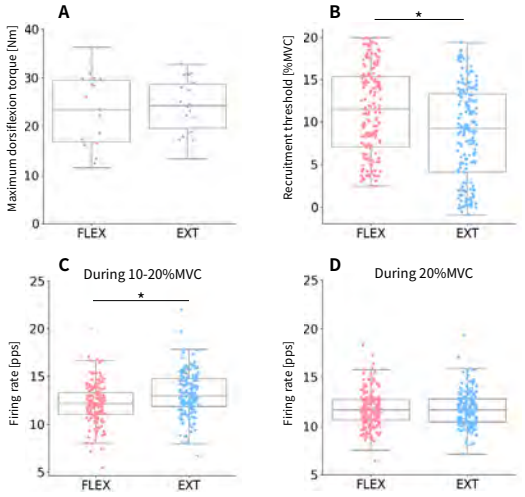

Figure 1 A. Maximum dorsiflexion torque. B. Recruitment threshold. C. Firing rate during 10-20%MVC in an ascending phase. D. Firing rate during 20%MVC in sustain phase. An asterisk represents a significant difference.

CONCLUSIONS

Peripheral nerve stretching, which was evaluated by measuring nerve conduction time by electrically stimulation, might increase motor unit recruitment thresholds and reduce the average firing rate of active motor units.

REFERENCES

[1] Andrade RJ et al. *Sci Rep* **8**(1): 14532, 2018.

[2] Andrade RJ et al. *J Appl Physiol (1985)* **129**(5): 1011-1023, 2020.

[3] Kantarci F et al. *Eur Radiol* **24**(2): 434-40, 2014.

[4] Dikici AS et al. *Radiology* **282**(2): 494-501, 2017.

[5] Watanabe K et al. *Muscle & Nerve* **48**(5): 806-813, 2013.

The difference in the precision of the soccer shot between dominant and non-dominant feet

Yusuke Shimotashiro[1], Masahiro Shinya[1]
[1]Graduate School of Humanities and Social Sciences, Hiroshima University, Higashi-Hiroshima, Japan.
Email: yu.shimo16@gmail.com

INTRODUCTION

In soccer, players are required to accurately shoot with both dominant and non-dominant feet. Precision or variability in kicking has been evaluated by Hunter et al. (2018) using 95% confidence ellipse [2]. However, the previous study measured shoots by the dominant foot only and did not focus on the difference between the dominant and non-dominant foot. Also, the study was limited to frontal shots and did not separately analyze straight (i.e., shooting rightward with the right foot and leftward with the left foot) and cross (i.e., shooting rightward with the left foot and leftward with the right foot) shooting direction. In light of the above, the purpose of this study was to determine the influence of the kicking foot and shooting direction on shooting precision.

METHODS

Sixteen right-footed players (male: 13, female: 3) with at least 6 years of soccer experience participated in the study. The participants were asked to make instep kicks aiming at a circular target (33 cm in diameter) as accurately as and as fast as possible as if it were a penalty kick. The target was placed at a height of 1.6 m inside the left and right goalposts. The distance from the participant to the goal was 11 m. In addition, the fastest possible shots, which did not require precision, were measured twice before the task. The number of trials was 80 in total, 20 trials for each of the four conditions of kicking foot (dominant/non-dominant foot) and shooting direction (straight/cross). A digital video camera (1920 × 1080 pixels, 120 fps) was used to measure the tangential velocity of the ball. Another camera (1920 × 1080 pixels, 60 fps) was set to measure the 2D location of the ball in the goal plane. The 20 ball locations for each condition were fitted by the bivariate normal distribution and a 95% confidence ellipse was calculated. The average velocity of the two shots taken before the task was used as the maximum shooting velocity, and the ball velocity during the task was calculated as a percentage of the maximum shooting velocity. A 2-way repeated measures ANOVA was conducted to detect the effects of kicking foot and shooting direction on the area of the 95% ellipse and the ball velocity relative to the maximum.

RESULTS AND DISCUSSION

The area of the 95% confidence ellipse with the dominant foot was 6.17 ± 1.93 m² in the straight direction and 6.62 ± 3.10 m² in the cross direction. The area of 95% confidence ellipse for the non-dominant foot was 10.22 ± 3.53 m² in the straight direction and 11.50 ± 4.81 m² in the cross direction. The 95% confidence ellipse area was significantly smaller for the dominant foot than for the non-dominant foot ($F(1,15) = 36.37$, $p < 0.001$, illustrated in Figure 1). There was no main effect of the kicking foot on the ratio of ball velocity during the task to maximum shooting velocity between the non-dominant and dominant foot.

The lack of the difference in the ball velocity relative to the maximum indicates that the observed difference in the kicking precision cannot be explained by the theory of speed-accuracy tradeoff. Antosiak-Cyrak et al. (2015) reported that the dominant foot took less time than the non-dominant foot in experienced soccer players using a task in which the foot passed through tubes of different sizes[1]. The observed difference in the kicking precision between the dominant and non-dominant foot might be interpreted as the difference in the dexterity or skill fullness.

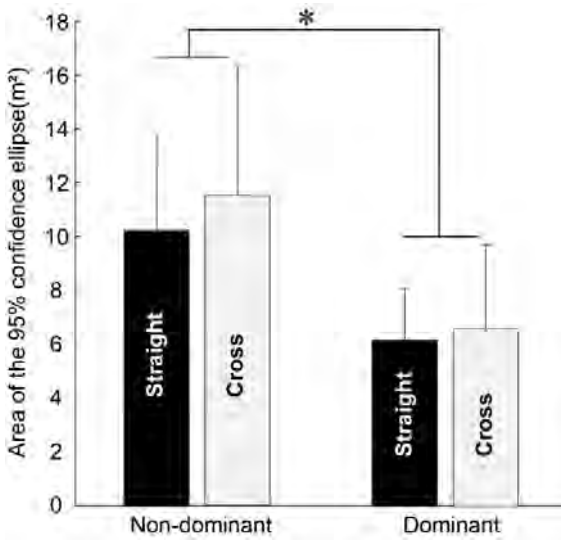

Figure 1 Comparison of 95% confidence ellipse area.
The main effect of the kicking foot was observed (* $p < 0.05$).
Error bars indicate standard deviation.

CONCLUSIONS

Shooting by the dominant foot was twice as precise as that by the non-dominant foot when the precision was quantified using the area of 95% confidence ellipse.

REFERENCES

[1]Antosiak-Cyrak, K.et al. (2015). TRENDS IN SPORT SCIENCES, 4(22), 207–215.
[2]Hunter, A. H.et al. (2018). Journal of Biomechanics, 72, 159–166.

Kinematic contribution to javelin velocity at different run-up velocities in male javelin throwers

Mizuki Makino[1], Koichi Nakayama[1], Yuka Ando[1] and Kenji Tauchi[2]
[1] Graduate School of Health and Sport Sciences, Chukyo University, Aichi, Japan.
[2] School of Health and Sport Sciences, Chukyo University, Aichi, Japan.
Email: m.mzk1011@gmail.com

INTRODUCTION

In daily training, many javelin throwers work on improving their throwing technique by throwing from a slower run-up velocity than in competitions. If the acquisition of javelin velocity in throws from a slower run-up velocity differs significantly from that of a full run-up throw, then throwers and coaches need to understand these differences and adjust the run-up velocity of throws in training. the purpose of this study was to clarify the differences in the contribution of each movement to javelin velocity caused by changes in the run-up velocity of an individual. We hypothesized that as the run-up velocity of an individual changes, the acquisition of javelin velocity would also change.

METHODS

Twelve collegiate male javelin throwers were included in this study. Participants performed the following two types of throws, two times each, at maximum effort; a one-cross throw that the thrower throws from a one-step run-up (Cross), and a full run-up throw that the thrower throws in the same way as in an actual competition (Run). Of the two throws of each type, the throw with the highest resultant velocity of the grip of the javelin at the time of release was used for the analysis. The coordinates of reflective markers affixed to anatomical landmarks on the body and javelin points during the experimental trials were recorded using a motion capture system (250 Hz). The mathematically method [1] was used to calculated the javelin velocity acquired by each joint movement and the percentage (contribution) of the javelin velocity acquired by each movement to the javelin velocity at the same moment was calculated. The analysis phase was from the last fore foot touchdown (L-on) to the javelin release (Rel). Differences in parameters between Cross and Run were confirmed using a paired t-test for those that followed a normal distribution and a Wilcoxon's signed rank test for those that did not ($\alpha = 0.05$). Differences in time series data were confirmed using a paired t-test in statistical parametric mapping ($\alpha = 0.05$).

RESULTS AND DISCUSSION

Cross had a lower forward release velocity than Run, and no significant difference was observed in the upward release velocity (Table 1). Therefore, the higher release angle observed in Cross than in Run may have been caused primarily by the decreased forward release velocity in Cross.

Despite the upward release velocity did not change significantly between the types of throwing, the contribution of trunk forward lean to upward javelin velocity was lower in Cross than in Run (Figure 1). The forward lean of the trunk in the javelin throw is caused by the converts the momentum of the whole body into trunk rotation after L-on [2]. Based on this, it is possible that less whole-body momentum was observed at L-on in Cross and that the forward lean of the trunk was subsequently less than in Run, with a concomitant decrease in their contribution to the upward javelin velocity.

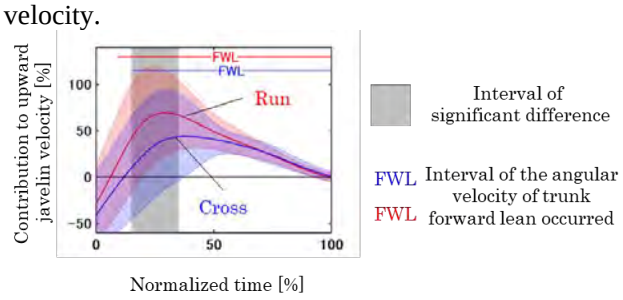

Figure 1: Contribution of the trunk forward lean to the upward javelin velocity.

CONCLUSIONS

Although no significant change in upward release velocity was observed between Cross and Run, there was a difference in the contribution of trunk forward lean. This result supports the hypothesis of the present study.

REFERENCES

[1] Elliott et al. *J Appl Biomech* **11**: 433-442, 1995.
[2] Morriss and Bartlett *Sports Med* **21**:438-446, 1996.

Table 1: The mean ± standard deviation of the various parameters in the Cross and Run (all parameters were normally distributed).

	Cross	Run	*r*	*p*
CG velocity at L-on [m/s]	3.3 ± 0.2	5.3 ± 0.5	0.98	<0.001
Forward release velocity [m/s]	15.7 ± 1.5	18.7 ± 1.6	0.95	<0.001
Upward release velocity [m/s]	10.1 ± 1.3	10.5 ± 1.0	0.46	0.115
Release angle [deg]	32.7 ± 4.5	29.4 ± 2.9	0.69	0.009

The intrinsic foot muscles contribute to controlling postural sway during single-leg stance

Momoka Nakamura[1], Moeka Samoto[1], Kei Masani[2] and Yasuhide Yoshitake[1]
[1] Graduate School of Science and Technology, Shinshu University, Ueda, Japan.
[2] Institute of Biomedical Engineering, University of Toronto, Toronto, Canada.
Email: nakamura.m.632@gmail.com

INTRODUCTION

It is well-known that the center of pressure (COP) fluctuation increases during single-leg stance compared to double-leg stance [e.g., 1]. During double-leg stance, the COP fluctuates mainly in the antero-posterior (AP) direction, which represents the ankle joint plantarflexor torque and is primarily controlled by the plantarflexor muscles [2]. However, during single-leg stance, the COP fluctuation in the medio-lateral (ML) direction becomes larger and close to the one in AP direction, which probably reflects ankle inversion/eversion torque, and/or foot deformation. It is unclear which muscles contribute to this control of the COP in the ML direction. The intrinsic foot muscles are assumed to largely contribute to it, because the muscle activities in intrinsic foot muscles were reported to remarably increase during single-leg stance compared to double-leg stance [3].

Here we investigated whether the intrinsic foot muscle and the plantarflexor muscle contribute to controlling the COP fluctuation in the ML and AP directions during single-leg stance. We analyzed temporal similarity between the COP and muscle activation measured using electromyography (EMG). Also, we analyzed the temporal similarity between the COP and fasicle length meausred using ultrasound technology. Recent progress of ultrasound technology has enabled successive tracking of the fasicle length. Since the fasicle length highly relates to muscle force [4], it is very likely that the temporal changes in the fasicle length highly relates to the COP fluctuation.

METHODS

Nine healthy young adults (5 females) participated in this study. Participants quietly stood barefoot with the single leg stance (SLS; right leg) on a force plate. Five trials were conducted, with each trial lasting approximately 10 s. The COP position in the medio-lateral (COP-ML) and antero-posterior (COP-AP) directions were calculated from the vertical and horizontal forces recorded by the force plate.

Ultrasound B-mode images and surface EMG were obtained from the abductor hallucis (AH) and the medial gastrocnemius (MG) of the right leg during single-leg stance. From ultrasound images (~150 fps), fascicle length was obtained by using a validated automatic tracking algorithm [5]. Interference EMG was full-wave rectified (rEMG). After adjusting sampling frequency and applying low-pass filtering at 5 Hz with zero-phase-lag, cross-correlation function (CCF) between COP and fascicle length and between COP and rEMG were calculated for the stead-state 8 s for each COP direction and each muscle. From CCF, a distinct peak above 95% confidence limit near time 0 was identified.

RESULTS AND DISCUSSION

In CCF between COP-ML and fascicle length of AH, a distinct positive peak (0.48 ± 0.20) was found for all participants. In CCF between COP-ML and rEMG of AH, a distinct negative peak (-0.57 ± 0.19) was found for almost all participants. In contrast, a distinct peak CCF between COP-AP and fascicle length of AH was found in a very few participants while a distinct peak CCF between COP-AP and rEMG of AH showed a smaller correlation of coefficient (-0.29 ± 0.14).

In CCF between COP-ML and fascicle length/rEMG of MG, a distinct peak was obtained for some participants. In contrast, in CCF between COP-AP and fascicle length of MG, a distinct negative peak was found for all participants (-0.46 ± 0.10). In CCF between COP-AP and rEMG of MG, a distinct positive peak was found for all participants (0.47 ± 0.11). These results suggest that muscle mechanical and electrical activities of AH and MG are temporally correlated with COP-ML and COP-AP, respectively during single-leg stance.

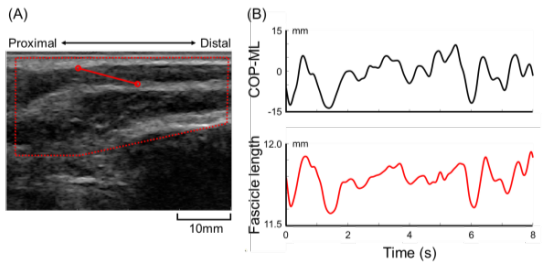

Figure 1 (A) A representative ultrasound image of AH with a fascicle (red line). (B) Example waveforms of COP-ML (upper) and fascicle length (bottom) of AH of a participant during SLS.

CONCLUSIONS

We demonstrated that AH highly contributes to controlling the COP fluctuation in the ML direction, while MG highly contributes to controlling the COP fluctuation in the AP direction during single-leg stance.

ACKNOWLEDGEMENTS

Supported in part by Grant-in-Aid for Scientific Research (B) in Japan to YY.

REFERENCES

[1] Błaszczyk et al. *J Biomech* **110**: 109982, 2020.
[2] Masani et al. *J Neurophysiol* **90**: 3774-3782, 2003.
[3] Kelly et al. *Clin Biomech* **27**: 46-51, 2012.
[4] Yoshitake et al. *J Sport Health Sci* **3**: 280-285, 2005.
[5] Cronin et al. *J Appl Physiol* **111**: 1491-1496, 2011.

MUSCLE SYNERGY ANALYSIS OF TWO SINGLE-LEG YOGA POSTURES: COMPARISON BETWEEN PRACTITIONERS AND NON-PRACTITIONERS

Luciano Luporini Menegaldo[1]*, Dafne Pires Pinto[1], Henrique Lelis C. de Oliveira[1] and Pedro Sarmet Moreira[1]
[1] Biomedical Engineering Program, COPPE, Federal University of Rio de Janeiro, Brazil.
Email: lmeneg@peb.ufrj.br

INTRODUCTION

Several effects on human physiology have been reported in the literature regarding Yoga practice. One is the increased inhibitory gamma amino-butyric acid (GABA) neurotransmitter system activity due to vagal stimulation mediated by the breath [1], which also influences feedforward cortical control on postural control [2]. In this work, we address whether habitual Yoga practitioners modulate muscle activity, releveled by EMGs, differently from non-practitioners while performing two simple single-leg Yoga postures.

Dimensionality reduction techniques, such as the non-negative matrix factorization (NMF), have been used to decompose m muscles' EMGs into a set of $n<m$ vectors called *synergies* multiplied by n time-varying neural commands [3]. Synergy analysis might reflect biological information processing and the generation of motor commands by the central nervous system. The number of synergies a subject uses in a motor task should be proportional to the complexity or richness of that motor execution related to skill. Fewer synergies, otherwise, might reflect a poorer task execution caused by disease or lack of training. However, by performing the Yoga postures (asanas), the subject aims to keep the center of mass as stable as possible, suppressing the body movement and, perhaps, decreasing complexity. Does Yoga training increase the number of synergies due to skill? Or, otherwise, might the increased inhibitory activity reduce the number of synergies while performing a learned asana?

METHODS

Eight yoga practitioners (YG) and eight healthy non-practitioner controls (CG) participated in the study, which was approved by Institution's Ethics Committee. The YG has practiced Yoga non-interruptedly for at least six months, at least two hours a week. The volunteers performed the Vrksasana for 45 seconds twice, with a 5 minutes rest interval. In the sequence, they performed the Natarajasana twice by the same time. Only the first stable 20s were considered in the analyses after the transient phase of the postures had decayed. EMGs from 11 muscles were collected using a BTS FreeEMG 300 device: gluteus medius, gluteus maximus, biceps femoris long head, semitendinosus, vastus lateralis, rectus femoris, tensor fasciae latae, gastrocnemius medialis, erector spinae iliocostalis, obliquus externus abdominis and soleus. EMG data were sampled at 1080 Hz and processed according to [4]. We used the variability accounted for (VAF) criterion (total VAF and per muscle >90%) to select the minimal number of synergies to reconstruct the original EMGs. The synergy vectors across subjects were gathered using k-means clustering. The synergy coordination index (SCI), which evaluates the size of the resulting synergy space or the coordination among the utilized synergies, was also assessed [5]. A larger SCI expressed a smaller synergy space size and was positively correlated to balance skills in a perturbed posture test. As data was identified as nonparametric, the Mann-Whitney U-test was used to compare groups; the Wilcoxon Signed Rank test was used to compare postures.

RESULTS AND DISCUSSION

Regarding the Vrksasana, the CG presented a median (interquartile range) number of synergies of 9.5 (3.25), while the YG was 6.5 (3.25) ($p=0.0365$*, $\eta^2=0.249$). In the Natarajasana, the number of synergies was 8 (2.5) vs. 9 (1) ($p=0.1675$, $\eta^2=0.116$) for the same groups. Comparing the postures, CG $p=0.3125$ ($\eta^2=0.092$) and YG $p=0.0547$ ($\eta^2=0.240$). Natarajasana presented a tendency for a smaller SCI compared with Vrksasana (YG: 0.157 x 0.209, $p=0.0391$* $\eta^2=0.276$; CG: 0.156 x 0.226, $p=0.1049$, $\eta^2=0.044$). When both groups were merged, the median values of SCI were 0.198 for Vrksasana and 0.158 for Vrksasana ($p=0.0299$*).

CONCLUSIONS

Yoga practitioners used fewer synergies than controls for the Vrksasana, suggesting a reduction of control complexity mediated by training. This effect was not observed for the Natarajasana. Additionally, the YG used more synergies (marginal p, but large effect size) for controlling the Natarajasana posture than the Vrksasana. When both groups merged, the SCI for Natarajasana was smaller than for Vrksasana, indicating that Natarajasana requires a larger synergy space and is a more demanding and complex postural task.

ACKNOWLEDGEMENTS

CNPq, CAPES, FINEP and FAPERJ.

REFERENCES

[1] Streeter CC et al. *Med Hyp* **78**: 571-579, 2012.
[2] Pinto DP et al., *Motor Control* **26**: 414-429, 2022
[3] Ting LH, *Prog Brain Res* **165**: 299-321, 2007
[4] Torres-Oviedo G and Ting, LH, *J Neurophysiol* **103**: 3084-3098, 2010
[5] Alnajjar F et al., *Front Comp Neurosc*: **7**, 136, 2013.

BREAK DANCE MOTION ANALYSIS THROUGH MOTOR SYNERGY

Keli Shen and Jun-ichiro Hirayama

National Institute of Advanced Industrial Science and Technology (AIST), Tsukuba, Japan.

Email: shen.keli@aist.go.jp

INTRODUCTION

Dance motion analysis is very challenging due to the complexity of movements as well as the large variety of motions across dance genres and choreographies. Motor synergy analysis is a powerful approach to understanding complex dance movements. Yet, most previous works [1, 2, 3] on dance synergies focused on simple dance motions with a limited variety in genres and choreographies. Thus, we aimed to newly analyze the motor synergies in break dance, a popular style of hip hop dance, especially their variability between choreographies.

METHODS

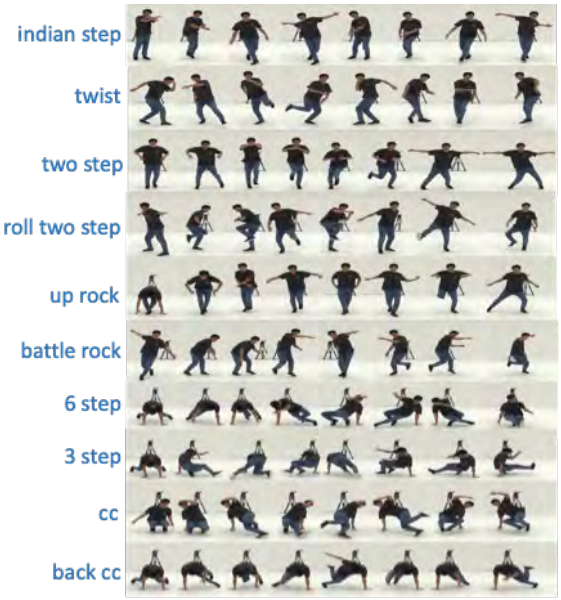

Figure 1 Key frames of ten break dance choreographies.

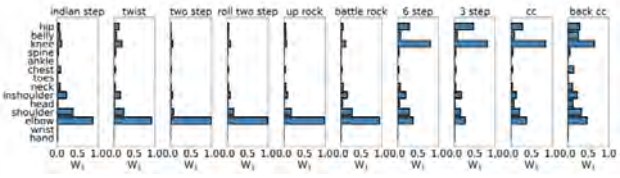

Figure 2 Motor synergy 1 of ten break dance choreographies with PCA.

Data were obtained from AIST Dance Video Database [4], and AIST++ dance datasets [5]. Three male dancers ageing in 20 − 30 years old had 6, 10, and 13 years of break dance experience. Each dancer performed four runs of ten dance choreographies shown in Figure 1. The music tempos of break dance were set to 80, 90, 100, 110, 120, and 130 beats per minute (BPM). The kinematic dance parameters were estimated [5]. First, we translated the 3D joint angles into the Euler-angle format. Then, the angle data of each choreography were segmented by the music beat timings. A root joint was discarded, and the remaining 23 joints (69 degrees of freedom) were considered in the synergy analysis. Motor synergy was computed with concatenated dance motion segments. PCA is used to minimize the following reconstruction error with respect to W and C:

$$E^2 = ||X - W \cdot C||_F^2 , \quad (1)$$

where $||\cdot||_F$ means the Frobenius norm, and X, W, and C depict the matrices of joint angles, motor synergies, and activation weights, respectively; W was taken to be orthonormal in columns.

RESULTS AND DISCUSSION

The modular motor synergy scores were summarized by taking the square root of the sum of squares of motor synergy weights in W within each body module. The 14 modules are given in Figure 2 (only the 1st PC is shown). The upper limb mainly contributes to the first six break dance choreographies, while the lower limb mainly contributes to the last four choreographies. The contribution of upper and lower limbs can be confirmed from movement key frames of dance choreographies depicted in Figure 1.

CONCLUSIONS

We recruited the modular motor synergy analysis by PCA and characterized a difference in the contributions of the upper and lower limbs. The ten choreographies were roughly divided into two groups based on the modular contributions. This synergy-based method may contribute to dance classification and motor coordination study.

ACKNOWLEDGEMENTS

This work was supported by New Energy and Industrial Technology Development Organization (NEDO) project JPNP20006, and JSPS KAKENHI Grant Number JP22K20519, Japan.

REFERENCES

[1] Toiviainen P et al. Music Perception,2010.
[2] Bronner S et al. Exp. brain, 233: 3565-3581, 2015.
[3] Toiviainen P et al. Music Perception,2022.
[4] Shuhei T et al. ISMIR 2019, pp.501-510, 2019.
[5] Ruilong L et al. ICCV, 2021.

LONG-LASTING VR-INDUCED POSTURAL CONTROL IMPAIRMENT AFTER MTBI

Gustavo Sandri Heidner[1,2], Zachary J. Domire[2], and Nicholas P. Murray[2]
[1] Department of Kinesiology, Montclair State University, Montclair, NJ, USA.
[2] Department of Kinesiology, East Carolina University, Greenville, NC, USA.
Email: heidnerg@montclair.edu

INTRODUCTION

Concussions often result in short-lived to long-lasting neurological function impairment, with symptoms appearing immediately, and possibly deteriorating into permanent neural damage. Several efforts have been made to quantify the incidence concussions and to improve diagnostic methods, which are still largely inconclusive and not always accurate. An absence of specific neuromuscular markers compromises diagnostic ability and reliability. For that purpose, we chose to investigate the neural correlates of oculomotor metrics (eye tracking) and corticomuscular coherence (EEG-EMG) metrics when participants are submitted to a virtual reality-implemented optical flow paradigm.

METHODS

The study cohort was comprised of thirty-three ($N = 33$, $n = 13$ concussed) young adults ($M_{age} = 21.6 \pm 3.0$ years), with a BMI < 30, with normal or corrected-to-normal vision that had or had not had a concussion in the past 8 years ($M_{time} = 33.8 \pm 26.0$ months since last concussion). Participants completed concussion history and physical activity levels surveys. They were then prepped with the wireless EEG cap and EMG electrodes and asked to stand in a relaxed position on a force plate (960 Hz). A 5-point calibration was then performed in the virtual reality (VR) environment and a set of mock targets was used to visually verify the calibration at the beginning of each trial. They completed three trials, each with a duration of 30 seconds. Data across all devices were time locked. Cross-spectra of delta, theta, alpha, beta, low gamma, and high gamma frequency bins were calculated for each individual trial, over each contralateral brain region, in relation to each one of the four leg muscles before being averaged across the three trials for each participant.

RESULTS AND DISCUSSION

For the solei muscles, there were significant main effects of concussion history on the beta, $F(1, 120) = 4.37$, $p = .039$, $\eta_p = .035$, and low gamma, $F(1, 120) = 7.35$, $p = .008$, $\eta_p = .058$, frequency bins. Similarly, for the tibiales anterior muscles, there were significant main effects of concussion history on the beta, $F(1, 120) = 4.49$, $p = .036$, $\eta_p = .036$, and low gamma, $F(1, 120) = 6.12$, $p = .015$, $\eta_p = .049$, frequency bins. In all cases, corticomuscular coherence in the beta and low gamma frequency bins increased in concussed participants when compared to their non-concussed counterparts (Figure 1). Neural modulations and muscle activity couplings were independent of limb dominance, and that the differences observed in the cerebral cortex between groups were similar across the frontal and sensorimotor cortexes. It is well-known that EMG amplitude increases with activation intensity[1] and that increased activation amplitude during dynamic loading is a product of faster cross-bridge cycling[2]. Similarly, cortical activity shifts towards greater frequencies during dynamic force tasks, especially when rapid integration of somatosensory and visual information is present[3].

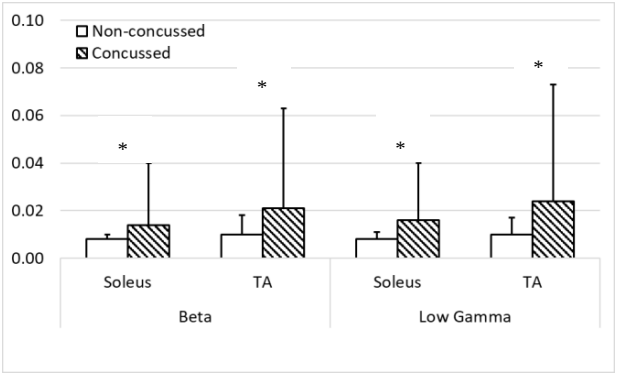

Figure 1. Means and standard deviations of corticomuscular coherence coefficient (y-axis) in β and low γ frequency bins for the solei and tibiales anterior of concussed and non-concussed groups. TA: tibialis anterior; β = 12-30 Hz; Low γ = 30-50 Hz; *: $p < .05$ between concussed and non-concussed.

CONCLUSIONS

Our results suggest that a link exists between cortical and lower extremity muscle activity dysfunction and concussion-related balance impairments persistence can be detected through a dual task visuomotor paradigm. These changes in corticomuscular coherence may predispose mTBI patients to musculoskeletal injury risk.

ACKNOWLEDGEMENTS

This project was supported by the Kinesiology Department at East Carolina University, and by the Matching Dissertation Grant from the International Society of Biomechanics.

REFERENCES

[1] Sakamoto A et al. *Eur J Appl Physiol* **112(3)**: 1015-25, 2012.
[2] Evetovich TK et al. *Med Sci Sports Exerc* **30(12)**: 1697-702, 199
[3] Omlor W et al. *Neuroimage* **34(3)**: 1191-8, 2007.

Awareness of Visual Offset Does Not Improve Shoulder Joint Position Sense in Virtual Reality Environment

Motoki Sakurai[1] and Andrew R. Karduna[1]
[1] Department of Human Physiology, University of Oregon, Eugene OR, USA
Email: motokis@uoregon.edu

INTRODUCTION

Humans integrate vision and proprioception to reach to a target (eg, grab a bottle), though they tend to weigh vision more heavily than proprioception [1]. Additionally, a motor learning study found that visual input could not be disregarded where participants were informed about visual offset and asked to ignore vision [2]. However, it remains unclear if humans can disregard visual input for a reaching task where motor adaption over trials is not involved. In the present study, we investigated the effect of visual offset when participants were instructed to ignore vision during a joint repositioning study. It was hypothesized that 1) induced visual offsets would result in repositioning errors consistent with the direction of the offset, and 2) the same trend in joint repositioning error would be observed even when participants were informed about offsets and asked to ignore vision.

METHODS

Sixteen healthy right-handed participants (female/male: 10/6, age: 23.3 ± 2.6 yr, height: 1.7 ± 0.1 m, weight: 68.3 ± 6.3 kg) performed a joint position sense (JPS) test in an immersive virtual reality environment (HTC VIVE, Taoyuan, Taiwan). Auditory cues guided the participants to reach to a target shoulder flexion angle (85, 90, 95, or 100º) to remember, and each target was presented three times for a total of 12 trials. Subjects were then instructed to replicate the target position as accurately as possible without auditory cues. A black marker represented a real-time hand position throughout the trial. There were total of 3 blocks of 12 trials. The first block was a familiarization block, where no visual offset was introduced for all 12 trials. Following the first block, two offset blocks (OB1 and OB2) were completed, where the task and settings were the same. The only difference between blocks was that participants were informed about the visual offset and instructed to ignore vision in OB2. In the two offset blocks, 4 out of 12 trials did not have a visual offset (0º offset) while either -8º or +8º vertical offset in the black marker position was caused for each of 4 target angles with a random order (12 trials per block – 3 offset angles x 4 target angles).

Constant error (CE) was calculated for each trial by taking a difference between a target angle and replicated angle with direction of error being taken into account. A two-way repeated measures ANOVA was performed to examine the main effect of visual offset and block as well as interactions of them on CE. Pairwise t-tests with the Bonferroni correction were performed for post-hoc testing when a significant effect or interaction was observed in the ANOVA. For all the statistical tests, an alpha level was set at 0.05. All statistical analyses were performed using R 4.2.2 (R Core Team)

RESULTS AND DISCUSSION

A significant main effect was found for visual offsets ($p < 0.001$), and a post-hoc pairwise t-test revealed that CE was larger when visual offsets were introduced ($p < 0.001$). Neither the effect of blocks nor the block-offset interaction was significant ($p > 0.05$). These results support the findings from a previous study in our lab which demonstrated that a visual offset causes an increase in reaching error [1]. It also demonstrated that awareness of visual offset did not increase an instant reaching task accuracy, similar to a motor adaptation study that involved reaching [2]. These results suggest that humans may rely on vision for reaching motions regardless of its accuracy when present.

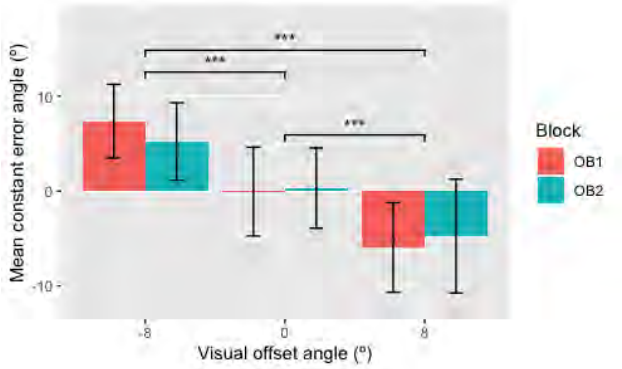

Figure 1. Mean CE with different visual offsets in OB1 and OB2 across participants. ***: $p < .001$

CONCLUSIONS

Our hypotheses were supported, with a non-significant block effect and significant visual offset effect. For shoulder flexion repositioning task, the awareness of visual offset did not help improve JPS.

REFERENCES

[1] Spitzley KA & Karduna AR. *J Motor Behavior*. **54(1)**: 92-101, 2022.

[2] Morehead JR et al. *J Cognitive Neurosciencey*. **29(6)**: 1061-107, 2017.

EFFECTS OF DUAL-TASK CHALLENGES ON THE MULTI-OBJECTIVE OPTIMAL CONTROL STRATEGIES DURING OBSTRUCTED GAIT

Yi-Chun Kuan[1,2,3,4], Shiuan-Huei Lu[1], and Tung-Wu Lu[1,5]
1 Department of Biomedical Engineering, National Taiwan University, Taiwan
2 Taipei Neuroscience Institute, Taipei Medical University, Taipei, Taiwan
3 Dementia Center and Department of Neurology, Taipei Medical University Shuang Ho Hospital, New Taipei City, Taiwan
4 Department of Neurology, School of Medicine, College of Medicine, Taipei Medical University, Taipei, Taiwan
5 Department of Orthopaedic Surgery, School of Medicine, National Taiwan University, Taiwan
Email: yckuang2@gmail.com

INTRODUCTION

Dual-task (DT) crossing is a more challenging activity that occupies cognitive resources than single-task (ST) crossing. Studies on cognitive-motor interference employing DT conditions have demonstrated that limited attentional resources are needed for gait, postural control and balance, resulting in a greater demand for the attentional load [1]. Lu et al. developed a customized planar model of the body for simulating ST obstacle-crossing [2]. Therefore, the current study aimed to identify the control strategy of DT obstacle-crossing of different heights using a multi-objective optimal control (MOOC) technique.

METHODS

Twelve healthy adults were asked to walk at a self-selected pace on an 8-meter walkway and to cross a height-adjustable obstacle (i.e., 10%, 20% and 30% of the subject's leg length) and two task conditions (i.e., ST and DT). During DT crossing conditions, each subject not only crossed the same obstacle as in the ST condition but also concurrently counted down by 3's from a randomly generated number between 90 and 100 and speak out loud. Marker trajectories were recorded using a motion capture system (Vicon MX T-40, OMG, UK) and the ground reaction forces were measured by two forceplates (OR6-7, AMTI, USA). Obstacle-crossing was formulated as an optimal control problem with two conflicting objectives: minimization of mechanical energy expenditure (f_1) and maximization of clearances of the swing heel (f_2) and toe (f_3) above the obstacle [2]. The resulting MOOC problem was solved using the weighting method, i.e. ($W_1f_1 + W_2f_2 + W_3f_3$). The crossing speed, end-point variables, and best-compromise weighting sets were averaged across all subjects for all tasks and height conditions. These weighting sets were compared between different tasks and obstacle heights using two-way repeated ANOVA.

RESULTS AND DISCUSSION

Compared to the ST obstacle-crossing, the DT obstacle-crossing condition showed an overall decreased crossing speed but increased leading and trailing toe-obstacle clearance. There were no significant between-task differences in leading heel-obstacle distance, trailing toe-obstacle distance, and best-compromise weighting sets (Figure 1) during both ST and DT tasks.

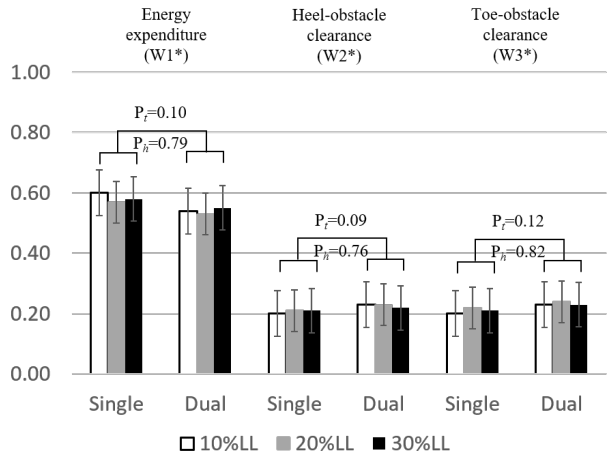

Figure 1: Means (standard deviations) of the best-compromise weighting sets (W1*, W2*, W3*), corresponding to the objective functions of mechanical energy expenditure, heel-obstacle clearance, and toe-obstacle clearance of the MOOC problem, for the single-task and dual-task crossing obstacles of three different heights: 10% (white), 20% (grey) and 30% (black) of individual subjects' leg length (LL). P-values for the main effects are also given (P_t: task effects; P_h: height effects).

CONCLUSIONS

Healthy adults were found to use similar control strategies during single-task and dual-task obstacle crossing, suggesting that the observed strategy was one at the central nervous system level. More studies shall assess the control strategy in patients with pathology.

ACKNOWLEDGEMENTS

This work was supported by the Ministry of Science and Technology, Taiwan (MOST 108-2314-B-038-057).

REFERENCES

[1] Bishnoi A et al. *Aging Ment Health*. 25: 1618-29, 2021
[2] Lu TW et al. *Gait & posture*. 36(3): 552-556, 2012

GENDER DIFFERENCES IN POSTURAL CONTROL DURING SINGLE-LEG SQUAT

Sakiko Nishimura[1,2], Tsutomu Fukui[23], Kazuyuki Mito[1]

[1] The Graduate School of Informatics and Engineering, The University of Electro-Communications / Tokyo, Japan.

[2] Sports Management Center, Bunkyo Gakuin University/ Tokyo, Japan

[3]Department of Physical Therapy, Bunkyo Gakuin University/ Saitama, Japan

Email: s-nishi@bgu.ac.jp

INTRODUCTION

The previous study showed when healthy people control posture using ankle and hip strategy there is some "trading off" between ankle and hip during single leg squat. In other word, when ankle moment is high hip is low, also when hip moment is high ankle is low. the study also suggested that postural control in the frontal plane was similar to it in the sagittal plane [1]. On the other hands, Gender differences in mutual relationship of lower extremity kinetics is unclear. The mutual relationship of lower extremity movement has been reported during single leg squat by Graci V et al [2]. The study suggested females show more knee abduction and hip adduction, than males in landing and single leg squat. But not including lower extremity moment. This study aimed to investigate the difference in lower extremity moment for posture control in frontal plane between genders during single leg squat.

METHODS

Subjects were 16 healthy adults (8 males and 8 females; 21.0 ± 1.5 yrs.) without history of orthopedic disease in lower limbs. They were asked to do a single-leg squat with their right leg. We asked that they bend their knee in 2 seconds and extend in 2 seconds and repeat three times. Kinematic and force plate data were collected with an eight-camera, three-dimensional motion capture system (VICON Nexus; Vicon Motion Systems Ltd., UK) and six force plates (AMTI, USA). Thirty-five reflective markers were attached to anatomical landmarks following the Vicon Plug-in-Gait marker placement protocol. Difference in frontal plane moments of lower extremity between male and female were analyzed using independent-samples t-test (significance at $p<0.05$).

RESULTS AND DISCUSSION

As a result of comparing frontal plane moment of lower extremities between males and females, hip moment of females is higher than males one and ankle moment of females is lower than males. Differences of Knee moment between gender are no significant (Table 1). That is, compared to males, females use hip strategy more ankle strategy for posture control. Also, focusing on the hip moment of each, while all males almost had the same values, females were divided into two groups, one with the same values as males and the other with higher values (Figure 1). In other words, females use a wider variety of postural control in than males. Some females use hip strategy more ankle and others use ankle strategy hipper like male.

Table 1: Gender differences in frontal plane moment of lower extremity

Joint	Joint Moment [Nm/kg]		*p-value*
	Male	Female	
Hip	15.5 ± 2.4	21.4 ± 4.1	$p<0.05$
Knee	13.1 ± 2.8	9.34 ± 7.1	*N.S*
Ankle	3.22 ± 0.5	2.41 ± 0.7	$p<0.05$

mean ± SD independent-samples t-test (n=16)

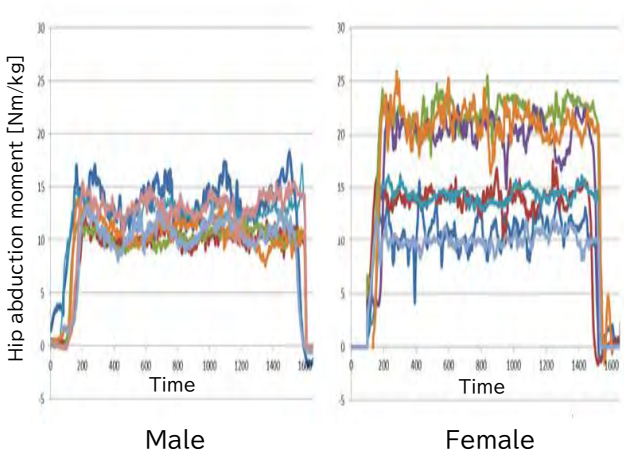

Figure 1 Gender differences in hip abduction moment during single-leg squat

CONCLUSIONS

These results demonstrate that females use a different movement strategy during single leg squat from males and that females showed more patterns of movement strategy between individual than males. We found some females employ a different movement strategy from males and such a strategy could expose females to a greater risk of hip and knee pain. For that reason, a postural control for female should be analyzed with attention to individual differences.

REFERENCES

[1] Nishimura S et al. *JPhysTherSci***30** :755-58,2015.

[2] V. Graci et al. *Gait Posture* **36**:461-466, 2012.

FORCE ENCODING IN MUSCLE SPINDLE SECONDARY ENDINGS

Jacob D. Stephens[1], Paul Nardelli[2], Lena H. Ting[1] and Timothy C. Cope[1,2]

[1] Coulter Department of Biomedical Engineering, Emory University and Georgia Institute of Technology, Atlanta, USA.[2] School of Biological Sciences, Georgia Institute of Technology, Atlanta, USA. *Email: jdstephens@gatech.edu

INTRODUCTION

Proprioception is a vital sense for the precise coordination of movement, however proprioception relies on feedback from multiple mechanosensors that are not fully-characterized. It has been postulated that length feedback from muscle spindles provide a mechanical description of the muscle tendon unit (MTU) state to the central nervous system. However, group IA afferents exhibit highly complex behavior that is not fully captured by muscle length and has been attributed to crossbridge binding properties of muscle fibers within the spindle [1]. Specifically, gr. IA firing in some passive stretch conditions can respond in part to muscle resistance to stretch, as shown by similarities to the muscle's force, as well as the yank (dF/dt), which give rise to initial bursts. On the other hand, muscle spindle gr. II afferents may be more singular in their encoding, as gr. II afferents do not terminate on the same fibers that give rise to initial bursts in IAs. We hypothesize that gr. II afferents respond to the resistive force on the muscle spindle and predict that, during imposed stretches of quiescent muscle, they can be modeled by estimates of the force on the muscle spindle.

METHODS

Preliminary data were collected from 11 afferents across 3 animals: 7 gr. IA and 4 gr. II. Length-controlled 20 mm/s ramp-hold-release stretches were applied to the triceps surae MTU in deeply anaesthetized rats. Action potentials were recorded via glass microelectrodes from the dorsal root of the spinal cord, and afferents were classified as either IA or II according to conduction velocity and responses to muscle twitch and vibration. Afferent firing profiles were fit to muscle force and yank using constrained optimization in MATLAB according to Blum et al in 2017 [1] and 2019 [2].

RESULTS AND DISCUSSION

As has been reported previously, gr. IA afferent firing rates could be reproduced with linear combinations of force and yank. Firing profiles were fit with a yank coefficient of 16 ± 14 pps/N/s (mean ± sd) and a force coefficient of 147 ± 81 pps/N, with a variance accounted for (VAF) of 0.74 ± 0.34. In comparison, gr. II afferents were best predicted with a similar force coefficient of 185 ± 56 pps/N and a smaller yank coefficient of 3 ± 2 pps/N/s, with a VAF of 0.89 ± 0.06. To ensure this small yank component was not a coincidence in the optimization, fits were run again without yank. In this iteration, the force component increased by 14 pps/N (p<1e-12, paired t-test) and the VAF decreased by 0.037 (p<1e-7, paired t-test), indicating yank did contribute to the model fit.

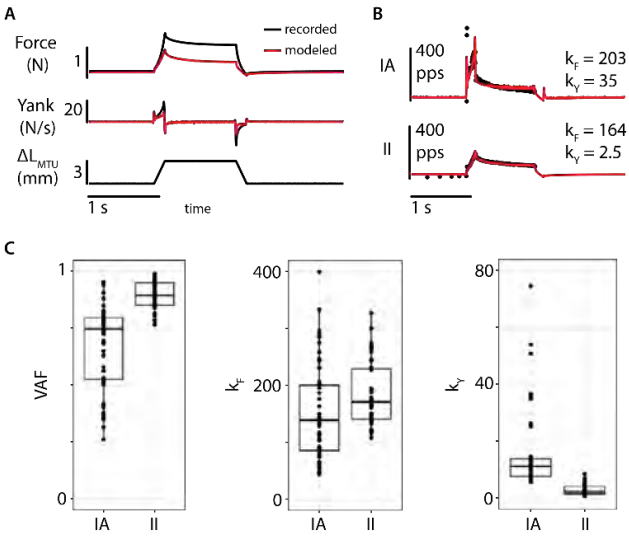

Figure 1 A) Example traces of recorded MTU length, MTU force, MTU yank, and IFR of a group IA afferent (black) and the estimated force and yank on contractile muscle tissues (red) according to the method described by Blum et al 2019 [2]. B) Example model fits using combinations of modelled force and yank in group IA, II, and IB afferents. C) Grouped data of model VAF, force component (k_F), and yank component (k_Y) of all afferent classes.

CONCLUSIONS

Although the yank sensitivity of gr. II afferents was non-zero, it was very low relative to the yank sensitivity of gr. IAs (means 3 and 16 pps/N/s, respectively). Thus, while gr. II afferents from muscle spindles do not appear to purely respond to forces on the spindle, the signal is biased towards force more so than gr. IAs. Considering gr. IAs and IIs together, it's possible that these afferents relay different components of imposed muscle stretches to the central nervous system.

ACKNOWLEDGEMENTS

This work was supported by the Georgia Tech/Emory NIH/NIBIB Training Program in Computational Neural-engineering (T32EB025816) and the National Institutes of Health Eunice Kennedy Shriver National Institute of Child Health and Human Development (NICHD) R01HD090642.

REFERENCES

[1] Blum KP et al. *PLoS Comput Biol* 2017 Sep 25;13(9).

[2] Blum KP et al. *J Exp Biol* 2019 Aug 2;222 (Pt 15)

Sex differences in laterality of motor unit firing behaviour of first dorsal interosseous muscle in young adults.

Yuichi Nishikawa[1] and Allison Hyngstrom[2]
[1] Faculty of Frontier Engineering, Kanazawa University, Kanazawa, Japan.
[2]Department of Physical Therapy, Marquette University, Milwaukee, United States.
Email: yuichi@se.kanazawa-u.ac.jp

INTRODUCTION

Human movement is coordinated by the central and peripheral factors. There is a sex differences in physical performance, in addition to muscle volume and muscle fiber composition as factors, sex differences in motor unit (MU) firing behabiour have recently reported [1]. Sex differences in central nervous system functions and hormonal influences have been pointed out as possible factors. Furthermore, hormones have been implicated in asymmetry of brain function, and high progesterone levels are known to weaken interhemispheric inhibition. These findings suggest that there are sex differences in asymmetries in motor nerve function, but sex differences in asymmetries of MU firing behaviour are not clear. The aim of this study was to examine the sex difference in laterality of MU firing behaviour during submaximal isometric contraction of first dorsal interosseous (FDI) musle in healthy young adults.

METHODS

Twenty-seven subjects (females, n = 14 and males, n = 13) were enrolled in this study. A grid of 64 multiple electrode was used to record the high-density surface electromyography (HD-EMG) from the FDI muscle. The participants were asked to perform maximum isometric voluntary contraction (MVC) of the bilateral pinch force. After MVC recording, all participants performed a submaximal isometric pinch force at 10%, 30%, and 60% MVC in a random order. Convolution blind source separation method was used to separate HD-SEMG recordings into individual MU discharge. To identify individual MUs, we used DEMUSE software [2]. A generalized linear mixed-effect model with random slopes, followed by Bonferroni multiple comparisons as a post hoc analysis, was applied to analyse the mean discharge rate. The explanatory variables were as follows; sex (female or male), side (dominant or nondominant), and MVC (10%, 30%, and 60%). The significance level was set at $p < 0.05$.

RESULTS AND DISCUSSION

We identified a total of 769 MUs (females: 318 MUs; Males: 451 MUs) that were considered for further analysis. The discharge rate showed a significant sex × side × MVC interaction ($F = 5.90$, $p = 0.0027$, $\eta^2 = 0.219$). The discharge rate showed significantly higher values at each torque level on females' dominant side than males' dominant side ($p < 0.0001$, respectively, Figure 1). Furthermore, at 60% MVC, male's nondominant side showed a significantly higher discharge rate than the dominant side ($p < 0.0001$, 95% CI = −5.516 to −2.295), but this pattern was not found in females.

Hormonal influences have been implicated in these sex differences is known to affect neurotransmitter function, and its has been reported that the MU discharge rate is higher after ovulation, when the progesterone level is high. On the other hand, a recent study reported that higher testosterone levels were associated with reduced MU action potential complexity. These findings indicate that sex hormones influence MU firing behaviour and may be one of the reasons for the observed sex differences in MU characteristics. It was also reported that high progesterone levels weakened interhemispheric inhibition, suggesting that such hormonal dynamics led to the asymmetry in the MU characteristics.

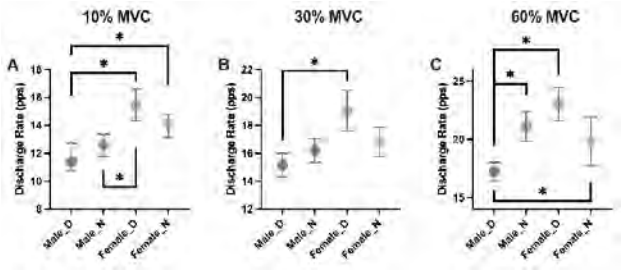

Figure 1. Comparison of discharge between dominant side and non-dominant side in females and males at 10%, 30%, and 60% MVC.

CONCLUSIONS

This study compared sex-specific MU firing behaviour and handedness in young adults using HD-SEMG. We found that males showed (1) significant asymmetry in discharge rate according to handedness at moderate and high force output and (2) a significantly lower discharge rate than females. Sex differences have been observed not only in motor function but also in disease severity, and clarification of neurophysiological sex differences will be an important finding in the rehabilitation medicine as well as in the sports science.

REFERENCES

[1] Lulic-Kuryllo T et al. *J Electromyogr Kinesiol* **66**: 102689, 2022.
[2] Holobar A et al. *Physiol Meas* **35**: 143-65, 2014

Kinematic analysis of controlling foot-ball acceleration at ball impact in Soccer Juggling

Kazuki Aoi[1], Takayuki Koike[1,2], and Masaaki Okauchi[1,2]
[1] Graduate school of Engineering, Oita University, Oita, Japan.
[2] Science and Technology, Oita University, Oita, Japan.
Email: t-koike@oita-u.ac.jp

INTRODUCTION

Previous studies investigated hand juggling and paddle juggling report that the vertical acceleration of the hand and paddle at the moment of ball impact shows negative values [1]. In a study of soccer juggling, vertical acceleration of the foot also showed a negative value at the ball impact [2]. However, it is not clear how the lower limb joints control this juggling when negative acceleration occurred. The purpose of this study was to investigate how the lower limb joints move when the foot acceleration shows negative at the moment of impact by instep kicking during juggling by experienced soccer players.

METHODS

Ten male students with experience in soccer participated in this study. We asked them to perform soccer juggling by instep kicking until the ball dropped to the ground. Subjects' whole-body kinematics during juggling was captured by four high-speed cameras (For-A inc. and Ditect inc., 250 fps). The coordinates of markers attached to the body surface were transformed by the 3D DLT method, and then the joint centers were acquired. The joint angles of both left and right lower limbs were calculated by Euler angles, and then angular velocities were calculated. The acceleration of the center of gravity of the foot was calculated, and the change in acceleration before and after the ball impact was obtained. At least five consecutive cycles of kinematic variables were analyzed, with 50 frames before and after the ball impact as one cycle. In this abstract, we report the results obtained from 6 of the 10 subjects.

RESULTS AND DISCUSSION

In this study, those who showed negative foot acceleration were classified as the negative group, and those whose acceleration values were not constant were classified as the positive group. The negative group had a higher ball height than the positive group (Table 1). The angular velocity of the hip joint on the side of the juggling leg moved in the direction of extension toward impact in the negative group, while it moved in the direction of flexion in the positive group. In the knee joint angle (Figure 2), the negative group was near full extension at impact and then flexed, while the positive group was in extension at impact and then extended. In the stance leg, the hip joint was always flexed in both groups. The knee joint was slightly flexed before impact and then extended toward impact, in the negative group. The positive group showed no change in angle and angular velocity. In the ankle joint, the negative group was always in the neutral position between plantar flexion and dorsiflexion, while the positive group was always in the plantar flexed position.

The negative foot acceleration at ball impact was caused by full extension of the knee joint and plantar flexion of the ankle joint of the kicking foot at impact, which was thought to be due to the gastrocnemius muscle, a biarticular muscle that mainly acts in knee flexion and plantar flexion, being stretched by knee extension.

Table 1: Ball height during soccer ball juggling.

	Mean height (m)
Negative group	1.28 ± 0.16
Positive group	0.78 ± 0.09

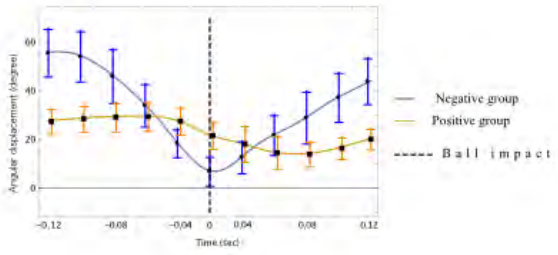

Figure 1 Angular displacement of the knee joint before and after ball impact.

CONCLUSIONS

The foot acceleration at the ball impact during soccer juggling was considered to be negative because of the coordinated movement of the joints on the leg side of the ball kicker, especially the multi-joint movement with full extension of the knee joint as the axis..

REFERENCES

[1] Sternad et al. *J Exp Psychol. Hum.Percept. Perform.*, **27**: 1163-1185, 2001.
[2] Tlili et al. *Neurosci. Lett* **360**: 45-48, 2004.

Sensorimotor learning of whole-body goal-directed movements with upper and lower extremities

Nagisa INUBASHIRI[1], Shota HAGIO[1] and Motoki KOUZAKI [1]
[1] Graduate School of Human Environmental Studies, Kyoto University, Kyoto, Japan.
Email: inubashiri.nagisa.22n@st.kyoto-u.ac.jp

INTRODUCTION

Imitation of the instructor's posture is one of the most common training methods for whole-body motor learning, which needs goal-directed movements with multiple effectors, such as the upper and lower extremities [1]. Previous studies have separately investigated sensorimotor learning process with either upper or lower limbs [2,3]. However, it has not been elucidated how the central nervous system learns the goal-directed movements with both the upper and lower extremities in a novel sensorimotor environment. Therefore, the purpose of this study was to examine sensorimotor learning in goal-directed upper and lower extremity movements using a novel point-to-point movement task with multiple effectors.

METHODS

Nine healthy men (age: 23.2 ± 1.3 years; height: 173.6 ± 5.0 cm; body mass: 68.2 ± 10.0 kg) participated in this study conducted over two days. On both days, goal-directed point-to-point movements were performed with the endpoint of both the upper and lower extremities. Participants were asked to simultaneously move four cursors corresponding to the frontal positions of both hands and feet to four targets on the screen. The positions of the hands and feet in the frontal plane were captured by the optical motion capture system and were mapped to the cursors on the screen in real-time. On Day 1, the tasks were conducted in 300 trials where the direction of the cursor movements corresponded to the direction of the hands and feet movements (normal mapping). On Day 2, after 60 trials in normal mapping, learning trials were implemented in 300 trials where the cursor movements in mediolateral directions were reversed to the direction of the hands and feet movements (mirror-reversed mapping). Mirror-reversed mapping induced learning of goal-directed hands and feet movements in a novel visuomotor environment. After learning trials, participants performed 60 trials in normal mapping as washout trials. One of thirty targets (6 directions × 5 distances) was randomly presented around each hand and foot. We measured reaction time in each of hands and feet and the elapsed time from movement onset to the time when all cursors moved within the targets (movement time).

RESULTS AND DISCUSSION

The mean movement time for the last 10 learning trials was significantly shorter than the time at the beginning of the learning trials for all end-effectors (Figure 1; Dominant hand: DH, 1.96 ± 0.74 vs 1.02 ± 0.62 s; Non-dominant hand: NH, 1.19 ± 0.73 vs 1.03 ± 0.34 s; Dominant foot: DF, 2.33 ± 0.30 vs 1.16 ± 0.33 s, the significance level was 0.05). Decrease in the movement time indicates that goal-directed movements both with the upper and lower extremities were learned in a novel mirror-reversed visuomotor environment. In learning trials, the movement time of DH and NH was similar to each other, whereas longer movement time was observed in DF. In addition, the reaction time of DF was significantly shorter than that of DH and NH during last 10 learning trials (p = 0.002, p < 0.001, respectively). These results indicate that visuomotor learning of whole-body goal-directed movements progressed in different learning processes between the upper and lower extremities.

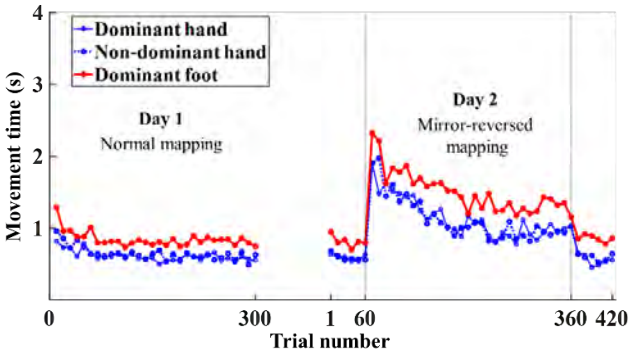

Figure 1 Movement time in each trial on Day 1 and Day 2. Movement time decreased over the course of the trials in mirror-reversed mapping. Each dot means average for all participants.

CONCLUSIONS

The goal-directed movements needed to control multiple end-effectors could be learned in a novel visuomotor environment. The process of learning would be similar in both hands but different between the upper and lower extremities.

ACKNOWLEDGEMENTS

This work was supported by Japan Society for the Promotion of Science (JSPS), Grant-in Aid for Scientific Research (B) (21H03343).

REFERENCES

[1] Pacheco M et al. *Front. Psychol* **10**: 1874, 2019.
[2] Shadmehr R et al. *J. Neurosci* **14**: 5, 1994.
[3] Moriyama M et al. *Front. Sports Act. Living* **4**: 883656, 2022.

Control of standing posture depends on adaptation of goal-directed lower extremity movements

Mai Moriyama[1], Motoki Kouzaki[1], and Shota Hagio[1]
[1] Graduate School of Human and Environmental Studies, Kyoto University, Kyoto, Japan.
Email: moriyama.mai.45u@st.kyoto-u.ac.jp

INTRODUCTION

How do sophisticated soccer players acquire skillful manipulation of a ball with their feet depending on ever changing environments? It was revealed that goal-directed movements with lower limb can be adapted to a novel visuomotor environment using a virtual ball-kicking task [1]. Since ball-kicking movements require single-leg stance posture, the support leg would be controlled in parallel with the adaptation of the kicking-leg movements to a novel environment. Previous study examining arm-reaching during standing posture demonstrated that anticipatory postural adjustments (APAs) to maintain postural equilibrium was learned in the process of adaptation of arm movements to novel dynamic environments [2]. Therefore, we aimed to clarify the postural adjustment in the support leg depending on sensorimotor adaptation of goal-directed kicking movements.

METHODS

Nine participants performed ball-kicking movements with their right foot, while standing with their left foot on a force plate. They were instructed to look at a monitor in front of them, which displayed a cursor and a target. The cursor represented participant's right foot position on the horizontal plane, and participants shot the target virtually located at 60 cm ahead of the start position. The foot trajectories were captured in real time using motion capture system. The experimental task was constructed by the baseline, learning and washout trials (140, 210 and 130 trials, respectively). During the learning trials, the cursor trajectory was rotated to 12° clockwise relative to the actual trajectory without telling the participants. This perturbation enabled us to investigate how ball-kicking movements are adapted to the novel visuomotor environment. In each trial, kicking angle was measured as the angular difference between the target and the right-foot position when the right foot exceeded target distance. APAs were also quantified as the medio-lateral deviation of the COP position of the left foot 50 ms before onset time of right foot movement.

RESULTS AND DISCUSSION

In the learning trials, kicking angle gradually shifted leftward to compensate for the rightward error induced by the 12-degree rotational perturbation (Figure 1). After the perturbation was removed in the washout trials, it took several dozen trials for the kicking angle to return to the baseline levels, indicating that participants adapted their right foot movements to the novel visuomotor environment. APAs during the learning trials also shifted leftward as kicking angle changed leftward. Once the perturbation was removed, APAs returned to the baseline level. These results suggest that postural control was modified following the adaptation of the goal-directed movements with the kicking leg.

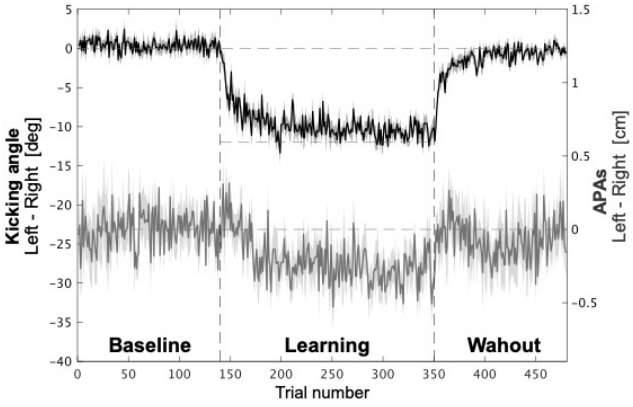

Figure 1 Time course of kicking angle and APAs.
This figure shows kicking angle (black line) and APAs (grey line) averaged across participants. A positive value of both data corresponds to the rightward deviation and vice versa. The shaded area represents the standard error of the mean. During the learning trials, the trajectories of the cursor were rotated to 12° clockwise relative to the actual trajectory. The middle horizontal line indicates the angle of 12 °, which is necessary to perfectly compensate for the perturbation.

CONCLUSIONS

We found that anticipatory postural response was modified in the process of adaptation of the focal goal-directed lower limb movements. The skilled manipulation of lower limb movements would be supported by the flexible adjustment of the postural control.

ACKNOWLEDGEMENTS

This work was supported by Japan Society for the Promotion of Science (JSPS), Grant-in Aid for Scientific Research (B) (21H03343).

REFERENCES

[1] Moriyama M et al. *Front. Sports Act. Living* **4**: 1-8, 2022.
[2] Ahmed A and Wolpert D. *J. Neurophisiol.* **102**: 2816-2824, 2009.

Effects of batting practice with pitch location feedback and peripheral vision on hitting variability in baseball

Masahiro Kokubu[1], Ryoichi Terahara[2], and Yudai Kawahara[2]
[1] Institute of Health and Sport Sciences, University of Tsukuba, Japan.
[2] Graduate School of Comprehensive Human Sciences, University of Tsukuba, Japan.
Email: kokubu.masahiro.gn@u.tsukuba.ac.jp

INTRODUCTION

In baseball batting, tracking fastballs with eyes and perceiving accurate pitch location are considered important. Visual feedback regarding bat-ball contact contributes to hitting accuracy [1]. However, the effects of concurrent feedback about the vertical and horizontal pitch locations on motor learning such as hitting velocity, accuracy, and variability have not been examined.

In addition, it is considered difficult for batters to keep their gaze on the ball until the moment of impact [2], so hitting practice using the peripheral visual field would be considered important.

Therefore, the purpose of the present study was to investigate the effects of batting practice with the feedback of pitch location and with using peripheral vision on hitting variability and velocity.

METHODS

Fifteen university baseball players (20.6±1.6 years; Mean±SD) participated in the present study. They were assigned into three groups: a practice group with pitch location feedback (FB group; n=5), a practice group with peripheral visual field (PV group; n=5), and a control group (CON group; n=5).

In the pre-test, the participants were asked to hit 15 straight pitches which were set at 120 km/h by a pitching machine. The strike zone was divided into five sections, in the high/low and inside/outside directions respectively. After each trial, they were asked to verbally answer the pitch location from the five sections for both directions. The contact position of the ball relative to the bat at impact was measured using a high-speed digital camera (480Hz), and the standard deviation of the bat-ball contact position (i.e., hitting variability) was calculated. The velocity of the ball at impact was also measured by a tracking system (Rapsodo®).

In the FB group, participants executed batting practice with straight pitches which were set at 120 km/h by the pitching machine 30 times per day. They received feedback on the pitch location in both directions immediately after each trial. Practice sessions consisted of three sessions a week for three weeks. In the PV group, participants executed front toss batting practice 40 times per day while directing their gaze at a certain point other than the ball. Practice sessions consisted of three sessions a week for two weeks. In the CON group, participants executed regular practice of the team as usual during this period. In the post-test, all participants were asked to execute the same measurement as in the pre-test.

RESULTS AND DISCUSSION

For the hitting variability, a two-way analysis of variance showed a significant interaction between group and time ($F(2,12)=4.05$, $p=.045$, $\eta_p^2=.40$). Subsequent analysis showed that the PV group showed significantly less standard deviation of the contact position in the post-test than in the pre-test ($p<.05$). There was also a tendency of less variability in the post-test compared to the pre-test in the FB group ($p<.10$). In the control group, there was no difference between the pre- and post-tests. These results suggest that practice using peripheral vision has an effect of less variability of the contact position.

In the FB group, the difference between the perceived and actual pitching position became smaller in the post-test than in the pre-test. Also, hitting velocity was larger in the post-test than in the post-test. These results suggest that there is a relationship between the ability to perceive the pitch location and the increase in batting average velocity.

CONCLUSION

Batting practice with the feedback of pitch location and with using peripheral vision would contribute to reducing hitting variability.

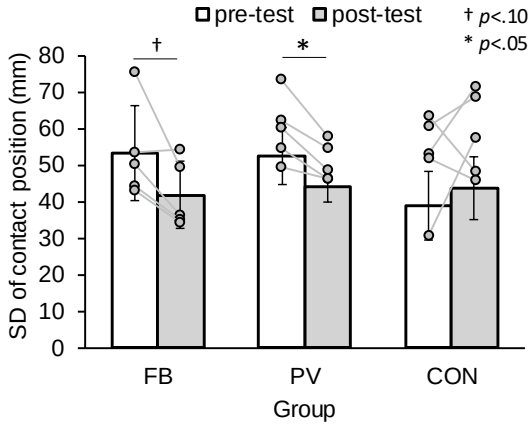

Figure 1 Hitting variability of each group in the pre- and post-test.

REFERENCES

[1] Gray R. *Res Q Exerc Sport* **80**: 491-501, 2009.
[2] Fogt N et al. Optom Vis Perform **8**: 129-34, 2020.

Direct measurements of tendon length changes during stretch-shortening cycles in rat

Atsuki Fukutani[1], Satoru Hashizume[1] and Tadao Isaka[1]
[1] Faculty of Sport and Health Science, Ritsumeikan University, Kusatsu, Japan.
Email: atsukifukutani@gmail.com

INTRODUCTION

The muscle force attained during concentric contractions is augmented by a preceding eccentric contraction. This phenomenon is called the stretch-shortening cycle (SSC). Although tendon elongation is considered the primary mechanism, we recently found that the magnitude of the SSC effect was not different even after removing the Achilles tendon [1]. To resolve these discrepant results, direct measurement of changes in Achille tendon length is required. Therefore, this study aimed to elucidate the influence of tendon elongation on the SSC effect by directly measuring the changes in Achilles tendon length.

METHODS

The rat soleus muscle (N = 9) was used in this experiment. The soleus was exposed and dissected from its surrounding connective tissues, and its blood and nerve supplies were left intact. To place the marker that can visualize the tenon length changes, a knot was placed on the aponeurosis (Figure 1, panel A). In the first experiment, isometric contraction with the maximal intensity was performed at the plateau region (optimal length), ascending limb (-2 mm from the optimal length), and descending limb (2 mm from the optimal length). During these contractions, the location of the silk knot was visualized using a stereomicroscope. In this experimental setting, the field of view was approximately 6 mm, and the number of pixels was 1,824. Thus, the pixel resolution was approximately 3.3 μm. In the second experiment, SSC and pure shortening trials were conducted. For the SSC trial, the isometric contraction was evoked at -2 mm. The muscle-tendon complex was then actively stretched to 2 mm in 1 s. Immediately after the end of the stretch, the muscle-tendon complex was actively shortened to -2 mm in 1 s. For the pure shortening trial, the isometric contraction was evoked at 2 mm, and then, a muscle-tendon complex was actively shortened to -2 mm in 1 s. During these contractions, the location of the silk knot was visualized using a video camera. In this experimental setting, the field of view was approximately 60 mm, and the number of pixels was 4,096. Thus, the pixel resolution was approximately 15 μm.

RESULTS AND DISCUSSION

For the first experiment, the magnitude of tendon elongation was 0.21 ± 0.17 mm for the optimal length, 0.14 ± 0.12 mm for the 2 mm, and 0.29 ± 0.25 mm for the -2 mm (panel B) ($p = 0.05$). Interestingly, the magnitude of tendon elongation was the largest in the smallest force condition (i.e., ascending limb condition). This result suggests that the observed tendon elongation was at least in part derived from eliminating the slack of the muscle-tendon complex. For the second experiment, the magnitude of tendon shortening attained during the shortening phase was not different significantly between SSC (0.20 ± 0.14 mm) and pure shortening trials (0.17 ± 0.09 mm) ($p = 0.322$) (Figure 1, panel C). This result indicates that the larger force attained in the SSC than in the pure shortening condition is difficult to be explained by the elastic energy stored in tendons or muscle-tendon interaction.

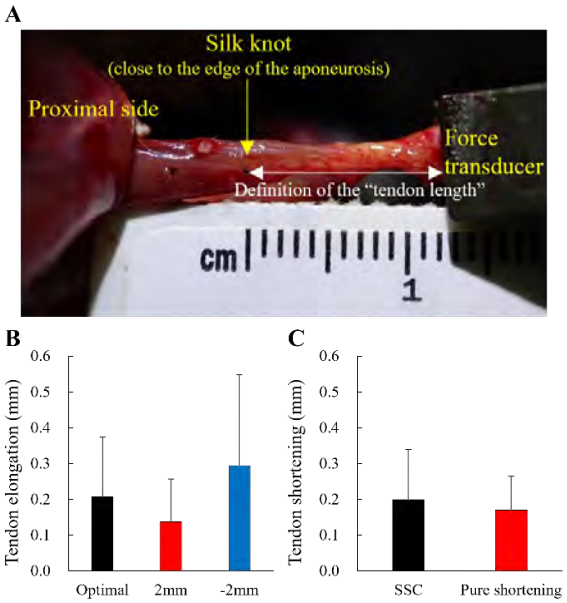

Figure 1 Experimental setting (panel A), the magnitude of tendon elongation attained during isometric contractions at different muscle lengths (panel B), and the magnitude of tendon shortening attained during the shortening phase in the SSC or pure shortening trials (panel C).

CONCLUSIONS

In conclusion, the contribution of Achilles tendon elongation to the SSC effect was negligible, at least in the case of the rat soleus and Achilles tendon. This is likely due to the small amount of tendon length changes attained during SSCs (e.g., 1.7% of the tendon length in the SSC trials). Based on our findings, tendon elongation does not necessarily explain the SSC effect, and factors other than tendon elongation can contribute to the SSC effect.

REFERENCES

[1] Fukutani A et al. *J Exp Biol* **222**: jeb204032, 2019.

Acute effects of dynamic versus static stretching in muscle architecture in adolescents

Zhiyu Tao[1,2], Dahua Ren[2], Tianchen Huang[2] and Mianfang Ruan [2]
[1] Graduate School of Design, Kyushu University, Fukuoka, Japan.
[2] Department of Physical Education and Health, Wenzhou University, Wenzhou, China.
Email: tao.zhiyu.277@s.kyushu-u.ac.jp

INTRODUCTION

Static stretching (SS) and dynamic stretching (DS) exercises are typically recommended to players of amateur and professional levels before performing any sport activities [1]. However, the number of studies on adolescents in this research field is still lacking. There is no research has used ultrasound to do the test for the lower limb stretching in adolescents now.

The purpose of this study is to summarize the acute changes in muscle structure such as the muscle fascicle length of the biceps femoris long head (BFlh) after lower limb stretching in adolescents.

METHODS

The subjects of the experiment were 10 primary school students. The sonographer used ultrasound to measure the middle region of the long head of the biceps femoris before and after DS and SS. In order to avoid interference between the two stretching methods, the subjects be separated by at least 72 hours between two tests. Since the entire muscle fascicle was not visible in the field of view of the probe, its length was estimated via the following validated equation from Blazevich et al. [2]and Kellis et al. [3]:

$FL=\sin(AA+90^{\circ})\times MT/\sin(180^{\circ}-(AA+180^{\circ}-PA))$.

AA = aponeurotic angle (the angle between the line markedas the aponeurosis and an intersecting horizontal line across the captured image); FL = muscle fascicle length; MT = muscle thickness; PA = pinnate angle (Figure 1).

RESULTS AND DISCUSSION

The changes in muscle architecture from both stretching conditions were compared (Table 1). Both FL and PA had significant interaction in the time main effect and intervention* time main effect ($p<0.01$), while MT in the above two main effects were not significantly interaction. The above results indicate that both SS and DS significantly altered PA and FL, but did not significantly altered the MT. Although there was no significant interaction between MT, PA and FL in intervention main effect ($p>0.05$), DS increased FL more significantly and reduced PA more significantly than SS.

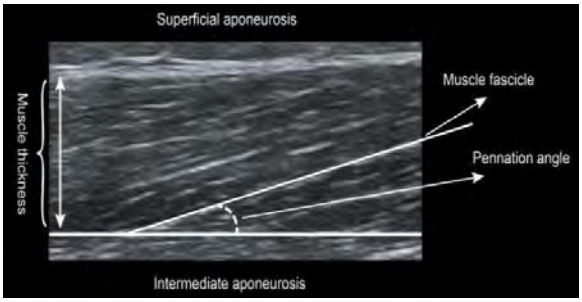

Figure 1 A two-dimensional ultrasound image of the BFlh.

CONCLUSIONS

Both dynamic stretching and static stretching can significantly change the muscle architecture of adolescents' BFlh, while static stretching has less effect on the muscle architecture than dynamic stretching.

REFERENCES

[1] Huang S et al. *J Biol* **11.3**: 374, 2022.
[2] Blazevich A et al. *J anat* **209.3**: 289-310, 2006.
[3] Kellis E et al. *J biomech* **42.15**: 2549-2554, 2009.

Table 1: Comparison of the effects of two stretching methods on muscle architecture.

	Before stretching		After stretching		Intervention		Time		Intervention* time	
	DS	SS	DS	SS	F	P	F	P	F	P
MT	13.92 ± 0.4	13.96 ± 0.6	14.12 ± 0.8	14.24 ± 0.8	0.07	0.78	2.48	0.13	0.06	0.79
PA	15.22 ± 1.2	14.71 ± 1.4	14.49 ± 1.3	14.62 ± 1.3	0.1	0.74	10.48	<0.01	6.38	0.021
FL	102.5± 6.8	102.75 ± 8.2	113.74± 5.5	106.1± 9.2	1.32	0.26	51.32	<0.01	14.67	0.01

Subtitle: (P): *p-value*, (F): *F-value*, (SS):*static stretching*, (DS):*dynamic stretching*.

TORQUE LOSS DURING SIMULTANEOUS ACTIVATION OF AGONISTIC MUSCLES

Michael Baggaley[1], Andrew Sawatsky[1], Heiliane de Brito Fontana[2] and Walter Herzog [1]
[1]Faculty of Kinesiology, University of Calgary, Calgary, Canada.
[2] Department of Morphological Sciences, Federal University of Santa Catarina, Florianopolis, Brazil.
Email: michael.baggaley1@ucalgary.ca

INTRODUCTION

The quadriceps muscles lose torque generating capacity when activated simultaneously [1]. In this study, we tested if this torque loss is unique to the quadriceps muscles or if it is a common phenomenon amongst agonistic muscle groups. To achieve this, experiments were performed in New Zealand white rabbits. The torque generating capacity of the plantarflexor muscles (Plantaris (PL), medial/lateral Gastrocnemius (MG/LG), and Soleus) were measured during simultaneous and individual activation of the muscles via direct nerve stimulation of the branches of the tibial nerve. The data presented herein represents preliminary findings of an ongoing investigation.

METHODS

Plantarflexor muscles of 3 skeletally mature, New Zealand white rabbits were analysed. Maximum isometric torque was measured at 90, 100, and 110 degrees of plantarflexion. The nerve branches of LG, MG, and PL were isolated and individually activated via nerve cuffs. The soleus was activated via stimulation of the LG nerve. One maximal activation (100 Hz) was performed at each ankle angle. Peak torque was determined for each muscle individually and summed to determine the difference in torque between individual muscle activation and activation of all muscles simultaneously. Simultaneous activation of all nerve branches was performed using the same joint angles and activation levels as was done foe the individual muscle activations. Mean and standard deviation for each angle and condition were calculated, and differences between simultaneous vs. summed activations were quantified.

RESULTS AND DISCUSSION

Simultaneous activation of the plantarflexor muscles resulted in reduced torque generating capacity compared to adding the torques produced during individual activation. Across all joint angles, a mean difference of -0.31 ± 0.14 Nm (26%) was observed between the summed torque for individual muscle activation compared to the simultaneous activation of the plantarflexor muscles. The largest difference was observed at 90° (37%; -0.60 Nm). The reduced torque generating capacity observed during simultaneous activation of agonistic muscles has been attributed to lateral forces applied to the muscles by each other resulting in lateral compression of individual muscles. Previous work in isolated muscles has demonstrated that controlled lateral compression of the rabbit medial gastrocnemius, impaired the force generating capacity of the muscle in a dose-dependent manner; more lateral force resulted in increased loss of force capacity [2].

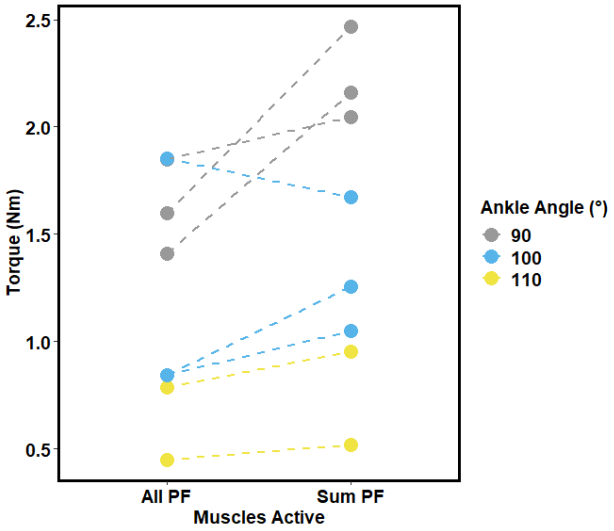

Figure 1. Plantarflexor torque produced during simultaneous activation of plantarflexor muscles (All PF) vs. summed torque of individual activation of plantarflexor muscles (Sum PF).

CONCLUSIONS

Plantarflexor torque generating capacity was impaired during simultaneous activation of the plantarflexor muscles compared to the summed torque produced during individual activation of the plantarflexor muscles. These preliminary results suggest that impaired torque generating capacity produced during simultaneous activation of agonistic muscles may be a common phenomenon of agonistic muscle groups.

REFERENCES

[1] Fontana H et al. *J Exp Biol* **223**: jeb213843, 2020.
[2] Siebert T et al. *J Biomech* 74:1822-1828, 2014.

Table 1: Plantarflexor torque produced when all muscles were activated simultaneously (All PF) vs. when the torque produced by individual muscles were summed (Sum PF)

	90°	100°	110°
All PF (Nm)	1.62 ± 0.22	1.17 ± 0.58	0.62 ± 0.24
Sum PF (Nm)	2.22 ± 0.22	1.32 ± 0.32	0.74 ± 0.31

Is force-generating capacity of the plantarflexor muscles affected by the surrounding skin mechanical property and orientation of gravity?

Yasuhide Yoshitake[1,2], Patricio Pincheira[2], Naokazu Miyamoto[3], Kosuke Hirata[4], Sohei Washino[5], and Hiroaki Kanehisa[6]
[1]Shinshu University, Nagano, Japan.[2] University of Queensland, Brisbane, Australia.[3]Juntendo University, Chiba, Japan, [4] Waseda University, Saitama, Japan. [5]National Institute of Advanced Industrial Science and Technology, Chiba, Japan. [6]National Institute of Fitness and Sports in Kanoya, Kagoshima, Japan.
Email: yasu_yoshitake@shinshu-u.ac.jp

INTRODUCTION

Since human soft tissues (e.g., facial skin, breasts) exhibit deformability to the force of gravity [1,2], gravity may also be a factor in deforming muscles. As muscle force-generating capacity is inherently dependent on muscle geometry, such as the force-length relationships, the orientation of gravitational force may also have an impact on muscle force. Cadaveric samples show that when laying in the prone position, removal of the skin results in a flattening of muscle and a reduction in muscle stiffness [3]. This suggests that the skin mechanical properties may play a significant role in the deformation of the muscle due to gravity and thereby in the force-generating capacity. Given that skin elasticity declines with age [4], alterations of muscle geometry caused by a decline in skin elasticity may contribute to a decrease in the force generation capacity seen with age. The current study aimed to clarify the systematic relationship between age, skin elasticity, the orientation of gravity force, muscle shape, and muscle force-generating capacity.

METHODS

Fifteen young adults (Young; 23.5 ± 1.5 yrs) and 15 old adults (Old; 64.0 ± 3.5 yrs) participated in this study. To explore the effect of muscle orientation with respect to the direction of gravity on the muscle geometry and force-generating capacity of the right medial gastrocnemius (MG) muscle, participants laid in the supine and prone positions during testing (Fig. 1). In both positions, the angle of the right ankle was fixed at 15 degrees of plantarflexion, and hip and knee joints were fully extended during measurements. The bare sole of the whole foot was attached to a flat foot pedal connected to a force transducer. Single electrical stimulation (with supramaximal intensity to the tibial nerve) was used to evoke plantar flexor torques. Then, peak torque (PT) was calculated to assess the muscle force-generating capacity. Ultrasound shear-wave elastography was used to assess skin mechanical properties (shear modulus) at the centre of MG. To measure muscle geometry, three-dimensional (3D) ultrasound recordings were utilized [5]. After reconstruction and segmentation of MG 3D geometry, MG anteroposterior (AP) length and transverse (ML) width were calculated in a 2D plane placed at 30% of the lower leg length (Fig. 1). ML/AP ratio was calculated to evaluate the representative MG 3D geometry.

RESULTS AND DISCUSSION

PT was smaller and ML/AP ratio was greater ($P < 0.05$) in the prone position compared to the supine position for both Young and Old groups. The position-related changes in PT and ML/AP ratio were greater in the Old group than the Young group ($P < 0.05$). The skin shear modulus (averaged across positions) of the Old group was smaller than that of the Young group ($P < 0.05$). There were correlations between the relative changes in ML/AP and PT (r = -0.78), between skin shear modulus and relative change in ML/AP (r = -0.69), and between skin shear modulus and relative changes in PT (r = 0.65). These results suggest that lower skin shear modulus with age promotes a flattening of the muscle shape in the prone position, which is accompanied by a greater reduction in muscle force-generating capacity.

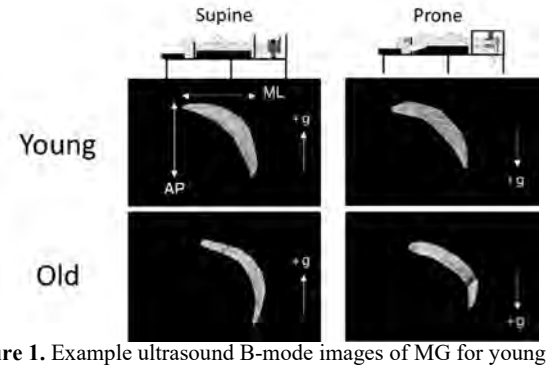

Figure 1. Example ultrasound B-mode images of MG for young (upper) and old adults (bottom) obtained by 3D ultrasound technique in the supine (left) and prone (right) positions.

CONCLUSIONS

In summary, age-related changes in skin mechanical properties affect gravity-dependent muscle shape and subsequently muscle force-generating capacity in MG.

ACKNOWLEDGEMENTS

Partly supported by JSPS KAKENHI (19H04018).

REFERENCES

[1] Chen et al. Biomarker Research **7**: 20, 2019.
[2] Flament et al. Int. J. Cosmet. Sci. **37**: 291, 2015.
[3] Yoshitake et al. Ultrasound in Med. & Biol **42**: 674, 2016.
[4] Cronin et al. J Appl Physiol **111**: 1491, 2011
[5] Barber et al. J Biomech **42**: 1313, 2009

MUSCULOTENDINOUS ARCHITECTURE AND STRENGTH OF SUPRASPINATUS AFTER TEAR AND ARTHROSCOPY REPAIR IN PATIENTS WITH FULL-THICKNESS TENDON TEAR

Yen-Ling Chou [1] , Yang-Hua Lin [1] , Chih-Hao Chiu [2], Hsiao-Yun, Chang [3] and Po-Tsun Chen*[1,2]
[1] School of Physical Therapy and Graduate Institute of Rehabilitation Sciences, College of Medicine, Chang Gung University, Taoyuan, Taiwan
[2] Department of Orthopedic Surgery, Linkou Chang Gung Memorial Hospital, Taoyuan, Taiwan
[3] Department of Athletic Training and Health, National Taiwan Sport University, Taoyuan, Taiwan
Email: ptchen@mail.cgu.edu.tw

INTRODUCTION

The tear occurring in supraspinatus tendon is more commonly than in other rotator cuff. After the tendon is torn, the altered musculotendinous architecture of supraspinatus can be found and may be associated with its dysfunctions. During the repairing surgery, tension was applied to re-attach the ends of torn tendon. Muscle fiber was then lengthened beyond the optimal length, which may compromise the contractile capacity[1]. In addition, supraspinatus stiffness which affects the extensibility of the musculotendon is one of the complications after tendon repair[2]. However, the changes in musculotendinous architecture of supraspinatus during shoulder movement are unknown in patients with supraspinatus tendon tears. Hence, this study aimed to evaluate the time-course changes and the difference between various shoulder postures in musculotendinous architecture of supraspinatus and shoulder strength in patients with full-thickness tear before and after tendon repairing.

METHODS

Six patients with unilateral full-thickness supraspinatus tendon tear were recruited for the evaluations before and three months after arthroscopic repair. The musculotendinous architecture of supraspinatus, including the fiber bundle length (FBL) and pennation angle (PA), was evaluated by sonography (ArtUs EXT-1H, Telemed, Italy) with a linear transducer (7.5- 15.0 MHz, Telemed, Italy) at the shoulder postures of resting (RS), active holding at 30° scaption (AH), and passively stretched (PS). The maximal strength of shoulder internal and external rotators, and supraspinatus muscles were evaluated by a hand-held dynamometer (MicroFET2, HOGGAN, USA). The Friedman's test with Wilcoxon signed-rank test as a post hoc test was used to compare the musculotendinous architecture between different postures, timings, and sides.

RESULTS

The FBL of supraspinatus on the affected side was shorter than that on the intact side across RS, AH, and PS postures either before or after repair. FBL in RS after repair (3.8±0.5 cm) was significantly increased with comparing to that before repair (3.7±0.6 cm). During PS, the FBL was also increased after repair (before repair: 3.8±0.5 cm, after repair: 3.9±0.5 cm). No significant difference in PA of supraspinatus was noticed between bilateral sides either before or after repair. However, PA was decreased on affected side after repair in RS (before: 12.3±1.5°, after: 11.2±1.2°) and AH (before: 13.2±1.5°, after: 12.4±1.4°). The shoulder muscle strength on the intact side was significantly larger than the affected side either before or after repair. The strength of internal rotator was increased significantly after repair (before: 5.2±2.7 kg, after: 6.7±4.1 kg), but no significant difference of strength after repair was found in external rotator and supraspinatus muscle.

CONCLUSIONS

The early or excessive mobilization after tendon repair may be helpful to avoid stiffness but may induce tendon re-tear. However, repaired tendons may receive over-stress or over-strain during shoulder movements and may thus increase the risk of re-tear. Therefore, the changes in musculotendinous architecture between contracting and stretched supraspinatus should be evaluated for the reference of the rehabilitation program and for the healing progress. Further study may be required to know the effects of rehabilitation on musculotendinous architecture of supraspinatus.

REFERENCES

[1] Sachdeva R et al. *Singapore Med J* **63**(2): 97-104, 2022.
[2] Itoigawa Y et al. *J Orthop Res* **38**(1): 219-227, 2020.

Mechanical Properties of The Achilles Tendon In Middle-aged Men and Its Relation to Jump Performance

Yoon-Hyung Cho[1,2], Hae-Dong Lee[2,3†]

[1] Department of Physical Education, Graduate School of Yonsei University / Seoul, Korea
[2] Department of Physical Education, College of Educational Sciences, Yonsei University, Seoul, Korea
[3] Frontier Research Institute of Convergence Sports Science, Yonsei University / Seoul, Korea
Email: xbridge1997@yonsei.ac.kr

INTRODUCTION

Interaction between muscle and elastic tendon enables us to perform flexible functions during locomotion; energy conservation, power amplification, and power attenuation [1]. Especially tendon's capability of storing and reusing elastic energy provides a mechanical advantage during the stretch-shortening cycle [2,3]. Even though the 50s is the population that needs to prepare for the elderly life, few studies on tendon mechanical and functional properties have been conducted, and the information is limited. Therefore, this study investigated the elastic properties of the Achilles tendon (AT) in their 50s. In addition, the association between the elastic properties of the AT and the jumping ability was studied.

METHODS

Healthy adult males in their 50s (n = 30; height 171.5 ± 5.5 cm, weight: 73.4 ± 10.6 kg, age: 54.5 ± 2.6yrs.) and in their 20s (n = 10; height: 176.5 ± 5.7 cm, weight: 79.3 ± 9.1 kg, age: 27.2 ± 1.1 yrs.) participated in this study. While subjects performed maximum plantar flexion (PF) on a custom-built dynamometer, maximum PF torque was measured, and the elongation of AT was measured using B-mode real-time ultrasound imaging. The countermovement (CMJ) and squat jump (SJ) were performed to measure their jumping and pre-stretch augmentation ability.

RESULTS AND DISCUSSION

As shown in Figure 1, the 50s (62.9 ± 12.1 mm^2) showed a larger Achilles tendon area than the 20s (51.0 ± 8.8 mm^2) ($p < .05$). In addition, Achilles tendon maximal elongation and stiffness were smaller in the 50s (15.5 ± 4.5 mm, 32.9 ± 16.0 Nmm^{-1}) than in the 20s (21.6 ± 3.8 mm, 46.1 ± 20.3 Nmm^{-1}) ($p < .05$). Hysteresis was higher in the 50s (20.5 ± 8.8%) than in the 20s (15.2 ± 6.3%) ($p < .05$). Both CMJ and SJ height were higher in 20s (43.0 ± 9.9 cm and 34.9 ± 8.3 cm) than in 50s (26.6 ± 5.4 cm and 23.5 ± 4.7 cm) (Figure 2) ($p < .05$). Achilles tendon properties were statistically significantly associated with CMJ and SJ performance (Table 1)

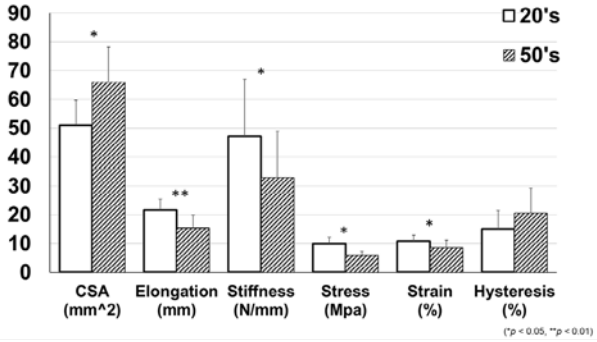

Figure 1 Comparison of the Achilles tendon properties between 50s and 20s. (*, $p < .05$; **, $p < .001$)

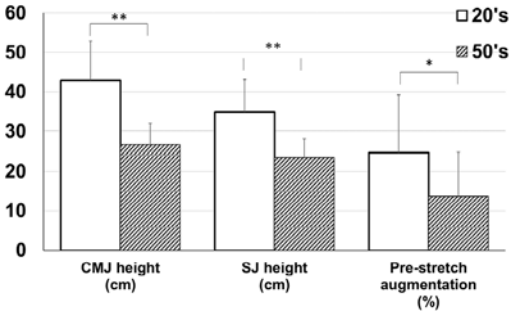

Figure 2 Jump performance and pre-stretch augmentation in the 50s and 20s. (*, $p < .05$; **, $p < .001$)

CONCLUSIONS

In conclusion, the changes in Achilles tendon elastic properties are prominent and significant from the 50s and affect jump performance. These results provide important basic information on aging, rehabilitation, and training.

REFERENCES

[1] Roberts T J et al. Science, 214(3), 353-361, 2011.
[2] Komi P V et al. Medicine and science in sports 10(4), 261-265, 1978.
[3] Kubo K et al. Acta Physiologica scandinavia, 178:25-32, 2003.
[4] Magnusson et al. Biological Sciences and Medical Sciences, 58(2), B123-B127, 2003.

Table 1 The association between jump performance and the elastic properties of the Achilles tendon.

	Maximal elongation (mm)	Hysteresis (%)	Strain (%)	Stress (Mpa)
SJ height (cm)	.394	-.388	.317	.498
CMJ height (cm)	.430	-.378	.337	.487

IN VIVO 3-DIMENSIONAL ULTRASONOGRAPHY OF HUMAN BICEPS FEMORIS REVEALS A TWISTED PROXIMAL APONEUROSIS

Carmela J. Mantecon Tagarro[1,2], Guido Weide [2],Takahashi Katsuki[1], Yasuo Kawakami[1], and Huub Maas[2]
[1] Faculty of Sport Science, Waseda University, Tokyo, Japan.
[2] Department of Human Movement Science, Vrije Universiteit Amsterdam, Amsterdam, The Netherlands.
Email: carme21_waseda@moegi.waseda.jp

INTRODUCTION

The biceps femoris long head (BFlh) has a complex fascicle architecture and is prone to strain injuries. Most of these injuries occur around the muscle-tendon junction, particularly in the proximal region. Battarmann et al. (1) associated the complexity of the proximal region of BFlh, i.e. a three-dimensional (3D) twist towards the origin, with the vulnerability to injury. However, information regarding the 3D musculo-tendinous geometry of BFlh is limited (2). Hence, the aim of this study is to identify the complexity of BFlh intramuscular aponeurosis by assessing its geometry with 3D ultrasonography.

METHODS

Series cross-sectional (CS) ultrasonograms of BFlh were taken from eleven healthy adults (mean ± SD = 22 ±2.5 years old) lying prone with the knee fully extended, while capturing the probe's 3D orientation (3). 3D volume of BFlh was reconstructed for each subject, and the intramuscular aponeurosis was identified in the CS view as a relatively flat, continuous, hyper-echogenic line. The outline of aponeurosis echo was traced along the length of BFlh to reconstruct its 3D geometry (Fig. 1). The angle of the aponeurosis relative to the global coordinate system in the CS plane was calculated using MATLAB along the aponeurosis length. The average angle (orientation) at different regions over the length i.e., 0%-20% (proximal), 40%-60% (middle) and 80%-100% (distal), were expressed relative to the angle at 50% of the aponeurosis length, with positive changes toward the lateral aspect (counter-clockwise in the proximal-distal direction) and negative toward the medial (clockwise).

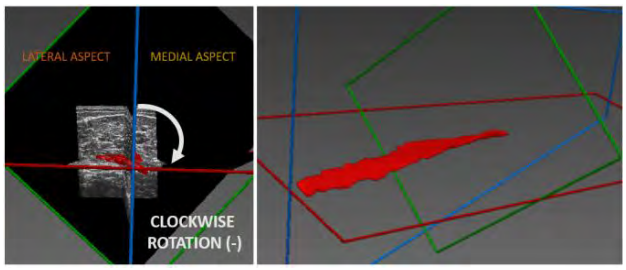

Figure 1: Aponeurosis 3D geometry reconstruction and medial and lateral twist representation.

RESULTS AND DISCUSSION

Reconstruction was successful in 7 out of 11 subjects (4 cases were discarded due to poor visualization of the aponeurosis). The average orientation of the aponeurosis differed between regions with different variations: proximal, +20º (95% CI [+5º, +36º]), middle, +1º (95% CI [-3º, +2º]), and distal, -4º (95% CI [-19º, +11º]). Considerable inter-individual differences were found (Table 1). In three subjects (no.3, no.5 no.7), the aponeurosis was systematically twisted medially (clockwise) from proximo-distally regions while in the other subjects (particularly no. 1), the aponeurosis twisted medial in the proximal-half and then from middle to distal change to lateral direction (counter-clockwise) or not at all (no.2, no. 4 and no.6).

Table 1: Average orientation of aponeurosis for three regions: proximal (0-20%) middle (40-60%), and distal (80-100%) expressed relative to the angle at 50% of the aponeurosis length.

Subject	Angle 0-20% (mean±SD) (º)	Angle 40-60% (mean±SD) (º)	Angle 80-100% (mean±SD) (º)
1	13±5	1±10	24±6
2	17±10	3±6	3±5
3	30±6	1±5	-9±4
4	-6±8	-3±4	-3±13
5	46±22	-2±3	-21±5
6	14±3	-4±5	0±5
7	27±10	-1±2	-23±3

CONCLUSIONS

The 3D orientation of BFlh intramuscular aponeurosis varies along its length to a greater extent in the proximal and distal regions. Significant inter-individual variations were observed. The twisted nature as well as inter-individual variation of the aponeurosis geometry may affect how mechanical strain and stress are distributed within and between muscle fibers, potentially affecting the susceptibility to strain injury.

ACKNOWLEDGEMENTS

This work was supported by JST SPRING, Grant Number JPMJSP2128. JSPS Kakenhi (Fostering Joint International Research B, 21KK0175).

REFERENCES

[1] Battarmann et al. 2011 Int J Sports Med 32(3):211-5.
[2] Rehorn MR and Blemker SS 2010 J Biomech.; 43(13): 2574–2581.
[3] Weide, G et al. 2017, J. Vis. Exp. (129)

Relationship between baseline flexibility and changes after chronic stretching intervention program

Masatoshi Nakamura[1], Kosuke Takeuchi[2], Riku Yoshida[3],
Kazuki Kasahara[3], Yuta Murakami[3] and Takamasa Mizuno[4]
[1] Faculty of Rehabilitation Sciences, Nishi Kyushu University, Saga, Japan.
[2] Department of Physical Therapy, Faculty of Rehabilitation, Kobe International University, Hyogo, Japan.
[3] Institute for Human Movement and Medical Sciences, Niigata University of Health and Welfare, Niigata, Japan
[4] Research Center of Health, Physical Fitness and Sports, Nagoya University, Nagoya, Japan
Email: nakamuramas@nisikyu-u.ac.jp

INTRODUCTION

Static stretching (SS) intervention programs are generally performed in sports and rehabilitation settings. Indeed, previous studies showed that SS intervention programs could increase the range of motion (ROM) and decrease muscle stiffness [1, 2]. Interestingly, the relationship between baseline flexibility and change after a single bout of SS intervention has been examined [3]. They showed that baseline flexibility had not been related to increased ROM or decreased muscle stiffness after a single bout of stretching. Still, the relationship between change after SS intervention programs and baseline flexibility is unknown. The relationship of change in SS intervention programs with baseline flexibility is expected to clarify the future adaptation of SS intervention programs. Thus, we aimed to investigate the relationship between baseline flexibility, i.e., ROM and muscle stiffness, and changes after SS intervention program.

METHODS

In this study, we reanalyze the results of our previous studies [1, 2]. We employed data from 44 healthy young males (age: 21.1±1.1 years, body mass: 62.3±7.1 kg, height: 170.6±7.1cm). Also, we adopted the dorsiflexion (DF) ROM and muscle stiffness before (baseline) and after 4 weeks SS intervention program. In these previous studies [1, 2], we measured the DF ROM and muscle stiffness during the passive stretching test via dynamometer and ultrasonography before and after 4 weeks SS intervention program. We calculated partial correlations between DF ROM or muscle stiffness at baseline and changes or rate of change (%) after SS intervention program adjusted for total stretching duration. A p-value of <0.05 indicated statistical significance.

RESULTS AND DISCUSSION

Our results showed that there was no significant association between DF ROM at baseline and changes in DF ROM (r=0.006, p=0.971, Figure 1-A), but a significant negative association between DF ROM at baseline and rate of change (%) in DF ROM after SS intervention program (r=-0.383, p=0.011, Figure 1-B). In addition, there was a significant negative association between muscle stiffness at baseline and changes in muscle stiffness after SS intervention program (r=-0.736, p<0.001, Figure 1-C). But there was no significant association between muscle stiffness at baseline and the rate of change (%) in muscle stiffness after SS intervention program (r=-0.298, p=0.053, Figure 1-D).

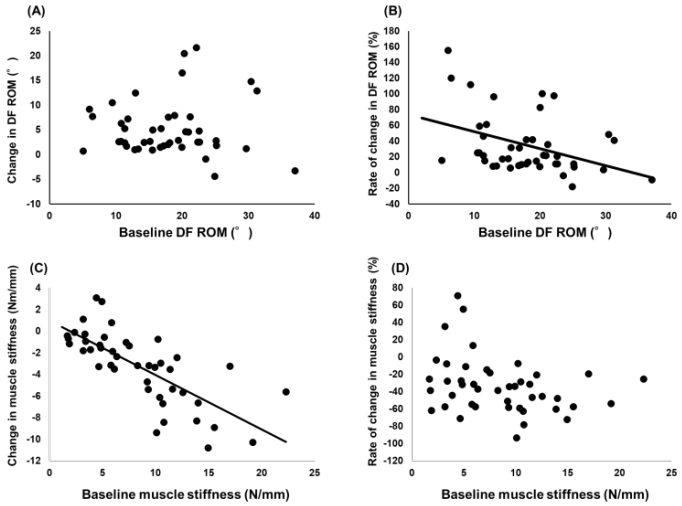

Figure 1. Association between dorsiflexion (DF) range of motion (ROM) or muscle stiffness at baseline and changes (A and C)or rate of change (%, B and D) after SS intervention program

The results of this study showed that The smaller in DF ROM before the SS intervention program, the greater increase in DF ROM after the SS intervention program. Also, the stiffer muscle stiffness before the SS intervention program, the greater decrease in muscle stiffness after the SS intervention program. Thus, our results suggested that the participants with lower flexibility (i.e., small ROM or stiff muscle stiffness) showed greater improvement in flexibility after the SS intervention program.

CONCLUSIONS

It is possible that the young male with lower flexibility before the SS intervention program had greater improvement in flexibility after the SS intervention program.

REFERENCES

[1] Nakamura M et al. *Front Physiol*. **17**;12:796497, 2021
[2] Nakamura M et al. *Front Physiol*. **1**;12:656579, 2021
[3] Takeuchi K et al. J Phys Ther Sci. **30**:1377-1380, 2018.

Force-generating capacity of plantarflexion force is lowered by gravity during standing positions

Kiichi Saji[1], Momoka Nakamura[1], Moeka Samoto[1] and Yasuhide Yoshitake[1]
[1] Graduate School of Science and Technology, Shinshu University / Ueda, Japan.
Email: mikuji5110@gmail.com

INTRODUCTION

External forces from our environment impose transverse loads on our muscles. Previous studies [e.g., 1] have demonstrated that transverse loads result in a decrease in the longitudinal muscle force. Changes in muscle architecture at rest and during contraction are suggested to contribute to the declined force. A most familiar external force for humans is gravity, which can play a role in pulling down soft tissues in humans [2]. Therefore, it is possible that the force-generating capacity of muscle is dependent on the orientation of the muscle relative to gravity, which is accompanied by the deformation of the muscle. The purpose of this study was to determine whether force-generating capacity and muscle geometry are influenced by the orientation of the muscle with respect to gravity. In this study, we especially focused on the standing posture as humans are primarily active in this posture.

METHODS

Force-generating capacity and muscle geometry were examined for the plantarflexor muscles in 16 healthy young adult males (21.5 ± 0.8 yrs, 5 female). Participants were positioned in a supine (SUPINE) and standing (STAND) posture, with the knee and hip joints fixed at ~180° and were instructed to avoid voluntary muscle activation throughout the experiment. In the standing position, special care was taken to ensure that participants did not impose their body weight onto their foot sole to prevent muscle activities in the plantarflexor muscles. The right ankle joint was set to -15° (DF15), 0° (N), and +15° (PF15) to explore the effect of length-dependent muscle stiffness.

The geometry of the right calf muscle at rest was measured using ultrasound B-mode images to determine the fascicle length of the medial gastrocnemius muscle (MG) at approximately 30% of the lower leg length. Doublet stimulus with a 20ms interstimulus interval at supramaximal intensity were delivered to the tibial nerve using a constant-current electrical stimulator to evoke maximal doublet-twitch torque from the plantarflexor muscles at each ankle position. Peak torque (PT) and rate of torque development (RTD) were subsequently determined.

The data were compared using a two-way ANOVA (2 positions × 3 ankle joint angles) with repeated measures and the rate of changes in these variables from SUPINE to STAND was also compared using a one-way ANOVA with repeated measures (3 ankle joint angles). When appreciate, a Bonferroni test was conducted for a post-hoc comparisons.

RESULTS AND DISCUSSION

PT and RTD were lower in STAND compared with SUPINE at PF15 and N ($P < 0.05$). The rate of these changes when posture was changed from SUPINE to STAND were most pronounced for PF15 (-25.9% and -23.5%) when compared to N (-16.0% and -13.3%) and DF15 (-1.3% and -0.5%). No difference in PT and RTD was observed in DF15 ($P > 0.05$).

The fascicle length was longer in SUPINE than STAND when collapsed across ankle joint angle ($P < 0.05$) with the effect of limb orientation on fascicle length being greater in PF15 (-14.8%) than DF15 (-8.2%). These results suggest that the standing posture causes a smaller peak torque, rate of torque development, and fascicle length than supine posture, especially at ankle joint angle of plantarflexed position.

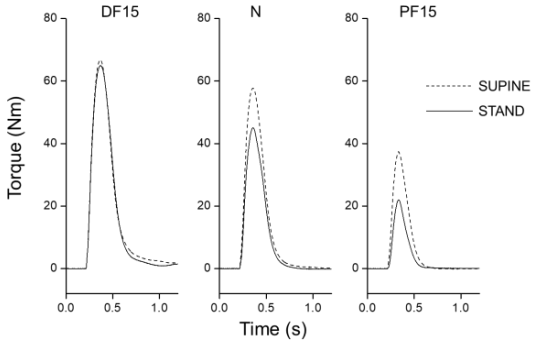

Figure 1 Representative torque signals evoked by doublet stimulation in supine (dot, SUPINE) and standing (solid, STAND) postures at DF15 (left), N (middle), and PF15 (right).

CONCLUSIONS

This study demonstrated that the orientation of muscle with respect to gravity influence both force-generating capacity and resting muscle geometry, with the largest effect seen at a plantarflexed ankle joint angle.

ACKNOWLEDGEMENTS

Supported in part by Grant-in-Aid for Scientific Research (B) in Japan to YY.

REFERENCES

[1] Ryan et al. *J Biomech* **86**: 160, 2019.
[2] Flament et al. *Int J Cosmet Sci* **37**: 291, 2015.

A BIOMECHANICAL 3D ANALYSIS OF A LAB RECORDED LATERAL ANKLE SPRAIN DURING A HANDBALL SPECIFIC FAKE-AND-CUT MANEUVER

Timo Bagehorn[1*], Kevin Bill[2], Patrick Mai[2], Tron Krosshaug[3], Uwe Kersting[2]
[1] Department of Health Science and Technology, Aalborg University, Denmark, * Email: tiba@hst.aau.dk
[2] Institute of Biomechanics and Orthopaedics, German Sport University Cologne, Germany
[3]Department of Sports Medicine, Norwegian School of Sports Sciences, Oslo, Norway

INTRODUCTION

Lateral ankle sprains are highly prevalent sport injuries which occur frequently in indoor and court sports (Gribble et al., 2016). Biomechanical measurements of accidental sprain injuries are rare but make important contributions to a more detailed understanding of the injury mechanism (Lysdal et al., 2022). In this case study, we present the kinematics and kinetics of a lateral ankle sprain that occurred in a force plate-equipped motion capture laboratory while studying handball-specific fake-and-cut maneuvers.

METHODS

The athlete affected was a female junior elite handball player (182 cm, 63 kg, 17 years, first Norwegian junior division). She could not continue with the measurements and could not participate in any sport for the next two days. She described a radiating calf pain and tenderness the week after the injury. She did not seek any further medical attention. The task was to perform a handball-specific fake-and-cut movement in front of a passive defender after accelerating for 6 meters and receiving a pass. Six trials performed before the injury served as reference for the analysis. The injury was recorded with a three-dimensional infrared motion capture system (82 whole-body marker set, 23 cameras, 200Hz, Qualisys AB, Sweden) and two force plates at 1000 Hz (AMTI, USA). Peak joint kinematics, kinetics, step length, and foot distance to COM were calculated.

RESULTS AND DISCUSSION

Important kinematics and kinetics are highlighted in Table 1. The injury showed excessive plantar flexion, inversion, and internal rotation of the ankle. Ankle inversion and internal rotation were higher at initial ground contact (IC), while plantarflexion was reduced. Furthermore, the injury is characterized by ankle internal rotation and inversion moments four to five times higher than the reference trials. Step length and foot distance to the COM were considerably smaller compared to the reference trials, indicating that the approach strategy was different in the preparatory phase with the foot airborne. Furthermore, a slip-catch shoe-surface interaction was observed after initial contact. This indicates an unexpected increase in shoe traction, possibly caused by the prevalent joint misalignment.

CONCLUSIONS

Preparatory maladjustment is the main contributor for injury in this particular case study.

Table 1: Peak ankle joint angles, foot kinematics, and moments.

	Injury	Time	Reference	Time
KINEMATICS	[°]	[ms]	[°]	[ms]
Plantarflexion	40.7	190	25.6 ± 1.3°	22 ± 10
Inversion	39.8	200	31.9 ± 7.1°	44 ± 56
Internal Rot.	62.8	195	11.9 ± 6.1°	-57 ± 82
(AT IC)	[cm]	[ms]	[cm] / [°]	[ms]
Step Length	42.1	0	66.6 ± 8.6	0
Foot-COM	39.9	0	50.7 ± 8.6	0
Inversion	9.4	0	4.1 ± 1.7	0
Internal Rot.	8.0	0	-0.5 ± 2.2	0
KINETICS	[Nm]	[ms]	[Nm]	[ms]
Inversion	89.9	179	17.2 ± 5.7	90 ± 26
Internal Rot.	42.9	176	9.3 ± 4.8	63 ± 50

ACKNOWLEDGEMENTS

This study is supported by Independent Research Fund Denmark (0136-00283B).

REFERENCES

[1] Gribble et al. *BJSM* **50(24)**:1496-1505, 2016.
[2] Lysdal et al. Sport Biom. **21(4)**:359-379, 2022.

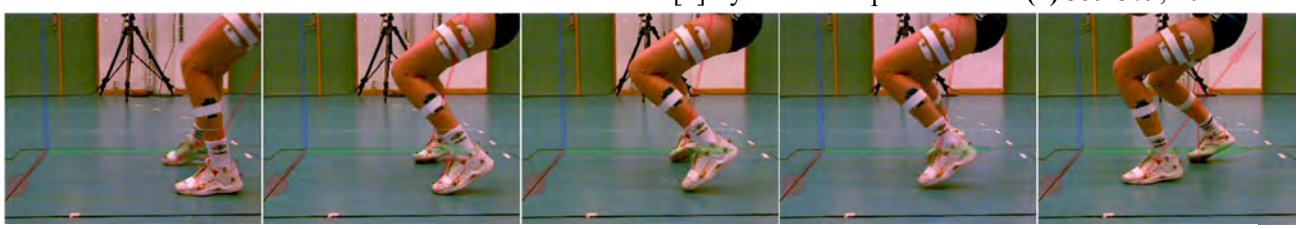

Figure 1: Images of the injury at 20, 105, 155, 195 (max .joint distortion) and 255 ms after IC.

A Novel Approach for Characterizing the Individual Plantar Intrinsic Foot Muscles: Cluster Analysis Based on Physiological Cross-Sectional Area and Muscle Fiber Length

Yuki Kusagawa[1], Toshiyuki Kurihara[2], Sumiaki Maeo[1], Takashi Sugiyama[1], Hiroaki Kanehisa[3] and Tadao Isaka[1]
[1] Faculty of Sport and Health Science, Ritsumeikan University, Kusatsu, Shiga, Japan.
[2] Faculty of Science and Engineering, Kokushikan University, Setagaya, Tokyo, Japan.
[3] National Institute of Fitness and Sports in Kanoya, Kanoya, Kagoshima, Japan.
Email: Kusagawayuki@gmail.com

INTRODUCTION

Plantar intrinsic foot muscles (PIFMs) consist of 10 muscles unilaterally and their morphological profiles differ individually [1, 2]. Theoretically, morphological profiles of a muscle determine its contractile properties: physiological cross-sectional area (PCSA) and muscle fiber length (FL) reflect maximal force production and shortening velocity, respectively. Thus, characterizing individual PIFMs from these morphological profiles may provide new insights into understanding the function of PIFMs. This study aimed to examine how individual PIFMs can be classified by the K-means cluster analysis based on the morphological parameters (PCSA and FL), which reflect the contractile properties.

METHODS

In 26 healthy young adult men, muscle volume and muscle length for each of seven PIFMs (abductor digiti minimi, ABDM; abductor hallucis, ABH; adductor hallucis oblique head, ADDH-OH; ADDH transverse head, ADDH-TH; flexor digitorum brevis, FDB; flexor hallucis brevis, FHB; quadratus plantae, QP) were measured using magnetic resonance imaging. The other three muscles (i.e., lumbricals, flexor digiti minimi, and plantar interossei) were excluded from the analysis due to their small size. PCSA and FL of each PIFM were estimated by using the measured data (muscle volume/length) and those previously reported in the cadaveric studies about pennation angle [1], FL to muscle length ratio [2], and FL [2]. After individually standardizing PCSA and FL by Z-score, K-means clustering was performed on 182 data samples (26 participants × 7 muscles) with PCSA and FL as attributes. The optimal number of clusters for K-means clustering was determined as four by the elbow method.

RESULTS AND DISCUSSION

Morphological profiles of each PIFM and the number of components classified into each cluster by the K-means clustering are summarized in Table 1. The relationship between PCSA and FL (standardized by Z-score) of individual PIFMs is shown in Figure 1. Cluster 1 consisted of all ADDH-OH and over half of FHB, indicating large PCSA and short FL (high force production at slow shortening velocity). Cluster 2 included all ABH and FDB, most of ABDM, and below half of FHB, indicating large PCSA and moderate FL (high force production at moderate shortening velocity). Cluster 3 included all QP with moderate PCSA and long FL (moderate force production at high shortening velocity). Cluster 4 consisted of all ADDH-TH and few ABDM, indicating small PCSA and moderate FL (small force production at moderate shortening velocity).

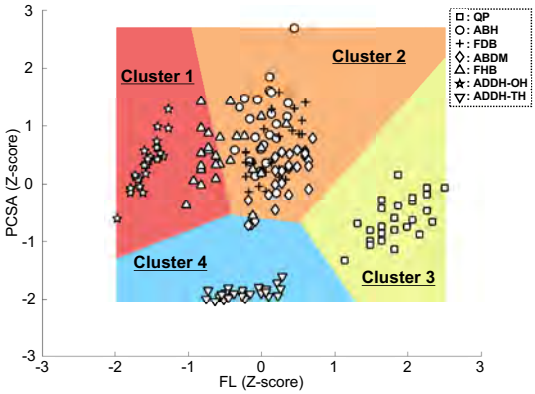

Figure 1 The relationship between PCSA and FL of individual PIFMs with the result of the K-means cluster analysis.

CONCLUSIONS

The K-means clustering based on morphological profiles (PCSA and FL) of individual PIFMs may become a novel approach for interpreting their function from viewpoint of maximal force production and shortening velocity.

REFERENCES

[1] Ledoux WR et al. *J Biomech.* **34**: 399-403, 2001.
[2] Kura H et al. *Anat Rec.* **249**: 143-51, 1997.

Table 1 The morphological profiles of individual PIFMs and the number of components classified into each cluster by the K-means clustering.

	Morphological profiles		Number of components classified into each cluster by K-means clustering			
	PCSA (cm^2)	FL (cm)	Cluster 1	Cluster 2	Cluster 3	Cluster 4
ABDM	6.35 ± 1.20	2.83 ± 0.26	–	23/26	–	3/26
ABH	8.70 ± 1.82	2.56 ± 0.19	–	26/26	–	–
ADDH-OH	6.89 ± 1.15	1.02 ± 0.16	26/26	–	–	–
ADDH-TH	0.70 ± 0.27	2.30 ± 0.32	–	–	–	26/26
FDB	7.49 ± 1.50	2.66 ± 0.26	–	26/26	–	–
FHB	7.42 ± 1.37	2.03 ± 0.34	15/26	11/26	–	–
QP	4.28 ± 1.02	4.32 ± 0.34	–	–	26/26	–

Values are means ± SD. Hyphens indicate no components classified into each cluster by K-means clustering.

PREDICTING CERVICAL SPINE DYNAMICS USING GAUSSIAN PROCESSES

Andrea Braschi[1,2], Neill D. F. Campbell[1,2], Keith Stokes[1] and Dario Cazzola [1,2]
[1] Department for Health, University of Bath, Bath, UK.
[2] Centre for the Analysis of Motion, Entertainment Research & Applications, University of Bath, Bath, UK.
Email: ab3758@bath.ac.uk

INTRODUCTION

Catastrophic cervical spinal (c-spine) injury is a life-altering condition that can occur in rugby union during misdirected tackles. The complex dynamics of the c-spine during such injurious scenarios has been studied via musculoskeletal forward dynamic (FD) simulations [1]. However, this can quickly become a computationally inefficient solution due to the set of ordinary differential equations (ODEs) that needs to be solved, and the simulation results can be biased by the study design and design variables chosen by the researcher. The aim of this study was to investigate whether a Gaussian Processes (GPs) generative model, trained using musculoskeletal FD simulations, can predict the external forces and the c-spine intervertebral joint motion and internal forces during theoretical head-first impacts without solving ODEs.

METHODS

A synthetic dataset was generated via 117 forward dynamic simulations in OpenSim 4.3 using a specific model for the rugby population that was previously validated for axial head impacts [1]. The c-spine kinematic patterns that were simulated were hyperextension of all the intervertebral joints and first order buckling, which results in extension of the first 5 intervertebral joints and flexion of the lower cervical spine. The Bayesian GP Latent Variable Model (GPLVM) [2] was employed to learn similarities and differences between simulations in a lower dimensional representation of the data, known as latent space. 94 of the simulations (~ 80%) were randomly selected to train the model and the rest was using to test it. At test time, the GPLVM generated c-spine dynamics and external forces based on other variables that were given to it, such as head rotational and linear kinematics.

RESULTS AND DISCUSSION

Figure 1 shows how the model grouped the three different head impacts in the latent space, while Table 1 illustrates the average RMSE between the model prediction and simulation results. The range of RMSE for all c-spine intervertebral joint angles in the sagittal plane was 0.06° - 0.24° (i.e 0.02% - 9.36%). The predicted c-spine internal forces across all c-spine joints had a RMSE that ranged from of 4.89 N – 31.38 N for the shear component (i.e. 0.39% - 124.51%) and 14.18 N – 105.64 N for the compressive (i.e. 0.07% - 0.48%). The average RMSE for the external forces ranged from 10.40 N to 61.31 N (i.e. 0.32% to 57.34%).
The high RMSE in percentage for the shear forces does not reflect a significant difference in absolute terms, as the range in Newtons shows.

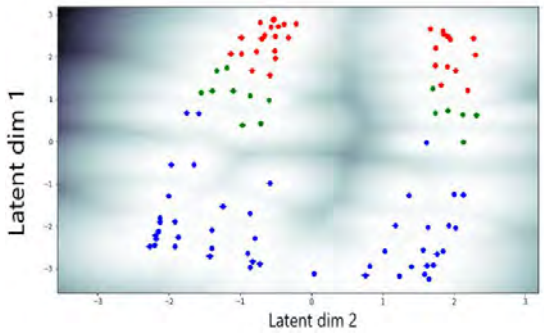

Figure 1 Representation of two dimensions of the latent space. The blue and red circles represent hyperextension and, respectively, whereas the green represent axial impacts.

CONCLUSIONS

The proposed framework is an encouraging starting point to implement probabilistic generative data-driven models as surrogate to mechanistic frameworks that rely on ODE solvers to investigate injury mechanisms. This approach will enable to run predictive simulations in future applications that are close to real-time.

ACKNOWLEDGEMENTS

This work was funded by the Centre for the Analysis of Motion, Entertainment Research & Applications (CAMERA).

REFERENCES

[1] Silvetsros P et al. *PLoS ONE* **14(5):** e0216663, 2019.
[2] Titsias M.K. and Lawrence N. D. *The International Conference on AISTATS,* 2010.

Table 1: Average RMSE between predicted and simulated time-series in absolute values and percentage (%).

Angles (deg)	0.2° ± 0.1°	0.8% ± 1.0%
Shear Force (N)	15.1 N ± 4.5 N	64.8 ± 64.5%
Compressive force (N)	69.2 N ± 3.5 N	0.2% ± 0.1%
External Force (N)	36.5 N ± 37.7 N	8% ± 5%

THE INFLUENCE OF BARIATRIC SURGERY ON POSTURAL STABILITY – A PILOT STUDY

Veronika Szabóová[1], Klára Daďová[1], Natálie Cibulková[1], Marcela Hašpicová[2], Martin Matoulek[3]
[1] Faculty of Physical Education and Sport, Charles University, Prague, Czech Republic,
[2] Second Faculty of Medicine, Prague, Czech Republic,
[3] First Faculty of Medicine, Charles University, Prague, Czech Republic.
Email: szaboo.v@gmail.com

INTRODUCTION

Recently, the rapidly increasing prevalence of sarcopenic obesity together with its serious consequences poses a critical health risk to the population. Muscle loss combined with the excessive amount of body fat that morbid obesity brings further enhances obesity accompanying comorbidities including reducing postural stability and thus significantly increasing the risk of fall with all the consequences [1, 2]. The best long-term results in the treatment of severe and morbid obesity are offered by bariatric surgery. Although bariatric surgeries lead to great and fast weigh loss, they are also followed by a significant loss of muscle mass which can also lead to other decline of postural stability. The aim of our study was to evaluate the influence of bariatric surgery on static postural stability.

METHODS

The research was designed as an experimental pilot study assessing postural stability before and after bariatric surgery. Eighteen subjects (13 females, 5 males) with obesity (body mass index 35–56 kg.m^{-2}), aged 27 to 67 years undergoing bariatric surgery participated in the study. The data collection was divided in two phases: pre-surgery and post-surgery. The pre-surgery measurements were performed approximately 2 weeks before the bariatric surgery and post-surgery measurements were performed 3 months after the surgery. Static and dynamic postural stability was measured and assessed using Tekscan MobileMat TM3140 pressure plate. Four postural stability parameters were evaluated: the total length of the COF sway, the length of antero-posterior and the medio-lateral COF range and the COF average speed. In four postural situations: natural stance with opened eyes, natural stance with closed eyes, maximal narrow stance with opened eyes and a maximal narrow stance with closed eyes. The measurement of each postural situation lasted 30s.

RESULTS AND DISCUSSION

The pilot study revealed statistically significant higher results (i.e. worse postural stability) after bariatric surgery for the total length of the COF sway in the natural stance with opened eyes, the total length of the COF sway in the maximal narrow stance with opened eyes and the COF average speed with opened eyes (Table 1). Our results suggest that bariatric surgery followed by fast weight loss may result into a decline in the static postural stability, mainly in more challenging situations. The natural stance may not be enough challenging to see statistically significant results. Maximal narrow stance with closed eyes might be on the other hand too challenging and therefore requiring more concentration which may lead to better results.

CONCLUSIONS

Although bariatric surgeries are considered as the most effective long-term management of morbid obesity, according to our study they may also have a negative impact on some musculoskeletal aspects such as postural stability. Further research in this topic is necessary. Our findings indicate a need for elimination of the negative effects by focusing on preservation of the muscle mass in pre-surgery and post-surgery regime.

ACKNOWLEDGEMENTS

This work was supported by the Cooperatio Program (Sport Sciences – Biomedical & Rehabilitation Medicine) and project MH CZ – DRO (General University Hospital in Prague – VFN, 00064165).

REFERENCES

[1] Benetti F A et al. Analyses of balance and flexibility of obese patients undergoing bariatric surgery. *Clinics* (Sao Paulo, Brazil), 71(2), 78–81, 2016.

[2] Rossi-Izquierdo M et al. Impact of obesity in elderly patients with postural instability. *Aging Clinical and Experimental Research*, 28(3), 423–428, 2016.

Table 1: Mean values (±SD) of weight, BMI, and postural stability parameters in all subjects (N = 18) pre and post-surgery.

	Pre-surgery	Post-surgery	*p-value*
Weight (kg)	138.11 ± 23.34	118.87 ± 19.52	$p = 0.013$
Body Mass Index (kg.m^{-2})	45.90 ± 7.03	39.65 ± 5.92	$p = 0.008$
COF sway - natural stance opened eyes (cm)	18.70 ± 4.64	21.22 ± 6.53	$p = 0.049$
COF sway - maximal narrow stance opened eyes (cm)	33.38 ± 9.78	41.29 ± 10.60	$p = 0.012$
COF - maximal narrow stance open eyes (cm.s^{-1})	1.15 ± 0.32	1.38 ± 0.35	$p = 0.012$

RELATIONSHIP OF JUMP PERFORMANCE AND GROUND REACTION FORCE VARIABLES BETWEEN YOUNG ADULTS AND DIFFERENT MATURITY ADOLESCENT SOCCER PLAYERS

Takahiro Namiki[1], Mina Samukawa[2], Itaru Chiba[3], Tomoya Ishida[2], Satoshi Kasahara[2], Yuta Koshino[2], Atsuhide Kida[1], Masayuki Inoue[4], Harukazu Tohyama[2]
[1] Rehabilitation Center, NTT Medical Center Sapporo, Sapporo, Japan.
[2] Faculty of Health Sciences, Hokkaido University, Sapporo, Japan.
[3] Nippon Sport Science University, Tokyo, Japan.
[4]Department of Orthopaedic Surgery, NTT Medical Center Sapporo, Sapporo, Japan
E mail: t.namiki.7373@gmail.com

INTRODUCTION

The countermovement jump (CMJ) is frequently used to assess physical performance. Jump height and reactive strength index (RSI) are the outcomes of CMJ performance. Jump height is associated with lower extremity work, power, and centre of mass (COM) displacement of the concentric phase. RSI is correlated with concentric COM displacement and lower extremity eccentric work calculated using ground reaction force (GRF) [1]. Age at peak height velocity (PHV) is an indicator of maturity in adolescents; at that age, height increases rapidly, and movement patterns such as jump movement are considered to change. Jump height and RSI have been reported to increase with maturity [2]. However, the relationship between jump performance and maturity, including GRF variables, has not yet been thoroughly investigated. Therefore, this study aimed to compare the characteristics of CMJ performance, including GRF variables, in adolescents of different maturity levels with those of adults.

METHODS

Ten young male soccer players (age: 22.1 ± 1.4 years; height: 171.1 ± 5.0 cm; body mass: 61.3 ± 6.0 kg) and forty-five male adolescent soccer players (age: 13.5 ± 0.9 years; height: 161.1 ± 9.0 cm; body mass: 50.3 ± 8.7 kg) participated in this study. Based on their maturity offset determined by age at PHV, adolescents were divided into the three following groups: pre-PHV (maturity offset ≤ –1.0), circa-PHV (–0.5 ≤ maturity offset ≤ 0.5) and post-PHV (1.0 ≤ maturity offset) [2]. CMJ was measured using a force plate (Ex-Jumper, DKH Co., Ltd., Japan) and divided into the following three phases. The unloading phase was defined from the start, when the vertical GRF decreased by more than 2.5% of the body weight value, to the time when the vertical GRF was at a local minimum. The eccentric phase was defined from the end of the unloading phase to the time when the COM velocity, which was calculated based on the GRF, reached 0. The concentric phase was defined from the end of the eccentric phase to takeoff time. Statistical analysis was performed using one-way analysis of variance (ANOVA), with Dunnett's t-test as a post-hoc analysis. The correlation between jump performance and the GRF variables was analysed using the Pearson product-moment correlation coefficient or Spearman's rank correlation coefficient. The significance level was set at $p < 0.05$.

RESULTS AND DISCUSSION

The adolescent group was divided into three groups with 13 adolescents pre-PHV, 24 in circa-PHV, and 8 in post-PHV group. Jump height, concentric displacement, and concentric work were significantly lower in the pre-PHV group than in young adults. However, no significant differences were found between circa- and post-PHV groups and young adults (Table 1). Jump height and concentric work were positively correlated in all the groups (r = 0.870–0.902, p = 0.002–0.001). Pre-PHV group had a lower jump performance than that of young adults. However, significant differences in jump performance were not detected in circa- and post-PHV groups and in young adults. These results suggest that adolescents in the pre-PHV phase are different from adults in jump performance. Pre-PHV group had lower concentric work than that of young adults; therefore, jump height was also lower than that in young adults.

CONCLUSIONS

In pre-PHV group, a lower jump height was found than in young adults. However, no significant differences were found between the other maturity groups and young adults. Maturity level should be considered when assessing adolescents' jump performance.

REFERENCES

[1] Sarvestan J, *Acta Gymnica* **48**: 9-14, 2018.
[2] Dobbs I, *Scand J Mes Sci Sports* **30**: 2143-53, 2020.

Table 1. Jump performance and ground reaction force variables.

	Pre-PHV	Circa-PHV	Post-PHV	Young adults	*p-value*[*]
Jump height (m)	0.28 ± 0.05	0.33 ± 0.05	0.36 ± 0.04	0.35 ± 0.05[†]	***p* = 0.013**
RSI (m/s)	0.52 ± 0.11	0.56 ± 0.10	0.58 ± 0.09	0.56 ± 0.12	p = 0.528
Concentric displacement (m)	0.29 ± 0.04	0.33 ± 0.05	0.35 ± 0.05	0.35 ± 0.05[†]	***p* = 0.020**
Concentric work (J/kgf)	0.52 ± 0.11	0.56 ± 0.10	0.58 ± 0.09	0.56 ± 0.12[†]	***p* = 0.002**

[*] One-way ANOVA's *p-value*.
[†] Significantly different from pre-PHV ($p < 0.05$).

QUANTIFYING THE CONTRALATERAL REPEATED BOUT EFFECT OF THE TRICEPS SURAE

Nicole Jones[1], Dean E. Mills[1], Patricio A. Pincheira[2], Ben W. Hoffman[1]
[1] School of Health & Medical Sciences, University of Southern Queensland, Ipswich, Australia.
[2] School of Human Movement and Nutrition Sciences, University of Queensland, Brisbane, Australia
Email: Nicole.Jones@usq.edu.au

INTRODUCTION

An initial bout of eccentric exercise induces soreness and muscle force decrement (exercise-induced muscle damage; EIMD) but is then followed by a protective adaptation for subsequent bouts of the same exercise (ipsilateral repeated bout effect; IL-RBE). Interestingly, this protective effect has been shown in the contralateral limb despite not performing an initial bout of exercise (contralateral repeated bout effect; CL-RBE) and has been shown for the elbow flexors and extensors as well as the knee flexors and extensors [1] but has yet to be observed in the triceps surae. Compared to other muscle groups, the magnitude of both the initial damage and the subsequent protection in the IL-RBE has been shown to be smaller for the triceps surae, likely because of the compliant Achilles tendon preventing large scale damage to active force generating structures [2]. As the CL-RBE doesn't require physical damage to the muscle fibres of the contralateral limb, this model may be useful in identifying the mechanism(s) that better explain EIMD and the RBE for the triceps surae (e.g., neural adaptations). However, as the CL-RBE has been shown to be ~50% in magnitude of the IL-RBE, and as the presence of EIMD and IL-RBE in the triceps surae is smaller, it is unclear if a CL-RBE can be induced in the triceps surae. Therefore, the aim of this study was to quantify the CL-RBE of the triceps surae in humans.

METHODS

Young, healthy participants (mean ± SD age: 34.3 ± 2.6 years, height: 1.70 ± 0.04 m, body mass: 83.6 ± 3.5 kg) performed a bout of eccentric exercise of the triceps surae (225 heel drops; ECC) on one leg (ECC1) followed by a repeated bout on the opposite leg two days later (ECC2). ECC was performed on the edge of a force plate through a 50^0 range of motion, while wearing a weighted vest (10% body weight). Markers of EIMD were assessed before (PRE) and 2 hours (2H), 24 hours (24H), and 48 hours (48H) after each ECC bout on both limbs. Plantar flexor torque was measured during the performance of three maximal voluntary isometric plantar flexor contractions (MVCs) via an isokinetic dynamometer. Muscle soreness was rated 0-10 (visual analogue scale) during 6 tasks (3 palpation and 3 active) for a total out of 60. The size of the protective effect (index of protection) for MVC torque and soreness was calculated using the values 48H after exercise: (ECC2 - ECC1)/ECC1×100 [3].

RESULTS AND DISCUSSION

Currently, data from four participants has been analysed. Muscle soreness increased from 2H-48H after ECC1, with a similar rise but faster recovery following ECC2 (Table 1).

Table 1. Mean (±SD) muscle soreness (/60) PRE, and 2H-48H after each eccentric exercise bout of the triceps surae.

		PRE	2H	24H	48H
Soreness	ECC1	0.3 ± 0.5	3.0 ± 2.0	8.3 ± 2.5	13.5 ± 4.4
	ECC2	0.3 ± 0.5	3.0 ± 4.1	8.3 ± 6.7	9.5 ± 9.1

MVC torque dropped 19%2H after ECC1 and had not recovered at 48H post-ECC1 (32% decrement). At 2H following ECC2 with the contralateral leg, torque dropped 15% and only a decrement of 14% remained at 48H (Figure 1). The index of protection at 48H for muscle soreness and MVC torque were 29.6 ± 6.8 % and 26.7 ± 18.8 %, respectively.

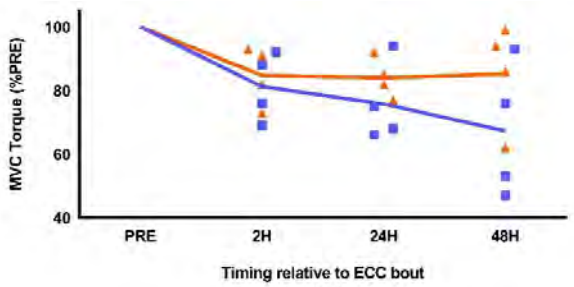

Figure 1. Mean MVC torque normalized to PRE before, and 2H–48H after the first (blue line) and second bouts (orange line) of triceps surae eccentric exercise. Participants used the opposite leg for the second bout two days after the first bout. Filled squares and triangles indicate individual data for ECC1 and ECC2, respectively.

CONCLUSIONS

Our preliminary analysis indicates that an initial bout of eccentric exercise using the triceps surae on one leg can provide protection for a subsequent bout of eccentric exercise for the contralateral limb. As such, the CL-RBE can be used for future work attempting to understand the mechanisms of EIMD/IL-RBE for this muscle group, where a large insult to the active force generating structures is absent.

REFERENCES

[1] Jeon S et al. *Res Sp Med* pp.1-20, 2021
[2] Pincheira P et al. *Sc J MSS* **28**(10): 2123-2134, 2018.
[3] Chen T et al. *MSSE* **48**(10): 2030–9, 2016.

INFLUENCE FROM WETSUIT ON THE ASSESSMENT OF BIOMECHANICAL PARAMETERS THROUGH IMU MEASUREMENTS

Alexander Weiss[1], Èric Lluch[2], Anne D. Koelewijn[1]
[1]Friedrich-Alexander-Universität Erlangen-Nürnberg (FAU), Machine Learning and Data Analytics Lab, Germany
[2]Siemens Healthineers, Digital Technology and Innovation, Erlangen, Germany
Email: alexander.aw.weiss@fau.de

INTRODUCTION

The use of biomechanical assessments in aquatic environments is essential for understanding and improving performance in sports such as swimming, diving, and surfing. However, established methods of biomechanical analysis, such as optical motion capture (OMC) systems, are not feasible for use in environments like the open sea. Inertial motion capture (IMC) systems that combine inertial measurement units with optimal control simulation of musculoskeletal models offer a potential solution, since such a system can accurately estimate kinetics and kinematics of walking and running [1]. However, natural aquatic environments are different than those in which IMC has been applied so far [2, 3]. For example, wetsuits are crucial in the ocean, and IMC sensors should be placed on the wetsuit to ensure a fixed location while practicing the sport. This could affect measurement accuracy. Therefore, we investigated the effect of wetsuits on the accuracy of IMC, by comparing the error between OMC and IMC with and without wearing a wetsuit.

METHODS

We conducted a pilot study with one participant, who walked and ran on a treadmill, while data was collected using both OMC and IMC. Each task was performed with and without a wetsuit. We then calculated joint angles and joint moments by solving optimal control problems for a sagittal plane musculoskeletal model. We created simulations by tracking the OMC and IMC data and evaluated the IMC system by comparing it to the simulation created with OMC data, both with and without the wetsuit. Joint angles from inverse kinematics, together with ground reaction forces, were tracked in the OMC simulations [4], while linear accelerations and angular velocities were tracked in the IMC simulations [1]. Here, we calculated the correlation coefficient and root mean squared error (RMSE) of the joint angles and moments of the hips, knees, and ankles, as well as of the ground reaction forces.

RESULTS AND DISCUSSION

We found that joint angles, joint moments, and ground reaction forces correlated well between the wetsuit and no-wetsuit condition, while RMSEs are similar to those in [1] (Tab. 1). The joint moment predictions with the IMC were even more similar to OMC when wearing the wetsuit than without the wetsuit (Tab. 1, Fig. 1). The correlation coefficient here was 0.95 for the recording without wetsuit and 0.98 for the recording with wetsuit.

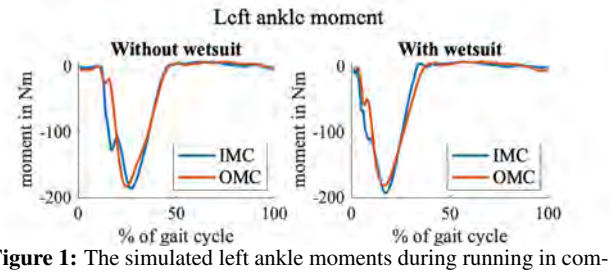

Figure 1: The simulated left ankle moments during running in comparison.

So far, we only analysed running data of one participants. We will further evaluate our methods on other participants, as well as for walking. We also plan to evaluate our algorithms by analysing motions recorded in a controlled aquatic environment.

CONCLUSIONS

In conclusion, our pilot study provides initial evidence that wearing a wetsuit does not affect the quality of motion analysis performed with IMC, meaning that there are no adverse affects when placing inertial sensors on a wetsuit instead of on the body. Future studies should assess movements recorded in an aquatic environment, to fully explore the potential of IMC in this environment.

REFERENCES

[1] Dorschky E et al. *J Biomech* **95**: 109276, 2019.
[2] Masumoto J et al. *Exerc Sport Sci Rev* **36(3)**: 160-169, 2008
[3] Wang Z et al. *IEEE Trans Hum Mach Syst* **49(2)**: 2168-2291, 2019
[4] Nitschke M et al. *PeerJ* **11**:e14852, 2023.

Table 1: Mean correlation coefficients (R) and root mean squared errors (RMSE), comparing the IMC to the OMC result, of all joint angles, joint moments and ground reaction forces (GRF) of the participant for wearing (WS) and not wearing (noWS) a wetsuit.

	R noWS	R WS	RMSE noWS	RMSE WS
Joint angles	0.94	0.93	11.03°	9.83°
Joint moments	0.88	0.92	25.70 Nm	19.99 Nm
GRF	0.93	0.93	0.14 BW	0.16 BW

EFFECT OF MOTOR SYNERGIES ON POSTURE AND PERFORMANCE STABILITY: A COMPARISON OF SELF- AND EXTERNAL TRIGGERED SHOOTING IN SIMULATED ARCHERY

Junkyung Song[1], Kitae Kim[3], Jaebum Park[1,2]
[1] Department of Physical Education, Seoul National University, Seoul, South Korea.
[2] Institute for Sports Science, Seoul National University, Seoul, South Korea.
[3] Department of Sports Science, Korea Institute of Sport Science, Seoul, South Korea.
Email: parkpe95@snu.ac.kr

INTRODUCTION

Successful archery performance requires stable drawing in force generation and standing in a vertical posture. Our current curiosities were about a mutual interaction of these two components, which may be affected by the trigger type of force release, e.g., release at a self-chose time or reaction to an external cue. Archery behaviors contain the actions of both upper and lower limbs, and several effectors (e.g., finger/hand forces, leg muscles) are involved in the shooting performance. Thus, the concept of synergies, which describes and quantifies the covariation patterns of multiple elements as an index of stability, would provide insight into archery performance from the perspective of biomechanics and motor control. This study employed a simulated archery shooting task in laboratory conditions and examined the effect of two release types on motor synergies and consequent archery performance consistency.

METHODS

We developed a customized bow frame that can measure the individual finger forces and frame angle. The subjects performed aim-releasing tasks on a force platform. Electrical activities of postural muscles were recorded using an electromyogram (Figure 1). In the self-triggered (ST) condition, the subjects released the target drawing force shown in the feedback screen in a self-paced manner. They released it by reacting to external signals in the external-triggered (ET) condition. We quantified postural sway indices by decomposing the center of pressure trajectories to rambling and trembling components. Uncontrolled manifold analysis was used to determine synergies (ΔV_z) in stabilizing upright posture and drawing force as stability indices. A target precision index (PRI) representing performance consistency was computed.

RESULTS AND DISCUSSION

The two synergy indices related to posture and drawing force stability were higher in the ST than in the ET condition (Table 1). We confirmed that co-contraction of the postural muscles during aim-release was relatively higher in the ET and negatively affected the postural stability. The small errors in multi-fingers force production could improve net drawing force stability in the ST condition. Further, the subjects showed relatively higher target precision under the ST condition (Table 1), which was significantly correlated with both posture and drawing force stability.

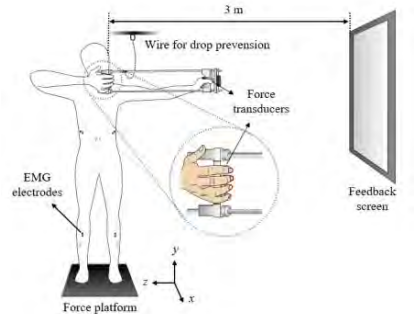

Figure 1 Experimental setup

CONCLUSIONS

The current findings suggested that the self-paced releasing with a feedforward control mechanism would be beneficial for archery performance consistency by increasing postural stability and reducing drawing force error. It can be applied in actual archery situations. Archers are generally known to use clickers and shoot in response, and a reduced reaction time to clickers was considered better archery performance [2]. Therefore, the strategy of predicting clicker drops, rather than reacting to them, could improve the consistency of archery performance.

ACKNOWLEDGEMENTS

This research was supported in part by the Basic Research Program through the National Research Foundation of Korea (NRF), funded by the MSIT (2022R1A4A503404611)

REFERENCES

[1] Kim et al. *Sci Rep* **8**: 12758, 2018.
[2] Ertan et al. *Hum Mov Sci* **22**: 37-45, 2003.

Table 1: Average synergy indices (ΔV_z) and target precision index (PRI) in the self- and external-triggered condition (mean ± SE).

Variables (normalized value)	ST	ET	Cohen's *d*	*p-value*
ΔV_z (postural stability)	0.80 ± 0.19	-0.02 ± 0.11	2.37	$p < 0.001$
ΔV_z (drawing force stability)	1.99 ± 0.15	1.69 ± 0.07	1.58	$p = 0.003$
PRI	0.17 ± 0.02	0.23 ± 0.03	1.24	$p = 0.01$

Muscle activity timing and amplitude in the early acceleration phase of curve sprinting

Benjamin Millot[1,2], Didier Pradon[3], Daniel Dinu[1], Paul Blache[1], Andras Hegyi[4], Axelle Arnould[1], Jean Slawinski[1]
[1] Laboratory Sport, Expertise and Performance (EA7370), French Institute of Sport (INSEP), Paris, France.
[2] French Athletics Federation (FFA), Paris, France.
[3]Pole Parasport – ISPC Synergies, CHU Raymond Poincaré, APHP, Garches, France.
[4]Laboratory "Movement, Interactions, Performance", Faculty of Sport Sciences, University of Nantes, France
Email: benjamin.millot@insep.fr

INTRODUCTION

Surface electromyography (sEMG) helps understand the muscular origin of sprinting technique. It has been shown that maximal hip flexion and maximal hip extension angles are reached later at maximal velocity in the curve than in the straight [1]. The hip flexors and extensors activation timings were shown to influence the step frequency both at maximal velocity [2]. Since the inside leg step frequency is reduced within the curve [1], this could result from delayed inside leg activation timings. Therefore, the aim of the present experimentation was to investigate the onset of muscle activity and the sEMG amplitude of hip flexors and extensors in straight-line and curve sprinting.

METHODS

9 (6 male and 3 female) experienced-to-elite curve sprinters (mean ± SD: age = 22.8 ± 3.0 years; body mass = 70.8 ± 5.7 kg; height = 177.3 ± 6.6 cm) volunteered to participate in this study. After a 45-min self managed warm-up, the participants performed 10 and 40-m sprints within two sprinting conditions: straight-line and curve on a reconstructed lane 5 (radius = 41.58 m).
sEMG (Delsys Inc., 2148 Hz) were positioned on the *Rectus Femoris* (RF) and *Biceps Femoris long head* (BF) of both left (L) and right (R) legs (3). After full-wave rectification and band-pass filtering (20-500 Hz), the onset timings (% of stance duration) of muscle activity were identified using Teager-Kaiser energy operator and Approximated Generalized Likelihood Ratio (4). Mean sEMG amplitudes were normalised to the maximal activity of the corresponding muscle detected over the straight-line 40-m sprints. Two-way RM ANOVAs were performed.

RESULTS

There were no significant effects for condition or side neither for the onsets of muscle activity of RF ($p > 0.283$) and BF ($p > 0.412$) (figure 1); nor for the sEMG amplitude of RF ($p > 0.718$) and BF ($p > 0.111$).

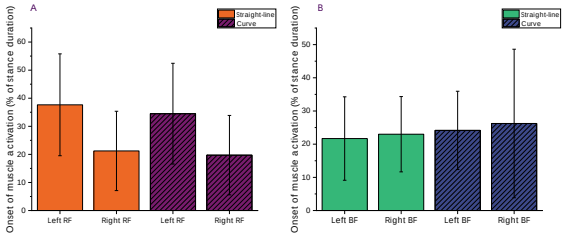

Figure 1 Mean ± *SD* onsets of muscle activity for A) *Rectus Femoris*, and B) *Biceps Femoris long head*.

CONCLUSIONS

The early acceleration phase of curve sprinting on a reconstructed lane 5 did not result in alterations of neither the onset timings nor the magnitudes of hip flexors and hip extensors muscular activity in comparison to the straight-line. Yet, this analysis only focussed on the first steps of a sprint. As already suggested by Judson et al. (5) regarding the ground reaction forces: the effect of the bend on the muscular activity during the acceleration phase could accumulate with the increasing velocity.

ACKNOWLEDGEMENTS

Benjamin Millot received a PhD scholarship (CIFRE contract n°2019/1904) founded by the French Athletics Federation and the French Agency of Research and Technology.

REFERENCES

[1] Churchill et al. (2015). Sports Biomechanics. 14(1):106-121.
[2] Kakehata et al. (2021). Med Sci Sports Exerc. 53(3):643-652.
[3] Hermens et al. (2000). J. Electromyogr. Kinesiol. 10(5):261-374.
[4] Solnik et al. (2010). Eur J Appl Physiol. 110 :489-498.
[5] Judson et al. (2019). Scand J Med Sci Sports. 29 :1563-1571.

Table 1: Mean ± *SD* of muscle activity amplitude for the *Rectus Femoris* and *Biceps Femoris long head* in straight-line and curve sprinting.

	Straight-line		Curve	
	Left	Right	Left	Right
Rectus Femoris	67.11 ± *34.14*	72.00 ± *29.02*	62.95 ± *38.88*	70.10 ± *38.97*
Biceps Femoris long head	52.86 ± *13.60*	54.59 ± *24.18*	45.95 ± *12.13*	59.33 ± *24.17*

Developing a simulation model considering frictional force during turning in dance

Akiko Imura[1], Sekiya Koike[2], Yoichi Iino[3], Fred Yeadon[4] and Sam Allen [4]
[1] Department of Health Promotion Sciences, Tokyo Metropolitan University / Hachioji, Japan.
[2] Faculty of Health and Sport Sciences, University of Tsukuba/ Tsukuba, Japan.
[3] Department of Sports Sciences, Graduate School of Arts and Sciences, University of Tokyo/ Tokyo, Japan.
[4] School of Sport, Exercise and Health Sciences, Loughborough University / Loughborough, UK.
Email: akikoimura17@gmail.com

INTRODUCTION

In the classical ballet turn, pirouette, the dancer swings upper limbs with both legs flexed, then stands on on one toe and turns. During the pirouette, the dancer utilize the frictional forces from the floor. The dancer generates the vertical angular momentum with the frictional force during swinging upper limbs, and then turns with the reduced frictional force due to standing on tiptoe.

The frictional force can be controlled by the joint motions. The limiting frictional force is the normal force acting on the floor multiplied by the static or dynamic frictional coefficients. Whether the force from the body is greater or less than the limiting frictional force determines the foot motions [1]. As the vertical ground reaction force (GRF) varies with joint motions, dancers would adjust their performance with the slipperness. A computer simulation of a turning model would reveal techniques dealing with friction during turning. The purpose of this study is to create a whole-body model which turns and slides.

METHODS

Coordinates of markers on the whole-body and GRFs were recorded using a motion capture system during pirouettes by a female ballet dancer. The foot markers were attached at; the toe, medial and lateral sides of the metatarsophalangeal (MP) joint, and the calcaneal process. The restoring forces (F) of the viscoelastic springs assumed at the location of the foot markers were calculated using the following the equation and the sum was the simulated GRF.

$$F = -Kd - Dv|d|,$$

where K and D are the stiffness and damping coefficients, d and v are the height of a marker from its reference and the d's diffrenciation, respectively [2]. The coefficients of the viscoelastic springs will be determined by minimizing the difference between the real and simulated GRF using a genetic algorithm [3].

Dynamic and static friction forces were applied to the foot in response to foot slippage. If the magnitude of each marker velocity exceeded a reference value, the maximum dynamic friction force will be applied along the opposite direction of the marker horizontal velocity vector, otherwise the forces to move the foot will be applied. Free moments were also assumed according to the friction forces.

RESULTS AND DISCUSSION

The total viscoelastic spring forces acting on each foot could simulate the vertical GRF of the experiment, except for the forces acting during turning of the supporting foot and during landing of the free leg. The root-mean-square difference between the experimental data and the viscoelastic spring forces was less than about 55 N, which is approximately 10% of the maximum GRF. The coefficients of dynamic and static friction were 0.18 and 0.17 for the supporting foot and 0.4 for the other foot (only for the dynamic). The frictional forces calculated from the simulated vertical forces were well matched for the supporting foot during rotation but not for the other foot during contacting on the floor.

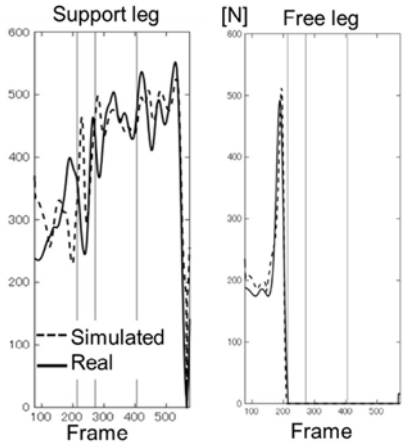

Figure 1 Simulated and real vertical GRF on feet.

CONCLUSIONS

These results suggest that to simulate the GRFs, it is necessary to assume not only viscoelastic springs assumed in the feet, but also springs in the body. With regard to the frictional forces acting on the foot while it is stationary needs appropriate estimates of the frictional coefficients.

ACKNOWLEDGEMENTS

This study is supported by JSPS KAKENHI (22K11553).

REFERENCES

[1] Imura A et al. *Hum mov sci.* **29**: 947-955, 2010.
[2] Allen SJ et al. *J Biomech* **43(16)**: 3156-3161, 2010.
[3] Goldberg DE et al. *Optimization and Machine Learning*, first ed. Addison-Wesley, Boston, MA, 1989.

COMPARISON OF THE DIFFERENCE BETWEEN COUNTERMOVEMENT AND SQUAT JUMP IN TRAINED AND UNTRAINED ADULTS

Cheng Ching-Feng [1, #], Chen Chu [2], Pan Chi-Hsueh [2], Chang Cheng-Hung [1], Lin Yi-Wun [2] and Yang Yun-Rong [2]
[1] Department of Athletic Performance, National Taiwan Normal University, Taipei, Taiwan.
[2] Department of Physical Education and Sport Sciences, National Taiwan Normal University, Taipei, Taiwan.
[#] Email: andescheng@ntnu.edu.tw

INTRODUCTION

Countermovement (CMJ) and squat (SJ) jumps are commonly used to monitor neuromuscular performance in athletes. Traditionally, the difference between SJ and CMJ can be used as an indicator for utilization of stretch-shorten cycle (SSC) [1]. However, it is unclear how CMJ and SJ performance differs between trained and untrained individuals after matching participants' characteristics. This study examined the differences in jumping performance between athletes and healthy individuals with similar physical characteristics.

METHODS

38 collegiate male athletes (ATH; included basketball, rugby, tennis, frisbee, taekwondo etc.) and 38 healthy and active collegiate male students (CON) were recruited in this cross-sectional study (Table 1). After 2 familiarization trials (to ensure the proper execution technique for each exercise test) and a 1RM half-squat test, all participants performed the vertical jumps (SJ and CMJ) and isometric mid-thigh pull (IMTP) test on a force platform (Ballistic Measurement System, Innervations, Australia). The vertical jumps consisted of 3 maximal trials for each type of jump with 10-s rest. A 2-min passive rest was allowed between SJ and CMJ tests. Jumping height was calculated from flight time. The difference between CMJ and SJ (**Diff** = CMJ–SJ), prestretch augmentation (**PA** = [CMJ–SJ]/SJ×100%), and eccentric utilization ratio (**EUR** = CMJ/SJ) were derived from jumping height.

For the IMTP test, participants performed three 5-s long attempts, separated by a 2-min passive rest, pulling a barbell clamped to the crash bars of the power rack in a standardized body position (knee angle of 125º and hip angle of 145º). The peak force, rate of force development (RFD at 0-30, 0-60, 0-90, 0-150 and 0-200 ms), and maximal RFD (RFDmax; 30-ms sampling windows) were obtained during IMTP test.

Table 1: Characteristics of participants (n = 76)

	Athletes	Healthy Adults	Cohen's *d*
Age (yrs)	21.0 ± 2.0	21.3 ± 1.9	0.16
Height (m)	1.75 ± 0.08	1.76 ± 0.04	0.18
Body mass (kg)	73.3 ± 13.1	70.3 ± 9.5	0.27
1RM (kg)	167 ± 35*	121 ± 18	1.65
1RM/BM	2.28 ± 0.30*	1.75 ± 0.32	1.73
CMJ (cm)	44.9 ± 4.9*	39.2 ± 5.0	1.16
SJ (cm)	35.8 ± 3.7*	31.9 ± 4.0	1.02

*$p < 0.05$, compared with healthy adults.

RESULTS AND DISCUSSION

The performance of SJ, CMJ, and 1RM in ATH were significantly greater than those in CON (Table 1). The peak force (ATH vs. CON, 1188 ± 335 vs. 966 ± 227 N, $d = 0.78$, $p < 0.05$) and RFDmax (ATH vs. CON, 7305 ± 2555 vs. 6001 ± 1615 N·s^{-1}, $d = 0.62$, $p < 0.05$) during IMTP in ATH were also significantly higher than those in CON. No significant differences between groups were found in RFD at other time-intervals during IMTP. Figure 1 indicated that the Diff in ATH group was significantly greater than that in CON ($d = 0.53$, $p = 0.026$). However, no significant differences were found on PA ($p = 0.317$) and EUR ($p = 0.325$) between groups.

Previous studies reported that Diff [2], PA [3], and EUR [4] might not be sensitive indicators for monitoring or distinguishing differences in athlete performance. Although the mechanisms (e.g., utilization of SSC, storage and utilization of elastic energy, uptake of muscle slack, buildup of stimulation) explained the difference between SJ and CMJ remain unclear [5], Diff might be a sensitive indicator of differences in jumping performance between trained and untrained individuals.

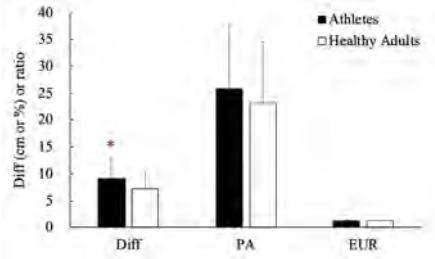

Figure 1 Differences between CMJ and SJ for the different groups. *$p < 0.05$, compared with healthy adults.

CONCLUSIONS

With matched participants' characteristics (age, height and body mass), Diff might be used as a good indicator of SSC efficiency to distinguish trained and untrained individuals. However, studies with a longitudinal design are needed to clarify the effect of chronic training on the utilization of SSC.

ACKNOWLEDGEMENTS

This study was funded by National Science and Technology Council (NSTC 112-2425-H-003-002).

REFERENCES

[1] McGuigan MR et al. *J Strength Cond Res* **20**: 992-5, 2006.
[2] Edwards T et al. *J Strength Cond Res* **in press**, 2022.
[3] Kozinc Ž et al. *Eur J Sport Sci* **22**: 985-93, 2022.
[4] Kozinc Ž et al. *Int J Environ Res Public Health* **18**: 11754, 2021.
[5] Van Hooren B et al. *J Strength Cond Res* **31**: 2011-20, 2017.

Get on Up; Relating Objective Hip-Hop Dance Biomechanics to Subjective Scoring

Joshua Alexander Vicente, M.S.[1], Belle Pearl Ponce de Leon, M.S.[1], Rudy Lua[1], Thomas "Rex" Ruswick[1], Makena Savola, M.S.[1], and Jacob W. Hinkel-Lipsker, Ph.D. [1]
[1] Kinesiology, California State University, Northridge, California, USA
Email: jhlipsker@csun.edu

INTRODUCTION

Hip-hop dance is a growing style of dance worldwide that typically involves an element of competition, where judges subjectively score dance performance[1]. To ensure competitive fairness, it is important to understand what judges are observing in dancers as part of the scoring process.[2] Such research would help elucidate whether judges' scores are more related to the objective biomechanics of dance moves, or other more subjective factors (e.g., attire). Therefore, the purpose of this study was to investigate the relationship between biomechanics of common dance moves among experienced dancers and how they are subjectively perceived by judges.

METHODS

Eighteen experienced adult-aged dancers were recruited for this study. Participants learned a choreographed routine, which contained two specific dance moves that were used for analysis: the arm wave, where the joints and segments of the arm move in a wave-like pattern from left to right, and inverted happy feet, where the feet move in opposition from one another alternating in transverse plane rotation. A 12-camera 3D motion capture system was used to record the coordinates of 28 retro-reflective markers at 240Hz, two force plates recorded ground reaction force data, and a separate camera provided video of each choreographed trial. These recorded video trials were be sent off sent to three professional judges for scoring.

For the arm wave, marker coordinate data were used to calculate metrics related to the displacement and velocity of arm joints and segments, as well as the shape deviation of an arm wave move from a sinusoidal wave pattern.[2] For the foot work, ground reaction force data were used to quantify the timing in forces between the two feet. Two stepwise linear regression models were then developed to test the degree to which: 1) arm wave kinematics and 2) foot work timing variables predicted judge's scores.

RESULTS AND DISCUSSION

Judges' scores for the arm wave were significantly predicted ($p < 0.001$, adjusted $R^2 = 0805$; Table 1) across all dancers by displacement of the right metacarpophalangeal (MCP) Joint (Figure 1; $p < .05$, **β** = -.331), as well as propagation velocity of the left forearm ($p < .05$, **β** = -.248) and right forearm ($p < .05$, **β** = -.891). Judges' scores for footwork were also significantly predicted by Timing Difference across all the dancers' performance ($p < .05$, **β** = -.535).

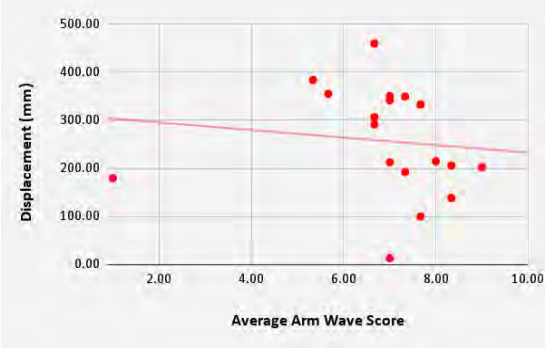

Figure 1 Right MCP Joint Displacement vs. Avg. Judges Scores.

CONCLUSIONS

Judges seemed to only focus on the beginning of the arm wave and seemed to rely on speed of both forearms to potentially show mastery & control. Using Biomechanical Analysis, this may prove fruitful to study other styles of dance or different movements common across styles to provide more predictors for performance and to catalog dance styles within academic literature.

REFERENCES

[1] Kojima et al., JMD, **6:**1, 1- 11, 2018

[2] Sato et al., *J. Appl. Biomech* **31**: 1, 1 – 7, 2015

Table 1: Results of regression model showcasing significant predictors for the arm wave & regression model for Footwork*.

	R	R^2	Adjusted R^2	RMSE	*p-value*
Right Forearm Velocity	.819	.670	.650	1.018	$p < 0.001$
Right MCP Joint	.882	.778	.748	.863	$p = 0.017$
Left Forearm Velocity	.916	.839	.805	.760	*P = .037*
*Time Difference	.535	.286	.242	1.028	*p = .022*

Changes in 5-10m elapse time in *kick start* of a swimming race at different back plate positionings

Masayuki UMEMOTO[1], Yasunori FUJITO[2], Hiroki HYODO[3], Natsumi FURUTA[2], Tadashi WADA[3], and Kazuo FUNATO[1]

[1] Kokushikan University / The Institute of Pyhsical Education, Japan.
[2] Kokushikan University / Graduate School of Sport System, Japan.
[3] Kokushikan University / Graduate School of Engineering, Japan.
Email: umemoto17@gmail.com

INTRODUCTION

Recent studies of the kick start have examined the differences in backplate position and reported on the relationship between the back plate position and the horizontal velocity at the start and the subsequent transit time[1) 2)]. However, there are no studies that have reported on the details of the movement on the platform, so there is no established index to indicate the optimal back plate position for on-site instruction.

The purpose of this study was to clarify the effects in the lower hip angle in different back plate positions has on the time of the 5m and 10m distances in a swim start.

METHODS

Seven male swimmers who were members of the national swimming team and university swimming clubs. Ten motion capture systems (PrimeX13 OptiTrack, Acuity Inc., Japan) were used to acquire kinematic data from the start signal to the entry into the water. Motion data was sampled at 180 Hz, and three-dimensional coordinate data were obtained from the subject's markers.

Each swimmer participated using three back plate positions; each dive using a different back plate position and recordings of time were made from the start to 15m. The back plate position was varied in three levels: Front (the position closest to the tip of the starting platform), Back (the position farthest from the tip of the starting platform), and Prefer (the position preferably used in practice and competitions).

RESULTS AND DISCUSSION

The results of this study showed that Back had the fastest 10m elapse time and significantly smaller than Front and Prefer ($p<0.05$) (Table 1). The take-off angles were Front, Prefer and Back, with significantly smaller values for Front and Back, Prefer and Back ($p<0.05$).

Figure 1 shows that the start of extension of each joint angle of the back leg tended to be earlier in the order of Front, Prefer, and Back. The hip joint angles at the starting position (0 sec) differed, with the Back showing the largest angle. In the start of a swimming race, the swimmers respond to the starting signal, kick the starting blocks with their legs, and simultaneously raise their upper bodies to jump off of the starting blocks. This is thought to have resulted in the swimmers being able to kick out smoothly. As a result, the swimmer had enough time to raise the upper body, and the take-off angle was close to being horizontal.

Table 1: Mean and Standard deviation of the variables of each back plate positions.

Variables (n=7)	unit	Front	Prefer	Back
		Mean±SD	Mean±SD	Mean±SD
Block Time	sec	0.71 ± 0.04	0.71 ± 0.03	0.70 ± 0.06
Entry Time	sec	1.08 ± 0.07	1.11 ± 0.05	1.13 ± 0.06
5m Time	sec	1.51 ± 0.10§	1.47 ± 0.07§	1.49 ± 0.09
10m Time	sec	4.48 ± 0.29¶	4.39 ± 0.22*	4.29 ± 0.23¶*
Horizontal take-off Velocity	m/s	4.24 ± 0.29	4.24 ± 0.31	4.25 ± 0.33
Vertical take-off Velocity	m/s	-0.33 ± 0.43	-0.32 ± 0.41	-0.17 ± 0.43
Resultant take-off Velocity	m/s	4.27 ± 0.30	4.27 ± 0.31	4.27 ± 0.32
Horizontal entry Velocity	m/s	5.06 ± 0.47	4.97 ± 0.40	5.03 ± 0.41
Vertical entry Velocity	m/s	-3.47 ± 0.72	-3.62 ± 0.41	-3.94 ± 0.41
Resultant entry Velocity	m/s	6.15 ± 0.72	6.15 ± 0.55	6.40 ± 0.64
Take-off angle	degree	-4.5 ± 5.8¶	-4.0 ± 5.7*	-2.1 ± 5.8¶*
Entry angle	degree	34.2 ± 4.7	36.1 ± 1.7	37.9 ± 3.3

Front vs.Perffer : p<0.05§ ,Front vs.Back : p<0.05¶ ,Perffer vs.Back : p<0.05*

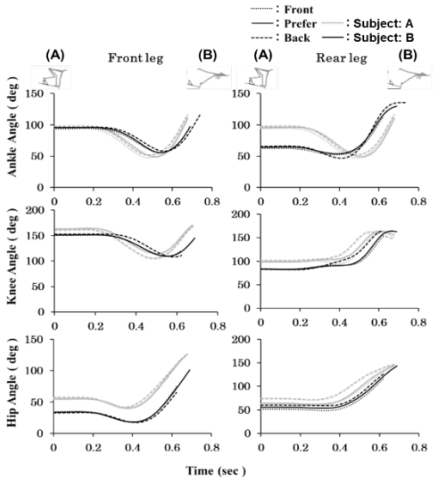

Figure 1 Joint angle at each back plate position. (A: statics posture at starting signal, B: posture at take-off)

CONCLUSIONS

The purpose of this study was to clarify the effect of the change in each joint angle of the lower limb from the start to the time of leg separation on the 5m and 10m elapse time due to the different positions of the back plate. The results showed that as the back plate position was moved backward, the take-off angle was significantly smaller and the 10m distance time was faster. The reasoning is the hip joint angle at the starting position was larger, and the timing of the start of extension of each joint angle of the back leg was earlier, which gave the swimmers enough time to raise their upper bodies.

REFERENCES

[1] Honda K et al. *30th Annual Conference of Biomechanics In Sports*: 72-75, 2012.

[2] Sakai S et al. *Jpn. Phys. Educ. Health Sport Sci.* **62**: 133-144, 2017

THE INFLUENCE OF PROJECTILE MASS ON THROW DISTANCE

John H Challis
Biomechanics Laboratory, The Pennsylvania State University
Email: jhc10@psu.edu

INTRODUCTION

In 1871 Darwin commented "To throw a stone with as true an aim as a Fuegian defending himself, or in killing birds, requires the consummate perfection in the correlated action of the muscles of the hand, arm, and shoulder, and, further, a fine sense of touch."[1]. Throwing has been implicated in the the evolutionary development of brain lateralization, encephalization, language, and intelligence [2]. Previous studies have examined the accurate timing of release on throw accuracy [e.g., 3], a crucial factor which hitherto has not received much attention is the influence of projectile mass on throw performance. In hunting and self-defense the projectile mass is important as it is a factor in a projectiles kinetic energy, which in turn has implications for the result of an accurate throw on its target. Therefore, the purpose of this study was to examine the influence of ball mass on throw distance, where throw distance reflects ball kinetic energy.

METHODS

A model of the upper limb was developed which simulated a simple throwing task. The model was used to examine the influence of ball mass on throw distance. The model was based on a previously published model [4]. The muscle moment (T_M) at each joint was determined from,

$$T_M = q(t).T_{Max}.T_\phi(\phi).T_{\dot\phi}(\dot\phi)$$

Where $q(t)$ is the active state at time t, T_{Max} is the maximum isometric moment, $T_\phi(\phi)$is the normalized moments produced at joint angle ϕ, and $T_{\dot\phi}(\dot\phi)$ is the normalized moment produced at joint angular velocity $\dot\phi$. Model parameters were tuned to the physical properties of two experimental subjects [4]. The optimal control problem was to find the active state time series which produced an instant of release which maximized throw distance (and therefore effectively release velocity and kinetic energy), for ball masses ranging in mass from 5.5 to 11 kg. The different mass balls were all assumed to be spheres of the same diameter, but with different densities to allow for a range of different ball inertial properties.

RESULTS AND DISCUSSION

As would be expected throw distance decreased with increasing ball mass (Figure 1). This pattern of results can be explained using geometric scaling principles. For a throw the muscles do work to move the mass of the ball. The work (W) performed by a muscle is a function of the muscle force (F_M) and the muscle change in length (ΔL_M), therefore $W = F_M.\Delta L_M$. The force produced by a muscle is a function of its cross-sectional area (CSA) which scales as a function of body mass (m), therefore $F_M \propto CSA \propto m^{2/3}$. While the change in muscle length will scale with body length (L), and therefore is also a function of body mass ($\Delta L_M \propto L \propto m^{1/3}$). The work done in a throw scales in proportion to body mass ($W = F_M.\Delta L_M \propto m^{2/3}.m^{1/3} \propto m$). At the instant of release the projectiles kinetic energy is $KE = \frac{1}{2}m_B.v_R^2$, where m_B is the ball mass, and v_R is the ball velocity at release. The ball's velocity will be due to the work done in the throw, therefore $m \propto m_P.v_R^2$. As throw distance is a function of release velocity squared, throw distance should be inversely proportional to ball mass, a relationship which demonstrates a good fit to the simulation data (non-linear model in Figure 1).

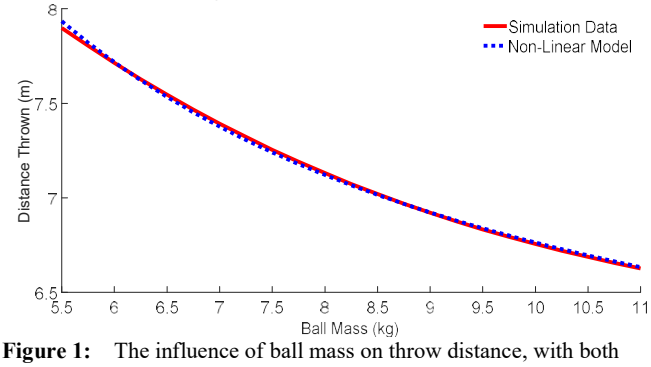

Figure 1: The influence of ball mass on throw distance, with both simulation results and geometric scaling model fit presented.

The geometric scaling non-linear model was fitted to world record shot put performances for different mass shots [5]. The error in predicting throw distance for shot put masses from 4 to 26 kg was 7%, providing further evidence in support of the veracity of the geometric scaling model of ball mass and throw distance.

CONCLUSIONS

In human throwing, throw distance is determined by the non-linear dynamics of the musculoskeletal system and ball mass, but the influence of ball mass on distance thrown can be explained by a simple relationship based on geometric scaling principles.

REFERENCES

[1] Darwin C. *The Descent of Man*. John Murray, London, 1871.
[2] Dunsworth H et al. In: *Upright Walking* (pp. 105-10), Senckenberg Institute, Frankfurt, 2003
[3] Chowdhary A G & Challis J H. *J Theor Biol*, **201**, 219-29, 1999.
[4] Chowdhary A G & Challis J H. *J Theor Biol*, **211**, 39-53, 2001.
[5] Willoughby D P. *The Super-Athletes*. South Brunswick, London, 1970.

CHANGES IN KINEMATIC PATTERNS IN RESPONSE TO BALL VELOCITY IN TENNIS FOREHAND DRIVE

Yoon-Seok Choi[1], Ji-won Park[1], Jiho Kim[1], Dong-Gyu Baek[1], Mukyeong Shin[1] and Jaebum Park [1,2,3]

[1] Department of Physical Education, Seoul National University.
[2] Institute of Sport Science, Seoul National University, Seoul, Korea.
[3]Advanced Institute of Convergence Science, Seoul National University, Seoul, Korea
Email: parkpe95@snu.ac.kr

INTRODUCTION

The forehand drive is one of the most critical skills in modern tennis. Among ball-hitting behaviors in sports, tennis stroke has a unique feature such that the player monitors the velocity and trajectory of the ball for the accuracy of hitting. "*Accurate hitting a movable ball with various speeds*" in tennis competitions is essential and the most critical, which would contrast novice and skilled players. In this regard, we examined and quantified the differences in the ability to adjust the forehand drive swing in response to ball speeds. Notably, the patterns of the sequential chain of the proximal to distal segments in the transverse plane were quantified and further compared between the professional and novice group.

METHODS

Seven expert tennis players and six novice players (under three years of tennis experience for leisure purposes) participated in this study. The device, which was manufactured for launching tennis balls with prescribed velocity (i.e., angle and speed), was used. There were three conditions of the velocity, including slow (7.54 ± 0.65 m/s;) medium (10.83 ± 0.59 m/s;) and fast (14.42 ± 0.50 m/s;). The experiment was composed of 5 repetitive sets, and five trials were given in each set for each velocity condition. The order of the prescribed ball projection was randomized. An infrared camera motion capture system measured the pelvis, shoulder, upper arm, and hand kinematic variables. Further, the angular variables were quantified, including angular displacement and maximum angular velocity of segments on the transverse plane. The mean value of trials for each condition was used as the representative value of that condition. Repeated-measures two-way ANOVAs with factors, ***Group*** (expert & novice) and ***Velocity*** (three levels), were performed.

RESULTS AND DISCUSSION

Both groups showed smaller angles in takeback and angular displacement of proximal segments (pelvis, shoulder) when a ball came fast. Contrary to these results, one of the distal segments - the angular displacement of the upper-arm, increased. Maximum angular velocity of the pelvis and shoulder showed a tendency to decrease according to increasing ball velocity. These results showed that participants tried to reduce the angle in takeback and angular displacement of proximal segments to get an accurate impact. In addition, they increased the angular displacement of the upper arm to compensate for decreasing usage of proximal segments. The maximum angular velocity of the shoulder showed significant ***Group*** × ***Velocity*** interaction. From this result, it is confirmed that the expert group changed their swing strategy adeptly, especially the maximum angular velocity of shoulder compared to novice group.

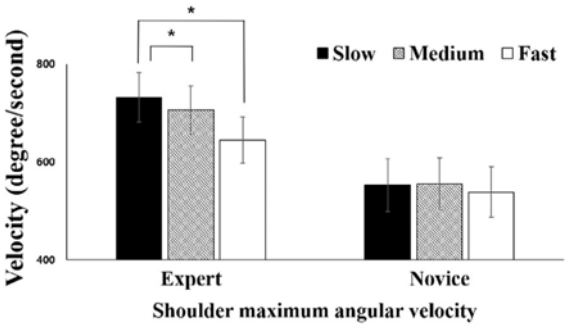

Figure 1 Averaged value of the maximum angular velocity of shoulder was shown for each group. It is also showed the statistical difference between velocity conditions. Asterisk indicates $p<0.01$.

CONCLUSIONS

Both groups changed their swing pattern according to ball velocity in a similar way reducing the usage of proximal segments and increasing that of distal segment. For the shoulder, the expert group modulated it linearly according to ball velocity, but the novice group did not. The results of this study elicited that players decrease their proximal segments. It also suggests that giving a commenting about maximum angular velocity of shoulder to the players who struggle with fast coming balls could be helpful.

ACKNOWLEDGEMENTS

This research was supported in part by the Basic Research Program through the National Research Foundation of Korea (NRF) funded by the MSIT (2022R1A4A503404611) and the Basic Science Research Program through the National Research Foundation of Korea (NRF) funded by the Ministry of Education (2021R1I1A4A01041781).

REFERENCES

[1] Landlinger, J et al. *Journal of sport science & medication* **9-4**: 643, 2010.

[2] Tresilian, J. R. et al *Exercise and sport sciences reviews* **32-4**: 20, 2004

CHARACTERISTICS OF THE STEPS IN EACH SECTION IN A TAILWIND SPRINT

Koichi Nakayama[1], Mizuki Makino[1], Masamichi Okudaira[2], Shota Enoki[2], Jun Koizumi[1] and Yoshiaki Manabe[2]
[1] Graduate School of Health and Sports Sciences, Chukyo University / Aichi, Japan.
[2] Health and Sports Sciences, Chukyo University / Aichi, Japan.
Email: kou493613@gmail.com

INTRODUCTION

One type of sprint training is called assisted training, which uses towing, downhill, and tailwind. This training is expected to improve sprinting ability by allowing the athlete to experience running faster than his or her maximum velocity by assisting during the sprint [1]. Previous studies have reported that supramaximum velocity can be experienced in towing and downhill, and that the external force of the assist causes the runner's movement to change differently from normal movement [2,3]. Studies on tailwind sprinting have reported higher sprint velocity than in no-wind conditions, based on simulation and competition data [4]. However, it is unclear what the factors increasing sprint velocity are for variables such as step frequency and step length. If we can identify the factors that cause changes in tailwind sprinting, we may gain insight to use in training. Therefore, the purpose of this study is to characterize the step that increase sprint velocity in tailwind sprint.

METHODS

Participants were 22 male students (100m PR: 10.73-12.03s) who belonged to a university track and field club. The experiment was conducted on a 120m indoor running track field lined with urethane rubber, and participants were asked to perform a 60m run. Experimental conditions were no wind and tailwind (2.0m/s) conditions. A tailwind was generated by 30 industrial fans installed on both sides at 4m intervals from the start to the finish. For data collection, a laser speed measuring machine and a high-speed camera were synchronized to capture the sprint. Laser measurement system (LDM301S; 100Hz) was placed behind the start, collected distance-time data. Velocity was calculated by differentiating the distance data. A high-speed camera (TS-5,100Hz) was installed on the side of the runway and panned to collect touchdown and take-off timing. One step was defined as the period between touchdown and take-off, and the support time, flight time, and step frequency for each step were calculated based on the time data. The average velocity from touchdown to take-off was used as the sprint velocity per step. The step length was calculated by dividing sprint velocity by step frequency. In this study, the distance from 0 m to 60 m was divided into 5 m intervals, and the average of two to three steps in that section was used as the representative value to compare no wind and tailwind. Normality of each data was checked by Shapiro-Wilk test. Since normality was not confirmed, the Wilcoxon rank-sum test was performed. The significance level was set at $p = 0.050$.

RESULTS AND DISCUSSION

In the 10-60m section, the sprint velocity was higher in tailwind than in no wind conditions (Fig.1). In the 25-30 m, 35-40 m, 45-50 m, and 50-55 m sections, the step length in the tailwind increased than no wind. In the 15-20 m and 40-45 m sections, the step frequency of the tailwind increased more than that of no wind. In the 25 m section, the tailwind flight time decreased more than no wind. In the present study, the sprint velocity increased after 10 m in the tailwind, suggesting that the sprinters were receiving tailwind-assisted changes from the acceleration phase. Although the increase in sprint velocity could be attributed to an increase in step length and step frequency, it could not be determined which variables have a dominant effect.

This may be due to a problem with the analysis method in which individual step are averaged for each section, or because the differences in step length and step frequency are small and the sprint velocity has been increased by a combination of factors. In the future, it may be necessary to examine each individual one-step change.

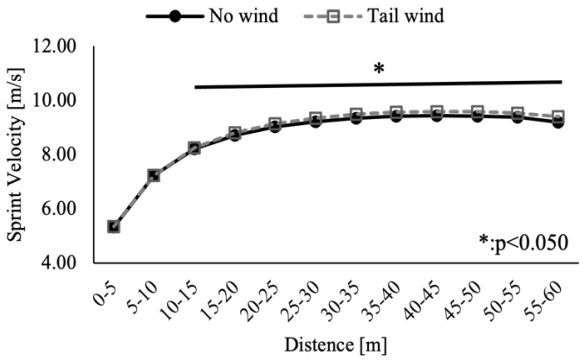

Figure 1 Change in sprint overall sprint velocity

CONCLUSIONS

In the 60m sprint with no wind and a tailwind, the sprint velocity was found to increase in the 10m to 60m section with the tailwind more than with no wind. Therefore, it was suggested that the training can be used as assisted training to experience supramaximum velocity even in an artificial tailwind.

REFERENCES

[1] Hicks D. *New studies in Athletics* 32: 35-52, 2018.
[2] Cecilia-Gallego et al, *J Sports Sci* 40:704-716,2022.
[3] Paradisis G P et al. *J Sports Sci* 19: 149-159, 2001.
[4] Moinat M et al. *Eur J Sport Sci* 18: 1185-1190, 2018.

EFFECTS OF STRENGTH TRAINING TARGETING MEDIAL QUADRICEPS/HAMSTRINGS ON KNEE JOINT BIOMECHANICS DURING SINGLE-LEG LANDING

Jiyoung Jeong[1], Dai-Hyuk Choi[2], and Choongsoo S. Shin[1]
[1] Mechanical Engineering, Sogang University, Seoul, Korea.
Email: cshin@sogang.ac.kr

INTRODUCTION

Anterior cruciate ligament (ACL) injury is one of the most frequent types of sports injuries. A previous study has demonstrated that the dynamic knee valgus and the peak valgus moment are thought to be important contributors to noncontact ACL injuries [1]. It has been documented that the lateral muscles of the lower extremity (e.g. vastus lateralis or biceps femoris) generated the knee valgus angle and moment, while the medial muscles (e.g. vastus medialis or semitendinosus/ semimembranosus) generated varus angle and moment [2,3]. Accordingly, strength training targeted at the medial quadriceps and hamstrings has been proposed previously [4], but no studies have investigated its effects on knee joint biomechanics with respect to ACL injury risk. Therefore, the purpose of this study was to examine the effect of novel strength training designed to strengthen the medial thigh muscles on knee joint kinematics and kinematics during single-leg landing.

METHODS

A total of 18 subjects without any current pain or history of lower extremity musculoskeletal injuries requiring surgery participated in the 8-week strength training targeting medial quadriceps and hamstrings (age: 22.1±1.8 yrs, height: 1.67±0.08 m, mass: 59.5±12.0 kg). This strength training program was developed based on the review of the literature and the consultation with an expert in athletic training [4].

Given that muscle thickness derived from ultrasound imaging can be an appropriate alternative to measure the individual thigh muscle strength [5], muscle thickness of individual quadriceps and hamstrings was measured using an ultrasound system. A motion capture system and a synchronized force plate were used to obtain the joint kinematics and kinetics during single-leg landing. Reflective markers were placed on the anatomical bony landmarks in the lower extremities. Kinematic and kinetic data were obtained during the stance phase from initial contact to toe-off. Joint moments were normalized to the body weight and height of each subject. Two-tailed paired *t*-tests were performed using MATLAB version R2021b. Significance levels were set at $P < 0.05$.

RESULTS AND DISCUSSION

After the strength training targeting the medial quadriceps and hamstrings, the muscle thickness of vastus medialis and semitendinosus increased by 7.9 % and 9.2 %, respectively ($P<0.001$ for both comparisons), thereby increasing M:L thigh muscle thickness ratio, as well ($P<0.001$). There were decreases in the varus-valgus excursion, the peak knee valgus, and the peak hip internal rotation moments during single-leg landing after training ($P=0.011$, $P=0.029$, and $P=0.006$, respectively, Table 1). Since previous prospective study reported that athletes who showed greater coronal plane knee angles at the time point of both initial contact and peak value sustained the ACL injury [1] and the peak knee valgus moment has been implicated to be a major mechanism of ACL injury occurring during simulated landing by inducing the high ACL strains [6], reduced knee varus-valgus excursion and peak knee valgus moment may decrease the potential risk of ACL injury.

Table 1: Kinematics/kinetics and mean EMG amplitudes both in pre- and post-training during single-leg landing (Mean ± SD).

	Pre	Post	p
Knee valgus at initial contact [deg]	1.3 ± 1.1	1.3 ± 1.2	0.991
Varus-valgus excursion [deg]	6.5 ± 1.5	5.8 ± 1.3	**0.011**
Peak hip internal rotation moment [Nm/(BW*Ht)]	0.072±0.012	0.068±0.009	**0.006**
Peak knee valgus moment [Nm/(BW*Ht)]	0.100±0.017	0.091±0.014	**0.029**

CONCLUSIONS

In conclusion, strengthened medial thigh muscles after targeted strength training altered the biomechanical risk factors of ACL injury by reducing the coronal plane knee excursion, peak knee valgus, and peak hip internal rotation moments during single-leg landing.

ACKNOWLEDGEMENTS

This work was supported by the National Research Foundation of Korea (NRF-2018S1A5A2A01035058).

REFERENCES

[1] Hewett T et al. *Am J Sports Med.* **49**: 183-92, 2005.
[2] Besier T et al. *Med Sci Sports Exerc.* **35**: 119-27, 2003.
[3] Zhang L et al. *Med Sci Sports Exerc.* **33**: 1194-9, 2001.
[4] Jeong J et al. *Trans Korean Soc Mech Eng B.* **44**: 575-82, 2020.
[5] Strasser E et al. *Age* **35**: 2377-88, 2013.
[6] Kiapour A et al. *Am J Sports Med.* **44**: 2087-96, 2016.

Effects of Wearing a Mask on Heart Rate Variability during Kendo Practice

Minato Kawaguchi and Kentaro Takahashi
[1] Department of Science and Engineering, Kanto Gakuin University, Yokohama, Japan.

Email: minato@kanto-gakuin.ac.jp

INTRODUCTION

The impact of masks on heart rate variability (HRV) has been scrutinized in various sporting events [1]. In Japan, the All Japan Kendo Federation has devised protocols to curtail the spread of the novel coronavirus during Kendo tournaments since 2020. These regulations mandate the usage of masks during Kendo matches. A previous investigation probed the influence of mask-wearing on Kendo swings and observed a significant trend in frontal swings. Nevertheless, this study only focused on a one-minute time frame and did not expound on the physiological impact of prolonged mask usage during practice. Consequently, this study aims to explicate the effect of mask-wearing on HRV while performing Kendo practice.

METHODS

Six male and one female university kendo club members participated. The subjects' ages ranged from 20 to 21 years, and their athletic experience ranged from 10 to 13 years. A three-dimensional polyurethane sports mask (Under Armour) was used. A wearable heart rate sensor, "myBeat" WHS-3 (Union Tool Co.), was used to measure body movement (acceleration) and electrocardiogram. Under the guidelines of the All-Japan Kendo Federation, a mouth shield was attached to the faceplate, and a mask was worn over the nose. Mouse shields were also worn for measurements without masks. The experiment was conducted in the following order: rest (1 minute of seated rest), *Kirikaeshi*, *Kakari-Keiko* (2 times for 20 seconds), rest, 4 minutes of *Gokaku-Keiko*, and rest. The experiments were conducted on separate days with and without wearing the mask, considering the effects of fatigue and other factors.

The data recorded by myBeat were the RR interval sequence of the electrocardiogram and the absolute acceleration. RMS values were derived for each period from the absolute acceleration time series, and if the RR interval was more significant than 1.2[s], it was excluded from the analysis as bradycardia. The RR interval mean and SD1 and SD2 of the Poincaré plot were obtained as heart rate variability indices. The frequency-domain indices, VLF, LF, and HF, were estimated based on the RR interval trend time series generated at a sampling frequency of 5 Hz. The mean values of each indicator for each phase were compared using a paired t-test. The significance level was set at 5%.

RESULTS AND DISCUSSION

There was no significant difference in RMS values between the masked and unmasked conditions during all periods. The mean RR interval was significantly smaller in the "with mask" condition in each of the later sessions of the experiment (Fig. 1). In HRV, SD1 and SD2 tended to be higher in the “without mask” condition at least after the second rest, and SD2/SD1 and LF were significantly higher in the masked condition at the last rest. These changes in HRV may be attributed to the fact that kendo is performed while observing the breathing of the opponent, resulting in a slower respiratory rhythm than in daily life and the wearing of a mask, which causes the body to take in more oxygen during inhaling.

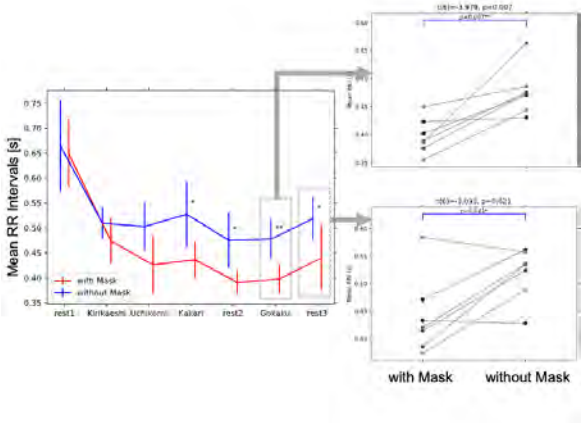

Figure 1 RR intervals [s] during Kendo practice with and without a mask. Error bar indicates the standard deviation (n=7). * = p<.05. ** = p<.01

CONCLUSIONS

During kendo practice, the presence or absence of a mask caused differences in heart rate activity, even though it did not cause differences in the magnitude of body movement. Especially in the latter half of the practice, the mask caused an increase in heart rate and a difference in heart rate variability indices (SD1, SD2, LF, and HF). One of the causes may be that the mask caused differences in breathing. In addition, since SD2/SD1 can be considered an index of sympathetic activation [2], wearing a mask may influence the autonomic nervous system.

REFERENCES

[1] Zheng, C. et al. *Sports Medicine*, **53**:125-150, 2023.
[2] Shaffer, F. and Ginsberg, *J.P. Front. Public Health*, **5**:258, 2017

Quantification of external work using mechanical crank power with a bicycle ergometer underestimates the net external work exerted by a human

Yuta Yamaguchi[1,2], Kosuke Taniguchi[3], Kanae Koguchi[1], Naoki Wada[2], and Tetsunari Nishiyama [1,2]
[1] Graduate School of Health and Sport Science, Nippon Sport Science University, Tokyo, Japan.
[2] Faculty of Sport Science, Nippon Sport Science University, Tokyo, Japan.
[3] Nippon Sport Science University, High Performance Center, Kanagawa, Japan.
Email: yuta_yamaguchi@outlook.jp

INTRODUCTION

The pedaling exercise has been widely used for the evaluation of endurance performance. Those studies utilized mechanical crank power to quantify the external work exerted by the rider. However, it is pointed out that this method fails to properly reflect the power exerted by the person, potentially leading to the misunderstanding of the data analysis and evaluation [1]. The mechanical crank power is the sum of the left and right crank powers (Figure 1). In general, the negative crank power is generated during the pulling phase [2]. Therefore, in order to maintain the mechanical crank power, surplus positive crank power is required during the pushing phase to compensate for the negative crank power [2]. The purpose of this study was to investigate the effect of the difference in methods, a conventional method of quantifying work by mechanical crank power and a method that considers surplus crank power, on endurance performance indices.

METHODS

Twenty cyclists (age: 19.7 ± 1.1 years old, height: 1.69 ± 0.04 m, body mass: 66.6 ± 7.4 kg) performed the incremental exercise test with an electromagnetically braked cycle ergometer (Excalibur Sport, Lode, Groningen, Nederland). The work rate was increased by 45W every 3 minutes. Expired gases were collected over the final 30 seconds of each stage (AE-310S, Minato medical science, Osaka, Japan). Both side crank powers were measured every 2 degrees of crank angle using a pedal force measurement system, and then the mechanical crank power ($P_{Mechanical}$) and net crank power (P_{Net}) considering surplus power were calculated (Figure 1). Relative exercise intensity, a commonly used measure of endurance performance, was quantified for mechanical crank power and net crank power, respectively. The surplus crank power ratio ($P_{Surplus}$) was calculated using the following equation.

$$P_{Surplus}\,[\%] = \frac{P_{Net}\,[W] - P_{Mechanical}\,[W]}{P_{Mechanical}\,[W]} \times 100 \qquad (1)$$

RESULTS AND DISCUSSION.

P_{Net} showed higher than $P_{Mechanical}$ for all relative exercise intensities, and $P_{Surplus}$ was shown to decrease with increasing exercise intensity (Table 1). Since the increase in $P_{Surplus}$ is related to the magnitude of negative crank power, the results of this study indicate that the rider generated less negative crank power as exercise intensity increased. This reflected the force application strategy of the rider to improve the force effectiveness by reducing the need for the propulsive leg to overcome the recovery leg (2).

On the other hand, the results of this study showed that low-intensity exercise may lead to a large underestimation (57% at $P_{50\%VO2peak}$). Negative crank power has been found to increase with decreasing exercise intensity (2, 3). Therefore, if the targeted relative exercise intensity is low, evaluation using P_{Net} is recommended.

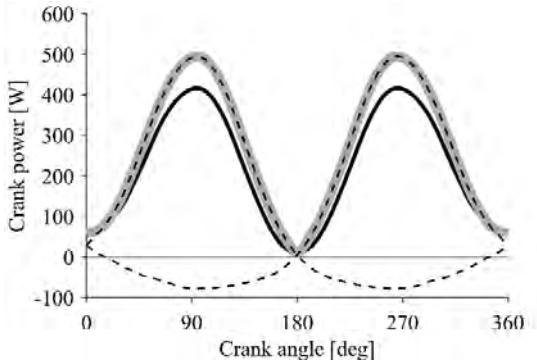

Figure 1 Typical example of the resultant force. The solid black line indicates mechanical crank power, the dashed black lines indicate crank power for each side, and the solid gray line indicates net crank power.

CONCLUSIONS

This study investigated the effect of the difference in methods that quantify the external work on endurance performance indices. The results of this study revealed that the quantification of work using $P_{Mechanical}$ underestimated net exerted work, which was more pronounced in low-intensity exercise.

Table 1 The crank power variable at each relative exercise intensity.

	$P_{Mechanical}$ [W/BW]	P_{Net} [W/BW]	$P_{Surplus}$ [%]
P_{Max}	5.0 ± 0.7	5.4 ± 0.6	9.5 ± 5.0
$P_{50\%VO2peak}$	1.9 ± 0.3	2.9 ± 0.3	57.0 ± 15.6
$P_{80\%VO2peak}$	3.7 ± 0.5	4.3 ± 0.4	20.5 ± 8.1

REFERENCES

[1] Cavanagh PR and Kram R. *Med Sci Sports Exerc.* **17**: 304-308, 1985.
[2] Sanderson DJ et al. *J. Sports Sci.* **18**: 173-181, 2000.
[3] Garcia-Lopez J et al. *J. Sports Sci.* **34**(17): 1619-1629, 2016.

Assessment of Strain Components for Kinesiology Taping Techniques with Digital Image Correlation

Chia-Han Hu[1], Shiuan-Huei Lu[1], Tsan-Yang Chen[1], Cheng-Hao Yu[1], and Tung-Wu Lu[1,2]
[1]Department of Biomedical Engineering, National Taiwan University, Taiwan, ROC
[2]Department of Orthopaedic Surgery, School of Medicine, National Taiwan University, Taiwan, ROC
Email: **twlu@ntu.edu.tw**

INTRODUCTION

Kinesiology Tape (KT) is a taping technique developed in the 1970s and has become popular and widely used by athletes and physicians of sports teams [1]. KT is constructed of breathable and stretchable material, which adheres to the skin with a medically approved adhesive. KT is designed to have the elasticity to avoid excessive restriction while providing enough pressure and support to facilitate muscle and tissue strength. However, a previous study showed that KT's application direction is not associated with improved performance and perceived the enhancement as essentially a placebo effect [2]. Furthermore, the effects on underlying force distributions of the skin attached to KT during motions are still unknown. Digital image correlation (DIC) is an optical technique based on image registration and tracking of the surface to obtain the distortion and deformation on the interested surface. It is hoped that the force distribution of the underlying skin surface aligned with taping direction can be clarified through the utilization of DIC. The purpose of the current study was to quantify the effect of KT on strain distribution under the surface skin with the DIC technique during motions using a dual-camera system.

MATERIALS AND METHODS

Fifteen healthy male individuals (age: 23.0 ± 1.5 years; height: 175.1 ± 3.4 cm; mass: 71.6 ± 8.5 kg) participated in the current study. All participants lay on the therapy bed in prone, and the examiner dotted on the surface skin of the biceps femoris muscle for image processing. Each participant was placed on an "I" strip of KT (1) with facilitation taping originating from the ischial tuberosity to the lateral femoral condyle, (2) and the inhibition taping in the opposite direction. Each participant performed isotonic knee flexion and extension under the dual-camera system (GRAS-50S5M, Point Grey, Canada). The strain distribution on the surface skin divided into fifteen regions were analyzed with principal strain using DIC analysis (Correlated Solutions, Columbia, U.S.A.). The stretch of tapes' applied strains to the underlying skin using MATLAB (Matlab R2019b) for calculating the subtraction of the corresponding regions between skin and tapes. One-way analysis of variance (ANOVA) was used to detect the differences in principal strain between two taping conditions in medial-lateral regions and proximal-distal regions. All statistical analyses were performed using SPSS 22.0 (SPSS Inc., Chicago. IL, U.S.A.) with the significance level set at $\alpha = 0.05$.

RESULTS AND DISCUSSION

The mean strain of each 15 regions between the two taping conditions was compared to identify the differences applied to the skin surface. The results showed significantly different strain distributions of KT between two taping conditions in the proximal-distal regions across medial, middle and lateral areas (Fig. 1). It would appear that the principal compressive strain of KT increased from proximal to distal end of the hamstrings on the surface skin during all tested knee flexion and extension angles. In addition, the results showed that the principal compressive strain of KT for all regions increased as the knee flexion angles increased. From the current results, the principal strain of KT showed non-homogeneous strain from the proximal to the distal region as well as with the change of knee flexion angles.

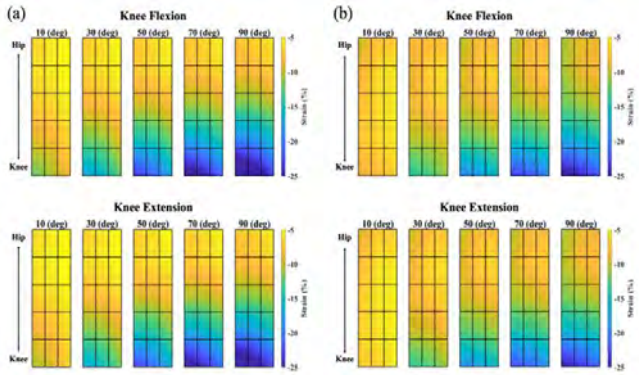

Figure 1. Average (%) principal strain distribution by using (a) facilitation (b) inhibition taping during knee flexion and extension. (The region of interest at taped muscle was divided into fifteen regions from proximal-distal regions across medial, middle and lateral areas.)

CONCLUSIONS

This is the first study to investigate the effects of KT on the principal strain of the surface skin during functional activities using a dual-camera system based on the DIC technique. The effect of KT tapping on the surface skin showed a non-homogeneous strain distribution from the proximal to the distal region at different knee flexion angles. The proposed new DIC-based method may be useful for the quantification of the effects of various KT techniques on other targeted muscles or joint movements in many patient populations and for those at different stages of rehabilitation.

REFERENCES

[1] Kase, et al. (2013). *Albuquerque*, 3rd Edition.
[2] Poon, et al. (2015). *Man Ther,* 20(1)130-133.

Contact force during maximal snatches

Mike Webb, Mark King, Matt Pain
School of Sport, Exercise and Health Sciences, Loughborough University, Loughborough, United Kingdom
Email: m.webb@lboro.ac.uk

INTRODUCTION

A key component of the snatch is the powerful contact that the hip makes with the barbell, despite this, the magnitude of this force has not been quantified in the literature. There has been a great breadth of research into the biomechanics of the snatch; most commonly barbell kinematics of elite weightlifters are investigated [1]. The barbell kinematic research comes without the context of a measurement of force applied to the barbell by contact with the hips during the second pull [2] of the lift. A common suggestion amongst the barbell trajectory research is the minimisation of anterior-posterior movement of the barbell [3]. Investigating the size of this force is essential to understand performance and the technique employed by weightlifters in the snatch.

METHODS

Ten weightlifters (6 male, 4 female; body mass: 49-113 kg; snatch 1RM: 47-142 kg) that had competed at a minimum of national level were recruited for the study; each had given informed consent of the protocol which had been approved by Loughborough University Ethical Advisory Committee. A Tekscan F-scan force sensor (Boston, MA) was fixed to the centre of Eleiko training, providing an effective measurement area covering the full circumference of the barbell. Pressure data were collected at 250 Hz for each lift. The testing protocol consisted of a series of snatch singles, with barbell mass increasing up to 90% of maximum. Participants were instructed to warm up as would be standard for competition and to select weights as such. Sensor data of the heaviest snatch single for each individual was exported and analysed. Duration of each of the contacts was analysed, with contact defined as starting with a total force of greater than 8 N and ending when force dropped below this threshold. Both peak force and 'contact impulse' were assessed. Impulse was calculated using the trapezoidal method to integrate the force curve over time. A regression analysis was performed to establish a relationship between barbell mass and each of the variables, across the group. A regression equation and R^2 value were used to evaluate the relationships.

RESULTS AND DISCUSSION

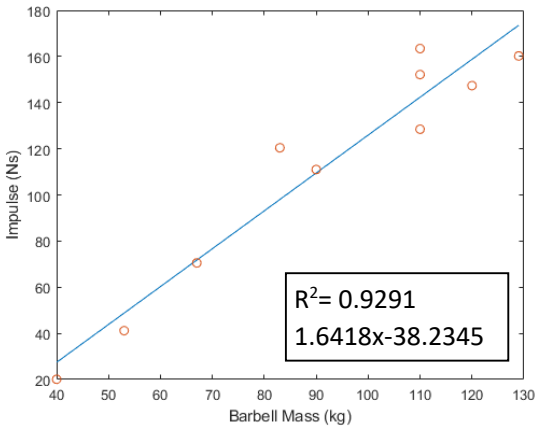

Figure 1 Contact impulse plotted against barbell mass.

The hypothesis that contact impulse increased as barbell mass increased was accepted (Figure 1). The lifters that lifted more weight generated larger impulse on the barbell, although did not necessarily apply larger impulse between their lifts as barbell mass increased. Peak force ranged from 260.1 N to 2682.5 N and contact duration ranged from 0.115 s to 0.170 s. When normalised using Sinclair total, lifters with a higher Sinclair also generated larger contact impulse with an R^2 of 0.8847.

CONCLUSIONS

The results of this study show that contact impulse on the barbell is a contributing factor in determining a lifter's ability to lift heavier loads, although varies within individuals. The Sinclair normalisation showed that even when body mass was accounted for, the 'better' lifters were able to produce larger contact impulse. Further research should look at technical aspects of the lift and the way these interact with contact force, and if possible, infer the direction of the force applied.

REFERENCES

1. Ho LKW et al. NSCA; 2014; 28:574–86.
2. Kipp K, Redden J, Sabick MB, Harris C.. J Strength Cond Res. 2012;26:1838–44.
3. Lester Ho KW, Williams MD, Wilson CJ, Meehan DL.. The Journal of Strength & Conditioning Research 2011;25.

HOW DO GRIP-ENHANCING AGENTS AFFECT FRICTION BETWEEN A FINGERTIP AND A BASEBALL?

Takeshi Yamaguchi[1,2], Daiki Nasu[3], Kei Masani[4,5]

[1] Department of Finemechanics, Graduate School of Engineering, Tohoku University, Sendai, Japan.
[2] Graduate School of Biomedical Engineering, Tohoku University, Sendai, Japan.
[3] Kashino Diverse Brain Research Laboratory, NTT Communication Science Laboratories, Kanagawa, Japan
[4] Institute of Biomaterials and Biomedical Engineering, University of Toronto, Toronto, Ontario, Canada
[5] KITE Research Institute, University Health Network, Toronto, Ontario, Canada
Email: takeshi.yamaguchi.c8@tohoku.ac.jp

INTRODUCTION

In June 2021, Major League Baseball (MLB) stepped up its crackdown on foreign substances (i.e. sticky substances), except for rosin, a mixture of magnesium powder and pine resin. The reason is that the increased friction between the fingertips and the ball is expected to increase the ball spin rate. However, it is currently unknown how applied substances influence friction coefficients. In this study, we investigated the effect of rosin and sticky substances on the friction coefficient between fingertips and MLB balls. Additionally, we compared the friction coefficient between MLB and Nippon Professional Baseball Organization (NPB) balls which are often thought to be less slippery than MLB balls. Our study aimed to determine the impact of grip-enhancing agents on friction between the ball and fingertips. This study has been published elsewhere [1].

METHODS

Nine healthy adult males participated in this study. The sliding friction test between an index finger and a baseball leather sheet was performed using a capacitive six-axis force sensor as shown in Fig. 1. The leather sheet with (Fig. 1(a)) or without seams (Fig. 1(b) was extracted from the official balls of MLB and NPB balls. The leather sheet adhered to the force sensor with adhesive tape. Each participant slid their index finger in the proximal direction over the leather sheet under eight different conditions, i.e. MLB ball with and without seam under no application (Fig. 1(c)), rosin powder application (Fig. 1(b)), and sticky substance application (Fig. 1(c)) (i.e., two ball conditions with three application conditions) as well as NPB ball with and without seams under no application. The moisture level of the fingertip under no application condition was measured using a skin sensor. The friction coefficient was calculated from normal and horizontal forces measured by the force sensor during the sliding test.

RESULTS AND DISCUSSION

Under no application condition, the friction coefficient varied among participants, which is due to individual differences in the moisture levels of finger skin among participants. The rosin application increased the friction coefficient between a finger and a ball surface by more than 20%. Furthermore, the rosin application significantly reduced the variation in the friction coefficient among participants. The rosin application also reduced the variation in the friction coefficient with respect to the applied normal force. The sticky substance application increased the friction coefficient by more than 50% compared to the no-application condition. NPB balls exhibited larger friction coefficients than MLB balls at approximately 20% in no-application conditions, which indicates that MLB balls are more slippery than NPB balls. This difference was also observed after mudding or sanding.

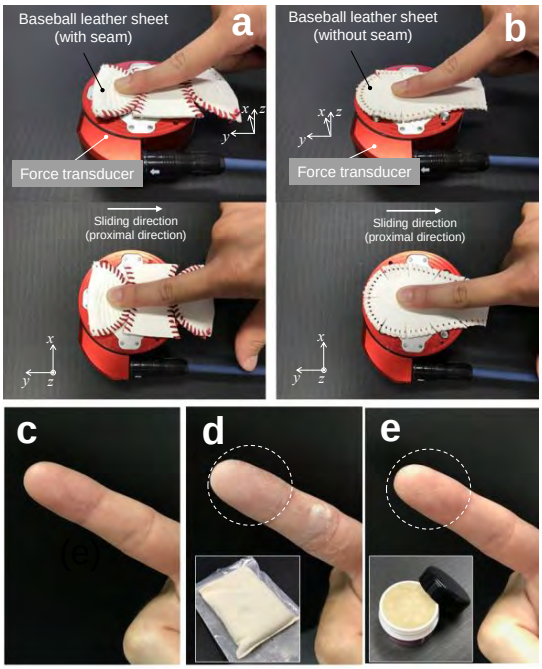

Figure 1 Experimental setup of sliding friction test for MLB ball leather sheet with seam (a) and MLB ball leather sheet without seam (b). Finger conditions: no application (c), rosin application (d), and sticky-substance application (e). [1]

CONCLUSIONS

We found that sticky substances increase friction which could positively affect the ball spin rate. The rosin application can help maintain constant friction against normal force and across pitchers, which could contribute to the fair playing field in baseball pitching in terms of friction between a finger and a ball. Our findings indicate that there is room for modification in the friction of MLB balls.

REFERENCE

[1] Yamaguchi T, Nasu D, Masani K. Commun Mater **3**: 92, 2022.

A PILOT STUDY ON THE PLANTAR PRESSURES IN FEMALES DURING SPRINTING ON NATURAL GRASS, 3G AND CORK SURFACES

Joanna Reeves, Daniel Rawson, and Sharon Dixon
Public Health and Sport Sciences, University of Exeter, Exeter, United Kingdom.
Email: j.e.reeves@exeter.ac.uk

INTRODUCTION

Artificial turf is commonly used as a playing surface due to its lower cost of maintainance compared to natural grass (grass). The third generation artificial surface (3G) has a rubber crumb infill made from recyled tyres. There are growing concerns that hazardous substances in the rubber crumb used in 3G may be harmful to the environment and/or human health and cork crumb may offer an environmentally friendly alternative [1]. However, the relative injury risk on a cork surface compared to 3G and grass has yet to be established. A stress fracture of the fifth metatarsal is a common injury in football (soccer) players, likely due to high loading of the forefoot during play [2]. The purpose of this pilot study was to compare the peak plantar pressure in the forefoot during sprinting on grass, 3G and cork in female team sport players.

METHODS

Five young female amateur team sport players (62.02 ± 8.41 kg) completed three successful 10 m sprinting trials on three surfaces (natural grass, 3G and cork) on separate days. A successful trial was considered to be within ±5% of the mean trial time. Testing on each surface was conducted on separate days with similar weather conditions and in a randomised order. All participants wore a football boot designed for female footballers (Ida Classica 22 Women's Soccer Cleat FG, Ida Sports, UK). Plantar pressure was recorded using insoles (Pedar-X®, novel GmbH, Munich, Germany). Data were processed using MATLAB (R2017b, Mathworks Inc.) with respect to the medial and lateral forefoot segments.

The peak pressure in three right foot steps per trial was averaged and the mean across trials was taken for further analysis. Effect size (Cohen's d) between conditions was calculated as the paired mean differences divided by the paired standard deviation.

RESULTS AND DISCUSSION

Data collection for participant 4 was not possible on the 3G surface due to availability. There was little to no difference in peak plantar pressure between surfaces in the medial forefoot. However, in the lateral forefoot, there was greater peak plantar pressure on the 3G surface compared to grass (d=0.5) and cork (d=0.7, Figure 1). There was no difference in peak plantar pressure between grass and cork in the lateral forefoot.

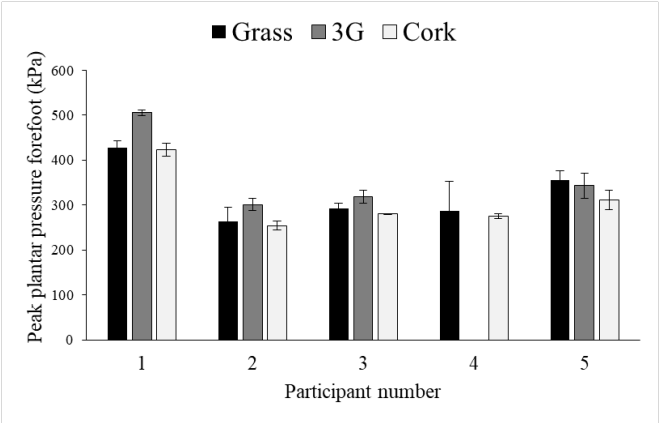

Figure 1. Mean ±SD of peak pressure in the lateral forefoot across three trials in each participant

CONCLUSIONS

Risk of lower limb injury, particularly fifth metatarsal stress fractures, may be similar on cork and grass surfaces and greater on 3G. However, future biomechanical and epidemiological studies using more participants, different populations and different movement tasks are needed to substantiate the findings of this pilot.

ACKNOWLEDGEMENTS

Ida Sports, UK supplied the boots for this project

REFERENCES

[1] Armada D et al. *Sci Total Environ* **812**, 2022.
[2] Shuen W et al. *The Surgeon* **7**(2): 86-88, 2009.

Relationship between Bilateral Asymmetry in Lower Limb Joint Biomechanics and Jumping Height during Single-leg Countermovement Jump

Shota Yamamoto[1], Munenori Murata[2], Rintaro Miyake[1] and Terumitsu Miyazaki[2]

[1]Graduate School of Physical Education, National Institution of Fitness and Sports in Kanoya, Kagoshima, Japan.
[2] National Institute of Fitness and Sports in Kanoya, Kagoshima, Japan.
Email: m226015@sky.nifs-k.ne.jp

INTRODUCTION

Larger bilateral asymmetry of jumping height of the single-leg countermovement jump (CMJ) was associated with smaller sprint performance [1]. Investigating the kinematics and kinetics characteristics, that cause the bilateral asymmetry of jumping height during the single-leg CMJ, might be valuable information to design training for improving sprint performance, as well as jumping performance. The previous study reported that the ankle joint kinematics were correlated with the bilateral asymmetry index of jumping height during the running single-leg jump [2], but these relationships during the single-leg CMJ remain unclear. Thus, we aimed to examine the relationships between the bilateral asymmetry in jumping height and the bilateral asymmetry in lower limb joint biomechanics during the single-leg CMJ.

METHODS

Twenty-two healthy male collegiate students (age, 20.3 ± 1.3 years; mass, 67.0 ± 9.2 kg; height, 1.71 ± 0.05 m) participated in this study. After a suitable warm-up, all participants performed five single-leg CMJs each on the right and left leg with their maximal effort in random order. Three-dimensional marker trajectories, placed on their whole body, and ground reaction force were measured using a motion capture system (250 Hz; Motion Analysis Corporation, USA) and a force plate (1000 Hz; Tech Gihan, Japan), respectively. The early and late phases of the single-leg CMJ were defined based on the vertical velocity of the center of mass (CoM): the early phase, from initiation of motion until the CoM reached zero vertical velocity, and the late phase, from the end of the early phase to take off. We calculated the bilateral asymmetry index of the lower limb joint angles and torques during the early and the late phases. We also calculated the bilateral asymmetry index of jumping height. We compared to the bilateral asymmetry index of the lower limb joint angles and torques between early and late phases using Wilcoxon's rank sum test. Additionally, Spearman's rank correlation coefficient was calculated between the bilateral asymmetry index of jumping height and the joint angles and torques. Statistical significance was defined as $p < 0.05$.

RESULTS AND DISCUSSION

The bilateral asymmetry index of jumping height was 4.02 ± 3.69 % (range, 0.08-13.98 %). The bilateral asymmetry index of lower limb joint angles and torques in the late phase was greater compared with the early phase (Figure 1). The knee extensor and ankle plantar flexor muscle groups act eccentrically during the early phase of the single-leg CMJ, while these muscle groups act concentrically during the late phase. A previous study reported that the bilateral asymmetry in muscle strength of the lower limb is greater during an eccentric contraction than during a concentric contraction [3]. However, our results (Figure 1) suggest that the findings of this previous study cannot be generalized to the single-leg CMJ. Moreover, we found that the bilateral asymmetry index of ankle joint torque during the late phase of the single-leg CMJ was significantly correlated with the bilateral asymmetry index of jumping height ($r = 0.44$, $p < 0.05$), whereas the other bilateral asymmetry index of the joint angles and torques in each phase was not significantly correlated with the bilateral asymmetry index of jumping height ($p > 0.05$). The findings imply that, during the single-leg CMJ, a reduction in bilateral symmetry of ankle plantar flexion torque, specifically during concentric contraction, might lead to a decrease in bilateral asymmetry of jumping height.

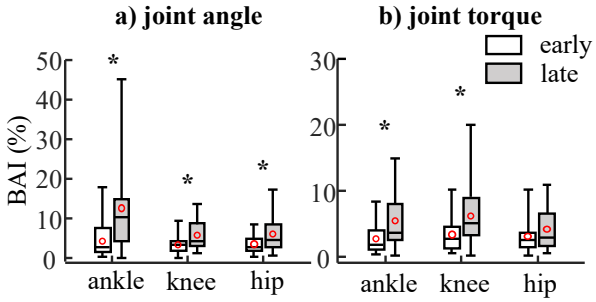

Figure 1 Bilateral asymmetry index of lower limb joint angles (a) and torques (b) during the early and late phases of the single-leg CMJ. (*: $p<0.05$)

CONCLUSIONS

We examined the relationship between the bilateral asymmetry of jumping height and the bilateral asymmetry of lower limb joint angles and torques in the early and late phases of single-leg CMJ. The results of this study showed that the bilateral asymmetry of the ankle joint torque in the late phase was positively correlated with the bilateral asymmetry of jumping height.

REFERENCES

[1] Bishop C et al. *J Strength Cond Res* **35(1)**: 56-63, 2021.
[2] Sugiyama T et al. *J Sports Sci Med* **13**: 951-7, 2014.
[3] Fousekis K et al. *J Sports Med Phys Fitness* **50**: 465-74, 2010.

A Biomechanical Study of Uchimata in Judo

- Comparison of different skill levels-

Kazuto Hamaguchi[1] , Sora Takeuchi[1], Taisei Wada[1], Takumi Furukawa[1] and Tatsuya Deguchi [1]
[1] Graduate school of Humanities and Social Sciences, Hiroshima University /Higashi-Hiroshima, Japan.
Email: kazuto_linear@yahoo.co.jp

INTRODUCTION

Although many biomechanical studies have been conducted in judo competitions, few studies have compared the biomechanics of experienced judo players at different levels of skill, such as competition level. Therefore, the biomechanical differences in *uchimata* (inner thingh throw) of skilled judo players and unskilled players have not yet been clarified, and there is room for further investigation into how body movements are performed during a throw. The purpose of this study was to compare the biomechanics of uchimata in two groups of skilled and unskilled judo competitors at different levels of competition, and to obtain suggestions for technical instruction.

Figure 1: Sequential photographs of uchimata.

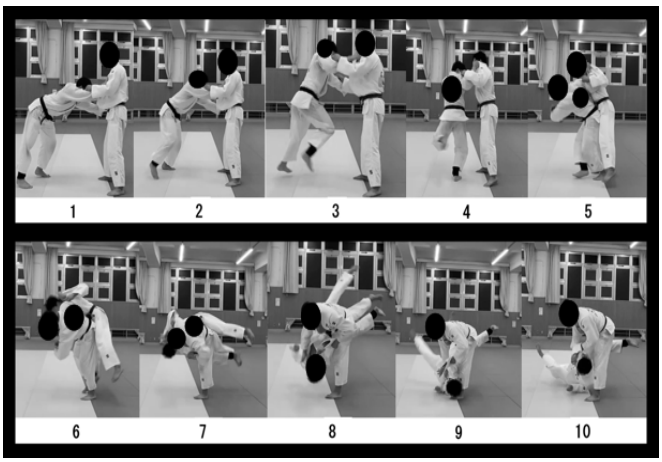

METHODS

The subjects were 20 male judo players belonging to a university judo club, 10 of whom had participated in national tournaments (hereafter referred to as "skilled players") and 10 of whom had not participated in national tournaments (hereafter referred to as "unskilled players"). Movements were recorded using an optical 3D movement analysis system, Mac3D (250 Hz). Forty-seven reflective markers were attached to the subjects with reference to Ishii et al. (2017) and Liu et al. (2022). Ground reaction forces acting on the feet during the movements were measured using a force plate (1000 Hz). After each trial, subjects introspectively rated their own performance on a 5-point scale (1=poor, 2=not so good, 3=normal, 4=good, 5=very good).

RESULTS AND DISCUSSION

In terms of movement time, athletes in the skilled group tended to have a shorter movement time than those in the unskilled group during the phase of body rotation. The maximum absolute velocity of the body center of gravity along the front-back direction was significantly greater for skilled athletes (0.87±0.23 m/s) than for the unskilled athletes (0.66±0.15 m/s) ($p=0.032$). The maximum angular velocity of the arms tended to be greater in skilled group (3.98±0.63 rad/s) than in unskilled group (3.59±0.69 rad/s), but the difference was not significant. The maximum angular velocity at the hip was significantly greater for the skilled group (1.80±0.20 rad/s) than for the unskilled group (1.39±0.19 rad/s) ($p<0.001$). The above results suggest that the speed of forward propulsion during the body rotation phase is a factor in the magnitude of the angular velocity of the hips and arms during the throwing phase.

CONCLUSIONS

In this study, skilled athletes tended to have higher angular velocity in all items compared to the unskilled athletes. The forward body center of gravity velocity of skilled athletes tended to be larger than that of unskilled athletes, and the movement time tended to be shorter.

REFERENCES

[1] Ishii T et al. Sports Biomechanics,17(2): 238-250,2021.
[2] Liu L et al. Sports Biomechanics,1-17,2022.

Table 1: Comparison of the timing of the maximum angular velocity between skilled and unskilled athletes, and the maximum at normalized time.

	Skilled		Unskilled			
	Max	Time(%)	Max	Time(%)	p-value	Cohen's d
Angular velocity of arm (rad/s)	3.98±0.63	160.2±12.4	3.59±0.69	163.0±23.3	0.227	0.69
Angular velocity of hip (rad/s)	1.80±0.20	94.8±32.4	1.39±0.19	105.5±23.0	<0.001***	0.21
COM (X-axis) velocity (m/s)	0.87±0.23	106.7±22.4	0.66±0.15	96.7±22.3	0.032*	0.40

Mean ± standard deviation
***p<0.001 *p<0.05 (n=20)
Time (% Normalised time)

EFFECTS OF NORDIC HAMSTRING EXERCISE ON HAMSTRING STIFFNESS, STRENGTH, AND FLEXIBILITY

Konstantinos Kaliarntas[1], Nelson Morais[1], Athanasios Souglis[2].

[1]School of Applied Sciences, Edinburgh Napier University, Edinburgh, UK

[2]School of Physical Education and Sports Science, National and Kapodistrian University of Athens, Greece

Email: k.kaliarntas@napier.ac.uk

INTRODUCTION

Hamsting injuries are among the most common injuries in athletes. Eccentric training has been shown to reduce hamstring injury rates. The Nordic Hamsting Exercise (NHE) is an eccentric exercise performed at short muscle length and has been shown to provoke changes in hamstring muscles. This study aims to assess the effects in eccentric hamstring strength, hamstring flexibility and biceps femoris long head muscle stiffness following a 6-week NHE intervention.

METHODS

Fifteen recreational male and female athletes were randomised into an NHE intervention group (n=7; 5 males and 2 females; age: 24.0±1.8y; height: 172.0±3.0cm; body mass: 85±5.1kg) and a control group (n=8; 4 males and 4 females; age: 24.3±1.3y; height: 172.0±3.0cm; body mass: 72.3±3.4kg). Isokinetic dynamometry (Cybex HUMAC2015, Massachusetts, USA) at 60º/s and 45º for eccentric and isometric peak torque respectively, myotonometry (MyotonPro, Myoton Ltd, Estonia) and manual goniometry were used to measure the outcomes. Each outcome was measured at baseline and after 6 weeks in both groups (5 days before and after the intervention programme). All data presented as means and standard error of the mean (SE). A two-way mixed ANOVA was used for all dependent variables and a level of $p < .05$ was used to accept significant differences.

RESULTS AND DISCUSSION

There was an 8% increase in eccentric peak torque and 6% increase in the isometric peak torque in the intervention group ($p < .05$), while both outcomes were reduced in the control group (time*group interactions $p<.05$). These results are in line with previously published evidence [1,2]. There was a 9% increase in hamstring flexibility in the control group while no changes observed in the intervention group (time*group interaction $p<.05$). No significant effects were observed in muscle stiffness in both groups (time*group interaction $p>.05$) (Table 1). Other studies have reported decrease in muscle stiffness after a similar intervention, however, methodological differences and limitations of the current study may be responsible for these differences [3].

CONCLUSIONS

A six-week NHE training programme may increase eccentric and isometric strength, which have both previously described as risk factors for hamstring injury. It seems that NHE has no significant effect in altering muscle flexibility and stiffness. The current evidence may inform training practice in recreational athletes as well as further research.

REFERENCES

[1] Delahunt et al. *EJAP*, **116(4):** 663–672,2016.

[2] Ribeiro-Alvares et al. *JSCR,* ***32*****(5):** 1254–1262, 2018.

[3] Uysal et al. *Scand J Med Sci Sports,* ***31*****(2):** 371–379, 2020.

Table 1. Assessed variables at pre- and post-training evaluations in control and intervention groups (mean ± SE).

	Control Group		Intervention Group	
	Pre	Post	Pre	Post
Muscle Strength				
Eccentric PT (Nm/Kg)	1.87 ± 0.11	1.74 ± 0.07	1.92 ± 0.18	2.08 ± 0.15
Isometric PT (Nm/Kg)	1.51 ± 0.07	1.33 ± 0.07	1.39 ± 0.09	1.47 ± 0.11
Flexibility				
Straight Leg Raise (º)	84.5 ± 4.67	92 ± 5.54	86.80 ± 3.71	87.25 ± 3.24
Muscle Stiffness				
MyotonPro (N/m)	258.38 ± 13.84	248.75 ± 19.86	240.88 ± 16.89	249.13 ± 16.14

PT: Peak Torque

Effect of the Upper Limb Joints on the Control of Ball Speed in Throwing Distance Control of Throw-in

Rintaro Miyake[1], Terumitsu Miyazaki[1], Shota Yamamoto[1] and Munenori Murata[1]
[1]National Institute of Fitness and Sports in Kanoya, Kanoya, Japan
Email: m226014@sky.nifs-k.ac.jp

INTRODUCTION

The throw-in in soccer requires distance control depending on the situation. However, most previous studies have focused on obtaining the maximum distance, and it has been reported that the upper limb was the primary contributor in generating ball speed [1]. A previous study on basketball, which investigated an accurate throwing distance coordination task similar to throw-in, has reported that the upper limb movement changes with an increase in throwing distance [2]. Therefore, it is believed that the throw-in would also require similar joint coordination; however, it has not been adequately discussed. This study aimed to determine the effect of each upper limb joint on the control of ball speed in throwing distance control in a throw-in.

METHODS

Five university male soccer players (height: 172.7 ± 6.0 cm; mass: 62.8 ± 4.3 kg; age: 20.6 ± 1.4 years) participated in this study. They performed standing throw-in to the targets on the ground that were placed at every 10% relative to the throw-in distance at each participant's maximum effort. Three-dimensional coordinates data of reflective markers on a body and ball were recorded using a motion analysis system (Mac3D system, Motion Analysis, 500Hz). We calculated the kinematic parameters of the body and ball, and the generated ball speed (GS) by each joint's angular velocity was calculated as follows [3]:

$$\mathrm{GS} = \hat{\mathbf{v}}_{\mathbf{Ball}} \cdot \left(\boldsymbol{\omega}_{\boldsymbol{Joint}} \times \boldsymbol{r}_{\boldsymbol{Joint \to Ball}}\right).$$

where $\hat{\mathbf{v}}_{\mathbf{Ball}}$ is the unit vector of the ball velocity, $\boldsymbol{\omega}_{\boldsymbol{Joint}}$ is the joint angular velocity, and $\boldsymbol{r}_{\boldsymbol{Joint \to Ball}}$ is the vector from joint to the ball. Furthermore, the same calculation was performed using the unit vector of the joint angular velocity ($\boldsymbol{\omega}_{\boldsymbol{Joint}}/\omega_{Joint}$) to evaluate the effect of the positional relationship between the ball and each joint on the ball speed ($\mathrm{GS}_{\hat{\omega}}$).

RESULTS AND DISCUSSION

The angular velocity of all joints increased with an increase in throw-in distance (Figure 1B). However, only the elbow generated more ball speed as throw-in distance increased, while the other joints did not contribute to the increase in the ball speed (Figure 1A). Due to the absence of the wrist's range of motion, the wrist angle is unchanged throughout all throw-in distances. Therefore, the distance from the elbow and wrist to the ball ($r_{Joint \to Ball}$) is generally unchanged between trials, and the $\mathrm{GS}_{\hat{\omega}}$ of the elbow and wrist were constant in all throw-in distances (Figure 1C). The $\mathrm{GS}_{\hat{\omega}}$ of the shoulder decreased with the increase in throw-in distance (Figure 1C). Because the ball is positioned forward to the shoulder at the release due to the regulation [4], the shoulder rotation always generates the downward and forward ball velocity. Therefore, as the release angle increased with throw-in distance, the difference in direction between the ball velocity generated by the shoulder and the actual ball velocity increased, and the shoulder's $\mathrm{GS}_{\hat{\omega}}$ would have decreased with increasing throw-in distance. However, considering that the angular velocity of the shoulder increases with throw-in distance, the shoulder may not directly contribute to the gain of ball speed but may contribute to the increase in the angular velocity of elbow extension and the adjustment of release angle.

CONCLUSIONS

This study aimed to determine the effect of each upper limb joint on the control of ball speed in throwing distance control in a throw-in. The main finding was that the elbow was the main contributor to control of the ball's flight distance in the throw-in.

REFERENCES

[1] Yumigeta et al., *The Japan journal of coaching studies*, **24(1)**:17-25, 2010.
[2] Ishikawa et al., *Jpn J. Phys. Educ. Health and Sport Sci*, **65**:1029-1039, 2020.
[3] Sprigings et al., *J. Biomech,***27(3)**:245-254, 1994.
[4] IFAB, *Laws of the Game 22/23*:122-124, 2022.

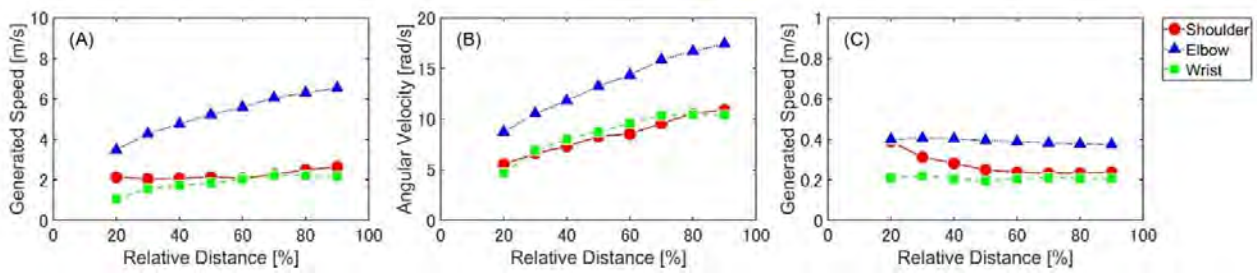

Figure 1 Generated ball speed by the upper limb joints at the moment of release, including the determining factors. (A) Generated speed (GS). (B) Joint angular velocity. (C) Generated speed per unit vector of angular velocity ($\mathrm{GS}_{\hat{\omega}}$).

Relationship between ball velocity and kinematics of pelvis and upper torso in female collegiate baseball players

Takuya Sekiguchi[2], Yuta Yamaguchi[1,2], Naoki Wada[1] and Tetsunari Nishiyama[1]
[1] Faculty of Sport Science, Nippon Sport Science University, Kanagawa, Japan.
[2] Graduate School of Health and Sport Science, Nippon Sport Science University, Tokyo, Japan.
Email: sekki.nine@gmail.com

INTRODUCTION

Among the factors determining a pitcher's ability, throwing with higher ball velocity is considered to be the most important [1]. Several previous studies showed that movement of trunk during pitching was related to ball velocity [2][3]. However, these studies have primarily focused on male subjects. Although there have been several studies on female baseball players, the relationship between kinematics of the trunk and ball velocity among female players has not been reported. The purpose of this study is to investigate the relationship between ball velocity and kinematics of pelvis and upper torso in female baseball players, and obtain knowledge for teaching and coaching of pitching motion for the female players.

METHODS

Ten female collegiate baseball players (age: 20.1 ±0.8 years old, height: 1.62 ± 0.06 m, body mass: 57.0 ± 7.0 kg) participated in this study. A three-dimensional motion analysis device (VICON MX40, Vicon motion systems, UK) was used to obtain kinematic data of the segments and joints at 200 Hz. Ball velocity was measured using a speed gun (SPORTS RADAR GUN Professional Sports HP-1, Mizuno, Tokyo, Japan). After warming up, the subjects threw fastballs from a portable pitching mound toward a catcher with maximal effort. Measurement was conducted at least ten times, and the data of the fastest pitches were analyzed. Baseball pitching was divided into two phases by three critical events. Spearman's rank correlation coefficient was used to assess significant differences between ball velocity and kinematic parameters of pelvis and upper torso ($p < 0.05$). All data were processed using MATLAB (Matlab2020b, Mathworks, MA, USA).

RESULTS AND DISCUSSION

Mean ball velocity was 96.2 ±7.4 km/h. Four kinematic parameters significantly correlated with ball velocity (Table1). Forward tilt angular velocity of the upper torso at the time of stride foot contact (SFC) and its peak value during arm cooking phase was positively correlated with ball velocity. This result showed that motion of upper torso forward tilt may provide a great momentum that can be translated into increased ball velocity from stride foot contact (SFC) to before maximum shoulder external rotation (MER). The relationship between sagittal plane motion of the trunk at the time of ball release and ball velocity was shown in the previous study on male baseball players [2]. Compared to results of this study, which showed differences by event. Lateral tilt angular velocity of the upper torso at the time of maximum shoulder external rotation (MER) and its peak value during arm acceleration phase was positively correlated with ball velocity. This result suggested that a motion of upper torso lateral tilt helped to increase ball velocity from maximum shoulder external rotation (MER) to before ball release (REL). This relationship between lateral lean motion of the trunk and ball velocity was similar to the previous finding for male baseball players [3]. In this study, there was no correlation between pelvic parameters and ball velocity.

Table 1: Angular velocity data and factors associated with ball velocity

	Mean ± SD	ρ
Ball velocity (km/h)	96.2 ± 7.4	
Stride Foot Contact (SFC)		
Upper torso forward tilt (°/s)	223.9 ± 159.6	0.673*
Arm cocking phase		
Maximum upper torso forward tilt（°/s）	432.8 ± 89.0	0.685*
Maximum Shoulder External Rotation (MER)		
Upper torso lateral tilt (°/s)	298.0 ± 117.1	0.758*
Arm acceleration phase		
Maximum upper torso lateral tilt (°/s)	305.1 ± 116.7	0.758*

ρ: correlation coefficient, *$p < 0.05$

CONCLUSIONS

Forward tilt angular velocity of the upper torso at the time of SFC and during arm cooking phase and lateral tilt angular velocity of upper torso at the time of MER and during arm acceleration phase was positively correlated with ball velocity. Comparison of our results with previous studies suggested that the phase and event of movement on the sagittal plane related to ball velocity may differ between male and female baseball players.

REFERENCES

[1] Takahashi et al. *Education Physics*, 2003.
[2] Solomito et al. *Orthop. J. Sports Med.* **6(10)**, 2018.
[3] Solomito et al. *Am J Sports Med*. **43(5)**, 2015

CHARACTERISTICS OF LEG MOVEMENTS THAT INDUCE RED CARDS IN RACE WALKING

Naoki Takahashi[1], Hironari Shinkai[2]
[1] The United Graduate School of Education, Tokyo Gakugei University, Tokyo, Japan.
[2] Arts and Sports Sciences Division, Tokyo Gakugei University, Tokyo, Japan.
Email: r208002f@st.u-gakugei.ac.jp

INTRODUCTION

In race walking rules, the advancing leg must be straightened from the heel contact until the vertical upright position with the ground (i.e. not bent at the knee) [3]. The referees may issue a red card to athletes with non-legal walking techniques, and three or more red cards will result in disqualification. Therefore, the judgment of the referees is significant to an athlete's performance. Several studies have been conducted on the judgment of referees [1,2]. However, these studies do not analyze the movement at the moment the referees make their decisions, so their accuracy may be questionable. To ensure proper verification, it is necessary to analyze the movements at the moment of the referee's decision. The aim of this study was to verify the movements that result in a red card as judged by the referees.

METHODS

The subjects were the 20 male athletes and the 3 referees who participated in the 2022 competitions. Video recordings (120fps) of the movements of 10 participants who received red cards from more than one referee (RC group) and 10 participants who did not receive any red cards during the competitions (NI group) were analyzed. We measured 4 step parameters (step frequency, step length, speed, and contact time) and the knee joint angle during the contact phase. The step parameters were analyzed using an independent t-test, and the knee joint angle was analyzed using Statistical Parametric Mapping (SPM). The significance level for all tests was set at 0.05.

RESULTS AND DISCUSSION

Table 1 showed that there were no significant differences in all step parameters, indicating that the competitive level of the two groups was similar. It is possible that these step parameters do not have a significant effect on the referees' judgments. The SPM analysis revealed that there was no marked difference in the knee joint angle between the RC and NI groups at heel contact and immediately after. However, from 22 to 77% of the contact phase, the RC group showed a significantly smaller knee joint angle compared to the NI group ($p < 0.001$) (Figure 1). Furthermore, the knee of the NI group was still extended after the vertical upright position, up to 44% of the contact phase, while the knee of the RC group was either flexed or kept still. The competitive rules state that the knee extension range is from heel contact to the vertical position. However, to avoid receiving a red card from referees, it is suggested by this study that athletes need to extend their knee from the moment of heel contact to the vertical upright position or immediately thereafter. Additionally, keeping a larger knee joint angle after the vertical upright position may also help athletes avoid receiving a red card.

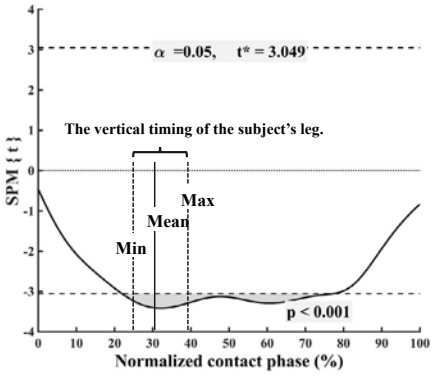

Figure 1. Results of SPM{t} for the knee joint angle. Mean, Max and Min are the instant when the subject's legs are vertical.

CONCLUSIONS

The knee joint was no marked difference at the heel contact and right after. However, our results suggests that athletes should extend their knee joint from heel contact to after the vertical upright position to avoid receiving a red card from the referees.

REFERENCES

[1] Hanley, B. et al, *Front Sports Act Living,* **8**: 1-9, 2019.
[2] Knicker, A. et al, NSA, 3: 25-38, 1990.
[3] World Athletics, Book of rules, 108-112, 2022.

Table 1: Results of t-tests for step parameters between the red card (RC) group and the no illegal (NI) group.

	RC group (n = 10)	NI group (n = 10)	Effect size	*p-value*
Step frequency (Hz)	3.25 ± 0.20	3.29 ± 0.17	0.25	$p = 0.59$
Step length (m)	1.06 ± 0.14	1.10 ± 0.12	0.33	$p = 0.47$
Speed (m/s)	3.44 ± 0.57	3.62 ± 0.47	0.35	$p = 0.45$

A Comparison of Rotation Sequences for Shoulder 3D Kinematics in the Volleyball Attack

Kiara Barrett, Hunter J. Bennett
Department of Human Movement Sciences, Old Dominion University / Norfolk, Virginia, United States.
Email: kbarr011@odu.edu

INTRODUCTION

The shoulder complex boasts a large range of motion, often causing issues with 3D kinematic calculations of joint angles. The international society of biomechanics (ISB) recommends the Euler YXY rotation sequence [1]. However, recent literature has found this rotation sequence produces complications in the tennis serve [2]. The disparity amongst the literature regarding a single "best" sequence for the shoulder supports the idea of individualizing the rotation sequence chosen for calculation based on the movement of the task. Previous investigations on rotation sequences have only included a few movements, mainly including tennis serves [2] and clinical tasks [3,4], leaving large gaps regarding movements relative to other sports. The volleyball attack, a prominent movement intrinsic to the sport, has yet to be evaluated. The purpose of this study was to determine the best rotation sequence for shoulder kinematics when performing a volleyball attack.

METHODS

Ten experienced (10 ± 3.74 yrs of experience) volleyball players were recruited to participate. After providing consent, participants completed a self-selected warmup followed by five overhead attacks aimed straight ahead. Participants were instructed to perform the attack with a follow-through where the arm crossed the body in the front, with the dominant hand ending on the contralateral side. A 12-camera motion capture system was used to record reflective markers placed on the humerus and upper trunk (thoracic and cervical). Shoulder angles were calculated in Visual3D software using six rotation sequences: ZXY, YXY, XZY, YXZ, ZYX, and XYZ (X: anteroposterior, Y: vertical, Z: mediolateral). The trial began at 'takeoff' from the ground and ended at the completion of the follow-through. Instances of gimbal lock and angle agreement with known shoulder ranges of motion (flexion/extension: 210°; abduction: 230°, and rotation: 190°) [2] were recorded.

RESULTS AND DISCUSSION

Group averages (mean(std)) for the YXY sequence were Y_1: 116.81(14.35); X_1: 110.63(11.29); Y_2: 94.75(14.63). All Tait-Bryan sequences are reported in Table 1. The YXZ and XZY sequences frequently presented with irreconcilable responses: rotations exceeded possible limits and never returned to anatomical position despite the participants doing so. Employing the ZYX and ZXY sequences resulted in unrealistic ranges of motion in three participants. The YXY and XYZ sequences produced no instances of gimbal lock or unreasonable ranges of motion in any participant. Despite instances of exceeding limits, group average range of motions were within those reported in literature.

The XZY sequence has previously shown better reliability than the YXY sequence [4] and was suggested to be better for calculating abduction and extension angles at the shoulder [3]. We found untenable angle calculations using this sequence and would not recommend it for use in examining the volleyball attack. This study provides support of both a Tait-Bryan and an Euler sequence. The XYZ may be preferred as the angles are anatomical terms that are frequently used in research/teaching. However, the YZY rotation sequence is more widely accepted, which improves cross-study comparisons.

CONCLUSIONS

We found two rotation sequences to be sufficient in calculating shoulder angles in the volleyball attack: YXY and XYZ. We recommend using the YXY rotation sequence in accordance with ISB recommendations to analyze this movement.

REFERENCES

[1] Wu G et al. *J Biomech* **38(5)**: 981-992, 2005.
[2] Bonnefoy-Mazure A et al. *J Biomech* **43(10)**: 2022-2025, 2010.
[3] Šenk M & Chèze L. *Clin Biomech* **21**: S3-S8, 2005.
[4] López-Pascual J et al. *J Biomech* **21**: 502-506, 2016.

Table 1: Average of range of motion in each rotation sequence.

	Flexion-Extension	Ad/Abduction	Int-Ext Rotation	GL	ROM Coherence
ZXY	165.57 (26.90)	76.54 (20.27)	121.07 (33.37)	No	Yes
ZYX	135.31 (45.16)	173.69 (29.28)	62.24 (62.24)	Yes	Yes
XZY	82.24 (11.29)	218.30 (57.71)	247.20 (72.58)	Yes	No
XYZ	129.86 (20.28)	128.64 (24.18)	125.27 (5.64)	No	Yes
YXZ	202.41 (78.24)	72.51 (11.27)	234.84 (75.36)	Yes	No

Averages reported as mean(SD). GL: Instance of gimbal lock; ROM Coherence: Range of Motion Coherence with reports in literature

Associations between Unilateral Drop Landing Mechanics and Diaphragmatic Contractility in Individuals with Recurrent Lateral Ankle Sprains

Shunya Nonoyama[1], Masafumi Terada[1], and Tadao Isaka[1]
[1] Faculty of Sport and Health Science, Ritsumeikan University, Kusatsu, Japan.
Email: sh0181ek@ed.ritsumei.ac.jp

INTRODUCTION

Lateral ankle sprains represent one of the most prevalent and frequent musculoskeletal injuries with the highest recurrence rate in athletic and general populations [1]. A variety of motor-behavioral impairments is hypothesized to contribute to the high rate of recurrent ankle sprains (RAS) and to the development of long-term negative consequences of lateral ankle sprains [2]. Altered landing mechanics following an initial ankle sprain is a significant motor-behavioral impairment that is a potential target for interventions aimed at preventing RAS [3]. A prospective cohort study has reported that altered landing strategies may increase the risk of re-injury [4]. Thus, it is crucial to identify clinical factors that is associated with changes in landing biomechanics in order to provide direction for targeted interventions. A previous investigation has identified altered diaphragmatic contractility in individuals with RAS [5]. The diaphragm plays a significant role in maintaining postural stability and executing functional movement by regulating intra-abdominal pressure [6]. Therefore, the alterations in diaphragm function observed previously among patients with RAS may be linked to altered landing mechanics in individuals with RAS. However, no study has explored association of landing mechanics and diaphragmatic contractility in individuals with RAS. Therefore, the purpose of this study was to investigate the association between drop landing kinetics and diaphragmatic contractility in individuals with RAS.

METHODS

Twenty-four participants with RAS volunteered for this cross-sectional study (age: 20.8±1.4 years, height: 170.5±7.8 cm, body mass: 61.8±6.7 kg, # of LAS history: 5.3± 9.7, Min: 2, Max: 50). Participants performed six trials of unilateral drop landing tasks on the force platform in their legs involved with RAS. The following kinetic measures were quantified: a rate of force development (RFD), peak ground reaction force (GRF) in vertical, posterior, and lateral directions. All kinetics were normalized to body weight. Diaphragm contractility of the right and left hemispheres was assessed using ultrasonography in a supine position while breathing quietly. The transducer was positioned perpendicularly at the midaxillary line, over the intercostal space between the 8th and 9th ribs on both sides. Diaphragm thickness at the end of resting inspiration and expiration was measured and used to calculate the degree of diaphragm contractility. Spearman's rank correlation coefficients were used to examine the association between kinetic variables and diaphragmatic contractility. Significance was set a priori at $P < 0.05$.

RESULTS

RFD was positively and moderately correlated with the degree of the right hemidiaphragm contractility (P=0.029). Peak posterior GRF was positively and moderately correlated with the degree of the right hemidiaphragm contractility (P=0.003). Peak vertical GRF was positively and moderately correlated with the degree of the right hemidiaphragm contractility but did not reach statistical significance (P=0.050). There were no significant correlations among other variables (P>0.05, Table 1).

CONCLUSIONS

There were moderate correlations between diaphragmatic contractility and landing kinetic measures. These findings indicate that RAS participants with greater diaphragmatic contractility may have a landing strategy to manipulate higher magnitude of GRF and RFD. Future investigations are required to determine effects of therapeutic intervention aimed to improve diaphragmatic contractility on landing mechanics in patients with RAS.

REFERENCES

[1] Gribble P et al. *Br J Sports Med* **50**: 1496-1505, 2016.
[2] Hertel J & Corbett R. *J Athl Train* **54**: 572-588, 2019.
[3] Simpson J et al., *Phys Ther Sport* **37**: 210-219, 2019
[4] Fransz D et al., *Am J Sports Med* **46**: 3454-3462, 2018.
[5] Terada M et al., *Med Sci Sports Exerc* **48**: 2040-5, 2016.
[6] Hodges P et al., *J Physiol* **522**：165-175, 1997.

Table1: Spearman's rank correlation coefficients between landing kinetic variables and diaphragmatic contractility.

ρ (P value)	RFD	Peak vertical GRF	Peak posterior GRF	Peak lateral GRF
The right hemidiaphragm contractility	0.445 (0.029)*	0.405 (0.050)	0.573 (0.003)*	0.078 (0.718)
The left hemidiaphragm contractility	0.281 (0.184)	0.324 (0.122)	0.263 (0.215)	-0.179 (0.402)

Abbreviations: RFD = rate of force development, GRF = ground reaction force. *Significant correlation coefficients ($P < 0.05$).

Grading of jumping height by quick movement

Yoshiho Muraoka[1], Hiroto Suzuki [1,2], and Keiji Kaneko [1]
[1] Department of Education, Meisei University, Tokyo, Japan.
[2] Nirayama Elementary School, Shizuoka, Japan.
Email: muraoka@ge.meisei-u.ac.jp

INTRODUCTION

According to previous research, grading of jumping height is done by adjusting joint angles and movement time, not by adjusting muscle strength [1]. However, in many sports competitions, not only "high" and "accurate" jumps, but also "quick and accurate" jumps are required in some situations. There are few studies that have clarified the jumping height, whole-body reaction time, and joint angle changes when a certain condition of jumping height is demanded in jumping "quickly and accurately".

The purpose of this study was to clarify the changes in jumping height, whole-body reaction time, joint angle, and angular velocity of grading by jumping movements with the awareness of jumping "quickly and accurately" in addition to jumping "quickly and high".

METHODS

Fifteen male university students were used as subjects. Vertical jumps were performed. First, the subjects performed a jump with unconditioned maximal effort (F100), followed by three sets of jumps at 100%, 70%, and 50% height in grading (R100, R70, and R50, respectively). Finally, F100 was performed again. In the grading jumps, subjects were told the target percentage of each grading before the test and instructed to jump quickly in response to the light stimulus. Subjects wore a suit with reflective markers attached, and displacement of each joint and site was measured by video recording. Whole-body reaction time was measured by measuring the time it took for the foot to leave the mat after the light stimulus was visible from the measuring device. From the videos, the body center of gravity was obtained using Flame DIAS55 software, and the jumping height was calculated. The jumping height was analyzed by comparing the target and measured values in grading. From the joint angles, changes and angular velocities of the hip, knee, and ankle joints were calculated. For angular velocity, the peak angular velocity during the jumping motion and the time of its peak appearance were calculated.

RESULTS AND DISCUSSION

Significant differences were found between F100 and R70, F100 and R50, and R100 and R50 in jumping height, and jumping height decreased with decreasing target values. Subjects may have been able to distinguish leap height in terms of effort between target values even in quick conditions such as those in this study. The target (F100, T70, T50) and measured (R100, R70, R50) values for each trial by grading are shown in **Figure 1**. As the target value decreased, the measured value exceeded the target value. A previous study reported that the difficulty of grading as the subjective effort was decreased was due to subjects' underestimation in grading, and that grading became more difficult the further away from the reference value the subjects moved [2]. The present study showed similar results.

The whole-body reaction time did not differ depending on the grading conditions, suggesting that it was not affected by the movement reaction time.

The joint angle changes and angular velocities revealed that the hip and knee joint flexion angles were significantly smaller in F100 than in R100, indicating that the range of motion of the joint angles from the preparatory movement to the take-off was greater in F100. It was thought that grading was performed by the extension movements of these two joints in the vertical jump by quick movements.

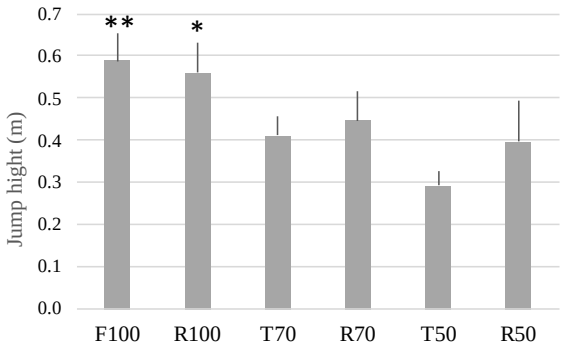

Figure 1 Target and measured values in grading (n=15). (**: R100 vs R50;P<0.05, **: F100 vs R70,R50; P<0.01)

CONCLUSIONS

It was found that in the rapid jumping motion, grading of jumping height was performed by the hip and knee joints by adjusting the amount of joint angle change.

REFERENCES

[1] Miyamoto T et al. *Japan J. Phys. Educ. Hlth. Sport Sci.***64**: 49-57, 2019.
[2] Ito K and Muraki Y. *The Jpn. J. Sports Method.* **10**: 17-24, 1997.

Acceleration Comparison between Peak Height Velocities in Male Youth Soccer Players

Kavon Bonakdar[1], Jake A. Melaro[1], Sean A. Brown[1], and Joshua T. Weinhandl[1]
[1] Kinesiology, Recreation, and Sport Studies, University of Tennessee, Knoxville, TN, USA.
Email: kbonakda@vols.utk.edu

INTRODUCTION

Sport-related injuries increase in males throughout high school, with ~68% of adolescent injuries occurring in the lower extremity [1, 6]. This is likely due to rapid, physiological changes during puberty such as bone growth and increased muscle mass, which can increase the forces experienced by the body and be a factor for higher prevalence of lower extremity injuries [2]. According to a recent study, growth-related injuries account for 30% of all severe injuries that require at least 40 days of participation time lost in soccer academies. Thus, the reduction of growth-related injuries can be important in the prevention of long-term repercussions and maximization players' potential development [5].

Investigating acceleration performance throughout puberty can provide insight into managing training load to reduce injury while also optimizing performance [3]. Therefore, the purpose of this study was to investigate the peak acceleration and acceleration integral in youth soccer players when performing various agility drills between maturation groups. It was hypothesized that peak height velocity (PHV) [4] could be estimated by peak accelerations and acceleration integrals.

METHODS

Sixty-six male youth soccer players were recruited from a local soccer club to voluntarily participate in this study (age: 12.7 ± 2.2 years). The Mirwald equation was used to determine how close the players were to their PHV. Inertial measurement units were placed on the participants bilaterally on the distal-medial tibia Participants completed a M-cone drill in which the participants ran in an M shape and made sharp cuts at each cone Data were analysed using Python v3.10.4 (Python Software Foundation, Beaverton, OR, USA). A simple linear regression was used to test if peak acceleration and an acceleration integral significantly predicted PHV (α = 0.05) using SPSS (IBM Corporation, Armonk, NY, USA).

RESULTS AND DISCUSSION

The results of the regression indicate that peak acceleration explained <0.01% of the variation in PHV [$F(1,64)=0.001$, $p=.981$]. The results of the second regression indicate that acceleration integrals explained 0.03% of the variation in PHV [$F(1,64)=0.216$, $p=.644$]. Our hypothesis that PHV could be estimated by peak accelerations and acceleration integrals was not supported. It was believed that the rapid physiological changes of increased bone and muscle mass would increase impact accelerations measured at the distal tibia. However, the results of this study emphatically refute that claim indicating the participants were able to adapt their impact attenuation along with their physiological changes.

Figure 1 Peak Height Velocity as a function of acceleration integral

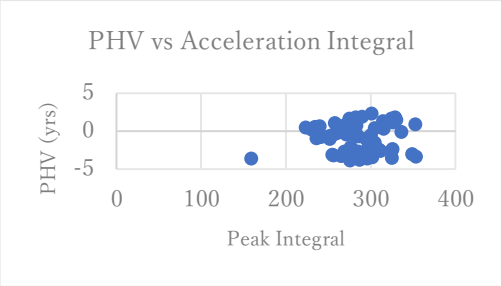

Figure 2 Peak Height Velocity as a function of peak acceleration

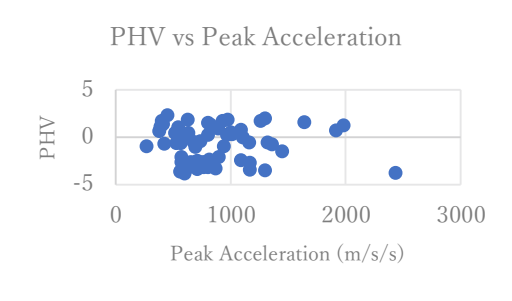

CONCLUSIONS

The results of this study provide the first evidence that acceleration performance does not increase throughout puberty. This does not align with the results of previous research [1,3,6], but our findings suggest that the changes in physiology and motor control during puberty might not be drastic enough to place players at a significantly higher risk of injury. Further research could track the acceleration performance in this age group throughout a whole practice.

REFERENCES

1. Comstock, R.D., Pierpoint, L.A.. National high school sports-related injury surveillance study 2018-2019. 2020
2. Dupré, T., & Potthast, W. *Sports Biomechanics*, 1-13, 2022
3. Gabbett, T. J. *BJSM* **50(5)**, 273-280. 2016
4. Mirwald, R. L. et al. *MSSE* , ***34*(4)**, 689-694. 2002
5. Monasterio, X., et al. *IJSM*. 2023
6. Verhagen, E. A. L. M., et al. *BJSM*, ***43*(13)**, 1031-1035. 2009

ELECTROMYOGRAPHIC ACTIVITY DURING DIFFERENT PHASES IN THE BENCH PRESS EXERCISE

Dusan Blazek[1], Anna Pisz[1], Artur Golas[2] and Petr Stastny [1]
[1] Faculty of Physical Education and Sport, Charles University, Prague, Czech Republic.
[2] Academy of Physical Education in Katowice, Poland.
Email: dusanmpk@seznam.cz

INTRODUCTION

The barbell bench press is a popular exercise for enhancing the strength of the upper limbs. Maximum strength development demands a high intensity training stimulus, such as 1-4 maximum repetitions (RM) per training session [1]. However, there are limited studies observing muscle activity in the different phases of the movement during bench press at 4RM intensity.

METHODS

A cross-sectional study with repeated measurements as part of the research project was used to examine differences in the electromyographic activity during different phases of 4RM bench press. Twenty three recreationally bench press practicing participants volunteered in the study (body mass: 84.8 ± 8.9 kg, age: 23.3 ± 2.5 years, height: 181.9 ± 5.0 cm). The study included three familiarization sessions and one testing session, with at least a 72-hour interval between each session. EMG activity was recorded using Musclelab 6000 (Ergotest Technology AS, Langesund, Norway) and was collected as an average during pre-sticking (pre stick) sticking (stick) and post-sticking (post stick) phase. Electrodes were placed according to SENIAM guidelines on the: Rectus Abdominis (RA), Obliquus Abdominis (OA), Triceps Brachii, caput longum (TB), Latissimus Dorsi (LD), Anterior Deltoideus (AD), Deltoideus Posterior (DP), Pectoralis Major, pars sternalis (PM_S), Pectoralis Major, pars clavicularis (PM_C). The raw EMG signals were transformed to the square root of the mean (RMS) value by a hardware peripheral network (frequency response 20-500 kHz, averaging constant 100 ms, total error ± 0.5%). Data were sampled at 1000 Hz. The one-way ANOVA was used to evaluate differences in muscle activation between the phases during all repetitions. A repeated measures ANOVA was used to calculate the differences between repetitions, phases, and muscle activation.

RESULTS AND DISCUSSION

There were significant differences in all muscle activity between the phases: RA, $F(4,1865)=12.34$, $p < 0.001$, OA, $F(4,1865)=15.6$, $p < 0.001$, TB, $F(4,1865)=20.09$, $p < 0.001$, LD, $F(4,1865)=10.71$, $p ,< 0.001$, AD, $F(4,1865)=29.62$, $p < 0.001$, DP, $F(4,1865)=44.5$, $p < 0.001$, PM_S, $F(4,1865)=31.88$, $p < 0.001$, PM_C, $F(4,1865)=25.05$, $p > 0.001$. A Tukey post hoc revealed that activation of all muscles differed between each of the phase statistically significantly $F(4,1864)=78.36$, $p < 0.001$. However, the highest difference occurred in the pre stick phase compared to the other phases in every repetition. There was also statistically significant difference in muscle activity between repetitions $F(3,1865)=69.4$, $p < 0.001$. However, there was no significant difference between the muscle activity in each of the phases and repetitions $F(12,1849)=1.54$, $p = 0.1$.

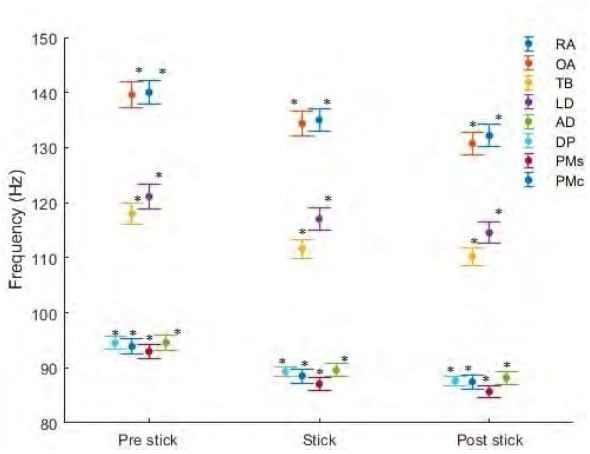

Figure 1 Frequency of discharge of individual muscles in each part of the movement phases in 4RM. *significant differences between the phases of the movement

CONCLUSIONS

Sticking phase is the most mechanically demanding point to surpass during a bench press exercise. Therefore, a decrease in muscle activity indicates exhaustion caused by overcoming this point which is observed in each of the 4RM. This exhaustion also remained in the post sticking phase.

REFERENCES

[1] Bird S P et al. Sports Med 35: 841-51, 2005.

WALTZ SWING CHARACTERISTICS OF THE COMPETITIVE BALLROOM DANCE WORLD CHAMPION COUPLE

Yasuyuki Yoshida[1], Arunas Bizokas[2], Katusha Demidova[2],
Shinichi Nakai[3], Rie Nakai[3] and Takuichi Nishimura[1,4]
[1] Human Augmentation Research Center, National Institute of Advanced Industrial Science and Technology, Chiba, Japan
[2] Non-affiliated
[3]Dance Jardin, Tokyo, Japan
[4]School of Knowledge Science, Japan Advanced Institute of Science and Technology, Ishikawa, Japan
Email: yasuyuki.yoshida@aist.go.jp

INTRODUCTION

Our research group has found the movement characteristics of a world champion couple in competitive ballroom dancing during waltz swing [1,2]. So far, forward movement in male and backward movement in female have been focused, but the reverse movement has not yet been analyzed. The purpose of this study is to find the movement characteristics of the world champion ballroom dance couple, focusing on backward movement for male and forward movement for female.

METHODS

Thirteen national level competitive ballroom dance couples participated. The age, height, and weight were, respectively, 24.3 ± 5.6 years, 173.4 ± 6.3 cm, and 61.1 ± 4.9 kg in males, and 22.6 ± 4.7 years, 161.2 ± 6.1 cm, and 47.6 ± 5.0 kg in females. In addition, A couple that had been champions in professional competitive ballroom dancing for 10 years participated. Age, height, and weight of the champion male dancer were 40 years, 183 cm, and 76 kg; those of the champion female dancer were 40 years, 169 cm, and 52 kg.

The movements were recorded at 240 Hz using the Xsens system (MVN, Xsens, Netherlands). The trial was performed as follows. 1. Preparation (123123); 2. Natural spin turn (123123); and 3. Second half of reverse turn (123). This method is the same as our previous research [1,2]. Statistical Parametric Mapping (SPM) [2] was performed on the height of the whole body center of mass of one swing in the second half of the natural spin turn (Figure 1).

RESULTS AND DISCUSSION

As a result of SPM, there was a significant difference in the first half between the champion male dancer and the male dancers. During the descending movement in the first half, the champion male dancers descended faster and reached a lower position than the male dancers. In the rise and fall movements, the champion male dancers were superior to the male dancers in descending dance skills. On the other hand, there was a significant difference in the last part of the second half between the champion female dancer and the female dancers.

CONCLUSIONS

Even when the male dancers moved backwards and the female dancers moved forwards, the movement characteristics of the champion male and female dancers appeared.

ACKNOWLEDGEMENTS

This work was supported by JSPS KAKENHI Grant Number 22K11491.

REFERENCES

[1] Yoshida Y et al. *J Dance Med Sci.* **24**: 168-174, 2020.
[2] Yoshida Y et al. *Balt. j., sport, health sci.* **120**: 4-12, 2021.

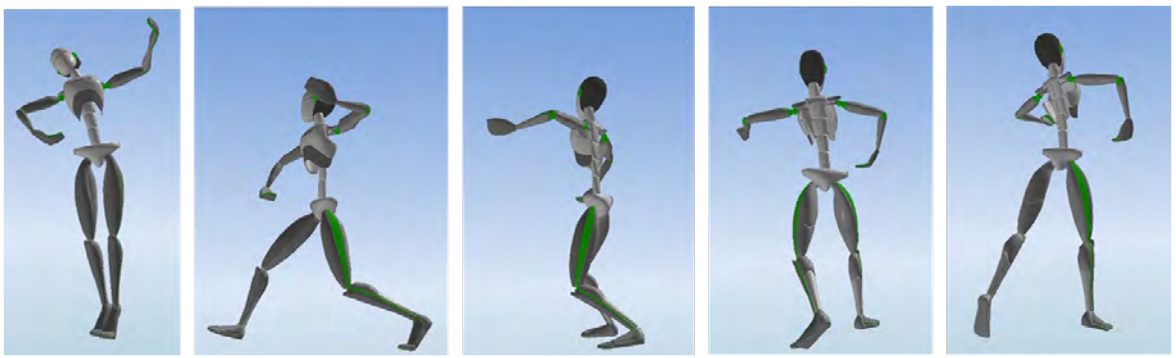

Figure 1 One swing for the second half of the natural spin turn for male.

VALIDITY OF SPRING-LIKE BEHAVIOUR PERFORMANCE DURING HOPPING USING A SMART WATCH

Atsuki Kageyama[1], Tadao Isaka[2], Tetsunari Nishiyama[1] and Mitsuo Otsuka[1]
[1] Faculty of Sport Science, Nippon Sport Science University, Kanagawa, Japan.
[2] Faculty of Sport and Health Science, Ritsumeikan University, Shiga, Japan.
Email: 20aa362@nittai.ac.jp

INTRODUCTION

Many dynamic sports motions are performed by the spring-like behaviours of the whole body. This can be usually assessed by leg stiffness during the hopping jump [1], that is conventionally measured by a force plate.
Recently, wearable technology has become widely prevalent in assessing sports performance. Particularly, accelerometers and gyrosensors in smartphones are used for the assessment of sports performance [2]. However, to the best of our knowledge, smart watches that can be easily attached to the wrist are still not used for assessing kinetics during dynamic sports motions. Therefore, the purpose of this study was to test the agreement between the spring-like behaviour performances during the hopping exercise calculated using two different methods: a method measured by force plates and a method measured by a smart watch.

METHODS

Forty active sports students participated in this study (71.9 ± 10.6 kg in mass). After a self-selected warm-up and familiarisation period, each participant completed five trials of five consecutive hops with maximal effort. Maximal effort was defined as the effort to try to achieve the maximal attainable height. Participants hopped in place with their arms akimbo. Data collected during three consecutive hops between the second and fourth hop of five hops were used in the analysis. A total of 600 hops were obtained.
During the experimental trials, the ground reaction force (GRF) and acceleration data were simultaneously collected at frequencies of 1,000 Hz and 100 Hz, respectively. GRFs of feet were sampled from two force plates (0.40 m X 0.40 m; TFP-404011B, Technology Service, Nagano, Japan). Acceleration data were sampled from a smart watch (Apple watch series 7, Apple, CA, USA). Actual peak vertical GRF (peak force), peak leg compression in the middle of the ground contact phase (COM displacement), and leg stiffness were calculated using the spring–mass model for each jump in each method [3]. The peak force and leg stiffness were normalised by body mass; so, they can be calculated using a smart watch without measuring the participant's mass. The predicted peak force, COM displacement, and leg stiffness were calculated from the acceleration data of a smart watch using a custom MATLAB program. The validity of the spring-like behaviour performance predicted with the smart watch was examined by the Brand-Altman analysis.

RESULTS AND DISCUSSION

The peak force predicted by the smartwatch was strongly correlated to the actual peak force predicted by the force plate (r = 0.708; Figure 1A). Bland-Altman upper and lower limits of agreement were −17.5 N/kg and 19.4 N/kg, respectively (Figure 1B). Both the fixed bias (1.0 N/kg of Figure 1B) and proportional bias (r = 0.229 of Figure 1B) were small.

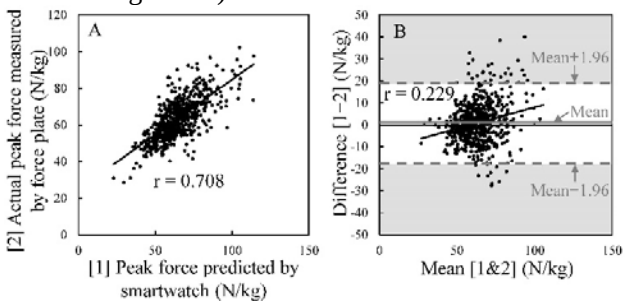

Figure 1 Panel A. Relationship between predicted peak force and actual peak force. Panel B. Bland-Altman plot for comparison of peak force between smart watch method and force plate method. The grey area indicates out of the limits of agreement.

The predicted leg stiffness by the smart watch was and moderately correlated with the actual leg stiffness by the force plate (r = 0.489). By Bland-Altman plot for comparison of leg stiffness, the random error (upper and lower limits of agreement: −0.303 N/m/kg and 0.214 N/m/kg) and proportional bias (r = −0.414) were not negligible. Therefore, during hopping, leg stiffness using the smart watch should be carefully assessed.

CONCLUSIONS

We conclude that force production, such as peak force during hopping, can be estimated by acceleration data measured by a smart watch. In contrast, the algorithm should be reconsidered and improved for the prediction of leg stiffness using a smart watch.

ACKNOWLEDGEMENTS

This work was supported by the Ministry of Education, Culture, Sports, Science, and Technology Grant-in-Aid for Scientific Research C (20611312).

REFERENCES

[1] Blickhan R. *J Biomech* **22**: 1217-27, 1989.
[2] Balsalobre-Fernández C. *J Sports Sci* **33**: 1574-9, 2015.
[3] Farley CT & Morgenroth DC. *J Biomech* **32**: 267-73, 1999.

CROSS-SECTIONAL AREA OF HAND INTRINSIC MUSCLES AND UPPER LIMB LENGTH ASSOCIATED WITH THROWING RECORD OF FEMALE DISCUS THROWERS

Yukiho Arano[1], Shigeo Hatakeyama[2], Toshiyuki Homma[3] and Mitsuo Otsuka[1,2]
[1] Graduate School of Health and Sport Science, Nippon Sport Science University, Yokohama, Japan.
[2] Faculty of Sport Science, Nippon Sport Science University, Yokohama, Japan.
[3] Faculty of Sports and Health Science, Daito Bunka University, Higashimatsuyama, Japan.
Email: 22sma27@nittai.ac.jp

INTRODUCTION

In the discus throw discipline, several previous studies on high performance have focused on analysing throwing motion and its relationship with the throwing record of the thrower [1]. In particular, the initial velocity of the discus at release is considered an important determinant of long throwing distance [2]. Before the release motion, the discus is gripped by the distal interphalangeal (DIP) joints of the throwing hand and moves around the thrower by his/her turning motion. Therefore, a larger centrifugal force is applied for greater throws, to the hand holding the discus, immediately before release.
Conversely, the magnitude of the centrifugal force decreases when the turning radius increasesd. Hence, hand muscularity and arm length would be related to the throwing record of discus throwers because of their specific adoptation. The purpose of this study was to clarify the relationship between the morphological characteristics of the upper limbs and the throwing records of discus throwers.

METHODS

Twenty female discus throwers (age 20.6 ± 1.5 y; body height 165.90 ± 3.71 cm; mass 71.4 ± 7.2 kg; personal record of discus throw 44.70 ± 5.20 m) participated in this study.
The cross-sectional area (CSA) of the dominant hand muscles was measured in the transverse plane using a 1.5-T magnetic resonance system (ECHELON OVAL, Hitachi Medical Corporation, Tokyo, Japan). Hand images were acquired using a knee coil positioned at the centre of the magnet. The location of the distal end of the first metacarpal bone was analysed to determine the CSAs of the hand muscles. The anatomical CSAs of the dorsal interosseous, palmar interosseous, opponens digiti minimi, abductor digiti minimi, lumbrical, adductor pollicis, flexor pollicis brevis, and abductor pollicis brevis muscles perpendicular to the third finger were calculated.
The dominant upper limb length from the midpoint of both clavicles to the distal end of the third distal phalanx was measured twice using measuring tape. The average value of the two measured lengths was used for further analysis.

RESULTS AND DISCUSSION

No significant relationships of the personal record were observed between the CSAs of the dorsal interosseous, palmar interosseous, opponens digiti minimi, abductor digiti minimi, adductor pollicis, flexor pollicis brevis, or abductor pollicis brevis muscles. The lack of significant relationships may be because we focused on female throwers who handled a light 1.0 kg compared to male throwers. In contrast, a significant relationship was observed between the personal record and the CSA of the lumbrical muscles ($r = 0.581$; $P < 0.05$; Figure 1). The lumbrical muscles have a many muscle spindles and produce not only metacarpophalangeal (MP) flexor forces but also DIP extensor forces. Therefore, the hand intrinsic muscles of greater throwers might play a role in manipulating the discus by flexing the MP joints during the faster turn, monitoring the discus motion, but fixing the DIP joints against a larger centrifugal force.
A significant relationship was observed between the length of the dominant upper limb and personal record ($r = 0.475$, $P < 0.05$). Hence, the longer upper limb length of greater throwers might lead the centrifugal force to reduce. Finally, it might lead the flexor digit muscles of intrinsic hand to not develop further.

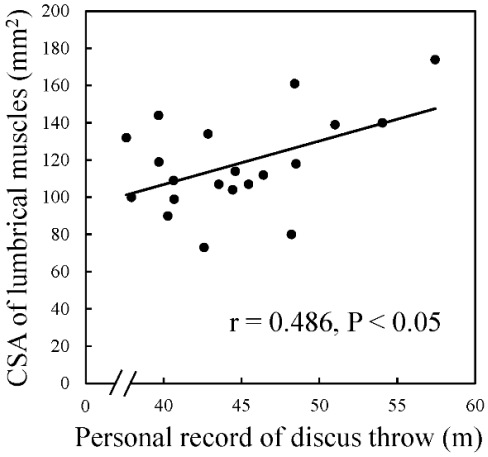

Figure 1 Correlation between the personal record of discus throw and cross-sectional area (CSA) of lumbrical muscles.

CONCLUSIONS

The dominant upper limb length was longer, and the CSA of the lumbrical muscle was larger in the greater discus throwers. Further research is required to clarify the CSA of the hand intrinsic muscles in other slice images and the relationship with the throwing record.

REFERENCES

[1] Yu B et al. *Sports Biomech* **1**: 25-45, 2002.
[2] Badura M. *New Studies Athl* **25**: 23-35, 2010.

Relationship between propulsive force and hip joint motion during eggbeater kick in Artistic Swimming

Hiroki Hyodo1, Ryoko Yamashita2, Koga Daiki3, Tadashi Wada1&2
1 Kokushikan University / Graduate School of Engineering, Tokyo, Japan.
2 Kokushikan University / School of Science and Engineering, Tokyo, Japan.
3 University of Tsukuba / Faculty of Health and Sport Sciences, Ibaraki, Japan.
Email: hyodo.h@kokushikan.ac.jp

INTRODUCTION

The egg beater kick is used in AS (Artistic Swimming) and water polo to keep the body in the water or lift it, and is a technique that generates propulsion in the vertical upward direction (buoyancy). Furthermore, in order to obtain more points for techniques, it is important not only to keep the body on the water surface, but also to raise the height above the water, so it is important to demonstrate a higher vertical propulsion force [1][2].

Optical motion capture systems, which are mainly used in recent years, use cameras to track markers attached to the body surface must be estimated. In this study, we estimated the center of the hip joint during the eggbeater kick, and investigated the relationship between each joint angle calculated from those points and the propulsive force in the vertical direction.

METHODS

The subjects were 8 females who had participated in AS (Age: 21.6, Height: 159.1cm, Mass: 55.6kg). Trials were performed 2 times at random in 3 trials. 1: Eggbeater kick with a weight of 2.5 kg (2.5kg). 2: Eggbeater kick with a weight of 5.0 kg (5.0kg). 3: Eggbeater kick in a normal state (Normal). In all trials, the weights and hands were instructed not to touch the surface of the water in order to avoid buoyancy on the weights. In addition, 18 self-luminous LED markers on the body (iliospinale anterius, iliosinale posterius, greater trochanter, outside the patella, inside the patella, lateral malleolus, medial malleolus, 5th metatarsal bone, left and right of the 1st metatarsal bone) affixed and obtained 3D motion. In the analysis phase, the right leg was targeted, and one cycle was defined as the time when the knee joint reaches maximum extension from the maximum flexion state and returns to maximum flexion again. In addition, the angle of the hip joint was determined by estimating the hip joint center using iliospinale anterius, iliosinale posterius, and greater trochanter landmarks [3]. Abduction and internal rotation were calculated (Figure1).

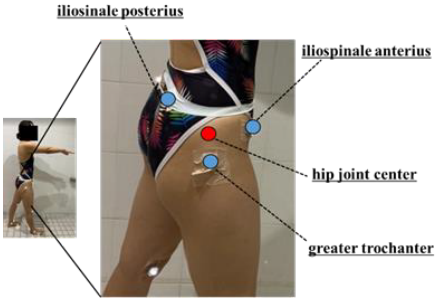

Figure 1 Estimation of Center of hip joint.

RESULTS AND DISCUSSION

During all trials, the duration of one cycle became larger and showed significantly lower values as the propulsive force increased (Normal: 0.64s, 2.5kg: 0.57s, 5.0kg: 0.54s). Table. 1 shows the average maximum and minimum values of hip flexion, abduction, internal rotation, knee flexion, and ankle plantar flexion in each trial. As a result, it was suggested that by increasing the abduction of the hip joint in the eggbeater kick, the water is captured from nearer the surface of the water and the propulsive force is increased. In addition, it is speculated that the knee joint is also flexed in the second half of one cycle, bringing the foot that catches the water closer to the water surface. However, although the hip joint abduction (HA) maximum value was significantly increased, the duration of one cycle was significantly shortened. This is thought to be due to an increase in the angular velocity of abduction. Therefore, swimmers may need to increase the contraction speed of the muscle groups around the hip joints to increase the angular velocity of abduction.

Table 1 Comparison of mean of each variable between trials.

		Normal (degree)			2.5kg (degree)			5.0kg (degree)		
		Mean	±	SD	Mean	±	SD	Mean	±	SD
Hip joint Flexion (HF)	Max	99.1	±	8.2	97.3	±	12.4	99.8	±	9.1
	Min	52.9	±	8.1	51.4	±	9.2	52.9	±	9.4
Hip joint Abduction (HA)	Max	61.7	±	6.4	66.8	±	6.4	70.1	±	9.2
	Min	51.0	±	5.8	51.3	±	6.1	53.7	±	5.9
Hip joint Internal rotation (HI)	Max	37.3	±	15.5	41.6	±	15.4	42.9	±	13.9
	Min	13.3	±	8.3	15.2	±	9.0	12.1	±	9.2
Knee joint Flexion (KF)	Max	108.9	±	13.6	107.6	±	9.9	108.9	±	14.1
	Min	39.2	±	6.7	36.3	±	4.5	34.0	±	3.2
Ankle joint Plantar flexion (AP)	Max	120.0	±	11.7	119.8	±	10.0	120.6	±	14.2
	Min	76.3	±	20.0	67.6	±	26.4	75.9	±	17.4

* p<o.o5, ** p<0.01

CONCLUSIONS

The results of this study suggested that increasing the abduction of the hip joint may be important in obtaining higher propulsive force in the eggbeater kick.

REFERENCES

[1] Eisuke Kawai. (2022). Biomechanics of eggbewter kicking – a review of motion and propulsive force -. Japanese Journal of Sciences in Swimming and Water Exercise, 25(1), 7-12.

[2] Sanders, R. H. (1999). Analysis of the eggbeater kick used to maintain height in water polo. Journal of Applied Biomechanics, 15(3), 284-291.

[3] Jun Kurabayashi et al., (2003). Validation of the estimation methods for the hip joint center. Journal of the Society of Biomechanisms, 27(1), 29-36.

DEVELOPMENT OF AN ADJUSTABLE SLEDGE FOR PARALYMPIC CROSS-COUNTRY SKIING WITH A PARTICULAR FOCUS ON NEUROLOGICAL AND PHYSIOLOGICAL IMPROVEMENT OF THE SITTING POSITION

Leonie Hirsch[1], Julia Suckrow[2], Ralf Rombach[2], Walter Rapp[2], Andres Jaramillo-Gonzalez[1] and Natalie Mrachacz-Kersting[1]
[1] Department of Neuroscience, Albert-Ludwigs Universität, Institute of Sports and Sports Science, Freiburg i.Br., Germany.
[2] Olympic Training Center Freiburg-Hochschwarzwald, Freiburg i.Br., Germany.
Email: natalie.mrachacz-kersting@sport.uni-freiburg.de

INTRODUCTION

In paralympic cross-country sit skiing, one of the main difficulties, in the beginning, is to find the most effective sitting position on the sledge. Athletes need an adjusted sledge optimised for their particular impairment [2]. The goal of this experiment was to develop a setup to define biomechanical and neurological parameters that help to construct individually adjustable sledges. Its requirements are to enable different sitting positions to meet different anthropometric and individual characteristics of athletes [2]. Biomechanical and neurological parameters were compared in the different positions with a special focus on forward propulsion and trunk muscle control.
The purpose of this pilot study was to understand the impact of the sitting position on the forward propulsion and therefore on the feature performance of the athletes.

METHODS

In the pilot phase of this experiment five healthy able-bodied subjects, without experience in nordic skiing participated (21 ± 4 years.; F). The Experiment was performed on a treadmill with a wheel-based adjustable sledge. The three positions of the sitting platform were defined as knee-high (KH), neutral (NT) and knee-low (KL), similar to the different classes defined by the para-nordic guidelines for sit skiing. Each participant was tested in every sitting position at the same individually chosen constant speed for six minutes, performing a double poling technique. Pole forces and bipolar surface electromyography (EMG) of three trunk muscles and three muscles of the upper limbs were simultaneously recorded on the dominant side. The propulsive pole force and the EMG activity of the recorded muscles in the different sitting positions were analysed and compared off-line.

RESULTS AND DISCUSSION

Using the exerted force as a variable to compare the different sitting positions, a trend towards the highest propulsive forces in the KH position and the lowest forces in the KL position is visible. This is also reflected in the poling frequency, which is higher in the KH position than in NT and KL. KL yields the lowest value. The KH position showed the shortest cycle lengths and KL the highest. Poling time per cycle was the shortest in the KH position. These results are in agreement with results found in the literature [1]. The activation of the *m. obliquus externus abdominis* was at a similar level of activation in all positions, the activation of the *m. erector spinae* was clearly reduced in the KH position (Figure 1). Activation of *m. rectus abdominis* was slightly higher in the KL in comparison to the NT positions, while the KH position, showed a reduced activation strength, which, however, extended into the recovery phase. A pre-activation of the *m. rectus abdominis* was seen towards the end in all positions.

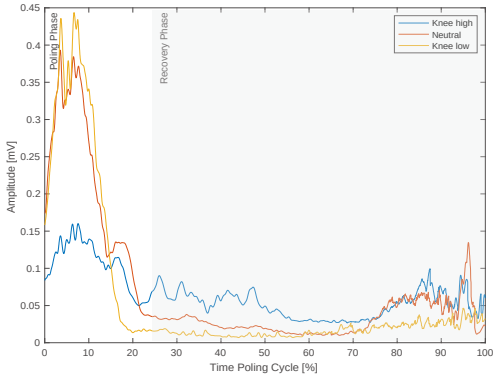

Figure 1: Mean EMG activation pattern of *m. rectus abdominis* in all sitting positions during the poling cycle

CONCLUSIONS

Visual differences between the three sitting positions were seen in the propulsive force output. Comparing the sitting positions, activation of trunk muscles responsible for flexion and extension differ in activation amplitude while the muscles that execute lateral tilt do not seem to differ. In further experiments this setup should be tested with paralympic athletes. Overall, the developed adjustable sledge and the measured biomechanical parameters offer an experimental setup that can provide insights into optimal sitting positions in paralympic cross-county sit skiing.

ACKNOWLEDGEMENTS

The authors would like to thank the Bundesinstitut für Sportwissenschaften for the financial support.

REFERENCES

[1] Karczewska-Lindinger M et al. *Journal of Science in Sport and Exercise* **3:281–291** (2021)
[2] Lajunen K et al. *Front. Sports Act. Living* **2:44** (2020)

EFFECTS OF TRUNK EXTENSION ON BODY AND WHEELCHAIR CENTERS OF GRAVITY DURING WHEELCHAIR PROPULSION MOVEMENTS

Koichi Kawabata[1], Takumi Tsukada[2], Hiroki Yoshimatsu[2], Rina Kato[2], Tatsuru Ibusuki[3], Toshihito Mitsui[4], and Yasunori Umemoto[5]

[1] Faculty of Wakayama Health Care Sciences, Takarazuka University of Medical and Health Care, Wakayama, Japan.
[2] Institute of Sports Science and Environmental Physiology, Wakayama Medical University, Wakayama, Japan.
[3] Rehabilitation Department, Akeno Central Hospital, Oita, Japan.
[4] Faculty of Sport Sciences, Nihon Fukushi University, Mihama, Japan.
[5] Department of Rehabilitation Medicine, Wakayama Medical University, Wakayama, Japan.
Email: k-kawabata@tumh.ac.jp

INTRODUCTION

In para-athletics wheelchair racing, trunk extension after pushing on the hand-rims reportedly increases wheelchair velocity. The present study was conducted to verify this phenomenon. Specifically, the centers of gravity (COGs) for the body and wheelchair were calculated and the relationship between trunk extension movements and change in each COG was investigated.

METHODS

The subject was one male wheelchair athlete in the T52 class as defined by World Para Athletics. A 12-camera Raptor-E motion capture system (MAC3Dsystem, Motion Analysis Corporation) was set up on an indoor straight course to capture propulsive movements in the final 10-m section during the 50-m sprint. Prior to the experiment, the athlete and wheelchair were affixed with 38 and 10 reflective markers, respectively. After an adequate warm-up, the athlete was instructed to run 50 m with maximum effort. The reflection markers were captured at 250 Hz during propulsive motion and the body COG was calculated from the 3D coordinates of the reflection markers. The wheelchair COG was calculated as follows. The wheelchair with reflective markers attached was suspended in two different postures and captured by camera from the side. The COG in the sagittal plane was defined as the intersection of the vectors from the suspended position to the vertical direction in the two different postures, and the COG in the frontal plane was defined as the same distance as the midpoint of the left and right rear wheel axles. The angle of trunk flexion/extension was defined as the angle between the y-axis (direction to the goal) and the vector pointing from the sacrum to C7, projected in the y–z plane of the global reference frame.

RESULTS AND DISCUSSION

The COG velocity of the wheelchair increased near the start of the push phase, and peak velocity was observed in the first half of the recovery phase. The COG velocity of the body also increased during the first half of the push phase, but showed a tendency to remain constant during the first half of the recovery phase. Peak angular velocities of trunk flexion and extension were observed in the first half of the push and recovery phases, respectively. Change in the COG velocity of the whole system (combined body and wheelchair) was similar to that of the body. The wheelchair COG velocity should have decreased during the recovery phase due to air and road resistance, but no such decrease was observed. This result suggests that extension of the trunk moved the COG of the body backwards, increasing the COG velocity of the wheelchair to maintain the COG velocity of the whole system.

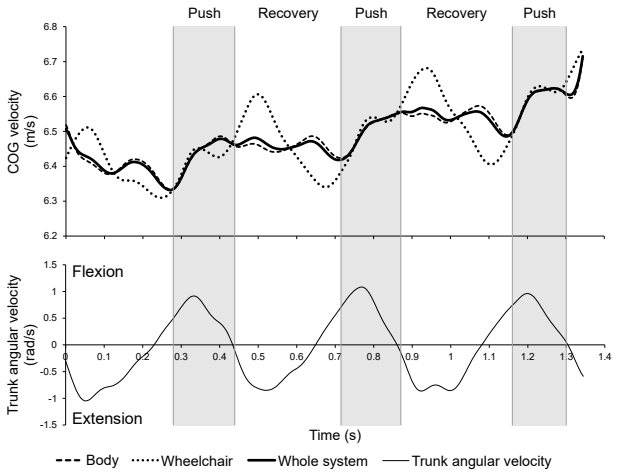

Figure 1 Velocity curves of COG and trunk angular velocity.

CONCLUSIONS

This study calculated body and wheelchair COGs and investigated the relationship between trunk extension movements and change in each COG. The results suggest that the increase in wheelchair COG velocity during the recovery phase contributes to maintaining constant COG velocity of the whole system.

ACKNOWLEDGEMENTS

This study received research grants from the Joint Usage/Research Center of Sports for Persons with Impairments, Wakayama Medical University (approval number: 2022-01).

REFERENCES

[1] Moss A D et al. *J Biomech* **38**: 15-22, 2005.

Effect of Short-term Combined Intervention Program on Erector Spinae Contractile Properties in Patients with Non-specific Chronic Low Back Pain

Hyungwoo Lee [1,2,5], Hojun Joo[1,5], and Kyoungkyu Jeon[1,2,3,4,5]
[1] Division of Sports Science, Incheon National University, Incheon, South Korea
[2] Department of Human Movement Science, Incheon National University, Incheon, South Korea
[3] Sport Science Institute, Incheon National University, Incheon, South Korea
[4] Health Promotion Center, Incheon National University, Incheon, South Korea
[5] Functional Rehabilitation Biomechanics Laboratory, Incheon National University, Incheon, South Korea
Email: jeonkay@inu.ac.kr

INTRODUCTION

Non-specific chronic low back pain (NSCLBP), which is reported to be unable to determine a specific diagnosis, has a multidimensional cause in which various factors are interrelated [1,2]. Core stabilization exercises aim to strengthen muscles in the transversus abdominis, lumbar multifidus, erector spinae, diaphragm, and back, which are important for maintaining neuromuscular control and dynamic spinal stability [3]. Therefore, the purpose of this study was to investigate the effect of a complex exercise including core stabilization exercise on the muscle contractile properties of the erector spinae muscles in patients with NSCLBP.

METHODS

This study was conducted with 16 women (age; 59.81±8.59 years, height; 158.16±5.58 cm, weight; 59.05±9.44 kg, visual analog scale; 5.94±1.01 points) suffering from NSCLBP. The subjects performed a complex exercise of 4 weeks. Tensiomyography (TMG, TMG-100 System electrostimulator, Slovenia) was used to compare and analyze the static contractile properties of erector spinae muscles. In order to compare and analyze the contraction characteristics of the measured muscle, measure-remeasurement and intra-rater reliability index (ICC) is the highest variable, maximal radial displacement (Dm, 0.91-0.99), a variable that records the maximum contraction displacement of the muscle, and contraction up to 10 to 90% of the maximum contraction displacement. A contraction time (Tc, 0.70-0.98), which is a time-consuming variable, was used [4]. In addition, velocity of contraction (Vc), a variable that can integrate the mechanical properties provided by TMG, was calculated and analyzed by the formula [$Vc\ (mm/ms) = Dm/Tc+Td$]. SPSS 26.0 (IBM, USA) was used for all data, and paired *t*-test was used to compare measurement result variables within the group. The significance level of all statistics was set at $P<.05$.

RESULTS AND DISCUSSION

After participating in the multimodal exercise intervention program, there was a significant difference between the measurements of Dm (P=0.016) and Vc (P=0.047), excluding Tc <Figure 1>. It is judged that Dm, which has a negative correlation with muscle stiffness, is likely to have risen as stiffness has decreased due to foam rollers and exercise [5]. In addition, it is judged that the activation of the erector spinae muscle increased due to exercise, and the muscle contraction speed variable Vc increased [6,7].

CONCLUSIONS

After participating in the complex exercise intervention program, muscle stiffness of the erector spinae muscles decreased and muscle contraction speed increased in subjects with non-specific chronic low back pain.

ACKNOWLEDGEMENTS

This study was supported by the University Innovation Support Project of Incheon National University.

REFERENCES

[1] Owen, P. J et al. *Br J Sports Med* **54**: 1279-1287, 2020.
[2] O'Sullivan, P et al. *J Orthop Sports Phys Ther* **46**: 932-937, 2016.
[3] Akhtar, M. W et al. *Pak J Med Sci* **33**: 1002, 2017.
[4] Martín-Rodríguez, S et al. *J Strength Cond Res* **31**: 3524-3536, 2017.
[5] Lee, H et al. *Appl Sci* **12**: 2501, 2022.
[6] Saeterbakken, A. H et al. *PLoS One* **14**: e0212216, 2019.
[7] Hvid, L et al. *Exp Gerontol* **80**: 51-56, 2016.

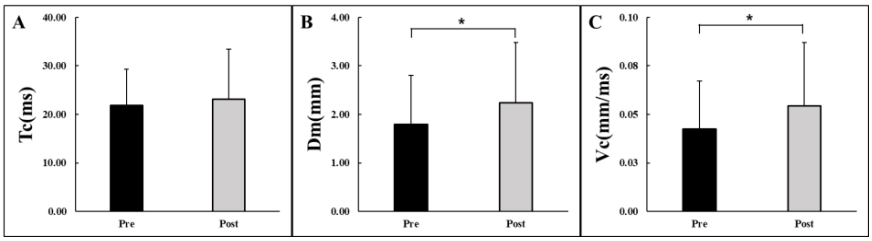

Figure 1. Analysis of pre-post findings
Note. Data are mean±standard deviation. Asterisk (*) indicates a significant difference at $P < 0.05$. A. Pre-post finding of contraction time (Tc). B. Pre-post finding of maximal radial displacement (Dm). C. Pre-post finding of velocity of contraction (Vc).

Biomechanics of Wheelchair Propulsion in Athletes of Wheelchair Racing

Mikito Hikosaka[1] and Noritaka Kawashima[1]
[1] Department of Rehabilitation for movement function, Research Institute of National Rehabilitation Center for Persons with Disabilities, Saitama, Japan.
Email: hikosaka-mikito-02@rehab.go.jp

INTRODUCTION

Highly-trained athletes of wheelchair racing show unique modalities and extraordinarily enhanced upper limb motor function that far exceed to daily use of wheelchair propulsion [1]. For the fairness of competition, wheelchair racing has a classification as their residual function. In the case of T54 class, the propulsive force is generated by the postural control and kinetic chain with the combination of upper limb and trunk functions. In contrast, racers classified as T51 have limited propulsive force due to the paralysis of their upper limb and trunk muscles but demonstrate particular compensatory upper limb movement. Such sort of residual function-depend strategy of propulsive force is worth trying to characterize biomechanical features for a better understanding of the performance of wheelchair racing. In order to deeply and precisely understand the mechanisms underlying wheelchair racing, we developed a testing simulator that enables us to measure the torque of the wheel and adjust various settings (e.g., camber angle, axle position). This study aimed to characterize the strategies of wheelchair propulsion based on the biomechanical evaluation for a wide range of residual functions and skill levels in athletes of wheelchair racing.

METHODS

Six wheelchair racers with variated ages, classifications and proficiency participated in this study. We recorded the kinematics of the upper limbs and trunk with a motion capture system (Optitrack, NaturalPoint inc., 240Hz), and the propulsive force were obtained by torque meter (UTM II, UNIPULSE corp., 1000Hz) implemented on the axle of the custom-developed simulator. The electromyography was recorded from 8 muscles on each left and right torso and upper limbs (Trigno, Delsys inc., 1000Hz). The subjects were asked to perform 20 to 30 strokes of propulsion while keeping approximately 80% of maximal effort. Ensemble averaged waveform was obtained from a chosen 10 to 15 strokes from the recorded trials.

RESULTS AND DISCUSSION

Figure 1 shows kinematic and kinetic profiles during wheelchair propulsion obtained from five athletes with spinal cord injury. The hand-rim angle at the contact and release timing gradually altered not only with the level of injury/classification but also skill level. For example, two Paralympians showed dynamic motion and higher torque exertion with relatively deep propulsion until 7 o'clock.

CONCLUSIONS

Comprehensive biomechanical analysis for wheelchair racers enables us to understand an individual's strategy for wheelchair propulsion. Our developed system has potentials to reveal mechanisms underlying wheelchair propulsion and then give athletes/coaches useful into for their training.

ACKNOWLEDGEMENTS

This work was supported by the Japan Society for the Promotion of Science KAKENHI Grant Number 22K21263. We thank RDS Co., Ltd. and fuRo for the joint research/development of the wheelchair simulator.

REFERENCE

[1] Vanlandewijck, Y. et al. *Sports Med* **31**: 5, 2001.

	Age / Gender	Level of injury	Classification
Subj. A	26yrs / M	C6 Complete SCI	T51 (Beginner)
Subj. B	29yrs / M	C6 Incomplete SCI	T52 (Athlete level)
Subj. C	27yrs / F	Th11 Complete SCI	T54 (Athlete level)
Subj. D	51yrs / M	C7 Incomplete SCI	T52 (Paralympian)
Subj. E	50yrs / M	Th4 Complete SCI	T53 (Paralympian)

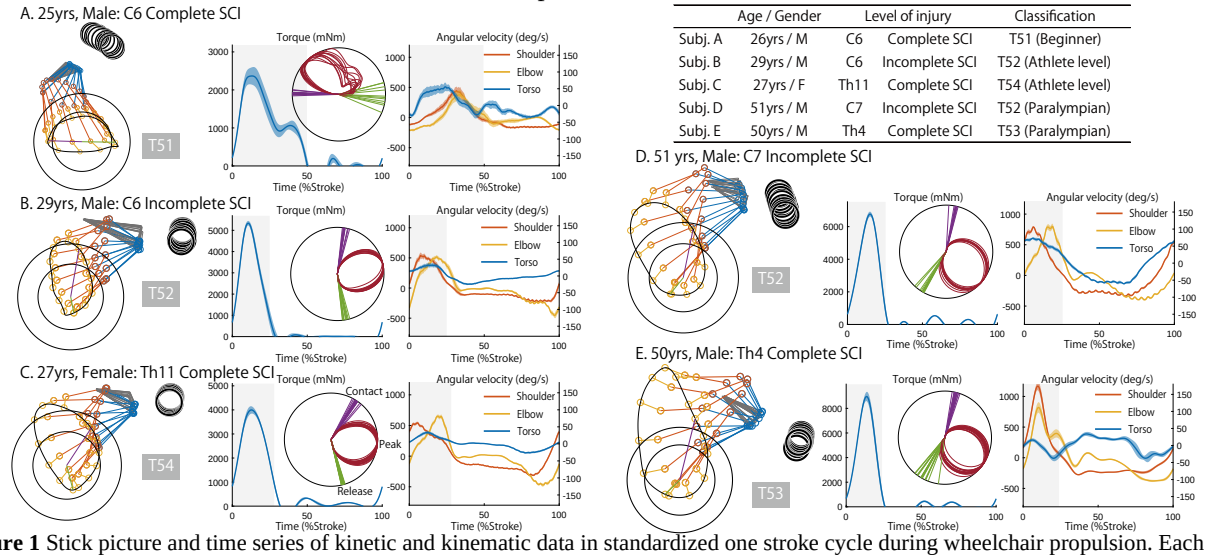

Figure 1 Stick picture and time series of kinetic and kinematic data in standardized one stroke cycle during wheelchair propulsion. Each stroke was divided into 2 phases, the push phase (a grey area) and the recovery phase. Circle diagrams suggest the hand-rim angle at the contact (purple), release (green), and torque exertion (red ellipse). Spinal cord injury, SCI.

INFLUENCE OF SEAT PAN ANGLE AND LOWER LEG STABILIZER ON LOWER LIMB MUSCLES ACTIVATION DURING SIMULATED SIT-SKI

Masashi Naoe[1], Shimada Yuji [2], and Ping Yeap Loh[3]
[1] Graduate School of Design, Kyushu University, Fukuoka, Japan.
[2] Department of Industrial Design, School of Design, Kyushu University, Fukuoka, Japan.
[3] Department of Human Life Design and Science, Faculty of Design, Kyushu University, Fukuoka, Japan
Email: py-loh@design.kyushu-u.ac.jp

INTRODUCTION

Individuals with lower limb disabilities may perform cross-country skiing in a sitting posture, where ski-skiers sit on a chair to perform a double-poling technique. In comparison to traditional skiing, chair design is considered as an important element that potentially influences the performance of sit-skiing. However, the research and development of cross-country sit skiing are hindered by the limited population. Previous studies recruited able-bodied to perform sit ski and, abled body and disabled body showed discrepancy and bias from ski economy and biomechanics perspectives [1,2,3]. Particularly, able-bodied is able to generate propulsion force from lower body even though in sitting posture [4]. In order to simulate sit-ski as similar as disabled body, this study investigated the effects of seat pan angle and lower leg stabilization on lower limb muscle activation (muscle onset) of hip flexors and extensors, namely rectus femoris and biceps femoris muscles during simulated sit-ski.

METHODS

Eight abled-bodied university male students belong to sports club were recruited for this study. This study was approved by Research Ethics Committee of the Faculty of Design at Kyushu University.

A ski ergometer (Concept2, USA) and a custom-made chair with an adjustable seat pan angle (0°, 10°, and 20°) and lower leg stabilizer were used to simulate double poling during sit-skiing. Next, surface EMG was recorded from the right rectus femoris and right biceps femoris muscles using surface bipolar active EMG electrodes (BA-U410m; Nihon Santaku, Osaka, Japan), which were amplified using a bio-instrumentation amplifier (BA1104m; Nihon Santeku, Japan), band-pass filtered (15-500 Hz), and full-wave rectified. The EMG data were A/D converted using a PowerLab 16/30 device (ADInstruments, New Zealand) and transmitted to a laptop computer. The participants were instructed to perform double poling in a total of seven conditions: standing and three seat pan angles (0°, 10°, and 20°) with lower leg stabilization conditions (with, without) (Figure 1a,b). The double-poling target was 50 strokes per minute with an output of 65 watts. Subsequently, EMG analysis period was set to 20 strokes after 30 s. Threshold-based method was utilized to determined muscle onset of both rectus femoris and hamstrings.

RESULTS & CONCLUSIONS

Both rectus femoris and biceps femoris showed activation during sit-ski (Figure 1c) at all seated condition. Additional muscle onset timing showed indicate the rectus femoris and bicep femoris were activated at double poling and recovery phase, respectively. Our results suggest that seat pan angle and without lower limb stabilizer could potentially minimize the muscles onset of rectus femoris but not biceps femoris.

ACKNOWLEDGEMENTS

The authors would like to thank the participants of the study for their participation.

REFERENCES

[1] Lajunen K et al. *Front Sports Act Living* **2**, 2020.
[2] Lindinger S.J. et al. *Eur J Appl Physiol* **111**:1103–1119, 2011
[3] Gastaldi L et al. Clin J Sport Med 22: 58–64, 2012
[4] Holmberg H-C et al. *Med Sci Sports Exerc* **37**: 807–818, 2005

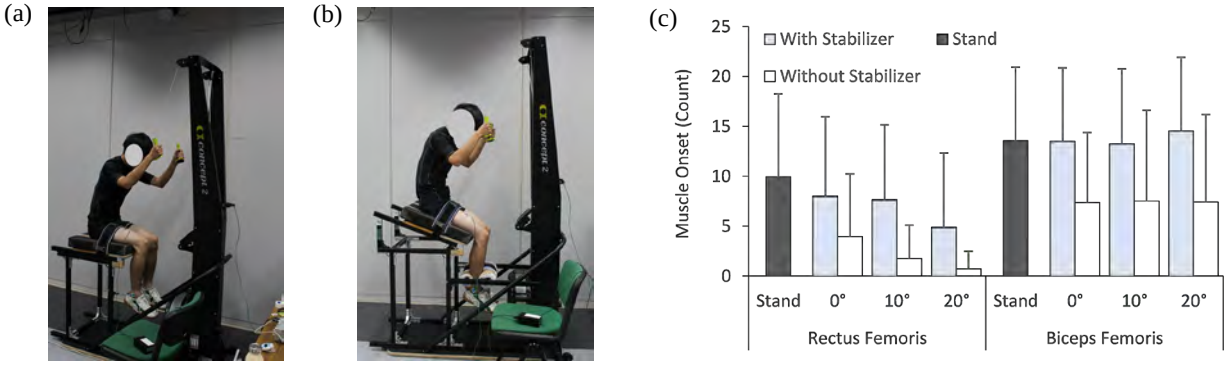

Figure 1 (a)seat pan 0° without stabilizer, (b) seat pan 20° with stabilizer, (c) muscle onset of rectus femoris & biceps femoris

SIZE DEPENDENT TRANSPORT DYNAMICS IN THE RAT ACHILLES TENDON

Jarod M. Forer[1,2], Yan Carlos Pacheco[1], Kait Link[1], Michael E. Hahn[2], and Nick J. Willett[1]
[1] Knight Campus for Accelerating Scientific Impact, University of Oregon, Eugene, Oregon, USA.
[2] Bowerman Sports Science Center, Dept. of Human Physiology, University of Oregon, Eugene, Oregon, USA.
Email: jforer@uoregon.edu

INTRODUCTION

The lymphatic system's capacity for clearing and recycling waste entities is essential in all aspects and stages of life. Near-infrared (NIR) imaging has been shown to accurately report lymphatic and vasculature fluid flow in an effort to better understand disease progression [1]. However, little is known about the *in vivo* drainage of tendons, especially Achilles tendons. Describing the size-dependent nature of drainage out of a region of interest is an essential first step in understanding the overall phenomenon of fluid transport, as shown previously in the rat knee joint [2]. This is exciting as previous work has demonstrated lymphangiogenesis to occur after injury to the Achilles tendon [3], meaning that a better knowledge of the mechanics at play can lead to future interventions in the healing process. We use an *in vivo* NIR imaging setup to compare the period in which the rat Achilles tendon clears out a lymphatic draining 20kDa PEG (Poly(ethylene glycol)) conjugated NIR dye, whose size prevents entry into blood vessels, to the drainage of NIR dye alone through the vasculature.

METHODS

Female Sprague-Dawley rats (Charles River Labs, 3-12 months old) received a 15µL intratendinous injection of either 20 kDa PEG conjugated with IR dye (n=5, 3 animals euthanized after 24 hours) or the IR dye alone (LI-COR, n=3) in one hind limb Achilles tendon. Subjects with missed injections were excluded. While under anesthesia, the subjects were imaged using an IVIS Spectrum (PerkinElmer) machine to measure the intensity of dye in the Achilles tendon region. At progressive timepoints after the injection (1, 3, 6, 24, 48, 72, and 96 hours), the subjects were once again anesthetized and imaged using the same settings to measure the intensity of dye remaining in the target region. The average radiance was calculated for an automatically generated freeform region of interest using the Living Image Software program (PerkinElmer) with a 4% threshold for all images. The radiance values were then normalized to the dye intensity at 1 hour. Calculations and data analysis were done in Prism (GraphPad).

RESULTS AND DISCUSSION

Normalized average radiance (the intensity of the dye remaining in the tendon space) is shown as a function of time after injection as both visualized and plotted data (Figure 1). The half-lives of the exponential fit lines to the data (2.98 hours for the conjugated dye, 2.19 hours for the dye alone) show that size-dependent clearance exists in the Achilles tendon space. Future studies involving histology of tissues and biodistribution of the dye are necessary. Experiments are also planned to observe the effects that exercise post-injection may have on the tendon space drainage kinematics in line with literature studying other regions [2]. Further, injury models may describe how lymphangiogenesis in the region might change the fluid transport properties.

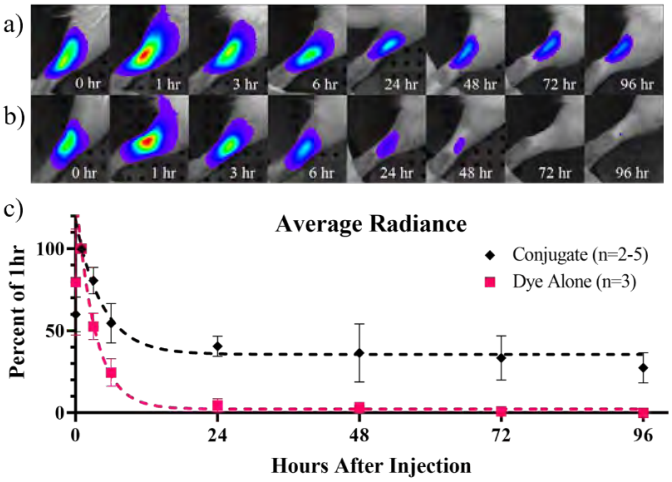

Figure 1: (a) Conjugate dye and (b) dye alone intensity decreasing over time in IVIS captures. (c) Average radiance of the two groups over time normalized to the value at 1 hour post injection.

CONCLUSIONS

In this study, we showed the rate and size dependency of biotransport of the rat Achilles tendon. Fluid transport of tendon tissue is a limited scientific space and the procedure described here helps lay the groundwork for future discoveries. Defining the kinematics of fluid transport is an essential first step to understanding the regenerative dynamics of tendons and potential interventions.

ACKNOWLEDGEMENTS

This material is based upon work supported by the National Science Foundation Graduate Research Fellowship under Grant No. 2022335756. The research is also supported by the Wu Tsai Human Performance Alliance and the Joe and Clara Tsai Foundation.

REFERENCES

[1] Weiler M et al. *J Biomed Optics* **17:** 066019, 2012.
[2] Bernard F et al. *J Biomed Optics* **26:** 126001, 2021
[3] Tempfer H et al. *Histochem and Cell Bio* **143:** 411-19, 2015

SENSITIVITY ANALYSIS OF FOUR GRAFT PARAMETERS ON KNEE KINEMATICS FOLLOWING PEDIATRIC ANTERIOR CRUCIATE LIGAMENT RECONSTRUCTION: A LINKED NEUROMUSCULOSKELETAL-FINITE ELEMENT MODELLING APPROACH

Ayda Karimi Dastgerdi[1], Christopher Carty[1,3], Azadeh Nasseri[1], Amir Esrafilian[2], Wayne Hall[1], Ivan Astori[3] and David John Saxby[1]

[1]Griffith Centre of Biomedical and Rehabilitation Engineering (GCORE), Griffith University, QLD, Australia
[2]Department of Technical Physics, University of Eastern Finland, Kuopio, Finland
[3]Department of Orthopedics, Children's Health Queensland Hospital and Health Service, QLD, Australia,
Email: ayda.karimidastgerdi@griffithuni.edu.au

INTRODUCTION

Optimizing anterior cruciate ligament (ACL) reconstruction (ACLR) surgery is an active research focus [1]. Given variations in graft insertion, pre-tension, type, and other parameters, the ACLR presents surgeons with many options to consider. Finite element (FE) simulations can provide insight into consequences of different surgical choices on post-operative knee biomechanics [2]. We developed a linked neuromusculoskeletal (NMSK)-FE model of the paediatric knee for pre-surgery planning. Here, we assessed the sensitivity of post-operative knee kinematics to four graft parameters: type, diameter, location, and pre-tension.

METHODS

For each of the four graft parameters, three variations were used, and consequently, 81 ACLR FE knee models were created based on the lower-limb geometry of an 11-year-old female acquired from magnetic resonance imaging. Three-dimensional motion (Vicon Motion Systems Ltd, UK), ground reaction loads (AMTI, Watertown, MA, USA), and 12 lower limb muscle electromyograms were acquired during walking. The FE boundary conditions and loading were estimated using OpenSim and calibrated EMG-assisted model, respectively. Knee flexion, abduction-adduction, internal-external rotation moments, and tibiofemoral and patellofemoral joint contact forces were used to drive FE models. Secondary knee kinematics (i.e., anteroposterior, and mediolateral femoral translations, abduction-adduction, and internal-external femoral rotations) were used to assess global sensitivity analysis through Sobol' indices at five timepoints across stance phase of gait.

RESULTS AND DISCUSSION

Figure 1 shows sensitivity of secondary kinematics to surgery parameters, which varies across stance. At foot contact, first order effects of the individual graft parameters on secondary kinematics were largest. As the knee progresses through stance, second order effects (i.e., surgical parameter interactions) on secondary kinematics increased in importance. Notably, graft type (i.e., gracilis, semitendinosus, and patellar tendon) had the highest first order effect on secondary kinematics compared to the other surgical parameters at certain timepoints. Graft diameter and location had the highest second order effects on secondary kinematics. The mediolateral translation is the secondary knee kinematic most sensitive to the variation in surgical parameters.

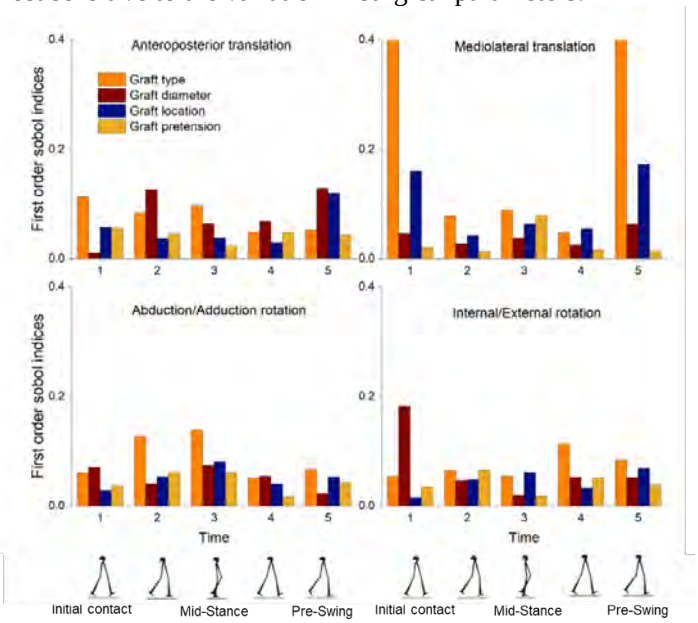

Figure 1. Global sensitivity analysis of four surgical parameters on the resulting secondary kinematics quantified by Sobol' indices for 5 timepoints of the stance phase of gait.

CONCLUSIONS

We used subject-specific FE models of the paediatric ACLR knee to assess the sensitivity of secondary knee kinematics to several surgical parameters. We found the effect of surgical parameters on secondary kinematics varies across the stance phase of gait. We will extend our analyses to encompass several additional patients with substantially different knee geometries for presentation at ISB 2023. This study will be the first comprehensive and practical sensitivity study examining the influence of paediatric ACLR surgical parameters on knee kinematics.

REFERENCES

[1] L. Benos, et al., Frontiers in Bioeng and Biotech, vol. 8, 2020.
[2] K. Halonen, et al., J. Biomech, vol. 49, 2016.

Effects of Different Carpal Tunnel Release Surgeries on Migration Patterns of Flexor Tendons

Hsiao-Feng Chieh[1,2], Chien-Ju Lin[1,2], Jyun-Da Lai[3] , Po-Ting Wu[4] , I-Ming Chou[5], Hsiu-An Chien[1], and Fong-Chin Su[1,2]

[1] Department of Biomedical Engineering, National Cheng Kung University, Tainan, Taiwan.
[2] Medical Device Innovation Center, National Cheng Kung University, Tainan, Taiwan.
[3] Department of Orthopedics, Tainan Municipal Hospital, Tainan, Taiwan
[4] Department of Orthopedics, College of Medicine, National Cheng Kung University, Tainan, Taiwan
[5] Department of Orthopedics, E-DA Hospital, Kaohsiung, Taiwan
Email: hfchieh@gmail.com

INTRODUCTION

Carpal tunnel syndrome (CTS) us a common disorder of the hand in clinics. For severe CTS patients, carpal tunnel release (CTR) surgery is recommended to decompress the median nerve by incising the transverse carpal ligament. Currently, the most adopted surgeries are open carpal tunnel release (OCTR) and endoscopic carpal tunnel release (ECTR). Recently, ultrasound-guided carpal tunnel release (UCTR) was developed with similar advantages of ECTR. Moreover, previous studies found the probability of Trigger Finger (TF) occurrence increased after transverse ligament release surgery.[1] However, the causes of the increased TF occurrence after different CTR techniques are seldom investigated. Thus, this study investigated the migration pattern of flexor digitorum tendon and the angle between the flexor tendon and the A1 pulley after UCTR and OCTR during different wrist angles to provide information about the risk of TF.

METHODS

Five fresh frozen cadaver hands were used in the experiments. In the experiment, the cadaver hand was secured to the customized frame in a palm-up posture and the wrist joint was mounted at the posture of neutral and flexion 30°, respectively. The index, ring, and little finger were fixed with splints in neutral position. The flexor digitorum superficialis (FDS) tendon of middle finger was applied 300 g and 500 g to simulate the finger motion at different force levels, and FDS tendons of index, ring and little fingers and flexor digitorum profrundus tendons of four fingers were applied 50 g each to maintain the tendon tension. UCTR, which can reduce the damage of anatomical structure in the carpal tunnel, was used in this study[2]. Images of tendon migration in the carpal tunnel and entrance angle at A1 pulley while applying force from 0 to 300/500 grams were recorded and measured with ultrasound transducer (TerasonTM). Friedman test were used to analyze the parameters of migrations between intact, UCTR and OCTR.

RESULTS AND DISCUSSION

Results of volar migration of FDS and changes of entrance angle at A1 pulley showed a tendency that with higher wrist flexion or increased applying force could cause higher volar migration and higher entrance angle after CTR, either OCTR or UCTR. In particular, the migration patterns of the FDS tendon of middle finger after OCTR at wrist neutral and flexion 30° and different force levels showed siginificant higher FDS volar migration comparing with intact condition. In addition, under lower applying force at wrist flexion 30°, a significant lower volar migration of FDS with UCTR was observed while comparing with those of OCTR. Therefore, UCTR might has a lower risk of inducing bowstring effect and developing trigger finger if operated under an appropriate load.

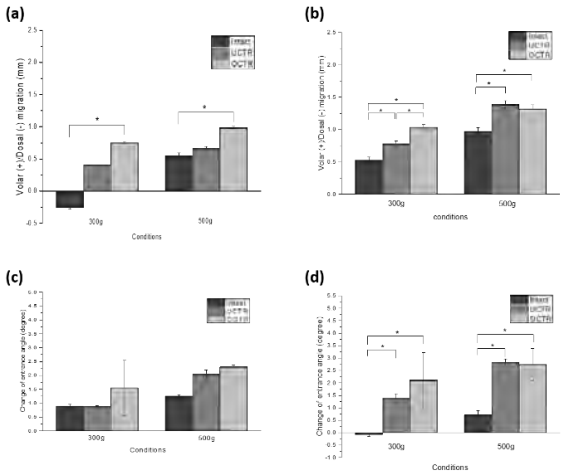

Figure 1 The volar migration at (a) wrist neutral posture and (b)wrist flexion 30˚; entrance angle of FDS at A1 pulley (c) wrist neutral posture and (d)wrist flexion 30˚ after different surgical treatments;

CONCLUSIONS

Our findings indicated that carpal tunnel release surgery strategy could influence the tendon gliding pattern in carpal tunnel and the entrance angle at A1 pulley. OCTR showed higher volar migration and change of entrance angle at each force levels and wrist postures indicated the higher risk inducing TF for CTS patients treated with OCTR than UCTR.

ACKNOWLEDGEMENTS

The study was supported by National Science and Technology Council in Taiwan (MOST 111-2635-E-006-002) and National Cheng Kung University and Show Chwan Health Care System (NCKUSCMH10715).

REFERENCES

[1] Lee, S.K., et al., J Hand Surg Eur, **39**: 694-698, 2014.
[2]Chern, T.C., et al., Arthroscopy, **31**: 2400-2410, 2015.

COMPRESSIVE FORCE INHIBITS EXCESSIVE VOLAR DISPLACEMENT OF THE FDS TENDON IN PATIENTS AFTER CARPAL TUNNEL RELEASE SURGERY

Chien-Ju Lin[1], Yi-Ching Chen[2], Hsiao-Feng Chieh[1], Li-Chieh Kuo[3], I-Ming Jou[4], Po-Ting Wu[5], Yen-Liang Lai[6], Chun-Ta Lai[6], and Fong-Chin Su [1,2]

[1] Medical Device Innovation Center, National Cheng Kung University, Tainan, Taiwan
[2] Department of Biomedical Engineering, National Cheng Kung University, Tainan, Taiwan
[3] Department of Occupational Therapy, College of Medicine, National Cheng Kung University, Tainan, Taiwan
[4] Department of Orthopedics, E-DA Hospital, Kaohsiung, Taiwan
[5] Department of Orthopedics, College of Medicine, National Cheng Kung University, Tainan, Taiwan
[6] Department of Orthopedics, Tainan Municipal Hospital, Tainan, Taiwan
Email: z10008088@email.ncku.edu.tw

INTRODUCTION

Carpal tunnel release (CTR) surgery is recommended for patients with severe carpal tunnel syndrome (CTS). However, volar displacement of the flexor digitorum superficialis (FDS) tendon increases due to absence of transverse carpal ligament restraint, which increases the potential incidence of trigger finger and affects hand function [1]. Clinically, therapists are eager to find solutions to prevent subsequent complications. This study aimed to elucidate whether compressive forces can attenuate the bowstring effect after CTR.

METHODS

15 healthy adults (age: 27±3.8 years) and 13 CTS patients underwent CTR surgery (age: 52±8.5 years) participated in the institutional review board-approved study. Tendon motion was recorded at the level of the metacarpophalangeal joint using an ultrasound system (ACUSON S2000, Siemens Medical Solutions) with a linear array transducer (6–18 MHz, 18L6HD). A load cell (MLP-25, Transducer Technique, Inc.) was used to adjust the compressive force applied to the carpal tunnel and to record changes in compressive fore and a custom-designed dynamometer was used to measure finger-applied torque. The target hand is secured to the support frame with the palm facing upward. The middle finger was maintained at 60° of flexion at the proximal interphalangeal joint. Maximal voluntary isometric contraction (MVIC) was performed with the wrist joint in a neutral position and 60° of flexion. Except for just contact force, 4N, and 8N of compressive force were additionally applied in CTS patients. Entrance angles of the FDS tendon and changes of compressive force were computed for further analysis.

RESULTS AND DISCUSSION

As shown in Table 1, significant differences were observed between the healthy condition and the CTS 4N condition and the healthy condition and the CTS 8N condition for both changes in entrance angle and compressive force. Compressive force of 4N and 8N significantly inhibited the volar displacement of the FDS tendon, which was reflected in a reduction in the change in the entrance angle in CTS patients. However, increased changes in compressive force might increase pressure in the carpal tunnel, which is detrimental for the median nerve. Under MVIC, compressive forces reached approximately 1.88 N and 3.58 N in healthy adults and CTS patients, respectively, due to the fixation of the load cell above the carpal tunnel, resulting in no significant difference in changes in entrance angle or compression force.

CONCLUSIONS

Compressive force of approximately 2N is able to inhibit excessive volar migration of the FDS tendon after CTR surgery.

ACKNOWLEDGEMENTS

The study was supported by National Cheng Kung University and Show Chwan Health Care System (NCKUSCMH10611), and National Science and Technology Council, Taiwan (MOST 104-2221-E-006-099-MY3).

REFERENCES

[1] Lee SK et al. *J Hand Surg Eur* **39**: 694-8, 2014.

Table 1: Average changes in the entrance angle of FDS tendon and compressive force

Conditions	Wrist Neutral				Wrist Flexed 30°			
	Healthy Just contact	CTS Just contact	CTS 4N	CTS 8N	Healthy Just contact	CTS Just contact	CTS 4N	CTS 8N
Change of Entrance Angel (degree)	1.52 (1.57)	1.28 (0.67)	1.01 (0.41)	0.95 (0.34)	2.25 (1.89)	1.56 (0.63)	1.27* (0.23)	1.10* (0.49)
Change of compressive force (N)	1.26 (1.18)	0.98 (1.49)	1.68 (1.25)	1.97 (1.71)	0.46 (1.03)	2.20 (2.08)	3.49* (2.40)	3.47* (1.85)

*significantly different from that of the healthy condition

Assistance of the paretic knee in the sit-to-stand motion of acute stroke survivors prevents their trunk overuse

Hiroki Hanawa[1], Keisuke Hirata[2], Taku Miyazawa [1]
[1] Department of Rehabilitation, University of Human Arts and Sciences, Saitama, Japan.
[2] Department of Rehabilitation, Tokyo Kasei University, Saitama, Japan.
Email: hiroki_hanawa@human.ac.jp

INTRODUCTION

Typical stroke survivors suffer from motor paralysis in their limbs. This makes it difficult for them to resist gravity and hold their posture. For example, in the sit-to-stand motion, they are unable to hold the squatting posture during the seat-off phase. Even in healthy elderly, almost maximum muscle strength is required at the knees for the seat-off. Therefore, chronic stroke patients transferred more mechanical energy from the trunk to the paretic knee [1]. This was viewed as a compensatory relationship between the less affected trunk and the paretic knee.

We hypothesized that (1) the compensatory relationship exists even in the acute phase of stroke, and (2) trunk compensations can be prevented by assisting the knee. The purpose of this study was to elucidate some of the validity of sit-to-stand exercises performed from the acute phase of stroke.

METHODS

The subjects were six acute stroke survivors. They were able to understand the study description, and signatures on a consent form were obtained. Small wireless inertial measurement units (IMU) and surface electromyography (sEMG) were used to measure their motion (both 1000Hz; Oisaka Electronics Co., Ltd.). The IMU was affixed to six locations on the body (thorax, pelvis, right and left thighs, and shanks). The electrodes of sEMG were affixed to seven muscles (right and left erector spinae, paretic gluteus maximus, long head of biceps femoris, vastus lateralis, tibialis anterior, and soleus). Subjects performed a sit-to-stand motion. The experimental conditions were two conditions: assisted and free knee joint hyperflexion prevention brace (90° restriction). We then converted the IMU data to segment angles and mechanical energy expenditure. The analyzed data were compared between the two conditions using a corresponding T-test. The significance level was set at $p = 0.05$.

RESULTS AND DISCUSSION

Mechanical energy expenditure in the thorax and pelvis up to seat-off was lower in the brace-assisted condition than in the free condition (both $p < 0.001$; Table 1). Activity in the paretic erector spinae was also smaller in the with assisted condition than in the free condition ($p < 0.001$; Figure 1). On the other hand, the posture (angle) of the six body segments was not significantly different at the start, at the end, or at seat-off.

Preventing hyperflexion of the knee resulted in decreased mechanical energy expenditure and erector spinae activity. Therefore, a compensatory relationship may have existed even in the acute phase of stroke. The fact that such assistance induces normal motor control could be a useful finding in clinical practice. On the other hand, since no kinematic changes were observed, evaluation by clinical observation is a future issue.

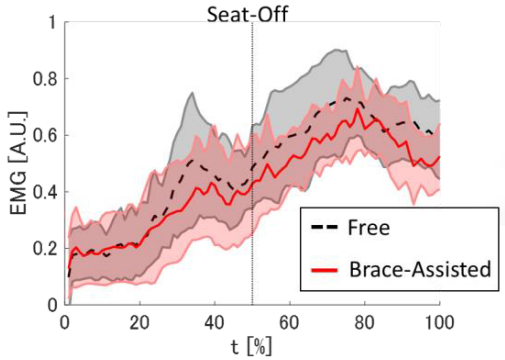

Figure 1 Muscle activity in the paretic erector spinae

CONCLUSIONS

After stroke, they adapt to motor paralysis from the acute phase and compensate with the less affected trunk. This compensatory relationship can lead to non-use of the paretic limb. The results of breaking this relationship by assisting their knee were clinically informative findings.

ACKNOWLEDGEMENTS

This work was supported by JSPS KAKENHI Grant Number 20K23260 & 21K17461,

REFERENCES

[1] Hanawa H et al. *Hum. Mov. Sci.* (In Press).

Table 1: Mechanical energy expenditure of trunk (thorax and pelvis)

	Brace-Assisted Knee Condition	Free Condition	*p-value*
Mechanical Energy of Thorax (J)	$22*10^{-4} \pm 29*10^{-4}$	$50*10^{-4} \pm 49*10^{-4}$	$p < 0.001$
Mechanical Energy of Pelvis (J)	$37*10^{-5} \pm 62*10^{-5}$	$13*10^{-4} \pm 15*10^{-4}$	$p < 0.001$

CLINICAL EFFICACY OF 3 DIFFERENT TYPES OF DIGITAL MIRROR THERAPY ON MOTOR AND DAILY FUNCTIONS IN STROKE SURVIVORS: A PRELIMINARY STUDY

Yu-Wei Hsieh[1*], Meng-Ta Lee[1] and Zih-Ming Syu[2]

[1] Department of Occupational Therapy and Graduate Institute of Behavioral Sciences, College of Medicine, Chang Gung University, Taoyuan City, Taiwan.

[2] Department of Physical Medicine and Rehabilitation, Lo-Sheng Sanatorium and Hospital, Ministry of Health and Welfare, Taoyuan City, Taiwan.

Email: ywhsieh@mail.cgu.edu.tw

INTRODUCTION

Stroke is one of the leading causes of death and disability worldwide. Upper-limb motor deficit is a common consequence after stroke, which causes difficulty in performing daily activities. Mirror therapy (MT), a promising and effective intervention for improving patients' functions, becomes the focus in stroke rehabilitation recently. Traditional MT provides visual illusions of the patient's normal intact hand movements as if it were the paralyzed one and generates mirror visual feedback (MVF) by using a mirror [1]. For optimizing the delivery of MT, we have developed an innovative digital MT system [2], which can provide 3 different types of MT in different MVF conditions and training modes: unilateral MVF with unimanual training (UM-UT), unilateral MVF with bimanual training (UM-BT), or bilateral MVF with bimanual training (BM-BT). The hardware of this innovative digital MT system includes a laptop, a computer screen, an adjustable monitor stand, and a webcam. This system has been programmed with modern web programming languages, including HTML5, CSS, and JavaScript, to administer multiple previews on a single webpage, to flip the preview horizontally, and to present a preview of the webcam and to record the webcam stream from the computer. This study aimed to examine the treatment efficacies of 3 different digital MT compared with traditional MT using a mirror box (Figure 1).

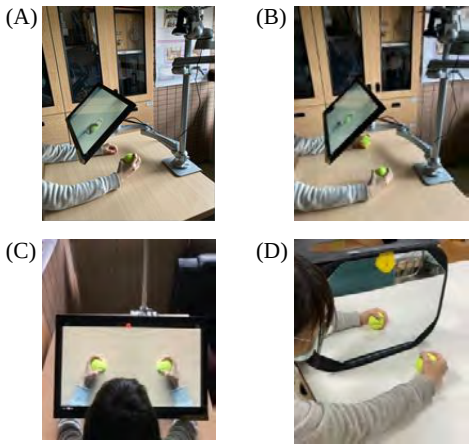

Figure 1 Conceptual illustration of 4 treatment groups: (A) uni-MVF condition and unimanual training (UM-UT); (B) uni-MVF condition and bimanual training (UM-BT); (C) bi-MVF condition and bimanual training (BM-BT); and (D) traditional MT using a mirror box.

METHODS

Twenty-two stroke patients were recruited and randomly allocated to 1 of 4 groups with a total of fifteen 1-hour therapy sessions. Outcome measures, including the Fugl-Meyer Assessment of the Upper Extremity (FMA-UE), Chedoke Arm and Hand Activity Inventory (CAHAI), and Motor Activity Log (MAL), were administrated at pre- and post-treatment. The nonparametric Kruskal–Wallis test and Wilcoxon signed-rank test were used, as appropriate.

RESULTS AND DISCUSSION

For the within-group changes, both the UM-UT and UM-BT groups had significant improvements on the FMA-UE-total and CAHAI scores. Additionally, the UM-UT and UM-BT had significant improvements respectively on the FMA-proximal and MAL scores. However, neither the BM-BT nor traditional MT groups did. For the between-group differences, no statistically significant differences but small to large effect sizes for different outcome measures were found. The preliminary results suggested that unilateral MVF with either unimanual or bimanual training delivered by the digital MT system showed significant within-group improvements in upper-limb motor and daily functions, and in the amount and quality of the affected arm and hand use in the real-world. However, more subjects need to be recruited to further validate the current results.

CONCLUSIONS

The preliminary study shows that the UM-UT and UM-BT groups of the digital MT system might be more promising as the alternative rehabilitation interventions for stroke survivors. Further large-scale study is suggested.

ACKNOWLEDGEMENTS

This work was supported by the National Science and Technology Council (NSTC 111-2628-B-182-009) and the Chang Gung Memorial Hospital (BMRPD25) in Taiwan.

REFERENCES

[1] Thieme H et al. *Cochrane Database Syst Rev* **7**: CD008449, 2018.

[2] Hsieh YW et al. *Sci Rep* **12**: 1868, 2022.

The effect of draw-in maneuver on knee joint function and thoracic kyphosis angle in patients with osteoarthritis of the knee

Y. Murakami[1,2], S. Ota[1,3], R. Fujita[3], H Ohko[3], S. Kawasaki[4]
[1]Graduate School of Health Care Studies, Seijoh University / Tokai, Aichi, Japan
[2]Department of Rehabilitation, Kamiiida daiichi General hospital / Nagoya, Aichi, Japan
[3]Department of Rehabilitation and Care, Seijoh University / Tokai, Aichi, Japan
[4]Fukinodai Orthopaedics Clinic / Tokai, Aichi, Japan
Email: yasuha.971009@gmail.com

INTRODUCTION

The knee adduction moment (KAM) is an index of mechanical stress during walking that affects the onset and progression of knee osteoarthritis (OA) [1]. Performing a draw-in maneuver (DI) during walking is a gait modification that reduces the KAM, but does not forcibly modify trunk or lower limb movements [2]. The long-term effects of this intervention, however, are not clear. To evaluate whether knee joint function would improve with a longer DI gait intervention in patients with knee OA.

METHODS

Studies were conducted in subjects aged ≥40 years with knee OA. A daily 20-minute DI gait was performed for 6 weeks. First, 10 minutes of DI gait instruction was given, and the normal posture and thoracic kyphosis angle during DI were measured at the beginning of the intervention. At baseline and after 6 weeks, we evaluated the Knee injury and Osteoarthritis Outcome Score (KOOS), knee pain, the MOS 8 item Short-Form Health Survey (SF-8), thoracic kyphosis angle, knee joint range of motion, knee extension muscle strength, hip abduction muscle strength, and activity level.

RESULTS AND DISCUSSION

Knee pain and the thoracic kyphosis angle were reduced in the 6-week pre- and post-intervention comparison (Table 1, Figure 1). No other parameters differed significantly after the intervention compared with baseline, and the implementation rate was 86±14%, with 20 minutes or more per day being 100%. In a previous study, it was reported that proper implementation of DI decreased thoracic kyphosis angle [3], increased muscle activity of the internal abdominal oblique, external abdominal oblique, and gluteus medius muscles in the first half of the stance phase during DI gait, and smooth center of mass to the stance side, resulting in decreased KAM [2]. In the present study, thoracic kyphosis angle decreased during DI posture, suggesting that DI was performed properly. The DI gait could be learned and practiced by patients with knee OA at an average age of 70 years. 20 minutes of DI gait per day decreased KAM during gait, which was thought to decrease knee pain. In addition, DI gait was effective in improving thoracic kyphosis.

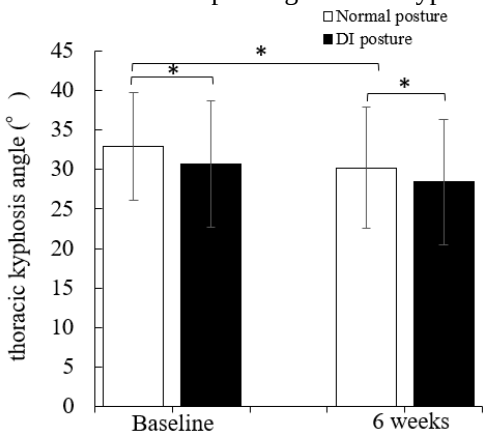

Figure 1 Effect of DI gait on the thoracic kyphosis angle.

CONCLUSIONS

After a 6-week intervention in patients with knee OA, KOOS and SF-8 scores did not improve significantly, but knee pain and thoracic kyphosis angle decreased. These results suggest that DI gait is useful as a gait modification for knee OA.

ACKNOWLEDGEMENTS

This work was supported by JSPS KAKENHI Grant Number 19H03970. The authors would like to thank the staff at Fukinodai Orthodaedics Clinic for their assistance in data collection and all the study participants for their contribution to the study.

REFERENCES

[1] Miyazaki T et al. Ann Rheum Dis **7**: 617-622, 2002.
[2] Fujita R et al. J Phys Ther Sci **33(4)**: 329-333, 2021.
[3] Ota S et al. J Phys Ther Sci **27(10)**: 3077-3079,2015.

Table 1: Effects of a 6-week DI gait intervention

	Baseline	6 weeks	P-value	Effect Size
VAS (mm)	41.5±2.14	33.1±24.6	0.03	0.47
KOOS (%)	59±16	63±13	0.07	0.95
SF-8 PCS	43.3±4.3	41.8±4.6	0.47	0.16
SF-8 MCS	49.2±7.5	51.2±7.1	0.43	0.17

VALIDITY AND RELIABILITY OF MOBILE APPLICATIONS IN PHYSICAL THERAPY: A SYSTEMATIC REVIEW

Ibiza Gonzaga[1], Keesha Bernice Blanco[1], Airen Margaret Magdalena[1], Agee Liezel Merquita[1], Dana Rae Santos[1], Kiara Nicole See[1], Tristan Isaiah Tolentino[1], Jannah Francine Tsai[1], Efren Louis Llanos[1], Cristine Rose Versales[1] and Ma. Roxanne Fernandez[1,2]

[1] Department of Physical Therapy, University of Santo Tomas / College of Rehabilitation Sciences, Manila, Philippines.

[2] Division of Health, Engineering, Computing and Science, University of Waikato / Te Huataki Waiora School of Health, Hamilton, New Zealand.

Email: ibizagonzaga@gmail.com

INTRODUCTION

The importance of the use of mobile applications in the health practice have grown increasingly over the years [1]. There is a need to assess if these applications can be validly and reliably used in the clinical setting as these are critical measures that evaluate the quality and effectiveness of a tool [2,3] to improve the delivery of health care in the physical therapy practice. This systematic review aimed to identify and synthesize existing studies on evidence of the concurrent validity and intra-rater, inter-rater, and test-retest reliability of mobile applications used in physical therapy.

METHODS

A literature search was conducted on nine databases: Web of Science®, PubMed®, Science Direct, Scopus®, Proquest, MEDLINE®, SPORTDiscus, and CINAHL on articles from inception to November 2021. Mendeley, Endnote and Rayyan were used for data management and screening. The methodological quality of all included studies was critically appraised using Brink and Louw Critical Appraisal Tool (CAT).

RESULTS AND DISCUSSION

Overall, 28 studies were included in the study (Figure 1). 17 articles assessed both validity and reliability, 10 assessed only reliability, and 1 assessed only validity. The apps were categorized into: apps for range of motion, balance, postural, sit-to-stand, and gait. Out of 28 studies, quality assessment scores show only 4 articles were considered poor quality, while 24 were considered good.

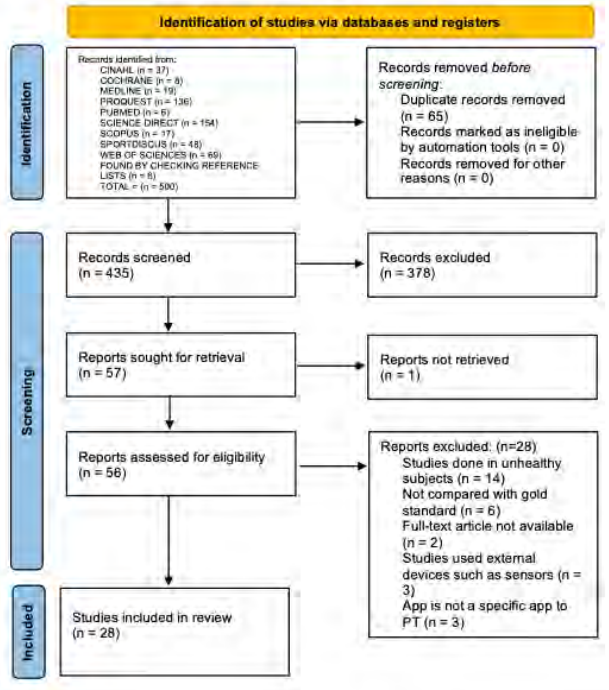

Figure 1 PRISMA Flow Diagram

CONCLUSIONS

A number of studies have demonstrated that mobile applications are valid and reliable for joint range of motion assessment, functional activity (i.e. sit to stand) and postural assessment. However, there was a wide range of results from mobile apps for measuring balance and gait; further research regarding their psychometric properties is needed.

REFERENCES

[1] Executive Board. *World Health Organization*. https://apps.who.int/iris/handle/10665/274134, 2017

[2] Atkinson G, Nevill A. *Sports Med* **26**: 4, 1998.

[3] Koo TK, Li MY. *J Chiropr Med* **15**: 2, 2016.

Change in ankle dorsiflexion motion during cycling generated by ankle assist ergometer

Keisuke Hirata [1,2], Hiroki Hanawa [3], Taku Miyazawa [2,3], Naohiko Kanemura [2], Kojiro Iizuka [4]
[1] Department of Rehabilitation, Tokyo Kasei University, Saitama, Japan.
[2] Graduate Course of Health and Social Services, Saitama Prefectural University, Saitama, Japan
[3] Department of Rehabilitation, University of Human Arts and Sciences, Saitama, Japan.
[4] Department of Machinery and Control Systems, Shibaura Institute of Technology, Saitama, Japan
Email: hirata-ke@tokyo-kasei.ac.jp

INTRODUCTION

During walking, motor commands coordinated between the joints in each leg (intralimb coordination) generate and contorol multi joint movement of leg [1]. By applying the underlying mechanisms of intralimb coordination, previous studies using split-belt treadmills (separated double-belt treadmills) have clarified the effect of changes in joint movement during walking on able-bodied people [2], [3] and patients suffering from movement disorders [4].

Ergometer training through cyclic movements such as walking can promote walking-like muscle activity and is associated with walking function improvement [5]. The common core hypothesis claims that upper- and lower-limb movements during walking, stepping, and ergometer exercises are controlled by a common rhythm and central pattern generator [6].

Our goal was to provide stimulation equivalent to a split-belt treadmill using an ergometer. We provided the same passive ankle joint motion at a specific crank angle per cycle during cycling movement using the Ankle Assit Ergometer (AAE) we developed. The purpose of this study was to verify the motor adaptation effect from before to after the passive assitance in the ankle joint motion on healthy young subjects.

METHODS

We developed the AAE by converted the pedals of a commercial ergometer into an ankle-assisting tool driven by a motor and brake. The AAE delivered ankle dorsiflexion assistance to 5 young adult participants from 90° after the top dead center until the bottom dead center of the crank angle during cycling. Electromyography (EMG) activity of the soleus (SOL) and tibialis anterior (TA) muscles was recorded bilaterally using surface electrodes (Trigno® Wireless System; DELSYS®, Natick, MA, USA). The opposite ankle angle was recorded using a goniometer (FAC-GM150; 4Assist, Tokyo, Japan). The recorded EMG and goniometer signals were digitized simultaneously along with the ergometer crank data.

The testing parameters were the dorsiflexion angular velocity (after - bofore) at the bottom dead center with ±25° and root-mean-square EMG activity (TA/SOL) at the bottom dead center with ±25°. To compare the results of ankle dorsiflexion muscle activation before and after assistance, we used a paired t-test between before and after assistance.

RESULTS AND DISCUSSION

We confirmed a significant difference in the ankle dorsiflexion angular velocity at the bottom dead center between before and immediately after assistance (after 2.52 ± 1.58, $p < 0.05$, figure 1 left). Moreover, we confirmed a significant increase in dorsiflexion muscle activation from before to immediately after assistance (before 1.18 ± 0.64, after 9.83 ± 6.06, $p < 0.05$, figure 1 right). These effects persisted after the removal of the assistance.

We confirmed the posssibility that the AAE activates the central pattern generator and induces motor adaptation of ankle movement by limb coordination during a motion cycle.

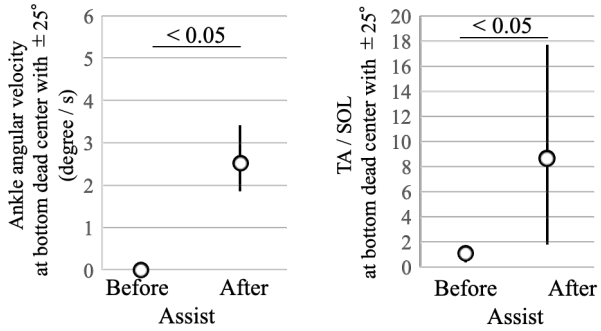

Figure 1 Ankle angular velocity and muscle activity before and after assistance

CONCLUSIONS

The developed AAE contributes to eliminating barriers to the clinical implementation of the rehabilitation tools delivering cyclic motion. As the next step, we are now going the application to stroke patients who have lost ankle joint motion.

ACKNOWLEDGEMENTS

[1]This work was supported by a Grant-in-Aid for Early-Career Scientists (20K19426) from the Japan Society for the Promotion of Science.

REFERENCES

[1] J. T. Choi et al., *Nat. Neurosci.,* 10, 8, 1055–62, 2007.
[2]R. Macalusoet al., *IEEE Trans. Neural Syst. Rehabil. Eng.,* 29, 508–516, 2021.
[3] U. Rashid, et al., *IEEE Access,* 7, 68469–68478, 2019.
[4] D. S. Reisman,et al., *Brain,*130, 7, 1861–1872, 2007.
[5] S. A. Kautzet al., *Neurorehabil. Neural Repair,* 19, 3, 250–258, 2005.
[6] E. P. Zehret al., *Exerc. Sport Sci. Rev.,* 33, 1, 54–60, 2005.

Virtual Reality Balance Training Improves Balance in Patients with Lumbar Spinal Stenosis: A Pilot Study

Po-Jung Chen[1], Phunsuk Kantha[1], Dar-Ming Lai[2] and Wei-Li[1,3*]

[1] School and Graduate Institute of Physical Therapy, National Taiwan University, Taipei, Taiwan.
[2] Division of Neurosurgery, Department of Surgery, National Taiwan University Hospital, Taipei, Taiwan.
[3] Physical Therapy Center, National Taiwan University Hospital, Taipei, Taiwan.
Email: wlhsu@ntu.edu.tw

INTRODUCTION

Lumbar spinal stenosis is a common degenerative condition and is often accompanied by pain and loss of balance. The common treatment methods for lumbar stenosis are rehabiltation exercise, and surgical intervention. In recent years, studies have shown that virtual reality (VR) training can help improve balance [1]. The aim of this study was to compare the balance ability of patients with unoperated lumbar spinal stenosis before and after VR skateboard training.

METHODS

The inclusion criteria of participants were 50-80 years old, diagnosed as patients with lumbar spinal stenosis and able to walk independently for more than 5 minutes. The measurement parameters included functional assessments and standing balance ability. The functional assessments included the Timed Up and Go test (TUG) and Five Times Sit-to-Stand test (5STS). To measure the quite standing balance ability, the center of pressure parameters such as mean distance, anteroposterior direction, and mediolateral direction on the force plate (Kistler 9286A, Kistler Instrument AG, CH) were used. The participants will receive virtual reality training for 6 weeks, 2 times a week, and 20 minutes each time (Figure 1). The content of the virtual reality training was skateboarding, and the hardware used HTC VIVE Pro (HTC Corporation, New Taipei City, Taiwan) and split belt treadmill (QQ-mill, Motekforce Link, The Netherlands).

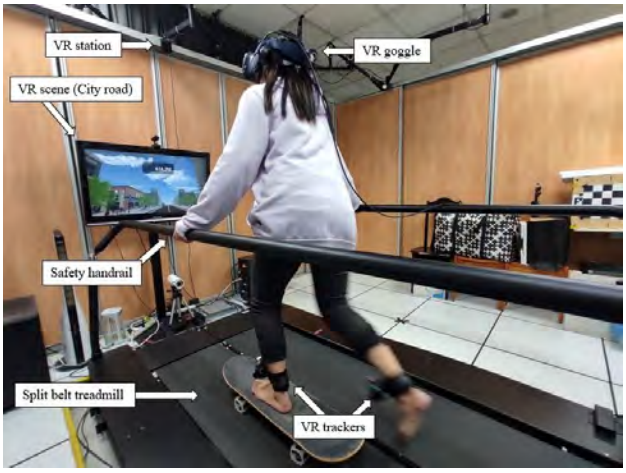

Figure 1 The VR skateboarding balance training system.

All data in this study were analyzed using IBM SPSS Statistics (19th Edition). The basic profile (age and sex) of the participants was analyzed by descriptive statistics. The Wilcoxon signed-rank test was used to compare differences within groups. Statistical significance level was set at p-value < 0.05.

RESULTS AND DISCUSSION

There are 4 participants (Age: 60.00 ± 9.40 years old), two males and two females in this pilot study. All functional assessments showed improvement, which represents an improvement in balance, but neither of them showed significant differences (Table 1). There are no significant differences in center of pressure parameters. Previous studies of virtual reality training have shown improvements in balance, and due to the small number of participants, it may be difficult to show statistical significance in this pilot study.

Table 1: The training results of No-surgery group

Measurements	Pre-training	Post-training	*p*-value
Functional assessments			
TUG (sec)	10.77 ± 3.71	9.23 ± 2.33	0.068
5STS (sec)	11.60 ± 4.79	7.10 ± 1.97	0.068
Center of pressure in quiet standing			
Total distance (cm)	0.38 ± 0.15	0.46 ± 0.22	0.465
AP distance (cm)	0.58 ± 0.29	0.56 ± 0.28	0.715
ML distance (cm)	0.23 ± 0.10	0.25 ± 0.10	0.465

AP / ML, in the anteroposterior / mediolateral direction.

CONCLUSIONS

Virtual reality skateboarding can improve balance performance in patients with lumbar spinal stenosis, and more patients will be recruited in the future to ensure the efficacy.

ACKNOWLEDGEMENTS

This work was supported by National Health Research Institutes (NHRI-EX112-11019EI), and National Science and Technology Council (MOST 111-2223-E-002-004-MY3) awarded to Dr. Wei-Li Hsu.

REFERENCES

[1] Kantha P et al. *Front. Bioeng. Biotechnol* **11**: 1136368, 2023.

Effect of increasing weight-bearing during the seat-off task with sit-to-stand training augmented feedback and epidural electrical stimulation in people with incomplete spinal cord injury: A preliminary study

Tzu-Ming Chang[1] Chich-Haung Richard Yang [1,2,3] Yu-Chen Chen[4] Ming-Yung Wu[4] Sheng-Tzung Tsai[2,4]
[1] Department of Physical Therapy; [2]Institute of Medical Sciences, Tzu Chi University, Hualien, Taiwan.
[3]Sports Medicine Center; [4]Department of Neurosurgery, Hualien Tzu Chi Hospital, Buddhist Tzu Chi Medical Foundation, Hualien, Taiwan
Email: 108317131 @ gms.tcu.edu.tw

INTRODUCTION

Functionally, increasing weight-bearing during the seat-off task is essential for patients with incomplete spinal cord injury (iSCI). It is logically associated with the assistance requiring momentum transfer during sit-to-stand (STS) and related to the ability to walk with minimal use of the upper extremities [1-2]. However, it is difficult for some severely neurological impaired patients to practice STS due to a lack of intrinsic feedback for movement control [3]. Recent literature has suggested that the mechanisms for the neuromodulation of epidural electrical stimulation (EES) combined with task-specific training may produce more substantial improvements in motor functions than functional electric stimulation [4-5]. Furthermore, some clinical studies have shown the effect of improving dynamic sitting balance and active standing with EES [5-6], but few studies investigated STS biomechanics with the EES intervention [4]. In this preliminary study, we aimed to examine the effect of increasing weight-bearing during the seat-off tasks with STS training augmented feedback and the EES in iSCI patients. We hypothesized that the patient's weight-bearing ability during the seat-off task would be enhanced after training, especially when EES turns on.

METHODS

One ASIA C subject at L2 level (age:54, BMI=27.47) undertook 16 sessions (2 days/week, total of eight weeks) of repetitive STS training & the EES. The dose of the training program is five times/ session, a total of 3 sets, with a rest period of 4-5 minutes between each set. The EES was turned on during the training. We instructed the subjects to sit on the customized body-weight support stand for safety and provided visual feedback (by two-bathroom scales) and verbal cues (by a trainer) to provide the loading feedback during training [3]. The vertical GRF and the three timing phases of STS (phase 1: the horizontal phase, phase 2: the transition phase, and phase 3: the vertical phase) were measured [7] as outcomes. We have measured both outcomes in both legs at on-off of EES condition in pre-training (0-week), 4-week, and 8-week STS training, respectively. The data showed mean ± standard deviation (SD) for the first peak force and slope and timing percentage for each STS phase.

RESULTS AND DISCUSSION

The result showed that the first peak force and slope gradually improved on the more affected leg, especially when EES was turned on; an increasing percentage was shown in phase 1, while there was no significance but variety in the percentage of phase 2 after training (Table 1). Previous studies have shown that some iSCI patients standing up with crutches [1] would reduce the trunk forward-leaning due to maintained balance and reduced weight-bearing during STS [2]. The results indicated that STS training augmented feedback contributed to the subject's weight-bearing control ability. Furthermore, the participant preferred a more 'trunk flexion impulse" strategy to stand up within the turn of EES, consistent with previous findings [5], showing that EES may enhance the reach performance in spinal cord injury.

CONCLUSIONS

STS training augmented feedback with EES could increase iSCI patients' weight-bearing ability. The effect of increasing weight-bearing by task-specific training with EES would be better than that using only EES protocol.

REFERENCES

[1] Khuna, L. et al. *Eur J Phys Rehabil Med* **53(4)**, 521-526, 2017.
[2] Saensook, W. et al. *Spinal cord* **56(3)**, 232-238, 2018.
[3] Nithiatthawanon, T. et al. *Spinal cord* **58(12)**, 1301-1309, 2020
[4] Hachmann, J. T. et al. *J Neurophysiol* **126(6)**, 1843-1859, 2021.
[5] Gill, M. et al. *Front Syst Neurosci* **14**, 79, 2020.
[6] Harkema, S. et al. *Lancet* **377(9781)**, 1938-1947, 2011.
[7] Nagasubramony A. et al. *European Conference on Cognitive Ergonomics*, April 26–29, 2021.

Table 1: The first peak force and slope of right leg, phase of STS between on-off of EES and before, after 4-week & 8-week STS training

		Pre-training	4-week off	4-week on	8-week off	8-week on
More affected leg	First peak force (%BW)	26.83 ±2.70	28.13 ±1.45	29.65 ±3.08	29.65 ±1.03	29.93 ±1.03
– Right leg	Slope (%BW/s)	148.93 ± 2.92	159.00 ± 3.38	170.06 ±18.51	169.06 ± 0.37	171.07 ± 4.31
Phase of STS	Phase 1 / 2 / 3 (%)	13 / 23 / 64	21 / 24 / 55	21 / 25 / 54	24 / 17 / 59	25 / 28 / 47

ACUTE EFFECTS OF DYNAMIC STRETCHING ON MUSCLE CONTRACTILE PROPERTIES OF ANKLE PLANTAR- AND DORSI-FLEXORS

Shuya Fukuoka[1], Kensuke Oba[2,3], Naoto Kyotani[1] and Mina Samukawa[2]
[1] Graduate School of Health Sciences, Hokkaido University, Sapporo, Japan.
[2] Faculty of Health Sciences, Hokkaido University, Sapporo, Japan.
[3] Department of Rehabilitation, Hitsujigaoka Hospital, Sapporo, Japan.
E-mail: syuya0127choco1219@eis.hokudai.ac.jp

INTRODUCTION

Dynamic stretching (DS) is commonly performed as a warm-up before playing sports. DS consists of repetitive motions throughout the joint range. Active stiffness is an outcome of exercise performance; however, no studies have shown active muscle stiffness with DS. Tensiomyography (TMG) is a non-invasive measurement device that assesses the contractile properties of skeletal muscles in response to electrical stimulation and can assess active stiffness. The purpose of this study was to investigate the effects of DS on the contractile properties of the ankle plantar flexors and dorsiflexors.

METHODS

Seventeen healthy males (22.0 ± 1.2 years) participated in the study. DS of the ankle plantar and dorsi-flexor muscles of the dominant leg was performed. The DS protocol consisted of four sets of 30 s, and 30-s rest was given in the standing position at a pace of 60 beats per min. The control condition was standing at rest for 210 s. Muscle contractile properties of the gastrocnemius medialis were measured using TMG (TMG-S1, TMG-BMC), a displacement sensor, and 5-cm diameter circular electrodes. Electrical stimulation was performed using a rectangular monophasic wave with a pulse duration of 1 ms. The stimulation intensity was gradually increased from 20 mA until the muscle radial displacement reached a plateau on the twitch response curve. From the maximal twitch response, the TMG parameters, which were maximal radial displacement amplitude (Dm), delayed time as the time from an electrical impulse to 10% of Dm (Td), contraction time as the time from 10 to 90% of Dm (Tc), and the index representing the velocity of contraction (Vc) as Dm divided by the sum of Td and Tc (Figure 1).

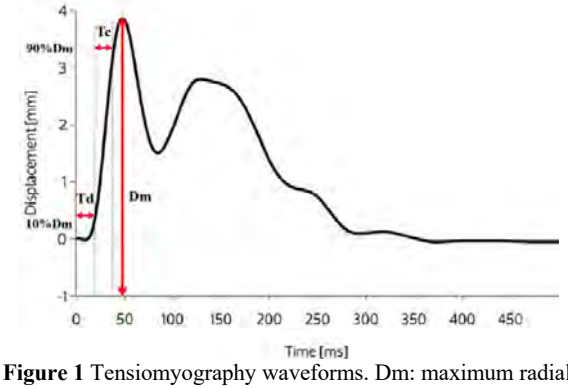

Figure 1 Tensiomyography waveforms. Dm: maximum radial displacement; Td: delayed time; Tc: contraction time.

RESULTS AND DISCUSSION

There were no significant main effects of condition, time, or interaction with Dm. There was a significant interaction for Td ($p < 0.01$). Post-hoc tests revealed that Td after DS was significantly lower than that before DS ($p < 0.01$). For Tc, a significant interaction was observed ($p < 0.05$). The post-hoc test revealed a significant decrease after DS compared with that before DS ($p < 0.01$). A significant interaction was observed for Vc ($p < 0.01$). The post-hoc test revealed a significant increase after DS compared with that before DS ($p < 0.01$). There was a significant decrease in delayed time (Td) and contraction time (Tc). A significant increase was observed in contraction velocity (Vc) after DS. A reduction in Td is indicated by an increase in muscle fibre conduction velocity. Hence, a decrease in Tc indicates an acceleration in the speed of force generation and an increase in Vc signifies an improvement in muscle performance [1, 2]. Increased muscle activity and jump performance after DS suggest an improvement in neuromuscular properties [3]. Muscle fibre conduction velocity is associated with muscle temperature [4]. It is inferred that neuromuscular properties were improved by an increase in muscle temperature after DS. Therefore, DS is effective in enhancing performance with changes in neuromuscular properties.

CONCLUSIONS

A significant reduction in delay and contraction time and a significant increase in contraction velocity were observed. These findings suggest that DS enhances neuromuscular properties without altering the mechanical muscle properties during contraction.

REFERENCES

[1] Simunič B et al. *Med Sci Sports Exerc* **43**: 1619-1625, 2011.
[2] Loturco I et al. *J Sports Sci Med* **15**: 483-491, 2016.
[3] Hough PA et al. *J Strength Cond Res* **23**: 507-512, 2009.
[4] Murakami K et al. *J Phys Ther Sci* **26**: 621-624, 2014.

CHARACTERISTICS OF TRUNK MUSCLE ACTIVITY IN CHILDREN WITH CEREBRAL PALSY DURING HORSEBACK RIDING –MULTIRESOLUTION ANALYSIS OF SEMG-

Kenichi Kaneko[1], Yoshiya Kawanori[2], Hitoshi Makabe [3], Kazuyuki Mito[4], Kiyoshi Yonemoto[5],
[1]Graduate School of Economics and Management System, Fuji University, Iwate, Japan
[2]Faculty of Social Welfare, Doho University, Nagoya, Japan
[3]Department of Physical Therapy, Juntendo University, Tokyo, Japan
[4]Department of Informatics, The University of Electro-Communications, Tokyo, Japan
[5]Faculty of Social Welfare, Iwate Prefectural University, Iwate, Japan
Email: kaneko@fuji-u.ac.jp

INTRODUCTION

Horseback riding therapy is one of the rehabilitation methods for spinal injury or brain damage. Our project team is studying to estimate for the benefits of horseback riding therapy in children with cerebral palsy (CP). The previous study showed the horseback riding therapy improved the gross motor function in the children with CP [1,2]. However little is known about the characteristic of activity of trunk muscles as the strategy of controlling the trunk posture during horseback riding. The purpose of this study was to estimate the characteristics of muscle activity pattern during the horseback riding from the view point of frequency domain of SEMG signals.

METHODS

The participants of this study were two low-birthweight children with CP (a 11-year old and a 3-month old girl, a 11-year old and a 3-month old boy, respectively) and two healthy children (a 10-year old and a 3-month old girl, an 9-year old and a 10-month old boy, respectively) as a control. Two subjects with CP had been receiving horseback riding therapy for over 9 years. The horseback riding therapy was approximately 30 minutes in duration and was performed once weekly in Iwate prefecture. SEMG signals were recorded simultaneously from eight trunk muscles during the horseback riding on the riding ground. A row SEMG signal was decomposed into five frequency bands (j = 1: 450-250 Hz, j =2: 250-125 Hz, j = 3: 125-62.5 Hz, j = 4: 62.5-31.25, and j = 5: 31.25-20 Hz, respectively) by the discrete wavelet transform [3]. Its wavelet transform coefficients were estimated by using the Daubechies-4 wavelet algorism and SEMG data of 512 points related to horseback riding. The activities of SEMG within the trunk muscle were compared by the values of the proportion of mean wavelet transform coefficient (%P_j).

RESULTS AND DISCUSSION

Figure 1 showed that the value of %P_j for the CP group at the low−frequency band (62.5-20 Hz) was smaller than that for the healthy group within the muscles of the lumbar region. The chi-square test for independence showed statistical differences of 1% for the muscles of the lumbar region. On the other hand, there was no statistical difference for the muscles of the cervical region. The activities of SEMG during horseback riding were different between the muscles of the lumbar region and the muscles of the cervical region. It was assumed that the spectral property of the surface EMG was altered by the volume conductor effects of the muscle fibers and the number of activated motor units (MUs). Recruitment strategies of lumbar region in children with CP might be higher MUs activities than the normal children during the horseback riding.

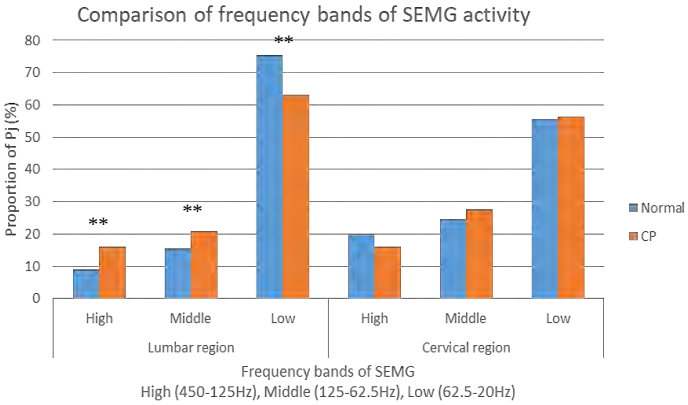

Figure 1 Comparison of frequency bands of SEMG activities. The mark ** indicates a significantly different level of 1 % of the chi-square test.

CONCLUSIONS

These results suggested that the characteristics of trunk muscle activities and the strategy of controlling the trunk posture during the horseback riding were difference between the children with CP and the healthy children. The activity of lower frequency of SEMG within the lumbar region might be suitable physiological index as an evaluation for the effect of horseback riding therapy.

ACKNOWLEDGEMENTS

This work was supported by KAKENHI (20H01709). We thank all the subjects who participated in the study.

REFERENCES

[1] Strashko EY et al. *Wiad Lek.* **69**: 527-9, 2016.
[2] Lucena-Antón D et al. *Complement Ther Clin Pract* **31**: 188-92, 2018.
[3]Kaneko K et al. *Gerontol Geriatr Med* doi: 10.1177/2333721420979800, 2020.

Statistical Shape Modelling and Reconstruction of Subject-Specific Foot Soles for Two-Point Discrimination Neuromuscular Sensory Tests

Yun-Chen Hsu[1], Mei-Ying Kuo[1], Tung-Wu Lu[2,3]

[1]Department of Physical Therapy, China Medical University, Taichung, Taiwan.
[2]Department of Biomedical Engineering, National Taiwan University, Taipei, Taiwan.
[3]Department of Orthopedic Surgery, School of Medicine, National Taiwan University, Taipei, Taiwan
Email: twlu@ntu.edu.tw

INTRODUCTION

Two-point discrimination (TPD) is the ability to consciously detect the minimum distance between two points on the skin, with the smaller distance indicating better acuity. This test has been administered in various ways, at multiple different body locations across a wide range of health conditions [1,2]. However, the test is time-consuming and lacked a reference standard for subject-specific TPD information for clinical examiners. By using the statistical shape model (SSM) method, the reconstruction of the subject-specific sole of foot shape and the TPD landmarks positions might be automated whilst improved in accuracy. The study aimed to propose an approach by SSM to predict personalized TPD landmarks based on the individual sole foot shape and provide a better understanding of the two-point discrimination sensation on sole of foot in healthy individuals.

METHODS

The training shape model was reconstructed from six out of twelve healthy subjects (age: 25.5±4.5 years, height: 1.7±0.1 m, mass: 63.5±12.0 kg, BMI: 21.9±2.2, foot length: 26.5 ± 1.1 cm) without any neuromusculoskeletal diseases in the lower limbs who participated in the current study. Twenty-one markers were equally distributed and attached to bony landmarks of the sole of the feet (i.e., head of first phalanx, navicular tuberosities, 5th metatarsal bases and heels). During the experimental procedure, each subject was asked to stand on the platform at the isocentre of a smartphone (iPhone 12 Pro, APPLE) camera's field of view. Subsequently, the subject-specific sole shape model and the TPD distribution landmarks were segmented from the mobile phone photograph after the camera calibration (Figure 1). All the training models were used to establish the correspondence trainset via Iterative Closest Point (ICP) registration and Coherent Point Drift (CPD) registration for reconstructing SSM-based sole shape models with TPD landmarks. These best-aligned models were used to analyze the shape differences with Principal Component Analysis (PCA) to obtain the shape coefficients and corresponding eigenvectors (i.e., top 7 in this study). The performance of the proposed SSM approach was evaluated using the leave-one-out cross-validation scheme. The reconstruction error of the two-dimensional model used the point-to-point mean error, and root mean square error (RMSE).

Table 1: Mean error and root mean square error of the leave-one-out cross-validation of the SSM-reconstructed model (unit: mm).

Mean Error	RMSE
2.44(0.77)	2.74(0.19)

RESULTS AND DISCUSSION

Mean errors and RMSE in shape accuracy of the leave-one-out-cross-validation of the subject-specific SSM-reconstructed models were 2.44±0.77 mm and 2.74±0.19 mm, respectively (Table 1). Submillimeter accuracies were found for all reconstructed subject-specific sole of foot shape models and the TPD landmarks by using the SSM approach. From the results, the accuracies of the two-dimensional (2D) shapes and TPD landmark positions showed high accuracies.

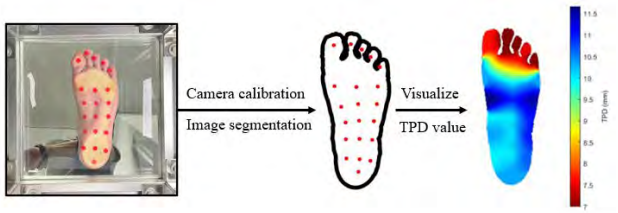

Figure 1 Experiment flowchart

CONCLUSIONS

The current study proposed a new approach that is able to reconstruct the 2D sole of the foot shape based on TPD landmarks. This approach may further set up a clear reference standard to assist clinical examiners in performing the clinical neurological assessments.

REFERENCES

[1] Ryan et al. BMC Musculoskeletal Disord. 15: 1-11, 2014.
[2] Won et al. J. Appl. Oral Sci., 25, 427-435, 2017

A SCOPING REVIEW ON EFFECTS OF EXERCISE TRAINING ON HAND DEXTERITY IN PATIENTS WITH PARKINSON

Ying-Ming Liu[1], Hsiao-Feng Chieh[2], Chien-Ju Lin[2]

[1] Division of Family Medicine, Sin Lau Medical Foundation, the Presbyterian Church of Taiwan, Tainan City, Taiwan

[2] Medical Device Innovation Center, National Cheng Kung University, Tainan, Taiwan

Email: z10008088@email.ncku.edu.tw

INTRODUCTION

Parkinson's disease is a common and complex neurological disease, which is also considered as a chronic, progressive neurodegenerative disease. The main clinical feature of Parkinson's disease is its characteristic motor symptoms. Major symptoms include rest tremor, bradykinesia, rigidity, and postural instability. In addition to Parkinson's disease, some other neurodegenerative diseases may also cause dopamine deficiency, leading to clinical manifestations similar to Parkinson's disease, so it is called Parkinsonism. Overall, motor symptoms in patients with Parkinson's disease tend to worsen as the disease progresses. Most previous studies have focused on examining lower extremity motor performance in patients with Parkinson's disease. However, it is inevitable that the movement disorders caused by Parkinson's disease are systemic, and the patient's hand function is also affected, which will become obvious in the later stage. Hand stiffness and tremor affect hand coordination, movement timing, fluidity of movement, and force control [1]. For patients with Parkinson's disease, dyskinesia is the symptom that most affects the functioning of daily life, but the number of previous studies related to upper limb rehabilitation is limited. Therefore, the aim of this review is to understand the effect of existing trainings on hand dexterity.

METHODS

The scoping review was based on a comprehensive literature search in PubMed, EMbase, Web of Science using key terms which included Parkinson*, hand function, dexterity, upper extremit*, upper limb*, fine motor, exercise*, and training. Studies were included if they (1)were written in English, (2)were original research articles, (3)randomly assigned the participants into groups, (4)recruited participants diagnosed with Parkinson's disease, (5)adopted exercise training for hands, (6)measured at least one outcome assessing hand dexterity, and (7)measured outcomes before and after intervention. Studies were excluded if the intervention was provided for only single session.

RESULTS AND DISCUSSION

Of the 290 studies retrieved from all databases, 8 studies met the criteria (Table 1). Five studies assess dexterity using Nine Hole Peg test, while three additional studies used the Purdue Pegboard test and Box & Block test. Different exercise types were adopted for intervention in these studies. According to one study, interactive video games for arm and hand exercises did not improve hand dexterity, despite improvements in game-playing performance. Other exercises including home-based dexterity exercise, virtual reality exergaming, Whqinxi exercise, Yang-ge dancing, and LSVT-BIG, have all improved hand dexterity in patients with Parkinson's disease.

Table 1: Exercises used for training in patients with Parkinson's disease

Study	Exercise type
Vanbellingen, 2017	Home-based dexterity exercise and Thera-band exercise
Allen, 2017	Exergames
Cikajlo, 2019	3D virtual reality and 2D non-immersive 2D exergaming
Wang, 2020	Wuqinxi exercise and stretching exercise
Choi, 2022	Task-based LSVT-BIG
Zare, 2022	Activity-based training and strengthening exercise
Hashemi, 2022	Upper limb virtual reality exercise
Li, 2022	Yang-ge dancing and conventional exercise

CONCLUSIONS

In recent years, there has been a growing body of research on exercise training to improve hand function in Parkinson's patients. From this review, we found that exercises involving finger movements have the potential to improve hand dexterity in people with Parkinson's disease. Therefore, there is still room for research to investigate which exercises, such as range of motion, stretching, coordination, and strengthening, will benefit patients more and make the outcomes durable.

ACKNOWLEDGEMENTS

The study was supported by National Science and Technology Council, Taiwan (MOST 111-2635-E-006-003).

REFERENCES

[1] Jankovic et al. *J. Neurol. Neurosurg. Psychiatry* **79**: 368-76, 2008

Towards crutch-less exoskeleton-assisted geriatric sit-to-stand motions – an experimental and optimization-based study

Jan C. L. Lau and Katja Mombaur
Canada Excellence Research Chair Human-Centred Robotics and Machine Intelligence, Systems Design Engineering and Mechanical & Mechatronics Engineering, University of Waterloo, Waterloo, Canada.
Email: jan.lau@uwaterloo.ca, katja.mombaur@uwaterloo.ca

INTRODUCTION

Most lower-limb exoskeletons are only powered along the sagittal plane and must be used with crutches for stability. To avoid falling backwards, users must push themselves forward with the crutches. Long-term crutch use can cause upper-limb joint deterioration [1], so a way to perform sit-to-stand (Sit2S) without crutches was investigated. A healthy young subject showed the possibility to do so even with motors disengaged, and the joint torques can be computed as a least-squares optimal control problem (OCP). The first goal of this study is to investigate Sit2S biomechanics with an exoskeleton. The second goal is to obtain the total required torques from least-squares OCP for the device to do crutch-less Sit2S with a frailer older adult, who cannot stand up by themselves and requires support.

METHODS

A healthy 25-year-old experienced TWIN user was recruited to perform Sit2S with the device under different conditions. Made for people with paraplegia, TWIN exoskeleton weighs 25 kg and has 4 active DOF in the hips and knees [2]. Biomechanics of Sit2S were observed at seat heights equal to and higher than the user's knee height. The following data, which are part of a larger experiment, are analyzed. Passive means the exoskeleton's motors are disengaged.

1. Active with crutches at seat height of 46 cm
2. Passive without crutches at seat height of 46 cm
3. Passive without crutches at seat height of 55.2 cm

Sit2S motions are recorded with the Vicon motion capture system. Forces exerted by crutches or feet are captured with Bertec force plates. Proven possible to use least-squares OCP to determine the required kinematics and actuation for exoskeleton walking [3], the OCP is formulated as a least-squares problem on Bioptim [4] to track Sit2S from cases 2 & 3. The system's state vector $[q\ \dot{q}\ \tau]^T$ contains joint positions $q \in \mathbb{R}^{13}$, joint velocities $\dot{q} \in \mathbb{R}^{13}$, and joint torques $\tau \in \mathbb{R}^{10}$. The controls are the first derivative of joint torques $u \in \mathbb{R}^{10}$. The model describes an elderly woman lumped with TWIN and assumes symmetry in the lower limbs. Translational position values are scaled to account for the height discrepancy between the reference data (young adult) and lumped model (older adult).

RESULTS AND DISCUSSION

In case 1, a peak combined crutch force of 330 N occurred when the subject is standing up. In cases 2 & 3, the subject first swings their arms forward and imposes a large trunk bend right before standing up. The vertical force exceeds the total weight of the human and TWIN, meaning that one must accelerate upwards to stand up from sitting. Table 1 shows the maximum torques at the xiphoid and lower limb joints in case 3, though upper-body joint torques are also computed. Full experimental results will be presented at the conference.

Table 1: Magnitude of maximum joint torque values at xiphoid, lumped hips, lumped knees, and lumped ankles in case 3.

	Xiphoid	Hips	Knees	Ankles
Torque (Nm)	34	130	109	47

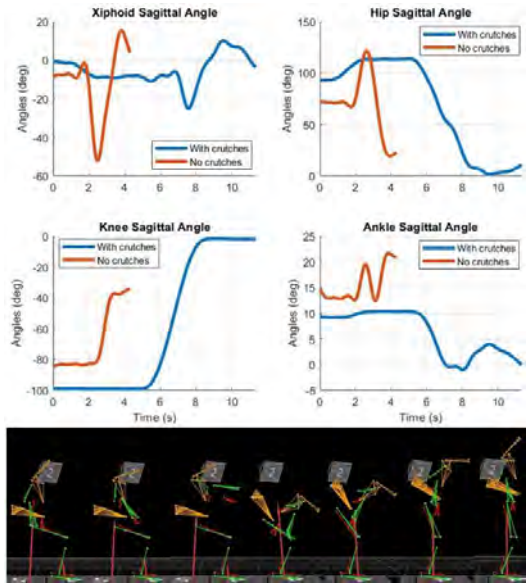

Figure 1 (Top) Joint angles of xiphoid, hip, knee, and ankle in cases 1 & 3. (Bottom) Motion capture recording of case 3.

CONCLUSIONS

The total torques computed would be the combined effort of the TWIN and older adult, and the split depends on the user's strength. This research is a preliminary step to obtain an optimal crutch-less Sit2S trajectory.

ACKNOWLEDGEMENTS

This research was undertaken thanks to funding from the Canada Excellence Research Chairs Program.

REFERENCES

[1] Opila et al. *J Biomech Eng*, **109**(4): 285-290, 1987
[2] Vassallo et al. *ICRA*, 1778-1784, 2020.
[3] Koch et al. *ICORR*, 113-118, 2015.
[4] Michaud et al. *IEEE TSMC*, **53**(1): 321-332, 2023.

A Usability Evaluation of the Powered-Wheelchair for severely Disabled in Korea

Eung-Pyo Hong[1], Yong-Cheol Kim[1], Dae-Jin Jang[1], Jungsun Kang[1], Yunhee Chang[1] and Ki-Tae Nam[1]
[1] Medical Convergence R&D Team, Rehabilitation Engineering Research Institute, Incheon, Korea.
Email: ephong@comwel.or.kr

INTRODUCTION

Powered-wheelchairs(PWs) have been provided to the disabled since 2005 trhough National Health Insurance Service(NHIS) in Korea. Accord to the survey, currently 5.9% of people with physical disabilities and cerebral palsy require PWs, but only 3.2% of people actually use PWs[1]. Many people have PWs but do not use them because they are not suitable for their physical conditions[2]. And this is due to the fact that most of the customized high-functioning PWs required for severely disabled people are expensive foreigh-made wheelchairs, so the purchase cost is excessive and maintenance and warranty services are limited. Accordingly, Rehabilitation Engineering Research Institute (RERI) is developing a powered-wheelchair with customized chairs, tilt, and recline functions for the localization of high-end powered wheelchairs. In this study, usability evaluation of the PW was conducted for the developed wheelchair in indoor and outdoor daily living environments.

METHODS

Ten people (60.4±15.0 years, 168.0±8.1cm, 73.5± 14.9kg) with spinal cord injury (Level C4~7) participated in this study and a sufficient explanation of the purpose and process of the study, voluntary written consent was obtained (IRB number of RERI-221108-2). The developed wheelchair can adjust the seat to suit the user's physical condition, and is equipped with tilt and recline functions. For usability evaluation, it was compared with commercially available wheelchair (KP-45.5, Karma Medical, Taiwan). The usability of the wheelchairs in daily life was evaluated in the living Lab of RERI. And the assigned tasks were performed according to driving scenarios in indoor and outdoor driving environments (carpets, rough roads, ramps, and obstacles). After completing all driving of a PW, the questionnaire was evaluated, and after sufficient rest, the evaluation of the next wheelchair was conducted. The questionnaire evaluation was conducted based on QUEST (Quebec User Evaluation of Satisfaction with assistive Technology) 2.0, usability evaluation of PW mechanical parts, and driving usability. The evaluation metrics were satisfaction with safety, adjustability, and convenience.

RESULTS AND DISCUSSION

As a result of device satisfaction of QUEST2.0, both wheelchairs showed relatively high satisfaction with an average of 4 points or more. And convenience showed similar satisfaction, but safety and operation & functionality were equally evaluated at 4.31 points, 3.5% and 7.9% lower than comparable products. As a result of the mechanical part, the stability was 4.21 points, 3.9% lower than the comparative product's 4.38 points, but the convenience was evaluated as 4.44 points, which was 19.4% higher than the comparative product.

Figure 1. Image of the wheelchair tests.

CONCLUSIONS

Localized powered-wheelchair showed high satisfaction with customized chairs, tilt and recline convenience. However, the wheelchair users who participated in the study had high manipulative proficiency, so there was a demand for finer control of the steering devices, and in the case of heavy users, there was a demand for a large torque at low speeds. In order to improve the control function and riding comfort in the future, we plan to improve the completeness of the product with the opinions of users presented in this usability evaluation and additional user monitoring.

ACKNOWLEDGEMENTS

This research was supported by the Assistive Technology R&D Project for People with Disabilities and the Elderly funded by the Ministry of Health & Welfare, Republic of Korea (#HJ20C0017).

REFERENCES

[1] 2020 Korea disability survey research report, Kim SH et al. *Korea Institute for Health and Social Affairs*, 2020.
[2] 2021 Cost-Effectiveness Analysis of Electric Wheelchair Distribution of Tilt Option, Kim JB et al. MPL Col., Ltd.

DEVELOPMENT OF AUTONOMOUS DRIVING SENSOR SYSTEM FOR WHEELCHAIR APPLICATION

Y.C.Kim[1], K.T.Nam[1], D.J.Jang[1], E.P.Hong[1]
[1] Rehabilitation Engineering Research Institute, Incheon, Korea.
Email: yckim@comwel.or.kr

INTRODUCTION

The purpose of this study is to develop an intelligent wheelchair that improves the convenience of operation to enable autonomous driving for indoor mobility support and daily life assistance in public facilities such as hospitals and museums for people with upper limb disabilities who lack wheelchair operation ability due to spasticity, tremors, and weakness. Especially, It is a study for optimizing sensor system equipment to improve autonomous driving performance and stability.

METHODS

A self-driving wheelchair is composed of RGBD(Intel REALSENSE D435), Webcam, 2D LiDAR(SICK TIM571) and RGBD for sensing rear driving environment. The self-driving wheelchair is composed of a wireless communication module(CNR-L600 Router) and a data processing device(Mini PC & Control power board Assembly) for environmental information processing and driving control. We check the problems through the track test of the autonomous wheelchair and the indoor driving test of the hospital, and carry out the complementary design to improve the performance.

RESULTS AND DISCUSSION

The self-driving wheelchair was tested in a track test simulating the indoor obstacle environment[3] and the driving test was conducted in the hospital indoor environment. The track test satisfies the driving safety without collision as a result of performance evaluation with a fixed obstacle, a movable obstacle, and a driving track of about 40m, which simulates a human model.

Figure 1 Autonomous driving Wheelchair Hospital Indoor Driving Test

In addition, it was confirmed that there is a problem in the detection of the movement obstacle in the front left and right diagonal direction in the driving test in the hospital room, and it is judged that the reason for this result is due to the limitation of the detection range of the RGBD located in the center. In addition, the table configured to locate the sensor in the center is inconvenient for the user to board, and it is judged that it is necessary to supplement the safety of the user against sudden stop or collision.

CONCLUSIONS

The use of the table is excluded for the boarding discomfort solution and safety assurance of the wheelchair user. In order to at the same time sense the dead zone and front of right and left to supplement the square of the front driving environment sensitive area RGBD of 2 is constituted in right and left. At this time, the 2D LiDAR is configured on the opposite side to which the controller is attached. Through this configuration, it is possible to prevent the accident risk by increasing the recognition performance of the movement obstacle in the diagonal area as well as the front.
yckim@comwel.or.kr

ACKNOWLEDGEMENTS

This study was funded by the government and supported by the R & D Center of the Ministry of Health, Labor and Welfare (Project No. 9991006832, KMDF_PR_200901_0162)

REFERENCES

[1] K.T. Nam et al. kspe_21AP04-004, 2021.
[2] Y.C. Kim et al. kspe_21AP04-005, 2021.
[3] K.T. Nam et al. kspe_22APP09-025, 2022.

Performance and Usability Evaluation of an Intelligent Wheelchair

Ki-Tae Nam[1], Yong Cheol[1] and Eung-Pyo Hong[1]
[1] Medical Convergence R&D Team, Rehabilitation Engineering Research Institute, Incheon, Republic of Korea.
Email: nkt798@comwel.or.kr

INTRODUCTION

The Intelligent Wheelchair combines robotic technology with conventional electric wheelchairs to provide autonomous driving to a destination with a robotic function, while allowing joystick steering like conventional electric wheelchairs. People with severe disabilities may not be able to use their upper limbs properly, making accurate joystick steering impossible. Therefore, an intelligent wheelchair is required. The Rehabilitation Engineering Research Institute (RERI) is designing and developing an intelligent wheelchair with autonomous driving function. In this study, the autonomous driving performance and usability evaluation were conducted on the developed intelligent wheelchair.

METHODS

The autonomous performance evaluation was conducted in accordance with the recently written standard "The Performance Evaluation of Autonomous Navigation for Powered Wheelchair". The test route was divided into two sections: the first section was a complex 2-meter-wide corridor with fixed obstacles. In the second section, four different types of moving obstacles were placed. The total length of the two sections is approximately 40 meters [1].

For the usability evaluation, six rehabilitation professionals (therapists, etc.) (31.5±8.5 years, 173.7±9.4 cm, 71.1±13.3 kg) participated in the study and provided full explanation of the study purpose and process and voluntary written consent (IRB number KCIRB-2022-0011). Tasks were created based on usage scenarios, and subjects performed tasks on the intelligent wheelchair for approximately 60 minutes. The results were collected and the subject's subjective feedback was obtained. The tasks consisted of two tasks to read and understand the product's user manual and four tasks to use the actual wheelchair.

RESULTS AND DISCUSSION

In the autonomous performance evaluation, the wheelchair completed 200 laps around the constructed track and avoided all obstacles and collisions during the test.

In the usability evaluation, the task of understanding the user manual was mostly trouble-free, while the task of operating the wheelchair often caused problems when driving the designated route (about 22.2%).

Figure 1 Designed and developed intelligent wheelchair

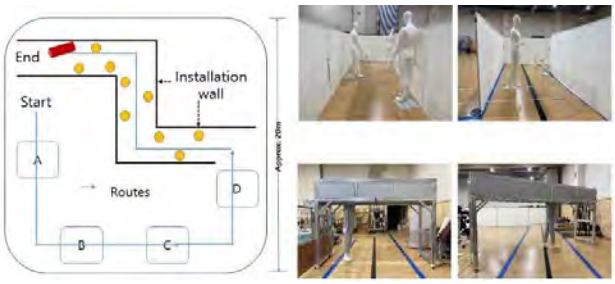

Figure 2 Autonomous Driving Performance Evaluation Track

CONCLUSIONS

Although the autonomous driving performance and safety of intelligent wheelchairs were satisfactory, they were often difficult to operate due to the complex user interface. Considering that the actual users of intelligent wheelchairs are severely disabled, there were many comments that a more intuitive and easy interface is needed. In addition, there were many comments that the table placed in front of the wheelchair made boarding inconvenient. In future studies, we plan to improve the product through additional user monitoring and feedback from usability evaluations.

ACKNOWLEDGEMENTS

This work supported by the Korea Medical Device Development Fund grant funded by the Korea government (the Ministry of Science and ICT, the Ministry of Trade, Industry and Energy, the Ministry of Health & Welfare, the Ministry of Food and Drug Safety) (Project Number: 9991006832, RS-2020-KD000162)

REFERENCES

[1] K.T.Nam et al. *Proc. of the KSPE Spring Conference*: 305, 2022.

A New Coupling Mechanics Model for Lower Limb Exoskeletons to Account for Initial Surface Forces

Christian Mele[1], James Tung[1], Katja Mombaur [1,2]
[1] Mechanical and Mechatronics Engineering, University of Waterloo, Waterloo, Canada.
[2] Systems Design Engineering, University of Waterloo, Waterloo, Canada.
Email: cmele@uwaterloo.ca

INTRODUCTION

Lower-limb exoskeletons are medical devices that aid in the ambulation of individuals with limited lower-limb mobility. To provide ambulatory assistance, force must be transferred from the exoskeleton to the user through coupling interfaces. These interfaces vary between devices and may contain materials that are rigid, soft, or a combination of the two. To predict and control the trajectory of the leg, the coupling mechanism must be well characterized [1].

Soft coupling mechanics are often represented as simple linear spring-damper systems that require experimental tuning or estimation to determine the coefficients. The least-squares fitting process leads to poor performance when predicting surface forces [1,2]. Recent studies also indicate initial strapping conditions influence reported coefficients [3]. This preliminary study details a new method of fitting spring coefficients in a piecewise approach for least squares approximation that does not sacrifice the simplicity and approachability that linear fitting provides.

METHODS

A case study was conducted to validate results from commonly used coupling models against experimental kinematic and force data collected at the exoskeleton's interface. We used a custom-made 3D printed mannequin leg to guarantee full predictability of the leg's behavior and the H3 exoskeleton (Technaid, Spain). VICON motion capture and Tekscan force-sensitive resistor (FSR) arrays were used to collect kinematic and force data, respectively (Fig. 1, bottom-left). Two models were simulated; the first operated using perfectly coupled assumptions (i.e. the mannequin leg and exoskeleton are assumed to move in union as one rigid body) and the latter assumed that the interface was represented by linear spring-damper.

A new framework of analysis was developed using results of this study to design a new simple spring-damper coupling equation, motivated by initial coupling forces and their influence on dynamics.

RESULTS AND DISCUSSION

Figure 1 (bottom-right) details the driving interface forces of recorded, commonly used linear-spring damper, and proposed coupled spring-damper. When in static contact, an initial pressure was observed that, a linear spring-damper model could not replicate. Figure 1 (top-center), highlights the difference between the old model and newly proposed model. This new model allows for initial coupling to influence mechanics.

The proposed model treats the system as starting initially coupled as a function of the combined spring coefficients. Separation occurs when the compressed surface reaches a displacement equal to the initial compressed length of the opposite surface, allowing for 4 total discrete phases (as opposed to the usual 2). When separation occurs, the system switches and is equivalent to the "Old" linear spring-damper. Dampening coefficient influence remain the same. Characterising this equation is slightly more complex, as direction is no longer the sole indicator for calculating coefficients. The simulated pseudo-static proposed model followed much closer to the recorded spring-values but could not account for drift likely caused by frictional influence.

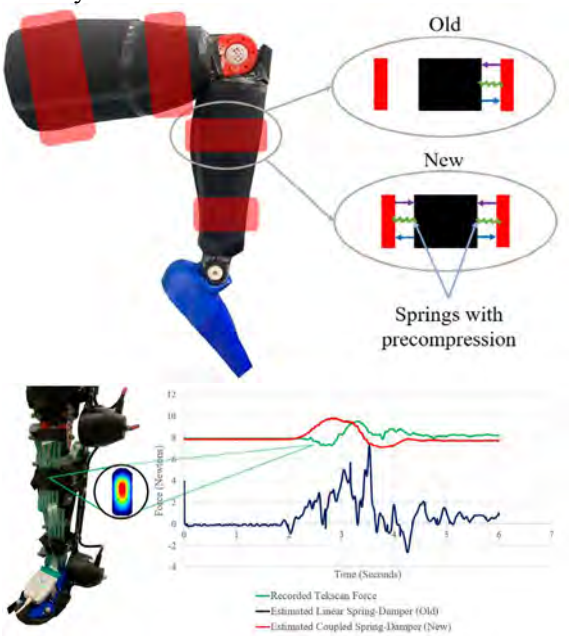

Figure 1 Graphic detailing the Proposed Coupled Spring-Damper model with loaded pre-compression against common models (Top). Testbench sensor setup (bottom-left). Recorded Tekscan force (Green) compared against highly stiff linear spring damper (Blue), and the proposed Coupled Spring-Damper (Red), (bottom-right).

CONCLUSIONS

The models used often in the characterisation of exo-user interactions lack the ability to describe non-linearities caused by initial coupling forces. The newly proposed model maintains the simplicity of linear spring-dampers, with consideration of multi-contact and single-contact stages to more accurately model force.

REFERENCES

[1]Massardi S. et al. *Sensors* **22,** no. 11: 3993, 2022.
[2]Mele C. et al. *WCB* **22**
[3]Langlois K. *et al*. *IEEE* **vol. 3**, no. 1,146-155, 2021.

Biomechanical Evaluation of Difference Between Customized Angled Abutments and Commercial Angled Abutment for Dental Implant in Maxillary Incisor Region

Heng Li Huang[1], Chih Ching Chi[1], Yen Wen Shen[1,2], Lih Jyh Fuh[1,2], Jui-Ting Hsu[1]
[1] School of Dentistry, China Medical University, Taichung City, Taiwan.
[2] Prosthetic Dentistry Department, China MedicalUniversity Hospital, Taichung City, Taiwan.
Email: henleyh@gmail.com

INTRODUCTION

Angled abutment is often required to achieve good esthetic and biomechanical function in immediate implant placement especially in the maxillary incisor region. In this study, finite element analysis and an in vitro experiment were used to investigate the biomechanical effects of the angled abutments with customized angles and the commercial 15°angled abutment in implant and surrounding bone in the region of maxillary incisors.

METHODS

The customized angles for angle abutments was referred from another clinical study by measuring the cone-beam computed tomography (CBCT) images of inclination angle of the incisors and lateral incisors from Taiwanese population from China Medical University Hospital (CMUH108-REC3-168). Therefore, there are four kinds of customized angled abutments (21.9°, 24.15°, 20.22°, 33°) were analyzed including all patients, patients under 20-23, 24-39 and 40-65 years old as compared with a commercial 15°angled abutment. The 3D models of customized angled abutments and a commercial 15°angled abutment were constructed by computer aided design software. For the 3D maxillary bone models, they were created from CBCT images of patients with medical imaging software. Then the computer simulation-finite element analysis (FEA) and in-vitro strain gauge experiment were employed with applying 100N or 50N of a axial force or an oblique force to evaluate the difference in stress/strain values of implant and surrounding bone between customized angled abutments and a commercial 15°angled abutment.\

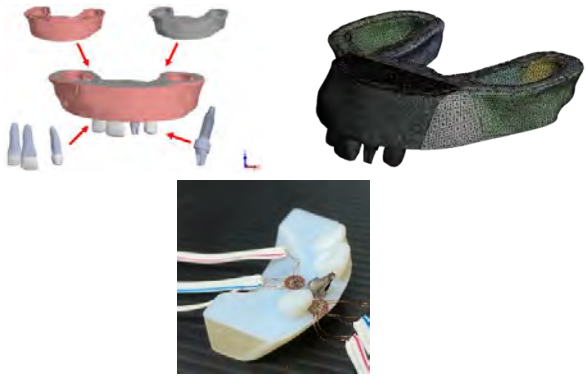

Figure 1. The left figure is the CAD models of maxillary bone (including cortical bone and cancellous bone), tooth and dental implant (including angled abutment and fixture) and the right figure is the mesh model for FEA. The middle figure is the sample for in-vitro strain gauge experiment.

RESULTS AND DISCUSSION

For the results of FEA, in the axial loading, because the angles of the customized angled abutments (21.9°, 24.15°, 20.22°, 33°) are relatively higher as compared with the commercial 15°angled abutment, the stress value in the dental implant and surrounding bone were also higher. However, in oblique loading the commercial 15° angled abutment showed higher stress value in implant and bone. For the results of the vitro experiment, there is no statically difference in bone strain between the customized 21.9° and the commercial 15° angled abutments. Nevertheless, in the oblique loading the use of a commercial 15°angled abutment induced the higher maximum and minimum principal bone strains.

Table 1. Maximum von-Mises stress of cortical bone, cancellous bone and implant under two kinds of loading conditions. (unit: MPa)

	Loading type	Abutment Angle	Cortical bone	Cancellous bone	Implant
All	Axial loading	15°	42.6	3.0	94.5
		21.9°	51.6	3.3	130.8
	Oblique loading	15°	55.8	4.2	327.2
		21.9°	51.1	4.0	223.3
20-23	Axial loading	15°	20.2	2.7	76.4
		24.15°	23.6	2.7	151.9
	Oblique loading	15°	38.1	3.3	301.5
		24.15°	37.8	3.1	204.0
24-39	Axial loading	15°	29.1	4.2	79.1
		20.22°	26.9	4.2	126.8
	Oblique loading	15°	43.4	4.3	302.3
		20.22°	45.0	4.1	201.1
40-65	Axial loading	15°	29.4	3.1	74.6
		33°	38.8	3.6	193.3
	Oblique loading	15°	116.79	7.69	400.1
		33°	100.23	6.89	223.4

CONCLUSIONS

The customized angled abutment show lower stress/strain in implant and surrounding bone in the oblique loading, but in the axial loading a commercial 15° angled abutment present higher stress/strain. It looks like that in terms of biomechanics, there seems to be no absolute benefit for using a customized angle abutment, and it is still related to the direction of the occlusal load.

ACKNOWLEDGEMENTS

This study was supported by the government organizations-Ministry of Science and Technology (Grant Nos. MOST 109-2221-E-039-002-MY2 & MOST 111-2221-E-039-008-MY2) in Taiwan.

GENERALISED LIGAMENT MODEL FOR FINITE ELEMENT MODELLING OF THE KNEE

Luca Kiener[1], and Michaela Nusser[1]
[1] Biomechanical Engineering, Zurich University of Applied Sciences/Institute of Mechanical Systems, Winterthur, Switzerland.
Email: luca.kiener@zhaw.ch

INTRODUCTION

A general ligament model for the tibiofemoral joint would pave the way for the use of finite element (FE) models in preoperative planning software as well as for the development of future implant designs for a variety of knee geometries. The aim was to develop a general ligament model applicable to knees from different specimens.

METHODS

A FE model of the knee was developed by segmenting MRI images containing the 3D geometries of the anterior and posterior cruciate ligaments (ACL, PCL) and the medial and lateral collateral ligaments (MCL, LCL). Beidokhti et al. [1] showed that modelling the ligaments as a continuum leads to more accurate contact modelling, which is important for the analysis of knee prostheses. The material model of the ligaments was a multilinear elastic model based on a tensile test on a LCL with a variable strain offset as calibration parameter. In addition, an initial strain was assigned to the ligaments to avoid compressive forces and provide stability to the knee. A holistic approach to the ligament model was to consider the ligament forces, which is the ligament's output affecting the tibiofemoral joint kinematics. Thus, the goal was to determine a set of forces as a general ligament model. Since there was only one calibration parameter per ligament, namely the strain offset, only one force value could determine this parameter. The target force for each ligament was defined during knee flexion from 0° to 90°. To obtain meaningful calibrating forces, they were selected in a position where the forces were high. The force set was based on seven different knee FE models that were independently calibrated based on robotic laxity testing of knee cadavers. The target forces were then applied to six new FE models.

RESULTS AND DISCUSSION

For the ACL, the LCL and the MCL, the calibration forces were defined at 0° flexion and were 15N, 49N and 23N, respectively. For the PCL, the force was 35N at 90° flexion. The target forces were iteratively calibrated for each FE model. Interestingly, the ligaments can exhibit large differences in forces at the flexion angles other than the one of calibration (Figure 1). There are several factors which may influence the behaviors of the ligaments. One factor being that the geometries of the ligaments may vary due to subject-specific differences and the challenges of proper segmentation. The definition of attachment points can also have an influence, as the definition is also subjective to a certain extent. Another factor is that the ligaments have different initial positions depending on the flexion angle during the MRI scan. A possible influence is also the position of the ligament within knee which means that for example larger knees produce a larger lever arm for the ligament. Although the calibrated force may be the same for the ligaments, the stresses in the ligament are higher the smaller the cross-section of the ligament is. This means that thinner ligaments have higher stresses and produce higher forces more quickly due to the curve behaviour. This may be a factor which determines if knee is generally stiff or loose. A viable strategy for preoperative planning would be to have a generative ligament geometry because segmenting the geometry is a time intensive procedure. This would be a compromise between subject-specific geometries and springs.

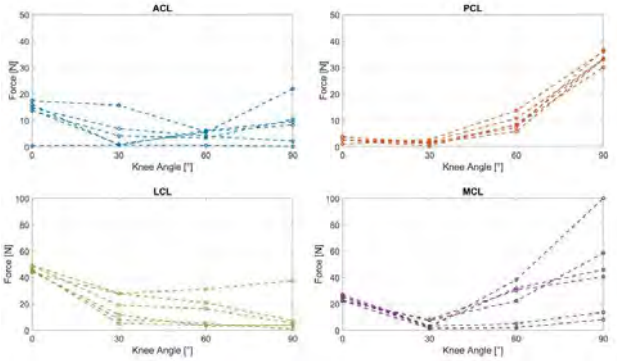

Figure 1 Ligament forces during a passive path flexion (0°-90°) of the ACL, PCL, MCL, LCL of six different FE models.

CONCLUSIONS

The pitfall of a generalized ligament model is that it is generalized and that it does not fit the subject as good as possible. Hence subject-specific properties need to be considered as it would improve the predicted kinematics already shown by Beidokhti et al. [1]. A possibility would be to have a loose and stiff ligament force set, which could be applied according to subject-specific laxity tests.

ACKNOWLEDGEMENT

We thank Innosuisse – Swiss Innovation Agency - for supporting this work.

REFERENCE

[1] Beidokhti HN et al. *J Biomech* **65**: 1-11, 2017.

IS COMPUTER VISION-BASED MOTION CAPTURE APPLICABLE FOR MUSCULOSKELETAL SIMULATION ?

Ryotaro Numata[1], Yasuaki Tsuyuki[1], Ryo Ueno[1,2]
[1]Department of Research and Development, ORGO Inc., Sapporo, Japan
[2]Faculty of Health Sciences, Hokkaido University, Sapporo, Japan.
Email: numata@orgo.co.jp

INTRODUCTION

Usually, several optical motion capture cameras and force plates are needed for musculoskeletal simulation. However, it is expensive and needs preparation time for the measurement. Vision-based monocular 3D human pose estimation is a suitable approach to overcome the above problems. It needs a single RGB camera for kinematics acquisition without any measuring devices. Therefore, the Vision-based approach has the possibility of reducing the cost and measuring time for the musculoskeletal simulation. In this study, we evaluated whether the kinematics data obtained from monocular 3D human pose estimation is applicable to musculoskeletal simulation.

METHODS

An open dataset [2] that was measured from 9 healthy subjects was used. It contains simultaneously recorded 6 types of motion capture data, RGB video and electromyography (EMG) from 9 dominant leg muscles (Soleus, Medial Gastrocnemius, Tibialis Anterior, Semimembranosus, Biceps Femoris, Vastus Lateralis, Rectus Femoris, Vastus Medialis). EMG data was high pass filtered at 25 Hz to remove wire artifacts, full-wave rectified, low pass filtered at 6 Hz and normalized by the maximum value of each trial. Two types of motion (Jump, Squat) from 7 subjects were used because estimated kinematics from 2 subjects were unsuccessful and pose estimation did not perform well for treadmill data. HuMoR [1], a computer vision-based monocular 3D human pose estimation method, is used to estimate the human pose from RGB video. HuMoR fits a human 3D mesh model to the sequential image by optimization with a conditional variational autoencoder.RGB videos that were used for HuMoR were captured at the frontal plane of participants. Markers used for simulation were extracted from the surface of a 3D human mesh as same as in the markerset of the above dataset. Ground reaction force estimation and muscle activation computation were performed with CusToM [3] with the musculoskeletal model consisting of 33 degrees of freedom and 82 muscles from the kinematics data from HuMoR. Out of 9 EMG records, lateral gastrocnemius was excluded from the analysis since it was not implemented in the musculoskeletal model. Spearman's rank correlation coefficient was computed between activation and EMG to examine estimated muscle activations accuracies. To evaluate the applicability of muscle activation from HuMoR, it was compared to the muscle activation computed with the motion capture data.

RESULTS AND DISCUSSION

Figure 1 shows the mean activation of each method in the jump trial over all subjects. Focusing on the knee extensors (Vastus Lateralis, Rectus Femoris, Vastus Medialis) that primarily work for the squat and jump, r_s scores between activation with HuMoR and EMG are equivalent to r_s score by activation with Mocap and EMG (Table1).

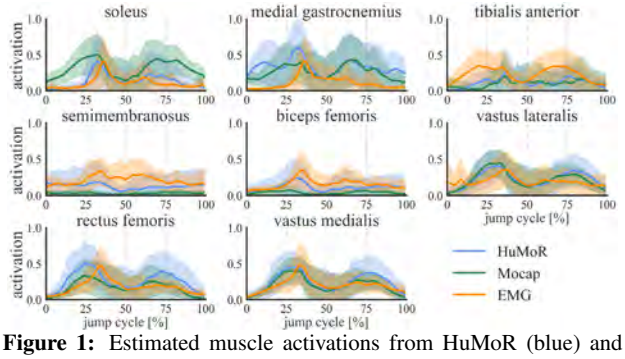

Figure 1: Estimated muscle activations from HuMoR (blue) and Mocap (green) as well as EMG (orange) averaged over the jump trials. The shaded area represents ± 1SD.

CONCLUSIONS

Preliminary results show the estimated kinematics from monocular video with a 3D human pose estimation algorithm is applicable for musculoskeletal simulation.

REFERENCES

[1] Rempe D et al. *ICCV*, 2019.
[2] Huawei W et al. *Zenodo*, 2022.
[3] Muller A et al. *J Open Source Softw*, 4(33), 927, 2022.

Table 1: r_s score between EMG and estimated activations from each method for the knee extensors

Task		Vastus Lateralis	Rectus Femoris	Vastus Medialis
Jump	Mocap vs EMG	0.54 ± 0.36	0.66 ± 0.07	0.74 ± 0.10
	Estimated vs EMG	0.50 ± 0.34	0.66 ± 0.03	0.73 ± 0.08
Squat	Mocap vs EMG	0.46 ± 0.45	0.68 ± 0.18	0.68 ± 0.15
	Estimated vs EMG	0.49 ± 0.41	0.67 ± 0.14	0.65 ± 0.16

CRITICAL REGIONS IN THE MANDIBLE DURING MASTICATION AND BLUNT IMPACT

Samrat Sagar[1], Rupesh Ghyar[1], B. Ravi[1] and Darshan Shah[1]
[1] Department of Mechanical Engineering, Indian Institute of Technology Bombay, Mumbai, India.
Email: samratsagar@iitb.ac.in

INTRODUCTION

There is a rise in the use of custom implants for the reconstruction of mandibles affected by osteosarcoma in order to restore facial aesthetics and oral functions. Custom implants have been known to offer better biomechanical fit and postoperative outcomes when compared to stock implants. However, there have been instances of postoperative implant fractures due to fatigue, where cracks were identified at stress concentration regions [1]. Additionally, blunt force trauma often causes mandible fractures [2], which could be to detrimental to the implant. Characterising potential regions of high stress in the native intact mandible could potentially direct design considerations while developing a custom implant. The aim of this study was to identify and characterise critical stress concentration regions in an intact mandible for simulated loading conditions during mastication and trauma.

METHODS

A finite element analysis was conducted on an edentulous intact mandible subjected to tasks replicating loading conditions from mastication and blunt impacts using Workbench 2020 R2 (Ansys Inc., PA, USA). The material of the model was assumed to be homogeneous and isotropic cortical bone. The condyles of the mandible were rigidly fixed. Forces of jaw-closing muscles were appropriately simulated in magnitude and line of action. For simulating mastication, the model was loaded under six unilateral clenching tasks – intercuspal (ICP), incisal (INC), canine (CAN), molar (MOL), left group (LGC) and left group with molar balancing (LGC+MB) – and one molar chewing task (MOL chew) [3]. Fist punches were simulated on four principal locations of the mandible – symphysis (SYM), parasymphysis (paraSYM), body (BOD) and ramus (RAM).

The critical stress for failure (σ_{cr}) was considered to be the fatigue shear strength of cortical bone (24 MPa) and yield strength of cortical bone (114 MPa) for the mastication tasks and blunt-impact tasks, respectively. Regions on the mandible exhibiting stress values over the critical stress were identified as critical regions. Critical regions appearing around the condyles were neglected following the St. Venant's principle.

RESULTS AND DISCUSSION

For all mastication tasks, except LGC and LGC+MB, critical regions were observed around the respective clenching points (Fig.1). In contrast, critical regions for fist punching tasks were found at the ipsilateral and contralateral condylar necks, with maximum stress values 1.75 to 6 times higher than σ_{cr} (Table 1). These findings were in agreement with the previous studies [2]. Critical regions thus identified on a native mandible could predict potential failure sites on a custom implant meant to replace it, allowing for improved design considerations apriori. Further improvements on the model will be directed towards using a dentate mandible with cortical and cancellous material.

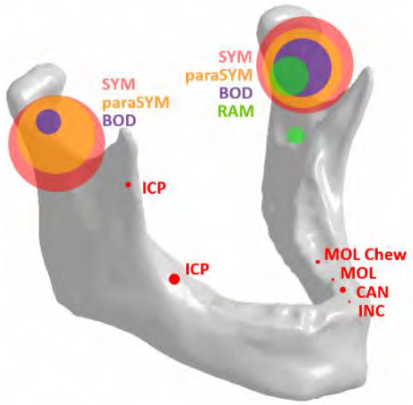

Figure 1 Critical regions on mandible for mastication and blunt-impact loads (circles indicate location and area of the critical region).

CONCLUSIONS

Critical regions during incisal clench, canine clench and molar chewing, which constitute the alternating bilateral mastication pattern [4], were predominantly observed on the body of the mandible. Therefore, while designing a mandibular implant for a body defect, designers should avoid stress concentration points, such as sharp edges or corners, which could lead to implant failure. In view of critical regions in condylar necks during blunt force trauma, similar care should be taken while designing temporomandibular joint implants.

REFERENCES

[1] Shi Q et al. *Engg Fail Anal* **124**: 105353, 2021.
[2] Torreira MG et al. *J Cran Max Surg* **32**: 303-7, 2004.
[3] Korioth TWP et al. *J Dent Res* **73**: 56-66, 1994.
[4] Reina JM et al. *J Biomech* **40**: 828–836, 2007.

Table 1: Maximum von Mises stress values (MPa) in the mandible for mastication and fist punching tasks.

Clenching						Chewing	Fist punching			
ICP	INC	CAN	MOL	LGC	LGC+MB	MOL chew	SYM	paraSYM	BOD	RAM
48.4	26.4	43.1	30.1	15.4	15.2	25.1	693.6	410.2	269.4	199.8

APPROPRIATE METRICS TO EVALUATE SPRING ASSISTANCE TO LOWER LIMBS FOR IMPROVING HUMAN GAIT

Rajbeer Singh Anand[1], Neeta Kanekar[2] and Anirban Guha[1]
[1] Department of Mechanical Engineering, Indian Institute of Technology Bombay, Mumbai, India.
[2] Department of Biosciences and Bioengineering, Indian Institute of Technology Bombay, Mumbai, India.
Email: rajbeer2007@iitb.ac.in

INTRODUCTION

Gait impairments in older adults severely increase their risk of disability, morbidity, and mortality. Wearable devices have been suggested for their gait assistance. Among wearable devices, passive exoskeletons have some advantages over active devices like lower weight and independence from power source. Before fabricating these passive devices, a designer often performs simulations to judge the performance of multiple designs. For comparing results of different simulations, researchers have mostly used two metrics - the peak value and the average of a parameter of interest over the Gait Cycle (GC) [1,2]. However, the questions of whether the chosen metrics lead to similar conclusions and capture the effect of the device in different phases of the GC remain unanswered. This study addresses these questions by evaluating these metrics separately in different phases of the GC. It also introduces another metric which is likely to be more representative of the performance of a device over the entire GC than the peak and average.

METHODS

OpenSim 4.4 was used for the simulations. The parameters evaluated were total metabolic rate (TMR) and right ankle moment (RAM). 7 metrics were considered for this study, peak, average, and area under the curve over the entire GC, the phase wise values of these three metrics, and the average of phase wise peaks. The GC was divided into 4 phases: initial stance (IS, 0-10% GC), mid stance (MS, 10-30% GC), terminal stance (TS, 30-60% GC), and swing (SW, 60-100% GC). Torsion springs with spring wire diameters of 2mm (TS_2, spring constant, k=0.023Nm/deg.), 3mm (TS_3, k=0.164Nm/deg.), and 5mm (TS_5, k=1.005Nm/deg.) at the ankles and linear springs replicating the path of soleus muscles with spring constants of 7kN/m (LS_7), 11kN/m (LS_11), and 15kN/m (LS_15) were used. The subject in this simulation weighed 72.6 kg with a standing height of 1.8 m and walked at a comfortable speed of 1.2 m/s on the treadmill. The spring assistance conditions were compared to the no spring (control) condition.

RESULTS AND DISCUSSION

Table 1 shows percentage changes in the parameters with spring versus the control condition. Positive values indicate an improvement. The greater detail captured through the phase wise representation was obvious. The fact that the IS and SW phases can show a deterioration in RAM in spite of the overall peak or average based data leading to the opposite conclusion, was significant. The magnitude of improvement in TMR with the use of torsion springs was severely underestimated by the peak compared to the other two metrics. Overall, predictions through the average and area under the curve metrics (in green) were much more closely correlated than those with the peak (in red).

CONCLUSIONS

Commonly used parameter metrics such as peak value over the entire GC may not be the best indicator of assessing the effectiveness of a device and in certain cases could even be misleading. Phase wise metrics provide a more nuanced indicator of the assistance (or the lack of it) provided by a device in different phases of the GC and could be more appropriate for guiding device development. This consideration becomes particularly important in the design of passive exoskeletons that may not have phase-wise control and act through the entire GC.

REFERENCES

[1] Cseke B et al. *IEEE Trans Biomed Eng.* **69(9)**: 2797-2805, 2022.
[2] Fang S et al. *Sensors (Basel).* **22(23)**: 9177, 2022.

Table 1: Percentage change in Total Metabolic Rate and Right Ankle Moment for spring vs no spring condition across different metrics.

Parameters \ Metrics		Peak for the GC	Phase wise peak				Average of phase wise peaks	Average for the GC	Phase wise average				Area under the curve for GC	Phase wise area under the curve			
			IS	MS	TS	SW			IS	MS	TS	SW		IS	MS	TS	SW
% Change in Total Metabolic Rate for Spring vs No Spring Condition	TS_2	11.93	11.93	9.56	29.79	35.70	22.27	21.08	9.22	11.85	29.05	24.25	22.48	9.88	14.03	29.41	24.75
	TS_3	11.79	11.79	8.22	30.51	34.65	21.87	21.12	9.28	11.30	29.47	24.04	22.45	9.82	13.54	29.58	24.74
	TS_5	11.34	11.34	7.36	17.73	16.27	13.47	18.09	9.21	9.92	25.61	19.43	19.83	9.59	12.48	26.93	20.26
	LS_7	-3.54	1.72	-1.19	-4.89	8.74	1.15	-3.15	-0.34	-6.78	-3.09	-3.07	-3.14	-0.50	-8.49	-3.14	-1.79
	LS_11	-8.48	-2.75	-3.50	-9.90	1.91	-3.61	-4.28	-4.40	-12.24	7.47	-15.75	-5.03	-4.67	-14.55	7.53	-14.73
	LS_15	-13.22	-13.22	9.85	0.11	2.23	-0.90	-4.90	-8.54	-2.73	-1.50	-9.58	-5.78	-7.35	-5.69	-1.75	-9.62
% Change in Right Ankle Moment for Spring vs No Spring Condition	TS_2	0.31	-1.25	0.39	0.31	3.62	0.35	0.26	0.22	1.00	-0.02	-4.27	0.26	0.13	0.95	-0.07	-7.60
	TS_3	1.60	1.33	1.73	1.60	5.96	1.56	1.69	3.01	2.93	1.33	-2.56	1.70	2.81	2.83	1.27	-6.77
	TS_5	9.36	16.34	9.66	9.36	-7.66	9.43	10.26	19.60	14.41	9.37	9.40	10.27	18.80	14.05	9.22	-1.89
	LS_7	5.65	-31.20	8.03	5.65	-91.91	11.42	15.68	-45.88	15.75	7.21	-388.89	15.48	-46.06	14.84	7.27	-417.27
	LS_11	8.88	-49.02	12.62	8.88	-144.47	17.97	24.63	-72.05	24.75	11.33	-611.11	24.33	-72.37	23.32	11.43	-655.71
	LS_15	12.11	-66.93	17.20	12.11	-196.81	24.50	33.57	-98.22	33.75	15.44	-832.48	33.18	-98.70	31.80	15.58	-894.14

Influence of Bone Inhomogeneity on Strain Calculation of CT-Based Vertebral Finite Element Models

Yen Cheng[1], Mu-Hsin Yin[2], Po-Liang Lai[3] and Hsiang-Ho Chen[2]
[1] School of Biomedical Engineering, Taipei Medical University, Taipei, Taiwan.
[2] Department of Biomedical Eng., Center for Biomedical Eng., Chang Gung University, Tauyuan, Taiwan.
[3] Department of Orthopedic Surgery, Linkou Chang-Gung Memorial Hospital, Tauyuan, Taiwan.
Email: hchen@mail.cgu.edu.tw

INTRODUCTION

Biomechanical computed tomography analysis can predict the bone strength and vertebral fracture risk in patients with low bone density. To automatically create a finite element model with inhomogeneous bone materials, a customized (MATLAB) program was designed for pre-processing CT images of each patient. This study will compare the vertebral strain in two models generated by using a MATLAB program (high inhomogeneity) and CAE software (low inhomogeneity).

METHODS

When modeling with MATLAB, the CT images are first stacked into a 3D array, and the pixel values are converted into Hounsfield units based on the RescaleSlope and RescaleIntercept in the CT image tag. The PixelSpacing is used to determine the actual imaging size. Using the Volume Segmenter, the general location of the image is marked for cropping. The bone segment is then separated based on the Hounsfield units, and the largest voxel group is marked for isolation, to separate the vertebrae to be analyzed[1].

According to the order of intensity values, the coordinates of each voxel's eight nodes are numbered and stored in a cell, which are then converted into three-dimensional coordinates. The intensity is converted into apparent density and elastic modulus using an empirical formula[2]. The maximum and minimum values of the y-coordinate are stored in an additional array to establish the node set for the upper and lower plane of the vertebral body. Strain calculation was conducted by LS-DYNA (LSTC, Livermore, CA, USA). A compression force was distributed perpendicularly on the upper endplate of the vertebral body. All nodes in the lower plane of the vertebral body are restricted. After renumbering the nodes, the solver can be utilized for computation.

For comparison, CAE software was utilized to create a vertebral body model. The 2D mesh model was extracted from the CT image using RETOMO (BETA CAE Systems, CH-6039 Root D4, Switzerland). Further processing of the 2D mesh model was performed using ANSA (BETA CAE Systems, CH-6039 Root D4, Switzerland), where the model was divided into 30 different materials through material mapping.

RESULTS AND DISCUSSION

The models were generated by using two methods (Figure 1). The time spent was 30.65minutes (customized) and 50.27 minutes (CAE software). The maximum and minimum values of the 1st Principal Strain-Infinitesimal and the 3rd Principal Strain-Infinitesimal were different (Table 1). However, there were ignorable differences between their means. The vertebral strains were similar in both models.

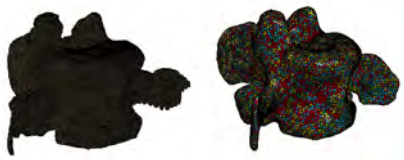

Figure 1 Left: customized; Right: CAE software

CONCLUSIONS

The modeling process used in this study can perform pre-processing and model meshing tasks automatically and saves time and labor costs in pre-processing. The result reveals that the customized program generates a model with more real bony distribution and similar strain as CAE model does. In the future, this modeling method can be used to predict the mechanical strengths and fracture risks of vertebrae.

REFERENCES

[1] Sheng Yue (2023). Label the largest pixel/voxel group in an image, MATLAB Central File Exchange.
[2] Rho JY, Hobatho MC, Ashman RB. Relations of Mechanical Properties to Density and CT Numbers in Human Bone. *Med Eng Phys* (1995) 17:347-55.

Table 1: Finite element analysis results of two models.

		Max	Min	Average
MATLAB Model	1st Principal Strain (tensile)	7.995e-05	-8.467e-06	3.0481e-05
	3rd Principal Strain (compressive)	1.961e-04	-8.467e-06	6.9164e-05
CAE Software Model	1st Principal Strain (tensile)	2.502e-03	-2.192e-07	3.7629e-05
	3rd Principal Strain (compressive)	5.674e-03	-5.976e-06	8.5826e-05

The Study of Tip-over Stability Analysis for Sitting Position Transition Wheelchair

Dae-Jin Jang[1], Yong-Cheol Kim[1], Eung-Pyo Hong[1] and Gyoo-Suk Kim[1]
[1] Rehabilitation Engineering Research Institute, Incheon, Korea
Email: rehajang@comwel.or.kr

INTRODUCTION

The sitting position transition power wheelchair is a mobile device used by the disabled who have difficulty in daily life by themselves. The sitting position trnsition power wheelchair is capable of backward tilt, recline, elevating legrest, lift, forward tilt, and stand. These postures are important for the prevention of various diseases in wheelchair users [1]. Some power wheelchairs reduce the movement speed or limit some postures when changing posture. However, there is no known criterion for limiting the posture, and there have been few studies on the tip-over risk evaluation when changing posture in power wheelchairs. In this study, ADAMS, a multi-body dynamics analysis program, the force-moment stability measurement method is used to calculate a stability metric when the posture of a power wheelchair is changed and the risk of tip-over in various postures is compared and analyzed.

METHODS

Force-moment stability measurement [2] is determined by the moment due to the inertial force and the moment due to the ground reaction force occurring at the center of gravity when the electric wheelchair moves or changes posture. The moment axes refer to a line connecting two adjacent points among the ground contact points of the power wheelchair, and the moment axes are equal to the number of wheels of the power wheelchair.

The stability measurement is calculated by the difference between the moment due to inertia and the moment due to ground contact force, and the equation is as follows.

$$SM_i = H_i^* r_i - \sum_{j=1}^{n}\left((p_j - p_i) \times F_j\right) r_i \quad (1)$$

Where when there are n ground contact points, r_i is a line (tip-over axis) connecting the i_{th} ground contact point and the next point, p_i is a three-dimensional vector connected to the i_{th} ground contact point at the center of gravity, and F_i is the ground contact force at i_{th} point. H_i^* in Eq. (1) is as follows.

$$H_i^* = I_b\dot{\omega} + \omega \times (I_b\omega) + (\dot{c} - \dot{p}_i + \omega \times (c - p_i)) \times mv_c \quad (2)$$

Wher I_b is the moment of inertia, ω is the angular velocity, c is the position of the center of gravity, and v_c is the movement speed of the center of gravity.

The stability metric refers to the value when the power wheelchair has the minimum value for all tip-over axes based on the most stable position. Therefore, if the power wheelchair is stationary, the stability metric value always has a positive value because only the ground reaction force was applied. However, when excessive acceleration or an external force is applied, the stability metric can become a negative value, and at this time, it can be considered to be inverted.

RESULTS AND DISCUSSION

For stability metric calculation, a posture transition power wheelchair is developed. The wheelbase of the power wheelchair is 525 mm, the height before the seat is lifted is about 580 mm from the ground, and the total weight of the power wheelchair is about 163 kg. The human body model was 175 mm and used two dummies weighing 75 kg and 100 kg. Stability metric values were compared and analyzed for tilt, recline, and lift operations. In the 45-degree tilt simulation, the stability metrics were 0.53 and 0.46 for the 75 kg and 100 kg models, respectively, and 0.51 and 0.46 for the 75 kg and 100 kg models, respectively, for the 90-degree recline. The stability metrics during lifting up to 380 mm were 0.95 and 0.92 for the 75 kg and 100 kg models, respectively.

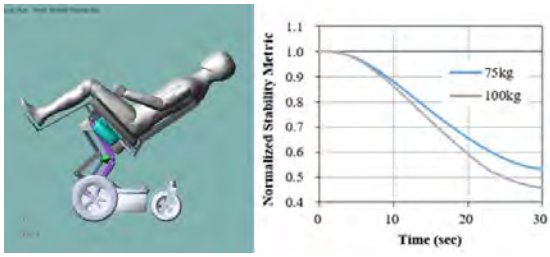

Figure 1 Stability metric in tilt simulation

CONCLUSIONS

As a result of the simulation, the stability metric was between 0.4 and 0.6 wheelchair during tilt and recline. This is not a condition for the wheelchair to overturn, but in this state, the wheelchair can be instantly overturned by losing the ground reaction force on either side due to a small stone, or outward extension of the user's arm. Under these conditions, the maximum speed of the wheelchair should be reduced and posture transition is restricted as a concerning step. In future research, we plan to compare the stability of wheelchairs by calculating the stability of each posture according to the movement speed of the wheelchair.

ACKNOWLEDGEMENTS

This work was supported by the Assistive Technology R&D Project for People with Disabilities and the Elderly funded by the Ministry of Health & Welfare, Republic of Korea (#HJ20C0017).

REFERENCES

[1] Dicianno B.E. et al. *Assist Technol*, **21**: 13-22, 2009.
[2] Peters S.C. et al. IEEE *Int. Conf. Robot. Autom.* 3711-6, 2006.

ANALYSIS OF POSTURE, SPINAL CURVATURES AND GAIT IN LUMBAR ARTHRODESIS PATIENTS

Guillaume Claus[1,2], Alessia Putzolu[3], Laurent Fabeck[3] and Véronique Feipel[1,2]

[1] Laboratory of Functional Anatomy, [2] Laboratory of Anatomy, Biomechanics and Organogenesis, [3] Department of Orthopaedics, Université Libre de Bruxelles (ULB), Belgium
Email: guillaume.claus@ulb.be

INTRODUCTION

The contribution of biomechanical analysis of the human spine regarding the diagnosis and therapeutic follow-up of patients suffering from low back pain is promising, but clinical studies supporting its relevance are rare. The aim of this study was to evaluate the clinical relevance of biomechanical parameters in persons with lumbar arthrodesis (LA) by studying static (vertebral curvatures) and dynamic (gait) parameters.

METHODS

A control group (CG, n=10) and an affected group with LA (n=13) volunteered aged 35 years and older for the study.

Data were collected using the A-palp technique [1] in a fourteen-camera optoelectronic system (T40s, VICON, Oxford, UK; sampling rate: 100Hz). Retro-reflective markers were placed on the anatomical landmarks organised for postural evaluation [2]. Additional landmarks were palpated according to a precise protocol [2] using the thermo-deformable splint of the A-Palp tool. This protocol allows to obtain a 3D model of the spine by continuously tracking the trajectory of the spinous processes from the external occipital prominence until the spinous process of S2. The landmarks were palpated in a controlled standing position. Lumbar lordosis (LL) and thoracic kyphosis (TK) were computed using the tangent method [2].

Consequently, participants walked barefoot on a 6m long ZENO instrumented walkway (ProtoKinetics, Havertown, PA, USA). Two trials were carried out at three randomized self-selected speeds (slow, fast and preferred [3]). Spatiotemporal variables were extracted using PKMas.

Mann-Whitney U tests and Pearson's correlation coefficients were used for statistical analysis.

RESULTS AND DISCUSSION

No group difference in LL and TK were found. During gait, the group with LA showed a greater toe out angle compared to CG. At preferred and/or fast speeds, step length, single support and gait velocity were lower, while stance phase, swing phase and step time increased in the LA group in comparison with CG.

These differences at preferred and fast speeds support that humans are better able to cope with postural instability and kinesiophobia at slow speed [4,5]. The use of adaptation mechanisms is stronger at higher gait speed.

In the CG, a strong negative correlation was found between LL and step length at fast speed (r=-0.77), indicating longer steps with lower LL. Moderate correlations existed between LL and stance, swing and single support phases at preferred speed in the CG (|r|≥0.50), increasing LL being associated with larger single support and swing phases and shorter stance phase. No correlation coefficient above 0.50 was found in the LA group, except for a moderate inverse relationship between TK and toe in/out angle (r=-0.53).

Table 1. Spatiotemporal gait parameters. Velocity in cm/s; Toe in/out angle in °; Step length, cycle length and step width in cm, Stance and single support phases in % of gait cycle. Significant different from CG in red.

Variable	**CG**			**LA**		
Speed	Slow	Preferred	Fast	Slow	Preferred	Fast
Velocity	72±25	120±12	171±20	73±27	110±22	139±35
Toe in/out angle	3±4	3±4	2±4	**9±5**	9±5	9±7
Step length	53±5	65±4	73±9	47±8	59±7	65±10
Cycle length	105±11	130±9	151±12	94±17	118±14	129±19
Step width	9±3	8±1	9±2	9±5	9±3	9±3
Stance phase	66±3	62±1	59±1	67±5	63±2	62±2
Single support	34±4	38±1	41±1	33±5	37±2	38±2

CONCLUSIONS

Patients with LA differed from controls in terms of spatiotemporal gait variables, but not of spinal curvatures. The absence of correlation between curvature and gait variables in the LA group and its clinical relevance needs further investigation, among others including larger samples.

REFERENCES

[1] Salvia P et al. *Gait Posture* **29**: 587-90, 2009.
[2] Salvia P et al. *Comput Methods Biomech Biomed Eng Imaging Vis* 2077236, 2022.
[3] Leyh C et al. *J Funct Morphol Kinesiol* **7**: 106, 2022.
[4] Henchoz Y et al. *Eur J Appl Physiol* **115**: 2433-43, 2015.
[5] Smith JA et al. *J Sport Health Sci* **11**: 450-65, 2022.
[6] Koch C et al. *Front Psychol* **9**: 2236, 2018.

Dependence of static compressive condition on breast support performance of sports bras during running

Yasuho Takii[1]
[1] Institute of Sport Science / ASICS Corporation, Kobe, Japan.
Email: yasuho.takii@asics.com

INTRODUCTION

The relationship between breast movement during running and breast support privided by sports bra has been studied previously. These studies have shown that the greater the support provided by a sports bra, the greater the reduction in breast movement during running[1,2]. In practical designing of sports bra, these research would be more fruiful if the detailed discussion as belows were added. (1)Comparison of breast movement in different sizes under the same compression of sports bra. (2)Understanding the critical contribution area in sports bra to controll the breast movement. (3)Relationshiop between breast movement and breast bounce perception.
Therefore, the aim of this study was to quantitatively examine the relationships between wearing compression of sports bras, breast movement during running and subjective breast bounce perception.

METHODS

Four females participated in this study (mean ± SD: 22.8 ± 4.6 years, 154.6 ± 2.7 cm, 46.4 ± 5.1 kg). Participants' breast sizes were 65A, 70A, 70C, 80C. Medium size bras were used for participants with 70C or 80C size breasts. Small size bras were used for participants with 65A or 70A size breasts. Six types of bras were used for this study. In these bras, two were low support types, one was medium support type, and two were high support types. Wearing compression was measured at ten points on each of their trunks in the static condition using an air-pack-type pressure sensor (AMI 3037-10, AMI Techno, Co., Ltd). Participants performed running trials (treadmill, 8 km/h), then 3D movement of the left nipple using the 3D motion analysis system (VICON Motion System, UK) and subjective breast bounce perception data during running using 10-cm visual analog scale were collected. The trajectory length in each bra condition compared to that of the nude condition was calculated as %Trajectory length (%Trj.). A multiple regression test was performed with %Trj. as the response variable and the pressure values at each point as the explanatory variables.

RESULTS AND DISCUSSION

The trajectory length of the left nipple during one cycle of running was longer for larger breast sizes and shorter for smaller breast sizes at all pressure levels. For each subject, there was a correlation between average pressure on the trunk and trajectory length. In terms of %Trj., values for all subjects were in the same range.
There was a correlation between average pressure on the trunk and %Trj. for each subject and for all subjects combined (Figure 1). The same level of breast bounce reduction was shown with increasing pressure. The multiple regression identified the pressure in the shoulder, lower breast and underbust areas to be important in describing %Trj. Subjects of all breast sizes had relatively low breast bounce perception when %Trj. was below 55%.
These results suggest that greater pressure is needed to bring the larger size breasts to the same level of breast bounce as the smaller size breasts. On the other hand, the rate of reduction in breast bounce required to feel less breast bounce and the wearing compression required to reach that rate of reduction are the same regardless of breast size. The results of the multiple regression analysis indicate a high contribution of forces controlling breast bounce in the vertical direction. This is a reasonable result given the large vertical displacement of the breast during bare-breast running[3]. Further analysis is needed to improve the accuracy of the multiple regression equation here, after adding information on the types of bra shapes and physical properties of the fabrics.

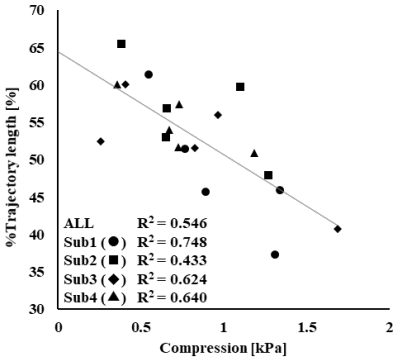

Figure 1 Relationship %Trj. and wearing compression.

CONCLUSIONS

For subjects with different breast sizes, it was required to provide higher wearing compression for subjects with lager breasts in order to achieve the same amount of breast bounce during running. If the rate of reduction in breast bounce was the same, the same wearing compression was required regardless of breast size. And pressure at the shoulders and lower breast area was important. Breast bounce perception was reduced when the reduction rate fell below a certain level.

REFERENCES

[1] Scurr J et al. J. Sports Sci. 29: 55-61, 2011.
[2] McGhee DE et al. Appl. Ergon. 44: 112-118, 2013.
[3] Scurr J et al. J. Appl. Biomech. 25: 322-329, 2009.

Comparison of scoliosis angles with and without menarche

Eunbi Park[1,2,5], Kyoungkyu Jeon[1,2,3,4,5], Wonbin Hyun[1,5], Hojun Joo[1,5] and Hyungwoo Lee[1,2,5]
[1] Division of Sports Science, Incheon National University, Incheon, South Korea
[2] Department of Human Movement Science, Incheon National University, Incheon, South Korea
[3] Sport Science Institute, Incheon National University, Incheon, South Korea
[4] Health Promotion Center, Incheon National University, Incheon, South Korea
[5] Functional Rehabilitation Biomechanics Laboratory, Incheon National University, Incheon, South Korea
Email: guddn318@inu.ac.kr

INTRODUCTION

Idiopathic scoliosis is the most common form and is characterized by its occurrence mainly in adolescence [1]. In particular, adolescent idiopathic scoliosis (AIS) is more common in girls, and women are at a 10-fold higher risk of developing than men [2,3]. In the case of adolescent idiopathic scoliosis, interest in estrogen as a potential factor for AIS has increased while the exact cause has not yet been identified [3]. In particular, in the case of women, since the secondary growth of menarche appears physiologically during adolescence, it is necessary to study the scoliosis angle according to the presence or absence of menarche. Therefore, the purpose of this study is to find out the scoliosis angle according to the presence or absence of menarche.

METHODS

A total of 130 elementary school female students were recruited for this study, and the group with menarche (age 12.35±0.58 years, height 154.22±6.87 cm, weight 45.03±11.46 kg) and the group without menarche (age 10.48±0.65 years, height 138.42±5.48 cm, weight 33.00±5.98 kg) were recruited. All subjects utilized spinal structural analysis (Formetric 4D, Diers Biomedical Solutions, Germany) using the rastersterography method to measure spinal deformity. This device is known as a device used to evaluate spinal divisions, and its validity and reliability have been demonstrated [4-6]. For measurement, a halogen light source was aimed at it, and a 3D model used for spinal deformity evaluation was constructed based on the image obtained, and scoliosis angle values were extracted by triangulation. For statistical analysis, an independent *t*-test was used for comparison within groups using the SPSS 26.0 (IBM, USA), and all variables were calculated as mean and standard deviation. The statistical significance level was set at $P < 0.05$.

RESULTS AND DISCUSSION

The scoliosis angle showed a significant difference between the groups according to menarche status <Figure 1>. Menarche in women is determined by the secretion rhythm of the ovarian hormones, estrogen, and progesterone [3]. Abnormal estrogen levels cause delayed menarche, which delays bone development and maturation, increasing the possibility of spinal deformities [7]. In addition, a higher risk of AIS in women is associated with delayed menarche, suggesting that low estrogen is an important factor in the onset of AIS [7].

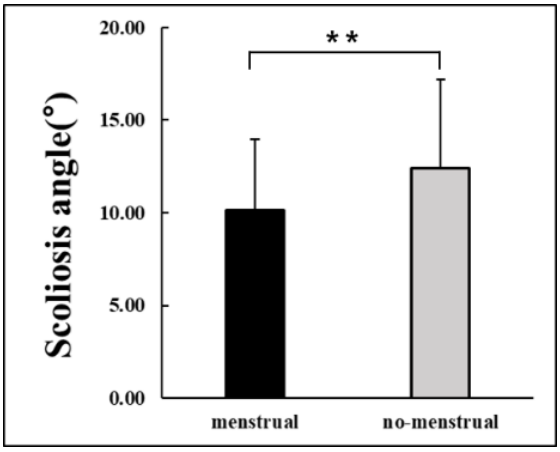

Figure 1. Result of scoliosis angle
Note. Data are mean ± standard deviation. Asterisk (**) indicates a significant difference between force level conditions at $P < 0.01$.

CONCLUSIONS

In addition to delayed menarche, one of the risk factors for AIS, the scoliosis angle was higher in the non-menarche group, which is highly likely to be due to abnormal estrogen levels, compared to the menarche group.

ACKNOWLEDGEMENTS

The authors would like to thank the participants for their time and commitment to this research. This study was supported by the University Innovation Support Project of Incheon National University.

REFERENCES

[1] Sung, S et al. *Int J Environ Res Public Health* **18**: 8152, 2021.
[2] Negrini, S et al. *Scoliosis* **1**: 1-14, 2006.
[3] Kulis, A et al. *Int Orthop* **39**: 1227-1236, 2015.
[4] Jeon, K et al. *Int J Environ Res Public Health* **15**: 2613, 2018.
[5] Frerich, J.M et al. *Open Orthop J* **6**: 261, 2012.
[6] Krott, N.L et al. *Eur Spine J* **29**: 2392-2401, 2020.
[7] Liang, Z.T et al. *FASEB J* **35**: e21839, 2021.

Effects of varying in load weight on spine kinematics in Deadlift

Kazuma Shoji[1], Koichi Nakayama[1], Masayo Shiouchi[1] and Yoshiaki Manabe[1,2]
[1]Graduate of Health and Sport Science, Chukyo University / Toyota, Aichi, Japan.
[2] School of Health and Sport Science, Chukyo University / Toyota, Aichi, Japan.
Email: decathlon0107@gmail.com

INTRODUCTION

Deadlift is a comprehensive training of the trunk and lower extremity muscles, and the load weight should be selected according to the targeted training effect [1]. Maximal and submaximal deadlift reported to have different lifting techniques and strategies [2]. However, no studies have yet comprehensive compared spinal kinematics of the spine between different load weights. In addition, the human spine, composed of 33 vertebral bones, has mobility, such as extension-flexion and rotation, similar to other joints. However, most biomechanical motion studies of deadlift simplify the human trunk to a single rigid-body segment, ignoring its motion. Recent studies have reported that using a segmented trunk model is able to measure detailed spinal kinematics [3]. This study utilized a trunk model with six rigid-body segments and compare spinal kinematic characteristics between different load weights.

METHODS

In this study, twelve university male track and field athletes performed traditional deadlifts. The maximum load weight (1RM: one repetition maximum) was estimated by a direct method for each subject, and the trials were performed at 60, 70, 80, 90% of the loads when 1RM was set at 100%. Using a 12-camera optical three-dimensional motion analysis (VICON MX, Oxford Metrics Group), we measured the three-dimensional coordinates of each reflective marker attached to a total of 27 physical feature points on the body. A force plate (Kistler) was used to simultaneously measure the ground reaction force. A link segment model, in which the trunk consisted of six regions, was constructed based on the method of Kudo et al. [3], and kinematic data for each region of the spine in the sagittal plane were calculated. Statistical processing was used for the statistical analysis software SPSS.26.0 (SPSS Inc., Chicago).

RESULTS AND DISCUSSION

The maximum flexion angle of the total spine angle was significantly greater for the 90% 1RM than for the other weights (60%: -52.05 ± 2.673deg vs. 70%: -53.47 ± 3.26deg vs. 80%: -55.19 ± 3.76 vs. 90%: -61.38 ± 3.96, P<.05). This result revealed that the increased load weight emphasizes the rounding of the trunk (Table 1). In particular, the differences in regional flexion angles of spine, when increased load weight, were significant at the lower regions of the spine (T12: at 0 to 100% normalized time, L3: at 0 to 60% normalized time, respectively; P <.05). And those increased flexion angles were found in the timing of the barbell passing through the knee (at 50% normalization time).

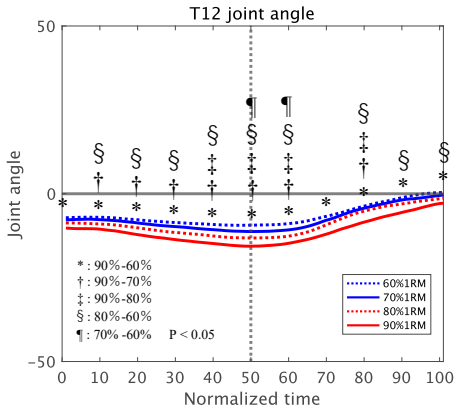

Figure 1 Time series data that show the lower thoracic spine angle during the ascending phase.

CONCLUSIONS

Concerning spinal kinematics in deadlift, we conclude that (1) flexion angle was larger with increasing load weight, (2) the difference in regional flexion angle, with increased load weight, were remarkable around the upper lumbar spine, (3) those region's flexion angle increased when the bar passes through the knee.

REFERENCES

[1] Rhea, MR et al. Med Sci Sports Exerc 35: 456-64, 2003.
[2] Hales, ME et al. J Strength Cond Res 23: 2574-80, 2009.
[3] Kudo, S et al. Gait and Posture 63: 119–123, 2018.

Table 1: Maximum flexion angle of total spine between different load weights (*: 90-60%, †: 90-70%, ‡:90-80%1RM, respectively; P<.05).

		60%1RM	70%1RM	80%1RM	90%1RM	
		Mean ± SD	Mean ± SD	Mean ± SD	Mean ± SD	
Maximum flexion angle	[°]	-52.05 ± 2.67	-53.47 ± 3.26	-55.19 ± 3.76	-61.38 ± 3.96	*, †, ‡
	95%CI	-57.90 ± -46.13	-60.65 ± -46.29	-63.46 ± -46.92	-70.09 ± -52.67	

LESS PAIN, BUT ONLY SMALL CHANGES IN SHOULDER KINEMATICS FOLLOWING TOPICAL ANESTHETIC IN PATIENTS WITH ONGOING SHOULDER PAIN

N.E. D'hondt[1,2]*, A.J.R. Leenen[2]*, H. Kiers[1,2], M.J.M. Hoozemans[2], T.D. Alta[3], N. Miedema[3], M.P. van de Borne[4], M.P.J. van der List[5], M.P.J. van den Bekerom[2,6], H.E.J. Veeger[7]

[1] Institute for Human Movement Studies, HU University of Applied Sciences Utrecht, Utrecht, The Netherlands
[2] Faculty of Behavioural & Movement Sciences, Vrije Universiteit Amsterdam, Amsterdam, The Netherlands
[3] Department of Orthopaedic Surgery, Spaarne Hospital, Haarlem, The Netherlands
[4] Department of Orthopaedic Surgery, Amphia Hospital, Breda, The Netherlands
[5] Department of Orthopaedic Surgery, Bergman Clinics, Naarden, The Netherlands
[6] Department of Orthopaedic Surgery, OLVG Hospital, Amsterdam, The Netherlands
[7] Department of Biomechanical Engineering, Delft University of Technology, Delft, The Netherlands
Email: norman.dhondt@hu.nl
* These authors contributed equally to this work

INTRODUCTION

Persistent shoulder pain involves a complex interaction between physiological and psychological factors. Still unknown is to what extent upper body movement behaviour in patients with shoulder pain is part of an ongoing nociception-based adaptive mechanism. The aim of this multicentre observational study was to observe the influence of immediate relief of nociception-based pain on shoulder and trunk kinematics during a semi-constrained painful overhead reach task in patients with ongoing shoulder pain.

METHODS

Symptomatic shoulders of 29 patients (mean age 59.0 SD 12.8 years; 16 males) were injected with corticosteroids and lidocaine by their attending orthopaedic surgeon. Immediately before and five minutes after the injection, patients had to reach ten consecutive times as high as possible to a target at the ceiling directly above. Pain intensity (VNRS-11) at each highest arm elevation, scapula, humerus and trunk kinematics (assessed using Xsens DOT, wireless inertial measurement units) were recorded. Shoulder motions were expressed as a helical angle rotation relative to their initial position. Pre- and post-injection motions were compared as the differences between those values.

RESULTS AND DISCUSSION

Generalized Estimating Equations analysis showed statistically significant reduction in pain during the reach task after the injection (n=27). Statistical Non-Parametrical Mapping did not identify differences in maximal shoulder and trunk helical angle contributions between conditions (Figure 1). Significantly lower angles for the post-injection condition were found for part of the descending phase (thoracohumeral [75.3%, 92.9%]; p<.001;scapulothoracic [73.7%, 93.1%]; p=.003; humeroscapular [71.4%, 92.3%]; p<.001).

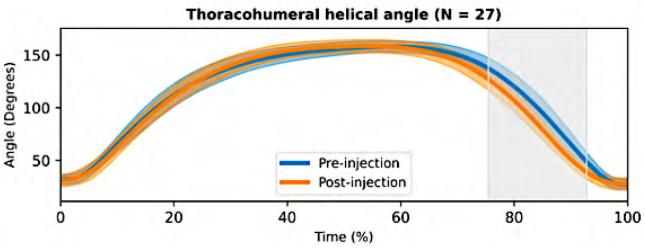

Figure 1 Results of Statistical non-Parametric Mapping (SnMP) of the elevation (helical) angle of the reach task within the normalized time domain (%). Mean (solid lines) and 95% confidence intervals (shaded band) of pre-injection are given in blue and post-injection in orange. Shaded grey areas indicate the significant differences.

CONCLUSIONS

Acute pain relief following topical anaesthetics does not result in immediate alterations in the maximal contribution of shoulder and trunk range of motion during a semi-constrained painful overhead reach task in patients with ongoing shoulder pain. At the group level, there appears to be no reason to alter shoulder and trunk kinematics when reaching for the target post-injection. However, there are small alterations in shoulder kinematics during the descending phase.

ACKNOWLEDGEMENTS

We thank all involved orthopaedics secretariats and colleagues of the Amphia Hospital, the Spaarne Hospital, the Bergman Clinics and the Onze Lieve Vrouwe Hospital (OLVG) for their help in organizing this study.

Motor unit behavior of the lower trapezius and serratus anterior in individuals with Scapular Dyskinesis

Masahiro Kuniki[1], Daisuke Kuwahara[1], Rei Konishi[1,2] and Nobuhiro Kito [2]

[1] Graduate School of Medical Welfare Sciences, Medical Engineering, Hiroshima International University / Hiroshima, Japan.

[2] Department of Rehabilitation, Faculty of Rehabilitation, Hiroshima International University / Hiroshima, Japan.

Email: n-kito@hirokoku-u.ac.jp

INTRODUCTION

Scapular dyskinesis (SD) is one of the factors that cause shoulder injuries [1]. Although the weakness of the lower trapezius and serratus anterior is associated with SD, these muscle thicknesses are not reduced in individuals with a shoulder injury, and muscle weakness due to muscle atrophy alone cannot explain the cause of SD. Muscle strength also depends on the number, size, and firing rate of recruited motor units (motor unit behavior, MU behavior) [2], but no studies have investigated MU behavior in the lower trapezius and serratus anterior of individuals with SD. The purpose of this study was to clarify the MU behavior of the lower trapezius and serratus anterior in individuals with SD.

METHODS

The Scapular Dyskinesis Test (SDT) was performed on 50 healthy young adults. The SDT is classified into Normal, Subtle, and Obvious by observing the scapular motion from the back during the raising and lowering of the upper limb [1]. The SDT results showed that 14 were Normal, 16 were Subtle, and 20 were Obvious. Of the Obvious, 9 who observed SD in the raising phase were considered as the SD group (SDG), and 11 who observed SD only in the lowering phase were excluded. Normal 14 was considered the Normal group (NG). The subject performed trapezoidal contractions with 70 % of the maximum voluntary contraction of the lower trapezius, serratus anterior at the position of manual muscle testing by Kendall. Muscle activity was measured with a Trigno Galileo sensor (Delsys, USA), and the EMG waveform was decomposed into MU action potential amplitude (MUAP-amp), mean firing rate (MFR), and recruitment threshold (RT) using a template-matching algorithm [3]. MFR was calculated as the mean of the firing rate during the 20-second plateau during trapezoidal contraction. The slope and y-intercept of the regression of MUAP-amp and MFR with RT were calculated. The MUs were divided into three groups by RT (< 20%, 20-40%, > 40%), and the average of MUAP-amp and MFR for each MU group was calculated. A two-sample t-test or Mann-Whitney test was used to compare each parameter between groups. The significance level was set at $p < 0.05$, and d or r was calculated as the effect size.

RESULTS AND DISCUSSION

The slope of the regression between MUAP-amp and RT was higher in the NG for both the lower trapezius (NG, 0.010 ± 0.003; SDG, 0.007 ± 0.002; $p = 0.010$, $d = 1.054$) and serratus anterior (NG, 0.009 ± 0.004; SDG, 0.004 ± 0.003; $p = 0.007$, $d = 1.272$). MUAP-amp of the lower trapezius is higher in the NG at all RTs, and the serratus anterior is higher in the NG at medium and high threshold MUs **(Figure 1).** The slope of the regression between MFR and RT was higher in the NG only for the serratus anterior (NG, 27.839 ± 3.515; SDG, 22.215 ± 5.069; p = 0.005, d = 1.347). In particular, the low firing rates of the medium and high threshold MUs **(Figure 1).** In addition to the size of the MU, the serratus anterior has a low firing rate, suggesting that the neural drive of the serratus anterior is reduced in individuals with SD.

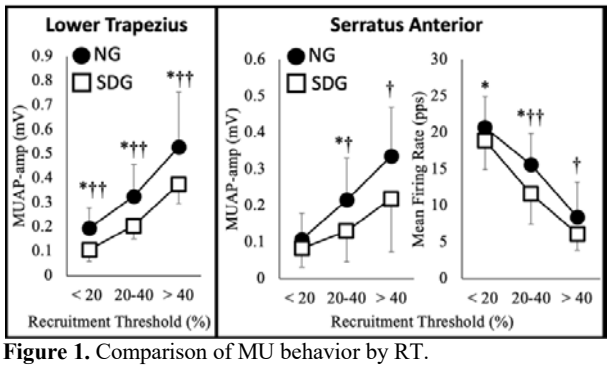

Figure 1. Comparison of MU behavior by RT.
* p <0.05; † medium effect size; †† large effect size
NG, Normal group; SDG, Scapular Dyskinesis group

CONCLUSIONS

Individuals with SD differ from individuals with normal scapular motion in MU behavior of the lower trapezius and serratus anterior. SD may be caused not only by muscle weakness due to muscle atrophy but also by neurophysiological factors such as recruited MU size and firing rate of the lower trapezius and serratus anterior.

ACKNOWLEDGEMENTS

The authors thank all individuals who participated in this study.

REFERENCES

[1] McClure P et al. *J Athl Train* **44**: 160-4, 2009.

[2] Enoka RM et al. Cold Spring Harb Perspect Med **7**: a029702, 2017.

[3] De Luca CJ et al. *J Neurophysiol* **113**: 1941-51, 2015.

Characteristics of Medial Elbow Pain in Professional and Amateur Baseball Players: Focusing on Valgus Instability and Ulnar Neuropathy

Issei Noda[1,2], Shintarou Kudo[1,3,4]

[1] Graduate School of Health Sciences, Morinomiya University of Medical Sciences/ Osaka, Japan.

[2] Ashiya orthopedics sports clinic, Hyogo, Japan.
[3] Inclusive medical science research institute, Morinomiya University of Medical Sciences/ Osaka, Japan
[4] AR-Ex medical research center/ Tokyo, Japan

Email: issei.noda@gmail.com

INTRODUCTION

Ulnar neuropathy is a common cause of medial elbow pain. Furthermore, valgus instability is known to be related to ulnar neuropathy. However, previous studies have not examined the effects of level of competition. Therefore, the purpose of this study was to examine the effect of level of competition on ulnar neuropathy.

METHODS

The subjects were 76 baseball players (32 professional baseball players and 44 amateur baseball players). The ulnohumeral joint space was measured at rest and during valgus stress loading using an ultrasonography. In addition, the presence of osteophytes on the medial epicondyle and sublime tubercle which was called insertion of the ulnar collateral ligament (UCL) was confirmed. Relative to the medial epicondyle, the arcade of Struthers was 5 cm proximal, the cubital tunnel was the posteo-medial part, and Osborne's ligament was defined as 3 cm distal. For statistical analysis, subjects were classified according to with or without of medial elbow pain. The CSA ratio were calculated as the CSA of the throwing side relative to the non-throwing side, respectively. The subjects were classified into four groups according to their level of competition and with or without of medial elbow pain. The ulnohumeral joint space and CSA ratio was compared among the four groups using a one-way analysis of variance and a multiple comparison test. The relationship between level of competition or medial elbow pain and osteophytes was examined using the X_2 test.

RESULTS AND DISCUSSION

Professional baseball players had 10 players with pain and 22 players without pain. Amateur baseball players had 24 players with pain and 20 players without pain.
The ulnohumeral joint space at rest was significantly wider in the professional with pain group than in the without pain group. The ulnohumeral joint space was significantly wider in the with pain group than in the without pain group in both professionals and amateurs during valgus stress. The CSA ratio of the ulnar nerve was significantly swelled in the with pain group compared to the without pain group in both the professional and amateur groups.
The relationship between medial elbow pain and osteophytes was significantly more in the with pain group. There was no significant difference between the level of competition and osteophytes.
Previous studies have reported ulnar neuropathy as a result of increased valgus instability and osteophytes in the ulnohumeral joint. Excessive valgus stress continues to be applied to the medial elbow, and repetitive mechanical stress of the UN increases. Osteophytes in the ulnohumeral joint may increase frictional stress on the ulnar nerve. These factors suggest that swelling of the ulnar nerve at the cubital tunnel and Osborne's ligament and osteophytes at the ulnohumeral joint are likely to be a factor in medial elbow pain.

CONCLUSIONS

Valgus instability, Osteophytes of the ulnohumeral joint and swelling of the ulnar nerve are factors for medial elbow pain. There was no significant difference between professionals and amateurs.

Effect of Multiplane Arm Elevations on Glenohumeral Kinematics and Contact Patterns

Chia-Ling Fan[1], Li-Wei Hung[2], Yi-Chen Wu[1], Yi-Ching Wang[1], Hsuan-Yu Lu[1], Cheng-Chung Lin[3], Tung-Wu Lu[1,4]

[1] Department of Biomedical Engineering, National Taiwan University, Taiwan, R.O.C.
[2] Department of Orthopedic Surgery, Shin Kong Wu Ho Su Memorial Hospital, Taiwan, R.O.C.
[3] Department of Electrical Engineering, Fu Jen Catholic University, Taiwan, R.O.C.
[4] Department of Orthopedic Surgery, School of Medicine, National Taiwan University, Taiwan, R.O.C.
Email: twlu@ntu.edu.tw

INTRODUCTION

The glenohumeral (GH) joint consists of the humeral head and the glenoid cavity of the scapula [1], however, previous studies have only been able to illustrate the rigid body kinematics of the GH joint without the contact pattern due to the lack of availability of a cartilage model [2]. The purpose of this study aimed to use 3D fluoroscopy and the virtual cartilage method to calculate the *in vivo* 3D GH rigid-body kinematics and the joint articular contact patterns during multiplane arm elevation.

METHODS

Twelve healthy adults (age: 25.5 ± 2.7 y/0; BMI: 23.8 ± 2.1 kg/m^2) performed arm elevation in the sagittal, frontal, and scapular planes under the surveillance of a biplane fluoroscopy system. A CT scan (Brilliance iCT 256, Philips) was firstly taken for each individual in supine to obtain subject-specific models of the humerus and scapula. By using 3D fluoroscopy to register the model projections to the corresponding x-ray images, the poses of the shoulder bone models were established [3]. The thickness of the virtual cartilage was defined as the mean distance of each vertex between the surface models of the glenoid and humeral head in the resting position. The contact region was then defined as the penetrated area between the glenoid cartilage and the humeral head cartilage. The contact point was established using the depth-weighted average over the contact region technique.

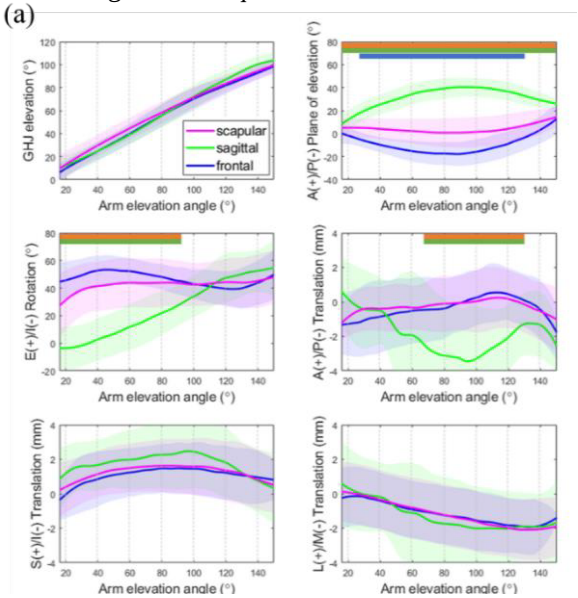

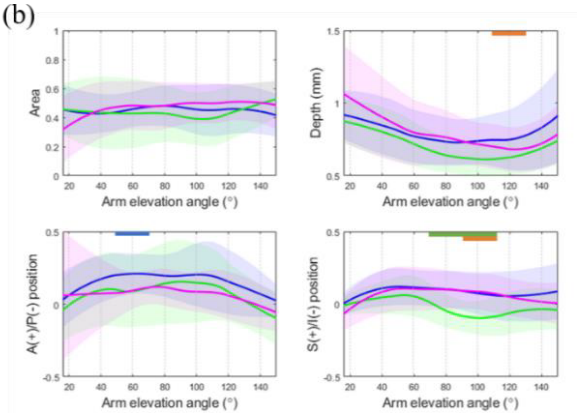

Figure 1 Means and standard deviations of the GH joint's (a) kinematics, (b) contact areas, depths and points during multiplane arm elevations. The orange horizontal line indicates a significant difference between the frontal plane and the sagittal plane; the blue horizontal line indicates a significant difference between the frontal plane and scapular plane; the green horizontal line indicates a significant difference between the sagittal plane and scapular plane.

RESULTS AND DISCUSSION

The greater anterior rotation was found during arm elevation in the sagittal plane, compared to that in the frontal or scapular plane (Fig 1a). Comparing arm elevation in the sagittal plane to that in the scapular or frontal planes, a larger external rotation was observed. The contact point of the GH joint typically remained in the immediate area (25% length of the glenoid) during arm flexion between 20° to 100°. The mean contact depth decreased during arm flexion between 20° to 100° but increased when arm flexion is greater than 100° among the three planes, which showed a similar trend of the contact area in the sagittal plane (Fig. 1b). The mechanical behaviour of the articular cartilages during arm elevation activities can be investigated by quantifying the interactions between the convex and concave surfaces of the GH joint.

CONCLUSIONS

This study successfully quantified the normative 3D GH kinematics in healthy young individuals and showed the coupled motions of the GH joint during multiplane arm elevation, which could serve as a recommendation for clinical practice guidelines.

REFERENCES

[1] Hess S.A. *Manual therapy*, **5**(2): 63-71, 2000.
[2] Giphart J.E. et al. *J Bone & Joint Surgery* **95**(3): 238-245, 2013.
[3] Lin C.C. et al. *Applied Sciences* **10**(23): 8426, 2020

PILOT FOLLOW UP OF A PATIENT WITH POST-STROKE HEMIPARESIS USING THE SSULF SCALE IN COMPARISON WITH OTHER CLINICAL ASSESSMENT.

Paris J Velasco Acosta[1,2], Leonardo E Anaya Campos[1], Ana Guadalupe Ramírez Nava[1], Ivett Quiñones Uriósteguí[1], Valeria Polet Olivares Gonzales[1, 3], Virginia Bueyes Roiz[1]
1 Instituto Nacional de Rehabilitación Luis Guillermo Ibarra Ibarra, Mexico City, Mexico
2 Universidad Iberoamericana CDMX, Mexico City, Mexico
3 Universidad Nacional Autónoma de México, Mexico City, Mexico
E-mail: parisvelasco.inr@gmail.com

INTRODUCTION

The use of clinical assessments, evaluation scales or metrics by physicians is one of the tools for the diagnosis of motor disabilities and for the preparation of a rehabilitation plan (1). These assessments (i.e. Ashworth, CUE-T, Grasp & Release, Fugl Meyer, Action Research Arm Test (ARAT), to name a few)(2) measure parameters like motor control, pain, movement range, coordination, strength, grip, object manipulation, etc.(3)(4), but that depend entirely on the training and ability of the physicians qualified to diagnose, rehabilitate, and treat patients with motor impairment.
From previous projects performed at the Instituto Nacional de Rehabilitación Luis Guillermo Ibarra Ibarra, an scale from collected SALM scores into 5 significative levels has been made, so patients can be classified by degree of impairment. Using the results from fuzzy classifiers The Smoothness-based Scale for the Upper Limb Function (SSULF) has been created, identifying level 1 as an unimpaired limb increasing the level of impairment until a level 5 being a severe impaired limb.

METHODS

The recruitment of a 68 year old male patient with right hemiparesis due to middle cerebral artery stroke of 2 years of evolution. Patient had a history of Diabetes Mellitus 2 and Hypertension of at least 10 years of diagnosis. During a period of six months the subject followed a rehabilitation program implemented by the group of Neurological Rehabilitation Physicians of the Institute. Along with this program the patient was evaluated with clinical scales; such as: ARAT, Motricity Index (from which only the superior extremity was accounted) and Modified Ashworth Scale; The methodology of the Sorting Block Box (SBB) system to acquire the smoothness data needed to obtain its SSULF score was also implemented.
The evaluations were placed at the beginning of the treatment, 3 months after its initiation, and at the end of the 6 months period.

RESULTS AND DISCUSSION

Each score obtained by the patient during the protocol was recorded to be compared within all the clinical scales performed, these values are show in Table1. The table shown has the values register by the SSULF classifications, ARAT, Motricity and Modified Ashworth. Scale.

CONCLUSIONS

The first Pilot using the SSULF scores to classify the function of the impaired limb of a patient being treated at the Institute showed that a correlation can be seen within the already performed scales by the group of Physicians, although an acknowledgment of the different skills needed for each clinical scales to be performed must be made to correlate the data along with a bigger sample of patients.
The continuation of testing the SSULF on as many patients as possible, must be an ongoing project to create a significant correlation of the scores obtained by this new tool.

REFERENCES

[1] Nesathurai, S. (2000). The rehabilitation of people with spinal cord injury. Boston: Blackwell Science .
[2] C. Metcalf. et al .(2007) A review of clinical upper limb assessments within the framework of the WHO ICF Main article. Musculoskeletal Care, vol. 5, no. 3, pp. 160– 173.
[3] T.L. Chelette. (1995) Enhanced metrics for identification of forearm rehabilitation. Rehabilitation Engineering, IEEE Transactions vol.3, no.1, pp.122-131.
[4] G.F. Harris. et al. (1990). Biomechanical assessment techniques in rehabilitation. Colloquium in South America, 1990, Proceedings of the 1990 IEEE, pp. 31-34.

Table 1: Scores obtained on each scale during the period of the study.

	SSULF		ARAT		Superior Motricity Index		Modified Ashworth Scale **	
Laterality	**Left**	**Right**	**Left**	**Right**	**Left ***	**Right**	**Left**	**Right**
Initial	1	2	57	24	-	73	0/0/0	0/1/0
3 months	1	2	57	35	-	73	0/0/0	0/1/0
6 months	1	2	57	38	-	73	0/0/0	0/1/0

.-** Motricity Index is only evaluated on the impaired limb. *.-** Scores are shown as follows shoulder/elbow/wrist

USING OUTDOOR CYCLING POWER OUTPUT AND HEART RATE TO ESTIMATE MAXIMAL OXYGEN CONSUMPTION

Tzyy-Yuang Shiang[1], Ting-Yu Yeh[1], Yin-Shin Lee[1] and Chen-Chang Tsai[2]
[1]Department of Athletic Performance, National Taiwan Normal University, Taipei, Taiwan
[2]Lifestyles of Health and Sustainability Executive Master of Business Administration, National Taiwan Normal University, Taipei, Taiwan
*E-mail: tyshiang@gmail.com

INTRODUCTION

Directly measured maximal oxygen consumption (VO_2max) was considered as the golden standard of performance and cardiorespiratory endurance. [1] However, measurement of VO_2max requires maximal efforts, which may pose health risks and also is restricted in laboratory condition [2]. Numerous submaximal cycling work tests exist for estimation of VO2max, such as the nomogram of Åstrand (*Å*-test). Much of the submaximal cycling tests have been performed indoors in laboratories, whereas little research has been performed outdoor cycling. Therefore, the purpose of the study was to investigate whether outdoor cycling data can be used to estimate VO_2max or not.

METHODS

In the study, nineteen male volunteers (6 non-experienced, 4 experienced and 9 professional) participated in 2 experimental trials consisting of 1 laboratory and 1 outdoor session and completed in two visits, at least 48 hours of rest between. They performed a graded exercise test (GXT) at first visit. After 5 minutes warm-up with 100W, power output increased 10W every minute until dropout [3]. The first visit aimed to obtain VO2max and the association between power output, heart rate and VO_2max. At the second visit, subjects performed outdoor cycling 20-kilometer time trial test with their maximal effort.

Data Analysis

In the indoor graded exercise test, power output and heart rate in the last 15 seconds of each stage of the official test were captured and conducted regression analysis. The slope of regression line was defined as indoor power/heart rate, (P/H) index. Since indoor P/H index had high correlation with VO2max, the index was fitted into regression equation to estimate VO_2max.

In the outdoor 20-kilometer time trial test, we removed the data that power is 0, power and heart rate were averaged over 60 seconds as output per minute. Linear regression was conducted between the power and heart rate per minute and the slope of the regression line was defined as outdoor P/H index. The outdoor P/H index were calculated to fit into regression equation to obtain predict VO_2max.

RESULTS AND DISCUSSION

VO_2max had high correlation with indoor P/H index ($r = 0.72$, $p < 0.01$). Standard error of estimation between estimated and measured VO_2max is 6.44 (ml/kg/min).

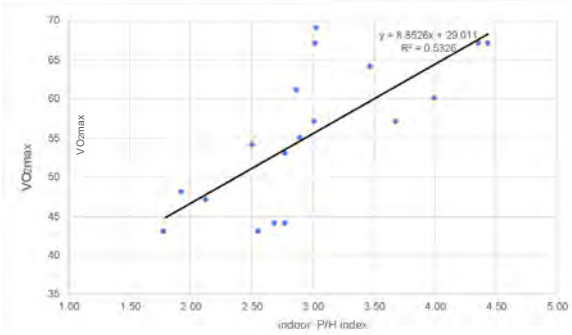

Figure 1 The linear regression of indoor P/H index and VO_2max

The predict VO_2max obtained from outdoor P/H index had medium correlation with VO_2max from indoor GXT ($r = 0.5$).

As the completing time of outdoor cycling varied among different subjects, the amount of data to derive outdoor P/H index also varied. Furthermore, since outdoor cycling test were largely influenced by the environmental conditions and cycling technique, more precise data cleaning or several times tests may be needed.

CONCLUSIONS

The predict VO2max obtained from outdoor P/H index had medium correlation with VO_2max from indoor graded exercise test. Hence, outdoor 20km cycling test may be used as the submaximal test to estimate VO_2max.

ACKNOLEDGEMENTS

The research was funded by Technology Development Program of Ministry of Economic Affairs.

REFERENCES

[1] Poole & Jones. *J Appl Physiol*, **122**:997-1002, 2017
[2] Ekblom-Bak et al. **24**:319-326, 2014.
[3] Vanhatalo, A et al. *Med & Sci in Sports & Exer,* **39**:548-555, 2007.
[4] Weyand, P et al. *J Applied Physio.,* **91**:451–458, 2001.
[5] Cink, RE & Thomas, TR. *Br. J. Sports Med.*, **15**:182-185, 1981.

Integrated Gaze Tracking and Motion Analysis During Walking

Zhaoyuan Wan[1], Xiaocheng Zhang[1], Yi-Xing Liu[1], and Ruoli Wang[1]
[1] Department of Engineering Mechanics, KTH Royal Institute of Technology, Stockholm, Sweden.
Email: zhaoyuan@kth.se

INTRODUCTION

Vision plays an important role in guidance for efficient human movement that often involves complex sensory integration, spatial orientation, balance, proprioception and haptic feedback [1]. With the development of mobile eye-tracking techniques, measurements of gaze patterns during movements have become more practical. However, most of the existing research analysed gaze and motion data separately due to the extra temporal and spatial synchronization has to be established, which is not always trivial [2]. In this study, we presented an integrated solution of a relatively low-cost eye tracking system and a marker-based Mocap system. Simultaneously recorded gaze data and gait patterns in different walking conditions were investigated.

METHODS

Five able-bodied participants with normal visual ability took part in the measurement. Participants were instructed to walk at their comfortable pace in two different settings: a plain path (level ground) and a complex path. The complex path consisted of a ramp, a plateau and a stair. Participants were asked to walk in both directions: from ramp to stair (RS), and from stair to ramp (SR). Reflective markers were placed on the bony landmarks according to CGM2.3 marker set. Ground reaction forces were also recorded. Gaze data was recorded by an eye-tracker (Pupil Core), which consists of one world camera (30Hz@1080p) and two pupil cameras (200Hz@192x192px). The marker trajectories were recorded with a 10-camera Mocap system (Vicon at 100Hz). The recorded gaze data was then transformed from the coordinate of the world camera to the global coordinate of the Mocap system using a marker cluster attached on the eye tracker. Arduino UNO was used to acquire time stamps for the eye tracker and the Mocap system, in order to achieve the temporal synchronization. The average gaze time distribution (proportions of gaze points falling in different areas) and gait parameters, i.e., step length and step time were calculated from 3 repeated trials and compared among different conditions.

RESULTS AND DISCUSSION

Regardless of the settings, the participants in general spent less than 50% of time looking at the walking path (Figure 1). Among 3 conditions, participants spent more time looking at the path during the RS trials. In particular, the plateau and stair attracted more visual attention than the ramp. During SR trials, the ramp occupied most of the gaze. As expected, gaze was always focused on the upcoming path, especially the downward path, possibly for better navigation and planning. Coupled with more gaze time on the pathway, participants had the longest step time and shortest step length in the RS trials, which led to the lowest walking speed (Table 1).

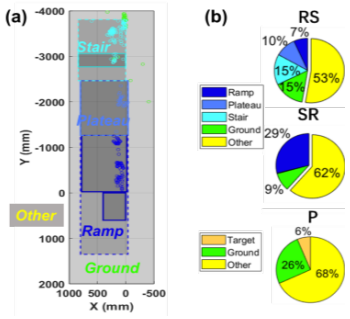

Figure 1 (a) Top view of transformed gaze points (circles) on the complex path from one example trial. Other refers to gaze points outside the walking path. (b) Average gaze time distribution from all participants. RS: from ramp to stair. SR: from stair to ramp. P: plain path (only 3 participants).

CONCLUSIONS

We proposed a feasible solution for simultaneous eye-tracking and motion analysis. Gaze point and motion data can be successfully synchronized spatially and temporally. Our preliminary results showed that people tended to look at the upcoming path during walking. As expected, gait parameters were found coupled with gaze time distribution, i.e., walking more slowly when looking at pathway more. The proposed integrated system can potentially benefit both research and clinical evaluation of sensory integration, spatial orientation, and proprioception during locomotion.

ACKNOWLEDGEMENTS

This project was generously funded by the Promobilia Foundation.

REFERENCES

[1] Madrid J & Hout M.C *Frontiers for Young Minds* **6**: 2018.
[2] Hunt R et al. *i-Perception* **13**: 5, 2022.

Table 1: Average gait cycle parameters from all participants. RS: from ramp to stair, calculated from the steps upward the ramp. SR: from stair to ramp, calculated from the steps downward the ramp. P: plain path (only 3 participants).

	RS	SR	P
Step time (ms)	568.2 ± 20.7	504.8 ± 22.2	511.2 ± 26.7
Step length (mm)	659.1 ± 69.6	702.5 ± 29.5	713.3 ± 53.4

CHANGES IN SPATIOTEMPORAL PARAMETERS DURING LONG DISTANCE RUNNING

Yuta Suzuki[1], Michael Hahn[2] and Yasushi Enomoto[3]
[1] Research Center for Urban Health and Sports, Osaka Metropolitan University, Osaka, Japan.
[2] Department of Human Physiology, University of Oregon, Eugene, USA
[3] Faculty of Health and Sport Sciences, University of Tsukuba, Tsukuba, Japan.
Email: ysuzuki@omu.ac.jp

INTRODUCTION

Observation of running performance with inertial mesurement units (IMUs) has become more popular in recent years. Monitoring runners during their training and races could be useful for improvement of runnning performance and reduction of running injury. The purpose of this study was to estimate the changes in spatiotemporal parameters during long distance running using a foot-mounted IMU.

METHODS

One university runner (female, 19 yrs, 1.63m, 50.9 kg) performed a 60-minute running trial at a self-selected speed (7 laps of a 1.8 km loop course). Linear accelerations and angular velocities of the right foot were measured with an IMU (Casio, Tokyo, Japan, 200 Hz) fixed to the dorsum of the foot.

Stride frequency and contact time were calculated from initial contact and toe-off events detected using acceleration data [1]. Additionally, stride length throughout the running trial was calculated [2]. Running speed of each stride was calculated from stride frequency and stride length. Calculated spatiotemporal variables of the 60-minute running trial were averaged for each of seven laps.

RESULTS AND DISCUSSION

The total number of detected strides in this study was 4689. Table 1 shows the average running speeds calculated from lap times and IMU data for seven laps. The results of this study demonstrate that gait events and stride lengths can be accurately estimated from IMU data during running.

Figure 1 shows changes in running speed, stride length, stride frequency and contact time during the 60-minute running trial. Running speed increased from 5th lap to 7th lap, and stride length also increased in this phase. Stride frequency increased and contact time decreased throughout the running trial, however the magnitudes of these changes were relatively small. These results indicate that the subject increased running speed during the latter part of running by increasing stride length.

CONCLUSIONS

This study attempted to estimate changes in spatiotemporal variables during long distance running. The results support the potential of monitoring runners and collecting longitudinal data during their training and races using IMUs.

ACKNOWLEDGEMENTS

This study was supported by JSPS KAKENHI (21K11334) and the CASIO SCIENCE PROMOTION FOUNDATION (K12-09). We would like to thank Casio for providing their IMUs for this study.

REFERENCES

[1] Benson L et al. *Sensors* **19**: 1483, 2019.
[2] Suzuki Y et al. *Sensors* **22**: 7129, 2022.

Table 1: Averaged running speed (m/s) calculated from lap times and IMU data.

	Lap time	IMU
Lap 1	3.83	3.90
Lap 2	3.91	3.97
Lap 3	3.99	3.96
Lap 4	3.91	3.94
Lap 5	4.06	4.01
Lap 6	4.10	4.08
Lap 7	4.10	4.13

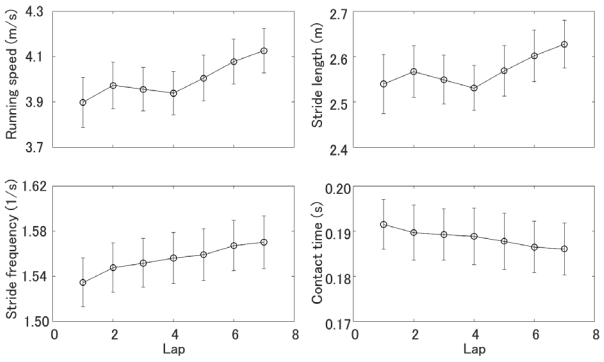

Figure 1 Changes in running speed, stride length, stride frequency and contact time during a 60-minute running trial.

CHANGES IN ACCELERATION LOAD DURING AN AGILITY TEST ON ARTIFICIAL TURF

Claudiane A. Fukuchi[1], Reyna Crawford[1], Anniek Vogel[2], Darren J. Stefanyshyn[1], and John W. Wannop[1]

[1] Human Performance Lab, Faculty of Kinesiology, University of Calgary, Canada

[2] The Hague University of Applied Sciences, Netherlands.

Email: claudiane.fukuchi@ucalgary.ca

INTRODUCTION

Artifical turf has been widely used in sports and has the advantage that the characterists of the turf can be modified to alter performance [1] and injury risk [2]. Due to the demands of practicing sports such as soccer, the participants are required to change their direction in response to external stimulus which could lead to increased loading rates. To quantify this, inertial sensors have been used in running [3] but the application in other sports contexts have been poorly described. Thus, the objective of this study was to investigate if altering the properties of artificial turf could attenuate peak accelerations measured with inertial sensors on the heel and shank segments when performing an agility test.

METHODS

Nineteen healthy males (age: 29.2 ± 6.0 years, height: 1.8 ± 0.1 m, body mass: 78.6 ± 9.4 kg) participated in this study after giving written consent. Two artificial turf conditions (FieldTurf, Tarkett Inc., Montreal, QC, Canada) installed in the laboratory were tested: 1) Control turf (shockpad: none; carpet fiber: poltethylene slit-film, infill: bottom = 1.0lbs/sqft sand, middle = 5.2lbs/sqft sand+2.6lbs/sqft 14-30 rubber, top = 0.4lbs/sqft 10-14 rubber) and 2) Shockpad (shockpad: 12mm thick Therma-plastic, carpet fiber: polyethylene monofilament, infill: bottom = 1.0lbs/sqft sand, middle = 5.2lbs/sqft sand+2.6lbs/sqft 14-30 rubber, top = 0.4lbs/sqft 10-14 rubber). All participants wore the same model of football cleats which were available in multiple sizes (Nike Vapor Edge Speed 360). During the data collection, each participant was required to perform a maximal effort agility test (3m-6m-3m) with athlete performance measured with photocells. The first cut of the agility test was considered for further analysis.

To measure the accelerations, two inertial measurement units (IMU, BlueTrident Vicon, Oxford, UK) at 225Hz were placed on the right heel cup of the shoe and right shank (shin bone). Additionally, ground reaction forces were measured with a force platform (Kistler) at 2400 Hz. The signals were filtered using a 4th order low-pass Butterworth filter at a cut-off frequency of 60-Hz. Maximum acceleration of the heel and shank, and maximum vertical ground reaction forces were selected for further analysis. Additionally, performance time was quantified based on the photocells. Paired *t*-tests were used to detect differences between the turf conditions (α=0.05). All data processing and statistical analyses were performed in Python.

RESULTS AND DISCUSSION

Comparing the two turfs, no difference in athlete performance was present (p=0.60). The shank medio-lateral acceleration (p<0.01); and both the heel (p=0.01) and shank (p<0.01) resultant acceleration presented lower values on the Shockpad turf compared with the Control turf (Figure 1).

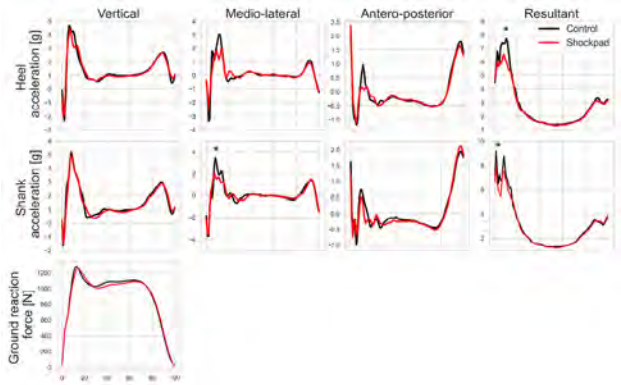

Figure 1 Ensemble average time-series across subjects of the heel and shank accelerations, and vertical ground reaction forces of the Control and Shockpad turf conditions

CONCLUSIONS

This preliminary study highlighted that the Shockpad artificial turf decreased the peak acceleration, particularly, in the shank segment. Altering components of artificial turf can influence acceleration of the body and might positively decrease the risk of injuries. Further studies with larger sample size and different drills are needed.

ACKNOWLEDGEMENTS

This work was supported by the Mitacs Accelerate Program (Postdoctoral Fellowship) and a Natural Sciences and Engineering Research Council of Canada Collaborative Research and Development Grant.

REFERENCES

[1] Kerdok AE et al. *J Appl Physiol* **92**: 469-478, 2002.

[2] Sanchez-Shancez J et al. *Sci Rep* **11**: 8625, 2021.

[3] Tenforde AS et al. *PM&R* **12**: 679-684, 2020.

DEVELOPMENT OF AN INSTRUCTIONAL SUPPORT SYSTEM FOR SKIING USING GNNS DATA

Hiroshi Hoshino[1] and Hidehiko Hayashi[2]
[1] Department of Economy, Hokusei Gakuen University / general education unit, Sapporo, Japan.
[2] Department of Economy, Hokusei Gakuen University / Institute of Management Information, Sapporo, Japan.
Email: h-hoshi@hokusei.ac.jp

INTRODUCTION

The utilization of Global Navigation Satellite System (GNSS) data in sports has increased rapidly in recent years. GNSS data for performance and team feature analysis is especially effective for ball game sports. GNSS data are commonly used to digitize the tracking information obtained by GNSS to aid in visualization.
The present study aimed to develop a ski instruction support system for technical alpine skiing training scenarios, in which the routes and speeds obtained from the GNSS tracking information were added and synthesized to video recordings of the trainees' skiing practice.

METHODS

1. Participants
The participants in this study were two adult males, one of whom (aged 58, 169 cm, 88 kg) passed the Level 2 Ski Test certified by the Ski Association of Japan (SAJ). The other (ski instructor: aged 56, 171 cm, 83 kg) had basic ski instructor certification. The participants were instructed to ski freely, as they would normally.The data obtained in this study were organized for use as basic references in the instruction scenarios as additional sensor visualizer items.
2. Ski Instruction Support System Development
(1) The ski instruction support system we are developing in this study aims to provide trainees with feedback images in which GNSS-derived speed and route data are added as sensor visualizer items on the skiing practice video recordings to create synthesized feedback for training. One of the advantages of this ski instruction support system is its instantaneous user (trainee) feedback. They can visually receive synthesized feedback from the video image and sensor information, while their kinesthesia from practice is still fresh. This would also enable them to share technical issues and progress in skill acquisition with the instructor.
As stated above, we are developing an effective tool for ski instruction. Here, we attempted to utilize GNSS and gyro sensors built into mobile terminals (smartphones) [1], which have recently become popular, to collect data during skiing practice. Two AQUOS sense 3 lite mobile terminals were used in this experiment. A preinstalled smartphone application was used. The system was modified to synchronize the video and sensor information obtained from the two mobile terminals automatically using GPS time.
(2) Participants placed the mobile terminal (AQUAS sense3 lite), which was pre-installed with the ski instruction support system, into their ski suits to collect the practice data. It was confirmed that wearing the device inside their clothes did not interfere with their performance or posture during skiing practice.

RESULTS AND DISCUSSION

A verification test of the ski instruction support system using GNSS data is conducted in this study. Figure 1 shows an example of the operation of the ski instruction support system. The image on the left (A) indicates the scenario of providing the participant with a practice image containing sensor visualizer items after practice. As shown in the image on the right (B), the recording was provided as a synthesized image of the participant's video recording, with data on speed, height evolution, body sway, and route.

CONCLUSIONS

As stated above, the ski instruction support system developed in this study provided users with video images containing sensor visualizer items immediately after skiing practice, suggesting that the use of GNSS data in the ski instruction support system is effective.

(A) (B)

Figure 1 The mobile terminal used in this study feeds back a video with a sensor visualizer item to the subject (A : left figure). At this time, both smartphones are connected via Bluetooth and the sensor information is displayed in sync with the video. The right figure shows a part of the image displayed to th e subject (B : right figure).

ACKNOWLEDGEMENTS

This work was supported by JSPS Grant-in-Aid for Early-Career Scientists. (Grant Number JP 20K19483, Hiroshi HOSHINO)

REFERENCES

[1] Hayashi H et al.International Conference on Advanced Applied Informatics (IIAIAAI) 540-543, 2021.

RELIABILITY OF THE LOADSOL INSOLE FOR MEASURING KINETICS DURING STATIONARY CYCLING

Walter Menke[1], Songning Zhang[1]
[1]Department of Kinesiology, Recreation and Sport Studies, University of Tennessee, Knoxville, USA
Email: wmenke@vols.utk.edu

INTRODUCTION

The loadsol insole is a commerical device used to measure in-shoe vertical ground reaction force (GRF). Traditionally, biomechanics research is conducted using force platforms or plantar pressure insoles/mats that require additional wires attached to equipment and usage of a laptop. This wireless insole enables free movement of the user without being restricted by wires. The reliability of the loadsol has not been examined in cycling [2]. The loadsol may be beneficial for clinical use because of its portability and cost reduction compared to a standard plantar pressure system. Therefore, the purpose of this study was to evaluate the reliability of GRFs measured by the loadsol device and vertical pedal reaction force (PRF) measured by the instrumented pedals during stationary cycling at different workloads.

METHODS

Ten healthy college aged students (age=22±4 years, height=1.70±0.1 m, mass=75.6±12.6 kg) were recruited from a local college campus. Customized instrumented 3D force pedals (1200Hz, Kistler) were used to measure PRF and vertical PRF was also concurrently measured with a 3-region, loadsol insole (100Hz, vertical force only, Novel) placed in a standard lab running shoes (Air Zoom Pegasus, Nike). Data collection was synchronized to Vicon Nexus by using loadsync device. Participants cycled on a stationary ergometer (Ergomedic 828E, Monark) at three workload conditions (1kg, 2kg, 3kg) at a cadence of 80 revolutions per minute for two minutes in each condition. PRF data were collected for the final 10 seconds of the two minutes and analyzed as a block consisting of the whole 10-second trial. Intraclass correlation coefficients (ICC) were computed using a Two-Way Mixed Effects model for Consistency with a 95% confidence interval (IBM Statistical Package for Social Science [1].

RESULTS AND DISCUSSION

The results showed that the loadsol consistently underestimated vertical peak reaction forces and produced systematically lower impulse values (Figure 1). ICC values ranged from 0.325 to 0.954 (Table 1). Overall, it appears that the loadsol showed better consistency with the instrumented pedals on peak vertical PRFs (ICC: 0.454 - 0.954, Table 1) as opposed to vertical PRF impulse (ICC: 0.325 – 0.850) for stationary cycling. PRFs are lower in cycling compared to other movement tasks with high loading such as jumping. The small differences measured by the two devices here may not be as easily identified in studies involving movements with high GRFs.

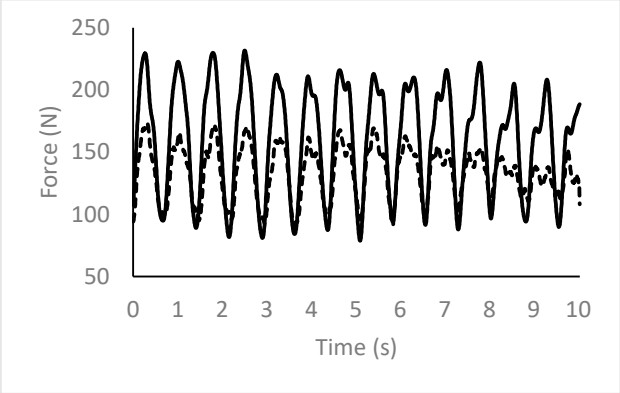

Figure 1 Ensemble reaction force curves for the right 3kg workload condition. Solid line represents instrumented pedals; dashed represents loadsol.

CONCLUSIONS

The loadsol can have wider clinical use for measuring patient kinetics without requiring specialized equipment, laboratory spaces, or highly trained personnel. This study provides evidence that the loadsol is consistent and reliable at measuring kinetics through a range of workloads for stationary cycling although it may underestimate peak forces. Further research may involve application to specific patient populations, especially those engaging in cycling activities as part of prevention or rehabilitative protocols.

REFERENCES

[1] Koo TK et al., *J Chirop Med*. **15**: 155-63, 2016
[2] Renner KE et al, *Sensors* **19**: 265, 2019

Table 1: Average measures ICC values for peak vertical GRF and total impulse between loadsol and instrumented pedals.

ICC Type	Right Side			Left Side		
	1kg	*2kg*	*3kg*	*1kg*	*2kg*	*3kg*
Peak PRFz	0.954	0.713	0.868	0.788	0.454	0.892
Impulse	0.325	0.663	0.754	0.549	0.531	0.850

In-Socket Pressure Sensor System for Lower Limb Prosthetic

Min Jo[1,3], Dong-young Ahn[1], Woo-sub Sim[1], Hee-seung Yang[2] and Chi-hwan An[2]
[1] Prosthetics and Orthotics Center, Veterans Health Service Medical Center, Seoul, Korea.
[2] Rehabilitation Center, Veterans Health Service Medical Center, Seoul, Korea.
[3] Department of Mechanical Engineering, Sejong University, Seoul, Korea.
Email: min8606@gmail.com

INTRODUCTION

A lower limb prosthesis is an indispensable device for lower limb amputees. It replaces the lost functions of the lower limb by combining and coordinating various parts such as the prosthetic foot, pins, pipes, and socket. The performance and user convenience of lower limb prostheses have improved with technological advances [1]. However, dissatisfaction among users remains[2, 3]. Because existing methods of evaluating lower limb prosthesis satisfaction are based on subjective elements such as user perception and psychological factors, quantitative evaluation is difficult. In particular, the socket, which connects the wearer of the lower limb prosthesis directly to the prosthesis frame, have a major influence on the satisfaction of prosthesis users. This study developed and evaluated a pressure sensor system for measuring interface pressure between the lower limb prosthetic socket and stump using up to 16 force-sensitive resistors (FSR).

METHODS

The developed pressure sensor uses 16 FSR channels and is aimed at enhancing user convenience through wireless communication, a data storage function, and a GUI. The gait simulator is designed to simulate the stance-phase motion. The movement of the gait simulator was limited to the anterior–posterior direction to observe the correlation between the tilt angle and sensor data, and the tilt angle ranged up to ±25°.

RESULTS AND DISCUSSION

The load change according to the tilt angle is shown to be out of phase in the C and G sensors, placed parallel to the gait simulator's direction of motion (Figure 1(A)). In contrast, the data for the A and E sensors, attached perpendicular to the direction of motion of the gait simulator, are in phase (Figure 1(B)). In addition, the difference between the maximum and minimum loads increased with an increase in the tilt angle (Table 1).

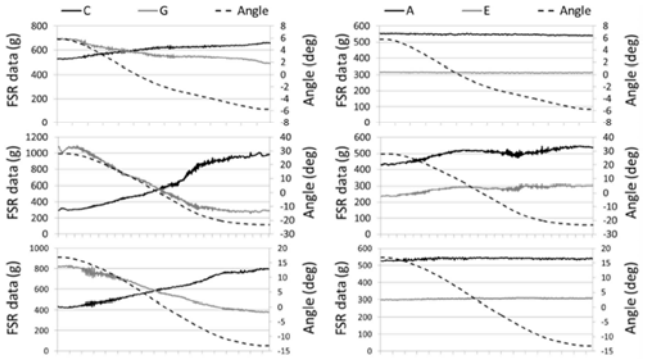

Figure 1 *The motion of the gait simulator at maximum tilt angles of ±5°, ±15°, and ±25°. (A: parallel sensor C and G, B: perpendicular sensors A and E).*

CONCLUSIONS

The lower limb prosthetic socket is pivotal in determining the comfort of the pros-thesis fit and its performance. The proposed pressure sensor system is designed to be worn with the prosthesis. Because it can measure changes in in-socket pressure during everyday use, it is expected to provide data that can be used to evaluate the wearer's intent or the walking environment.

ACKNOWLEDGEMENTS

This work was supported by the Korea Medical Device Development Fund grant funded by the Korea government (the Ministry of Science and ICT, the Ministry of Trade, Industry and Energy, the Ministry of Health & Welfare, the Ministry of Food and Drug Safety) (Project Number: 1711135029, KMDF_PR_20200901_0158)

REFERENCES

[1] Jia X. et al. *J Biomech* **37**: 1371-1377, 2004
[2] Dillingham, T.R. et al. *Am. J. Phys. Med. Rehabil* **80**:536-571, 2001
[3] Ali, S. et al. *Arch. Phys. Med. Rehabil* **93**:1919-1923, 2012

Table 1: Difference between the maximum and minimum load at tilt angles of ±5°, ±15°, and ±25°

(Unit: g)

Tilt angle	Load measurement	A	B	C	D	E	F	G	H
±5°	Max. − Min.	16	127	139	32	7	154	208	145
±15°	Max. − Min.	24	333	378	64	16	397	450	339
±25°	Max. − Min.	100	652	713	103	75	830	832	580

WEARABLE INTRA-FOOT TEMPERATURE GRADIENTS DURING FREE-LIVING CONDITIONS

Emily Matijevich[1,2]
[1] Human Performance Laboratory, Faculty of Kinesiology, University of Calgary, AB, Canada
[2] Orpyx Medical Technologies, Calgary, AB, Canada
Email: em.matijevich@gmail.com

INTRODUCTION

Core body temperature has long been considered a key vital sign – an objective measure of an individual's physiological status. Distal skin temperatures have also been shown to reveal health insights. For example, foot temperatures assessed with thermography have been used to evaluate foot health in individuals with diabetes [2]. While single time point, static thermograms have proven clinically useful, the development of sensory insoles embedded with temperature sensors allows for continuous foot temperature monitoring. Prior to continuous foot temperatures being leveraged for digital health monitoring opportunities, a fundamental understanding of foot temperatures during free-living conditions is necessary.

Intra-foot temperature gradients have been well characterized during static thermograms; a decrease in temperature moving from proximal to distal is observed in healthy feet [3]. However, it is not well established how this relationship changes throughout the day, and if this relationship is individual specific. Therefore, the purpose of this pilot study was to evaluate intra-foot temperature gradients across healthy individuals during ambulatory, free-living conditions.

METHODS

Five healthy volunteers participated in a 2-week wear session. Participants wore a sensory insole (Orpyx® SI) in a self-selected footwear 5+ hours per day during their free-living activities. The sensory insole measured temperature at five foot locations (heel, metatarsal 1, 3, and 5, and the big toe, **Figure 1**) at a rate of 1/60 Hz. An individual's intra-foot temperature gradient was evaluated as the difference in temperature versus the metatarsal 3 temperature (the most central location).

RESULTS AND DISCUSSION

As expected, across all five individuals, the heel was typically warmer than the metatarsal 3 (1.2±0.6 ºC for the left foot), the big toe was typically cooler (-1.8±0.8 ºC), and metatarsals 1 and 5 were similar in temperature to metatarsal 3 (-0.4±0.3 -0.5±0.3 for metatarsal 1 and 5, respectively). Foot temperature gradients were similar between the left and right foot (**Figure 1**). However, the magnitude of this intra-foot gradient varied across individuals. For example, in one individual (P04) the big toe was typically 0.9 ºC cooler, whereas in another individual the big toe was typically 3.1 ºC cooler (P05). Results suggest individuals have a personal foot temperature "fingerprint".

In these healthy participants, intra-foot temperature gradients remained consistent throughout free-living conditions (**Figure 1**). While activity and behaviour will change the absolute magnitude of foot temperatures, the intra-foot temperature gradient is likely consistent.

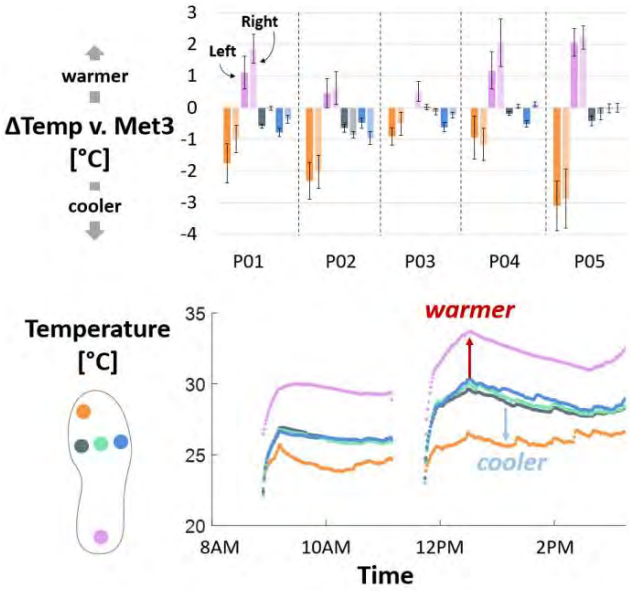

Figure 1 Upper: Intra-foot temperature differences versus metatarsal 3 (Met3) across five participants. Bars = average, error bars = standard deviation across days. Lower: Example of time-series foot temperature

CONCLUSIONS

Wearable, effortless distal skin temperature monitoring is an exciting, emerging digital health opportunity. During free-living conditions, healthy participants exhibit an expected proximal to distal foot temperature decrease, but the magnitude of this gradient is individual specific. Absolute foot temperatures vary throughout the day, but the foot temperature gradient likely remains consistent. These preliminary findings in healthy individuals may guide interpretation of both healthy and pathological time continuous foot temperatures.

ACKNOWLEDGEMENTS

Funding provided by Orpyx Medical Technologies.

REFERENCES

[1] Maijala et al. *BMC Women's Health* **19**: 150, 2019
[2] Roback *Expert Review of Med* **7**:5, 711-718, 2010
[3] Sun et al. *Foot & Ankle* **26**: 10, 2005

Is a wirelessly-charged implant safe?

Maedeh Amirpour[1], Eryn Kwon[2], Kristi Fechney[1]
[1] Department of Engineering Science, University of Auckland, Auckland, New Zealand.
[2] Department of Anatomy and Medical Imaging, University of Auckland, Auckland, New Zealand.
Email: m.amirpourmolla@auckland.ac.nz

INTRODUCTION

Subdermal wirelessly-charged implantable sensors and devices induce electromagnetic waves between the charging and receiving systems, causing damaging effects on the tissue in-between. The electromagnetic energy is converted to thermal energy, which increases the tissue temperature. Heat transfer and its effect on tissue is unknown as it involves a range of varying physical parameters and the tissue complex morphology. We aim to understand the thermal response of tissue with different morphologies to mitigate tissue overheating during wireless charging process. The tissue thermal insult will be modelled by a multi-physics bio-heat mathematical formulation and validated against computational models.

Heat dissipation in living tissues undergoing wireless radio frequency electromagnetic field is a complex phenomenon since it highly depends on tissue size and involves multiple physics such as the heat conduction in solid tissue, heat convection between fluid (blood) and solid tissue, internal heat generation during electromagnetic loss and blood circulation[1-2]. This coupled multi-physics challenge prevents the widespread adoption of Wirelessly-charged implantable devices and sensors which operate under radio frequency electromagnetic field (kHz-MHz). One of the biggest barriers is the danger of tissue overheating from heat dissipation during wireless charging process. We hypothesise that tissue with its full complexity at various scales, from capillary vessels to large tissue layers such as muscle, play a major role in thermal dissipation. However, understanding of the multi-physics nature of heat dissipation including thermal, electromagnetic, structural, fluid and blood flow interactions within tissue underlying wireless electromagnetic stimulation is still unknown.

METHODS

The research will be carried out in two phases. In the first phase, we will generate biofidelic anatomical models with a range of tissue layers and blood vessels based on Magnetic Resonance Imaging (MRI) scans of human tissue with different sizes that encompass reasonable range of typical implant recipient. The second phase will extend the author's previously developed multi-physics, 3-dimensional, high-fidelity finite element (FE) model for high frequency electromagnetic stimulators. The computational model will first apply high frequency electromagnetic fields on the tissue model developed from the phase one to quantify key parameters of thermal dissipation. Moreover, tissue hot spots and temperature distribution will be modelled as electromagnetic loss within tissue leads to temperature rise. In this project, we will answer the below research questions to generate knowledge on a bio-heat mathematical model with considering diffrent tissue morphologies:

1. How does the geometry, size and density of tissue impact the tissue thermal insult?
2. What is the relationship between factors like temperature, pressure, electromagnetic field, strength and chemical potential of living tissue undergoing radio frequency electromagnetic stimulation?
3. How does the interaction between the factors above determine heat dissipation in tissue?

RESULTS AND DISCUSSION

In the first phase, MRI scans and image processesing of a chest area of a 32-year old man was perfromed in order to derived a 3D cad model for the next step which is multiphysics computational simulation of the tissue under wireless elactromagnetic charging (Figure 1).

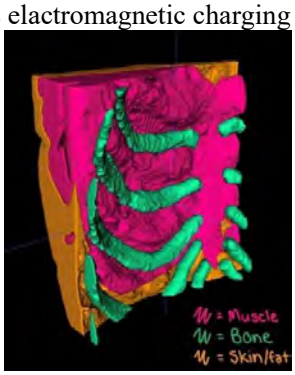

Figure 1: 3D cad model of MRI scan and image prosessing of a right chest area

CONCLUSIONS

This project will give clear insight into the heat dissipation mechanism in variable tissue morphologies undergoing high electromagnetic field exposure and thermal impact.

ACKNOWLEDGEMENTS

The authors would like to thank Transdiciplinary Ideation Fund (TIF) at the University of Auckland to provide financial support on this project.

REFERENCES

[1] Zhang, Q., Sun, Y. & Yang, J. Bio-heat response of skin tissue based on three-phase-lag model, Scientific Reports, Nature Research, 10, 16421, 2020.
[2] Bocan, K.N., M.H. Mickle, and E. Sejdi´c, Multi-disciplinary challenges in tissue modeling for wireless electromagnetic powering: a review. IEEE Sensors, 17, 6498–6509, 2017

DEVELOPMENT AND VALIDATION OF A METHOD TO DETECT INITIAL CONTACT DURING GRADED RUNNING USING A SACRAL MOUNTED INERTIAL MEASUREMENT UNIT

Aida Chebbi[1], Seth Donahue[2], Rachel Robinson[1], Mike Hahn[1]
[1] Department of Human Physiology, University of Oregon, Eugene, USA
[2] Northwestern University Prosthetics-Orthotics Center, Chicago, USA
Email: achebbi@uoregon.edu

INTRODUCTION

Wearable sensors including inertial measurement units (IMUs) allow in-field monitoring and produce an affordable alternative to three-dimensional optical motion capture. Accurate detection of gait events (GEs) is critical for analyzing running biomechanics. Foot mounted IMUs have been used to perform GE detection [1], however it is unknown whether GE can be determined using only a sacral mounted IMU. The purpose of this study was to develop and validate an initial contact (IC) detection method using a sacral mounted IMU. Additionally, we developed a technique to determine whether the IC is from the left or the right foot, based on angular velocity of the sacral mounted IMU. We compare the new method against an IC detection method using foot-mounted IMUs while running on a force instrumented treadmill across a range of speeds and grades.

METHODS

Ten healthy recreational runners (8 F, 2M, 23 years, 169 cm, 59 kg) were equipped with IMUs (Casio, Tokyo, Japan) mounted bilaterally on the dorsal aspect of the foot and at the sacrum. Each participant ran on a force instrumented treadmill (Bertec, Columbus, OH, USA) at three grades: level ground (LG), incline (INC) and decline (DEC) at ±7.5 deg. The total range of speeds across participants was 2.55–4.48 m s−1. For the IMU-based algorithm, first, maxima and minima of sacral angular velocity about the anterior-posterior axis (Sacral ω_y) is found. Then the location of the first maximum and first minimum is compared to determine the sign of the first extrema. Once sign is defined, the second extrema is determined within a 3 ms window. The maximum allowed time between two successive minima / maxima was set to a criterion value of 5 ms. Left initial contact (LIC) was identified as the first peak of the sacral resultant acceleration (Sacral Res Acc) after the minimum of Sacral ω_y. Right initial contact (RIC) was identified as the first peak of Sacral Res Acc after the maximum of Sacral ω_y.

RESULTS AND DISCUSSION

Wada et al [2] compared pelvic orientation angles using a single lower back-mounted inertial sensor during sprinting with a 3D motion capture system. They noted that mediolateral pelvis angles increased at the beginning of the right leg support phase, and started to decrease at the left leg support phase with a difference of 4.1 ± 1.2 deg. Our results (Figure 1) show that during the right impact, sacral angular velocity increased, and the RIC was identified as the first peak after maximum Sacral ω_y. During the left impact, sacral angular velocity increased in the negative direction, and the LIC was identified as the first peak after minimum Sacral ω_y. The time difference between RIC, LIC Foot and Sacrum was between 6.1 ± 2.2 and 2.8 ± 1.6 ms for right side and between 5.8 ± 1.8 and 3.1 ± 1.5 ms for left side (Table 1).

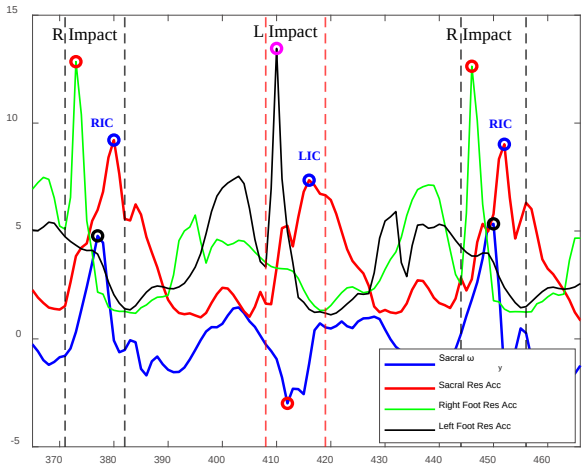

Figure 1 RIC and LIC identification from Sacral Res Acc using the maximum and minimum Sacral ω_y.

Table 1: Time differences between RIC and LIC Foot and Sacrum (ms); Mean ± SD.

	LG	INC	DEC
Right	3.7 ± 1.7	6.1 ± 2.2	2.8 ± 1.6
Left	3.8 ± 1.8	5.8 ± 1.8	3.1 ± 1.5

CONCLUSIONS

The results of this study support the idea that a single inertial sensor at the sacrum can be used to detect initial contact and distinguish between left and right contacts. The algorithm developed in this study will be expanded to include toe off from sacral IMU as part of GE detection in indoor and outdoor running.

ACKNOWLEDGEMENTS

This work was supported in part by an industry sponsored research agreement with Casio, the Wu Tsai Human Performance Alliance and the Joe and Clara Tsai Foundation.

REFERENCES

[1] Donahue S et al. *Sensors*, **22**(9), 3452, 2022.
[2] Wada T et al. *MDPI*, **49**(1)**,** 10, 2020.

Two hands gesture control for a robotic hand

Atheer Khalaf[1], Haidar Khalaf[2], Amdjed Belgacem[2] and Senol Piskin[1*]
[1]Dept. of Mechanical Engineering, Faculty of Eng. and Natural Sciences, Istinye University Istanbul, Turkey.
[2]Department of Computer Engineering, Arel University, Istanbul, Turkey.
[3]Department of Computer Engineering, Kadir Has University, Istanbul, Turkey.
[*]Speaker and corresponding author. Email: senol.piskin@istinye.edu.tr

INTRODUCTION

For years, robots have played a role in society, handling tasks from manufacturing and industry to delicate medical procedures. The safety restrictions and physical limitations of robots have hindered their potential. keyboard and mouse are the standard means of human-computer interaction [1]. Wearable haptic gloves based on flexible sensors are used lately to control similar robotic hands however, they are costly and may not be comfortable for every user. This paper presents an easier method to control a robotic hand using hand gestures by utilizing computer vision (CV). The open-source framework MediaPipe is used to detect human hands through a webcam[2].MediaPipe employs image processing and machine learning to infer landmarks of the real-time captured hand, once the hand model is captured, it can be used to control the robotic hand.

METHODS

CV captures input data at 24 frames per second. The user controls the robotic hand using hand gestures, CV collects the user's hand coordinates, and based on the user's hand motion the robotic hand is controlled. The robotic hand has 6 Degrees of Freedom (DOF), and each finger can move independently as well as the wrist. Arduino chip is used to control the motors of the robotic hand. Since the MediaPipe program was written in python code, Pyfirmata (a python interface) is used to establish a connection between CV & Arduino therefore, Arduino will receive orders from CV based on the detected user's hands to actuate the motors that will allow for the robotic fingers and wrist motion. Once the user's hand is detected by the webcam, CV will automatically display the overlay of the hand and execute the orders according to our algorithm. By displaying their right hand to the webcam, the user can independently control each robotic finger by flexing and unflexing their own fingers. The user can twist the robotic wrist to 170 deg from its origin by contracting their left hand. The Robotic fingers and wrist are controlled at the same time when both hands are displayed.

RESULTS AND DISCUSSION

A recently published paper discussed a robotic hand control system using flexible sensors attached to a haptic glove [3]. Both projects serve a similar purpose however, our system has more DOF, since not only the fingers are controlled but the wrist as well. Our system is less complex and more user-friendly as it has fewer components. It doesn't require any signal transmission modules to provide a wireless connection and no wearable devices are used. As shown in Figure 1. The system has little equipment (a computer that can be replaced by a Raspberry pi board, and a robot). The method was manually evaluated by various users and found to be user-friendly. The accuracy of the system is influenced by the camera quality however, thanks to the MediaPipe framework, it achieved an average accuracy of 95% when standard webcams were employed.

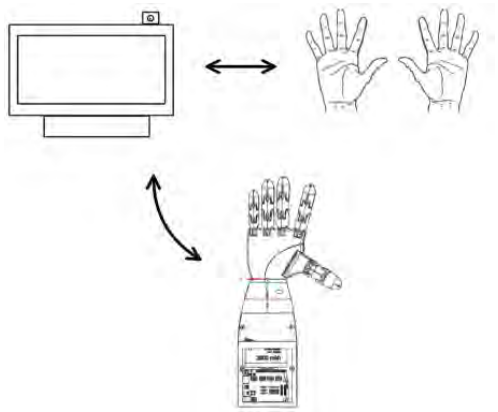

Figure 1 System of CV-controlled robotic hand.

CONCLUSIONS

Gestures can make robots accessible to people with disabilities and can be used to control robots wirelessly. This technique is very simple and easier to control than other complex control systems. More features have been developed and are now being processed in patent work. These features will allow the user to have a more human-like finger motion experience as well as the ability to control the robotic hand with the help of virtual reality (VR).

ACKNOWLEDGEMENTS

This research has received funding from the European Research Executive Agency, Marie-Sklodowska Curie Actions - Global Individual Fellowship (101038096), and from Istinye University, BAP project (2019B1).

REFERENCES

[1] Hassanpour R et al. *IADIS Int Conf Interf*, 2008.
[2] https://mediapipe.dev (accessed Jan. 30, 2023).
[3] Salman F et al. Sens Act. A Phys **309**: 112004, 2020.

WHOLE-BODY KINEMATICS PREDICTION WHILE WALKING AND RUNNING USING A VIRTUAL ACCELEROMETER ON VARIOUS POSITIONS

Gunwoo Park[1], Seungbum Koo[1*]

[1] Department of Mechanical Engineering, Korea Advanced Institute of Science and Technology, Daejeon, Republic of Korea.
Email: skoo@kaist.ac.kr

INTRODUCTION

In addition to transportation, the purpose of locomotion is various such as recreation, sports, or therapy. Poses during walking and running, represented by kinematic gait parameters, affect the performance or injury risk. Previous studies predicted lower body joint kinematics using an inertial sensor on the lower back [1] and shank [2]. The studies showed the feasibility of using a single sensor and artificial neural network (ANN) for specific motion in a database. Nevertheless, further research about the effect of the sensor position is needed. This study is about predicting three-dimensional motion of a whole body with an accelerometer. We compared three sensor positions, left wrist, lower back, and right shank.

METHODS

The motion capture dataset includes data from 198 subjects, 157 males and 41 females (mean and standard deviation of age 28.0 ± 9.8). Motion capture was done on a treadmill with four walking and running speeds, 4 km/h, 8 km/h, 10 km/h, and 12 km/h. Using the inverse kinematics function in OpenSim [3], 28 gait parameters were calculated. Accelerations were calculated at the three body segments, left radius, pelvis, and right tibia. The virtual accelerometer measures three-dimensional acceleration of each segment as a wearable sensor does. The gait parameters were segmented into a gait cycle using ground reaction force and temporally normalized to 100Hz. The dataset was split into training, validation, and test set with 160, 19, and 19 subjects. We trained ANN with two linear layers to predict a gait parameter from a virtual accelerometer data (Figure 1). The ANN has batch normalization with a momentum of 0.9 at the input layer and a dropout function with a probability of 0.5 at the hidden layer.

RESULTS AND DISCUSSION

We compared root-mean-squared error (RMSE) from three positions with an analysis of variance and Tukey's test (Table 1). P-values were obtained for each pair of sensor positions.

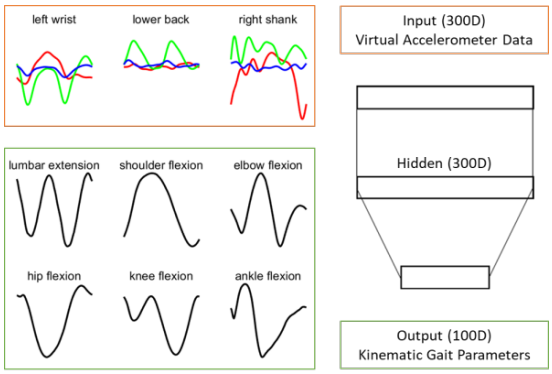

Figure 1 ANN description with input and output.

The sensors were effective in predicting the motion of adjacent joints in the kinematics tree. Upper and lower body movements are mutually related while walking and running [4]. It may be possible to predict a whole-body movement with a single sensor. The virtual accelerometer method may be applied to any motion capture dataset without sensor data.

CONCLUSIONS

This study found an effect of the sensor position on prediction accuracy. Our results will benefit selecting devices to implement the ANN for motion prediction.

ACKNOWLEDGEMENTS

This study was supported by the National Research Foundation (MSIT Project No. 2022M3C1A3080598) and by Institute of Information & Communications Technology (MSIT Project No. 2022-0-00025) funded by the Korea government. This study was supported by Samsung Electronics MX division.

REFERENCES

[1] Lim et al. *Sensors* **22(1)** 53, 2019.
[2] Gholami et al. *Sensors* **20(10)**: 4633, 2020.
[3] Seth et al., *PLoS Comput Biol* **14(7)**, 2018.
[4] Pontzer et al., *J Exp Biol* **212(4)**: 523-534, 2018.

Table 1: The mean and standard RMSE (unit in degrees) of three sensor positions for each gait parameter. The underlined RMSE values are significantly lower than not underlined values for the same gait parameter ($p > 0.001$), and p-values were not shown if $p < 0.001$.

	Left wrist (1)	Lower back (2)	Right shank (3)	*p-value*
Lumbar extension	5.46 ± 3.75	3.66 ± 2.30	5.53 ± 3.57	$p = 0.149$ (1, 3)
Right shoulder flexion	7.01 ± 4.79	6.66 ± 3.88	7.80 ± 4.50	
Right elbow flexion	7.48 ± 4.51	9.53 ± 6.03	9.32 ± 5.54	$p = 0.001$ (2, 3)
Right hip flexion	5.36 ± 2.57	4.47 ± 2.04	4.46 ± 1.90	$p = 0.979$ (2, 3)
Right knee flexion	6.24 ± 2.95	5.19 ± 2.86	2.89 ± 1.15	
Right ankle flexion	7.71 ± 2.66	7.42 ± 2.91	6.61 ± 2.62	

REAL-TIME MUSICAL FEEDBACK FROM PRESSURE-SENSING INSOLES FOR ANKLE FRACTURE REHABILITATION: A CASE REPORT

Markus A. Wimmer[1], Luisa Cedin[1], Christopher Knowlton[1]
[1] Department of Orthopedics, Rush University Medical Center / Chicago, United States.
Email: markus_a_wimmer@rush.edu

INTRODUCTION

Ankle fracture often leads to gait impairments in kinetics, kinematics, and temporospatial parameters several months later[1]. Patient adopts an avoidance behaviour which may cause detrimental impact on contralateral limb and body stability. Gait retraining can be challenging due to continuous therapist guidance. Biofeedback could offer uninterrupted instruction while allowing patients to perceive their performance and adjust it accordingly. Studies have shown that auditory feedback is a promising approach to rehabilitation and gait retraining [2,3], however, they offered only negative stimulus and no engagement. Our aim was to target ankle fracture rehabilitation and gait retraining by using a musical, progressive, and reward-based auditory feedback based on a wireless pressure-sensing insole.

METHODS

A 56-year-old male who suffered a trimalleolar fracture on the right ankle was recruited two months post-op after being released for full weight-bearing. Lack of mobility during walking was evident. Real-time pressure data from sensors under the hallux and second toe and total force were obtained with Insole3 (OpenGo, Moticon) - a 16-sensor pressure insole with an embedded six-axis inertial measurement unit - and transmitted to Max 8 (Cycling '74). A 50N threshold of total force triggered a Musical Instrument Digital Interface chord to play, followed by a second chord when the pressure of the toe sensors exceeded a pre-adjusted threshold (Pachelbel's *Canon in D* four-bar progression). Listening to whether the second chord played would indicate the patient if he applied sufficient pressure on his toes; timing between heel-strike and toe-off would cue the rhythm of the chords. Training consisted of 6 sessions of 12 min, preceded by 5-min warm-up and practice. Health limb practice demonstrated how the music should sound. 3D gait analysis (Qualisys) was conducted at baseline (BL) and after one month of practice (1M) at a self-selected speed to evaluate ankle and foot kinematics. Ankle joint ankle and was determined on Visual 3D (C-Motion).

RESULTS AND DISCUSSION

Higher cadence (BL = 47.7 strides/min; 1M = 50.6) and longer stride lengths (Table 1) were seen after practice. Mean fraction of stance phase was significantly different ($p < 0.001$) between limbs and significantly increased on the affected leg after training ($p = 0.003$). Less plantar flexion during swing phase on the affected side at baseline and range of motion seems more closely related to healthy side after training (Figure 1). Mean pressure under toes nearly doubled on the affected side after training and was distributed more evenly in-between sides but did not reach the level of the healthy limb.

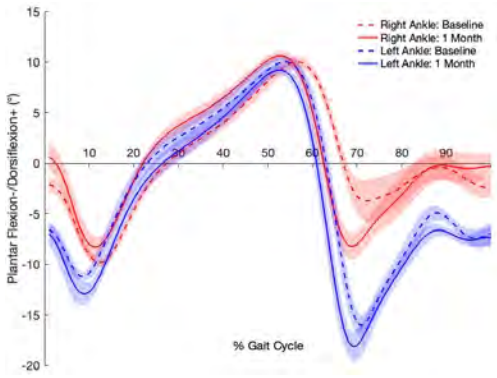

Figure 1 Ankle joint angle at baseline and after one month of training.

CONCLUSIONS

Reward-based and progressive musical auditory feedback resulted in more resemblance on kinematics and symmetric distribution of forces and less pressure avoidance of toe region. Our developed technology has potential to be an evaluation, intervention, and compliance monitoring tool in real-world settings. Further studies are in progress to validate and demonstrate its effects on other clinical conditions.

REFERENCES

[1] Mirando M et al. *Diagnostics* **12**: 199, 2022.
[2] He J et al. *Gait & Posture* **70**: 2019.
[3] Donovan L et al. *Gait & Posture* **40**: 2016.

Table 1: Gait parameters of the healthy (left) and affected (right) side at baseline and after one-month of biofeedback training.

	Baseline		1-Month	
	Left	Right	Left	Right
Mean stride length (m)	1.23 ± 0.03	1.23 ± 0.04	1.36 ± 0.04	1.37 ± 0.05
Stance % of gait cycle	65.6 ± 1.3	60.0 ± 1.4	64.1 ± 3.8	60.8 ± 2.6
Mean pressure - hallux and second toe (terminal stance) (N/cm^2)	16.03	5.85	14.32	9.27

A Hybrid LSTM-ANN Model for Predicting Balance Variables and Spatiotemporal Parameters During Gait Using A Single Waist-Worn IMU

Chih-Ching Yeh[1], Cheng-Hao Yu[1], Yi-Fu Lu[2], Frank Yeong-Sung Lin[2] and Tung-Wu Lu[1]
[1] Department of Biomedical Engineering, National Taiwan University, Taipei, Taiwan
[2] Department of Information Management, National Taiwan University, Taipei, Taiwan
Email: twlu@ntu.edu.tw

INTRODUCTION

Monitoring dynamic balance during gait is critical for fall prevention in the elderly. A well-developed method is by quantifying the inclination angles (IA) of the body's centre of mass (COM) relative to the centre of pressure (COP) and their rates of change (RCIA) in standard gait laboratories [1]. Inertial Measurement Units (IMUs) have become more widely used for gait monitoring in domestic environments owing to the reduction in size and costs [2]. For IA and RCIA, several IMUs would be needed for the complete measurement of the body segments, making it infeasible for daily monitoring. Artificial neural networks (ANN) can potentially reduce the number of sensors, but multiple sensors are still needed in estimating gait parameters [3]. Monitoring balance and spatial-temporal parameters during gait using a single sensor remains challenging. The current study aimed to develop a new approach based on a long short-term memory network (LSTM) and an ANN for predicting IA and RCIA and spatial-temporal parameters using a single waist-worn IMU and to evaluate its accuracy against data obtained using 3D motion analysis systems.

METHODS

Ten healthy young and ten older adult males wearing 50 skin markers and an IMU on the waist walked on a 10-meter walkway while the ground reaction forces were measured with four forceplates and marker data by a motion capture system. The body's COM position was calculated as the weighted sum of the positions of the COM's of all the body segments using the marker data and segmental inertial properties. The COP position was calculated using forces and moments measured from the forceplates. These data were used to calculate gold standard IA, RCIA [1], and spatial-temporal parameters over a gait cycle, which, together with the low-pass filtered IMU data, were used to train the proposed hybrid LSTM-ANN model (Figure 1). The two LSTM layers extracted the IA and RCIA features, which were passed onto the ANN layers with data on body height and leg length to estimate the spatial-temporal parameters. Data from 229 gait cycles were used to train the LSTM-ANN model, and 10% of trials were used to test the model. The model predictions were compared to the gold standard, giving percentage relative root-mean-squared errors (rRMSE). Independent t-tests were used to compare the groups for measured and model-predicted parameters, respectively.

RESULTS AND DISCUSSION

The means (standard deviations) of the rRMSEs of the sagittal IA, sagittal RCIA, frontal IA, and frontal RCIA were 4.17 (0.90), 8.35 (1.40), 6.10 (2.20), 4.60 (0.90), respectively. Those for stride length, speed, cadence and contralateral toe-off and contralateral heel-strike and toe-off were 4.42 (4.30), 7.57 (7.56), 6.86 (6.17), 1.78 (1.63), 1.45 (1.34), 1.52 (1.39), respectively. The proposed LSTM-ANN model accurately predicted balance parameters, giving rRMSE of less than 5% and 8% for sagittal and frontal IA and RCIA, respectively (Table 1). It was also very accurate in predicting gait events and spatial-temporal parameters (Table 1). Such error levels were smaller than between-group differences reported in the literature [1]. Similar between-group effects were also obtained using measured and model-predicted data. Further training of the new model with a bigger dataset, including people with fall risks, will be helpful to improve the prediction accuracies and its application in balance monitoring and fall prevention.

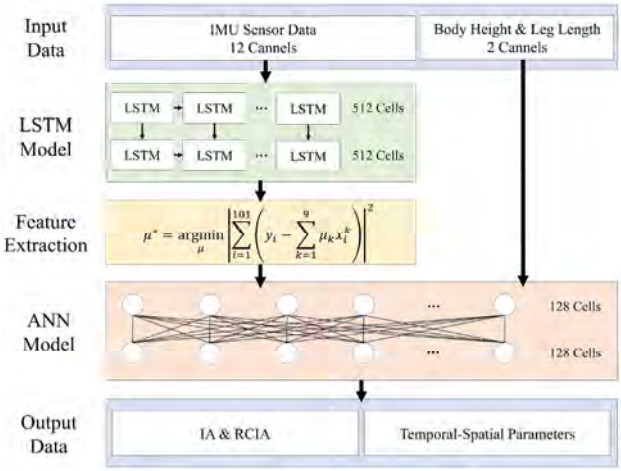

Figure 1 The structure of the proposed LSTM-ANN neural network model.

CONCLUSIONS

This study was the first in the literature to show the feasibility of predicting whole-body balance variables and spatiotemporal parameters during gait based on a single IMU on the pelvis. The current LSTM-ANN model was shown to have reasonably high accuracy and great potential for real-life monitoring of dynamic balance in people with fall risks.

REFERENCES

[1] Hong, S.W., et al. *Gait Posture* **42(4)**: 523-528, 2015.
[2] Atrsaei, A., et al. *NPJ Parkinsons Dis.* **7(1)**, 24, 2021.
[3] Yu, S., et al. *Ann Biomed Eng*. 1-14, 2023.

PROPHYLACTIC CERCLAGE FIXATION FOR PREVENTION OF PERIPROSTHETIC FEMORAL FRACTURES: THE SIGNIFICANCE OF CABLE LOCATION

Kartik I. Reddy[1], Jonathan E. Gold[1], Sabir K. Ismaily[1], David Rodriguez-Quintana[1], and Shuyang Han[1]
[1] Department of Orthopaedic Surgery, McGovern Medical School, UTHealth Houston, Texas, USA.
Email: shuyang.han@uth.tmc.edu

INTRODUCTION

Periprosthetic femoral fracture is a common complication of total hip arthroplasty (THA). Prophylactic cerclage cable has been advocated for preventing propagation of cortical cracks during THA and postoperative activities [1,2]. Clinical studies have recommended placement of prophylactic cables at levels ranging from 0-20mm below the fracture, while definitive biomechanical data guiding the location of prophylactic cables is still lacking. Therefore, this biomechanical study was performed to examine two research questions:

(1) What is the acceptable cerclage cable location in order to effectively prevent fracture propagation?
(2) How does the cable tension change during loading?

METHODS

Femoral shafts of five fresh-frozen cadavers were prepared in this study. In each femoral shaft, five tests were performed sequentially with a CoCr prophylactic cable placed at varying distances (i.e., 5mm, 10mm, 15mm, 20mm, and cableless) from a longitudinal fracture. The fracture was initiated prior to each test using a surgical saw. The cerclage cable was outfitted with a compressive load cell in order to achievethe same cable tension across different tests and to measure the cable tension changes during subsequent loading.

To prepare for testing, the femoral canal was reamed, and then a 4° taper was advanced with an MTS machine at a rate of 10mm/min (Figure 1A). The test was terminated when crack propagation occurred or at 15mm displacement. The fracture was stained with blue ink to facilitate visualization. The ultimate force and cable tension were compared between different groups with a repeated measure ANOVA and post hoc analysis using Fisher's PLSD test.

RESULTS AND DISCUSSION

Compared to the control group, a cerclage placed at 5mm below the initial fracture increased the ultimate force by 2.4-fold to about 3 times the bodyweight (p=0.02). As the cerclage was placed further away, the ultimate force continuously decreased. When the distance reached 20mm, the cerclage did not provide any resistance to fracture propagation (Table 1).

The cable tension changed in different patterns between groups. With the cable at 5-10mm, the tension first remained flat and then increased rapidly in the late stage (Figure 1B). However, when the cable was 15-20mm below the fracture, there was minimal change in the cable tension throughout the test (Figure 1C), indicating that the cable was not effective.

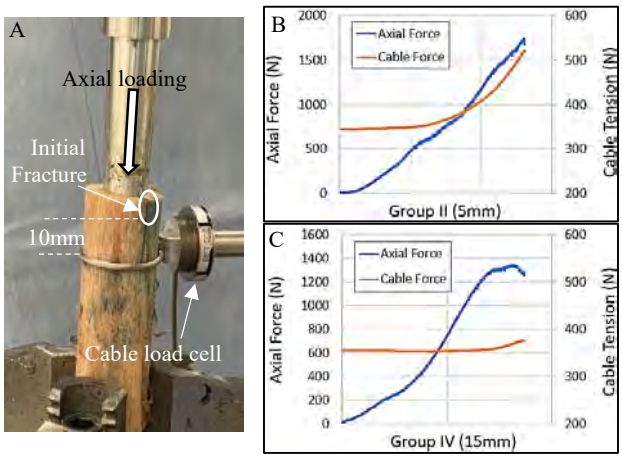

Figure 1. Test setup (A) and typical graphs (B and C) showing variations of the axial force and cable tension during loading.

CONCLUSIONS

The results of this biomechanical study supported the use of a prophylactic cerclage cable for periprosthetic femoral fractures. More importantly, the closer the cerclage to the fracture, the better the performance for preventing fracture propagation. When a prophylactic cerclage cable was placed 20mm below the fracture, the biomechanical response of the bone was similar to that without a cerclage.

ACKNOWLEDGEMENTS

The cerclage cables were donated by ZimmerBiomet.

REFERENCES

[1] Kuster L et al. *J Arthroplasty* **34**: 987-90, 2019.
[2] Gkiatas I et al. *J Arthroplasty* **36**: 3333-9, 2021.

Table 1: The ultimate force and increase in cable force in different groups. p.s. * significant difference compared to the control group.

Variables	Group I (Control)	Group II (5mm)	Group III (10mm)	Group IV (15mm)	Group V (15mm)
Ultimate force (N)	705.6±110.6	1798.6±370.6*	1263.8±222.8*	1081.2±193.1*	650.2±111.7
Cable force increase (N)	N/A	133.9±52.9	81.9±26.3	43.4±13.1	3.4±6.6

PASSIVE COLLAR STIFFNESS OF A CUSTOM-DESIGNED HIGH-COLLAR SHOE

Alireza Nasirzadeh[1], Jaeha Yang[1], Seung-Tae Yang[1], Juseok Yun[1], Young Yoon Bae[2], Juyeon Park[2], Jooeun Ahn[3] and Giuk Lee[1]

[1] Department of Mechanical Engineering, Chung-Ang University, Seoul, Republic of Korea.
[2] Department of Textiles, Merchandising, and Fashion, Seoul National University, Seoul, Republic of Korea.
[3] Department of Physical Education, Seoul National University, Seoul, Republic of Korea.
Email: giuklee@cau.ac.kr

INTRODUCTION

High-collar shoes should provide enough collar stiffness (CS) to protect the ankle during high-demand activities such as running. The primary purpose of this study was to introduce a high-collar running shoe that allows regulating CS and a new method to measure CS.

METHODS

To fabricate a flexible running shoe (figure 1, C), neoprene fabric was used for the upper part, and thermoplastic polyurethane and rubber were used for the midsole and outsole, respectively. Two Boa® ratcheting reels (Boa Technology Inc, USA) were implemented on the lateral sides of the collar wired to a 3D-printed top cover which allowed adjusting CS (figure 1, A & B). To measure passive CS, the force generated by a 200W motor at a constant velocity of 10 cm/s was applied to the shaft of a foot prosthesis (figure 1, D). Starting from 90°, the motor pulled the shaft to 60° and 110° for dorsi-flexion and plantar flexion, respectively. By reaching the end range angle, the motor released the wire with the same velocity to measure collar recoil movement. An IMU sensor (MTi-630, Xsens, Netherland) controlled the motor by measuring the shaft's angular position. The force in the wire was measured using a load cell (LSB205, Futek Inc., USA) synchronized with the Vicon motion capture system that tracked collar movement and wire angle by reflective markers.

At the 90° shaft position, two pressure-measuring sensors (Kikuhime, TT Medi Trade, Denmark) were placed at the level of the medial and lateral malleolus of the prosthesis. Then, the Boa® ratcheting reels were regulated until both sensors reached the same levels of 10-, 30-, and 60-mmHg, representing the low, medium, and high CS conditions, respectively.

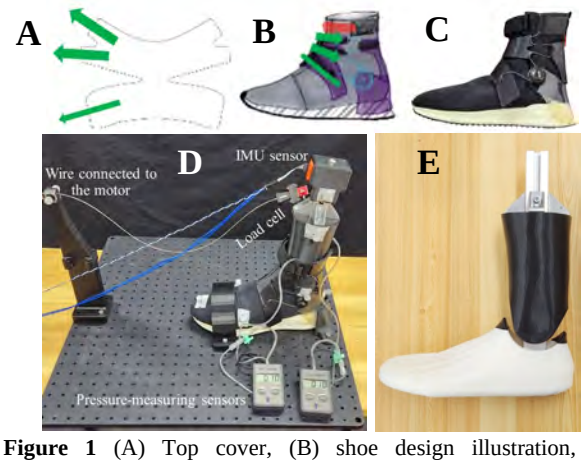

Figure 1 (A) Top cover, (B) shoe design illustration, (C) manufactured prototype of the custom-designed high-collar shoe, (D) collar stiffness measurement setup, and (E) foot prosthesis.

All data were filtered using a fourth-order low-pass Butterworth filter with a cut-off frequency of 10 Hz. The moment-angle curve was calculated using the component of the wire's force perpendicular to the shaft. The slopes from 90° to 60° and 110° characterized the dorsiflexion and plantar flexion CSs, respectively [1]. The area between the pulling and recoiling curves indicates the mechanical energy lost [1].

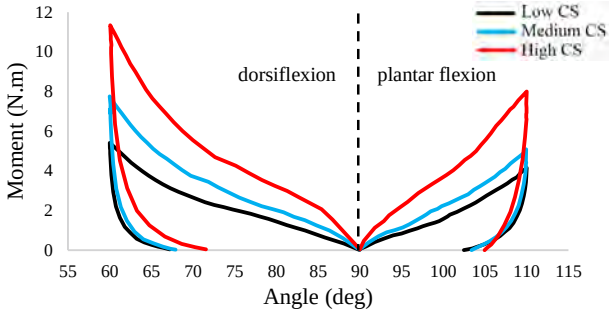

Figure 2 Moment-angle diagram for three CS conditions.

RESULTS AND DISCUSSION

The stiffness characteristics for three CS conditions are presented in Figure 2. The CS ($Nm.deg^{-1}$) for low, medium, and high conditions were -1.8, -2.57, and -3.78 for dorsiflexion and 2.04, 2.53, and 3.98 for plantar flexion, respectively. Also, energy loss (%) for low, medium, and high CS conditions were 90.2, 89.9, and 85.8 for dorsiflexion and 82.1, 84.3, and 87.5 for plantar flexion, respectively.

The main issue with similar studies that tried to measure CS is that they did not solely measure the CS but the whole shoe's bending stiffness [2], applied a range of constant forces to the shaft that makes it unclear how the high-collar reacted during different ankle angles [3] or applied the force to the shaft manually [1]. The presented method addressed these problems.

CONCLUSIONS

Mechanical testing of the high-collar shoe revealed nonlinear moment-angle relations for all conditions, which is typical for the material used for the high-collar shoe. Compared to the low CS condition, the stiffer collars required higher forces to deform to the same end range and returned lower percentages of energy for dorsiflexion and higher percentages for plantar flexion during recoiling.

REFERENCES

[1] Kersting UG et al. *J Biomech* **126**: 110643, 2021.
[2] Cikajlo I et al. *Ergonomics* **50**: 2171-82, 2007.
[3] Böhm H et al. *J Biomech* **43**: 2467-72, 2010.

MOUSE HORIZONTAL AIMING PERFORMANCE BETWEEN TWO GAMING MICE OF DIFFERENT SLANTED DESIGN

Yu-Lin Chen[1,2], Winny Chang[1], and Kuang-Wei Lin[1]
[1] BenQ Corporation, Taipei City, Taiwan.
[2] National Taiwan Sport University, Taoyuan City, Taiwan.
Email: a6984802@gmail.com

INTRODUCTION

In the past, studies pointed out that lightweight mouse may effectively optimize performance while minimizing discomfort [1][2]. However, the shape of the mouse is the first point of contact with the human body, and it is the key that directly affects the feel of the movement. But how the shape of the gaming mouse affects the horizontal target acquisition skills is unknown. Therefore, the purpose of this study was to explore the difference of slanted design in gaming mice which e-sport players use. In this study, it was hypothesized that all variables in given e-sport players would be significantly different between the two designs.

METHODS

Eight male e-sport professional players of first-person shooter game volunteered as participants. The data collection was done in an indoor experimental area with a dedicated "ZOWIE ZONE" gaming table. The kinematics data include hand horizontal velocity, and metacarpophalangeal (MCP) and proximal interphalangeal (PIP) angle of index finger, which were detected by Motion Analysis System with Cortex 9.0.0.44. The muscle activation signals of the 1st dorsal interossei (1st DI), 4th dorsal interossei (4th DI), abductor digiti minimi (ADM), extensor indicis (EI), flexor carpi radialis (FCR) and extensor carpi ulnaris (ECU) were recorded with the Delsys-16 EMG system. A nonparametric statistical procedure Wilcoxon was used to test differences.

RESULTS AND DISCUSSION

This study shows that the MCP joint angle of the index finger and the other parameters between two slanted design during horizontal task were not significantly different (Table 1). The MCP joint angle of the index finger, which may affect the comfort of moving your palm horizontally and clicking, indicates the angle between the first knuckle of the index finger and the palm when the palm rests on the back of the mouse. In horizontal target acquisition skills, reaching the target quickly and accurately are achieved by muscle coordination and joint movement from upper arm to forearm, and finally to the mouse. There was no significant difference in hand velocity and upper extremity muscle activation signals between the two design during horizontal aiming task. The reason may be that not all players' movements are consistent. For example, the wrist-aiming gamers have more wrist angular displacement, while the arm-aiming gamers use more upper arm and forearm to move quickly.

CONCLUSIONS

The kinematic data in this study shows that the MCP joint angle of the index finger and the horizontal aiming performance were affected by mouse slant. It is recommended to investigate whether other shape designs of the mouse have impacts on performance in the future, which could help know more clearly how to effectively design the shape to enhance the performance.

REFERENCES

[1] Yishu Y et al. *Proc Hum Factors Ergon Soc Annu Meet* 66: Issue 1, 2022.
[2] Eoin C et al. *Appl Ergon* 99: 103637, 2022.

Table 1: Deference of the kinematics and muscle activation signals data between two frontal inclination design.

	Mouse A	Mouse B	*p-value*
Kill per minute	80.71 ± 11.92	87.68 ± 9.70	0.078
Maximum medial-lateral velocity (m/s)	5.38 ± 1.06	5.55 ± 1.06	0.945
MCP joint angle of index finger (°)	142.15 ± 8.82	145.75 ± 8.30	0.008*
PIP joint angle of index finger (°)	146.22 ± 10.81	145.5 ± 10.44	0.547
1st dorsal interossei (%)	8.40 ± 5.36	8.42 ± 4.69	0.109
Extensor indicis (%)	16.43 ± 9.01	16.56 ± 9.57	0.945
Extensor carpi radialis (%)	9.36 ± 7.14	9.52 ± 6.81	0.844
Extensor carpi ulnaris (%)	23.77 ± 11.29	23.20 ± 11.24	0.547

Compare of the clinical efficacy of volar plating with the pronator quadratus preservation versus the pronator quadratus repair or transection for distal radius fractures in different age groups

Kazuya Umeyama[1], Takuya Kawai[1], Yuki Takahashi[1], Aoi Kawachi[1], Hiroki Matsukawa[1], Yoshiki Nishikawa[1], Moe Andou[1], Kanato Haruuchi[1] and Yasutaka Yoshinaka[2]

[1] Department of Rehabilitation / Daito chuou Hospital, Daito, Japan.
[2] Department of Orthopedic Surgery / Daito chuou Hospital, Daito, Japan.
Email: b5108949@kio.ac.jp

INTRODUCTION

Distal radius fractures (DRF) are one the most common upper limb injuries requiring open reduction and internal fixation in an orthopaedic setup. Over the last decade, volar plating has become the treatment of choice for such fractures, as it results in better functional outcomes with greater fragment stability and low complication rates as compared to other means of management. The pronator quadratus (PQ) muscle covers the distal radius metaphysis and needs to be released from the radial end to visualise the fracture and subsequent fixation of the volar plate. Considerable controversy exists if post-fixation, the muscle needs to be repaired or not. Clinicians have reported contrasting opinions, with some favouring PQ repair while others demonstrating no beneficial role of the same. The purpose of this study was to evaluate and compare the clinical efficacy of volar plating with PQ preservation versus PQ repair or transection for DRF in different age groups.

METHODS

In this study, (a) range of motion (ROM) and (b) grip strength meter (TTM, Tokyo, Japan) were used.

(a) ROM was performed as long as there was no pain, and ROM of palm flexion, dorsi flexion, radial flexion, ulnar flexion, internal rotation, and external rotation was evaluated in the sitting position.

(b) In an upright position, the patient gripped the grip strength meter and adjusted it so that the second joint of the index finger was at 90 degrees. The upper limbs were held in a posture with the upper limbs drooping toward the body, and the measurement was performed without swinging the grip strength meter. Since grip strength is affected by body size and other factors, the value on the affected side was divided by body weight to obtain the body weight ratio.

All consecutive fractures of the distal radius surgically treated with the Vollard plate were assigned to a group with PQ preservation versus PQ repair or transection and grouped according to age. Groups were divided into 60s, 70s, and 80s (Group A: 60-69 years, 5 patients, Group B: 70-79 years, patients, Group C: 80-89 years, 6patients). 22 patients had complete 4 week follow-up (1,2,3,4 weeks) and were included in this study. 22 patients who were between September 2018 and December 2022, there with DRF underwent open reduction and internal fixation using the volar locking palmar plates (Synthes or MEIRA companies). Written informed consents were obtained from all subjects prior to the experiments. The range of motion and grip strength at each week were compared between groups with and without PQ restoration by age.

RESULTS AND DISCUSSION

ROM and grip strength for each group at each week were determined using a t-test. There were no differences among the groups in the 60s. In the 70s, range of motion was better in dorsiflexion and palmar flexion at 1 week in the PQ muscle preservation group (Table 1). In the 80s, the grip strength to body weight ratio was stronger in the PQ muscle preservation group in grip strength at 1, 3, and 4 weeks (Table 1).

CONCLUSIONS

In this study, dorsiflexion and palmar flexion was better at 1 week in the 70s PQ muscle sparing group, and grip strength to weight ratio was better at 1, 3, and 4 weeks in the 80s PQ muscle sparing group. The results of this study revealed that age influences the decision to preserve or not preserve the PQ muscle for DRF in the early postoperative period.

Table 1: Comparison of ROM and grip strength between volar plating with PQ preservation versus PQ repair or transection for DRF in different age groups

	PQ preservation	PQ repair or transection	*p-value*
Group B dorsal flexion (1week)	29.167° ± 6.6646°	47.500° ± 10.607°	$p = 0.024$
Group B palm flexion (1week)	34.167° ± 5.845°	50.000° ± 14.142°	$p = 0.049$
Group C grip strength (1week)	0.067 ± 0.054	0.161 ± 0.038	$p = 0.033$
Group C grip strength (3week)	0.111 ± 0.055	0.227 ± 0.070	$p = 0.028$
Group C grip strength (4week)	0.122 ± 0.063	0.282 ± 0.066	$p = 0.009$

The optimal tunnel entry point in cranial cruciate ligament reconstruction for dogs: a simulation analysis for femoral tunnel placement

Ching-Ho Wu[1], Tsai-Yu Lee[1], Shih-Wen Wang[1], and Cheng-Chung Lin[2]
[1]Institute of Veterinary Clinical Science, National Taiwan University, Taipei, Taiwan
[2]Department of Electrical Engineering, Fu Jen Catholic University, New Taipei City, Taiwan
Email: chinghowu@ntu.edu.tw

INTRODUCTION

Intraarticular reconstruction of the cranial cruciate ligament (CCL) aims to repair stifle stability and physiological function in dogs. However, to date, its poor postoperative outcomes made it less favorable among veterinary surgeons, and tunnel malpositioning was one of the most common causes of complications [1]. For instance, insufficient tunnel length was shown to result in weak fixation strength [2]. There is no consensus on the position/orientation of tunnel placement in canine CCL reconstruction. Thus, the study aimed to explore the potential femoral tunnel entry points (FTEPs) on the lateral femoral condyle by simulation analysis of commonly utilized criteria for human ACL reconstruction, namely femoral length, footprint coverage, and tunnel-face angle.

METHODS

The computed tomography (CT) scans of hindlimbs from 10 median-breed adult dogs (7 females and 3 males; body weight: 15.2–22.6 kg) were collected, from which 18 femoral bone models, free from bone and articular abnormalities, were reconstructed (9 left and 9 right). The FTEPs were determined on femoral model surfaces using an approach modified from the study by Hodel et al. [3](Figure 1A). The simulated femoral tunnels were placed by creating 4.5-mm diameter hollow cylinders from the candidate FTEPs toward the centroid of the CCL footprint on the femur. The femoral aperture was defined as the intersection area between the simulated tunnel and the medial surface of the lateral femoral condyle. The tunnel length was defined as the distance between the centroid of the femoral CCL footprint to the FTEP. The footprint coverage was defined as the similarity between the CCL footprint and the apertures as follows:

$$\text{Similarty} = \frac{\text{intersection of areas}}{\text{union of areas}} 100\% \quad (1)$$

The tunnel-face angle was defined as the angle between the central axis of the tunnel and the tangent surface at each FTEP.

RESULTS AND DISCUSSION

The results showed that the FTEP A7 has the highest footprint similarity (Figure 1B). The more cranial FTEPs possess longer tunnel lengths. Since a tunnel length <15 mm was found to affect graft strength [2], the FTEPs caudal to A4, B5, C5, D5, E4, and F3 should be avoided (Figure 1B). In clinical practice, a smaller tunnel-face angle is challenging to drill tunnels even for experienced surgeons. An adequate tunnel-face angle was never suggested in the literature. In the present study, to our surgical experience, we recommend a tunnel-face angle >30° to ensure successful tunnel drilling. As a result, the FTEPs other than A11, C9, C10, D8, D9, and E8 were feasible for tunnel placement (Figure 1B). In summary, FTEP A7 gives the highest footprint similarity and satisfies the demands for sufficient tunnel length and tunnel-face angle.

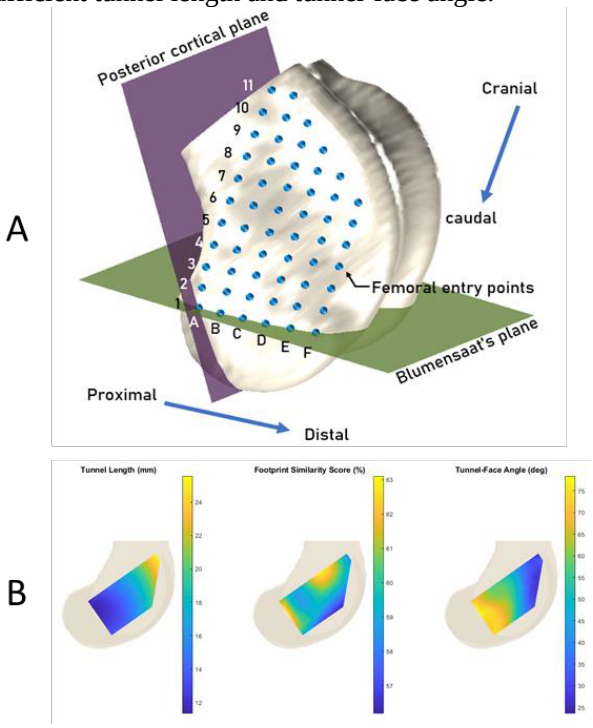

Figure 1 (A) The candidate FTEPs (B) Heatmaps on the lateral condyle show averaged tunnel length (mm), footprint similarity (%), and tunnel-face angle (°) of each FTEP.

CONCLUSIONS

The study recommends the FTEP, A7, for the outside-in drilling of the 4.5-mm-diameter femoral tunnel on the lateral femoral cortex in canine CCL reconstruction as it can yield the highest footprint similarity and satisfy the criterion of tunnel length and tunnel-face angle.

REFERENCES

[1] C. Sommer et al., Knee Surgery, Sports Traumatology, Arthroscopy, vol. 8, no. 4, pp. 207-213.
[2] L. Qi, et al., Arthroscopy: The Journal of Arthroscopic & Related Surgery, vol. 27, no. 6, pp. 825-833.
[3] S. Hodel et al., Journal of Experimental Orthopaedics, vol. 8, no. 1, p. 44.

CHANGES IN LOWER LEG KINEMATIC FREQUENCY CONTENT DURING PRE-GROUND CONTACT AND WEIGHT ACCEPTANCE PHASES OF ACL INJURY RISK SCREENING TASKS

Simon Augustus[1] and Neal Smith[2]

[1] Applied and Human Sciences, Kingston University, London, UK.
[2] Institute of Sport, University of Chichester, Chichester, UK.
Email: s.augustus@kingston.ac.uk

INTRODUCTION

Change of direction (COD) and single leg drop jump (SLDJ) tasks are often used to assess non-contact ACL injury risk. Kinematic and force data are combined in 3D motion analysis to derive biomechanical proxies of injury risk (e.g. peak knee abduction moment during weight acceptance; WA). However, the extent to which foot-ground collisions induce expansion of lower leg frequency content is unknown. Understanding these changes is important if researchers are to optimise use of contemporary low-pass filter techniques that vary the magnitude of noise reduction over different phase of a task (i.e. transition from aerial to ground contact) [e.g., 1,2]. The aim of this study was thus to assess changes in foot and shank marker frequency content during the pre-ground contact phase, WA and post-WA phases of COD and SLDJ tasks.

METHODS

Three-dimensional lower limb kinematics were collected from 16 recreational athletes (77 ± 12 kg, 1.76 ± 0.09 m, 26.8 ± 4.5 years) performing unanticipated COD (approach velocity = 4-5 m/s) and SLDJ (drop height = 0.3 m) tasks (250 Hz; Oqus 300, Qualysis Medical AB, Sweden). Marker trajectories from the ground contacting leg (Table 1) were exported to Matlab (R2022a, Mathworks, USA) where frequencies corresponding to 95% cumulative signal power were determined for each: pre-ground contact (peak vertical position to vGRF > 10N), WA (vGRF > 10N to first trough following the vGRF impact peak) and post-WA phases (first trough following the vGRF impact peak to vGRF < 10 N). This analysis was performed in each X (medial/lateral), Y (anterior/posterior) and Z (vertical) planes and comparisons between phases made using pairwise effect sizes (Cohen's *d*; 0.2 - 0.5 small, 0.5 - 0.8 medium, > 0.8 large).

RESULTS AND DISCUSSION

COD and SLDJ tasks both showed large expansions in marker frequency content between pre-ground contact to WA, then reductions between WA and post-WA (d = 0.5 – 4.0; Table 1). This was likely due to the sudden deceleration of the markers after foot-ground collision. For COD, while frequencies expanded in all planes following ground contact, this was most pronounced in the vertical plane (d > 2.0) and these changes were similar irrespective of marker location. For SLDJ, frequency content was generally lower than for COD, and thus expansion and reduction was less pronounced (d = 0.3 – 3.0). This was likely due to a slower ground-contact velocity. However, like COD, the largest expansions during WA were in the vertical plane and were most evident for the foot markers (Table 1).

CONCLUSIONS

COD and SLDJ ACL injury risk screening tasks induce abrupt expansion and then reduction of lower leg kinematic frequency content following foot-to-ground collision. Given proxies of injury risk are often derived after transition to the higher frequencies during WA (e.g., peak knee abduction moment), researchers might consider using low-pass filter methods that vary the magnitude of noise reduction in different phases of a movement [e.g., 1,2]. The data presented here can help inform cut-off frequency selection and optimise signal-to-noise ratios when using such methods for COD and SLDJ tasks. However, it remains to be seen whether adopting such techniques would offer improvements for identifying individuals at risk from non-contact ACL injury.

REFERENCES

[1] Augustus S et al. *J Biomech* **101**: 109639, 2020.
[2] Davis D & Challis J. *J Biomech* **101**: 109619, 2020

Table 1: Mean ± SD frequencies (Hz) at 95% cumulative signal power for lower leg markers in different phases of the COD and SLDJ tasks.

	Pre-Ground Contact			Weight Acceptance			Post-Weight Acceptance		
	x (med/lat)	y (ant/post)	z (vert)	x (med/lat)	y (ant/post)	z (vert)	x (med/lat)	y (ant/post)	z (vert)
COD									
5th Met. Head	16.8 ± 6.9	26.4 ± 7.7	15.4 ± 7.1	34.9 ± 14.3	35.6 ± 15.5	49.0 ± 11.2	5.6 ± 4.9	8.3 ± 5.5	8.9 ± 4.1
Calcaneus	16.9 ± 6.8	30.4 ± 13.3	20.5 ± 9.0	34.3 ± 14.3	35.7 ± 15.6	26.7 ± 14.2	4.8 ± 4.7	10.1 ± 5.5	6.3 ± 2.7
Distal Shank	19.2 ± 8.3	29.6 ± 12.8	14.6 ± 7.6	35.8 ± 14.8	41.0 ± 18.9	35.4 ± 13.8	5.7 ± 5.0	7.0 ± 3.4	3.7 ± 1.5
Proximal Shank	18.8 ± 7.2	32.3 ± 15.8	15.1 ± 7.4	35.5 ± 14.4	43.1 ± 19.5	34.8 ± 13.9	5.6 ± 4.5	6.5 ± 2.9	3.4 ± 1.4
SLDJ									
5th Met. Head	13.9 ± 4.9	13.0 ± 4.9	14.8 ± 5.3	20.0 ± 9.1	19.9 ± 9.5	29.9 ± 11.8	3.2 ± 1.7	4.1 ± 3.1	11.2 ± 4.8
Calcaneus	14.5 ± 5.1	13.1 ± 4.5	13.2 ± 4.6	23.3 ± 8.4	18.3 ± 9.3	31.5 ± 6.5	4.5 ± 2.4	2.8 ± 1.3	8.5 ± 3.4
Distal Shank	13.4 ± 3.7	13.5 ± 4.6	12.9 ± 4.2	20.3 ± 9.2	20.0 ± 10.8	22.9 ± 8.3	3.3 ± 1.4	3.0 ± 1.2	4.3 ± 1.4
Proximal Shank	12.9 ± 4.0	13.8 ± 5.4	12.7 ± 4.2	20.0 ± 9.2	23.7 ± 13.3	22.3 ± 8.3	3.0 ± 1.6	3.0 ± 1.1	4.1 ± 1.4

The effect of racket mass on effective striking mass in tennis

Yoshiyuki Kawano[1], Masahiro Ikenaga[2], Nobue Okuma[2] and Hiroyuki Nunome[1]
[1] Faculty of Sports and Health Science, Fukuoka University, Fukuoka, Japan.
[2] Advanced Research and Development, YONEX CO., LTD, Nagaoka, Japan.
Email: k.yoshiyuki0729@gmail.com

INTRODUCTION

The initial ball velocity can be enhanced in tennis by increasing the racket's momentum at ball impact. However, due to the game's characteristics, increasing the racket's momentum by increasing the racket's mass would not always provide an advantage for players.
At the moment of ball impact in tennis, the racket's momentum is imparted to the ball where a part of the racket's mass is utilized as effective striking mass. Currently, many amateur tennis players tend to select a racket of 300g because the mass has been recognized as the "gold standard". However, it is still unknown whether the gold standard racket is the best in terms of effective striking mass. Thus, the purpose of this study was to clarify whether the mass of the gold standard racket (300g) is a reasonable mass for tennis rackets from the perspective of effective striking mass.

METHODS

Twenty-three experienced and right-handed tennis players (19 males and 4 females, height: 170.91 ± 8.81cm, weight: 62.96 ± 6.93kg) participated.
Rackets with five different masses (Racket_1(272g); Racket_2(285g); Racket_3(300g); Racket_4(315g); Racket_5(330g)) were prepared and the subjects were instructed to strike six balls delivered from a ball launcher (Slinger Bag, Slinger Inc.), as hard as possible so that the ball goes into the opponent's court.
An eight-camera motion capture system (Vicon Vero, Vicon Ltd.) was used to capture the subject's body and racket movements at 250 fps. The initial velocity of the ball after ball impact was measured using a TrackMan (TrackMan Inc.).
Of the five markers attached to the racket, the midpoint of two markers on either side of the racket was used to define the point where the participants hit the ball.
Applying the law of conservation of momentum with the assumption of the centrifugal collision happens between the racket and ball, effective striking mass during tennis hard strokes was calculated.

RESULTS AND DISCUSSION

We aimed to clarify the effect of gross racket mass on effective striking mass to examine whether the gold standard racket has some rationale from the perspective of effective striking mass.
On average, the striking masses of Racket_1–5 corresponded to 76.18 ± 6.90%, 75.86 ± 6.40%, 74.41 ± 6.42%, 73.44 ± 6.96%, and 72.10 ± 5.49% of the racket masses, respectively. The racket masses always exceeded the striking masses in all conditions (Figure 1). This finding supported the previous finding [1] and indicates that the mass required for ball impact (striking mass) can be provided by the mass of the racket alone under the given conditions in this study. In this study, we could not find any scientific rationales for the gold standard mass (300g) generally applied for conventional tennis rackets, suggesting tennis rackets could be lighter.

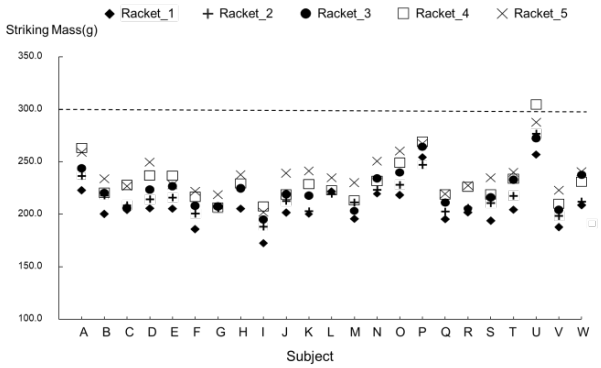

Figure 1. Effective striking masses during groundstrokes in tennis.

CONCLUSIONS

For tennis groundstrokes (hard shots), effective striking mass was found to be lighter than the racket's "gold standard" (300g), suggesting that tennis rackets could be even lighter.

ACKNOWLEDGEMENTS

This study was supported by YONEX CO., LTD.

REFERENCES

[1] Watanabe T et al. *Medicine and Science in Sports* **11(4)**: 359–361, 1979.

WHEELCHAIR OPERATING CAPABILITIES OF ELDERLY CAREGIVERS

Misono Sakai[1], Makoto Ikeda [1], Taisei Yamamoto[1], Tsubasa Kawasaki[1], Satoshi Sugimoto[1], Syogo Ninomiya[1], Akio Kobe[1], and Takenobu Inoue[2]

[1] School of Health Science, Tokyo International University,Saitama, Japan

[2] Department of Assistive Technology, Research Institute of the National Rehabilitation Center for Persons with Disabilities, Saitama, Japan. Email: msakai@tiu.ac.jp

INTRODUCTION

The population of older people has been increasing in Japan. As a result, an increasing number of elderly people are caring for other people of the same generation. How safe it is for elderly caregivers to operate a wheelchair on mainly barrier-free roads is unknown. The purpose of this study is to investigate the wheelchair operating capabilities of elderly people based on their body function.

METHODS

A total of 56 community-dwelling women participated in this study. Of this, 36 were considered elderly (average age: 79.4±3.8 years, height 149.5±5.4 cm, and weight 51.8±7.1 kg), and 20 were young adults (average age 18.9±1.0 years, height 159.8±4.8 cm, and weight 54.8±6.9 kg). The study was approved by the ethics community of Tokyo International University. All participants gave written and signed informed consent. We evaluated participants using the two-step test, stand-up test, and 25-question Geriatric Locomotive Function Scale to detect locomotive syndrome, which the Japanese Orthopaedic Association defines as a condition of reduced mobility. We also evaluated normal and fast walking times over a 5-m distance with and without a 75 kg dummy-weighted wheelchair, Timed Up and Go test (TUG), timed one-leg stand (eyes open and closed), grip strength (both hands), wheelchair operation test (time to tip caster to 10-cm height, travel up a 4.39-m longitudinal slope, go through a left-inclined 4.14-m course, and recovery from one forward-wheel dropping). For the statistical analysis, we used the Mann-Whitney *U* test or a two-sample *t*-test to compare performances between the two groups. Additionally, we used multiple regression analysis for wheelchair operation ability and logistic analysis for the property of tip caster (stepwise selection method).

RESULTS AND DISCUSSION

Of the 36 older people, 24 had Stage 1 locomotive syndrome, six people had Stage 2, two people had Stage 3, and four people did not have locomotive syndrome. The Stage of locomotive syndrome increases as mobility decreases. The older participants scored lower than the younger adults in 5-m walking time (fast), one-leg stand, TUG, grip power of both side strength, and wheelchair operation (Table 1). Eight (22%) of the older participants were unable to tip the caster up to a 10 cm height. From the multiple regression analysis, the grip strength of the left hand and the stage of locomotive syndrome predicated the longitudinal walking time and slope traversing ability. We were unable to determine a prediction factor using logistical analysis for the ability to tip a wheelchair back. We hypothesized that weak grip strength and locomotive function of elderly people influences wheelchair operating ability. Furthermore, tipping a wheelchair back needs not only muscular strength but also the acquisition of how to use power.

CONCLUSION

Most elderly people (over 75 years) have locomotive syndrome, which influences their ability to operate a wheelchair. In addition to barrier-free roads, we suggest that older caregivers use assistive technology when operating a wheelchair. In addition, they are needed to improve their body function.

ACKNOWLEDGEMENTS

This study received funding from the Foundation for Promoting Personal Mobility and Ecological Transportation.

Table 1: Comparison of wheelchair operating capabilities between younger and elderly participants

	Young	Elderly	Effect size (r)	*p-value*
5-m walking time (fast speed) (s)	2.62± 0.30	2.90± 0.57	0.30	p <0.05
Walking time on longitudinal slope (normal speed) (s)	7.31± 1.37	13.15± 6.89	0.65	p <0.001
Walking time on longitudinal slope (fast speed) (s)	4.80± 0.54	8.81± 4.35	0.77	p <0.001
Walking time traversing a slope (normal speed) (s)	5.60± 0.84	6.49± 1.48	0.34	p <0.01
Walking time traversing a slope (fast speed) (s)	3.80± 0.36	4.60± 0.81	0.58	p <0.001
Tipping a wheelchair back (s)	2.72± 0.42	4.32± 1.74	0.63	p <0.001
Recovery from one forward-wheel drop (s)	2.49± 0.54	3.27 ± 1.28	0.40	p <0.01

EIGHT-WEEK OF CONCURRENT AND TRADITIONAL TRAINING ENHANCES SPECIFIC ADAPTIONS OF INDIVIDUALS WITH SUB-HEALTHY SEDENTARY ADULTS

Chia-Lun Lee[1], Liang-Ying Yu[1], Nai-Jen Chang[2]
[1]Center for Physical and Health Education / National Sun Yat-sen University, Kaohsiung City, Taiwan
[2]Department of Sports Medicine / Kaohsiung Medical University, Kaohsiung City, Taiwan
Email: karenlee1129@gmail.com

INTRODUCTION

Dr. Robert Hickson [1] demonstrated impaired strength gains with traditional concurrent strength and endurance training the "interference effect". There are most of studies confirm that gains in muscle hypertrophy and strength are compromised when strength- and endurance-based training are undertaken concurrently. However, the interference effects of high-intensity aerobic exercise (HIAT) combined with high-intensity resistance exercise (HIRT) on strength development and endurance performance are unknown. The purpose of the study was to investigate the responses to eight-week of concurrent and traditional training on physiological and cardiovascular function, and one-repetition maximum [1-RM] strength capacity in sedentary adults with suboptimal health.

METHODS

Forty-one unhealthy and sedentary adults were recruited to complete this eight-week concurrent training or traditional training study in randomized order. After a familiarization trial, all participants performed a graded exercise test for determining VO_{2max}. Participants were assigned to either for eight-week training: (1) Concurrent training A (CTA)- Two bouts of HIAT (12 movements at 80–90%HRmax) before a single bout of HIRT (8 exercises at 20% – 60% of 1-RM) a day three time a week. (2) Concurrent training B (CTB)- A single bout of HIRT before two bouts of HIAT a day three times a week. (3) Traditional training (TT)- Two bouts of HIAT a day three times per week and two bouts of HIRT a day two times per week. A single bout of HIAT consists of 3 sessions, each separated by 1-min of the rest; each session includes four segments. Each whole-body exercise in a segment was done for 30-s at high effort, followed by 15-s of downtime, then repeated. Participants were evaluated on cardiovascular parameters, energy expenditure and maximal muscular capacity. The level of statistical significance is set at $p < 0.05$.

RESULTS AND DISCUSSION

There were significant increases in VO_{2max}, VE at VO_{2max}, O_2 plus, and endurance time on the ergometer in CTA and CTB groups ($p < .05$), with higher decreases in body fat percentage in CTA and CTB groups ($p < .05$). Only VE at VO_{2max} and endurance time increased in TT group ($p < .05$), with no significant difference among three groups. Furthermore, there were significant increases in energy expenditure and excess post-exercise oxygen consumption during post-exercise 30 minutes in CTB group compared with CTA and TT groups ($p < .05$). Significant increases in maximal strength after training in bench press of 1-RM (Figure 1) and back squat of 1-RM (Figure 2) among CTA, CTB, and TT groups, as well as increase by 9.2% – 12 .7% in the hand grip strength ($p < .05$). The interference effect of this study was not existed likely explained by methodological differences [2].

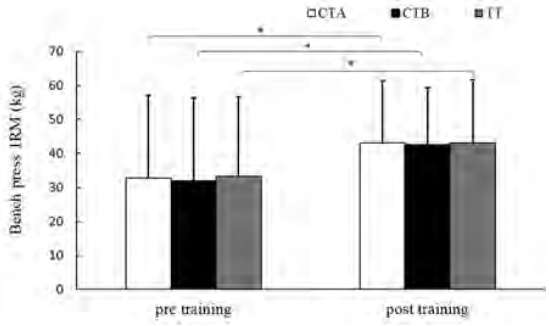

Figure 1 Change in bench press of 1-RM before and after training.

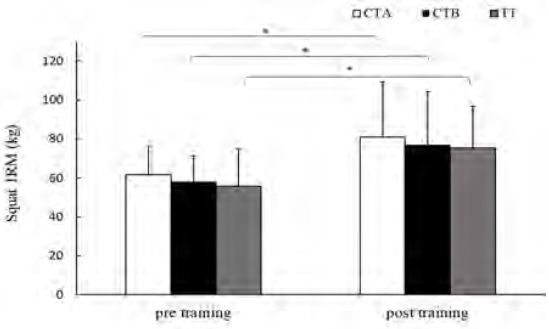

Figure 2 Change in squat of 1-RM before and after training.

CONCLUSIONS

In sub-healthy sedentary individuals, TT improves chest, hands, and leg muscle performance. However, concurrent HIAT combined with HIRT further improves body fat percentage, cardiovascular function at VO_{2max}, and muscle strength performance.

ACKNOWLEDGEMENTS

The project was supported by the National Science and Technology Council (MOST-110-2410-H-110-007-MY2).

REFERENCES

[1] Hickson RC. *Eur J Appl Physiol Occup Physiol* **45**: 255-263, 1980.
[2] Fyfe et al. *Sports Med* **48**: 289-297, 2018.

KINEMATIC CHARACTERISTICS OF THE SWING MOVEMENT IN COMTEMPORARY DANCE

Mayumi Kuno-Mizumura[1], Riko Mizushima[1], and Yui Kawano [2]
[1] Graduate school of Humanities and science, Ochanomizu University, Tokyo, Japan.
[2] Japanese Institute of Sports Science, Tokyo, Japan.
Email: mizumura.mayumi@ocha.ac.jp

INTRODUCTION

In contemporary dance, the natural movement patterns of the body and its relation to gravity had been incorporated into dance. The movement called the swing which could be often seen in Limón Technique would be one of basic movement in modern or contemporary dance. Limón Technique by José Limón is one of common basic modern dance techniques originated from 20th century. Previous study reported that strong associations between higher beauty scores and certain kinematic parameters, especially those related to amplitude of movements in contemporary dance (Torrents et al.,2017). Although dance students perform the swing movement in their classes as well as rehearsals, kinematic characteristics of the swing movement are still unknown. So, the purpose of this study was to investigate the swing movement in contemporary dance by 3D motion analysis and its relation with the qualitative evaluation of the movement by experienced dance instructors.

METHODS

Twenty young female dancers participated in our study. Their mean age was 20.9 years old with 7.1 years of contemporary or modern dance training as the average. Dancers were asked to perform the swing movement to the right side which could be frequently seen in modern or contemporary dance such as Limon technique. The swing motion (Fig. 1) was captured with 8 optical cameras at 120 Hz. Three-dimensional motion analysis system (VICON, Motion Analysis, USA) was used to calculate the center of mass (COM) and other kinematic variables. After motion analysis, we also investigated how three experienced dance instructors perceived the swing movements by using VAS scale as well as impression of gravity, relaxation and COM displacement viewing the images of the stick pictures from the movement analysis.

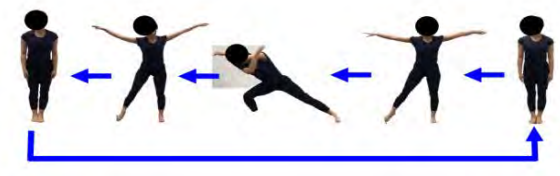

Figure 1 The images of one sequence of the swing movement.

RESULTS AND DISCUSSION

Average score of the swing movement was 6.52 ± 0.56 ranged from 5.3 to 7.3. Then, dancers were divided into two groups by the average score. Significant correlations were obtained between VAS scale of the swing movement and the impression of relaxation, that of gravity (Fig.2), that of downward displacement of COM, and that of movement amplitude evaluated by big to small. During the swing movement, lateral displacement to the right side of COM appeared with downward displacement of COM. High score group (HG) showed significant greater displacement of the head, the neck, and the shoulder compared to Low score group (LG). HG also showed significant larger angle of trunk lateral rotation on both sides, thoracic lateral tilt angle on both sides, elbow flexion/extension angle, and right hip angle of adduction/abduction. There was no significant difference in COM displacement between two groups. As for movement speed, during first half of the movement, HG showed significantly faster velocity of the head and the neck displacement as well as faster angular velocity of hip flexion. During latter half of the movement, HG also showed significantly faster velocity of the head, the neck and the shoulder as well as faster angular velocity of lateral tilt of the trunk.

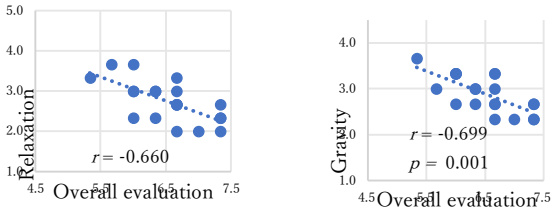

Figure 2 Correlations between impressions of relaxation and that of the gravity by the movement and overall evaluation of the swing movement

CONCLUSIONS

From the results of this study, it is indicated that dancers evaluated as high presentation in the swing movement would perform the swing movement with larger displacement of the upper body, while there was no significant difference in COM displacement between high- and low-score swing movement.

REFERENCES

[1] Torrents C et al. *Perception* **42**: 447-458, 2013

Effect of measurement approach on jawbone density for the dental implant evaluation

Shiuan-Hui Wang[1], Lih-Jyh Fuh [1,2], Jui-Ting Hsu[1,3*,]
[1] School of Dentistry China Medical University, Taichung, Taiwan
[2]Department of Dentistry China Medical University and Hospital, Taichung, Taiwan
[3]Department of Biomedical Engineering, China Medical University, Taichung, Taiwan
Email: jthsu@mail.cmu.edu.tw; richard@ms32.url.com.tw

INTRODUCTION

Bone quality evaluation is essential for dental implant programs. Dental cone-beam computed tomography (CBCT) is suitable for jawbone quality assessment. Many scholars have used dental CBCT or medical CT to measure cancellous bone density.[1-2] However, there has yet to be a unified measurement method in the past, and there needs to be a discussion on the correlation between different measurement methods. The aim of this study is to investigate the relationship between two different measures of cancellous bone density by using dental cone-beam computed tomography.

METHODS

Two hundred preoperative dental CBCT images, which were obtained from China Medical University Hospital, were input into the medical image software MIMICS.
To establish 3D virtual dental implants at the potential implant sites. The length and diameter of the virtual cylinder were set as 11mm and 3.5mm. Different regions of interest (ROI) were used in two measurement methods, "inside cylinder" and "outside cylinder," was used to measure cancellous bone density. The repeated measures ANOVA was conducted to analyze the difference between the different methods. The Pearson correlation coefficient was used to analyze the correlation between the two methods.

RESULTS AND DISCUSSION

The results showed that the measurement result of the "outside cylinder" (527.03±227.97 grayscale value, GV) was significantly higher than that of the "inside cylinder" (496.53±233.52 GV). According to the Kolmogorov–Smirnov normality test analysis, the three measurement results showed normal distribution (P value>0.05). In addition, there was a high correlation between the two methods (r=0.970; p<0.001).(Table 1.)

The bone density measured in the "outside cylinder" group was significantly higher than in the "inside cylinder" group. We speculate that the main reason is that the ROI of the "outside cylinder" is more peripheral than the "inside cylinder." These may cause the cortical bone area to be included in the ROI, resulting in overestimating the cancellous bone density. Although the "outside cylinder" is the bone area actually connected with the dental implant, the cortical bone should be excluded when the cancellous bone density measurement is performed. Cortical bone and cancellous bone have different effects on implant stability, the two of which should discuss separately.[3] According to the above research results, if the "outside cylinder" is used for density assessment, more careful evaluation is required to avoid overestimating bone density.

CONCLUSIONS

Two measurement methods of cancellous bone density did not affect the magnitude trend of the results. The "outside cylinder" was significantly higher than the "inside cylinder."

REFERENCES

[1]Norton MR et al. Clin Oral Implants Res . 2001, 12(1):79-84.
[2] Hao Y et al. Eur Rev Med Pharmacol Sci . 2014, 1:D1.
[3] Hsu JT et al. Clin Implant Dent Relat Res . 2013, 15(2):251-261.

Table 1: The measurement result and the relationship between the two methods.

Measurement methods		All region	Anterior Maxilla	Posterior Maxilla	Anterior Mandible	Posterior Mandible	Kolmogorov-Smirnov
Mean density (GV)	Inside cylinder	496.53±233.52	582.93±229.49	403.09±206.44	661.13±211.43	525.63±225.22	p>0.05
	Outside cylinder	527.03±227.97	627.72±228.40	425.14±195.67	698.81±210.93	569.92±209.42	p>0.05
Pearson correlation coefficient (r)		0.970 (p<0.01)	0.965 (p<0.01)	0.975 (p<0.01)	0.931 (p<0.01)	0.966 (p<0.01)	--

A DIGITAL, DIVERSE, ASSEMBLABLE INTELLIGENT MOVEMENT EVALUATION AND TRAINING SYSTEM FOR INDIVIDUALS WITH DISABILITIES.

Yan-Ying Ju[1], Wann-Yun Shieh[2,3], Yu-Chun Yu[4], Yu-Huei Chien[5] and Hsin-Yi Kathy Cheng [3,5,*]

[1] Department of Adapted Physical Education, National Taiwan Sport University, Taoyuan, Taiwan.
[2] Department of Computer Science and Information Engineering, Chang Gung University, Taoyuan, Taiwan.
[3]Department of Physical Medicine and Rehabilitation, Chang Gung Memorial Hospital, Taoyuan, Taiwan.
[4]Taoyuan Municipal Taoyuan Special School, Taoyuan, Taiwan.
[5]Graduate Institute of Early Intervention, Chang Gung University, Taoyuan, Taiwan.
[*]Correspondence email: kcheng@gap.cgu.edu.tw

INTRODUCTION

The special education population exhibits great individual differences. Effective training for this population needs to be personalized with specific movement indicators. They are also less motivated to participate in activities, hence adaptive games with diversities are needed to attract their attention. To date, with many intelligent movement evaluation and training systems available for typically developed individuals, a system specially designed for the special education population is scarce. The current multidisciplinary project aims to construct a digital, diverse, assemblable intelligent movement evaluation and training system for individuals with disabilities. This project was divided into three stages: 1. Evaluate the needs of the target group, analyze functional indicators to create the decision tree, and design the multi-functional assemblable modules; 2. Carry out content and structure planning, define movement parameters, and introduce AIoT technology; 3. Identify featured characteristics, plan for data collection and inclusive training activities (Fig. 1).

METHODS

To identify the unmet needs of this group, the team performed a literature review with keywords including "assistive devices, physical and mental disabilities, motion analysis, machine learning, system development", etc., summarized the pros and cons of the current-available functional assessment tools and devices, and ran them through multiple expert meetings. The performance indicators of the target population and the needs of special education schools were then identified.

The project is expected to design and develop an integrated assessment and training system for institutions with individuals with physical and intellectual disabilities. The assemblable system includes functional assessment modules for both the upper and lower limb (U/E and L/E). These modules are capable of measuring the control of arms and legs, eye-hand/foot coordination, attention. The module is equipped with a control circuit with a wireless transmission function. Sensors including micro switches, accelerometers, gyroscopes, and pressure gauges are installed on the circuit.

RESULTS AND DISCUSSION

Here we present 1. The prototype of the plug-in geometric block module and its corresponding application for the U/E. There are several different shapes of bases and plugs on the panel, and the participant must pair all specific shape plugs into the same shape base to complete the test. This is the most direct way to test the shape identification and manipulation function of the hand, including pickup, rotation, and eye-hand coordination. The app will first beep first at the start, and when the participant finishes pairing the last plug with the base, it will be considered as the stop of the test. 2. The prototype of the smart ball module and the smart mat for the L/E. Data will be collected and transmitted via wifi to the integrated system. The participant performed several desired movements according to the instructions on the screen of the assessment system. The signals measured by the sensors inside the smart ball and the smart mat collected the performance parameters via a self-developed signal collection gateway, processed, and sent to the computer for real-time calculation. School teachers and sports coaches can use mobile phones to receive data and upload the signal-processing results to the cloud for storage and formulate training plans accordingly.

Figure 1 The purposed assessment and training system

CONCLUSIONS

The intelligent system developed can not only objectively and efficiently evaluate the target population and provide specific features for personalized training design; moreover, through the diverse, assemblable design, it can facilitate the participation of these individuals and encourage them to interact with the peers. Results can also be used for reference by related professionals for teaching/rehab program design, scientific communication, product development and technology transfer, etc..

REFERENCES

[1] Cabeza-Ruiz R et al. *Journal of Intellectual Disability Research*, **64:** 612-628, 2020.

[2] Shieh WY et al. *Sensors*, **20(18)**: 5444, 2020.

MULTIVARIATE KINEMATIC ANALYSIS OF PIANO PERFORMANCE : A CASE STUDY OF A PROFESSIONAL PIANIST

Dawon Park[1], Taegyun Kwon[4], Joonhyung Bae[4], Jonghwa Park[3], Juhan Nam[4] and Jaebum Park [1,2]

[1] Department of Physical Education, Seoul National University, Seoul, South Korea
[2]Institute of Sport Science, Seoul National University, Seoul, South Korea
[3]College of Music, Seoul National University, Seoul, South Korea
[4]Graduate School of Culture Technology, Korea Advanced Institute of Science and Technology, Daejeon, South Korea
Email: parkpe95@snu.ac.kr

INTRODUCTION

The music performance by professional pianists is remarkable from the perspectives of aesthetics, i.e., beautiful sounds, and human movement science as well. In particular, the complex and dexterous actions by the hands and fingers during a piano performance are feasible due to the structural advantage of the hands and fingers, such as high mechanical degrees of freedom. In other words, high-quality piano performance may be associated with the ability to coordinate high-dimensional elements, including hands, fingers, and trunk. By general consensus from the current control theories, the strategy of the central nervous system (CNS) toward the high dimensionality of the elements is to reduce the degrees of freedom in such a way that the elements are classified into a limited number of groups (i.e., dimension reduction) that are latent variables as to the performance skills or coordination [1]. The purpose of this study was to examine the patterns of coordinative patterns and dimension reduction of a piano performance by a professional pianist.

METHODS

One professional pianist who has worked performer and instructor for at least 20 years participated in this study. The participant played a Computer Controlled Piano (Disklavier C7, Yamaha Inc., Hamamatsu, Japan) for 30 repertories which were composed of four techniques. (1) pulling arm legato: up, down, pronation and supination motion of wrist with released in the shoulder, (2) upper-arm gravity drops: a portion of the pulling arm cycle with a low- and high-wrist form, (3) forward gravity drops-rebounds: control of lower arm to maintain wrist height, and (4) hand bounce: produce faster and lighter repetitions of hands [2]. Spherical reflective markers were attached to the hand and each finger joint. Kinematics of upper body segments were captured using eight infrared cameras at 100Hz (OptiTrack, Natural Point Inc., Corvallis, OR). The geometric model consisting of 24 segmental angles was used for the quantification of mechanical properties of body kinematics. Principal component analysis (PCA) was performed to investigate the strategy of dimension reduction during the piano performance.

RESULTS AND DISCUSSION

(1) In pulling arm legato technique showed that the wrist, thumb, and little fingers were performed in one mode. (eigen value=14.99, variance=34.95%) by PCA. Also, upper limb elements were grouped into one mode (eigen value=1.89, variance=4.39%). These results suggest that the group of thumb and little finger and fixed upper arm play a role in the frame for hand circle motion. (2) upper arm gravity drops were shown that upper limb elements were separated into different modes. This technique is characterized by controlling the wrist movement with the motion of the upper arm. That is, it is shown that harmony can be played continuously by using the coordination of the upper and lower arm to control the movement of the wrist. (3) Forward gravity drops-rebounds showed that the wrist and forearm were one mode (eigen value=16.13, variance=37.50%), and the index-middle, ring-little, and thumb fingers of both hands represented as independent groups. It suggested that wrist and forearm motion and finger independence play an important role in short continuous hitting motions. (4) Hand bounce was shown that the index, middle, and ring fingers of each hand were played in one mode (left hand: eigen value=11.46, variance=26.64%; right hand: eigen value=9.68, variance=22.51%). This result reflected that the character of this technique which is by playing notes quickly and lightly for a long time while fixed wrist position.

CONCLUSIONS

The current results showed the existence of a common mode (i.e., latent variable) across different piano techniques. Further, the kinematics of the thumb, little finger, and wrist joint played a significant role in the overall frame. To sum up, the control ability of wrist position and independent motions of fingers may be a contributor to the professional piano performance, albeit these should not be all about the “beauty” of the piano performance.

ACKNOWLEDGEMENTS

This research was supported in part by the Basic Research Program through the National Research Foundation of Korea (NRF) funded by the MSIT (2022R1A4A503404611)

REFERENCES

[1] Danna-dos-Santos, Alessander, et al. *Exp Brain Res* **179**: 533-550, 2007.
[2] Fink, Seymour. *Hal Leonard Corporation*: 1992.

PROGRESSIVE ENERGIZATION EVALUATION AND BENEFITS OF GROUP EXERCISE SESSION FOR SENIORS – POST-EVENT MOVEMENT OBSERVATION AND ANALYSIS METHOD

Ying-Ting Hsueh[1,2], Shih-Chung Cheng[1], Yen-Kuang Lin[1], Wen-Chih Tseng[3]
[1] Graduate Institute of Athletics and Coaching Science, National Taiwan Sport University, Taoyuan, Taiwan.
[2] JV Fitness, Hsinchu, Taiwan.
[3] Dr. SAFe, Hsinchu, Taiwan.
E-mail: 1110503@ntsu.edu.tw

INTRODUCTION

According to the definition of the World Health Organization (WHO), when the population over 65 years old exceeds 14%, it is called an Aged Society. Taiwan is estimated to enter a super-aged society by 2025, making health and aging issues urgently needed to be taken seriously. As the elderly grow older, their physical functions gradually decline, including decreased muscle strength, decreased cardiorespiratory endurance, decreased nerve conduction velocity, decreased muscle flexibility, and decreased activity, which in turn leads to decreased physical fitness. Therefore, this study aimed at enhancing physical activity through group exercise instruction in the elderly population.

METHODS

The target population of the current study was the elderly who are over 65 years old and rarely do exercise. First, a doctor will diagnose and confirm whether the physical condition is suitable for participation. After the diagnosis, There were 15 people (age: 71.53±5.06) met the inclusion criteria; then, a qualified group sports coach provided group sports guidance. The courses were held 4 times a week, two hours each time, for a period of three months, with a total of 48 training sessions. The content of the courses were listed as follows: Weeks 1 to 4: Warm up with low-impact aerobics (20 min), operate a series of isokinetic training machines (50 min), stand balance (20 min), and flexibility (20 min); weeks 5 to 8: high-low impact aerobic (50 min), muscle strength and coordination training (20 min), chair yoga (40 min); weeks 9 to 12: high-low impact aerobic added agility and interval running training (50 min), combined with cognitive function and memory training (30 minutes), chair yoga (30 minutes). The evaluation method of this study adopts the post-event movement observation based on recording video, and three observation time points (the first week, the sixth week, and the 12th week) were used to evaluate and analyze the movement ability Four perspective of cardiorespiratory, resistance, flexibility and balance divided into 21 indicators were scored.

RESULTS AND DISCUSSION

Analysis of the movement ability in the three periods showed that all the indicators in the 6th week were significantly better than the 1st week; all the indicators in the 12th week were significantly better than the 1st and 6th weeks (p<0.001), and all indicators had the greatest effect (3.18~5.18). (Table 1) only lists the index results with effect size >4. **Important findings:** (1) Immediately hear the rhythm and respond to the action, (2) Being able to correct themself when there is a wrong rhythm, (3) Capable of memorizing the action to achieve the ability of the action combination, (4) After coordination and agility training, flexibility and dynamic balance ability were improved. This gradual and diversified guidance to safely and effectively enhance the physical activity ability of seniors, could be an appropriate method.

CONCLUSIONS

This study demonstrates that the physical function and cognitive function of the participants could be improved through progressive energy enhancement, Keeping up with the rhythm of the music as a whole, combining high and low impact, forward and backward and sideways movement, and dynamic and static balance control, intermittent intensity are the keys to improve heart rate and agility performance, and flexibility. A documentary is attached to this study for future relevant professionals to serve as a reference for the guidance of senior sports.

REFERENCES

[1] Neil-Sztramko SE et al. *BMC Geriatr* **29**: 539, 2022.

Table 1: Significant difference and benefit value of important indicators

	Pre-test	Mid-test	Post-test	*p-value*	Effect size
ROM	3.93±0.96	5.73±0.96#	7.60±0.74*	<0.001	4.29
displacement	5.33±0.72	6.80±0.68#	8.13±0.64*	<0.001	4.09
action plane	6.20±0.41	7.33±0.48#	8.60±0.50*	<0.001	5.18
interval	0.00±0.00	2.13±0.51#	4.53±1.30*	<0.001	4.92
isokinetic	5.27±0.45	6.27±0.45#	7.93±0.79*	<0.001	4.08
balance	4.00±1.00	5.87±0.83#	7.80±0.77*	<0.001	4.24
reflexes	5.27±0.70	6.40±0.50#	8.20±0.67*	<0.001	4.24

α=0.05 **#:**Mid-test is better than Pre-test ***:**Post-test is better than Pre-test and Mid-test

Age-related differences in knee and ankle dynamic joint stiffness during walking

Haruki Toda[1,2], Hiroaki Hobara[2,3] and Mitsunori Tada[2]

[1] Robot Rehabilitation Center, The Hyogo Institute of Assistive Technology, Hyogo, Japan.
[2] Artificial Intelligence Research Center, National Institute of Advanced Industrial Science and Technology (AIST), Tokyo, Japan.
[3] Department of Medical and Robotic Engineering Design, Faculty of Advanced Engineering, Tokyo University of Science, Tokyo, Japan
Email: toda@assistech.hwc.or.jp

INTRODUCTION

An appropriate vertical center of mass (CoM) displacement during walking allows efficient mechanical energy exchange and reduces the amount of mechanical work demands. However, older adults tend to have flatter and smaller vertical CoM displacements than younger adults. Knee and ankle dynamic joint stiffness, which is defined as the change in joint moment divided by the change in joint angle [2], are important for providing body support while preventing excessive downward CoM motion [1]. However, little is known about the age-related changes in knee and ankle DJS during walking. Thus, the aim of this study was to investigate the differences in vertical CoM displacement and knee and ankle DJS between the young and the older adults.

METHODS

We used a public dataset from the National Institute of Advanced Industrial Science and Technology Gait Database 2019 [3]. From the Gait Database, 107 healthy young adults aged 20 to 39 years old (44 men and 63 women) and 129 healthy older adults aged 65 years or older (69 men and 60 women) were used for the analysis. The marker trajectories and ground reaction forces were collected using 15 infrared cameras and six force plates. Then, inverse kinematics and kinetics were analysed by a house development software 'DhaibaWorks'. The vertical CoM displacement during early to mid-stance was calculated, and normalized subject's body height (%BH). Knee and ankle DJS were expressed by the linear regression slope of the flexion-extension moment vs. flexion-extension angle during the power absorption phase. Analysis of covariance was performed to compare the CoM displacement and the DJS of the knee and ankle between the young and the older adults using walking speed and gender as covariates.

RESULTS AND DISCUSSION

Our results showed that older adults had significantly smaller knee DJS and vertical CoM displacement (Figure 1). In contrast, there was no difference in ankle DJS between the young and the older adults (Figure 1). Knee joint in early stance to mid-stance plays a role in elevating CoM. However, older adults may be unable to shift their CoM upward in this phase due to small knee DJS. On the other hand, ankle DJS did not appear to be an age-related change.

CONCLUSIONS

Our study indicates that older adults have a small knee DJS with a flat CoM displacement during walking. Our findings suggest that interventions to increase knee DJS in the early stance are necessary to improve vertical CoM displacement in older adults.

ACKNOWLEDGEMENTS

This study was supported by the JST-Mirai Program Grant Number JPMJMI21H5, Japan.

REFERENCES

[1] Santos RT et al. *J Biomech* **129**: 110803, 2021.
[2] Akl AR et al. Gait Posture **82**:294-300, 2020.
[3] Kobayashi Y et al. AIST Gait Database, 2019

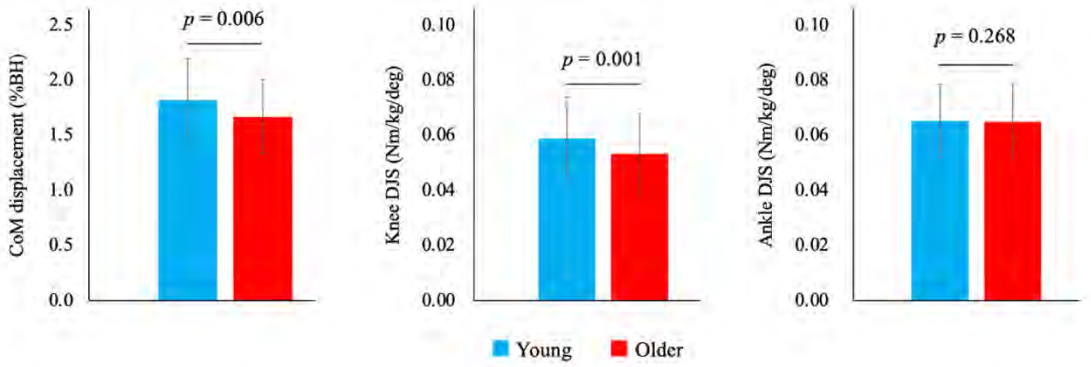

Figure 1 Bar plots of the vertical center of mass (CoM) displacement normalized body height (%BH), and the knee and ankle dynamic joint stiffness (DJS) in young and older adults.

Gait modification after verbal instruction of “knee extension” or “hip extension” at early stance phase to knee flexed gait.

Shinya Ogaya[1], Rena Yano[1], Asahi Sekine[1], Ryosuke Momose[1], Shiuba Kudo[1], Rena Yamamoto[1] and Aoi Uchida[1]

[1] Department of Physical Therapy, Saitama Prefectural University / Koshigaya, Japan.
Email: ogaya-shinya@spu.ac.jp

INTRODUCTION

Many patients with knee osteoarthritis walk with their knees flexed greatly. Physical therapists may employ verbal commands to extend the patient’s knee in some cases. The verbal instruction seemed to be effective as the patient's knee was extended. Although the knee is extended, ankle and hip may lead to an unexpected change in motion. Because the knee joint is formed by the thigh and shank, change in knee joint motion is always accompanied by changes in either or both hip and ankle joint motion. The thigh and shank tilt directly affect the hip and ankle angle, respectively. Based on this concept of multi-joint kinematics, similar changes can be observed by instructing hip extension. Verbal movement instructions are commonly used in clinical practice; however, there are few reports on their effectiveness.

It has been reported that when walking on a split-belt treadmill at different walking speeds, the knee at the side of the slower speed flexes in the early stance phase [1]. Therefore, this study examined how lower limb joint motion was changed by the verbal instructions of “knee extension” and “hip extension” during knee-flexed gait using a split-belt treadmill.

METHODS

The subjects were twenty three healthy young adults (mean age:20.5 years). This study was approved by the Research Ethics Committee of the University. Eighteen reflex markers were attached to the subjects according to the plug-in-gait lower limb model. The VICON motion analysis system was used to measure three-dimensional motion data. The subjects walked on a split-belt treadmill with two ground floor reaction forces (Kistler). Initially, walking at 1.0 km/h for both sides was measured (normal gait: NG), and subsequently, speed was increased to 1.5 km/h only on the left side (baseline split-belt gait: BS). Next, the participants were instructed verbally to extend their right knee after heel contact (knee extension gait: KE) and to extend their right hip after heel contact (hip extension gait: HE), in random order.

The joint angles and body joint moments normalized by body weight (BW) were calculated. One-way ANOVA and multiple comparisons (Bonfferoni) were used to compare the peak values at each gait phase for the three conditions BS, KE, and HE.

RESULTS AND DISCUSSION

Peak knee flexion at the early stance was 15.0° in the NG and 19.9° in the BS, simulating the flexed knee gait on the split treadmill. Peak knee flexion was 11.7° in KE and 15.5° in HE, with significant differences among all three conditions (BS, KE, and HE). As expected, the knee was extended by both verbal instructions. Peak ankle dorsiflexion and hip extension in the late stance showed significant differences among the three conditions. These results indicate that hip extension instruction facilitated more hip extension in the late stance phase than knee extension instruction, while strongly limiting ankle dorsiflexion.

Knee extension moment showed significant differences among all three conditions (SG:8.6 Nm/BW, HE:5.7 Nm/BW, KE:7.3 Nm/BW). The knee extension moment decreases when the knee is extended.

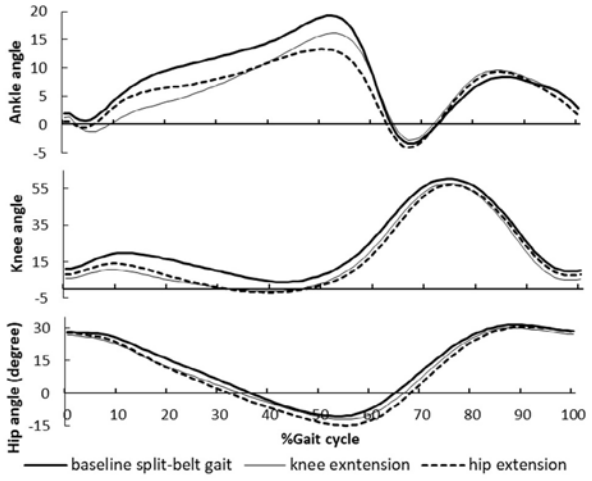

Figure 1 Joint Angle in 3 gait conditions.

CONCLUSIONS

Appropriate verbal instruction differs depending on whether the aim is to encourage more hip extension or maintain ankle dorsiflexion as much as possible.

ACKNOWLEDGEMENTS

Non

REFERENCES

[1] Hirata K et al. *J Med Biol Eng* **39**: 693-701, 2019

Association of Muscle Function with Gait Ability based on Various Speeds in Older Women over 75 years

Bohyun Kim[1,2], Changhong Youm[1,2*], Hwayoung Park[1], Hyejin Choi[1,2], Juseon Hwang[1,2], Minsoo Kim[1], and Byungjoo Noh[3]

[1] Biomechanics laboratory, Dong-A University / Busan, Republic of Korea
[2] Department of Health Sciences, Graduate School, Dong-A University / Busan, Republic of Korea
[3] Department of Kinesiology, College of Natural Sciences, Jeju National University / Jeju, Republic of Korea
Email: chyoum@dau.ac.kr

INTRODUCTION

Loss of motoneurons with aging is associated with decreased muscle fiber number and size and leads to reduced muscle function (MF). MF is a comprehensive measure of muscle strength, power, and fatigue and can be assessed for decreased gait ability, which contributes to decreased physical performance as well as sarcopenia. However, few studies have investigated the association between MF and gait variables, and it is limited to preferred speed gait test. Therefore, it is necessary to examine the association between MF with gait ability at continuous and various speeds using inertial sensors in older women over 75 years.

METHODS

The participants of this study were 144 older women aged≥75 years. MF measure was performed five times sit-to-stand test. The gait test was performed at three speeds by modifying the preferred walking speed (PWS; slower walking speed [SWS, 80% of PWS]; faster-walking speed [FWS, 120% of PWS]) on a straight 19 m-overground walkway. Multicollinearity was used to select gait variables related to muscle function, and linear regression analysis was performed to identify the MF that explains the decrease in gait ability. Furthermore, gait variables were classified into quantile, and binary logistic regression analysis was performed to determine the classification between groups 1 (first quantile) and 3 (third quantile), according to MF. To investigate the classification accuracy of groups 1 and 3, areas under the curve (AUCs), sensitivity, specificity, and cut-off values were calculated using receiver operating characteristic curve analysis.

RESULTS AND DISCUSSION

MF was significantly associated with step length at SWS (R^2=0.266) and FWS (R^2=0.298), single support phase at PWS (R^2=0.196) and FWS (R^2=0.245), total steps at PWS (R^2=0.145), and stance phase at PWS (R^2=0.242) and FWS (R^2=0.269). As binary logistic regression of groups 1 and 3, MF of group 3 exhibited 2.8 times in step length at SWS (R_N^2: 0.459; AUC: 0.758), 3.5 times in step length at FWS (R_N^2: 0.432; AUC: 0.794), 2.8 times in single support phase at PWS (R_N^2: 0.441; AUC: 0.713), and 2.8 times in single support phase at FWS (R_N^2: 0.343; AUC: 0.746), which was greater than group 1 (Figure 1). In previous studies, changes in step parameters in older adults were associated with impaired balance and compensation for lower limb muscle weakness during gait, leading to shorter single support and longer stance phases to maintain dynamic stability[1]. Furthermore, it is suggested that older women with reduced MF are challenged to maintain symmetry to secure dynamic stability when gaiting under objective and various speed conditions[2].

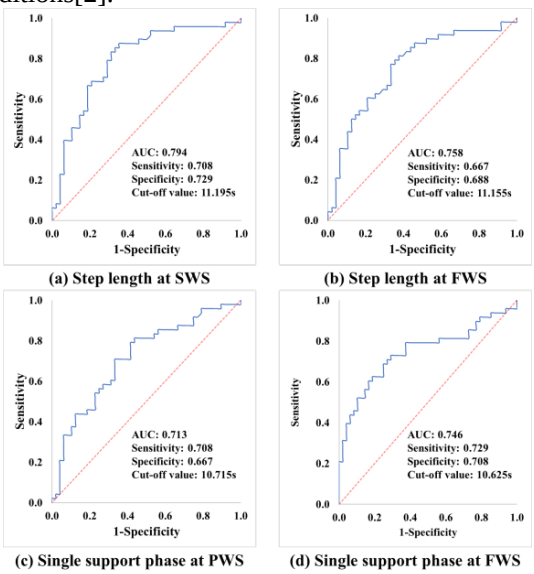

Figure 1. Receiver operating characteristic (ROC) curves for classification between groups 1 and 3

CONCLUSIONS

Our study indicated that a decrease in MF is associated with a decrease in gait ability, and MF in older women over 75 years may predict a reduction in step length at SWS and FWS and single support phase at PWS and FWS. Therefore, we suggest that MF is useful for evaluating gait tasks under continuous and various speed conditions, which are essential for the daily life activities of older women and assessing health status.

ACKNOWLEDGEMENTS

This study was supported by the Dong-A University Research Fund.

REFERENCES

[1] Aboutorabi et al. *Aging Clin Exp Res*. **28**, 393–405, 2016.
[2] Nasirzade et al. *Phys. Treat. -Specif. Phys. Ther. J.* **7**, 3–12, 2017.

GENDER DIFFERENCES IN TRUNK AND LOWER EXTREMITY KINEMATICS DURING HURDLE STEP AND SQUAT LIFTING

Ganbat Danaa[1], Batlkham Dambadarjaa[2], Tserenchimed Purevsuren[1], Munkh-Erdene Bayartai[2] and Batbayar Khuyagbaatar[1]
[1]Department of Technical Mechanics, Mongolian University of Science and Technology, Ulaanbaatar, Mongolia
[2]Department of Physical Therapy, Mongolian National University of Medical Sciences, Ulaanbaatar, Mongolia
Email: ganbatda@must.edu.mn

INTRODUCTION

Movement pattern differences exist between sexes and influence the rates of musculoskeletal injuries as well as treatment and rehabilitation strategies [1]. The deficiencies in the trunk and lower extremity movement can be examined by functional tasks, where squatting is the most commonly used while the hurdle step (HS) movement provides unique contrast relative to the squat because it tests bilateral functionality [2]. However, there are few studies have investigated gender differences during functional activities. In this study, we compared the trunk and lower extremity kinematics between males and females during the squat lifting (SL) and HS movements.

METHODS

Thirty-six healthy Mongolian adults (14 males, age 23.7±6.4 years, height 168.8±6.0 cm, weight 62.7±11.1 kg, and 22 females, age 25.1±8.6 years, height 160.3±7.1 cm, weight; 58.1±9.4 kg) were recruited. The Xsens wearable motion capture system (MVN, Xsens technologies, Netherlands) was used to record full body movements during the HS and SL at 120 Hz. Participants completed 3 repetitions of the HS, followed by 3 repetitions of the SL. The trunk and right lower extremity joint angles in the sagittal plane were calculated, normalized, and averaged for male and female groups. The trunk joint angle was calculated using a relative orientation between the pelvis and thorax segments. An independent sample t-test was used to compare the mean values of joint angles between the groups.

RESULTS AND DISCUSSION

The trunk, hip, knee, and ankle joint angles were compared between males and females during HS and SL (Figure 1). The hip, knee, and ankle flexions were similar, while the trunk flexion was significantly different between the males (4.9±7.7° in HS; 10.2±16.7° in SL) and females (2.3±5.1° in HS; 2.4±11.3° in SL) regardless of functional tasks ($p<0.001$). It was similar to previous studies, where they reported that trunk motion was significantly larger for men during the lifting movements [3]. The current results showed that gender differences in trunk mobility and men tend to bend more forward during both HS and SL.

CONCLUSIONS

The results demonstrated the gender difference in the trunk and lower extremity kinematics between males and females during HS and SL. A significant difference was observed for trunk flexion between males and females but no differences for hip, knee, and ankle joint angles during functional tasks. Therefore, different trunk kinematics between males and females should be considered during clinical examination and functional activities.

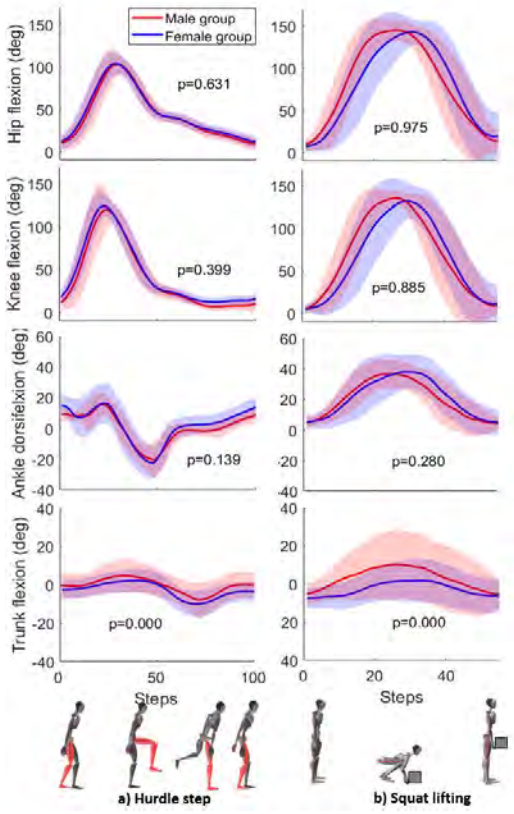

Figure 1 Hip, knee, ankle, and trunk flexion during HS and SL.

ACKNOWLEDGEMENTS

This work was supported by the "Mongolia-Japan Engineering Education Development" project (J24C16) and the Mongolian University of Science and Technology (mfund-052022).

REFERENCES

[1] Mauntel TC et al. *J App Biomech* **31**: 244-9, 2015.
[2] Remedios T et al. *Front Bioeng Biotechnol* **8**: 364, 2020
[3] Lingbeck L et al. *Ergonomics,* **44**: 202-14, 2001.

Effect of lower limb joints pain on toe area of foot pressure during walking in the elderly

Kazuya Imaizumi[1], Yumi Iwakami[1]
[1] Tokyo Healthcare University, Tokyo, Japan.
Email: k-imaizumi@thcu.ac.jp

INTRODUCTION

Gait is one of the most basic physical movements for human. Declining gait function impacts not only to various physical functions but also activities of daily living and quality of life for the elderly. In our previous study, we developed an evaluation method for toe function based on the plantar pressure distribution while walking and revealed the relationship between age-related decline and gait parameters [1]. In this study, we will examine the relationship between lower extremity pain and the plantar pressure parameter, which is thought to be related to the decline in gait function.

METHODS

Plantar pressure data were obtained from 33 female and 10 male adults more than 65 years who reported having no difficulty walking without support in Japan. Experimental setup and data analysis were conducted according to the previous study [1]. Toe Are Ratio (TAR) was calculated as the quotient of the toe area divided by the whole foot area. General gait parameters were also obtained using the attached software.

Participants were asked to respond to pain on a scale of none, mild pain, moderate pain, and severe pain in low back, knee, and foot.

Correlation analysis was conducted to evaluate the relationship between the plantar pressure parameter and various gait parameters. Ordinal logistic regression analysis was also used with the objective variable as pain in each part. A probability level of 0.05 was considered to indicate statistical significance.

RESULTS AND DISCUSSION

For 43 elderlies, 46.5% had pain in low back, 55.8% had in knee, 20.9% have in foot (Table 1).

The results of correlation analysis indicate that the TAR had moderate positive correlations with walking speed (r=0.411, p=0.0069) and weak positive correlations with step length (r=0.334, p=0.0029) and stride time (r=0.336, p=0.027).

Figure 1 shows the logistic regression plots of pain in low back and knee. The results of the logistic regression had significant effect on the degree of knee pain (p=0.0189), and back pain (p=0.007).

As a consideration, the TAR was correlated with three gait parameters which reflect age-related decline in gait function. Furthermore, the TAR may be affected by changes in gait due to lower extremity pain. On the other hand, as no significant effect on the TAR was observed for foot pain, so further investigation is needed.

Table 1: Number of participants with back, knee, and foot pain

	Low Back	*Knee*	*Foot*
Pain	**Number (%)**	**Number (%)**	**Number (%)**
No	24 (54.5%)	20 (54.5%)	33 (75.0%)
Light	15 (34.1%)	19 (34.1%)	7 (15.9%)
Moderate	4 (9.1%)	4 (9.1%)	1 (2.3%)
Severe	1 (2.3%)	1 (2.3%)	1 (2.3%)

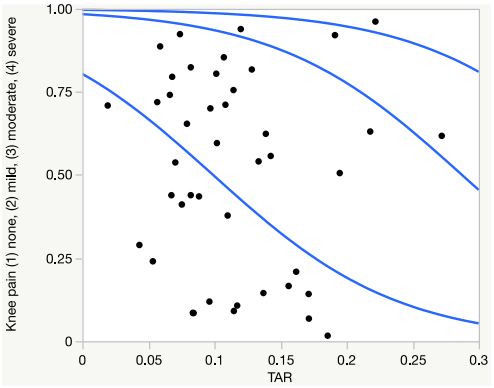

a) Knee pain

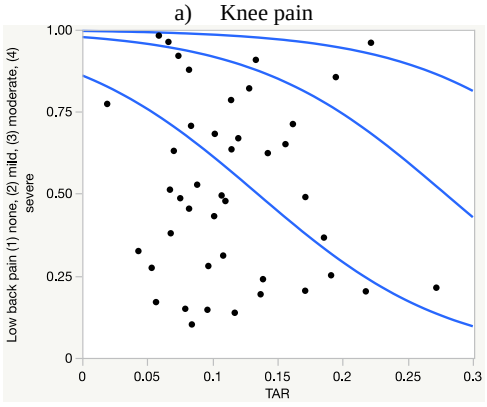

b) Low back pain

Figure 1 Logistic regression plots of TAR and pain in low back and knee.

CONCLUSION

The toe ratio parameter may be useful in assessing the impact of pain on gait in older adults with reduced gait function.

ACKNOWLEDGEMENTS

This work was supported by JSPS KAKENHI Grant Number 17K01588.

REFERENCES

[1] Imaizumi K et al. *IEEE EMBC* **2019**: 2434-2438, 2019.

Effect of light touch on inappropriate mediolateral foot placement

Toyoda Y[1], Iwamoto Y[1,2], Ishii Y[1,2], Mizutani M[1], Ono I[1], Takahashi M[1,2]
[1] Department of Biomechanics, Graduate School of Biomedical and Health Sciences, Hiroshima University / Hiroshima, Japan.
[2] Center for Advanced Practice and Research of Rehabilitation, Graduate School of Biomedical and Health Sciences, Hiroshima University, Hiroshima, Japan
Email: m226107@hiroshima-u.ac.jp

INTRODUCTION

Stable gait requires an estimation of the kinematic state of the body centre of mass (CoM) and a corresponding control of the mediolateral (ML) foot placement. Proprioceptive information derived from the hip abductor muscles (HA) of the stance leg contributes to the estimation of the CoM state. Perturbing proprioception from the hip abductor muscles due to muscle vibration can lead to misidentification of CoM, resulting in inappropriate foot placement [1]. Light touch may be beneficial for inappropriate foot placement that occurs in this way. Light touch adds somatosensory information, which may improve the accuracy of CoM estimation and correct for the foot placement. In this study, we investigated whether light touch is effective against inappropriate foot placement caused by perturbing proprioception from the HA.

METHODS

Eight healthy young adults volunteered to participate in this experiment. Participants walked on treadmill with comfortable speed. They walked under 4 conditions: normal gait (N), vibration gait (V), light touch gait (LT), and vibration gait with light touch (VLT). In V and VLT, vibration was applied to the left HA during the left stance phase, which was intended to perturb proprioception from the HA. To quantify the dynamics on the frontal plane during walking, the foot placement, the CoM displacement and the margin of stability (MOS) were calculated. In the two conditions with vibration, the right heel contact after the vibratory stimulation was defined vibration step and before the vibratory stimulation was defined non-vibration step. The difference of each parameter of the non-vibration step with vibration step was calculated. For all parameters, the Shapiro-Wilk test was used to check for normality of the data. As normality was observed for all parameters, paired t-test was used. Sequential Bonferroni correction coefficients were used to adjust alpha levels for multiple comparisons. The significant level was set at 5%.

RESULTS AND DISCUSSION

In V, the vibration step was placed more medially than non-vibration step (Figure 1), but the displacement of CoM was not altered (Table1). This caused reduced the MOS (Table 1). In VLT, there was no significant defeference in dynamics on the frontal plane (CoM displacement, foot placement, MOS) compared vibration step to non-vibration step (Figure 1, Table 1). Thus, the HA vibration caused an illusory shift of CoM and foot was placed more medially [2], but the ML foot placement was modified by light touch. This suggests that by obtaining information about their position in the external environment through light touch [3], which corrects the error in displacement of CoM recognition caused by the HA vibration and the foot was properly placed.

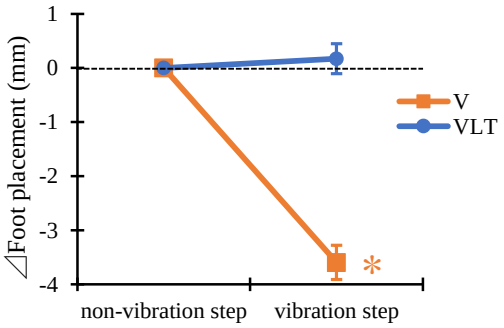

Figure 1 Effect of vibration on foot placement. The asterisk (*) indicates significance ($p < 0.05$).

CONCLUSIONS

We found that light touch can correct inappropriate foot placement caused by perturbing proprioception from the HA. Light touch may be a effective approach for in individual with walking balance deficits.

REFERENCES

[1] Arvin M et al. *Front Physiol* **9**: 1134, 2018.
[2] DevinC et al. *J Neurophysiol* **114**: 2220-9, 2015.
[3] Bingenheimer K et al. *Neurosci Lett* **589**: 176-80, 2015.

Table 1: Effect of vibration on CoM displacement and MOS. mean ± SD, * : significant at $p < 0.05$

	V	VLT
⊿CoM displacement (mm)	1.0 ± 2.4	1.4 ± 1.9
⊿MOS (mm)	-3.6 ± 3.2 *	0.2 ± 2.7

CLASSIFICATION OF YOUNG ADULT MOTOR FLUCTUATION PHENOTYPES IN GAIT

Christopher A. Bailey[1], Alexandre Mir-Orefice[1], Julie Nantel[1] and Ryan B. Graham[1]
[1] School of Human Kinetics, University of Ottawa, Ottawa, Canada.
Email: cbailey2@uottawa.ca

INTRODUCTION

Stride-to-stride motor fluctuations (i.e. motor variability) are natural in human gait. Excess or insufficient fluctuations in gait are well-linked to fall risk, yet, even healthy young adults show high inter-individual variability in motor fluctuations [1]. In materials handling tasks, the inter-individual variability can be explained by different motor phenotypes (i.e., low fluctuation "repeaters" and high fluctuation "replacers") with trait-like similarity over time [2,3]. This suggests that similar motor fluctuation phenotypes could exist in gait, although this remains untested. The purpose of this study was to determine if gait motor fluctuation phenotypes exist in young adults.

METHODS

Young adults (N = 51, 27 females) completed seven-minutes of constant-speed treadmill gait at their preferred speed. Marker-based inverse kinematics during 200 consecutive right-leg strides were computed in OpenSim 4.2 using a full body model [4]. Three motor fluctuation features were quantified from 32 degrees of freedom (3D angles of the lower and upper limb joints, trunk, pelvis): (i) magnitude of variability (mean standard deviation [meanSD]); (ii) local dynamic stability (local divergence exponent [λ_{max}]); (iii) regularity (sample entropy [SaEn]). Principal components (PCs) of features were computed by principal components analysis. PCs were interpreted by the loading vectors, then input into machine learning-based clustering using the k-means method for 5000 iterations to test cluster sizes of 1 to 15. The optimal number of clusters across iterations was selected by the number that was the most common elbow in the k-means inertia curve. Cluster differences in PC scores were analyzed using one-way ANOVAs.

RESULTS AND DISCUSSION

Two PCs explained 32.3% of variance in the 96 motor fluctuation inputs. Higher PC1 score was interpreted as more fluctuation across all joints (e.g. significant positive loadings showing higher meanSD of hip and wrist flexion) and higher PC2 score as more fluctuation of upper limb joints with less fluctuation of lower limb joints (e.g. significant positive loading showing higher wrist flexion meanSD and significant negative loading showing lower hip flexion meanSD). Using the k-means method, PC scores were optimally partitioned into 4 clusters for 98.4% of iterations (Figure 1). Table 1 shows that clusters differed by PC1 score ($p < 0.001$; Cluster 1 < Cluster 2 < Cluster 3 < Cluster 4) and PC2 score ($p < 0.001$; Clusters 1,2,4 < Cluster 3). Unlike in materials handling [2,3], 4 motor fluctuation phenotypes characterized gait. We interpret these as “full-body repeaters” (Cluster 1), “full-body replacers” (Cluster 4), “moderates” (Cluster 2), and “upper limb replacers, lower limb repeaters” (Cluster 3).

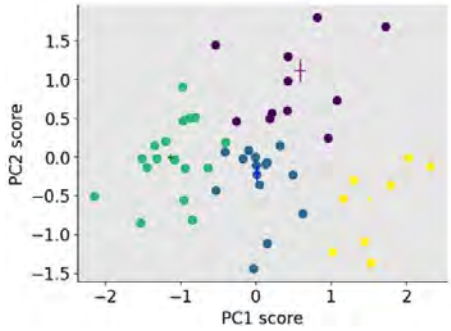

Figure 1: Clusters (k = 4) identified by the k-means method. Cluster centroids and standard deviations (+) are shown.

CONCLUSIONS

Young healthy adults can be classified into four distinct motor fluctuation phenotypes during treadmill gait at preferred speed. Further work is needed to see how these extend to other populations and locomotor tasks, and whether phenotype can help better assess fall risk.

ACKNOWLEDGEMENTS

This study was supported by NSERC and the Ontario Early Researcher Award Program.

REFERENCES

[1] Bailey et al. *J Biomech* **130**: 110855, 2022.
[2] Sandlund et al. *Hum Mov Sci* **51**: 17-26, 2017.
[3] Oomens et al. *Appl Ergonomics* **100** : 103668, 2022.
[4] Rajagopal et al. *IEEE Trans Biomed Eng* **63**: 2068-79, 2016.

Table 1: Sample sizes and principal component (PC) scores (mean ± SD) for each cluster. Colour descriptors match those in Figure 1.

	Cluster 1 (green)	Cluster 2 (blue)	Cluster 3 (purple)	Cluster 4 (yellow)	One-way ANOVA p
Sample size	17; 8 females	15; 8 females	11; 5 females	8; 6 females	
PC1 (a.u.)	-1.16 ± 0.38	0.02 ± 0.30	0.58 ± 0.66	1.51 ± 0.46	$p = 3.2 * 10^{-9}$
PC2 (a.u.)	0.04 ± 0.49	-0.20 ± 0.49	1.13 ± 0.49	-0.54 ± 0.57	$p = 6.3 * 10^{-5}$

VERY SHORT BOUT DURATIONS DECREASE THE EFFICIENCY OF WALKING UP STAIRS

Francesco Luciano[1], Luca Ruggiero[1], Gaspare Pavei[1] and Alberto E. Minetti[1]
[1]Department of Pathophysiology and Transplantation, University of Milan, Italy.
Email: francesco.luciano1@unimi.it

INTRODUCTION

The metabolic demands of locomotion are generally examined at steady-state conditions, which last several minutes; however, in everyday life, people mostly walk for shorter bouts [1]. Previous research hinted that shorter bouts of walking up stairs may have a lower ratio of mechanical to metabolic power, also known as locomotor (apparent) efficiency, compared to longer ones [2]. As mechanical power in stair climbing is primarily done to raise and accelerate the body center of mass [2], this is a suitable model for studying the efficiency of short bouts of walking while minimizing the bias due to elastic storage, negative power, and internal power. The aim of the present study was to examine how an extensive combination of standardized bout durations and power outputs impacted locomotor efficiency.

METHODS

Mechanical power. Three participants (1 female; age 27±5 years; mass 73±12 kg; mean±SD) walked on a Technogym Climb Excite escalator at incline 78% and diagonal speeds of 0.20, 0.25 and 0.36 m/s while an eight-camera Vicon system recorded the position of 18 bilateral markers. Total mechanical power (P_{mech}; W kg^{-1}) was calculated by summing the power to raise and accelerate the body center of mass and the power to swing limbs [3].

Metabolic power and efficiency. Eight participants (4 female; age 26±5 years; mass 72±14 kg) walked on the escalator at the same speeds for 10, 30, 60, 90, and 240 second bouts in randomized order. Oxygen consumption ($\dot{V}O_2$; mL min^{-1} kg^{-1}) was measured by a Cosmed K5 metabograph. The oxygen volume consumed for each bout ($VO2_{integ}$; mL kg^{-1}) was calculated by integrating net (above resting) $\dot{V}O_2$ over time, from bout start to the end of a 7-min recovery. Average net metabolic power ($P_{met;}$ W kg^{-1}) was then calculated as $VO2_{integ}$ divided by bout duration and multiplied by the energy equivalent of oxygen in aerobic respiration. Locomotor efficiency was then given by P_{mech} / P_{met} and regressed over bout duration with a linear mixed model.

RESULTS AND DISCUSSION

At all speeds, the positive mechanical power to raise and accelerate the body center of mass was more than 95% of P_{mech}; bout duration correlated negatively with P_{met}, and hence positively with efficiency (Table 1, Figure 1). The efficiencies were in line with previous research on walking up stairs [2] and in the range of those of isolated concentric muscular contractions.

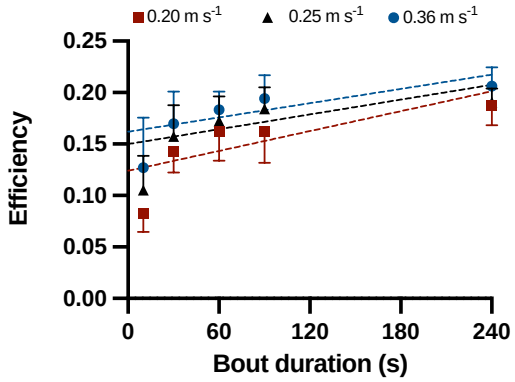

Figure 1 Efficiency versus bout duration and speed (mean±SD). Dashed lines: fixed effects from linear mixed model.

CONCLUSIONS

Short bouts of uphill stair walking are less efficient than longer ones, as they require a higher average metabolic power to produce the same mechanical power. Changes in the metabolic O_2 equivalent at the onset of exercise, the constant amount of energy consumed during the cardiodynamic phase of $\dot{V}O_2$ on-kinetics, and the relatively higher 'weight' of increased system entropy could have a role in these findings.

REFERENCES

[1] Orendurff et al. *J Rehabil Res Dev* **45**, 2008.
[2] Minetti et al. *J Exp Biol* **223**, 2020.
[3] Minetti et al. *J Physiol* **471**, 1993.

Table 1: P_{mech}, P_{met} (means±SD), and regression coefficient for efficiency versus bout duration ($ß_{efficiency}$; mean[95% CI]).

Speed (m s^{-1})	P_{mech} (W kg^{-1})	P_{met} (W kg^{-1})					$ß_{efficiency}$
		10-s bout	30-s bout	60-s bout	90-s bout	240-s bout	
0.20	1.31±0.04	15.8±3.5	9.2±1.3	8.1±1.4	8.1±1.5	7.0±0.7	$3.2•10^{-4}$ [$1.9•10^{-4}$; $4.5•10^{-4}$]
0.25	1.62±0.04	15.4±4.9	10.3±2.0	9.4±1.3	8.8±1.0	8.5±0.6	$2.4•10^{-4}$ [$1.1•10^{-4}$; $3.6•10^{-4}$]
0.36	2.31±0.04	18.2±7.0	13.6±2.5	12.6±1.2	11.9±1.4	11.2±1.0	$2.3•10^{-4}$ [$1.1•10^{-4}$; $3.3•10^{-4}$]

Open dataset for bipedal locomotion on an instrumented treadmill

Dominik Krumm[1], Jayant Wakode[2], Daniel Koska[3] and Stephan Odenwald[1]
[1] Sports Equipment and Technology, Chemnitz University of Technology, Germany.
[2] Neuromotor Behavior, University of Münster, Germany.
[3] Research Methodology and Data Analysis in Biomechanics, Chemnitz University of Technology, Germany.
Email: dominik.krumm@mb.tu-chemnitz.de

INTRODUCTION

Research on power output in running is limited. Unlike in cycling, there are no machines to which force is applied, making it difficult to measure power output. Existing portable devices estimate mechanical power output in running as a function of a runner's anthropometry, temporal-spatial parameters, and/or wind speed [1]. Our overall goal is to determine the mechanical power during running based on kinetic data. As a first step, we have performed long-duration measurements and uploaded them as a freely available dataset that allow us and the scientific community to estimate ground reaction forces based on plantar pressure. In this abstract, we present the experiments performed and give a brief overview of normalised individual runners' ground reaction forces and their temporal parameters.

METHODS

The study was approved by the Institute's Ethics Committee (#101525731). Seventeen persons (age: 29 ± 7 y, height 179 ± 9 cm, body weight 75 ± 13 kg) participated in the study. Data were collected simultaneously using a two-belt treadmill with integrated force plates (1000 Hz) and two pressure insoles with eight pressure sensors each (100 Hz). The experiment included three runs with a total duration of 40 minutes for each participant. The runs included two-minute warm-up and cool-down periods at a speed of 3 km·h^{-1}, three-minute running intervals at speeds of 4 km·h^{-1}, 6 km·h^{-1}, 9 km·h^{-1}, and 12 km·h^{-1}, and one-minute rest periods. Ground reaction forces were filtered using a 4th order zero-lag Butterworth filter with a cut-off frequency of 10 Hz and 30 Hz for the anterior-posterior forces and vertical forces, respectively. Only steps without a foot strike across the two force plates were selected for further analysis. Gait events were determined from the vertical force signals, with a force threshold of 50 N. In this abstract, only the results for 9 km·h^{-1} and 12 km·h^{-1} are displayed.

RESULTS AND DISCUSSION

The ground reaction forces measured in more than 500 hours of running showed different patterns across participants and running speeds (Figure 1).

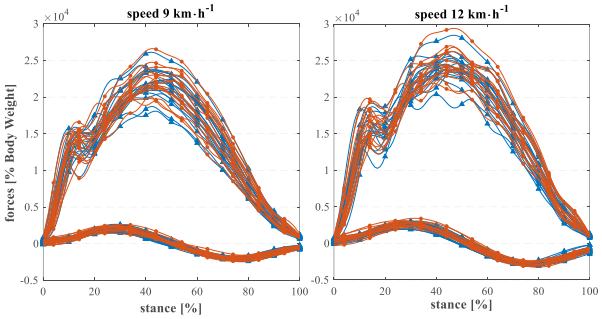

Figure 1 Left (blue '▲') and right (red 'o') mean values of normalised vertical and anterior-posterior ground reaction forces of participants (n = 17) running at speeds of 9 km·h^{-1} and 12 km·h^{-1}.

Participants completed a total of 31,874 steps at 9 km·h^{-1} and 11,572 steps at 12 km·h^{-1}. Due to cross-plate strikes, 47% and 61% of these steps were discarded, respectively. Table 1 summarizes the statistics for selected temporal parameters.

Table 1 Mean and standard deviation of the temporal parameters cadence, flight phase and stance phase across all valid steps.

	9 km·h^{-1}	12 km·h^{-1}
cadence (steps·min^{-1})	157 ± 9	166 ± 8
flight phase (ms)	89 ± 26	122 ± 18
stance phase (ms)	294 ± 31	240 ± 18

CONCLUSIONS

The data collected for this study is available as an open dataset at https://osf.io/kcqtf/ [2]. We are currently working on estimating ground reaction forces based on the measured plantar pressure. This will allow us in the future to determine the mechanical power during running based on the kinetic data.

ACKNOWLEDGEMENTS

Funded by the Deutsche Forschungsgemeinschaft (DFG, German Research Foundation) – Project-ID 416228727 – SFB 1410.

REFERENCES

[1] Cerezuela-Espejo V et al. *Physiol Behav* **223**: 112972, 2020.
[2] Krumm D et al. (2022, April 29). https://doi.org/10.17605/OSF.IO/KCQTF

HAS THE KNOWLEDGE OF BAREFOOT GAIT IN HEALTHY ADULTS CHANGED WITH TECHNOLOGICAL ADVANCEMENTS? – A SYSTEMATIC REVIEW

Alycia Fong Yan[1], Allan Chak Lun Fu[1], and Adrienne Hunt[1]
[1] Faculty of Medicine and Health, The University of Sydney, Sydney, Australia.
Email: alycia.fongyan@sydney.edu.au

INTRODUCTION

Despite the longevity and amount of research into human walking biomechanics, and technological advances in data acquisition, the current knowledge base used to teach gait analysis continues to refer to early theoretical work rather than drawing on original research. Since most published gait studies focus on a particular area of the body, outcome measures from a single study tend to be limited, and therefore tertiary educators seeking to use an evidence-based approach must source multiple individual studies to support the description of kinematics and kinetics across phases of gait and different joints in the body. Commensurate with advances in motion capture technology over the past 50 years, the conduct of research has become more rigorous, and so there now exists a vast and extensive pool of contemporary data from across the world that has the potential to enhance our understanding of healthy gait.The aim of this systematic review of human walking was to provide a thorough, evidence-based, and confident description of the kinematics and kinetics of healthy adult barefoot walking.

METHODS

A systematic search of the major databases from inception to June 2019 was conducted to collect all papers that investigated kinematics and/or kinetics of healthy, barefoot, human walking. Studies were included if they were a full original study investigating level, straight line walking. Participants needed to be healthy humans, aged 18-65 years, performing barefoot walking trials. Studies must have investigated kinematic and/or kinetic variables including angular displacement of all segments of the body, ground reaction forces (GRF), joint moments, and joint power in any of three planes. For inclusion in this review the data must have been presented in time series format or with respect to key time points in the gait (e.g., initial contact, foot flat, mid swing, terminal swing, heel off, toe off). Three independent reviewers screened the articles, analysed the quality, and extracted the data of the included papers. Due to the heterogeneity of the methodologies used and data presentation, a narrative synthesis was adopted. A rigorous quality assessment process was undertaken to ensure that the data were produced from valid and reliable measurements and provided an accurate and trustworthy representation of the results obtained. The process was based upon the JBI Critical Appraisal Checklist for Analytical Cross-Sectional Studies [1].

RESULTS AND DISCUSSION

161 papers met the inclusion/exclusion criteria. 26% were of sufficient quality to enable quantitative synthesis. The quality of studies included in this review was highly variable, with 12% of the eligible papers inaccessible to the reader due to unclear data presentation; data variability was reported in only 68% of the papers; and data normality was rarely described.
A clear consensus was reached for all characteristic sagittal plane movements of the hip, knee and ankle joints, the transverse plane of the pelvis and the hip joint, and the GRF in all three planes; however, it was challenging to determine the typical frontal and transverse plane movements for all other joints.
The authors could not draw any conclusions about the inter-relationships between the upper extremities and the head with other body parts during the gait cycle, or kinetics data in the frontal and transverse planes for all body regions, as no relevant studies were eligible for analysis.
The lack of clarity on the key events, such as stance and swing phase, made drawing fair and confident comparisons among studies, challenging. Lack of consensus in the frontal and transverse planes can be attributed to large variability, due to within or between participant differences, or as a result of different modelling selections, or a range of motion that crosses zero, since conflicting directions of the movement were reported. This was particularly evident for the foot and ankle.

CONCLUSIONS

Despite technological advancements in motion capture, healthy adult gait sagittal plane motion of the major joints and GRF are still the variables that can be described confidently. Improvement in the consistency of how gait analysis is conducted and reported may reduce the incongruency found in the frontal and transverse planes, and within the foot. This will enable future meta-analyses and multi-centre studies.

REFERENCES

[1] A. Moola, et al. *Joanna Briggs Institute Reviewer's Manual, The Joanna Briggs Institute*, 2017

MUSCLE ACTIVATION PATTERNS IN DECOUPLED STRIDE FREQUENCY AND DUTY FACTOR

Germán Pequera[1,2], Ignacio Ramirez Paulino[3], Carlo Biancardi[2]
[1]Ingeniería Biológica, CENUR Litoral Norte, Universidad de la República, Paysandú, Uruguay
[2]Biomechanics Lab., Dept. de Ciencias Biológicas, CENUR Litoral Norte, Universidad de la República, Paysandú, Uruguay
[3]Instituto de Ingeniería Eléctrica, Facultad de Ingeniería, Universidad de la República, Montevideo, Uruguay
Email: gpequera@cup.edu.uy

INTRODUCTION

The duty factor (*DF*) is defined as the fraction of the duration of a gait cycle for which each foot remains on the ground, and is inversely related to the peak ground reaction forces [1]. The difficulty of isolating *DF* from stride frequency (*SF*) during locomotion makes it hard to evaluate the impact of this parameter. An elegant experimental design suggested that reducing the *DF* maintaining the same average force and *SF* would imply the activation of more muscular fibres, with higher energy expenditure [2]. The asymmetries of unilateral skipping make an experimental model for decoupling *DF* from *SF* during locomotion, providing the basis to explore how muscles behave in these conditions. The aim of this work was to determine how *DF* changes alone, independently of *SF*, would affect the muscle activity, by analyzing the muscle activation patterns in the time-frequency domain during skipping gait at controlled speed.

METHODS

Fourteen volunteers (age: 25.3 ± 3.7 years, mass: 78.15 ± 13.8 kg, height: 1.76 ± 0.09 m) performed unilateral skipping at 9 km/h recording electromyographic activity (EMG) with a Delsys Trigno electromyograph at 2000 Hz on Biceps Femoris (BF), Vastus Medialis (VM), Tibialis Anterior (Tib), Soleus (Sol), Gastrocnemius Medialis (GasMed), Rectus Femoris (RF) and Gluteus Medius (GluM) of each leg. Also, the position of 18 markers located on the body was recorded at 100 Hz using 8 Vicon Bonita cameras to reconstruct an 11-segment body model. *DF* and *SF* was calculated by identifying the landing and takeoff times from the heel and fifth metatarsal markers. EMG signals were processed using a filter-bank generated from 11 Wavelets with center frequencies from 6.9 to 395.4 Hz to estimate EMG power (intensity) [3].

RESULTS

The *DF* in trailing leg was smaller than *DF* in leading leg (Table 1). In order to clarify the obtained results, Figure 1 shows an overview of the sum of the EMG intensity in one muscle per joint, at each of the four highest frequency bands (218, 271, 331 and 395 Hz). Wavelet analysis displayed greater intensity at high frequencies in GluMed of the trailing leg, while GasMed and RF showed the same activation patterns in both legs, despite the different *DF*.

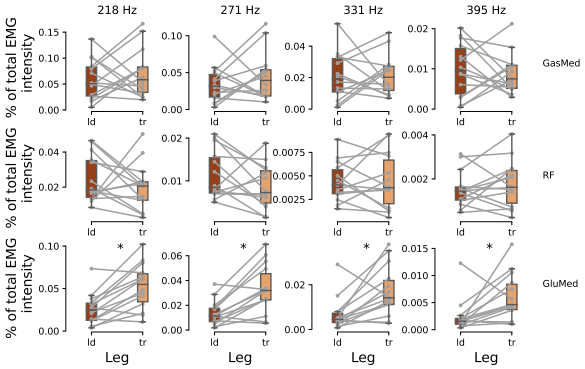

Figure 1: EMG intensity sum in frequency bands with center frequency of 218, 271, 331 and 395 Hz in leading leg (ld) and trailing leg (tr) during skipping. Asterisks (*) indicate significance at 0.05.

CONCLUSIONS

Changes in *DF* were related with greater intensity in high frequencies in GluMed, a muscle that execute high force during locomotion. Short *DF*s could trigger a switch to fast-twitch fiber recruitment in GluMed as strategy to perform high force development in short times during gait cycle. GasMed and RF maintained inaltered recruitment patterns despite the spatiotemporal constraint. This behaviour could be associated to gait selection or *SF* modification.

ACKNOWLEDGEMENTS

We acknowledge to Comisión Sectorial de Inevestigación Científica (CSIC) for funding this work.

REFERENCES

[1] Minetti AE *J Biomech* **31**: 463-468, 1998.
[2] Beck ON et al. *Proc. Royal Soc. B* **287**: 20200431, 2020.
[3] Von Tscharner V *J Electromyogr Kinesiol* **10**: 433-445, 2000.

Table 1: Mean ± standard deviation and results from comparison of both legs in stride frequency (*SF*) and duty factor (*DF*). α was set at 0.05.

	Trailing leg	Leading leg	p-value
SF (Hz)	1.76 ± 0.24	1.76 ± 0.24	$p = 0.90$
DF	0.24 ± 0.04	0.40 ± 0.06	$p < 0.001$

STANDING BALANCE REPONSES TO PHYSICAL AND VISUAL PERTURBATIONS

Calaina Brooke[1,2], Stephanie Tran[2], Stephen D. Perry[1,2,3]
[1] Rehabilitation Sciences Institute, University of Toronto, Toronto, Canada.
[2] KITE, University Health Network, Toronto, Canada.
[3] Kinesiology, Wilfrid Laurier University, Waterloo, Canada.
Email: c.brooke@mail.utoronto.ca

INTRODUCTION

Stable upright balance requires sensory and motor systems to effectively process stimuli from the surrounding environment and provide the corresponding downstream motor responses[1,2]. External perturbations can be applied to disturb the centre of mass (COM) and disrupt balance when the COM exceeds the base of support (BOS)[3]. External perturbations can be applied in the form of a physical or visual stimuli. To maintain stability, a reactive sequence of postural movements are required following physical perturbations while visual perturbations cause a perceived need to adjust balance.

The purpose of the present study was to evaluate the responses to visual and physical perturbations during quiet stance. It was hypothesized that standing balance will be more unstable in the anterior-posterior (AP) than mediolateral (ML) direction in response to physical and visual perturbations and perturbations in the AP direction will increase instability.

METHODS

The present study consisted of young adults (n=12; age = 18-40 years). All testing sessions took place in the FallsLab of the Toronto Rehabilitation Institute. The experiment used a 6m x 3m moveable platform, with four AMTI force plates, a 12-camera VICON motion tracking system, and the HTC Vive Pro Virtual Reality Head Mounted Display. The experiment consisted of 12 45-second quiet standing trials. There were five randomized conditions: no perturbations (None), AP visual shift (AP_VS) or ML visual shift (ML_VS), AP physical shift of the platform (AP_PS), and ML physical shift (ML_PS). Visual shifts of the virtual environment were applied at 2 m/s^2. Physical shifts of the physical platform were applied at 2 m/s^2. The perturbations were delivered at random times after 30 seconds of standing. Centre of Pressure (COP) path length was calculated by summing the Euclidean distance between successive data points over a 4 second analysis period starting at the onset of the perturbation.

RESULTS AND DISCUSSION

A Generalized Linear Mixed Model (GLMM) analysis was conducted on the length of the COP path length for the 12 healthy subjects (8F:4M, 24.6 +/- 1.1 years). Subject ID was considered as a random factor, and perturbation type (visual vs. physical) and perturbation direction (AP vs. ML) were examined as fixed factors. There was a significant effect of perturbation type ($p < 0.001$). Physical Perturbations in the ML and AP direction (19422.83cm +/- 11706.04cm; 4070.26cm+/-42455cm) induced larger COP path lengths compared to visual perturbations in the ML and AP direction (4396.7cm+/-5050.86cm;2793.40cm+/-2457cm). There was no significant effect of perturbation direction ($p=0.790$). ML direction did not produce significantly different COP Path Lengths compared to AP direction in physical ($p=0.419$) or visual ($p=0.256$) conditions. Mean Max COP excursions in the AP direction were analysed, and a significant effect of perturbation type was found ($p<0.001$). Physical perturbations resulted in larger COP excursions in the ML and AP perturbations (11.54cm+/-5.53cm;411.65cm+/-1770.9cm) when compared to ML and AP visual perturbations (2.25cm+/-1.34cm; 2.38cm+/- 2.12cm).

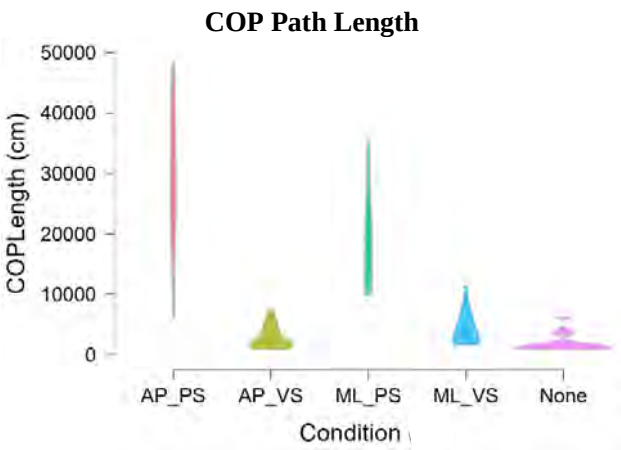

Figure 1. COP Path Length (cm) for all conditions for the 4 second analysis window. (AP_PS – Anterior Posterior Physical Shift, AP_VS – Anterior Posterior Visual Shift, ML_PS – Medio-lateral Physical Shift, ML_VS – Medio-lateral Visual Shift)

CONCLUSIONS

Physical perturbations resulted in larger COP path lengths compared to visual perturbations, and there was no significant difference between COP Path Lengths in the medio-lateral and anterior-posterior directions for each visual and physical perturbations. Physical perturbations also resulted in increased maximum COP excursion in the AP direction with greater effects observed in response to the physical perturbations.

REFERENCES

[1] Cripps A et al. *Brain Inj* **32**:1566-1575, 2018
[2] O'Connor SM et al. *Journal of Neurophysiology* **102**:1411-1419, 2009
[3] Rogers MW et al. *Handbook of Clinical Neurology*: 85-105, 201

THE EFFECT OF DIFFERENT WALKING SPEED ON GAIT STABILITY BETWEEN YOUNG AND ELDERLY POPULATION ANLAYSED BY A ZERO MOMENT POINT METHOD

S. K. Han[1], Y.W. Yoo[2], H.W. Choi[1] and K.K. Lee[2]

[1] AI·Robotics department, Korea Institute of Industrial Technology, Ansan, Korea.
[2] College of Physical Education, Kookmin University, Seoul, Korea.
Email: shan@kitech.re.kr

INTRODUCTION

A fall is one of the main health problems in the elderly population, because it causes traumatic injury [1] and is associated with increased morbidity and mortality [2]. Compromised stability is considered a major fall risk factor for older adults. Since a dynamic stability in a biped model can be defined by a zero mement point method (ZMP), the stability analysis of human walking can be simplified with the ZMP method despite of its complexity. The aim of this study was to compare the effect of walking speed on the dynamic gait stability between the elderly and the young population using a ZMP method. It was hypothesized that increased walking speed in the elderly greater affects their giat stability than in the young.

METHODS

The subjects for the young (n= 24, a mean age of 22.2 ± 1.0 years, YG) and elderly group (n= 24, a mean age of 69.9 ± 1.0 years, EG) with no musculoskeletal disorders and fall experience were recruited for walking experiments. The experiments were approved by the Korea National Institute for Bioethics Policy Review Board. Each participant was monitored using a Helen Hayes full-body marker set. Each participant was asked to walk at a self-selected speed (SWS), 110 % of SWS and 120 % of SWS on 10 m flat ground. A three-dimensional motion capture system (Motion Analysis, USA) was used to record and analyze marker trajectories. Gait stability is defined by the percentage of ZMP values inside of base of support during one gait cycle. Results are shown as means ± standard error of the mean. Comparisons of ZMP values were conducted using a repeated measured ANOVA (SPSS 21.0, SPSS Inc.).

RESULTS AND DISCUSSION

An average SWS, 110 % and 120 % of SWS were 1.34 ± 0.06 m/s, 1.48 ± 0.07 m/s and 1.62 ± 0.07 m/s for the YG, and 1.19 ± 0.03 m/s, 1.31 ± 0.03 m/s and 1.44 ± 0.03 m/s for the EG, respectively. At 110% of SWS, the gait stabilities in the anterior-posterior (AP) direction were decreased by 2.1 % and 10.8 % for the EG and YG, respectively, and at 120% of SWS, those were decreased by 4.3 % and 3.9 % for the EG and YG, respectively. The gait stabilities at 110% of SWS in the medial-lateral (ML) direction were decreased by 9.0 % and 18.1 % for the EG and YG, respectively, and at 120% of SWS, those were decreased by 10.1 % and 8.3 % for the EG and YG, respectively. However, at the same walking speed of 1.34 m/s, there is a tendency of a greater decrease of gait stability in EG compared to YG (Figure 1).

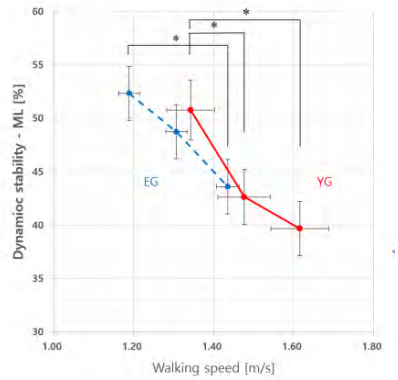

Figure 1. Gait stability in the ML direction at the different walking speed between young and elderly group. Data in the figure are shown as means ± standard error of the mean. (* p = 0.05).

CONCLUSIONS

Gait stability were similar in both the YG and EG at the SWS, but the pattern of change with increasing speed was greatly different. Namely, the gait stability gradually decreased through 120% SWS in the EG, but in the YG, the gait stability decrease rapidly at 110% of SWS and then the decrease rate reduced at 120 % SWS. Overall, it is anticipated that the gait stability of the YG is more affected by an increases of walking speed than that of the EG at the certain speed range.

ACKNOWLEDGEMENTS

This project was supported by the Technology Innovation Program (Industrial Strategic Technology Development Program) (20007058, Development of safe and comfortable human augmentation hybrid robot suit) funded by the Ministry of Trade, Industry & Energy (MOTIE, Korea).

REFERENCES

[1] Baker and Harvey. *Clin Geriatr Med* 1: 501-12, 1985.
[2] Nevitt et al. JAMA **261**: 2663-2668, 1989.

Table 1: Gait stability in the AP direction at the different walking speed between the YG and EG.

	SWS	SWS × 110%	SWS × 120%
EG	77.6 ± 2.3	76.0 ± 2.1	72.9 ± 2.5
YG	77.1 ± 3.5	69.6 ± 3.2	67.0 ± 3.3

EFFECT OF MIDSOLE HARDNESS ON THE CENTER OF PRESSURE DURING WALKING

Yohei Yamazaki[1,2], Hiroaki Noro[3], Keiichiro Hata[1,2], Shota Akahoshi[1], Shuta Matsui[1], Lee Rou You[1], Kazuyuki Kanosue[2] and Toshio Yanagiya[1,2]
[1] *Graduate school of Health and Sports Science, Juntendo University, Chiba, Japan*
[2] *Institute of Health and Sports Science & Medicine, Juntendo University, Chiba, Japan*
[3] *Faculty of Health and Sports Science, Juntendo University, Chiba, Japan*
Email: sh4222010@juntendo.ac.jp

INTRODUCTION

One of the functions of shoes is to improve postural stability and prevent injuries. Postural stability is affected by the mechanical properties of shoe midsole material. The trajectory of center of pressure (COP) is a parameter which evaluates dynamic balance control during gait. The "butterfly diagram" which depicts the COP trajectory during gait enables us to confirm visually the length and sway of COP, and step width [1,2]. The purpose of this study was to compare the postural stability during gait in different midsole materials and hardness by using the "butterfly diagram".

METHODS

Seven males (28.1±4.1 years, 1.72±0.05 m, 71.1±7.9 kg) who had no lower limb injuries participated in this study. The participants walked for 50 s at 4 km/h on a split-belt force-instrumented treadmill (Tec Gihan Co. Ltd, Uji, Japan, 1kHz) with two walking shoes conditions of different midsole and hardness. One was Softer midsole shoes （SS） with Ethylen-Vinyl Acetate (EVA) midsole and lower hardness. The other was Harder midsole shoes （HS) with Polyurethane (PU) midsole and higher hardness. Ground reaction force and COP coordinates during walking were collected by the force-instrumented treadmill. Butterfly diagram was produced using obtained COP coordinates (Figure 1). Displacements of anterior-posterior and lateral COP were calculated during single and double support stance phase. Step width was the difference of lateral COP coordinate between both legs.

RESULTS AND DISCUSSION

It is possible to compare the difference of COP displacement and step width between the shoe conditions visually. Lateral COP displacement of SS was significantly greater than of HS throughout the stance phase. On the other hand, there was no significant difference in lateral COP during the single support stance phase (Table 1). Therefore, HS may decrease the sway of lateral COP especially during the double support stance phase.

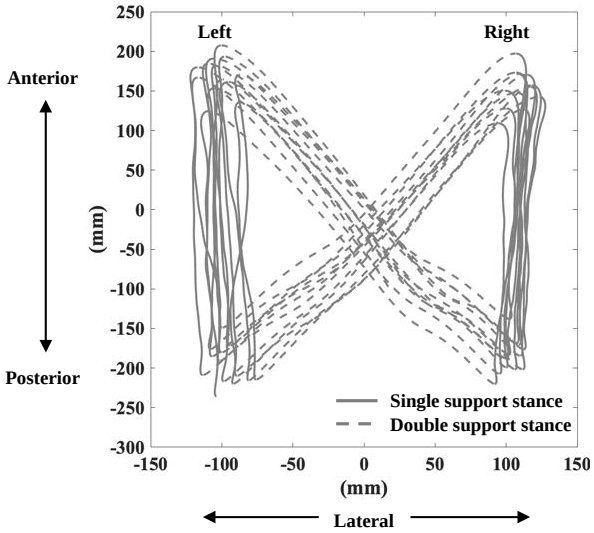

Figure 1: Typical result of the butterfly diagram.

CONCLUSIONS

Different midsole materials and hardness affects the COP displacement. Harder midsole made of PU decreases lateral COP displacement, which would provide more stability in walking.

REFERENCES

[1] Kalron A et al. *J Neurol Sci* **358**: 92-100, 2015.
[2] Lee Y et al. *Gait Posture* **76**: 157-161, 2020.

Table 1: Results of COP displacement and step width.

	SS	HS	*p-value*	Effect size
Lateral COP displacement of the single and double support stance phase (mm)	138.2 ± 14.2	129.3 ± 15.6	$p = 0.02$	0.65
Lateral COP displacement of the single support stance phase (mm)	18.74 ± 4.75	17.01 ± 2.93	$p = 0.33$	0.47
Step width (mm)	236.19 ± 19.03	229.52 ± 23.88	$p = 0.30$	0.33

A.R.G! AUGMENTED REALITY AND GAIT: CUES ELICIT GAIT ADAPTATIONS IN AR

Wendy Pham[1], Gwendolyn Retzinger[1], Borna Golbarg[1], Kyle Dang[1], and Jacob Hinkel-Lipsker[1]
[1] Kinesiology, California State University, Northridge, California, USA.
Email: jhlipsker@csun.edu

INTRODUCTION

Use of augmented reality (AR) technology for rehabilitation has drastically increased in recent years. Evidence has shown that visual and auditory cues alter spatial and temporal gait parameters, respectively [1]. Through providing visual and auditory cues while walking, AR can be used to cue spatiotemporal gait adaptations with applications to clinical populations such as those with Parkinson's disease [2-4]. However, given the novelty of the technology it is unknown how cues delivered through AR drive gait adaptations. The purpose of this study is to assess the feasibility of visual and auditory cues delivered through AR on altering spatiotemporal gait outcomes in a healthy, young population.

METHODS

20 healthy participants (7 F/13 M; 25.5 + 4 yrs) were recruited to walk for 10 steps in four different cueing conditions using an AR headset: No Cues (NC) (i.e., natural gait), Visual (V), Auditory (A), and Visual + Auditory (VA). Each condition was completed three times in a random order for a total of 12 trials. An Inertial Measurement Unit (IMU) system with integrated footswitches was used to collect spatiotemporal gait data at 200 Hz. A System Usability Survey (SUS) was administered afterwards to determine the usability of our novel application and linear regressions were performed to determine the relationship between reported usability and gait variability.

RESULTS AND DISCUSSION

All cueing conditions exhibited a significantly faster cadence (V, A, VA = 0.67, 0.68, 0.68 steps/sec, respectively) compared to NC trials (0.63 steps/sec; p <0.05). Surprisingly, cadence variability was significantly higher for A trials (coefficient of variation (CV) = 0.11) compared to the other three groups (NC, V, AV = 0.1, 0.09. 0.09; p <0.05). V trials exhibited significantly decreased stride lengths (2.13 m) compared to NC (2.3 m; p < 0.05). Increased reported system usability was significantly correlated with decreased stance time across A trials (adj R^2 = 0.262, β = -0.549, p = 0.012).

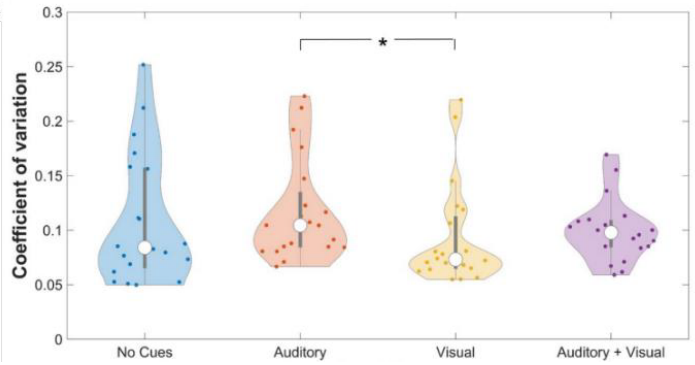

Figure 1 Violin plots demonstrating the mean and distribution of individual data points in each cueing condition for cadence variability.

CONCLUSIONS

Our findings reinforced that certain visual and auditory cues affect gait parameters, albeit in a direction opposite of what was hypothesized (e.g., greater cadence variability with auditory cues). These results provide insight into how healthy populations respond to cues delivered through AR, providing a foundation for future studies to implement AR with clinical populations such as those with Parkinson's disease.

ACKNOWLEDGEMENTS

Thanks to Alex Krause, Nicholas Cando, Joshua Vicente, Rabbani Nzeza, and other members of the Move-Learn Lab (MLL) and Positive Augmented Research and Development (PAR-D) Lab for assistance with app development and data collection. This work was supported by the Department of Defense (Contract # W911NF2110273).

REFERENCES

[1] Vaz J.R. et al. *Phsyiol*. **11**:1-10, 2020.
[2] Ginis P et al. *Ann. Phys. Rehabil. Med.* **61**:407-413, 2018.
[3] Dibble L.E. et al. *Gait Posture* **19**:215-225, 2004.
[4] Wittwer J.E. et al. *Gait Posture* **37**:219-222, 2013

EFFECTS OF ARTIFICIAL KNEE JOINT CONSTRAINT ON SHARED NEURAL DRIVE OF ANKLE PLANTAR FLEXORS DURING GAIT

Carlos Cruz-Montecinos[1], Claudio Tapia[1], Sofia Pérez-Alenda[2], Mauricio Cerda[3] and Huub Maas[4]
[1] Department of Physical Therapy, University of Chile, Santiago, Chile
[2] Department of Physiotherapy, University of Valencia, Valencia, Spain
[3]Programme of Anatomy and Developmental Biology, ICBM, University of Chile, Santiago, Chile.
[4]Department of Human Movement Sciences, Vrije Universiteit Amsterdam, Amsterdam, Netherlands
Email: carloscruz@uchile.cl

INTRODUCTION

Synergistic muscles receive common descending drive from the CNS [1]. It is unknown how a joint range of motion constraint affects this shared neural drive between neighboring synergistic muscles. We aimed to investigate how an artificial knee joint constraint affects the shared neural drive of ankle plantar flexors during gait. As the gastrocnemius muscle (GAS) length depends on knee angle, we hypothesize that artificial knee constraint decreases the shared neural drive between GAS and soleus (SOL), which does not cross the knee joint.

METHODS

Fifteen healthy subjects walked overground at 1 m/s with an articulated knee brace limiting knee between 20° to 40° degrees (simulating a knee flexion contracture). Muscle activity of plantar flexors was collected through surface electromyography. Ten cycles corresponding to the middle 10 meters of a 30-meter corridor were used for data analysis (20 cycles in total). Shared neural drive was assessed using nonlinear method based on the ensemble empirical mode decomposition and instantaneous phase dependence of time series in bi-directional causality [2]. To estimate the intensity of shared neural drive, mutual predictability was assessed using approximate cross-entropy [3]. This method has been recently proposed to assess the synergistic action between pairs of synergistic muscles. [3].

RESULTS AND DISCUSSION

Artificial restriction of knee extension results in indicate that the direction of causality of shared neural drive is affected. ($p<0.05$) (Figure 1). Our results may be explained by potential changes in length-dependent and force-dependent feedback due to the restriction of knee extension during gait [4]. Our results agree with those of animal studies where the manipulation of muscle length and the connective tissue interface between neighboring muscles have been shown to change intermuscular coordination during locomotion [5].

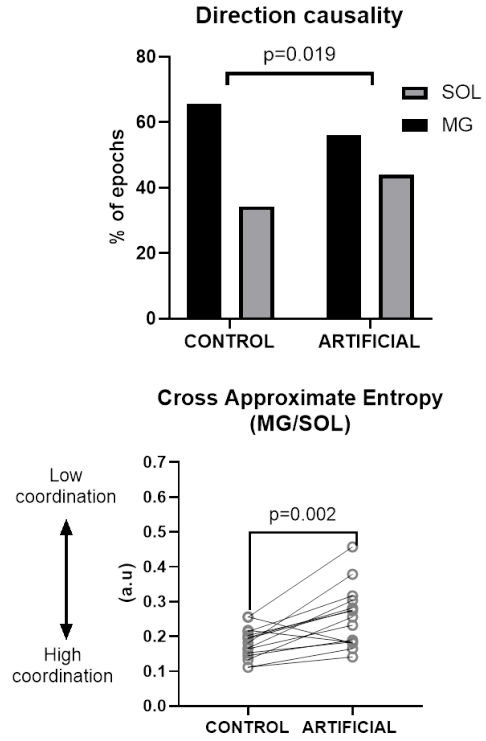

Figure 1. *Top. Direction of causality between medial gastrocnemius to soleus (MG) and Soleus to MG (SOL). Bottom. Mutual predictability between MG and SOl.*

CONCLUSIONS

The artificial restriction of knee extension changes the interaction from the gastrocnemius muscle to the soleus and their coordination. These results support the presence of excitatory length-dependent feedback from gastrocnemius to soleus during locomotion.

REFERENCES

[1] De Luca CJ. *J Neurophysiol*,87: 2200-2204., 2002.
[2] Yang AC et al. *Nat Commun, **9**: 3378, 2018.*
[3] Cruz-Montecinos C. *Med Biol Eng Comput*: **1-13**, 2022.
[4] Nichols, T. R.et al. *J Neurophysiol* **81**: 467-478, 1999
[5] Bernabei, M et al. *J Neurophysiol* **118:** 1677-1689, 201

DETRENDED FLUCTUATION ANALYSIS OF RUNNING STRIDE TIME AT AND NEAR THE MAXIMAL LACTATE STEADY STATE

van Rassel, C.R. [1], Dimmick, H.L. [1], Ferber, R.[1], & MacInnis, M.J. [1]
[1] Faculty of Kinesiology, University of Calgary, Calgary, AB, Canada.
Email: crvanras@ucalgary.ca

INTRODUCTION

Fluctuations in running stride time (ST) may represent complex and rhythmic changes to the neuromuscular control of human gait [1]. Detrended fluctuation analysis (DFAα1) of ST has been used to quantify long range correlations (LRC) of the locomotor system. DFAα1 typically yields a scaling exponent between 0.5 and 1.0 and an alteration in ST-DFAα1 has been associated with acute fatigue, overreaching, and injury history [2]. Thus, ST-DFAα1 may provide utility as a running training metric. Maximal lactate steady state (MLSS), which represents the boundary between sustainable and unstustainable exercise, is commonly used to prescribe exercise intensity. Despite evidence that ST-DFAα1 may be altered during prolonged continuous exercise, it remains unknown whether similar fractal responses occur during constant-intensity exercise at/near the MLSS threshold. The purpose of this investigation was to determine the variation of ST-DFAα1 responses at and within 5% of MLSS and to determine the repeatability of ST-DFAα1 at MLSS.

METHODS

Sixteen (9M, 7F) recreational runners (mean [SD]; 30.1 [4.2] yrs, $\dot{V}O_{2max}$ 54.6 [6.3] ml·kg^{-1}·min^{-1}) performed an incremental exercise test and four, 30-min, constant-speed running trials at running speeds 5% below (B), at (M), and 5% above (A) MLSS, and a final repeat trial at MLSS (R). Participants were fitted with an inertial measurement unit (Blue Trident, Vicon, Oxford, UK; 1125 Hz, ±16 g) positioned between the posterior superior iliac spines, coincident with the inferior aspect of the iliac crest. Acceleration data were sectioned into three 8-min segments at the beginning (S1; 0.5-8.5min), middle (S2; 12.5-20.5min), and end (S3; 22-30min) of the 30-min running trials. Vertical axis acceleration data were low-band pass filtered before calculating ST as the sum time between consecutive peak accelerations. ST-DFAα1 was calculated for each 8-min section with window size 16 to N/9, where N is the number of STs within each respective segment. Differences in ST-DFAα1 across intensities and duration for the B, A, and M trials were examined using a linear mixed effects model (LMM), and repeatability of ST-DFAα1 at MLSS (R and M trials) was determined via LMM, intra-class correlation coefficients (ICCs) and Bland-Altman limits of agreement (LOA).

RESULTS AND DISCUSSION

Runners completed 30 min of running at B, M, and R, but not A (n=7) due to volitional exhaustion. 682 [35] strides were recorded per segment. There was no significant duration × intensity interaction effect ($p = 0.17$) or main effects for duration ($p = 0.66$) or intensity ($p = 0.76$) for ST-DFAα1 (Figure 1). On average ST-DFAα1 measures were lower during R compared to M trials, ICCs were moderate, and LOA were wide, suggesting that ST-DFAα1 measures between trials were not repeatable at MLSS (Table 1). As R was the final trial, it is possible that multiple bouts of prolonged treadmill running alter neuromuscular control of running gait, potentially indicating differences in fatigue or fitness, or the need for a "learning phase."

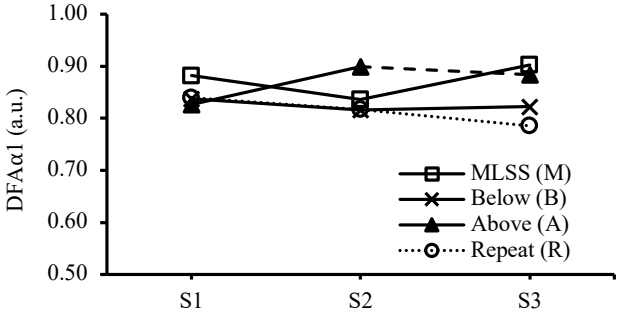

Figure 1 Mean ST-DFAα1 measures.

CONCLUSIONS

Although not significant, our preliminary analysis suggests that running intensities above MLSS may produce greater ST LRCs and that ST-DFAα1 measures between trials were not repeatable at MLSS.

ACKNOWLEDGEMENTS

This work was funded by NSERC, NSERC Wearable Technology Research and Collaboration (WeTRAC) CREATE Training Program, and Alberta Innovates.

REFERENCES

[1] Hausdorff J.M. *Hum Mov Sci* **26(4)**: 555-589, 2007.
[2] Mo S et al. *Gait & Posture* **64**: 7-11, 2018.

Table 1: Results of LMM (n = 16) and between-day reliability (n = 12) of ST-DFAα1 during M and R trials.

	Trial	Mean (95% CI)	Main effect of trial	ICC (95% CI)	Mean difference (LOA)
ST-DFAα1	MLSS	0.874 (0.817 to 0.931)	$p < 0.002$	0.662 (0.354 to 0.820)	0.066 (-0.066 to 0.198)
	Repeat	0.812 (0.755 to 0.870)			

Frontal forefoot strike patterns and its associations with 100-m sprint performance in male sprinters

Haruto Arai[1], Tadashi Suga[1], Masafumi Terada[1], Yuki Kusagawa[1], Keishi Kuroki[1], and Tadao Isaka[1]
[1] Faculty of Sport and Health Sciences, Ritsumeikan University / Shiga, Kusatsu, Japan.
Email:gr0573rr@ed.ritsumei.ac.jp

INTRODUCTION

Foot strike patterns during running in long-distance runners have been typically classified into three patterns based on foot positionings in the sagittal plane and are related to their running performance [1]. In contrast, few studies have reported the usage trend of sagittal foot strike patterns in sprinters because most sprinters use the forefoot strike pattern [2]. To the best of our knowledge, no study has investigated the classification of forefoot strike patterns in sprinters. Utilizing the forefoot strike pattern classification may provide insight into understanding of how sprint performance differs among sprinters. Therefore, in this field study, we examined the usage trend of forefoot strike patterns based on foot positioning in the frontal plane during a 100-m sprint in male sprinters and then its associations with their 100-m sprint performance.

METHODS

Frontal video in 613 male sprinters who finished a 100-m sprint race were recorded from seven track and field events in the 2022 season using high-speed cameras placed behind the finish line. To ensure as much frontal video as possible, the video was acquired with one camera per sprinter. Of these, 417 male sprinters, who used the forefoot strike pattern and whose the corrected 100-m sprint time (see below) was less than 12.00 s, were included in the analyses of this study. The classification of the frontal forefoot strike pattern of the first leg stepping after the start was performed at a passage of 60 m (i.e., maximum speed phase) during a 100-m sprint. The frontal forefoot strike patterns were first classified into the non-inversion strike (NIVS) and inversion strike (IVS). NIVS was defined as a pattern in which the medial and lateral portions of the forefoot contacted with the ground almost simultaneously, whereas in IVS, the lateral edge of the forefoot contacted with the ground. Further, the NIVS pattern was subclassified into the flat strike (FS) and abduction strike (AS) and the IVS pattern was subcategorized into the inversion strike (IS) and abduction and inversion strike (AIS). FS was defined as a pattern in which the tip of the forefoot contacted the forward direction to the ground, whereas in AS, it contacted the outward direction to the ground. IS was defined as a pattern in which the lateral edge of the forefoot contacted the forward direction to the ground, whereas in AIS, it contacted the outward direction to the ground. To calculate the corrected 100-m sprint time for each sprinter, the official 100-m sprint time was corrected for the effect of wind speed using a windless conversion [3]. The Mann-Whitney U or Kruskal-Wallis test were used to compare the corrected 100-m sprint times between the different forefoot strike pattern groups.

RESULTS

The usage rates of NIVS and IVS patterns were 13.7 and 86.3%, respectively (Figure 1A). The corrected 100-m sprint time was significantly shorter in the NIVS group than in the IVS group (Figure 1B: $P = 0.002$). Additionally, the usage rates of four sub-patterns were the highest for the AIS (73.6%), followed by the IS (12.7%), AS (8.2%), and FS (5.5%). The corrected 100-m sprint time was significantly shorter in the FS and AS groups in the AIS group ($P < 0.05$). Furthermore, the corrected 100-m sprint time in the FS group was significantly shorter than that in the IS group ($P = 0.041$).

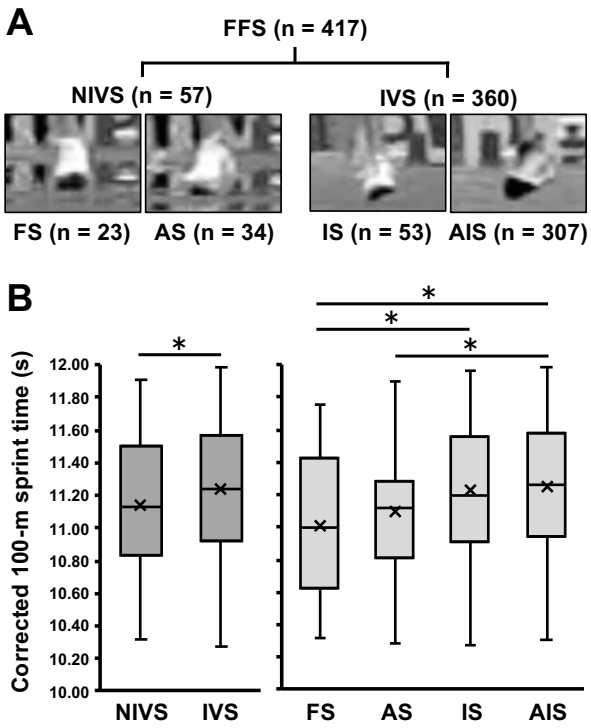

Figure 1. Frontal forefoot strike patterns and its associations with 100-m sprint performance in 417 male sprinters. A: classification and usage trends of forefoot strike patterns, B: comparisons of the corrected 100-m sprint time among the different forefoot strike pattern groups. *Significant difference ($P < 0.05$) between groups.

CONCLUSIONS

This study demonstrated that forefoot strike patterns based on the frontal plane can be classified into two or four patterns in male sprinters and may be related to their 100-m sprint performance. Therefore, these findings indicate that the frontal forefoot strike patterns may be an important biomechanical factor contributing to superior 100-m sprint performance in sprinters.

REFERENCES

[1] Lieberman DE et al. *Nature* **463**: 531-535, 2010.
[2] Krell JB et al. *J Sports Sci* **14**:175-180, 2006.
[3] Moinat M et al. *Eur J Sport Sci* **18**:1185-1190, 2018.

Can an Accelerometer Replace Lower Extremity Joint Moment upon Running?

Young-Seong Lee[1], JiSeon, Ryu[1], Sukhoon Yoon[1], Sang-Kyoon Park [1†]
[1]Motion Innovation Centre, Institute of Sport Science, Korea National Sport University, Seoul, Korea
Email: spark@knsu.ac.kr

INTRODUCTION

High impact occuridng from the ground upon running causes injuries to the lower extremities, and the relationship beteen the impact and injuries has been investigated through ground reaction force (GRF) and joint moment. Fore foot strike causes ankle injuries by increasing plantar flexion moment at the ankle joint in running and delivers high impact shock to the fore foot, therefore, it increases fracture rate of toes. Meanwhile, the rear foot stike increaes the knee joint's extension moment, and thus causes knee injuries and delivers high impact shock to the tibia, so it incresases the stress fracture rate of the tibia [1]. To investigate the impact characteristics, accelerometers are recently used. Very high correlations between the accelerometer attached to the tibia and the impact variables of vertical GRF was investigated, so the accelerometer is used as one of the impact variables[2]. However, research investigating relation-ship between the accelerometer attached to the lower extremity segmenaation and the joint moment is really insufficient. Accordingly, this research aims to examine relationships between joint moments and the peak accelerations on the tibia, thigh, and 5th lumbar (L5) during running.

METHODS

This research recruited 60 males in their 20s to 30s, and they conducted artificial fore foot strike and rear foot strike running. In doing so, they used a treadmill embedded with eight infrared cameras and GRF. Each accelerometer was attached to the distal tibia (8cm above the medial ankle), thigh (50% site from the greater trochanter of femur to the later epicondyle), and L5. The participants performed running on the treadmill through measurement of each participant's preferred velocity. They ran for 3 minutes depending on each strike pattern (RFS vs. FFS), and each participant's 20 steps were analyzed through one-minute video recording, respectively. Strike patterns were selected on the basis of the strike pattern scope proposed by previous researches, and the participants with improper strike patterns were excluded. The joint moment was computed through Visual 3D, and the 2nd lowpass filtering was carried out along with the accelerometer data (camera sf: 100Hz, GRF & Acc. sf: 1,000Hz). Correlation between the acceleration and joint moment were determined using the pearson correlation coefficient with a confidence level of $p < 0.05$.

RESULTS AND DISCUSSION

According to the research results, the plantar flexion moment of ankle joint showed a correlation with the vertical and resultant acceleration of the distal tibia upon rear foot strike (p<.05, table 1). The extension moment of hip joint revealed a correlation with the vertical and resultant acceleration of L5 upon fore foot strike and rear foot strike (p<.05, table 1). The result means that the accelerometer attached to the lower extremity segmentation affects the lower extremity joint moment during rear foot strike running. The reason why no correlation was revealed between the accelerometer attached to the thigh and knee joint moment is skin movement artifact. Therefore, it is judged that accelerometers need to be attached to the site close to bones, not skin, when attaching an accelerometer.

CONCLUSIONS

Our findings suggest that peak accelerations by using accelerometers are significantly correlated with joint moments at the ankle and hip joint during rear foot strike running. However, some consideration would be required when applying this approach to forefoot strike running due to weak correlation.

REFERENCES

[1] Goss, D. L. & Gross, M. T. *US army medical department Journal*, **62-71**, 2012.
[2] Hennig, E. M. & Lafortune, M. A. *ISBS*, **7(3)**, 1991

Table 1: Mean (standard deviation) and correlation between joint moment and acceleration (unit: moment [BWs], Acc. [g]

mean±SD r(p)	Ankle			Knee			Hip		
	Joint moment	Vertical Acc. (g)	Resultant Acc. (g)	Joint moment	Vertical Acc. (g)	Resultant Acc. (g)	Joint moment	Vertical Acc. (g)	Resultant Acc. (g)
Rear foot strike	2.52±0.37	7.92±2.58	9.03±2.68	1.83±0.38	10.32±4.37	12.10±4.43	1.19±0.27	5.17±2.68	5.55±2.66
		.54 (.01)*	**.49 (.01)***		.05 (.74)	.02 (.91)		**.29 (.03)***	**.27 (.04)***
Fore foot strike	3.29±0.35	6.74±1.40	13.77±3.88	1.50±0.37	7.71±2.67	9.46±2.77	1.20±0.20	6.15±2.56	6.40±2.55
		.16 (.23)	.18 (.18)		-.02 (.90)	-.06 (.68)		**.35 (.01)***	**.33 (.02)***

*: indicates significant difference (p<.05).

Foot medial longitudinal arch deformation and plantar load distribution pattern during running

Akira KIUCHI, Tomoya HIRANO, Natsumi FURUTA and Kazuo FUNATO
Graduate School of Sport System, Kokushikan University / Tokyo, Japan
Email: s1dd002x@kokushikan.ac.jp

INTRODUCTION

As one of the important foot functions, medial longitudinal arch (MLA) play spring-like action far braking and accelerating of movement. During the stance phase, MLA changes in response to load, absorbing shock at foot contact and generating propulsive force during push off phase [1]. The load applied to the foot during contact is called plantar load, and to date has been evaluated using a plantar pressure measurement plate. One of the problems in evaluating plantar load is how to divide the foot into sections and quantify the load at each plantar region. It is difficult to quantify and evaluate how much load is applied to any section of the foot, because the anthropometry of the foot differs from person to person.

To overcome this problem, automated and objective footprint masking based on anatomical structures of the foot was developed [2]. The running has a high incidence of foot-related injuries, and the evaluation of plantar load based on the foot anatomical structures and the shock absorption of MLA are considered to predict and prevent sports injuries. Therefore, the purpose of this study was to quantify changes in MLA and the plantar load distribution during running.

METHODS

Eight healthy male subjects participated in this study (Age 20.8±3.4 years; Height 174.2±4.7 cm; Mass 69.9±5.6 kg). Plantar pressure measurement plate (Novel GmbH®, 100Hz), motion capture system (Oxford, 100Hz) and force plate (Kistler, 1KHz) were synchronized. Using this system, subjects performed running trial at 2.78m/s. Plantar load distribution was divided into five sub-area based on anatomical measurement points [2]. MLA angle was calculated as the angle between the distal first metatarsal, navicular tuberosity and calcaneus, and first metatarsophalangeal joint (MTPJ) angle as the angle between the hallux, distal and proximal first metatarsal.

RESULTS AND DISCUSSION

Plantar loads were observed on the medial and lateral hindfoot and the lateral forefoot at foot contact, followed by the medial forefoot and the midfoot after 10% of the normalized time from foot contact to toe off (Fig. 1A). Lateral forefoot and total plantar loads showed maximum values at 40%, followed by a gradual decrease (Fig. 1A). The medial forefoot load tended to increase after 40%, reaching a maximum value at 50% and then gradually decreasing (Fig. 1A). The load shift from the lateral to medial forefoot observed in this study may be a function of the foot's ability to increase foot stiffness during push off (Fig. 1A). MLA angle showed the greatest amount of change around 40%, when the maximum load value was shown (Fig. 1A, B). At this point, a large load was applied to the forefoot, and MLA seems to play a role in absorbing the load to the foot (Fig. 1A, B). Hick's [3] windlass mechanism is that dorsiflexion of MTPJ tightens the plantar aponeurosis and, thereby, pulls the calcaneus and metatarsal heads towards each other and stiffens the foot. In this study, there was also a tendency for MLA angle to decrease with MTPJ dorsiflexion (Fig. 1B, C). In addition, ground reaction force (GRF) tended to increase in the anterior direction after 60%, when MTPJ was dorsiflexed (Fig. 1C, D). From these results, it is assumed to dorsiflexion of MTPJ increased the stiffness of the foot and forward propulsion.

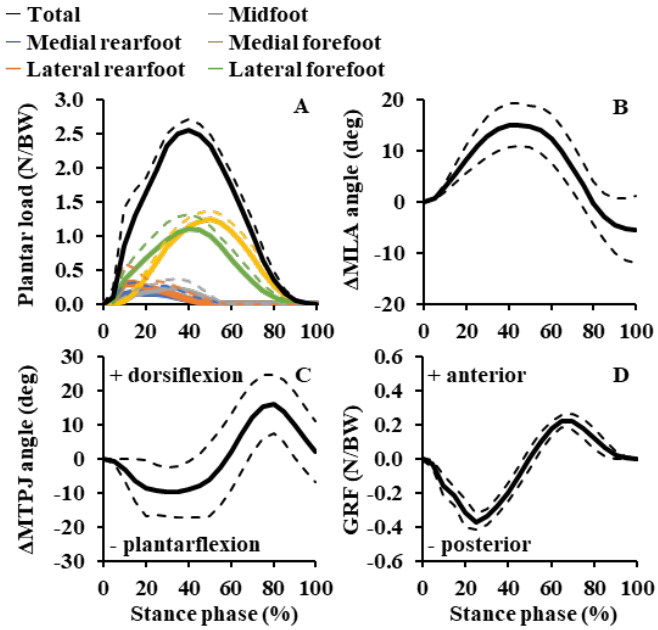

Figure 1 Temporal changes (A) 5 sub-area plantar loads distribution (B) MLA angle (C) GRF (D) MTPJ angle during running

CONCLUSIONS

MLA is a flexible structure that absorbs plantar load during foot contact, and it was assumed that the dorsiflexion of MTPJ during push off contributed to the increase in foot stiffness to support forward propulsion from the forefoot.

ACKNOWLEDGEMENTS

This study was funded by the Descente and Ishimoto Memorial Foundation for the Promotion of Sports Science.

REFERENCES

[1] C. Mahieu et al. *Int Biomech* **6**: 75-84, 2019.
[2] J. Stebbins et al. *Gait Posture* **22**: 372-376, 2005.
[3] J. Hicks. *J Anat* **88**: 25-30, 1954.

Biceps Femoris Shortens Actively during the Late Swing Phase of High-speed Running

Junhee Yoon[1,3], Hae-Dong Lee[2,3]
[1] Department of Physical Education Graduate School, Yonsei University / Seoul, Korea.
[2] Department of Physical Education, College of Educational Sciences, Yonsei University/ Seoul, Korea
[3] Frontier Research Institute of Convergence Sports Science, Yonsei University/ Seoul, Korea
Email: beargom_@yonsei.ac.kr

INTRODUCTION

Hamstring strain injury (HSI) commonly occurs in sports involving high-speed running [1]. HSI primarily happens in the late swing phase due to the hamstring muscle-tendon unit (MTU) reaching its maximum length [2]. Recent studies showed that accuracy in predicting muscle behavior through joint kinematics could not be guaranteed because of the interaction between muscle and elastic tendon within an MTU [3]. Thus, in the swing phase of high-speed running, the hamstring muscle behavior may act differently from the MTU behavior.

This study investigated the fascicle and MTU behavior and the activation of the biceps femoris long head (BFlh) during the swing phase of high-speed running.

METHODS

Nine recreationally active males (age 24 ± 1.7 years; height 178.7 ± 6.1 cm; weight 78.8 ± 6.3 kg) ran at 70, 80, and 90% of their maximum running speed on a treadmill. Kinematics of the hip and knee joints were collected during running. Muscle activation of BFlh was also recorded using surface electromyography (sEMG). The fascicle length of BFlh was monitored using a B-mode real-time ultrasound imaging system.

During the swing phase, one-way repeated measures ANOVA was performed to investigate the differences in the hip and knee joint angle, fascicle behavior, MTU behavior, and muscle activation of BFlh between each speed.

RESULTS AND DISCUSSION

The MTU length changes of the BFlh during the swing phase increased significantly as the speed increased ($p < .05$), from 70% to 80%. There was no significant difference in fascicle length change during the swing phase when the running speed increased. Unlike MTU behavior, the fascicle was actively lengthened with weak activation during the early to the middle swing phase but actively shortened with strong activation during the late swing phase.

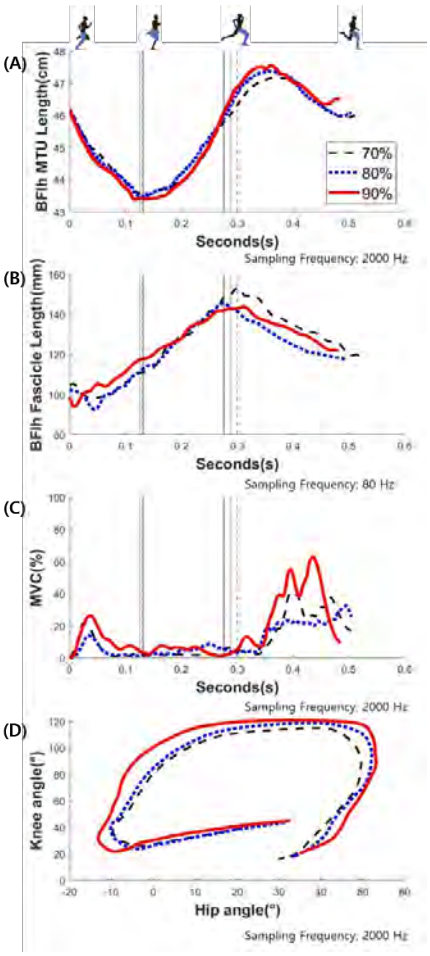

Figure 1 Sample raw data for a representative subject. (A) BFlh MTU behavior, (B) BFlh fascicle behavior, (C) BFlh muscle activation, and (D) hip angle to knee angle during the swing phase. Vertical lines represent the phase divisions 70% (broken line), 80% (dotted line), and 90% (solid line).

CONCLUSIONS

In this study, the BFlh fascicle actively shortens during the late swing phase. Also, during the swing phase, fascicle behavior was asynchronous with the MTU behavior in BFlh. The MTU length and muscle activation significantly increased as the speed increased, but the fascicle length behaved isometrically.

REFERENCES

[1] Dalton et al. *The American journal of sports medicine* **43.11**: 2671-2679, 2015.

[2] Chumanov et al. *Medicine and science in sports and exercise* **43.3**: 525, 2011

[3] Fukunanga et al. *Exercise and sport sciences reviews* **30.3**: 106-110, 2002

PROSPECTIVE IDENTIFICATION OF MUSCULOSKELETAL INJURY RISK IN ELITE COLLEGE DISTANCE RUNNERS USING GROUND REACTION FORCES

Harper E. Stewart[1], Michael E. Hahn[4], Rodger Kram[5], Alena M. Grabowski[5], Rand R. Wilcox[3], and Jill L. McNitt-Gray[1,2]
[1]Biomedical Engineering, [2]Biological Sciences, [3]Psychology, University of Southern California, Los Angeles, USA. [4] Human Physiology, University of Oregon, Eugene, USA. [5]Integrative Physiology, University of Colorado Boulder, Boulder, USA.
Email: hestewar@usc.edu

INTRODUCTION

Previous studies have reported contradicting results about biomechanical factors contributing to running-related injuries.[1] We sought to prospectively identify runners at risk for injury using ground reaction force (GRF)-time characteristics. We hypothesized that runners with a subsequent musculoskeletal injury would have more GRF characteristics outside statistical boundaries of non-injured runners.

METHODS

Thirty-three National Collegiate Athletic Association Division I endurance runners (22 F, 11 M) provided informed consent in this IRB approved multi-institutional study. GRFs were measured for multiple foot contacts at 1000Hz using over-ground force plates (Kistler) or instrumented treadmills (Treadmetrix and Bertec). Athletes ran at 7 min/mi (3.83 m/s). Data were filtered with a low-pass 4th-order Butterworth recursive filter (50Hz treadmill, 75Hz over-ground) using custom Python and R scripts. Nine (out of 33) athletes experienced a musculoskeletal injury. We selected ten GRF variables for each leg in the vertical and anterior-posterior directions. These included contact time, braking time, average vertical GRF during braking and propulsion (Avg $_V$GRF Brake, Avg $_V$GRF Prop), average anterior-posterior GRF during braking and propulsion (Avg $_{AP}$GRF Brake, Avg $_{AP}$GRF Prop), change in vertical velocity during braking and propulsion (Δv_V Brake, Δv_V Prop), change in anterior-posterior velocity during braking and propulsion (ΔvAP Brake, ΔvAP Prop). We established boundaries for all non-injured athletes as Median +/- Scaled Median Absolute Deviation (MADN) [2] (Table 1).

Table 1: Median (MADN) GRF variables in uninjured runners.

Median (MADN)	*Braking*	*Propulsion*
Avg GRF_V (BW)	1.951 (0.140)	1.329 (0.147)
Avg GRF_{AP} (BW)	-0.200 (0.024)	0.219 (0.027)
Δv_V (m/s)	0.955 (0.123)	0.328 (0.134)
Δv_{AP} (m/s)	-0.195 (0.022)	0.210 (0.029)
Time (ms)	Braking: 98 (9)	Contact: 198 (12)

We used a robust distance measure (RDM) [2] to determine if a GRF variable was within the boundaries of non-injured runners (Fig 1). Cliff's method was used to test the probability that an injured runner would have more variables outside the non-injured boundaries.[2]

RESULTS AND DISCUSSION

The median number of variables outside the boundaries was 3 for non-injured and 4 for injured athletes. We found no statistically significant difference (p=0.17) between injured and non-injured legs, which may be due to low power from the small sample size.

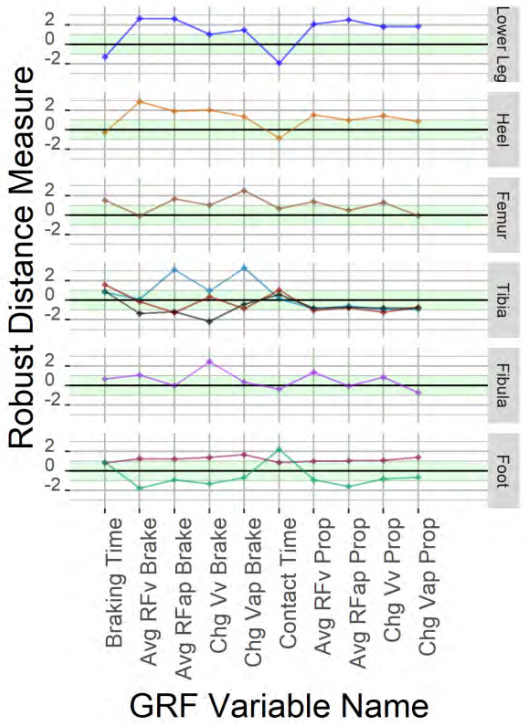

Figure 1: Robust Distance Measures (RDM) of GRF variables for nine injured athletes. Green indicates Median +/- MADN. Individuals are ordered by soft tissue injury (top 2 rows) and by bone stress response location. (+ = higher force/velocity/time).

CONCLUSIONS

Our new method identifies GRF variables that may contribute to running-related injuries.

ACKNOWLEDGEMENTS

Supported by the Pac12 SAHWB Grant Program (#3-03_PAC-12-Oregon-Hahn-17-02), ARCS Foundation, & USC WiSE.

REFERENCES

[1] Schmida E A et al. *MSSE* 1;54(8):1382-1388, 2022

[2] Wilcox R, *Modern Statistics for the Social and Behavioral Sciences*, 2nd Ed, 2017

GRADED RUNNING DOES NOT IMPACT JOINT WORK ASYMMETRY IN HEALTHY RUNNERS

Rachel Robinson[1], Seth Donahue[2], Aida Chebbi[1], Michael Hahn[1]
[1] Department of Human Physiology, University of Oregon, Eugene, OR, USA.
[2] Northwestern University Prosthetics-Orthotics Center, Northwestern University, Chicago, IL, USA.
Email: rrobins3@uoregon.edu

INTRODUCTION

Between-limb asymmetry of running biomechanics is often examined as a running related injury risk factor and consideration for return to training after injury. Additionally, higher levels of asymmetry have been associated with reduced mechanical efficiency which would impact running performance [1]. While expected levels of asymmetry have been characterized for level ground (LG) running across a range of speeds in healthy runners [2], the amount of expected asymmetry during incline (INC) and decline (DEC) running is unknown. Determining the effect of graded surfaces on asymmetry would inform return to run prescription and training program design. Furthermore, establishing expected values for healthy runners will inform future studies that aim to examine the effect of asymmetry on injury risk and performance. Therefore, the purpose of this study is to determine the effect of graded running on joint work asymmetry at the hip, knee, and ankle.

METHODS

Eleven healthy, recreational runners (7 females, age: 25 years, mass: 63 kg, height: 170 cm) completed thirteen 30s running trials at 5 speeds across 3 grades (LG, 7.5° INC and 7.5° DEC). Kinematic data were collected at 200 Hz using an 8-camera motion capture system (Motion Analysis Corp.) and kinetic data were collected at 1000 Hz using a force-instrumented treadmill (Bertec). Each participant's slowest speed (1:30 min/mile slower than self-reported 5k pace; average 3.20 m/s) was utilized for analysis, as this was the estimated speed at which participants performed the majority of their training volume. Sagittal plane hip, knee, and ankle power were calculated using inverse dynamics in Visual 3D (C-Motion, Inc.). Stance phase positive and negative work were calculated for each joint by integrating the positive and negative portions of the power-time curves, respectively (Figure 1). Symmetry angle was utilized to calculate between-limb asymmetry for each variable [3]. Repeated-measures ANOVAs were performed using SPSS (IBM) to determine the effect of grade on joint work asymmetry.

RESULTS AND DISCUSSION

Across grades, asymmetry was lowest at the ankle (<3.5%), followed by the knee (5.5-10.25%) and hip (6.79-19.25%), which is consistent with previous LG studies [2]. Inter-subject variability of joint work asymmetry was high (Table 1). No significant effect of grade was detected for between-limb asymmetry of negative or positive ankle and knee work or negative hip work ($p > 0.05$). However, positive hip work asymmetry was significantly higher in the DEC condition compared to INC ($p = 0.003$). Since positive hip work is minimal in DEC running (Figure 1), small absolute differences in hip work result in a large relative asymmetry.

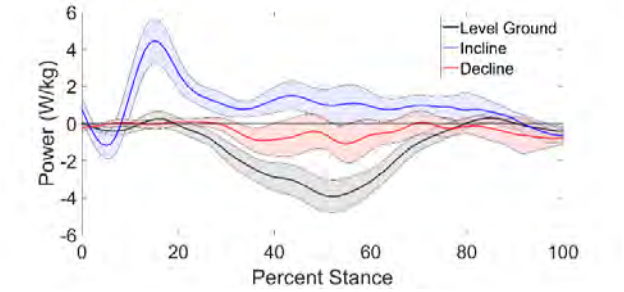

Figure 1 Hip power across grades for one exemplar participant. Work is calculated as the area under the power-time curve (J/kg). Shaded areas represent ± 1 standard deviation.

CONCLUSIONS

Joint work asymmetry changes minimally in response to graded running. While positive hip work asymmetry is higher in DEC running, this appears to be due to the minimal amount of positive hip work performed while running downhill and is not likely clinically significant.

ACKNOWLEDGEMENTS

This work was supported by the Wu Tsai Human Performance Alliance and the Joe and Clara Tsai Foundation.

REFERENCES

[1] Melo C et al. *J Biomech* **109**:1-5, 2020
[2] Stiffler-Joachim M et al. *MSSE* **53**:945-950, 2021
[3] Zifchock R et al. *Gait & Posture* **27**:622-627, 2008

Table 1: Joint work asymmetry across level ground, incline, and decline conditions

	Level Ground	Incline	Decline
Stance Phase Negative Work Asymmetry (%)			
Hip	9.46 (9.42)	16.17 (8.77)	12.90 (11.56)
Knee	5.59 (3.53)	5.28 (4.71)	6.32 (3.82)
Ankle	2.95 (4.38)	3.85 (1.6)	2.99 (1.57)
Stance Phase Positive Work Asymmetry (%)			
Hip	17.06 (15.74)	6.79 (5.02)*	19.24 (11.48)*
Knee	5.50 (4.75)	7.05 (4.98)	10.25 (9.10)
Ankle	1.76 (1.84)	2.76 (1.54)	3.3 (2.86)

* significantly different ($p = 0.003$)
Data are presented as mean (standard deviation)

SPEED DEPENDENT CHANGES TO ANKLE JOINT MECHANICS DURING INCLINE RUNNING

Hidetaka Hayashi [1], Rachel Robinson[1], Seth Donahue[2], Aida Chebbi[1], Michael Hahn[1]
[1] Department of Human Physiology, University of Oregon, Eugene, USA.
[2] Northwestern University Prosthetics-Orthotics Center, Northwestern University, Chicago, USA
Email: hhayash7@uoregon.edu

INTRODUCTION

Uphill running is characterized by an increased demand for work performed and is often incorporated in a runner's training regimen. Previous studies have reported an increase in ankle joint work and power with grade during stance phase, while joint moment remained unchanged [1, 2]. This suggests that an increase in joint angular velocity is the source of increased power, and thus increased work. Indeed, it has been shown that the shortening velocity of the gastrocnemius muscle-tendon unit (MTU) increases with grade [3], leading to an effective increase in joint angular velocity. While the effect of grade has been well documented, the role of speed on the mechanical properties of the ankle joint is still unclear. Therefore, the purpose of this study was to clarify the effect of speed on ankle joint mechanics during incline treadmill running.

METHODS

Seven healthy, recreational runners (2M, 5F; age: 24.5 years, height: 176.8 cm, mass: 67.7 kg) completed 30s running trials at 4 speeds with a grade of 7.5˚ incline on a force-instrumented treadmill (Bertec). Speeds were relative to each participant's self-reported 5k pace (Speed 4), where Speeds 1, 2, and 3 were 1:30, 1:00, and 0:30 min/mile slower, respectively. Kinematic data were collected using an 8-camera motion capture system at 200 Hz (Motion Analysis Corp.), and force data were collected at 1 kHz. Peak plantar flexion (PF) and dorsiflexion (DF) angular velocity was calculated from joint kinematic data. Ankle joint power was calculated using an inverse dynamics approach in Visual3D (C-motion), and work was defined as the time-integral of power (Figure 1). The effect of speed on dependent variables was assessed with a one-way repeated measures ANOVA using SPSS (IBM Corp.).

RESULTS AND DISCUSSION

Both peak positive and negative power increased with speed ($p < .001$), while there was no significant effect of speed on net work ($p = .235$). Peak PF and DF angular velocity increased with speed ($p < .001$; $p = .022$, respectively). Post-hoc pairwise comparisons with Bonferroni correction are summarized in Table 1.

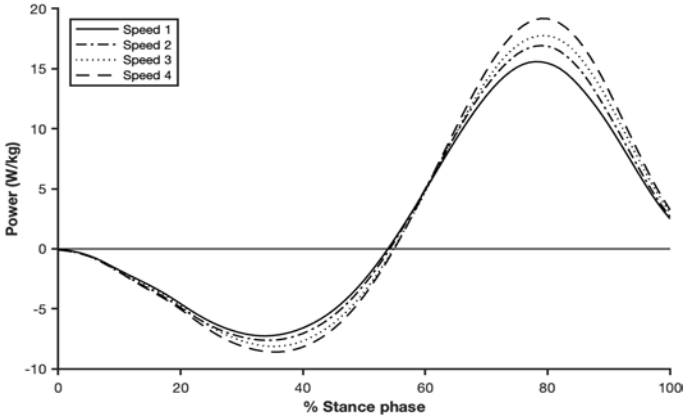

Figure 1 Ankle joint power (W/kg) during stance (average of 7 subjects).

CONCLUSIONS

No change in ankle joint net work was observed, while peak positive and negative power increased. This increase in power may be attributed to the observed increase in joint angular velocity, suggesting greater stretch and recoil of tendinous tissue. Future work should clarify further the contribution of the whole MTU to joint power, specifically about the ankle joint.

ACKNOWLEDGEMENTS

This work was supported by the Wu Tsai Human Performance Alliance and the Joe and Clara Tsai Foundation.

REFERENCES

[1] Roberts & Belliveau *J Exp Biol* **208**: 1963-70, 2005
[2] Nuckols et al. *PLoS One* **15**(8): e0231996, 2020
[3] Lichtwark & Wilson *J Exp Biol* **209**: 4379-88, 2006

Table 1. Average values of ankle joint work, power, and angular velocity across 4 speeds (n = 7)

	Speed 1	Speed 2	Speed 3	Speed 4	*p-value*
Net work (J/kg)	0.54 ± 0.13	0.56 ± 0.15	0.57 ± 0.12	0.59 ± 0.14	$p = .235$
Peak positive power (W/kg)	15.83 ± 1.37	17.15 ± 1.92	18.01 ± 1.84[a]	19.40 ± 1.66[a,b,c]	$p < .001$
Peak negative power (W/kg)	-7.49 ± 1.8	-7.82 ± 1.63	-8.29 ± 1.85[a]	-8.82 ± 1.84[a,c]	$p < .001$
Peak PF velocity (˚/sec)	-612.68 ± 43.74	-642.64 ± 50.24[a]	-666.45 ± 49.07[a,b]	-690.60 ± 46.86[a,b,c]	$p < .001$
Peak DF velocity (˚/sec)	242.71 ± 47.23	249.53 ± 40.82	254.63 ± 40.15	259.78 ± 35.86	$p = .022$

Values are mean ± SD. a: difference between Speed 1; b: difference between Speed 2; c: difference between Speed 3.

The effects of foot torsional stiffness on foot kinematics and impact force during running

Tomohito Nakatsugawa[1], Yuya Ezawa[1] and Takeo Maruyama[2]
[1] Department of Social and Human Sciences, School of Environment and Society, Tokyo Institute of Technology, Tokyo, Japan.
[2] Institute for Liberal Arts, Tokyo Institute of Technology, Tokyo, Japan.
Email: nakatsugawa.t.aa@m.titech.ac.jp

INTRODUCTION

Foot torsional stiffness evaluates foot complex motion in three planes and viscoelasty of the midfoot. Previous studies have shown that abnormal foot torsional stiffness exhibits abnormal foot kinematics during gait, which is associated with a history of overuse injuries [1,2]. However, no study examines the influence of foot torsional stiffness on foot kinematics and kinetics during running. The purpose of this study was to investigate the relationship among foot torsional stiffness, multi-segment foot kinematics, and kinetics during running.

METHODS

Twenty-nine healthy adults participated in this study and 12 subjects (7 females and 5 males) who ran with rearfoot strike were analyzed. We simultaneously measured midfoot passive resistance torque and forefoot frontal plane motion relative to rearfoot from forefoot maximum pronation to supination (Figure 1). Foot torsional stiffness was calculated by dividing the torque change by segmental excursion between forefoot 5° of eversion to 5° of inversion. This range corresponds to the forefoot frontal plane range of motion measured during the stance phase of gait [3]. Subjects ran barefoot at 3.3 m/s ± 10% along the 10-m runway and collected ground reaction force and three-dimensional kinematics of the shank, rearfoot, and forefoot. We calculated the peak fore-/rearfoot angle and excursion in the absorption and propulsive phases. We also calculated the impact peak, active peak, initial loading rate, and second loading rate as variables of impact force [4]. The relationships among foot torsional stiffness, kinematics, and kinetics were explored using Pearson's correlation coefficients ($\alpha = 0.05$).

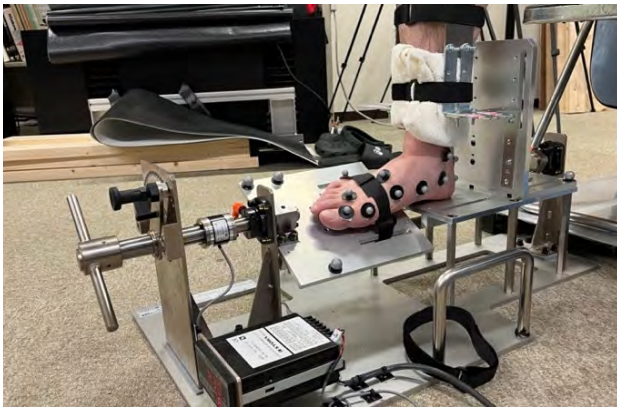

Figure 1 Measurement of midfoot passive resistance torque and three-dimensional foot kinematics.

RESULTS AND DISCUSSION

The foot torsional stiffness was significantly correlated with peak rearfoot inversion ($r = 0.65$, $p = 0.02$) in the propulsion phase and active peak ($r = 0.62$, $p = 0.03$), respectively. High foot torsional stiffness was associated with greater rearfoot inversion. The medial longitudinal arch elevation that occurs in the propulsive phase would increase the foot stiffness, which makes it possible to generate propulsive force efficiently. Considering rearfoot inversion is part of foot supination, it is possible that the foot with high foot torsional stiffness contributes to generating propulsive forces efficiently by elevating the arch in running. Moreover, high foot torsional stiffness was also associated with a higher active peak. Because the foot arch is depressed by the load at foot flat where active peak occurs, the value of active peak is considered to be an index of shock absorption by foot arch [4]. Thus, high foot torsional stiffness may prevent efficient shock absorption. Foot torsional stiffness depends on soft tissues such as intrinsic foot muscles, ligaments, and plantar aponeurosis across the midfoot. These soft tissues contribute to shock absorption in early to mid-stance, while they also contribute to energy return and the rigidity of the medial longitudinal arch in late stance. In particular, intrinsic foot muscles contract concentrically or eccentrically according to the magnitude of the load, which provides proper rigidity of the foot. Increasing the stiffness of the foot in propulsive phase allows the foot to transmit force to the ground efficiently and potentially reduces excessive strain on the soft tissues of the foot [5].

CONCLUSIONS

Foot torsional stiffness affects the foot kinematics and impact force during running as well as walking. High foot torsional stiffness appears to be effective for generating propulsion, while it may be inefficient from the point of view of shock absorption. This finding suggests that evaluating foot torsional stiffness may help in the selection of footwear and foot orthoses for rearfoot strikers.

REFERENCES

[1] Gomes, R.B. et al. *Gait Posture* **70**: 20-3, 2019.
[2] Magalhães, F.A. et al. *J Biomech* **119**: 110328, 2021.
[3] Levinger, P. et al. *Gait Posture* **32**: 519-23, 2010.
[4] Williams III, D.B. et al. *J Athl Train* **49**: 290-6, 2014.
[5] Kelly, L.A. et al. *J R Soc Interface* **12**: 20141076, 2015

The Influence of Fast Running Speed on Joint Coupling Angle between Ankle and Knee Joints in Unilateral Patellofemoral Pain

Chia-Li Hsu[1], Tunpisith Jeamsupakorn[2,5], Chich-Haung Richard Yang[2,4,5], Kuan-Lin Liu[2,3]
[1] Department of Physical Medicine &Rehabilitation; [2]Sports Medicine Center; [3]Department of Orthopedic Surgery, Hualien Tzu Chi Hospital, Buddhist Tzu Chi Medical Foundation, Hualien, Taiwan.
[4]Department of Physical Therapy; [5]Institute of Medical Science, College of Medicine, Tzu Chi University, Hualien, Taiwan.Email: r.chyang@gms.tcu.edu.tw

INTRODUCTION

Patellofemoral pain (PFP) is the most common condition that often increases compression forces and loads over the patella during dynamic activities such as stairs ascending and descending, jumping, running, and squatting [1]. A common cause is multifactorial, including biomechanical problems, muscle dysfunction, and overuse injury [2]. Changes in neuromotor control in running patterns could be a precursor to persistent symptoms, such as pain, in runners with PFP. An increase in running speed may contribute to moderate alterations in the frequency of joint coupling movement patterns [3]. We aimed to examine whether changes in the joint coupling angle of the knee and ankle joints during fast appear in individuals with PFP compared to healthy controls.

METHODS

15 recreational runners with PFP (age 36.5±9.9 years, BMI 22.3±2.9 kg/m^2) and 15 healthy controls (age 27.4±8.4 years, BMI 22.4±2.5 kg/m^2) were recruited. The PFP group has reported unilateral anterior or retropatellar knee pain during functional activity, pain on patellar palpation, and symptoms lasting at least 3 months on and off, with pain VAS of at least 3/10. We collected data during fast running (120% of self-selected speed) on the treadmill at a fast speed. Using vector coding technique to calculate the joint coupling angle between ankle and knee joint in the sagittal plane at fast running speed. The result was shown in the mean joint coupling angle of both groups, SPM1d t-test and p-value bar graph. In the mean joint coupling angle graph, the left y-axis is the degree of joint coupling angle, the right y-axis is the coordination pattern (proximal (knee) phase, in phase, distal (ankle) phase, and anti-phase) [4].

RESULTS AND DISCUSSION

In fast running speed during the initial stance phase of running, the PFP group showed increased knee flexion while ankle dorsiflexion (Anti-phase distal dominance). Then, from the mid-stance to the terminal stance of the running cycle, the PFP group showed decreased knee flexion while ankle dorsiflexion with knee extension while ankle plantar-flexion (In proximal phase dominance). In the terminal stance phase, the PFP group showed increased knee flexion while ankle plantar flexion to knee extension while ankle plantar flexion. In the early float phase, the PFP group showed an increase in knee extension during ankle dorsiflexion. During the swing phase, the PFP group showed a decrease in knee flexion while ankle dorsiflexion for knee extension during ankle flexion. During the late float, the PFP group showed a decline in knee extension in the late phase to increase knee extension during ankle dorsiflexion. (Figure 1). These findings have shown a significant impact on the understanding the neuromuscular control of knee and ankle coupling angles during fast running in runners with PFP.

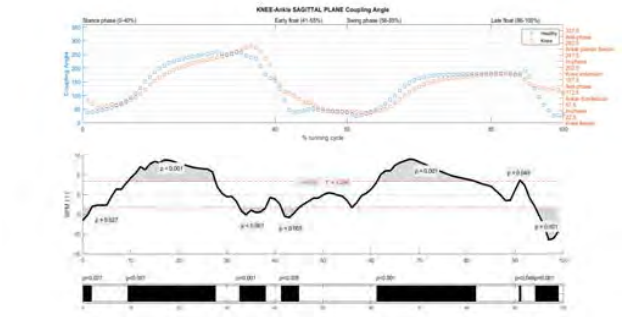

Figure 1. Knee-Ankle coupling angle in the sagittal plane during fast speed running

CONCLUSIONS

Individuals with PFP may employ a compensatory motor strategy in the knee and ankle coupling angle to adapt their functional movements, such as fast running. These findings could provide a further understanding of impairments in movement control to improve optimal rehabilitation for these populations.

ACKNOWLEDGEMENTS

We express our thanks to the financial support from Intramural research grant (TCRD109-49), the Buddhist Tzu Chi Medical Foundation, Taiwan.

REFERENCES

[1] Powers CM et al., J Orthop Sports Phys Ther, 42(6), A1-54, 2012.
[2] Lankhorst NE et al., Br J Sports Med, 47(4), 193-206, 2013.
[3] Floría, P et al., Human Movement Science, 66, 449-458, 2019.
[4] Needham RA et al., ISBS Proceedings Archive, 35(1), 131, 2017.

STEP-TO-STEP CHANGES IN LOWER LIMB MUSCLE ACTIVITY DURING THE ACCELERATION STAGE OF SPRINTING

Keiichiro Hata[1,2], Hiroaki Noro[3], Yohei Yamazaki[1,2], Tetsuo Fukunaga[2], Ryu Nagahara[4] and Toshio Yanagiya[1,2]
[1] *Graduate school of Health and Sports Science, Juntendo University, Chiba, Japan*
[2] *Institute of Health and Sports Science & Medicine, Juntendo University, Chiba, Japan*
[3] *Faculty of Health and Sports Science, Juntendo University, Chiba, Japan*
[4] *National Institute of Fitness and Sports in Kanoya, Kanoya, Japan*
Email: kichiro.ht@gmail.com

INTRODUCTION

Power output onto the ground is necessary during the human accelerated sprinting. Previous studies indicated that the contractile component of the muscles is responsible for the power output during low-velocity running, whereas the stored elastic energy in the series elastic elements enhances power output during high-velocity running [1, 2]. Based on these concepts, it was expected that the lower limb muscle activation pattern would vary with increasing running velocity during sprint acceleration. This study aimed to determine the electromyogram (EMG) of the lower limb muscles during the acceleration stage of sprinting.

METHODS

Four male sprinters (Table 1) performed 70-m sprinting from starting blocks in the indoor track. EMGs for lower limb 16 muscles (rectus femoris [RF], vastus medialis [VM] and lateralis [VL], biceps femoris [BF], gastrocnemius medialis [GM] and lateralis [GL], soleus [SOL], and tibialis [TA] muscles of both right and left lower limbs) were recorded at each step using telemetric surface EMG system (Noraxon, USA, Inc., Scottsdale, AZ, 2kHz). EMG signals were filtered using a band-pass filter (20–450 Hz) and smoothed using root mean squared analysis (Time window: 25 ms). The maximum muscle activation obtained during the sprinting was used to normalize EMG. Ground reaction forces in each step were measured using a 50-m force plate system (Tec Gihan Co. Ltd, Uji, Japan, 1 kHz). The integral EMG (iEMG) and the ratio of iEMG during the braking and propulsive phases (iEMG ratio) were calculated.

Table 1: Characteristics of participants

	Age (years)	Height (m)	Mass (kg)	100-m personal best (s)
Sprinter A	21	1.69	68.9	10.36
Sprinter B	27	1.82	70.0	10.62
Sprinter C	22	1.73	64.3	11.30
Hurdler D	21	1.67	65.5	10.81
Mean	23.5	1.73	67.2	10.77
SD	2.6	0.59	2.3	0.34

RESULTS AND DISCUSSION

The iEMG was the highest immediately after the block clearance and gradually decreased with increasing velocity until a certain activation level in the acceleration stage was achieved and maintained (Figure 1). Participants reached 80% of their maximum running velocity (80%V_{max}) at 7-10 steps. Greater iEMG was observed in the propulsive phase, compared with braking phase until 80%Vmax. This suggest that concentric force production by the lower limb muscles can be important for initial accelerating the human body. In contrast, with increasing running velocity above 80%V_{max}, iEMG gradually decreased in the propulsive phase and increased in the braking phase. In this high-velocity acceleration stage, the elastic energy stored in a series elastic element would enhance the power output, possibly resulting in a decrease in iEMG in the propulsive phase.

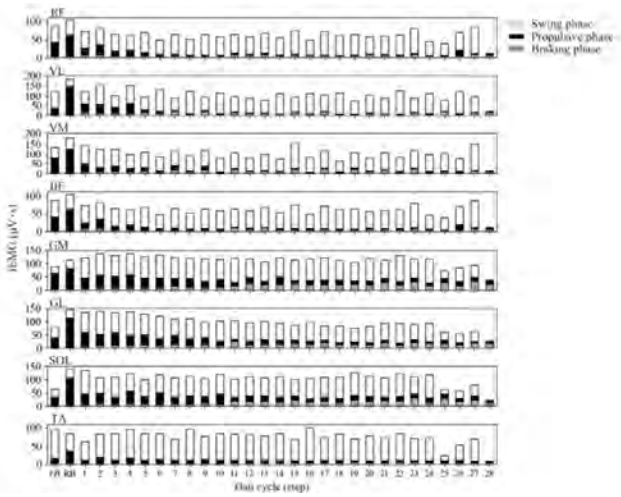

Figure 1 Results of iEMG of support leg across each step during sprinting for sprinter A. FB and RB indicated the front and rear block clearance, respectively. Over 80%V_{max} was reached at step 10.

CONCLUSIONS

From the block clearance to 80%V_{max}, iEMG in the propulsive phase accounts for the majority of the total iEMG in the stance phase. As the running velocity increased, the rate of iEMG in the braking phase increased.

REFERENCES

[1] Cavagna et al. *The Journal of Physiology 217*(3): 709–72, 1971.
[2] Matsuo et al. *Journal of Experimental Biology* 222(5): 2019

KINEMATICS OF MAXIMAL VELOCITY RUNNING: FACTORS TO FURTHER ENHANCE STEP LENGTH AND FREQUENCY

Takeo Matsubayashi[1], Mai Kameda[1], Takafumi Kageyuki[1] and Amane Zushi[1]
[1] Department of Sport Science and Research, Japan Institute of Sports Sciences, Tokyo, Japan.
Email: takeo.matsubayashi@jpnsport.go.jp

INTRODUCTION

Kinematics of maximal velocity running and its relation to maximal runing velocity have been investigated in several studies. However, it is not fully understood how it relates to the two components of running velocity independently, i.e., step length (SL) and step frequency (SF). To enhance maximal running velocity, one have to improve either or both SL and SF depending on their trainability. Therefore, it is important to understand the running kinematics required to improve each component separately. The aims of this study were 1) to examine the relation between SL, SF, and running kinematics, and 2) to elicit what kind of running motion would be required to improve SL and SF.

METHODS

Japanese male track and field athletes (n=102, including sprinters, hurdlers, long jumpers, decathletes; maximal running velocity, 10.17±0.32 m/s) participated in this study. Their maximal velocity running was captured using a 250-Hz optical motion capture system. Spatiotemporal and kinematic parameters, e.g., contact time (CT), flight time (FT), contact length (CL), segment/joint angles and angular velocities in the sagittal plane, were obtained from two consecutive left and right steps of each athlete. Multiple regression analysis was used to examine the relation between SL, SF, and the running kinematics: it can elicit the effect of one explanatory variable with those of the others standardized, allowing the kinematics related to SL and SF to be examined independently. Regression models were developed with each spatiotemporal and kinematic parameter as a dependent variable and with SL, SF, and leg length as explanatory variables. Leg length was included to standardize the effect of body dimensions. The effects were determined based on the statistical significance (α=0.05) of the standardized partial regression coefficients (β).

RESULTS AND DISCUSSION

SL and SF were both found to be negatively related to CT (β=-0.44 and -0.98 for SL and SF, respectively), implying that an increase in maximal running velocity should be accompanied by a reduction in CT, irrespective of whether SL or SF is improved. However, it should be noted that the effect of SL was smaller than that of SF. This may reflect the inherent demand of longer CT for longer SL: longer SL should be accompanied by longer FT (β=0.34), which may require a greater impulse during the stance phase, and longer CT would be preferred for this. This is also supported by the positive relation between SL and CL (β=0.28), suggesting that a slightly longer CT can be achieved with a longer CL. Correspondingly, the kinematics of the stance-leg knee joint was found to be related to SL (Figure 1 top). Longer SL was accompanied by a more extended stance-leg knee joint (β=0.25) and a more forward swung stance-leg shank segment (β=0.34) at toe-on; the knee joint was largely flexed after toe-on (β=0.30), although its maximum flexion angle was not marked (β=0.03, $p>0.05$). This stance knee joint motion may play an important role in achieving a longer CL. SL was also found to be related to the forward lean angle of the trunk at toe-on (β=0.32) and toe-off (β=0.28). Due to this forward leaned trunk, the extended knee joint was not associated with a larger center-of-mass (CoM) -toe distance at toe-on (β=0.09, $p>0.05$). On the other hand, the distance at toe-off was larger for longer SL (β=0.44). As for SF, it was found to be negatively related to CL (β=-0.27) and CoM-toe distance at toe-on (β=-0.47), which was mainly due to a more forward leaned trunk at the toe-on (β=0.46, larger effect than SL, Figure 1 bottom). Smaller CoM-toe distance at toe-on suggests that a breaking impulse may be smaller, and this may be a key to keeping SL unshortened. SF was also related to the angular velocity of the swing-leg knee flexion (β=0.54), suggesting that a lower moment of inertia would allow faster forward recovery of the swing leg and higher SF.

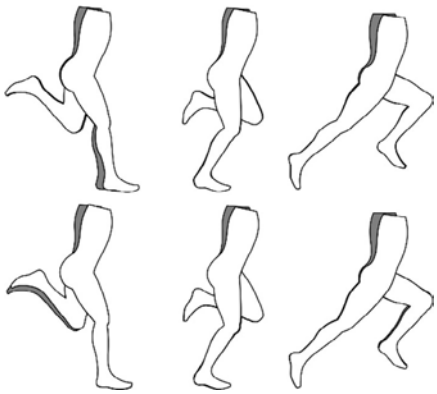

Figure 1 Running motions related to longer SL (top) and higher SF (bottom) respectively, plotted over the average running motion derived from the present data (dark silhouette).

CONCLUSIONS

The current study successfully elicited the motions related to greater SL and SF separately: longer SL was mainly related to longer CL and larger stance-leg knee movement, whereas higher SF was related to smaller CoM-toe distance at toe-on with forward leaned trunk and faster swing leg knee flexion. Acquisition of these motions would help to enhance maximal running velocity with improved SL and/or SF.